F 1103

04
REFERÁLVA

REVUE ROUMAINE DE CHIMIE

Hommage à I. G. MURGULESCU pour son 70e anniversaire

TOME 17
Nos 1, 2
Janvier-Février 1972

ÉDITIONS DE L'ACADÉMIE DE LA RÉPUBLIQUE SOCIALISTE DE ROUMANIE

Rev. Roumaine Chim.

17, *1*, *2*, 1 – 420 (1972) Bucarest

COMITÉ DE RÉDACTION

Rédacteur en chef :

I. G. MURGULESCU, membre de l'Académie de la République Socialiste de Roumanie

Rédacteurs en chef adjoints :

A. T. BALABAN et V. E. SAHINI, membres correspondants de l'Académie de la République Socialiste de Roumanie

Collège de rédaction :

C. DRĂGULESCU, RALUCA RIPAN, CR. SIMIONESCU, membres de l'Académie de la République Socialiste de Roumanie; EM. BRATU, membre correspondant de l'Académie de la République Socialiste de Roumanie; Pr G. OSTROGOVICH, MARGARETA AVRAM, F. BADEA, I. D. MARCHIDAN, D. NEGOIU et D. SĂNDULESCU

La *Revue Roumaine de Chimie* paraît 12 fois par an. Toute commande de l'étranger (fascicules ou abonnements) sera adressée à Întreprinderea de comerţ exterior — Rompresfilatelia P. O Box 2001, Bucarest, Roumanie

Les manuscrits, les livres et les revues proposés en échange, ainsi que toute correspondance seront envoyés à la rédaction :

REVUE ROUMAINE DE CHIMIE
23, str. Dumbrava Roşie, Bucarest, Roumanie

REVUE ROUMAINE
DE
CHIMIE

ORSZÁGOS MŰSZAKI KÖNYVTÁR ÉS DOKUMENTÁCIÓS KÖZPONT

Tome 17, Nos 1, 2 Janvier-Février 1972

Page

Hommage à I. G. MURGULESCU 5–7

ALEXANDRU T. BALABAN, Determination of hyperfine coupling constants from ESR spectra of organic free radicals 9–24

P. BALTĂ, L. DOLLINGHER and MARIA CÎRSTEA, Phototropic glasses on B_2O_3 basis . . . . 25–28 R

HERMANN BEYER, DÉNES KALLÓ und GÉZA SCHAY, Zur kinetischen Untersuchung der katalytischen Krackung von Propan . . . . 29–33 R

G. BLIZNAKOV, S. DELINESHEV, On the binding energy of small clusters of atoms 35–39

D. BRATLAND, G. H. BØE, K. GRJOTHEIM, H. RENSVIK and E. AAMLAND, Some introductory investigations on electrolytic deposition of Y-Al and Y-Mg alloys . . . . 41–48 R

EM. A. BRATU and GHEORGHIȚA I. JINESCU, Heat transfer in vibrated fluidized layers . . . . 49–56 R

J. BRENET, P. DANTZER, P. MIRABEL et J. GUION, Évaluation de la nature des interactions ioniques dans les mélanges binaires de sels fondus à anion commun et comportant des cations polarisables 57–62

M. CHEMLA, Relation diffusion-conductivité dans les solutions d'électrolytes et applications structurales 63–67

D. CISMARU and C. RADOVICI, Kinetic equations for reactions taking place in powders. I. Complete form of the equation for spheric particles . . . . . 69–75 bef

GERDA COMȘA and W. GROTH, The influence of gas adsorption on the surface recombination of nitrogen atoms on stainless steel 77–82

MIHAELA CONSTANTINESCU and E. SEGAL, Memory effects in oxygen and hydrogen photosorption on thin zinc oxide films 83–93

G. COSTEANU et CORNELIA MATEESCU, L'influence du solvant sur la vitesse de réaction. L'hydrolyse alcaline de l'acétate, du propionate et du butyrate de *n*-butyle dans le solvant mixte eau-acétone 95–102

TH. DELEANU, I. V. IONESCU, VALERIA NAHORNIAK et D. A. ISĂCESCU, Déduction d'une classification des transitions de phase 103–109

Ю. К. ДЕЛИМАРСКИЙ, А. В. ГОРОДЫСКИЙ и В. А. БАГРИЙ, Исследование дифференциального сопротивления электрода при больших поляризациях 111–114

Page

CĂTĂLINA DEMETRESCU et IOANA ŞARAMET, Recherches sur la cyclisation des acyl-aryl-thiosemicarbazides 1,4-disubstituées. V. Nouveaux N_1-diphénylsulfonyl-N_4-aryl-thiosemicarbazides et 1,2,4-mercapto-triazoles à action antivirale . . . . 115—124

ALEXANDRU DUCA et CLEOPATRA CALU, Méthodes de détermination du rhénium dans les molybdénites. La détermination polarographique du rhénium à côté des traces de molybdène . . . . 125—129

GUY EMSCHWILLER, Sur la production de tétracyanoferrates . . . . 131—135 R

TIBOR ERDEY-GRÚZ, ELVIRA KUGLER, ILONA NAGY-CZAKÓ und KATALIN BALTHAZÁR-VASS, Überführungszahlen und Temperaturkoeffizienten der Leitfähigkeit einiger Elektrolyte in Gemischen von Dioxan mit Wasser . . . . 137—143 R

PAOLO FERLONI, CRISTIAN TELEA, PAOLO FRANZOSINI and MARIO ROLLA, Demixing phenomena in methyl formate + paraffinic or olefinic hydrocarbon binary mixtures . . . . 145—153

A. N. FRUMKIN, E. V. STENINA, N. V. NIKOLAEVA-FEDOROVICH, G. N. PETUKHOVA, V. A. YUSUPOVA, Polarographic maxima of the third kind. II. Borneol . . . . 155—160

Я. М. КОЛОТЫРКИН, Г. М. ФЛОРИАНОВИЧ и Г. С. РАСКИН, Влияние состава раствора на кинетику растворения хрома в кислых средах при катодной поляризации. . . . . 161—166

V. N. KONDRATIEV, On the mechanism of the nitrogen atom reaction with ethylene . . . . 167—170

J. KORYTA, M. BŘEZINA and N. KŘÍŽ, Electrode processes of hydrogen peroxide on platinum electrode in alkaline and acid medium . . . . 171—178

MIRCEA IONESCU, MAGDA IVĂNESCU and MARIANA FERANDO, Chemical changes in cereals by shrivelling . . . . 179—186 R

G. J. JANZ and K. BALASUBRAHMANYAM, Some applications of laser Raman spectroscopy in fused salt studies . . . . 187—194

D. I. MARCHIDAN and SPERANŢA MATEI, Thermodynamic data for some non-stoichiometric uranium oxides by solid-state EMF technique . . . 195—202

B. F. MARKOV, Calcul des énergies d'excès intégrales libres des systèmes ternaires de sels fondus sur la base des systèmes binaires . . . . 203—208

А. Б. НАЛБАНДЯН, О некоторых результатах исследования реакции окисления метана, инициированного азотной кислотой . . . . . 209—212

TATIANA ONCESCU, M. CONTINEANU and G. BĂLĂCEANU, Kinetics and mechanisms of the thermal decomposition of diphenyldiazomethane in the absence of solvent. I . . . . 213—223

G. PANNETIER et D. FĂTU, Étude de la morphologie des produits de la décomposition thermique du coprécipité : $Ag_2CO_3-CdCO_3$ . . . . 225—229

SEPTIMIA POLICEC, T. SIMONESCU and C. DRĂGULESCU, Simultaneous spectrophotometric determination of gallium and indium . . . . 231—237

MARCEL POURBAIX, Signification du potentiel de protection lors de la corrosion par piqûres, de la corrosion intergranulaire et de la corrosion fissurante sous tension . . . . 239—251

O. RADOVICI, N. BONCIOCAT and VERONICA POPESCU-TUCSEK, Some kinetic aspects of the anodic oxidation of silicon in ethylene glycol . . 253—257

Page

RALUCA RIPAN und CS. VÁRHELYI, Über α-Dioximinkomplexe der Übergangsmetalle. XXXV. Kobalt (III)-bis-dimethylglyoximin-Chelate mit *cis*-geometrischer Konfiguration . . . . 259—265
FREDERICK D. ROSSINI, Compilations of data for chemical thermodynamics 267—271
V. EM. SAHINI and LILIANA CIUREA, Infrared spectra of carbonyl aromatic ion radicals. I. Carbonyl stretching frequency and force constant changes due to the formation of anion radicals from benzophenone, fluorenone, phenanthrenequinone and anthraquinone . . . . 273—284
MANLIO SANESI, The heats of adsorption of some hydrocarbons on zirconia 285—290
I. A. SCHNEIDER, Über die dynamische Thermogravimetrie bei komplexen Abbauprozessen . . . . 291—301
CR. SIMIONESCU, SVETLANA DUMITRESCU, M. LEANCĂ, M. DĂRÎNGĂ und MARIA GROVU, Studium der Polymerisation von Acetylenderivaten. XV. Die übermolekulare Struktur der Polymere . . . . 303—309
S. SOLACOLU, R. DINESCU und MARIA ZAHARESCU, Die thermischen Phasengleichgewichte des Systems $SrO\text{-}V_2O_5$ . . . . 311—317
S. SOLACOLU et D. POPESCU-HAŞ, Coordination de l'ion Al^{3+} dans les structures vitrocéramiques du système $Na_2O-MgO-Al_2O_3-SiO_2$ ayant le fluor comme agent de nucléation . . . . 319—327
JAVIER SORIA and JOHN TURKEVICH, Electron paramagnetic resonance study of nitroxides in dioxane water system . . . . 329—333
P. SPACU and C. I. LEPĂDATU, Molecular orbital patterns for *f*-clusters . . 335—341
S. STERNBERG and CONSTANŢA HERDLICKA, Interdiffusion coefficient of the silver ion in molten alkali chlorides by the chronopotentiometric method . . . . 343—352
G. C. SUCIU, Notes on pyrolysis . . . . 353—356
A. R. UBBELOHDE, Ionic melts as model liquids . . . . 357—360
R. VÎLCEANU und P. SCHULZ, Kinetische Untersuchung basischer Esterverseifungen in wäßriger Lösung mit einem pH-metrischen Titrationsverfahren. Basische Hydrolyse der Dialkylphosphite in wäßriger Lösung . . . . . 361—366
RODICA VÎLCU and ZOICA CENUŞE, Thermodynamic excess functions in liquid-vapour equilibria in the *n*-heptane—toluene system . . . . . . 367—377
I. VLAGIU and V. STANNETT, Initial studies on the radiation induced grafting of styrene to polyethylene terephthalate fibers . . . . 379—383 R
ŞTEFANIA ZUCA and MARIELLA CONSTANTINESCU, The self-diffusion coefficients in some molten nitrates . . . . 385—396
I. ZUGRĂVESCU, MAGDA PETROVANU, MARIA CAPROŞU et I. DRUŢĂ, Sur le méthyl-1-phtalazinium-carbéthoxyméthylure. III . . . . 397—403
WOON kie PAIK and JOHN O'M. BOCKRIS, Ellipsometric and reflectance measurements for the determination of optical properties and thickness of a light-absorbing thin film . . . . 405—410
CLAUDE NICOLAU, Short-lived free radicals in aqueuous solutions of purines 411—420

MŰSZAKI KÖNYVTÁR ÉS
…ÁCIÓS KÖZPONT

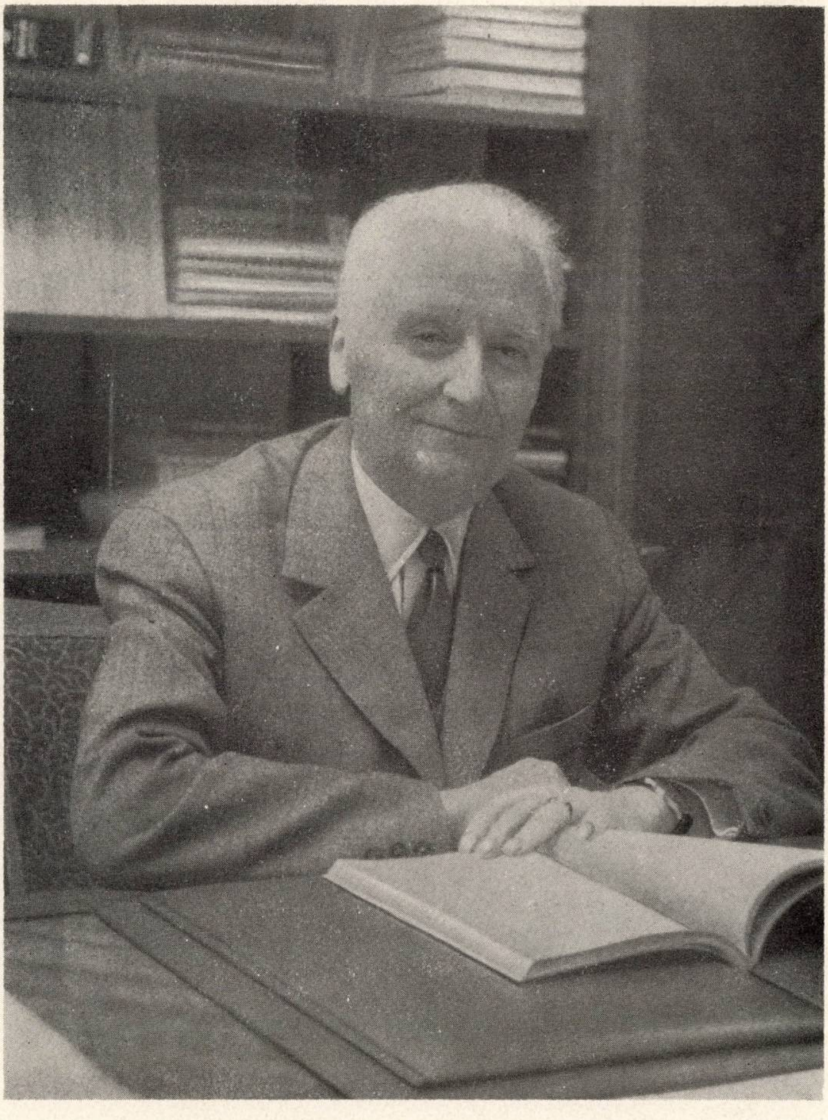

I. G. Murgulescu

MŰSZAKI KÖNYVTÁR ÉS DOKUMENTÁCIÓS KÖZPONT 1883

PROFESSOR I. G. MURGULESCU

Professor Dr. I. G. MURGULESCU, member of the Academy of the Socialist Republic of Romania, professor of Physical Chemistry at the Bucharest University, and Director of the Centre of Physical Chemistry, is seventy years old on January 27, 1972.

His scientific personality, his important contribution in creating a modern school of physical chemistry in Romania, and his multiple activities in teaching and scientific research are unanimously recognized and appreciated.

This special issue of *Revue Roumaine de Chimie* containing papers of Romanian and foreign scientists is dedicated to his anniversary.

Professor Dr. I. G. MURGULESCU was born at Cornu, Oltenia. He studied at the elementary school in his native village and he followed the high school in Craiova. Being a student at the Science Faculty of the Cluj University he proved many times his ingenuity.

He started his didactic activity at the Science Faculty of the Cluj University where, in 1928, he was appointed as assistant after having graduated from the same Faculty with the highest honours. In 1930 he obtained his Ph. D. degree. His Ph. D. thesis on Copper Thiosulphate Complexes, was approved with "Magna Cum Laude" by the Cluj University.

His scientific personality has been noted by the late Professor G. Spacu, head of the chair of Inorganic Chemistry in Cluj University. Professor I. G. MURGULESCU spent the years 1932–1933 at the Institute of Physical Chemistry of the Leipzig University working with Professor F. Weigert on photochemical problems.

Returning home in 1934, Professor I. G. MURGULESCU became reader in Analytical Chemistry and Physical Chemistry at the Timişoara Polytechnic Institute, and he held this position until he was appointed full professor at the same Institute in 1944. In 1949 he was appointed professor of physical chemistry at the Bucharest University where he lectured ever since then.

Professor MURGULESCU's researches cover a wide field : kinetics, thermodynamics, electrochemistry, spectroscopy, inorganic and analytical chemistry, molten salt chemistry.

Starting from the studies of complex combinations he identified new types of complex silver and copper thiosulphates in the presence of ammonium, potassium and sodium, and extended these investigations spectrophotometric, cryoscopic, and conductometric measurements ;

he determined thus the composition of Durrand's salt. He also investigated spectrophotometrically the copper and cobalt salts in solution and the type of the chemical bond of complex chromium, manganese, iron and cobalt oxalates.

The study of the refractometric properties of aqueous solutions of electrolytes allowed him to elaborate new methods for calculating the refractive index of electrolytes and the individual ionic refractions. One of these methods has been applied to obtain the refractive indices of ferricyanide and ferrocyanide ions.

In photochemistry, he studied the quantum efficiency and the mechanism of the photochemical decomposition of potassium cobaltic oxalate and of diphenyldiazomethane in solution. Also the kinetics of the thermal decomposition of diphenyldiazomethane has been studied by Professor MURGULESCU and his coworkers.

Professor I. G. MURGULESCU studied the kinetics of the alcoholysis of benzyl chloride, and decomposition of the cobaltic oxalate in aqueous solution.

Another problem in which Professor I. G. MURGULESCU became interested was the anodic passivation of metals and alloys. His studies on the electrochemical behaviour of thin films and on the determination of electrode potentials are well known.

His contribution to chemical thermodynamics dealt mainly with thermal decomposition of calcium carbonate, thermodynamic activity of solutions and alloys and free energy of chemical substances. By ebullioscopy he obtained the dissociation constant of α-nitroso-β-naphthol in solution. By calorimetry he obtained the heat of dissolution of sodium iodate, both anhydrous and hydrated.

In analytical chemistry Professor I. G. MURGULESCU has elaborated new analytical methods for mercury and he used for the first time *ortho*-chlorobenzoic acid in alkalimetry and acidimetry. He elaborated a new conductimetric method for titrating molybdates and wolframates using silver nitrate, and also for complex iron cyanides enriching the theory of precipitation processes in the physico-chemical analysis.

He has published studies on the theory of the equivalence point in titrimetry, and the determination of normal electrode potentials.

In 1957 Professor I. G. MURGULESCU turned toward the area of research for which he became best known, the physical chemistry of molten salts. His contributions to this field are both theoretical and experimental. Professor MURGULESCU's researches in molten salts cover a wide field : thermodynamic properties of binary mixtures of molten salts by the methods of electromotive forces ; cryometry and vapour pressure measurements ; transport properties of molten salts, namely viscosity, electric conductivity ; optical properties of molten salts (refractive indices) ; heat of mixture of molten salts etc.

In 1948 Professor I. G. MURGULESCU was elected Member of the Academy of the Socialist Republic of Romania. As a recognition of his merits he was elected Vicepresident between 1959–1963 and President of the Academy of the Socialist Republic of Romania between 1963–1966.

Under Professor MURGULESCU's leadership, in 1963, was formed the Centre of Physical Chemistry of the Academy of the Socialist Republic of Romania (now belonging to the Ministry of Education), where he is Director ever since.

The stimulating atmosphere which prevails in Professor MURGULESCU's activity at the Centre of Physical Chemistry and the Bucharest University, provided an excellent starting point for many young scientists who are now engaged in research and teaching in diferent fields of physical chemistry. The same atmosphere has been beneficial for a few young scientists from abroad during their affiliation with the Centre of Physical Chemistry.

As a recognition of his remarkable organizing aptitudes, Professor I. G. MURGULESCU was designated Rector of the Timişoara Polytechnic Institute (1947–1949), Rector of the Bucharest University (1949–1950), Deputy Minister of Education and then Minister of Education (1950–1956 and 1960–1963).

In carrying out his duties, Professor MURGULESCU gave an example of perseverance and tenacity to all his co-workers and pupils. His attachment to the teaching and research, which he succeeded in combining throughout his career, was the most characteristic work of his multilateral activity. Among the public offices he detained or detains one may quote : member of the Grand National Assembly since 1948 : Vice President of the Grand National Assembly since 1967 ; Vice President of the State Council (1965–1967).

As an international recognition of his scientific merits, he was elected member of the USSR Academy of Sciences and Czechoslovak Academy of Sciences. He is a member of the editorial board of several scientific journals : *Electrochimica Acta*, *Corrosion Science*, *The Journal of Chemical Thermodynamics*. He is editor-in-chief of the chemical scientific journals *Revue Roumaine de Chimie* and *Studii* şi *Cercetări de Chimie*.

For his scientific and public activity, Professor I. G. MURGULESCU was awarded several distinctions, medals and prizes such as : Romanian State Prize (1963), Emeritus Professor (1964), Emeritus Scientist (1969), the Gold Medal of the 39th Congress of Industrial Chemistry (1970), Hero of Socialist Labour (1971).

Professor MURGULESCU's personality is an example for Romanian scientists who hold him in high esteem. We wish him a long and fruitful life serving high scientific and patriotic ideals.

Revue Roumaine de Chimie, **17**, *1*, *2*, 9–24 (1972)

Dedicated to professor I. G. MURGULESCU
in honour of his 70 th birthday

DETERMINATION OF HYPERFINE COUPLING CONSTANTS FROM ESR SPECTRA OF ORGANIC FREE RADICALS

ALEXANDRU T. BALABAN

Institute of Atomic Physics, P.O.B. 35, Bucharest, Romania

Received October 6, 1971

To find coupling constants from complex ESR spectra of free radicals with known structure presenting hyperfine splittings, a general procedure is presented, involving : (i) summation of line intensities giving the number of coupled nuclei ; (ii) evaluation of the sum of coupling constants from the number of lines and the extent of the spectrum ; (iii) writing of this sum as all possible partitions ; (iv) examination of the spectra reconstructed from these partitions. This procedure is exemplified for the frequently occurring case of ESR spectra to be analyzed in terms of nitrogen and proton coupling constants : N-nitroso-phenyl-nitroxide (I), N-nitroso-*p*-tolyl-nitroxide (II), N-methoxy- (III) and N-ethoxy-2,4,6-tricarbomethoxyphenylaminyl (IV), 2,2-diphenyl-1-benzenesulfonylhydrazyl (V) and N-nitroso-*p*-nitrophenyl-nitroxide (VI).

INTRODUCTION

Electron spin resonance (ESR) spectra originate in the absorption of electromagnetic energy E of microwave frequencies by substances possessing unpaired electron spins. In an external magnetic field H, only two orientations of a free electron spin are allowed ; the energy difference between spins of different orientations is $E = h\,\nu = g\,\beta\,H$. Here $\beta = eh/4\pi m_e c$ is the Bohr magneton, and g is the spectroscopic splitting factor. These g-factors offer precious information on the nature of the free radicals and can be readily determined from an experimental ESR spectrum.[1,2]

However, the present paper is concerned with other informations which can be obtained from ESR spectra, namely, the hyperfine coupling constants. In molecules where there is a non-zero electronic spin density at one or more nuclei X possessing a nuclear spin I_X, the electronic energy levels will be split by interaction (coupling) with the nuclear

---

[1] E. Klein, K. Möbius and H. Winterhoff, *Z. Naturforsch.*, **22 a**, 1704 (1967).

[2] M.S. Blois, Jr. (editor), "Free Radicals in Biological Systems", Academic Press, New York, 1961.

spin. Since there are $2I + 1$ allowed orientations of the nuclear spin in the external magnetic field H, there will be as many resonance energies which will give rise to as many lines in the ESR spectrum. A free radical with one hydrogen atom ($I_H = 1/2$) will therefore give rise to two lines of equal intensity (amplitude); their spacing or splitting is the hyperfine coupling constant a_H (usually measured in units of magnetic field) proportional to the spin density ρ at the hydrogen nucleus. The proportionality constant Q in McConnell's relationship $a = Q\rho$ depends on the nature of the free radical and averages —22.5 to —30 gauss.[3]

Two hydrogen atoms equally coupled with the unpaired electron give rise to three lines in the ESR spectrum; the intensity of the middle line is twice that of the outer lines (1 : 2 : 1 triplet). A number n_H of hydrogen atoms gives rise to $n_H + 1$ lines whose intensities are the binomial coefficients of the series $(x + 1)^{n_H}$ i.e. the combinatorial coefficients from Pascal's triangle. The sum of these intensities is 2^{n_H}, as shown by a well-known combinatorial theorem.

A nitrogen-14 nucleus ($I_N = 1$) coupled with the odd electron gives rise to a 1 : 1 : 1 triplet; two equally coupled nitrogens give rise to a 1 : 2 : 3 : 2 : 1 quintet, three equally coupled nitrogen give rise to a 1 : 3 : : 6 : 7 : 6 : 3 : 1 septet and so on. These coefficients form a generalized numerical triangle (Table 1), where each number is the sum of I_x adjacent numbers from the line above it. [4] The sum of the intensities is, in the case of n_N nitrogen-14 atoms, 3^{n_N}, and the intensities are the trinominal coefficients of the series $(x^2 + x + 1)^{n_N}$.

The situation is more complex when, as occurs frequently in practice, there are several unequally coupled nuclei posssessing nuclear spins. There

Table 1

Generalized numerical triangles

n	Pascal's triangle, $I = 1/2$														
1							1		1						
2						1		2		1					
3					1		3		3		1				
4				1		4		6		4		1			
5			1		5		10		10		5		1		
6		1		6		15		20		15		6		1	
7	1		7		21		35		35		21		7		1

n	Generalized numerical triangle, $I = 1$														
1							1	1	1						
2						1	2	3	2	1					
3					1	3	6	7	6	3	1				
4				1	4	10	16	19	16	10	4	1			
5			1	5	15	30	45	51	45	30	15	5	1		
6		1	6	21	50	90	126	141	126	90	50	21	6	1	
7	1	7	28	77	161	266	357	393	357	266	161	77	28	7	1

---

[3] H.M. Mc Connell, *J. Chem. Phys.*, **24**, 632 (1956).

[4] F. Gerson, "High Resolution ESR Spectroscopy", Wiley-Verlag Chemie, Weinheim, 1970.

are very few indications in the published literature [4-20] and no standard procedure for analyzing a given experimental ESR spectrum, where overlapping of lines, unsatisfactory resolution and lack of salient features assisting in the interpretation, make the operation tedious and dependent on intuition and/or luck. Deuterations [4,21] are not always possible. Even with spectrum simulators or computer programs for simulating ESR spectra, approximate coupling constants are necessary at the start for further refinement.

PROCEDURE OF ANALYSING ESR SPECTRA OF FREE RADICALS IN SOLUTION

Spectra must be recorded with sufficient amplification and resolution to allow all lines (especially the marginal ones) to be visible. Variation of concentration to enable the weakest and strongest lines to appear is often necessary; of course the settings of the ESR spectrometer can be varied but this is not always sufficient. Since high concentrations of the free radical give a better signal-to-noise ratio but deteriorate the resolution, a compromise must be reached.

Starting from the assumption that an ESR spectrum of a single free radical with known structue must be analyzed in terms of coupling constants, the following procedure is proposed (the ESR spectrum is supposed to be symmetrical relative to its centre).

1. Frequently, spurious impurities give rise to weak lines in an ESR spectrum. To ascertain whether weak lines belong to the spectrum, i.e. are caused by the same free radical, the intensity ratio between the strongest

[5] A.R. Forrester, J.M. Hay and R.H. Thomson, "Organic Chemistry of Stable Free Radicals", Academic Press, London – New York, 1968.

[6] A. Carrington and A.D. Mc Lachlan, "Introduction to Magnetic Resonance with Applications to Chemistry and Chemical Physics", Harper and Row, New York, 1967.

[7] M. Bersohn and J.C. Baird, "An Introduction to Electron Paramagnetic Resonance", W.A. Benjamin, New York, 1966.

[8] D.J.E. Ingram, "Free Radicals as Studied by ESR", Butterworths, London, 1958; "Spectroscopy at Radio and Microwave Frequencies", 2nd ed., Butterworths, London, 1967.

[9] C.P. Slichter, "Principles of Magnetic Resonance", Harper and Row, New York, 1963.

[10] A.L. Buchachenko, "Stable Radicals", Consultants Bureau, New York, 1965.

[11] P.M. Ayscough, "Electron Spin Resonance in Chemistry", Methuen, London, 1967.

[12] H.M. Assenheim, "Introduction to Electron Spin Resonance", Hilger and Watts Ltd, London 1966.

[13] G. Schoffa, "Elektronenspinresonanz in der Biologie", Verlag G. Braun, Karlsruhe, 1964.

[14] S.A. Altshuler and B.M. Kozyrev, "Electron Paramagnetic Resonance", Academic Press, New York-London, 1964.

[15] L.A. Bliumenfeld, V.V. Voevodskii and A.G. Semenov, "Primenenie ESR v Khimii", Izd. Sibirskogo Otdel. Akad., Nauk S.S.S.R., Novosibirsk, 1962.

[16] W.A. Pryor, "Free Radicals", McGraw-Hill, New York, 1966; "Introduction to Free Radical Chemistry", Prentice-Hall, New Jersey, 1966.

[17] C.J.M. Stirling, "Radicals in Organic Chemistry", Oldbourne Press, London, 1965.

[18] I. Ursu, "La résonance paramagnetique électronique", Dunod, Paris, 1968.

[19] Z. Simon, în "Rezonanța paramagnetică electronică. Aplicații în chimie și biologie" (C. Nicolau, editor), Ed. Tehnică, Bucharest, 1966.

[20] K. Scheffler and H.B. Stegman, "Electronespinresonanz", Spinger, Berlin, 1970.

[21] A.T. Balaban, F. Cuiban and I. Pascaru, *J. Magn. Resonance*, (in press).

line and the weak line under consideration is measured. In the absence of fortuitous line overlap, this ratio can be calculated from the structural formula of the free radical. If there are m_i equivalent nuclei with nuclear spin I_i, then the overlap-free ratio is the product extended over all i's of the largest number in the line corresponding to m_i nuclei in the generalized Pascal triangle for I_i. If the intensity of the weak line under consideration is much lower relative to the strongest line than this calculated ratio (taking into account the possibility of fortuitous overlap, a factor of 3—4 must be allowed), then the weak line does not belong to the spectrum.

If, as usual, first derivative ESR spectra are recorded, in the folowing discussion by line intensities we will mean ratios between the heights of each line and the height of the first, weakest, line belonging to the spectrum (this line is the outermost line at the left of the spectrum). Line width variations may sometimes considerably alter the intensities and even the number of lines.[22]

2. Summation of intensities of all lines belonging to the spectrum gives an approximate sum, A, which serves to estimate the number of all n_i nuclei with nuclear spin I_i interacting with the unpaired electron, since $A = \prod_i (2 I_i + 1)^{n_i}$. In conjunction with the formula of the free radical, this relationship shows whether all atoms with a non-zero nuclear spin from the structural formula interact, or whether some couplings are too small to be observed. If, as will be discussed below, the free radical has n_N nitrogen atoms and n_H hydrogens interacting with the odd electron then $A = 2^{n_H} \cdot 3^{n_N}$. This equation must yield integer values for n_H and n_N based on the approximate value for A.

3. If a spectrum consists of separate equal subgroups of lines which, as judged by their intensities, are due to splitting by a nucleus (or a few nuclei) with a larger coupling constant than the remaining constants, then the discussion is simplified if only one (usually the first, left, better resolved) subgroup of lines is considered. This is often the case in nitrogen free radicals. Owing to the symmetry of the splitting, this subgroup of lines must also have intensities with a symmetric disposition relatively to its centre. The centre can be on a line or on an interval between lines. If overlaps distort intensities on the right side of the centre, the undistorted intensities can by written by symmetry if the symmetry centre is precisely located.

4. If the intervals between lines are unequal, then the smallest interval is taken as unit and the total span D of the spectrum is expressed as an integer in terms of d units (which may be converted into units of magnetic field). The equation

$$D = 2 \sum_i I_i\, n_i\, a_i ,$$

where nuclear spins I_i and numbers of nuclei n_i are known, must be solved in integer values for a_i. This is straightforward for one or two unknown a_i's (in the latter case, the Diophantine equation is solved by using continuous fractions, congruences or Euclid's algorithm).[23,24] For more than two unknown a_i' s the non-determined equation is solved as follows.

---

[22] A. Hudson and G.R. Luckhurst, *Chem. Rev.*, **69**, 191 (1969).

5. The partitions* of D into exactly $2\sum_i I_i n_i$ non-zero integers, or all partitions of $D - 2\sum_i I_i n_i$ into at most $2\sum_i I_i n_i$ integers, can easily be calculated. The numbers of the latter partitions may be calculated using Euler's function and can be found in mathematical tables.[26] The former partitions can be found from the latter by adding 1 to each of the terms of the latter partitions (including zeros to yield $2\sum_i I_i n_i$ terms).

Table 2[a,b]

Numbers p(n, m) of ways in which a number n can be written as a sum of m positive integers, or as a sum of positive integers the largest being at most m

n	m												p (n)
	1	2	3	4	5	6	7	8	9	10	11	12	
1	1												1
2	1	1											2
3	1	1	1										3
4	1	2	1	1									5
5	1	2	2	1	1								7
6	1	3	3	2	1								11
7	1	3	4	3	2	1	1						15
8	1	4	5	5	3	2	1	1					22
9	1	4	7	6	5	3	2	1	1				30
10	1	5	8	9	7	5	3	2	1	1			42
11	1	5	10	11	10	7	5	3	2	1	1		56
12	1	6	12	15	13	11	7	5	3	2	1	1	77

[a] Partitions of n are $p(n) = \sum_m p(n, m)$.

[b] The recurrence relationships on which this table is based are: $p(n, m) = \sum_{i=1}^{m} p(n-m, i)$ and $p(n, m) - p(n-1, m-1) = p(n-m, m)$.

For $m > n$, $p(n, m) = 0$. Numbers right of the zig-zag line are equal to p(n) and repeat themselves on the diagonals.

---

[*] The partitions[25] p(n) of an integer n are all distinct ways in which n can be written as a sum of positive integers (Table 2).

[23] A.O. Gelfond, "Rezolvarea ecuaţiilor în numere întregi", translation from Russian, Biblioteca Societăţii Ştiinţelor Matematice şi Fizice, Bucharest, 1954.

[24] R. Courant and H. Robbins, "What is Mathematics?" Oxford Univ. Press, London, 1941.

[25] G.H. Hardy and E.M. Wright, "An Introduction to the Theory of Numbers", 3rd., Oxford Univ. Press, London, 1954, chapter 19.

[26] J.A. Todd, *Proc. London Math. Soc.*, **48**, 229 (1943/4); H. Gupta, E.E. Gwyther and J.C.P. Miller, "Tables of Partitions", Royal Society Math. Tables vol. 4, 1958.

6. From the list of the former partitions, those ones are retained which contain reasonable coupling constants (expressed in terms of d units). By reasonable we mean compatible with the formula of the radical, both in relative magnitude, and in number of equal coupling constants : in the case of a free radical having m_i magnetically equivalent atoms with nuclear spin I_i, e.g. the three hydrogens of a freely rotating methyl group, only those partitions will be retained which possess at least $2 \sum_i I_i m_i$ equal couplings (3 in the above example).

From the set of integers in the partition, each nucleus with nuclear spin I_i uses up $2I_i$ equal integers into one coupling constant.

7. With the retained partitions, theoretical intensities are calculated, which may be used for "stick diagrams" of the ESR spectrum. These are then compared with the actual spectrum. By using spectrum simulators the coupling constants and line widths can be further adjusted to account for minor differences in intensities.

EXAMPLES

As examples we will discuss the published N-nitroso-phenyl-nitroxide (I)[27] and the unpublished N-nitroso-*p*-tolyl-nitroxide (II),[28] 2,4,6-tricarbomethoxyphenyl-methoxyaminyl (III) and -ethoxyaminyl radicals (IV)[29]; the 2,2-diphenyl-1-benzenesulfonylhydrazyl (V)[30] presents a fairly complex ESR spectrum, whereas N-nitroso-*p*-nitrophenyl-nitroxide (VI)[28] illustrates degeneracy in assigning coupling constants.

Example I.[27] The successive steps in the analysis of the ESR spectrum of I are presented in the following :

1. No spurious lines are present, the ESR spectrum has 42 lines all belonging to radical I. The highest-to-lowest overlap-free intensity ratio is calculated from the equivalence of the two *m*- and the two *o*-protons to be $2^2 = 4$.

2. Approximate intensities for the left hand half of the spectrum are 1 : 2 : 1 : 3 : 7 : 5 : 4 : 9 : 9 : 3 : 3 : 10 : 11 : 5 : 7 : 14 : 7 : 5 : 11 : 10 : 4 : .. (corrected for the gradual decrease in intensity from left to right). Summation of all line intensities yields $A = 262 \cong 3^2 \cdot 2^{n_H}$. The integer n_H from this equation is 5 hydrogen atoms, i.e. all hydrogens of the radical.

3. There are no subgroups of lines evident in the spectrum at a cursory inspection.

4. All intervals being approximately equal to d, the total span between the 42 lines is $D = 41$ d ($d = 0 \cdot 95$ Gauss). The resulting equation is therefore $D = 2 \cdot 1 \cdot a_N + 2 \cdot 1 \cdot a_{NO} + 2 \cdot 2 \cdot 1/2 \cdot a_{m-H} + 2 \cdot 2 \cdot 1/2 \cdot a_{o-H} +$ $+ 2 \cdot 1/2 \cdot a_{p-H} = 2\,a_N + 2a_{NO} + 2a_{m-H} + 2a_{o-H} + a_{p-H}$.

5. From partitions of 41 into 9 non-zero integers, or of $(41-9)$ into 9 integers, we select $41 = 11 + 11 + 4 + 4 + 3 + 3 + 3 + 1 + 1$,

---

[27] A.T. Balaban, N. Negoiţă and I. Pascaru, *Rev. Roumaine Chim.*, **16**, 721 (1971).

[28] A.T. Balaban, N. Negoiţă and R. Baican, *J. Magn. Resonance* (in press). (Abstracts of International Symposium on Magnetic Resonance, Rehovoth, 24–31 Aug. 1971).

[29] A.T. Balaban, N. Negoiţă, M. Frangopol and P.T. Frangopol, to be published.

[30] A.T. Balaban and N. Negoiţă, *Rev. Roumaine Chim.* (in press).

respectively $41-9 = 10 + 10+3+3+2+2+2+0+0$ since they fulfill criteria 4 and 6.

6. The above partition affords the following hyperfine coupling constants : $a_N = 11$ d, $a_{NO} = 4$ d, $a_{o-H} = 3$ d, $a_{p-H} = 3$d, $a_{m-H} =$ d ; the values in Gauss are seen on fig. 1.

7. The calculated intensities compare favorably with those under item 2 :

1 : 2 : 1 : 3 : 7 : 5 : 4 : 9 : 10 : 6 : 6 : 11 : 11 : 5 : 8 : 14 : 8 : 5 : 11 : 11 : 6 : . . .
The coupling constants could be further refined to account both for the differing intensities and for the imperfect overlap observed for the third and tenth line in the spectrum, which have larger half-widths and/or double maxima (fig. 1).

Alternatively, a closer inspection reveals the triplet whose centers are characterized by intensities ca. 10 :10 :6 :6 :10 :10 in fig. 1. Then the subgroup of 20 lines has intensities (for the left half of the subgroup) 1 : 2 : 1 : 3 : 7 : 5 : 4 : 9 : 9 : 3 : . . . .

The 19 intervals must be partitioned into 7 non-zero integers subject to the condition $A = 19\ d = 2\ a_{NO} + 2a_{o-H} + 2a_{m-H} + a_{p-H}$. The 65 partitions of $(19-7)$ into at most 7 integers afford as the only reasonable

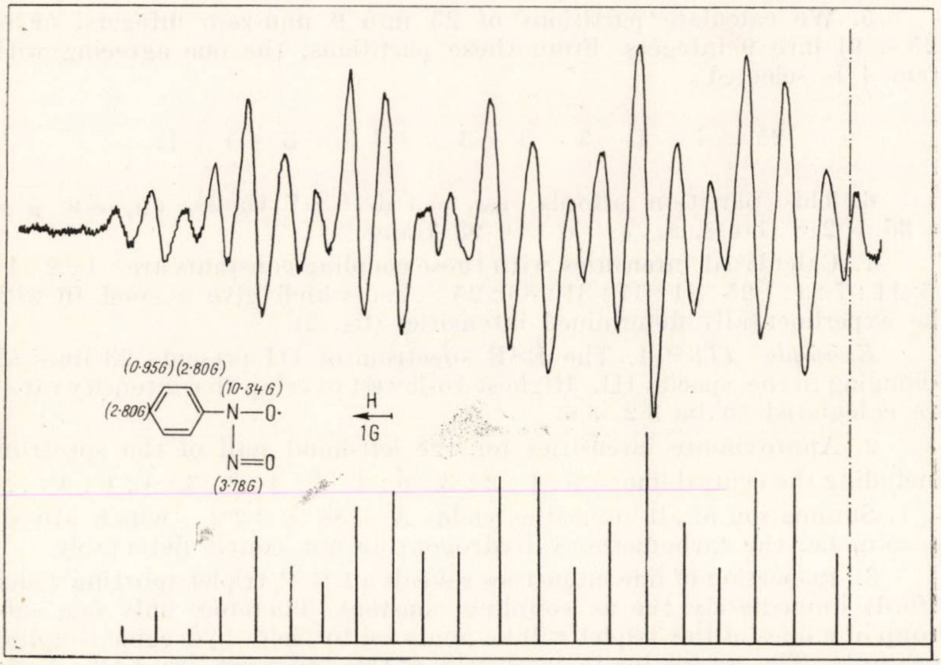

Fig. 1. – Right half of experimental ESR first-derivative spectrum of N-nitroso-phenylnitroxide (I) in dioxane and stick diagram of reconstructed spectrum.

solutions

$$19 = 3 + 3 + 3 + 3 + 3 + 2 + 2 = 4 + 4 + 5 + 2 + 2 + 1 + 1 =$$

$$= 5 + 5 + 3 + 2 + 2 + 1 + 1 = 4 + 4 + 3 + 3 + 3 + 1 + 1,$$

only the last one leading to an intensity pattern agreeing with the experiment.

Example II. [28] The ESR spectrum of II is more complicated, as seen in fig. 2, with 48 lines.

1. No spurious lines are present. The calculated highest-to-lowest overlap-free intensity ratio is $3.2^2 = 12$.

2,3. One can recognize a pattern of lines which is repeated three times, yielding the larger nitrogen coupling constant (the centers of the three multiplets are indicated on the experimental spectrum in fig. 2). The line intensities for the first half of the subgroup of 26 lines are approximately : 1 : 2 : 1 : 4 : 11 : 6 : 7 : 23 : 20 : 10 : 27 : 32 : 20 : . . . (corrected for the gradual intensity decrease from the left to the right of the spectrum). Summation of these intensities affords $A = 328 \cong 3.2^{n_H}$, whence $n_H = 7$, i.e. all hydrogens.

4. All intervals d are equal ($d = 0\cdot93$ Gauss). The span of the subgroup of lines is $D = 25\ d = 2a_{NO} + 3a_{Me} + 2a_{o-H} + 2a_{m-H}$.

5. We calculate partitions of 25 into 9 non-zero integers, or of (25 − 9) into 9 integers. From these partitions, the one agreeing with item 4 is selected :

$$25 = 4 + 4 + 3 + 3 + 3 + 3 + 3 + 3 + 1 + 1.$$

6. This partition affords $a_{NO} = 4\ d = 3\cdot7$ Gauss, $a_{Me} = a_{o-H} = 3d = 2\cdot8$ Gauss, $a_{m-H} = d = 0\cdot93$ Gauss.

7. Calculated intensities with these coupling constants are : 1 : 2 : 1 : : 5: 11 : 7 : 11 : 25 : 21 : 17 : 31 : 35 : 25 : . . . . which give a good fit with the experimentally determined intensities (fig. 2).

Example III. [29] 1. The ESR spectrum of III presents 23 lines all belonging to the species III. Highest-to-lowest overlap-free intensity ratios are calculated to be $3.2 = 6$.

2. Approximate intensities for the left-hand half of the spectrum (including the central line) are : 1 : 2 : 3 : 6 : 4 : 6 : 4 : 3 : 3 : 4 : 6 : 4 : . . .

Summation of all intensities yields $A = 88 \cong 3.2^{n_H}$ which affords $n_H = 5$, i.e. the carbomethoxy hydrogens do not couple detectably.

3. Inspection of line intensities reveals a 1 :1 :1 triplet splitting which affords immediately the a_N coupling constant. Therefore only one subgroup of 9 lines of the triplet will be analyzed to yield hydrogen coupling constants. The approximate intensities of this subgroup are 1 : 2 : 3 : 6 : : 4 : 6 : 3 : 2 : 1 (by symmetry, since there is overlap between subgroups).

4. All intervals are equal to d ($d = 1\cdot43$ Gauss). The span is $D = 8d$ intervals. The resulting equation, $D = 3a_{Me} + 2a_{m-H}$, is a diophantine equation $3x + 2y = 8$ which can be easily solved to afford

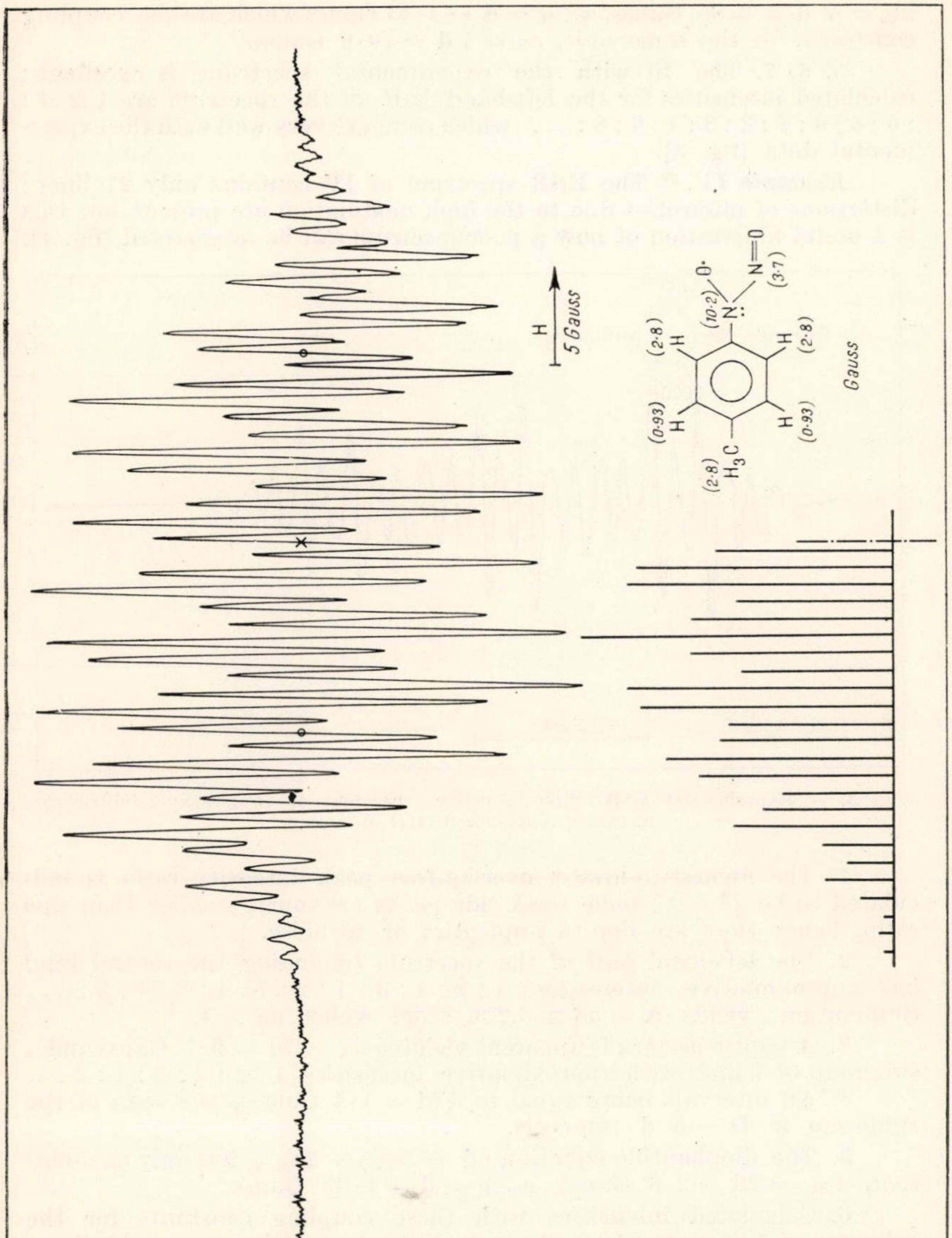

Fig. 2. — Experimental ESR first-derivative spectrum of N-nitroso-*p*-tolyl-nitroxide(II) in dioxane and stick diagram of reconstructed spectrum.

$a_{Me} = 2\ d = 2 \cdot 85$ Gauss, $a_{m-H} = d = 1 \cdot 43$ Gauss which are the coupling constants. In the same unit, $a_N = 7\ d = 10 \cdot 0$ Gauss.

5, 6, 7. The fit with the experimental spectrum is excellent: calculated intensities for the left-hand half of the spectrum are 1 :2 :4 : : 6 : 6 : 6 : 4 : 3 : 3 : 4 : 6 : 6 : . . . which compare very well with the experimental data (fig. 3).

Example IV. [29] The ESR spectrum of IV contains only 21 lines; distortions of intensities due to the high modulation are present but this is a useful illustration of how a poor spectrum can be interpreted (fig. 4).

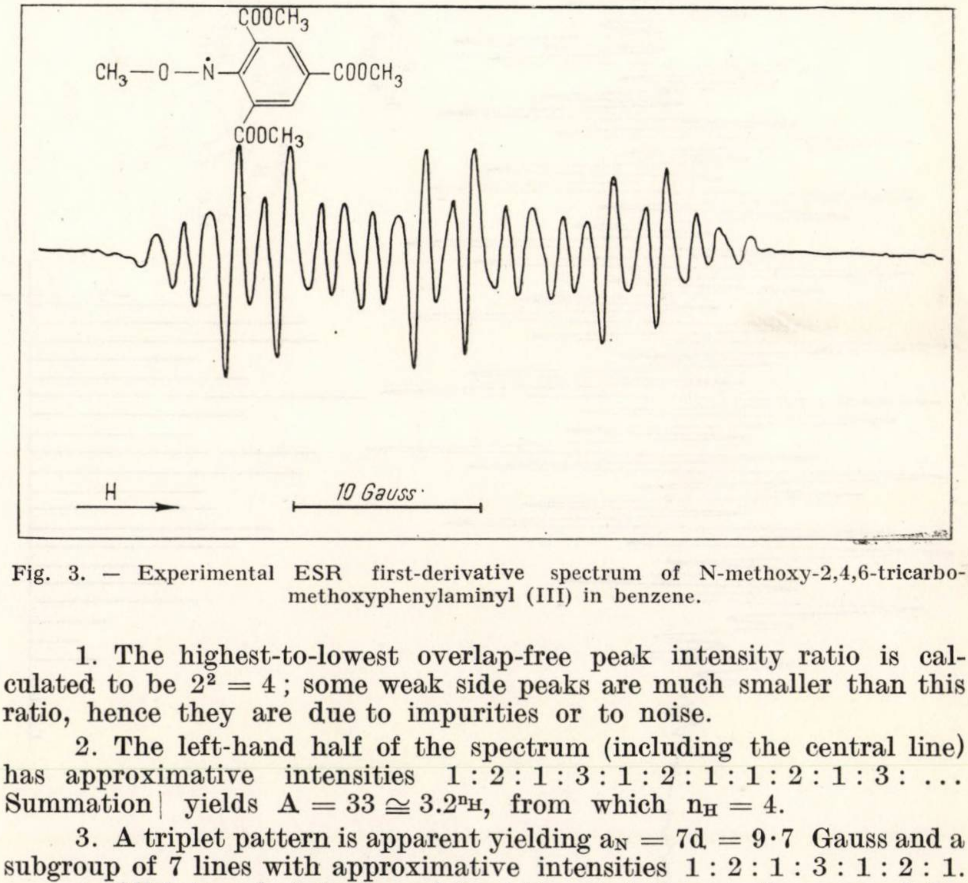

Fig. 3. — Experimental ESR first-derivative spectrum of N-methoxy-2,4,6-tricarbomethoxyphenylaminyl (III) in benzene.

1. The highest-to-lowest overlap-free peak intensity ratio is calculated to be $2^2 = 4$; some weak side peaks are much smaller than this ratio, hence they are due to impurities or to noise.

2. The left-hand half of the spectrum (including the central line) has approximative intensities 1 : 2 : 1 : 3 : 1 : 2 : 1 : 1 : 2 : 1 : 3 : . . . Summation yields $A = 33 \cong 3.2^{n_H}$, from which $n_H = 4$.

3. A triplet pattern is apparent yielding $a_N = 7d = 9 \cdot 7$ Gauss and a subgroup of 7 lines with approximative intensities 1 : 2 : 1 : 3 : 1 : 2 : 1.

4. All intervals being equal to d ($d = 1 \cdot 4$ Gauss), the span of the subgroup is $D = 6$ d intervals.

5. The diophantine equation $6d = 2a_{CH_2} + 2a_{m-H}$ has only one solution, $a_{CH_2} = 2d = 2 \cdot 8$ Gauss, $a_{m-H} = d = 1 \cdot 39$ Gauss.

6. Calculated intensities with these coupling constants for the subgroup of 7 lines are : 1 : 2 : 3 : 4 : 3 : 2 : 1, which differ appreciably from the experimental data, but represent the only solution compatible with them. The good agreement with the coupling constants of III lends further confidence in this interpretation.

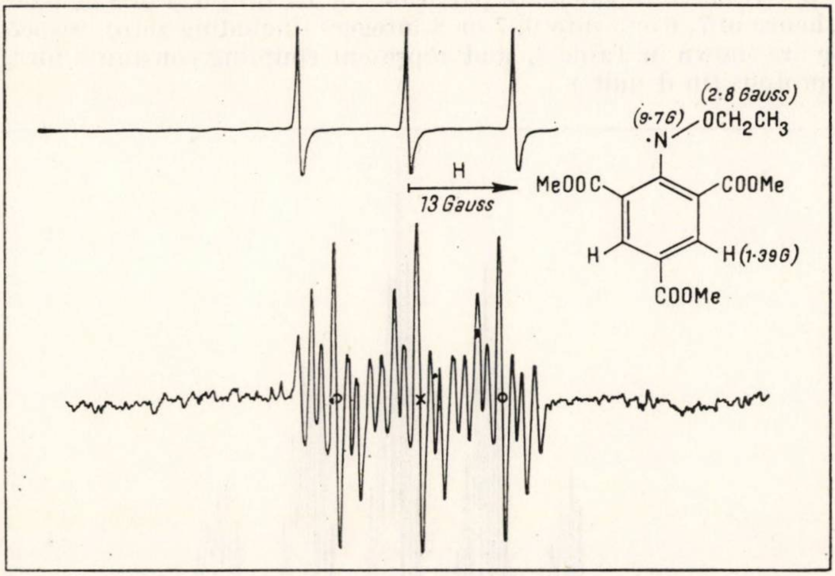

Fig. 4. — Experimental ESR first-derivative spectra of N-ethoxy-2,4,6-tricarbomethoxyphenyl-aminyl (IV) in benzene (lover trace) and of Frémy salt in water (upper trace).

Example V.[30] The spectrum of 1-benzenesulfonyl-2,2-diphenyl-hydrazyl (V) is rather complex, presenting 50 lines (the two marginal lines appear only under high sensitivity) shown in fig. 5.

1. No spurious lines are present.

The highest-to-lowest overlap-free intensity ratio is difficult to estimate (even knowing that no coupling with the arenesulfonyl group is present) because *a priori* the two phenyl groups of the diphenylamino moiety can be assumed to be freely rotating hence equivalent or on the contrary non-equivalent as in the crystal of diphenylpicrylhydrazyl.[31]

2. Approximate intensities for the first group of 14 lines at the left of the spectrum (completed by symmetry) are for the left half: 1 : 2 : 4 : 6 : 10 : 18 : 14 : ... However, the first line being very weak, errors in the evaluation of intensities are likely to be rather large. Summation of intensities gives $A = 110 \cong 2^x$; this leads to values $x = 6{,}7$ or 8 to be considered.

3. Since the hydrazyl has two nitrogens with high spin density, if nitrogen coupling constants are equal, a 1 : 2 : 3 : 2 : 1 major quintet should appear. This is indeed the case, affording immediately an approximative $a_{N_1} = a_{N_2} = 9d$ coupling constant.

4. All intervals d are taken as equal, $d = 1 \cdot 05$ Gauss. The span of the subgroup of lines is $D = 13\ d = \sum_i a_{H_i}$

---

[31] D.E. Williams, *J. Amer. Chem. Soc.*, **89**, 4280 (1967).

5. We have to calculate partitions of 13 into 6, 7 or 8 non-zero integers, hence of 7, 6 or 5 into 6, 7 or 8 integers (including zero), respectively. These are shown in Table 3, and represent coupling constants for the 6, 7 or 8 protons (in d units).

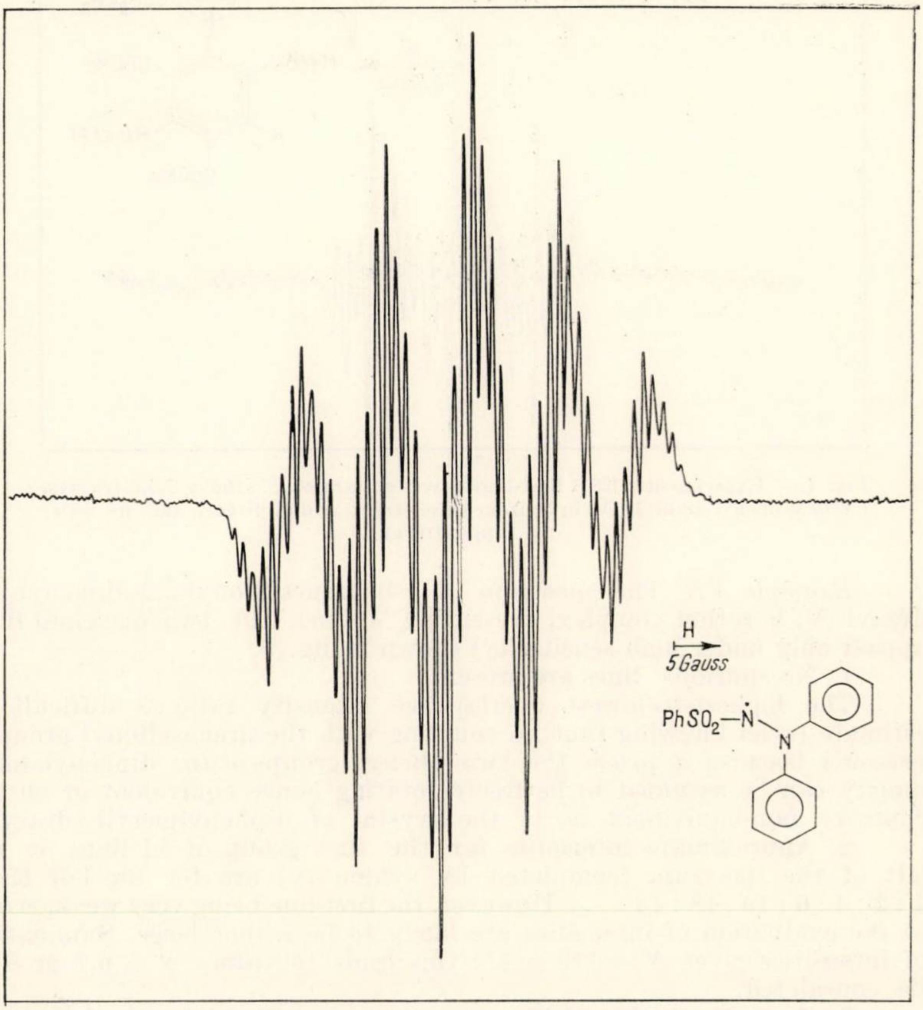

Fig. 5. — Experimental ESR first-derivative spectrum of 1-benzene-sulfonyl-2,2-diphenylhydrazyl in dioxane.

6. From the 32 possibilities, only partitions 4, 5, 6, 13, 14, 15, 17, 25 and 31 can be taken into account, according to their intensity pattern. The closest fit with the experimental spectrum is provided by partitions numbered 4, 14 and 17, but partition 4 of table 3 gives both a fair agreement with the experiment, and a resonable collection of coupling constants. The most interesting conclusion is that the two phenyl groups of the diphenylamino moiety cannot be equivalent (this follows directly from

Table 3

For ESR spectrum of V, partitions of 13 into x non-zero integers

No	Partition into a_H								Calculated intensities (left half)						
x = 8															
1	6	1	1	1	1	1	1	1	1	7	21	35	35	21	8
2	5	2	1	1	1	1	1	1	1	6	16	26	30	27	22
3	4	3	1	1	1	1	1	1	1	6	15	21	22	27	36
4	4	2	2	1	1	1	1	1	1	5	12	20	27	31	32
5	3	3	2	1	1	1	1	1	1	5	11	17	25	33	36
6	3	2	2	2	1	1	1	1	1	4	9	17	26	33	38
7	2	2	2	2	2	1	1	1	1	3	8	16	25	35	40
x = 7															
8	7	1	1	1	1	1	1		1	6	15	20	15	6	1
9	6	2	1	1	1	1	1		1	5	11	15	15	11	6
10	5	3	1	1	1	1	1		1	5	10	11	10	12	15
11	4	4	1	1	1	1	1		1	5	10	10	7	11	20
12	5	2	2	1	1	1	1		1	4	8	12	14	13	12
13	4	3	2	1	1	1	1		1	4	7	9	12	15	16
14	3	3	3	1	1	1	1		1	4	6	7	13	18	15
15	4	2	2	2	1	1	1		1	3	6	10	13	15	16
16	3	3	2	2	1	1	1		1	3	5	9	13	15	18
17	3	2	2	2	2	1	1		1	2	5	9	12	17	18
18	2	2	2	2	2	2	1		1	1	6	6	15	15	20
x = 6															
19	8	1	1	1	1	1			1	5	10	10	5	1	—
20	7	2	1	1	1	1			1	4	7	8	7	4	1
21	6	3	1	1	1	1			1	4	6	5	5	6	5
22	5	4	1	1	1	1			1	4	6	4	2	6	10
23	6	2	2	1	1	1			1	3	5	7	7	5	4
24	5	3	2	1	1	1			1	3	4	5	6	6	7
25	4	4	2	1	1	1			1	3	4	4	5	7	8
26	4	3	3	1	1	1			1	3	3	3	7	9	6
27	5	2	2	2	1	1			1	2	4	6	6	7	6
28	4	3	2	2	1	1			1	2	3	5	6	7	8
29	3	3	3	2	1	1			1	2	2	5	7	6	9
30	4	2	2	2	2	1			1	1	4	4	7	7	8
31	3	3	2	2	2	1			1	1	3	5	5	9	8
32	3	2	2	2	2	2			1	—	5	1	10	5	10

the odd number of intervals D). The tentative assignment[30] of coupling constants according to partition 4 ($a_{N_1} = a_{N_2} = 9 \cdot 4$ Gauss ; for one phenyl group $a_{o-H} = 2 \cdot 1$ Gauss, $a_{m-H} = 1 \cdot 0$ Gauss, $a_{p-H} = 4 \cdot 2$ Gauss ; for the second phenyl group, $a_{o-H} = a_{p-H} = 1 \cdot 0$ Gauss) is suported by the ESR spectrum of 2,2-di-(*p*-bromophenyl)-1-benzenesulfonylhydrazyl,[32] but further confirmations are needed.

Example VI [28]. The ESR spectrum of VI is poorly resolved, therefore the intensities of lines are only tentative, especially in the right part of the spectrum ; there are 41 lines.

---

[32] N. Negoiţă and A.T. Balaban, to be published.

1. No spurious lines are seen; the overlap-free intensity ratio is $2^2 = 4$.

2,3. A triplet with $a_N = 11$ d is clearly visible simplifying the task to a subgroup of 19 lines with approximative intensities 1 : 2 : 2 : 4 : 8 : 7 : : 10 : 10 : 8 : 7 : . . . . . for the left half of the subgroup including the centre line. Summation of intensities yields $A = 96 = 3^2 \cdot 2^{n_H}$, hence $n_H = 4$ hydrogens.

4. All intervals d are taken as equal, d = 0·81 Gauss. The span of the subgroup of lines is D = 18 d.

5. Instead of examining the 40 partitions of 18 into 8 non-zero integers (or of 10 into up to 8 integers), we will assume free rotation, therefore $18\ d = 2a_{NO} + 2a_{NO_2} + 2a_H + 2a_H'$. Partitions of 9 into 4 non-zero integers (or of 5 into up to 4 integers) are shown in Table 4.

6. Here a difference from the previous cases arises, since one can assign differently the coupling constants to a_N or a_H', the resulting intensity pattern being different.* All possibilities are considered in table 4,

Table 4

Partitions of 18 and calculated spectra for VI

No	Partition of 18								Coupling const.						Intensities									
									a_{NO}	a_{NO_2}	a_H	a_H	a_H	a_H										
1	6	6	1	1	1	1	1	1	6	1	1	1	1	1	1	5	11	14	11	5	2	5	11	14
2									1	1	6	6	1	1	1	4	8	10	8	4	3	8	16	20
3	5	5	2	2	1	1	1	1	5	2	1	1	1	1	1	4	7	8	8	9	11	11	9	8
4									5	1	2	2	1	1	1	3	6	9	10	10	9	9	10	10
5									2	1	5	5	1	1	1	3	5	6	6	8	11	19	25	24
6									1	1	5	5	2	2	1	2	5	6	8	8	9	12	13	16
7	4	4	3	3	1	1	1	1	4	1	3	3	1	1	1	3	4	5	11	11	11	10	12	14
8									3	1	4	4	1	1	1	3	4	4	6	10	12	12	13	14
9									1	1	4	4	3	3	1	2	3	4	7	10	11	12	14	16
10									4	3	1	1	1	1	1	4	6	5	6	10	11	10	12	14
11	4	4	2	2	2	2	1	1	4	2	2	2	1	1	1	2	4	6	8	10	11	12	12	12
12									4	1	2	2	2	2	1	1	5	4	11	7	15	8	16	8
13									2	2	4	4	1	1	1	2	3	4	7	10	9	8	11	14
14									2	1	4	4	2	2	1	1	4	3	9	6	15	9	19	10
15	3	3	3	3	2	2	1	1	3	3	2	2	1	1	1	2	3	6	7	8	12	12	13	16
16									3	2	3	3	1	1	1	2	2	5	8	8	11	14	14	14
17									3	1	3	3	2	2	1	1	3	5	6	10	11	13	15	14
18									2	1	3	3	3	3	1	1	2	5	6	9	11	14	16	14
19	3	3	2	2	2	2	2	2	3	2	2	2	2	2	1	—	5	1	11	5	15	11	16	14
20									2	2	3	3	2	2	1	—	4	2	8	8	11	16	12	02

---

* In some cases ambiguities occur, e.g. an ESR spectrum consisting of six equal equidistant lines can be interpreted as being due either to $a_N = 2d$ and $a_H = d$, or to $a_N = d$ and $a_H = 3d$.

resulting in 20 intensity patterns to be compared with the experimental spectrum. Cases 7, 8 and 11 come close to the observed pattern but the best agreement is given by case 16 in table 4, yielding the coupling constants indicated on fig. 6.

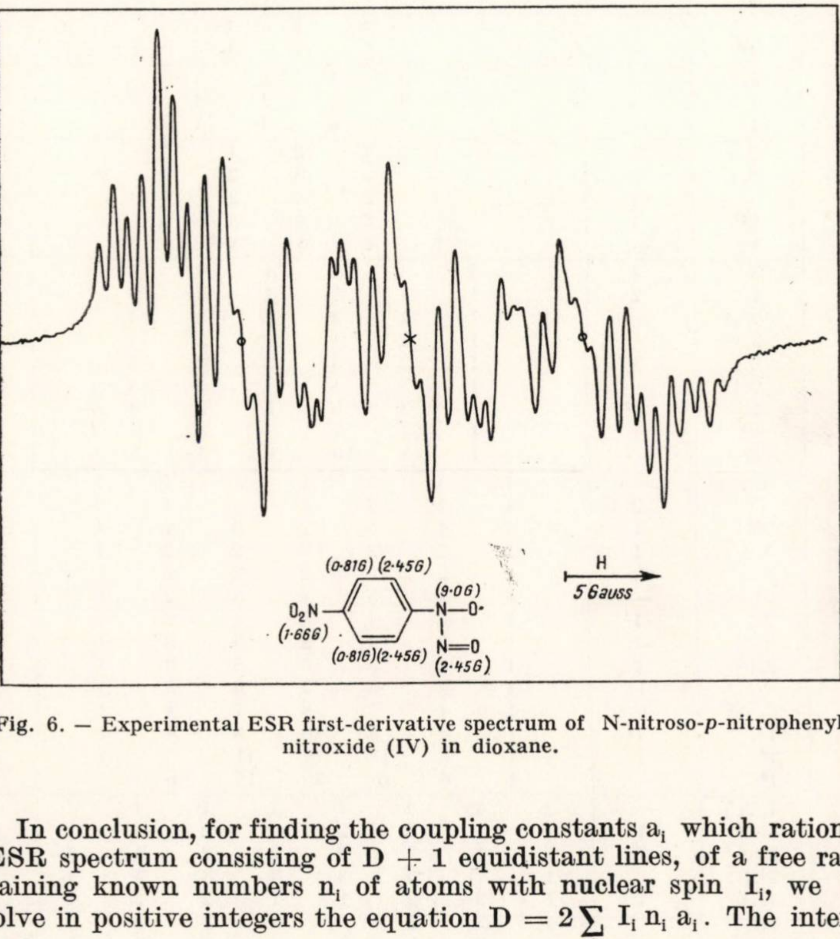

Fig. 6. — Experimental ESR first-derivative spectrum of N-nitroso-*p*-nitrophenylnitroxide (IV) in dioxane.

In conclusion, for finding the coupling constants a_i which rationalize an ESR spectrum consisting of $D + 1$ equidistant lines, of a free radical containing known numbers n_i of atoms with nuclear spin I_i, we have to solve in positive integers the equation $D = 2\sum_i I_i n_i a_i$. The intensity distribution pattern is equivalent to providing $\sum n_i - 1$ non-explicit equations so as to make the solution unique. In order to assist in interpreting such ESR spectra, table 5 presents all possible intensity distribution patterns for free radicals containing H and N atoms and presenting from 2 to 8 equidistant lines (and no missing lines in between). The table can be easily expanded but space limitations only allow us to mention that there are respectively 32 and 53 possibilities of such 9-and 10-line ESR spectra.

Table 5[a]

All possible ESR spectra with 2 – 8 equally spaced lines due to hydrogen and/or nitrogen atoms

Number of lines	Coupling constants		Intensities I_i								$\sum_i I_i$
	a_H	a_N									
2	1	—	1	1							2
3	—	1	1	1	1						3
	1^2	—	1	2	1						4
4	2,1	—	1	1	1	1					4
	1	1	1	2	2	1					6
	1^3	—	1	3	3	1					8
5	2	1	1	1	2	1	1				6
	$2,1^2$	—	1	2	2	2	1				8
	—	1^2	1	2	3	2	1				9
	1^2	1	1	3	4	3	1				12
	1^4	—	1	4	6	4	1				16
6	3	1	1	1	1	1	1	1			6
	1	2	1	1	1	1	1	1			6
	$2^2,1$	—	1	1	2	2	1	1			8
	$3,1^2$	—	1	2	1	1	2	1			8
	2,1	1	1	2	3	3	2	1			12
	$2,1^3$	—	1	3	4	4	3	1			16
	1	1^2	1	3	5	5	3	1			18
	1^3	1	1	4	7	7	4	1			24
	1^5	—	1	5	10	10	5	1			32
7	3, 2, 1	—	1	1	1	2	1	1	1		8
	—	2, 1	1	1	2	1	2	1	1		9
	2^2	1	1	1	3	2	3	1	1		12
	3, 1	1	1	2	2	2	2	2	1		12
	1^2	2	1	2	2	2	2	2	1		12
	$2^2,1^2$	—	1	2	3	4	3	2	1		16
	2	1^2	1	2	4	4	4	2	1		18
	$3, 1^3$	—	1	3	3	2	3	3	1		16
	$2,1^2$	1	1	3	5	6	5	3	1		24
	—	1^3	1	3	6	7	6	3	1		27
	$2, 1^4$	—	1	4	7	8	7	4	1		32
	1^2	1^2	1	4	8	10	8	4	1		36
	1^4	1	1	5	11	14	11	5	1		48
	1^6	—	1	6	15	20	15	6	1		64
8	4, 2, 1	—	1	1	1	1	1	1	1	1	8
	3, 2	1	1	1	2	2	2	2	1	1	12
	2, 1	2	1	1	2	2	2	2	1	1	12
	$2^3,1$	—	1	1	3	3	3	3	1	1	16
	4, 1	1	1	2	2	1	1	2	2	1	12
	$3,2,1^2$	—	1	2	2	3	3	2	2	1	16
	3	1^2	1	2	3	3	3	3	2	1	18
	1	2,1	1	2	3	3	3	3	2	1	18
	$2^2, 1$	1	1	2	4	5	5	4	2	1	24
	$4, 1^3$	—	1	3	3	1	1	3	3	1	16
	$3, 1^2$	1	1	3	4	4	4	4	3	1	24
	1^3	2	1	3	4	4	4	4	3	1	24
	$2^2, 1^3$	—	1	3	5	7	7	5	3	1	32
	2, 1	1^2	1	3	6	8	8	6	3	1	36
	$3, 1^4$	—	1	4	6	5	5	6	4	1	32
	$2, 1^3$	1	1	4	8	11	11	8	4	1	48
	1	1^3	1	4	9	13	13	9	4	1	54
	$2,1^5$	—	1	5	11	15	15	11	5	1	64
	1^3	1^2	1	5	12	18	18	12	5	1	72
	1^7	—	1	7	21	35	35	21	7	1	128

[a] The number of lines is $\Sigma\,(2a_N + a_H) + 1$, and the sum of intensities is $\sum_i I_i = 2^{n}H . 3^{n}H$. Coupling constants a_H aand a_N are in d units (d being the spacing between adjacent lines.)

Revue Roumaine de Chimie, **17**, *1*, *2*, 25 – 28 (1972)

Dedicated to Professor I. G. MURGULESCU
on his 70th birthday

PHOTOTROPIC GLASSES ON B_2O_3 BASIS

P. BALTĂ*, L. DOLLINGHER** and MARIA CÎRSTEA*

* Polytechnic Institute, Str. Polizu 1, Bucharest
** Centre of Physical Chemistry, Str. Galaţi 31, Bucharest, Romania

Received September 4, 1971

Continuing some previous works, phototropic glasses on a B_2O_3 basis have been studied, establishing first of all synthesis conditions of their possible obtention. The results allow to deduce the way in which AgCl is placed in a B_2O_3 lattice and to point out some structural parameters on the photosensitivity of these glasses.

In one of the previous papers [1] the authors have discussed a simple energetic model of the processes taking place in phototropic glasses. Experiments have been made to gather experimental data that could materialize some characteristics of the process. Since usual phototropic glasses have complex compositions with too many variable parameters, we have looked for a glass as simple as possible. Having in view that B_2O_3 holds a considerable share in all varieties of phototropic glass, a pure B_2O_3 glass has been selected containing silver salt conferring photosensitivity.

The following is part of the original results of this study which is in progress.

THE OBTENTION OF PHOTOTROPIC GLASSES ON A B_2O_3 BASIS

One can find in the literature only a slight hint at some characteristics of the phototropic glass on a B_2O_3 basis,[2] but no data on its synthesis.

For this reason we had to try several theoretically possible ways. The direct method of melting a mixture of boric acid and fresh silver chloride came to a dead end. Silver was reduced while melting and glass was coloured but with no sensitivity to light after cooling. After several experiments, we reached the conclusion that it was possible to obtain a phototropic glass from boric anhydride by melting it in two stages. In the first one a chemically pure boric acid was dehydrated by heating for six hours at 800° and then for two hours at about 1400°. According to the literature data,[3] a B_2O_3 glass with less than 0.2% water could be obtained under such circumstances. This glass was granulated by powdering and mixed with fresh silver chloride. In a second stage this mixture melted at about 500°. When this temperature was exceeded, silver reducing and glass degradation could not be avoided, probably owing to the well-known sensitivity of AgCl to light and heat. About an hour later a glass of satisfactory quality was obtained, but it was difficult enough to extract it from the crucible as well as to process it because of its high viscosity. The composition of the mixture from which this glass was obtained (denoted by 1) is shown in table 1.

---

[1] P. Baltă, E. Baltă and L. Dollingher, *Rev. Roumaine Chim.*, **16**, 1315 (1971).

[2] G. Gliemeroth, *Glass Email Keram. Techn.*, **8**, 269 (1968).

[3] P. Baltă and V. Burghelea, *Ind. Uşoară*, **8**, 539 (1969).

Table 1

Composition of the mixtures used to obtain the glasses under study

Compounds in the mixture (grams)	Glass		
	1	2	3
B_2O_3	100	100	—
$B(OH)_3$	—	—	220
AgCl	1.4	—	—
$AgNO_3$	—	1.7	1.7
NaCl	—	3.95	—
HCl (conc.)	—	—	10

Another experiment was based on the idea of introducing into the glass a silver less sensitive to light and heat, thus creating proper conditions to secure AgCl only in the molten glass. With this end in view, $AgNO_3$ and NaCl were introduced into the initial mixture (table 1, glass 2). A double exchange reaction took place at high temperatures, after which $NaNO_3$ decomposed, finally remaining only silver chloride and sodium borate. Thus, the melting temperature could be increased up to 800° or even more by obtaining a glass with phototropic characteristics. Unfortunately this glass had sodium impurities that determined a separation of some vitreous microphases of sodium borate, and the samples were therefore opalescent.

The third way tried differs substantially from the preceding ones. We started with a solution in water of boric acid and silver nitrate, and after steady stirring, hydrochloric acid was added (table 1, glass 3) . The solution was evaporated until dryness and the resulting powder was dehydrated gradually and melted at a temperature not exceeding 600°. Under such circumstances a glass having phototropic features was obtained. A too advanced dehydration could however not be obtained and the remaining boric acid brought about a separation of microphases leading to glass opalescence. The complex microstructure of the glass can be seen on figure 1.

All glasses were molten in platinum crucibles in electric furnaces with resistance. The samples were thermally treated at 250, 275 and 300° for 15 and 30 minutes, then ground on both sides, so that transparency variation could be tested according to the UV irradiation time with constant intensity.

The process of spontaneous and thermal decoloration was also studied.

EXPERIMENTAL RESULTS

Figure 2 shows some results that point out the influence of the composition on the photosensitivity of the glasses obtained. Considering the initial transparency equal to 100% the particular influence of irradiation could be analysed. The purest glass number 1 darkens relatively slowly by lowering its transparency to about 60% after 5 minutes. Glasses containing alien cations are more sensitive, reaching about 57% as in the case of the variety with sodium (No. 2) and about 41% for the one with hydrogen (No. 3), for the same irradiation time. A marked differentiation of glass varieties as far as the influence of thermal treatment on photosensitivity is concerned, could also be noted. It is well known that thermal treatment causes a separation of vitreous microphases, which influences the characteristics of these glasses. In the case of glass No. 1 the treatments for 15 minutes at different temperatures have as a matter of fact no influence at all. But for a longer time an increase of sensitivity could be ascertained, at the same time with the growth of temperature and length of time.

The influence of the duration of the treatment at 275° on this glass is shown in figure 3. The glasses with the numbers 2 and 3 have a higher sensitivity to thermal treatment. Generally speaking, an increase of sensitivity according to both parameters can be noted.

Figure 4 for instance presents the influence of temperature on the variation of transparency of glass No. 2 in accordance with the irradiation time. Sometime an extension of duration at high temperature (such as 30 minutes at 300°) brings about a decrease of sensitivity.

As regards the return of transparency to the initial value, these glasses have a considerable inertia. Spontaneous bleaching takes place very slowly so that it cannot practically be taken into account. That is why thermal fading has been examined. At a temperature over 100° irradiated glasses fade approaching initial transparency. Figure 5 shows for instance the values of the transparency reached by glass No. 1 after 7 minutes of fading at various temperatures. Bleaching develops relatively slowly even under these energetic conditions.

DISCUSSIONS OF RESULTS

The above mentioned results are leading to some useful ideas about the processes taking place in these glasses.

Different influence of thermal treatment on glass sensitivity in accordance with its composition has to be correlated to the separation of the vitreous microphases. But this process depends on the chemical compounds included in the glass. Probably some complex substance that could be called "chloro-borates" forms in glass No. 1 lacking foreign cations. The possibility of the appearance of such compounds is due to the donor character of chlorine and the acceptor one of boron. Non-participating chlorine electrons, using the free orbital of boron, determine an increase in its coordination from 3 to 4, and isolated tetrahedra of $[BO_3Cl]$ appear in the bidimensional B_2O_3 lattice. The concentration of these tetrahedra during thermal treatment, for the building up of AgCl granules, big enough to be sensitive to light, is slow because other peaks are linked to the lattice. In the presence of sodium or hydrogen in higher concentrations, some compounds of the $[BO_3Cl]$ Na_3Ag, $-[BO_2Cl]$ Na_2Ag, $>[BOCl]$ NaAg as well as $>[BOCl]$ HAg type develop, so that the tetrahedron is not bound at all or has less peaks bound in the B_2O_3 lattice. The separation of the microphases takes place faster under these circumstances. First of all, molecules with more Na and Ag will concentrate in microphases. Then, microphases will be diluted into Ag and glass sensitivity will decrease at higher temperatures and after a longer treatment.

Another interesting phenomenon is the rise in sensitivity from pure glass (No. 1) to glass with Na^+ (No. 2) and that with H^+ (No. 3). It is obviously a matter of influence of these cations on the transfer of charge that takes place under UV irradiation. If we assumed the existence of the above compounds, such an influence is to be expected. The innermost mechanism of this process is still to be examined.

The high stability of coloured glasses indicates the close connection of the halogen with the B_2O_3 lattice after neutralization of Ag^+. The halogen can be dislocated for a new interaction with silver only by heating at highly enough temperatures.

CONCLUSIONS

Synthesis conditions that allow the obtention of some phototropic glasses on B_2O_3 basis have been established.

The characteristics of the examined glasses allow to infer the AgCl placing in the B_2O_3 lattice and point to the influence of some structural parameters on the sensitivity of phototropic glasses.

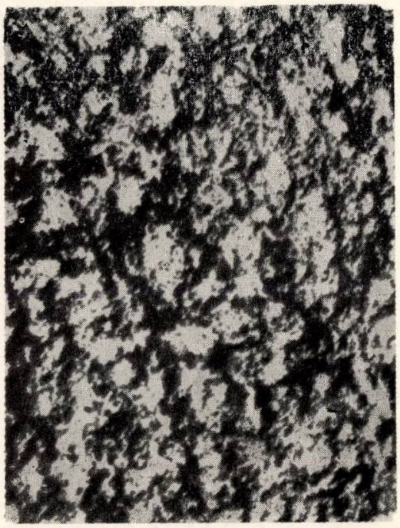

Fig. 1. — Aspect on the electron microscope of glass No. 3 molten at 600°.

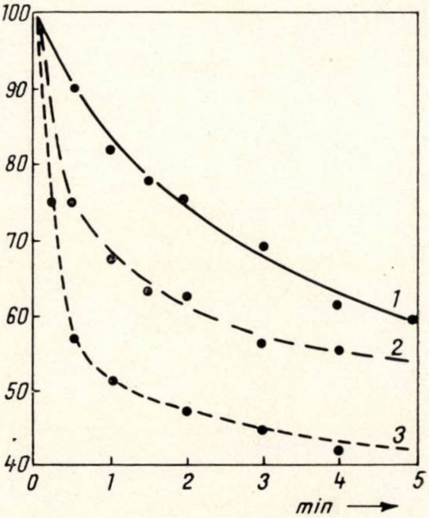

Fig. 2. — Variation of transparency according to the irradiation time. Figures on the curves (1, 2, 3), show glass composition as in table 1. Samples have been thermally treated for 15 minutes at 300°.

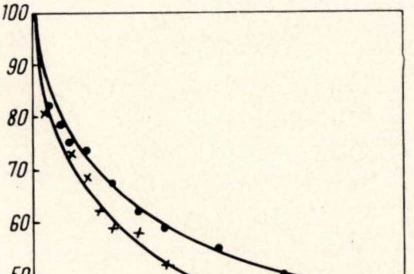

Fig. 3. — Influence of the duration of thermic treatments on glass No. 1 sensitivity: *1)* **15** min. at 275°; *2)* 30 min. at 275°.

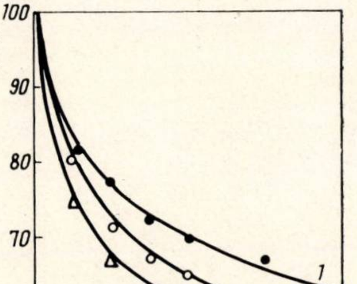

Fig. 4. — Influence of the temperature of thermal treatment on photosensitivity of glass No. 2: *1)* 15 min. at 250°; *2)* 15 min. at 275°; *3)* 15 min. at 300°.

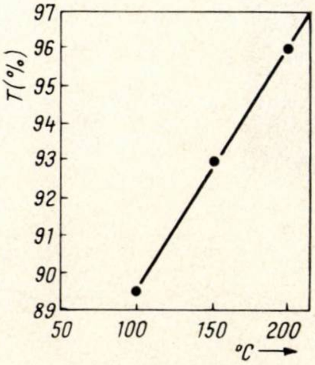

Fig. 5. — Influence of temperature of the fading treatment on glass transparency after 7 minutes. Samples of glass No. 1 previously treated for 30 minutes at 300° and irradiated for 10 minutes.

Revue Roumaine de Chimie, 17, 1, 2, 29–33 (1972)

Herrn Professor I. MURGULESCU
zum 70. Geburtstag

ZUR KINETISCHEN UNTERSUCHUNG DER KATALYTISCHEN KRACKUNG VON PROPAN

HERMANN BEYER, DÉNES KALLÓ und GÉZA SCHAY

vom Zentralforschungsinstitut für Chemie der Ungarischen Akademie der Wissenschaften,
Budapest, II, Pusztaszeriút, 57–69

Eingegangen am 13. September 1971

Es wurde die Kinetik der primären Reaktionen bei der Krackung des Propans untersucht. Um die aufgrund störender Folgereaktionen auftretenden Olefine zu entfernen, wurde ein selektives Ab- bzw. Desorptionssystem verwendet. Als Krackkatalysator wurde ein natürlich vorkommender, bei 500° dekationisierter Klinoptilolit eingesetzt. Es wurden die Geschwindigkeitskonstanten und die Aktivierungsenergien der Krackung und Dehydrierung von Propan bei 460° für verschiedene thermische Vorbehandlungen des Katalysators ermittelt. Aktivität und Selektivität des Katalysators hängen von der Anzahl und Temperatur der Ausheizvorgänge ab. Die Aktivierungsenergien hingegen sind unabhängig von der thermischen Vorbehandlung und für beide primären Reaktionen gleich.

Die unter üblichen Reaktionsbedingungen durchgeführte katalytische Krackung paraffinischer Kohlenwasserstoffe ist chemisch gesehen ein sehr komplizierter und komplexer Prozeß. Neben den Primärreaktionen, d.h. den unter Aufsprengung von C-C-Bindungen und Bildung von niederen Olefinen und Paraffinen verlaufenden eigentlichen Krackreaktionen und der damit stets einhergehenden Substratdehydrierung, verlaufen nämlich noch viele, auf mannigfaltige Weise ineinandergreifende Folgereaktionen der primären Reaktionsprodukte, von denen sich besonders die Olefine als störend erweisen. Bei einem so komplexen, durch Variation der Versuchsbedingungen nicht zu vereinfachenden Reaktionsgeschehen ist eine kinetische Auswertung von Versuchsergebnissen von vornherein aussichtslos.

Unseres Erachtens können aber nur dann Erkenntnisse über die Mikrokinetik der primären Reaktionen des Krackprozesses gewonnen und eine Überprüfung der zahlreich in Vorschlag gebrachten, sich oft auch widersprechenden Vorstellungen über den Reaktionsmechanismus und die chemische Natur der aktiven Zentren vorgenommen werden, wenn experimentell mit ausreichender Genauigkeit bestimmte kinetische Parameter der einzelnen primären Reaktionen zur Verfügung stehen. Unser Ziel war deshalb, die Kinetik der primären Reaktionen unter Ausschaltung aller störenden Folgereaktionen zu untersuchen.

Als Substrat haben wir Propan verwendet. Bei diesem hinsichtlich der Krackung einfachsten paraffinischen Kohlenwasserstoff ist noch am ehesten ein zu übersehendes Reaktionsbild zu erwarten, da neben der Dehydrierreaktion

$$C_3H_8 \rightleftarrows C_3H_6 + H_2 \tag{1}$$

nur eine einzige Krackreaktion

$$C_3H_8 \rightarrow C_2H_4 + CH_4 \tag{2}$$

abläuft und das dabei auftretende gesättigte Reaktionsprodukt (Methan) nicht weiter gespalten werden kann.

Um die störenden Folgereaktionen der nach den Reaktionsgleichungen (1) und (2) auftretenden Olefine auszuschalten, wurden die Versuche in einer Zirkulationsapparatur (geschlossener integraler, statischer Reaktor) vorgenommen, wobei durch entsprechende Wahl der Zirkulationsgeschwindigkeit die Kontaktzeit für einen Reaktordurchlauf und damit die während dieser Zeit gebildete Olefinmenge genügend klein gehalten und die Olefine hinter dem Krackreaktor aus dem zirkulierenden Gasstrom selektiv entfernt wurden.

Die Entfernung der Olefine aus dem Zirkulationssystem kann auf zwei verschiedenen Wegen erfolgen. Bei der einen Methode, die schon an anderer Stelle beschrieben wurde,[1] erfolgt eine Hydrierung der Olefine zu gesättigten Kohlenwasserstoffen in einem in den Zirkulationskreis eingebauten Hydrierreaktor. Bei Zusatz von Wasserstoff zum Substrat kann so unter geeigneten Reaktionsbedingungen die Dehydrierreaktion (1) im Gesamtsystem praktisch vollständig zurückgedrängt und die Stoffumwandlung im System infolge der Hydrierung des nach (2) gebildeten Äthylens durch die Bruttogleichung

$$C_3H_8 + H_2 \rightarrow C_2H_6 + CH_4$$

beschrieben werden. Auf diese Weise können jedoch nur die eigentlichen Krackreaktionen, nicht aber die stets als Begleitreaktion ablaufende Substratdehydrierung untersucht werden. In der vorliegenden Arbeit wurden die sich gemäß der Reaktionsgleichungen (1) und (2) bildenden Olefine nach einem zweiten, auf selektiver Ad- bzw. Absorption dieser Verbindungen beruhenden Verfahren aus dem Zirkulationssystem entfernt. Bisher wurden derartige Versuche nur von Fejes und Emmett[2] vorgenommen, die allerdings zu Fehlschlüssen führten, da das dabei als Sorptionsmittel verwendete Quecksilberperchlorat mit Kohlenwasserstoffen unter Bildung von Radikalen reagiert, die bereits bei den für die katalytische Krackung erforderlichen Reaktionstemperaturen eine schnelle thermische Spaltung des Substrates bewirken (Keulks und Emmett[3]).

---

[1] H. Beyer, *Acta Chim. Acad. Sci. Hung.*, im Druck.

[2] P. Fejes und P.H. Emmett, *J. Catalysis*, **5**, 193 (1966).

[3] G.W. Keulks und P.H. Emmett, *J. Catalysis*, **6**, 153 (1966).

Wir haben die Versuche mit der schon früher beschriebenen [1] Apparatur ausgeführt, bei der lediglich der Hydrierreaktor gegen ein Sorptionsgefäß ausgetauscht wurde. Als Krackkatalysator wurden etwa 15 g eines in ungefähr 70–80 %iger Reinheit natürlich vorkommenden, nach Austausch der Kationen gegen Ammoniumionen (1,6 mMol/g) bei 500° dekationisierten Klinoptilolits eingesetzt. Der Katalysator wurde vor jeder aus 5–8 halbstündigen Versuchen bestehenden Versuchsserie im Reaktor bei 540° mit Sauerstoff regeneriert, danach zur Reduktion gewisser Katalysatorverunreinigungen (z.B. Fe_2O_3) mit Wasserstoff behandelt und anschließend etwa 4 Stunden im Vakuum bei 540 bzw. 630° ausgeheizt.

Das Volumen des Zirkulationssystems betrug etwa 250 ml, die Volumengeschwindigkeit der Gasströmung ungefähr 70 ml/s und der Propandruck zu Versuchsbeginn 100–400 torr. Die Reaktionstemperaturen wurden so gewählt, daß eine 50%ige Konversion im allgemeinen in 30–90 Minuten erreicht wurde. Die Olefine wurden in auf Bimsstein im Gewichtsverhältnis von etwa 1 : 1 aufgebrachter, 3% Silbersulfat enthaltender konzentrierter Schwefelsäure absorbiert. Das Sorptionsgefäß war mit etwa 80 g dieses Sorptionsmittels beschickt und wurde zur Verbesserung des Sorptionseffektes auf 0°C abgekühlt.

Propylen war bei den unter den angegebenen Versuchsbedingungen durchgeführten Krackversuchen hinter dem Sorptionsgefäß gaschromatographisch nicht nachweisbar, d.h., daß der Partialdruck unter 0,005 torr lag. Der Äthylenpartialdruck ist abhängig von der bereits sorbierten Äthylenmenge und betrug im allgemeinen nur einige hundertstel torr. Beim Auftreten höherer Äthylenpartialdrücke wurde frisches Sorptionsmittel eingesetzt.

Von Äthanspuren abgesehen, die auf eine Hydrierung des im System in sehr geringen Konzentrationen vorliegenden Äthylens zurückzuführen sind und bei der Auswertung rechnerisch berücksichtigt werden können, treten bei den so ausgeführten Versuchen als Reaktionsprodukte erwartungsgemäß nur Wasserstoff und Methan in der Gasphase auf. Der Katalysator zeigt über relativ lange Versuchszeiten hinweg keine Ermüdungserscheinungen, auch sind keine Kohlenstoffablagerungen auf der Katalysatoroberfläche festzustellen. Die Konversionskurven des gebildeten Wasserstoffs bzw. Methans lassen sich also ohne weiteres zur Bestimmung der Kinetik der Reaktion (1) bzw. (2) heranziehen.

Die Kinetik der katalytischen Krackung von Propan haben unseres Wissens bisher nur Franklin und Nicholson [4] untersucht. Die Versuche wurden in einem einfachen statischen System ausgeführt, in dem natürlich auch die Folgereaktionen der Olefine abliefen. Die kinetische Auswertung beschränkt sich auf die Propankonversion, für die innerhalb der natürlich sehr großen Fehler (vergleichbare Geschwindigkeitskonstanten zeigen Abweichungen von bis zu 25%) ein Verlauf nach erster Ordnung gefunden wurde. Wir konnten aufgrund der speziellen Art unserer Versuchstechnik wesentlich genauere Untersuchungen (1–2 % Fehler) vornehmen und feststellen, daß sowohl die Krackung (Aufsprengung der C-C-Bindung) als auch die Dehydrierung des Propans nach genau erster Ordnung verläuft.

---

[4] F.L. Franklin und D.E. Nicholson, *J. Phys. Chem.*, **60**, 59 (1956).

Wie aus Tabelle 1, in der die Reaktionsgeschwindigkeitskonstanten k für eine Reaktionstemperatur von 460° und die aus der Temperaturabhängigkeit der Geschwindigkeitskonstanten berechneten Aktivierungsenergien $E^{\neq}$ angegeben sind, und den in Abb. 1 dargestellten Arrheniusdiagrammen zu ersehen ist, hängen Aktivität und Selektivität des Katalysators von der Zeitdauer der Ausheizung bzw. Anzahl der Ausheizvorgänge und — in wesentlich größerem Maße — auch von der Ausheiztemperatur ab. Die Aktivierungsenergien sind hingegen unabhängig von der thermischen Vorbehandlung des Katalysators und — was besonders bemerkenswert ist — für die beiden primären Reaktionen (1) und (2) gleich.

Tabelle 1

Geschwindigkeitskonstanten und Aktivierungsenergien der Krackuug nnd Dehydrierung von Propan bei 460^2

Vers.-Serie*	Aush. - Temp. (°C)	k bei 460°C [Mol.g^{-1} Torr^{-1} s^{-1}]$\times 10^{10}$		$E^{\neq}$ [kcal/Mol]	
		Krackung	Dehydr.	Krackung	Dehydr.
1	540	3.69	0.73	33.7	34.1
6	540	2.28	0.59	33.5	34.2
7	630	0.55	0.31	34.2	34.2

* Vor den mit n- und i-Butan als Substrat ausgeführten Versuchsserien 2–5 wurde der Katalysator ebenfalls bei 540° C ausgeheizt.

Aus den bisherigen experimentellen Feststellungen lassen sich hinsichtlich des Reaktionsmechanismus einige interessante Schlußfolgerungen ziehen. Die Tatsache, daß zwei so verschiedenartige Reaktionen wie die Aufsprengung der C-C-Bindung und die Dehydrierung die gleiche Aktivierungsenergie erfordern, läßt den Schluß zu, daß beide Reaktionen über einen gemeinsamen aktiven Komplex verlaufen und die Bildung dieses Komplexes, also die Substratchemisorption der geschwindigkeitsbestimmende Schritt ist. Die Kinetik erster Ordnung weist auf eine geringe Bedeckung der aktiven Oberfläche durch diesen Komplex hin. Im Verlaufe der weiteren Reaktion zerfällt der gemeinsame aktive Komplex — vielleicht über Zwischenstufen — unter Aufsprengung der C-C-Bindung oder Dehydrierung. Da sich aber die Selektivität des Katalysators mit der thermischen Vorbehandlung verändert, muß im Mechanismus einer der beiden Reaktionen auch noch ein zweites aktives Zentrum eine Rolle spielen.

Aus den bisherigen Ergebnissen kann noch kein vollständiges Bild über den Reaktionsmechanismus und die chemische Natur der beiden aktiven Zentren erhalten werden. Das ist das Ziel weiterer Untersuchungen. Die festgestellte Abhängigkeit der Aktivität und Selektivität von der thermischen Vorbehandlung des Katalysators läßt jedoch vermuten, daß Brönsted- und Lewis-Zentren am Reaktionsmechanismus beteiligt sind.

Schließlich soll noch bemerkt werden, daß sich die Geschwindigkeit beider primärer Reaktionen nicht verändert, wenn die Zirkulationsgeschwindigkeit und damit auch der im Reaktor herrschende, in der Größenordnung von 0,01—0,1 torr liegende Partialdruck des sich bildenden Propylens variiert wird. Wir können somit der mehrfach vertretenen Meinung (vgl. z.B. Eastwood[5]), daß Olefine die Paraffinkrackung initiieren, nicht zustimmen.

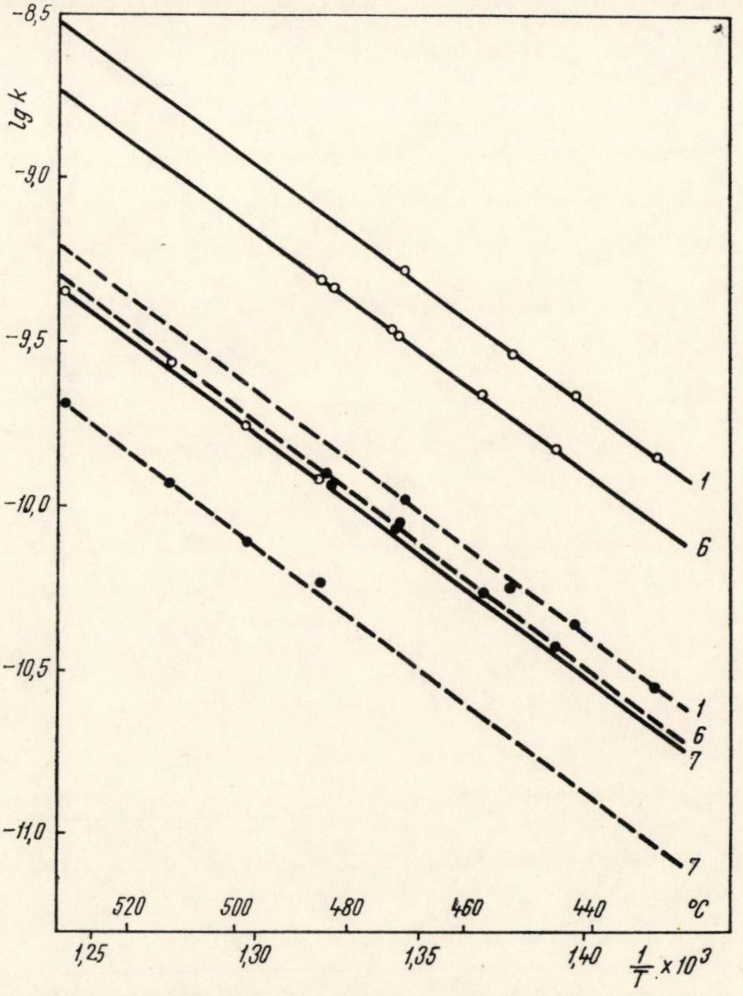

ARRHENIUS-Diagramme für Krackung (ausgezogene Gerade) und Dehydrierung (gestrichelte Gerade) von Propan an bei 540° (Versuchsserien 1 und 6) und 630° (Versuchsserie 7) ausgeheiztem, dekationisiertem Klinoptilolit.

---

[5] S.C. Eastwood, Preprint of the Proceedings of the 8th World Petroleum Congress, Moscow, 1971.

Revue Roumaine de Chimie, 17, 1, 2, 29–33 (1972)

Schließlich soll noch bemerkt werden, daß sich die Geschwindigkeit beider genannter Reaktionen nicht verändert, wenn die Zirkulationsgeschwindigkeit und damit auch der im Reaktor herrschende, in der

[illegible]

Grenzschichtung von [illegible] und [illegible] liegende Partialdrücke des sich bildenden Propylens verändert wird. Wir können somit der [illegible] Annahme [illegible], daß [illegible] die Partialdruckverteilung [illegible] nicht einstellen.

[illegible] Proceedings of the 5th World [illegible]

[illegible]

Revue Roumaine de Chimie, **17**, *1, 2*, 35–39 (1972)

Dedicated to Professor I. G. MURGULESCU
on his 70th birthday

ON THE BINDING ENERGY OF SMALL CLUSTERS OF ATOMS

G. BLIZNAKOV, S. DELINESHEV

Institute of General and Inorganic Chemistry, Bulgarian Academy of Sciences, Sofia, Bulgaria

Received September 15, 1971

With the aid of the LCAO-MO method it was shown that the energy of a bond in a small cluster of atoms changes with the change in configuration of the cluster and in the number of the cluster atoms. This should be taken into consideration in calculating the energy parameters characterizing clusters of different configurations and sizes.

The LCAO-MO method was used in studying the growth of a lithium crystal. It was shown that in spite of the presence of a sufficient number of atoms needed for the formation of a three-dimensional crystal, the two-dimensional crystal with the same number of atoms and a structure corresponding to that of the most dense plane (110) of the lithium lattice, is the stabler one.

The classical fluctuation theory of nucleation was developed in the papers of Gibbs, [1] Volmer, [2] Kossel,[3] Stranski and Kaischew, [4] Becker and Doering. [5] According to this theory, fluctuations in density of the initial phase cause the formation of clusters of molecules which are in labile equilibrium with their environment and represent nuclei of the new phase. The sizes of the nuclei depend on the supersaturations at which they are formed. Nuclei formed at high supersaturations are smaller than those appeared at low supersaturations.

The experimental data available in the literature show that at high supersaturations, the number of molecules in the nucleus appeared as a result of homogeneous nucleation is of the order of several tens. [6] There is a similar situation with heterogeneous nucleation. The number of mercury atoms forming the nucleus is, according to Mutafchiev and Kaischew, [7] about 20. Kaischew and Gutsov [8] have found the number of iron atoms in the critical nucleus to be 1 to 1.5. According to the calculations of Toshev and Markov, [9] the critical nucleus of cadmium contains about 2 atoms. The above results concern electrolytic nucleation. Kenty [10] has calculated the radii of the critical nuclei of silver and gold formed on a substrate. They are of the order of 2 to 4 Å.

---

[1] J.W. Gibbs, "Thermodynamische Studien", Leipzig, 1892.

[2] M. Volmer and A. Weber, *Z. Phys. Chem.*, **119**, 277 (1926) ; M. Volmer, *Z. Elektrochem.*, **35**, 555 (1929) ; M. Volmer and M. Marder, *Z. phys. Chem. (A)*, **154**, 97 (1931) ; H. Brandes. and M. Volmer, *Z. Phys. Chem. (A)*, **155**, 466 (1931) ; M. Volmer and W. Schultze, *Z. phys. Chem. (A)*, **156**, 1 (1931) ; M. Volmer and H. Flood, *Z. Phys. Chem. (A)*, **170**, 273 (1934).

[3] W. Kossel, *Nachr. Gött. Ges.*, **1927**, 135 ; *Naturwiss.*, **18**, 901 (1930).

[4] I.N. Stranski and R. Kaishev, *God. Sof. U-tet fiz.-mat. f-t*, **32**, 171 (1935/36) ; *Uspekhi. fiz. nauk*, **21**, 408 (1939).

[5] R. Becker and W. Doering, *Ann. Phys.*, **24**, 719 (1935).

[6] J.P. Hirth and G.M. Pound, "Condensation and Evaporation", Pergamon Press, New York, 1963.

In the papers of Galashin, Senchenkov and Chibissov [11–13] on the nucleation of silver on/in crystals of silver bromide, critical nuclei containing about 60 silver atoms each are discussed. The small number of atoms in the critical nuclei shows that when the nucleation theory is applied in its usual form, significant difficulties arise. This is due to the fact that constants (such as the free surface energy) characterizing the bulk phase are used in calculating small complexes of atoms. For that reason, the thermodynamics of small phases with the greater part of molecules lying on the surface is being studied intensively.[14–20] The stability of a small cluster of atoms is directly associated with its binding energy. The determination of this quantity as the sum of the nearest-neighbour bonds (the bond energy being a constant independent of the number of atoms, or the number of bonds, respectively), seems not to be reliable. [21]

On the basis of experimental data for some metals it could be shown that the energy of bonds in the smallest crystal complex, i.e. in a two-atom molecule, D_0, is more than twice as large as the energy, ε_s, found for an infinitely large crystal (see Table 1).

Model calculations were carried out with a simple model (a crystal having a simple cubic lattice) by the LCAO-MO method. [21] The results show that the energy of a bond between nearest neighbours has its highest value in the case of a two-atom complex (Fig. 1). When the crystal increases, the energy of the bond decreases and tends to a constant value which is different for one-, two- and three-dimensional crystals.

Recently Borovinskii and Klyuchnikov [22] calculated the binding energy of small crystals with a simple cubic lattice by the LCAO-MO

[7] B. Mutafchiev and R. Kaishev, *Izvest. Inst. fizikokhimya*, **1**, 43 (1960).

[8] R. Kaishev and I. Gutsov, *Izvest. Inst. fizikokhimya*, **2**, 77 (1962).

[9] S. Toshev and Iv. Markov, *Izvest. Inst. fizikokhimya*, **6**, 21 (1967).

[10] J.L. Kenty, *J. Chem. Phys.*, **47** 3120, (1967); *Surface Science*, **20**, 349 (1970).

[11] E.A. Galashin, *Zhur. fiz. Khim.*, **42**, II 61 (1968).

[12] E.A. Galashin and E.P. Senchenkov, *Doklady Akad. Nauk S.S.S.R.*, **185**, II 5 (1969).

[13] E.A. Galashin, E.P. Senchenkov and K.B. Chibistov, *Doklady Akad. Nauk. S.S.S.R.*, **185**, 428 (1969).

[14] F.P. Buff and J.J. Kirkwood, *J. Chem. Phys.*, **18**, 991 (1950).

[15] L.M. Shcherbakov, *Kolloid. Zhur.*, **14**, 379 (1952); **20**, 759 (1958); **23**, 215 (1961).

[16] L.M. Shcherbakov, "Issledovaniya v oblasti poverkhnostnykh sil", Izd. A.N. S.S.S.R., Moskva, 1961.

[17] L.M. Shcherbakov and V.I. Rykov, *Kolloid. Zhur.*, **23**, 221 (1961).

[18] L.M. Shcherbakov, P.P. Ryazantsev and N.P. Filippova, *Kolloid. Zhur.*, **23**, 338 (1961).

[19] A.S. Rusanov, "Fazovye ravnovesiya i poverknostnye yavleniya", Khimya, L, 1967.

[20] T. Hill, "Thermodynamics of Small Systems", N.Y. Amsterdam, 1963 P.1.; 1969 P.2.

[21] G. Bliznakov and S. Delineshev, *Kristall und Technik* (in press).

[22] L.A. Borovinskii and U.G. Klyuchnikov, Uch. zapiski N.G.P.I., t. 431, "Isledovaniya protseov kristalizatsii", Novgorod, 1961, p. 44.

method. They showed that the binding energy could be represented as the sum of volume, surface and edge energies only if the number of atoms in the three-dimensional crystal complex is larger than 10^3 atoms.

Table 1

Ratio between bond energy in a two-atome molecule and energy for an infinite crystal

Metal	$\frac{D_0}{\varepsilon_s}$
Lithium	2.56 – 2.78
Sodium	2.64
Potassium	2.21
Rubidium	2.33
Caesium	2.25
Copper	3.81
Silver	3.63
Gold	3.65
Nickel	4.07

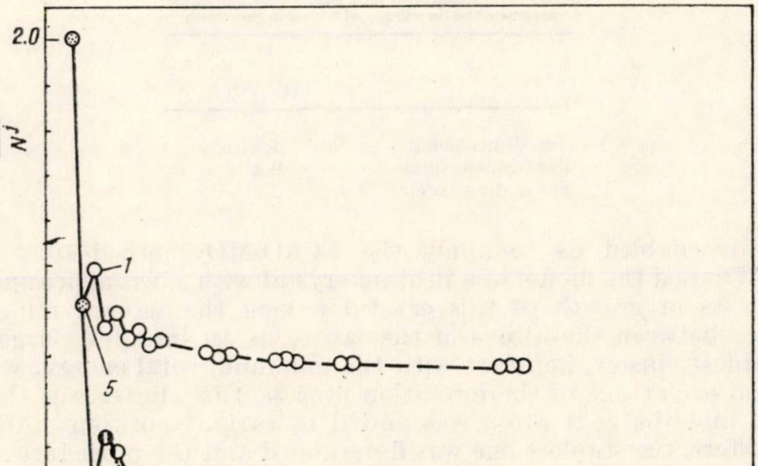

Fig. 1. — Dependence of the average energy of a bond on the number of atoms in the crystal.

E, binding energy of the crystal (in β units) ; N^J, number of bonds in the crystal ; N, number of atoms in the crystal ; 1 one-dimensional crystals ; 2, two-dimensional crystals ; 3, three-dimensional crystals ; 4, a point corresponding to two- and three-dimensional crystals ; 5, a point corresponding to the three types of crystals ; 6, according to data of Borovinskii and Klyutchnikov.

Our results are in agreement with those of Borovinskii and Klyuchnikov. As evident from the curve of a three-dimensional crystal, the energy of a bond is almost independent of the size of the three-dimensional crystal when the number of atoms in the crystal is larger than 10^3 atoms.

The ratio $\left(\frac{E_2}{(E/N^j)_i}\right)$ between the energy, E_2, of a bond in the two-atom molecule and the energy, $(E/N^j)_i$, of a bond in a crystal in which the energy of a bond depends but very little on its size, is given in table 2 with respect to the different cases. The energies are calculated by the above LCAO-MO method.[21]

A comparison of tables 1 and 2 shows that the results obtained by model calculations give a qualitatively correct picture of the situation, and there is at least no discrepancy between experimental and theoretical results.

Table 2

Ratio between energies of a bond in the two-atome molecule and the energy of a bond in the crystal

i	$\frac{E_2}{(E/N^j)_i}$
One-dimensional	1.57
Two-dimensional	2.41
Three-dimensional	2.81

This enabled us to apply the LCAO-MO method to a concrete case.[23] We used the model of a lithium crystal with a bcc lattice and studied the process of growth of this crystal having the same symmetry and distances between the atoms in the lattice as an infinitely large crystal. The stablest cluster, i.e., that with the minimum total energy, was determined on each stage of the formation process, this cluster was then taken as basis and the next atom was added in various positions. Among the new clusters, the stablest one was determined and the procedure repeated. We used a method analogous to that applied by Tyutyulkov and Hiebaum [24] in studying the growth of a hypothetic two-dimensional model of a square-shaped crystal lattice taking into consideration the interactions of up to second neighbours in the two-dimensional lattice plane. In contrast to them, we considered the interactions of up to 6th neighbours in the three-dimensional crystal lattice of lithium. Besides, in the process of growth of the crystal we took into consideration all possible positions (two- and three-dimensional ones) of the new atom.

Figure 2 contains part of the results. It is evident that in spite of the presence of a sufficient number of atoms needed for the formation of a three-dimensional crystal, the two-dimensional crystal with the same number of atoms and a structure corresponding to that of the most dense plane, 110, of the lithium lattice, is the stabler one.

---

[23] G. Bliznakov, D. Lazarov and S. Delineshev (to be published).

[24] N. Tyutyulkov and G. Khibaum, private communication.

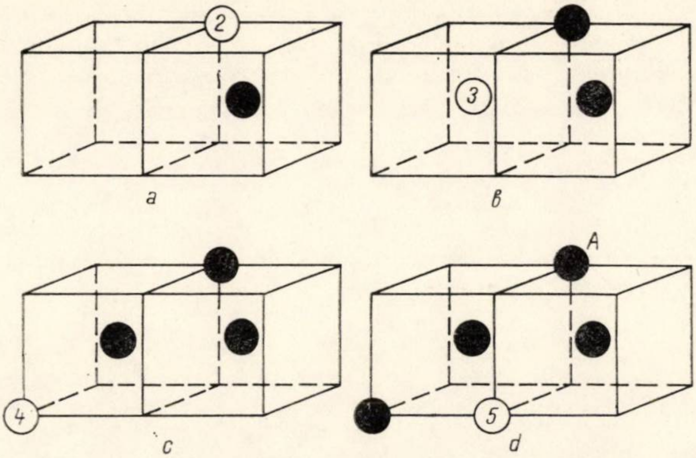

Fig. 2. — Stages of growth (*a*, *b*, *c*, *d*) of a lithium crystal
A, the stablest cluster of *n* atoms ;

The authors express their thanks to the Computing Center of the Mathematical Institute of the Bulgarian Academy of Sciences where part of the problems were solved.

Revue Roumaine de Chimie, **17**, *1*, *2*, 41–48 (1972)

Dedicated to Professor I. G. MURGULESCU
on his 70th birthday

SOME INTRODUCTORY INVESTIGATIONS ON ELECTROLYTIC DEPOSITION OF Y-Al AND Y-Mg ALLOYS

D. BRATLAND, G. H. BØE, K. GRJOTHEIM, H. RENSVIK and E. AAMLAND
Institute of Inorganic Chemistry
The Technical University of Norway
Trondheim, Norway

Received September 22, 1971

Yttrium-magnesium and yttrium-aluminium were produced by electrolysis of Y_2O_3 in $LiF-YF_3$ melts using floating cathodes of liquid magnesium and liquid aluminium, respectively. The maximum concentrations of yttrium obtained wer 48.8 wt% for Y-Mg alloy and 22.0 wt% for Y-Al alloy. The density of the electrolyte determined the upper limit of yttrium concentration in the alloys. It was also found that cathode current efficiency decreased with increasing yttrium content of the alloys.

INTRODUCTION

Electrolytic production of alloys from molten salt electrolytes is a comparatively new field of research, although electrodeposition of alloys has been studied extensively at lower temperatures during the past 100 years. When discussing electrochemical alloy deposition it is convenient to distinguish between codeposition of metals and the deposition of one alloy component on a substrate metal. The electrodeposition of yttrium in a liquid aluminium cathode and in a liquid magnesium cathode, respectively, were investigated in the present work.

A mixture of lithium fluoride and yttrium fluoride was used as the electrolyte. Yttrium oxide was added to this mixture. Fluorides have several advantages as electrolytes. They are less hygroscopic than most chlorides, and therefore, are more readily prepared in the pure state. They have a pronounced ability to dissolve compounds, particularly oxides, which are virtually insoluble in other molten salts. Because the decomposition potential of an oxide is usually lower than that of the corresponding fluoride, addition of the oxide to the electrolyte reduces the operational voltage.[1,2]

The rare-earth metals, including yttrium, are so reactive that molten salt electrolysis is one of the very few methods to produce them. Half of their number, however, have melting points above 1,300°, so that reduction to the pure, liquid metal imposes severe construction and materials

---

[1] W.J. Hamer, M.S. Malmberg, and B. Rubin, *J. Electrochem. Soc.*, **112**, 750 (1965).

[2] W.J. Hamer, *J. Electroanalyt. Chem.*, **10**, 140 (1965).

problems. In many cases, however, one is not primarily interested in the pure metal, but rather in master alloys with other metals. The electrodeposition of such alloys has been studied at the Reno Metallurgy Research Center, U.S. Bureau of Mines, Reno, Nevada, USA. [3–5] Recently the study of electrolytic production of yttrium-light metal alloys has been initiated at our Institute of Inorganic Chemistry in connection with our general interest in molten salt systems.

EXPERIMENTAL

Because graphite was not attacked by the fluoride melt, a graphite crucible was used for the electrolytic cell. Both liquid aluminium and liquid magnesium float on the surface of the electrolyte so it was convenient to use the graphite crucible as the anode. The essential features of the yttrium-aluminium cell are shown in figure 1. The corresponding yttrium-magnesium cell is shown in figure 2. In both cells, the molten metal was confined

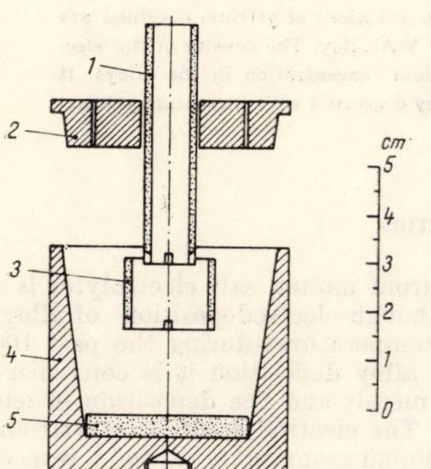

Fig. 1. — Electrowinning cell for production of yttrium-aluminium alloys. (Exploded view)

1, Cathode compartment with cuts in bottom end; *2*, Crucible lid with holes for escape of anode gas; *3*, Sleeve with cuts in bottom end. Prevents anode gas from entering the cathode compartment; *4*, Crucible (anode); *5*, Alumina disk. Prevents gas evolution in cells bottom; *6*, Hole for thermocouple.

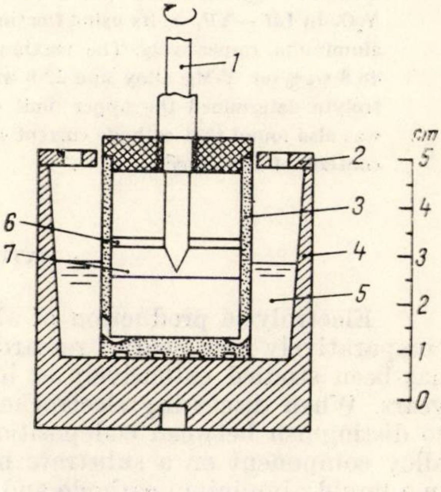

Fig. 2. — Electrowinning cell for production of yttrium-magnesium alloys.

1, Cathode wire, 5 mm silver steel, bottom end shaped as a blade. *2*, Crucible lid with holes for escape of anode gas. *3*, Cathode compartment with holes in wall near bottom. *4*, Crucible (anode). *5*, Electrolyte. *6*, Molten salt flux. *7*, Floating magnesium cathode.

---

[3] E. Morrice, E.S. Shedd, and T.A. Henrie, Bu Mines Rept. of Inv. **1968**, 7146.

[4] E. Morrice, E.S. Shedd, M.M. Wong, and T.A. Henrie, *J. Metals*, **21**, 34 (1969).

[5] E. Morrice, J.E. Murphy, and M.M. Wong, Bu Mines Rept. of Inv., **1969**, 7308.

within a tube of refractory material supported on the cell bottom. It was necessary for this material to be electrically nonconductive as well as to be resistant chemically to the electrolyte and the alloy produced. Both alumina and magnesia met these requirements. An alumina tube was used as the cathode compartment in preparing Y-Al alloys and a magnesia tube was used for Y-Mg alloys. To prevent the anode gases (carbon monoxide and carbon dioxide) from getting into the cathode compartment and oxidizing the metal product, the bottom of the cell was covered by a nonconducting material. In the Y-Al cell an alumina disk was used, while in the Y-Mg cell the cathode compartment was a closed end magnesia tube. To promote efficient mixing of the catholyte and anolyte, there were holes in the wall of the cathode compartment. The cell was covered by a lid to reduce the evaporation of the electrolyte. It was observed that the vapor pressure above the electrolyte increased with an increasing amount of lithium fluoride in the electrolyte.

Oxidation of magnesium by CO_2 in the anode gas was a problem in the Y-Mg cell because of the high vapor pressure of magnesium. Significant amounts of finely divided carbon present in the cell after electrolysis were evidence of this reaction. The problem was minimized by using a molten salt flux to cover the liquid cathode.

The electrowinning cells were mounted in vertical tube furnaces. The furnaces were gas-tight and contained pure argon during the experiments to prevent contamination of the reactive metals by oxygen and nitrogen. To enhance mass transport of yttrium metal into the alloy, the liquid cathode metal was mechanically stirred during electrolysis in most experiments.

MATERIALS

Lithium fluoride, Baker Analyzed Reagent, J. T. Baker. Yttrium fluoride, anhydrous, 99.9% pure, from various sources. Yttrium oxide, 99.9% pure, from various sources. Barium fluoride, Baker Analyzed Reagent, J. T. Baker. Aluminium, 99.999% pure, A/S Vigeland Brug, Vennesla, Norway. Magnesium, 99.98% pure Norsk Hydro A/S. — Alumina tubes: Alsint quality, Haldenwanger, Berlin, Germany. Magnesia tubes: Degussit MG 25 quality, Degussa, Frankfurt am Main, Germany. Graphite: AUC quality, from Union Carbide Norden, Trollhättan, Sweden.

RESULTS AND DISCUSSION

a) YTTRIUM-MAGNESIUM ALLOYS

The electrolyte used in the experiments had a molar ratio of LiF to YF_3 of 3 : 1. Yttrium oxide (7 wt%) was added to this electrolyte. The electrolyte temperature used in all experiments was 760°.

Cathodic current efficiency has been measured as a function of current density and the amount of current consumed (figs. 3 and 4). There seems to be an optimum current density around 0.5 amp cm^{-2} (fig. 3). Above this density, the rate at which yttrium metal is formed is probably higher than the rate at which the metal is transported into the liquid cathode. Inspection of the electrolyte subsequent to the experiment revealed a gray layer of metal particles below the cathode. Analysis of samples by means of X-ray microprobe has shown that the particles have a high content of yttrium.

Figure 4 indicates that the current efficiency decreases with increasing amount of current applied per gram magnesium. This is probably due to increasing viscosity of the alloy with increasing concentration of yttrium, causing the mass transport into the alloy to decrease.

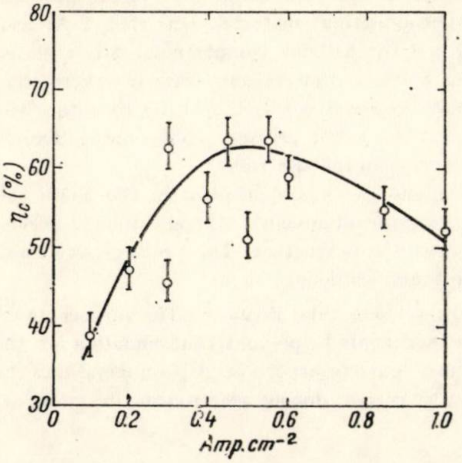

Fig. 3. — Cathodic current efficiency *vs.* current density. Magnesium cathode.

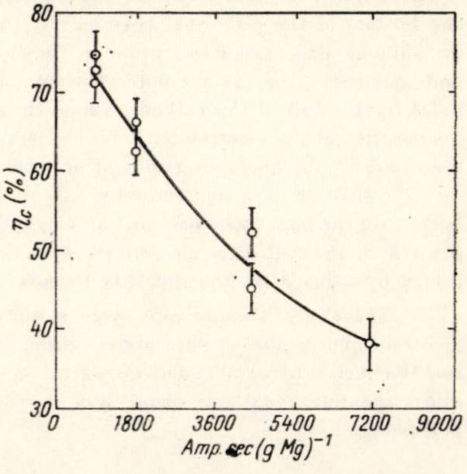

Fig. 4. — Cathodic current efficiency *vs.* amount of current. Cathodic current density 0.5 amp cm^{-2}. Magnesium cathode. Electrolyte : 3LiF·YF$_3$.

Alloys containing up to 48.8 wt% yttrium have been obtained by the liquid Mg cathods method. According to the phase diagram of the system Mg-Y [6] the first trace of solid YMg$_2$ will precipitate from the liquid alloy at 760° when the content of yttrium exceeds 53 wt%. The alloy will be completely solid when the composition YMg$_2$ is reached (65 wt%).

b) YTTRIUM-ALUMINIUM ALLOYS

Electrolytes of two different compositions were employed. In one the molar ratio of LiF to YF$_3$ was 3 : 1, and in the other 1 : 2. Yttrium oxide, usually 7 wt%, was added to both electrolytes. In some experiments BaF$_2$ was added.

The electrolyte 3LiF.YF$_3$ was used in the temperature range 725° — 815° and at 1,000°. The electrolyte LiF.2YF$_3$ was used at 1,000° only. The phase diagram of the LiF-YF$_3$ system has been determined by Thoma et al. [7]

---

[6] J.F. Smith, D.M. Bailey, D.B. Novotny, and S.E. Davison, Acta Metallurgica, **13**, 889, (1965).

[7] R.E. Thoma, C.F. Weaver, H.A. Friedman, H. Insley, L.A. Harris, and H.A. Yakel Jr., *J. Phys. Chem.*, **65**, 1096 (1961).

Figure 5 shows the relationship between current density and current efficiency at 760°. The liquid metal cathode was not stirred in these experiments.

In order to increase the rate of alloy formation, the temperature was raised to 1,000° and mechanical stirring was introduced. Cathode current efficency was measured as a function of the amount of current at various cathode current densities. In figure 6 it is shown that the current effi-

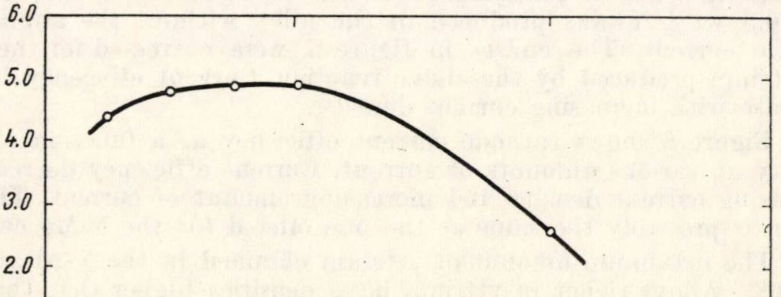

Fig. 5. — Weight percent yttrium in the alloy *vs.* total current, at 760°. Aluminium cathode, 3LiF.YF_3 electrolyte.

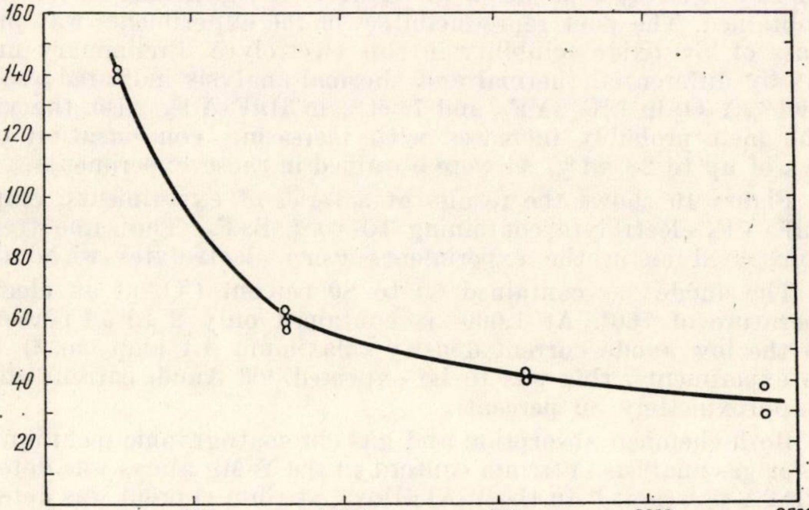

Fig. 6. — Cathodic current efficiency *vs.* amount of current per gram aluminium. Cathodic current density : 0.74 amp cm^{-2}. Aluminium cathode. Not corrected for metal-salt reactions. Electrolyte : 3LiF·YF_3.

ciency exceeds 100 percent at low current values. This is probably due to a reaction between aluminium metal in the cathode and yttrium ions in the electrolyte :

$$\text{Al(alloy)} + \text{Y}^{3+} = \text{Y(alloy)} + \text{Al}^{3+}$$

This reaction was investigated quantitatively at 1,000°. It was found that 3.5 ± 0.5 wt% Y was produced in the alloy without the application of electric current. The curves in figure 7 were corrected for the amount of yttrium produced by the above reaction. Current efficiency is seen to decrease with increasing current density.

Figure 8 shows cathode current efficiency as a function of current density at various amounts of current. Current efficiency decreases with increasing current density and increasing amount of current. The explanation is probably the same as the one offered for the Y-Mg cell.

The maximum amount of yttrium obtained in the Y-Al alloys was 22 wt%. Alloys richer in yttrium have densities higher than that of the electrolyte so they will not float. A higher concentration of YF_3 or the addition of BaF_2 would increase the density of the electrolyte.

According to the phase diagram [8] of the system Al-Y, the first trace of solid YAl_2 appears in the liquid alloy at 1,000° as the concentration of yttrium exceeds 31 wt%, and the alloy solidifies when the composition YAl_2 (62 wt% Y) is reached.

Current efficiency as a function of the amount of current in the $LiF \cdot 2YF_3$ electrolyte is shown in figure 9. A significant correlation was not obtained. The poor reproducibility of the experiments was probably because of low oxide solubility in this electrolyte. Preliminary measurements by differential thermal and thermal analysis indicated a solubility of 5 wt% Y_2O_3 in $LiF \cdot 2YF_3$, and 7 wt% in $3LiF \cdot YF_3$. Also, the viscosity of the melt probably increases with increasing concentration of YF_3. Alloys of up to 28 wt% Al were obtained in these experiments.

Figure 10 shows the results of a series of experiments, employing a $3LiF \cdot YF_3$ electrolyte containing 10 wt% BaF_2. The same trend was demonstrated as in the experiments using electrolytes without BaF_2.

The anode gas contained 60 to 80 percent CO_2 at an electrolysis temperature of 760°. At 1,000° it contained only 2 to 10 percent CO_2. With the low anode current density (maximum 0.1 amp cm^{-2}) used in these experiments, this was to be expected. [9,10] Anode current efficiency was approximately 80 percent.

Both chemical absorption and gas chromatographic techniques were used for gas analysis. Yttrium content in the Y-Mg alloys was determined by EDTA titration. [11] In the Y-Al alloys, yttrium content was determined by spectrophotometry [12] and X-ray fluorescence.

---

[8] R.L. Snyder, Dissertation, Iowa State University, 1960, 85 p.

[9] J. Thonstad, *J. Electrochem. Soc.*, **111**, 955 (1964).

[10] J. Thonstad, *ibid.*, 111, 959 (1964).

[11] J.S. Fritz, *Analyt. Chem.*, **30**, **1111** (1958).

[12] C.M. Budanova and S.N. Pinaeva, *Zhur. analit. Khim.*, **20**, 320 (1965).

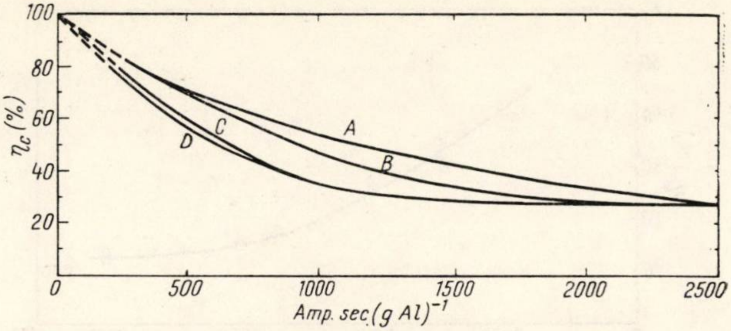

Fig. 7. — Cathodic current efficiency *vs.* amount of current.
Cathodic current densities :
A: 0.24 amp cm^{-2}, B: 0.48 amp cm^{-2}
C: 0.74 amp cm^{-2}, D: 1.00 amp cm^{-2}.
Corrected for metal-salt reactions.
Electrolyte: $3LiF \cdot YF_3$.

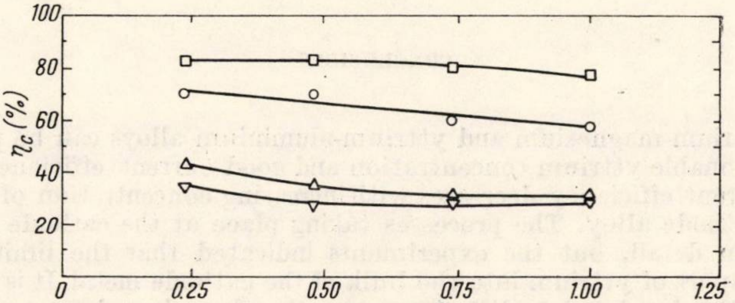

Fig. 8. — Cathodic current efficiency *vs.* current density.
Amount of current:
□ 250 amp sec (g Al)$^{-1}$ ○ 500 amp sec (g Al)$^{-1}$ △ 1500 amp sec (g Al)$^{-1}$ ▽ 2000 amp sec (g Al)$^{-1}$ Electroyte: $3LiF \cdot YF_3$.

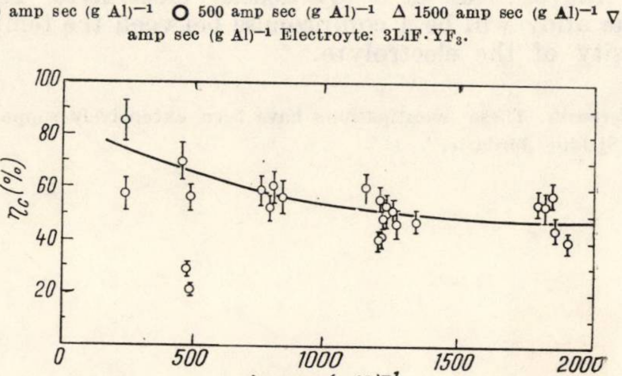

Fig. 9. — Cathodic current efficiency *vs.* amount of current per gram aluminium. Electrolyte : $LiF \cdot 2YF_3$.

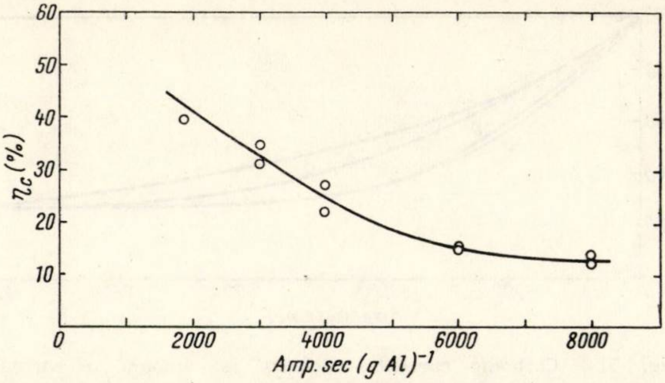

Fig. 10. — Cathodic current efficiency *vs.* amount of current per gram aluminium. Cathodic current density 0.75 amp cm^{-2}. Corrected for metal-salt reactions. Electrolyte : $3LiF \cdot YF_3$ containing 10wt % BaF_2.

CONCLUSIONS

Yttrium-magnesium and yttrium-aluminium alloys can be produced with reasonable yttrium concentration and good current efficiency. However, current efficiency decreases with increasing concentration of yttrium in the cathode alloy. The processes taking place at the cathode were not studied in detail, but the experiments indicated that the limiting step was transport of yttrium into the bulk of the cathode metal. It is not clear whether this is related to diffusion across the phase boundary, or to transport within the bulk metal. Also, when the rate of deposition of yttrium metal exceeds the rate of transport into the alloy, yttrium separates more readily from the cathode in a low-density electrolyte. The content of yttrium in the alloy will be a compromise between the temperature used and the density of the electrolyte.

Acknowledgements. These investigations have been extensively supported by "Forskningsgruppe for Sjeldne Jordarter".

Revue Roumaine de Chimie, **17**, *1*, *2*, 49−56 (1972)

Dedicated to Professor I. G. MURGULESCU
on his 70th birthday

HEAT TRANSFER IN VIBRATED FLUIDIZED LAYERS

EM. A. BRATU and GHEORGHIȚA I. JINESCU

Poliytechnic Institute, Str. Polizu 1, Bucharest 8, Romania

Received September 21, 1971

Vertical vibrations, improving the structure of the fluidized layer (homogenization), have a positive effect on the heat transfer between the fluidized particles and the gas. This process depends essentially on the circulation of the phases. Experimental determinations show an increase of the heat transfer coefficient for the vibrated layer as compared to non-vibrated ones. To characterize the effect of vertical vibrations on the structure of the fluidized layer a homogeneity number is defined. This parameter varies exponentially with the vibrational acceleration.

The intensity of heat transfer in the fluidized layer depends on the circulation, the mixing degree of the phases in the layer and the structure of the fluidized layer. Literature data [1−7] referring to fluid − solid particles heat transfer, show that the low values obtained for the heat transfer coefficient in the layer fluidized by gases (of the order of 1 kcal/m^2.h.degree) as compared to the layer fluidized by liquids (600−3000 kcal/m^2.h.degree) are mainly due to the presence of stable non-homogeneities in the structure of the layer fluidized by gases.

Since in most industrial processes fluidized layers are exploited at velocities of the fluidization gas 50 to 100 times the minimum fluidization velocity, which confers the layer a strongly non-homogeneous aspect, the efforts of the research workers have been lately directed towards the obtention of a more homogenous structure of the layers fluidized by gases. The use of vertical vibrations, [7−18] is one of the methods tried to improve the qualities of the layer fluidized by gases.

[1] E. Ruckenstein and I. Teoreanu, *Rev. Chim.* (*București*), **11**, 137 (1960).
[2] E. Ruckenstein and I. Teoreanu, *Rev. Chim.* (*București*), **11**, 296 (1960).
[3] E. Ruckenstein, *Rev. Chimie* (*București*), **10**, 45 (1949).
[4] E. Ruckenstein, *Stud. și Cercetări Energ. Acad. R.S.R.*, **11**, 23 (1961).
[5] I. Teoreanu, Doctoral Thesis, Bucharest, 1961.
[6] K. Lewis, E. R. Gilliland and H. Griouard, *Chem. Eng. Progr. Symp.*, **58**, 87 (1962).
[7] Gh. I. Jinescu, Doctoral Thesis, Bucharest, 1970.
[8] R. S. Narsimha and K. Ramalingam, *Chem. Eng. Sci.*, **12**, 166 (1960).
[9] T. M. Reed and M. R. Fenske, *Ind. Eng. Chem.*, **47**, 275 (1955).
[10] V. A. Cilenov and N. V. Mihailov, *Inzh. fiz. Zhur.*, **9**, 196 (1965).
[11] Tetsuo Yoshida, *Kagaku Kogaku*, **29**, 875 (1965); *Chem. Abstr.*, **64**, 4626 (1966).
[12] J. Biaggi, *Ind. Chemist*, **54**, 472 (1967).
[13] Em. A. Bratu, Gh. I. Jinescu and E. Ruckenstein, Vibrated fluidized bed, Communication at the Congress of the fluidization, Warsaw, 1964.
[14] V. A. Cilenov and N. V. Mihailov, *Zhur. fiz. Khim.*, **39**, 473 (1965).
[15] Em. A. Bratu and Gh. I. Jinescu, *Studii și Cercetări Chim. Acad. R.S. Romania*, **17**, 699 (1969).
[16] Em. A. Bratu and Gh. i. Jinescu, *Rev. Chim.* (*București*), **20**, 547 (1969).
[17] Em. A. Bratu and Gh. I. Jinescu, *Génie Chim.*, **104**, 1657 (1971).
[18] Em. A. Bratu and Gh. i. Jinescu, *Brit. Chem. Eng.*, **16**, 691 (1971).

The conditions in which incipient fluidization appears in vertical vibration of the fluidization column and the homogenizing effect of the vibrations, were established in previous papers. [7,13,15–18] From these papers we mention the following results :

— the decrease of the minimum fluidization velocity with the increase of the ratio of the vibrational acceleration, $a\omega^2$, to the gravitational acceleration, g, as a function of the solid particles' characteristics ;

— evidence for two types of layers : 1) the *vibrofluidized layer* in which the fluidization of the layer is due to both : the force due to vibration and the force exerted by the gas on the solid particle, and 2) *the vibrated fluidized layer*, in which the force exerted by the gas is sufficient to achieve the fluidization, the vibrations having a homogenizing role for the structure of the layer.

The present paper deals with the heat transfer of gas-solid particles in the vibrated fluidized layer in comparison with the non-vibrated fluidized layer, in order to establish the effect of the vertical vibrations which homogenize the structure of the fluidized layer.

1. APPARATUS AND PROCEDURE FOR EXPERIMENTAL MEASUREMENTS

The apparatus (figure 1) consists of the usual devices employed in fluidization (1,6-8) to which a system for heating and maintaining a constant temperature of the fluidization gas (9, 9′, 10—12) was added. The air temperature at the basis of the layer and after leaving it

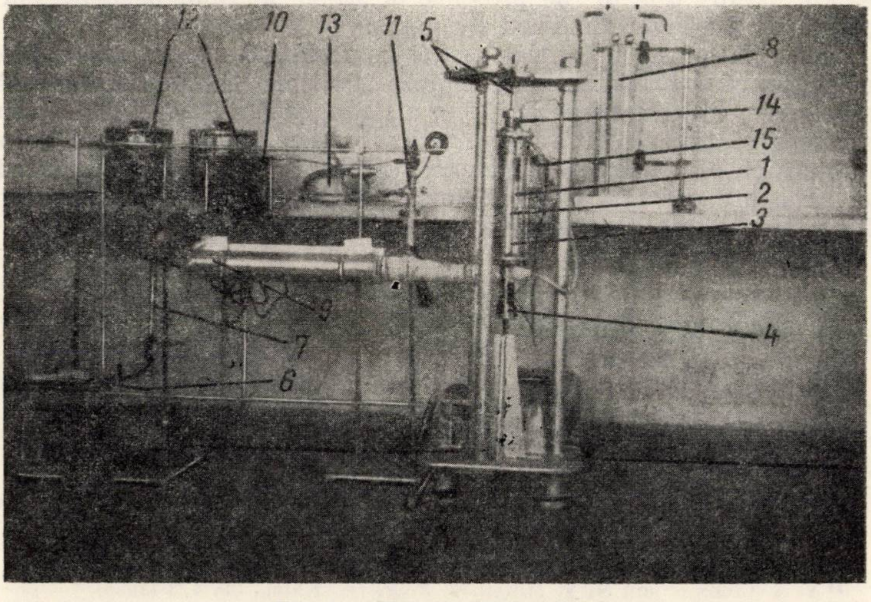

Fig. 1. — Experimental set-up.

1, Fluidization column ; *2*, Layer of solid particles ; *3*, Thermal insulation ; *4*, Mechanical vibrator ; *5*, Guide way ; *6*, Filter ; *7*, Rotameter ; *8*, Differential pressure gauge ; *9,9′*, Resistances ; *10*, Relay ; *11*, Resistance thermometer ; *12*, Autotransformers ; *13*, Galvanometer ; *14*, Thermocouple ; *15*, Cold welding of the thermocouple.

was measured by means of two cromel-copel thermocouples (14) which, by means of the mirror galvanometer (13), give the temperature with a 0.1°C accuracy. The apparatus permits a vertical vibration of the column in the frequency field $\nu \in 0-50$ Hz and amplitude $a \in 0-3$ mm through a mechanical vibrator.

The fluidization agent (air heated to the desired temperature) flows at a constant rate in the empty column, until stationary thermal conditions are established. At this moment, considered as the starting point, cold solid particles are introduced, and in conditions stated for simple or vibrated fluidization, the temperature of the air as it leaves the layer is read continuously. The temperature of the air entering the layer is kept constant. As the temperature of the solid particles increases — the heat is transmitted from the gas to the particles — the temperature difference between the gas and the particles becomes smaller and smaller. The temperature of the gas leaving the column increases in time, finally tending to an equilibrium value, when the gas temperature becomes practically identical to that of the particles of the layer.

Because of the complex phenomena, the conditions of the experimental measurements involved : (i) — constant parameters : the characteristics of solid particles (marble, $\rho_p = 2.66$ g/cm^3, $d_p = 0.175$ mm), the air temperature as it enters the layer ($t_i = 60°$), the size of the fluidization column ($D = 50$ mm) and of the particle layer ($H_0 = 80$ mm) ; (ii) — independent variables : the gas flow capacity and vibration characteristics ($a \in 1-3$ mm amplitude $\nu \in 0-50$ Hz frequency), and — (iii) variables depending on the vibrational acceleration, $a\omega^2$: the minimal fluidization velocity, u_{mv} and the fluidization degree $u/u_{mv} \in 1-40$.

2. RESULTS AND DISCUSSION

According to the biphasic model of the non-homogeneous fluidized layer one considers the fluidized layer as made of a continuous phase formed by gas particles and a dispersed bubble phase. The existence of the gas bubbles, wheter coalescing or not, diminishes the contact between the phases, the gas of the dispersed phase participating to a small extent in the transfer processes, which reduces the efficiency of these processes.

The small values obtained for the heat transfer coefficient α', defined by the relation :

$$q = \alpha'(t - T) \tag{1}$$

where t is the temperature of the gas leaving layer and T is the temperature of the solid particles, are explained by Ruckenstein and Teoreanu [1] by the existence of stable gas bubbles in the non-homogeneous fluidized layer. The above authors prove that most of the heat passes from the gas to the solid particles in the continuous homogeneous phase of the layer. In this phase the solid particles and the gas have practically the same temperature t', differing from the average temperature t, of the gas leaving the layer. The fraction of the gas flow capacity passing through the layer in bubble form, transfers a negligible amount of heat to the solid particles, and the temperature of this gas fraction is therefore equal to the temperature t_i, at which the gas enters the fluidized layer.

It results therefore that t is an average of the temperatures of both phases (continuous and bubble) expressed by relation (2):

$$t = \xi t' + (1 - \xi) t_i \tag{2}$$

where ξ is the fraction of the gas flow capacity passing through the continuous phase of the layer.

The vertical vibrations, improving the structure of the layer fluidized by gases, have a favorable influence on the gas — solid particles heat transfer.

Out of 30 measurements, we give as examples in figures 2 and 3, the curves obtained by representing the temperature of the gas leaving the layer *versus* time, in six cases in which the amplitude (fig. 2) or vibration frequency (fig. 3) varies.

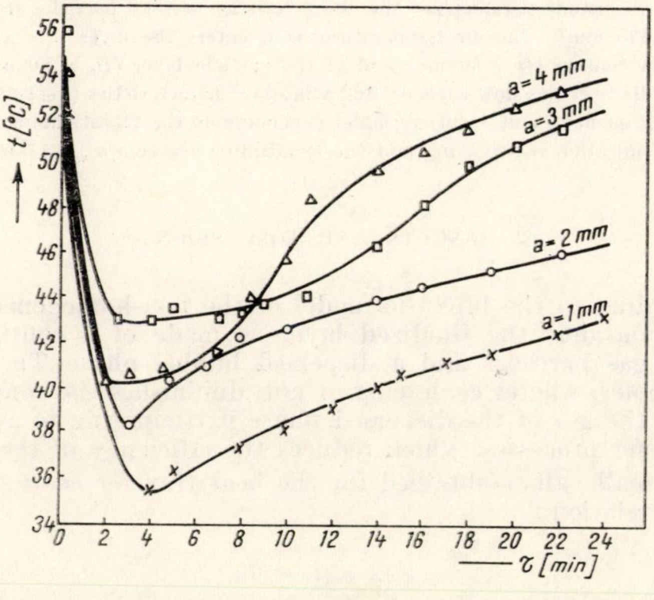

Fig. 2. — Temperature of fluidizing gas leaving the layer *vs.* time for several values of amplitude of vibration at the constant frequency of vibration, $\nu = 28$ Hz.

The heat transfer coefficient α, between gas and solid particles in the continuous homogeneous phase, is very high, $10^2 - 10^3$ kcal/m^2,h.degree. Therefore the form of the curves $t - \tau$ is not affected by the coefficient α, but especially by the gas fraction passing through the layer as bubbles. The slope of the temperature curves of the gas is steeper in the vibrated layer, and therefore the time in which the solid particles will reach the same temperature as that of the gas entering the layer (the heating time of a batch of material) is smaller than in the unvibrated fluidized layer.

The general conclusion, resulting from the variation in time of the exit temperature of the fluidizing air, is the improvement of the heat transfer, hence the achievement of more homogeneous fluidized structures in the whole volume of the layer.

By maintaining a constant flow of the fluidizing gas (hence a constant thermal flow) the increase of the acceleration of the vibrations has two antagonistic effects on the structure of the fluidized layer, namely :

— it increases the fluidization degree, hence the quantity of gas bubbles passing through the layer, by lowering the minimal fluidization velocity ; this has theoretically a negative effect ;

— the dispersion of the bubbles in the layer is increased up to their "dissolution" in the layer, a more homogeneous structure being achieved due to the impact forces transmitted to the solid particles lowering the interparticle forces. This makes it possible for the hydrostatic pressure of the bubbles to overpower the interparticle forces, hence the bubbles to "dissolve" as they are formed in the continuous phase.

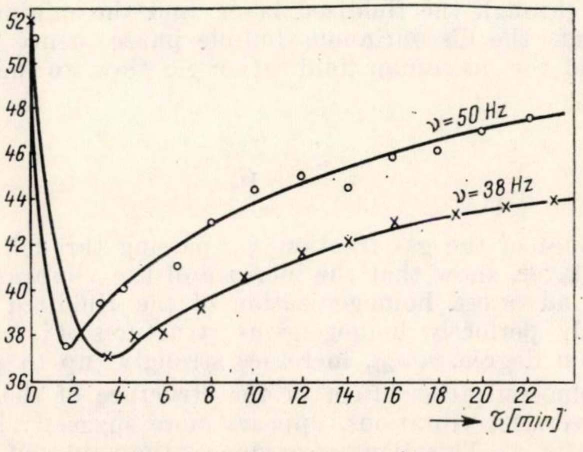

Fig. 3. — Temperature of fluidizing gas leaving the layer vs. time for two values of frequency of vibration, at the constant amplitude of vibration, $a = 1\text{mm}$.

To estimate the influence of the vibrations on the gas-solid heat transfer (hence on the structure of the layer) it is necessary to define a parameter taking into account the increase of the fluidization degree. We have calculated a homogenization number, I_v, given by equation (3) :

$$I_v = \frac{\xi_v - \xi_v'}{\xi_v} 100 \tag{3}$$

where ξ_v is the fraction of the gas flow passing through the continuous phase of the vibrated fluidized layer, and ξ_v' is the theoretical fraction of the gas flow passing through the continuous phase of the vibrated fluidized layer, if the vibration would not "dissolve" the gas bubbles.

For the calculation of ξ_v we used the relation deduced by Ruckenstein and Teoreanu[1] :

$$\ln \frac{(t_i - t)_\tau}{(t_i - t)_{\tau=0}} = -\left(\frac{G_s c_s}{A \alpha} - \frac{G_s c_s}{G_g c_g} \frac{1}{\xi_v} \right)^{-1} \tag{4}$$

in which α, the heat transfer coefficient in the continuous phase is calculated from the equations valid in the case of the homogeneous fluidization ; the values of the temperature t as a function of τ are determined experimentally.

Theoretically it is assumed that the difference between the gas flow passing through the fluidized layer, and the minimum fluidization flow, represents the discontinuous bubble phase, hence that it is given by the ratio of the maximum fluidization gas flow, to the total gas flow :

$$\xi_v' = \frac{G_{g,m}}{G_g} \tag{5}$$

The values of the gas fraction ξ_v, passing through the continuous phase of the layer, show that the increase of the vibrational acceleration results in an advanced homogenization of the fluidized state, tending towards nearly perfectly homogeneous structures ($\xi_v = 0.95$), through the fluidization degree, u/u_{mv}, increases strongly (up to 40).

This homogenization effect of the structure of the fluidized layer achieved by vertical vibrations, appears more suggestively in a diagram $I_v = I_v(a\omega^2)$ (fig. 4). This diagram evidences the values of the vibrational

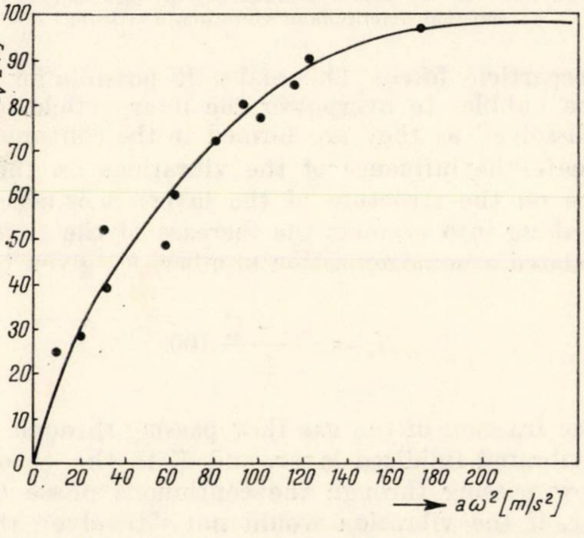

Fig. 4. — Homogeneity number, I_v, *vs.* vibratory acceleration, $a\omega^2$.

acceleration from which the layer tends towards a total homogenization ($I_v = 95\%$).

Visual observation performed simultaneously with the thermal transfer confirm these conclusions. As the vibratorial acceleration increases, the number, dimensions and frequency of the gas bubbles decreases. Since the gas bubbles are small or absent the aspect of the vibrated fluidized layer approaches the aspect of a layer fluidized with liquid.

CONCLUSIONS

The use of vertical vibrations in fluidization leads to interesting results owing to the fact that the force transmitted by the vibration to the solid particle displaces the gas velocity range allowing the existence of a fluidized layer towards small gas velocities and improves the structure of the layer fluidized by gases through (i) the reduction of the gas fraction passing through the layer in bubble form, (ii) the pulsation of the gaseous phase and (iii) the intensification of the local disorderly movement of the solid particles.

This explains the intensification of the gas-solid particle heat transfer, since one obtains increases from 1 to 10^2—10^3 kcal/m^2.h.degree for the heat transfer coefficient, α', corresponding to the homogeneous structure of the layer.

It is a useful result for the practical technique of gas-fluidized layers that one can use vibrations to improve the structure of non-homogeneous fluidized layers (through the decrease of the interparticle forces as a result of the vibrations) countering the factors determining the non-homogeneity such as high degree offluidization, electrostatic forces, or granulometry of the solid particles.

Symbols

a — amplitude of vibration,
A — area of solid particles,
c_s — heat capacity of solid particles,
c_g — heat capacity of fluidizing gas,
d_p — mean diameter of solid particles,
D — diameter of column,
g — gravitational acceleration,
G_g — gravimetric flow rate of fluidizing gas,
$G_{g,m}$ — minimum gravimetric flow rate of fluidizing gas,

G_s — weight of layer of solid particles,
H_0 — height of fixed layer,
I_v — homogeneity number,
t_i — temperature of fluidizing gas on entering the layer,
t — temperature of fluidizing gas leaving the layer,
t' — temperature of fluidizing gas in the continuous phase of the layer,
T — temperature of solid particles,
u — fictitious velocity of gas,
u_{mv} — minimum velocity of fluidization under vibrational conditions,
ρ_p — density of solid particles,
ν — frequency of vibration,
ω — angular velocity,
$a\omega^2$ — vibrational acceleration.

Revue Roumaine de Chimie **17**, *1*, *2*, 57–62 (1972)

En l'honneur du 70e anniversaire du
Professeur I. G. MURGULESCU

ÉVALUATION DE LA NATURE DES INTERACTIONS IONIQUES DANS LES MÉLANGES BINAIRES DE SELS FONDUS À ANION COMMUN ET COMPORTANT DES CATIONS POLARISABLES

J. BRENET, P. DANTZER, P. MIRABEL et J. GUION *

Laboratoire d'Electrochimie et Chimie Physique du Corps Solide, Université Louis Pasteur, 4, rue Blaise Pascal, 67, Strasbourg France

Reçu le 22 septembre 1971

Nous cherchons à tester la validité de la théorie des solutions conformes pour les mélanges (Cu-M) Cl ou Br avec M = Li, Na, K, Rb. Les résultats sont comparés à ceux obtenus pour les mélanges correspondants à base de chlorure ou de bromure d'argent.

L'étude expérimentale des solutions binaires de sels fondus abordée par des techniques variées et élaborées telles que la microcalorimétrie à haute température, piles de formation ou de concentration, diagrammes de phases..., etc, a donné lieu au développement de nombreuses analyses théoriques permi lesquelles la méthode des solutions conformes reste la plus féconde. [1,2,3]

En conservant le formalisme proposé par Davis et Rice, [3] l'enthalpie de mélange d'une solution $A-B$ s'exprime :

$$\Delta H^M = N_A N_B [U_0 + U_1 \delta_{AB} + U_2 \delta^2_{AB}] \tag{1}$$

où

N_A, N_B désignent les fractions molaires respectives des constituants A et B. δ_{AB} représente le paramètre de distance défini par :

$$\delta_{AB} = \frac{\mathrm{d}_{AX} - \mathrm{d}_{BX}}{\mathrm{d}_{AX}\,\mathrm{d}_{BX}}$$

d_{AX} et d_{BX} étant les distances internucléaires pour les sels purs AX et BX respectivement.

---

* Adresse actuelle: Laboratoire de Chimie Physique, Université de Nice, Parc Valrose, 06–Nice

[1] H. Reiss, J.L. Katz, O.J. Kleppa, *J. Chem. Phys.*, **36**, 144 (1962).
[2] M. Blander, *J. Chem. Phys.*, **37**, 172 (1962).
[3] H.T. Davis, S. Rice, *J. Chem. Phys.*, **41**, 14 (1964).

U_0, U_1 et U_2 sont des fonctions d'un paramètre de couplage ξ, associé aux divers types de forces : Van der Waals, ion-dipôle induit..., etc.

La relation (1) est encore présentée sous la forme utilisée par Kleppa.[4]

$$\Delta H_M = N_A N_B [a + bN_A + cN_A N_B] \tag{2}$$

a, b et c désignent des fonctions polynomiales de δ_{AB}. La forme la plus simple développée originellement par Reiss et al.[1] est donnée par :

$$\Delta H^M = N_A N_B \, \Omega(T, p) \, \delta^2_{AB} \tag{3}$$

Dans le cas où les interactions de dispersion dépendant des paramètres ξ sont petites par rapport aux interactions de type coulombien, les quantités U_0, U_1 deviennent négligeables par rapport à U_2 et les résultats peuvent être exprimés à l'aide de la relation (3).

Dans le cas contraire, les termes U_0 et U_1 deviennent importants ; ceci est généralement le cas des mélanges comportant des cations polarisables tels que Ag^+, Tl^+ ...[5].

Un certain nombre de questions relatives aux développements théoriques pour cette classe de mélange restent à résoudre, en particulier. Les données expérimentales relatives aux distances interioniques, polarisabilités, potentiels d'ionisation nécessaires aux calculs sont relativement incertaines.

Par ailleurs ces solutions ont été surtout étudiées par calorimétrie, alors que l'analyse théorique des solutions conformes reste entièrement valable pour les enthalpies libres d'excès de mélange. L'influence de la température sur ces fonctions thermodynamiques, l'évaluation des entropies d'excès de mélange ont reçu peu d'attention.

Dans cette catégorie de mélanges, nous avons entrepris l'étude des solutions d'halogénures de cuivre (I), halogénures alcalins. L'ion Cu^+ isostructural de Ag^+, mais plus petit, permettait de prévoir des interactions de mélange plus importantes.

Nous avons réalisé deux approches expérimentales à l'aide de cellules de concentration de types différents.

Dans une première partie nous avons constitué des cellules avec jonction liquide — liquide à travers une paroi de verre fritté.[6,7] En l'absence de données relatives aux propriétés de transport, nous avons négligé l'influence possible d'un potentiel de jonction.[8] Dans une deuxième partie, nous avons réalisé des cellules avec membranes de verre du type utilisé par Ostvold[9] et Thulin.[10]

Nos derniers résultats ont démontré l'influence très importante du potentiel de jonction, et ont été considérés seuls valables pour l'exploitation présentée ici. Ils sont présentés sous forme analytique dans le tableau 1.

---

[4] L.S. Hersh, O.J. Kleppa, *J. Chem. Phys.*, **42**, 1309 (1965).

[5] L.S. Hersh, A. Navrotsky, O.J. Kleppa, *J. Chem. Phys.*, **42**, 3752 (1965).

[6] P. Mirabel, Thèse 3ème Cycle Strasbourg, 1968.

[7] P. Mirabel P. Dantzer, J. Guion, J. Chim. phys. (1971) (sous presse)

[8] I.G. Murgulescu, S. Sternberg, *Discuss. Faraday Society*, **32**, 107 (1961).

[9] Østvold, Thèse University of Trondheim (Norway), 1971.

[10] L.U. Thulin, Thèse University of Trondheim (Norway), 1971.

Nous avons observé pour les systèmes de chlorures et bromures Cu — K et Cu — Rb, que les variations de ΔG^E_M avec la température sont très importantes.

Tableau 1

Valeur des paramètres *a*, *b*, *c* de l'expression $\Delta G^E_M = N_A N_B (a + bN_A + cN_A N_B)$ (N_A, fraction molaire de l'halogénure de cuivre)

Système	a	b	c
(Cu-Li) Cl	1395	255	—
(Cu-Na) Cl	−1475	−288	—
(Cu-K) Cl	700°C−4067 600°C−3094	232	−3687
(Cu-Rb) Cl	700°C−4980 600°C−3980	− 21	−3240
(Cu-Na) Br	−1200	—	—
(Cu-K) Br	700°C−3390	−1200	−952

Ces résultats sont comparés aux résultats relatifs aux systèmes (Ag—M) Cl ou Br, correspondants [11–14] fig. 1 et 2 sous la forme

$$\overline{G}^E_A = f(1 - N_A)^2 \tag{4}$$

A désignant CuCl ou AgCl.

Nous constatons que les interactions sont nettement plus importantes pour les systèmes à base d'halogénures de cuivre. Les effets d'asymétrie apparaissent également nettement plus marqués.

Toutefois, avec une incertitude inférieure à 10 %, les résultats présentés, pour une température déterminée, peuvent être analysés comme si l'on avait des solutions régulières. Ceci nous permet en particulier de suivre le processus adopté par Kleppa et al. [4,5]

Nous avons donc calculé les quantités

$$\Delta G^E_{Alk} = N_A N_B (U_0^{++} - 340\ \delta^2_{AB}) \simeq \Delta H^M_{\text{calculé}}. \tag{5}$$

Les données relatives aux calculs pour les systèmes (Ag — M) Cl ou Br et (Cu — M) Cl ou Br sont indiquées tableau 2.

Nous avons ensuite testé la relation

$$\left(\frac{\Delta G^E_{\text{exp}} - \Delta G^E_{Alk}}{N_A N_B}\right)_{0,5} = f(\delta_{AB}) \tag{6}$$

---

[11] M.B. Panish, F.F. Blankenship, W.R. Grimes, R.F. Newton, *J. Phys. Chem.*, **62**, 1325 (1958).

[12] J. Guion, M. Blander, D. Henstenberg, K. Hagemark, *J. Phys. Chem.*, **72**, 2086 (1968).

[13] I.G. Murgulescu, S. Sternberg, *Rev. Chim. Acad. R.P. Roumaine*, **2**, 251 (1957).

[14] J.H. Hildebrand, E.J. Salstrom, *J. Amer. Chem. Soc.*, **54**, 4257 (1932).

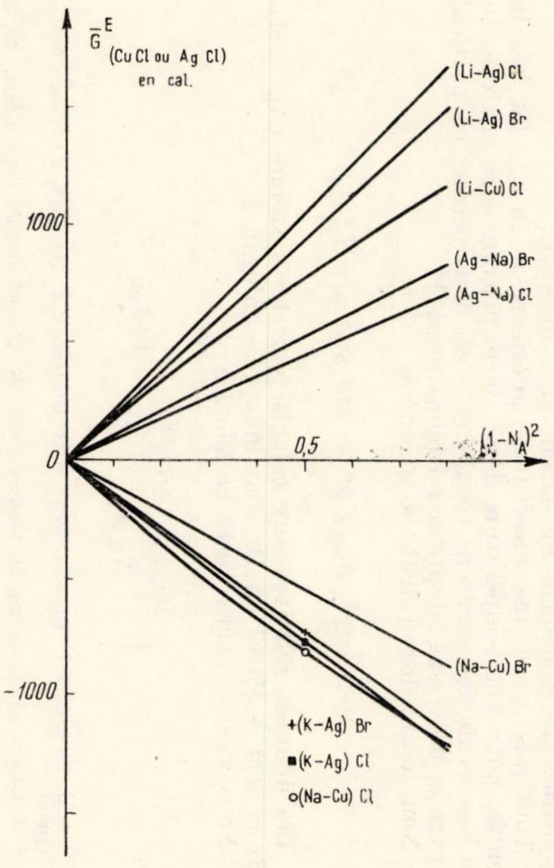

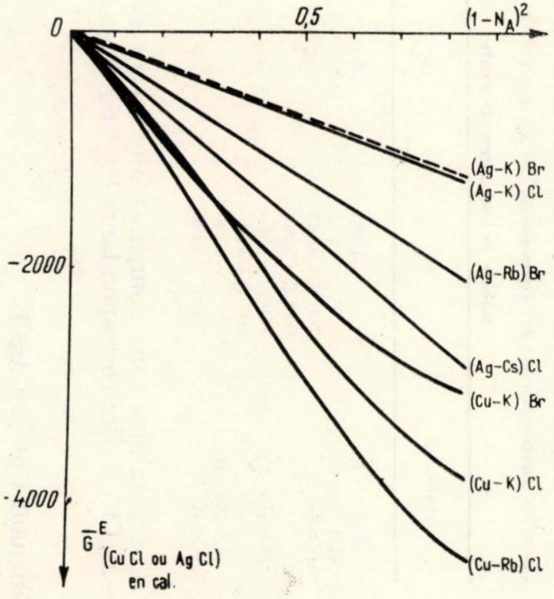

Figures 1 et 2. Comparaison entre les enthalpies libres partielles molaires d'excès de CuCl CuBr, AgCl et AgBr dans les mélanges (Cu-M)Cl ou Br, (Ag-M)Cl ou Br.

Tableau 2

Données utilisées pour le calcul des termes de la relation (5).

$$(5)\quad \Delta G^{E}_{Alk} = N_A N_B (U_0^{++} - 340\,\delta^2_{AB})$$

	Polarisabilités α 10^{24} cm^3	Potentiel d'ionisation I 10^{12} ergs. molécule^{-1}
Ag^+	1,72[16]	30,9[15c]
Cu^+	1,2**	29,3
Li^+	0,030[17]	90,9
Na^+	0,182	56,8
K^+	0,844	38,2
Rb^+	1,42	33,0

Distances interioniques cation-anion [15a,b] en Å.

$d_{AgCl}{}^* = 2,76$ $d_{LiCl} = 2,47$
$d_{CuCl}{}^* = 2,60$ $d_{NaCl} = 2,80$ $d_{NaBr} = 2,98$
$d_{AgBr}{}^* = 2,90$ $d_{KCl} = 3,10$ $d_{KBr} = 3,29$
$d_{CuBr}{}^* = 2,70$ $d_{RbCl} = 3,30$

* Nous avons choisi arbitrairement la valeur de $r_{Cu^+} \simeq 0,80$ Å, comme pour r_{Ag^+} qui a été choisi tel que $r_{Ag^+} \simeq 0,95$ Å (voir réf. [14]).

** Nous avons également choisi cette valeur arbitrairement. Dans la littérature nous avons trouvé deux valeurs 0,43 [17] et 1,6 [18] qui nous ont semblé être des valeurs extrêmes. Rappelons que pour Ag^+, la valeur retenue est 1,72 et que la référence [17] donnait 2,4.

La figure (3) sur laquelle nous avons indiqué une marge d'erreur correspondant à ± 50 % de la valeur de U_0^{++} calculée, indique aux approximations près, une relation linéaire de type proposé par Kleppa. La pente approximative de cette droite serait toutefois proche de 50 kcal.Å/mole au lieu de 40 kcal.Å/mole pour les systèmes à base d'halogénures d'Argent.

On retrouve donc à propos des systèmes d'halogénures (Cu—M), l'impossibilité d'expliquer l'ensemble des résultats par l'intervention des interactions coulombiennes et de dispersion seules.

Si l'on doit également envisager l'influence de la nature covalente des sels AgCl et CuCl, comme le suggère Kleppa, l'importance de ce facteur devrait être plus marqué pour les systèmes à bases d'halogénures de cuivre, ce qui correspond à l'observation d'une pente plus importante.

Il est évident que ce point mérite un développement plus large et nécessite d'autres résultats expérimentaux.

---

[15] M. Blander ed., Molten Salt Chemistry, 1964 :
a) p. 118—119 ;
b) p. 622 ;
c) p. 162.

[16] E. Kordes, W. Bergmann, W. Vogel, *Z. Elektrochem.*, **55**, 600 (1951).

[17] L. Pauling, *Proc. Roy. Soc.*, **A 114**, 181 (1927).

[18] J.R. Tessmann, A.H. Kahn, W. Schockley, *Phys. Rev.*, **92**, 890 (1953).

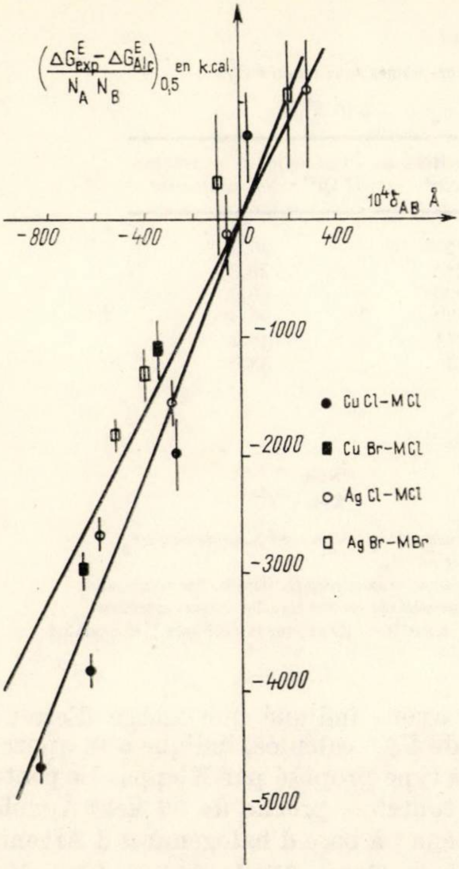

Figure 3. Variation de $\left(\frac{\Delta G^E_{\text{exp}} - \Delta G^E_{Alk}}{N_A\, N_B}\right)_{0,5}$ en fonction du paramètre de distance δ_{AB}.

Une étude calorimétrique relative à l'ensemble de ces systèmes apparaît également indispensable pour une meilleure compréhension de l'ensemble de nos résultats, et pour analyser l'influence de la température sur les propriétés thermodynamiques de mélange.

Revue Roumaine de Chimie, **17**, *1*, *2*, 63–67 (1972)

En l'honneur du 70e anniversaire du
Professeur I. G. MURGULESCU

RELATION DIFFUSION-CONDUCTIVITÉ DANS LES SOLUTIONS D'ÉLECTROLYTES ET APPLICATIONS STRUCTURALES

M. CHEMLA

Laboratoire d'Electrochimie, Université de Paris VI, 8, Rue Cuvier, Paris- 5e, France

Reçu le 24 septembre 1971

On met en évidence l'intérêt général de la détermination des processus de transport dans les électrolytes, en relevant le rôle essentiel des mesures d'autodiffusion dans l'étude des interactions ioniques. Une voie nouvelle est ainsi ouverte dans la connaissance de la structure des solutions électrolytiques.

INTRODUCTION

Les mesures de coefficient de diffusion et de conductivité dans les électrolytes sont extrêmement anciennes mais ne sont relatives qu'aux propriétés de transport global de l'électrolyte et ne mettent pas en évidence le comportement individuel des ions.

Cependant, depuis la découverte et l'application des isotopes comme traceurs, il est possible d'atteindre les coefficients de diffusion individuels des ions et de mettre ainsi en évidence leur déplacement spontané, connu sous le nom d'autodiffusion.

C'est la détermination de ces coefficients d'autodiffusion ionique dans les électrolytes qui constitue le thème central de notre étude. Nous nous proposons dans ce travail d'étudier les divers facteurs structuraux qui déterminent la variation du coefficient de diffusion ionique, de montrer les conséquences que l'on peut en déduire sur la nature et les propriétés de transport des électrolytes en solution.
Nous envisagerons également la relation entre le phénomène de diffusion ionique et les autres propriétés de transport particulièrement de conductivité.

RELATION DIFFUSION-CONDUCTIVITÉ

La diffusion est définie par la première loi de Fick le flux de particules J est proportionnel au gradient de concentration :

$$J = -D\frac{\partial C}{\partial x} \tag{1}$$

Le coefficient D est appelé coefficient de diffusion.

On déduit de (1), l'équation aux dérivées partielles décrivant le phénomène de diffusion :

$$\frac{\partial C}{\partial t} - D\frac{\partial^2 C}{\partial x^2} = 0 \tag{2}$$

Cette équation met en évidence les dimensions du coefficient de diffusion qui sont celles du carré d'une longueur multipliée par l'inverse d'un temps.

Il existe donc deux points de vue possibles pour interpréter les coefficients de diffusion :

— Soit le point de vue macroscopique : Réponse d'un système à la contrainte constitué par un gradient de concentration ; le mode de description correspondant est la thermodynamique phénoménologique des processus irréversibles.

— Soit le point de vue microscopique : déplacement spontané des particules du milieu du fait de l'agitation thermique ; le mode de description est alors la mécanique statistique.

a) *Dilution Infinie.* Dans le cas de l'autodiffusion d'ions en solution, on relie à diffusion infinie le coefficient d'autodiffusion D à la mobilité u suivant la relation :

$$\frac{D}{u} = \frac{kT}{Ze} \tag{3}$$

où k est la constante de Boltzmann,
T — la température absolue,
Z — le nombre de charges portés par l'ion,
e — la charge élémentaire.

L'équation (3) porte le nom de relation de Nernst-Einstein. Elle a permis par la mesure d'un des deux coefficients u ou D l'évaluation de l'autre. En particulier dans le cas des ions en solution aqueuse, jusqu'à la découverte des isotopes, la mesure de mobilités ioniques a été le seul moyen général d'évaluation des coefficients de diffusion. Il est à remarquer que la relation (3) n'est valable qu'à dilution infinie et que pour des valeurs finies de la concentration, des écarts à cette loi sont observés.

b) *Lois Limites.* La loi limite en $\sqrt{C}$ pour les écarts a été établie et vérifiée expérimentalement. [1,2]

Comme les mobilités ne sont pas en général connues on définit le rapport :

$$\frac{D^+ + D^-}{\Lambda} = \frac{RT}{F^2} \quad \text{à dilution infinie.} \tag{4}$$

---

[1] P. Turq, F. Lantelme et M. Chemla. *Electrochimica Acta*, **14**, 1081 (1969).

[2] P. Turq, F. Lantelme et Y. Roumegous, M. Chemla, *J. Chim. Phys.*, **68**, 527 (1971)

Le nombre φ sans dimension, défini par :

$$\varphi = \frac{D^+ + D^-}{\Lambda} \Big/ \frac{RT}{F^2} \tag{5}$$

est égal à 1 à dilution infinie.

Les variations de φ chiffreront donc les écarts à la relation de Nernst-Einstein et mettront en évidence les modifications structurales du milieu.

A titre d'exemple signalons que les variations de φ seront très importantes lors de la formation d'associations ioniques puisque dans le cas d'associations neutres ne conduisant pas le courant il y a une diminution très importante de la conductivité sans variations corrélatives des coefficients de diffusion.

LOIS LIMITES

$$\Lambda = \Lambda_0 - (\alpha\Lambda_0 + \beta)\sqrt{C} \tag{6}$$

$$D = D_0(1 - \alpha\sqrt{C}) \tag{7}$$

La figure 1 représente d'une part les variations de φ du bromure de césium dans l'eau et d'autre part les variations de φ dans des mélanges eau-dioxanne [3] de basse constante diélectrique, pour le même sel. (82, 82 % de dioxanne), mélange pour lequel existe une très forte proportion de paires neutres CsBr.

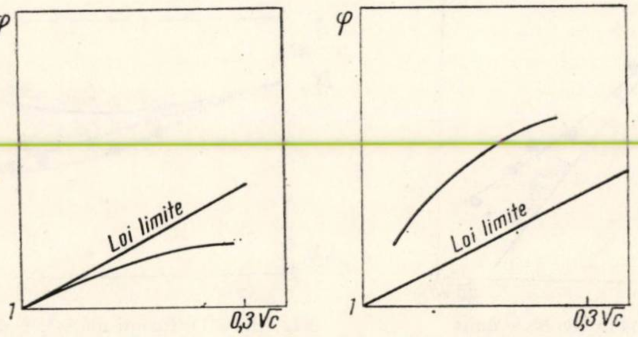

Fig. 1. — *a*, Variation de φ du CsBr en solution aqueuse ; *b*, dans les mélanges eau-dioxanne.

c) *Termes d'ordre supérieur*. La variation des conductivités avec la concentration a été déterminée jusque pour des termes d'ordre $C^3/^2$ depuis les travaux de Fuoss et Onsager, [4,5] de Fernandez-Prini [6], de Jus-

---

[3] H. Latrous Thèse de Doctorat de 3ème Cycle — Orsay 1970.

[4] R.M. Fuoss et F. Acascina, « Electrolytic Conductance », Interscience New-York, 1959.

[5] R.M. Fuoss et L. Onsager, *Proc. Nat. Acad. Sci. U.S.A.*, **47**, 818 (1961).

[6] R. Fernandez-Prini, *Trans. Faraday, Soc.*, **64** 2146 (1968).

tice. [7] L'intérêt de cette extension est de permettre :

— d'une part d'expliquer la variation des conductivités des électrolytes en l'absence d'associations.

— d'autre part puisque l'association fait intervenir en premier ordre des termes en C, il est nécessaire, pour avoir une description quantitative des phénomènes, de connaître la contribution correspondante des termes d'interactions électrostatiques.

Ces développements de la théorie de la conductivité ont permis l'étude d'un grand nombre de milieux.

Dans notre laboratoire nous avons développé récemment [8,9] la théorie correspondante pour les coefficients d'autodiffusion.

LOIS ÉTENDUES

Sans associations

$$\Lambda = \Lambda_0 - S\sqrt{C} + JC + EC \log C + J_2 C^{3/2} \tag{8}$$

$$\begin{aligned} D = D_0 (1 - S'\sqrt{C} + JC + E'\, C \log C + J'_2\, C^{3/2} + \\ + E'_3\, C^{3/2} \log C) = D_0 (1 + \varepsilon\,(C)) \end{aligned} \tag{9}$$

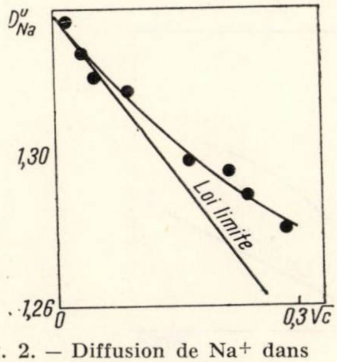

Fig. 2. — Diffusion de Na^+ dans les solutions de NaCl.

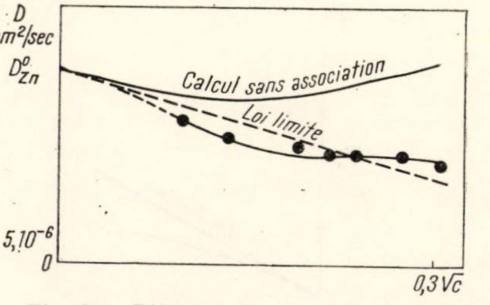

Fig. 3. — Diffusion de $SO_4^{=}$ dans les solutions aqueuses de $ZnSO_4$.

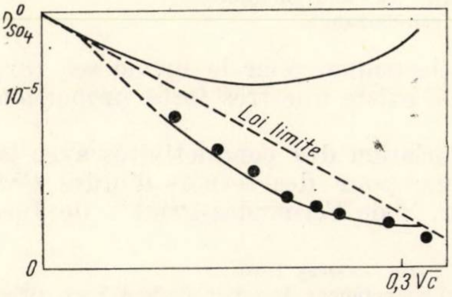

Fig. 4. — Diffusion de Zn^{++} dans les solutions aqueuses de $ZnSO_4$.

---

[7] J.-C. Justice, *Electrochim. Acta*, **16** 701 (1971).

[8] P. Turq, *J. Phys. Chim.* (à paraître).

[9] P. Turq, R. Deloncle et M. Chemla, *J. Chim. Phys.*, octobre 1971.

Avec associations. Si γ est la proportion d'associations

$$\Lambda = (1-\gamma)(\Lambda_0 - S\sqrt{\mu} + J\mu + E\mu\log\mu + J_2\,\mu^{3/2} \tag{10}$$

$$D = D_0(1+\varepsilon(\mu))(1-\gamma) + \gamma\,Dp \tag{11}$$

Dp — le coefficient de diffusion des paires.
μ — la force ionique du milieu.

Rappelons que jusqu'à présent seules étaient connues les lois limites, qui ont d'ailleurs été retrouvées dans le cadre de la mécanique statistique.[10] Nous disposons maintenant d'un système cohérent pour l'interprétation des mesures de coefficient d'autodiffusion et de conductivité qui nous permet de prévoir quantitativement les écarts à la relation de Nernst-Einstein en solution, avec ou sans phénomène d'association.

A titre d'exemple, nous donnons dans les figures 2—4 les variations du coefficient d'autodiffusion dans des solutions aqueuses d'électrolytes 1—1[11] et également dans le cas d'un électrolyte 2—2.

CONCLUSION

L'étude des écarts à la relation de Nernst-Einstein et la mesure des coefficients d'autodiffusion dans les électrolytes permettent d'élucider un nombre important de problèmes physico-chimiques.[12] En ce qui concerne la structure des solutions électrolytiques, il est possible d'obtenir des informations quantitatives sur la nature, les propriétés d'association et les coefficients de transport des diverses espèces existant en solution. Il est à remarquer que ceci n'est possible que grâce à la séparation des termes électrostatiques qui sont calculés à l'aide de la loi limite et des termes d'ordre supérieur.

Nous confirmons donc, l'intérêt général de la détermination des processus de transport dans les électrolytes, mettant en relief le rôle essentiel des mesures d'autodiffusion dans l'étude des interactions ioniques. Nous pensons qu'une voie nouvelle est ainsi ouverte dans la connaissance de la structure des solutions électrolytiques.

---

[10] P. Turq, *Chemical Physics Letters*, **5** (7) 432 (1970).

[11] R. Mills, *J. Phys. Chim.*, **63** 1973 (1959).

[12] M. Olsztajn, P. Turq et M. Chemla, *Electrochim. Acta*, **14** 1081 (1969).

Revue Roumaine de Chimie, **17**, *1*, *2*, 63—67 (1972)

Revue Roumaine de Chimie, 17, 1, 2, 69–75 (1972)

Dedicated to Professor I. G. MURGULESCU
on his 70th birthday

KINETIC EQUATIONS FOR REACTIONS TAKING PLACE IN POWDERS. I COMPLETE FORM OF THE EQUATION FOR SPHERIC PARTICLES

D. CISMARU and C. RADOVICI

Research Center of Physical Chemistry Str. Galaţi 31, Bucharest, Romania

Received September 7, 1971

A new equation for the kinetics of reactions in solid media, in powder form, is deduced.

I. INTRODUCTION

The equation formerly suggested by Cismaru for reactions in solids in powder form [1,2] has been explained for the case of spheric particles, without taking into account the fact that generally speaking the volume of the reacting compound differs from that of the resulting compound. The present paper aims at eliminating this approximation and an equation of a wider range is deduced, still based on the initial reasoning.

II. DEDUCTION OF THE EQUATION

The initial starting conditions are : one mole B, having a molar volume V_B, reacts to n moles A, having a molar volume V_A and a molar weight μ_A, giving m moles AB, with a molar volume V_{AB}, so that :

1. the diffusion coefficient of reactant A towards the surface AB is much higher than the diffusion coefficient through the layer AB. On the surface of AB, the concentration of A may be taken for constant and uniform till its exhaustion. We shall denote this concentration C_1,

2. the growing rate of the layer of reaction product is the same all over the surface of B,

3. the rate at which A diffuses through B is much smaller than the rate at which it reacts with B, so that at the $B-AB$ border the concentration of A is practically equal to 0,

---

[1] D. Cismaru, *Studii şi Cercetări Fiz. Acad. R.P.R.*, **4**, 435 (1955).

[2] D. Cismaru, *Studii şi Cercetări de Chim. Acad. R.P.R.*, **2**, 113 (1957).

4. particles B are spheric.

With these initial conditions the deduction of the equation is given below.

The transformation degree of particles B may be expressed as the ratio of the consumed weight to the initial one, or of the consumed volume to the initial one :

$$z = \frac{V_i \rho - V \rho}{V_i \rho} = \frac{V_i - V}{V_i} = \frac{V_c}{V_i} \tag{1}$$

where : V_i = the initial volume ; V = the current volume and V_c = the consumed volume, ρ = density.

As the growing rate of the reaction product layer is everywhere the same, the rate at which reactant B is consumed will also be the same, so that, neglecting product $\mathrm{d}S\mathrm{d}x_B$ one may write :

$$\mathrm{d}V_c = S\mathrm{d}x_B \tag{2}$$

and

$$\frac{\mathrm{d}V_c}{\mathrm{d}t} = S\frac{\mathrm{d}x_B}{\mathrm{d}t} \tag{3}$$

where S is the surface of B and x is the thickness of layer B to be consumed. The transformation rate of B will be :

$$\frac{\mathrm{d}z}{\mathrm{d}t} = \frac{1}{V_i} S \frac{\mathrm{d}x_B}{\mathrm{d}t} \tag{4}$$

Between the thickness of the consumed layer in B and the thickness of the formed layer AB (x_{AB}), there exists, for even layers, the relationship :

$$\frac{V_B}{x_B} = \frac{mV_{AB}}{x_{AB}} \tag{5}$$

from which one deduces :

$$x_B = \frac{1}{m}\frac{V_B}{V_{AB}} x_{AB} ; \quad \frac{\mathrm{d}x_B}{\mathrm{d}t} = \frac{1}{m}\frac{V_B}{V_{AB}}\frac{\mathrm{d}x_{AB}}{\mathrm{d}t} \tag{6}$$

The differential form of relation (6) – the case of very thin layers – is also valid, with a precision range of a superior order differential, for all forms of layers. Introduced into relationship (4), it gives :

$$\frac{\mathrm{d}z}{\mathrm{d}t} = \frac{1}{V_i}\cdot\frac{V_B}{V_{AB}} S \frac{\mathrm{d}x_{AB}}{\mathrm{d}t} \tag{7}$$

This equation was deduced only based on condition 2 and may therefore be applied to all reactions in which this condition is satisfied, explicitely depending on the concrete conditions of the respective reaction.

We shall show explicitely equation (7) for reactions in which particles B have a spheric form (fig. 1) and conditions 1 and 3 are satisfied.

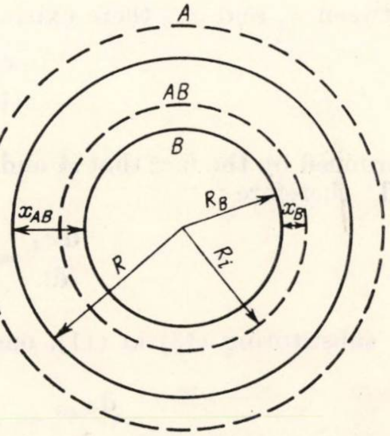

Fig. 1. – Reaction scheme between A and B.

In this case the quantity of A (expressed in moles) passing during a time-unit through the surface of any sphere having its center in the center of particle B, is constant for a given thickness (x_{AB}) of the reaction product layer :

$$\frac{\mathrm{d}C_A}{\mathrm{d}t} = -DS\frac{\mathrm{d}C}{\mathrm{d}r} = -4\pi r^2 D\frac{\mathrm{d}C}{\mathrm{d}r} = Q\,(x_{AB}) \tag{8}$$

Making use of this equation, we shall calculate $\frac{\mathrm{d}x_{AB}}{\mathrm{d}t}$ *versus* the quantity of A diffused through the reaction product layer AB.

$$C_A\,(\text{moles}) = \frac{V\rho_A}{\mu_A} = \frac{V_{AC}}{V_A} \tag{9}$$

where V_{AC} is the total volume of A consumed in the reaction, and V_A, ρ_A and μ_A are respectively : the molar volume, the density and the molecular weight of A. By differentiating we obtain :

$$\frac{\mathrm{d}C_A}{\mathrm{d}t} = \frac{1}{V_A}\frac{\mathrm{d}V_{Ac}}{\mathrm{d}t} = \frac{1}{V_A}S\frac{\mathrm{d}x_A}{\mathrm{d}t} \tag{10}$$

where x_A is the thickness of the hypothetical layer of A which would disappear at the surface $B-AB$ if the reaction did not take place. By introducing (10) into (8), we obtain :

$$\frac{dx_A}{dt} = - D V_A \frac{dC}{dr} \tag{11}$$

Between x_A and x_{AB} there exists the relation :

$$\frac{x_A}{n V_A} = \frac{x_{AB}}{m V_{AB}} \tag{12}$$

(dermined by the fact that A and AB must extend on the same surface S) and therefore :

$$\frac{dx_A}{dt} = \frac{n V_A}{m V_{AB}} \cdot \frac{dx_{AB}}{dt} \tag{13}$$

By substituting (13) in (11), one obtains :

$$\frac{dx_{AB}}{dt} = - D \frac{m}{n} V_{AB} \frac{dC}{dr} \tag{14}$$

The gradient $\frac{dC}{dr}$ may be determined from equation (8). By integrating, one obtains :

$$C \Big|_{0}^{C_1} = \frac{Q(x_{AB})}{4\pi D} \cdot \frac{1}{r} \Big|_{R - x_{AB}}^{R}$$

(where C_1 is the concentration of A at the outer surface of AB, and R is the radius of the sphere at the $AB-A$ border) and therefore

$$C_1 = \frac{Q(x_{AB})}{4\pi D} \left(\frac{1}{R} - \frac{1}{R - x_{AB}} \right) = - \frac{Q(x_{AB})}{4\pi D} \frac{x_{AB}}{R(R - x_{AB})}$$

$$Q(x_{AB}) = - \frac{4\pi D C_1 R (R - x_{AB})}{x_{AB}} \tag{15}$$

By replacing (15) in (8) one obtains :

$$4\pi r \; D \frac{dC}{dr} = \frac{4\pi D C_1 R (R - x_{AB})}{x_{AB}}$$

$$\frac{dC}{dr} = \frac{C_1 R (R - x_{AB})}{r^2 x_{AB}} = \frac{C_1 R (R - x_{AB})}{R_B^2 x_{AB}} \tag{16}$$

By replacing (16) in (14), one obtains :

$$\frac{\mathrm{d}x_{AB}}{\mathrm{d}t} = -D\frac{m}{n}V_{AB}\,\frac{C_1 R\,(R - x_{AB})}{x_{AB}\,R_B^2} \tag{17}$$

which introduced into (7) gives :

$$\frac{\mathrm{d}z}{\mathrm{d}t} = -\frac{1}{V_i}\,\frac{V_B}{nV_{AB}}\cdot S.D\frac{m}{n}V_{AB}\,\frac{C_1 R\,(R - x_{AB})}{x_{AB}\,R_B^2}$$

$$\frac{\mathrm{d}z}{\mathrm{d}t} = -\frac{3V_B DC_1}{4\pi R_i^3 n}\cdot 4\pi R_B^2\,\frac{R\,(R - x_{AB})}{R_B^2\,x_{AB}}$$

$$\frac{\mathrm{d}z}{\mathrm{d}t} = -\frac{3DV_B C_1}{nR_i^3}\cdot\frac{R\,(R - x_{AB})}{x_{AB}} \tag{18}$$

To be able to compare equation (18) with the similar equations found in literature [3,4] we shall express R and x_{AB} as a function of R and z, using the relations suggested in figure 1.

$$R_B = R_i\sqrt[3]{1 - z} \tag{19}$$

$$R = R_i\sqrt[3]{z\left(\frac{mV_{AB}}{V_B} - 1\right) + 1} = R_i\sqrt[3]{K_1 z + 1} \tag{20}$$

where

$$K_1 = \frac{mV_{AB}}{V_B} - 1$$

$$x_{AB} = R - R_B = R_i\sqrt[3]{K_1 z + 1} - R_i\sqrt[3]{1 - z} \tag{21}$$

By introducing (19, 20, 21) into (18), one obtains :

$$\frac{\mathrm{d}z}{\mathrm{d}t} = -\frac{3V_B DC_1}{nR_i^2}\,\frac{\sqrt[3]{(1 - z)(K_1 z + 1)}}{\sqrt[3]{K_1 z + 1} - \sqrt[3]{k - z}} = K\,\frac{\sqrt[3]{(1 - z)\,(K_1\,z + 1)}}{\sqrt[3]{K_1 z + 1} - \sqrt[3]{1 - z}} \tag{22}$$

---

[3] A.M. Ghintsling and B.I. Brounstein, *Zhur. priklad. Khim.*, **23**, 1249 (1950).

[4] R.E. Carter, *J. Chem. Phys.*, **34**, 2010 (1961).

where :

$$K = \frac{3V_B DC_1}{nR_i^2}$$

For $K_1 = 0$, that is for $mV = V_B$, equation (22) is reduced to :

$$\frac{dz}{dt} = -K\frac{\sqrt[3]{1-z}}{1-\sqrt[3]{1-z}} \tag{23}$$

which by integration gives :

$$(1-z)^{2/3} + \frac{2}{3}z - 1 = \frac{2}{3}Kt = K't \tag{24}$$

namely exactly Ghistling-Brounstein's equation [3] in which the reaction constant is thus expressed. As was shown [1,2] this equation is reduced to Jander's equation [5] in the case of very thin layers (films) of reaction product.

By integrating equation (22) one obtains :

$$-\frac{3}{2}(1-z)^{2/3} - \frac{3}{2K_1}(K_1 z + 1)^{2/3} = -Kt + c \tag{25}$$

For $t = 0$, $z = 0$, so that $c = -\frac{3}{2}\left(1 + \frac{1}{K_1}\right)$

Equation (25) becomes :

$$(1-z)^{2/3} + \frac{1}{K_1}(K_1 z + 1)^{2/3} - \frac{1}{K_1} - 1 = K_2 t \tag{26}$$

where :

$$K_2 = \frac{2}{3}K = \frac{2V_B DC_1}{nR_i^2}$$

Equation (26) is identical to Carter's equation [4,6] with the difference that here the reaction constant appears in an explicite form. One may therefore consider that the experimental checking of Carter's equation is also valid for equation (26).

---

[5] W. JANDER, *Z. anorg. Chem.*, **163**, 30 (1927).

[6] R.E. CARTER, *J. Chem. Phys.*, **35**, 1137 (1961).

III. CONCLUSIONS

A simple kinetic equation is deduced in differential (18), (22) as well as in integral (26) form, taking into account the evolution of the curvature of the surfaces, as well as the ratio of the reacting volume to the resulting volume, which is explained in the case of spherical particles encompassed in the initially formulated conditions 1—4. The suggested equations contain Jander and Ghinstling equations as particular cases, and are deduced based on the more general equation (7) which may, in principle, be explained for any form of particles.

Revue Roumaine de Chimie, **17**, *1*, *2*, 77–82 (1972)

Dedicated to Professor I. G. MURGULESCU
on his 70th birthday

THE INFLUENCE OF GAS ADSORPTION ON THE SURFACE RECOMBINATION OF NITROGEN ATOMS ON STAINLESS STEEL

GERDA COMŞA and W. GROTH
Institute of Physical Chemistry, Bucharest, Romania
and
Institute of Physical Chemistry of the University of Bonn

Received July 26, 1971

The influence of impurity layers upon the wall recombination of nitrogen atoms on a stainless steel surface was studied in connection with the work carried out with the "big sphere" at the Institute of Physical Chemistry in Bonn. The wall recombination coefficient was determined using the nitrogen afterglow decay method. This technique had to be improved in order to be applied to the very short decay times and the extremely small intensities involved in our experiments. It was thus possible to measure the recombination coefficient of nitrogen atoms for a stainless steel surface cleaned by outgassing and iongetter pumping and to study sistematically the influence of different surface treatments on this parameter.

INTRODUCTION

The recombination of nitrogen atoms in the gas-phase is a three-body process between two nitrogen atoms and a carrier gas molecule [1] (nitrogen or noble gas molecules), i.e. a second order reaction with respect to the atom concentration, N. As known from the literature [2–4] and observed also in our experiments, the wall recombination on metals is a first order process, which can be explained on account either of an adsorption mechanism [2,3] or of a mechanism involving the formation of a surface nitrid. [5] Thus the disappearance rate of nitrogen atoms in a closed metallic reaction vessel can be written :

$$-\frac{\mathrm{d}N}{\mathrm{d}t} = k_v N^2 p + k_s N \tag{1}$$

---

[1] A.N. Wright and C.A. Winkler, in "Active Nitrogen", Academic Press, New York, 1968, pp. 161–170.

[2] K.E. Shuler and K.J. Laidler, *J. Chem. Phys.*, **17**, 1212 (1949).

[3] R. Kelley and C.A. Winkler, *Canad. J. Chem.*, **37**, 62 (1959).

[4] R.A. Young, *J. Chem. Phys.*, **34**, 1292 (1961).

[5] M.L. Rahman and J.W. Linnett, *Trans. Faraday Soc.*, **67**, 183 (1971).

where p is the total pressure and k_v and k_s are the rate constants of the volume and surface recombination processes. The parameter k_s is connected to the wall recombination coefficient γ by the relationship [2]:

$$k_s = \gamma \frac{\bar{v} S}{4V} \tag{2}$$

where $\bar{v}$ is the average atom velocity and S and V are the surface and volume of the reaction vessel. The recombination coefficient γ is the fraction of colliding atoms which react on the surface.

By adequately choosing the reaction vessel dimensions, the total pressure, the atom concentration and the nature of the wall, one may arrange the prevailling of either the second or the first order process. For instance, when simulating chemiluminiscence reactions which occur in the upper atmosphere the process to be studied is the volume recombination at low pressures. Accordingly, the reaction vessel has to be large for the undesirable wall recombination to be negligible. At the Institute of Physical Chemistry of the University of Bonn such simulation experiments are carried out in a 7.5-meter stainless steel sphere. In spite of the favourable value of the S/V ratio and the relatively inactive wall material the surface recombination was, in some experiments, quite important and dependent on the history of surface treatment. It seemed therefore useful to study the nitrogen atom recombination on stainless steel as such, under suitable conditions, and to find out, what kind of treatment a stainless steel surface needs to become inactive against nitrogen recombination.

When the wall recombination coefficient is to be measured the gas-phase recombination has to be negligible. In the case of the nitrogen atom recombination and of usual vessel dimensions this occurs at pressures below several torrs and it is the more marked as the S/V ratio is higher. Equation (1) reduces then to

$$-\frac{\mathrm{d}N}{\mathrm{d}t} = k_s N \tag{1'}$$

respectively

$$N = N_0 \, \mathrm{e}^{-k_s t} \tag{3}$$

As the total light intensity of the nitrogen afterglow (a phenomenon following the gas-phase recombination of the nitrogen atoms) is proportional to the square of the atom concentration:

$$I \sim N^2 = N^2 \, \mathrm{e}^{-2k_s t} = N_0^2 \, \mathrm{e}^{-\frac{\gamma \bar{v} S}{2V} t} \tag{4}$$

one can determine γ by recording the intensity decay of the afterglow:

$$I = I_0 \, \mathrm{e}^{-t/\tau} \tag{5}$$

and computing the decay time τ from the slope of the straight line $\log I = f(t)$. The recombination coefficient is then given by the expression :

$$\gamma = \frac{2V}{\bar{v}S\tau} \tag{6}$$

EXPERIMENTAL

The decay time can be measured by introducing a certain quantity of "active nitrogen" (that is a mixture of molecular and atomic nitrogen, obtained, for instance, by means of a microwave discharge) into the reaction vessel previously evacuated and by recording the decay of the afterglow intensity with a suitable photomultiplier. On account of the relatively active surface (even in case of cleaning with iongetter pumping only) the decay times in our experiments were very short (shorter than the time needed for operating a usual valve) and the intensities very low. The short decay time required a rapid interruption of the flux of atoms into the vessel, while the low intensity a periodic repetition of the process. In other words, the flux of nitrogen atoms had to be interrupted periodically. This was achieved by the periodic interruption of the microwave discharge. A detailed description of the apparatus used is given in a previous paper.[6] The reaction vessel was a stainless steel cylinder of 170 mm in diameter and 400 mm in length.

With the method improved in this way we measured the decay time for several "states" of the stainless steel surface :

1) "Cleaned", that is after several hours of outgassing at 250° and iongetter pumping (final pressure 10^{-8} torr);

2) "Cleaned" + covered with a gas layer: after cleaning as in (1), one of the following gases (O_2, CO_2, CO, H_2O or air) was introduced into the reaction vessel at a pressure of several torrs and evacuated again after some time, by preliminary and diffusion pumping;

3) After a several days exposure to atmospheric air, followed by preliminary and iongetter pumping;

4) Covered with teflon foil and cleaned by preliminary and iongetter pumping.

After each of these "treatments" the surface was exposed to the active nitrogen, whereby the total pressure in the reaction vessel was in the range of $10^{-2} \ldots 10^{-1}$ torr.

RESULTS

The measured decay time shows a clear dependence upon the kind of surface treatment and is, as expected, the shortest when the surface is cleaned by outgassing and the longest when the surface is covered with teflon. Figure 1 gives a semilog plot of four decay curves, obtained after outgassing. The curves were recorded at different moments from the beginning of the periodic atom introduction, without having it interrupted meanwhile. One can see, that the decay time increases with the length of time passed from the beginning of the experiment, Δt_A. In other words, the active nitrogen produces a passivating of the surface. The same observation had been made by Rahman and Linnett [5] during the nitrogen atom recombination on thin evaporated iron films.

---

[6] G.H. Comşa and W. Groth, *Ber. Bunsengesellschaft Phys. Chem.*, **75**, 1066 (1971), (in print).

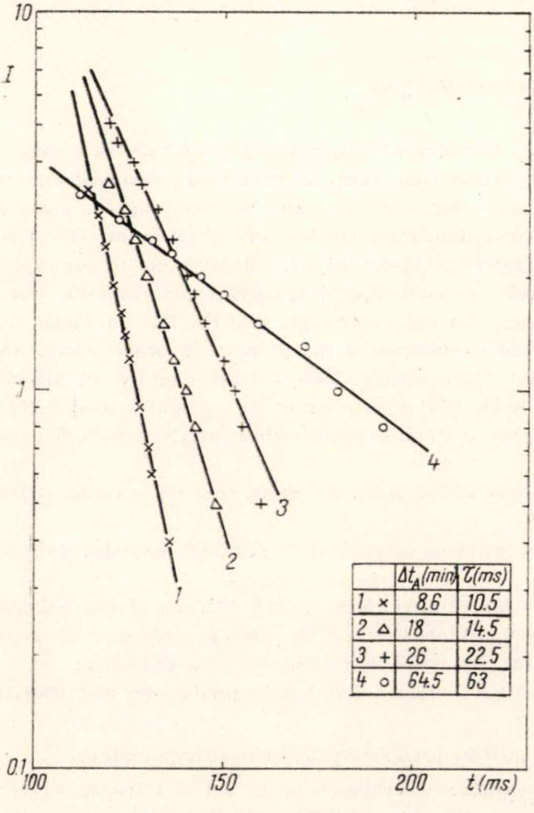

Fig. 1. — Semilog plots of four afterglow decay curves for the surface cleaned by outgassing and iongetter pumping.

By computing the decay time τ from the slope of the straight lines in fig. 1 and plotting log τ against Δt_A there results the straight line *1* in figure 2. By extrapolating it to $\Delta t_A = 0$, one gets the decay time $\tau_0 = 8$ ms, which corresponds to the clean surface. The curves *2* and *3* in figure 2 were obtained for the surface treated as in (2), namely for the surface cleaned and covered with a CO_2, respectively air-layer. The extrapolation of these straight lines gives the decay time $\tau_0 = 37$ ms for the covered surface.

The measured decay times for the different states of the surface and the corresponding computed rate constants and recombination coefficients are summarized in table 1. In the case of the surface-cleaned by outgassing the recombination coefficient is of the order of magnitude 10^{-2}, while in case of the gas covered surface only 10^{-3}. Prolongued exposure to atmospheric air produces a further passivating by one order of magnitude. After teflon coating — whereby 3% of the stainless steel surface area remained uncovered —

Table 1

Recombination coefficient of nitrogen atoms on a stainless steel cylinder for various surface treatments

PRESENT WORK				COMPARATIVE VALUES		
Surface treatment	τ (s)	k_s (s^{-1})	γ	Nature of surface	γ	Authors
Outgassing and iongetter pumping	8×10^{-3}	6.3×10^{1}	2.3×10^{-2}			
Outgassing, Gas introduction (CO_2, CO, O_2, air, H_2O) Evacuating	$3 \times 10^{-2}..6\times10^{-2}$	$1.7 \times 10^{1}..$ $..0.8 \times 10^{1}$	$6.2 \times 10^{-3}..$ $..3.1 \times 10^{-3}$	Evaporated iron films	2.1×10^{-3} 1.0×10^{-3} 3.9×10^{-4}	Rahman and Linnett (1970)[5]
Several days exposure to air, Evacuating, Iongetter pumping	$1.2 \times 10^{-1}..$ $..3 \times 10^{-1}$	4.2 ... 1.7	1.2×10^{-3} .. ..4.6×10^{-4}	Polished stainless steel plate	1.6×10^{-3}	Buschmann (1965)[8]
Coating with Teflon-foil (97 % of the surface covered with Teflon) * Evacuating, Ionget*-ter pumping	8	6.3×10^{-2}	1.7×10^{-5}	Stainless steel (exposed to a prolongued oil back diffusion)	4×10^{-7}	Becker, Elzer, Groth and Kley (1968)[7]
			4×10^{-6}	Teflon-tube	5×10^{-7} 5×10^{-6}	Evenson and Burch (1966)[9]

* Teflon-foil

the overall recombination coefficient was 1.7×10^{-5}. From this value we computed the recombination coefficient for teflon foil : 4×10^{-6}.

For the sake of comparison some γ-values given in literature are also listed in table 1. There exist only two values for the recombination of nitrogen atoms on stainless steel.[7,8] One refers to a polished plate of stainless steel, [8] which had not been subjected to any special outgassing. This value can therefore be compared with the one we obtained after a longer exposure of the reaction vessel to the atmosphere. The other value of 4×10^{-7} had been found in the simulation apparatus [7] after months of operation. It is not yet clear, if this value, which is unexpectedly low for a metal, is due to the prolongued action of active nitrogen and other gases or to an impurification of the surface with diffusion pump oil DC-705 (caused by back-diffusion).

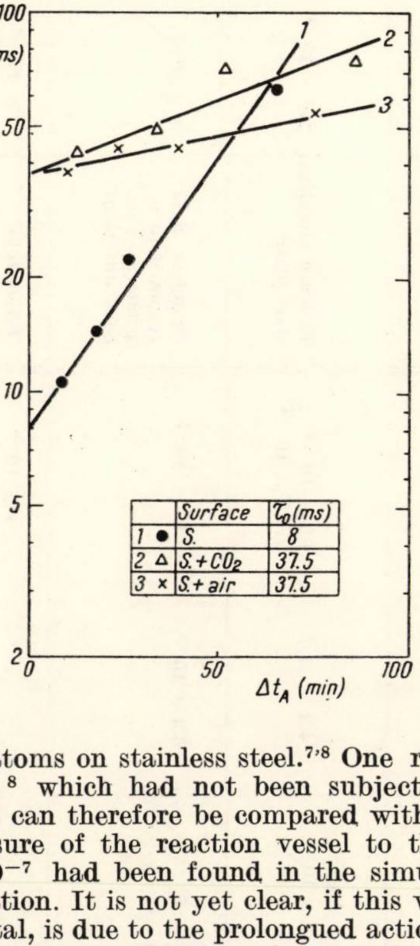

Fig. 2. — Dependence of the decay time τ on the length of time, Δt_A, of the surface exposure to active nitrogen.

The sequence of the three values concerning the nitrogen atom recombination on evaporated iron films [5] shows the above mentioned passivating of the surface. Finally, we notice that the recombination coefficient obtained for teflon may well compare with that found by Evenson and Burch. [9]

---

[7] K.H. Becker, A. Elzer, W. Groth and D. Kley, Forschungsbericht SHA-2, University Bonn, 1968.

[8] H.W. Buschmann, Private Communication.

[9] K.H. Evenson and D.S. Burch, *J. Chem. Phys.*, **45**, 2450 (1966).

Revue Roumaine de Chimie, **17**, *1, 2*, 83–93 (1972)

Dedicated to Professor I. G. MURGULESCU
on his 70th birthday

MEMORY EFFECTS IN OXYGEN AND HYDROGEN PHOTOSORPTION ON THIN ZINC OXIDE FILMS

MIHAELA CONSTANTINESCU and E. SEGAL

Institute of Physical Chemistry, Str. Dumbrava Roşie 23, Bucharest, Romania

Received May 20, 1971

Some results obtained in the study of photosorptive properties of zinc oxide films *versus* oxygen and hydrogen are presented in the light of the electronic theory of memory effects.

The theory of the phenomena conditioned by the memory effect presented by semiconductors with photosorptive properties was developed by Volkenstein and Baru.[1] Considering the memory effect as an adsorption on nonequilibrium centers – generated by irradiation and localized on the biographical defects of the surface – the above authors have established the general equation describing the changing in time of the surface concentrations corresponding to the adsorption centers $X(t)$ and adsorbed particles $N(t)$ respectively :

$$X(t) = \mu X^* - (\mu X^* - X_i)\,\mathrm{e}^{-a(t-t_i)} \tag{1}$$

$$N(t) = Ae^{-a(t-t_i)} + Be^{-(b+c)(t-t_i)} + C \tag{2}$$

where :

$$\mu = \frac{1}{1+\nu} \tag{3}$$

and :

$$\nu = \frac{a_3 + a_4}{a_1 + a_2} \tag{4}$$

$$a = a_1 + a_2 + a_3 + a_4 \tag{5}$$

---

[1] F.F. Volkenstein and V.G. Baru, *Zhur. fiz. Khim.*, **42**, 1317 (1968).

$$\left.\begin{aligned} A &= \frac{b}{a-b-c}(\mu X^* - X_i) \\ B &= N_i - \frac{b}{a-b-c}(\mu X^* - X_i) - \frac{b}{b+c}\mu X^* \\ C &= \frac{b}{b+c}\mu X^* \end{aligned}\right\} \quad (6)$$

X^* is the surface concentration of the structural defects of the same type, t is the time and the subscript i refers to the initial value of the represented variable : a_1, a_2, a_3 and a_4 are the real or apparent kinetic constants of the charging or discharging processes of a neutral defect A°, respectively a negative one A^- :

$$A^\circ + e \xrightarrow{a_1} A^-$$

$$A^\circ \xrightarrow{a_2} A^- + p$$

$$A^- \xrightarrow{a_3} A^\circ + e$$

$$A^- + p \xrightarrow{a_4} A^\circ$$

and b and c represent the kinetic constants for adsorption, respectively desorption.

For acceptor type defects, which could be in neutral electrical state A°, or positively charged A^+, one can easily demonstrate that equations (1) and (2) are formally valid, the only change being in the significance of the constants a_1, a_2, a_3, a_4. In these conditions, the above constants refer to the following processes :

$$A^\circ + P \xrightarrow{a_1} A^+$$

$$A^\circ \xrightarrow{a_2} A^+ + e$$

$$A^+ \xrightarrow{a_3} A^\circ + P$$

$$A^+ + e \xrightarrow{a_4} A^\circ$$

The study of the electrical resistance variation of a thin zinc oxide film, previously saturated with oxygen, during irradiation at room temperature [2] has led to the results shown in figure 1.

The first irradiation determines an important decrease of the electrical resistance down to a constant value. Stopping irradiation results in an increase of the electrical resistance up to a constant value, which is lower as the original one. During the second irradiation the electrical resistance decreases again with a quantity corresponding to the dark variation. Continuing with alternative dark and irradiation periods, the phenomenon shows itself perfectly reversible.

---

[2] E. Segal and M. Teodorescu, *Rev. Roumaine Chim.*, 12, 75 (1967).

Analysing the shape of the dark and irradiation curves (excepting the first irradiation), one can see that the electrical resistance varies faster under irradiation and slower in the dark period. One can also observe (for the case of first irradiation, too) that the parts of the curves corresponding to the dark periods have the concavity directed towards the negative values of the electrical resistance, while the parts of the curves corresponding to the irradiation periods have the concavity directed towards the positive values of the electrical resistance.

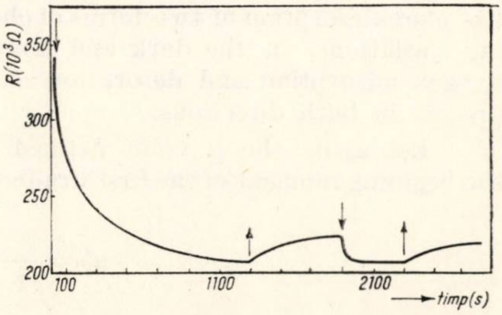

Fig. 1. — Electrical resistance variation of zinc oxide film *versus* time for oxygen photosorption :
↓ – under irradiation ;
↑ – in the dark.

The irreversibility of reaching again the initial value of the electrical resistance of the zinc oxide film in the first dark period, shows like a memory effect of the film due to previous irradiation. This phenomenon can be explained by the following considerations :

As a result of the film treatment, prior to chemisorption, on the zinc oxide surface there are different chemisorbed forms of charged oxygen ($\underline{O}_2^{--}$, $\underline{O}_2^{-}$),[3] which have resisted thermal degassing. At room temperature — the temperature of the experiments — the oxygen is adsorbed especially under the form $\underline{O}_2^{--}$.[4] On the surface to be irradiated there are then at least two types of chemisorbed oxygen (the lines under the chemical symbols are for the adsorbed states).

The irradiation can realize the desorption of both forms of chemisorbed oxygen. The oxygen adsorbed at room temperaure can be desorbed according to the process :

$$\underline{O}_2^{-} + h\nu \rightarrow O_2 + e \qquad \text{(I)}$$

---

[3] V.F. Kiselev, "Poverknostnyie iavlenia v poluprovodnikah i dielektrikah", "Izd Nauka" Moscow, 1970, p. 331–337.

[4] I.P. Solonitin, *Kinetika i Kataliz*, **7**, 128 (1966).

Also after irradiation the form $\underline{O}_2^{--}$ can pass into the form $\underline{O}_2^{-}$:

$$\underline{O}_2^{--} + h\nu \rightarrow \underline{O}_2^{-} + e \tag{II}$$

which afterwards could be released following a type (I) process.

Considering the above facts, one can say that the more marked variation of the electrical resistance, after the first irradiation, is due to the photodesorption of two forms of chemisorbed oxygen, while the following variations, in the dark and under irradiation, are due only to the oxygen adsorption and desorption at room temperature by the type (I) process in both directions.

Let μ_0' be the μ value defined by equation (3), corresponding to the begining moment of the first irradiation. Following relations (3) and (4) :

$$\mu_0' = \frac{1}{1 + \nu_0'} \tag{3'}$$

$$\nu_0' = \frac{(a_3)_0' + (a_4)_0'}{(a_1)_0' + (a_2)_0'} \tag{4'}$$

In these conditions, the calculations lead to the following formulae for the initial concentration of the adsorbed particles, and for the respective adsorption centers :

$$N_i = \frac{b}{b + c} \mu_0' X^* \tag{7}$$

$$X_i = \mu_0' X^* \tag{8}$$

Taking into account relations (7) and (8), eq. (6) becomes :

$$\left.\begin{aligned} A &= \frac{b}{a - b - c} (\mu - \mu_0') X^* \\ B &= - \frac{ab}{(b + c)(a - b - c)} (\mu - \mu_0') X^* \\ C &= \frac{b}{b + c} \mu X^* \end{aligned}\right\} \tag{9}$$

Assuming that irradiation results in the disappearance of the adsorption centers ($\mu < \mu_0'$) the evolution of the surface concentration of the particles adsorbed during irradiation may be described by eq. (2), the constants A, B and C being expressed by eq. (9). In this way, one can obtain :

$$N(t) = \frac{ab}{a-b-c}(\mu - \mu_0')X^*\left[\frac{1}{a}\,e^{-a(t-t_i)} - \frac{1}{b+c}\,e^{-(b+c)(t-t_i)}\right] + \\ + \frac{b}{b+c}\,\mu X^* \qquad (10)$$

The discussion of the eq. (10) can be easily made for two particular cases, namely :

1) when : $b + c \gg a$.

Then : $\frac{1}{a}\,e^{-a(t-t_i)} \gg \frac{b}{b+c}\,e^{-(b+c)(t-t_i)}$

and :

$$N(t) = \frac{b}{b+c}(\mu_0' - \mu)X^*\,e^{-a(t-t_i)} + \frac{b}{b+c}\,\mu X^* \qquad (10\,a)$$

Taking into account that $\mu_0' > \mu$, eq. (10a) states a decrease in time of the number of adsorbed particles under the influence of the irradiation, down to the value :

$$N(\infty) = \frac{b}{b+c}\,\mu X^* \qquad (11)$$

2) when : $b + c \ll a$.

Then : $\frac{1}{a}\,e^{-a(t-t_i)} \ll \frac{1}{b+c}\,e^{-(b+c)(t-t_i)}$

and :

$$N(t) = \frac{b}{b+c}(\mu_0' - \mu)X^*\,e^{-(b+c)(t-t_i)} + \frac{b}{b+c}\,\mu X^* \qquad (10\,b)$$

Based on eq. (10b) one can also determine a decrease in time of the chemisorbed particles concentration until the value given by eq. (11).

Assuming that the electrical resistance variations determined by us (figure 1), are proportional to the variations of the surface concentration of chemisorbed oxygen particles, it results that eq. (10) and its simplified forms (10a) and (10b), describe in a satisfactory manner the electrical resistance variation of the covered zinc oxide film during the first irradiation.

Eq. (2) describes also the film behaviour during the dark period which succeeds to the irradiation period. In such conditions :

$$a = a_0 \tag{12}$$

$$\mu = \mu_0$$

$$N_i = \frac{b}{b+c}\mu X^* \tag{13}$$

$$X_i = \mu X^* \tag{14}$$

and the constants A, B and C have respectively the forms :

$$A = \frac{b}{a_0 - b - c}(\mu_0 - \mu) X^* \tag{15}$$

$$B = -\frac{a_0 b}{(b+c)(a_0 - b - c)}(\mu_0 - \mu) X^*$$

$$C = \frac{b}{b+c}\mu_0 X^*$$

Taking into account conditions (12), (13) and (14) and also relations (15), eq. (2) becomes :

$$N(t) = \frac{a_0 b}{a_0 - b - c}(\mu_0 - \mu) X^* \left[\frac{1}{a_0} e^{-a_0(t-t_i)} - \frac{1}{b+c} e^{-(b+c)(t-t_i)}\right] + \tag{16}$$

$$+ \frac{b}{b+c}\mu_0 X^*$$

Like in the previous case, eq. (16) should be discussed for two particular cases :

1) when : $b + c \gg a_0$.

Then : $\frac{1}{a_0} e^{-a_0(t-t_i)} \gg \frac{1}{b+c} e^{-(b+c)(t-t_i)}$

and :

$$N(t) = \frac{b}{b+c}(\mu - \mu_0) X^* e^{-a_0(t-t_i)} + \frac{b}{b+c}\mu_0 X^* \tag{16a}$$

Because $\mu < \mu_0$, eq. (16 a) shows that the number of particles adsorbed on the surface unity increases in time up to the value :

$$N(\infty) = \frac{b}{b+c}\mu_0 X^* \tag{17}$$

2) when : $b + c \ll a_0$.

Then : $\frac{1}{a_0} e^{-a_0(t-t_i)} \ll \frac{1}{b+c} e^{-(b+c)(t-t_i)}$

and :

$$N(t) = \frac{b}{b+c}(\mu - \mu_0) X^* e^{-(b+c)(t-t_i)} + \frac{b}{b+c}\mu_0 X^* \tag{16b}$$

For this case too, the adsorbed particles concentration increases in time up to the constant value given by eq. (17). The experimental data resulted from figure 1, are in good agreement with these consequences of the theory.

Starting irradiation after this value is reached leads to desorption. The phenomenon is described by the same eq. (2), where :

$$N_i = \frac{b}{b+c}\mu_0 \tag{18}$$

$$X_i = \mu_0 X^* \tag{19}$$

$$A = \frac{b}{a-b-c}(\mu - \mu_0) X^* \tag{20}$$

$$B = -\frac{ab}{(b+c)(a-b-c)}(\mu - \mu_0) X^*$$

$$C = \frac{b}{b+c}\mu X^*$$

Comparing eqs (18), (19) and (20), with eqs (6), (7) and (8), one can see that the results can be obtained by replacing μ_0' by μ_0 in eqs (10), (10a) and (10b).

Thus :

$$N(t) = \frac{ab}{a-b-c}(\mu - \mu_0) X^* \left[\frac{1}{a} e^{-a(t-t_i)} - \frac{1}{b+c} e^{-(b+c)(t-t_i)}\right] + \frac{b}{b+c}\mu X^* \tag{21}$$

$$N(t) = \frac{b}{b+c}(\mu_0 - \mu) X^* e^{-a(t-t_i)} + \frac{b}{b+c} \mu X^* \tag{21a}$$

$$N(t) = \frac{b}{b+c}(\mu_0 - \mu) X^* e^{-(b+c)(t-t_i)} + \frac{b}{b+c} \mu X^* \tag{21b}$$

Taking into account that $\mu_0 > \mu$, it results that eqs (21), (21a) and (21b) show the decrease of the chemisorbed particles surface concentration during irradiation. It should be remarked, that in this case, too, the concentration of the constant value, reached after prolonged irradiation is given also by eq. (11). As it results from figure 1, our experimental data are also in accordance with this prevision of the theory.

The curves showing the concentrations variation of chemisorbed particles during irradiation, according to eqs (10) and (21), must have the concavity directed towards the positive values of the electrical resistance because $\frac{d^2 N}{d t^2} > 0$. In the case of the dark adsorption the curve $N(t)$ has the concavity directed towards the negative values of the electrical resistance, because in this case $\frac{d^2 N}{d t^2} < 0$. This prevision of the theory, has been also experimentally checked (see figure 1).

If we take into account that[1]:

$$(a_1) > (a_1)_0$$

$$(a_4) > (a_4)_0$$

it results that: $a > a_0$.

Because under irradiation, the values of the surface concentration of electrons and holes are higher than in the dark, it follows that the variation in time of the surface concentration will be more marked during irradiation than in the dark. This provision of the theory is experimentally verified, too.

Memory effects, are also recorded in the study of hydrogen photosorption on thin zinc oxide films.[5] According to our experimental data, the introduction of hydrogen over a thin zinc oxide film at the same moment with the beginning of the irradiation, produces a negative variation (a decrease) of the electrical resistance, smaller than when the hydrogen is introduced under irradiation over a film previously irradiated in vacuum until a constant value of the electrical resistance had been reached (figure 2).

A simple qualitative explanation of the process is that irradiation generates adsorption centers for hydrogen; it is evident that the previously irradiated film will dispose of more adsorption centers for hydrogen than the film whose irradiation begins simultaneously with the gas introduction.

---

[5] M. Constantinescu and E. Segal, *Rev. Roumaine Chim.*, **16**, 1703 (1971).

We shall try to describe the variation in time of the chemisorbed particles concentration using the same eq. (2), but, this time, assuming that irradiation generates adsorption centers.

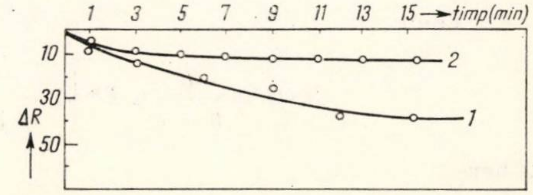

Fig. 2. — Electrical resistance variation of zinc oxide film *versus* time for hydrogen photosorption :
1, previously irradiated film ;
2, previously nonirradiated film.

When introducing the gas simultaneously with the beginning of irradiation, the initial conditions are :

$$X_i = 0 \tag{22}$$

$$N_i = 0$$

For these conditions, the constants *A*, *B* and *C* from eq. (6) will have the following expression :

$$A = \frac{b}{a-b-c}\mu X^* \tag{23}$$

$$B = \frac{a b}{(b+c)(b+c-a)}\mu X^*$$

$$C = \frac{b}{b+c}\mu X^*$$

Eq. (2) with the constants given by (23) becomes :

$$N(t) = \frac{a b}{a-b-c}\mu X^* \left[\frac{1}{a}\mathrm{e}^{-a(t-t_i)} - \frac{1}{b+c}\mathrm{e}^{-(b+c)(t-t_i)}\right] + \frac{b}{b+c}\mu X^* \tag{24}$$

As for the previous cases, it is more advantageous to discuss eq. (24) on the basis of simplified conditions :

1) when : $b + c \gg a$

Then :

$$N(t) = \frac{b}{b+c}\mu X^* \left[1 - \frac{1}{1-\delta}\mathrm{e}^{-a(t-t_i)}\right] \tag{24 a}$$

where :

$$\delta = \frac{a}{b+c} \quad \text{and} \quad \delta \ll 1 \tag{25}$$

2) when : $b + c \ll a$

Then :

$$N(t) = \frac{b}{b+c}\,\mu\,X^{*}\left[1 - \frac{1}{1-\delta}\,\mathrm{e}^{-(b+c)(t-t_i)}\right] \tag{24 b}$$

Where :

$$\delta = \frac{b+c}{a} \quad \text{and :} \quad \delta \ll 1 \tag{26}$$

Eq. (24) and its simplified forms (24a) and (24b) show an increase in time of the photoadsorbed particles concentration up to the limit value $N(\infty)$ given by the equation :

$$N(\infty) = \frac{b}{b+c}\,\mu\,X^{*} \tag{27}$$

For the case of gas introduction over a previously irradiated film until reaching a constant electrical resistance value, the initial conditions are :

$$X_i = \mu\,X^{*} \tag{28}$$

$$N_i = 0$$

For these conditions, the constants A, B and C from eq. (6) will have the following expressions :

$$A = 0 \tag{29}$$

$$B = -\frac{b}{b+c}\,\mu\,X^{*}$$

$$C = \frac{b}{b+c}\,\mu\,X^{*}$$

and eq. (2) becomes :

$$N(t) = \frac{b}{b+c}\,\mu\,X^{*}\left[1 - \mathrm{e}^{-(b+c)(t-t_i)}\right] \tag{30}$$

Eq. (30) describes the variation in time of the photoadsorbed particles concentration on a previously irradiated film.

If we compare eq. (30) with eqs (24a) and (24b), taking into account the evident inequalities :

$$\frac{1}{1-\delta} > 1$$

$$e^{-a(t-t_i)} > e^{-(b+c)(t-t_i)} \qquad \text{(for 24 a)}$$

it results that any moment after the gas introduction, the photoadsorbed particles concentration for the previously irradiated film is higher, and :

$$[N(t)]_{(30)} > [N(t)]_{(24\ a)}$$

$$[N(t)]_{(30)} \gg [N(t)]_{(24\ b)}$$

and this is in a good qualitative agreement with the experimental data.

Eqs (24) and (30) give the same limit value for the photoasdsorbed particles concentration in both cases, that is :

$$N(\infty) = \frac{b}{b+c}\mu X^*$$

In other words, the experimental curves must be concurrent for very high values of the time. As it results from figure 2, considering that the electrical resistance variations represent the variation of adsorbed particles concentration, the experiment does not confirm this conclusion.

The disagreement is due to the fact that the surface of nonirradiated zinc oxide films contains adsorption centers for hydrogen in acceptor form, as already discussed in a previous note. [6] The hydrogen introduced in the system at the same moment with the beginning of irradiation can be adsorbed on these centers, so that a part of the adsorption centers does not realize the photoadsorption in donor form.

For this reason the limit value corresponding to the donor form is lower than that determined by eq. (24).

---

[6] M. CONSTANTINESCU and E. SEGAL, Rev. Roumaine chim., **16**, 801 (1971).

Revue Roumaine de Chimie, **17**, *1*, *2*, 95 – 102 (1972)

Hommage au Professeur I. G. MURGULESCU
à l'occasion de son 70e anniversaire

L'INFLUENCE DU SOLVANT SUR LA VITESSE DE RÉACTION

L'HYDROLYSE ALCALINE DE L'ACÉTATE, DU PROPIONATE ET DU BUTYRATE DE *n*-BUTYLE DANS LE SOLVANT MIXTE EAU-ACÉTONE

G. COSTEANU et CORNELIA MATEESCU

Chaire de Chimie-Physique, Institut Polytechnique, Bucarest, 132, Calea Griviței

Reçu le 8 octobre 1971

Les auteurs étudient l'hydrolyse alcaline de l'acétate, du propionate et du butyrate de *n*-butyle dans le solvant mixte eau-acétone à 20, 30, 40 et 50°. Les résultats obtenus sont mis en corrélation avec la constante diélectrique du solvant. On attribue la variation de la constante de vitesse de la réaction, ainsi que la variation des fonctions thermodynamiques d'activation au phénomène de solvatation.

En poursuivant nos recherches sur l'influence du milieu sur la vitesse de réaction nous avons étudié l'hydrolyse alcaline de l'acétate, du propionate et du butyrate de *n*-butyle dans un mélange de deux solvants , eau-acétone, de constantes diélectriques différentes, en proportions variables.

Dans ces conditions on peut faire varier la constante diélectrique du milieu et suivre l'évolution des réactions déjà mentionnées.

PARTIE EXPÉRIMENTALE

Les esters ont été préparés et purifiés d'après les méthodes déjà connues. [1]

L'acétone *p.a.*, traitée d'abord par du permanganate de potassium jusqu'à la coloration rose, est distillée, puis desséchée sur du carbonate de potassium et ensuite redistillée.

La concentration de l'ester, approximativement égale à 0,01 M, est déterminée par saponification totale. La concentration de l'hydroxyde de sodium, constante dans tous les essais, est égale à 0,01N.

Les déterminations ont été effectuées à 20, 30, 40 et 50° par la méthode des « tubes scellés ».[2]

---

[1] A.I. Vogel, « A Text Book of Practical Organic Chemistry », vol. III, IIIe éd., Langmans, Green and Co., London-New York, 1956, p. 382.

[2] G. Costeanu, O. Landauer et C. Mateescu, *Rev. Roumaine Chim.*, **13**, 155 (1968).

RÉSULTATS EXPÉRIMENTAUX

Les constantes de vitesse de l'hydrolyse alcaline des esters étudiés par nous, calculées au moyen de l'équation cinétique des réactions du second ordre pour différents mélanges eau-acétone, sont réunies dans les tableaux 1, 2 et 3.

Tableau 1

Valeurs des constantes de vitesse en 1 mole $^{-1}$ s $^{-1}$, à 20, 30, 40 et 50° de l'hydrolyse alcaline de l'acétate de *n*-butyle dans l'eau-acétone

X acétone	10^2k 20°C	$10^2\,k$ 30°C	$10^2\,k$ 40°C	10^2k 50°C
0,041	6,05	9,92	17,25	28,32
0,056	5,22	8,73	14,00	21,79
0,091	4,21	7,04	11,08	17,30
0,132	3,22	5,52	9,22	14,66
0,182	2,45	4,43	7,70	12,83
0,244	1,70	3,55	6,30	11,04
0,325	1,29	2,92	5,42	9,86
0,374	1,11	2,35	5,09	9,60

Tableau 2

Valeurs de *E*, *A*, ΔS^*, ΔH^* et ΔG^* de l'hydrolyse alcaline de l'acétate de *n*-butyle calculées pour différents mélanges eau-acétone

X acétone	*E* *k*cal/mole	log *A*	ΔS^* u.e.	ΔH^* *k*cal/mole	ΔG^* *k*cal/mole
0,041	9,838	6,1133	−35,14	9,246	19,899
0,056	9,198	5,5948	−37,48	8,606	19,968
0,091	8,900	5,2858	−38,90	8,308	20,101
0,132	9,678	5,7430	−36,84	9,086	20,254
0,182	10,342	6,1147	−35,09	9,750	20,387
0,244	11,646	6,9749	−31,16	11,054	20,500
0,325	12,698	6,6510	−32,67	12,106	22,010
0,374	13,705	8,2862	−25,17	13,113	20,744

Tableau 3

Valeurs des constantes de vitesse, en 1 mole $^{-1}$ s $^{-1}$, à 20, 30, 40 et 50° de l'hydrolyse alcaline du propionate de *n*-butyle dans l'eau-acétone

X acétone	10^2k 20°C	10^2k 30°C	10^2k 40°C	10^2k 50°C
0,056	2,93	5,12	9,06	14,20
0,091	2,46	4,27	7,47	12,30
0,132	2,09	3,50	5,96	9,32
0,182	1,70	2,87	5,14	8,46
0,244	1,17	2,25	4,38	7,70
0,325	0,72	1,70	3,61	6,37
0,374	0,68	1,50	3,09	5,95

Sur les tableaux 2, 4 et 6 figurent les énergies d'activation (*E*), les facteurs préexponentiels (*A*), les enthalpies d'activation (ΔH^*), les entropies d'activation (ΔS^*), et les enthalpies libres d'activation (ΔG^*), calculées pour différents mélanges eau-acétone.

On observe que les constantes de vitesse diminuent à mesure que la teneur en acétone du solvant augmente, donc avec la diminution de la constante diélectrique du milieu.

Tableau 4

Valeurs de *E*, *A*, ΔH^*, ΔS^* et ΔG^* de l'hydrolyse alcaline du propionate de *n*-butyle calculées pour différents mélanges eau-acétone

X acétone	*E* *k*cal/mole	log *A*	ΔS^* u.e.	ΔH^* kcal/mole	ΔG^* kcal/mole
0,056	14,637	9,2976	−20,55	14,045	20,275
0,091	10,047	5,8984	−36,10	9,455	20,399
0,132	9,427	5,3653	−38,53	8,835	20,515
0,182	10,047	5,1541	−39,49	9,455	21,426
0,244	11,188	6,4455	−33,59	10,595	20,778
0,325	12,538	7,3003	−29,69	11,946	20,946
0,374	13,270	7,7757	−27,50	12,678	21,015

Tableau 5

Valeurs des constantes de vitesse, en 1 mole $^{-1}$ s^{-1}, à 20, 30, 40 et 50°C l'hydrolyse alcaline du butyrate de *n*-butyle dans l'eau-acétone

X acétone	10^2k 20°C	10^2k 30°C	10^2k 40°C	10^2k 50°C
0,091	1,00	2,11	4,35	8,79
0,132	0,93	1,96	3,98	7,69
0,182	0,72	1,43	2,85	5,93
0,244	0,48	1,08	2,22	4,80
0,325	0,34	0,70	1,71	3,62
0,374	0,29	0,61	1,55	3,17

Tableau 6

Valeurs de *E*, *A*, ΔH^*, ΔS^* et ΔG^* de l'hydrolyse alcaline du butyrate de *n*-butyle calculées pour différents mélanges eau-acétone

X acétone	*E* *k*cal/mole	log *A*	ΔS^* u.e.	ΔH^* *k*cal/mole	ΔG^* *k*cal/mole
0,091	13,956	8,4207	−24,57	13,364	20,812
0,132	13,389	7,9776	−26,59	12,797	20,858
0,182	13,270	7,7548	−27,59	12,679	21,043
0,244	14,506	8,5270	−24,07	13,914	21,211
0,325	15,421	9,0066	−21,87	14,829	21,451
0,374	15,696	9,1371	−21,28	15,104	21,555

Ceci pourrait être attribué soit aux interactions des molécules d'eau et des molécules du constituant organique du solvant mixte, [3] soit à la diminution du pouvoir ionisant du milieu de réaction. [4]

On doit remarquer aussi qu'à la même température et à la même concentration du solvant mixte la constante de vitesse diminue de l'acétate au butyrate de *n*-butyle.

La diminution de la constante de vitesse de l'acétate au butyrate de *n*-butyle est attribuée à l'effet inductif-positif du groupement alkyle dont l'action croît dans le même sens. [5]

Toujours dans un but de comparaison nous avons calculé la variation des constantes de vitesse (Δk) entre $X = 0{,}124$ et $X = 0{,}377$ pour toutes les températures de nos déterminations. On a choisi ce domaine de concentrations, pour comparer l'influence du solvant eau-acétone avec celle du solvant eau-dioxanne. [6]

On observe que Δk varie dans le sens $\Delta k_a > \Delta k_p > \Delta k_b$, c'est-à-dire dans le même sens que les moments dipolaires des esters.

En faisant le rapport $\frac{\Delta k_i}{\Delta k_j}$ (i et j étant les symboles des ésters considérés) on remarque que ce rapport tend vers l'unité quand la température augmente. On est tenté d'admettre que le phénomène de solvatation des différentes espèces moléculaires s'atténue avec la température.

Tableau 7

Variation des constantes de vitesse (Δk)

T°C	Δk acétate	Δk propionate	Δk butyrate	$\frac{\Delta k_a}{\Delta k_b}$	$\frac{\Delta k_a}{\Delta k_p}$	$\frac{\Delta k_p}{\Delta k_b}$
20	2,40	1,40	0,55	4,36	1,71	2,54
30	3,55	1,30	1,28	2,77	2,73	1,08
40	4,30	3,25	2,27	1,89	1,32	1,43
50	5,40	3,95	4,40	1,23	1,37	0,90

L'influence du facteur électrostatique sur la constante de vitesse s'exprime, soit par l'équation d'Amis $\ln k = \ln k_0 + \frac{Ze\mu}{k\mathrm{T}r^2 D}$ si l'on admet le mécanisme d'une réaction de type ion-molécule dipolaire, [7,8]soit par l'équation de Laidler-Eyring [9]

---

[3] D.E. Evans et I.I. Gordon, *J. Chem. Soc.*, **1938**, 1434.

[4] E.H. Hughes et G.K. Ingold, *J. Chem. Soc.*, **1935**, 244.

[5] G. Akerlög, *J. Amer. Chem. Soc.*, **54**, *4125* (1932).

[6] G. Costeanu, C. Mateescu, *Rev. Roumaine Chim.*, **17**, 1803 (1971).

$$\ln k = \ln k_0 - \frac{1}{kT}\left(\frac{D-1}{2D+1}\right)\left[\frac{\mu_A^2}{r_A^3} + \frac{\mu_B^2}{r_B^3} - \frac{\mu_{AB}^2}{r_{AB}^3}\right]$$

en supposant, au contraire, que la réaction a lieu entre la molécule de l'ester et la molécule de l'eau, c'est-à-dire une réaction du type dipôle-dipôle.

En représentant graphiquement la variation de log k en fonction de $\frac{1}{D}$ et $\frac{D-1}{2D+1}$, on trouve, dans les deux cas, une variation linéaire seulement dans un domaine de concentrations assez limité.

Il faut croire que les deux équations n'expriment que partiellement les interactions entre les réactifs et le milieu de réaction.

Cependant on trouve une variation linéaire en représentant graphiquement le log k en fonction de D (fig. 1—9).

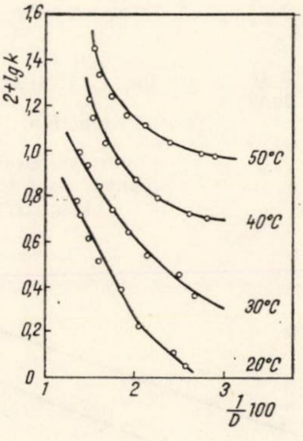

Fig. 1. — Variation de log k en fonction de $\frac{1}{D}$ de l'hydrolyse alcaline de l'acétate de n-butyle dans l'eau-acétone.

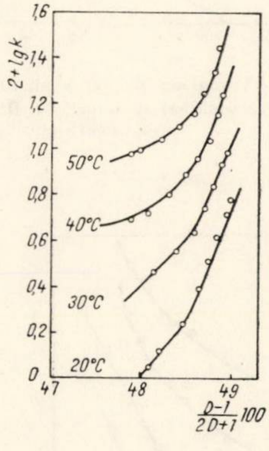

Fig. 2. — Variation de log k en fonction de $\frac{D-1}{2D+1}$ de l'hydrolyse alcaline de l'acétate de n-butyle dans l'eau-acétone.

Nous avons trouvé que l'énergie d'activation des trois esters varie avec la teneur en acétone du solvant mixte et passe par un minimum qui se déplace de l'acétate au butyrate de n-butyle (fig. 10).

---

[7] E.S. Amis, *J. Chem. Educ.*, **29**, 337 (1952).

[8] E.S. Amis, *J. Chem. Educ.*, **30**, 351 (1953).

[9] K.J. Laidler et H. Eyring, Ann. New York Acad. Sci., **39**, 303 (1940).

On admet qu'au minimum de l'énergie d'activation le complexe activé, étant un agrégat très polaire, est bien plus solvaté que les molécules réagissantes.

Comme prévu, au minimum d'énergie d'activation correspond, à la même concentration du solvant mixte, une valeur minimale de l'entropie

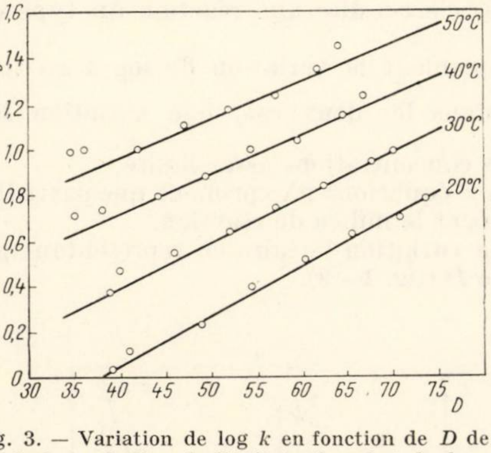

Fig. 3. — Variation de log k en fonction de D de l'hydrolyse alcaline de l'acétate de n-butyle dans l'eau-acétone.

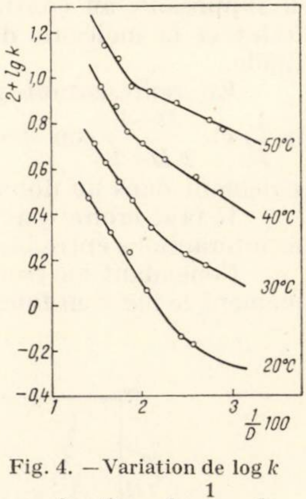

Fig. 4. — Variation de log k en fonction de $\frac{1}{D}$ de l'hydrolyse alcaline du propionate de n-butyle dans l'eau-acétone.

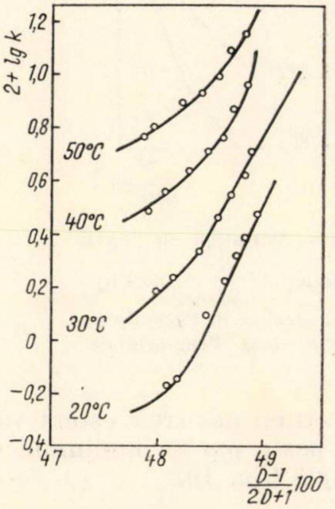

Fig. 5. — Variation de log k en fonction de $\frac{D-1}{2D+1}$ de l'hydrolyse alcaline du propionate de n-butyle dans l'eau-acétone.

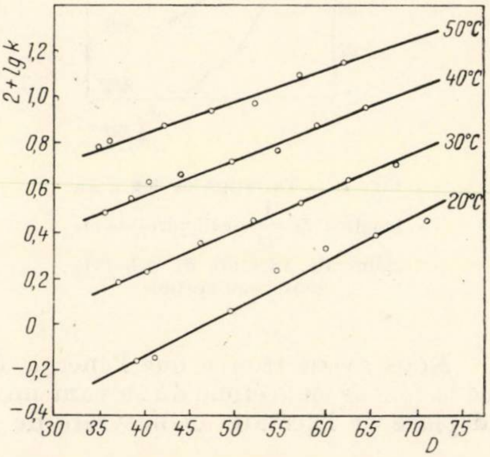

Fig. 6. — Variation de log k en fonction de D de l'hydrolyse alcaline du propionate de n-butyle dans l'eau-acétone.

d'activation. On doit supposer que la solvatation du complexe activé est accompagnée d'un arrangement régulier des molécules du solvant autour de ce complexe. Les forces électrostatiques du complexe activé, assez puissantes, orientent les molécules du solvant, font diminuer leur liberté de mouvement, et par conséquent l'entropie d'activation diminue.

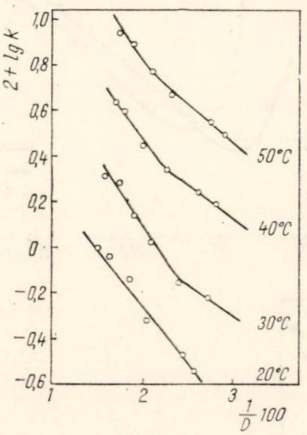

Fig. 7. — Variation de log k en fonction de $\frac{1}{D}$ de l'hydrolyse alcaline du butyrate de n-butyle dans l'eau-acétone.

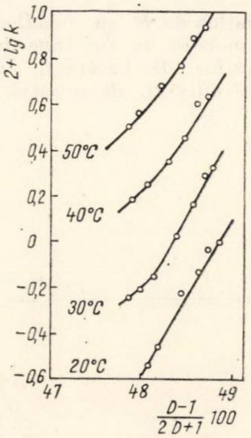

Fig. 8. — Variation de log k en fonction de $\frac{D-1}{2D+1}$ de l'hydrolyse alcaline du butyrate de n-butyle dans l'eau-acétone.

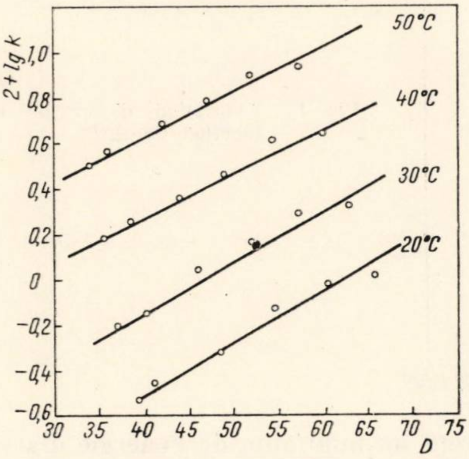

Fig. 9. — Variation de log k en fonction de D de l'hydrolyse alcaline du butyrate de n-butyle dans l'eau-acétone.

La fraction molaire de l'acétone, correspondant au minimum de l'énergie d'activation, croît de l'acétate au butyrate de n-butyle, c'est-à-dire dans l'ordre décroissant de la solubilité des esters.

La corrélation entre l'enthalpie d'activation et l'entropie d'activation est exprimée graphiquement par les courbes $T\Delta S^* = f(\Delta H^*)$ (fig. 11). On

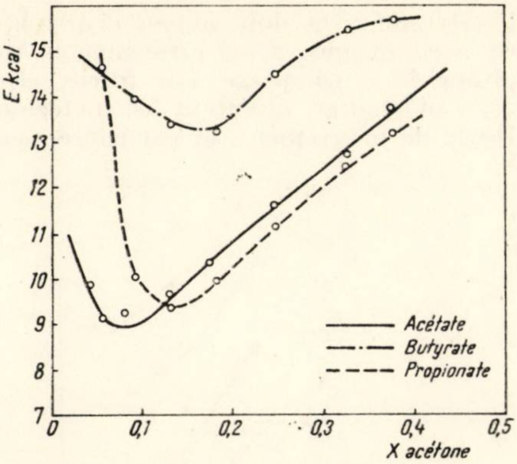

Fig. 10. — Variation de *E* en fonction de la fraction molaire de l'acétone de l'hydrolyse alcaline de l'acétate, du propionate et du butyrate de *n*-butyle.

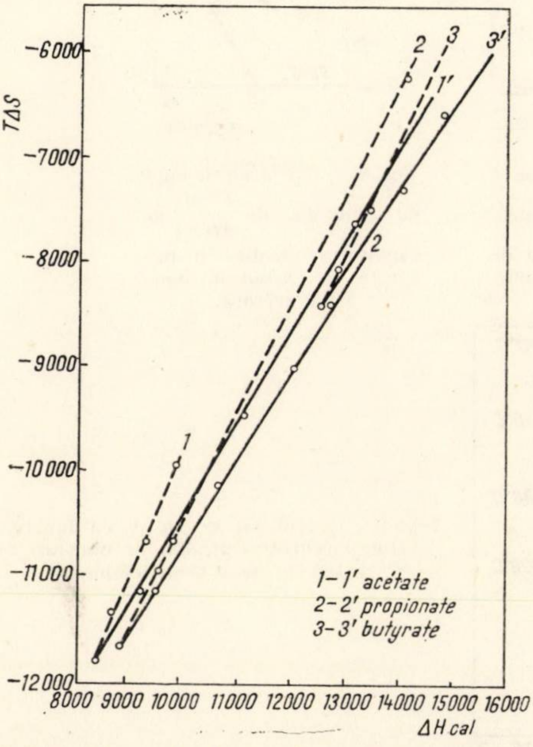

Fig. 11 — Variation de $T\Delta S^*$ en fonction de ΔH^*.

obtient deux droites qui se rencontrent au minimum de l'énergie d'activation ; elles vérifient l'équation $T\Delta S^* = \alpha\Delta H^* + \beta$. La pente de la droite a une valeur supérieure à l'unité ($\alpha = 1,09$) dans le solvant riche en eau ; elle est inférieure à l'unité ($\alpha = 0,83$) dans le solvant riche en acétone.

On attribue ces résultats à une solvatation plus forte du complexe activé dans le solvant riche en eau ; les molécules d'eau subissent alors unei certaine orientation autour du complexe activé.

Revue Roumaine de Chimie, 17, 1, 2, 103–109 (1972)

Hommage au Professeur I. G. MURGULESCU
à l'occasion de son 70e anniversaire

DÉDUCTION D'UNE CLASSIFICATION DES TRANSITIONS DE PHASE

TH. DELEANU, I. V. IONESCU, VALERIA NAHORNIAK et D. A. ISĂCESCU

Institut de Chimie Macromoléculaire P. Poni
Bucarest, 18, Str. Dumbrava Roșie

Reçu le 15 septembre 1971

A l'aide de certaines considérations théoriques très simplifiées on propose une illustration des transitions de phase possibles. On met en évidence le cas où la matière ne mémorise pas une grande partie des transitions successives. Alors, aux points des transitions de phase existent d'importantes variations des grandeurs de transport, tandis que les variations des grandeurs qui caractérisent l'état d'équilibre restent petites. Si la matière mémorise la majorité des transitions successives on a les transitions de phase de premier ou de second ordre. On montre que même si les transitions de phase aux polymères ne diffèrent pas, en principe, des transitions de phase communes, leur complexité est plus grande, pouvant ainsi être considérées formellement comme une catégorie à part.

I. INTRODUCTION

Le contraste entre la simplicité et la similitude de diverses transitions de phase et la complexité des études théoriques effectuées seulement sur des catégories restreintes de tels processus, ont attiré l'attention sur l'insuffisance de la connaissance du mécanisme intime général qui les caractérise.[1] Récemment Roy [2] a présenté une tentative de classification des phases des solides non cristallins.

Le premier essai d'interprétation du mécanisme des transitions de phases a été fait par Lindemann. [3] Ces dernières années ont apparu plusieurs développements à son point de vue. [4–6] Einstein a apporté une importante contribution à la connaissance du mécanisme des transitions de phase observant qu'un gaz Bose présente un point de condensation. L'interprétation des transitions de phase aux solides a été basée sur les études du modèle Ising effectuées spécialement par Yang et Lee [7] et par Onsager. [8,9]

---

[1] L.P. Kadanoff, W. Götze, D. Hamblen, R. Hecht, E.A.S. Lewis, V.V. Palciauskas, M. Rayl et J. Swift, *Rev. Mold. Phys.*, **39**, 395 (1967).

[2] R. Roy, *J. Non-cryst. Solids*, **3**, 33 (1970).

[3] F.A. Lindemann, *Phys. Z.*, **11**, 609 (1910).

[4] M. Ross, *Phys. Rev.*, **184**, 233 (1969).

[5] K.H. Krebs, *Phys. Rev.*, **138A**, 143 (1965).

[6] A.K. Singh et P.K. Sharma, *Canad. J. Phys.*, **46**, 1677 (1965).

La première tentative de classification des transitions de phase a été faite par Ehrenfest. [10] Le point de vue thermodynamique a été développé ultérieurement notamment par Tizsa.[11–12] On a longtemps considéré que les transitions de phase aux systèmes unidimensionnelles ne sont pas possibles. [13,14] Une contradiction est apparue lorsqu'on a découvert les transitions de phase optiques aux solutions diluées des polypeptides, qui ne pouvaient être interprétées qu'à l'aide des transitions de phase unidimensionnelles. Un nouvel examen des hypothèses sur la possibilité d'existence des transitions de phases des systèmes unidimensionnelles a fait l'objet de nombreuses recherches. [15] Dans plusieurs travaux on a utilisé des concepts liés à la polymérisation.[15–17] Sauf le cas des polypeptides, les transitions de phase aux polymères ne sont pas encore bien comprises. De légères inflexions, qui peuvent apparaître à deux ou trois températures, de la courbe qui caractérise la dépendance du volume spécifique en fonction de température, sont considérées des transitions de phases. Donc, on peut entendre par transition de phase la variation relativement rapide de certains paramètres en fonction d'autres au voisinage de certaines valeurs de ces derniers. La définition n'est pas précise du point de vue mathématique mais elle est particulièrement suggestive.

L'analyse de divers comportements possibles des substances à la proximité des transitions de phase basée sur l'hypothèse de quelques transitions successives nécessite une fondamentation à l'aide de la mécanique quantique. Cette fondamentation fait l'objet d'un autre travail * dans lequel on démontre qu'on peut résoudre les problèmes de la mécanique quantique à l'aide d'un formalisme utilisé dans la cinétique chimique, ce qui signifie qu'on peut traiter stochastiquement la mécanique quantique. L'étape suivante est représentée par l'analyse de l'approximation de plusieurs transitions successives par une transition unique. La troisième étape a pour but l'illustration des transitions de phase possibles. Dans ce qui suit on développe seulement cette dernière étape.

---

[7] C.N. Yang et T.D. Lee, *Phys. Rev.*, **87**, 404, 410 (1952).

[8] L. Onsager, *Phys. Rev.*, **65**, 117 (1944).

[9] K. Huang, «Statistical Mechanics», Wiley, New York, 1963.

[10] H.B. Callen, «Thermodynamics», Wiley, New York, 1960, p. 180.

[11] L. Tisza, «On the General Theory of Phase Transitions», en: «Phase Transitions in Solids», ed. R. Smoluchowski, J.E. Mayer, W.A. Weyl John Wiley & Sons, New York, 1957.

[12] L. Tisza, «Generalized Thermodynamics», The M.I.T., Press Cambridge Mass., 1966.

[13] L. Landau et E. Lifchitz, «Physique Statistique», Ed. MIR, Moscou 1967.

[14] L. van Hove, *Physica*, **16**, 137 (1950).

[15] M.E. Baur, et L.H. Nosanow, *J. Chem. Phys.*, **37**, 153 (1962).

[16] Ayao Amemiya et O. Saito, *J. Phys. Soc. Japan*, **26**, 1264 (1969).

[17] P. Whittle, *Proc. Cambridge Phil. Soc.*, **61**, 475 (1965).

* En cours de publication.

II. LA DESCRIPTION LA PLUS SIMPLE DU MODÈLE

Soit $\mathcal{G}_r$ la concentration des centres actifs dans un état r, par exemple d'un polymère à r mères au moment t ; $\mathcal{M}$ représente la concentration d'initiateur. L'équation cinétique de la polymérisation réversible s'écrit :

$$\frac{\mathrm{d}}{\mathrm{d}t}\mathcal{G}_{r+1} = P\mathcal{M}(\mathcal{G}_r - \mathcal{G}_{r+1}) + \overline{P}(\mathcal{G}_{r+2} - \mathcal{G}_{r+1}) \tag{1}$$

où P et $\overline{P}$ représentent respectivement la constante de vitesse de polymérisation et de dépolymérisation. Cette manière d'étude a été utilisée aux études des processus de nucléation [18] et de la polycondensation. [19,20] On se propose dans cette section de mettre en évidence les propriétés générales de ce système d'équations :

Si on note par $\mathcal{G} = \sum \mathcal{G}_r$ et par $\mathcal{G}_v = \sum r\,\mathcal{G}_r$ on déduit de (1)

$$\frac{1}{P}\frac{\mathrm{d}}{\mathrm{d}t}(\mathcal{G} - \mathcal{G}_1) = \alpha\mathcal{G}_1 - \mathcal{G}_2 \,;\; \frac{1}{\overline{P}}\frac{\mathrm{d}}{\mathrm{d}t}(\mathcal{G}_v - \mathcal{G}_1) = \alpha\,(\mathcal{G} + \mathcal{G}_1) - \mathcal{G} - \mathcal{G}_2 - \mathcal{G}_1 \tag{2}$$

où $\alpha = P\,\mathcal{M}/\overline{P}$. A l'équilibre $\mathrm{d}\mathcal{G}_r/\mathrm{d}t = 0$ et on constate que la série $\sum\mathcal{G}_r$ est convergente si $\alpha < 1$.

On suppose que l'initiation est un processus bimoléculaire caractérisé par les constantes de vitesse P^x et $\overline{P}^x$:

$$\frac{\mathrm{d}\mathcal{G}_1}{\mathrm{d}t} = P^x\,\mathcal{M}\,\mathcal{I} - P\,\mathcal{M}\,\mathcal{G}_1 + \overline{P}^x\,\mathcal{G}_1 \tag{3}$$

Si on se limite à un processus d'initiation homogène résulté par activation du monomère avec les constantes de vitesse A et $\overline{A}$, on a

$$\frac{\mathrm{d}}{\mathrm{d}t}\mathcal{I} = -\,P^x\mathcal{M}\mathcal{I} + A\mathcal{M} - \overline{A}\mathcal{I} + \overline{P}^x\mathcal{G}_1 \tag{4}$$

L'équation qui donne la consommation du monomère est

$$\frac{\mathrm{d}}{\mathrm{d}t}\mathcal{M} = -\,P^x\,\mathcal{M}\mathcal{I} - P\,\mathcal{M}\mathcal{G} + \overline{P}\,(\mathcal{G} - \mathcal{G}_1) + \overline{P}^x\,\mathcal{G}_1 - A\mathcal{M} + \overline{A}\mathcal{I} \tag{5}$$

---

[18] W. G. Courtney, *J. Chem. Phys.*, **36**, 2018 (1962); *J. Phys. Chem.*, **72**, 421 (1967).

[19] A. V. Tobolski, «Properties and Structure of Polymers», John Wiley, & Sons, New York, 1960.

[20] A. V. Tobolski et W. J. Mackight, «Polymeric Sulfur and Related Polymers», John Wiley &Sons, New York, 1965.

Les équations (2—5) conduisent à l'identité

$$\frac{d\mathfrak{J}}{dt} = 0 \text{ où } \mathfrak{J} = \mathcal{G}_1 + \mathcal{M} + \mathcal{I} + \mathcal{G}_v \tag{6}$$

A l'équilibre, on obtient

$$y(\alpha) = 1 \tag{7}$$

$$\text{où } y(\alpha) \equiv a\alpha + b\alpha^2\left(\frac{1}{1-\alpha} + \frac{1}{(1-\alpha)^2}\right) \tag{8}$$

$$a = \frac{\vec{P}}{P\mathfrak{J}}\left(1 + \frac{A}{\overline{A}}\right) \quad \text{et } b = \frac{A}{\overline{P}}\,\frac{P^x}{\overline{P}^x}\left(\frac{P}{P}\right)^2/\mathfrak{J}$$

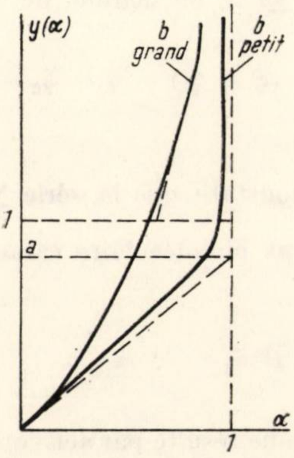

Fig. 1. — La fonction $y(\alpha)$ d'après la relation (8).

Si P et $\overline{P}$ suivent la loi d'Arhenius, il existe une température à laquelle $\alpha \simeq 1$ et le comportement de la substance se modifie d'une manière d'autant plus brusque dans le voisinage de cette température que b est plus petit (fig. 1). Cette température correspond juste à la transition de phase de la substance respective.

Si on entend par monomère un solvant moléculaire à petites molécules, alors dissolvant une substance étrangère on a une variation de la concentration du solvant $\Delta\mathcal{M}$ et il résulte un abaissement ΔT de la température de solidification d'après la relation

$$\frac{E}{R\,T^2}\Delta T = \frac{\Delta\mathcal{M}}{\mathcal{M}} \tag{9}$$

Cette relation résulte par la différentiation de la relation $\alpha = 1$. On reconnaît ici l'expression bien connue de la constante cryoscopique à l'aide de laquelle on détermine le poids moléculaire. Si on suppose par exemple l'entropie molaire de fusion égale à 2 cal/(mole. degré), le nombre moyen n de molécules constituant le microcristal, c'est-à-dire le degré moyen de polymérisation (si on le suppose analogue à un polymère), est :

$$\frac{\Delta T}{T} \simeq \frac{1}{n}$$

où T est la température de fusion du monocristal et $\Delta T + T\ (>T)$ est une température voisine à celle du point de fusion. Pour ce domaine de témpératures $y(\alpha) = 1 \simeq a$ et l'équation (8) se réduit à la relation approximative

$$b/a = (1 - \alpha)^3$$

III. DISCUSSION

L'emploi habituel de la cinétique chimique dans les applications suppose l'existence des sortes de molécules ci-dessus :

— molécules actives, qui prennent part effectivement dans un certain processus et

— molécules inactives, qui ne participent pas effectivement dans un certain processus mais qui ont le rôle de gêner l'activité des molécules actives.

Les études concernant les transitions de phase supposent l'emploi dans les équations cinétiques d'une troisième catégorie de molécules :

— molécules écranées, qui ne sont ni actives ni inactives dans le sens mentionné. C'est, par exemple, le cas des molécules de l'intérieur d'un cristal.

Les transitions d'un état r à un autre état $r+1$ d'après la relation (1) ne doivent pas correspondre nécessairement toutes à des additions effectives, c'est-à-dire à une mémorisation par la matière de toutes les transitions élémentaires indiquées. Il peut exister d'importantes variations de la viscosité, par exemple, sans qu'il existe des variations importantes des grandeurs qui caractérisent l'équilibre, comme c'est le cas des chaleurs spécifiques, du volume spécifique ou de l'entropie du système, c'est-à-dire du degré d'ordre respectif. Quelques-unes de ces transitions de phase justifient pleinement ce point de vue aux cristaux liquides.

La principale différence entre une vraie polymérisation et une transition de phase, pour laquelle la matière mémorise la transition respective, consiste seulement dans la valeur beaucoup plus grande de l'énergie de liaison dans le premier cas que dans le second. Ainsi , en général, dans le cas de la vraie polymérisation prennent naissance des branches filiformes d'abord, qui se réticulisent parfois ultérieurement. Mais aux transitions de phase analogues aux polymérisations la réticulisation doit être nécessairement concomitante à la croissance. Justement cette concomitance des deux processus conduit à la formation du microcristal. Cette réticulisation peut être bidimensionnelle ou tridimensionnelle. L'existence de la réticulisation bidimensionnelle n'est pas encore bien mise en évidence. Les propriétés analogues aux cristaux de certains liquides pourraient être dues à un empilement labile des disques. Aux températures un peu plus basses ces empilements cesseraient d'être labiles. Ainsi on pourrait expliquer les formes, quelquefois de rosette d'autrefois de cône,[21] des germes obtenus aux cristaux liquides. Un autre argument de l'existence des germes bidimensionnels a été obtenu indirectement par la vérification expérimentale des propriétés du modèle Ising traité par Onsager.[22]

Si ces germes formés d'après la cinétique de la relation (1) favorisent l'initiation à leur surface d'autres germes similaires, alors on a des transitions de phase de premier ordre. Les transitions de phase du second ordre correspondent au cas où les germes ne favorisent pas l'initiation d'autres germes similaires sur leur surface. Ainsi les transitions de phase d'ordre supérieur conforme au critère analytique d'Ehrenfest sont dépourvues de sens physique. La croissance des germes uniques ne peut physiquement continuer infiniment. Les diverses causes de désactivation de ces germes ont une probabilité d'apparition d'autant plus grande que l'énergie de liaison entre les molécules du germe est plus petite. Une des causes de ces désactivations est l'apparition des empêchements stériques accidentelles. Si cet empêchement stérique est dû à la contraction, alors à l'aide d'une compression il serait possible de passer d'une transition de phase de second ordre à une de premier ordre. Ce processus n'a pas été encore mis en évidence expérimentalement. Aux transitions de phase de premier ordre l'initiation d'un nouvel germe peut être favorisé aux sommets, aux arêtes ou à la surface du germe. On obtient ainsi des cristaux en forme d'aiguilles, de lames ou de polyèdres réguliers respectivement.

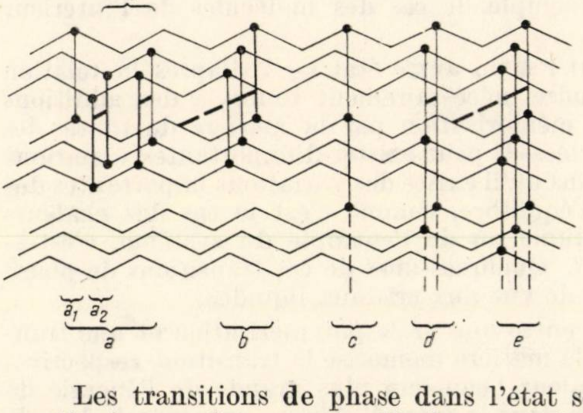

Fig. 2. — Possibilités de réticulation des polymères à l'état amorphe.

Les transitions de phase dans l'état solide amorphe de la matière constituée par des macromolécules conduisent à l'établissement de certaines liaisons de réticulisation représentées dans la figure 2, pour lesquelles la réticulisation d'un second ordre n'est plus obligatoire. La représentation sous forme de macromolécules parallèles est exclusivement schématique. On n'a pas représenté le cas ou la réticulisation d'un atome de la chaîne favorise la réticulisation de son voisin. Pour la macromolécule pliable ce processus conduit à la formation d'un microcristal d'une macromolécule unique. Dans la figure 2 on a représenté aussi quelques réticulisations qui ne conduisent pas à une réaction en chaîne. Celles-ci se développent donc dans un domaine de températures plus large. L'établissement des liaisons de réticulisation conduit aussi à une variation de volume, c'est-à-dire à la disparition de certaines lacunes. Les polymères filiformes avec des liaisons intercaténaires relativement énergiques conduisent aussi à l'apparition d'importantes tensions due à l'apparition ou à la disparition d'une lacune. On doit s'attendre qu'il existe des temps de relaxation d'ordres de grandeur très variés. L'existence des lacunes d'origines variées peut conduire à certaines déviations de la loi WLF,[23] comme c'est le cas de la viscosité à la proximité du point de solidification. On devrait s'attendre qu'en principe la théorie de Cohen et Turnbull[24] reste vraie sous une forme généralisée pour plusieurs types de lacunes. L'origine de la complexité des transitions de phase aux polymères résulte de la variété des types des lacunes correspondant aux liaisons représentées dans la fig. 2. Justement cette complexité permet d'utiliser des formalismes mathématiques très variés. On peut mentionner celui d'Appelquist[25] qui utilise les transitions de phase d'ordre supérieur pour interpréter les propriétés des macromolécules.

---

[21] G.W. GRAY, «Molecular Structure and Properties of Liquid Crystals», Academic Press, London, 1962.

[22] «Critical Phenomena», Proceedings of a Conference Held in Washington, édité par M. S. Green et J.V. Stengers, National Bureau of Standars Miscellaneous publ., 273, 1966.

L'étude exclusive de l'état d'équilibre ne peut pas caractériser complètement le mécanisme des transitions de phase. Pour obtenir une information plus ample il est nécessaire d'étudier les temps de relaxation. Leurs valeurs peuvent être étudiées en substituant dans la relation (1) $\mathcal{G}_r$ par $G_r \exp(-\tau t)$, où G_r et τ sont des constantes par rapport au temps ; τ représente l'inverse du temps de relaxation. On vérifie que pour la convergence de la série $\sum G_r$ sont nécessaires des conditions analogues à celle déduite pour l'état d'équilibre ($\alpha<1$). Ces conditions conduisent à la délimitation d'un contour dans le plan complexe de la grandeur τ dans lequel on assure la convergence de la série $\sum G_r$. Ces considérations justifient l'intérêt qu'on doit accorder à l'utilisation des signaux en forme de dents de scie pour certaines fréquences et certaines formes des dents correspondant au composant réel du temps de relaxation.

---

[23] M.L. Williams, R.F. Landel et J.D. Ferry, *J. Amer. Chem. Soc.*, **77**, 3701 (1955).

[24] M.H. Cohen et D. Turnbull, *J. Chem. Phys.*, **31**, 1164 (1959).

[25] J. Applequist, *J. Chem. Phys.*, **50**, 600 (1969).

Revue Roumaine de Chimie, 17, 1, 2, 111–114 (1972)

К 70-летию проф. И. Г. МУРГУЛЕСКУ

ИССЛЕДОВАНИЕ ДИФФЕРЕНЦИАЛЬНОГО СОПРОТИВЛЕНИЯ ЭЛЕКТРОДА ПРИ БОЛЬШИХ ПОЛЯРИЗАЦИЯХ

Ю. К. ДЕЛИМАРСКИЙ, А. В. ГОРОДЫСКИЙ и В. А. БАГРИЙ

Институт общей и неорганической химии,
Академия наук Украинской ССР, Киев

Получена 4 сентября 1971 г.

La mesure de la résistance différentielle à la surface électrode/électrolyte en courant alternatif entre deux cathodes peut se faire si le courant continu est séparé par des résistances de 0,5 mohm. Ce schéma a été employé pour déterminer la surtension de l'hydrogène sur l'argent et le nickel. Une résistance différentielle nulle correspond au moment de transition linéaire de la courbe voltamétrique. Ainsi, l'extrapolation de cette section linéaire à des courants nuls fournit la valeur de la surtension limite.

Довольно большое число экспериментальных данных по вольтамперным измерениям в расплавленных и водных электролитах указывают на одну общую особенность поляризационных кривых, проявляющуюся в том, что при достаточном перенапряжении логарифмическая зависимость переходит в хорошо выраженную прямую линию[1].

Одной из удобных позиций, пытавшихся трактовать линейные участки на поляризационных кривых, является точка зрения о предельном перенапряжении[2]. Согласно этой концепции, при больших плотностях тока перенапряжение стремится к некоторому пределу, а линейные участки на поляризационных кривых являются асимптотами, наклон которых к осям координат определяется омическими потерями в электролите или какими-либо другими сопротивлениями в ячейке.

В экспериментальном отношении предельное перенапряжение означает достижение нулевого дифференциального сопротивления межфазовой границы. До настоящего времени это последнее обстоятельство не имело четкого опытного подтверждения. Это связано с принципиальными трудностями измерения перенапряжения или потенциала электрода без омических потерь в электролите. В сущности, единственным методом, претендующим на полное исключение этих потерь, является коммутаторный метод. Поскольку электрохимическая система представляет собой (рис. 1 *а*), комбинацию параллельной RC-цепи (электрод) и активного сопротивления β (электролит), то напряжение на клеммах *1* и *2* этой цепи после

---

[1] Я. В. Дурдин, Л. Киш и В. И. Кравцов, « Тр. IV Совещания по электрохимии », Изд-во АН СССР, Москва, 1959, стр. 102; О. К. Кудра, « Тр. II Всесоюзной конференции по теоретической и прикладной электрохимии », Изд-во АН УССР, Киев, 1949, стр. 47; С. В. Карпачеб, А. Т. Филяеб и С.Ф. Палъгуеб, *Тр. Ин-та электрохимии УФАН СССР*, *3*, 161 (1962).

[2] S. Glasstone, *J. Chem. Soc.*, **125**, 250, 2414, 2646 (1924); A. Hickling и F. Salt, *Trans. Faraday Soc.*, **37**, 224, 319, 333, 450 (1941); S. Schuldiner и J. P. Hoare, *J. Phys. Chem.*, **61**, 705 (1957).

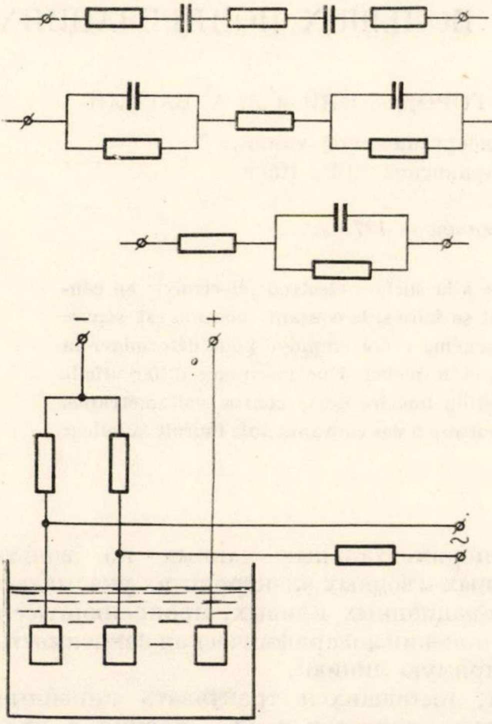

Рис. 1. — Объединенная электрохимическая ячейка.

прерывания тока будет представлять собой потенциал, до которого заряжена емкость *C*, т.е. чистое падение напряжения на межфазовом сопротивлении *R*.

Коммутаторные измерения весьма однозначно демонстрируют существование предельного перенапряжения[3]. Но к коммутаторному методу всегда может быть предъявлена претензия, что емкость *C* начинает разряжаться на сопротивление *R* раньше, чем измеряется ее потенциал. Хотя совпадение данных различных авторов, полученных на различных установках при различной скорости коммутации и говорит в пользу этого метода, тем не менее его нельзя рассматривать как безусловно доказательный.

В предложенном нами ранее методе[4] дается еще один из вариантов исключения омических потерь. Измерение дифференциального сопротивления производится переменным током на двух катодах (рис. 1, *г*), разделенных со стороны постоянного тока сопротивлениями в 0,5 Мом. Эквивалентная схема катодов со стороны переменного тока представлена на рис. 1, *б* где ß—сопротивление электролита. На фазочувствительном вольтметре измеряется активное U_a и емкостное U_c падение напряжения между клеммами *3* и *4* при заданном переменном токе. Это обозначает переход к последовательной эквивалентной $r\,C$-схеме (рис. 1, *в*). Этот переход соответствует формулам

---

[3] А. В. Городыский и И. К. Делимарский, *Collection*, **36**, 877 (1971).

[4] А. В. Городыский, И. К. Делимарский и В. А. Багрий, ТЭХ, **7**, вып. 4 (1971).

$$\beta + 2r = \beta + \frac{2R}{1+\omega^2C^2R^2}, \qquad (1)$$

$$2/\omega C = \frac{2\,\omega C R^2}{1+\omega^2C^2R^2}, \qquad (2)$$

где $\beta + 2r$—активное сопротивление между клеммами *3* и *4* и $2/\omega\ C$—емкостное.

В условиях предельного перенапряжения величина R должна стремиться к нулю. Тогда

$$\lim_{R\to 0}(\beta + 2r) = \beta, \qquad (3)$$

$$\lim_{R\to 0}\frac{2}{\omega C} = 0. \qquad (4)$$

С помощью описанной схемы нами проведены исследования реакции выделения водорода на серебре и никеле:

$$\mathrm{Ag/2N\,(NH_4)_2\,SO_4+1NH_3BO_3/}, \qquad \mathrm{Ni/2N\,(NH_4)_2SO_4+1NH_3BO_3/}.$$

В обоих случаях с ростом поляризации величина активной составляющей напряжения (сопротивления) асимптотически приближается к постоянной величине, а величина емкостной — к нулю (рис. 2 и 3). Это, во-первых, согласуется с теоретическими формулами (1)—(4), во-вторых, демонстрирует достижение предельного перенапряжения в этих реакциях. Интересно отметить, что достижение практически нулевого дифференциального сопротивления межфазовой границы совпадает с моментом достижения линейного участка на вольт-амперной характеристике. Таким образом, величина предельного перенапряжения может определяться по экстраполяции этого линейного участка на нулевой ток.

Перегибы в начальных участках кривых связаны с тем, что при применявшейся нами частоте переменного тока электрокапиллярные свойства системы отражаются на импедансных кривых. Эти перегибы не связаны с вольт-амперными кривыми. При высоких поляризациях электрокапиллярные свойства перестают отражаться на импедансных кривых, уступая место фарадеевским процессам.

Менее важным результатом полученных данных является корреляция между величинами предельного перенапряжения H_2 на серебре и

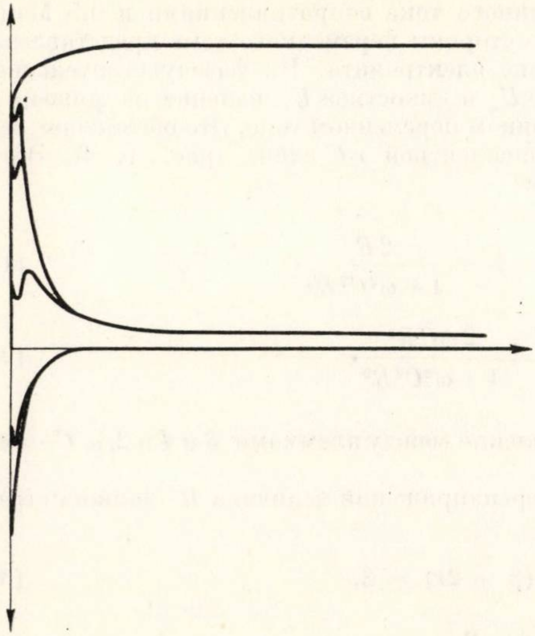

Рис. 2. — Выделение водорода на серебре.

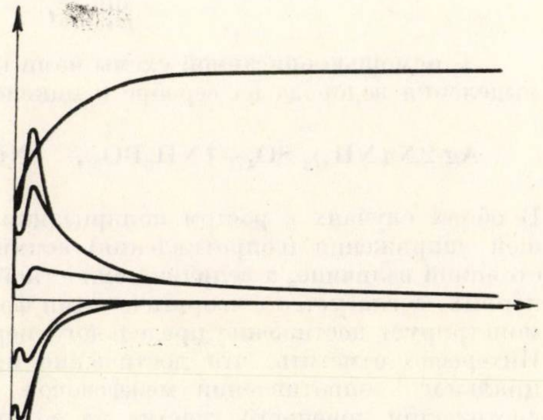

Рис. 3. — Выделение водорода на никеле.

никеле (1,3 в и 1 в) и параметром *a* в уравнении Тафеля (0,95 в и 0,64 в соответственно для серебра и никеля [5]). Это указывает на связь предельного перенапряжения с токами обмена.

---

[5] А. Н. Фрумкин, В. С. Багоцкий, З. А. Иофа и Б. Н. Кабанов, « Кинетика электродных процессов », Изд-во МГУ, Москва, 1952, стр. 126.

Revue Roumaine de Chimie, **17**, *1*, *2*, 115–124 (1972)

Hommage au Professeur I. G. MURGULESÇU
à l'occasion de son 70e anniversaire

RECHERCHES SUR LA CYCLISATION DES ACYL-ARYL-THIOSEMICARBAZIDES 1,4-DISUBSTITUÉES. V

NOUVEAUX N_1-DIPHÉNYLSULFONYL-N_4-ARYL-THIOSEMICARBAZIDES ET 1,2,4-MERCAPTO-TRIAZOLES À ACTION ANTIVIRALE *

CĂTĂLINA DEMETRESCU et IOANA ŞARAMET

Laboratoire de Chimie Organique, Faculté de Pharmacie, Institut de Médecine et de Pharmacie, Bucarest, 19–21, str. Alex. Sahia

Reçu le 26 juillet 1971

En partant de l'analyse de la stéréoisomérie éthylénique des formes tautomères thioliques, présentées par les diphényl-sulfonyl-carboxy-aryl-thiosemicarbazides 1,4-disubstituées, les auteurs ont réalisé de nouvelles classes de 3-mercapto-1, 2, 4-triazoles, dérivés de la diphénylsulfone, par cyclisation déshydratante, en catalyse basique de ces thiosemicarbazides. On a ainsi synthétisé 16 nouveaux composés doués d'action antivirale sur le virus du mosaïque du tabac (V.M.T.), dans des doses pratiquement non toxiques. La structure des nouveaux composés a été vérifiée avec précision par analyse chimique et par étude comparée de leur spectres de vibration moléculaire en IR.

Au cours des recherches systématiques sur la corrélation de la structure chimique et l'action antituberculeuse des sulfamides de la classe du sulfathiadiazole on a esquissé l'idée que les thiosemicarbazides 1,4-disubstituées, employées comme intermédiaires dans la synthèse, devraient être, elle-mêmes, douées d'un intense effet antibacillaire [1–3]. Comme la plupart de ces thiosemicarbazides possèdent une haute toxicité, on a entrepris de nombreuses études afin de modifier leur structure de base et d'abaisser leur toxicité.

Ces dernières années on a accordé beaucoup d'attention à l'étude de la réaction de cyclisation déshydratante des thiosemicarbazides 1,4-disubstituées, capables de mener à de nouvelles classes d'hétérocycles pentaatomiques : 3-mercapto-1,2,4-triazoles (III) et 2-arylamino-1,3,4-thiadiazoles (IV), selon les conditions de réaction utilisées. [4–6]

---

* IVe partie : C. Demetrescu, Al. Mavrodin, 7e Rencontres de Chimie Thérapeutique, Lyon, 8–10 sept. 1971.

[1] R. Behnisch, F. Mietzsch et H. Schmidt, *Angew. Chem.*, **60**, 113 (1948).

[2] M.M. Girard et M.J. Laroche, *Ann. pharm. fr.*, **XV**, 9–10, 556 (1957).

[3] E. Ciorănescu, ''Médicaments de Synthèse'', IIe Ed., tehnică, Bucarest, 1966, p. 637.

[4] E. Hoggarth, **J. Chem. Soc.**, **1949**, 1160, 1163 ; **1950**, 612.

[5] F. Russo et M. Ghelardoni, *Boll. chim. farm.*, **108**, 128 (1969).

[6] M.M. Girard, *Compt. rend.*, **225**, 458 (1947).

Inspirés par les résultats spectaculaires, obtenus dans ce domaine, [7–9] nous avons synthétisé dans le présent ouvrage de nouvelles thiosemicarbazides 1,4-disubstituées de la classe des diphénylsulfones, par addition nucléophile des hydrazides des acides diphényl-sulfonyl-carboxyliques aux isothiocyanates d'*o*-tolyl et d'α-naphthyle :

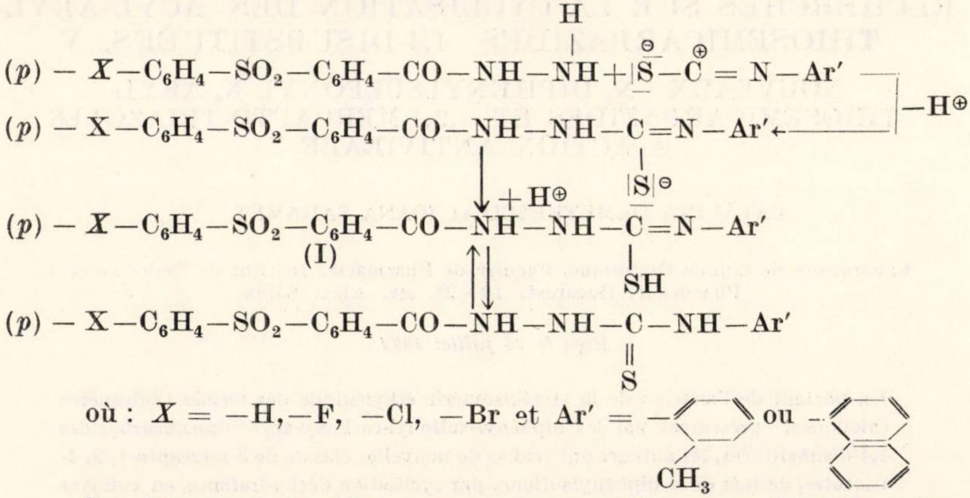

$$(p)-X-C_6H_4-SO_2-C_6H_4-CO-NH-\overset{H}{\overset{|}{N}}H+|\overset{\ominus}{\underline{S}}-\overset{\oplus}{C}=N-Ar'$$

$$(p)-X-C_6H_4-SO_2-C_6H_4-CO-NH-NH-\underset{|\overline{S}|^{\ominus}}{\underset{|}{C}}=N-Ar' \xleftarrow{-H^{\oplus}}$$

$$\downarrow +H^{\oplus}$$

$$(p)-X-C_6H_4-SO_2-C_6H_4-CO-NH-NH-\underset{SH}{\underset{|}{C}}=N-Ar' \quad (I)$$

$$\uparrow\downarrow$$

$$(p)-X-C_6H_4-SO_2-C_6H_4-CO-NH-NH-\underset{S}{\underset{\|}{C}}-NH-Ar'$$

où : $X = -H, -F, -Cl, -Br$ et $Ar' =$ ou

Ces thiosemicarbazides peuvent être cyclisées par déshydratation en catalyse basique ou acide, avec obtention de nouveaux composés hétérocycliques pentagonaux du type (III) et (IV), suivant le schéma de réaction :

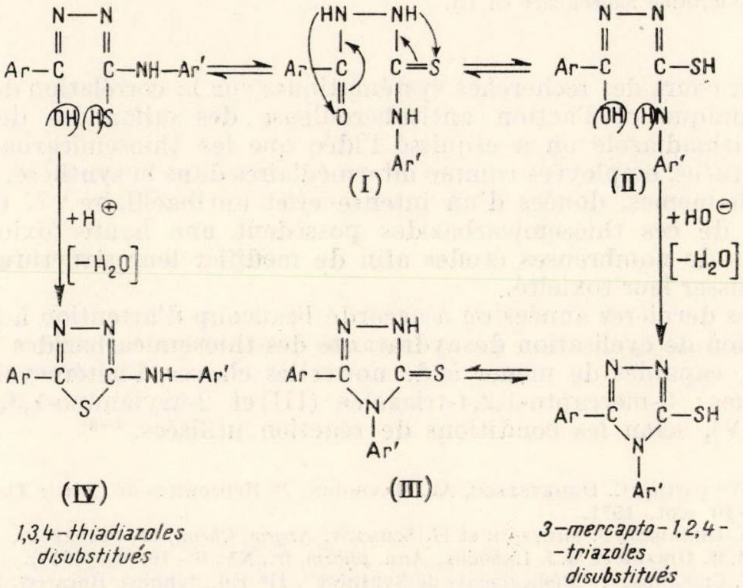
(I)
(II)
+H⊕
[−H₂O]
+HO⊖
[−H₂O]
(IV)
(III)
1,3,4-thiadiazoles disubstitués
3-mercapto-1,2,4-triazoles disubstitués

---

[7] C. Demetresco, *Rev. Roumaine Chim.* (1971) (sous presse).

[8] C. Demetresco et V. Manu, *Pharmazie-Berlin*, 1971 (sous presse).

[9] C. Demetresco, *Arhiv. für Pharm.*, 1971 (sous presse).

où : Ar$=(p)-X-C_6H_4-SO_2-C_6H_4-$; X étant : $-$H, $-$F, $-$Cl, $-$Br et

Ar′ =

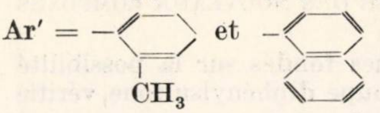

Pour mettre en évidence les deux formes tautomères (I) et (II), nous nous sommes basés dans nos recherches sur les conclusions intéressantes obtenues en 1947 par Girard,[6] qui reprend les études de Freund et de son école,[10] confirmées deux années plus tard par Hoggarth,[4] ainsi que par les chercheurs roumains Budeanu et Ciugureanu,[11] en 1968.

Nous avons ainsi admis que pour la cyclisation déshydratante en catalyse basique ou acide — des diphénylsulfonyl-carboxy-thiosemicarbazides, N_4-substituées avec les groupes *o*-tolyl, respectivement α-naphtyl, la forme thiolique (II) de celle-ci peut exister sous deux formes stéréoisomères, l'une *cis* (II_A) et l'autre *trans* (II_B), c'est-à-dire :

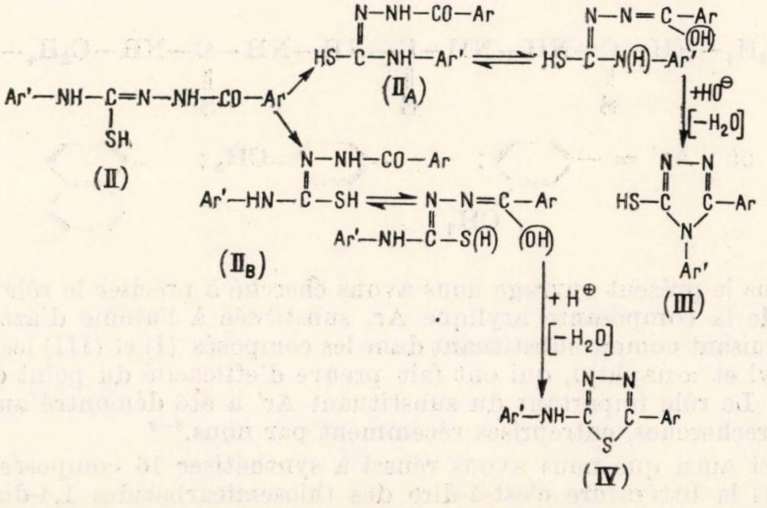

L'explication des bases théoriques du mécanisme de réaction, en catalyse basique et acide, de ces types de cyclisations déshydratantes a été analysée par nous, antérieurement.[7]

L'isomérie de ce type, *cis* et *trans*, serait donc responsable de la manière dont la synthèse peut être dirigée par deux voies, dans la réaction de cyclisation déshydratante. Ainsi, à partir de la forme II_A-en catalyse basique — la fermeture des cycles du type 3-thyol-1, 2,4,-triazolique (III) devient possible, tandis que pour la forme II_B — en catalyse acide — on aboutit à des cycles du type 2-arylamino-1,3,4-thiadiazolique (IV).

Dans le présent ouvrage, nous avons conduit la réaction de cyclisation déshydratante en catalyse basique, en utilisant une solution d'hydroxyde de sodium 2 N. L'étude détaillée des hétérocycles du type (IV) feront l'objet d'un travail prochain (Note VI).

---

[10] M. Freund, *Ber.*, **29**, 2483 (1896).

[11] C. Budeanu, *Anal. Şt. Univ., I.C. Cuza — Iaşi, Chimie*, **XIII** (1), 178 (1967) ; **XIV** (1), 81 (1968).

DISCUSSION SUR LA STRUCTURE ET L'ACTIVITÉ DES NOUVEAUX COMPOSÉS

Dans nos recherches nous nous sommes fondés sur la possibilité de développer l'effet thérapeutique, dû au groupe diphénylsulfone, vérifié par nous du point de vue thérapeutique.[12]

D'autre part, nous avons considéré les résultats intéressants obtenus en 1955 par Buu-Hoi, Loc et Xuong.[13] qui ont introduit les groupes actifs *m*-, respectivement *p*-tolyl et α-naphtyl dans la molécule des carbohydrazides, composés à structure thio-uréique $(-NH-\underset{\underset{S}{\|}}{C}-NH-)$, à l'aide de la méthode de Guha et De, utilisée pour l'obtention des dianilides des acides thiocarbohydrazo-bis-thiocarboxyliques—(1,5) :

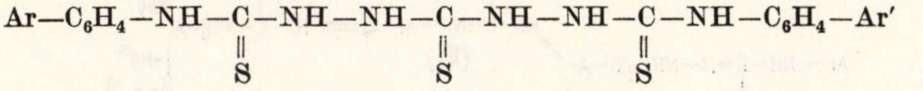

$$Ar-C_6H_4-NH-\underset{\underset{S}{\|}}{C}-NH-NH-\underset{\underset{S}{\|}}{C}-NH-NH-\underset{\underset{S}{\|}}{C}-NH-C_6H_4-Ar'$$

où : Ar′ =

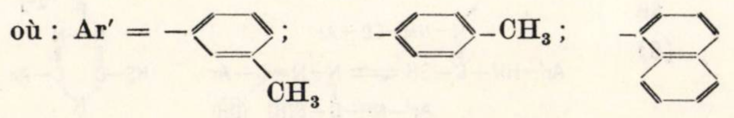

Dans le présent ouvrage nous avons cherché à préciser le rôle déterminant de la composante arylique Ar, substituée à l'atome d'azote N_4, en introduisant comme substituant dans les composés (I) et (III) les groupes *o*-tolyl et α-naphtyl, qui ont fait preuve d'efficacité du point de vue pratique. Le rôle important du substituant Ar′ a été démontré aussi par d'autres recherches, entreprises récemment par nous.[6–9]

C'est ainsi que nous avons réussi à synthétiser 16 composés, non-cités dans la littérature c'est-à-dire des thiosemicarbazides 1,4-disubstituées et des 1, 2, 4-mercaptotriazoles 2,5-disubstitués, dans lesquels l'Ar est représenté par le radical *p*-*X*-diphényl-sulfonyl ($X = -H, -F, -Cl, -Br$) et Ar′ est l'*o*-tolyl, respectivement l'α-naphtyl.

Nous avons confirmé la structure exacte de ces composés par l'analyse des éléments (le microdosage de l'azote et le semi-microdosage du soufre) et par une étude complète des spectres d'absorption en IR.[14] Les attributions des bandes spectrales sont rendues dans le tableau 1 et confirment avec exactitude la structure chimique proposée.

En comparant la structure des thiosemicarbazides (II) avec celle des mercapto-triazoles (III), résultant de leur cyclisation déshydratante en catalyse basique, on constate que dans leur molécule se trouve le groupe

---

[12] AL. MAVRODIN, C. DEMETRESCO, C. CHIRITZA et O. MACOVSCHI, « Travaux des IIIe Rencontres Nationales des Pharmaciens » Bucarest, 7–9 nov. 1968, p. 19.

[13] N.P. BUU-HOÏ, T.B. LOC et N.D. XUONG, *Bull. Soc. chim. France*, I, 694 (1955) ; II, 363 (1956).

[14] D. BIRCĂ-GĂLĂŢEANU, C. DEMETRESCU et D. IORDACHE, « Travaux de la Session Scientifique Jubilaire de l'Institut Polytechnique de Bucarest », 1970 ; *Rev. Roumaine Phys.* (1971) (sous presse).

$\rangle C=N-\overset{|}{N}-C$ = déterminant de l'activité tuberculostatique, proposé par la chimiste soviétique Sciukina et son école :[15]

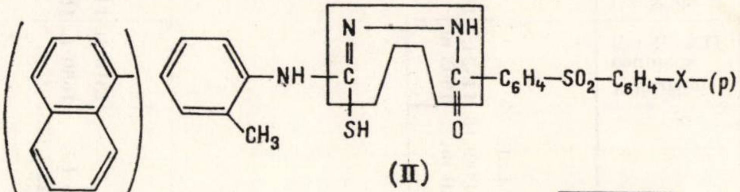

(II)

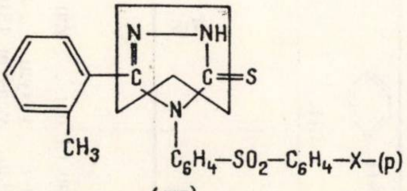

(III)

De nombreuses recherches récentes relèvent la corrélation de l'action antituberculeuse et de celle antifungique, pour les dérivés des thiosemicarbazides. On constate souvent une augmentation de l'effet antibacillaire et antifungique, comme suite à la cyclisation, avec obtention des triazoles, ou bien l'apparition d'autres effets intéressants comme : l'action hypoglycémiante, antiinflammatoire, cytostatique antipyrétique, inhibitrice de la monoaminoxydasé (M.A.O.), analgésique, etc.[5,16–19].

DONNÉES SUR L'ACTION ANTIVIROTIQUE

On a expérimenté l'action antivirotique sur des plantes de tabac : *Nicotiana glutinosa* et *Nicotiana Xanthi*, qui présentent comme symptomes des lésions locales (nécroses), après l'infection par le virus du mosaïque du tabac (V.M.T.).

Tous les composés ont été actifs, présentant une forte inhibition du développement des nécroses (compris entre 50–75%). Le composé au N° XVI ($X = -H$, Ar' = α-naphtyl) a présenté une activité très intense. Administré préventif, deux heures avant l'infection expéri-

---

[15] M.N. Schiukina, T.N. Perşhin, O.O. Makeeva, E.S. Sazonova, E.S. Nikitskaya, A.D. Yanina et A.N. Iakovleva, *Doklady Acad. Nauk* SSSR, **84**, 981 (1952).

[16] A.K. Bhat, R.P. Bhamaria, R.A. Bellare et C.V. Deliwala, *Indian J. Chem.*, 5 (9), 397 (1967).

[17] P.N. Buu-Hoï et D.N. Xuong, *J. Chem. Soc.*, 1955, 1573, **1956**, 2160 ; Compt. Rend., **238**, 295 (1954) ; Compt *Rend.*, **235** 1952.

[18] M.T. Shah, M.J. Mhasalka, N.A. Varaya, R.A. Bellare et C.V. Deliwala, *Indian J. Chem.*, **5**, (8), 391 (1967).

[19] Al. Mavrodin et F. Gagiu, *Pharmazie*, **22**, 434 (1967).

ANNEXE 1

Tableau 1

indiquant les attributions pour les bandes des groupements actifs en IR

(cm^{-1})

C—Cl	N—C=S	N=C—S	SH	O=C—NH	C_6H_5	SO_2	Vibrations couplées C=S, NH	C=N de l'anneau hétérocycl.	Phényle bisubstitué
I. 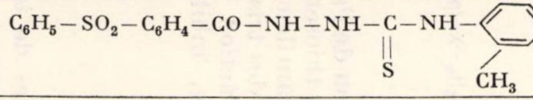									
—	645 m. 687 t.i. 1300 t.i. 1490 i.	1535 t.i.	2605 f.	C=O, Am. I ......1670 t.i. (NHδpl.) Am. II ....1535 t.i.) δ(C—N) Am.III ... {1265 i. / 1305 m. δ (O=C—N) ... 755 t.i. Am. V, ... 725 t.i. NH v. ..... 3320 m.	ν_4 : (C—H) δ ⊥ pl. 690 t.i. ν_{14} :(C—H)δ ‖ pl. 1020 i. ν_{12} :(C—H) ν ... 3100 m. ν_{13} : (C—C) v ... 1490 i.	déf. ... 520 infl. v_1 sym. ... 1160 t.i. v_2 asym. 1310 m.	1452 i. 1505 m.	1490 i.	850 i.
XIV. 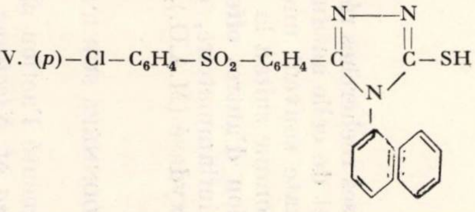									
785 t.i.	680 t.i. 1550 m.	1550 m.	2570 infl.	(NHδpl.) Am. II ..... 1535 i. δ(C—N) Am.III ... {1325 t.i. / 1280 i. Am. V ..... 710 i. NH v. .....3300 i.	ν_4 :(C—H)δ⊥pl. ...680 t.i. ν_{14} :(C—H) δ ‖ pl. 1020 t.i. ν_{12} :(C—H) v .... 3100 m. ν_{13} : (C—C) v ... 1485 i.	déf. ... 530 f. v_1 sym. 1165 t.i. v_2 asym. 1325 t.i.	1510 m. 1630 f.	1480 i. 1605 m.	850 m.

Légende

i. = intense	pl. = vibration dans le plan
t.i. = très intense	v. = vibration de valence
m. = intensité moyenne	sym. = vibration symétrique
infl. = inflexion	déf. = vibration de déformation

mentale, il a réduit le nombre de nécroses de 75%. Le composé au n° XV (X = —Cl, Ar' = *o*-tolyl) réduit le nombre des nécroses de 50% et s'il est administré de manière curative, c'est-à-dire deux heures après l'infection des plantes, son action croît de telle sorte que le nombre de nécroses est réduit de 75%. Toutes les substances sont pratiquement exemptes de toxicité.

PARTIE EXPÉRIMENTALE

Synthèse des nouvelles acyl-aryl-thisemicarbazides 1,4-disubstituées V. N_1-[p-(p'-chlore-phénylsulfonyl)-benzoyl]-N_4-(o-tolyl)-thiosemicarbazide :

$$(p)-Cl-C_6H_4-SO_2-C_6H_4-CO-NH-NH-(C{=}S)-NH-C_6H_4-CH_3-(o)$$

On dissout 2 g (0,0064 moles) d'hydrazide de l'acide *p*-chloré-diphénylsulfonyl-*p'*-carboxylique, au chaud, en 180 ml (excès) d'éthanol absolu et on filtre la solution très chaude. On fait tomber, goutte à goutte, 0.96 g (0,0064 moles) d'isothiocyanate d' *o*-tolyl et on refluxe, pendant 3 heures. Après 15 minutes de l'ébullition, des cristaux aciculaires, billants de thiosemicarbazide (V) apparaissent dans la masse de réaction au P.f. 217° (de l'éthanol). Ces cristaux sont très solubles dans le diaméthylformamide, l'acide acétique et la pyridine, solubles au chaud dans l'éthanol, le méthanol, le propylènglycol et la glycérine, insolubles dans l'éther de pétrole, la ligroïne, le toluène et l'eau. Rend. 63%.

$C_{21}H_{18}O_3N_3S_2Cl$ *Calculé* : N 9,14 ; S 13,94

Trouvé : N 9,22 ; S 13,86%

Synthèse des nouveaux mercapto-triazoles 2,5-disubstitués. XVI. 1-[(α-naphtyl-3-mercapto)-5-p-brome-phényl-sulfonyl)-phényl]-1,2 4-triazole

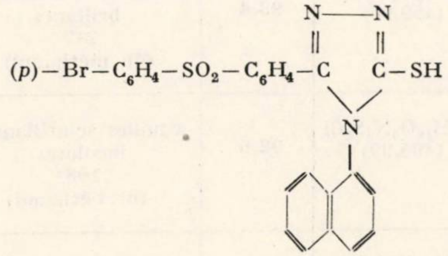

1 g (0,0016 mole') de N_1-[*p*-(*p'*-brome-phénylsulfonyl)-benzoyl]-N_4-(α-naphtyl)-thiosemicarbazide est dissous, par agitation, dans 31,2 ml d'une solution de NaOH 2N. Après éclaircissement de la solution, on refluxe légèrement pendant 15 minutes et puis on ajoute 40 ml d'eau. On filtre ensuite la solution chaude et on neutralise avec du HCl 10%, goutte à goutte, jusqu'à pH = 3. A ce moment, la précipitation du triazole (XVI) est complète. Il se dépose un précipité abondant qui est essoré, lavé à l'eau jusqu'à réaction neutre et recristallisé du méthanol. Il se présente sous forme de microcristaux incolores, au p.f. 270°, très solubles dans l'acétone, la pyridine et le chloroforme, solubles dans l'éthanol, le méthanol et

ANNEXE 2

Tableau synoptique 2

des nouveaux composés synthétisés

$(p)-X-C_6H_4-SO_2-C_6H_4-COHN-NH-(C{=}S)-NH-Ar$

Nº	X	Ar′	Formule et poids moléculaire	Rend. %	Point de fusion et solvant de cristallisation	N %	S %
						Calculé Trouvé	Calculé Trouvé
I	H	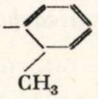	$C_{21}H_{19}O_3N_3S_2$ (425,51)	92,2	aiguilles incolores 210° (de l'éthanol)	9,88 10,03	15,07 15,01
II	H	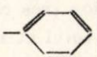	$C_{21}H_{18}O_3N_3S_2$ (461,54)	73,3	paillettes incolores éclatantes 181° – 2° (de l'éthanol abs.)	9,10 9,24	13,89 13,88
III	F	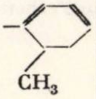	$C_{21}H_{18}O_3N_3S_2F$ (443,39)	61,7	microcristaux jaune pâle 158° (de l'éthanol abs).	9,47 9,51	14,46 14,37
IV	F	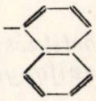	$C_{24}H_{18}O_3N_3S_2F$ (479,53)	60,5	aiguilles incolores 162° (décomp.) (de l'éthanol)	8,76 8,90	13,37 13,29
V	Cl	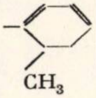	$C_{21}H_{18}O_3N_3S_2Cl$ (459,96)	93,4	feuillets incolores brillants 217° (du méthanol)	9,14 9,22	13,94 13,86
VI	Cl	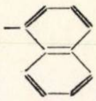	$C_{24}H_{18}O_3N_3S_2Cl$ (495,99)	92,6	aiguilles scintillants incolores 198° (de l'éthanol)	8,47 8,50	12,93 12,87
VII	Br	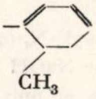	$C_{21}H_{18}O_3N_3S_2Br$ (504,42)	93,8	feuillets incolores éclatants 236° (du méthanol	8,33 8,44	12,71 12,65
VIII	Br	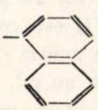	$C_{24}H_{18}O_3N_3S_2Br$ (540,45)	90,9	feuillets incolores scintillants 200° (de l'éthanol abs.)	7,78 7,85	11,87 11,89

(suite) Annexe 2

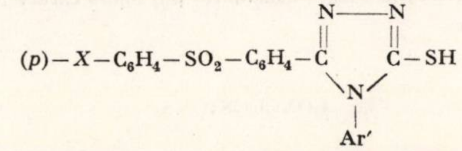

N°	X	Ar'	Formule et poids moléculaire	Rend. %	Point de fusion et solvant de cristallisation	N % Calculé Trouvé	S % Calculé Trouvé
IX	H	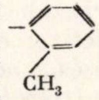 CH$_3$	$C_{21}H_{17}O_2N_3S_2$ (407,50)	72,5	microcristaux incolores 242° (de l'éthanol)	10,31 10,32	14,74 15,66
X	H	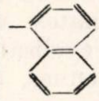	$C_{24}H_{16}O_2N_3S_2$ (442,52)	71,8	microcristaux incolores 275° (de l'éthanol abs.)	9,49 9,58	14,49 14,34
XI	F	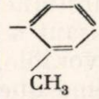 CH$_3$	$C_{21}H_{16}O_2N_3S_2F$ (425,49)	62,3	aiguilles incolores 178° (de l'éthanol)	9,88 9,96	15,07 15,01
XII	F	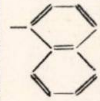	$C_{24}H_{16}O_2N_3S_2F$ (461,52)	58,9	aiguilles incolores 201° (du méthanol)	9,10 9,22	13,89 13,77
XIII	Cl	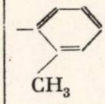 CH$_3$	$C_{21}H_{16}O_2N_3S_2Cl$ (441,95)	84,7	microcristaux incolores 259° (de l'éthanol abs.)	9,50 9,66	14,51 14,49
XIV	Cl	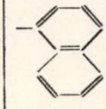	$C_{24}H_{16}O_2N_3S_2Cl$ (477,98)	85,3	microcristaux incolores 285° (de l'éthanol)	8,79 8,87	13,43 13,40
XV	Br	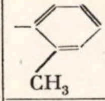 CH$_3$	$C_{21}H_{16}O_2N_3S_2Br$ (486,41)	88,9	aiguilles incolores 181° (de l'éthanol abs.)	8,64 8,79	13,20 13,12
XVI	Br	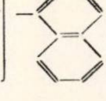	$C_{24}H_{16}O_2N_3S_2Br$ (522,44)	89,2	aiguilles incolores 270° (de l'éthanol)	8,04 8,16	12,28 12,19

l'acide acétique glacial, insolubles dans l'eau, le benzène, le xylène et la ligroïne. Rend. = = 83.80 %.

$C_{24}H_{16}O_2N_3S_2Br$ *Calculé* : N 8,04 ; S 12,28
Trouvé : N 8,16 ; S 12,19 %.

Les autres composés, synthétisés par voies analogues, sont indiqués dans le tableau synoptique 2 où sont comprises ainsi leurs constantes physiques caractéristiques et les données analytiques correspondantes.

CONCLUSIONS

Basés sur les considérations théoriques sur la stéréoisométrie éthylénique de quelques nouvelles diphénylsulfonyl-thiosemicarbazides, substituées à N_4 avec les composantes l'*o*-tolyle, respectivement l'α-naphtyle, nous avons synthétisé 16 nouveaux composés : acyl-arylthiosemicarbazides 1,4-disubstituées et 1,2,4-mercapto-triazoles 2,5-disubstitués. La réaction a eu lieu par l'addition nucléophyle des hydrazides des acides diphénylsulfonyl-carboxyliques aux isothiocyanates aryliques de l'*o*-tolyl et respectivement de l'α-naphtyl, suivie d'une cyclisation déshydratante en catalyse basique des thiosemicarbazides obtenues, conduisant à des 3-mercapto-1, 2, 4-triazoles.

Les composés obtenus ont montré une action antivirotique intense sur le VMT. La cyclisation des thiosemicarbazides conduisant à de nouveaux mercapto-triazoles s'est montrée particulièrement favorable.

Nos recherches dans ce domaine continuent, de même que l'étude approfondie des effets pharmacodynamiques, qui est en cours.

Revue Roumaine de Chimie, **17**, *1*, *2*, 125–129 (1972)

Hommage au Professeur I. G. MURGULESCU
à l'occasion de son 70e anniversaire

MÉTHODES DE DÉTERMINATION DU RHÉNIUM DANS LES MOLYBDÉNITES*

LA DÉTERMINATION POLAROGRAPHIQUE DU RHÉNIUM À CÔTÉ DES TRACES DE MOLYBDÈNE

ALEXANDRU DUCA et CLEOPATRA CALU

Institut Polytechnique de Jassy, Faculté de Chimie industrielle, chaire de Chimie analytique, 11, Calea 23 August

Reçu le 19 juillet 1971

On présente la séparation, la concentration et le dosage du rhénium dans les molybdénites. On réanalyse la détermination colorimétrique du rhénium en présence de petites concentrations de molybdène. On présente également une variante extractive-polarographique de la détermination du rhénium des molybdénites, comme méthode de contrôle. Le principal avantage de cette variante consiste dans la spécificité de la détermination polarographique du rhénium, en présence de quantités minimales molybdène.

A. CONTRIBUTION AU PROBLÈME DE LA SÉPARATION, DE LA CONCENTRATION ET DU DOSAGE DU RHÉNIUM DANS LES MOLYBDÉNITES

Les recherches de R.Ripan et des collaborateurs ont visé dès 1943 l'identification et le dosage du rhénium dans la molybdénite indigène.[1] En raison de l'absence d'un étalon de rhénium, celui-ci a été dosé seulement en 1953[2] et un an plus tard le collectif a publié aussi une méthode originale polarographique pour la détermination du rhénium dans la molybdénite et les concentrés de rhénium.[3] L'identification, le dosage et l'extraction des concentrés de rhénium[4–8] font partie du problème de la valorisation de la molybdénite indigène.[9–12] Il est bien connu, que la majorité des méthodes colorimétriques de dosage du rhénium dans les molybdénites présente une série d'inconvénients.[13–24] En étudiant le grillage de la molybdénite en fonction de différents facteurs, pour surveiller la sublimation quantitative du rhénium avec les moindres pertes de molybdène, on est arrivé à un procédé satisfaisant pour les fins analytiques et pour la préparation du rhénium. Cette méthode thermique est une méthode de désagrégation, de concentration et de séparation du rhénium et du molybdène. Du rapport initial 1 part Re pour 10 000 parts Mo (dans des concentrés de molybdène à 40% Mo) après le grillage en courant d'air ou d'oxygène on arrive à un rapport de 1 part Re pour 3–5 parts Mo ou même 1 part Re : 1 part Mo. Le produit de sublimation, lavé quantitativement et philtré est transporté dans un ballon jaugé. Dans une quote-part (correspondant à 5–10 μg Re) on fait le dosage polarographique[3,4,25,26] ou photocolorimétrique ($SnCl_2+KSCN$)[4,27] du rhénium. La méthode de désagrégation thermique suivie du dosage polarographique ou photocolorimétrique du rhénium (sans la séparation du molybdène) est recommandée pour les analyses de série.[4] La méthode recommandée a été vérifiée sur des concentrés de molybdène et des concentrés de cuivre, comparativement à la méthode de Tribalat[13] modifiée par Beeston.[14]

---

* Travail présenté au 39e Congrès International de Chimie Industrielle, Bucarest, 7–11 septembre 1970.

[1] R. Ripan, N. Erös et Al. Duca, Travaux de laboratoire 1943–44.

[2] Al. Duca, *Studii și Cercetări Chim. Fil. Cluj*, **5**, 83 (1954).

[3] Al. Duca et D. Stănescu, *Studii și Cercetări Chim. Fil. Cluj*, **6**, 123 (1955).

[4] Al. Duca, D. Stănescu et M. Pușcașu, *Studii și Cercetări Fil. Cluj*, **13**, 197 (1962).

[5] Al. Duca, M. Pușcașu et D. Stănescu, *Studii și Cercetări Chim. Fil. Cluj*, **14**, 351, (1963).

[6] Al. Duca, D. Stănescu et M. Pușcașu, *Rev. Roumaine Chim.*, **11**, 833 (1966).

[7] Al. Duca, D. Stănescu et M. Pușcașu, *Rev. Roumaine Chim.*, **11**, 839 (1966).

[8] Al. Duca, M. Pușcașu et D. Stănescu, *Rev. Roumaine Chim.*, **11**, 829 (1966).

En milieu basique de NaCl 2N, dans des systèmes réels, on peut doser par polarographie jusqu'à une part Re pour 300 parts Mo. Si le rapport Mo : Re > 300, on a besoin d'une séparation préalable du molybdène. Le rhénium peut être dosé par polarographie à côté de petites quantités de molybdène aussi en milieu acide (H_2SO_4), partant de la réduction du tellure (H_6TeO_6) catalysée par des traces de rhénium.[25] La sensibilité des réactions de réduction polarographique du rhénium est grande aussi, du fait que le rhénium se réduit de 7^+ à 1^- c'est-à-dire dans la réaction d'électrode participent 8 électrons.[28] Par la méthode polarographique de réduction du tellure catalysée par les traces de rhénium (en milieu de H_2SO_4) on peut déterminer jusqu'à 0,05 μg Re/ml de solution ; dans NaCl2N

---

[9] R. Ripan et Al. Duca, *Bul. Acad. R.P.R.*, **2**, 381 (1950).

[10] R. Ripan et Al. Duca, *Bul. Acad. R.P.R.*, **4**, 379 (1952).

[11] Al. Duca, *Studii si Cercetări Chim. Fil. Cluj*, **3**, 42 (1952).

[12] Al. Duca et Gh. Marcu, *Rev. Roumaine Chim.* (*numéro hommage à R Ripan*), 235 (1966).

[13] S. Tribalat, I. Pam et H.M. Iungfeich, *Analyt. Chim. Acta*, **6**, 142 (1952).

[14] J.H. Beeston et J.R. Lewis, *Analyt. Chem.*, **25**, 651 (1953).

[15] E.B. Sandell, « Colorimetric Determination of Traces of Metals », Interscience Publishers, New-York-London, 1959, p. 750–766.

[16] D.I. Ryabchikov et A.I. Lazarev, *Trudy Kom. po analit. khim.*, VII (X), 61 (1956).

[17] V. Patrovsky, *Chem. listy*, **51**, 1295 (1957).

[18] S.A. Fischer et W.V. Meloche, *Analyt. Chem.*, **24**, 1100 (1952).

[19] V. W, Meloche et A.F. Preuss, *Analyt. Chem.*, **26**, 1911 (1954).

[20] Ranski, *Zavodskaya Lab.*, **24**, 803 (1958).

[21] Jen-Yin Yen et Tseng-Ning Tao, *Sci. Sinica* (Peking), **7**, 730 (1958).

[22] D.I. Riabchikov et L.V. Borisova, *Zhur analit. Khim.*, **13**, 155 (1958).

[23] J.L. Kassner, Shih-Fan Ting et E.L. Grove, *Talanta*, **8**, 269 (1961).

[24] V.M. Taraian, « Analiticheskaya khimiya reniya », Izd. « Mitk », Erevan, 1966.

[25] K. Györbiro, *Acta Chim. Acad. Sci. Hung.*, **27**, 121 (1961).

[26] K.S. Pachomova et L.P. Volkova, *Zavodskaya Lab.* **25**, 1291 (1959).

[27] M.L. Nichols et J.H. Rogers, *Iod. Eng. Chem. Analyt,. Ed.*, **16**, 137 (1944).

[28] J.J. Lingane, *J. Amer. Chem. Soc.*, **64**, 1005 (1942).

au pH $\sim$ 11 + Na_2SO_3, jusqu'à 0,5 μg Re/ml et en NaCl 2N au pH $\sim$ 11 avec barbotage d'hydrogène jusqu'à 1 μg Re/ml solution. Pour le dosage des traces de molybdène dans les concentrés de rhénium (obtenus de la molybdénite indigène) nous avons utilisé la méthode polarographique en réalisant des déterminations dans les solutions de base suivantes : $HNO_3 + NH_4 . NO_3$ [27] et complexon III.[29,30] Après les épreuves nous avons observé que le rhénium ne gène pas la détermination du molybdène dans ces solutions de base et qu'il est donc possible de déterminer par polarographie les traces de molybdène dans les concentrés de rhénium. Dans la solution de $NO_3H + NH_4 . NO_3$ on peut déterminer jusqu'à 0,01% Mo en 99,99% Re. La sensibilité de la méthode est de 0,02 μg Mo/ml de solution. Dans la solution de complexon III on peut déterminer jusqu'à 0,1% Mo en 99,9% Re. La sensibilité de la méthode est de 1 μg Mo/ ml de solution.

B. LA POSSIBILITÉ DE DÉTERMINATION COLORIMÉTRIQUE DU RHÉNIUM À CÔTÉ DE PETITES CONCENTRATIONS DE MOLYBDÈNE

Dans un travail publié[4] nous avons précisé la possibilité de déterminer le rhénium dans les produits de volatilisation en présence de petites quantités de molybdène. À cause de plusieurs critiques récentes sur l'extraction des traces de molybdène à côté du rhénium avec du chlorure de tetraphénylarsonium (TPA) dans du chloroforme, d'après la méthode Tribalat, Pam, Iungleich,[13] modifiée par Beeston et Lewis,[14] nous avons repris cette méthode pour apporter quelques éclaircissements : 1) le contrôle de la présence ou de l'absence des traces de molybdène dans l'extrait chloroformique et 2) la possibilité de détermination colorimétrique du rhénium à côté de petites concentrations de molybdène.

1. Le contrôle des traces de molybdène dans l'extrait chloroformique a été réalisé sur une série d'épreuves exécutées d'après la méthode citée,[13,14] après avoir éloigné le chloroforme sur bain de sable, repris le résidu avec 6 ml $HNO_3 + NH_4 . NO_3$ et polarographié dans le domaine 0,0 — 1,0 V, $S = 1/50$. Tous les résultats polarographiques ont indiqué l'absence des traces de molybdène dans l'extrait chloroformique. On peut constater cela aussi par spectrophotométrie, mais avec une moindre précision.

À cette occasion nous soulignons qu'il est important pour la désagrégation de la molybdénite à l'acide nitrique, après l'éloignement de l'acide nitrique avec l'acide chlorhydrique, de ne pas aller jusqu'au séchage et aussi que la séparation des traces d'eau du chloroforme avec du $CaCl_2$ anhydre soit faite 2 ou 3 fois avec la plus grande attention. Toutes ces précautions prises la méthode donne de très bons résultats.

2. La possibilité de détermination colorimétrique du rhénium en présence de petites concentrations de molybdène-thiocyanate est fondée sur la différence des spectres d'absorption et sur la différence de stabilité des thiocyanates complexes du rhénium et du molybdène. Dans la figure 1 on présente les spéctres d'absorption des thiocyanates complexes de rhénium et de molybdène. Les lectures ont été faites après

---

[29] R. Pribil et B. Blažek, *Chem. listy*, **45**, 430 (1951).

[30] A. Stern, *Ind. Eng. Chem. Analyt. Ed.*, **14**, 64 (1942).

30 minutes. Dans la figure 2 on présente l'absorption (A)-fonction de diverses concentrations du rhénium, à trois longueurs d'onde (425—500 nm). On peut observer que la sensibilité de la détermination du rhénium présente un maximum à $\lambda = 425$ nm, moindre à 455 nm et plus petite encore à 500 nm. Les déterminations du rhénium à $\lambda = 500$ nm sont pourtant satisfaisantes si à côté du rhénium il y a les mêmes ou de plus grandes concentrations de molybdène, ainsi que le montre la fig. 3.

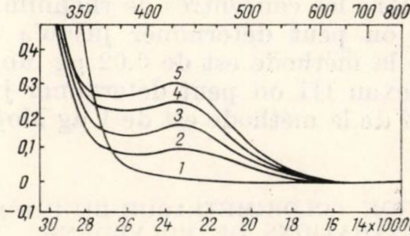

Fig. 1. — Spectres d'absorption des thiocyanates complexes de rhénium et de molybdène.

1, 30 μg Mo; *2–5*, 30—120 μg Re.

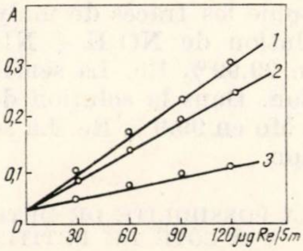

Fig. 2. — Courbe d'étalonnage rhénium — tiocyanate à trois longueurs d'onde.

1, $\lambda=425$ nm; *2*, $\lambda=455$ nm; *3*, $\lambda = 500$ nm.

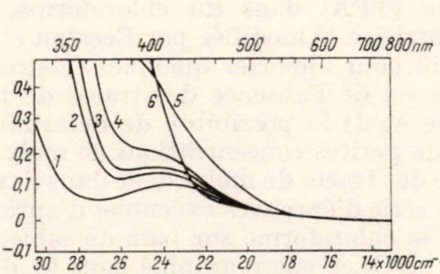

Fig. 3. — Spectres d'absorption rhénium—thiocyanate à côté de molybdène.

1, 30 μg Re; *2–4*,30 μg Re+50—100—200 μg Mo; *5*, 60 μg Re+600 μg Mo; *6*, 1200 μg Mo.

L'analyse des spectres d'absorption dans le domaine de 350 à 600 nm suggère la possibilité de déterminer les petites quantités de rhénium et de molybdène par une seule courbe d'absorption, sur la base des courbes-étalon pour le rhénium et le molybdène et la corrélation des valeurs d'absorption à deux longueurs d'onde (385 et 425 nm).

C. UNE VARIANTE EXTRACTIVE-POLAROGRAPHIQUE POUR LA DÉTERMINATION DU RHÉNIUM DANS LES MOLYBDÉNITES

1. Le contrôle polarographique (dans la solution de base de NaCl2N, pH ~ 11 + Na_2SO_3) démontre la possibilité de faire des déterminations avec le tétraphénylarsonium (TPA). Une étude systématique de cette détermination polarographique sera faite dans un autre travail.

2. Pour la détermination polarographique du rhénium dans l'extrait chloroformique d'après la méthode citée [13,14] il faut chasser le TPA sans pertes de rhénium. L'éloignement quantitatif du TPA sans pertes de rhénium a été réalisé sur une résine cationique fortement acide (Amberlite IR-120, forme H). Après l'éloignement du chloroforme par séchage sur bain de sable, on reprend l'extrait avec 4 ml d'eau, on ajoute 0,5 g d'Amberlite IR-120 forme H, on agite (avec un agitateur magnétique) de 2 à 5 minutes. En ces conditions le TPA est retenu quantitativement par la résine, tandis que le rhénium reste dans la solution aqueuse. On prend 1 ml de solution, on ajoute 5 ml de NaCl2N au pH $\sim 11 + Na_2SO_3$ et on polarographie dans l'intervalle 1,0–1,6 V, S = 1/10. L'interprétation quantitative du rhénium se fait d'après une courbe-étalon ou d'après la méthode de l'additif. Dans les tableaux 1 et 2 on présente quelques résultats qui démontrent l'éloignement quantitatif du TPA avec la résine et la possibilité de déterminer le rhénium dans l'extrait chloroformique, traité d'après la méthode.[13,14]

Tableau 1

Contrôle polarographique de l'élimination quantitative du TPA sur une résine cationique

Re + TPA	La hauteur du palier polarographique h (mm)
10 μg Re	50
10 μg Re + 200 μg TPA	51
10 μg Re + 400 μg TPA	50
10 μg Re + 800 μg TPA	51

Tableau 2

Détermination polarographique du rhénium d'après la variante proposée (dans le présent ouvrage) en comparaison de la méthode colorimétrique. [13,14]

Nº de l'épreuve	μg Re/g MoS_2 déterminé polarographiquement	μg Re/g MoS_2 déterminé par colorimétrie	Erreur en regard de la valeur moyenne
I	92	91	±2 %
II	92	91	
III	93	93	
IV	93	92	

Ainsi que le démontrent nos essais et études répétés on peut appliquer avec confiance les méthodes colorimétrique et polarographique pour la détermination du rhénium dans les molybdénites en respectant les précautions recommandées.

Revue Roumaine de Chimie, 17, 1, 2, 131 – 135 (1972)

En l'honneur du 70e anniversaire
du Professeur I. G. MURGULESCU

SUR LA PRODUCTION DE TÉTRACYANOFERRATES

GUY EMSCHWILLER

Laboratoire de Chimie physique, Ecole Supérieure de Physique et de Chimie, 10, rue Vauquelin, 75-Paris 5e

Reçu le 4 septembre 1971

La photolyse et la thermolyse des solutions aqueuses d'aquopentacyanoferrate (II) de sodium sont susceptibles de produire un tétracyanoferrate, dont la présence a été établie en mettant à profit sa réaction sur le nitrosobenzène qui donne naissance à un complexe coloré en bleu, le dinitrosobenzène-tétracyanoferrate (II) de sodium. Des essais effectués à des pH compris entre 3 et 10 il résulte que c'est dans les milieux les plus acides que le tétracyanoferrate est le plus stable.

Le temps est révolu où les ferrocyanures ou hexacyanoferrates (II) étaient considérés comme des complexes parfaits, parce qu'on n'avait pas réussi à trouver trace, dans leurs solutions aqueuses, d'ions ferreux ni d'ions cyanés, comme cela aurait été le cas s'ils avaient été susceptibles de se dissocier conformément à la réaction d'équilibre :

$$Fe(CN)_6^{4-} \rightleftharpoons Fe^{2+} + 6CN^-$$

En vérité, il ne s'agit là que d'une réaction globale, car il n'est pas douteux qu'une telle dissociation procède par étapes, le départ séparé de chacun des ions cyanés pouvant s'accompagner de la production successive d'ions complexes pentacyanés, tétracyanés, . . ., tels que $Fe(CN)_5(H_2O)^{3-}$, $Fe(CN)_4(H_2O)_2^{2-}$, . . ., jusqu'à aboutir à l'ion ferreux.

Il a été établi que la réaction primaire de dissociation de l'ion hexacyanoferrate (II) est :

$$Fe(CN)_6^{4-} + H_2O \rightleftharpoons Fe(CN)_5(H_2O)^{3-} + CN^-$$

Cette dissociation a été observée dans des circonstances diverses, par photolyse, par thermolyse, par action des sels mercuriques, etc.[1] Divers pentacyanoferrates ont été préparés et isolés ; c'est ainsi qu'une méthode de préparation de l'aquopentacyanoferrate (II) de sodium a été décrite par Hofmann[2] et elle demeure la seule valable.

---

[1] voir en particulier : G. EMSCHWILLER, « Contributi teorici e sperimentali di polarografia », Vol. 3o, supplemento a *La Ricerca Scientifica*, **27**, 164 (1957).

[2] K. A. HOFMANN, Liebigs *Ann. Chem.*, **312**, 1 (1900).

La première seule des différentes étapes de dissociation de l'ion hexacyanoferrate (II) avait donc été clairement reconnue. J'ai réussi à mettre en évidence la seconde, en étudiant la photolyse [3] et la thermolyse des solutions aqueuses d'aquopentacyanoferrates (II), qui peuvent s'accompagner de la production de tétracyanoferrates (II).

Pour caractériser la présence de tétracyanoferrates, j'ai eu recours au nitrosobenzène, qui permet non seulement de les déceler, mais aussi de les doser. Baudisch [4] avait reconnu que l'aquopentacyanoferrate (II) réagit sur le nitrosobenzène pour donner le nitrosobenzène-pentacyanoferrate (II) $Fe(CN)_5(C_6H_5NO)^{3-}$ coloré en violet, et j'ai mis à profit cette réaction pour doser les pentacyanoferrates [5]. De même, j'ai découvert que le nitrosobenzène était susceptible de donner avec les tétracyanoferrates le dinitrosobenzène-tétracyanoferrate (II) $Fe(CN)_4(C_6H_5NO)_4^{2-}$ coloré en bleu [6], et j'ai pu tirer profit de cette réaction pour doser les tétracyanoferrates.

1. PRODUCTION DU DINITROSOBENZÈNE-TÉTRACYANOFERRATE (II) À PARTIR DU NITROSOBENZÈNE-PENTACYANOFERRATE (II)

Si l'on traite une solution d'hexacyanoferrate (II) par du chlorure mercurique en quantité ménagée, en présence de nitrosobenzène en excès, il se produit une réaction stœchiométrique impliquant la transformation de deux ions complexes par ion mercurique, [7] conformément à l'équation :

$$2\ Fe(CN)_6^{4-} + Hg^{2+} + 2\ C_6H_5NO \rightarrow 2\ Fe(CN)_5(C_6H_5NO)^{3-} + Hg(CN)_2$$

De la même manière, si l'on traite une solution de nitrosobenzène-pentacyanoferrate (II) par du chlorure mercurique en quantité limitée, en présence de nitrosobenzène à la température ordinaire, on voit aussitôt la couleur virer du violet au bleu et le changement peut être complet en peu de temps. Ici encore, se produit une réaction stœchiométrique impliquant la transformation de deux ions complexes par ion mercurique,[6] conformément à l'équation :

$$2\ Fe(CN)_5(C_6H_5NO)^{3-} + Hg^{2+} + 2\ C_6H_5NO \rightarrow 2\ Fe(CN)_4(C_6H_5NO)_2^{2-} + \\ + Hg(CN)_2$$

J'ai pu déterminer quantitativement le spectre d'absorption de ce nouveau complexe coloré en bleu, dans la région du visible. A cette fin, a été dissous dans l'eau du nitrosobenzène-pentacyanoferrate (II) de sodium solide, pur, à des concentrations variables, 10^{-4}, 2.10^{-4}, 3.10^{-4}, 4.10^{-4}, 5.10^{-4} M, puis additionné de nitrosobenzène de telle sorte que le mélange final renferme 30% en volume d'une solution éthanolique de nitrosobenzène à 7,5 g/l, enfin de chlorure mercurique à des concentrations diverses, soit, comptées dans le mélange final, 10^{-5}, 2.10^{-5}, 3.10^{-5}, 4.10^{-5}, 5.10^{-5} et 8.10^{-5} M. La formation du complexe coloré bleu se manifeste par l'apparition d'une bande d'absorption dont le maximum est à 640 nm. Pour chacune des concentrations de chlorure mercurique, les valeurs obtenues pour les densités optiques à 640 nm sont pratiquement les mêmes, quelle que soit la concentration du nitrosobenzène-pentacyanoferrate ; la production du dinitrosobenzène-tétracyanoferrate est bien proportionnelle à la concentration du chlorure mercurique, à la condition que le nitrosobenzène-pentacyanoferrate soit présent en excès.

---

[3] G. Emschwiller, *Compt. rend.*, **270** ,1362 (1970).

[4] O. Baudisch, *Berichte dtsch. Chem. Ges.*, **55**, 2698 (1922) ; **62**, 2706 (1929).

[5] G. Emschwiller, *Compt. rend.*, **236**, 72 (1953.)

[6] G. Emschwiller, *Compt. rend.* **247**, 1115 (1958).

[7] G. Emschwiller, *Compt. rend.*, **242**, 1610 et 1883 (1956).

Les mêmes résultats spectrométriques ont été retrouvés en produisant le complexe violet *in situ* dans la solution par action du nitrosobenzène sur l'amminopentacyanoferrate (II) en milieu tamponné au pH 3,9.

Le complexe violet présente un maximum d'absorption à 530 nm (coefficent d'extinction 6460 mole^{-1} cm^{-1}) ; le complexe bleu présente un maximum d'absorption à 640 nm (coefficient d'extinction molaire 6800) et un second situé lui aussi vers 530 nm (coefficient d'extinction 5700).

Il importe de remarquer que, tandis que la production du complexe violet à partir du pentacyanure ne nécessite qu'un excès relativement faible de nitrosobenzène, de telle sorte qu'il suffit d'utiliser une solution aqueuse de ce réactif, par contre la production du complexe bleu n'est totale que si le nitrosobenzène est présent en très grand excès, de l'ordre de 200 à 250 moles de nitrosobenzène par mole de tétracyanoferrate ; c'est la raison pour laquelle il faut recourir à une solution alcoolique de nitrosobenzène suffisamment concentrée. Aussi bien, en employant une solution aqueuse, même saturée, de nitrosobenzène, la production du complexe bleu à partir de tétracyanoferrate est-elle négligeable, tandis que la transformation du pentacyanure en complexe violet est totale. En conséquence, le nitrosobenzène en solution aqueuse permet de doser, dans un mélange de pentacyanoferrate et de tétracyanoferrate, le pentacyanoferrate seul, tandis que la solution éthanolique de nitrosobenzène à 7,5 g/l permet de déterminer tout à la fois les teneurs en pentacyanoferrate et en tétracyanoferrate.

2. PRODUCTION DE TÉTRACYANOFERRATE (II) PAR PHOTOLYSE DE SOLUTIONS AQUEUSES D'AQUOPENTACYANOFERRATE (II)

Les solutions aqueuses d'aquopentacyanoferrate (II) de sodium ont été obtenues à partir du produit solide préparé selon la méthode indiquée par Hofmann. [1] Mais j'ai reconnu que ce produit renferme, en réalité, deux constituants [8] ; l'un est bien l'aquopentacyanoferrate correspondant à l'ion $Fe(CN)_5(H_2O)^{3-}$, tandis que l'autre est un dimère correspondant à l'ion binucléaire di-μ-cyano-octacyanodiferrate (II) $Fe_2(CN)_{10}^{6-}$.[9] Ces deux constituants sont susceptibles de coexister en équilibre en solution aqueuse, [10] et l'on peut mettre à profit les déplacements d'équilibre pour préparer des solutions enrichies en l'un ou en l'autre. C'est ainsi que, pour préparer des solutions très enrichies en complexe uninucléaire, il suffit d'abandonner pendant 4 heures, à la température de 10°C, une solution du produit d'Hofmann à une concentration de l'ordre de 10^{-3} M, en prenant la précaution d'opérer sous atmosphère d'azote. On peut ainsi atteindre des teneurs dépassant 95% et atteignant jusqu'à 98 ou même 100%, en aquopentacyanoferrate (II) vrai.

---

[8] G. Emschwiller, *Compt. rend.*, **238**, 341 (1954).

[9] G. Emschwiller, *Compt. rend.*, **265**, 281 (1967).

De telles solutions ont été soumises à l'action de la radiation 366 nm de l'arc au mercure, à une température comprise entre 0 et 2°C pour éviter toute décomposition thermique, dans des cuves cylindriques à faces parallèles de 2,5 cm de diamètre et 1,5 cm d'épaisseur. Les irradiations ont duré de 5 mn à 3 h. La disparition de l'aquopentacyanoferrate a été suivie par colorimétrie en mettant à profit la réaction sur la solution aqueuse de nitrosobenzène. La formation du tétracyanoferrate a été suivie spectrométriquement, pour la radiation 640 nm, en utilisant la réaction sur le nitrosobenzène en solution alcoolique. Les essais ont porté d'abord sur des solutions aqueuses non tamponnées, puis sur des solutions tamponnées.

Les rendements quantiques ont été rapportés à l'aquopentacyanoferrate disparu. Ils ont été trouvés égaux à 0,35 en milieu non tamponné (pH de l'ordre de 6,5), et, pour les milieux tamponnés, 0,30 au pH 3,53 – 0,31 au pH 3,95 – 0,38 au pH 4,45 – 0,48 au pH 5,9 – 0,58 au pH 6,0 – 0,47 au pH 7,7 – 0,36 au pH 8,9 – 0,30 au pH 9,9. Ainsi le rendement quantique semble passer par un maximum pour un pH de l'ordre de 6.

La réaction primaire de photolyse libère un ion cyané avec formation d'ion tétracyanoferrate, qui doit d'adjoindre deux molécules d'eau pour respecter la coordinance 6 du fer :

$$\mathrm{Fe(CN)_5(H_2O)^{3-} + H_2O + h\nu \rightarrow CN^- + Fe(CN)_4(H_2O)^{2-}}$$

Des réactions secondaires s'ensuivent, en particulier la combinaison d'ions cyanés et pentacyanés en ions hexacyanés, comme aussi une décomposition du tétracyanoferrate aboutissant à la production d'ions ferreux.

La stabilité du complexe tétracyané apparaît variable avec les conditions de milieu. Voici quels ont été, après une heure d'irradiation, les rendements en complexe tétracyané rapportés au pentacyanure disparu : 26% en solution non tamponnée, et, pour les milieux tamponnés, 38% au pH 3,53 – 39% au pH 3,95 – 24% au pH 4,45 – 14% au pH 5,9 – 13% au pH 6,0 – 10% au pH 7,7 – 7% au pH 8,9 – 3% au pH 9,9. C'est donc dans les milieux les plus acides que la production du tétracyanoferrate se révèle la plus forte.

Le rendement en tétracyanoferrate est variable au cours du temps et tend en général à décroître au fur et à mesure que se poursuit l'irradiation ; c'est ainsi que, pour le pH 3,95, le rendement en tétracyanoferrate, rapporté au pentacyanoferrate disparu, a été de 64% après 15 mn, 48% après 30 mn, 39% après 1 h.

---

[10] G. Emschwiller, *Compt. rend.*, **259**, 4281 (1964).

3. PRODUCTION DE TÉTRACYANOFERRATE (II) PAR THERMOLYSE DE SOLUTIONS AQUEUSES D'AQUOPENTACYANOFERRATE (II)

Comme pour l'étude de la photolyse, les expériences ont porté sur des solutions aqueuses étendues d'aquopentacyanoferrate (II) de sodium, à peu près exemptes du complexe binucléaire. La disparition de l'aquopentacyanoferrate a été suivie par la méthode colorimétrique au nitrosobenzène et aussi spectrométriquement par mesure de l'intensité de la bande d'absorption dont le maximum est à 445 nm. Les essais ont été effectués, en présence ou en l'absence de tampons, à des températures comprises entre 15 et 35°. L'allure des cinétiques est d'ailleurs variable avec le pH et aussi, éventuellement, avec la nature des tampons. Dans les cas les plus simples, la réaction apparaît d'ordre un jusqu'à des taux de décomposition de l'aquopentacyanoferrate pouvant atteindre ou même dépasser 80 % ; il en est ainsi pour les milieux non tamponnés ou à tampons citrate-acide chlorhydrique (pH 2,97—3,53—3,95—4,45), ou tamponnés aux phosphates (pH 5,9 et 6,8). On calcule alors des constantes de vitesse ayant respectivement pour valeurs à 35° : $11{,}9.10^{-3}$ mn^{-1} au pH 2,97— $14{,}4.10^{-3}$ au pH 3,53—$15{,}9.10^{-3}$ au pH 3,95—$21{,}4.10^{-3}$ au pH 4,45— $17{,}3.10^{-3}$ au pH 5,9—$11{,}1.10^{-3}$ au pH 6,8 et aussi pour la solution non tamponnée. Il y aurait ainsi une vitesse maximale de décomposition pour le pH 4,45. Les résultats cinétiques sont plus complexes dans les autres milieux tamponnés (tampons aux phosphates de pH 7,7 et tampons aux borates de pH 8,3—8,9 et 9,9), la réaction de décomposition allant alors s'accélérant au cours du temps.

Les produits de la réaction sont les mêmes que pour la photolyse, à savoir : tétracyanoferrate (II), hexacyanoferrate (II), ions ferreux, ions cyanés ou acide cyanhydrique. En ce qui concerne la production du tétracyanoferrate, elle n'atteint ou dépasse un rendement de 20 % par rapport à l'aquopentacyanoferrate disparu que pour les pH au plus égaux à 4. La concentration du tétracyanoferrate va alors régulièrement croissant au cours du temps, de telle sorte qu'elle peut égaler et dépasser celle du pentacyanoferrate restant. C'est ainsi, par exemple, que, dans un essai ayant porté sur une solution $0{,}9.10^{-3}$ M d'aquopentacyanoferrate de sodium à 96,5 % de complexe uninucléaire, tamponnée au pH 3,95 et maintenue à 35°C, la concentration du tétracyanoferrate a été $0{,}24.10^{-3}$ M au bout de 6 heures, alors que celle du pentacyanoferrate n'était plus que $0{,}06.10^{-3}$ M. Un tel résultat témoigne que, dans certaines conditions de milieu, le tétracyanure est plus stable que le pentacyanure. Pour les pH supérieurs à 4, les rendements en complexe tétracyané peuvent n'être que de quelques % ou même à peu près nuls ; dans les solutions non tamponnées, le rendement croît d'abord jusqu'à près de 15 %, au bout de 2 h à 35°, pour décroître ensuite.

Ces recherches ont été effectuées avec la participation expérimentale de Madame Claude Friedrich.

Revue Roumaine de Chimie, 17, 1, 2, 131 – 135 (1972)

Revue Roumaine de Chimie, 17, *1*, *2*, 137–143 (1972)

Herrn Professor I. G. MURGULESCU
zum 70. Geburtstag

ÜBERFÜHRUNGSZAHLEN UND TEMPERATURKOEFFIZIENTEN DER LEITFÄHIGKEIT EINIGER ELEKTROLYTE IN GEMISCHEN VON DIOXAN MIT WASSER

T. ERDEY-GRÚZ, ELVIRA KUGLER, ILONA NAGY-CZAKÓ
und KATALIN BALTHAZÁR-VASS

vom Lehrstuhl für physikalische Chemie und Radiologie der Eötvös Loránd Universität, Budapest, VIII, Puskin u. 11–13

Eingegangen am 6. September 1971

Es wurden die Überführungszahlen von LiCl, KCl und HCl in Gemischen von Dioxan und Wasser (0–60 Mol %) bei 5° und 25° sowie die elektrische Leitfähigkeit einiger Lösungen von LiCl, $LiClO_4$, KCl und HCl in demselben Lösungsmittelgemisch (60–71 Mol %) bei Temperaturen zwischen 5° und 70° gemessen. Die Änderung der Kationenbeweglichkeit mit der Zusammensetzung des Lösungsmittels und mit der Temperatur sowie die anomale Temperaturabhängigkeit der Leitfähigkeit lassen sich an Hand des hydrodynamischen und prototropen Mechanismus aufgrund des von den verschiedenen Parametern des Solvats und des Solventen (Größe, Form und elektrisches Feld der Ionen, Viskosität und Struktur des Solventen, Wanderung der prototropen Ladungen usw.) ausgeübten Einflusses und unter Besichtigung der stattfindenden Vorgänge (Solvatation, Änderung, der Struktur des Wassers, Bildung von intermolekularen Komplexen, Inonenpaarbildung usw). deuten. Man erhält auf diese Weise Aufschlüsse über den Mechanismus der Ionenwanderung und über die Struktur der Lösungen.

Die Leitfähigkeit der Elektrolytlösungen bzw. die Beweglichkeit gelöster Ionen hängt u.a. auch vom Mechanismus der Ionenwanderung ab. Gelten die Gesetzmäßigkeiten der Hydrodynamik für die Wanderung der Ionen, so ist die Beweglichkeit hauptsächlich durch die Größe bzw. die Gestalt der Ionen und die Viskosität der Lösung bestimmt. Kommt auch der Protonenaustausch zwischen den Lösungsmittelmolekülen dem hydrodynamischen Mechanismus hinzu, wie es bei Wasserstoff- und Hydroxydionen oft der Fall ist, so spielt auch die Art und Weise bzw. das Ausmaß der prototropen Ladungswanderung in der Leitfähigkeit eine wesentliche Rolle. Beide Arten des Wanderungsmechanismus stehen auch mit der Flüssigkeitsstruktur des Lösungsmittels in Zusammenhang. Im Fall der hydrodynamischen Wanderung beeinflußt das Lösungsmittel einerseits durch Solvatation die Größe der wandernden Ionen, andererseits die Viskosität. Und zwar in dieser Hinsicht ist nicht die makroskopisch meßbare Viskosität ausschlaggebend, sondern die – durch den Umfang und das elektrische Feld der Ionen veränderte – lokale Viskosität (Mikroviskosität) in unmittelbarer Nähe der Ionen. Der prototrope Mechanismus der Elektrizitätsleitung hängt in noch größerem Maße von der Struktur der Flüssigkeit ab. [1] Dementsprechend lassen die Untersuchungen der Leitfähigkeit und der Überführungszahlen in Lösungsmittelgemischen gewisse Folgerungen auf den Mechanismus der Ionenwanderung und auf die Struktur der Flüßigkeit zu.

I. Die Messungen der Überführungszahlen einiger Elektrolyte in Lösungsmittelgemischen von Wasser mit ein- und mehrwertigen Alkoholen [1,2] haben ergeben, daß sich die Überführungszahlen des K^+-, F^-- und Cl^-- Ionen (t) mit der Zusammensetzung des Lösungsmittelgemisches zwar in charakteristischer Weise ändern, jedoch sind diese Änderungen verhältnismäßig klein ($\Delta t < 0,04$). Die Überführungszahlen des Wasserstoffions ändern sich dagegen wesentlich. (Unter „Wasserstoffionen" verstehen wir hier die in Lösung vorhandenen Oxoniumionen bzw. ihre eventuellen Substitutionsprodukte.) So wird z. B. die Überführungszahl des Wasserstoffions von HCl in einem Lösungsmittelgemisch von 95 Mol% Propanol mit Wasser bei 25° von $t_{\text{H-Wasser}} = 0,83$ auf $t_{\text{H}} = 0,51$ (bei 5° sogar auf $t_{\text{H}} = 0,48$) herabgesetzt, obwohl in reinem Propanol $t_{\text{H}} = 0,65$ ist. In Gemischen von Glyzerin mit Wasser wird dagegen t_{H} auf etwa 0,94 erhöht. Diese Änderungen werden durch Bildung von verschieden substituierten Oxoniumionen bzw. durch die verschiedene Affinität des Protons zu den Lösungsmittelmolekülen erklärt. Es spielt auch die Beeinflussung der Struktur der Flüssigkeit durch das elektrische Feld der Ionen eine Rolle.

Im folgenden wird über Messungen der Überführungszahlen von LiCl, KCl, KF und HCl berichtet, die in Lösungsmittelgemischen von 1,4-Dioxan mit Wasser ausgeführt worden sind. Dioxan enthält – im Gegensatz zu den Alkoholen – keine Hydroxylgruppen, und seine Gemische mit Wasser haben eine wesentlich andere Struktur, als die Gemische der Alkohole mit Wasser. Die bei 5° und 25° ausgeführten Messungen – deren Einzelheiten an anderer Stelle beschrieben sind [3] – ergaben Überführungszahlen, die in Abb. 1 angegeben sind.

Es ist bemerkenswert, daß die Überführungszahlen der hydrodynamisch leitenden Li^+-, K^+-, F^-- und Cl^-- Ionen zwar wenig durch Dioxan verändert werden, doch weisen diese kleine Änderungen gewisse charakteristische Züge auf. Die kleinsten Änderungen verursacht Dioxan in den Lösungen von KF, und zwar die Änderungen der Überführungszahlen bei 5° verlaufen parallel mit denen bei 25°. Das Verhältnis der Beweglichkeiten der K^+- und der F^--Ionen wird also durch Dioxan nur geringfügig verändert. Dies steht wohl damit im Zusammenhang, daß die nichtsolvatisierten K^+- und F^--Ionen gleichgroß sind (ihr Radius im Kristallgitter beträgt $r_F = r_K = 1,33$ Å). Allerdings folgt aus den Überführungszahlen, daß die Beweglichkeit der F^--Ionen gegenüber der der K^+-Ionen durch das Dioxan etwas erhöht wird.

---

[1] S. zusammenfassend: T. ERDEY-GRÚZ, E. KUGLER und L. MAJTHÉNYI, *Electrochimica Acta*, **13**, 947 (1968).

[2] T. ERDEY-GRÚZ, L. MAJTHÉNYI und I. NAGY-CZAKÓ, *Acta Chim. Acad. Sci. Hung.*, **53**, 29 (1967).; ebenda Zusammenstellung der früheren Untersuchungen.

[3] T. ERDEY-GRÚZ und I. NAGY-CZAKÓ, *Acta Chim. Acad. Sci. Hung.*, **67**, 283 (1971).

In den Lösungen von KCl und LiCl liegen die Verhältnisse merklich anders. Einerseits zeigen die Kurven der Überführungszahlen des Kations Extremwerte, andererseits überschneiden sich die auf 5° und auf 25° bezogenen Kurven. Diese Tatsachen weisen darauf hin, daß die Änderungen der Ionenbeweglichkeiten durch mehrere – teilweise entgegengesetzte – Einflüsse bedingt sind, die wohl infolge der unterschiedlichen Ionenradien ($r_{\mathrm{Li}} = 0{,}68$ Å, $r_{\mathrm{Cl}} = 1{,}81$ Å) in Vorschein treten.

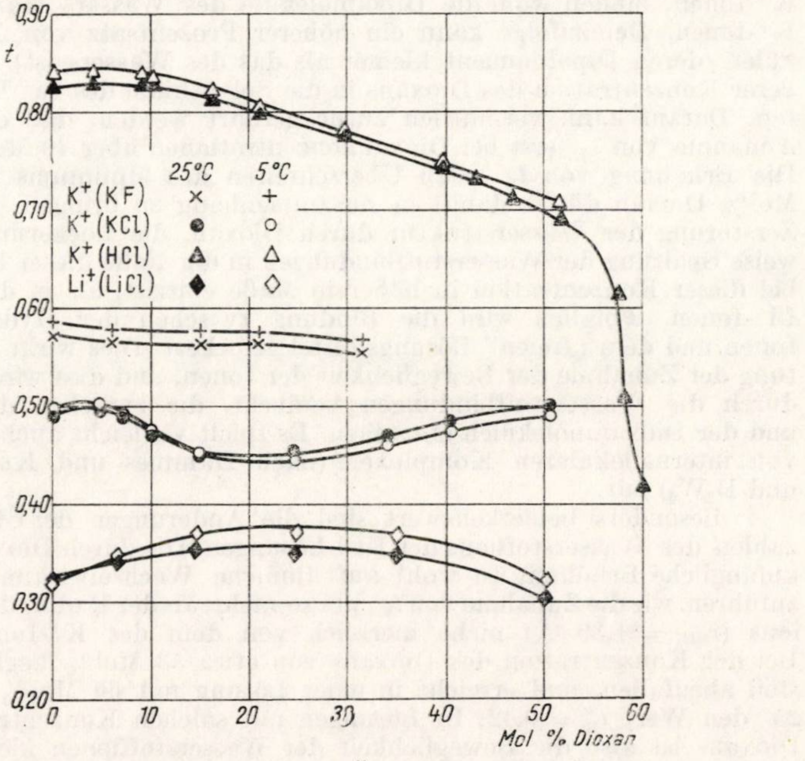

Abb. 1. – Die Abhängigkeit der Überführungszahlen (t) vom Dioxangehalt des Lösungsmittels.

Die anfängliche Zunahme von t_{Li} und t_{K} steht vermutlich damit im Zusammenhang, daß die äußere Hydrathülle dieser Ionen durch Dioxan verringert wird, und daß dieser Einfluß bei den kleineren und stärker hydratisierten Li^+-Ionen stärker ist, als beim größeren und weniger hydratisierten K^+-Ionen. In beiden Fällen wird die Beweglichkeit des kleineren Kations im Gebiet geringer Konzentrationen des Dioxans im Verhältnis zum Anion gesteigert. Mit steigender Konzentration des Dioxans tritt jedoch einerseits die Solvatation der Ionen, andererseits die Zerstörung der Wasserstruktur immer mehr in Vordergrund. Die Abnahme der Überführungszahlen der Li^+- und K^+-Ionen in Lösungsmittelgemischen mit höherem Dioxangehalt ist wohl hauptsächlich dadurch bestimmt, daß die Größe der Kationen verhältnismäßig stärker zunimmt, als die der größeren Cl^--Ionen. Und zwar die kleinen Li^+-Ionen (an deren Grenzen eine höhere Feldstärke herrscht, als an den Grenzen der größeren K^+-Ionen, binden wohl die Dipolmoleküle des Wassers stärker, als die K^+-Ionen. Demzufolge kann ein höherer Prozentsatz von Dioxanmolekülen (deren Dipolmoment kleiner als das des Wassers ist) erst bei größerer Konzentration des Dioxans in die Solvathülle des Li^+-Ionen eintreten. Darauf kann vermutlich zurückgeführt werden, daß eine stärkere Abnahme von t_{Li} erst bei Dioxankonzentrationen über 40 Mol% beginnt. Die Erhöhung von t_K nach Überschreiten des Minimums bei etwa 25 Mol% Dioxan dürfte damit in Zusammenhang zu bringen sein, daß die Zerstörung der Wasserstruktur durch Dioxan, die Lockerung bzw. teilweise Spaltung der Wasserstoffbindungen in der Nähe dieser Ionen bereits bei dieser Konzentration in höherem Maße eintritt, als in der Nähe der Li^+-Ionen. Folglich wird die Bindung zwischen der Hydrathülle der Ionen und dem „freien" Lösungsmittel gelockert. Dies wirkt in der Richtung der Zunahme der Beweglichkeit der Ionen, und dies wird wohl nicht durch die Wasserstoffbindungen verdeckt, die zwischen den Wasser- und der Dioxanmolekülen entstehen. Es spielt vielleicht auch die Bildung von intermolekularen Komplexen (nach Hammes und Knoche[4] DW_2 und D_2W_2) mit.

Besonders bemerkenswert sind die Änderungen der Überführungszahlen des Wasserstoffions der HCl-Lösungen. Die durch Dioxan bewirkte anfängliche Erhöhung ist wohl auf ähnliche Wechselwirkungen zurückzuführen, wie die Zunahme von t_K, um so mehr, als der Radius des Oxoniumions ($r_{OH_3} = 1{,}39$ Å) nicht merklich von dem des K^+-Ions abweicht. Bei der Konzentration des Dioxans von etwa 53 Mol% beginnt aber t_H steil abzufallen, und erreicht in einer Lösung mit 60 Mol% Dioxan bei 25° den Wert $t_H = 0{,}42$. In Lösungen mit solchen Konzentrationen des Dioxans ist also die Beweglichkeit der Wasserstoffionen kleiner, als die der Chlorionen. Die Erklärung dieser Erscheinung ist wohl darin zu suchen, daß die Flüssigkeitsstruktur des Wassers in diesem Konzentrationsbereich durch Dioxan bereits in hohem Maße zerstört wird, und vielleicht die Bildung von D_2W_2 Komplexen in den Vordergrund tritt. Unter diesen Bedingungen sind durch Wasserstoffbindungen gebildete „Wasserpolymere" nicht mehr in genügender Häufigkeit zugegen, um merkliche prototrope Ladungsverschiebung zu ermöglichen. Dieser Befund ist zugleich ein Argument dafür, daß für das Zustandekommen des prototropen Leitungsmechanismus das Vorhandensein von genügend großen Komplexen aus Wassermolekülen, die durch Wasserstoffbindungen zusammengehalten werden, eine Vorbedingung ist. Monomere Wassermoleküle bzw. kleinere Oligomere und Dioxan-Wasser-Komplexe bewirken keine merkliche prototrope Leitung. Letztere können dagegen zur Vergrößerung der Solvathülle der Oxoniumionen beitragen, wodurch das Absinken der Überführungszahl auf $t_H < 0{,}5$ bewirkt wird.

II. Die Abhängigkeit der Leitfähigkeit verschiedener Elektrolyte in Gemischen von Wasser mit Dioxan ist von mehreren Forschern eingehend untersucht worden. [5] Über den Temperaturkoeffizienten der Leitfähigkeit in breiten Gebieten der Temperatur und der Konzentration des Dioxans ist dagegen viel weniger bekannt.

---

[4] G.G. Hammes und W. Knoche, *J. Chem. Phys.*, **45**, 4041 (1966).

Bei der Untersuchung der Leitfähigkeit von LiCl, $LiClO_4$, KCl und HCl in Lösungsmittelgemischen haben wir beim Dioxangehalt von 60 bis 71 Mol% (Dielektrizitätskonstante $\varepsilon = 7,7-5,6$) und im Temperaturgebiet von 5°C–70°C Temperaturkoeffizienten gefunden, [5] die nennenswert von den allgemein bekannten abweichen. Die Äquivalentleitfähigkeit der 0,001 molaren Lösungen dieser Elektrolyte in den genannten Lösungsmittelgemischen wächst anfänglich mit wachsender Temperatur, erreicht ein Maximum, und nimmt bei weiterer Temperaturerhöhung wieder ab. In Abb. 2 sind die relativen Änderungen der Äquivalentleitfähigkeiten

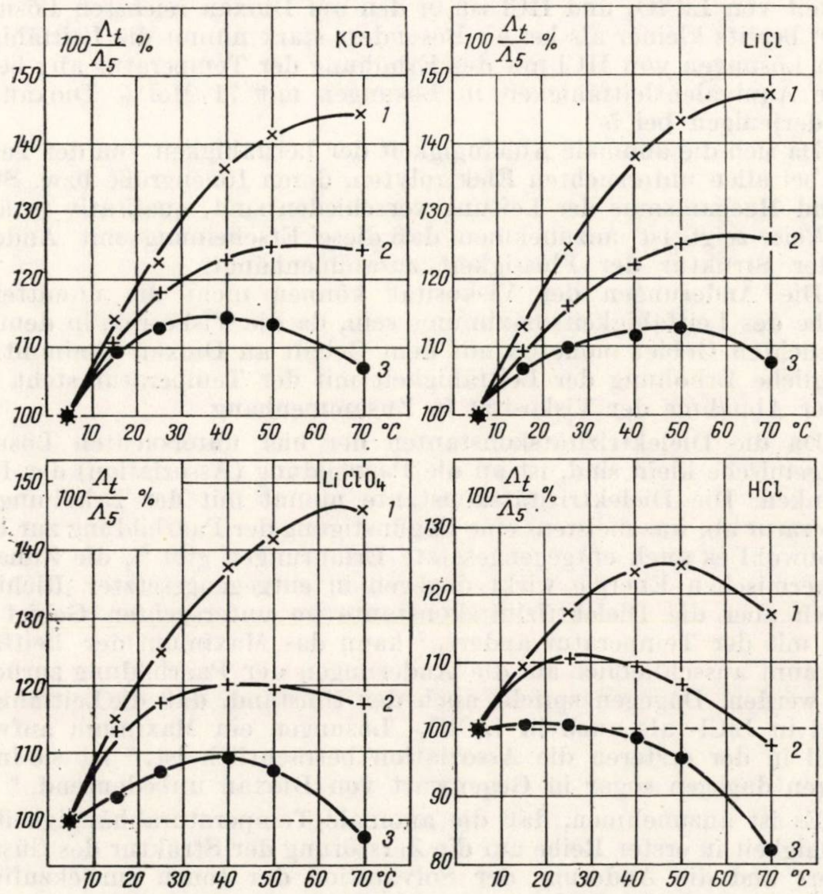

Abb. 2. – Die Abhängigkeit der Leitfähigkeit von der Temperatur
1. – 60,17 Mol % Dioxan; 2. – 65,77 Mol % Dioxan; 3 – 70,99 Mol % Dioxan

---

[5] T. Erdey-Grúz, E. Kugler, I. Nagy-Czakó und K. Balthazár-Vass: *Acta Chim. Acad. Sci. Hung.*, im Druck. Ebenda Zusammenstellung der früheren Untersuchungen.

bei t °C bezogen auf die Leitfähigkeit bei 5° in Prozenten $\left(100 \frac{\Lambda_t}{\Lambda_5} \%\right)$ angegeben. (Abb. 2). Wie ersichtlich, ist bei gegebenem Elektrolyt das Maximum um so mehr ausgeprägt, und es liegt bei um so niedrigerer Temperatur, je höher der Dioxangehalt des Lösungsmittels ist. Die Leitfähigkeit von $LiClO_4$ und HCl ist in den am Dioxan reichsten Lösungen bei 70° bereits kleiner als bei 5°. Besonders stark nimmt die Leitfähigkeit in den Lösungen von HCl mit der Erhöhung der Temperatur ab; bei 70° ist die Äquivalentleitfähigkeit in Lösungen mit 71 Mol% Dioxan nur 82% derjenigen bei 5°.

Da sich die anomale Abhängigkeit der Leitfähigkeit von der Temperatur bei allen untersuchten Elektrolyten, deren Ionengröße bzw. Struktur und Mechanismus der Leitung verschieden sind, qualitativ in ähnlicher Weise zeigt, ist anzunehmen, daß diese Erscheinung mit Änderungen der Struktur der Flüssigkeit zusammenhängt.

Die Änderungen der Viskosität können nicht die unmittelbare Ursache des Leitfähigkeitsmaximums sein, da die Viskosität in dem hier untersuchten Gebiet monoton mit dem Gehalt an Dioxan abnimmt. Die anfängliche Erhöhung der Leitfähigkeit mit der Temperatur steht wohl mit der Abnahme der Viskosität in Zusammenhang.

Da die Dielektrizitätskonstanten der hier untersuchten Lösungsmittelgemische klein sind, ist an die Paarbildung (Assoziation) der Ionen zu denken. Die Dielektrizitätskonstante nimmt mit der Erhöhung der Temperatur ab, was meistens eine Begünstigung der Paarbildung zur Folge hat (obwohl es auch entgegengesetzte Erfahrungen gibt [6]), die Zunahme der thermischen Energie wirkt dagegen in entgegengesetzter Richtung. Da sich aber die Dielektrizitätskonstante im untersuchten Gebiet nur wenig mit der Temperatur ändert, [7] kann das Maximum der Leitfähigkeit kaum ausschließlich auf die Änderungen der Paarbildung zurückgeführt werden. Dagegen spricht auch der Umstand, daß die Leitfähigkeit sowohl in LiCl- als auch in $LiClO_4$- Lösungen ein Maximum aufweist, obwohl in der ersteren die Assoziation beträchtlich ist, [8] ist sie in den letzteren dagegen sogar in Gegenwart von Dioxan unbedeutend. [9]

Es ist anzunehmen, daß die anomale Temperaturabhängigkeit der Leitfähigkeit in erster Reihe auf die Zerstörung der Struktur des flüssigen Wassers und die Änderung der Solvatation der Ionen zurückzuführen sind, wobei auch die Bildung von Dioxan-Wasser Komplexe eine Rolle spielen kann. Nach unseren oben geschilderten Erfahrungen über die Überführungszahlen des Wasserstoffions sind wohl in Lösungen mit mehr als 60 Mol% Dioxan keine ausgedehntere, durch Wasserstoffbindungen zusammengehaltene Komplexe von H_2O-Molekülen vorhanden, sondern vorwiegend monomere Moleküle bzw. oligomere Komplexe. Jedenfalls ist die Bindung zwischen den Wassermolekülen dermaßen gelockert, daß eine Übergabe von Protonen zwischen den Wassermolekülen praktisch nicht mehr möglich ist. Man kann auch daran denken, daß Dioxanmoleküle infolge der Auflockerung der Wasserstruktur bzw. der Bildung von Dioxan-Wasser Komplexe mit steigender Temperatur zunehmend in die sekundäre Hydratationssphäre der Ionen einbezogen werden. Als Hinweis darauf kann die Tatsache betrachtet werden, daß das anfängliche Anwachsen der Leitfähigkeit bei steigender Temperatur um so kleiner ist, bzw. das Maximum der Leitfähigkeit liegt bei um so niedrigerer Temperatur, je höher die Konzentration des Dioxans ist. Die Fähigkeit des Dioxans Ionen zu solvatisieren geht auch aus den Untersuchungen von Grunwald[10] bzw. Atkinson und Mori [11] hervor.

---

[6] Nach A. d'ARPANO und R.M. FUOSS, *J. Phys. Chem.*, **73**, 400 (1969), nimmt die Assoziation der Pikrinsäure in Mischungen von Azetonitril und Methanol bzw. Äthanol mit abnehmender Dielektrizitätskonstante ab.

[7] F.E. CRITCHFIELD, J.A. GIBSON und J.L. HALL, *J. Amer. Chem. Soc.*, **75**, 1991 (1953).

[8] L. FABRY und R.M. FUOSS, *J. Phys. Chem.*, **68**, 971 (1964).

[9] F. ACCASCINA, G. PISTOIA und S. SCHIAVO, *Ricerca sci.*, **34**, 6 (1964); F. ACCASCINA und S. SCHIAVO, „Chemical Physics of Ionic Solutions" ed. B.E. Conway and R. G. Barradas, New York, 1966, S. 515.

Die besonders starke Abnahme der Leitfähigkeit der HCl in den dioxanreichsten Lösungen steht vielleicht mit der starken Solvatation der Oxoniumionen in Zusammenhang. Bereits die Tatsache, daß die Überführungszahl des Wasserstoffions im Lösungsmittel mit 60,3 Mol% Dioxan $t_H = 0{,}42$ ist, weist darauf hin, daß die Solvatation des OH_3^+-Ions, bzw. ihre Bindung mit den Molekülen der Umgebung stark ist. Vermutlich wird durch Temperaturerhöhung die Bindung der Moleküle des Lösungsmittels miteinander stärker gelockert bzw. aufgehoben, als die Bindung der Lösungsmittelmoleküle mit den Wasserstoffionen. In einer Umgebung mit vielen „freien" Dioxanmolekülen können viel leichter größere Solvatkomplexe gebildet werden, als wenn die Lösungsmittelmoleküle miteinander verbunden sind. [12] Allerdings können obige Vermutungen die anomalen Temperaturkoeffizienten bei weitem nicht abschließend klären.

---

[10] E. GRUNWALD, G. BAUGHMAN und G. KOHNSTAM, *J. Amer. Chem. Soc.*, **82**, 5801 (1960).

[11] G. ATKINSON und J. MORI, *J. Chem. Phys.*, **45**, 4717 (1966).

[12] E. FORSLIND, Proc. Internat. Congr. Rheol., Oxford, 1953, 151 (1954); L. J. KAVANAU, „Water and Solute-Water Interactions", San Francisco, 1964, S. 54.

Revue Roumaine de Chimie, 17, 1, 2, 145–153 (1972)

Dedicated to Professor I. G. MURGULESCU
on his 70th birthday

DEMIXING PHENOMENA IN METHYL FORMATE+PARAFFINIC OR OLEFINIC HYDROCARBON BINARY MIXTURES *

PAOLO FERLONI, CRISTIAN TELEA, PAOLO FRANZOSINI and MARIO ROLLA
Institutes of Physical Chemistry and Electrochemistry, University of Pavia, Italy

Received September 4, 1971

The miscibility gaps (MG's) in the binaries formed with methyl formate (component *1*) and several alkanes and alkenes were measured. The newly collected data were discussed together with previous results in order to prove that a satisfactorily accurate prediction of the MG features in a still unknown system is possible even when a different *1* is used.

1. INTRODUCTION

For years our research group has been performing a rather extensive investigation on liquid-liquid equilibria in binaries where *1* was methyl acetate (MeOAc), nitromethane ($MeNO_2$) or acetone (Me_2CO), and *2* was a (C_5-C_9)-hydrocarbon. [1]

A comparative inspection of the results obtained allowed us to point out some connections we summarized in a number of semi-empirical rules, according to which a reasonable forecast of the features of the MG's in still unknown systems (characterized by the same *1*) is now possible.

Thus, before discussing the new data on the title mixtures, an abridged exposure of the above rules seems to be worthy.

2. BINARIES WHERE *1* IS FIXED AND *2* IS AN ALKANE

2.1. DEPENDENCE OF THE CRITICAL SOLUTION TEMPERATURE (CST, T_{max} °K) ON THE NATURE OF *2*.

a) When the mixtures formed with a fixed *1* and the (C_5-C_9)-n-alkanes are considered, the CST's increase with the number, n_C, of the n. alkane carbon atoms, and the experimental data drawn on the (T_{max},

---

* Work carried out with the financial aid of the Italian National Research Council (Rome).

[1] a) M. Rolla, P. Franzosini, R. Riccardi and L. Bottelli, *Z. Naturforsch.*, **21a**, 601 (1966); b) P. Franzosini, R. Riccardi and M. Rolla, "Thermodinamica Chimica" (Convegno CNR tenuto a Roma, 30–31 marzo 1967); c) M. Rolla, P. Franzosini, R. Riccardi and L. Bottelli, *Z. Naturforsch.*, **22a**, 48 (1967); d) P. Franzosini, R. Riccardi and M. Rolla, *Ricerca sci.*, **38**, 123 (1968); e) R. Riccardi, P. Franzosini and M. Rolla, *Z. Naturforsch.*, **23a**, 1816 (1968); f) P. Franzosini, A. Geangu-Moisin and P. Ferloni, *ibid.* **25a**, 457 (1970); g) P. Ferloni, A. Geangu-Moisin, P. Franzosini and M. Rolla, *ibid.*, in press.

n_C)-plane are usually satisfactorily interpolated by slightly bent parabolas *.

b) The replacement of a n-alkane with a branched isomer causes a more or less marked CST depression, dependent on the branch number and nature. E.g., concerning a group of C_8-alkanes studied, the CST's were progressively decreasing when (*1* being the same) n-octane, 2-methyl-heptane, 3-methyl-heptane, 2,5-dimethyl-hexane, 2,2-dimethyl-hexane and 2,2,4-trimethyl-pentane were successively taken into account.

Within a certain alkane series (e.g., the series of the 2-methyl-alkanes) the CST dependence on n_C seems to be once more of a parabolic type.

c) Whatever the alkane series may be, the CST's can be rather satisfactorily foreseen on the basis of a procedure formerly applied by Tatevskii et al. [2] to several physico-chemical alkane properties.

We checked in fact that, in a group of systems formed with the same *1* and any (C_5-C_9)-alkane, the CST's may be expressed as:

$$T_{\max} = n_{12}T_{12} + n_{13}T_{13} + n_{14}T_{14} + n_{22}T_{22} + n_{23}T_{23} + n_{24}T_{24} + n_{33}T_{33} + n_{34}T_{34} + n_{44}T_{44} \qquad (1)$$

where n_{ij} = number of the C − C bonds type $C_i - C_j$ in the alkane molecule, and T_{ij} = empirical parametric value attributed to an Avogadro's number of C_i-C_j bonds.

It is apparent that, in order to evaluate the nine T_{ij} parameters in eq. (1), the CST's in the mixtures formed with *1* and nine properly selected alkanes are to be measured.

2.2. DEPENDENCE OF THE CRITICAL COMPOSITION (CC, $N_{2,\max}$) ON THE NATURE OF *2*

a) As for mixtures of a fixed *1* with a given alkane series, the greater n_C is, the lower $N_{2,\max}$ will be: the function $N_{2,\max}(n_C)$ seems to be of a parabolic type, too.

b) Within different alkane series, close $N_{2,\max}$ values correspond to equal n_C values **.

3. THE "GENERALIZED" DEMIXING CURVE

On the (T, N)-plane a demixing curve usually looks unsymmetrical, which is in any case implicit in what we said at point 2.2.

---

* In a first approximation assumed as straight lines at point c).

** It is noteworthy that the presence of a double bond in the hydrocarbon molecule, though affecting the CST, does not affect the CC.

[2] V.M. TATEVSKII, V.A. BENDERSKII and S.S. YAROVOI, "Rules and Methods for Calculating the Physico-Chemical Properties of Paraffinic Hydrocarbons", Pergamon Press, London, 1961.

Drawing a "generalized" curve, symmetrical with respect to $z = 0.5$ and common to a large system group where *1* is the same, is still possible according to Malesinska [3]) when reduced demixing temperatures, $T/T_{\max}$, and fractions z, defined as :

$$z_1' = N_1'q_1/(N_1'q_1 + N_2'q_2) \qquad z_2' = 1 - z_1' \qquad (2a)$$

$$z_1'' = N_1''q_1/(N_1''q_1 + N_2''q_2) \qquad z_2'' = 1 - z_1'' \qquad (2b)$$

are employed. In eq.'s (2) the apexes ′ and ″ refer to solutions of *1* into *2* and of *2* into *1*, respectively, while the ratio :

$$Q = q_2/q_1 = N_{1,\,\max}/N_{2,\,\max} \qquad (3)$$

is an asymmetry factor, in the following assumed as T-independent for the sake of simplicity.

It is now to be remarked that rather similar generalized demixing curves were always obtained when studying the alkane containing system groups where *1* was everytime MeOAc, $MeNO_2$ or Me_2CO.

4. EXPERIMENTAL

Apparatus and procedure were detailed elsewhere.[4]

The chemicals used were Fluka methyl formate ($>$ 98%), 2-methyl-pentane ($\geqslant$99.9), 3-methyl-pentane ($\geqslant$99.8), 2,2-dimethyl-hexane ($\geqslant$99), 2,3,4-trimethyl-pentane ($\geqslant$99.5), 2,3,5-trimethyl-hexane ($\geqslant$99), 2,2,4-trimethyl-hexane ($\geqslant$ 98), 1-octene ($\geqslant$99.7), *trans*-2-octene ($\geqslant$99), *trans*-3-octene ($\geqslant$99), *trans*-4-octene ($\geqslant$99).

As a specimen of the results obtained, we report in Table 1 and Fig. 1 the data collected on the (MeOF + octene)-mixtures, while in Table 2 the CST's concerning all of the systems studied are summarized.

5. DISCUSSION

5.1. As for (MeOF + alkane)-systems, it is first to be said that all of the rules given in sections 2 and 3 are still obeyed : in particular eq. (1) applies successfully.

Thus, assuming as correct the CST's taken on the n. hexane, [1f] 2-methyl-pentane, 3-methyl-pentane, n-octane, [1f] 2,2-dimethyl-hexane and

---

[3] B. Malesinska, *Bull. Acad. polon. Sci., Ser. Sci. Chim.*, **8**, 53 (1960).

[4] P. Franzosini, *Z. Naturforsch.*, **18a**, 224 (1963).

Table 1

Binaries formed with methyl formate and isomeric octenes

Octene (*2*)	N_2	T (°K)
1-octene	0.042	220.7
	0.116	241.5
	0.133	243.3
	0.143	244.0
	0.161	244.9
	0.222	246.5
	0.245	246.8
	0.353	246.6
	0.419	246.2
	0.554	242.6
	0.618	239.0
	0.623	238.0
	0.744	226.7
	0.755	227.0
trans-2-octene	0.025	214.2
	0.041	223.7
	0.084	239.1
	0.113	244.5
	0.114	245.2
	0.129	247.1
	0.152	249.0
	0.203	250.7
	0.231	250.9
	0.309	251.3
	0.373	250.8
	0.403	250.9
	0.497	248.5
	0.580	246.2
	0.614	244.1
	0.617	243.4
	0.644	241.6
	0.732	232.8
	0.759	230.1
	0.804	223.6
trans-3-octene	0.056	233.9
	0.105	247.3
	0.106	247.6
	0.141	251.3
	0.186	253.3
	0.247	254.3
	0.317	254.5
	0.327	254.5
	0.427	253.5
	0.430	253.7
	0.536	250.8
	0.543	249.4
	0.612	247.1
	0.663	243.0
trans-4-octene	0.023	214.3
	0.038	225.1
	0.047	230.6
	0.058	236.8
	0.096	247.2
	0.111	249.1
	0.121	250.1
	0.213	254.9
	0.342	255.4
	0.372	255.3
	0.507	253.1
	0.539	251.5
	0.624	247.2
	0.693	241.7
	0.773	234.0
	0.817	226.4
	0.852	222.1

Table 2

CST's in binaries formed with methyl formate and a number of alkanes and alkenes

Hydrocarbon	$T_{\max}$ (°K)
2-methyl-pentane	263.8
3-methyl-pentane	262.6
2,2-dimethyl-hexane	273.0
2,3,4-trimethyl-pentane	271.2
2,3,5-trimethyl-hexane	277.8
2,2,4-trimethyl-hexane	275.6
1-octene	246.8
trans-2-octene	251.0
trans-3-octene	254.5
trans-4-octene	255.4

2,3,4-trimethyl-pentane containing binaries, the following T_{ij} values:

$$\begin{aligned} T_{12} &= +122.4 & T_{13} &= +\ 83.2 \\ T_{22} &= +\quad 7.4 & T_{23} &= -\ 32.7 \\ T_{33} &= -\ 72.4 & 3T_{14} + T_{24} &= +135.8 \end{aligned}$$

can be easily obtained.

Then, for (MeOF + 2,3,5-trimethyl-hexane)- and (MeOF + 2,2,4-trimethyl-hexane)-mixtures the above data allow to deduce CST values respectively equal to 278.2 and 276.0°K, in fair agreement with the experimental ones (277.8 and 275.6 °K).

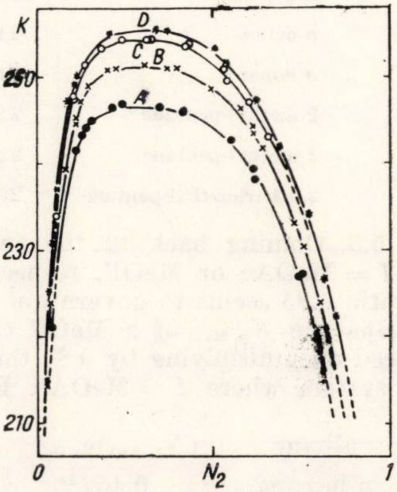

Fig. 1. — Liquid-liquid equilibria in binaries formed with MeOF and 1-, *trans*-2-, *trans*-3- and *trans*-4-octene (curves *A*, *B*, *C* and *D*, respectively).

5.2. We are, however, chiefly interested here in comparing the MeOF containing mixtures with those previously studied, formed with the same alkanes and a different *1*, in particular when the latter is MeOAc.[1a]

A few years ago Riccardi et al. [5] studied the miscibility gaps in the systems MeOAc + CS_2 and MeOF + CS_2, where the CST-ratio is

$$R = \frac{(T_{\max})_{\mathrm{MeOAc}}}{(T_{\max})_{\mathrm{MeOF}}} = \frac{221.5}{260.6} = 0.85_0$$

It is now interesting to note that the same (or nearly the same) ratio is still holding in the (ester + alkane)-mixtures, as the figures reported in Table 3 prove.

Should the $(T_{\max})_{\mathrm{MeOF}}$'s be compared with the CST's taken on analogous systems where *1* is either $MeNO_2$[1cd] or Me_2CO[1b], *R* values respectively equal to ~ 1.4 and 0.9 would be found.

This new regularity clearly allows a CST forecasting in binaries with different *1*, while those reported at point 2.1 concerned only systems where *1* was the same.

---

[5] R. Riccardi and M. Sanesi, *Gazz. chim. Ital.*, **96**, 542 (1966).

Table 3

CST ratio for all the binaries available where MeOAc or MeOF are mixed with the same alkane

Alkane	$(T_{\max})_{\mathrm{MeOAc}}$	$(T_{\max})_{\mathrm{MeOF}}$	R
n-pentane	220.6^{1a}	259.1^{1f}	0.85_1
n-hexane	228.0^{1a}	266.9^{1f}	0.85_4
n-heptane	235.1^{1a}	274.4^{1f}	0.85_7
n-octane	241.9^{1a}	281.8^{1f}	0.85_8
n-nonane	248.2^{1a}	288.8^{1f}	0.85_9
2-methyl-pentane	224.6^{1a}	263.8	0.85_1
3-methyl-pentane	223.0^{1a}	262.6	0.84_9
2,3,4-trimethyl-pentane	228.8^{1a}	271.2	0.84_4

5.3. Coming back to the two mixture groups where *2* = alkane and *1* = MeOAc or MeOF, respectively, it may still be observed that the ratio 0.85 seems to govern not only the CST's, but the CC's too, inasmuch as the $N_{2.\max}$ of a MeOF containing system can be immediately deduced on multiplying by 0.85 the $N_{2.\max}$ value measured on the analogous system where *1* = MeOAc. E.g.:

alkane	$(N_{2.\max})_{\mathrm{MeOAc}}$	$0.85 \cdot (N_{2.\max})_{\mathrm{MeOAc}}$	$(N_{2.\max})_{\mathrm{MeOF}}$
n-hexane	$0.45_0\ ^{1a}$	0.38_3	$0.38_2\ ^{1f}$
n-octane	$0.36_5\ ^{1a}$	0.31_0	$0.30_6\ ^{1f}$

5.4. The following conclusions may be drawn

a) Should the demixing curves concerning a number of (MeOAc + alkane)-systems be known, an appropriate use of the factor 0.85 enables to deduce the CST's and CC's of the analogous systems where *1* = MeOF.

b) As for the latter binaries, an *a priori* forecast of the whole demixing region boundaries is also possible on the basis of the generalized demixing curve proper to the previously mentioned (MeOAc + alkane)-mixtures, since, as a matter of fact, a sufficiently close coincidence exists between the generalized demixing curves proper to both groups of systems (see Fig. 2), and since the asymmetry factors, Q_{MeOF}, are easily evaluated from the above deduced $(N_{2.\max})_{\mathrm{MeOF}}$ values.

As an example, the described procedure was applied to the (MeOF + 3-methyl-pentane)-mixtures: the results are shown in Fig. 3, where the calculated curve is compared to the pertinent experimental points.

c) It may further be observed that the CST's concerning binaries formed with MeOF and an alkane other than those whose mixtures with MeOAc were studied may anyhow be deduced with the help of eq. (1).

E.g., if we desire to know the CST of the system (MeOF + 2,3,5-trimethyl-hexane) when the corresponding one containing MeOAc was not investigated, eq. (1) allows to calculate for the latter a CST equal

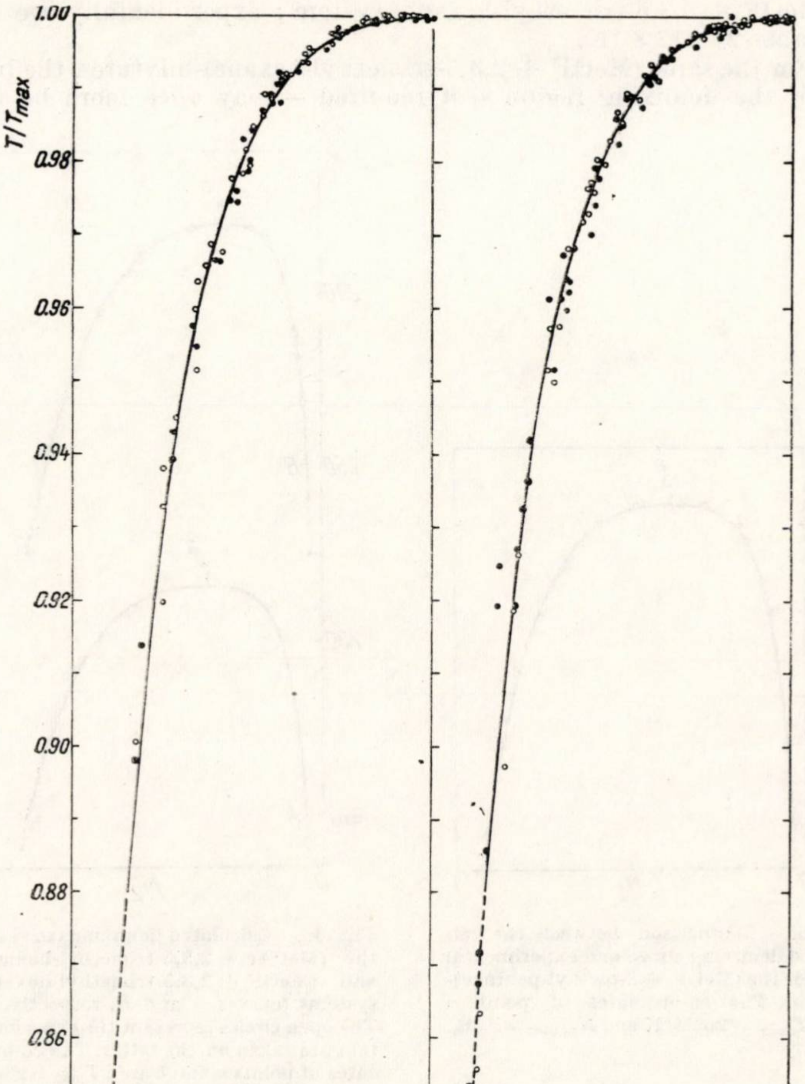

Fig. 2. — In the left section the data [1a] taken on mixtures formed with MeOAc and n-pentane, n-hexane, n-heptane, n-octane, n-nonane, 2-methyl-pentane, 3-methyl-pentane and 2,3,4-trimethyl-pentane are drawn on the ($T/T_{\max}$ *vs.* z)-plane together with the interpolating curve. In the right section the same curve is compared with data taken on mixtures formed with MeOF and the same alkanes (open circles : z_2'' ; full circles : z_1').

to 236.4 °K *, which, divided by 0.85, suggests 278.1 °K as the CST of the (MeOF + 2,3,5-trimethyl-hexane)-system : experimentally we found (see Table 2) 277.8 °K.

For the same (MeOF + 2,3,5-trimethyl-hexane)-mixtures, the boundaries of the demixing region – if required – may once more be traced by taking into account a CC $= 0.33_0 . 0.85 = 0.28_1$ **, an asymmetry factor $Q = 0.71_9/0.28_1 = 2.5_6$, and the generalized curve proper to the (MeOAc + alkane)-binaries : the results are shown in Fig. 4.

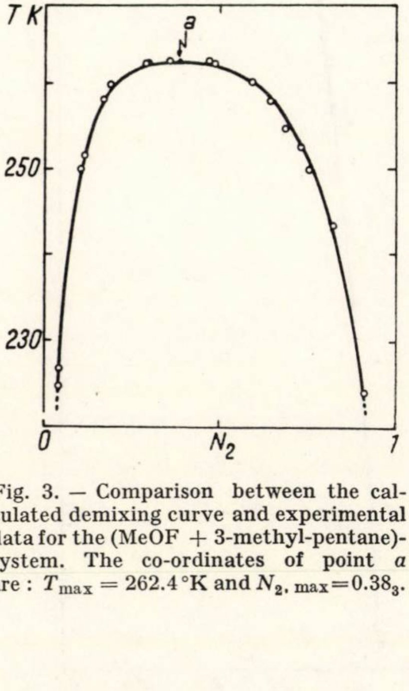

Fig. 3. – Comparison between the calculated demixing curve and experimental data for the (MeOF + 3-methyl-pentane)-system. The co-ordinates of point *a* are : $T_{\max} = 262.4$ °K and $N_{2,\max} = 0.38_3$.

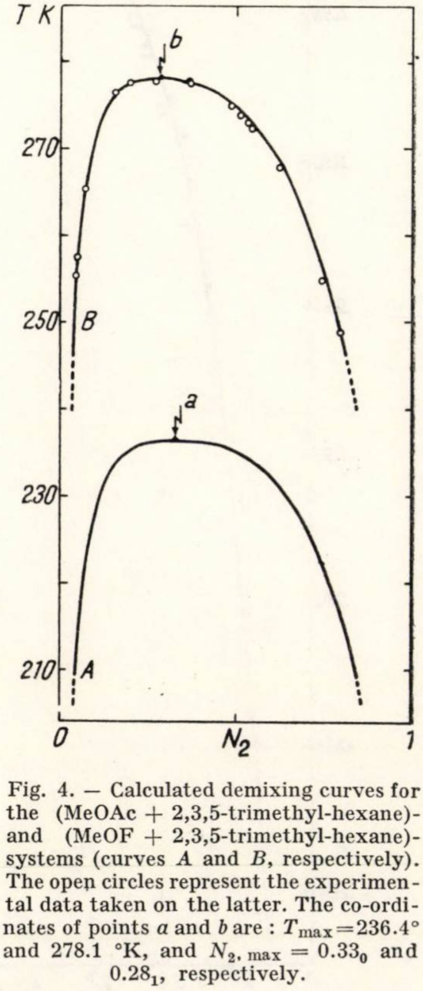

Fig. 4. – Calculated demixing curves for the (MeOAc + 2,3,5-trimethyl-hexane)- and (MeOF + 2,3,5-trimethyl-hexane)-systems (curves *A* and *B*, respectively). The open circles represent the experimental data taken on the latter. The co-ordinates of points *a* and *b* are : $T_{\max} = 236.4°$ and 278.1 °K, and $N_{2,\max} = 0.33_0$ and 0.28_1, respectively.

---

* The parametric values are taken from. [1a]

** Concerning the (MeOAc+alkane)-binaries, the function $N_{2,\max}(n_C)$ may be written[1a] :

$$N_{2,\max} = 0.825 - 0.077_5\, n_C + 0.002_5\, n_C^2$$

Since 2,3,5-trimethyl-hexane is a C_9-alkane, 0.33_0 is the expected $(N_{2,\max})_{\text{MeOAc}}$ value.

5.5. According to point 2.2, a noteworthy coincidence between the CC of the (MeOF + octane)-system ($N_{2,\,\mathrm{max}} = 0.30_6$) and those of the binaries formed with MeOF and 1-octene (0.30_9), *trans*-2-octene (0.30_7), *trans*-3-octene (0.31_0) and *trans*-4-octene (0.31_3) was found.

Moreover, a comparison between the latter four systems and the analogous ones where $\bar{1} = \mathrm{MeNO_2}$ * allows to obtain *R* ratios respectively equal to 1.4_3, 1.4_3, 1.4_3 and 1.4_2, in a satisfactory agreement with the figure (~1.4) mentioned at point 5.2.

---

* Other data are lacking.

Revue Roumaine de Chimie, 17, 1, 2, 155–160 (1972)

Dedicated to Professor I. G. MURGULESCU
on his 70th birthday

POLAROGRAPHIC MAXIMA OF THE THIRD KIND. II

BORNEOL

A.N. FRUMKIN, E.V. STENINA, N.V. NIKOLAEVA-FEDOROVICH, G.N. PETUKHOVA, V.A. YUSUPOVA

Moscow State University, USSR

Received September 24, 1971

It was shown that in the presence of borneol well defined maxima of the third kind appear on the current-voltage curve of the 10^{-3} M $AgNO_3$ + M Na_2SO_4 solution. The maxima can be obtained at any potential but only as long as the coverage of the mercury surface by the surfactant does not exceed a certain limit.

INTRODUCTION

In [1] the polarographic maxima, which are due to tangential motions caused by the adsorption process itself, were called polarographic maxima of the third kind. For the first time current maxima on the current-potential (I, φ) curves and tangential motions of the mercury drop surface were observed at the desorption potentials of a surfactant by Doss. [2] Current maxima at the desorption potentials were observed in solutions in which butyl and octyl alcohols were emulgated. [3] In [3] it was suggested that the appearance of the current maxima at the adsorption-desorption potentials is related to the presence of a concentration gradient of surfactants, which results from the adsorption process itself. Sathyanarayana [4] for the first time obtained well-defined and reproducible current maxima in the case of reduction of Cu^{2+} and Cd^{2+} in the presence of camphor additions. Comparing the I, φ—and the differential capacity-potential (C, φ) curves he showed that the largest maximum corresponds to the desorption potential of camphor. In, [1] at the desorption potentials of

---

[1] A.N. Frumkin, E.V. Stenina and N.V. Fedorovich, *Elektrokhimiya*, **6**, 1572 (1970).

[2] K. Doss and D. Venkatesan, *Proc. Indian Acad. Sci*, **49**, 129 (1959).

[3] A.N. Frumkin, S. Sathyanarayana and N.V. Nikolaeva-Fedorovich, *Izvest. Akad. Nauk S.S.S.R., Otdel. khim. Nauk*, **1962**, 1977.

[4] S. Sathyanarayana, *J. Electroanalyt. Chem.*, **10**, 56 (1965).

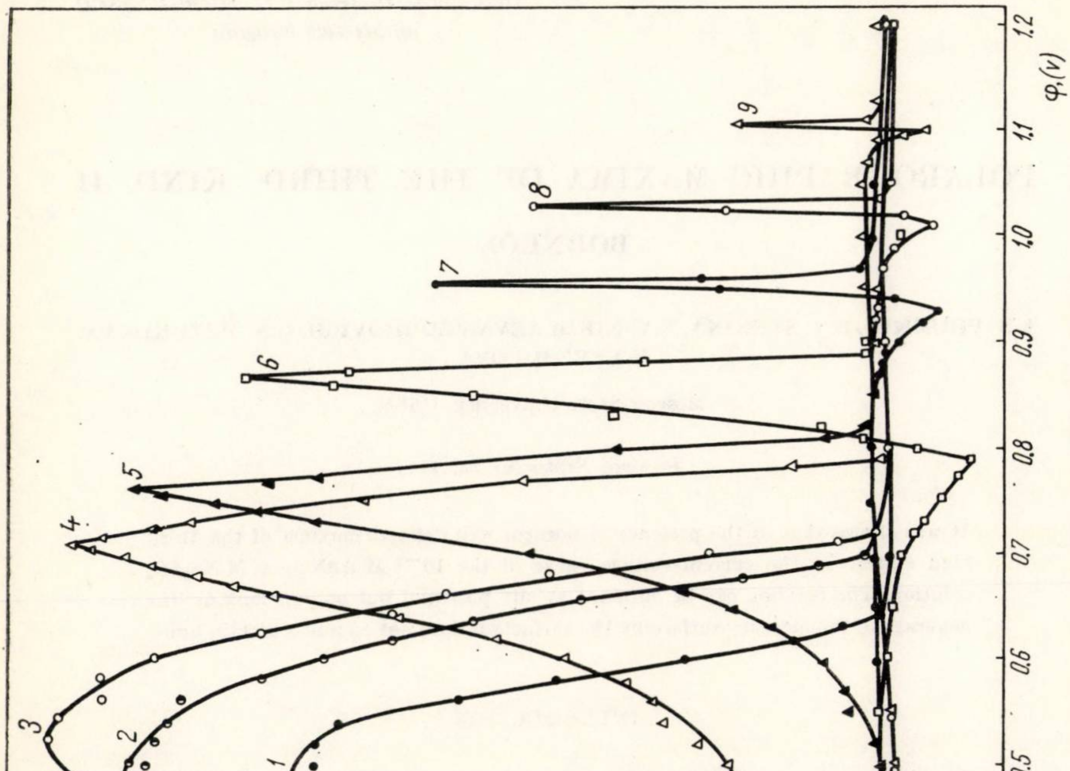

Fig. 1. — Polarization curves of the reduction of 10^{-3} M $AgNO_3$ in M Na_2SO_4 with borneol additions:

camphor, positive and negative current maxima were obtained for the reduction reaction of Cu^{2+}, Ag^{+} and Tl^{+}, but at small camphor concentrations the current increase was observed over the whole range of adsorption potentials.

Thus, so far well defined polarographic maxima of the third kind have been obtained only in the case of camphor adsorption. For further investigation of these maxima we studied their appearance in the case of adsorption of other substances whose structure is similar to that of camphor, such as borneol, for example. In this investigation we used the experimental technique described in. [1]

DISCUSSION

Figure 1 shows the I, φ-curves for 10^{-3} M $AgNO_3 + $ M Na_2SO_4 with different borneol additions. The most positive part of the I, φ-curves where a polarographic maximum of the first kind appears is not reproduced in the figure. Introduction of 3×10^{-5} M borneol leads to a current increase in the region of the potential of zero charge (pzc) (Fig. 1, curve 1). With rising borneol concentration, the current at the maximum increases and the potential range in which the polarographic maximum is observed widens. Further increase of borneol concentration leads first to a splitting of the maximum and then to a decrease in the current at the maximum and even to a complete disappearance of the maximum in the pzc range (Fig. 1, curves 3—5). At borneol concentrations in excess of a certain limit, maxima appear only at relatively large positive and negative charges of mercury surface.

We have also measured the dependence of the current on the drop growth time (I, t-curves). In the range of potentials of the maxima of the third kind we found considerable distortions of the I, t-curves in the form of irregular oscillations, which suggests that the current maxima observed are associated with irregular mercury surface motions. [5]

To establish the relation between the appearance of the maxima and the surface coverage we measured the C, φ-curves in M Na_2SO_4 in the presence of borneol (Fig. 2). The shape of the C, φ-curves in these solutions is similar to that of the C, φ-curves in solutions with camphor additions. [6] There are no pronounced capacity peaks on the C, φ-curves at the adsorption-desorption potentials, which is characteristic of adsorp-

---

[5] A.B. ERSHLER, D.I. DZHAPARIDZE and G.A. TEDORADZE, *Zhur. fiz. Khim.*, **37**, 666 (1963).

[6] S. SATHYANARAYANA and K. BAIKERIKAR, *J. Electroanalyt. Chem.*, **21**, 449 (1969).

tion processes which follow the Frumkin isotherm with a value of the attraction constant a $\geqslant 2$.[7] If we compare the I, φ and the, C, φ-curves, we see that at small borneol concentrations the potential range in which

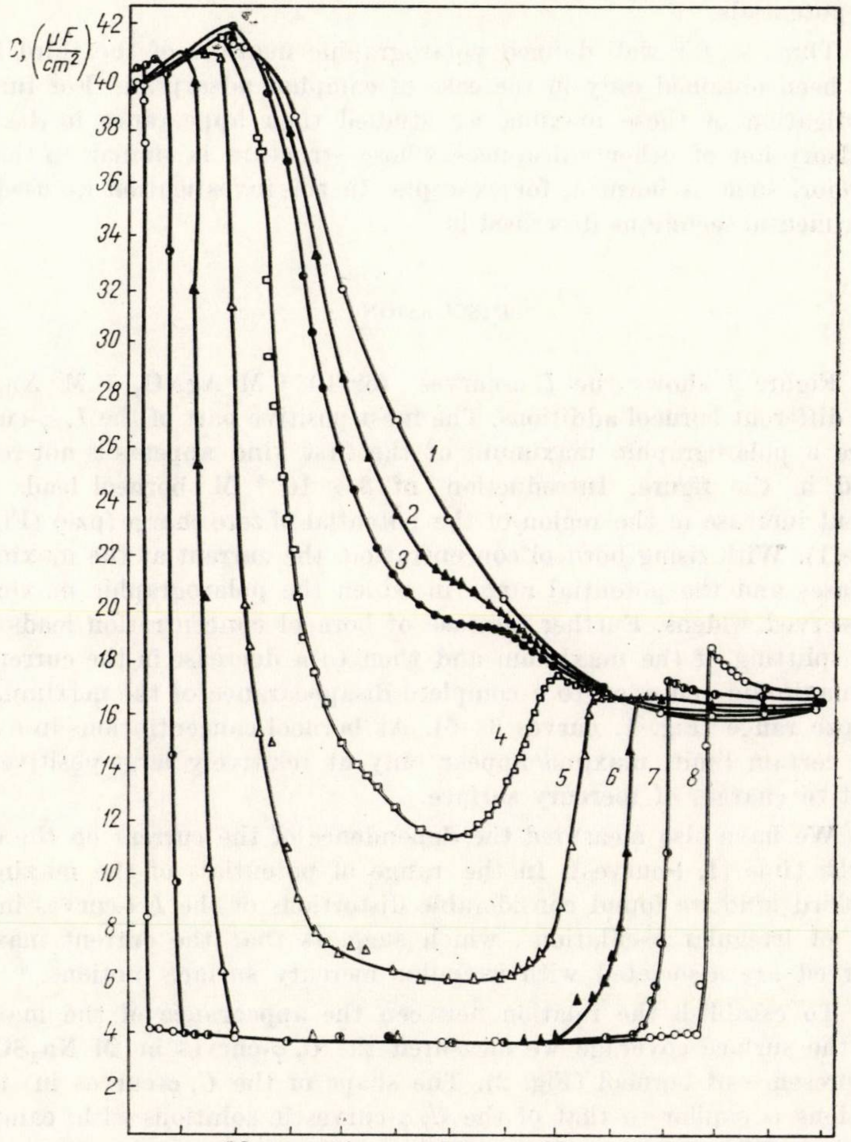

Fig. 2. — Differential capacity -potential curves in M Na_2SO_4 solutions (1) with borneol additions :

2, 3×10^{-5} M; *3*, 4×10^{-5} M; *4*, 6×10^{-5} M; *5*, 10^{-4} M; *6*, 1.8×10^{-4} M; *7*, 3×10^{-4} M; *8*, 6×10^{-4} M.

---

[7] A.N. Frumkin and B.B. Damaskin, "Sovremenniye aspekti elektrokhimii", J.O'M. Bockris ed. 1967, Moscow, "Mir", p. 170.

the current increases in excess of the diffusion current coincides with the potential range in which borneol is adsorbed (Fig. 3), the highest current maximum corresponding to the greatest adsorption of borneol. At these borneol concentrations the surface coverage θ is much less than unit at all potentials. With increasing borneol concentrations, when the surface coverage in the pzc region increases, the tangential motions of mercury surface caused by nonuniform borneol adsorption diminish and when a certain surface coverage value is reached, the maxima of the third kind disappear. At these, and higher, borneol concentrations the maxima are observed only at the desorption potential (Fig. 4), as was the case with camphor.

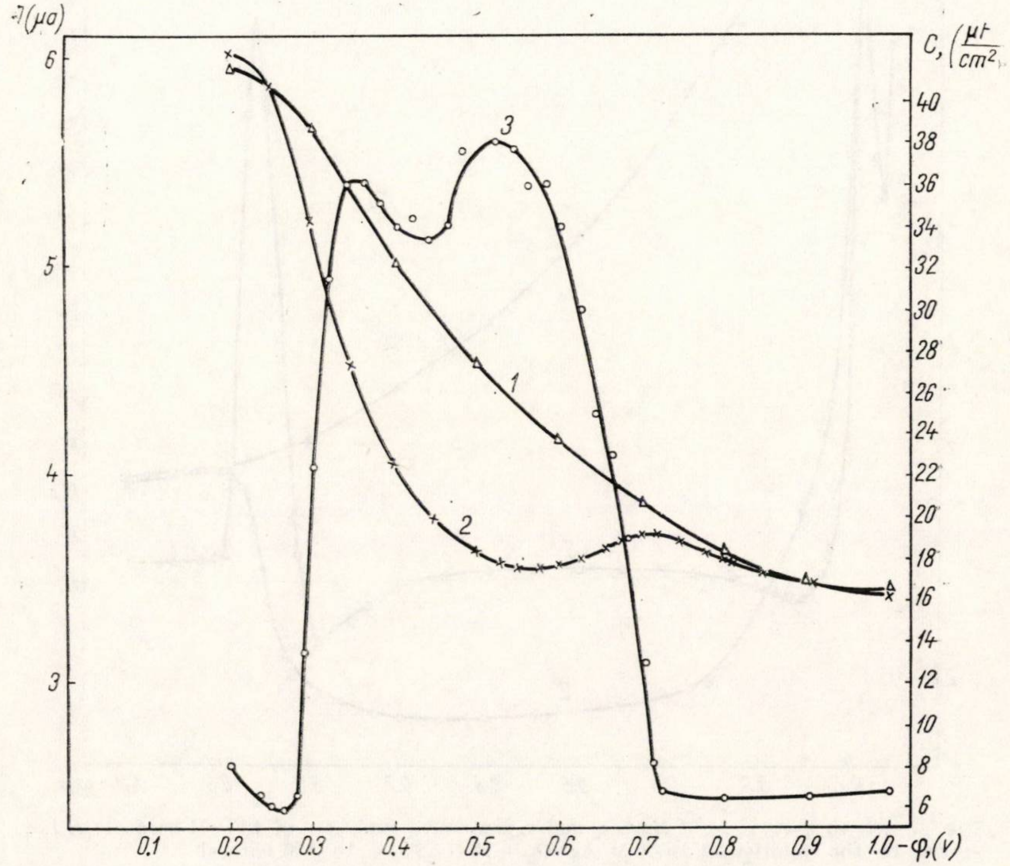

Fig. 3. — *1*, *C*, φ-curve in MNa_2SO_4 and *2*, same with borneol addition in the concentration 4×10^{-5} M; *3*, *I*, φ-curve in the solution 10^{-3} M $AgNO_3$ + M Na_2SO_4 + 4×10^{-5} M borneol.

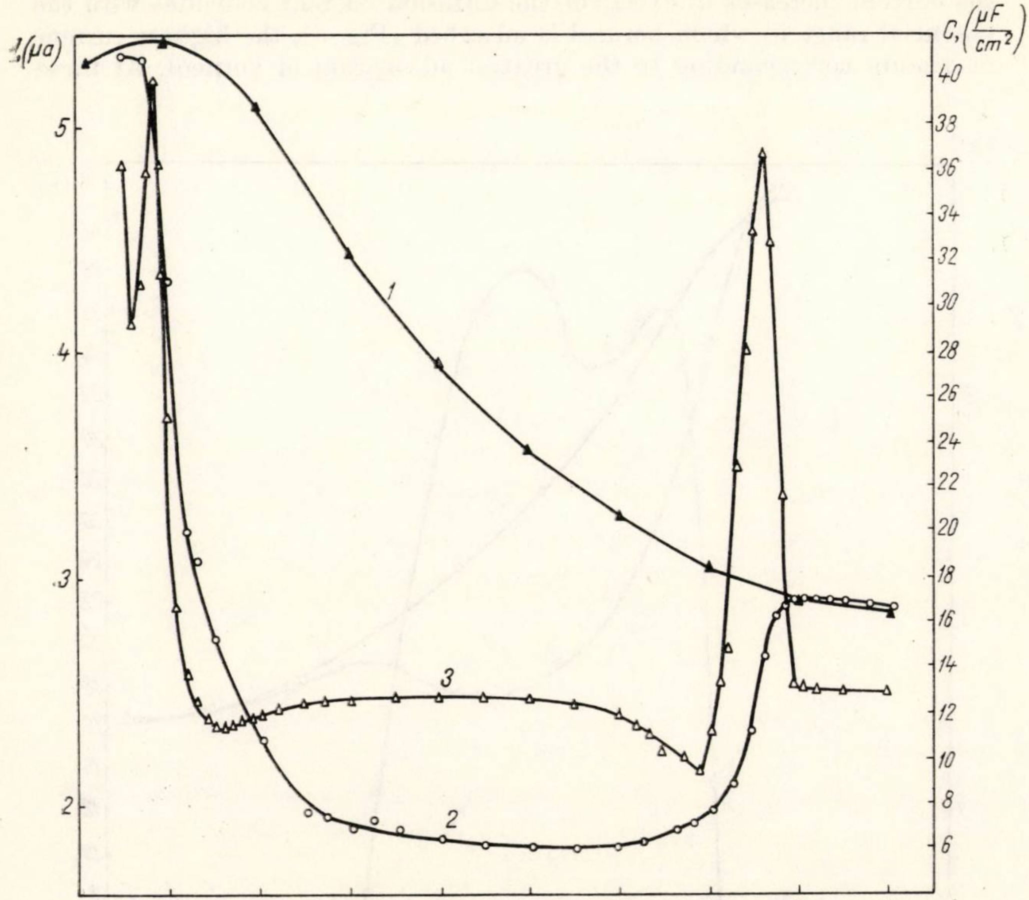

Fig. 4. — *1*, *C*, φ-curve in M Na_2SO_4 and *2*, same with addition of 10^{-4} M borneol; *3*, *I*, φ-curve in the solution of 10^{-3} M $AgNO_3$ + M Na_2SO_4 + 10^{-4} M borneol.

CONCLUSIONS

From the above it results that the appearance of the sharp polarographic maxima of the third kind at the adsorption-desorption potentials is associated only with the fact that at these potentials the surface coverage can assume any value from zero to unit in a narrow potential range.

As will be shown in a subsequent paper the disappearance of the maxima at higher surfactant concentration is caused by the inhibition of the tangential motions under the action of the adsorbed layer.

Revue Roumaine de Chimie, **17**, *1, 2*, 161–166 (1972)

К 70-летию проф. И. Г. МУРГУЛЕСКУ

ВЛИЯНИЕ СОСТАВА РАСТВОРА НА КИНЕТИКУ РАСТВОРЕНИЯ ХРОМА В КИСЛЫХ СРЕДАХ ПРИ КАТОДНОЙ ПОЛЯРИЗАЦИИ

Я. М. КОЛОТЫРКИН, Г. М. ФЛОРИАНОВИЧ и Г. С. РАСКИН

Научно-исследовательский физико-химический институт им. Л. Я. Карпова,
Москва

Получена 24 сентября 1971 г.

Изучается связь между скоростью растворения хрома при повышенной температуре и катодной поляризации и анионным составом электролита. Измерения показали, что ионы Cl^-, SO_4^{2-} и ClO_4^- не оказывают специфического действия на процесс. Скорость растворения хрома возрастает с ростом кислотности раствора. Окислители (перекись водорода, бихромат, нитрат) оказывают тормозящее действие на растворение хрома. Высказаны предположения о возможных причинах этого действия. В кислых средах хром растворяется по химическому механизму с участием ионов водорода.

При растворении хрома в серной кислоте в области катодной поляризации свойственное металлам закономерное снижение скорости растворения при смещении потенциала в отрицательном направлении нарушается: скорость растворения перестает зависеть от потенциала[1–3]. Одним из возможных объяснений такого явления может быть предположение о том, что хром в этих условиях растворяется по химическому механизму [2, 3], то есть путем непосредственного взаимодействия атомов хрома с окислительными компонентами раствора.

Для заключения о природе частиц, участвующих в химической реакции растворения хрома, нами изучалась связь между скоростью растворения этого металла при катодной поляризации и анионным составом электролита.

Опыты проводились на хроме вакуумной выплавки (чистота 99,95 %) в деаэрированных растворах при температуре 90°. Электрод помещался в трехэлектродную ячейку и выдерживался в ней в течение определенного времени при заданном потенциале, после чего раствор сливался и анализировался на содержание ионов хрома фотоколориметрическим и радиохими-

---

[1] В. М. Княжева, « Электрохимическое поведение хрома », Кандидатская диссертация, Физ.-хим. ин-т им. Карпова, Москва, 1958.

[2] Г. М. Флорианович и Я. М. Колотыркин, *Докл. АН СССР*, **157**, 422 (1964).

[3] Я. М. Колотыркин и Г. М. Флорианович, *Защита металлов*, **1**, 7 (1965).

ческим [4] методами (в последнем случае применялся гамма-радиоактивный хром). В части опытов с помощью специальной ячейки измерялось количество выделяющегося водорода. При работе с окислителями определялись также парциальные скорости восстановления окислителей, для чего применялись соответствующие аналитические методы.

Опыты проводились в растворах серной, хлорной и соляной кислот без добавок и в присутствии соответствующих солей щелочных металлов, а также в азотной кислоте и в серной и хлорной кислотах, содержащих окислители — перекись водорода, бихромат, и нитрат.

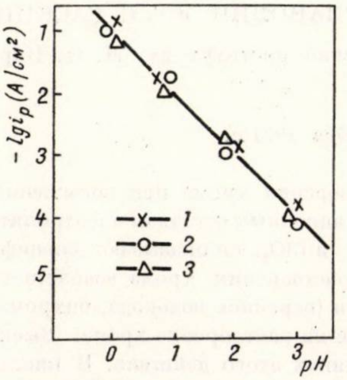

Рис. 1. — Зависимость скорости растворения хрома при катодной поляризации и 90° от pH в растворах хлорида (*1*), перхлората (*2*) и сульфата (*3*) при суммарной 1 N концентрации анионов.

Измерения показали, что во всех исследованных растворах в области потенциалов от — 0,3 до — 0,6 в по н.в.э. скорость растворения хрома с точностью до 30% не зависит от потенциала. В приведенных ниже данных через i_p обозначены усредненные скорости растворения хрома во всем исследованном интервале потенциалов, а через i — опытные значения скорости растворения при заданных потенциалах.

В кислых растворах хлоридов, перхлоратов и сульфатов с постоянной ионной силой величина i_p является линейной функцией pH (рис. 1). Для всех этих растворов указанная зависимость характеризуется одной и той же прямой с наклоном $(\partial \lg i_p/\partial \mathrm{pH})_\varphi = 1{,}1$. Это дает основание сделать вывод, что ионы Cl^-, SO_4^{2-} и ClO_4^- не оказывают специфического действия на процесс растворения хрома в рассматриваемой области потенциалов и pH.

Учитывая найденный нами первый порядок реакции растворения хрома по ионам водорода (рис. 1), а также принимая во внимание независимость скорости этого процесса от концентрации воды в растворе [5], можно предположить, что частицами, участвующими в химической реакции растворения хрома в кислых растворах сульфатов, перхлоратов и хлоридов, являются ионы водорода:

$$Cr + H_3O^+ \rightarrow Cr^+ + H + H_2O. \tag{1}$$

---

[4] М. А. Демброоский и Г. Н. Флорианович, *Защита металлов*, 1, 115 (1965).

[5] Л. А. Соколоба, « Исследование механизма активного растворения железа в кислых растворах », Кандидатская диссертация, Физ.-хим. ин-т им. Карпова, Москва, 1969.

Реакция (1) протекает, по-видимому, через промежуточные стадии образования и разложения гидридов хрома (образование гидридов при катодной поляризации хрома в серной кислоте экспериментально доказано[6]) и сопровождается последующими реакциями в растворе:

$$Cr^{+} + H_3O^{+} \rightarrow Cr^{2+} + H + H_2O,$$
$$2H \rightarrow H_2.$$

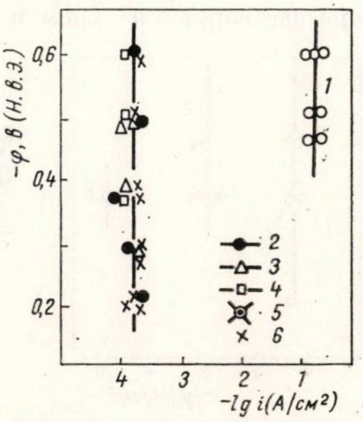

Рис. 2.— Зависимость скорости растворения хрома от потенциала в растворах:
1 – 1 N H_2SO_4, *2* – 1 N HNO_3, *3* – 1 N H_2SO_4 + 10N $NaNO_3$, *4* – 1N H_2SO_4 + 1 M H_2O_2, *5* – 1N H_2SO_4 ± $K_2Cr_2O_7$, *6* – 1N $HClO_4$ + 10N $NaNO_3$.
Температура 90°.

Участие ионов водорода можно представить и иной схемой:

$$Cr + H_3O^{+} \rightarrow Cr\ (H_3O^{+}), \tag{2}$$
$$Cr(H_3O^{+}) + H_3O^{+} \rightarrow Cr\ [(H_2O)_2]^{++} + H_2, \tag{3}$$

предположив, что стадия (2) протекает быстро, но не равновесно, а стадия (3) лимитирует скорость всего процесса.

В отличие от рассмотренных выше анионов, ионы нитрата оказывают специфическое действие на растворение хрома. Как видно из рис. 2, переход от 1 N H_2SO_4 к 1 N HNO_3 (кривые 1 и 2) сопровождается уменьшением скорости растворения примерно на три порядка. Тот же эффект наблюдается и при введении в серную или хлорную кислоты нитрата натрия достаточно высокой концентрации (кривые 3 и 6). Существенно, что тормозящее действие на растворение хрома в серной кислоте оказывают также добавки перекиси водорода и бихромата калия (кривые 4 и 5).

Тот факт, что все найденные замедлители растворения являются окислителями, наводит прежде всего на мысль о возможной связи между обнаруженным эффектом и окислительным действием добавки. Можно предположить, что в присутствии окислителя происходит его взаимодействие с атомами металла с образованием поверхностных слоев типа окисных. Такие слои могут, по-видимому, препятствовать непосредственному взаимодействию атомов хрома с ионами H_3O, подобно тому, как действуют на химическое растворение пассивирующие слои, образующиеся при анодной пассивации [2,3].

---

[6] W. H. Smith, *J. Electrochem. Soc.*, **103**, 51 (1956).

Вероятность взаимодействия металла с окислителем в значительной мере определяется природой металла. Очевидно, что чем выше сродство металла к кислороду, тем легче металл может окисляться. В согласии с этим находятся результаты сопоставления действия окислителей на растворение металлов различной природы. На рис. 3 сопоставлены кривые потенциал — логарифм скорости растворения для железа (по данным[5]), хрома и хромистых сталей IX13 и X28) (содержание хрома соответственно 13 и 28%) в азотной кислоте. С наименьшей скоростью в этом растворе растворяются хром и содержащая большое количество хрома сталь X28. Скорость растворения железа, обладающего меньшим сродством к кислороду, максимальна (и даже превышает скорость его растворения в серной кислоте при том же pH раствора [5]). Сталь IX13 занимает промежуточное положение.

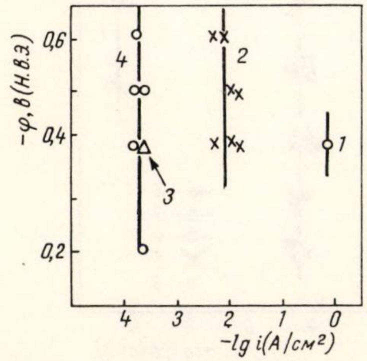

Рис. 3.— Зависимость от потенциала скоростей растворения железа (*1*), сталей IX13 (*2*) и X23 (*3*), а также хрома (*4*) в 1 N азотной кислоте при температуре 90°.

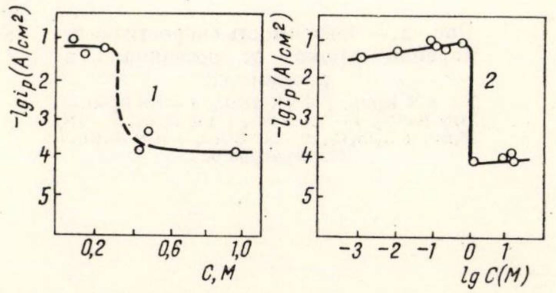

Рис. 4. — Влияние концентрации окислителя на скорость растворения пнри катодной поляризации и температуре 90° врастворах 1 N H_2SO_4 с добавками $NaNO_3$ (*1*) и H_2O_2 (*2*).

Другим возможным объяснением тормозящего действия окислителей на растворение хрома может быть предположение о том, что катодное восстановление окислителей в условиях химического растворения хрома протекает с участием поверхностного комплекса $Cr(H_3O^+)$, образующегося по реакции (2). В результате концентрация $Cr(H_3O^+)$ снижается, что и вызывает тормозящий эффект. При таком предположении можно ожидать, что действие окислителей должно проявляться лишь при некоторой достаточной их концентрации в растворе. С этим согласуются результаты по влиянию концентрации окислительных добавок на скорость растворения хрома по химическому механизму. Как следует из рис. 4, с ростом содержания перекиси водорода и нитрата натрия в растворе серной кислоты величины i_p сначала почти не изменяются, а затем, при некоторой критической концентрации окислителя $C_{кр}$, резко падают*.

---

* Эффект, подобный представленному на рис. 4, характерен и для обычной пассивации металлов под действием окислителей. В этом случае также требуется определенная концентрация окислителя для торможения растворения. Явление это, однако, имеет совсем иную природу [Н. Я. Бунэ и Я. М. Колотыркин, *Журн. физ. хим.*, *35*, 1544 (1961)].

В связи с полученным результатами может возникнуть вопрос, не связано ли торможение растворения с влиянием окислителей на процесс катодного выделения водорода. В самом деле, если принять, что растворение хрома при катодной поляризации происходит не по химическому механизму, а связано с разрушением металла под действием катодно выделяющегося водорода, то торможение растворения под действием окислителей можно было бы объяснить их тормозящим влиянием на процесс выделения водорода. Для проверки такого предположения нами измерялась парциальная скорость электрохимического выделения водорода на хроме в серной кислоте без добавок и в присутствии перекиси водорода и бихромата калия. Опыты проводились в 1 N серной кислоте при 90°. Продолжительность опытов — 15 мин. Результаты приведены на рис. 5. Здесь *1* — скорость растворения хрома в чистой серной кислоте, *2* — то же в присутствии 0,32 М перекиси водорода, *3* и *4* — катодная и анодная поляризационные кривые, измеренные в серной кислоте без окислителя, *5* и *6* — парциальные скорости выделения водорода в присутствии соответственно 0,32 М H_2O_2 скорости восстановления перекиси водорода в растворе серной кислоты с 0,32 М H_2O_2.

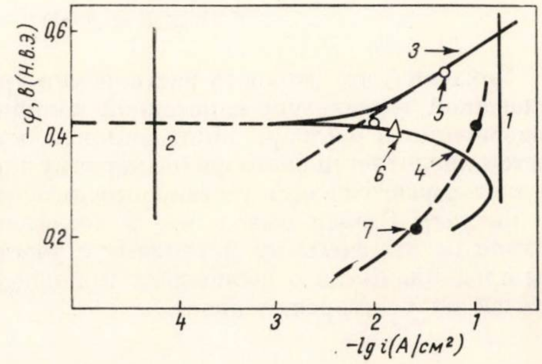

Рис. 5. — Результаты измерения парциальных скоростей растворения хрома (*1* и *2*), выделения водорода (*5* и *6*) и восстановления окислителя (*7*) на хроме в растворах 1 N H_2SO_4 без добавок (*1*) и с H_2O_2 (*5* и *7*) и $K_2Cr_2O_7$. Кривые (*3*) и (*4*)—катодная и анодная поляризационные кривые, измеренные в 1 N H_2SO_4.

Сопоставление катодной поляризационной кривой (*3*) для раствора без окислителей со скоростью выделения водорода в присутствии перекиси и бихромата (*5* и *6*) позволяет заключить, что в условиях эксперимента скорость электрохимического выделения водорода не зависит от наличия в растворе окислителя*. Это означает, что торможение растворения хрома под действием окислителей, по-видимому, нельзя связать с их влиянием на скорость катодного выделения водорода.

Данные рис. 5 позволяют сделать и другое интересное заключение. Из сравнения анодного тока растворения хрома в чистой серной кислоте (*4*) и скорости растворения в присутствии H_2O_2 (*2*) следует, что под действием окислителя имеет место замедление не только химического растворения хрома, но и его активного растворения по электрохимическому механизму.

---

* Следует отметить, что это справедливо только для начального периода эксперимента (10—15 мин.). Затем выделение водорода в присутствии окислителя (H_2O_2) замедляется. Катодный ток при этом остается неизменным, расходуясь на восстановление перекиси водорода.

Поскольку при катодной поляризации хрупкого хрома в серной кислоте на его поверхности могут появляться трещины [6], возникает вопрос, не связано ли растворение хрома в исследованных нами условиях с этим явлением. Опыты, проведенные с ковким хромом (легированным 1% иттрия) позволили ответить на этот вопрос отрицательно. Было установлено, что хром с иттрием растворяется в серной кислоте при катодной поляризации с той же скоростью, что и чистый хром.

ВЫВОДЫ

Показано, что скорость растворения хрома в кислых растворах при повышенной температуре и катодной поляризации не зависит от природы и содержания в растворе таких анионов, как Cl^-, SO_4^{2-},ClO_4^-, возрастает с ростом кислотности раствора (по первому порядку относительно ионов H^+) и резко тормозится в присутствии окислителей (перекись водорода, бихромат, нитрат). Сделан вывод, что в исследованных условиях хром растворяется по химическому механизму с участием ионов водорода. Высказаны предположения о возможных причинах тормозящего действия окислителей на растворение хрома.

Revue Roumaine de Chimie, 17, 1, 2, 167 – 170 (1972)

Dedicated to Professor I.G. MURGULESCU
on his 70th birthday

ON THE MECHANISM OF THE NITROGEN ATOM REACTION WITH ETHYLENE

V.N. KONDRATIEV

Institute of Chemical Physics, Academy of Sciences of the USSR Moscow

Received August 20, 1971

Taking into account the structure of the transition state, the first step in the reaction of nitrogen atoms with ethylene is probably $N + C_2H_4 \rightarrow NCH_2 + CH_2$, resulting in a new reaction mechanism. On this basis rate constants are calculated.

The first step of the reaction between atomic nitrogen and ethylene is always considered to be

$$N + C_2H_4 = HCN + CH_3 \tag{1}$$

followed by

$$N + CH_3 = HCN + 2H(\text{or } H_2) \tag{2}$$

(for references see [1]). Later on Herron [2] took into account some specific features of this reaction, in particular the increase in HCN, the main reaction product, in the presence of atomic hydrogen, and introduced the following steps into the overall reaction mechanism :

$$H + C_2H_4 = C_2H_5 \tag{3}$$

$$H + C_2H_5 = 2CH_3 \tag{4}$$

$$N + C_2H_5 = NH + C_2H_4 \tag{5}$$

$$N + NH = N_2 + H \tag{6}$$

However, reaction (1) does not seem to be of a high probability in view of the transition complex structure, and step

$$N + C_2H_4 = NCH_2 + CH_2 \tag{1'}$$

is conceived as more probable.

---

[1] V. N. KONDRATIEV, "Konstanty Skorosti Gazofaznykh Reaktsii", Izd. Nauka, Moscow, 1970, p. 57.

[2] J. T. HERRON, *J. Phys. Chem.*, **69**, 2736 (1965) ; **70**, 2803 (1966).

The somewhat modified Herron [3] mechanism will then be expressed as :

$$N + C_2H_4 = NCH_2 + CH_2 \qquad (1')$$

$$NCH_2 + C_2H_4 = HCN + C_2H_5 \qquad (2')$$

$$NCH_2 + N = HCN + NH \qquad (2'')$$

$$NCH_2 + H = HCN + H_2 \qquad (2''')$$

$$CH_2 + N = HCN + H \qquad (3')$$

$$H + C_2H_5 = 2CH_3 \qquad (4)$$

$$CH_3 + N = HCN + 2H \qquad (2)$$

$$N + C_2H_5 = NH + C_2H_4 \qquad (5)$$

$$N + NH = N_2 + H \qquad (6)$$

As the reactions between nitrogen atoms and olefins yielding HCN occur at a temperature close to 20°, it is essential that all elementary steps be at least thermoneutral. In order to estimate the enthalpy of (1′) and (2′) (all other steps being exothermal), it is first necessary to determine the NCH_2 radical energy.

Denoting by D_1 the energy of NCH_2 dissociation to $N + CH_2$, and by D_2 that of dissociation to $HCN + H$, we obtain $\Delta H_{1'} = 167.5 - D_1$ ($2CH_2 = C_2H_4 + 167.5 \pm 10$ kcal/mole) for enthalpy of (1′), and $\Delta H_{2'} = D_2 - 39$ ($H + C_2H_4 = C_2H_5 + 39 \pm 1$ kcal/mole) for (2′). Since, following from the enthalpy of reaction $N + CH_2 = HCN + N$, D_1 and D_2 are related as $D_2 = D_1 - 119 \pm 5$ kcal/mole, the above conditions for thermoneutrality of (1′) and (2′) reduce to a single one, namely $39 \pm 1 > D_2 > 49 \pm 15$, i.e. $D_2 = 37 \pm 3$ kcal/mole *.

The value D_2 that corresponds to process

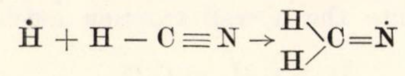

$$\dot{H} + H - C \equiv N \rightarrow H_2C = \dot{N}$$

can be taken as approximately equal to the energy of H atom addition to an acetylene molecule

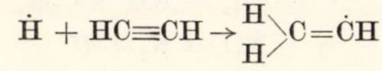

$$\dot{H} + HC \equiv CH \rightarrow H_2C = \dot{C}H$$

From the enthalpy of processes $H + C_2H_3 = C_2H_4(-102 \pm 2)$ and $2H + C_2H_2 = C_2H_4(-146)$ we find for this energy $146 - 102 \pm 2 = 44 \pm$

---

* All thermochemical data given here were kindly supplied by V.A. Medvedev. Calculation by the group equivalent procedure [4] yielded $D_2 = 35$ kcal/mole.

[3] J. T. Herron and R. E. Hui, *J. Phys. Chem.*, **72**, 2538 (1968).

[4] J. L. Franklin, J. G. Dillard, H. M. Rosenstock, J. T. Herron, K. Draxl and F. H. Field, "Ionization Potentials, Appearance Potentials and Heats of Formation of Gaseous Positive Ions", Nat. Bureau Standards (USA), 1969.

$\pm 2 = D_2$. Comparing this D_2 value with the thermoneutrality condition for process $NCH_2 + C_2H_4 = HCN + C_2H_5$ (2′) ($D_2 = 37 \pm 3$) and taking into account the approximation made in estimating D_2, one will see that this condition could take place in reality. In the same manner we obtain $\Delta H_1 = 167.5 \pm 10 - 161 \pm 3 = 6.5 \pm 13$ for enthalpy of (1).

In accordance with the proposed mechanism and taking the NH, C_2H_5 and NCH_2 concentrations as steady, the expression for the rate constant of (1′) will be

$$k_1' = \frac{\ln(C_2H_4)_0/(C_2H_4)_t}{\int_0^t (N)\mathrm{d}t} - \frac{\int_0^t \frac{k_1'k_4(H)(N)}{k_4(H)+k_5(N)} \frac{k_2'(C_2H_4)\mathrm{d}t}{k_2'(C_2H_4)+k_2''(N)+k_2'''(H)}}{\int_0^t (N)\mathrm{d}t}$$

It differs in its second term from that obtained by Herron :

$$k_1 = \frac{\ln(C_2H_4)_0/(C_2H_4)_t}{\int_0^t (N)\mathrm{d}t} - \frac{\int_0^t \frac{k_3\, k_4(H)^2\, \mathrm{d}t}{k_4(H)+k_5(N)}}{\int_0^t (N)\mathrm{d}t} .$$

The latter assumes steady C_2H_5 and NCH_2 concentrations.

The following equations are obtained for N and HCN concentrations, respectively :

$$\frac{\mathrm{d}(N)}{\mathrm{d}t} = -\,2k_1'(C_2H_4)(N)\left[1 + \frac{k_2'(C_2H_4)+k_2''(N)}{k_2'(C_2H_4)+k_2''(N)+k_2'''(H)}\right],$$

$$\frac{\mathrm{d}(HCN)}{\mathrm{d}t} = 2k_1'(C_2H_4)(N)\left[1 + \frac{k_4(H)}{k_4(H)+k_5(N)}\,\frac{k_2'(C_2H_4)}{k_2'(C_2H_4)+k_2''(N)+k_2'''(H)}\right],$$

whence

$$-\frac{\mathrm{d}(N)}{\mathrm{d}(HCN)} = \frac{1+\dfrac{k_2'(C_2H_4)+k_2''(N)}{k_2'(C_2H_4)+k_2''(N)+k_2'''(H)}}{1+\dfrac{k_4(H)}{k_4(H)+k_5(N)}\,\dfrac{k_2'(C_2H_4)}{k_2'(C_2H_4)+k_2''(N)+k_2'''(H)}} .$$

At $k_4(H) << k_5(N)$ and $k'''(H) << k_2'(C_2H_4) + k_2''(N)$ we have $(N)/(HCN) \simeq 2$, in agreement with Herron's results [2].*

---

* This can be obtained from the Herron mechanism as well, provided $k_4(H) < < k_5(N)$, and with the additional condition $k_3(H) \simeq k_1(N)$.

Herron has also found that 2% of H_2 added into discharge approximately doubles the HCN yield. Assuming then that $k_4(H) >> k_5(N)$ and $k'''(H) >> k_2'(C_2H_4) + k_2''(N)$, we obtain from the above equations

$$\frac{\Delta(N)}{(HCN)} \simeq 1$$

also in fair agreement with experiment *. The same mechanism seems to be valid for N atom reactions with other olefins[3] .

The agreement between the ratios $\Delta N/(HCN)$ obtained from the above mechanism and the experimental values cannot be considered as a convincing argument in favour of the mechanism validity.

The mechanism of the atomic nitrogen reaction with ethylene (and with olefins in general, as well as with acetylens)[3] must be further investigated. The proposed elementary reaction (1′) also needs experimental verification.

It is assumed here, just as in most other papers, that excited nitrogen molecules which might be formed in discharge or as a result of nitrogen atom recombination are absent. Reaction (7)

$$N_2^* + C_2H_4 = 2NCH_2 \tag{7}$$

followed by the above secondary processes may assumed by occur in the presence of excited N_2^* molecules.

---

* This can be obtained from the Herron mechanism as well, provided $k_4(H) >> k_5(N)$.

Revue Roumaine de Chimie, 17, 1, 2, 171–178 (1972)

Dedicated to Professor I.G. MURGULESCU
on his 70th birthday

ELECTRODE PROCESSES OF HYDROGEN PEROXIDE ON PLATINUM ELECTRODE IN ALKALINE AND ACID MEDIUM

J. KORYTA, M. BŘEZINA and N. KŘÍŽ

J. Heyrovský Institute of Polarography, Czechoslovak Academy of Sciences,
Prague, Czechoslovakia

Received August 2, 1971

Reduction of H_2O_2 alone takes place rapidly at a rotating platinum disc in the potential range of oxygen reduction and probably the irreversibility is caused by the fact that oxygen is reduced to water according to the reaction scheme :

$$O_2 \overset{K_1}{\rightleftarrows} HO^- \xrightarrow{K} 2OH^-$$

Similarly to this process at Ag electrode, in view of this result, it may be assumed that the main current-forming processes in the anodic-cathodic wave of H_2O_2 are the reactions :

$$O_2 \xleftarrow{K_1} HO_2^- \xrightarrow{K_2} 2OH^-$$

In contrast to numerous papers dealing with reduction of oxygen on platinum electrodes the interest about the processes of hydrogen peroxide alone at the same electrode [1–3] is rather small in spite of the fact that H_2O_2 is a possible intermediate in oxygen reduction.

EXPERIMENTAL

A rotating platinum disc (3 mm diameter) was used in most experiments. The details of the electrode assembly are given in.[4] For cyclic voltammetry a PO 4 Polarograph (Radiometer Co., Copenhagen) was used (scan rate 0.4 V/min). Polarization from positive to negative potentials will be indicated by (+ –), polarization in the reverse sense by (– +). The $I-E$ curves were corrected for the $I-R$ drop[4] and for the liquid junction potential.

[1] L. Müller and L. Nekrassov, *J. Electroanalyt. Chem.*, **9**, 282 (1965).
[2] W. Vielstich, "Brennstoffelemente", Verlag Chemie, Weinheim 1965, p. 125–126.
[3] M. R. Tarassievich and K. A. Radyushkina, *Elektrokhimiya*, **6**, 376 (1970).
[4] M. Březina, J. Koryta and M. Musilová, *Coll. Czech. Chem. Comm.* **33**, 3397 (1968).

PRETREATMENT OF THE ELECTRODE

The electrode was first polished with emery paper (6/0, SIA; Switzerland), then a triangular voltage sweep (scan rate 0.4 V/min) was applied to the electrode and finally the current-potential curve was recorded in the same potential range. The influence of different procedures for pretreatment of the electrode was described elsewhere.[5] The roughness factor determined by means of hydrogen adsorption was about 2.0.

A mercury (II) oxide electrode in 1M – KOH was used as a reference, but all values of electrode potentials are referred to S.H.E.

Analytically pure sulphuric acid and potassium hydroxide (Lachema, Brno, Czechoslovakia) were used. All solutions were prepared from redistilled water. Solutions were deaerated with pure argon (Moravské chemimické závody, Ostrava, Czechoslovakia). The electrolytic vessel was cleansed with a mixture of 3 parts of 96% H_2SO_4 and 1 part of 30% H_2O_2.

RESULTS

At low speed of rotation (64 rpm) hydrogen peroxide dissolved in H_2SO_4 as well as KOH solutions give in (+ –) polarization a S-shaped anodic-cathodic $I-E$ curve when the polarization starts at a potenial by about 0.35 V more positive than the potential of zero current of the $I-E$ curve (see Fig. 1). The curves were corrected for the residual current (see Fig. 2) which was due to the reduction of the surface oxide and the discharge of H_3O^+ connected with chemisorption (cathodic branch) and to the oxidation of adsorbed hydrogen and formation of surface oxide (anodic branch). On reverse polarization a distorted anodic-cathodic curve is obtained in 0.5 M H_2SO_4 while in 0.1 M KOH the $I-E$ curve is S-shaped (see Fig. 1).

When increasing the speed of rotation so that a larger portion of the $I-E$ curve is controlled by the rate of surface processes on the electrode, which is shown in figure 3, indicating also the influence of the initial potential in (+ –) polarization upon the $I-E$ curve at 512 r.p.m., the larger participation of surface processes as rate-controlling steps follows from a larger potential range where no limiting current is observed. The more oxide is originally present on the electrode, the more separated are the anodic and cathodic electrode processes in (+ –) polarization.

In figure 4 the $I-E$ curves of hydrogen peroxide are compared with those of oxygen for 0.5 M H_2SO_4 and 1 M KOH.

DISCUSSION

As shown in figure 4 the cathodic wave of oxygen in 0.1 M KOH is situated at more negative potentials than the anodic-cathodic wave of hydrogen peroxide. However, in the case of platinum, this potential difference is smaller than with a silver electrode.[4] Thus, at 512 rpm.

---

[5] M. Březina, J. Koryta and N. Kříž, *J. Electroanalyt. Chem.*, in preparation.

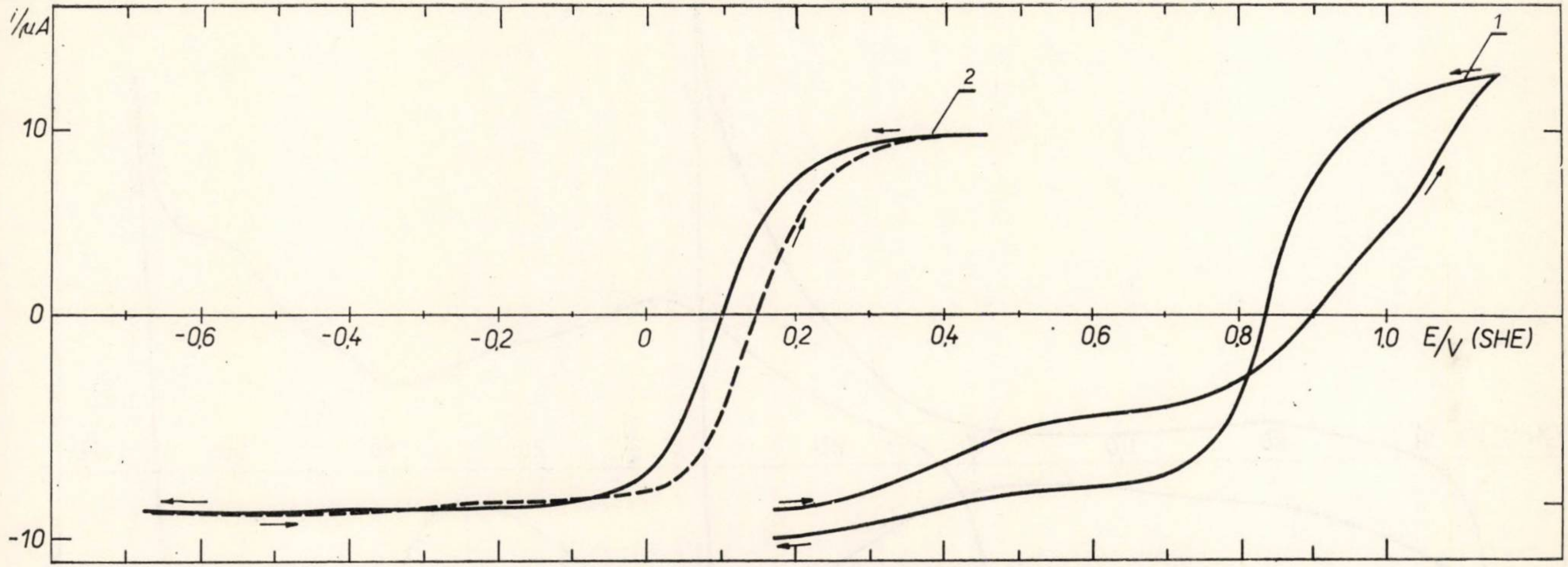

Fig. 1. — Cyclic voltammetric curves of 5×10^{-4} M H_2O_2 in 0.5 M H_2SO_4 (curve *1*) and 0.1 M KOH (curve *2*), corrected for the residual current. Arrows show the sense of the potential scan 64 rpm. Electrode polished with emery paper.

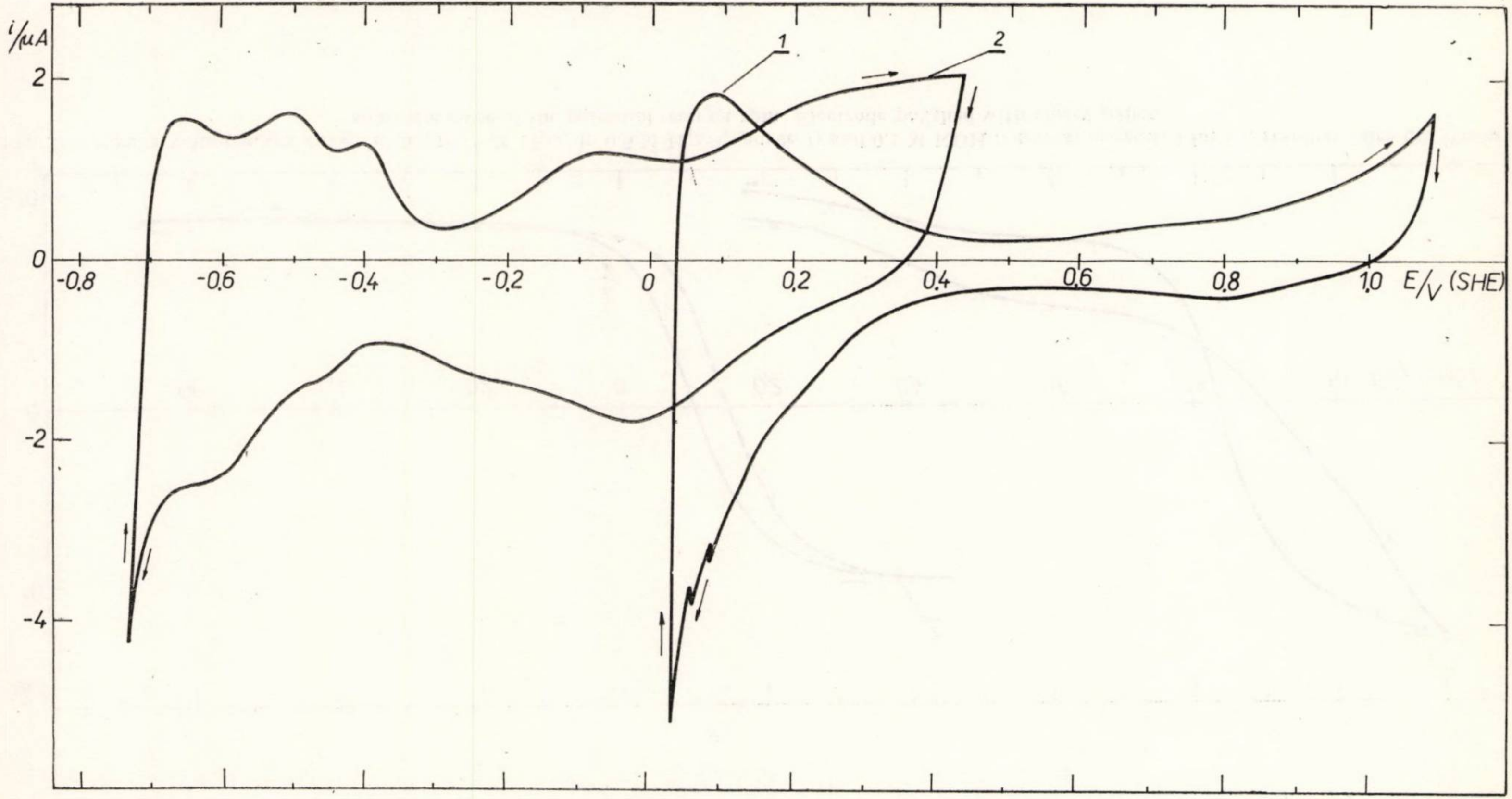

Fig. 2. — Residual current, Cyclic voltammetric curves of 0.5 M H_2SO_4 (curve *1*) and 0.1 M KOH (curve *2*). Arrows show the sense of the potential scan. Electrode polished with emery paper.

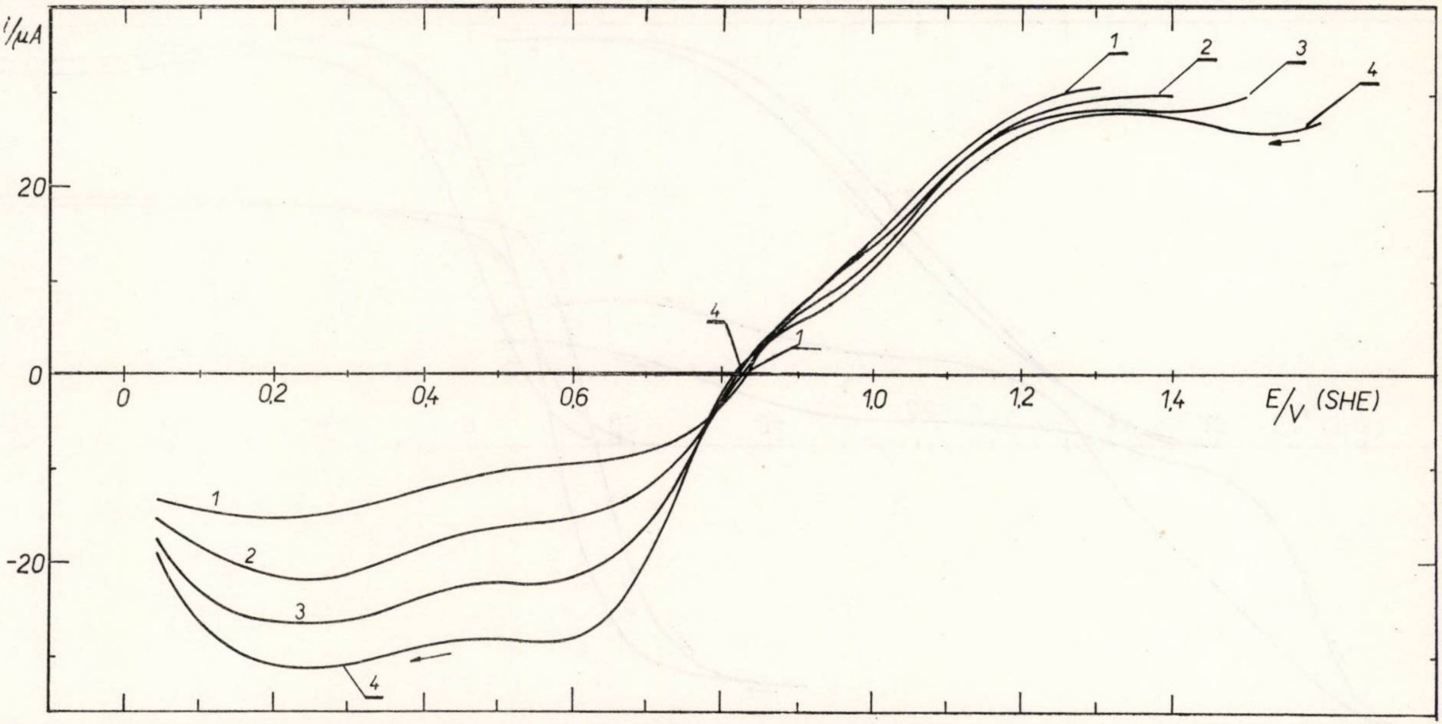

Fig. 3. — Influence of initial potential E_i on $I-E$ curve of 5×10^{-4} M H_2O_2 in 0.5 M H_2SO_4; the initial potentials are *1*, + 1.3 V; *2*, +1,4V ; *3*, + 1.5 ; *4*, + 1,6 V. Speed of rotation 512 rpm.

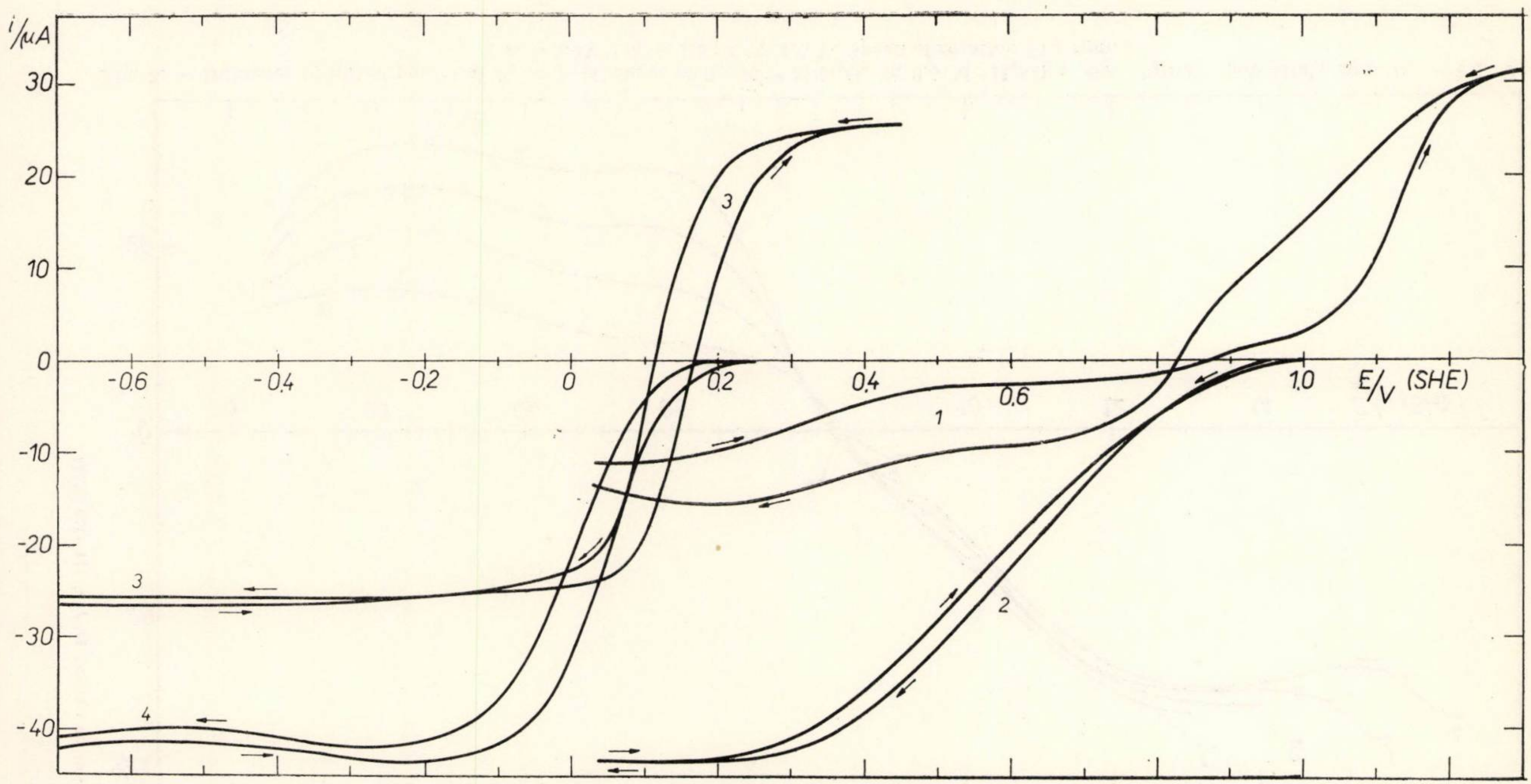

Fig. 4. — Comparison of $I-E$ curves of 5×10^{-4} M H_2O_2 (curves *1, 3*) and O_2 (saturated solution with air — curves *2, 4*) in 0.5 M H_2SO_4 (curves *1, 2*) and 0.1 M KOH (curves *3, 4*). Speed of rotation 512 rpm.

the half-wave potential of oxygen reduction wave at Pt is $E_{\frac{1}{2}} = -0.003$ V $(+-)$ and $E_{\frac{1}{2}} = +0.045$ V $(-+)$ and the potential of zero current of the anodic-cathodic wave of H_2O_2 $E_m = +0.113$ V $(+-)$ and $E_m = = +0.167$ V $(-+)$ whereas at Ag these quantities are $E_{\frac{1}{2}} = -0.046$ V $(+-)$, $E_{\frac{1}{2}} = -0.027$ V $(-+)$, $E_m = +0.196$ V $(+-)$ and $E_m = = +0.208$ V $(-+)$, respectively.

The half-wave potential of the oxygen wave is close to the thermodynamic value of the pH-dependent standard potential of the $H_2O_2-O_2$ couple in 0.1 M KOH which is $E^\circ = +0.060$ V (this value was obtained in the same electrolyte and electrolytic assembly as the value of $E_{\frac{1}{2}}$ of oxygen at Pt but a Hg-dropping electrode was used [6,7]). In spite of this fact even at Pt the oxygen reduction is almost completely irreversible which follows from the large value of the reciprocal slope of the wave. This quantity is defined as $\partial E/\partial \log (I/I_d-I)/$ where I_d is the limiting current of oxygen. The value of the reciprocal slope lies between 0.07 and 0.12 V instead of 0.029 V for a reversible wave. The irreversibility is caused by the fact that oxygen is reduced to water according to the reaction scheme

$$O_2 \overset{k_1'}{\rightleftharpoons} HO_2^- \xrightarrow{k_2} 2OH^- \tag{I}$$

Obviously there is $k_1 \ll k_2$. This explanation is supported by the fact that reduction of H_2O_2 alone takes place rapidly in the potential range of oxygen reduction.

In view of this result it may be assumed that the main current-forming processes in the anodic-cathodic wave of H_2O_2 are, similarly to this process at Ag electrode, [4] the reactions

$$O_2 \xleftarrow{k_1} HO_2^- \xrightarrow{k_2} 2OH^- \tag{II}$$

with some contribution of oxygen reduction to water according to the scheme (I). However the catalytic decomposition of H_2O_2

$$H_2O_2 \xrightarrow{k_3} \frac{1}{2} O_2 + H_2O \tag{III}$$

may not be overlooked as it was done in our preceding paper [4] but it should be stressed that it is only to a small extent a current-forming reaction (cf. ref[3]).

In a rough approximation we shall neglect completely the electrochemical reduction of oxygen and deduce an equation for the anodic-cathodic wave of H_2O_2 under following assumptions :

[6] V. S. Bagotsky and D. L. Motov, *Doklady Akad. Nauk S.S.S.R.*, **71**, 501 (1950).

[7] J. Koryta, *Coll. Czech. Chem. Comm.*, **18**, 21 (1953).

i. The surface process which determines the concentration of H_2O_2 in the neighbourhood of the electrode and thus its supply from the bulk is characterized by the sum of all k_1, k_2 and k_3.

ii. The current is given only by the difference of the current-forming rate constants i.e. of the anodic rate constant k_1 and of the cathodic rate constant k_2.

Defining $\mathscr{H} = 0.62 \,.\, 2\,FD_{H_2O_2}^{2/3} \,.\, \nu^{-1/6} \,.\, \omega^{1/2}$ where $D_{H_2O_2}$ is diffusion coefficient of H_2O_2, ν kinematic viscosity of the solution and ω angular velocity of the disc [8] we obtain the equation [9]

$$(I_d - I)/(I_d + I) = (\mathscr{H}/2F + 2k_2 + k_3)/(\mathscr{H}/2F + 2k_1 + k_3) \tag{1}$$

where I_d is anodic limiting current. For fast surface processes $\mathscr{H} \ll 2k_1 + k_3$, $\mathscr{H} \ll 2k_2 + k_3$, so that

$$(I_d - I)/(I_d + I) = (2k_2 + k_3)/(2k_1 + k_3). \tag{2}$$

Thus, the right-hand side is independent of $\mathscr{H}$. This is possible only in the case when I is proportional to $\mathscr{H}$ in the similar way as I_d. Thus, I is a transport-controlled current. On the other hand, the shape of the $I-E$ curve depends on the values of surface reaction rate constants k_1, k_2 and k_3. From this we may conclude that here we have a remarkable case of a $I-E$ curve with convective diffusion-controlled currents in all points of the curve whereas the form of $I-E$ curve depends on the rate constants of surface reactions.

For a detailed discussion of eq. (1) we may assume (similarly as in ref. [4]) an exponential dependence of k_1 and k_2 on electrode potential

$$k_1 = k \exp\left[\quad \beta z_1(E - E_m)/RT\right] \tag{3}$$

$$k_2 = k \exp\left[-\alpha z_2(E - E_m)/RT\right] \tag{4}$$

where E_m is the zero current potential, $k_1 = k_2 = k$ for $E = E_m$ and α, β, z_1 and z_2 have the usual significance.

A numerical calculation shows that smooth anodic-cathodic wave (cf. Fig. 1) is obtained, if $\mathscr{H}/2F + k_3 \ll k$. On the other hand if $\mathscr{H}/2F + k_3 \gg k$, one separate anodic and one separate cathodic wave should be obtained. This is the case in figure 3. However, the inflection point does not coincide with the line of zero current. This is probably caused by the uncertainty in the correction for the residual current.

There are also other complications in the electrode process connected with the decrease of current in the cathodic part of the $I-E$ curves shown in figure 3. These complications are most probably connected with the presence of varying quantities of oxides on the electrode.

---

[8] V. G. Levich, "Chemical Hydrodynamics", Prentice Hall, Englewood Cliffs, 1962.

[9] M. Březina, A. Hofmanová, J. Koryta, N. Kříž and M. Musilová, Extend. Abstr. 21st CITCE Meet., Prague, 1970, p. 326.

Revue Roumaine de Chimie, 17, 1, 2, 179–186 (1972)

Dedicated of Professor I.G. MURGULESCU
on his 70th birthday

CHEMICAL CHANGES IN CEREALS BY SHRIVELLING

MIRCEA IONESCU, MAGDA IVĂNESCU and MARIANA FERANDO
Agronomical Institute, Bd. Mărăşti 59, Bucharest, Romania

Received September 8, 1971

The percentage changes of the chemical content of wheat and corn grains matured under normal conditions and submitted to shrivelling are analysed and commented.

We have shown in former papers [1] that through shrivelling the corn and the wheat grain becomes smaller and its starch and protein content decreases due to the incomplete accumulation of these substances in the grain. As starch decreases more than protein, the proportion of the former in the grain also decreases while that of the latter increases, so that shrivelled wheat appears to be richer in protein than the one matured under normal conditions.

The present paper presents new biochemical data on shrivelled corn and wheat and the same plants matured under normal conditions. These new data are referring to :

a) The content in crude protein, pure protein and genuine proteins of some wheat (table 1) and corn varieties (table 2) matured under normal conditions or affected by atmospheric drought and high temperature (shrivelling).

b) The content in crude protein, free amino acids, proteolytic enzymes and the ribonuclease activity of some corn grains, normally matured or shrivelled (table 3).

c) The content in different types of phosphorous components of some corn grains matured normally and under unfavourable conditions, i.e. shrivelled (table 4).

The data included in tables 1 and 2 lead to the following conclusions :

1. In the grains of different wheat varieties, matured under normal conditions, the proportion of pure protein is of 91.96–94.25 % (average 93.45 %) of the crude protein content, and in shrivelled grains of the same wheat varieties, the proportion of pure protein is generally lower, viz. 87.37–94.99 % (average 90.21 %) of the crude protein content. These data show that shrivelling, in the case of wheat, not only results in a decrease of the content in nitrogenous substances, because of the

---

[1] M. V. Ionescu, N. N. Săulescu, M. Ivănescu and M. Bîrsan, *Stud. Cercet. Biochim. Acad. R.S.R.*, **4**, 487 (1961) ; M. V. Ionescu, N. N. Săulescu, M. Ferando, M. Visarion and M. Ivănescu, *Rev. Roumaine Biochim.*, **1**, 19 (1967).

Table 1

Content in crude protein, pure protein and different genuine proteins of some wheat varieties matured under normal and unfavourable conditions

(expressed per 100 g of dry matter)

VARIETY	Shrivelling degree	Crude protein (N × 6.25)	Pure protein		Albumins-globulins		Prolamins-gliadins (alcohols-soluble)		Glutelines (alkali-soluble)	
			%	% of crude protein	%	% of pure protein	%	% of pure protein	%	% of pure protein
TRIUMPH 1961 crop Carei	Normal	12.82	11.79	91.96	2.71	22.98	3.70	31.37	5.16	43.76
	Shriv. I	14.24	12.72	89.32	3.56	27.98	3.77	29.63	4.98	39.14
	Shriv. II	16.07	14.24	88.61	3.78	26.54	4.21	29.56	6.10	42.93
TRIUMPH 1964 crop Dîlga	Normal	15.88	14.82	93.32	3.86	26.04	6.41	43.25	5.19	35.02
	Shriv. I	15.56	15.47	87.37	3.89	25.20	7.27	46.99	4.64	29.99
PONCA 1961 crop Carei	Normal	15.87	14.69	94.25	3.38	22.00	5.52	30.77	5.10	34.71
	Shriv. I	16.98	16.13	94.99	3.74	23.18	5.71	35.39	5.71	35.39
SCOROSPELCA 1964 crop Dîlga	Normal	16.72	15.76	94.25	3.71	23.50	6.59	41.80	5.12	32.4
	Shriv. I	17.98	16.32	90.76	3.45	21.50	7.52	46.07	5.26	32.23

Table 2

Content in crude protein, pure protein and different genuine proteins of some corn varieties grown at Dilga under normal and unfavourable condition

(expressed per 100 g dry matter)

Sub species	VARIETY	Shrivelling degree	Crude protein (N × 6.25)	Pure-protein %	Pure-protein % of crude protein	Albumins-globulins (salt-soluble) %	Albumins-globulins (salt-soluble) % of raw protein	Prolamins (alcohol-solub) %	Prolamins (alcohol-solub) % of crude protein	Glutelines (alkali-soluble) %	Glutelines (alkali-soluble) % of crude protein
INDENTATA	PIONEER 383	Normal	11.48	10.92	95.14	1.72	15.72	3.73	35.96	4.84	44.30
		Shriv. I	12.40	11.95	96.40	2.26	18.94	3.88	32.43	5.38	45.0
		Shriv. II	13.19	12.47	94.87	1.88	15.10	3.28	25.90	6.87	53.71
	ICAR 54	Normal	11.32								
		Shriv. I	11.82	11.29	95.55	1.26	9.40	5.76	51.02	4.27	37.82
		Shriv. II	11.79	11.20	95.00	1.06	9.46	5.50	49.11	4.64	31.40
	MINHIBRID 511	Normal	11.31	10.69	94.53	1.026	9.60	5.29	49.50	4.41	41.24
		Shriv.	11.66	11.33	97.20	1.84	16.15	4.70	41.50	4.80	42.35
Indurata	M.D. 0213	Normal	10.85	10.20	94.00	0.813	7.97	4.40	43.18	4.99	48.92
		Shriv.	10.69	10.30	96.32	1.246	12.10	4.02	39.06	5.02	48.75

Table 3

Crude protein, free amino acids, ribonuclease activity, proteolytic enzymes of some normal and shrivelled corn grains

VARIETY	Shrivelling degree	Crude protein (N × 6.25) gr % d.s.	Total free amino acids (in g per 100 of dry material) *	Ribonuclease activity (units per 1 g of initial material)	Proteolytic enzymes (mg. of aminic nitrogen released by hydrolysis)**	Propotion of free amino acids *versus* protein
PIONEER 383	Normal	11.48	0.150	128.13	0.0896	1.3
	Shrivelled I	12.40	0.185	204	0.0784	1.5
	Shrivelled II	13.19	0.200	180	0.1212	1.5
ICAR 54	Normal	11.32	0.150	82.5	0.600	1.3
	Shrivelled I	11.82	0.180	140	0.486	1.5
	Shrivelled II	11.79	0.245	142	0.634	2.1

* expressed in leucin

** under standard working conditions.

Table 4

Content in different phosphorous components of some corn grains matured under normal and unfavourable conditions

Sample	Shrivelling degree	Total phosphorous	Liposoluble phosphorous	Acid-soluble phosphorous	Mineral phosphorous	Phosphorous esters and glucides	Phytic phosphorous	A.R.N. phosphorous	A.D.N. phosphorous
PIONEER 383	Normal	1.10	0.303	0.124	0.012	0.027	0.084	0.238	0.048
	Schriv. I	1.14	0.290	0.122	0.012	0.030	0.078	0.245	0.049
	Shriv. II	1.11	0.279	0.113	0.011	0.030	0.071	0.236	0.047
MINIHIBRID 511	Normal	1.027	0.614	0.106	0.012	0.071	0.022	—	—
	Shriv.	0.94	0.465	0.103	0.011	0.047	0.043	—	—
ICAR 54	Normal	1.10	—	0.118	0.012	0.056	0.049	—	—
	Shriv. I	1.16	0.617	0.137	0.011	0.053	0.071	—	—
	Shriv. II	1.120	0.634	0.123	—	0.052	0.059	—	—

incomplete filling of the grain, but it also renders the formation of protein in the grain more difficult.

2. In the grains of different corn varieties, normally matured, the proportion of pure protein is of 94.00—95.14 % of the crude protein content, and in the shrivelled grains of the same corn varieties, the proportion of pure protein is higher, viz. 95.55—97.20 % of the crude protein content. These data show that in the case of corn, the shrivelling has for consequence only a decrease of the protein content (owing to the incomplete filling of the grain), but without rendering the formation of protein in the grain more difficult, as in the case of wheat. We ascribe the fact that the formation of protein in the corn grain is not made more difficult by shrivelling — as in the case of wheat — either to the accumulation period, or to the lower protein content of corn. Indeed, protein formation in a cereal grain slows down and becomes more difficult when a certain concentration (a certain content) is exceeded.

Shrivelling renders hence the formation of proteins more difficult only when a certain concentration, which in our case is 12 %, is exceeded.

3. Simultaneously with the decrease of the protein content in the grain there also appears a change in the ratio between the different types of genuine proteins, due to shrivelling. Thus, in wheat, shrivelling has for consequence an increase in the proportion of albumins and prolamins and a slight decrease of the glutelins. In corn the phenomenon takes place conversely, that is the proportion of prolamins decreases, while that of glutelins increases. The differences appearing between prolamins and glutelins are nevertheless, in our opinion, not of a kind that could endanger, after shrivelling, the panification qualities of wheat flour and therefore the formation of a gluten with good elastic qualities; this is due to the fact that prolamins are insoluble in water and do not coagulate at higher temperatures.

On the other hand the decrease of prolamins and the increase of glutelins shows that, for corn, shrivelling increases the alimentary value of protein, especially as a result of the increase in the lysine proportion.

4. The proportion of free amino acids in the shrivelled corn grain is practically the same as in the normally matured one. This shows that the formation of protein from synthetized amino acids is actually not hindered by shrivelling. These conclusions thus confirm those of point (2) above which show that the only consequence of shrivelling is a more difficult formation of the amino acids, but not their conversion into proteic substance (a fact which appears to be perfectly logical).

5. As a consequence of shrivelling, the hydrolytic activity of proteolytic enzymes decreases by 10—30 % in corn. This is probably due to the partial denaturation of the enzymes owing to atmospheric drought, high temperatures, or other causes occurring at the time of grain filling and determining deep changes in the molecular structure of grains.

6. The case of ribonucleases is different. The activity of ribonucleases increases as a result of shrivelling, thus bringing about a degradation to mononucleotides, and even further, of ribonucleic acids, which diminishes their vital qualities.

7. The different phosphoric compounds appearing in the corn grain do not undergo essential changes subsequent to shrivelling. Only the lipo-

phosphoric compounds decrease generally due to the shrivelling of corn grains ; this leads to the conclusion that shrivelling results in a reduction of the breathing processes, during which the phosphotrioses appear that lead to the formation of lipidic compounds.

EXPERIMENTAL

The measurements given in the present paper were carried out :

a) For crude protein by the Andersen Jensen [2] method.

b) For pure protein by the Bernstein [2] method.

c) For different types of genuine proteins by fractionating proteins according to their solubility after Ermacov's method.[3]

d) For ribonuclease activity, Amfinsen's method as modified by Willson.[4] The ribonuclease activity unit was considered the quantity of enzyme determining an absorption change of 0.1 per 260 milimicrons in the experimental conditions specified by this method.

CONCLUSIONS

Atmospheric drought, high temperature, strong rust attacks are the main causes of grain shrivelling in cereals.

Shrivelling determines a number of morphological, physiological and biochemical changes, namely :

1) The corn and wheat grain becomes smaller and its starch and protein content decreases due to the incomplete accumulation of these substances in the grain. Starch decreasing more than protein, its proportion in the grain decreases, while that of protein increases, so that shrivelled wheat appears more proteic than the one matured under normal conditions.

2) In wheat shrivelling not only results in a decrease of the content in nitrogenous substances, but it also renders more difficult the process of protein formation in the grain, a fact not encountered in the case of corn shrivelling.

3) In the case of wheat, shrivelling brings about an increase in the prolamin proportion and a slight decrease of the gliadins in the grain ; in corn the phenomenon takes place conversely. We assume that the changes appearing in the ratio between prolamins and glutelins are due to the enzymatic system, and maybe to the nucleic acids which after the shrivelling of corn acquire the quality of repressing the synthesis of zein and concomitantly favouring the synthesis of glutelin, which is richer in lysine. Shrivelling thus appears as a process of chemical variability, preceding sometimes mutation. However, the changes appearing in the ratio prolamins : glutelins are not of a kind that could endanger or diminish, after shrivelling, the panification qualities of wheat flour or the alimentary value of corn protein.

---

[2] I. Bömer, A. Jüchenack and G. Tillmans, "Handbuch der Lebensmittelchemie", vol. 2, J. Springer, Berlin, 1938.

[3] A. I. Ermacov and V. V. Aresimovici, "Metody biokhimiceskovo issledovania rastenyi", Moscow, 1952.

[4] G. M. Willson, *J. Biolog. Chem.*, **248**, 2260 (1967).

4) The formation of protein from synthetized amino acids is not hindered through shrivelling in the case of corn. This conclusion shows therefore that shrivelling has for consequence only a greater difficulty in the formation of amino acids, but not in their conversion into proteic substance.

5) As a consequence of shrivelling the hydrolytic activity of the proteolytic enzymes decreases down to 30% in the case of corn. This activity has not been studied by us in the case of wheat.

6) Through shrivelling the nucleic acids of protoplasm are more easily degraded in corn ; in wheat they have not been studied.

7) The breathing processes are reduced through shrivelling and lipidic compounds are therefore formed is smaller quantity.

Shrivelling appears thus as a process of incomplete and abnormal development of the grain, in which the breathing processes are reduced, and the vital potential of protoplasm, especially of nucleic acids, is weaker, due to the unfavourable environmental conditions.

Revue Roumaine de Chimie, 17, 1, 2, 187–194 (1972)

Contributed in honor of Academician
Professor I.G. MURGULESCU on the
occasion of his 70th birthday

SOME APPLICATIONS OF LASER RAMAN SPECTROSCOPY IN FUSED SALT STUDIES

G.J. JANZ and K. BALASUBRAHMANYAM

Rensselaer Polytechnic Institute
Troy, New York, U.S.A.

Received September 4, 1971

The present communication reports three studies in which molten ionic salts may be used to explore the properties of ultraconcentrated electrolytes : molten $AgNO_3$ and $AgNO_3-CH_3CN$ mixtures; molten $LiClO_3$, and $LiClO_3-H_2O$ mixtures; molten $Ca(NO_3)_2 . 4H_2O$ and its mixtures with KNO_3. These examples are part of a more general system of two component mixtures in which the component in excess is a molten salt and the second component is a molecular solvent. The results of the laser Raman studies are examined from the practical viewpoint of the second component as a trace contaminant, and from the structural changes in the transition from molten salt to an ultraconcentrated solution.

This communication reports the results of some of our studies, using laser Raman spectroscopy, of two component mixtures in which the component in excess is a molten salt and the second component is a molecular solvent such as CH_3CN or H_2O. The interest in such systems stems both from practical and theoretical viewpoints, i.e., as trace contaminants and from the viewpoints of ultraconcentrated electrolyte solutions.

EXPERIMENTAL

All measurements were made with a Jarrell-Ash laser Raman spectrometer (model 25–300) having a resolution of 0.4 cm^{-1} (in the first order) using diffraction gratings of 1180 g/mm, and two lasers as excitation sources (He–Ne laser, 55 mw; Ar^+ ion laser, 125 mw). A duPont model 310 analogue computer was used to resolve the band contours (Lorentzian and/or Gaussian components).

$AgNO_3 - CH_3CN$: In the present work the spectra of $AgNO_3$ in the molten state (235°) and of $AgNO_3$ dissolved in CH_3CN (at 25° concentration range, ~ 3 moles l^{-1} to ~ 13 moles l^{-1}) were investigated. Owing to the relatively high melting point of $AgNO_3$ (m. 210°), the direct solution of CH_3CN in molten $AgNO_3$ was not attempted.

$LiClO_3-H_2O$: The details of our studies on $LiClO_3 - H_2O$ system are found elsewhere.[1] Molten $LiClO_3$ and molten $LiClO_3$ with increasing amounts of H_2O (132°) were investigated.

---

[1] B. G. Oliver and G. J. Janz, *J. Phys. Chem.*, **75** October issue, (1971).

$Ca(NO_3)_2.4H_2O-KNO_3$, molten mixtures : The molten tetrahydrate (m. 42.7°) and with increasing amounts of KNO_3 (up to 70 mole %) were investigated. The mixtures were studied at 100°.

RESULTS AND DISCUSSION

$AgNO_3-CH_3CN$: For the free NO_3^- ion (D_{3h}, point group symmetry) the generalized vibrational assignments are : $\nu_1(A_1') \sim 1050\ cm^{-1}$, $\nu_2(A_1'') \sim 825\ cm^{-1}$; $\nu_3(E') \sim 1384\ cm^{-1}$ and $\nu_4(E') \sim 719\ cm^{-1}$ (ν_1 mode is inactive in the infrared spectrum, and ν_2 mode is inactive in the Raman spectrum). The salient features in the present investigation of molten $AgNO_3$ and for an ultraconcentrated solution of $AgNO_3$ in CH_3CN are shown in Figure 1. The resolution of the band contours shows clearly that the symmetry of the NO_3^- ion has been lowered from that of the free ion symmetry (D_{3h}), i.e., in addition to the appearance of the Raman forbidden mode ν_2 as a weak band, the degeneracies of the ν_3 and ν_4 modes have been lifted. The asymmetric shape of the band due to the symmetrical stretching mode (ν_1) suggests a coupling of vibrations of the nearest NO_3^- ion neighbours. From the earlier studies [2,3] ionic associa-

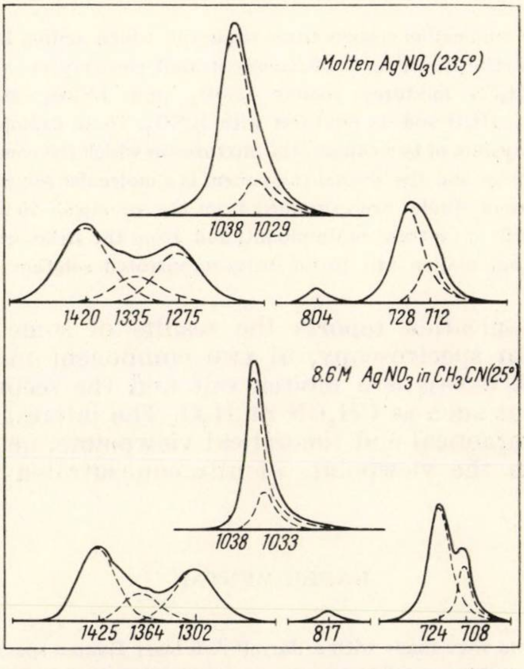

Fig. 1. — Raman spectrum of molten $AgNO_3$ (235°C) and of $AgNO_3$ in CH_3CN (25°C). The asymmetric shape of the ν_1 band is illustrated, and the resolution of the band contours in the ν_3 and ν_4 regions.

---

[2] G. E. Walrafen and D. E. Irish, *J. Chem. Phys.*, **40**, 911 (1964).

[3] J. P. Devlin, K. Williamson and G. Austin, *J. Chem. Phys.*, **44**, 2203 (1966).

tion had been proposed in molten $AgNO_3$; the present results are additional support for the presence of a weak association (sensed through the coupling vibrations). From this viewpoint the structural impact through the dilution effect with a molecular solvent, such as CH_3CN, is of particular interest. In Figure 2, the band due to the symmetrical stretching mode (ν_1) for an ultraconcentrated solution (12.2 moles 1^{-1} $AgNO_3$) is compared with the same band in molten $AgNO_3$. Also shown in the same figure, are the changes as CH_3CN is added to dilute the ultraconcentrated mixture. One notes the close similarity in the band contours for the molten salt and the ultraconcentrated solution, and the decrease in the intensity of the band attributed to the coupling interactions as CH_3CN dilutes this mixture. At $\sim$ 3 moles 1^{-1}, the 1037 cm^{-1} band is symmetrical in shape, and one may assume that the vibrational interactions are virtually decoupled. This concentration region corresponds with the region in which the inner coordination sphere of the Ag^+ ions contains approximately 2 to 4 CH_3CN molecules, [4] and this apparently is sufficient for vibrational decoupling.

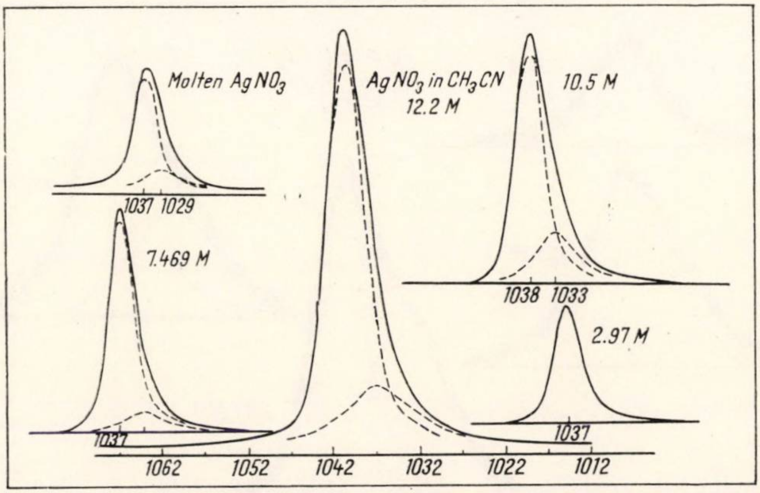

Fig. 2. — Asymmetric shape of the ν_1 band in $AgNO_3-CH_3CN$ (12.2 M) in molten $AgNO_3$ and in $AgNO_3-CH_3CN$ solutions of various concentration. The gradual disappearance of the low frequency component with dilution is shown.

$LiClO_3-H_2O$: The point group symmetry of the unperturbed ClO_3^- ion is C_{3v}, and the generalized assignments are: $\nu_1(A_1) \sim 950$ cm^{-1}; $\nu_2(A_1) \sim 620$ cm^{-1}; $\nu_3(E) \sim 1000$ cm^{-1} and $\nu_4(E) \sim 480$ cm^{-1}. In Figure 3, the results are shown for the ν_4 band of molten $LiClO_3$ (21.3 moles 1^{-1}) and for molten $LiClO_3$ containing increasing amounts of water. One notes the loss of degeneracy of the ν_4 mode; in the ν_3 region also similar

---

[4] K. Balasubrahmanyam and G. J. Janz, *J. Amer. Chem. Soc.*, **92**, 4189 (1970).

results are found. The lifting of these degeneracies indicates that the symmetry of the ClO_3^- ion in molten $LiClO_3$ has been lowered from that of the unperturbed ion (C_{3v}), and this may be attributed to enhanced ion-ion interactions (most probably due to the close packing or association). Inspection of Figure 3 shows that this degeneracy is restored if the molten salt is diluted with water (e.g. ~ 5 moles l^{-1} of $LiClO_3$, the band contour is symmetrical). The water band region ($3000-3800$ cm^{-1}) was examined to see what additional information could be gained. Some of the results are illustrated in Figure 4, together with a comparison of the Raman spectrum of pure water at the same temperature.

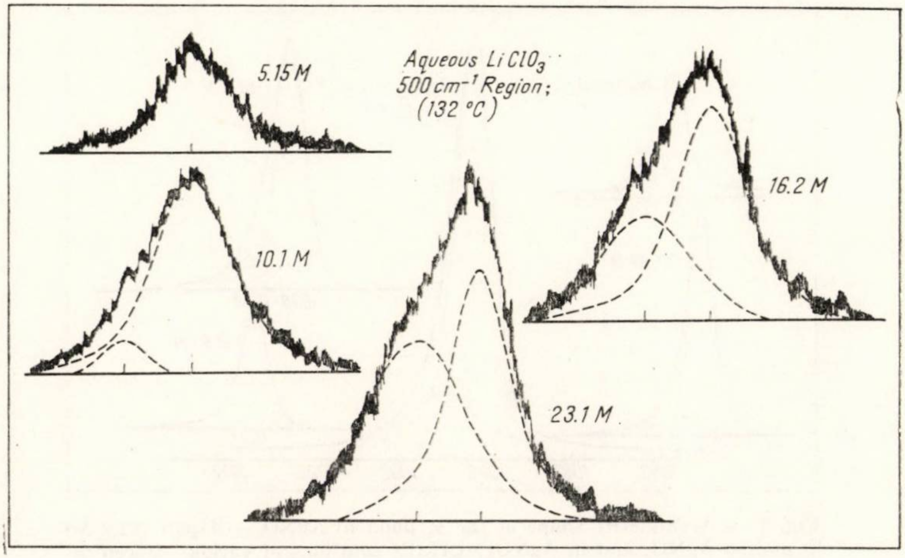

Fig. 3. — The ν_4 band in molten $LiClO_3$ (23.1 M), and in $LiClO_3-H_2O$ solutions of various concentrations. The disappearance of the high frequency component with dilution is illustrated.

Relative to the pure water spectrum the following points should be noted. The band contour has been resolved into four components, after Walrafen [5]; (i.e., 3630, 3520, 3420 and 3250 cm^{-1}). The two intense bands at 3250 and 3420 cm^{-1} in water spectrum are attributed to the H-bonded network of the water structure; while the weak bands at 3520 and 3630 cm^{-1} to the non H-bonded H_2O molecules. Addition of an electrolyte to water decreases the intensity of the 3250 and 3420 cm^{-1} bands relative to the intensity of the other two higher frequency components, [6,7] and this is interpreted as due to the breaking up of the hydrogen bonding in the bulk water structure.

Inspection of the results (see Figure 4) shows the decreasing intensities, as the salt content is increased, of the bands attributed to the H-bonded structure of bulk water. It is also apparent that these changes are accompanied by the increase in the intensity of the bands assigned to non H-bonded water molecules. In the ultraconcentrated region (~12.5 mole 1^{-1}, $LiClO_3$) very little bulk water structure remains. Further, the sharpening of the water band spectrum at high concentrations may be due to the trapping of water molecules in the $LiClO_3$ bulk structure, and is thus subjected to high electric field strengths. It is of interest to note that the thermodynamic activity of water in such highly concentrated $LiClO_3$ solutions has been quantitatively accounted [8] for by a modified B.E.T. equation (physical adsorption model) rather than on the basis of the theory of interionic attraction for electrolytes.

---

[5] G. E. Walrafen, *J. Chem. Phys.*, **47**, 114 (1967).

[6] T. T. Wall and D. F. Hornig, *J. Chem. Phys.*, **47**, 784 (1967).

[7] G. E. Walrafen, *J. Chem. Phys.*, **36**, 1035 (1962).

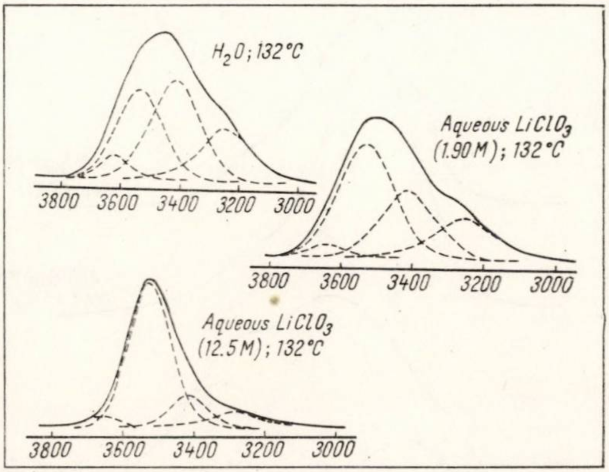

Fig. 4 — Band contour analysis of the O—H stretching mode region in bulk water and for two concentrations of $LiClO_3-H_2O$ mixtures. The diminution in intensity of the low frequency components with increasing concentrations of $LiClO_3$ is shown.

$Ca(NO_3)_2 . 4H_2O-KNO_3$, molten mixtures : The results of electrical conductance measurements [9] of molten $Ca(NO_3)_2 . 4H_2O$ and of molten mixtures of $Ca(NO_3)_2 . 4H_2O-KNO_3$ have been explained on the basis of the large hydrated multivalent cations $Ca^{2+}(H_2O)_4$, i.e., the hydrated ion behaves as a weak field dipositive cationic species. Additional support for this comes from the subsequent molar volume [10] and NMR studies. [11] In the latter, however, there is a modest water resonance shift at high temperatures as KNO_3 is added, and this would correspond with a displace-

---

[8] A. N. Campbell and B. G. Oliver, *Canad. J. Chem.*, **47**, 2671 (1969).

[9] C. A. Angell, *J. Electrochem. Soc.*, **112**, 1224 (1965).

[10] J. Braunstein, L. Orr and W. MacDonald ; *J. Chem.* Engg. Data, *12*, 415 (1967).

[11] C. T. Moynihan and A. Fratiello, *J. Amer. Chem. Soc.*, **89**, 5546 (1967).

ment of H_2O from the $Ca^{2+}(H_2O)_4$ ionic species. The present work was undertaken to see what additional information could be gained by the laser Raman technique. The salient results are illustrated in Figures 5

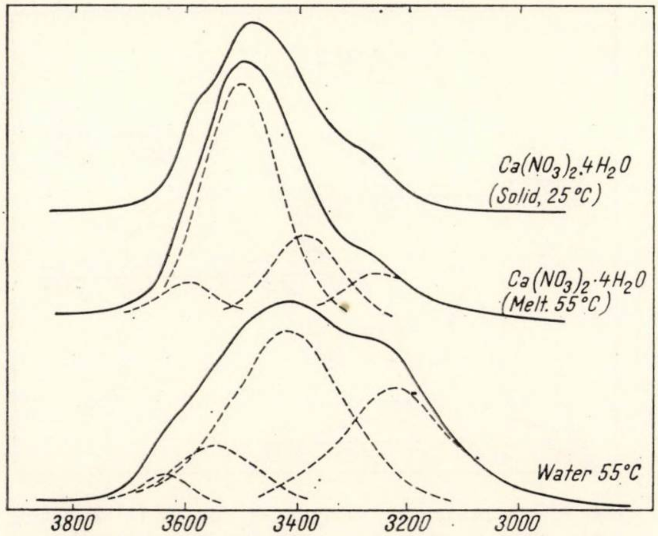

Fig. 5. — Raman band contours for water in the 3000—3800 cm^{-1} region, for bulk water (55°C), for molten $Ca(NO_3)_2 \cdot 4H_2O$ (55°C) and for solid $Ca(NO_3)_2 \cdot 4H_2O$ (25°C). The resolution of the band contour into four components, and the similarity in the spectra of molten and crystalline $Ca(NO_3)_2 \cdot 4H_2O$ is illustrated.

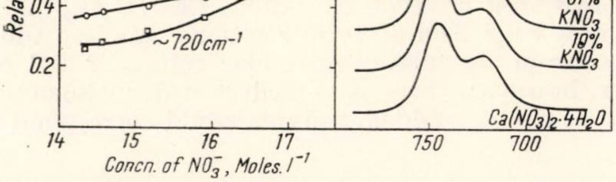

Fig. 6. — Raman bands due to the NO_3^- ion in the ν_4 region, for $Ca(NO_3)_2 \cdot 4H_2O$ and for molten mixtures of $Ca(NO_3)_2 \cdot 4H_2O - KNO_3$ (at 100°C). The relative intensity variations of the component bands is shown relative to the total band intensity as a function composition.

and 6. Shown in Figure 5 is the water band region (3000—3800 cm^{-1}) for the solid hydrate, the molten hydrate and for bulk water. The marked diminution of the intensities of the bands associated with the H-bonded water structure (in bulk water) is evidence that the H_2O is bound in the first coordination sphere of the Ca^{2+} ion. The general features of these spectra are virtually unchanged as the temperature is increased to 100°.

Exploratory studies of the molten mixtures of $Ca(NO_3)_2.4H_2O$—KNO_3, showed that the most significant spectral changes occurred in the ν_4 vibrational region of the NO_3^- ion spectrum. Some of the results for this region are illustrated in Figure 6, together with the changes in the relative intensities of the component bands for various concentrations of added KNO_3 [$Ca(NO_3)_2 . 4H_2O$ corresponds to a solution containing 14.4 moles l^{-1} of NO_3^{-1}; 30% $Ca(NO_3)_2.4H_2O$—70% KNO_3 corresponds to a solution containing 16.92 moles l^{-1} of NO_3^{-1}]. The quantitative intensity measurements show clearly that the relative intensities of the 740 and 717 cm^{-1} bands are not linear functions of molar concentration of the NO_3^- ion in the melt. A corresponding study of the water band region shows that with increasing KNO_3 concentrations the 3520 cm^{-1} band increases in intensity. These observations are understood if there is a penetration of the primary solvation sphere of the Ca^{2+} by the NO_3^- ions as KNO_3 is added to the molten hydrate. An attempt was made to establish whether the water thus displaced is bound to K^+, but this proved outside the capabilities of our spectral techniques.

Another interesting feature in the Raman spectrum of molten $AgNO_3$, molten $LiClO_3$ and in 12.2 molar solution of $AgNO_3$ in CH_3CN is the presence of a low frequency band (i.e., 120 cm^{-1} in $AgNO_3$ melt, and in $AgNO_3$—CH_3CN solution; 140 cm^{-1} in $LiClO_3$ melt). Such low frequency modes have been assigned to the lattice-like motions of ions.[12,13] On dilution of the ultraconcentrated solutions these bands disappear. The presence of such bands in the molten salts and in the ultraconcentrated solutions, thus, may be an additional criterion for ionic association and/or vibrational coupling of ions in such electrolyte systems.

CONCLUSIONS

The present observations have been limited to three examples in which the molten ionic salts may be used to explore the properties of ultraconcentrated electrolytes. The spectral evidence is in accord with the views of pronounced vibrational coupling (molten nitrates) and ionic clustering (molten chlorates). The analysis of the water band region (3000—3800 cm^{-1}) clearly supports the view advanced earlier by Samoilov,[14] i.e., the structures of very concentrated electrolytes apes that of the crystal hydrates. The Stokes-Robinson "physical adsorption"

---

[12] J. H. R. Clarke, *Chem. Phys. Letters*, 4, 39 (1969).

[13] G. H. Wegdam, R. Bonn, and J. Van der Elsken, *Chem. Phys. Letters*, 2, 182 (1968).

[14] O. Y. Samoilov, "Structure of Aqueous Electrolyte Solutions and the Hydrations of Ions". (Transl. from Russian by D. J. G. Ives, London, Consultants Bureau Publ., New York 1965.)

model,[15] and the more general quasi-lattice model of Braunstein [16] in which the water molecules and the solute anions compete for sites in the coordination sphere of the solute cations, are significant for their quantitative account of the observed physico-chemical properties of such ultraconcentrated electrolytes, and these warrant further attention. The marked similarities in the spectra of molten salts and ultraconcentrated solutions encourage the viewpoint that studies of the latter may provide the bridge between theories of electrolyte solutions and fused salt structure.

Acknowledgments. We thank B. G. Oliver for reference to the $LiClO_3-H_2O$ studies (in publication), and for the continued interest of S. C. Wait and B. G. Oliver in this work at Rensselaer. Support from the National Science Foundation for our programs in molten salt spectroscopy and structure is acknowledged with pleasure.

---

[15] R. H. Stokes and R. A. Robinson, *J. Amer. Chem. Soc.*, **70**, 1870 (1948).
[16] J. Braunstein, *J. Phys. Chem.*, **71**, 3402 (1967).

Revue Roumaine de Chimie, 17, 1, 2, 195–202 (1972)

Dedicated to Professor I.G. MURGULESCU on his 70th birthday

THERMODYNAMIC DATA FOR SOME NON-STOICHIOMETRIC URANIUM OXIDES BY SOLID-STATE EMF TECHNIQUE

D.I. MARCHIDAN and SPERANŢA MATEI
Centre of Physical Chemistry
Str. Galaţi 31, Bucharest, Romania

Received April 2, 1971

Electromotive force measurements on high-temperature galvanic cells containing solid electrolyte have been made in order to obtain thermodynamic data for uranium oxides with O/U ratio 2.04 ; 2.11 ; 2.19 and 2.21. Partial molar free energies, enthalpies and entropies of solution of oxygen in these oxides, the corresponding relative integral quantities, as well as the equilibrium pressures of oxygen as a function of the temperature have been calculated.

In order to clarify the phase relations between the stable high-temperature non-stoichiometric uranium oxides, accurate and complete data referring to their thermodynamic properties are necessary. Although non-stoichiometric uranium oxides have been the object of many investigations, many of the thermodynamical data of the stable high-temperature oxide phases are not reliable or have not been determined yet.

The use of solid electrolyte electrochemical cells proved to be an efficient method for determining thermodynamic data of the uranium compounds at elevated temperatures. [1–5]

In our laboratory an investigation concerning the thermodynamic properties of uranium oxides comprised between UO_2 and U_3O_8 in the temperature range of 1073 to 1373 K by EMF measurements was initiated. [6] Carrying on these studies, determinations were made for the following oxides having a non-stoichiometric composition : $UO_{2.04}$, $UO_{2.11}$, $UO_{2.19}$ and $UO_{2.21}$.

To this purpose EMF measurements were carried out on electrochemical cells with solid electrolyte of the type :

$$\text{Fe, wüstite} \,|\, (0.85\ ZrO_2 + 0.15\ CaO) \,|\, UO_{2+x}$$

---

[1] S. Aronson and J. Belle, *J. Chem. Phys.*, **29**, 151 (1958).

[2] K. Kiukkola, *Acta Chem. Scand.*, **16**, 327 (1962).

[3] T. L. Markin, L. E. Roberts and A. Walter, "Thermodynamics of Nuclear Materials", Ed. I.A.E.A., Vienna, 1962, p. 693.

[4] * * * "Thermodynamics of Ceramic Systems". Ed. British Ceramic Society (Proceedings 8) Stoke-on-Trent, 1967, p. 51.

[5] W. A. Yuill, Thesis, The University of Iowa, Ph. D., 1967.

[6] D. I. Marchidan and S. Matei, *Rev. Roumaine Chim.*, **15**, 1491 (1970).

EXPERIMENTAL

The cell assembly consisting of the electrolyte tablet between the two electrode tablets was inserted into a quartz cell, the form and construction of which have been minutely described in previous papers.[6,7]

The EMF measurements were carried out in a vacuum installation at a residual gas pressure of about 133×10^{-6} N.m^{-2}. The installation and experimental procedure have been previously shown.[6,7]

MATERIALS

The uranium oxide $UO_{2.04}$ was prepared from reactor grade uranium dioxide powder Merck, and the uranium oxides $UO_{2.11}$, $UO_{2.19}$ and $UO_{2.21}$ from the hexahydrate uranyl nitrate powder Chemapol *p.a.* The uranium oxide tablets were prepared by pressing the powder with the known composition into cylindrical tablets and by their sintering at 1523–1573°K in nitrogen atmosphere. After each run the oxygen-to-uranium ratios of the electrodes were determined by the usual method of oxidizing the weighed electrode at about 1073–1173°K in air,[2] when the obtained product is assumed to be U_3O_8.[8–10] It was stated that during an EMF experiment the change in the composition of the electrodes did not exceed the limits of the analytical accuracy and that no oxidation of the tablets had occurred during the EMF measurements.

The cells involve an iron-wüstite reference electrode and a solid electrolyte which, as previously shown,[4,11] acts as a purely ionic conductor. The technique of preparing the electrolyte and reference electrode tablets was described in the above mentioned paper.[6]

RESULTS AND DISCUSSION

Thermodynamic data for $UO_{2.04}$ and $UO_{2.11}$

The oxides with the atomic ratio 2.04 and 2.11 are part of the series of non-stoichiometric oxides UO_{2+x}, comprised between UO_2 and U_4O_9, which make up a single phase at high temperature, with the fluorite-type structure.

The EMF measurements were effected within the temperature range of 1073–1373°K and we found that in this range EMF linearly varied with the temperature (figures 1 and 2). By the least squares analysis we obtained the equations which gave the dependence of EMF on temperature, from 1073 to 1373°K :

$$UO_{2.04} \quad E(\mathrm{V}) = 0.656 - 0.220 \times 10^{-3}T \tag{1}$$

$$UO_{2.11} \quad E(\mathrm{V}) = 0.563 - 0.083 \times 10^{-3}T \tag{2}$$

The partial molar free energy of oxygen in equilibrium with the uranium oxide (tables 1 and 2) may be obtained by combining the stan-

---

[7] D. I. Marchidan and S. Matei, *Studii și Cercetări Chim. Acad. R.S.R.*, **18**, 617 (1970).

[8] F. Grønvold, *J. Inorg. and Nuclear Chem.*, **1**, 357 (1955).

[9] H. R. Hoekstra, S. Siegel, L. H. Fuchs and J. J. Katz, *J. Phys. Chem.*, **59**, 136 (1955).

[10] P. E. Blackburn, *J. Phys. Chem.*, **62**, 897 (1958).

[11] K. Kiukkola and C. Wagner, *J. Electrochem. Soc.*, **104**, 308 (1957).

dard free energy of formation of wüstite, known from equilibrium measurements in gas [12], with the measured free energy change of the cell, as it results from the equations :

$$\Delta G_{\text{cell}} = 2\,\Delta G^{\circ}_{\text{wüstite}} - \Delta\overline{G}_{O_2} \tag{3}$$

Table 1

Thermodynamic data for $UO_{2.04}$

Temp. °K	$-\Delta\overline{G}_{O_2}$ (kJ.mol^{-1})	$-\Delta G$ (kJ.mol^{-1})	$-\Delta G/n_{UO_2}$ (kJ/g. atom uranium)	$-\log p_{O_2}$ (N.m^{-2})
1073	226.856	4.447	4.535	6.046
1123	224.513	4.401	4.489	5.446
1173	222.923	4.368	4.455	4.926
1223	220.203	4.313	4.401	4.406
1273	217.442	4.259	4.347	3.926
1323	215.099	4.213	4.301	3.496
1373	213.132	4.175	4.259	3.106

$-\Delta\overline{H}_{O_2}$ (kJ.mol^{-1}) = 277.206
$-\Delta H$ (kJ.mol^{-1}) = 5.435
$-\Delta H/n_{UO_2}$(kJ/g atom uranium) = 5.542

$-\Delta\overline{S}_{O_2}$ (kJ.K^{-1}.mol^{-1}) = 0.046
$-\Delta S$ (kJ.K^{-1}.mol^{-1}) = 0.00091
$-\Delta S/n_{UO_2}$ = 0.00093

where :

$$\Delta G_{\text{cell}} = -4\mathcal{F}\text{E} \tag{4}$$

$$(\mathcal{F} = 96.508 \text{ kJ/volt.equiv.*})$$

As follows from equation (4) an uncertainty of 0.001 V in the EMF corresponds to an uncertainty of 386.032 J in ΔG_{cell}.

Table 2

Thermodynamic data for $UO_{2.11}$

Temp. °K	$-\Delta\overline{G}_{O_2}$ (kJ.mol^{-1})	$-\Delta G$ (kJ.mol^{-1})	$-\Delta G/n_{UO_2}$ (kJ.g.atom uranium)	$-\log p_{O_2}$ (N.m^{-2})
1073	206.396	10.731	11.330	5.046
1123	200.957	10.447	11.029	4.346
1173	195.894	10.183	10.752	3.726
1223	190.874	9.924	10.476	3.156
1273	185.811	9.660	10.200	2.626
1323	181.125	9.418	9.941	2.156
1373	176.481	9.175	9.685	1.716

$-\Delta\overline{H}_{O_2}$ (kJ.mol^{-1}) = 312.879
$-\Delta H$ (kJ.mol^{-1}) = 16.301
$-\Delta H/n_{UO_2}$(kJ/g atom uranium) = 17.213

$-\Delta\overline{S}_{O_2}$ (kJ.K^{-1}.mol^{-1}) = 0.099
$-\Delta S$ (kJ.K^{-1}.mol^{-1}) = 0.0052
$-\Delta S/n_{UO_2}$ = 0.00549

---

* Throughout this paper, 1 cal = 4.184 J and 1 atm. = 101325 N.m $^{-2}$.

[12] K. Kiukkola and C. Wagner, *J. Electrochem. Soc.*, **104**, 379 (1957).

We found that the temperature dependence is given by the equations :

$$UO_{2.04}\ \Delta\overline{G}_{O_2}\ (\mathrm{kJ.mol^{-1}}) = -\ 277.206 + 0.046\ T \qquad (5)$$

$$UO_{2.11}\ \Delta\overline{G}_{O_2}\ (\mathrm{kJ.mol^{-1}}) = -\ 312.879 + 0.099\ T \qquad (6)$$

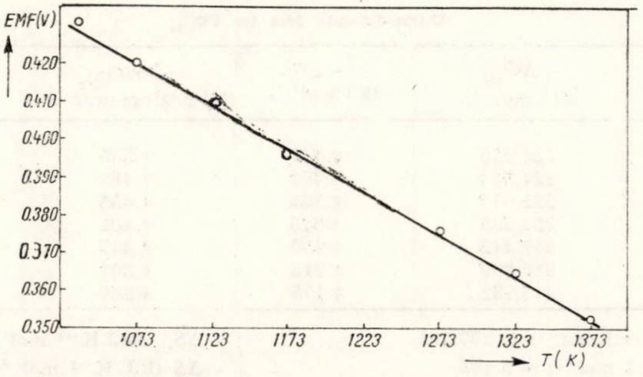

Fig. 1. — Variation of EMF with the temperature for $UO_{2.04}$.

The fact that $\Delta\overline{G}_{O_2}$ linearly varies with the temperature is in accordance with the results previously found for other non-stoichiometric oxides that are part of the same single-phase region [1].

Partial molar free enthalpies and entropies may be calculated from the thermodynamic relations :

$$\frac{\partial\left(\dfrac{\Delta\overline{G}_{O_2}}{T}\right)}{\partial T} = -\ \frac{\Delta H_{O_2}}{T^2} \qquad (7)$$

$$\Delta\overline{G}_{O_2} = \Delta\overline{H}_{O_2} - T\,\Delta\overline{S}_{O_2} \qquad (8)$$

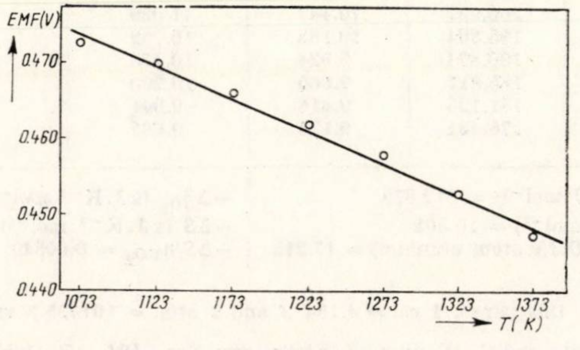

Fig. 2. — Variation of EMF with the temperature for $UO_{2.11}$.

Since the partial molar free energy is a linear function of the temperature at constant composition, that means that the partial molar enthalpy and entropy are independent of the temperature.

The integral molar thermodynamic quantities were calculated from partial molar quantities according to the known formulas [2,6]. Tables 1 and 2 include a list of the thermodynamic data of these oxides.

A comparison of the experimental data can be made by calculating the $\Delta\overline{G}_{O_2}$ isotherm (at 1150°K) from our results, for the oxides $UO_{2.04}$, $UO_{2.11}$ and $UO_{2.125}$, [1] and inscribing on the same diagram (figure 3) the molar partial free energies values, corresponding to some non-stoichiometric oxides which are part of the same single-phase region UO_{2+x}, reported by Aronson and Belle, [1] as well as those calculated from the equations related by Rand and Kubaschewski. [13] The results are in accordance.

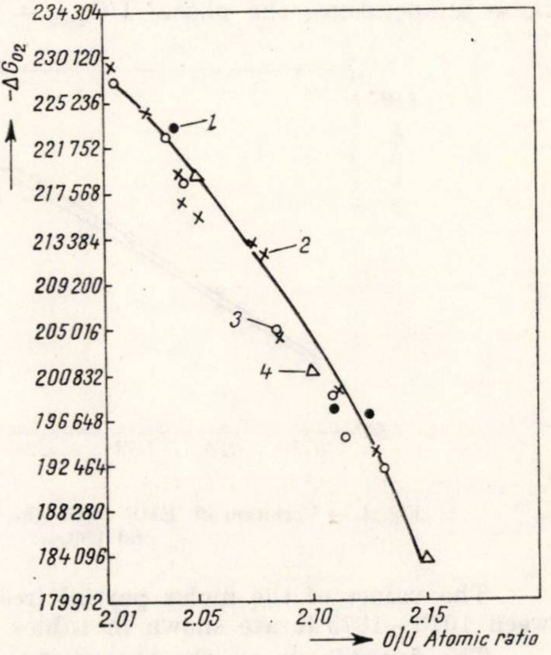

Fig. 3 – $\Delta\overline{G}_{O_2}$ *versus* O/U ratio:
1, Obtained by authors for $UO_{2.04}$, $UO_{2.1}$, and $UO_{2.125}$; *2*, Obtained by Aronson and Belle[5] at 1150°K; *3*, Obtained by Kiukkola[3] at 1173°K; *4*, Calculated from the equations related by Rand and Kubaschewski [13].

The equilibrium oxygen partial pressures (in atm.) may be calculated from the equations:

$$\Delta\overline{G}_{O_2} = RT \ln p_{O_2} = 2.303\, RT \log p_{O_2} \tag{9}$$

---

[13] M. H. Rand and O. Kubaschewski, "The Thermochemical Properties of Uranium Compounds", Oliver and Boyd, Edinburgh, 1963, p. 26.

Passing to the International System we take into account that 1 atm = 101325 $N.m^{-2}$ and $R = 8.314$ $J.K^{-1}.mol^{-1}$. Making all the necessary transformations one obtains the partial pressure of oxygen in $N.m^{-2}$ (Tables 1 and 2).

Thermodynamic data for $UO_{2.19}$ *and* $UO_{2.21}$

With the oxides having the atomic ratios 2.19 and 2.21 one obtains for EMF a dependence on the temperature having the form shown in figure 4. For these compositions one can observe a definite break in the EMF *vs.* temperature curve at about 1233°K and, respectively 1283°K which indicates a phase transformation at these temperatures; the homogeneous UO_{2+x} phase prevails above these temperatures, while below these temperatures the phases $UO_{2+x} + U_4O_{9-y}$ coexist.

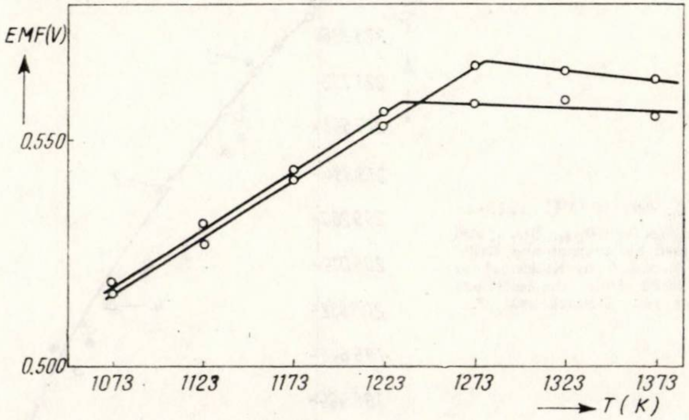

Fig. 4. — Variation of EMF with the temperature for $UO_{2.19}$ and $UO_{2.21}$.

The values of the molar partial free energy for temperatures between 1073—1373°K are shown in tables 3 and 4.

The dependence on the temperature of $\Delta\overline{G}_{O_2}$ must be separately calculated for temperature ranges situated on each side of the transformation point. As a matter of fact, the relationships of the type:

$$\Delta\overline{G}_{O_2} = \Delta\overline{H}_{O_2} - T\,\Delta\overline{S}_{O_2}$$

are available for temperature ranges in which phase transformations do not take place, since a phase change would entail an ethalpy and entropy change.

Thus, for the temperature range in which there is a single phase UO_{2+x} we determined the relationships:

$$UO_{2.19} \qquad \Delta\overline{G}_{O_2}\ (kJ.mol^{-1}) = -\,306.268 + 0.128\ T \qquad (10)$$

$$UO_{2.21} \qquad \Delta\overline{G}_{O_2}\ (kJ.mol^{-1}) = -\,296.695 + 0.131\ T \qquad (11)$$

Table 3

Thermodynamic data for $UO_{2.19}$

Temp °K	$-\Delta\bar{G}_{O_2}$ (kJ.mol^{-1})	$-\Delta G$ (kJ.mol^{-1})	$-\Delta G/n_{UO_2}$ (kJ/g.atom uranium)	$-\log p_{O_2}$ (N.m^{-2})	$-\Delta\bar{H}_{O_2}$ (kJ.mol^{-1})	$-\Delta H$ (kJ.mol^{-1})	$-\Delta H/n_{UO_2}$ (kJ/g.atom uranium)	$-\Delta\bar{S}_{O_2}$ (kJ.K^{-1} mol^{-1})	$-\Delta S$ (kJ.K^{-1} mol^{-1})	$-\Delta S/n$
1073	188.991	16.233	17.323	4.276	435.972	37.781	41.379	0.230	0.019	0.021
1123	177.401	15.271	16.694	3.256	435.972	37.781	41.379	0.230	0.019	0.021
1173	166.104	14.267	15.648	2.396	435.972	37.781	41.379	0.230	0.019	0.021
1223	154.389	13.263	14.560	1.596	435.972	37.781	41.379	0.230	0.019	0.021
1273	147.193	12.635	13.849	1.036	306.268	26.526	29.078	0.128	0.011	0.012
1323	140.624	12.091	13.221	0.556	306.268	26.526	29.078	0.128	0.011	0.012
1373	135.352	11.631	12.761	0.156	306.268	26.526	29.078	0.128	0.011	0.012

Table 4

Thermodynamic data for $UO_{2.21}$

Temp. °K	$-\Delta\bar{G}_{O_2}$ (kJ.mol^{-1})	$-\Delta G$ (kJ.mol^{-1})	$-\Delta G/n_{UO_2}$ (kJ/g.atom uranium)	$-\log p_{O_2}$ (N.m^{-2})	$-\Delta\bar{H}_{O_2}$ (kJ.mol^{-1})	$-\Delta H$ (kJ.mol^{-1})	$-\Delta H/n_{UO_2}$ (kJ/g.atom uranium)	$-\Delta\bar{S}_{O_2}$ (kJ.K^{-1}. mol^{-1})	$-\Delta S$ (kJ.K.$^{-1}$. mol^{-1})	$-\Delta S/n$
1073	189.786	18.028	19.940	4.246	435.930	41.379	45.772	0.229	0.021	0.024
1123	178.949	16.999	18.802	3.306	435.930	41.379	45.772	0.229	0.021	0.024
1173	166.941	15.857	17.539	2.436	435.930	41.379	45.772	0.229	0.021	0.024
1223	155.728	14.794	16.393	1.656	435.930	41.379	45.772	0.229	0.021	0.024
1273	144.096	13.690	15.141	0.906	435.930	41.378	45.772	0.229	0.021	0.024
1323	137.904	13.100	14.489	0.446	296.695	28.200	31.170	0.131	0.012	0.013
1373	132.088	12.547	13.878	0.026	296.695	28.200	31.170	0.131	0.012	0.013

and for the temperature range in which UO_{2+x} is disproportionally found in $UO_{2+x} + U_4O_{9-y}$ it has been stated that:

$$UO_{2.19} \qquad \Delta\bar{G}_{O_2}\,(\mathrm{kJ.mol^{-1}}) = -\,435.972 + 0.230\ T \tag{12}$$

$$UO_{2.21} \qquad \Delta\bar{G}_{O_2}\,(\mathrm{kJ.mol^{-1}}) = -\,435.930 + 0.229\ T \tag{13}$$

We can observe that in the two-phase region $\Delta\bar{G}_{O_2}$ does not practically change with the composition. The values obtained by us for this region are near to those related by Perron [14] who, by reviewing the data pertaining to the two-phase region $UO_{2+x} + U_4O_{9-y}$ and by the use of elementary statistical analysis, found that:

$$\Delta\bar{G}_{O_2}\,(\mathrm{kJ.mol^{-1}}) = -\,430.466 + 0.229\ T \tag{14}$$

The values of $\Delta\bar{H}_{O_2}$ and $\Delta\bar{S}_{O_2}$ for the single-phase and for the two-phase ranges are listed in tables 3 and 4.

It is found that the passage from the single-phase to the two-phase region is accompanied by a strong decrease in the relative partial molar heat of solution of oxygen in uranium oxide and in the relative partial molar entropy of oxygen. This statement is in accordance with the result obtained by other authors [1,2] and was interpreted as indicating a continuous increase of the order in the oxygen lattice with the dissolution of oxygen in the UO_{2+x} phase. As a matter of fact, the passage from the UO_{2+x} to the U_4O_9 phase is achieved by incorporating oxygen ions into interstitial positions in its fluorite lattice leading to a more stable configuration of atoms. The attractive interactions between interstitial oxygen ions will cause the decrease of the value of the partial molar enthalpy of solution of oxygen with the increase in oxygen content.

From the determinations effected one can easily see that the region of stability of the UO_{2+x} phase is dependent on temperature, namely it increases with the temperature increase.

Acknowledgements. This work was performed under contract No. 695/RI/RB with the International Atomic Energy Agency. The authors are grateful to the IAEA for permission to publish this paper. We wish to express our deep gratitude to Professor I. G. Murgulescu for his interest in our work. We also wish to express our thanks to the Laboratory of Nuclear Materials, Institute of Atomic Physics, Bucharest.

---

[14] P. O. PERRON, "Thermodynamics of Non-stoichiometric Uranium Dioxide", Chalk River, Ontario, 1968.

Revue Roumaine de Chimie, **17**, *1*, 2, 203–208 (1972)

Hommage au Professeur I.G. MURGULESCU
à l'occasion de son 70e anniversaire

CALCUL DES ÉNERGIES D'EXCÈS INTÉGRALES LIBRES DES SYSTÈMES TERNAIRES DE SELS FONDUS SUR LA BASE DES SYSTÈMES BINAIRES

B.F. MARKOV

Institut de Chimie générale et inorganique de l'Académie des Sciences de l'Ukraine,
32–34, Rue Novo-Belischanskaia, Kiev 142

Reçu le 27 septembre 1971

On présente une nouvelle forme de calcul des propriétés thermodynamiques d'excès d'un système ternaire, basé sur les propriétés intégrales d'excès des systèmes binaires qui constituent le système ternaire. On donne les résultats obtenus pour les systèmes ternaires : AgCl + KCl + NaCl ; AgCl + NaCl + CsCl et $MgCl_2$ + KCl + NaCl.

Les diagrammes des énergies d'excès intégrales libres de Gibbs des alliages liquides des systèmes métalliques sont utilisés depuis longtemps pour la présentation concrète des relations des composants d'alliage.

Cette méthode de la présentation des résultats expérimentaux pour les systèmes ternaires de sels fondus ne s'est pas répandue largement puisque les propriétés thermodynamiques de ces systèmes sont étudiées insuffisamment.

Le mode de calcul des propriétés thermodynamiques intégrales du système ternaire ne se basant que sur la propriété partielle de l'un des composants (définie directement dans l'expérience) a été envisagé à plusieurs reprises dans la littérature. La version la plus réussie a été donnée par Darken.[1]

Pour donner une caractéristique parfaite du système ternaire, outre la détermination de la propriété partielle de l'un des composants dans les deux systèmes binaires, il est nécessaire de la déterminer pour une série de sections du système ternaire. C'est un travail difficile et probablement c'est pourquoi les systèmes ternaires sont peu étudiés.

Il est intéressant de vérifier la possibilité de calcul de la propriété d'excès des mélanges fondus ternaires sur la base des propriétés d'excès intégrales des trois systèmes binaires faisant le système ternaire.

---

[1] L. S. Darken, *J. Amer. Chem. Soc.*, **72**, 2909 (1950).

L'équation correspondante peut être obtenue de la manière suivante : L'énergie d'excès intégrale libre pour le système ternaire peut être représentée comme la somme de contributions des combinaisons binaires,

$$G^E_{1,2,3} \cong |G^E_{1,2}| + |G^E_{1,3}| + |G^E_{2,3}| \tag{1}$$

Pour le système binaire 1—2 $G^E_{1,2}$ est proportionnel au produit des fractions molaires des composants $G^E_{1,2} = k\, x_1\, x_2$, où x — les fractions molaires dans les systèmes binaires.

La contribution des combinaisons 1—2 dans le système ternaire est aussi proportionnelle au produit des fractions molaires au mélange ternaire $|G^E_{1,2}| = k'\, N_1\, N_2$, où N — les fractions molaires dans le système ternaire.

Sans tenir compte de l'influence du troisième composant, on admet que $K = K'$, alors

$$|G^E_{1,2}| = G^E_{1,2}\frac{N_1 . N_2}{x_1 x_2} = G^E_{1,2}\,(N_1 + N_2)^2$$

puisque

$$x_1 = \frac{N_1}{N_1 + N_2}; \quad x_2 = \frac{N_2}{N_1 + N_2}$$

Par substitution des valeurs correspondantes dans l'equation (1) nous aurons

$$G^E_{1,2,3} = G^E_{1,2}\,(N_1 + N_2)^2 + G^E_{1,3}\,(N_1 + N_3)^2 + G^E_{2,3}\,(N_2 + N_3)^2 \tag{2}$$

quand

$$x_1 = \frac{N_1}{N_1 + N_2} \quad x_1 = \frac{N_1}{N_1 + N_3} \quad x_2 = \frac{N_2}{N_2 + N_3}$$

Pour calculer l'énergie d'excès intégrale libre du système ternaire à partir de l'équation (2) il est nécessaire d'avoir les énergies d'excès intégrales libres des trois systèmes binaires faisant le système ternaire. Si dans les systèmes binaires ont lieu les fonctions régulières, c'est-à-dire les courbes énergie d'excès libre — composition sont représentées par les paraboles symétriques :

$$G^E_{1,2} = b_{1,2} \cdot x_1 x_2\,;\; G^E_{1,3} = b_{1,3}\, x_1\, x_3\,;\; G^E_{2,3} = b_{2,3}\, x_2\, x_3$$

l'équation (2) devient alors,

$$G^E_{1,2,3} = b_{1,2}\, N_1\, N_2 + b_{1,3}\, N_1\, N_3 + b_{2,3}\, N_2\, N_3 \tag{3}$$

Il est à noter que l'équation (3) a été déjà citée dans la littérature.

Maintenant nous avons la possibilité de vérifier la précision avec laquelle l'équation (3) rend les données expérimentales pour les systèmes

AgCl−KCl−NaCl et AgCl−NaCl−CsCl obtenues par Guion et coll. [2] et l'équation (2) pour le système $MgCl_2$−KCl−NaCl d'après Neil et coll. [3]

Le schéma de vérification est le suivant :

1. En appliquant l'équation de Darken, on définit l'énergie d'excès intégrale libre pour la section du système ternaire correspondant à 50 moles % du système binaire 2−3.

Par extrapolation proche de cette courbe, on calcule :

2. A partir des valeurs de $G^E_{1,2}$, $G^E_{1,3}$ et $G^E_{2,3}$, on calcule $G^E_{1,2,3}$ (cal.)
3. D'après la courbe $G^E_{1,2,3}$ (cal.) — composition, on définit graphiquement l'énergie d'excès partielle libre du composant 1 $\overline{G}^E_1$ (cal.) et on la trace en fonction de la composition (ligne continue).
4. Les valeurs expérimentales $\overline{G}^E_1$ (cercles) sont comparées avec la courbe calculée.

La fig. 1 présente des courbes de l'énergie d'excès intégrale libre de la G^E — section AgCl−KCl.NaCl à 800° en fonction de la composition et les courbes de l'énergie d'excès partielle libre AgCl, $\overline{G}^E_{AgCl}$ trouvées par calcul. Les valeurs expérimentales de $\overline{G}^E_{AgCl}$ sont désignées par des cercles.

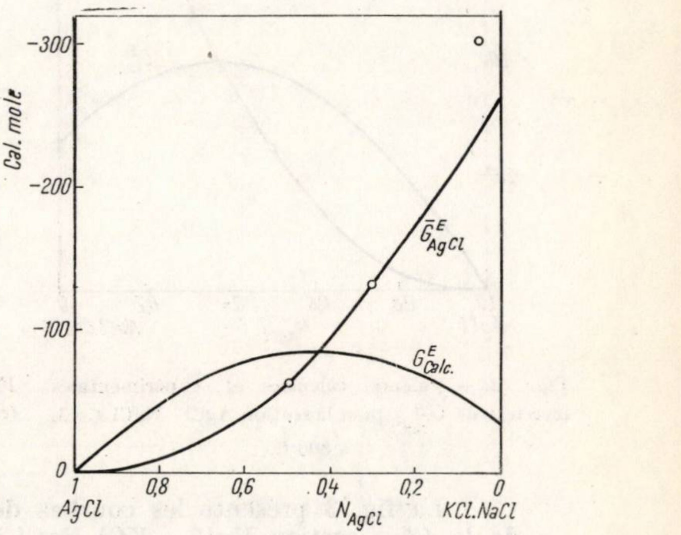

Fig. 1. — Valeurs calculées et expérimentales (cercles) de $\overline{G}^E_{AgCl}$ pour la section AgCl−KCl.NaCl, à 800°C.

La fig. 2 présente les courbes de l'énergie d'excès intégrale libre de la G^E — section AgCl−NaCl.CsCl à 800° en fonction de la composition et les courbes de l'énergie d'excès partielle libre AgCl, $\overline{G}^E_{AgCl}$ trouvées par calcul.

---

[2] J. Guion, M. Blander, D. Hengstenberg et K. Hagemark, *J. Phys. Chem.*, **72** 2086 (1968).

[3] D. E. Neil et H. M. Clark, *J. Chem. Eng. Data*, **10**, 21 (1965).

Les valeurs expérimentales $\overline{G}^E_{\mathrm{AgCl}}$ sont désignées par cercles. Aux teneurs hautes en AgCl les valeurs expérimentales et calculées coïncident bien dans les deux systèmes. Les déviations sensibles ont lieu seulement à 5 moles % AgCl.

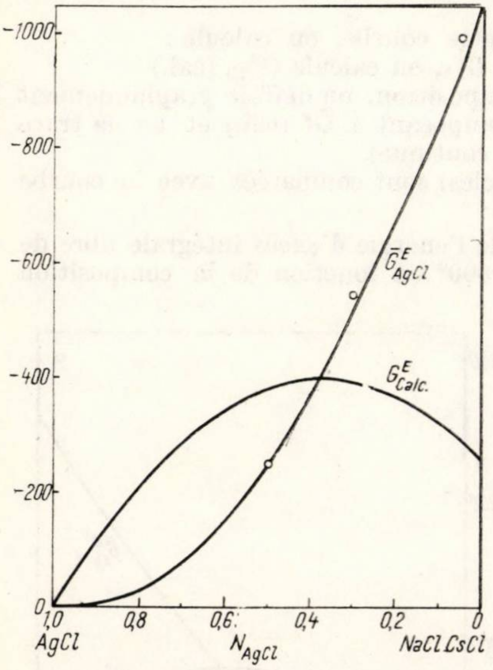

Fig. 2. — Valeurs calculées et expérimentales (cercles) de $\overline{G}^E_{\mathrm{AgCl}}$ pour la section AgCl—NaCl. CsCl, à 800°C.

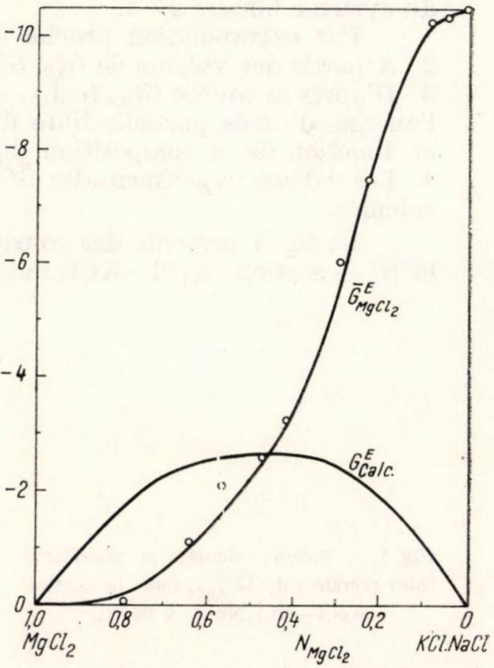

Fig. 3. — Valeurs calculées et expérimentales (cercles) de $\overline{G}^E_{\mathrm{MgCl_2}}$ pour la section $\mathrm{MgCl_2}$—KCl.NaCl, à 800°C.

La fig. 3 présente les courbes de l'énergie d'excès intégrale libre de la G^E — section $\mathrm{MgCl_2}$—KCl.NaCl à 800° en fonction de la composition et les courbes de l'énergie d'excès partielle libre $\mathrm{MgCl_2}$, $\overline{G}^E_{\mathrm{MgCl_2}}$ trouvées par calcul.

Les valeurs expérimentales de $\overline{G}^E_{\mathrm{MgCl_2}}$ désignées par les cercles coïncident bien avec la courbe calculée.

Cela confirme que l'énergie d'excès intégrale libre de mélange ternaire peut être en bonne approximation évaluée sur la base des mêmes paramètres des systèmes binaires faisant le système ternaire.

Il est nécessaire une vérification expérimentale d'application des équations (2) et (3) pour l'estimation du degré d'approximation.

Pour l'étude expérimentale des systèmes ternaires il serait désirable de savoir d'avance les types possibles de diagrammes des propriétés d'excès des systèmes ternaires représentant les relations des composants du système.

Ce problème peut être résolu sur la base de l'équation (3) en utilisant les valeurs différentes du coefficient *b*.

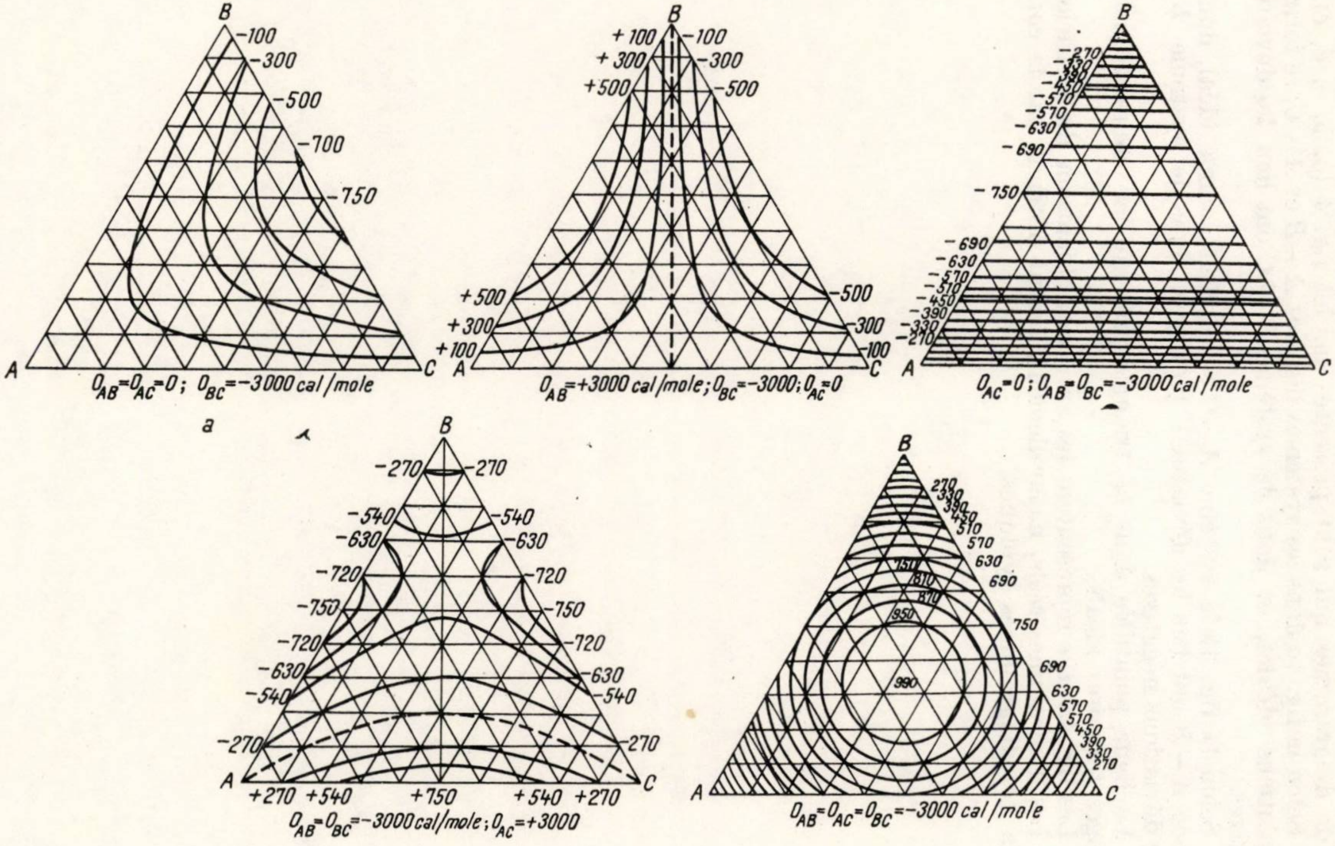

Fig. 4. — Diagrammes typiques d'énergie d'excès libre-composition des systèmes ternaires.

Les recherches réalisées dans ce domaine ont donné 5 types essentiels de diagrammes qui sont présentés sur les fig. 4 (*a*, *b*, *c*, *d*, *e*).

Selon la fig. 4*a* dans les systèmes binaires $A-B$ et $A-C$, se forment les solutions idéales, et dans le système $B-C$ ont lieu les déviations négatives.

Selon la fig. 4*b* le système $A-C$ se conduit comme idéal, dans le système $A-B$ ont lieu les déviations positives, dans le système $B-C$ — les déviations négatives.

La ligne pointillée dans le triangle présente les compositions de mélanges ternaires idéals.

Les fig. 4*c*, *d*, *e* représentent les autres combinaisons de coefficients.

Les diagrammes réels, naturellement, seront obtenus par la combinaison des diagrammes typiques.

Revue Roumaine de Chimie, 17, 1, 2, 209–212 (1972)

К 70-летию проф. И. Г. МУРГУЛЕСКУ

О НЕКОТОРЫХ РЕЗУЛЬТАТАХ ИССЛЕДОВАНИЯ РЕАКЦИИ ОКИСЛЕНИЯ МЕТАНА, ИНИЦИИРОВАННОГО АЗОТНОЙ КИСЛОТОЙ

А. Б. НАЛБАНДЯН

Лаборатория химической физики АН Армянской ССР, Ереван, ул. Московская, 22

Получена 18 сентября 1971 г.

Кратко излагаются результаты, полученные в лабораториях Бухарестского Центра физической химии под руководством академика профессора И. Г. Мургулеску, и в лабораториях Московского института химической физики Академии наук СССР под руководством автора данной статьи, в области окисления метана, инициированного азотной кислотой. Особое внимание уделяется новым явлениям, открытым в процессе этого сотрудничества, а также успехам, достигнутым впоследствии в Бухаресте в вопросе « холодного пламени метана », и в Москве в вопросе исследования кинетики разложения паров азотной кислоты.

Более 10 лет назад профессор Мургулеску — руководитель Института физической химии Академии Социалистической Республики Румынии командировал в нашу Лабораторию окисления углеводородов Института химической физики АН СССР одного из своих многочисленных молодых способных учеников. Им оказался Шнайдер И. А., ныне профессор, заведующий кафедрой физической химии Ясского университета. Целью командировки была постановка совместной работы в области химического использования природного газа-метана. Как известно, большие запасы этого газа в Социалистической Республике Румынии и в Советском Союзе делают метан весьма ценным объектом теоретических исследований, могущих в перспективе иметь важное народнохозяйственное значение. До этого одним из направлений, развиваемых профессором Мургулеску с сотрудниками, было исследование термического распада метана в ацетилен. Работа проводилась с целью выяснения механизма этой реакции. Предложенный авторами механизм термического образования ацетилена широко известен и обсуждается в литературе. С одобрения профессора Мургулеску была поставлена задача частичного, селективного окисления метана в формальдегид широко используемого в химической промышленности для получения синтетических смол, пластических масс, а также различных полимерных материалов, обладающих ценными свойствами. Начатая в то время совместная работа успешно продолжается в Институте физической химии, руководимом профессором Мургулеску, в Ясском университете, а также в Институте химической физики АН СССР и Лаборатории химической физики АН Армянской ССР.

Хотелось бы коротко остановиться на первых интересных результатах, полученных в совместных исследованиях, а также на развитии этих работ в указанных организациях, поскольку они тесно связаны с именем профессора Мургулеску. Принимая во внимание большую инертность метана к окислению, было решено инициировать реакцию парами азотной кислоты. Исследования показали, что в одинаковых условиях пары азотной кислоты являются более эффективным инициатором, чем окись и двуокись азота. В присутствии азотной кислоты одинаковый выход формальдегида достигается при температуре почти на 100° ниже, чем при инициировании окислами азота. В ходе работы было обнаружено новое явление: скачок температуры, который наблюдается начиная с определенной критической скорости потока реагирующих газов [1]. В этом скачке, температура превышала температуру стенок реактора (500—520°) на несколько десятков градусов. Оказалось, что величина скачка сильно зависит от скорости потока. По мере ее увеличения он растет и в оптимуме достигает 200—250°. Времена контакта в этих условиях составляют несколько сотых и тысячных долей секунды. Была обнаружена тесная связь между величиной температурного скачка и выгодом ценных кислородсодержащих продуктов. Параллельно со скоростью струи наблюдается рост амплитуды скачка и вместе с ним выхода формальдегида. В оптимальных условиях выход формальдегида в 1,5—2 раза превышает максимальный выход, получаемый при инициировании окислами азота. Если в последнем случае наряду с формальдегидом наблюдается образование равных количеств окиси углерода, то в условиях инициирования парами азотной кислоты в оптимальном режиме конечные продукты практически отсутствуют. Наряду с формальдегидом был обнаружен нитрометан, количество которого в противоположность формальдегиду падало с ростом скорости потока реагирующих газов [2,3]. Для объяснения столь необычного влияния паров азотной кислоты было высказано предположение, что при высоких температурах молекула азотной кислоты распадается гомогенно с образованием свободного радикала OH и NO_2. В результате повышения концентрации активных центров возрастает и скорость реакции. Большие скорости потока требуются для того, чтобы успеть вынести радикалы OH из зоны подогрева в зону высокой температуры, где длина цепи большая. Возникающий при распаде HNO_3 свободный гидроксил легко реагирует с метаном образуя цепь реакций

$$OH+CH_4 \rightarrow H_2O+CH_3,$$

$$CH_3+O_2 \rightarrow CH_2O+OH.$$

В последующих работах образование значительных количеств радикалов OH при высокотемпературном распаде паров азотной кислоты непосредственно было доказано методом, электронного парамагнитного резонанса[3–6]. В продуктах распада было установлено также наличие радикалов NO_3. Их образование, по-видимому, связано с взаимодействием гидроксильного радикала с HNO_3: $OH + HNO_3 = H_2O + NO_3$. В согласии с результатами предыдущих исследователей, был установлен бимолекулярный характер реакции распада азотной кислоты. На основании этих данных и некоторых других наблюдений следовало ожидать, что скорость распада HNO_3 должна зависеть от природы частицы, с которой сталкивается молекула HNO_3. Были поставлены специальные опыты по исследованию кинетики распада паров азотной кислоты в широком температурном интервале (500—800°) в присутствии азота и метана. Концентрация HNO_3 в атмосфере этих газов составляла 0,5%. Опыты проводились при атмосферном давлении в струе в кварцевом реакторе ($d \simeq 0{,}14$ см, $l = 8$ см). Времена пребывания газов изменялись в пределах от 0,0006 до 0,004 сек. Изучался распад безводной азотной кислоты (98—99% концентрации). Кинетика распада азотной кислоты при различных температурах в атмосфере азота представлена на рис. 1. Видно, что при 500° и максимальном времени контакта $t_k = 0{,}004$ сек. азотная кислота распадается лишь на 3%; при том же времени контакта и 600, 650, 700, 750 и 800° на 58; 65; 81, 88 и 92% соответственно. Картина распада кислоты в атмосфере метана резко изменяется. На рис. 2 приведена кинетика распада при различных температурах. Из рисунка видно, что при $t_k = 0{,}004$ сек и 500° пары азотной кислоты распадаются на 90%. Для получения такого процента превращения в атмосфере азота необходимо температуру повысить до 750°. При $t_k = 0{,}001$ сек. и 600° в инертной среде кислота распадается на 38%, а в атмосфере метана почти на 90%. Результаты, полученные в этих опытах, говорят о том, что метан скорее всего вступает в химическую реакцию с

---

[1] И. А. Шнайдер, О. А. Иванов и А. Б. Налбандян, *ДАН СССР*, **180**, 626 (1968).

[2] A. B. Nalbandyan, I. Iosif и I. A. Schneider, *Rev. Roum. Chimie*, **13**, 671 (1968).

[3] I. Iosif, K. A. Schneider и A. B. Nalbandyan, *Rev. Roum. Chimie*, **13**, 857 (1968).

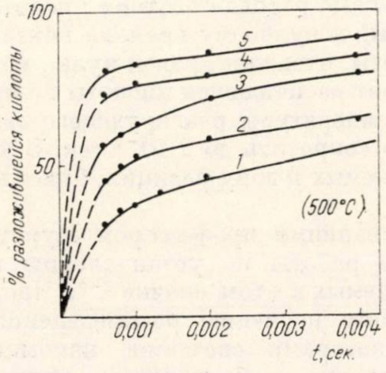

Рис. 1

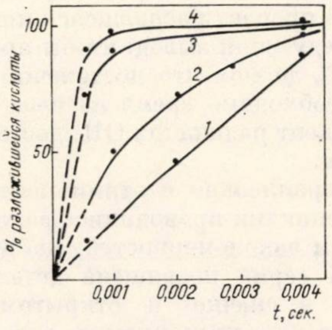

Рис. 2

---

[4] Ю. М. Гершензон, А. П. Дементьев и А. Б. Налбандян, *ДАН СССР*, **180**, 1147 (1968).

[5] Ю. М. Гершензон, А. П. Дементьев и А. Б. Налбандян, *Изв. АН СССР, серия хим.*, 2808 (1969).

[6] Е. А. Овсоян и А. Н. Налбандян, *Арм. хим. жур.*, **22**, 1057 (1969).

молекулой HNO_3. Об этом свидетельствует также формальдегид, обнаруженный в продуктах реакции. Из анализа результатов, представленных на рис. 2, становится ясно, почему для получения скачка температуры с максимальной амплитудой необходимо опыты проводить при очень малых временах контакта, т.е. при больших скоростях потока реагирующей метано-воздушной смеси. При большом времени контакта, составляющем, например, 0,004 сек. для 500° практически вся азотная кислота распадается в зоне подогрева смеси и образующиеся радикалы OH успевают рекомбинировать раньше, чем попадают в зону высокой температуры и длинных цепей.

Рассматривая кинетические кривые распада азотной кислоты в присутствии метана, экстраполированные к нулевому времени контакта, при котором процент распавшейся кислоты, очевидно, равен нулю, можно сделать следующий вывод: чтобы процент распавшейся кислоты не превышал 25—35 % до момента достижения температуры реагирующего газа 600—650°, необходимо время нагрева его сократить до 2.10^{-4} сек. В этом случае процент радикалов OH, доставляемых в зону реакции, будет наиболее высоким.

Параллельно с этими исследованиями профессором Мургулеску и его учениками проводились важные работы по установлению природы скачка и закономерностей, наблюдаемых в этом скачке [7–9]. Часть работ из этой серии посвящена детальному изучению распределения температуры в скачке и открытому авторами свечения, напоминающего свечение холодных пламен, возникающих в определенных условиях при окислении высших углеводородов. Показано, что в зависимости от условий опыта обнаруженное холодное пламя может иметь стационарный или пульсирующий характер. Установлено также, что положение пламени в реакторе и его протяженность являются функциями скорости потока реагирующих газов и концентрации инициатора. При больших скоростях струи и малых концентрациях паров азотной кислоты пламя стабилизируется у выхода прореагировавших газов из реакционного сосуда. Для выяснения природы пламени большое значение имела бы постановка опытов со спектральным анализом свечения. Измерения температуры в скачке позволило установить, что максимальная температура достигается не мгновенно, а в течение длительного времени, составляющего несколько десятков минут. После установления максимальной температуры последняя может сохраниться сколь угодно долго при условии непрерывной подачи свежей смеси постоянного состава.

---

[7] D. P. Lazăr и I. A. Schneider, *Rev. Roum. Chimie*, 13, 1285 (1968).

[8] I. Iosif, D. P. Lazăr и I. A. Schneider, « Intern. Symposium on Gas Kinetics », 1969, Szeged, Ungary.

[9] I. G. Murgulescu, I. A. Schneider и I. Iosif, « The second Intern. Symposium on Gas Kinetics », 1971, Dep. of Chem. Univ. College of Swansea, England.

Revue Roumaine de Chimie, **17**, *1*, *2*, 213–223 (1972)

Dedicated to Professor I.G. MURGULESCU
on his 70th birthday

KINETICS AND MECHANISM OF THE THERMAL DECOMPOSITION OF DIPHENYLDIAZOMETHANE IN THE ABSENCE OF SOLVENT. I

TATIANA ONCESCU, M. CONTINEANU and G. BĂLĂCEANU

Department of Physical Chemistry, University of Bucharest
Bd. Republicii 13, Bucharest, Romania

Received August 2, 1971

From the kinetic study of thermal decomposition of diphenyldiazomethane in the absence of solvent, at different temperatures, there results a reaction mechanism which involves the appearance of the diphenylcarbene radical, which starts further reactions.

The thermal decomposition of diphenyldiazomethane in solution was studied by several researchers. [1–5] They all agree that the first reaction stage is the formation of diphenylcarbene, which also is confirmed by the photolysis [6–8] of the diazo compound.

In this paper we deal with the decomposition of the diphenyldiazomethane in the absence of the solvent in the temperature range 30°–100°, at which this compound is molten.

EXPERIMENTAL

In several reaction vessels fitted with stoppers, samples of 0.1 g diphenyldiazomethane were weighed. The weighing was caried out as quickly as possible at a temperature of about 20°, protecting the substance from light. This precaution was necessary because the diphenyldiazomethane melting point is about 30° and even over 25° the substance softens, being very difficult to handle.

---

[1] W. E. Parham and W. R. Hasek, *J. Amer. Chem. Soc.*, **76**, 935 (1954).

[2] I. G. Murgulescu and T. Oncescu, *J. Chim. phys.*, **58**, 508 (1961).

[3] W. Kirmse, *Liebigs Ann. Chem.*, **666**, 9 (1963).

[4] H. Reimliger, *Chem. Ber.*, **97**, 339 (1964).

[5] D. Bethell, B. Whittaker and J. D. Callister, *J. Chem. Soc.*, **1965**, 2466.

[6] R. W. Murray, A. M. Trozzolo, E. Wasserman and W. A. Jeger, *J. Amer. Chem. Soc.*, **34**, 3213 (1962).

[7] R. W. Brandon, G. L. Closs and C. Hutchison Jr., *J. Chem. Phys.*, **37**, 1878 (1962).

[8] T. Oncescu, D. Bogdan, M. Contineanu and G. Bălăceanu, *Ber. Bunsengesellschaft Phys. Chem.*, **72**, 247 (1968).

Then the samples were introduced into the thermostat at the required temperature. At time intervals the vessels were suddenly dipped into a cooling mixture, after which 20 cm^3 of cool solvent (*o*-xylene) were added.

The values of the optical densities necessary for the computation of the rate constants were determined by recording the absorption of these solutions with a Unicam SP 800 Spectrophotometer.

The final products of the reaction were analysed by means of their infrared spectra, using the potassium bromide disk method, on a UR 10 Zeiss Jena Spectrophotometer.

To watch the evolving of N_2 during the reaction the chromatographic method was also used.

For this, the reaction was studied on a Perkin Elmer Chromatograph. We worked with a chromatographic column of 1 m, $\Phi_i = 4$ mm and $\Phi_e = 6$ mm, filled with molecular sieve of 5 Å, thermostated at 80°. We have proceeded in the following way :

— through the reaction vessel which contained 1 g of diphenyldiazomethane, H_2 was bubbled for about an hour (100 ml/min at room temperature)

— the H_2 stream was reduced up to 8 ml/min and the reaction vessel was introduced into the thermostat at a working temperature of 80°

— a sample of 1 ml was taken out of the gas resulted from the reaction, by means of the gas tap, at time intervals of 3 minutes

— the same was repeated, using O_2 as carrying gas, in whose presence the thermal decomposition of diphenyldiazomethane was carried out at the same temperature

— the recording chromatograms were estimated with the usual method of measuring the peak surfaces, corresponding to the N_2 evolved in the two cases studied.

RESULT AND DISCUSSION

In the absence of the solvent the most plausible reaction mechanism should be the following, supported by the formation of benzophenone azine in high amounts, separated and rendered evident by its infrared absorption spectrum and its melting point.

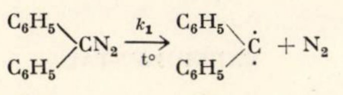

$$(C_6H_5)_2CN_2 \xrightarrow[t^\circ]{k_1} (C_6H_5)_2\dot{C}\cdot + N_2 \qquad \text{(a)}$$

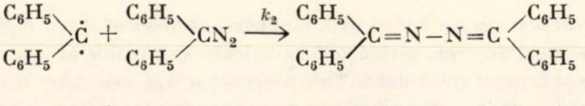

$$(C_6H_5)_2\dot{C}\cdot + (C_6H_5)_2CN_2 \xrightarrow{k_2} (C_6H_5)_2C{=}N{-}N{=}C(C_6H_5)_2 \qquad \text{(b)}$$

As the reaction vessels were not degassed, the following sequence of reactions certainly takes place in parallel (first mentioned by Bartlett and Traylor [9] at the photolysis of diphenyldiazomethane in alcoholic solution) :

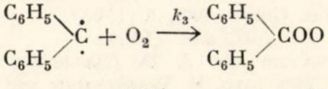

$$(C_6H_5)_2\dot{C}\cdot + O_2 \xrightarrow{k_3} (C_6H_5)_2COO \qquad \text{(c)}$$

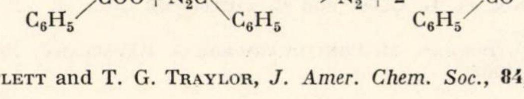

$$(C_6H_5)_2COO + N_2C(C_6H_5)_2 \xrightarrow{k_4} N_2 + 2\,(C_6H_5)_2CO \qquad \text{(d)}$$

---

[9] P. D. Bartlett and T. G. Traylor, *J. Amer. Chem. Soc.*, **84**, 3408 (1962).

In our case benzophenone still forms and we rendered evident by the presence of the $>C{=}O$ frequency in the infrared spectrum at about 1665 cm^{-1}.

In figure 1 are presented the infrared spectra of pure benzophenone (I) and of a diphenyldiazomethane sample decomposed at 80°, in air (II). Another proof in this sense is the infrared spectrum obtained from a diphenyldiazomethane sample also decomposed at 80°, but this time by bubbling O_2 through the molten diazo compound (III).

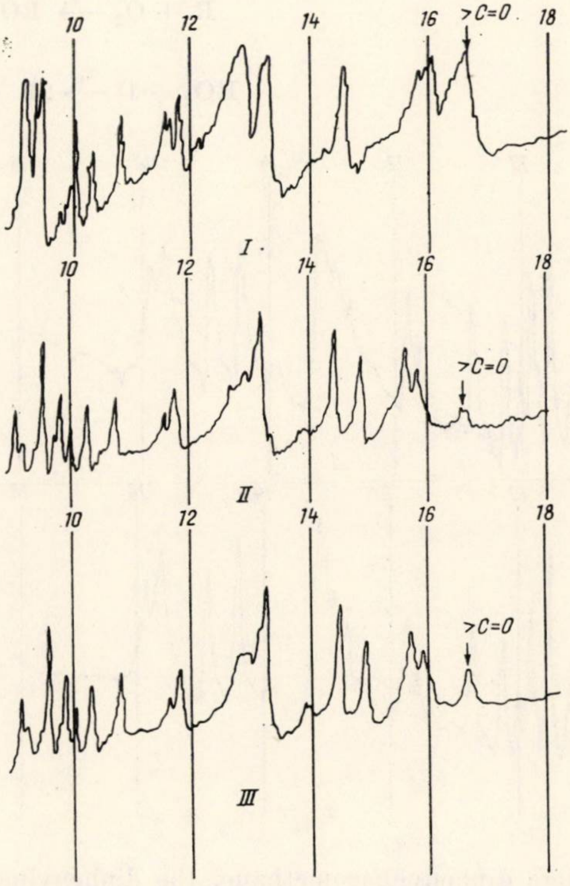

Fig. 1. — Infrared spectrum of: I) pure benzophenone II) decomposed diphenyldiazomethane sample at 80° in air III) decomposed diphenyldiazomethane sample at 80°, by bubbling O_2.

One can notice that transmission at a frequency of about 1665 cm^{-1} (III) is higher than that obtained from the sample decomposed in air (II), where the reaction with O_2 is limited only to the contact surface between the molten diphenyldiazomethane and atmospheric oxygen.

The infrared spectrum of diphenyldiazomethane sample decomposed at the same temperature, but in vacuum, is further proof in favour of the proposed reaction mechanism, with the formation only of benzophenone azine as final product (fig. 2)

Under these conditions the general reaction scheme is the following :

$$2D \xrightarrow{k_1} 2R + 2N_2 \tag{a}$$

$$R + D \xrightarrow{k_2} C \tag{b}$$

$$R + O_2 \xrightarrow{k_3} RO_2 \tag{c}$$

$$RO_2 + D \xrightarrow{k_4} 2B + N_2 \tag{d}$$

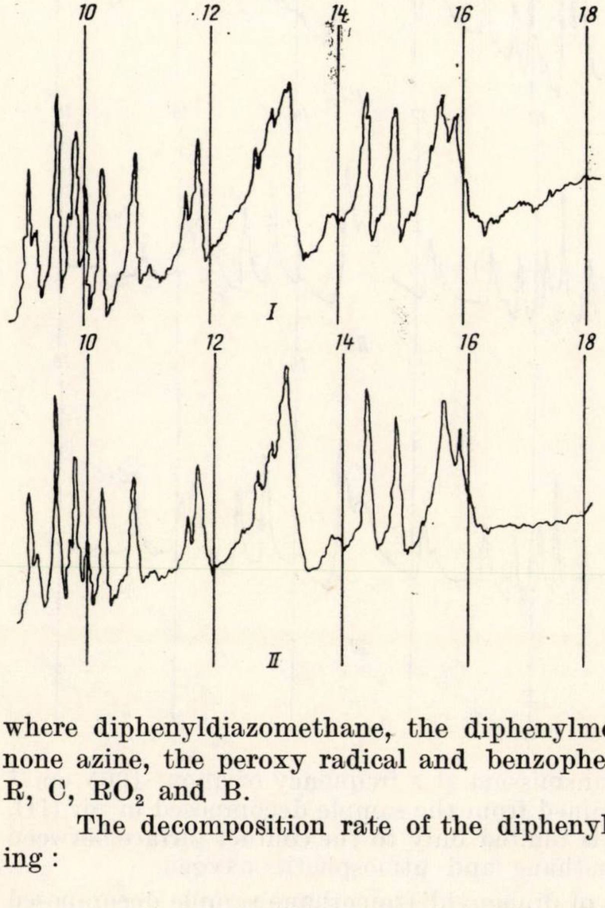

Fig. 2. — Infrared spectrum of I) pure benzophenone azine II) decomposed diphenyldiazomethane sample at 80°, in vacuum.

where diphenyldiazomethane, the diphenylmethylene radical, benzophenone azine, the peroxy radical and benzophenone were denoted by D, R, C, RO_2 and B.

The decomposition rate of the diphenyldiazomethane is the following :

$$-\frac{dC_D}{dt} = 2k_1C_D + k_2C_RC_D + k_4C_DC_{RO_2} \tag{1}$$

Applying the stationarity approximation to the intermediate radicals, we get :

$$\frac{dC_R}{dt} = 2k_1C_D - k_2C_RC_D - k_3C_RC_{O_2} = 0 \qquad (2)$$

$$C_R = \frac{2k_1C_D}{k_2C_D + k_3C_{O_2}} \qquad (3)$$

$$\frac{dC_{RO_2}}{dt} = k_3C_RC_{O_2} - k_4C_{RO_2}C_D = 0 \qquad (4)$$

$$k_3C_RC_{O_2} = k_4C_{RO_2}C_D \qquad (5)$$

Introducing (5) in equation (1) we get :

$$-\frac{dC_D}{dt} = 2k_1C_D + k_2C_RC_D + k_3C_RC_{O_2} = 2k_1C_D + C_R(k_2C_D + k_3C_{O_2}) \qquad (6)$$

in which, substituting eq. (3) we get :

$$-\frac{dC_D}{dt} = 4k_1C_D = kC_D \qquad (7)$$

which is characteristic of first order reactions, and which is verified by our experimental data calculated by the integral equation :

$$k = \frac{2.303}{t}\lg\frac{C_{Do}}{C_D} \qquad (8)$$

In table 1 are presented our results as an example for one of the working temperatures. In the second column are given the optical densities for the wavelength λ = 526 nm, for which diphenyldiazomethane presents the highest absorption.

In the next table the rate constant determined in the same way, for all the working temperatures are given.
The last but one column of the table contains the rate constants k_1 of the unimolecular thermal decomposition process (a) derived from the simple relation (7) :

$$k_1 = \frac{k}{4} \qquad (9)$$

An activation energy of 22.3 ± 0.4 kcal/mol was calculated with these data, as it results from figure 3.

The preexponential coefficient computed for unimolecular reaction (a) is given in the last column of table 2 which leads to a value of about

Table 1

Rate constant of diphenyldiazomethane decomposition at 70°; $l = 1$ cm

t sec	E_{526}	$k \times 10^4$ sec^{-1}
0	2.52	—
840	2.30	1.07
1800	1.98	1.33
3600	1.60	1.26
9000	1.02	1.00
10800	0.78	1.07
14400	0.50	1.10
18000	0.40	1.02
25200	0.14	1.05
36000	0.06	1.05
	Average :	1.11×10^{-4} sec^{-1}

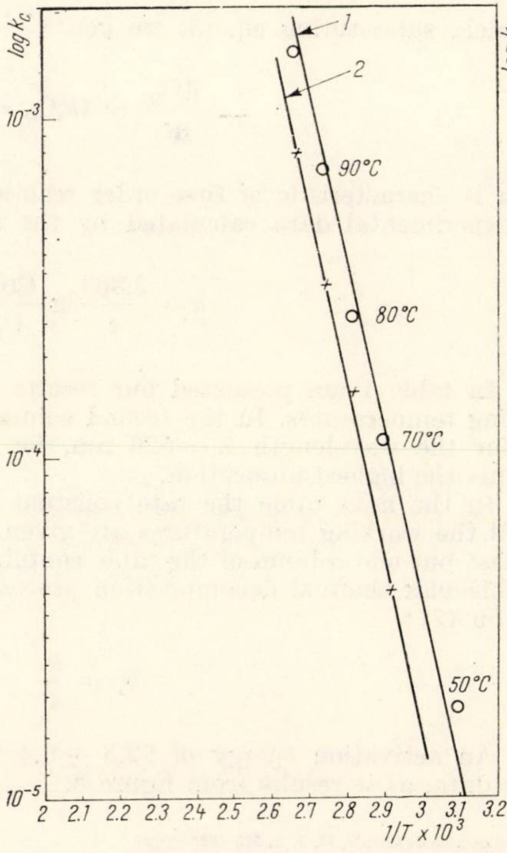

Fig. 3. — 1) Variation of log k *versus* $1/T$ for the thermal decomposition in air 2) variation of log k_C *versus* $1/T$ for the reaction of benzophenone azine formation.

10^{10} s^{-1}. This order of magnitude is approximately one thousand times smaller than for unimolecular processes. The discrepancy can be explained in the light of Z. Simon's [10] theory, according to which the diphenyldiazomethane thermal decomposition may be a nonadiabatic reaction which takes place with change of multiplicity. This means that in the activated complex a transition takes place from the ground singlet state to the excited triplet one, and the radical $(C_6H_5)_2\dot{\underset{\cdot}{C}}$ resulting from the reaction is in a ground state [6].

To verify the reaction mechanism suggested for the reaction which takes place in the presence of athmospheric O_2, we determined the molecular N_2 evolving during the reaction. Indeed, if reactions (a) and (b) are taken into consideration on the one hand, and reactions (a), (c), (d) on the other hand, in the latter case a double amount of N_2 would be obtained.

Table 2

Rate constants of diphenyldiazomethane decomposition at different temperatures

T^{o}	k $\sec^{-1}$	k_1 $\sec^{-1}$	$\log A_1$
32	1.88×10^{-6}	4.7×10^{-7}	—
50	1.56×10^{-5}	3.9×10^{-6}	9.7
70	1.11×10^{-4}	2.8×10^{-5}	9.6
80	2.60×10^{-4}	6.5×10^{-5}	9.6
90	6.90×10^{-4}	1.7×10^{-4}	9.6
100	1.56×10^{-3}	3.9×10^{-4}	9.7

In figure 4 are given the two chromatograms obtained for one of the reaction moments ($t = 41$ minutes).

It is obvious that in the presence of O_2, the amount of N_2 evolved from the reaction is double as compared to that evolved in its absence (the device sensitivity is reduced to half as compared to the previous case). This behaviour is verified only in the first part of the reaction, where the contact between the bubbled O_2 and the molten diphenyldiazomethane is close. The diffusion of O_2 is hindered by the formation on benzophenone azine in greater amounts, as it is in the solid state at this temperature.

For this reason the amount of N_2 evolved for the next intervals of the reaction is smaller than its double and decreases continuously as the sample solidifies.

Alongside with the diphenyldiazomethane decomposition we also studied the formation kinetics of the main final product benzophenone azine. For this purpose the determination of the optical densities of the same samples for which the extinctions E for $\lambda = 526$ nm were measured, was carried out also for $\lambda = 380$ nm.

The visible and UV absorption spectra of the diphenyldiazomethane and benzophenone azine in *o*-xylene are given in figure 5.

---

[10] Z. Simon, *Studii și Cercetări Chim. Acad. R.P.R.*, **11**, 271 (1963); Disertation (1965).

Because when the decomposition takes place in air, the amount of the benzophenone formed is very low (see figure 1.II) and the molar absorption coefficient of the benzophenone in *o*-xylene $k^{\mathrm{B}}_{380} = 26$ is also very small in comparison with that of benzophenone azine $k^{\mathrm{C}}_{380} = 563$, one can neglect the absorption of benzophenone at the considered wavelength without any significant error.

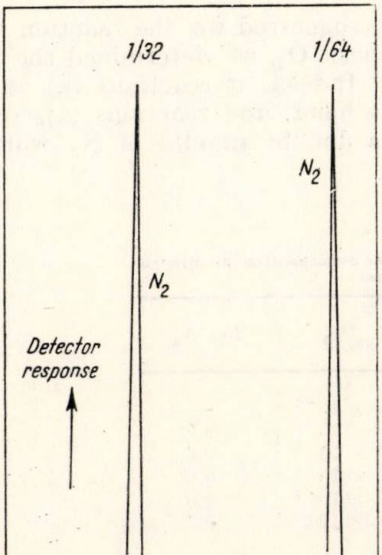

Fig. 4. — Chromatograms of N_2 obtained from the thermal decomposition of diphenyldiazomethane in the presence (II) and absence of O_2 (I).

Under these conditions the concentration of the forming benzophenone azine during the reaction can be calculated with the simplified equation (1 = 1 cm) :

$$C_{\mathrm{C}} = \frac{E_{380} - \dfrac{k^{\mathrm{D}}_{380}}{k^{\mathrm{D}}_{526}} E_{526}}{k^{\mathrm{C}}_{380} - \dfrac{k^{\mathrm{D}}_{380}}{k^{\mathrm{D}}_{526}} k^{\mathrm{C}}_{526}} \qquad (10)$$

The rate constant of the benzophenone azine formation is given by the equation :

$$\frac{\mathrm{dC_C}}{\mathrm{d}t} = k_2 \mathrm{C_R C_D} \qquad (11)$$

in which

$$C_D = \frac{E^D_{526}}{k^D_{526}} \tag{12}$$

It immediatly results that :

$$k_2 C_R = k_C = \frac{dC_C/dt}{C_D} \tag{13}$$

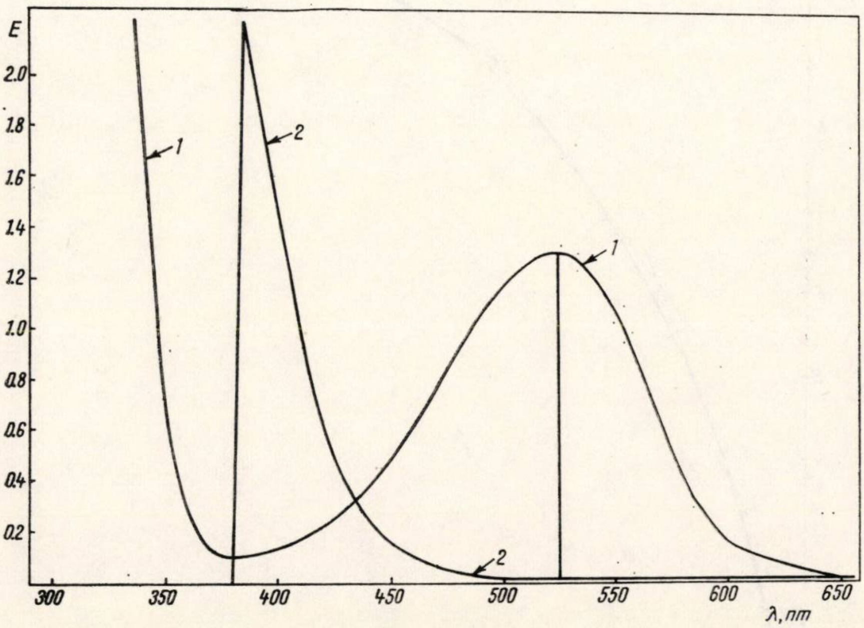

Fig. 5. — Absorption spectra of diphenyldiazomethane (1) and benzophenone azine (2) in *o*-xylene.

By plotting the concentration of the benzophenone azine versus the time *t* and using the tangent method in the various points of the curve, corresponding to varied moments of the reaction, we determined the reaction rate $\frac{dC_C}{dt}$

Thus we calculated the k_2C_R product which must be a constant value, because C_R in the stationarity approximation is a very low and constant concentration of the radical $(C_6H_5)_2\dot{C}$.

Table 3 lists these computations, for one of the working temperatures, 70°.

The third column shows that at the end of the reaction, benzophenone azine concentration is 0.0125 mol 1^{-1} practically corresponding to the quantitative transformation of diphenyldiazomethane in benzophenone azine.

In table 4 are listed the values of the product k_2C_{rk} for all the working temperatures. The last column shows that for each temperature, the rate constant of the diphenyldiazomethane decomposition is approximately double in comparison with that of benzophenone azine formation, which is another confirmation of the proposed mechanism.

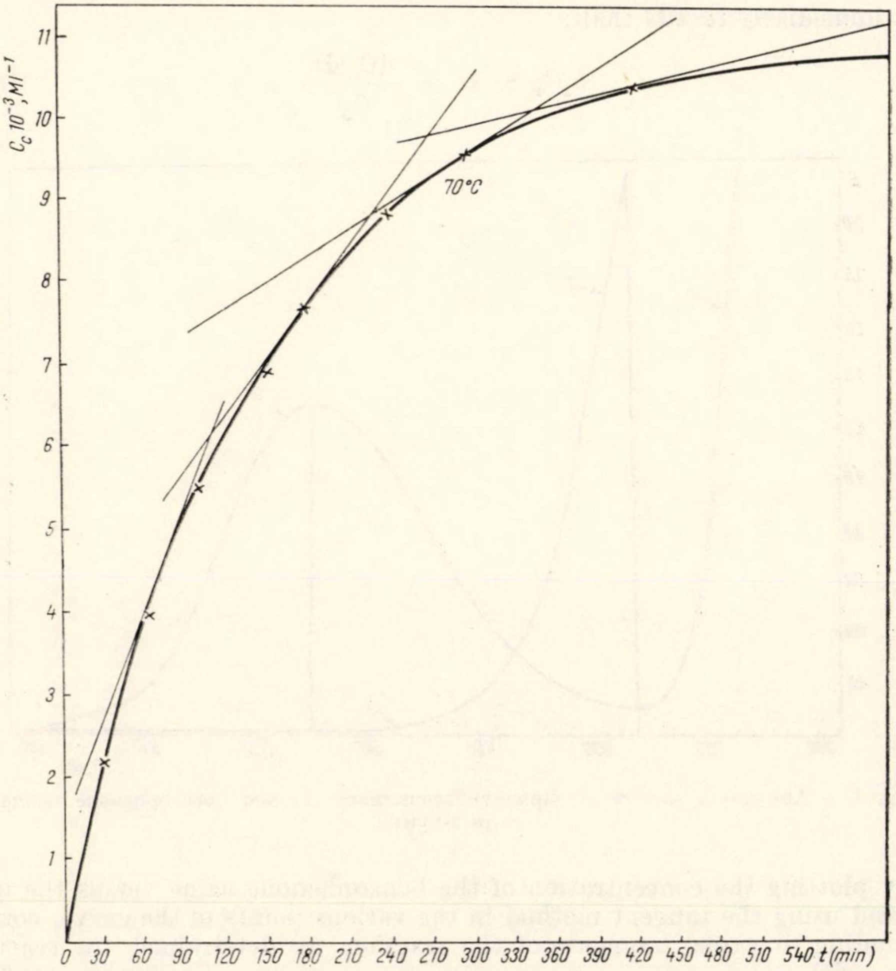

Fig. 6. — Plotting of the benzopheone azine concentration against time, during the reaction.

With these data we plotted log k_C against $1/T$ (figure 3) and calculated the activation energy. As seen this has the same value as that calculated for the diphenyldiazomethane decomposition (both straight lines have the same slope) which is in good agreement with the reaction mechanism.

Singer and Lewis [11] studying the pyrolysis of 5% diphenyldiazomethane in diphenyl, at higher temperatures (140°—170°) in the absence of O_2, emphasized by ESR spectra the formation of some intermediates, out of which they identified one as being the fragment, $(C_6H_5)_2\overset{|}{C}-N\langle$ · Working under the conditions of the above authors we reproduced the same ESR spectrum ; however, in our working conditions, that is, in pure molten diphenyldiazomethane, it was impossible to obtain ESR signals.

Table 3

Kinetics of the benzophenone azine formation at 70° (l = 1 cm)

t sec	E_{380}	$C_C \times 10^3$ Ml^{-1}	$\frac{dC_C}{dt} = tg\alpha \times 10^6$	$C_R k_2 \times 10^5$ sec^{-1}
0	0.2	0	— —	— —
840	0.8	1.05	— —	— —
1800	1.6	2.52	1.01	4.8
3600	2.4	4.00	0.733	4.3
9000	4.0	6.94	0.450	4.2
10800	4.4	7.69	0.360	4.3
14400	=.0	8.80	0.238	4.5
18800	5.4	9.52	0.162	3.8
25000	5.8	10.3	0.073	5.2
36000	6.0	10.6	— —	— —
50400	6.3	12.4	— —	— —
				Average : 4.5×10^{-5}

Table 4

Rate constants of benzophenone azine formation at different temperatures

T°	$k_2 C_R$ sec^{-1}	k/k_C
70	4.5×10^{-5}	2.5
80	1.6×10^{-4}	2.0
90	3.1×10^{-4}	2.2
100	7.0×10^{-4}	2.0

---

[11] L. S. Singer and I. C. Lewis, *J. Amer. Chem. Soc.*, **90**, 4212 (1968).

Revue Roumaine de Chimie, 17, *1, 2*, 225–229 (1972)

En l'honneur du 70e anniversaire
du Professeur I.G. MURGULESCU

ÉTUDE DE LA MORPHOLOGIE DES PRODUITS DE LA DÉCOMPOSITION THERMIQUE DU COPRÉCIPITÉ : $Ag_2CO_3—CdCO_3$

G. PANNETIER et D. FĂTU *

Laboratoire de Cinétique Chimique de l'Université de Paris VI, Equipe de Recherche Associée au C.N.R.S. nº 24, 1, rue Guy de la Brosse, 75-Paris 5e, France

Reçu le 13 septembre 1971

La morphologie du mélange pulvérulent argent métallique et oxyde de cadmium, obtenu en pyrolysant le coprécipité $Ag_2CO_3-CdCO_3$, est influencée d'une manière évidente par les conditions dans lesquelles on prépare et décompose les carbonates. L'expérience montre que les dimensions et la forme des grains de la poudre obtenue varient en fonction de la concentration et de la température des solutions de nitrate d'argent et de cadmium utilisées pour précipiter les carbonates, de la nature de l'atmosphère gazeuse et de la vitesse de chauffage pendant la pyrolyse. Si, au préalable, on réduit le carbonate d'argent à l'état d'argent métallique, les dimensions des grains de la poudre, ainsi obtenue, varient selon la nature du réducteur utilisé.

INTRODUCTION

Les décompositions thermiques de l'oxyde d'argent [1] et des carbonates d'argent [2] et de cadmium, [3,4] comptent parmi les premières réactions à l'état solide dont la cinétique a été étudiée.

Lewis [1] a établi que la réaction :

$$2Ag_2O \rightarrow 4\ Ag + O_2\uparrow \qquad (1)$$

présente un caractère autocatalytique de sorte que sa vitesse passe par un maximum.

---

* Adresse habituelle : Chaire de Cinétique Chimique, Université de Bucarest, Bd. Republicii 13, Roumanie

[1] G. W. Lewis, *Z. phys. Chem.*, **32**, 310 (1905).

[2] N. Centnertzwer et B. Bruzs, *Z. phys. Chem.*, **123**, 111 (1926).

[3] J. Zawadski et S. Bretsznajder, *Z. phys. Chem.*, **22**, 60 (1938).

[4] M. M. Pvlyuchenko et E. A. Prodan, "Geterogenye Khimiheskie reactii", Izd. Nauka i tekhnika Minsk, 1965, p. 79.

Prodan et Pavlyuchenko [4] ont montré que l'énergie d'activation de la réaction de décomposition du carbonate de cadmium dépend des conditions de préparation et de vieillissement des réactifs.

Actuellement, le nombre des travaux consacrés à l'étude de la décomposition thermique des carbonates d'argent et de cadmium et d'oxyde d'argent continue à croître, étant donné l'intérêt présenté par ces produits pour l'industrie électrotechnique. [5,6]

Dans ce qui suit, nous allons présenter l'influence des conditions de préparation et de décomposition thermique de coprécipité $Ag_2CO_3-CdCO_3$ sur la morphologie de la poudre Ag—CdO ainsi obtenue.

PROTOCOLE EXPÉRIMENTAL

MODE DE PRÉPARATION

Le coprécipité $Ag_2CO_3-CdCO_3$ contenant 7,1% de carbonate de cadmium a été préparé en ajoutant lentement, sous agitation, une solution de nitrate d'argent et de cadmium à une solution de carbonate de sodium. Le coprécipité a été filtré, lave, séché et calciné à 450°C.

Les réactifs utilisés sont les nitrates d'argent et de cadmium et le carbonate de sodium Prolabo R.P.

TECHNIQUES UTILISÉES

Les produits de décomposition thermique ont été identifiés par leur diagramme de diffraction des rayons X. Les dimensions des cristallites du produit de décomposition étant de l'ordre de 1000 Å nous avons été dans l'impossibilité d'appliquer la méthode Scherrer. [7] En effet celle-ci ne donne des résultats satisfaisants que pour des diamètres de particules inférieurs à 1000 Å. Dans ces conditions nous avons eu recours à la microscopie électronique, en utilisant un appareil JEOL type JEM-120. Les échantillons ont été réalisés en déposant sur une grille de cuivre, une suspension dans l'eau, des produits de décomposition dispersés par ultra-sons.

La grille de cuivre a été préalablement recouverte d'une membrane de carbone d'une épaisseur de l'ordre de 100—150 Å.

Les conditions et les étapes des processus de pyrolyse ont été établies à l'aide d'une thermobalance UGINE-EYRAUD type B 60 et d'un microanalyseur A.T.D. M3 licence CNRS.

Les gaz dégagés lors de la décomposition ont été identifiés en couplant un chromatographe CHROMODAM à un dispositif A.T.D. [8]

Les traces de sodium contenues dans les produits solides de décomposition ont été mises en évidence par absorption atomique (appareil PERKIN-ELMER).

---

[5] G. M. Areand, *Sci Rech. Aerosp. Rep.*, **6** (23), 4009 (1968); ref. *Chem. Abstr.*, **71**, 76654 C (1969).

[6] M. Sato, M. Hijikata et I. Morimoto, *Nippon Kizoku Gakkaishi*, **33** (8), 954 (1969); ref. *Chem. Abstr.*, **71**, 96017 a (1969).

[7] B. D. Cullity "Elements of X-Ray Diffraction", Addison-Wessley Publishing Company Inc. London-England, 1959, p. 99.

[8] G. Pannetier et G. Vjega-Mariadassou, *J. Gas. Chromatgr.*, **1967**, 441.

OBSERVATIONS PRÉLIMINAIRES

Bien que l'analyse thermogravimétrique montre seulement deux étapes pendant la décomposition du coprécipité $Ag_2CO_3-CdO_3$ contenant 7,1% de carbonate de cadmium, ce processus s'avère plus complexe.

La première étape correspond à la décomposition du carbonate d'argent :

$$Ag_2CO_3 \rightarrow Ag_2O + CO_2 \uparrow \qquad (I)$$

avec départ de dioxyde de carbone.

La seconde étape conduit au dégagement de dioxyde de carbone et d'oxygène : celle-ci correspond donc à la superposition de deux processus, conformément au schéma réactionnel suivant :

$$CdCO_3 \rightarrow CdO + CO_2 \uparrow \qquad (II)$$

$$Ag_2O \rightarrow 2Ag + \frac{1}{2} O_2 \uparrow \qquad (III)$$

La partie initiale de la courbe d'A.T.D. correspondant à la première étape de décomposition (schéma réactionnel I) montre un léger épaulement qui indique un processus de nucléation bien individualisé. En effet l'étude cinétique done pour la période initiale de décomposition ($0 < \alpha^* < 0{,}06$) une énergie d'activation $E = 18{,}2$ *k*cal/mole, tandis que le processus de croissance des germes ($0{,}06 \leqslant \alpha \leqslant 0{,}9$) est caractérisé par une valeur légèrement inférieure (16,4 *k*cal/mole).

RÉSULTATS ET DISCUSSION

On prépare les précipités en ajoutant une solution contenant 0,3 M/l $AgNO_3$ et 0,03 M/l $Cd(NO_3)_2$ à une solution de carbonate de sodium 0,5 M/l ; la solution est agitée pendant une demi-heure et le précipitat est filtré et séché jusqu'à 440° avec une vitesse de 5°/mn. La poudre d'argent métallique et d'oxyde de cadmium obtenue présente un diamètre moyen de particules de 0,18 μ. Un examen attentif montre que la variation de la vitesse de chauffage ($\Delta T / \Delta t$) affecte sensiblement le paramètre morphologique (voir fig. 1*a*).

Ce résultat peut être expliqué du point de vue cinétique, par les valeurs différentes de l'énergie d'activation correspondant respectivement aux processus de nucléation et de croissance des germes.

Si l'on utilise une vitesse de chauffage réduite (2,4°/mn) la décomposition commence et se déroule dans un domaine de température moins élevé.

Dans ces conditions, le processus de nucléation, ayant une énergie d'activation supérieure (18,2 *k*cal/mole), il se déroule avec une vitesse

* α — degré de décomposition.

plus faible que celui de la croissance des germes (E = 16,4 *k*cal/mole) ; il y a donc apparition d'un nombre assez limité de noyaux qui se développent plus rapidement. On observe alors la formation de grains de diamètre d'environ 2,5 μ.

Au contraire, quand on utilise des vitesses de chauffage peu importantes (19,5°/ mn) le phénomène de pyrolyse se déplace vers des températures élevées.

Dans ces conditions, le processus de nucléation bien qu'ayant une énergie d'activation plus élevée, commence à se dérouler à une vitesse importante. Donc dans ce cas, les germes qui se forment seront nombreux et de faibles dimensions (Ø = 0,16 μ)

De même, il est logique de considérer, au cours d'une pyrolyse rapide, l'éclatement des grains initiaux provoqué par l'accumulation, puis le dégagement initial de gaz émis ($CO_2 + O_2$).

La poudre d'argent métallique et d'oxyde de cadmium est susceptible de frittage quand on la chauffe. Comme le montre la figure 1*b*, ce processus est très net au-dessus de 500°.
En chauffant à 600°C, il y a prise en masse compacte de l'échantillon. La température de précipitation et la concentration de la solution de nitrate, semblent aussi influencer la morphologie du produit final (voir fig. 1*c* et *d*) mais dans des limites assez étroites.

En général, il est convenable d'utiliser de faibles concentrations de réactifs pour obtenir un produit final plus pur.

La concentration de la solution de carbonate de sodium ne semble pas influencer la morphologie de la poudre, mais seulement sa pureté. L'analyse par absorption atomique montre que le produit de pyrolyse contient 0,05% Na quand on précipite les carbonates en utilisant une solution de concentration 0,5 M/l Na_2CO_3. Si l'on accroît la concentration jusqu'à 1 M/l Na_2CO_3, le produit ainsi obtenu est moins pur, contenant 0,16% Na.

Si avant de calciner le précipité simultané on réduit le carbonate d'argent à l'aide d'hydrate d'hydrazine, on obtient une poudre plus pure (0,03% Na) et contenant des grains de forme plus régulière (voir fig. 2*a*) et de dimension plus importante (Ø = 0,3 μ) que dans le cas où l'on pyrolyse directement le coprécipité (fig. 2*b*).

Pour réduire le carbonate d'argent, on peut utiliser aussi l'aldéhyde formique qui est un agent moins actif que l'hydrate d'hydrazine et permet d'obtenir des grains ayant des dimensions plus importantes (Ø = 0,5 μ).

L'utilisation des réducteurs précédents permet d'obtenir directement dans la solution le mélange $Ag-CdCO_3$ qui, par pyrolyse conduit au produit final : $Ag-CdO$ en dégageant seulement une faible quantité de dioxyde de carbone. Dans ce cas, le processus de décomposition est simplifié et correspond au schéma réactionnel II. Enfin, notons que le processus de pyrolyse est sensible à la présence de vapeur d'eau qui abaisse la température correspondant au début de la décomposition, d'environ 20°C.

La poudre obtenue en décomposant le coprécipité $Ag_2CO_3-CdCO_3$ en présence de vapeur d'eau est plus dispersée que celle préparée dans l'air (Ø = 0,12 μ).

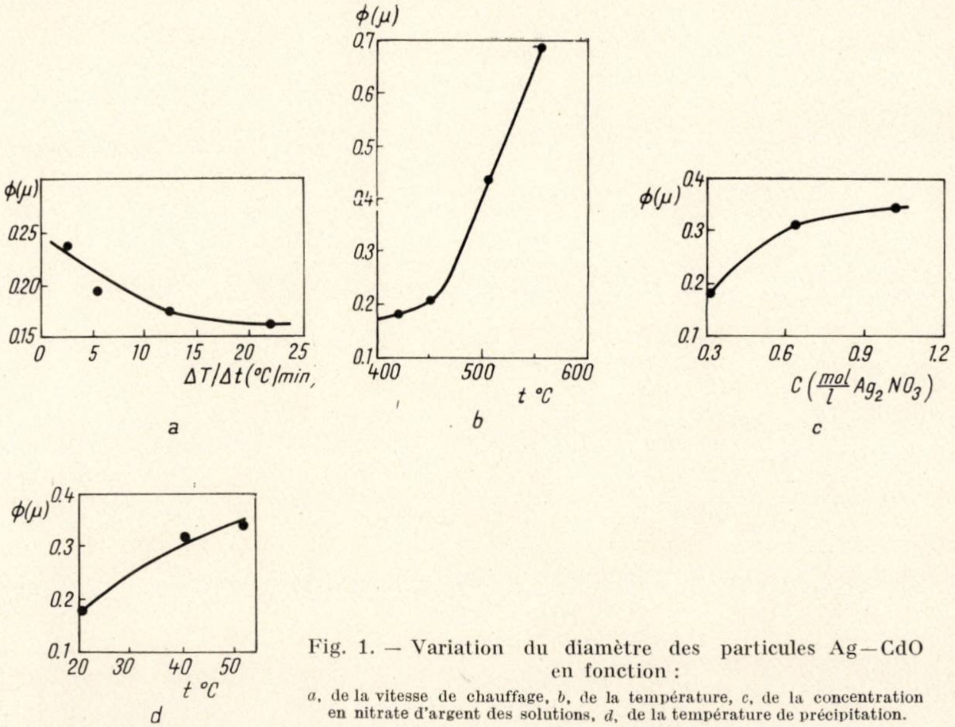

Fig. 1. — Variation du diamètre des particules Ag—CdO en fonction :

a, de la vitesse de chauffage, *b*, de la température, *c*, de la concentration en nitrate d'argent des solutions, *d*, de la température de précipitation.

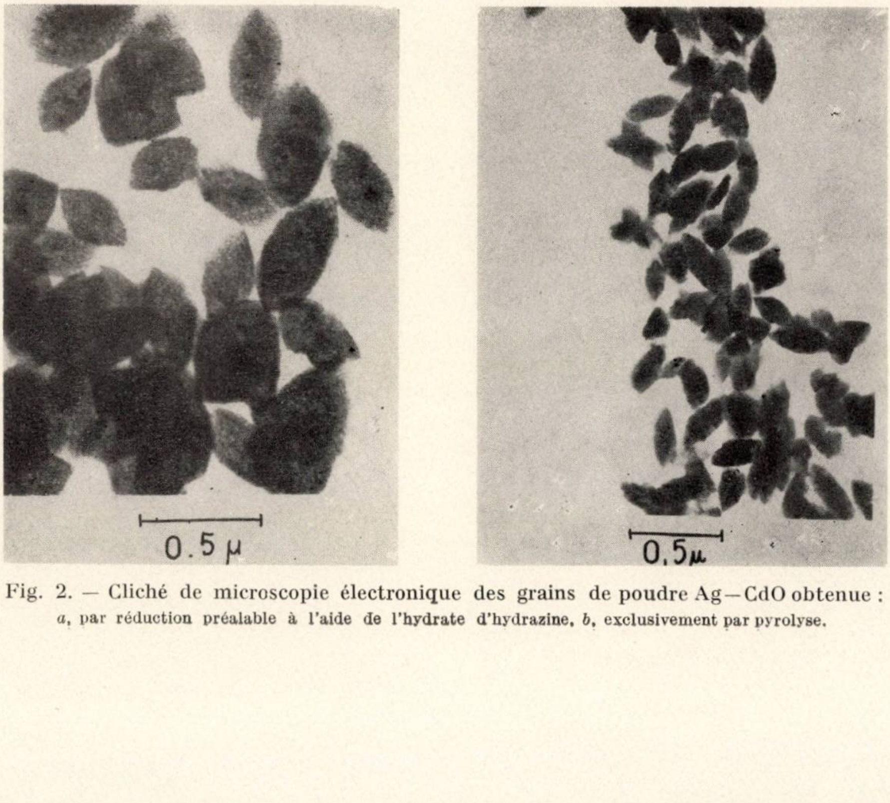

Fig. 2. — Cliché de microscopie électronique des grains de poudre Ag—CdO obtenue :
a, par réduction préalable à l'aide de l'hydrate d'hydrazine, *b*, exclusivement par pyrolyse.

La présence de vapeur d'eau semble faciliter le processus de nucléation.

Cette observation est en accord avec les résultats de Spencer et Topley [9] qui ont trouvé que la vapeur d'eau accélère la réaction de décomposition du carbonate pur.

CONCLUSION

La morphologie de la poudre Ag—CdO obtenue en pyrolysant les précipités simultanés $Ag_2CO_3-CdCO_3$ est contrôlée non seulement par les conditions de décomposition (vitesse de chauffage, atmosphère gazeuse, température de pyrolyse), mais aussi par les conditions de précipitation des carbonates (température et concentration des solutions des réactifs).

L'utilisation d'hydrate d'hydrazine ou l'aldéhyde formique pour réduire en solution le carbonate d'argent permet d'obtenir après pyrolyse une poudre Ag—CdO plus pure ayant une remarquable capacité de frittage.

---

[9] W. D. Spencer et B. Topley, *J. Chem. Soc.*, **1929**, 2633.

Revue Roumaine de Chimie, 17, 1, 2, 231–237 (1972)

Dedicated to Professor I.G. MURGULESCU
on his 70th birthday

SIMULTANEOUS SPECTROPHOTOMETRIC DETERMINATION OF GALLIUM AND INDIUM

SEPTIMIA POLICEC, T. SIMONESCU and C. DRĂGULESCU

Centre of Chemistry, Blv. Mihai Viteazul 24, Timişoara, Romania

Received August 18, 1971

The UV spectrophotometric determination of gallium in the presence of indium was carried out at the two In-ANDA system isosbestic points wavelengths, $\lambda = 260$ nm and 316.5 nm. The determination of indium in the presence of gallium was accomplished at 289.5 nm, the wavelength of one of the two isosbestic points of the Ga-ANDA system. There are two possible ways of performing these determinations, the former by using water as reference and the latter, with a blank solution; 2–40 μg Ga/cm^3, representing 5–85% Ga mixed with indium were thus determined, as well as 11–90% In. The average relative percent error did not exceed 3%.

Complex compounds of the anthranil-N,N-diacetic acid, ANDA, with Ga^{3+} and In^{3+} have been investigated in the laboratory [1]. The study has been carried out spectrophotometrically in the UV range. The equimolar composition and the stability of the respective chelates have been established.

Attempts to determine Ga^{3+} and In^{3+} spectrophotometrically, using ANDA as a reagent proved rather unsatisfactory from the selectivity point of view.

In a previous paper [2] a method dealing with simultaneous spectrophotometric determination of pairs of elements has been described. The same principle is applied in the present work to the determination of both Ga^{3+} and In^{3+} from mixtures of the two elements.

EXPERIMENTAL

Apparatus

A Unicam SP 800 spectrophotometer was used for absorbance measurements; pH determinations were carried out on a Clamann and Grahnert model MV 11, pH-meter.

---

[1] C. Drăgulescu, S. Policec and T. Simonescu, *Talanta*, **13**, 1451 (1966).

[2] S. Policec, T. Simonescu and C. Drăgulescu, *Talanta*, **17**, 567 (1970).

Reagents

1×10^{-2} M solutions of the disodium salt of anthranil-N,N-diacetic acid, ANDA, (synthetized in this laboratory[3]) were prepared by neutralization of a known weight of the acid with standard NaOH.

Gallium nitrate, a 5×10^{-3}M solution, was prepared dissolving London Matthey "Specpure" $Ga/NO_3/_3.8H_2O$ in 1×10^{-1}N nitric acid.

Indium nitrate, the 5×10^{-3}M solution, was obtained with "Serva" Heidelberg *p.a* metallic indium dissolved in 1×10^{-1}N nitric acid.

The concentration of gallium and indium of both reactant solutions was checked complexometrically [4].

1×10^{-1}N nitric acid solution was used as solvent; a U C B Brussels 70% HNO_3, was the product we made use of.

RESULTS AND DISCUSSION

Experimental evidence on the possibility of the simultaneous spectrophotometric determination of Ga^{3+} and In^{3+} with ANDA as reagent, is given by diagrams A, A′ and B, B′ in figure 1.

In diagram A absorption curves of the Ga-ANDA system, are presented. They are obtained with constant ligand excess (curve 1) together with variable amounts of metal ion (curves 2–5). The formation of two isosbestic points at roughly 270 nm and 290 nm proves an equilibrium to be established among the present species.

Diagram B expresses the same for the In-ANDA system, its isosbestic points being located at about 260 and 316 nm. In the 271–273 nm range curves are also crossing but there is no distinct intersection point.

The existence of isosbestic points in two systems formed by different metal ions and the same ligand, under identical experimental conditions, is an evidence of the possibility of a simultaneous determination of the two metal ions in each other's presence.

The same isosbestic points in diagram A and B are present also in the corresponding A′ and B′ diagrams. The latter ones represent another mode of recording spectrophotometrically the same samples which led to diagrams A and B. The only difference is the reference solution used : in A, B this is water and in A′, B′, the ligand solution (the one which has the absorption curve 1, in both diagrams A and B). Diagrams A′ and B′ have thus eliminated the ligand's absorption. The zero line (which is in fact the absorption curve of the ligand recorded against itself) will pass through the corresponding isosbestic points which are obviously located at the same wavelengths. In the A′, B′ plot type, the isosbestic point absorbance of all the complexes, irrespective of their formation degree, appears to be zero. It is but proportional to the metal ion present at other wavelengths.

---

[3] C. Drăgulescu, T. Simonescu and R. Anton, *Studii şi Cercetări, Sti. Chim., Baza Cercetări Sti. Timişoara,* **1**, 21 (1959).

[4] J. Doležal, V. Patrovský, Z. Šulcek and J. Švasta, *Chem. listy,* **49**, 1517 (1959).

The Ga-ANDA and In-ANDA complexes being equimolar, the isosbestic points will be net up to a 1 :1 = Me : Ligand combination ratio. A ligand excess is recommended.

If diagrams A′ and B′ in figure 1 are superposed, as shown in figure 2, a suggestive plot is obtained. At 260 and 316 nm, the isosbestic points of the In-ANDA system (curves 2′–5′), the absorption of the latter is constantly zero while that of the Ga-ANDA system (curves 2–5) is proportionally variable to the Ga^{3+} concentration. The same is true for the isosbestic point of the Ga-ANDA system, when at 290 nm the In-ANDA system only, exhibits variable absorption with the metal ion concentration present. The 270.5 nm Ga-ANDA isosbestic point cannot be used as it is too closely located to the 271–273 nm crossing range of the In-ANDA system. It herefrom results that, if the absorbance of a Ga + In mixture is measured at the isosbestic points of the IN-ANDA system, this can be totally attributed to the Ga-ANDA system (the In-ANDA one appearing as zero at this particular wavelength). If the absorbance of the same mixture is measured at the 290 nm isosbestic point of the

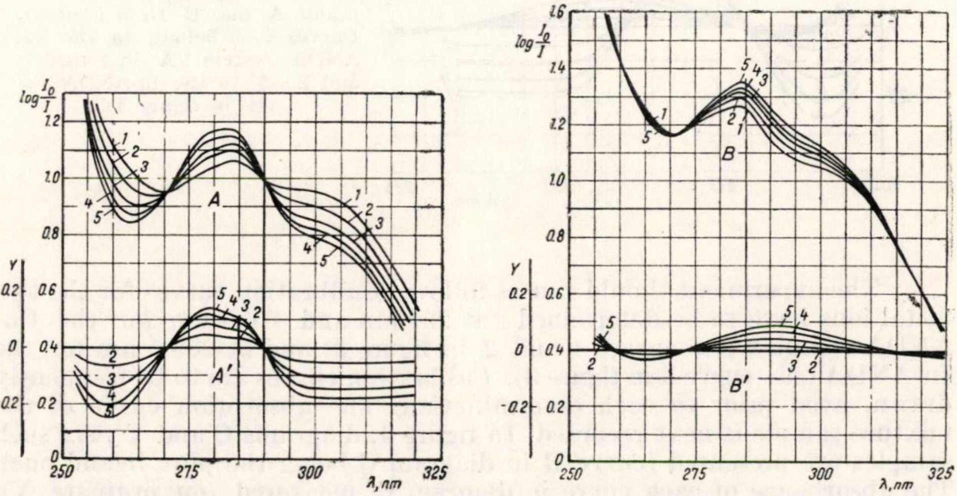

Fig. 1. — Absorption curves of the Ga-ANDA (diagram A) and In-ANDA system (B), with water as reference. Ga^{3+} concentration, in A: O (curve 1), 2×10^{-4}M (2), 4×10^{-4}M (3), 6×10^{-4}M (4) and 8×10^{-4}M (5). In^{3+} concentrations in B are identical to the corresponding ones in A, except that of curve 5 which is 7.6×10^{-4}M. ANDA concentration is constant for each of the two diagrams: 8×10^{-4}M diagram A and 1×10^{-3}M diagram B.

Diagrams A′ and B′ are identical with A respectively B except for the reference which is here the blank solution. Cell length: 1 cm.

Ga-ANDA system, the whole absorbance is to be attributed to the In-ANDA complex present. A ligand excess over the Ga + In sum has to be used.

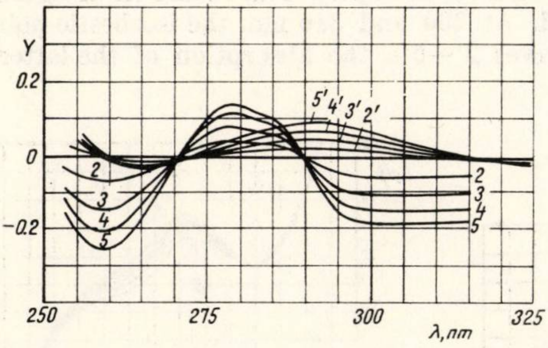

Fig. 2. — Superposition of diagrams A′ and B′ from figure 1. Curves 2—5 belong to the Ga-ANDA system (A′ in figure 1) and 2′—5′ to the In-ANDA one (B′ in figure 1).

The experiment should run as follows. Calibration curves for the two metal ions have to be determined : at 260 nm and 316.5 nm for the Ga-ANDA complex (see curves 1 and 2 in figure 3) and at 289.5 nm for the In-ANDA one (curve 3 in figure 3). Calibration curves are to be frequently drawn, even prior to each determination. The absorption curve of the mixture sample is next recorded. In figure 4, diagrams C and C′, six such samples are presented (curve R in diagram C being the pure ligand one). The absorbance of each curve in diagram C′ measured (on ordinate Y), at $\lambda = 260$ nm, is the contribution of Ga^{3+}. The corresponding concentrations are presently obtained from calibration curve 1 in figure 3. We may check these results by reading the absorbance of the same absorption curves in C′, figure 4 at the 316.5 nm wavelength, and subsequently evaluating the concentration from calibration curve 2 (figure 3). This is shown, by columns c and e, in Table 1 A, for the six curves in figure 4. In the same figure 4 the absorbance corresponding to the 289.5 nm wavelength is due to the In^{3+} concentration and it should be evaluated from calibration curve 3 in figure 3. For the six samples recorded in figure 4 the obtained values are presented in table 1 B column c. The relative percent error does not, in the average, exceed 3%.

When C type diagrams are preferred to C′ ones, the whole procedure is identical except that the absorbance corresponding to particular curve is measured as a difference against the reference curve R and this value is then used to determine the concentration from the respective calibration curve.

There is another fact connected with some preliminary investigation in this work. In order to detect the most adequate solvent to be used, several tests have been made. An aqueous medium adjusted to pH 2.9 with HNO_3 did not lead to clear-cut isosbestic points. A 1×10^{-1} N perchloric acid medium as well as a 1×10^{-1} N nitric acid one, both yielded clear-cut isosbestic points. The isosbestic points location seems to have been influenced by the pH, but not by the nature of the anions present in the reaction medium.

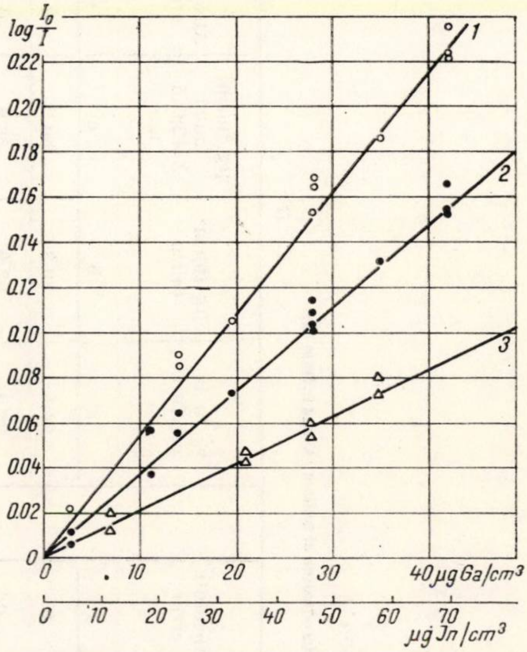

Fig. 3. — Calibration curves for Ga-ANDA: curve 1 (at $\lambda = 260$ nm) and 2 (316.5 nm) and for In-ANDA: curve 3 ($\lambda = 285.5$ nm). ANDA concentration, constant 253.09 μ g/cm³. Blank reference. Cell length: 1 cm.

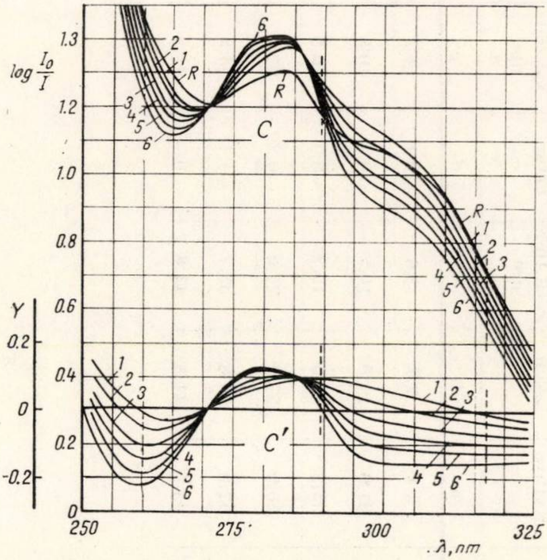

Fig. 4. — Absorption curves of the (Ga + In)-ANDA system: in diagram C the reference is water and in C′, the blank solution. The Ga^{3+} concentration is: 0 (curve R), 0.4×10^{-4}M (1), 1.6×10^{-4}M (2), 2.8×10^{-4}M (3), 4×10^{-4}M (4), 5×10^{-4}M (5), 6×10^{-4}M (6). The In^{3+} concentration is: 0 (curve R), 1×10^{-4} M(1), 3×10^{-4}M(2), 4×10^{-4}M(3), 5×10^{-4}M(4), 6×10^{-4} (5), 7×10^{-4}M(6), ANDA concentration constant = 1×10^{-3}M. Cell length: 1 cm.

The experimental procedure of the simultaneous spectrophotometric determination of Ga^{3+} and In^{3+} at $\lambda = 260$ nm, respectively 289.5 nm, is next going to be briefly described.

Table 1

Simultaneous spectrophotometric determination of gallium (A) and indium (B)

	A						B			
Sample no	% Ga in mixture	μg Ga/cm^3 taken	μg Ga/cm^3 found $\lambda = 3.16.5$ nm	Absolute error	μg Ga/cm^3 found $\lambda = 260$ nm	Absolute error	% In in mixture	μg In/cm^3 taken	μg In/cm^3 found $\lambda = 289.5$ nm	Absolute error
	a	b	c	d	e	f	a	b	c	d
1	5.4	2.7	2.6	−0.1	2.7	0	94.6	80.3	80.3	0
2	21.0	11.0	10.7	−0.4	10.8	−0.3	78.9	68.9	68.9	0
3	35.9	19.5	19.2	−0.3	19.5	0	64.0	57.4	55.8	−1.6
4	50.0	27.8	27.0	−0.8	27.0	−0.8	50.0	45.9	47.3	1.4
5	62.5	34.8	33.7	−1.1	34.8	0	37.0	34.4	34.0	−0.4
6	85.7	41.8	41.8	0	41.8	0	14.0	11.0	11.9	0.4

Absorption curves of a calibration series for Ga^{3+} are recorded as an A′ type diagram. Six samples (or even less) are prepared starting with 0.2 cm^3 up to 3 cm^3 $Ga(NO_3)_3$, a $5 \times 10^{-3}M$ solution in $1 \times 10^{-1}N$ HNO_3 as solvent, to which 2.5 cm^3 of an $1 \times 10^{-2}M$ aqueous ANDA solution are constantly added and finally brought to the mark in 25 cm^3 flasks with HNO_3, a $1 \times 10^{-1}N$ solution, as solvent. Their absorption spectra are recorded against the ligand solution as reference (2.5 cm^3 of $1 \times 10^{-2}M$ aqueous ANDA diluted to 25 cm^3 with HNO_3 $1 \times 10^{-1}N$). The absorbance measured at 260 nm (on the Y ordinate) is used to draw the calibration plot for Ga^{3+} at $\lambda = 260$ nm. Another calibration plot for Ga^{3+} may be drawn on the basis of the same curves' absorbances measured at 316.5 nm.

An analogous procedure is repeated for the In^{3+} calibration curve determination. The same 1×10^{-1} M HNO_3 solvent is used (to make up the final 25 cm^3 volume of six samples) as well as the same constant volume (2.5 cm^3) of the $1 \times 10^{-2}M$ aqueous ligand solution (ANDA) and consequently the same reference solution. Variable amounts of In $(NO_3)_3$ as $5 \times 10^{-3}M$ solution (in the same $1 \times 10^{-1}N$ HNO_3 solvent) are measured (by means of a microburette), ranging from 0.5 to 3.5 cm^3. Absorbances measured for each curve at $\lambda = 289.5$ nm led to the In^{3+} calibration curve plot.

The absorption curve of a mixture of say 2.0 cm^3 Ga^{3+} and 2.5 cm^3 In^{3+} solution, together with 2.5 cm^3 of ANDA, prepared under identical conditions (reactants' and reagent's stock solutions concentration, final volume, solvent) as the calibration samples, is next recorded against the same blank reference. The absorbance measured at 260 nm is converted from the corresponding calibration curve into Ga^{3+} concentration. The absorbance measured at 316.5 nm converted into Ga^{3+} concentration from the second Ga^{3+} calibration curve, is a check of the previously obtained value. The absorbance red at 289.5 nm is to be used for the In^{3+} concentration evaluation from the respective In^{3+} calibration curve.

Revue Roumaine de Chimie, 17, 1, 2, 239–251 (1972)

En l'honneur du 70° anniversaire
du Professeur I. G. MURGULESCU

SIGNIFICATION DU POTENTIEL DE PROTECTION LORS DE LA CORROSION PAR PIQÛRES, DE LA CORROSION INTERGRANULAIRE ET DE LA CORROSION FISSURANTE SOUS TENSION *

MARCEL POURBAIX

CEBELCOR, Avenue Paul Héger, Grille 2, Bruxelles 5, Belgique

Reçu le 9 septembre 1971

D'une manière générale, les solutions qui existent à l'intérieur de piqûres actives et de fissures de corrosion sous tension de nombreux métaux et alliages passivables sont localement acides, du fait même de phénomènes d'hydrolyse ; et, s'il existe du chlorure dans la solution corrodante ou dans le métal, cet acide est de l'acide chlorhydrique qui est particulièrement agressif. Ceci se produit aussi dans d'autres cas où la corrosion se produit dans des conditions de diffusion restreinte, telles que la corrosion intergranulaire ou la corrosion caverneuse. Dans tous ces cas, une connaissance complète des données électrochimiques (de natures thermodynamique et cinétique) concernant à la fois le comportement des cavités actives qui existent à l'intérieur de piqûres ou fissures (anodes), qui sont généralement acides, et le comportement de surfaces passives extérieures à ces cavités (cathodes), qui sont généralement alcalines, aide à obtenir une connaissance complète du mécanisme de ces corrosions ; ceci aide donc à maîtriser ces corrosions. En règle générale, la corrosion par piqûres, la corrosion fissurante sous tension, la corrosion intergranulaire et la corrosion caverneuse peuvent être annihilées par maintien du potentiel d'électrode en dessous d'une valeur critique déterminée, appelée « potentiel de protection ». Ce potentiel de protection (en dessous duquel des piqûres préexistantes, des fissures et des cavernes de corrosion ne peuvent grandir) ne peut pas être confondu avec le potentiel de « rupture » ou de « piqûration » (au-dessus duquel des piqûres peuvent être formées). Ce popotentiel de protection est approximativement égal au potentiel existant à l'intérieur de piqûres ou fissures acides. On considère le cas du cuivre, de fer, d'aciers inoxydables, d'aciers à haute résistance, d'alliages de titane et d'aluminium. On signale l'utilité d'un programme de recherches à long terme pour l'étude électrochimique systématique de phénomènes de corrosion qui se produisent dans des conditions de diffusion restreinte : piqûration, corrosion intergranulaire, corrosion fissurante sous tension, corrosion caverneuse.

---

* Mémoire présenté lors de la «1970 Corrosion Research Conférence de la National Association of corrosion Engineers». NACE, Philadelphie, 2–4 mars 1970.

1. POTENTIEL DE PIQÛRATION ET POTENTIEL DE PROTECTION

La figure 1*a* représente schématiquement cinq courbes de polarisation potentiocinétiques relatives au comportement du fer Armco dans des solutions exemptes de chlorure, de pH, 5, 7, 9, 11, et 13 ; il est aisé de déduire de ces courbes de polarisation la figure 1*b* qui représente, en fonction du pH et du potentiel d'électrode, les conditions expérimentales d'immunité, de corrosion généralisée et de passivité.[1]

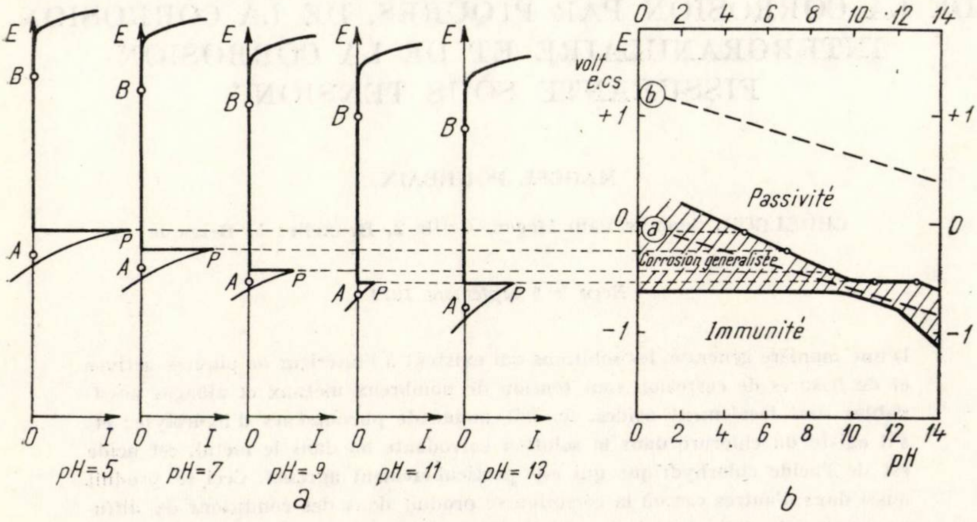

Fig. 1. — Comportement du fer en solution exempte de chlorure (Schéma).

a, Courbes de polarisation en présence de solutions de pH 5 à 13. *b*, Circonstances expérimentales d'immunité, de corrosion généralisée et de passivité.

Les potentiels qui séparent les régions d'immunité et de corrosion généralisée sont les *potentiels d'équilibre C* de la réaction de corrosion, en dessous desquels cette réaction est thermodynamiquement impossible. Les potentiels qui séparent les régions de corrosion généralisée et de passivité sont les *potentiels de passivation P*, au-dessus desquels un film protecteur est formé sur le métal.

La figure 2*a* représente schématiquement cinq courbes de polarisation en solutions de même pH 5 à 13, mais contenant 10^{-2} ion. g Cl^- par litre (355 p.p.m. Cl^-). Nous rappelons que *r* est le *potentiel de rupture* ou *potentiel de piqûration* au-dessus duquel le film passivant devient localement non protecteur, ce qui conduit à la formation de piqûres ; *p* est le *potentiel de protection* en dessous duquel les piqûres ainsi formées ne grandissent plus et deviennent donc inoffensives. La figure 2*a* permet de tracer la figure 2 *b* qui montre, outre les domaines d'immunité, de corrosion généralisée et de passivité mentionnés ci-dessus, un domaine de piqûration (situé au-dessus du potentiel de rupture *r*, lequel dépend fortement du pH et de la teneur en chlorure) ; la ligne qui représente le potentiel de protection *p* (qui est presque indépendant du pH et de la teneur en chlorure) divise le domaine de passivité en une région supérieure où les piqûres éventuellement préexistantes grandissent (la passivité est alors imparfaite) et une région inférieure où les piqûres préexistantes ne grandissent pas (la passivité est alors parfaite). La figure 2*b* montre aussi que, pour des pH inférieurs à 6, il ne se produit pas de passivation ; seule une corrosion généralisée est alors possible.

---

[1] M. Pourbaix, *a) Recent Applications of Electrode-Potential Measurements in the Thermodynamics and Kinetics of Corrosion of Metals*, Corrosion **25**, 267—281 (1969) ; Rapports Techniques CEBELCOR, **112**, RT. 167 (1970).

b) Recherches en corrosion. Résultats de travaux récents. Voyage aux Etats-Unis d'Amérique, Rapports Techniques CEBELCOR, **109**, RT. 157 (1969).

c) Bases fondamentales de la protection cathodique et applications, Rapports Techniques CEBELCOR, **111**, RT. 166 (1969).

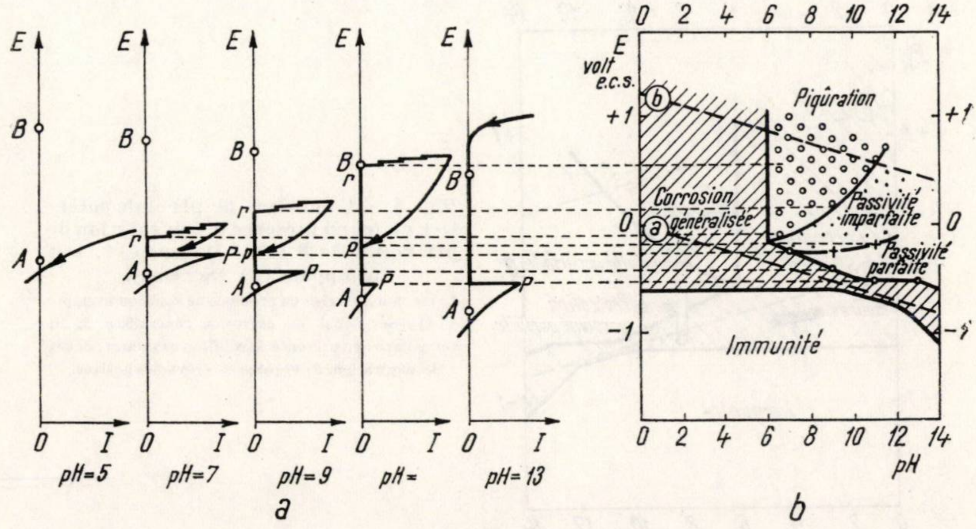

Fig. 2. — Comportement du fer en solution chlorurée (10^{-2} ion.g par litre, soit 355 ppm Cl^-) (Schéma).

a, Courbes de polarisation en présence de solutions de pH 5 à 13. *b*, Circonstances expérimentales d'immunité, de corrosion généralisée, de passivités parfaite et imparfaite et de piqûration.

La figure 3, qui est semblable à la figure 2*a*, montre les conditions de potentiel possibles pour du fer en présence d'une solution de pH 8, 10^{-2} M en Cl^-. Si la solution est exempte d'oxygène et d'autres oxydants, le potentiel d'électrode de fer non polarisé se situera au point *l* et il se produira une corrosion généralisée avec dégagement d'hydrogène ; si de telles conditions exemptes d'oxygène n'existent que sur une partie de la structure en fer, la corrosion généralisée ainsi initiée conduira à une corrosion caverneuse (crevice corrosion). Si la solution renferme de l'oxygène, le potentiel d'électrode peut s'élever jusqu'au point *2*, et ceci conduit à une piqûration. Etant donné que, dans ces deux cas (avec ou sans oxygène) , les produits de corrosion stables ne sont pas les ions dissous Fe^{++} et Fe^{+++} formés primairement, mais des oxydes ou hydroxydes tels que Fe_3O_4 et $Fe(OH)_3$, il se produit une hydrolyse à l'intérieur des crevasses et des piqûres selon les réactions :

$$3Fe^{++} + 4H_2O \rightarrow Fe_3O_4 + 8H^+ + 2e^-$$

et

$$Fe^{+++} + 3H_2O \rightarrow Fe(OH)_3 + 3H^+$$

et si, ainsi que c'est généralement le cas, les crevasses et piqûres sont fermées du fait de la déposition de produits de corrosion solides, cette hydrolyse conduit à une acidification locale à l'intérieur des crevasses et piqûres ; si du chlorure est présent, cet acide est de l'acide chlorhydrique, lequel est particulièrement agressif.

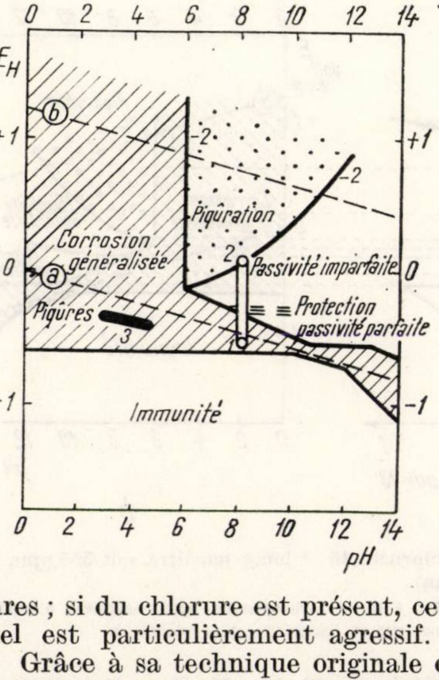

Fig. 3. — Conditions de pH et de potentiel du fer en présence d'une solution de pH voisin de 8 (10^{-2} M dans Cl^-, soit 355 ppm Cl^-) (Schéma).

1, fer non polarisé en présence de solution exempte d'oxygène : début de corrosion généralisée. *2*, fer non polarisé en présence de solution oxygénée : début de piqûration. *2*, Piqûres et crevasses actives.

Grâce à sa technique originale de solidification par refroidissement dans l'azote liquide, B. F. Brown [2a, b] a observé le premier que de telles conditions acides (pH 3,8) existent réellement à l'extrémité de fissures de corrosion sous tension de nombreux aciers, dans une solution à 3 % NaCl. En utilisant le dispositif représenté à la figure 5, nous avons étudié avec J. Van Muylder les conditions de potentiel et de pH existant à l'intérieur de crevasses d'acier au carbone, dans des conditions d'aération différentielle et nous avons observé les valeurs représentées par la zone noire *3* de la figure 3 : pH variant entre 4,7 et 2,7 selon les conditions d'aération différentielle entre une cathode aérée passive (pH environ 10) et l'anode active non aérée. Il n'y a pas de raison pour que, pour un même métal en corrosion, les conditions existant à l'intérieur de piqûres dif-

---

[2] B. F. Brown, *a*) In collaboration with C. T. Fujii and E. Ph. Dahlberg, *Methods for Studying the Solution Chemistry within Stress-Corrosion Cracks*, J. Electrochemical Soc., **116**, 218–219 (1969).

b) *On the Electrochemistry of Stress-Corrosion Cracking of High Strength Steels*, Publication CEBELCOR, E. 76. (1969).

c) *The Role of the Occluded Cell in Stress-Corrosion Cracking of High Strength Steels*, Rapports Techniques CEBELCOR, **112**, RT. 170 (1970).

fèrent des conditions existant à l'intérieur de crevasses, de fissures ou au long de joints de grain en corrosion, ou de toute autre cellule de corrosion fermée.

Si par conséquent, du fait par exemple de la présence d'oxygène dans une solution contenant du chlorure, le potentiel de piqûration *2* (figure 3) est atteint sur une surface passive de fer, la piqûre ainsi formée provoque l'apparition dans le système considéré d'une surface acide fermée indiquée par *3* à cette figure. Cette figure montre aussi que le « *potentiel de protection* » en dessous duquel nous avons observé que des piqûres deviennent inactives et inoffensives est approximativement égal au (ou légèrement supérieur au) potentiel *3* à l'intérieur de ces piqûres. Et ceci rend très claire la signification scientifique de ce potentiel de protection, signification qui n'était pas apparente lorsque l'existence d'un tel potentiel a été observée pour la première fois en 1961, dans le cas d'aciers inoxydables[3] : ainsi qu'il a été observé en 1962 pour des piqûres de cuivre [4,5], des piqûres de fer et d'acier deviennent inactives et inoffensives si le potentiel d'électrode à l'extérieur des piqûres devient inférieur à une valeur critique bien définie qui est approximativement égale au potentiel d'électrode à l'intérieur des piqûres actives. Pour le *cuivre*, ce *potentiel de protection* est approximativement égal à $+270$ à $+420$ $\mathrm{mV_{ehs}}$; pour des *aciers*, il est d'environ -400 à -200 $\mathrm{mV_{ehs}}$. La connaissance de tels potentiels de protection, qui doivent exister pour tout métal ou alliage passivable susceptible de subir des piqûres, rend donc possible d'établir des techniques à base scientifique pour la protection cathodique de métaux et alliages contre la corrosion par piqûres, ainsi que probablement contre d'autres formes de corrosion se produisant dans des conditions de diffusion restreinte : corrosion caverneuse, corrosion fissurante sous tension, corrosion intergranulaire.

La figure 4 montre schématiquement, pour quatre concentrations en chlorure (10^{-3}, 10^{-2}, 10^{-1} et 10^{0} M), les données déjà présentées à la figure 3 pour une solution 10^{-2}. On peut voir que le potentiel de piqûration dépend fortement à la fois du pH et de la teneur en chlorure ; le potentiel de protection est sensiblement indépendant du pH et de la teneur en chlorure.

A titre d'illustration de la validité expérimentale de ces concepts, nous reproduisons à la figure 6 [3a,b] des résultats obtenus précédemment lors de tests potentiostatiques conduits sur un acier au chrome AISI 410 poli au carborundum, placé dans une solution saturée en oxy-

---

[3] M. Pourbaix, L. Klimzach-Mathieu, J. Meunier et Cl. Vanleugenhaghe, *a*) *Sur le comportement électrochimique d'aciers alliés en solution chlorurée.* Rapports Techniques CEBELCOR, R T. 103, RT. 104, RT. 105, RT. 120 (1962).

b) *Potentiokinetic and corrosimetric Investigations on the Corrosion Behaviour of Alloy Steels*, Corrosion Science, **3**, 239–259 (1963).

[4] J. Van Muylder, M. Pourbaix, P. Van Laer et N. de Zoubov, *a*) *Sur la tension d'électrode de cuivre en présence d'eau de Bruxelles. Influence de la lumière et des conditions de circulation de l'eau*, Rapport Technique CEBELCOR, RT. 125 (1965).

b) *Electrochemical Nature of the Pitting of Copper in Water and in Aqueous Solutions*, Publication CEBELCOR, E. 61 (1967).

[5] M. Pourbaix, *On the Effect of Chlorides on the Behaviour of Metals and Alloys in the Presence of Aqueous Solutions*, Proc. Symposium on the Coupling of Basic and Applied Corrosion Research. A. Dialogue (Washington D. C. and Gaithersburg Md., March 21–22, 1966), Publ. NACE, Houston (1969).

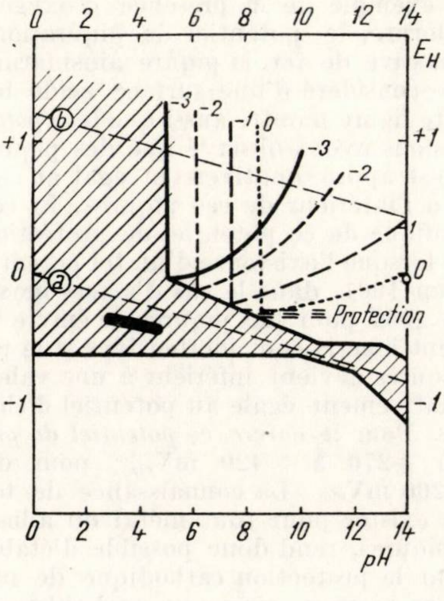

Fig. 4. — Influence de la teneur en chlorure sur les potentiels de rupture et de protection du fer ($Cl^- \ 10^{-3}$ à 10^0 M) (Schéma).

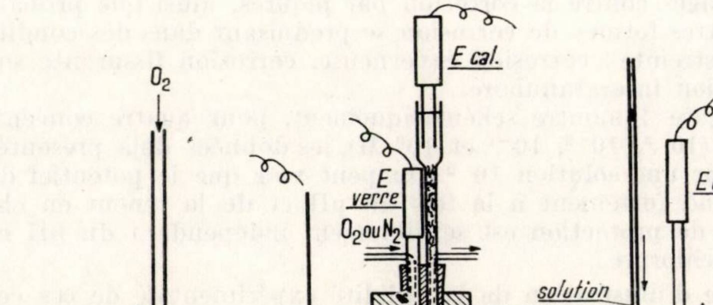

Fig. 5. — Dispositif pour l'étude de la corrosion caverneuse.

gène (8,3 g/l $NaHCO_3$ et 200 g/l NaCl), à 20°C ; les potentiels critiques étaient :

potentiel de piqûration —150 mV_{ecs}

potentiel de protection —300 mV_{ecs}

Lors de leur immersion dans cette solution, les échantillons d'acier présentaient un potentiel libre (sans application de courant) variant entre

-150 et $+300$ mV_{ecs} ce qui, étant donné que ces valeurs sont supérieures au potentiel de piqûration, implique l'initiation de piqûres. Après une minute de maintien sans courant deux des échantillons furent polarisés anodiquement à des potentiels constants supérieurs à -150 mV_{ecs} (soit -100 et 0 mV_{ecs}), deux échantillons furent polarisés cathodiquement entre -150 et -300 mV_{ecs} (à -200 et -250 mV_{ecs}). Un échantillon fut polarisé à -300 mV_{ecs}. La figure 6 (ainsi que des courbes courant-temps enregistrées au cours de l'expérience mais non reproduites ici) * montrent que, comme prédit pour le cas de surfaces préalablement endommagées par piqûres :

1. En cas de maintien au-dessus du potentiel de piqûration (-150 mV_{ecs}), il se produit une piqûration intense,
2. En cas de maintien entre le potentiel de piqûration et le potentiel de protection, il se produit aussi une piqûration, mais pas aussi intense,
3. En cas de maintien en dessous du potentiel de protection, les piqûres préalablement formées, ne grandissent pas.

Par ailleurs, dans le cas d'échantillons polarisés immédiatement entre le potentiel de piqûration et le potentiel de protection, sans avoir été maintenus préalablement sans courant dans la solution, aucune corrosion n'a été observée.

2. PROTECTION CATHODIQUE

La figure 7 représente, d'après B. F. Brown [2r, 1c] l'effet d'une polarisation cathodique sur le pH existant à l'intérieur d'une fissure et sur la vitesse de fissuration d'aciers soumis à un effort de tension mécanique dans une solution à 3,5% NaCl. Comme l'a dit Brown [1c] cette figure montre que « si l'on abaisse le potentiel successivement à des valeurs de plus en plus négatives, le pH à l'intérieur de la cellule fermée s'élève. Lorsque le potentiel est abaissé à environ $-0{,}85$ $volts_{ecs}$ ($-0{,}60$ $volts_{ehs}$), il n'y a plus de dissolution du fer dans la crevasse, et la vitesse de propagation de la crevasse est minimale. A des potentiels encore plus negatifs, la vitesse de fissuration augmente à nouveau, et à tous les potentiels la combinaison du potentiel imposé et du pH dans la fissure place le point représentatif dans la région favorable d'une formation cathodique d'hydrogène à l'intérieur de la fissure ».

Rappelons que, dans des diagrammes tels que celui qui est représenté à la partie gauche de la figure 7, la distance verticale entre un potentiel expérimental et le potentiel d'équilibre de deux réactions électrochimiques déterminées mesure l'affinité de cette réaction dans les conditions expérimentales considérées. L'affinité de la dissolution de fer, dont la valeur est 300 mV à pH 3, devient 0 à pH 9 ; l'affinité de dégagement d'hydrogène, qui demeure sensiblement constante et voisine de 100 mV pour tous les pH inférieurs à 9, croît aux pH plus élevés et atteint 500 mV à pH 14. Par conséquent, comme l'a dit Brown, lorsque le potentiel d'électrode est sensiblement plus élevé que $-0{,}60$

---

* Voir [3a] Rapport Technique CEBELCOR R. T., 103, fig. 17.

$\text{volts}_{\text{ehs}}$, la propagation de la fissure est due principalement à une dissolution du fer (soit à une « active path corrosion »), ainsi qu'à une légère fragilité d'hydrogène. Lorsque le potentiel d'électrode est abaissé en dessous de $-0{,}60$ $\text{volts}_{\text{ehs}}$, la dissolution du fer devient nulle, et la fragilité d'hydrogène est accrue.

Afin d'examiner davantage le mécanisme de la protection cathodique contre la corrosion caverneuse et les autres formes de corrosion dans des conditions de diffusion restreinte, nous avons utilisé avec J. Van Muylder le dispositif représenté à la figure 5, avec addition d'une anode auxiliaire en platine, afin de permettre de polariser cathodiquement la cathode aérée externe.

Une même solution (NaOH, 0,001 M et NaCl 0,001 M) a été introduite dans la partie externe ouverte et dans le compartiment interne fermé.

On a alors fait barboter de l'oxygène dans la solution externe, et on a fait passer de l'azote pur dans le compartiment interne afin de promouvoir une aération différentielle laquelle a conduit progressivement, à l'intérieur de ce compartiment, à une diminution du potentiel et du pH, ainsi qu'à une certaine corrosion. Après plusieurs jours, le pH à l'intérieur du compartiment interne (qui était en fait une crevasse artificielle) s'est stabilisé à environ 4,7 avec quelques chutes soudaines jusqu'à environ 2, 7, spécialement lors d'un remplacement temporaire de l'azote par de l'oxygène ; la surface externe aérée est demeurée non corrodée. Ces conditions externes et internes de l'échantillon en cas d'absence de polarisation sont indiquées à la figure 8 par les points marqués *O*.

Ensuite la surface externe a été polarisée cathodiquement avec des intensités de courant croissantes ; les points *1* à *9* indiquent à titre d'exemple les caractéristiques des surfaces externes et internes correspondant à des valeurs croissantes du courant de polarisation. Ces résultats ne sont pas très reproductibles, et dépendent de la vitesse à laquelle l'expérience est conduite ; toutefois, on peut voir que :

— lorsque le potentiel de protection (environ — 400 mV_{ehs} point *3*) est atteint sur la surface externe, la solution à l'intérieur de la crevasse n'est plus acide (pH 7) et le potentiel d'électrode y est voisin du potentiel d'immunité (environ -500 à -600 mV_{ehs}),

— lorsque le potentiel extérieur devient inférieur à environ -800 mV_{ehs}, la solution à l'intérieur de la crevasse devient sensiblement alcaline (pH 10 à 11), par suite d'une réduction importante de l'eau avec dégagement d'hydrogène,

— les potentiels internes sont inférieurs aux potentiels externes si ceux-ci sont supérieurs à environ -600 à -700 mV ; ils leur sont supérieurs dans les autres cas.

3. COMPORTEMENT ÉLECTROCHIMIQUE DE MÉTAUX ET ALLIAGES EN PRÉSENCE DE CHLORURES

Les diagrammes tels que les figures 3, 4 et 8 existent pour tout métal ou alliage passivable, ou, plutôt, pour tout constituant de tels métaux et alliages (ferrite, austénite, cémentite, etc) ; étant bien entendu que, pour chacun de ces constituants, les données indiquées sur ce dia-

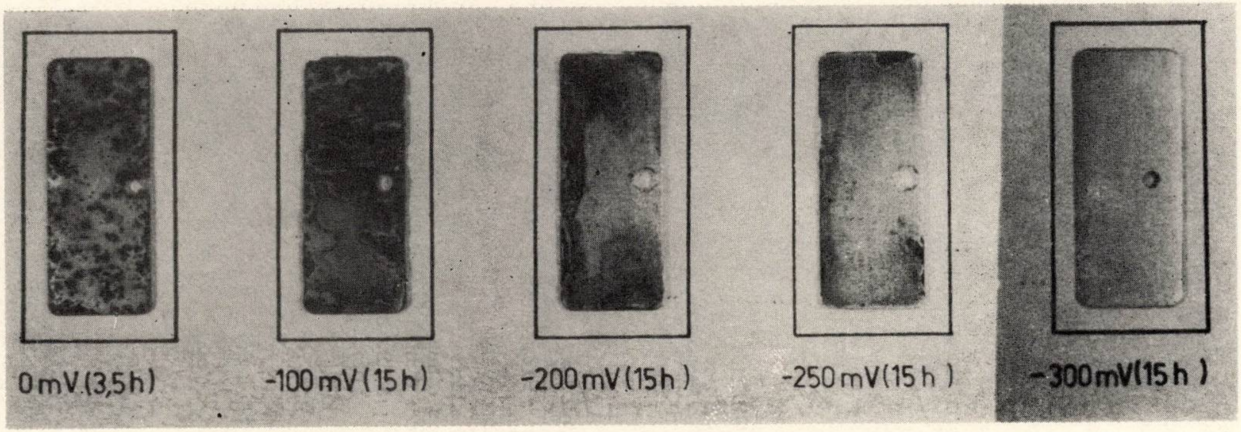
0 mV (3,5 h)
-100 mV (15 h)
-200 mV (15 h)
-250 mV (15 h)
-300 mV (15 h)

Fig. 6. — Essais corrosimetriques potentiostatiques sur acier type AISI 410.

Solution : 8.3 g/l $NaHCO_3$ et 200 g/l NaCl. Gaz : O_2. Température : 20°C. Polissage : carborundum 180 A. Prépolarisation : 1 mn à la tension libre. Potentiel de piqûration : $-150\ mV_{ecs}$. Potentiel de protection : $-300\ mV_{ecs}$

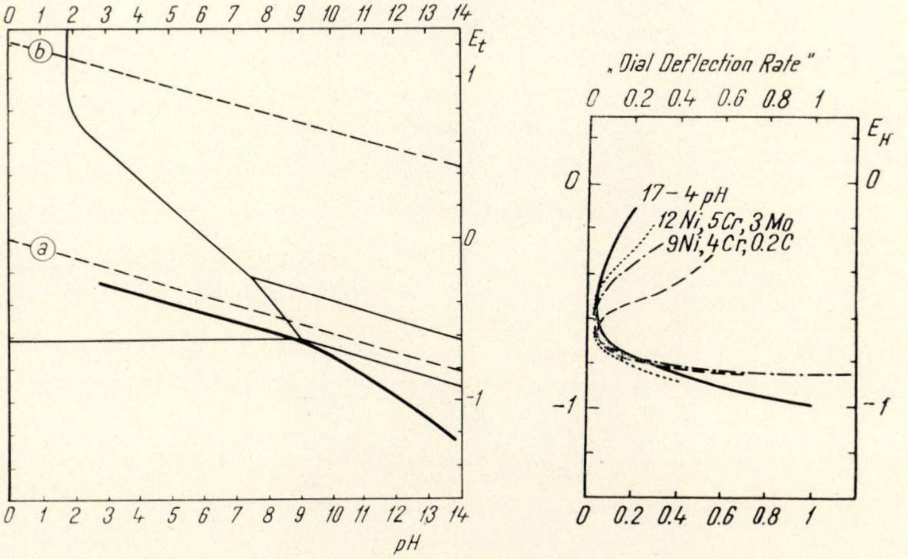

Fig. 7.— Influence d'une polarisation cathodique sur les caractéristiques électromiques et sur la vitesse de propagation d'une fissure de corrosion sous tension. (Acier au chrome AISI 4340 en présence d'une solution de NaCl 3 %.) (D'après B.F. Brown.)

Le « dial deflexion rate » indiqué dans la partie de droite de la figure mesure la vitesse de propagation de la fissure.

gramme dépendent de plusieurs facteurs, tels que : état de surface, anions en solution, température, etc.

On ne connaît actuellement que très peu de chose au sujet de ces diagrammes ; par conséquent, nous nous contenterons d'indiquer ici différentes formes de tels diagrammes, afin d'illustrer leur interprétation possible. Pour chacun de ces diagrammes, nous avons considéré le comportement du métal quand il est en contact avec une eau de pH voisin de 8 contenant du chlorure.

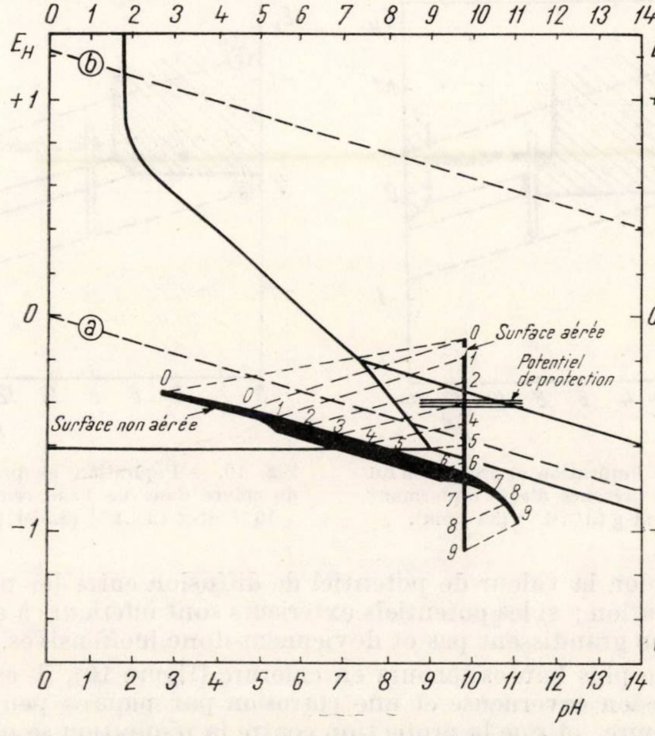

Fig. 8. — Influence d'une polarisation cathodique sur les caractéristiques électrochimiques d'une piqûre (ou caverne) de corrosion. (Acier au carbone ordinaire en présence de solution aérée de NaOH 0,001 M et NaCl 0,001 M.) (Schéma)

On a réuni par des traits pointillés les caractéristiques simultanées de la surface non aérée (piqûre) et de la surface aérée. Les points marqués 0 correspondent à une absence de polarisation ; les points 1 à 9 correspondent à des polarisations cathodiques de la surface aérée.

Les figures 9 et 10 montrent schématiquement les conditions de piqûration et de protection de cuivre, dans des eaux environ 10^{-3} et 10^{-1} M en Cl^- (35 et 3550 p.p.m.).

Dans le cas de la concentration en chlorure la plus faible (figure 9), aucune corrosion caverneuse ne peut se produire, mais s'il se forme des piqûres sur le métal, ces piqûres ont un pH voisin de 3,5 par suite de l'hydrolyse de CuCl formé primairement, hydrolyse qui conduit à la formation de Cu_2O et de HCl. Le potentiel d'équilibre du cuivre dans ces piqûres est voisin de $+270\ mV_{ehs}$. Ces piqûres grandissent si le potentiel à l'intérieur des piqûres est supérieur à cette valeur d'équilibre, et ceci correspond à un potentiel extérieur aux piqûres variant entre +350 et

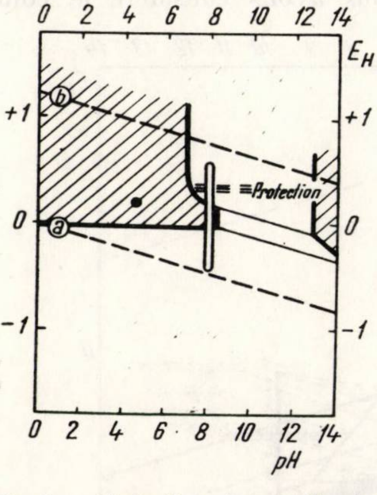

Fig. 9. — Piqûration et protection du cuivre en présence d'eau renfermant 10^{-3} at-g Cl^-. 1^{-1} (35 ppm).

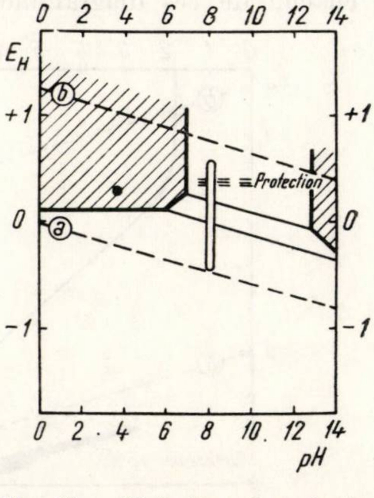

Fig. 10. — Piqûration et protection du cuivre dans de l'eau renfermant 10^{-1} at-g $Cl^-.1^{-1}$ (3.550 ppm).

+400 mV selon la valeur de potentiel de diffusion entre les piqûres et le sein de la solution ; si les potentiels extérieurs sont inférieurs à ces valeurs, les piqûres ne grandissent pas et deviennent donc inoffensives.

Pour de plus hautes teneurs en chlorure (figure 10), il est probable qu'une corrosion caverneuse et une corrosion par piqûres peuvent toutes deux se produire, et que la protection contre la piqûration se produit dans à peu près les mêmes conditions que celles qui sont observées pour les teneurs plus faibles en chlorure (potentiel extérieur inférieur à environ $+350$ à $+ 450\ mV_{ehs}$). Une protection totale contre toute forme de corrosion (piqûration et cavernes) est obtenue à des potentiels inférieurs à $+ 100\ mV_{ehs}$.

La figure 11 montre une section à travers une piqûre de cuivre en présence d'eau froide. A l'intérieur de la piqûre existe une solution de HCl imprégnant des dépôts de CuCl blanc et de CuO_2 rouge, couverts par de la malachite verte. Si le potentiel à l'intérieur de la piqûre est supérieur au potentiel d'équilibre, du cuivre se dissout dans la piqûre, laquelle est active et croît rapidement ; si le potentiel est inférieur, du cuivre se dépose dans la piqûre , qui est inactive et inoffensive.

La figure 12 concerne le cas de *fer* en présence de solutions 10^{-1}M en Cl^-. Comme indiqué précédemment, un tel diagramme révèle la possibilité d'une corrosion caverneuse dans les régions non aérées, et de piqûration dans les régions aérées, étant entendu que les piqûres deviennent inactives en dessous d'un potentiel de protection voisin de -200 à -400 mV_{ehs}.

La figure 13 est un schéma provisoire pour un acier au chrome, établi suite à quelques travaux expérimentaux initiés à Bruxelles avec le soutien de la U. S. Atomic Energy Commission et de l'Euratom, et à l'Université de Floride, à Gainesville dans le cadre du programme ARPA.

Fig. 11. — Piqûre de cuivre.
Section montrant la présence de Cu_2O rouge et de CuCl blanc sous une couche de malachite verte.

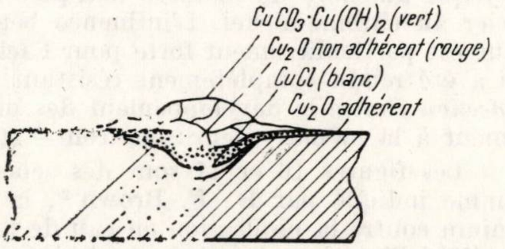
$CuCO_3 \cdot Cu(OH)_2$ (vert)
Cu_2O non adhérent (rouge)
CuCl (blanc)
Cu_2O adhérent

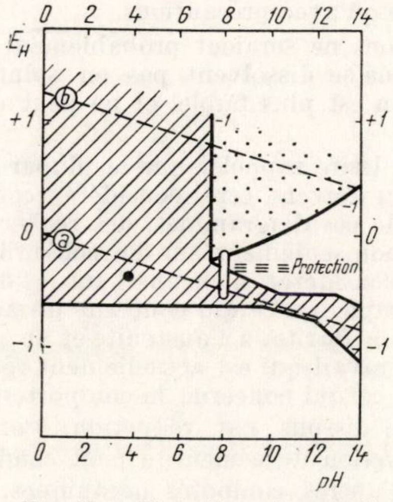
0 2 4 6 8 10 12 14
E_H
b
+1
-1
+1
-1
0
a
0
Protection
-1
1
0 2 4 6 8 10 12 14
pH

Fig. 12. — Piqûration et protection du fer (Cl^- 10^{-1} M) (Schéma).

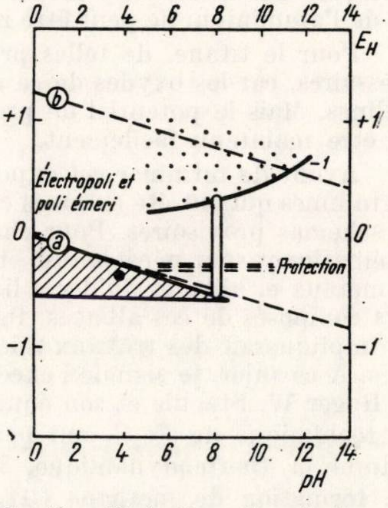
0 2 4 6 8 10 12 14
E_H
b
+1
+1
-1
Électropoli et poli émeri
0
a
0
Protection
-1
-1
0 2 4 6 8 10 12 14
pH

Fig. 13. — Piqûration et protection d'acier au chrome AISI 410 (Cl^- 10^{-1} M) (Schéma).

Il semble que l'addition de chrome à l'acier réduit le domaine de corrosion généralisée et conduit à une élévation du potentiel de piqûration. Il y a donc pour ces aciers une moindre tendance à la corrosion caverneuse et un moindre danger de formation de piqûres. Cependant, ces types de corrosion, cavernes et piqûres, existent encore tous deux. Le potentiel de protection n'est pas modifié de manière sensible. Nous avons observé les mêmes potentiels de piqûration pour de l'acier *poli à l'émeri* et pour de l'acier *poli électrolytiquement*.

Les figures 14 et 15 sont des schémas provisoires pour des aciers au chrome-nickel et au chrome-nickel-molybdène. Selon ces deux schémas, il n'y aurait pas de danger de corrosion caverneuse pour aucun de ces deux aciers dans les solutions utilisées pour ces essais. Ces aciers sont tous deux plus résistants à la piqûration que l'acier au chrome. *Le polissage électrolytique* améliore de manière marquée la résistance à la piqûration de l'acier au chrome-nickel. L'influence bénéfique d'un polissage électrolytique est particulièrement forte pour l'acier au chrome-nickel-molybdène, qui a été rendu complètement résistant à la piqûration. *Le potentiel de protection* contre le développement des piqûres est demeuré approximativement à la même valeur : environ -200 à -400 mV_{ehs}.

Les figures 16 et 17 sont des schémas provisoires pour du titane. Comme indiqué par B. F. Brown ^{2c}, la protection cathodique de l'aluminium contre la piqûration en eau de mer est due à la suppression de l'acidité à l'intérieur des piqûres. Ceci se produit conformément à un mécanisme semblable au mécanisme montré dans le cas du fer à la figure 8. Il est cependant important, à cause de la nature amphotère de l'oxyde d'aluminium, d'éviter des conditions trop alcalines, lesquelles peuvent provoquer une dissolution de cet oxyde. De ce fait, la protection cathodique de l'aluminium ne peut être réalisée qu'avec précautions.

Pour le titane, de telles précautions ne seraient probablement pas nécessaires, car les oxydes de ce métal ne se dissolvent pas en solutions alcalines. Mais le potentiel de protection est plus faible, et ne peut donc pas être maintenu facilement.

Avant de terminer cet exposé, je désire rappeler que la plupart des diagrammes qui ont été montrés ci-dessus doivent être considérés comme des schémas provisoires. Pour chacun de ces diagrammes, des recherches systématiques sont nécessaires, et ceci non seulement sur des échantillons des métaux et alliages qu'il y a lieu de considérer, mais aussi sur les différents composés de ces alliages. Par exemple, en ce qui concerne les aciers ceci impliquerait des travaux relatifs à la ferrite, à l'austénite et aux carbures. A ce sujet, je signale l'excellent travail qui est actuellement réalisé par Roger W. Staehle et son équipe en ce qui concerne le comportement électrochimique de Fe_3C, qui peut être dissous par réduction. Comme l'indique la thermodynamique, la réduction de cémentite peut conduire à la formation de méthane CH_4 ou d'autres composés organiques, et, étant donné que l'hydrogène peut être dissous dans le fer et que le méthane ne peut pas l'être, il est probable que ce que l'on considère actuellement comme « fragilité d'hydrogène » peut être, en fait, tout au moins dans certains cas, une « fragilité de méthane » résultant de la réduction de carbures existant le long de joints de grains. Ceci pourrait être une contribution importante à la compréhension de la corrosion fissurante sous tension et de la fragilité d'hydrogène.

De telles études systématiques devraient, et cela va sans dire, faire usage non seulement de techniques électrochimiques, mais aussi d'autres techniques, notamment de métallurgie physique, microscopie ordinaire et électronique, microscopie à la sonde de Castaing, ellipsométrie, etc. Si de telles études pouvaient être réalisées sur tous les métaux et alliages industriels et sur leurs constituants, il en résulterait des résultats extrêmement utiles. Une telle entreprise serait longue et peu facile, et nécessiterait une équipe de 10 à 20 chercheurs travaillant pendant 100 ans, ou mieux, une équipe de 100 à 200 chercheurs travaillant pendant 10 ans ; mais un tel effort serait rentable, car les formes les plus insidieuses de la corrosion pourraient finalement être maîtrisées.

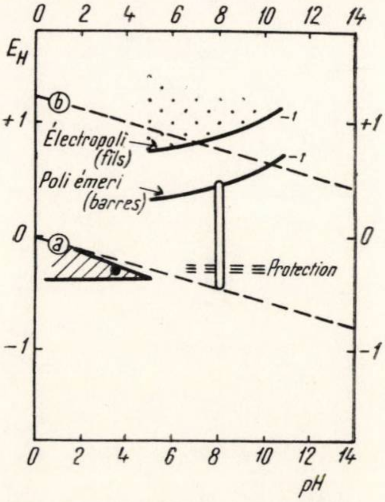
0 2 4 6 8 10 12 14
E_H
+1
0
−1
ⓑ
ⓐ
Électropoli (fils)
Poli émeri (barres)
−1
−1
Protection
pH

Fig. 14. — Piqûration et protection d'acier chrome-nickel AISI 304 (Cl^- 10^{-1} M) (Schéma).

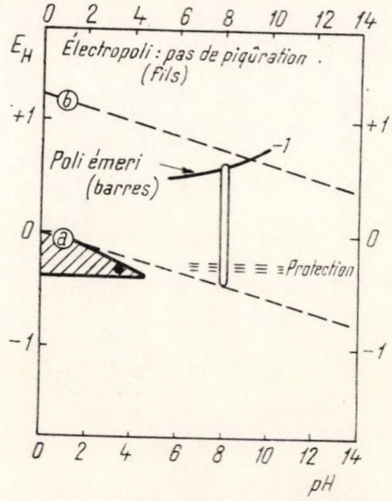
0 2 4 6 8 10 12 14
E_H
Électropoli : pas de piqûration. (Fils)
+1
0
−1
ⓑ
ⓐ
Poli émeri (barres)
−1
Protection
pH

Fig. 15. — Piqûration et protection d'acier chrome-nickel-molybdène AISI 316 (Cl^- 10^{-1} M) (Schéma).

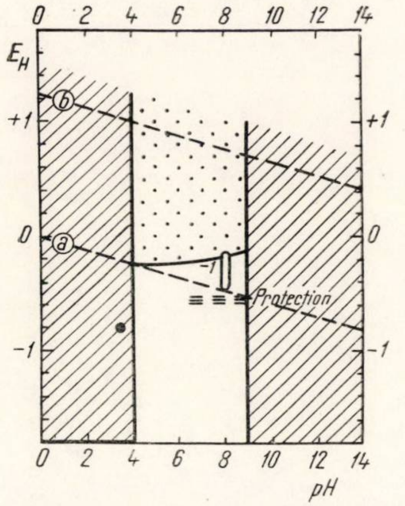
0 2 4 6 8 10 12 14
E_H
+1
0
−1
ⓑ
ⓐ
−1
Protection
pH

Fig. 16. — Piqûration et protection de l'aluminium (Cl^- 10^{-1} M) (Schéma).

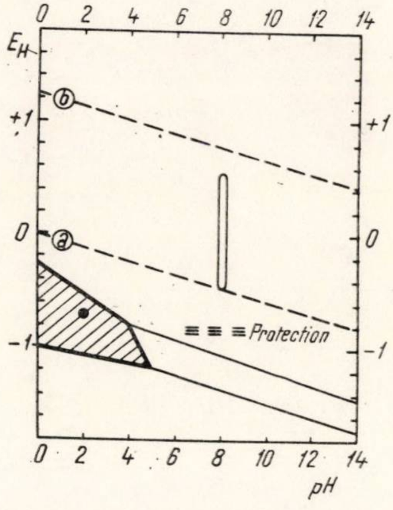
0 2 4 6 8 10 12 14
E_H
+1
0
−1
ⓑ
ⓐ
Protection
pH

Fig. 17. — Fissuration et protection du titane (absence de piqûration) (Schéma)

Revue Roumaine de Chimie, **17**, *1*, *2*, 253 – 257 (1972)

Dedicated to Professor I.G. MURGULESCU
on his 70th birthday

SOME KINETIC ASPECTS OF THE ANODIC OXIDATION OF SILICON IN ETHYLENE GLYCOL

O. RADOVICI, N. BONCIOCAT and VERONICA POPESCU-TUCSEK

Centre of Physical Chemistry, Str. Galați 31, Bucharest, Romania

Received August 12, 1971

Specimens of Si-p and Si-n were exposed to the anodic treatment in ethylene glycol + 0.04 N KNO_3 solutions in order to obtain thick passive films. Based on the experimental results and on Mott and Cabrera's equation, a relationship was derived in order to obtain the thickness of the film (δ) at a given value of the cell voltage (U) at time t : $\delta(t) = R_{current}\ (M/zFsS)\ U(t)$.

INTRODUCTION

The anodic oxidation of silicon has been the subject of many experimental studies, among which we mention the works of Schmidt and Michael,[1] Politychi and Fuchs,[2] Turner,[3] etc. These works have shown that the growing process of the oxide film on the silicon surface is governed by the same laws as for valve metals : Al, Zr, Ta, etc.

The problems related to the interpretation of the kinetics of film growth have been emphasized empirically by Günterschulze and Betz[4] and theoretically by Verwey,[5] Mott [6,7] and Cabrera.[8,9]

Mott and Cabrera derived a well known equation which expresses the relationship between ionic current density (i) and field strength $\Delta\varphi/\delta$ through the thin anodic films :

$$i = i_0 \exp\left((\alpha zF/RT)\, a\, (\Delta\varphi/\delta)\right) \qquad (1)$$

where i_0 = the exchange current density ; δ = film thickness ; α = transfer coefficient ; a = jump distance in the film.

---

[1] P. F. Schmidt and W. Michel, *J. Electrochem. Soc.*, **104**, 230 (1957).

[2] A. Politychi and E. Fuchs, *Nature*, **A 14**, 271 (1959).

[3] D. R. Turner, "Electrochemistry of Semiconductors", Academic Press (editor P. J. Holmes), New York, 1962, p. 179.

[4] A. Günterschulze and H. Betz, *Z. Physik*, **91**, 70 (1934).

[5] E. J. W. Verwey, *Physica*, **2**, 1059 (1933).

[6] N. F. Mott, *Trans. Faraday Soc.*, **43**, 429 (1947).

[7] N. F. Mott, *J. Chem. Phys.*, **44**, 172 (1947).

[8] N. Cabrera, *Phil. Mag.*, **40**, 175 (1949).

[9] N. Cabrera and N. F. Mott, *Reports Progr. Phys.*, **12**, 163 (1949).

In the present work, a correlation is made between the thickness of the film (δ) and the cell voltage (U) at time (t) starting from Mott and Cabrera's equation (1). The experimental results obtained during anodic oxidation of Si-n and Si-p electrodes were in good agreement with this theoretical equation.

THEORETICAL CONSIDERATIONS

Equation (1) shows that an increase of the film thickness at constant current density, assumes an increase of the potential difference so that ratio $\Delta\varphi/\delta$ is constant.

If we assume that the ionic current density is used in the film growing process (no corrosion of the silicon) it follows :

$$\mathrm{d}\,\delta/\mathrm{d}t = (M/zFs)i \tag{2}$$

where z represents the number of Faradays (F) consumed when one mole of oxide is formed, and s is the density of the oxide film.

If E is the strength of the electric field, with constant value during the film growth, under galvanostatic conditions we have :

$$\mathrm{d}(\Delta\varphi)/\mathrm{d}t = E(\mathrm{d}\,\delta/\mathrm{d}t) = (M/zFs)Ei \tag{3}$$

Equation 3 shows a linear dependence between $\Delta\varphi$ and t and a proportional slope of the curve to the product Ei.

However to a great increase of i (tenfold) it corresponds but an insignificant increase of E (10%).

Consequently, in a first approximation the slope of straight lines representing the dependence of the potential drop through the growing oxide film and time is proportional to the current density if the anodic oxidation proceeds under galvanostatic conditions.

On the other hand, the ohmic drop ($\Delta\varphi_{\mathrm{sol}}$) of solution (between Si and Pt electrodes) has a low and constant value in comparison with the ohmic drop of the oxide film at over 200 Å. In such conditions there is a linear dependence between cell voltage and time $U(t) \approx \Delta\varphi\ (t)$ excepting the beginning of the oxidation process when the mass transfer through the film is not determining step of the reaction rate. So we can write :

$$\mathrm{d}U\,(t)/\mathrm{d}t \approx \mathrm{d}\,(\Delta\varphi\,(t))/\mathrm{d}t = \lambda i \tag{4}$$

where :

$$\lambda = (M/zFs)\,E \tag{4'}$$

If R_{current} is the current efficiency of the electrolytic process, we can replace i by $R_{\mathrm{current}}\,(I/S)$, where I is the intensity of applied current and S is the area of the Si electrode.

We have then :

$$\mathrm{d}U\,(t)/\mathrm{d}t \approx \lambda^*\, I \tag{5}$$

$$\lambda^* = R_{\text{current}}\,(M/zFsS)\,E \tag{5'}$$

Replacing in eq. (5′) the value of E by expression

$$\Delta\varphi\,(t)/\,\delta\,(t) = (U\,(t) - \Delta\varphi_{\text{sol}})/\,\delta(t) \approx U(t)/\,\delta\,(t)$$

we obtain :

$$\delta\,(t) = R_{\text{current}}\,(M/zFsS\;\lambda^*)\,U\,(t) \tag{6}$$

Consequently the film thickness at the time t is (in a first approximation) proportional to the cell voltage at time t.

Eq. (6) can be verified by optical (interferometric) or electrical (capacity) methods which give directly the thickness of the oxide films.

Rearranging eq. (6) we obtain the following relationship :

$$\delta\,(t_1)/\,U(t_1) \approx \delta\,(t_2)/\,U\,(t_2) \approx \ldots\; R_{\text{current}}\,(M/zFsS\lambda^*) \tag{7}$$

which is equivalent with analytical expression :

$$\delta\,(t) \approx \text{Const.}\;U\,(t) \tag{7'}$$

Utilizing eq. (7′) we may calculate the final voltage in order to obtain an oxide film of a given thickness. Of course, the constant in this equation depends on the experimental conditions.

From the physical point of view the constant in eq. (7′) is the reciprocal of the strength of electric field E. This means that E can be obtained from experimental data.

If E is known, it is possible to get the current efficiency from the relationship :

$$R_{\text{current}} \approx zFsS\lambda^*/ME \tag{8}$$

because λ^* is obtained from the experimental curve $U = U\,(t)$.

These relations are valid for values of polarizing voltage lower than breakdown potential i.e. under 450 V.

RESULTS AND DISCUSSIONS

In order to check the above equations numerous anodic oxidations experiments of Si-n and Si-p electrodes, were carried out in ethylene glycol

$+ 0.04$ N KNO_3 solutions. The electrical arrangement of electrodes polarization is shown in figure 1.

Some experimental results obtained are presented in Fig. 2 and figure 3.

Figure 2 shows the time dependence of anodic potential of Si-p (1.13 cm^2 area) for given values of electrolytic current. One can observe a linear dependence of the curves and the slope are proportional to the values of the anodic oxidation currents. This behaviour is in agreement with equation (5) and (5′). The same results were obtained for Si-n.

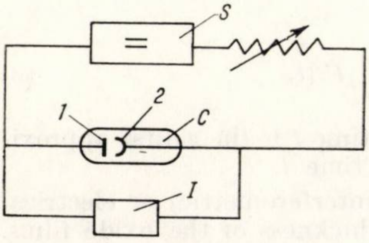

Fig. 1. — Experimental circuit: S — power supply 500 V/240 mA; I — recorder; C — electrolytic cell; 1 — silicon electrode; 2 — platinum electrode.

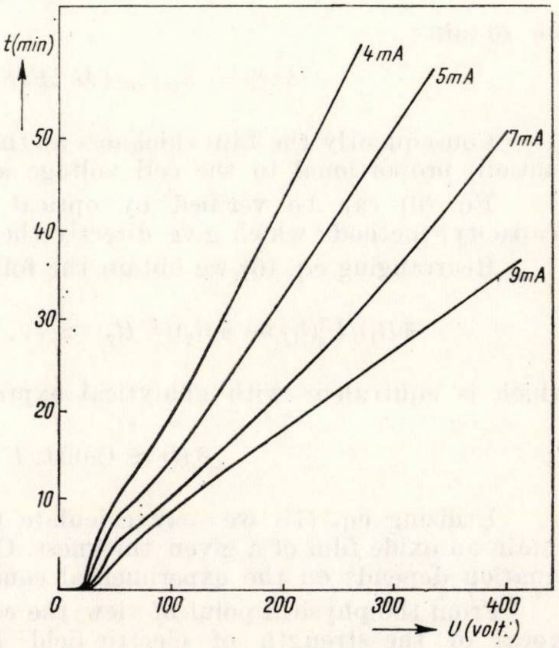

Fig. 2. — Dependence of $U = U(t)$ curve on the intensity of oxidation current for Si-p.

Therefore one can obtain controllable growths of the oxide films on Si utilizing anodic currents between 4 and 9 mA (1.13 cm^2 area of electrode). The most convenient oxidation current which we found was at 7 mA (low dissipation power and sufficiently short oxidation time).

The electrochemical behaviour of anodic oxide film has been studied by anodic polarization technique. The experiments were carried out in the same solutions and immediately after the formation of the oxide film.

Figure 3 shows anodic polarization curves of Si-n electrodes which were previously oxidized at final voltage: $U_1 = 100$ V; $U_2 = 150$ V; $U_3 = 200$ V; $U_4 = 250$ V; $U_5 = 300$ V; $U_6 = 440$ V. Abscissa represents the voltage of Si electrode against calomel electrode (i.e. the potential drop through the film), and the ordinate represents the current in μA.

The dependences $I = I(\Delta\varphi)$ are exponentials according to Mott-Cabrera's equation (1). This equation shows that for $i = R_{\text{current}} I/S =$

constant, we may get the following ratios :

$$\Delta\varphi_1/\delta_1 \simeq \Delta\varphi_2/\delta_2 \simeq \ldots \simeq \Delta\varphi_6/\delta_6$$

If it is assumed that equation (7′) were reliable, the thickness of oxide films would be proportional to final voltage of 6 electrodes :

$$\Delta\varphi_1/U_1 \simeq \Delta\varphi_2/U_2 \simeq \ldots \approx \Delta\varphi_6/U_6 \qquad (I = \text{const.})$$

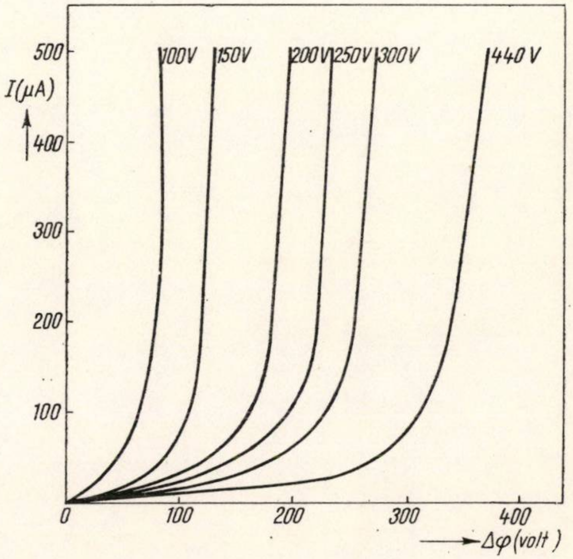

Fig. 3. — Polarization curves for 6 Si-n electrodes, oxidized at $U_1 = 100$ V; $U_2 = 150$ V; $U_3 = 200$ V; $U_4 = 250$ V; $U_5 = 300$ V; $U_6 = 440$ V.

Figure 2 shows that the condition is satisfied in a first approximation, and this represents an additional experimental proof of the reliability of the equations derived in the first part of this paper.

Revue Roumaine de Chimie, 17, *1*, *2*, 253–257 (1972)

17–C. 3101

Revue Roumaine de Chimie, 17, 1, 2, 259 – 265 (1972)

Herrn Professor I. G. MURGULESCU
zum 70. Geburtstag

ÜBER α-DIOXIMINKOMPLEXE DER ÜBERGANGSMETALLE. XXXV

KOBALT (III)-bis-DIMETHYLGLYOXIMIN-CHELATE MIT *cis*-GEOMETRISCHER KONFIGURATION

RALUCA RIPAN und CS. VÁRHELYI
vom Lehrstuhl für Anorganische Chemie der Babeş-Bolyai-Universität, Cluj,
Str. Arany János, 11.

Eingegangen am 12. August 1971

Die Oxydation von Kobalt (II)-salz-Lösungen in Gegenwart von Dimethylglyoxim (DH_2) und Äthylendiamin, bzw. *o*-Phenanthrolin führt zur Bildung von einwertigen Komplexkationen mit *cis*-geometrischer Konfiguration $[Co(DH)_2en]^+$ und $[Co(DH)_2(o\text{-}Phen)]^+$. Die analoge Reaktion mit aromatischen *ortho*-Diaminen erfordert Chelate mit *trans*-geometrischer Anordnung : $[Co(DH)_2(Amin)_2]^+$. Die Komplexanionen : $[Co(DH)_2CO_3]^-$ und $[Co(DH)_2(C_2O_4)]^-$ entstehen durch Substitutionsreaktionen aus $[Co(CO_3)_3]^{3-}$. Die Zusammensetzung der obenerwähnten Chelate wurde durch eine Reihe von doppelten Umsetzungsreaktionen bestätigt.

Die Kobalt (III)-bis-dimethylglyoximin-Chelate vom Typ : $Co(DH)]_2AB]$ mit zwei einzähnigen Liganden können je nach der gegenseitigen Stellung der A- und B-Liganden, in zwei geometrisch isomeren Modifikationen : *cis* und *trans*, auftreten.

Wie aus UV- und IR-spektroskopischen Untersuchungen hervorgeht, gehören die meisten, bis heute erhaltene Verbindungen von dieser Klasse zu der *trans*-Reihe. Die zwei sehr kurzen, in diesen Verbindungen auftretenden O—H.. O Wasserstoffbindungen stabilisieren die planare $Co(DH)_2$-Gruppe, bzw. die *trans*-$[Co(DH)_2AB]$-Komplexe. [1–3] Die für das Zerlegen der O—H..O Brücken nötige erhebliche Bindungsenergie erschwert die *trans-cis* geometrische Umlagerung und deshalb sind die *trans*-$Co(DH)_2AB$-Chelate für die Untersuchung der Kinetik von vielen Substitutionsreaktionen sehr geeignet. Die Ligandenaustauschreaktionen mit einzähnigen Liganden verlaufen nur entlang der A-Co-B Axen und, im Gegensatz zu den $[Co(en)_2XA]^{2+}$-Komplexen,[4,5] *trans-cis* geometrische

---

[1] A. NAKAHARA, *Bull. Chem. Soc. Japan*, **28**, 473 (1955).

[2] R. RIPAN, CS. VÁRHELYI und E. HAMBURG, *Studii şi Cercetări Chim. Fil. Cluj*, **14**, 227 (1963).

[3] R. RIPAN, CS. VÀRHELYI und E. HAMBURG, *Stud. Univ. Babeş-Bolyai, Chem.* **9**, (2), 33 (1964).

[4] M. L. TOBE, *J. Chem. Soc.*, **1959**, 3776.

[5] J. BAILAR und L. B. CLAPP, *J. Amer. Chem. Soc.*, **67**, 171 (1945).

Umwandlungen komplizieren die Substitutionsvorgänge nicht. Die erhebliche Stabilität der koplanaren $Co(DH)_2$-Atomgruppe ermöglichte für Ablov und Mitarbeiter[6,7] die Erörterung des *trans*-Effektes im Falle der Substitutionsreaktionen der oktaedrischen Kobalt (III)-Komplexe.

Die erste Verbindung mit nicht koplanar angeordneten Dimethylglyoximin-Resten ist [8] das Nichtelektrolyt : $[Co(DH)_3]$ mit dem $[Co(en)_3]^{3+}$ ähnlicher asymmetrischer Struktur. Ablov und Mitarbeiter [9,10] behauptet, daß bei der Einwirkung von konz. KOH auf $[Co(DH)_2(H_2O)Cl]$, bzw. auf $[Co(DH)_2(H_2O)NO_2]$ eine *cis*-Dihydroxo-Verbindung: $K[Co(DH)_2(OH)_2]$ entsteht. Diese Verbindung dient nach ihrer Meinung als Ausgangssubstanz für die Herstellung von *cis*-$[Co(DH)_2AB]$.

Zur Bestätigung der *cis*- Konfiguration der $[Co(DH)_2AB]$-Komplexe berufen sich diese Verfasser auf die Ähnlichkeit der UV-Spektren der $[Co(DH)_3]$ und einiger $[Co(DH)_2AB]$. Für die planare geometrische Anordnung der $Co(DH)_2$-Gruppe, bzw. für die *trans* -$Co(DH)_2AB$ charakteristische UV-Bande bei 250 nm erscheint beim $[Co(DH)_3]$ und bei einigen „*cis*"-Hydroxo-Verbindungen um 260–270 nm. Ablov und Mitarbeiter lassen aber außer Betracht, daß diese Hydroxo-Verbindungen in alkalischem Medium entstehen, wo parallel auch Deprotonierungsreaktionen : $[Co(DH)_2AB]^- = [Co(D_2H)AB]^{2-} + H^+$ stattfinden. In Folge dieser Reaktion verschiebt sich die UV Absorptionsbande von 250 nm nach 260–270 nm. Bis-dimethylglyoximin-kobalt(III)-Chelate mit *cis* geometrischer Konfiguration entstehen wahrscheinlich in Anwesenheit von zweizähnigen Liganden, wie Diamine (Äthylendiamin, Propylendiamin, α, α'-Dipyridyl, *o*-Phenanthrolin, Kohlensäure, Oxalsäure Malonsäure, usw.) und α-Aminosäure, wie Glycocoll, Alanin.

Einige Derivate aus dieser Klasse wurden von Ablov und Mitarbeiter [11,12] aus $[Co(DH)_2(H_2O)_2]NO_3$ erhalten.

In dieser Arbeit haben wir die Oxydation von Kobalt(II)-salz-Lösungen in Gegenwart von Dimethylglyoxim und von einigen zweizähnigen Liganden, wir *o*-Phenylendiamin, Äthylendiamin und *ortho*-Phenanthrolin untersucht. Diese Amine treten leicht in die innere Koordinationssphäre der Kobalt (III)-dioximine.

Das aromatische *o*-Phenylendiamin besetzt nur eine Koordinationsstelle und bildet das $[Co(DH)_2(o\text{-Phenylendiamin})_2]^+$ mit *trans* geometrischer Anordnung. Die Gewinnung von 5 neuen Komplexsalzen bestätigt die von Nakatsuka und Iinuma [13] angegebene Formel.

---

[6] A. V. Ablov, *Doklady Akad. Nauk. S.S.S.R.*, **97**, 1010 (1954).

[7] A. V. Ablov, N. M. Samush und M. S. Popov, *Doklady Akad. Nauk. S.S.S.R.*, **106**, 665 (1956).

[8] A. Nakahara und R. Tschuchida, *J. Amer. Chem. Soc.*, **76**, 3103 (1954).

[9] A. V. Ablov und N. M. Samush, *Doklady Akad. Nauk. S.S.S.R.*, **113**, 1265 (1957).

[10] A. V. Ablov, M. P. Filippov und N. M. Samush, *Doklady Akad. Nauk. S.S.S.R.*, **133**, 575 (1960).

[11] A. V. Ablov, N. M. Samush und O. A. Bologa, *Zhur. neorg. Khim.*, **8**, 860 (1963).

[12] A. V. Ablov, O. A. Bologa und N. M. Samush, *Zhur. neorg. Khim.*, **11**, 2632 (1966).

[13] Y. Nakatsuka und H. Iinuma, *Bull. Chem. Soc. Japan*, **11**, 48 (1936).

Tabelle 1

Neue Derivate von $[Co(DH)_2$ (*o*-Phenylendiamin)$_2]$ X [a]

Formel	Ausgangssubstanzen	Ausb. (%)	Charakteristik	*Analyse* *ber. gef.*
A. Pikrat	20 ml „A" 50 ml 1% Pikrinsäure	75	Gelbbraune mikrokrist. Masse	Co 8,03 7,90 N 17,18 17,40
A. $[Cr(NH_3)_2(HCS)_4]$. . 2 H_2O	20 ml "A" +100 ml 1% Reineckesalz	50	Braune mikrokrist. Masse	S 14,91 14,54 $1/3Co_3O_4+1/2Cr_2O_3$ 18,17 18,15
A. [Cr.(Anilin)$_2$ – –(NCS)$_4$]	20 ml "A" + lg NH_4[Cr-(Anilin)$_2$NCS)$_4$] in 30 ml Metanol (1 : 1)	50	Braune mikrokrist. Masse	S 13,14 12,87 $1/3\ Co_3O_4+1/2Cr_2O_3$ 16,01 16,28
A. [Cr(*p*-Toluidin)$_2$– – (NCS)$_4$]	Analogerweise	60	Rotbraune, mikrokrist. Masse	S 12,77 12,58 $1/3\ Co_3O_4+1/2Cr_2O_3$
$A_3[Cr(NCS)_6]$	20 ml "A" +lg$K_3[Cr(NCS)_6]$ in 100 ml. W.	75	Braune mikrokrist. Masse	S 10,03 10,14 N 17,54 17,33

[a] "A" = $[Co(DH)_2$ (*o*-Phenylendiamin)$_2]^+$

In Anwesenheit von Äthylendiamin und *o*-Phenanthrolin erhielten wir aber tricyclische Chelate mit der Zusammensetzung : $[Co(DH)_2(en)]^+$ und $[Co\,(DH)_2$(*o*-Phenanthrolin)$]^+$. Diese leichtlösliche Chelate können aus der Lösung durch doppelte Umsetzungsreaktionen mit voluminösen Komplexanionen ausgeschieden werden.

Durch Einwirkung von Dimethylglyoxim auf $Na_3[Co(CO_3)_3]$ erhielten wir durch eine Substitutionsreaktion das $[Co(DH)_2\,CO_3]^-$.

$$Na_3[Co(CO_3)_3]+2\ DH_2=Na[Co(DH)_2CO_3]+Na_2CO_3+H_2O+CO_2$$

Aus der wäßrigen-alkoholischen Lösung des Natriumsalzes erhielten wir eine Reihe wohl kristallisierender Produkte vom Typ : $[Co(DH)_2(Amin)_2]\ [Co(DH)_2CO_3]$. Die Charakterisierung dieser binären Salze ist in der Tabelle 3 wiedergegeben.

Das Carbonatsalz : $Na[Co(DH)_2CO_3]$ zersetzt sich bei niedrigeren pH-Werten, analogerweise mit den wohlbekannten $[Co(NH_3)_4CO_3]$ X und $[Co(en)_2CO_3]$X. Beim Erwärmen mit Oxalsäurelösung entstehen — zum Beispiel — $[Co(NH_3)_4C_2O_4]$ X und $[Co(en)_2C_2O_4]$X aus den letzten Verbindungen.

Tabelle 2[a]

Neue Derivate von $[Co(DH)_2\ en]\ X$ (B) und $[Co(DH)_2\ (o\text{-}Phen)]\ X$ (C)

Formel	Ausgangssubsstanzen	Ausb. (%)	Charakteristik	*Analyse*		
					ber.	*gef.*
B. Piktra	20 ml "B" + 75 ml 1% Pikrinsäure	50	Gelbbraune Prismen	Co	10,21	10,34
C. Pikrat	Analogerweise	80	Braune mikrokrist. Masse	Co N	8,40 17,96	8,33 18,10
B. $[Cr(NH_3)_2(NCS)_4]$	20 ml "B" 100 ml 1% Reineckesalz	60	Rotbraune mikrokrist. Masse	S $1/3\ Co_3O_4+1/2Cr_2O_3$	19,21 23,41	19,40 23,60
C. $[Cr(NH_3)_2(NCS)_4]\cdot 2\,H_2O$	Analogerweise	60	Rotbraune mikrokrist. Masse	S N	15,88 20,80	16,00 20,62
B. $[Cr(Anilin)_2-(NCS)_4]$	20 ml "B" + 100 ml 1% $NH_4[Cr(Anilin)_2-(NSC)_4$ [in verd. Methanol (1 : 1)	50	Rotbraune mikrokrist. Masse	S $1/3\ Co_3O_4+1/2Cr_2O_3$	15,64 19,06	15,70 19,23
C. $[Cr(Anilin)_2-(NCS)_4]$	Analogerweise	70	Rotbraune, lange Nadeln	S N	13,59 17,80	13,17 17,65
B. $[Cr(p\text{-}Toluidin)_2-(NSC_4)]$	Analogerweise	60	Rotbraune Prismen	S $1/3\ Co_3O_4+1/2Cr_2O_3$	15,12 18,43	15,27 18,31
C. $[Cr(p\text{-}Toluidin)_2-(NCS)_4]$	Analogerweise	77	Rotbraune Tafeln	S N	13,20 17,28	13,06 17,20
$B_3.[Cr.(NCS)_6]$	20 ml "B" +1 g $K_3[Cr(NCS)_6]$ in 50 ml. W	70	Braune mikrokrist. Masse	S N	13,28 23,22	13,44 22,97
$C_3.Cr(NCS)_6]$	Analogerweise	70	Braune mikrokrist. Masse	S N	10,61 18,53	10,29 18,27

[a] "B" = $[Co\ (DH)_2\ en]^+$, "C" = $[Co(DH)_2\ (o-Ph)en)]^+$

Im Falle des $Na[Co(DH)_2CO_3]$ führt die Reaktion mit Oxalsäure zur Bildung von $Na[Co(DH)_2C_2O_4]$:

$$Na[Co(DH)_2CO_3]+H_2C_2O_4=Na[Co(DH)_2C_2O_4] + CO_2 + H_2O$$

Dieses Oxalato-dimethylglyoximino-kobaltiat ist auch leicht löslich in wässriger-alkoholischer Lösung.

Durch doppelte Umsetzungsreaktionen könnten wir aber einige binäre Salze vom Typ : $[Co(DH)_2\ (Amin)_2]\ [CO(DH)_2C_2O_4]$ isolieren und charakterisieren.

Tabelle 3 [a]

Derivate von Typ : $[Co(DH)_2(Amin)_2]\,[Co(DH)_2CO_3]$

Formel	Ausgangssubstanzen	Ausb. (%)	Charakteristik	*Analyse*		
					ber.	*gef.*
$[Co(DH)_2(Pyridin)_2]$. D	5 mMol $Na[Co(DH)_2-CO_3]$ 50 ml W+5 mMol $[Co(DH)_2Py_2]$-acetat/50ml	20	Kleine braune Prismen	Co N	14,79 17,59	14,53 17,66
$[Co(DH)_2(\beta$-Picolin$)_2]$. D	Analogerweise	10	Braune Tafeln	Co N	14,30 16,99	14,39 17,20
$[Co(DH)_2(Anilin)_2]\cdot D$	Analogerweise	15	Braune Nadeln	Co	14,30	14,47
$[Co(DH)_2$(p-Chloranilin$)_2]$.D.$2H_2O$	Analogerweise	22	Braune mikrokrist. Masse	Co H_2O N	12,68 3,87 15,07	12,67 4,50 15,20
$[Co(DH)_2$(*p*-Bromanilin$)_2]$.D	Analogerweise	18	Braune mikrokrist. Masse	Co N	12,17 14,25	12,10 14,10

[a] "D" = $[Co(DH)_2CO_3]^-$

Tabelle 4 [a]

Derivate von Typ $[Co(DH)_2(Amin)_2]\,[Co(DH)_2\,C_2O_4]$.

Formel	Ausgangssubstanzen	Ausb. (%)	Charakteristik	*Analyse*		
					ber.	*gef.*
$[Co(DH)_2(Pyridin)_2]\cdot E$	10 mMol $Na[Co(DH)_2C_2O_4]$ in 15 ml W+5 mMol $[Co(DH)_2Py_2]$ acetat/50 ml	25	Braune Prismen	Co N	14,30 16,99	14,15 16,60
$[Co(DH)_2(\beta$-Picolin$)_2]\cdot E$	Analogerweise	20	Braune krist. Masse	Co	13,83	13,60
$[Co(DH)_2(Abilin)_2]\cdot E$	Analogerweise	25	Braune Prismen	Co N	13,83 16,43	13,65 16,19
$[Co(DH)_2$(*p*-Br-Anilin$)_2]$. E	Analogerweise	30	Braune mikrokrist. Masse	Co N	11,66 13,86	11,51 13,43

[a] "E" = $[Co(DH)_2C_2O_4]^-$

Diese präparative Arbeit bestätigt die Zusammensetzung der $[Co(DH)_2\ en]^+$, $[Co(DH)_2\ (o\text{-Phenanthrolin})]^+$, $[Co(DH)_2CO_3]^-$ und $[Co(DH)_2C_2O_4]^-$.

Alle zweizähnigen Liganden können wegen sterischer Hinderung in diesen Chelaten nur vicinale, *cis*-Stellungen in den oktaedrischen Kobalt(III)-komplexen besetzen. Sowohl in der Molekülstruktur der obenerwähnten *cis*-Chelate, als auch in jener des $[Co(DH)_3]$ fehlen die starken, intramolekularen O-H .. O-Wasserstoffbrückenbindungen. Diese Erscheinung könnte man sehr leicht durch IR-spektroskopische Untersuchungen beweisen. Es ist uns bis jetzt nicht gelungen Derivate der obenerwähnten *cis*-Chelate mit einfachen Ionen (K, Na, Cl, J) zu erhalten, welche für IR-spektroskopische Messungen nötig sind.

EXPERIMENTELLER TEIL.

$[Co(DH)_2$ (o-Phenylendiamin)$_2]$ acetat, $[Co(DH)_2$ (en)$]$ acetat- und $[Co(DH)_2$ (o-Phenanthrolin)$]$ acetat-Lösungen

40 mMol Dimethylglyoxim und 20 mMol *o*-Phenanthrolin, Äthylendiamin, bzw. 25—30 mMol *o*-Phenylendiamin in 100 ml Äthahol werden mit 20 mMol $Co(CH_3-COO)_2 . 4\ H_2O$ in 25 ml Wasser gemischt. Die Mischung beider Lösungen wird mit einem starken Luftstrom 4—5 Stunden oxydiert. Die braunen Flüssigkeiten werden abfiltriert und für doppelte Umsetzungsreaktionen verwendet.

Je 10 ml von diesen Stammlösungen enthalten :

"A" 2 mMol $[Co(DH)_2$ (*o*-Phenylendiamin)$_2]$ acetat

"B" 2 mMol $[Co(DH)_2\ en]$ acetat

"C" 2 mMol $[Co(DH)_2$ (*o*-Phen)$]$ acetat

$Na[Co(DH)_2CO_3]$-Lösung : 50 mMol $CoCl_2$ werden mit Perhydrol in Gegenwart von überschüssigem $NaHCO_3$ oxydiert und das gebildete $Na_3[Co(CO_3)_3]$ mit 10 mMol Dimetylglyoxim in 500 ml heißem Äthanol behandelt. Es entsteht eine braune Lösung unter Kohlendioxidentwicklung. Nach Filtrierung wird die Stammlösung zu doppelten Umsetzungsreaktionen verwendet. 50 ml Lösung enthalten : 5 mMol Na $[Co(DH)_2CO_3]$.

$Na[Co(DH)_2C_2O_4]$-Lösung : 100 mMol $Na[Co(DH)_2CO_3]$ in 150 ml Wasser werden mit 100 mMol Oxalsäure unter Erwärmen auf dem Wasserbade behandelt. Nach Aufhören der Kohlensäureentwicklung wird die Lösung abgekühlt und zur doppelten Umsetzungsreaktionen verwendet. Je 15 ml aus dieser Stammlösung enthalten 10 mMol $Na[Co(DH)_2C_2O_4]$. Es ist bemerkenswert, daß die Wechselwirkung zwischen Dimethylglyoxim und $K_3[Co(C_2O_4)_3] . 3H_2O$ keine Menge von $K[Co(DH)_2C_2O_4]$ erzielt. Wegen der Reduktion des Komplexes fällt rosafarbenes CoC_2O_4 aus.

Für die doppelten Umsetzunsgsreaktionen haben wir $[Co(DH)_2(Amin)_2]$. acetat- Lösungen (mit Amin = Pyridin, Picolin, Alkyl-Aniline, usw.) [14—16] Picrinsäure, $NH_4[Cr(NH_3)_2(NCS)_4]$,

---

[14] R. Ripan, Cs. Várhelyi und B. Böhm, *Stud. Univ. Babeş-Bolyai, Chem.*, **7**, (1), 77 (1962).

[15] R. Ripan, Cs. Várhelyi und B. Böhm, *Studii şi Cercetări Chim. Fil. Cluj*, **13** (2), 145 (1962).

[16] R. Ripan, Cs. Várheryi und J. Urmösi, *Z. anorg. Chem.*, **332**, 95 (1964).

$K_3[Cr(NCS)_6]$ und Amin.$H[Cr(Amin)_2-(NCS)_4]$ in wässriger, oder verd. alkoholischer Lösung verwendet.

Analyse. Der Kobaltgehalt der Proben wurde volumetrisch mit Komplexon III in Anwesenheit von Murexid bestimmt. Die organischen Bestandteile wurden vorher mit konz. H_2SO_4 und etwas KNO_3 zerstört. Nach dem Aufschluß wurden die Proben verdünnt und mit Natriumacetat und Ammoniaklösung neutralisiert. Die Stickstoffgehalt wurde nach Dumas ermittelt. Die Summe : $Co_3O_4 + Cr_2O_3$ durch glühen bei 900°, und der Schwefelgehalt als $BaSO_4$ bestimmt.

Die $[Co(DH)_2(Amin)_2]$ $[Co(DH)_2CO_3]$ und $[Co(DH)_2(Amin)_2]$ $[Co(DH)_2C_2O_4]$ Verbindungen sind schwer löslich im Wasser und in höheren aliphatischen Alkoholen, sie lösen sich leicht in Pyridin, Aceton und Methyl-äthylketon.

Revue Roumaine de Chimie, 17, 1, 2, 267 – 271 (1972)

Dedicated to Professor I.G. MURGULESCU
on his 70th birthday

COMPILATIONS OF DATA FOR CHEMICAL THERMODYNAMICS *

FREDERICK D. ROSSINI

Department of Chemistry, Rice University, Houston, Texas 77001, U.S.A.

Received September 4, 1971

This is a brief summary report on the status of compilations of data for thermodynamics, with a short statement about CODATA in this connection.

First, however, let me make a few remarks to indicate the importance of the work in calorimetry and thermodynamics. One of man's greatest capabilities is that of making observations and measurements. Science is based upon observation and measurement. The better and more accurately we can observe and measure, the better and more effectively we can exercise control over the matter and the energy of the world in which we live. The control and development of energy have accompanied almost every significant advance in science and technology. Records indicate that the technological advancement of a country goes hand in hand with its production and consumption of energy. Thermodynamics is the science that is concerned with energy. Therefore, it is important that we have a good understanding of thermodynamics if we are to advance man's condition in the world.

To me, thermodynamics is one of the most interesting and most powerful subjects that can be studied by man. I think we are all fortunate to be working in this field, and I wish each of you much success in your individual observations and measurements in calorimetry and thermodynamics.

Now to the matter of compilations of data for chemical thermodynamics. To an audience such as this, and at this stage of our development in science, I think it is unnecessary to justify our need for authoritative compilations of data.

The fact is that a working experimental thermodynamicist would have neither the time nor the inclination to compile all the numerical data he might need. Instead, our present day plan interposes, between the original investigator who created the data and the end investigator who uses the data, a system of review, appraisal, and compilation of the data by qualified experts. Many advantages result from having such funda-

---

*** Taken from a talk presented at the Second International Conference on Calorimetry and Thermodynamics, Orono, Maine, U.S.A., July 13, 1971.**

mental work on thermodynamic tables performed systematically and consistently in a cooperative program by qualified experts, rather than incidentally and sporadically at the time of need by workers in different laboratoiries whose main interests are in other matters.

In addition to the obvious advantage of producing a complete, accurate, and self-consistent set of values of thermodynamic properties, such a cooperative program results in a considerable saving in overall cost, particularly in manpower of high intellectual capacity, which is our most precious resource.

Now let me discuss with you specific compilations of data for chemical thermodynamics. Because of my limited time, I will simply report on those compilations that most workers consider to be the principal ones.

First, I will give a brief historical review. Then I will present the current status of these principal compilation projects as reported to me within the past two months by their respective Directors.

One of the earliest tables of heats of formation of chemical compounds was put together by Julius Thomsen of Denmark, published from 1882 to 1886.

Tabulations of some principal thermodynamic properties came out in the Landolt-Bornstein Tables of Germany, which first appeared in 1883 and have continued ever since, although these tables cover all sorts of physical properties.

Also, some tabulations of miscellaneous thermodynamic data came out in the Annual Tables of France , which first appeared in 1910 and have continued since, although the emphasis has been more on other properties.

In 1923, Lewis and Randall, of the U.S.A., published their tables of the heats and free energies of some chemical substances.

In the years 1926 to 1930 appeared the International Critical Tables of Numerical Data of Physics, Chemistry, and Technology. This was the largest single compilation job in history, and, although its headquarters were in the U.S.A., the seven volumes of 3,500 pages involved the work of 408 scientists from 18 different countries. Included in these tables were many compilations of thermodynamic data, particularly the one on heats of formation in Volume V, by Bichowsky. This was the first really comprehensive, critical, and self-consistent table of heats of formation.

In 1936 appeared the book of Bichowsky and Rossini on the "Thermochemistry of the Chemical Substances". This work revised and extended considerably the compilation which appeared in Volume V of the International Critical Tables.

Meanwhile, over the years 1934 to 1962, appeared the compilations of K. K. Kelley, of the U. S. Bureau of Mines, on the thermodynamic properties of metallurgically important substances.

In 1944, appeared the first tables of thermodynamic properties of hydrocarbons and related compounds of the American Petroleum Institute Research Project 44, under Rossini and later Zwolinski. These loose-leaf tables came out in book form in 1947 with a second volume in 1953. Essentially all thermodynamic properties of hydrocarbons and related compounds are covered in these tables, which constitute the most comprehensive work in this field ever published.

In 1952, appeared the large National Bureau of Standards Circular 500, on Selected Values of Chemical Thermodynamic Properties, by Rossini, Wagman, Evans, Levine and Jaffe. This was a revision and extension of the book of Bichowsky and Rossini.

In 1955 appeared the first of the loose-leaf data sheets on Selected Values of the Thermodynamic Properties of Metals and Alloys, under Hultgren at the University of California-Berkeley.

In 1956, appeared the first of the loose-leaf data sheets of the Manufacturing Chemists Association Research Project under Rossini and Zwolinski, later becoming the Thermodynamics Research Center Data Project, on "Selected Values of Properties of Chemical Compounds".

In 1960, under Stull at the Dow Chemical Company, came the first of the loose-leaf tables of the thermodynamic properties of properties of propellants and related substances, under the JANAF label.

In 1962, in the U.S.S.R., appeared the volume entitled "Thermodynamic Properties of Chemical Substances", by Glushko, Gurvich, Medvedev, and others, on propellants and related substances.

In 1965, in the U.S.S.R., appeared the volume entitled "Thermodynamic Constants of Substances", by Glushko, Medvedev, Gurvich, and others. Three volumes have so far been published. This work parallels that of NBS Circular 500.

So much for the history. Now I would like to give the present status of several of these works that are still going on.

The American Petroleum Institute Research Project 44 is continuing its work in the Thermodynamics Research Center at the Texas A and M University, College Station, Texas, under Zwolinski and coworkers. Also associated with this work is the Thermodynamics Research Center Data Project on chemical substances other than hydrocarbons. These data are issued in losse-leaf form, and, in total, cover over 14,000 sheets, of which about 2,200 relate to thermodynamic properties. Of the sheets containing thermodynamic data, 1,600 are from the API Research Project 44 and 600 are from the Thermodynamics Research Center Data Project. Work on both projects is actively continuing.

At the National Bureau of Standards, work is continuing on the revision of NBS Circular 500 on "Selected Values of Chemical Thermodynamic Properties", under Wagman, Evans and coworkers. So far, NBS Technical Notes 1, 2, 3, 4, and 5 have been published, containing 422 pages of data covering the thermodynamic properties of the first 61 elements, and their compounds, in the standard order of arrangement. Work on an additional 103 pages of data on the six alkaline earth metals and their compounds has been completed and is ready for publication. Work on the 15 lanthanide elements, and their compounds, in the standard order of arrangement, is well along. This makes a total of 82 elements, and their compounds, in the standard order of arrangement, that will have been reported. This work is actively continuing.

The project on "Selected Values of the Thermodynamic Properties of Metals and Alloys", by Hultgren and coworkers at the University of California-Berkeley, continues until June 30, 1972, when Hultgren will retire and the project will be discontinued. The final volume will contain revisions of material previously issued as well as new data. These will be covering 66 elements, on 435 pages, and 222 alloy systems, on 779 pages, making a total of 288 systems on 1,214 pages. The bibliography comprises about 8,800 entries. At the conclusion of the work, the file of references, the search system, and the microfiche collection will be under the custody of Don Stevens of the Atomic Energy Commission.

The JANAF Thermochemical Tables Project at the Dow Chemical Company, Midland, Michigan, under Stull until 1969, now under Prophet, is funded by the U.S. Air Force Office of Scientific Research and support is expected to continue. So far, 34 supplements of tables have been issued, with the total number of species covered now being 1,120. The coverage includes the following elements and certain of their compounds : O, H, F, Cl, Br, I, S, N, ,P, C, Si, Pl, Hg, Cu, Fe, Mo, W, Ti, Zr, B, Al, Be, Mg, Ca, Sr, Ba, Li, Na, K, electron. The compounds covered are normally the oxides, hydroxides, and halides, with emphasis on the smaller species, including ions, likely to exist at hight temperatures. The latest publicly available set of tables is NSRDS-NBS-37 "JANAF Thermochemical Tables", Second Edition, which contains 1,099 species. This work is actively continuing.

The project in the U.S.S.R. on the "Thermodynamic Properties of Chemical Substances" is actively continuing under Glushko, Gurvich, Medvedev, and coworkers, supported by the Academy of Sciences of the U.S.S.R. The compounds selected are those important in propellant and combustion processes. In 1971, the third volume will be started, with work on the thermodynamic properties of about 800 substances from 100K to very high temperatures. Plans for work through 1975 are on the books for this project.

The project in the U.S.S.R. on the "Thermodynamic Constants of Substances" is actively continuing under Glushko, Medvedev, Gurvich, and coworkers, supported by the Academy of Sciences of the U.S.S.R. Four volumes have so far been published in this work, which uses the standard order of arrangement and follows the pattern of NBS Circular 500, including all inorganic compounds and organic compounds with 1 and 2 carbon atoms. The fourth volume contains data on 4,500 substances, in 920 pages with 7,000 references. The fifth volume is in press and will appear in the fall of 1971, covering about 2,500 substances in about 500 pages, with 3,500 references. The sixth volume, in preparation, will go to the printer in the fall of 1971, covering about 2,400 substances, with 8,000 references.

Now for the conclusing part of my report, let me make a few remarks about CODATA and its interest in the data of chemical thermodynamics. CODATA is the acronym invented by Guy Waddington for the Committee on Data for Science and Technology of the International Council of Scientific Unions or ICSU. ICSU is the umbrella for 15 international unions, and, as such, is a good vehicle to obtain accord on certain scientific matters among several scientific unions.

CODATA was established in 1966 by ICSU and was given the following assignments on a world-wide basis : (1) To ascertain what data-compiling work is going on and what the needs are ; (2) To achieve coordination among and provide guidance for data-compiling projects; (3) To encourage support for data-compiling projects by appropriate private, governmental, and intergovernmental agencies; (4) To encourage the use of internationally approved constants, units, and symbols; (5) To produce a compendium-directory-survey of continuing data-compiling projects and related work; (6) To encourage and coordinate research on new forms for preparing and distributing critically evaluated numerical data.

One of the most important tasks of CODATA is producing a world-wide compendium of data-compiling projects. The first edition of this work, which appeared in the fall of 1969, was greatly benefitted by the existence of the similar compendium issued several years earlier by the Office of Critical Tables of the National Research Council, U.S.A., under Guy Waddington. This CODATA Compendium reports on all data-compiling projects throughout the world. It had been planned to have this compendium brought up to date every two years, but it appears that this target will not be met this year. We are hopeful, however, that the second edition of the CODATA Compendium will appear in 1972.

Among the Tasks Groups established by CODATA to carry out certain of its responsibilities are three of interest to this Conference:

1. Task Group on Computer Use. Concerned with coordination and compatibility of programs and equipment.
2. Task Group on Fundamental Constants. Concerned with developing and maintaining a recommended list of fundamental constants for world-wide use.
3. Task Group on Key Values for Thermodynamics. Concerned with developing agreement on values for key substances involved in thermodynamic calculations.

As the then President of CODATA, I had the privilege of appointing the membership of the Task Group on Key Values for Thermodynamics about two years ago. Professor Stig Sunner is the Chairman of this Task Group.

Revue Roumaine de Chimie, **17**, *1*, *2*, 273–284 (1972)

Dedicated to Professor I. G. MURGULESCU
on his 70th birthday

INFRARED SPECTRA OF CARBONYL AROMATIC ION RADICALS. I

CARBONYL STRETCHING FREQUENCY AND FORCE CONSTANT CHANGES DUE TO THE FORMATION OF ANION RADICALS FROM BENZOPHENONE, FLUORENONE, PHENANTHRENEQUINONE AND ANTHRAQUINONE

V. EM. SAHINI and LILIANA CIUREA

University of Bucharest, Laboratory of Physical Chemistry, Bd. Republicii 13,
Bucharest, Romania

Received September 11, 1971

The infrared spectra changes of the above mentioned carbonyl compounds due to the anion radical formation during their reduction with alkali metals are studied. The influence of both, reduction agent and solvent, on the carbonyl stretching frequency is examined. The decrease of the carbonyl frequency in anion radical in comparison with its value in neutral molecule was correlated to the decrease of the carbonyl force constant. The carbonyl force constants were obtained from MO calculations using Coulson and Longuet-Higgins formula, which had been adjusted to the systems with unpaired electrons.

The anion radicals formed the object of abundent research works dealing with their electronic and ESR spectra. In the infrared region the anion radicals were studied to a small extent, and only a few papers appeared recently on this subject in the literature.[1–3] The first study about the infrared spectra of the anion radicals was made by Kacikurova[1] on some aromatic hydrocarbon anions. In the spectra of anion radicals obtained from hydrocarbons, a decrease of all the vibrational band frequencies in comparison with the corresponding frequencies of the hydrocarbon bands was observed. The differences between the hydrocarbon band frequencies and those of the corresponding anions became smaller as the number of aromatic rings increased. This fact was connected to the decrease of the odd electron density on the carbon atoms.

The existence of a relation between the odd electron density ρ on different atom groups and the shifts of the group frequencies $\Delta\nu$ due to the ionization was also found by Eargle and Cox[2,3] in the case of some aromatic hydrocarbons, ketones and compounds containing a nitrile or sulfone group. Based on the relations between ρ and $\Delta\nu$, established by these authors, knowing the $\Delta\nu$ values of IR spectra, the spin densities on different functional groups could be estimated and compared to the results obtained from the ESR spectra. As proportional constant between ρ and $\Delta\nu$ for certain functional groups one has considered the half average frequency shift which had been observed for some compounds where the bond multiplicity in neutral molecules decreased with one unit. For instance, for the carbonyl group, the $\Delta\nu$ shift of the carbonyl frequency passing from the neutral molecule to the anion is $\rho \cdot 500/2$, where ρ is the odd electron density on carbonyl, and 500 represents the average shift observed in some compounds where a modification from a double bond structure to a single bond between carbon and oxygen atoms took place.

---

[1] I. IA. KACIKUROVA, *Doklady Akad. Nauk, S.S.S.R.*, **163**, 1198 (1965); *Teor. Eksp. Khim.*, **3**, 498 (1967).

[2] D. H. EARGLE, JR. and E. W. COX, *Chem. Soc.*, Spec. Publ. No. 22, 117 (1967).

[3] D. H. EARGLE, Jr., *J. Chem. Soc. (B)*, **8**, 1556 (1970).

The present work gives the infrared spectra of anion radicals obtained from benzophenone, fluorenone, phenanthrenequinone and anthraquinone, studying the way in which the existence of the odd electron influences the vibration spectrum of the molecule, especially the position of the carbonyl vibration band, the most characteristic band of the infrared spectra of the carbonyl compounds. The change of the carbonyl electronic density through the introduction into the system of an additional electron leads to the decrease of the double bond character and implicitly of the carbonyl force constant. This was verified by the carbonyl force constants calculated by the MO method for the neutral molecule and for its anion.

EXPERIMENTAL

The studied anion radicals (metal ketyls) were prepared by the reduction of ketones or quinones with alkali metals (Li, Na or K) in an inert atmosphere using tetrahydrofuran (THF), 1,2-dimethoxyethane (DME) and dimethylformamide (DMF) as solvents. The substances were purified by repeated recrystallization or sublimation and the solvents were purified by refluxing and fractional distillation over Na or P_2O_5.

The infrared spectra were recorded with a Unicam SP 100 spectrophotometer in the $375-2150$ cm^{-1} range using an air-tight NaCl cell ($0.05-1$ mm path length) to prevent the decomposition of the solution in contact with the atmosphere. The concentration range used was $10^{-3}-10^{-1}$ M/l. The spectra of ketone or quinone were recorded first, before adding the reduction agent, then at the different reduction times till complete reduction was achieved and finally the decomposed solution. Compared to the electronic and ESR spectroscopy, in the infrared region we had to use the higher concentrations of the anion radicals to make its bands detectable in the spectra. In the case of metal ketyls a concentration-dependent equilibrium generally exists in solution between the monomeric radical ions and the dimer species. It was therefore not possible, in some cases, to detect in the IR spectra of anion radicals, the monomeric species, but only the dimeric ones (for example in the case of phenanthrenequinone in ethereal solvents). The IR spectra of anthraquinone anions in DME and THF could not be recorded, on the one hand due to the low solubility of anthraquinone in these solvents, a fact entailing the low concentration of the anion, and on the other hand, to the low solubility even of the anion forming in these solvents. The anion solubility increases if sodium tetraphenyl boride is added, but the carbonyl band can be only obtained as an inflexion.

RESULTS AND DISCUSSIONS

The characteristic bands of the anions were easily recognized in the infrared spectra of the ketone or quinone solutions after the new bands which appeared in the spectrum subsequent to addition to the reduction agent. The intensity of these bands increased gradually as the reduction time rose and they disappeared when the solutions came in contact with air. In figures 1—5 are given some of the infrared spectra of alkali-metal reduced compounds obtained from benzophenone, fluorenone and phenanthrenequinone as also the spectra of initial and decomposed compounds.

In most cases the spectra of partially reduced ketone or quinone have been recorded, as may be seen in the spectra by the presence of the unreduced carbonyl compound band. After completion of the reduction reaction this band disappeared (see spectrum d of figure 1). In the presented spectra the corresponding bands of the anions are denoted by an asterix. To establish the position of all anion bands we had to record the spectra in different solvents, with different absorption regions, so that the regions in which they can be used should complete one another. Unfortunately there are few solvents in which the studied anions are soluble. The IR anion bands in the 1000—1400 cm^{-1} region, could not be detected because the three solvents used present strong absorption bands in this region. Figures 2 and 3 show spectra of benzophenone anions in DME and DMF in the regions where these solvents have no strong peaks. The new bands appearing in the spectra of alkali-metal reduced benzophenone, and which belong to its anion are : 611, 628, 693, 750, 858, 889, 995, 1400 and 1560 cm^{-1} . In the presence of an excess of alkali metal the spectrum in figure 2c was obtained, different from the one in figure 2b. In this case the colour of the solution also changed from blue to red, indicating the formation of the dianion.[4]

The new bands appearing in the infrared spectra of the reduced fluorenone which were assigned to the corresponding anion are : 628, 644, 726, 770, 782, 1410, 1542, 1558 and 1587 cm^{-1}. Through the decomposition of the fluorenone anion the initial fluorenone is restored (see figure 4).

The bands corresponding to reduced phenanthrenequinone in the region under study are : 756, 1400, 1532, 1570 and 1606 $\mathrm{cm.}^{-1}$ In this case, in the concentration range of recorded spectra, the equilibrium existing in solution between anion (the "red" species) and dimer (the "green" species) is shifted toward the dimer as shown by electronic[5] and ESR [6] spectra. Electronic and ESR spectra studies of the alkali metal reduction products of the phenanthrenequinone and anthraquinone have shown the possible formation in solution of a larger number of reduction i.e. forms : anion radicals, dimers, dianions [5-7] and trianion radicals. [8,9]

---

[4] H. V. Carter, B. J. McClelland and E. Warhurst, *Trans. Faraday Soc.*, **56**, 455 (1960).

[5] T. L. Staples and M. Szwarc, *J. Amer. Chem. Soc.*, **92**, 5022 (1970).

[6] K. Maruyama, *Bull. Chem. Soc. Japan*, **37**, 553 (1964).

[7] V. E. Sahini and L. Ciurea, *Rev. Roumaine Chim.*, **14**, 1093 (1969).

[8] N. L. Bauld, *J. Amer. Chem. Soc.*, **86**, 3894 (1964).

[9] T. E. Gough, *Trans. Faraday Soc.*, **66**, 2420 (1970).

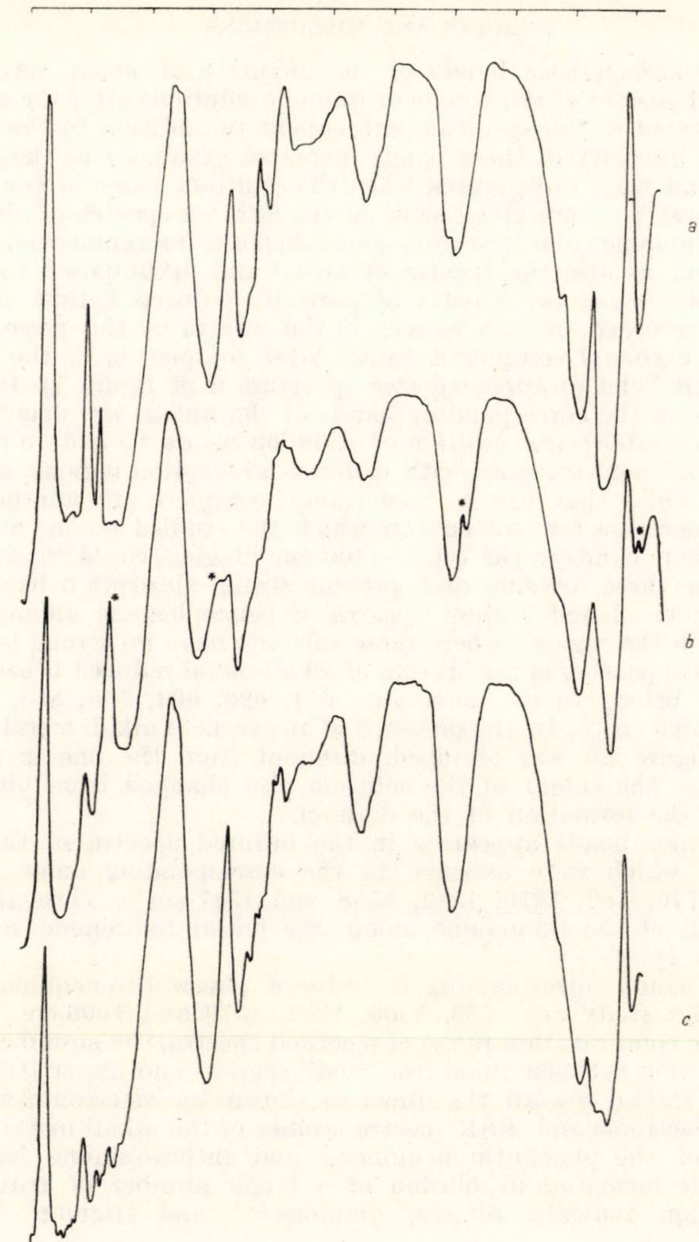

Fig. 1. — IR spectra of :
a, benzophenone in THF ; *b*, partially reduced benzophenone with Li in THF ; *c*, partially decomposed sample ;

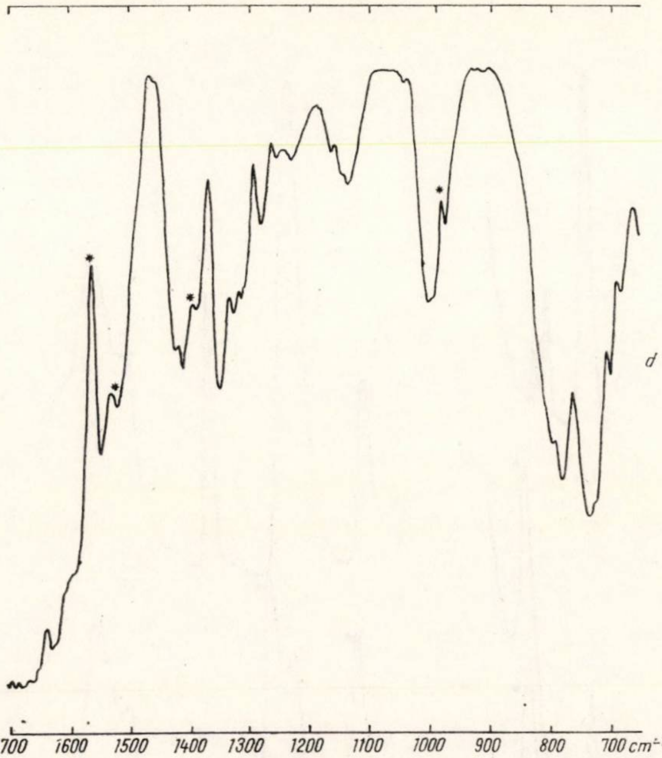

Fig. 1 d,
d, fully reduced benzophenone with Na in THF.

Infrared spectral study of different reduction forms of the carbonyl compounds will be disscused in a forthcoming paper.

The important change observed in the spectra of the reduction products was the shift of the carbonyl band from 1660—1730 cm^{-1} corresponding to the initial carbonyl compounds in the 1540—1570 cm^{-1} region. For several carbonyl compounds Eargle and Cox have assigned the vibration band belonging to the carbonyl of the anion based on the great intensity of this band. The same shifts of the carbonyl frequency were also observed in other cases where a decrease of the double bond character took place due to the intramolecular electronic displacements, as was the case for ketone complexes with different electronic acceptors.[10]

[10] P. Chalandon and B. P. Susz, *Arch. Sci.*, **9**, 461 (1956); *Helv. Chim. Acta*, **41**, 1332 (1958); D. Cassimatis and B. P. Susz, *Helv. Chim. Acta*, **43**, 852 (1960), **44**, 943 (1961); B. P. Susz, *Rev. Chim.*, **7**, 579 (1962); J. Göhring, G. P. Rossetti and B. P. Susz, *Helv. Chim. Acta*, **46**, 2639 (1963); G. P. Rossetti and B. P. Susz, *Helv. Chim. Acta*, **47**, 289, 299, 2053, (1963); G. Duyckaerts, *Cron. Chim.*, **1967**, 5; G. Olofsson, *Acta Chem. Scand.*, **22**, 377 (1968); G. Leclère-*zur* Nedden and G. Duyckaerts, *Bull. Soc. chim. belges*, **79**, 479 (1970).

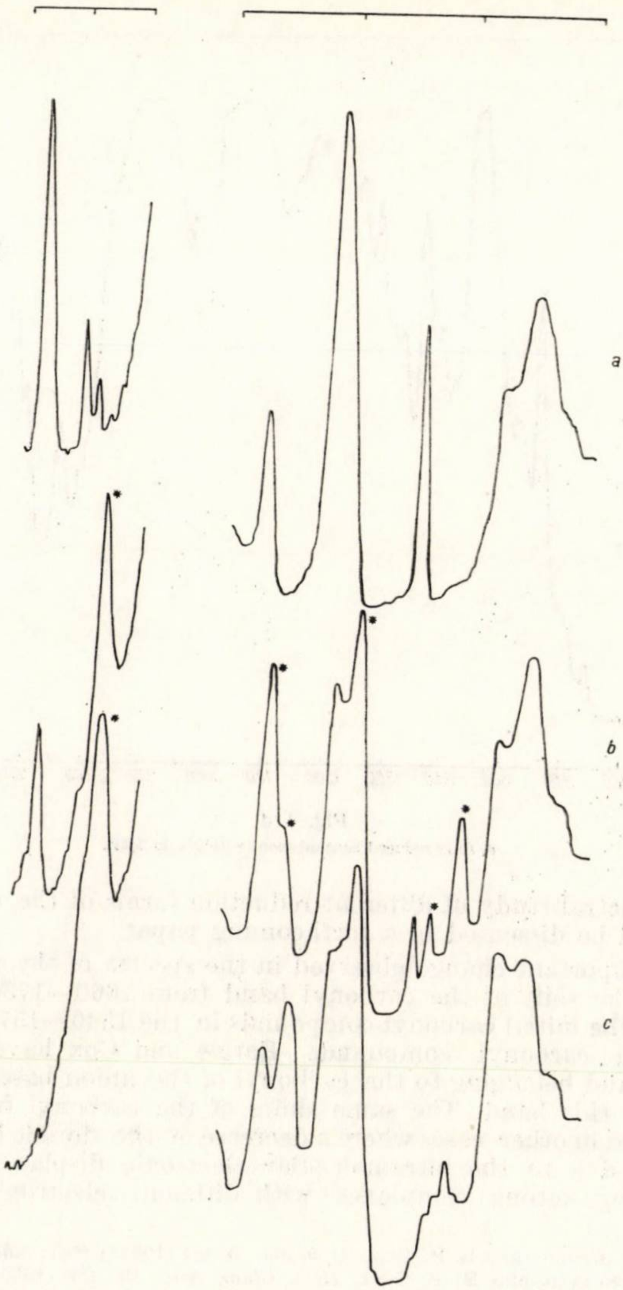

Fig. 2. — IR spectra of :

a, benzophenone in DME ; *b*, partially reduced benzophenone with Na (blue) ;
c, partially reduced benzophenone with excess Na (red).

The values of the anion carbonyl frequencies in comparison with those corresponding to the studied neutral molecules are given in table 1, their dependence on the solvents being also presented. The measurement of the anion carbonyl frequencies in DMF was made with less accuracy because the respective bands were placed between two strong peaks of the solvents. The results in table 1 were obtained using Na as reduction agent. With other alkali metals used for the reduction, the position of carbonyl band has not changed, as seen, for instance, from the spectra b and d from the figure 1.

The shift of the carbonyl frequencies to the smaller values in the anions as compared to its values in the neutral molecules (the frequency differences being between 100 and 180 cm $^{-1}$) is due to decrease of the double bond character of the carbonyl, as a result of the existence in the anion of an additional electron. If the relation proposed by Eargle and Cox between $\Delta\nu$ and ρ and verified by them in the case of benzophenone and fluorenone were applied to phenanthrenequinone, one would obtain for ρ the value of 0.515 against its value calculated according to Hückel theory and which was of 0.590.

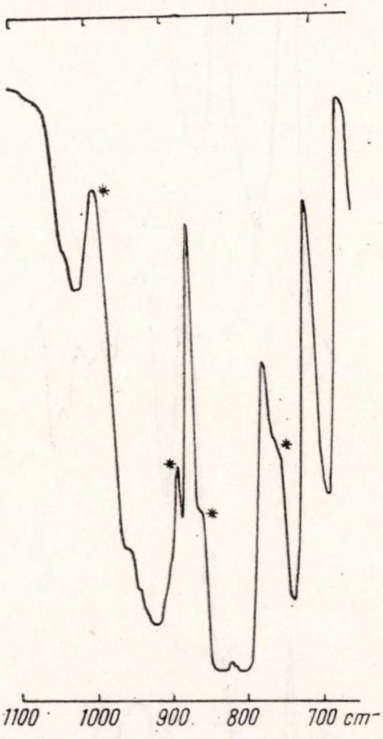

Fig. 3. — IR spectra of : partially reduced benzophenonein DMF

The decrease of the double bond character in the anion carbonyl group must be reflected in the smaller value of the carbonyl force constant, confirmed by the calculated values of the force constants for anions and neutral molecules. In table 2 are given the values of the carbonyl force constants *K*, as well as the values of the bond orders *p* and the self-polarizabilities π necessary for the MO calculation of the force constants for neutral molecules and their corresponding anions and dianions. The specific parameters for each molecule are given in table 3, the MO calculation being carried out with the relationships : $\alpha_X = \alpha_C + h_X \beta_{CC}$ and $\beta_{CX} = k_{CX} \beta_{CC} \beta$, where α, β, h and k have the significance known from Hückel theory.[11] The bond order and self-polarizability values corresponding to the neutral molecule given in table 2 are those calculated by Berthier[12] with the same parameters for all molecules, namely the

---

[11] A. Streitwieser, Jr., "Molecular Orbital Theory for Organic Chemists", John Wiley, New York — London, 1961.

[12] G. Berthier, B. Pullman and J. Pontis, *J. Chim. phys.*, 49, 367 (1952).

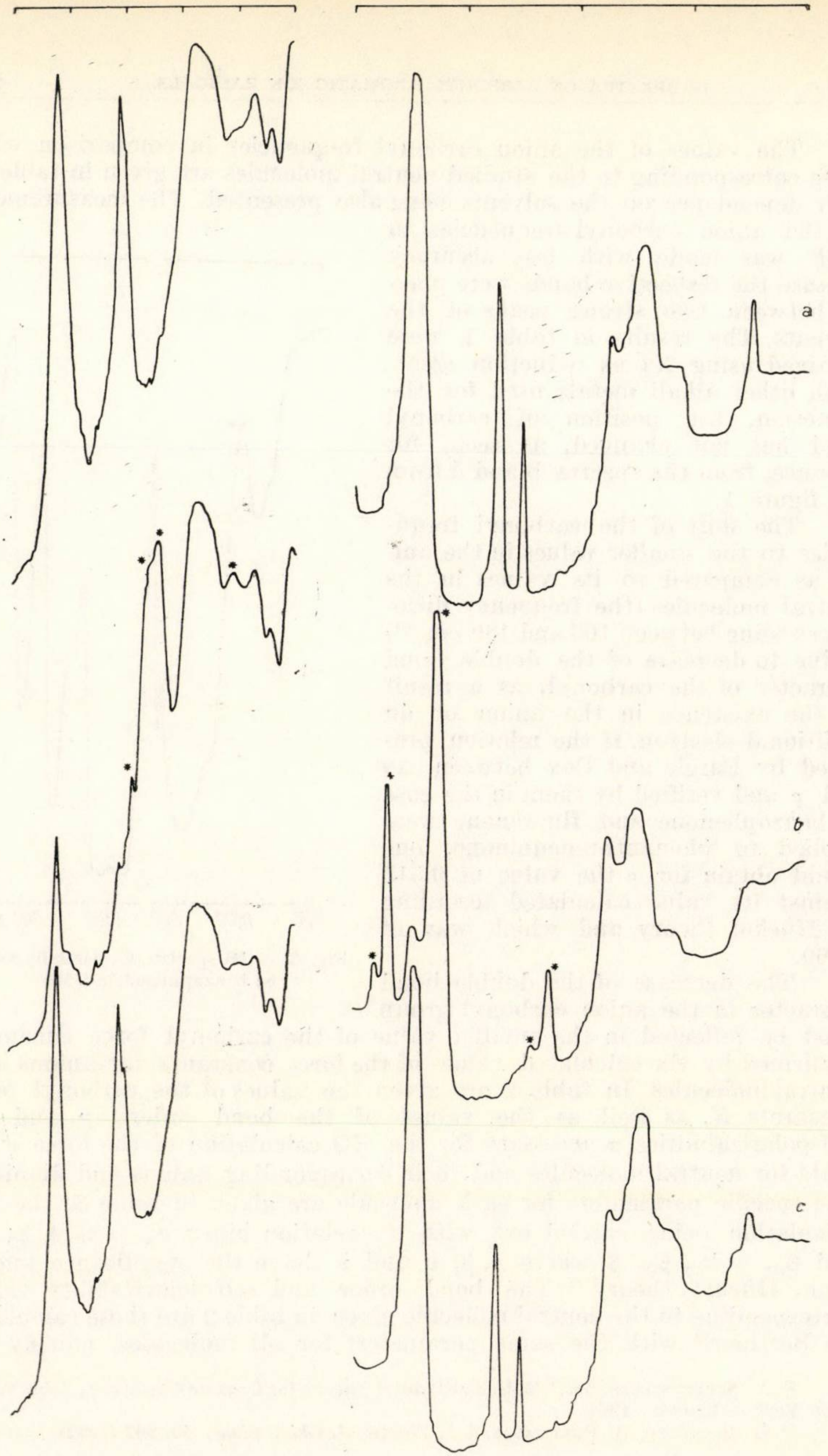

Fig. 4. — IR spectra of:
a, fluorenone in DME; *b*, partially reduced fluorenone with Na in DME; *c*, decomposed sample.

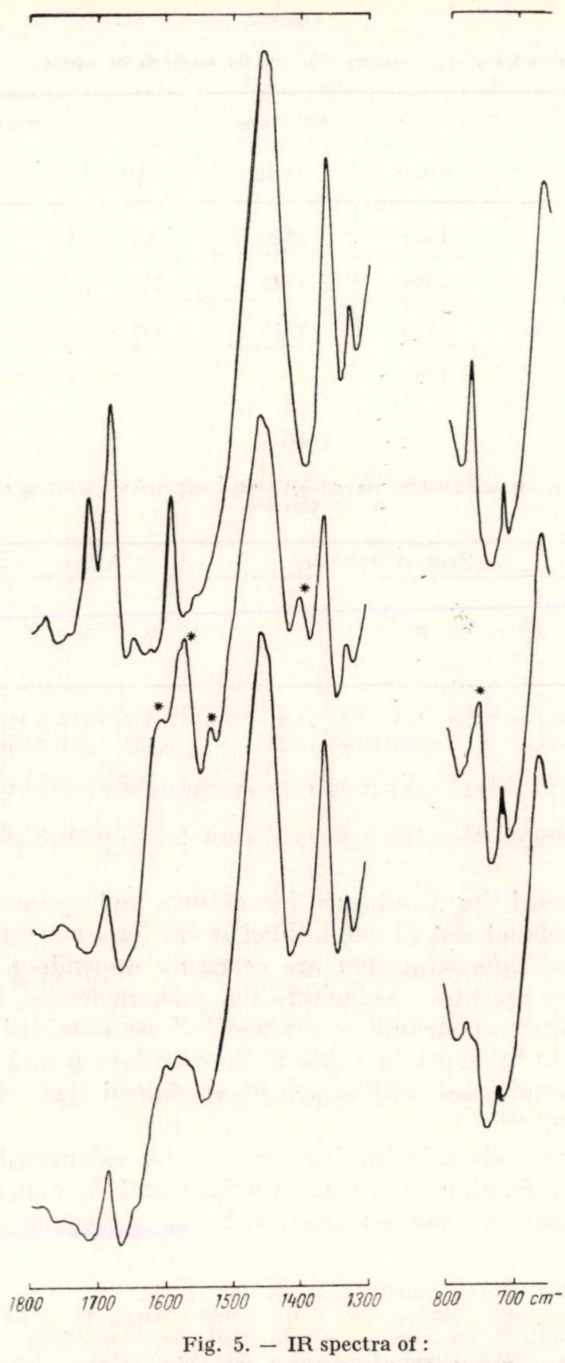

Fig. 5. — IR spectra of :
a, phenanthrenequinone in THF ; *b*, partially reduced phenanthrenequinone with Na in THF ; *c*, partially decomposed sample.

Table 1

Dependence of ν_{CO} frequency (cm^{-1}) of the anions on the solvent

Molecule	ν_{CO} (anion)			ν_{CO} (neutral molecule)
	DMF	DME	THF	THF
Benzophenone	1560	1560	1653	1669
Fluorenone	1558	1542	1540	1726
9,10-Phenanthrenequinone	1555	1575	1570	1686
Anthraquinone	1560			

Table 2

Mobile bond orders p, self-polarizabilities for carbonyl bonds π and carbonyl stretching force constants K (10^5 dyne.cm^{-1})

Molecule	Neutral Molecule				Anion			Dianion		
	p	π	K		p	π	K	p	π	K
			A	B						
Benzophenone	0.857 (0.762)	0,105	10.82	11.21 (10.63)	0.594	0.284	8.42	0.397	0.330	6.61
Fluorenone	0.871	0.092	10.95	11.29	0.524	0.267	7.93	0.345	0.278	6.40
9,10-Phenanthrene quinone	0.885 (0.712)	0.082	11.06	11.38 (10.33)	0.638	0.597	7.78	0.491	0.774	5.72
9,10-Anthraquinone	0.860 (0.724)	0.102	10.85	11.22 (10.40)	0.728	0.494	8.86	0.606	0.716	7.11

parameters proposed by Coulson[13] for ketone and quinone : $h_0 = 1.2$ and $k_{CO} = 2$. The bond orders and implicitly the force constants evaluated within the Hückel approximation are certainly dependent on the parameters used. With specific parameters for each molecule, as those used in the study of their electronic structureo[14-17] we obtained for p and K the values given in brackets in table 2. To calculate p and π for anions we used the parameter set with which we explained their electronic spin resonance spectra.[15,18]

The carbonyl self-polarizability $\pi_{co,co}$ was calculated for neutral molecules and its dianions after the Coulson and Longuet-Higgins formula[19] with respect to the energies and the molecular orbital coefi-

---

[13] C. A. Coulson, *Trans. Faraday Soc.*, **42**, 106 (1946).
[14] C. Parkanyi and V. Horac, *Coll. Czech. Chem. Comm.*, **31**, 835 (1966).
[15] R. Dehl and G. K. Fraenkel, *J. Chem. Phys.*, **39**, 1793 (1963).
[16] A. Kuboyama, *Bull. Chem. Soc. Japan*, **32**, 1226 (1959).
[17] A. Kuboyama, *Bull. Chem. Soc. Japan*, **31**, 752 (1958).
[18] V. E. Sahini and L. Ciurea, *Rev. Roumaine Chim.*, **14**, 689 (1969).
[19] C. A. Coulson and H. C. Longuet-Higgins, *Proc. Roy. Soc.*, **191 A**, 39 (1947),

Table 3

Parameter values

Molecule		Coulomb integrals		Resonance integrals			
		h_O	$h_{C(O)}$	k_{CO}	k_{C-CO}	k_{OC-CO}	$k_{CC'}$
Benzophenone	Neutral	1.3	0,2	1.41			
	Anion	1.5		1.6	0.9		
Fluorenone	Neutral						
	Anion	1.6	0.16	1.5	1.2		0.8
9,10-Phenanthrenequinone	Neutral	1.3	0.2	1	0.8	0.8	
	Anion	1.3		1.5	1.2		0.8
9,10-Anthraquinone	Neutral	1.3	0.2	1	0.8		
	Anion	1.2		1.6	0.8		

cients. For a system made up of m doubly occupied orbitals and $n-m$ free orbitals. $\pi_{co,co}$ is given by the following relation :

$$\pi_{co,co} = 2 \sum_{j=1}^{m} \sum_{k=m+1}^{n} \frac{(C_{cj} C_{ok} + C_{oj} C_{ck})^2}{\varepsilon_j - \varepsilon_k} \tag{1}$$

For the anion where the first m orbitals are doubly occupied, the $m+1$ orbital is singly occupied and the following $m+2 \ldots n$ are free orbitals, the self-polarizability may be calculated with the relation :

$$\pi_{co,co} = 2 \sum_{j=1}^{m} \sum_{k=m+2}^{n} \frac{(C_{cj} C_{ok} + C_{oj} C_{ck})^2}{\varepsilon_j - \varepsilon_k} + \tag{2}$$
$$+ 2 \sum_{j=1}^{m} \frac{(C_{cj} + C_{o,m+1} + C_{oj} C_{c,m+1})^2}{\varepsilon_j - \varepsilon_{m+1}} + \sum_{k=1}^{n}{}' \frac{(C_{c,m+1} C_{ok} + C_{o,m+1} C_{ck})^2}{\varepsilon_{m+1} - \varepsilon_k}$$

where the ′sign of the last sum indicates the exclusion of the term $k = m+1$. The relation (2) could also be written :

$$\pi_{co,co} = 2 \sum_{j=1}^{m} \sum_{k=m+2}^{n} \frac{(C_{cj} C_{ok} + C_{oj} C_{ck})^2}{\varepsilon_j - \varepsilon_k} + \tag{3}$$
$$+ \sum_{j=1}^{m} \frac{(C_{cj} C_{o,m+1} + C_{oj} C_{c,m+1})^2}{\varepsilon_j - \varepsilon_{m+1}} + \sum_{k=m+2}^{n} \frac{(C_{c,m+1} C_{ok} + C_{o,m+1} C_{ck})^2}{\varepsilon_{m+1} - \varepsilon_k}$$

With the self-polarizability calculated according to relation (3) and the bond order calculated for anions with :

$$p_{co} = 2 \sum_{j=1}^{m} C_{cj} C_{oj} + C_{c,m+1} C_{o,m+1} \tag{4}$$

one may obtain the force constants of the anion carbonyl applying Coulson and Longuet-Higgins formula.[20] For the force constants of the single and respectively double bond one has taken the values: 5.5×10^5 dyne/cm and respectively 12×10^5 dyne/cm and for the length of the single and respectively double bond, the values 1.43 Å and 1.23 Å were taken. β has been considered equal to 3×10^{-12}erg. For neutral molecules, besides the force constants calculated with Coulson and Longuet-Higgins formula, given in column A of table 2, the force constants were also calculated with the formula proposed by Jensen.[21] The values obtained with Jensen formula, where for the carbonyl bond order of the formaldehyde 0.988 has been taken, are given in column B of table 2. The values of the force constant from column B are higher than those from column A, because the simple form of Jensen formula is equivalent to the neglecting of the self-polarizability term in Coulson and Longuet-Higins formula.

Comparing the force constants of carbonyl bonds in the compounds under study, as expected we observed a decrease in these values on passing from the neutral molecule to the anion and then to the dianion, since the additional electrons occupied the lowest antibonding orbital of the molecule. In the case of quinone, the value $\Delta\nu$ as well as the change in the force constant ΔK from the neutral molecule to the anion, is greater for the phenanthrenequinone than for the anthraquinone. This fact may be correlated to the greater value of the carbonyl spin density, namely 0.590 for phenanthrenequionone in comparison with 0.489 for anthraquinone. The above values of the spin densities were calculated by the Hückel method.

---

[20] C. A. Coulson and H. C. Longuet-Higgins, *Proc. Roy. Soc.*, **193A**, 460 (1948).
[21] H. H. Jensen, *Acta Chem. Scand.*, **23**, 3163 (1969).

Revue Roumaine de Chimie, 17, 1, 2, 285–290 (1972)

Dedicated to Professor I. G. MURGULESCU
on his 70th birthday

THE HEATS OF ADSORPTION OF SOME HYDROCARBONS ON ZIRCONIA*

MANLIO SANESI

Institute of Physical Chemistry of the University Pavia, Italy

Received September 11, 1971

The heats of adsorption on ZrO_2 in the temperature range 90–220° were evaluated at zero surface coverage by gas-solid chromatography for some *n*-alkanes, the corresponding 1-alkenes and the cyclic compounds cyclohexane, cyclohexene and benzene. Among the results it can be particularly remarked that the heats of adsorption of both *n*-alkanes and 1-alkenes are linear functions of the carbon atom number, having the same value of the slope : this confirms the previous conclusion that these molecules are likely adsorbed in a "lying-down" position, and that the adsorption interaction mainly involves dispersion forces for the aliphatic CH_2- and CH_3-groups, while an additional contribution of electrostatic nature should be taken into account for the double-bond Π-electron system.

The heats of adsorption of some saturated and unsaturated hydrocarbons on γ-Al_2O_3 and MgO were reported in previous papers,[1] and it was then concluded that with saturated hydrocarbons, dispersion forces only are mainly responsible for the adsorption interaction, whereas specific contributions principally of electrostatic nature are recognizable in the adsorption of unsaturated or aromatic compounds. Further, it was found that the above oxides, as well as silica gel, behave in a strictly similar way for both the specific and the non-specific interactions, thus allowing to infer that the interacting centres of the adsorbing solids are in each case the large O^{2-} surface ions (as regards the dispersion interaction) and the partly protonized surface hydroxyls (as regards the interaction with the π-electron systems of unsaturated adsorbate molecules).

In order to acquire more experimental data, a substantial enlargement of the research to other oxidic adsorbants (such as TiO_2, ZrO_2, BeO, etc.) has been planned. In the present work the heat of adsorption on zirconia has been determined for five linear chain hydrocarbons (from C_5 to C_9), for the corresponding 1-mono-olefins and for the cyclic compounds cyclohexane, cyclohexene and benzene. The gas chromatographic method was again employed, which allows to attain very low surface coverages and to extrapolate the measured values to zero surface coverage.

---

* Work performed at the "Centro di studio per la termodinamica ed Elettrochimica dei sistemi salini fusi e solidi" of the *Consiglio Nazionanale delle Ricerche*, operating within the Institute of Physical Chemistry of Pavia University.

[1] a) M. SANESI and V. WAGNER, *Z. Naturforsch.*, 23 *a*, 979 (1968) ;
b) *Idem, ibid.*, 25 a, 688 (1970) ; c) *Idem, ibid.*, 25 a, 693 (1970).

EXPERIMENTAL

Materials. The *n*-alkanes, 1-pentene and 1-hexene were all FLUKA products of the "Puriss" grade (stated purity > 99.9%); 1-heptene, 1-octene and cyclohexene were C. ERBA "RS" for gas chromatography (99.97%); 1-nonene was FLUKA "Purum" (97%); cyclohexane was C. ERBA "RS" for spectroscopic use and benzene was C. ERBA "RS" for cryoscopy. These two latter were sodium dried and repeatedly distilled before use; all the remaining were employed without further treatments. No attempt was made to purify 1-nonene, because of the small available amount: in the experimental conditions however, it gave a single sharp peak, so that the final extrapolated results were not liable to be affected by the small impurity content. As for 1-heptene, a duplicate run was carried out with a sample from B.D.H.; this was sodium dried and redistilled to constant refractive index: $n_D^{20°} = 1.39982$ (lit.: $n_D^{20°} = 1.39980$ [2]).

The adsorbent was a sample of monoclinic zirconia, prepared from a C. ERBA "RP" product [3] in a similar way as that employed in previous dielectric constant measurements. [4] A fraction with grain size ranging from 125 to 250 μ proved satisfactory for gas-solid chromatography. The specific surface area, as measured by the AREA-METER (Ströhlein & Co., Düsseldorf) according to Haul and Dümbgen's method, [5] was of ca. 3.2 m^2/g. The adsorbent was oven heated at 200 °C before packing the column; the packed column was then flushed with the carrier gas at 150 °C for 6–8 hours. The flushing process was occasionally repeated between different runs.

Apparatus and procedure. Details of the apparatus (essentially a gas chromatograph by C. ERBA S.p.A., mod. B/f) and of the procedure were given previously. [1a] The column was stainless steel (length 1 m, i.d. 1 cm), the carrier gas electrolytic hydrogen.

For each compound, retention times at several different temperatures and at constant flow rate were measured with increasing amounts of injected sample (from about 0.5×10^{-6} to 20×10^{-6} mole). The temperature intervals (40–50°) ranged from a lower limit of 90° with *n*-pentane to an upper one of 220° with 1-nonene, with flow rates of 30–40 ml/min and pressure drops across the column of 0.1–0.3 atm. The retention times, referred to those of injected samples of non-adsorbed air, were corrected for the pressure drop and for the temperature difference between the column and the flow meter, according to James and Martin. [6]

For all the adsorbates, except *n*-pentane, *n*-hexane and cyclohexene, duplicate independent runs were carried out.

RESULTS AND DISCUSSION

The decimal logarithms of the corrected retention times always showed a linear dependence on the reciprocal absolute temperature: a set of these plots is reported as an example in figure 1. The heats of adsorption, Q_a, were then evaluated from the slopes of the straight lines by the least square method and the standard deviations of Q_a were calculated according to Beers[7]: these were generally of the order of $\pm 0.1-0.2$ kcal/mole and only exceptionally (n-nonane, run 1; benzene, run 1) reached ± 0.5 kcal/mole.

---

[2] A. F. Forziati, D. J. Camin and F. D. Rossini, *J. Res. Nat. Bur. Stand.*, **45**, 406 (1950).

[3] This was in the form of a very fine powder, not suitable for gas chromatography.

[4] M. Sanesi G. Cremante, S. Pizzini and V. Wagner, *Z. Naturforsch.*, **26 a**, 159 (1971).

[5] R. Haul and G. Dümbgen, *Chem.-Ing.-Techn.*, **35**, 586 (1963).

[6] A. T. James and A. J. Martin, *Biochem. J.*, **50**, 679 (1952).

With all the adsorbates, in each experimental run the Q_a values showed a slight increase with decreasing injected amount: from the plots as those reported as a specimen in figure 2, the heats of adsorption at zero surface, coverage, $Q_{a,0}$, were graphically extrapolated. The results for each run are reported in table 1, together with the mean values, $\overline{Q}_{a,0}$.

Fig. 1. — Plot of log retention time (min) *vs.* $1/T$ for different injected amounts of n-heptane.

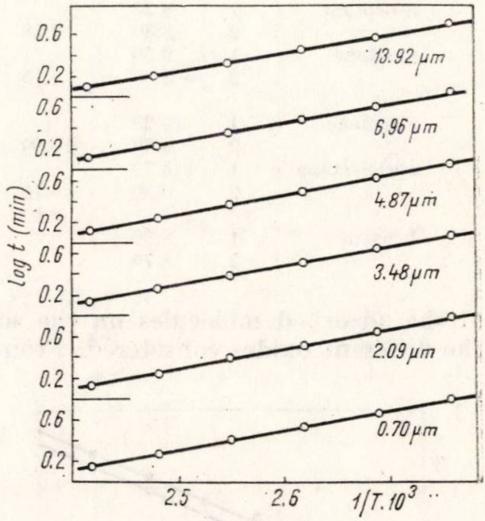

Fig. 2. — Dependence of Q_a on the injected amount (in mole × 10^{-6}) for the n-alkanes.

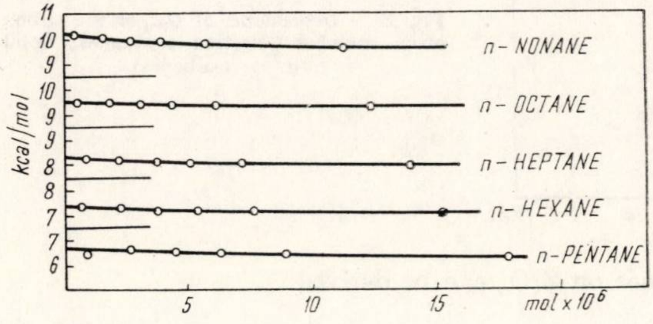

The heats of adsorption in ZrO_2 are always lower by about 2 kcal/mole than those previously found with the same adsorbates on γ-Al_2O_3 and MgO.[1] As in the latter cases, however, the heat of adsorption of the n-alkanes on ZrO_2 shows a straight line dependence on the carbon atom number, n_c, (Fig. 3) thus suggesting that both the interaction mechanism involved in the adsorption of these saturated compounds and the position of the adsorbed molecules on the solid surface have similar features on the different oxides considered. From the present results the straight line equation for the n-alkanes on ZrO_2 can be derived

---

[7] Y. BEERS, "Theory of Error", Addison Wesley Publ. Co., Reading, Mass., 1958, p. 37 ff. See also ref. 1-a, note 7.

Table 1

Heat of adsorption (kcal/mole) on ZrO_2 at zero surface coverage

Adsorbate	Run	$\overline{Q}_{a,o}$	$\overline{Q}_{a,o}$	Adsorbate	Run	$Q_{a.o}$	$\overline{Q}_{a,0}$
n-pentane	1	6.70	6.70	1-pentene	1	6.90	
n-hexane	1	7.35	7.35		2	6.90	6.90
n-heptane	1	8.25		1-hexene	1	8.30	
	2	8.30	8.28		2	8.20	8.28
n-octane	1	9.50			3	8.35	
	2	8.80	9.15	1-heptene	1	8.60	
					2	8.90	8.75
n-nonane	1	10.20		1.-octene	1	9.50	
	2	9.80	10.00		2	9.60	9.55
cyclohexane	1	6.70					
	2	6.80	6.75	1-nonene	1	10.60	
			8.60		2	10.35	10.48
benzene	1	8.50		cyclohexene	1	8.20	8.20
	2	8.70					

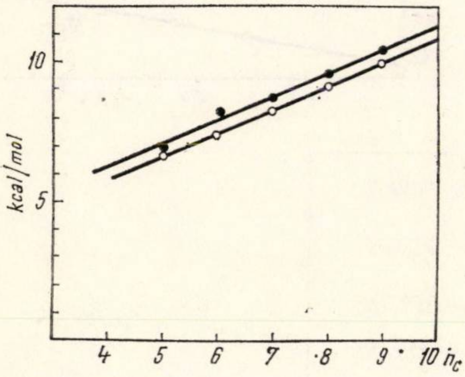

Fig. 3. – Dependence of $Q_{a,0}$ on the carbon atom number (circles: n-alkanes; solid points: 1-alkenes).

$$Q_{a.0}(\text{kcal/mole}) = 2.41 + 0.84\ n_C \qquad (1)$$

whose slope means the adsorption potential per CH_2-group, as due to dispersion forces only ($P_{d,\ CH_2}$). Remembering the equation previously obtained[1-a,c] for γ-Al_2O_3 ($Q_{a.\ 0} = 2.12 + 1.21\ n_C$) and for -MgO ($Q_{a.\ 0} = 1.85 + 1.17\ n_C$), and also the one reported by Kiselev[8] for a silica gel ($Q_a = 1.50 +$

---

[8] A. V. Kiselev, "Proc. 2nd Int. Congr. Surface Activity", Butterworths Sci. Publ., London 1957, p. 179.

1.24 n_C), it can be seen that the order of magnitude of $P_{d,\,CH_2}$ is still preserved and an average value $P_{d,\,CH_2} = 1.1 \pm 0.1$ kcal/mole might be confidently assumed for the four oxides. A still better agreement is obtained if one evaluates the dispersion interaction potential per CH_3-group-P_{d,CH_3} : following the way indicated in one of the previous papers,[9] and assuming a mean temperature of 410 °K, one now obtained $P_{d,\,CH_3} = 1.64$ kcal/mole for ZrO_2, whereas the values found for Al_2O_3, MgO and SiO_2 were respectively 1.82, 1.64 and 1.69.[9]

The heats of adsorption of 1-alkenes are as expected higher than those of the corresponding n-alkanes. Here again the dependence of $Q_{a,\,0}$ on n_C is given by a straight line (Fig. 3). The corresponding equation is

$$Q_{a,\,0}(\text{kcal/mole}) = 2.90 + 0.84\ n_C \tag{2}$$

which has exactly the same slope as eq. (1). This rather striking result strongly supports the assumptions previously made about the adsorption of n-alkanes on the considered oxides. In this case, indeed, assuming that the alkane molecule are adsorbed in a "lying-down" position[10] and that dispersion forces only are mainly involved in the adsorption interaction, it was shown [1-b] that the heat of adsorption in a homologous alkane series (from C_4 up) can be expressed in terms of the dispersion potential contributions for the CH_3 – and CH_2-groups, i.e.,

$$Q_a = 2\ (P_{d,\,CH_3} - P_{d,\,CH_2}) + RT + n_C\, P_{d,\,CH_2} \tag{3}$$

which, at constant T, establishes the linear relation experimentally verified. Considering now the 1-alkene homologous series, it seems highly probable that these molecules be adsorbed in a similar lying-down position. If the aliphatic portion of such unsaturated molecules maintains the same average equilibrium distance from the surface as a wholly saturated molecule, then the $P_{d,\,CH_3}$ and $P_{d,\,CH_2}$ contributions for this portion should also remain unchanged. For the initial unsaturated portion, one should take into account the contribution from the electrostatic interaction between the surface hydroxyls and the double-bond π-electron system, P_e, besides the dispersion potential contributions for the CH_2- and CH-groups joined in the double bond, $P^*_{d,\,CH_2}$ and $P^*_{d,\,CH}$. On the whole, the heat of adsorption of an 1-alkene ($n_C > 4$) might be written, in a merely formal way, as

$$Q_a = P_e + P^*_{d,\,CH_2} + P^*_{d,\,CH} + P_{d,\,CH_3} + (n_C - 3)\, P_{d,\,CH_2} + RT. \tag{4}$$

Although the values of the terms P_e, $P^*_{d,\,CH_2}$ and $P^*_{d,\,CH}$ remain unknown, it seems likely that they are not or only slightly affected by the length of the aliphatic portion. Therefore, after rearrangement and putting $P_e + P^*_{d,CH_2} + P^*_{d,\,CH} + P_{d,\,CH_3} - 3P_{d,\,CH_2} + RT = \text{const} = A$, eq. (4) becomes

$$Q_a = A + n_C\, P_{d,\,CH_2} \tag{5}$$

where $P_{d,\,CH_2}$ has just the same value as in eq. (3).

---

[9] See ref. 1-c, p. 695.

[10] S. E. Hoory and J. M. Prausnitz, *Trans. Faraday Soc.*, 63, 455 (1967).

As for the cyclic molecules, it can be finally remarked that : 1) the heat of adsorption of cyclohexane is lower than that of n-hexane by 0.6 kcal/mole (on γ-Al_2O_3, $\Delta Q_a = -0.9$) ; 2) a remarkable increase ($\Delta Q_a =$ $= + 1.45$ kcal/mole) is shown on passing from cyclohexane to cyclohexene (on $\gamma-Al_2O_3$ and MgO, $\Delta Q_a = +1.40$) ; 3) a much lower increase ($\Delta Q_a =$ $= + 0.40$ kcal/mole) is observed when passing from cycohexene to benzene (on γ-Al_2O_3, $\Delta Q_a = +0.6$). Thus, some features of a general behaviour already pointed out in the preceding paper $^{1-c}$ are clearly apparent also through the results of the present experiments.

Revue Roumaine de Chimie, **17**, *1*, *2*, 291–301 (1972)

Herrn Professor I. G. MURGULESCU
zum 70. Geburtstag

ÜBER DIE DYNAMISCHE THERMOGRAVIMETRIE BEI KOMPLEXEN ABBAUPROZESSEN

I. A. SCHNEIDER

vom Lehrstuhl für physikalische Chemie der „Al. I. Cuza"-Universität, Iași

Eingegangen am 4. September 1971

Auf Grund von kinetischen Überlegungen wird gezeigt, daß unter thermisch dynamischen Bedingungen komplizierte Abbaureaktionen von Polymeren einen Umsatzeinfluß der Aktivierungsenergie aufweisen werden. Dieser Umsatzeinfluß bedingt auch einen Einfluß der Aufheizgeschwindigkeit, so daß im allgemeinen Standardbedingungen angewendet werden müssen, um eine thermische Charakterisierung von Polymerabbaureaktionen zu ermöglichen. Die berechneten kinetischen Parameter besitzen deshalb nur eine relative Bedeutung und erst nach Extrapolation lassen sich zur Kennzeichnung des Reaktionsmechanismus brauchbare Werte ableiten.

Die dynamische Thermogravimetrie (d-TG), d.h. der gravimetrisch verfolgte thermische Abbau von Festkörpern bei konstanter Aufheizgeschwindigkeit ermöglicht eine Auftrennung der verschiedenen Abbauetappen, wobei das Temperaturgebiet einer Abbaustufe umso tiefer liegt, je geringer die Thermostabilität der Substanz, bzw. je kleiner die Gesamtaktivierungsenergie der Abbaureaktion ist. Die Möglichkeit einer Auftrennung der verschiedenen Abbaustufen bietet auch große Vorteile für das Studium des thermischen Abbaus von Polymeren, da von vornherein Depolymerisationsreaktionen (deren Ablauf in einer Stufe erfolgt) von Abbaureaktionen, die in mehreren Stufen erfolgen, unterschieden werden können.

Seitdem in der Literatur auch verschiedene Methoden zur Berechnung der kinetischen Parameter und insbesondere der Aktivierungsenergie vorgeschlagen worden sind, wird die d-TG in steigendem Maße zur Charakterisierung der Thermostabilität von Polymeren und zum kinetischen Studium ihrer Abbaureaktionen herangezogen.

Die Vielzahl der Methoden zur Berechnung der kinetischen Parameter aus Thermogrammen erklärt sich zum Teil daraus, daß die kinetische Grundgleichung der thermischen Abbaureaktionen von Festkörpern

$$A_{\text{fest}}\ B \longrightarrow_{\text{fest}} + C_{\text{gasförmig}}$$

die in d-TG Bedingungen bei einer konstanten Aufheizgeschwindigkeit (*Hr*) von $\frac{\mathrm{d}T}{\mathrm{d}t} =$ $= a$°C/Min durch den Ausdruck

$$-\frac{\mathrm{d}x}{\mathrm{d}T} = \frac{A}{a} \exp\left(-E/RT\right) x^{n} \tag{1}$$

wiedergegeben ist, nicht unmittelbar lösbar ist. Aus diesem Grunde können sie, je nachdem ob die kinetische Grundgleichung direkt oder nach Integration verwendet wird, in die zwei großen Klassen von differentiellen oder integralen Methoden eingereiht werden. [1–5]

Ein Versuch diese Methoden zum Studium der thermischen Dehydrochlorierung von PVC heranzuziehen zeigte aber, wie aus Tabelle 1 hervorgeht, daß die verschiedenen Berechnungsmethoden zu unterschiedlichen Werten für E führen.

Tabelle 1

Dehydrochlorierung von PVC in thermisch dynamischen Bedingungen Probeumenge : 20 mg ; Atmosphäre : Luft ; Thermowaage : Derivatograph MOM - Budapest

Untersuchungs-methode Literatur-hinweis)	Aktivierungsenergie E (kcal/Mol)	*Hr* °C/Min
[6]	50,4	18,3
[7]	49,2	,,
[8]	variabel 65—29,8 (verschiedene Probenmengen)	,,
[9] und [10]	bis w_M 51,0 nach w_M 15,8	,,
[11]	variabel 64,6—43,3	verschiedene
[12]	29,6	,,
[13]	32,3	,,
[14]	variabel 33,1—26,1	,,

Dabei ergab sich, daß die so berechnete ,,Aktivierungsenergie'' zusätzlich sowohl vom Umsatzgrad, als auch von der verwendeten *Hr* abhängig ist. [3]

Weitere Untersuchungen zeigten, daß die Einflüsse auch an anderen Polymeren zu beobachten sind. [15–17]

Auch aus anderen veröffentlichen Arbeiten [18,19] ergeben sich diesbezügliche Hinweise, wenn auch von einem Einfluß der *Hr* nicht direkt gesprochen wird und die Werte gemittelt worden sind.

[1] P. E. Slade und L. T. Jenkis ,,Techniques and Methods of Polymer Evaluation, Vol. I. Thermal Analysis'' Edward Arnold, 1966.

[2] J. H. Flynn und L. A. Wall, *J. Res. Nat. Bur. Stand.*, **70 A**, 487 (1966).

[3] D. Furnică und I. A. Schneider, *Makromol. Chem.*, **108**, 182 (1967).

[4] G. G. Cameron und J. D. Fortune, *Europ. Polymer J.*, **4**, 333 (1968).

[5] J. H. Flynn, "Thermal Analysis" Vol. II. Academic Press, 1969, S. 1111.

[6] L. Reich, H. T. Lee und D. W. Levi, *J. Appl. Polymer Sci.*, **9**, 351 (1965) ; *Polymer Letters*, **1B**, 515 (1963).

[7] E. S. Freeman und B. Carroll, *J. Phys. Chem.*, **62**, 394 (1958) ; *J. Polymer Sci.*, 54, 299 (1961).

[8] G. K. Chatteryée, *J. Polymer Sci.*, **A 3**, 4523 (1965).

[9] A. W. Coats und J. T. Redfern, *Nature*, **201**, 68 (1964).

[10] Ch. D. Doyle, *Makromol. Chem.*, **83**, 220 (1964) ; *Nature*, **207**, 102 (1963).

[11] L. Reich, *Polymer Letters*, **2**, 621 (1964).

[12] D. W. van Krevelen, C. van Heerden und F. Y. Hantjes, *Fuel*, **30**, 253 (1951).

[13] H. E. Kissinger, *Analyt. Chem.*, **29**, 170 (1957).

[14] L. Reich, *Makromol. Chem.*, **66**, 102 (1963).

[15] I. A. Schneider, C. Vasile, D. Furnică und A. Onu, *Makromol. Chem.*, **117**, 41 (1968).

[16] N. Hurduc, I. A. Schneider und Cr. Simionescu, *Cellulose Chem. and Technol.*, **2**, 569 (1968).

[17] C. N. Caşcaval, C. Vasile und I. A. Schneider, *Makromol. Chem.*, **131**, 55 (1970).

[18] L. Reich und D. W. Levi, ,,Macromolecular Reviews'' Vol. I. Intersci. Publ. Corp., N.Y., 1967, S. 183.

[19] H. L. Friedman, *J. Polymer Sci.*, **C6**, 183 (1964).

Der Umsatzeinfluß ist des öfteren beobachtet worden und in Abb. 1 zeigen wir als Beispiel unsere Ergebnisse für den thermischen Abbau von α-Cellulose bei verschiedenen *Hr*.

Die Berechnungen wurden dabei nach Reichs Oberflächenmethode[11] und nach Flynn und Wall [20] ausgeführt.

Audebert und Aubineau, [21] die sich näher mit dem Umsatzeinfluß befaßt haben, sind der Meinung, daß dieser vom Mechanismus der Polymerabbaureaktion bedingt ist. Auch aus anderen Arbeiten ergibt sich ein Umsatzeinfluß, obwohl die Autoren selbst diese Möglichkeit nicht erwogen haben. [22–24]

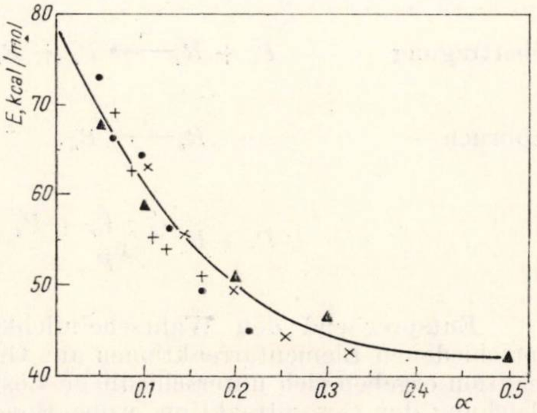

Abb. 1. — Der Einfluß des Umsatzgrades auf die Aktivierungsenergie der zweiten Abbaustufe α-Cellulose unter d-TG Bedingungen Berechnungen nach der "Oberflächenmethode" [11] (*Hr* — — 2,4 ; Δ—4,8 und+12,4°C/Min) und der Flynn-Wallschen Methode (x)[20]

Durch Änderung der experimentellen Untersuchungsbedingungen konnten wir belegen, daß die beobachteten Einflüsse nicht auf physikalische Ursachen, wie Diffusion, Wärmeübertragung u.ä. zurückzuführen sind, da wir bei der thermischen Dehydrochlorierung von PVC dieselben Ergebnisse an zwei Thermowaagen unterschiedlicher Konstruktion, in Luft, Stickstoff oder Vakuum und mit verschiedenen Probenmengen erhalten haben. [15]

Somit aber ergab sich auch für uns der wichtige Schluß, daß die Deutung nur in den Besonderheiten des thermischen Abbaumechanismus von Polymeren unter d-TG Bedingungen zu suchen ist.

Um näher auf die beobachteten Einflüsse eingehen zu können, nehmen wir im folgenden z. B. an, daß der thermische Abbau eines Polymeren durch Depolymerisation erfolgt, an der nach Boyd[25] folgende Elementarreaktionen beteiligt sein können:

---

[20] J. H. Flynn und L. A. Wall, *Polymer Letters*, **4**, 323 (1966).

[21] R. Audebert und C. Aubineau, *Europ. Polymer. J.*, **6**, 965 (1970).

[22] D. A. Anderson und E. S. Freeman, *J. Polymer Sci.*, **54**, 253 (1961).

[23] H. C. Andersen, *J. Polymer. Sci.*, **C6**, 175 (1964).

[24] J. R. MacCallum und J. Tanner, *Europ. Polymer J.*, **6**, 907 (1970).

[25] R. H. Boyd, *J. Chem. Phys.*, **31**, 321 (1959); **45**, 773 u. 778 (1966); *J. Polymer Sci.*, **5**, 1573 (1967).

Start	$P_n \begin{array}{l} \overset{k_0}{\nearrow} R_r + R_{n-r} \\ \underset{k_0'}{\searrow} R_n + R_1\,(M_1) \end{array}$	statistisch Endgruppenstart
Depropagierung	$R_n \xrightarrow{k_1} R_{n-1} + P_1(M)$	
Übertragung	$P_n + R_s \xrightarrow{k_3} P_r + R_{n-r} + P_s$	
Abbruch	$R_n \xrightarrow{k_2} P_n$	erster Ordnung
	$R_r + R_s \begin{array}{l} \overset{k_2'}{\nearrow} P_r + P_s \\ \searrow P_{r+s} \end{array}$	zweiter Ordnung

Entsprechend den Wahrscheinlichkeiten für die Beteiligung der verschiedenen Elementarreaktionen am Gesamtmechanismus der Abbaureaktion ergeben sich unterschiedliche Lösungen für die Geschwindigkeitsgleichung der Gesamtreaktion, wobei Boyd selbst 11 Grenzfälle bespricht.

All diese Lösungen gelten nur für quasistationäre Reaktionszustände, bzw. für $\Sigma \mathrm{d}R_i/\mathrm{d}t = 0$, d.h. für den Fall, wenn die Geschwindigkeit der Radikalbildung in der Startreaktion der des Verschwindens in den Abbruchreaktionen gleich ist ($v_{\mathrm{st}} = v_{\mathrm{Abbr}}$).

Diese kinetische Grundbedingung ist aber unter den thermisch dynamischen Bedingungen der d-TG infolge des stetigen Temperaturanstieges nicht erfüllt, so daß im allgemeinen drei Stadien unterschieden werden können.

1. Bis zum Geschwindigkeitsmaximum gilt: $v_{\mathrm{st}} > v_{\mathrm{Abbr}}$
2. Bei Geschwindigkeitsmaximum ist die Bedingung $v_{\mathrm{st}} = v_{\mathrm{Abbr}}$ erfüllt, d.h. es werden quasistationäre Zustände vorgetäuscht, und
3. Nach dem Geschwindigkeitsmaximum gilt: $v_{\mathrm{st}} < v_{\mathrm{Abbr}}$

Somit ergibt sich aber unter der Annahme, daß der Abbruch erster Ordnung vernachlässigbar ist und daß die Geschwindigkeitskonstante der Startreaktion gleich k_0 ist, d.h. daß der Start statistisch erfolgt, für die Reaktionsgeschwindigkeit bei Geschwindigkeitsmaximum die bekannte kinetische Grundgleichung für stationäre Reaktionszustände, die unter isothermen Bedingungen Anwendung findet.

$$(\mathrm{d}M/\mathrm{d}t)_M = k_1 R = k_1 (2k_0 P/k_2')^{1/2}$$

d.h. die Geschwindigkeitskonstante der Polymerabbaureaktion bei Geschwindigkeitsmaximum ist durch den Ausdruck

$$(k)_M = k_1\,(2k_0/k_2')^{1/2} \tag{2}$$

gekennzeichnet.

Da unter thermisch dynamischen Bedingungen sich der quasistationäre Reaktionszustand nur auf das Geschwindigkeitsmaximum begrenzt, kann entsprechend der allgemeinen Theorie von Kettenreaktionen[26] angenommen werden, daß bis dahin die Radikalkonzentration entsprechend :

$$R = W_0 \tau \exp(-t/\tau)$$

zunehmen wird, worin W_0 die Geschwindigkeit der Startreaktion und τ die mittlere Lebensdauer der Radikale bedeuten.

Damit ergibt sich, daß unter thermisch dynamischen Bedingungen die Reaktionsgeschwindigkeit nach

$$\mathrm{d}M/\mathrm{d}t = 2k_{st}k_1\,\tau \exp(-t/\tau)\,P \tag{3}$$

$$\text{d.h. } \mathrm{d}M/\mathrm{d}T = \frac{2}{a} k_{st}k_1\,\tau \exp(-aT/\tau)\,P$$

stetig mit dem Umsatz bzw. mit der Temperatur exponentiell ansteigen wird und der für quasistationäre Zustände charakteristischen maximalen Reaktionsgeschwindigkeit zustrebt.

Für Reaktionsbeginn ergibt sich aus (3) für $t \to 0$

$$(\mathrm{d}M/\mathrm{d}t)_{\alpha=0} = 2k_{st}k_1\,\tau\,P$$

und

$$(k)_{\alpha=0} = 2\tau\,k_{st}k_1 \tag{4}$$

worin α den Umsatz der Reaktion darstellt.

Entsprechend wird auch die Aktivierungsenergie eine Umsatzabhängigkeit aufweisen und bei Depolymerisationsreaktionen ausgehend vom Anfangswert $(E)_{\alpha=0} = E_{st} + E_1$ stetig abnehmen und bei Geschwindigkeitsmaximum dem Werte $(E)_M = 1/2\,E_{st} + E_1 - E_{\mathrm{Abbr}}$ zustreben.

Ähnliche Überlegungen sind auch für andere komplizierte Abbaureaktionen von Polymeren gültig, so daß im allgemeinen angenommen werden kann, daß unter thermisch dynamischen Bedingungen der thermische Abbau von Polymeren immer einen mehr oder weniger deutlichen Umsatzeinfluß der Aktivierungsenergie aufweisen wird, was ja auch experimentell bestätigt worden ist.

Unter Berücksichtigung dieser Tatsache können wir nun etwas näher auf die Kinetik des thermischen Abbaues von Polymeren eingehen. Wird Gleichung (1) in Abhängigkeit von der Gewichtsänderung umgeschrieben so gelangt man zum Ausdruck :

$$\mathrm{d}w_T/\mathrm{d}T = \frac{A}{a} \exp(-E/RT)\,w_r^n \tag{5}$$

---

[26] V. N. Kondratiev, "Kinetika khimicheskih gazovykh reaktsii" Izd. Akad. Nauk., Moskau, 1968, S. 481.

worin, wie erwähnt, a die konstante Hr, w_T den Gewichtsverlust bei T, w_∞ den Gewichtsverlust am Ende einer Abbaustufe und $w_r = w_\infty - w_T$ das Polymergewicht bei T bedeuten. A, E und n haben den üblichen physikalischen Sinn. Oft wird in der kinetischen Grundgleichung (5) auch der Umsatzgrad $\alpha = w_T/w_\infty$ an Stelle der Gewichtsverluste verwendet.

Eine der verbreitetsten differentiellen Methoden wurde von Freeman und Carroll[7] vorgeschlagen, welche bei konstanter Hr die kinetischen Parameter aus dem Ausdruck

$$\frac{\Delta \log \mathrm{d}w_T/\mathrm{d}T}{\Delta \log w_r} = n - \frac{E}{2{,}3R} \cdot \frac{\Delta(T)^{-1}}{\Delta \log w_r} \tag{6}$$

ableitet. Grundsätzlich kann diese Methode auch bei einer Umsatzänderung von E angewendet werden, nur müssen dann die Differenzen Δ zwischen nahe liegenden Punkten gemacht werden. Trotzdem werden in diesem Falle die erhaltenen Werte nur Mittelwerte von relativer Bedeutung sein.

Bei den integralen Methoden tauchen gleich zwei Schwierigkeiten auf. Erstens muß n bekannt sein, damit die Umsatzintegrale $\int \mathrm{d}w_T/w_r^n = F(c)$ gelöst werden kann, so daß im allgemeinen mathematische Näherungsmethoden angewendet werden müssen.

Zweitens kann die exponentielle Integrale $\int \frac{A}{a} \exp\,(-E/RT)\,\mathrm{d}T$ nicht direkt gelöst werden, wodurch eine Erklärung der verschiedenen in der Literatur vorgeschlagenen Ausdrücke gegeben ist. Doch all diese annähernden Lösungen setzen voraus, daß A, a und E konstant sind, so daß von vornherein die Anwendung dieser Methoden für die Untersuchung von Polymerabbaureaktionen unter thermisch dynamischen Bedingungen in Frage gestellt ist.

Aus diesem Grunde können zur Untersuchung des thermischen Abbaues von Polymeren im Prinzip nur die Methoden herangezogen werden, die entwickelt worden sind, um die kinetischen Parameter für konstante Umsätze zu berechnen, d.h. die eine mögliche Umsatzänderung der Aktivierungsenergie zu berücksichtigen erlauben.

Zwei von diesen Methoden scheinen eine größere Bedeutung zu haben: die sogenannte „Oberflächenmethode" von Reich[11] und die Methode von Flynn und Wall.[24]

Unter Verwendung von Doyles Lösung für die exponentielle Integrale

$$\log F(c) = \log\,(AE/R) - \log\,a + p\,(E/RT)^{15} \tag{7}$$

$$\text{worin } p\,(E/RT) \cong -2{,}135 - (E/2{,}303\,R)\,(T)^{-1} \tag{8}$$

falls $E/RT \gg 20$ ist, was in den meisten Fällen für Polymerdestruktion zutrifft, und mit der Annahme, daß E denselben Wert für gleiche Umsätze unabhängig von der verwendeten *Hr* hat, gelangen Flynn und Wall zum Ausdruck

$$d\,(\log a)/d\,(T)^{-1} \cong -E/2{,}303R \tag{9}$$

der bei konstanter *E* zu einer Familie von parallelen Geraden für verschiedene Umsätze führt. Je geringer die Aktivierungsenergie ist, umso kleiner wird die Neigung dieser Geraden, und somit umso größer die Temperaturverschiebung des Zersetzungsbereiches mit der *Hr* zu höheren Temperaturen sein.[27]

Gleichung (9) kann aber auch benützt werden um den Einfluß des Umsatzgrades auf *E* zu verfolgen, obwohl die Autoren der Methode diesen Fall nicht in Erwägung ziehen. Wird aber ein Umsatzeinfluß angenommen, so verlaufen die Flynn-Wall-Geraden nicht mehr parallel, sondern fächerförmig auseinander. Dieses führt aber neben der erwähnten Temperaturverschiebung des Zersetzungsbereiches auch zu einer Verbreiterung des Temperaturbereiches in dem die Zersetzung stattfindet (Abb. 2).

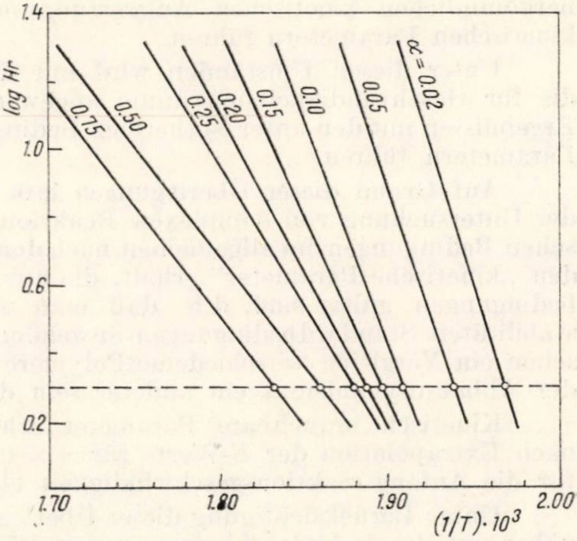

Abb. 2. – Hypothetische Flynn-Wall Darstellung für eine Umsatzabhängigkeit der Aktivierungsregie (E=70 kcal/Mol bei α=0,02 und 29 kcal/Mol bei α = 0,75)

Eine Verbreiterung des Temperaturbereiches bedeutet aber eine scheinbare Verringerung des Temperaturkoeffizienten der Zersetzungsreaktion, d.h. eine scheinbare Abnahme der Aktivierungsenergie mit Erhöhung der *Hr*.

Diese Schlußfolgerung kann ausgehend von Gleichung (7) auch mathematisch belegt werden. Werden zwei aufeinanderfolgende Umsatzgrade bei derselben *Hr* in Betracht gezogen, so ergibt sich aus (7)

$$[\Delta \log F(c)]_a \cong [\Delta\,(-E/2{,}303\;R)\;(T)^{-1}]_a \tag{10}$$

---

[27] C. Duval, „Inorganic Thermogravimetric Analysis", Elsevier Publ. Comp., Amsterdam, 1963, S. 133.

da eine mögliche Änderung von E das logarithmische Glied log (AE/R) weniger beeinflussen wird.

Wird jetzt derselbe Umsatzbereich für zwei verschiedene Hr in Erwägung gezogen, so gilt entsprechend

$$[\Delta \log F(c)]_{a_1} = [\Delta \log F(c)]_{a_2}$$

auch

$$[\Delta(ET^{-1})]_{a_1} = [\Delta(ET^{-1})]_{a_2} \tag{11}$$

Da aber bei einer Umsatzänderung der Aktivierungsenergie infolge der Verbreiterung des Temperaturbereiches $\Delta(T)_{a_1}^{-1} \neq \Delta(T)_{a_2}^{-1}$ gilt, muß auch $(E)_{a_1} \neq (E)_{a_2}$ sein, damit die Bedingungen (11) erfüllt bleiben. Somit läßt sich schließen, daß eine mögliche Umsatzänderung der Aktivierungsenergie immer von einem mehr oder weniger deutlichen Einfluß der Hr auf die Aktivierungsenergie gekennzeichnet ist und die herkömmlichen kinetischen Auswertungsmethoden nur zu scheinbaren kinetischen Parametern führen.

Unter diesen Umständen wird nur die Methode von Kissinger,[13] die für Geschwindigkeitsmaximum angewendet wird, zu vergleichbaren Ergebnissen mit den unter isothermen Bedingungen erhaltenen kinetischen Parametern führen.

Auf Grund dieser Überlegungen läßt sich schließen, daß man bei der Untersuchung von komplexen Reaktionen unter thermisch dynamischen Bedingungen im allgemeinen nach den üblichen Berechnungsmethoden „kinetische Parameter" erhält, die nur für die verwendeten Arbeitsbedingungen gültig sind, d.h. daß man zum Vergleich von Thermostabilitäten Standardbedingungen anwenden muß, wobei wahrscheinlich schon ein Vergleich verschiedener Polymere wieder fraglich sein kann, da der Abbaumechanismus ein anderer sein dürfte.

Kinetisch brauchbare Parameter erhält man wahrscheinlich erst nach Extrapolation der E-Werte für $\alpha = 0$ bzw. $a = 0$, da diese Werte für die Anfangsreaktionsgeschwindigkeit charakteristisch sein dürften.

Unter Berücksichtigung dieser Überlegungen wollen wir nun etwas näher auf die Dehydrochlorierung von PVC eingehen.

Um nähere Aussagen machen zu können fraktionierten wir ein „Geon" Suspensions-PVC nach Benevisse[28] und charakterisierten die Fraktionen viskosimetrisch und durch Lichtstreuung in CH bei 25°.[29]

In Abb 3 und 4 ist die Abhängigkeit der Aktivierungsenergie der Dehydrochlorierung in d-TG Bedingungen vom Umsatz bzw. der Hr für die erhaltenen PVC-Fraktionen wiedergegeben. Die zugehörigen extrapolierten E-Werte, zusammen mit den nach Kissinger[13] berechneten E-Werten für Geschwindigkeitsmaximum sind in Tabelle 2 zusammengestellt.

---

[28] J. P. Benevisse, Thèse de doctorat, Universitée de Lion, 1960.

[29] A. Onu, C. Vasile und I. A. Schneider, *Rev. Roumaine Chim.*, **15**, 1935 (1970).

Wie aus Abb. 5 ersichtlich ist, ändern sich die extrapolierten E-Werte mit $1/M_w$ proportional. Wird nun angenommen, daß die Dehydrochlorierung nach einer Kettenreaktion ähnlich einer Depolymerisation

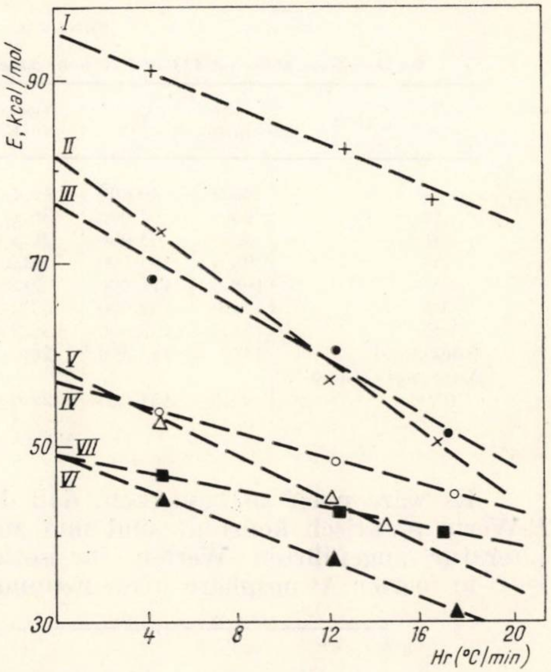

Abb. 3. — Der Einfluß der Hr auf die Aktivierungenergie der Dehydrochlorierung von PVC-Fraktionen in d-TH Bedingungen.

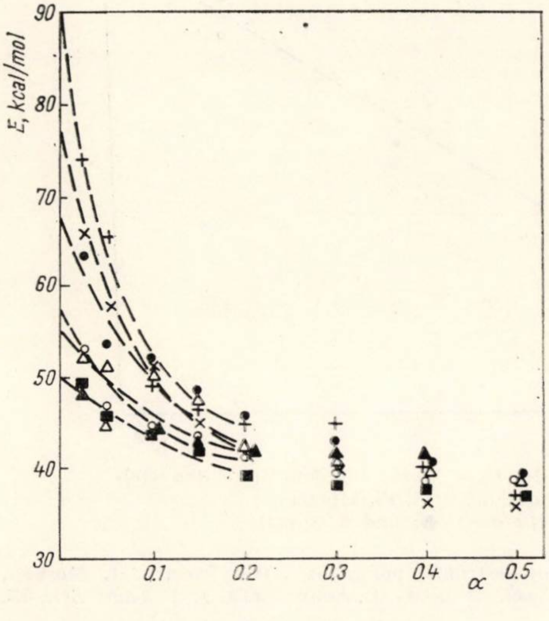

Abb. 4. — Der Einfluß des Umsatzgrades auf die Aktivierungenergie der Dehydrochlorierung von PVC-Fraktionen in d-TG Bedingungen. + — I ; x — II ; ● — III ; o — IV ; Δ — V ; ▲ — VI und ■ — 7. Fraktion

verläuft, so deutet nach Boyd diese Abhängigkeit auf statistischen Start und sehr langen „Reißverschluß"; ein Reaktionsmechanismus der für die Dehydrochlorierung von PVC annehmbar scheint.

Tabelle 2

Der thermische Abbau von PVC in d-TG Bedingungen; die Dehydrochlorierungsreaktion

Fraktion	$[\eta]$ ml/g	$\overline{M}_w$	$E_{\text{Kissinger}}$ kcal/Mol	$E_{a=0}$ kcal/Mol	$E_{\alpha=0}$ kcal/Mol
I	49,9	49.000	$30{,}4 \pm 2{,}6$	95	90
II	63,0	67.000	$30{,}4 \pm 2{,}7$	81,2	77,5
III	55,0	63.000	$29{,}3 \pm 1{,}2$	76	68,2
IV	93,0	108 000	$32{,}2 \pm 2{,}8$	56,5	57
V	108,0	117.000	$29{,}3 \pm 2{,}1$	58	55
VI	119,0	152.000	$32{,}2 \pm 2{,}6$	48,5	50
VII	138,5	173.000	$32{,}2 \pm 2{,}7$	48,5	50
Rückstand	119	143.000	$28{,}6 \pm 3{,}0$	—	—
Ausgangs-„Geon" PVC	99,5	151.000	$29{,}6 \pm 2{,}6$	74,5	74,5
			Mittel: $30{,}8 \pm 2{,}8$		

Es wäre noch zu bemerken, daß die nach Kissinger berechneten E-Werte praktisch konstant sind und zufriedenstellend mit den in der Literatur angeführten Werten für isotherme Dehydrochlorierung von PVC in inerter Atmosphäre übereinstimmen.[28,30]

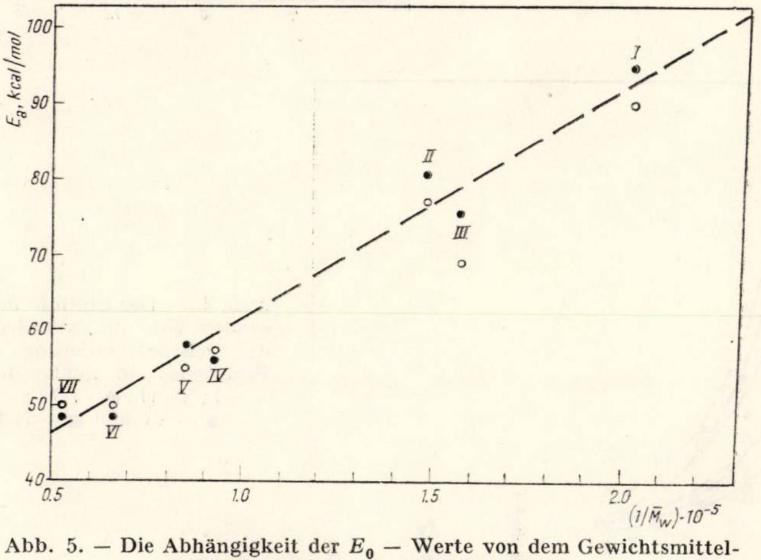

Abb. 5. — Die Abhängigkeit der E_0 — Werte von dem Gewichtsmittelmolekulargewicht der PVC-Fraktionen. E_0 extrapoliert für $a=0$ (●) und $\alpha=0$ (○)

---

[30] N. Grassie, „Khimia protsessov destruktii polimerov", Izd. Inostr. Lit. Moskau, 1959 S. 156; s.a. R. S. Stromberg, S. Strauss und G. B. Achhammer, *J. Polymer. Sci.*, **35**, 355 (1958).

Eine mögliche Erklärung wäre, daß infolge des großen Austrittspotentials der gasförmigen Produkte in thermisch dynamischen Bedingungen der PVC-Abbau, unabhängig von der umgebenden Atmosphäre in HCl-Atmosphäre erfolgt, wofür auch dieselben Ergebnisse in Luft, Stickstoff und Vakuum sprechen.[15]

Abschließend wäre zu bemerken, daß kinetisch brauchbare Ergebnisse nur bei einer kritischen Anwendung der d-TG Methode erhalten werden können. Die üblichen Auswertungsmethoden liefern meistens nur relative Aktivierungsenergien, die aber bei Verwendung von Standardbedingungen zu einer Charakterisierung der Thermostabilität von Polymeren herangezogen werden können.

Revue Roumaine de Chimie, 17, 1, 2, 303–309 (1972)

Herrn Professor I. G. MURGULESCU
zum 70. Geburtstag

STUDIUM DER POLYMERISATION VON ACETYLENDERIVATEN. XV*

DIE ÜBERMOLEKULARE STRUKTUR DER POLYMERE

CR. SIMIONESCU, SVETLANA DUMITRESCU, M. LEANCĂ, M. DĂRÎNGĂ
und MARIA GROVU
von der Technischen Hochschule, Calea 23 August 11, Iaşi

Eingegangen am 25. August 1971

Es wurde ein Studium der übermolekularen Struktur von Polyphenylazethylen und seiner Derivate durch Substitution von -NO_2, -Cl, -CH_3 im Benzolring, mittels der Röntgenbeugung und der Elektronenmikroskopie durchgeführt. Zu diesem Zwecke wurde der Ordnungsgrad und die Symmetrieklasse der Kristallite für einen Teil der untersuchten Polymere bestimmt. Mit Hilfe des Elektronenmikroskops wurden verschiedene Typen von morphologischen Gebilden studiert, die aus den Benzollösungen der betreffenden Polymere erhalten wurden.

1. EINFÜHRUNG

Es ist bekannt, daß die elektrophysikalischen Eigenschaften von Halbleiter-Polymeren in großem Maße von ihrer Molekularstruktur und vor allem von ihrem übermolekularen Bau abhängen.

Die übermolekulare Struktur ergibt sich als Folgeerscheinung der gegenseitigen Lage der Ketten, der intra- und intermolekularen Zwischenwirkungen, der Biegsamkeit der Ketten, der Natur der makromolekularen Konformationen und Konfigurationen, ihrer gegenseitigen Ausrichtung, des Auftretens von sekundären Überbauelementen wie auch des Aufbaues der Polystruktur der Polymere.

Die Einführung der verschiedenen Substituenten (-NO_2, -Cl, -CH_3 Gruppen) in den Benzolkern des Phenylazetylens hat neben der Veränderung der chemischen Struktur des Polymers die Schaffung von Makromolekülen mit konjugierten Doppelbindungen zur Folge, die das Auftreten von gegenseitigen Einwirkungen verschiedener Intensität zur Folge haben können.

Die gegenseitige Anordnung der Makromoleküle und demgemäß die übermolekulare Struktur des Polymeren ist von seht vielen Faktoren abhängig. Ein Studium der übermolekularen Struktur ist notwendig, wenn man die Festsetzung der günstigsten Bedingungen verfolgt, um Polymere mit vorbestimmten Eigenschaften zu erhalten.

---

* XIV.: Mitt. CR. SIMIONESCU, SV. DUMITRESCU, T. LIXANDRU, S. VASILIU und B. SIMIONESCU, *Plaste und Kautschuk* (im Druck)

Die Untersuchungen im Bereiche der übermolekularen Struktur der Polymeren im allgemeinen befinden sich in einem fortgeschrittenen Stadium dank der Vielfältigkeit und Genauigkeit der Methoden, die zu diesem Zwecke angewendet werden : Röntgenbeugung, Elektronenmikroskopie, Mikrokalorimetrie, Dilatometrie, densitometrische Studien usf.

Im Rahmen der vorliegenden Arbeit haben wir uns die Aufgabe gestellt, einige Gesichtspunkte der übermolekularen Struktur von Phenylazetylenpolymeren mittels Röntgenbeugung und Elektronenmikroskopie zu studieren.

Wir weisen darauf hin, daß die Fachliteratur wenig Arbeiten über den Kristallinitätsgrad des Polyphenylazetylens und seiner Derivate aufweist [1-3] ; was die morphologischen Typen der übermolekularen Strukturen angeht, sind uns keine Veröffentlichungen bekannt.

2. STUDIUM DER ÜBERMOLEKULAREN STRUKTUR DURCH RÖNTGENBEUGUNG

2a. EXPERIMENTELLER TEIL

Unsere Untersuchungen erstreckten sich über folgende Arten von Halbleiterpolymeren in Pulverform aus der Azetylenklasse :

1. Polyphenylacetylen, welches durch Ionen-Koordinations-Polymerisations-Mechanismen in Gegenwart des katalytischen Systems $Al(iC_4H_9)/VO(C_5H_7O_2)_2$ erhalten wird und das wir konventionell mit (PFAi) notieren.
2. Polyphenylacetylen, welches auf dem Wege photochemischer Auslösung entsteht (PFAf) ;
3. Poly-methyl-phenylazetylen (PmFA) und
4. Poly-chlor-phenylazetylen (PClFA)

Polymere mit den Substituenten Methyl und Chlor in *para*-Stellung des Benzolrings wurden unter denselben Bedingungen wie das ionische Polyphenylazetylen erhalten.

Man beobachtet, daß bei allen Polymeren, mit Ausnahme des PFAf, je zwei Fraktionen abgetrennt wurden : eine in den üblichen organischen Lösungsmitteln lösliche und eine unlösliche Fraktion.

Die Beugungsbilder (siehe Tabellen 1, 2, 3, 4) wurden an einer TUR-M61 Einrichtung mit Goniometer Modell HZG-1 aufgenommen. Die Strahlungen kamen aus einer Röntgenröhre mit Kupferanode, die mit 30 kV und 20 mA gespeist wurde, und wurden durch einen Nickelfilter monochromatisiert ($\lambda_{Cu-K\alpha} = 1537{,}4$).

Für eine Anzahl von 3 Produkten (siehe Abb. 1, 2, 3) wurde das Spektrum der Röntgenbeugung photographisch aufgenommen. Zu diesem Zwecke wurde eine Beugungsvorrichtung TUR M-60 mit einem Aufnahmegerät, Type DEBYE-SCHERRER mit einem Durchmesser von 57,3 mm benützt ; die verwendete Strahlung war dieselbe ($\lambda_{Cu-K\alpha}$).

---

[1] Sv. Dumitrescu, Doktorarbeit, Technische Hochschule Iași (1968).

[2] P. Ehrlich, R, J. Kern, E. D. Pierron und T, Provder, *Polymer Letters*, **5**, 911 (1967).

[3] A. A. Berlin, M. I.Tscherfaschin, P. P. Kissilitza und M. Ia. Kuschnerov, *Vysokomol. Soedineniya*, **9**, 45 (1967).

2b. ERGEBNISSE UND DISKUSSIONEN

Die erhaltenen Versuchsangaben werden in den nachfolgenden Tabellen und Abbildungen festgehalten:

Tabelle 1

PFAi – unlösliche Fraktion

Linien Nr. I	$d^{*}_{Å}$	$I/I_1\,\%$**
1	5,95	24
2	4,67	49
3	3,31	39
4	2,34	41
5	2,08	49
6	1,47	7
7	1,235	100
8	1,167	17
9	0,93	12
10	0,907	32
11	0,827	12

* $d_{Å}$ – stellt die Netzebenenabstände dar.

** $I/I_1\,\%$ – stellt die relative Intensität des Beugungsmaximums dar.

Tabelle 2

PFAf – lösliche Fraktion

Linien Nr.	$d_{Å}$	$I/I_1\,\%$
1	4,87	diffuses Maximum*[1]
2	2,37	100
3	2,04	37
4	1,435	15
5	1,32	66
6	1,175	16

*[1] Das diffuse Maximum ist durch $R = 1{,}25$ xd gekennzeichnet R stellt Durchschnittswert der Trennungsabstände der diffundierenden Einheiten dar[4]

Die auf den Bereich 5—70° (θ) beschränkten Messungen zeigen im allgemeinen eine klare Trennung der amorphen Beugungsdiffusion in den geordneten Bereichen.

Zur quantitativen Kennzeichnung des Koordinationsgrades der untersuchten Polymere berechnete man die relativen Werte des Kristallinitätsgrades nach Hermans.[5]

---

[4] H. P. Klug und L. E. Alexander, „X-Ray Diffraction Procedures for Polycristalline and Amorphous Materials", John Wiley, New York, 1954, S. 911.

[5] P. H. Hermans, *J. Polymer Sci.*, **4**, 709 (1949).

Tabelle 3

PmFA – lösliche Fraktion

Linien Nr.	d Å	I/I_1 %
1	6,845	11
2	4,805	10
3	3,470	3
4	2,370	100
5	2,040	44
6	1,435	18
7	1,225	65
8	1,173	6
9	1,012	6
10	0,910	23
11	0,888	52
12	0,864	3
13	0,850	75
14	0,816	38

Tabelle 4

PmFA – unlösliche Fraktion

Linien Nr.	d Å	I/I_1 %
1	7,04	7
2	4,76	15
3	2,26	65
4	2,04	29
5	1,44	6
6	1,22	100
7	1,173	6
8	0,930	4
9	0,827	9

Tabelle 5

Kristallinitätsgrade der untersuchten Polymere

Lfd. Nr.	Bezeichnung des Polymeren	Kristallinitätsgrad %
1	PFAi — unlösliche Fraktion	41
2	PFAi — lösliche Fraktion	amorph
3	PFAf	<10
4	PmFA — unlösliche Fraktion	30
5	PmFa — lösliche Fraktion	27
6	PClFA — unlösliche Fraktion	60
7	PClFA — lösliche Fraktion	amorph

Die durchschnittlichen Ausmaße der Kristallite wurden mittels der Analyse der Form der Beugungslinien bestimmt.

Bei einer relativ vollkommen kristallinen Verbindung im Pulverzustand kann die durchschnittliche Dimension der Kristallite mittels der bekannten Scherrerschen Beziehung bestimmt werden:

$$D_{hkl} = \frac{K\lambda}{\beta_{0.} \cos \theta}$$

wobei D_{hkl} den Mittelwert der Kristallitenausmaße in senkrechter Richtung auf die Ebenen h, k, l, darstellt; β_0 ist die integrale Breite oder die Breite bei halber Maximalintensität der Kurve, welche das Beugungsmaximum beschreibt, das in rad gemessen wird, und K ist eine Konstante, deren Wert gewöhnlich gleich der Einheit angenommen wird.

Die Scherrersche Formel wird von einigen Autoren dazu verwendet, einen Schätzwert der Ausmaße der kristallinen Bereiche bei Polymeren zu berechnen.[6] Es ist zu bemerken, daß die auf diesem Wege erhaltenen zahlenmäßigen Resultate nicht den tatsächlichen Werten entsprechen; dies wegen des bedeutenden Beitrages der Gitterverzerrungen und der Geometrie der experimentellen Montage bei der Breite der Reflexe.

Im Zusammenhang mit den polymeren Systemen schließt der gegenwärtige Zustand der Verzerrungstheorie und der Beugungsreflexe beträchtliche Elemente von Unsicherheit und Kontroversen ein.

Unter Verwendung der Scherrerschen Beziehung wurden die durchschnittlichen Kristallitenausmaße der untersuchten Polymeren bestimmt (siehe Tabelle 6).

Das Indizieren der Beugungsbilder eines Teiles der untersuchten Polymeren zeigt das Vorhandensein von Kristallen mit tetragonaler Symmetrie an. Bei der unlöslichen Fraktion von PFAi sind die Parameter der Elementarzelle durch folgende Werte gekennzeichnet: $a = 4{,}67$ Å ± ± 0,01 und $c = 5{,}95$ Å ± 0,01: für PmFA unlösliche Fraktion: $a = 4{,}76$ Å ± 0,01 und $c = 7{,}04$ Å ± 0,01.

Tabelle 6

Durchschnittliche Ausmaße der Kristallite

Lfd. Nr.	Natur des Polymeren	Durchschnittsausmaß des Kristalliten (Å)
1	PFAi – unlösliche Fraktion	300
2	PFAf	290
3	PmFA-unlösliche Fraktion	275

Es wird festgestellt, daß die unlöslichen Anteile der untersuchten Polyphenylazetylene einen höheren Ordnungsgrad als die löslichen aufweisen. Die geringen Unterschiede des Kristallinitätsgrades zwischen den beiden Typen von Fraktionen bei sämtlichen Polymeren gestatten die Folgerung, daß die unlöslichen Fraktionen der Polyphenylazetylene vernetzte Ketten enthalten, was ihre Unlöslichkeit rechtfertigt. Diese Annahme stimmt mit den Ergebnissen der IR-Spektralanalyse überein, die in einer früheren Arbeit veröffentlicht wurden.[7] Man beobachtet gleichfalls, daß die Lage der Beugungslinien bei allen Phenylazetylenpolymeren ungefähr die gleiche bleibt; dies beweist die Erhaltung der mittleren Periodizitätsabstände.

---

[6] L. E. Alexander, „X-Ray Diffraction Methods in Polymer Science", John Wiley, New York, 1969, S. 631.

3. STUDIUM DER ÜBERMOLEKULAREN STRUKTUR DURCH ELEKTRONENMIKROSKOPIE

3.a. EXPERIMENTELLER TEIL

Unsere Untersuchungen der übermolekularen Struktur wurden an einem Elektronenmikroskop TESLA BS 513-A angestellt.

Es wurden die Strukturen verfolgt, die man durch Absetzung aus Lösungen erhielt; dies gilt für die löslichen Fraktionen folgender Polymere: PFA; PFAf; PmFA und PClFA.

Man arbeitete mit Benzollösungen von Polymeren bei Gehalten von 0,1...0,0001%. Da man bei Konzentrationen von 0,1% Molekülagglomerate erhielt, verzichtete man auf diese unschlüssigen Proben.

3.b. ERGEBNISSE UND DISKUSSIONEN

Gemäß den Literaturempfehlungen[8] muß jedes Studium der übermolekularen Struktur von Polymeren mit der Untersuchung des übermolekularen Baues der amorphen Phase beginnen, ohne Rücksicht darauf, ob das Polymer kristallin ist oder nicht.

Es wurden zuerst Ablagerungen aus Lösungen von 0,005% Konzentration auf Gittern mit Kolloxylinträgern bei Zimmertemperatur erhalten. Nach Abdampfen des Lösungsmittels wurden die Proben mit Germanium unter einem Winkel von 45° beschattet. In diesem Fall erhielt man kugelförmige Strukturen für PClFA (Bild 4) und PFAi (Abb. 5).

In einer andern Probenreihe wurden Lösungen von 0,005% Gehalt im Trockenschrank 3 Stunden lang bei 50° gehalten, dann wurde die Temperatur langsam ($\sim 0{,}2°/\text{min}$) bis auf 23° abgekühlt. Unter diesen Arbeitsbedingungen erhielt man gleichfalls kugelförmige Strukturen für PFAf (Abb. 6) und PmFA (Abb. 7).

Eine Lösung von PClFA von 0,005% Konzentration, die 2 Stunden lang bei 50° gehalten und dann langsam auf 23° abgekühlt wurde, ergab nach Ablagerung auf Kohleträgern im mikroskopischen Bild eine spezifische kugelförmige Makrostruktur, welche sich aus der Assoziation von Einzelkügelchen ergaben (Abb. 8). Die Proben wurden in diesem Fall mit Ag unter einem Winkel von 45° beschattet.

Aus der Lösung derselben Polymere von 0,005% Gehalt, die 4 Stunden lang bei 40° gehalten, auf Gittern mit Kolloxylinträgern abge-

---

[7] Cr. Simionescu, Sv. Dumitrescu, T. Lixandru, S. Vasiliu und B. Simionescu, *Plaste und Kautschuk* (im Druck).

[8] W. A. Kargin und G. L. Slonimski, „Kratkije otcherki po fisikokhimii polimerov", Izd. Khim., Moskau, 1967, S. 24.

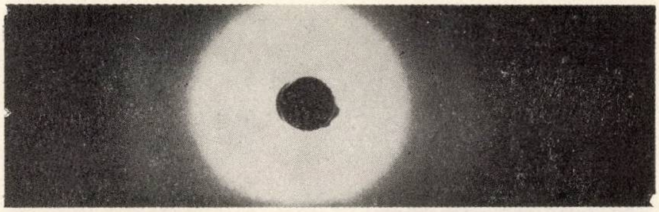

Abb. 1. — Beugungspektrum von PClFA (lösliche Fraktion).

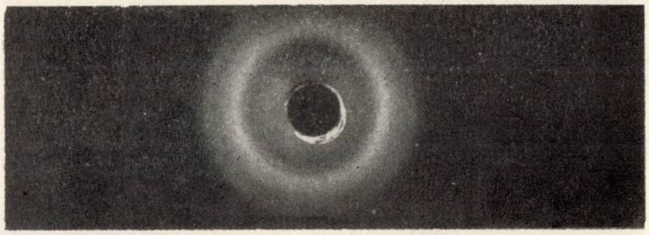

Abb. 2.—Beugungsspektrum von PClFA (unlösliche Fraktion).

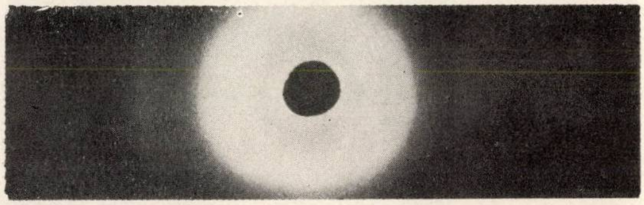

Abb. 3. — Beugungsspektrum von PFAi (lösliche Fraktion).

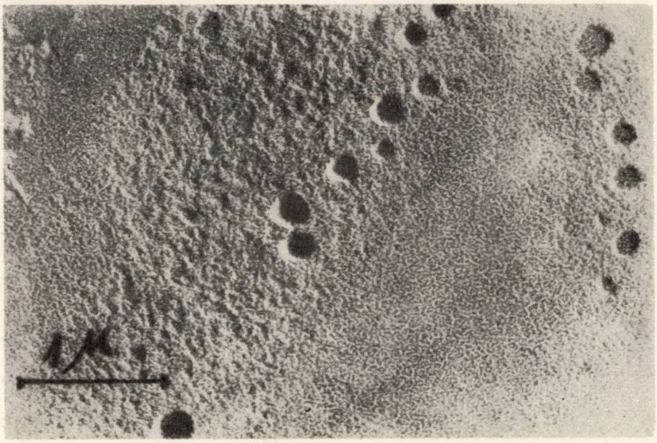

Abb. 4. — Kugelförmige Struktur von PClFA.

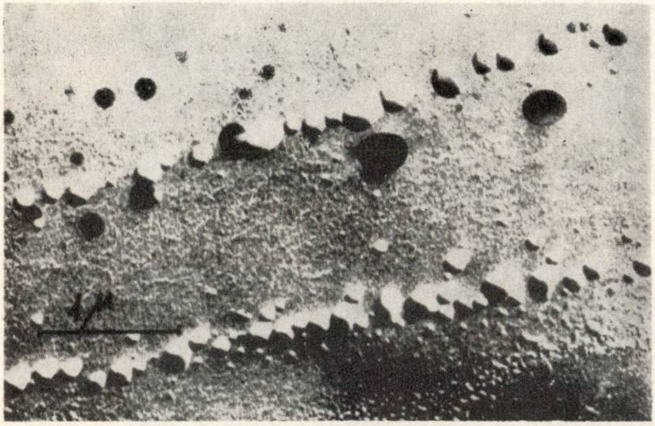

Abb. 5. — Kugelförmige Struktur von PFAi.

Abb. 6. — Kugelförmige Struktur von PFAf.

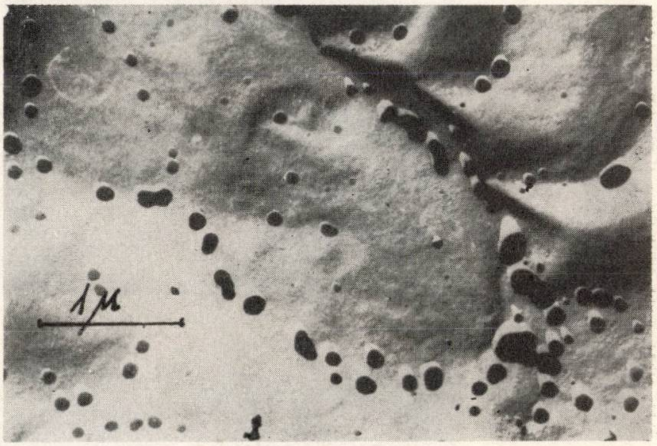

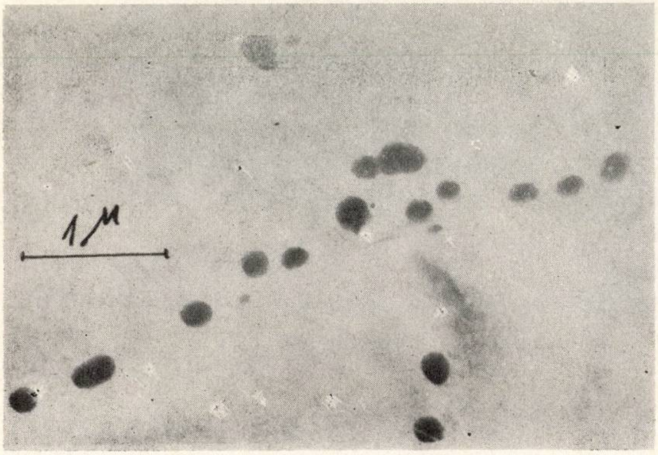

Abb. 7. — Kugelförmige Struktur von PmFA.

Abb. 8. — Makroglobulare Struktur von PClFA.

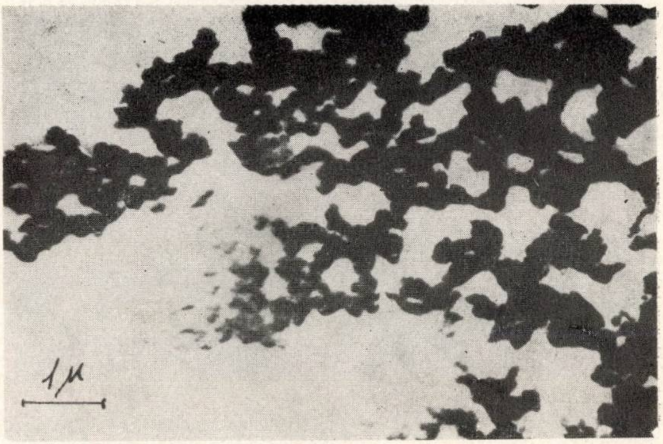

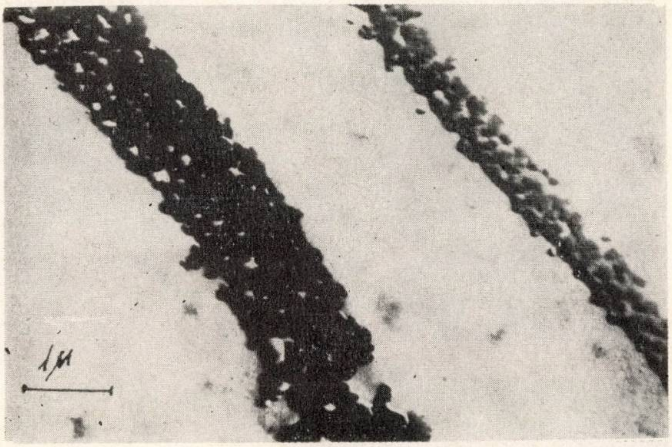

Abb. 9. — Komplexe kugelförmige Aggregate von PClFA.

Abb. 10. — Kugelförmige Struktur von PFAf.

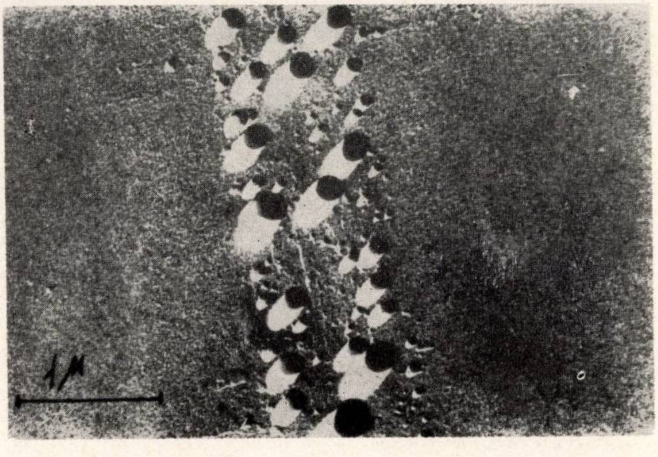

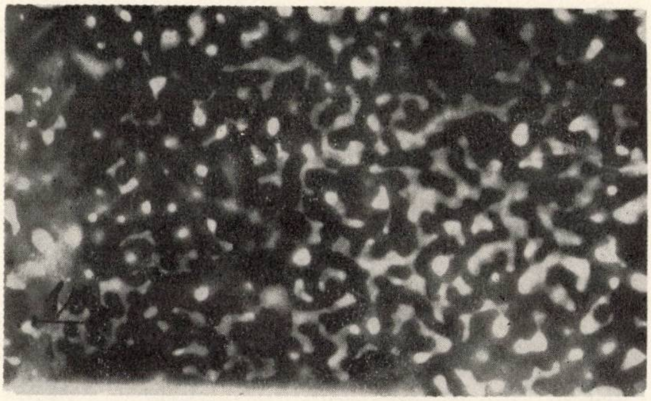

Abb. 11. — Komplexe Strukturen von PClFA.

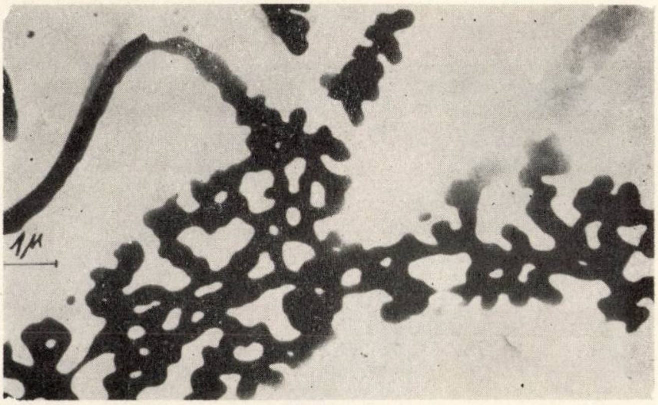

Abb. 12. — Komplexe Strukturen von PFAf.

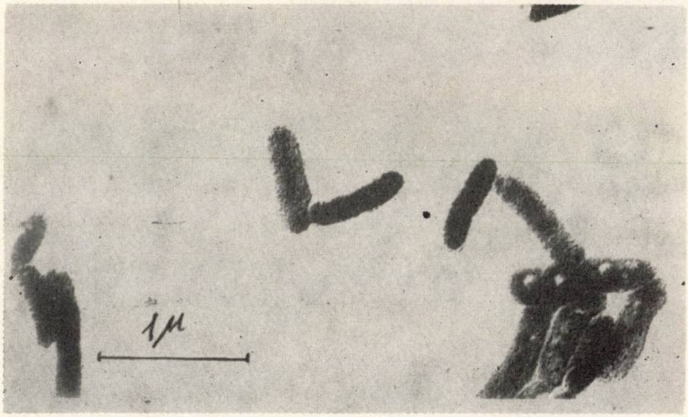

Abb. 13. — PmFA — Strukturen die Paketen ähneln.

lagert und bei dieser Temperatur noch 2 Stunden gehalten wurden, erhielt man komplexe Strukturen, die sich durch einen Aggregationsvorgang der Kügelchen ergaben (Abb. 9).

Im Falle einer PFAf-Lösung von 0,0005 % Gehalt, welche 3 Stunden lang bei 45° gehalten, auf Kolloxylinfilmen abgelagert und bei Zimmertemperatur verdampft wurde, erhielt man typisch kugelförmige Strukturen (Abb. 10).

PClFA von 0,005 % Gehalt weist durch einfache Ablagerung auf Kolloxylinfilmen bei Zimmertemperatur komplexe Strukturen auf (Abb. 11). Ähnliche Strukturen erhielt man auch bei PFAf, dessen 0,005 %ige Lösung 2 Stunden lang bei 50° gehalten und dann auf einen Kohleträger bei Zimmertemperatur abgelagert wurde (Abb. 12).

Durch Ablagerung auf Kohlenmembranen bei Zimmertemperatur einer PmFA-Lösung von 0,005 % Gehalt, welche 3 Stunden lang bei 45° gehalten wurde, erhielt man eigentümliche morphologische Strukturen, von verlängerter Form, ungefähr gleicher Ausmaße, die mit den Formationen von der Art der Kettenpakete ähneln (Abb. 13).

Es ergibt sich, daß alle Polymeren die Tendenz aufweisen vorzüglich kugelförmige Strukturen zu bilden ; dies war zu erwarten, wenn man ihre chemische Darstellung in Betracht zieht, mit umfangreichen seitlichen Substituenten an der Grundkette. In Abhängigkeit von der Konzentration der Benzollösungen der Polymeren und von der angewendeten thermischen Behandlung, erhielt man sowohl kugelförmige Einzelstrukturen (Abb. 4, 5, 6, 7, 10) als auch Kugelassoziationen in der Form komplexerer Gebilde (Abb. 8, 9, 11, 12).

Um festzustellen, ob man auch andere morphologische Formen erzielen kann, wäre es zweckmäßig, die übermolekularen Strukturen zu studieren, zu welchem Zwecke Polymerlösungen verwendet werden müßten, die auch mit anderen Lösungsmitteln als Benzol erhalten werden, wobei natürlich andere Temperaturbedingungen einzuhalten wären.

4. SCHLUSSFOLGERUNGEN

Es wurde die übermolekulare Struktur der durch Polymerisation von Phenylazetylen und seiner Derivate erhaltenen Polymere, wie auch die Morphologie der aus Benzollösungen derselben erhaltenen Konformationen studiert.

1. Bei allen erwähnten Polymeren stellt man kleine Koordinationsgrade fest.
2. Die mittleren Periodizitätszahlen sind ungefähr bei allen untersuchten Polymeren gleich.
3. Man stellt eine tetragonale Symmetrie der Kristallite von PFA und PmFA fest.
4. Bei allen untersuchten Polymertypen beobachtet man, daß der unlösliche Anteil durch einen höhern Koordinationsgrad als der lösliche gekennzeichnet ist.
5. Man stellt fest, daß die Phenylazetylenpolymere eine geringe Fähigkeit aufweisen, übermolekulare Strukturen höherer Koordination zu bilden.

Revue Roumaine de Chimie, 17, 1, 2, 303–309 (1972)

gelegt und bei dieser Temperatur noch 2 Stunden gehalten wurden, erhielt man komplexe Strukturen, die sich durch einen Aggregationsvorgang der Kügelchen ergeben (Abb. 9).

Im Falle einer PVAF-Lösung von 0,005% Gehalt, welche 3 Stunden lang bei 40° gehalten, auf Koffeinkristallen abgelagert und bei Zimmertemperatur verdampft wurde, erhielt man typisch kugelförmige Strukturen (Abb. 10).

PVFA von 0,005% Gehalt zeigt durch einfache Ablagerung auf Kohle bei der Zimmertemperatur komplexe Strukturen auf (Abb. 11).

Ähnliche Strukturen erhielt man auch bei PVAL, deren 0,005%ige Lösung 3 Stunden lang bei 50° gehalten und dann auf einen Kohleträger bei Zimmertemperatur abgelagert wurde (Abb. 12).

Durch Ablagerung auf Kohlenmembranen bei Zimmertemperatur einer PVFA-Lösung von 0,005% Gehalt, welche 3 Stunden lang bei 45° erhalten wurde, erhielt man eigentümliche morphologische Strukturen, von verschiedener Form, ungefähr gleicher Ausmasse, die mit den Formationen von der Art der Kettenpakete ähneln (Abb. 13).

Es ergibt sich, daß alle Polymeren die Tendenz aufweisen vorzüglich kugelförmige Strukturen zu bilden; dies war zu erwarten, wenn man ihre chemische Darstellung in Betracht zieht, mit umfangreichen seitlichen Substituenten an der Grundkette. In Abhängigkeit von der Konzentration der Behandlungen der Polymeren und von der angewendeten thermischen Behandlung erhielt man sowohl kugelförmige Einzelstrukturen (Abb. 4, 5, 6, 7, 10), als auch Kugelassoziationen in der Form komplexer Gebilde (Abb. 8, 9, 11, 12).

Um festzustellen, ob man auch andere morphologische Formen erzielen kann, wäre es zweckmäßig, die übermolekularen Strukturen zu studieren, zu welchem Zwecke Polymerlösungen verwendet werden müßten, die auch mit anderen Lösungsmitteln als Benzol erhalten werden, wobei natürlich andere Temperaturbedingungen einzuhalten wären.

4. SCHLUSSFOLGERUNGEN

Es wurde die übermolekulare Struktur der durch Polymerisation von Vinylacetat und seiner Derivate erhaltenen Polymere, wie auch die Morphologie der aus Benzollösungen derselben erhaltenen Koagulationen studiert.

1. Bei allen erwähnten Polymeren stellt man kleine Koordinationsgrade fest.
2. Die mittleren Parakristallgrößen sind ungefähr bei allen untersuchten Polymeren gleich.
3. Man stellt eine ausgesprochene Symmetrie der Kristallite von PVA und PVF fest.
4. Bei allen untersuchten Polymertypen bemerkt man, daß der amorphe Anteil durch einen höheren Koordinationsgrad als der kristalline gekennzeichnet ist.
5. Man stellt fest, daß die Phasenbildungskinetik eine geringe Fähigkeit aufweisen, übermolekulare Strukturen höherer Koordination zu bilden.

Revue Roumaine de Chimie, 17, 1, 2. 311–317 (1972)

Herrn Professor I. G. MURGULESCU
zum 70, Geburtstag

DIE THERMISCHEN PHASENGLEICHGEWICHTE DES SYSTEMS $SrO-V_2O_5$

S. SOLACOLU, R. DINESCU und MARIA ZAHARESCU

vom Institut für Physikalische Chemie, Bukarest, str. Dumbrava Roșie, 23

Eingegangen am 14. August 1971

Es wurden die thermischen Phasengleichgewichte des binären Systems SrO-V_2O_5 untersucht. Die Bildung von drei binären Verbindungen, und zwar : $SrO.V_2O_5$, welche bei 658° kongruent schmilzt, $2SrO.V_2O_5$ und $3SrO.V_2O_5$ mit unkongruenten Schmelzpunkten bei 1010° bzw. 1250° wurde festgestellt. Die Verbindungen wurden röntgenographisch, lichtmikroskopisch und durch IR-Spektroskopie charakterisiert.

1. EINLEITUNG

Die Massen der binären Systeme vom Typus RO-V_2O_5 ($R = Mg$, Ca, Sr, Ba) wurden besonders wegen ihren elektrischen und mineralisierenden Eigenschaften untersucht. Von Futaki[1] wurde die Zugehörigkeit der oben genannten Systeme mit hohem V_2O_5-Gehalt den „Kritischen Temperatur-Widerständen" zugeordnet. Diese Massen sind durch einen starken elektrischen Widerstandsabfall bei 68° (mit 2—4 Größenordnungen) und einem negativen Temperaturkoeffizienten des elektrischen Widerstandes charakterisiert.

Die Untersuchungen die sich auf diese Systeme beziehen, wurden durch Bestimmung der thermischen Phasengleichgewichtsdiagramme theoretisch begründet.

Die thermischen Phasengleichgewichte der Systeme $MgO-V_2O_5$[2–6] $CaO-V_2O_5$[7] und $BaO-V_2O_5$[2,8] waren vorher untersucht worden.

Den Gegenstand dieser Arbeit bilden die thermischen Phasengleichgewichte im System $SrO-V_2O_5$, worüber in der Fachliteratur keine Aufschlüsse vorliegen.

---

[1] H. Futaki, *Japan J. Appl. Phys.*, **4**, 28 (1965).

[2] R. Kohlmuller und J. Perraud, *Bull. Soc. chim. France*, **1964**, 642.

[3] A. J. Pollard, *Sci. Aerospace Rept.*, **3**, 1095 (1965); *Chem. Abstr.*, **64**, 1405 e.

[4] V. A. Matveevicheva, Z. I. Ejkova, B. E. Zaitsev und A. G. Lyubarski, *Zhur. fiz. Khim.*, **43**, 263 (1969).

[5] R. Wollast und A. Tazairt, *Silicat. Ind.*, **34**, 27 (1969).

[6] S. Solacolu, R. Dinescu und M. Zaharescu, *Rev. Roumaine Chim.*, **16**, 851 (1971).

[7] A. N. Morozov, *Metallurg.*, **13**, 24 (1938).

[8] S. Solacolu, R. Dinescu und M. Zaharescu, *Rev. Roumaine Chim.*, **15**, 401 (1970).

2. VERSUCHSDURCHFÜHRUNGEN

Die verwendeten Reagenzien waren analysenrein : V_2O_5—99,60 % und $SrCO_3$—99,7%. Zur Aufbereitung der untersuchten Massen wurden die jeweiligen Stoffe als Pulver von 60 μm Korngröße 5 Std. lang als Wassersuspension geschüttelt. Auf diesem Weg wurde die Reaktion zwischen der durch Auflösung des V_2O_5 erhaltenen Vanadiumsäure und $SrCO_3$ verwirklicht.

2.1. BESTIMMUNG DER SCHMELZTEMPERATUREN

Die Bestimmung der Liquidustemperaturen wurde mit einem Zeiss-Hochtemperaturmikroskop, mit horizontalem Ofen ausgeführt. Das Mikroskop gibt die Möglichkeit Temperaturen bis 1600° zu erreichen. Die Versuchstechnik wurde in vorangehenden Arbeiten [6,8] beschrieben.

2.2. BESTIMMUNG DES BILDUNGSMECHANISMUS DER CHEMISCHEN VERBINDUNGEN

Die Untersuchung des Bildungsmechanismus der chemischen Verbindungen wurde durch Differentialthermoanalyse und Thermogravimetrie ausgeführt, wobei ein Erdey-Paulik Derivatograph mit einer Aufheizgeschwindigkeit von 10°/min, bis zu einer Temperatur von 1000° verwendet wurde.

2.3. PHASENANALYSE

Die Phasenanalyse wurde durch die statische Methode, in einem Superkanthalofen auf thermisch behandelten Proben ausgeführt. Zur Identifizierung der Phasen wurde die röntgenographische, lichtmikroskopische und IR-spektroskopische Methode benützt.

Die röntgenographischen Bestimmungen wurden nach Debye-Scherrer mit einem TUR Gerät und $Cu_{K\alpha}$ -Strahlen ausgeführt.

Die lichtmikroskopischen Bestimmungen wurden im polarisierten Licht, auf dünnen Schliffen durchgeführt.

Die IR-spektroskopischen Bestimmungen wurden mit dem Zeiss Spektrograph in dem Frequenzgebiet 1800—400 cm^{-1} durchgeführt.

3. VERSUCHSERGEBNISSE

3.1. CHEMISCHE VERBINDUNGEN IM SYSTEM

Die Phasenanalyse der untersuchten Massen führte zur Identifizierung der folgenden 5 kristallinen Phasen im thermischen Gleichgewicht : V_2O_5, SrO, $SrO.V_2O_5$, $2SrO.V_2O_5$ und $3SrO.V_2O_5$. Die identifizierten binären Verbindungen wurden bisher in der Fachliteratur nicht beschrieben.

Die drei binären Verbindungen, die durch Reaktion im festen Zustand bei den Temperaturen von 600°, 800° und 900° entstanden, sind durch Röntgenbeugungslinien, welche in Tabelle 1 wiedergegeben sind, charakterisiert.

Tabelle 1

Röntgenbeugungslinien der Verbindungen des Systems $SrO-V_2O_5$

$SrO \cdot V_2O_5$		$2\,SrO \cdot V_2O_5$		$3\,SrO \cdot V_2O_5$	
d	I	d	I	d	I
3,626	s. sch.				
		3,463	st.		
3,309	s. st.				
		3,184	s. st.		
3,054	st.			3,082	s.st.
		2,986	m. st.		
		2,838	m. st.		
		2,728	m. st.	2,798	s. st.
		2,519	st.		
2,352	m. st.	2,378	s. sch.	2,357	sch.
		2,241	m. st.	2,228	st.
2,187	m. st.			2,186	sch.
		2,130	sch.	2,145	sch.
2,087	m. st.	2,004	s.sch.	2,078	st.
1,901	sch.				
1,883	sch.			1,856	m. st.
1,8276	sch.				
1,808	m. st.				
				1,671	st.
				1,620	st.

s.sch. = sehr schwach
sch. = schwach
m.st. = mittelstark
st. = stark
s.st. = sehr stark

Die mikroskopischen Aufnahmen der $SrO.V_2O_5$, $2SrO.V_2O_5$ und $3SrO.V_2O_5$ sind in Abbildung 1 (a, b, c) gezeigt.

Die Verbindung $SrO.V_2O_5$ bildet prismatische, gestreckte, gelblichbraune Kristalle.

Die Verbindung $2SrO.V_2O_5$ ergibt kleine, prismatische gestreckte, gelblichweiße Kristalle.

Die Verbindung $3SrO_2O_5$ bildet prismatische, hexagonale, durchsichtige Kristalle

Die IR-Spektren der genannten Verbindungen sind in Abbildung 2 (a, b, c) wiedergegeben. Die Untersuchung der Spektren zeigt, daß sie keine charakteristischen Absorptionsbanden für V_2O_5[9] und $SrCO_3$[10,11] enthalten.

---

[9] B. E. Zaitsev, Z. I. Ejkova und I. I. Joffe, *Kinetika i Kataliz*, **7**, 4 (1966).

[10] J. H. Hunt, M. P. Wisherd und L. C. Bohnam, *Analyt. Chem.*, **22**, 1478 (1950).

[11] H. Moenke, „Mineralspektren", Berlin, **1962**, 3.15.

Die Verbindung $SrO.V_2O$ besitzt Absorptionsbanden bei 490, 530, 570, 670, 855, 905, 950 und 965 cm^{-1}.

Die Verbindung $2SrO.V_2O_5$ zeigt Absorptionsbanden bei 570, 730, 825, 855, 885, 905, 920 und 940 cm^{-1}.

Die Verbindung $3SrO.V_2O_5$ zeigt Absorptionsbanden bei 760, 825, 835, 880, 985, 910, 920, 1110 und 1150 cm^{-1}.

3.2. BILDUNGSMECHANISMUS DER CHEMISCHEN VERBINDUNGEN

Der Bildungsmechanismus wurde für die Fälle des trockenen und des in wässeriger Suspension homogenisierten Ausgangmaterials untersucht.

Die Aufeinanderfolge der Erscheinungen, welche zur Bildung der binären Verbindungen führen, konnte dadurch festgestellt werden, daß die Anzahl und Temperatur, bei welcher thermische Effekte auftreten, mit den Gewichtsvariationen und der röntgenographischen Analyse im untersuchten System in Verbindung gebracht wurden. Für die Massen die trocken homogenisiert wurden, war folgende thermische Entwicklung zu bemerken (Abbildung 3 a, b, c):

Die Ausgangsmischung welche zur Verbindung $SrO.V_2O_5$ führt, weist zwei endotherme Effekte bei 400° und 555° auf, die von einer Gewichtsabnahme, gemäß dem Zerfall von $SrCO_3$, begleitet ist.

Die Ausgangsmischung, welche der Verbindung $2SrO.V_2O_5$ entspricht, weist ihrerseits Effekte bei 400° und 555° auf, denen andere zwei endotherme Effekte bei 670° und 1010° folgen. Daraus folgt, daß in diesem Fall $SrO.V_2O_5$ gebildet wird, welches bei 670° mit dem in Überschuß befindlichen $SrCO_3$ reagiert. Dabei wird $2SrO.V_2O_5$ gebildet und CO_2 abgegeben. Der endotherme Effekt bei 1010° wird dem unkongruenten Schmelzen des $2SrO.V_2O_5$ zugeschrieben.

Die Verbindung $3SrO.V_2O_5$ bildet sich in drei Stufen: bei 555° bildet sich $SrO.V_2O_5$, welches bei 670° mit $SrCO_3$ im Überschuß reagiert und $2SrO.V_2O_5$ bildet. Diese Verbindung bildet bei 895° mit dem Rest des $SrCO_3$ das $3SrO.V_2O_5$.

Folglich bildet sich, unabhängig vom $SrO : V_2O_5$-Verhältnis, zuerst $Sr.O.V_2O_5$, welches bei $SrCO_3$-Überschuß bei höheren Temperaturen in $2SrO.V_2O_5$, bzw. $3SrO.V_2O_5$ übergeht. Diese Reaktionen finden mit $SrCO_3$-Zerfall statt, was den endothermen Charakter der verzeichneten thermischen Effekte erklärt.

Gleichartigen Reaktionsmechanismus kann man bei den in wässerigen Suspensionen homogenisierten Proben feststellen. In diesen Fällen ist die Auswertung der verzeichneten thermischen Effekte schwieriger,

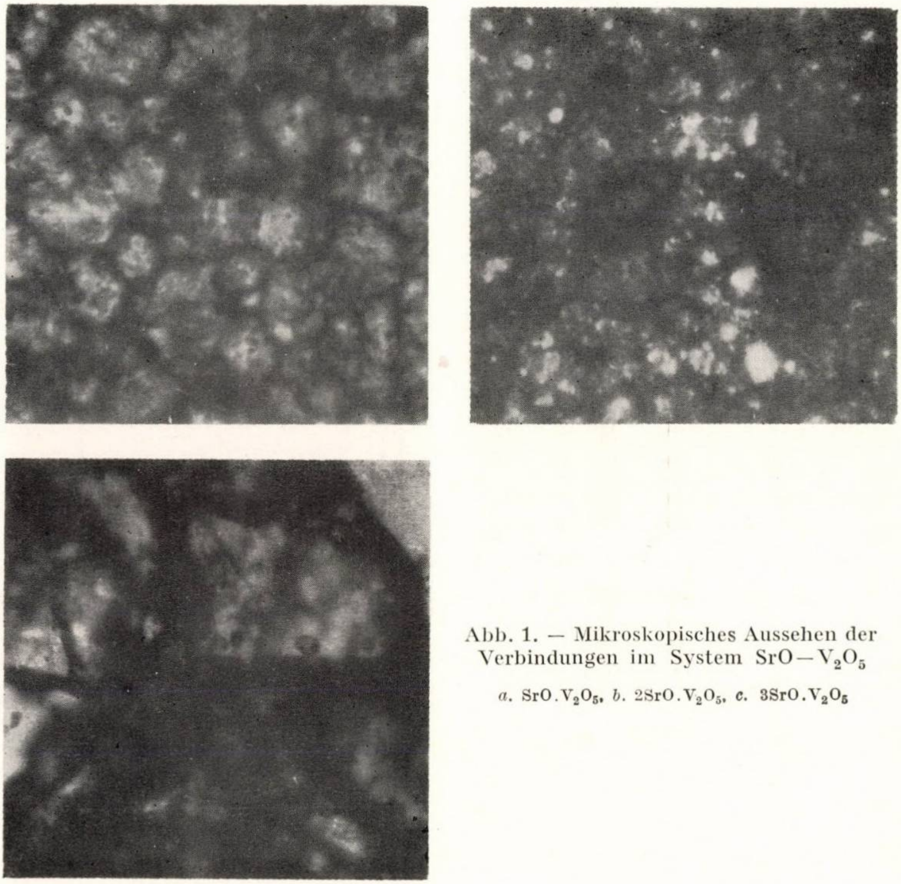

Abb. 1. — Mikroskopisches Aussehen der Verbindungen im System $SrO-V_2O_5$

a. $SrO.V_2O_5$, *b*. $2SrO.V_2O_5$, *c*. $3SrO.V_2O_5$

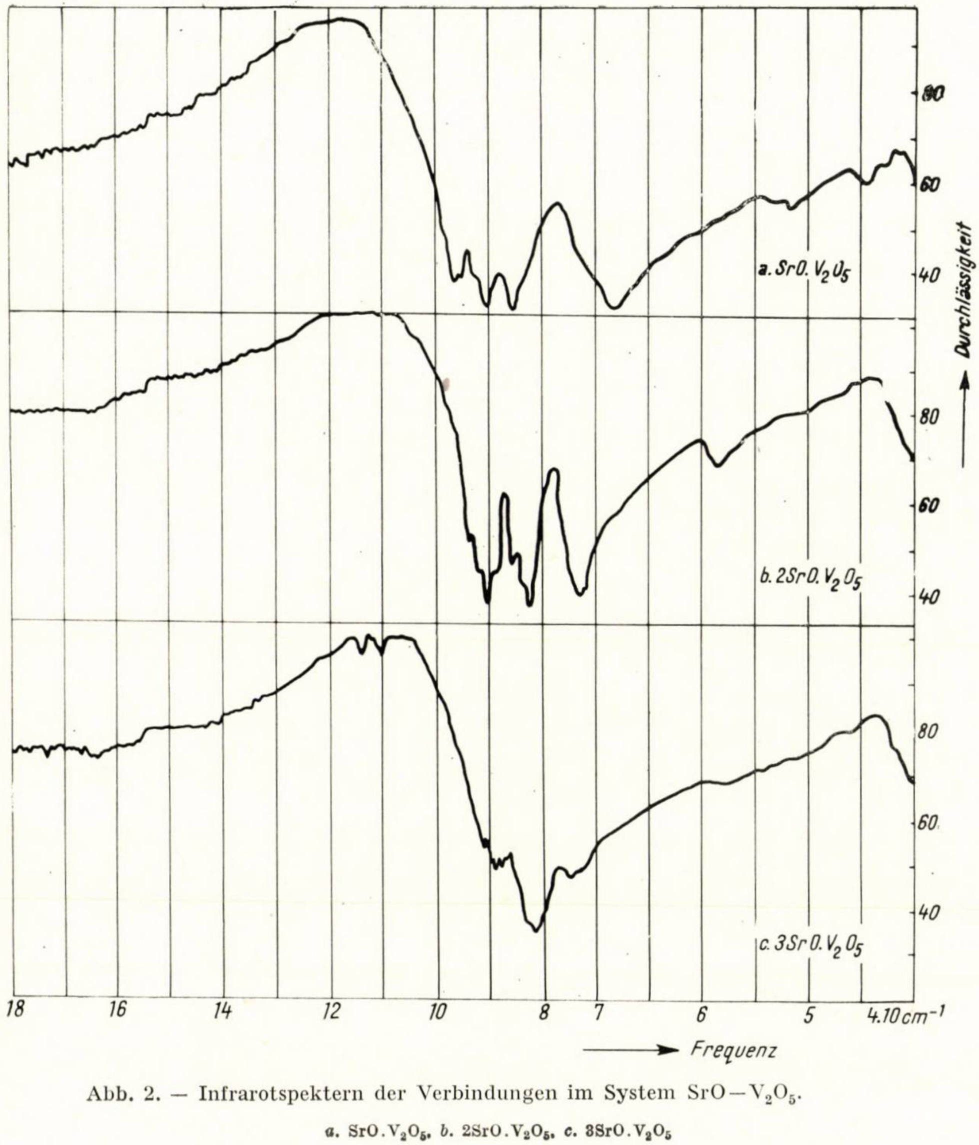

Abb. 2. — Infrarotspektern der Verbindungen im System $SrO-V_2O_5$.

a. $SrO.V_2O_5$, *b.* $2SrO.V_2O_5$, *c.* $3SrO.V_2O_5$

wegen den Zwischenprodukten welche sich auf Grund der Reaktion zwischen V_2O_5 und $SrCO_3$ in wässerigem Medium bilden.

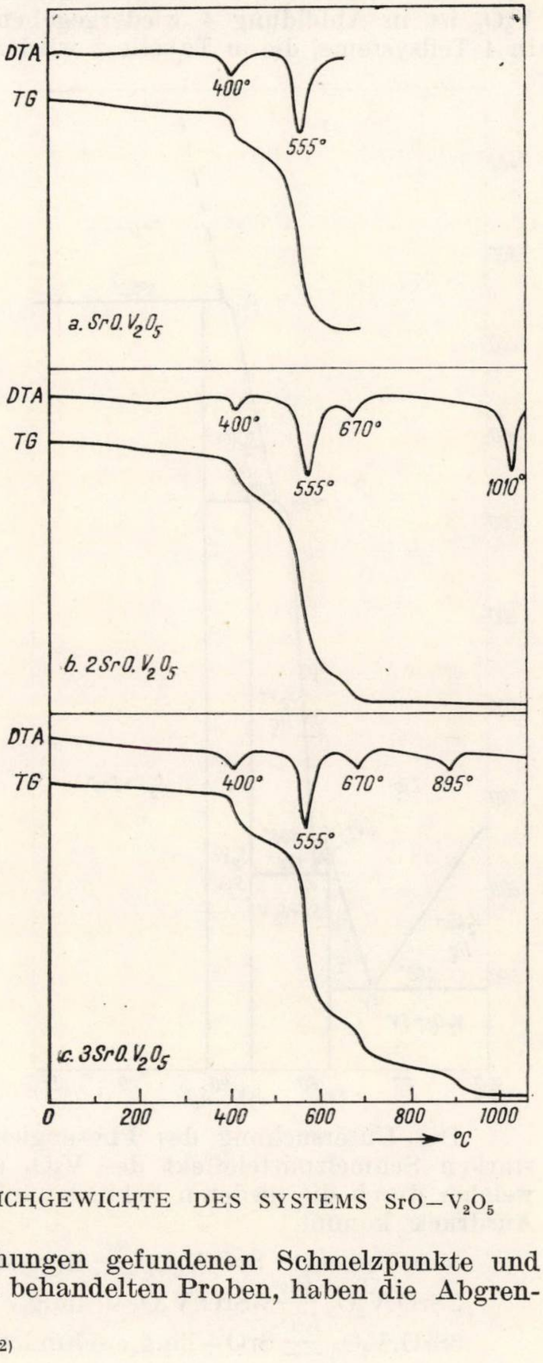

Abb. 3. — Thermogravimetrische und thermodifferentielle Kurven der Verbindungen in System $SrO-V_2O_5$
a. $SrO.V_2O_5$, b. $2SrO.V_2O_5$, c. $3SrO.V_2O_5$

3.3. THERMISCHE PHASENGLEICHGEWICHTE DES SYSTEMS $SrO-V_2O_5$

Die für die binären Mischungen gefundenen Schmelzpunkte und die Phasenanalyse der thermisch behandelten Proben, haben die Abgrenzung der primären Kristallisationsfelder der einzelnen Phasen ermöglicht, sowie die Bestimmung der invarianten Punkte.

Das thermische Phasengleichgewichtsdiagramm des Systems SrO-V_2O_5 ist in Abbildung 4 wiedergegeben. Das binäre System teilt sich in 4 Teilsysteme, die in Tabelle 2 wiedergegeben sind.

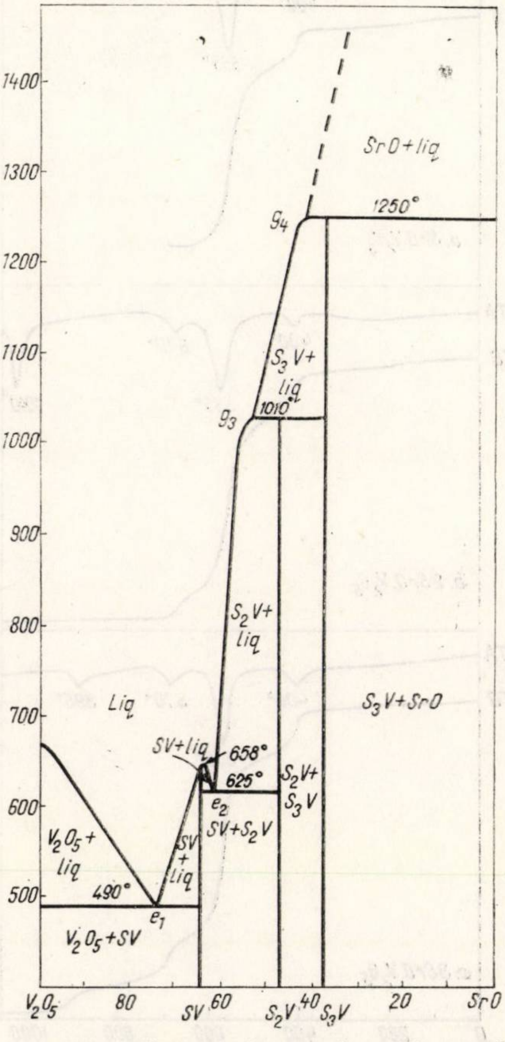

Abb. 4. – Thermisches Phasengleichgewichtsdiagramm des Systems SrO – V_2O_5.

Die Untersuchung des Phasengleichgewichtsdiagramms zeigt den starken Schmelzmitteleffekt des V_2O_5 auf die Massen dieses Systems, welcher durch die niederen Schmelzpunkte der invarianten Punkte zum Ausdruck kommt.

Man bemerkt : $SrO.V_2O_5 \overset{658^0}{\rightleftharpoons}$ liq., schmilzt kongruent

$2SrO.V_2O_5 \overset{1010^0}{\rightleftharpoons} 3SrO.V_2O_5 + liq.g_3$, schmilzt unkongruent

$3SrO.V_2O_5 \overset{1250^0}{\rightleftharpoons} SrO + liq.g_4$, schmilzt unkongruent

Tabelle 2

Die Teilsysteme des binären Systems $SrO-V_2O_5$

Das Teilsystem	Inv. Punkt	Zusamensetzung %		Schmelzpunkt, °C
		SrO	V_2O_5	
I $V_2O_5-SrO\cdot V_2O_5$	e_1	26,00	74,00	490
II $SrO.V_2O_5-2SrO\cdot V_2O_5$	e_2	38,50	71,50	625
III $2SrO.V_2O_5-3SrO\cdot V_2O_5$	g_3	46,00	54,00	1010
IV $3SrO_2.V_2O_5-SrO$	g_4	61,50	38,50	1250

4. SCHLUSSFOLGERUNGEN

1. Es wurde das thermische Phasengleichgewichtsdiagramm des binären Systems $SrO—V_2O_5$ aufgestellt.

2. Es wurde das Vorhandensein der drei binären chemischen Verbindungen, und zwar : $SrO.V_2O_5$, welches bei 658° kongruent schmilzt, $2SrO.V_2O_5$ und $3SrO.V_2O_5$ mit dem unkongruenten Schmelzpunkt bei 1010°, bzw. 1250° im System festgestellt.

3. Der Bildungsmechanismus der drei binären chemischen Verbindungen, welche röntgenographisch, lichtmikroskopisch und IR-spektroskopisch charakterisiert wurden, ist erörtert worden.

Revue Roumaine de Chimie, **17**, *1*, *2*, 311–317 (1972)

Revue Roumaine de Chimie, **17**, *1*, *2*, 319–327 (1972)

Hommage au Professeur I. G. MURGULESCU
à l'occasion de son 70° anniversaire

COORDINATION DE L'ION Al^{3+} DANS LES STRUCTURES VITROCÉRAMIQUES DU SYSTÈME $Na_2O-MgO-Al_2O_3-SiO_2$ AYANT LE FLUOR COMME AGENT DE NUCLÉATION

S. SOLACOLU et D. POPESCU-HAŞ
Institut Polytechnique de Bucarest, Chaire de Physico-Chimie des Silicates et Composés Oxydiques, 1, str. Polizu

Reçu le 4 août 1971

On a étudié les spectres d'absorption en infrarouge de certains composés de la section à 10% Na_2O du système $Na_2O-MgO-Al_2O_3-SiO_2$ sans fluor et, dans une seconde version, en ajoutant 6,00% fluor, en poursuivant :
— la variation de la proportion des groupements $[AlO_4]$ dans les verres contenant une proportion égale de SiO_2, le contenu de Al_2O_3 étant variable et la variation de la proportion des groupements $[AlO_4]$ dans les verres, en fonction de la température du traitement thermique de cristallisation. On a constaté que l'absorption dans le cadre de la bande ayant le numéro d'onde de 750 cm^{-1}, caractéristique aux groupements $[AlO_4]$,varie conjointement avec le compartiment de cristallisation indiquant la variation des structures quasi cristallines, avec les compartiments de cristallisation primaire.
Celle-ci varie aussi avec la température de traitement de cristallisation, les maxima devenant plus « aiguës », ce qui dénote que par le traitement thermique il s'établit l'ordre à distance.

INTRODUCTION

Les masses fondues de verre de la zone inférieure des compartiments de cristallisation primaire de l'enstatite et de la cordiérite, situées dans la section de 10% Na_2O du système Na_2O-MgO-Al_2O_3-SiO_2, quoique avec un contenu relativement petit de SiO_2 (45...55% mole), présentent une tendance réduite de cristallisation et l'on en peut obtenir des structures vitreuses à de très bonnes aptitudes au façonnage. En ajoutant 6,00... 6,50% de fluor, l'on élargit le domaine d'obtention des structures vitreuses, en l'élargissant aussi vers les masses fondues avec un contenu de $SiO_2 <$ 45% mole, situées dans le compartiment de cristallisation primaire du spinelle. Ces verres présentent, par comparaison avec les verres techniques habituels la particularité d'un très grand contenu de Al_2O_3 en présence de l'ion Mg^{2+}, lequel peut à son tour coordiner tétraédriquement, et de cette façon les groupements $[MgO_4]$ participeront à la formation de la structure vitreuse.[1,2,3]

Les recherches effectuées pour l'obtention de structures vitrocéramiques en faisant cristalliser les verres du système Na_2O-MgO-Al_2O_3-SiO_2 ont montré qu'aussi bien leur capacité de cristallisation que le degré de cristallinité des masses vitrocéramiques obtenues varient en fonction du contenu de Al_2O_3.[4]

Compte tenu du fait que les processus déterminant ces comportements sont conditionnés en grande mesure par la position et la coordination que l'ion Al^{3+} possède, aussi bien dans les structures vitreuses que dans celles vitrocéramiques, on a effectué dans le présent travail des recherches concernant la variation du numéro de coordination de l'ion Al^{3+} par les spectres d'absorption en infrarouge de certains verres du système Na_2O-MgO-Al_2O_3—SiO_2.

1. TECHNIQUE EXPÉRIMENTALE

La fusion des verres étudiés a été effectuée dans un creuset en platine-rhodium, dans un four à silites de construction personnelle, en matériaux isoréfractaires superalumineux. La température de fusion a été de 1500°, avec un palier de 120 minutes pour les verres sans fluor, et de 1450° avec un palier de 60 minutes pour les verres à contenu de fluor.

Le façonnage des corps d'essais sous forme de pastilles d'un diamètre de 20 mm et 5 mm d'épaisseur a été réalisé par compression dans des formes métalliques. Les corps d'essais, après compression, ont été refroidis brusquement jusqu'à 500° et après, la vitesse de refroidissement a été contrôlée dans un four électrique, en éliminant les tensions internes.

Le traitement thermique de cristallisation a été réalisé dans un four électrique à une vitesse d'augmentation de 15°/mn, à des températures différentes, de 100 en 100°, entre 650° et 1150°, avec des paliers, à chaque température, compris entre 60 et 240 minutes. Les spectres d'absorption en infrarouge ont été déterminés à un spectrophotomètre pour infrarouge, UR. 20 Karl Zeiss-Jéna, sur des échantillons pulvérulents pastillés dans du bromure de potassium.

2. RÉSULTATS EXPÉRIMENTAUX

2.1. MASSES VITROCÉRAMIQUES DU SYSTÈME D'ÉQUILIBRE DE PHASES $Na_2O-MgO-Al_2O_3-SiO_2$

Les recherches ont été effectuées sur des compositions de la section à 10% Na_2O du système Na_2O-MgO-Al_2O_3-SiO_2 (figure 1), sans fluor, étant notées avec les symboles S_1-S_8, et celles où l'on a ajouté 6,00% de fluor, étant notées avec les symboles 1F-9F, s'encadrant dans les sous-systèmes : IX: $NAS6-MA-M_2S-NAS_2$ et X: $NAS6-M_2S-NAS_2-NM_2S_6$

---

[1] E. I. Galiant, *Doklady Akad. Nauk S.S.S.R.*, **137**, 1424 (1961).

[2] A. Petzoldt, G. F. Wishmann et O. Hennig, *Glastechn. Ber.*, **34**, 56 (1961).

[3] L. Ainsworth, *J. Soc. Glass Technol.*, **38**, 479 (1954).

[4] D. Popescu Haş, « Thèse », Inst. Polytechnique, Bucarest, 1971, p. 59.

Le système quaternaire Na_2O-MgO-Al_2O_3-SiO_2 n'ayant pas constitué jusqu'à l'heure présente l'objet d'une recherche scientifique, on n'a pas pu préciser les volumes de cristallisation primaire des composants. Compte tenu des points d'invariance des systèmes ternaires composants et du fait que la section de 10% Na_2O est très rapproché de ce système quaternaire, du système ternaire de base : MgO-Al_2O_3-SiO_2, on a admis la probabilité que la position des compositions recherchées dans les volumes de cristallisation primaire du système quaternaire correspond aux compartiments de cristallisation primaire des composants du système ternaire de base.

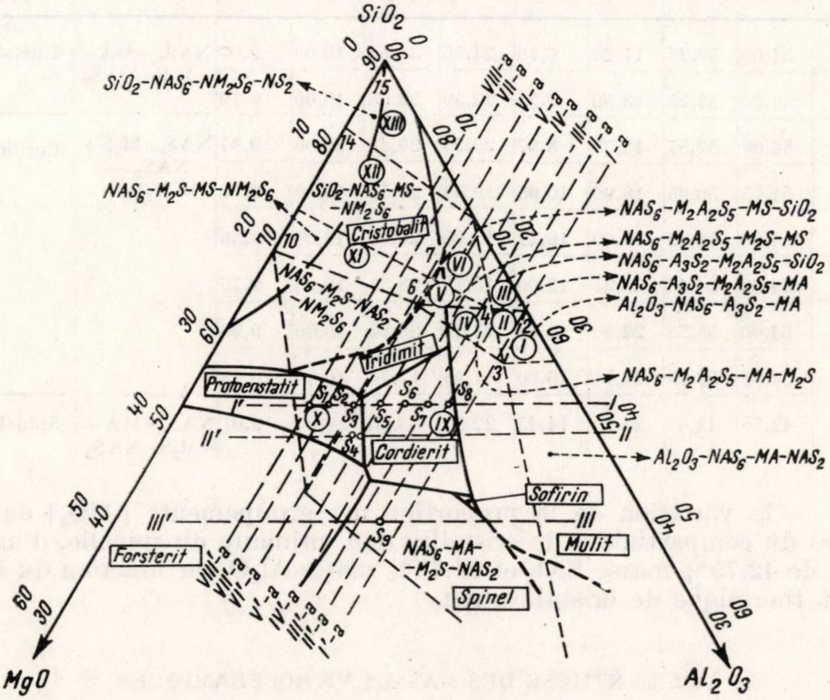
SiO2
MgO
Al2O3
SiO2-NAS6-NM2S6-NS2
NAS6-M2S-MS-NM2S6
SiO2-NAS6-MS-
-NM2S6
NAS6-M2S-NAS2-
-NM2S6
NAS6-M2A2S5-MS-SiO2
NAS6-M2A2S5-M2S-MS
NAS6-A3S2-M2A2S5-SiO2
NAS6-A3S2-M2A2S5-MA
Al2O3-NAS6-A3S2-MA
NAS6-M2A2S5-MA-M2S
Al2O3-NAS6-MA-NAS2
NAS6-MA-
-M2S-NAS2
Cristobalit
Tridimit
Protoenstatit
Cordierit
Sofirin
Mulit
Forsterit
Spinel
I
II
III
IV
V
VI
IX
X
XI
XII
XIII
S1
S2
S3
S4
S5
S6
S7
S8
S9
I'
II'
III'
I-a
II-a
III-a
IV-a
V-a
VI-a
VII-a
VIII-a
I'-a
II'-a
III'-a
IV'-a
V'-a
VI'-a
VII'-a
VIII'-a
2
3
4
6
7
10
14
15
0
10
20
30
40
50
60
70
80
90

Fig. 1. — Section correspondant à 10% Na_2O dans le système Na_2O-MgO-$Al_2O_3-SiO_2$ et les compositions étudiées.

En étudiant les spectres d'absorption en infrarouge des compositions indiquées dans le tableau 1, on a poursuivi deux aspects, à savoir :

— la variation de la proportion des groupements $[AlO_4]$ dans les verres ayant des compositions situées sur une ligne correspondant à un contenu égal de masse de SiO_2, laquelle parcourt les compartiments de cristallisation de l'enstatite et de la cordiérite, le contenu de Al_2O_3 variant entre 11,25% masse et 24,75% masse ;

Tableau 1

Masses vitrocéramiques du système $Na_2O-MgO-Al_2O_3-SiO_2$

Le verre	SiO_2		Al_2O_3		MgO		Na_2O		Sous-système d'équilibre phasique	Compartiment de cristallisation primaire
	% masse	% mole	% masse	% mole	% masse	% mole	% masse	% mole		
S_1	54,00	50,27	11,25	6,16	24,75	34,56	10,00	9,07	NAS_6-MA- $-M_2S-NAS_2$	Enstatite
S_2	54,00	51,25	13,50	7,53	22,50	32,03	10,00	9,19		
S_3	54,00	52,57	15,75	8,97	20,25	29,40	10,00	9,37	NAS_6-M_2S- $-NAS_2-$ $-NM_2S_6$	Cordiérite
S_4	51,75	50,95	18,90	10,95	19,35	28,57	10,00	9,53		
S_5	54,00	53,32	18,00	10,42	18,00	26,66	10,00	9,56		
S_6	54,00	54,43	20,25	12,00	15,75	23,31	10,00	9,76		
S_8	54,00	55,58	22,50	13,62	13,50	20,84	10,00	9,96		
S_9	54,00	56,78	24,75	15,30	11,25	17,74	10,00	10,18		
S_{10}	42,75	42,44	24,75	14,45	22,50	33,50	10,00	9,61	NAS_6-MA- $-M_2S-NAS_2$	Spinelle

— la variation de la proportion des groupements $[AlO_4]$ dans les verres du compartiment de cristallisation primaire du spinelle, d'un contenu de 42,75% masse SiO_2 et 24,75% masse Al_2O_3 en fonction du traitement thermique de cristallisation.

2.2. SYNTHÈSE DES MASSES VITROCÉRAMIQUES

Lors de la synthèse des verres étudiés, on a utilisé comme matière première du quartz filonaire, d'un contenu de 99,75% de SiO_2, broyé à une finesse correspondant au passage intégral sans résidu par le tamis de 0,1 mm, de l'alumine calcinée pure Carlo-Erba — Italie, de l'oxyde de magnésium *p.a.* E. Merck — R.F. d'Allemagne, du carbonate de soude *p.a.* I.I.S. Reactivul — Roumanie et de la cryolithe pure, provenant de l'Union Soviétique.

Les mélanges dosés gravimétriquement ont été homogénéisés avant la fusion dans des broyeurs à boulets de porcelaine, pendant 60 minutes et séchés à l'étuve, à 110°.

Afin d'obtenir des masses fondues plus homogènes, chaque mélange a été soumis à la fusion deux fois, la masse fondue étant frittée dans l'eau. On a façonné des corps d'essais à partir de verres fondus une troisième fois. Une partie des corps d'essais a été refroidie brusquement entre les plaques d'acier inoxydable jusqu'à la température ambiante, et une autre partie a été recuite, afin d'éliminer les tensions internes et ensuite, traitée thermiquement pour cristallisation.

2.3. PROPRIÉTÉS SPECTRALES DANS L'INFRAROUGE ET DISCUSSION DES RÉSULTATS

Les maxima des bandes d'absorption dans le spectre infrarouge des verres sans fluor S_1-S_4 et du compartiment de l'enstatite avec addition de fluor 1.F−4.F, ainsi que des verres exempts de fluor S_5-S_8 et les verres avec du fluor 5.F−8.F du compartiment de cristallisation primaire de la cordiérite, sont présentés dans les figures 2 et 3. Tous ces

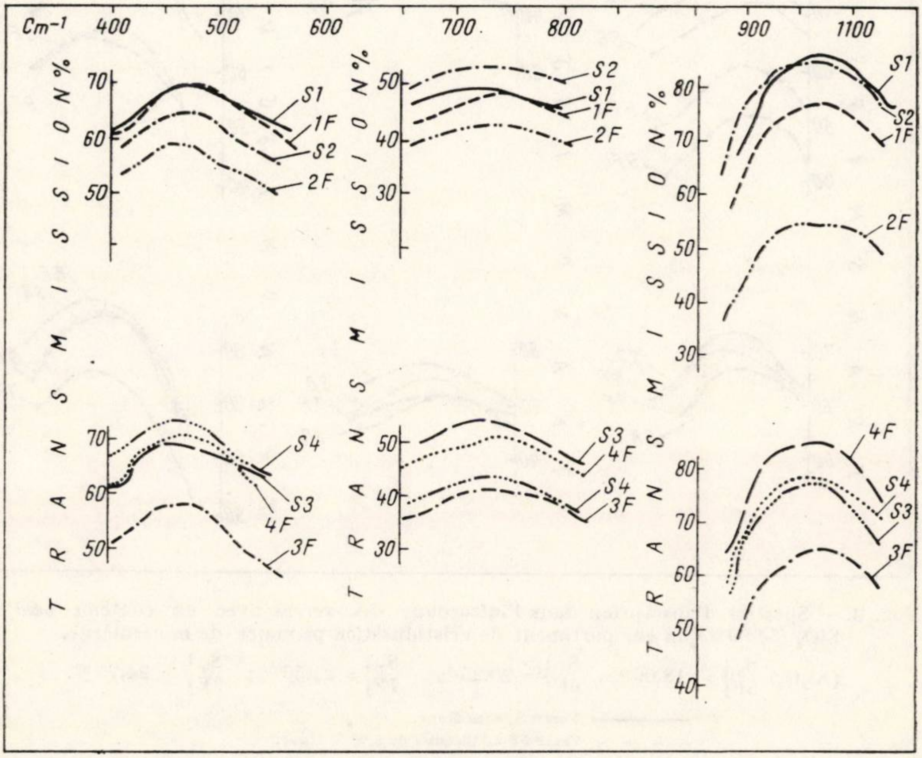

Fig. 2 — Spectres d'absorption dans l'infrarouge des verres avec un contenu égal de SiO_2 (54,00 %), du compartiment de cristallisation primaire de l'enstatite et les compositions étudiées.

$$(Al_2O_3)\ \left.\begin{matrix}S_1\\1F\end{matrix}\right\} = 11{,}25\,\%\,;\quad \left.\begin{matrix}S_2\\2F\end{matrix}\right\} = 13{,}50\,\%\,;\quad \left.\begin{matrix}S_3\\3F\end{matrix}\right\} = 15{,}75\,\%\,;\quad \left.\begin{matrix}S_4\\4F\end{matrix}\right\} = 18{,}90\,\%.$$

———————	Verre S_1 sans fluor.
— — — —	Verre 1F additionné de 6,00% fluor.
—·—·—·—	Verre S_2 sans fluor.
— ·· — ·· —	Verre 2F additionné de 6,00% fluor.
——— ———	Verre S_3 sans fluor.
— · — — ·	Verre 3F additionné de 6,00% fluor.
···· —····	Verre S_4 sans fluor.
···············	Verre 4F additionné de 6,00% fluor.

verres, sauf celui du S_4, respectivement 4.F, ont les compositions situées sur la ligne du contenu égal de masse de SiO_2 et la quantité de Al_2O_3 variant entre 11,25% et 24,75% masse.

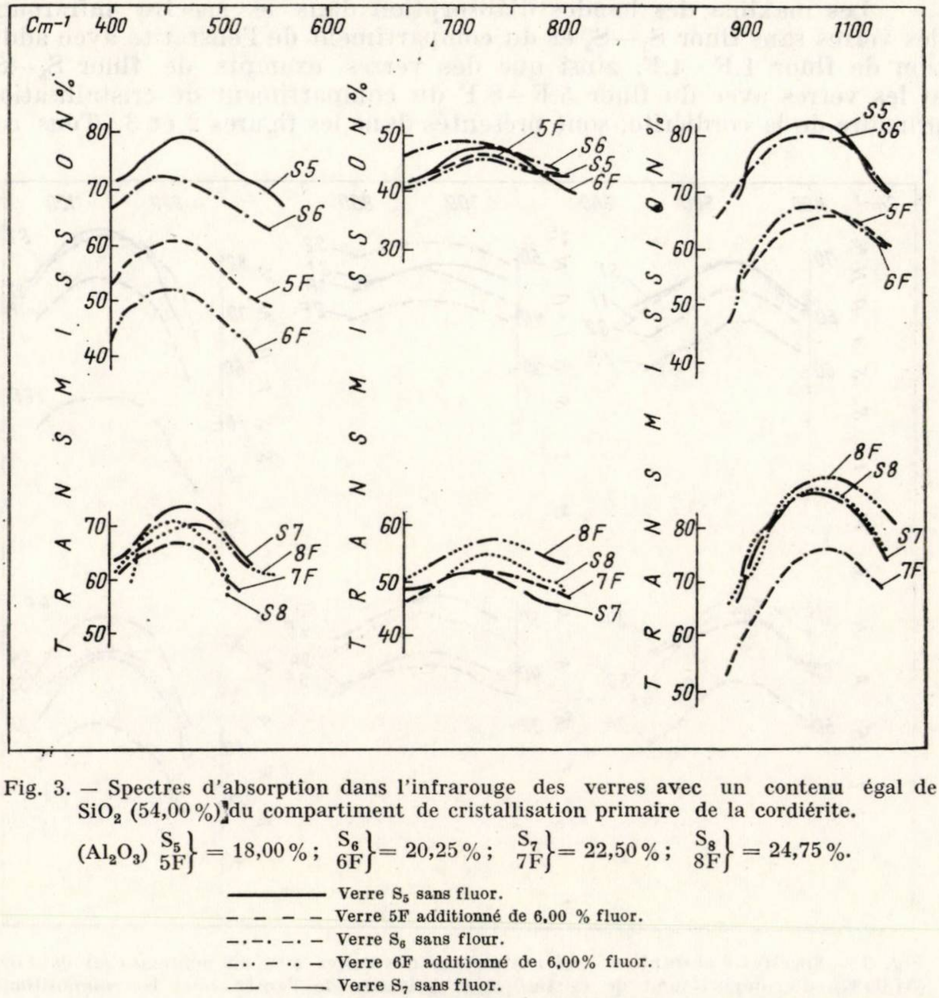

Fig. 3. — Spectres d'absorption dans l'infrarouge des verres avec un contenu égal de SiO_2 (54,00 %) du compartiment de cristallisation primaire de la cordiérite.

$(Al_2O_3)\ \left.\begin{matrix}S_5\\5F\end{matrix}\right\} = 18{,}00\,\%;\ \left.\begin{matrix}S_6\\6F\end{matrix}\right\} = 20{,}25\,\%;\ \left.\begin{matrix}S_7\\7F\end{matrix}\right\} = 22{,}50\,\%;\ \left.\begin{matrix}S_8\\8F\end{matrix}\right\} = 24{,}75\,\%.$

——————— Verre S_5 sans fluor.
— — — — Verre 5F additionné de 6,00 % fluor.
—.—. —. — Verre S_6 sans flour.
—.. — .. — Verre 6F additionné de 6,00% fluor.
—— —— Verre S_7 sans fluor.
— — . — — . Verre 7F additionné de 6,00% fluor.
.... Verre S_8 sans fluor.
... ——— ... Verre 8F additionné de 6,00% fluor.

En examinant la variation du maximum de la bande d'absorption avec le numéro d'onde 750 cm^{-1}, correspondant aux groupements $[AlO_4]$, [5] on observe les suivants :

Dans les verres $S_1 - S_3$ du compartiment de l'enstatite, l'absorption du spectre infrarouge croît avec l'augmentation de la quantité de Al_2O_3, d'où il résulte que le nombre des groupements [AlO_4] qui participent à la structure du verre augmente.

---

[5] O. Ghirin, « Stekloobraznoye sostoyanye », Ier vol., Izd. Akad. S.S.S.R., Moscou—Leningrad, 1963, p. 99.

Dans le cas du verre S_4 qui est le plus rapproché de la surface limite entre les compartiments de cristallisation primaire de l'enstatite et de la cordiérite, quoique le contenu de Al_2O_3 soit supérieur aux autres verres, pourtant l'absorption diminue. En ce qui concerne la bande d'absorption comprise entre les numéros d'onde de 400 cm^{-1} et 600 cm^{-1}, correspondant aux groupements [AlO_6], leur intensité diminue dans le cas des 3 premières compositions ($S_1 - S_3$), et croît dans le cas de la composition S_4. Il faut remarquer aussi que les pics des compositions avec additions de fluor (1.F—4.F) paraissent plus aplatis que ceux des mêmes compositions, exemptes de fluor. Cela constitue une indication que dans les compositions contenant du fluor, l'ordre à distance manque dans un plus fort degré.

Pour les verres $S_5 - S_8$ ayant des compositions situées dans le compartiment de cristallisation primaire de la cordiérite, on observe une augmentation de l'absorption dans le cadre de la bande correspondant au numéro d'onde 750 cm^{-1} caractéristique des groupements [AlO_4]. L'augmentation commence à partir de S_5 où l'absorption se trouve au niveau du verre S_4 du compartiment de l'enstatite, et croît continuellement jusqu'à S_8, ayant le maximum de contenu de Al_2O_3 (24,75% masse). Ainsi dans la série des verres avec addition de fluor de ce compartiment (5.F-8.F), on observe l'aplatissement des pics par rapport aux pics des verres équivalents de la série sans fluor. L'explication est la même, pareillement au cas des compositions du compartiment de cristallisation de l'enstatite, respectivement de l'augmentation du degré de désordre provoqué par l'introduction du fluor.

En examinant la variation de l'absorption dans le spectre infrarouge pour l'ensemble entier, les compositions, situées sur la ligne d'un contenu égal de SiO_2, on observe qu'elle ne croît pas continuellement avec l'augmentation du contenu de Al_2O_3, le long de la ligne des compositions traversant le compartiment de cristallisation primaire de l'enstatite et de la cordiérite.

L'absorption dans le spectre infrarouge croît le long de la ligne des compositions du compartiment de l'enstatite, mais lors du passage dans le compartiment de la cordiérite, il se produit une diminution.

Après le passage dans le compartiment de la cordiérite, l'absorption dans le spectre de l'infrarouge, dans le cadre de la bande des groupements (AlO_4), croît de nouveau, le long de la ligne des compositions.

Le mode de variation de l'absorption dans le spectre infrarouge des verres étudiés constitue une indication du fait que les structures quasi cristallines présentes dans le verre varient d'un compartiment de cristallisation à l'autre. Ces résultats concordent avec les résultats obtenus par S. Solacolu et ses collaborateurs, [6,7] dans les études effectuées concernant l'hétérogénéité phasale des verres.

---

[6] S. Solacolu et D. Totoescu, *Bul. Şti. al Academiei Seria Şt. tehnice şi chimice*, **5**, 99 (1953).

[7] S. Solacolu et P. Baltă, *Rev. de Mat. de Constr. et de Trav. Publ.*, **583**, 95 (1964).

Les pics des bandes d'absorption du verre, avec addition de fluor 9.F (verre S_9 additionné de 6,00 % fluor), du compartiment de cristallisation primaire du spinelle avec un contenu important de Al_2O_3 (24,75 % masse), ayant subi un traitement thermique de cristallisation à différentes températures sont présentés dans la figure 4.

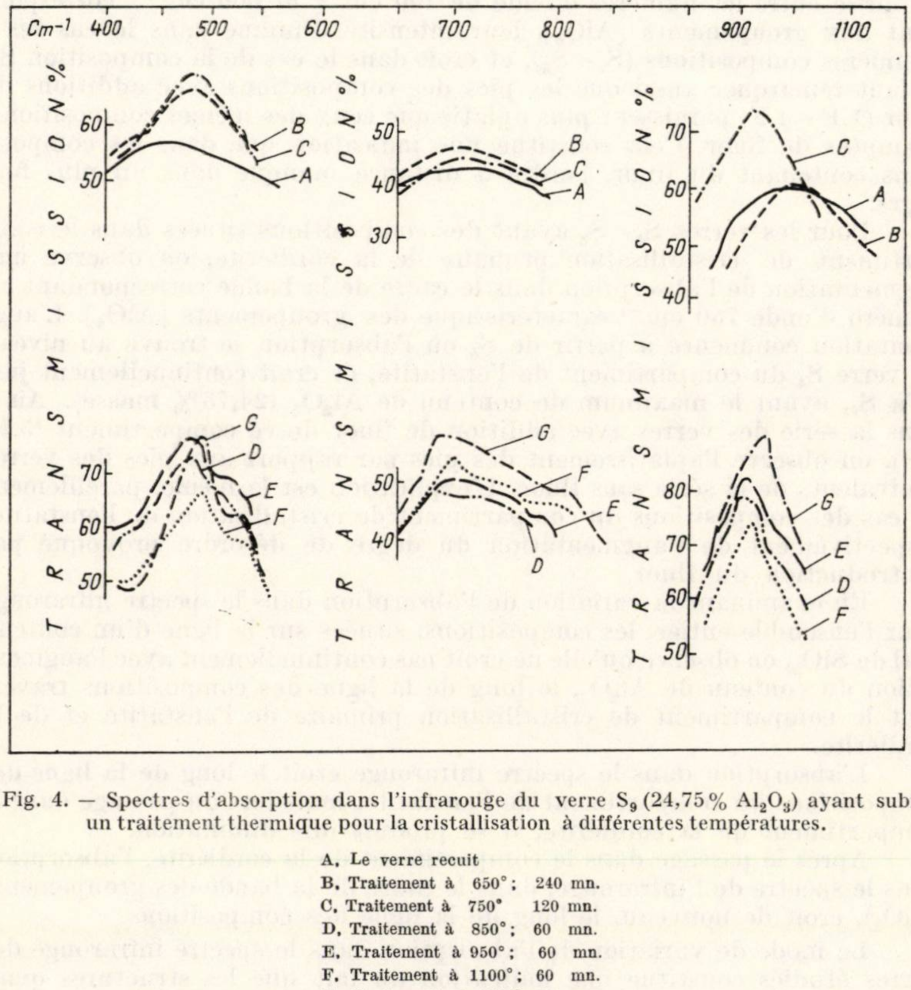

Fig. 4. — Spectres d'absorption dans l'infrarouge du verre S_9 (24,75 % Al_2O_3) ayant subi un traitement thermique pour la cristallisation à différentes températures.

A. Le verre recuit
B. Traitement à 650° ; 240 mn.
C. Traitement à 750° 120 mn.
D. Traitement à 850° ; 60 mn.
E. Traitement à 950° ; 60 mn.
F. Traitement à 1100° ; 60 mn.
G. Traitement à 1150° ; 60 mn.

L'étude de la bande du numéro d'onde de 750 cm^{-1}, correspondant au groupement [AlO_4], révèle que par l'élévation de la température de traitement, l'intensité de l'absorption augmente, respectivement le nombre de groupements [AlO_4]. De même, aussi bien les maxima des bandes [AlO_6], que celles des bandes [SiO_4] deviennent plus aiguës, à mesure que la température s'accroît, ce qui démontre que par la cristallisation des structures vitreuses, il s'établit de plus en plus l'ordre à distance.

L'augmentation du nombre des groupements $[AlO_4]$ dans les réseaux cristallins qui se forment par suite du traitement thermique correspond parfaitement à la microstructure des masses vitrocéramiques.

CONCLUSIONS

1. On a établi que la proportion des groupements $[AlO_4]$, dans le verre du système $Na_2O-MgO-Al_2O_3-SiO_2$, exempt de fluor et avec addition de fluor, varie au passage d'un compartiment de cristallisation à l'autre, ce qui démontre que les structures quasi cristallines existant dans les verres, varient avec les compartiments de cristallisation primaire.

2. On a établi que dans les compositions contenant du fluor, l'ordre à distance manque dans un degré plus fort que dans les compositions exemptes de fluor.

3. On a établi que la proportion de groupements $[AlO_4]$ croît avec le traitement thermique, et cela avec l'établissement concomitant de plus en plus prononcé de l'ordre à distance. L'augmentation de la proportion des groupements $[AlO_4]$ avec la température correspond à la microstructure des masses vitrocéramiques.

Les auteurs expriment leurs vifs remerciements à l'Ingénieur Elian Mihail, du Centre de Recherches de Chimie Organique, pour la collaboration aux recherches spectrographiques.

Revue Roumaine de Chimie, **17**, *1, 2*, 329–333 (1972)

Dedicated to Professor I. G. MURGULESCU
on his 70th birthday

ELECTRON PARAMAGNETIC RESONANCE STUDY OF NITROXIDES IN DIOXANE WATER SYSTEM

JAVIER SORIA* and JOHN TURKEVICH**

Princeton University, Princeton, N. J. 08540

Received September 1971

ESR spectra of two nitroxides were studied in dioxane-water mixtures of various concentrations. Variations in hyperfine coupling constants, line intensities and spin lattice relaxation times are used to interpret the properties of the mixed solvent.

Solvent effects on the electron paramagnetic resonance (EPR) parameters of the nitroxides [1] have important implications in spin labeling studies. In particular, the polarity of the immediate environment of the label molecule can express itself in the intensity, the hyperfine constant and relaxation time of the spin label molecule.

Since the polar character of the solvent is related to its dielectric constant, it was of interest to determine the effect of the dioxane water systems (whose dielectric constant can be varied continuously from values of 2 to 80) on the EPR behaviour of the nitroxide.

Infrared, [2] NMR [3] proton spin-lattice relaxation time, [4] Raman shift [5,6] studies support the hypothesis that small amounts of dioxane enhance the strength of the water-water hydrogen bonds in the vicinity of the dioxane molecule. This undoubtedly facilitates the organization of water into cages. However at 60% volume of dioxane (V_a) the system changes from a dispersion of dioxane molecules in water matrix to a dispersion of clusters of water molecules in a dioxane matrix. This is indicated by changes in many properties, especially density and viscosity [7] which occur near 60% V_a. It is proposed to follow the changes in the EPR

---

* Present address: Instituto de Quimica Fisica "Rocasolano" Madrid, Spain.

** Work supported by the U. S. Atomic Energy Commission.

[1] R. Briere, H. Lemaire and A. Rassat, *Bull. Soc. chim. France*, 1965, 3273.

[2] A. Fratiello and J. P. Luengo, *J. Amer. Chem. Soc.*, **85**, 3072 (1963).

[3] A. Fratiello and C. Douglass, *J. Mol. Spectroscopy*, **11**, 465 (1963).

[4] C. J. Clemett, *J. Chem. Soc.*, (*A*) **1969**, 455; *ibid.*, 1969, 761.

[5] C. Faucomier and M. Harrand, *Ann. Phys.*, **1**, 5 (1956).

[6] Yu. I. Naberukhin and S. I. Shuiskii, *Zhur. struk. Khim.*, **8**, 606 (1967).

[7] A. M. Shkohin, N. K. Lenitskaya and V. A. Lozhnikov, *Zhur. Obschei. Khim.*, **38**, (1968).

characteristics of the nitroxide to see whether there are any discontinuities at this composition of dioxane-water system.

EXPERIMENTAL

Tetramethylpiperidone oxide isothiocyanate (I) and tetramethyl carboxypyrroline oxyl (II) were obtained from Varian Associates. The *p*-dioxane was Matheson, scintillation grade. The water was de-ionized and distilled.

The X band EPR spectrometer (Varian 4500) had a modulation frequency of 100 khz and maximum klystron power of 300 mW. A special thin quartz cell was used for all measurements. The high resolution proton resonance measurements were made on the Varian H-60. A Cary spectrometer was used for ultraviolet studies.

The nitroxides were dissolved in pure water and dioxane to give a concentration of 2.5×10^{-4}M. True solution was insured either by stirring for over an hour or by heating to higher temperature and then cooling. Proportionality of the signal intensity with concentration was used as a check of true solubility.

RESULTS

The EPR spectra consisted of three equally spaced hyperfine lines of approximately the same intensity, with the peak at high field side being significantly smaller. The signal parameters in water were $g = 2.0057$, $A = 16$ gauss, and the width of the individual lines $\Delta H = 1.2$ gauss, while in dioxane the values are $g = 2.0065$, $A = 14.2$ gauss and $\Delta H = 1.7$ gauss. These values are in agreement with those previously reported[1]. The hyperfine structure of the EPR spectrum of three lines indicates that the unpaired spin density is mainly concentrated at the nitrogen atom of the nitroxide and the solvent affects the distribution of spin density.

A plot of the intensity of the central peak (Fig. 1a) and of the hyperfine constant A (Fig. 1b) against the dioxane concentration shows a break in the curve at 80% dioxane. Furthermore there is no linear dependence of these parameters on the dielectric constant of the system. The intensity measurements were carried out at low klystron power to avoid saturation effects in the measurements. Saturation measurements were used to calculate $T_1 - T_2$ and width measurements to calculate T_2, the spin-spin relaxation time. This permitted the calculation of T_1, the spin-lattice relaxation time [8]. The variation of these parameters with concentration shows a maximum in T_1 at 60% dioxane (Fig. 2). The ratio of the height of the central peak to the high field peak permits the calculation of the correlation time τ for the fast tumbling of the nitroxides in the different solvent environment [9] and this shows a maximum in the same region (Fig. 3)-

The ultraviolet absorption spectrum of the nitroxide (I) shows a peak at 2400 Å, the plot of whose intensity with concentration shows a break at 70%.

---

[8] C. P. Poole, "Electron Spin Resonance", Interscience, **1967**, 709.

[9] T. J. Stone, T. Buckman, P. L. Nordio and H. M. McConnell, *Proc. Nat. Acad. Sci. U.S.A.*, **54**, 1010 (1965).

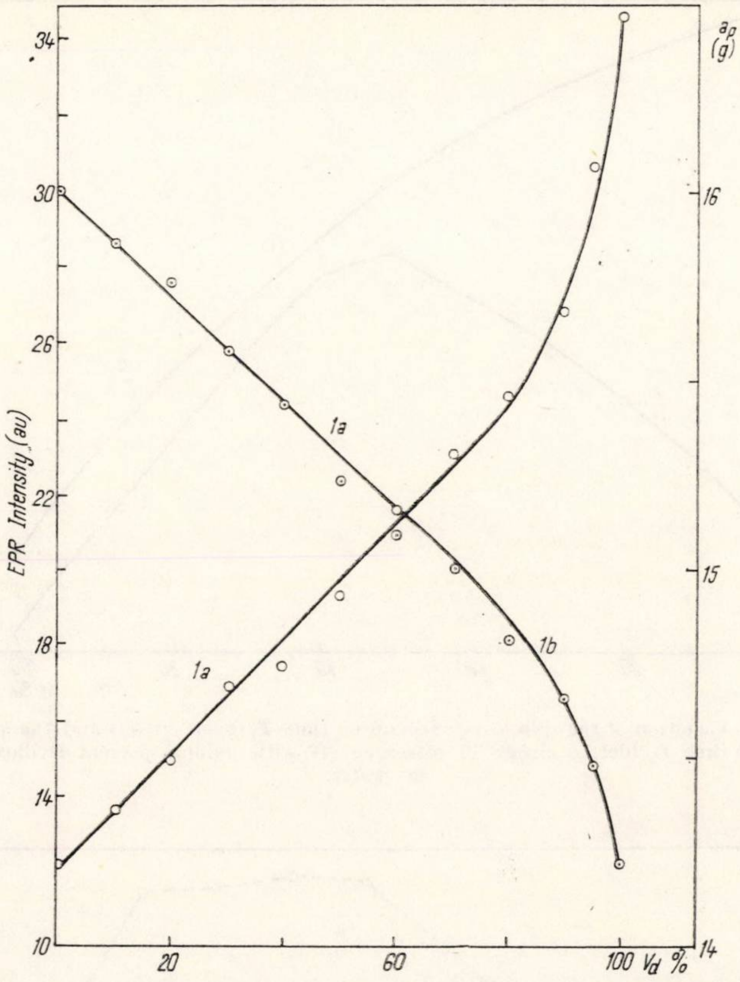

Fig. 1. — a) Variation of the intensity of the EPR line of nitroxide (II) ; b) the hyperfine constant A with volume percent of dioxane V_d in water.

Results obtained on the high resolution of the proton lines of water and dioxane were similar to those previously reported [3,4] ; an increase in the relaxation time of the two lines was observed as the dioxane concentration increased to about 6% V_d, after which there was a decrease. Similar result has been observed in the Raman spectrum [6]. Dissolution of the nitroxide shortened the relaxation time but to a lesser degree than some paramagnetic ions. The maximum observed at 6% V_d disappears when the system contains the nitroxide.

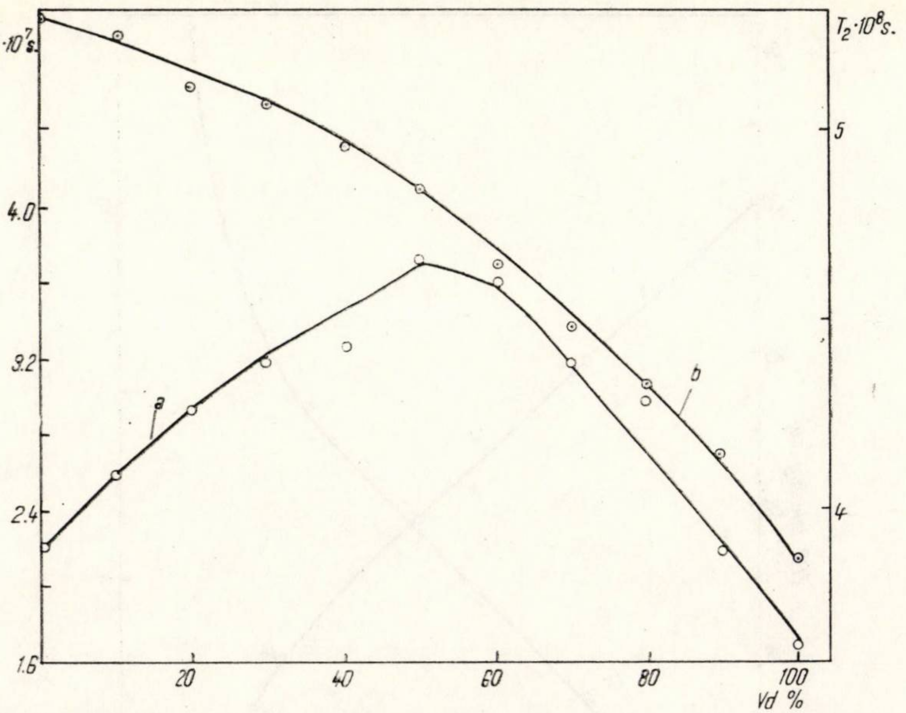

Fig. 2. — Variation of the spin lattice relaxation time T_1 (open circles) and the spin-spin relaxation time T_2 (dotted circles of nitroxide (II) with volume percent of dioxane V_d in water.

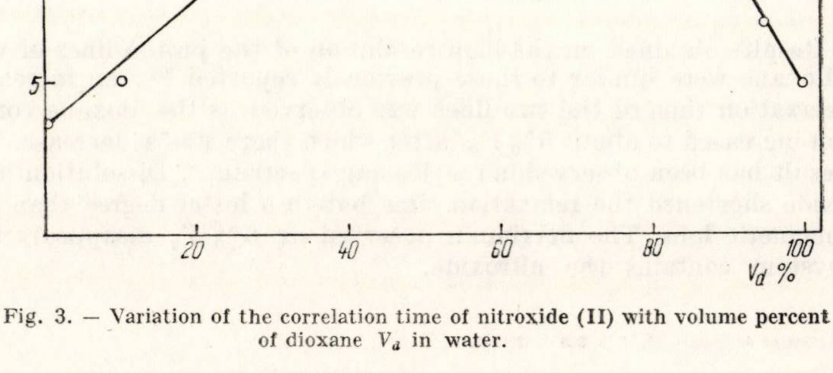

Fig. 3. — Variation of the correlation time of nitroxide (II) with volume percent of dioxane V_d in water.

DISCUSSION

The EPR measurements support the point of view that in spite of the complete mutual solubility of water-dioxane, the system does not form a perfect solution. Although the nitroxide is more soluble in dioxane than in water, the hyperfine structure constant indicates that it is soluble in water in low dioxane concentrations. As the concentration of dioxane increases, the nitroxide becomes associated in water causing a decrease in signal intensity over what would be expected from an additivity relation. Further increase in the dioxane concentration produces a breakdown of the water structure and all the EPR parameters approach linearly those of the nitroxide in pure dioxane.

The present results support the model proposed [4,6] for the water-dioxane system and offer a new sensitive way to study on a molecular basis homogeneity of liquid systems.

Revue Roumaine de Chimie, **17**, *1, 2*, 335 – 341 (1972)

Dedicated to Professor I. G. MURGULESCU
on his 70th birthday

MOLECULAR ORBITAL PATTERNS FOR *f*-CLUSTERS

P. SPACU and C. I. LEPĂDATU

Center of Chemical Physics, Dumbrava Roşie 23, Bucharest, Romania

Received October 2, 1971

Molecular orbital patterns for f-shell in different coordination geometries are presented, using the generalized angular overlap model. The results take into account the chemical bonding effects on the *f*-orbital set, being useful in the interpretation of phenomena related to the molecular electronic structure of lanthanide and actinide clusters.

These last years, the chemistry of lanthanides and actinides enjoyed a flourishing development impelled by the last laser researches, the f^n ions being considered as ideal materials for optical pumping [1] as well as by the older controversy on the *f*-orbital participation in the chemical bonding. [2]

As far as the second problem is concerned, recent data have undoubtedly demonstrated that the *f*-orbitals do contribute to the formation of coordination bonds, their symmetry properties playing, to a certain extent, a significant role in the choice of the coordination geometries. [3] It is obvious in this context, that a lot of phenomena related to *f*-clusters cannot be cleared up without a correct splitting of the *f*-shell produced by the chemical bonds and electrostatic ligand field. Various procedures [4] have been proposed in order to get *f*-orbital patterns in different geometries, all being conceived in the framework of electrostatic ligand field theory. Besides their tedious handling when applied to lower symmetries, partly due to the complexity of *f*-wavefunctions, unpleasant complications arise in those cases where the covalent contribution required a careful estimation.

It is the aim of this note to present a collection of *f*-orbital patterns using the angular overlap model (AOM) [5] in a LCAOMO alternative recently described.[6] We chose this method since it has proved particularly powerful in explaining the spectral behaviour [7,8], and the topological properties [9,10] of the clusters, as well as because the approach works for any covalency degree considered.

---

[1] P. Görlich, H. Karras, G. Kötiz and R. Lehmann, "Spectroscopic Properties of Activated Laser Crystals", Physica Status Solidi, vol. 5 suppl. 3 ; vol. 6, suppl. 2 (1964) ; and vol. 8 suppl. 2 (1965), Akademie-Verlag, Berlin.

[2] S. P. Sinha, "Complexes of the Rare Earths", Pergamon Press, Oxford, 1966.

[3] S. P. Sinha, "Structure and Bonding in Lanthanide Complexes with High Coordination Number" (preprint).

[4] W. Low, "Paramagnetic Resonance in Solids", Solid State Physics, suppl. 2, Acad. Press., New York, 1960.

[5] C. E. Schäffer and C. K. Jørgensen, *Mol. Phys.*, **9**, 401 (1965).

According to the generalized AOM[6], the molecular energies are given by

$$E = \varepsilon_0 + \sum_k \sum_j {}^kD_{ij}^2\, e^k_{\lambda(j)} + \sum_k \sum_{k'} \sum_j {}^kD_{ij}\, {}^{k'}D_{ij}\, e^{kk'}_{\lambda(j)} + \ldots \tag{1}$$

where ε_0 is the zero-order energy, i, $k \neq k'$ run over all central atom and ligand orbitals involved in chemical bonding, e^k_λ, $e^{kk'}_\lambda$ describe the central atom-ligand and the interbond interactions respectively, λ showing the bonding type. Explicit formulas for the last two quantities may be found in the cited paper.[6] ${}^kD_{ij}$'s from (1) represent the angular matrix elements of the rotation necessary to bring the central atom orbital set from its proper coordinate system to that of the k-th ligand, the indices i, j running over former central atom orbital set.

We give below the *f*-MO patterns for several meaningful idealized coordination geometries, typical or possible for lanthanide and actinide clusters (examples are given for higher coordination numbers), in a model with independent bonds ($e^{kk'} = 0$) and assuming that only the "σ" bonding is operative. Real *f*-orbitals, fundamental and cubic, have been used, group-theoretically classified according to Eisenstein's notations.[11] The angular matrix elements D_{ij} are given in the Appendix. The calculations have been performed for coordination number N up to 12.

$N = 3$ (trigonal, D_{3h})

$E(e'', a_2', a_2'') = \varepsilon_0$

$E(e') = \varepsilon_0 + 9/16\, e_\sigma$

$E(a_1') = \varepsilon_0 + 15/8 e_\sigma$

$N = 4$ (tetrahedral, T_d)

$E(t_1) = \varepsilon_0$

$E(t_2) = \varepsilon_0 + 16/27 e_\sigma$

$E(a_1) = \varepsilon_0 + 20/9 e_\sigma$

$N = 5$ (trigonal bipyramid, D_{3h}, $LnCl_5^{2-}$ in fused salts)

$E(e'', a_2') = \varepsilon_0$

$E(e') = \varepsilon_0 + 9/16 e_\sigma$

$E(a_1') = \varepsilon_0 + 15/8 e_\sigma$

$E(a_2'') = \varepsilon_0 + 2e_\sigma$

$N = 6$

— Octahedron, O_h; eg. $L_n(\text{Halide})_6^{3-}$ in non-aqueous solvents

$E(t_{2u}, a_{2u}) = \varepsilon_0$

$E(t_{1u}) = \varepsilon_0 + 2e_\sigma$

— Trigonal prism, D_{3h}; $Yb(CH_3COO)_3$

$E(a_2') = \varepsilon_0$

$E(a_2'') = \varepsilon_0 + 3/16 e_\sigma$

$E(a_1') = \varepsilon_0 + 15/32 e_\sigma$

$E(e') = \varepsilon_0 + 81/64 e_\sigma$

$E(e'') = \varepsilon_0 + 45/32 e_\sigma$

---

[6] C. I. Lepădatu, *Z. phys. Chem. (Frankfurt)*, **73**, 249 (1970).

[7] P. Spacu and C. I. Lepădatu, *J. Amer. Chem. Soc.*, **88**, 3221 (1966).

[8] C. I. Lepădatu, *Z. phys. Chem. (Frankfurt)*, **60**, 205 (1968).

[9] P. Spacu and C. I. Lepădatu, *Z. phys. Chem. (Frankfurt)*, under press.

[10] C. I. Lepădatu, accepted to *J. Cryst. and Mol. Structure*.

[11] J. C. Eisenstein, *J. Chem. Phys.*, **25**, 142 (1956).

$N = 7$

— Pentagonal bipyramid, D_{5h}; eg. CeF_7^{3-}, UF_7^{3-}

$E(e_2'') = \varepsilon_0$

$E(e_1') = \varepsilon_0 + 15/16 e_\sigma$

$E(e_2') = \varepsilon_0 + 25/16 e_\sigma$

$E(a_2'') = \varepsilon_0 + 2 e_\sigma$

— Capped trigonal prism, C_{2v}; Sm_2O_3

$E(b_2) = \varepsilon_0$

$E(a_1) = \varepsilon_0 + 3/16 e_\sigma$

$E(b_1) = \varepsilon_0 + 35/32 e_\sigma$

$E(a_1, a_2) = \varepsilon_0 + 45/32 e_\sigma$

$E(b_1, b_2) = \varepsilon_0 + 93/64 e_\sigma$

$N = 8$

— Hexahedron (Cube), O_h

$E(t_{2u}) = \varepsilon_0$

$E(t_{1u}) = \varepsilon_0 + 32/27 e_\sigma$

$E(a_{2u}) = \varepsilon_0 + 40/9 e_\sigma$

— Square anti-prism Archimedian cube), D_{4d}; eg. UF_4

$E(e_1) = \varepsilon_0 + 4/9 e_\sigma$

$E(e_3) = \varepsilon_0 + 20/27 e_\sigma$

$E(b_2) = \varepsilon_0 + 32/27 e_\sigma$

$E(e_2) = \varepsilon_0 + 20/9 e_\sigma$

— Bicapped trigonal prism, C_{2v}; eg. $TbCl_3$

$E(b_2) = \varepsilon_0$

$E(a_1) = \varepsilon_0 + 3/16 e_\sigma$

$E(a_1, a_2) = \varepsilon_0 + 45/32 e_\sigma$

$E(b_1, b_2) = \varepsilon_0 + 105/64 e_\sigma$

$E(b_1) = \varepsilon_0 + 55/32 e_\sigma$

— Hexagonal bipyramid, D_{6h}; eg. $[UO_2(O_2)_3]^{4-}$

$E(e_{2u}, b_{2u}) = \varepsilon_0$

$E(e_{1u}) = \varepsilon_0 + 9/8 e_\sigma$

$E(a_{2u}) = \varepsilon_0 + 2 e_\sigma$

$E(b_{1u}) = \varepsilon_0 + 15/4 e_\sigma$

$N = 9$ (Tricapped trigonal prism, D_{3h}; eg. $[Nd(OH_2)_9]^{3+}$

$E(a_2') = \varepsilon_0$

$E(a_2'') = \varepsilon_0 + 3/16 e_\sigma$

$E(e'') = \varepsilon_0 + 45/35 e_\sigma$

$E(e') = \varepsilon_0 + 117/64 e_\sigma$

$E(a_1') = \varepsilon_0 + 75/32 e_\sigma$

$N = 12$ (Tetradecahedron, O_h)

$E(a_{2u}) = \varepsilon_0$

$E(t_{1u}) = \varepsilon_0 + 1/4 e_\sigma$

$E(t_{2u}) = \varepsilon_0 + 15/4 e_\sigma$

The bonding molecular levels have $e_\sigma < 0$ and zero-order energies from the ligand, and the antibonding ones $e_\sigma > 0$ and ε_0 corresponding to the valence state of the free central atom. The results obtained actually represent the first steps in an *ab initio* treatment (bringing of interacting orbitals to the bond coordinate system, double diagonalization, factorization and expansion of the secular equation including overlap in the Brillouin-Wigner-Löwdin formalism), but e_σ may be well considered as an energetical parameter, the covalent part being naturally included into its explicit formulation [6]. The semiempirical approach thus obtained works well because the bonding/antibonding effects are essentially localized in the region of each central atom-ligand bond, the e_σ values depending only on the nature of these bonds, irrespective of the coordination number and topology of the cluster (principle of holohedrized symmetry [12]). These properties allow the comparison between clusters by means of a single parameter, an evident advantage on the crystal field results, being useful in the interpretation of EPR, electronic spectra and stereochemical properties.

---

[12] P. Spacu and C. I. Lepădatu, *Z. phys. Chem.* (*Frankfurt*), **73**, 255 (1970).

APPENDIX

The angular matrices so far published [5,13,14] dealt with real orbitals having $l \leqslant 2$. We give below the matrix elements of the irreducible representation for $l = 3$ (fundamental set indexed according to $C_{\infty v}$, $D_{\infty h}$ groups), obtained in a right-handed system under Eulerian angles (α β, γ)

$$(1) \qquad |i| = [D_{ij}^{(f)}(\alpha\beta\gamma)]\ |j|$$

$$(2) \qquad D^{(f)}(\alpha\beta\gamma) = D_{Z}^{(f)}(\alpha)\, D_{Y}^{(f)}(\beta)\, D_{Z'}^{(f)}(\gamma)$$

where $|i|$ (former set), $|j|$ (new set) are column matrices with matrix elements

$$\sigma = Y_3^0\,;\ \bar{\pi} = \frac{i}{\sqrt{2}}(Y_3^{-1} + Y_3^{+1})\,;\ \pi = \frac{1}{\sqrt{2}}(Y_3^{-1} - Y_3^{+1})\,;$$

$$\bar{\delta} = \frac{i}{\sqrt{2}}(Y_3^{-2} - Y_3^{+2})\,; \quad \delta = \frac{1}{\sqrt{2}}(Y_3^{-2} + Y_3^{+2})\,;$$

$$\bar{\Phi} = \frac{i}{\sqrt{2}}(Y_3^{-3} + Y_3^{+3})\,; \quad \Phi = \frac{1}{\sqrt{2}}(Y_3^{-3} - Y_3^{+3}),$$

$Y_l^{|m|}$ being harmonics normalized to 4π in the Condon-Shortley phase convention.

The D-matrices were obtained using the homomorphism of spinor and point groups [15] and checked up in the way recommended by C.E. Schäffer[14]. The total irreducible representation matrix $D^{(f)}(\alpha\beta\gamma)$ is the final result of the generally noncommutative multiplication (2), having the following 7×7 D_{ij} elements :

$$D_{\sigma\sigma} = \frac{1}{8}\,[5\cos 3\beta + 3\cos\beta]\,; \qquad D_{\sigma\bar{\pi}} = -\frac{\sqrt{6}}{16}\,[5\sin 3\beta + \sin\beta]\,(-\sin\gamma)\,;$$

$$D_{\sigma\pi} = -\frac{\sqrt{6}}{16}\,[5\sin 3\beta + \sin\beta]\cos\gamma\,; \qquad D_{\sigma\bar{\delta}} = -\frac{\sqrt{15}}{8}\,[\cos 3\beta - \cos\beta](-\sin 2\gamma)\,;$$

---

[13] H.-H. SCHMIDTKE, *Z. Naturforsch.*, **19 a**, 1502 (1964).

[14] C. E. SCHÄFFER, *Structure and Bonding*, **5**, 68 (1968).

[15] E. P. WIGNER, "Group Theory and its Applications in Quantum Mechanics", Acad. Press. Inc., New York, 1959.

$$D_{\sigma\delta} = -\frac{\sqrt{15}}{8}[\cos 3\beta - \cos\beta]\cos 2\gamma\,; \quad D_{\sigma\bar{\Phi}} = \frac{\sqrt{10}}{16}[\sin 3\beta - 3\sin\beta](-\sin 3\gamma)\,;$$

$$D_{\sigma\Phi} = \frac{\sqrt{10}}{16}[\sin 3\beta - 3\sin\beta]\cos 3\gamma\,; \quad D_{\bar{\pi}\sigma} = \frac{\sqrt{6}}{16}[5\sin 3\beta + \sin\beta]\sin\alpha\,;$$

$$D_{\bar{\pi}\bar{\pi}} = \frac{1}{8}[3 + 5\cos 2\beta]\cos\alpha\cos\gamma + \frac{1}{16}[15\cos 3\beta + \cos\beta]\sin\alpha(-\sin\gamma)\,;$$

$$D_{\bar{\pi}\pi} = \frac{1}{8}[3 + 5\cos 2\beta]\cos\alpha\sin\gamma + \frac{1}{16}[15\cos 3\beta + \cos\beta]\sin\alpha\cos\gamma\,;$$

$$D_{\bar{\pi}\bar{\delta}} = -\frac{\sqrt{10}}{4}\sin 2\beta\cos\alpha\cos 2\gamma - \frac{\sqrt{10}}{16}[3\sin 3\beta - \sin\beta]\sin\alpha(-\sin 2\gamma)\,;$$

$$D_{\bar{\pi}\delta} = -\frac{\sqrt{10}}{4}\sin 2\beta\cos\alpha\sin 2\gamma - \frac{\sqrt{10}}{16}[3\sin 3\beta - \sin\beta]\sin\alpha\cos 2\gamma\,;$$

$$D_{\bar{\pi}\bar{\Phi}} = \frac{\sqrt{15}}{8}(1 - \cos 2\beta)\cos\alpha\cos 3\gamma - \frac{\sqrt{15}}{16}[\cos 3\beta - \cos\beta]\sin\alpha(-\sin 3\gamma)\,;$$

$$D_{\bar{\pi}\Phi} = \frac{\sqrt{15}}{8}(1 - \cos 2\beta)\cos\alpha\sin 3\gamma - \frac{\sqrt{15}}{16}[\cos 3\beta - \cos\beta]\sin\alpha\cos 3\gamma\,;$$

$$D_{\pi\sigma} = \frac{\sqrt{6}}{16}[5\sin 3\beta + \sin\beta]\cos\alpha\,;$$

$$D_{\pi\bar{\pi}} = \frac{1}{8}[3 + 5\cos 2\beta](-\sin\alpha)\cos\gamma + \frac{1}{16}[15\cos 3\beta + \cos\beta]\cos\alpha(-\sin\gamma)\,;$$

$$D_{\pi\pi} = \frac{1}{8}[3 + 5\cos 2\beta](-\sin\alpha)\sin\gamma + \frac{1}{16}[15\cos 3\beta + \cos\beta]\cos\alpha\cos\gamma\,;$$

$$D_{\pi\bar{\delta}} = -\frac{\sqrt{10}}{4}\sin 2\beta(-\sin\alpha)\cos 2\gamma - \frac{\sqrt{10}}{16}[3\sin 3\beta - \sin\beta]\cos\alpha(-\sin 2\gamma)\,;$$

$$D_{\pi\delta} = -\frac{\sqrt{10}}{4}\sin 2\beta(-\sin\alpha)\sin 2\gamma - \frac{\sqrt{10}}{16}[3\sin 3\beta - \sin\beta]\cos\alpha\cos 2\gamma\,;$$

$$D_{\pi\bar{\Phi}} = \frac{\sqrt{15}}{8}(1 - \cos 2\beta)(-\sin\alpha)\cos 3\gamma - \frac{\sqrt{15}}{16}[\cos 3\beta - \cos\beta]\cos\alpha(-\sin 3\gamma)\,;$$

$$D_{\pi\Phi} = \frac{\sqrt{15}}{8}(1 - \cos 2\beta)(-\sin\alpha)\sin 3\gamma - \frac{\sqrt{15}}{16}[\cos 3\beta - \cos\beta]\cos\alpha\cos 3\gamma\,;$$

$$D_{\bar{\delta}\sigma} = -\frac{\sqrt{15}}{8}[\cos 3\beta - \cos\beta]\sin 2\alpha\,;$$

$$D_{\bar{\delta}\bar{\pi}} = \frac{\sqrt{10}}{4}\sin 2\beta\cos 2\alpha\cos\gamma + \frac{\sqrt{10}}{16}[3\sin 3\beta - \sin\beta]\sin 2\alpha\,(-\sin\gamma)\,;$$

$$D_{\bar{\delta}\pi} = \frac{\sqrt{10}}{4}\sin 2\beta\cos 2\alpha\sin\gamma + \frac{\sqrt{10}}{16}[3\sin 3\beta - \sin\beta]\sin 2\alpha\cos\gamma\,;$$

$$D_{\bar{\delta}\bar{\delta}} = \cos 2\beta\cos 2\alpha\cos 2\gamma + \frac{1}{8}[5\cos\beta + 3\cos 3\beta]\sin 2\alpha\,(-\sin 2\gamma)\,;$$

$$D_{\bar{\delta}\delta} = \cos 2\beta\cos 2\alpha\sin 2\gamma + \frac{1}{8}[5\cos\beta + 3\cos 3\beta]\sin 2\alpha\cos 2\gamma\,;$$

$$D_{\bar{\delta}\bar{\Phi}} = -\frac{\sqrt{6}}{4}\sin 2\beta\cos 2\alpha\cos 3\gamma - \frac{\sqrt{6}}{16}[\sin 3\beta + 5\sin\beta]\sin 2\alpha\,(-\sin 3\gamma)\,;$$

$$D_{\bar{\delta}\Phi} = -\frac{\sqrt{6}}{4}\sin 2\beta\cos 2\alpha\sin 3\gamma - \frac{\sqrt{6}}{16}[\sin 3\beta + 5\sin\beta]\sin 2\alpha\cos 3\gamma\,;$$

$$D_{\delta\sigma} = -\frac{\sqrt{15}}{8}[\cos 3\beta - \cos\beta]\cos 2\alpha\,;$$

$$D_{\delta\bar{\pi}} = \frac{\sqrt{10}}{4}\sin 2\beta\,(-\sin 2\alpha)\cos\gamma + \frac{\sqrt{10}}{16}[3\sin 3\beta - \sin\beta]\cos 2\alpha\,(-\sin\gamma)\,;$$

$$D_{\delta\pi} = \frac{\sqrt{10}}{4}\sin 2\beta\,(-\sin 2\alpha)\sin\gamma + \frac{\sqrt{10}}{16}[3\sin 3\beta - \sin\beta]\cos 2\alpha\cos\gamma\,;$$

$$D_{\delta\bar{\delta}} = \cos 2\beta\,(-\sin 2\alpha)\cos 2\gamma + \frac{1}{8}[5\cos\beta + 3\cos 3\beta]\cos 2\alpha\,(-\sin 2\gamma)\,;$$

$$D_{\delta\delta} = \cos 2\beta\,(-\sin 2\alpha)\sin 2\gamma + \frac{1}{8}[5\cos\beta + 3\cos 3\beta]\cos 2\alpha\cos 2\gamma\,;$$

$$D_{\delta\bar{\Phi}} = -\frac{\sqrt{6}}{4}\sin 2\beta\,(-\sin 2\alpha)\cos 3\gamma - \frac{\sqrt{6}}{16}[\sin 3\beta + 5\sin\beta]\cos 2\alpha(-\sin 3\gamma)\,;$$

$$D_{\delta\Phi} = -\frac{\sqrt{6}}{4}\sin 2\beta\,(-\sin 2\alpha)\sin 3\gamma - \frac{\sqrt{6}}{16}[\sin 3\beta + 5\sin\beta]\cos 2\alpha\cos 3\gamma;$$

$$D_{\bar{\Phi}\sigma} = -\frac{\sqrt{10}}{16}[\sin 3\beta - 3\sin\beta]\sin 3\alpha;$$

$$D_{\bar{\Phi}\bar{\pi}} = \frac{\sqrt{15}}{8}(1-\cos 2\beta)\cos 3\alpha\cos\gamma - \frac{\sqrt{15}}{16}[\cos 3\beta - \cos\beta]\sin 3\alpha\,(-\sin\gamma);$$

$$D_{\bar{\Phi}\pi} = \frac{\sqrt{15}}{8}(1-\cos 2\beta)\cos 3\alpha\sin\gamma - \frac{\sqrt{15}}{16}[\cos 3\beta - \cos\beta]\sin 3\alpha\cos\gamma;$$

$$D_{\bar{\Phi}\bar{\delta}} = \frac{\sqrt{6}}{4}\sin 2\beta\cos 3\alpha\cos 2\gamma + \frac{\sqrt{6}}{16}[\sin 3\beta + 5\sin\beta]\sin 3\alpha\,(-\sin 2\gamma);$$

$$D_{\bar{\Phi}\delta} = \frac{\sqrt{6}}{4}\sin 2\beta\cos 3\alpha\sin 2\gamma + \frac{\sqrt{6}}{16}[\sin 3\beta + 5\sin\beta]\sin 3\alpha\cos 2\gamma;$$

$$D_{\bar{\Phi}\bar{\Phi}} = \frac{1}{8}[5 + 3\cos 2\beta]\cos 3\alpha\cos 3\gamma + \frac{1}{16}[15\cos\beta + \cos 3\beta]\sin 3\alpha\,(-\sin 3\gamma);$$

$$D_{\bar{\Phi}\Phi} = \frac{1}{8}[5 + 3\cos 2\beta]\cos 3\alpha\sin 3\gamma + \frac{1}{16}[15\cos\beta + \cos 3\beta]\sin 3\alpha\cos 3\gamma;$$

$$D_{\Phi\sigma} = -\frac{\sqrt{10}}{16}[\sin 3\beta - 3\sin\beta]\cos 3\alpha;$$

$$D_{\Phi\bar{\pi}} = \frac{\sqrt{15}}{8}(1-\cos 2\beta)(-\sin 3\alpha)\cos\gamma - \frac{\sqrt{15}}{16}[\cos 3\beta - \cos\beta]\cos 3\alpha\,(-\sin\gamma);$$

$$D_{\Phi\pi} = \frac{\sqrt{15}}{8}(1-\cos 2\beta)(-\sin 3\alpha)\sin\gamma - \frac{\sqrt{15}}{16}[\cos 3\beta - \cos\beta]\cos 3\alpha\cos\gamma;$$

$$D_{\Phi\bar{\delta}} = \frac{\sqrt{6}}{4}\sin 2\beta\,(-\sin 3\alpha)\cos 2\gamma + \frac{\sqrt{6}}{16}[\sin 3\beta + 5\sin\beta]\cos 3\alpha\,(-\sin 2\gamma);$$

$$D_{\Phi\delta} = \frac{\sqrt{6}}{4}\sin 2\beta\,(-\sin 3\alpha)\sin 2\gamma + \frac{\sqrt{6}}{16}[\sin 3\beta + 5\sin\beta]\cos 3\alpha\cos 2\gamma;$$

$$D_{\Phi\bar{\Phi}} = \frac{1}{8}[5 + 3\cos 2\beta](-\sin 3\alpha)\cos 3\gamma + \frac{1}{16}[15\cos\beta + \cos 3\beta]\cos 3\alpha\,(-\sin 3\gamma);$$

$$D_{\Phi\Phi} = \frac{1}{8}[5 + 3\cos 2\beta](-\sin 3\alpha)\sin 3\gamma + \frac{1}{16}[15\cos\beta + \cos 3\beta]\cos 3\alpha\cos 3\gamma.$$

Revue Roumaine de Chimie, 17, 1, 2, 343–352 (1972)

Dedicated to Professor I.G. MURGULESCU
on his 70th birthday

INTERDIFFUSION COEFFICIENT OF THE SILVER ION IN MOLTEN ALKALI CHLORIDES BY THE CHRONOPOTENTIOMETRIC METHOD

S. STERNBERG and CONSTANŢA HERDLICKA

Institute of Physical Chemistry, str. Galaţi 31, Bucharest, Romania

Received August 6, 1971

The interdiffusion coefficient of silver ion in molten LiCl, NaCl, KCl, RbCl, CsCl and NaCl + KCl (1 :1) at different temperatures has been measured by the chronopotentiometric method.

The interdiffusion coefficient of Ag^+ decreases from LiCl to CsCl. The activation energies of diffusion were found to be approximately equal to the energies of holes formation in the solvent. The Stokes-Einstein and Nernst-Einstein equations are discussed.

The chronopotentiometric method has been used by us in determining the interdiffusion coefficient and activation energy of diffusion of silver ion in pure molten alkali nitrates. [1,2]

In this work we have extended the diffusion measurements by the chronopotentiometric method to higher temperatures characteristic of alkali halides.

Most chronopotentiometric studies investigate the interdiffusion of metallic ions in molten salts the migration medium being an eutectic mixture of LiCl—KCl and the measurements were carried out at 450° [3–8]; only in a few cases are measurements performed within a wider temperature range whose upper limit does not exceed 730°. [9–11] Relatively few

---

[1] S. Sternberg and C. Herdlicka, *Rev. Roumaine Chim.*, **14**, 991 (1969).

[2] S. Sternberg and C. Herdlicka, *Rev. Roumaine Chim.*, **15**, 343 (1970).

[3] H. A. Laitinen and W. S. Ferguson, *Analyt. Chem.*, **29**, 4 (1957).

[4] H. A. Laitinen and H. C. Gaur, *Analyt. Chim. Acta*, **18**, 1 (1958).

[5] B. Scrosati, *Analyt. Chem.*, **38**, 1588 (1966).

[6] H. A. Laitinen and D. R. Rhodes, *J. Electrochem. Soc.*, **109**, 413 (1962).

[7] B. Scrosati and H. A. Laitinen, *Analyt. Chem.*, **38**, 1894 (1966).

[8] J. D. Van Norman, *Analyt. Chem.*, **33**, 946 (1961).

[9] C. E. Thalmayer, S. Bruckenstein and D. M. Gruen, *J. Inorg. Nuclear Chem.*, **26**, 347 (1964).

[10] F. Caligara, L. Martinot and G. Duyckaerts, *J. Electroanalyt. Chem.*, **16**, 335 (1968).

[11] T. Suzuki, *Electrochim. Acta*, **15**, 303 (1970).

diffusion measurements have been carried out in the equimolecular NaCl-KCl mixture [12−15] at temperatures exceeding 700°. The single alkali halides have not yet been used as interdiffusion media.

The present paper reports the results of interdiffusion measurements of the silver ion in single alkali halides media as well as in the equimolecular NaCl—KCl mixture, at different temperatures within a range of over 100°.

EXPERIMENTAL

The device and the procedure of recording the potential-time curves have been described in previous papers. [1,2].

The high temperatures imply experimental conditions different from those used at low temperatures. The specific conditions of obtaining correct chronopotentiograms are extensively described elsewhere [16].

The working electrode [16] was a platinum plate with surface areas between 0.4 and 0.7 cm^2. Its potential was measured across a reference electrode of the Ag/AgCl (0.1 m) + solvent.

The potential-time curves have been recorded for current densities between 30—80 mA/cm^2 and AgCl concentrations in solvent of $3-8\times10^{-5}$ mol/cc. The high temperatures favour the convention ; to prevent the superposition of convection over mass diffusion, the transition times were maintained between 0.6 and 1.5 sec.

All the chemicals used in experiments were p.a. grade recrystallized and melted in HCl. To remove gaseous HCl solved in the melt, purified and dried argon has been passed through the melt for several hours.

In LiCl and NaCl the greatest part of water retained in the salt was eliminated by vacuum pumping (2—3 hours) followed by the above mentioned operations. The potential-time curves recorded for the solvents purified in the above conditions showed no trace of impurities.

RESULTS

The interdiffusion coefficients of the silver ion have been determined within a wide temperature range in : LiCl (638—816°), NaCl (823—915°), KCl (790—916°), RbCl (735—876°), CsCl (663—865°) and the equimolecular mixture NaCl—KCl (710—880°).

In table 1 are given the interdiffusion coefficients of Ag^+ at different temperatures for each solvent studied.

The temperature dependence of interdiffusion coefficient is well represented by an Arrhenius type equation

$$D = D_0 \exp\ [-E/RT]$$

---

[12] Y. K. Delimarskii, A. V. Gorodyskii and V. V. Kuzmovitch, *Coll. Czech. Chem. Comm.*, **25**, 3056 (1960).

[13] A. N. Baraboshkin, M. V. Smirnov and N. A. Saltykova, "Electrockhimia Rasplavlenikh Solevikh i Tviordikh Electrolitov", Inst. Electrokhim. Akad. Nauk, U.R.S.S.-Uralsk Filial nr. 2, 1961, p. 53.

[14] O. V. Skiba, M. V. Smirnov and T. F. Khazemova, "Electrochemistry of Molten and Solid Electrolytes", translation of Constultants Bureau, New York, Ed. by M. V. Smirnov, 1964, p. 7.

[15] T. Sakakura, *J. Electrochem. Soc. Japan*, **35**, 75 (1967).

[16] S. Sternberg and C. Herdlicka, *Rev. Roumaine Chim.* (in press).

Table 1

The interdiffusion coefficient of silver ion in molten alkali chlorides.

LiCl

Temp °C	638	665	694	697	718	746	752	790	795	816
$D \times 10^5$ $cm^2 . sec^{-1}$	11.41	12.96	14.20	14.38	14.99	15.59	15.42	19.35	18.12	19.10

NaCl

Temp °C	823	825	840	844	855	864	886	905	915
$D \times 10^5$ $cm^2 . sec^{-1}$	9.87	9.99	10.30	10.76	10.87	11.22	12.04	13.12	13.37

KCl

Temp °C	790	793	801	811	830	835	848	861	873	880	887	890	906	916
$D \times 10^5$ $cm^2 . sec^{-1}$	8.61	8.62	8.82	9.47	9.61	9.97	10.55	10.99	11.04	11.12	11.40	11.57	12.76	12.70

RbCl

Temp °C	735	745	767	773	782	806	837	876
$D \times 10^5$ $cm^2 . sec^{-1}$	6.31	6.84	6.98	7.33	7.83	8.59	8.73	10.04

CsCl

Temp °C	663	684	693	698	735	765	794	822	833	865
$D \times 10^5$ $cm^2 . sec^{-1}$	4.82	5.40	5.45	5.88	6.49	7.17	7.74	8.73	8.92	9.76

NaCl + KCl

Temp °C	710	736	742	750	780	792	813	819	834	854	880
$D \times 10^5$ $cm^2 . sec^{-1}$	6.94	7.40	8.09	8.53	9.10	9.21	9.76	10.10	10.08	11.12	11.42

where E is the activation energy for diffusion and D_0 the pre-exponential factor, both of them temperature-independent.

Figure 1 shows this dependence. The numerical values of E and D_0 determined by the least squares method are given in tables 2 and 3.

In table 2 are given the interdiffusion data of Ag^+ in NaCl—KCl (1: 1) which we obtained together with the results other authors obtained by the chronopotentiometric method, too.

Table 2

Diffusion constants of Ag^+ in NaCl+KCl (1 : 1) obtained by us and other authors

$D \times 10^5 cm^2. sec^{-1}$ 710°C	$D_0 \times 10^3$ $cm^2. sec^{-1}$	E cal. mol^{-1}	Temperature range °C	Reference
6.94±0.35	1.91±0.48	6411±517	710—880	our results
7.06	1.29	5700	700—800	Smirnov [13]
4.5±0.2	—	—	710	Delimarskii [12]

Table 3

Activation energy, E and pre-exponential factor, D_0 for silver ion diffusion in simple molten alkali chlorides

Solvent	$D_0 \times 10^3$ $cm^2.sec^{-1}$	E cal. mol^{-1}	Temperature range C°
LiCl	2.46±0.48	5516±389	638—816
NaCl	4.66±0.31	8404±150	823—915
KCl	3.30±0.51	7709±344	790—916
RbCl	1.87±0.16	6712±220	735—876
CsCl	2.38±0.27	7223±182	663—865

It should be noteworthy that our results agreed with those found by Smirnov and collab. [13]

DISCUSSION

The interdiffusion coefficient of the silver ion in alkali chlorides decreases as the cation radius increases. At the melting point of the solvent this decrease is evident as seen in figure 2. A similar behaviour is remarked for the equivalent conductivity [17] and the cationic self-diffusion of the solvent [18,19] which are also represented in figure 2.

---

[17] St. Zuca and M. Olteanu, *Rev. Roumaine Chim.*, **15**, 357 (1970).

[18] J. O'M. Bockris and G. W. Hooper, *Discuss. Faraday Soc.*, **32**, 218 (1961).

[19] J.O'M. Bockris, S. R. Richards and L. Nanis, *J. Phys. Chem.*, **69**, 1627 (1965).

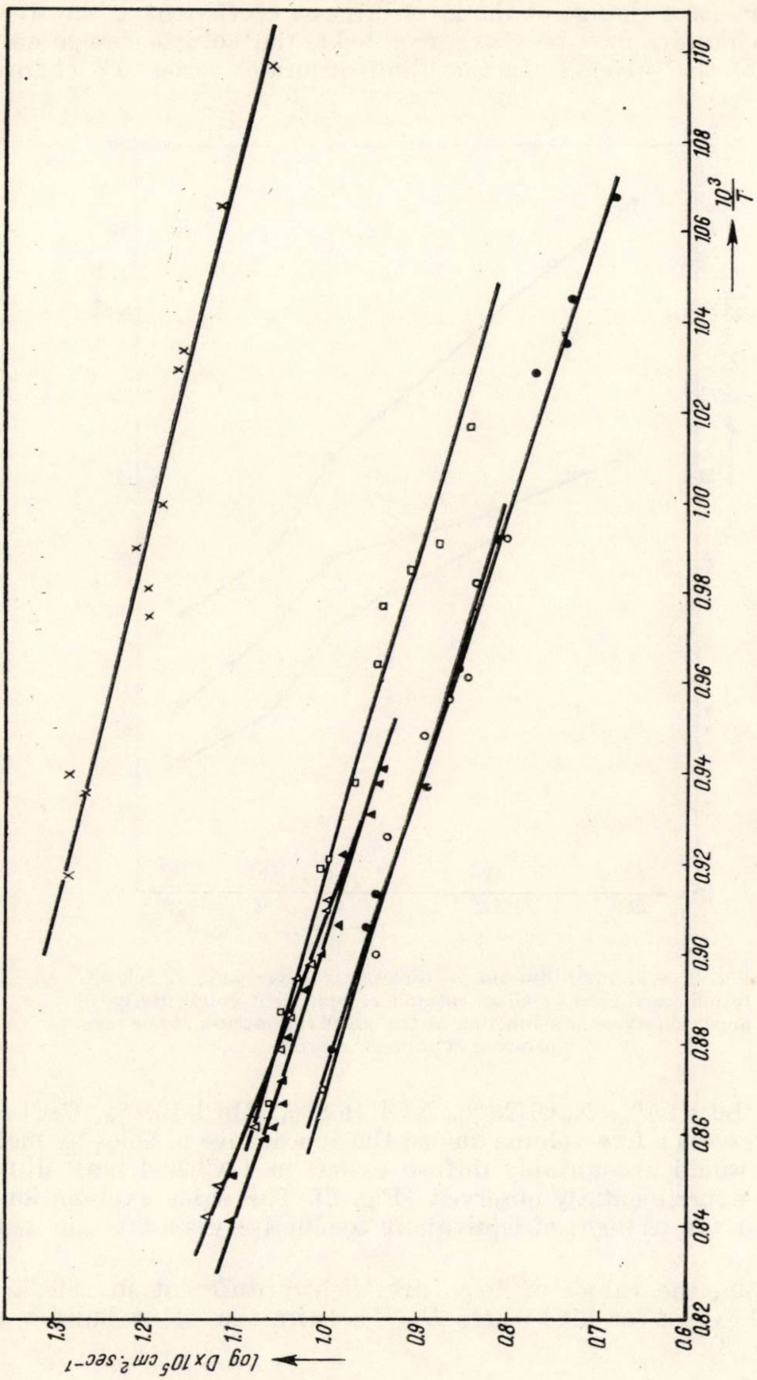

Fig. 1. — Arrhenius plots of the silver ion interdiffusion coefficient in :
X -LiCl; Δ - NaCl; ▲ - KCl; ○ - RbCl; ● - CsCl; □ - NaCl + KCl.

The relative change of the interdiffusion coefficient in the five molten alkali chlorides may be also correlated to the volume change on melting, ΔV, of the solvents. In the alkali chlorides series ΔV changes as follows[20]: LiCl 25%, NaCl 23%, KCl 16.8%, RbCl 13.4%, CsCl 9.8%. If ΔV represents a free volume due to the appearance of holes by melting, then Ag^+ would accountably diffuse easiest in LiCl and most difficulty in CsCl, as experimentally observed (Fig. 2). The same explanation may be given for the changes of equivalent conductivity *versus* the cationic radius.

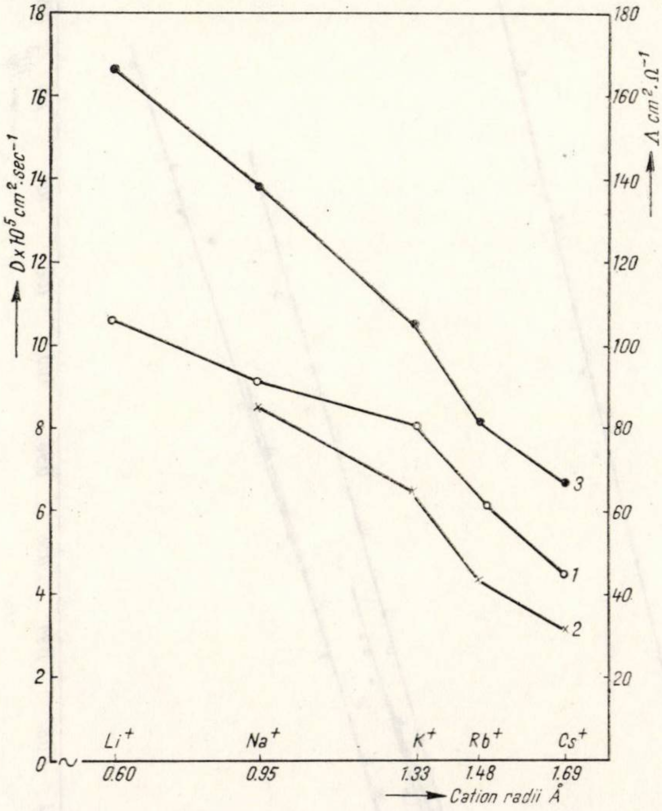

Fig. 2. — *1*, Interdiffusion coefficient of silver ion; *2*, Self-diffusion coefficient of alkali cation; *3*, equivalent conductivity of alkali chlorides as a function of the alkali cation radii at the temperature of solvent melting.

At 850°, the values of D_{Ag^+} are slightly different in NaCl, KCl, RbCl, CsCl except for LiCl where D_{Ag^+} is twice the other halides under study (Fig. 3).

---

[20] H. Spindler and F. Sauerwald, *Z. anorg. Chem.*, **335**, 267 (1965).

If we compare our results with the self-diffusion coefficients of solvent cations, the LiCl being unfortunately absent, D_{Ag^+} in the same solvent is higher than the cationic self-diffusion coefficient and the difference increases proportionally to the radius of alkali cation. The lowest difference between values is between D_{Ag^+} and D_{Na^+} in NaCl due to the fact that the radii of silver and sodium ions are very close to each other. We can state, as in the case of alkali nitrates, that the ratio of the interdiffusion coefficient of a foreign cation to the self-diffusion coefficient of the solvent cation is higher than unit when the radius of the foreign cation is smaller than the radius of the solvent cation.

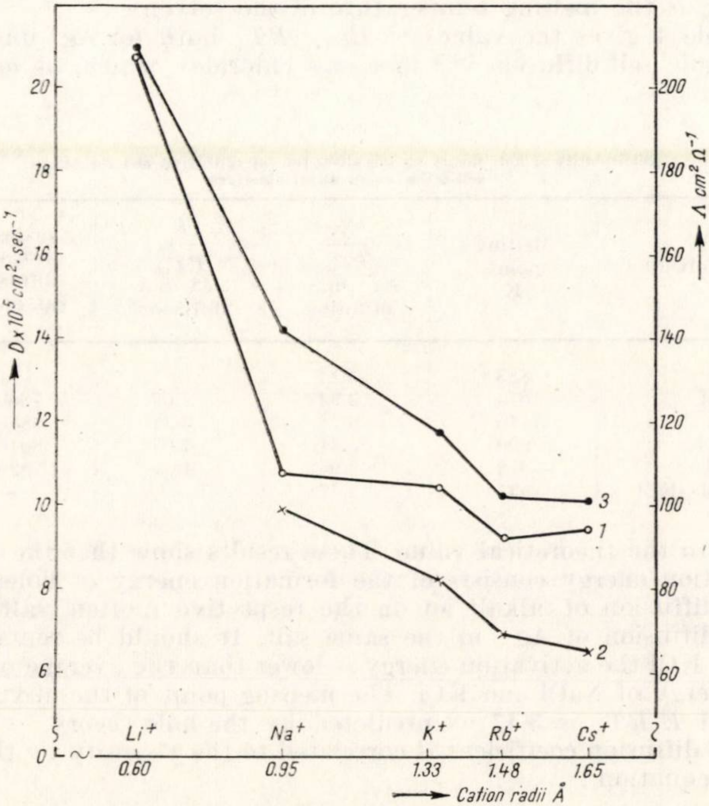

Fig. 3. — *1*, Interdiffusion coefficient of silver ion ; *2*, self-diffusion coefficient of alkali cation ; *3*, equivalent conductivity of alkali chlorides as a function of the alkali cation radii at 850°.

The activation energies for the diffusion of Ag^+ are higher as the melting point of alkali chloride is higher. Bockris and co-workers [19] explained the results of their self-diffusion measurements on the basis of Fürth's holes theory. Starting from the hole theory for liquids Bockris and coworkers [19] found for the formation energy of holes the equation :

$$E_h = 3.74\ RT_m$$

where T_m is the melting temperature of the solvent.

Table 4 gives the values of $E_{\text{exp.}}\ /RT_m$ both for Ag^+ interdiffusion and cationic self-diffusion [18,19] in alkali chlorides which, as easily seen, are close to the theoretical value. These results show that the main part of activation energy consists of the formation energy of holes both for the self-diffusion of alkali ion in the respective molten salt and for the interdiffusion of Ag^+ in the same salt. It should be remarked that in NaCl—KCl the activation energy is lower than the average of the activation energy of NaCl and KCl. The melting point of the mixture is also lower and E/RT_m is 3.47 as predicted by the hole theory.

Table 4

Applicability of hole theory on the silver ion interdiffusion and the cation self-diffusion in alkali chlorides

Solvent	Melting point °K	$\frac{E}{RT_m}$ Ag^+ interdiffusion	$\frac{E}{RT_m}$ Me^+ self-diffusion	E (experim.) Me^+ self-diffusion cal. mol^{-1}
LiCl	883	3.14	—	—
NaCl	1074	3.94	3.68	7860[18]
KCl	1045	3.71	3.31	6880[19]
RbCl	990	3.41	4.07	8010[18]
CsCl	918	3.96	4.01	7320[18]
NaCl+KCl	931	3.47	—	—

The diffusion coefficient is correlated to the viscosity by the Stokes-Einstein equation :

$$D_i = \frac{KT}{a\pi\eta r_i}$$

where r_i is the radius of the diffusing ion (cm) and η is the viscosity of the solvent (gr. cm^{-1}. sec.$^{-1}$). For the constant "a" we took 4.6, found for alkali nitrates by us[2] and by other authors. [21] In the classical equation a is 6 for the diffusion of a large particle and 4 for a small particle. The solutions being very diluted in AgCl the viscosity of the liquid is that of the alkali halide.

The radius of the silver ion used in calculation is, according to Pauling, 1.13 Å and viscosity was taken from Murgulescu and Zuca's paper. [22]

Table 5 gives the results of the calculation according to Stokes-Einstein equation at 850° and melting point of the solvent. Examination of data in table 5 shows that at the melting point of the solvent, excepting LiCl and NaCl, a satisfactory agreement between the calculated and experimental values is found, while at 850° there are great differences between the two series of data, the agreement existing only for KCl and RbCl.

---

[21] S. Forcheri and V. Wagner, *Z. Naturforsch*, **22a**, 1171 (1967).

[22] I. G. Murgulescu and St. Zuca, *Z. Phys. Chem.*, **220**, 300 (1963).

Table 5

Comparison between the experimental and calculated interdiffusion coefficient according to Stokes-Einstein equation for silver ion in alkali chlorides

Solvent	850°C			Solvent melting point		
	η^{20} cp	$D \times 10^5$ (exp.) $cm^2 . sec^{-1}$	$D \times 10^5$ (calc.) $cm^2 . sec^{-1}$	η^{20} cp	$D \times 10^5$ (exp.) $cm^2 . sec^{-1}$	$D \times 10^5$ (calc.) $cm^2 . sec^{-1}$
LiCl	0.763	20.79	12.44	1.804	10.62	4.14
NaCl	1.203	10.79	7.89	1.436	9.09	6.32
KCl	0.956	10.43	9.93	1.190	8.06	7.42
RbCl	0.939	0.23	10.11	1.354	6.17	6.18
CsCl	0.768	9.35	12.36	1.372	4.54	5.66

Stokes-Einstein equation applies better in alkali nitrates [2,21] than in alkali halides.

A general qualitative confirmation of the S.E. equation may be obtained if the interdiffusion coefficients of Ag^+ in alkali halides and nitrates are compared. Their ratio D_{Ag^+} (halide)/D_{Ag^+} (nitrate) is, at melting point the same as the ratio $\left(\frac{T_m}{\eta}\right)$ halide / $\left(\frac{T_m}{\eta}\right)$ nitrate except for the lithium salts for which the diffusion coefficients ratio is higher, as seen in table 6. In alkali halides, excepting LiCl and CsCl, D_{Ag^+} is 4–5 times higher than in alkali nitrates, this situation being related to the higher melting temperatures and the lower diffusion coefficients of alkali halides.

Table 6

Comparison between the interdiffusion coefficient of Ag^+ in alkali halides and nitrates

Solvent	$\frac{(D_{Ag^+}) \text{ halide}}{(D_{Ag^+}) \text{nitrate}}$	$\frac{(T_m/\eta) \text{ halide}}{(T_m/\eta) \text{ nitrate}}$
Li^+	13.3	5.5
Na^+	4.7	3.7
K^+	4.4	3.8
Rb^+	4.1	4.8
Cs^+	1.7	2.3

It was qualitatively observed that the interdiffusion coefficients of Ag^+ in single alkali chlorides are proportional to the equivalent conductivity, their dependence on the cation nature being similar (Figs. 2 and 3). This proportionality is mathematically expressed by Nernst-Einstein equation which correlates the diffusion coefficient and the equivalent electric conductivity λ_i.

$$D_i = \frac{\lambda_i RT}{F^2} \tag{1}$$

or the ionic mobility u_i

$$\frac{D_i}{RT} = \frac{u_i}{zF} \tag{2}$$

The lack of experimental data for the ionic mobilities of Ag^+ in alkali halides prevented us from testing this equation.

In general, the literature contains only few data on the ionic mobilities of foreign ions in alkali halides and therefore the N.E. equation was mainly used for checking the self-diffusion data.

For the interdiffusion we may apply the N.E. equation to the diffusion of Ag^+ in single alkali nitrates since, except for $LiNO_3$, the ionic mobilities of Ag^+ in these solvents are known. [23]

Table 7 gives the results obtained with eq. 2; the interdiffusion coefficients of Ag^+ are taken from our previous papers [1,2] and mobilities of Ag^+ from Murgulescu and Topor's paper. [23] Table 7 shows that deviations from N.E. equation are high.

Table 7

Comparison between the experimental and calculated interdiffusion coefficient according to Nernst-Einstein equation for silver ion alkali nitrates at 450°

Solvent	U_{Ag^+} (exp.)[22] cm^2.sec^{-1} volt	D_{Ag^+}(exp.)[1,2] cm^2. sec^{-1}	D_{Ag^+} (calc.) cm^2.sec^{-1}
$LiNO_3$	—	6.59×10^{-5}	—
$NaNO_3$	3.68×10^{-4}	4.22×10^{-5}	2.29×10^{-5}
KNO_3	3.73×10^{-4}	3.17×10^{-5}	2.32×10^{-5}
$RbNO_3$	3.34×10^{-4}	3.37×10^{-5}	2.08×10^{-5}
$CsNO_3$	1.72×10^{-4}	3.25×10^{-5}	1.07×10^{-5}

Arstdalen and collab. [24] proved that N.E. equation is not valid also for self-diffusion in single alkali nitrates.

The Nernst-Einstein eq. does not apply to molten salts and the general explanation given by various authors is that not all ionic groups, which contribute to the mass transport, also contribute to the charge transport and therefore various conduction mechanisms may be suggested.

From our above calculations it results that there is a similitude between the self-diffusion and interdiffusion mechanisms. As for the Ag^+ ion transport in alkali solvents it is likely that some kinetic entities which participate in interdiffusion do not participate in electromigration. This accounts for the lower interdiffusion coefficient calculated from silver ion mobilities in alkali nitrates as compared to the experimental one.

---

[23] I. G. Murgulescu and D. Topor, *Rev. Roumaine Chim.*, **13**, 979 (1968).

[24] A. S. Dworkin, R. B. Escue and E. R. Van Arstdalen, *J. Phys. Chem.*, **64**, 872 (1960).

Revue Roumaine de Chimie, **17**, *1*, *2*, 353–356 (1972)

Dedicated to Professor I.G. MURGULESCU
on his 70th birthday

NOTES ON PYROLYSIS

G. C. SUCIU

Institute of Petroleum, Gas, and Geology str. Av. Traian Vuia 6, Bucharest, Romania

Received October 5, 1971

Recent developments in coil pyrolysis with special stress on chemical engineering problems are presented. Some aspects on the correlation of lab and plant scale data are outlined.

The increase in world wide requirements of ethylene has led to the necessity to crack heavier feed stocks for its manufacture, such as naphthas and gas oils, particularly in countries with small or no crude production and attendant scarcity or lack of light alkanes (C_2, C_3.)

The success of the process for handling heavier stocks is largely determined by the performance of the pyrolysis heater.

Considerable progress has been realized in the design and operation of pyrolysis reactors during the last few years by a better understanding of the cracking reactions and by the availability of improved high-temperature alloys.

Cracking of hydrocarbons is an essentially endothermal high temperature, free radical mechanism process, leading to primary decomposition products consisting mainly of olefines, methane, and hydrogen and to secondary reactions additionally producing aromatics and coke.

In the cracking of pure hydrocarbons yields of ethylene decrease from ethane, to propane, to n-butane etc. and are higher for n-alkanes than for equal molecular weight iso-alkanes, the difference decreasing with an increase in molecular weight. Naphthenes decompose to less ethylene and to more butadiene than the alkanes, the yield difference decreasing with chain length. Monocyclic aromatic rings remain unconverted while polycyclic aromatics tend to polymerize. In mixtures of hydrocarbons, such as in naphthas, the individual components with the highest reaction rates provide free radicals to the more refractory constituents thus speeding up their decomposition.

For chemical engineering kinetics purposes, pyrolysis is being considered as a first order reaction with an activation energy decreasing from approximately 3×10^8 J/kmole for ethane to about $2.1-2.3 \times 10^3$ J/kmole for n-pentane and heavier alkanes. For naphthas, the reaction velocity constant is about equal to that of an iso-alkane having the same, or a slightly higher C-atom number in the molecule. There is a determined time-temperature range, for each feed stock, for maximum ethylene yield or for a given products distribution.

Although numerous types of pyrolysis reactors have been industrially tested, such as pebble heating in moving beds, sand-contacting in fluidized beds, regenerative heating etc., the tube heater is still the most widely used reactor to-day.

Short residence time and high cracking temperatures are characteristic features of present day units. Newer heaters provide for a reisdence time of 0.3 seconds and less, compared to over one second in the early sixties (Table 1). This has required higher operating temperatures, in the range of 860° in naphtha cracking, and has more than doubled radiant section heat fluxes. Heat densities of 70000 w/m^2 are being currently attained and, 90000 w/m^2 have been reported in tests run on semicommercial units on gas oil feed stocks. In order to avoid premature coking and ensure longer runs between coil decoking, mass velocities were increased to 120−150 kg/m^2s. High severity, short residence time cracking results in considerable ethylene yield improvement (fig. 1) [3]

Table 1

Recent developments in tubular heater design [1]

	1962	1964	1966	At present
Tube arrangement	2-pass horiz.	4-pass horiz.	6-pass vert.	Vert.
Hydrocarbon thruput t/hr	4.5	10.0	17.0	—
Steam/hydrocarbon ratio, wt.	0.45	0.50	0.50	—
Max. coil outlet temperature °C	760	817	855	(870)
Ethylene yield, wt % (40−180°C− B. R. Naphtha)	17−24	20−26	22−28	—
Average heat flux w/m^2	35000	38000	57000	(80000)
Residence time (sec. above 600°C)	1.8	1.2	0.8	(0.3)
Max. firebox temperature[2] C°	1040	1100	1150	1260
Tube material	18-8Cr-Ni or 20-35Cr-Ni	20-35Cr-Ni	20-35Cr-Ni or 25-20Cr-Ni	—

Designing a competitive pyrolysis heater for a given feed stock implies optimizing the value of a large number of physical variables and parameters controlling the yield pattern and the thruput in relation to construction restraints, such as maximum tube metal and firebox temperatures, and limiting mass velocities.

The yield pattern is determined by the nature of the feed, the conversion, the temperature (coil outlet temperature and temperature profile along the coil) and the partial pressure of the hydrocarbons. The overall conversion, temperature curve (heat flux) and pressure drop is obtained by a stepwise calculation procedure involving local solution of the $\int k.dt$ function for a first order reaction.

---

[1] S. B. Zdonik, E. J. Green and L. P. Hallee; *Oil and Gas Journ.*, **1969** 221.

[2] S. B. Zdonik, E. J. Green and L. P. Hallee, *ibid.* **1969**, 89.

[3] M. J. Maddock and R. K. Dorn; *ibid.*, **1971**, 67.

The intricated relationships relating physical and design variables, the many steps and iterations required in order to obtain an optimum solution for a given feed stock, yield pattern and thruput, has made the use of a computer indispensable.

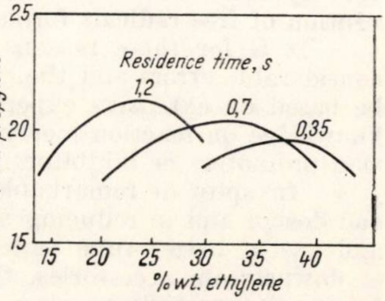

Fig. 1[3]. – Ethylene-propylene yields from light naphtha pyrolysis.

A fundamental problem to be solved before proceeding to a coil design for a given feedstock is the knowledge of the yield pattern and of the reaction velocity constant, which have to be determined experimentally. Correlation of pilot plant and industrial coil data in this field is quite a problem.

At the high mass velocities practiced in industrial coils, with Reynolds numbers ranging between 10^5 and 10^6, relative film thickness is negligible and temperature drop across the boundary layer is low. Therefore film cracking accounts for only a few percent of the overall reaction.

In pilot coils, operating at low Reynolds numbers, film thickness may account for a large percentage of the total cross-section of the tube, and temperature drops across the film may run into figures of 100°, even at moderate heat densities (fig. 2) [4]. Thus in a di = 10 mm coil fed with

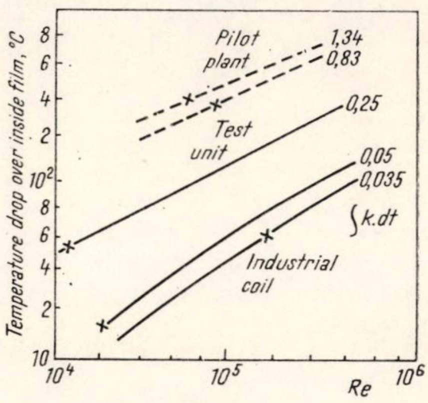

Fig. 2[4]. – Effect of Re on temperature drop and $k.dt$ over inside fluid film.

---

[4] J. L. De Blieck and A. G. Groossen, *Hydroc. Processing*, **1971**, 78.

naphtha at an average gas velocity of 11 m/s, the temperature drop across the boundary layer may exceed 100° and the cross-section of the film may amount to over 1/4 of the cross-section of the tube. Evidently, even at low Reynolds number there is a positive radial material flow from the wall, due to the volumetric expansion of the feed, accompanying the reaction. Under these conditions the integration of $\int k.dt$ along the tube will yield very approximate results. The matter is further complicated by the intervention of free radicals formed within the boundary layer.

It is for these reasons that pilot plant data may be affected by considerable errors and their extrapolation to industrial size units has to be based on extensive experimentation. Laboratory studies may further knowledge on reaction mechanism revealing new aspects on specific reaction promoters or inhibitors.

In spite of remarkable improvements brought about in pyrolysis coil design and in reducing maintenance difficulties, by the manufacture and use of better tube material, vertical tube arrangement and design of downstream accessories, there is a sustained effort to develop new types of pyrolysis reactors capable of processing heavier feed stocks (heavy distillates and residues).

Pyrolysis by direct contact with 1800 – 2000°C steam [5], by submerged burning and plasma jet cracking [6] is being experimented on at present in pilot plants and in semicommercial units. It is believed however, that at this moment there is no new process in sight that might economically justify the replacement of coil pyrolysis within the next few years.

---

[5] S. Gomi and S. Araki, Proceedings 8th World Petr. Congress, 1971, vol. 4, paper 4.

[6] K. Gehrman and H. Schmidt, *ibid.*, vol. 4 paper 5.

Revue Roumaine de Chimie, 17, 1, 2, 357 – 360 (1972)

Dedicated to Professor I. G. MURGULESCU
on his 70th birthday

IONIC MELTS AS MODEL LIQUIDS

A. R. UBBELOHDE

Imperial College, Department of Chemical Engineering and Chemical Technology, Prince Consort Road, London S.W. 7, UK

Received July 4, 1971

The general physical chemistry of solutions was enormously developed in the nineteenth and early twentieth centuries ; in particular various aspects of electrolytes received much attention. Interest in these ionic solutions was stimulated partly by their relevance for a variety of scientific problems, including biological situations, and partly by the discovery of elegant model laws for dilute electrolytes, including improvements such as the Debye Hückel theory.

Growth of the physical chemistry of ionic melts is comparatively much more recent. Technical and experimental difficulties arising from the need to work with ionic melts at temperatures above ambient, and from the corrosive action of many ionic melts, have been obstacles to growth. These obstacles are gradually being overcome, through the work of many schools, including that of Dr. Murgulescu. A further obstacle to progress stems from the need for flexible model laws of really wide applicability to ionic melts. With ions of simple inert gas type of electronic structure, prospects for applying well known physico-chemical generalisations, such as corresponding-state theories, might seem particularly hopeful. However, even attempts to calculate properties such as melting points T_f or surface energies σ_f as a function of the mean ion contact radius r_x^1 for ionic melts of the inert gas type, illustrate basic difficulties in extending any conventional generalisations along familiar lines. One such difficulty arises from the long range interaction forces between charged ions. These demand "many-body" formulations in the development of statistical thermodynamics of ionic melts. Furthermore peculiarities are indicated for the micro-polarisability of ions not of the inert gas type, even when they are monatomic. These limit the usefulness of treating such ions in melts as simple charged spheres, even when the ionic mixtures are dilute. As one illustration, the partial molal volume of thal-

---

[1] H. Reiss, S. W. Mayer and J. L. Katz, *J. Chem. Phys.*, **35** 820 (1961).

lium ions in a mixture with inert gas ions such as K^+ and B_r^- seems to demand the assumption of non-spherical symmetry of properties of individual ions.[2]

Considerations of this general nature have prompted a distinctive line of attack in most of my own researches. One basic principle underlying these researches has been that all ionic melts are much closer in structure to crystalline state(s), than to any *quasi-gaseous* model.

Examination of individual crystal structures assumed by the ions, and of melting parameters of these crystals, serve to tell us what mechanisms of melting operate in producing ionic liquids. Clearly model theories of ionic melts must conform to these mechanisms as one requirement. A second basic consideration is that some physical properties are much more structure-sensitive than others ; this is particualarly evident for condensed assemblies such as ionic melts. By way of illustration, transport properties such as viscosity and ionic conduction appear to be considerably more sensitive to local structure in mixed ionic melts of nitrates [3] than is the case for properties such as the molar volume.[4] Quite often the most comprehensive mathematical theories deal with properties that are unfortunately not particularly sensitive to local structure in mixed ionic melts. To use such theories properly makes it specially important to develop experimental measurements of excess functions of mixed ionic melts of sufficiently high precision to provide real tests of physico-chemical theory. Considerable progress in determining excess functions of mixtures of ionic melts has been made in recent years [5] though there is still urgent need for further advances in precision.

Because of the importance of detailed knowledge about their melting mechanisms, it is highly desirable to enlarge the range and variety of ionic melts, available for experimentation. In the realm of inorganic chemistry, most simple monatomic ions have already been studied in melts, though by extending temperatures of measurement more information should undoubtedly be obtainable concerning monatomic ions of valency higher than unity. Polyatomic inorganic ions are known in much greater diversity, but a prime consideration is the valence-bond stability of any such ion when in strong non-compensated electrostatic fields, such as arise in ionic melts. Amongst a few well known examples, researches with nitrate ions, have made good use of adequate stability of the NO_3^- polyatomic structure. Other inorganic polyatomic ions with different repulsion envelopes, and even with higher ionic charges, would help to extend and generalise the substantial progress already made with inorganic nitrate melts.

The realm of organic chemistry offers much wider synthetic opportunities for making small changes of structure within a given type of molecule, than is possible for inorganic compounds. If all the salts known to organic chemists gave stable ionic melts, this would of itself greatly enlarge the field for study and for technical applications of this distinctive class of liquids. However, even a preliminary survey showed that stable organic ionic melts are far less common than the crystalline states of the same compounds.[6] With some salts, one reason may of course be that their melting points are rather high. At high temperatures, chemical activation energy for various decomposition process is usually readily available. A more subtle consideration is that when rates of thermal decomposition within a crystal and within its melt are compared by extrapolating observations up to T_f for the solid, and down to T_f for the liquid, a large increase in decomposition rates is found on passing from crystal to liquid. This may probably be expected in ionic assemblies, since powerful local electrostatic fields due to the charged ions are to some extent compensated for ionic *crystals* by the crystal symmetry. But as soon as the crystal melts, this symmetry compensation is lost and any ionic influences on mechanisms of bond-rearrangement can exert their maximum power.

---

[2] E. R. Buckle, P. E. Tsaoussoglou and A. R. Ubbelohde, *Trans. Faraday Soc.*, **60**, 496 (1964).

[3] E. Rhodes, W. E. Smith and A. R. Ubbelohde, *Proc. Roy. Soc.*, **A 285** 263 (1965); *Trans. Faraday Soc.*, **63** 1943 (1967).

[4] W.J. McAuley, E. Rhodes and A.R. Ubbelohde, *Proc. Roy. Soc.*, **A 289**, 151 (1966).

[5] A.R. Ubbelohde, *Nature*, **206**, 246 (1965).

To some extent one can meet the general expectation that ionic melts are less stable than their ionic crystals by choosing to work with organic ionic crystals of low melting points. For various reasons my own researches in this direction have recently concentrated on carboxylate salts of fairly low molecular weights. In favorable examples these combine fairly low melting points, with a fairly high ratio of ionic charges to atoms, about the same as in other better known ionic melts, such as nitrates. Alkali metal acetates, propionates, butyrates, and valerates have received our particular attention.

A very useful discovery was that it is essential rigorously to exclude molecular oxygen from systems containing this class of organic ionic melts. Uncharged hydrocarbon molecules of structure similar to the organic anions being investigated, do of course show more or less pronounced chemical interaction with oxygen at temperatures similar to those used with even low melting organic salts. It might perhaps have been expected that the ionic charge on the carboxylate anion might confer some additional stability. This is not the case. Other evidence suggests that to avoid the decomposition of organic ionic melts it is essential to suppress charge transfer reactions, which may be symbolised quite generally $R\mathrm{COO}^- + M \rightarrow M^- + R^-\mathrm{COO}$ (free radical). In this equation, the electron acceptor impurity M may be molecular oxygen, but may also be a transitional metal ion of fairly low oxidation reduction potential such as Fe^{++} or $\mathrm{Cu}.^{++}$

All impurities capable of easy charge transfer can be readily suppressed using modern procedures. However, a further catalytic impurity is the presence of free OH^- ion.[7] Free hydroxyl is unavoidably present in ionic melts prepared from organic acids, unless a small excess of acid is added during the preparation. Such excess can be readily removed subsequently using vacuum methods.

---

[6] A.R. Ubbelohde, a *J. chim. phys.*, **1969**, 59 ; b *Chemistry & Industry*, **1969**, 64 ; *Chemistry & Industry*, **1968**, 311, 313.

F.J. Hazlewood, E. Rhodes and A.R. Ubbelohde, *Trans. Faraday Soc.*, **62** 3101 (1966).

[7] J.J. Duruz, H.J. Michels and A.R. Ubbelohde, Chemistry & Industry, **1969**, 1386.

Organic ionic melts stabilised by suppression of all these parasite chemical reactions appear to be stable up to at least 350°C[8]. The decomposition which is observed above this temperature appears not to depend on impurities but to be related to thermal cracking reactions of corresponding uncharged organic molecules. When descomposition does occur, differences in cracking due to the presence of the charge on the ion, and to the local ionic environment of the molecule undergoing cracking in the melt, offer situations of great chemical interest. They present an unexplored sector of reaction kinetics. Below 350° C, it appears wholly practicable to study a variety of stable organic ionic melts with all the resources of modern physical chemistry, after taking the precautions described, to exclude parasitic decomposition reactions. This conclusion opens up many new possibilities of extending and diversifying researches on ionic melts.

---

[8] J.J. Duruz, H.J. Michels and A.T. Ubbelohde, *Proc. Roy. Soc.*, **A 322**, 281 (1971).

Revue Roumaine de Chimie, 17, 1, 2, 361–366 (1972)

Herrn Professor I. G. MURGULESCU
zum 70. Geburtstag

KINETISCHE UNTERSUCHUNG BASISCHER ESTERVERSEIFUNGEN IN WÄSSRIGER LÖSUNG MIT EINEM pH-METRISCHEN TITRATIONSVERFAHREN

BASISCHE HYDROLYSE DER DIALKYLPHOSPHITE IN WÄSSRIGER LÖSUNG

R. VÎLCEANU und P. SCHULZ

Vom Chemischen Zentrum des Unterrichtsministeriums, Timişoara, Bd. Mihai Viteazul, 24

Eingegangen am 27. August 1971

Es wird ein einfaches und bequemes Verfahren vorgeschlagen, die Geschwindigkeitskonstanten basischer Esterverseifungen in wäßrigem Mittel zu bestimmen. Die Methode beruht auf pH-metrischer Titration verdünnter wäßriger Lösungen der Ester mit Alkalihydroxyd und ergibt charakteristische Titrationskurven, die unmittelbare Rückschlüsse auf die Reaktionskinetik gestatten. Aufgrund dieser Kurven ist eine Berechnung der Geschwindigkeitskonstanten möglich. Ihre Temperaturabhängigkeit erlaubt über die Aktivierungsparameter einen Einblick in den Reaktionsmechanismus. Vorliegende Untersuchung beschränkt sich auf die Reihe der Dialkyl-phosphite (Alkyl = methyl, äthyl, propyl, i-propyl, butyl, 2-butyl, tert.-butyl, pentyl.)

Untersuchungen betreffend die Reaktivität der Dialkylphosphite in wäßriger Lösung haben zu einem einfachen und bequemen Verfahren geführt, aufgrund der Titration mit Alkalihydroxyd die Geschwindigkeitskonstanten der basischen Hydrolyse von Estern zu bestimmen, z.B.

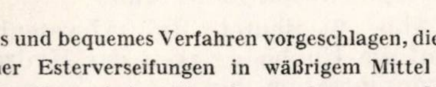

$$(RO)_2P \rightarrow + OH^{\ominus} \rightarrow (RO)(^{\ominus}O)P(\rightarrow O)H$$

Findet obige Reaktion in verdünnter wäßriger Lösung statt, indem das Alkalihydroxyd mit konstanter Titrationsgeschwindigkeit hinzugefügt wird, wobei eine Glaselektrode den pH-Wert laufend mißt, ändert sich der pH-Wert nach charakteristischen Kurven, deren Verlauf in hohem Maße von der Titrationsgeschwindigkeit abhängt.

Man erhält im allgemeinen zwei Kurventypen, die wir mit A und B bezeichnen wollen (Abb. 1. und 2.). Dabei sind v_1, v_2, v_3 und v_4 die Titrationsgeschwindigkeiten in steigender Folge.

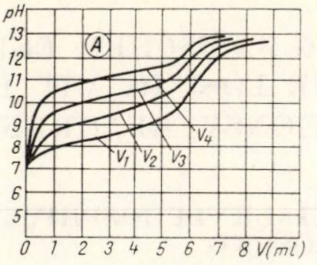

Abb. 1. — Titrationskurven vom Typ A.

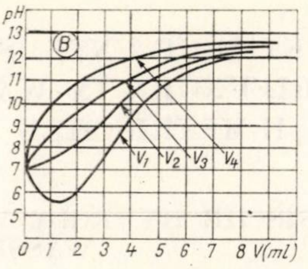

Abb. 2. — Titrationskurven vom Typ B.

Im Falle der Kurven vom Typ A (Abb.1) steigt der pH-Wert verhältnismäßig langsam und beschreibt einen charakteristischen Inflexionspunkt, der das Ende der Hydrolyse kennzeichnet. Dieses ist nur dann möglich, wenn die Erhöhung der OH-Ionenkonzentration zur Erhöhung der Hydrolysegeschwindigkeit führt.

Im Falle B (Abb. 2) deutet die Abwesenheit eines analogen Inflexionspunktes auf die Unabhängigkeit der Hydrolysegeschwindigkeit von der OH-Ionenkonzentration hin.

Ein weitergehendes Studium hat erwiesen, daß die Kurven im Falle A im allgemeinen einer bimolekularen Kinetik und einem SN2-Mechanismus zugeordnet werden können, während sie im Falle B monomolekularer Kinetik und gewöhnlich einem SN1-Mechanismus entsprechen (Abb. 3).

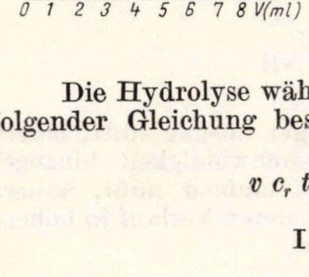

Abb. 3. — Gegenüberstellung der Titrationskurven Typ A und B.

Die Hydrolyse während der Titration läßt sich quantitativ mit Hilfe folgender Gleichung beschreiben:

$$\underset{\mathrm{I}}{v\,c_r\,t} + \underset{\mathrm{II}}{\int_{m_{eo}}^{m_e} dm_e} = \underset{\mathrm{III}}{c_{\mathrm{OH}}\,(V_0 + v\,t)} \qquad (1)$$

In Gleichung (1) stellt I die bis zum Zeitpunkt t hinzugegebene Hydroxydmenge, II die durch Hydrolyse verbrauchte und III die augenblicklich in der Lösung befindliche Alkalihydroxydmenge dar.

Die ursprüngliche OH-Ionenmenge in der wäßrigen Esterlösung ist im allgemeinen vernachlässigbar.

In Gleichung (1) ist:

v die Titrationsgeschwindigkeit, l NaOH-Lsg/Sek.
c_r die Molarität der NaOH-Lösung.
t die seit Beginn der Titration verflossene Zeit, Sek.
m_e die im Augenblick t in der Lösung befindliche Estermenge, Mol.
c_{OH} die OH-Ionenkonzentration im Zeitpunkt t, Mol/l.
V_0 das Initialvolumen der Esterlösung, l.

Im Falle bimolekularer Kinetik folgt weiter:

$$m_e = c_e\,(V_0 + v\,t)$$

$$\mathrm{d}m_e = (V_0 + vt)\,\mathrm{d}c_e + c_e\,v\mathrm{d}t$$

$$\mathrm{d}c_e = -\,k_{II}\,c_e\,c_{OH}\,\mathrm{d}t$$

$$v\,c_r\,t + \int_0^t [\,-(V_0 + vt)\,k_{II}\,c_e\,c_{OH} + c_e\,v]\,\mathrm{d}t = c_{OH}\,(V_0 + vt)$$

k_{II} ist die Geschwindigkeitskonstante der bimolekularen Hydrolyse.

Für pH-Werte zwischen 8 und 9 können die Hydrolysebedingungen so gewählt werden, daß III in Gleichung (1) vernachlässigt werden kann, da:

$$\frac{(V_0 + vt)\,c_{OH}}{v\,c_r\,t} < 10^{-3}$$

Wird dann die Summe von Term I und II in Gleichung (1) gleich Null gesetzt und abgeleitet, ergibt sich folgender Ausdruck für k_{II}:

$$k_{II} = \frac{v\,(c_r + c_e)}{(V_0 + vt)\,c_e\,c_{OH}} \tag{2}$$

Nimmt man c_{OH} in halber Entfernung zum Inflexionspunkt (s. Abb. 3), ergibt Ausdruck (1):

$$k_{II} = 2\,\frac{v\left[c_r + \dfrac{m_{e0}}{2\,(V_0 + vt_{1/2})}\right]}{m_{e0}\cdot c_{OH1/2}} \tag{3}$$

m_{e0} ist die Estermenge zu Beginn der Titration, Mol.
$c_{OH1/2}$ ist die OH-Ionenkonzentration in halber Entfernung zum Inflexionspunkt, Mol/l.
$t_{1/2}$ ist die halbe Titrationsdauer, Sek.

Eine entsprechende Wahl der Titrationsgeschwindigkeit im Falle A (Abb. 1), führt zu Titrationskurven, die eine optimale Berechnung der Geschwindigkeitskonstanten k_{II} in jedem gegebenen Falle gestatten.

Handelt es sich um Kurven vom Type B, dann ergibt eine adäquate Titrationsgeschwindigkeit im ersten Abschnitt absteigende Kurven (s. Abb. 2). Eine solche Kurve ermöglicht die Berechnung der Geschwindigkeitskonstanten k_1 erster Ordnung, da im Abschnitt ON (Abb. 3) die gesamte hinzugefügte Alkalihydroxydmenge durch Hydrolyse verbraucht wurde :

$$k_I = 2{,}303\; t_N \log \frac{m_{e0}}{m_{eN}} \tag{4}$$

t_N ist die Zeit bis Punkt N (Abb. 3), Sek.

m_{eN} ist die im Zeitpunkt t_N in der Lösung befindliche Estermenge, Mol.

In gewissen Fällen führt eine Titration unter gleichen Bedingungen zu einem von A und B verschiedenen Kurventyp C (Abb. 4). Im Sinne des oben Ausgeführten ließe sich ein solcher Fall als parallel verlaufende mono- und bimolekulare Hydrolyse betrachten. Es besteht unter gewissen Umständen die Möglichkeit, aufgrund dieser Kurven die beiden parallellaufenden Reaktionen getrennt zu erfassen. Findet die bimolekulare Hydrolyse bei mittleren pH-Werten bedeutend langsamer statt als die monomolekulare, dann gestattet der erste, absteigende Kurvenabschnitt die Berechnung von k_1 unter Vernachlässigung des bimolekularen Anteils, mit Formel (4). Die Berechnung von k_{II} erfolgt mit :

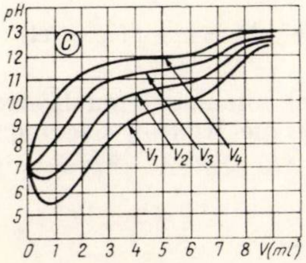

Abb. 4. — Titrationskurven vom Typ C.

$$k_{II} = \frac{v\,(c_e + c_r) - k_I\, c_e\,(V_0 + vt)}{c_e\, c_{OH}\,(V_0 + vt)} \tag{5}$$

Formel (5) läßt sich von (1) analog ableiten, wenn man dabei den monomolekularen Abteil berücksichtigt :

$$dc_e = -\,k_{II}\; c_e\; c_{OH}\; dt - k_I\, c_e\; dt.$$

Das beschriebene Verfahren eignet sich besonders gut zur Erfassung hoher Hydrolysegeschwindigkeiten, denn in diesem Falle ist die Auswertung der Titrationskurven einfacher und genauer. Bei kleinen Reaktionsgeschwindigkeiten sind entsprechend kleine Titrationsgeschwindigkeiten erforderlich, und der Inflexionspunkt verlagert sich nach hohen pH-Werten. Die Kurve befindet sich dann in einem pH-Bereich, der die bei Berechnung von Ausdruck (2) vorgenommene Näherung verschlechtert.

Versuche in der Reihe der Dialkylphosphite haben Titrationskurven aller beschriebenen Typen ergeben (s. Tabelle 1).

Die Bestimmungen wurden bei drei verschiedenen Temperaturen im Bereich 20—50° ausgeführt. Daraus egaben sich die Aktivierungsparameter. Die Ergebnisse sind in Tabelle 2 zusammengefaßt. Die Aktivierungsparameter sind mit den von den Kurvenverläufen abgeleiteten Mechanismen im Einklang.[1,2]

Tabelle 1

Titrationskurven der Dialkyl-phosphite

Dialkylphosphit	Titrationskurve, Abb. 1, 2, 4.
Dimethylphosphit	A
Diäthylphosphit	A
Dipropylphosphit	A
Dibutylphosphit	A
Dipentylphosphit	A
Diisopropylphosphit	A
Di-2-butylphosphit	C
Di-tert.-butylphosphit	B

Tabelle 2

Geschwindigkeitskonstanten und Aktivierungsparameter

$(RO)_2POH$	$k_{II}^{20°}$ $Sek^{-1}Mol^{-1}$	$k_{I}^{20°}$ Sek^{-1}	$S^{\neq}$ Cal. $Mol.^{-1}$ $Grd.^{-1}$	$H^{\neq}$ Kcal
R = methyl	1240	—	— 1,9	—13,4
R = äthyl	95,5	—	—24,3	— 8,8
R= propyl	38,7	—	—27,5	— 8,8
R = butyl	36,2	—	—28,0	— 8,8
R = pentyl	8,30	—	—31,1	— 8,8
R = isopropyl	3,57	—	—32,9	— 8,4
R=2-butyl	1,03	—	—34,8	— 6,4
R=tert.-butyl	—	$7{,}35.10^{-5}$	+24,3	—29

Ein $\Delta S^{\neq}$ — δ^*- Diagramm zeigt deutlich, daß im Falle der Dialkylphosphite mit normalen aliphatischen Resten die Hydrolyse ohne maß-

---

[1] S.L. Friess, E.S. Lewis and A. Weissberger, Technique of Organic Chemistry, VIII/I, Interscience Publishers, New York, 1961, Kap. VI.

[2] E.S. Gould, Mechanismus und Struktur in der organischen Chemie, Verlag Chemie, Weinheim, 1962, Kap. 6.

gebliche sterische Einflüsse über SN2 verläuft. Bei verzweigten Resten, vor allem bei Di-2-butylphosphit scheint aufgrund der Titrationskurve eine SN1-Beteiligung wahrscheinlich (Typ C, Abb. 4). Das Diagramm

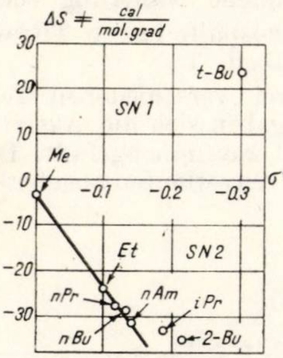

Abb. 5. – Diagramm $\Delta S^{\neq} - \sigma^*$.

Abb. 5 unterstützt diese Annahme, da die Aktivierungsentropie in diesem Falle nach höheren Werten abweicht.[1,2]

Eine Berechnung von k_I nach (4) führte leider zu keinem eindeutigen Ergebnis.

Bei Di-tert.-butylphosphit entsprechen sowohl die Titrationskurve, als auch die Aktivierungsparameter einem SN1-Mechanismus.

BESCHREIBUNG DER VERSUCHE

Die nach einem verbesserten Verfahren hergestellten Dialkylphosphite wurden gaschromatographisch auf Reinheit geprüft[3]. Es wurden jeweils Proben von 10–20 mg Ester in 40 ml Wasser bei konstantgehaltener Temperatur und intensiver Rührung mit 0,1–0,25-normaler Natriumhydroxydlösungen automatisch in Gegenwart einer Glaselektrode titriert (Titriergerät : Potentiograph Metrohm, Herisau). Die Einführung der Esterprobe geschah mit Hilfe einer automatischen Hamilton-Präzisionsspritze im Augenblick des Titrationsbeginns.

Die Glaselektrode wurde mit geeigneten Pufferlösungen für jede gewünschte Temperatur geeicht.[4].

---

[3] R. VILCEANU, P. SCHULZ, L. KURUNCZI und Z. SZABADAI, Unveröffentlichte Versuche.

[4] J.J. LINGANE, Electroanalytical Chemistry, II. Ed. Interscience Publishers, New York, 1958, Kap. IV.

Revue Roumaine de Chimie, **17**, *1 2*, 367–377 (1972)

Dedicated to Professor I. G. MURGULESCU
on his 70th birthday

THERMODYNAMIC EXCESS FUNCTIONS IN LIQUID-VAPOUR EQUILIBRIA IN THE *n*-HEPTANE–TOLUENE SYSTEM

RODICA VÎLCU and ZOICA CENUŞE

University of Bucharest, Chair of Chemical Thermodynamics and Electrochemistry. Bd. Republicii 13, Bucharest, Romania

Received June 26, 1971

The free excess enthalpy of the n-heptane – toluene system as well as the activity coefficients of the components for various compositions of the system have been calculated in accordance with isobaric data of the liquid – vapour equilibrium. The introduction of corrections required by the nonideal behaviour of the system phases under consideration grants a marked thermodynamical consistency to the data obtained for the liquid – vapour equilibrium of the system to be studied.

INTRODUCTION

The separation of various hydrocarbons by distillation is facilitated by the addition of a third component of either polar or nonpolar nature which forms with the hydrocarbons under consideration, solutions with varied degrees of nonideality. The n-heptane-toluene system is of special interest from this standpoint, being related to the separation of toluene from other hydrocarbons.

The system has been investigated by Steinhauser and White,[1] who, under constant pressure conditions up to ± 0.1 mm Hg, have calculated the activity coefficients supposing that the vapour phase enjoys an ideal behaviour at 760 mm Hg according to an equation of the form :

$$\log \gamma_i = \log P^{g}_{xi}/P_i x^l_i = 2.8808 - \log P_i + \log x^g_i/x^l_i \tag{1}$$

They have also checked up the thermodynamic consistency of the liquid-vapour equilibrium data obtained experimentally according to

$$\log \gamma_2 = -\int_{x_1=0}^{x_1=x_2} x^l_1/x^l_2 \, \mathrm{d} \log \gamma_1 \tag{2}$$

---

[1] H.H. Steinhauser and R.H. White, *Ind. Eng. Chem.*, **41**, 2112 (1949).

The obtained data have been compared to those of Bromiley and Quiggle[2] and equilibrium temperatures smaller by about 1°, have been found out.

The liquid-vapour equilibrium data obtained by Sierg[3] have been processed in the same way.

For the sake of comparison, Rose and Williams[4] have put forward a liquid-vapour equilibrium curve using the trial and error method, and concluded that accurate experimental data are within a range of ±0.002 molar fraction and ± 0.2° as against the predicted curve.

Hipkin and coworkers[5] have calculated the activity coefficients of this system using a Margules equation of the form

$$\log \gamma_1 > b\,(1-x_1^l)^2 + (1-x_1^l)^3 \tag{3a}$$

$$\log \gamma_2 = b\,(x_1^l)^2 + 3/2c x_1^{l2} - c x_1^{l3} \tag{3b}$$

and in parallel a Van Laar equation under the form utilized by Gilliland

$$\log \gamma_1 = B/T\ [1 + A x_1^l/(1-x_1^l)]^2 \tag{4a}$$

$$\log \gamma_2 = AB/T\ [A + (1-x_1^l)/x_1^l]^2 \tag{4b}$$

while the constants of eqs. (3a, 3b) and (4a, 4b) have been determined out of experimental data by Gilliland's graphical method with the following values for the n-heptane – toluene system : $b = 0.022$; $c = 0.133$, $A = 1.37$, $B = 54.3$

Hipkin's values for the activity coefficients, assuming an ideal behaviour of the vapour phase, are smaller than Rose's consistency limit for n-heptane and exceed the admissible limit for toluene.

This fact prompted Garner and coworkers[6] to take into account the nonideality of the vapour phase of the system under study, in order to obtain both reproducible and of high thermodynamic consistency data.

They have introduced the nonideality correction of the vapour phase and have correlated the liquid-vapour equilibrium data by Li-Coull[7] equation of the form

$$T \log \gamma_{C_7H_{16}} = 43.9\ x^l_{C_7H_{16}}/(x^l_{C_7H_{16}} + 0.987\ x^l_{C_7H_8})]^2 \tag{5a}$$

$$T \log \gamma_{C_7H_8} = 45.6/(x^l_{C_7H_8} + 1.013\ x^l_{C_7H_{16}})^2 \tag{5b}$$

Taking account of this correlation of the experimental data it has been concluded that an enhancement of the deviation from ideality, by introducing some corrections into the calculation of activity coefficients, leads to a very good agreement between calculated values and experimental data.

---

[2] E.C. Bromley and D. Quiggle, *Ind. Eng. Chem.*, **25**, 1136 (1933).

[3] L. Sierg, *Chem. Ing. Techn.*, **22**, 322 (1950).

[4] A. Rose and E.T. Williams, *Ind. Eng. Chem.*, **49**, 1528 (1955).

[5] H. Hipkin and H.S. Myers, *Ind. Eng. Chem.*, **46**, 2524 (1954).

[6] F.H. Garner, O.B.E. Fellow and R.T.W. Hall, *J. Inst. Petrol.*, **4**, 1 (1955).

[7] Y. Li and Y. Coull, *J. Inst. Petrol.*, **34**, 692 (1948).

The rigorous treatment of phases present within the equilibrium characterized by certain temperature and pressure values, has been, therefore, carried out, taking account of the vapours nonideality. In the vapour phase, even at relatively small pressure, the existence of molecular interactions, enhanced with the pressure increase, brings about their nonideal behaviour. The nonideality corrections of the vapour phase may be represented by the fugacity [8] coefficients ; however more often on the thermodynamic processing of the experimental data of the liquid-vapour equilibrium, corrections are being introduced which take account also of the nonideality of the liquid phase. Such widely applied method is that developed by Scatchard and Raymond,[9] based on the application of the state equation with the virial coefficients both for pure vapours and for mixtures. For mixtures, the second virial coefficient is given by equation

$$\beta_m = \sum_{i=1}^{n} \sum_{k=1}^{n} x_i^g x_k^g \beta_{ik} \qquad (6)$$

where

n — number of components in the mixture
x_i^g, x_k^g — molar fractions of components i and k in gaseous phase
β_{ik} — virial interaction coefficient among the molecules of components i and k in vapour phase.

For binary systems eq. (6) assumes the form :

$$\beta_m = x_1^{g^2} \beta_{11} + 2 x_1^g x_2^g \beta_{12} + x_2^{g^2} \beta_{22} \qquad (7)$$

Here, β_{11} and β_{22} stand for the second virial coefficient within the state equations of the pure components, while β_{12} considers the interactions of the two components' molecules. For the calculation of the activity coefficient of the component l within the binary system, Scatchard and Raymond obtained the following equation :

$$\log \gamma_1 = \log P x_1^g / P_1^0 x_1^l + (\beta_{11} - v_1)(P - P_1^0)/RT +$$
$$+ (1 - x_1^g)^2 (2\beta_{12} - \beta_{11} - \beta_{22}) P/RT$$

where voume v_1 represent the molar volume of the first component in liquid phase.

The hypotheses that molar volumes in liquid phase were additive and that the liquid volume does not depend on the pressure within a small variation range of it, underlie the above equation.

To calculate the activity coefficients according to eq. (8), the second virial coefficient should be known.

---

[8] C.N. Lewis and M. Randall, ,,Химическая термодинамика", Химтеоретиздат, 1936, p. 74.

[9] G. Scatchard and C.D. Raymond, *J. Amer. Chem. Soc.*, **60**, 1278 (1938).

Generally, for pure substances the virial coefficients are known, unlike the experimental data for the coefficients of gaseous mixtures which are limited.

If the component's molecules do not show up any inclination to the specific interaction, magnitude β_{ik} may be approximately calculated as the arithmetic mean of values β_{ii} and β_{kk} of eq. (8) and then, for the calculation of the activity coefficients of the binary system's components the following equation is obtained

$$\log \gamma_1 = \log P x_1 / P_1^0 x_1^l + (\beta_{11} - v_1)(P - P_1^0)/2.303RT \tag{9}$$

The calculation according to the above equation is possible only for systems made up of nonpolar substances.

On processing the liquid-vapour equilibrium data in binary systems, the nonideality of the vapour phase is expressed as a correction to the value of the activity coefficient.

$$\log \gamma_1 = \log P x_1^g / P_1^0 x_1^l + \log z_1 \tag{10}$$

$$\log z_1 = (\beta_{11} - v_1)(P - P_1^0)/2.303\ RT \tag{11}$$

Within determinations under isobaric conditions, P is a constant, while P_1^0, v_1 and β_{11} are temperature functions. The corrections become significant at pressures higher than the atmospheric pressure; they are, however, also important when the differences between the boiling points of the system's components are great.[10]

EXPERIMENTAL DATA

The liquid-vapour equilibrium data have been obtained under isobaric conditions by means of the apparatus and with the procedure previously described.[11]

The substances have the characteristics listed in table 1.

Table 1

Physical properties of n-heptane and toluene

Substance	n-Heptane	Toluene
Source	Carlo-Erba (reagente puro) Division chimica industriale Milano	Bruxelles (purum exempt de thiophéne)-Belgium
Boiling point	98.31 compared to 98.4_4	110.62 compared to 110.634
Refraction indices	1.386 compared to 1.3878_4	1.4930 compared to 1.4969_4
Density	0.684 compared to 0.6795_5	0.870 compared to 0.8620_5
Molecular weight	100.200	92.142

---

[10] ED. G. SCHEIBEL, *Ind. Eng. Chem.*, **41**, 1076 (1949).

[11] R. VÎLCU and Z. CENUȘE, *Rev. Roumaine Chim.*, (in press).

Based on experimental liquid-vapour equilibrium data we have calculated the vapour tensions of both components of the mixture, using Antoine equation of the form

$$\log P = A - B/(c + t) \tag{12}$$

where constants A, B, C for both substances, given by Garner and coworkers[6], are shown in table 2.

Table 2

Constants of Antoine eq. for the vapour tension of n-heptane and toluene

	A	B	C
n-Heptane	6.90319	1268.586	216.954
Toluene	6.95334	1343.943	219.377

The experimental liquid-vapour equilibrium data of the n-heptane — toluene system are given in table 3.

Table 3

Experimental equilibrium date of the n-heptane – toluene system and vapour tensions calculated by Antoine's equation

$x^e_{C_7H_{16}}$	$x^g_{C_7H_{16}}$	$\overset{\circ}{t}_{bcorr}$	$\overset{\circ}{P}_{C_7H_{16}}$	$\overset{\circ}{P}_{C_7H_8}$
0.0350	0.0580	109.68	1045.63	740.09
0.0710	0.1140	108.92	1007.83	710.09
0.1080	0.1596	107.92	995.40	703.37
0.1460	0.2046	106.64	953.12	677.68
0.1915	0.2648	105.76	931.60	660.52
0.2350	0.3154	105.16	922.30	644.51
0.2800	0.3890	104.74	911.46	640.97
0.3260	0.4138	103.34	875.36	615.14
0.3745	0.4715	103.02	867.96	609.21
0.4175	0.5158	102.43	853.56	598.51
0.4720	0.5734	102.02	838.10	591.22
0.5250	0.6073	101.29	825.30	577.94
0.5775	0.6450	100.87	816.00	577.11
0.6325	0.6874	100.40	807.40	563.17
0.6915	0.7475	100.00	796.74	556.32
0.7480	0.7780	99.97	795.04	555.79
0.8090	0.8297	99.28	780.85	544.28
0.8775	0.8882	98.85	769.42	537.18
0.9426	0.9528	98.45	760.50	526.82

The temperature-composition diagram and the equilibrium diagram are given in figures 1 and 2.

PROCESSING OF EXPERIMENTAL DATA

To calculate the activity coefficients of the n-heptane-toluene system we have considered the deviation from ideality of the vapour phase, in accordance with eq. (9).

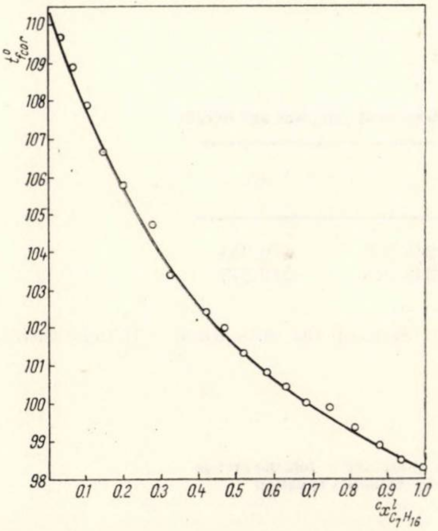

Fig. 1. — Dependence of boiling temperature (t^0_f) of the n-heptane-toluene system with respect to the molar fraction of -heptane in liquid phase ($x^l_{C_7H_{16}}$).

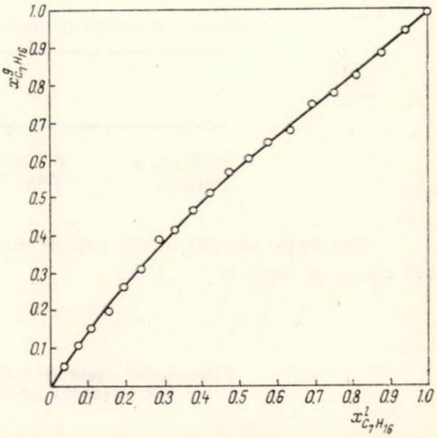

Fig. 2. — Equilibrium diagram of the n-heptane-toluene system.

It has been shown that P^0_1, v_1 and β_{11} are temperature functions. For the calculation of virial coefficients we have used Wohl's [6] method by applying expression

$$B = RT_c/P_c \cdot (0.197 - 0.012\ T_r - 0.4/T_r - 0.146/T_r^{3.27}) \tag{13}$$

while for the calculation of the critical temperature we have used Meissner's and Reading's [12] equation for aromatic substances

$$T_c = 1.41\ T_f + 66 - r\ (0.383\ T_f - 93) \tag{14}$$

where r — is the ratio of the total number of acyclic atoms and the total number of carbon in the molecule, while for hydrocarbons we applied equation

$$T_c = 1.027\, T_f + 159 \tag{15}$$

[12] H.P. Meissner and E.M. Reading, *Ind. Eng. Chem.*, **34**, 521 (1942).

for the calculation of the critical pressure the same research workers have put forward equation

$$P_c = 20.8\ T_c / (V_c - 8) \tag{16}$$

the critical volume (V_c) being calculated from the parachor of the substance, according to equation

$$V_c = (0.377[P] + 11.0)^{1,25} \tag{17}$$

The reduced and critical values of the state parameters obtained for both substances are given in table 4.

Table 4

Critical and reduced values of n-heptane and toluene

	$T_c^0 k$	T_r	$[P]^{13}$	V_c (cm^3/mol)	P_c (atm)	P_r
n-Heptane	540.499	0.6872	310.8	431.22	26.56	0.0376
Toluene	599.416	0.6402	246.9	289.15	44.34	0.0225

In the calculation of the z_i value, given by eq. (11) it also occurs the value of the liquid's molar volume, not known at the boiling point, but that can be determined by Meisner and Reading[12] general relation, where they give the values of μ_L for various reduced temperatures and pressures, μ_L being a universal, adimensional function of reduced vapour tension (P_r^0) and reduced temperature (T_r).

The density of the saturated liquid is calculated by equation

$$D_1 = P_1\ M_1 / \mu_L\ RT \tag{18}$$

The representation of μ_L related to the constant reduced pressure (P_r) and reduced temperature (T_r) points to almost straight lines whose slopes have a value very close to unit.

It has been noticed that $\mu_L / P_r = f(T_r)$ and the values of M_L / P_r determined from the preceding correlation have been represented function of T_r. From eq. (18) the value of the molar volume is

$$v_1 = M_1 / D_1 = RTf(T_r) / P_c \tag{19}$$

while introducing it into eq. (11) another expression of the deviation z_1 is obtained

$$\log z_1 = (P_1^0 - P)[f(T_r) - 0.197/T_r + 0.012 + 0.400/T_r^2 + 0.146/T_r^{4,27}]/P_c \tag{20}$$

with the essential requirement of the knowledge of critical temperature and pressure for each component. The values of z_1 calculated in this way have been represented by Scheibel[10] in a nomogram.

---

[13] "Manualul inginerului chimist", vol. 2, Ed. Tehnică, Bucharest, 1952, p. 1857.

To facilitate the calculation of z_1 and because of the lack of critical data for the various molar fractions of the system, Garner and coworkers[6] have plotted the representation of z_1 related to temperature in the range 100–160°, from experimental critical data. Their values have been compared to those of Scheibel's nomogram and a perfect agreement has been found. These are listed in table 5.

Table 5

Deviation magnitude z for the n-heptane – toluene system

Temperature °C	z_n-heptane	z toluene
100	1.002	0.988
120	1.037	1.012
140	1.077	1.040
160	1.126	1.070

From the $z_1 = f(t°C)$ plot we have taken the z_1 values for experimental boiling temperatures.

The activity coefficients of both components of the system have been thus calculated.

Table 6

Activity coefficients of the n–heptane – toluene system

$x^l_{C_7H_{16}}$	$Z_{C_7H_{16}}$	$Z_{C_7H_{16}}$	$\gamma_{C_7H_{16}}$	$\gamma_{C_7H_8}$
0.0350	1.0189	0.9996	1.227	1.002
0.0710	1.0164	0.9978	1.200	1.002
0.1080	1.0152	0.9970	1.145	1.015
0.1460	1.0135	0.9958	1.32	1.021
1.1915	1.0130	0.9955	1.143	1.041
0.2350	1.0121	0.9948	1.119	1.049
0.2800	1.0112	0.9947	1.117	1.050
0.3260	1.0103	0.9937	1.111	1.060
0.3745	1.0092	0.9929	1.111	1.066
0.4175	1.0082	.09922	1.111	1.069
0.4720	1.0076	0.9919	1.110	1.077
0.5250	1.0060	0.9907	1.082	1.082
0.5775	1.0049	0.9900	1.045	1.123
0.6325	1.0048	0.9899	1.027	1.136
0.6915	1.0030	0.9887	1.018	1.061
0.7480	1.0019	0.9879	0.999	1.190
0.8090	1.0006	0.9872	0.998	1.230
0.8775	1.0001	0.9867	0.98[illegible]	1.274
0.9426	0.9997	0.9864	0.98[illegible]	1.335

Figure 3 plots the activity coefficients of the n-heptane - toluene system with respect to the molar fraction of n-heptane in liquid phase. The obtained values agree with Garnes's ones showing a deviation in the range $0 < x^l_{C_7H_{16}} < 0.25$.

Based on the expression given by Scatchard and collab., the excess chemical potentials of both components have been calculated according to Brzostowski S[14] equation

$$\mu_1^E = RT \log P x_1^g / P_1^0 x_1^l + C (V_1 - \beta_1)(P - P_1^0) \qquad (21)$$

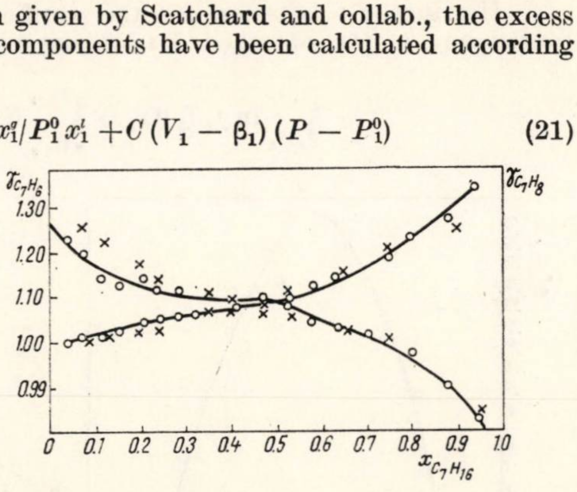

Fig. 3. — Diagram of the activity coefficients of the system function of molar fraction of the heptane in liquid phase ($x^l_{C_7H_{16}}$)
1,0 experimental data;
2,x comparative data. [4]

and the excess thermodynamic potential by relation

$$G^E = x_1^l \mu_1^E + x_2^l \mu_2^E \qquad (22)$$

expressions which may be used when the system's components have no associated molecules in any vapour phase.

The excess thermodynamic functions are listed in table 7 and plotted in figure 4.

Table 7

Chemical excess potentials and free excess enthalpy

$x^l_{C_7H_{16}}$	$\mu^E_{C_7H_{16}}$	$\mu^E_{C_7H_8}$	G^E	$\mu^E_{C_7H_{16}}\ \mu^E_{C_7H_8}$
0.0350	67.58	0.66	2.90	66.92
0.0710	60.00	0.91	5.11	59.09
0.1080	44.52	4.88	9.16	39.63
0.1460	40.63	6.81	11.75	33.82
0.1945	43.70	13.13	18.98	30.57
0.2350	36.70	15.62	20.50	21.08
0.2800	36.08	15.91	21.55	20.17
0.3260	34.43	18.93	23.97	16.50
0.3745	34.37	20.74	25.84	13.63
0.4175	34.20	21.63	26.87	12.57
0.4720	33.78	24.02	28.62	9.76
0.5250	22.46	25.47	23.88	− 3.01
0.5775	12.40	37.34	23.87	−23.14
0.6325	8.58	41.11	20.42	−32.53
0.6915	5.74	48.42	18.85	−42.68
0.7480	−0.029	56.01	14.09	−56.03
0.8090	−0.038	73.93	13.80	−74.31
0.8775	−3.63	76.98	6.22	−80.61
0.9426	−5.33	94.[illegible]2	0.388	−99.75

---

[14] W. Brzostowski, Bull. Acad. Polonaise des Science, **8**, 6 (1960).

Herrington's criterion for the verification of the thermodynamic consistency of the obtained data is expressed as

$$\int_{x_1=0}^{x_1=1} \ln f_1/f_2 \, \mathrm{d}x_1 = \int_{T=t_2}^{T=t_1} H^E/RT^2 \, \mathrm{d}T \tag{23}$$

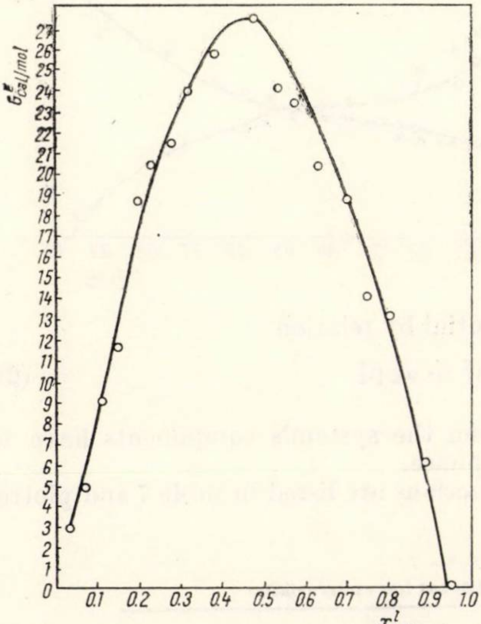

Fig. 4. — Diagram of the excess thermodynamic potential G^E, of the system function of $x^l_{C_7H_{16}}$.

and for our system we use the following simplifying :

$$\int_{T=t_2}^{T=t_1} H^E/RT^2 \, \mathrm{d}T = 0$$

DISCUSSION AND CONCLUSIONS

Applying Herington's criterion we have pointed to the consistency of experimental data obtained within the study of the liquid-vapour equilibrium of the n-heptane — toluene system. They acquire an even more marked thermodynamic consistency by introducing the corrections required by the nonideal behaviour of phases.

Our experimental data for vapour tensions compared to Steinhauser and Sierg measurements confirm to a greater extent Garner's values.

These have been used with a view to establishing the imperfection degree of both the vapour and the liquid phase, also stating the values for the activity coefficients of the system component, their chemical excess potentials and the free excess enthalpy of the system. Since some reference data for excess magnitudes are lacking, our data for such functions of deviation from ideality had no comparison terms.

It has been found that in the case of the system under investigation the concentration where the maximum of the free excess energy is located, is shifted with respect to the position $x_1^l = x_2^l = 05$, to $x_1^l = 0.472$ i.e. towards the composition richer in toluene. The asymmetry of the parabola respresenting the dependence $G^E = G^E(x_1^l)$ confirms intuitively the nonideal behaviour of the system, also stressed by the values calculated for varied deviation magnitudes. With the change in the components' proportion, a change in the intensity of interactions is also found, thrown into prominence by the various values of the functions of deviation from ideality of the system.

Without being able to sort out the different types of interaction energies on overall estimation of their magnitude occurs for various proportions among components.

Revue Roumaine de Chimie, 17, 1, 2, 379 – 383 (1972)

Dedicated to Professor I. G. MURGULESCU
on his 70th birthday

INITIAL STUDIES ON THE RADIATION INDUCED GRAFTING OF STYRENE TO POLYETHYLENE TEREPHTHALATE FIBERS

I. VLAGIU* and V. STANNETT

Department of Chemical Engineering, North Carolina State University, Raleigh, North Carolina, 27607 U.S.A.

Received September 15, 1971

The kinetics of the radiation induced grafting of styrene to polyethylene terephthalate fibres has been studied. A dose rate of 0.72 Mrads per hour of Cobalt 60 radiation was used throughout at temperatures between 30 – 80°C. Dimethyl sulfoxide and water were used as swelling agents. The grafting rate was found to increase with temperature with an activation energy of 13.7 kcal/mole but reached a maximum in the vicinity of the glass transition temperature. The mechanism and kinetics of the grafting reaction are discussed in some detail.

INTRODUCTION

The modification of textile fibers with ionizing radiation is interesting from both the theoretical and practical points of view. Grafting to fibers is particularly interesting since it enables the superposition of the group of properties of the grafted side chains on the fiber without necessarily disturbing the peroperties of the parent fiber. The whole field of the radiation modification of textile fibers has been reviewed in detail by Stannett and Hoffman[1] and more recently by Hoffman. [2]

Studies of the radiation grafting of styrene to polyethylene terephthalate film have been reported by Ballantine and Glines.[3] The radiation grafting of itaconic acid, acrylamide and 4-vinyl pyridine has been discussed by Hoigné and Schamberg[4,5] together with the chemical grafting of styrene. The radiation grafting of acrylic acid and other monomers to polyester fibers has been studied in detail by Zielinski,[6] Blin[7] and by Sakurada [8] and their coworkers.

---

* National Science Foundation Visiting Scientist, Institute of Physical Chemistry, Bucharest, Romania.

[1] V.T. Stannett and A.S. Hoffman, American Dyeshruff Reporter, **57**, 91 (1968).

[2] A.S. Hoffman, Isotopes and Radiation Technology, **8**, 84 (1970).

[3] D.S. Ballantine and A. Glines, Brookhaven National Labs. Report, B.N.L. 7573.

[4] J. Hoigné, E. Schamberg, Textilveredlung *5*, 400 (1970).

[5] E. Schamberg and J. Hoigné, Polymer Sci., Part A-1, **8**, 693 (1970).

[6] W. Zielinski, T. Achmatowicz and A. Robalewski, Proc. of the 2nd Tihany Symp. on Rad. Chem., **1967**, 733.

[7] M.F. Blin, R. Candon, G. Gaussens and F. Lemaire, Proc. of Symp. "Large Radiation Sources for Ind. Proc.", München, S 319, 1969, IAEA, Vienna.

[8] I. Sakurada, Y. Kada and T. Kawahara, JAERI, 5026, **3**, 150 (1970).

In this paper the effect of temperature and of dimethyl sulfoxide and water as swelling agents on the radiation induced grafting of styrene to polyethylene terephthalate fibers will be discussed.

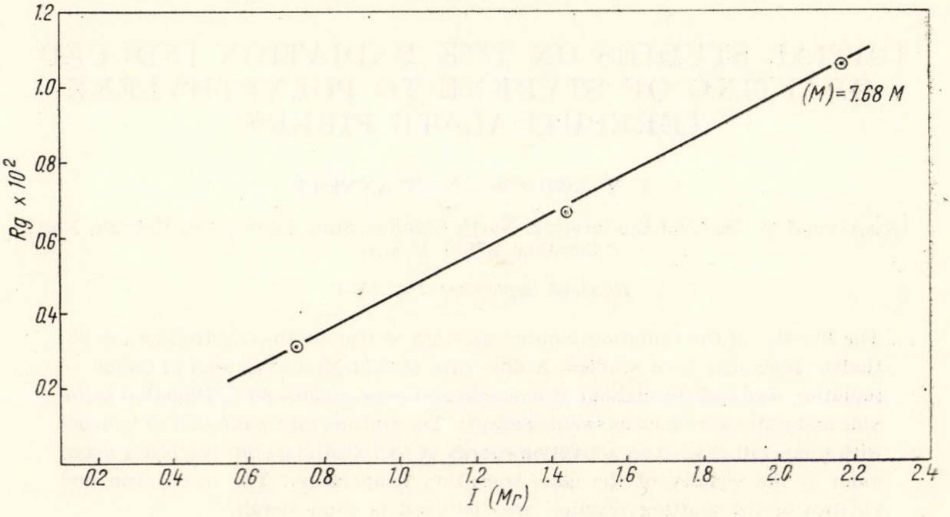

Fig. 1. — Effect of dose on radiation grafting yield (percent)

EXPERIMENTAL

Materials. Monsanto Chemical Co., U.S.A., *polyethylene terephthalate fibers* in the form of drawn multifilament tire cord yarn was used. The crystallinity was 58 %.

The yarn was treated in a soxhlet with methanol and acetone and dried under vacuum to constant weight before use. The styrene, dimethyl sulfoxide and other reagents were obtained from the Fisher Scientific Company and purified by distillation before use.

Procedures. 0.5—1.0 grams of fibers were placed in glass ampoules together with the monomer and solvents and degassed by several freeze-thaw cycles at 10^{-5} torr and sealed under vacuum. The irradiations were carried out at 0.72 Mrads per hour in a Cobalt 60 radiation source. The fibers were washed with benzene and dried to constant weight. The weight increase was recorded as the grafting yield.

RESULTS

(a) *Effect of Dose.* The percent graft was found to increase linearly with dose with negligible induction periods as shown for example in figure 1.

(b) *Effect of Monomer Concentration.* The effect of the monomer concentration on the rate of grafting obtained with various concentrations of styrene monomer in dimethyl sulfoxide are presented in figure 1 as log-log plots. It can be seen that the initial rates of grafting vary to the 1.52 power of the monomer concentration at 30°.

(c) *Effect of Dimethyl Sulfoxide Concentration.* The effect of dimethyl sulfoxide on the grafting rate over a wide range of concentrations is illustrated in figure 3. The addition of small amounts to the styrene increases the grafting yield considerably, a maximum is reached and then the rate falls steadily in the manner shown in figure 2. The initial rise is undoubtedly due to a swelling effect followed by the kinetic consequence of dilution of monomer in the manner discussed later.

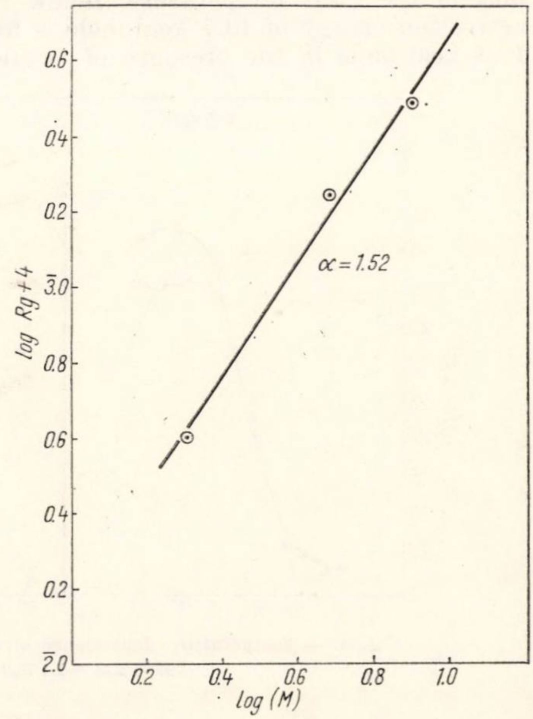

Fig. 2. — Effect of monomer concentration on rate of grafting (% per hour)

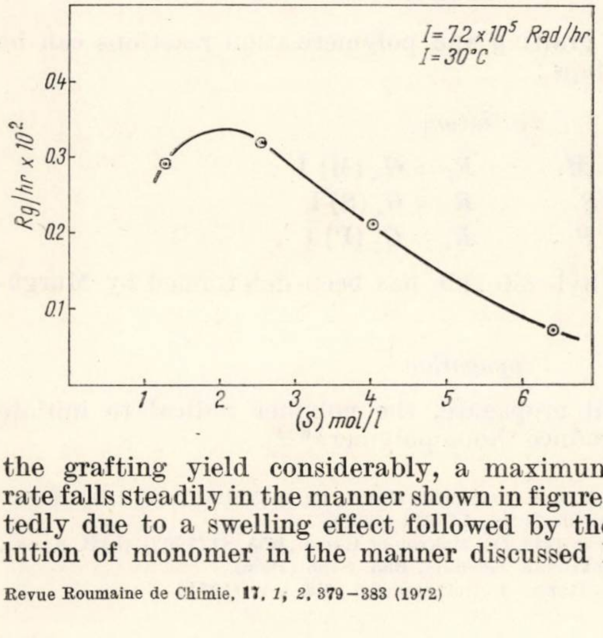

Fig. 3. — Effect of solvent (dimethyl sulfoxide) on rate of grafting (% per hour)

(d) *The Effect of Temperature.* The effect of temperature with styrene solutions is illustrated in figure 4. It can be seen that, in agreement with the results of Hoigné and Schamberg[4,5] a maximum is reached in the vicinity of the glass temperature. Below the glass temperature an overall activation energy of 13.7 kcal/mole is found in the absence of water and 12.4 kcal/mole in the presence of water.

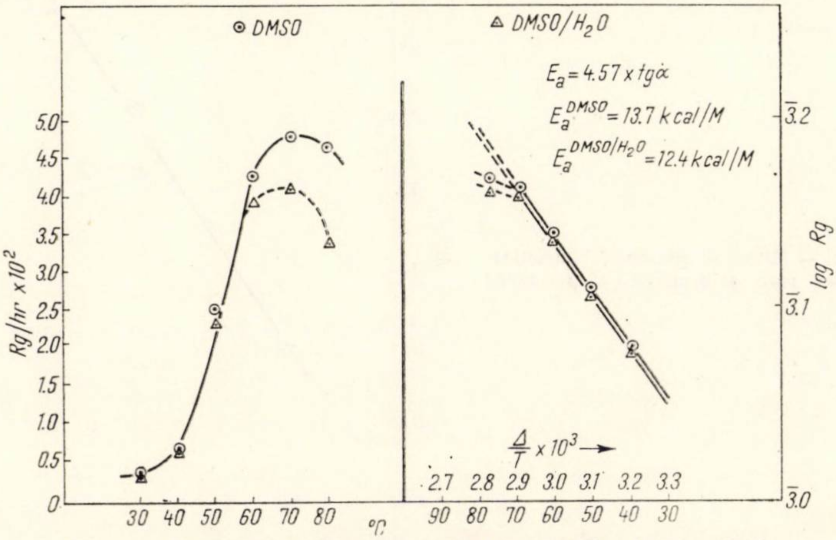

Fig. 4. — Temperature dependence of rate of grafting (% per hour).
DMSO 2.55 M/L; H_2O 0.92 M/L.

DISCUSSION

The overall radiation grafting and polymerization reactions can be expressed in the following steps:

Initiation

(Monomer)	$M \rightsquigarrow M.$	$R_i = G_m\,(\mathrm{M})\,\mathrm{I}$
(Solvent)	$S \rightsquigarrow S.$	$R_i = G_s\,(\mathrm{S})\,\mathrm{I}$
(Polymer)	$P \rightsquigarrow P.$	$R_i = G_p\,(\mathrm{P})\,\mathrm{I}$

The $G\,(R\cdot)$ value for dimethyl sulfoxide has been determined by Murgulescu and Vlagiu as 1.28.[9]

Propagation

All three radicals will propagate, the polymer radical to initiate grafting the others to produce homopolymer.[10,11]

---

[9] (a) I. Vlagiu and J. Păun, Rev. Roumaine de Chim., **12**, 1085 (1967); (b) I.G. Murgulescu and I. Vlagiu, Rev. Roumaine de Chim., **14**, 411 (1969).

[10] (a) R.E. Kesting and V. Stannett, Die Makromol. Chem., **B55**, S1 (1962). (b) K. Araki, H. Kiho and V. Stannett, Die Makromol. Chemie., **B95**, S106 (1966).

[11] A.J. Restaino and W.N. Reed, J. Polymer Sci., **36**, 499 (1959).

Termination

In principle the growing chains can be terminated by another growing chain or by any of the three primary radicals.[10,11]

Chain Transfer

Chain transfer of the growing chains to monomer, polymer or solvent can also occurr. The value for the chain transfer constants for styrene is 6.0×10^{-5}, the value for polyethylene terephthalate is probably higher. Murgulescu and Vlagiu [9] have measured the chain transfer constant of dimethyl sulfoxide and found it to be 6.93×10^{-5}, quite comparable to styrene in value.

The detailed kinetics of the grafting reaction including the chain transfer steps have been derived by Vlagiu and Stannett [12] for the steady state reaction. Very little post effect was found in the present work so steady state kinetics may be a good approximation. The final equation derived was : Rate of grafting, $R_g =$

$$\frac{K_p}{2K_t^{1/2}} (G_m I)^{1/2} (M)^{3/2} \left[1 + \frac{G_s(S) + G_p(P)}{G_m(M)}\right]^{1/2} \left[\frac{K_t^1 K_{\text{trs}}(S)}{K_t K_p^1(M)} + 1\right]^{-1/2}$$

K_t and K_p are the normal termination and propagation rate constants. K_t^1 is for the termination of growing chains with solvent radicals and K_p^1 for the initiation of chains by solvent radicals. K_{trs} is for the transfer reaction with solvent

The equation predicts the order of the rate on monomers to be between 1.0 and 1.5. (We found 1.5) and a 0.5 order of the rate on dose rate. This dependency is presently being studied in this laboratory.

The effect of temperature is interesting. The maximum has been discussed in detail by Hoigné and Schamberg and is probably due to the interaction of diffusion of monomer and gel effects. In our work the additional complications of the swelling and sensitizing effects of the dimethyl sulfoxide are introduced. These and other features of the grafting reaction are being studied further and will be discussed in a later publication.

---

[12] I. Vlagiu and V. Stannett, to be published.

Revue Roumaine de Chimie, 17, *1*, 2, 385–396 (1972)

Dedicated to Professor I. G. MURGULESCU
on his 70th birthday

THE SELF-DIFFUSION COEFFICIENTS IN SOME MOLTEN NITRATES

ŞTEFANIA ZUCA and MARIELLA CONSTANTINESCU

Institute of Physical Chemistry Str. Galaţi 31, Bucharest, Romania

Received August 12, 1971

The self-diffusion coefficients of the cation in molten $NaNO_3$, KNO_3, $RbNO_3$, $CsNO_3$ and $AgNO_3$ were determined by the improved "diffusion-into-the-capillary" method. The results can be summarized in Arrhenius equations :

$$D_{Na^+} = (1.29 \pm 0.04)10^{-3} \exp \quad (-4350 \pm 220)/RT$$

$$D_{K^+} = (1.48 \pm 0.19)10^{-3} \exp \quad (-5670 \pm 180)/RT$$

$$D_{Rb^+} = (1.16 \pm 0.10)10^{-3} \exp \quad (-5480 \pm 125)/RT$$

$$D_{Cs^+} = (1.32 \pm 0.03)10^{-3} \exp \quad (-5810 \pm 320)/RT$$

$$D_{Ag^+} = (0.47 \pm 0.02)10^{-3} \exp \quad (-3680 \pm 80)/RT$$

The agreement with the results obtained by other authors and the correlation existing between the ionic size and the self-diffusion coefficient in these melts are discussed.

In recent years, the interest aroused by self-diffusion coefficient studies has increased extensively. A large number of different experimental techniques have been applied for this purpose :

1. — the impregnated paper strip method, first used by Arnikar and Chemla[1] and developed by Honig [2] and Kwak[3] ;

2. — the porous frit technique used by Djordjevic and Hills [4] and developed by Sjöblom[5] ;

3. — the vanishing bubble technique, used by Angell and Bockris [6] ;

---

[1] M. Chemla and H.J. Arnikar, *Ann. Phys.*, **16**, 1291 (1959).

[2] E.P. Honig ,Thesis, Amsterdam 1964.

[3] I.C. Th. Kwak, Thesis, Amsterdam 1967.

[4] I. Djordjevic and G.J. Hills, *Trans. Faraday Soc.*, **56**, 269 (1960).

[5] C.A. Sjöblom, Thesis, Göteborg, 1968.

[6] C.A. Angell and J.O'M. Bockris, *Electrochim. Acta*, **1**, 308 (1959).

4. — the capillary method widely used by different authors.[7–15]

Among these methods, only the capillary method has been proved to be suitable for a very large temperature range (up to 1100°) and even in very corrosive melts when the capillaries were of platinum or gold.[9,14,15] The two variants of the method are:

— the "diffusion-out-of-the-capillary" method where the capillaries are filled with radioactive molten salt and the bath consists of inactive salt. The method involves a complicated filling technique, (by means of a needle connected to a syringe[7–9]) and a long diffusion time (1—3 days).

Recently Koster[10] improved the method by adapting a vacuum technique for filling the capillaries.

— the "diffusion-into-the-capillary" method where the bath contains the radioactive salt and the capillaries are filled with inactive molten salt. The method was initiated by Bockris and co-workers.[11–13] The advantages of the method are the very simple filling procedure by means of a vacuum technique and the relatively short time (1—3 h) asked for diffusion. Therefore, we have chosen for our experiments "the diffusion-into-the-capillary" method. Firstly we decided to establish the experimental working conditions in connection with the "immersion" and "Δl" effects, the main problems met with the capillary method.

A reinvestigation of self-diffusion coefficients of molten nitrates seemed to us suitable for this purpose as it allowed a comparison of our results with those obtained by completely different methods which are independent of the systematic errors characteristic of the capillary measurements. On the other hand, we have aimed at obtaining a self-consistent and perhaps a more accurate set of data.

We report in the following the experimental data on the self-diffusion coefficients of cation in the molten $NaNO_3$, KNO_3, $RbNO_3$, $CsNO_3$ and $AgNO_3$.

EXPERIMENTAL

Apparatus

The diffusion cell is shown in figure 1. and consists of a Pyrex glass tube (*A*) (⌀50 mm) which contains at the bottom the molten radioactive salt (*B*). In the vessel (*A*) there is a second Pyrex glass vessel (*C*) containing the inactive salt; the vessel (*C*) may be turned so as to superimpose over (*B*) by help of the glass handle (*D*).

After the filling of the capillaries with inactive salt the reservoir (*C*) could be removed and the capillaries immersed into the radioactive bath (*B*).

---

[7] A.S. Dworkin, R.B. Escue and E.R. van Arstdalen, *J. Phys. Chem.*, **64**, 872 (1960).

[8] F. Lantelme, Thesis, Paris, 1965.

[9] P.L. Spedding and R. Mills, *J. Electrochem. Soc.*, **112**, 594 (1965).

[10] J. Koster, Thesis, Amsterdam, 1971.

[11] J.O'M. Bockris and G. Hooper, *Discuss, Faraday Soc.*, **32**, 218 (1961).

[12] L. Nanis, S.R. Richards and J.O'M. Bockris, *Rev. Sci. Instr.* **36**, 673 (1965).

[13] S.R. Richards, Thesis, 1967.

[14] K. Grjotheim and S. Zuca, *Acta Chem. Scand.*, **22**, 531 (1968).

[15] D. Harari, F. Lantelme and M. Chemla, *J. Chim. phys.*, **66**, 1286 (1969).

The four silica capillaries (*E*), with inner diameter 1 mm, length 30 mm, were placed on the holder (*F*) which could be rotated around its vertical axis by a shaft (*G*) attached to a adjustable stirrer motor. The calibrated Pt-Pt-10 Rh thermocouple (*H*) dipping into the molten salt served for temperature measurement.

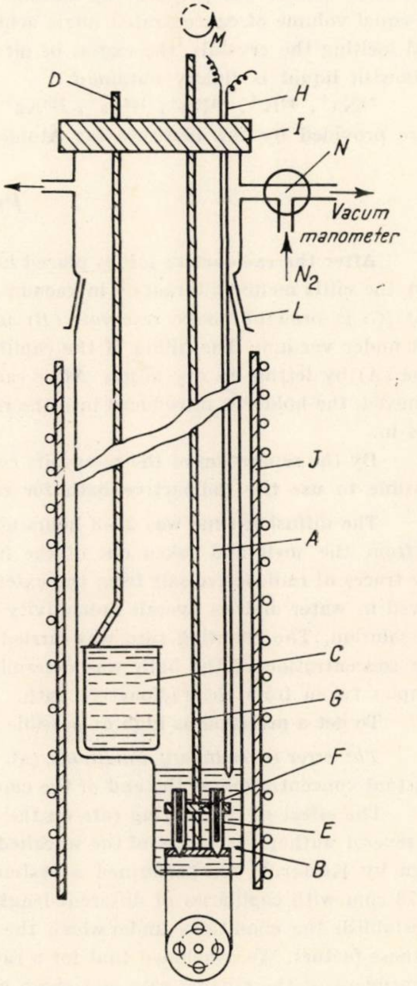

Fig. 1. — Diffusion apparatus.

A – diffusion tube; *B* – reservoir with radioactive salt; *C* – reservoir with inactive salt; *D* – glass handle; *E* – silica capillaries; *F*, *G* – capillary holder; *I* – metal lid; *J* – furnace; *H* – thermocouple Pt–Pt/10 Rh; *L* – joint; *M* – stirrer motor; *N* – stopcock.

The open end of the diffusion tube was tightened with a metal lid (I) so as to ensure a controlled atmosphere inside the cell. For the same purpose (*D*) (*F*) and (*H*) moved in a precision slip-joint. A vacuum of 3 – 5 mm Hg could be obtained inside the tube (*A*).

The diffusion cell was placed in a vertical Kanthal resistance furnace. A constant temperature of the furnace, within ±0.5° was obtained by means of a photothermoregulator. A temperature gradient of 5° on 10 cm distance was ensured as to avoid the immersion effect associated with the immersion of the capillaries into the bath.

Chemicals

The alkali nitrates were Merck or BDH *p.a.* degree reagents. They were purified by single recrystallization from distilled water, dried for 24 h at 150° and melted alternately under vacuum and in a dried argon atmosphere. The melts were a clear colourless liquid. Highly purified silver nitrate was prepared by adding, to a saturate solution of *p.a.* reagent silver nitrate, an equal volume of concentrated nitric acid to effect the crystallization of the salt. By drying and melting the crystals, the excess of nitric acid is completely removed and a clear, slightly yellowish liquid is finally obtained.

$^{24}Na^+$, $^{42}K^+$, $^{86}Rb^+$, $^{134}Cs^+$, $^{110}Ag^+$ radioactive isotopes were used as tracers. They were provided by the Institute for Atomic Physics, Bucharest, Romania.

Procedure

After the radioactive salt is placed in (*B*) and inactive salt in (*C*), the furnace is heated and the saltis melted alternately in vacuum and in inert atmosphere of argon gase. The reservoir (*C*) is brought above reservoir (*B*) and the capillary holder is immersed into the liquid salt under vacuum. The filling of the capillaries is performed by increasing the pressure in the tube (*A*) by letting in dry argon. After raising the capillaries from the melt, reservoir (*C*) is removed, the holder is introduced into the radioactive bath (*B*) and the stirring rate of 33 rpm sets in.

By the separation of the reservoirs containing active and inactive molten salt it became possible to use the radioactive bath for carrying out several experiments.

The diffusion time was 2–3 hours after which the holder and the capillaries were lifted from the melt and taken out of the furnace. After cooling they were washed to remove any traces of radioactive salt from the external walls, then the content of each capillary was solved in water and its overall radiactivity was measured with a G.M. counter immersed in the solution. The counting rate was carried out with a NR 108 Orion type electronic counted The concentration of the bath was determined by measuring the activity of two weighed samples taken from the radioactive bath.

To get a precision as high as possible some precautions have been taken :

The error in boundary conditions. (a). The stirring was initiated in order to maintain a constant concentration at the end of the capillary.

The effect of the stirring rate on the measured diffusion coefficients has been discussed by several authors in terms of the so-called "$\Delta 1$" effect. A general survey of the problem is given by Koster.[10] We performed a systematic investigation at various stirring rates from 0–78 rpm with capillaries of different lengths (3–5 cm) and various diffusion times (2–6 h) to establish the conditions under which the measured self-diffusion coefficient is not affected by these factors. We concluded that for a rate below 3 mm/sec the self-diffusion coefficient is independent of the stirring rate and chose as working rate 33 rpm.

(b). To diminish the immersion effect the capillaries filling was carried out at a temperature by 5° lower than the diffusion temperature. Some zero experiments have also been carried out as to make evident the transport of matter on introducing and removing the capillaries from the bath. When circumstances demanded it, this effect was calculated and the respective corrections were made.

(c). Quartz capillaries were used in order to avoid the volume change and also to reduce the isotopic $^{24}Na-Na$ exchange in glass.

(d). The capillary diameter was measured by an ordinary comparator with a 5×10^{-3} mm precision.

(e). The diffusion coefficient does not depend on the capillary length but for a better reproducibility the capillary ends were all in the same plane to ensure the same hydrodynamic conditions.

A discussion of the errors which determine the accuracy of the experimental self-diffusion coefficients will be presented below.

— *The precision of the analysis.* (1). The most important error sources in the diffusion coefficient were the counting statistics which proved to be :

— at activities of 6000—8000 c.p.m. —— ± 1.5% and

— at activities of 1000—2000 c.p.m. —— ± 2.3%.

(2). The wahhing error was ± 0.5%.

(3). The geometry reproducibility error was ± 2%.

— The average error in boundary conditions and in analysis was 3%.

— Another source of error was the imprecision of the temperature measurement : ±0.4%.

The overall error of the diffusion coefficient was obtained by taking into account the error sources :

$$E = \sqrt{E^2_{\text{boundary conditions}} + E^2_{\text{analysis}} + E^2_{\text{temperatures}}} =$$

$$= \sqrt{(3.)^2 + (0.4)^2} = \pm 3.04\,\%.$$

RESULTS AND DISCUSSION

The self-diffusion coefficient was calculated by the equation :

$$Q = 2C_0 A \sqrt{Dt/\pi} \tag{1}$$

where Q(c.p.m.) is the total radioactivity of diffusate, C_0 (c.p.m. cm^{-3}) the concentration of the radioactive species in the bulk of the salt ; A (cm^2) the cross-section of the capillary, and t(sec) the time of the experimental run.

For each investigated salt the self-diffusion coefficients of the cation have been measured over a temperature range of about 150° above their melting point.

The results obtained are given in table 1.

The present data are compared to the values obtained by other workers in figs. 2—6.

From the data illustrated in figure 2 it is evident that in molten $NaNO_3$ there is a close agreement between different authors. [16,7,8,9] The highest percent differences (—10%) are between our data and Sjöblom's[20] data, and (+10%) between our data and Nagarajan's.[19]

---

[16] C.A. Angell and J.W. Tomlinson, *Discuss. Faraday Soc.*, **32**, 237 (1961).

Table 1

Self-diffusion coefficients of the cation in molten nitrates

NaNO$_3$		KNO$_3$		RbNO$_3$		CsNO$_3$		AgNO$_3$	
t°C	$D_{Na^+} \cdot 10^5 cm^2 sec^{-1}$	t°C	$D_{K^+} \cdot 10^5 cm^2 sec^{-1}$	t°C	$D_{Rb^+} \cdot 10^5 cm^2 sec^{-1}$	t°C	$D_{Cs^+} \cdot 10^5 cm^2 sec^{-1}$	t°C	$D_{Ag^+} \cdot 10^5 cm^2 sec^{-1}$
327	1.99 ± 0.09	342	1.45 ± 0.02	327	1.13 ± 0.01	432	2.03 ± 0.03	224	1.12 ± 0.02
343	2.30 ± 0.07	350	1.54 ± 0.02	340	1.29 ± 0.01	449	2.28 ± 0.02	245	1.32 ± 0.03
366	2.51 ± 0.02	364	1.66 ± 0.04	361	1.48 ± 0.02	458	2.39 ± 0.02	260	1.45 ± 0.02
366	2.59 ± 0.04	366	1.74 ± 0.01	390	1.82 ± 0.03	474	2.65 ± 0.03	268	1.48 ± 0.02
366	2.56 ± 0.02	378	1.82 ± 0.03	421	2.09 ± 0.03	478	2.72 ± 0.08	287	1.69 ± 0.05
380	2.74 ± 0.15	383	1.90 ± 0.09	439	2.37 ± 0.03	492	2.93 ± 0.02	294	1.76 ± 0.02
398	2.92 ± 0.11	384	1.93 ± 0.06	466	2.75 ± 0.02			318	2.10 ± 0.01
		409	2.27 ± 0.01					352	2.38 ± 0.09
		426	2.69 ± 0.06						

Examination of figure 3 shows that for D_+ in molten KNO_3 there is a satisfactory agreement between the data obtained by Dworkin[7] with "out-of-the-capillary method" and our data.

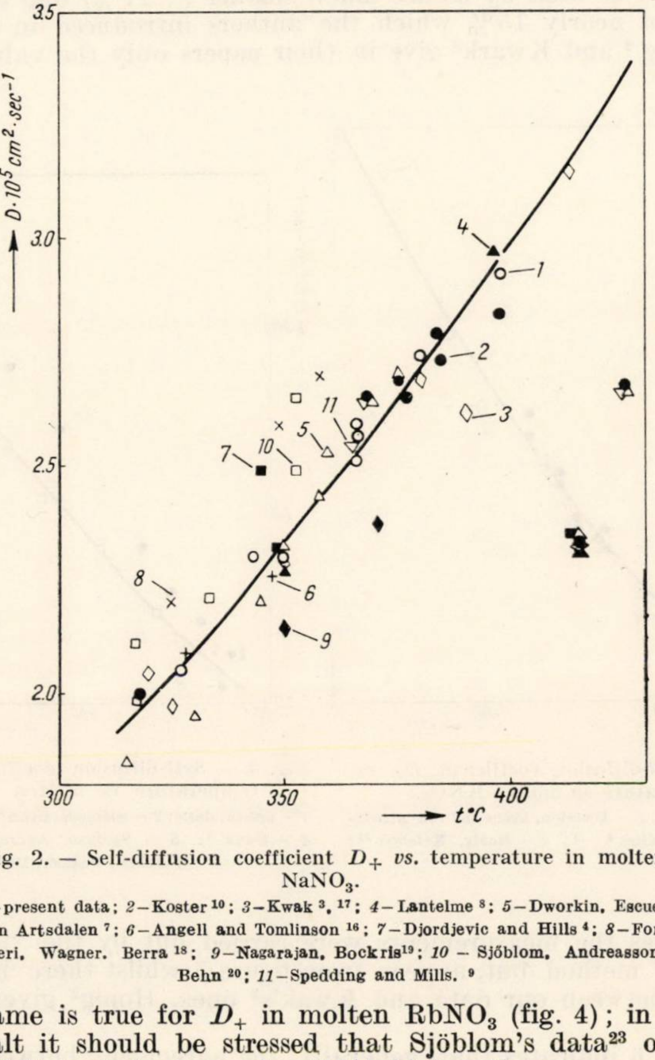

Fig. 2. — Self-diffusion coefficient D_+ vs. temperature in molten $NaNO_3$.

1 — present data; 2 — Koster[10]; 3 — Kwak[3, 17]; 4 — Lantelme[8]; 5 — Dworkin, Escue, van Artsdalen[7]; 6 — Angell and Tomlinson[16]; 7 — Djordjevic and Hills[4]; 8 — Forcheri, Wagner. Berra[18]; 9 — Nagarajan, Bockris[19]; 10 — Sjöblom, Andreasson, Behn[20]; 11 — Spedding and Mills.[9]

The same is true for D_+ in molten $RbNO_3$ (fig. 4); in connection with this salt it should be stressed that Sjöblom's data[23] obtained by the porous frit technique are by (9%) higher than ours and those of Honig[2] obtained by the "impregnated paper strip" method are by 9% lower than ours.

---

[17] J.A.A. KETELAAR and J.C. TH. KWAK, *J. Phys. Chem.*, **71** (4), 1149 (1967).
[18] S. FORCHERI, V. WAGNER and E. BERRA, *Electrochim. Metall III*, **2**, 123 (1968).
[19] M.K. NAGARAJAN and J.O'M. BOCKRIS, *J. Phys. Chem.*, **70**, 1854 (1966).
[20] C.A. SJÖBLOM, D. ANDREASSON, A. BEHN, *Z. Naturforsch.* **25a**, 700 (1970).

Figure 5 illustrates that the agreement for D_+ in molten $CsNO_3$ between our data and those obtained by Dworkin[7] by the "out-of-the-capillary" method is perfect. The data obtained by Nagarajan[19] by the same method as used by us are much smaller (—17%) due to the "Δl" correction of nearly 15% which the authors introduced in their calculation. Honig [2] and Kwark[3] give in their papers only the values at 450°.

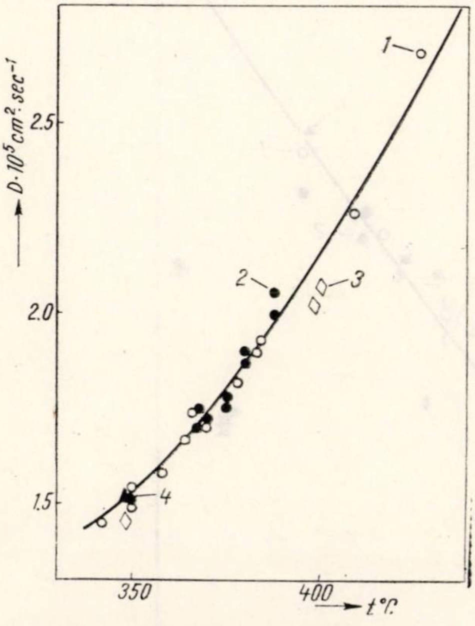

Fig. 3. — Self-diffusion coefficient D_+ *vs.* temperature in molten KNO_3.

1 — present data; *2* — Dworkin, Escue and van Artsdalen [7]; *3* — Lantelme [21]; *4* — Honig, Ketelaar [22];

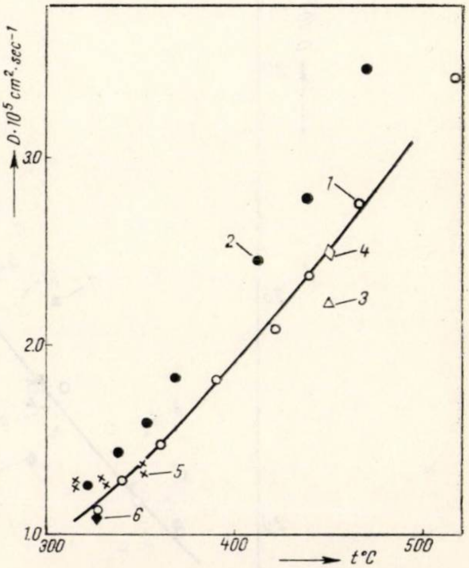

Fig. 4. — Self-diffusion coefficient D_+ *vs.* temperature in molten $RbNO_3$.

1 — present data; *2* — Sjöblom, Behn [23]; *3* — Honig [2]; *4* — Kwak [3]; *5* — Sjöblom, Andreasson, Behn [20]; *6* — Forcheri, Wagner, Berra [13].

In both cases the measurements were carried out by the "impregnated paper strip" method but, as seen from figure 5 whilst there is a perfect agreement between our data and Kwak's[3] ones, Honig[2] gives values by 11% lower.

Figure 6 indicates that, generally, the agreement between different techniques is very poor in molten $AgNO_3$. While our data agree very well (less than ±3%) with Dworkin's[7] and Richard's[13] data, the results obtained by Sjöblom[20] using an improved version of the gravimetric interdiffusion technique are by 25% higher and those of Sjöblom[24] by the porous frit technique, by 19% lower than ours.

---

[21] F. Lantelme and M. Chemla, *Bull. Soc. chim. France*, **1963** 969.

[22] E.P. Honig and J.A.A. Ketelaar, *Trans. Faraday Soc.*, **62**, 190 (1966).

[23] C.A. Sjöblom and A. Benn, *Z. Naturforsch.*, **24a**, 464 (1969).

[24] C.A. Sjöblom and J. Andersson, *Z. Naturforsch.*, **21a**, 276 (1966).

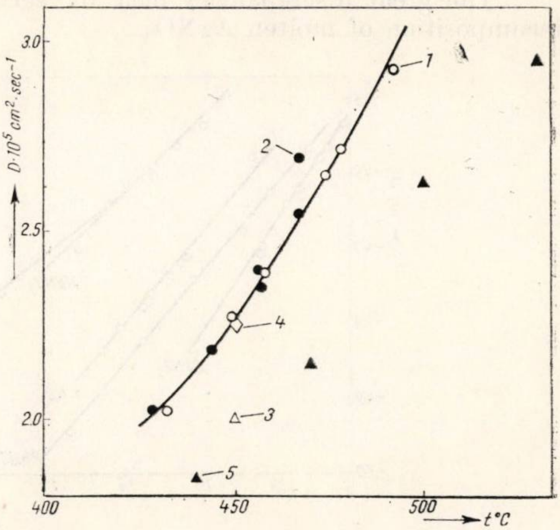

Fig. 5. — Self-diffusion coefficient D_+ *vs.* temperature in molten $CsNO_3$.

1 – present data; *2* – Dworkin, Escue, van Artsdalen [7]; *3* – Honig [2]; *4* – Kwak [3,17]; *5* – Nagarajan, Bockris. [19]

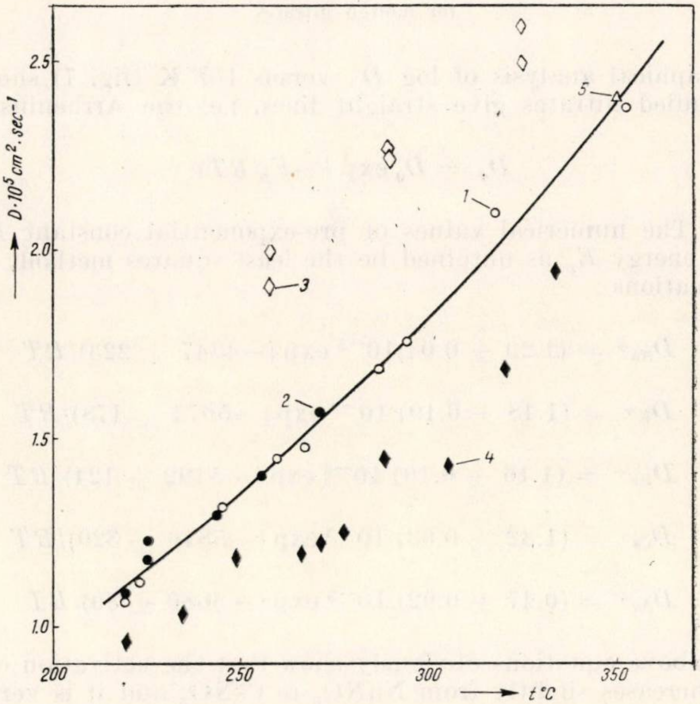

Fig. 6. — Self-diffusion coefficient of D_+ *vs.* temperature in molten $AgNO_3$.

1 – present data; *2* – Dworkin, Escue and van Artsdalen [7]; *3* – Sjöblom, Andreasson, Behn [20]; *4* – Sjöblom, Andersson [24]; *5* – Richards [13].

The great discrepancies may by certainly attributed to the slight decomposition of molten $AgNO_3$.

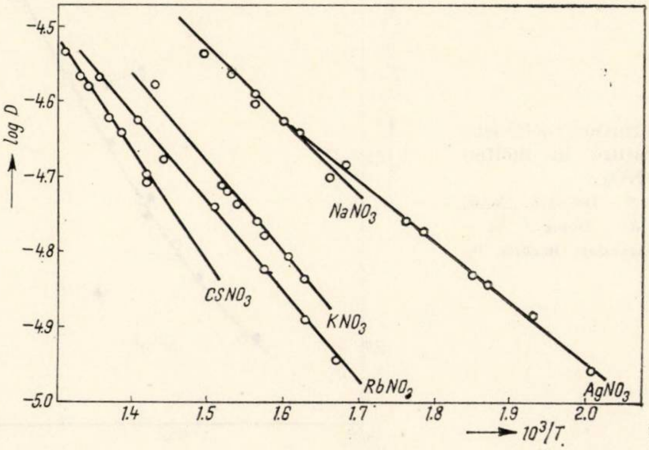

Fig. 7. — Log D_+ against reciprocal of the absolute temperature for molten nitrates.

A graphical analysis of log D_+ versus $1/T$°K (fig. 7) showed that all the studied nitrates give straight lines, i.e. the Arrhenius equation

$$D_+ = D_0 \exp\left(-E_D/RT\right) \tag{2}$$

is obeyed. The numerical values of pre-exponential constant D_0 and of activation energy E_D as obtained be the least squares method, are given in the equations:

$$D_{\mathrm{Na}^+} = (1.29 \pm 0.04) 10^{-3} \exp\left(-4347 \pm 223\right)/RT \tag{3}$$

$$D_{\mathrm{K}^+} = (1.48 \pm 0.19)\, 10^{-3} \exp\left(-5674 \pm 178\right)/RT \tag{4}$$

$$D_{\mathrm{Rb}^+} = (1.16 \pm 0.10)\, 10^{-3} \exp\left(-5492 \pm 124\right)/RT \tag{5}$$

$$D_{\mathrm{Cs}^+} = (1.32 \pm 0.03)\, 10^{-3} \exp\left(-5810 \pm 320\right)/RT \tag{6}$$

$$D_{\mathrm{Ag}^+} = (0.47 \pm 0.02)\, 10^{-3} \exp\left(-3680 \pm 80\right)/RT \tag{7}$$

The above equations obviously show that the activation energy for diffusion increases slightly from $NaNO_3$ to $CsNO_3$ and it is very low for $AgNO_3$.

This behaviour may be explained if we take into account the prediction of the hole theory[25] according to which E_D depends directly of melting temperature (T_m) by the relation :

---

[25] R. FÜRTH, *Proc. Cambridge Phyl. Soc.*, **37**, 252 (1941).

$$E_D = 3.74 \ RT_m \qquad (8)$$

where T_m is expressed in °K.

Although the E_D development in the serie of the studied nitrates is correctly given by hole theory, the agreement between the numerical values calculated by eq. (8) and the experimental data is somewhat poorer. The differences are small in molten $NaNO_3$ and $AgNO_3$ ($+ 0.3\%$ and respectively $+ 2.5\%$), but they reach $+ 25\%$ in the remaining nitrates of the series. As it was already stated [7] the $D_+ r_+$ product is constant in molten nitrates. The present results do not alter this conclusion.

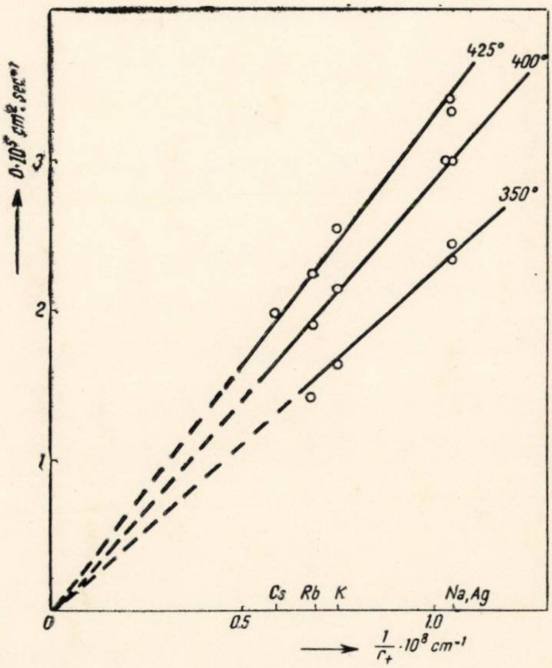

Fig. 8. — Dependence of D_+ against $1/r_+$ in molten nitrates.

Figure 8 illustrates in a convincing way that making allowance for the relative error in D_+, a straight line can be drawn through the obtained points and the origin of coordinates. A special remark has to be made for the radius of Ag^+ in its molten nitrate. In a previous paper by Zuca and Borcan[26] it has been pointed out that there are many experimental data proving that the ionic radius in the crystal, as given by Pauling, does not express the real size occupied by the silver ion in molten $AgNO_3$. On that occasion, it was concluded that Ag^+ has an ionic size equal to that of the Na^+ ion. We consider that the results in figure 8 support this interpretation.

---

[26] St. Zuca and R. Borcan, *Electrochim. Acta*, **15**, 1817 (1970).

Regarding the Nernst-Einstein equation we recall that, as already stated by many researchers, it was proved not to hold in molten salts. We only note the following regularities observed for the Nernst-Einstein coefficient defined as $\alpha = RTu_+/FD_+$ where u_+ is the ionic mobility. This coefficient is smaller than unit for all the nitrates and decreases as the cationic radius increases, namely it is 0.82 in $NaNO_3$; 0.66 in KNO_3 ; 0.57 in $RbNO_3$; 0.55 in $CsNO_3$.

We consider that this evolution pleads for the idea that, as we shift toward $CsNO_3$, the degree of association in the melt increases.

Revue Roumaine de Chimie, 17, 1, 2, 397 – 403 (1972)

Hommage au Professeur I. G. MURGULESCU
à l'occasion de son 70e anniversaire

SUR LE MÉTHYL-1-PHTALAZINIUM-CARBÉTHOXYMÉTHYLURE. III[1]

I. ZUGRĂVESCU, MAGDA PETROVANU, MARIA CAPROŞU et I. DRUŢĂ

Université « Al. I. Cuza »
Laboratoire de Chimie organique, Jassy, 11, str. 23 August

Reçu le 25 août 1971

Poursuivant des recherches concernant les ylures carbone-azote on a étudié les conditions d'obtention et la réactivité du méthyl-1-phtalazinium-carbéthoxyméthylure. L'élimination de l'acide bromhydrique à partir du bromure de N^3-carbéthoxyméthyl-1-méthyl-phtalazinium (V) conduit au méthyl-1-phtalazinium-carbéthoxyméthylure très stable. Par cycloaddition dipolaire 1,3 de l'anhydride maléique, du N-phényl maléimide et de l'acétylène dicarboxylate de méthyle sur le méthyl-1-phtalazinium-carbéthoxyméthylure (VI) on obtient les composés azabicycliques XII_a, XII_b et XIII.

Dans un travail précédent,[1] en étudiant l'action du bromure de phénacyle sur la méthyl-1-phtalazine on a obtenu le bromure de N-phénacyl-1-méthyl-phtalazinium qui, en milieu alcalin, donne naissance au phtalazinium-phénacylure II. L'ylure II subit spontanément un procesus d'inactivation conduisant au dimère III :

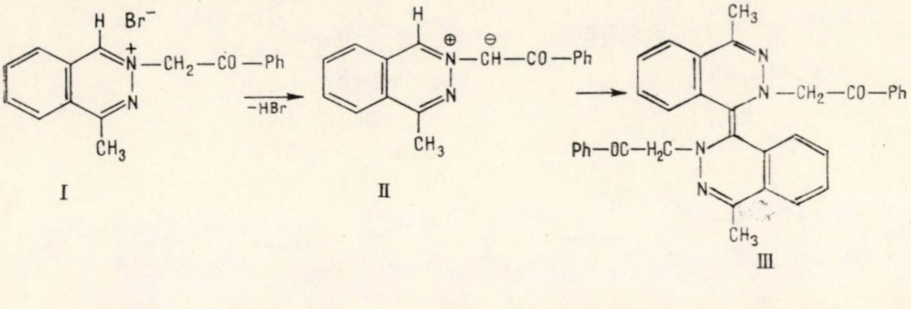

La formation du dimère III peut être expliquée par l'apparition d'un intermédiaire carbénique IV formé, à son tour, par suite de l'arrachement du proton 4 du cycle phtalazinique, par le carbanion. La capacité du centre anionique d'accepter le proton constitue un facteur essentiel et déterminant pour le processus de dimérisation.

---

[1] M. Caproşu, M. Petrovanu, I. Druţă et I. Zugrăvescu, *Bull. Soc. chim. France*, **1971**, 1834.

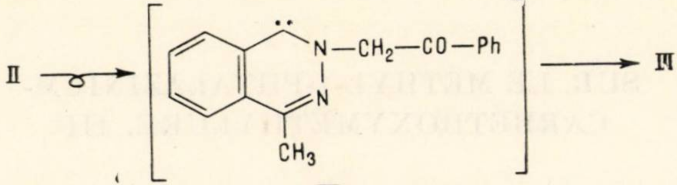

IV

Poursuivant les recherches concernant l'obtention de méthyl-1-phtalazinium ylures stables nous avons envisagé d'étudier les composés yluriques résultés au cours de la déhydrobromation des sels obtenus par l'action d'autres réactants α-halogénocarbonylés sur la méthyl-1-phtalazine.

Tenant compte du fait que, dans d'autres travaux précédents I. Zugrăvescu et ses coll.[2,3] ont obtenu des carbéthoxyméthylures stables (incapables de dimérisation) dérivés de la phtalazine[2] et de l'isoquinoléine[3], dans le présent travail nous avons arrêté nos recherches sur le méthlyl-1-phtalazinium-carbéthoxyméthylure, analogue du point de vue structurel à l'ylure II.

En traitant la méthyl-1-phtalazine par le bromoacétate d'éthyle on a obtenu le bromure de N^3-carbéthoxyméthyl-1-méthylphtalazinium V qui, par élimination d'acide bromhydrique en milieu alcalin donne naissance au méthyl-1-phtalazinium-carbéthoxyméthylure VI :

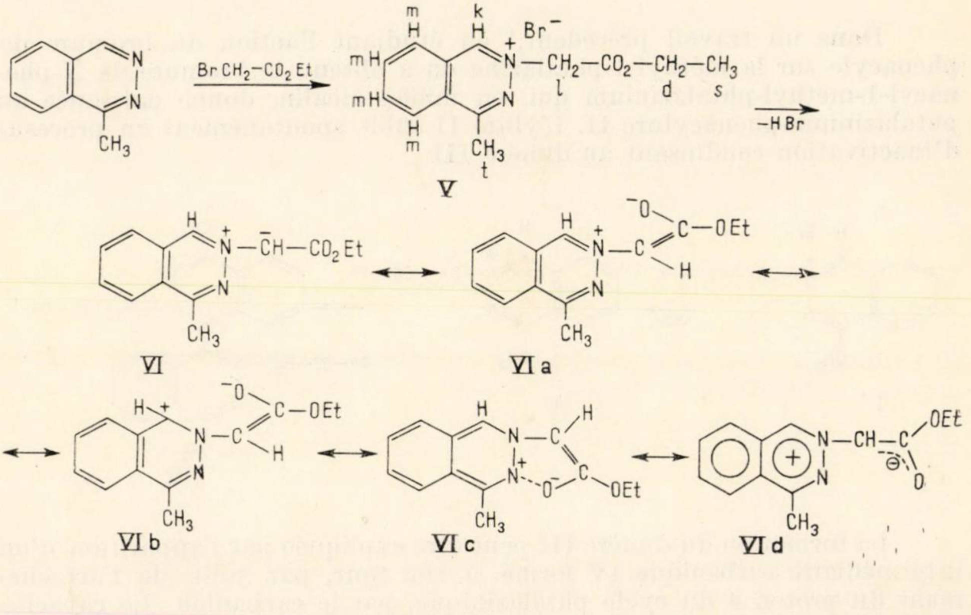

V

VI

VI a

VI b

VI c

VI d

---

[2] M. Petrovanu, A. Sauciuc et I. Zugrăvescu, *An. sti. Univ. « Al. I. Cuza » Iaşi*, **16**, 65 (1970).

[3] I. Zugrăvescu, E. Rucinschi et G. Surpăţeanu, *An. sti. Univ. « Al. I. Cuza » Iaşi*, **16**, 41 (1970).

L'ylure VI apparaît beaucoup plus stable que le méthyl-1-phtalazinium-phénacylure II. Ainsi, d'une part, le produit VI ne subit aucun processus de dimérisation conduisant à un analogue du composé III, même dans des conditions expérimentales très diverses, d'autre part, l'ylure VI est incapable de fixer le CO_2 (IX), réaction qui pourtant se produire spontanément dans le cas de l'isoquinoléinium-carbéthoxy-méthylure VII[3] qui, par addition du CO_2 conduit au produit bétaïnique VIII :

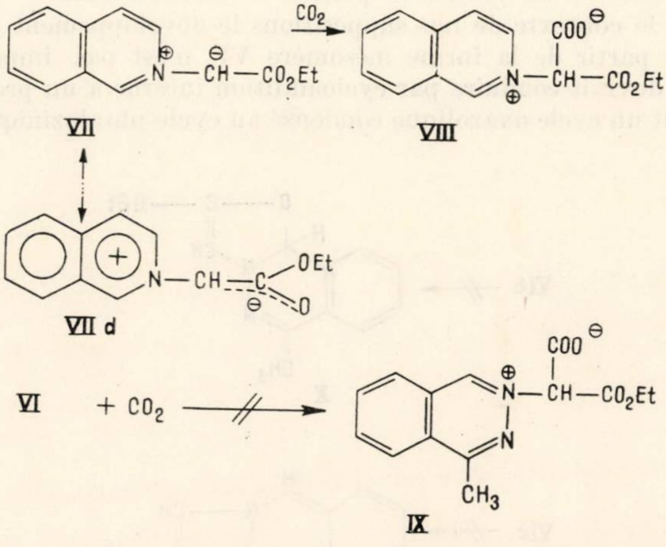

La stabilité remarquable de l'ylure VI en comparaison de l'ylure II pourrait être expliquée de la façon suivante :

Les structures énol-bétaïniques du type VI_a, VI_b, VI_c .... deviennent prioritaires par rapport à la structure VI grâce à l'effet +E exercé par le groupement éthoxylique, par suite duquel la charge anionique est poussée vers l'oxygène. Dans l'ylure II la charge anionique est attirée par le noyau phénylique ce qui explique la priorité de la forme carbanionique. Les structures énol-bétaïniques pour VI expliquent aussi le manque de couleur du produit en comparaison des autres ylures du type C—N qui sont colorés. Le fait que le produit VI ne subit pas de processus d'hydratation et n'additionne pas le CO_2 plède aussi en faveur des formes oxanioniques. Parmi les structures énol-bétaïniques mentionnées, VI_c explique le mieux les propriétés chimiques du méthyl-1-phtalazinium-carbéthoxyméthylure. L'incapacité de l'oxoanion, dans la structure VI_c considérée, de capter le proton de la position 4 du cycle 1-méthylphtalazinique, rend impossible l'apparition d'un intermédiaire carbénique analogue à IV, donc celle d'un dimère analogue à III.

Comme, en général, on admet la contribution prioritaire de la structure VI$_c$ dans laquelle les deux charges sont fortement compensées grâce à l'interaction électrostatique, l'apparition de la forme carbanionique rien qu'en présence d'un faible réactant électrophyle tel que le CO_2 devient peu probable. Dans le cas de l'isoquinoléinium-ylure VII l'oxoanion ne subit pas une telle attraction électrostatique — et en ceci consiste la différence essentielle entre VII et VI — le déplacement des électrons dans la structure mésomère VII$_d$ vers l'atome de carbone sous l'influence du CO_2 devient possible et on obtient le produit d'addition VIII.

Dans le contexte de nos suppositions le développement d'une structure VI$_b$ à partir de la forme mésomère VI$_d$ n'est pas improbable. La forme VI$_b$ devrait conduire par cycloaddition interne à un produit X qui contiendrait un cycle oxazolique condensé au cycle phtalazinique :

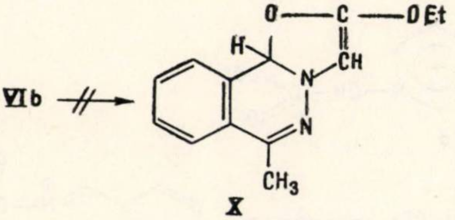

X

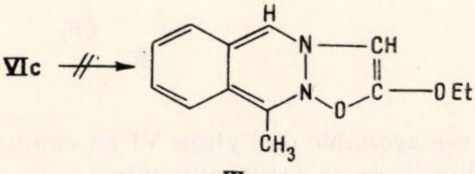

XI

Malgré la grande tendance de la position 4 du cycle 1-méthyl-phtalazinique à devenir positive on n'a pas observé la formation d'un produit X. Il est possible que l'hybridation sp^2 des atomes de carbone liés par une double liaison éthylénique, qui ne permet pas l'approche suffisante du carbanion par l'oxoanion, soit l'une de causes qui empêchent la fermeture d'un cycle de cinq atomes. On peut envisager les mêmes considérations pour le composé azabicyclique XI qui lui aussi n'a pas été obtenu.

Le caractère dipolaire du produit VI a été toutefois mis en évidence par sa participation directe aux réactions de cycloadditions 1,3-dipolaires. En présence d'agents diénophyliques énergiques tels que l'anhydride maléique et le N-phényl-maléimide la formation d'une structure carbanionique VI à partir du mésomère VI$_d$, qui est seule capable de former par cycloaddition un noyau de cinq atomes, devient possible XII$_a$, XII$_b$. On observe que dans ce cas, les formes énol-bétaïniques de type VI$_b$ devraient donner naissance à un cycle de sept atomes dont la formation est difficile à réaliser tenant compte des raisons stériques.

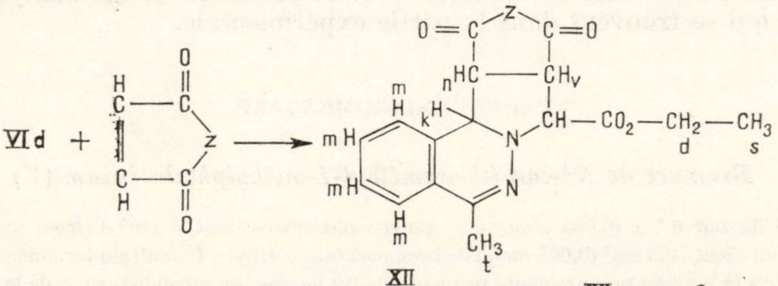
VI d
Z
m H
k H
n HC
CH v
CH—CO₂—CH₂—CH₃
d
s
N
CH₃
t

XII

XII a Z=O
XII b Z=N—Ph

D'une façon analogue sous l'action de l'acétylènedicarboxylate de méthyle il se forme, par suite d'une cycloaddition suivie par un processus de déhydrogénation, le cycloadduct XIII.

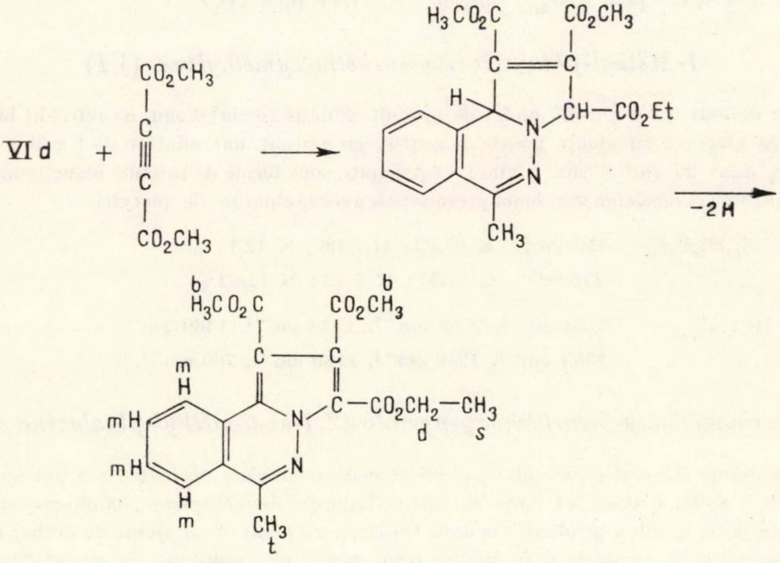
VI d
CO₂CH₃
H₃CO₂C
CO₂CH₃
CH—CO₂Et
N
CH₃
−2H
b
C—CO₂CH₂—CH₃
d
s
m H
t

XIII

Les mêmes produits de cycloaddition, XII_a, XII_b et XIII ont été obtenus avec l'ylure *in situ* à partir du sel quaternaire de cycloimmonium V en présence de triéthylamine et des agents philodiéniques susmentionnés. Le fait qu'on obtient les mêmes produits à partir de l'ylure VI et du sel V constitue un argument en plus en faveur de la structure dipolaire du composé VI.

La structure des produits de cycloaddition XII_a, XII_b et XIII a été mise en évidence à l'aide des spectres IR, RMN et des analyses chimiques qui se trouvent dans la partie expérimentale.

PARTIE EXPÉRIMENTALE

Bromure de N^3-carbéthoxyméthyl-1-méthylphtalazinium (V)

On dissout 0.7 g (0.005 mole) de méthyl-1-phtalazine dans 30 cm³ d'alcool méthylique absolu et on ajoute 0,6 cm³ (0,005 mole) de bromoacétate d'éthyle. L'addition terminée on laisse le mélange à la température ambiante pendant 10 – 12 heures. Au refroidissement de la solution on ajoute de l'éther éthylique jusqu'à la précipitation complète du sel quaternaire. Produit beige, p.f. 165° (avec décomposition), rend. 70 %.

Analyse : $C_{13}H_{15}O_2N_2Br$ *Calculé* : C 50,16 ; H 4,82 ; N 9,00 %
P.M. 311 *Trouvé* : C 49,82 ; H 4,94 ; N 9,34 ; 9,30 %.

RMN : Triplet $\delta = 1{,}35$ ppm ($3H_s$), J = 7,5 cps ; singlet $\delta = 3{,}17$ ppm ($3H_t$) ; quadruplet $\delta = 4{,}35$ ppm ($2H_d$), J = 7,5 cps ; singlet $\delta = 6{,}12$ ppm ($2H_1$) ; multiplet central à $\delta = 8{,}7$ ppm ($4H_m$) ; singlet $\delta = 11{,}84$ ppm (H_k).

1-Méthyl-phtalazinium-carbéthoxyméthylure (VI)

On dissout 0,7 g (0,0025 mole) de produit V dans 20 cm³ d'eau, on refroidit la solution avec de la glace et on ajoute goutte à goutte, en agitant, une solution de 1 g (0,0025 mole) de K_2CO_3 dans 20 cm³ d'eau. L'ylure VI précipite sous forme de produit blanc jaunâtre. P.f. 125°. Rend. 50 %. Coloration vert foncé presque noir avec le chlorure de picryle.

Analyse : $C_{13}H_{14}O_2N_2$ *Calculé* : C 67,82 ; H 6,08 ; N 12,17 %
Trouvé : C 67,31 ; H 6,23 ; N 12,62 %.

Spectres IR : ν'_{max} : 3480 cm^{-1}, 2998 cm^{-1}, 1728 cm^{-1}, 1460 cm^{-1},
1385 cm^{-1}, 1240 cm^{-1}, 1180 cm^{-1}, 760 cm^{-1}.

1,2-Dicarbométhoxy-3-carbéthoxy-pyrrolo-(2,1-a)-6-méthyl-phtalazine (XIII)

On ajoute 0,7 cm³ (0,005 mole) d'acétylènedicarboxylate de méthyle à une solution de 1,1 g (0,005 mole) d'ylure VI dans 40 cm³ de chlorure de méthylène ; on observe un échauffement ; on porte à reflux pendant 3 heures. On laisse refroidir et on ajoute de l'éther éthylique jusqu'à précipitation complète d'un produit brun rougeâtre. Le produit est recristallisé dans de l'alcool méthylique. Cristaux blancs fusibles à 143°. Rend. 30 %.

Le même produit peut être obtenu comme suit : on ajoute 0,7 cm³ (0,005 mole) d'acétylène dicarboxylate de méthyle et 0,7 cm³ (0,005 mole) de triéthyl-amine et à une suspension de 1,4 g (0,005 mole) de bromure de N-carbéthoxy méthyl-1-méthyl-phtalazinium dans 40 cm³ de chlorure de méthylène.

Analyse : $C_{19}H_{18}O_6N_2$: *Calculé* : C 61.62 ; H 4,86 ; N 7,56 ;
Trouvé : C 61,70 ; 61,34 ; H 5,08, 5,05 ; N 7,86 %.

RMN : Triplet $\delta = 1{,}41$ ppm ($3H_s$), $J = 7{,}5$ cps ; singlet $\delta = 2{,}78$ ($3H_t$) ; singlet $\delta = 3{,}88$($6H_b$) ; quadruplet $\delta = 4{,}4$ ($2H_d$), $J = 7{,}5$ cps ; multiplet $\delta = 7{,}65$ ($4H_m$).

1,2-anhydride de l'acide 3-carbéthoxy-10bH-pyrolino-(2,1-a)-6-méthyl-phtalazine-1,2-dicarboxylique (XII_a), $Z = 0$

A une solution de 1,15 g (0,005 mole) d'ylure VI dans 30 cm³ de chlorure de méthylène on ajoute une solution de 0,5 g (0,005 mole) d'anhydride maléique dissous dans 10 cm³ de chlorure de méthylène. On porte à reflux le mélange réactionnel pendant 2 heures. On chasse la plus grande partie du solvant. Au refroidissement de la solution le produit brut se sépare quantitativement ; on recristallise dans du benzène. Produit blanc, p.f. 159–160°, rend. 40 %

Le même produit a été obtenu à partir du sel V.

Analyse : $C_{17}H_{16}N_2O_5$ *Calculé* : C 62,19 ; H 4,93 ; N 8,53 %
Trouvé : C 62,14 ; H 5,15 ; N 8,45 %.

Spectres IR ν'_{max} : 3200 cm^{-1} : 1835 cm^{-1}, 1755 cm^{-1}, 1730 cm^{-1}, 1463 cm^{-1}, 1378 cm^{-1}, 1222 cm^{-1}, 1200 cm^{-1} ; 1075 cm^{-1}, 1035 cm^{-1}, 958 cm^{-1}, 921 cm^{-1}.

RMN : Triplet $\delta = 1{,}34$ ppm ($3H_s$), $J = 7{,}5$ cps ; singlet $\delta = 2{,}18$ ppm ($3H_t$) ; triplet $\delta = 3{,}6$ ppm ($1H_v$), $J = 8{,}5$ cps ; doublet $\delta = 4{,}1$ ppm ($1H_n$), $J = 8{,}5$ cps ; quadruplet $\delta = 4{,}3$ ppm ($2H_d$), $J = 7{,}5$ cps ; doublet $\delta = 4{,}82$ ppm ($1H_1$), $J = 8{,}5$ cps ; singlet $\delta = 5{,}21$ ppm ($1H_k$) ; multiplet $\delta = 7{,}47$ ppm ($4H_m$).

Il résulte que l'angle diédrique entre H_k et H_n a une valeur approximative de 90°, donc J = O. La constante de couplage entre H_1 et H_v étant égale à celle entre H_n et H_v on obtient un triplet pour H_v.

N-phényl-imide de l'acide 3-carbéthoxy-10bH-pyrolino-(2,1-a)-6-méthyl-phtalazine-1,2-dicarboxylique (XII_b). $Z = -N-C_6H_5$

On dissout 0,7 g (0,0025 mole) de bromure de N³-carbéthoxy-méthyl-1-phtalazinium dans 30 cm³ de chlorure de méthylène, on ajoute une solution de 0,4 g (0,0025 mole) de N-phénylmaléimide dans 10 cm³ de chlorure de méthylène et 0,3 cm³ (0,0025 mole) de triéthylamine. On porte à reflux le mélange pendant 4 heures. On laisse refroidir et on extrait à l'eau le bromhydrate de la triéthylamine. On sèche ensuite la solution de chlorure de méthylène sur du Na_2SO_4 sicc. et on chasse le solvant. Le produit brut brun obtenu est recristallisé dans du benzène. On obtient un produit blanc p.f. 168–9°, rend. 40 %.

Analyse : $C_{23}H_{21}N_3O_4$: *Calculé* : C 68,48 ; H 5,21 ; N 10,42 %
Trouvé : C 68,58 ; H 5,85 ; N 10,50 %.

Spectres IR : ν'_{max} : 3000 cm^{-1}, 1775 cm^{-1}, 1707 cm^{-1}, 1737 cm^{-1}, 1505 cm^{-1}, 1388 cm^{-1}, 1234 cm^{-1}, 1175 cm^{-1}, 1040 cm^{-1}, 980 cm^{-1}, 957 cm^{-1}.

RMN : Triplet $\delta = 1{,}35$ ppm ($3H_s$), $J = 7{,}5$ cps ; triplet $\delta = 3{,}58$ ppm ($1H_v$), $J = 8{,}5$ cps ; doublet $\delta = 4$ ppm ($1H_n$), $J = 8{,}5$ cps ; quadruplet $\delta = 4{,}35$ ppm ($2H_d$), $J = 7{,}5$ cps ;

doublet $\delta=4{,}95$ ppm ($1H_b$), $J=8{,}5$ cps ; singlet $\delta=5{,}3$ ppm ($1H_k$) ; multiplet central à $\delta=7{,}43$ $9H_m$.

Il résulte que l'angle diédrique entre H_k et H_n a une valeur approximative de 90° donc J=O. La constate de couplage entre H_1 et H_v étant égal à celle entre H_n et H_v on obtient un triplet pour H_v.

RMN : triplet, δ = 1,41 ppm (CH$_3$, J = 7 Hz) ; singlet, δ = [illegible] ; [illegible], δ = [illegible] ; quadruplet, δ = [illegible] (CH$_2$, J = 7 Hz) ; [illegible].

[illegible] de l'acide 3-carbéthoxy-10bH-pyrazolo-[illegible]-1,2-dicarboxylique (VII, 1, R = [illegible])

[illegible] solution de [illegible] mole [illegible] une solution de [illegible] dans [illegible]. On porte à reflux [illegible] mélange [illegible] pendant [illegible] heure. On [illegible] le produit [illegible] dans [illegible] et on obtient [illegible].

Analyse : [illegible] Calculé : C [illegible] ; H [illegible] ; N [illegible]

Trouvé : C [illegible] ; H [illegible] ; N [illegible]

Spectre IR [illegible] : [illegible] cm^{-1} ; [illegible] cm^{-1} ; [illegible] cm^{-1} ; [illegible]

RMN : [illegible] δ = [illegible] ppm (CH$_3$, J = 7 Hz) ; singlet, δ = [illegible] ; [illegible] ; quadruplet, δ = [illegible] ; doublet, δ = [illegible] ; [illegible].

Il résulte que l'angle dièdrique entre H$_1$ et H$_2$ a une valeur voisine [illegible] de 90°, [illegible]. La constante de couplage entre [illegible] et [illegible] [illegible] on obtient [illegible] pour H$_2$.

N-phényl-imide de l'acide 3-carbéthoxy-10bH-pyrazolo-[illegible]-1,2-dicarboxylique (XII, 1, R = [illegible] C$_6$H$_5$)

On dissout [illegible] de N-carbéthoxy-[illegible] dans [illegible] de chlorure de méthylène, on ajoute une solution de [illegible] de N-phényl-maléimide dans 10 cm^3 de [illegible] et [illegible] On porte à reflux le mélange pendant [illegible] heures. On laisse refroidir et on [illegible] de la [illegible]. On sèche ensuite la solution de chlorure de méthylène sur du Na$_2$SO$_4$ sec et on chasse le solvant. Le produit brut [illegible] est recristallisé dans le [illegible]. On obtient un produit [illegible] F. [illegible] ; Rendement [illegible] %.

Analyse : [illegible] Calculé : C [illegible] ; H [illegible] ; N [illegible]

Trouvé : C [illegible] ; H [illegible] ; N [illegible]

Spectre IR [illegible] : [illegible] cm^{-1} ; [illegible] cm^{-1} ; [illegible] cm^{-1} ; [illegible] cm^{-1} ; [illegible] cm^{-1} ; [illegible] cm^{-1} ; [illegible] cm^{-1} ; [illegible] cm^{-1}.

RMN : Triplet δ = [illegible] ppm (CH$_3$, J = 7 Hz) ; triplet δ = [illegible] ppm (CH, J = [illegible] cps) ; doublet δ = [illegible] ppm (CH, J = [illegible] cps) ; quadruplet δ = [illegible] ppm (CH$_2$, J = 7 cps) ;

doublet δ = [illegible] ppm (CH, J = [illegible] cps) ; singlet δ = [illegible] ppm (CH) ; massif centré à δ = [illegible] (H$_{ar}$).

Il résulte que l'angle dièdrique entre H$_1$ et H$_2$ a une valeur approximative de 90° [illegible]. La constante de couplage entre H$_2$ et H$_3$ [illegible] entre H$_2$ et H$_3$, on calcule [illegible] pour H$_3$.

[illegible]

Revue Roumaine de Chimie, 17, 1, 2, 405–410 (1972)

Dedicated to Professor I. G. MURGULESCU
on his 70th birthday

ELLIPSOMETRIC AND REFLECTANCE MEASUREMENTS FOR THE DETERMINATION OF OPTICAL PROPERTIES AND THICKNESS OF A LIGHT-ABSORBING THIN FILM

WOON KIE PAIK and JOHN O'M. BOCKRIS

Department of Chemistry University of Pennsylvania
Philadelphia, Penna. 19014

Received September 22, 1971

The ellipsometry is in difficulty for light absorbing films because there are three unknowns to be determined from only two equations. The measurement of the intensity change in addition to the conventional ellipsometric data, Δ and Ψ, enables to determine the optical constants and the thickness of a very thin conducting film.

INTRODUCTION

One of the powerful, broadly applicable, techniques of observing film covered surfaces (particularly those in solution) is ellipsometry. In ellipsometry, one measures the change in state of a polarized light on reflection from a surface. When a linearly polarized light is reflected from a surface at an oblique angle, the reflected beam is, in general, elliptically polarized, (hence, the name of the field).

Ellipsometry has been applied to the measurements of the optical constants of a material with a bare surface, the refractive index and thickness of a dielectric film, or of the thickness of a conducting film when its optical properties are known. The vigor of the workers involved in this field is evidenced by the two symposiums on the subject of ellipsometry held in the past decade[1,2] and the symposium on optical studies of adsorbed layers [3] held in 1970, as well as the numerous papers published recently.

However, in its conventional form, ellipsometry has been an insufficient technique for the measurement of thickness and optical constants of an unknown conducting film. The limitation comes from the fact that

---

[1] "Ellipsometry in the Measurement of Surfaces and Thin Films, Symposium Proceedings", E. Passaglia, R.R. Stromberg, and J. Kruger, Ed., Natl. Bur. Std. Misc. Publ. 256, Washington, D.C. 1964.

[2] "Proceedings of the Symposium on Recent Developments in Ellipsometry", N. Bashara, A. Buckman, and A. Hall ed., North Holland, 1969. see also *Surface Sci.*, **16**, 1–446 (1969).

[3] "Optical Studies of Adsorbed Layers at Interfaces, Reading Symposium", Faraday Society, 1970.

the measured change of polarization state gives us *two* equations, while there are *three* unknown variables to be determined; the thickness and the real and imaginary parts of the optical constant of the film, $n_f = n - i\,k$.

Therefore, in attacking problems involving electronically conducting films, such as surface films on metals which are frequently encountered in electrochemical systems, arbitrary assumptions or auxiliary measurements had to be made to obtain the information on the film, even approximately.

It is the purpose of this paper to explain how some recent improvements on this optical technique made by the authors[4] have resolved this difficulty.

THEORY

The propagation of any polarized light can be described by the behavior of the two mutually perpendicular components of the light.

The component that is parallel to the plane of incidence is reflected at an interface between the ith and j^{th} medium with the reflection coefficient, $r_{ij}^{\parallel}$, given by the Fresnel equation,

$$r_{ij}^{\parallel} = \frac{n_i \cos \Phi_j - n_j \cos \Phi_i}{n_i \cos \Phi_j + n_i \cos \Phi_i} \tag{1}$$

where n_i and n_j are the refractive index of the ith and j^{th} medium respectively,. Φ's are the angles of incidence in those mediums. The Fresnel reflection coefficient for the component that is perpendicular to the plane of incidence is:

$$r_{ij}^{\perp} = \frac{n_j \cos \Phi_j - n_i \cos \Phi_i}{n_j \cos \Phi_j + n_i \cos \Phi_i} \tag{2}$$

When light is incident from a transparent medium, medium 1, onto medium 3 covered with a film of medium 2, the two components are reflected with the resultant reflection coefficients given as follows:

$$r^{\parallel} = \frac{r_{12}^{\parallel} + r_{23}^{\parallel} \exp(-iD)}{1 + r_{12}^{\parallel} r_{23}^{\parallel} \exp(-iD)} \tag{3}$$

$$r^{\perp} = \frac{r_{12}^{\perp} + r_{23}^{\perp} \exp(-iD)}{1 + r_{12}^{\perp} r_{23}^{\perp} \exp(-iD)} \tag{4}$$

---

[4] W. Paik and J. Bockris, to be published in *Surface Sci.*

where D is related to the thickness of the film, τ and the wavelength, λ, of the light as

$$D = (4\pi \tau n_2/\lambda) \cos \Phi_2 \tag{5}$$

When the medium 2 or 3 is light absorbing, the n's and Φ's are complex numbers in those mediums. Thus, for a light-absorbing film, $n_2 = n - i$ where $i = \sqrt{-1}$. The complex angles Φ's are defined by :

$$n_1 \sin\Phi_1 = n_2 \sin\Phi_2 = n_3 \sin\Phi_3 \tag{6}$$

where Φ_1 is the (real) angle of incidence in the transparent medium.

Each of $r^{\parallel}$ and $r^{\perp}$ is, therefore, a complex function, i.e.,

$$r^{\parallel} = |r^{\parallel}| e^{i\delta_{\parallel}} \tag{7}$$

$$r^{\perp} = |r^{\perp}| e^{i\delta_{\perp}} \tag{8}$$

Their phase shifts, $\delta_{\parallel}$ and $\delta_{\perp}$, cannot be determined, but the relative phase shift, $\Delta = \delta_{\parallel} - \delta_{\perp}$, can be measured by an ellipsometer.

Therefore, conventional ellipsometry consists of measurement of the parameters Δ and ψ defined by the ratio of $r^{\parallel}$ to $r^{\perp}$:

$$\tan \psi \cdot e^{i\Delta} = \frac{r^{\parallel}}{r^{\perp}}, \tag{9}$$

$\tan\psi$ being the ratio of the absolute magnitudes of the two reflection coefficients. Formula (9) consists in fact of two equations since both sides have real and imaginary parts. Thus,

$$\tan\psi \cos \Delta = \text{Real}\left(\frac{r^{\parallel}}{r^{\perp}}\right) \tag{9a}$$

$$\tan\psi \sin \Delta = \text{Imag}\left(\frac{r^{\parallel}}{r^{\perp}}\right) \tag{9b}$$

We will concern ourselves here with the cases where all the n's for the 1st and 3rd medium as well as the angle of incidence in the first medium are known and n_2 and τ of the film is to be determined from observation. Where the film is not light-absorbing, i.e., k is zero, as is the case with the dielectric films, there are only two unknowns, n and τ, to be determined. Determination of n and τ is, in this case, straightforward if Δ and ψ are measured since we have two simultaneous equations (9a) and (9b), although the actual calculation requires the setting up of a computer programme.

It is when k is non-zero or unknown that the ellipsometry is in difficulty because there are *three* unknowns to be determined from only *two* equations.[5–8] Each of equations (9a) and (9b) is a function of three unknown variables, n, k, and τ.*

Here, we notice the fact that there are three measurable quantities $|r^{\parallel}|$, $|r^{\perp}|$ and Δ, each of which is a function of n, k and τ, but that a sacrifice is made in the number of measurable quantities, and hence in the number of usable equations, because only the *ratio* $|r^{\parallel}|/|r^{\perp}|$ ($= \tan \psi$) is taken along with Δ.

Therefore, if we measure $|r^{\parallel}|$ and $|r^{\perp}|$, along with Δ, we have three simultaneous equations, which are sufficient for the determination of n, k and τ. A better alternative is to measure the reflection coefficient of the total light instead of the two components, and to measure ψ and Δ. When the azimuth of the incident beam is 45°, as is usual in ellipsometry, the recflection coefficient of the total light is an average of those of the two components, i.e.,[9]

$$|r|^2 = 1/2\,(|r^{\parallel}|^2 + |r^{\perp}|^2) \tag{10}$$

Therefore, equations (9a) (9b) and (10) are the convenient 3 equations to use : from them, the three unknown parameters can be obtained without resort to extra-ellipsometric techniques.

Variation of $|r|$ with n, k or τ can be measured by measuring the intensity change of the reflected beam since the intensity of the reflected light I is proportional to the square of $|r|$:

$$I = AI_i\,|r|^2 \tag{11}$$

and

$$\frac{\delta(|r|^2)}{|r|^2} = \frac{\delta I}{I} \tag{12}$$

where I_i is the intensity of the incident beam and A is the attenuation constants due to the optical elements in the path.

CONSIDERATIONS OF EXPERIMENTAL CONDITIONS

The usual practice in ellipsometry is to use an angle of incidence that is near the principal angle of incidence where the sensitivity in Δ measurement is greatest. However, the change in the reflectance is usually very small at such an angle. One can calculate the changes in Δ, ψ and $|r|$

---

[5] F.L. McCrackin and J.P. Coulson, in ref. 1.

[6] R.J. Archer, *J. Electrochem. Soc.*, **104**, 619 (1957).

[7] J.O'M. Bockris, A.K.N. Reddy and B. Roa, *ibid.*, **113**, 1132 (1966).

[8] R.S. Sirohi and M.A. Genshaw, *ibid.*, **116**, 910 (1969).

* Of course, by taking two different angles of incidence, two more equations can be generated. However, McCrackin and Coulson[5] showed that it is impractical to use the method of multiple angle of incidence. It is too insensitive.

[9] M. Born and E. Wolf, "Principles of Optics", Pergamon Press, 1965.

for a hypothetical film with assumed values of n, k and τ as functions of angle of incidence. Such a preliminary calculation guides the proper choice of the angle of incidence at which variation in $|r|$ is large enough for experimental determination with reasonable accuracy with a small sacrifice in the sensitivity in Δ. For example, a calculation[4] for cobalt surface immersed in an aqueous solution showed that a presence of a surface film of refractive index of $2.6 - i\ 0.4$ would give about 1.5% decrease in reflected light intensity, and 2.2° and 0.17° decreases in Δ and ψ respectively, at the angle of incidence of 58°. At an angle of incidence that is near the principal angle ($\sim 75°$), the change in $|r|$ would be an order of magnitude smaller and accurate measurement would have been impossible.

Unlike conventional ellipsometry, where only Δ and ψ are measured, well stabilized light sources and intensity measuring equipments, e.g. photomultiplier tubes, and a regulated power supply in a well thermostated environment, are required.

In conclusion, a measurement of the intensity change in addition to the conventional ellipsometric data, Δ and ψ enables us to determine the optical constants and the thickness of a very thin conducting film. This approach should be particularly useful for thin films that cannot grow continuously or change their structural and electronic properties as they grow, since other approaches fail for such cases.

ACKNOWLEDGEMENTS. This work was financially supported by the Office of Naval Research, Contract No. N00014-67-0216-0016. The authors are thankful for helpful discussions with Dr. J. Kruger and Mrs. C. L. McBee.

Revue Roumaine de Chimie, 17, 1, 2, 411–420 (1972)

Dedicated to Professor I. G MURGULESCU
on his 70th birthday

SHORT-LIVED FREE RADICALS IN AQUEOUS SOLUTIONS OF PURINES

CLAUDE NICOLAU

Department of Molecular Biology, Faculty of Medicine, University of Craiova, Romania

Received November 2, 1971

Following reaction with chemically generated OH radicals in a flow-system, paramagnetic transients were detected by means of ESR spectroscopy, in aqueous solutions of purines. The adducts formed were addition products at C (8) in the imidazole ring. The same type of adducts were observed when amino radicals instead of OH radicals were reacted with the organic molecules. Aliphatic alcohol free radicals were generated by reaction with OH' and then subsequently reacted with caffeine. The splitting constants and g-factors together with computer simulation of the ESR spectra allowed the elucidation of the structure of the adducts and of their mechanism of formation. In the same three-way flow system the fast reaction of molecular repair of free radicals by sulfhydryls and disulfides were followed and their mechanism discussed.

The radiation damaging of biochemical and biological structures occurs through a direct and an indirect mechanism.[1] Both cases show common features, but there are also a number of specific aspects which are worthwhile investigating. The direct effect of radiation on biomolecules has been extensively investigated[2,3] while the indirect one received more recently special attention, mainly due to pulse-radiolysis techniques.[4]

The development of flow techniques, used in conjunction with Electron Paramagnetic Resonance (EPR) spectroscopy allowed a direct assay of the short-lived paramagnetic species arising during radiolysis of aqueous systems or in sytesms simulating them.

Among the main products of water radiolysis are $OH^{\cdot}$ radicals and Θ_{aq}^{-}, hydrated electrons, both of which are exceptionally reactive towards organic molecules. A number of systems have been devised in order to produce $OH^{\cdot}$ radicals under controlled conditions.

---

[1] H. Dertinger and H. Jung, "Molecular Radiobiology", Springer Verlag, New York, 1971.

[2] A Müller, *Progr. Biophys. Mol. Biol.*, **17**, 101 (1961).

[3] W. Gordy, *Ann. New York Acad. Sci.*, **161**, 100 (1969).

[4] G.E. Adams and B.D. Michael, in "Energetics and Mechanisms in Radiation Biology", ed. by G.O. Phillips, Academic Press, London, New York, 1968, p. 333.

We have been using the Dixon-Norman system[5] consisting of a titanous salt reacted with hydrogen peroxide according to the reaction :

$$Ti^{+3} + H_2O_2 \rightarrow Ti^{+4} + OH^{\cdot} + OH^-$$

The hydroxyls thus produced were reacted in a flow system with a number of biomolecules, such as amino acids,[6,7] pyrimidine,[7,8,9] nucleosides,[9] all of which yielded paramagnetic species, whose identification became possible due to their EPR spectra. The experimental methods are described elsewhere.[8,10]

Not only free radicals produced during the attack of various biomolecules with $OH^{\cdot}$ or NH_2 radicals ($T_i^{+3} + NH_2OH \rightarrow Ti^{+4} + NH_2 + OH^-$) were investigated, but also the fast reactions underlying the mechanism of molecular repair by sulfhydryls and disulfides.[10] This molecular repair or restitution — when the initial chemical structure may be restored — is the first step in chemical radioprotection. In order to simulate this phenomenon, a three-way flow system was used, where through arms 1 and 2 the abstraction or addition radical of the biomolecule was produced and mixed about 20 ms later with the sulfhydryl or disulfide solution flowing through arm 3.[10]

In another series of three-way flow experiments, through arms 1 and 2 $OH^{\cdot}$ and alcohols were flowed (CH_3OH, C_2H_5OH, $i-C_3H_7OH$) so as to produce the abstraction alcohol radicals. These radicals were mixed, about 20 ms later with a 10^{-2} M aqueous solution of caffeine flowing through arm 3. Addition radicals were produced which will be discussed further below.

a) OH AND NH_2 ADDUCTS

The purines, as a whole, show definitely lower reactivities towards $OH^{\cdot}$ and $NH_2^{\cdot}$ than do pyrimidines. Caffeine (1, 3, 7-trimethyl purine) yielded, nevertheless, clear-cut spectra of adducts with those radicals. When reacted with $OH^{\cdot}$ it showed an overlapping doublet of quintets due to interaction with one proton and two nitrogens (fig. 1).

The splitting by the β-proton was 28.5 G and that by $N_{(9,7)}$ 9.5 G. The g-factor value is within the expected limits for such a type of radical. The adduct with HN_2 shows a splitting of 9 lines with the intensity-ratios 1:2:3:2:2:2:3:2:1 suggesting an interaction with two equally coupled N's and one proton. The splittings are $a_H = 31$ G and $a_N = 7.7$ G.

---

[5] W.T. Dixon and R.O.C. Norman, *J. Chem. Soc.*, **1963**, 3119.

[6] W.A. Armstrong and W.G. Humphreys, *Canad. J. Chem.*, **45**, 2589 (1961).

[7] H. Paul and H. Fischer, *Ber. Bunsengesellschaft Phys. Chem.*, **73**, 972 (1969).

[8] Cl. Nicolau, M. McMillan and R.O.C. Norman, *Biochim. Biophys. Acta*, **174**, 413 (1969).

[9] H. Dertinger and Cl. Nicolau, *Biochim. Biophys. Acta*, **199**, 316 (1970).

[10] Cl. Nicolau and H. Dertinger, *Radiation Res.*, **42**, 62 (1970).

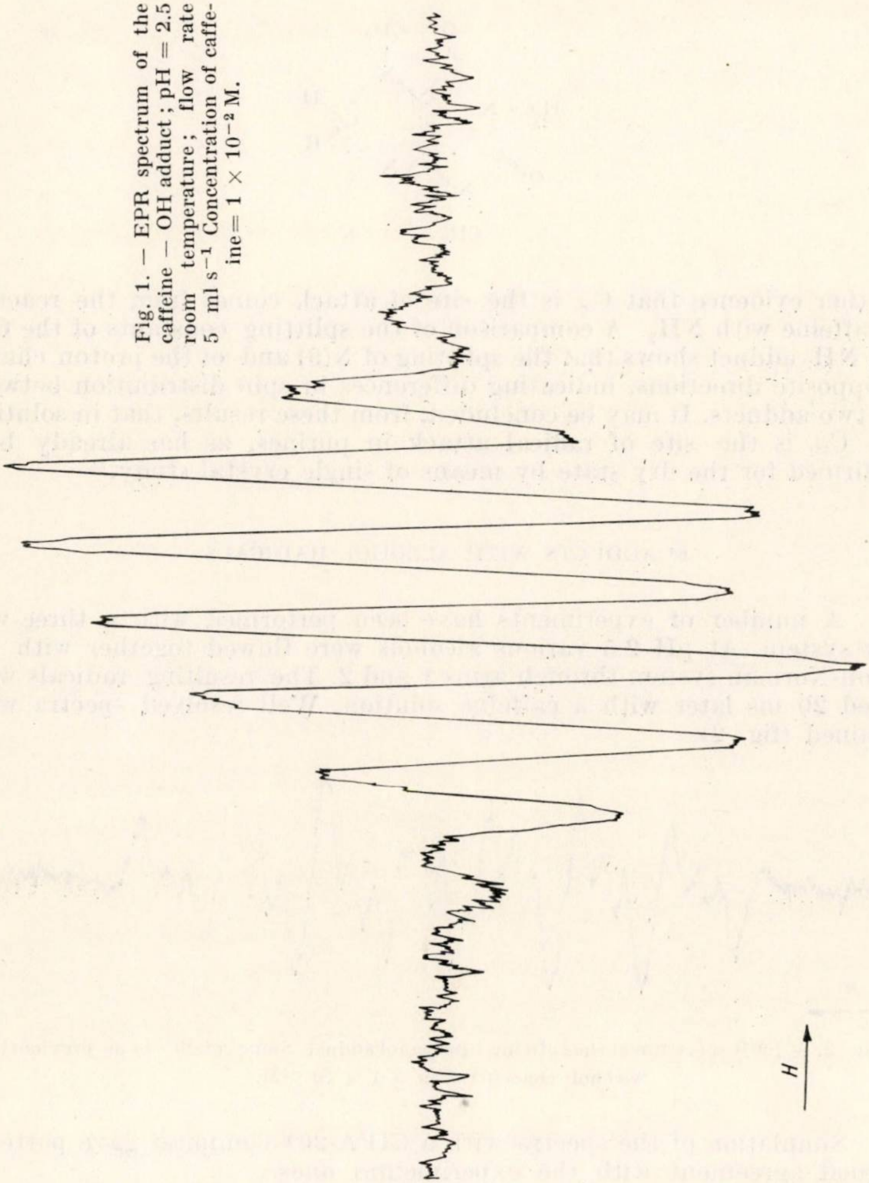

Fig. 1. – EPR spectrum of the caffeine – OH adduct ; pH = 2.5 room temperature ; flow rate 5 ml s^{-1} Concentration of caffeine = 1 × 10^{-2} M.

Both spectra are attributed to $C_{(8)}$ adducts in which the unpaired spin is centered at $N_{(9)}$.

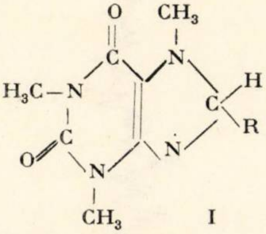

I

Further evidence that $C_{(8)}$ is the site of attack comes from the reaction of caffeine with NH_2. A comparison of the splitting constants of the $OH^{\cdot}$ and $NH_2^{\cdot}$ adduct shows that the splitting of N(9) and of the proton change in opposite directions, indicating differences in spin distribution between the two adducts. It may be concluded, from these results, that in solution, too, $C_{(8)}$ is the site of radical attack in purines, as has already been confirmed for the dry state by means of single crystal study.[11]

b) ADDUCTS WITH ALCOHOL RADICALS

A number of experiments have been performed with a three-way flow system. At pH 2.5 various alcohols were flowed together with the Dixon-Norman system through arms 1 and 2. The resulting radicals were mixed 20 ms later with a caffeine solution. Well resolved spectra were obtained (fig. 2).

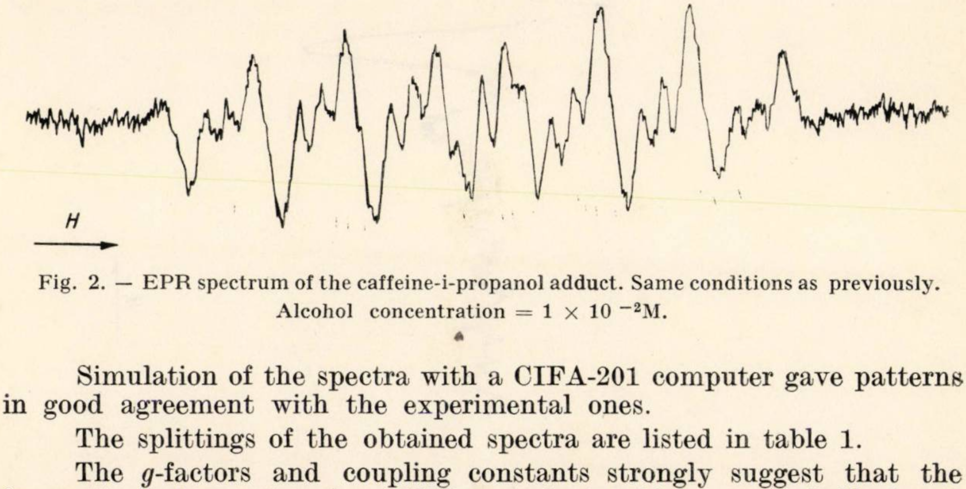

Fig. 2. — EPR spectrum of the caffeine-i-propanol adduct. Same conditions as previously. Alcohol concentration = 1 × 10^{-2}M.

Simulation of the spectra with a CIFA-201 computer gave patterns in good agreement with the experimental ones.

The splittings of the obtained spectra are listed in table 1.

The *g*-factors and coupling constants strongly suggest that the free radicals detected ar $C_{(8)}$ addition products which are, probably intermediates in a longer reaction sequence. Attack with OH· of the alcohols lead to the formation of the known radical :

---

[11] C. Alexander and W. Grody, *Proc. Nat. Acad. Sci. U.S.A.*, **58**, 1279 (1967).

$$(CH_3)_2\,CHOH + OH^{\cdot} \rightarrow (CH_3)_2\,\dot{C}OH + HOH$$

and smaller amounts of a radical resulted from hydrogen abstraction at the methyl.

Table 1

g-factors and spllitting (gauss) of the EPR spectra shown by the adducts of caffeine with· CH_2 OH and with ·C $(CH_3)_2$ OH

Adduct	H(8)	N(9)	(N(7)	(N(1)	CH_2	*g*-factor
with $\dot{C}H_2OH$	31	9.5	9.5		4	2.0028
with $\dot{C}(CH_3)_2OH$	30	9.5	9.5	3		2.0030

Reaction with caffeine leads then to the following adduct :

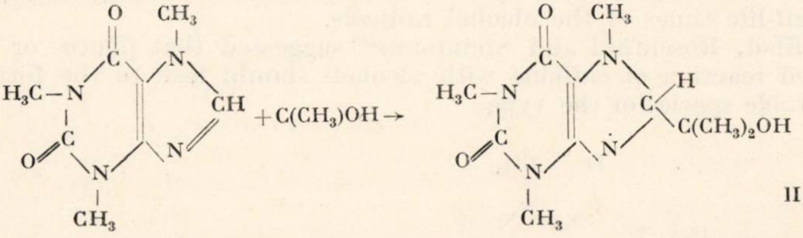

II

The splitting from $H_{(8)}$ of 30 gauss is in good agreement with the values found in the NH_2 and OH· adducts of caffeine.[9] It is the kind of value one would expect for a β-proton. The same holds for the $N_{(9)}$ splitting, but a number of new features appear regarding the other splittings.

For instance, in the methanol adduct :

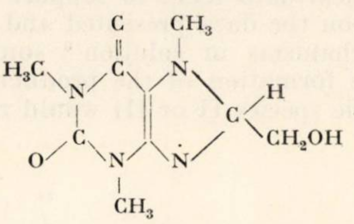

III

a splitting of 4 gauss is observed in a 1 :2 :1 pattern superimposed on the main splitting. This has been assigned to the methylene protons added at $C_{(8)}$ and such a value for this splitting is normal. The spectrum is much alike that of the OH adduct.

In the i-propanol adduct a number of new observations were made. First the two imidazole nitrogens show equivalent splittings (9.5 gauss).

The equivalence of the $N_{(7)}$ and N(9) splittings is somewhat surprising since $N_{(7)}$ is substituted; substitution, in the case of deoxyadenosine led to widely differing couplings of the two nitrogens in the $C_{(8)}$ addition radical.[12]

The difference between the coupling constants both of the two nitrogens and of the CH_2 hydrogens in guanine and adenosine was accounted for by Gordy[3] as being evidence for the non-identity of the radicals obtained with the two bases. While in the case of guanine a $C_{(8)}$ adduct is being postulated, in that of adenosine a $C_{(2)}$ adduct was held responsible for the appearance of ESR spectra.[3,11,12]

In caffeine reacted with CH_2OH or with $C(CH_3)_2OH$, $C_{(8)}$ adducts are found. This affirmation is supported by the splitting of the $C_{(8)}H$ hydrogen (28—31 gauss) which can be hardly accounted for in another way.

In the i-propanol adduct a third nitrogen splitting (3 gauss) was observed; it is not possible to account for it, unambigously at present.

The paramagnetic species, resulted from the reaction of the alcohol radicals with caffeine have specific half-life times depending largely upon the half-life times of the alcohol radicals.

Elad, Rosenthal and Steinmaus[13] suggested that photo- or radio-induced reaction of caffeine with alcohols should lead to the formation of a stable species of the type

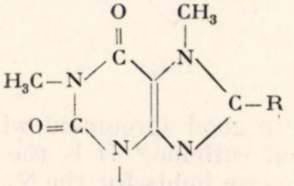

IV

$R=CA_2OH$, CH_2CH_2OH, etc.

NMR and chemical data seem to support this formulation of the end product. Based upon the data presented and on those concerning the molecular repair mechanisms in solution[10] some speculation might be allowed regarding the formation of the product.

The paramagnetic species II or III would react with further alcohol radicals to give:

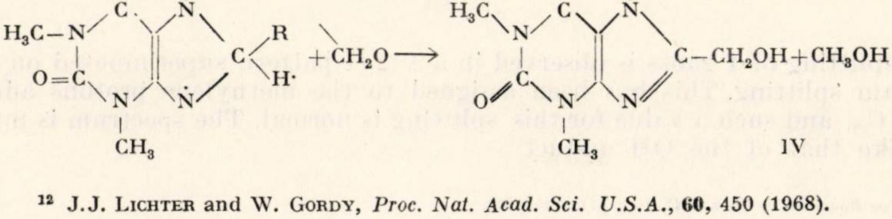

---

[12] J.J. Lichter and W. Gordy, *Proc. Nat. Acad. Sci. U.S.A.*, **60**, 450 (1968).

An alternative possibility would be :

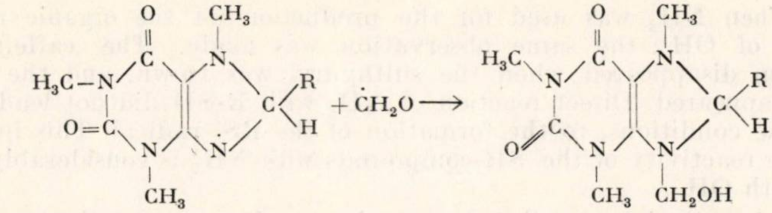

V

Besides being sterically and energetically not favoured, the formation of V may be ruled out by the D-exchange experiments of Elad et al.[14] showing that there were no exchangeable protons in the purine ring of the adduct. Should V have been formed one exchangeable proton would have been observed. The same held for other adducts, like adenosine-2-propanol.[14]

Of course, a last alternative should not be forgotten, namely the abstraction of $H_{(8)}$ by remaining, unreacted $OH^{\cdot}$ radicals. Anyway, their concentration should be quite low since they :

a) reacted with alcohols,

b) had a rather long dead time before coming in contact with the caffeine solution (20 ms),

c) could have still reacted with caffeine ($k \sim 10^{9}\ mol^{-1}\ s^{-1}$).

Even if, despite all that the hydroxyls could have reacted with II or III, this could hardly have been the case in the UV experiments of Elad and his associates. [13,14]

With purine, things seem to look differently. Linschitz and Connolly[15] showed, based upon spectrophotometric and NMR evidence, that alcohols add photochemically to purine at position 6. Experiments are in progress now, in our laboratory we investigate the structure of the paramagnetic adduct of purine reacted with alcohol radicals.

c) MOLECULAR REPAIR MECHANISMS [10]

I. *Repairing by RSH compounds*

If the solution containing the SH-compound was introduced after the reaction of the $OH^{\cdot}$ radicals with the target organic molecule in a three-way flow experiment, two characteristic observation were made :

1. The ESR spectrum of the organic radicals produced by $OH^{\cdot}$ attack disappeared completely.

2. The triplet pattern of the sulfur radical ($g = 2.0105$; $a_H = 90$ gauss) became observable.

---

[13] D. Elad, I. Rosenthal and H. Steinmaus, *Chem. Comm.*, **1969**, 305.

[14] H. Steinmaus, I. Rosenthal and D. Elad, *J. Amer. Chem. Soc.*, **91**, 4922 (1969).

[15] H. Linschitz and J.S. Connolly, *J. Amer. Chem. Soc.*, **90**, 2979 (1968).

This happens not only in the case of abstraction radicals [4] but also when adding radicals[10] like caffeine.

When NH_2 was used for the production of the organic radicals instead of $OH^{\cdot}$, the same observation was made. The caffeine-NH_2 spectrum disappeared when the sulfhydryl was flown, and the sulfur radical appeared. Direct reaction of NH_2 with R-SH did not lead under the same conditions, to the formation of the RS′ radical. This indicates that the reactivity of the SH-compounds with $NH_2^{\cdot}$ is considerably lower than with OH.

It is essential to notice that results 1 and 2 are not observed if the role of the organic and the SH-compounds is interchanged. This means that sulfur radicals, once produced, are not altered if the solution of the organic molecule is added after the reaction of the SH- compound with $OH^{\cdot}$ or NH_2.

II. *Repairing by R′SSR compounds*

The same set of experiments was also performed with the disulfides cystamine and cystine. The direct reaction of these two compounds with $OH^{\cdot}$ leads to the production of the same sulfur radical as in the case of the SH-compounds. With $NH_2^{\cdot}$, however, no signal could be observed. The reaction of the disulfides with the organic radicals produced by $OH^{\cdot}$ or $NH_2^{\cdot}$ attack does not lead to the production of the triplet signal as in the case of the sulfhydryls. The general observation made is that the spectrum of the organic radical disappears. In some cases especially in the experiments with $OH^{\cdot}$ hints of a signal seemed to appear, however, being neither entirely reproducible nor identifiable. This indicates that another reaction mechanism is working in this case.

In aqueous solutions the formation of the RS radical is due to the reaction :

$$RSH + OH^{\cdot} \rightarrow RS^{\cdot} + H_2O$$

The results of the three-way flow experiments with cysteine or cysteamine as the third reactant being the disappearance of the spectrum of the organic radical and the appearance of the sulfur triplet may be formulated in the following equation :

$$RSH + X^{\cdot} \rightarrow RS^{\cdot} + XH$$

In this case $X^{\cdot}$ is the organic radical produced by $OH^{\cdot}$ or $NH_2^{\cdot}$ attack. This means that the repair process effected by SH-compounds consists in the donation of a hydrogen atom to the organic radical.

The two typical reactions of OH radicals with organic molecules are abstraction of atomic hydrogen as in the case of alcohols (Dixon and Norman[5]) and addition to a double bond.[8] Our results indicate that hydrogen donation is independent of the radical to be repaired even if the radical is nitrogen centered as in the case of caffeine, where the unpaired spin is located at position $N_{(9)}$ of the imidazole ring. Finally, from the energetic point of view the hydrogen donation seems to be favoured by the relatively low energy of the SH bond (87–89 kcal/mole) as compared to the NH or CH bond.

SS-compounds

As already pointed out OH radicals react with cystine and cystamine to produce the radical RS·. However, no reaction with $NH_2^{\cdot}$ leading to a defined and detectable e.s.r. signal was observed. In contrast to the situation with SH compounds three-way flow experiments with disulfides did not lead to the detection of a RS·. signal. Only traces of such a signal could be observed in three-way experiments with OH· resulting probably from its direct reaction with the disulfide. However, the introduction of the SS-containing solution always led to a complete disappearance of the spectrum of the organic radical as observed with the SH compounds. This indicates that a repair mechanism different from that of the sulfhydryls is operating. Remembering that the experiments were performed at acid pH the following reaction sequence between the disulfide and the organic radical X· was suggested.[10]

$$RSSR + X^{\cdot} \rightarrow ([RSSR^{+}] + X^{-}$$

$$X^{-} + H^{+} \rightarrow XH$$

$$[RSSR^{+}] \rightarrow RS^{+} + RS^{\cdot}$$

In this reaction scheme the protecting mechanism is primarily an electron donation to the organic radical, the intermediate anion X^{-} being neutralized by the H^{+} ions to yield XH. This means that if X· is a hydrogen abstraction radical the disulfide under these conditions effects its repair as in the case of sulfhydryls. The radical RS· is, however, a secondary product resulting from the decay of the disulfenium cation $RSSR^{+}$.[16] The resulting low RS· concentration might explain why we fail to detect the triplet signal in the three-way flow experiments with disulfides (Nicolau and Dertinger).[9,10] In two -way flow experiments when the disulfides react directly with OH·, however, the RS radical reaches detectable concentrations. In this case the reaction scheme postulated above may be used replacing X· by OH·. These findings are in agreement with the mechanism proposed by Owen et al.[16] to describe the initiation of the radiolytic decay of aerated cystine solutions. Although the disulfenium cation is a paramagnetic species its ESR spectrum could not be observed. The reason for this might be the instability of this species which is assumed to decay yielding the sulfenium cation and the radical RS·.

---

[16] T.G. Owen, M. Rodriguez, B.G. Johnson and J.S.H. Roach, *J. Amer. Chem. Soc.*, **90**, 196 (1968).

The results reported are believed to be relevant for the problems of radioprotection. Compared with other techniques the flow method has the unique advantage that the loci of target radical formation and their reaction with the sulfur compounds are spatially and temporally separated. This is, in fact, necessary to confirm that the most significant property of the sulfur compound is really repair capability rather than ordinary scavenging ability

NOTE POUR LES AUTEURS

La *Revue Roumaine de Chimie* publie des articles en anglais, français, russe, allemand ou espagnol. Les auteurs sont priés d'envoyer des articles, notes, communications et comptes rendus inédits.

Les manuscrits seront dactylographiés à deux intervalles. Les tableaux seront dactylographiés sur feuilles séparées, de même que la légende des figures. Les diagrammes seront tracés à l'encre de Chine sur papier calque. Les tableaux et les figures seront numérotés par des chiffres arabes, en nombre strictement nécessaire. Prière de ne pas inscrire les mêmes données dans les tableaux et les figures. Les formules chimiques seront incluses dans le texte; en outre, elles seront transcrites sur des feuilles séparées. Les auteurs sont priés d'indiquer les caractères italiques (en soulignant les lettres au crayon), ainsi que tout autre caractère spécial. L'ordre des références bibliographiques sera celui de leur mention dans le texte; le nom de l'auteur sera précédé de l'initiale du prénom; les publications périodiques seront présentées suivant les prescriptions internationales. Les références seront ajoutées à la fin de l'article; elles paraîtront comme des notes, au bas de la page. Le texte sera précédé d'un résumé comprenant 15 lignes au maximum.

L'entière responsabilité du contenu des articles appartient aux auteurs. On publie des articles dus aux collaborateurs roumains ou étrangers. Les auteurs recevront 50 tirés à part.

PRINTED IN ROMANIA

TRAVAUX PARUS AUX ÉDITIONS DE L'ACADÉMIE DE LA RÉPUBLIQUE SOCIALISTE DE ROUMANIE

I. ZUGRĂVESCU et L. STOICESCU-CRIVETZ, **Polimeri heterociclici** (Polymères hétérocycliques), 1971, 190 p., 9,50 lei.

CORNEL BODEA et collab., **Tratat de biochimie vegetală**, partea I, **Fitochimie** (Traité de biochimie végétale, Ire partie, Phytochimie), Ier vol., 1964, 747 p. + 4 annexes + 2 pl., 41 lei ; IIe vol., 1965, 1962 pl., 1 pl., 56 lei ; IIIe vol., 1967, 773 p., 35 lei.

V. GHEȚIE et V. MICUȘAN, **Analiza imunochimică. Teorie și practică** (Analyse immunochimique. Théorie et pratique), 1966, 369 p., 28 lei.

SILVIA IONESCU, **Reacții chimice induse de radiațiile ionizante** (Réactions chimiques produites par les radiations ionisantes), 1963, 271 p., 15 lei.

MARIETA NICOLAE, **Fizico-chimia proceselor fotografice** (Physico-chimie des processus photographiques), 1964, 426 p. + 4 pl., 35 lei.

R. PORTOCALĂ et L. POPA, **Acizii ribonucleici celulari și virali** (Les acides ribonucléiques cellulaires et viraux), 1966, 375 p., 8 pl., 26 lei.

D. PURDELA et R. VÎLCEANU, **Chimia compușilor organici ai fosforului și ai acizilor lui** (La chimie des composés organiques du phosphore et de ses acides), 1965, 540 p., 37 lei.

CRISTOFOR SIMIONESCU, MARGARETA GRIGORAȘ et AGATA CERNĂTESCU-ASANDEI, **Chimia lemnului din R.P.R.** (La chimie du bois en Roumanie), 1964, 239 p. + 3 pl., 27 lei.

CRISTOFOR SIMIONESCU et CLEOPATRA VASILIU-OPREA, **Mecanochimia compușilor macromoleculari** (La mécanochimie des composés macromoléculaires), 1967, 344 p., 23,50 lei.

I.V. MAXIM, **Materiale nucleare** (Matériaux nucléaires), 1969, 444 4 pl., 30 lei.

1972 MAI 1

I.P.I. c. 310^{1}

43 426

Lei 25.—

F 1103

R

04-001

REVUE ROUMAINE DE CHIMIE

TOME 17
N° 3
Mars 1972

ÉDITIONS DE L'ACADÉMIE DE LA RÉPUBLIQUE SOCIALISTE DE ROUMANIE

Rev. Roumaine Chim.

17, 3, 421—592 (1972)

COMITÉ DE RÉDACTION

Rédacteur en chef :

I. G. MURGULESCU, membre de l'Académie de la République Socialiste de Roumanie

Rédacteurs en chef adjoints :

A. T. BALABAN et **V. E. SAHINI**, membres correspondants de l'Académie de la République Socialiste de Roumanie

Collège de rédaction :

C. DRĂGULESCU, RALUCA RIPAN, CR. SIMIONESCU, membres de l'Académie de la République Socialiste de Roumanie; **EM. BRATU**, membre correspondant de l'Académie de la République Socialiste de Roumanie; Pr G. **OSTROGOVICH, MARGARETA AVRAM, F. BADEA, I. D. MARCHIDAN, D. NEGOIU** et **D. SĂNDULESCU**

La *Revue Roumaine de Chimie* paraît 12 fois par an. Toute commande de l'étranger (fascicules ou abonnements) sera adressée à Întreprinderea Rompresfilatelia, Boîte postale 2001 Telex 011631 Bucarest, Roumanie

Les manuscrits, les livres et les revues proposés en échange, ainsi que toute correspondance seront envoyés à la rédaction :

REVUE ROUMAINE DE CHIMIE
23, str. Dumbrava Roşie, Bucarest, Roumanie

ÉDITIONS DE L'ACADÉMIE DE LA RÉPUBLIQUE SOCIALISTE DE ROUMANIE
3 bis, str. Gutenberg, Bucarest, Roumanie

REVUE ROUMAINE
DE
CHIMIE

ORSZÁGOS MŰSZAKI KÖNYVTÁR ÉS DOKUMENTÁCIÓS KÖZPONT 1883

Tome 17, N° 3 Mars 1972

	Page
I. G. MURGULESCU, TATIANA ONCESCU and S. G. IONESCU, On the photolysis of $[Mn(C_2O_4)_2(H_2O)_2]K$ in dimethylformamide. I	423–429
I. G. MURGULESCU and MARILENA ŞERBAN, On the viscosity of molten metals	431–440 R
LUCIA ODOCHIAN and I. A. SCHNEIDER, Some aspects of methane cracking kinetics in static conditions. III. The influence of the coal deposit . . .	441–445
RODICA VÎLCU and ST. PERIŞANU, Application of the Allen-Skinner bond energy scheme to aromatic hydrocarbons and to amines	447–453
V. PRISSIAJNYI and V. VASILESCU, Ultrasonic velocity and compressibility in reciprocal fused salts systems: Cd, Pb‖Cl, Br	455–460
|R. PIONTELLI,| On some definitions and conventions in electrochemistry . .	461–465
H. A. SKINNER and Y. VIRMANI, High-temperature microcalorimetry: the thermal decomposition of $Cr(CO)_6$ and of $Mo(CO)_6$	467–470 R
I. TEOREANU und ANNEMARIE PURI, Studium der Anregung der Hochofenschlacke mit Natronsilikat und Natronfluosilikat	471–475
VIJAY MOHAN BHATNAGAR, Spectroscopic observations on nickel (II) perchlorate complexes	477–480
N. S. BIRADAR and V. H. KULKARNI, A spectroscopic study of oxovanadium (V) complexes with multidentate Schiff bases. II	481–487
GH. MARCU und V. SĂCELEAN, Indirekte Bestimmungen mit Hilfe der β^--Rückstrahlung. IV. Die Bestimmung von K^+ und NH_4^+ mit $Na_2Pb[Me^{II}(NO_2)_6]$	489–495
C. LITEANU, S. GOCAN, T. HODIŞAN, H. NAŞCU and C. MĂRUŢOIU, The influence of the temperature gradient on the form of the elution curves and of the height of the theoretical plate in column chromatography with ion exchangers	497–503
N. PASCU, V. SĂCELEAN, LIVIA CRIVEI, ERNA KISS und N. BOJAN, Studium des Verhaltens von Fe^{3+}, Co^{2+} und Ni^{2+} auf dem Kationenaustauscher Vionit CS-3 im Medium von organischem Lösungsmittel – $HCl-H_2O$	505–509
A. POPESCU, A. SZABO und P. FINK, IR-Untersuchungen der Adsorption an Mischoxid-Katalysatoren	511–518
JEAN-MARIE LEROY et GABRIEL TRIDOT, Applications de la microanalyse par sonde électronique à la catalyse hétérogène	519–524

Page

R GEORGETA CSOMONTANYI et A. PANOVICI, Étude de la déshydratation du méthylphénylcarbinol sur diverses masses de contact 525–532

КОРНЕЛИЯ КОРИЧУК, ДЖОРДЖЕТА ЧЁМОНТАНИ и СПЕРАНЦА ПОПА, Исследование зауглероживания некоторых катализаторов дегидрирования алкилароматических углеводородов 533–538

A. KRAUSE, Über zwei verschiedene katalytische Hydrierungsreaktionen des Naphthols und deren Mechanismen 539–541

A. KRAUSE, Mechanismus der katalytischen Bildung von langkettigen Kohlenwasserstoffen und oxidischen organischen Nebenprodukten aus CO und H_2 543–546

CRISTOFOR SIMIONESCU, SVETLANA DUMITRESCU et MARIA GROVU, Étude sur la polymérisation des dérivés acétyléniques. XII. Cinétique de la photopolymérisation du phénylacétylène 547–558

R I. GAVĂT, VICTORIA DIMONIE, D. DONESCU, MARIANA MUNTEANU, IOANA ISĂCESCU, Polymérisation rapide de l'ε-caprolactame en présence de composés organo-métalliques 559–564

AMALIA CRUSOS, CONSTANTIN UGLEA et ION AGHERGHINEI, Étude de la polydispersité du polychlorure de vinyle par chromatographie sur gel perméable pendant la destruction mécano-chimique 565–570

GH. MANDRIC and VALENTINA ȚĂRANU, Synthesis of polyurethane elastomers, starting materials and intermediates. XI. Synthesis of nitrodiisocyanates 571–572

Z. SIMON, MARIA NUȚIU and G. OSTROGOVICH, The study of the biuret reaction. VI. Electronic spin resonance of some copper(II)-complexes with cyanuric acid and succinimide 573–579

J. VODNÁR, Hydroperoxidation of organic compounds at the liquid/gas interface. III. Hydroperoxidation of phenylcyclohexane with oxygen ... 581–588

COMPTES RENDUS 589–591

Revue Roumaine de Chimie, **17**, *3*, 423–429 (1972)

ON THE PHOTOLYSIS OF $[Mn(C_2O_4)_2(H_2O)_2]$ K IN DIMETHYLFORMAMIDE. I

I. G. MURGULESCU, TATIANA ONCESCU and S. G. IONESCU

Department of Physical Chemistry, University of Bucharest,
Bd. Republicii 13, Bucharest, Romania

Received August 2, 1971

We have investigated the photolysis of $[Mn(C_2O_4)_2(H_2O)_2]$ K in DMF, on irradiation with wavelengths from the visible and ultraviolet absorption bands of the complex. In both cases the kinetics of the photolysis verifies a zero molecular order. The quantum yields determined agree with the proposed mechanism of the photolysis. The intermediates which were supposed to appear in the different stages of the reaction could be identified by their characteristic ESR signals.

A systematical study of the photolysis of $[Mn(C_2O_4)_2(H_2O)_2]$K from the kinetic point of view is not to be found in literature, as in aqueous solutions thermal decomposition occurs rather fast at room temperature,[1] overlapping the photochemical decomposition which can no longer be accurately studied. That is why we have changed the reaction medium replacing it by DMF in which the complex dissolves and the thermal decomposition is significantly slowed down ($k^{25°}_{DMF} = 1.06 \times 10^{-5}\ s^{-1}$; $k = {}^{25°}_{H_2O} = 7 \times 10^{-4}\ s^{-1}$).

Under these conditions, the correction of the photolysis data concerning the thermal contributions can be accurately made.

EXPERIMENTAL

The yellow complex $[Mn(C_2O_4)_2(H_2O)_2]$ K – presumed as the *trans*-isomer[2] – was prepared according to the literature.[3]

Its absorption spectrum as well as the optical density measurements for $\lambda = 450$ nm at different photolysis intervals, were carried out at a SP 800 Unicam spectrophotometer. The molar absorption coefficient found was equal to $166 \pm 4\ M^{-1}\ cm^{-1}$.

DMF p.a. Riedel de Haën was used as solvent. The complex solutions in DMF had concentrations ranging from 1×10^{-3} M to 3×10^{-3} M.

---

[1] I. G. Murgulescu and T. Oncescu, *Rev. Roumaine Chim.*, **10**, 3 (1965).
[2] T. Oncescu and V. Sahini, *Rev. Chim. Acad. R.P.R.*, **1**, 73 (1963).
[3] G. H. Cartledge and W. K. Erichs, *J. Amer. Chem. Soc.*, **58**, 2063 (1936).

The irradiation equipment used for the determination of the quantum yield is shown in figure 1.

For the irradiation in visible, a high pressure mercury lamp HBO 500 was used as well as a Y M-2 monochromator, while for the ultraviolet, a HBO 50 mercury lamp, a Zeiss Jena glass filter for λ = 366 nm and a solution filter [4] ($NiSO_4 + CoSO_4$) for λ = 312–3 nm. The irradiation cell was thermostated at 25°.

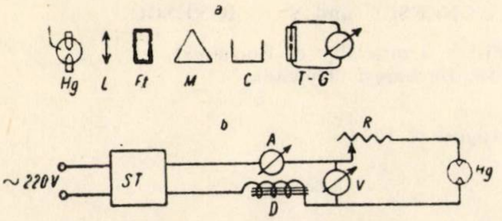

Fig. 1. — a) Equipment used for the irradiation and light energies measurements; Hg — mercury lamp; L — lens; Ft — thermal filter (H_2O); M — monochromator; C — thermostated irradiation cell; T—G — thermoelement-galvanometer. b) Mercury lamp power supply; ST — stabilized power supply; A — ampermeter; V — voltmeter; Hg — mercury lamp; R — variable resistence; D — choke.

The light intensity measurements were made according to the indications given by literature [5] by the thermoelement-galvanometer system (Vacuum Thermoelement ThV1 and a mirror galvanometer Göttingen, $C_V = 1.2 \times 10^{-6}$ V/mm/m; $R_i = 59\ \Omega$) calibrated in advance (the calibration constant $TC = 0.58$ erg/s.cm² per 1 mm deflection of the galvanometer).

Chemical actinometry with $[(Fe(C_2O_4)_3]K_3$ was used in parallel.[6–8] In the cell the actinometric solution and the $[Mn(C_2O_4)_2(H_2O)_2]K$ solution in DMF, were irradiated alternately in order to determine the number of moles photolysed ΔN_m^A, ΔN_m^R respectively, as well as the light fraction $\overline{F}_R$ absorbed by the Mn (III) complex solution. The quantum yield is given by the equation:

$$\Phi_R = \frac{\Delta N_m^R}{t_R} \frac{t_A}{\Delta N_m^A} \frac{\Phi_A}{\overline{F}_R} \tag{1}$$

in which t_R and t_A represent the irradiation time in minutes, of the Mn (III) complex and actinometric solutions; Φ_A is the quantum yield of the photolysis of the actinometric solution whose value is known from literature for different wavelengths used on irradiation.

The ESR spectra of the intermediates which appeared during the photolysis were recorded on a spectrometer working in X band, with a modulated magnetic field at high frequency (171 Kc/s). The spectra were recorded at 77°K, the temperature at which the irradiation was also carried out.

RESULTS AND DISCUSSION

The absorption spectrum of $[Mn(C_2O_4)_2(H_2O)_2]K$ in DMF has two absorption bands as it can be seen from figure 2 : one of lower intensity in visible, due to the absorption of the central ion, with an absorp-

---

[4] C. R. Masson, V. Bockelheide and W. Noyes Jr., "Technique in Organic Chemistry", vol. 2, 2nd ed., ed. by Weissberger, New York, 1948, p. 250.

[5] J. G. Calvert and J. N. Pitts, Jr., "Photochemistry", John Wiley and Sons, Inc. New York, London, Sydney, 1966, p. 771–780.

[6] C. A. Parker, *Proc. Roy. Soc.*, **A 220**, 104 (1953).

[7] C. G. Hatchard and C. A. Parker, *Proc. Roy. Soc.*, **A 235**, 518 (1956).

[8] J. Lee and H. H. Seliger, J. *Chem. Phys.*, **40**, 519 (1964).

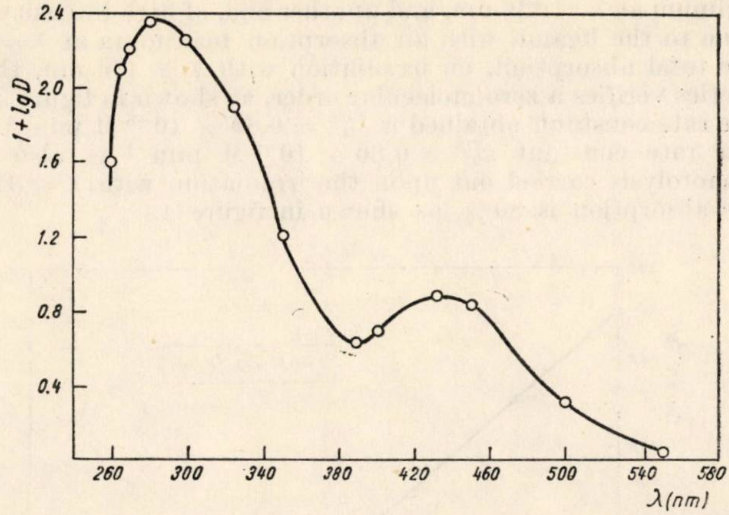

Fig. 2. – Absorption spectrum of $[Mn\ (C_2O_4)_2(H_2O)_2]$ K in DMF.

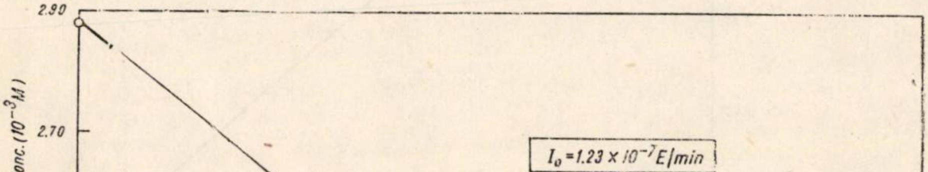

Fig. 3. – Zero molecular order kinetics of the photolysis of $[Mn(C_2O_4)_2(H_2O)_2]K$ in DMF at 25° on irradiation with λ = 436 nm.

tion maximum at λ = 436 nm, and another one, of high intensity in ultraviolet, due to the ligand, with an absorption maximum at λ = 290 nm.

For total absorption, on irradiation with λ = 436 nm, the photolysis kinetics verifies a zero molecular order, as shown in figure 3.

The rate constant obtained is $k_0^{436} = 0.80 \times 10^{-5}$ M min^{-1}. A zero molecular rate constant $k_0^{313} = 0.86 \times 10^{-5}$ M min^{-1} is also obtained for the photolysis carried out upon the irradiation with λ = 312−3 nm when the absorption is 80%, as shown in figure 4.

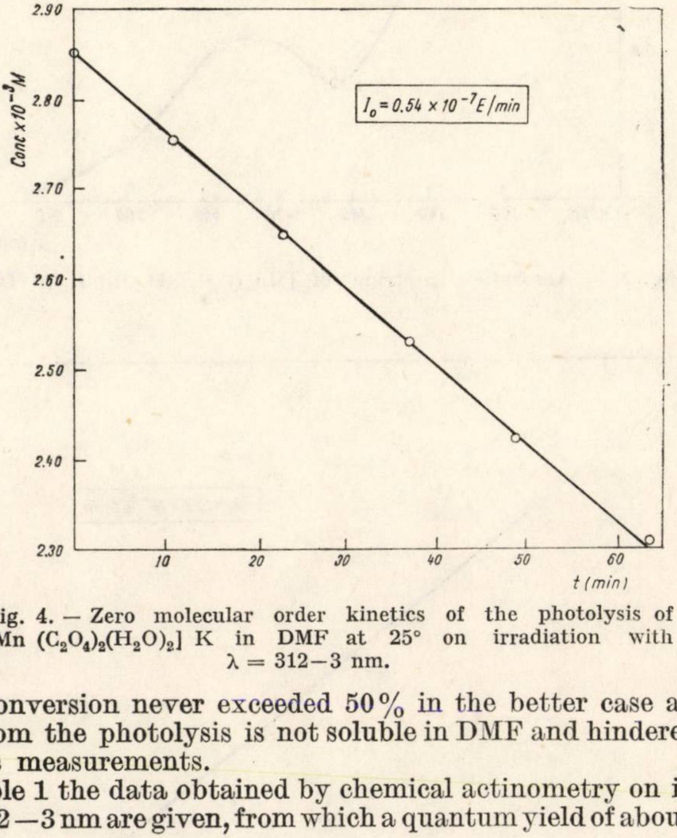

Fig. 4. — Zero molecular order kinetics of the photolysis of [Mn $(C_2O_4)_2(H_2O)_2$] K in DMF at 25° on irradiation with λ = 312−3 nm.

The conversion never exceeded 50% in the better case as MnC_2O_4 resulting from the photolysis is not soluble in DMF and hindered spectrophotometric measurements.

In table 1 the data obtained by chemical actinometry on irradiation with λ = 312 −3 nm are given, from which a quantum yield of about 2 results.

Table 1

Photolysis of [Mn $(C_2O_4)_2(H_2O)_2$] K in DMF λ = 312−3 nm; $I_0 = 1.23 \times 10^{-7}$ E/min; $c = 2.88 \times 10^{-3}$ M; T = 25°

t, min	$V \times 10^8$ moles/min	Φ_R
11	10.47	1.94
23	10.50	1.95
37	10.20	1.89
49	10.80	2.00
63	10.30	1.91
		Average 1.94

The same result is obtained on irradiation with $\lambda = 366$ nm.

On irradiation with $\lambda = 436$ nm, also by chemical actinometry, a quantum yield was determined, equal to 0.74. The same photolysis, this time investigated by measuring the light by the thermoelement-galvanometer system leads to $\Phi_R = 0.72$, therefore in good agreement with the first value.

The irradiation with ultraviolet which excites a CT state must lead to an intermediate complex by the transfer of an electron from one of the oxalic groups to the central ion:

$$[\overset{III}{Mn}(C_2O_4)_2(H_2O)_2]^- \xrightarrow{h\nu} [\overset{II}{Mn}(C_2O_4)(C_2O_4)^{\cdot -}(H_2O)_2]^- \quad (a)$$

$$[\overset{II}{Mn}(C_2O_4)(C_2O_4)^{\cdot -}(H_2O)_2]^- \rightarrow MnC_2O_4 + (C_2O_4)^{\cdot -} + 2H_2O \quad (b)$$

$$[\overset{III}{Mn}(C_2O_4)_2(H_2O)_2]^- + (C_2O_4)^{\cdot -} \rightarrow MnC_2O_4 + C_2O_4^{--} + 2H_2O + 2\,CO_2 \quad (c)$$

The value, of about 2, of the quantum yield supports the idea of such a reaction mechanism. Moreover, similar mechanisms, based upon other experiments, have been supposed to take place on the photolysis of the aqueous solutions of $[Me(C_2O_4)_3]K_3$ in which Me can be Co (III),[9] Fe (III),[10] Cr (III)[11] and Mn (III).[12]

The fact that the photolysis of $[Mn(C_2O_4)_2(H_2O)_2]K$ performed by us on irradiation with visible light leads to the same final reaction products, justifies us in supposing the existence of the same reaction sequences. Of course, since the absorption of $\lambda = 436$ nm excites a state with a marked dd character, $[Mn(C_2O_4)(C_2O_4)^{\cdot -}(H_2O)_2]^-$ can appear only as a result of a nonradiative transition dd → CT, as previously discussed.[13] Besides, the value of the quantum yield 0.74 obtained in this case supports the idea of such a process, which occurs with a significant probability, competing with other nonradiative transitions.

The formation of another type of a Mn (II) intermediate complex was emphasized by Pozniak, Shagisultanova and Neokladnova[12] at the photolysis of an aqueous solution of $[Mn(C_2O_4)_3]K_3$, by a new absorption band in visible ($\lambda = 400$ nm) obtained at low temperatures. Its intensity grows as the intensity of the absorption band of $[Mn(C_2O_4)_3]K_3$ decreases, the latter disappearing from the system. The absence of an ESR signal from such a paramagnetic intermediate seems to have no explanation. The only signal obtained by these authors was that corresponding to ion radical $(C_2O_4)^{\cdot -}$ resulting from the decomposition of the former intermediate. This signal is located between the third and fourth component in the spectrum of the Mn^{+2} free ion.

---

[9] A. W. Adamson and A. H. Sporer, *J. Amer. Chem. Soc.*, **80**, 3865 (1958).

[10] C. A. Parker and C. G. Hatchard, *J. Phys. Chem.*, **63**, 22 (1959).

[11] M. A. Malati, M. W. Raphael, *J. Inorg. Nuclear Chem.*, **28**, 915 (1966).

[12] A. L. Pozniak, G. A. Shagisultanova and L. N. Neokladnova, *Teoreticeskaya i eksperimental'nayakhimiya*, **4**, 567 (1968).

[13] I. G. Murgulescu, T. Oncescu, Z. Simon, *Rev. Roumaine Chim.*, **12**, 737 (1967).

In our investigations on the photolysis of $[Mn(C_2O_4)_2(H_2O)_2]K$ in DMF carried out at 77°K we obtained an ESR spectrum in which the singlet corresponding to the ion radical $(C_2O_4)^{\cdot -}$ can be very clearly observed too. Besides, the existence of this radical ion was also emphasized at the thermal decomposition in aqueous solutions of $[Mn(C_2O_4)_2(H_2O)_2]K$ by other physical and chemical methods.[14]

Figure 5 gives the ESR spectrum obtained by us.

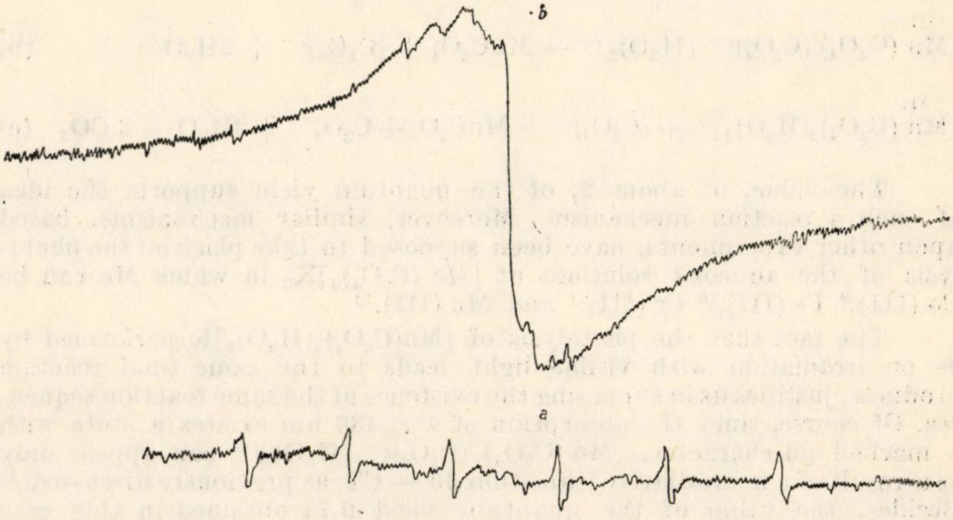

Fig. 5. — ESR spectrum of :
a) Mn^{+2} sample; b) irradiated $[Mn(C_2O_4)_2(H_2O)_2]K$ in DMF at 77°K.

Here, other six lines can be noticed besides the radical ion $(C_2O_4)^{\cdot -}$ singlet. We ascribe these lines to the charge transfer complex $[Mn(C_2O_4)(C_2O_4)^{\cdot -}(H_2O)_2]K$ which appears in the primary photochemical process (a).

We reached this conclusion also due to the fact that the splitting of these six lines is smaller than in the case of the free Mn^{+2} ion. Besides, dissolving MnC_2O_4 in an aqueous solution of $C_2O_4K_2$ when an oxalic complex of Mn (II) is certainly formed, an ESR spectrum with six lines is also obtained whose splitting can be compared to that obtained from the photolysis of $[Mn(C_2O_4)_2(H_2O)_2]K$ in DMF at 77°K. If the sample is kept at room temperature for a few seconds, the signals intensity of the intermediates decreases as the secondary reaction takes place. If longer kept at room temperature, only the large signal of Mn^{+2} from the MnC_2O_4 formed as final product can be noticed.

---

[14] T. Oncescu, *Rev. Roumaine Chim.*, **2**, 209 (1970).

Other investigations for the confirmation of the above mentioned hypotheses are in progress.

We are indebted to Mr. O. Constantinescu from the Institute of Atomic Physic for his help in obtaining the ESR spectra.

Revue Roumaine de Chimie, **17**, *3*, 431–440 (1972)

ON THE VISCOSITY OF MOLTEN METALS

I. G. MURGULESCU and MARILENA ŞERBAN
Physical Chemistry Department, Bucharest University,
Bd. Republicii 13, Bucharest, Romania

Received November 15, 1971

The present work is meant to investigate the applicability of Batschinski's equation for metallic liquids and liquified rare gases. It can be noticed that all these liquids obey this law within temperature ranges of a few hundreds degrees above the melting point. Trying to establish the significance of the molecular constant Ω, we conclude that the viscous flow which occurs in liquified rare gases and the melts of metals, having close-packed crystalline structures in the solid state, takes place by means of particles whose radius lies between the corresponding atomic and ionic radius. In the case of Ga, Sn, Sb, Bi, Hg, Zn and Cd melts, the presence of certain associated particles, especially dimers, can be noticed to a greater or smaller extent.

INTRODUCTION

The viscosity of molten metals is comparable to the viscosity of molecular liquids and that of molten salts, as regards its order of magnitude. Hence, the attempt to extend to molten metals the viscosity theories and equations valid for molecular liquids.

According to this tendency, we shall start by taking into consideration the viscosity of a group of molten metals, as well as that of a few liquified rare gases. Both systems are made up of monoatomic particles, with spheric symmetry.

The viscosity equations can be divided into two groups : equations having but a summary theoretical foundation and equations with a more elaborate theoretical foundation.

The equations of the first group usually have two adjustable parameters, alongside with experimental magnitudes such as : density, molecular mass, temperature. Such are Batschinski's [1] and da C. Andrade's [2] equations.

Equations whose theoretical character is more marked have only one adjustable parameter alongside with experimental magnitudes and molecular constants such as : molecular diameter, particle vibration frequency and so on. Equations based upon Eyring's theory [3] belong to this group.

---

[1] A. I. Batschinski, *Z. phys. Chem.*, **84**, 643 (1913).

[2] E. N. da C. Andrade, *Phil. Mag.*, **17**, 698 (1934).

Attempts have been made to establish equations of the viscosity coefficient which should contain only experimental magnitudes and molecular constants but no adjustable parameter. This is the case of Panchenkov's equation.[4]

In the present work we are going to deal in particular with the applicability of Batschinscki's equation to metallic liquids and liquified rare gases. To this end, molten metals from different groups were studied, whose viscosity coefficients and densities are known for greater or smaller temperature ranges: Li,[5,6] Na,[6–8] K,[6–8] Rb,[5] Cs[5]; Cu,[9] Ag,[9] Au,[9,10]; Mg,[11] Zn,[8,12,13] Cd,[8,13] Hg[14]; Al,[12,15] Ga [16]; Sn,[11,17–20] Pb [20]; Sb,[20] Bi [21]; Fe,[22–24] Co,[22,24] Ni.[22,24]

It must be pointed out that judging by the lattice complexity and the high values of electrical resistance, Hg, Ga, Sn, Sb and Bi are no ideal metals and they occupy an intermediate position between metallic and valence lattices. This is made evident in the case of Ga, Sn, Sb and Bi also by the fact that instead of expanding, their volume decreases when they are melting.

We have also extended our study to three liquified rare gases: Ar,[25] Kr,[25] Xe.[25]

All these metallic and non-metallic liquids, being made up of monoatomic particles, make possible an easier deduction of the molecular significance of the parameters in the corresponding viscosity equations.

---

[3] S. Glasstone, K. J. Laidler and H. Eyring, "The Theory of Rate Processes", New York, London, 1941, p. 480–485.

[4] G. M. Panchenkov, *Doklady Akad. Nauk S.S.S.R.*, **50**, 329 (1945); **63**, 701 (1948); **79**, 985 (1951); *Zhur. fiz. Khim.*, **20**, 811 (1946); **24**, 1390 (1950).

[5] E. N. da C. Andrade and E. R. Dobbs, *Proc. Roy. Soc.*, **211** A, 12 (1952).

[6] Landolt-Börnstein, "Zahlenwerte und Funktionen aus Physik, Chemie, Astronomie, Geophysik und Technik", 6. Auflage, 4. Bd., Technik, 2. Teil, Bandteil c, 1965, p. 326, 352–353.

[7] C. T. Ewing, J. A. Grand and R. R. Miller, *J. Phys. Chem.*, **58**, 1086 (1954).

[8] C. J. Smithels, "Metals Reference Book", vol. II, 2nd ed., London, 1955, p. 639.

[9] E. Gebhardt and G. Wőrwag, *Z. Metallkde.*, **42**, 358 (1951).

[10] E. Gebhardt and G. Wőrwag, *Z. Metallkde.*, **43**, 106 (1952).

[11] E. Gebhardt, M. Becker and H. Sebastian, *Z. Metallkde.*, **46**, 669 (1955).

[12] E. Gebhardt and K. Detering, *Z. Metallkde.*, **50**, 379 (1959).

[13] K. Detering and F. Sauerwald, *Z. anorg. Chem.*, **223**, 204 (1935).

[14] "Handbook of Chemistry and Physics", 41st ed., 1959–1960, p. 2185.

[15] E. Gebhardt, M. Becker and S. Dorner, *Z. Metallkde.*, **44**, 510 (1953).

[16] K. E. Spells, *Proc. Phys. Soc.*, **48**, 299 (1936).

[17] E. Gebhardt, M. Becker and S. Schäfer, *Z. Metallkde.*, **43**, 292 (1952).

[18] E. Gebhardt, M. Becker and E. Trägner, *Z. Metallkde.*, **44**, 379 (1953).

[19] E. Gebhardt, M. Becker and K. Köstlin, *Z. Metallkde.*, **47**, 684 (1956).

[20] E. Gebhardt and K. Köstlin, *Z. Metallkde.*, **48**, 636 (1957).

[21] E. Gebhardt and K. Köstlin, *Z. Metallkde.*, **48**, 601 (1957).

[22] G. Cavalier, *Compt. rend.*, **256**, 1308 (1963).

[23] H. Schenck, M. G. Frohberg and K. Hoffmann, *Arch. Eisenhuettenw.*, **34**, 93 (1963).

[24] H. Hiebler and H. Trenkler, *Berg-u. Huettenmännische Monatshefte*, **112**, 150 (1967).

[25] J. P. Boon, J. C. Legros and G. Thomaes, *Physica*, **33**, 547 (1967).

BATSCHINSKI'S EQUATION

Batschinski's equation :

$$\eta = \frac{c}{v - \omega} \tag{1}$$

expresses the relationship between the liquid viscosity coefficient η and its specific volume v. The equation contains two adjustable parameters — c and ω — typical of each liquid.

The significance of constant ω, called the limiting specific volume, is easily obtained, if we notice that when v tends to ω, the viscosity becomes infinite ; the liquid solidifies. The limiting specific volume therefore represents the rigid portion of the liquid, while the difference $(v - \omega)$ can be considered the free volume, accessible to the particle motion in the viscous flow.

Constant c represents an internal friction coefficient, whose dimension is : viscosity x volume.

Multiplying the denominator and the numerator of equation (1) by the molecular weight, we get :

$$\eta = \frac{C}{V - \Omega}, \tag{2}$$

in which V, Ω and C represent the corresponding molecular magnitudes. In the sequel we shall frequently refer to this equation.

For a first check of the applicability of equation (1) for the viscosity of the above liquids, the fluidity $1/\eta$ is plotted against the specific volume v (figures 1—2). In the cases in which the equation is obeyed, the relation between the two magnitudes is represented by a straight line, whose slope is $1/c$ and the intercept is $(-\omega/c)$.

As it can be seen from figures 1 and 2, equation (1) is obeyed almost for all molten metals mentioned above, as well as for the liquified rare gases. A certain departure from linearity occurs only in the case of Na, K, Hg, Ga and Sn melts (we cannot state the same thing for Li, as data from two different sources were used for its plotting). Still, within temperature ranges of a few hundreds of degrees above the melting point, equation (1) practically holds good for all liquids made up of monoatomic particles, with the exception of Hg, for which this range is only of a few scores of degrees.

The temperature ranges with available viscosity coefficients are given in table 1, together with the melting and boiling temperatures of the elements under study. These ranges are particularly wide just in the case of Na, K, Ga and Sn, which enables us to notice their slight departure from the conditions of equation (1).

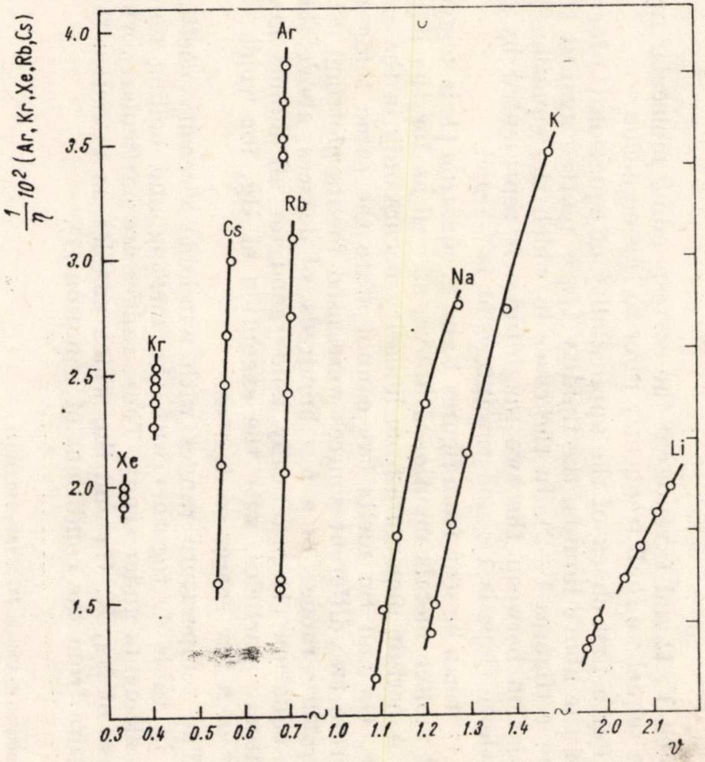

Fig. 1. — Fluidity of molten alkali metals and liquified rare gases.

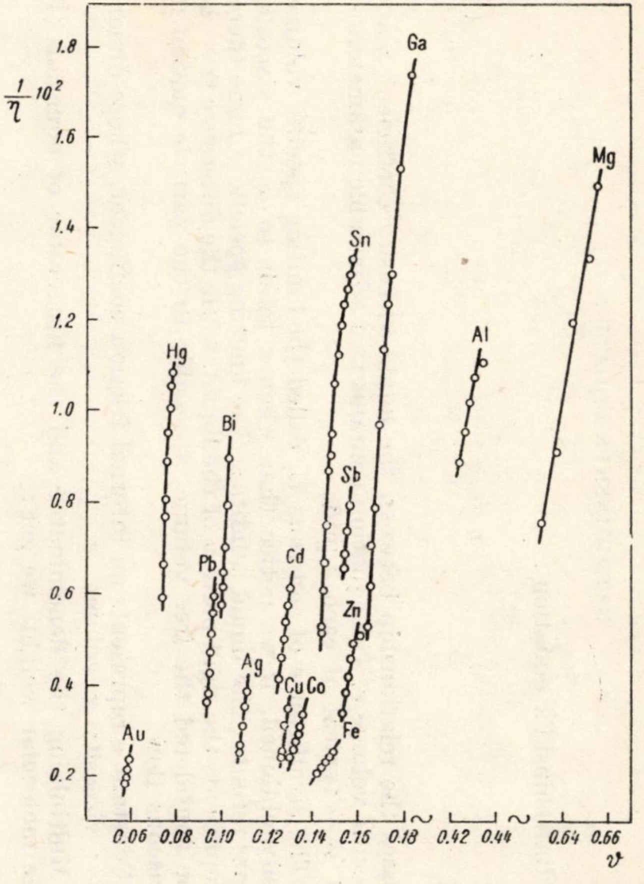

Fig. 2. — Fluidity of molten metals from IB, IIB, IIIB, IVB, VB and VIII groups

To illustrate the excellent applicability of Batschinski's equation for the estimation of the viscosity of molten metals, the values of the viscosity coefficient of liquid Ag are given in table 2.

Table 1

Temperature ranges for which viscosity coefficients are given.

Element	T_m °C	T_b °C	Temperature range °C
Li	180	1370	183.3 – 285.3 ; 300–700
Na	97.8	892	97.8 – 700
K	63.6	775	63.7 – 700
Rb	38.8	680	38 – 220
Cs	28.5	700	28.4 – 210.9
Cu	1083	2590	1083 – 1300
Ag	960.8	2210	960.5 – 1300
Au	1063	2950	1063 – 1300
Mg	650	1103	650 – 900
Zn	419.5	907	419 – 700
Cd	321	765	350 – 600
Hg	−38.9	357	−10 – 340
Al	660	2480	658 – 900
Ga	29.8	2250	52.9 – 1100
Sn	231.9	2450	232 – 1300
Pb	327.4	1740	327 – 600
Sb	630.5	1440	630.5 – 750
Bi	271	1560	271 – 560
Fe	1537	3070	1500 – 1750
Co	1492	2900	1450 – 1750
Ni	1453	3000	1350 – 1700
Ar	−189.4	−186	−189.22 – −186.02
Kr	−157.2	−153.2	−157.07 – −152.73
Xe	−111.8	−108	−109.85 – −107.93

Table 2

Viscosity of liquid silver. $\omega = 0.09981$ cm^{3}g^{-1}; $c = 2.959 \times 10^{-4}$ Poise × cm^{3}g^{-1}

T °C	ρ g cm^{-3}	v cm^{3}g^{-1}	$\eta \times 10^2$ Poise Exp.	$\eta \times 10^2$ Poise Calc.
960.5	9.301	0.10752	3.88	3.84
1000	9.27	0.10787	3.66	3.67
1100	9.17	0.10905	3.19	3.20
1200	9.07	0.11025	2.83	2.83
1300	8.98	0.11136	2.59	2.56

The agreement between the experimental values and those calculated by means of equation (1) is very good, the differences do not exceed the limits of experimental errors, within a temperature range of 300°.

The values of parameters ω, Ω, c and C for the elements under study are given in table 3.

Table 3

Parameters in Batschinski's equation.

Element	ω $cm^3\ g^{-1}$	Ω $cm^3\ gat^{-1}$	$c \times 10^4$ Poise × $cm^3\ g^{-1}$	$C \times 10^2$ Poise × $cm^3\ gat^{-1}$	Observations : ΔT°C
Li	1.8317	12.71	7.291	0.506	183.3−285.3
Na	1.023	23.53	3.848	0.885	100 −300
K	1.136	44.42	3.808	1.489	100 −200
Rb	0.6398	54.69	2.627	2.245	
Cs	0.5070	67.38	2.352	3.126	
Cu	0.1190	7.56	2.798	1.778	
Ag	0.0998	10.77	2.959	3.192	
Au	0.0542	10.68	1.951	3.843	
Mg	0.6078	14.78	3.214	0.781	
Zn	0.1425	9.32	2.864	1.872	
Cd	0.1157	13.01	2.285	2.569	
Hg	0.0701	14.06	0.575	1.154	−10 − 40
Al	0.3952	10.66	3.333	0.899	
Ga	0.1587	11.06	1.110	0.774	52.9−402
Sn	0.1379	16.37	1.106	1.313	232 −600
Pb	0.0890	18.44	1.250	2.590	
Sb	0.1442	17.56	1.456	1.773	
Bi	0.0937	19.58	1.030	2.152	
Fe	0.1250	6.98	9·027	5.042	
Co	0.1175	6.93	6.372	3.756	
Ni	0.1163	6.83	6.381	3.745	
Ar	0.6183	24.70	2.321	0.927	
Kr	0.3499	29.29	2.519	2.108	
Xe	0.2988	39.23	2.083	2.735	

RESULTS AND DISCUSSION

Out of the two parameters in Batschinski's equation — i.e. C and Ω — the latter can be easily deduced both from other experimental data and the molecular constants. This enables the determination of its corpuscular significance. To this end, the values of the limiting atomic volume Ω, for the studied liquids, were given in table 4. In column three the atomic volume V_1 of the solid is given, estimated graphically, at the melting point, by taking into account the corresponding expansion coefficient, according to the equation :

$$V_1 = V_0 (1 + \beta t)$$

The values of the same volume are given in the next column, this time estimated by means of the atomic volume of the liquid and of the volume change ΔV, both measured at the melting point. Finally, V_3 is the solid atomic volume, determined experimentally at the melting point.

Table 4

Limiting atomic volumes Ω and atomic volumes at the melting point.

Element	Ω cm³ gat⁻¹	V, cm³ gat⁻¹			Observations : ΔT°C
		V_1	V_2	V_3	
Li	12.71	13.37	13.41	—	183.3 — 285.3
Na	23.53	24.13	24.14	—	100 — 300
K	44.42	45.97	46.10	—	100 — 200
Rb	54.69	56.50	56.68	—	
Cs	67.38	70.86	70.42	—	
Cu	7.56	7.53	7.68	7.64	
Ag	10.77	10.90	11.14	10.85	
Au	10.68	10.69	10.84	10.66	
Mg	14.78	14.72	14.73	—	
Zn	9.32	9.54	9.54	9.56	
Cd	13.01	13.37	13.39	13.38	
Hg	14.06	14.13	14.12	—	−10 — 40
Al	10.66	10.50	10.68	10.52	
Ga	11.06	11.77	11.82	—	52.9—402
Sn	16.37	—	17.53	—	232 —600
Pb	18.44	18.76	18.76	18.81	
Sb	17.56	18.75	18.93	18.51	
Bi	19.58	21.58	21.47	21.44	
Fe	6.98	—	—	—	
Co	6.93	7.07	—	—	
Ni	6.83	7.05	—	—	
Ar	24.70	25.10	24.70	—	
Kr	29.29	28.44	29.64	—	
Xe	49.23	38.06	38.47	—	

Table 4 shows that for most of the elements there is a good agreement between the limiting volume Ω and the atomic volume at the melting point, irrespective of the method by which the latter was estimated. More important differences, without being exaggerated, occur in the case of alkali metals, Ga, Sn, Sb and Bi, reaching up to 9 % (for Bi).

Let us try, now, to establish a connection between Ω and the molecular magnitudes on which it depends. We should like to mention that, in a previous work,[26] it was shown that for binary ionic liquids (molten alkali halides) the limiting molecular volume Ω can be calculated according to the relation :

---

[26] I. G. Murgulescu, *J. Chim. phys.*, **Oct. (special no.)**, 43 (1969).

$$\Omega = 8N\,(r_+^3 + r_-^3),$$

r_+ and r_- being the radii of the constituent ions and N — Avogadro's number. The equation is obtained by admitting that each ion reduces the volume allowing the viscous flow by the volume of a cube, whose side is equal to its diameter.

Admitting the same hypothesis for molten metals, the following relation would result :

$$\Omega = 8\,Nr^3,$$

r being the radius of the metallic atom. As it could be expected, the values calculated by means of this equation prove to be much to great as compared to the experimental ones.

Indeed, in the liquids studied by us, we do not deal with free ions, like in the case of ionic liquids, but with more complex structures, in which the distances between particles are estimated with difficulty. From our calculations, it was found that, by replacing the radius in the previous equation by 0.91 r, an intermediate value between the atomic and ionic radius, a useful relations can be obtain :

$$\Omega = 6.028\,Nr^3 \tag{3}$$

The numerical coefficient in this relation can be approximated to 6.0, without significant error.

As it can be seen from table 5, the limiting volumes Ω, calculated from the equation (3), agree well with those found experimentally for the melts of the elements from the following groups : IA, IB, IIA, III B-Al, IVB-Pb, VIII, and for the liquified rare gases. In the solid state, all these elements have close-packed crystalline structures : cubic face-centered, hexagonal and cubic body-centered.

The following elements, in the molten state, present differences between the calculated and experimental limiting volumes. They belong to group IIB, IIIB-Ga, IVB-Sn and VB.

Elements in group IIB crystallize in distorted hexagonal lattices, the others, generally, forming complex crystalline structures. The viscosity properties of their melts, perfectly agreeing with their other properties, show that these elements depart from the ideal metallic state.

The limiting volumes Ω, determined experimentally, being greater than those calculated from equation (3), prove that in the viscous flow of the molten metals Ga, Sn, Sb and Bi, bigger particles are involved ; they have resulted from the association of particles whose radius is 0.91 r. If this hypothesis is admitted, then the association degree existing in the melts of these elements can be determined from the differences between the limiting volumes Ω, calculated by means of equation (3), and the experimentally measured volumes.

Supposing that mostly dimers result from the association, the value $3r$ can be taken as the average diameter of the particles involved in the flow.

Table 5

Limiting atomic volume: experimental and calculated values. Association degree.

Element	r[27] Å	Ω, cm^3 gat^{-1}		x
		Exp.	Eq. (3)	
Li	1.519	12.71	12.73	—
Na	1.858	23.53	23.29	—
K	2.272	44.42	42.58	—
Rb	2.475	54.69	55.04	—
Cs	2.654	67.38	67.87	—
Cu	1.278	7.56	7.58	—
Ag	1.444	10.77	10.93	—
Au	1.442	10.68	10.89	—
Mg	1.598	14.78	14.82	—
Zn	1.332	9.32	8.58	0.125
Cd	1.486	13.01	11.99	0.124
Hg	1.502	14.06	12.30	0.208
Al	1.432	10.66	10.66	—
Ga	1.221	11.06	6.61	0.980
Sn	1.405	16.37	10.07	0.910
Pb	1.750	18.44	19.46	—
Sb	1.450	17.56	11.07	0.853
Bi	1.547	19.58	13.44	0.665
Fe	1.241	6.98	6.94	—
Co	1.253	6.93	7.14	—
Ni	1.246	6.83	7.02	—
Ar	1.91	24.70	25.30	—
Kr	2.01	29.29	29.48	—
Xe	2.20	39.23	38.66	—

Denoting by x the fraction of associated particles out of the whole number of atoms in a gram-atom, we get:

$$6.028\,(1 - x)\,Nr^3 + \frac{x}{2}\,N\,(3 \times 0.91\,r)^3 = \Omega_{\mathrm{exp}}$$

or

$$6.028\,(1 - x)\,Nr^3 + 10.17\,Nr^3x = \Omega_{\mathrm{exp}}\,,$$

---

[27] "Tables of Interatomic Distances and Configuration in Molecules and Ions", Special Publication No. 11, London, 1958, p. S3–11.

hence

$$x = \frac{\Omega_{\mathrm{exp}} - \Omega_{\mathrm{calc}}}{4.142\ Nr^3} \tag{4}$$

The values of the association degree x, for the elements in whose case the association takes place, are given in the last column of table 5. As it can be seen, the viscous flow in molten Ga takes place almost only through dimers; the association degree comes very close to 1. Association decreases going from Sn to Sb and Bi. For the metals in group IIB association decreases, only 10—20% of the particles being associated.

It is interesting to notice that through the extrapolation of ω at temperatures higher than those given for some of these elements in our tables, smaller values are obtained. In this way, according to eq. (4), the association degree will decrease with the temperature increase.

This phenomenon explains why, studies dealing with the dependence of liquid viscosity on the specific volume at high pressures [28] prove that viscosity does not depend on the volume alone.

The nature of the association products cannot be easily determined. Labile structures of the type $\mathrm{Me^+\ Me^-}$, breaking up and renewing themselves at very high rates in comparison with the displacement rate of particles in viscous flow, are highly likely.

---

[28] P. W. Bridgman, "The Physics of High Pressure", London, 1949, p. 330—356.

Revue Roumaine de Chimie, **17**, *3*, 441–445 (1972)

SOME ASPECTS OF METHANE CRACKING KINETICS IN STATIC CONDITIONS. III.

THE INFLUENCE OF THE COAL DEPOSIT

LUCIA ODOCHIAN and I. A. SCHNEIDER
Department of Physical Chemistry, "Al. I. Cuza" University,
Calea 23 August 11, Jassy, Romania

Received May 17, 1971

This paper deals with the influence of the coal deposit on the reactor surface on the reaction kinetics of methane cracking at 913, 943 and 973°K and a pressure varying from 40 to 760 mm Hg. The experimental results indicate a serious breaking action of the deposited coal suggesting a homogeneous-heterogeneous character of the reaction.

Considering the available scarce information regarding the influence on the reaction rate of the coal deposit formed on the inner vessel surface during methane cracking, the aim of this paper was to study this influence at different temperatures and pressures varying from 40 to 760 mm Hg in the static system previously described.[1]

Some of the results have been published in an earlier paper [2] the present one dealing especially with the influence of the coal deposit of the cracking process within a larger temperature range.

EXPERIMENTAL AND DISCUSSION

The methane cracking process has been carried out at three different temperatures (913,943 and 973°K) and over a large pressure range, (40 to 760 mm Hg) in a quartz vessel having a S/V ratio of 1.22 cm^{-1}. The cracking process rate was followed by recording of the thermal conductivity variation of the gaseous reaction mixture.

Since the scope of this paper was not to establish absolute reaction rate values, we have renounced to the calibration of the conductivity cell.

Because our main purpose was to find out the influence of the coal deposit on the inner surface of the reaction vessel during the cracking process, the reaction rate measurements were carried out for transformation degrees smaller than 1–2%.

---

[1] Part I: L. Odochian and I. A. Schneider, *Rev. Roumaine Chim.*, **11**, 1647 (1970).
[2] Part II: L. Odochian and I. A. Schneider, *Rev. Roumaine Chim.*, (in press).

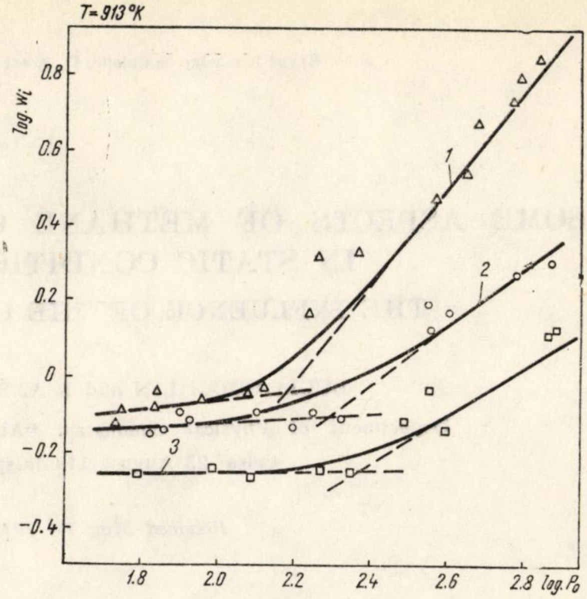

Fig. 1. — Coal deposit influence on the initial reaction rate of methane cracking at 913°K.

1 — clean surface; *2* — influence of the coal deposited during a 20 min. reaction period; *3* — influence of the coal deposited during 2 × 20 min. reaction periods.

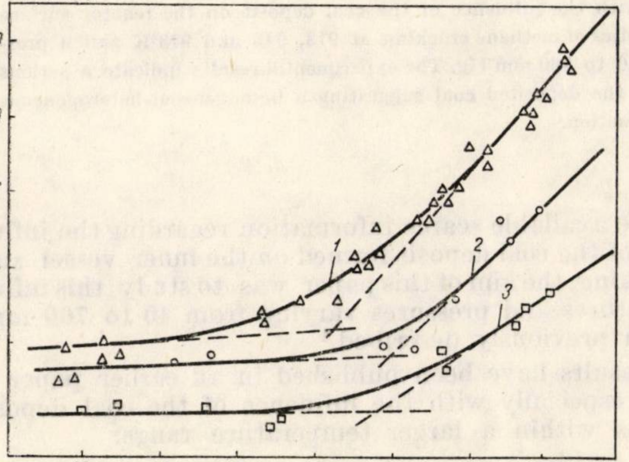

Fig. 2. — Coal deposit influence on the initial reaction rate of methane cracking at 943°K.

1 — clean surface; *2* — influence of the coal deposited during a 20 min. reaction period; *3* — influence of the coal deposited during 2 × 20 min reaction periods.

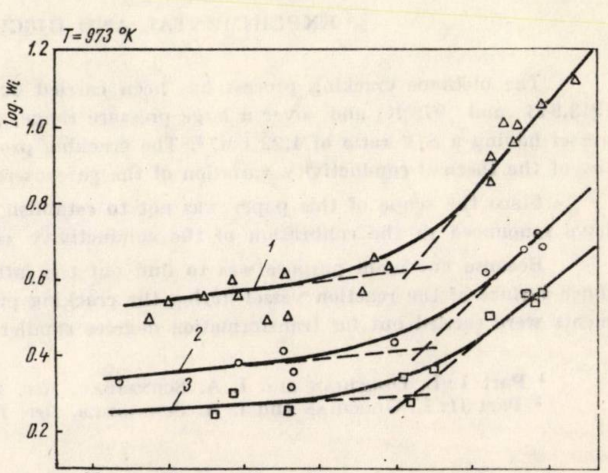

Fig. 3. — Coal deposit influence on the initial reaction rate of methane cracking at 973°K.

1 — clean surface; *2* — influence of the coal deposited during a 20 min. reaction period; *3* — influence of the coal deposited during 2 × 20 min. reaction periods.

The acquired results enabled us to distinguish two reaction stages, function of the initial rate variation with the initial pressures of the reaction mixture.

Thus, there is a high pressure region and a low pressure region, the latter being characterized by a reaction order tending to zero, thus proving a heterogeneous occurrence of the cracking reaction.

This is clearly illustrated by the following figures (1, 2 and 3) where the initial reaction rate is plotted in semi-logarithmic coordinates as function of the system pressure for three different kinetic situations : when the reaction vessel surface has no coal deposit (curves 1), when it has a coal deposit formed during a single twenty minutes cracking reaction period (curves 2) and finally, when the surface is covered by a coal deposit formed along two successive twenty minutes reactions period (curves 3).

As it can be seen, the coal deposit has a pronounced retarding effect on the initial rate of the cracking process.

The concomitant diminishing tendency of the overall reaction order permits to conclude that the coal deposit has a heterogeneous role, favouring the breaking process of H atoms on the wall.

The conclusion is in good accordance with the results reported by Quinn and Purnell [3] who noted a heterogeneous breaking reaction of the chain reactions having H atoms as chain carriers, when the cracking process occurs in a reaction vessel with inner coal deposit.

Similar considerations were reported by Gordon [4] who suggested a change in the reaction order when the H atoms breaking process occurs on the reactor's walls.

Table 1 illustrates this reaction order change more clearly by showing the limiting values of the overall reaction orders for both high and low pressures domains.

Table 1

Limiting values of the overall reaction orders for the methane cracking reaction in reaction vessel with different sizes of coal deposits

The state of the surface	913°K		943°K		973°K	
	P_{high}	P_{low}	P_{high}	P_{low}	P_{high}	P_{low}
Clean surface	0.99	0.15	1.15	0.08	1.16	0.13
Coal deposited for 20 min.	0.80	0.08	0.88	0.05	0.94	0.087
Coal deposited for 2 × 20 min.	0.70	0.00	0.78	0.019	0.78	0.055

---

[3] G. I. Quinn and I. N. Purnell, "Photochemistry and Reaction Kinetics", Cambridge, University Press, 1967, p. 330.

[4] A. S. Gordon, Symposium Kinetics of Pyrolytic Reactions, Chemical Institute of Canada, Ottawa, 1964.

We wish to remark that the overall reaction order variation is more pronounced at lower temperatures which can be explaind by the decreasing collision frequency in gaseous phase.

Another conclusion is that the effect of the coal deposit is cumulative. This results, on the one hand, from the stronger reaction rate diminution caused by a thicker coal deposit and on the other hand, from the reproducibility of the experimental results irrespective of the formation of the coal deposit in two successive twenty-minute cracking periods or in a single 40-minute cracking period (figure 4).

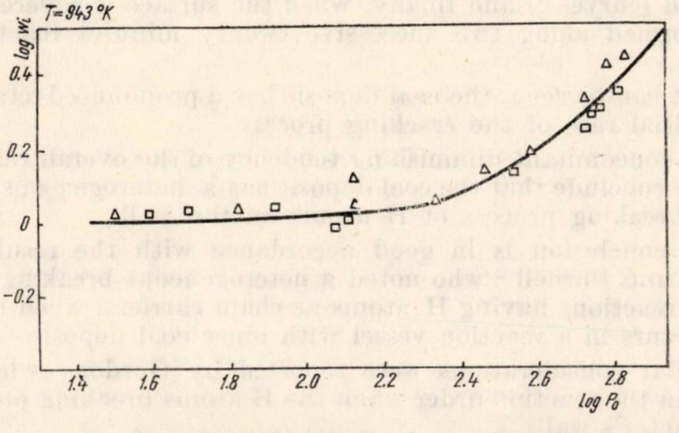

Fig. 4. — Reproducibility on a full coal-covered surface formed during 40 min. cracking reaction at 943°K.

□ — coal deposited during 2 × 20 min. cracking reaction
△ — coal deposited during a continuous 40 min. cracking reaction.

It must be noted that between the two twenty-minute cracking periods the reaction vessel was connected to a high vacuum system in order to remove the gaseous reaction mixture.

The critical pressure value at which the transition from the kinetical homogeneous stage to the heterogeneous stage could be observed, was strongly dependent both on the reaction temperature and especially on the coal deposit size as it results from values in table 2.

However, the heterogeneous domain enlargement, along with the coal deposit size, confirms its heterogeneous effect on the chain breaking reaction.

Using the reaction rates dependent on the initial pressure for the coal-covered surfaces, an activation energy of about 35.4—42.3 kcal/mol can be estimated. These values are in good agreement with those calculated by other authors [5–7] for the same reaction, using different expe-

---

[5] J. L. Mar'yasin and P. A. Tesner, *Doklady Akad. Nauk S.S.S.R.*, **140**, 1121 (1961).

[6] P. A. Tesner, *Trudy Vsesoyuz. Nauchn. Issled. Inst. Prirodn. Gazov*, **49**, 195 (1961).

[7] I. G. Petrenko, *"Gasificatsiya i Piroliz Topliv"*, Akad. Nauk S.S.S.R., Gos. Kom. po Topliv Prom. pri Gosplane SSSR, Inst. Goryuch. Iskop., Sb. Statei, 1964, p. 45.

rimental methods. This activation energy can be admitted as valid for fully covered surfaces, as in the case of many other gaseous hydrocarbons.[8-9]

Table 2

Critical initial pressures in mm Hg at which a transition from homogeneous to heterogeneous reaction can be observed.

The state of the surface	913°K	943°K	973°K
Clean surface	148	180	276
Coal deposited for 20 min.	196.5	230	292.5
Coal deposited for 2 × 20 min.	234	248	299.5

At the same time, the activation energy of 42 kcal/mol is very close to the theoretical activation energy for the hydrogen chemosorption on the coal surfaces,[10] this being an additional argument in favour of the assumption, that the methane cracking process presents a chain-ending reaction mainly based on the heterogeneous recombinations of the H atoms.

All these considerations constitute as many arguments in favour of a homogeneous-heterogeneous mechanism for the methane cracking reaction in quartz vessels, taking into account that the coal deposit causes a diminution of the overall reaction order, and also that the activation energy has a value whose size agrees with those found in literature for the heterogeneous recombination of the H atoms on the carbon surfaces.

---

[8] N. A. Sargert and K. J. Laidler, *Canad. J. Chem.*, **41**, 838 (1963).

[9] I. N. Purnell and G. J. Quinn, *J. Chem. Soc.*, **4128**, 1961.

[10] R. N. Barrer, *J. Chem. Soc.*, **1256**, 1936.

Revue Roumaine de Chimie, **17**, *3*, 441–445 (1972)

Revue Roumaine de Chimie, 17, 3, 447–453 (1972)

APPLICATION OF THE ALLEN-SKINNER BOND ENERGY SCHEME TO AROMATIC HYDROCARBONS AND TO AMINES

RODICA VÎLCU and ST. PERIŞANU

Chair of Chemical Thermodynamics and Electrochemistry
University of Bucharest, Bd. Republicii 13, Bucharest, Romania

Received September 3, 1971

The heat of atomization has been calculated for a great number of aromatic hydrocarbons and primary, secondary and tertiary amines and diamines, according to the Allen-Skinner method. The agreement between calculated values and those inferred from experimental data, generally lies within experimental errors. Most deviations appear for compounds with radicals ethyl and isopropyl in their molecule. An explanation of the errors has been attempted and the correlation with similar deviations of the halogenated derivatives has been carried out.

In recent years a calculation method of the formation heats based on additivity, introduced by Allen [1] and improved by Skinner [2] gained recognition in thermochemistry. Besides the good agreement with experimental results, the method still presents the advantage of a physical support since the summing up terms correspond to the interactions among neighbouring atoms of order 1 and 2.

The interactions under consideration are those occurring in the calculation method of molecular orbitals as a linear combination of bond orbitals (MO – LCBO)[3,4] i.e : binding energies (among neighbouring atoms), interactions energies among next nearest neighbour atoms and trigonal interactions.

Skinner [2] showed that for saturated compounds, the terms may be grouped so that corrections occurring after summing up the binding energies, should not take account of hydrogen neighbourhoods greater than order 1, which greatly simplifies the problem. For the sake of exemplification we shall proceed to the calculation of the atomization heat of monoamines.

---

[1] T. L. Allen, *J. Chem. Phys.*, **31**, 1039 (1959).
[2] H. A. Skinner, *J. Chem. Soc.*, **1962**, 4396.
[3] J. Brown, *J. Chem. Soc.*, **1953**, 2615.
[4] J. Brown, *J. Chem. Soc.*, **1954**, 1625.

$$\begin{aligned}
H^a(C_n\, H_{2n+1}\, NH_{2,g}) &= (n-1)E_{CC} + (2n+1)E_{CH} + E_{CN} + \\
&+ 2E_{NH} + b_{CCC}P_{CCC} + b_{CCH}P_{CCH} + b_{HCH}P_{HCH} + b_{CCN}P_{CCN} + \\
&+ P_{HNH} + 2P_{CNH} + b_{HCN}P_{HCN} + c\begin{pmatrix} & H & \\ & C & \\ H & & H \end{pmatrix} T\begin{pmatrix} & H & \\ & C & \\ H & & H \end{pmatrix} + \\
&+ c\begin{pmatrix} & C & \\ & C & \\ H & & H \end{pmatrix} T\begin{pmatrix} & C & \\ & C & \\ H & & H \end{pmatrix} + c\begin{pmatrix} & C & \\ & C & \\ C & & H \end{pmatrix} T\begin{pmatrix} & C & \\ & C & \\ C & & H \end{pmatrix} + c\begin{pmatrix} & C & \\ & C & \\ H & & H \end{pmatrix} T\begin{pmatrix} & C & \\ & N & \\ H & & H \end{pmatrix} + \\
&+ c\begin{pmatrix} & N & \\ & C & \\ H & & H \end{pmatrix} \cdot T\begin{pmatrix} & N & \\ & C & \\ H & & H \end{pmatrix} + c\begin{pmatrix} & N & \\ & C & \\ C & & H \end{pmatrix} T\begin{pmatrix} & N & \\ & C & \\ C & & H \end{pmatrix} + c\begin{pmatrix} & C & \\ & C & \\ C & & N \end{pmatrix} T\begin{pmatrix} & C & \\ & C & \\ C & & N \end{pmatrix}
\end{aligned} \tag{1}$$

Here we denote by E the bond energies, by P — the interaction energies of the next nearest neighbour atoms (or among neighbouring bonds) by T — the interaction energies of atoms triangles located around a central atom, while b and c respectively, are the number of neighbouring bonds of a certain type and the number of atoms trios with a certain configuration. If we introduce the following notations :

$$B_{CC} = E_{CC} - 3P_{HCH} + 6P_{CCH} - 4T\begin{pmatrix} & H & \\ & C & \\ H & & H \end{pmatrix} + 6T\begin{pmatrix} & C & \\ & C & \\ C & & H \end{pmatrix}$$

$$B_{CH} = E_{CH} + 3/2P_{HCH} + T\begin{pmatrix} & H & \\ & C & \\ H & & H \end{pmatrix}$$

$$\begin{aligned}
B_{CN} &= E_{CN} + 3P_{HCN} - 2P_{HNH} + 2P_{CNH} - 3/2\, P_{HCH} + \\
&+ 3T\begin{pmatrix} & H & \\ & C & \\ H & & N \end{pmatrix} - T\begin{pmatrix} & H & \\ & N & \\ C & & H \end{pmatrix} - 2T\begin{pmatrix} & H & \\ & C & \\ H & & H \end{pmatrix}
\end{aligned}$$

$$B_{NH} = E_{NH} + 3/2\, P_{HNH} + T\begin{pmatrix} & H & \\ & N & \\ C & & H \end{pmatrix}$$

$$\Gamma_{CCC} = P_{HCH} - 2P_{CCH} + P_{CCC} + 2T\begin{pmatrix} & H & \\ & C & \\ H & & H \end{pmatrix} - 4T\begin{pmatrix} & C & \\ & C & \\ H & & H \end{pmatrix} + 2T\begin{pmatrix} & C & \\ & C & \\ C & & H \end{pmatrix}$$

$$\begin{aligned}
\Gamma_{CCN} &= P_{HCH} - P_{CCH} + P_{CCN} - P_{NC_H} + 2\Bigg[T\begin{pmatrix} & H & \\ & C & \\ H & & H \end{pmatrix} - T\begin{pmatrix} & C & \\ & C & \\ H & & H \end{pmatrix} - \\
&- T\begin{pmatrix} & N & \\ & C & \\ H & & H \end{pmatrix} + T\begin{pmatrix} & N & \\ & C & \\ C & & H \end{pmatrix}\Bigg]
\end{aligned}$$

$$\Delta\begin{pmatrix} & \mathrm{C} & \\ & \mathrm{C} & \\ \mathrm{C} & & \mathrm{C}\end{pmatrix} = -T\begin{pmatrix} & \mathrm{H} & \\ & \mathrm{C} & \\ \mathrm{H} & & \mathrm{H}\end{pmatrix} + 3T\begin{pmatrix} & \mathrm{C} & \\ & \mathrm{C} & \\ \mathrm{H} & & \mathrm{H}\end{pmatrix} - 3T\begin{pmatrix} & \mathrm{C} & \\ & \mathrm{C} & \\ \mathrm{C} & & \mathrm{H}\end{pmatrix} + T\begin{pmatrix} & \mathrm{C} & \\ & \mathrm{C} & \\ \mathrm{C} & & \mathrm{C}\end{pmatrix}$$

$$\Delta\begin{pmatrix} & \mathrm{C} & \\ & \mathrm{C} & \\ \mathrm{C} & & \mathrm{N}\end{pmatrix} = -T\begin{pmatrix} & \mathrm{H} & \\ & \mathrm{C} & \\ \mathrm{H} & & \mathrm{H}\end{pmatrix} + 2T\begin{pmatrix} & \mathrm{C} & \\ & \mathrm{C} & \\ \mathrm{H} & & \mathrm{H}\end{pmatrix} + T\begin{pmatrix} & \mathrm{N} & \\ & \mathrm{C} & \\ \mathrm{H} & & \mathrm{H}\end{pmatrix} - T\begin{pmatrix} & \mathrm{C} & \\ & \mathrm{C} & \\ \mathrm{C} & & \mathrm{H}\end{pmatrix} -$$

$$-2T\begin{pmatrix} & \mathrm{N} & \\ & \mathrm{C} & \\ \mathrm{C} & & \mathrm{H}\end{pmatrix} + T\begin{pmatrix} & \mathrm{N} & \\ & \mathrm{C} & \\ \mathrm{C} & & \mathrm{C}\end{pmatrix}$$

eq. (1) may be considerably simplified as :

$$H^a\,(C_n\,\mathrm{H}_{2n+1}\,\mathrm{NH}_2, g) = (n-1)\,B_{\mathrm{CC}} + (2n+1)\,B_{\mathrm{CH}} + B_{\mathrm{CN}} + \qquad (2)$$
$$+ 2B_{\mathrm{NH}} + b_{\mathrm{CCC}}\,\Gamma_{\mathrm{CCC}} + b_{\mathrm{CCN}}\,\Gamma_{\mathrm{CCN}} + c\begin{pmatrix} & \mathrm{C} & \\ & \mathrm{C} & \\ \mathrm{C} & & \mathrm{C}\end{pmatrix}\Delta\begin{pmatrix} & \mathrm{C} & \\ & \mathrm{C} & \\ \mathrm{C} & & \mathrm{C}\end{pmatrix} + c\begin{pmatrix} & \mathrm{C} & \\ & \mathrm{C} & \\ \mathrm{C} & & \mathrm{N}\end{pmatrix}\Delta\begin{pmatrix} & \mathrm{C} & \\ & \mathrm{C} & \\ \mathrm{C} & & \mathrm{N}\end{pmatrix}$$

Similarly we also find the expressions for the calculation of the atomization heats of other substances.

CALCULATION OF THE ATOMIZATION HEATS OF AROMATIC COMPOUNDS

In applying the Allen-Skinner bond energy scheme to the aromatic compounds, we have not used the method envisaged for olefines by Skinner,[2] who had distinguished between the contributions of σ and π bonds, but we have considered instead the carbon atoms from the aromatic cycle as differing from the aliphatic ones and we have calculated different energetic contributions for them.

To check up the applicability of the bond energy scheme we have compared the atomization heats calculated by equation :

$$H^a\,(\text{subst.}, g) = \sum_i n_i\,\Delta H_f\,(\mathrm{A}_i, g) - \Delta H_f^0\,(\text{subst.}, g) \qquad (3)$$

where n_i = number of atoms of species A in the respective molecule
$\Delta H_f\,(\mathrm{A}_i, g)$ = formation heat of the A_i atom in gaseous state
$\Delta H_f^0\,(\text{subst.}, g)$ = formation heat of the respective substance in ideal gas state, under standard conditions, inferred from experimental data

with those calculated by summing up the atoms interactions in the molecule, according to eq. (2).

We have used some values selected or calculated by Skinner[5] i.e. : $\Delta H_f(\mathrm{C}, g) = 170.9$; $\Delta H_f\,(\mathrm{H}, g) = 52.10$; $\Delta H_f\,(\mathrm{N}, g) = 113.0$; $B_{\mathrm{CC}} =$

---

[5] H. A. Skinner and G. Pilcher, *Quart. Rev.*, **17**, 264 (1963).

$= 78.84$; $B_{CH} = 99.29$; $\Gamma_{CCC} = 2.58$. The values are expressed in kcal and are related to 1 mole or atom gram of substance as required. The contributions $\Gamma_{CC^{(a)}C^{(a)}}$ and $\Gamma_{CCC^{(a)}}$ have been interpolated between Γ_{CCC} and $\Gamma_{C^{(a)}C^{(a)}C^{(a)}}$, while the value of $\Delta\begin{pmatrix} & C & \\ & C & \\ C & & C \end{pmatrix}$ has been considerd constant and equal to -0.55, irrespective of the carbon atoms implied.[*]

We still had to calculate $B_{C^{(a)}C^{(a)}}$, $B_{C^{(a)}C}$, $B_{C^{(a)}H}$ and $\Gamma_{C^{(a)}C^{(a)}C^{(a)}}$. In view of their determination we have set up an equation system for the atomization heats of benzene, toluene, n-butyl benzene and naphthalene. The formation heats used by us for these substances as well as for the forthcoming ones were selected by Stull, Westrum and Sinke.[6] We give as an example the equation for benzene

$$H^a(C_6H_6,\ g) = 6B_{\overline{C^{(a)}}C^{(a)}} + 6B_{\underline{C^{(a)}}H} + 6\Gamma_{C^{(a)}C^{(a)}C^{(a)}} \qquad (4)$$

On solving the system we found the following values: $B_{C^{(a)}C^{(a)}} = 102.61$; $B_{C^{(a)}H} = 112.86$; $B_{C^{(a)}C} = 91.16$; $\Gamma_{C^{(a)}C^{(a)}C^{(a)}} = 4.23$; $\Gamma_{C^{(a)}C^{(a)}C} = 3.68$ and $\Gamma_{C^{(a)}CC} = 3.13$ are then calculated. We notice that as expected every energetic contribution is greater than the corresponding values for the aliphatic carbon.

With these data we can calculate the atomization heats of other aromatic hydrocarbons. Table 1 shows a good agreement with the respective values deduced from experimental data. However, for xylenes, according to the scheme used, the formation heats ought to have identical values. Indeed, for *meta*- and *para*-xylene they differ by less than 0.2 kcal/mole, while for *ortho*-xylene a correction $\varepsilon = -0.5$ kcal/mole had to be introduced. This calculation route has been generalized for all polyalkylsubstituted benzenes and naphthalenes in the sense that ε corrections have been applied where there were radicals in neighbouring positions. The method led to good results both for the substances in the table and for other substances with greater molecules, which we omitted for restricted space purposes.

The attempt to calculate the atomization heat of hydrocarbons with three benzene cycles led to a value almost equal to the mean between the atomization heat of anthracene and phenanthrene:

H^a_{exp} (anthracene, g) = 2858.43 kcal/mole,
H^a_{exp} (phenanthrene, g) = 2864.14 kcal/mole,
H^a_{calcd} ($C_{14}H_{10}$, g) = 2861.22 kcal/mole.

This fact may be correlated to the respective resonance energies. Their values in the series benzene, naphthalene, anthracene, phenanthrene (expressed in β units, calculated by the molecular orbital method without overlap) are respectively: 2.00; 3.613; 5.314; 5.448. The resonance energy of anthracene is smaller than that corresponding to a linear increase with the number of cycles, while that of phenanthrene is greater.

---

[*] We have denoted by $C^{(a)}$ the carbon atom in aromatic cycle.

[6] D. R. STULL, E. F. WESTRUM and G. C. SINKE, "The Chemical Thermodynamics of Organic Compounds", Wiley, Inc. New York, 1969 p. 367–395 and 461–467.

Table 1

Experimental and calculated heats of atomization of aromatic hydrocarbons

Aromatic compound	H^a_{exp}	$H^a_{calcd.}$	$H^a_{exp}-H^a_{calcd}$
Benzene	1318.18	1318.18	0.00
Toluene	1601.16	1601.15	0.00
Ethyl benzene	1881.08	1881.71	−0.63
n-Propyl benzene	2161.43	2161.71	−0.28
i-Propyl benzene	2162.36	2164.29	−1.93
n-Butyl benzene	2441.70	2441.71	−0.01
i-Butyl benzene		2444.28	
1-Pentyl benzene	2721.71	2721.71	0.00
1-Hexyl benzene	3001.75	3001.71	0.04
1-Heptyl benzene	3281.78	3281.71	0.07
o-Xylene	1883.66	1883.66	0.00
m-Xylene	1884.08	1884.16	−0.08
p-Xylene	1883.91	1884.16	−0.25
1, 2, 3-Trimethylbenzene	2165.59	2166.14	−0.55
1, 2, 4-Trimethylbenzene	2166.63	2166.64	−0.01
1, 3, 5 Trimethylbenzene	2167.14	2167.14	0.00
1, 2, 3, 4-Tetramethylbenzene	2448.42	2448.62	−0.20
1, 2, 3, 5-Tetramethylbenzene	2449.11	2449.12	−0.01
1, 3, 4, 5-Tetramethylbenzene	2449.22	2449.12	0.10
Pentamethylbenzene	2731.86	2731.12	0.18
Hexamethylbenzene	3013.86	3013.10	0.76
Naphthalene	2089.72	2089.71	0.01
α-Methyl naphthalene	2372.97	2372.69	0.28
β-Methyl naphthalene	2373.15	2372.69	0.46
o-Diethyl benzene	2442.93	2444.22	−1.29
m-Diethyl benzene	2443.62	2444.72	−1.10
p-Diethylbenzene	2443.72	2444.72	−1.00
1, 2, 3-Triethylbenzene		3007.01	
1, 2, 4-Triethylbenzene		3007.51	
1, 3, 5-Triethylbenzene		3008.01	

CALCULATION OF ATOMIZATION HEAT OF AMINES

Skinner[2] has checked up Allen's energy scheme for some primary amines. He used, besides the above mentioned parameters, also the following values : $B_{CN}=64.73$; $B_{NH}=93.45$; $\Gamma_{CCN} = 4.10$; $\Delta\begin{pmatrix} & C & \\ & C & \\ C & & N \end{pmatrix} = -1$. Working with more recent values[6,7] and extending the calculations to several compounds, we had to make use of a corrected value for B_{CN} equal to 65.13 and to introduce parameters $\Gamma_{CNC} = 4.55$ and $\Delta\begin{pmatrix} & C & \\ & N & \\ C & & C \end{pmatrix} = -1.16$. The last two values are deduced from the atomization heats of dimethylamine and trimethylamine.

As seen (table 2), for diamines we noticed rather great positive deviations, most likely due to the steric repulsion of the NH_2 groups belong-

---

[7] D. W. Good and R. T. Moore, *J. Chem. Eng. Data.*, **15**, 150 (1970).

ing to neighbouring carbon atoms. Similar observations were made by Lacher and Skinner [8] for polyhalogenated ethanes.

Table 2

Experimental and calculated heats of atomization of amines

Amine	H^a_{exp}	$H^a_{\text{calcd.}}$	$H^a_{\text{exp}}-H^a_{\text{calcd.}}$
Methylamine	549.90	549.90	0.00
Ethylamine	830.50	831.42	−0.92
n-Propylamine	1111.90	1111.42	0.48
i-Propylamine		1114.52	
n-Butylamine	1391.70	1391.42	0.28
i-Butylamine	1394.60	1394.52	0.08
1-Amino 2-methylpropane	1393.27	1393.45	−0.18
2-Amino 2-methylpropane	1398.35	1398.65	−0.30
Dimethylamine	824.00	824.00	0.00
Diethylamine	1387.00	1387.04	−0.04
Trimethylamine	1100.30	1100.3	+0.00
Triethylamine	1943.70	1944.86	−1.16
Ethylene 1,2-diamine	988.70	988.26	0.44
1,2-Propylenediamine	1272.51	1271.37	1.15
1,2-Diamino-n-butane	1552.48	1551.36	1.12
1,2-Diamino-2-methylpropane	1556.37	1555.49	0.88

CONCLUSIONS

Although the parameters Γ and Δ introduced by us are no averaged values, as in Allen's [1] and Skinner's [2] works and the range of the compounds where calculations have been carried out, by using the same parameters is large enough, the deviation of calculated values with respect to those inferred from experience is, for most compounds, smaller than experimental errors or the differences in the data of various authors. Obviously, the calculations are liable to improvements along with the ever increasing accuracy of experimental data.

Unusually great deviations are noticed for the compounds with the ethyl radical (this is also the reason of not using them for the calculation of Γ parameters). A possible explanation might be the differing effect of the atom, or group of atoms replacing one hydrogen in ethane on the non-neighbouring carbon atom, as against the case when the same atom or group replaces one hydrogen in a longer paraffin chain. We also looked for the appearance of similar situations for other classes of compounds. We have only found such deviations for halogenated derivatives (see table 3); for sulphur compounds we established that those with the ethyl radical show calculated formation heats greater, in absolute value, than those deduced from experimental data. [9] As regards the

---

J. R. Lacher and H. A. Skinner, *J. Chem. Soc.*, **A 1968**, 1034.

[9] J. P. McCullough and W. D. Good, *J. Phys. Chem.*, **65**, 1430 (1961).

oxygen compounds, no conclusions could be drawn because of the great discrepancies among the data of the various authors, especially those referring to alcohols. We note that in table 3, $\Delta H^{0}_{f.\,\mathrm{calcd.}}$ in the last but one column have been obtained by us using equation :

$$\Delta H^{0}_{f.\,\mathrm{calcd.}} = -\,6.65 - 2.35\,n - 2.58\,b_{\mathrm{CCC}} - 4.63\,b_{\mathrm{CCBr}} + \\ +\,0.55\,c\begin{pmatrix} & \mathrm{C} & \\ & \mathrm{C} & \\ \mathrm{C} & & \mathrm{C} \end{pmatrix} + 1.77\,c\begin{pmatrix} & \mathrm{C} & \\ & \mathrm{C} & \\ \mathrm{C} & & \mathrm{Br} \end{pmatrix} \qquad (5)$$

Table 3

Comparison between the heats of formation of monobrominated alifatic hydrocarbons according to different authors

Bromoalkane	$\Delta H^{0*}_{f.\mathrm{exp.1}}$	$\Delta H^{02}_{f.\mathrm{calcd}}$	$\Delta H^{02}_{f.\mathrm{calcd}} - \Delta H^{0}_{f\,\mathrm{exp.1}}$	$\Delta H^{0**}_{f\,\mathrm{exp.2}}$	$\Delta H^{0***}_{f.\mathrm{calcd.}}$	$\Delta H^{0}_{f.\mathrm{calcd}} - \Delta H^{0}_{f\,\mathrm{exp.2}}$
Bromomethane	− 9.60	− 9.85	−0.25	− 9.00	− 9.00	0.00
Bromoethane	−15.30	−16.20	−0.90	−15.30	−15.98	−0.68
1-Bromopropane	−21.10	−21.13	−0.03	−21.00	−20.91	0.09
2-Bromopropane	−23.55	−23.73	−0.18	−23.20	−23.77	−0.57
1-Bromobutane	−26.01	−26.06	−0.05	−25.65	−25.84	−0.19
2-Bromobutane	−28.66	−28.66	0.00	−28.70	−28.70	0.00
1-Bromo-2-methyl-propane	−28.40	−28.09	0.31		−27.87	
2-Bromo-2-methyl-propane	−31.20	−31.89	−0.69	−32.00	−31.82	0.18
1-Bromopentane	−31.13	−30.99	0.14	−30.87	−30.77	0.10
1-Bromohexane	−35.88	−35.92	0.04		−35.70	
1-Bromoheptane	−40.69	−40.85	−0.16		−40.63	

* $\Delta H^{0}_{f\,\mathrm{exp1}}$ are experimental values selected by Skinner[3]

** $\Delta H^{0}_{f\,\mathrm{exp2}}$ are experimental values selected by Stull, Westrum and Sinke[6]

*** Data calculated by means of equation (5)

The above hypothesis is strengthened by the fact that similar deviations also appear for the compounds with i-propyl radical where there are two CCX interactions with the marginal carbon atoms.

By means of the obtained data we can predict the formation heat of other substances of the respective classes.

Thus, according to our calculations for isobutyl-benzene, e.g. : $\Delta H^{0}_{f.}\,(\mathrm{g}) = -\,5.88$ kcal/mole, while for isopropyl amine $\Delta H^{0}_{f.}\,(\mathrm{g}) = -19.5$ kcal/mole.

In accordance with isopropyl benzene, n-propylamine, 1,2,3-trimethylbenzene data, it also appears that some experimental values adopted nowadays, will have to be corrected.

Revue Roumaine de Chimie, 17, 3, 455–460 (1972)

ULTRASONIC VELOCITY AND COMPRESSIBILITY IN RECIPROCAL FUSED SALTS SYSTEMS: Cd, Pb || Cl, Br

V. PRISSIAJNYI * and V. VASILESCU

Institute of Physical Chemistry
Str. Galaţi 31, Bucharest, Romania

Received August 2, 1971

The velocities of ultrasonic waves in $PbBr_2-PbCl_2$, $CdCl_2-CdBr_2$, $CdBr_2-PbBr_2$, $CdCl_2-PbCl_2$, $PbCl_2-CdBr_2$ and $PbBr_2-CdCl_2$ mixtures have been measured and adiabatic and isothermal compressibilities have been calculated. The excess volume – excess compressibility correlation previously established is not valid in the reciprocal salts mixtures. This might be explained by the ionic exchange reaction which takes place in these systems.

1. INTRODUCTION

The fused mixtures containing components with layer structure [1-4] are interesting since they frequently show volume effects opposite to those found in alkali-halide and complex forming mixtures. This is explained by the layer destruction which occurs on mixing.

In systems containing one of this kind of salts (Cd, Mg, Zn halides) and another bivalent salt the layer structure destruction is the main process and gives the most important effect upon volume as well as upon other physical properties. That is why these systems represent a good field for checking to what extent the excess compressibility – excess volume correlation which was proved to exist [5-9] has a general character; there are already indications that in such mixtures this corelation does not hold.[10,11] The new data obtained in this paper allow us to get more ample conclusions. This explains our choice for $PbBr_2 - PbCl_2$(I), $CdCl_2 - CdBr_2$(II), $CdBr_2 - PbBr_2$(III), $CdCl_2 - PbCl_2$(IV), $PbCl_2 - CdBr_2$(V), $PbBr_2 - CdCl_2$(VI) mixtures; we also intended to establish the relationship between the compressibility of binary and reciprocal salts systems.

---

* Permanent address: Inst. of General and Inorganic Chemistry, Academy of Sciences, Kiev, U.S.S.R.

[1] W. Bues, *Z. anorg. Chem.*, **279**, 104 (1955).

[2] M. Tanaka, K. Balasubrahmanyam and J. O'M. Bockris, *Electrochim. Acta*, **8**, 621 (1963).

[3] D. E. Irish and T. F. Young, *J. Chem. Phys.*, **43**, 1765 (1965).

[4] K. Balasubrahmanyam, *J. Chem. Phys.*, **44**, 3270 (1966).

[5] S. Sternberg and V. V. Vasilescu, *Rev. Roumaine Chim.*, **12**, 1187 (1967).

[6] S. Sternberg and V. V. Vasilescu, *Rev. Roumaine Chim.*, **13**, 265 (1968).

[7] S. Sternberg and V. V. Vasilescu, *Rev. Roumaine Chim.*, **15**, 1665 (1970).

[8] S. Sternberg and V. V. Vasilescu, *Rev. Roumaine Chim.*, in press.

[9] S. Sternberg and V. V. Vasilescu, *J. Chem. Thermodynamics*, in press.

[10] S. Sternberg and V. V. Vasilescu, *J. Chem. Thermodynamics*, **1**, 595 (1969).

[11] V. V. Vasilescu, S. Volkov and S. Sternberg, *Rev. Roumaine Chim.*, **15**, 1819 (1970).

II. EXPERIMENTAL

A pulse interference method was used (20 μs pulses with 200 Hz repetition frequency) the ultrasounds of 1 MHz being passed into the melt and picked up by silica rods.[5,12] The maximum error in velocity determinations was ± 5 $m.s.^{-1}$; the error in adiabatic compressibility did not exceed 1 %. The temperature gradient in the furnace was less than 0.5 K cm^{-1}; the temperature was maintained within ± 0.5 K. Measurements have been carried out under dry argon.

All Cd halides were prepared from Merck reagents by recrystallization and pre-melting in a strong stream of the respective pure dry hydrogen halide; $CdBr_2$ has been obtained by distillation in quartz retort, the salt being caught in Pyrex ampoules. The Pb halides have been prepared from Pb nitrate and acetate by exchange reaction with the corresponding hydrogen halide acids. The handling of salts took place in dry box under nitrogen atmosphere.

III. RESULTS

A linear dependence of velocity (u) on temperature was recorded in all 6 mixtures and the simple salts:

$$u = u_0 - at \tag{1}$$

(t is the temperature in Celsius degrees; we preserved the Celsius scale only for eq. (1), to be able to compare our data in simple salts with Bockris' data [15]).

The values of a and u_0 for simple salts and mixtures (I)—(VI) are given in table 1. Our data for $CdCl_2$ and $CdBr_2$ compare with Bockris'values [13]; the value of u in pure $PbCl_2$ was determined earlier.[5] Since no ultrasonic measurement was carried out on $PbBr_2$ there is no comparison term for it. As expected the velocity values are the same at the inversion point of mixtures (V) and (VI); this is a good proof for the reproducibility of our data. The density data were available in reference [14] for systems (I), (II) and (IV) and in reference [15] for the remaining ones. The heat capacities (C_p) of pure salts needed for calculations [5] were taken from references[13,16] and the volume changes on melting for pure

---

[12] J. O'M. Bockris and N. E. Richards, *Proc. Roy Soc. A.*, **241**, 44 (1957).

[13] J. O'M. Bockris, A. Pilla and J. L. Barton, *Rev. Chim. Acad. R.P.R.*, **2**, 69 (1962).

[14] N. K. Boardman, F. H. Dorman and E. Heymann, *J. Phys. Colloid. Chem.*, **53**, 375 (1949).

[15] B. F. Markov, V. D. Prissiajnyi and G. P. Prihod'ko, unpublished data.

[16] O. Kubashewski, E. L. Evans and C. B. Alcock, "Metallurgical Thermochemistry", Pergamon Press, New York, 1967, p. 403.

$CdCl_2$ and $CdBr_2$ from paper [13]; the volume changes on melting for $PbCl_2$ and $PbBr_2$ have been calculated from molar volumes of liquid and solid.[17]

Table 1

Temperature dependence of ultrasonic velocities for the fused Cd, Pb || Cl, Br system

X_2 mole fraction of the second salt	$-a$ m.s^{-1}K^{-1}	u_0 m.s^{-1}	X_2	$-a$	u_0	X_2	$-a$	u_0
$PbBr_2-PbCl_2$			$CdCl_2-CdBr_2$			$CdBr_2-PbBr_2$		
0.0	0.667	1458	0.0	0.380	1290	0.4	0.461	1181
0.4	0.688	1528	0.0**	0.381	1280	0.5	0.517	1237
0.5	0.740	1584	0.4	0.280	1095	0.6	0.517	1265
0.6	0.763	1616	0.5	0.306	1088			
1.0*	0.796	1739	0.6	0.317	1072			
			1.0	0.280	970			
			1.0**	0.300	984			
$CdCl_2-PbCl_2$			$CdCl_2-CdBr_2$			$PbBr_2-CdCl_2$		
0.4	0.760	1609	0.3	0.687	1538	0.3	0.599	1390
0.5	0.737	1625	0.4	0.679	1487	0.4	0.579	1376
0.6	0.767	1660	0.5	0.577	1377	0.5	0.578	1376
			0.6	0.469	1260	0.6	0.554	1365
			0.7	0.445	1201	0.7	0.488	1327

* According to reference [5];
** According to reference.[13]

The values of γ (C_p/C_V), adiabatic (β_S) and isothermal (β) compressibility ($\beta = \gamma\beta_S$), excess isothermal compressibility (β^E), excess volume (V^E), molecular ultrasonic velocity (R), calculated and experimental β^E/β_0 (β_0 is the ideal isothermal compressibility) are listed in tables 2 and 3.

---

[17] ⁂ "International Critical Tables of Numerical Data. Physics, Chemistry and Technology", Vol. 3, McGraw-Hill Book Comp., New York and London, 1928, p. 50.

Table 2

Excess quantities for mixtures (I) – (III), 873°K

Mixture	$PbBr_2-PbCl_2$					$CdCl_2-CdBr_2$					$CdBr_2-PbBr_2$		
X_2	0.0	0.4	0.5	0.6	1.0	0.0	0.4	0.5	0.6	1.0	0.4	0.5	0.6
$10^{11}\cdot\beta_S$, $m^2\cdot N^{-1}$	16.7	15.5	15.1	14.7	13.1	26.4	31.7	32.8	33.9	38.6	26.6	24.5	22.5
γ	1.306	1.331	1.337	1.343	1.368	1.126	1.109	1.104	1.099	1.082	1.171	1.194	1.217
10^{11} β, $m^2\cdot N^{-1}$	21.8	20.6	20.2	19.7	17.9	29.7	35.1	36.2	37.3	41.8	31.1	29.2	27.4
10^{11} β^E, $m^2\cdot N^{-1}$	0	0.2	0.2	0.1	0	0	−0.1	−0.2	−0.2	0	−2.6	−2.5	−2.2
$10^6 V^E$, $m^3\cdot mole^{-1}$	0	0	0	0	0	0	0	0	0	0	−0.45	−0.52	−0.52
10^3 R, S.I. units	7.07	6.89	6.88	6.84	6.76	5.67	5.67	5.69	5.72	5.82	6.29	6.40	6.51
$(\beta^E/\beta_0)\cdot 100$ calc.	0	0	0	0	0	0	0	0	0	0	−3.3	−3.9	−3.9
$(\beta^E/\beta_0).100$ exp.	0	1	1	0	0	0	0	−1	−1	0	−8.4	−8.6	−8.0

Table 3

Excess quantities for mixtures (IV) – (VI) ; 873°K

Mixture	$CdCl_2-PbCl_2$			$PbCl_2-CdBr_2$					$PbBr_2-CdCl_2$				
X_2	0.4	0.5	0.6	0.3	0.4	0.5	0.6	0.7	0.3	0.4	0.5	0.6	0.7
$10^{11}\cdot \beta_S$, $m^2\cdot N^{-1}$	18.8	17.2	16.2	17.1	19.0	21.2	23.8	26.7	19.0	20.3	21.2	22.0	23.1
γ	1.223	1.247	1.271	1.277	1.248	1.219	1.191	1.163	1.255	1.238	1.219	1.202	1.183
$10^{11}\cdot \beta$, $m^2\cdot N^{-1}$	23.0	21.4	20.6	21.8	23.7	25.8	28.3	31.0	23.8	25.1	25.8	26.4	27.3
$10^{11}\cdot \beta^E$, $m^2\cdot N^{-1}$	−1.8	−2.2	−1.8	−1.7	−2.0	−2.3	−2.3	−2.2	−2.2	−2.9	−2.3	−2.3	−2.0
$10^6\cdot V^E$ m^3 mol^{-1}	−0.51	−0.53	−0.52	−0.10	−0.12	−0.12	−0.35	−0.31	−0.27	−0.38	−0.20	−0.27	−0.20
10^3 R, S.I. units	6.09	6.22	6.32	6.50	6.41	6.32	6.18	6.09	6.61	6.42	6.30	6.17	6.03
(β^E/β_0). 100 calc.	−5.9	−6.0	−5.7	−0.9	−1.1	−1.1	−3.0	−2.6	−2.8	−3.2	−1.8	−2.6	−2.0
(β^E/β_0). 100 exp.	−7.3	−9.3	−8.0	−8.0	−8.4	−8.9	−8.1	−7.1	−9.2	−12.0	−8.9	−8.7	−7.3

IV. DISCUSSION

The parallelism between the sign of V^E and β^E which was shown to exist in binary systems with common anion[5-9] is also present in the (I)—(IV) binary mixtures studied. Characteristic of these mixtures as of other molten mixtures containing components with layer structure[10, 11] is that both V^E and β^E are negative. The binary mixtures with common cation (I), (II) have compressibilities, as expected, very close to the ideal values.

It is remarkable that the reciprocal salts mixtures (V) and (VI) have also negative V^E and β^E. This demonstrates that in reciprocal salts mixture formation the layer structure destruction plays an important role. The β^E/β_0 ratio may be calculated by the equation:

$$\beta^E/\beta_0 = \frac{V_0}{V}\,\frac{\Delta V + V^E}{\Delta V} - 1 \tag{2}$$

which was obtained[10] on the basis of Furth's[18,12] hole theory; the compressibility of liquid lattice was disregarded. In reciprocal salts V_0, ΔV and β_0 were calculated in the way indicated elsewhere.[18]

Examination of tables 2 and 3 shows that calculated (eq. (2)) β^E/β_0 for binary systems (III), (IV) are not very different from the experimental value (in systems (I) and (II) β^E/β_0 is very small and the comparison is senseless). This means that the volume effect on mixing may be approximately described by the hole model.

In reciprocal salts mixtures β^E takes values which are very close to the ones in binary mixtures; meanwhile β^E/β_0 has a different behaviour. One of the causes for this may be the influence of exchange reactions which are known to be present. The ultrasonic molecular velocity in these systems is not so sensitive to the mixing effects; its deviations from additivity are very low and no general conclusions could have been drawn.

In conclusion, to understand the behaviour of systems of the type studied here, more of them should be investigated and the compressibility (which is more sensitive than molecular sound velocity) of binary and reciprocal systems as well as the correlation between them established. This sort of correlation has been attempted for other systems.[18]

---

[18] V. D. Prissiajnyi, V. V. Vasilescu and S. Sternberg, *J. Chem. Thermodynamics*, in press.

Revue Roumaine de Chimie, 17, 3, 461–465 (1972)

ON SOME DEFINITIONS AND CONVENTIONS IN ELECTROCHEMISTRY

R. PIONTELLI

Cattedra di Chimica Fisica, Politecnico di Milano, Milan, Italy

Received July 24, 1971

The main quantities characterizing the properties and work conditions of a galvanic chain are "pseudoscalar" whose sign is correlable with the conventional choice of a positive circulation sense into the chain. In this manner the "Stockholm convention" may acquire a more rational foundation. For the particular case of a tensiometric chain formed by coupling a studied electrode with a reference electrode, one may consider both: an e.m.f. or "electrode voltage" $\mathcal{E}$ (with a sign corresponding to the so called European convention) and an "oxidation affinity" (with a sign corresponding to the "American convention").

I) The present crisis of the theoretical electrochemistry is largely acknowledged.[1] On the other hand, the disease diagnosis is still a very controversial matter, thus making also the cure difficult and remote. In the opinion of the present author, there subsists the need of a rather radical re-examination of the fundamental concepts and methods, starting from the definitions* and conventions.

In the present paper, some considerations, concerning the quantities suitable to characterize the galvanic cells, are developed.

We shall consider a "complete" chain one, in which the extremity conductors are homogeneous-isotropic electronic conductors having identical chemical-physical properties (the electric status excepted). Let us call L and L' respectively the points (poles) by means of which the chain** is connected with external conductors in a way to be able to exchange electromagnetic work with the surrounding. We shall assume the axis LL' to be and isotropy axis for the cell.*

---

[1] R. Piontelli, *Comptes rendus de la deuxième réunion de CITCE*, **1950**, 344.

* In spite of the exterior optimism of many treatises, whose leading criterium is the one of avoiding all the difficulties and of omitting the areas where the difficulties themsel ves cannot be ignored. Unfortunately these areas include a large part of the ones of applied interest and in general all those in which the existing experimental evidence and the phenomenological knowledge do not allow space for speculations.

** Which can be assimilated to an omo-thermal, omo-baric system, chemically isolated and whose electric-charge-exchanges with the surrounding are, on the whole, compensated in the steady or quasi-steady conditions here considered.

We shall assume for the sake of simplicity that chemical modifications occur in the cells when and only when a current is circulating, strictly following the Faraday laws, and that they may be completely described by a single reaction equation.

The quantities which characterize the working conditions of the cell, at any given time, when provisionally considered in absolute value (after an individual choice of unit) are:

1) the electric potential difference between the poles, or "cell voltage" E (Volt)**;

2) the circulated charge q (coulombs);

3) the advancement degree of the chain reaction ξ (the absolute value of the changes of q and ξ are bound by the equation: $|d\xi| \equiv |dq|/n\mathcal{F}$, where $\mathcal{F}$ is the "Faraday constant" while the definite positive number n (sometimes written z and called: charge number or reaction equivalence) gives the number of $\mathcal{F}$ involved by unit change of ξ);***

4) the current intensity: $\mathcal{I} \equiv dq/dt$;

5) the extensive thermodynamic properties of the chain (in particular: H, S, G);

6) their partial derivatives in respect to ξ (at constant T and P) (that is to say the "differential thermodynamic reactions effects"):****

$$\left(\frac{\partial H}{\partial \xi}\right)_{T_1P} \equiv \triangle H; \left(\frac{\partial S}{\partial \xi}\right)_{T_1P} \equiv \triangle S; \left(\frac{\partial G}{\partial \xi}\right)_{T_1P} \equiv \triangle G$$

7) the electromotive force (e.m.f.) of the chain, expressive of the internal thermodynamic affinity involved by the circulation of the unit (conventional) charge, and given (in absolute value) by $|\mathcal{E}| = |\triangle G|/n\mathcal{F}$.

The quantities: E, q, $\mathcal{I}$, ξ, $\triangle H$, $\triangle S$, $\triangle G$, $\mathcal{E}$ are defined as a rule in algebraic value by means of a conventional sign choice. This is often explicitely considered only for $\mathcal{E}$.

The choice of the sign convention for $\mathcal{E}$ has been however, a very controversial matter, the subject of a semi-secular conflict between the so-called "european" and "american" conventions, a battle officially settled* by the: "Stockholm convention" (1953)**, whose content is too universally known to deserve to be recalled it here.

---

* By assuming, as we do, the extremity conductors to be identical, E may be operationally defined without ambiguity and it corresponds either to the "Volta potential difference" or to the ,,Galvani" one, and it may be determined by the usual tensiometric methods.

** The LL' axis being an isotropy axis, the distribution of the current is uniform along any of the cross-sections normal to this axis.

*** When utilizing ξ as the chemical evolutive coordinate, one must recall the conventional choices associated with it: a) origin (that is the chemical configuration, in which we conventionally assume: $\xi \equiv 0$); b) unitary change (choosen when the absolute values of the stoichiometric coefficients, containing an arbitrary common numerical factor, are selected); c) the sign attributed to the changes according to the reaction direction.

**** By defining the thermodynamic reaction effects as the result of the application to the extensive quantities of the system of the differential operator: $\triangle \equiv (\partial/\partial\xi)_{T,P}$, these effects may be defined in rigorous manner also when the relative composition is changing and the effects are functions of ξ. The usually considered effects $\triangle H$, ΔG a.s.o. concern the case in which reactants and producs are taken in standard reservoirs.

The main disadvantage of this convention is the fact that the convention is made to depend on another artificial and unnecessary conventional choice of a scheme for the chain, in which "left" and "right" poles are distinguished, while the general physical basis, which must correlate the signs of all the above quoted quantities are ignored.

The author of the present paper has proposed, since a long time,[1] his own solution to the problem, in view of giving to the sign convention a basis resting on intrinsic characteristics, extended to all the "pseudoscalar" quantities characterizing the chain.

The present paper gives more explicit a formulation of the same ideas, avoiding, moreover, the formerly introduced notations, which were criticized, at the time, as being "typographically heavy" and leading to interference between the superscripts introduced to recall the sign conventions and those indicating standard conditions and others.

II) We shall consider, first of all, two classes of chains according to the presence or, on the contrary, absence of a cross-section in respect to which the chain is symmetric as far as the nature and succession order of the phases*** are concerned.

For the chains of the first class (that is possessing this plane) the senses in which we may run along internally are not intrinsically distinguished.

These chains, however, are also devoid of e.m.f.; while any practical work condition imposes a distinction among the circulation senses or extremities.

We shall no longer therefore consider the chains of this class.

For the chains of the other class the extremities of the $L-L'$ axis and the opposite senses: from L to L', or viceversa, are intrinsically distinguished, independently of any conventional representation scheme, or in other words these chains possess an intrinsic, physical polarity.

The adoption of a sign convention for the quantities which characterize the work conditions of the chain is simply an abridged way to correlate these quantities with this intrinsic polarity of the chain, that is to express for instance that the considered "conventional charge" is circulating into the chain from L towards L' a.s.o.

---

* At least for the IUPAC followers.

** This convention was the result of a very laborious compromise among the subcommissions IUPAC for Chemical-Physic and Electrochemistry. The present author was a Vice-President of the Electrochemistry sub-commission at the time, and he was explicitely contrary to not a few of the implications of the final text. It is perhaps superfluous to state that present author shares the universally accepted conventions concerning: 1) the sign attributed to the charge of the "negative electron"; 2) the consideration of "conventional" electric currents (that is considered due to the flowing of positive charges).

*** Also if not in respect to the form and size of the phases themselves (no relevant circumstances for our present purposes). We shall thus consider here the existence of a symmetry plane for the chain "scheme".

By attributing to these quantities a sign, correlated to this circulation sense (or substitutive of a precision on their polarity), we make them to be "pseudoscalar", that is to be quantities defined in algebraic value, with a conventional sign correlated to a conventional sense.

Let us now assume as positive the internal displacements : from the pole L'[*] (thus assumed as the *origin* of the positive displacements) towards the other L (terminal).

On the basis of this choice, we may attribute a positive sign :

a) to the (conventional) charges q, circulating in the chain from L' towards L ;

b) to the current intensity $\mathcal{I}$ when, carrying the (conventional) charges from L' towards L ;

c) to the $\triangle\xi$ corresponding to a charge circulation in the positive sense[**] ;

d) to the applied voltage E, when it represents the work of the electrostatic forces when the unit of (conventional) charge passes from L' to L (that is when the electric potential of L' is greater than the one in L) that is : $E \equiv V_{L'} - V_L$;

e) to the e.m.f. $\mathcal{E}$ when it represents the thermodynamic affinity made available when the unit of (conventional) charge passes from L' to L (that is G decreases).

We shall then have : $\mathrm{d}q = \mathcal{I}\,\mathrm{d}t = n\mathcal{F}\,\mathrm{d}\xi$ and :

$$\mathcal{E} \equiv -\left(\frac{\partial G}{\partial q}\right)_{T,P} = -\left(\frac{\partial G}{\partial \xi}\right)_{T,P}\frac{\mathrm{d}\xi}{dq} = -\frac{\triangle G}{n\mathcal{F}}$$

Elementary thermodynamics indicates that the (algebraic) sum $E + \mathcal{E}$ represents the total (or electrochemical) affinity available for the circulation of the unit charge into the chain from L' towards L.

At equilibrium we thus have :

$$E_{\mathrm{Eq}} = (V_{L'} - V_L)_{\mathrm{Eq}} = -(V_L - V_{L'})_{\mathrm{Eq}} = -\mathcal{E} = \frac{\triangle G}{n\mathcal{F}}$$

or also : $\mathcal{E} = (V_L - V_{L'})_{\mathrm{Eq}}$.

In other words, in the frame of the choice of L' as the origin of the positive displacements into the chain, when $\mathcal{E} > 0$, $(V_L - V_{L'})_{\mathrm{Eq}} > 0$ that is L is the positive pole of the chain, or also the *sign of $\mathcal{E}$ gives directly the electric polarity of the chain terminal L.*

---

[*] Irrespective of the position (left or right) attributed to L' in the representative scheme.

[**] This choice for the $\triangle\xi$ sign does not depend on the particular form attributed to the reaction equation. One may, however, consider as especially suited the form :

$$a_1A_1 + a_2A_2 + \dots \xrightarrow{\Delta\xi} b_1B_1 + b_2\,B_2 + \dots$$

(A being the species consumed and B the formed ones when the reaction is due to the circulation of charge in the positive sense).

In the above considerations we had no "a priori" reasons for choosing L' instead of L as the origin.

A reason for suggesting such a choice intervenes for instance when comparing the thermodynamic properties of the (tensiometric) chains formed by a series of "electrodes" to be investigated coupled with a given "reference electrode".

We shall then denote by L' the pole inherent to the reference electrode, and thus by L the one inherent to the electrode under study.

When one chooses to define the e.m.f. of the tensiometric cell so that to make it express the excess (in absolute value and sign) of the electric level of the pole L in respect to L' at equilibrium (a choice corresponding to the Stockholm convention*, one should adopt L' as the origin, or the $L' \rightarrow L$ circulation sense as positive.

The sign of $\mathcal{E}$ then expresses the polarity of the studied electrode in the tensiometric chain at equilibrium.

Instead of considering the electric potential difference between the poles L and L' of the chain at equilibrium, we may consider, on the contrary, the "oxidation affinity" ** of the partial reaction occurring at the studied electrode (L), given in relative value in respect to the one of the reaction occurring at the reference electrode (L').

This choice (which corresponds to the Lewis convention) may be realized either by assuming L as the origin of the positive displacement in the cell, or by maintaining the precedent choice of L' as the origin, but by considering instead of $\mathcal{E}$ the quantity :

$$\mathcal{P} \equiv \left(\frac{\partial G}{\partial q}\right)_{T,P} = \frac{\triangle G}{n\mathcal{F}} = -\mathcal{E}.$$

The above considerations lead to the following conclusions.

1) the conflict between the so-called european and american conventions arises from the confusion between two different concepts, for which also two different conventional choices of sign are admissible ;

2) it is, however, logically necessary to put the conventions concerning the e.m.f. in a general convention system inherent to the whole of the pseudoscalar quantities characterizing the properties and work conditions of a galvanic chain ;

3) it should be very opportune to eliminate the diction "electrode potential" as entirely unfit and confusing as far as this is utilized for both $\mathcal{E}$ and $\mathcal{P}$, which should be called : electrode voltage (in respect to the given reference electrode) and oxidation affinity, respectively ***.

The extension of the above convention system to the general case (including non-equilibrium conditions) has been discussed elsewhere.[3]

---

* According to which L becoms the left end in the chain scheme.

** A name opportunely proposed by the CND of CITCE :

*** Of course, the name of "electrochemical potential" for either $\mathcal{E}$ or $\mathcal{P}$ is even more unsuitable being already utilized to indicate the thermodynamic quantity $\bar{\mu}$ (see ref.[2]).

[2] R. Piontelli, *Electrochim. Metallorum*, 4, 85 (1969).

[3] R. Piontelli, *Electrochim. Metallorum*, 4, 11 (1969).

Revue Roumaine de Chimie, 17, 3, 461 – 465 (1972)

In the above considerations we had no a priori reason for choosing L instead of R as the origin.

A reason for suggesting such a choice may occur for instance when considering the thermodynamic properties of the (conventional) chain formed by a series of "electrodes" to be investigated coupled with a given "reference electrode".

We shall then denote by L the pole relative to the reference electrode and thus by R the one inherent to the electrode under study.

When one chooses to define the e.m.f. of the thermodynamic cell so as to make it express the excess (in absolute value and sign) of the electric level of the pole R in respect to L at equilibrium, a choice corresponding to the Stockholm convention, one should adopt L as the origin of the [illegible] excursion sense as positive.

The sign of E then expresses the polarity of the studied electrode in the thermodynamic chain at equilibrium.

Instead of considering the electric potential difference between the poles R and L of the chain at equilibrium, we may consider, in the same way, the corresponding affinity A' of the partial reaction occurring at the studied electrode (i.e. given a relative value in respect to the one of the reaction occurring at the reference electrode) [illegible].

This choice, which corresponds to the [illegible] convention, may be realized either by assuming as the origin [illegible] the positive direction [illegible] of the cell, or by maintaining the previous choice of L as the origin, but by considering instead of E the quantity

$$[illegible]$$

The above considerations lead to the following conclusions.

1) The content of the so-called European and American conventions [illegible] the equations between two different concepts, for which also two different conventions of sign are admissible.

2) It is, however, generally desirable to avoid [illegible] conventions concerning the [illegible] of [illegible] system in regard to the choice of the fundamental quantities characterizing the properties and work conditions of a galvanic chain.

3) It should be very opportune to eliminate the term "electrode potential" as [illegible] used and confusing as far as this is utilized for E and E', which should be called "electrode voltage (in respect to the given reference electrode) and oxidation affinity", respectively [**].

The extension of the above convention system to the general case (including non-equilibrium conditions) has been discussed elsewhere [*].

---

[*] According to which [illegible]

[**] [illegible] proposed by the [illegible]

[***] Of course, the use of [illegible] thermodynamic potentials [illegible] is even more [illegible] to indicate the thermodynamic quantity [illegible].

[illegible]

[*] R. Piontelli, [illegible]

Revue Roumaine de Chimie, 17, 3, 467–470 (1972)

HIGH-TEMPERATURE MICROCALORIMETRY. THE THERMAL DECOMPOSITION OF $Cr(CO)_6$ AND OF $Mo(CO)_6$

H. A. SKINNER and Y. VIRMANI
Chemistry Department, University of Manchester, Manchester, M13 9PL

Received December 13, 1971

The Calvet high temperature microcalorimeter was used to measure the endothermic heats of thermal decomposition of the hexacarbonyls of chromium and molybdenum, in the temperature range 240–260°. The calorimeter, used as a "drop" calorimeter, was calibrated by using the vaporization of iodine as standard process. From the measured decomposition heats, the enthalpies of formation, ΔH_f^0 [Cr (CO_6, *c*] = − 223.5 ± 3 and ΔH_f^0 [Mo $(CO)_6$, *c*] = −229.5 ± ± 3 kcal mol^{-1} were derived. The latter (uncorrected for the thermal effects from surface adsorption of CO on the metal formed) may be slightly less negative than the true values.

The Calvet high temperature microcalorimeter is finding increasing usage for thermal studies in the range 200–1000°, in particular by metallurgical thermochemists.[1] There would seem to be ample scope for the Calvet instrument in the study of a variety of chemical reactions occurring at high temperatures, notably those involving thermal decomposition, although little has as yet been done. In the present work, the Calvet instrument was used as a drop calorimeter to measure the enthalpy of thermal decomposition of the hexacarbonyls of molybdenum, tungsten, and chromium. The measurements were made at fixed temperatures in the range 200–300°, on samples of carbonyl weighing only a few milligrams.

EXPERIMENTAL

The Calvet high temperature microcalorimeter (Setaram, Lyon) was the twin cel model, operating range from 100°–800°. The heat sink, made of Kanthal, contained two cavities, lined with twin thermopiles (each of 198 Pt–Pt/Rh thermocouples), wherein the twin cylindrical cells (Kanthal; 1.7 cm diameter, 8.5 cm ht) fitted closely. Temperature

---

[1] Colloques Internationaux du C.N.R.S., No. 201, "Thermochimie", Marseille, 30 June–2 July, 1971.

control of the calorimeter was achieved by use of the Setaram RT64 temperature regulator. The output from the thermopiles, which were connected in opposition, was fed to a sensitive galvanometer (Sefram), the mirror movement of which was followed and recorded by a Photodyne spot-follower. Each Kanthal cell was loaded with a close-fitting Pyrex glass reaction vessel, which was supported off the base of the cell on a table made from a short piece of glass tubing (14 mm high) with a platinum disc acting as table top. Samples were dropped from outside the calorimeter into the Pyrex reaction vessel via the inlet chute (length 70 cm, o.d. 0.4 cm). Carbonyl samples were contained in thin glass capillary tubes, 1cm long, made from Drummond Microcaps. In a ,,drop" experiment, a carbonyl-packed capillary was let fall into the "live" cell at the same time as a similar, but empty, glass capillary was dropped into the "reference" cell. In this way, the thermal effects of the glass capillaries entering the cells cancelled out, so that the recorded thermogram related solely to the thermal decomposition of the carbonyl sample.

The hexacarbonyls used were commercial products (B.D.H. Ltd.; R. N. Emanuel, Ltd.; Alfa Inorganics, Inc.), and were purified before use by repeated fractional sublimation *in vacuo*. The Pyrex reaction vessels were thoroughly dried by gentle heating *in vacuo*, and then charged with argon gas (Puragon: O_2 impurity 3 parts per million) before placing in position in the microcalorimeter.

Preliminary test experiments showed that thermal decomposition of $Cr(CO)_6$ begins at *ca.* 140°, of $Mo(CO)_6$ at *ca.* 150°, and of $W(CO)_6$ at *ca.* 170°. To achieve rapid and total decomposition within the Pyrex reaction bulb, it proved necessary to regulate the hot zone at *ca.* 100° above onset temperatures. Measurements were therefore made with the calorimeter temperature set at fixed values within the range 240°—300°. It proved necessary to limit the quantity of carbonyl introduced at one time to a few milligrams (usually 2 to 3 mg), otherwise vapour escaped the hot zone, and decomposition occurred to some extent in the inlet chute. Thus, whereas 10 mg $Mo(CO)_6$ introduced into the reaction vessel (at 260°) in four doses of 2.5 mg decomposed completely *within* the cell, a sample dose of 10 mg gave some metal deposits forming *outside* the reaction cell, and produced a ,,dirty" inlet tube. A molybdenum mirror deposited in the reaction vessel was easily dissolved in nitric acid, and the resulting solution was perfectly clear, without trace of carbonaceous dust. Tungsten mirrors formed from $W(CO)_6$ could be dissolved in warm hydrochloric acid, giving perfectly clear solutions. We were, however, unable to dissolve chromium mirrors in acid, even after prolonged boiling.

The calorimeter was calibrated electrically (Joule heating) in the recommended manner at selected temperatures in the range 200—300°. Electrical calibration, however, was not accepted as final in view of our usage of the calorimeter for ,,drop" experiments, and we have given main weight to calibrations based directly on ,,drop" measurements using iodine as standard substance. In these check experiments, identical iodine samples were dropped simultaneously into ,,live" and ,,reference" cells to evaluate the out-of-balance of one side with respect to the other; iodine samples were also dropped separately on each side to evaluate the individual cell calibration constants.

The temperature pick-up by a sample during the ,,drop" was estimated from drop experiments with samples of tin, and of platinum wire, encased in glass capillaries. There is some variability in pick-up from one drop to another, but the error arising from this is thought to be small.

Drop experiments with metal carbonyls frequently gave an abnormally low endothermic effect for the first sample, compared with subsequent drops of samples 2, 3, and 4 into the same reaction cell. The initial release of free metal on the glass surface may have acted as "getter" for trace impurities on the reactor surface, and the initial formation of metal film is also surface active for adsorption of CO. Both factors act in the same way thermally, reducing the true value of ΔH (decomposition). The thermograms given by the first drop in a series were discounted in evaluating the heats of decomposition.

RESULTS

Preliminary results are available on the heats of decomposition of Cr (CO)$_6$ at 514 K, and of Mo (CO)$_6$ at 534 K. The measured ΔH_{obs} refer to the processes

$$\text{(i)}\ \mathrm{Cr(CO)_6},\ c\ [T_1 \sim 320\ \mathrm{K}] \rightarrow \mathrm{Cr}\ (c) + 6\mathrm{CO}\ (g)\ [T_2 = 514\ \mathrm{K}]$$

$$\Delta H_{\text{obs}} = 74 \pm 3\ \mathrm{kcal\ mol^{-1}}$$

and

$$\text{(ii)}\ \mathrm{Mo(CO)_6},\ c\ [T_1 \sim 325\ \mathrm{K}] \rightarrow \mathrm{Mo}\ (c) + 6\ \mathrm{CO}\ (g)\ [T_2 = 534\ \mathrm{K}]$$

$$\Delta H_{\text{obs}} = 81 \pm 3\ \mathrm{kcal\ mol^{-1}}$$

Corrected to 298 K, the enthalpies of decomposition become

(i) $\Delta H = 65 \pm 3$ kcal mol^{-1} for Cr (CO)$_6$, and

(ii) $\Delta H = 71 \pm 3$ kcal mol^{-1} for Mo (CO)$_6$.

Ignoring for the moment the thermal corrections arising from surface adsorption of CO on the metallic films produced by decomposition, these ΔH values lead to standard enthalpies of formation as follows : —

$$\Delta H_f^0\ [\mathrm{Cr(CO)_6},\ c] = -\ 223.5 \pm 3\ \mathrm{kcal\ mol^{-1}}$$

and

$$\Delta H_f^0\ [\mathrm{Mo(CO)_6},\ c] = -\ 229.5 \pm 3\ \mathrm{kcal\ mol^{-1}}$$

The current literature values,[2] based on heat of combustion measurements by Cotton, Fischer and Wilkinson [3] are −257.4 and −234.9 kcal mol^{-1} respectively. Bearing in mind that static bomb combustion measurements on organometallic compounds are often difficult to interpret because of incomplete oxidative combustion of the metal, the present result for Mo (CO)$_6$ may be said to be in fair agreement with that obtained from combustion calorimetry. The discrepancy in the case of Cr (CO)$_6$, however, is much larger, and indicates that there may be a large error in the currently recommended ΔH_f^0 value for Cr(CO)$_6$.

It is clear that the thermal decomposition results need correction to allow for the exothermic effects arising from surface adsorption of CO gas on the metal formed. Surface adsorption heats per mol CO adsorbed are substantial,[4] but even on the micro-scale we have used, it seems unlikely that correction for this effect should amount to more than a few kcal mol^{-1} metal, provided that adsorption is limited to those metal atoms at, or near to, the surface of the metal film. Measurements are in progress on the heat of the decomposition reaction:

---

[2] National Bureau of Standards, Washington, Technical Report 270—4, 1969.

[3] F. A. Cotton, A. K. Fischer and G. Wilkinson, *J. Amer. Chem. Soc.*, **78**, 5168 (1956).

$$Cr(CO)_6 + \frac{3}{2} I_2(g) \rightarrow CrI_3(c) + 6CO(g)$$

which, it is hoped, will eliminate this uncertainty, present in the direct thermal decomposition studies. Preliminary results strongly indicate that the ΔH_f^0 value from combustion calorimetry is too negative, although perhaps not by such a large margin as the present results from thermal decomposition (uncorrected for CO adsorption) would suggest.

---

[4] D. Brennan and F. H. Hayes, *Phil. Trans. Royal Soc.*, A (London), **258**, 347 (1965).

Revue Roumaine de Chimie, 17, 3, 471–475 (1972)

STUDIUM DER ANREGUNG DER HOCHOFENSCHLACKE MIT NATRONSILIKAT UND NATRONFLUOSILIKAT

I. TEOREANU und ANNEMARIE PURI

von der Polytechnischen Hochschule, Lehrstuhl-Technologie der Silikate und Oxyde, Bukarest
str. Polizu, 1

Eingegangen am 7. September 1971

An Hand von Röntgenanalysen und pH-messungen werden die physikalisch-chemischen Prozesse untersucht, welche bei der Erhärtung einer mit Zusätzen von Natronsilikat (allein oder zusammen mit Natronfluosilikat) angeregten industriellen Hochofenschlacke stattfinden. Auf Grund der Versuchergebnisse wird erachtet, daß sich der Einfluß der Anreger (in den in der Arbeit verwendeten Quantitäten) hauptsächlich auf die im erhärtenden System auftretenden Ionengleichgewichte und auf den Polykondensationsgrad des erhärteten Zementsteines auswirkt.

1. EINLEITUNG

Die Möglichkeit der Anregung des Erhärtungsprozesses der Schlacken durch Natronsilikat wird von einigen Autoren angezeigt.[1–4] Durch diese Art der Anregung kann man, besonders wenn sie von geeigneten hydrothermalen Behandlungen begleitet wird, bedeutende mechanische Festigkeiten erreichen. In einer früheren Arbeit[4] haben wir, an Hand von Messungen der plastischen Widerstandsfähigkeit, das Vorhandensein von zwei Etappen in der Bildung der räumlichen Erhärtungsstruktur festgestellt; in der ersten Etappe (welche von Rebinder[5] Induktionsperiode genannt wurde) tritt in dem Komplex der hydratisierten Teilchen ein Struktur und Konkretionskontakte bildender Prozeß auf; in der folgenden Etappe wachsen diese Kristalle, verfilzen sich untereinander und bilden die räumliche Erhärtungsstruktur. Die Gegenwart von Natronsilikat und noch mehr von Natronsilikat und Natronfluosilikat zusammen, bewirkt eine bedeutende Abkürzung der Induktionsperiode und beschleunigt die Entwicklung der räumlichen Erhärtungsstruktur in der

---

[1] V. V. Constantinov und G. I. Pujanov, *Stroit. mat.*, **6**, (8), 33 (1960).

[2] A. P. Tarasova u.a., Za stoikie beton. i zhelezobeton. stroit., Dokl. Sovetsk. Moskva, 1965 (1966), S. 74.

[3] B. S. Dobrov, Izdel. met. shlacov, Ural. Nauchn. - Issled. Proekt. Inst. Stroit. Mat., Moskau, 1965.

[4] I. Teoreanu, A. Puri und P. Baltă, *Bul. Inst. Polit. București*, **30** (5–6), 85 (1968).

[5] E. E. Segalova und P. A. Rebinder, *Stroit. mat.*, **6**, (7), 21 (1960).

zweiten Etappe. Die vorliegende Arbeit soll Informationen über die Art des Einflusses der oben genannten Anreger bringen.

Es wurde eine industrielle Hochofenschlacke aus Hunedoara, deren Zusammensetzung unten angegeben ist, verwendet :

Oxid	SiO_2	Al_2O_3	Fe_2O_3	Mn_3O_4	CaO	MgO	S	Unlösl.	Fe_{Metall}
%	37,52	7,80	0,24	0,66	48,18	4,30	0,73	0,25	0,21

Es wurde sowohl mit Mörtel (Schlacke : Sand = 1 : 3) als auch mit Schlacke allein gearbeitet; das Verhältnis Wasser: Festkörper betrug in beiden Fällen 0,4. Die Anregung wurde mit 2%, 5% und 8% Natronsilikat sowie mit 8% Natronsilikat und 2% Natronfluosilikat zusammen, durchgeführt.

Die Schlacke und der Sand wurden zu einer Feinheit entsprechend einem Rest von 6% auf dem 4900 Maschen/cm²-Sieb vermahlen, das Modul „n" (Verhältnis zwischen Mole SiO_2 und Mole Na_2O) des Natronsilikates war 3,45 (es scheint bemerkenswert daß, auf Grund der in der Arbeit [4] gefundenen Werten, bei der unter normalen Zuständen erhärteten, mit Natronsilikaten mit kleineren Modulen angeregten Hochofenschlacke, größere mechanische Festigkeiten erzielt werden); das Natronfluosilikat war chemisch rein.

Die Proben wurden bis zu den verschiedenen Untersuchungsterminen in Behältern mit feuchtigkeitsgesättigter Atmosphäre aufbewahrt. Als Untersuchungsmethoden wurden Röntgenographie (Debyegramme mit $Cu_{K\alpha}$-strahlung) und pH-messungen (mit einer Molybdänelektrode) verwendet. Um die intergranuläre Lösung der Pasten zu extrahieren (zwecks pH-messungen) wurden diese in einer speziellen Matritze mit 400 daN/cm² gepreßt.

2. DARSTELLUNG UND DISKUSSION DER ERGEBNISSE

Die Debyegramme der nichtangeregten Schlacken weisen, nach sieben Tagen Hydratationsdauer, keine, den Hydratationsprodukten charakteristischen Linien auf, obwohl die Interferenzen der nichthydratisierten Schlacke nicht mehr zu erkennen sind. Zu diesem Zeitpunkt ist der pH-Wert der Probe nur 10,15, also niedriger als der für die Bildung von tobermoritähnlichen Hydrosilikaten bekannte Gleichgewichtswert von pH = 10,65.[6] Das langsame Anwachsen der pH-Werte gestattet, nach 28 Tagen Hydratationsdauer, die Bildung von Kalciumhydrosilikaten; röntgenographisch kann man die Linien von weniger basischen Hydrosilikaten — CSH (I) — feststellen.

Bei der nicht angeregten Schlacke kann man, nach drei Monaten Hydratationsdauer, klar die Interferenzen der Hydrosilikate feststellen. Es treten die Linien 2,678 Å und 3,021 Å auf, welche von Schwiete und Mitarbeitern [7] den Hydrosilikaten der Art (C, M) SH (ähnlich dem von Sweet [8] entdeckten, natürlichen, tobermoritischen Mineral — Tacharanit — mit 3,2% MgO im Gitter) zugeschrieben werden. Die Verschiebung einiger, den Hydrosilikaten charakteristischen Interferenzen, weisen auf die Möglichkeit einer teilweisen Ersetzung der Si^{4+}-ionen durch Al^{3+}-ionen hin; diese Tatsache wird auch in einer Arbeit [9] bezüglich der Hydratation der mit Klinker angeregten Gehlenit- und Anortitschlacke, bei Anortit sogar ohne Anreger, festgestellt. Die Möglichkeit einer teilweisen Ersetzung der Si^{4+}-ionen des Tobermoritgitters mit Al^{3+}-ionen wurde von Kalousek [10] schon 1957 angezeigt. Die Linie bei 3,58 Å (welche auch bei den angeregten Proben auftritt) könnte das Vorhandensein von hexagonalen Aluminathydraten der Art $2CaO.Al_2O_3.8H_2O$, anzeigen. Es ist wahrscheinlich, daß die restlichen Interferenzen (3,9716 Å, 4,337 Å und 5,065 Å) der gegebenen Schlacke charakteristischen Hydraten, welche in den gegebenen pH-Gebieten stabil sind, angehören.

---

[6] V. I. Babuşhkin, G. M. Matveev und O. P. Mcedlov-Petrosian — „Termodinamika silikatov", Izd. Lit. Stroit., Moskau, 1965.

[7] H. E. Schwiete, U. Ludwig, K. E. Würth und G. Grieshammer, *Zement-Kalk-Gips* **22**, 154 (1969).

[8] J. M. Sweet, *Minerolog. Mag.*, **1961**, 745.

Es ist interessant hervorzuheben, daß aus den Debyegrammen der drei Monate lang hydratisierten, plastischen Mörtelproben, die den tobermoritähnlichen Hydrosilikaten und den Hydrosilikaten mit eingebauten Mg^{2+}-ionen charakteristischen Interferenzen fehlen.

An Hand von röntgenographischen Untersuchungen wird festgestellt, daß der Einfluß des Natronsilikates auf den Erhärtungsprozeß der untersuchten Schlacke hauptsächlich ,,physikalischer'' Natur ist. Die Debyegramme weisen keine neuen, der angeregten Schlacke charakteristischen Linien, auf, welche chemischen Verbindungen aus dem System Schlacke-Anreger-Wasser zugelegt werden könnten.

Bei den mit Natronsilikat angeregten Schlackenproben erscheinen, schon nach sieben Tagen Hydratationsdauer, schwache Linien, welche das Vorhandensein von Hydrosilikaten CSH (I) oder (C, M) SH andeuten.

Es ist wahrscheinlich, daß diese Hydrosilikate sich auch in den angeregten Mörtelproben bilden, aber unter den gegebenen Arbeitsbedingungen röntgenographisch nicht identifiziert werden konnten.

Bei den mit 5% und 8% Natronsilikat angeregten Schlackenproben treten, nach drei Monaten Hydratationsdauer, Interferenzen auf, welche das Vorhandensein von Hydrosilikaten sowohl der Art CSH (I) als auch CSH (II) und (C, M) SH anzeigen. Das Vorhandensein einer Linie bei 3,58 Å entspricht wahrscheinlich, wie schon gezeigt wurde, der Verbindung $2CaO.Al_2O_3.8\,H_2O$. Diese Linien fehlen in den angeregten Mörtelproben; für die mit 8% Natronsilikat angeregten Mörtelproben erscheinen Linien welche weiter oben Hydraten der gleichen Zusammensetzung mit der nichthydratisierten Schlacke zugeschrieben wurden (3,972 Å, 4328 Å und 4,962 Å).

Die mit Natronsilikat und Natronfluosilikat zusammen angeregte Schlacke weist qualitative Unterschiede auf. Die Intensität der, den Hydrosilikaten (C, M) SH charakteristischen Linien, welche nach 7 Tagen Hydratationsdauer gut sichtbar sind, wird nach 28 Tagen Hydratationsdauer bedeutend schwächer, während man diese Linien bei den drei

---

[9] I. Teoreanu und M. Georgescu, *Rev. Roumaine Chim.*, **16**, 33 (1971).

[10] G. L. Kalousek, *J. Amer. Ceram. Soc.*, **40**, 127 (1957).

Monate lang hydratisierten Proben überhaupt nicht mehr erkennen kann. In den Debyegrammen der drei Monate alten Proben erscheinen andererseits zwei starke Linien (3,72 Å und 4,137 Å), welche bei den nicht angeregten oder nur mit Natronsilikat angeregten Proben nicht vorkommen und welche ein Hinweis auf das Vorhandensein eines ausgeprägten Polykondensationsprozesses oder von chemischen Reaktionen im System Schlacke-Anreger-Wasser sein könnten; eine isomorphe Ersetzung der Ca^{2+}-Ionen der Hydrosilikate durch Na^{+}-Ionen ist ebenfalls möglich. Die Bildung von Natronkalziumhydrosilikaten ist, gemäß den Arbeiten von Pujanov[11] auch in Abwesenheit von Natronfluosilikat möglich; daß sie in unserem Fall röntgenographisch nicht identifizierbar sind, ist wahrscheinlich ihrem gelartigen Charakter zuzuschreiben; aus demselben Grunde können eventuell vorhandene Natronhydrosilikate röntgenographisch nicht nachgewiesen werden.

In einer früheren Arbeit[4] wurden die größten meschanischen Widerstandsfähigkeiten für Massen mit 8% Natronsilikat und 2% Natronfluosilikat erhalten. Die mechanische Widerstandsfähigkeit eines erhärteten Bindemittels hängt bedeutend von dem Kondensationsgrad und der Verschiedenheit der Hydratationsstrukturen (welche von der chemisch-morphologischen Zusammensetzung bestimmt werden), von der Entwicklungskinetik der Erhärtungsstruktur, von deren Kompaktität und inneren Spannungen, ab.

Es scheint, daß die Gegenwart des Natronfluosilikates den Kondensationsgrad der Hydratationsstrukturen hebt.[12,13] Außerdem ist es möglich, daß die vom Natronfluosilikat ausgelösten Ionengleichgewichte optimale Verhältnisse zwischen den verschiedenen chemisch-morphologischen Formationen des hydratisierten und erhärteten Systems bewirken und zu einer Entwicklungskinetik, welche die inneren Spannungen auf ein Mindestmaß herabsetzt, führen; die pH-Werte der Masse mit 8% Natronsilikat und 2% Natronfluosilikat befinden sich an der unteren Grenze der für die angeregten Proben erhaltenen Werte—Abb. 1, Kurve 3.

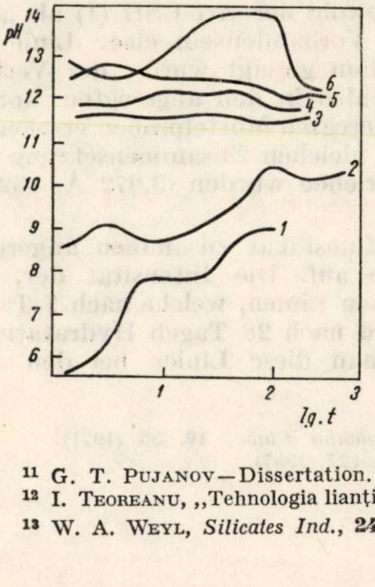

Abb. 1. — Änderung der pH-Werte mit der Hydratationszeit.

1, nichtangeregter Mörtel; *2*, nichtangeregte Schlacke; *3*, mit 8% $Na_2O.nSiO_2$ und 2% Na_2SiF_6 angeregter Mörtel; *4*, mit 8% $Na_2O.nSiO_2$ und 2% Na_2SiF_6 angeregte Schlacke; *5*, mit 8% $Na_2O.nSiO_2$ angeregter Mörtel; *6*, mit 8% $Na_2O.nSiO_2$ angeregte Schlacke.

---

[11] G. T. Pujanov—Dissertation. M. H. T. I. M. Moskau 1960.

[12] I. Teoreanu, „Tehnologia lianţilor şi betoanelor", E.D.P., Bukarest 1967, S. 371.

[13] W. A. Weyl, *Silicates Ind.*, 24, 88 (1959).

3. SCHLUSSFOLGERUNGEN

Aus den Versuchsergebnissen kann man nachstehende Folgerungen ziheen :

Es scheint, daß das Natronsilikat hauptsächlich durch eine Änderung des Ionengleichgewichtes der intergranulären Lösung wirkt, welche sowohl eine Beschleunigung der Hydratationsgeschwindigkeit, als auch Änderungen der chemisch-morphologischen Struktur der Hydrate zur Folge hat.

Zusätze von Natronsilikat mit Natronfluosilikat zusammen beschleunigen die Hydratationsprozesse in größerem Maße. Es scheint, daß die Bildung einer Erhärtungsstruktur mit einem hohen Kondensationsgrad und einer dichten Textur, welche gleichzeitig niedrige innere Spannungen hat, stattfindet. Eine chemische Interaktion oder eine teilweise isomorphe Einschließung der Na^+ - Ionen in das Gitter der Hydratationsprodukte der Schlacke scheint ebenfalls glaubhaft.

Revue Roumaine de Chimie, 17 3, 477–480 (1972)

SPECTROSCOPIC OBSERVATIONS ON NICKEL (II) PERCHLORATE COMPLEXES

VIJAY MOHAN BHATNAGAR *, **

Department of Chemistry, University of New Brunswick, Fredericton, New Brunswick, Canada

Received July 20, 1971

The regular tetrahedral structure for the ClO_4^- ion requires that it should possess two vibration frequencies, ν_3(1090, 1140 cm.$^{-1}$) and ν_4 (621 cm.$^{-1}$) which are active in the infrared spectrum. The appearance of the non-degenerate frequency, ν1 (938 cm^{-1}) in nickel (II) perchlorate complexes may be due to the distortion of the ion in a crystal field of lower symmetry than itself. The appearance of new bands, splitting of the degenrate modes, frequency shifts of the bands, etc., in nickel (II) perchlorate complexes are discussed.

In connection with the interesting contribution of Sun and Brewer [1] on the nickel (II)-γ-picoline-perchlorate complex system, some observations on the infrared spectra of nickel (II) perchlorate complexes are now reported.

The perchlorate ion, as a regular tetrahedral molecule AB_4, has nine vibrational degrees of freedom. These are distributed over one non-degenerate, one doubly-degenerate, and two triply degenerate vibrations as shown in Table 1.

Table 1

Normal vibrations of regular tetrahedral molecule ClO_4^-

Number	Class	Description
1	A_1	Totally symmetrical, stretching
2	E	Doubly degenerate, bending
3	F_2	Triply degenerate, stretching
4	F_2	Triply degenerate, bending

---

* X-ray and infrared work on nickel (II) perchlorate hexahydrate was carried out at University of New Brunswick during 1969–70.

** Permanent address: P.O. Box 399, Cornwall, Ontario, Canada.

[1] M. S. Sun and D. G. Brewer, *Canad. J. Chem.*, 49, 1502 (1971).

All four vibrations are allowed in the Raman spectrum and are assigned as follows.[2,3] The number in parentheses indicate the degeneracy of the vibration.

(1) A_1	(2) E	(3) F_2	(4) F_2
938	461	1080, 1130	627

Their position in the infrared spectrum is shown as follows :

Forbidden	Forbidden	1090, 1140	621 cm^{-1}

Until new X-ray evidence, complimented with detailed infrared and other spectroscopic studies, is reported, it is difficult to assume that the perchlorate in all the reported complexes [1] would be ionic. Also, only the infrared spectra would not reveal with certainty if the normal tetrahedral symmetry of ClO_4^- is distorted. Probably, it is not distorted very much if at all.[4] However, the presence of the totally symmetric vibration (ν_1, 938 cm^{-1}) as a weak band in the infrared spectra [1] shows that either the ClO_4^- is distorted from its usual T_d symmetry or else the environment around the ClO_4^- is not symmetrical. As the infrared spectra are generally concerned with inter-atomic vibrations, the mechanical interaction between the atoms can be adequately described by a model which is ionic. It is probable that while the atoms of the ClO_4 group are charged they may not be completely ionised. Sun and Brewer [1] have assumed ionisation within the group.

There is clear evidence of ν_1, ClO_4^-(938 cm^{-1}), several new bands and splitting of the degenerate modes, frequency shifts of the bands, and intensification of the spectra in the work of Sun and Brewer (1). The authors have assumed the activation of ν_1, (938 $cm.^{-1}$) mode and splitting of the ν_3 (1090, 1140 cm^{-1}.) mode due to the low site symmetry of the crystal lattice. The authors did not elaborate their point further nor they focussed any attention to the frequency shitfs of the ligand fundamentals caused by complex formation.

In general, the triply degenerate frequencies ν_3, (1090, 1140 cm^{-1}) and ν_4 (621 cm^{-1}) are observed in the infrared spectra of ionic perchlorates ; the former appearing as a very broad strong band with a poorly defined maxima, which is occasionally split.[5] The non-degenerate frequency ν_1, (938 cm^{-1}) is theoretically forbidden in the infrared. It seems, that in the work of Sun and Brewer (1) this absorption has become weakly allowed owing to the distortion of the ion in the crystal field of lower symmetry than itself.

Sun and Brewer [1] have observed a frequency near 1089 cm^{-1} in all the reported complexes. This frequency has not been shown either in Nujol or in $CHCl_3$ or CH_2Cl_2 spectra. It is probable that this frequency near 1089 $cm.^{-1}$ in the solid perchlorates constitutes the simplest type of

---

[2] G. HERZBERG, "Infrared and Raman Spectra of Polyatomic Molecules", D. Van Nostrand Co. New York, 1945.

[3] K. NAKAMOTO, "Infrared Spectra of Inorganic and Coordination Compounds," John Wiley and Sons, New York (1963).

[4] N. COLTHUP, personal communication.

[5] F. A. MILLER and C. H. WILKINS, *Analyt. Chem.*, **24**, 1253 (1952).

result that can arise from the combination tone $\nu_2 + \nu_4$ ($461 + 627 = 1088$ cm^{-1}). This is close enough to the unperturbed fundamental frequency ν_3 (1090, 1140 cm^{-1}).

Sun and Brewer [1] have observed free ligand peaks in Nujol and $CHCl_3$ or CH_2Cl_2 but they are not well defined in KBr. I would guess that the absorption bands arising from the coordinated γ-picoline should be almost identical in all complexes. However, 485 cm.$^{-1}$ ($\nu_{16\ b}$) of γ-picoline in $NiL_4(ClO_4)_2$ splits into two strong bands 514 and 500 cm^{-1}. This frequency shift of the ligand fundamental may be caused by the complex formation.

Furthermore, the infrared spectra of the solid complexes and of the solutions in $CHCl_3$ or CH_2Cl_2 are not identical. It may be due to slight interaction with KBr matrix or with organic solvents. This shift of frequencies may also be due to a change in the symmetry of the free perchlorate ion. In the spectra of these complexes, a shift to lower frequencies is observed on passing from the solid to the $CHCl_3$ or CH_2Cl_2 solution spectra. This may be attributed to the interactions of the solvent molecules with the Ni (II) ion along with z-axis of the square-planar complexes.[6] Sun and Brewer [1] have assumed a square planar arrangement of four γ-picoline molecules for all three perchlorate complexes.

The observed splitting of ν_3 (1090, 1140 cm^{-1}) and ν_4 (621 cm^{-1}) in the work of Sun and Brewer [1] is consistent with the loss of the T_d symmetry. The correlation (Table 2) shows the effect of this lowering of symmetry on the degeneracy of the vibration.[7]

Table 2

Correlation between T_d, C_{3v}, C_{2v} and C_s

T_d	C_{3v}	C_{2v}	C_s
A_1	A_1	A_1	A'
E	E	$A_1 + A_2$	$A' + A''$
F_2	$A_1 + E$	$A_1 + B_1 + B_2$	$A' + A' + A''$

The possible causes of the observed splitting of ν_3 (1090, 1140 cm^{-1}) and ν_4 (621 cm^{-1}) may be : 1 : distortion of the ClO_4^- tetrahedron in the crystal lattice : 2 : covalent bonding of the ClO_4^- to the metal through one or more of the oxygen atoms, and : 3 : a non-uniform field due to the water or ligand molecule round the cation. This perturbing effect of the ligand field, covalent bonding with structures, and some distortion of the perchlorate ion in the lattice may be the cause of the appearance of ν_1 (938 cm^{-1}) in all perchlorate complexes reported by Sun and Brewer.[1]

It also seems likely that instead of each cause acting alone, all three possible causes may be responsible together for the appearance of

---

[6] J. Chatt, G. A. Gramlen and L. E. Orgel, *J. Chem. Soc.*, **1958**, 486.

[7] S. D. Ross, *Spectrochim. Acta*, **18**, 225 (1962).

ν_1 (938 cm^{-1}) and the lowering of the symmetry. Certainly only the ligand fields could not cause the lowering of the symmetry as, if it were true, anhydrous compounds e.g., $NiL_4(ClO_4)_2$ should show ν_3 (1090, 1140 cm^{-1}) and ν_4(621 cm^{-1}) as singlets and ν_1 (938 cm^{-1}) should be absent. Similarly, it seems unlikely that covalent bonding could attribute to such an extent. The observed spectra are not consistent with lowering of the symmetry merely to C_{3v} when ν_3 (1090, 1140 cm^{-1}) and ν_4 (621 cm^{-1}) would be doublets. In fact, a triplet is also found for ν_3 (1090, 1140 cm^{-1}) which would imply the symmetry C_{2v}. The presence of ν_3 (1090, 1140 cm^{-1}) as a triplet, and ν_1 (938 cm^{-1}) in the spectra shows that some other factors also must be involved e.g., distortion due to the size of the cation or lattice.

Thus, it seems that the appearance of ν_1, (938 cm^{-1}) and splitting of ν_3 (1090, 1140 cm^{-1}) and ν_4 (621 cm^{-1}) in these compounds (1) may be due to the combined effect of the several causes as discussed above. Hathaway and Underhill [8] have also stated that while the effect of coordination of the perchlorate group is likely to bring about major differences in the infrared spectra, minor shifts or splittings may result from a lowering of the site symmetry of the group, from coupling of vibrations between perchlorate groups in the same unit cell or by a purely isotopic effect within the group.

Thus, until a detailed X-ray structural investigation is published, it may be assumed from the infrared spectra of the solid perchlorate complexes that the T_d symmetry of the ClO_4 ion has been reduced to C_{3v} or C_{2v}.

It is obvious that there is a great deal of work still to be done in this area of research. This is particularly true concerning the detailed and accurate infrared and X-ray data of these interesting complexes. Since the ν_1(938 cm^{-1}) mode is infrared active only for point groups compatible with a molecular dipole moment i.e., when centres of positive and negative charges of the molecule do not coincide, its appearance in nickel (II) perchlorate complexes is indicative of a lowering of the molecular symmetry from T_d to either C_{3v}, C_{2v}, etc. However, the infrared data suggest that there is probably slight deviation from C_{3v} or C_{2v} symmetry. It is difficult to suggest definitely whether the symmetry has been lowered to C_{3v} or C_{2v}. As the number of infrared active bands in the T_d, C_{3v} and C_{2v} forms are 2, 6, and 8, respectively [9]; it is possible to distinguish between these different environments of the ClO_4^- group by the number of infrared bands observed. However, the infrared data of Sun and Brewer [1] do not coincide either with T_d symmetry or with C_{3v} or C_{2v}. On the basis of infrared study, it is difficult to accept a lower symmetry with precision as the infrared spectra allow us to draw conclusions as to the highest possible symmetry of a molecular group but not regarding the lowest possible symmetry because of the difficulty of obtaining complete resolution of all bands.

---

[8] B. J. HATHAWAY and A. E. UNDERHILL, *J. Chem. Soc.*, **1961**, 3091.

[9] V. M. BHATNAGAR, *Arch. Oral Biol.*, **15**, 469 (1970).

Revue Roumaine de Chimie, 17, 3, 481–487 (1972)

A SPECTROSCOPIC STUDY OF OXOVANADIUM (V) COMPLEXES WITH MULTIDENTATE SCHIFF BASES. II

N. S. BIRADAR and V. H. KULKARNI,

Department of Chemistry, Karnatak University, Dharwar-3, India

Received June 17, 1971

The complexes of $VOCl_3$ with multidentate Schiff bases have been prepared in carbon tetrachloride medium and characterized by elemental analyses. The complexes are dark coloured amorphous substances and non-electrolytes in DMF. The IR spectra of the complexes are discussed and probable structures have been proposed.

INTRODUCTION

In this phase of our investigation on oxovanadium (V) Schiff base complexes we wish to report the syntheses and characterization of oxovanadium (V) complexes with the following multidentate Schiff bases.

EXPERIMENTAL

The chemicals used in the reactions were of reagent grade. Salicylaldehyde was distilled before use.

The Schiff bases were prepared by the method known in the literature. Vanadium-oxy-trichloride was prepared by the standard method,[1] and extracted with carbon tetrachloride after storing over metallic sodium.

Preparation of complexes

The carbon tetrachloride solution of $VOCl_3$ was treated with a slight excess of Schif base dissolved in the same solvent with vigorous shaking, and left at room temperature with occasional shaking till the evolution of HCl gas ceased. The precipitated complex was filtered, washed with carbon tetrachloride then with ether and finally dried at 45–50°.

The dry mass was powdered and extracted with carbon tetrachloride in a Soxhlet apparatus. The complex was once again washed with ether and dried at 45–50°.

Analysis

Vanadium in these complexes was estimated volumetrically [2] and chloride was determined gravimetrically as AgCl. Nitrogen was estimated by Kjeldalh method. Results of the elemental analysis are shown in table 1.

---

[1] G. BRAUER, "Handbook of Preparative Inorganic Chemistry", Vol. II, Academic Press, New York, 1965, p. 1264.

[2] A. I. VOGEL, "Quantitative Inorganic Analysis", Longmans Green, London, 1961.

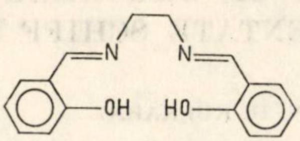

I.

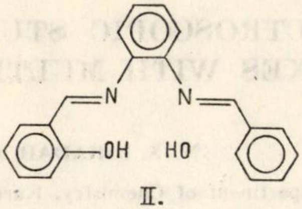

II.

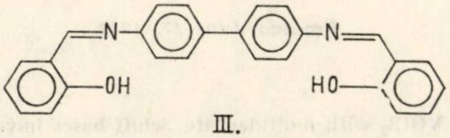

III.

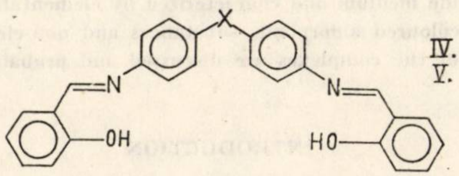

IV. X = NH
V. X = S

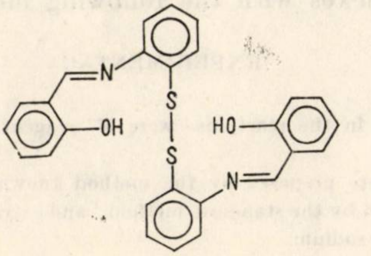

IV

Table 1

Elemental analysis of oxovanadium (V) Shiff base complexes

Lig. No.	Comp. No.	% V		% N		% Cl		Empirical formula
		Found	Calc.	Found	Calc.	Found	Calc.	
I	VII	13.41	13.83	7.45	7.60	9.40	9.63	$(C_{16}H_{14}N_2O_2)VOCl$
II	VIII	12.30	12.25	7.00	6.74	8.72	8.53	$(C_{20}H_{16}N_2O_2)VOCl$
III	IX	10.34	10.35	5.74	5.75	7.18	7.18	$(C_{26}H_{18}N_2O_2)VOCl$
IV	X	9.74	9.72	5.28	5.31	6.70	6.74	$(C_{26}H_{18}SN_2O_2)VOCl$
V	XI	9.98	10.04	8.18	8.28	6.85	6.99	$(C_{26}H_{19}N_3O_2)VOCl$
VI	XII	9.00	9.12	4.92	5.01	6.27	6.36	$(C_{26}H_{18}S_2N_2O_2)VOCl$

Physical Measurements

The conductances of the complexes in DMF were determined on an ELICO conductivity bridge C.M. 82 having cell of a cell constant 0.829 cm^{-1} manufactured by Electronic Industrial Instruments Co., Hyderabad. The infrared spectra of the ligands and the complexes in nujol mull were recorded on a Perkin Elmer infracord.

RESULTS AND DISCUSSION

The elemental analyses in table 1 show that $VOCl_3$ forms complexes with the Schiff bases (I—VI) by loosing two of its three chlorides. The molar conductances determined in DMF at the concentration 10^{-3}M make us to predict that these are non-electrolytes in DMF.

Electronic Spectra

The intense bands in the region 300—380 mμ of the ligands are replaced by more complicated broad bands of varying intensity in the oxovanadium (V) complexes. The spectra of the complexes do not resemble the spectra of the ligands. This can be taken as an evidence for the complex formation.

The band in the region 240—260 mμ appears in the ligands as well as in their complexes, and it is attributed to the $\pi-\pi^*$ benzenoid band in view of the previous work.[3]

The spectra of the ligands I—III show an increase in the intensity from I—III. This can be interpreted as a consequence of replacing CH_2-CH_2 hydrocarbon bridge successively by a phenyl ring and a biphenyl ring. This results in the increase of double bonds, and conjugation. Hence, there is an increase in the intensity. The ligands IV, V and VI show altogether different spectra because of the electron donating NH, S groups, but the intensity of the spectra almost remains the same as that of III. This suggests that NH, S and S—S groups cannot function as the conjugation transmittors.

The same trend is observed in the oxovanadium (V) complexes VII, VIII and IX of the ligands I, II and III. However, the complexes X, XI and XII show slight decrease in the intensity. This may be due to the steric hindrance of the bridging groups.

Infrared Spectra

The infrared frequencies of the ligands and their complexes are given in table 2 along with their assignments.

The presence of a broad and weak band in the region 2800—2700 cm^{-1} in the ligands (I—VI) is due to the intramolecular hydrogen bonded —OH. This band disappears in the complexes (VII—XII) indicating that the metal oxygen bond is formed with the hydroxy groups of the base.

---

[3] K. K. Chatterjee and B. E. Douglas, *Spectrochim. Acta*, **21**, 1625 (1965).

Table 2

Infrared frequencies (in cm^{-1}) of Schiff bases and their oxovanadium (V) complexes

	I	VII	II	VIII	III	IX	IV	X	V	XI	VI	XII	Assignments
1	2976	2985	3012	2985	2985	2985	2985	2985	2941	2924	2941	2985	Aromatic CH and = CH stretching
2	2632	—	2778	—	2646	—	2703	—	2564	—	2564	—	Intramolecular H-bonded-OH
3	1618	1608	1616	1613	1618	1639	1616	1613	1621	1634	1613	1613	C = N stretching vibration
4	1592	1587	1587	—	1600	1613	1587	1575	1550	1587	1587	1575	
	1565	1538	1563	1550	1575	1538	1563	1563	1520	1527	1563	1563	Aromatic C = C stretching vibrations
	1488	—	1481	1481	1497	—	1481	1493	1497	—	1493	1460	
5	1274	1316	1274	1292	1280	1295	1282	1292	1285	1370	1274	1287	Phenolic C—O stretching
6	—	961	—	970	—	1001	—	990	—	990	—	1000	V = 0 stretching
						980							

The strong band around 1280 cm^{-1} assignable to the phenolic C—O stretch in these Schiff bases (Table 2) is slightly shifted to the higher frequency.

A strong band found around 1618 cm^{-1} in the ligands is attributed to the C = N stretch in view of the previous assignments.[4,5] This band in the complexes shows a considerable shift suggesting the possible coordination of the Schiff base through the azomethine nitrogen.

All the complexes (VII—XII) show strong band around 980 cm^{-1} due to the V = 0 stretch. This indicates the high π-bond order of vanadium-oxygen bond of VO^{3+} species. The complex IX shows two strong bands (Table 2) in the VO stretching region. This helps us to infer that the complex IX may exist in the dimeric form. Ginsberg and co-workers [6] have also made similar observations in the case of oxovanadium (IV) Schiff base complexes.

The IR interpretation has revealed that the coordination bond has been formed between oxovanadium and two azomethine groups of the Schiff bases, and Vanadium-oxygen bonds have been formed between oxovanadium and ligand oxygen atoms. It is known that the ligand I is sterically very flexible and can encompass the metal moiety strainlessly. It is also reported that the ligand I, always prefers to have *cis* configuration.[7] It has been established in the case of oxovanadium (IV) that V = 0 bond is normal to the plane of the molecule.[8] In view of all these observations, and the observed non-electrolytic nature of the complex, the complex VII can be regarded as having coordination number six.

When the $CH_2—CH_2$ hydrocarbon bridge is replaced by a phenyl ring, a more rigid tetradentate II results. This ligand favours the forma-

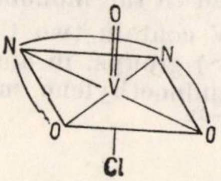

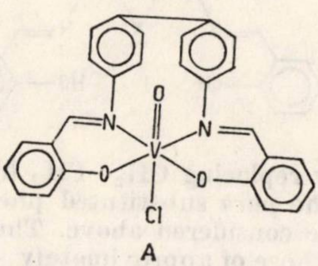

A

---

[4] N. S. Biradar, V. H. Kulkarni and N. N. Sirmokadam, *Monatsh.*, **101**, 551 (1970).

[5] N. S. Biradar and V. H. Kulkarni, *Rev. Roumaine Chim.*, **15**, 1993 (1970).

[6] A. P. Ginsberg, E. Koubeck and H. J. Williams, *Inorg. Chem.*, **5**, 1656 (1966).

[7] A. E. Martell and M. Calvin, "Chemistry of the Metalchelate Compounds", Printice Hall, New York, 1959.

[8] M. M. Jones, *J. Amer. Chem. Soc.*, **76**, 5995 (1954). R. T. Clounch, T. W. Martin, and M. M. Jones, *J. Amer. Chem. Soc.*, **83**, 1073 (1961).

tion of *cis* complexes. The oxovanadium (V) complex formed with this ligand (VIII) is a non-electrolyte and hence has coordination number six. In the light of the previous findings it may be concluded that the ligand II favours *cis* configuration in the case of oxovanadium (V).

In the case of ligand III, one can expect the following two structures for the oxovanadium (V) complex of this ligand.

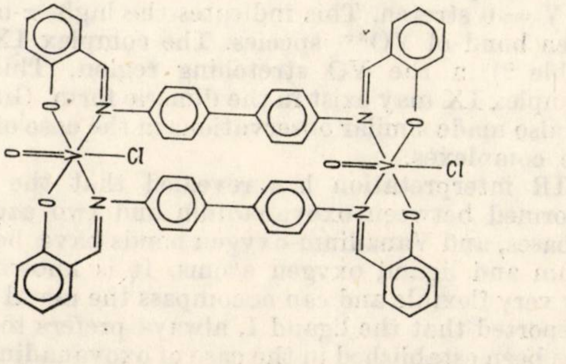

On the steric grounds, and in analogy with the known dimeric complexes[9,10] it can be predicted that the complex IX can exist in the dimeric form. Because of its limited solubility in the organic solvents the molecular weight could not be determined. However, the doublet observed in the V—O stretching region of the complex IX makes us believe that the dimeric form is preferred to the monomeric form.

The ligands IV and V contain two C = N, two —OH and one X (where X is either NH or S) groups, in analogy with the known Schiff bases *bis* (salicylidene) diaminoethylene sulphide and *bis* (salicylidene) diaminodiethylene amine.[10–12]

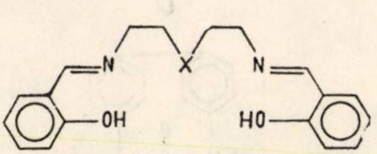

The ligands resulted by replacing CH_2-CH_2 hydrocarbon bridges in the above Schiff base by the *para* substituted phenyl rings are bulkier and more rigid than the one considered above. The pyramidal disposition of the sulphur bonds and those of approximately $-sp^{3-}$ hybridised —NH— will allow the two C = N and two —OH groups to surround a single metal ion. This results in removing the —X— far away from the position suitable for the coordination construction of the models also shows

---

[9] N. S. BIRADAR and V. H. KULKARNI, *J. Inorg. Nucl. Chem.* **33**, 3781 (1971).

[10] CONST. G. MACAROVICI, E. PERTE and E. MOTIU, *Rev. Roumaine Chim.*, **11**, 53 (1966).

[11] H. GOODWIN, "Chelating Agents and Metal Chelates", Ed. by F. P. DWYER and D. P. MELLOR, Academic Press, New York, 1964.

[12] B. DAS SARMA and J. C. BAILAR JR., *J. Amer. Chem. Soc.*, **77**, 5476 (1955).

that the C = N and —OH can encompass the metal but the molecule is much strained to involve —X— in the coordinate bond formation. The IR spectra of the complexes show only one strong band in the V—O stretching region (table 2), suggesting the monomeric nature of the complexes. The further confirmation of non-coordonation of X comes from the IR study of the complex X. The ligand IV shows a broad band around 3300 cm^{-1} and is attributed to the NH stretch. This band in the oxovanadium (V) complex X does not show any splits. The coordination of —NH— to the metal should increase the multiplicity resulting in the splitting of the —NH— band into several bands. Non-splitting of the —NH— in the complex X is suggestive of the non-coordination of the —NH— to the central oxovanadium (V). Similar observations have been reported by Bailar and Das Sarona[12] in the case of the copper (II) complex with *bis* (salicylidene) diethylene tetramine. The complexes X and XI are non-electrolytes in DMF and hence have coordination number six.

Ligand VI is more flexible than ligands IV and V, and can surround the metal without much strain. This is due to the presence of the —S—S— bridge, present in the *ortho* position. However, there may not be any coordinate bond between vanadium and di-sulphide bridge. The complex XII, formed of this ligand, is non-electrolyte in DMF and shows only one strong band for V—O stretch. This complex has also a coordination number six.

ACKNOWLEDGEMENT. The authors wish to thank Prof. D. K. Banerjee, I. I. Sc., Bangalore for the IR spectra. One of the authors (V.H.K.) is grateful to the Karnatak University for the financial assistance.

Revue Roumaine de Chimie, 17, 3, 489–495 (1972)

INDIREKTE BESTIMMUNGEN MIT HILFE DER β^--RÜCKSTRAHLUNG. IV[1-3]

DIE BESTIMMUNG VON K^+ UND NH_4^+ MIT $Na_2Pb[Me^{II}(NO_2)_6]$

GH. MARCU und V. SĂCELEAN

aus dem Chemischen Institut Cluj, str. Donáth, 63–105

Eingegangen am 9. Juli 1971

Es wurden neue Methoden für die indirekte Bestimmung von K^+ und NH_4^+ aus Chloridlösungen mit Hilfe von $Na_2Pb\,[Me^{II}\,(NO_2)_6]$ (wo $Me^{II} = Co^{2+}$ – nur im Falle von NH_4^+, Ni^{2+}, Cu^{2+}), unter Anwendung der β^--Rückstrahlung ausgearbeitet. Die statistische Verarbeitung der experimentellen Daten hat bewiesen, daß die vorgeschlagenen Methoden für die Bestimmung von 0,070–0,294 g K^+, beziehungsweise 0,0323–0,1357 g NH_4^+, gleich gut sind.

In den vorhergehenden Arbeiten[1-3] wurde gezeigt, daß die Analysenmethode mit Hilfe der β^--Rückstrahlung erfolgreich auch für die Bestimmung von Elementen mit niedriger Ordnungszahl verwendet werden kann.

Wenn ein konstantes Volumen einer Lösung mit effektiv hoher Ordnungszahl mit einem konstanten Volumen einer Lösung, die ein Element mit niedriger Ordnungszahl enthält, in verschiedenen Konzentrationen, vermischt wird, so wird nach der Fällung des Elementes mit niedriger Ordnungszahl mit einem oder mehreren Ionen mit hoher Ordnungszahl eine entsprechende Änderung der effektiven Ordnungszahl der Lösung hervorgerufen.

Auf Grund der verkehrt proportionalen Abhängigkeit, die es zwischen der Intensität der rückgestrahlten β^--Strahlen und der effektiven Ordnungszahl der Lösung gibt, kann die Konzentration des Elementes mit niedriger Ordnungszahl aus der untersuchten Lösung bestimmt werden.

Je mehr sich die effektive Ordnungszahl einer Lösung für dieselbe Konzentration eines Elementes mit niedriger Ordnungszahl verringert, desto empfindlicher ist die Methode.

Es ist bekannt, daß bei Hinzufügen einer Lösung, die K^+ und NH_4^+ enthält, zu einem Überschuß einer $Na_2Pb\,[Me^{II}\,(NO_2)_6]$-Lösung sich kristalline Niederschläge bilden, die schnell ausfallen:

$$2\,Me^+ + Na_2Pb\,[Me^{II}(NO_2)_6] = Me^I_2Pb\,[Me^{II}(NO_2)_6] + 2Na^+ \qquad (I).$$

wo $Me^+ = K^+$, NH_4^+ und $Me^{II} = Co^{2+}$, Ni^{2+}, Cu^{2+}.

---

[1] Gh. Marcu und V. Săcelean, *Rev. Roumaine Chim.*, **13**, 1463 (1968).

[2] Gh. Marcu und V. Săcelean, *Stud. Univ. Babeş-Bolyai Chem.*, **14**, 19 (1969).

[3] Gh. Marcu und V. Săcelean, *Stud. Univ. Babeş-Bolyai, Chem.*, **14**, 139 (1969).

Für die gewählten Arbeitsbedingungen eignet sich die Bestimmung von K^+ mit $Na_2Pb\,[Co\,(NO_2)_6]$ nicht.

Mit Hilfe der erwähnten Methode wurde K^+ und NH_4^+ aus konzentrierten Chlorid- und Sulfat-Lösungen mit $Na_2Pb[Cu\,(NO_2)_6]$[2] bestimmt.

In dieser Arbeit wurde dasselbe Verfahren für die Bestimmung von K^+ und NH_4^+ mit $Na_2Pb[Ni(NO_2)_6]$, von NH_4^+ mit $Na_2Pb[Co(NO_2)_6]$ untersucht, so wie eine neue Variante, die sich auf das Lösen der $Me_2^IPb[Me^{II}(NO_2)_6]$-Niederschläge und auf das Messen der von der Lösung rückgestrahlten β^--Strahlen stützt.

Es ist ersichtlich, daß in diesem Fall die effektive Ordnungszahl der erhaltenen Lösungen, beziehungsweise die Intensität der rückgestrahlten β^--Strahlen, direkt proportional mit der Quantität des gelösten Niederschlages ist und implizite mit der Konzentration des Elementes mit niedriger Ordnungszahl.

Für die Berechnung der Quantität von K^+ oder NH_4^+ aus den untersuchten Proben kann die graphische Methode (siehe Abb. 1—4), oder die vorher vorgeschlagene Formel[1] verwendet werden:

$$C_x = \frac{C_1(\Lambda_2 - \Lambda_x) + C_2(\Lambda_x - \Lambda_1)}{\Lambda_2 - \Lambda_1}$$

wo C_x die Konzentration der unbekannten Probe ist, Λ_x—die Intensität der von dieser rückgestrahlten β^--Strahlen, C_1 und C_2—die Konzentrationen zweier Standardproben, und Λ_1 und Λ_2—die Intensität der von den Standardproben rückgestrahlten β^--Strahlen.

Es wurde mit KCl- und NH_4Cl-Lösungen gearbeitet, deren Titer gravimetrisch mit Natriumtetraphenylborat bestimmt wurde.[4]

ARBEITSWEISE

Fällungsreagens mit Cobalt. Es werden 84 g $Co\,(NO_3)_2 \cdot 6H_2O$ in Wasser gelöst und die Lösung wird auf 200 ml gebracht. Es werden 90 g $Pb\,(NO_3)_2$ und 350 g $NaNO_2$ genommen, in Wasser gelöst und die Lösung wird bis auf 800 ml gebracht. Vor der Verwendung werden die beiden Lösungen gemischt. Die erhaltene Lösung wird bei Kühle in einer dunkeln Flasche aufbewahrt und ist ~24 Stunden stabil.

Fällungsreagens mit Nickel. Es werden 84 g $Ni\,(NO_3)_2 \cdot 6H_2O$ in ~100 ml Wasser gelöst, 90 g $Pb\,(NO_3)_2$ und 350 g $NaNO_2$ in ~350 ml Wasser. Die beiden Lösungen werden gemischt und mit Wasser auf 1 l gebracht. Die bei Kühle in dunkler Flasche aufbewahrte Lösung behält den Titer unverändert wenigstens einen Monat.

Fällungsreagens mit Kupfer. Seine Darstellung wurde vorher beschrieben.[2]

Verfahren. In einen Kolben von 50—100 ml gibt man genau 25 ml Fällungreagens, kühlt bis auf 0° ab; es werden 5 ml von der neutralen Lösung des zu analysierenden Salzes hinzugefügt, es wird geschüttelt und 4—5 Min. stehen gelassen (vorzugsweise immer bei 0°). Der gebildete Niederschlag wird filtriert, vom Filtrat nimmt man 25 ml und bestimmt die Intensität der rückgestrahlten β-Strahlen.

---

[4] M. Kohler, *Z. analyt. Chem.*, **138**, 9 (1953).

Im Falle der Verarbeitung der Niederschläge wird folgenderweise vorgegangen: Zu höchstens 5 ml der zu analysierenden Salzlösung werden auf einmal ~25 ml bis auf 0° gekühltes Fällungsreagens hinzugefügt, es wird geschüttelt, man läßt die Proben 4–5 Min. stehen (immer bei 0°), die Lösung wird auf einem Trichter mit einem kleinen Filterpapier abgeschüttet (weil ein kleiner Teil des Niederschlages von der Lösung mitgenommen wird), der Niederschlag wird dreimal mit je 3 ml kaltem Wasser gewaschen und jedesmal wird der Überstand auf demselben Trichter abgeschüttet.

In den Kolben mit dem Niederschlag gibt man auch das Filterpapier mit dem nach dem Abschütten erhaltenen Niederschlag und zerstört den Niederschlag mit 10 ml HNO_3 8M (es wird leicht erwärmt, bis kein NO_2 mehr entweicht). Die erhaltenen Nitrate gibt man in einen Meßkolben und füllt mit Wasser auf 25 ml auf. Dieser Lösung bestimmt man die Intensität der rückgestrahlten β-Strahlen.

Apparatur. Für die Bestimmung der Intensität der von den Lösungen rückgestrahlten β^--Strahlen wurde eine Batterie von zwei in parallel geschalteten GM-Zählern, des Typs STS-6, die an einen Nuklearzähler geschaltet wurde, verwendet. Der Abstand zwischen den GM-Zählern war 3 cm, und der Abstand zwischen den Zählern und der Lösungsfläche war 0,8 cm. Die β^--Strahlenquelle, die ~ 1 mCi $^{204}TlNO_3$ enthielt, wurde zwischen die zwei GM-Zähler angebracht. Die radioaktive Substanz wurde auf die innere Fläche eines Kegels mit dem Durchmesser der Grundfläche von 1,2 cm und einer Höhe von 0,2 cm gegeben. Der Abstand zwischen der Grundfläche des Kegels und der Fläche der Lösung war 0,7 cm.

Die zu analysierende Lösung wurde in einen zylindrischen Plexiglasbehälter mit einem Durchmesser von 3,7 cm und einer Höhe von 1,2 cm gegeben.

Experimentelle Daten. Um die vorgeschlagenen Varianten für die Bestimmung von K^+ und NH_4^+ mit $Na_2Pb[Me^{II}(NO_2)_6]$ zu überprüfen, wurden die Eichkurven aus Abb. 1–4 gezogen und es wurde eine statistische Verarbeitung der bei der Bestimmung von 0,070–0,294 g K^+, beziehungsweise 0,0323–0,1357 g NH_4^+, erhaltenen Ergebnissen durchgeführt (Tabellen 1–4)

Tabelle 1

Ergebnisse der statistischen Verarbeitung experimenteller Daten, erhalten bei der Bestimmung von 0,070–0,294 g K^+ auf Grund der β^--Rückstrahlung

Methode	Experimentelle Indexe	Statistische Parameter	n	$\overline{X}$	σ	e
1	$Na_2Pb[Ni(NO_2)_6]$	Differenz	12	0,0005	0,0016	0,0004
	Lösungsüberschuß	Prozente	12	100,24	0,90	0,26
2	$K_2Pb[Ni(NO_2)_6]$	Differenz	12	−0,0004	0,0016	0,0004
	Gelöst	Prozente	12	99,80	0,82	0,24
3	$K_2Pb[Cu(NO_2)_6]$	Differenz	12	−0,0003	0,0014	0,0004
	Gelöst	Prozente	12	99,85	0,79	0,23

Differenz = Differenz zwischen der in Probe genommenen und der experimentell gefundenen Me^+-Menge.
Prozente = Prozentual ausgedrücktes Verhältnis zwischen der experimentell gefundenen und der in Probe genommenen Me^+-Menge
n = Anzahl der Bestimmungen.
$\overline{X}$ = Arithmetischer Mittelwert.
σ = Mittlere quadratische Abweichung.
e = Mittlerer statischer Fehler des Mittelwertes.

Revue Roumaine de Chimie, 17, 3, 489–495 (1972)

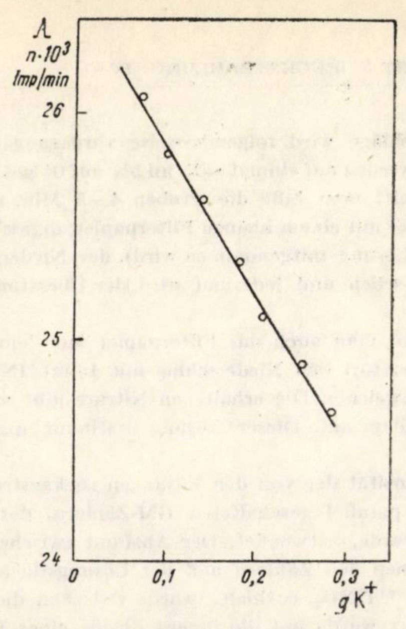

Abb. 1. — Änderung der Intensität (Λ) der β^--Strahlen, die von 25 ml Lösung, erhalten nach der Fällung von K^+ mit einem Überschuß von $Na_2Pb[Ni(NO_2)_6]$, rückgestrahlt wurden.

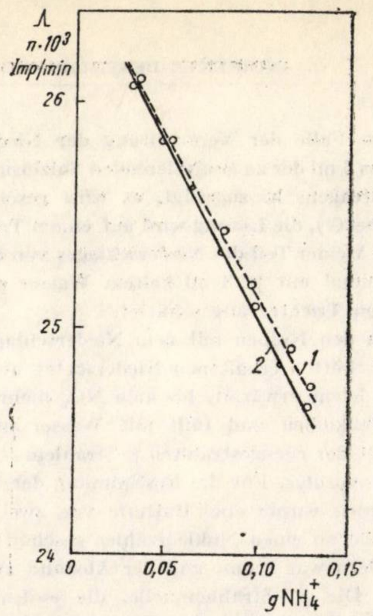

Abb. 2. — Änderung der Intensität (Λ) der β^--Strahlen, die von 25 ml Lösung, erhalten nach der Fällung von NH_4^+ mit einem Überschuß von $Na_2Pb[Co(NO_2)_6]$ (*1*) und einem Überschuß von $Na_2Pb[Ni(NO_2)_6]$ (*2*) rückgestrahlt wurden.

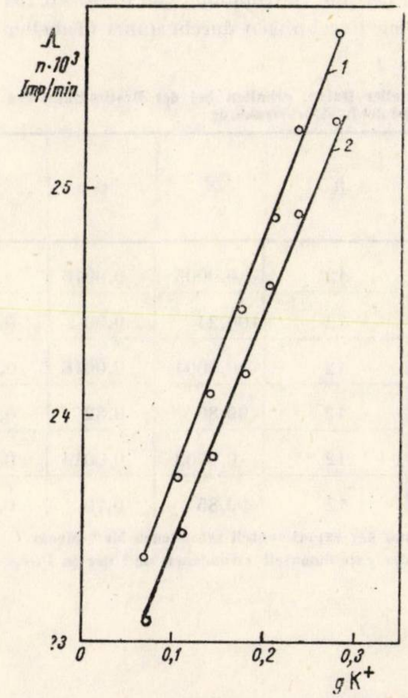

Abb. 3. — Änderung der Intensität (Λ) der β^--Strahlen, die von 25 ml Lösung erhalten durch Lösen der Niederschläge von $K_2Pb[Ni(NO_2)_6]$ (*1*) und $K_2Pb[Cu(NO_2)_6]$ (*2*) rückgestrahlt wurden.

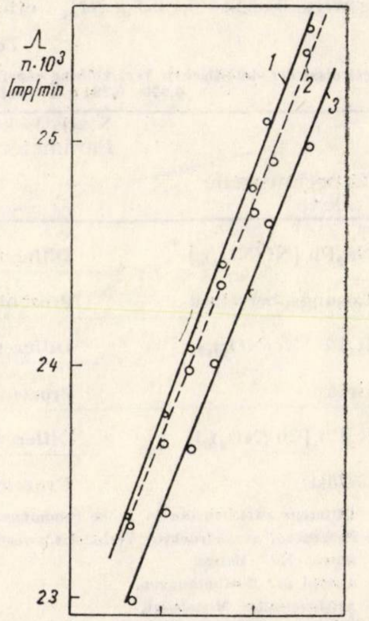

Abb. 4. — Änderung der Intensität (Λ) der β^--Strahlen, die von 25 ml Lösung, erhalten durch Lösen der Niederschläge von $(NH_4)_2Pb[Ni(NO_2)_6]$ (*1*), von $(NH_4)_2Pb[Co(NO_2)_6]$ (*2*) und von $(NH_4)_2Pb[Cu(NO_2)_6]$ (*3*), rückgestrahlt wurden.

Tabelle 2

Studententest *(t)* für die Bestimmung von 0,070 – 0,294 g K^+ auf Grund der β -Rückstrahlung

Experimentelle Indexe / Studententest	$t_{1.2}$	$t_{1.3}$	$t_{2.3}$
Differenz	1,231	1,160	0,124
Prozente	1,197	1,075	0,145

Tabelle 3

Ergebnisse der statistischen Verarbeitung experimenteller Daten, erhalten bei der Bestimmung von 0,0323 – 0,1357 g NH_4^+, auf Grund der β$^-$-Rückstrahlung

Methode	Experimentalle Indexe	Statistische Parameter	*n*	$\bar{x}$	σ	*e*
4	$Na_2Pb\,[Ni\,(NO_2)_6]$ Lösungsüberschuß	Differenz	12	0,00003	0,0007	0,0002
		Prozente	12	99,91	0,94	0,27
5	$Na_2Pb\,[Co\,(NO_2)_6]$ Lösungsüberschuß	Differenz	12	0,0001	0,0007	0,0002
		Prozente	12	100,22	0,90	0,26
6	$(NH_4)_2Pb\,[Ni\,(NO_2)_6]$ Gelöst	Differenz	12	0,00008	0,0008	0,0002
		Prozente	12	100,03	0,88	0,25
7	$(NH_4)_2Pb\,[Co\,(NO_2)_6]$ Gelöst	Differenz	12	0,00003	0,0007	0,0002
		Prozente	12	100,08	0,81	0,23
8	$(NH_4)_2Pb\,[Cu\,(NO_2)_6]$ Gelöst	Differenz	12	–0,00013	0,0008	0,0002
		Prozente	12	99,85	1,04	0,30

Tabelle 4

Studententest *(t)* für die Bestimmung von 0,0323 – 0,1357 g NH_4^+ auf Grund der β$^-$-Rückstrahlung

Experimentelle Indexe / Studententest	$t_{4.5}$	$t_{4.6}$	$t_{4.7}$	$t_{4.8}$	$t_{5.6}$	$t_{5.7}$	$t_{5.8}$	$t_{6.7}$	$t_{6.8}$	$t_{7.8}$
Differenz	0,497	0,531	0,023	0,477	0,055	0,077	0,714	0,161	0,637	0,509
Prozente	0,792	0,569	0,454	0,142	0,502	0,383	0,894	0,139	0,439	0,579

DISKUSSION

Da die Lösung, die das Ion $[Co(NO_2)_6]^{4-}$ enthält, sich mit der Zeit durch Oxidation mit $[Co(NO_2)_6]^{3-}$, welches verschiedene Ammoniummischpräzipitate sowohl mit Na^+ als auch mit Pb^{2+}, die sich in der Lösung befinden, bilden kann, selbst verunreinigt, wird empfohlen, die $Pb(NO_3)_2-NaNO_2$-Lösung und die $Co(NO_3)_2$-Lösung getrennt aufzubewahren. Um das Fällungsreagens zu erhalten, werden sie nur am betreffenden Tag gemischt, so wie vorher gezeigt wurde.

Sicherlich, da die Fällungsreagenzien einen Überschuß von NO_2^- enthalten, findet neben der Bildungsreaktion $(NH_4)_2Pb[Me^{II}(NO_2)_6]$ auch folgende Reaktion statt:

$$NH_4^+ + NO_2^- = N_2 + 2H_2O \qquad (II).$$

Wie aus Abb. 1 und 2 ersichtlich ist, haben die Intensitäten der vom Lösungsüberschuß rückgestrahlten β^--Strahlen im Falle der Präzipitation von äquivalenten Mengen von K^+ und NH_4^+ mit $Na_2Pb[Ni(NO_2)_6]$, beziehungsweise von NH_4^+ mit $Na_2Pb[Co(NO_2)_6]$, ähnliche Werte.

Ähnliche Werte wurden auch in der vorhergehenden Arbeit [2] bei der Bestimmung von K^+ und NH_4^+ mit $Na_2Pb[Cu(NO_2)_6]$ erhalten. Dieses beweist, daß die Reaktion (II) in den beschriebenen experimentellen Bedingungen mit einer sehr kleinen Geschwindigkeit stattfindet und so die Bestimmung von NH_4^+ mit $Na_2Pb[Me^{II}(NO_2)_6]$ praktisch nicht stört.

Zwischen den Intensitäten, der von den Lösungen, die durch Zerstörung der Niederschläge, gebildet aus äquivalenten Mengen von K^+ und NH_4^+ (für dasselbe Fällungsreagens), mit HNO_3 erhalten wurden, rückgestrahlten β-Strahlen, tritt eine etwas größere Differenz auf. Dieses ist dem Umstand zuzuschreiben, daß NH_4^+ komplett entweicht, entsprechend der Reaktion (II), während das gebildete KNO_3 zu einem leichten Anwachsen der effektiven Ordnungszahl führt (Abb. 3 und 4).

Nach der Berechnung des Parameters t und in Abhängigkeit der Anzahl der Freiheitsgrade wurde festgestellt, daß die Differenz zwischen den Mittelwerten nicht bedeutend ist, woraus hervorgeht, daß die drei vorgeschlagenen Methoden für die Bestimmung von K^+, beziehungsweise fünf für die Bestimmung von NH_4^+, vom Standpunkt der Präzision indentisch sind, demnach sind sie gleich gut.

Die angeführten Methoden beziehen sich auf reine KCl und NH_4Cl-Lösungen.

So wie in der vorhergehenden Arbeit [2] bei der Bestimmung von äquivalenten Mengen von K^+ aus KCl und K_2SO_4, beziehungsweise NH_4^+ aus NH_4Cl und $(NH_4)_2SO_4$, mit $Na_2Pb[Cu(NO_2)_6]$ (auf Grund des Überschusses der Fällungslösung) gezeigt wurde, stellt man fest, daß für das gleiche Ion die Intensität der rückgestrahlten β-Strahlen im Falle der Chloride größer ist.

Diese Tatsache wird durch die Differenz der Ordnungszahlen der entsprechenden Anionen, die nach der Fällung in der Lösung bleiben, erklärt, $Z_{Cl} = 17$ und $Z_{SO_4} = 10{,}67$.

Daraus kann man den Schluß ziehen, daß für die Bestimmung von K^+ und NH_4^+ auf Grund des Überschusses von $Na_2Pb[Me^{II}(NO_2)_6]$ nur reine Lösungen empfohlen werden oder solche, die kleine Mengen fremder Ionen mit niedriger Ordnungszahl enthalten.

Im Falle der Anwesenheit fremder Ionen, die die Fällung nicht stören, die aber zum Anwachsen der effektiven Ordnungszahl der Lösung beitragen, wird die Bestimmung von K^+ und NH_4^+ auf Grund der durch Lösen von $Me_I^2Pb\,[Me^{II}(NO_2)_6]$ erhaltenen Lösungen empfohlen.

Die durchgeführten Versuche haben bewiesen, daß Na^+, Mg^{2+}, Cl^-, NO_3^- und SO_4^{2-} die Fällungen nicht stören.

Aus obigem ergibt sich, daß die für die Bestimmung für K^+ und NH_4^+ vorgeschlagenen Methoden einfach sind, hinreichend schnell und genau, so daß sie besonders für Serienanalysen einiger Lösungen, die die erwähnten Ionen enthalten, verwendet werden können.

Revue Roumaine de Chimie, **17**, *3*, 497–503 (1972)

THE INFLUENCE OF THE TEMPERATURE GRADIENT ON THE FORM OF THE ELUTION CURVES AND OF THE HEIGHT OF THE THEORETICAL PLATE IN COLUMN CHROMATOGRAPHY WITH ION EXCHANGERS

C. LITEANU, S. GOCAN, T. HODIŞAN, H. NAŞCU and C. MĂRUŢOIU

Chair of Analytical Chemistry of the "Babeş-Bolyai" University, Str. Arany Janos 11, Cluj, Romania

Received September 18, 1971

The paper presents results on the influence of the temperature gradient $\left(\frac{60-40}{30} = 0.66°/\text{cm} \text{ and } \frac{80-60}{30} = 0.66°/\text{cm}\right)$ on the form of the elution curves as well as on the height, *H*, of the plate, compared to the effect of temperature (20°, 60° and 80°) for the elution of Zn^{2+} and Co^{2+} ions. Lower values were obtained in the case of the temperature gradient than in isothermal conditions.

The influence of temperature on the shape of the elution curves, of the distribution constant and of the height of the theoretical plate in chromatographic separations on ion exchangers column was studied in numerous papers.[1–9]

The temperature gradient technique was successfully applied to open column chromatography (strips) [10,11] and in the case of closed column, only to the fractionation of the polymers.[12,13] In gas chromatography the temperature gradient as well as the programmed temperature gradient [14,15] is successfully applied.

---

[1] P. B. Hamilton, D. C. Bogue and R. A. Anderson, *Analyt. Chem.*, **32**, 1782 (1960).

[2] Ulla-Britt Larson, I. N. Norstedt and O. Samuelson, *J. Chromatog.*, **22**, 102 (1966).

[3] K. A. Kraus and R. J. Raridon, *J. Amer. Chem. Soc.*, **82**, 3271 (1960).

[4] R. Dybczynski, *Roczniki Chem.*, **37**, 1411 (1963).

[5] J. Minczewski and R. Dybczynski, *Chem. Analit*, **10**, 1113 (1965).

[6] G. Brunisholtz and R. Roulet, *Chimia* (Basel), **21**, 188 (1967).

[7] R. Dybczynski, *J. Chromatog.*, **14**, 79 (1964).

[8] R. Dybczynski, *J. Chromatog.*, **31**, 115 (1967).

[9] R. Dybczynski and Ludmila Wodkiewicz, *J. Inorg. Nuclear Chem.*, **31**, 1495 (1969).

[10] C. Liteanu and S. Gocan, *Stud. Univ. Babeş-Bolyai. Chem.*, **6**, 99 (1961).

[11] C. Liteanu and S. Gocan, *Bull. Soc. chim. France*, **1970**, 4527.

[12] C. A. Baker and R. J. P. Williams, *J. Chem. Soc.*, **1956**, 2352.

[13] G. V. Shultz, G. Berger and A. G. R. Scholtz, *Ber. Bunsenges. Physik. Chem.*, **69**, 856 (1956).

[14] N. M. Turkeltaub, *Zhur. fiz. Khim.*, **27**, 1827 (1953).

[15] M. H. Guermouche, M. Fotscher and J. M. Vergnand, *J. Chromatog.*, **52**, 9 (1970).

Temperature, as a parameter in chromatography on closed column with ion exchangers, is nowadays more and more often used to improve chromatographic separations. Meanwhile we must mention the fact that modern chromatographs are able to work at the desired temperature.

As known from the theory of ion exchanger chromatography the expression HETP has the following form [1,16] :

$$H = 1.64\, r + \frac{K_d}{(K_d + F_I)^2} \cdot \frac{0.142\, r^2 v}{D_S} + \frac{K_d^2\, 0.266\, r^2 v}{(K_d + F_I)^2 F_{II}\, D_L (1 + 70\, rv)} \tag{1}$$

where : r — represents the ray of the resin granules ;
v — the flowing velocity of the eluent ;
K_d — the distribution coefficient at the equilibrium state ;
D_S — the diffusion coefficient in the resin ;
D_L — the diffusion coefficient in the solution ;
F_I — the free fraction of the column ;
$F_{II} = (1 - F_I)$ — the fraction of the colum occupied by the resin.

If the longitudinal diffusion is also taken into account in the two phases, two more terms [17] are added to equation (1).

These relationships show that the value of HETP is made up of three terms : the first one represents the contribution of the particles size, the second one represents the contribution of the diffusion in the particle of the resin, and the third represents the contribution of the diffusion in the film of the liquid around the particle of the resin having a thickness of 10^{-3} cm.

The temperature reacts on the value of HETP by means of the distribution coefficient K_d and of the diffusion coefficients D_L and D_S. The relation expressing the dependence of the distribution coefficient K_d on temperature has the following form [18] :

$$\ln K_d = \ln \frac{\gamma_B}{\gamma_A} + \ln \frac{\bar{\gamma}_{AR}}{\bar{\gamma}_{BR}} + \frac{P}{RT} (\bar{V}_{AR} - \bar{V}_{BR}) \tag{2}$$

where : γ_A, γ_B — are the activity coefficients of ions A and B,
$\bar{\gamma}_{AR}, \bar{\gamma}_{BR}$ — are the activity coefficients of compounds AR, BR in the hypothesis that the resin is infinitely diluted,
P — the swelling pressure of the resin,
$\bar{V}_{AR}, \bar{V}_{BR}$ — the partial molar volumes of compounds AR, BR,
R — the general constant of the gases,
T — the temperature in Kelvin degrees.

---

[16] E. Glueckauf, "Ion Exchange and its Applications", Society of Chemical Industry, London, 1955, p. 34.

[17] R. Dybczynski, *J. Chromatog.*, **50**, 487 (1970).

[18] G. E. Myers and G. E. Boyd, *J. Phys. Chem.*, **60**, 521 (1956).

The diffusion coefficients D_L and D_S depend on temperature according to the following expression [19]:

$$D = D_0 e^{-\frac{E}{RT}} \tag{3}$$

where E represents the activation energy (needed for the passing of the molecule from an initial to a neighbouring position),

D_0 — is a coefficient slightly changing with the temperature.

It results that the action of the temperature on the value of HETP is very complex, although certain qualitative remarks can be made. As seen from equation (1), the diffusion coefficients being at the denominator, and growing exponentially with the temperature (3), it results that the value of HETP must be strongly enough influenced by the temperature while decreasing. As the distribution coefficient K_d may increase, decrease or stay constant with the temperature, in certain cases the height of the theoretical plate might grow with the temperature.[6]

We may therefore conclusively state that the increase of the temperature has generally a positive effect on the shape of the elution curves, and apparently on the whole separation process.

The action of the temperature gradient (along the column) on HETP, and respectively on the shape of the elution curves, will be more complex, since the exchange process always takes place at other temperatures as the spot shifts on the column. This will evidently lead to a continuous variation of the ionic exchange rate along the column. The exchange rate is a function of the diffusion processes in the solution film covering the grain, but especially of the diffusion in the grain. The exchange rates in the frontal part of the spot, and in its tail will therefore be different. By accordingly choosing the temperature gradient one can act favourably on the shape of the elution curves, especially on the asymmetric curves with long tails.

In the present study we have purposely chosen the chromatographic system giving very broad elution curves in istothermal conditions at 20° so as to better broad the action of temperature as well as that of the temperature gradient.

EXPERIMENTAL

The isothermal elution at different temperatures was carried out by means of a column with double walls for thermostating.

The temperature gradient was achieved by means of the device shown in figure 1, made of copper (1) and with an inner diameter approximately equal to the outer diameter of the glass column (2). The metallic tube is provided with circular chambers *a* and *b* through which water flows from a thermostat at temperature t_1 in the lower chamber and at temperature t_2 in the upper chamber ($t_2 > t_1$). The glass column (2) is equipped at its lower part with a frit (3) on which the ionite (4) is put.

---

[19] J. C. Giddings, "Dynamics of Chromatography" Part 1, "Principles and Theory" vol. 1 of "Chromatographic Science Series", Marcel Dekker, New York, 1965, p. 232.

As known from the theory of thermal conductivity of a metallic bar with temperatures t_1 and t_2 at both ends ($t_2 > t_1$), the temperature along the bar decreases from t_2 to t_1 according to an exponential law of the form : $t_1 = t_2 e^{-aL}$, in which L is the distance and a is a constant equal to $a = \sqrt{\alpha p / \lambda S}$, where α-is the outer conductivity of the bar, p — the perimeter of the bar, λ — the thermal conductivity of the bar, S — the cross-section of the bar. The appearance of the temperature variation along the column is given in figure 2. The law according to which the temperature gradient varies will therefore also have an exponential form.

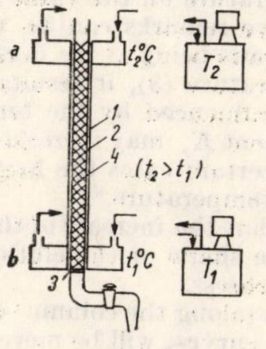

Fig. 1. — Design of the device.

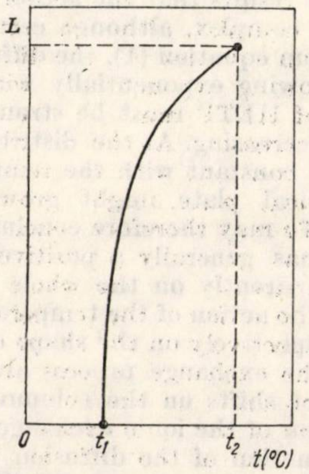

Fig. 2. — Variation of temperature along the column.

We used a column having length $L = 30$ cm and diameter $d_i = 1$ cm, filled with ion exchanging resin Dowex 50—X8, in H—R form; the Zn^{2+}, Cd^{2+} and Co^{2+} were eluted from the column by HCl, 0.5 N, 5 ml $ZnCl_2$ with a 17 mg Zn/ml, 2 ml $CoCl_2$ with a 19.5 mg Co/ml and 0.1 ml $CdCl_2$ with a 77.7 mg Cd/ml were introduced into the column.

The flowing velocity of the eluent through the column was 2.5 ml/min. The concentrations in Zn^{2+}, Cd^{2+} and Co^{2+} of the eluent fractions were determined by titration with complexon III.

RESULTS AND CONCLUSIONS

The results concerning the elution curves obtained at different temperatures, as well as in temperature gradient, for Zn^{2+} and Co^{2+} ions are given in figures 3—6.

The figures point to the fact that smaller retention volumes are obtained with the rise in temperature while the elution curves grow narrower (figs. 3 and 4). We also notice that as the temperature gradient is obtained at higher temperatures the retention volume as well as the total elution volume are smaller and consequently the time of analysis will be shortened (fig. 5 and 6).

Fig. 3. — Influence of temperature on elution curves.

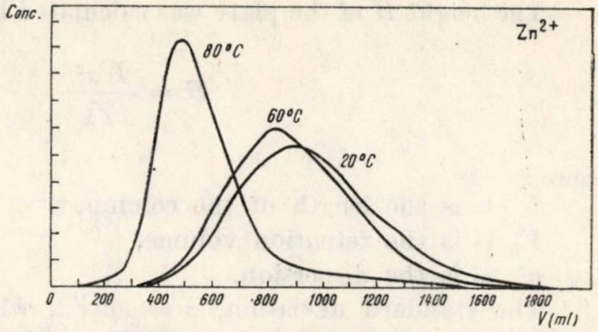

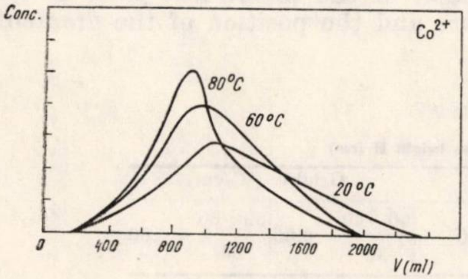

Fig. 4. — Influence of temperature on elution curves.

Fig. 5. — Influence of temperature gradient on elution curves.

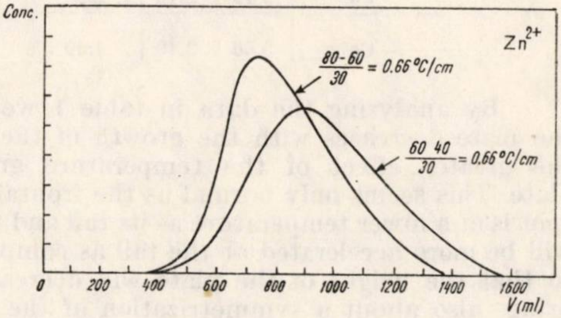

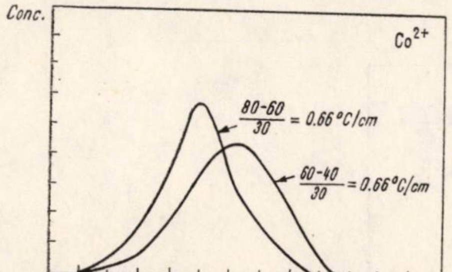

Fig. 6. — Influence of temperature gradient on elution curves.

The height H of the plate was calculated by means of relationship [7]:

$$H = \frac{L\,\sigma^2}{V_R^2} \tag{4}$$

where:

L = is the length of the column,

V_R = is the retention volume,

σ^2 = is the dispersion.

The standard deviation, $\sigma = w/2\sqrt{2}$, where w is the breadth of the peak measured at 0.368 × maximum height.

The values obtained for the height of the theoretical plate H for Zn^{2+} and Co^{2+} ions *versus* temperature and the position of the gradient are given in table 1.

Table 1

Values of the plates height H (cm)

Ion	Temperature			Grad.t. (°C/cm)	
	20	60	80	$\frac{60-40}{30} = 0.66$	$\frac{80-60}{30} = 0.66$
Zn^{2+}	2.40	2.18	2.06	1.92	1.75
Co^{2+}	5.66	3.40	1.90	1.88	1.80

By analysing the data in table 1 we notice that the height H of the plate decreases with the growth of the temperature. We also notice the greater effect of the temperature gradient on the height of the plate. This seems only normal as the frontal part of the chromatographic spot is at a lower temperature as its tail and therefore the exchange process will be more accelerated at the tail as compared to the front of the spot, so that the height of the plate will decrease. The temperature gradient brings also about a symmetrization of the elution curves.

Figures 7 and 8 give the elution curves on the separation of $Cd^{2+} + Zn^2$ and $Cd^{2+} + Co^{2+}$ ions.

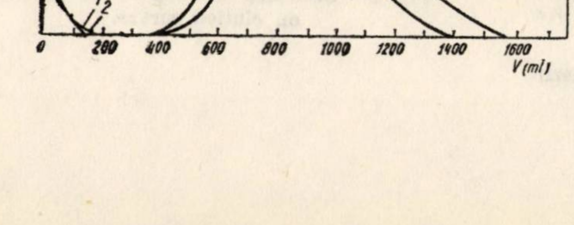

Fig. 7. — Influence of temperature gradient on the separation of Cd^{2+} and Zn^{2+}.

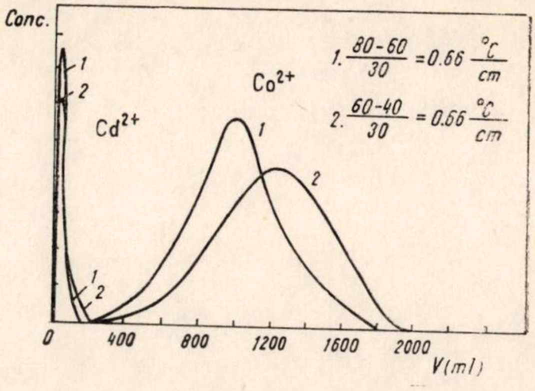

Fig. 8. — Influence of temperature gradient on the separation of Cd^{2+} and Co^{2+}.

Figures 7 and 8 show that the separation of $Cd^{2+} + Zn^{2+}$ and $Cd^{2+} + Co^{2+}$ may be achieved at any chosen temperature interval, but for higher temperatures the retention volumes are smaller, and consequently the analysis time, shorter.

This study is the first attempt to apply the temperature gradient to closed column chromatography with ion exchangers, and in further research this technique will be also applied to other chromatographic separations.

Revue Roumaine de Chimie, 17, 3, 505–509 (1972)

STUDIUM DES VERHALTENS VON Fe^{3+}, Co^{2+} UND Ni^{2+} AUF DEM KATIONENAUSTAUSCHER VIONIT CS-3 IM MEDIUM VON ORGANISCHEM LÖSUNGSMITTEL – $HCl-H_2O$

N. PASCU, V. SĂCELEAN, LIVIA CRIVEI, ERNA KISS und N. BOJAN
vom Chemischen Institut Cluj, str. Donáth, 63–105

Engegangen am 9. Juli 1971

Es wurden die Verteilungskoeffizienten von Fe^{3+}, Co^{2+} und Ni^{2+} auf dem Kationenaustauscher Vionit CS-3 in den Medien Azeton – $HCl-H_2O$, Äthanol – $HCl-H_2O$ bestimmt, und auf Grund dieser wurde eine rapide Trennung des Gemisches $Fe^{3+}-Co^{2+}-Ni^{2+}$ auf der Mikrosäule durchgeführt.

In letzter Zeit werden die Gemische organisches Lösungsmittel – Mineralsäure – Wasser für die Trennung verschiedener Ionen sowohl auf Anionenaustauschern als auch auf Kationenaustauschern immer öfter verwendet.

Die bedeutendste Rolle des Ionenaustausches in Mischlösungsmitteln spielt die Solvatation und die Komplexbildung.

Die stufenweise Ersetzung des Wassers durch ein organisches Lösungsmittel führt zu einer Verringerung des Hydratationsgrades der hydratierten Ionen und zu einer Vergrößerung der Ioneninteraktion.

Wegen der Eigenschaft, die sie besitzt, Komplexverbindungen zu bilden, wird die Salzsäure häufig zu Trennungen auf Ionenaustauschern sowohl in wäßrigem Medium als auch im Medium von organischen Lösungsmitteln oder in gemischten Medien verwendet.

Von den organischen Lösungsmitteln, die mit Wasser mischbar sind, wird häufig Azeton und Äthylalkohol verwendet.

Bezüglich den Trennungen einiger Kationen auf stark sauren Kationenaustauschern mit HCl-Mischlösungsmitteln, wurde festgestellt, daß die Selektivitätskoeffizienten im allgemeinen mit dem Anwachsen des organischen Lösungsmittelgehaltes wachsen.

So sind Fritz und Rettig [1], nachdem sie die Verteilungskoeffizienten mehrer Kationen auf Dowex-50W-X8 gemessen haben, zur Schlußfolgerung gelangt, daß die Differenzen zwischen den Verteilungskoeffizienten für dieselbe HCl-Konzentration im Medium Azeton—Wasser größer sind als im wäßrigen Medium.

---

[1] J. S. Fritz und T. A. Rettig, *Analyt. Chem.*, 34, 1562 (1962).

Auf Grund dieser Daten haben sie mehrere Kationen aus verschiedenen Gemischen getrennt.

Auf demselben Kationenaustauscher haben Korkisch und Ahluwahlia [2] die Adsorptionscharakteristiken und die Trennungsmöglichkeiten von 20 Elementen im Medium organisches Lösungsmittel — $HCl-H_2O$ (Azeton, Äthanol, Methanol, n-Propanol usw.) untersucht.

Nachdem sie das Verhalten einiger Metalle auf dem Kationenaustauscher Zeo-Karb 225 untersucht haben, ist es Kember, Macdonald und Wells [3], gelungen, Cu^2 von Ni^{2+} durch Elution mit Azeton — $HCl-H_2O$ zu trennen.

Die Trennung von Cu^{2+}, Co^{2+} und Ni^{2+} mit HCl — Mischlösungsmitteln wurde von Lásztity und Beljavskaja [4] auf dem Kationenaustauscher KU-2 durchgeführt.

Zu erwähnen ist noch die Verwendung von Azeton — $HCl-H_2O$ bei der selektiven Elution einiger Kationen, [5-6] sowie bei rapiden Trennungen von radioaktiven Isotopen.[7]

Weiter werden die Arbeitsweise und die experimentellen Ergebnisse, die beim Studium der Trennung von Fe^{3+}, Co^{2+} und Ni^{2+} auf dem Kationenaustauscher Vionit CS-3 (sulfonisch stark saurer Kationenaustauscher auf Grund von Polystyroldivinylbenzol, mit 7% DVB), in den Medien Azeton — $HCl-H_2O$ und Äthanol — $HCl-H_2O$ erhalten wurden, angeführt.

ARBEITSWEISE

Für die Bestimmung der Verteilungskoeffizienten (Kd) wurde mit Genauigkeit ungefähr 1 g Ionenaustauscher (Granulation 0,150—0,075 mm) gewogen. Vorher wurde er mit diammoniakalischer Zitratlösung 0,5 M gereinigt, in H Form mit HCl 10% gebracht und an der Luft getrocknet.

Der Ionenaustauscher wurde in einen 100 ml-Kolben gegeben, es wurden 3 ml Nitratlösung 0,05M des betreffenden Metalls hinzugefügt und es wurde mit Lösungen von organischem Lösungsmittel — $HCl-H_2O$ bis auf 50 ml so aufgefüllt, um die Arbeitskonzentrationen zu erhalten. Der Kolben wurde mechanisch 24 Stunden geschüttelt, es wurde ein Anteil von der Flüssigkeit genommen, es wurde fast bis zur Trockne eingedämpft und dann wurde die Metallionenmenge mit Hilfe der Methode von Takamoto [8] bestimmt.

---

[2] J. Korkisch und S. S. Ahluwalia, *Talanta*, **14**, 155 (1967).

[3] N. F. Kember, P. S. Macdonald und R. A. Wells, *J. Chem. Soc.*, **1955**, 2273.

[4] A. Lásztity und T. A. Belyavskaya, *Proc. III. Analyt. Chem. Conf. Budapest*, **1**, 59 (1970).

[5] S. K. Majumdar und A. K. De, *Analyt. Chim. Acta*, **25**, 452 (1961).

[6] J. S. Fritz und J. E. Abbink, *Analyt. Chem.*, **37**, 1274 (1965).

[7] S. P. Peterson, F. Terra und G. H. Morrison, *J. Radioanalyt. Chem.*, **2**, 115 (1969).

[8] S. Takamoto, *Japan Analyst*, **4**, 178 (1955).

Die Verteilungskoeffizienten wurden mit Hilfe folgender Formel berechnet:

$$\mathrm{Kd} = \frac{\dfrac{\text{Millimol Metallionen auf dem Austauscher}}{\text{Gramm getrockneter Austauscher}}}{\dfrac{\text{Millimol Metallionen in der Lösung}}{\text{Gesamtes Lösungsvolumen}}}$$

Die Lösungen wurden so dargestellt, daß die Menge vom organischen Lösungsmittel und vom Wasser in Volumenprozenten ausgedrückt wird und die Konzentration von HCl in Molaritäten. Zum Beispiel, 1 l HCl 0,9 M in 90 % Azeton wurde folgendermaßen dargestellt: 900 ml Azeton wurden mit 72 ml konzentrierter HCl und 28 ml Wasser vermischt. Die Änderung des Volumens, die beim Mischen auftritt, kann vernachlässigt werden.

Für die Trennung des Gemisches von $^{55+59}\mathrm{Fe} + {}^{60}\mathrm{Co} + {}^{63+65}\mathrm{Ni}$ wurde eine Mikrosäule von 2 × 15 mm, die den Kationenaustauscher Vionit CS-3 (H Form) mit der Granulation von $\sim 25-30\,\mu$ enthielt, verwendet.

Das Volumen eines Tropfens im Falle der Elution mit HCl 2,5 M war 0,03 ml, die Durchflußgeschwindigkeit 1 Tropfen/43 sec; für das Gemisch organisches Lösungsmittel — $\mathrm{HCl-H_2O}$ war das Volumen eines Tropfens 0,013 ml und die Durchflußgeschwindigkeit im Falle des Gemisches mit Azeton 1 Tropfen/5 sec. und im Falle des Gemisches mit Äthanol 1 Tropfen/15 sec.

ERGEBNISSE UND DISKUSSION

Der Effekt des organischen Lösungsmittels und der Salzsäurekonzentration auf die Verteilungskoeffizienten von $\mathrm{Fe^{3+}}$, $\mathrm{Co^{2+}}$ und $\mathrm{Ni^{2+}}$ auf dem Kationenaustauscher Vionit CS-3 kann in den Abb. 1—6 verfolgt werden.

Aus Abb. 1—3 ist ersichtlich, daß die Verteilungskoeffizienten von $\mathrm{Fe^{3+}}$ und $\mathrm{Co^{2+}}$ mit dem Steigen des Azetongehaltes bis zu einer bestimmten Grenze anwachsen, bei einer größeren Konzentration fallen sie steil ab, als Folge der Bildung von Chlorokomplexen. Im Falle von $\mathrm{Ni^{2+}}$ nehmen die Verteilungskoeffizienten nur in HCl 1,1M und großen Azetonkonzentrationen ab.

Im Falle der Gemische Äthanol — $\mathrm{HCl-H_2O}$, Abb. 4—6, ist ein stetiges Anwachsen der Adsorption von $\mathrm{Co^{2+}}$ und $\mathrm{Ni^{2+}}$ mit dem Anwachsen der Alkoholkonzentration festzustellen. Bei größeren Alkoholkonzentrationen fallen die Verteilungskoeffizienten des $\mathrm{Fe^{3+}}$ steil ab.

Aus den Abb. 1—6 geht hervor, daß für eine konstante organische Lösungsmittelkonzentration die Vergrößerung der Salzsäurekonzentration zu einer Verringerung der Verteilungskoeffizienten führt.

Gestützt auf die experimentell erhaltenen Ergebnisse wurde eine rapide Trennung des Gemisches $\mathrm{Fe^{3+}-Co^{2+}-Ni^{2+}}$ auf einer Mikrosäule mit dem Kationenaustauscher Vionit CS-3 (Abb. 7) durchgeführt.

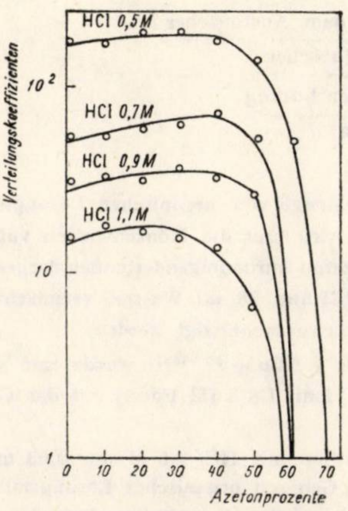

Abb. 1. – Änderung der Kd von Fe^{3+} in Funktion der Azeton- und der Salzsäurekonzentration.

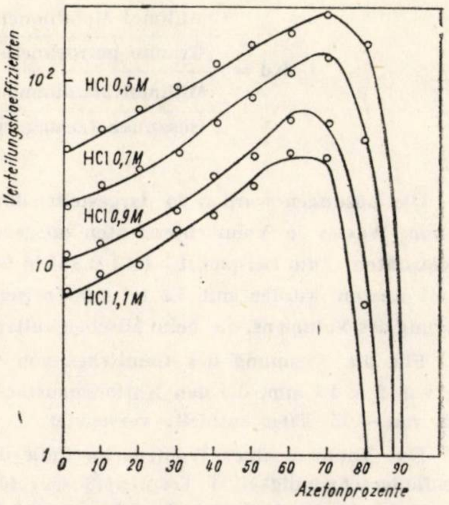

Abb. 2. – Änderung der Kd von Co^{2+} in Funktion der Azeton- und der Salzsäurekonzentration.

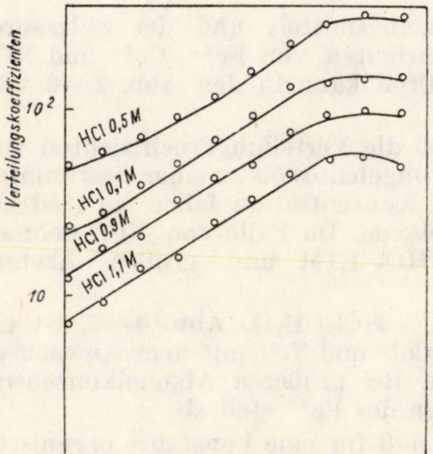

Abb. 3. – Änderung der Kd von Ni^{2+} in Funktion der Azeton- und der Salzsäurekonzentration.

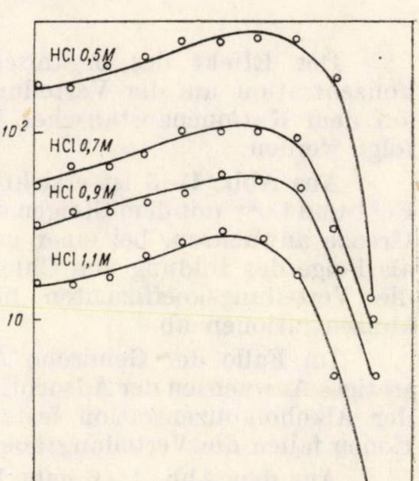

Abb. 4. – Änderung der Kd von Fe^{3+} in Funktion der Äthanol- und der Salzsäurekonzentration.

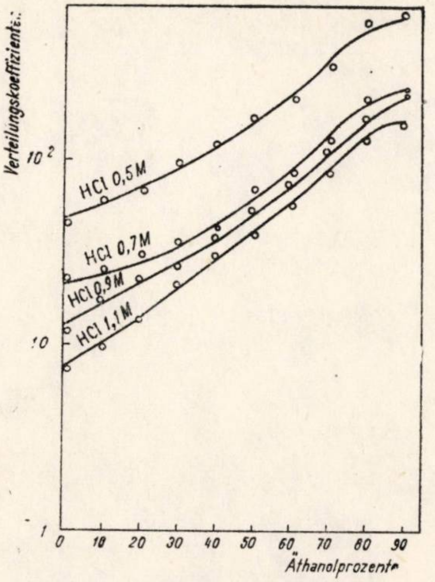

Abb. 5. — Änderung der Kd von Co^{2+} in Funktion der Äthanol- und der Salzsäurekonzentration.

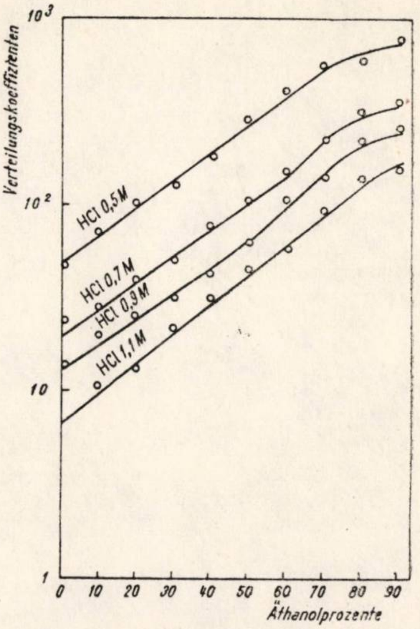

Abb. 6. — Änderung der Kd von Ni^{2+} in Funktion der Äthanol- und der Salzsäurekonzentration.

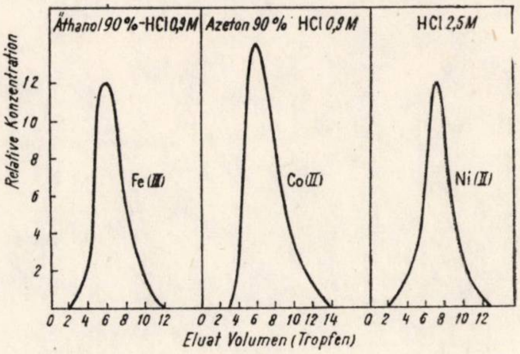

Abb. 7. — Chromatographische Trennung des Gemisches Fe^{3+}, Co^{2+} und Ni^{2+} auf der Mikrosäul e mit dem Kationenaustauscher Vionit CS-3.

SCHLUSSFOLGERUNGEN

Es wurden die Verteilungskoeffizienten von Fe^{3+}, Co^{2+}, Ni^{2+} auf dem Kationenaustauscher Vionit CS-3 im Medium von Azeton — HCl—H_2O und Äthanol — HCl—H_2O bestimmt.

Aus den dargestellten experimentellen Ergebnissen läßt sich schließen, daß der einheimische Kationenaustauscher Vionit CS-3 mit Erfolg für die Trennung des Gemisches von Fe^{3+}—Co^{2+}—Ni^{2+} verwendet werden kann.

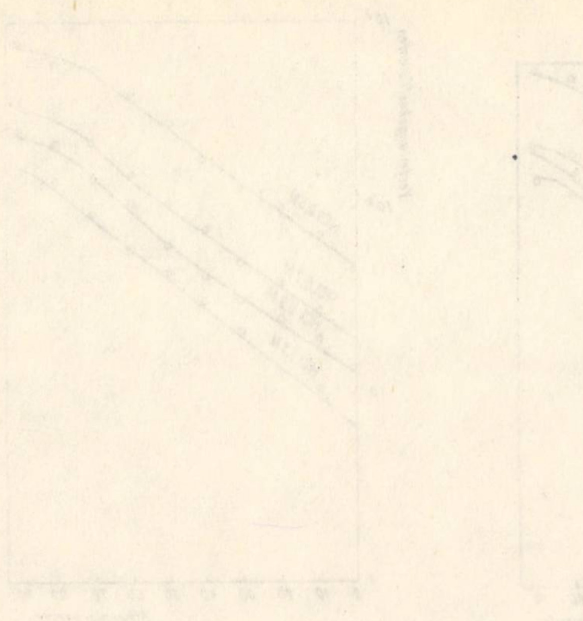

Abb. [illegible]. — Änderung der Kd von Ni²⁺ in Funktion der Äthanol- und der Salzsäurekonzentration.

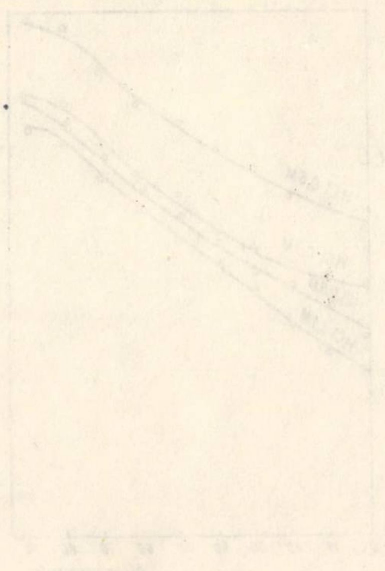

Abb. [illegible]. — Änderung der Kd von Co²⁺ in Funktion der Äthanol- und der Salzsäurekonzentration.

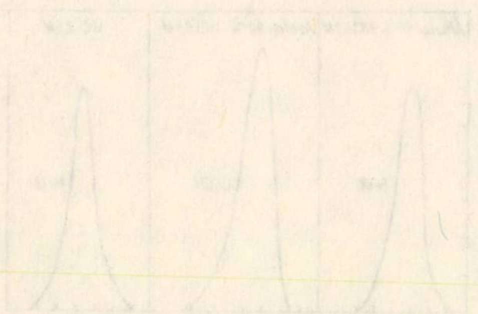

Abb. [illegible]. — Chromatographische Trennung des Gemisches Fe³⁺, Co²⁺ und Ni²⁺ auf der Mikrosäule mit dem Kationenaustauscher Vionit CS-3.

SCHLUSSFOLGERUNGEN

Es wurden die Verteilungskoeffizienten von Fe^{3+}, Co^{2+}, Ni^{2+} auf dem Kationenaustauscher Vionit CS-3 im Medium von Azeton — HCl — H_2O und Äthanol — HCl — H_2O bestimmt.

Aus den dargestellten experimentellen Ergebnissen läßt sich schließen, daß der einheimische Kationenaustauscher Vionit CS-3 mit Erfolg für die Trennung des Gemisches von Fe^{3+}—Co^{2+}—Ni^{2+} verwendet werden kann.

Revue Roumaine de Chimie, 17, 3, 511–518 (1972)

IR-UNTERSUCHUNGEN DER ADSORPTION AN MISCHOXID-KATALYSATOREN

A. POPESCU *, A. SZABO * und P. FINK **

*von der Universität Bukarest, Chemische Fakultät, Bukarest, Splaiul Independenţei 89
**von der Universität Jena, Sektion Chemie, 69 Jena, Am Steiger 3, D.D.R.

Eingegangen am 15. September 1971

Es wurden IR-Untersuchungen an $MoO_3-Fe_2O_3$, $MoO_3-Bi_2O_3$ und $MoO_3-Bi_2O_3-Fe_2O_3$ Katalysatoren in Form von dünnen selbsttragenden Tabletten durchgeführt. In speziellen Küvetten wurde die Adsorption von Ammoniak, Pyridin und Methanol IR-spektroskopisch beobachtet. Die Methode der Transmission erwies sich auf Grund der großen IR-Absorption und Streuung der Proben nur bedingt geeignet. Mit Hilfe der Ammoniak-Adsorption konnten Lewis-Säurezentren und Brönsted-Säurezentren an den oxidierten Katalysatoren nachgewiesen werden, während die Brönsted-Acidität an den reduzierten Katalysatoren fehlte. Es war ebenfalls eine schwache Pyridin-Adsorption festzustellen, die allerdings auf nicht zu starke Säurezentren schließen ließ. Die Methanoladsorption und Adsorption der Oxidationsprodukte war im Rahmen der Beobachtungsgrenze völlig reversibel.

EINLEITUNG

IR-Untersuchungen haben sich in den letzten Jahren als sehr wertvolle Methode zur Charakterisierung der Struktur der Katalysatoren selbst und vor allem zur Charakterisierung der möglichen adsorptiven Wechselwirkungen an Katalysatoroberflächen bewährt.[1,2] Dabei werden einmal die Wechselwirkungen aller Reaktanden unabhängig voneinander an den Katalysatoroberflächen studiert. Zum anderen ist es jedoch auch möglich, die zu Tabletten gepreßten Katalysatoren unter katalytischen Bedingungen, zum Beispiel im Flow-System, zu untersuchen. Nicht zuletzt spielen vorkatalytische Untersuchungen, die der Aufklärung der Natur und der Verteilung der Zentren dienen, eine große Rolle.

In dieser Arbeit soll der Versuch unternommen werden, die Wechselwirkung von Ammoniak, Pyridin und Methanol an speziellen Mischoxid-Katalysatoren zu charakterisieren.

---

[1] G. K. Boreskov, G. D. Kolovertnov, L. M. Kefeli, L. M. Pleasova, L. G. Karokchiev, V. N. Mostikhin, B. I. Popov, V. A. Dzisko und D. V. Tarasova, *Kinetika i Kataliz*, **7**, 144 (1966).

[2] F. Trifiro, V. De Vecchi und I. Pasquon, *J. Catalysis*, **15**, 8 (1969).

EXPERIMENTELLE TECHNIK

Die IR-spektroskopischen Untersuchungen wurden an selbsttragenden Tabletten durchgeführt. Die Katalysatortabletten (Ø 20 mm, Dicke 200 μm) wurden mittels einer Dezimalpresse in einem speziellen Preßwerkzeug unter einem Druck von 6000 Kp/cm^2 gepreßt. In einer IR-Küvette aus Quarz wurden die Untersuchungen der Tabletten durchgeführt. Die Küvette (Abb. 1) besteht aus einem Quarzrohr (Ø$_{\text{innen}}$ 22 mm, 135 mm lang), das mit einer Heizung und an den beiden Enden mit Metallkühlringen versehen ist. Das Quarzrohr hat zwei Zuführungen, damit auch im Gasstrom gearbeitet werden kann. Die planparallel angeschliffenen Quarzrohre werden beiderseitig mit CaF$_2$- oder KBr-Scheiben abgedichtet, die mit zähem Hochvakuumfett aufgeklebt werden. Radial eingesägte Quarzrohrstückchen halten die Katalysatortabletten senkrecht in den Küvetten. Mit einer Öldiffusionspumpe können die Küvetten auf 10^{-4} bis 10^{-6} Torr evakuiert werden. Diese Küvetten können mit einem einfachen Dosiersystem in Verbindung gebracht werden, es kann aber auch die Adsorption im

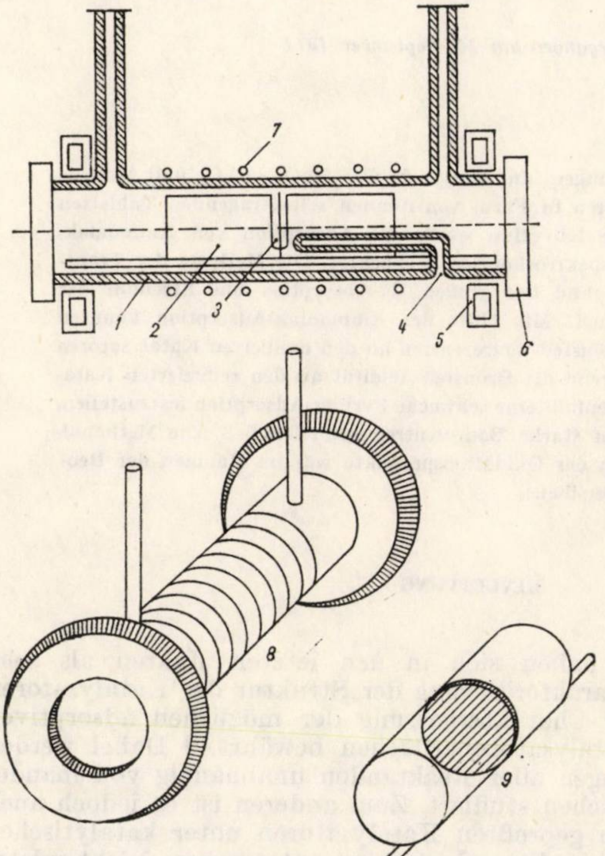

Abb. 1. — IR-Küvette für Sorptionsuntersuchungen.

1, Quarzrohr; *2*, Quarzhalterung für Probetabletten; *3*, Tablette; *4*, Hülse für Thermoelement; *5*, Kühlung; *6*, KBr-Fenster; *7*, Heizwicklungen; *8*, Küvette; *9*, Halterung mit Probetablette.

Inertgasstrom (Stickstoff, Argon) durchgeführt werden. Dazu wird der Inertgasstrom in einem Sättiger mit dem Sorptiv, z.B. Methanol, Pyridin beladen.

Vor den Adsorptionsexperimenten wurden die Proben in der Küvette 2 Stunden bei 400° und 10^{-5} Torr evakuiert. Im Anschluß an die Dehydratation schloß sich entweder eine Oxidation mit O_2 bei 400° oder eine Reduktion mit Methanol bei 300°, an, um den oxidierten oder reduzierten Kontakt beim Experiment einzusetzen. Nach dem Abkühlen der Probe unter Vakuum wurde das Grundspektrum registriert und dann in Abhängigkeit von der Sorptivzugabe jede Veränderung verfolgt. Das Arbeiten im Flow-System, d.h. im Inertgasstrom, erwies sich als vorteilhaft, da man hier im Spektrometer selbst alle möglichen Prozesse, wie Oxidation, Reduktion, Dehydratation oder Adsorption im Inertgasstrom kontinuierlich beobachten konnte. Das Flow-System ist in Abbildung 2 schematisch dargestellt. Über den Sättiger 1 oder den Sättiger 2 konnten verschiedene Sorptive zugeführt werden.

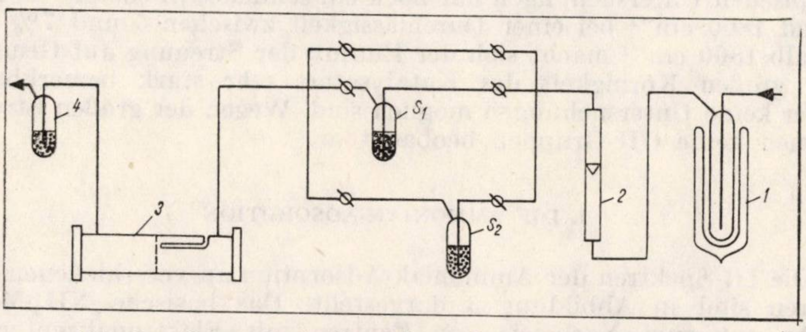

Abb. 2. — Schematische Darstellung der Strömungsapparatur.
1, Kühlfalle; *2*, Rotameter; *3*, IR-Küvette; *4*, Blasenzähler; S_1, S_2-Sättiger.

Als IR-Spektrometer stand das Ultrarotspektralphotometer UR 20 (VEB Carl Zeiss, Jena) zur Verfügung. Wegen der geringen Durchlässigkeit der verwendeten Proben wurde bei relativ großer Spaltbreite (Spaltbreite 8) und optimalen Verstärkerbedingungen gearbeitet.

Die als Adsorptive verwendeten Flüssigkeiten, Methanol und Pyridin, wurden sorgfältig getrocknet und mehrmals destilliert. Ammoniak lag in sehr reine Form vor und wurde noch einmal über aktiviertem Zeolith getrocknet.

In Tabelle 1 ist die chemische Zusammensetzung der verwendeten Mischoxid-Katalysatoren dargestellt. Sie wurden durch Mischfällung und anschließende thermische Behandlung erhalten.[3,4]

Tabelle 1

Chemische Zusammensetzung der Katalysatoren

Kat. Nr.	% MoO_3	% Bi_2O_3	% F_2O_3
1	52,2	42,3	5,5
2	55,3	44,7	—
3	85,4	—	14,6

---

[3] A. Popescu, A. Szabo und I. V. Nicolescu, *Rev. Chim. (Bucureşti)*, **17**, 602 (1966),

[4] A. Popescu, A. Szabo und A. Ionescu, *Analele Univ. Bucureşti. Ser. St. Nat. Chimie.* **16** (2), 33 (1967).

MESSERGEBNISSE

Sämtliche präparierte Katalysatortabletten zeigten trotz minimaler, für die mechanische Stabilität erforderlicher Dicke nur eine Durchlässigkeit zwischen 5 und 7%. Auf der anderen Seite ist die spezifische Oberfläche der Katalysatoren relativ gering (4,5–5,5 m^2/g) so daß man eine möglichst große Katalysatormenge durchstrahlen müßte, um das Spektrum der adsorbierten Moleküle zu beobachten. Unter diesen erschwerten Bedingungen mußten die optimalsten Bedingungen gesucht werden. Auf Grund der Eigenabsorption der Katalysatoren blieb für die IR-spektroskopischen Untersuchungen nur noch ein schmales „Fenster" zwischen 900 und 1800 cm^{-1} bei einer Durchlässigkeit zwischen 5 und 7% offen. Oberhalb 1800 cm^{-1} macht sich der Einfluß der Streuung auf Grund der relativ großen Körnigkeit des Katalysators sehr stark bemerkbar, so daß hier keine Untersuchungen möglich sind. Wegen der großen Streuung sind auch keine OH-Gruppen beobachtbar.

1. DIE AMMONIAK-ADSORPTION

Die IR-Spektren der Ammoniak-Adsorption an verschiedenen Katalysatoren sind in Abbildung 3 dargestellt. Das basische NH_3-Molekül ist sehr gut zum Nachweis von Zentren mit Elektronakzeptoreigenschaften (Lewis-Säurezentren) oder auch zum Nachweis von Protonen (Brönsted-Säurezentren) auf dispersen Oxiden.[5] Auf Grund seiner ein. fachen symmetrischen Struktur sind die Spektren sehr einfach zu deuten- Das NH_3-Molekül hat folgende Grundschwingungen (Tabelle 2).

Tabelle 2

Das NH_3-Molekül. Grundschwingungen

	ν (NH_3) cm^{-1}	$\delta\delta$ (NH_3) cm^{-1}	δs (NH_3) cm^{-1}
NH_3, Gas	3414 3336	1628	932 968
NH_3, flüssig	3375 3285	1632	1035 1066

Im Beobachtungsbereich können wir nur die Deformationsschwingungen von NH_3 und von NH_4^+ beobachten. Das IR-Spektrum des gasförmigen NH_3 (935, 970 cm^{-1}) ist bei allen Experimenten deutlich zu sehen, es bleibt jedoch auch nach 1stündigem Evakuieren noch NH_3 irreversibel an der Katalysatoroberfläche gebunden.

Katalysator Nr. 1, oxidiert. Nach dem Evakuieren (1 h bei 23°,10^{-4} Torr) bleiben die Banden bei 1480 cm^{-1} und 1625 cm^{-1} mit geringer Extinktion (Spektrum 3). Diese Banden charakterisieren NH_4^+ (1480 cm^{-1}; δ_{as} NH_4) und koordinativ gebundenes NH_3 (1625 cm^{-1}; δ_d NH_3). Wir müssen also die Existenz von Brönsted-Säurezentren und Lewis-Säurezentren in geringer Konzentration feststellen.

---

[5] H. DUNKEN, P. FINK und E. PILZ, *Chem. Techn.*, **18**, 490 (1966).

Katalysator Nr. 1, reduziert. Nach dem Evakuieren unter den gleichen Bedingungen bleibt hier nur die Bande bei 1625 cm^{-1} (Spektrum 6), die koordinativ gebundenen NH_3 an Lewis-Säurezentren zugeschrieben wird. Bei der Anwesenheit von gasförmigen NH_3 wird noch eine Bande bei 1500 cm^{-1} beobachtet, die jedoch beim Evakuieren verschwindet.

Katalysator nr. 2, oxidiert. Hier werden nach dem Evakuieren unter den gleichen Bedingungen die Banden bei 1420 cm^{-1} und bei 1630 cm^{-1} sehr deutlich beobachtet (Spektrum 9). Auf Grund der Extinktionsverhältnisse muß man hier auf deutlich mehr NH_4^+ schließen, d.h. die Konzentration der Brönsted-Säurezentren ist hier gegenüber der des Katalysators Nr. 1 wesentlich größer. Über das Verhältnis der Brönsted-Säurezentren zu den Lewis-Säurezentren läßt sich wegen der unbekanten Extinktionskoeffizienten aus diesen Experimenten keine Aussage machen.

Katalysator Nr. 2, reduziert. Hier ist nach der Einwirkung von NH_3 und dem Evakuieren nur eine schwache Andeutung der Bande bei 1625 cm^{-1} zu beobachten (Spektrum 12). Es sind also nur noch sehr schwache Lewis-Säurezentren, oder Lewis-Säurezentren in geringer Konzentration vorhanden.

Katalysator Nr. 3, reduziert. Nach Ammoniakeinwirkung und Evakuieren ist nur eine Andeutung von koordinativ gebundenen NH_3 vorhanden (Spektrum 15).

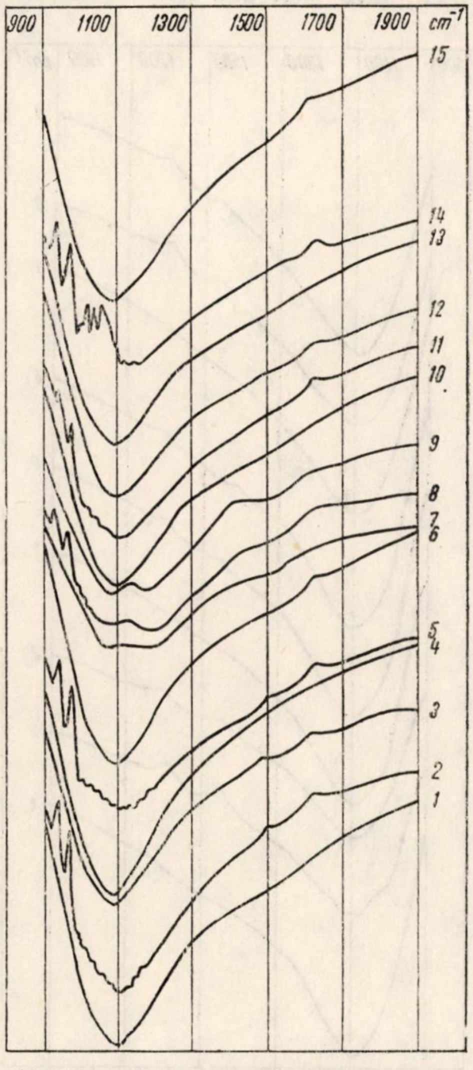

Abb. 3. — IR-Spektren der NH_3-Adsorption.

Spektren 1, 2, 3 — Katalysator Nr. 1 in oxidierter Form
Spektren 4, 5, 6 — Katalysator Nr. 1 in reduzierter Form
Spektren 7, 8, 9 — Katalysator Nr. 2 in oxidierter Form
Spektren 10, 11, 12 — Katalysator Nr. 2 in reduzierter Form
Spektren 13, 14, 15 — Katalysator Nr. 3 in reduzierter Form
Grundspektren (1, 4, 6, 10, 13), Spektren in NH_3-Atmosphäre (2, 5, 8, 11, 14), Spektren der evakuierten Proben (3, 6, 9, 12, 15).

2. DIE PYRIDIN-ADSORPTION

Besonders interessant für die Diskussion der Bindungsverhältnisse des Pyridins ist der C—C-stretching-Bereich. Parry[6] konnte als erster zeigen, daß sich aus den Informationen des Spektrums zwischen 1400 und 1700 cm^{-1} sehr aufschlußreiche Informationen über die Bindungsverhältnisse des Pyridins bei der Adsorption an der Katalysatoroberfläche erhalten lassen.

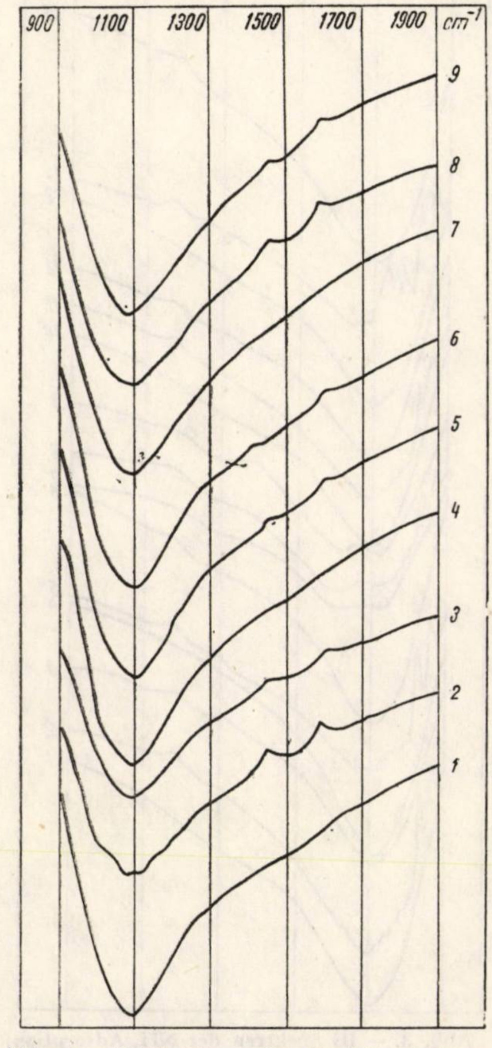

Abb. 4. — IR-Spektren der Pyridin Adsorption an Katalysatoren Nr. 1, 2 und 3 im oxidierten Zustand.

Spektren 1, 2, 3 — Katalysator Nr. 1; Spektren 4, 5, 6 — Katalysator Nr. 2; Spektren 7, 8, 9 — Katalysator Nr. 3. Grundspektren (1, 4, 7), Spektren in Pyridin Atmosphäre (2, 5, 8), Spektren der evkuiaerten Proben (3, 6, 9).

Bei der Pyridinabsorption (Abb. 4), an dem Katalysator Nr. 1 treten deutliche Banden bei 1450 und 1590 cm^{-1} und schwächere Banden im Bereich um 1100 cm^{-1} herum auf. Nach dem Evakuieren (1 h bei 23°, 10^{-4} Torr) sind nur noch kleine Andeutungen bei 1450 und 1590 cm^{-1} zu beobachten. Auf Grund des Auftretens dieser Banden kann man nur auf relativ schwach gebundenes Pyridin schließen (Spektrum 3). Bei stärkeren Bindungen des Pyridins an Lewis-Säurezentren müßten Banden bei 1610—1630 cm^{-1} auftreten. Die Katalysatoren Nr. 2 und 3 (Abb. 4) zeigen die gleichen Erscheinungen, nach dem Evakuieren sind nur noch sehr schwache Andeutungen der Banden bei 1450 und 1590 cm^{-1} vorhanden (Spektrum 6 und 9).

3. DIE METHANOL-ADSORPTION

Die Methanoladsorption an den untersuchten Katalysatoren ist vollkommen reversibel. Es treten die typischen IR-Banden des dampfförmigen Methanols auf (1020, 1040 und 1070 cm^{-1}), die den ν_{C-O} und ν_{CH_3}-Schwingungen zugeordnet werden. Nach dem Evakuieren (1/2 h bei 23°, 10^{-4} Torr) sind diese Banden nicht mehr zu erkennen. Man muß konstatieren, daß die Methanoladsorption nahezu reversibel ist (Abb. 5). Erhitzt

---

[6] E. P. Parry, *J. Catalysis*, **2**, 371 (1963).

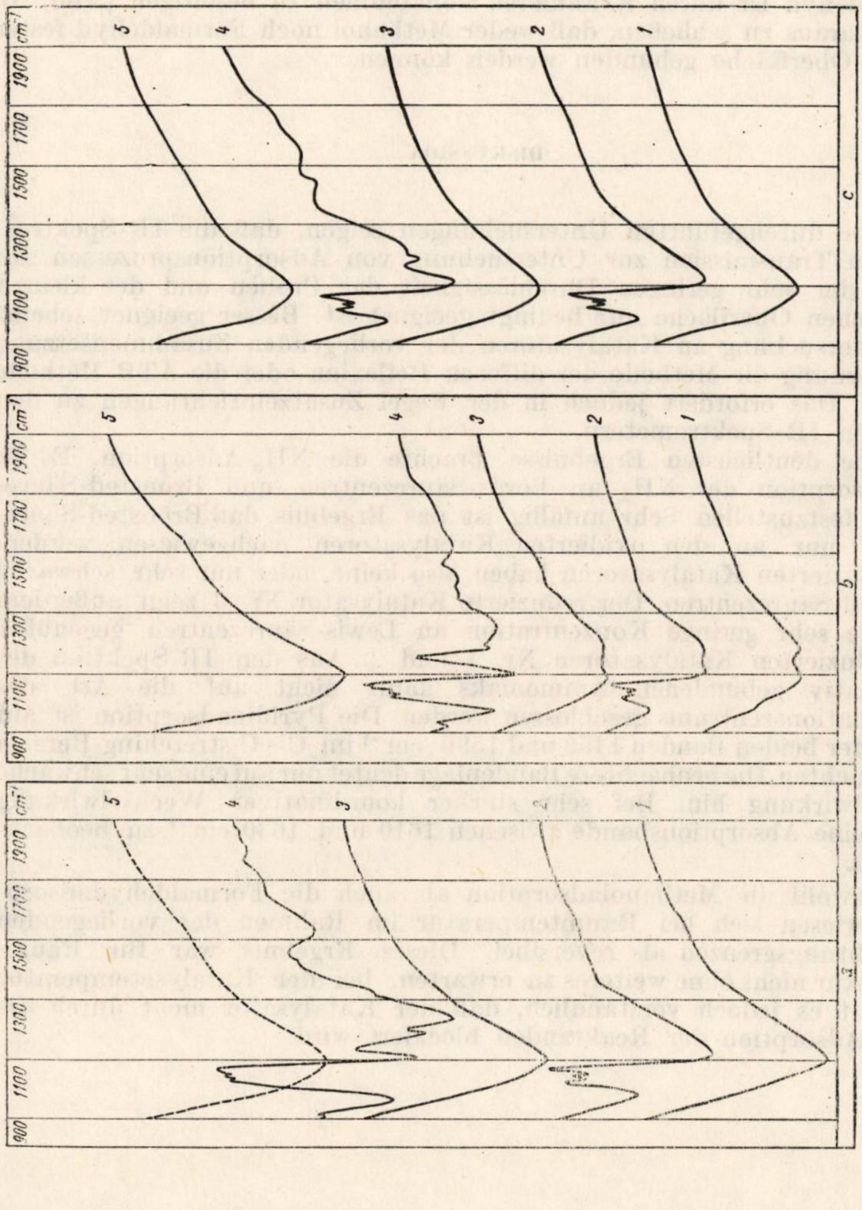

Abb. 5. — Spektren der Methanol und Formaldehyd Adsorption.

Grundspektren (1), Spektren in Methanol Atmosphäre (2), Spektren in Formaldehyd und Methanol Atmosphäre (4), Spektren der evakuierten Proben (3 und 5). *a*. Katalysator Nr. 1; *b*. Katalysator Nr. 2; *c*. Katalysator Nr. 3

man die Proben bei 300° 10 Minuten lang in der Methanolatmosphäre, so beobachtet man neue IR-Banden bei 940, 1065, 1155, 1200 cm^{-1}, einige kleinere Banden zwischen 1300 und 1400 cm^{-1} und bei 1460 cm^{-1}, die auf die Bildung von Formaldehyd weisen. Aber auch das gebildete Formaldehyd ist durch Evakuieren vollkommen zu beseitigen (Abb. 5). Es ist daraus zu schließen, daß weder Methanol noch Formaldehyd fester an der Oberfläche gebunden werden können.

DISKUSSION

Die durchgeführten Untersuchungen zeigen, daß die IR-Spektroskopie in Transmission zur Untersuchung von Adsorptionsprozessen auf Grund der sehr geringen Durchlässigkeit der Proben und der kleinen spezifischen Oberfläche nur bedingt geeignet ist. Besser geeignet scheint zur Untersuchung an Katalysatoren der vorliegenden Zusammensetzung und Körnung die Methode der diffusen Reflexion oder die ATR-Methode zu sein. Das erfordert jedoch in der Regel Zusatzeinrichtungen zu den normalen IR-Spektrometern.

Die deutlichsten Ergebnisse brachte die NH_3-Adsorption. Es ist die Adsorption des NH_3 an Lewis-Säurezentren und Brönsted-Säurezentren festzustellen. Sehr anfällig ist das Ergebnis, daß Brönsted-Säurezentren nur an den oxidierten Katalysatoren nachgewiesen werden. Die reduzierten Katalysatoren haben also keine, oder nur sehr schwache Brönsted-Säurezentren. Der reduzierte Katalysator Nr. 3 zeigt außerdem nur eine sehr geringe Konzentration an Lewis-Säurezentren gegenüber den reduzierten Katalysatoren Nr. 1 und 2. Aus den IR-Spektren des koordinativ gebundenen Ammoniaks kann nicht auf die Art des Koordinationszentrums geschlossen werden. Die Pyridinadsorption ist auf Grund der beiden Banden 1450 und 1590 cm^{-1} im C—C-stretching-Bereich zu beobachten. Die beobachtete Bandenlage deutet nur auf eine sehr schwache Wechselwirkung hin. Bei sehr starker koordinativer Wechselwirkung müßte eine Absorptionsbande zwischen 1610 und 1630 cm^{-1} zu beobachten sein.

Sowohl die Methanoladsorption als auch die Formaldehydadsorption erwiesen sich bei Raumtemperatur im Rahmen der vorliegenden Beobachtungsgrenzen als reversibel. Dieses Ergebnis war für Raumtemperatur nicht ohne weiteres zu erwarten, bei der Katalysetemperatur (300°) ist es jedoch verständlich, daß der Katalysator nicht durch die starke Adsorption der Reaktanden blockiert wird.

Revue Roumaine de Chimie, 17, 3, 519 – 524 (1972)

APPLICATIONS DE LA MICROANALYSE PAR SONDE ÉLECTRONIQUE À LA CATALYSE HÉTÉROGÈNE*

JEAN-MARIE LEROY et GABRIEL TRIDOT
École Nationale Supérieure de Chimie de Lille

Reçu le 19 janvier 1971

L'examen de la morphologie d'un catalyseur constitue une étape primordiale dans l'étude exhaustive d'une catalyse hétérogène. La microanalyse par sonde électronique, utilisée parallèlement avec les autres techniques physicochimiques, doit permettre de surmonter les difficultés dues à la complexité et à la mauvaise cristallinité des échantillons. Cette méthode, particulièrement intéressante pour l'examen de la surface de phases mixtes, est peu employée dans le cas de solides sous forme de poudres non conductrices.

L'échantillon jouant le rôle d'anticathode dans une sonde électronique, la préparation du spécimen exige des conditions spéciales et doit être effectuée avec les plus grands soins. Nous avons adopté deux modes de préparation :

— dans la première le catalyseur est préalablement mélangé à de la poudre de graphite puis comprimé à 250 bars sous un vide de 10^{-2} Torr.

— dans la seconde, le catalyseur est mélangé avec de l'araldite puis enrobé dans une résine. La pastille obtenue est ensuite polie au carbure de silicium avec lubrification à l'alcool puis à la poudre diamant de 1μ. L'échantillon est alors nettoyé aux ultra sons puis métallisé sous vide.

Afin d'éviter la détérioration des échantillons nous avons travaillé avec une tension accélératrice de 20 kV et une intensité de sonde de 10 nano A. Ceci correspond à une pénétration comprise entre 1 et 1,5 μ pour nos échantillons. La microsonde CAMECA MS 46 utilisée possède un dispositif combinant l'action d'un piège refroidi à l'azote liquide avec l'introduction d'une fuite d'oxygène dans la chambre objet, qui permet d'éviter toute contamination de l'échantillon pendant le bombardement électronique.

Nous nous sommes bornés à traiter trois exemples d'applications de la microanalyse par sonde électronique à la catalyse hétérogène.

---

* Extrait de la Conférence présentée à la Conférence Républicaine de Chimie-Physique pure et appliquée, Bucarest, septembre 1970.

ÉTUDES DE LA RÉPARTITION SUPERFICIELLE ET D'AGGLOMÉRATS

Le but initial de l'étude est de déterminer la répartition du fer et du molybdène à la surface des grains du catalyseur. En effet, toute anomalie dans la concentration de surface des solides fausse l'interprétation des résultats relatifs à l'examen des propriétés superficielles et catalytiques. Il est donc intéressant d'obtenir pour chaque composé la distribution des concentrations métalliques superficielles, d'en déterminer les concentrations métalliques moyennes et enfin de les comparer aux concentrations métalliques massiques obtenues par analyse chimique classique.

CALCULS DE CORRECTION

— *Choix des témoins*. Les catalyseurs pouvant être considérés, dans une certaine mesure, comme un mélange d'oxydes Fe_2O_3 et MoO_3, les calculs de correction sont établis à partir des témoins suivants : fer et molybdène d'une part, oxydes Fe_2O_3 et MoO_3 d'autre part.

— *Etude statistique du catalyseur*. Sur chaque catalyseur, cent mesures différentes donnant les concentrations en molybdène et en fer sont effectuées et corrigées chacune séparément afin de pouvoir tracer l'histogramme du rapport atomique Mo/Fe.

— *Correction d'absorption*. Toutes ces corrections sont effectuées suivant les méthodes de Castaing[1] et Philibert.[2] Nous donnons toutefois à la constante de Lenard les valeurs préconisées par Duncumb et Shields.

— *Correction de fluorescence par raie caractéristique*. L'utilisation des raies $K\alpha_1$ du fer et $L\alpha_1$ du molybdène rend cette correction tout à fait négligeable.

— *Correction de fluorescence par spectre continu*. C'est la plus délicate à résoudre et la plus controversée. Dans nos expériences l'effet dû à la fluorescence du fond continu est négligeable grâce à l'angle d'émergence des rayons X relativement faible (voisin de 18° sur la microsonde CAMECA) et au bon pouvoir de résolution du spectrographe.

— *Erreurs instrumentales*. Les erreurs sont de plusieurs types : statistiques (émission de photons), spectrales (bruit de fonds, superposition des raies, déplacement des raies)... Il convient d'y ajouter les erreurs liées à l'échantillon, au compteur et au faisceau électronique. Nous avons imposé des conditions expérimentales permettant de négliger ces divers paramètres. Par conséquent, seules les corrections d'absorption nécessitent un soin particulier dans cette étude.

DÉTERMINATION DES CONCENTRATIONS MÉTALLIQUES SUPERFICIELLES

Les catalyseurs 1 à 6 donnent une courbe de répartition du type de Gauss, très étroite (fig. 1), il en va tout autrement pour le catalyseur 7 (fig. 2). Sur l'ordonnée, k est le rapport des intensités d'une raie caractéristique engendrée respectivement par le spécimen et le témoin pur.

---

[1] R. Castaing, Thèse, Paris, 1952.

[2] J. Philibert, *Métaux Corrosion Industrie*, **40**, (465) 157 (1964).

Tableau 1

Comparaison des concentrations métalliques superficielles avec les concentrations métalliques massiques

Cata. N°	Rapport global Mo/Fe (analyse chimique)	Rapport Mo/Fe (microsonde) témoins Fe et Mo	Diff. relat. en %	Rapp. Mo/Fe (microsonde) témoins Fe_2O_3 et MoO_3	Diff. relat. en %
1	0,28	0,27	4	0,27	4
2	0,40	0,42	5	0,42	5
4	0,90	0,85	6	0,86	5
5	1,34	1,24	7,5	1,26	6
6	1,66	1,65	0,5	1,66	0
7	3	2,76	8	2,79	7

INTERPRÉTATION DES RÉSULTATS

— La différence relative sur le rapport atomique Mo/Fe obtenu, soit par microanalyse par sonde électronique soit par analyse chimique, est au maximum de 7%, ce qui représente une différence relative maximale de 3,5% pour une concentration métallique massique (Fig. 3). Ces résultats sont très satisfaisants pour une étude quantitative de poudre. [3]

— Les témoins Fe et Mo et les corrections réalisées à partir de ces témoins donnent des résultats très légèrement inférieurs à ceux obtenus à partir des oxydes Fe_2O_3 et MoO_3.

— L'histogramme par micron carré, des catalyseurs 1, 2, 4, 5 et 6 en fonction du rapport atomique Mo/Fe, montre les différences de rapport atomique obtenues par volume irradié. Ces différences sont plus difficilement détectables sur les images X.

— Les images électroniques présentent un aspect semblable, elles permettent de situer la taille des grains entre 15 et 30 μ. Ces images et les courbes de répartition correspondantes permettent d'envisager les grains de catalyseurs formés par des agglomérats dont le rapport Mo/Fe varie d'une manière continue suivant une courbe du type de Gauss.

— Pour le catalyseur 7, il en va tout autrement et chaque grain, de taille moyenne 20 μ, se présente sous forme d'agglomérats de deux types différents (Fig. 4). L'image électronique met en évidence des taches grisâtres que nous appellerons agglomérats du type I et des taches blanches, agglomérats du type II, dont certaines ont des dimensions très nettement supérieures aux précédentes. Le même phénomène se trouve sur l'image X de répartition du fer et sur l'enregistrement des intensités respectives du fer et du molybdène (fig. 5) effectué suivant la ligne de balayage *xy* matérialisée sur la figure 4.

L'hétérogénéité des grains nous a conduit à travailler avec une sonde défocalisée d'un diamètre de 50 μ. Ceci nous permet d'obtenir les concentrations superficielles moyennes du Fe et du Mo par un nombre de tests relativement peu important (100 tests). Chaque type d'agglomérat est ensuite analysé avec une sonde focalisée de diamètre gaussien 1 μ.

---

[3] G. Brau, *Rev. Chim. Miné.*, **6**, 441 (1969).

La répartition du rapport atomique Mo/Fe est figurée par deux courbes de Gauss dont les moyennes statistiques ont respectivement les valeurs 4,24 et 1,69 pour les types I et II. Les agglomérats de type I présentent une concentration plus élevée en molybdène et un domaine de répartition du rapport Mo/Fe très large. L'étendue du domaine pour le rapport Mo/Fe peut s'expliquer par une participation de plusieurs agglomérats touchés par l'impact de la sonde.

Les agglomérats de type II, plus facilement analysés à cause de leurs dimensions, présentent un rapport atomique Mo/Fe moyen égal à 1,69. Cette valeur correspond, compte tenu des erreurs expérimentales, à celle de la phase molybdate ferrique.

MISE EN ÉVIDENCE ET INTERPRÉTATION DU PHÉNOMÈNE DE DÉSACTIVATION

Le solide testé est le catalyseur 7 qui s'est révélé le plus actif pour l'oxydation du méthanol en formaldéhyde.[4] Dans les conditions opératoires du réacteur dynamique différentiel et pour la température de 285°C l'activité du catalyseur, stable après 2 heures de mise en régime, demeure constante pendant 8 heures puis décroît assez rapidement. Un dépôt bleuâtre se forme vers le bas du réacteur où se produit une baisse sensible de température. Nous nous sommes proposé d'étudier à la microsonde électronique les variations morphologiques du catalyseur concomitantes avec la perte d'activité.

Les images électroniques et les histogrammes du catalyseur « neuf » et « usagé » sont représentées sur la figure 6. Rappelons que l'étude statistique du catalyseur « neuf » fait apparaître deux maximums du rapport atomique Mo/Fe, situés à 1,69 et 4,24 et attribués respectivement aux phases molybdate ferrique et oxyde de molybdène MoO_3.

L'histogramme du catalyseur « usagé » montre la présence d'un maximum pour un rapport Mo/Fe = 1,4. Le pic unique et la nouvelle valeur du rapport Mo/Fe indiquent la disparition de la phase MoO_3 et la destruction partielle du molybdate ferrique.

Nous nous sommes d'abord intéressés au dépôt obtenu en bas du réacteur. Une partie du tube est prélevée, enrobée dans la résine puis analysée à la sonde électronique. La figure 7 qui représente les images électroniques et X, met en évidence la présence des éléments Mo et O et l'absence de Fe dans ce dépôt. L'analyse quantitative fait apparaître un rapport O/Mo légèrement inférieur à 3, il s'agit donc d'oxyde de molybdène communément dénommé « bleu de molybdène ». Ce phénomène explique la disparition du pic attribué à la phase MoO_3 dans l'histogramme du catalyseur « usagé ».

Nous avons ensuite examiné à la microsonde électronique divers échantillons en fonction de leur temps de travail. La disparition du pic attribué à la phase MoO_3 intervient la première, elle est sans effet sur l'activité du catalyseur. Par contre, dès que la valeur du deuxième pic, attribué à la phase molybdate ferrique, commence à décroître la désacti-

---

[4] S. Peirs, Thèse, Lille, 1970.

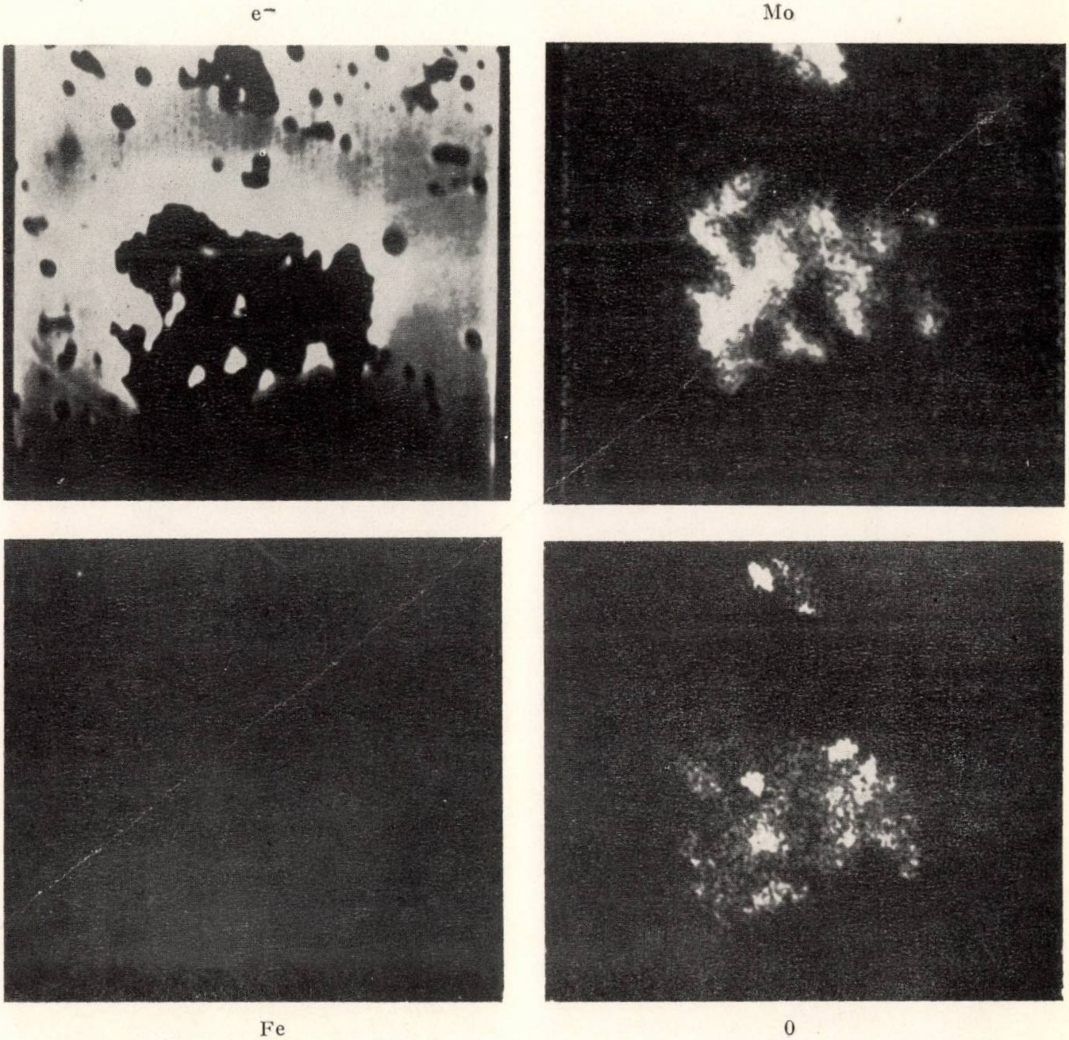

Fig. 7. — Images électronique et *X* du dépôt obtenu en bas du réacteur.

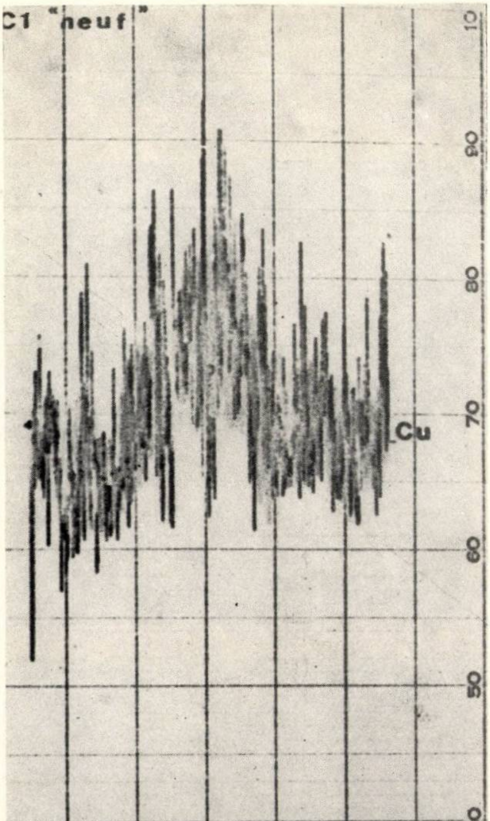

Fig. 8. — Répartition du cuivre et du manganèse suivant l'axe central d'une pastille de catalyseur « neuf » (enregistrement à vitesse constante).

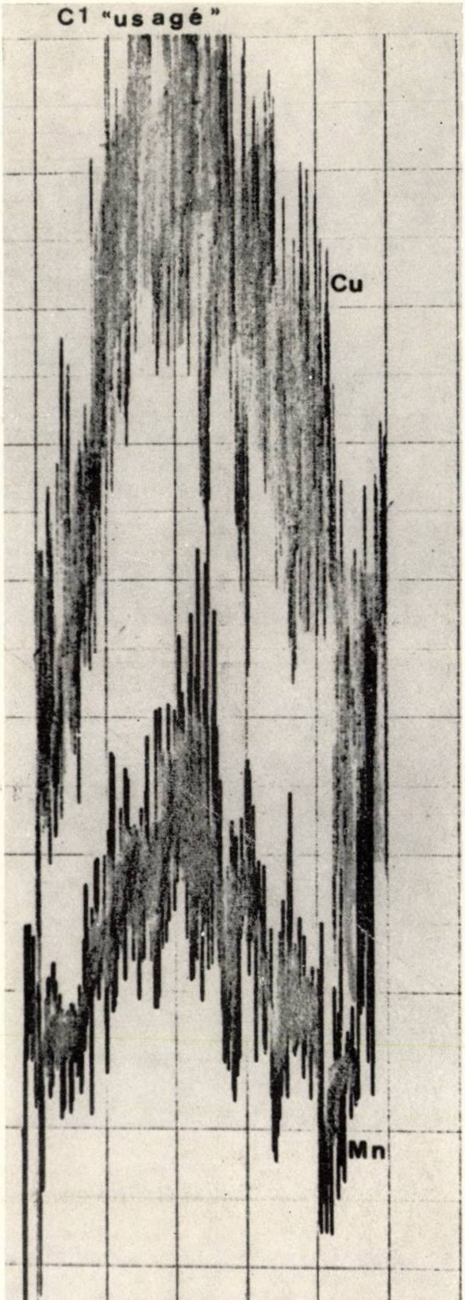

Fig. 9. — Répartition du cuivre et du manganèse suivant l'axe central d'une pastille de catalyseur « usagé » (enregistrement à vitesse constante).

vation suit une loi colinéaire. La désactivation est donc liée à la destruction de molybdate ferrique et ceci confirme qu'il s'agit bien de la phase active du catalyseur.

Pourtant si la phase MoO_3 ne semble pas intervenir directement dans l'activité du catalyseur il est incontestable qu'un échantillon initialement constitué par la phase molybdate ferrique pure est beaucoup moins actif. Ce phénomène peut s'expliquer par une dispersion plus grande de la phase active molybdate ferrique dans un catalyseur contenant également du MoO_3. Cette hypothèse semble confirmée par les images électroniques des échantillons 7 et 6. En effet, les dimensions des grains du spécimen 6, correspondant à la phase ferromolybdate pure, sont bien plus importantes que celles relatives au catalyseur 7. L'image électronique de l'échantillon 6 est représentée sur la figure 1.

ÉTUDE DE LA RÉPARTITION DE LA PHASE ACTIVE DANS DES PASTILLES DE CATALYSEUR

Nous avons pris comme exemple un catalyseur de conversion basse température, constitué par un mélange d'oxydes de cuivre et de manganèse sur support alumine. La préparation du spécimen est effectuée par imprégnation de l'alumine par une solution des nitrates puis calcination à l'air. Lors de l'imprégnation il se produit des phénomènes de chromatographie qui sont différents suivant le type d'alumine.

Les dosages chimiques fournissent un résultat global, nous avons déterminé la présence de gradient de concentration à l'intérieur de certaines pastilles par balayage à la microsonde :

— soit automatiquement à vitesse constante ce qui donne l'allure générale du phénomène.

— soit en déplaçant manuellement l'échantillon ce qui permet d'effectuer plusieurs comptages sur une même surface et d'obtenir ainsi le nombre d'impulsions moyen.

CATALYSEUR « NEUF »

L'enregistrement à vitesse constante (fig. 8) suivant l'axe central de la pastille montre que le Cuivre et le Manganèse ont une très légère tendance à migrer vers le centre de la pastille.

L'enregistrement manuel confirme ce fait. La répartition du Cuivre est beaucoup moins homogène que celle du Manganèse, les écarts sur le Cuivre sont de ± 17%.

CATALYSEUR « USAGÉ »

La figure 9 montre que le Cuivre et le Manganèse, ont migré vers le centre de la pastille mais la répartition reste symétrique. Le rapport $\frac{[\mathrm{Mn}]\ \text{périphérie}}{[\mathrm{Mn}]\ \text{centre}}$ passe de la valeur 1,3 dans le catalyseur « neuf » à 1,6 dans l'échantillon « usagé ».

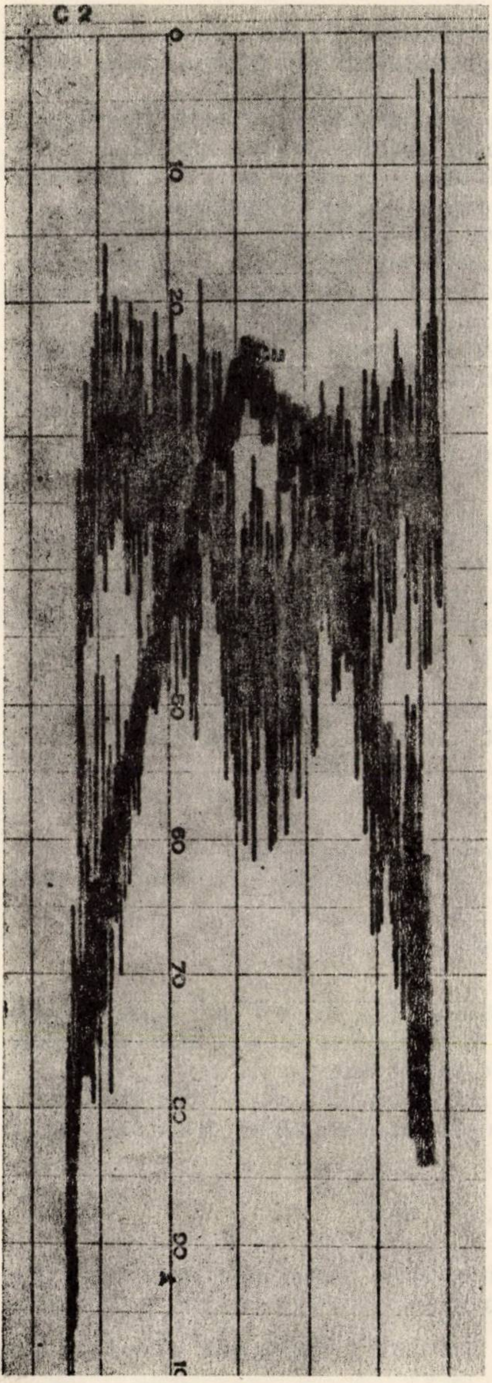

Fig. 10. — Répartition du cuivre et du manganèse suivant l'axe central d'une pastille d'échantillon présentant une activité catalytique médiocre.

Une étude plus approfondie de catalyseurs ayant travaillé pendant des temps différents montre que les baisses d'activité suivent une loi colinéaire à celle de la migration du Cuivre et du manganèse à l'intérieur de la pastille.

Pour des raisons économiques tous avons tenté de changer le type d'alumine constituant le support. Tous les matériaux utilisés ont donné des résultats défavorables concernant l'activité des catalyseurs. Afin d'élucider le phénomène nous avons analysé par microsonde électronique un spécimen présentant une activité médiocre.

L'enregistrement (fig. 10) montre que dans un tel échantillon la répartition du Cuivre et du Manganèse est tout à fait contraire : le Cuivre migre vers le centre et le Manganèse vers la périphérie. Pour palier à cet inconvénient nous avons modifié les techniques d'imprégnation et de calcination. Les concentrations des éléments actifs sont alors équilibrées dans la masse de contact et l'activité catalytique est satisfaisante.

Deux phénomènes intéressants se dégagent de cette étude :

— l'évolution de la répartition de la phase active du catalyseur lors de son travail et la relation entre cette évolution et l'activité catalytique.

— l'influence considérable de la « qualité » du support sur la loi de répartition de la phase active.

Nous pourrions citer d'autres exemples d'applications de la microanalyse par sonde électronique mais nous pensons que les problèmes traités permettent d'entrevoir et d'envisager le nouveau et vaste champ d'application de cette technique qui doit largement contribuer à la connaissance de la morphologie des catalyseurs.

Revue Roumaine de Chimie, 17, 3, 525–532 (1972)

ÉTUDE DE LA DÉSHYDRATATION DU MÉTHYLPHÉNYLCARBINOL SUR DIVERSES MASSES DE CONTACT*

GEORGETA CSOMONTANYI et A. PANOVICI
Institut PETROCHIM, Ploieşti, 251, B-dul Republicii

Reçu le 15 février 1971

Quoique, du point de vue thermodynamique, la réaction de formation du styrène à partir du méthylphénylcarbinol soit exceptionnellement favorable, les vitesses pour atteindre des conversions élevées sont réduites, fait qui impose l'utilisation des catalyseurs sélectifs. On étudie la réaction de formation du styrène à partir du méthylphénylcarbinol, en caractérisant au point de vue cinétique par les énergies d'activation et les facteurs préexponentiels une série de catalyseurs et en établissant une corrélation linéaire entre les énergies d'actication et le logarithme des facteurs préexponentiels. A l'aide des coefficients relatifs d'adsorption on détermine les fonctions thermodynamiques de remplacement du réactant, par adsorption du produit sur la surface catalytique active.

La déshydratation du méthylphénylcarbinol (MPhC) en styrène constitue une étape du nouveau procédé pour l'obtention concomitante du propèneoxyde et du styrène à partir du propène et de l'éthylbenzène. Le procédé consiste dans l'oxydation en phase liquide de l'éthylbenzène en hydroperoxyde d'éthylbenzène, ce dernier, étant l'agent d'époxydation du propène dans la deuxième phase du procédé se transformant, après avoir cédé l'oxygène au propène, en MPhC. Présenté par la firme Halcon International au VIIe Congrès Mondial du Pétrole,[1] le nouveau procédé offre des rendements et des sélectivités élevées (plus de 95% mole), rapporté tant au propène, qu'à l'éthylbenzène.

Le présent travail se propose une étude thermodynamique et cinétique de la transformation du MPhC, le but poursuivi étant le choix et la caractérisation cinétique de certains systèmes catalytiques qui dirigent d'une manière sélective la réaction vers la formation du styrène.

La littérature recommande pour la déshydratation du MPhC des oxydes métalliques : Al_2O_3, TiO_2, bauxite, argile.[2–6] Une série d'auteurs font des études sur la cinétique de la déshydratation de certains alcools primaires, secondaires et tertiaires, en présence de Al_2O_3, $SiO_2-Al_2O_3$ et d'autres catalyseurs, pour élucider le mécanisme de la déshydratation catalytique et la nature des centres actifs responsables de cette réaction.[7–11] Balandin et ses collaborateurs,[12–15] en étudiant la déshydratation et la déshydrogénation de certains alcools ayant des structures différentes, déterminent des fonctions thermodynamiques de remplacement par adsorption, démontrant l'effet catalytique par la corrélation géométrique des centres actifs et des molécules réactantes.

---

* Communication faite au 39e Congrès International de Chimie Industrielle, Bucarest, 1970.

[1] VIIe Congrès Mondial du Pétrole, Mexique, 1967, — Petrochemistry, vol. 5, 1967, p. 67.

[2] A. A. Vansheidt et V. M. Zeltzer, *Zhur. priklad. Khim.*, **21**, 512 (1948).

[3] P. G. Sergheev et B. D. Crujalov, *Khim. Prom.*, **1957**, 201.

[4] L. C. Shriver et W. Charleston (to Carbide and Carbon Chemicals Corporation), U.S.A. Pat. 2 399 395, 23 sept. 1943.

[5] E. I. Korchak et N. I. Hachensack (to Halcon International Inc.), U.S.A. Pat. 3 442 963, 24 mai 1967.

[6] J. Kollar (to Halcon International Inc.), Belg. Pat. 657 833, 30 juin 1965.

CONSIDÉRATIONS THERMODYNAMIQUES

Les réactions chimiques prises à l'étude, à partir du MPhC sont :

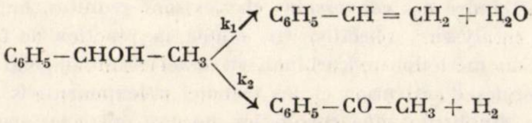

$$C_6H_5-CHOH-CH_3 \xrightarrow{k_1} C_6H_5-CH=CH_2 + H_2O$$
$$C_6H_5-CHOH-CH_3 \xrightarrow{k_2} C_6H_5-CO-CH_3 + H_2$$

Au point de vue thermodynamique, les deux réactions sont caractérisées par les fonctions indiquées dans le tableau 1, dont il ressort que les deux réactions sont thermodynamiquement possibles, même dans des conditions standard, les enthalpies de réaction (ΔH_r) montrant pour la réaction de déshydrogénation un caractère faiblement endothermique, tandis que la réaction de déshydratation avec formation du styrène devient exothermique à des températures dépassant 500°K. Les constantes d'équilibre et les conversions à l'équilibre ont des valeurs très élevées, les équilibres étant pratiquement totalement déplacées dans la direction de la formation du styrène, respectivement de l'acétophénone.

Quoique, au point de vue thermodynamique, la réaction de formation du styrène à partir du MPhC soit exceptionnellement favorable, les vitesses qui permettent d'atteindre des conversions élevées sont réduites, fait qui impose le choix de certains systèmes catalytiques adéquats qui, en dehors du rôle d'accélération de la vitesse de déshydratation au styrène, dirigent sélectivement la transformation du MPhC, en réduisant, au minimum possible, la vitesse de réaction non désirée de déshydrogénation à l'acétophénone.

---

[7] R. Figueras, A. Mohl et Y. Trambouse, *Compt. rend.*, Ser. C, **1968**, 1123.

[8] J. D. Butler, *J. Chem. Soc.*, **1968**, 905.

[9] F. Blac et H. Pines, *J. Org. Chem.*, **33**, 2035 (1968).

[10] J. M. Parera et S. N. Figoli, *J. Catalysis*, **14**, 303 (1969).

[11] R. Figueras, L. De Mourgues et Y. Trambouse, *J. Catalysis*, **14**, 107 (1969).

[12] A. A. Balandin, O. Bogdanova et A. T. Scheglova, *Izvest. Akad. Nauk. SSSR, Otdel. khim. Nauk*, **1955**, 723.

[13] O. Bogdanova, A. A. Balandin et A. T. Scheglova, *Izvest. Akad. Nauk. SSSR., Otdel. khim. Nauk*, **7**, 795 (1957).

[14] A. A. Balandin et A. A. Tolstopyatova, *Zhur. fiz. Khim.*, **XXX**, **6**, 1367 (1956).

[15] A. A. Balandin, O. K. Bogdanova et J. P. Belomestnic, *Doklady. Akad. Nauk S.S.S.R.*, **38**, 595 (1961).

Tableau 1

Fonctions thermodynamiques pour les réactions de déshydratation et déshydrogénation du MPhC

$C_6H_5-CHOH-CH_3 \rightarrow C_6H_5-CH=CH_2+H_2O$

Fonctions thermo-dynamiques / T°K	$\Delta H_r \frac{\text{cal}}{\text{mole}}$	$\Delta S_r \frac{\text{cal}}{\text{mole.grad}}$	$\Delta G \frac{\text{cal}}{\text{mole}}$	K_p	α % mole
298	9222	42,78	− 3278	$3{,}95.10^2$	99,65
400	3390	43,3	−13930	$6{,}1\ .10^7$	100,0
500	− 2946	43,59	−24491	$5.51.10^{10}$	
600	− 9985	43,76	−36241	$1{,}76.10^{13}$	
700	−17132	43,03	−47253	$6{,}36.10^{14}$	

$C_6H_5-CHOH-CH_3 \rightarrow C_6H_5-CO-CH_3 + H_2$

Fonctions thermo-dynamiques / T°K	$\Delta H_r \frac{\text{cal}}{\text{mole}}$	$\Delta S_r \frac{\text{cal}}{\text{mole.grad}}$	$\Delta G \frac{\text{cal}}{\text{mole}}$	K_p	α % mole
298	10300	37,41	− 850	4,21	90,0
400	9500	36,36	− 5040	$5{,}82.10^2$	99,0
500	8590	36,77	− 9800	$1{,}97.10^4$	100,0
600	6820	36,69	−15200	$3{,}59.10^5$	
700	6330	35,23	−18330	$5{,}03.10^5$	

PARTIE EXPÉRIMENTALE

Les expériences de déshydratation ont été effectuées dans un réacteur intégral en courant continu, en utilisant une couche fixe de catalyseur, dans le domaine de la cinétique de réaction.

Les conditions ont été telles que les phénomènes de diffusion soient négligeables.

Les matières premières utilisées dans cette étude ont été :

– le MPhC d'une pureté dépassant 99,5% poids,

– le styrène, d'une pureté de 99,75% poids.

Les matières premières et les produits de réaction ont été analysés par chromatographie gaz-liquide, à l'aide d'un chromatographe muni d'un détecteur de thermoconductibilité et d'une colonne d'un mètre de longueur, remplie de cellite C_{22}, imprégnée de Reoplex 12%, en régime isotherme.

Dans une étude préliminaire, on a poursuivi la transformation du MPhC dans la phase de vapeurs, sur une couche fixe de matériau inerte (grains de quartz) dans le domaine de températures de 300° à 400°, pour divers temps de contact. La formation du styrène découle dans ces conditions à des vitesses extrêmement réduites, le rendement ne dépassant pas 3% mole, à des temps de contact de plus de 20 secondes. La transformation du MPhC a aussi lieu dans la direction de la déshydrogénation à l'acétophénone, toujours avec des rendements faibles, qui ne dépassent pas 1% mole.

L'emploi de certaines masses de contact à base d'oxyde (Al_2O_3, TiO_2, $SiO_2-Al_2O_3$) mène à une augmentation considérable de la vitesse de déshydratation, la transformation ayant lieu à des sélectivités élevées. Tel qu'il résulte du tableau 2, dans des conditions de température de 300–400°, pour des temps de contact de 1–3 secondes, on obtient des rendements de 50 à 95% mole styrène, avec des sélectivités au-dessus de 90% mole, les meilleures performances étant obtenues en présence des catalyseurs $TiO_2-Al_2O_3$, à savoir : des conversions dépassant 90% mole à des sélectivité supérieures à 95% mole, à 350° et temps de contact de 1—2 s.

Tableau 2

Résultats de la déshydratation du MPhC sur diverses masses de contact

Masse de contact	Conditions de réaction		Performances	
	Temp. °C	τ s	Rendement % mole	Sélectivité % mole
Quartz	350	23,0	2,7	80,2
	400	2,4	1,7	82,0
$SiO_2-Al_2O_3$	350	3,0	60,0	85,7
	400	1,9	62,0	90,1
$\alpha-Al_2O_3$	350	1,56	63,2	94,0
	400	1,2	74,1	92,3
Tamis moléculaires S.M.	300	1,02	50,2	92,3
	350	2,1	76,5	96,4
TiO_2	350	3,0	90,5	96,0
	350	1,0	56,6	98,5
$TiO_2-Al_2O_3$	300	2,0	85,0	96,5
	350	1,2	90,2	96,5
	350	2,0	95,0	95,5

Dans ces conditions, en l'absence du catalyseur, on n'a observé pratiquement aucune transformation du MPhC.

Dans l'étude cinétique effectuée on a considéré la réaction de déshydratation du MPhC en styrène comme une réaction monomoléculaire, irréversible, découlant selon le schéma :

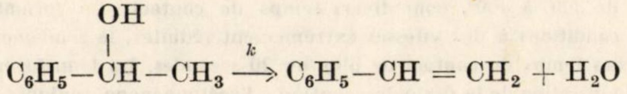

$$C_6H_5-\underset{}{\overset{\displaystyle OH \atop |}{CH}}-CH_3 \xrightarrow{k} C_6H_5-CH=CH_2+H_2O$$

dont la constante de vitesse k a été déterminée par la relation de Balandin et ses collaborateurs.[15]

$$k = 2{,}303\,(Z_2+Z_3)\,A_1\cdot\log\frac{A_1}{A_1^{-m}} - m(Z_2+Z_3-1)$$

où :

A_1 — débit d'alimentation moles/l.cat.s
m — conversion molaire en produit désiré
Z_2 — coefficient relatif d'adsorption du styrène, par rapport au MPhC
Z_3 — coefficient relatif d'adsorption de l'eau, par rapport au MPhC.

Pour la détermination des coefficients d'adsorption relatifs Z_2 et Z_3, on a employé la relation :

$$Z = \frac{m_0/m - 1}{100/p - 1}$$

où :

m_0 — conversion en styrène à l'alimentation en MPhC pur,
m — conversion en styrène à l'alimentation en MPhC en mélange avec du styrène, respectivement de l'eau,
p — pour cent molaire de MPhC dans l'alimentation.

En faisant varier la vitesse molaire de passage du MPhC sur la couche fixe de catalyseur, dans le domaine de températures de 250° à 350°, on a poursuivi la variation de la conversion du MPhC en styrène. Des isothermes conversion-temps de contact sur le catalyseur $TiO_2-Al_2O_3$, représentées dans la figure 1, on a calculé les constantes de vitesse de déshydratation dans le domaine de température étudié, dont la représentation logarithmique dans le système de référence Arrhenius (fig. 2) nous a permis de déterminer l'énergie d'activation (11 540 cal/mole) et le facteur préexponentiel ($\log k_0 = 4{,}12$).

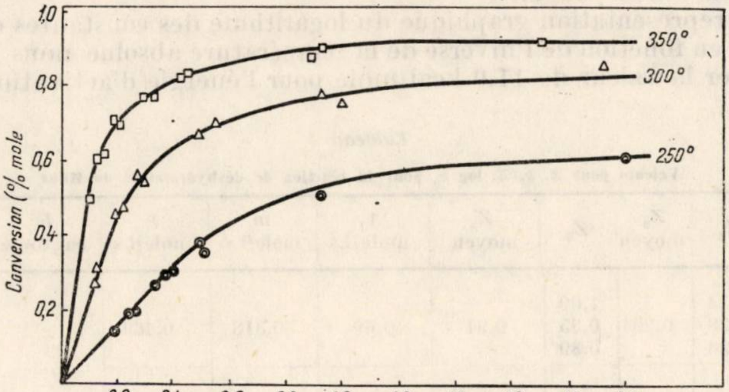

Fig. 1. — Isothermes conversion-temps de contact à la déshydratation du MPhC en présence du catalyseur $TiO_2-Al_2O_3$.

Pour vérifier si les valeurs de l'énergie d'activation et du facteur préexponentiel, déterminées par la méthode graphique, sont réelles, et non apparentes, nous avons eu recours à la détermination de la constante de vitesse selon la relation de Balandin et ses collaborateurs, indiquée ci-dessus. Les valeurs des coefficients relatifs d'adsorption Z_2 et Z_3 dans le domaine de températures 275—350° ont été déterminées en poursuivant la conversion du MPhC en styrène à l'alimentation du MPhC pur et à l'alimentation du MPhC en mélange de 15%, 30% et 50% mole styrène, et respectivement de l'eau. Ces valeurs ont été utilisées pour la détermination des constantes de vitesse k, par la détermination des valeurs m, à diverses vitesses molaires d'alimentation A. Tel qu'il résulte du tableau 3, les valeurs des coefficients relatifs d'adsorption styrène-MPhC augmentent avec la température à partir de 0,294 à 275° à 2,55 pour 350°, tandis que, dans le même domaine de températures, les valeurs des coefficients relatifs d'adsorption pour l'eau-MPhC se maintiennent pratiquement constants à la valeur de 0,9.

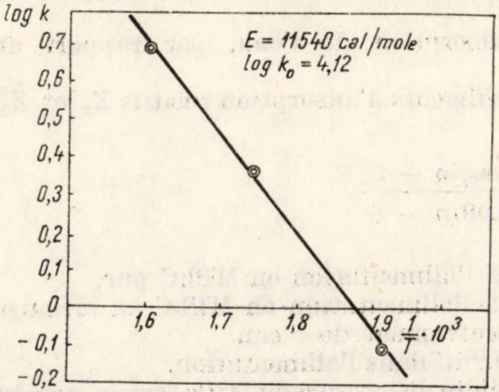

Fig. 2. — Variation du log. k avec $\frac{1}{T}$ pour la réaction $C_6H_5-CHOH-CH_3 \rightarrow C_6H_5-CH=CH_2 + H_2O$.

La représentation graphique du logarithme des constantes de vitesse calculées en fonction de l'inverse de la température absolue nous a permis de trouver la valeur de 11,0 kcal/mole pour l'énergie d'activation et 4,05

Tableau 3

Valeurs pour Z, k, E, log k_0 pour la réaction de déshydratation du MPhC

T°C	Z_2	Z_2 moyen	Z_3	Z_3 moyen	A_1 mole/l.s	m mole/l.s	k mole/l.s	E cal/mole	log k_0 mole/l.s
275	0,34 0,28 0,26	0,294	1,09 0,85 0,89	0,94	0,69	0,318	0,469	11000	4,05
300	0,94 1,15 0,91	1,0	0,94 0,78 0,88	0,87	0,69	0,394	0,755		
350	2,64 2,50 2,51	2,55	0,90 0,98 0,82	0,90	0,69	0,428	1,551		

$Z_2 = a\,(styrène)/_{a(MPhC)}$ $\qquad$ $Z_3 = a\,(\text{eau})/a\,(\text{MPhC})$

$$k = 2{,}303(Z_2 + Z_3)A_1 \log.\ \frac{A_1}{A_1 - m} - m(Z_2 + Z_3 - 1)$$

pour le logarithme du facteur préexponentiel, les valeurs trouvées étant très rapprochées de celles déterminées par méthode graphique.

On a caractérisé, au point de vue cinétique, par la même méthode, quelques oxydes métalliques dans la réaction de déshydratation du MPhC en styrène, les valeurs trouvées pour les énergies d'activation variant entre 8 kcal/mole pour le TiO_2 et 16 kcal/mole pour l'α—Al_2O_3 et log k_0 entre 2,5 et 6.

La représentation graphique du log k_0 en fonction de l'énergie d'activation est donnée dans la figure 3. On observe une variation linéaire du log k_0 avec l'énergie d'activation pour tous les catalyseurs étudiés dans la réaction de déshydratation du MPhC en styrène.

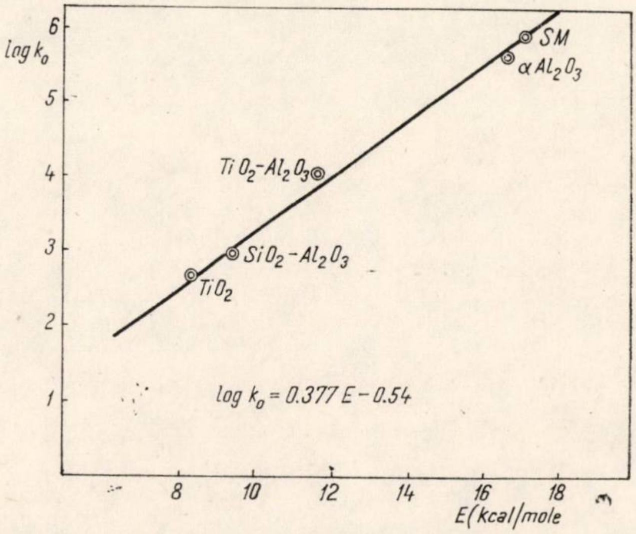

Fig. 3.—Variation du facteur log k_0 avec l'énergie d'activation E, pour divers catalyseurs dans la réaction :

$$C_6H_5-CHOH-CH_3 \rightarrow C_6H_5-CH=CH_2 + H_2O$$

Tableau 4

Fonctions thermodynamiques de remplacement par adsorption pour les systèmes styrène-MPhC et H_2O – MPhC

T°C	Z_{2_m}	Z_{3_m}	Log Z	ΔG cal/mole	ΔH cal/mole	ΔS cal/ mole. grad
275	0,294		−0,582	1332	−19 650	−38,3
300	1,0		0,0	0	−19 650	−35,6
350	2,55		0,406	−1156	−19 650	−29,7
275		0,9	−0,046	115	0	− 0,21
300		0,9	−0,046	120,4	0	− 0,21
350		0,9	−0,046	131	0	− 0,21

$Z_2 = a(\text{styrène})/a(\text{MPhC.})$

$Z_3 = a(\text{eau})/a\text{MPhC.}$

$$Z = \frac{m^0/m - 1}{100/P - 1}$$

$\Delta G = -RT.\ln Z$

$\Delta S = (\Delta H - \Delta G)/T$

Les valeurs trouvées pour les coefficients relatifs d'adsorption Z_2-styrène-MPhC et, Z_3-eau-MPhC dans le domaine de températures de 275° à 350° ont permis la détermination, conformément aux relations connues, des fonctions thermodynamiques de remplacement par adsorption du MPhC avec du styrène, respectivement avec de l'eau. Les résultats sont donnés dans le tableau 4.

Revue Roumaine de Chimie, 17, *3*, 533 – 538 (1972)

ИССЛЕДОВАНИЕ ЗАУГЛЕРОЖИВАНИЯ НЕКОТОРЫХ КАТАЛИЗАТОРОВ ДЕГИДРИРОВАНИЯ АЛКИЛАРОМАТИЧЕСКИХ УГЛЕВОДОРОДОВ*)

КОРНЕЛИЯ КОРИЧУК, ДЖЕОРДЖЕТА ЧЁМОНТАНИ и СПЕРАНЦА ПОПА

Институт Петрохим
Бул. Републичий, № 291, Плоешть, Румыния

Поступила в редакцию: 15 февраля 1971 г.

Установлено, что при работе окиснометаллических катализаторов в реакции дегидрирования алкилароматических углеводородов происходит падение их активности за счет углеотложения на каталитически активной поверхности. В настоящей работе процесс падения активности катализатора типа $Fe_2O_3-Cr_2O_3-K_2CO_3$ вследствие углеотложения на его каталитически активной поверхности в реакции дегидрирования этилбензола, характеризуется энергией дезактивации. Определено эмпирическое соотношение вида $\Omega = \beta(-\alpha q)$, описывающее изменение активности катализатора в зависимости от количества углистых отложений на его поверхности. Отмечено, что отложение кокса с течением времени на этих катализаторах описывается соотношением вида $q = ht^n$.

В результате протекания побочных реакций в процессе каталитического дегидрирования алкилароматических углеводородов, поверхность катализаторов постепенно покрывается углистыми отложениями, так называемым « коксом », отвечающим общей формуле $(CHx)_n$, а содержание водорода снижается пропорционально с временем отложения [1]. Вследствие углеотложения на каталитически активной поверхности и, следовательно, блокировки активных центров катализатора, его активность снижается и восстановление ее до первоначальной величины требует проведения процесса периодической регенерации. Ввиду усиления использования каталитически активной поверхности, наряду с испытанием катализатора в желаемой реакции необходимо уделять должное внимание и зауглероженности его поверхности за счет протекания побочных реакций. Многие авторы[2,3] изучали процесс зауглероженности различных катализаторов (глиноземных, алюмосиликатных и т.д.) при их применении в процессах дегидрирования, крекинга и др. На основе полученных экспериментальных данных было установлено, что процесс углеотложения может быть описан разнообразными математическими соотношениями. Таким образом, для каталитического крекинга углеводородов рекомендуются соотношения вида:

---

[1] G. Froment, *Ind. chim. belge*, **27**, 1041 (1962).

[2] И. Тюряев, *Ж. физ. хим.*, **31**, 93 (1957).

[3] Yuichi Ozawa и K. B. Bischoff, *Ind. End. Chem. Process Design and Developement*, **7**, 1 (1968).

*) Работа была представлена на 39-ом Конгрессе индустриальной химии, Бухарест, 1970 г.

$$q = ht^n,^4 \qquad q = At + B\,(1 - e^{-Dt}),^5$$

где:

q — г кокса/г катализатора;

A, B, D, h, n, — постоянные, связанные с сырьем, катализатором и температурой;

t — время отложения.

Шендрик и сотр.[6] описывают зауглероженность (q) алюмохромового катализатора в реакции дегидрирования бутана во время t соотношением $q = A + Bt$, где: A, B — постоянные, связанные с конверсией и объемной скоростью. Другие авторы, например Тюряев и сотр.[2] отмечают, что зауглероженность катализатора при дегидрировании бутана описывается функцией: $q = ht^n$. Многие авторы описывают изменение активности катализатора в зависимости от углеотложения на его поверхности математическими соотношениями, установленными эмпирически. Таким образом, по мнению авторов работы[7], функция $\Omega = f(q)$, где Ω — дезактивация катализатора за счет углеотложения, q — количество углистых отложений, линейнообразна: $\Omega = 1 - q/q_0$, где q_0 — количество кокса, полностью дезактивирующее катализатор.

Гуген и Ватсон[8] предлагают гиперболическое соотношение вида: $\Omega = 1/(1 + \beta q)$, где β — постоянная, а Фромент и Бишофф[9] связывают Ω и q экспоненциальным соотношением $\Omega = \exp(-\alpha q)$, где α — постоянная.

ЭКСПЕРИМЕНТАЛЬНАЯ ЧАСТЬ

Вопрос зауглероженности катализатора был изучен в процессе превращения этилбензола в присутствии окисножелезного катализатора с добавками, на лабораторной проточной установке. Снижение парциального давления этилбензола было достигнуто разбавлением азотом. В качестве сырья применяли этилбензол нефтехимического происхождения, с чистотой более 99,6 % вес., а в качестве разбавителя — азот, с чистотой не менее 99,8 % вес. Применяемому катализатору типа $Fe_2O_3 - K_2CO_3 - Cr_2O_3$ с удельной поверхностью около 10 м²/г характерна макропористая структура и распределение большинства (80 %) пор в области радиусов свыше 1000 Å; с кинетической точки зрения он характеризуется энергией активации 31,0 ккал/мол по реакции дегидрирования этилбензола в стирол. Характеристика катализатора, применяемого на адиабатической установке дегидрирования этилбензола следующая: $T_{\text{ср}}$ — 610°,

---

[4] A. Voorhies, *Ing. Eng. Chem.*, **37**, 318 (1945).

[5] Г. М. Панченков, « Кинетика и Катализ », Акад. наук СССР, 1960.

[6] М. Н. Шендрик и А. Н. Боресков, *Кинетика и катализ*, **6**, 313 (1965).

[7] S. Masamune и J. M. Smith, *Amer. Inst. Chem. Engineers J.*, **12**, 384 (1966).

[8] S. A. Hougen и K. M. Watson, « Chemical Process Principles », W.N.Y.

[9] G. Froment и K. B. Bischoff, *Chem. Eng. Sci.*, **16**, 189 (1961).

объемная скорость — 0,5 ч$^{-1}$, кратность разбавления углеводород/H_2O 1/2,6 (вес.); выход 38—40 % вес., при избирательности около 88 % вес. Анализ активности катализатора был проведен путем дозировки компонентов газообразного и жидкого катализата от дегидрирования этилбензола газожидкостной хроматографией. Процесс углеотложения исследовали как гравиметрическим определением отложений в пересчете на единицу веса катализатора, так и элементарным анализом углистых отложений.

ОБСУЖДЕНИЕ ПОЛУЧЕННЫХ РЕЗУЛЬТАТОВ

При исследовании поведения катализатора типа $Fe_2O_3—Cr_2CO_3—K_2O_3$ в реакции дегидрирования этилбензола в промышленном адиабатическом реакторе в течение около 2000 часов, было установлено, что хотя этот катализатор и обладает свойством саморегенерации и присутствие воды в реакторе способствует удалению углистых отложений с поверхности катализатора, все же активность последнего постепенно снижается. Поддерживание постоянства конверсии этилбензола без изменения парциального давления осуществляют постепенным повышением температуры реакционной смеси таким образом, чтобы сохранить постоянство не только конверсии, но и селективности (в данном случае — конверсия 40—45 вес. %, а селективность около 88 вес. %). Рост термического уровня реакции на слое катализатора в зависимости от времени реакции при одном цикле между двумя регенерациями ввиду сохранения показателей катализатора (рис. 1), является мерой обратимой дезактивации за счет его зауглероженности. Прекращение реакции для сжигания углеотложений приводит к восстановлению первоначальной активности катализатора.

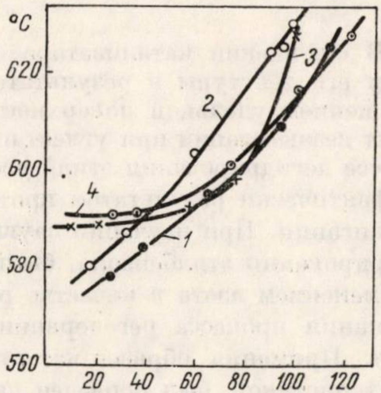

Рис. 1. — Циклическое повышение температуры для поддерживания постоянства конверсии:
1, I-ый цикл,
2, II-ой цикл,
3, III-ий цикл,
4, IV-ый цикл.

Падение активности катализатора в результате зауглероженности его поверхности при одном цикле между двумя регенерациями дало возможность представить явление дезактивации соотношением[10]

$$\mathrm{d}T/\mathrm{d}\tau = (kp_0/Ea)\, RT^2 \exp\,(-Ep/RT),$$

---

[10] В. А. Хохлов, Г. С. Яблонский и С. В. Вепрева, *Хим. пром.*, *10* (1968).

Revue Roumaine de Chimie, 17, *3*, 533–538 (1972)

где: $dT/d\tau$ — зависимость изменения температуры от длительности цикла при постоянной конверсии;

k_{p0} — предэкспоненциальный фактор, $ч^{-1}$;

E_p — энергия дезактивации катализатора, кал/мол;

E_a — 31000 кал/мол, энергия активации реакции дегидрирования этилбензола в стирол.

С течением времени энергия дезактивации в процессе дегидрирования увеличивается (табл. 1) и реакция коксообразования становится все более некаталитическим термическим процессом.

Таблица 1

Зависимость энергии (E) дезактивации и $\lg k_{p0}$ от времени работы катализатора типа $F_2O_3-Cr_2O_3-K_2CO_3$ в процессе дегидрирования этилбензола в стирол

Номер цикла	Длительность работы, ч.	E дезактив. E_p кал/мол	Предэксп. фактор k_{p0}, $ч^{-1}$	$\lg k_{p0}$
I	1—115	26306,25	$2{,}40.10^{4}$	4,38
II	132—227	48850,00	$1{,}10.10^{10}$	10,041
III	231—335	72356,25	$5{,}80.10^{15}$	15,764
IV	1484—1624	103775,00	$2{,}06.10^{23}$	23,314

В отношении катализатора, указанное явление объясняется изменением его текстуры в результате рекристаллизации, сопровождаемой уменьшением удельной поверхности и количества активных центров. Эффект дезактивации при углеотложении, наблюдаемый в промышленном процессе дегидрирования этилбензола в присутствии годяного пара является фактически результатом протекания процессов коксообразования и его сжигания. При изучении зауглероженности катализатора в процессе дегидрирования этилбензола, были проведены лабораторные испытания с применением азота в качестве разбавителя ввиду подавления явлений протекания процесса регенерации одновременно с процессом углеотложения. Применяя образец катализатора с предварительно установленной характеристикой, был проведен ряд испытаний по дегидрированию этилбензола при 580, 600, 620°, с поддержанием постоянства объемной скорости углеводорода и кратности разбавления этилбензол-азот. Превращение этилбензола было испытано при различной длительности опыта. Было установлено, что дезактивация катализатора непосредственно связана с временем испытания; как вытекает из рис. 2, эффект дезактивации оценивают по снижению конверсии и увеличению количества углеотложений. Степень конверсии при трех рабочих температурах снижается до значений, соответствующих термической конверсии этилбензола, когда можно считать, что катализатор полностью дезактивирован (речь идет об обратимой дезактивации, т.к. после регенерации зауглероженной поверхности активность восстанавливается до первоначального значения).

Из соответствующих экспериментальных данных (табл. 2) вытекает, что активность катализатора (q) связана с количеством углеотложений (q) на его поверхности экспоненциальным соотношением вида, представленного Фрометом и Бишоффом[9]: $\Omega = \beta \exp(-\alpha q)$.

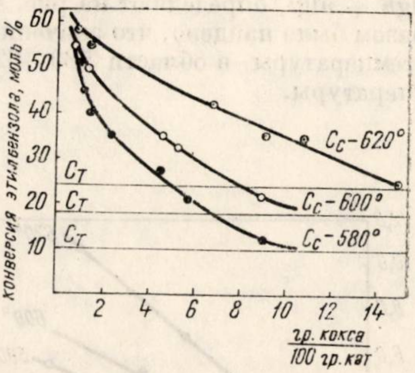

Рис. 2. — Зависимость изменения конверсии от зауглероженности катализатора типа $Fe_2O_3-Cr_2O_3-K_2CO_3$ при дегидрировании этилбензола (об. скорость — 0,5ч$^{-1}$; $P_{ЭБ}$ — 0,05 ат), C_C — каталитическая конверсия, C_T — термическая конверсия.

Таблица 2

Контроль соотношения $\Omega=\beta\exp(-\alpha q)$ в отношении изменения активности катализатора в зависимости от его зауглероженности

Темп., °C	Время исп., ч.	q	Рассч. lg Ω	Найден. lg. Ω	α	β
500	1,0	1,17	1,650	1,653	0,162	54
	2,0	1,36	1,634	1,602		
	3,0	2,38	1,565	1,544		
	5,5	4,58	1,410	1,431		
	7,0	5,75	1,328	1,322		
600	0,6	0,82	1,725	1,732	0,1105	58
	1,0	1,20	1,706	1,699		
	4,0	4,50	1,548	1,544		
	5,0	5,21	1,514	1,518		
620	0,5	0,80	1,715	1,763	0,0528	60
	1,0	1,42	1,747	1,740		
	4,0	6,82	1,623	1,623		
	6,3	10,84	1,530	1,544		
	8,0	14,86	1,438	1,477		

Ω– активность катализатора при конверсии этилбензола, мол.%: конверсии

q– г кокса/100 г катализатора;

α,β– постоянные.

С целью изучения кинетики коксообразования на поверхности катализатора в процессе превращения этилбензола при постоянных объемных скоростях и кратности разбавления, было исследовано изменение количества кокса в пересчете на вес.% катализатора, в зависимости от времени отложения (t, ч.), при температурах 580, 600 и 620° (см. рис. 3).

При помощи экспериментальных данных было проверено соотношение $q = ht^{n2}$, связывающее количество углеотложений (q) с временем отложения (t), где h и n — постоянные, зависящие от свойств катализатора и сырья, а также от температуры. Путем изображения функции $\lg q = \lg h + n \lg t$, определяют на рис. 4 значения постоянных h и n; таким образом было найдено, что значения h не превышают единицы, независимо от температуры в области 580—620°, а значение n возрастает с ростом температуры.

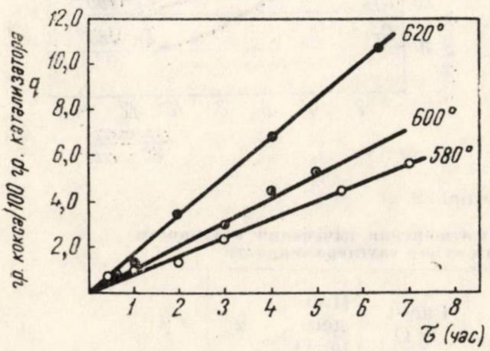

Рис. 3. — Зависимость изменения количества углеотложений от времени отложения.

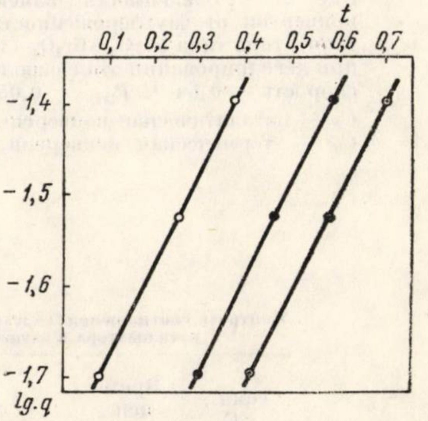

Рис. 4.—Определение постоянных h и n в соотношении $q=ht^n$:

1, $q = -$ 1,774;
2, $q = -$ 1,99;
3, $q = -$ 2,104.

Таблица 3

Зависимость соотношения C/H в углеотложениях от длительности отложения и температуры при конверсии этилбензола на катализаторе $Fe_2O_3-Cr_2O_3-K_2CO_3$

Темп., °C	Длитель. отлож., ч.	г отлож./100 г кат. всего % вес.	C вес. %	H_2 вес. %	C/H	г угл. 100 г отлож.
580	0,5	1,23	0,9	0,33	0,96	73,5
	1,0	1,39	1,17	0,22	1,62	84,5
	3,0	2,62	2,38	0,24	3,17	89,0
	5,0	5,47	5,21	0,26	6,20	95,0
620	0,5	1,19	0,97	0,22	1,46	79,5
	1,0	1,67	1,42	0,25	1,96	85,2
	4,0	7,10	6,82	0,28	8,10	95,8
	8,0	15,41	14,86	0,55	9,55	96,1

Из химического анализа углеотложений на поверхности катализатора вытекает, что отложенный кокс отвечает формуле $(CHx)_n$ где x изменяется в зависимости от времени отложения, а отношение C/H резко возрастает с повышением температуры, таким образом, что примерно за 5 часов содержание углерода в отложении превышает 95% вес. (табл. 3).

Revue Roumaine de Chimie, **17**, *3*, 539–541 (1972)

ÜBER ZWEI VERSCHIEDENE KATALYTISCHE HYDRIERUNGSREAKTIONEN DES NAPHTHOLS UND DEREN MECHANISMEN

A. KRAUSE

Aus dem Institut für Anorganische Chemie der Universität Poznań (Polska)

Eingegangen am 4. März 1971

Die Hydrierung am Nickelkatalysator des 2-Naphthols kann entweder an dessen Benzol- oder Phenolring stattfinden. Letzteres erfolgt, wenn man Ni mit einem alkalischen Zuschlag dotiert, wodurch die Bildung von atomarem Wasserstoff unterbunden und die von Hydridwasserstoff gefördert wird.

Nach Adkins und Krsek[1] ist die katalytische Hydrierung des 2-Naphthols eine recht eigentümliche und komplizierte Reaktion. Am Nickelkatalysator erfolgt die Hydrierung vorwiegend an dem Benzolring, der nicht die Hydroxylgruppe umfaßt. Wenn aber Ni durch kleine Mengen NaOH verstärkt ist, so wird in erster Linie der andere Ring durch die Hydrierung beansprucht. Wahrscheinlich handelt es sich dabei um zwei verschiedene Reaktionsmechanismen, worüber im folgenden berichtet wird.

Der Ni-Katalysator hat, da Nickel kein Edelmetall ist, überschüssige latent kationische Donatorzentren (don.) mit quasifreien Elektronen, im Vergleich mit seinen defektelektronischen (def.), latent anionischen Akzeptorradikalen.[2] Da Naphthol, ähnlich wie Phenol, saure Eigenschaften hat, so werden nach dessen Chemisorption die don. Ni-Zentren, die eine Lewis-Base sind,[2] blockiert. Andererseits dürfte der andere, OH-freie Benzolring des Naphthols eher latent kationisch sein, so daß er sich in Richtung des latent anionischen def.-Zentrums orientiert. Damit befände sich das Naphthol sozusagen in einem Zangenkomplex zwischen den beiden Zentren des Katalysators, die demzufolge ihre normale Funktion, nämlich die der Wasserstoffaktivierung, nicht mehr ausüben könnten. Nun wird aber der am def. - Zentrum chemisorbierte Benzolring (s. oben) zugleich aktiviert (radikalisch), so daß nunmehr der molekulare Wasserstoff für die Hydrierung offenbar ausreicht, umso mehr, als derselbe an dem zuvor radikalisierten Benzolring aktiviert werden kann. Da die latent kationischen Eigenschaften des aktivierten atomaren Wasserstoffes ausgeprägter sind als diejenigen des Benzolrings, so dürfte dieser während seiner Hydrierung gleichzeitig durch die H-Atome verdrängt, d.h. desorbiert werden:

---

[1] H. Adkins und G. Krsek, *J. Amer. Chem. Soc.*, **70**, 412 (1948).
[2] A. Krause, *Monatsh. Chem.*, **96**, 1134 (1965).

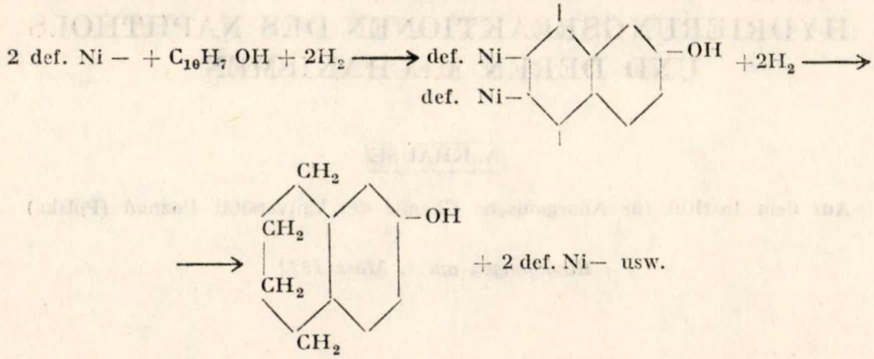

Damit sind nun die def.-Zentren z.T. wieder frei und können den molekularen Wasserstoff aktivieren, so daß die soeben beschriebene Hydrierungsreaktion sich noch reibungsloser abwickeln dürfte. Es ist nicht ausgeschlossen, daß bei der Gelegenkeit die latent kationischen H-Atome das schwächer latent kationische don.-Zentrum verdrängen und obendrein noch die Naphthol-OH-Gruppe, d.h. ihr latent anionisches O-Atom, hydrierend angreifen können, was als eine unerwünschte Nebenreaktion zu bezeichnen wäre. Wenn das zutreffen sollte, so würde jedoch an den soeben entblockierten don.-Zentren Hydridwasserstoff erzeugt werden, der den atomaren Wasserstoff rekombinationsähnlich — wenigstens teilweise — wegfängt [3] und so dessen schädliche Wirkung bremst:

$$\text{def.} - + H_2 \rightarrow \text{def.} - H + H \text{ und don.} - + 1/2\ H_2 \rightarrow \text{don.} + H^- ;$$

$$\text{don.} + H^- + \text{def.} - H \rightleftharpoons H_2 + \text{don.} - + \text{def.} -$$

Die Situation ist eine andere, wenn der Ni-Katalysator kleine Mengen NaOH enthält, welche die def.-Zentren, die eine Lewis-Säure [2] sind, blokkieren und damit die Bildung von atomarem Wasserstoff unterbinden, so daß solchenfalls nur Hydridwasserstoff an den don.-Zentren entstehen kann. Letztere sind übrigens diesmal durch das Substrat nicht versperrt, da dieses mit seinem phenolischen Ring an dem mit NaOH belegten def.-Zentrum Platz sucht. Das H^--Anion steuert nun, ohne das latent anionische O-Atom der phenolischen OH-Gruppe anzugreifen, auf deren H-Atom zu, das am stärksten kationisch unter den H-Atomen des Naphthols ist, und würde es infolge Dehydrierung [3] auffangen:

$$\text{don.} + H^- + H \text{ (vom Substrat)} \rightarrow H_2 + \text{don.} -$$

Doch ist die genannte OH-Gruppe durch die auf der Ni-Oberfläche adsorbierte NaOH festgehalten, sozusagen geschützt, ohne daß es gleich zu einer chemischen Wechselwirkung zwischen den beiden Partnern kommt. Nichtsdestoweniger setzt aber der Hydridwasserstoff gerade an dieser Stelle seine Arbeit fort, indem er mit einer Art Krackwirkung [3] den Phenolring hydriert, wobei die H^--Leitungselektronen sich zwischen die $C = C$ Doppelbindungen einschieben, wonach die OH-Phenolgruppe zu einer Alkoholgruppe wird, was auch mit den experimentellen Befunden von Adkins und Krsek [1] im Einklang steht (s. oben). Wenn aber übermäßig viel Hydridwasserstoff entstehen sollte, so würde durch dessen Hydrierwirkung ebenso der andere Ring (der Benzolring) in Mitleidenschaft gezogen werden. Auch könnte an dem bereits hydrierten Phenolring u.U. eine teilweise Rückreaktion einsetzen, da der Hydridwasserstoff, wie schon erwähnt, auch dehydrierend wirken kann. Man wird also, um das nach Möglichkeit zu vermeiden, die Wasserstoffzufuhr im Verlauf der katalytischen Umsetzung genau regulieren müssen. Dennoch läßt sich wohl kaum vermeiden, daß während der Naphtholhydrierung im Sinne des einen oder des anderen Reaktionsmechanismus der bewußte Nachbarring völlig intakt bleibt, was übrigens auch von Adkins und Krsek [1] zugegeben wird.

---

[3] A. KRAUSE, *Roczniki Chem.*, 43, 130 (1969).

Revue Roumaine de Chimie, 17, 3, 533 – 541 (1972)

Revue Roumaine de Chimie, 17, 3, 543–546 (1972)

MECHANISMUS DER KATALYTISCHEN BILDUNG VON LANGKETTIGEN KOHLENWASSERSTOFFEN UND OXIDISCHEN ORGANISCHEN NEBENPRODUKTEN AUS CO UND H₂

|A. KRAUSE|

Aus dem Institut für Anorganische Chemie der Universität Poznań (Polska)

Eingegangen am 4. März 1971

Die Bildung von langkettigen C–H-Stoffen aus CO und H_2 erfordert aktivierten Wasserstoff, und zwar atomaren und Hydridwasserstoff. Der optimale alkalische Zuschlag zum Eisenkatalysator reguliert die Aktivierung der beiden Wasserstofftypen, obschon eine völlige Ausschaltung von oxidischen Nebenprodukten sich dabei nicht umgehen läßt.

Bei der Fischer-Tropsch-Synthese wurden oft Eisenkatalysatoren mit einem K_2CO_3-Zuschlag verwendet. Dabei zeigte es sich, daß die C–H-Ausbeute bei einem Optimum des letzteren (0,4–0,6% K_2O) am güngstigsten ist, während mit steigender Kalimenge die Bildung oxidischer Produkte, wie z.B. die von Alkoholen und Säuren mehr und mehr überwiegt.[1] Diese lassen sich übrigens auch bei der C–H-Produktion mit optimaler Kalimenge nicht ganz ausschalten, so daß man es solchenfalls mit einer unerwünschten Nebenreaktion zu tun hat, worüber in der Praxis oft Klage geführt wurde. Aus dem nachfolgend entwickelten Reaktionsmechanismus geht jedoch hervor, daß man die genannte Nebenreaktion mit in Kauf nehmen muß, wenn man bei der C–H-Produktion nicht beim Methan stehen bleiben will.

Dem an sich komplizierten System kommt man näher, wenn man die beiden Aktivierungsmöglichkeiten des Wasserstoffes berücksichtigt. Nach einer vom Verf. angegebenen Theorie wird an den Fe-Donatorzentren (don.) des Katalysators, die latent kationisch sind und quasifreie Elektronen haben,[2] der Wasserstoff unter Hydridbildung aktiviert.[3] Dieser Hydridwasserstoff kann nun, wie vor kurzem erkannt wurde,[3] hydrierend und auch dehydrierend wirken, was für die Entwicklung des Reaktionsmechanismus von besonderer Bedeutung ist. Die dehydrierende Wirkung des Hydridwasserstoffs ist so zu verstehen, daß das H^--Anion ein latent kationisches H-Atom der Substratmolekel unter H_2-Bildung aufgreift. An den defektelektronischen (def.) Fe-Akzeptorradikalen, die latent anionisch sind, wird atomarer Wasserstoff erzeugt, der latent kationisch ist. Man vergleiche hierzu die folgenden Gleichungen : $\text{don. Fe}- + 1/2\ H_2 \rightarrow \text{don.Fe}^+H^-$ und $\text{def.Fe}- + H_2 \rightarrow \text{def.Fe}-H + H$. Beide Wasserstofftypen können sich rekombinationsähnlich zwar auslöschen, jedoch nur teilweise, da die betr. Reaktion umkehrbar ist :

---

[1] F. Fischer und H. Tropsch, *Ber. dtsch. chem. Ges.*, **56**, 2428 (1923); H. H. Storch, N. Golumbic und R. B. Anderson, "The Fischer-Tropsch and Related Syntheses", New York, 1951.

[2] A. Krause, *Z. physik. Chem. (Leipzig)*, **30**, 233 (1961); *Monatsh. Chem.*, **96**, 1134 (1965).

[3] A. Krause, *Roczniki Chem.*, **43**, 1917, 2047, 2167 (1969).

$$\text{don.} + H^- + \text{def.} - H \rightleftarrows H_2 + \text{don.} - + \text{def.} - \text{usw.}$$

H^- ist hier ein dehydrierendes Agens.

Wenn man mit einem hohen Alkalizuschlag die def.-Zentren, die eine Lewis-Säure sind, völlig blockiert, so wird nur Hydridwasserstoff auftreten können. Das H^--Anion greift zwar das latent anionische O-Atom des CO nicht direkt an, kann aber mit seinen Leitungselektronen die $C = O$ Doppel — (oder Dreifachbindung) lösen und sich dann an O anlagern d.h. hydrierend wirken. Das so entstehende Radikal $\underset{\diagup}{\overset{\diagdown}{-}}C-OH$ nimmt ohne weiteres Wasserstoff auf :

$$4\ \text{don.} - + 2H_2 + CO \rightarrow 4\ \text{don.} + 4H^- + CO \rightarrow CH_3OH +$$
$$+ 4\ \text{don.} - \text{usw.}$$

Falls aber einem daran gelegen ist, den Sauerstoff des CO zu entfernen, so eignet sich dafür besser der latent kationische atomare Wasserstoff, der an den def.-Zentren aufkommt. Dieser reagiert mit O unter H_2O-Bildung, so daß ein C—H-Stoff in Sicht kommt: $3\ \text{def.} - + 3H_2 + CO \rightarrow 3\ \text{def.} - H + 3H + CO \rightarrow H_2O + CH_4 + 3\ \text{def.} - \text{usw.}$

Hier genügt also der atomare Wasserstoff, so daß man zu diesem Zweck die def.-Zentren offenhalten und die don.-Zentren (eine Lewis-Base) evtl. mit sauren Zuschlägen blockieren sollte. Wenn man aber beim Methan nicht stehen bleiben will, sondern zu benzinartigen C—H-Stoffen gelangen möchte, so muß man außerdem noch den Hydridwasserstoff mobilisieren (s. unten). Dann ist auch zuviel atomarer Wasserstoff, der den ersteren rekombinationähnlich deprimieren würde, nicht am Platze, so daß nunmehr der optimale Kalizuschlag (s. oben) verständlich wird.

Man kann aber die C—H-Kettenbildung nicht aus CH_2-Radikalen entwickeln, da diese, auch wenn sie noch so nahe beieinander ständen,[4] schon durch molekularen Wasserstoff vernichtet d.h. hydriert würden. Auch dürfen nicht zuviele Zentren des Katalysators durch die Methylenradikale belegt werden,[4] da ebenso für die Wasserstoffaktivierung einige übrigbleiben müssen. Hier hilft nun der Hydridwasserstoff, der an den don.-Zentren entsteht (s. oben) und das Methan angreift. Er kann das CH_4 natürlich nicht hydrieren, wohl aber dehydrieren. In dem Moment, wo das am don.-Zentrum geschieht, lagert sich an diesem das soeben entstandene CH_3-Radikal nach Art von Metallalkylverbindungen an, wodurch die CH_3-Gruppe geschützt wird. Sie könnte zwar noch weiter, sogar bis zum radikalen Carbid dehydriert werden, doch würde dieses sofort hydriert werden, so daß die Methylgruppe wieder aufkommt, wozu selbst der molekulare Wasserstoff ausreichen dürfte, der im Verlauf dieser Umsetzungen entsteht. Wenn nun ein CH_4-Molekel sich in der Nähe des Metallalkyls befindet, so ist jetzt eine gemeinsame Dehydrierung der beiden Partner ohne Rückreaktion möglich, und das führt zur Bildung einer langen C—H-Kette. Hierfür genügt zahlenmäßig nur ein don.-Zentrum, an welchem die wachsende C—H-Kette zunächst hängen bleibt. Es sind demnach noch genügend aktive Zentren vorhanden, die für die Wasserstoffaktivierung benötigt werden. Folgende Gleichungen geben über das Wachstum der C—H-Kette Auskunft: don. $Fe— + 1/2H_2 + CH_4 \rightarrow$ don. $Fe^+H^- + CH_4 \rightarrow H_2 +$ don. $Fe—CH_3$; don. $Fe—CH_3 + CH_4 + 2$ don. $Fe— + H_2 - 2$ don.$Fe^+2H^- + CH_4 + H_3C—Fe$don. $\rightarrow$

---

[4] Vgl. E. F. G. Herington, *Trans. Fraday Soc.*, **37**, 361 (1941).

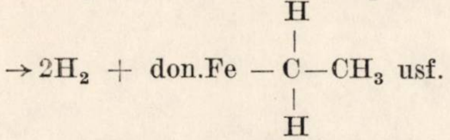

$$\rightarrow 2H_2 + \text{don.}Fe - \overset{\displaystyle H}{\underset{\displaystyle H}{\overset{|}{\underset{|}{C}}}} - CH_3 \text{ usf.}$$

Solange CH_4-Molekeln vorhanden sind, hat der Hydridwasserstoff mit dieser Dehydrierungsarbeit zu tun. Wenn aber die CH_4-Molekeln verbraucht werden, dann wendet er sich einer anderen Aufgabe, nämlich der Hydrierung zu, wodurch die Krackung in die Wege geleitet wird, die möglicherweise schon während des C—H-Kettenwachstums ihr Spiel treibt. Die Krackung wird durch die H^--Leitungselektronen bewerkstelligt, die sich zwischen die C—C-Bindungen einschieben und diese lösen. Bei einer teilweisen Krackung und zusätzlichen Liquidierung eines anderweitigen H-Atoms durch H^- formt sich eine Seitenkette. Ausführlich wurde darüber an anderer Stelle berichtet.[3]

Wie steht es nun mit der Desorption der C—H-Kette vom don. Fe-Zentrum? Auch hier greift der Hydridwasserstoff ein, der weit stärker anionisch ist als Alkyl und daher dieses verdrängt und sich gleichzeitig an der Bruchstelle anlagert. Desgleichen könnte der atomare Wasserstoff diese Arbeit verrichten, da er stärker latent kationisch ist als don.Fe- und dessen Verdrängung verursacht.

Die Bildung von oxydischen Produkten in diesem System (s. oben) vollzieht sich ebenfalls nach den gleichen Richtlinien wie zuvor. So entstehen höhere Alkohole wie folgt: 2 don.$Fe— + H_2 \rightarrow 2$ don.$Fe^+ 2H^- + CH_3 \cdot OH + CH_4 \rightarrow C_2H_5OH + 2\ H_2 + 2$ don.Fe—. Schließlich kann der Alkohol (eine latente Säure) an den Lewis-basischen don.Fe-Zentren dehydriert werden,[3] so daß Aldehydbildung erfolgt: don.$Fe— + C_2H_5OH \rightarrow$ don.$Fe^+H^- + C_2H_5O— \rightarrow H_2 + CH_3.COH +$ don.Fe—. Die Lewis-basischen don.Fe-Zentren sowie der alkalische K_2O-Zuschlag (s. oben) und das im Reaktionsmedium vorhandene Wasser fördern des weiteren die Dismutation des Aldehyds, was u.a. zur Bildung einer entsprechenden Säure führt. Diese könnte allerdings die don.Fe-Zentren mit der Zeit teilweise blockieren, so daß der Katalysator sukzessive an Aktivität verlieren würde.

Zum Abschluß noch ein Wort über die mögliche Chemisorption des CO, das als latent kationischer Partner am def.-Zentrum, oder auch unter Carbonylbildung am don.-Zentrum Platz nehmen könnte, womit möglicherweise eine Blockade der beiden Zentren zu befürchten wäre. Bei dieser CO/H_2-Konkurrenzwirkung hat aber die Chemisorption und Aktivierung des Wasserstoffes sicher den Vorrang.

Revue Roumaine de Chimie, 17, 3, 547–558 (1972)

ÉTUDE SUR LA POLYMÉRISATION DES DÉRIVÉS ACÉTYLÉNIQUES. XII*

CINÉTIQUE DE LA PHOTOPOLYMÉRISATION DU PHÉNYLACÉTYLÈNE

CRISTOFOR SIMIONESCU, SVETLANA DUMITRESCU et MARIA GROVU

Institut Polytechnique de Jassy, 11, str. 23 August

Reçu le 18 août 1971

On établit la cinétique et le mécanisme concernant la polymérisation radicalique du phénylacétylène par voie photochimique. La cinétique de la photopolymérisation du phénylacétylène (PhA) est étudiée à l'aide d'une méthode originale photocolorimétrique. Cette méthode s'avère sensible, permettant d'apprécier des variations et des degrés de conversion aussi petits que possible.

1. INTRODUCTION

L'attention d'un nombre toujours croissant de chercheurs a été attirée ces derniers temps par l'étude des processus de polymérisation des hydrocarbures acétyléniques, laquelle constitue une voie d'obtenir des polymères à doubles liaisons conjuguées dans la chaîne de base.

Les lois gouvernant ces processus diffèrent de celles de la polymérisation vinylique, tout en étant moins connues. La majorité des travaux publiés sur ces phénomènes sont consacrés à la polymérisation du phénylacétylène.[1–5]

Le polyphénylacétylène est un polymère dont les liaisons conjuguées de la chaîne aliphatique sont coplanaires. Cette structure assure le dépla-

---

[*] voir XI : Cr. Simionescu, Sv. Dumitrescu, T. Lixandru, M. Dărîngă, B. Simionescu et M. Viță, V. Sahini et J. Weisberg, Isledovanie polimerizatsii Proizvodnykhatsetilena. XI. Polimery fenilatsetilena *o*- i *p*-zameschionie. Sootnochenie mejdu rezultatami poluchenami sposobom raschiota moleculiarnykhorbitalei pokliukeliu i experimentalnymi danami, *Vysokomol. Soedineniya* (sous presse).

[1] A. A. Berlin et V. P. Parini, *Izvest. Vysshei Scoly, Khimia i khimiches. Tehn.*, **1**, 122 (1958).

[2] A. A. Berlin, L. A. Blimenfeld, M. I. Chercaskhin, A. E. Calmanson et O. G Seliscaya, *Vysokomol. Soedineniya*, **1**, 1361 (1959).

[3] I. M. Barkalov, A. A. Berlin, V. I. Golidanskii et B. S. Dzantiev, *Vysokomol. Soedineniya*, **2**, 1103 (1960).

[4] V. V. Korshak, A. M. Poliakova et M. D. Suchicov, *Vysokomol. Soedineniya*, **2**, 1205 (1960).

[5] P. S. Shantarovich et I. A. Sliapicova, *Vysokomol. Soedineniya*, **3**, 363 (1961).

cement des électrons π de la double liaison le long de la chaîne de base et conditionne en même temps le renforcement de la liaison C—C, la croissance de la stabilité thermique des liaisons chimiques, de même que la réduction de l'énergie d'excitation à l'état de triplet, ce qui explique la semi-conductibilité et les propriétés paramagnétiques, optiques et chimiques de ce produit. Mais la continuité de la structure coplanaire, tout comme les dimensions du fragment de chaîne conjuguée sont déterminées aussi par les facteurs cinétiques qui dirigent le développement des réactions au cours du processus d'obtention du polymère. C'est pourquoi l'étude de la cinétique et du mécanisme de la formation des polymères se caractérisant par un tel système de liaisons doubles conjuguées, de même que la connaissance de leur structure moléculaire et surmoléculaire, présentent un intérêt tout particulier tant au point de vue théorique que pratique.

2. PARTIE EXPÉRIMENTALE

Ce travail se propose d'établir les paramètres cinétiques concernant la polymérisation radicalique du phénylacétylène par voie photochimique.

La cinétique de la photopolymérisation du PhA a été étudiée à l'aide d'une méthode originale, à savoir la méthode photocolorimétrique. Le processus de la photopolymérisation se déroule avec de petites conversions et la méthode photocolorimétrique — méthode analytique — permet l'enregistrement des variations de conversion aussi petites que possible, sous la forme de variations de densité optique du milieu de réaction, sans que la séparation du polymére soit nécessaire.[6] On a utilisé un photocolorimètre du type ФЭК—М.

Dans le cas des composés macromoléculaires se caractérisant par une polydispersité plus grande ou plus petite, le choix d'un filtre idéal, permettant le passage uniquement des radiations absorbées par la solution et retenant toutes les autres, présente certaines difficultés.

Pour le cas PPhA des diagrammes des niveaux d'énergie du monomère et des oligomères (dimères, trimère) on a calculé par la méthode MO—LCAO — Hückel l'énergie de transition de l'ordre I[7] pour chacun des produits mentionnés. On a établi qu'elle baisse du monomère vers les oligomères, dans le sens de croissance du degré de polymérisation, ce qui, théoriquement, devrait conduire du maximum de la bande d'absorption du spectre électronique vers des longueurs d'ondes de plus en plus grandes. Le phénomène du déplacement bathochrome a été confirmé expérimentalement.[7] Toutes ces considérations nous ont déterminé à employer un grand nombre de filtres en vue d'établir les paramètres cinétiques ; aussi les constantes cinétiques obtenues représentent-elles la moyenne des valeurs trouvées pour chaque filtre à part.

Dans le cas de la polymérisation radicalique du PhA il semble que le degré moyen de polymérisation ne change pratiquement pas avec la durée de réaction, en présentant uniquement de petites variations avec la température, même si les polymérisations sont effectuées à des intervalles de température assez grands. C'est ce qui confirme que la polymérisation de l'acétylène et ses dérivés découle selon des lois différentes de celles de la polymérisation vinylique.

---

[6] Cr. Simionescu, Sv. Dumitrescu et M. Grovu, Rev. Roumaine Chim. (sous presse).

[7] Sv. Dumitrescu, C. Ghirvu, Cr. Simionescu et V. Sahini, *Bul. Inst. Politeh. Iaşi*, **19**, *1—2*, 407 (1968).

Pour confirmation on présente dans le tableau 1 les données expérimentales concernant la variation de la masse moléculaire du polymère fonction des paramètres de la polymérisation radicalique du PPhA effectuée par voie purement thermique.

Tableau 1

Variation de la masse moléculaire du polyphénylacétylène fonction des paramètres de polymérisation (durée et température)

Température de polymérisation, °C	Durée de polymérisation, h	Masse moléculaire moyenne, $\overline{M}$
150	1	510
	2	480
	5	588
	10	563
170	1	417
	2	457
	5	523
	10	414
190	1	323
	2	387
	5	374
	10	320

L'invariabilité de la masse moléculaire du PPhA obtenu dans les conditions expérimentales mentionnées nous a permis d'adopter la méthode photocolorimétrique en vue d'apprécier les conversions dans le processus de la photopolymérisation du PhA.

Dans quelques travaux antérieurs on a étudié la cinétique et le mécanisme de la polymérisation radicalique du PhA en présence du tri-isopropyle-bore.[8,9] Par cette voie on a pu établir que l'activité des macroradicaux croissants de PPhA baisse au fur et à mesure que la longueur de la chaîne augmente, à cause de la croissance du degré de délocalisation de l'électron libre. Il s'ensuit que chaque étape de croissance de la chaîne macromoléculaire peut être considérée comme une étape d'arrêt de la croissance de la chaîne. Il en résulte que les deux étapes bien distinctes dans le cas de la polymérisation vinylique, à savoir l'étape de croissance et celle d'arrêt de la chaîne moléculaire, peuvent être remplacées par un seul processus « d'amortissement ». Le mécanisme de la polymérisation radicalique du PPhA pourra alors être conventionnellement représenté par le schéma :

1) Initiation de la chaîne : $$M^{\cdot} + I^{\cdot} \xrightarrow{k_1} M_1^{\cdot} \qquad (1)$$

(I˙ — radical d'initiateur de tri-isopropyle-bore)

2) Croissance de la chaîne : $$M + M^{\cdot} \xrightarrow{k_2} M_2^{\cdot} \qquad (2)$$

$$\cdot\ \cdot\ \cdot\ \cdot\ \cdot\ \cdot\ \cdot\ \cdot$$

$$M + M_{n-1}^{\cdot} \xrightarrow{k_2} M_n^{\cdot} \qquad (3)$$

---

[8] Cr. Simionescu, Sv. Dumitrescu, *Rev. Roumaine Chim.*, **12**, 407 (1967).

[9] Cr. Simionescu et Sv. Dumitrescu, *Plaste und Kautschuk*, **2**, 84 (1968).

3) Arrêt de la croissance de la chaîne :

$$M + M_n^{\cdot} \xrightarrow{k_3} A \qquad (4)$$

$$M + M_n^{\cdot} \xrightarrow{k_4} M_n - H \qquad (5)$$

$$M_n^{\cdot} + M_m^{\cdot} \xrightarrow{k_5} M_{n+m} \qquad (6)$$

A — est la forme inactive de la macromolécule qui résulte dans le processus d'amortissement de l'activité des macroradicaux.

En jugeant d'après les valeurs des masses moléculaires du PPhA obtenu par cette voie, c'est la réaction (4) qui semble avoir la plus grande probabilité.

Afin de confirmer l'hypothèse de l'amortissement des macroradicaux de PPhA on a calculé la valence libre des atomes de carbone terminaux de la chaîne polyphénylacetylénique. On sait que l'indice de valence libre indique la capacité de réaction radicalique, l'atome le plus réactif au point de vue de la réaction radicalique étant celui qui a le plus grand indice de valence libre. L'étude des diagrammes moléculaires du monomère Pha et des oligomères correspondant à des degrés de polymérisation 2 et 3 montre que l'indice de valence libre enregistre un abaissement au cours de la croissance du degré de polymérisation. (fig. 1). La moyenne des coefficients de valence libre sera donc 0,6175 pour le monomère, pour les dimères 1,3 et 1,4 — 0,6041 et 0,5171 pour le trimère 1, 4, 6.

Mais l'étude de la cinétique de la polymérisation radicalique du Pha présente aussi des avantages expérimentaux et beaucoup plus de rigueur si on l'effectue par voie photochimique.

On a utilisé dans ce but des lampes de type AS 500 et l'on a réalisé les irradiations dans des fioles en quartz de construction spéciale qui ont permis à thermostater le mélange de réaction. Les polymérisations se sont produites dans l'intervalle de température compris entre +12—+42°. On a introduit chaque fois dans les fioles des quantités constantes de monomère. Les conversions ont été effectuées par photocolorimétrie à partir des courbes d'étalonnage de l'appareil (fig. 2).

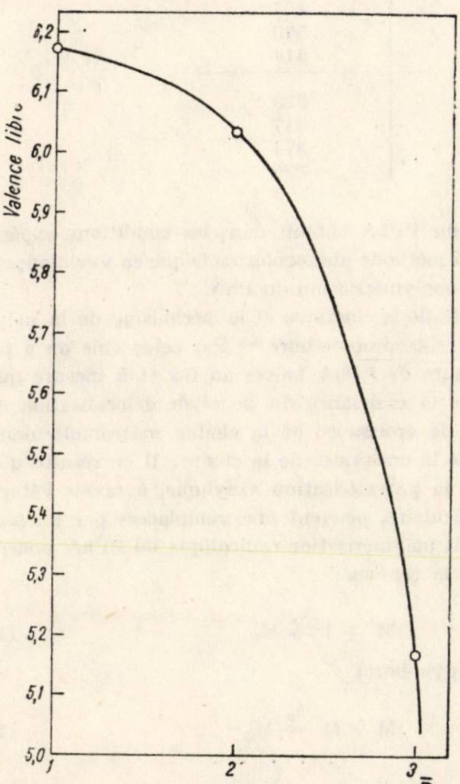

Fig. 1. — Variation de la valence libre des atomes de carbone terminaux en fonction du degré de polymérisation du polyphénylacétylène.

La durée maximale d'irradiation a été de 5 heures, le degré de transformation maximal obtenu étant petit (2,35 %) par rapport aux conversions qu'on peut réaliser pendant la

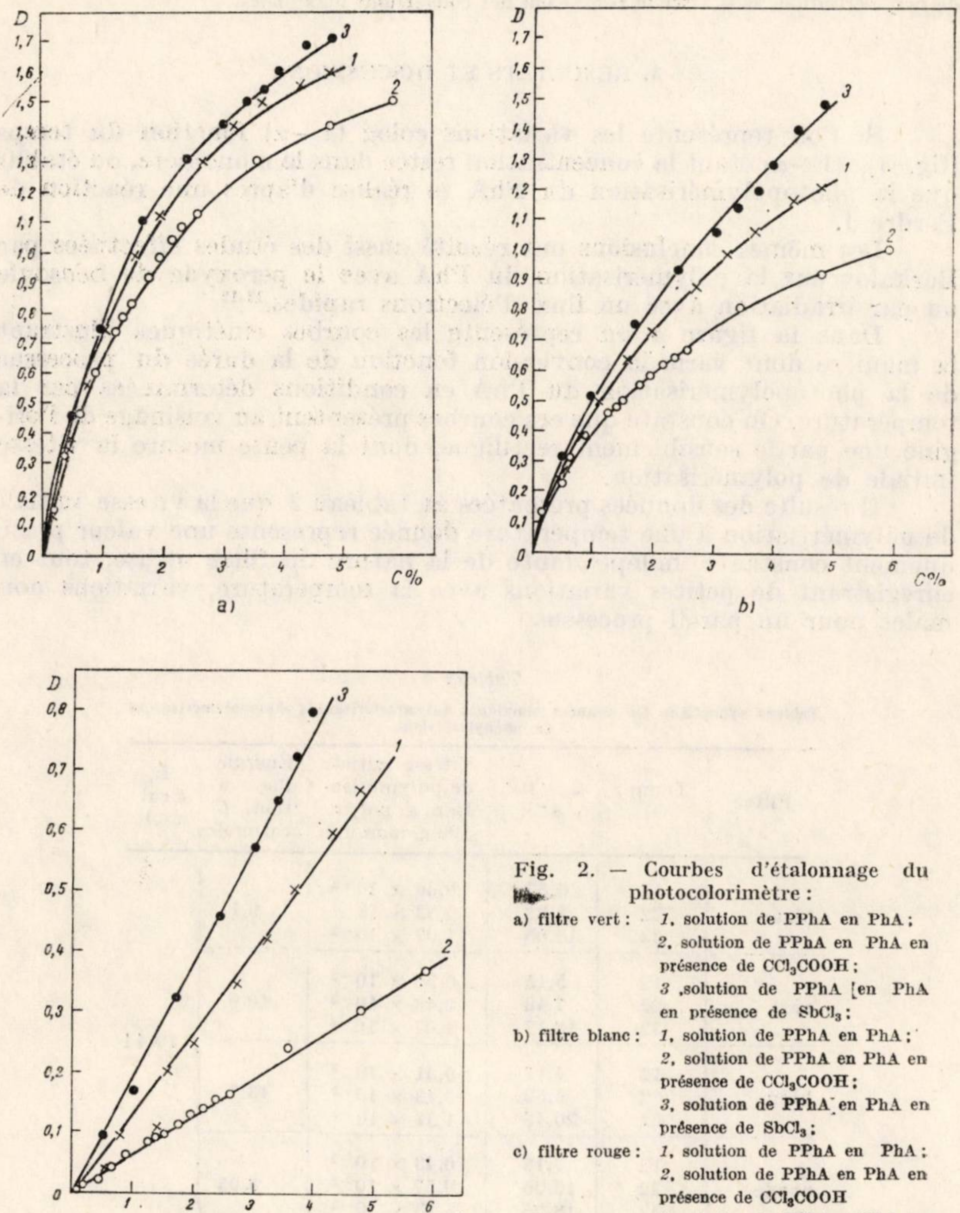

Fig. 2. — Courbes d'étalonnage du photocolorimètre :

a) filtre vert : *1*, solution de PPhA en PhA ; *2*, solution de PPhA en PhA en présence de CCl_3COOH ; *3* ,solution de PPhA en PhA en présence de $SbCl_3$;

b) filtre blanc : *1*, solution de PPhA en PhA ; *2*, solution de PPhA en PhA en présence de CCl_3COOH ; *3*, solution de PPhA en PhA en présence de $SbCl_3$;

c) filtre rouge : *1*, solution de PPhA en PhA ; *2*, solution de PPhA en PhA en présence de CCl_3COOH *3*, solution de PPhA en PhA en présence de $SbCl_3$.

polymérisation du PhA avec tri-isopropyle-bore.[10] Il faut mentionner que dans toutes les expériences effectuées par photochimie on a étudié seulement l'étape initiale du processus de polymérisation, sans viser la réalisation des conversions maximales.

3. RÉSULTATS ET DISCUSSIONS

Si l'on représente les variations colog $(1-\alpha)$ fonction du temps (fig. 3), $(1-\alpha)$ étant la concentration restée dans le monomère, on établit que la photopolymérisation du PhA se réalise d'après une réaction de l'ordre I.

Les mêmes conclusions ont résulté aussi des études effectuées par Barkalov sur la polymérisation du PhA avec le peroxyde de bensoyle ou par irradiation avec un flux d'électrons rapides.[11,12]

Dans la figure 4 on représente les courbes cinétiques illustrant la manière dont varie la conversion fonction de la durée du processus de la photopolymérisation du PhA en conditions déterminées par la température. On constate que ces courbes présentent au voisinage de l'origine une partie sensiblement rectiligne, dont la pente mesure la vitesse initiale de polymérisation.

Il résulte des données présentées au tableau 2 que la vitesse initiale de polymérisation à une température donnée représente une valeur pratiquement constante, indépendante de la nature du filtre utilisé, tout en enregistrant de petites variations avec la température, variations normales pour un pareil processus.

Tableau 2

Tableau synoptique des données cinétiques qui caractérisent la photopolymérisation du phénylacétylène

Filtre	Temp., °C	$k_m \times 10^7$ s^{-1}	Vitesse initiale de polymérisation, g. polym. /100 g. mon.min.	Énergie d'activation, E $k$cal/mole	E_n k cal mole
blanc	12	5,57	$0,36 \times 10^{-2}$	9,1	10,44
	22	8,22	$0,53 \times 10^{-2}$		
	32	16,05	$1,07 \times 10^{-2}$		
vert	12	5,15	$0,35 \times 10^{-2}$	10,9	
	22	7,46	$0,46 \times 10^{-2}$		
	32	18,17	$1,07 \times 10^{-2}$		
bleu	12	4,17	$0,31 \times 10^{-2}$	13,7	
	22	6,62	$0,43 \times 10^{-2}$		
	32	20,48	$1,31 \times 10^{-2}$		
rouge	12	7,18	$0,43 \times 10^{-2}$	8,05	
	22	10,06	$0,57 \times 10^{-2}$		
	32	18,25	$1,13 \times 10^{-2}$		

---

[10] CR. SIMIONESCU et SV. DUMITRESCU, Patent 50973, décembre 18 1967.

[11] I. M. BARKALOV, A. A. BERLIN, V. I. GOLIDANSKII et GO MIN-GAO, *Vysokomol. Soedineniya*, **3**, 368, (1968).

[12] I. M. BARKALOV, V. I. GOLIDANSKII, L. I. KOTOVA et S. S. KUZMINA, *Vysokomol. Soedineniya*. **3**, 373 (1963).

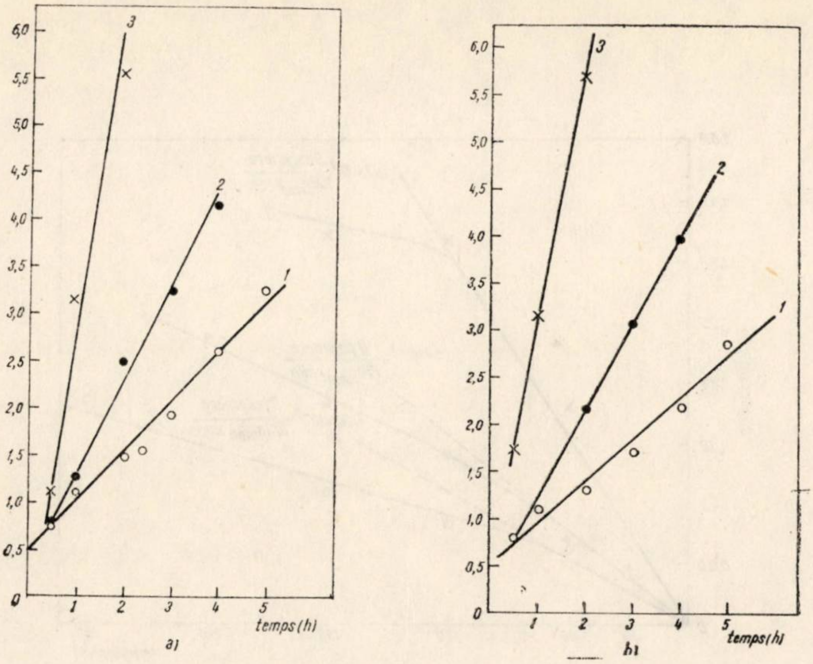

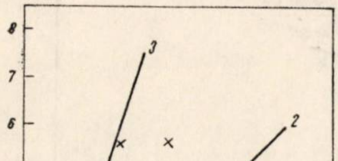

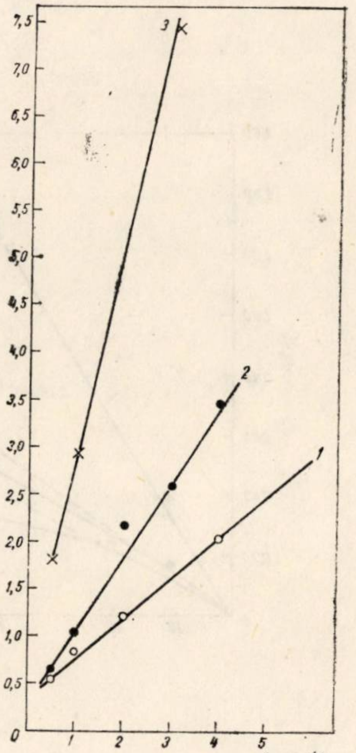

Fig. 3. — Détermination de l'ordre de réaction dans le processus de la photopolymérisation du PhA :

a) filtre blanc : *1*, −12°C ; *2*, −22°C ; *3*, −33°C ;
b) filtre vert : *1*, −12°C ; *2*, −22°C ; *3*, −33°C ;
c) filtre rouge : *1*, −12°C ; *2*, −22°C ; *3*, −33°C ;
d) filtre bleu : *1*, −12°C ; *2*, −22°C ; *3*, −33°C.

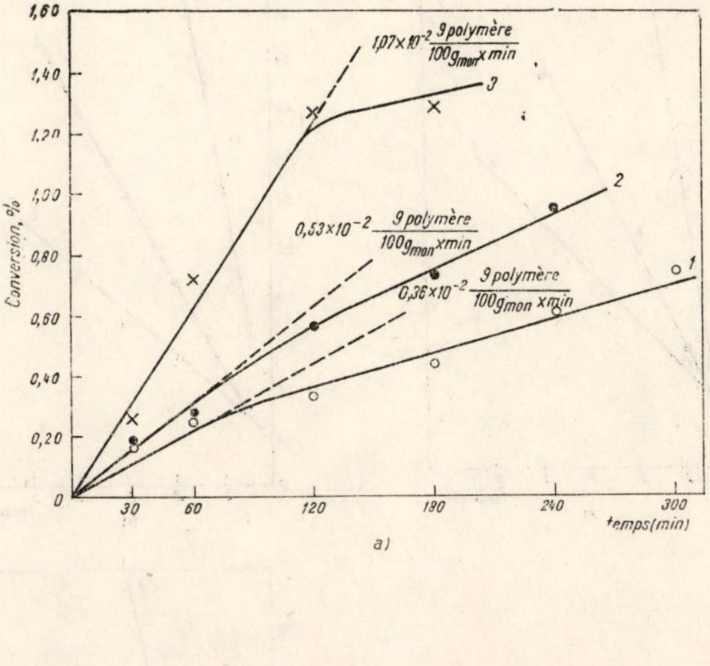
1,60
1,40
1,20
1,00
0,80
0,60
0,40
0,20
0
Conversion, %
30
60
120
180
240
300
temps (min)
$1{,}07\times10^{-2}\ \frac{g\ polymère}{100g_{mon}\times min}$
3
2
$0{,}53\times10^{-2}\ \frac{g\ polymère}{100g_{mon}\times min}$
$0{,}36\times10^{-2}\ \frac{g\ polymère}{100g_{mon}\times min}$
1
a)
1,50
1,40
1,20
1,00
0,80
0,60
0,40
0,20
0
Conversion, %
30
60
120
180
240
300
temps (min)
$1{,}07\times10^{-2}\ \frac{g\ polymère}{100g_{mon}\times min}$
$0{,}46\times10^{-2}\ \frac{g\ polymère}{100g_{mon}\times min}$
$0{,}35\times10^{-2}\ \frac{g\ polymère}{100g_{mon}\times min}$
b)

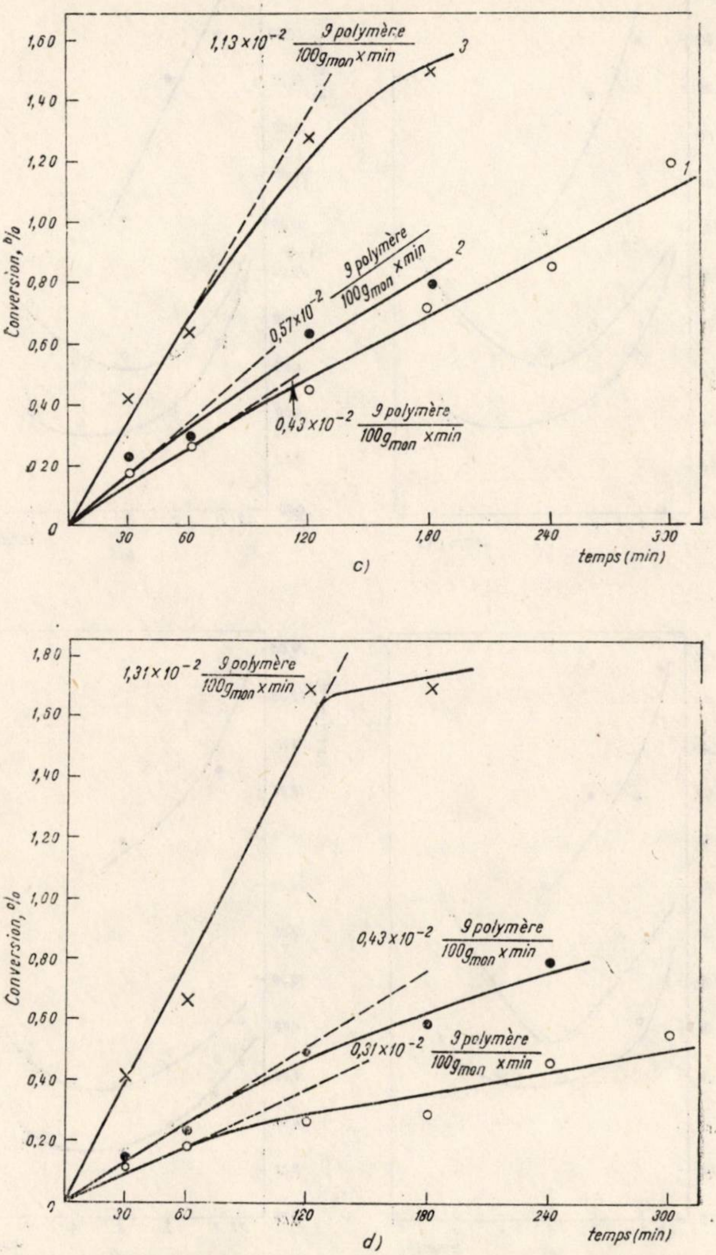

Fig. 4. — Cinétique de la photopolymérisation du phénylacétylène :
a) filtre blanc : *1*, −12°C ; *2*, −22°C ; *3*, −32°C ;
b) filtre vert : *1*, −12°C ; *2*, −22°C ; *3*, −32°C ;
c) filtre rouge : *1*, −12°C ; *2*, −22°C ; *3*, −32°C ;
d) filtre bleu : *1*, −12°C ; *2*, −22°C ; *3*, −32°C.

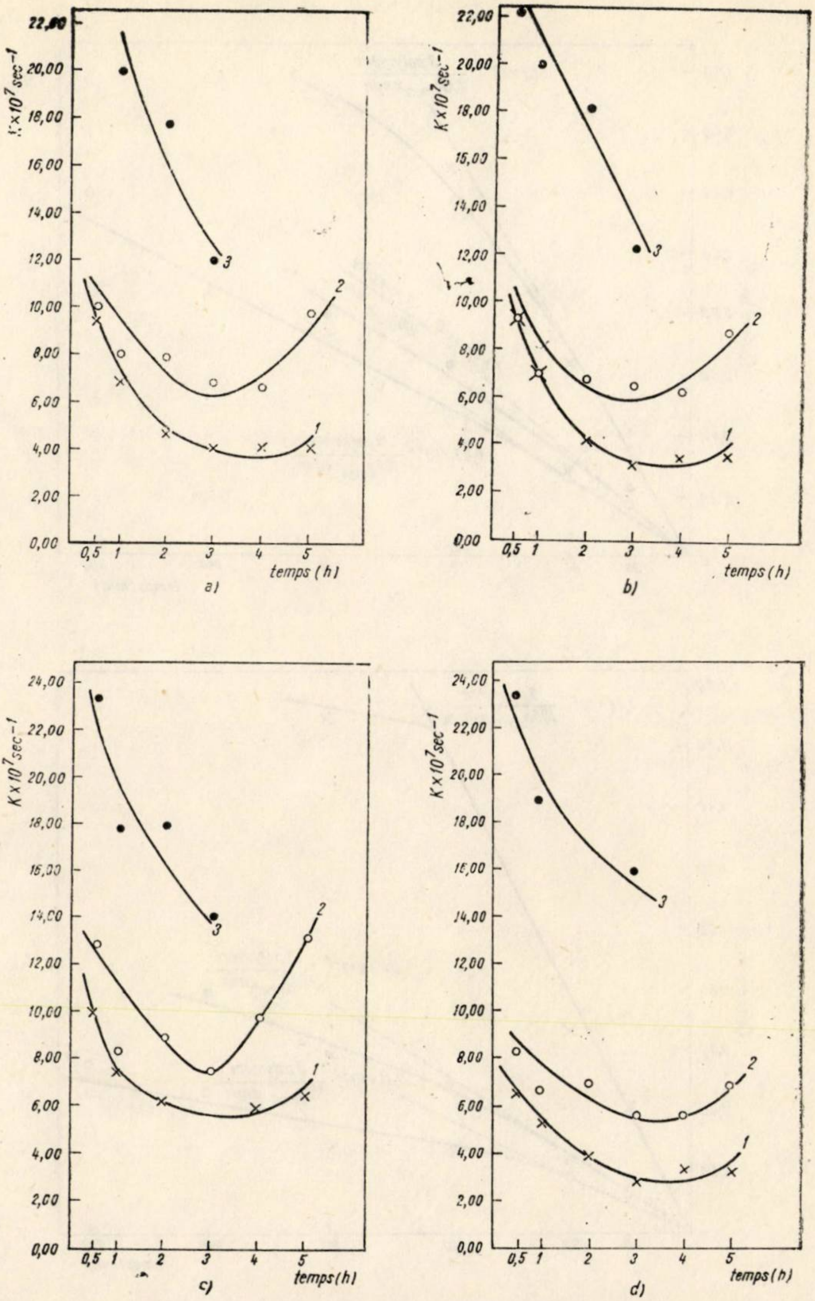

a) b) c) d)

Fig. 5. — Variation dans le temps de la constante de la vitesse de photopolymérisation du phénylacétylène :

a) **filtre blanc** : *1*, −12°C ; *2*, −22°C ; *3*, −32°C ;
b) **filtre vert** : *1*, −12°C ; *2*, −22°C ; *3*, −32°C ;
c) **filtre rouge** : *1*, −12°C ; *2*, −22°C ; *3*, −32°C ;
d) **filtre bleu** : *1*, −12°C ; *2* −22°C ; *3*, −32°C.

Il résulte des valeurs des conversions enregistrées dans la fig. 4 que la photopolymérisation du PhA cesse à de petits degrés de transformation du monomère à cause des réactions secondaires qui peuvent avoir lieu pendant l'irradiation. On sait en même temps que H de la liaison acétylénique du PhA est suffisamment mobile.

Compte tenu de toutes ces considérations on peut admettre l'hypothèse de l'existence des réactions de transfert de chaîne vers le monomère, capables de conduire à la formation de radicaux inactifs ayant la forme :

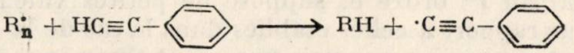

On observe que les valeurs de la constante de vitesse de la réaction de photopolymérisation du PhA enregistre d'abord une décroissance dans le temps, suivie d'une croissance (fig. 5) qu'on pourrait attribuer à l'accroissement du nombre de centres actifs du milieu de réaction. Ce phénomène constitue une particularité du processus de polymérisation photochimique du PhA.

Les données cinétiques obtenues dans le processus de photopolymérisation du PhA, introduites dans l'équation classique d'Arrhénius, permettent de déterminer l'énergie d'activation de la polymérisation. Si l'on représente graphiquement la fonction log $k_m = f(1/T)$, on constate que les points correspondant aux diverses températures de travail se placent sur une droite (fig. 6).

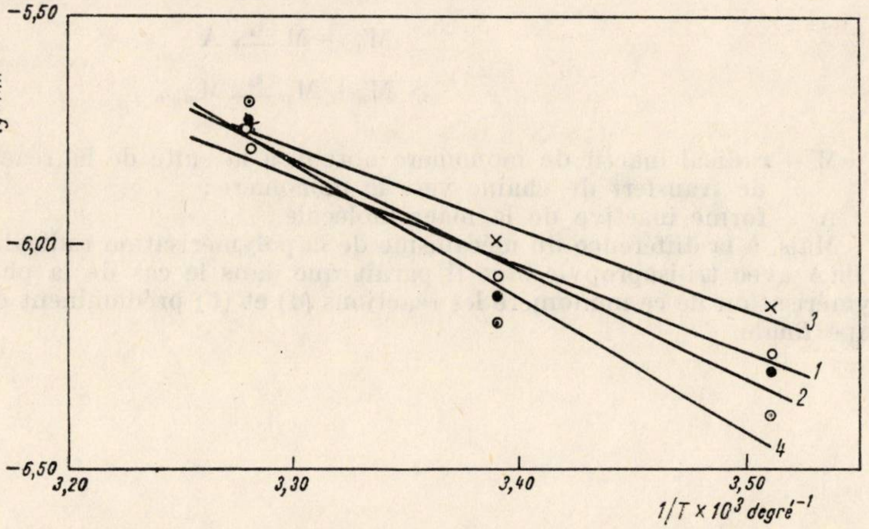

Fig. 6. — Détermination de l'énergie d'activation dans la photopolymérisation du phénylacétylène :

1, filtre blanc ;
2, filtre vert ;
3, filtre rouge ;
4, filtre bleu.

Revue Roumaine de Chimie, 17, *3*, 547 – 558 (1972)

On a pu calculer par cette voie l'énergie d'activation, en trouvant une valeur moyenne de 10,44 kcal/mole. En utilisant des sources de rayons UV à forte intensité on a pu établir des énergies d'activation encore plus petites (2,88 kcal/mole).

4. CONCLUSIONS

En concluant on peut affirmer que la photopolymérisation du PhA est une réaction du Ier ordre et suppose de petites valeurs de l'énergie d'activation, par rapport à celles établies dans le cas de la polymérisation radicalique de ce monomère par voie purement thermique (3,7 kcal/mole)[5] ou initiée par tri-isopropyle-bore (29 kcal/mole)[8] et le peroxyde de bensoyle.[11]

Le mécanisme de la photopolymérisation peut être exprimé conventionnellement à l'aide du schéma suivant :

1) Initiation de la chaîne :

$$M \xrightarrow{h\nu} M^{x} \xrightarrow{k_1} M^{\cdot} \qquad (1)$$

2) Croissance de la chaîne :

$$M + M^{\cdot} \xrightarrow{k_2} M_2^{\cdot} \qquad (2)$$

$$\cdot\ \cdot\ \cdot\ \cdot\ \cdot\ \cdot\ \cdot\ \cdot$$

$$M + M_n^{\cdot} \xrightarrow{k_2} M_{n+1} \qquad (3)$$

3) Arrêt de la croissance de la chaîne :

$$M_n^{\cdot} + M \xrightarrow{k_3} M_n - H + M^{\cdot} \qquad (4)$$

$$M_n^{\cdot} + M \xrightarrow{k_4} A \qquad (5)$$

$$M_n^{\cdot} + M_m^{\cdot} \xrightarrow{k_5} M_{m+n} \qquad (6)$$

où :

$M^{\cdot}$ — radical inactif de monomère obtenu à la suite de la réaction de transfert de chaîne vers le monomère ;

A — forme inactive de la macromolécule.

Mais, à la différence du mécanisme de la polymérisation radicalique du PhA avec tri-isopropyle-bore il paraît que dans le cas de la photopolymérisation de ce monomère les réactions (4) et (6) prédominent dans l'étape finale.

Revue Roumaine de Chimie, 17, 3, 559–564 (1972)

POLYMÉRISATION RAPIDE DE L'ε-CAPROLACTAME EN PRÉSENCE DE COMPOSÉS ORGANO-MÉTALLIQUES

I. GAVĂT,
VICTORIA DIMONIE
D. DONESCU,
MARIANA MUNTEANU,
IOANA ISĂCESCU

Institut de Chimie macromoléculaire « P. Poni », Jassy, Section « Processus de polymérisation », Bucarest, 18, str. Dumbrava Roșie, Bucarest, Roumanie

Reçu le 19 juillet 1971

On a étudié la polymérisation de l'ε-caprolactame en présence du sel d'Al obtenu par la réaction triéthylaluminium-monomère. On a suivi l'influence de la concentration du catalyseur, pendant la polymérisation, et en même temps, sur les poids moléculaires. On a obtenu des polymères solubles aussi bien que des polymères insolubles. On a étudié l'influence des additifs cocatalytiques : eau, isocyanate de phényle, chlorure de benzoyle, acétylacétone sur l'activité du système catalytique.

On connaît que la polymérisation rapide de l'ε-caprolactame s'effectue en présence des métaux alcalins et de leurs sels, respectivement des sels des métaux alcalino-terreux.

La plupart des fois la polymérisation est fortement activée par des dérivés imidiques, des dérivés acylés de l'ε-caprolactame, comme l'acétylcaprolactame [1–3] ou des composés qui peuvent former « in situ » de tels dérivés comme le chlorure de benzoyle,[4] des isocyanates,[5,8] etc. On connaît aussi la polymérisation de l'ε-caprolactame en présence des catalyseurs organoaluminiques [9–11] qui a lieu en l'absence des activateurs au

---

[1] J. Sebenda et J. Kralicek, *Chem. listy*, **52**, 788 (1968).

[2] J. Kralicek, J. Sebenda, Z. Zodak et O. Wichterle, *Chem. promysl.*, **11**, 377 (1961).

[3] T. Konomi et H. Tani, *J. Polymer Sci. A*–1, **7**, 2255 (1969).

[4] Foster Grant Co., Brevet Brit. 640 558, 1964 ; *Chem. Abstr.*, **62**, 16464 (1965).

[5] Mohamed Abdelmoneim El Azmirli, V. V. Korshak, V. A. Sergeev et Z. F. Saikina, *Vysokomol. Soedineniya Ser. A*, **9**, 944 (1967).

[6] Mohamed Abdelmoneim El Azmirli, V. V. Korsak et V. A. Sergeev, *Vysokomol Soedineniya Ser. A*, **9**, 950 (1967) :

[7] Mohamed Abdelmoneim El Azmirli, V. V. Korsak et V. A. Sergeev, *Vysokomol. Soedineniya Ser. A*, **10**, 640 (1968).

[8] N. I. Antropova, K. N. Vlasova, A. V. Samokhvalov et G. I. Pavlova, *Plast. Massy*, **12**, 18 (1967).

[9] T. Konomi, H. Tani, *J. Polymer Sci. A–1*, **7**, 2269 (1969).

[10] V. V. Korshak, T. M. Frunze, L. B. Danilevskaya, et V. V. Kurashev, *Izvest. Akad. Nauk SSSR, Otdel khim. Nauk*, **3**, 63 (1968).

[11] O. Fukumoto (Toyo Rayon Co Ltd), Brevet Japonais 10 540 (1960) ; *Chem. Abstr.*, **55**, 8939b (1961) ;

températures au-dessus du point de fusion du polymère ou à des températures plus basses, avec addition supplémentaire de métaux alcalins ou de sels de ces métaux avec le caprolactame.[3,9,12–15]

Dans le présent travail nous nous sommes proposé d'étudier la cinétique de polymérisation de l'ε-caprolactame, polymérisation catalysée par le triéthylaluminium, ainsi que l'influence de différents additifs pour élucider le mécanisme de polymérisation.

PARTIE EXPÉRIMENTALE

1. **Matières premières.** *Caprolactame* : produit des Usines de Fibres Synthétiques Săvineşti, distillé en atmosphère d'argon et séché sous vide (3.10^{-2} mm Hg), pendant une heure avant la polymérisation.

Triéthylaluminium (Schering A. G.) : utilisé sous forme de solution 1,7 M dans du benzène anhydre (séché par tamis moléculaires).

Isocyanate de phényle p.a. (Merck) : utilisé non purifié.

Acétylacétone : séchée et rectifiée à une pression réduite.

Chlorure de benzoyle : utilisé fraîchement distillé.

2. **La préparation du catalyseur** a été réalisée dans des fioles de polymérisation par réaction entre le triéthylaluminium et le caprolactame dans un rapport moléculaire aluminium : caprolactame = 1 : 6. La réaction a eu lieu à la température ordinaire et après que le dégagement du gaz cesse, on évapore le solvant pendant 30 minutes à 80° sous vide.

3. **La polymérisation** a été réalisée à 220° après homogénéisation du catalyseur avec le monomère à 80—100°. Si on utilise le cocatalyseur celui-ci s'introduit dans le mélange monomère-catalyseur sous agitation.

Au cas des polymérisations effectuées dans des dilatomètres le système catalyseur — monomère — cocatalyseur se solidifie à la température ordinaire. Au-dessus du polymère dans le bulbe du dilatomètre on introduit l'huile de paraffine séchée sur du sodium métallique, sous vide (5 mm Hg) et en atmosphère d'argon. Pour tous les essais on a chargé le dilatomètre avec 8 g de caprolactame ; le dilatomètre a un capillaire de $\Phi = 3{,}73$ mm. Le dilatomètre a été thermostaté dans un bain d'huile de silicone (la température a été mesurée avec une précision de ± 0,15°. Toutes les opérations ont été exécutées en atmosphère inerte d'argon sec et exempt d'oxygène. Les viscosités intrinsèques des polymères ont été déterminées en employant des solutions dans le méthacrésol à 25°. La formule de calcul[16] a été la suivante :

$$[\eta] = \frac{\sqrt{1{,}34 \times \eta_{sp} + 1} - 1}{0{,}67 \times C}$$

Brevet Japonais 13 794 (1962) ; *Chem. Abstr.*, 59, 6539b (1963).

M. Ito (Toyo Rayon Co Ltd), Brevet Japonais 18 590 (1960) ; *Chem. Abstr.*, **55**, 21662e (1961).

[12] Y. Tanaka, F. Kogata (Kanegofuchi Spinning Co Ltd), Brevet Japonais 29 033, 1965, *Chem. Abstr.*, **64**, 9842b (1966) ; Brevet Japonais 1621 (1968), *Chem. Abstr.*, **68**, 105675 (1968).

[13] R. Blain (Société Rhodiaceta), Brevet Fr. 1 457 548 (1965), *Chem. Abstr.*, **67**, 3346 (1967).

[14] H. Tani et T. Konomi, *J. Polymer Sci. A*-1, **4**, 301 (1966).

[15] R. Blain et H. Sekiguchi, *Compt. rend.*, **261**, 3414 (1965).

[16] S. Zaharovsky, *Chem. Promysl*, **17**, 30 (1967)

RÉSULTATS ET DISCUSSIONS

a) *L'influence de la concentration du catalyseur.* On a étudié l'influence du catalyseur sur la conversion et les caractéristiques du polymère. Du tableau 1, il résulte qu'il existe une dépendance directe entre le rendement en polymère et l'augmentation de la concentration du catalyseur jusqu'à la valeur approximative de 1 mole % $AlEt_3$, après quoi la conversion en polymère est pratiquement constante; [17] pour toutes les expériences le temps de réaction a été de 3 heures.

Tableau 1

Polymérisation du caprolactame à l'aide du triéthylaluminium à 220° (temps de réaction 3 heures)

Exp. n°	Concentration $AlEt_3$ mole/100 mole monomère	Solubilité dans l'eau % (en poids)	[η]
1	0,35	25,3	2,84
2	0,5	14,7	3,95
3	0,75	12,7	4,3
4	0,85	11	insoluble
5	1,0	11,5	insoluble
6	1,5	12,4	3,64
7	1,8	11,3	2,44
8	2,0	11,4	2,1
9	3,0	11,8	1,41

La figure 1 illustre l'évolution en fonction du temps du processus de polymérisation du caprolactame. La polymérisation commence après une période d'induction de 10—15 minutes, suivie d'une étape d'autoaccélération. On arrive au maximum de conversion après 2 heures de réaction.

Les viscosités intrinsèques des polymères dépendent directement de l'augmentation de la concentration du triéthylaluminium jusqu'à une valeur de 1 mole % quand on obtient des polymères insolubles, après quoi, l'augmentation de la concentration du catalyseur conduit à une décroissance brusque de [η]. Les polymères insolubles dans le *m*-crésol sont solubles dans l'acide formique à l'ébullition.

Konomi et Tani [9] ont trouvé que pour obtenir des polymères insolubles il est nécessaire d'employer en même temps le sel d'aluminium et le sel alcalin du monomère respectif. Les résultats de nos expériences (tableau 1 et fig. 2) démontrent qu'en fonction des conditions de travail on peut obtenir (seulement avec des sels d'aluminium) des polymères solubles, ainsi que des polymères insolubles.

---

[17] O. Wichterle, *Makromol. Chem.*, **35**, 174 (1960).

b) *L'influence des additifs cocatalytiques.* Pour élucider les causes de la formation de ces polymères insolubles à une concentration de 1 mole % $AlEt_3$, on a effectué des essais de polymérisation en présence de différents additifs : l'eau, l'isocyanate de phényle et l'acétylacétone (tableau 2).

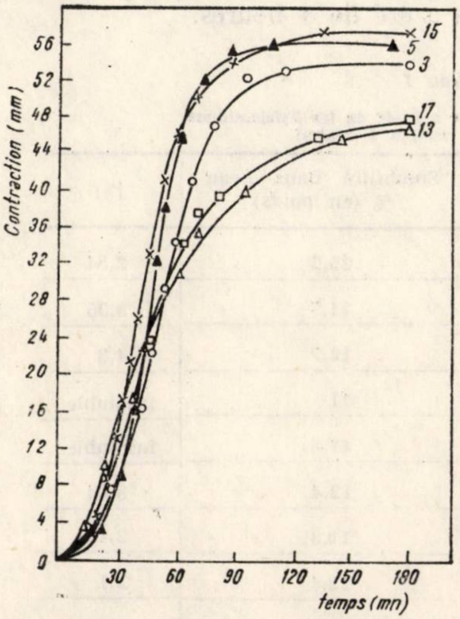

Fig. 1. — Évolution du processus de polymérisation de l'ε-caprolactame avec le temps, polymérisation réalisée dans un dilatomètre (température de polymérisation 220°, temps de réaction 3 heures).
15—1 mole % $AlEt_3$; 0,5 mole % d'eau ; 5—1 mole % $AlEt_3$; 3—0,75 mole % $AlEt_3$; 17—1 mole % $AlEt_3$; 1 mole % isocyanate de phényle ; 13—1 mole % $AlEt_3$; 1 mole d'eau.

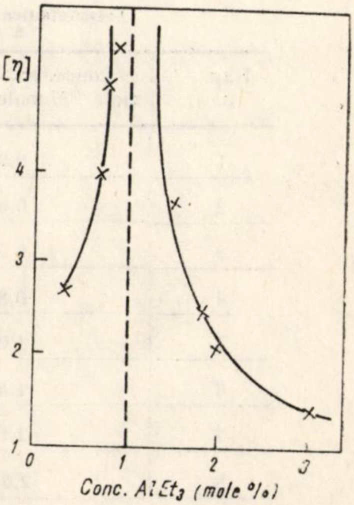

Fig. 2. — Dépendance des viscosités intrinsèques de la concentration du catalyseur.

À une concentration de 1 mole % triéthylaluminium vis-à-vis de celle du monomère, l'addition de l'eau dans des rapports moléculaires de 0,25 : 1 et 0,5 : 1 ($H_2O : AlEt_3$) conduit à la décroissance de la conversion en dépendance directe de l'augmentation de la quantité d'eau, mais on obtient toujours des polymères insolubles (exp. 15, 16).

À des rapports moléculaires de 0,75 : 1 et 1 : 1 ($H_2O : AlEt_3$), la conversion baisse aussi, en fonction de l'augmentation de la quantité d'eau, les polymères obtenus dans ces cas étant solubles (exp. 13, 14). En présence de quantités plus grandes d'eau, a lieu une désactivation du catalyseur, dont la conséquence est la décroissance de la conversion, au-dessous de celle d'équilibre.

Tableau 2

Influence des additifs sur la polymérisation du caprolactame avec $AlEt_3$ à 220° (temps de réaction, 3 heures)

Exp. n°	Conc. $AlEt_3$ mole/100mole monomère	Additifs		Solubilité dans l'eau % (en poids)	[η]
		substance	conc. mole /100 mole monomère		
10 a	1,0	—	—	11,3	insoluble
11	0,5	eau	0,5	59	1,39
12	0,75	,,	0,75	55,91	,,
13	1	,,	1	22,4	2,3
14	1	,,	0,75	13,7	2,83
15	1	,,	0,5	12,3	insoluble
16	1	,,	0,25	11,8	,,
17	1	isocyanate de phényle	1	22	1,0
18 c	1	chlorure de benzoyle	1	—	—
19 c	1	acétylacétone	1	—	—

a. On a effectué la polymérisation en utilisant la technique du vide poussé (10^{-4} mm Hg).
b. Insoluble dans le méta-crésol.
c. La polymérisation ne se produit pas.

L'existence d'une corrélation entre l'augmentation de la quantité d'eau du système et la formation des polymères solubles confirme l'hypothèse que par la réaction $Al(Cpl)_3 - H_2O$, un des groupes Al—N—CO est hydrolysé et les possibilités de croissance de la chaîne sont limitées seulement dans deux directions.

Pour vérifiér si les cocatalyseurs, efficaces dans la polymérisation alcaline, ont le même effet dans ce système catalytique on a effectué des polymérisations en présence de l'isocyanate de phényle et du chlorure de benzoyle.

Si pendant la polymérisation on ajoute l'isocyanate de phényle en rapport équimoléculaire vis-à-vis d' $AlEt_3$, à des concentrations du catalyseur de 1 mole %, la conversion et en même temps la viscosité intrinsèque du polymère baissent en comparaison des résultats obtenus au cas de la polymérisation sans catalyseur (fig. 1, exp. 17).

Si on ajoute du chlorure de benzoyle la polymérisation ne se produit pas.

De même, la polymérisation ne se produit pas si on ajoute des complexants forts comme l'acétylacétone en rapport équimoléculaire vis-à-vis de l'aluminium.

Les effets négatifs de l'addition de l'isocyanate de phényle et de l'acétylacétone n'apparaissent pas au cas des polymérisations de l'ε-caprolactame en présence des métaux alcalins.

On observe du tableau 3 que la conversion d'équilibre est atteinte dans tous les trois cas.[17]

À cause de la basicité réduite de l'aluminium par rapport à celle du sodium la dissociation du sel aluminium — caprolactame se produit à des températures supérieures aux températures nécessaires pour la polymérisation alcaline.[18]

---

[18] E. Sittler et J. Sebenda, *J. Polymer Sci. Pt C*, **16**, 67 (1967).

Donc les polymérisations à des températures inférieures à 200°C ont lieu seulement en présence des sels des métaux alcalins de caprolactame, le triéthylaluminium étant dans ce cas un cocatalyseur.

Tableau 3

Polymérisation du caprolactame en présence du Na métallique à 220° (temps) de réaction 1,5 h)

Exp. n°	Concentration Na mole/100 mole monomère	Additifs		Solubilité dans l'eau % (en poids)	[η]
		Substance	Concentration mole/100 mole monomère		
20	1,4	—	—	10,86	1,53
21	1	isocyanate de phényle	1	10,3	1,28
22	0,85	acétylacétone	1	13	1,08

Tous les résultats mentionnés prouvent que la polymérisation du caprolactame en présence du triéthylaluminium est différente de la polymérisation alcaline.

Par son caractère déficitaire d'électrons, l'aluminium produit une labilisation de la liaison cyclique, amidique de l'ε-caprolactame et fournit en même temps des centres actifs nécessaires dans la polymérisation.

Dans ce cas la présence des cocatalyseurs usuels dans la polymérisation alcaline n'est plus efficace.

Revue Roumaine de Chimie, 17, 3, 565 – 570 (1972)

ÉTUDE DE LA POLYDISPERSITÉ DU POLYCHLORURE DE VINYLE PAR CHROMATOGRAPHIE SUR GEL PERMÉABLE PENDANT LA DESTRUCTION MÉCANO-CHIMIQUE

AMALIA CRUSOS, CONSTANTIN UGLEA et ION AGHERGHINEI

Institut de Chimie Macromoléculaire « Petru Poni », Jassy, 41 A, Aleea Gr. Ghica Vodă

Reçu le 24 mars 1971

Les auteurs étudient la modification de la polydispersité du polychlorure de vinyle, pendant le processus de destruction mécano-chimique, par chromatographie sur gel perméable. En utilisant la méthode des moindres carrés, on calcule la constante de vitesse de destruction et le poids moléculaire limite du polymère dans des conditions mécaniques données. On détermine aussi le nombre total des macroradicaux formés dans le processus.

I. INTRODUCTION

La destruction mécano-chimique des polymères est conditionnée par l'interaction de quelques facteurs de base qui s'influencent réciproquement déterminant l'efficacité de la rupture des chaînes macromoléculaires.

Parmi ces facteurs, le poids moléculaire initial et la polydispersité du matériau soumis à la destruction ont un rôle très important.

L'étude expérimentale de la scission des chaînes macromoléculaires sous l'action de différentes sollicitations mécaniques prouve la diminution progressive de la polydispersité en fonction de la durée de l'action mécanique jusqu'à l'établissement dans les conditions données du poids moléculaire limite possible (M_∞).

La détermination des relations entre les caractéristiques cinétiques expérimentales et les constantes élémentaires de destruction aux molécules de différentes longueurs présente une grande importance.

La littérature de spécialité comprend peu de données sur la variation de la polydispersité moléculaire des hauts polymères pendant le processus mécano-chimique. Booth[1] étudie le comportement du polyisoprène avec une distribution moléculaire étroite, à l'action de différents processus mécano-chimiques, alors que Baramboim[2] détermine les courbes intégrales de distribution de la gélatine et du polyvinyle (alcool) en fonction de la durée de l'action mécanique.

---

[1] C. Booth, *Polymer*, 4, 471 (1963).

[2] N. K. Baramboim, « Mehanokhimiia polimerov », Izd. nauchino-tekhn. lit. SSSR, Moscou, 1961, p. 43, 55.

Grohn et ses collaborateurs et Bischof étudient la dégradation mécano-chimique du polychlorure de vinyle (PVC) sans traiter des aspects de la polydispersité.[3,4]

En partant du PVC avec une large polydispersité, le rapport MW/Mn = 4,8, nous nous sommes proposé de suivre par une technique de bonne résolution, telle la chromatographie sur gel perméable, la modification de la polydispersité en fonction de l'augmentation progressive de la durée du broyage jusqu'à l'établissement du poids moléculaire limite.

II. DONNÉES EXPÉRIMENTALES

Pour les expérimentations on a utilisé le PVC, un produit industriel avec un poids moléculaire gravimétrique moyen initial $\overline{Mw} = 147\,000$ et un poids moléculaire moyen numérique initial $Mn = 36\,000$.

La destruction mécano-chimique a été effectuée dans un broyeur vibratoire L.S.-60 (Veb-Kefama-Katzhütte) avec les vases et les boulets confectionnés en acier inoxydable V_2A, ayant une capacité de 1 l et munis d'une chemise de réchauffage et de refroidissement pour le maintien d'une température constante.

Une destruction optimale est soumise aux conditions mécaniques suivantes : rapport de remplissage des vases de broyage 0,4 % ; amplitude des oscillations 2 mm ; nombre de tours : 1 450 tours/mn. Le broyage a été conduit en présence de l'air à la température ambiante de 16 ± 2°.

La durée de l'action mécanique a varié entre 6 et 48 heures.

La modification de la distribution moléculaire du PVC pendant le processus de mécano-destruction a été suivie par chromatographie sur gel perméable à l'aide d'un appareil WATERS-200. Les déterminations ont été effectuées en solution de cyclohexanone (0,4 %) à 50°. La vitesse d'élution a été de 1 ml/mn.

III. RÉSULTATS ET DISCUSSIONS

Dans les processus de destruction mécano-chimique la diminution de la polydispersité, Mw/Mn, est une conséquence de l'accumulation des fractions avec le poids moléculaire faible qui tend vers M_∞ moyen, c'est-à-dire vers un produit plus homogène en ce qui concerne le poids moléculaire.

Par suite des déterminations expérimentales, pratiquement, on a constaté une diminution continue du domaine de la variation du poids moléculaire. Dans l'intervalle de M_0 (le poids moléculaire moyen initial), jusqu'à M_∞, la vitesse de modification est différente et diminue à mesure que le poids du polymère s'approche de M_∞.

---

[3] H. Grohn et K. Bischof, *Wissenschaftliche Zts. der T.H. für Chemie, Leuna, Merseburg*, 4, 153 (1961/1962).

[4] K. Bischof, *Rev. Chim. (București)*, 4, 205 (1962).

Les résultats expérimentaux que nous avons obtenus au broyage vibratoire du PVC mettent en évidence la baisse prononcée du poids moléculaire (figure 1) aux durées comprises entre 6—24 heures. L'augmentation continue de l'action destructive produit une diminution moins sensible du poids moléculaire qui tend vers M_∞ moyen.

A mesure que le poids moléculaire diminue, la polydispersité du polymère se modifie. Dans la figure 2 on observe que le rapport Mw/Mn décroît de façon accentuée jusqu'à 24 heures. Ultérieurement, à mesure que le processus de destruction avance et tend à s'établir M_∞, Mw/Mn se modifie moins sensiblement sans atteindre la valeur 1.

Dans la chromatographie sur gel perméable on a établi que, entre le logarithme du poids moléculaire des fractions séparées et le volume d'élution, il y a une relation linéaire. Ainsi, les portions au poids moléculaire supérieur se séparent les premières. Dans la figure 3 on observe que parallèlement à la croissance de la durée du processus de destruction la courbe différentielle de distribution subit deux modifications importantes : 1) un déplacement de la position de maximum à gauche (le

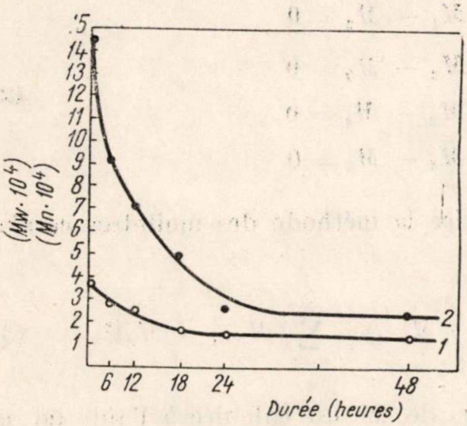

Fig. 1. — Variation du poids moléculaire moyen gravimétrique (courbe *1*) et numérique (courbe *2*) en fonction de la durée de broyage.

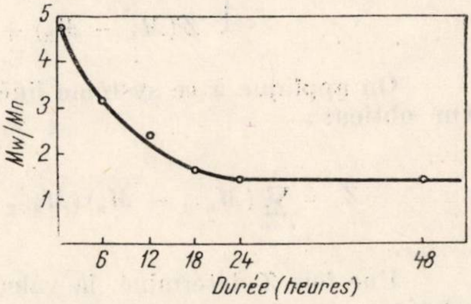

Fig. 2. — Modification du rapport Mw/Mn en fonction de la durée de broyage.

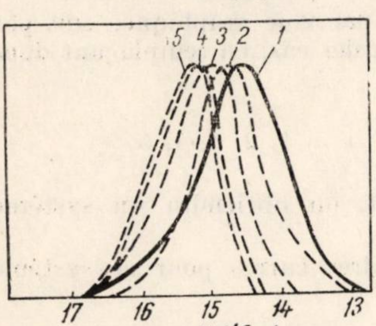

Fig. 3. — Gel-chromatogrammes. PVC produit initial (*1*). PVC soumis au broyage pendent 6 heures (*2*), 12 heures (*3*), 24 heures (*4*) et 48 heures (*5*).

volume d'élution plus grand) et 2) un continuel rétrécissement, fait qui se reflète aussi dans la figure 2 qui représente la variation du rapport Mn/Mw en fonction de la durée de broyage.

Conformément aux données fournies par chromatographie sur gel perméable a été calculée la constante de la vitesse de destruction, K, à l'aide de la relation établie par Baramboim :[2]

$$M_{\tau} = (M_0 - M_{\infty})\, e^{-k\tau} + M_{\infty} \tag{1}$$

Pour éliminer les incertitudes qui sont presque inévitables dans la méthode graphique de détermination nous avons utilisé la méthode des moindres carrés.

Si on note avec $M_0, M_1, M_2 \ldots M_5$ les masses moléculaires respectives au moment $t = 0, t_1 = 6$ h, $t_2 = 12$ h... $t_5 = 30$ h et $Z = e^{-6k}$ l'équation (1) nous conduit au système linéraire :

$$\begin{cases} Z(M_1 - M_0) + M_1 - M_2 = 0 \\ Z(M_2 - M_1) + M_2 - M_3 = 0 \\ Z(M_3 - M_2) + M_3 - M_4 = 0 \\ Z(M_4 - M_3) + M_4 - M_5 = 0 \end{cases} \tag{2}$$

On applique à ce système linéaire la méthode des moindres carrés. On obtient :

$$Z = \sum_{n=0}^{3} (M_{n+1} - M_n)(M_{n+2} - M_{n+1}) \Big/ \sum_{n=0}^{3} (M_{n+1} - M_n)^2 \tag{3}$$

Une fois Z déterminé, la valeur de K est calculée à l'aide de la relation :

$$K = -1/6 \ln Z. \tag{4}$$

La valeur de M_{∞} est déterminée soit par voie graphique, soit par la méthode des moindres carrés. Dans ce dernier cas, en remplaçant dans le système d'équation :

$$M_n = (M_0 - M_{\infty}) Z^n + M_{\infty}, \quad \text{où} \quad n = 1, 2, 3, 4, 5,$$

la valeur du Z déterminée antérieurement, on obtiendra un système d'équations linéaires pour M_{∞}.

En appliquant la méthode des moindres carrés pour ce système linéaire, il résulte :

$$M_{\infty} = \sum_{n=1}^{5} (1 - Z^n)(M_n - M_0 Z^n) \Big/ \sum_{n=1}^{5} (1 - Z^n)^2 \tag{5}$$

Après les calculs on obtient les valeurs :

— la constante de la vitesse de destruction, $K = 0{,}125\ \mathrm{h}^{-1}$;

— le poids moléculaire moyen limite, $M_\infty = 30\,700$.

Sur la base du M_∞ qui a été calculée on a déterminé le coefficient φ_1, qui représente le rapport entre la diminution du poids moléculaire à un moment donné, τ, et la diminution limite possible :

$$\varphi_1 = (M_0 - M_\tau)/(M_0 - M_\infty) \tag{6}$$

La représentation graphique de φ_1 en fonction de la durée du processus mécano-destructif permet une expression plus étendue du degré de destruction (figure 4).

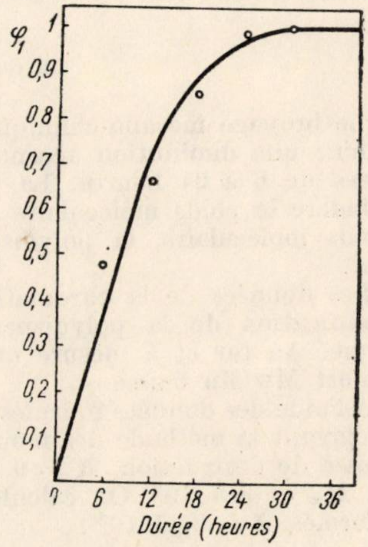

Fig. 4. — Variation du degré de destruction exprimée par l'intermédiaire du φ_1, en fonction de la durée de broyage.

Le nombre total des macroradicaux formés pendant le processus de destruction peut être calculé avec la relation évidente :

$$L = N_\infty - N_0 \tag{7}$$

où on a noté avec L le nombre de liaisons rompues pendant le processus de destruction, N_0, le nombre initial de macromolécules, N_∞, le nombre final de macromolécules.

Le nombre de macromolécules contenues par m grammes de polymère ayant la masse moléculaire moyenne numérique M_i est donné par la relation :

$$N_i = \mathrm{m} \cdot \mathrm{N}/M_i\ (i = 0,\infty) \tag{8}$$

où on a noté avec N le nombre d'Avogadro.

Compte tenu de la relation (8) on peut écrire la relation (7) sous la forme (9).

$$L = mN(1/M_\infty - 1/M_0) \tag{9}$$

Cette dernière relation permet la détermination du nombre total de macroradicaux formés pendant la destruction Z :

$$Z = 2L = 2\,mN\left(\frac{1}{M_\infty} - \frac{1}{M_0}\right) \tag{10}$$

La relation (10) a été proposée par Baramboim.[2] En remplaçant les valeurs on obtient : $Z = 2{,}43 . 10^{20}$.

III. CONCLUSIONS

Le broyage mécano-chimique du PVC dans les conditions données détermine une diminution accentuée du poids moléculaire à des durées étendues de 6 à 24 heures. La continuation de la destruction permet d'atteindere le poids moléculaire limite. Parallèlement à la modification du poids moléculaire, la polydispersité du polymère décroît progressivement.

Les données de la chromatographie sur gel perméable confirment la modification de la polydispersité pendant la destruction mécanochimique. Au fur et à mesure que le processus de destruction avance, le rapport Mw/Mn baisse.

A l'aide des données fournies par chromatographie sur gel perméable en employant la méthode des moindres carrés, on détermine la constante de vitesse de destruction, $K = 0{,}125\ \text{h}^{-1}$ et le poids moléculaire moyen limite, $M_\infty = 30{,}7 . 10^3$. On calcule aussi le nombre total de macroradicaux formés, $Z = 2{,}43 . 10^{20}$.

Revue Roumaine de Chimie, 17, 3, 571–572 (1972)

SYNTHESIS OF POLYURETHANE ELASTOMERS, STARTING MATERIALS AND INTERMEDIATES. XI
SYNTHESIS OF NITRODIISOCYANATES

GH. MANDRIC and VALENTINA ŢĂRANU

Institute of Macromolecular Chemistry "P. Poni" Aleea Gr. Ghica Vodă 41 A, Jassy, Romania

Received June 14, 1971

The paper presents the conditions for the synthesis of two new aromatic nitrodiisocyanates (I and II).

In a previous paper [1] the synthesis of two nitrodiisocyanates has been reported. To continue this work we have prepared two other nitrodiisocyanates : 2,2′-dinitro-4,4′-diphenyldiisocyanate (I) and 3,3′-dimethyl-6,6′-dinitro-4,4′-diphenylmetanediisocyanate (II).

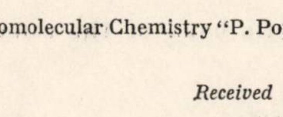

(I)

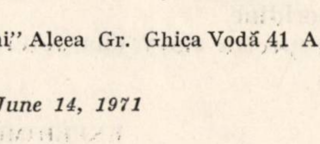

(II)

Both nitrodiisccyanates were prepared by the phosgene treatment of the corresponding dinitrodiamine dihydrochlorides. Benzidine was used as starting material for the first diisocyanate (I) and *o*-toluidine for the second diisocyanate (II). *o*-Toluidine was converted into 3,3′-dimethyl-4,4′-diaminodiphenylmethane.

Both diamines were nitrated and then converted into their dihydrochlorides.

3,3′-Dimethyl-4,4′-diamino-6,6′dinitrodiphenylmethane is not known in literature and it was identified by elemental analysis and by conversion into 3,3′-dimethyl-4,4′-6,6-′tetraaminodiphenylmethane (which is known with m.p. lit.[2] 203—204°; found 202—204°);

---

[1] Part XII : I. Matei, Gh. Mandric and V. Ţăranu, *Rev. Roumaine Chim.*, **11**, 843 (1966).

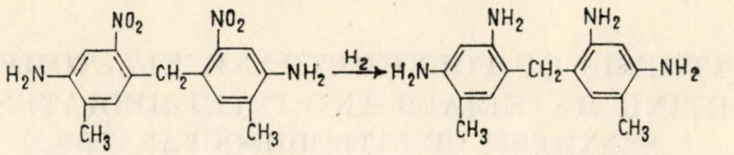

The nitrodiisocyanates were purified by recrystallization from tetralin and were characterized by elemental analysis and by their reaction with piperidine.

Infrared spectra show characteristic band of the isocyanate group at 2250 cm^{-1}.

EXPERIMENTAL

In order to synthesize the nitrodiisocyanate (I), 2,2′-dinitro-benzidine (III) was obtained by the nitration of benzidine sulfate with kalium nitricum and sulfuric acid (yield, 62%, m.p. lit.[3] 214°; m.p. found 213—214°).

By passing a stream of hydrochloric acid through an alcoholic solution of product (III) the corresponding dihydrochloride (IV) was obtained.

To obtain the second nitrodiisocyanate (II), the following compound was synthesized: 3,3′-dimethyl-4,4′-diaminodiphenylmethane (V) which was prepared by condensation of *o*-toluidine with formaldehyde (yield 78%, m.p.$_{\text{lit.}}$[4] 155°; m.p. found 154—155°).

3,3′-Dimethly-4,4′-diamino-6,6′-dinitrodiphenylmethane (VI) was obtained by nitration of product (V) with kalium nitricum and sulfuric acid (yield, 34.18% m.p. found 212—213°). The dihydrochloride of 3,3′-dimethyl-4,4′-diamino-6,6′dinitrodiphenylmethane (VII) was prepared by passing a stream of hydrochloric acid through the ethanolic solution of product (VI).

2,′-Dinitro-4,4′-diphenyl diisocianate (*I*). The product (IV) 10 g, well dried, in tetralin (100 ml) was treated with phosgene for 2 hr, maintaining the temperature between 130—150°, phosgene treatment was continued at 150—180° for 1 hr. By passing a stream of nitrogen through the installation,[5] the excess of phosgene was evacuated. After filtering, the nitrodiisocyanate was recrystallized from tetralin (m.p. 135—136°)

$C_{14}H_6N_4O_6$ *Calcd.*: N, 17.17; *Found*: N, 17.22.

The adduct of nitrodiisocyanate (I) with piperidine is an yellow product with m.p. 148—150°.

$C_{24}H_{28}N_6O_6$ *Calcd.*: C, 58.06; H, 5.64; N, 16.93;
Found: C, 58.15; H, 5.20; N, 16.61.

3,3′-Dimethyl-6,6′-dinitro-diphenylmethane-diisocyanate (*II*). The product (VII), well dried, was phosgene-treated in the same conditions as described for the nitrodiisocyanate I. The nitrodiisocyanate (II) was also recrystallized from tetralin (m.p. 134—136°)

$C_{17}H_{12}N_4O_6$, *Calcd.*: N, 15.22; *Found*: N, 14.85.

The adduct of nitrodiisocyanate (II) with piperidine is a yellow product (m.p. 204°)

$C_{27}H_{34}N_6O_6$ *Calcd.*: C, 60.24; H, 6.32; N, 15.61;
Found: C, 61.21; H, 6.31; N, 15.85.

---

[2] F. Ullman and E. Naef, *Ber. dtsch. chem, Ges.*, **33**, 915 (1900).

[3] E. Täuber, *Ber. dtsch. chem. Ges.*, **23**, 795 (1890).

[4] O. Ya. Fedotova, M. A. Askarov and I. P. Losev, *Zhur. obschei Khim.*, **27**, 775 (1957).

[5] E. Cocea, A. Caraculacu, G. Mărculescu, A. Petruş and I. Matei, *Studii şi Cercetări St. Chim. Fil. Iaşi*, **10**, 261 (1959).

Revue Roumaine de Chimie, **17**, *3*, 573–579 (1972)

THE STUDY OF THE BIURET REACTION. VI

ELECTRONIC SPIN RESONANCE OF SOME COPPER(II)-COMPLEXES WITH CYANURIC ACID AND SUCCINIMIDE

Z. SIMON *, MARIA NUŢIU and G. OSTROGOVICH

The "Traian Vuia" Polytechnic Institute, Department of Organic Chemistry, str. Bocşa 6,
Timişoara, Romania

Received May 24, 1971

The electronic spin resonance spectra, at room temperature for the following Cu (II)-complexes of the cyanuric acid (**1**) and the succinimide (**2**) were recorded : $CuCyur^{II}.Py_2.\ H_2O$, $CuCyur^{I}_{2}.2\,NH_3$, $CuCyur^{II}.\ LiCyur^{I}.2H_2O$, $Na_2[CuCyur^{I}_{4}].\ .\ 6H_2O$, α-$Na_2\ [CuCyur^{I}_{4}]$, β–$Na_2\ [CuCyur^{I}_{4}]$, $K_2\ [CuCyur^{I}_{4}].\ 6H_2O$, $K_2[CuCyur^{I}_{4}]$ and $M_2[CuSu_4]nH_2O$, where Cyur is a cyanuric acid anion (I-mono, II-dibasic), Su is a succinimide anion, while $M = Li^+, Na^+, K^+, Rb^+, Cs^+$ and $n = 1, 6, 6, 2$ and 2 respectively. Starting from the obtained *g*-values, the symmetry of the ligand field, the nature of the Cu (II)–N bond and the partition of the unpaired electron between the Cu (II) ion and the ligands are evaluated.

★

At the 1st National Chemistry Conference (Cluj, 1962) G. Ostrogovich expressed the opinion, confirmed also by other authors,[1,2] that the biuret reaction can be characterized by the formation of the complexes by the Cu^{2+} and Ni^{2+} ions with a dsp^2 hybridization and a tetragonal coordination, with certain organic nitrogen compounds, complexes with an unusual colour, while most Cu^{2+}-complexes are blue.

Cambi and Tremolada [3] studied the magnetic properties and the X-ray spectra of Cu^{2+} and Ni^{2+}-succinimide complexes and concluded that they have the same structure. Accordingly, the Cu^{2+} ion is in the dsp^2 hybridization, like the Ni^{2+} ion in this case, rather than in the sp^3 hybridization.

The mentioned colours for the Cu^{2+} complexes should thus correspond to two different steric arrangements of the ligands. Indeed, from the point of view of the crystal field, the tetragonal structure corresponds to a splitting into four energy levels of the atomic 3d orbitals, with one electron on the highest level for the Cu^{2+} ion. This would explain the

---

* University of Timişoara, Department of Organic Chemistry.

[1] H. C. Freeman, J. E. W. L. Smith and J. C. Taylor, *Acta Cryst.*, **14**, 407 (1961).

[2] A. W. McLellan and G. A. Melson, *J. Chem. Soc.* (A), **1967**, 137.

[3] L. Cambi and E. Tremolada, *Gazz. Chim. Ital.*, **65**, 322 (1935).

"anomalous" colour for the tetragonal Cu^{2+} complexes, as in the case of tetrahedral complexes the 3d orbitals are split into only two levels, the triple degenerated upper one with 5 electrons. The tetragonal (planar, axial) structure would be favoured by strong field ligands, as there is only 1 electron on the very high 3d level, but as all four coordinated atoms are in the same plane, the steric requirements would be more severe.

In this paper we studied the ESR spectra for anionic complexes of the Cu^{2+} ion with cyanuric acid (**1**) and succinimide (**2**), which exhibit both the red-violet colour, characteristic of the biuret reaction and the blue colour characteristic of "normal" complexes, depending on the alkaline cation.

Our aim was to obtain information concerning the steric structure from the ESR spectra, a rather difficult task, as these complexes are completely unsoluble in water or other solvents, or if they dissolve (the succinimide complexes) they undergo complete decomposition. Therefore the ESR spectra could be recorded only on polycrystalline powders.

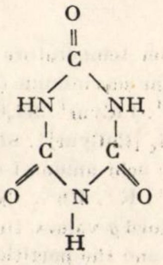

(1)

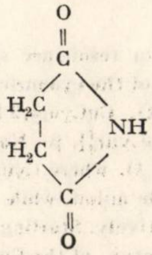

(2)

EXPERIMENTAL

The substances, listed in table 1, were prepared according to the indications given in notes.[4–8]

The ESR spectra were recorded on a JES-3B spectrometer (from IFA-Cluj), at room temperature, for polycrystalline powder. The differential spectra obtained (figures 1–3) do not exhibit hyperfine structure, have a single, asymmetric pair of peaks and some of them, also a shoulder. The gyromagnetic factors $g_{\perp}$ and $g_{||}$ were calculated out of the position of these peaks and of the shoulder, respectively, the integral intensities ($A_E = A_{\perp} + A_{||}$) out of the height of these peaks. All these values are listed in table 1, together with the half-widths ΔH_1, ΔH_2 of the peaks and the colour of the complexes. The ESR spectrum of

[4] G. Ostrogovich and M. Nuţiu, *Bul. St. Tehn. I.P. "Traian Vuia"* Timişoara, **15**, 29 (1970)

[5] G. Ostrogovich and A. Nemeş, *Studii şi Cercet. Sti. Chim., Baza Cercetări Sti. Timişoara*, **7**, 285 (1960).

[6] L. A. Tschugaeff, *Chem. Ber.*, **40**, 1973 (1907).

[7] G. Ostrogovich and M. Nuţiu, Rev. Roumaine. Chim., **16**, 1487 (1971).

[8] A. Ostrogovich and G. Ostrogovich, *Atti del V Congresso Nazionale di Chimica Pura ed Applicata*, Sardegna, Maggio e Giugno, **1935**, 431; *Chem. Zentr.*, **1937**, I, 2146.

a polycrystalline copper-oxalate (CuC_2O_4) powder at room temperature was also recorded, as a check. A symmetric spectrum resulted without hyperfine structure and with a $g_\perp$-factor value, $g_\perp = 2.0792$ in good agreement with $g_\perp = 2.0780$ of Kivelson and Neiman.[9]

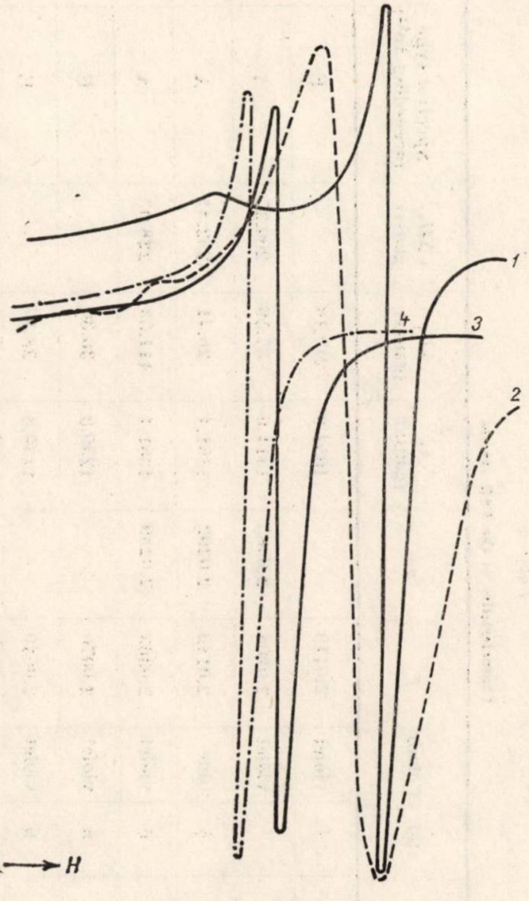

Fig. 1. — ESR spectra of polycrystalline powders at room temperature for the complexes:
(1) $Na_2[CuSu_4]5H_2O$ (5.87 gauss/mm);
(2) $K_2[CuSu_4]6H_2O$ (5.87gauss/mm);
(3) $Rb_2[CuSu_4]2H_2O$ (6.26 gauss/mm) and
(4) $Cs[CuSu_4]2H_2O$ (6.26 gauss/mm).

We tried to obtain the electronic spectra by the reflexion method on a UNICAM SP-800 spectrograph. The reflexion spectra obtained in this way show two shallow maxima in the regions 500—600 mμ and 280—300 mμ for the violet complexes and in the regions 650—800 mμ and 220—300 mμ for the blue ones.

The polycrystalline powders of complexes 2—4 and 10—14 (table 1) were tested for semiconductivity tablets at room temperature. All tested substances show an infinite resistivity.

---

[9] D. Kivelson and R. Neiman, *J. Chem. Phys.*, **35**, 149 (1964).

Table 1

Characteristics of the ESR spectra

No	Substance	Ref.	Colour	$g_\perp$	$g_\parallel$	A_E (gauss)	ΔH_1 (gauss)	(ΔH_2 gauss)	Spectral type (according to[12])	$G = \frac{g_\parallel - 2}{g_\perp - 2}$
1	$CuCyur^{II}.\ Py_2.\ H_2O$	4	violet	2.0113	—	1054.8	219.10	—	E	—
2	$CuCyur_2^{I}.\ 2NH_3$	4	violet	2.0006	2.0085	1314.6	37.56	209.37	A	14
3	$Na_2[CuSu_4].\ 5H_2O$	6	blue	2.0149	2.0292	1361.4	26.41	252.41	A	1.89
4	$K_2[CuSu_4].\ 6H_2O$	6	violet	2.0363	2.0289	1361.4	111.53	228.93	A	0.80
5	$Rb_2[CuSu_4].\ 2H_2O$	6	violet	2.0070	—	1230.0	36.30	—	E	—
6	$Cs_2[CuSu_4].\ 2H_2O$	6	violet	2.0649	—	1439.8	28.17	—	E	—
7	$Li_2[CuSu_4].\ H_2O$	6	blue	—	—	—	—	—	E	—
8	$Li\ [CuCyur^{III}].\ 2H_2O$	7	blue	No ESR-signal						
9	$Li\ [CuCyur^{I}Cyur^{II}].\ 2H_2O$	7	violet	2.0006	2.0292	1258.2	90.98	146.75	A	49
10	$Na_2[CuCyur_4^{I}].\ 6H_2O$	8	violet	2.0149	2.0292	1095.5	26.41	252.41	A	1.96
11	$K_2[CuCyur_4^{I}].\ 6H_2O$	7	blue	2.0220	2.0363	851.3	243.60	126.20	A	1.65
12	$\alpha-Na_2[CuCyur_4^{I}]$	8	violet	2.0149	2.0292	1430.4	17.61	258.28	A	1.96
13	$\beta-Na_2\ [CuCyur_4^{I}]$	8	blue	2.0149	—	1205.0	117.69	—	E	—
14	$K_2[CuCyur_4^{I}]$	7	pink	2.0149	—	2088.5	17.61	—	E	—

Cyur = cyanuric acid anion (I, II, III, mono-, di- and respectively tri-basic)

Su = succinimide anion (monobasic)

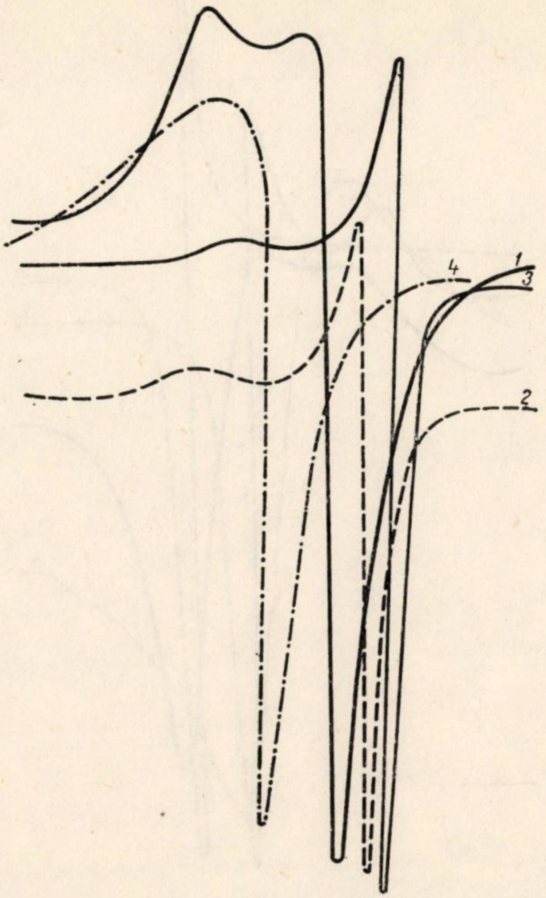

Fig. 2. – ESR spectra of polycrystalline powders at room temperature for the complexes:

(*1*) $Li[CuCyur^{II}\ Cyur^{I}]\ 2H_2O$;
(*2*) $Na_2\ [CuCyur^{I}_{4}]\ 6H_2\ O$,
(*3*) $\alpha-Na_2[CuCyur^{I}_{4}]$ and
(*4*) $\beta-Na_2[CuCyur^{I}_{4}]$ (5.87 gauss/mm).

RESULTS AND DISCUSSION

Our $g_{\perp}$ and $g_{||}$ values of table 1, in comparison with those for copper (II) complexes of other authors,[10] are sensibly lower and nearer to the $g = 2.0023$ value for the unpaired electron on atoms without angular moment (C, N, O). Thus our $g_{\perp}$ values are in the 2.007–2.0065 range as compared to the range 2.040–2.090 indicated by Wiersema and Windle [10] and our $g_{||}$ values in the 2.007–2.077 range as compared to 2.150–2.240. For certain complexes (1, 5, 6, 13 and 14, table 1) we obtained a single, also low, g-value. A similar result was obtained by Macarovici et al.[11] for some Cu^{2+} complexes with benzidine and other

---

[10] A. K. Wiersema and J. J. Windle, *J. Phys. Chem.*, **68**, 2316 (1964).

[11] A. Nicula, R. Micu-Semeniuc and C. Gh. Macarovici, *Rev. Roumaine Chim.*, **13**, 1329 (1968).

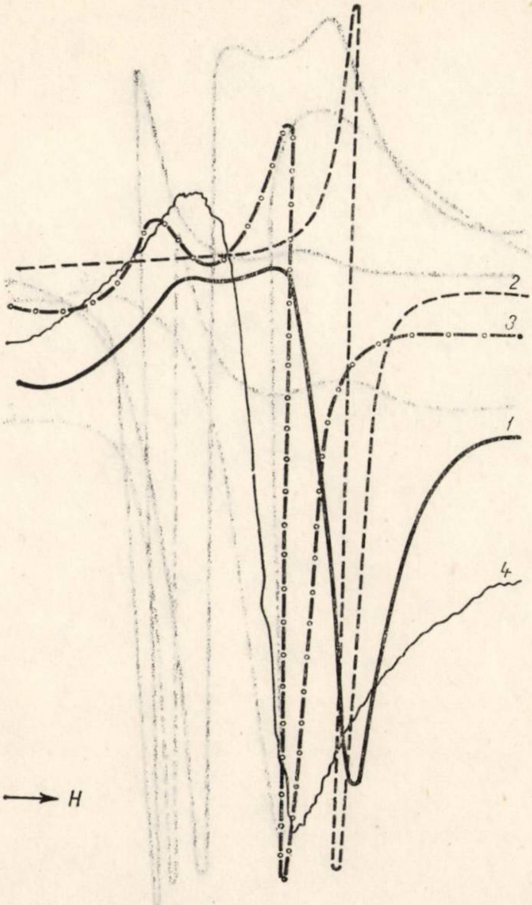

Fig. 3. — ESR spectra of polycrystalline powders at room temperature for the complexes:

(*1*) $K_2[CuCyur^{I}_{4}]\,6H_2O$ (5.87gauss/mm);

(*2*) $K_2[CuCyur^{I}_{4}]$ (5.87 gauss/mm);

(*3*) $Cyur^{I}_{2}Cu\,2NH_3$ (6.26 gauss/mm) and

4) CyurII Cu Py_2H_2O (6.26 gauss/mm).

ligands and was explained, by those authors, as due to the formation of a semiquinonic benzidine radical (Bzd^+) in the corresponding complexes.

In comparison with the classification of ESR spectra for the Cu^{2+}-complexes (polycrystalline powder) of Hathaway and Billing,[12] our spectra correspond either to the type shown by figure 7A, or to the one in figure 7E (page 169 in [12]). Following Hathaway and Billing, type "*E*" spectra correspond to a regular tetrahedral symmetry — a rather rare case — or more often, to a very distorted symmetry. Type "*A*" spectra correspond to an axial symmetry (tetragonal in our case), more or less distorted as the factor $G = (g_{||} - 2)/(g_{\perp} - 2)$ is lower than $G = 4.0$.

The information given by these ESR spectra on the geometry of the complexes is thus rather meagre. An inspection of table 1 still allows to draw some conclusions. The blue complexes, with a supposed tetrahedral symmetry, have either spectra of type "E" (7 and 13), i.e. possibly tetrahedral, or of type "A" (3 and 11) but with a very low *G* factor, i.e. a very distorted symmetry. The spectra of the violet complexes, whose symmetry is supposed tetragonal, correspond in most cases to the type "A" with *G* factors higher than for the blue complexes. Exceptions are the substance no 1 which must be a polymer because of the dibasic Cyur anion, no 14, with an "anomalous" colour (rather pink than violet), and no 5 and 6.

---

[12] B. J. HATHAWAY and D. E. BILLING, *Coordin. Chem. Rev.*, **5**, 143 (1970).

Substance no 8 (Li [CuCyur]. $2H_2O$) does not give any ESR signal. In this case, each Cyur-ligand must coordinate two Cu^{2+} ions, a fact able to produce a strong interaction between the upper 3d-levels of these ions and pairing of electrons on the resulting "bonding" energy band. A similar explanation was given by Melson [2] for the low paramagnetism of the binuclear complex of Cu^{2+} with the biuret:

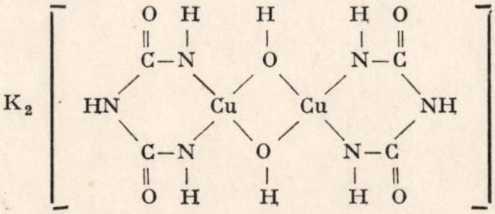

The partition of the unpaired electron between the Cu^{2+} ion and the ligands can be calculated by the formulae of Kivelson and Newman,[9] out of the $g_{\|}$ and $g_{\perp}$ values. Some parameters from the electronic spectra or from finer details of the ESR spectra, are also needed, but could not be obtained from our powder spectra. The relatively low $g_{\perp}$ and $g_{\|}$ factors of our complexes indicate only a high degree of covalency for the Cu (II)-N bonds.

Our very low $g_{\|}$ values, if they are not due to errors inherent to the use of polycrystalline powders, indicate even a partial "reduction" of the Cu^{2+} ion by the ligands. A transition of the unpaired electron on the π-electron system of the ligands should produce an electronic conductivity: the Cyur ligands of nearby complexes are hydrogen-bonded and partially occupied energy bands would result. Electrons shifted from the ligands towards the Cu^{2+}-ion, should thus result from the nonbonded electron pairs of the coordinated N-atoms.

A strong covalent character for the Cu (II)—N bond can in any case be inferred from our ESR spectra. In the crystalline field approximation this is tantamount to a high Δ-splitting parameter, which according to the considerations in the first part of this note, should favour a geometry of planar, tetragonal type, characteristic of the biuret reaction. The strong shift of the nonbonded electron pairs of the N-atoms towards the Cu^{2+}-ion can be due to the fact that at least part of the coordinated N-atoms, whose electronegativity is not too high, have a formal negative charge in our complexes.

Revue Roumaine de Chimie, 17, 3, 573–579 (1972)

Revue Roumaine de Chimie, 17, 3, 581–588 (1972)

HYDROPEROXIDATION OF ORGANIC COMPOUNDS AT THE LIQUID/GAS INTERFACE. III*)[1]

HYDROPEROXIDATION OF PHENYLCYCLOHEXANE WITH OXYGEN

J. VODNÁR

"Babes-Bolyai University of Cluj, Department of Chemical Technology, str. Arany János 11, Cluj, Romania

Received November 25, 1970

The paper presents the experimental results obtained by hydroperoxidation of phenylcyclohexane at the liquid/gas interface,[1–3] using purified technical oxygen as hydroperoxidizing agent and cumene hydroperoxide as initiator. Hydroperoxidation has been studied dependening on different parameters. On the basis of the experimental results obtained, the maximum reaction rates were determined concerning both the classical and the liquid/gas interface methods. The kinetics of the process and the activation energy were determined. The necessary time to achieve maximum concentration of hydroperoxide was reduced by 50% and the rate of the hydroperoxidation is by 75% higher than those in the normal types of systems used for such reactions.

The experimental results obtained by the hydroperoxidation of cumene at the liquid/gas interface were presented in a previous paper.[1]

Owing to the technological importance, the hydroperoxide of phenylcyclohexane could have — beside that of the cumene — in producing Relon type synthetic fibres, the author considered important to study the hydroperoxidation of phenylcyclohexane; by the decomposition of phenylcyclohexane hydroperoxide in acid catalysis, cyclohexanone could be obtained beside phenol.

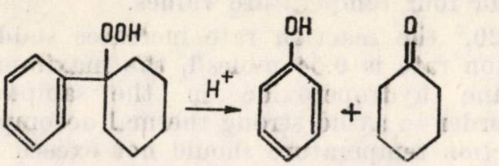

Scheme 1. Decomposition of phenylcyclohexane hydroperoxide in acidic catalysis.

---

*) Paper presented at the 39 th International Congress of Industrial Chemistry, Bucharest, 1970.

[1] I. VODNÁR, *Stud. Univ. Babeş-Bolyai, Chem.*, **2**, 91 (1970).

[2] I. VODNÁR, *J. Appl. Chem.*, **20**, 99 (1970). London.

[3] I. VODNÁR, *Patent of S. R. Romania*, Nr. **51928** (1969).

At present, the raw material used in producing polyamides of relon type is phenol, obtained by the decomposition of cumene hydroperoxide in acid catalysis.

Relon may be obtained in three stages (oximation, Beckmann rearrangement and polymerization) if we use cyclohexanone as raw material, instead of five (hydrogenation, oxidation, oximation, Beckmann type rearrangement and polymerization) necessary when using phenol.

This article present the experimental results obtained in hydroperoxidation of phenylcyclohexane, applying the method of liquid/gas interface.[2,3] On the basis of the experimental results the kinetics of the process was plotted. The maximum reaction rates and activation energy were determined, the optimal conditions of hydroperoxidation of phenylcyclohexane being also described.

APPARATUS AND PROCEDURE

Hydroperoxidation of phenylcyclohexane was made in a laboratory chemical reactor, described in the first article of this series.[3] Purified technical oxygen has been used as hydroperoxidizing agent. The process has been studied in accordance with different parameters (temperature, flow of oxygen, type of initiator, concentration of initiator, phenylcyclohexane and natrium adipate).

The phenylcyclohexane used as raw material, was synthesized from benzol and cyclohexene by the Friedel-Crafts method.[4] It was purified with concentrated sulphuric acid and a water solution of sodium hydroxide.[5] The volume of phenylcyclohexane samples subjected to hydroperoxidation was 25 ml.

Hydroperoxidation is achieved by bubbling the purified technical oxygen through phenylcyclohexane sample. Tests for dosing hydroperoxide [6] are taken from the reaction mixture, periodically.

RESULTS AND DISCUSSION

The results obtained are illustrated in figures 1—10. The first parameter studied was the hydroperoxidation temperature. The flow of oxygen was 7.2 l/h and the initial cumene hydroperoxide content of the sample, used as initiator, was 0,329 moles/l. Figure 1 illustrates the kinetic curves for four temperature values.

Beyond 120,° the reaction rate increases suddenly. But at 132,° when the reaction rate is 0.54 moles/l, the maximum concentration of phenylcyclohexane hydroperoxide in the sample does not exceed 1.6 moles/l. In order to avoid strong thermal decomposition of hydroperoxide, the reaction temperature should not exceed 126°.

With a view to comparing the efficiency of the liquid/gas interface method with the classical one, a series of experiments are made in a

---

[4] D. Bodroux, *Ann. Chim. (France)*, **11**, 561 (1929).

[5] B. A. Redoshkin, V. A. Shushunov and N. I. Kurochkin, *Trudy po khim. i khim. tekhnol.*, **1**, 3 (1960), Gorkij.

[6] H. Raley, F. Rust and W. Vaughan, *J. Amer. Chem. Soc.*, **70**, 1336 (1948).

The curves of two experiments carried out at 127°, by using 0,329 moles/l (curve 1) and 0,107 moles/l (curve 2) cumene hydroperoxide as initiator, as well as 0,1% sodium adipate, in both cases, are presented in figure 7.

In the presence of sodium adipate the reaction rate appears almost the same in all experiments, if cumene hydroperoxide as initiator, is used in amounts of 0,10–0,329 moles/l.

In the following two experiments a different flow of oxygen was applied: 7,2 and 5,6 l/h. Cumene hydroperoxide 0,329 moles/l was used as initiator. The temperature was maintained at 120° (figure 8).

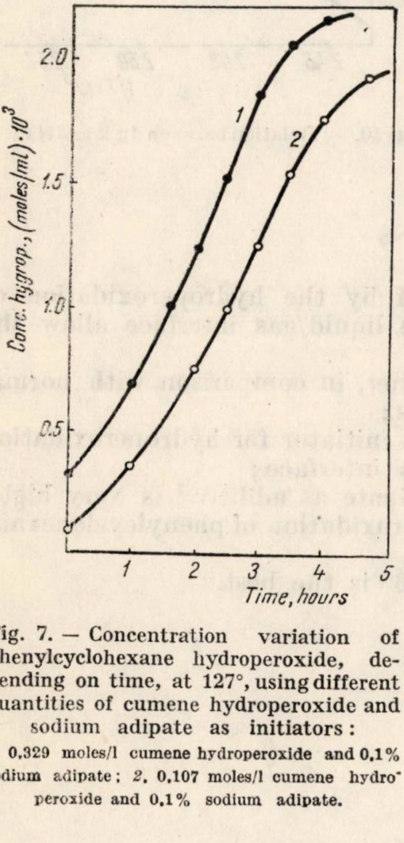

Fig. 7. — Concentration variation of phenylcyclohexane hydroperoxide, depending on time, at 127°, using different quantities of cumene hydroperoxide and sodium adipate as initiators:

1, 0,329 moles/l cumene hydroperoxide and 0,1% sodium adipate; 2, 0,107 moles/l cumene hydroperoxide and 0,1% sodium adipate.

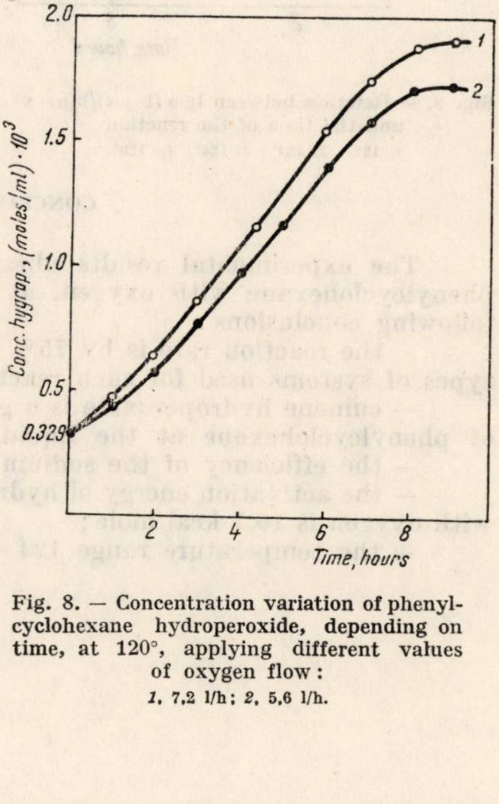

Fig. 8. — Concentration variation of phenylcyclohexane hydroperoxide, depending on time, at 120°, applying different values of oxygen flow:

1, 7,2 l/h; 2, 5,6 l/h.

Figure 8 shows that the hydroperoxidation rate depends only to a small extent on the oxygen flow.

On the basis of the experimental results obtained, the kinetics of the process is plotted, using a kinetic relation characteristic of autocatalysed reactions.[1] Figure 9 shows the linearized curves by means of the above mentioned relation.

The activation energy of the hydroperoxidation process calculated from pairs of lg k and $1/T$ values (figure 10), corresponding to the three chosen temperatures, is equal to 10,7 kcal.

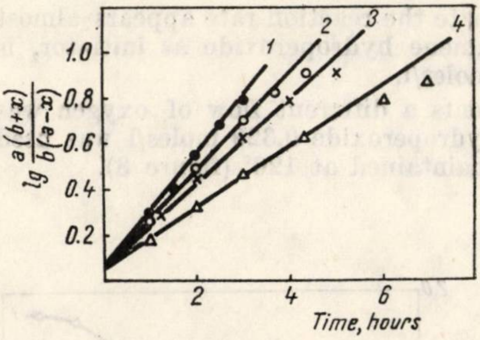

Fig. 9. — Relation between lg a (b+x)/b(a—x) and the time of the reaction
1, 132°; *2*, 127°; *3*, 124°; *4*, 120°.

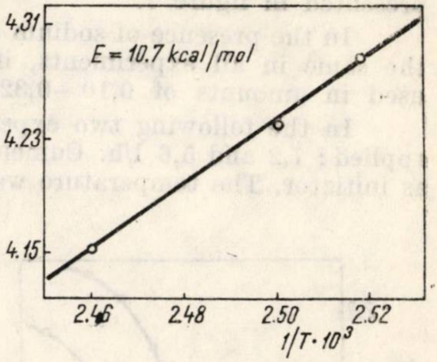

Fig. 10. — Relation between lg k and1/T.

CONCLUSIONS

The experimental results obtained by the hydroperoxidation of phenylcyclohexane with oxygen, at the liquid/gas interface allow the following conclusions :

— the reaction rate is by 75% higher, in comparison with normal types of systems used for such reactions ;

— cumene hydroperoxide is a good initiator for hydroperoxidation of phenylcyclohexane at the liquid/gas interface ;

— the efficiency of the sodium adipate as additiv [7] is very high ;

— the activation energy of hydroperoxidation of phenylcyclohexane with oxygen is 10,7 kcal/mole ;

— the temperature range 124—126° is the best.

M. VON ARDENNE, K. STEINFELDER, and R. TÜMMLER, *Elektronanlagerungs-Massenspektrographie organischer Substanzen*, Springer-Verlag Berlin, Heidelberg, New York 1971, VIII + p. 403.

Negatively-charged ions usually receive very cursory treatment in the standard works on mass spectrometry. Apart from an old monograph by Massey (1950), and a brief chapter in McLafferty (1963), four pages is the maximum devoted to the subject in the textbooks at present available to the reviewer. There are several reasons for this, but principally it is because, with the usual electron-impact sources of commercial spectrometers, the yield of negatively-charged ions is very low – smaller than that of positive ions by a factor of 10^{-3} to 10^{-4}. As a consequence, their study has not followed the rapid development seen with the positive ions, but has remained a rather quiet backwater, fished principally, since 1957, by Professor Manfred von Ardenne and his associates in Dresden. The catch is laid out for inspection in the volume under review.

Probably all that the average organic chemist knows – or thinks that he knows – about the mass spectra of negative ions is that, besides being weak and difficult to obtain, they tend to contain relatively few peaks, usually the $(M-1)^-$ and a few fragments, and therefore they provide little structural information. The Dresden group have overcome the former problem by constructing a source ("Elektronanlagerungs (EA)-Ionenquelle", which, to preserve the initials, we may as well call the electron-addition ion source) operating under a relatively high pressure (ca. 10^{-2} torr) of argon. The details of the construction and operation of the instrument, together with some introductory theory and technical details of the processing of the results, occupy the first hundred pages of the book, and there is no need to elaborate on them here. Ten pages of this deal with the practical problem of counting – assigning to each line its correct mass number, and other details receive similarly thorough treatment in the first five chapters.

Chapters 6–8 (185 pp.), and a further 90 pages of tables, are concerned with the spectra, and abundantly show that the charge of lack of usefulness cannot stand. At present, an EA mass spectrometer, producing negative ion spectra rapidly and routinely, and with the counting problem solved in some automatic fashion, seems to be some way away. Until then, chemists may learn from this book what to look forward to – and what pitfalls to avoid. Some spectra are superficially very similar to those of positive ions, with abundant fragmentation. Prominent M^- peaks are frequently observed. Compounds giving rise to these spectra usually have low-lying vacant orbitals: those which give stable radical anions will be familiar to ESR spectroscopists, although the field is much wider than this. More commonly, a hydrogen atom is lost, and the principal peak appears at $(M-1)^-$. Then there are traps for the uninitiated, as for instance the $(M+15)^-$ $(M-H+O)$ peaks of aromatic compounds, often found unless traces of oxygen are excluded; the M_2^- ions of acids; the $(M+69)^-$ peaks of trifluoroacetates; and species defying the normal rules of valency – the $(M+17)^-$ $(M.OH^-)$ ion-molecule pairs, which are all that is generally to be found in the EA spectra of saturated hydrocarbons and other molecules otherwise reluctant to accept an electron or lose a proton. Fragment ions are usually assigned what the organic chemist would regard as sensible and reasonable structures (which is not always the case with the positive ion electron-impact spectra, in which the more energetic processes often give rise to some rather bizarre formulations).

One question which should be asked is: is the book not a little premature in its appearance? Contrasting with the thoroughness of the technical description, which could no doubt have been written at any time in the last ten years, is the rather perfunctory treatment of the results, from the chemical standpoint. A very heterogeneous collection of compounds are listed as having been investigated, and frequently hoped for data on simple compounds are not available. There are no simple saturated ethers, for instance, besides tetrahydrofuran (not mentioned in the index, but to be found on p. 301). Nitrophenols are there, but not nitrobenzene; nor is benzophenone. In the opinion of this reviewer, a systematic study of the various structural elements of common organic compounds is most desirable. Perhaps this deficiency will be remedied in a later edition.

Less defensible, perhaps, although also less serious, is the very large number of minor errors the book contains. Table 10.3, for instance, is in a very bad state. Compounds are stated to be in alphabetical order, which they are not, and the various classes into which they are divided seem to bear little relation to their structures. Phthalonitrile, for example, is among the "O-containing compounds", while ten of the "N-containing compounds" contain no nitrogen. Three of the ten "O-heterocycles" have missing bonds. Two of the "N-heterocycles" have incorrect formulae, and two other structures are transposed. Two of the three "S-heterocycles" are transposed. The first of the "Steroids" is either wrongly named or the structure is wrongly drawn (probably both). The structures for cymarin and helveticoside are identical, but differ in molecular formula. And so on. The table is only useful, in that it gives formulae for some of the more esoterically-named compounds appearing in Table 10.4, but one wishes one could have a little more confidence in them.

Table 10.4 is very extensive (68 pp.), listing up to ten principal peaks in the EA-mass spectra of 737 compounds (here, mercifully, in the usual formula-index order). A few positive-ion spectra are also included, for comparison, both here and in the text (although it is difficult to justify the name "electron-addition" mass spectra when applied to the positive ions). The reviewer feels that the table would have been of more value if it contained say 200 of the simpler compounds, with at least the majority having both negative and positive ion spectra shown.

It would be easy to continue in this critical vein, but to do so would be to present an unbalanced, and unfair, picture. In its present form the book is a fascinating account of the possibilities afforded by negative ion mass spectrometry, as a result of the development of the EA source. If the reviewer has used considerable space in indicating where there is room for improvement, it is because he feels that the book is indeed well worth improving.

A. J. Boulton

KARL HÖLL, *Water: analysis, estimate, processing, chemistry, bacteriology, biology*, 5th ed. Walter de Gruyter & Co. Berlin, 1970, XVIII + p. 423

The author, assisted by Dr. Helmut Peter and Dr. Dietrich Lüdemann presents an entirely revised and much completed fifth edition of his thorough study on water in all its implications and connections with human life in modern society.

The work is divided into three main parts:

I — Chemistry, analysis, estimate and processing of water is dealt with in the first ten chapters of the book. Thus chapter I relates drilling methods and sampling water for different uses.

normal type apparatus and, simultaneously, in one permitting the application of the new method. The initial cumene hydroperoxide (initiator) content of the phenylcyclohexane sample was 0.329 moles/l. Two of these experiments are illustrated in figure 2.

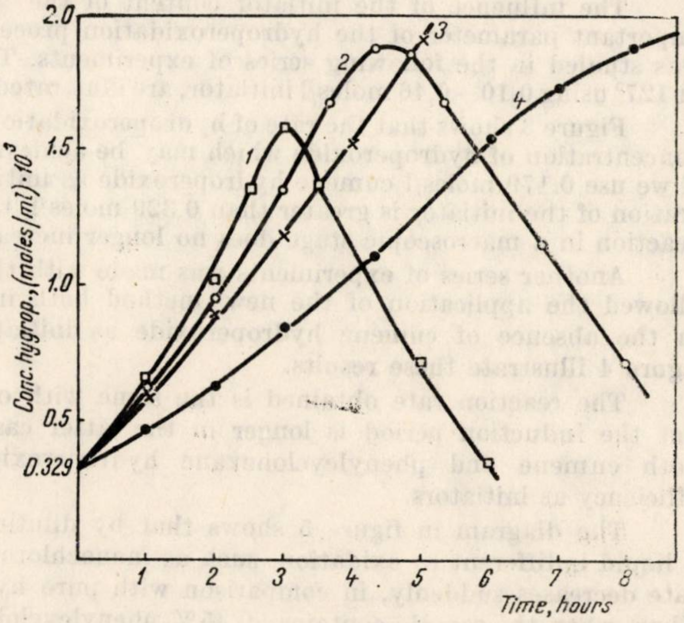

Fig. 1.— Concentration variation of phenylcyclohexane hydroperoxide, depending on time, at different temperatures :
1, 132° ; *2*, 127° ; *3*, 124° ; *4*, 120°.

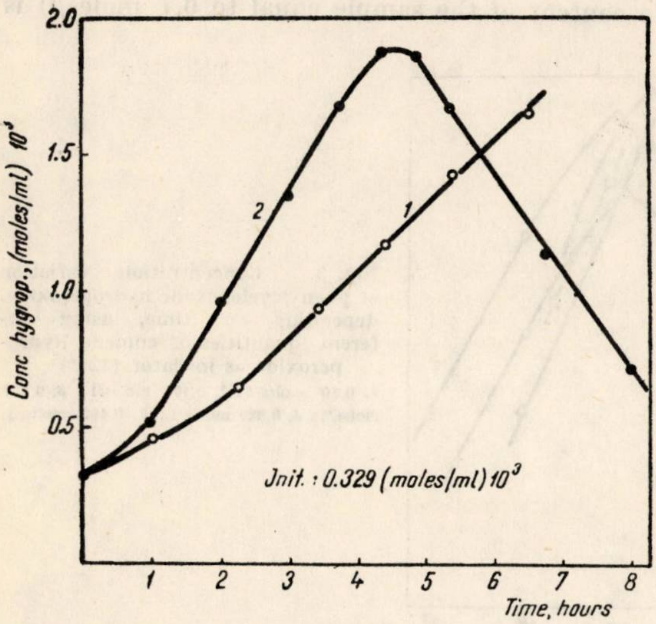

Fig. 2. — Concentration variation of phenylcyclohexane hydroperoxide, depending on time, by applying different methods (127°) :
1, classical method ; *2*, the method of "liquid/gas interface".

By applying the method of "liquid/gas interface", the reaction rate at 127° is by 75% higher, as compared to the classical method. These experimental data demonstrate the economic advantages of the new method.

The influence of the initiator content of the sample, which is an important parameter of the hydroperoxidation process of hydrocarbons, was studied in the following series of experiments. The results obtained at 127° using 0,10 – 0,46 moles/l initiator, are illustrated in figure 3.

Figure 3 shows that the rate of hydroperoxidation and the maximum concentration of hydroperoxide which may be achieved, are high enough if we use 0.179 moles/l cumene hydroperoxide as initiator. If the concentration of the initiator is greater than 0.329 moles/l, the mean rate of the reaction in a macroscopic stage does no longer increase but it decreases.

Another series of experiments was made with the apparatus which allowed the application of the new method both in the presence and in the absence of cumene hydroperoxide as initiator. The curves in figure 4 illustrate these results.

The reaction rate obtained is the same with or without initiator, but the induction period is longer in the latter case. This shows that both cumene and phenylcyclohexane hydroperoxide have the same efficiency as initiators.

The diagram in figure 5 shows that by diluting the sample with a liquid indifferent to oxidation, such as monochlorobenzol, the reaction rate decreases suddenly, in comparison with pure hydrocarbon samples. Thus, when the sample contains 89.45% phenylcyclohexane, the reaction rate (at a hydroperoxide content of the sample equal to 0,7 moles/l) is

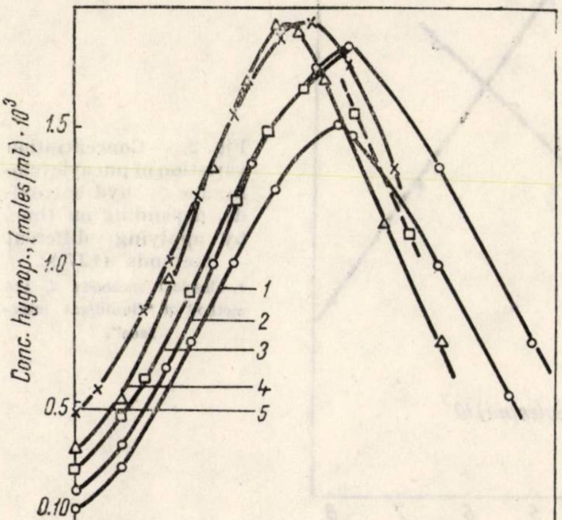

Fig. 3. — Concentration variation of phenylcyclohexane hydroperoxide, depending on time, using different quantities of cumene hydroperoxide as initiator (129°):
1, 0,107 moles/1; *2*, 0,175 moles/1; *3*, 0,257 moles/1; *4*, 0,329 moles/1; *5*, 0,462 moles/1.

Fig. 4. — Kinetic curves of phenylcyclohexane hydroperoxidation process, in the presence and in the absence of the initiator:
1, in absence of the initiator; *2*, using 0,329 moles/l initiator t = 127°

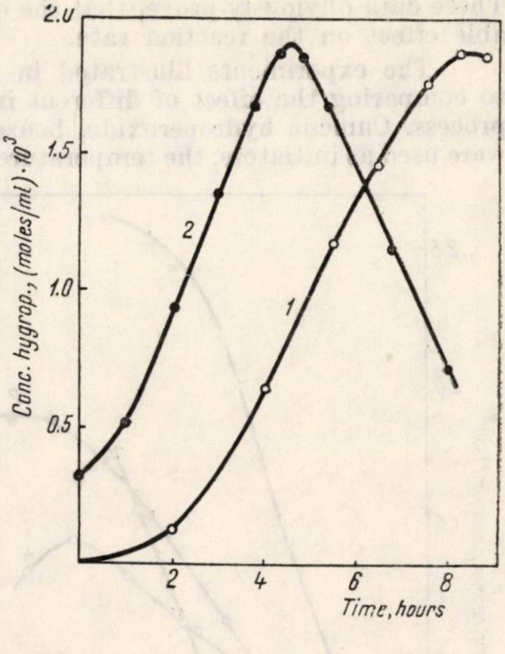

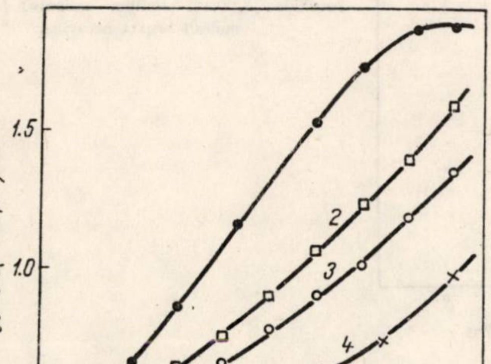

Fig. 5. — Kinetic curves of hydroperoxidation of phenylcyclohexane at 120°, by applying different concentrations of phenylcyclohexane:
1, 100% ph.c.h.; *2*, 89,45% ph.c.h.; *3*, 78,8% ph.c.h.; *4*, 57,8% ph.c.h.

0.135 moles/l.h; when the sample contains 78,8 and 57,8% phenylcyclohexane, the reaction rates are 0,118 and 0,105 moles/l.h. If the sample is formed of pure phenylcyclohexane, the reaction rate is 0,193 moles/l.h.

These data obviously prove, that the quality of the solvent has a remarkable effect on the reaction rate.

The experiments illustrated in figure 6 were made with a view to comparing the effect of different initiators on the hydroperoxidation process. Cumene hydroperoxide, benzoyl peroxide and sodium adipate [7] were used as initiators, the temperature being maintained at 120°.

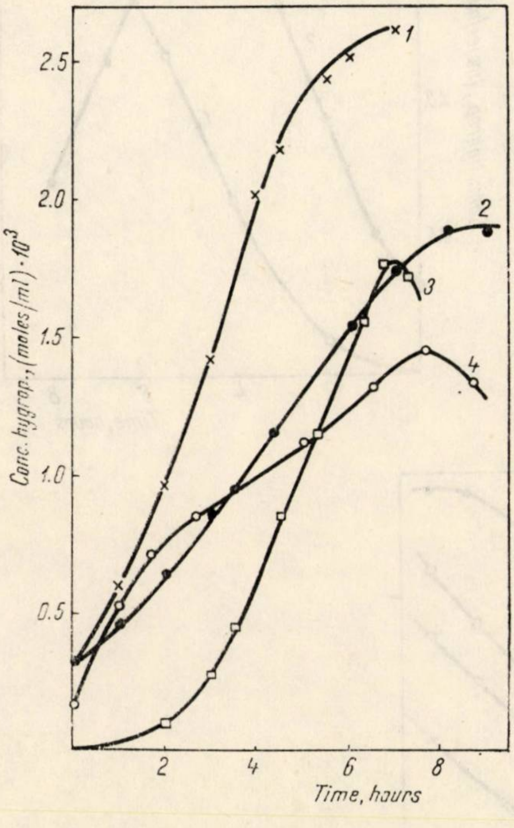

Fig. 6. — Concentration variation of phenylcyclohexane hydroperoxide, depending on time, at 120°, using different initiators:

1, 0,329 moles/l cumene hydroperoxide and 0,1% sodium adipate; *2*, 0,329 moles/l cumene hydroperoxide; *3*, 0,1% sodium adipate; *4*, 0,1645 moles/l benzyl peroxide.

When using 0,329 moles/l cumene hydroperoxide together with sodium adipate as initiators (curve 1), the reaction rate increases to 0,6 moles/l.h, whereas in the presence of cumene hydroperoxide alone, the rate is no more than 0,243 moles/l.h. When sodium adipate alone is used as additiv, the same reaction rate can be reached as in the presence of cumene hydroperoxide, but the induction period is higher (about 2,5 hours). In the experiment illustrated by curve 4 benzoyl peroxide was used as initiator, in quantities of 0,1645 moles/l, twice less than cumene hydroperoxide. The reaction is highest at the beginning, and it afterwards suddenly decreases. The phenomena may be attributed to the fast thermal decomposition of the benzoyl peroxide which generates products able to decompose the accumulated hydroperoxide.

---

[7] I. Vodnár, *Patent of S.R. Romania*, Inreg. nr. 60195 (1969).

Chapter II and III relate physical and chemical methods of analysis, the reactives to be used to determine gravimetrically, volumetrically and colorimetrically the amonium salts, nitrates, nitrites, phosphates, polyphosphates, sulphates, chlorine and organic matters contained by different sorts of waters.

Chapter IV treats the sanitary problems related to water for human consumption and different antigerminative methods. The role of the silver ion is emphasized as well as the UV irradiation of water, both producing a perfect purifying effect for a very low cost.

However, the latter method can be used only for small quantities of water because of its long duration, while the former takes a very short time.

Chapters V to VII present the physical and chemical characteristics of drinking and industrial water, and their determination by chemical reactants or measuring of the redox potential.

Chapter VIII deals with the analysis of mineral waters, with emphasis laid specially on the methods of determining the elements to be found in very small quantities such as iron, copper, zinc, cobalt, mangan, iodine, so-called inorganic vitamins, which lend therapeutic value to water.

Chapter IX lists reactants for water analysis and chapter X a questionnaire for the same, as well as a rich bibliography.

The second part, the "bacteriology of drinking water" by H. Peter presents the action of the main bacteries and viruses infecting water and the most efficient methods to deal with them. A special bibliography of "water bacteriology" is added to the chapter.

In the third part of the book usually employed chemical reactants for a biological purification of drinking as well as of industrial or swiming pool water are given. The best suited reactants for a biological purification of water are: chlorine and some of its chemical combinations, copper sulphate, amonium salts, organometallic compounds, antibiotics, insecticides, herbicides, etc. The concentration of reactants is given according to the species of micro-animals, as well as seaweed and myceliae to be dealt with for a biologically pure water.

An alphabetical index completes the book.

All the complex problems regarding water treatment to obtain the necessary purity for domestic, industrial or common use, at an acceptably low cost are examined at a high scientific level and backed by a rich documentary material.

Al. Fruma

ORSZÁGOS MŰSZAKI KÖNYVTÁR ÉS DOKUMENTÁCIÓS KÖZPONT
A 1883

[illegible]

Chapter II and III deal [illegible] physical and chemical [illegible], the [illegible] [illegible] determining [illegible], colorimetrically and [illegible] the [illegible] [illegible] [illegible] chlorine and organic matter [illegible] [illegible] of waters.

Chapter IV [illegible] problems [illegible] water [illegible] and [illegible] [illegible]. The [illegible] is [illegible] the [illegible] of waters [illegible] a [illegible] for a very [illegible] [illegible]. However, [illegible] method can be used [illegible] [illegible] of [illegible] [illegible] takes a very short time.

Chapters V to VIII present the [illegible] [illegible] of drinking and [illegible] water, and their [illegible] by [illegible] [illegible] of the [illegible].

Chapter VIII deals with the analysis of [illegible] [illegible], with [illegible] [illegible] on the [illegible] [illegible] the elements [illegible] to be found in very small quantities such as [illegible] [illegible] [illegible] [illegible] [illegible] [illegible] [illegible] [illegible] in water.

Chapter IX [illegible] of water analysis and [illegible] X [illegible] on the [illegible] as well as a [illegible].

The second part [illegible] bacteriology of drinking water by [illegible] [illegible] presents the action of the [illegible] [illegible] of the water and the [illegible] efficient methods to deal with [illegible]. [illegible] water bacteriology is added to the chapter.

In the third part of the book [illegible] employed [illegible] [illegible] for a biological purification of [illegible] as well as of industrial or [illegible] water are given. The best [illegible] for a biological purification of water [illegible] [illegible] the [illegible] of its chemical [illegible] [illegible] [illegible] [illegible] salts, [illegible] components, [illegible] [illegible], etc. The concentration of [illegible] is given according to the species of [illegible], as well as [illegible] to [illegible] for a biologically pure water.

An alphabetical index completes the [illegible].

[illegible] [illegible] water [illegible] [illegible] [illegible] the [illegible] [illegible] industrial or [illegible] use at an [illegible] cost [illegible] [illegible] [illegible] and [illegible] [illegible] laboratory [illegible].

[illegible]

NOTE POUR LES AUTEURS

La *Revue Roumaine de Chimie* publie des articles en anglais, français, russe, allemand ou espagnol. Les auteurs sont priés d'envoyer des articles, notes, communications et comptes rendus inédits.

Les manuscrits seront dactylographiés à deux intervalles. Les tableaux seront dactylographiés sur feuilles séparées, de même que la légende des figures. Les diagrammes seront tracés à l'encre de Chine sur papier calque. Les tableaux et les figures seront numérotés par des chiffres arabes, en nombre strictement nécessaire. Prière de ne pas inscrire les mêmes données dans les tableaux et les figures. Les formules chimiques seront incluses dans le texte; en outre, elles seront transcrites sur des feuilles séparées. Les auteurs sont priés d'indiquer les caractères italiques (en soulignant les lettres au crayon), ainsi que tout autre caractère spécial. L'ordre des références bibliographiques sera celui de leur mention dans le texte; le nom de l'auteur sera précédé de l'initiale du prénom; les publications périodiques seront présentées suivant les prescriptions internationales. Les références seront ajoutées à la fin de l'article; elles paraîtront comme des notes, au bas de la page. Le texte sera précédé d'un résumé comprenant 15 lignes au maximum.

L'entière responsabilité du contenu des articles appartient aux auteurs. On publie des articles dus aux collaborateurs roumains ou étrangers. Les auteurs recevront 50 tirés à part.

PRINTED IN ROMANIA

TRAVAUX PARUS AUX ÉDITIONS DE L'ACADÉMIE DE LA RÉPUBLIQUE SOCIALISTE DE ROUMANIE

I. ZUGRĂVESCU et L. STOICESCU-CRIVETZ, **Polimeri heterociclici** (Polymères hétérocycliques), 1971, 190 p., 9,50 lei.

CORNEL BODEA et collab., **Tratat de biochimie vegetală, partea I, Fitochimie** (Traité de biochimie végétale, Ire partie, Phytochimie), Ier vol., 1964, 747 p. + 4 annexes + 2 pl., 41 lei ; IIe vol., 1965, 1962 p., 1 pl., 56 lei ; IIIe vol., 1967, 773 p., 35 lei.

V. GHEŢIE et V. MICUŞAN, **Analiza imunochimică. Teorie şi practică** (Analyse immunochimique. Théorie et pratique), 1966, 369 p., 28 lei.

SILVIA IONESCU, **Reacţii chimice induse de radiaţiile ionizante** (Réactions chimiques produites par les radiations ionisantes), 1963, 271 p., 15 lei.

MARIETA NICOLAE, **Fizico-chimia proceselor fotografice** (Physico-chimie des processus photographiques), 1964, 426 p. + 4 pl., 35 lei.

R. PORTOCALĂ et L. POPA, **Acizii ribonucleici celulari şi virali** (Les acides ribonucléiques cellulaires et viraux), 1966, 375 p., 8 pl., 26 lei.

D. PURDELA et R. VÎLCEANU, **Chimia compuşilor organici ai fosforului şi ai acizilor lui** (La chimie des composés organiques du phosphore et de ses acides), 1965, 540 p., 37 lei.

CRISTOFOR SIMIONESCU, MARGARETA GRIGORAŞ et AGATA CERNĂTESCU-ASANDEI, **Chimia lemnului din R.P.R.** (La chimie du bois en Roumanie), 1964, 239 p. + 3 pl., 27 lei.

CRISTOFOR SIMIONESCU et CLEOPATRA VASILIU-OPREA, **Mecanochimia compuşilor macromoleculari** (La mécanochimie des composés macromoléculaires), 1967, 344 p., 23,50 lei.

I. V. MAXIM, **Materiale nucleare** (Matériaux nucléaires), 1969, 444 p., 30 lei.

1972 MAI 1 8

I.P.I. c. 1033

43 426

LEI 25.—

F 1103

04
REFERÁLVA

REVUE ROUMAINE DE CHIMIE

TOME 17
Nº 4
Avril 1972

RRCHAX, 17 4, 593–770 (1972)

ÉDITIONS DE L'ACADÉMIE DE LA RÉPUBLIQUE SOCIALISTE DE ROUMANIE

Rev. Roumaine Chim. 17, 4, p. 593 – 770 (1972) Bucarest

COMITÉ DE RÉDACTION

Rédacteur en chef :

I. G. MURGULESCU, membre de l'Académie de la République Socialiste de Roumanie

Rédacteurs en chef adjoints :

A. T. BALABAN et V. EM. SAHINI, membres correspondants de l'Académie de la République Socialiste de Roumanie

Collège de rédaction :

C. DRĂGULESCU, RALUCA RIPAN, CR. SIMIONESCU, membres de l'Académie de la République Socialiste de Roumanie; EM. BRATU, ECATERINA CIORĂNESCU-NENITZESCU, P. SPACU, membres correspondants de l'Académie de la République Socialiste de Roumanie; MARGARETA AVRAM, D. I. MARGHIDAN, G. NIAC et D. SĂNDULESCU

La *Revue Roumaine de Chimie* paraît 12 fois par an. Toute commande de l'étranger (fascicules ou abonnements) sera adressée à Întreprinderea de comerţ exterior — Rompresfilatelia B.P 2001, telex 011631, Bucarest, Roumanie

Les manuscrits, les livres et les revues proposés en échange, ainsi que toute correspondance seront envoyés à la rédaction :

REVUE ROUMAINE DE CHIMIE
23, str. Dumbrava Roşie, Bucarest, Roumanie

ÉDITIONS DE L'ACADÉMIE DE LA RÉPUBLIQUE SOCIALISTE DE ROUMANIE,
3 bis, str. Gutenberg, Bucarest

ORSZÁGOS MŰSZAKI KÖNYVTÁR ÉS DOKUMENTÁCIÓS KÖZPONT
1883

TRENTE-ET-UNIÈME CONGRÈS DU GROUPEMENT POUR L'AVANCEMENT DES MÉTHODES PHYSIQUES D'ANALYSE
(G.A.M.S.)

tenu avec la participation de la SOCIÉTÉ CHIMIQUE DE FRANCE

Le 31e Congrès du G.A.M.S. aura lieu à Paris du

Lundi 5 au Vendredi 9 Juin 1972

Il sera consacré à des exposés et discussions sur les :

MÉTHODES SPECTROGRAPHIQUES ET CHROMATOGRAPHIQUES D'ANALYSE

De plus, la journée du vendredi **9** juin, placée sous l'égide de la Division de Chimie Analytique de la Société Chimique de France, sera consacrée à une mise au point sur diverses méthodes modernes d'analyse.

Les séances se tiendront à la salle d'Iéna, 10, avenue d'Iéna, PARIS-16°, où sera présentée simultanément une exposition d'appareils.

Les propositions de communications concernant le G.A.M.S. doivent parvenir, accompagnées du titre et d'un résumé (une page dactylographiée), avant le *15 février 1972*, à l'adresse suivante :

Secrétariat du G.A.M.S. (Congrès)
10, rue du Delta
75-PARIS-9 ème

Pour tous renseignements complémentaires, envoyer la correspondance à la même adresse.

REVUE ROUMAINE DE CHIMIE

ORSZÁGOS MŰSZAKI KÖNYVTÁR ÉS DOKUMENTÁCIÓS KÖZPONT 1883

Tome 17 N° 4 Avril 1972

Page

I. G. MURGULESCU and IOANA DEMETRESCU, Kinetics of reactions of benzhydryl chloride and benzyl bromide with secondary alcohols . . . . . 595–601 R
I. G. MURGULESCU and EUGENIA SĂLĂGEANU, Some physico-chemical properties of simple molten salts. III 603–610
B. HESSETT and P. G. PERKINS, The reorganisation energy of $TiCl_4$ . . . 611–616
V. EM. SAHINI, VERONICA TUFOI and AL. IVANOV, Some considerations about the stability of complex combinations of cobalt. 617–620
D. I. HERȚIA and AL. IVANOV, About the exact development of atomic and molecular wave functions 621–631
E. SEGAL, Cinétique des réactions superficielles en courant, accompagnées d'une augmentation du nombre des molécules. IV 633–642
R. DINESCU et M. CERCHEZ, Formules de calcul du nombre des sous-systèmes contenus dans les systèmes chimiques binaires, ternaires et quaternaires 643–646
LUIGI CAMPANELLA, ERNESTO CHIACCHIERINI and MAURIZIO PALCHETTI, Polarographic and oscillopolarographic behaviour of dipicolinic acid . . . . 647–660 R
S. GOCAN and C. LITEANU, Some considerations about the resolution by paper and thin layer chromatography with temperature gradient . . . 661–667
S. GOCAN, C. LITEANU, T. HODIȘAN, H. NAȘCU and ȘTEFANIA BÎNDEANU, Temperature gradient chromatography as compared to unidimensional multiple chromatography 669–674
F. MÁNOK, CS. VÁRHELYI und MINERVA GĂLĂȚEANU-TITIENI, Polarographische Untersuchung des UO_2^{2+}-Oxalsäure-Systems 675–682
R. MIHAIL, External catalytic reactions on bluff surfaces 683–695
P. SPACU and SILVIA PLOȘTINARU, Mixed ligand lanthanide chloromandelates containing *o*-phenanthroline and 5,6-dimethylphenanthroline 697–703
GH. MARCU und V. SĂCELEAN, Indirekte Bestimmung von K^+ und NH_4^+ durch die β^--Strahlen Absorption . . . . 705–709 R
GH. MARCU, CS. VÁRHELYI und ILDIKÓ MÜLLER, Neue Kobalt(III)-Chelate mit einem vierzähnigen Komplexbildner 711–717
N. VOICULESCU et I. POPESCU, Réactions des ligands coordinés. I. L'action des composés organoaluminiques sur les bisdiméthylglyoximates de nickel, palladium et cuivre et sur la diméthylglyoxime non coordinée 719–726

Rev. Roumaine Chim. **17, *4*, 593 – 770 (1972), Bucarest**

Page

IG. POINESCU, Transformations chimiques du polychlorure de vinyle. II. Synthèses de polyélectrolytes réticulés avec des groupes sulfoniques à base de polychlorure de vinyle arylé avec des polyalkylbenzènes 727–740

I. NANU and C. ANDREI, Copolymers of conjugated dienes with maleic acid monoesters. V. Copolymerization of isoprene with monocyclohexylmaleate and monobenzylmaleate . . . . 741–746 R

R. BACALOGLU, FL. NEAMŢIU, ILSE BACALOGLU and G. OSTROGOVICH, Infrared spectra of amidic derivatives of carbonic acid. VI. Substituted 1,5-benzylidine guanylureas (free bases and sulphates) 747–754

CASANDRA NICOLAU, Méthode microbiologique de détermination quantitative de l'acide *para*-aminobenzoïque, vitamine H_1 755–764

COMPTES RENDUS

S. H. DOSS, Sources of information in steroid chemistry (Part 1) 765–770

Revue Roumaine de Chimie, **17**, *4*, 595 – 601 (1972)

ORSZÁGOS MŰSZAKI KÖNYVTÁR ÉS DOKUMENTÁCIÓS KÖZPONT
1883

KINETICS OF REACTIONS OF BENZHYDRYL CHLORIDE AND BENZYL BROMIDE WITH SECONDARY ALCOHOLS

I. G. MURGULESCU and IOANA DEMETRESCU

Physical Chemistry Department, Bucharest University
Bd. Republicii 13, Bucharest

Received November 26, 1971

The systems formed by benzyl bromide with propyl and butyl secondary alcohols, as well as those formed by benzhydryl chloride with the same alcohols were studied. Viscosity of alcohols at the working temperatures was determined, as well as the energy of activation of the viscous flow, in order to try to establish the role of viscosity in the kinetics of these reactions. The obtained results were compared with the data concerning systems formed by the same halides with normal and isoalcohols.

INTRODUCTION

Kinetics of the reactions between benzyl bromide [1-4] and benzhydryl chloride [5-9] with alcohols was frequently cited in the literature. Because the systems with secondary alcohols were less studied, as well as in order to supplement with new data our image about the kinetics of dipole-dipole reactions in solution, the present study was carried out

EXPERIMENTAL

Schuchardt benzyl bromide was used; the benzhydryl chloride was prepared in our laboratory starting from benzophenone. The water in alcohols was determined by Karl Fisher's method, the following quantities being found: 0.19% in secondary propyl alcohol, and 0.35% in secondary butyl alcohol.

---

[1] H. van Halban and W. Gast, *Z. phys. Chem.*, **91**, 591 (1916).

[2] J. W. Baker, *J. Chem. Soc.*, **1934** (987).

[3] I. G. Murgulescu and I. Demetrescu, *Rev. Roumaine Chim.*, **15**, 141 (1970); *ibidem*, **16**, 1483 (1971).

[4] C. W. L. Bevan, E. D. Hughes and C. K. Ingold, *Nature*, **171**, 301 (1953).

[5] J. F. Norris and A. Morton, *J. Amer. Chem. Soc.*, **50**, 1795 (1928);
J. F. Norris and C. Banta, *J. Amer. Chem. Soc.*, **50**, 1804 (1928).

[6] J. A. Ward, *J. Chem. Soc.*, **1927**, 2285 (1927);
F. G. Kiy and J. A. Ward, *J. Amer. Chem. Soc.*, **57**, 2394 (1935).

[7] T. Farinacci and L. Hammet, *J. Amer. Chem. Soc.*, **59**, 2542 (1937).

[8] D. Hughes, C. K. Ingold and N. A. Taher, *J. Chem. Soc.*, **1940**, 949.

[9] I. G. Murgulescu and F. Bărbulescu, *Rev. Roumaine Chim.*, **8**, 153 (1963).
I. G. Murgulescu and I. Demetrescu, *Rev. Roumaine Chim.*, **16**, 781 (1971).

The reactions were followed up conductometrically, the concentrations being evaluated from calibration curves previously plotted; for reactions between benzyl bromide and alcohols also titrimetric determinations were carried out.

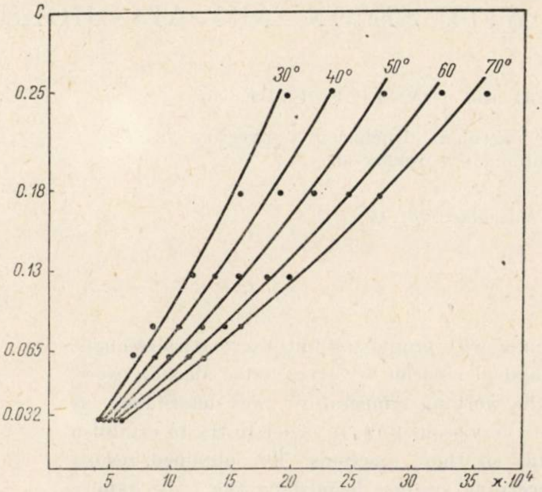

Fig. 1. — Calibration curves for HBr in secondary propyl alcohol at various temperatures.

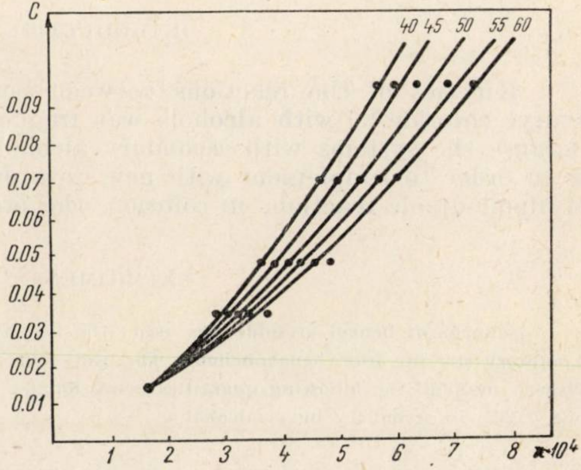

Fig. 2. — Calibration curves for HCl in secondary propyl alcohol at various temperatures.

In the case of reactions with benzhydryl chloride, the calibration was carried out in the reaction medium; for the reactions between benzyl bromide and secondary alcohols, because they last very long, the calibration was effected separately, using solutions of hydrobromic acid in secondary alcohols. The way of obtainig these solutions and their concentrations for the titration was described in a previous paper.[3] We specify only the concentrations of sodium methoxide which was used for dosing the acid: 0.025, 0.033, and 0.066, selected by probing, according to the possible concentration of the solution to be dosed. We give as examples in figures 1 and 2 plots of specific conductivity *versus* the concentration of hydrochloric and hydrobromic acid in secondary alcohols, at various temperatures.

RESULTS

The systems benzhydryl chloride — alcohols and benzyl bromide — alcohols are typically bimolecular ones, but using one reactant in excess, the alcohol, the reactions become pseudomonomolecular and the rate constant is given by :

$$k = \frac{2.303}{bt} \log \frac{a}{a - x},$$

where a and b are the initial concentrations of the reactants. In table 1 we give, as an example, the values we obtained for the reaction between benzyl bromide and secondary propyl alcohol at 75°.

Table 1

Rate constants of the reactions between benzyl bromide and secondary propyl alcohol
a = **0.000165 mol/cm^3** ; b = **0.0121 mol/cm^3** ; T = **75°**

t sec	$\varkappa . 10^4$ $\Omega^{-1}\,cm^{-1}$	x mol cm^{-3}	$a - x$ mol cm^{-3}	$k \times 10^3$ cm^3 mol^{-1} s^{-1}
0	—	0	0.000165	—
14700	7.483	0.000041	124	1.60
17100	8.416	0.000047	118	1.54
18000	8.832	48	117	1.59
19500	9.493	53	112	1.62
20400	9.920	56	109	1.67
21600	10.13	57	108	1.61
22800	10.4	59	106	1.59
25200	10.9	63	102	1.58
34200	16.1	79	086	1.54
36000	16.9	85	080	1.64
39000	17.7	98	067	1.74

The values of the rate constants are not a function of the initial concentration of the reactants.

In table 2 the rate constants and energies of activation of the reactions between benzyl bromide and secondary alcohols are listed ; in table 3 we give the same quantities for the alcoholysis of benzhydryl chloride.

Table 2

Rate constants for the system : $C_6H_5CH_2Br$ + ROH
$k \times 10^3$ cm^3 mol^{-1} s^{-1}

ROH	60°	65°	70°	75°	80°	85°	A_{exp}	$E_{cal/mol}$
sec C_3H_7OH	0.638	0.825	1.30	1.63	—	—	5.98×10^7	16500
sec C_4H_9OH	—	0.421	0.631	0.84	1.01	1.50	1.17×10^7	16200

Table 3

Rate constants for the system: $(C_6H_5)_2CHCl + ROH$
$k \times 10^2 cm^3\ mol^{-1}\ s^{-1}$

ROH	40°	45°	50°	55°	60°	A_{exp}	$E_{cal/mol}$
sec C_3H_7OH	0.210	0.331	0.510	0.767	1.21	1.48×10^{10}	17400
sec C_4H_9OH	0.155	0.241	0.384	0.545	0.883	6.19×10^{9}	17600

In figure 3 log k is plotted as a function of $1/T$, according to the equation of Arrhenius.

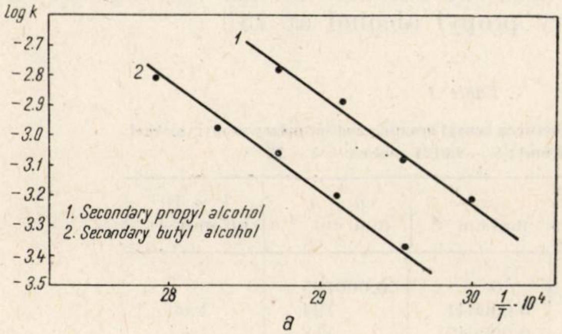

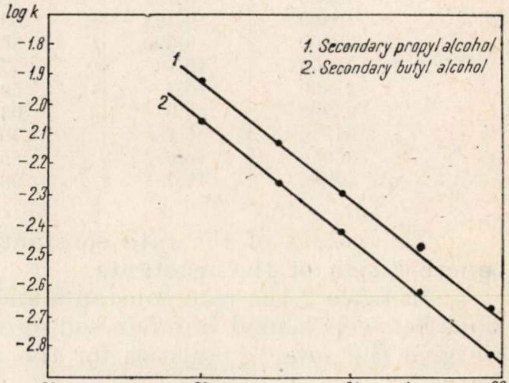

Fig. 3. — *a*. Alcoholysis reactions of benzyl bromide ; *b*. Alcoholysis reactions of benzhydryl chloride.

Comparing these energies of activation with those in the case of the same halides with normal [2-9] and isoalcohols [3,9] we notice that the reactions with secondary alcohols have a much smaller activation energy ; the corresponding pre-exponential factors are much smaller too.

As regards the solvent effect, besides electrostatic effects [2,3,8] reflected in the dielectric constant and having a small weight, we thought useful, because these alcohols have many carbon atoms, to evaluate the viscosity of solvents.

Determination of viscosity at various temperatures allowed the calculation of the energy of activation of the viscous flow and the correction of the experimental activation energy by taking into account the solvent viscosity.

The viscosity was determined at four temperatures by using an Ostwald apparatus ; as reference liquid with known viscosity, water [10] was used.

According to Poiseuille's law, the viscosity of the liquid is given by :

$$\eta_1 = (t_1/t_a)\,(\rho_1/\rho_a)\,\eta_a$$

where t_1 and ρ_1 represent the duration of flow and the density of the liquid under study and t_a and ρ_a the same quantities for water. In table 4 we present the results.

Table 4

Viscosity of the alcohols at various temperatures

Compound	$\eta_{10°}$	$\eta_{15°}$	$\eta_{20°}$	$\eta_{25°}$	$\eta_{40°}$	$\eta_{50°}$	$\eta_{60°}$
water	1.3077	1.1404	1.005	0.8937	0.6560	0.5494	0.4688
sec C_3H_7OH	3.41	2.93	2.44	2.133	—	—	—
sec C_4H_9OH	5.42	4.22	3.55	2.995	—	—	—
sec $C_5H_{11}OH$	5.50	4.78	3.91	3.275	2.032	—	—
iso C_4H_9OH	—	4.75	3.92	2.834	—	—	—
iso $C_5H_{11}OH$	6.18	5.11	4.32	3.681	2.337	—	—
iso $C_8H_{17}OH$	—	—	—	8.331	5.032	3.817	2.826

The obtained values permit a linear representation for the dependence $\log\eta$ as a function of $1/T$, according to the equation of de Guzman :

$$\eta = B\exp\left(\frac{E_{\text{visc}}}{RT}\right).$$

In figure 4 we give the straight lines representing this dependence and the values obtained in the literature for the viscosity of the same alcohols.[11-13]

By means of de Guzman's equation we can evaluate the energy of activation of the viscous flow, and, under the simple assumption that the energy of activation of the reaction in solution is the sum of the experimental energy and various corrections, we have :

---

[10] "Handbook of Chemistry and Physics", 41st edition, editor-in-chief CHARLES D. HODGMAN, Chemical Rubber Publishing Co., Cleveland, Ohio, 1959—1960.

[11] K. DRÜKER and R. KASSEL, *Z. phys. Chem.*, **76**, 367 (1911).

[12] J. TIMMERMANS and F. MARTINS, *J. Chem. Phys.*, **25**, 411 (1928), *Chem. Abstr.*, **1928**, 4024.

[13] J. TIMMERMANS and Y. DELCOURT, *J. Chem. Phys.*, **31**, 85—124 (1934), Chem. Abstr., **1934**, 3958.

$$E_a = E_{exp} + E_{visc}$$

According to this equation, we present in table 5 corrections for viscosity and corrected energies for the studied systems.

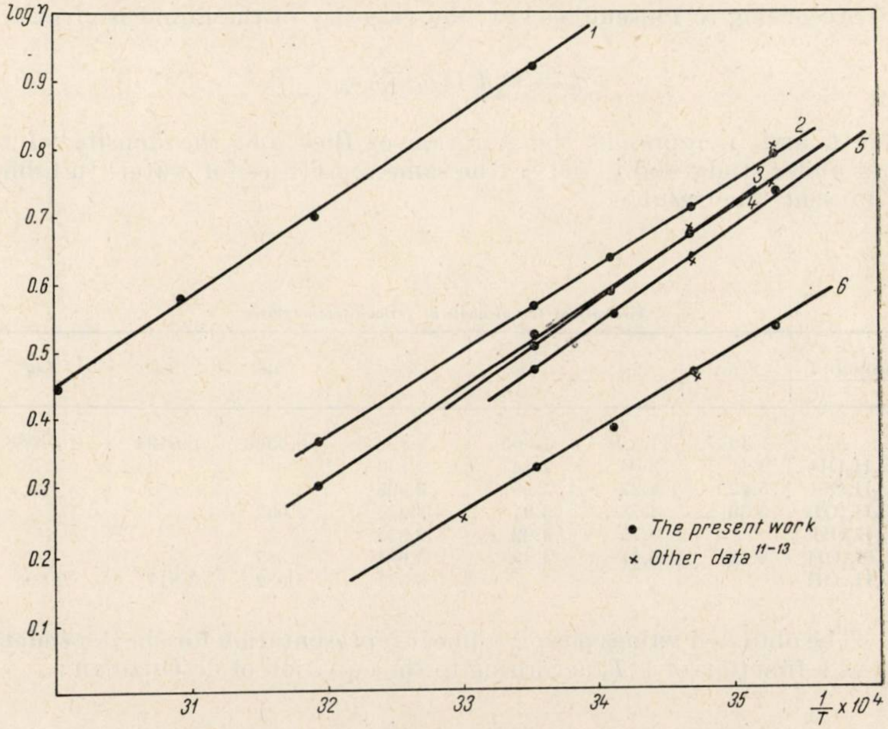

Fig. 4. — Dependence viscosity as a function of temperature

1, isooctyl alcohol; *2*, isopentyl alcohol; *3*, secondary pentyl alcohol; *4*, isobutyl alcohol; *5*, secondary butyl alcohol; *6*, secondary propyl alcohol.

It could be noticed that, in comparison with the normal alcohols, the energy of activation of the viscous flow is greater in the case of secon-

Table 5

Energy of activation and corrected energies for the studied systems

Alcohol	E_{visc}	System $ROH+(C_6H_5)_2CHCl$		System $C_6H_5CH_2Br+ROH$	
		E	$E_{correct.}$	E	$E_{correct.}$
sec — C_3H_7OH	5700	17400	23100	16500	22200
sec — C_4H_9OH	5900	17600	23500	16200	22100
sec — $C_5H_{11}OH$	5700	—	—	—	—
iso — C_4H_9OH	5050	20370	25420	20100	25450
iso — $C_5H_{11}OH$	5020	19610	24630	19200	24220
iso — $C_8H_{17}OH$	6100	18190	24290	18500	24600

dary and isoalcohols; because in these cases the experimental energy of activation is smaller, using the viscosity corrections the differences disappear. The uniform values of the total activation energy point out the similitude of these alcoholysis reactions, and the corrected value, of about 24000 cal/mol, corresponds to usual values of activation energies for this kind of reactions.

Of course, taking into account the viscosity in the way described above is rather superficial, but for alcoholysis reactions between dipoles, where other effects are small, and especially for alcohols with high viscosity,[14] we think this correction as justified.

---

[14] E. A. Moelwyn-Hughes, "The Kinetics of Reactions in Solution", Oxford, Clarendon Press, 2nd edition, 1947, p. 204, 272.

Revue Roumaine de Chimie, 17, 4, 603–610 (1972)

SOME PHYSICO-CHEMICAL PROPERTIES OF SIMPLE MOLTEN SALTS. III

I. G. MURGULESCU and EUGENIA SĂLĂGEANU

Institute of Physical Chemistry Str. Galaţi 31, Bucharest
and
III Department of Physical Chemistry
University of Bucharest, Romania

Received November 23, 1971

A modified form of the Buehler, Hirschfelder and Curtis' equation has been elaborated. Using a cellular model, the equation has been applied to the study of the structure of some molten salts. The expansion coefficients α and compressibility coefficients β_T have been evaluated and compared with the experimental data, determining in this way if a molten salt has a cubic, face-centered cubic or body-centered cubic structure.

Buehler, Hirschfelder and Curtis'equation

$$PV\left(1 - \frac{\sigma}{a}\right) = RT$$

can be successfully applied to the molten salts study.[1,2] In order to use this equation to the structure determination of the molten salts, it is preferable to write a more general relation for a,

$$a = \gamma^{1/3}\left(\frac{V}{\nu N}\right)^{1/3} \tag{1}$$

where V is the molar volume, N is the Avogadro number, and ν represents the number of ions resulting from the dissociation of a molten salt molecule. It is well known that γ can take the following values,

$$1, \quad \frac{3}{4}\sqrt{3}, \quad \sqrt{2}$$

for cubic, body-centered cubic or face-centered cubic and hexagonal close-packed structure, respectively.

---

[1] I. G. Murgulescu, *Rev. Roumaine Chim.*, 11, 965 (1969): 15, 1463 (1970).

[2] J. O. Hirschfelder, C. F. Curtis and R. Byron Bird, "Molecular Theory of Gases and Liquids", John Wiley & Sons, New York, London, 1954, p. 286.

For a simple molten salt, dissociating in ν ions, Buehler's equation is :

$$PV\left(1-\frac{2\nu^{1/3}N^{1/3}}{\gamma^{1/3}V^{1/3}}\bar{r}\right)=\nu RT \tag{2}$$

where $\bar{r}$ is the average radius of the constituent ions ($\sigma = 2\bar{r}$). All the other symbols have their usual meanings.

STRUCTURE OF THE SIMPLE MOLTEN SALTS

From eq. (2), it is possible to calculate the expansion coefficient α

$$\alpha=\frac{1}{V}\left(\frac{\partial V}{\partial T}\right)_P=\frac{1}{T}\,\frac{1-\dfrac{2\nu^{1/3}N^{1/3}}{\gamma^{1/3}V^{1/3}}\bar{r}}{1-\dfrac{2}{3}\dfrac{2\nu^{1/3}N^{1/3}}{\gamma^{1/3}V^{1/3}}\bar{r}} \tag{3}$$

Some comparative data of the experimental and calculated expansion coefficient (eq. 3), for some molten salts, are given in table 1. All possible values of the γ, mentioned above, were considered.

The experimental values of the expansion coefficients were obtained from density measurements, using the relation,

$$\alpha=-\frac{1}{\rho}\frac{d\rho}{dT} \qquad (4$$

as shown in a previous paper.[1]

As it can be observed from table 1, molten halides of K, Rb and Cs, have the same face-centered cubic structure in both crystalline and molten state. A simple cubic structure is more likely for sodium halides. There is no agreement between experimental and calculated values for lithium halides (for all values of γ), the calculated expansion coefficient being higher than expected. This is probably due to the big difference between the radius of the lithium ions and that of the halogen ions. We should bear in mind that Buehler's equation can be applied to the molten salts study, using an average ion radius, only when we are dealing with ions of comparable radii. In all the other cases, large differences between calculated and experimental values are expected : the larger the anion radius, the bigger the difference.

The calculated expansion coefficient values for $\gamma = 1$ beginning with potasium halides, were disregarded because they are in complete disagreement with the experimental results.

Molten silver halides have a face-centered cubic structure ; two of them — silver chloride and silver bromide — have the same structure in the solid state.

Table 1

Expansion coefficients of some simple molten salts at the melting point

Salt	T_f K	V cm³	$\bar{r}$ Å	$\alpha \times 10^4$ degree^{-1}			
				Calculated			Experimental
				$\gamma = 1$	$\gamma\ \frac{3}{4}\ \overline{3}$	$\gamma = \sqrt{2}$	
LiF	1121	14.2	0.98	2.93	3.92	4.25	2.71
LiCl	883	28.2	1.21	3.94	5.20	5.61	2.87
LiBr	823	34.3	1.28	4.45	5.81	6.13	2.59
LiI	742	43.1	1.38	4.96	6.47	7.09	2.96
NaF	1268	21.0	1.16	2.04	3.16	3.42	2.89
NaCl	1073	37.6	1.38	3.15	3.97	4.25	3.49
NaBr	1020	44.0	1.45	2.96	4.23	4.52	3.50
NaI	933	54.7	1.56	3.22	4.62	4.92	3.48
KF	1131	30.4	1.35	—	3.11	3.51	3.41
KCl	1043	48.9	1.57	—	3.57	3.90	3.84
KBr	1007	56.0	1.64	—	3.72	4.08	3.91
KI	954	67.8	1.75	—	3.91	4.27	3.89
RbCl	995	53.8	1.65	—	3.46	3.85	3.95
RbBr	965	60.9	1.72	—	3.70	3.96	3.95
RbI	920	73.4	1.82	—	3.84	4.24	3.96
CsF	976	41.6	1.53	—	3.36	3.78	3.52
CsCl	918	60.3	1.75	—	3.40	3.85	3.84
CsBr	909	67.9	1.82	—	3.70	3.85	3.89
CsI	899	81.8	1.93	—	3.53	3.99	3.74
CuCl	695	26.4	1.14			2.11	3.18
AgCl	728	29.4	1.53		1.32	2.21	1.74
AgBr	707	33.7	1.61		1.13	2.11	1.86
AgI	829	92.1	1.71		1.41	2.17	1.81
TlCl	703	42.6	1.65		2.93	3.68	3.19
$CaCl_2$	1045	53.3	1.54		2.11	2.65	2.03
$SrCl_2$	1146	58.1	1.58		2.01	2.43	2.13
$BaCl_2$	1235	65.6	1.66		2.08	2.14	2.16
$BaBr_2$	1126	74.8	1.75		1.71	2.21	2.33
$ZnCl_2$	535	54.1	1.45		6.31	7.05	2.12
$CdCl_2$	841	73.5	1.53		4.80	3.50	2.42
CdI_2	661	82.3	1.76		3.72	4.56	2.53
$PbCl_2$	774	73.7	1.63		3.70	4.92	3.98
$PbBr_2$	646	80.3	1.73		4.05	5.23	3.23

There is a good agreement between calculated and experimental expansion coefficients of the barium halides for a face-centered cubic structure. On the contrary, for the Ca and Sr chlorides there is a better agreement for the body-centered cubic structure. In the solide state none of these halides presents a cubic structure.

Usually, experimental expansion coefficients of Zn, Cd and Pb halides are much lower than theoretical ones, for all the values of the γ. Bockris, Delimarsky and Markov have explained this discrepancy by admitting the complex anion formation.

We shall now consider the compressibility coefficient. Buehler's equation yields :

$$\beta_T = -\frac{1}{V}\left(\frac{\partial V}{\partial P}\right)_T = \frac{V}{\nu RT}\,\frac{1-\left(\dfrac{2\,\nu^{1/3}\,N^{1/3}}{\gamma^{1/3}\,V^{1/3}}\,\bar{r}\right)^2}{1-\dfrac{2}{3}\,\dfrac{2\,\nu^{1/3}\,N^{1/3}}{\gamma^{1/3}\,V^{1/3}}\,\bar{r}} = \frac{V}{\nu R}\left(1-\frac{2\,\nu^{1/3}\,N^{1/3}}{\gamma^{1/3}\,V^{1/3}}\,\bar{r}\right)\alpha \quad (5)$$

where β_T is the compressibility coefficient.

The experimental values for β_T were obtained by ultrasound velocity measurements using the equation

$$\beta_T = \frac{\gamma}{U_S\,\rho} \quad (6)$$

where γ is now the ratio C_p/C_v of the molar heat capacities and ρ is the density. The necessary data were taken from Janz's papers.[3]

Examination of the experimental and calculated compressibility coefficient values given in table 2 shows that the agreement between them is not so good as for the expansion coefficient. With a few exceptions, the calculated values are lower than experimental ones, specially for elements from the II A and II B groups.

The best agreement between experimental and theoretical values is for a face-centered cubic structure, therefore for $\gamma = \sqrt{2}$.

BUEHLER'S EQUATION APPLIED TO THE MOLTEN SALTS

Buehler's equation has been obtained assuming that the molecules from liquid state are similar with rigid spheres without interactions. To be able to apply this equation to the molten salts, where there are interactions among the particles, we have to add the internal presure P_i, to the pressure value, hence

$$P = p + P_i$$

where p is the applied pressure. Therefore, the equation (2) becomes

$$(p + P_i)\,V\left(1-\frac{2\,\nu^{1/3}\,N^{1/3}}{\gamma^{1/3}\,V^{1/3}}\,\bar{r}\right) = \nu RT \quad (7)$$

But

$$P_i = \left(\frac{\partial E}{\partial V}\right)_T$$

---

[3] G. Janz, "Molten Salts Handbook", Academic Press, New York-London, 1967, p. 249.

Table 2

Compressibility coefficients of some simple molten salts

Salt	T_f K	V cm^3	$\bar{r}$ Å	$\beta_T \times 10^{11}$cm^2 Dyne^{-1}			Salt	T_f K	V cm^3	$\bar{r}$ Å	$\beta_T \times 10^{11}$cm^2 Dyne^{-1}		
				Calculated		Experimental					Calculated		Experimental
				$\gamma = \frac{3}{4}\sqrt{3}$	$\gamma = \sqrt{2}$						$\gamma = \frac{3}{4}\sqrt{3}$	$\gamma = \sqrt{2}$	
LiCl	883	28.2	1.21	2.10	2.40	2.14	CsCl	973	61.6	1.75	1.67	2.22	4.29
	1073	29.9		1.97	2.50	2.47		1073	64.1		1.84	2.35	5.12
	1273	31.8		1.71	2.21	3.30		1173	66.8		1.99	2.90	6.27
LiBr	973	35.3	1.28	2.54	2.92	2.58	CsBr	973	89.3	1.82	5.20	5.93	5.58
	1073	36.3		2.53	2.85	2.95		1073	93.0		5.17	6.03	6.71
	1173	37.2		—	2.20	3.36		1173	97.1		5.36	6.20	8.27
NaCl	1073	37.6	1.38	1.77	2.10	2.87	$MgCl_2$	1073	57.6	1.42	1.53	1.88	7.8
	1173	38.9		1.80	2.14	3.38	$MgBr_2$		71.5	1.52	1.98	2.11	9.9
	1273	40.4		1.87	2.20	4.00	MgI_2		94.5	1.66	2.71	3.26	13.7
NaBr	1073	44.8	1.45	2.24	2.65	3.36	$CaCl_2$	1073	53.5	1.54	0.40	0.66	1.40
	1173	46.4		2.30	2.69	3.86	$CaBr_2$		64.9	1.63	0.56	0.84	1.80
	1273	48.2		2.35	2.76	4.49	CaI_2		85.8	1.77	0.87	1.28	2.80
NaI	973	55.4	1.56	2.55	3.58	3.84	$SrCl_2$	1073	58.5	1.58	0.43	0.66	1.99
	1073	57.5		3.07	3.61	4.57	$SrBr_2$		68.9	1.68	0.48	0.78	2.37
	1173	59.6		3.15	3.65	5.47	SrI_2		83.6	1.82	0.67	0.84	2.53
KCl	1073	49.5	1.57	1.73	2.16	3.84	$BaCl_2$	1273	66.2	1.66	0.38	0.60	1.50
	1173	51.4		1.84	2.26	4.57	$BaBr_2$	1173	75.2	1.75	0.38	0.64	2.00
	1273	53.5		1.96	2.36	5.47	BaI_2	1073	93.7	1.89	0.47	0.83	2.10
KBr	1073	57.4	1.64	2.12	2.62	4.38	$ZnCl_2$	873	60.8	1.45	1.94	2.39	4.90
	1173	59.3		2.27	2.75	5.21	$ZnBr_2$		77.9	1.55	2.81	3.41	7.10
	1273	62.4		2.41	2.90	6.21	ZnI_2		87.0	1.69	2.06	2.65	8.10
KI	954	67.8	1.75	2.59	3.27	4.87	$CdBr_2$	873	67.4	1.62	0.96	1.36	4.30
	1073	71.1		2.79	3.40	5.99	CdI_2		88.2	1.76	1.37	1.92	6.00
	1173	74.2		3.22	3.57	7.20							

and Buehler's equation reads

$$\left[p + \left(\frac{\partial E}{\partial V}\right)_T\right] V \left(1 - \frac{2\,\nu^{1/3}\,N^{1/3}}{\gamma^{1/3}\,V^{1/3}}\,\bar{r}\right) = \nu RT. \tag{8}$$

The same equation can be obtained by using a statistical approach. According to the cellular model, the energy E_s of a molten salt, is given by the following relation

$$E_s = E + \sum[\Psi(\bar{r}_i) - \Psi(0)] \tag{9}$$

where E is the potential energy of the liquid when all the particles are placed in the center of the respective cell and $\Psi(\bar{r}_i) - \Psi(0)$ is the potential energy difference required to carry a particle i from the center of the cell i to the $\bar{r}_i$ coordinate, while all the other particles remain fixed.

By using the well-known relation for the free volume v_f

$$v_f = \int e^{-\frac{\Psi(\bar{r}_i) - \Psi(0)}{kT}}\,d\bar{r}_i \tag{10}$$

the configuration integral Q, for a molten salt, dissociating in ν ions, takes the form

$$Q(N, V, T) = v_f^{\nu N}\,e^{-\frac{E}{kT}} \tag{11}$$

According to Lennard-Jones and to Devonshire's approximation, the potential energy change is given by a spherical symmetric function, $\Psi(\rho) - \Psi(0)$, the new variable depending only on the distance ρ, from the center. Applying this approximation, one has,[4]

$$\Psi(\rho) - \Psi(0) = \sum_n m_n \frac{1}{2}\int_0^{\pi}\left[\varphi\left(\sqrt{a_n^2 + \rho^2 - 2a_n\rho\cos\theta}\right) - \varphi(a_n)\right]\sin\theta\,d\theta$$

where m_n is the number of particles from the n-shield and a_n is the distance from the center of the cell under consideration. Substituting $\cos\theta = u$ the previous equation becomes

$$\Psi(\rho) - \Psi(0) = \sum_n m_n \frac{1}{2}\int_{-1}^{+1}\left[\varphi\sqrt{a_n^2 + \rho^2 - 2a_n\rho u} - \varphi(a_n)\right] du \tag{12}$$

---

[4] J. A. Barker, "Lattice Theories of the Liquid State", The Macmillan Company, New York, 1966, p. 50.

Considering, in a first approximation, only the coulombian forces, for a binary salt, one has

$$\varphi(a_n) = \frac{n_+ n_- e^2}{a_n}$$

where n_+ and n_- are the numbers of charges carried by adjacent particles. Thus, eq. (12) becomes

$$\Psi(\rho) - \Psi(0) = \sum_n m_n \frac{1}{2} \int_{-1}^{+1} \frac{n_+ n_- e^2}{a_n} \left[\frac{1}{\sqrt{1 + \left(\frac{\rho}{a_n}\right)^2 - 2\frac{\rho}{a_n} u}} - 1 \right] du \tag{13}$$

Since the integral is zero, for the free volume, one obtains

$$v_f = \frac{4\pi}{3}(a - \sigma)^3 \tag{14}$$

and the configuration integral becomes

$$Q(N, V, T) = \left\{ \frac{4\pi}{3} \left[\gamma^{1/3} \left(\frac{V}{\nu N} \right)^{1/3} - \sigma \right]^3 \right\}^{\nu N} e^{-\frac{E}{kT}} \tag{15}$$

It is easy to see that, for the pV product, one has

$$pV = \nu N k T \frac{1}{1 - \frac{2\nu^{1/3} N^{1/3}}{\gamma^{1/3} V^{1/3}} \bar{r}} - V \left(\frac{\partial E}{\partial V} \right)_T \tag{16}$$

and, therefore the equation of state, reads

$$\left(p + \frac{\partial E}{\partial V} \right) V \left(1 - \frac{2\nu^{1/3} N^{1/3}}{\gamma^{1/3} V^{1/3}} \bar{r} \right) = \nu N k T \tag{17}$$

from where the internal pressure P_i, is then found to be,

$$P_i = \left(\frac{\partial E}{\partial V} \right)_T$$

As was pointed out in a previous paper,[1] for a molten salt vapor, containing mono- and n-mers, the internal pressure becomes

$$P_i = \frac{\lambda}{nV} \tag{18}$$

For alkali halides ($\nu = 2$), when dimers are formed in vapor phase ($n = 2$), eq. (17) reads

$$\left(p + \frac{\lambda}{2V}\right) V \left(1 - \frac{2^{4/3} N^{1/3}}{\gamma^{1/3} V^{1/3}} \bar{r}\right) = 2\,RT \tag{19}$$

At the melting point, p can be neglected compared to P_i and therefore one has

$$\lambda \left(1 - \frac{2^{4/3} N^{1/3}}{\gamma^{1/3} V^{1/3}} \bar{r}\right) = 4RT \tag{20}$$

which has been examined in detail in a previous paper.[1]

Revue Roumaine de Chimie, **17**, *4*, 611–616 (1972)

THE REORGANISATION ENERGY OF $TiCl_4$

B. HESSETT and P. G. PERKINS

Department of Pure and Applied Chemistry
University of Strathclyde, Glasgow, C.1, UK

Received November 15, 1971

The reorganisation energies of titanium tetrachloride from the tetrahedral to the square planar, *cis* octahedral, and trigonal bipyramidal configurations are calculated by the self-consistent molecular orbital method. The energy order for the processes is *cis* $O_h >$ trigonal bipyramidal $>$ square planar.

A large number of coordination complexes of titanium tetrachloride are now known.[1] These are of 1 : 1 and 1 : 2 stoichiometries and, in them, the symmetry of the titanium site is either trigonal bipyramidal [2] or octahedral.[3] We have recently carried out an experimental study of the thermodynamics of formation of these complexes [4] but were not able to calculate the intrinsic bond dissociation energies of the titanium-ligand bonds, since the reorganisation energies [5,6] of $TiCl_4$ from tetrahedral to trigonal bipyramidal and octahedral symmetries were not known.

In a separate study we have modified the all-electron self-consistent field molecular orbital method for use with transition elements [7] and have applied it to the calculation of the ground and lower excited states of titanium tetrachloride.[8] We reserve complete discussion of the latter calculations until a later date but, because of the importance of the reorganisation energy in donor-acceptor thermodynamics, we consider it worthwhile to report on these particular results now.

---

[1] R. J. H. Clark, "The Chemistry of Titanium and Vanadium", Elsevier, London, Chapter 3.

[2] G. W. A. Fowles and R. A. Hoodless, *J. Chem. Soc.*, **1963**, 33; I. R. Beattie and T. Gilson, *J. Chem. Soc.*, **1965**, 6595.

[3] C. I. Brändten, *Acta. Chem. Scand.*, **16**, 1806 (1962).

[4] B. Hessett and P. G. Perkins, *J. Chem. Soc.*, (A), **1970**, 3229; *J. Chem. Soc.*, (A), **1970**, 3331.

[5] F. A. Cotton and J. R. Leto, *J. Chem. Phys.*, **30**, 993 (1959).

[6] D. R. Armstrong and P. G. Perkins, *J. Chem. Soc.*, (A), **1967**, 1217.

[7] P. G. Perkins, I. C. Robertson and J. M. Scott, *Theor. Chim. Acta*, **22**, 299 (1971).

[8] D. R. Armstrong, P. G. Perkins, and J. J. Stewart, to be published.

CALCULATIONAL METHODS

Construction of Fock Matrix. The scheme is based on the work of Pople, Segal, and Santry [9] and some of the modifications used in the present work have been discussed by one of us previously. [10,11] We used explicit orbital one-centre repulsion integrals between electrons and set the diagonal core Hamiltonian matrix elements equal to the appropriate valence-state ionisation potentials for the orbitals in the usual way. These two parameters for the chlorine and titanium orbitals are set out in Table 1. The 3*d* orbitals of chlorine were included in all models, although we do not believe that the results would have been significantly affected by their neglect.

Table 1

Input data

Atom		Orbital exponent	VSIP ($H_{\mu\mu}$)	One-centre repulsion integral ($\gamma_{\mu\mu}$)
Ti	4*s*	1.075	6.07	9.00
	4*p*	0.725	3.35	
	3*d*	2.280	5.58	
Cl	3*s*	2.183	25.29	15.33
	3*p*	1.733	13.99	13.20
	3*d*	1.000	2.20	7.52

In constructing the Fock matrix elements we propose a new and improved approach [8] over that which has hitherto been employed.

The diagonal element of the Fock matrix

$$F_{\mu\mu} = H_{\mu\mu} + \sum_{\lambda\sigma} P_{\lambda\sigma}[\langle \mu\mu \mid \lambda\sigma \rangle - \frac{1}{2} \langle \mu\lambda \mid \mu\sigma \rangle]$$

becomes under zero differential overlap

$$F_{\mu\mu} = H_{\mu\mu} + \sum_{\lambda} P_{\lambda\lambda} \langle \mu\mu \mid \lambda\lambda \rangle - \frac{1}{2} P_{\mu\mu} \langle \mu\mu \mid \mu\mu \rangle$$

Now when all the atoms are completely separated

$$P_{\lambda\sigma} = 0, \qquad P_{\lambda\lambda} = p^{0}_{\lambda\lambda}$$

i.e., the occupancy of orbital λ in the isolated atom and $F_{\mu\mu}$ is then the self-consistent energy of an electron in orbital μ. Now, for an atom of configuration $n\,s^p\ n\,p^q\ n\,d^r$, we have the following expression for the energy of an electron in any orbital λ

---

[9] J. A. Pople, D. P. Santry, and G. A. Segal, *J. Chem. Phys.*, **43**, S129 (1963).

[10] K. A. Levison and P. G. Perkins, *Theor. Chim. Acta*, **17**, *1* (1970).

[11] D. R. Armstrong, P. G. Perkins, and J. J. Stewart, *J. Chem. Soc.* (A), in the press.

$$E_\lambda = \frac{1}{2}\,P^g_{\lambda\lambda}(U^0_{\lambda\lambda}) + \left(1 - \frac{1}{2}\,P^g_{\lambda\lambda}\right)(U^{-1}_{\lambda\lambda})$$

where $U^0_{\lambda\lambda}$ and $U^{-1}_{\lambda\lambda}$ are the valence-state ionisation potentials of the same orbital in the neutral atom at negative ion respectively. This expression has the correct behaviour at values of $P^g_{\lambda\lambda}$ of 0, 1, and 2 and we assume that the E_λ obtained by interpolating non-integral values of $P^g_{\lambda\lambda}$ are physically sensible.

If we now write

$$\gamma_{\lambda\lambda} = U^{-1}_{\lambda\lambda} - U^0_{\lambda\lambda}$$

then

$$E_\lambda = \frac{1}{2}\,P^g_{\lambda\lambda}(U^0_{\lambda\lambda}) + \left(1 - \frac{1}{2}\,P^g_{\lambda\lambda}\right)(U^0_{\lambda\lambda} + \gamma_{\lambda\lambda})$$

thus

$$F_{\mu\mu} = U^0_{\mu\mu} + \gamma_{\mu\mu}\left(1 - \frac{1}{2}\,P^g_{\mu\mu}\right)$$

$$= H_{\mu\mu} + \sum_\lambda P^g_{\lambda\lambda}\,\gamma_{\lambda\mu} - \frac{1}{2}\,P_{\mu\mu}\,\gamma_{\mu\mu}$$

If the atoms are now considered to be at positions where there is significant interaction, then the orbital occupancy $P^g_{\lambda\lambda}$ will deviate from that of the ground state of the atom (*i.e.*, an integral number). Thus we have

$$F_{\mu\mu} = U^0_{\mu\mu} - \sum_\lambda P^g_{\lambda\lambda}\,\gamma_{\lambda\mu} + \gamma_{\mu\mu} + \sum_\lambda P_{\lambda\lambda}\,\gamma_{\lambda\mu} - \frac{1}{2}\,P_{\mu\mu}\,\gamma_{\mu\mu}$$

$$\text{i.e.}\quad F_{\mu\mu} = U^0_{\mu\mu} + \sum_\lambda (P_{\lambda\lambda} - P^g_{\lambda\lambda})\,\gamma_{\lambda\mu} + \left(1 - \frac{1}{2}\,P_{\mu\mu}\right)\gamma_{\mu\mu}$$

and this is the form of Fock diagonal which is employed in the present series of calculations. In passing, it is worth noting that, if the equation above is rewritten using the Pople-type "atomic" repulsion integrals, then

$$F_{\mu\mu} = U^0_{\mu\mu} + \sum_\lambda (P_{\lambda\lambda} - P^g_{\lambda\lambda})\,\gamma_{AB} + \left(1 - \frac{1}{2}\,P_{\mu\mu}\right)\gamma_{AA}$$

the middle term

$$\sum_{\lambda} (P_{\lambda\lambda} - P^{g}_{\lambda\lambda})\, \gamma_{AB} = \sum_{B} \sum_{\lambda}^{B} (P_{\lambda\lambda} - P^{g}_{\lambda\lambda})\, \gamma_{AB}$$

$$= \sum_{B} (P_{BB}\ P'_{BB})\, \gamma_{AB}$$

$$= \sum_{B} (P_{BB} - Z_{B})\, \gamma_{AB}$$

$$= \sum_{B \neq A} (P_{BB} - Z_{B})\, \gamma_{AB} + (P_{AA} - Z_{A})\, \gamma_{AA}$$

The final term

$$\left(1 - \frac{1}{2}\, P_{\mu\mu}\right) \gamma_{AA}$$

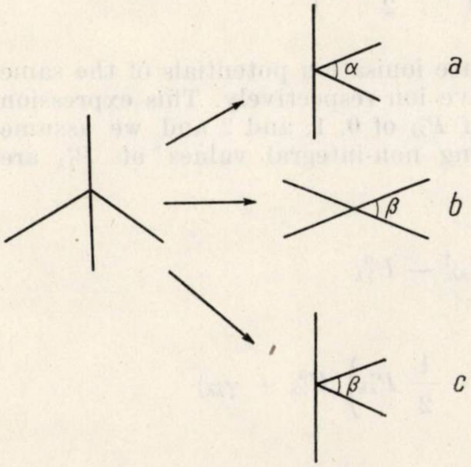

Fig. 1

so, taken together, we have

$$F_{\mu\mu} = U^{0}_{\mu\mu} + \sum_{B \neq A} (P_{BB} - Z_{B})\, \gamma_{AB} + \left(P_{AA} - \frac{1}{2}\, P_{\mu\mu} + 1 - Z_{A}\right) \gamma_{AA}$$

which is identical with Pople Segal-Santry equation 2.16 in ref. [9].

The energies required to bring about reorganisation of the $TiCl_4$ may be obtained by calculating the minimum *total* molecular energy of the molecule in all its geometrical forms. The particular processes which are thought to be most interesting, and which have therefore been studied, are shown in Figure 1. Because it is necessary to *minimise* the energy, in each particular geometry, a series of calculations was run in which the Ti—Cl bond lengths were varied over a range so as to obtain the minimum total energy of the model. For the trigonal bipyramidal model (*a*) the angle α was kept at 120° whilst in cases (*b*) and (*c*) the angle β was fixed at 90°.

RESULTS

Calculational methods such as this, which is not an *ab initio* technique, are not capable of producing, reliably, absolute energy quantities, although a strong point of the method is its differential prediction of stable geometries. However, some idea of the absolute energy quantities involved is highly desirable, and so we have calibrated the energy scale by carrying out a parallel calculation, by the same method, of the planar → pyramidal reorganisation energy of boron trifluoride. Here again, minimisation of total energy with B—F bond length was achieved for the two geometries. The reorganisation energy thus calculated for this molecule enables a calibration to be effected, since a prior non-empirical calculation of the reorganisation energy of BF_3 has been carried through.[12]

The calculated energy quantities for BF_3 and the different geometries of $TiCl_4$ are given in Table 2. By using the *ab initio* and semi-empirical reorganisation energies for BF_3, we arbitrarily set 1 eV = 37.7 kJ mol^{-1}. This leads to the conclusion that reorganisation from the tetrahedral to the trigonal bipyramidal form of $TiCl_4$ requires 84.0 kJ mol^{-1}, when the same energy scaling is applied. The transformation from the tetrahedral to the quasioctahedral form having the two vacant positions *cis* to each other is almost half as much again as this, being 113.4 kJ mol^{-1}. The square planar model, which is formed by an extreme tetragonal distortion of the tetrahedron, has some 64.4 kJ mol^{-1} more energy than tetrahedral titanium tetrachloride. An examination of the energy components making up the total is revealing : with regard to the electronic energies the stability order is *cis* octahedral > trigonal bipyramidal > square planar > tetrahedral. However, the nuclear repulsion energies of the configurations dominate and are ordered in the opposite sense. This produces the latter order of overall stability. In view of this, it is rather surprising that 1 : 2 complexes appear in general to favour *cis* geometry. The geometry of the final complex, however, is not necessarily determined by the reorganisation energy, since the latter does not take into account the energy of the new bonds formed. With regard to the 1 : 1 trigonal bipyramidal and 1 : 2 *cis* octahedral conformations, it seems that the reduction in nuclear repulsion energy between the equatorial chlorines

Table 2

Calculated minimum energies for various geometries (eV)

		Electronic energy	Nuclear repulsion energy	Total energy
$TiCl_4$	Trigonal bipyramidal	−2712.74	972.31	−1740.43
	cis octahedral	−2732.81	993.16	−1739.65
	square planar	−2703.07	962.12	−1740.95
	tetrahedral	−2690.89	948.22	−1742.66
BF_3	planar	−3461.83	1288.66	−2173.17
	pyramidal	−3470.47	1301.10	−2169.37

The *ab initio* reorganisation energy of BF_3 is 143.1 kJ mol^{-1} (ref.12).

---

[12] D. R. Armstrong and P. G. Perkins, *Theor. Chim. Acta.*, **15**, 413 (1969).

which occurs on going from a six-coordinate to a five-coordinate complex is the dominant factor which operates in determining geometry.

If the appropriate reorganisation energies are inserted into an energy cycle for the gas-phase formation of 1 : 1 and 1 : 2 titanium complexes, then the mean intrinsic bond dissociation energies ($-\Delta H_D$) of some titanium-ligand bonds can be computed. The cycle is :

$$\begin{tikzcd}
\mathrm{TiCl_4}\,n\mathrm{L}\,(g) \arrow[r, "-\Delta H_D"] & \mathrm{TiCl_4}^*\,(g) + n\mathrm{L}\,(g) \arrow[d, "-\Delta H_{\mathrm{reorg.}}"] \\
 & \mathrm{TiCl_4}\,(g) + n\mathrm{L}\,(g) \arrow[ul, "-\Delta H_g"]
\end{tikzcd}$$

where the asterisk denotes the appropriate reorganised form of $\mathrm{TiCl_4}$. The value of the intrinsic bond dissociation energy will depend on the geometrical structure of the dissociating complex, since this determines the path of reorganisation. However, if we assume that 1 : 1 complexes of which the structures are unknown are simple five-coordinate monomers and that the 1 : 2 complexes are *cis* octahedral, then the reorganisation energies can be combined with data from ref. [4]. Table 3 lists the mean

Table 3

Mean titanium-ligand bond dissociation energies

Ligand	1 : 1 complex (kJ mol^{-1})	1 : 2 complex (kJ mol^{-1})
Tetrahydrofuran	262	180
Tetrahydropyran	222	148
Tetrahydrothiophen	233	154
Benzophenone	232	176
Acetophenone	212	144
Acetonitrile	192	146

titanium-ligand bond dissociation energies for a number of complexes and it is clear in all cases the bonds are weaker in the 1 : 2 adducts. This point is consistent with experimental observations made on the same type of coordination complexes of the Group III trihalides.[13] Of course, not all the structures of the complexes have yet been elucidated and some revision of Table 3 may become necessary as and when more structural information is forthcoming.

One of us (B.H.) thanks the University of Strathclyde for the award of a James Young Scholarship.

---

[13] N. N. Greenwood and P. G. Perkins, *J. Chem. Soc.*, **1960**, 1145.

Revue Roumaine de Chimie, **17**, *4*, 617–620 (1972)

SOME CONSIDERATIONS ABOUT THE STABILITY OF COMPLEX COMBINATIONS OF COBALT

V. EM. SAHINI, VERONICA TUFOI and AL. IVANOV
Center of Physical Chemistry, str. Galaţi 31, Bucharest, Romania

Received December 14, 1971

By considering the electronic ground state of a molecule perturbed by the small vibrations of its nuclei, the second order perturbation theory is used in order to compare the stability of several complex combinations of Co(II) and Co(III). Some considerations about applicability of this method are made.

INTRODUCTION

Some relatively recent works [1-3] deal with the problem of examining the reaction possibilities of complex molecules by using the second order perturbation theory and symmetry considerations. The perturbation operator used in these calculations is the potential energy variation with respect to nuclear displacements produced by the small vibrations. Such considerations are suitable in order to analyse the possibilities of decomposition of complex molecules.

In the following we study the stability of Co(II) hexacoordinated compounds in respect to corresponding compounds of Co(III), by changing to a certain extent the formalism employed in references.[1-3] By considering the tetracoordinated (tetrahedral) compounds of Co(II) too, we will make some observations about the validity of this method.

In the first section the general method is exposed; in the second one the above concrete applications are given.

1. THE DESCRIPTION OF THE METHOD

Let us consider an n-electron molecule, described in its ground state by an antisymmetrized function Φ_0. If the Hamiltonian of this molecule is perturbed by a W-operator, the shift of the ground level is given by the well-known formulas:

$$\Delta E = < \Phi_0 | W | \Phi_0 > + \sum_{\substack{K \\ K \neq 0}} \frac{< \Phi_0 | W | \Phi_k > < \Phi_k | W | \Phi_0 >}{E_0 - E_k} \qquad (1.1)$$

where Φ_k are the wave functions corresponding to E^k energies and E_0 is the energy of the ground state.

---

[1] R. Bader, *Canad. J. Chem.*, **40**, 1164 (1962).
[2] R. Pearson, *J. Amer. Chem. Soc.*, **91**, 1252 (1969).
[3] R. Pearson, *Theor. Chim. Acta*, **16**, 107 (1970).

We consider the perturbation operator due to the small vibrations in the following form:

$$W = \sum_{\alpha} \frac{\partial V}{\partial Q_\alpha} Q_\alpha + \sum_{\alpha,\beta} \frac{\partial^2 V}{\partial Q_\alpha \, \partial Q_\beta} Q_\alpha Q_\beta \tag{1.2}$$

where Q_k are the symmetry coordonates and V the interaction energy between the nuclei and between the electrons and nuclei. By using the notations:

$$\frac{\partial}{\partial Q_\alpha} \equiv Q_\alpha, \quad \frac{\partial^2}{\partial Q_\alpha \, \partial Q_\beta} \equiv \partial^2_\alpha \, \beta$$

We can write the second order perturbation energy as follows:

$$E^{2)} = \sum_{\alpha,\beta} < \Phi_0 \,|\, \partial^2_{\alpha\beta} \,|\, \Phi_0 > Q_\alpha Q_\beta +$$

$$+ \sum_{\alpha,\beta} \left\{ \sum_{K \neq 0} \frac{< \Phi_0 \, \partial_\alpha V \,|\, \Phi_k > < \Phi_k \,|\, \partial_\beta V \,|\, \Phi_0 >}{E_0 - E_k} \right\} Q_\alpha Q_\beta \tag{1.3}$$

In order to calculate the matrix elements that appear in this expression, we will consider the next observations:

(a) $\Phi_0, \Phi_1, \ldots, \Phi_k$ are constructed as n-electronic antisymmetrized functions by using a given energy-level diagram.

b) The V operator may be represented as a summ of n monoelectronic operators $V(i)$, where i denotes the coordinate set of the i-electron.

(a) and (b) result in:

$$\partial_\alpha V = \sum_{i=1}^{n} \partial_\alpha V(i) \, ; \; \partial_{\alpha\beta} V = \sum_{i=1}^{n} \partial^2_{\alpha\beta} V(i) \tag{1.4}$$

and

$$< \Phi_0 \,|\, \partial^2_{\alpha\beta} V \,|\, \Phi_0 > = \sum_{i=1}^{n} < \varphi_i(i) \,|\, \partial^2_{\alpha\beta} V(i) \,|\, \varphi_i(i) > \tag{1.5}$$

$$< \Phi_0 \,|\, \partial_\alpha V \,|\, \Phi_k > = < \varphi(i) \,|\, \partial_\alpha V(i) \, \varphi'(i) > \tag{1.5'}$$

where $\varphi(i)$ are molecular orbitals and φ, φ' denote the differing orbitals of Φ_0 and Φ_k, respectively (it is well known that if Φ_0 and Φ_k posess more than two different orbitals, the matrix element (1.5′) vanishes).

The symmetry properties of $\partial_\alpha V$ and $\partial^2_{\alpha\beta} V$ operators with respect to those of molecular orbitals φ_i permit us to say whether or not the matrix elements (1.5) vanish. The relation (1.3) gives the total energetic shift. Using the symmetry considerations it may be established which of the vibrational modes may contribute to break down the molecule in question.

2. APPLICATIONS TO COMPLEXES OF Co(II) AND Co(III)

We shall apply the above method in order to compare the stability of the octahedral complexes of Co(III) and Co(II).

The antibonding levels in the energetic diagrams were calculated by using the parametric method from.[4] According to reference [2] we shall compare the values of the negative term:

$$\Delta E^{(2)} = \sum_{\alpha,\beta} \left\{ \sum_{\substack{K \\ K \neq 0}} \frac{<\Phi_0\, \partial_\alpha V \,|\, \Phi_k> < \Phi_k \,|\, \partial_\beta V \,|\, \Phi_0>}{E_0 - E_k} \right\} Q_\alpha Q_\beta \tag{2.1}$$

for the studied complexes. A large value of $|\Delta E^{(2)}|$ indicates a slight decomposition of the complex molecule.

For comparison we have chosen on the one hand the $[Co(NH_3)^6]^{3+}$ and $[Co(NH_3)_6]^{2+}$ complex ions and on the other hand the $[CoF_6]^{3-}$, $[CoF_6]^{2-}$ pair. The approximate energy levels diagrams are given in figs. 1 and fig. 2 respectively:

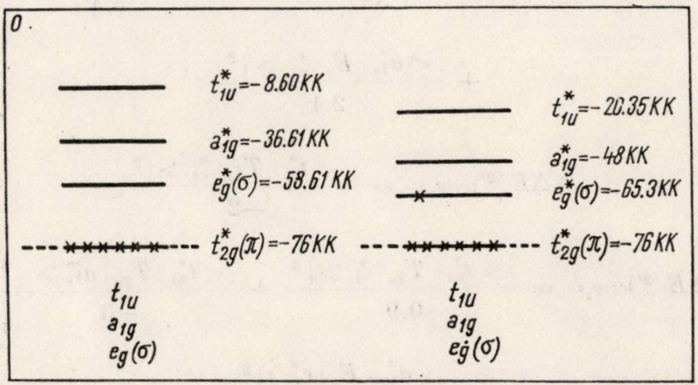
0.
$t^*_{1u}=-8.60KK$
$a^*_{1g}=-36.61KK$
$e^*_g(\sigma)=-58.61 KK$
$t^*_{2g}(\pi)=-76KK$
t_{1u}
a_{1g}
$e_g(\sigma)$
$t^*_{1u}=-20.35KK$
$a^*_{1g}=-48KK$
$e^*_g(\sigma)=-65.3KK$
$t^*_{2g}(\pi)=-76KK$
t_{1u}
a_{1g}
$e_g(\sigma)$

Fig. 1. — Electronic energy levels $[Co(NH_3)_6]^{3+}$; $[Co(NH_3)_6]^{2+}$.

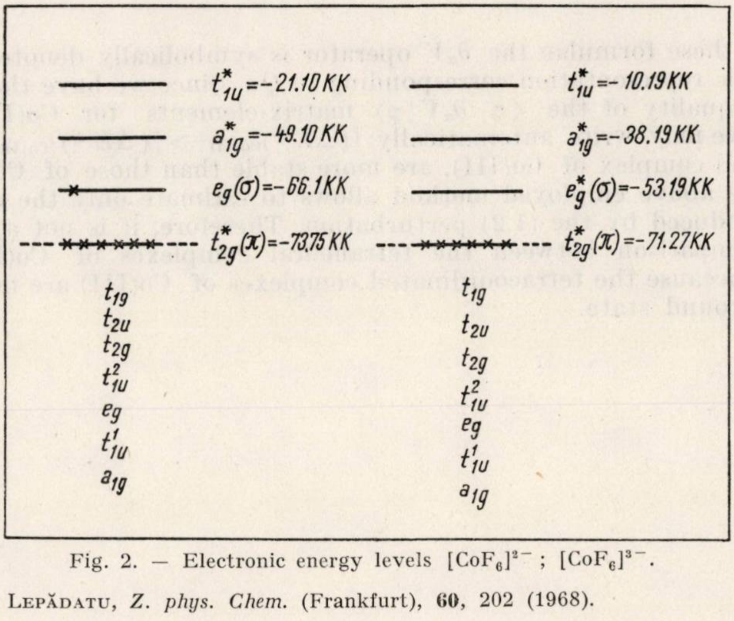
$t^*_{1u}=-21.10KK$
$a^*_{1g}=-49.10KK$
$e_g(\sigma)=-66.1KK$
$t^*_{2g}(\pi)=-73.75KK$
t_{1g}
t_{2u}
t_{2g}
t^2_{1u}
e_g
t^1_{1u}
a_{1g}
$t^*_{1u}=-10.19KK$
$a^*_{1g}=-38.19KK$
$e^*_g(\sigma)=-53.19KK$
$t^*_{2g}(\pi)=-71.27KK$
t_{1g}
t_{2u}
t_{2g}
t^2_{1u}
e_g
t^1_{1u}
a_{1g}

Fig. 2. — Electronic energy levels $[CoF_6]^{2-}$; $[CoF_6]^{3-}$.

---

[4] C. Lepădatu, *Z. phys. Chem.* (Frankfurt), **60**, 202 (1968).

For the sake of convenience we have denoted in these diagrams the energy differences between those levels which we use in our calculations. Considering that differences $|E_0 - E_k|$ must be smaller than 4 eV[2] so that the contribution of Φ_k – configuration in the (2.1) should be sufficiently important and considering also the symmetry properties of the $Q\ V$ operator, we can write symbolically:

$$(\Delta E^{(2)})_{\mathrm{CO(NH_3)_6{}^{3+}}} = \frac{|<t^*_{2g}|\,T_{2g}\,|{}^{*}_{eg}>|^2}{2.77}$$

$$(\Delta E^{(2)})_{\mathrm{CO(NF_3)_6{}^{2+}}} = \frac{|<t^*_{2\gamma}|\,T_{2g}\,|_{eg}>|^2}{1.32} + \frac{|<t^*_{2\gamma}|\,T_{2g}\,|\,a^*_{1\gamma}>|^2}{3.4} +$$

$$+\frac{|<a^*_{1g}|\,E_g|\,{}^{*}_{eg}>|^2}{2.1}$$

$$(\Delta E^{(2)})_{\mathrm{COF_6{}^{3-}}} = \frac{|<t^*_{2g}|\,T_{2g}\,|{}^{*}_{eg}>|^2}{-2}$$

$$(\Delta E^{(2)})_{\mathrm{COF_6{}^{4-}}} = \frac{|<t^*_{2g}|\,T_{2g}\,|{}^{*}_{eg}>|^2}{-0.9} + \frac{|<t^*_{2g}|\,T_{2g}\,|\,a^*_{1g}>|^2}{-3} +$$

$$+\frac{|\langle a^*_{1g}\,|\,E_g\,|\,e^*_g\rangle|^2}{-2.1}.$$

In these formulae the $\partial_\alpha V$ operator is symbolically denoted as the irreducible representation corresponding to $Q\alpha$. Since we have the approximate equality of the $\langle\varphi|\ \partial_\alpha V\,|\varphi\rangle$ matrix-elements for Co(III) and Co (II), we may write automatically $|(\Delta E^{(2)})_{\mathrm{Co(III)}}| > |(\Delta E^{(2)})|_{\mathrm{Co(II)}}$ i.e. the octahedral complex of Co(III), are more stable than those of Co(II).

The above employed method allows to estimate only the energetic shifts produced by the (1.2) perturbation. Therefore, it is not applicable for a comparison between the tetrahedral complexes of Co(III) and Co(II), because the tetracoordinated complexes of Co(III) are not stable in the ground state.

Revue Roumaine de Chimie, 17, 4, 621–631 (1972)

ABOUT THE EXACT DEVELOPMENT OF ATOMIC AND MOLECULAR WAVE FUNCTIONS

D. I. HERŢIA and AL. IVANOV

Institute of Physical Chemistry
str. Galaţi 31, Bucharest, Romania

Received November, 9,1971

The paper presents from a unitary point of view some ways of writing the exact wave functions of N-electron systems, showing that the form of the approximate wave functions used in some current quantum chemical calculations is justified through the existence of these exact series developments. The developments of the exact wave function into infinite series of products of mono-, bi- or n- ($n < N$)-electronic functions (the independent particles, pairs or groups models) are corollaries of one and the same theorem connected with the spaces of functions with integrable squares. Hence, an expression of the type of that used by Sinanoğlu (M.E.T.) is rigorously derived, as well as the properties of its terms.

INTRODUCTION

Let be a N-electrons system, an associated ${}^{N}\mathcal{H}$ space of the wave functions, and a Hamiltonian H, defined as a linear and closed operator over ${}^{N}\mathcal{H}$, whose precise form is determined by the physical circumstances. The conditions imposed upon the wave functions in order to describe the states of the system allow organisation of the ${}^{N}\mathcal{H}$ space as a separable Hilbertian space. Once the H-operator is defined, one can always get a variational principle which could allow finding its eigen-functions through an iteration process. For this purpose, it is necessary to choose test functions-elements of ${}^{N}\mathcal{H}$ or, more exactly, a subset of ${}^{N}\mathcal{H}$ in which we may appreciate we will find the interesting eigen-functions with a reasonable good approximation. Of course, the conditions *a priori* imposed to these test functions may vary to a large extent, but since the resolution of a concrete physical problem is considered, we may require for the test functions tu fulfil the following two conditions :

1°. To assure a maximum convergence of the iteration process connected with the chosen variational calculation;

2°. To offer an intuitive physical interpretation (this condition is frequently not fulfilled, e.g. for the James-Coolidge type functions).

In this paper we intend to analyse various forms of test functions as proposed in a series of methods for the estimation of correlation effects, without making concrete suppositions with regard to the form of H-operator. The basic idea is to make use of a number of ways for representing the ${}^N\mathcal{H}$ states-space which might be grouped under two headings :

a) To write down ${}^N\mathcal{H}$ as a closure, in the topological sense, of a number of subsets of ${}^N\mathcal{H}$ which justifies the configurations superposition and the methods of independent pairs (or groups).

b) To write down ${}^N\mathcal{H}$ as a direct sum of a finite family of closed orthogonal subspaces — which leads to the writing of test functions in terms of cluster — type functions.

These ways of representing the ${}^N\mathcal{H}$ space lead to exact expressions, for the wave functions, which serve as a basis for choosing the test functions to be used in the calculation. This approach allows also a rigurous proof of the equivalence between various ways of writing down the wave functions, implicitly indicating at the same time, the manner in which they can be obtained, from each other.

Section II deals with the first of these ways. A configurational basis in ${}^N\mathcal{H}$ is chosen, which allows to get, in section III a decomposition of ${}^N\mathcal{H}$ into a direct sum of subspaces, as mentioned in b).

The Appendix presents a demonstration of T 1 which can be correlated, by those who are interested, with reference. [1]

I. THE DEVELOPMENT OF WAVE FUNCTION IN AN INFINITE SERIES

We will begin by presenting in an adequate form the superposition of the configurations.[2] Let the N-particle system be. To each particle "i" a configuration space $\mathcal{X}_i$ is ascribed, with the coordinate element $(r_i, \theta_i, \varphi_i), (r_i, \theta_i, \varphi_i)$ being the spherical coordinates of a given point). For N-particles we will have a set of configuration space

$$\mathcal{X}_1, \mathcal{X}_2, \ldots, \mathcal{X}_i, \ldots, \mathcal{X}_N$$

Let $\mathcal{K}$ be the field of the complex numbers.

D_1. We call a wave function for an N-particle ystem, the mapping :

$$\Psi^N : \overset{N}{\underset{j=1}{\times}} \mathcal{X}_j \to \mathcal{K} \tag{1.1}$$

which fulfills the following conditions :

1. it is square integrable,
2. it is continuous,
3. it is derivable with continuous derivatives.

The set of all Ψ^N functions spans a linear space associated with the N-particle system denoted as ${}^N\mathcal{H}$. Let us consider in the following the set of linear spaces associated with each particle :

$$h_1, h_2, \ldots, h_i, \ldots, h_N$$

---

[1] N. Bourbaki, "Intégration", Herman & Cie, Paris, cap. 3.

[2] P. O. Löwdin, *Adv. Chem. Phys.*, **2**, 207 (1959) ; *Phys. Rev.*, **97**, 1509 (1955).

obviously $\Phi_i \in h_i$ is a mapping:

$$\Phi_i : \mathscr{X}_i \to \mathcal{K} \tag{1.1'}$$

From each h_i space there is a denumerable and orthonormalized basis $b_i = \{\Phi_i^\alpha\}_{\alpha \in N}$ (where $\mathbb{N}$ is the set of natural numbers).

Let us construct the set

$$\mathscr{B} = \left\{ \bigotimes_{i=1}^{N} \Phi_i^\alpha \, ; \;\; \Phi_i^\alpha \in b_i \, , \;\; i = 1, 2 \ldots, N \right\} \tag{1.2}$$

The set $\mathscr{B}$ is orthonormalized and denumerable. Generally, a linear space spanned by an orthonormal set $\mathscr{L}$ will be denoted by $\mathrm{Sp}(\mathscr{L})$. In $\mathrm{Sp}(\mathscr{L})$ will be considered all infinite linear combinations of elements from $\mathscr{L}$

Obviously,

$$\mathrm{Sp}(\mathscr{B}) \subset {}^N\mathscr{H} \tag{1.3}$$

Throughout, $\mathrm{Sp}(\mathscr{B})$ will be denoted as ${}^N\mathscr{H}_0$

T_1 $\mathscr{B}$ is a basis in ${}^N\mathscr{H}$ (see Appendix).

Each element of ${}^N\mathscr{H}$ can be represented through an infinite series generated on the basis $\mathscr{B}$. Let us denote by Φ_K an element from $\mathscr{B}$; consequently for each $\Psi^N \in {}^N\mathscr{H}$ one may write

$$\Psi^N = \textstyle\sum_{K=0}^{\infty} C_K \, \Phi_K \;\; ; \;\; C_K \in \mathcal{K}, \; \Phi_K \in \mathscr{B} \tag{1.4}$$

This notation is nothing but the representation of the function in the S.C. method.

Ψ^N might be expanded into an infinite series of pair particle functions in a similar manner as in (1.4). Indeed, let us consider the following choice of pairs of configuration spaces (the choice is quite arbitrary) $(N = 2n)$:

$$\mathscr{X}_1, \mathscr{X}_2, \ldots\ldots\ldots\ldots, \mathscr{X}_{i-1}, \mathscr{X}_i, \ldots\ldots\ldots\ldots, \mathscr{X}_{N-1}, \mathscr{X}_N.$$

$${}^2\mathscr{X}_{12} = \mathscr{X}_1 \times \mathscr{X}_2, \ldots, {}^2\mathscr{X}_{i-1,i} = \mathscr{X}_{i-1} \times \mathscr{X}_i, \ldots, {}^2\mathscr{X}_{N-1,N} = \mathscr{X}_{N-1} \times \mathscr{X}_N \tag{1.5}$$

D_1 should be modified in such a way that

$$\Psi^N : \underset{(ij)\;(i \neq j)}{\times} {}^2\mathscr{X}_{ij} \to \mathcal{K} \tag{1.1''}$$

In this case $\Psi^N \in {}^N\mathscr{H}$ can be represented in a series:

$$\Psi^N = \textstyle\sum_{m=0}^{\infty} C_m \left(\bigotimes_{(ij)} \Psi^2_{(ij)} \right)_m \tag{1.6}$$

where $\Psi^2_{(ij)}$ functions are definite for the configuration space ${}^2\mathscr{X}_{ij}$. In a similar way we may divide the sequence of N configuration spaces into a series of arbitrary subsystems :

$$\mathscr{X}_1, \mathscr{X}_2, \ldots, \mathscr{X}_k, \mathscr{X}_{k+1}, \ldots, \mathscr{X}_l, \ldots, \mathscr{X}_m, \ldots, \mathscr{X}_N$$

$$ {}^{K}\mathscr{X}_{G_1} = \mathop{\times}_{i=1}^{k} \mathscr{X}_i,\ {}^{l-k}\mathscr{X}_{G_2} = \mathop{\times}_{i=k+1}^{l} \mathscr{X}_i, \ldots,\ {}^{N-m}\mathscr{X}_{G_n} = \mathop{\times}_{i=m}^{N} \mathscr{X}_i \qquad (1.7)$$

where

$$k + h + \ldots + g = N\ (h = l - k, \ldots, g = N - m)$$

The wave functions Ψ^N may be considered defined on the set $\mathop{\times}_{i=1}^{n} {}^{\Upsilon_i}\mathscr{X}_{G_i}$ (where ${}^{\Upsilon_i}\mathscr{X}_{G_i}$ represents the general notation for the Cartesian products in (1.7)) :

$$\Psi^N : \mathop{\times}_{i=1}^{n} {}^{\Upsilon_i}\mathscr{X}_{G_i} \to \mathcal{K} \qquad (1.1''')$$

The series corresponding to such a re-arrangement of the configuration spaces is

$$\Psi^N = \sum\nolimits_m C_m \left(\bigotimes_{i=1}^{n} \Psi^{\Upsilon_i}_{(G_i)} \right)_m \qquad (1.8)$$

For physical reasons one may choose different possibilities for dividing the set of configuration spaces in pairs, or groups, which are adequate for a given system (for instance the separation in pairs of electrons described by the same space orbital; in pairs of electrons for the same chemical bond; in groups of electrons localized in the same regions of the space; $\sigma - \pi$ separability; the separability of atoms in a molecule).

To this partitioning, it will correspond an accelerated convergence of series (1.6) and (1.8). This is so since using wave functions of pairs or groups which describe well the correlation effects inside pairs or groups, we can limit the development to one term. The remaining terms will describe the correlation effects between different pairs respectively groups, these effects being sufficiently small to be neglected.

If in (1.8), (1.6) and (1.4) we resort only to the first term in the series, we get models of independent groups, pairs, or particles. These are models because if the functions for particles, pairs, or groups are written as linear combinations of elements from the corresponding bases, this assumes that to each pair or group is associated a basic set which does not contain functions from the basic set of other pairs or groups. This is not, obviously always possible.

II. THE EXACT DEVELOPMENT OF A WAVE FUNCTION IN FINITE SERIES

Let b be an orthonormal basis in a linear space h and $\Phi_k \in b$. To the b basis corresponds a $\mathcal{B}$ basis in ${}^N\mathcal{H}_0$ with $\Phi_k \in \mathcal{B}$.

D_2. We call reference set associated with a Ψ^N function a subset $\beta \subset b$ which contains N elements from b. Then we may write b in the form :

$$b = \beta \cup \gamma \qquad \gamma = \complement\beta \tag{2.1}$$

We denot by Φ_0 the functions of ${}^N\mathcal{H}_0$ which is a product of all elements of β.

Let be the subspace

$$\mathrm{Sp}(\Phi_0) = \{C\,\Phi_0;\quad C \in \mathcal{K}\} = \mathcal{H}_0 \subset {}^N\mathcal{H} \tag{2.2}$$

The set $\mathcal{B} \setminus \{\Phi_0\}$ is linear independent. It spans the subspace

$$\mathrm{Sp}\,(\mathcal{B}\setminus\{\Phi_0\}) = \mathcal{H}^{\mathrm{corr}} \subset {}^N\mathcal{H} \tag{2.3}$$

We call this subspace correlation space.

P_1. $\mathcal{H}^{\mathrm{corr}}$ is the orthogonal complement of $\mathcal{H}_0$.

Proof. Indeed, let $\chi \in \mathcal{H}^{\mathrm{corr}}$ be a function of this subspace. Then

$$\langle C\Phi_0, \chi\rangle = \langle C\Phi_0, \textstyle\sum_{k\neq 0} C_k\,\Phi_k\rangle = \displaystyle\sum_{k\neq 0} C^* C_k \langle \Phi_0, \Phi_k\rangle = 0. \tag{2.4}$$

But according to T_1, $(\forall)\,\Psi^N \in {}^N\mathcal{H}$ one may write

$$\Psi^N = \textstyle\sum_{k=0}^{\infty} C_k\,\Phi_k = C_0\,\Phi_0 + \displaystyle\sum_{k\neq 0} C_k\,\Phi_k = C_0\,\Phi_0 + \chi \tag{2.5}$$

From this it follows

$${}^N\mathcal{H} = \mathcal{H}_0 \oplus \mathcal{H}^{\mathrm{corr}} \tag{2.6}$$

$\mathcal{H}_0$ and $\mathcal{H}^{\mathrm{corr}}$ are closed sub spaces. Then, for every subspace we can define a projector :

$$\mathrm{P}_0 : {}^N\mathcal{H} \to \mathcal{H}_0 \tag{2.7}$$

$$\mathrm{P}_1^{\mathrm{corr}} : {}^N\mathcal{H} \to \mathcal{H}^{\mathrm{corr}} \tag{2.8}$$

The sum of these projectors is a new projector. This new projector is just the identical mapping :

$$I : \mathcal{H}^N \to \mathcal{H}^N \tag{2.9}$$

$$I = \mathrm{P}_0 + \mathrm{P}^{\mathrm{corr}} \qquad \text{(see L-2, L-3)} \tag{2.10}$$

We note

$$\frac{\Phi_0}{(i_1, \ldots, i_k)} = \bigotimes_{\Phi_{i_j} \in \beta,\, i_j \neq i_1, \cdots, i_k} \Phi_{ij} \tag{2.11}$$

We can further define the linear independent sets as follows :

$$\mathcal{B}_i^1 = \left\{ \frac{\Phi_0}{(i)} \otimes \Phi_\mu ; \quad \Phi_\mu \in \gamma \right\}$$

$$\mathcal{B}_{ij}^2 = \left\{ \frac{\Phi_0}{(ij)} \otimes \Phi_\mu \otimes \Phi_r ; \Phi_\mu, \Phi_r \in \gamma \right\} \tag{2.12}$$

$$\mathcal{B}_{i_1 \ldots i_k}^k = \left\{ \frac{\Phi_0}{(i_1 \ldots i_k)} \otimes \Phi_{\mu_1} \otimes \ldots \otimes \Phi_{\mu_k} ; \; \Phi_{\mu_1}, \ldots, \Phi_{\mu_k} \in \gamma \right\}$$

with corresponding closed subspaces :

$$\begin{aligned} &\mathrm{Sp}\,(\mathcal{B}'_i) = \mathcal{H}_i^1 \\ &\mathrm{Sp}\,(\mathcal{B}_{ij}^2) = \mathcal{H}_{ij}^2 \\ &\vdots \\ &\mathrm{Sp}\,(\mathcal{B}_{i_1 \ldots i_k}^k) = \mathcal{H}_{i_1 \ldots i_k}^k \end{aligned} \tag{2.13}$$

The associated projectors will be :

$$\begin{aligned} &P'_i : {}^N\mathcal{H} \to \mathcal{H}_i^1 \\ &P_{ij}^2 : {}^N\mathcal{H} \to \mathcal{H}_{ij}^2 \\ &\vdots \\ &P_{i_1 \ldots i_k}^k : {}^N\mathcal{H} \to \mathcal{H}_{i_1, \ldots, i_k}^k \end{aligned} \tag{2.14}$$

This projector maps the space ${}^N\mathcal{H}$ into the corresponding closed subspaces. It is easy to show that every subspace of this set is orthogonal to each other (see P-1). Hence

$$\mathcal{H}^{\mathrm{corr}} = \bigoplus_{k=1}^{N} \Big(\bigoplus_{(i_1 \ldots i_k)} \mathcal{H}_{i_1 \ldots i_k}^k \Big) \tag{2.15}$$

Further we use the following lemmas :

L.1 For any two projectors P' and P'' associated with two orthogonal subspaces A and B of the same space, we have :

$$P'P'' = P''P' = 0 \tag{2.16}$$

(this lemma is true for any n projectors $P_1, \dots, P_n$ associated with a orthogonal subspaces of the same space, i.e. :

$$P_i P_j = P_j P_i = 0 \quad i \neq j). \tag{2.16'}$$

L.2 If two projectors P' and P'' fulfil the condition :

$$P'P'' = P''P' = 0$$

then

$$Q = P + P' \tag{2.17}$$

is a projector (this lemma is true for n projectors

$$P_1, \dots, P_n, \; (P_i P_j = P_j P_i = 0)$$
$$Q = \sum_i P_i) \tag{2.17'}$$

L.3. If $P' : x \to x'$ and $P'' : x \to x''$ fulfil lemma 2, then

$$(P' + P'')\, x = P'\,(x) \oplus P''\,(x) = x' \oplus x'' \tag{2.18}$$

For n projectors $P_1, \dots, P_n$ which fulfil L.2 we have :

$$(\sum_i P_i)\,(x) = \bigoplus_{i=1}^{n} P_i\,(x) \tag{2.18'}$$

With these lemmas we can write further :

$$P^{\text{corr}} = \sum_{k=1}^{N} \sum\nolimits_{(i_1 \dots i_k)} P^k_{i_1 \dots i_k} \tag{2.19}$$

In other words, the identical mapping of ${}^N\mathcal{H}$ has the form :

$$I = P_0 + \sum_{k=1}^{N} \sum\nolimits_{(i_1 \dots i_k)} P^k_{i_1 \dots i_k} \tag{2.20}$$

T_2. In a given decomposition of the space ${}^N\mathcal{H}$ in a finite direct sum of orthogonal subspaces, for every element $\Psi^N \in {}^N\mathcal{H}$ we can find one and only one decomposition in a finite series.

The proof follows immediately from L.1 – L.3 and the unicity results from the fact that every projector is a mapping.

Furthermore it follows from T-2 that for our decomposition of space:

$$^{N}\mathcal{H} = \mathcal{H}_0 \oplus \left\{ \bigoplus_{k=1}^{N} \Big(\bigoplus_{(i_1 \ldots i_k)} \mathcal{H}^k_{i_1 \ldots i_k} \Big) \right\} \tag{2.21}$$

every $\Psi^N \in {}^N\mathcal{H}$ can be put in the following form:

$$\Psi^N = I\,\Psi^N = P_0\,\Psi^N + \sum_{k=1}^{N} \sum_{i_1 \ldots i_k} P^k_{i_1 \ldots i_k}\,\Psi^N \tag{2.22}$$

As a next step we have explicitly

$$\begin{aligned} &P_0\,\Psi^N = C_0\,\Phi_0 \\ &P'_i\,\Psi^N = \Sigma^{\infty}_{\mu}\, C^i_{\mu}\,\frac{\Phi_0}{(i)} \otimes \Phi_{\mu} = \frac{\Phi_0}{(i)} \otimes \Big(\sum_{\mu} C^i_{\mu}\,\Phi_{\mu}\Big) \\ &\vdots \\ &P^k_{i_1 \ldots i_k}\,\Psi^N = \sum_{\mu_1 \ldots \mu_k} C^{i_1 \ldots i_k}_{\mu_1 \ldots \mu_k}\,\frac{\Phi_0}{(i_1 \ldots i_k)} \otimes \Big(\bigotimes_j \Phi_{\mu_j}\Big) \end{aligned} \tag{2.23}$$

where

$$\Phi_{\mu_j} \in \gamma$$

We introduce the new functions:

$$\begin{aligned} &U(i) = \sum_{\mu} C^i_{\mu}\,\Phi_{\mu} \\ &U(ij) = \Sigma_{\mu,\nu}\, C^{ij}_{\mu\nu}\,\Phi_{\mu} \otimes \Phi_{\nu} \\ &\vdots \\ &U(i_1 \ldots i_k) = \Sigma_{\mu_1 \ldots \mu_k}\, C^{i_1 \ldots i_k}_{\mu_1 \ldots \mu_k} \bigotimes_{\mu_1 \ldots \mu_k} \Phi_{\mu_j}. \end{aligned} \tag{2.24}$$

From T.1 it follows that these functions are elements of the spaces h_i, $^2\mathcal{H}, \ldots,$ $^k\mathcal{H}$ respectively, i.e. they describe $1, 2 \ldots k$ particles.

With this notation the exact expansion of Ψ^N in a finite serie becomes:

$$\Psi^N = C_0\,\Phi_0 + \sum_{k=1}^{N} \Sigma_{(i_1 \ldots i_k)}\,\frac{\Phi_0}{(i_1 \ldots i_k)} \otimes U(i_1 \ldots i_k) \tag{2.25}$$

Obviously for every choice of reference set β we have another decomposition of the space, of the form (2.21). The decomposition (2.25) results from the choice of Φ_0. In other words we can begin series (2.25) with any

$\Phi_m \in \mathcal{B}$. It is of interest to choose the β set so that the corresponding function have the greatest weight, i.e.

$$|C_0|^2 > \Sigma_{l \neq 0} |C_l|^2 \, {}^{*)} \tag{2.26}$$

For the sake of simplicity we choose the normalization [3] of the Ψ^N function as follows

$$\langle \Psi^N, \ \Phi_0 \rangle = 1$$

With this normalization we get $C_0 = 1$ and (2.25) becomes:

$$\Psi^N = \Phi_0 + \sum_{k=1}^{N} \sum\nolimits_{(i_1 \dots i_k)} \frac{\Phi_0}{(i_1 \dots i_k)} \otimes U(i_1 \dots i_k) \tag{2.25'}$$

development which is similar to Sinanoğlu's formula for the exact wave function.[4]

Here the so-called correlation function is

$$\chi = \left(\sum_{k=1}^{N} \sum\nolimits_{(i_1 \dots i_k)} \frac{\Phi_0}{(i_1 \dots i_k)} \otimes U(i_1 \dots i_k) \right) \tag{2.27}$$

T_3. All the functions $U(i \dots i_k)$ and $\Phi_l \in \beta$ fulfill the orthogonality relations:

$$\langle U(i), \ \Phi_l \rangle = 0$$
$$\vdots$$
$$\langle U(i_1 \dots i_k), \ \Phi_l \rangle = 0 \tag{2.28}$$

Proof. We come back to the definition of the functions

$$U(i), \dots \ U(i_1 \dots i_k)$$
$$U(i) = \Sigma_\mu C^i_\mu \Phi_\mu$$
$$\vdots$$
$$U(i_1 \dots i_k) = \sum\nolimits_{\mu_1 \dots \mu_k} C^{i_1 \dots i_k}_{\mu_1 \dots \mu_k} \left(\bigotimes_j \Phi_{\mu_j} \right)$$

---

*) In the open shell system where it is impossible to find a Φ_0 function with condition (2.26), we may choose a reference set β' consisting of $N' > N$ elements from b. For this reference set we have:

$$\sum_{l=0}^{\binom{N}{N'}} |C_l|^2 > \sum\nolimits_{R > \binom{N}{N'}}^{\infty} |C_l|^2 \qquad (\beta' = \{\Phi_l; 1 \leqslant l \leqslant N'\})$$

[3] O. SINANOĞLU, *J. Chem. Phys.*, **36**, 706 (1962).

[4] O. SINANCĞLU, *Proc. Nat. Acad. Sci. U.S.A.*, **47**, 1217 (1961); *Proc. Roy. Soc.*, **A-260**, 379 (1961); *J. Chem. Phys.*, **36**, 706 (1962); *Rev. Mod. Phys.*, **35**, 517 (1963); *Adv. Chem. Phys.*, **6**, 315 (1964).

Since $\beta \cap \gamma = \emptyset$ (the empty set) and since b is an orthogonal set, we have

$$\langle U(i),\ \Phi_i \rangle = 0 \qquad\qquad \Phi_i \in \beta.$$
$$\vdots$$
$$\langle U(i_1 \ldots i_k),\ \Phi_i \rangle = 0 \ {}^{*)}$$

Obviously we may introduce in the formalism the antisymmetrization as a projector in ${}^{N}\mathcal{H}$

$$\mathcal{A} : {}^{N}\mathcal{H} \to {}^{N}\widetilde{\mathcal{H}}$$

The decomposition of ${}^{N}\widetilde{\mathcal{H}}$ gives the development of an antisymmetric wave function. The use of the antisymmetrized unctions leads to the original form of the ${}^{N}\Psi$ development given by Sinanoğlu as a finite series

$$\Psi^N = \mathcal{A}\left\{\Phi_0 + \sum_{i=1}^{N} \frac{\Phi_0}{(i)} \otimes U(i) + \frac{1}{\sqrt{2\,!}} \sum_{i>j} \frac{\Phi_0}{(ij)} \otimes U(ij) + \ldots\right\}$$

Whence, for the $U(i_1, \ldots, i_k)$ functions it results the property

$$U(i_1, \ldots, i_l, \ldots, i_j, \ldots, i_k) = -\,U(i_1, \ldots, i_j, \ldots, i_l, \ldots\, i_k)$$

This form of the exact function may be used as a test function, by limiting the choice to some of the series terms (mainly of the $U(ij)$ type).

CONCLUSIONS

We wish to emphasize here some of the general conclusions of our work.

1. Any model of independent particles, pairs or groups, necessarily leads to the formal consideration of a tensorial product space of more Hilbert spaces — the latter ones representing the sets of states of the particles, pairs or groups initially considered. This tensorial product has a closure equal to that of ${}^{N}\mathcal{H}$, that is for any $\Psi \in {}^{N}\mathcal{H}$ and for any $\varepsilon > 0$, we find an element Φ of the tensorial product space such that $\| \Psi - \Phi \| < \varepsilon$ ($\| \cdot \|$ being the norm in ${}^{N}\mathcal{H}$).

Very important seems to be the fact that all the above considerations remain valid for any distribution of the N electrons into pairs or groups. Practically, we are being interested that the series of elements of the tensorial product should converge as quickly as possible towards the function we are looking for; this also accounts for the distribution into groups on the basis of physico-chemical arguments.

2. Starting from a model of independent particles, pairs, or groups, one can always draw a Sinanoğlu-type relationship by choosing a suitable

---

*) These are the so-called "orbital-orthogonality" relations!

representation of the ${}^{N}\mathcal{H}$ space as a direct sum of some of its subspaces. This procedure is of particular interest in the case of the independent particles model. Of course, irrespective of the function-product of N monoelectronic functions we are starting from, we can develop exactly any function into a finite series in which this product-function appears as a first term (2.25′). Nevertheless, it is easy to see that we cannot take into account but a few of the terms of this series, although it is finite. In order to be able to use successfully this development, it is necessary that the starting product function be a Hartree-Fock function, which is precisely the procedure used by Sinanoğlu.

Appendix

The treatment given in our paper is, in fact, in the $\mathcal{L}^2$ space of the square integrable functions, which is a Hilbert space. Here we want to give a sketch for a rigorous proof of T-1.

We shall denote the space of the square integrable functions for the i particle by $\mathcal{L}^2_i$.

The functions in $\mathcal{L}^2_i$ are square integrable with respect to a measure μ_i and those in $\mathcal{L}^2$ with respect to the product measure $\mu = \bigotimes_i \mu_i$.

Obviously the tensorial product $\bigotimes \mathcal{L}^2_i \subset \mathcal{L}^2$. The elements of this tensorial product are just the Φ_K "configurations". Then T-1 follows from the fact that $\bigotimes \mathcal{L}^2_i$ is dense in $\mathcal{L}^2$.[1]

Revue Roumaine de Chimie, 17, 4, 621–631 (1972)

Revue Roumaine de Chimie, **17**, 4, 633 – 642 (1972)

CINÉTIQUE DES RÉACTIONS SUPERFICIELLES EN COURANT, ACCOMPAGNÉES D'UNE AUGMENTATION DU NOMBRE DES MOLÉCULES. IV[1]

EUGEN I. SEGAL
Chaire de Théorie cinétique de la matière et de Cinétique chimique, Université de Bucarest,
13, Bd. Republicii

Reçu le 11 novembre 1971

On présente un calcul formel-cinétique des réactions superficielles d'ordre quelconque, accompagnées d'une augmentation du nombre de molécules.

Dans trois notes antérieures,[1] on a présenté le résultat des calculs cinétiques concernant les réactions superficielles d'ordre 1 et 2 en courant, accompagnées d'une augmentation du nombre de molécules. Le but de cette étude est d'étendre les résultats mentionnés pour des réactions superficielles d'ordre quelconque. Pour cette généralisation, on a utilisé le modèle de Balandin,[2] Frost [3] et Pantchenkov.[4]

On considère une réaction superficielle générale de la forme :

$$\begin{aligned} \nu_1 A_1 + \nu_2 A_2 + \ldots + \nu_i A_i + \ldots + \nu_l A_l \to \nu_1' A_1' + \nu_2' A_2' + \ldots + \\ + \nu_i' A_i' + \ldots \nu_l' A_l' \end{aligned} \tag{I}$$

Les calculs cinétiques formels sont basés sur les hypothèses suivantes :

1. la réaction a lieu en phase adsorbée ;
2. comme étape limitante, on a considéré la réaction superficielle ;
3. l'adsorption des réactants et des produits de réaction est langmuirienne ;
4. chaque molécule a besoin, pour être adsorbée, d'un seul centre superficiel ;
5. la vitesse de la réaction superficielle, définie par la quantité de substance qui entre en réaction dans l'unité de temps sur une unité de

---

[1] Ire – IIIe Parties. E. I. Segal, *Rev. Roumaine Chim.*, **16**, 183 (1971) ; **16**, 495 (1971) ; **16**, 1297 (1971).

[2] A. A. Balandin, *Zhur. obskhchei Khim.*, **12**, 153 (1942) ; *Vestnik MGU*, **1957**, 137.

[3] A. V. Frost, « Trudy po kinetike i katalizu », Izdatelstvo Akademii Nauk SSSR, Moscou, 1956, p. 210 ; I. P. Lapin et A. V. Frost, *Zhur. fiz. Khim.*, **15**, 971 (1951).

[4] G. M. Pantchenkov, « Gueteroguennyi kataliz v Khimicheskoi promyshlennosti », Goskhimizdat, Moscu 1955, p. 291.

surface, ω, peut être exprimée par la relation générale :

$$\omega = k_n \prod_{i-1}^{l} \theta_{A_i}^{\nu_i} \theta_0^{\left(\sum\limits_{i=1}^{l} \nu_i' - \sum\limits_{i=1}^{l} \nu_i\right)} \tag{1}$$

où k_n représente la constante cinétique correspondant à un ordre de réaction n $\left(\text{évidemment } n = \sum\limits_{i=1}^{l} \nu_i\right)$, Π — l'opérateur produit, θ_{A_i} — le degré de recouvrement de la surface par le réactant A_i et θ_0 — la fraction de surface libre.

La dernière hypothèse n'a pas été prise en considération dans les calculs cinétiques effectués par Balandin et collab.[2], Frost [3] et Pantchenkov [4] pour les réactions en courant. Si on néglige l'effet de la fraction de surface libre dans l'équation cinétique, les résultats obtenus seront en contradiction avec le IIe principe de la thermodynamique et seront exprimés, dans certains cas, par des expressions intégrales qui ne mettent pas en évidence la dépendance de la constante cinétique de certains paramètres importants du processus.[1,5]

L'hypothèse 3 permet d'exprimer comme suit la concentration superficielle du réactant A_i et la fraction de surface libre :

$$\theta_{A_i} = \frac{b_{A_i} p_{A_i}}{1 + \sum\limits_{i=1}^{l} b_{A_i} p_{A_i} + \sum\limits_{i=1}^{l} b_{A'} p_{A'}} \tag{2}$$

$$\theta_0 = \frac{1}{1 + \sum\limits_{i=1}^{l} b_{A_i} p_{A_i} + \sum\limits_{i=1}^{l} b_{A_i'} p_{A_i'}} \tag{3}$$

où b_{A_i} et b_{A_i}' représentent les coefficients d'adsorption du réactant A_i et, respectivement, du produit de réaction A_i', tandis que p et p' représentent les pressions partielles correspondantes.

Pour la suite des calculs, on note avec l — la longueur du réacteur tubulaire où est supposée avoir lieu la réaction I, v_0 — la vitesse spatiale et y — le degré de transformation.

La quantité de substance qui entre dans la réaction dans l'unité de temps sur une portion infinitésimale de longueur dl du réacteur est exprimée par :

$$v_0 \mathrm{d}y = \omega \frac{\mathrm{d}S}{\mathrm{d}l} \tag{4}$$

---

[5] S. L. KIPERMAN, « Vvedenie v kinetiku gueteroguennykh katalitichestikh reactsii », Izdatelstvo Nauka, Moscou 1964, p. 134—138.

où ω est défini par :

$$\omega = \frac{\partial^2 x}{\partial t \, \partial S} \tag{5}$$

x étant la quantité de substance, exprimée par les mêmes unités que v_0, qui entre dans la réaction, et $\mathrm{d}S$ — la surface du catalyseur correspondant à une portion de longueur $\mathrm{d}l$ du réacteur.

Soit $S_0 = \frac{\mathrm{d}S}{\mathrm{d}l}$.

Evidemment, S_0 représente la surface du catalyseur correspondant à l'unité de longueur du réacteur. Dans ces conditions, en intégrant l'équation (4), on obtient :

$$S_0 1 = v_0 \int_0^v \frac{\mathrm{d}y}{\omega} \tag{6}$$

Il faut ensuite déterminer la dépendance $\omega = \omega\,(y)$ et intégrer l'expression (6).

Dans ce but, on considère les expressions déduites par Frost [3] et, en généralisant, on obtient pour le nombre de moles des réactants n_{A_1}, $n_{A_2}, \ldots, n_{A_i}, \ldots, n_{A_l}$, et des produits de réaction, $n'_{A_1}, n'_{A_2}, \ldots n'_{A_i}, \ldots, n'_{A_l}$ les relations suivantes :

$$\begin{aligned}
n_{A_1} &= v_0 - \nu_1 v_0 y = v_0(1 - \nu_1 y) \\
n_{A_2} &= f_2 v_0 - \nu_2 v_0 y = v_0(f_2 - \nu_2 y) \\
&\cdots\cdots\cdots\cdots\cdots\cdots \\
n_{A_i} &= f_i v_0 - \nu_i v_0 y = v_0(f_i - \nu_i y) \\
&\cdots\cdots\cdots\cdots\cdots\cdots \\
n_{A_l} &= f_c v_0 - \nu_l v_0 y = v_0(f_l - \nu_l y) \\
n_{A'_1} &= \delta_1 v_0 + \nu'_1 v_0 y = v_0(\delta_1 + \nu'_1 y) \\
n_{A'_2} &= \delta_2 v_0 + \nu'_2 v_0 y = v_0(\delta_2 + \nu'_2 y) \\
&\cdots\cdots\cdots\cdots\cdots\cdots \\
n_{A'_i} &= \delta_i v_0 + \nu'_i v_0 y = v_0(\delta_i + \nu'_i y) \\
&\cdots\cdots\cdots\cdots\cdots\cdots \\
n_{A'_l} &= \delta_l v_0 + \nu'_l v_0 y = v_0(\delta_l + \nu'_l y)
\end{aligned} \tag{7}$$

où

$$f_i = \frac{v_i}{v_0} \text{ et } \delta_i = \frac{v_i'}{v_0}$$

On considère le cas général $f \neq 1$ et $\delta_i \neq 1$. En additionnant, on obtient de (7) le nombre total de moles des réactants et des produits de réaction du système, exprimé par

$$n_{A_1} + n_{A_2} + \ldots + n_{A_i} \ldots . + n_{A_l} + n_{A_1'} + n_{A_2'} + \ldots + n_{A_i'} + \ldots + n_{A_l'} =$$

$$= \left(1 + \sum_2^l f_i + \sum_1^l \delta_i + my\right) v_0 \tag{8}$$

où

$$m = \sum_1^l \nu_i' - \sum_1^l \nu_i \tag{9}$$

Les pressions partielles des réactants en fonction de la pression totale P sont exprimées par :

$$p_{A_1} = \frac{1 - \nu_1 y}{1 + \sum_2^l f_i + \sum_1^l \delta_i + my} P$$

$$p_{A_2} = \frac{f_2 - \nu_2 y}{1 + \sum_2^l f_i + \sum_1^l \delta_i + my} P$$

$$\ldots\ldots\ldots\ldots\ldots$$

$$p_{A_i} = \frac{f_i - \nu_i y}{1 + \sum_2^l f_i + \sum_i^l \delta_i + my} P \tag{10}$$

$$\ldots\ldots\ldots\ldots$$

$$p_{A_l} = \frac{f_l - \nu_l y}{1 + \sum_2^l f_i + \sum_1^l \delta_i + my} P$$

De même, pour les pressions partielles des produits de réaction, on obtient les relations

$$
\begin{aligned}
p_{A_1'} &= \frac{\delta_1 + \nu_1' y}{1 + \sum\limits_2^l f_i + \sum\limits_1^l \delta_i + my} P \\
p_{A_2'} &= \frac{\delta_2 + \nu_2' y}{1 + \sum\limits_2^l f_i + \sum\limits_1^l \delta_i + my} P \\
&\cdots\cdots\cdots\cdots \qquad\qquad (11) \\
p_{A_i'} &= \frac{\delta_i + \nu_i' y}{1 + \sum\limits_2^l f_i + \sum\limits_1^l \delta_i + my} P \\
&\cdots\cdots\cdots\cdots \\
p_{A_l'} &= \frac{\delta_l + \nu_l' y}{1 + \sum\limits_2^l f_i + \sum\limits_1^l \delta_i + my} P
\end{aligned}
$$

Compte tenu de (2), (3), (10) et (11) t de la notation $n' = \sum\limits_{i=1}^{l} \nu_i'$, l'expression (1) de la vitesse de réaction devient

$$
\begin{aligned}
\omega &= \\
&= k_n \frac{(b_{A_1}P)^{\nu_1}(b_{A_2}P)^{\nu_2}\ldots(b_{A_i}P)^{\nu_i}\ldots(b_{A_l}P)^{\nu_l}(1-\nu_1 y)^{\nu_1}(f_2-\nu_2 y)^{\nu_2}\ldots(f_i-\nu_i y)^{\nu_i}\ldots(f_l-\nu_l y)^{\nu_l}}{\left[1 + \sum\limits_2^l f_i + \sum\limits_1^l \delta_i + my + b_{A_1}P(1-\nu_1 y) + \sum\limits_2^l b_{A_i}P(f_i-\nu_i y) + \sum\limits_1^l b_{A_i'}P(\delta_i + \nu_i' y)\right]^{n'}} \\
&\quad \times \left(1 + \sum_2^l f_i + \sum_1^l \delta_i + my\right)^m \qquad (12)
\end{aligned}
$$

Pour simplifier cette expression, on note :

$$b_{A_i}P = \beta_i \qquad b'_{A_i}P = \beta_i' \tag{13}$$

$$a = 1 + \sum_2^l f_i + \sum_1^l \delta_i - b_{A_1}P + \sum_2^l b_{A_i}Pf_i + \sum_1^l b_{A_i'}P\delta_i \tag{14}$$

$$b = m - \sum_1^l b_{A_i}P\nu_i - \sum_1^l b_{A_i'}P\nu_i' \tag{15}$$

$$c = 1 + \sum_{2}^{l} f_i + \sum_{1}^{l} \delta_i \tag{16}$$

et on obtient :

$$\omega = k_n \prod_{1}^{l} \beta_i \frac{(1 - \nu_1 y)^{\nu_1} (f_2 - \nu_2 y)^{\nu_2} \ldots (f_i - \nu_i y)^{\nu} \ \ldots (f_l - \nu_l y)^{\nu_l}}{(a + by)^{n'}} \times$$

$$\times (c + my)^m \tag{17}$$

En introduisant ce dernier résultat dans (6), on obtient :

$$k_n S = \frac{v_0}{\prod_{1}^{l} \beta_i^{\nu_i}} \int_0^y \frac{(a + by)^{n'}}{(1 - \nu_1 y)^{\nu_1} \prod_{2}^{l} (f_i - \nu_i y)^{\nu_i} (c + my)^m} \,\mathrm{d}y \tag{18}$$

En examinant séparément l'intégrale

$$I_{(y)} = \int_0^y \frac{(a + by)^{n'}}{(1 - \nu_1 y)^{\nu_1} \prod_{2}^{l} (f_i - \nu_i y)^{\nu_i} (c + my)^m} \,\mathrm{d}y \tag{19}$$

on remarque, qu'il est avantageux pour la suite des calculs d'exprimer l′ intégrand sous la forme suivante :

$$\frac{(a + by)^{n'}}{(1 - \nu_1 y)^{\nu_1} (f_2 - \nu_2 y)^{\nu_2} \ldots (f_i - \nu_i y)^{\nu_i} \ldots (f_l - \nu_l y)^{\nu_l} (c + my)^m} =$$

$$= \frac{b^{n'}}{(1 -)^n \, \nu_1^{\nu_1} \nu_2^{\nu_2} \ldots \nu_i^{\nu_i} \ldots \nu_l^{\nu_l} \, m^m} + \tag{20}$$

$$+ \frac{(a + by)^{n'} - \dfrac{b^{n'}}{(-1)^n \, \nu_1^{\nu_1} \, \nu_2^{\nu_2} \ldots \nu_i^{\nu_i} \ldots \nu_l^{\nu_l} \, m^m} (1 - \nu_1 y) \prod_{2}^{l} (f_i - \nu_i y)^{\nu_i} (c + my)^m}{(1 - \nu_1 y)^{\nu_1} \prod_{2}^{l} (f_i - \nu_i y)^{\nu_i} (c + my)^m}$$

En notant

$$\frac{b^{n'}}{(-1)^n \, \nu_1^{\nu_1} \, \nu_2^{\nu_2} \ldots \nu_i^{\nu_i} \ldots \nu_l^{\nu_l} \, m^m} = \alpha \tag{21}$$

le second terme du membre II de la relation (20) peut être écrit de la façon suivante :

$$\frac{(a+by)^{n'}-\dfrac{b^{n'}}{(-1)^{n}\,\nu_1^{\nu_1}\,\nu_2^{\nu_2}\ldots\nu_i^{\nu_i}\ldots\nu_l^{\nu_l}\,m^{m}}(1-\nu_1 y)^{\nu_1}\prod_2^{l}(f_i-\nu_i y)^{\nu_i}(c+my)^{m}}{(1-\nu_1 y)^{\nu_1}\prod_2^{l}(f_i-\nu_i y)^{\nu_i}\,(c+my)^{m}}=$$

$$=\frac{(a+by)^{n'}-b^{n'}\left(y-\dfrac{1}{\nu_1}\right)^{\nu_1}\left(y-\dfrac{f_2}{\nu_2}\right)^{\nu_2}\ldots\left(y-\dfrac{f_l}{\nu_l}\right)^{\nu_l}\left(y+\dfrac{c}{m}\right)^{m}}{\dfrac{b^{n'}}{\alpha}\left(y-\dfrac{1}{\nu_1}\right)^{\nu_1}\left(y-\dfrac{f_2}{\nu_2}\right)^{\nu_2}\ldots\left(y-\dfrac{f_l}{\nu_l}\right)^{\nu_l}\left(y+\dfrac{c}{m}\right)^{m}} \tag{22}$$

Cette expression peut être à son tour développée en fractions simples[6] :

$$\frac{(a+by)^{n'}-b^{n'}\left(y-\dfrac{1}{\nu_1}\right)^{\nu_1}\left(y-\dfrac{f_2}{\nu_2}\right)^{\nu_2}\ldots\left(y-\dfrac{f_l}{\nu_l}\right)^{\nu_l}\left(y+\dfrac{c}{m}\right)^{m}}{\dfrac{b^{n'}}{\alpha}\left(y-\dfrac{1}{\nu_1}\right)^{\nu_1}\left(y-\dfrac{f_2}{\nu_2}\right)^{\nu_2}\ldots\left(y-\dfrac{f_l}{\nu_l}\right)^{\nu_l}\left(y+\dfrac{c}{m}\right)^{m}}=$$

$$\begin{aligned}
=\frac{\alpha}{b^{n'}}\Bigg[&\frac{A_1^1}{y-\dfrac{1}{\nu_1}}+\frac{A_1^2}{\left(y-\dfrac{1}{\nu_1}\right)^2}+\ldots+\frac{A_1^{\nu_1}}{\left(y-\dfrac{1}{\nu_1}\right)^{\nu_1}}+\\
&+\frac{A_2^1}{y-\dfrac{f_2}{\nu_2}}+\frac{A_2^2}{\left(y-\dfrac{f_2}{\nu_2}\right)^2}+\ldots+\frac{A_2^{\nu_2}}{\left(y-\dfrac{f_2}{\nu_2}\right)^{\nu_2}}+]\\
&+\ldots\ldots\ldots\ldots\ldots\ldots+\\
&+\frac{A_i^1}{y-\dfrac{f_i}{\nu_i}}+\frac{A_i^2}{\left(y-\dfrac{f_i}{\nu_i}\right)^2}+\ldots+\frac{A_i^{\nu_i}}{\left(y-\dfrac{f_i}{\nu_i}\right)^{\nu_i}}+]\\
&+\ldots\ldots\ldots\ldots\ldots\ldots\\
&+\frac{A_l^1}{y-\dfrac{f_l}{\nu_l}}+\frac{A_l^2}{\left(y-\dfrac{f_l}{\nu_l}\right)^2}+\ldots+\frac{A_l^{\nu_l}}{\left(y-\dfrac{f_l}{\nu_l}\right)^{\nu_l}}+]\\
&+\frac{A_{l+1}^1}{y+\dfrac{c}{m}}+\frac{A_{l+1}^2}{\left(y+\dfrac{c}{m}\right)^2}+\ldots+\frac{A_{l+1}^{m}}{\left(y+\dfrac{c}{m}\right)^{m}}\Bigg]
\end{aligned} \tag{23}$$

---

[6] V. Smirhov, « Cours de mathématiques supérieures », Tome I, Ed. Mir., Moscou, 1969, p. 481.

Soit

$$f(y) = \frac{(a+b)^{n'} - b^{n'}\left(y-\frac{1}{\nu_1}\right)^{\nu_1}\left(y-\frac{f_2}{\nu_2}\right)^{\nu_2}\cdots\left(y-\frac{f_i}{\nu_i}\right)^{\nu_i}\cdots\left(y-\frac{f_l}{\nu_l}\right)^{\nu_l}\left(y+\frac{c}{m}\right)^{m}}{\left(y-\frac{1}{\nu_1}\right)^{\nu_1}\left(y-\frac{f_2}{\nu_2}\right)^{\nu_2}\cdots\left(y-\frac{f_l}{\nu_l}\right)^{\nu_l}\left(y+\frac{c}{m}\right)^{m}} \tag{24}$$

Les coefficients A_k^r du développement (23) peuvent être déterminés comme suit[6] :

$$A_1^{\nu_1-i} = \frac{1}{i\,!}\frac{\mathrm{d}^i}{\mathrm{d}y^i}\left[f(y)\left(y-\frac{1}{\nu_1}\right)^{\nu_1}\right]\Bigg|_{y=\frac{1}{\nu_1}} \qquad i = 0,\ 1,\ 2, \ldots\ \nu_1 - 1$$

$$A_2^{\nu_2-i} = \frac{1}{i\,!}\frac{\mathrm{d}^i}{\mathrm{d}y^i}\left[f(y)\left(y-\frac{f_2}{\nu_2}\right)^{\nu_2}\right]\Bigg|_{y=\frac{f_2}{\nu_2}} \qquad i = 0, 1, 2, \ldots\ \nu_2 - 1$$

$$\cdots\cdots\cdots\cdots\cdots\cdots\cdots\cdots \tag{25}$$

$$A_l^{\nu_l-i} = \frac{1}{i\,!}\frac{\mathrm{d}^i}{\mathrm{d}y^i}\left[f(y)\left(y-\frac{f_l}{\nu_l}\right)^{\nu_l}\right]\Bigg|_{y=\frac{f_l}{\nu_l}} \qquad i = 0, 1\ , 2\ \ldots\ \nu_l - 1$$

$$A_{l+1}^{m-i} = \frac{1}{i\,!}\frac{\mathrm{d}^i}{\mathrm{d}y^i}\left[f(y)\left(y+\frac{c}{m}\right)^{m}\right]\Bigg|_{y=-\frac{c}{m}} \qquad i = 0\ , 1, 2\ \ldots\ m - 1$$

En connaissant ces coefficients, on peut facilement calculer l'intégrale (9) de l'expression (19). En effet, en tenant compte de (20),

$$I = -\frac{b'_n}{(-1)^n \prod\limits_1^l \nu_i^{\nu_i}\, m^m} - y +$$

$$+ \frac{1}{(-1)^n \prod\limits_1^l \nu_i^{\nu_i}\, m^m}\left[A_1^1 \ln\left(y-\frac{1}{\nu_1}\right) - \frac{A_1^2}{y-\frac{1}{\nu_1}} - \frac{A_1^3}{2\left(y-\frac{1}{\nu_1}\right)^2} - \ldots -\right.$$

$$- \frac{A_1^{\nu_1}}{(\nu_1-1)\left(y-\frac{1}{\nu_1}\right)^{\nu_1-1}} + A_2^1 \ln\left(y-\frac{f_2}{\nu_2}\right) - \frac{A_2^2}{y-\frac{f_2}{\nu_2}} - \frac{A_2^3}{2\left(y-\frac{f_2}{\nu_2}\right)^2} - \ldots -$$

$$- \frac{A_2^{\nu_2}}{(\nu_2-1)\left(y-\frac{f_2}{\nu_2}\right)^{\nu_2-1}} + \ldots\ldots\ldots\ldots\ldots +$$

$$+A_l^1 \ln\left(y-\frac{f_l}{\nu_l}\right)-\frac{A_l^2}{y-\dfrac{f_l}{\nu_l}}+\frac{A_l^3}{2\left(y-\dfrac{f_l}{\nu_l}\right)^2}-\dots-\frac{A_l^{\nu_l}}{(\nu_l-1)\left(y-\dfrac{f_l}{\nu_l}\right)^{\nu_l-1}}+ \tag{26}$$

$$+A_{l+1}^1 \ln\left(y+\frac{c}{m}\right)-\frac{A_{l+1}^2}{y+\dfrac{c}{m}}\,\frac{A_{l+1}^3}{2\left(y+\dfrac{c}{m}\right)^2}-\dots-\frac{A_{l+1}^m}{(m-1)\left(y+\dfrac{c}{m}\right)^{m-1}}$$

En introduisant ce résultat dans (18), on obtient :

$$k_nS=\frac{v_0}{\prod\limits_1^l \beta_i^{\nu_i}}\left\{\frac{b^{n'}}{(-1)^n\prod\limits_1^l \nu^{\nu_i}\, m^m}\,y+\dots\right.$$

$$+\frac{1}{(-1)^n\prod\limits_1^l \nu_i^{\nu_i}\dots m^m}\left[A_1\ln\left(y-\frac{1}{\nu_1}\right)-\frac{A_1^2}{y-\dfrac{1}{\nu_1}}-\frac{A_1^3}{2\left(y-\dfrac{1}{\nu_1}\right)^2}-\dots-\right.$$

$$-\frac{A_1^{\nu_1}}{(\nu_1-1)\left(y-\dfrac{1}{\nu_1}\right)^{\nu_1-1}}+A_2^1\ln\left(y-\frac{f_2}{\nu_2}\right)-\frac{A_2^2}{y-\dfrac{f_2}{\nu_2}}+\frac{A_2^3}{2\left(y-\dfrac{f_2}{\nu_2}\right)^2}-$$

$$-\frac{A_2^{\nu_2}}{(\nu_2-1)\left(y-\dfrac{f_2}{\nu_2}\right)^{\nu_2-1}}+\dots\dots\dots\dots \tag{27}$$

$$+A_l^1\ln\left(y-\frac{f_l}{\nu_l}\right)-\frac{A_l^2}{y-\dfrac{f_l}{\nu_l}}-\frac{A_l^3}{2\left(y-\dfrac{f_l}{\nu_l}\right)^2}-\dots-\frac{A_l^{\nu_l}}{(\nu_l-1)\left(y-\dfrac{f_l}{\nu_l}\right)^{\nu_l-1}}+$$

$$\left.\left.+A_{l+1}^1\ln\left(y+\frac{c}{m}\right)-\frac{A_{l+1}^2}{y+\dfrac{c}{m}}-\frac{A_{l+1}^3}{2\left(y+\dfrac{c}{m}\right)^2}-\dots-\frac{A_{l+1}^m}{(m-1)\left(y+\dfrac{c}{m}\right)^{m-1}}\right]\right\}$$

En appliquant cette relation à des cas particuliers, on retrouve les formules de calcul des constantes cinétiques pour des réactions d'un certain ordre. La comparaison des formules de calcul déduites ainsi et de celles établies sans tenir compte de l'effet de la fraction de surface libre a déjà été présentée dans les notes antérieures.[1]

CONCLUSIONS

1. On a effectué un calcul cinétique formel des réactions superficielles isolées en courant, accompagnées d'une augmentation du nombre de molécules.

2. La particularisation des résultats ainsi obtenus conduit à des formules de calcul correctes et en principe fondées pour la description cinétique des différents processus superficiels.

Revue Roumaine de Chimie, **17**, *4*, 643–646 (1972)

FORMULES DE CALCUL DU NOMBRE DES SOUS-SYSTÈMES CONTENUS DANS LES SYSTÈMES CHIMIQUES BINAIRES, TERNAIRES ET QUATERNAIRES

R. DINESCU et M. CERCHEZ

Centre de Chimie Physique, Bucarest, 23, Str. Dumbrava Roșie

Reçu le 14 décembre 1971

On a calculé par analyse combinatoire toutes les formules pour la détermination du nombre des sous-systèmes qui se forment dans les systèmes chimiques binaires, ternaires et quaternaires ayant des composants chimiques.

La connaissance du nombre des sous-systèmes qui composent un système chimique polynaire ayant des composants chimiques simplifie l'obtention des diagrammes d'équilibre de phase, étant donné que ce nombre fournit des indications sur les paragenèses d'équilibre.

Les formules de détermination du nombre des sous-systèmes du même ordre pour les systèmes binaires, ternaires et quaternaires sont connues.[1–3] Les formules de calcul du nombre des sous-systèmes d'un ordre inférieur (par exemple la détermination dans le cas des systèmes quaternaires du nombre des sous-systèmes binaires et ternaires), pour les systèmes des composants chimiques, ne sont pas connues.

Dans ce qui suit, on présente toutes les formules nécessaires pour la détermination complète du nombre des sous-systèmes qui se forment dans les systèmes des composants chimique binaires, ternaires et quaternaires.

DÉTERMINATION DES FORMULES DE CALCUL DU NOMBRE DES SOUS-SYSTÈMES

Le nombre des sous-systèmes possible qui se forment dans un système avec n composants ayant des composants définis de l'ordre n et des composants de l'ordre $n' \leqslant n - 1$ se déduit en considérant le fait qu'un composant défini peut coordiner seulement avec les composants du sous-système de l'ordre du système donné — qui résultent par son élimination.

---

[1] N. S. Curnacov, « Vvedenie v fizico-khimicheskii analiz », Izd. N.A.S.S.S.R. Moscou—Leningrad, 1940, p. 62.

[2] N. S. Dombrovscaya, *Izv. sect. fiz. khim. analiza*, **19**, 1949, 103.

[3] A. S. Berejnoi, « Mnogocomponentyie sistemy ochislov », Izd. Naucova dumca, Kiev, 1970, p. 18, 243—264.

Dans ce but on a recours à l'analyse combinatoire, utilisée usuellement aussi pour d'autres types de déterminations dans la géométrie thermodynamique, par exemple dans le cas des équilibres polyphasiques hétérogènes.[4]

Dans le tableau 1 sont données en détail, les formules de détermination du nombre des sous-systèmes en fonction des composants binaires, ternaires et quaternaires qui peuvent se former dans les systèmes binaires, ternaires et quaternaires. On mentionne que les formules ne s'appliquent que pour les composants qui font partie des sous-systèmes limites du système initial et la position de trois ou plusieurs composants ternaires ne doit pas être colinéaire et de quatre ou plusieurs composants quaternaires ne doit pas être coplanaire.

Tableau 1

Nombre des sous-systèmes binaires ternaires et quaternaires qui peuvent se former dans les systèmes binaires ternaires et quaternaires suivant le type des composés chimiques du système

Systèmes quaternaires *Q* — nombre de composants quaternaires	*Sous-systèmes quaternaires* $C_4^4 + Q(C_5^4 - C_4^4 - 1) = 1 + 3Q^*)$ *Sous-systèmes ternaires* $C_4^3 + Q(C_5^3 - C_4^3) = 4 + 6Q$ *Sous-systèmes binaires* $C_4^2 + Q\,(C_5^2 - C_4^2) = 6 + 4Q$
Systèmes quaternaires *T* — nombre de composants ternaires	*Sous-systèmes quaternaires* $C_4^4 + T(C_5^4 - C_4^4 - 2) = 1 + 2T^*)$ *Sous-systèmes ternaires* $C_4^3 + T(C_5^3 - C_4^3 - 1) = 4 + 5T$ *Sous-systèmes binaires* $C_4^2 + T(C_5^2 - C_4^2) = 6 + 4T$
Systèmes quaternaires *B* — nombre de composants binaires	*Sous-systèmes quaternaires* $C_4^4 + B(C_5^4 - C_4^4 - 3) = 1 + B^*)$ *Sous-systèmes ternaires* $C_4^3 + B(C_5^3 - C_4^3 - 3) = 4 + 3B$ *Sous-systèmes binaires* $C_4^2 + B(C_5^2 - C_4^2 - 1) = 6 + 3B$

[4] E. M. Levin, C. R. Robbins, H. F. Mc.Murdie, « Phase Diagrams for Ceramists », Ed. The American Ceramic Society inc., Columbus-Ohio, 1964, p. 26—246.

Tableau 1 (suite)

Systèmes quaternaires Q — nombre de composants quaternaires T — nombre de composants ternaires B — nombre de composants binaires	*Sous-systèmes quaternaires* $3C_4^4 + Q(C_5^4 - C_4^4 - 1) + T(C_5^4 - C_4^4 - 2) + B(C_5^4 - C_4^4 - 3) = 1 + B + 2T + 3Q^{*})$ *Sous-systèmes ternaires* $3C_4^3 + Q(C_5^3 - C_4^3) - T(C_5^3 - C_4^3 - 1) + B(C_5^3 - C_4^3 - 3) = 1 + 3B + 5T + 6Q$ *Sous-systèmes binaires* $3C_4^2 + Q(C_5^2 - C_4^2) + T(C_5^2 - C_4^2) + B(C_5^2 - C_4^2 - 1) = 6 + 3B + 4T + 4Q$
Systèmes ternaires T — nombre de composants ternaires	*Sous-systèmes ternaires* $C_3^3 + T(C_4^3 - C_3^3 - 1) = 1 + 2T^{*})$ *Sous-systèmes binaires* $C_3^2 + T(C_4^2 - C_3^2) = 3 + 3T$
Systèmes ternaires B — nombre de composants binaires	*Sous-systèmes ternaires* $C_3^3 + B(C_4^3 - C_3^3 - 2) = 1 + B^{*})$ *Sous-systèmes binaires* $C_3^2 + B(C_4^2 - C_3^2 - 1) = 3 + 2B$
Systèmes ternaires T — nombre de composants ternaires B — nombre de composants binaires	*Sous-systèmes ternaires* $2C_3^3 + T(C_4^3 - C_3^3 - 1) + B(C_4^3 - C_3^3 - 2) = 1 + B + 2T^{*})$ *Sous-systèmes binaires* $2C_3^2 + T(C_4^2 - C_3^2) + B(C_4^2 - C_3^2 - 1) = 3 + 2B + 3T$
Systèmes binaires B — nombre de composants binaires	*Sous-systèmes binaires* $C_2^2 + B(C_3^2 - C_2^2 - 1) = 1 + B^{*})$

---

*) Formules démontrées aussi par Curnacov[1] et Dombrovscaya[2]

Les vérifications effectuées pour quelques systèmes oxydiques sont indiquées dans le tableau 2 ; il résulte un accord parfait avec les déterminations expérimentales.

Tableau 2

Vérification du nombre des sous-systèmes dans les systèmes oxydique binaires, ternaires et quaternaires

Système	Bibliographie	Composants		Sous-systèmes		
		Binaires	Ternaires	Binaires	Ternaires	Quaternaires
Na_2O-SiO_2	4	4	—	1+4 = 5	—	—
$CaO-SiO_2$	4	4	—	1+4 = 5	—	—
$Al_2O_3-SiO_2$	4	1	—	1+1 = 2	—	—
$MgO-SiO_2$	4	2	—	1+2 = 3	—	—
$CaO-Al_2O_3-SiO_2$	4	10	2	3+2.10+3.2 = 29	1+10+2.2 = 15	—
$MgO-Al_2O_3-SiO_2$	3	4	2	3+2. 4+3.2 = 17	1+4+2.2 = 9	—
$Al_2O_3-TiO_2-MgO$	3	5	—	3+2.5 = 13	1+5 = 6	—
$ZrO_2-TiO_2-SiO_2$	3	2	—	3+2.2 = 7	1+2 = 3	—
$CaO-MgO-FeO-ZrO_2$	3	1	—	6+3.2 = 12	4+3.2 = 10	1+1= 2
$CaO-MgO-FeO-Fe_2O_3$	3	5	—	6+3.5 = 21	4+3.5 = 19	1+5= 6
$CaO-MgO-ZrO_2-TiO_2$	3	8	1	6+3.8+4 = 34	1+3.8+5 = 30	1+8+2=11
$CaO-MgO-FeO-TiO_2$	3	9	—	6+3.9 = 33	4+3.9 = 3	1+9=10

CONCLUSIONS

On a présenté les formules complètes pour la détermination du nombre des sous-systèmes qui se forment dans les systèmes chimiques binaires, ternaires et quaternaires ayant des composants chimiques.

Revue Roumaine de Chimie, 17, 4, 647 – 660 (1972)

POLAROGRAPHIC AND OSCILLOPOLAROGRAPHIC BEHAVIOUR OF DIPICOLINIC ACID*

LUIGI CAMPANELLA, ERNESTO CHIACCHIERINI and MAURIZIO PALCHETTI

Institute of Analytical Chemistry, University, Rome, Italy

Received May 27, 1971

The polarographic and oscillopolarographic behaviour of dipicolinic acid was studied in various media and at 25°. Five reduction processes were evidenced and interpreted on the basis of the equilibria among the six species under which the acid can exist in aqueous solutions. The only species neither polarographically nor oscillopolarographically active resulted to be the completely deprotonated bivalent anion.

The polarographic behaviour of dipicolinic acid (2,6-pyridinedicarboxylic acid or 2,6$-$H$_2$PC) at the dropping mercury electrode (DME) has been qualitatively studied by Volke and Volkova,[1] who looked for the polarographic separation of pyridine carboxylic acids. The authors found that dipicolinic acid gives two polarographic waves in acid medium, the first wave being higher than the second one; on increasing the pH, the two waves decrease, the first one disappears at pH 10, while the second one at pH $\cong$ 5; in neutral medium (pH $\cong$ 7) a third wave appears. Oscillopolarographic behaviour shows two peaks; the peak characterized by a more positive peak potential is also more pronounced than the other; if pH is 7 neither peak is observed.

Considering that dipicolinic acid can exist in several forms depending on the pH of the solution, we have examined its polarographic and oscillopolarographic behaviour, in order to properly correlate them and also to determine the values of equilibria constants. The study was carried out in aqueous solutions, whose free acidity varied from very high values ($\sim$ 6 M HClO$_4$) up to pH 10, and in different media usually used as buffers.

EXPERIMENTAL

MATERIALS

Dipicolinic acid supplied by Aldrich Chemical Co. Inc., was purified by recrystallyzation from water and controlled by melting point determination[2] and by its spectrophotometric characteristics.[3] The solutions were prepared by dissolving in distilled water weighed amounts of the anhydrous acid (dried at 115°). The known equilibrium constants of proton-transfer reactions in water of the acid are reported in Table 1. Citric and Britton-Robinson buffers were prepared in the usual way. All chemicals used were analytically pure.

---

* Work carried out by aid of Italian National Researches Council (C.N.R.) — Rome — Italy.

[1] J. Volke and V. Volkova, *Coll. Czech. Chem. Comm.*, 20, 908 (1955).

[2] E. P. Oliveto "Pyridine and its derivatives", part III, E. Klingsberg, New York, 1962, p. 267.

Table 1

Successive apparent equilibrium constants of proton transfer reactions in water: $H_3B^+ + H_2O \rightleftarrows H_2B + H_3O^+$ (1) $H_2B + H_2O \rightleftarrows HB^- + H_3O^+$ (2) $HB^- + H_2O \rightleftarrows B^{2-} + H_3O^+$ (3)

$pK_{a,1}$	$pK_{a,2}$	$pK_{a,3}$	Ionic strength M	T°C	References
—	2.10 (a)	4.68 (a)	0.1 $NaNO_3$	20°	4
—	2.17 (a)	4.96 (a)	—	—	5
—	2.16 (a)	4.76 (a)	0.1 KCl	30°	6
—	2.09 (b)	4.53 (b)	0.5 $NaClO_4$	25°	7
<0.5 (a)	2.35 (a)	4.80 (a)	$\simeq 5.10^{-4}$	—	8

(a) pH-concentration quotient ("mixed" constant)
(b) concentration quotient

APPARATUS AND PROCEDURE

E. Leybold's Nachfolger (Köln) polarograph with photographic recording and equipped with a DME, whose characteristics (in $KClO_4$ 0.1 M and at open circuit) were: $m = 2.377$ mg sec^{-1}, $t = 3.56$ sec, $l = 21$ cm, $r = 0.032$ mm.

Amel (Milan) polarograph (mod. 461) with pen recording and with a DME having the following characteristics: $m = 0.865$ mg sec^{-1}, $t = 3.00$ sec (obtained by a hammer), $l = 25$ cm, $r = 0.050$ mm. Satured calomel electrode (SCE) was always employed as reference electrode. connected to the measurement cell by means of an agar-KNO_3 or $KClO_4$ conductivity bridge Oscillopolarograph Amel mod. 448; dropping time = 8 sec, waiting time = 6 sec; measurement time = 2 sec.

pHmeter Radiometer "PHM-22r" equipped with usual electrodes and agar-KNO_3 or $KClO_4$ bridges.

The solutions for the polarographic analyses were deareated by N_2 deoxygenated and opportunely humified.

All the measurements were carried out at 25.0 ± 0.5°.

The highest acidities of solutions were expressed by Hammett H_0 function[9,10] for perchloric acid.

The results are the mean of at least five values; the $E_{1/2}$ values resulted to agree within 2 mV (the ohmic drop due to the resistance of the cell circuit being taken into account).

RESULTS

2.6—H_2PC shows different reduction steps or peaks depending on pH. They are numbered according to increasing negative potential.

---

[3] R. M. Acheson and G. A. Taylor, *J. Chem. Soc.*, **4**, 4140 (1959).
[4] G. Anderegg, *Helv. Chim. Acta*, **43**, 414 (1960).
[5] V. D. Canic, *Ber. Chem. Crs. Beograd*, **20**, 29 (1957).
[6] R. M. Tichane and W. E. Bennett, *J. Amer. Chem. Soc.*, **79**, 1293 (1957).
[7] A. Napoli, *Talanta*, **15**, 189 (1968).
[8] J. Faucherre, C. Petitfaux and B. Charletier, *Bull. Soc. chim. France*, **1967**, 1091.
[9] H. B. Kuivila, *J. Phys. Chem.*, **59**, 1028 (1955).
[10] M. A. Paul and F. A. Long, *Chem. Rev.*, **57**, 1626 (1960).

FIRST PROCESS

The first (more positive) polarographic wave (fig. 1) appears in about all the range of acidity examined: only in very acid solutions

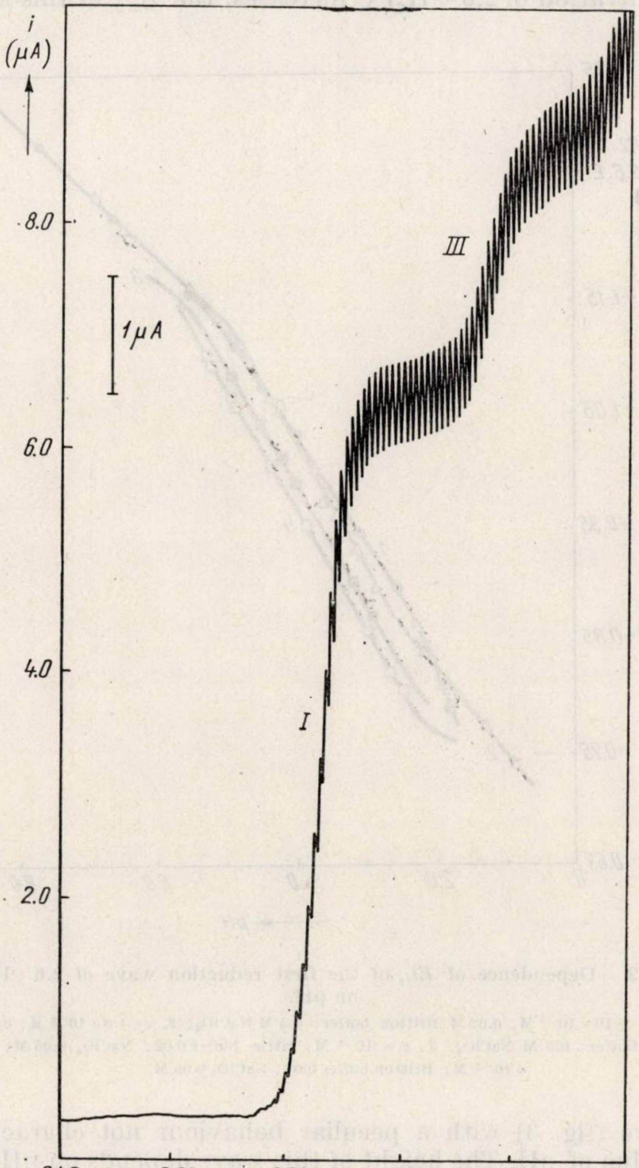

Fig. 1. — Polarographic behaviour of 2,6$-H_2PC$ solution in 0.02 M citric buffer and 0.5 M $NaClO_4$. $c = 1.0 \times 10^{-3}$ M; pH $= 2.40$ (For the III wave see below).

(~5 M in $HClO_4$) or at pH about 10 it is absent; its $E_{1/2}$ is a nonlinear function of pH and becomes more negative with increasing pH; no marked differences of $E_{1/2}$ values were observed in different electrolytes (fig. 2); as the concentration of $2,6-H_2PC$ increases, the $E_{1/2}$ of this step becomes more negative (fig. 3) with a peculiar behaviour not characteristic of a particular value of pH. The height of this wave depends on pH and reaches its maximum value at pH ~ 3 (fig. 4); at this pH value, in the concentration range $10^{-4} + 10^{-3}$ M, there is a proportion between the height of the wave and the concentration of the reducible species.

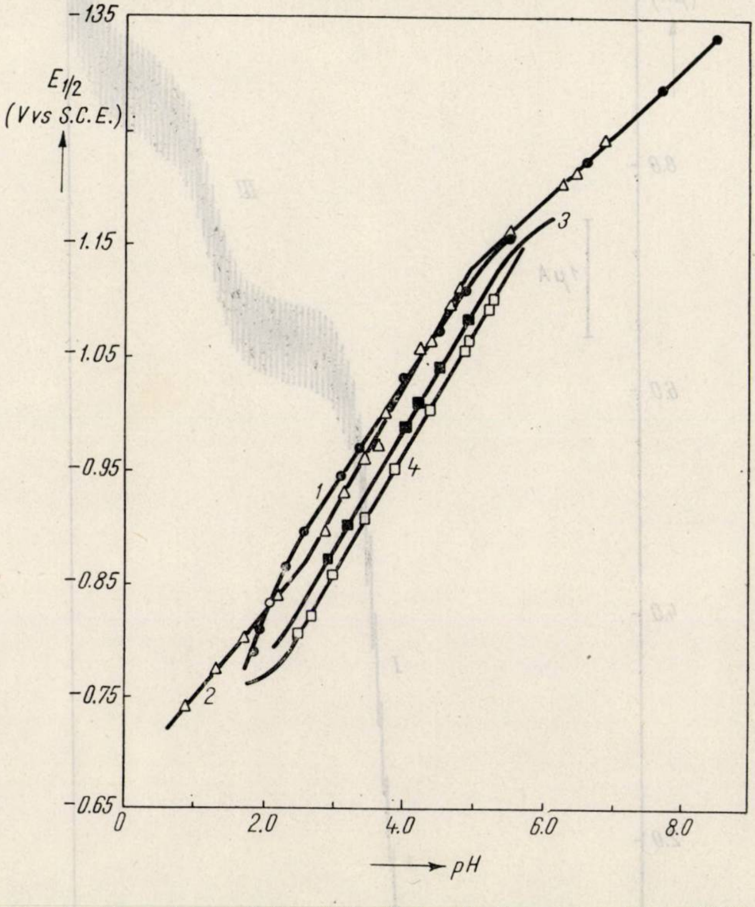

Fig. 2.—Dependence of $E_{1/2}$ of the first reduction wave of $2,6-H_2PC$ on pH.

1, $c = 1.10 \times 10^{-3}$ M; 0.02 M Britton buffer; 0.5 M $NaClO_4$; *2*, $c = 1.0 \times 10^{-3}$ M; 0.02 M citric buffer; 0.5 M $NaClO_4$; *3*, $c = 10^{-3}$ M; citric buffer 0.02; $NaClO_4$ 0.05 M; *4*, $c = 10^{-3}$ M; Britton buffer 0.02; $NaClO_4$ 0.05 M.

The reversibility was tested up to 2×10^{-2} M acid concentration by the semilogarithmic curve $\log i/(i_d - i) = f(V$ vs. SCE) and the first

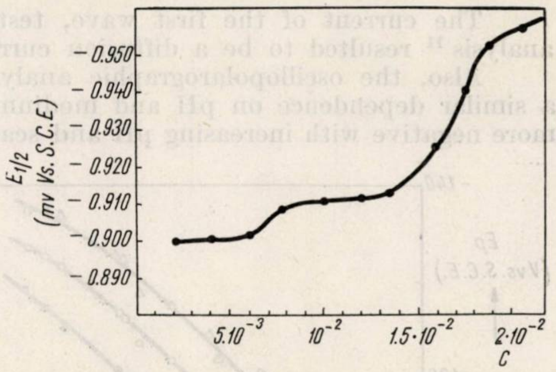

Fig. 3. — Dependence of $E_{1/2}$ of the first reduction process of 2,6 − H_2PC on acid concentration; 0.02 M citric buffer 0.5 M $NaClO_4$.

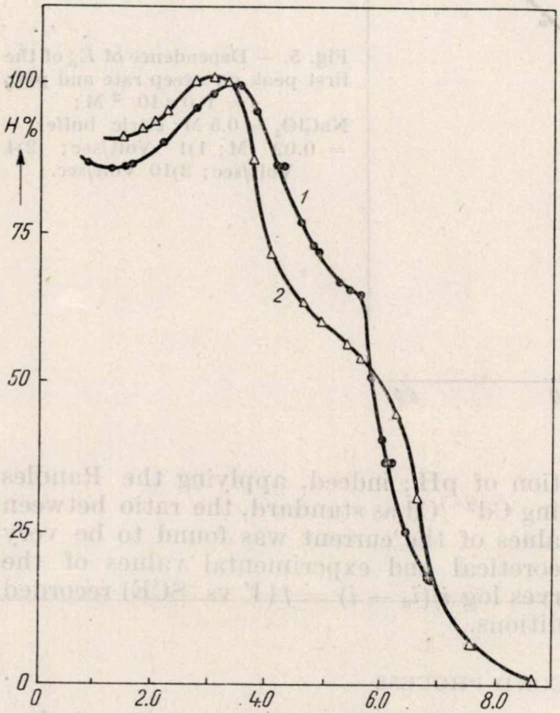

Fig. 4. — Dependence of height, as percentage value of the first reduction wave of 2,6 − H_2PC on pH; *1*, $c = 1.0\times10^{-3}$ M; 0.02 M citric buffer; 0.5 M $NaClO_4$; *2*, $c = 1.0\times10^{-3}$ M; 0.02 M Britton buffer; 0.5 M $NaClO_4$

wave was found to be a reversible one-electron wave only in a narrow range of pH depending on medium:

MEDIUM	pH range for reversibility
0.02 M citric buffer, 0.5 M $NaClO_4$	2.4 ÷ 2.7
0.05 M ,, ,, 0.5 M $NaClO_4$	1.7 ÷ 3.0
0.25 M ,, ,, 0.5 M $NaClO_4$	1.4 ÷ 3.2
0.05 M ,, ,, 0.05M $NaClO_4$	3.1 ÷ 4.5
0.02 M Britton-Robinson buffer, 0.5 M $NaClO_4$	2.0 ÷ 2.3
0.25 M ,, ,, 0.5 M $NaClO_4$	1.7 ÷ 2.5

The current of the first wave, tested by linear and logarithmic analysis [11] resulted to be a diffusion current.

Also, the oscillopolarographic analysis of the first process shows a similar dependence on pH and medium of solution. The E_p becomes more negative with increasing pH and scanning rate (fig. 5). Also in this case the reversibility is a function of pH; indeed, applying the Randles and Sevcik [12,13] equation and using Cd^{2+}/Cd as standard, the ratio between theoretical and experimental values of the current was found to be very near to the ratio between theoretical and experimental values of the slope in the semilogarithmic curves $\log i/(i_d - i) = f(V \text{ vs. SCE})$ recorded in the same experimental conditions.

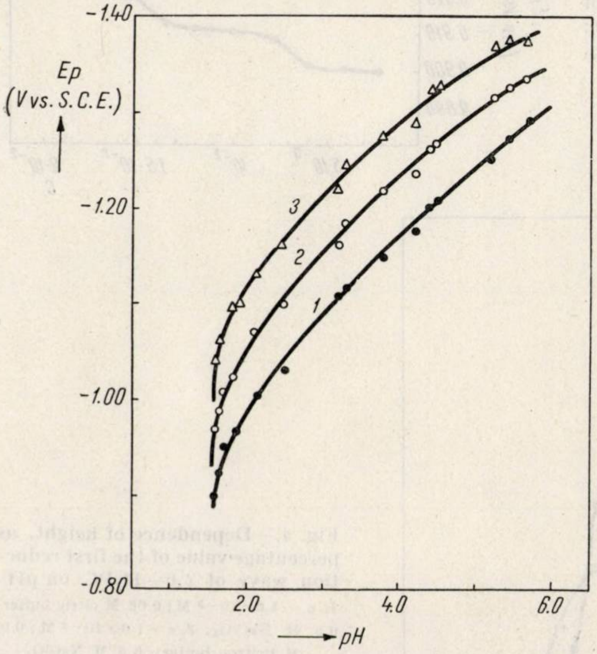

Fig. 5. — Dependence of E_p of the first peak on sweep rate and pH; $c = 1.0 \times 10^{-3}$ M; $NaClO_4 = 0.5$ M; citric buffer = = 0.02 M; 1)1 Volt/sec; 2)4 Volt/sec; 3)10 Volt/sec.

SECOND PROCESS

The second step appears when the pH values of solution is less than 1, but also at pH = 2.0 the presence of this step has its influence on the logarithmic analysis of the first step.

The height of the second step increases with the acidity of the solution while the height of the first step is decreasing; when the acidity is very high (~5 M in $HClO_4$) only the second step is observed (fig. 6,7). The $E_{1/2}$ of this step is about −0.74 V vs. SCE. The corresponding oscillopolarographic peak is clearly evidenced by the derivative oscillopolarograms, recorded for solutions at pH less than 1 (fig. 8).

---

[11] L. Ya. Kheifets, *Zhur. analit. Khim.*, **20**, 355 (1965).

[12] A. Sevcik, *Coll. Czech. Chem. Comm.*, **13**, 349 (1948).

[13] J. E. B. Randles, *Trans. Faraday Soc.*, **44**, 327, 334 (1948).

On the basis of the observed polarographic and oscillopolarographic behaviour, we can propose that different polarographically active species of $2.6-H_2PC$ exist in aqueous solutions.

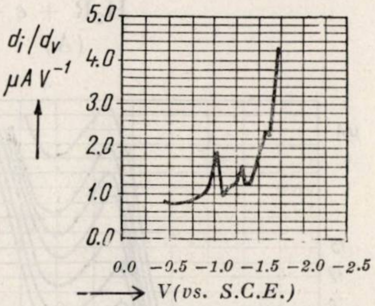

Fig. 8. — Derivative oscillopolarographic curve $di/dV = f(V)$ of $2,6-H_2PC$ solution.

$c = 1.0 \times 10^{-3}$ M; citric buffer = 0.02 M; pH = 0.20; $NaClO_4$ = 0.5 M; voltage sweep rate = 1 V/sec.

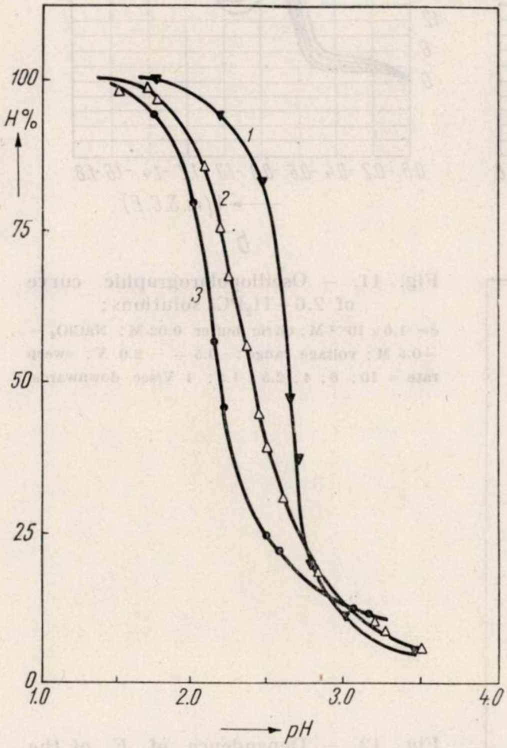

Fig. 9. — Dependence of height, as percentage of the maximum value of the third reduction wave of $2,6-H_2PC$ on pH; $c - 1.0 \times 10^{-3}$M; $NaClO_4 = 0.5$ M.

1, Britton buffer 0.02 M; *2*, citric buffer 0.02 M.

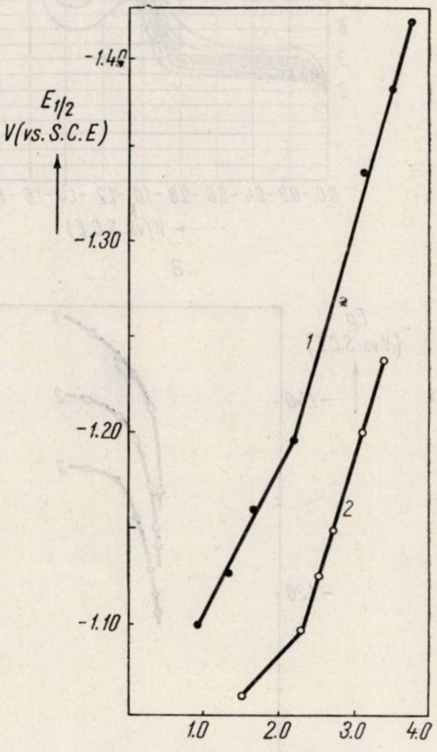

Fig. 10. — Dependence of $E_{1/2}$ of the third reduction wave of $2,6-H_2PC$ on pH.

1, $c = 1.0 \times 10^{-3}$ M; citric buffer 0.02 M; $NaClO_4 = 0.5$ M; *2*, $c = 1.0 \times 10^{-3}$ M; Britton buffer 0.05 M; $NaClO_4 = 0.5$ M.

The results show that the first wave (I) is present in about all our experimental conditions; in very acid medium and also in alkaline medium;

this fact can induce that the process of the first wave should be the reduction of the undissociated diprotic acid:

$$\underset{(A)}{H_2R} + e \rightarrow \underset{(B)}{HR^-} + 1/2\, H_2 \qquad (1)$$

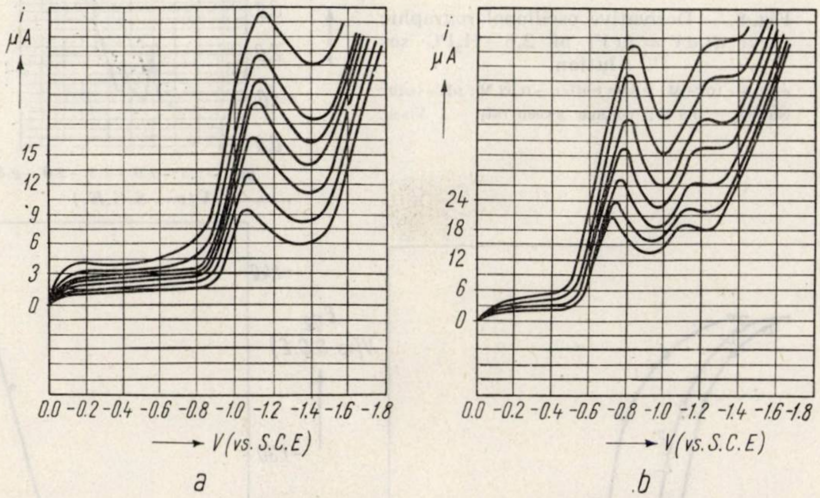

Fig. 11. — Oscillopolarographic curve of 2,6—H_2PC solutions; $c = 1.0 \times 10^{-3}$ M; citric buffer 0.02 M; $NaClO_4$ = 0.5 M; voltage range: $-0.5 \div -2.0$ V; sweep rate = 10; 6; 4; 2.5; 1.5; 1 V/sec downwards.

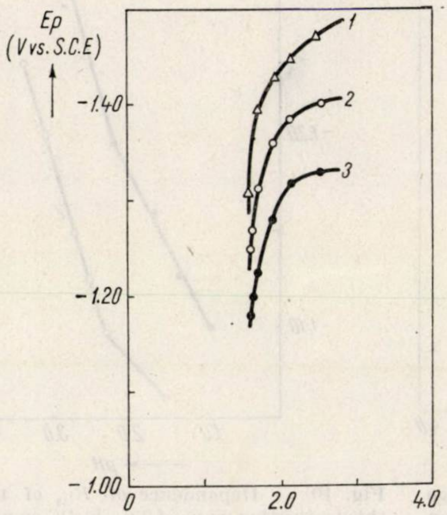

Fig. 12. — Dependence of E_p of the third peak on sweep rate and pH. $c = 1.0 \times 10^{-3}$ M; citric buffer = 0.25 M; *1*, 1 V/sec; *2*, 4 V/sec; *3*, 10 V/sec.

Because the height of this wave is a particular function of pH with maximum value at pH about 3 or 3.5 (Fig. 4), we have to suppose the existence of some competing equilibria; therefore we could not calculate the exact value of the acid-base constant for the equilibrium (I) by variation of the height of the wave with pH. Nevertheless, the approximated equilibrium constant deduced by the analysis of fig. 4 resulted to be depending on the electrolyte medium, but anyway about 2.1, and therefore very near to the values previously reported (table 1) in literature.

The existence of an adsorption component of the current of this wave, is evidenced by the curve of figure 15. The increase of the height of the wave with increasing acidity of the solution, can be explained by the protonation of undissociated species H_2R to H_3R^+ in very acid medium in agreement with other authors [8]; in fact, as it is shown in picture 8 a new wave (II) occurs in very acid solutions. In this case the reduction can occur as

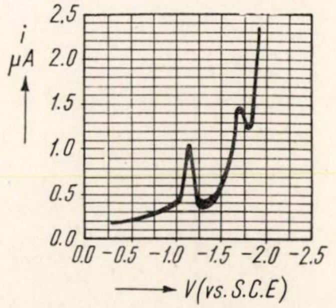

Fig. 13. — Oscillopolarographic curve of 2,6−H_2PC solution.
$c = 1.0 \times 10^{-3}$ M; citric buffer = 0.02 M; pH = 5.20; voltage sweep rate = 1 V/sec.

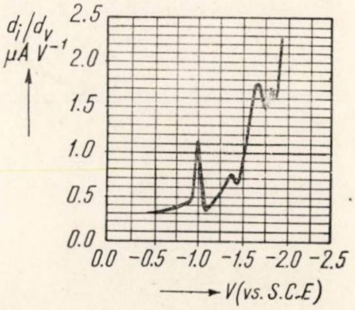

Fig. 14. — Derivative oscillopolarographic curve $di/dV = f\ (V)$ of 2,6−H_2PC solution.
$c = 1.0 \times 10^{-3}$M; citric buffer = 0.02 M; pH = 4.20; $NaClO_4$ = 0.5 M; voltage sweep rate = 1 V/sec.

$$\underset{(C)}{H_3R^+} + 1\,e \rightarrow \underset{(A)}{H_2R} + 1/2\,H_2 \qquad (2)$$

For this equilibrium we could find the protonation constant in perchloric acid by Hammett's function [9,10] (Fig. 16); the calculated value results to be −1.5.

The assignment of this wave and of the corresponding peak to the reduction of protonated species, is confirmed by the fact that both disappear by treating the solutions with cationic exchanger.

The existence of the following equilibrium must be also considered :

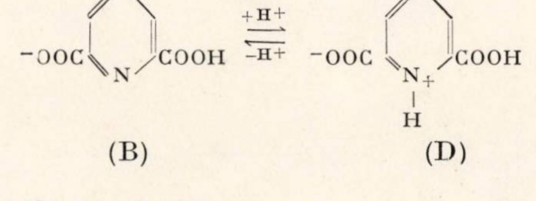

(B) (D) (3)

its real extent is confined by the third wave (III) (Fig. 1), the reduction process being :

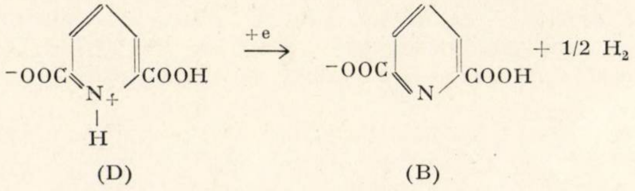

(4)

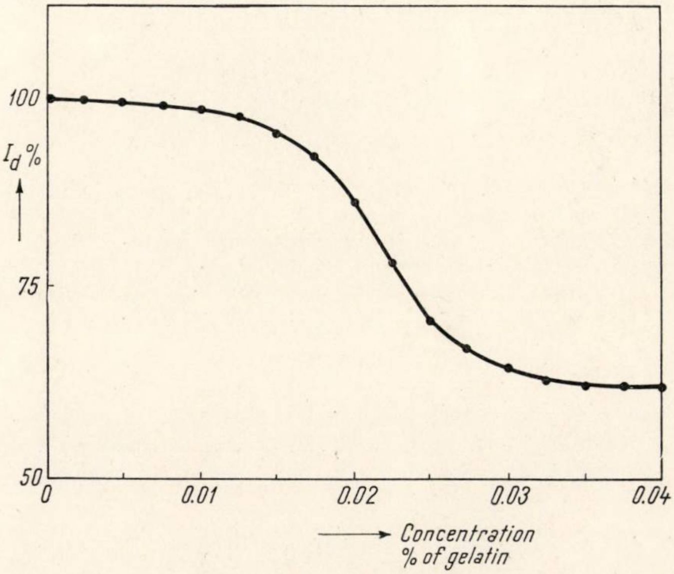

Fig. 15. — Influence of gelatin additions on the height of the first reduction wave of 2,6$-H_2PC$; citric buffer = 0.02 M; pH = 2.40; $NaClO_4$ = 0.5 M; c = 1.0×10^{-3} M

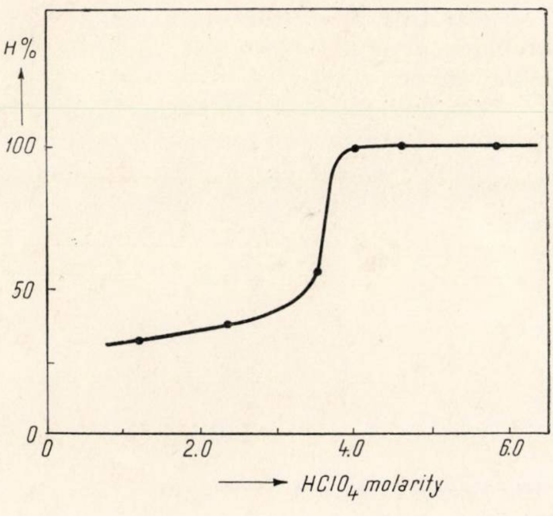

Fig. 16. — Dependence of height of the reduction wave of 2,6$-H_3PC^+$ on $HClO_4$ concentration ; $c = 1.0 \times 10^{-3}$M; $HClO_4 + NaClO_4 = 5$M

The equilibrium constant of the zwitterionic species and univalent anion, can be evaluated by the curve where the height of the wave is plotted against the pH (Fig. 9) and resulted to be 2.2 in citric buffer 0.02 M, 2.6 in citric buffer 0.05 M and 2.4 in Britton buffer 0.02 M.

The value is influenced by the nature of the medium, confirming in this way the zwitterionic nature of the species reduced in this process.[15] When the pH reaches the value of 3.5 + 4, a new wave (IV) occurs at more negative potentials (ws. S.C.E.) than the previous one (Fig. 14). This wave disappears at pH about 10; for this fact and also according to the mechanism of reduction proposed for similar substances,[16] we can propose the electrodic reaction:

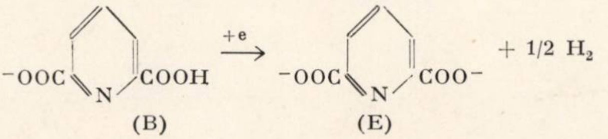

(5)

The values of the above equilibrium constants determined by the analysis in figure 4 resulted to be 4.5 in citric buffer 0.02 M, 4.7 in citric buffer 0.05 M and 4.0 in Britton buffer 0.02 M, the dependence on medium being still observed.

By increasing the pH of solutions, the (B) species can change in (F) as:

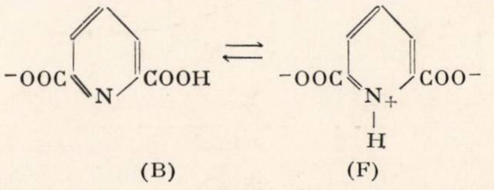

(6)

The presence of different polarographically active species in solutions of 2,6$-H_2PC$, as above said, is also pointed out by the shape of the curve represented in figure 4: the different inflexion points of this curve can be ascribed respectively to the equilibria (1), (5) and (6); the presence of different electrolytes can affect the position of the inflexion points.

Also, the species (F) is polarographically active, but the corresponding wave (V) occurs only under particular conditions. In this case we can suppose the reduction of (F) species as

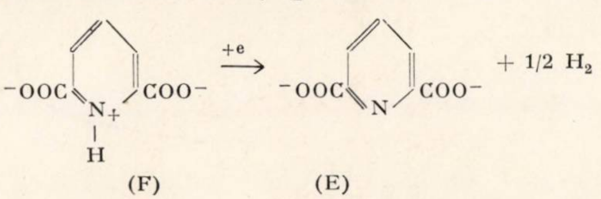

(7)

---

[16] J. Volke, *Coll. Czech. Chem. Comm.*, **22**, 1777 (1957).

All equilibria concerning 2,6$-H_2PC$ are finally collected in figure 17, showing their dependence on pH.

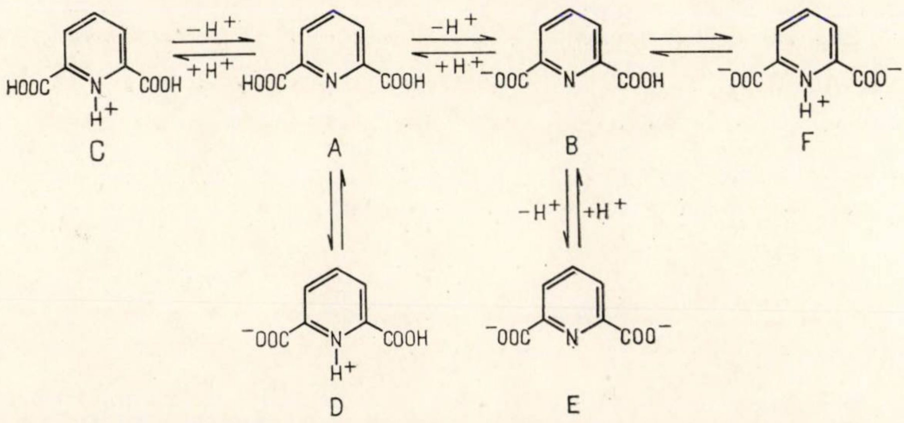
HOOC
COOH
N
H+
C
−H+
+H+
HOOC
N
COOH
A
−H+
+H+
⁻OOC
N
COOH
B
⁻OOC
N
COO⁻
H+
F
−H+
+H+
⁻OOC
N
COOH
H+
D
⁻OOC
N
COO⁻
E

Fig. 17. — Equilibria among the different species under which 2,6$-H_2PC$ can exist in aqueous solutions.

Revue Roumaine de Chimie, **17**, *4*, 661–667 (1972)

SOME CONSIDERATIONS ABOUT THE RESOLUTION BY PAPER AND THIN LAYER CHROMATOGRAPHY WITH TEMPERATURE GRADIENT

S. GOCAN and C. LITEANU

Chair of Analytical Chemistry of the "Babeş-Bolyai" University
Str. Arany János 11, Cluj, Romania

Received September 18, 1971

In the present paper an equation was deduced for the resolution in the chromatography with temperature gradient. The reaction of the temperature gradient on the magnitudes determining the resolution is also discussed.

Several criteria were suggested to characterize the separability of the two components on an open column (paper or thin layer). Dixon [1] suggests the notion of resolution power P of a chromatographic separation having the following expression:

$$P = \frac{\sqrt{N}}{k}\sqrt{1 - R_f} \qquad (1)$$

where N stands for the number of theoretical plates, R_f — the relative velocity of the component on the column, k a constant; for $k = 4$ the maximum of mutual fouling of the two components is 2.3%.

Duncan [2] gives a relation for thin layer chromatography and shows that the separation of two substances can take place if the value of r in equation (2) is higher than the unit:

$$r = \frac{a}{b + 0.1\ a} \qquad (2)$$

where: $a = R_{f_1} > b = R_{f_2}$. As shown before, [3] the condition that the value of $r > 1$, is not enough to characterize the separation conditions of two substances.

---

[1] H. B. F. Dixon, *J. Chromatog.*, **7**, 467 (1962).

[2] G. R. Duncan, *J. Chromatog.*, **8**, 37 (1962).

[3] C. Liteanu and S. Gocan, *Talanta*, **17**, 1115 (1970).

De Ligny and co-workers[4,5] introduce the notion of efficiency to characterize the chromatographic process regarding the separation of two components :

$$E = \frac{(\beta - 1)^2}{4\beta}(1 - R_{f_1})(1 - R_{f_2})\frac{1}{\sqrt{H_1 H_2}} = \frac{R_s^2}{\sqrt{l_1 l_2}} \tag{3}$$

where : $\beta = \alpha_1/\alpha_2$ — the ratio of the repartition coefficient of the two components, H — the height of the theoretical plate, and R_f — the relative migration rate of the chromatographic zone, R_s — the resolution, and l — the distance measured on the densitogram from the start to the center of the zone.

The notion of efficiency introduced by De Ligny is in fact nothing else than the separation function F ascribed to the unit of length, as it may easily be demonstrated. The separation function[6,7] is equal to the square of the resolution[8,9] and therefore according to equation (3), $E = F/1$.

Snyder and Sanders[10] have inferred, for the resolution in case of two adjacent and very narrow chromatographic zones, assumed to have equal standard deviations $\sigma_1 = \sigma_2$ and very close repartition coefficients of the two substances $\alpha_1 \approx \alpha_2$, the following equation :

$$R_s = \underset{(a)}{\frac{1}{4}\left(\frac{\alpha_1}{\alpha_2} - 1)\right)}\underset{(b)}{\sqrt{R_f N}}\,\underset{(c)}{\frac{\alpha_2}{1 + \alpha_2}} \tag{4}$$

The chromatographic separation is ultimately determined by the dynamics of the processes going on in the column [the efficiency of the column (b), i.e., the number of theoretical plates], by the thermodynamic features of the phases and components [the separation selectivity (a)] as well as by the repartition coefficient of component 2.

In the present paper we intend to find an expression of the resolution for an open column in the temperature gradient chromatography. We will therefore start from the well-known relationships[8,9] such as :

$$R_s = \frac{t_2 - t_1}{2(\sigma_1 + \sigma_2)} \tag{5}$$

---

[4] C. L. De Ligny, H. M. Schmidt and W. De Vries, *Rec. trav. chim.*, **82**, 1061, 1071, 1076 (1962).

[5] C. L. De Ligny and A. G. Remijnse, *Rec. Trav. chim.*, **86**, 421 (1967).

[6] J. C. Giddings, *Analyt. Chem.*, **32**, 1707 (1960).

[7] H. Svensson, *J. Chromatog.*, **25**, 256 (1966).

[8] T. E. Ellerington, "Gas Chromatography", D. H. Desty (ed.), Butterworths, London, 1958.

[9] W. L. Jones and R. Kieselbach, *Analyt. Chem.*, **30**, 1590 (1958).

[10] R. L. Snyder and D. L. Sanders, *J. Chromatog.*, **44**, 1 (1969).

where t_2 and t_1 are the necessary times for the elution of components 2 and 1, respectively σ_2 and σ_1 standard deviations, or

$$R_s = 2 \frac{\Delta z}{X_1 + X_2} \tag{6}$$

where X_1 and X_2 represent the breadth of the basis of the two peaks determined by the intersection with the tangents drawn through the inflexion points of the elution curve.

Let us consider two chromatographic zones on the paper band or the chromatographic plate and meanwhile the respective densitogram (fig. 1).

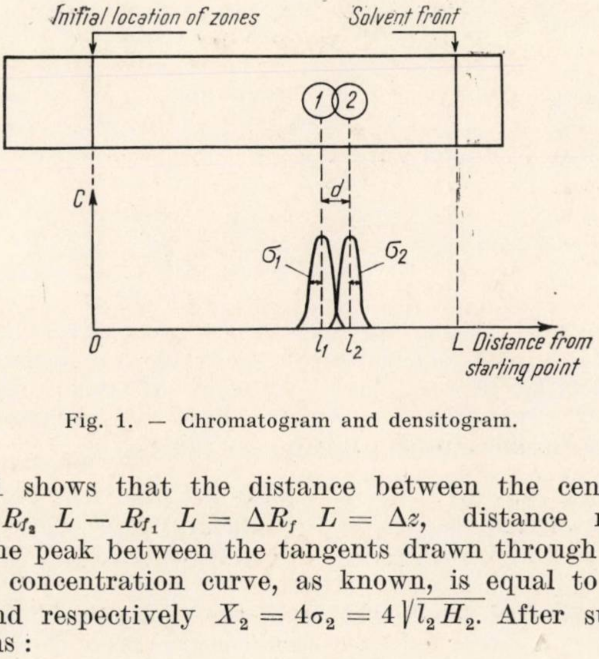

Fig. 1. — Chromatogram and densitogram.

Figure 1 shows that the distance between the centers of zones $d = l_2 - l_1 = R_{f_2}\ L - R_{f_1}\ L = \Delta R_f\ L = \Delta z$, distance measured at the basis of the peak between the tangents drawn through the inflexion points of the concentration curve, as known, is equal to $X_1 = 4\,\sigma_1 = 4\sqrt{l_1 H_1}$ and respectively $X_2 = 4\sigma_2 = 4\sqrt{l_2 H_2}$. After substitution in (6) one obtains :

$$R_s = \frac{\Delta R_f L}{2\left(\sqrt{l_1 H_1} + \sqrt{l_2 H_2}\right)} \tag{7}$$

or

$$R_s = \frac{\Delta R_f\ \sqrt{L}}{2\left(\sqrt{R_{f_1} H_1} + \sqrt{R_{f_2} H_2}\right)} \tag{8}$$

But, as shown,[11] the values of R_f and ΔR_f in the temperature gradient, have the following expressions :

$$(R_f)_{\text{grad.t}} = (R_f)_{\text{iso}} \frac{V + \Delta V}{V} \tag{9}$$

$$(\Delta R_f)_{\text{grad}} = (\Delta R_f)_{\text{iso}} \frac{V + \Delta V}{V} \tag{10}$$

Equation (8) representing the resolution of two components on an open column in temperature gradient chromatography becomes :

$$(R_s)_{\text{grad.t}} = \frac{(\Delta R_f)_{\text{iso}} \sqrt{L}}{2\left(\sqrt{(R_{f_1})_{\text{iso}} (H_1)_{\text{grad.t}}} + \sqrt{(R_{f_2})_{\text{iso}} (H_2)_{\text{grad.t}}}\right)} \sqrt{\frac{V + \Delta V}{V}} \tag{11}$$

If the chromatographic zones are close and equal as surface, one can write : $(R_{f_1})_{\text{iso}} = (R_{f_2})_{\text{iso}} = (R_f)_{\text{iso}}$ and $(H_1)_{\text{grad.t}} = (H_2)_{\text{grad.t}} = (H)_{\text{grad.t}}$, equation (11) taking a simpler form :

$$(R_s)_{\text{grad.t}} = \frac{\sqrt{L}}{4\sqrt{(H)_{\text{grad.t}}}} \left(\frac{\Delta R_f}{\sqrt{R_f}}\right)_{\text{iso}} \sqrt{\frac{V + \Delta V}{V}} \tag{12}$$

We shall now discuss the reaction of the temperature gradient on the improvement of the separation, respectively the increase of the resolution. The temperature gradient reacts on all terms which determine the resolution, excepting the length (the distance start-front) if the expansion due to the temperature is not considered.

1. THE ACTION OF THE TEMPERATURE GRADIENT ON THE HEIGHT OF THE THEORETICAL PLATE $(H)_{\text{grad.t}}$

The problem of the height H of the theoretical plate in the case of paper and thin layer chromatography has been discussed in a series of papers.[12-21] Generally, in all these papers the height of the theoretical plate is made up of three terms : the first represents the contribution of turbulent diffusion, the second, the contribution of molecular diffusion, and the third the contribution of local nonequilibrium. For instance, Stewart [14] shows, that the first term in paper chromatography may be neglected, and the second becomes important only for high values of $z_f^2 = kt$, that is, the distance from the level of the eluent to the front. The equation given for the height of the plate is the following :

---

[11] C. Liteanu and S. Gocan, *Bull. Soc. chim. France*, **1967**, 3836.

[12] K. L. Mallik and J. C. Giddings, *Analyt. Chem.*, **34**, 760 (1962).

[13] C. L. De Ligny and D. Bax, *Z. analyt. Chem.*, **205**, 22 (1964).

[14] G. H. Stewart, "Advances in Chromatography" J. C. Giddings and R. A. Keller (eds) vol. 1, E. Arnold, Publisher, London, 1965, p. 107.

[15] G. H. Stewart, *Separ. Sci.*, **1**, 135 (1966).

[16] C. L. De Ligny and W. Van De Meent, *J. Chromatog.*, **53**, 469 (1970).

[17] C. L. De Ligny and A. G. Remijnse, *J. Chromatog.*, **33**, 242 (1968).

[18] C. L. De Ligny and A. G. Remijnse, *J. Chromatog.*, **35**, 257 (1968).

[19] C. L. De Ligny, *J. Chromatog.*, **49**, 393 (1970).

[20] C. L. De Ligny and A. G. Remijnse, *Rec. Trav. chim.*, 86, 410, 421 (1967).

[21] G. H. Stewart, *Separ. Sci.*, **1**, 747 (1966).

$$H_{\text{obs}} = A + \frac{BR_f z_f}{\theta k} + \frac{C\theta k}{2z_f} \ln \frac{R_f z_f}{z_0} \tag{13}$$

where $R_f = A_M/(A_M + \alpha A_s)$ that is the relative velocity of the spot, z_0 — the distance from the level of the eluent to the start line, θ — the ratio of the velocity of the solvent to the spot and front, and A, B and C are constants.

The temperature gradient reacts on the term representing the local nonequilibrium by lowering the values of θ and k (the constant of the flow equation of the eluent) owing to the evaporation of the eluent in the column. In the temperature gradient a much better equilibrium is achieved than in the isotherm chromatography, first owing to the increase in temperature as the spot advances, and secondly because the shifting velocity of the spot becomes smaller and smaller due to the stronger evaporation as the spot migrates (fig. 2). The form of the spot is initially circular, and at the end of the cromatography becomes elliptical, with the small axis in the flowing direction of the eluent, as one can notice in the case of Mn^{2+} (fig. 3). This is explained by the fact that in the front part of the spot evaporation is more important and therefore the shifting velocity of the eluent and of the spot will be smaller.

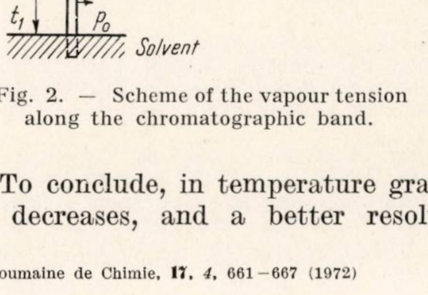

Fig. 2. — Scheme of the vapour tension along the chromatographic band.

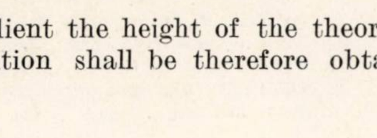

Fig. 3. — Spot shape after development.

To conclude, in temperature gradient the height of the theoretical plate decreases, and a better resolution shall be therefore obtained.

2. CHANGES OF VALUES R_f AND ΔR_f OWING TO THE VARIATION OF THE REPARTITION COEFFICIENT

We must admit that a variation of the repartition coefficient α takes place in the temperature gradient, owing to the action of two factors: the temperature and the loss of homogeneity of the eluent.

2.1. Change of the repartition coefficient and of the value of R_f with the temperature. As well-known, the relative velocity of the spot is given by relationship:

$$R_f = \frac{1}{1 + \frac{A_s}{A_M}\alpha}, \text{ and } \alpha = e^{-\frac{\Delta G^\circ}{RT}}$$

where ΔG° is the free repartition energy, R — the general constant of the gases, and T — the absolute temperature.

For all substances for which $\Delta G^\circ < 0$, the value of R_f will increase with the temperature. The effect of temperature has been studied in literature in a series of papers. [22–24]

Also, for a series of cases[25–27] it has been ascertained that ΔR_f increases too with the raise of temperature, and therefore the ratio $\Delta R_f / \sqrt{R_f}$ may increase with the temperature and the resolution improve.

2.2. *Change of the repartition coefficient with the loss of homogeneity of the eluent.* The loss of homogeneity of the mobile phase is known in isothermal chromatography. [28–30] In the temperature gradient the loss of homogeneity of the eluent is accentuated because of the additional evaporation. [25,31,32] The eluent being generally a mixture, undergoes a more marked loss of homogeneity than in isothermal conditions. To illustrate these statements we give in figure 4 the distribution of HCl on the chromatogram. [32] The temperature of the eluent in the tank was 20° in all cases.

The increase of the concentration of HCl on the chromatogram leads generally to the change of α, respectivelly of the values R_f, a well -known fact in isothermal chromatography. [33,34]

---

[22] C. S. Knight, *Nature*, 200, 1314, (1963).

[23] G. Parissakis and D. Vrandi-Piscou, "Journées hellènes de séparation immédiate et de chromatographie" (IIIèmes J.I.S.I.C.) 1965, p. 61.

[24] F. Geiss and H. Schlitt, *J. Chromatog.*, **33**, 208 (1968).

[25] C. Liteanu and S. Gocan, *Rev. Chim. Acad. R.P.R.*, **7**, 1041 (1962).

[26] C. Liteanu and S. Gocan, *Stud. Univ. Babeș-Bolyai, Chem.*, **11**, 71 (1966).

[27] S. Gocan and C. Liteanu, *Bull. Soc. chim. France*, **1969**, 1409.

[28] A. Grün, *Chimia*, **11**, 173 (1951).

[29] L. Horner, W. Emerich and A. Kischner, *Z. Electrochem.*, **56**, 987 (1952).

[30] J. Dixmier, P. Dupuis and M. Hortz, *Chim. analyt.*, **38**, 129 (1956).

[31] C. Liteanu, and S. Gocan, *Stud. Univ. Babeș-Bolyai, Chem.*, **7**, 99, (1962).

[32] C. Liteanu and S. Gocan, *Bull. Soc. chim. France*, **1967**, 2836.

[33] T. Născuțiu, *Rev. Roumanie Chim.*, **9**, 273 (1964); **10**, 989 (1965); **12**, 839 (1967).

[34] G. de Carvalho, *Analyt. Chim. Acta.*, **16**, 555 (1957).

We can therefore state that through this loss of homogeneity, generated by the action of the temperature gradient, due to continuous evaporation a gradient of pH, concentration, polarization, ionic strength is achieved in each case.

To conclude, in the temperature gradient chromatography the effect of temperature is combined with the effect of these gradients obtained through the loss of homogeneity of the eluent, and thus the resolution will increase.

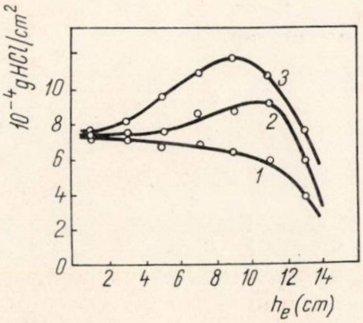

Fig. 4. — Distribution of HCl on the chromatogram. Eluent : propanol + HCl (d = 1.19) + H_2O (80 + 10 + 10 v/v). Whatman paper no. 4.
1, Isotherm : 20° ; *2*, With temperature gradient ; 0.5°/cm ; *3*, with temperature gradient : 1.0°/cm.

3. THE GROWTH OF THE VALUE OF THE RESOLUTION DUE TO THE SUPPLEMENTARY VOLUME OF ELUENT ΔV PASSING THROUGH THE EVAPORATION COLUMN

In the temperature gradient chromatography a volume $V + \Delta V$ of eluent passes through the column. The quantity of eluent leaving the column, ΔV, depends on the evaporation rate, which in its turn depends on the size of the temperature gradient, of the saturation degree of the chamber, as well as on the duration of the chromatographical process. [35] By ΔV one understands only that part of the eluent's volume which has evaporated from the column and is participating in the chromatographic repartition process.[35] Anyhow, the duration of the chromatographic process may be as long as possible (when the evaporation is compensated by the flow of eluent entering the column) and we can obtain for ΔV any value, therefore an increased resolution as may be seen from eqs (8) and (9).

---

[35] S. Gocan, C. Ciupală-Costea, T. Hodişan and C. Liteanu, *Rev. Roumaine, Chim.*, **16**, 873 (1971).

Revue Roumaine de Chimie. 17, 4, 669–674 (1972)

TEMPERATURE GRADIENT CHROMATOGRAPHY AS COMPARED TO UNIDIMENSIONAL MULTIPLE CHROMATOGRAPHY

S. GOCAN, C. LITEANU, T. HODIŞAN, H. NAŞCU and ŞTEFANIA BÎNDEANU

Chair of Analytical Chemistry of the Babeş-Bolyai University, Str. Arany Janos 11, Cluj, Romania

Received September 18, 1971

The present paper shows that the temperature gradient chromatography has certain common characteristics with the unidimensional multiple chromatography (UMC). In fact, what is discontinously achieved in unidimensional multiple chromatography, is achieved continuously in the temperature gradient chromatography (the temperature gradient is applied along the open chromatographic column). Compared to the multiple chromatography, the temperature gradient also increases the separation efficiency by the loss of homogeneity of the eluent and the action of the temperature. From the practical point of view, temperature gradient chromatography presents the advantage of simplifying the operations.

The multiple unidimensional chromatography (UMC) is a chromatographic technique which is part of the repeated chromatographical methods and consists of the repeated irrigation of the same support (paper or thin layer) with the same eluent in the same direction. Each elution is followed by the removal and drying of the support from the chromatographic chamber.

The method was first used by Jeanes, Wise and Dimler, [1] to separate some carbon hydrates. Though UMC presents a high resolution capacity [1,2] owing to the size of the effective length of the chromatographic support and therefore of the number of theoretical plates, the exceedingly long time required by the numerous developments as well as the operations needed by the lack of continuity of the process have restrained its use.

---

[1] A. Jeanes, C. S. Wise and R. J. Dimler, *Analyt. Chem.*, **23**, 415 (1951).

[2] D. French and G. H. Wild, *J. Amer. Chem. Soc.*, **75**, 2612 (1953).

The theoretical bases of UMC were a matter of concern for several research-workers. [2-12] It was shown [1] that the theoretical distance, $h_z^{(n)}$, on which the center of the chromatographic spot of a component in any development n shifts, is given by relationship :

$$h_z^{(n)} = LR_f(1 - R_f)^{n-1} \tag{1}$$

where L represents the distance between the starting line and the front of the eluent, and n the number of developments. The total distance $H_z^{(n)}$ covered by the center of the spot after n developments, will be :

$$H_z^{(n)} = L[1 - (1 - R_f)^n] \tag{2}$$

This relationship shows that if $n \to \infty$, $H_z^{(n)} \to L$ and therefore $R_f \to 1$, meaning that the spot was obliged to cover the whole length of column L.

The distance covered by the center of the spot after the first development is :

$$h_z^{(1)} = LR_f \tag{3}$$

so that the total length of the column shall be $L^{(n)} = \sum_{i=1}^{n} L_i$, and the distance covered after n developments will be :

$$H_z^{(n)} = \sum_{i=1}^{n} h_{z_i} = L^{(n)} R_f \tag{4}$$

supposing that the R_f of the component considered remains practically constant. But in non-repeated chromatography a length $L^{(n)}$ would be necessary for the spot to cover the distance $H_z^{(n)}$ achieved in UMC after n developments. Therefore $L^{(n)} > L$, as $H_z^{(n)} > h_z^{(1)}$. Thus, $L^{(n)} = L + \Delta L$, where ΔL is the "supplementary length" achieved in UMC. As shown [13] out of the whole eluent volume which enters the column in n developments, only a part (between spot — front) contributes to the chromatographic repartition process. Let this volume be $\Delta V^{(n)}$, and A_M the cross-section of the mobile phase in the column. Evidently $\Delta L = \Delta V^{(n)}/A_M$.

---

[3] J. A. Thoma, *Analyt. Chem.*, **35**, 214 (1963).

[4] J. A. Thoma, *J. Chromatog.*, **12**, 441 (1963).

[5] H. C. Chakrabortty and D. P. Burma, *Analyt. Chim. Acta*, **15**, 451 (1956).

[6] L. Starka and R. Hampl, *J. Chromatog.*, **12**, 347 (1963).

[7] R. Rüdiger and H. Rüdiger, *J. Chromatog.*, **17**, 186 (1965).

[8] H. P. Lank, *Z. analyt. Chem.*, **184**, 107 (1961).

[9] G. Goldstein, *Analyt. Chem.*, **42**, 140 (1970).

[10] D. S. Galanos and V. M. Kapoulos, *J. Chromatog.*, **13**, 128 (1964).

[11] E. Sala and P. Fromageot, *J. Labelled Compds.*, **6**, 298 (1970).

[12] E. Salla, "Ve Symp. International Chromatographic-Electrophorese", Bruxelles, Presses Académiques Européennes, 146, 1969.

[13] S. Gocan, C. Ciupală-Costea, T. Hodişan and C. Liteanu, *Rev. Roumaine Chim.*, **16**, 873 (1971).

The relationship expressing the resolution for an open column (paper, thin layer)[14] has the following form :

$$R_s = \frac{\Delta R_f \sqrt{L}}{2(\sqrt{R_{f_1} H_1} + \sqrt{R_{f_2} H_2})} \qquad (5)$$

where $\Delta R_f = R_{f_2} - R_{f_1}$, H_1 and H_2 — the equivalent height of the theoretical plate for the two considered components, and L — is the length of the column.

This formula shows that the resolution of the separation of the two components considered grows with the length of the chromatographic column. Also H_1 and H_2 decrease as the shape of the spots changes passing from a circular to an elliptic one, with the small axis in the migration direction of the eluent. This is explained by the fact that in the second development the front of the eluent reaches at the beginning the lower edge of the spot, which starts advancing, and as a result, the diameter of the spot on this direction decreases tending to take the form of an ellipse. By increasing the number of developments, the excentricity of the ellipse will increase.

As demonstrated,[1] the values of ΔR_f according to the number of developments pass through a maximum for $n = \frac{1}{R_f} - 1$, after which they decrease again, and after a very high number of repetitions, both components reach the front.

Three cases can be met :

a) $(\Delta R_f)_{\max} > (\Delta R_f)_{\text{sep}}$, separation possible at $n_{\text{sep}} < n_{\max}$

b) $(\Delta R_f)_{\max} = (\Delta R_f)_{\text{sep}}$, separation possible at $n_{\text{sep}} = n_{\max}$

c) $(\Delta R_f)_{\max} < (\Delta R_f)_{\text{sep}}$, separation impossible,

where $(\Delta R_f)_{\text{sep}}$ is the difference between the values R_f for a column of length L, after n developments, and corresponding to a resolution $R_s = 1$ (corresponding to a separation degree of 98%). In practice one must also take into account the minimum analysis time necessary to obtain a resolution $R = 1$ and not more, and therefore case *b* shall be chosen.

We have tried to see how much of the characteristics of the stationary phase (respectively of the paper) is changed by the number of elutions. We have therefore eluted a strip of chromatographic paper without spots which was dried and then the spot was applied and it was again eluted. By comparing the values R_f thus obtained, to the values R_f obtained after the first development, one noticed a difference located within bonds of experimental errors ± 0.02.

The reaction mechanism in the temperature gradient chromatography is by far more complex. An important part of this mechanism[15] is just the possibility of realizing a supplementary volume of eluent passing through the column without a greater length of the column being necessary. This supplementary volume of eluent ΔV is achieved due to the fact that the temperature gradient creates inside the chromatographic chamber a gradient of the eluent's vapour tension directed upwards. Owing to this, a diffusion of the vapours of the eluent takes place downwards with their condensation on the surface of the eluent. In these conditions of non-saturation of the inner atmosphere and of evaporation of the eluent on the column, new quantities of eluent penetrate into the column, so that the volume of eluent in the column, V is smaller than the volume V' of eluent penetrating into the column, that is to say $V' = V + \Delta V$, in which ΔV is the volume of eluent which has left the column through evaporation. Evidently, as shown before, [13] not the whole quantity of eluent contributes to the chromatographic repartition process, but only a part. In fact, the supplementary eluent volume ΔV which is achieved without continuity in multiple chromatography, is achieved continuously in temperature gradient chromatography.

---

[14] S. Gocan and C. Liteanu, Rev. Roumaine Chim., **17**, 661 (1972).

[15] C. Liteanu and S. Gocan, *Bull. Soc. chim. France*, **1970**, 4527.

We have established [14] a relationship expressing the resolution in temperature gradient chromatography for an open column (paper or thin layer) in the following form :

$$(R_s)_{\text{grad.t}} = \frac{(\Delta R_f)_{\text{iso}} \sqrt{L}}{2\left(\sqrt{(R_{f1})_{\text{iso}} H_1} + \sqrt{(R_{f_2})_{\text{iso}} H_2}\right)} \sqrt{1 + \frac{\Delta V}{V}} \qquad (6)$$

and the resolution grows therefore with the increase of the volume of supplementary eluent V taking part in the chromatographic repartition process, and this volume, as shown, [13] is a function of the duration of the development.

EXPERIMENTAL RESULTS

The multiple developements have been achieved in a series of test-tubes with double walls and thermostats, by sending a water current from a thermostat.

The system Ni^{2+}, Co^{2+} and Mn^{2+} which for the eluent and paper chosen present separation difficulties were selected.

The results obtained in UMC regarding the variation of the R_f values *versus* the number of developments are given in figures 1—3 we have also denoted on the figure the effective time necessary to the corresponding number of developments cummulated in hours. The distance start-front was in all cases 14 cm. Through the vertical lines we have denoted the size of the spot in R_f value units.

By examining figures 1—3 we notice that for 20°, even after $n_{\max} = 7$ no separation is achieved; at 30° the existence of three spots for $n = 6$, though overlapping, is put into evidence, but for $n_{\max} = 7$ a separation is noticed; at 40° one notices the existence of three zones after $n = 5$, but their separation becomes possible also after $n_{\max} = 7$ developments.

The developments in temperature gradient were achieved in a chromatographic chamber[15] of 30×20×40 cm. The thermal regime inside the chromatographic chamber is given in figure 4. The distance between the level of the eluent in the bath and the heating eluent was of 32 cm,

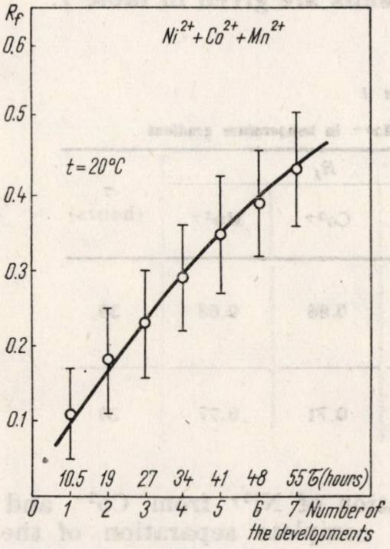

Fig. 1. — Variation of R_f values *versus* the number of developments. Eluent: n-butanol sat. HCl 4 N, Whatman paper no. 3.

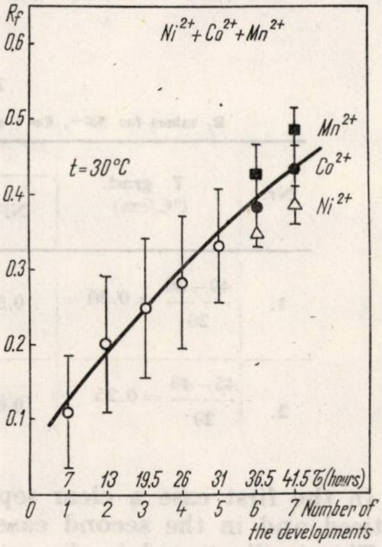

Fig. 2. — Variation of R_f values *versus* the number of developments. Eluent: n-butanol sat. HCl 4 N, Whatman paper no. 3.

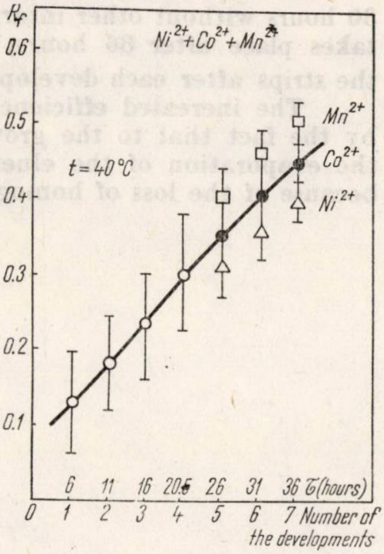

Fig. 3. — Variation of R_f values versus the number of deveolpments. Eluent: n-butanolsat. HCl 4 N, Whatman paper no. 3.

the contact thermometer for thermosetting being set at that level, and the control thermometer t_2 which measured the higher temperature at the column's end was placed at a distance of 20 cm.

We have worked at two gradients, with the same eluent and paper as in the case of UMC. The results are given in table 1.

Table 1

R_f values for Ni^{2+}, Co^{2+} and Mn^{2+} in temperature gradient

Nr.	T. grad. (°C/cm)	R_f			τ (hours)
		Ni^{2+}	Co^{2+}	Mn^{2+}	
1.	$\frac{40-30}{20} = 0.50$	0.53	0.66	0.68	30
2.	$\frac{45-40}{20} = 0.25$	0.63	0.71	0.77	30

In the first case a clear separation of Ni^{2+} from Co^{2+} and Mn^{2+} is noticed and in the second case a complete separation of the three ions. This is illustrated in figure 5. As not all colours appear on the white-black film, the outline of these spots has been marked with a pencil. The migration direction of the eluent and the zones is marked by an arrow.

In conclusion, we have succeeded in separating these ions within 30 hours without other intermediary operations. In UMC, the separation takes place after 36 hours, to which, if the necessary time for drying the strips after each development is added, one reaches about 45 hours.

The increased efficiency of the temperature gradient is explained by the fact that to the growth of the effective column ΔL , owing to the evaporation of the eluent (ΔV), an elution gradient is also added because of the loss of homogeneity of the eluent.

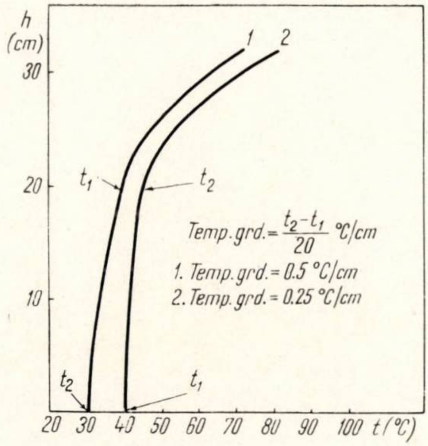

Fig. 4. — Thermal regime in the chromatographic chamber.

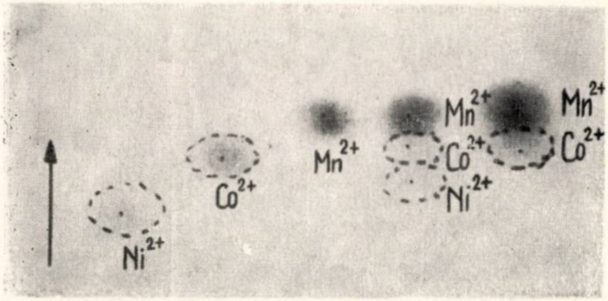
Ni^{2+}
Co^{2+}
Mn^{2+}
Mn^{2+}
Co^{2+}
Ni^{2+}
Mn^{2+}
Co^{2+}

Fig. 5. — Chromatogram.

Revue Roumaine de Chimie, **17**, *4*, 675–682 (1972)

POLAROGRAPHISCHE UNTERSUCHUNG DES UO_2^{2+}-OXALSÄURE-SYSTEMS

F. MÁNOK, CS. VÁRHELYI und MINERVA GĂLĂŢEANU-TITIENI

vom Lehrstuhl für Anorganische Chemie der Babeş-Bolyai-Universität, Cluj,
str. Arany János, 11

Eingegangen am 5. Oktober 1971

Es wurde das UO_2^{2+}-Oxalsäure-System in 5.10^{-2} n $HClO_4$ auf polarographischem Wege untersucht. Die Zunahme der Stufenhöhe nach Zugabe von Oxalsäure wird von den Verfassern — in Gegensatz zu der monoelektronischen Reduktion des UO_2^{2+} — mit einer zweielektronischen Reduktion der Oxalato-uran(VI)-Komplexe erklärt. Die Messung der Änderung der polarographischen Stufenhöhen des U(VI) bei einer bestimmten UO_2^{2+}-Ionkonzentration in Funktion der Oxalsäuremenge ermöglichte die Berechnung der Bildungskonstanten des U(ox) und $U(ox)_2$: $\beta_1 = 1{,}0.10^5$ und $\beta_2 = 5{,}6.10^9$ in guter Übereinstimmung mit den auf potentiometrischem Wege erhaltenen Werten. Die logarithmische Analyse der in Oxalsäureüberschuß aufgenommenen Polarogramme zeigt, daß der Elektrodenvorgang ein einheitlicher Prozeß ist. Aus den Untersuchungen geht hervor, daß die polarographische Reduktion der oxalato-Komplexe des Urans (VI) ein irreversibler Prozeß ist.

Das Uran ergibt mit Oxalsäure verschiedene Komplexe. Die potentiometrischen Untersuchungen des $UO_2^{2+} - H_2C_2O_4$-Systems von Rajan und Martell[1] zeigen die Bildung eines beständigen Oxalato-Uran-Komplexes mit der Zusammensetzung : UO_2^{2+} : Oxalat $= 1 : 2$.

Die polarographische Reduktion des Urans(VI) in Anwesenheit von Oxalsäure wurde hauptsächlich vom analytischen Standpunkt verfolgt. Es ist empfehlenswert nach Legge[2] die Bestimmung des Urans(VI) in Oxalsäurestammlösungen auszuführen. Die erste polarographische Stufe des Urans(VI) in einem großen Überschuß von Oxalsäure ist annähernd zweimal so hoch als in Salzsäure- oder Perchlorsäure-Lösungen.

Alekperov und Zhdanov[3] erwähnen, daß sich in verd. Salzsäure, die Gegenwart von F^- oder Oxalsäure die erste polarographische Stufe des Urans(VI) erhöht und bei erheblichen Konzentrationen von diesen Substanzen die Stufenhöhe einen Grenzwert erreicht.

---

[1] K. S. Rajan und A. E. Martell, *J. Inorg. Nuclear Chem.*, **29**, 523 (1967).
[2] D. I. Legge, *Analyt. Chem.*, **26**, 1617 (1954).
[3] A. I. Alekperov und C. I. Zhdanov, *Zhur. neorg. Khim.*, **5**, 1743 (1960).

Es ist ansonsten bekannt, daß die erste polarographische Stufe des Urans in salzsäure- oder perchlorsäurehaltigen Lösungen eine monoelektronische Reduktion : $U(VI) \xrightarrow{e} U(V)$ zeigt.

Das entstehende UO_2^+ mit fünfwertigem Uran erleidet eine Disproportion nach der Gleichung :

$$2\,UO_2^+ + 4\,H^+ \rightleftarrows UO_2^{2+} + U^{4+} + 2\,H_2O$$

Nach Alekperov und Zhdanov nimmt die Konzentration des UO_2^{2+} infolge dieser Reaktion in der Nähe der Elektrode zu und damit wächst auch der Grenzstrom. In Anwesenheit von F^- oder $C_2O_4^{2-}$ bilden sich beständige Fluoro-, bzw. Oxalato-Komplexe des Urans(IV) und diese Erscheinung beschleunigt die Disproportionierungsreaktion.

Bei einem großen Überschuß von diesen Anionen erreicht die Disproportionierungsgeschwindigkeit so erhebliche Werte, daß die Reduktion des Urans(VI) von einem monoelektronischen Prozeß in einen zweielektronischen Vorgang übergeht.

Die obere Erklärung ist aber nicht widerspruchfrei. Die aus den Redoxpotentialwerten ($UO_2^{2+} \xrightarrow{+0,063} UO_2^+ \xrightarrow{+0,58} U^{4+}$) berechnete Gleichgewichtskonstante der Disproportion ($K = 10^{8,8}$) zeigt, daß die Reaktion nach rechts stark verschoben ist.

Die Konzentrationsänderung des U^{4+} durch Komplexbildung kann die Disproportionierungsgeschwindigkeit nicht erheblich beeinflussen.

Zur Erklärung des obenerwähnten Elektrodenvorganges in Gegenwart von Oxalsäure haben wir eine neue Hypothese aufgestellt.

Unserer Meinung nach bildet das UO_2^{2+}-Ion wahrscheinlich Oxalato-Komplexe, welche an der Quecksilbertropfelektrode in einem zweielektronischen Prozeß reduziert werden.

Für die Bestätigung dieser Annahme haben wir eine polarographische Untersuchung über das UO_2^{2+}-Oxalsäure-System in perchlorsaurem Medium durchgeführt.

EXPERIMENTELLES

Die polarographischen Messungen wurden mit einem Polarograph Typ OH—102 (Radelkis) durchgeführt. Es wurde eine thermostatierte polarographische Zelle mit zwei Elektroden : eine Quecksilbertropfelektrode und eine gesättigte Kalomelelektrode verwendet. Meßtemperatur : 20°. Die nötigen Lösungen wurden aus $UO_2.(CH_3-COO)_2.2H_2O$, 70%ige $HClO_4$, $NaClO_4$ und $H_2C_2O_4.2H_2O$ analysenrein gefertigt. $C_{NaClO_4} = 0{,}2$ M, $C_{HClO_4} = 5.10^{-2}$ M. Die Konzentration der Oxalsäure wurde zwischen 6.10^{-3}—0,2 M geändert. Der pH-Wert der Lösungen wurde mit Perchlorsäure auf pH = 1,20 eingestellt. Es wurden zwei Serien von Messungen mit $C_{UO_2^{2+}} = 4.10^{-4}$, bzw. $1{,}6.10^{-3}$ ermittelt. Zur Beseitigung der Maxima wurde eine 0,02%ige Gelatinelösung verwendet. Der Sauerstoff wurde mit Hilfe eines kräftigen Methanstromes aus den Lösungen entfernt (etwa 10 Min.).

Die Ergebnisse der Messungen (die Änderung der Stufenhöhen in mm, in Funktion der Oxalsäurekonzentration) sind in Tabelle 1 und 2 zusammengestellt.

Tabelle 1

Änderung der polarographischen Stufenhöhe des Urans (VI) mit zunehmender Oxalsäurekonzentration bei $C_{U(VI)} = 4.10^{-4}$

Nr.	C_{oxH_2} $.10^{-3}$M	h mm
1.	6,35	69,0
2.	22,21	90,0
3.	25,38	94,0
4.	31,73	97,5
5.	38,08	100,0

Grenzwert der Stufenhöhe : $h_{lim} = 110$ mm

Tabelle 2

Änderung der polarographischen Stufenhöhe des Urans(VI) mit zunehmender Oxalsäurekonzentration bei $C_{U(VI)} = 1{,}6.10^{-3}$

Nr.	C_{oxH_2} 10^{-3}M	h mm
1.	6,35	112,0
2.	12,69	129,5
3.	15,86	135,5
4.	19,04	141,0
5.	28,55	158,0

Grenzwert der Stufenhöhe : $h_{lim} = 180$ mm

Bei großem Überschuß von Oxalsäure (0,2 Mol) erreichen die Stufenhöhen einen Grenzwert.

$h_{lim} = 110$ mm, wenn $C_{U(VI)} = 4.10^{-4}$ M
$h_{lim} = 180$ mm, wenn $C_{U(VI)} = 1.6.10^{-3}$ M

Deutung der Ergebnisse

Die Bildungsreaktionen der Oxalato-Uran-Komplexe kann man schematisch folgendermaßen darstellen :

$$U + ox \rightleftarrows Uox \tag{I}$$

$$U + 2\,ox \rightleftarrows U\,(ox)_2 \tag{II}$$

wo „ox" = COO —
|
COO —

Für die entsprechenden Gleichgewichte sind die folgenden Bildungskonstanten gültig :

$$\beta_1 = \frac{[Uox]}{[U]\,[ox]} \tag{1}$$

$$\beta_2 = \frac{[U\,(ox)_2]}{[U]\,[ox]^2} \tag{2}$$

Für die Gesamtkonzentration des U(VI) : C_U haben wir :

$$C_U = [U] + [Uox] + [U(ox)_2] \tag{3}$$

Aus den Gleichungen (1) — (3):

$$C_{\mathrm{U}} = [\mathrm{U}] + \beta_1 \cdot [\mathrm{U}]\,[\mathrm{ox}] + \beta_2 \cdot [\mathrm{U}] \cdot [\mathrm{ox}]^2 \tag{4}$$

bzw.

$$C_{\mathrm{U}} - [\mathrm{U}] = U_C = \beta_1\,[\mathrm{U}]\,[\mathrm{ox}] + \beta_2 [\mathrm{U}] \cdot [\mathrm{ox}]^2 \tag{5}$$

U_C ist die Summe der Konzentrationen der zwei Oxalato-Komplexe. Aus (5) kann man leicht die folgende Gleichung ermitteln:

$$\frac{[\mathrm{U}_C]}{[\mathrm{U}]\,[\mathrm{ox}]} = \beta_1 + \beta_2\,[\mathrm{ox}] \tag{6}$$

Die linke Seite der Gleichung ist eine lineare Funktion der Oxalatkonzentration.

Die graphische Darstellung von $\frac{[\mathrm{U}_C]}{[\mathrm{U}]\,[\mathrm{ox}]}$ in Funktion der [ox]-Konzentration ermöglicht die Bestimmung von β_1 und β_2.

Die Konzentrationen des komplexierten und nichtkomplexierten Urans ($[\mathrm{U}_C]$ und $[\mathrm{U}]$) können aus unseren experimentellen Daten nach folgender Vorstellung erhalten werden.

Mit der Annahme, daß die verschiedenen Formen des Urans(VI) gleiche Diffusionskoeffizienten haben, unterscheiden sich die Konstanten der Diffusionsströme des komplexierten und nichtkomplexierten Urans nur in der Zahl der austauschbaren Elektronen bei dem Reduktionsvorgang voneinander.

Folglich kann man schreiben:

$$k_1\,[\mathrm{U}] + k_2\,[U_c] = h \tag{7}$$

wo k_1 und k_2 die entsprechenden Konstanten des Diffusionsstromes bezeichnen. Das Verhältnis k_2/k_1 ist gleich 2.

Bei großem Überschuß von Oxalsäure ist die ganze Menge des U(VI) komplexiert. Den Grenzwert der Stufenhöhe erhalten wir in diesem Falle nach Gl. (8)

$$k_2\,[C_{\mathrm{U}}] = h_{\mathrm{lim}} \tag{8}$$

Mit Hilfe dieser Beziehungen errechnet man die Endgleichung (9):

$$[\mathrm{U}] = 2\,[C_{\mathrm{U}}]\left(\frac{h_{\mathrm{lim}} - h}{h_{\mathrm{lim}}}\right) \tag{9}$$

welche die Berechnung der [U]- und [U_C]-Konzentrationen ermöglicht (7. und 8. Spalte der Tabelle 3).

Tabelle 3

Die berechneten Konzentrationswerte in der ersten und zweiten Annäherung

C_U M.10^{-3}	Erste Annäherung			Zweite Annäherung				$\frac{[U_C]}{[U][ox]} \cdot 10^5$
	C_{oxH_2} M.10^{-3}	C_{oxH_2} M.10^{-6}	[ox] M.10^{-6}	C_{oxH_2} M.10^{-3}	[ox] M.10^{-6}	[U] M.10^{-3}	[U_C] M.10^{-3}	
0,400	6,35	6,24	3,06	6,23	3,05	0,296	0,104	1,17
	22,21	21,95	10,77	21,86	10,72	0,145	0,255	1,62
	25,38	25,11	12,32	24,99	12,26	0,128	0,272	1,70
	31,73	31,43	15,42	31,29	15,35	0,102	0,298	1,88
	38,08	37,76	18,53	37,59	18,44	0,082	0,318	2,06
1,600	6,35	5,96	2,93	5,91	2,90	1,205	0,395	1,15
	12,69	11,99	5,88	11,82	5,80	0,900	0,700	1,33
	15,86	15,05	7,39	14,82	7,27	0,790	0,810	1,41
	19,04	18,14	8,90	17,84	8,75	0,697	0,903	1,49
	28,55	27,34	13,42	26,63	13,10	0,387	1,213	1,74

Die nichtkomplexierte Oxalation-Konzentration wurde durch einige Näherungen ermittelt. In der ersten Näherung wurden die Oxalsäurekonzentrationen durch Subtraktion der berechneten [U_C]-Werte korrigiert. Diese Werte wurden dann für die Berechnung der [ox] mit Hilfe der Gleichung (10) verwendet.

$$[ox] = \frac{C_{oxH_2}}{\frac{[H^+]^2}{K_1 K_2} + \frac{[H^+]}{K_2}} \tag{10}$$

Die erste und zweite Dissoziationskonstante der Oxalsäure wurden aus der Literatur genommen: ($K_1 = 6{,}5 . 10^{-2}$, bzw. $K_2 = 6{,}1 . 10^{-5}$); Wasserstoffionenkonzentration: $[H^+] = 6{,}3 . 10^{-2}$.

Die [ox]-Werte sind in der 4. Spalte der Tabelle 3 dargestellt. Wie aus Tabelle 3 ersichtlich, ist die Oxalsäure in den Proben Nr. 2–5 in großem Überschuß vorhanden, und ihre Konzentrationswerte sind unmittelbar für die Berechnung des β_1-Wertes mit Hilfe der Gleichung (6) zu verwenden.

Die graphische Darstellung von $\frac{[U_C]}{[U]\,[ox]}$ gegen [ox] ist in Abb. 1 wiedergegeben.

Der Schnitt der Geraden mit der Ordinatenachse liefert den β_1-Wert: $1{,}05 . 10^5$.

Für die zweite Näherung wurden die Konzentrationen der in den beiden Komplexformen gebundenen Oxalsäure mit Hilfe der in der ersten Näherung erhaltenen [ox]-Werte, bzw. mit dem durch graphische Darstellung erhaltenen β_1-Wert ermittelt.

$$[\text{Komplexierte Oxalsäure}] = \beta_1 \cdot [U][ox] + 2\,([U_C] - \beta_1 [U]\,[ox]) \quad (11)$$

Mit Hilfe dieser korrigierten C_{oxH_2}-Werte wurden die korrigierten [ox]-Konzentrationen berechnet (die 5. und 6. Spalte in Tabelle 3). Die letzten Konzentrationswerte dienten zur graphischen Darstellung der Funktion (6) (Abb. 2).

Wie aus Abb. 2 ersichtlich, liegen die erhaltenen $\frac{[U_C]}{[U]\,[ox]}$-Werte in der Nähe einer Geraden. Diese Erscheinung spricht für die Gültigkeit unserer Annahme in Bezug auf die Zunahme des Grenzstromes in Gegenwart von Oxalsäure.

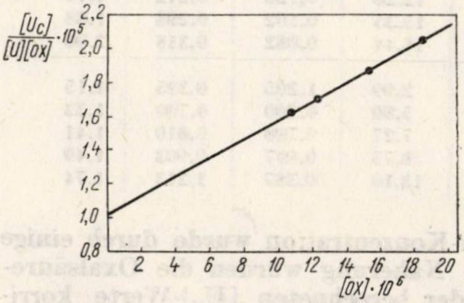

Abb. 1. — Graphische Darstellung von $\frac{[U_C]}{[U]\,[ox]}$ in Funktion von [ox] (Erste Näherung).

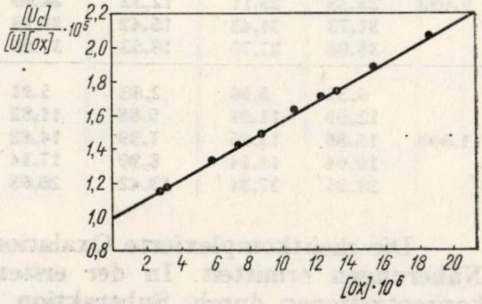

Abb. 2. — Graphische Darstellung von $\frac{[U_C]}{[U]\,[ox]}$ in Funktion von [ox] (Zweite Näherung).

Die β_1- und β_2-Werte wurden mit Hilfe der Methode der kleinsten Quadrate unter Verwendung der korrigierten [ox]-Werte berechnet.

$$\beta_1 = 1{,}0 . 10^5 \qquad \beta_2 = 5{,}6 . 10^9$$

Die gute Übereinstimmung des von uns erhaltenen β_2-Wertes mit den aus potentiometrischen Messungen ($1{,}3 . 10^9$) berechneten, unterstützt unsere Annahme bezüglich der UO_2^{2+}-Oxalsäure-Gleichgewichte.

Die Bestimmung der Bildungskonstanten der Oxalato-Uran(VI)-Komplexe hat auch eine besondere analytische Wichtigkeit, bei der polarographischen Bestimmung des Urans. Mit Hilfe dieser Werte können wir leicht die für die völlige Überführung des UO_2^{2+} in Oxalato-Derivat nötige Oxalsäuremenge berechnen.

Es ist aber bemerkenswert, daß sich die Linearität zwischen der Stufenhöhe und der Gesamtkonzentration des Urans bei konstanten pH-Werten auch bei niedrigerem Transformationsgrad bewährt.

Die Eichkurven für UO_2^{2+} : $0{,}4-4 . 10^{-4}$, bzw. $1-12 . 10^{-4}$ M sind in Abb. 3 und 4 ersichtlich.

Versuchsbedingungen : $C_{NaClO_4} = 0{,}1$ M, $C_{HClO_4} = 5 . 10^{-2}$ M, $C_{oxH_2} = 3{,}17 . 10^{-2}$ M, Gelatine : 0,02 %, pH = 1,2.

Wie aus den Abbildungen hervorgeht, ändern sich die Stufenhöhen linear mit der Gesamtkonzentration des Urans, obwohl der Transformationsgrad $\frac{[U_C]}{[C_U]}$ unter diesen Bedingungen nur 0,797 beträgt.

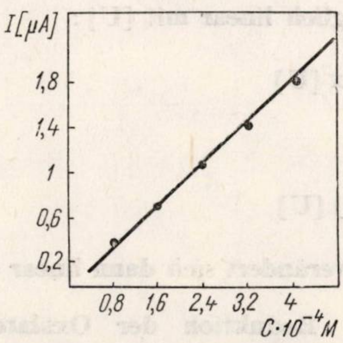

Abb. 3. — Eichkurve für die polarographische Bestimmung des Urans(VI) in Anwesenheit von Oxalsäure im Konzentrationsbereiche :

U(VI) = 0,5 – 4.10⁻⁴ M (C_{NaClO_4} = 0,1 M, C_{oxH_2} = 3,17.10⁻² M, Gelatine :0,02 %).

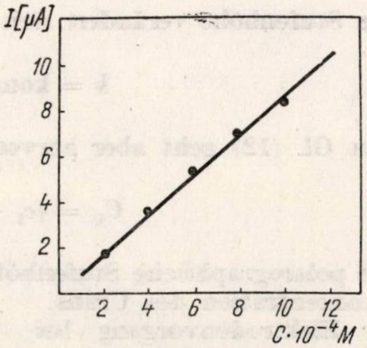

Abb. 4. — Eichkurve für die polarographische Bestimmung des Urans (VI) in Anwesenheit von Oxalsäure im Konzentrationsbereiche :

U(VI) = 1 – 12.10⁻⁴ M (C_{NaClO_4} = 0,1 M, $C_{ox.H_2}$ = 3,17.10⁻² M, Gelatine : 0,02 %).

Die lineare Änderung des Grenzstromes mit der Gesamtkonzentration des Urans bei nicht vollständiger Überführung in Oxalato-Komplex kann man folgenderweise erklären :

Wie aus Gl. (6) hervorgeht, ist das Verhältnis $\frac{[U_C]}{[U]}$, bei einem bestimmten pH-Wert von der freien Oxalation-Konzentration, bzw. der Oxalsäure-Konzentration abhängig. Die letzten Größen verändern sich bei kleinen Urankonzentrationen praktisch nicht.

So bleibt das $\frac{[U_C]}{[U]}$-Verhältnis konstant.

$$\frac{[U_C]}{[U]} = c_1 = \frac{[C_U] - [U]}{[U]} \tag{12}$$

Wie erwähnt bleibt folgende Gleichung für die Stufenhöhe gültig :

$$h = k_2 [U_C] + \frac{k_2}{2} [U] \tag{13}$$

Durch Teilung dieser Gleichung durch [U] erhalten wir :

$$\frac{h}{[\mathrm{U}]} = k_2\, C_1 + k_2/2 \tag{14}$$

Die Stufenhöhe verändert sich folglich linear mit [U] :

$$h = \text{konst. x } [\mathrm{U}] \tag{15}$$

Aus Gl. (12) geht aber hervor :

$$C_{\mathrm{U}} = (c_1 + 1)\,[\mathrm{U}] \tag{16}$$

Die polarographische Stufenhöhe verändert sich dann linear mit der Gesamtkonzentration des Urans.

Der Elektrodenvorgang bei der Reduktion der Oxalato-Uran-Komplexe ist nicht reversibel.

Abb. 5 stellt die logarithmische Analyse einer polarographischen Kurve in folgenden Versuchsbedingungen dar :
$C_{\mathrm{U}} = 1{,}6 . 10^{-3}$ M ; $C_{\mathrm{NaClO_4}} = 0{,}2$ M ; $C_{\mathrm{HClO_4}} = 5 . 10^{-2}$ M ; $C_{\mathrm{oxH_2}} = 0{,}2$ M ; Gelatine = 0,02 %.

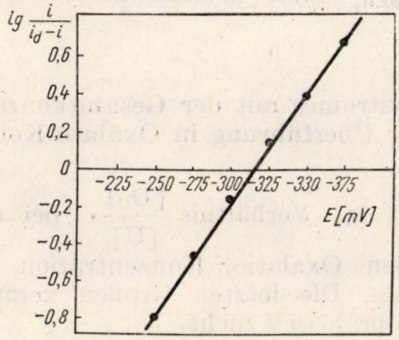

Abb. 5.—Logarithmische Analyse der polarographischen Reduktionsstufe des Urans(VI) in Oxalsäureüberschuß. (C_{U} = 1,6.10^{-3} M, $C_{\mathrm{oxH_2}}$ = 0,2 M, $C_{\mathrm{NaClO_4}}$ = 0,2 M, $C_{\mathrm{HClO_4}}$ = 5.10^{-2} M, Gelatine : 0,02 %).

Wie aus Abb. 5 ersichtlich, ist die Änderung von log $\frac{i}{i_d - i}$ in Funktion von E linear. Der aus der Neigung der Geraden berechnete Durchtrittsfaktor beträgt : $\alpha = 0{,}34$.

Die Linearität der Kurve bestätigt, daß der Elektrodenprozeß einheitlich ist.

Revue Roumaine de Chimie, **17**, *4*, 683 – 685 (1972)

EXTERNAL CATALYTIC REACTIONS ON BLUFF SURFACES

R. MIHAIL

Polytechnic Institute str. Polizu 1, Bucharest, Romania

Received September 29, 1971

A numerical study was performed to investigate boundary layer flow with external chemical reactions on bluff surfaces. The convective diffusion equation together with a kinetic law were solved numerically for the reactant surface concentration, in terms of local mass transfer coefficient and of a delay factor for a surface with step change in concentration. Some examples are given to illustrate the present technique. Local surface concentrations are computed for circular and elliptical cylinders.

1. INTRODUCTION

External catalytic reactions are encountered in numerous commercial processes as ammonia oxidation, methanol dehydrogenation, synthesis of cyanhidric acid, and others.

Mathematical models which describe the spatial history of the reactant concentration along the catalyst surface have been proposed only for flat plates, but no work has been done on reactions which occur on bluff surfaces, though these represent the usual shape of industrial catalysts.

Among the earliest works on the subject of external catalytic reactions are those of Chambré[1] and Rosner [2] mainly based on the use of shear stress as an independent variable and thus they are inadequate for bodies which present boundary layer separation. The analysis of Acrivos [3] refers to reaction in the boundary layer and that of Kusik and Happel [4] to a catalytic fixed bed with spherical particles, but assuming a constant concentration over sphere surface seems unrealistic.

In this work a theoretical analysis is carried out on isothermal external catalytic reactions on single bodies with bluff surface in boundary layer flow. The flow field is assumed to be laminar.

---

[1] P. L. CHAMBRE, *Appl. Sci. Research*, **A 6**, 97 (1956).
[2] E. D. ROSNER, *J. Aerospace Sci.*, **26**, 281 (1959).
[3] A. ACRIVOS, *Chem. Eng. Sci.*, **13**, 57 (1960).
[4] L. C. KUSIK and J. HAPPEL, *Ind. and Eng. Chem.*, **1**, 163 (1962).

The analysis of the problem involves the simultaneous solution of the momentum and diffusion equations, the kinetic law of the surface reaction being introduced as a boundary condition. The solution is developed as a superposition integral equation whose versatility was proved in analogous circumstances.[5]

Numerical results obtained and presented for cylinders demonstrate the influence of catalyst shape on the reaction rate.

2. ANALYTICAL STATEMENT OF THE PROBLEM

Consideration is given to an arbitrary surface with pressure gradient on which a catalytic reaction occurs. The system equations which describe the hydrodynamics and mass transport is subject to the conventional boundary layer assumptions and neglect viscous dissipation and the variation of properties with the dependent variables

$$\frac{\partial u}{\partial x} + \frac{\partial v}{\partial y} = 0 \tag{1}$$

$$u \frac{\partial u}{\partial x} + v \frac{\partial u}{\partial y} = - \frac{1}{\rho} \frac{dp}{dx} + \nu \frac{\partial^2 u}{y^2} \tag{2}$$

$$u \frac{\partial C}{\partial x} + v \frac{\partial C}{\partial y} = D \frac{\partial^2 C}{\partial y^2} \tag{3}$$

The usual boundary conditions which apply are

$$\begin{aligned} y = 0 \quad & u = 0 \quad v = 0 \\ y = \infty \quad & u = U(x) \quad C = C_\infty \\ x = 0 \quad & u = U(0) \quad C = C_\infty \end{aligned} \tag{4}$$

The rate expression is introduced as boundary condition on C

$$y = 0 \quad D \frac{\partial C(x, 0)}{\partial y} = - aR, \quad i = 1, \quad 2, \ldots ,s \tag{5}$$

where

$$R = R \quad [C_1 (x, 0), \ldots, C_s (x, 0)] \tag{6}$$

is the rate of transformation of a significant reactant due to reaction.

---

[5] R. Mihail, *Chem. Eng. Sci.*, **25**, 461 (1970).

As it was first formulated by Chambré, [1] since the diffusion equation (3) is linear the principle of superposition may be used to obtain solutions which satisfy the boundary condition (5). Thus if C_i represents particular solutions of eq. (3), then

$$C_i(x,\ y) - C_{i\infty} = \int_0^x \psi(x,\ y,\ z)\,\frac{\mathrm{d}C(z,\ 0)}{\mathrm{d}z}\,\mathrm{d}z \tag{7}$$

where ψ is the solution to the diffusion eq. (3) for the case of a step-surface concentration distribution. The function ψ $(x,\ y,\ z)$ satisfies the following set of boundary conditions :

$$\begin{array}{ll} \begin{matrix} x > z \\ x < z \end{matrix} & \psi(x,\ 0,\ z) = \begin{cases} 1 \\ 0 \end{cases} \\ y \neq 0 & \psi(x,\ \infty,\ z) = 0 \\ & \psi(z,\ y,\ z) = 0 \end{array} \tag{8}$$

Since the functional form of the derivative $\mathrm{d}C\,(z,\ 0)/\mathrm{d}z$ is not known the formal solution of equations system (5) — (8) can be formulated by differentiating eq. (5) and inserting the derivatives in eq. (7). There results

$$R(C_O) = -\int_0^x D\left(\frac{\partial\psi}{\partial y}\right)_{y=0}\cdot\frac{\mathrm{d}C(z,\ 0)}{\mathrm{d}z}\,\mathrm{d}z \tag{9}$$

Taking into account the discontinous conditions (8) it follows

$$-D\left(\frac{\partial\psi}{\partial y}\right)_{y=0} = k_m(x,\ z) \tag{10}$$

and thus

$$R(C_O) = \int_0^x k_m(x,\ z)\,\frac{\mathrm{d}C(z)}{\mathrm{d}z}\,\mathrm{d}z \tag{11}$$

which is a Stjeltes integral and where $k_m\,(x,\ z)$ is the local mass transfer coefficient following a step change in surface concentration. An equivalent form of eq. (11) was deduced by Lindberg and Schmitz, eq. (10) in ref. [6]

---

[6] R. C. Lindberg and R. A. Schmitz, *Chem. Eng. Sci.*, **24**, 1113 (1969).

If $k_m(x, z)$ is referred to the mass transfer coefficient of a surface with locally constant concentration

$$\frac{k_m(x, z)}{k_m(x)} = \Phi(x, z) \tag{12}$$

than eq. (11) may be written as :

$$R(x) = k_m(x)\left[\Delta C_O(0) + \int_0^x \Phi(x, z)\frac{\mathrm{d}C_O(z)}{\mathrm{d}z}\,\mathrm{d}z\right] \tag{13}$$

The first term inside the bracket indicates that the only concentration discontinuity occurs at the leading edge.

The integral eq. (13) can be solved numerically by subdividing the x axis into n equal intervals of length Δx and approximating the derivative $\mathrm{d}C_O/\mathrm{d}z$ in each interval Δx by the expression

$$\frac{\mathrm{d}C_O(z)}{\mathrm{d}z} = \frac{1}{\Delta z}\left[C_O(i\,\Delta x) - C_O((i-1)\,\Delta x)\right] \tag{14}$$

for $(i-1)\,\Delta x \leqslant z \leqslant i\,\Delta x$, which allows its removal from the integral sign. eq. (13) may now be expressed as

$$R(x) = k_{mi}(x)\left[\Delta C_O(0) + \sum_{i=1}^{n}\left(\frac{\mathrm{d}C_O(z)}{\mathrm{d}z}\right)_{x_{i-1}-x} - x\int_{x_{i-1}}^{x_i}\Phi(x, z)\,\mathrm{d}z\right] \tag{15}$$

By normalizing the x space, the general form of the integral in this equations becomes :

$$\int_{x_{i-1}}^{x_i}\Phi(x, z)\,\mathrm{d}z = x\left[\int_0^{x_i/x}\Phi(x, z)\,\mathrm{d}\left(\frac{z}{x}\right) - \int_0^{x_{i-1}/x}\Phi(x, z)\,\mathrm{d}\left(\frac{z}{x}\right)\right] \tag{16}$$

Performing calculations of reactant surface concentration with eq. (15) implies the knowledge of the delay factor $\Phi(x, z)$, the local mass transfer coefficient $k_{mi}(x)$ and the kinetic law of the surface reaction $R(x)$.

3. THE DELAY FACTOR

As it is seen, at the heart of superposition lies the delay factor for a step change in surface concentration, $\Phi(x, z)$, defined by eq. (12).

Since $k_m \propto 1/\delta_c$, an analytical form of $\delta_c(x)$ is needed in order to express the delay factor. As usual solutions to the integral diffusion equation, giving δ_c, are numerical, it was attempted to use wedge solutions in order to simulate flow past cylinders or spheres. Advantage was taken of the following expression for the delay factor

$$\Phi(x, z) = \left[1 - \left(\frac{z}{x}\right)^{3/4(m+1)}\right]^{-1/3} \tag{17}$$

first deduced by Bond[7] for wedge-shaped bodies, on the assumption that velocity near wall is linear in y. The velocity $U(x)$ on the edge of the boundary layer is given by

$$U(x) = u_1\, x^m \tag{18}$$

For pure wedge flow $m = \text{const.}$ but for arbitrary two-dimensional profiles m will vary with position along the surface. Thus, eq. (17) applies to any two-dimensional surface, viz. elliptical cylinders. The elliptical profile is determined by the ratio a/b of its semiaxes, a being parallel to the oncoming flow, fig. 1. The reference length will be defined by $L = a$.

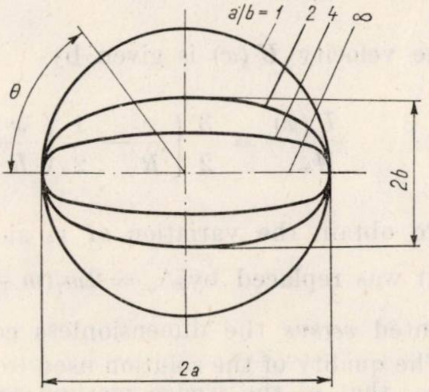

Fig. 1. — Elementary shapes of catalytic bodies.

In order to be able to express the variation of m with position along an elliptical cylinder surface the wedge variable, Λ_w, is introduced; thus following Meksyn[8]:

$$\Lambda_w = 2\left(\frac{L}{r}\,\frac{U_\infty}{U(x)}\right)^2 \left\{\frac{r^2}{L^2}\,\frac{U(x)}{U_\infty}\,\frac{\mathrm{d}x}{L}\right\} \frac{\mathrm{d}U(x)/U_\infty}{\mathrm{d}x/L} \tag{19}$$

For two-dimensional flow $r = L$, and for pure wedge flow

$$\Lambda_w = 2m/(m+1) = Ct.$$

---

[7] R. Bond, "Heat transfer to a laminar boundary layer with nonuniform free stream velocity and nonuniform wall temperature", Inst. of Engrg. Res., Univ. of Calif., Berkeley, 1950.

[8] D. Meksyn, "New methods in laminar boundary-layer theory", Pergamon Press, Oxford, 1961.

The velocity at the edge of the boundary layer of an elliptical cylinder results from the potential theory

$$\left(\frac{U(x)}{U_\infty}\right)^2 = 1 + \left(\frac{a}{b}\right)^2 \frac{1 - \cos 2\theta}{1 + (a/b)^2 + [1 - (a/b)^2] \cos 2\theta} \tag{20}$$

where θ is the angular coordinate. Therefore, from equation (19) and (20) the following equation is obtained

$$\Lambda_w = \frac{4}{1 + (a/b)^2 + [1 - (a/b)^2] \cos \theta} \cdot \frac{\cos \theta}{1 + \cos \theta} \tag{21}$$

For spheres $L = 2r$, so we have

$$r/L = \frac{1}{2} \sin \theta = \frac{1}{2} \sin\left(\frac{2x}{L}\right) \tag{22}$$

and the velocity $U(x)$ is given by

$$\frac{U(x)}{U_\infty} = \frac{3}{2}\left[\frac{x}{R} - \frac{1}{2}\left(\frac{x}{R}\right)^3 + \frac{1}{40}\left(\frac{x}{R}\right)^5 \ldots\right] \tag{23}$$

To obtain the variation of m along surface the left-hand side of eq. (20) was replaced by $\Lambda_w = 2m/(m+1)$. In fig. 2, $\alpha = \frac{3}{4}(m+1)$ is represented *versus* the dimensionless coordinate x/L.

The quality of the solution used to obtain the delay factor is, in last instance, that of the wedge method propunted by Meksyn for transfer calculations for boundary layers with longitudinal pressure gradient. The application of a pure wedge method to arbitrary two-dimensional profiles or rotationally symmetrical bodies is legitimate if $d\Lambda_w/d(x/L)$ is small, i. e. in the vicinity of the forward stagnation point. However, comparing the results obtained in the boundary layer theory it was found [8] that its accuracy is of the same order of magnitude as that of the others.

4. LOCAL MASS TRANSFER COEFFICIENTS

Since the superposition integral eq. (15) is to be solved by a purely numerical scheme both theoretical expressions and experimental results can be used for the local mass transfer coefficient. A considerable amount of work has been carried out in the problem of local transport from spheres and cylinders. Many boundary layer solutions are now known in literature and experimental work is also available. The subject was thoroughly reviewed by Spalding and Pun [9] for cylinders and Galloway and Sage for spheres. [10]

The theoretical solutions apply only to the forward flow, while in the region of separated flow an adequate theoretical treatment is lacking and recourse must be made to semiempirical solutions.

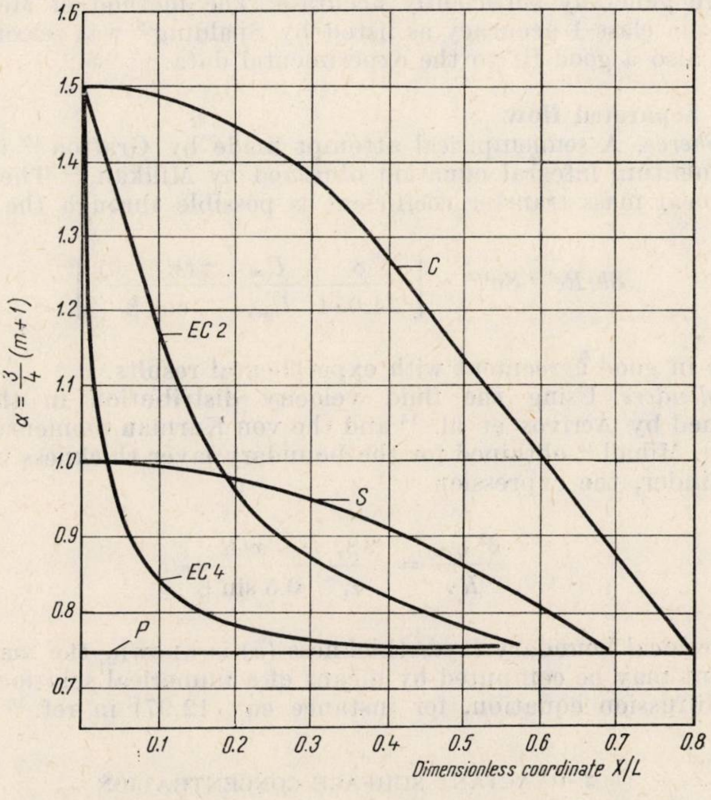

Fig. 2. — Exponent α *vs.* dimensionless coordinate x/L. C = circular cylinder ; $EC\ 2$ = elliptical cylinder $a/b = 2$; $EC\ 4$ = elliptical cylinder $a/b = 4$; S = sphere ; P = flat plate.

a) **Forward flow**

Spheres. From statistical analysis of both theoretical and experimental data the following expression resulted [10] :

$$Fs_\infty = A + B\ Re^{1/2}\ Sc^{1/6} \tag{24}$$

where the Frössling number *Fs* indicates the variation of the local transport from that at stagnation.

---

[9] D. B. Spalding, and H. L. Evans, *Int. J. Heat Mass Transfer*, **5**, 239 (1962).

[10] R. T. Galloway and B. H. Sage, *Int. J. Heat Mass Transfer*, **11**, 539 (1968).

The values of the coefficients in eq. (33) depend slightly on the *Re* number and are represented in figure 8, of the afore mentioned reference, as a function of polar angle.

Cylinders. The analysis of various methods for predicting laminar transport coefficients have shown that the methods using similar solutions are generally sufficiently accurate. The method of Merk [11] which falls in the class 1 accuracy as listed by Spalding [9] was selected because it gives also a good fit to the experimental data.

b) **Separated flow**

Spheres. A semiempirical attempt made by Grafton [12] is based on the momentum integral equation obtained by Milikan. [13] The prediction of the local mass transfer coefficient is possible through the expression

$$Sh/Re^{1/3}\,Sc^{1/2} = \left[\frac{8}{34.054}\,\frac{U_\infty}{U_{\text{rev}}}\,\frac{\tau(\pi-\theta)}{\cos\beta}\right]^{1/2} \tag{25}$$

which is in good agreement with experimental results.

Cylinders. Using the fluid velocity distribution in the wake as determined by Acrivos et al. [14] and the von Karman momentum integral equation, Mihail [15] obtained for the boundary layer thickness in the wake of a cylinder, the expression

$$\frac{\delta^2 U_\infty}{R\nu} = \frac{2\beta_1}{\alpha_1}\,\frac{x/R}{0.5\sin\beta} \tag{26}$$

Once the local boundary layer thickness (x) is known, the mass transfer coefficient may be computed by means of a numerical solution to the integral diffusion equation, for instance eq. (12.97) in ref. [16]

5. REACTANT SURFACE CONCENTRATION

The kinetic expression (6) may be written as

$$R\,[C_0^*(x)] = k\,\Omega[C_0^*(x)] \tag{27}$$

thus enabling one to display in eq. (15) the local Damköhler number:

$$D_a(x)\,\Omega[C_0^*(x)] = \left[\Delta C_0^*(0) + \sum_{i=1}^{n}\left(\frac{\mathrm{d}C_0^*}{\mathrm{d}z}\right)_{x_{i-1}-x_i}\int_{x_{i-1}}^{x_i}\Phi(x,\,z)\,\mathrm{d}z\right] \tag{28}$$

---

[11] J. H. Merk, *J. Fluid Mechanics*, **5**, 460 (1959).

[12] R. W. Grafton, *Chem. Eng. Sci.*, **8**, 457 (1963).

[13] C. B. Millikan, *Amer. Soc. Mech. Engrs. Trans.*, **54**, A.P.M. 29 (1932).

[14] A. Acrivos, D. D. Snowden, S. A. Grove and E. E. Petersen, *J. Fluid Mechanics*, **21**, 737 (1965).

[15] R. Mihail, *Chem. Eng. Sci.*, **24**, 1186 (1969).

[16] H. Schlichting, "Boundary layer theory", 5 the ed., McGraw-Hill, New York, 1968.

Replacing the differential ($\mathrm{d}C_0^*/\mathrm{d}z$) by formula (14) there results :

$$Da(x)\,\Omega[C_0^*(x)] = \left[\Delta C_0^*(0) + \sum_{i=1}^{n}\left(\frac{C_0^*(i\,\Delta x) - C_0^*(i-1)\,\Delta x}{\Delta z}\right)\int_{x_{i-1}}^{x_i}\Phi(x,\ z)\,\mathrm{d}z\right] \tag{29}$$

If the kinetic expression Ω is not too complicated, eq. (29) may be solved for $C_0^*(x)$ and a step by step numerical integration can proceed provided that $Da(x)$ and $\Phi(x, z)$ are known functions of x.

In solving eq. (29) the spatial direction was divided into n equal sections ; alternatively a generalized spatial coordinate was used, expressed as the Damköhler number. For computer calculation eq. (29) must be explicited in respect of $C_0^*(n)$ and transformed in a recurrence formula.

To illustrate the computational properties of this equation a number of examples were worked in detail.

For an irreversible first-order reaction

$$A \rightarrow \text{products}$$

the reactant surface concentration C_0 in eq. (29) may be explicited as follows :

$$C_0^*(n) = \frac{C_0^*(n-1)\left[\int_0^1 \Phi(u)\,\mathrm{d}u - \int_0^{\frac{n-1}{n}} \Phi(u)\,\mathrm{d}u\right]}{1 + \left[\int_0^1 \Phi(u)\,\mathrm{d}u - \int_0^{\frac{n-1}{n}} \Phi(u)\,\mathrm{d}u\right]} + \frac{\sum_{i=1}^{n-1}\left\{[C_0^*(i-1) - C_0^*(i)]\left[\int_0^{\frac{i}{n}} \Phi(u)\,\mathrm{d}u - \int_0^{\frac{i-1}{i}} \Phi(u)\,\mathrm{d}u\right]\right\}}{1 + \left[\int_0^1 \Phi(u)\,\mathrm{d}u - \int_0^{\frac{n-1}{n}} \Phi(u)\,\mathrm{d}u\right]} \tag{30}$$

Note that for bluff surfaces the last condition (4), with respect to C_O, is in error at the origin since the stagnation concentration is less than C_∞, due to finite thickness of the boundary layer. However, the error disappears quickly since the solution decays very rapidly and the flow is symmetrical.

Using the relevant parameters shown in table 1, the reactant surface concentration distribution for a first order irreversible reaction, computed as described in the foregoing, is presented in figure 3 and figure 4. For the flat plate catalyst, figure 3, the Damköhler number is used as spatial coordinate. In figure 4, where various cylindrical surfaces are considered, with the ratio of the semi-axes *a*/*b* as parameter, use is done of the dimensionless physical coordinate *x*/*L*.

Due to the nature of hydrodynamic mathematical solution, which vanishes in the vicinity of the separation point, the curves are extrapolated in this area.

Table 1

Mass transfer coefficients (Sh Re$^{-1/2}$) used in computation of surface concentration
Sc = 1

$\frac{a}{b}$ / $\frac{x}{L}$	1	2	4
0.000	18.3	34.8	65.4
0.100	—	28.3	31.0
0.174	17.9	—	—
0.200	—	22.6	17.4
0.300	—	20.4	12.6
0.349	17.4	—	—
0.400	—	17.6	10.9
0.500	—	13.6	9.2
0.523	16.6	—	—
0.600	—	10.9	8.7
0.698	15.3	—	—
0.700	—	8.26	7.8

For plat plate Sh $Re_x^{-1/2} = 0.33$.

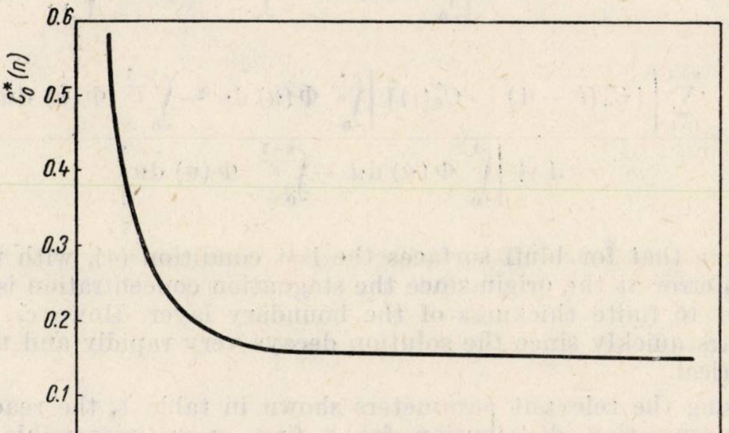

Fig. 3. — First order irreversible surface reaction on a flat plate; reactant concentration C_0^* *vs.* Damköhler number.

As it is seen, for given flow regime and diffusional properties, the shape of the catalyst surface influences in a definite manner the surface concentration distribution. The thinner the boundary layer, the higher the reactant surface concentration is. At the stagnation point, where mass transfer is more effective, the reaction displays the maximum rate. The competition between reactant transfer by diffusion in the boundary layer and reactant consumption by reaction at the catalyst surface determines a lower rate towards ths boundary layer separation point. Thus a catalyst is more efficient and better utilized in the stagnation area.

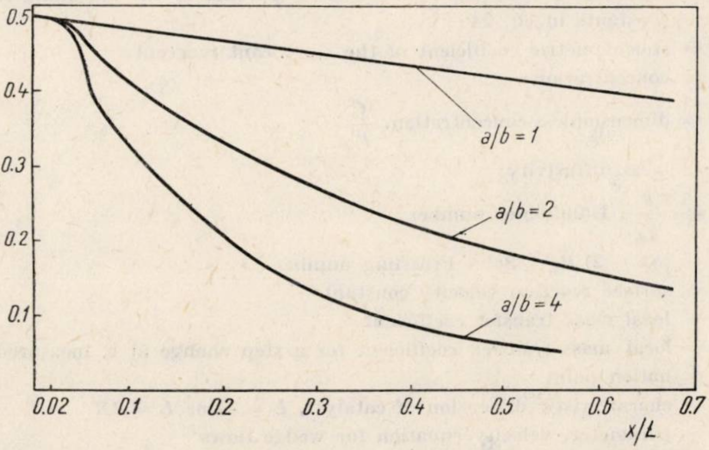

Fig. 4. — First order irreversible surface reaction on cylindrical surfaces. C = circular cylinder; $EC2$ = elliptical cylinder $a/b = 2$; EC 4 = elliptical cylinder $a/b = 4$.

The same computational procedure applies for any other two—dimensional surfaces and for various kinetic expressions.

CONCLUSION

Quantitative behaviour of external surface reactions may be estimated by the superposition integral equation advanced in this study.

The computational technique may be extended to catalytic surfaces of arbitrary shape in two-dimensional boundary layer flow and for varied kinetic schemes.

The solution of the integral equation describing the reactant surface concentration for a first-order irreversible reaction indicates the competing effects of diffusion in the boundary layer and surface kinetics and stresses the non-uniform effectiveness of the catalyst surface.

This suggests that in ordered array of catalyst particles an optimal shape may be found giving the greatest production rate per unit catalytic surface.

Notation

a, b = semi-axes of elliptical cylinder, a — parallel to the oncoming flow

A, B constants in eq. 24

a = stoichiometric coefficient of the significant reactant

C = concentration

C^* = dimensionless concentration, $\frac{C}{C_\infty}$

D = mass diffusivity

Da = $\frac{k}{k_m}$, Damköhler number

Fs = $(Sh - 2)\, Re^{1/2}\, Sc^{1/3}$, Frössling number

k = surface reaction velocity constant

$k_m(x)$ = local mass transfer coefficient

$k_m(x, z)$ = local mass transfer coefficient for a step change at z, measured from stagnation point

L = characteristic dimension of catalyst, $L = a$, or $L = 2R$

m = parameter, velocity equation for wedge flows

R = reaction rate function

Re = $U_\infty L/\nu$ Reynolds number,

Re_x = local Reynolds number for flat plate $U_\infty x/\nu$

Sc = ν/D Schmidt number,

Sh = $k_m(x)\, L/D$ Sherwood number,

r = radial distance from the center of the sphere

R = radius of the cylinder of the sphere

u = velocity in x or z direction in the boundary layer, or else dummy variable in eq. (30).

u_1 = constant, velocity equation for wedge flows

$U(x)$ = velocity at edge of boundary layer

U_{rev} = maximum back flow velocity in wake

v = velocity in y direction

x = distance along surface, from stagnation point

y = distance measured perpendicular to catalytic surface

z = distance at which a step change in concentration occurs

Greek letters

α = $\frac{3}{4}(m + 1)$

β = angle between wake contour near surface and the surface, Ref. (12) and (15)

δ = boundary layer thickness

δ_c = concentration boundary layer thickness

σ_e = a function of θ

θ = angle from forward stagnation point

Λ_w = wedge variable, eq (18)

ν = kinematic viscosity of fluid

ρ = density of fluid

$\Phi(x, z)$ = $k_m(x/z)/k_m(x)$, eq. (12)

$\psi(x, y, z)$ = step—surface concentration function
$\Omega\,[C_{io}(x)]$ = a function of surface concentration, eq. (27)

Subscripts

i — the ith species of a chemical reaction
O — surface conditions
∞ — undisturbed flow conditions

Superscript

0 — at forward stagnation point

Revue Roumaine de Chimie, 17, 4, 697–703 (1972)

MIXED LIGAND LANTHANIDE CHLOROMANDELATES CONTAINING *o*-PHENANTHROLINE AND 5,6-DIMETHYLPHENANTHROLINE

P. SPACU and SILVIA PLOŞTINARU

Institute of Physical Chemistry, Dumbrava Roşie, 23
Bucharest, Romania

Received November 27, 1971

The paper deals with a new series of mixed ligand complexes of Ce, Pr, Nd, Sm, Eu, Dy containing *o*-phenanthroline or 5,6-dimethylphenanthroline and chloromandelic acid. The photoelectron and IR spectra gave information on the coordinative chemical bonding, the covalency degree (nephelauxetic ratio) being calculated from the red shift of the absorption bands in the visible range. It was shown that the Eu complexes exhibit an intense fluorescence when UV irradiated light.

These last years, the lanthanide complexes with ligands containing heterocyclic nitrogen have been intensively studied either for theoretical or practical reasons. Mixed ligand complexes of lanthanide ions with chlorides, nitrates, thiocyanates, acetates, chloroacetates and phenanthroline have been already reported.[1–3]

The lanthanide ions give with *o*-phenanthroline in aqueous media cationic species $[\mathrm{Ln(phen)_2}]^{3+}$, which can form insoluble products with different acids, especially oxycarboxylic ones. The complex $\mathrm{Sm(phen)_2(salicylate)_3}$ has been prepared,[4] the spectral data indicating the decacoordination for this compound. Coordinative complexes of rare earth with benzoic and *p*-OH benzoic acids have been similarly prepared and characterized.[5]

The present paper deals with the synthesis and the chemical and physical properties of a new series of coordination compounds of the type $\mathrm{Ln(phen)_2(ClMand)_3}$ and $\mathrm{Ln(DMPh)_2(ClMand)_3}$, where:
Ln = Ce, Pr, Nd, Sm, Dy, Eu.
phen = *o*-phenanthroline

---

[1] F. A. Hart and F. P. Laming, *J. Inorg. Nuclear Chem.*, **26**, 579 (1964); **27**, 1605 (1965).

[2] L. R. Melby, N. J. Rose, E. Abramson and J. C. Caris, *J. Amer. Chem. Soc.*, **86**, 5117 (1964).

[3] P. Spacu and E. Antonescu, *Z. Chem.*, **7**, 163 (1967).

[4] K. K. Rohatgi and S. K. Sen Gupta, *J. Inorg. Nuclear Chem.*, **31**, 1203 (1969).

[5] S. P. Sinha, *Mol. Phys.*, **16**, 285 (1969).

DMPh = 5,6 dimethylphenanthroline

ClMand = chloromandelic acid ($Cl-C_6H_4-CHOH-COOH$)

In some previous papers [6,7] the simple lanthanide chloromandelates have been studied, the products obtained being white precipitates, practically insoluble in water or alcohol, suitable for quantitative analyses and separation of lanthanide ions.[8,9]

The new compounds herein reported are solid anhydrous substances, stable and insoluble in water, less soluble in ethanol and methanol, but easily soluble in dimethylformamide (DMF) and dimethylsulfoxide (DMSO).

EXPERIMENTAL

Reagents. For the preparation of lanthanide complexes the following reagents have been used: oxides (Ln_2O_3) of spectral purity (Matthey and Johnson); Ce $(NO_3)_3$ (E. Merck-puriss); *o*-phenanthroline (E. Merck p. a.); 5,6-dimethylphenanthroline (Fluka AG-Switzerland); chloromandelic acid (Fluka AG-Switzerland).

Preparation. Ln $(phen)_2(ClMand)_3$ were prepared by treating aqueous solutions of ammonium chloromandelate with a mixture in aqueous solution of hydrated $Ln(NO_3)_3$ and *o*-phenanthroline in the ratio 3 : 1 : 2. The solution is left to stand a few hours, the settled precipitate being then filtered and washed repeatedly with water and finally with benzene. The products thus obtained were dried in a dessiccator on H_2SO_4. We must point out that a rigorous control of pH for each component should be made in such a way that the pH of the final solution should not exceed the value 5.8–6. The coordination compounds containing 5,6-dimethylphenanthroline have been prepared using a 0.1 M HCl solution to solve the reagent. The preparation is that described above. As far as the elemental analysis is concerned, the metal was determined as oxide by ignition and C, H, N by direct micro-combustion.

The analytical data and the chemical formulas for the products obtained are given in Table 1.

Apparatus. Absorption spectra in solution for UV and visible range have been recorded on a VSU-2 Zeiss-Jena spectrophotometer, while the reflectance spectra at room temperature on a spectrophotometer VSU-1 using MgO as a standard.

IR spectra in the range 700–4000 cm^{-1} have been recorded on a spectrophotometer UR-10 using pellets of KCl.

RESULTS AND DISCUSSION

ELECTRONIC SPECTRA

The absorption UV spectra for rare earth complexes and free ligands have been recorded using ethanolic and methanclic solutions ($C = 10^{-5}M$).

---

[6] P. Spacu, E. Antonescu, M. Mavrodin and S. Şerban, *Studii şi Cercetări Chim. Acad. R.P.R.*, **10**, 163 (1962).

[7] P. Spacu, E. Antonescu, M. Mavrodin and S. Şerban, *Studii şi Cercetări Chim. Acad. R.P.R.*, **11**, 385 (1963).

[8] P. Spacu, E. Antonescu, M. Mavrodin and S. Şerban, *Studii si Cercetări Chim. Acad. R.P.R.*, **10**, 91 (1962).

[9] P. Spacu and S. Ploştinaru, *Rev. Roumaine Chim.*, **12**, 672 (1967).

Table 1

Analytical data

Formula of the compound	Ln %		N%		C%		H%	
	Calc.	Found	Calc.	Found	Calc.	Found	Calc.	Found
$Ce(phen)_2(ClMand)_3$	13.13	13.54 13.37	5.25	5.84 5.52	54.07	53.92 54.14	3.18	3.52 3.61
$Pr(phen)_2(ClMand)_3$	13.33	13.46 13.58	5.30	5.63 5.48	54.49	54.75 54.06	3.21	3.40 3.73
$Nd(phen)_2(ClMand)_3$	13.60	13.65 13.81	5.28	5.14 5.64	54.34	54.45 54.12	3.20	3.41 3.75
$Sm(phen)_2(ClMand)_3$	14.10	14.33 14.28	5.25	5.34 5.76	54.03	54.16 54.28	3.19	3.32 3.87
$Eu(phen)_2(ClMand)_3$	14.20	14.63 14.34	5.26	5.43 5.40	53.93	53.88 53.76	3.33	3.46 3.58
$Dy(phen)_2(ClMand)_3$	15.06	15.19 15.24	5.19	5.30 5.46	53.38	53.56 53.08	3.15	3.32 3.41
$Ce(DMPh)_2(ClManD)_3$	12.59	12.65 12.80	5.03	5.54 5.62	56.11	55.98 56.03	3.77	3.99 4.05
$Nd(DMPh)_2(ClManD)_3$	12.92	13.03 13.11	5.01	5.18 5.46	55.91	55.49 55.40	3.76	3.98 4.31
$Eu(DMPh)_2(ClManD)_3$	13.52	13.60 13.48	4.98	5.30 5.18	55.51	55.08 55.00	3.73	4.14 4.06
$Dy(DMPh)_2(ClManD)_3$	14.32	14.51 14.28	4.93	4.90 5.25	54.97	54.57 54.50	3.70	4.22 3.86

The absorption bands for chloromandelic acid were reported in a previous note.[6]

Figure 1 shows the absorption spectra for Eu(III) and Dy(III) complexes and free phenanthroline. As may be seen, all absorption bands occurring in the UV range are due to the organic ligand, namely at 230 nm and 264 nm. The last band is somewhat shifted in the reflectance spectra at 270 nm, this shift being probably caused by the lattice effects.

The absorption spectra between 220 – 300 nm for Nd(III) and Ce(III) complexes with 5,6 dimethylphenanthroline and that of the free ligand are plotted in figure 2. As may be seen, the ands observed at 228 nm and 271 nm could be assigned to the π-electron system of the organic ligand.

As far as the electronic spectra in the visible range are concerned, the Pr(III) and Nd(III) complexes have absorption bands proper to the central metal ion, assigned to transitions from the ground state $^3H_4$, $^4I_{9/2}$ respectively, to the excited J levels of the $4f^n$ configuration.

Table 2 presents spectral data for Nd(III) and Pr(III) complexes containing *o*-phenanthroline and 5,6-dimethylphenanthroline in solution of dimethylformamide. The absorption spectra for Nd(III) and Pr(III) nitrates in aqueous solutions have been taken as standards. As may be seen from Table 2, practically insignificant changes in intensity or frequency occurred in the spectra of the Nd(III) complexes when compared with the Nd(III) aquocomplex, except for the hypersensitive transition $^4I_{9/2} \rightarrow {}^4G_5$ for which an obvious increase in its intensity should be noted from 7.08 in aquocomplex to 13.75 and 15.69 in the complexes containing *o*-phenanthroline and 5,6-dimethylphenanthroline, respectively. The minor changes observed would indicate that the 4f orbitals are not too much involved in the chemical bond formation, otherwise changes in intensity and frequencies of the f-f transitions caused by the vibronic coupling should take place to a greater extent in the electronic spectra.

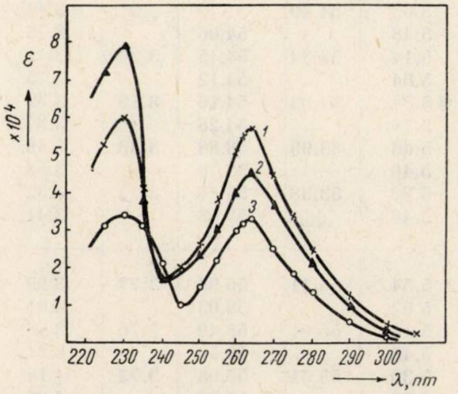

Fig. 1. — Absorption spectra in the UV range for:

1, $Eu(phen)_2(ClMand)_3$; 2, $Dy(phen)_2(ClMand)_3$; 3, *o*-phenanthroline.

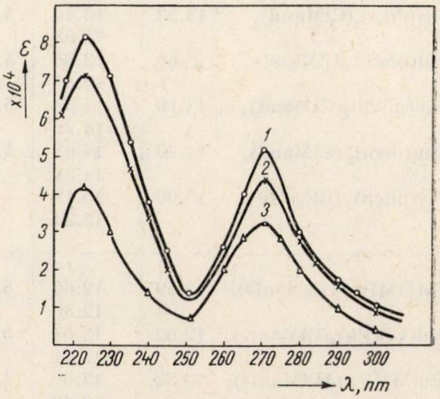

Fig. 2. — Absorption spectra in the UV range for:

1, $Nd(DMPh)_2(ClMand)_3$; 2, $Ce(DMPh)_2(ClMand)_3$; 3, 5,6-dimethylphenanthroline.

For the Pr(III) complex no increase in the intensity of the molar extinction was observed (Table 2).

The nephelauxetic ratio taken as a measure of the covalency degree of metal-ligand bonds in which f-metal orbitals were involved, has been estimated from

$$1 - \beta = \frac{\bar{\nu}_{\text{aquo}} - \bar{\nu}_{\text{complex}}}{\bar{\nu}_{\text{aquo}}}\ ^{10,11}$$

Table 2 shows that the value $1 - \beta$ takes low values, which means that the metal-ligand bonds in the complexes herein considered are almost similar with those of aquocomplexes taken as standards. The positive value of $1-\beta$ shows that the chemical bonds are however more covalent than those of the aquoions. The covalency degree has been calculated from

$$\delta = \frac{1 - \beta}{\beta} \cdot 100.\ ^{12}$$

---

[10] C. K. Jørgensen, R. Pappalardo and E. Ritterhaus, *Z. Naturforsch.*, **19A**, 424 (1964).

[11] N. K. Dutt and S. Rahut, *J. Inorg. Nuclear Chem.*, **32**, 2905 (1970).

[12] S. P. Sinha, *Spectrochim. Acta*, **22**, 57 (1966).

Table 2

Visible spectral data

$Nd(NO_3)_3$ in water			$Nd(phen)_2(ClMand)_3$ in DMF				
λ nm	$\bar{\nu}$ cm^{-1}	ε	λ nm	$\bar{\nu}$ cm^{-1}	ε	$1-\beta$	$\delta\%$
512	19,531	1.83	512	19,531	2.87	0	0
520	19,231	3.58	524	19,084	5.80	0.764×10^{-2}	0.7699
575	17,391	7.08	582	17,182	13.75	1.202×10^{-2}	1.2166
755	13,245	6.40	755	13,245	7.91	0	0
805	12,422	7.41	810	12,346	9.83	0.612×10^{-2}	0.6157
$Nd(NO_3)_3$ in water			$Nd(DMPh)_2(ClMand)_3$ in DMF				
512	19,531	1.83	512	19,531	6.88	0	0
520	19,231	3.58	524	19,084	10.12	0.764×10^{-2}	0.7699
575	17,391	7.08	582	17,182	15.69	1.202×10^{-2}	1.2166
755	13,245	6.40	755	13,245	8.88	0	0
805	12,422	7.41	810	12,346	11.42	0.612×10^{-2}	0.6157
$Pr(NO)_3$ in water			$Pr(phen)_2(ClMand)_3$ in DMF				
444	22,523	9.04	446	22,422	9.57	0.448×10^{-2}	0.450
468	21,368	4.62	471	21,231	4.96	0.641×10^{-2}	0.6451
481	20,790	3.01	484	20,661	3.28	0.620×10^{-2}	0.6238
588	17,007	1.90	595	16,807	2.02	1.176×10^{-2}	1.1899

As may be seen from Table 2, both Nd(III) complexes containing *o*-phenanthroline and 5,6 dimethylphenanthroline have the same "δ", which means that the methyl groups in positions 5,6 on the aromatic ring have no influence on the coordination bonds between heterocyclic nitrogen and lanthanide ion.

IR SPECTRA OF $Ln(phen)_2(ClMand)_3$

The IR spectrum of free phenanthroline and different coordination compounds have been discussed by Schilt and Taylor [13] and for the lanthanide complexes by Hart and Laming,[1] Sinha,[14] Carassiti [15] and others.

The IR pectra for $Ln(phen)_2$ $(ClMand)_3$ in the range $400-1600$ cm^{-1} show a lot of absorption bands proper to the *o*-phenanthroline and chloromandelic acid. Table 3 gives the absorption maxima in cm^{-1} units and the most probable assignment for coordinated and free phenanthroline. As may be seen, strong absorption bands should be observed in three ranges of frequencies namely 700−900 cm^{-1}; 1100−1250 cm^{-1} and 1400−1650 cm^{-1}.

---

[13] H. A. Schilt and R. C. Taylor, *J. Inorg. Nuclear Chem.*, **9**, 211 (1959).

[14] S. P. Sinha and H. M. N. H. Irving, *Analyt. Chim. Acta*, **52**, 193 (1970).

[15] V. Carassiti, A. Seminara and A. Seminara-Musumeci, *Ann. Chim.* (Ital.), **54**, 1025 (1964).

The maxima lying in the first range could be assigned to the out-of-plane vibration of the hydrogen atoms. The strong absorption maximum at 730 cm^{-1} should be ascribed to the out-of-plane motions of heterocyclic hydrogen atoms, and the absorption at 850 cm^{-1} to the same motions of the hydrogen atoms on the centre ring. It should be noted that the last absorption band is split in the IR spectra of the complexes (850 cm^{-1}; 865 cm^{-1}). This splitting is probably due to the perturbations produced by the crystal lattice or neighbour molecules on the moving in phase of the hydrogens.

The observed bands in the range 1100−1250 cm^{-1} are of less importance for the characterization of the metal-ligand bonding, these being assigned to the in-plane bending motions C−H or to other possible ring vibrations.

The absorption maxima arisen from the skeletal frequencies occurring in the region 1400−1650 cm^{-1} [16] are of particular interest, because changes in their position or intensities can prove the coordination of the heteroatom. Three absorption bands appearing in this region, namely at

Table 3

IR spectral data

Free phen	$Nd(phen)_2(ClMand)_3$	$Eu(phen)_2(ClMand)_3$	ClMand acid	Assignment
710 w	705 sh	705 sh		
740 s	740 s	740 s		C−H out of plane bend
774 m	782 m	782 m		
820 vw	820 w	820 w	820 s	C−H out of plane bend
850 s	850 s	850 s		
	865 m	865 m		
870 m	870 w	870 w	870 m	
	935 w	935 w	942 m	
	958 w	958 w	955 m	
1040 vw	1026 m	1025 m	1022 m	
1100 m	1098 s	1098 s	1080 s	
1145 w	1150 w	1149 w		
1222 w	1200 vw	1200 vw	1200 s	
	1230 vw	1230 vw	1235 s	
1350 w	1358 s broad	1350 s broad	1350 m sh	
1425 s	1420 s	1432 s	1420 m	Ring vibration
1513 s	1510 s	1505 s	1500 m	Ring vibration
	1535 s	1530 s		
1600 m	1610 vs ; v broad	1605 vs ; v broad	1605 w	OCO asymm. stretch and Ring vibrations
1628 w	1630 vs ; sh	1630 vs ; sh		

s = strong, m = medium, w = weak, sh = shoulder

---

[16] E. B. Wilson Jr., J. K. Decius and P. C. Cross, "Molecular Vibrations", chap. X McGraw-Hill Publishing Company Ltd., New York, 1955.

1425 cm^{-1}, 1500 cm^{-1} and 1600 cm^{-1} are more intense and shifted towards higher frequencies. It should be mentioned that the band at 1513 cm becomes more intense and split in the coordinated phenanthroline, the distance between the two components depending on the nature of the lanthanide ion. As may be earlier observed[13] the magnitude of the separation varied with the ionic radius of the central metal ion. For Nd(III) and Eu(III) complexes the splitting is practically the same (25 cm^{-1}), both elements being close enough in the 4f series.

The very strong absorption band at 1600 cm^{-1} could be assigned most likely to the ring vibrations of the phenanthroline, the asymmetric frequency absorption OCO of the chloromandelic acid appearing in the same region being very weak and probably masked by the first one.

FLUORESCENCE

The Eu(III) mixed ligand chloromandelates containing *o*-phenanthroline and 5,6-dimethylphenanthroline exhibit an intense fluorescence when UV irradiated.

The fluorescence could be explained by a radiative intramolecular energy transfer from organic ligand to the lanthanide ion *via* a metastable triplet state of the ligand, as shown for other lanthanide coordination compounds.[17]

[17] S. P. Sinha, *Z. Naturforsch.*, **25a**, 665 (1970).

Revue Roumaine de Chimie, 17, 4, 705–709 (1972)

INDIREKTE BESTIMMUNG VON K^+ UND NH_4^+ DURCH DIE β^--STRAHLENABSORPTION

GH. MARCU und V. SĂCELEAN
vom Chemischen Institut Cluj, str. Donáth, 63–105

Eingegangen am 24. Juli 1971

Es wurden zwei indirekte Bestimmungsmethoden für K^+, beziehungsweise drei im Falle von NH_4^+, auf Grund der Absorption der β^--Strahlen von den durch Lösen der Niederschläge $Me_2^IPb[Me^{II}(NO_2)_6]$ (wo $Me^I = K^+, NH_4^+$ und $Me^{II} = Co^{2+}$ — nur für NH_4^+, Ni^{2+}, Cu^{2+}) erhaltenen Lösungen ausgearbeitet. Durch die statistische Verarbeitung der experimentellen Ergebnisse wurde festgestellt, daß die Bestimmungsmethoden für 0,070–0,294 g K^+, beziehungsweise für 0,0323–0,1357 g NH_4^+, aus ihren Chloridlösungen, dieselbe Präzision haben.

Wenn zwischen β^--Strahlenquelle und Detektor eine Substanz eingeschoben wird, findet eine Abschwächung der Strahlenintensität nach folgender Beziehung statt:

$$\Lambda = \Lambda_0 e^{-\mu x}$$

wo Λ die Intensität der austretenden Strahlen darstellt, Λ_0 — die Intensität der einfallenden Strahlen, μ — den liniaren Absorptionskoeffizienten und x — die Dicke der durchquerten Schicht.

Im Falle einer Lösung für unveränderliche Arbeitsbedingungen, hängt die Intensität der austretenden Strahlen nur von der Natur und der Anzahl der Atome aus der Volumeneinheit ab.

Die Abschwächung der Intensität der austretenden Strahlen ist umso stärker je größer die Ordnungszahl der Atome ist.

Gestützt auf diese Betrachtungen, wurde die Anwendungsmöglichkeit der β^--Strahlenabsorption für die indirekte Bestimmung von K^+ und NH_4^+ durch ihre Fällung mit $Na_2Pb[Me^{II}(NO_2)_6]$ untersucht:

$$2Me^+ + Na_2Pb[Me^{II}(NO_2)_6] = Me_2^I Pb[Me^{II}(NO_2)_6] + 2Na^+ \qquad (I)$$

wo $Me^I = K^+, NH_4^+$ und $Me^{II} = Co^{2+}$ — nur im Falle von NH_4^+, Ni^{2+}, Cu^{2+}.

Für die Bestimmung von Me^+ können zwei Varianten verwendet werden und zwar: es wird ein Anteil von der Lösung, die nach dem Fällen von Me^+ bleibt, genommen, oder man löst den gebildeten Niederschlag, die Lösung wird auf ein konstantes Volumen gebracht und man mißt die Intensität der aus der Lösung austretenden Strahlen. Aus der Abhängigkeit, die es zwischen der Me^+-Menge und der Intensität der austretenden Strahlen gibt, kann der Me^+-Gehalt der untersuchten Probe bestimmt werden.

In diesem Sinne wurden die Eichkurven aus Abb. 1—4 gezogen und aus Rücksichten, die weiter unten erörtert werden, wurden Me^+-Bestimmungen nur durch Verarbeitung der $Me^I_2 Pb[Me^{II}(NO_2)_6]$-Niederschläge durchgeführt (Tabellen 1—3).

Um den Me^+-Gehalt der untersuchten Probe zu finden, kann die graphische Methode verwendet werden (Abb. 1—2), oder die Formel, die aus der Bedingung der Koliniarität von drei Punkten herrührt:

$$\begin{vmatrix} C & \lg\Lambda & 1 \\ 0 & \lg_{H_2O} & 1 \\ C_x & \lg\Lambda_x & 1 \end{vmatrix} = 0$$

wo:

$$C_x = \frac{C \lg \dfrac{\Lambda_{H_2O}}{\Lambda_x}}{\lg \dfrac{\Lambda_{H_2O}}{\Lambda}}$$

und wo C_x die Me^+-Menge der unbekannten Probe darstellt, Λ_x — die Intensität der aus dieser ausgetretenen Strahlen, C — die Konzentration einer Eichprobe, Λ und Λ_{H_2O} — die Intensität der aus der Eichprobe, beziehungsweise Wasser, ausgetretenen Strahlen.

ARBEITSWEISE

Im ersten Fall wird $Me^I_2Pb[Me^{II}(NO_2)_6]$ in HNO_3 gelöst, die Lösung wird in einen Meßkolben von 25 ml gegeben und es wird mit Wasser bis zur Marke aufgefüllt, während im zweiten Fall 25 ml von der nach der Fällung gebliebenen Lösung genommen werden.

Die Fällungsreagenzien und die Arbeitsbedingungen wurden ausführlich in der Arbeit [1] beschrieben.

Die Lösungen wurden in eine zylindrische Plexiglasschale gegeben, die eine untere Wanddicke von 0,03 cm, einen Durchmesser von 5,5 cm und eine Höhe von 1,3 cm hatte. Unter die Schale wurde die β^--Strahlenquelle von $\sim$ 2mCi eigenschoben, erhalten aus $^{204}TlNO_3$, welches auf die innere Fläche eines Kegels mit einem Grundflächendurchmesser von 1,2 cm und einer Höhe von 0,3 cm gegeben wurde.

Um die Intensität der aus der Lösung austretenden β^--Strahlen zu messen, wurde ein GM-Zähler des Typs STS-6, der über die Schale mit der Lösung (in einem Abstand von 1,5 cm von der Lösungsfläche) genau über die Strahlenquelle montiert wurde, an einen Nuklearzähler geschaltet.

---

[1] GH. MARCU und V. SĂCELEAN, *Rev. Roumaine Chim.*, unter Druck.

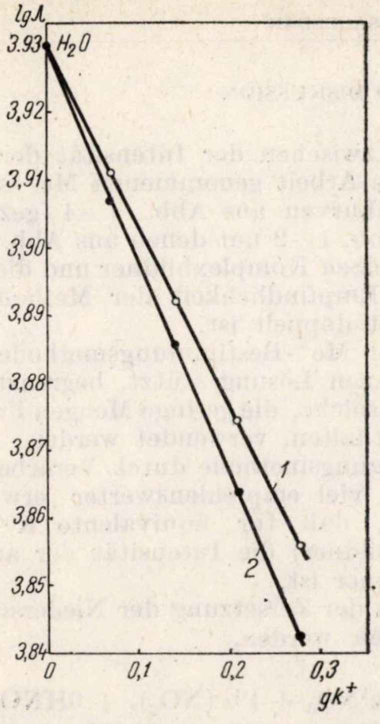

Abb. 1 — Änderung der Intensität (lgΛ) der aus 25 ml Lösung, erhalten durch Lösen der $K_2Pb[Cu(NO_2)_6]$ (*1*) und $K_2Pb[Ni(NO_2)_6]$-Niederschläge (*2*), austretenden β^--Strahlen.

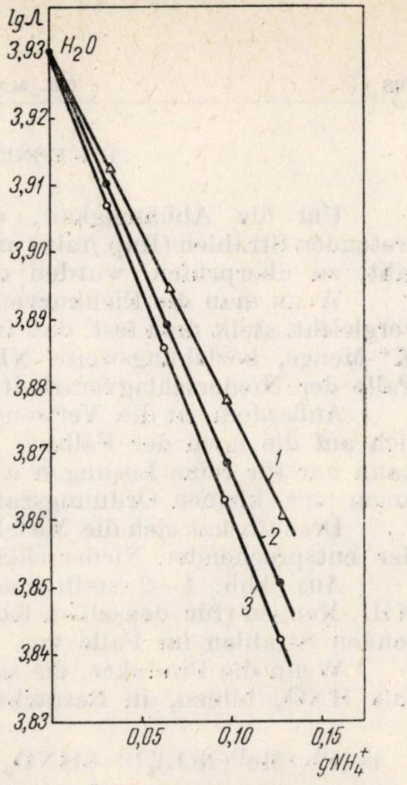

Abb. 2 — Änderung der Intensität (lgΛ) der aus 25 ml Lösung, erhalten durch Lösen der $(NH_4)_2Pb[Cu(NO_2)_6]$ (*1*), $(NH_4)_2Pb[Co(NO_2)_6]$ (*2*) und $(NH_4)_2\cdot Pb[Ni(NO_2)_6]$-Niederschläge (*3*), austretenden β^--Strahlen.

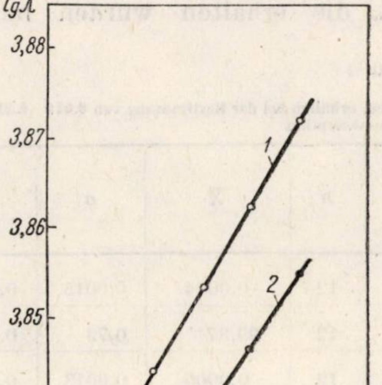

Abb. 3 — Änderung der Intensität (lgΛ) der aus 25 ml Lösung, erhalten bei der Fällung von K^+ mit einem Überschuß von $Na_2Pb[Ni(NO_2)_6]$ (*1*) und $Na_2Pb[Cu(NO_2)_6]$ (*2*), austretenden β^--Strahlen.

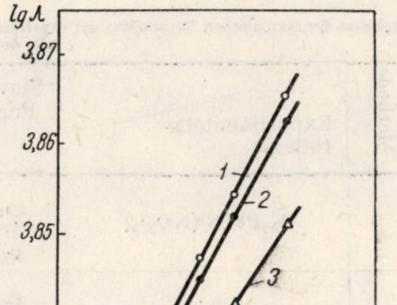

Abb. 4 — Änderung der Intensität (lgΛ) der aus 25 ml Lösung, erhalten bei der Fällung von NH_4^+ mit einem Überschuß von $Na_2Pb[Ni(NO_2)_6]$ (*1*), $Na_2Pb[Co(NO_2)_6]$ (*2*) und $Na_2Pb[Cu\cdot(NO_2)_6]$ (*3*), austretenden β^--Strahlen.

ERGEBNISSE UND DISKUSSION

Um die Abhängigkeit, die es zwischen der Intensität der austretenden Strahlen (Imp./min) und der in Arbeit genommenen Me^+-Menge gibt, zu überprüfen, wurden die Eichkurven aus Abb. 1—4 gezogen.

Wenn man die Eichkurven aus Abb. 1—2 mit denen aus Abb. 3—4 vergleicht, stellt man fest, daß für denselben Komplexbildner und dieselbe K^+-Menge, beziehungsweise NH_4^+, die Empfindlichkeit der Methode im Falle der Niederschlagverarbeitung fast doppelt ist.

Außerdem ist die Verwendung der Me^+-Bestimmungsmethode, die sich auf die nach der Fällung gebliebenen Lösung stützt, begrenzt. Sie kann nur für reine Lösungen oder für solche, die geringe Mengen Fremdionen mit kleinen Ordnungszahlen enthalten, verwendet werden.

Deshalb hat sich die Me^+-Bestimmungsmethode durch Verarbeitung der entsprechenden Niederschläge als viel empfehlenswerter erwiesen.

Aus Abb. 1—2 stellt man fest, daß für äquivalente K^+- und NH_4^+-Mengen (für denselben Komplexbildner) die Intensität der austretenden Strahlen im Falle von K^+ kleiner ist.

Wenn die Produkte, die sich nach der Zersetzung der Niederschläge mit HNO_3 bilden, in Betracht gezogen werden,

$$Me^I_2Pb\,[Me^{II}(NO_2)_6] + 6HNO_3 = 2\,Me^INO_3 + Pb\,(NO_3)_2 + 6HNO_2 \quad (II)$$

$$NH_4^+ + NO_2^- = N_2 + 2H_2O \quad (III)$$

stellt man fest, daß im Falle der Niederschläge mit K^+ sich auch KNO_3 bildet, was die vergrößerte Absorption der Strahlen erklärt.

Weiter unten werden die Daten der statistischen Verarbeitung der experimentellen Ergebnisse angegeben, die erhalten wurden bei der

Tabelle 1

Ergebnisse der statistischen Verarbeitng der experimentellen Daten, erhalten bei der Bestimmung von 0,070 – 0.294 g K+ mit der β⁻-Strahlenabsorption

Methode	Experimentelle Indexe	Statistische Parameter	n	$\overline{X}$	σ	e
1.	$K_2Pb[Ni(NO_2)_6]$	Differenz	12	—0,0004	0,0015	0,0004
		Prozente	12	99,87	0,73	0,21
2.	$K_2Pb[Cu(NO_2)_6]$	Differenz	12	0,0005	0,0013	0,0004
		Prozente	12	100,22	0,68	0,20

Differenz = Differenz zwischen der in Probe genommenen und der experimentell gefundenen Me^+ Menge.
Prozente = Prozentual ausgedrücktes Verhältnis zwischen der experimentell gefundenen und der in Probe genommenen Me^+ Menge.
n = Anzahl der Bestimmungen.
$\overline{X}$ = Arithmetischer Mittelwert.
σ = Mittlere quadratische Abweichung.
e = Mittlerer statistischer Fehler des Mittelwertes.

Bestimmung von K^+ und NH_4^+ auf Grund der Absorption der β^--Strahlen von Lösungen, die durch Lösen der $Me_2^IPb[Me^{II}(NO_2)_6]$-Niederschläge erhalten wurden.

Es wird erwähnt, daß sowohl bei den Bestimmungen als auch beim Ziehen der Eichkurven mit reinen KCl- und NH_4Cl-Lösungen gearbeitet wurde.

Tabelle 2

Ergebnisse der statistischen Verarbeitung der experimentellen Daten, erhalten bei der Bestimmung von 0,0323 – 0,1357 g NH_4^+ mit der β^--Strahlenabsorption

Methode	Experimentelle Indexe	Statistische Parameter	n	$\bar{X}$	σ	e
3	$(NH_4)_2Pb[Co(NO_2)_6]$	Differenz	12	–0,0002	0,0007	0,0002
		Prozente	12	99,71	0,82	0,24
4	$(NH_4)_2Pb[Ni(NO_2)_6]$	Differenz	12	0,00003	0,0008	0,0002
		Prozente	12	100,02	0,78	0,23
5	$(NH_4)_2Pb[Cu(NO_2)_6]$	Differenz	12	–0,00013	0,0007	0,0002
		Prozente	12	99,83	0,67	0,19

Tabelle 3

Studententest (t) für den Vergleich der Analysenmethoden

Experimentelle Indexe	Studenttest	$t_{1,2}$	$t_{3,4}$	$t_{3,5}$	$t_{4,5}$
	Differenz	1,501	0,687	0,237	0,490
	Prozente	1,151	0,919	0,367	0,631

Aus der Berechnung des Parameters t und in Abhängigkeit von der Anzahl der Freiheitsgrade stellt man fest, daß die Differenz zwischen den Mittelwerten nicht bedeutend ist, und demnach haben die zwei Bestimmungsmethoden für K^+ durch die β^--Strahlenabsorption, beziehungsweise drei im Falle von NH_4^+, dieselbe Präzision.

Andererseits zeigt der Vergleich der bei der Bestimmung von K^+ und NH_4^+ durch die β^--Rückstrahlung erhaltenen Ergebnisse mit denen, die durch β^--Strahlenabsorption erhalten wurden, im Falle der durch Lösen der $Me_2^IPb[Me^{II}(NO_2)_6]$-Niederschläge erhaltenen Lösungen, daß beide Verfahren gleich gut sind.

Revue Roumaine de Chimie, 17, 4, 705–709 (1972)

Revue Roumaine de Chimie, **17**, *4*, 711–717 (1972)

NEUE KOBALT(III)-CHELATE MIT EINEM VIERZÄHNIGEN KOMPLEXBILDNER

GH. MARCU, CS. VÁRHELYI und ILDIKÓ MÜLLER

vom Lehrstuhl für Anorganische Chemie der
Babeş-Bolyai Universität, Cluj, str. Arany János 11

Eingegangen am 4. September 1971

Es wurden drei neue Kobalt(III)-amin-Komplexe durch Luftoxydation von Kobalt(II)-Salzen in Anwesenheit von einem vierzähnigen Komplexbildner, der Schiffschen Base Äthylendiimino-bis-acetylaceton : $C_{12}H_{20}N_2O_2$, und von primären organischen Aminen erhalten. Die Formeln der entstehenden Komplexkationen: [Co ec (*o*-Anisidin)$_2$]$^+$, [Co ec (*p*-Phenetidin)$_2$]$^+$ und [Co ec (Cyclohexylamin)$_2$]$^+$ wurden auf präparativem Wege bestimmt. Wechselwirkung der Schiffschen Base mit $Na_3[Co(NO_2)_6]$ führt zur Bildung von [Co ec $(NO_2)_2$]$^-$. Es wurden 30 neue Komplexsalze in kristallisierter Form isoliert. Zur Klärung einiger Strukturfragen wurden auch spektrophotometrische Untersuchungen im UV- und IR-Bereich durchgeführt.

Die Schiffsche Base : Äthylendiimino-bis-acetylaceton ($C_{12}H_{20}N_2O_2$) entsteht durch Kondensierung von 1 Mol Äthylendiamin mit 2 Mol Acetylaceton nach der Gleichung :

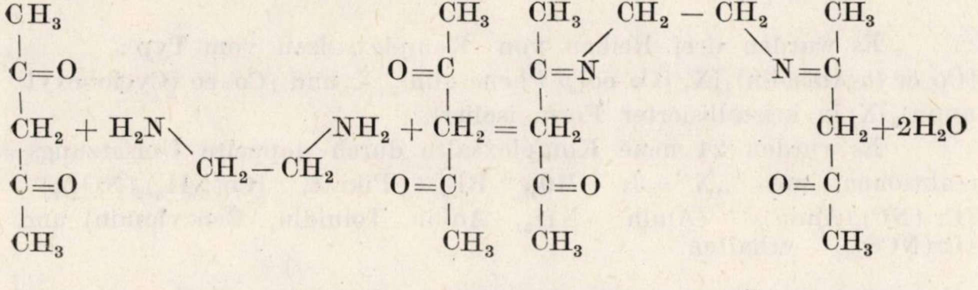

Dieser vierzähnige Chelatbildner tritt mit Salzen der Übergangsmetalle leicht in Wechselwirkung. Die ersten bis-Acetyl-aceton-äthylendiiminchelate mit Kupfer(II) wurden von Combes[1] dargestellt. Später haben Morgan und Smith[2,3] einen Nichtelektrolyt-Komplex des zweiwertigen

---

[1] A. Combes, *Compt. rend.*, **108**, 1252 (1889).

[2] G. T. Morgan und D. M. Smith, *J. Chem. Soc.*, **125**, 1996 (1924).

[3] G. T. Morgan und D. M. Smith, *J. Chem. Soc.*, **127**, 2030 (1925).

Kobalts [Co ec $(H_2O)_2$] und eine Reihe von Komplexsalzen des Typus [Co ec $(NH_3)_2$] X beschrieben. („ec" bezeichnet die koordinierte Schiffsche Base Äthylendiimino-bis-acetylaceton : $C_{12}H_{18}N_2O_2$). Die letzten Verbindungen entstehen bei der Oxydation von [Co ec $(H_2O)_2$] in Gegenwart von NH_3 und Ammoniumsalzen.

Theoretisch ist es möglich, sämtliche aromatischen und heterocyclischen Amine in die innere Koordinationssphäre der Kobalt-(III)-Komplexverbindungen, wie im Falle der Dimethylglyoximine: $[Co(DH)_2(Amin)_2]$ X und $[Co(DH)_2(Amin)\ X]$[4,5] oder im Falle der bis-Äthylendiamin-acido-amin-Co(III)-Verbindungen : $[Co(en)_2\ X\ Amin]\ Y_2$[6,7] einzuführen.

In früheren Arbeiten [8–10] berichteten wir über die Bildung der Chelate vom Typus $[Co\ ec\ Amin)_2]^+$ mit Amin = Pyridin, Picolin, Anilin.

In Fortsetzung dieser Versuche haben wir eine Reihe von aromatischen, alycyclischen und aliphatischen Monoaminen in dieser Hinsicht untersucht.

Die Derivative mit Pyridin und Picolin wurden aus dem Nichtelektrolyt [Co ec $(H_2O)_2$] durch Oxydation mit H_2O_2 in Gegenwart einer Mischung von Amin und Aminchlorhydrat erhalten :

$$2[Co\ ec\ (H_2O)_2] + 4Amin + H_2O_2 + 2H^+ = 2[Co\ ec\ Amin)_2]^+ + 6\ H_2O$$

Die Synthese der Diaquoverbindung [Co ec $(H_2O)_2$] führt nur zu schlechten Ausbeuten. Aus dieser Ausgangssubstanz konnten wir keine einheitlichen [Co ec $(Amin)_2$] X-Derivate mit aliphatischen und aromatischen Aminen darstellen. Wir konnten aber feststellen, daß die [Co ec $(Amin)_2$]X-Chelate mit diesen Aminen sehr leicht aus den Komponenten durch Luftoxydation in wäßrigen-alkoholischen Lösungen mit guter Ausbeute entstehen.

$$2Co^{2+} + 2\ ec.H_2 + 4Amin + 1/2\ O_2 = 2[Co\ ec\ (Amin)_2]^+ + H_2O + 2\ H^+$$

Es wurden drei Reihen von Komplexsalzen vom Typ : [Co ec (*o*-Anisidin)$_2$]X, [Co ec(*p*-Phenetidin)$_2$]X und [Co ec (Cyclohexylamin)$_2$]X in kristallisierter Form isoliert.

Es wurden 24 neue Komplexsalze durch doppelte Umsetzungsreaktionen mit „X"=J, $C10_4$, BF_4, Pikrat, $[Co(NH_3)_2(NO_2)_4]^-$, $[Cr\ (NC)_4(Amin)_2]^-$ (Amin = NH_3, Anilin, Toluidin, Benzylamin) und $[Cr(NCS)_6]^{3-}$ erhalten.

---

[4] A. V. Ablov, *Bull. Soc. chim. France*, **1940**, 151.

[5] J. Nakatsuka und H. Iinuma, *Bull. Chem. Soc. Japan*, **11**, 48 (1936).

[6] H. Meisenheimer und E. Kiderlen, *Liebigs Ann. Chem.*, **438**, 238 (1924).

[7] J. Baylar und L. B. Clapp, *J. Amer. Chem. Soc.*, **67**, 17 (1945).

[8] R. Ripan, Cs. Várhelyi und J. Csorvási, *Studii și Cercetări Chim., Fil. Cluj*, **12**, 191 (1961).

[9] R. Ripan, Cs. Várhelyi und A. Nyesö, *Z. anorg. Chem.*, **341**, 103 (1965).

[10] Cs. Várhelyi, C. Stanisav und E. Hamburg, *Stud. Univ. Babeș-Bolyai, Chem.*, **14**, (2) 71 (1969).

Andererseits wurde die Wechselwirkung von dieser Schiffschen Base mit $Na_3[Co(NO_2)_6]$ untersucht. In acetatgepufferter Lösung führt die Reaktion zur Substitution von vier Nitro-Gruppen :

$$Na_3[Co(NO_2)_6] + ec.\,H_2 = Na[Co\,ec\,(NO_2)_2] + 2\,NaNO_2 + 2\,HNO_2$$

Dieses Komplexanion bildet im allgemeinen sehr leicht lösliche Komplexsalze. Es wurden doch einige Derivate vom Typ $[Co\,ec\,(Amin)_2]$, $[Co\,ec\,(NO_2)_2]$ dargestellt und charakterisiert. Doppelte Umsetzungsreaktionen mit Metallsalzen und Komplexen der Hexamin- und Monoacido-pentamin-Reihe geben keine wohldefinierten schwer löslichen Produkte.

Die $[Co\,ec\,(Amin)_2]^+$ und $[Co\,ec\,(NO_2)_2]^-$ sind gemischte Chelate mit zwei hexaatomischen und mit einem pentaatomischen Ringen

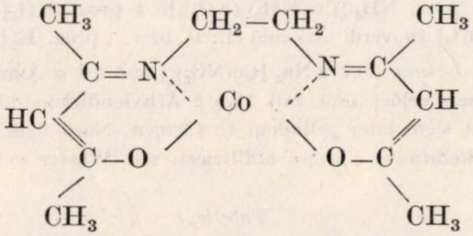

Die oktaedrischen Kobalt(III)-Verbindungen mit Athylendiimino-bis-Acetylaceton können in fünf stereoisomeren Formen auftreten. Diese Komplexformen umfassen zwei Paare von optischen Antipoden und eine inaktive Modifikation (Abb. 1.)

Morgan und Smith[3] haben zwei sehr unbeständige optisch aktive Modifikationen des $[Co\,ec\,(NH_3)_2]^+$-Ions mit D-Camphersulfonat isoliert. Diese aktiven Modifikationen gehen aber sehr schnell in die inaktive *trans*-Modifikation über.

Unsere Bemühungen optisch aktive Salze durch fraktionierte Kristallisation der entsprechenden D-Tartrate und D-Camphersulfonate zu isolieren, waren wegen der sehr großen Löslichkeit dieser Derivate erfolglos. Wir nehmen an, daß bei der Synthese von den fünf Stereoisomeren nur die inaktive *trans*-Form entsteht, welche vom energetischen Standpunkt die beständigste Form ist.

Zur Klärung einiger Strukturfragen wurden auch spektrophotometrische Untersuchungen im UV- und IR-Bereich durchgeführt.

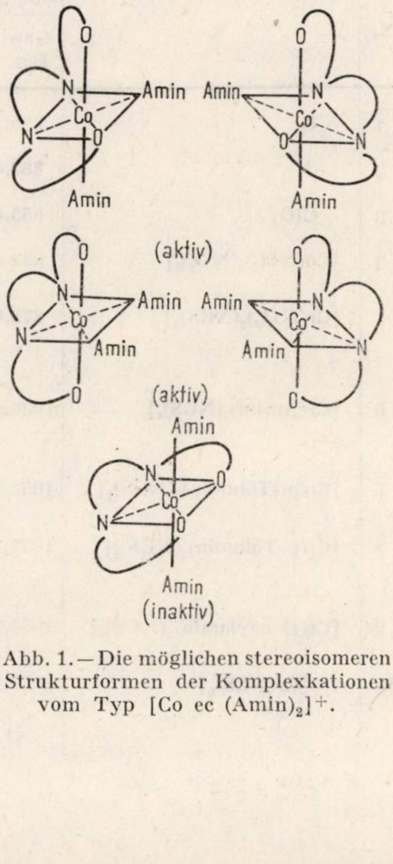

Abb. 1. — Die möglichen stereoisomeren Strukturformen der Komplexkationen vom Typ $[Co\,ec\,(Amin)_2]^+$.

EXPERIMENTELLES

$[Co$ ec (o-Anisidin)$_2]$-acetat, $[Co$ ec (p-Phenetidin)$_2]$-acetat und $[Co$ ec (Cyclohexylamin)$_2]$-acetat-Lösungen

7,5 g (30 mMol) $Co(CH_3-COO)_2 . 4 H_2O$ werden in 50 ml Wasser aufgelöst und mit einer Mischung von 6,75 g Äthylendiimino-bis-acetylaceton (ec. H_2) (30 mMol) und 60 mMol Amin (7 g *o*-Anisidin, 7,2 g *p*-Phenetidin und 6,3 g Cyclohexylamin) in 125 ml Äthanol versetzt. Die so entstandene braune Flüssigkeit wird mit einem starken Luftstrom 4–6 Std. lang oxydiert, dann von den Oxydationsnebenprodukten abfiltriert und mit 50 proz. Äthanol auf 200 ml aufgefüllt. 50–50 ml von diesen Stammlösungen enthalten 7,5 mMol $[Co$ ec $(Amin)_2]$-acetat. Aus den so hergestellten Stammlösungen erhält man die übrigen Salze durch doppelte Umsetzung.

Für diese Umsetzungsreaktionen verwendet man 5 proz. NaBr, KJ, 4 proz. $NaClO_4$, 1 proz. Pikrinsäure, 1 proz. $NH_4 [Co (NH_3)_2(NO_2)_4]$, 1 proz. $NH_4[Cr(NH_3)_2(NCS)_4]$, 1 proz. Amin. $H[Cr(NCS)_4(Amin)_2]$ in verd. Äthanol (1 : 1), bzw. 1 proz. $K_3[Cr(NCS)_6]$ in Überschuß.

$Na[Co$ ec $(NO_2)_2]$-Lösung 20,2 g $Na_3 [Co(NO_2)_6]$ und 10 g Ammoniumacetat (50 mMol) werden in 100 ml Wasser gelöst und mit 11,5 g Äthylendiimino-bis-acetylaceton versetzt. Die Schiffsche Base löst sich unter gelindem Erwärmen. Nach dem Aufhören der NO_2-Entwicklung wird die dunkelbraune Lösung abfiltriert, mit Wasser auf 150 ml aufgefüllt und

Tabelle 1

Neue Komplexsalze vom Typ $[Co$ ec $(p\text{-Phenetidin})_2]X$

Nr.	X	Mol. Ausbeute		Charakteristik	Analyse		
		Gew. Ber.	%			*Ber.*	*Gef.*
1	Br	635,4	15	Rotbraune rhomb. Platten	Co	9,27	9,30
2	J	682,4	30	Braune Nadeln	Co	8,64	8,42
					N	8,22	8,42
3	ClO_4	655,0	35	Unregelmäßige rotbraune Platten	Co	9,00	8,70
4	$[Co(NH_3)_2(NO_2)_4]$	832,5	40	Braune Platten	Co	14,16	13,94
					N	16,82	16,74
5	$[Cr(NH_3)_2(NCS)_4]$	873,9	40	Braune mikrokrist.	1/3 Co_3O_4 + 1/2 Cr_2O_3		
				Masse		17,88	17,90
					N	16,03	15,80
6	$[Cr(Anilin)_2(NCS)_4]$	1026,1	50	Braune mikrokrist.	1/3 Co_3O_4 + 1/2 Cr_2O_3		
				Masse		15,23	14,99
					N	13,65	13,20
7	$[Cr(m\text{-Toluidin})_2(NCS)_4]$	1054,1	50	Braune mikrokrist. Masse	N	13,29	13,41
8	$[Cr(p\text{-Toluidin})_2(NCS)_4]$	1054,1	50	Braune Mikrokrist.	1/3 Co_3O_4 + 1/2 Cr_2O_3		
				Masse		14,82	14,66
					N	13,29	13,10
9	$[Cr(Benzylamin)_2(NCS)_4]$	1054,1	55	Dunkelbraune mikrokrist. Masse	N	13,29	13,45
10	$1/3[Cr(NCS)_6]$	2067,1	40	Braune mikrokrist.	Co_3O_4 + 1/2 Cr_2O_3		
				Masse		15,32	15,01
					N	12,20	11,90

Tabelle 2

Neue Komplexsalze vom Typ [Co ec (Cyclohexylamin)$_2$]X (A.X) und [Co ec (*o*-Anisidin)$_2$]X (B. X)

Nr.	X	Mol. Ausbeute Gew. Ber.	(%)	Charakteristik	Analyse Ber.	Gef.
11	A.J.	606,4	25	Gelbbraune feine Nadeln	Co 9,72 N 9,24	10,00 9,18
12	A.ClO_4	579	20	Gelbbraune Platten	Co 10,18	10,37
13	A. Pikrat	697,6	20	Gelbbraune mikrokrist. Masse	Co 8,45 N 14,07	8,29 14,20
14	A.$[Co(NH_3)_2(NO_2)_4]$	756,6	25	Aggregate aus gelben Tafeln	Co 15,58 N 18,47	15,84 18,70
15	A.$[Cr(NH_3)_2(NCS)_4]$	798,0	35	Kleine gelbe Nadeln	1/3 Co_3O_4+1/2 Cr_2O_3 19,58 N 17,55	 19,20 17,06
16	A.[Cr(Anilin)$_2$(NCS)$_4$]	950,1	40	Gelbbraune Platten	1/3 Co_3O_4+1/2 Cr_2O_3 16,45 N 14,74	 16,64 14,49
17	$A_3[Cr(NCS)_6]$	1839,2	50	Unregelmäßige kleine braune Prismen	Co_3O_4 + 1/2 Cr_2O_3 17,23 N 13,71	 17,03 13,50
18	B.J.	654,4	20	Glänzende rote Prismen	Co 9,00	8,89
19	B.ClO_4	627	25	Rote Prismen	Co 9,40	9,20
20	B.BF_4.H_2O	632,3	40	Rechteckige braune Platten	Co 9,32 H_2O 2,89	9,60 2,93
21	B.$[Co(NH_3)_2(NO_2)_4]$	804,5	50	Rotbraune Prismen	Co 14,65 N 17,41	14,40 17,60
22	B. $[Cr(NH_3)_2(NCS)_4]$	845,9	50	Braune mikrokrist. Masse	1/3 Co_3O_4+ 1/2 Cr_2O_3 18,47 N 16,56	 18,19 16,30
23	B. [Cr (Anilin)$_2$ NCS)$_4$]	998,1	55	Braune mikrokrist. Masse	N 14,03	13,86
24	B_3. $[Cr(NCS)_6]$	1,983,1	50	Braune mikrokrist. Masse	Co_3O_4 + 1/2 Cr_2O_3 15,97 N 12,71	 15,66 12,60

zu doppelten Umsetzungsreaktionen verwendet. 30 ml Lösung enthält annähernd 10 m Mol Na [Co ec $(NO_2)_2$]. Diese Lösungsmenge wird mit je 10 mMol [Co ec (Amin)$_2$] acetat vereinigt.

Spektroskopische Untersuchungen. Die Lichtabsorption von [Co ec (Amin)$_2$]X wurde im Wasser gemessen. Die Spektren der obenerwähnten Chelate sind dem des [Co ec (β-Picolin)$_2$]J[9] sehr ähnlich und zeigen vier Maxima oder Schultern. Die erste und die dritte Absorptionsbande sind von der Natur der Aminkomponenten beeinflußt.

Die Ultrarotspektra von [Co ec (Amin)$_2$]X wurden in KBr-Preßlingen untersucht.

Nach Ueno und Martell[11,12] ist die im Spektrogramm des freien nichtkoordinierten Äthylendiimino-bis-acetylaceton bei 1550 cm^{-1} auftretende Bande der $\nu_{C=N}$-Valenzschwingungsfrequenz zuzuordnen. Diese Bande ist bei den Ni, -Pd- und Cu-Chelaten gegen

---

[11] K. Ueno und A. E. Martell, *J. Phys. Chem.*, **59**, 998 (1955).
[12] K. Ueno und A. E. Martell, *J. Phys. Chem.*, **60**, 1270 (1956).

1520—1530 cm^{-1} zu verschoben. Diese Valenzschwingung ist bei den [Co ec $(Amin)_2$]X Chelaten um 1521—1522 cm^{-1} erkennbar. Die bei der freien „ec. H_2" um 1143 cm^{-1} auftretende Bande entspricht den ν_{C-O}-Valenzschwingungsfrequenzen. Diese Frequenzen treten bei Cu(II)- und Ni(II)-Derivaten um 1113, bzw. 1122 cm^{-1} auf. Im Falle der obenerwähnten Kobalt(III)-Chelate erscheinen sie um 1120 cm^{-1}.

Tabelle 3

Neue Komplexsalze vom Typ [Co ec $(Amin)_2$] [Co ec $NO_2)_2$]

Nr.	Formel	Mol. Ausbeute		Charakteristik	Analyse		
		Gew. Ber.	(%)		*Ber.*		*Gef.*
25	[Co ec $(NH_3)_2$]. X	688,5	10	Braune unregelmäßige Tafeln	Co N	17,12 16,28	168,6 16,44
26	[Co ec $(Pyridin)_2$].X	812,6	12	Braune Platten	Co N	14,50 13,79	14,33 13,90
27	[Co ec (β-$Picolin)_2$].X	840,6	10	Braune Tafeln	Co N	14,02 13,33	13,80 13,50
28	[Co ec (γ-$Picolin)_2$].X	840,6	14	Braune Plättchen	Co	14,02	13,96
29	[Cp ec (*p*-$Phenetidin)_2$].X	928,8	10	Dunkelbraune unregelmässige Tafeln	Co N	12,70 12,06	12,50 11,70
30	[Co ec $(Anilin)_2$].X	840,6	15	Braune Platten	Co N	14,02 13,33	13,76 13,19

$X = [Co\ ec\ (NO_2)_2]^-\ Co(C_{12}H_{18}N_2O_2)\ (NO_2)_2$ —

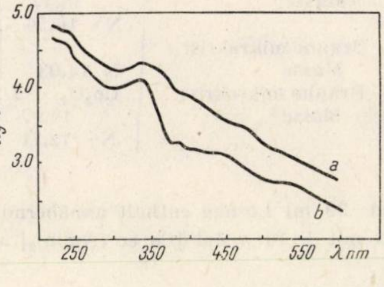

Abb. 2. — Absorptionsspektren
a, [Co ec (*p*-$Phenetidin)_2$]Br;
b, [Co ec $(Cyclohexylamin)_2$]CO_4

Tabelle 4

Spektraldaten von [Co ec $(Amin)_2$]-Verbindungen

Verbindung	λ_1 nm	log ε_1	λ_2 nm	log ε_2	λ_3 nm	log ε_3	λ_4 nm	log ε_4
[Co ec $(Pyridin)_2$] J	420—430	2,79	—	—	330	3,79	250_i	4,22
[Co ec (p-$Phenetidin)_2$]Br	400—420	3,70	385_i	3,90	340	4,33	270_i	4,39
[Co ec $(Cyclohexylamin)_2$] ClO_4	415—430	3,20	385_i	3,27	332	4,10	270_i	4,10

„i" = Inflexionspunkt

Diese Erscheinung ist ein direkter Beweis für den kovalenten Charakter der Co-N-(Schiffsche Base) und Co-O-Bindung.

In diesen Spektrogrammen liegen die ν_{N-H}-Valenzschwingungsfrequenzen um 3250–3300 und 3170–3190 cm^{-1} (die Verschiebung gegen die freien Amine um 100–150 cm^{-1}). Die Co-N (Amin)-Bindung hat also kovalenten Charakter.

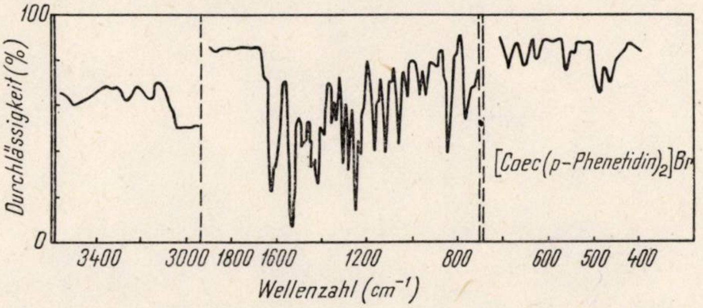

Abb. 3. – Ultrarotspektrum von [Co ec (*p*-Phenetidin)$_2$]Br.

Tabelle 5

Charakteristische IR-Schwingungsfrequenzen einiger Komplexe vom Typ [Co ec (Amin)$_2$]X

Schwingungs-frequenz	Amin	
	o-Anisidin	*p*-Phenetidin
ν_{N-H}	3205 (m)	3270 (m)
	3120 (m)	3180 (m)
δ_{NH_2}	1560 (m)	1530 (s.s.)
$\nu_{C=N}$	1520 (s.s.)	1521 (s.s.)
δ_{CH_3}	1470 (s)	1470 (s)
δ_{CH_2}	1350 (m)	1360 (m)
δ_{NH_2}	1320 (m)	1320 (m)
γ_{C-O}	1115 (s.s.)	1120 (s.s.)
γ_{NH_2}	830 (s)	830 (s)
ν_{Co-O}	570 (m)	563 (m)
ν_{Co-N}	478 (m)	485 (m)

m – mäßig
s.s – sehr stark
– stark

Revue Roumaine de Chimie, **17**, *4*, 719–726 (1972)

RÉACTIONS DES LIGANDS COORDINÉS. I
L'ACTION DES COMPOSÉS ORGANOALUMINIQUES SUR LES BISDIMÉTHYLGLYOXIMATES DE NICKEL, PALLADIUM ET CUIVRE ET SUR LA DIMÉTHYLGLYOXIME NON COORDINÉE

N. VOICULESCU et I. POPESCU

Institut de Chimie Macromoléculaire «P. Poni», 41 A, Aleea Gr. Ghica Vodă, Jassy

Reçu le 7 juin 1971

On décrit les méthodes de préparation et les propriétés des dérivés organoaluminiques des bisdiméthylglyoximates de Ni(II), Pd(II), Cu(II) et de la diméthylglyoxime non coordinée. Ces nouveaux complexes organométalliques sont plus instables que les dérivés similaires du bore, mais ils sont plus stables que les composés organiques de l'aluminium. Dans le cas des bisdiméthylglyoximates de nickel et de palladium les produits ont été obtenus par substitution de l'hydrogène dans la liaison OH. . .O avec les groupes AlX_2 (X=isobutyle, éthyle, phényle et chlore). Les produits ont été caractérisés par analyses chimiques, spectrales et röntgénographiques.

L'étude de la réactivité des oximes coordinées avec des ions métalliques est connue il y a presque 50 ans. Ainsi, en 1925, Barker [1] a essayé une réaction entre le $Ni(II)(DMGH)_2$ (DMGH = le radical diméthylglyoxime coordinée) et l'iodure de méthyle, en obtenant des produits méthylés du $Ni(II)(DMGH)_2$. En 1929, Thilo et Friedrich [2] ont étudié une réaction semblable. Mais leurs résultats infirment l'existence de l'éther oximique coordinée, dans la réaction directe entre l'iodure de méthyle et le $Ni(II) (DMGH)_2$.

Les essais ultérieurs pour l'éthérification et l'estérification du groupe OH de $Ni(II) (DMGH)_2$ avec l'isocyanate de phényle,[3] anhydride acétique, [4] ainsi que la réaction avec l'iodure de méthylmagnésium dans l'éther amylique, [5] ont mis en évidence la dissimulation des propriétés caractéristiques de ce groupe en comparaison de celui des oximes libres.

$Ni(II)(DMGH)_2$ et $Pd(II)(DMGH)_2$ donnent avec le chlorure d'acétyle des composés de formule $Me(II)(DMGH)Cl_2$ et le ligand acétylé libre.[6] Les halogénures d'alkyle dans la réaction avec Ni(II) $(DMGH)_2$ conduisent à des produits qui correspondent à la formule I.[7]

---

[1] M. F. Barker, *Chem. News*, **130**, 99 (1925).

[2] E. Thilo et K. Friedrich, *Ber. dtsch. chem. Ges.*, **62 B**, 2990 (1929).

[3] L. A. Chugaev, *J. Chem. Soc.*, **105**, 2187 (1914).

[4] R. C. Voter, C. V. Banks, V. A. Fassel et P. W. Kehres, *Analyt. Chem.*, **23**, 1730 (1951).

[5] O. L. Brady et M. M. Muers, *J. Chem. Soc.*, **1930**, 1599.

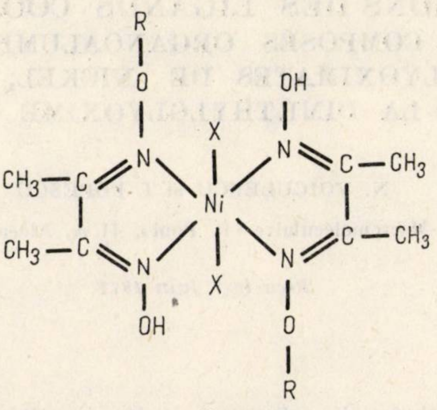

Formule I

Sharpe et Wakefield[8] ont étudié l'action de l'acide chlorhydrique sur le Ni(II) $(DMGH)_2$ et le Pd(II) $(DMGH)_2$. Ils ont aussi communiqué ultérieurement que les produits de cette réaction dans le cas du chélate de palladium se comporte d'une manière différente de ceux de nickel dans la réaction avec le chlorure d'acétyle.[9] La résistance à l'éthérification et l'estérification du groupe OH de la diméthylglyoxime coordinée a été attribuée à la liaison OH...O qui se réalise dans les chélates de la diméthylglyoxime avec les ions des métaux transitionnels. La liaison en pont réalisée par le proton, entre ces deux atomes d'oxygène (formule II) est considérée comme l'une des plus courtes (2,40 Å dans le chélate de nickel et 2,59 Å dans celui de palladium[10]) et des plus puissantes liaisons de l'hydrogène. Toutefois les deux protons des ponts sont réactifs.

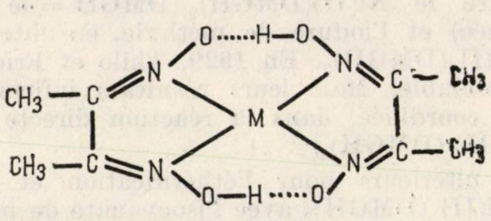

Formule II

---

[6] R. A. Krause, D. C. Jicha et D. H. Busch, *J. Amer. Chem. Soc.*, **83**, 528 (1961).

[7] M. M. Jones, « Ligand Reactivity and Catalysis », Academic Press, New York and London, 1968, p. 125.

[8] A. G. Sharpe et D. B. Wakefield, *J. Chem. Soc.*, **1957**, 496.

[9] A. G. Sharpe et D. B. Wakefield, J. Chem. Soc., **1957**, 3323.

[10] D. E. Williams, G. Wohlauer et R. E. Rundle, *J. Amer. Chem. Soc.*, **81**, 755 (1959).

En 1962 Schrauzer[11] a trouvé que le Ni(II)(DMGH)$_2$ et d'autres complexes similaires réagissent avec les dérivés du bore du type BX_3, où X peut être le fluor, le chlore, ou les radicaux des hydrocarbures aliphatiques. Les produits obtenus font partie d'une nouvelle classe de combinaisons et correspondent à la formule III. Des composés semblables ont été obtenus par Umland et Thierig.[12]

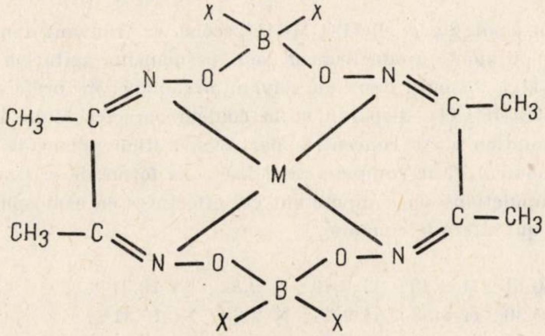

Formule III

On ne rencontre pas dans la littérature des dérivés des bisdiméthylglyoximates de Ni(II), Pd(II) et Cu(II) avec les composés organoaluminiques. Les composés synthétisés par nous en partant du Ni(II)(DMGH)$_2$ et du Pd(II)(DMGH)$_2$ correspondent à la formule IV dans laquelle l'atome de bore de III est remplacé par l'atome d'aluminium.

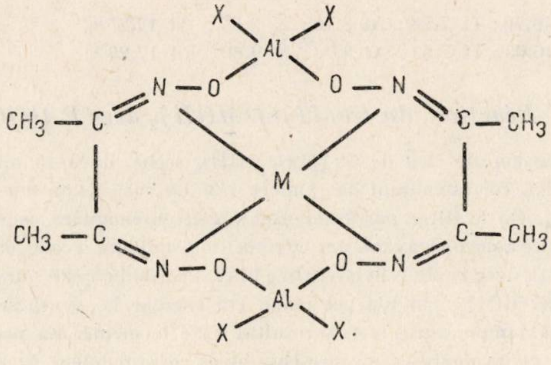

Formule IV

Le Cu(II)(DMGH)$_2$ avec triisobutylaluminium se comporte différemment.

---

[11] G. N. Schrauzer, *Chem. Ber.*, **95**, 1438 (1962).
[12] F. Umland et D. Thierig, *Angew. Chem.*, **74**, 388 (1962).

Revue Roumaine de Chimie, **17**, *4*, 719–726 (1972)

PARTIE EXPÉRIMENTALE

Les bisdiméthylglyoximates de Ni(II), Pd(II) et Cu(II) ont été préparés selon la méthode de Basu, Cook et Belford.[13] Le complexe de cuivre a été préparé suivant les indications de Fleischer et Freiser.[14]

Le tétraisobutylaluminium-bisdiméthylglyoximate de nickel

A une suspension de 2 gde $Ni(II)(DMGH)_2$ séché, se trouvant dans 15 ml de *n*-heptane fraîchement distillé, on ajoute graduellement, sous permanente agitation, une quantité correspondante de $Al(iC_4H_9)_3$ dissoute dans un solvant organique, de préférence le *n*-heptane. La suspension du $Ni(II)(DMGH)_2$ disparaît et la couleur caractéristique du chélate change en rouge-orange. La solution a été concentrée par évaporation sous vide et refroidie avec de la glace jusqu'au moment où le composé cristallise sous forme de cristaux rouges-oranges. La réaction et les manipulations du composé ont été effectuées en atmosphère d'azote séché afin d'éviter l'humidité qui altère le composé.

Analyses :

Calculé : C 50,61 ; H 8,43 ; Al 9,49 ; N 9,84 ; Ni 10,31 %

Trouvé : C 50,30 ; H 8,58 ; Al 9,45 ; N 9,69 ; Ni 10,31 %

Le poids moléculaire a été déterminé par cryoscopie dans du benzène :

Calculé : 569 ; *Trouvé* : 587.

Le tétraisobutylaluminium-bisdiméthylglyoximate de palladium

Il a été obtenu d'une manière semblable à celui du nickel, par traitement d'une suspension de 2 g de $Pd(II)(DMGH)_2$ séché, en 15 ml de *n*-heptane avec une quantité correspondante de $Al(iC_4H_9)_3$ aussi dissoute dans le *n*-heptane. On a procédé ensuite comme pour le composé de nickel, en obtenant une poudre jaune verdâtre.

Analyses :

Calculé : C 46,70 ; H 7,78 ; Al 8,75 ; N 9,07 ; Pd 17,25 %

Trouvé : C 46,63 ; H 7,63 ; Al 8,70 ; N 9,30 ; Pd 17,29 %

Réaction du $Cu(II)(DMGH)_2$ avec l'$Al(iC_4H_9)_3$

A une suspension de 2 g de $Cu(II)(DMGH)_2$ séché, dans 15 ml de *n*-heptane on a ajouté de l'$Al(iC_4H_9)_3$ correspondant au rapport 1/2. La suspension n'a pas disparu ni avec excès de $Al(iC_4H_9)_3$. On le filtre par un creuset G2 et en éloignant complètement le solvant, on obtient une poudre amorphe ayant une composition similaire à celle obtenue par la réaction directe de l'$Al(iC_4H_9)_3$ avec la diméthylglyoxime libre. Le résidu resté sur le filtre contient du CuO et du $Cu(II)(DMGH)_2$ qui n'a pas réagi. On cherche la synthèse dans d'autres solvants et à diverses températures mais le résultat a été le même. La poudre obtenue ne contient pas de cuivre et les analyses physico-chimiques correspondent à celles données pour le dérivé obtenu par réaction de l'$Al(iC_4H_9)_3$ avec la diméthylglyoxime.

Réaction de la diméthylglyoxime avec l'$Al(iC_4H_9)_3$

A 5 g de diméthylglyoxime on ajoute lentement, sous agitation, la solution de $Al(iC_4H_9)_3$ dans le *n*-heptane. Toujours en agitant, on le chauffe à reflux pendant deux heures. La solution change de couleur en orange sans faire consommer toute la quantité de diméthylglyoxime, même avec excès d'$Al(iC_4H_9)_3$. Par filtration et éloignement du solvant on obtient un produit solide orange.

---

[13] C. Basu, G. M. Cook et R. L. Belford, *Inorg. Chem.*, **3**, 1361 (1964).

[14] D. Fleisher et H. Freiser, *J. Phys. Chem.*, **66**, 389 (1962).

Analyses :

Calculé : C 60,60 ; H 10,60 ; Al 13,63 ; N 7,07 %.
Trouvé : C 59,63 ; H 10,60 ; Al 13,80 ; N 7,16 %.

Le poids moléculaire déterminé par cryoscopie dans du benzène :
Calculé : 792 ; *Trouvé* : 740.

Analyse röntgénographique

Les images de diffraction des nouveaux composés ont été obtenues par la méthode des poudres avec un appareil TUR M60 en utilisant la radiation CuK_α et un filtre de nickel. Les poudres ont été introduites dans des capillaires de verre Lindemmann de 0,5 mm de diamètre et ont été exposées à 40 kV et 14 mA durant 6 heures. Les résultats des mesures röntgénographiques sont donnés dans le tableau 1. Les intensités des lignes ont été évaluées d'une manière visuelle des images de diffraction.

Tableau 1

Données röntgénographiques

Line	$Pd(DMG)_2Al_2(C_4H_9)_4$		$Ni(DMG)_2Al_2(C_4H_9)_4$	
	d(Å)	I/I_0	d(Å)	I/I_0
1	4548	20	6787	90
2	4085	100	5380	40
3	3526	30	4502	70
4	3206	40	4116	100
5	2649	60	3247	30
6	2414	50	2646	80
7	2047	10*	2416	10
8	1779	20	2127	30
9	1702	10	1750	10
10	1619	10	1657	10

* Les lignes d'intensité plus faible ne sont pas insérées dans le tableau.

Spectre IR

Les spectres IR des composés obtenus ont été enregistrés avec un appareil Unicam SP-200 dans le KBr. Les absorptions caractéristiques des « chélates » et des composés synthétisés par nous sont présentées dans le tableau 2.

Tableau 2

Absorptions IR caractéristiques

Produit	OH	OH	C=N	NO	OH
$Ni(II)(DMGH)_2$	2350	1780	1560	1235	900
$NiAl_2(DMG)_2(C_4H_9)_4$	—	—	1600	1230	—
$Pd(II)(DMGH)_2$	2340	1710	1550	1250	910
$PdAl_2(DMG)_2(C_4H_9)_4$	—	—	1595	1240	—
$Al_4(DMG)_2(C_4H_9)_8$	—	—	1630	1250	—

DISCUSSIONS

Les nouvelles combinaisons résultées par le changement de l'hydrogène de la liaison OH...O de $Ni(II)(DMGH)_2$ et $Pd(II)(DMGH)_2$ avec des groupes $Al(iC_4H_9)_2$ mettent en évidence le fait que l'atome d'aluminium s'intercale entre les deux atomes d'oxygène en montrant qu'il est tétracoordiné par la réalisation d'une liaison sp^3. La réaction du $Ni(II)(DMGH)_2$ et du $Pd(II)(DMGH)_2$ avec l'$Al(iC_4H_9)_3$ peut être représentée par le schéma de réaction :

$$M(II)(DMGH)_2 + 2Al(iC_4\,H_9)_3 \rightarrow M(II)(DMG)_2\,Al_2\,(iC_4\,H_9)_4 + 2C_4\,H_{10}$$

qui conduit à la formation de combinaisons complexes aluminium-organiques et dégagement d'isobutane. L'exothermicité et la rapidité avec laquelle se produit la réaction infirment l'inertie chimique des hydrogènes glyoximiques de ces chélates.

Les déterminations magnétiques, effectuées par la méthode de Gouy, montrent que les nouveaux produits sont diamagnétiques. Ainsi, les liaisons hybrides dsp^2 réalisées par le métal dans les chélates ne sont pas modifiées, la structure plane se conservant.

L'utilisation du *n*-heptane comme solvant nous a été suggérée par les études des solubilités de ces chélates dans divers solvants.[14-16] Dans le *n*-heptane les composés étudiés par nous sont pratiquement insolubles. Au contraire, les dérivés aluminium-organiques des chélates sont très solubles en *n*-heptane et dans autres solvants organiques qui ne contiennent pas d'atomes de chlore ou d'autres groupes fonctionnels qui pourraient réagir avec les composés. L'eau, ainsi que l'alcool décomposent les produits en libérant le chélate. Les acides et les bases les décomposent avec violence. Chauffés en mélange avec K_2CO_3 et KNO_3 ils font explosion.

Les spectres IR (tableau 2) mettent en évidence que les vibrations de valence de la liaison $C = N$ des dérivés aluminium-organiques du $Ni(II)(DMGH)_2$ et du $Pd(II)(DMGH)_2$, en comparaison de celles des produits de départ, sont déplacées vers des fréquences plus grandes avec une approximation de 40 ± 5 cm^{-1}. Ce déplacement montre une croissance de la densité électronique aux ions de Ni(II) et Pd(II) et diminuent la capacité pour la formation des adducts avec les bases.

Les résultats de nos essais pour obtenir des adducts avec la pyridine ou avec ses dérivés ont été négatifs. Les composés se dissolvent dans la pyridine avec l'intensification des couleurs mais l'isolation des adducts n'a pas été possible. La disparition des régions d'ondes habituelles des maximums d'absorption des groupes OH de $Ni(II)(DMGH)_2$ et $Pd(II)(DMGH)_2$ montre que ceux-ci ont changé d'identité par la formation de nouvelles combinaisons. Il faut remarquer que les déplacements, survenus dans les fréquences $C = N$ et $N - O$ des produits organoaluminiques des chélates, sont en bonne concordance avec ceux obtenus par Blink et Hadzi pour les formes deutérées des $Ni(II)(DMGH)_2$ et $Pd(II)(DMGH)_2$.[17]

---

[15] J. E. Caton Jr. et C. V. Banks, *Talanta*, **13**, 967 (1966).

[16] R. E. Rundle et C. V. Banks, *J. Phys. Chem.*, **67**, 508 (1963).

[17] R. Blinc et D. Hadzi, *J. Chem. Soc.*, **1958**, 4536.

Les données röntgénographiques présentées dans le tableau 1 montrent que les composés ont une structure cristalline différente de celle des produits de départ, probablement avec une symétrie orthorombique, par analogie avec ceux du bore.[11] Les complexes plan-quadratiques tels que le Ni(II) $(DMGH)_2$ et le Pd(II) $(DMGH)_2$ ont conformément à la théorie des orbitaux moléculaires un excès d'orbitaux « d » qui peuvent être utilisés à la formation de liaison métal-métal.[18]

Dans les nouvelles combinaisons obtenues, ainsi que dans les complexés à bore, les répulsions métal-métal sont beaucoup plus grandes que dans les chélates et le dichroïsme caractéristique des composés Ni(II) $(DMGH)_2$ et Pd(II) $(DMGH)_2$[19,11] est diminué.

Le groupe OH de Cu(II) $(DMGH)_2$ se comporte différemment du groupe similaire des chélates de nickel et de palladium, avec les réactifs caractéristiques.

Ainsi, les cristaux marron de Cu(II) $(DMGH)_2$ forment un precipité bleu après avoir réagi sur l'anhydride acétique.[20] De même avec l'isocyanate de phényl et le sulfate de méthyl.[20] La réaction a lieu instantanément avec la formation des produits de couleur bleu ou vert. Ce comportement peut être attribué au caractère différent de la liaison de l'hydrogène de ce chélate. Dans le manomère de Cu(II) $(DMGH)_2$ qui se trouve seulement en solution, la longueur des liaisons de l'hydrogène est de 2,70 Å et 2.53 Å,[21] mais le composé cristallisé a les liaisons beaucoup plus grandes qui sont affaiblies à cause de la présence des liaisons Cu—O réalisées dans le dimère.[16]

Le Cu(II) $(DMGH)_2$ a un comportement différent dans la réaction avec l'$Al(iC_4H_9)_3$ par laquelle nous avons essayé d'obtenir un dérivé semblable à ceux obtenus au cas du Ni(II) $(DMGH)_2$ et du Pd(II) $(DMGH)_2$. Le produit solide obtenu dans cette réaction ne contient pas de cuivre et a une composition chimique identique au composé obtenu par réaction directe entre l'$Al(iC_4H_9)_3$ et la diméthylglyoxime. La représentation structurelle de ce composé est assez difficile, nous nous sommes arrêtés à la formule cyclique V où l'atome d'aluminium réalise une liaison sp^3, mais une représentation linéaire n'est pas exclue, ou une autre où il y ait des liaisons Al—N.

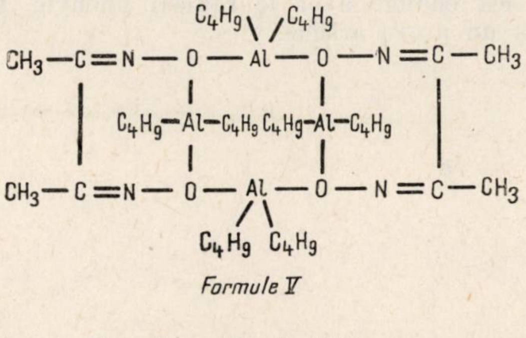

Formule V

---

[18] R. E. RUNDLE, *J. Phys. Chem.*, **61**, 45 (1957).

[19] S. YAMADA, *J. Amer. Chem. Soc.*, **75**, 6351 (1953).

[20] J. E. CATON JR. et C. V. BANKS, *Inorg. Chem.*, **6**, 1670 (1967).

[21] E. FRASSON, E. BARDI et S. BEZZI, *Acta Cryst.*, **12**, 201 (1959).

L'image de diffraction de ce composé est caractéristique des composés partiellement cristallins. On ne rencontre plus dans le spectre IR du composé les bandes d'absorption caractéristiques du groupe OH, mais le maximum d'absorption de la liaison C=N est déplacé à des fréquences plus grandes que dans les composés avec nickel et palladium. La solubilité, ainsi que le comportement chimique sont similaires aux composés décrits auparavant.

Recherches orientatives pour obtenir des complexes organo-métalliques avec d'autres dérivés d'aluminium

Les bisdiméthylglyoximates de nickel et palladium réagissent aussi avec l'$Al(C_2H_5)_2Cl$ et donnent des composés correspondant à la formule VI. Dans ces composés on conserve la liaison Al—Cl

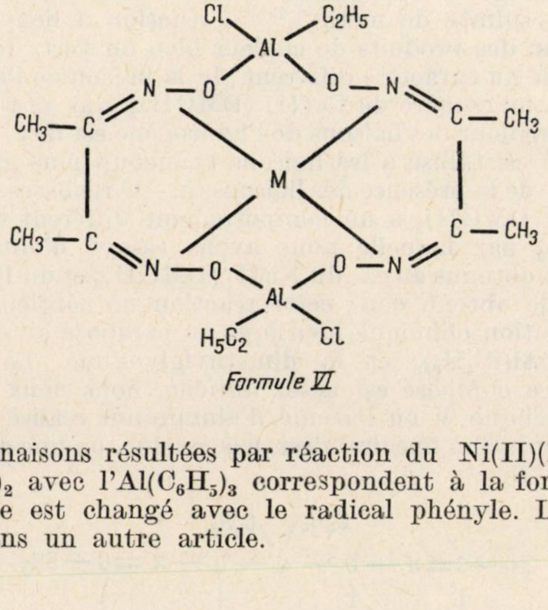

Formule VI

Les combinaisons résultées par réaction du Ni(II)$(DMGH)_2$ et du Pd(II) $(DMGH)_2$ avec l'$Al(C_6H_5)_3$ correspondent à la formule IV où le radical isobutyle est changé avec le radical phényle. L'étude détaillée sera donnée dans un autre article.

Revue Roumaine de Chimie, **17**, *4*, 727–740 (1972)

TRANSFORMATIONS CHIMIQUES DU POLYCHLORURE DE VINYLE. II *

SYNTHÈSES DE POLYÉLECTROLYTES RÉTICULÉS AVEC DES GROUPES SULFONIQUES À BASE DE POLYCHLORURE DE VINYLE ARYLÉ AVEC DES POLYALKYLBENZÈNES

IG. POINESCU
Institut de Chimie Macromoléculaire
41 A, Aleea Grigore Ghica Vodă, Jassy

Reçu le 8 février 1971

On étudie la synthèse de nouveaux polyélectrolytes réticulés, avec des groupes sulfoniques, en partant du polychlorure de vinyle dont on a substitué partiellement au chlore les noyaux du toluène, des xylènes, du mésitylène et du pseudocumène. L'introduction de groupes fonctionnels capables d'un échange d'ions a été effectuée avec de l'H_2SO_4 monohydrate et de l'HSO_3Cl, en présence de 1,2-dichloréthane.

Ces dernières années les transformations chimiques des polymères connaissent un développement tout particulier,[1] et ont pour but l'obtention de nouveaux composés macromoléculaires ayant des propriétés physiques et chimiques supérieures. Dans ce sens, nous rappelons les transformations chimiques du polystyrène,[2] des copolymères styrène-divinylbenzène,[3] pour la préparation des polyélectrolytes solubles ou insolubles, largement utilisés dans l'industrie et l'agriculture.[4,5]

Le présent ouvrage nous fait part de l'étude de l'introduction de groupes alkylarylsulfoniques dans la chaîne macromoléculaire du polychlorure de vinyle (PCV).

La synthèse de ces polyélectrolytes comporte deux phases distinctes : dans la première phase le PCV est arylé avec des polyalkylbenzènes,[6] et dans la seconde le polychlorure de vinyle arylé (PCVA) et est sulfoné avec de l'H_2SO_4 monohydraté, ou de l'HSO_3Cl.

---

* Ire partie : Ig. Poinescu, *Rev. Roumaine Chim.*, **14**, 373 (1969).

[1] W. Kern et R. C. Schultz, *Angew. Chem.*, **69**, 153 (1957).

[2] C. R. Raha, *J. Proc. Inst. Chem.*, **38**, 78 (1966).

[3] S. Sevcik et J. Stamberg, *Coll. Czech. Chem. Comm.*, **32**, 4232 (1967).

[4] K. Gärtner et K. Efer, *Makromol. Chem.*, **36**, 133 (1960).

[5] H. Kurt, *VDI-Zeitschrift*, **102** (1960), Nr. 22S. 1061/67 et Nr. 23S. 1103/09.

[6] Ph. Teyssié et G. Smets, *J. Polymer Sci.*, **20**, 351 (1956).

Le polychlorure de vinyle a été arylé avec : toluène (PCVT), *o*-xylène (PCV *o*-X), *m*-xylène, (PCV *m*-X.), *p*-xylène (PCV *p*-X.), mésitylène (PCVM) et pseudocumène (PCVP).

La structure chimique des produits arylés, ainsi que le degré de substitution du chlore du PCV par les polyalkylbenzènes dépendent des conditions de la réaction, d'arylation Friedel-Crafts.

Ces composés macromoléculaires, ayant une structure initiale très complexe, forment la base de départ pour la synthèse de nouveaux polyélectrolytes réticulés avec des groupes sulfoniques dont les méthodes de préparation sont présentées dans cet ouvrage.

Les indications dans la littérature de spécialité se réfèrent seulement à la synthèse des polyélectrolytes avec des groupes sulfoniques à base de polyvinyltoluène, polyvinylxylène, ou de leurs copolymères.[7-15]

PARTIE EXPÉRIMENTALE

La réaction d'arylation du PCV a été effectuée conformément aux indications de Teyssié et Smets,[6] à 0°. On a obtenu des polymères arylés avec : toluène, *o*-xylène, *m*-xylène, *p*-xylène, mésitylène et pseudocumène, dont le contenu en chlore, après arylation, était compris entre 5,26% et 54,2%, ce qui correspond à un degré de substitution "apparent" calculé d'après le contenu en chlore, de 4,40 jusqu'à 90,70 %.

La sulfonation des polymères arylés a été effectuée avec de l'H_2SO_4 monohydrate, ou de l'HSO_3Cl en présence de 1,2-dichloréthane, comme solvant du PCVT.

L'opération de sulfonation a été effectuée dans un ballon à plusieurs cols munis de thermomètres, un agitateur et réfrigérant ascendant, ayant à son côté supérieur un tube à $CaCl_2$ anhydre.

On introduit dans le ballon le 1,2-chloréthane anhydre et le PCVT en quantités calculées de sorte qu'une solution concentrée à 4% en résulte, après quoi on y joint l'agent de sulfonation, en agitant énergiquement. Le polyélectrolyte est formé et se sépare de la solution, étant insoluble dans le solvant. Après sulfonation le contenu du ballon est transvasé, sous forte agitation, dans de l'eau froide. Le produit de réaction est lavé à l'eau jusqu'à l'élimination totale de l'acide sulfurique, et séché sous vide à 50° pendant 24 heures. Le polyélectrolyte sulfonique ainsi préparé a été caractérisé du point de vue physico-chimique.

---

[7] H. H. Roth, *Ind. Eng. Chem.*, **46**, 2435 (1954).

[8] H. H. Roth, (Dow Chemical Co.), U.S. 2 691 644, 12.10.1954 ; *Chem. Abstr.*, **49**, 1365 (1955).

[9] H. H. Roth, *Ind. Eng. Chem.*, **49**, 1820 (1957).

[10] Tsutomu Kuwata et Sadao Yoshkawa, (Asahi Glass Co.), Japan 4590 ('57), 06.07 ; *Chem. Abstr.*, **52**, 14032 (1958).

[11] Wm. C. Bauman et H. H. Roth (Dow Chemical Co.), U. S. 2 835 655, 20.05.1958 ; *Chem. Abstr.*, **52**, 15966 (1958).

[12] A. S. Teot, (Dow Chemical Co.), U. S. 2 836 578, 27.05.1958 ; *Chem. Abstr.*,**52**, 16794 (1958).

[13] H. H. Roth (Dow Chemical Co.) Brit. 823 113, 04.11.1959 ; *Chem. Abstr.*, **54**, 9367 (1967).

[14] Yoshio Tsunoda et Maomi Seko, (Asahi Chemical Industry Co. Ltd) Ger. 1 082 406, 25.05.1960 ; *Chem. Abstr.*, **55**, 27704 (1961).

[15] A. B. Davankov, O. A. Vitol et V. A. Faingor, *Vysokomol. Soedineniya*, **3**, 1566 (1961).

Les conditions de la réaction de sulfonation ont été établies d'après le PCVT *. On a soumis à la sulfonation le polymère contenant, après arylation, 25,35 % de chlore, pour étudier le mode de comportement des unités structurelles chlorovinyliques et vinylalkylbenzéniques pendant la réaction de sulfonation.

Les déterminations analytiques du contenu en chlore, soufre, des capacités d'échange et des titrages potentiométriques ont été exécutées de la même manière que dans notre ouvrage antérieur *.

RÉSULTATS ET DISCUSSIONS

On a effectué des réactions d'arylation dans les mêmes conditions (tableau 1) pour établir l'ordre de la réactivité des polyalkylbenzènes par rapport au PCV. Les résultats obtenus, calculés en pourcentage du poids des unités structurelles de chlorure de vinyle, montrent une différence dans la réactivité des polyalkylbenzènes en fonction du nombre et de la position des substituants méthyle dans le noyau benzénique. Le toluène, les *o*- et *p*-xylènes sont les plus réactifs, suivis par le *m*-xylène, le mésitylène et le pseudocumène. L'obtention de certaines petites valeurs pour les degrés de substitution, dans le cas des composés trisubstitués, est due à l'influence des facteurs stériques.

Tableau 1

Arylation du PCV par polyalkylbenzènes*

N°	Hydrocarbure aromatique	PCV/$AlCl_3$ mole	PCV/ hydrocarbure aromatique mole	Chlore %	Contenu d'unités structurelles de chlorure de vinyle dans 100 g de polymère arylé %
1	Benzène	1,0/0,5	1,0/17,6	28,42	50,12
2	Toluène	1,0/0,5	1,0/17,6	2,43	4,28
3	*o*-Xylène	1,0/0,5	1,0/17,6	5,72	10,09
4	*m*-Xylène	1,0/0,5	1,0/17,6	20,91	36,87
5	*p*-Xylène	1,0/0,5	1,0/17,6	5,81	10,24
6	Mésitylène	1,0/0,5	1,0/17,6	44,25	78,04
7	Pseudocumène	1,0/0,5	1,0/17,6	46,30	81,65

* Hydrocarbure aromatique – 0,2813 mole; P.C.V. – 0,016 mole; Concentration de la solution de PCV – 4,0 %; Température de la réaction d'arylation – 0°; Durée de la réaction d'arylation – 90 mn.

---

* Le PCVT ayant un contenu en chlore de 25,53 % a été obtenu dans les conditions suivantes : PCV — 1 g; 1,2-dichloréthane-25 ml; toluène-25 ml. La durée de la réaction d'arylation-60 minutes. Température — 0°. PCV/$AlCl_3$—1/0,25 mole.

L'acide sulfurique réagit seulement avec le noyau benzénique, tandis que l'acide chlorosulfonique, selon la température à laquelle la réaction de sulfonation a lieu, agit soit seulement sur le noyau aromatique, soit simultanément sur le noyau benzénique et sur les unités structurelles de chlorure de vinyle existant dans le polymère après son alkylation.

Nous devons souligner que la réaction de sulfonation par HSO_3Cl est très énergique, étant accompagnée de réactions secondaires, non désirées, comme l'oxydation, la déshydrochloruration, la dégradation du polymère, etc.

La réaction de sulfonation est influencée par le rapport agent de sulfonation/polymère, la concentration de la solution du polymère, la température, le degré de substitution du chlore du PCV par le polyalkylbenzène. Les résultats obtenus ont été représentés graphiquement ou sous forme de tableau.

Etant donné que par sulfonation on obtient des produits insolubles, réticulés, à structure tridimensionnelle, à groupes fonctionnels capables d'échange ionique, dénommés échangeurs de cations, on a exprimé le degré de sulfonation par la capacité d'échange sulfonique qui est directement proportionnelle au contenu de groupes sulfoniques du polyélectrolyte.[16]

LA CAPACITÉ D'ÉCHANGE SULFONIQUE

— *L'influence de la quantité de l'agent de sulfonation.* La valeur de la capacité d'échange sulfonique (K_{SO_3H}) augmente avec la quantité d'acide sulfurique utilisée pour la sulfonation et est de 1,90 méq/g pour le rapport H_2SO_4/polymère de 3/1 (fig. 1, courbe 1). La croissance de la quantité d'acide sulfurique au-dessus de la valeur du rapport mentionné n'influence plus le degré de sulfonation que dans une très faible mesure (1,97 méq/g).

La sulfonation par HSO_3Cl découle en quelque sorte différemment par rapport à l'acide sulfurique monohydrate (fig. 1, courbe 2). La courbe de la dépendance de la capacité d'échange sulfonique du rapport HSO_3Cl/polymère présente un maximum pour le rapport 3/1, après quoi on observe une diminution de la capacité d'échange sulfonique de 2,32 méq/g à 1,39 méq/g.

On obtient les valeurs maximales pour les capacités d'échanges sulfoniques des PCVT sulfonés pour les rapports agent de sulfonation/polymère plus petits que dans le cas PCV/aryles-benzène*.

Le polyvinyltoluène est sulfoné approximativement cinq fois plus rapidement que le polystyrène,[9] et montre une plus forte tendance à former des structures tridimensionnelles.

Cela indique l'existence d'une analogie structurelle entre le polyvinyltoluène et le polychlorure de vinyle arylé par du toluène.

La sulfonation du PCVT par HSO_3Cl à partir des rapports 7/1 est accompagnée d'une forte dégradation du polymère avec formation de groupes carboxyliques [la capacité d'échange carboxylique 0,2—0,4 méq/g

---

[16] T. G. Moralli, *J.C.N.R.S.*, **26**, 265 (1954).

(fig. 1), courbe 3)], ce qui explique en partie le fait que la capacité d'échange sulfonique diminue dans la seconde branche de la courbe.

— *Influence de la concentration de la solution de polymère.* La quantité de solvant utilisée pour dissoudre le polymère influence le degré de sulfonation (fig. 2). La capacité d'échange sulfonique augmente avec la dilution du milieu de réaction jusqu'à une concentration de 5 % du polymère dans le 1,2-dichloréthane. Des plus fortes dilutions dépassant cette valeur ont un effet négatif sur le degré de sulfonation, respectivement sur la capacité d'échange sulfonique, à la suite de la diminution de l'agent de sulfonation, c'est-à-dire de la vitesse de la réaction de sulfonation.

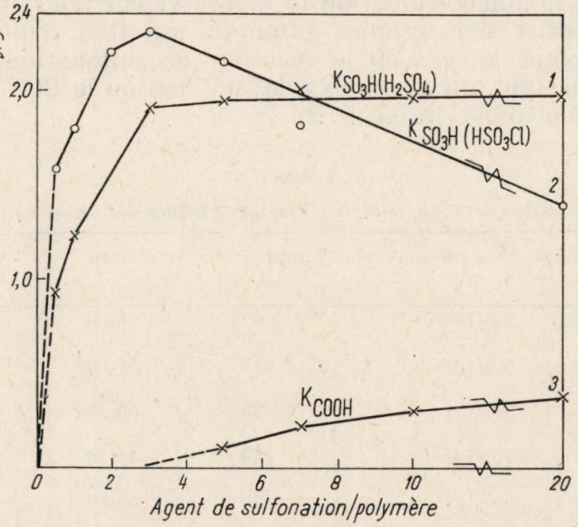

Fig. 1. — Influence de la quantité d'agent de sulfonation sur la capacité d'échange sulfonique, K_{SO_3H} (*1* et *2*) et carboxylique K_{COOH} (*3*) ; température — 25° ; durée — 5 heures.

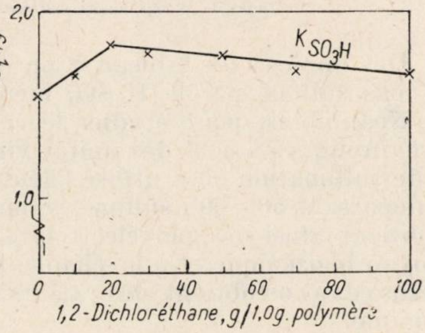

Fig. 2. — Influence de la concentration de la solution de polymère sur la capacité d'échange sulfonique, K_{SO_3H} ; H_2SO_4 monohydrate/polymère — 5/1 ; température — 25° ; durée — 5 heures.

— *Influence de la température de sulfonation.* La sulfonation du PCVT par H_2SO_4 à différentes températures donne des produits dont la capacité d'échange sulfonique augmente avec la température : 1 méq/g à 0° et 1,92 méq/g à la température de 120° (fig. 3, courbe 1), la croissance étant accentuée dans la première partie de la courbe jusqu'à 40°. La capacité d'échange sulfonique obtenue par sulfonation du PCVT à 120° est de 1,92 méq/g, supérieure approximativement de 14 % à sa valeur pour 40°.

Pour vérifier si le groupe sulfonique est fixé seulement au noyau benzénique, même au cas où la réaction de sulfonation, s'effectue à la température de 120°, on a soumis à la sulfonation le PCV non arylé, dans les mêmes conditions (tableau 2).

Tableau 2

Action de l'H_2SO_4 monohydrate sur le PCV à différentes températures*

N°	H_2SO_4 monohydr./ P.C.V.	Température °C	Chlore %	Soufre %
1	5,0/1,0	0	56,65	—
2	5,0/1,0	15	56,60	—
3	5,0/1,0	25	56,32	—
4	5,0/1,0	50	55,70	—
5	5,0/1,0	75	55,10	—
6	5,0/1,0	90	54,37	—
7	5,0/1,0	120	53,81	—

* Concentration de la solution de PCV en 1,2-dichloréthane – 4 % ;
Durée de la réaction de sulfonation – 5 heures.

Des données du tableau 2 on observe que le polychlorure de vinyle n'est pas sulfoné par le H_2SO_4 même à 120°.

Néanmoins, pour étudier le comportement des unités structurelles chlorovinyliques à côté des unités vinylalkylbenzéniques pendant la réaction de sulfonation on a utilisé l'acide chlorosulfonique qui, à la température dépassant 50—60°, sulfone également la principale chaîne aliphatique. On obtient ainsi des polyélectrolytes avec des groupes sulfoniques fixés au noyau benzénique et à la chaîne principale aliphatique (fig. 3, courbe 2). Dans ce cas on obtient des valeurs supérieures pour la capacité d'échange sulfonique.

— *Influence de la durée de la réaction de sulfonation.* La valeur de la capacité d'échange sulfonique est fonction de la durée, de la température et de la nature de l'agent de sulfonation (fig. 4). Ainsi, pour la sulfonation par H_2SO_4, la capacité d'échange sulfonique croît d'une manière appréciable pendant les deux premières heures (1,86 méq/g), pour que, après une durée de 10 heures de sulfonation, la valeur de celle-ci n'augmente que de 0,17 méq/g (fig. 4, courbe 1).

Pour la sulfonation par HSO_3Cl à 25°, les valeurs des capacités d'échange sulfonique se situent sur une droite approximativement parallèle à l'abscisse (fig. 4, droite 2). La différence entre les valeurs des capacités sulfoniques après 15 minutes et 10 heures est de seulement 0,07 méq/g.

De la valeur des capacités d'échanges sulfoniques on déduit que le HSO_3Cl est un agent de sulfonation beaucoup plus énergique que le H_2SO_4 et que la réaction de sulfonation est complète après 15 minutes.

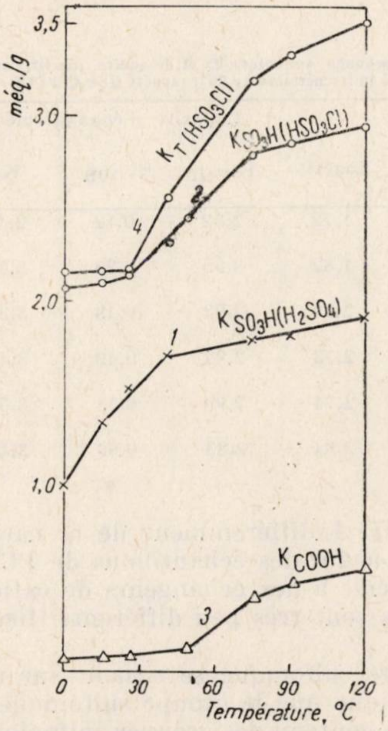

Fig. 3. — Influence de la température sur la capacité d'échanges sulfoniques, K_{SO_3H} (*1* et *2*), carboxyliques K_{COOH} (*3*) et totales K_T (*4*) ; le rapport agent de sulfonation/polymère 5/1 ; durée : 5 heures.

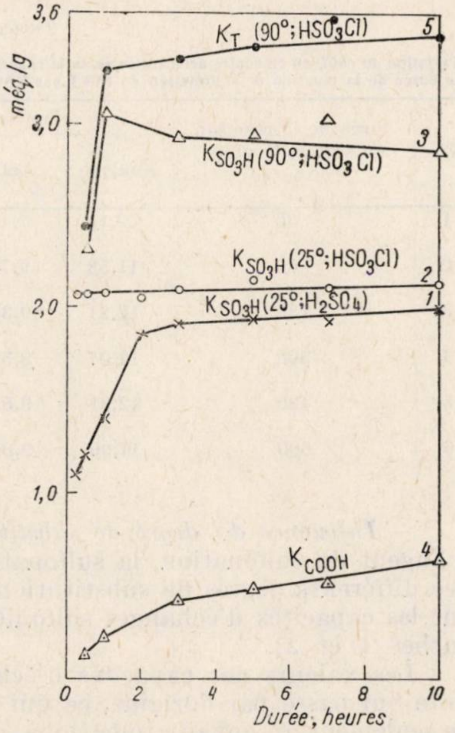

Fig. 4. — Influence de la durée de réaction de sulfonation sur la capacité d'échanges sulfoniques, K_{SO_3H} (*1, 2* et *3*), carboxyliques, K_{COOH} (*4*) et totales, K_T (*5*) ; le rapport agent de sulfonation/polymère-5/1.

Dans le cas de la sulfonation par HSO_3Cl à la température de 90°, la capacité d'échange sulfonique varie de la manière suivante : pendant les 60 premières minutes elle croît jusqu'à la valeur de 3,05 méq/g, après quoi elle décroît jusqu'à 2,83 méq/g, ce qui représente approx. 7% (fig. 4, courbe 3).

Pour les échangeurs de cations préparés par la sulfonation du PCVT par HSO_3Cl, on a trouvé une différence appréciable entre le contenu de soufre déterminé expérimentalement et celui calculé à partir de la valeur de la capacité d'échange sulfonique.[16] Nous croyons que ce soufre, appelé « soufre inactif » se trouve dans l'échangeur de cations sous forme de groupes $-SO_2-$, ou même de groupes $-SO_3H$, lesquels pour des motifs stériques ne peuvent pas participer au processus d'échange ionique. De même, la quantité de soufre inactif croît avec la durée de la réaction de sulfonation, expliquant ainsi la diminution de la capacité d'échange sulfonique observée (tableau 3).

Tableau 3

Variation du contenu en soufre actif (calculée de la capacité d'échange sulfonique [16]) et du soufre inactif, avec la durée de la réaction de sulfonation du PCVT par HSO_3Cl, à la température de 96°; rapport $HSO_3Cl/PCVT - 5/1$

N°	Durée de la réaction de sulfonation en minutes	Soufre %			Capacité d'échange méq/g		
		Analyse	Actif	Inactif	K_{SO_3H}	K_{COOH}	K_T
1	30	9.14	7,42	1,72	2,32	0,12	2,44
2	60	11,58	9,76	1,82	3,05	0,23	3,28
3	180	12,21	9,34	2,89	2,92	0,43	3,35
4	300	12,07	9,34	2,73	2,92	0,49	3,41
5	420	12,31	9,57	2,74	2,99	0,53	3,51
6	600	11,90	9,05	2,84	2,83	0,64	3,47

— *Influence du degré de substitution.* Indifféremment de la nature de l'agent de sulfonation, la sulfonation à 25° des échantillons de PCVT avec différents degrés de substitution mène à des échangeurs de cations dont les capacités d'échanges sulfoniques sont très peu différents (fig. 5, courbes 1 et 2).

Les valeurs des capacités d'échange sulfonique se situent sur une droite qui passe par l'origine, ce qui indique que le groupe sulfonique se fixe seulement au noyau aromatique, et le contenu des groupes sulfoniques est directement proportionnel au degré de substitution, respectivement à la quantité d'hydrocarbure aromatique qui s'est substituée au chlore du PCV.

La sulfonation par acide chlorosulfonique à 90° est différente de celle à 25°, étant donné que parallèlement à la sulfonation des noyaux benzéniques, une partie des unités structurelles de chlorure de vinyle non arylées (non substituées) sont également sulfonées.

Les échangeurs de cations obtenus ont des valeurs des capacités d'échange sulfonique entre 3,50 et 3,90 méq/g (fig. 5, courbe 3).

La sulfonation du PCVT, ayant un degré de substitution supérieur à 85—90%, mène à des polyélectrolytes à groupes sulfoniques solubles dans l'eau. Cette exception, déviant de la règle générale, s'explique ainsi : les polymères ayant des degrés de substitution élevés, possèdent un nombre relativement réduit d'unités structurelles chlorovinyliques. Celles-ci, pendant l'opération de sulfonation ne subissent qu'une réaction de déhydrochloruration intramoléculaire avec formation de doubles liaisons. Les réactions de déhydrochloruration intermoléculaire ne peuvent être réalisées et, en conséquence, des structures spatiales tridimensionnelles, menant à l'obtention de polyélectrolytes insolubles, ne peuvent pas se former.

De même, l'augmentation du nombre de groupes sulfoniques dans le polymère augmente la capacité de celui-ci de se dissoudre dans l'eau.[17]

On a montré que, indifféremment de la nature de l'agent de sulfonation, la réalisation de la réaction de sulfonation à 25 % a pour conséquence l'introduction de groupes sulfoniques seulement dans le noyau benzénique, tandis qu'à 90°, l'acide chlorosulfonique sulfone le noyau aromatique, ainsi que la principale chaîne aliphatique. En calculant la différence entre les capacités d'échanges sulfoniques aux deux températures, on obtient les valeurs des capacités d'échange sulfonique données par les groupes $-SO_3H$ fixées seulement sur la chaîne aliphatique principale, $K'_{SO_3H'}$ (fig. 5, droite 6). La valeur $K'_{SO_3H'}$ décroît en même temps que le degré de substitution (du contenu en noyaux benzéniques), étant donné que le degré de substitution est proportionnel au nombre d'unités structurelles vinylalkylbenzéniques.

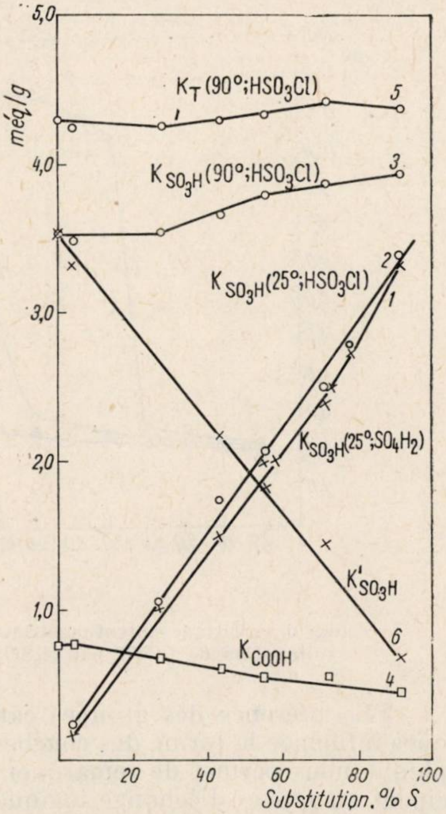

Fig. 5. — Dépendance de la capacité d'échanges sulfoniques K_{SO_3H} (*1*, *2* et *3*), carboxyliques, K_{COOH} (*4*) et totales, K_T (*5*) du degré de substitution du chlore du PCV par polyalkylbenzènes. K'_{SO_3H} — capacité d'échange sulfonique donnée par les groupes — SO_3H fixés sur la chaîne principale aliphatique (6). Rapport HSO_3Cl/polymère — 5/1 ; durée — 5 heures.

LA CAPACITÉ D'ÉCHANGE CARBOXYLIQUE

La capacité d'échange carboxylique (K_{COOH}) est donnée par la présence des groupes $-COOH$, dans la structure de la chaîne macromoléculaire. Ce type de capacité d'échange a été identifié pour les échangeurs de cations obtenus par sulfonation du PCVT par HSO_3Cl à une température au-dessus de 50° et est une conséquence des réactions d'oxydation des polymères. La valeur de la capacité d'échange carboxylique dépend du rapport HSO_3Cl/polymère, de la température et de la durée de la réaction de sulfonation (fig. 1 et 3), ainsi que du degré de substitution du chlore (fig. 5, courbe 4). La capacité d'échange carboxylique décroît avec l'augmentation du degré de substitution, ce qui nous fait supposer l'existence d'une liaison de dépendance entre la grandeur et la fréquence des segments de chaîne macromoléculaire de polychlorure de vinyle restés dans le polymère après son arylation, et le contenu de groupes carboxyliques.

---

[17] R. Singer et Demagistri, *J. Chem. Phys.*, **47**, 704 (1950).

Les groupes carboxyliques ont été mis en évidence par des déterminations de capacité d'échange par acétate de calcium, solution $2^0/_{00}$ et titrage potentiométrique des échangeurs de cations (fig. 6).

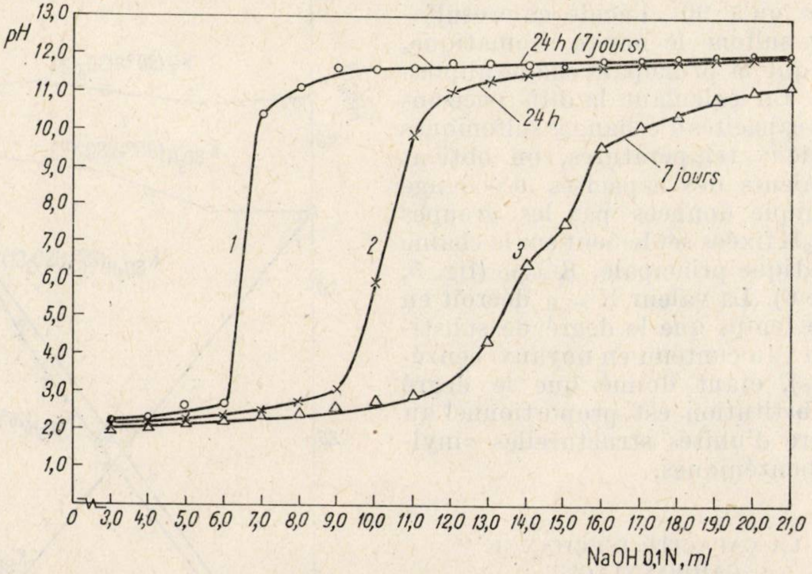

Fig. 6. — Titrage potentiométrique des échangeurs de cations obtenus par sulfonation de PCVT par H_2SO_4 monohydrate (*1*) et HSO_3Cl (*2* et *3*).

La présence des groupes carboxyliques à côté des groupes sulfoniques influence la forme des courbes de titrage potentiométriques. Le graphique nous permet de remarquer que les groupes carboxyliques participent au procès d'échange ionique à partir de pH >6,5.

Les produits de sulfonation du PCV arylé au xylène, mésitylène et pseudocumène présentent un intérêt tout particulier du point de vue théorique.

La sulfonation de ces polymères arylés a été effectuée seulement avec de l'acide chlorosulfonique, à 25° et 90°, pour les mêmes raisons que celles signalées pour la sulfonation du PCVT.

Les conditions de réaction pour l'obtention des polyélectrolytes sulfoniques sont données dans le tableau 4.

Des données de ce tableau on peut tirer les conclusions suivantes :

— La température à laquelle la réaction de sulfonation a été effectuée influence sensiblement le degré de sulfonation, augmentant en même temps les vitesses des réactions d'oxydation (avec formation de groupes carboxyliques), la déhydrochloruration des unités chlorovinyliques, et d'autres.

— La sulfonation des polymères arylés à haut degré de substitution du chlore du PCV par hydrocarbures aromatiques mène, comme

Tableau 4

Sulfonation par HSO_3Cl du PCV arylé par polyalkylbenzènes*

N°	PCV arylé par	Température de la réaction de sulfonation °C	Chlore, %		Pertes en chlore % P	Capacité d'échanges — méq/g		
			Avant sulfonation	Après sulfonation		Sulfonique K_{SO_3H}	Carboxylique K_{COOH}	Totale K_T
1	*ortho*-Xylène	25	7,10	6,90	3,00	8,82 % soufre	(soluble dans l'eau)	
2	*ortho*-Xylène	90	7,10	4,82	32,00	10,73 % soufre	(soluble dans l'eau)	
3	*méta*-Xylène	25	27,14	25,77	5,00	1,04	0,14	1,18
4	*méta*-Xylène	90	27,14	3,50	87,10	2,08	0,34	2,46
5	*para*-Xylène	25	11,65	10,17	12,00	2,50	0,27	2,77
6	*para*-Xylène	90	11,65	3,25	72,10	2,37	0,57	2,94
7	Mésitylène	25	34,30	32,10	6,41	0,83	0,13	0,96
8	Mésitylène	90	34,30	5,00	85,42	1,80	0,22	2,02
9	Pseudocumène	25	23,04	21,50	6,68	0,83	0,26	1,09
10	Pseudocumène	90	23,04	3,92	83,02	2,17	0,56	2,74

* HSO_3Cl/polymère — 5/1 ; Durée de la réaction de sulfonation — 5 heures.

dans le cas du PCVT à des produits solubles dans l'eau, c'est-à-dire à des polyélectrolytes sulfoniques à structure linéaire.

La sulfonation des PCV arylés par polyalkylbenzènes est un procès très complexe, dû au fait que l'on part d'un composé macromoléculaire ayant une structure compliquée, un polymère formé de différentes unités structurelles, chaque unité ayant un comportement différent par rapport à l'agent de sulfonation, ainsi que par le fait que la réaction de sulfonation est accompagnée par toute une série de réactions secondaires (réactions de déhydrochloruration, oxydation, dégradation, etc.).

Parmi toutes ces réactions secondaires, la réaction de déhydrochloruration est la plus importante, étant donné qu'elle modifie fortement la structure du polymère. Comme conséquence des réactions de déhydrochloruration des unités structurelles chlorovinyliques existant dans le polymère après son arylation, il résulte des polyélectrolytes réticulés, contenant de doubles liaisons dans leur structure.

L'intensité des réactions de déhydrochloruration a été suivie par l'analyse du chlore pour les produits obtenus dont on a calculé les pertes de chlore en pourcentage (%P) pour chaque échangeur de cations synthétisé. Les valeurs obtenues ont été représentées graphiquement selon leur dépendance de divers facteurs dans les figures 7—11, ce qui nous permet de conclure comme suit :

— La valeur des pertes de chlore (% P) est approximativement constante, étant comprise entre 25,0 et 26,4 % pour le PCVT sulfoné par H_2SO_4, ou HSO_3Cl à la température de 25° (figures 7—10).

— Les pertes de chlore sont influencées dans une faible mesure par la quantité d'agent de sulfonation (fig. 7), en révanche la dilution du milieu de réaction, c'est-à-dire la diminution de la concentration du système, mène à la réduction de l'intensité des réactions de déshydrochloruration (fig. 9, droite 1).

— Les pertes de chlore dépendent de la durée de la réaction de sulfonation, dans le cas où le HSO_3Cl est utilisé comme agent de sulfonation, et l'on obtient des valeurs dépassant approximativement de 10 % celles de la sulfonation par H_2SO_4 monohydrate (fig. 10, courbes 1 et 2).

— Indépendamment de la nature de l'agent de sulfonation, la valeur des pertes de chlore est proportionnelle au degré de substitution du PCVT, les courbes ayant la même forme (fig. 11, courbes 1 et 2).

— Si l'action du H_2SO_4 monohydrate sur le PCVT ne dépend pas de la température, en révanche le HSO_3Cl réagit différemment par rapport au polymère arylé, en fonction de la température à laquelle la sulfonation est réalisée (fig. 9, courbe 2). Ainsi que l'on constate, la courbe 2 de la figure 9 peut être divisée, d'après l'angle de la pente rapporté à l'abscisse, en trois segments, l'inclinaison de chacune étant directement liée à la vitesse de la réaction de déshydrochloruration. On observe de même que cette réaction s'intensifie à partir de 75°, ce qui concorde aussi avec les observations faites pour la sulfonation du PCV par HSO_3Cl. [18]

---

[18] M. Dima, I. Scondac, Ig. Poinescu, A. Carpov et Gh. V. Cotruţ, *Studii Cercetări Şti. Chim. Fil. Iaşi*, **15**, 233, 255, 265 (1963).

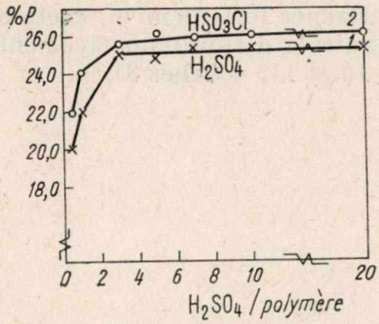

Fig. 7. — Influence de la quantité d'agent de sulfonation sur les pertes de chlore (%P). Durée de la réaction de sulfonation — 5 heures ; température — 25°.

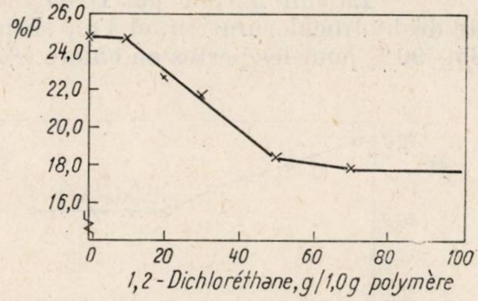

Fig. 8. — Influence de la concentration de la solution de PCVT en 1,2-dichloréthane sur les pertes de chlore (%P). Rapport H_2SO_4/PCVT — 5/1 ; durée — 5 heures ; température — 25°.

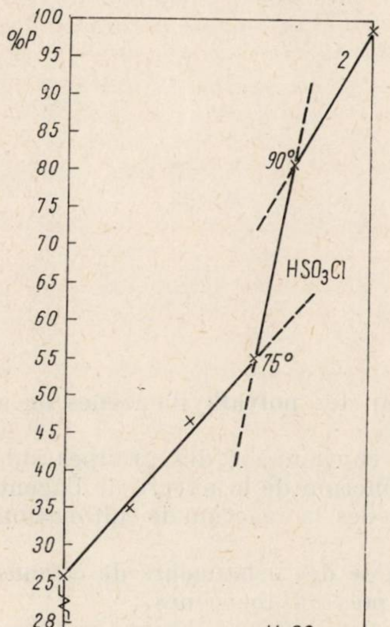

Fig. 9. — Influence de la température sur les pertes de chlore (%P) pendant la réaction de sulfonation du PCVT par H_2SO_4 (1) et HSO_3Cl (2). Rapport agent de sulfonation/PCVT — 5/1 ; durée — 5 heures.

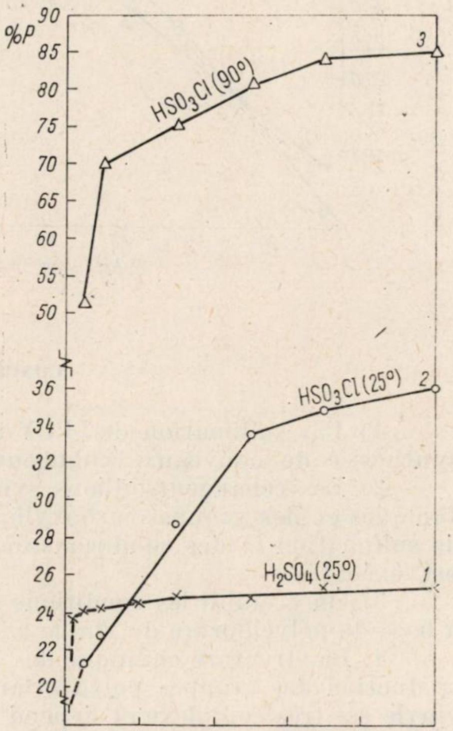

Fig. 10. — Dépendance des pertes de chlore (%P) de la durée de la réaction de sulfonation et de la nature de l'agent de sulfonation. Rapport agent de sulfonation PCVT — 5/1.

— La sulfonation par HSO_3Cl à 90° influence fortement la réaction de déshydrochloruration, et l'on obtient des valeurs d'approximativement 85—90 % pour les pertes en chlore (%P) (fig. 10 et 11, courbes 3).

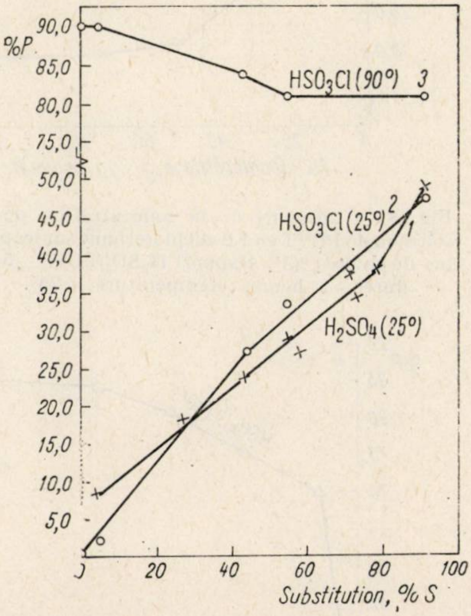

Fig. 11. — Dépendance des pertes de chlore (% P) du degré de substitution (%S) du chlore du PCV par le toluène. Rapport agent de sulfonation/PCVT— 5/1 ; durée — 5 heures.

CONCLUSIONS

1) Par sulfonation des PCV arylés par des polyalkylbenzènes on a synthétisé de nouveaux échangeurs d'ions.

2) Les échangeurs d'ions synthétisés contiennent des groupes sulfoniques et des groupes carboxyliques en fonction de la nature de l'agent de sulfonation et des conditions dans lesquelles la réaction de sulfonation est exécutée.

3) On a établi les conditions de synthèse des échangeurs de cations à base de polychlorure de vinyle arylée par polyalkylbenzènes.

4) La structure chimique des échangeurs de cations obtenus par l'introduction des groupes polyalkylarylsulfoniques dans le polychlorure de vinyle est très complexe et dépend des conditions de la réaction de sulfonation et de la nature de l'agent de sulfonation.

Revue Roumaine de Chimie, **17**, *4*, 741–746 (1972)

COPOLYMERS OF CONJUGATED DIENES WITH MALEIC ACID MONOESTERS. V

COPOLYMERIZATION OF ISOPRENE WITH MONOCYCLOHEXYLMALEATE AND MONOBENZYLMALEATE

IOAN NANU* and CONSTANTIN ANDREI **

* Chair of Macromolecular Chemistry, Polytechnic Institute,
Timişoara, Romania,
and
** Research Laboratory, Ploieşti Petrochemical Industrial Group,
Brazi, Prahova County, Romania

Received October 29, 1971

A study was carried out on copolymerization of isoprene with monocyclohexylmaleate and monobenzylmaleate in presence of (A.I.B.N.) azo-isobutyronitrile, determining the reactivity ratios at 70°.

For isoprene (M_1)-monocyclohexylmaleate (M_2)
$r_1 = 0.135 \pm 0.025$, $r_2 = 0$ (according to Mayo-Lewis) and
$r_1 = 0.121$, $r_2 = 0$ (according to Fineman-Ross).

For isoprene (M_1)-monobenzylmaleate (M_2)
$r_1 = 0.075 \pm 0.025$, $r_2 = 0$ (according to Mayo-Lewis) and
$r_1 = 0.055$, $r_2 = 0$ (according to Fineman-Ross).

The apparent activation energy determined for copolymerization of isoprene with monocyclohexylmaleate was 27.31 kcal/mol, whereas for copolymerization of isoprene with monobenzylmaleate it was of 21.40 kcal/mol.

INTRODUCTION

Copolymerization of isoprene with maleic acid monoesters obtained with alcohols of the normal aliphatic series, was studied in previous works.[1–4] Thereby, the influence of the alcoholic radical of the monoester on the reactivity ratios was remarked.

The applicability of the copolymer composition equation was also studied, which takes into account the effect of the terminal unit (ultimate model) in comparison with the penultimate model equation, the fact being remarked that the latter does not verify the experimental results.

The value of the reactivity ratios indicated the fact that all the systems studied are typical cases of heterocopolymerization.

---

[1] I. Nanu and C. Andrei, *Rev. Roumaine Chim.*, **15**, 1883 (1970).

[2] I. Nanu and C. Andrei, *Rev. Roumaine Chim.*, **16**, 75 (1971).

[3] I. Nanu and C. Andrei, *Bul. St. Tehnic I.P. Timişoara*, (in print).

[4] I. Nanu and C. Andrei, *Makromol, Chem.*, (in print).

The purpose of the present work is to observe the behaviour of monocyclohexylmaleate and monobenzylmaleate in the copolymerization reaction with isoprene.

Reactivity ratios and apparent activation energy are determined in this work.

EXPERIMENTAL

MATERIALS

Monocyclohexylmaleate was prepared in laboratory from analytical grade maleic anhydride (Union Chimique Belge) and analytical grade cyclohexanol (Reactivul, Bucharest) in a molar ratio of 1 : 1 at 80°. After two recrystallizations from acetone, the monoester had the following characteristics: solid (transparent rectangular lamella), 60—61.5° melting point and 283—285 acid number.

Monobenzylmaleate was prepared from analytical grade maleic anhydride and benzyl alcohol (E. Merck) in molar ratio of 1 : 1 at 90°. The monoester thus obtained had the following characteristics: solid (needle-like crystals), 49—50° melting point and 272—275 acid number.

Isoprene, cyclohexanone and α,α'-azobisisobutyronitrile (A.I.B.N.) showed the same characteristics as communicated in previous works.[1,2]

METHOD OF WORK

The process of copolymerization of isoprene with monocyclohexylmaleate and monobenzylmaleate was carried out in homogeneous medium, cyclohexanone being used as solvent and A.I.B.N. (azo-isobutyronitrile) as initiator.

The copolymerization, separation and purification of the copolymers was achieved in the same manner as used in copolymerization of isoprene with other monoesters and described previously.[1,2,4]

The analysis of the copolymer composition was carried out by elementary microanalysis.

RESULTS AND DISCUSSIONS

REACTIVITY RATIOS

In all cases, copolymerization was carried out at conversions below 5%. The experimental results are shown in table 1.

With the help of these results, using Mayo and Lewis[5] intersection method, as well as Fineman and Ross[6] linearized composition equation method, (r_1 and r_2) reactivity ratios were determined.

---

[5] F. R. Mayo and F. M. Lewis, *J. Amer. Chem. Soc.*, **66**, 1594 (1944).

[6] M. Fineman and S. D. Ross, *J. Polymer Sci.*, **5**, 259 (1950).

Table 1

Copolymerization of isoprene with monocyclohexylmaleate and monobenzylmaleate in the presence of free radicals

Test	Feed composition (mole frac.)		Copolymer composition (mole frac.)		Conversion %	Copolymer analysis	
	$[M_1^\circ]$	$[M_2^\circ]$	m_1	m_2		C, %	H, %
	Isoprene (M_1) — Monocyclohexylmaleate (M_2)						
L_1	0.738	0.262	0.500	0.500	2.02	67.65	8.32
L_2	0.896	0.104	0.673	0.327	2.63	72.00	9.07
L_3	0.372	0.628	0.500	0.500	2.08	67.65	8.32
L_4	0.942	0.058	0.760	0.240	2.60	75.00	9.58
L_5	0.982	0.018	0.784	0.216	3.28	75.90	9.74
L_6	0.133	0.867	0.500	0.500	3.45	67.66	8.32
L_7	0.497	0.503	0.484	0.516	2.65	67.65	8.32
	Isoprene (M_1) — Monobenzylmaleate (M_2)						
M_1	0.745	0.255	0.505	0.595	1.37	70.10	6.59
M_2	0.900	0.100	0.626	0.374	2.13	72.70	7.36
M_3	0.381	0.619	0.502	0.498	1.55	70.13	6.63
M_4	0.944	0.056	0.638	0.362	2.37	73.00	7.15
M_5	0.982	0.018	0.710	0.290	2.57	74.85	7.99
M_6	0.137	0.863	0.504	0.496	4.24	70.15	6.63
M_7	0.496	0.504	0.501	0.499	1.90	70.07	6.81

– Reaction temperature, 70°

– Initiator : $[AIBN] \times 10^3 = 0.91$ moles

In figures 1 and 2 Mayo-Lewis representation for isoprene—monocyclohexylmaleate and isoprene—monobenzylmaleate systems was indicated and in figure 3 Fineman-Ross representation for both systems. The reactivity values obtained from these diagrams are presented in table 2.

A good agreement can be observed between the values obtained by the two methods.

The value of r_1 for isoprene—monocyclohexylmaleate system is greater than for isoprene—monobenzylmaleate system.

The fact that in the indicated reaction conditions $r_1 > 0$ but subunitary and $r_2 = 0$, means that both systems tend towards a regular alternance.

Both monocyclohexylmaleate and monobenzylmaleate are incapable of homopolymerization in these conditions and are therefore typical cases of heterocopolymerization, similar to the copolymerization of isoprene with maleic acid monoesters obtained with normal alcohols of the aliphatic series.[1,4]

In figure 4 composition diagrams of copolymers are represented for both systems, plotted with the aid of the established reactivity ratios (isoprene-monocyclohexylmaleate : $r_1 = 0.135$, $r_2 = 0$ and isoprene-monobenzylmaleate : $r_1 = 0.075$, $r_2 = 0$), in comparison with the experimental results.

A good agreement is noticed between the results obtained from the calculation with the help of the reactivity ratios and the experimental results.

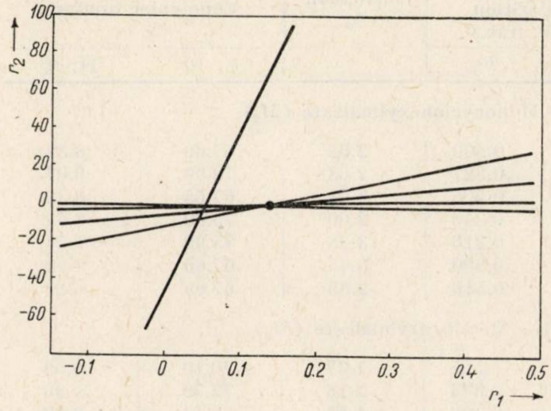

Fig. 1. — Determination of reactivity ratios by the Mayo-Lewis method for isoprene — monocyclohexylmaleate.

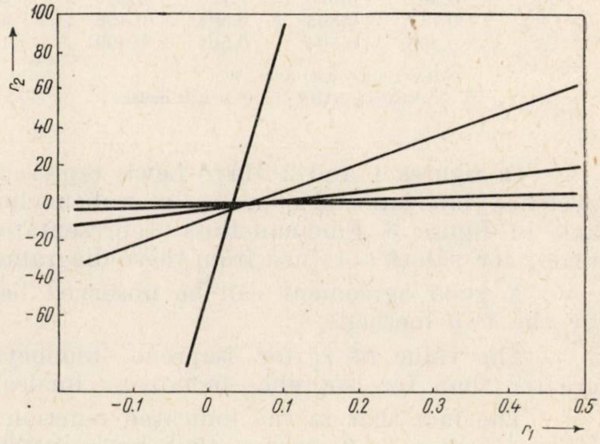

Fig. 2. — Determination of reactivity ratios by the Mayo-Lewis method for isoprene — monobenzylmaleate.

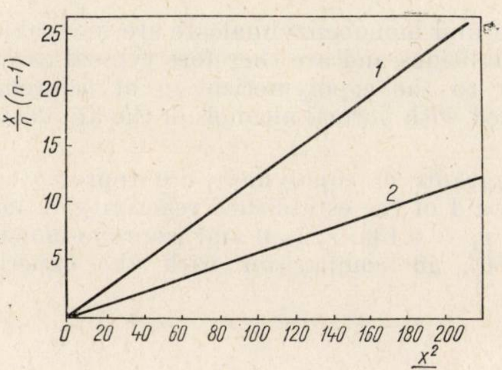

Fig. 3. — Fineman-Ross representation for the determination of the reactivity ratios of isoprene with :
1, monocyclohexylmaleate; *2*, monobenzylmaleate.

Table 2

Reactivity ratios in the copolymerization of izoprene (M_1) with monocyclohexylmaleate and monobenzylmaleate at 70°

M_2	Method			
	Mayo-Lewis		Fineman-Ross	
	r_1	r_2	r_1	r_2
Monocyclohexylmaleate	0.135±0.025	0	0.121	0
Monobenzylmaleate	0.075±0.025	0	0.055	0

It is noteworthy that for very high values of $[M_1^\circ]/[M_2^\circ]$, the experimental values do not agree with the copolymer composition equation, which takes into account the effect of the ultimate group (ultimate model). This fact is not easily distinguished from figure 4, but is emphasized by Barb's [7] representation of copolymer composition equation ($r_2 = 0$):

$$n - 1 = r_1 x$$

where $x = [M_1^\circ]/[M_2^\circ]$ and $n = m_1/m_2$.

From the representation of $n-1$ experimental values as a function to x for isoprene–monocyclohexylmaleate system (fig. 5) a deviation can be observed from linearity for very high values of x. This deviation was also observed in the representation of isoprene–monobenzylmaleate system for very high values of x.

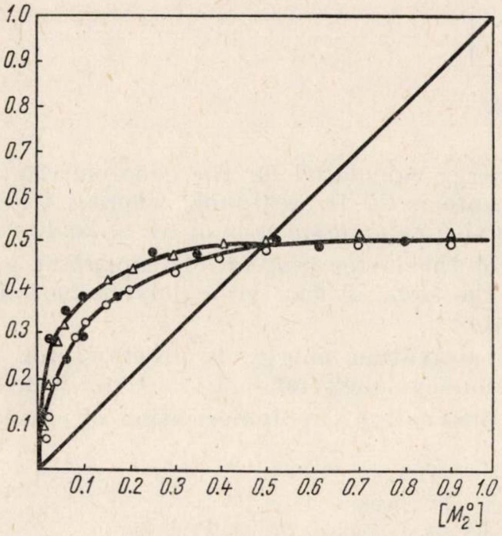

Fig. 4. — Copolymer composition diagram:
1, ○ isoprene – monocyclohexylmaleate ($r_1 = 0.135$; $r_2 = 0$);
2, △ isoprene – monobenzylmaleate ($r_1 = 0.075$; $r_2 = 0$);
3, • experimental result for both systems.

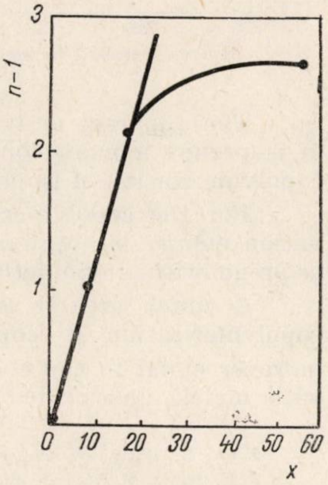

Fig. 5. — Barb representation for the isoprene — monocyclohexylmaleate system.

On verifying whether these experimental results agree with the copolymer composition equation, which admits the effect of the penultimate unit, obtained by Merz, Alfrey and Goldfinger [8] and reduced by Barb [7] the conclusion has been drawn of the inapplicability of this equation.

The deviations in the application of the classical copolymerization equation for very high values of x, were explained in an earlier work.[4]

ACTIVATION ENERGY

The influence of temperature on the copolymerization of isoprene with monocyclohexylmaleate and monobenzylmaleate is given by the Arrhenius representation in figure 6.

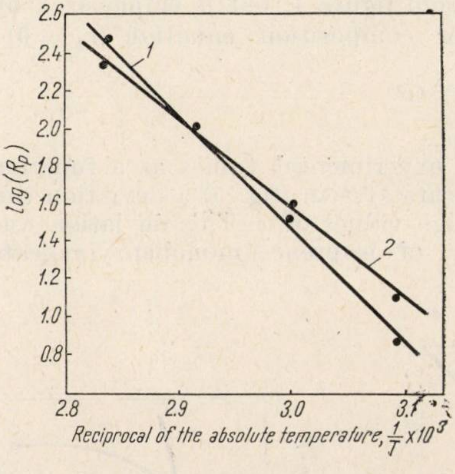

Fig. 6. — Effect of temperature on the reaction rate on the copolymerization of isoprene with :
1, monocyclohexylmaleate ; 2, monobenzylmaleate.

The apparent activation energy calculated for the copolymerization of isoprene—monocyclohexylmaleate is 27.31 kcal/mol, whereas for the copolymerization of isoprene-monobenzylmaleate it is of 21.40 kcal/mol.

For the copolymerization of the latter system, the apparent activation energy is approximately the same as for the copolymerization of isoprene with monomethylmaleate.[1]

A much greater apparent activation energy is observed for the copolymerization of isoprene—monocyclohexylmaleate system, which is however equal to the energy of alternating copolymerization of ethylene with maleic anhydride.[9]

---

[7] W. G. Barb, *J. Polymer Sci.*, **11**, 117 (1953).

[8] E. Merz, T. Alfrey and G. Goldfinger, *J. Polymer Sci.*, **1**, 75 (1946).

[9] S. Machi, T. Sakai, M. Gotoda and T. Kagiya, *J. Polymer Sci., Part A — 1*, **4**, 821 (1966).

Revue Roumaine de Chimie, 17, 4, 747 – 754 (1972)

INFRARED SPECTRA OF AMIDIC DERIVATIVES OF CARBONIC ACID. VI[1]

SUBSTITUTED 1,5-BENZYLIDINE GUANYLUREAS (FREE BASES AND SULPHATES)

R. BACALOGLU, FL. NEAMŢIU, ILSE BACALOGLU and G. OSTROGOVICH

Department of Organic Chemistry, Polytechnic Institute "Traian Vuia" Timişoara, Str. Bocşa 6, Timişoara, Romania

Received June 28, 1971

By examining the infrared spectra of some substituted 1,5-benzylidine guanylureas and their sulphates, the characteristic bands have been tentatively assigned to the oxo-amino-tetrahydro-s-triazine system. It has thus been established that in the crystalline lattice there is either a tautomer B or an association of tautomers A and B, depending on the type of substituent. In the salts of these compounds, protonation occurs at the endocyclic double bonded nitrogen.

This paper is part of our studies which aim the elucidation of the fine structure and configuration aspects of some dioxo-, oxo-amino-, and diamino-hydro-s-triazine derivatives by their infrared absorption spectra.

RESULTS AND DISCUSSIONS

a) *Free bases.* Table 1 is presenting the interpretations given to the most significant infrared spectra bands of a series of 6-aryl-2-amino-4-oxo-tetrahydro-s-triazine compounds (as an example see figures 1 and 2). In the 1630 – 1720 cm^{-1} range there is a series of bands which have been attributed to the carbonyl group stretching vibrations. For these vibrations the 1690 – 1780 cm^{-1} range has been ascribed to di-oxo-tetrahydro-s-triazines,[2–5] the 1680 – 1740 cm^{-1} one to di-oxo-hexahydro-s-triazines[2] and the 1690 – 1800 cm^{-1} one to cyanuric acid and its tri-N-methyl-derivative.[6–11] Ammeline and ammelide exhibit these bands at 1710 – 1740 cm^{-1}.[11]

---

[1] Part V., R. Bacaloglu, E. Catalina and G. Ostrogovich, *Spectrochim. Acta* **23 A**, 1571 (1967).

[2] I. Flament, R. Prornel and R. H. Martin, *Helv. Chim. Acta*, **42**, 485 (1959).

[3] J. Jonas, M. Horak, A. Piskala and J. Gut, *Coll. Czech. Chem. Comm.*, **27**, 2754 (1962).

[4] A. Piskala, *Coll. Czech. Chem. Comm.*, **28**, 2365 (1963).

[5] G. Ostrogovich, I. Bacaloglu, M. Safta and R. Bacaloglu, unpublished data.

[6] A. Rosens, *Bull. Soc. chim. belges*, **59**, 377 (1950).

[7] R. Newman and R. M. Badger, *J. Amer. Chem. Soc.*, **74**, 3545 (1952).

[8] A. I. Finkelstein, *Optica i spectr.*, **5**, 264 (1958).

[9] G. Ostrogovich, R. Bacaloglu and E. Catalina, *Studii şi cercet. Sti. Chim., Baza Cercetări Sti. Timişoarc*, **10**, 143 (1963).

[10] M. Cignitti and L. Paoloni, *Rend. Inst. Sup. Sanita*, **23**, 1037 (1960).

[11] W. M. Padgett and W. F. Hemner, *J. Amer. Chem. Soc.*, **80**, 803 (1958).

Table 1

Characteristic bands of 1,5-benzylidine guanylureas substituted in benzene nucleus (cm^{-1})

No	Substituent	CO stretching	CN stretching	NH_2		NH_2 stretching		NH guanidine stretching	NH ureic stretching	CN stretching and NH deformation coupled
				shearing	twisting-	asymm.	symm.			
I	$p-N(CH_3)_2$	1630	1570	1550	1025	3370	3270	3100	3150	1460 1370 1280
II	$p-CH_3$	1650	1620	1560	1025	3320	3230	3080	3150	1440 1380 1280
III	$-H$	1670 1700	1630 1650	1590 1560	1025 1050	3300	3170	2900	3140	1420 1365 1280 1470 — 1290
IV	$p-Cl$	1685 1710	1625 1655	1595 1560	1020 1045	3300	3190	2900	3160	1450 1390 1275 1420 1370 1290
V	$m-Cl$	1690 1720	1635 1660	1590 —	1030 1045	3250	3180	2900	3130	1420 1360 1265 1440 1390 —
VI	$o-Cl$	1680 1710	1635 1660	1595 1560	1040 1050	3300	3170	2900	3150	1430 1375 1280 1480 — —
VIII	$p-NO_2$	1670 1720	1630 1660	1590 —	1020 —	3370	3250	2800	3180	1410 1390 1290 1440 — 1270
IX	$m-NO_2$	1660	1630	1560	1020	?	?	3000	3240	1415 1380 1280
X	$o-NO_2$	1650	1620	1560	1030	3340	3260	3050	3050	1420 1395 1280

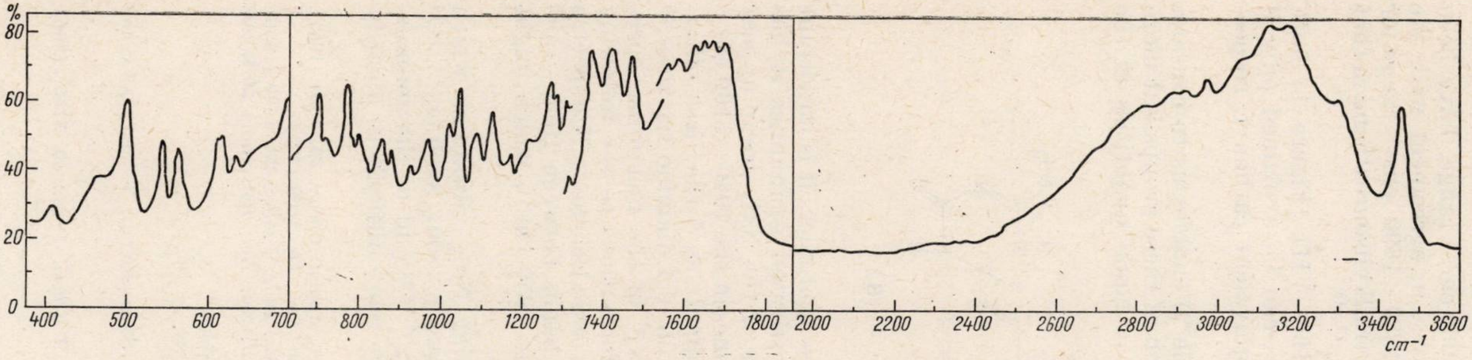

Fig. 1. — IR spectrum of 1,5-benzylidine guanylurea (nujol and hexachlorbutadiene mulls).

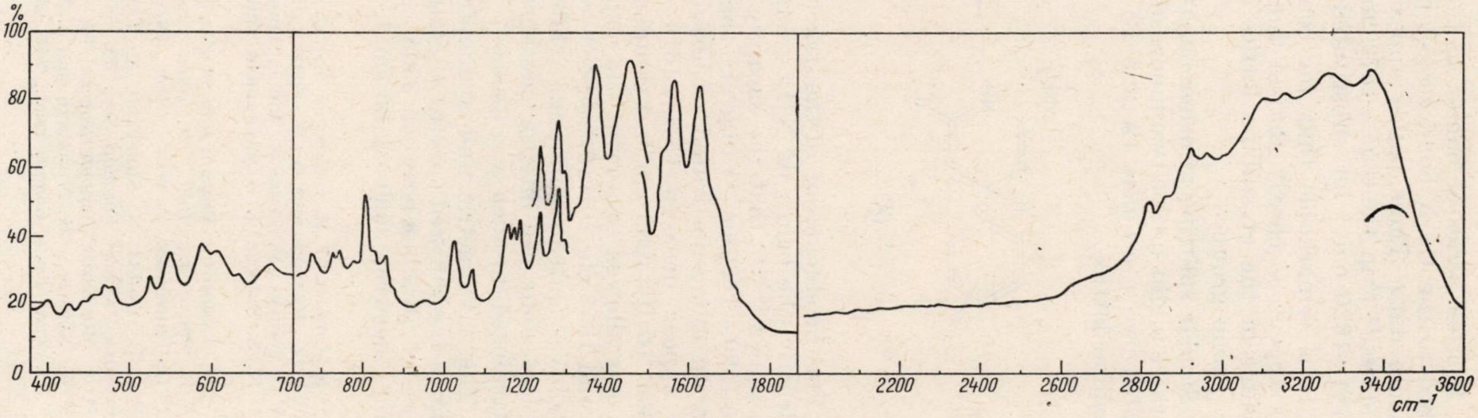

Fig. 2. — IR spectrum of *p*-dimethylamino-benzylidine guanylurea (nujol and hexachlorbutadiene mulls).

Another series of bands, in the 1570—1660 cm^{-1} range, have been ascribed to the C=N bond stretching vibrations, in agreement with the literature data. These bands appear in the 1530—1690 cm^{-1} range for guanidines,[12–16] in the 1655—1672 cm^{-1} for one trialkylisourea[14] and in that of 1580—1620 cm^{-1} for substituted amidines.[17–18]

It is remarkable that for compounds III—VIII (Figure 1) both bands appear as clearly shaped doublets. This can be explained only if we admit in the crystalline lattice two nonequivalent carbonyl, respectively imine groups.

Similar splitting of other bands (see Table 2) enables us to consider that these might not be two modes of association of these groups but more probable two tautomers (A and B) existing in equal quantities in the crystalline lattice.

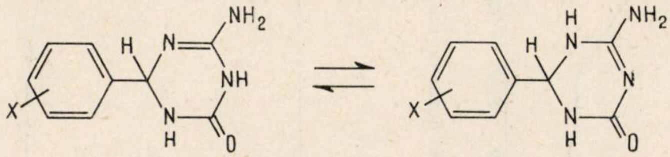

(A) (B)

For the elucidation of the structure of these tautomers it is important to identify the bands of NH_2 groups. In substituted guanidines it has been shown [15,16,19] that the shearing vibrations of the NH_2 group appear in the 1590—1660 cm^{-1} range and the twisting ones in the 1040—1100 cm^{-1} range. In monosubstituted or unsubstituted amidines [18] the first vibrations appear between 1570—1610 cm^{-1} and in 2,4-diamino-triazines,[20] between 1610—1680 cm^{-1}. A complete analysis [21] of the melamine spectrum has allowed to ascribe the respective deformations to the following 1627 and 1653 cm^{-1} bands respectively to 1178 and 1194 cm^{-1}. The spectra of the investigated compounds exhibit intense bands between 1530—1590 cm^{-1} and some less intense ones between 1020—1050 cm^{-1}, which might be attributed to such vibrations.

The asymmetric and symmetric stretching NH_2 vibrations which appear in the infrared spectra of guanidines between 3200—3400 cm^{-1}, [12,14] in those of amidines between 3300—3500 cm^{-1}, [17,18,22] and of the amino-s-triazines between 3000—3400 cm^{-1}, [11,16,20,21] are more difficult to identify

---

[12] E. LIEBER, D. R. LEVERING, and L. J. PATTERSON, *Analyt. Chem.*, **23**, 1594 (1951).

[13] P. L. PICKARD and G. W. POOLY, *J. Amer. Chem. Soc.*, **76**, 5169 (1954).

[14] J. FABIAN, M. LEGRAND and P. POIRIER, *Bull. Soc. chim. France*, **23**, 1499 (1956).

[15] K. S. SURESH, J. RAMACHADRAN and C.N.R RAO, *J. Sci. Ind. Res.* India **20 B**, 203 (1961).

[16] M. TAKIMOTO, *Nippon Kagaku Zasshi*, **85**, 168 (1964).

[17] D. PREVORSEK, *Bull. Soc. chim. France*, **1958**, 788.

[18] D. PREVORSEK, *J. Phys. Chem.*, **66**, 769 (1962).

[19] C. L. ANGELL, N. SHEPPARD, A. YAMAGUCHI, T. SHIMANOUCHI, T. MIYAZAWA and S. MITZUSHIMA, *Trans Faraday Soc.*, **53**, 589 (1957).

[20] G. MORIMOTO, *Nippon Kagaku*, **87**, 797 (1966).

[21] W. SAWODNY, K. NIEDENTH and J. W. DAWSON, *J. Chem. Phys.*, **45**, 3155 (1966).

[22] D. PREVORSEK, *Compt. rend.*, **244**, 2599 (1957).

in our compounds due to the superposition with other NH existing vibrations, as well as with crystallyzation alcohol OH vibrations. In the case of I—VI, VIII and X compounds two bands or shoulders in the 3250—3370 and 3170—3270 cm^{-1} range have been attributed to these vibrations.

To the NH bond vibrations which appear in amidines between 3100—3250 cm^{-1},[17,18,22] in cyanuric acid and cyanuric bases between 3000—3200 cm^{-1},[6-11] we ascribed two bands between 3120—3240 cm^{-1} and 2800—3100 cm^{-1}. For compounds III—X both bands, but especially the last one, are expressing, by their position as well as by their width, a very strong association by proton bonds (Figure 1).

In view of the above discussed data, we may admit that in the crystalline lattice compounds III—VI and VIII are in an equimolecular association of the two tautomers through triple hydrogen bonds :

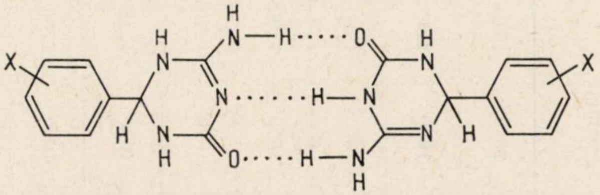

Such an association has been ascribed by us [23] to the mixtures of cyanuric acid-melamine and ammelide-ammeline in order to explain their properties. It is evident that each of the two tautomers is not able to bear a similar association.

We do ascribe the lower band frequencies of both CO and CN groups to the B tautomer, due to the direct conjugation of these groups. Examining the frequencies for compounds I, II, IX and X it may be admitted that they are exclusively in the B tautomer form. Table 1 presents also some C—N stretching vibrations and N—H bending vibrations. They are situated in the range usually attributed to vibrations of this kind (e.g. amidines 1200—1570 cm^{-1}).[17,18,22] They are, undoubtedly, characteristic of the amino-oxo-s-triazine system in the respective tautomer form, and consequently more difficult to compare with those of some related systems.

b) *Monoprotonated compounds* (*sulphates*). Table 2 shows the interpretation given to the most significant bands of the monoprotonated compounds (see for exemplification Figure 3).

The stretching vibrations of the carbonyl group are shifted towards greater wavenumbers due to the positivation of the nitrogen atom from its close vicinity.

In the NH bond vibrations range (2700—3300 cm^{-1}) there is an exceedingly broad band which tells, besides a very strong association through proton bonds, about an important positivation of the nitrogen

---

[23] G. Ostrogovich and R. Bacaloglu, *Studii şi Cercet. Sti. Chim., Baza Cercetări Sti. Timişoara*, **9**, 273 (1962).

Table 2

Characteristic bands of 1,5-benzylidine guanylurea sulphates substituted in benzene nucleus (cm^{-1})

No	Substituent	CO stretching	NH guanidine stretching	NH ureic stretching	NH_2 stretching		NH_2 shearing	Guanidine bands		CN stretching and NH deformation coupled
					assymm	symm.		I	II	
I	$p-N(CH_3)_2$	1740	2820	3200	3100	3300	1670	1710	1705	1450 1370 1280
II	$p-CH_3$	1735	2840	3170	3050	3300	1670	1715	1700	1470 1390 1290
III	$-H$	1735	2780	3170	3080	3220	1655	1700	1685	1460 1390 1280
IV	$p-Cl$	1730	2830	3150	3100	3220	1650	1720	1695	1460 1390 1280
V	$m-Cl$	1735	2840	3130	3030	3210	1670	1710	1700	1480 1410 1290
VI	$o-Cl$	1730	2830	?	3050	3280	1660	1715	1690	1480 1380 1290
VII	$o-COOH$	1740	2780	3100	3020	3200	1650	1705	1690	1460 1380 1290
VIII	$p-NO_2$	1730	2800	3200	3080	3300	1650	1720	1695	1480 1385 1260
IX	$m-NO_2$	1730	2830	3220	3150	3300	1670	1710	?	1470 ? 1280
X	$o-NO_2$	1745	2790	?	3090	3300	1650	1715	1690	1430 1360 1270

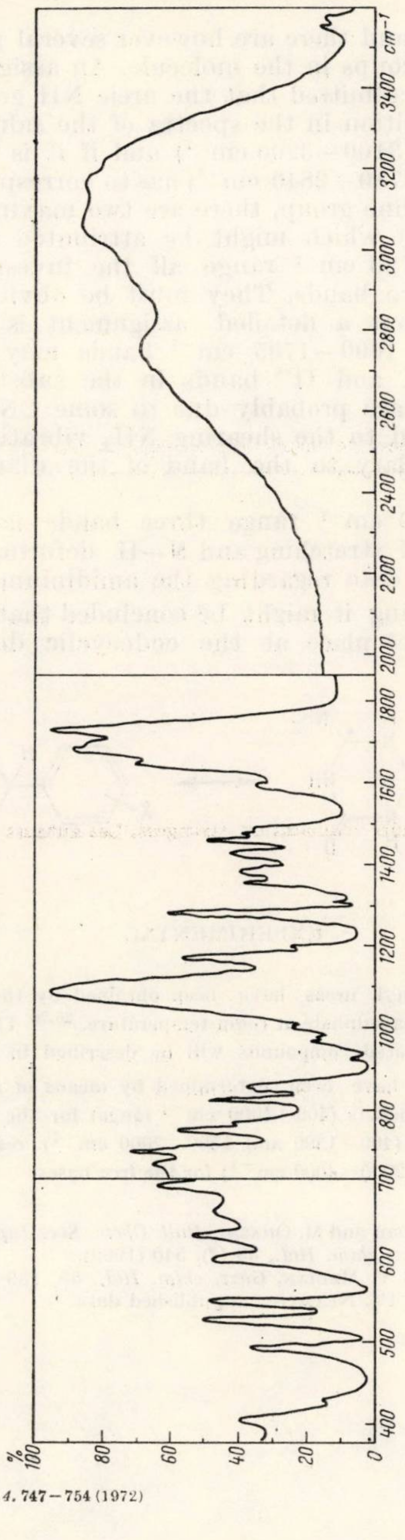

Fig. 3. IR spectrum of 1,5-benzylidine guanylurea sulphate (KBr pellet).

atom. On this broad band there are however several peaks corresponding to the different NH groups in the molecule. An assignment is of course more difficult. If it is admitted that the ureic NH group does not considerably change its position in the spectra of the salts compared to that in free bases (around 3100—3200 cm^{-1}) and if it is taken into account that the lowest band (2780—2840 cm^{-1}) has to correspond to the strongly positivated NH guanidine group, there are two maxima left (3200—3300 and 3020—3150 cm^{-1}) which might be attributed to the NH_2 group.

In the 1650—1720 cm^{-1} range all the investigated compounds exhibit a group of two bands. They must be obviously related to the guanidinium system but a detailed assignment is also difficult. The 1700—1715 cm^{-1} and 1690—1705 cm^{-1} bands may correspond to the so-called "guanidine I and II" bands in the substituted guanidinium salts spectra,[24] which are probably due to some CN vibrations.

We have ascribed to the shearing NH_2 vibration a band between 1650—1670 cm^{-1}, similary to the band of the diamino-s-triazine salts (1640—1680 cm^{-1}).[20]

In the 1200—1500 cm^{-1} range three bands have been attributed to some coupled C—N stretching and N—H deformation vibrations, in agreement with some data regarding the amidinium salts.[21]

From the foregoing it might be concluded that benzylidine guanyl ureas protonation takes place at the endocyclic double bond carrier nitrogen atom:

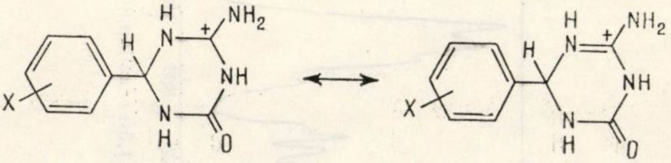

EXPERIMENTAL

The benzylidine guanyl ureas have been obtained by the reaction of substituted benzaldehydes and guanyl urea sulphate at room temperature.[25,26] The syntheses and the characterizations of the examinated compounds will be described in a forthcoming paper.[27]

The infrared spectra have been determined by means of a UR-10 type Carl Zeiss Jena Spectrograph in KBr pellets (400—4000 cm^{-1} range) for the benzylidine guanyl urea sulphates and in nujol mulls (400—1300 and 1500—2000 cm^{-1}), respectively hexachlorbutadiene mulls (1200—1500 and 2000—4000 cm^{-1}) for the free bases.

---

[24] T. Goto, K. Nakanishi and M. Ohashi, *Bull. Chem. Soc. Japan*, **30**, 723 (1957).

[25] A. Ostrogovich, *Gazz. chim. Ital.*, **39** (I), 540 (1909).

[26] A. Ostrogovich and V. Median, *Gazz. chim. Ital.*, **59**, 189 (1929).

[27] G. Ostrogovich and Fl. Neamțiu, unpublished data.

Revue Roumaine de Chimie, 17, 4, 755–764 (1972)

MÉTHODE MICROBIOLOGIQUE DE DÉTERMINATION QUANTITATIVE DE L'ACIDE *PARA*-AMINOBENZOÏQUE, VITAMINE H_1*

CASANDRA NICOLAU

Institut « Prof. Dr I. Cantacuzino », 103, Splaiul Independenţei, Bucarest

Reçu le 15 juin 1971

On a employé dans les recherches le streptocoque hémolytique ensemencé dans le milieu de culture Trüche épuisé et régénéré, dans lequel on a mit du sérum ou du plasma humain et on a poursuivi la vitesse de consommation du glucose du milieu, dosé chaque heure pendant 11 heures après l'ensemencement. Sur la base des données numériques représentant la consommation du glucose du milieu, on a construit une courbe pour chaque épreuve d'analyse. Cette courbe est comparée aux courbes standard obtenues auparavant sur la culture, dont le milieu comprend des concentrations variables de 1 mg $^0/_{00}$ à 1000 mg $^0/_{00}$ d'acide P.A.B., ce qui permet de déterminer à quelle courbe à concentration connue d'acide P.A.B. correspond l'épreuve d'analyse. La méthode est spécifique de l'acide P.A.B. qui est le facteur de croissance et le métabolite essentiel pour le streptocoque hémolytique.

A. INTRODUCTION

L'acide *para*-amino-benzoïque (P.A.B.), la Vitamine H_1, a été synthétisé pour la première fois par Fischer en 1863, par réduction de l'acide paranitrobenzoïque par sulfure d'ammonium.

Il a été obtenu plus tard comme produit intermédiaire dans la synthèse des anesthésiques locaux tels que la novocaïne et l'anesthésine.

L'acide P.A.B. (Vitamine H_1) forme avec la biotine (Vitamine H) le groupe des substances vitaminiques, présentes dans certains systèmes enzymatiques, qui interviennent dans le transfert de carboxyle.[1–3]

---

* Ouvrage expérimental effectué à l'Institut Prof. Dr Cantacuzino, Bucarest.

[1] L. Harris, S. N. Ray et A. Ward, *J. Biochem.*, **27**, 2011 (1933).

[2] T. W. Birch et L. Harris, *J. Biochem.*, **28**, 602 (1934).

[3] D. S. Rubo et M. J. Gillespie, *Nature*, **146**, 838 (1940).

Woods et Fischer [4] constatent en 1940 expérimentalement à l'extrait de levure de bière l'existence d'un facteur antagoniste sulfamidique, l'acide P.A.B., dont les propriétés chimiques suggèrent une liaison chimique étroite avec le sulfamide.

La science roumaine a contribué à l'étude de l'acide P.A.B. par les recherches de Danielopolu et Rudeanu [5] (1940) concernant sa propriété d'antagoniste sulfamidique.

Dans leurs travaux sur le thème : «Régénération des milieux de culture», Angelescu, Dîmboviceanu, Roth et Nicolau [6–10] ont relevé la propriété de l'acide P.A.B. en tant que facteur de croissance et métabolite essentiel pour le streptocoque hémolytique.

Des résultats identiques ont été obtenus dans les expériences avec deux dérivés de l'acide P.A.B., à savoir : l'ester éthylique (anesthésine) et l'ester à diméthylaminoéthanol (novocaïne).

Les données expérimentales ont permis aux auteurs d'aboutir à certaines conclusions, quelques-unes apportant une importante contribution théorique et pratique au problème de la régénération des milieux de culture,[11] d'autres ouvrant de nouvelles perspectives pour des applications pratiques en biochimie et thérapeutique de l'acide P.A.B. et de ses dérivés, tels que : la novocaïne et l'anesthésine.[12]

L'une des applications pratiques en biochimie est la méthode microbiologique de détermination quantitative de l'acide P.A.B. dans le milieu organique qui fait d'ailleurs l'objet de cet ouvrage.

B. PARTIE EXPÉRIMENTALE

Dans notre ouvrage sur le thème : « La méthode microbiologique de détermination quantitative de l'acide P.A.B. » nous avons utilisé comme étalon le diagramme fig. 1.

Ce diagramme $v = f(t)$ a été établi sur la base des données expérimentales obtenues dans les recherches antérieures, en poursuivant par doses répétées à une heure d'intervalle, pendant (t) 11 heures, [13] la vitesse (v) de consommation du glucose, sur un milieu synthétique Trüche épuisé et régénéré, ensemencé de streptocoque hémolytique, isolé d'une septicémie. Ce milieu a été régénéré par correction du pH à 7 et en ramenant le glucose au chiffre initial, $2^0/_{00}$ ml de milieu. [14]

---

[4] D. D. Woods, *Biol. J. exp. Pathol.*, **21**, 74 (1940).

[5] D. Danielopolu et A. Rudeanu, *Bull. Acad. Med. Roum.*, **185**, 199 (1943).

[6] A. Dîmboviceanu, H. Roth et E. Angelescu, *Biochem. Z.*, **136**, 215 (1944).

[7] E. Angelescu, A. Dîmboviceanu, H. Roth et C. Nicolau, *Acad. Roum. Bull. Sec. Sci.*, **2**, 94 (1945).

[8] E. Angelescu, A. Dîmboviceanu, H. Roth et C. Nicolau, *Rev. Chim. Acad. R.P.R.*, **3**, 87 (1958).

[9] E. Angelescu, A. Dîmboviceanu, H. Roth et C. Nicolau, *Rev. Chim. Acad. R.P.R.*, **4**, 207 (1959).

[10] C. Nicolau, Thèse de doctorat Fac. Sc. Ph. Chimiques, Univ. de Bucarest (1949).

[11] A. Besredka, *Compt. rend. Soc. Biolog.*, **89**, 7 (1923).

[12] F. E. Möller et K. Schwarz, *Ber.*, **74**, 1612 (1941).

[13] I. Buchanan, *J. Infect. Dis.*, **26**, 190 (1927).

[14] E. Angelescu, A. Dîmboviceanu, H. Roth et C. Nicolau, *Hommage à Traian Săvulescu.*, **1959**, 969.

Avant l'ensemencement, on a ajouté au milieu de culture de l'acide P.A.B. en concentrations variant de 1 mg $^0/_{00}$ à 1000 mg $^0/_{00}$.

Dans des conditions expérimentales identiques à celles utilisées pour le diagramme étalon, nous avons déterminé la concentration de l'acide P.A.B. dans le sérum et le plasma, à un groupe de 75 malades, répartis en deux lots dont le premier formé de malades au régime alimentaire et apport habituel de vitamines, le deuxième comportant des malades auxquels on a administré de l'acide P.A.B. par dose thérapeutique (6—10 g en 24 h).

MATÉRIAUX ET MÉTHODES

Nous avons utilisé les matériaux suivants :

1. Milieu Trüche épuisé et régénéré, maintenu au frais.
2. Streptocoque hémolytique entraîné et activé jusqu'à l'obtention d'une culture abondante, par plusieurs passages pendant 24 heures sur le milieu Trüche frais.
3. Sang stérile récolté, environ 25 ml.
4. Acide P.A.B., sol. 1 g%, dans des fioles stériles.
5. Courbes étalon, pour la comparaison des résultats.

MODE DE TRAVAIL

Chaque épreuve a été analysée selon la même technique, en respectant le même ordre d'opérations, comme suit : dans deux ballons stériles ont été répartis 150 ml de milieu synthétique Trüche épuisé et régénéré, préparé pour l'expérience. Dans le premier ballon on a introduit 15 ml de sérum sanguin ou plasma pour analyse, le second ballon servant de témoin. Au témoin a été ajouté de l'acide P.A.B., afin d'obtenir dans le milieu de culture une concentration de 1 mg $^0/_{00}$. Tous les deux ont été ensemencés d'un ml de culture de streptocoque hémolytique de 24 heures et mis au thermostat à 37°.

Une heure après on a prélevé stérilement de chaque ballon 10 ml de milieu en filtrant immédiatement par Seitz E. K. Le filtrat a été conservé pour le dosage du glucose, tout en maintenant les ballons à 37°. Des prélèvements ont été faits par 10 ml à une heure d'intervalle, pendant 11 heures, après l'ensemencement. La quantité de glucose de chaque échantillon filtrée est dosée.

Au prélèvement de chaque échantillon, on a simultanément noté l'intensité de développement du streptocoque hémolytique, selon le degré d'opacité du milieu de culture. Le glucose a été dosé après défécation au réactif Patein, suivant la méthode de Bertrand. Nous avons ainsi déterminé, quantitativement, la vitesse de consommation du glucose du milieu, en indiquant dans un tableau les donneés en pour cent, et représenté graphiquement la vitesse de consommation du glucose du milieu, pendant 11 heures ; sur l'abscisse apparaît le temps en heures à partir de l'ensemencement et sur l'ordonnée le glucose en pour cent consommé. Les deux courbes obtenues, représentant l'épreuve d'analyse et le témoin, sont comparées au graphique étalon étant ainsi déterminé quantitativement l'acide P.A.B. à $^0/_{00}$ ml dans le produit étudié (sérum sanguin ou plasma).

COURBES ÉTALON POUR LA COMPARAISON DES RÉSULTATS

Dans la fig. 1 est représenté le graphique étalon avec une concentration d'acide P.A.B. de 1 mg $^{0}/_{00}$ à 1000 mg $^{0}/_{00}$ dans le milieu Trüche épuisé et régénéré.

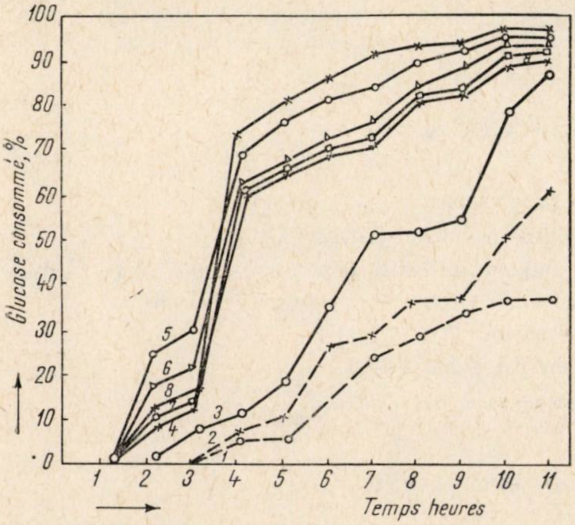

Fig. 1. — Les courbes standards, cultures sur le milieu Trüche épuisé et régénéré. *1*,0 $^{0}/_{00}$, *2*, 1 mg $^{0}/_{00}$, *3*,10 mg $^{0}/_{00}$, *4*, 100 mg $_{0}/_{00}$, *5*, 250 mg $^{0}/_{00}$, *6*, 500 mg $^{0}/_{00}$, *7*, 750 mg $^{0}/_{00}$, *8*, 1000 mg $^{0}/_{00}$.

On remarque la 4ᵉ courbe, qui est la plus évidente : elle indique la consommation de glucose la plus élevée et le développement rapide de la culture de streptocoque hémolytique. La période stationnaire est beaucoup raccourcie et le développement logarithmique est énormément accéléré. On a obtenu cette courbe sur des cultures à 100 mg $^{0}/_{00}$ d'acide P.A.B. dans le milieu épuisé et régénéré ($= 7{,}10^{-7}$ mole/cm^{3}), ce chiffre étant considéré le biostimulent optimal pour le streptocoque hémolytique.

La courbe 1 la moins développée représente la culture témoin sans acide P.A.B. dans le milieu. Entre ces deux courbes sont situées les autres courbes correspondant à 1000 mg $^{0}/_{00}$ 750 mg $^{0}/_{00}$, 500 mg $^{0}/_{00}$, 250 mg $^{0}/_{00}$, 10 mg $^{0}/_{00}$ et 1 mg $^{0}/_{00}$.

Les échantillons soumis à l'analyse avec des quantités en dessous de 1 mg $^{0}/_{00}$ d'acide P.A.B. peuvent être inscrits entre les courbes *1* et *2* qui représentent l'espace avec les microgrammes de 0 mg $^{0}/_{00}$ acide P.A.B. à 1 mg $^{0}/_{00}$ acide P.A.B.

C. EXPÉRIENCES POUR LA DÉTERMINATION QUANTITATIVE DE L'ACIDE P.A.B. — VITAMINE H_1

1. EXPÉRIENCES EFFECTUÉES DANS LE SÉRUM SANGUIN ET LE PLASMA DES MALADES AU RÉGIME ALIMENTAIRE ET APPORT NORMAL DE VITAMINES (PREMIER LOT)

a) *Expériences dans le sérum sanguin*

Le tableau 1 donne les résultats des expériences — le témoin — et le tableau 2 l'échantillon analysé — avec le chiffre moyen obtenu dans le dosage du glucose chez 40 malades du premier lot. La première colonne — temps heures—indique l'heure à laquelle on a fait le prélèvement du milieu, et le dosage du glucose ; dans la deuxième colonne sont inscrits les chiffres indiquant le glucose contenu en 1000 ml de milieu ; dans la troisième colonne — le glucose consommé à 100 ml, les chiffres indiquant la consommation du glucose obtenu au dosage, à une heure d'intervalle, pendant 11 heures, rapportés à 100 de glucose initial ; dans la dernière colonne on a désigné par le signe + l'intensité du développement de la culture estimée d'après le degré de perturbation du milieu.

Tableau 1

Le témoin en présence de 1 mg $^0/_{00}$ d'acide P.A.B.

Temps heures	Glucose dans 1000 ml	Glucose consommé %	Développement
0	2,41	—	—
1	2,41	0	—
2	2,41	0	— +
3	2,41	0	+
4	2,25	6,6	+
5	2,17	10,0	+
6	1,80	25,3	+
7	1,74	27,9	+ +
8	1,32	45,3	+ +
9	1,32	45,3	+ +
10	1,20	50,2	+ +
11	0,90	62,6	+ +

Tableau 2

L'épreuve d'analyse dans le sérum sanguin (Ier lot)

Temps heures	Glucose dans 1000 ml	Glucose consommé %	Développement
0	2,41	—	—
1	2,41	0	— +
2	2,41	0	+
3	2,30	4,5	+
4	2,10	12,4	+
5	1,65	31,1	+
6	1,60	33,0	+ +
7	1,50	37,7	+ +
8	1,22	49,4	+ +
9	1,22	49,4	+ +
10	0,90	62,6	+ +
11	0,60	75,1	+ +

Avec les données représentées dans les deux tableaux et la courbe étalon, nous avons construit la figure 2.

En comparant les résultats obtenus dans l'épreuve analysée — la courbe de l'épreuve — au graphique représentant les courbes des valeurs standard de l'acide P.A.B., il est évident que la courbe du témoin se superpose étroitement à la courbe étalon avec 1 mg ‰ d'acide P.A.B. et la courbe représentant l'épreuve se situe entre le témoin et la courbe de 10 mg ‰ ml.

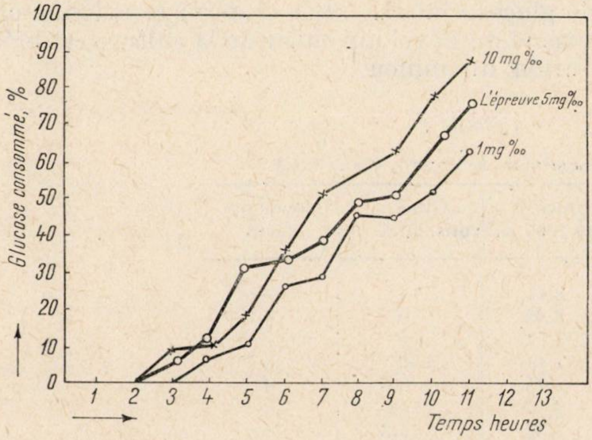

Fig. 2. — Graphique comparatif : courbe de l'épreuve dans le sérum sanguin (Ier lot) — courbe standard.

On estime que la concentration de l'acide P.A.B. dans l'épreuve de l'analyse du sérum sanguin est d'environ 5 mg‰ ml.

b. *Expériences dans le plasma*

Les données expérimentales de l'épreuve d'analyse de l'acide P.A.B. dans le plasma sont indiquées, toujours en chiffre moyen de l'entier lot de malades (premier lot), dans le tableau 3 ; sur la base des données de l'épreuve et de la courbe étalon, nous avons construit la figure 3.

Tableau 3

L'épreuve d'analyse dans le plasma (Ier lot)

Temps heures	Glucose dans 1000 ml	Glucose consommé %	**Développement**
0	2,41	—	—
1	2,41	0	—+
2	2,41	0	—+
3	2,20	8,7	+
4	2,12	12,0	+
5	1,90	21,2	++
6	1,50	33,2	++
7	1,20	50,6	++
8	1,17	51,4	++
9	0,90	62,6	++
10	0,48	80,0	+++
11	0,30	87,5	+++

Dans la figure 3 sont inscrits les résultats des analyses dans le plasma, comparés à l'étalon acide P.A.B. ; on observe que la courbe de l'épreuve dans le plasma se superpose à l'étalon, ayant 10 mg $^0/_{00}$ ml d'acide P.A.B. Nous pouvons apprécier que l'épreuve de plasma contient environ 10 mg$^0/_{00}$ ml d'acide P.A.B.

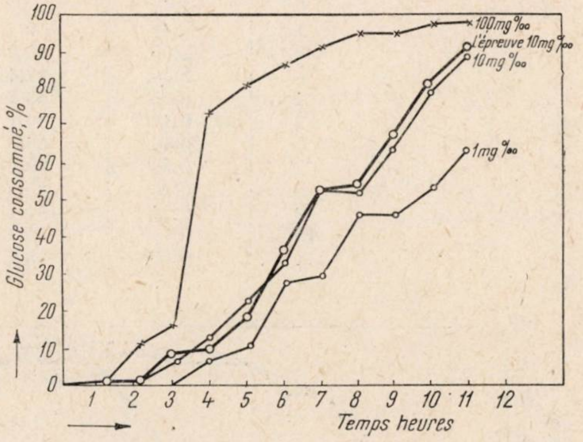

Fig. 3. — Graphique comparatif : courbe de l'épreuve dans le plasma (Ier lot) — courbe standard.

2. EXPÉRIENCES EFFECTUÉES DANS LE SÉRUM SANGUIN ET DANS LE PLASMA CHEZ LES MALADES AU RÉGIME ALIMENTAIRE ET APPORT DE VITAMINES NORMAUX SATURÉS THÉRAPEUTIQUEMENT D'ACIDE P.A.B. (IIe LOT)

Le dosage de l'acide P.A.B. dans le sérum sanguin et le plasma a été expérimenté à ce lot de 35 malades quand on administrait dans la thérapeutique appliquée l'acide P.A.B., en doses de 6 — 10 g en 24 heures, la substance pure en prises de 0,50 g, ou le paraminol comprimé.

a) *Expériences dans le sérum sanguin*

La vitesse de consommation du glucose dans les cultures de streptocoque hémolytique auxquelles on a ajouté le sérum des malades du deuxième lot est donnée dans le tableau 4.

A l'aide des résultats inscrits dans le tableau 4 et de la courbe étalon on a obtenu la figure 4.

L'allure de la courbe marquant l'épreuve d'analyse dans le sérum sanguin représente une parallèle très rapprochée de l'étalon à 100 mg $^0/_{00}$. d'acide P.A.B.

Tableau 4

L'épreuve d'analyse dans le sérum sanguin (IIe lot)

Temps heures	Glucose dans 1000 ml	Glucose consommé %	Développement
0	2,41	–	–
1	2,41	0	+
2	2,05	15,0	++
3	2,00	17,4	+++
4	0,75	68,8	+++
5	0,48	80,1	+++
6	0,48	80,1	+++
7	0,26	89,2	+++
8	0,26	89,2	+++
9	0,24	90,1	+++
10	0,15	93,7	+++
11	0,15	93,7	+++

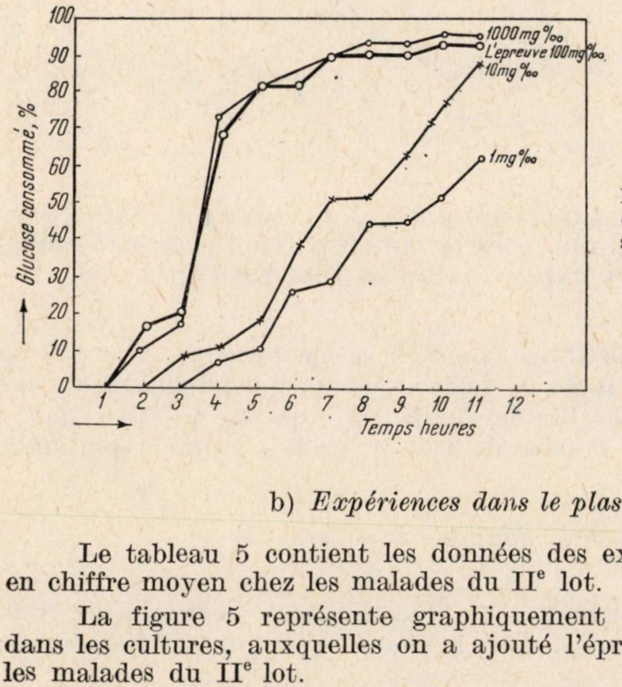

Fig. 4. — Graphique comparatif : courbe de l'épreuve dans le sérum sanguin (IIelot)—courbe standard.

b) *Expériences dans le plasma*

Le tableau 5 contient les données des expériences dans le plasma en chiffre moyen chez les malades du IIe lot.

La figure 5 représente graphiquement les résultats des dosages dans les cultures, auxquelles on a ajouté l'épreuve dans le plasma chez les malades du IIe lot.

Les expériences effectuées sur le IIe lot de malades saturés thérapeutiquement d'acide P.A.B. démontrent une croissance de la vitesse de consommation du glucose dans les cultures de streptocoque hémolytique, auxquelles on a ajouté des épreuves d'analyse, le sérum sanguin ou le plasma de ce lot de malades.

L'étude des données inscrites dans les tableaux 4 et 5 et des figures 4 et 5 révèle une croissance évidente de la concentration de l'acide P.A.B. dans le sérum sanguin et surtout dans le plasma ; l'allure de la courbe marquant

Tableau 5

L'épreuve d'analyse dans le plasma (IIe lot)

Temps heures	Glucose dans 1000 ml	Glucose consommé %	Dévelop-pement
0	2,41	—	—
1	2,41	0	+
2	2,17	10,0	++
3	2,04	15,3	+++
4	0,95	51,0	+++
5	0,44	81,3	+++
6	0,44	81,3	+++
7	0,38	84,2	+++
8	0,28	88,4	+++
9	0,25	90,0	+++
10	0,12	95,0	+++
11	0,10	95,9	+++

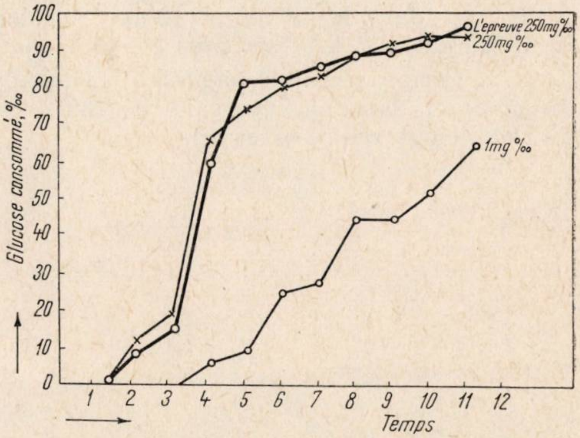

Fig. 5. — Graphique comparatif : courbe de l'épreuve dans le plasma (IIe lot) — courbe standard.

l'épreuve d'analyse dans le sérum sanguin est très rapprochée de la courbe étalon à 100 mg $^{0}/_{00}$ ml et la courbe représentant l'épreuve dans le plasma s'inscrit sur la figure à proximité de la courbe étalon à 250 mg $^{0}/_{00}$ ml d'acide P.A.B. Par conséquent, nous avons constaté qu'au IIe lot de malades on trouve l'acide P.A.B. à une concentration de 100 mg $^{0}/_{00}$ ml dans le sérum sanguin et à une concentration de 250 mg $^{0}/_{00}$ ml dans le plasma.

CONCLUSIONS

1. La détermination quantitative de l'acide P.A.B. dans le sang (sérum et plasma) est possible en employant la méthode microbiologique de dosage. La méthode est basée sur la propriété de facteur de crois-

sance que possède l'acide P.A.B. pour le streptocoque hémolytique, ensemencé au milieu de culture Trüche épuisé et régénéré.

2. Le critère d'appréciation de la concentration de l'acide P.A.B. dans le milieu de culture contenant l'épreuve d'analyse est la vitesse (v) de consommation du glucose du milieu dosée chaque heure, pendant (t) 11 heures dès l'ensemencement et la croissance plus ou moins abondante de la culture, observée macroscopiquement. La courbe $v = f(t)$ de la consommation de glucose résultée de l'épreuve à analyser est comparée aux courbes étalon obtenues antérieurement sur des cultures dont le milieu comprend des concentrations variables (entre 1 mg $^0/_{00}$ et 1000 mg $^0/_{00}$) d'acide P.A.B.

3. Les données expérimentales, ont permis à déterminer la concentration de l'acide P.A.B. dans le sang (sérum et plasma) et formuler cette nouvelle méthode microbiologique de dosage de l'acide P.A.B. (Vitamine H_1). Ces données indiquent une concentration d'acide P.A.B. plus élevée au IIe lot des malades, auxquels on a administré de l'acide P.A.B. (Vitamine H_1) pendant les expériences, à savoir : 100 mg $^0/_{00}$ dans le sérum et 250 $^0/_{00}$ dans le plasma, tandis qu'au Ier lot de malades, seulement 5 mg $^0/_{00}$ dans le sérum et 10 mg $^0/_{00}$ dans le plasma. La concentration de l'acide P.A.B. est plus élevée dans le plasma que dans le sérum.

4. Cette méthode spécifique de l'acide P.A.B. peut être appliquée aisément et dans un intervalle de temps réduit, présentant, également, un coefficient réduit d'erreurs.

Revue Roumaine de Chimie, **17**, *4*, 765–770 (1972)

SOURCES OF INFORMATION IN STEROID CHEMISTRY (Part 1)

S. H. DOSS*

Steroids are compounds containing the perhydrocyclopentanophenanthrene nucleus. They include sterols, bile acids, sex hormones, adrenocortical hormones, cardiac glycosides, sapogenins, and some alkaloids.

The evolution of the steroid literature is shown by the following statistics of publications per year[1]:

1910–1925	10
1926–1932	10–40
1933–1939	40–100
1940–1945	80–50
1946–1948	90–120
1949–1953	150–130, 210, 290, 320

The purpose of these series of articles is to guide the researcher to the leading articles, textbooks, physical measurements, catalogs and patents in the steroid literature.

One of the important sources of information in this field is Elsevier's Encyclopaedia of Organic Chemistry, General description of the contents of the series.

Series I. Aliphatic compounds
  vol. 1 Hydrocarbons, halogen and nitrogen compounds
  vol. 2 Hydroxy- and keto-compounds
  vol. 3 Carboxylic acids, S-, Se-, Te-, P-, As- and metal compounds.

Series II. Carboisocyclic Non'-Condensed Compounds
  vol. 4. Compounds with 3-, 4-, 5-, 7-membered or larger rings
  vol. 5–11. Compounds with 6-membered rings

A. Monocyclic six-membered ring compounds

vol. 5. Hydrocarbons and halogen compounds.
vol. 6. Nitro-, nitroso, hydroxylamino-, amino, azo-, azoxy-, diazo-, hydrazino-, triazeno-,triazo-, and other nitrogen compounds.
vol. 7. Hydroxy-compounds.
vol. 8. Keto-compounds
vol. 9. Carboxylic acids
vol. 10. S-, Se-, Te-, P-, As- and metal compounds

---

* B. Sc., M. Sc., Ph. D., Ed. Dip. Psy. Dip. L.L.B. and L.L.M. Present address: Organisch-chemisches Institut der Universität Bonn, W/Germany.

[1] W. Klyne, "The Chemistry of the Steroids", Methuen & Co., London 1965, p. 21.

B. Polycyclic non-condensed six-membered ring compounds

vol. 11. Biphenyl, diphenyl methane, etc. terphenyl, triphenyl methane, etc. Compounds with 4 phenyl groups etc.

Series III. Carboisocyclic condensed compounds
vol. 12. Bicyclic compounds.
vol. 13. Tricyclic compounds
vol. 14. Tetra and higher-cyclic compounds.

Series IV. Heterocyclic compounds
vol. 15. Heterocyclic compounds with 1 N.
vol. 16. Heterocyclic compounds with 2 and more N.
vol. 17. Heterocyclic compounds with 1 and more 0.
vol. 18. Heterocyclic compounds with N and 0 with S, Se and Te.

General Indexes
vol. 19. General subject Index and Group Index.
vol. 20. General Formula Index.

Only volumes 12, 13 and 14, dealing with condensed carboisocyclic compounds, have appeared. Once the right volume has been chosen, it is easy to find the compound, either from the alphabetical index and the formula index at the end of the volume or with the aid of the table of contents of the volume or of the individual skeleton system; or by using the ring index at the beginning of each volume of the first edition (generically summarized on the binding)*.

Characteristics of the Eycyclopaedia

1. The system of classification is based on the structure (carbon skeleton) of compounds so that those which are most closely related are placed together. Within each series (aliphatic, carbocyclic and heterocyclic), the structural skeleton determines the arrangement.

2. Compounds within each section are always arranged in the same order; hydrocarbons, halogen nitrogen-, hydroxy-, keto-compounds; carboxylic acids, sulphur compounds, etc.

3. In connection with each compound its derivatives (additive compounds, esters, ethers, phenylurethanes, hydrazones... etc.) are described. Thus, anhydrides of dicarboxylic acids and lactones of hydroxy-acids are dealt with immediately after the corresponding acid.

4. References are arranged at the end of each chapter according to the year of publication in an ascending order.

5. In addition to the information on the individual compounds, it contains a separate survey for the methods of preparations of the more important ring systems.

6. The following order of radical substituents is used in the names: alkyls and alkylidenes: methyl, ethyl, vinyl, ethynyl, propyl... methylene, ethylidene... phenyl, tolyl, benzyl..., benzylidene... anthryl... phenanthryl, etc.

Halogen: fluoro, chloro, bromo, iodo;

Nitrogen-containing functions: c. g., nitro, amino (acetamino, anilino) hydroxylamino, azo, hydrazino, etc.

Keto:

Carboxy (cyano);

Thio (mercapto).

7. As a rule, esters, ethers, acyl derivatives, oximes, hydrazones, etc. are not included in the subject index but only in the formula index.

8. The prefixes epi- and iso-, when referring to configuration, are disregarded in the alphabetical index.

---

* Dr. Herman Skolnik, private communication.

Volume 14 and its classification

Vol. 14 deals with tetracyclic and higher cyclic compounds according to the following classification :

1. Compounds with 3 five-membered rings and 1 six-membered ring.
2. Compounds with 2 five-membered and 2 six-membered rings.
3. Compounds with 1 five- and 3 six-membered rings from page 12—211.
4. Compounds with 4 six-membered rings.
5. Compounds with seven-membered rings.
6. Tetracyclic compounds containing carbon bridged rings.
7. Tetracyclic spiro-compounds.

From page 12—311 (volume 14 of series III) — pages not in brackets — steroid information is classified and due to the tremendous expansion of the literature, each item is subdivided into more specialized classified compounds. This additional information constitutes the supplements of vol. 14 — pages in brackets, followed by an "s" — another advantage of the supplements is that the patent literature has been incorporated.

1.2. Cyclopentenophenanthrene

	main volume p.	supplement p.
A. Hydrocarbons	15[2]	(1382 S)[3]
B. Halogen compounds	25	(1449 S)
C. Nitrogen compounds	27	(1478 S)
D. Hydroxy compounds	30	(1487 S)
I. Hydroxy compounds with OH attached to a side chain	30	(1487 S)
II. Hydroxy compounds with OH directly attached to a ring	30	(1494 S)
a) Monohydroxy compounds	30	(1494 S)
b) Dihydroxy compounds	95	(1917 S)[4]
c) Tri- and tetrahydroxy compounds	107	(1952 S)
E. Ketones	113	
I. Compounds with CO in a side chain	113	(2215 S)[5]
a) Compounds with 1 CO group in a side chain	113	(2215 S)
b) Compounds with 2 CO group in a side chain	117	(2378 S)
II. Compounds with CO in a ring	118	(2383 S)
1. Compounds with 1 CO group in a ring	118	
a) Ketones without any other function	118	(2383 S)

---

[2] E. Josephy and F. Radt, "Elsevier's Encyclopaedia of Organic Chemistry", vol. 14 (Tetracyclic and Higher-Cyclic Compounds) of Series III (Carboisocydic and Higher-Cyclic Compounds) of Series III (Carboisocydic Condensed Compounds), Elsevier Publishing Co. Inc., New York, Amsterdam (1949). In this volume the literature up to and including 1936 has been consulted.

[3] F. Radt (Edited by A. Georg with the assistance of M. Georg Plant); "Elsevier's Encyclopaedia of Organic Chemistry", vol. 14 Supplement III (Steroid, part 1) pp. 1347 s — 1868 s (1954).

[4] F. Radt (ed.), "Elsevier's Encyclopaedia of Organic Chemistry", volume 14, Supplement IV, steroids, part 2, p. p. 1869 s — 2214 s (1956).

[5] F. Radt (ed.) "Elsevier's Encyclopaedia of Organic Chemistry" : volume 14, Supplement V (1959), Steroids, part 3, pp. 2215 s — 2990 s Oxo-steroids.

b) Chloro-ketones, e. g. Dehydroandrosteryl	128	(24735)
c) Hydroxy-ketones	132	(2510 S)
*Hydroxy-ketones with OH attached to a side chain	132	
**Hydroxy-ketones with OH directly attached to a ring	133	
d) Compounds with 1 CO in a ring and in side chains, e.g. Progesterone, corticosterone	150	(2777 S)
2. Compounds with 2 CO groups in rings, e. g. androstenediones, cholestanediones, dehydrocorticosterone	155	(2872 S)
3. Compounds with 3 CO groups in rings, e. g. adrenosterone	165	(2979 S)
Tetraketosteroids		(2985 S)
F. Carboxylic acids	166	
I. Carboxylic acids without other functions	166	(2991 S)[6]
2. Halogeno-carboxylic acids	172	(3012 S)
3. Hydroxy-carboxylic acids	173	(3017 S)
4. Keto-carboxylic acids	199	(3339 S)
5. Degradation products of bile acids	215	(3528 S)
G. Sulphur compounds	224	(3629 S)
Metal derivatives		(3644 S)
Bi-steroids		(3645 S)
H. Cyclopentenophenanthrene with an ethylene oxide ring in a side chain, e. g. Schymnol	224	(cf. supplement steroid part 5) [7]
I. Cyclopentenophenanthrene attached to a γ-lactone	225	
1. Compounds with 2 OH groups attached to rings, e. g. digitoxigenin, thevetigenin, uzarigenin	225	
2. Compounds with 3 OH groups attached to rings, e. g. periplogenin, sarmentogenin, digoxigenin, gitoxigenin	234	(cf. supplem. steroid part 6)[8]
3. Compounds with 4 or more OH groups attached to rings	249	
4. Compounds with an aldehyde group, e. g. strophanthidin	252	

---

[6] F. Radt (ed.), "Elsevier's Encyclopaedia of Organic Chemistry", volume 14, Supplement VI, steroids, part 4, pp. 2991 s — 3672 s — 2672 s acids ; sulfur and metal derivatives ; Bi-steroids (1962).

[7] F. Radt (Edited with the assistance of A. Georg and Dora Stern) "Elsevier's Encyclopaedia of Organic Chemistry", volume 14, Supplement VII, steroids, part 5, pp. 3673 a — 4376 a (1965).

[8] F. Radt (Edited with the assistance of Dora Stern, "Elsevier's Encyclopaedia of Organic Chemistry", volume 14, Supplement VIII, steroids, part 6, pp 4377 s — 5177 s (1969).

NOTE POUR LES AUTEURS

La *Revue Roumaine de Chimie* publie des articles en anglais, français, russe, allemand ou espagnol. Les auteurs sont priés d'envoyer des articles, notes, communications et comptes rendus inédits.

Les manuscrits seront dactylographiés à deux intervalles. Les tableaux seront dactylographiés sur feuilles séparées, de même que la légende des figures. Les diagrammes seront tracés à l'encre de Chine sur papier calque. Les tableaux et les figures seront numérotés par des chiffres arabes, en nombre strictement nécessaire. Prière de ne pas inscrire les mêmes données dans les tableaux et les figures. Les formules chimiques seront incluses dans le texte; en outre, elles seront transcrites sur des feuilles séparées. Les auteurs sont priés d'indiquer les caractères italiques (en soulignant les lettres au crayon), ainsi que tout autre caractère spécial. L'ordre des références bibliographiques sera celui de leur mention dans le texte; le nom de l'auteur sera précédé de l'initiale du prénom; les publications périodiques seront présentées suivant les prescriptions internationales. Les références seront ajoutées à la fin de l'article; elles paraîtront comme des notes, au bas de la page. Le texte sera précédé d'un résumé comprenant 15 lignes au maximum.

L'entière responsabilité du contenu des articles appartient aux auteurs. On publie des articles dus aux collaborateurs roumains ou étrangers. Les auteurs recevront 50 tirés à part.

PRINTED IN ROMANIA

TRAVAUX PARUS AUX ÉDITIONS DE L'ACADÉMIE DE LA RÉPUBLIQUE SOCIALISTE DE ROUMANIE

I. ZUGRĂVESCU et L. STOICESCU-CRIVETZ, **Polimeri heterociclici** (Polymères hétérocycliques), 1971, 190 p., 9,50 lei.

CORNEL BODEA et collab., **Tratat de biochimie vegetală**, partea I, **Fitochimie** (Traité de biochimie végétale, Ire partie, Phytochimie), Ier vol., 1964, 747 p. + 4 annexes + 2 pl., 41 lei ; IIe vol., 1965, 1262 p., 1 pl., 56 lei, IIIe vol., 1967, 773 p., 35 lei.

V. GHEŢIE et V. MICUŞAN, **Analiza imunochimică. Teorie şi practică** (Analyse immunochimique. Théorie et pratique), 1966, 369 p., 28 lei.

SILVIA IONESCU, **Reacţii chimice induse de radiaţiile ionizante** (Réactions chimiques produites par les radiations ionisantes), 1963, 271 p., 15 lei.

MARIETA NICOLAE, **Fizico-chimia proceselor fotografice** (Physico-chimie des processus photographiques), 1964, 426 p. + 4 pl., 35 lei.

R. PORTOCALĂ et L. POPA, **Acizii ribonucleici celulari şi virali** (Les acides ribonucléiques cellulaires et viraux), 1966, 375 p., 8 pl., 26 lei.

D. PURDELA et R. VÎLCEANU, **Chimia compuşilor organici ai fosforului şi ai acizilor lui** (La chimie des composés organiques du phosphore et de ses acides), 1965, 540 p., 37 lei.

CRISTOFOR SIMIONESCU, MARGARETA GRIGORAŞ et AGATA CERNĂTESCU-ASANDEI, **Chimia lemnului din R.P.R.** (La chimie du bois en Roumanie), 1964, 239 p. + 3 pl., 27 lei.

CRISTOFOR SIMIONESCU et CLEOPATRA VASILIU-OPREA, **Mecanochimia compuşilor macromoleculari** (La mécanochimie des composés macromoléculaires), 1967, 344 p., 23,50 lei.

I. MAXIM, **Materiale nucleare** (Matériaux nucléaires), 1969, 444 p., 30 lei.

1972 JUL 29

I.P.I. e. 1150

43 426

Lei 25.—

F 1103

04

REVUE ROUMAINE DE CHIMIE

TOME 17
Nº 5
Mai 1972

RRCHAX, 17, *5*, 771–944 (1972)

ÉDITIONS DE L'ACADÉMIE DE LA RÉPUBLIQUE SOCIALISTE DE ROUMANIE

Rev. Roumaine Chim. 17, *5*, 771–944 (1972).

COMITÉ DE RÉDACTION

Rédacteur en chef:

I. G. MURGULESCU, membre de l'Académie de la République Socialiste de Roumanie

Rédacteurs en chef adjoints:

A. T. BALABAN et V. EM. SAHINI, membres correspondants de l'Académie de la République Socialiste de Roumanie

Collège de rédaction:

C. DRĂGULESCU, RALUCA RIPAN, CR. SIMIONESCU, membres de l'Académie de la République Socialiste de Roumanie; EM. BRATU, ECATERINA CIORĂNESCU-NENITZESCU, P. SPACU, membres correspondants de l'Académie de la République Socialiste de Roumanie; MARGARETA AVRAM, D. I. MARCHIDAN, G. NIAC et D. SĂNDULESCU

La *Revue Roumaine de Chimie* paraît 12 fois par an. Toute commande de l'étranger (fascicules ou abonnements) sera **adressée à Întreprinderea Rompresfilatelia** Boîte postale 2001, **telex** 011631, **Bucarest, Roumanie**

Les manuscrits, les livres et les revues proposés en échange, ainsi que toute correspondance seront envoyés à la rédaction:

REVUE ROUMAINE DE CHIMIE

23, str. Dumbrava Roşie, Bucarest, 9, Roumanie

ÉDITIONS DE L'ACADÉMIE DE LA RÉPUBLIQUE SOCIALISTE DE ROUMANIE
3 bis, str. Gutenberg, Bucarest, Roumanie

ORSZÁGOS MŰSZAKI KÖNYVTÁR ÉS DOKUMENTÁCIÓS KÖZPONT

REVUE ROUMAINE DE CHIMIE

Tome 17, N° 5 Mai 1972

Page

P. G. PERKINS, The electronic structure of some molecules and ions containing carbon, silicon, oxygen and sulphur. I 773–780

Ю. А. КРУГЛЯК, Г. ХИБАУМ и Н. Е. РАДОМЫСЕЛЬСКАЯ, Электронная структура основного состояния бензильного радикала в равновесной конфигурации 781–799

K. MATIAŠOVSKÝ, MARTA PAUČÍROVÁ and M. MALINOVSKÝ, Contribution to the study of the structure and the thermodynamic properties of molten compounds of the type M_3AlF_6. I. Structure . . . . 801–808 R

MARTA PAUČÍROVÁ, M. MALINOVSKÝ and K. MATIAŠOVSKÝ, Contribution to the study of the structure and the thermodynamic properties of molten compounds of the type M_3AlF_6. II. Thermodynamic properties 809–817

К. ГРЙОТХЕЙМ, К. МАТИАШОВСКИ и П. ФЕЛЛНЕР, Получение сплавов кремния посредством электролиза криолито-кремнеземного расплава 819–829

LETIȚIA TOPOR and J. WYPARTOWICZ, Vapor pressures of molten cadmium bromide and cadmium iodide 831–834

C. N. CAȘCAVAL et I. A. SCHNEIDER, Étude par chromatographie pyrolytique de quelques polymères vinyliques . . . . 835–840 R

V. P. KUDESIA, Kinetics and mechanism of bromination of crotonic acid by aqueous bromine . . . . 841–846 R

CONST. GH. MACAROVICI et GH. MORAR, L'obtention de combinaisons complexes mixtes des Ti(IV) et Bi(III) avec les acides oxalique et tartrique pour leur conversion aux oxydes mixtes correspondants 847–853

AGNETA BÂTCĂ-CERBU, Study on the behaviour of the NaA type zeolite in the presence of nitrates of some bivalent cations dissolved in molten sodium nitrate 855–861

C. I. LEPĂDATU, An MO approach to the stabilization problem of the coördination clusters 863–864

A. T. BALABAN, Chemical graphs. XIV. Valence isomers of [12] annulene . . 865–881

A. T. BALABAN, Chemical graphs. XV. Degenerate Cope rearrangements of valence isomers of annulenes 883–896

FL. CUIBAN, Reductive cyclization of α- and β-(*o*-nitrophenyl)-substituted amides 897–903

S. H. DOSS, The proton magnetic resonance spectra of sultams 905–914

Rev. Roumaine Chim. **17**, *5*, 771–944 (1972) București

R

I. FLOREA, Spektrophotometrische Dosierung des Benzidins mit Natriumhypochlorit und mit Unterchloriger Säure 915–923

V. ARMEANU, STELA OANCEA, STANA RUSENESCU and L. M. BĂLOIU, Determination of the partition constant of compounds used in spectrophotometric analysis 925–930

VIORICA PELLONI-TAMAŞ, NORA RĂDULESCU and ROCSANDRA SIMIONOVICI, The solvent effect on UV spectra of some aminopyridine derivatives 931–936

LUCREŢIA I. POPA et IOANA ARSENIE, Recherches sur l'obtention du hafnium de pureté nucléaire. I 937–944

Revue Roumaine de Chimie, 17, 5, 773–780 (1972)

THE ELECTRONIC STRUCTURE OF SOME MOLECULES AND IONS CONTAINING CARBON, SILICON, OXYGEN AND SULPHUR. I

PETER G. PERKINS

Department of Pure and Applied Chemistry, University of Strathclyde
Glasgow, C. 1, Scotland

Received December 30, 1971

The electronic structures of molecular CO_2 and SiO_2 and the ions CO_3^{2-}, SiO_3^{2-}, CO_4^{4-}, and SiO_4^{4-} have been studied by a self-consistent molecular orbital method including all valence electrons. It is shown that a crystal field effect occurs in the anions. This is due to the "extra" electrons possessed by the moiety and has the effect of linearly shifting the energy levels upwards. The 3*d* orbitals of silicon participate in the bonding and lower the total molecular energies by 0.5–1.0%, the greatest effect being manifest in the SiO_4^{4-} ion. The *d* orbitals also have the effect of evening out the charge separation between the silicon and the oxygen atoms. The relative stabilities of corresponding pairs of anions can be explained by a reverse crystal field effect from the associated cations : thus, CO_4^{4-} is shown to possess a number of weakly bonded electrons, where as the orbital levels in the analogous SiO_4^{4-} ion are strongly bonding.

INTRODUCTION

As is well known, the chemical behaviour of silicon and its compounds is frequently markedly different from that of the corresponding carbon systems. This statement is also true for the pair of elements, oxygen and sulphur, and the differences are often attributed to the participation of 3*d* orbitals. In this and forthcoming papers, we will investigate the point and will attempt to rationalise some of the observed chemical differences between silicon and carbon, firstly when in combination with oxygen and secondly, when sulphur is substituted for oxygen. Furthermore, we shall study the series of links which silicon forms with halogens and with nitrogen in order to try and discover what rôle the 3*d* orbitals play in the bonding in these compounds.

The present paper is concerned with problems appertaining to the C–O and Si–O bonds and, in this context, a number of interesting points arise ; (1) for carbon the most stable oxide at ordinary temperatures is the simple, linear, gaseous dioxide, CO_2, whereas for silicon, the most stable form of the dioxide, SiO_2, is a solid composed of linked SiO_4 tetrahedra. This does not mean that the linear, gaseous molecule, SiO_2, cannot exist but that the three-dimensional solid is thermodynamically the more stable. The *fundamental* reason for the difference between the two is not, however, revealed by such thermodynamic arguments; (2) in the anion series the carbonate ion is stable in association with a variety of cations but the simple, trigonal $SiO_3^=$ ion does not appear to exist; metasilicate ions are always built from linked SiO_4 units with the appropriate charges on the whole moiety; (3) when we pass to the XO_4^{4-} series the pattern is reversed: here the discrete tetrahedral SiO_4^{4-} ion is well known (and linked forms are ubiquitous in silicate minerals) but the simple CO_4^{4-} is not and ions of this stoichiometry are thought to correspond to peroxy salts.

In order, therefore, to throw light on these problems, we have calculated the electronic structures of a representative series of systems by an all-valence electron self-consistent field method[1,2] and we here examine the results of this treatment.

CALCULATIONAL METHODS

The calculational method was essentially an adaptation of the Pople-Segal-Santry technique[1]; this has been modified by us for explicit inclusion of orbital rather than atomic parameters.[2] Thus, in constructing the elements of the Fock matrix to be diagonalised, we explicitly used the Hamiltonian matrix elements ($H_{\mu\mu}$) and one-centre electron repulsion integrals ($\gamma_{\mu\mu}$) for the orbitals themselves. This also leads to a scaling of the orbital off-diagonal elements of the Hamiltonian matrix by the Mulliken-Wolfsberg-Helmholtz principle rather than by the assumption of standard atomic parameters for this purpose.[1] It is also convenient to evaluate the two-centre repulsion integrals by an adaptation of the Mataga method.[3]

In general, calculations of the CNDO type have been shown to be reliable for compounds composed of first-row atoms [4] and the work which has been carried out to date on those in which second-row atoms figure, although necessarily more tentative, promises equally well.

The present work studied the effects of including the 3*d* orbitals on silicon in a systematic way and three series of calculations, *a*, *b* , and *c*, were carried through. In *a* the 3*d* orbitals were neglected, whilst in *b* and *c* they were included in "diffuse" or "contracted" form ("diffuse" and "contracted" 3*d* orbitals have different radial exponents[2] and this point has been discussed fully previously). Insufficient evidence (in the form of *ab initio* calculations) exists for silicon compounds which might indicate, with some degree of finality, which orbital exponent is generally the more appropriate for silicon in its compounds, although the parameter will almost certainly vary to some extent, depending on the groups attached to silicon. However, it is worthy of note that, in similar calculations on phosphorus-oxygen compounds,[5,6] the *contracted* form of radial function seems to yield a superior description of the electronic structure of the systems. Hence, until and unless further evidence comes to light, we regard the series of calculations *c* as the most realistic in each group.

---

[1] J. A. Pople, D. P. Santry and G. A. Segal, *J. Chem. Phys.*, **43**, S 129 (1965).

[2] K. A. Levison and P. G. Perkins, *Theor. Chim. Acta*, **17**, 1 (1970).

[3] K. A. Levison and P. G. Perkins, *Theor. Chim. Acta*, **14**, 206 (1969).

[4] D. R. Armstrong, B. J. Duke and P. G. Perkins, *J. Chem. Soc.* (*A*) **1969**, 2566.

The input data for the present work are shown in Table 1. Bond lengths and bond angles were abstracted from standard compilations [7] and they are listed in Table 2. No bond lengths are known for gaseous SiO_2 and here a scaling procedure was employed. The bond length assumed for Si—O in $SiO_3^=$ is somewhat arbitrary but the value scaled from the known data for $CO_3^=$, CO and SiO turned out to exceed that in α-quartz. We do not expect any significant error to result from the assumption of 1.57 Å for this bond length, since geometrical data affect *total* molecular energies rather more severely than eigenvalues or electronic charge distribution. The latter results are of most importance in this paper.

Table 1

Input parameters for core Hamiltonian matrix ($\mathbf{H}_{\mu\mu}$) and electron repulsion matrix ($\gamma_{\mu\mu}$)

Atom	Orbital Exponent			$H_{\mu\mu}$ (eV)			$\gamma_{\mu\mu}$ (eV)		
	s	*p*	*d*	*s*	*p*	*d*	*s*	*p*	*d*
C	1.550	1.325	—	−19.44	−10.67	—	15.60	14.37	—
O	2.200	1.975	—	−32.38	−15.85	—	22.14	21.42	—
Si*	1.533	1.083	0.500	−15.15	− 7.62	−1.10	10.77	8.25	3.76
Si+	1.533	1.083	0.667	−15.15	− 7.62	−2.05	10.77	8.25	5.64

* parameters appropriate to "diffuse" 3*d* orbitals.
+ parameters appropriate to "contracted" 3*d* orbitals.

Table 2

Geometric parameters

Species	Data
CO_2	linear, C—O, 1.16 Å, Ref. 7
SiO_2	linear, Si—O, 1.55 Å, scaling from CO, SiO, and CO_2. Ref. 7
$CO_3^=$	trigonal, C—O, 1.31 Å, Ref. 7
$SiO_3^=$	trigonal, Si—O, 1.57 Å, (scaling from $CO_3^=$ and CO gives a value > Si—O in $SiO_4^{==}$)
$CO_4^{==}$	tetrahedral, C—O, 1.46 Å [incremented by 0.15 Å, Δ ($CO_3^=$ − CO_2)]
$SiO_4^{==}$	tetrahedral, Si—O, 1.61 Å as in α-quartz, Ref. 7

---

[5] R. M. ARCHIBALD and P. G. PERKINS, *Rev. Roumaine Chim.*, **16**, 1137 (1971).

[6] B. J. McALOON and P. G. PERKINS, *Theor. Chim. Acta*, **22**, 304 (1971).

[7] "Interatomic Distances in Molecules and Ions", Chem. Soc. Special Publ. No. 11, London, 1958.

RESULTS AND DISCUSSION

The principal results obtained from the calculations are presented in Tables 3, 4, 5 and 6. It is convenient to mention one or two points first and then to discuss the systems comparatively in pairs.

Table 3

Eigenvalues for CO_2, CO_3^{2-} and $CO_4{}^{4-}$ (eV)

$1\Sigma_g^+$	−42.40	$1a_1'$	−23.88	$1a$	−6.23
$1\Sigma_u^+$	−40.50	$1e'$	−15.92	$1t$	1.82
$2\Sigma_g^+$	−19.16	$2a_1'$	1.59	$2a$	17.32
$1\Pi_u$	−17.41	$1a_2''$	2.64	$2t$	20.48
$2\Sigma_u^+$	−12.73	$2e'$	4.81	$1e$	22.89
$1\Pi_g$	−11.11	$1a_2'$	8.43	$3t$	24.04
		$1e''$	9.34	$4t$	26.87
$2\Pi_u$	5.39	$3e'$	10.74	$3a$	43.19
$3\Sigma_g^+$	10.05	$2a_2''$	24.50	$5t$	44.67
$3\Sigma_u^+$	11.66	$3a_1'$	28.29		
		$4e'$	30.57		

It is seen first of all (Tables 3 and 4) that, in all cases, the ground-state electronic structure is that of a closed shell : hence, in each case, the determinantal wave-function belongs to $^1\Gamma_1$, the totally symmetric irreducible representation of the group. This is a result which could not have been anticipated and, indeed, it might have been that the species at present unknown were radicals, since in all cases there is inherent orbital degeneracy conferred by the symmetry of the systems.

A second, most striking, feature of the results for the anions is that, in all cases, a number of the occupied energy levels have *positive* energies. This is a feature of calculations on anions in general when electron repulsion is included (it does not appear in extended Hückel calculation) and stems from the fact that the "extra" electrons associated with an anion exert a repulsive potential on the neutral species which is totally symmetric. This acts as a crystal field of the same symmetry as the neutral species and so displaces the eigenvalues linearly upwards in the energy scale. A readjustment of the situation can readily be brought about by attaching cations to the anionic species. If the anionic charge is thus neutralised by a series of positive charges arranged around the ion in a totally symmetric manner, then the eigenvalues are shifted linearly to lower energies. The magnitude of the shift can be calculated easily using an ionic model, since two charges of opposite sign situated apart at a distance of 1 Å exert a force of attraction of 14.4 eV. In the real physical situation, *e.g.*, in a crystal, the cations will not usually occupy positions with respect to the anion which conform to a totally symmetric array. Hence, in the series expansion of the potential, terms higher than the constant first one will contribute and splitting of the degeneracy of the energy levels of the anion, if present, may occur. This "*reverse crystal field effect*" of the cations is of considerable significance with respect to cation effects in salts.

Table 4

Eigenvalues for SiO_2 and SiO_4^{4-} (eV)

	SiO_2				SiO_3^{2-}				SiO_4^{4-}		
	a	*b*	*c*		*a*	*b*	*c*		*a*	*b*	*c*
$1\Sigma_g^+$	−35.60	−36.33	−37.49	$1a_1'$	−20.60	−20.52	−22.06	$1a$	− 6.76	− 7.28	− 7.57
$1\Sigma_u^+$	−35.51	−35.74	−36.11	$1e'$	−16.19	−17.17	−18.23	$1t$	− 0.21	− 0.83	− 1.83
$2\Sigma_g^+$	−16.05	−16.70	−17.50	$2a_1'$	1.54	0.86	− 0.04	$2a$	17.27	16.83	16.33
$1\Pi_u$	−12.62	−12.92	−13.26	$1a_2''$	3.50	3.31	2.68	$2t$	20.22	19.20	18.22
$1\Pi_g$	− 9.70	−10.32	−11.40	$2e'$	5.23	4.97	2.98	$1e$	22.12	21.20	19.70
$2\Sigma_u^+$	− 6.21	− 6.61	− 7.24	$1a_2'$	6.88	6.22	6.07	$3t$	22.83	22.36	22.19
				$1e''$	8.31	7.63	6.52	$4t$	26.05	25.33	24.22
$2\Pi_u$	3.79	3.52	3.30	$3e'$	10.45	8.70	8.57				
$3\Sigma_g^+$	5.14	4.63	3.68					$3a$	38.74	38.01	37.03
$3\Sigma_u^+$	10.04	9.70	9.28	$2a_2''$	20.59	20.28	19.72	$5t$	39.74	38.62	37.36
$1\Delta_g$	—	13.66	10.08	$3a_1'$	22.87	23.25	20.59	$2e$	—	40.75	39.00
$2\Pi_g$	—	13.97	10.98	$4e'$	25.11	24.07	22.93	$6t$		41.54	40.86
$4\Sigma_g^+$	—	14.67	12.59	$2e''$	—	27.17	24.61				
				$4a_1'$	—	27.37	25.03				
				$5e'$	—	27.91	26.53				

It is intrinsically obvious that the energy levels of *isolated* anions in the gas-phase would be positive since, if they were not, then it would mean that a neutral species like CO_3 or SiO_4 would have a strong affinity for two and four electrons, respectively and, if these were expected to be bound and to correspond to high negative eigenvalues, then the electronegativity of these neutral groups would exceed by far that of fluorine or chlorine.

Table 5

Charge distribution in CO_2, CO_3^{2-} and CO_4^{4-}

	CO_2	CO_3^{2-}	CO_4^{4-}
C 2*s*	1.29	1.20	1.23
2*p*	2.25	2.64	2.81
Nett charge on C	+ 0.46	+0.16	−0.04
O 2*s*	1.65	1.72	1.80
2*p*	4.58	5.00	5.19
Nett charge on O	−0.23	−0.72	−0.99

Table 6

Charge distribution in SiO_2, SiO_3^{2-} and SiO_4^{4-}

	SiO_2			SiO_3^{2-}			SiO_4^{4-}		
	a	*b*	*c*	*a*	*b*	*c*	*a*	*b*	*c*
Si 3*s*	1.56	1.54	1.52	1.39	1.42	1.29	1.30	1.27	1.19
3*p*	1.69	1.66	1.57	2.36	2.21	2.17	2.47	2.44	2.22
3*d*	—	0.13	0.36	—	0.28	0.81	—	0.41	1.05
Nett charge on Si	+0.75	+0.67	+0.55	+0.25	+0.09	−0.27	+0.23	−0.12	−0.46
O 2*s*	1.75	1.73	1.70	1.71	1.69	1.66	1.71	1.69	1.65
2*p*	4.62	4.61	4.58	5.04	5.01	4.92	5.35	5.28	5.24
Nett charge on O	−0.37	−0.34	−0.28	−0.75	−0.70	−0.58	−1.06	−0.97	−0.89

If the geometry of the appropriate salt is known and orbital overlap between anion and cation ignored, then it is a simple matter to correct for the reverse crystal field. A later paper will consider the whole problem and its chemical implications in detail : for the present purpose, all that is needed is the sequence of eigenvalues for the species. These can be corrected approximately where necessary.

The effect of including 3*d* orbitals on the total molecular energies of all the silicon species is to stabilise them with respect to the situation where the *d* orbitals are neglected. In this context the "contracted" *d* orbital (calculations *c*) produces a more marked energy lowering. This stabilisation increases slowly over the series SiO_2, SiO_3^{2-}, SiO_4^{4-} and amounts to 1.0% for the contracted and $\frac{1}{2}$% for the diffuse *d* orbital when expressed as a proportion of the total energy. With one or two minor exceptions, the eigenvalues for the systems are stabilised by *d* orbital addition and the five new eigenvalues in which the $3d$ functions are mainly weighted appear as the highest antibonding group.

With regard to the charge distributions, it is noteworthy that, for both the carbon and silicon anions, the bulk of the "extra" electronic charge is located on the oxygen atoms. In Si compounds the d orbitals exert an important effect on charge distribution in that, by becoming occupied, they tend to level out the polarity across the Si–O bonds. This effect is clearly shown in the present results and it has also been noted in an analogous series of phosphate ions.[6] The d orbitals of silicon become occupied at the expense of all other orbitals in the system : this contrasts with the situation in some phosphorus and aluminium compounds[2,5,6] where the orbitals remove electrons preferentially from the $3p$ levels.

It is striking that the d orbital occupation of silicon rises almost linearly as the number of attached O atoms is increased. This observation is consistent with early suggestions of the role of d orbitals in sulphur and phosphorus bonding.[8]

CO_4^{4-} *and* SiO_4^{4-}

We can estimate the approximate linear shift in energy levels based on a sodium salt, using the following geometry : we take the four Na^+ ions to form a second superimposed tetrahedron which utilises the vacant sites of the XO_4^{4-} unit and we set the Na–O distance at 2.44 Å for both anions. The calculated charge distributions can then be used to compute the reverse crystal field effect. If we take four Na–O and four Na–X interactions which just neutralise the crystal field effect of the four electrons, then we find that the highest bonding level for CO_4^{4-} lies at +2.6 eV. (The assumption of purely coulombic interactions between sodium and the anion is, of course, an approximation, since it neglects a minor degree of covalency.)[9] It is now clear why this ion should be unstable in solution and why it should so easily lose electrons. Moreover, there are six electrons lying at this level in the $4t$ orbitals which are localised between the oxygens and the central carbon, and hence oxygen is readily lost, reverting to the stable CO_3^{2-} anion. The ion SiO_4^{4-} presents a far more stable situation : here the reverse crystal field effect lowers the eigenvalues to a much greater extent (all become strongly bonding) and the d orbitals, being strongly filled, add to the crucial stability of the $4t$ orbitals yet more. Indeed, these molecular orbitals exhibit one of the largest decreases in energy brought about by the d bases. It would hence seem that the SiO_4^{4-} system owes a significant measure of its stability to the participation of d orbitals.

CO_3^{2-} *and* SiO_3^{2-}

Using a simple D_{3h} model with Na^+ ions lying axial to the $XO_3^=$ plane with Na–O distances equal to 2.44 Å, a similar correction of the eigenvalues for the presence of cations can be made. This leads to values of -1 eV and -3.2 eV for the highest bonding orbitals of CO_3^{2-} and SiO_3^{2-} respectively. We now see why the CO_3^{2-} is known, because its oxidation product, CO_4^{4-} is labile whilst the CO_3^{2-} ion itself is intrinsically too stable for it to tend to lose oxygen and form CO_2. It seems that the simple planar ion, SiO_3^{2-}, should also be intrinsically stable, as the eigenvalue pattern is rather similar to that for CO_3^{2-}. Here, again, the $3d$ orbitals produce a marked lowering of the highest bonding e' type orbital (by ~ 2 eV). The reason for its non-existence is probably the high stability of the SiO_4 unit. A linking of two SiO_3^{2-} units to give $Si_2O_6^{4-}$ entities in which the Si atom is tetrahedrally surrounded by oxygens will displace the energy levels favourably. On the other hand, the instability of CO_4 units makes the dimerisation path $2CO_3^{2-} \rightarrow C_2O_6^{4-}$ less attractive. Calculations on the dimer systems would be revealing.

---

[8] D. P. Craig and C. Zauli, *J. Chem. Phys.*, **37**, 601 (1962)

[9] R. Fortune and P. G. Perkins, unpublished work.

CARBON DIOXIDE AND SILICON DIOXIDE

We now seek reasons for the known chemical differences between these oxides; CO_2 is a stable gas with a linear structure, whilst SiO_2 is usually encountered as a very stable solid in which (e.g., in crystalline α quartz) each silicon atom occupies a tetrahedral site and is linked by bridging oxygens to other similar units. *Gaseous*, molecular SiO_2 should also be linear but there still remains the problem of why CO_2 does not give rise to a solid form similar to SiO_2. Any rationalisation of these differences should really take account both of the electronic structures of molecular SiO_2 and of CO_2 and of solid-state structures in which both are tetrahedrally coordinated. Unfortunately, the latter treatments are not yet available and recourse must be made to comparison of the molecular electronic structures with those of the SiO_4^{4-} and COO_4^{4-} anions.

A particularly interesting feature of the SiO_2 structure which emerges is that the highest bonding orbital is of σ type (Σ_u^+) and is built from the set of three collinear p functions. A set of π orbitals also appears, as in CO_2. Hence, whereas the latter molecule has effectively no electron donor properties, it may be that linear SiO_2 could act as an electron donor

The fact that, *a* the orbital energies for SiO_2 are greater than those. of CO_2 and *b* there is a stable SiO_4 tetrahedral unit helps to explain why the favoured form in the solid state is that of an infinite net of linked tetrahedra. Of course, the SiO_4^{4-} anion is not strictly analogous to solid SiO_2 and, as stated above, band-structure calculations on the XO_2 tetrahedral solids need to be carried through. Undoubtedly, however, the linear $\rightarrow$ angular reorganisation energy must play a cogent part and the energy level picture presented suggests that this quantity will be greatest for CO_2.

Revue Roumaine de Chimie, **17**, *5*, 781 – 799 (1972)

ЭЛЕКТРОННАЯ СТРУКТУРА ОСНОВНОГО СОСТОЯНИЯ БЕНЗИЛЬНОГО РАДИКАЛА В РАВНОВЕСНОЙ КОНФИГУРАЦИИ

Ю. А. КРУГЛЯК, Г. ХИБАУМ и Н. Е. РАДОМЫСЕЛЬСКАЯ

Институт физической химии им. Л. В. Писаржевского АН УССР, Киев
Институт органической химии Болгарской Академии наук, София

Получена 20 октября 1971 г.

На примере бензильного радикала предложен способ оценки равновесной конфигурации сопряженных углеводородов. Как и следовало ожидать, экзоциклическая связь в бензильном радикале получилась наиболее длинной. Вычислена волновая функция основного состояния бензильного радикала с учетом широких наборов конфигураций, включая их полный набор в π-электронном приближении, который соответствует точному решению модельного гамильтониана Паризера-Парра. Приведены результаты расчета энергии корреляции, проекции приближенной функции на точную, электронной и спиновой заселенности связей и атомов бензильного радикала, естественных спин-орбиталей и их чисел заполнения, а также дана оценка погрешности вычисления длин связей С—С и констант сверхтонкого расщепления на протонах за счет приближенного вычисления волновой функции. Показано, что как бы точно ни была вычислена волновая функция в π-электронном приближении для равновесной конфигурации бензильного радикала, как и для его равносвязной конфигурации, невозможно получить даже правильный знак разности спиновой заселенности *пара*- и *орто*-атомов углерода.

1. ВВЕДЕНИЕ

Главная причина всестороннего теоретического исследования свойств бензильного радикала в основном состоянии связана с давно известным расхождением между экспериментальными значениями сверхтонких расщеплений на *орто*- и *пара*-протонах бензильного радикала и их теоретическими значениями, вычисленными посредством простого уравнения Мак-Коннела[1] из π-спиновых заселенностей соответствующих атомов углерода. Согласно экспериментальному спектру ЭПР,[2] расщепления на указанных выше протонах равны соответственно 5,14 и 6,14 э, тогда как известные полуэмпирические π-электронные схемы расчета приводят к меньшему значению расщепления на *пара*-протоне. Не спасает положения полуэмпирический учет всех валентных электронов в схеме метода INDO. [3] Авторы работы [3] обращают внимание на то, что причина этого расхождения до сих пор не найдена.

---

[1] H. M. McConnell, *J. Chem. Phys.*, **24**, 632, 764 (1956).

Может быть несколько причин, потенциально способных объяснить сформулированное выше противоречие, которое носит качественный характер. Одна из них могла быть связана с вычислением π-спиновой заселенности атомов углерода на недостаточно точной собственной функции π-электронного модельного гамильтониана для бензильного радикала. Это предположение себя не оправдало, что стало ясно после детального исследования свойств основного состояния бензильного радикала [4-7] с использованием при построении пробной волновой функции большого числа возбужденных конфигураций вплоть до учета их полного набора, который соответствует точной собственной функции использованного в работе [4-7] модельного гамильтониана Паризера-Парра. Кроме того, в [8-9] показано, что желаемое отношение π-спиновой заселенности *орто*- и *пара*-атомов углерода получается в одноконфигурационном приближении, а также в многоконфигурационном приближении с учетом только тех пяти однократно возбужденных конфигураций, которые согласно теореме, доказанной в [10,11], смешиваются с основной конфигурацией, если в обоих случаях базисные орбитали удовлетворяют вариационному принципу только для замкнутых оболочек радикала. Однако дальнейшее, даже незначительное увеличение числа конфигураций при построении пробной волновой функции снова приводит к неправильному отношению указанных заселенностей.

Известны результаты неэмпирического расчета бензильного радикала неограниченным методом самосогласованного поля (ССП) на гауссовом базисе с учетом всех электронов.[12-14] Вычисление спиновой заселенности непосредственно на протонах привело к удовлетворительному не только качественному, но и количественному согласию с экспериментальными значениями расщеплений. Неясным остается влияние проектирования неограниченной по спину волновой функции на отношение спиновой заселенности на *орто-* и *пара*-протонах бензильного радикала. Также открытым остается вопрос об отказе от использования простого уравнения Мак-Коннела [1] и переходе к его обобщенному варианту.[15]

---

[2] A. Carrington и I. C. P. Smith, *Molec. Phys.*, **9**, 137 (1965).

[3] J. A. Pople, D. L. Beveridge и P. A. Dobosh, *J. Amer. Chem. Soc.*, **90**, 4201 (1968).

[4] Ю. А. Кругляк, Е. В. Моздор и В. А. Куприевич, *Укр. физ. журнал*, **15**, 48 (1970).

[5] V. A. Kuprievich, Yu. A. Kruglyak и E. V. Mozdor, *Intern. J. Quantum Chem.*, **4**, 73 (1970).

[6] Ю. А. Кругляк, Е. В. Моздор и В. А. Куприевич, *Доклады Болгарской АН*, **23**, 89 (1970).

[7] Е. В. Моздор, В. А. Куприевич и Ю. А. Кругляк, *Литовский физический сборник*, **10**, 219 (1970).

[8] Yu. A. Kruglyak и E. V. Mozdor, *Theor. Chim. Acta*, **15**, 365 (1969).

[9] Е. В. Моздор и Ю. А. Кругляк, *Теор. и экспер. хим.*, **5**, 731 (1969).

[10] Yu. A. Kruglyak, E. V. Mozdor и V. A. Kuprievich, *Croat. Chem. Acta*, **42**. *4* (1970).

[11] Е. В. Моздор, Ю. А. Кругляк и В. А. Куприевич, *Теор. эксперим. хим.*, **5**, 723 (1969).

[12] Ю. А. Кругляк, Х. Прейсс и Р. Яношек, *Укр. физ. журнал*. **15**, 980, 1578 (1970).

[13] Ю. А. Кругляк, Х. Прейсс и Р. Яношек, *Ж. структур. хим.*, **12** (1971).

[14] Ю. А. Кругляк, И. И. Украинский, Х. Прейсс и Р. Яношек, *Теор. эксперим. хим.*, **7** (1971).

До сих пор речь шла о расчетах бензильного радикала с одинаковыми длинами связей С—С (равносвязная модель). Счастнев и Жидомиров [16] и вслед за ними Новаковский [17] выполнили согласование резонансных интегралов $\beta_{\mu\nu}$ и порядков связей $P_{\mu\nu}$ бензильного радикала в рамках обычного метода Хюккеля, оценили « равновесные » значения длин связей $R_{\mu\nu}$, пользуясь функциональной зависимостью $R_{\mu\nu}$ от $P_{\mu\nu}$ Коулсона-Голебиевского, [18] и рассчитали распределение π-спиновой заселенности обычным [19] и модифицированными [17] методами Мак-Лаклана. Оказалось, что расщепления, вычисленные затем по простой формуле Мак-Коннела,[1] хорошо согласуются с их экспериментальными значениями, тогда как этот же метод [19] в применении к равносвязной модели бензильного радикала приводит к неправильному отношению расщеплений на *орто-* и *пара*-протонах.[17,19]

Таким образом, создалось впечатление, что причина обсуждаемого расхождения между экспериментальными и теоретическими значениями расщеплений на *орто-* и *пара*-протонах бензильного радикала кроется в пренебрежении реальной геометрической конфигурацией этого радикала.

Настоящее сообщение посвящено расчету спиновой заселенности и других характеристик электронного строения основного состояния бензильного радикала в его равновесной геометрической конфигурации, оцененной путем одновременного согласования $P_{\mu\nu}$, $R_{\mu\nu}$, $\beta_{\mu\nu}$ и кулоновских интегралов $\gamma_{\mu\nu}$ в рамках одноконфигурационного приближения теории ССП для состояний с открытой оболочкой. При вычислении свойств бензильного радикала волновая функция его основного состояния строилась в многоконфигурационном приближении с учетом большого числа конфигураций вплоть до их полного набора для модельного гамильтониана Паризера-Парра.

2. ОЦЕНКА РАВНОВЕСНОЙ ГЕОМЕТРИЧЕСКОЙ КОНФИГУРАЦИИ БЕНЗИЛЬНОГО РАДИКАЛА

Для π-электронной оболочки бензильного радикала использовалась традиционная модель Паризера-Парра.[20] Соответствующий гамильтониан имеет вид

---

[15] H. M. McConnell, *J. Chem. Phys.*, **28**, 1188 ; **29**, 244 (1958).

[16] П. В. Счастнев и Г. М. Жидомиров, *Теор. и эксперим. хим.*, **3**, 541 (1967).

[17] J. Nowakowski, *Theor. Chim. Acta*, **18**, 133 (1970).

[18] C. A. Coulson и A. Golebiewski, *Proc. Phys. Soc.*, **78**, 1310 (1961).

[19] A. D. McLachlan, *Molec. Phys.*, **3**, 233 (1960).

[20] R. Pariser и R. G. Parr, *J. Chem. Phys.*, **21**, 466, 767 (1953).

$$\boldsymbol{H} = \sum_{\mu\nu\sigma} H^{\text{ост}}_{\mu\nu}\, \boldsymbol{a}^{+}_{\mu\sigma}\, \boldsymbol{a}_{\nu\sigma} + \frac{1}{2} \sum_{\mu\nu\sigma\sigma'} \gamma_{\mu\nu}\, \boldsymbol{a}^{+}_{\mu\sigma}\, \boldsymbol{a}^{+}_{\nu\sigma'}\, \boldsymbol{a}_{\nu\sigma'}\, \boldsymbol{a}_{\mu\sigma}, \tag{1}$$

где $\boldsymbol{a}^{+}_{\mu\sigma}$ и $\boldsymbol{a}_{\mu\sigma}$ — операторы рождения и уничтожения электрона со спином σ на атоме μ, кулоновские интегралы $\gamma_{\mu\nu}$ вычислялись по формуле Оно[21], потенциал ионизации I_C взят равным 11,16 эв, а сродство к электрону равным 0,03 эв[22], так что $\gamma_{\mu\mu} = 11{,}13$ эв. Диагональные элементы матрицы остова вычислялись без учета интегралов проникновения, а именно :

$$H^{\text{ост}}_{\mu\mu} = - I_{\mu} - \sum_{\substack{\nu \\ \nu \neq \mu}} n_{\nu}\, n_{\mu}\, \gamma_{\mu\nu}, \tag{2}$$

где n_{μ} — число π-электронов, поставляемое атомом μ и равное в нашем случае единице. Недиагональные элементы $H^{\text{ост}}_{\mu\nu}$ полагались равными константам $\beta_{\mu\nu}$ для соседних атомов и нулю для несоседних.

Резонансные интегралы $\beta_{\mu\nu}$ и соответствующие им длины связей $R_{\mu\nu}$, следуя схеме, предложенной в [23,24], вычислялись путем взаимного согласования по методу, подробно изложенному и обоснованному в [25,26]. В настоящем сообщении достаточно сформулировать основные положения этого метода и привести аргументы в пользу применимости его к нейтральным альтернантным радикалам.

Полную энергию нейтрального альтернантного радикала разобъем на две части

$$E^{T} = E^{\pi} + E^{\sigma}. \tag{3}$$

Для вычисления первого слагаемого E^{π}, представляющего собой энергию π-электронов, обратимся к выражению для энергии системы с открытыми оболочками, находящейся при заданном числе неспаренных электронов в состоянии с максимальным спином.

$$E = S_p(\boldsymbol{H}\boldsymbol{P}^{T}) + \frac{1}{2} S_p(\boldsymbol{J}^{T}\boldsymbol{P}^{T}) - \frac{1}{4} S_p(\boldsymbol{K}^{T}\boldsymbol{P}^{T}) + \frac{1}{4} S_p(\boldsymbol{K}^{o}\boldsymbol{P}^{o}), \tag{4}$$

где H — матрица операторов кинетической энергии электрона и взаимодействия его с остовом системы. Полная матрица плотности $\boldsymbol{P}^{T}$ разбивается на вклады от замкнутых (c) и открытых (o) оболочек

$$\boldsymbol{P}^{T} = 2\boldsymbol{P}^{c} + \boldsymbol{P}^{o}, \tag{5}$$

---

[21] K. Ohno, *Theor. Chim. Acta*, **2**, 219 (1964).

[22] J. Hinze и H. H. Jaffé, *J. Amer. Chem. Soc.*, **84**, 540 (1953).

[23] M. J. S. Dewar и H. N. Schmeising, *Tetrahedron*, **11**, 96 (1960).

[24] A. L. H. Chung и M. J. S. Dewar, *J. Chem. Phys.*, **42**, 756 (1965).

[25] В. И. Лутошкин, Г. Г. Дядюша и Ю. А. Кругляк, В сб. « Строение молекул и квантовая химия », « Наукова думка », Киев, 1970, с. 132.

[26] В. И. Лутошкин, Ю. А. Кругляк и Г. Г. Дядюша, *Теор. эксперим. хим.*, **7**, (1971).

и аналогичные выражения справедливы для матриц кулоновского $\boldsymbol{J}^T$ и обменного K^T операторов.

В приближении нулевого дифференциального перекрывания для π-электронов

$$J^T_{\mu\nu} = \delta_{\mu\nu} \sum_{\varkappa} \gamma_{\mu\varkappa} P^T_{\varkappa\varkappa}, \tag{6}$$

$$K^{T(o)}_{\mu\nu} = \gamma_{\mu\nu} P^{T(o)}_{\mu\nu}. \tag{7}$$

Тогда справедливы равенства

$$S_p (\boldsymbol{J}^T \boldsymbol{P}^T) = \sum_{\mu\nu} \gamma_{\mu\nu} P^T_{\mu\mu} P^T_{\nu\nu}, \tag{8}$$

$$S_p (\boldsymbol{K}^{T(o)} \boldsymbol{P}^{T(o)}) = \sum_{\mu\nu} \gamma_{\mu\nu} (P^{T(o)}_{\mu\nu})^2. \tag{9}$$

Подставляя (8) и (9) в (4), получаем

$$\begin{aligned} E^\pi = \sum_{\mu\nu} H^{\text{ост}}_{\mu\nu} P^T_{\mu\nu} + \frac{1}{2} \sum_{\mu\nu} \gamma_{\mu\nu} P^T_{\mu\mu} P^T_{\nu\nu} - \\ - \frac{1}{4} \sum_{\mu\nu} \gamma_{\mu\nu} (P^T_{\mu\nu})^2 + \frac{1}{4} \sum_{\mu\nu} \gamma_{\mu\nu} (P^o_{\mu\nu})^2. \end{aligned} \tag{10}$$

Для нечетных альтернантных радикалов

$$P^T_{\mu\mu} = 1, \quad P^o_{\mu,\mu+1} = 0, \quad P^o_{\mu\mu} P^o_{\mu+1,\mu+1} = 0, \quad P^T_{\mu\nu} = P^c_{\mu\nu}. \tag{11}$$

Прибавляя к (10) энергию остова

$$E^{\text{ост}} = \sum_{\mu<\nu} \gamma_{\mu\nu} P^T_{\mu\mu} P^T_{\nu\nu} \tag{12}$$

и учитывая свойства (11) матриц плотности, получаем окончательно

$$E^\pi = 2 \sum_q \beta_q P^c_q - \frac{1}{2} \sum_q \gamma_q (P^c_q)^2 + F, \tag{13}$$

где суммирование ведется по связям, а величина F слабо зависит от порядков связи. Аналогичное выражение справедливо также и для альтернантных молекул, [25,27] для которых в одноконфигурационном при-

---

[27] S. de Bruijn, *Theor. Chim. Acta.*, **18**, 34 (1970).

ближении, как доказано в [27], можно без большой ошибки пользоваться линейным соотношением Коулсона-Голебиевского [18] между равновесной длиной $\widetilde{R}_{\mu\nu}$ и соответствующим ей равновесным порядком связи $\widetilde{P}_{\mu\nu}$, предполагая наличие между ними взаимно однозначного соответствия

$$\widetilde{R}_{\mu\nu} = 1{,}517 - 0{,}180\, \widetilde{P}_{\mu\nu}. \tag{14}$$

Таким образом, приведенные выше аргументы свидетельствуют о применимости линейных соотношений типа (14) и к нейтральным альтернантным радикалам. При оценке в одноконфигурационном приближении равновесной конфигурации бензильного радикала в основном состоянии мы пользовались соотношением (14).

Следуя Лонге-Хиггинсу и Сейлему, [28] энергию σ-электронов представим как сумму энергий отдельных связей

$$E^{\sigma} = \sum_{q} E_{q}^{\sigma} \tag{15}$$

и предположим, что E_q^{σ} зависит только от R_q. Тогда для E^T имеем*

$$\frac{\mathrm{d}E^{T}}{\mathrm{d}R_{q}} = \frac{\partial E^{\pi}}{\partial P_{q}} \cdot \frac{\mathrm{d}P_{q}}{\mathrm{d}R_{q}} + \frac{\partial E^{\pi}}{\partial \beta_{q}} \cdot \frac{\mathrm{d}\beta_{q}}{\mathrm{d}R_{q}} + \frac{\partial E^{\pi}}{\partial \gamma_{q}} \cdot \frac{\mathrm{d}\gamma_{q}}{\mathrm{d}R_{q}} + \frac{\mathrm{d}E_{q}^{\sigma}}{\mathrm{d}R_{q}}. \tag{16}$$

В приближении ССП первый член в (16) тождественно равен нулю. Воспользуемся условием минимума полной энергии для всех связей

$$\left(\frac{\mathrm{d}E^{T}}{\mathrm{d}R_{q}}\right)_{R_{q}=\widetilde{R}_{q}} = 0. \tag{17}$$

Тогда из (17), (16) и (13) следует, что для выбранной функции γ_q от $\widetilde{R}_q$ или $\widetilde{P}_q$ задание зависимости β_q от $\widetilde{R}_q$ или $\widetilde{P}_q$ предполагает справедливым для всех связей

$$\frac{\mathrm{d}E_{q}^{\sigma}}{\mathrm{d}\widetilde{R}_{q}} = \left(-\,2\widetilde{P}_{q}\,\frac{\mathrm{d}\beta_{q}}{\mathrm{d}\widetilde{P}_{q}} + \frac{1}{2}\,\widetilde{P}_{q}^{2}\,\frac{\mathrm{d}\gamma_{q}}{\mathrm{d}\widetilde{P}_{q}}\right) \Big/ \frac{\mathrm{d}\widetilde{R}_{q}}{\mathrm{d}\widetilde{P}_{q}} \tag{18}$$

и наоборот, если задана зависимость $E_q^{\sigma}\,(\widetilde{P}_q)$, то

$$\beta_{q} = \int \left(\frac{1}{4}\,\widetilde{P}_{q}\,\frac{\mathrm{d}\gamma_{q}}{\mathrm{d}\widetilde{P}_{q}} - \frac{1}{2\widetilde{P}_{q}} \cdot \frac{\mathrm{d}E_{q}^{\sigma}}{\mathrm{d}\widetilde{P}_{q}}\right) \mathrm{d}\widetilde{P}_{q}. \tag{19}$$

---

* Индексы T, o и c при P_q опускаем, поскольку из (11) и (13) следует, что в альтернантных нейтральных радикалах открытая оболочка не вносит вклада в матрицу плотности.

[28] H. C. Longuet-Higgins и L. L. Salem, *Proc. Royal Soc.*, **A251**, 172 (1959).

Для второй вариации энергии E^{π} имеем

$$\delta^2 E^{\pi} = \sum_{\mu\nu} (P_{\mu\nu}\, \delta^2 H_{\mu\nu}^{\text{ост}} + \delta P_{\mu\nu}\, \delta H_{\mu\nu}^{\text{ост}}) +$$

$$+ \frac{1}{4} \sum_{\mu\nu\varkappa\eta} [P_{\mu\nu}\, P_{\varkappa\eta} (2\,\delta^2 < \mu\nu|\varkappa n > - \,\delta^2 < \mu\varkappa|\nu\eta >) + \tag{20}$$

$$+ 2P_{\mu\nu}\, \delta P_{\varkappa\eta} (2\,\delta < \mu\nu|\varkappa\eta > - \,\delta < \mu\varkappa|\nu\eta >)].$$

Тогда для силовой константы

$$k_q = \left(\frac{\mathrm{d}^2 E^T}{\mathrm{d} R_q^2}\right)_{R_q = \widetilde{R}_q} \tag{21}$$

можно получить следующее выражение:

$$k_q = \left(\widetilde{P}_q \frac{\mathrm{d}\gamma_q}{\mathrm{d}\widetilde{P}_q} - 2\,\frac{\mathrm{d}\beta_q}{\mathrm{d}\widetilde{P}_q}\right)\left[1 - \left(\frac{\partial P_q}{\partial R_q}\right)_{R_q = \widetilde{R}_q} \left(\frac{\mathrm{d}\widetilde{R}_q}{\mathrm{d}\widetilde{P}_q}\right)\right] \Big/ \left(\frac{\mathrm{d}\widetilde{R}_q}{\mathrm{d}\widetilde{P}_q}\right)^2. \tag{22}$$

Для оценки β_q можно воспользоваться выражением (19), выбрав конкретный вид функций $\gamma_q\ (R_q)$ и $E_q^{\sigma}\ (R_q)$, как это сделано в [29]. Мы же поступили следующим образом. Согласно [30], $k_{\text{C}-\text{C}}$ практически линейно зависит от порядка связи в ряду C_2H_6, C_2H_4, C_2H_2. Можно думать, что для $P_q < 1$ линейная зависимость k_q от P_q будет выполняться еще более строго. Выберем β_q в виде полинома по $\widetilde{P}_q$

$$\beta_q = \beta_0 + \beta_1\left(\widetilde{P}_q - \frac{1}{2}\right) + \beta_2\left(\widetilde{P}_q - \frac{1}{2}\right)^2 \tag{23}$$

и подставим (23) в (22). Тогда для этана $(\widetilde{P} = 0)$ и этилена $(\widetilde{P} = 1)$ получим

$$k^{(0)} = \frac{2}{\omega^2}(\beta_2 - \beta_1), \quad (\widetilde{P} = 0) \tag{24}$$

$$k^{(1)} = \frac{2}{\omega^2}\left[\left(\frac{\mathrm{d}\gamma}{\mathrm{d}\widetilde{P}}\right)_{\widetilde{P}=1} - (\beta_1 + \beta_2)\right], \quad (\widetilde{P} = 1) \tag{25}$$

---

[29] K. Nishimoto, *Theor. Chim. Acta*, **7**, 207 (1967).
[30] Е. М. Попов и Г. А. Каган, *Теор. эксперим. хим.*, **1**, 295 (1965).

где

$$\omega = -\frac{\mathrm{d}\widetilde{R}_q}{\mathrm{d}\widetilde{P}_q}. \tag{26}$$

Воспользовавшись экспериментальными значениями силовых констант связи С—С в этане и этилене $k^{(0)} = 7{,}02 \cdot 10^6$ см$^{-2}$ и $k^{(1)} = 14{,}2 \times 10^6$ см$^{-2}$,[31] а также указанным выше конкретным видом функций $\gamma_q(\widetilde{R}_q)$ и $\widetilde{R}_q\ (\widetilde{P}_q)$, Дядюша и Лутошкин[32] получили из (24) и (25) $\beta_1 = -0{,}55$ эв и $\beta_2 = -0{,}10$ эв. Ими же для β_0 найдено значение $\beta_0 = -2{,}7$ эв, которое обеспечивает хорошее согласие между экспериментальными и расчетными значениями равновесных длин связей и энергий возбуждения $S_0 \to S_1$ и $S_0 \to T_1$ в молекулах бутадиена, гексатриена и октатетраена.[33] Эти же значения параметров β_0, β_1 и β_2 оправдали себя при оценке силового поля бензола, бутадиена и гексатриена,[32] нафталина,[34] антрацена, пирена и коронена[35] и использованы нами для расчета равновесной конфигурации бензильного радикала.

Равновесные порядки связей вычислялись на самосогласованных решениях фокиана $\boldsymbol{\Omega}$ для состояний с полуоткрытыми оболочками без орбитального вырождения. В отличие от [36,37] использовался другой частный случай общего выражения для фокиана такого типа,[38] а именно:

$$\boldsymbol{\Omega} = \boldsymbol{H}^{\text{ост}} + \boldsymbol{J}^{T} - \frac{1}{2}\boldsymbol{K}^{T} + \frac{1}{2}(\boldsymbol{I} - \boldsymbol{P}^{T})\boldsymbol{K}^{o}(\boldsymbol{I} - \boldsymbol{P}^{T}) - $$
$$- (\boldsymbol{I} - \boldsymbol{P}^{T} + \boldsymbol{P}^{o})\,\boldsymbol{K}^{o}\,(\boldsymbol{I} - \boldsymbol{P}^{T} - \boldsymbol{P}^{o}), \tag{27}$$

где I — единичная матрица.

В качестве начального приближения для расчетов с варьированием геометрии (ВГ) брались результаты, полученные стандартным методом Паризера-Парра (ПП) с фокианом (27). Длина связи R_{CC} принималась равной 1,4 Å, все углы $\angle$ССС равными 120°, а интеграл β равным β_0 в (23). Нумерация атомов соответствует присоединению метиленовой группы $\text{C}_{(7)}\text{H}_2$ к атому C_1.

Согласование по геометрии выполнялось двумя методами без изменения первоначальных углов $\angle$ССС. Согласно Дьюару и Глейчеру (ДГ),[39] проводилось согласование $\beta_{\mu\nu}$ и $P_{\mu\nu}$ при неизмененных начальных значениях $\gamma_{\mu\nu}$ и $R_{\mu\nu}$ (метод ПП-ДГ). Согласовывались также все параметры — $\beta_{\mu\nu}$, $R_{\mu\nu}$ и $\gamma_{\mu\nu}$ в зависимости от $P_{\mu\nu}$ (метод ПП-ВГ) без изменения первоначальных углов $\angle$ ССС. В последнем случае фенильная группа бензильного радикала получалась незамкнутой. Для усреднения этого эффекта расчет методом ПП-ВГ проводился для трех разных последовательностей задания координат атомов: 1234567 (нормальная последовательность), 3456127 и 4561237. Результаты расчетов показывают, что остальные возможные последовательности (без прерывания порядка следования атомов в кольце) сводятся к трем указанным выше. Вычисления проводились посредством программы PPP-4 на машине М-220 Института кибернетики АН УССР. Результаты расчета энергии и порядков связи указанными методами приведены в табл. 1.

---

[31] Г. А. Каган и Е. М. Попов, *Изв. АН СССР, Отд. хим. наук*, 1393 (1964).

[32] Г. Г. Дядюша и В. И. Лутошкин, *Теор. эксперим. хим.*, **7**, 3 (1971).

[33] Г. Г. Дядюша и В. И. Лутошкин, *Литовский физический сборник*, **10** (1970).

[34] В. И. Лутошкин и В. Ф. Головко, *Теор. эксперим. хим.*, **7**, (1971).

[35] В. И. Лутошкин, В. Ф. Головко, Г. Г. Дядюша и Ю. А. Кругляк, *Теор. эксперим. хим.*, **7**, (1971).

[36] Yu. A. Kruglyak и G. G. Dyadyusha, *Theor. Chim. Acta*, **12**, 18 (1968).

[37] Ю. А. Кругляк, *Ж. структ. хим.*, **10**, 28 (1969).

[38] Г. Г. Дядюша и В. А. Куприевич, *Теор. эксперим. хим.*, **1**, 460 (1963).

[39] M. J. S. Dewar и G. L. Gleicher, *J. Amer. Chem. Soc.*, **87**, 685 (1965).

Таблица 1

Заселенность связей $P_{\mu\nu}$ и π-электронная энергия бензильного радикала, рассчитанные разными методами в одноконфигурационном приближении для состояний с одной открытой оболочкой

Метод	$-E^{\pi}$, эв	$P_{\mu\nu}$						
		1—2	1—6	1—7	2—3	5—6	3—4	4—5
ПП	214,508	0,5883	0,5883	0,4730	0,6824	0,6824	0,6564	0,6564
ПП—ДГ	215,125	0,5913	0,5913	0,4626	0,6831	0,6831	0,6561	0,6561
ПП-ВГ 1234567	214,902	0,5918	0,5951	0,4559	0,6844	0,6813	0,6549	0,6576
ПП-ВГ 3456127	214,753	0,5931	0,5929	0,4569	0,6832	0,6832	0,6560	0,6562
ПП-ВГ 4561237	214,614	0,5914	0,5941	0,4572	0,6854	0,6817	0,6537	0,6580
PPP-2	214,740	0,5930	0,5930	0,4568	0,6832	0,6832	0,6560	0,6560

Полученные результаты позволяют оценить пределы отклонения углов между связями от 120° и относительный вклад углов в изменение геометрии по сравнению с длинами связей. Для этой цели используем выражение из [40] для отклонения $\delta\varphi$ угла $\angle$ССС от 120°, образованного сторонами с длиной $R_0 + \delta R_1$ и $R_0 + \delta R_2$ и опирающегося на расстояние между атомами через один, равное $2\sqrt{3}\,R_0 + \delta\angle$,

$$\delta\varphi = [2\,\delta\angle - \sqrt{3}\,(\delta R_1 + \delta R_2)/R_0 \tag{28}$$

или для эквивалентных по симметрии связей ($\delta R_1 = \delta R_2 = \delta R$)

$$\frac{\delta\varphi}{\delta R} = \frac{2}{R_0}\left(\frac{\delta\angle}{\delta R} - \sqrt{3}\right). \tag{29}$$

Воспользовавшись порядками связей, рассчитанными методом ПП-ВГ (табл. 1), и соотношением (14), получим $0{,}0011 \leqslant |\delta R_1|\,(|\delta R|) \leqslant 0{,}0104$ и $0{,}0060 \leqslant |\delta R_2| \leqslant 0{,}0350$. Величину $\delta\angle$ оценим как различие в длинах, эквивалентных по симметрии связей. Тогда аналогичным образом получим $0{,}000010 \leqslant |\,\delta\angle\,| \leqslant 0{,}000774$. В результате из (28) и (29) при $R_0 = 1{,}4$ Å получаются следующие пределы возможного изменения $\delta\varphi$ и $\delta\varphi/\delta R$: $23' \leqslant |\delta\varphi| \leqslant 3°\,13'$ и $0{,}026 \leqslant |\delta\varphi/\delta R| \leqslant 0{,}043$. Последнее неравенство указывает на пренебрежимо малую роль углов в изменении геометрии сравнительно с длинами связей. Полученная оценка возможных пределов изменения углов не противоречит многочисленным экспериментальным данным по геометрии сопряженных углеводородов (см. также[40]).

---

[40] И. А. Мисуркин и А. А. Овчинников, *Ж. структ. хим.*, **5**, 888 (1964).

На основании сказанного выше равновесные длины связей в бензильном радикале вычислялись из соответствующих порядков, усредненных по результатам трех расчетов методом ПП-ВГ (табл. 1). Окончательные результаты приведены в табл. 2. Однозначное определение углов выполнить труднее (см. однако [40]) и в свете результатов предыдущего абзаца в этом нет настоятельной необходимости. Мы поступили следующим образом. Предполагалось, что наибольшему возмущению подвергались либо углы $\angle C_2C_1C_6$ и $\angle C_1C_2C_3$, либо $\angle C_1C_2C_3$ и $\angle C_2C_3C_4$. Остальные углы, не эквивалентные указанным по симметрии, полагались равными 120°. Критерием для выбора между двумя возможными моделями наибольших возмущений углов служила энергия бензильного радикала, вычисленная в том же приближении, как и в методе ПП-ВГ, но с оператором $\mathbf{\Omega}$ из [36,37], который для физически измеримых величин приводит к тем же результатам, что и оператор (27). Расчет проводился по программе РРР-2.[41] Оказалось, что первая модель (возмущение углов $\angle C_2C_1C_6$ и $\angle C_1C_2C_3$) менее устойчива, чем вторая на 0,03%. Малость этой величины подтверждает выводы, полученные в предыдущем абзаце. Результаты расчета энергии и порядков связи для второй модели, принятой окончательно в качестве равновесной конфигурации бензильного радикала приведены в последней строке табл. 1. Значения соответствующих возмущенных углов получаются равными $\angle C_1C_2C_3 = 119°\,37'$ и $\angle C_2C_3C_4 = 120°\,23'$. Отклонения от 120° не превосходят пределы, оцененные выше. В табл. 3 даны окончательные координаты атомов углерода бензильного радикала. Коэффициенты $C_{\mu i}$ базисных орбиталей равновес-

Таблица 2

Длины связей $C_\mu - C_\nu$ в безильном радикале, вычисленные разными методами, Å

C_1-C_2	C_2-C_3	C_3-C_4	C_1-C_7	Лит-ра
1,410	1,380	1,390	1,380	43
1,430	1,386	1,406	1,391	16
1,395	1,395	1,395	1,440	42
1,417	1,391	1,401	1,401	44
1,420	1,398	1,406	1,424	4–7
1,417	1,393	1,403	1,422	12–14
1,410	1,394	1,399	1,435	наст. статья

---

[41] Ю. А. Кругляк, Г. Г. Дядюша, В. А. Куприевич, Л. М. Подольская и Г. И. Каган, « Методы расчета электронной структуры и спектров молекул », » Наукова думка », Киев, 1969.

ной конфигурации бензильного радикала, используемые далее для расчетов в многоконфигурационном приближении, даны в табл. 4.

Известные нам результаты вычисления длин связей в бензильном радикале собраны в табл. 2. По-видимому, первая оценка была сделана Пинни и Кинчем в 1938 г. [43] на основе простейших вариантов методов Хюккеля и валентных схем. Наиболее длинной оказалась связь $C_1—C_2$. Аналогичный результат получен Счастневым и Жидомировым. [16] Недавно Ватман-Грайкар,[44] воспользовавшись хюккелевскими порядками связей и зависимостью $R_{\mu\nu}$ от $P_{\mu\nu}$ по Коулсону, [45] пришла к такому же выводу. Выполненные нами расчеты указывают на то, что наиболее длинной связью в бензильном радикале должна быть связь $C_1—C_7$. По-видимому, это так и должно быть, поскольку эта связь является экзоциклической. На это обстоятельство обратили внимание Шаг и Филлипс [42] при реинтерпретации электронного спектра поглощения бензильного радикала и она подтверждается (см. табл. 2) как полуэмпирическими расчетами с сильно расширенным (вплоть до полного) КВ,[4–7] так и неэмпирическим

Таблица 3

Декартовы координаты атомов углерода бензильного радикала в равновесной конфигурации

μ	x, Å	y,Å
1	2,79850	0
2	2,09350	−1,22105
3	0,69950	−1,21153
4	0	0
5	0,69950	1,21153
6	2,09350	1,22105
7	4,23350	0

Таблица 4

Коэффициенты $C_{\mu i}$ базисных орбиталей равновесной конфигурации бензильного радикала, вычисленные мотодом ССП для состояний с одной открытой оболочкой (оператор Ω из 36,37,41*

i / μ	1	2	3	4	7
4	0	−0,285024	0	0,226000	0,886818
3	0	−0,5	−0,5	0	0
2	0,536921	0,199241	−0,325358	−0,586192	0,277460
1	0,460126	0,411926	0,379661	0,361719	0,172606

* Остальные коэффициенты определяются симметрией орбиталей и свойствами альтернантности бензильного радикала

расчетом бензильного радикала неограниченным методом ССП с учетом всех электронов на гауссовом базисе.[12–14]

---

[42] J. C. SCHUG и D. H. PHILLIPS, *J. Chem. Phys.*, **49**, 3734 (1968).
[43] W. G. PENNEY и G. J. KYNCH, *Proc. Royal Soc.*, **A164**, 409 (1938).
[44] L. WATMANN-GRAJCAR, *J. chim. Phys.*, **66**, 1018 (1969).
[45] C. A. COULSON, *Proc. Royal Soc.*, **A169**, 413 (1939).

3. МНОГОКОНФИГУРАЦИОННОЕ ПРИБЛИЖЕНИЕ

Приведенные в п. 2 данные полностью определяют гамильтониан (1). Расчеты в многоконфигурационном приближении удобнее выполнять, перейдя предварительно в представлении вторичного квантования от атомных орбиталей к молекулярным

$$\boldsymbol{a}_{\mu\sigma} = \sum_i C_{\mu i} \boldsymbol{A}_{i\sigma} \tag{30 а}$$

$$\boldsymbol{a}^+_{\mu\sigma} = \sum_i C^*_{\mu i} \boldsymbol{A}^+_{i\sigma}. \tag{30 б}$$

Подставив (30) в (1), получим

$$\boldsymbol{H} = \sum_{ij\sigma} h_{ij} \boldsymbol{A}^+_{i\sigma} \boldsymbol{B}_{j\sigma} + \frac{1}{2} \sum_{ijkl\sigma\sigma'} (ij \mid kl) \boldsymbol{A}^+_{i\sigma} \boldsymbol{A}^+_{j\sigma'} \boldsymbol{A}_{l\sigma'} \boldsymbol{A}_{k\sigma}, \tag{31 а}$$

где

$$h_{ij} = \sum_{\mu\nu} C^*_{\mu i} C_{\nu j} H^{\text{ост}}_{\mu\nu}, \tag{31 б}$$

$$(ij|kl) = \sum_{\mu\nu} C^*_{\mu i} C^*_{\nu j} C_{\mu k} C_{\nu l} \gamma_{\mu\nu}. \tag{31 в}$$

Гамильтониан (31) взят в качестве исходного в наших расчетах. Входящие в него молекулярные орбитали C_i (табл. 4) минимизируют энергию основной конфигурации бензильного радикала. Такой выбор базисных орбиталей представляется наиболее естественным, обеспечивая выполнение теорем альтернантности не только для полного, но и для определенных усеченных наборов конфигураций, содержащих все конфигурации заданной кратности возбуждения. Кроме того, такие орбитали обращают в нуль ряд элементов матрицы КВ[10,11] между основной конфигурацией и одновозбужденными в силу соотношений, аналогичных теореме Бриллюэна для молекул.

Многоконфигурационное приближение на фиксированном орбитальном базисе разработано достаточно полно. Волновая функция записывается в виде разложения по слэтеровским детерминантам с последующим определением коэффициентов разложения путем диагонализации матрицы КВ. Улучшение аппроксимации волновой функции достигается простым расширением набора учитываемых конфигураций. Если волновая функция разложена по полному набору конфигураций, в который в нашем случае входит их конечное число, то получается точная собственная функция данного модельного гамильтониана. Порядок матрицы КВ существенно понижается, если от детерминантов перейти к их ортонормированным линейным комбинациям заданной симметрии и мультиплетности. Эта общая схема была реализована ранее [46–48,41,10,11] на основе последовательного использования формализма вторичного квантования и применялась при расчете основного и возбужденных состояний бензильного радикала, [8,9,49,50] молекул глицина, тирозина и их нейтральных и заряженных радикалов [46,51] и пептидных фрагментов [52] с ограниченным КВ, а также с полным учетом КВ для основного состояния равносвязного бензильного радикала. [4–7] Мы также воспользовались этой схемой в настоящей работе для расчета основного состояния бензильного радикала в равновесной конфигурации.

Основная конфигурация бензильного радикала относится к представлению B_2 группы симметрии C_{2v}. В π-электронном приближении имеется еще 212 возбужденных конфигураций, относящихся к тому же представлению. Из них одновозбужденных 9, двух — 40, трех — 69, четырех — 64, пяти — 25, шестивозбужденных 5. Возбужденные конфигурации могут содержать 1, 3, 5 и 7 неспаренных электронов. Соответственно этому число различных спин-конфигураций равно 1, 3, 10 и 35, из которых можно построить 1, 2, 5 и 14 взаимно ортогональных базисных векторов. Распределение их в зависимости от кратности возбуждения следующее: 14, 74, 150, 122, 38, 5. Расчеты проводились с семью наборами базисных векторов — *G*, *I*, *II*, *III*, *IV*, *V*, и *F*. Тривиальный набор *G* содержит только основную конфигурацию, следующий набор *I* наряду с ней включает все одновозбужденные конфигурации, набор *II* пополнен всеми двухвозбужденными и т.д. Набор *F* соответствует полному ряду КВ для рассматриваемой задачи. В соответствии с этим размерности наборов *G* ,*I*, . . ., *V*, *F* таковы: 1, 15, 89, 239, 361, 399, 404. Использованные нами коэффициенты перед спин-конфигурациями даны в [4,5]. Там же и в [46–48,41,10,11] имеются подробные сведения о построении базисных векторов в представлении вторичного квантования.

Ввиду громоздкости матриц КВ и сложности выражений для матричных элементов, возрастающей по мере увеличения числа неспаренных электронов, в использованном нами комплексе программ CI-3 (авторы — В. А. Куприевич, Ю. А. Кругляк, Е. В. Моздор) не используются аналитические выражения для матричных элементов. Запрограммированы лишь несложные правила для их вычисления в представлении вторичного квантования, вытекающие из теорем Вика [53,47,48] и в равной

---

[46] Ю. А. Кругляк, « О расчете электронной структуры сопряженных молекул и радикалов методами самосогласованного поля и конфигурационного взаимодействия », В кн. Л. П. Каюшин, К. М. Львов, М. К. Пулатова: « Исследование парамагнитных центров облученных белков », Изд-во « Наука », Москва, 1970, гл. 6.

[47] Ю. А. Кругляк, В. А. Куприевич и Е. В. Моздор, В сб. « Строение молекул и квантовая химия », « Наукова думка », Киев, 1970, стр. 121.

[48] V. A. Kuprievich, Yu. A. Kruglyak и E. V. Mozdor, *Croat. Chem. Acta*, **43**, *1* (1971).

[49] Yu. A. Kruglyak и E. V. Mozdor, *Theor. Chim. Acta*, **15**, 374 (1969).

[50] Е. В. Моздор и Ю. А. Кругляк, *Теор. и эксперим. хим.*, **5**, 740 (1965).

[51] Ю. А. Кругляк, М. К. Пулатова, Е. В. Моздор, Е. Н. Судьбина, В. Г. Пасоян и Л. П. Каюшин, *Биофизика*, **13**, 401 (1968).

[52] Е. Н. Судьбина, М. К. Пулатова, Л. П. Каюшин и Ю. А. Кругляк, *Биофизика*, **15**, 1124 (1970).

[53] G. C. Wick, *Phys. Revs*, **80**, 268 (1950).

мере, пригодные для конфигураций произвольной структуры. Числа заполнения одночастичных состояний для электронов равны 0 или 1. Поэтому машинный код идеально приспособлен для записи конфигураций в представлении вторичного квантования. Ряд логических операций, например, свертки операторов, также несложно реализовать машинными командами. Все необходимые построения подробно описаны в [41,47,48].

Комплекс CI-3 включает три основных программы и ряд вспомогательных. Программа CI-3M вычисляет элементы матрицы КВ с последующей записью их построчно на магнитную ленту. Программа CI-3D предназначена для нахождения первых собственных значений матрицы КВ и соответствующих собственных векторов методом Несбета. [54] Программа CI-3P вычисляет матрицы электронной и спиновой заселенности. Вспомогательные программы TRANSFER, CHECK и OVERLAP предназначены для переписи и контроля записи на ленту матрицы КВ и для вычисления интеграла перекрывания S многоконфигурационных волновых функций. Естественные спин-орбитали и соответствующие им числа заполнения вычислялись путем диагонализации матриц плотности посредством программы ХЮККЕЛЬ-А.[55]

Отклонение энергии основного состояния бензильного радикала, вычисленной с разными наборами конфигураций, от точного значения иллюстрируется данными табл. 5. Энергия корреляции (см. также рисунок) в принятой модели равна — 0,786185 эв, что ощутимо меньше, по сравнению с энергией корреляции для равносвязного бензильного радикала.[4–7] Объясняется это прежде всего тем, что в случае равновесной конфигурации для $|\beta_{CC}|$ использовано большее значение по сравнению с равносвязной моделью. Из табл. 5 также следует, что при уточнении пробной волновой функции за счет одно-, двух- и трехвозбужденных конфи-

Таблица 5

Изменение энергии E^π основного состояния бензильного радикала в равновесной конфигурации по мере уточнения пробной волновой функции.

Ψ	E^π, эв*
G	0,786185
I	0,631662
II	0,035619
III	0,012193
IV	0,000156
V	0,000031
F	0

* За ноль отсчета принята энергия бензильного радикала, вычисленная на точной волновой функции модельного гамильтониана (31) и равная −215,525771 эв.

---

[54] R. K. Nesbet, *J. Chem. Phys.*, **43**, 311 (1965).

[55] Ю. А. Кругляк, В. С. Квакуш, Г. Г. Дядюша и В. И. Хильченко, «Методы вычислений в квантовой химии. Расчет π-электронной структуры молекул простыми методами молекулярных орбиталей», «Наукова думка», Киев, 1967, гл. 2, § 2.

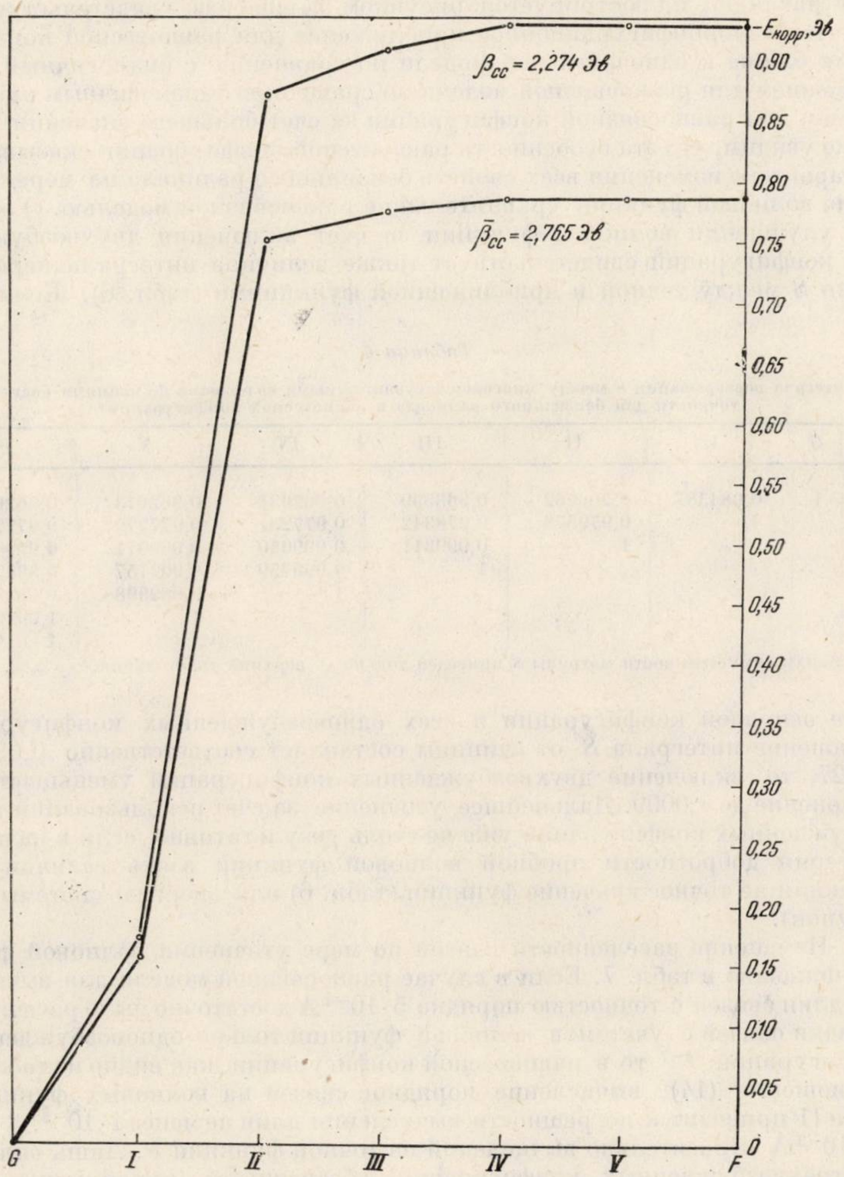

Рис. 1.—Изменение энергии корреляции бензильного радикала в зависимости от точности пробной волновой функции для равносвязной конфигурации (β_{CC} = — 2,274 эв) [4–7] и для равновесной ($\overline{\beta}_{CC}$ = — 2,765 эв).

гураций энергия корреляции учитывается соответственно на 20,95 и 98%, т.е. в несколько большей степени, чем для равносвязной модели. [4–7] Этот факт наглядно иллюстрируется рисунком и еще раз свидетельствует о том, что одноконфигурационное приближение для равновесной конфигурации ближе к одночастичной модели по сравнению с аналогичным приближением для равносвязной модели по сравнению с аналогичным приближением для равносвязной конфигурации за счет большего значения $|\overline{\beta}_{\text{CC}}|$. Ниже увидим, что эта особенность равновесной конфигурации сказывается на характере изменения всех свойств бензильного радикала по мере уточнения волновой функции сравнительно с равносвязной моделью. О заметном улучшении волновой функции за счет включения двухвозбужденных конфигураций свидетельствует также величина интеграла перекрывания S между точной и приближенной функциями (табл. 6). Если при учете основной конфигурации и всех одновозбужденных конфигураций отклонение интеграла S от единицы составляет соответственно 0,0374 и 0,0227, то включение двухвозбужденных конфигураций уменьшает это отклонение до 0,0009. Дальнейшее уточнение за счет использования трехвозбужденных конфигураций уже не столь результативно, если в качестве критерия добротности пробной волновой функции взять величину ее проекции на точное значение функции (табл. 6) или энергию системы (см. рисунок).

Таблица 6

Интеграл перекрывания S между многоконфигурационными волновыми функциями разной точности для бензильного радикала в равновесной конфигурации*

Ψ	*G*	I	II	III	IV	V	*F*
G	I	0,984387	0,966962	0,963599	0,962638	0,962613	0,962610
I		I	0,979678	0,978342	0,977281	0,977270	0,977266
II			1	0,999311	0,999080	0,999071	0,999070
III				1	0,999759	0,999757	0,999755
IV					1	0,999998	0,999998
V						1	1,000000
F							1

* Ввиду симметричности матрицы S приведен только ее верхний треугольник.

Изменение заселенности связей по мере уточнения волновой функции показано в табл. 7. Если в случае равносвязной модели для вычисления длин связей с точностью порядка $5 \cdot 10^{-4}$ Å достаточно было рассчитать порядки связей с учетом в волновой функции только одновозбужденных конфигураций, [4–7] то в равновесной конфигурации, как видно из табл. 7 и соотношения (14), вычисление порядков связей на волновых функциях G, I и II приводит к погрешности вычисления длин не менее $1 \cdot 10^{-2}$, $3 \cdot 10^{-3}$ и $1 \cdot 10^{-3}$ Å относительно вычислений на точной функции F. Лишь включение трехвозбужденных конфигураций обеспечивает приемлемую точность оценки длин связей порядка $2 \cdot 10^{-4}$ Å.

Как и в случае равносвязной модели спиновая заселенность атомов и связей (табл. 8) существенно изменяется по мере уточнения волновой функции. Из табл. 8 и уравнения Мак-Коннела [1] с константой $Q_{\text{CH}}^{\text{H}} = 22$ э[3] следует, что в одноконфигурационном приближении погрешность оценки расщепления на протоне за счет приближенного вычисления волновой

Таблица 7

Недиагональные элементы одночастичной матрицы плотности $P_{\mu\nu}$ бензильного радикала в равновесной конфигурации, вычисленные на волновых функциях разной точности*

$\mu\nu$	Ψ						
	G	I	II	III	IV	V	*F*
12	0,5930	0,5605	0,5524	0,5478	0,5472	0,5471	0,547120
14	−0,2966	−0,2680	−0,2570	−0,2525	−0,2516	−0,2516	−0,251603
17	0,4568	0,5201	0,5096	0,5171	0,5164	0,5165	0,516478
23	0,6831	0,6915	0,6752	0,6743	0,6732	0,6732	0,673219
25	−0,3169	−0,3037	−0,2846	−0,2814	−0,2802	−0,2802	−0,280227
34	0,6561	0,6447	0,6308	0,6285	0,6276	0,6275	0,627524
37	−0,0495	−0,0701	−0,0661	−0,0676	−0,0674	−0,0674	−0,067377

* Остальные элементы либо строго равны нулю, либо совпадают с приведенными значениями по соображениям симметрии. Электронная заселенность каждого атома $P_{\mu\mu}$ строго равна единице.

Таблица 8

Элементы матрицы спиновой заселенности $\rho_{\mu\nu}$ бензильного радикала в равновесной конфигурации, вычисленные на волновых функциях разной точности*

$\mu\nu$	Ψ						
	G	I	II	III	IV	V	*F*
11	0	−0,0835	−0,0885	−0,0945	−0,0951	−0,0951	−0,095112
22	0,0812	0,1585	0,1547	0,1641	0,1639	0,1640	0,163993
33	0	−0,0473	−0,0489	−0,0550	−0,0552	−0,0552	−0,055212
44	0,0511	0,1440	0,1387	0,1472	0,1472	0,1473	0,147255
77	0,7864	0,7171	0,7381	0,7291	0,7304	0,7303	0,730295
13	0	0,0162	0,0177	0,0183	0,0183	0,0183	0,018299
24	−0,0644	−0,1085	−0,0995	−0,1021	−0,1016	−0,1016	−0,101600
26	0,0812	0,0994	0,0874	0,0872	0,0868	0,0868	0,086802
26	−0,2528	−0,2371	−0,2292	−0,2278	−0,2272	−0,2272	−0,227197
35	0	0,0054	0,0067	0,0081	0,0080	0,0080	0,007995
47	0,2004	0,1992	0,1853	0,1843	0,1833	0,1833	0,183340

* Остальные элементы либо строго равны нулю, либо совпадают с приведенными значениями по соображениям симметрии.

функции может достичь значения 2,1 э. Учет одновозбужденных конфигураций уменьшает эту погрешность до 0,3 э, а двухвозбужденных — лишь до 0,2 э и только включение в волновую функцию трехвозбужденных конфигураций обеспечивает оценку расщепления с приемлемой точностью порядка 0,03 э.

Разность «экспериментальных» значений спиновой заселенности *пара-* и *орто-*атомов углерода $\rho_{44} - \rho_{22}$ составляет примерно $+0{,}45$.[2] Одноконфигурационный расчет дает для нее значение с противоположным знаком, равное $-0{,}030$. Это означает, что простое уравнение Мак-Коннела [1] может привести к погрешности оценки расщепления, равной 1,6 э, если спиновая заселенность вычислена в одноконфигурационном приближении. Вместе с ранее сделанной оценкой погрешности за счет одноконфигурационной аппроксимации волновой функции это составит 3,7 э. Уточнение волновой функции путем включения одно-, двух- и трехвозбужденных конфигураций снижает суммарную погрешность соответственно до 1,6; 1,5 и 1,4 э. Дальнейший учет конфигураций более высокой кратности возбуждения уже ничего не изменяет. Разность остается отрицательной.

Таблица 9

Естественные α-спин-орбитали бензильного радикала в равновесной конфигурации, вычисленные на волновых функциях разной точности *

Ψ	μ	$5b_2$	$2a_2$	$4b_2$	$3b_2$	$2b_2$	$1a_2$	$1b_2$
I	1	0,29271	0,00000	−0,67929	−0,05356	−0,61039	0,00001	0,27827
	2	−0,33352	0,48578	0,27183	−0,29580	−0,33268	−0,51382	0,34161
	3	0,46406	−0,51383	0,21422	0,01742	0,18805	−0,48579	0,45065
	4	−0,50399	−0,00000	−0,41876	0,24418	0,48513	−0,00002	0,52503
	7	−0,08450	−0,00000	0,35162	0,87287	−0,31623	0,00000	0,08557
II	1	0,42417	−0,00000	−0,60845	−0,32663	0,21370	0,00000	0,54545
	2	−0,38270	0,48376	0,20003	−0,40741	−0,17121	−0,51573	0,34385
	3	0,41141	−0,51573	0,30463	0,14404	−0,38801	−0,48376	0,25815
	4	−0,40694	0,00000	−0,51302	0,53804	−0,46829	0,00000	0,24985
	7	−0,15179	−0,00000	0,31777	0,47996	0,61262	0,00000	0,51992
III	1	0,42554	−0,61058	−0,00000	−0,30666	0,25108	−0,00000	0,53762
	2	−0,38114	0,19643	0,48138	−0,40834	−0,14355	−0,51795	0,35889
	3	0,41219	0,30585	−0,51795	0,13679	−0,37699	−0,48138	0,27519
	4	−0,40627	−0,50911	0,00000	0,53359	−0,46892	−0,00000	0,26674
	7	−0,15340	0,32210	−0,00000	0,50034	0,62580	−0,00000	0,48037
IV	1	0,42991	−0,60781	−0,00000	−0,31669	0,21983	−0,00000	0,54509
	2	−0,38249	0,19376	0,48131	−0,40857	−0,16772	−0,51802	0,34799
	3	0,41009	0,30884	−0,51802	0,14179	−0,38628	−0,48131	0,25909
	4	−0,40255	−0,51189	−0,00000	0,54039	−0,47036	−0,00000	0,25034
	7	−0,15552	0,32045	0,00000	0,48334	0,61299	−0,00000	0,51357
V	1	0,42999	−0,60779	−0,00000	−0,31651	0,22009	−0,00000	0,54506
	2	−0,38249	0,19370	0,48129	−0,40857	−0,16753	−0,51803	0,34812
	3	0,41008	0,30888	−0,51803	0,14174	−0,38621	−0,48129	0,25919
	4	−0,40249	−0,51190	−0,00000	0,54035	−0,47040	−0,00000	0,25041
	7	−0,15556	0,32047	0,00000	0,48353	0,61305	−0,00000	0,51429
F	1	0,42998	−0,60779	−0,00000	−0,31655	0,21986	−0,00000	0,54513
	2	−0,38249	0,19370	0,48129	−0,40858	−0,16769	−0,51803	0,34803
	3	0,41008	0,30888	−0,51803	0,14175	−0,38630	−0,48129	0,25905
	4	−0,40248	−0,51190	−0,00000	0,54037	−0,47046	−0,00000	0,25026
	7	−0,15556	0,32046	0,00000	0,48347	0,61288	−0,00000	0,51356

* Коэффициенты для остальных атомов определяются из соображений симметрии.

Таким образом, как бы точно ни была вычислена волновая функция в π-электронном приближении ни для равносвязной конфигурации бензильного радикала, [4–7] ни для равновесной невозможно получить правильный знак разности спиновой заселенности *пара*- и *орто*-атомов углерода. Успех, достигнутый в этом направлении Счастневым и Жидомировым,[16] по-видимому, следует признать случайным.

В заключение рассмотрим свойства естественных спин-орбиталей $N^{\sigma}_{\mu i}$ бензильного радикала в равновесной конфигурации, которые можно использовать для ускорения сходимости ряда КВ. Для спина α они приведены в табл. 9 в зависимости от точности волновой функции, на которой вычислялись матрицы плотности. Естественные спин-орбитали для одноконфигурационной аппроксимации волновой функции не приведены, поскольку они совпадают с хартри-фоковскими орбиталями (табл. 4) с точностью до унитарного преобразования.[56] Расположив орбитали (табл. 9) в порядке последовательного увеличения соответствующих чисел заполнения n_{σ} (табл. 10) и сравнив их с аналогичными данными для равносвязной модели бензильного радикала (в [4–7] приведены $N^{\alpha}_{\mu i}$ и n_{α} только для точной волновой функции), можно заметить, что для равносвязной модели в отличие от равновесной хартри-фоковская последовательность расположения орбиталей по симметрии—$1b_2$, $2b_2$, $1a_2$, $3b_2$, $2a_2$,$4b_2$, $5b_2$ восстанавливается, начиная с учета при построении волновой функции трехвозбужденных конфигураций. Для равновесной конфигурации эта последовательность нарушена вплоть до полного КВ (см. табл. 9, 10). Это обстоятельство нужно учитывать при записи β-спин-естественных орбиталей (см. [4–7], особенно табл. VIII в [5]), в частности, при выполнении КВ в базисе естественных орбиталей. По сравнению с равносвязной моделью бензильного радикала[4–7] числа заполнения для разных спинов в меньшей степени отличаются для разрыхляющих и связывающих орбиталей, заполненных в одноконфигурационном приближении одинаково. Точно так же учет КВ в равновесной модели меньше влияет на отклонение чисел заполнения от единицы или нуля.

Таблица 10

Числа заполнения n_{α} естественных спин-орбиталей бензильного радикала в равновесной конфигурации, вычисленные на волновых функциях разной точности

Орбиталь	Ψ I	Орбиталь	Ψ II	III	IV	V	*F*
$5b_2$	0,0011	$5b_2$	0,0066	0,0072	0,0075	0,0075	0,00754
$2a_2$	0,0032	$2a_2$	0,0221	0,0244	0,0255	0,0255	0,02548
$4b_2$	0,0116	$4b_2$	0,0238	0,0257	0,0267	0,0267	0,02667
$3b_2$	0,9841	$3b_2$	0,9742	0,9718	0,9708	0,9708	0,97077
$2b_2$	1,0000	$1a_2$	0,9838	0,9826	0,9815	0,9815	0,98151
$1a_2$	1,0000	$2b_2$	0,9931	0,9923	0,9921	0,9921	0,99205
$1b_2$	1,0000	$1b_2$	0,9964	0,9961	0-9960	0,9960	0,99597

Авторы благодарят В. А. Куприевича за полезные замечания, В. В. Лобанова за помощь в проведении расчетов и И. Петре за проявленный им интерес к нашим исследованиям и существенную помощь в подготовке рукописи.

---

[56] P.-O. Lowdin, *Phys. Revs*, **97**, 1474 (1955).

Revue Roumaine de Chimie, 17, 5, 801–808 (1972)

CONTRIBUTION TO THE STUDY OF THE STRUCTURE AND THE THERMODYNAMIC PROPERTIES OF MOLTEN COMPOUNDS OF THE TYPE M_3AlF_6. I STRUCTURE

KAMIL MATIAŠOVSKÝ, MARTA PAUČÍROVÁ and MILAN MALINOVSKÝ
Institute of Inorganic Chemistry of the Slovak Academy of Sciences, Dúbravská cesta,
Bratislava, Czechoslovakia

Received December 25, 1971

Various dissociation patterns of the complex anion AlF_6^{3-} in molten Na_3AlF_6 and Li_3AlF_6 which were calculated from the thermodynamic data, cryoscopic measurements and density data, are discussed. It has been found that the ions M^+, AlF_6^{3-}, AlF_4^- and F^- are present in molten M_3AlF_6. The existence of the complex anion $Al_3F_{14}^{5-}$ and of the cation Al^{3+} seems to be highly improbable.

In the phase diagrams of the systems $MF-AlF_3$ ($M = Li$ and Na, resp.) there exists a pronounced maximum, which is consistent with the formation of a congruently melting compound of the type M_3AlF_6. However the flattened shape of this maximum indicates a partial decomposition, or dissociation of this compound on melting.

Considering the different possible dissociation patterns, the degree of dissociation of the complex anion AlF_6^{3-} in fused M_3AlF_6 was calculated on the basis of thermodynamic data, from the cryoscopic measurement and from density data.

A. DISSOCIATION MECHANISM OF MOLTEN M_3AlF_6

1. DISSOCIATION OF M_3AlF_6 to MF and AlF_3

The phase diagram of molten $MF-AlF_3$ mixtures [1,2] allows for the assumption that MF and AlF_3 are the most probable products of the dissociation of molten M_3AlF_6. This assumption prevailing especially in the previous literature.

---

[1] K. Grjotheim, J. L. Holm, C. Krohn and J. Thonstad, in "Selected Topics in High Temperature Chemistry", T. Förland, K. Grjotheim, K. Motzfeldt, S. Urnes, eds. Universitetsforlaget, Oslo, 1960, p. 151.

[2] M. Malinovský, I. Čakajdová and K. Matiašovský, *Chem. Zvesti*, **21**, 794 (1967).

Pearson and Waddington[3] made the first attempts to determine the degree of dissociation of the complex anion AlF_6^{3-} in molten $Na_3\,AlF_6$. They assumed that cryolite partly dissociates at melting point (m.p.) according to the equation

$$Na_3AlF_6 \rightleftharpoons 3NaF + AlF_3 \qquad (1)$$

From the free energy changes they calculated that about 15% Na_3AlF_6 dissociates at 1000 °C and the dissociation increases with increasing temperature. Their results, however, are principally incorrect since the authors committed an error in calculation.

In the above paper[3] a method of calculation of the degree of dissociation of molten Na_3AlF_6 based on the measured density data of molten $NaF - AlF_3$ mixtures was used. Assuming the additivity of the molar volumes in this system (the hypothetical density values of molten AlF_3 and of undissociated Na_3AlF_6 were obtained by extrapolation), the authors calculated a curve which is in good agreement with the experimental data for the dependence density *vs.* composition and they assumed that about 20% and 30% of sodium cryolite dissociate at 1000 °C and 1100° respectively.

In his later work[4] Pearson corrected the incorrect value of the degree of dissociation of the complex anion AlF_6^{3-} calculated in his previous work.[3] On the basis of the thermodynamic data which were available at that time, the equilibrium constants for the equation (1) were obtained, $K = 1.7 \times 10^{-5}$ at 1000° and $K = 4.6 \times 10^{-5}$ at 1100°. These revised values for the equilibrium constants were too low to explain the experimentally determined dependence of density of molten $NaF - AlF_3$ mixtures on the concentration. For this reason Pearson suggested that these discrepancies between the degree of dissociation determined on the basis of measured density data and that calculated from the thermodynamic considerations could be ascribed to the formation of a complex which by its presence increased the dissociation of molten sodium cryolite.

By the same method as Pearson and Waddington, Abramov [5] determined the degree of dissociation of molten Na_3AlF_6 on the basis of the isotherms of molar volumes. The calculated values are : $\alpha = 0.15$ at 1000° and $\alpha = 0.20$ at 1100°. The authors point to the fact that these are only approximate values which, however, allow for quantitative estimation of the degree of dissociation of the thermal dissociation of molten Na_3AlF_6.

Mashovets and Novikova [6] also calculated the degree of dissociation of molten Na_3AlF_6 on the basis of thermodynamic data. For the scheme (1) they reported the equilibrium constant $K = 1.22 \times 10^{-5}$ at 1027° and the degree of dissociation 0.058. However, this last value is incorrect, since to the reported equilibrium constant corresponds the value 0.028.

---

[3] T. G. Pearson and J. Waddington, *Discuss. Faraday Soc.*, **1**, 307 (1947).

[4] T. G. Pearson, "The Chemical Backround of the Aluminium Industry", Royal Institute of Chemistry, No 3 (1955).

[5] G. A. Abramov, M. M. Vetyukov, I. P. Gupalo and A. A. Kostyukov, L. N. Lozhkin, „Teoreticheskie osnovy elektrometallurgii alyuminia", Metallurgizdat, Moscow 1953, p. 216.

[6] V. P. Mashovets and N. A. Novikova, Izv. Vysshikh Ucheb. Zav. Tsvet. Met., **2** (*4*), 83 (1959).

Later Mashovets and Novikova [7] calculated the equilibrium constant to be $K = 2.23 \times 10^{-5}$. The corresponding degree of dissociation would be then 0.032 and not 0.068 as it is reported in the work.[7]

For the calculation of the degree of dissociation of the complex anion AlF_6^{3-} Frank[8] used thermodynamic values for Na_3AlF_6, NaF and AlF_3 reported by.[9,10] Since the melting point reported in[9] is too high when compared with other available data, Frank corrected the used thermodynamic data for a lower value of the melting point. The calculated values are as follows: $K = 3 \times 10^{-5}$, $\alpha = 0.033$ at 1006°, $K = 4 \times 10^{-5}$, $\alpha = 0.036$ at 1100°.

On the basis of cryoscopic measurements of molten $NaF-AlF_3$ mixtures [11,12] the proposed scheme (1) was verified as possible dissociation scheme for molten Na_3AlF_6. In these considerations, NaF and AlF_3 were supposed to be completely dissociated to the ions Al^{3+}, Na^+ and F^-. The best agreement between the calculated liquidus curve and the experimental data in the temperature range from 940 to 1080° was obtained for the equilibrium constant $K = 3.0 \times 10^{-5}$ and $\alpha = 0.07$. For this calculation the value of the heat of fusion of Na_3AlF_6 $\Delta H_f = 20.85$ kcal./mole was used.

Frank and Foster, [13] using the dissociation scheme (1), calculated the density values of molten $NaF - AlF_3$ mixtures in the concentration range from 0 to 30 mole % AlF_3. In their paper they did not report the value of the equilibrium constant they used and also the agreement reported between the measured and calculated density data was not satisfactory.

Using a scheme analogous to the scheme (1), Jenssen [14] studied the degree of dissociation of the complex anion AlF_6^{3-} in molten Li_3AlF_6. Calculation procedure proposed by Grjotheim [11] was applied. The calculated value of the equilibrium constant K is 0.11 at the temperature of the melting point of Li_3AlF_6.

On the basis of the measured density data Matsushima et al. [15] calculated the degree of dissociation of molten Li_3AlF_6 according the scheme (1). They report the values $K = 6.537 \times 10^{-3}$ and $\alpha = 0.1606$ at 1000°.

From the above it follows that the degree of dissociation of molten Na_3AlF_6 according to the scheme (1), calculated on the basis of the thermodynamic data is smaller than 0.4. However, the degree of dissociation which would account for the lowering of the temperature of the primary crystallization of molten $NaF-AlF_3$ mixtures ($\alpha = 0.07$[11]) and for the density data of this system is higher than the value calculated from the thermodynamic data. The higher value of the degree of dissociation of molten Na_3AlF_6 calculated on the basis of measured density data is most probably caused by the fact that for the hypothetical density of AlF_3 an extrapolated value was accepted. It should be stressed here that the dependence of the density of molten $NaF-AlF_3$ mixtures on the concentration was studied only in the concentration range up to 40 mole% AlF_3.[5,16] On the other hand, the cryoscopic investigations assumed the presence of the cation Al^{3+} in molten Na_3AlF_6. The transport numbers measurements in the system $Na_3AlF_6-Al_2O_3$[17] have proved that the prevailing part (appr. 95%) of current in the melt was transported by the ions Na^+. The value of the transport number of sodium ion may not be that high; anyway, this value indicates that the Al^{3+} ions cannot be present in molten Na_3AlF_6 in an appreciable concentration. Hence it may be assumed that the extensive dissociation of molten Na_3AlF_6 verified by thermodynamic calculations and experimental measurements cannot follow the proposed scheme (1) and that the dissociation mechanism must be quite different.

---

[7] V. P. Mashovets and N. A. Novikova, *Izvesti*; *Vysshikh Ucheb. Zav. T svet. Met.*, **5**, 78 (1962).

[8] W. B. Frank, *J. Phys. Chem.*, **65**. 2081 (1961).

[9] C. J. O'Brien, K. K. Kelley, *J. Amer. Chem. Soc.*, **79**, 5616 (1957).

[10] E. G. King, *J. Amer. Chem. Soc.*, **79**, 2056 (1957).

[11] K. Grjotheim, "Contribution to the Theory of Aluminium Electrolysis", Det. Kgl. Norske Videnskabers Selskabs Skrifter Nr. 5 Bruns Bokhandel, Trondheim 1956.

[12] J. Brynestad, K. Grjotheim and S. Urnes, *Z. Elektr.-Ber. Bunsenges. Phys. Chem.*, **63**, 707 (1959).

[13] W. B. Frank and L. M. Foster, *J. Phys. Chem.*, **64**, 95 (1960).

[14] B. Jenssen, "Thesis", Technical University of Norway, Trondheim 1969.

[15] T. Matsushima, Y. Yoshida and N. Takahashi, *Denki Kogaku*, **39**, 102 (1971).

2. DISSOCIATION OF Na_3AlF_6 TO $Na_5Al_3F_{14}$ AND NaF

Frank and Foster[13] considered the following dissociation scheme for molten Na_3AlF_3 :

$$3Na_3AlF_6 \rightleftharpoons Na_5Al_3F_{14} + 4NaF \tag{2}$$

The experimentally determined density data are in a good agreement with the values calculated according to this scheme of dissociation in the concentration range 0 to 20 mole% AlF_3; at higher concentration of AlF_3, however, there are rather big discrepancies between the measured and calculated values.

The dissociation scheme (2) is based on the assumption of the presence of complex $Al_3F_{14}^{5-}$ anion in molten $NaF-AlF_3$ mixtures. However, the compound $Na_5Al_3F_{14}$ (chiolite) which is known as a crystalline substance, is decomposed at 739 ° by a peritectic reaction.[11] Hence it follows that the existence of this ionic species in the melt at about 1000° is highly improbable. This was confirmed also by spectroscopic measurement.[18]

3. DISSOCIATION OF M_3AlF_6 TO MF AND $MAlF_4$

Recently, the following dissociation scheme of molten Na_3AlF_6 was considered to be most probably

$$Na_3AlF_6 \rightleftharpoons NaAlF_4 + 2NaF \tag{3}$$

---

[16] J. D. Edwards, C. S. Taylor and A. S. Russel, *J. Electrochem. Soc.*, **100**, 508 (1953)

[17] W. B. Frank and L. M. Foster, *J. Phys. Chem.*, **61**, 1531 (1957).

[18] C. Solomons, J. H. R. Clarke and J. O'M. Bockris, *J. Chem. Phys.*, **49**, 445 (1968).

The compound $NaAlF_4$ was identified by Howard[19] in quenched vapours over the molten $NaF-AlF_3$ mixtures close to the equimolar composition. In a solid state at temperatures below 500° this compound decomposed according to the equation : $5NaAlF_4 \rightleftharpoons Na_5Al_3F_{14}+2AlF_3$. The assumption on the existence of $NaAlF_4$ in the melt is supported by the results of the investigation of the vapour composition,[20-22] vapour pressure[21,23] and X-ray diffraction of quenched vapour.[24] The existence of the complex AlF_4^- anion in the melt was determined by cryoscopic[25] and spectroscopic[18] measurements. Considerations on electron structure and electrical conductivity of molten sodium cryolite[26,27] also corroborate this assumption.

$LiAlF_4$ was identified in quenched vapours by spectroscopic methods[22,28] by X-ray powder diffraction[29] and the presence of the anion AlF_4^- in molten Li_3AlF_6 was confirmed by cryoscopic measurement.[30]

Grjotheim[11] performed for the first time quantitative estimation of the degree of dissociation according to scheme (3) on the basis of cryoscopic measurements in the system $NaF-AlF_3$. In his work Grjotheim considered several possible mechanisms of dissociation and after having compared the measured and calculated liquidus curves he found the scheme (3) with the equilibrium constant $K = 0.06$, $\alpha = 0.3$ to be the most suitable for the molten sodium cryolite. The heat of fusion used for these calculations was $\Delta H_f = 20.85$ kcal/mole. Brynestad et al.[31] used in their calculations of the equilibrium constant the value $\Delta H_f = 27.64$ kcal/mole reported by.[9] Close to the m.p. of cryolite (1009°) $K = 0.0297$ and $\alpha = 0.23$.

Using an analogous proceeding Rolin,[32,33] determined the following values for the dissociation of sodium cryolite in the proximity of the m.p. : $K = 0.177$ and $\alpha = 0.44$ for $\Delta H_f = 20$ kcal/mole, $K = 0.02$ and $\alpha = 0.204$ for $\Delta H_f = 24.6$ kcal/mole.

In the calculation of theoretical liquidus curves both Grjotheim and Rolin expressed the ionic activities in the melt on the basis the Temkin's model. More recently Rolin and Rey[34] using classic thermodynamics calculated the degree of dissociation of Na_3AlF_6 $\alpha = 0.2$.

---

[19] E. H. Howard, *J. Amer. Chem. Soc.*, **76**, 2041 (1954).

[20] H. Ginsberg and A. Bohm, *Z. Elektrochem.*, **61**, 315 (1957).

[21] A. Vajna and R. Bacchiega, *Met. ital.*, **52**, 481 (1960).

[22] L. D. McCory, R. C. Paule and J. L. Margrave, *J. Phys. Chem.*, **67**, 1086 (1963).

[23] M. M. Vetyukov, M. L. Bliustein and V. P. Poddymov, *Zav. Tsvet. Met.*, **2**, 126 (1959).

[24] H. Ginsberg and K. Resch, *Z. Erzbergbau u. Metallhüttenw.*, **13**, 523 (1960).

[25] K. Grjotheim, T. Halvorsen and S. Urnes, *Canad. J. Chem.*, **37**, 1170 (1959).

[26] G. J. Landon and A. R. Ubbellohde, *Proc. Roy. Soc. (London)*, **240**, 160 (1957).

[27] G. J. Landon, "The Melting Mechanism of Cryolite, Na_3AlF_6 ", Cong. Intern. Chim. Pure et Appl. 16, Paris, 1957.

[28] R. F. Porter and E. E. Zeller, *J. Chem. Phys.*, **33**, 858 (1960).

[29] G. Garton and B. M. Vanklyn, *J. Inorg. Nucl. Chem.*, **27**, 2461 (1965).

[30] K. Matiašovský and M. Malinovský, *Chem. Zvesti*, in press.

[31] J. Brynestad, K. Grjotheim and S. Urnes, *Met. italicna*, **52**, 495 (1960).

[32] M. Rolin, *Bull. Soc. Chim. France*, 1960, 677, 681.

[33] M. Rolin and M. Bernard, *Bull. Soc. Chim. France*, 1962, 429.

[34] M. Rolin and M. Rey, *Bull. Soc. Chim. France*, 1966, 2785.

The calculated and the experimentally determined liquidus curves are in good agreement in the concentration range up to 25 mole % AlF_3, at higher concentrations there are, however, considerable differences between the calculated and measured values. Cochran[35] assumes that this discrepances may be explained by the presence of a further complex anion, $Al_3F_{14}^{5-}$, besides the anions AlF_6^{3-} and AlF_4^- in the melt. He proposes the following dissociations schemes :

$$Na_3AlF_6 \rightleftharpoons NaAlF_4 + 2NaF \tag{4}$$

$$Na_5Al_3F_{14} \rightleftharpoons Na_3AlF_6 + 2NaAlF_4 \tag{5}$$

According to Cochran, the corresponding equilibrium constants are $K_{(4)} = 0.0194$ and $K_{(5)} = 0.0877$. However, these dissociation schemes are very improbable since $Na_5Al_3F_{14}$ is unstable in the liquid phase, as mentioned above. This was also confirmed by Paučírová et al.[36]

Frank and Foster [13] considered three different dissociation schemes and compared the mesaured and calculated density values of molten $NaF-AlF_3$ mixtures. They confirmed the high probability of the dissociation scheme (3) with the corresponding values $K = 0.09$ and $\alpha = 0.35$ at 1000°.

Vetyukov[37] determined the degree of dissociation of molten Na_3AlF_6 on the basis of the isotherm of molar volumes of melts in the system $NaF-NaAlF_4$ at 1000°. This method was used before by Pearson and Waddington[3] and by Abramov et al.[5]. The calculated value of the degree of dissociation was $\alpha = 0.25$. However, Paučírová et al.[36] found that the method proposed by Vetyukov is not the most suitable for the calculation of the degree of dissociation of molten cryolite.

On the basis of the experimentally determined density values of molten $NaF-AlF_3$ mixtures, Paučírová et al.[36] calculated the degree of dissociation of molten Na_3AlF_6 $\alpha = 0.30-0.32$ and the equilibrium constant $K = 0.06-0.08$ at 1000°. The calculated density values are in good agreement with the measured values in the concentration range up to 20 mole % AlF_3. At higher concentrations of AlF_3 the differences between calculated and measured values are relatively higher. These differences are most probably caused by the fact that the calculation of the density involves the assumption of the additivity of molar volumes. The density data of molten $NaF-AlF_3$ mixtures calculated by Frank and Foster[13] are in good agreement with the experimental results in the concentration range up to 30 mole % AlF_3, most probably because of a rather high value of density of $NaAlF_4$ used for the calculation (1.873 $g.cm^{-3}$). The experimentally determined value of density[38] for $NaAlF_4$ is 1.63 $g.cm^{-3}$ which agrees with the data obtained by extrapolation of the dependence of densities of molten $NaF-AlF_3$ mixtures on the concentration at 1000° which range from 1.60 to 1.72 $g.cm^{-3}$ [39,40].

---

[35] C. N. Cochran, *Trans. Metallurg. Soc. AIME*, **239**, 1056 (1967).

[36] M. Paučírová, K. Matiašovský and M. Malinovský, *Rev. Roumaine Chim.*, **15**, 201 (1970).

[37] M. M. Vetyukov, "Fizicheskaya khimia rasplavlennykh solei i shlakov", Trudy vsesoyuznogo soveshchania po fizicheskoi khimii solei i shlakov, Metallurgizdat, Moscow, 1962, p. 77.

[38] M. Paučírová, K. Matiašovský and M. Malinovský, *Rev Roumaine Chim.*, **15**, 33 (1970).

Using scheme (3) Mashovets and Yudin[41] found on the basis of the interaction of compounds Na_3AlF_6, $NaAlF_4$ and AlF_3 with water vapour the value of the equilibrium constant of dissociation of molten Na_3AlF_6 at 1027°, $K = 7.64 \times 10^{-4}$, this corresponding to $\alpha = 6.1 \times 10^{-2}$. From this calculation it follows that only 6% Na_3AlF_6 dissociate into NaF and $NaAlF_4$. The degree of dissociation of the reaction

$$NaAlF_4 \rightleftharpoons 1/3Na_3AlF_6 + 2/3AlF_3 \qquad (6)$$

was calculated by a similar method. The calculated values are : $K = 0.990$, $\alpha = 0.651$. Thus, according to Mashovets and Yudin, molten Na_3AlF_6 is dissociated only to a minor extend.

Yudin and Mashovets[42] assume that the dissociation of sodium cryolite occurs according to two parallel schemes :

$$Na_3AlF_6 \rightleftharpoons NaAlF_4 + AlF_3,\ K = 7.64.10^{-4} \qquad (7)$$

$$Na_3AlF_6 \rightleftharpoons 3NaF + AlF_3,\ K = 2.23.10^{-5} \qquad (8)$$

On the basis of the equilibrium constants determined in previous works,[7,41] they calculated the following values of the molar fractions of constituents : $N_{NaAlF_4} = 0.044$, $N_{AlF_3} = 0.010$. Hence it follows that in molten Na_3AlF_6 at 1027° there are only about 1% AlF_3 and 4.4% $NaAlF_4$.

On the other hand, the investigation of Raman spectra[18] showed that at 1030° . Na_3AlF_6 is dissociated to anions AlF_6^{3-}, AlF_4^-, F^- and the degree of dissociation is somewhere between 0.6 and 0.8, the higher value being more probable. This value differs considerably from values calculated by means of indirect methods and it is, most probably too high.

In comparison with Na_3AlF_6, less attention was devoted to the investigation of the dissociation of the complex anion AlF_6^{3-} in molten Li_3AlF_6. Papers dealing with this dissociation appeared only in recent years and in these, the dissociation scheme similar to the scheme (3) was considered.

On the basis of cryoscopic measurements using a method suggested by Grjotheim,[11] Jenssen[14] calculated the degree of dissociation of molten Li_3AlF_6 $\alpha = 0.2$, this corresponding to the equilibrium constant $K = 0.023$. Using a similar procedure, Rolin et al.[43] determined the values $K = 0.06$ and $\alpha = 0.3$. Malinovský and Vrbenská[44] succeeded to attain

---

[39] G. A. Abramov and P. A. Kozunov, *Trudy Leningrad. politekhn. inst. Razdel Metallurgia*, **1**, 60 (1939).

[40] A. Vajna, *Alluminio*, **19**, 541 (1950).

[41] V. P. Mashovets and B. Yu. Yudin, *Izv. Vysshikh Ucheb. Zav. Tsvet. Met.*, **5** (4), 95 (1962).

[42] B. Yu. Yudin and V. P. Mashovets, *Zhur. Prikl. Khim.*, **36**, 1244 (1963).

[43] M. Rolin and H. Latreille, H. Pham, *Bull. Soc. Chim. France*, 2271 (1969).

[44] M. Malinovský and J. Vrbenská, *Collection Czech. Chem. Com.*, **36**, 567 (1971).

a good agreement between the measured and calculated values of the liquidus curve using the values $K = 0.09$ and $\alpha = 0.35$.

For the calculation of the degree of dissociation of molten lithium cryolite on the basis of density data of molten $LiF-AlF_3$ mixtures which was carried out by Paučírová et al.[36] the method proposed by Frank and Foster[13] was used. The calculated values at 1000° are $K = 0.06$ and $\alpha = 0.3$. Matsushima et al.[15] obtained by the same method the values $K = 0.038$ and $\alpha = 0.25$.

B. TEMPERATURE DEPENDENCE OF THE DEGREE OF DISSOCIATION OF COMPLEX ANION AlF_6^{3-} IN MOLTEN M_3AlF_6

On the basis of scheme (3), Frank and Foster[13] determined, using the experimental density data, the dependence of the degree of dissociation of molten Na_3AlF_6 on the temperature. From this dependence they determined the heat of dissociation to be $\Delta H_{dis} = 22$ kcal/mole. Matiašovský et al.[45] calculated the heat of dissociation of sodium cryolite $\Delta H_{dis} = 10.7$ kcal/mole , which is approximately one half of the value presented in.[13] Brynestad et al.[31] calculated the theoretical liquidus curve for two different values of the heat of dissociation of Na_3AlF_6 : 22.0 kcal/mole according to[13] and an arbitrary chosen value 10.0 kcal/mole. A good agreement between the calculated and experimental values was found for the heat of dissociation $\Delta H_{dis} = 10.0$ kcal/mole, which is close to the value presented by Matiašovský et al.

The values of the heat of dissociation, ΔH_{dis} of molten Li_3AlF_6, determined by Matiašovský et al.[45] and by Matsushima et al.[15] 11.2 kcal/mole and 13.0 kcal/mole, respectively, are in a good agreement with respect to the accuracy of the calculation. According to Malinovský,[46] from the thermodynamic point of view Li_3AlF_6 and Na_3AlF_6 may be considered as thermodynamically analogous compounds with a virtually equal values of the entropy of fusion. Therefore, the values of the heat of dissociation may be expected to be close to each other ; data presented by Matiašovský et al.[45] confirm this assumption.

---

[45] K. Matiašovský, M. Paučírová and M. Malinovský, *Coll. Czech. Chem. Comm.*, in press.

[46] M. Malinovský, *Chem. Zvesti*, **21**, 783 (1967).

Revue Roumaine de Chimie, 17, 5, 809 – 817 (1972)

CONTRIBUTION TO THE STUDY OF THE STRUCTURE AND THE THERMODYNAMIC PROPERTIES OF MOLTEN COMPOUNDS OF THE TYPE M_3AlF_6. II[1]

THERMODYNAMIC PROPERTIES

MARTA PAUČÍROVÁ, MILAN MALINOVSKÝ and KAMIL MATIAŠOVSKÝ

Institute of Inorganic Chemistry of the Slovak Academy of Sciences, Dúbravska cesta,
Bratislava, Czechoslovakia

Received December 25, 1971

On the basis of the temperature dependence of the degree of dissociation of the complex AlF_6^{3-} anion in molten Na_3AlF_6 and Li_3AlF_6 and assuming that the dissociation is described by the scheme $M_3AlF_6 \rightleftharpoons 2MF + MAlF_4$, the thermodynamic properties for undissociated liquid cryolites and molten $MAlF_4$ were calculated.

INTRODUCTION

The experimentally determined heat contents of molten compounds of the type M_3AlF_6 (where M denotes Li or Na) and also the thermodynamic functions calculated for these compounds do not respresent pure liquidus cryolites. They correspond to the mixtures in which M_3AlF_6 is in equilibrium with the products of its dissociation according to the equation

$$M_3AlF_6\,(s) \rightleftharpoons (1-\alpha)M_3AlF_6(l) + \alpha MAlF_4(l) + 2\alpha MF\,(l) \qquad (1)$$

where α is the degree of dissociation of the complex AlF_6^{3-} anion in molten M_3AlF_6. The thermodynamic values for the hypothetical undissociated M_3AlF_6 can be calculated since the temperature dependence of the degree of dissociation α is known.

The thermodynamic data for the compounds MF and M_3AlF_6 which were used in this paper are listed in Table 1.

---

[1] K. Matiašovský, M. Paučírová and M. Malinovský, *Coll. Czech. Chem. Comm.*, in press.

Table 1

Thermodynamic data for MF and M_3AlF_6 compounds

Compound	Melting point (°K)	$-\Delta H^\circ_{298}$ kcal. mole^{-1}	S°_{298} cal. mole^{-1} deg.$^{-1}$	ΔH_f kcal. mole^{-1}	C_p cal·mole^{-1}·deg^{-1}			Range °K
					a	$b \cdot 10^3$ T	$c \cdot 10^{-5}$ T^{-2}	
LiF (s)	1121	146.3 [2]	8.5 [2]	6.4 [2]	9.14	5.19	— [2]	298−m.p.
LiF (1)					15.5	—	— [2]	m.p.−1500
NaF (s)	1268	137.53 [3]	12.3 [2]	7.92 [4]	8.412	6.23	1.963 [4]	298 − m.p.
NaF (1)					16.866		[4]	m.p.−1400
Li_3AlF_6(s)	1055	805.0 [5]	46.4 [5]	21.5 [5]	74.2		[6]	873 − m.p.
Li_3AlF_6(1)					82.7		[6]	m.p.−1153
Na_3 AlF_6(s, α)	833.5*	792.4 [3]	57.0 [7]	2.22** [4]	45.51	0.32	1.755 [4]	298 − 833.5
Na_3AlF_6(s, β)	1279			26.71 [4]	36.4	24.28	[4]	833.5−m.p.
Na_3AlF_6 (1)					96.814		[4]	m.p.−1350

* Transition temperature α → β

** Heat of transition

---

[2] O. Kubashewski, E. Ll. Evans and C. B. Alcooch, "Metallurgical Thermochemistry", Pergamon Press, New York, 4th ed. 1967.

[3] E. W. Dewing, *Met. Trans.*, **1**, 2211 (1970).

[4] W. B. Frank, *J. Phys. Chem.*, **65**, 2081 (1961).

[5] P. D. Green, P. Gross and C. Hayman, *Trans. Faraday Soc.*, **64**, 633 (1968).

[6] H. Latreille, "Thesis", Lyon, 1968.

[7] E. G. King, *J. Amer. Chem. Soc.*, **79**, 2056 (1957).

1. THERMODYNAMIC PROPERTIES OF UNDISSOCIATED Na_3AlF_6

The heat content of the undissociated Na_3AlF_6 can be obtained from the equation:

$$(H_T - H_{298})_n = (H_T - H_{298})_d - \alpha\,\Delta H_d \qquad (2)$$

where $(H_T - H_{298})_n$ is the heat content of the hypothetical undissociated molten Na_3AlF_6,

$(H_T - H_{298})_d$ is the heat content of the solution of cryolite and the products of its dissociation,

ΔH_d is the heat of dissociation for reaction (1), 10.7 kcal./mole.[1]

The heat of mixing, ΔH_{mix}, of dissociation products equals zero, since the calculations are carried out for an ideal solution. The calculated values for the heat content of undissociated cryolite at three temperatures are presented in Table 2.

Table 2

Heat content of molten Na_3AlF_6

Temperartue °K	Degree of dissociation	$(H_T - H_{298})_d$ kcal. mole^{-1}	$(H_T - H_{298})_n$ kcal. mole^{-1}
1279	0.32	94.97	91.55
1329	0.34	99.81	96.17
1379	0.36	104.65	100.80

On the basis of the values given in Table 2, the temperature dependence for the heat content of undissociated Na_3AlF_6 was derived:

$$(H_T - H_{298})_n = 92.5T - 26808 \text{ (cal. mole}^{-1}\text{)} \qquad (3)$$

Differentiating equation (3) by temperature we obtained the heat capacity of the undissociated cryolite:

$$C_p = 92.5 \text{ cal. deg}^{-1}\text{. mole}^{-1} \qquad (4)$$

The heat of fusion of undissociated cryolite was calculated according to the equation:

$$\Delta H_{f,n} = \Delta H_{f,d} - \alpha\,\Delta H_d \qquad (5)$$

where $\Delta H_{f,n}$ is the heat of fusion of undissociated molten Na_3AlF_6 $\Delta H_{f,d}$ is the heat of fusion of the solution of cryolite with the products of its dissociation.

The calculated value is :

$$\Delta H_{f,n} = 23.3 \text{ kcal.mole}^{-1} \tag{6}$$

The temperature dependence of the entropy of undissociated Na_3AlF_6 can be obtained from the equations :

$$(S_T - S_{298})_n = (S_{1279} - S_{298})_s + \Delta S_{f,n} + (S_T - S_{1279})_n \tag{7}$$

$$\text{according to}^4 \ (S_{1279} - S_{298})_s = 96.6 \text{ cal. mole}^{-1}\text{. deg}^{-1} \tag{8}$$

$$\text{hence, } \Delta S_{f,n} = 18.17 \text{ cal. mole}^{-1}\text{. deg.}^{-1} \tag{9}$$

$$\text{and } (S_T - S_{1279})_n = \int_{1279}^{T} 92.5 \, \mathrm{d}T/T = 213.03. \log T - 661.46 \tag{10}$$

Substituting from Eqs (8—10) into Eq. (7) we obtain :

$$(S_T - S_{298})_n = 213.03 \log T - 546.54 \tag{11}$$

From Eqs (3) and (11) and the value $S^0_{298} = 57$ cal. mole^{-1}. deg^{-1}, the function $(G_T - H_{298})$ for undissociated molten cryolite can be derived :

$$G_T = H_T - TS_T \tag{12}$$

$$(G_T - H_{298})_n = (H_T - H_{298})_n - T(S_T - S_{298} + S_{298})_n \tag{13}$$

$$(G_T - H_{298})_n = 582.04 \ T - 213.03 \ T \log T - 26808 \tag{14}$$

Since Na_3AlF_6 is partially dissociated at its melting point (m.p.), the experimentally determined m.p. is lower than the hypothetical m.p. of undissociated cryolite. This hypothetical m.p. can be calculated from the La Chatelier-Schrödervan Laar equation :

$$\ln a = \frac{\Delta H_{f,n}}{R} \left(\frac{1}{T_0} - \frac{1}{T} \right) \tag{15}$$

where $a = 0.419$, is the activity of the undissociated Na_3AlF_6 in the melt at the m.p. (this value was calculated from the degree of dissociation),

$T = 1279$°K, is the experimentally determined m.p. of Na_3AlF_6,

T_0 is the hypothetical m.p. of undissociated Na_3AlF_6.

The calculated value for m.p. of undissociated cryolite according to the equation (15) is :

$$T_0 = 1424 \ {}^\circ\text{K} \tag{16}$$

The values T_0 for pure Na_3AlF_6 determined by different authors are presented in Table 3.

Table 3

Melting point of undissociated Na_3AlF_6

Melting point		Degree of dissociation	Author	Method
°K	°C			
1425	1152	0.23	Brynestad[8]	cryoscopy
1472	1199	0.35	Frank[9]	density
1355	1085	0.204	Rolin[10]	cryoscopy
1424	1151	0.32	this work	density

2. THERMODYNAMIC PROPERTIES OF UNIDOSSOCIATED Li_3AlF_6

The calculation of the thermodynamic properties of the undissociated molten Li_3AlF_6 was carried out using a similar method as in the case of molten sodium cryolite. The heat content of the undissociated lithium cryolite was calculated according to the equation (2), where $\Delta H_d = 11.2$ kcal.mole⁻¹. The calculated data are given in Table 4.

Table 4

Heat content of molten Li_3AlF_6

Temeperature °K	Degree of dissociation	$(H_T-H_{298})_d$ kcal. mole^{-1}	$(H_T-H_{298})_n$ kcal/Δmole^{-1}
1055	0.21	71.20	68.85
1100	0.32	74.92	72.34
1150	0.25	79.05	76.25

The dependence of the heat content of undissociated Li_3AlF_6 on the temperature is described by the equation :

$$(H_T - H_{298})_n = 77.94 \ T - 13375 \ (\text{cal. mole}^{-1}) \qquad (17)$$

From Eq. (17) it follows that

$$C_p = 77.94 \ \text{cal. mole}^{-1}. \text{deg}^{-1} \qquad (18)$$

The heat of fusion of undissociated Li_3AlF_6, calculated by means of the Eq. (5), is

$$\Delta H_{f,n} = 19.15 \ \text{kcal.mole}^{-1} \qquad (19)$$

---

[8] J. Brynestad, K. Grjotheim and S. Urnes, *Met. Ital.*, **52**, 495 (1960).
[9] W. B. Frank and L. M. Foster, *J. Phys. Chem.*, **64**, 95 (1960).
[10] M. Rolin and M. Bernard, *Bull. Soc. Chim. France*, **1962**, 429.

The entropy of the undissociated molten lithium cryolite is given by equations :

$$(S_T - S_{1055})_n = \int_{1055}^{T} 77.94\,\mathrm{d}T/T = 179.57 \log T - 543.02 \tag{20}$$

$$(S_T - S_{298})_s = \int_{298}^{T} 74.18\,\mathrm{d}T/T = 170.83 \log T - 422.62 \tag{21}$$

From Eq. (21) for the temperature $T = 1055$ °K it follows that

$$(S_{1055} - S_{298})_s = 93.8 \text{ cal. mole}^{-1}.\ \text{deg}^{-1}$$

From Eqs (7), (20) and (21) and for the value $\Delta S_{f,n} = 18.15$ cal. mole^{-1}. deg^{-1} the following equation can be obtained :

$$(S_T - S_{298})_n = 179.57 \log T - 431.07 \tag{22}$$

The function $(G_T - H_{298})_n$ for undissociated Li_3AlF_6 may be written :

$$(G_T - H_{298})_n = 462.61\,T - 179.57\,T \log T - 13375 \tag{23}$$

The hypothetical m.p. of undissociated lithium cryolite was calculated from the Eq. (15). The calculated value is

$$T_0 = 1130.8\ \text{°K} \tag{24}$$

The values of the melting points of Li_3AlF_6, determined by different authors, are listed in Table 5.

Table 5

Melting point of undissociated Li_3AlF_6

Melting point		Degree of dissociation	Author	Method
°K	°C			
1145	872	0.3	Rolin [11]	cryoscopy
1119	846	0.2	Jenssen [12]	cryoscopy
1070.1	878.1	0.35	Malinovský [13]	cryoscopy
1130.8	857.8	0.21	this work	density

The thermodynamic values for hypothetical undissociated Na_3AlF_6 were calculated also by Frank.[4] The reported data are compared with those calculated in this work in Table 6, where also the data for undissociated

---

[11] M. Rolin, H. Latreille and H. Pham., *Bull. Soc. Chim. France*, 2271 (1969).

[12] B. Jenssen, "Thesis", Trodheim, 1969.

[13] M. Malinovský and J. Vrbenská, *Coll. Czech. Chem. Comm*, **36**, 567 (1971).

Li_3AlF_6 are presented. It is evident that the data which have been determined in the present work are higher than those reported in [4], which is most probably caused by the high value of the heat of dissociation which was used for the calculation by Frank. In the calculation of the theoretical liquidus curve for the system NaF — AlF_3, Brynestad et al. [8] utilized two values of the heat of dissociation : the value 22 kcal. $mole^{-1}$ published by Frank and Foster [9] and the arbitrary selected value 10 kcal. $mole^{-1}$. They obtained a good agreement between the experimentally determined and calculated values for the last value which is very close to the value used in this work.

Table 6

Calculated thermodynamic data for molten undissociated Na_3AlF_6 and Li_3AlF_6

Thermodynamic data	Na_3AlF_6 according to [4]	Na_3AlF_6 this work	Li_3AlF_6 this work
$\Delta H_{f,n}$ (kcal, $mole^{-1}$)	18.76	23.25	19.15
$S_{f,n}$(cal. $mole.^{-1}$ deg^{-1})	14.67	18.17	18.15
$(H_T - H_{298})_n$ cal. $mole^{-1}$	76.12T − 10330	92.5T − 26808	77.94T − 13375
C_p (cal. $mole.^{-1}$ deg^{-1})	76.12	92.5	77.94
$(S_T - S_{298})_{nl}$ cal. $mole.^{-1}$ deg^{-1}	175.304 logT − 433.358	213.03 logT − 661.46	179.57 logT − 431.07
$(G_T - H_{298})_n$ kcal. $mole^{-1}$	452.478T − 10330 − − 175.304T logT	582.04T − 26808 − − 213.03 T log T	462.61T − 13375 − − 179.57 T log T

As it was mentioned in Part I, Li_3AlF_6 and Na_3AlF_6 may be regarded as thermodynamically analogous compounds with virtually equal entropies of fusion.[14] From Table 6 it follows that this condition is satisfied for the heat of dissociation of Na_3AlF_6 10.7 kcal. $mole^{-1}$, while it does not hold for the higher values.

3. CALCULATION OF THE HEAT CAPACITIES OF MOLTEN $MAlF_4$

The heat capacities of molten $MAlF_4$ were calculated according to the method proposed by Frank,[4] who expressed the total heat content change, following the temperature increase and the change in the composition, in two steps :

$$\begin{tikzcd}
T_1\,{}^\circ K & T_1\,{}^\circ K & T_2\,{}^\circ K \\
n_{1,T_1}\ M_3AlF_6 & n'_{1,T_1}\ M_3AlF_6 & n'_{1,T_2}\ M_3AlF_6 \\
n_{2,T_1}\ MF \arrow[r, "\Delta H_2"] & n'_{2,T_1}\ MF \arrow[r, "\Delta H_3"] & n'_{2,T_2}\ MF \\
n_{3,T_1}\ MAlF_4 \arrow[rr, bend right, "\Delta H_1"'] & n'_{3,T_1}\ MAlF_4 & n'_{3,T_2}\ MAlF_4
\end{tikzcd}$$

---

[14] M. Malinovský, *Chem. Zvesti*, **21**, 783 (1967).

According to this scheme :

$$\Delta H_1 = \Delta H_2 + \Delta H_3 \tag{25}$$

$$\Delta H_1 = (H_{T_2} - H_{298})_{d,\alpha_1} - (H_{T_1} - H_{298})_{d,\alpha_2} \tag{26}$$

$$\Delta H_2 = \Delta n_{\mathrm{M_3AlF_6}} \, \Delta H_d \tag{27}$$

$$\Delta H_3 = (n_{\mathrm{M_3AlF_6}} \, C_{p,\mathrm{M_3AlF_6}} + n_{\mathrm{MF}} \, C_{p,\mathrm{MF}} + n_{\mathrm{MAlF_4}} C_{p,\mathrm{MAlF_4}} \,) \; T \tag{28}$$

where $\Delta n_{\mathrm{M_3AlF_6}}$ is the number of moles of M_3AlF_6 dissociating according to Eq. (1),

$n_{i,T}$ is the number of moles of each constituent,

$C_{p,i}$ is the heat capacity of each constituent,

$$T = T_2 - T_1 \,.$$

By solving Eqs. (25—28) for the heat capacities of molten $MAlF_4$ the values are obtained :

$$C_{p,\mathrm{NaAlF_4}} = 58.8 \text{ cal. mole}^{-1}.\,\text{deg}^{-1}$$

$$C_{p,\mathrm{LiAlF_4}} = 45.9 \text{ cal. mole}^{-1}.\,\text{deg}^{-1}$$

In the calculation of the heat capacities of $MAlF_4$ an analogous scheme can be applied :

$$\begin{tikzcd}
\mathrm{T_1} \; {}^\circ\mathrm{K} & \mathrm{T_2} \; {}^\circ\mathrm{K} & T_2 \; {}^\circ\mathrm{K} \\
n_{1,T_1} \, \mathrm{M_3AlF_6} & n_{1,T_2} \, \mathrm{M_3AlF_6} & n'_{1,T_2} \, \mathrm{M_3AlF_6} \\
n_{2,T_1} \, \mathrm{MF} \arrow[r, "\Delta H_2"] & n_{2,T_2} \, \mathrm{MF} \arrow[r, "\Delta H_3"] & n'_{2,T_2} \; \mathrm{MF} \\
n_{3,T_1} \, \mathrm{MAlF_4} \arrow[rr, bend right, "\Delta H_1"'] & n_{3,T_2} \;\; \mathrm{MAlF_4} & n'_{3,T_2} \, \mathrm{MAlF_4}
\end{tikzcd}$$

in this case, ΔH_2 and ΔH_3 are given by the equations :

$$\Delta H_2 = (n_{\mathrm{M_3AlF_6}} \, C_{p,\mathrm{M_3AlF_6}} + n_{\mathrm{MF}} \, C_{p,\mathrm{MF}} + n_{\mathrm{MAlF_4}} \, C_{p,\mathrm{MAlF_4}}) \; T \tag{29}$$

$$\Delta H_3 = \Delta n_{\mathrm{M_3AlF}} \;\; \Delta H_d \tag{30}$$

The calculated heat capacities values are :

$$C_{p,\mathrm{NaAlF_4}} = 58.8 \text{ cal. mole.}^{-1} \text{ deg}^{-1}$$

$$C_{p,\mathrm{LiAlF_4}} = 45.8 \text{ cal. mole.}^{-1} \text{ deg}^{-1}$$

It is evident that both methods yield practically the same value of the heat capacities of molten $MAlF_4$ compounds.

4. CALCULATION OF THE STANDARD FREE ENERGY OF FORMATION OF $MAlF_4$

The thermodynamic properties of molten $MAlF_4$ cannot be expressed in the conventional form, because the heat of formation from the elements at room temperature and the heat content values at low temperatures (up to 500°) are not available. (Below 500°, $NaAlF_4$ decomposes to $Na_5Al_3F_{14}$ and AlF_3).[15] However, the temperature dependence of the equilibrium constant for the dissociation reaction (1) is known, and hence it is possible to calculate the free energy of formation of $MAlF_4$. The change of the free energy for the scheme (1) can be express by the equation :

$$\Delta G^0_r = -RT \ln K = 2\,\Delta G^0_{MF} + \Delta G^0_{MAlF_4} - \Delta G^0_{M_3AlF_6} \qquad (31)$$

where ΔG^0_r is the change of free energy for reaction (1),

K is the equilibrium constant for reaction (1),

ΔG^0_i is the standard free energy of formation of MF, $MAlF_4$ and undissociated M_3AlF_6.

The values of the free energy of formation are calculated according to the equation :

$$\Delta G^0_i = (G_T - H_{298})_{\text{compound}} - (G_T - H_{298})_{\text{element}} + \Delta H^0_{298} \qquad (32)$$

The values $(G_T - H_{298})$ for undissociated M_3AlF_6 are calculated from Eqs. (14) and (22). The values of $(G_T - H_{298})$ for NaF are given in[4], $(G_T - H_{298})_{\text{element}}$ and $(G_T - H_{298})$ for LiF are calculated according to,[16] ΔH^0_{298} are presented in Table 1.

The calculated values of the standard free energy of formation of $MAlF_4$ are :

$NaAlF_4$: $\Delta G^0_{1279°K} = -410.174$ kcal

$\Delta G^0_{1329°K} = -404.999$ kcal

$\Delta G^0_{1379°K} = -401.876$ kcal

$LiAlF_4$: $\Delta G^0_{1055°K} = -436.543$ kcal

$\Delta G^0_{1100°K} = -434.838$ kcal

$\Delta G^0_{1150°K} = -432.619$ kcal

The authors are highly thankful to Dr. I. Proks for helpful discussions and suggestions

---

[15] E. H. Howard, *J. Amer. Chem. Soc.*, **76**, 2041 (1954).

[16] "Termodinamicheskie svoistva individualnykh veshchestv", Akademia Nauk S.S.S.R. Moscow, 1962.

Revue Roumaine de Chimie, **17**, *5*, 819–829 (1972)

ПОЛУЧЕНИЕ СПЛАВОВ КРЕМНИЯ ПОСРЕДСТВОМ ЭЛЕКТРОЛИЗА КРИОЛИТО-КРЕМНЕЗЕМНОГО РАСПЛАВА

К. ГРЙОТХЕЙМ,

Институт неорганической химии Норвежской высшей технической школы, Трондхейм, Норвегия

К. МАТИАШОВСКИ и П. ФЕЛЛНЕР,

Институт неорганической химии Словацкой Академии наук, Братислава, Чехословакия

Получена 21 декабря 1971 г.

В работе приводятся результаты исследований, направленных на изучение возможности получения сплавов Si—Al, Si—Cu и Si—Al—Cu. Изучались химические свойства расплавов системы $Na_3AlF_6-SiO_2-Al_2O_3$ и измерялись напряжения разложения составных частей электролита. Электролиз реализовался посредством применения графитового анода и алюминиевого или же медного катода. Были рассчитаны изменения свободной энтальпии для возможных реакций, а также исследованы плотности и электропроводности как двухкомпонентных, так и трехкомпонентной систем в концентрационном интервале 0—5 % SiO_2 и 0—12 % Al_2O_3. Напряжения разложения электролита измерялись по методу I-E кривых. Во всех использованных электролитах рассматривалось влияние плотности тока на выделение металлов. Был также рассчитан как теоретический, так и экспериментальный выход по току.

Получение сплавов кремния посредством электролиза интересно как с теоретической, так и с практической точек зрения. Идея эта не новая. В литературе уже был опубликован целый ряд работ, в которых рассматривались:

— электролиз SiO_2, растворенной в расплавленной смеси окислов щелочноземельных металлов и других металлов; [1–11]

---

[1] П. В. Гельд и О. А. Есин, *Докл. АН СССР*, **70**, 43 (1950).

[2] О. А. Есин и П. М. Шуригин, *Докл. АН СССР*, **94**, 1145 (1954).

[3] О. А. Есин и Л. К. Гаврилов, *Жур. физ. хим.* **29**, 556 (1955).

[4] О. А. Есин и В. А. Чечулин, *Докл. АН СССР*, **113**, 109 (1957).

[5] О. А. Есин и Г. А. Топорищев, *Жур. физ. хим.*, **31**, 474 (1957).

[6] О. А. Есин и В. А. Чечулин, *Жур. физ. хим.*, **32**, 2 (1958).

[7] В. И. Мусихин и О. А. Есин, *Изв. ВУЗов, Черная металлургия*, *12*, 3, (1959).

[8] A. E. Martin и J. Derge, *Metall. Techn.*, **10**, 1 (1943).

[9] J. O'M. Bockris, J. Kitchener и H. Daves, *Trans. Faraday Soc.*, **48**, 536 (1952).

[10] R. Sato и R. Sakagami, *J. Electrochem. Soc. Japan*, **26**, 173 (1958).

[11] R. Dickson и E. B. Dismukes, *Trans. Metall. Soc. AIME*, **224**, 505 (1962).

— электролиз SiO_2, растворенной в расплавленной смеси окислов и фторидов щелочных металлов и щелочноземельных металлов; [12,13]

— электролиз SiO_2, растворенной в расплавленном криолите; [14–16]

— электролиз фторосиликатов. [17–20]

Из анализа результатов вышеперечисленных работ, проведенного, в работах [21,22], вытекает, что для получения Si и его сплавов наиболее выгоден электролиз расплавов на базе криолита. С точки зрения возможности использования в промышленности, в первую очередь интерес представляет возможность получения сплава Si—Al посредством электролиза криолито-кремнеземных расплавов или же расплавов системы Na_3AlF_6—SiO_2—Al_2O_3, с применением алюминиевого катода. Можно предполагать, что при электролизе расплавов Na_3AlF_6—SiO_2 будет выделяться кремний, а при электролизе расплавов системы Na_3AlF_6–SiO_2–Al_2O_3 – кремний или же, в определенных условиях, одновременно кремний и алюминий. Особый интерес представляет последний случай, который открывает возможность получения сплава Si—Al в единственном процессе, и который весьма схож с известным методом производства алюминия. При применении другого металла в качестве катода, могут быть получены соответствующие сплавы Si, которые могут представлять интерес с промышленной точки зрения.

В данной работе приводятся результаты исследований, направленных на изучение возможности получения сплавов Si—Al, Si–Cu и Si—Al—Cu. В первой части работы изучались химические и физико-химические свойства расплавов системы Na_3AlF_6—SiO_2—Al_2O_3 и измерялись напряжения составных частей электролита. Во второй части работы электролиз реализовался посредством применения графитового анода и алюминиевого или же медного катода.

ХИМИЧЕСКИЕ РЕАКЦИИ В СИСТЕМЕ Na_3AlF_6–SiO_2

Кремнозем, введенный в расплавленный криолит может реагировать с Na_3AlF_6 или с AlF_3 согласно реакциям:

$$3SiO_2 + 4Na_3AlF_6 = 3SiF_4 + 12NaF + 2Al_2O_3, \tag{1}$$

$$3SiO_2 + 4AlF_3 = 3SiF_4 + 2Al_2O_3. \tag{2}$$

Изменение свободной энтальпии при 1300°K для реакции (1) и (2), вычисленное на основе термодинамических данных, соответственно равно — 19 ккал и —42 ккал. Из этого следует, что с точки зрения термодинамики,

---

[12] M. Dodero, *Bull. Soc. chim. France*, Memoires 5 ser., **6**, 209 (1939).

[13] B. Lotto, *Vetro e silicati*, **10**, 5 (1966).

[14] R. Monnier и D. Barakat, *Helv. Chim. Acta*, **40**, 2041 (1957).

[15] R. Monnier и Ph. Grandjean, *Helv. Chim. Acta*, **43**, 2163 (1960).

[16] К. П. Баташев и А. И. Журин, *Металлург*, **2**, 66 (1933).

[17] M. Dodero, Compte rend., **208**, 799 (1939).

[18] H. von Wartenberg, *Z. anorg. Chem.* **B. 265**, 168 (1951).

[19] M. Rolin, *J. fours electr.* **62**, 83 (1953).

[20] F. Olstowski, U. S. Pat. 2,909.471, October, 1959.

[21] K. Grjotheim и K. Matiašovský, *Hutnické listy*, **25**, 876 (1970).

[22] K. Grjotheim, K. Matiašovský, P. Fellner и A. Silný, *Canad. Metall. Quarterly*, 9 (1971).

возникновение SiF_4 является вероятным, однако в соответствии с данными [23,24], скорость этой реакции настолько незначительна, что изменения в химическом составе могут не учитываться.

С применением металлического алюминия может протекать и следующая реакция:

$$3SiO_2 + 4Al = 2Al_2O_3 + 3Si, \qquad (3)$$

для которой, при 1300°K, соответствует изменение свободной энтальпии $\Delta G^\circ = -139{,}55$ ккал. Эта реакция может оказывать существенное влияние на параметры электролиза, например на выход по току.[21,25]

При изучении реакции (3) были применены Na_3AlF_6 — природный гренландский криолит (т.п. 1006 ± 1°, 54,72%F), SiO_2 — осадочный, т.н. « чистый », Al — гранулированный, т.н. « чистый » (99,9%). Измерение проводилось в графитовом тигеле (сечение ∅ 45 мм, высота 80 мм), с навеской 40 г Al и 100 г смеси 95% Na_3AlF_6 с 5%SiO_2. Для поддержания в расплаве постоянной концентрации SiO_2 была применена кварцевая футеровка (трубка), которая плотно прилегала к стенке графитового тигеля. Измерение было проведено в атмосфере аргона, при температуре 1000°. Для измерения температуры был применен термоэлемент Pt/Pt 10 Rh. Были проведены две серии опытов без перемешивания, а также с перемешиванием расплава, используя поток аргона, который подводился посредством графитовой трубки под поверхность расплава. После измерений графитовый тигель был разбит, а полученный расплав Si—Al был подвергнут анализу.

Результаты измерений приведены на рис. 1. Полученные результаты говорят о том, что равновесие для реакции (3), при данных экспериментальных условиях, сдвинуто к образованию металлического кремния. Из дальнейшего сравнивания найденных зависимостей видно, что скорость реакции гораздо больше при перемешивании расплава, а если его не перемешивать, при продолжении эксперимента скорость реакции постепенно снижается. Можно предполагать что решающим для скорости реакции является активность кремния (который, вероятно, связан в форме комплексного иона) в границах фазового раздела между расплавом и жидким алюминием, и решающим же фактором, определяющим кинетику реакции, является передвижение ионов к поверхности, содержащих кремний. Необходимо считаться с тем, что Al_2O_3, возникающая в результате реакции (3), будет концентрироваться на поверхности раздела, что при электролизе может существенно повлиять на напряжение разложения SiO_2 и Al_2O_3, а тем самым и осаждение обоих металлов.

---

[23] R. Monnier и D. Barakat, *Ind. chim. belge, Suppl. 1, Compt. rend.* Congr. intern. chim. ind. 31e, Liège 1958.

[24] D. F. Weill и W. J. Fyfe, *J. Electrochem. Soc.*, **111**, 582 (1964).

[25] K. Grjotheim и K. Matiašovský, *Chemické zvesti*, **25** (1971).

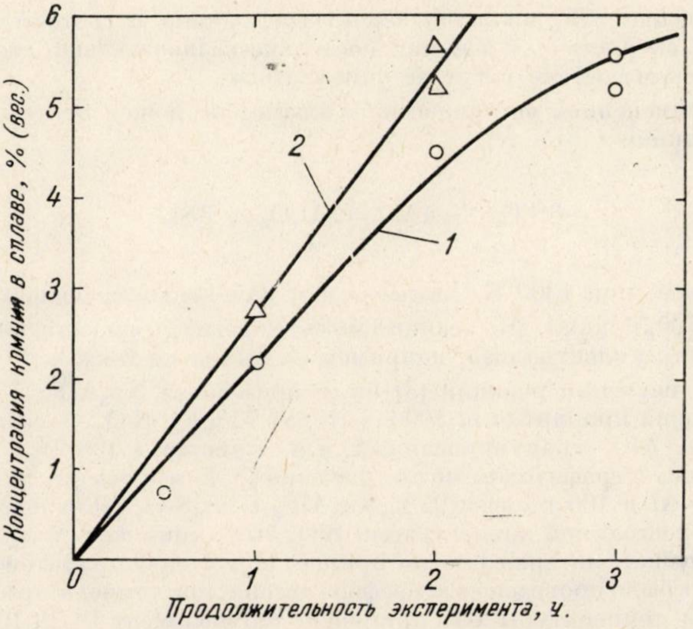

Рис. 1. — Зависимость количества кремния, выделенного по реакции $3\ SiO_2 + 4Al = 3\ Si + 2\ Al_2O_3$, от длительности эксперимента:

1, без перемешивания расплава, *2*, с перемешиванием расплава.

ФИЗИКО-ХИМИЧЕСКИЕ СВОЙСТВА РАСПЛАВОВ СИСТЕМЫ $Na_3AlF_6 - SiO_2 - Al_2O_3$

Из двухкомпонентных систем, являющихся сторонами концентрационного треугольника приведенной трехкомпонентной системы, с особым вниманием была изучена система $Na_3AlF_4 - Al_2O_3$, являющаяся основным электролитом при производстве алюминия (см., например, [26]). Для системы $Na_3AlF_6 - SiO_2$ пока что была составлена фазовая диаграмма системы [16] и измерялась электропроводность[27]. Также рассматривались равновесия фаз в системе $Na_3AlF_6 - SiO_2 - Al_2O_3$ при 800 и 1010°.[24]

В предлагаемой работе были исследованы плотность и электропроводность расплавов трехкомпонентной системы в концентрационном интервале 0—5% SiO_2 и 0—12% Al_2O_3. Для приготовления образцов, кроме вышеприведенных реактивов, была применена Al_2O_3 типа « Реанал », для хроматографии. При измерении плотности был применен метод гидростатического взвешивания, описанный в работе [28], при измерении же электропроводности — двойной мост Томсона и дискообразные электроды из гладкой платины. [29] точность измерений при определении плотности была ±0,2%, при определении электропроводности ±3%.

---

[26] Г. А. АБРАМОВ и др., « Теоретические основы электрометаллургии алюминия ». Металлургиздат, Москва, 1954.

[27] А. И. БЕЛЯЕВ, « Физико-химические основы электрометаллургии алюминия». Металлургиздат, Москва, 1947.

На рис. 2 изображена изотерма плотности расплавов системы $Na_3AlF_6-SiO_2-Al_2O_3$ при 1000°. Из положения линий одинаковой плотности можно заключить, что кремнозем практически не оказывает влияния на плотность расплавленного криолита, а повышает плотность криолито-глиноземных расплавов, главным образом, в области более высоких концентраций Al_2O_3. Изменения же плотности в исследуемой области концентрации могут быть не приняты во внимание.

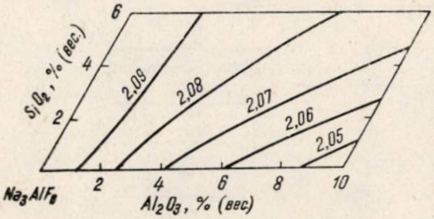

Рис. 2. — Изотерма плотности ($г.см^{-3}$) расплава системы $Na_3AlF_6-SiO_2-Al_2O_3$ при 1000°.

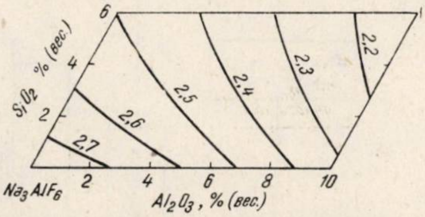

Рис. 3. — Изотерма электропроводности ($ом^{-1}.см^{-1}$) расплавов системы $Na_3AlF_6-SiO_2-Al_2O_3$ при 1000°.

Изотерма электропроводности расплавов трехкомпонентной системы, при 1000° , изображена на рис. 3. Составленная диаграмма показывает, что с повышением концентрации SiO_2 и Al_2O_3, электропроводность расплавов рассматриваемой системы понижается. В отношении бинарной системы $Na_3AlF_6-SiO_2$, необходимо обратить внимание, что измеренные величины электропроводности значительно выше величин, приведенных в работе Беляева.[27]

НАПРЯЖЕНИЕ РАЗЛОЖЕНИЯ SiO_2 И Al_2O_3

Стандартные напряжения располсжения E_r^0 кремнозема, а также глинозема, вычисленные на основе табличных значений, в соответствии с изменением свободной энергии Гиббса, при 1300°К,[30] соответственно равны 1,675 и 2,170 в. При применении графитового анода и, исходя из предположения, что соответствующим продуктом анодной реакции является CO_2, на основе термодинамических данных, при 1300°К, были вычислены следующие значения напряжения разложения:

$$SiO_2 + C = Si + CO_2\,; \quad \Delta G^\circ = 59{,}75 \text{ ккал}; \; E_r^0 = 0{,}65 \text{ в};$$

$$Al_2O_3 + 3/2C = 2Al + 3/2CO_2\,; \quad \Delta G^\circ = 159{,}4 \text{ ккал}; \; E_r^0 = 1{,}15\text{в}.$$

---

[28] K. Matiašovský, A. Jászová и M. Malinovský, *Chemické zvesti*, **17**, 605 (1963).

[29] V. Daněk, M. Malinovský и K. Matiašovsky, *Chemické zvesti*, **22**, 707 (1968).

[30] « Термодинамические свойства индивидуальных веществ ». Изд-во АН СССР, Москва, 1962.

Из проведенных вычислений вытекает, что при предположении единичной активности составных частей, на катоде в соответствующем количестве выделяется кремний. Если вместо индифферентного графитового катода будет применен алюминиевый или медный катод, можно ожидать, что в результате образования сплава Si–Al или же Si–Cu наступит деполяризация, что может существенно повлиять на процесс электролиза. Решающее влияние может также оказать активность растворенных Al_2O_3 или SiO_2.

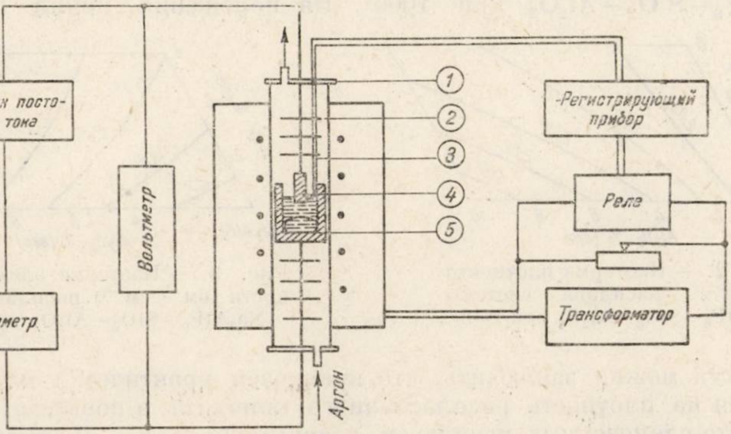

Рис. 4. – Схема прибора для измерения напряжения разложения и для электролиза:

1, фланец печи охлаждаемый водой, *2*, корундовое радиационное кольцо, *3*, термопара, *4*, графитовый электрод, *5*, графитовый тигель.

Напряжения разложения составных частей эктролита измерялись по методу I–E кривых. При измерениях была применена подобная установка, как при непосредственном электролизе (рис. 4). При измерениях в качестве катода поочередно были применены графит, алюминий, медь, сплав Si–Al. При применении металлического катода непосредственно перед проведением измерений был проведен предварительный электролиз, для того чтобы исключить возможную деполяризацию вследствие растворимости металлов при электролите, главным образом Al. Результаты приведены в табл. 1.

На основании сопоставления вычисленных и экспериментально установленных значений напряжения разложения, можно заключить, что при электролизе SiO_2, важную роль играет анодное напряжение, подобно тому как это имеет место при электролитическом разложении Al_2O_3 .[31] Из сопоставления измеренных значений напряжения разложения также очевидно, что наиболее низкое напряжение разложения было измерено при применении графитового катода. Можно предполагать, что в данном случае, вследствие образования на поверхности катода карбида кремния SiC, наступила деполяризация. Значения напряжения разложения при применении алюминиевого или медного катода существенно бóльшие, во-

---

[31] K. Grjotheim, J. L. Holm, C. Krohn и K. Matiašovský, *Svensk Kemisk Tidskrift*, **78**, 547 (1966).

Таблица 1

Напряжения разложения кремнезема и глинозема для различных экспериментальных условий

Состав электролита % (вес.)	Анод	Катод	Темп. °C	E_d (SiO_2) в	E_d (Al_2O_3) в
95% Na_3AlF_6+5% SiO_2	графит	графит	1000±2	1.00±0.05	—
95% Na_3AlF_6+5% SiO_2	графит	Al	1000±2	1.15±0.05	—
95% Na_3AlF_6+5% SiO_2	графит	Cu	1030±2	1.10±0.05	—
90% Na_3AlF_6+10%Al_2O_3	графит	Al	1000±2	—	1.45±0.05
90% Na_3AlF_6+10% Al_2O_3	графит	87.5%Al 12.5%Si	1000±2	—	1.25±0.05
90% Na_3 AlF_6+10% Al_2O_3	графит	Cu	1030±2	—	1.50±0.05
90% Na_3 AlF_6+5%SiO_2 + +5% Al_2O_3	графит	Cu	1030±2	1.18±0.05	—
85% Na_3 AlF_6+5% SiO_2+ + 10% Al_2O_3	графит	Cu	1030±2	1.30±0.05	—
85% Na_3 AlF_6+5%SiO_2 + +10% Al_2O_3	графит	Al	1000±2	1.25±0.05	—

преки тому, что в результате образования сплава Si–Al или Si–Cu также наступает деполяризация. Неожиданным оказалось то, что в случае Al_2O_3 напряжение разложения при применении медного катода выше, чем при применении алюминиевого катода. По-видимому, при выделении на металлическом катоде Si, с точки зрения деполяризации, решающим фактором является скорость диффузии кремния внутрь катода с поверхности катода. Эта проблема подробно освещена в работе [32].

Проведенные измерения подтверждают также тот факт, что между образовавшимися потенциалами кремния и алюминия разница весьма небольшая, так что в определенных условиях, на катоде одновременно могут выделяться оба металла. Ввиду того, что в настоящее время мы не располагаем необходимыми термодинамическими и электрохимическими данными, условия для одновременного отложения Si и Al приходится устанавливать экспериментальным путем.

ЭЛЕКТРОЛИЗ С АЛЮМИНИЕВЫМ КАТОДОМ

При электролизе применяется графитовый анод, с эффективной поверхностью равной 10 см^2, при жидком алюминиевом катоде весом в 40 г. Были проведены измерения с электролитом следующих составов: 95% Na_3AlF_6 + 5%SiO_2 или 85% Na_3AlF_6 + 5% SiO_2 + 10%Al_2O_3. В обоих случаях при электролизе была применена кварцевая футеровка. Электролиз был осуществлен в атмосфере аргона. После электролиза и охлаждения тигель с электролитом разбивался, после чего взвешивался катод и анализировался. Средний состав сплава был определен путем количественного химического анализа, а распределение Si в катодном сплаве было

---

[32] G. Boe, K. Grjotheim, K. Matiašovský и P. Fellner, *Canad. Metall.Quarterly*, **9** (1971).

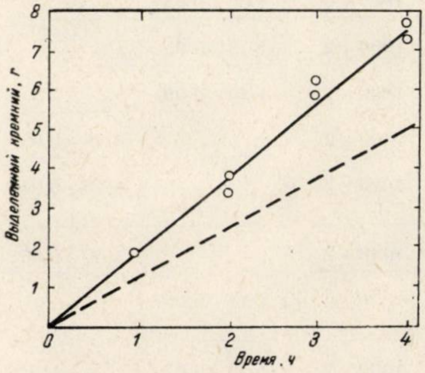

Рис. 5. — Выделение кремния электролизом кремнезема, растворенного в криолите при применении алюминиевого катода. $I = 5$ а.

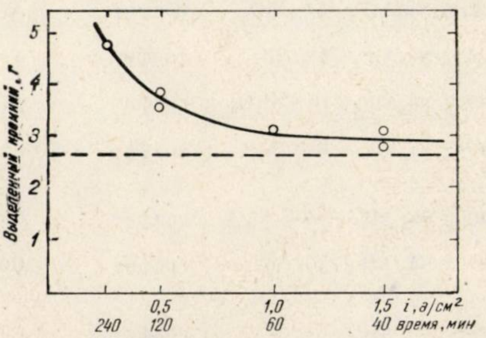

Рис. 6. — Электролитическое выделение кремния при различных плотностях тока при применении алюминиевого катода.

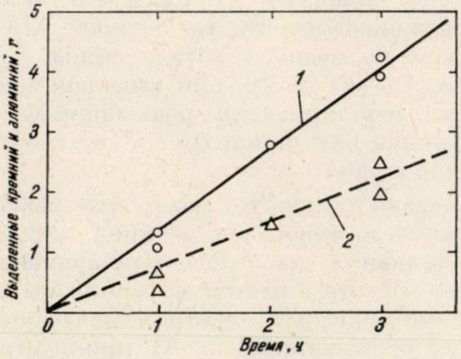

Рис. 7. — Электролитическое выделение кремния и алюминия при применении алюминиевого катода:
1, количество выделенного кремния, 2, количество выделенного алюминия.

определено путем спектрального анализа поверхности отдельных сечений катода.

За один ампер-час теоретически выделяется 0,2617 г Si или 0,335 г Al. При электролизе расплавленных солей выход по току существенно ниже теоретического, особенно в отношении потерь материала, что является следствием реакции выделенного металла с электролитом или с анодными продуктами. Эти потери (а тем самым и выход по току) зависят, главным образом, от температуры, плотности тока и факторов, вытекающих из конструкции и размеров электролизера. Однако, в данном случае можно ожидать, что при электролизе расплавов системы $Na_3AlF_6-SiO_2$ с применением алюминиевого катода мнимый выход по току по кремнию будет повышаться, ввиду реакции расплавленной SiO_2 с металлическим алюминием, вследствие чего, кроме Si, выделенного электролитическим путем, в катодном сплаве будет также присутствовать кремний, выделенный в результате реакции химического обмена (3).

Это предположение было подтверждено экспериментальным путем. В первой серии измерений подвергался электролизу криолито-кремнеземный расплав током в 5 а ($i_a = 0{,}5$ а/см²). Результаты измерений приведены на рис. 5. Прерывистая линия соответствует 100%-ному выходу по току. На рисунке показано, что количество выделенного Si (или мнимый выход по току) во всех случаях выше теоретически выделяемого количества при 100%-ном выходе по току.

В следующей серии экспериментов электролиз проводился при различных плотностях тока, причем количество поступившего электричества во всех случаях было одинаково (10 ампер-часов). Результаты проведенных измерений приведены на рис. 6 (прерывистая линия соответствует 100%-ному выходу по току), из которого видно, что при увеличении плотности тока количество выделяемого кремния в общем снижается, что, по-видимому, происходит от уменьшения количества Si, выделенного исключительно вследствие химической реакции. Установить же действительное количество выхода по току невозможно, поскольку, мы не располагаем данными, относящимися к количеству кремния, выделяющегося в результате химической реакции обмена. Можно считать, что экспериментальные условия при изучении реакции (3) и при электролизе — различны, в особенности если дело касается концентрации кремния на поверхности катода.

В последующей серии опытов, электролизу подвергался расплав системы $Na_3AlF_6-SiO_2-Al_2O_3$ под действием постоянного тока 5 а с применением алюминиевого катода. Было обнаружено, что при таком составе электролита на катоде одновременно выделяется кремний и алюминий. Результаты измерений показаны на рис. 7.

На основе анализа измерений можно заключить, что при электролизе криолитового расплава, одновременно содержащего в различных пропорциях кремнозем и глинозем, могут быть приготовлены сплавы Al—Si различного состава.

ЭЛЕКТРОЛИЗ С ПРИМЕНЕНИЕМ МЕДНОГО КАТОДА

Были проведены 3 серии измерений электролитов, содержавших 95%Na_2AlF_6+5%SiO_2, 90%Na_3AlF_6+5%SiO_2+5%Al_2O_3, 85% Na_3AlF_6+ +5%SiO_2+10%Al_2O_3. Электролиз проводился при 1030°, при расстоянии между полюсами 23—25 мм, током в 3 и 5 а. В качестве катода вначале был применен медный цилиндр (⌀20 мм, ь = 10мм). В этом случае жидкий сплав Si—Cu или Si—Al—Cu образовался только на поверхности катода. В дальнейших опытах поэтому были применены медные стружки весом около 3 г, которые в результате образования сплава плавились сразу же в начале электролиза, так что при дальнейшем электролизе был получен гомогенный сплав. Кварцевая футеровка была применена только при электролизе криолито-кремнеземных расплавов.

Из значений напряжения разложения, полученных при измерениях, проведенных с применением медного катода, можно заключить, что с повышением концентрации глинозема, в электролите повышается напряжение разложения SiO_2. Напряжение разложения кремнезема также повышается при повышении плотности тока. Таким образом, можно предполагать, что в определенных условиях, на медном катоде будут выделяться оба металла. Это предположение подтверждено результатами проведенных опытов.

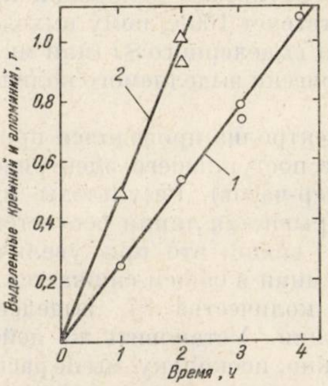

Рис. 8. — Выделение кремния при применении медного катода как функция продолжительности электролиза.

1, общий ток 3а, *2*, общий ток 5а.

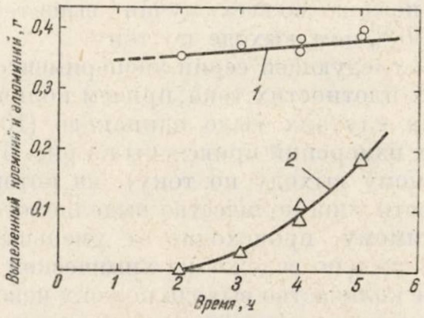

Рис. 9. — Зависимость количества выделенного кремния от плотности тока (85 % криолита, 5 % кремнезема, 10 % глинозема). Общее количество электричества, прошедшего через электролизер в каждом эксперименте составляло 5 ампер-часов.

, выделенный алюминий, *2*, выделенный кремний.

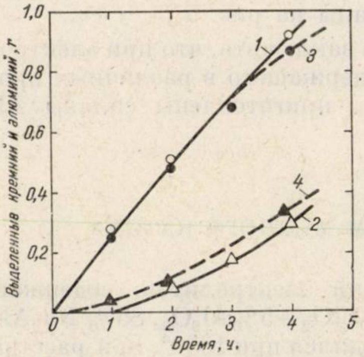

Рис. 10. — Выделение кремния и алюминия при применении медного катода. $I = 3$ а.

1, выделенный Si (5 вес. % SiO_2, 5 вес. % Al_2O_3); *2*, выделенный Al (5 вес. SiO_2, 5 вес. % Al_2O_3); *3*, выделенный Si (5 вес. % SiO_2, 10 вес. % Al_2O_3); *4*, выделенный Al (5 вес. % SiO_2, 10 вес. % Al_2O_3).

На рис. 8 приведены результаты измерений при электролизе криолито-кремнеземного расплава с током 3 и 5 а. Полученные путем измерений значения свидетельствуют о том, что зависимость выделенного количества Si от продолжительности электролиза — в обоих случаях линейная. Выход по току, на основании установленного количества кремния в сплаве Cu—Si для токов 3 и 5 а, соответственно равен 33,2% и 37,4%.

Относительно низкие значения получены, вероятно, вследствие небольшого расстояния между полюсами, а также от сравнительно высокой температуры электролиза; тем не менее здесь ясно, что с повышением плотности тока повышается и выход по току.

В дальнейшей серии опытов рассматривалось влияние плотности тока на одновременное выделение кремния и алюминия при электролизе расплава, состоящего из 85% $Na_3AlF_6 + 5\% SiO_2 + 10\% Al_2O_3$. При отдельных опытах время электролиза определялось таким образом, чтобы во всех случаях через электролизер проходило одинаковое количество электричества, равное 5 а-час. Результаты измерений приведены на рис. 9. Площадь поверхности жидкого медного катода не удалось определить (равнялась она приблизительно 10 $см^2$), и поэтому вместо плотности тока были приведены соответствующие значения тока. Из рисунка видно, что при низких катодных плотностях тока (приблизительно ниже 0,2 $а. см^{-2}$), на катоде осаждается только кремний, в то время как при более высоких плотностях тока одновременно осаждаются оба металла, причем доля алюминия возрастает с возрастанием плотности тока. Данный случай подтвердил, что выход по току возрастает при повышении плотности тока.

В последней серии опытов электролиз расплава системы $Na_3AlF_6 - SiO_2 - Al_2O_3$ проводился под током 3 и 5 а. (См. рис. 10). Результаты измерений показали, что с повышением концентрации глинозема в электролите увеличивается количество выделяемого алюминия. С продолжительностью электролиза растет количество выделяемого алюминия, а количество выделяемого кремния, по причине понижения концентрации кремнозема в электролите, падает.

ВЫВОДЫ

Из анализа результатов проведенных измерений вытекает, что при электролизе криолито-кремнеземных расплавов, с применением подходящего металлического катода, могут получаться соответствующие сплавы, с требуемой концентрацией кремния. При электролизе расплавов системы $Na_3AlF_6 - SiO_2 - Al_2O_3$ и при правильном выборе экспериментальных условий можно добиться одновременного выделения кремния и алюминия, что может быть использовано для приготовления сплавов Si—Al. Преимущество получения сплава непосредственно электролизом заключается в том, что по сравнению с существующими в настоящее время методами получения сплава посредством смешивания составных элементов в чистом виде, при электролизе могла бы применяться подходящая для этого смесь SiO_2 и Al_2O_3, например, смесь кремнезема и глинозема, полученных в качестве промежуточного продукта при производстве Al_2O_3 из боксита.

Авторы благодарят фирму Электрокемиск за помощь при реализации этой работы.

Revue Roumaine de Chimie, 17, 5, 831–834 (1972)

VAPOR PRESSURES OF MOLTEN CADMIUM BROMIDE AND CADMIUM IODIDE

LETIŢIA TOPOR and J. WYPARTOWICZ *

Centre of Physical Chemistry, P.O. Box 2103, Bucharest, Romania

Received January 13, 1972

Vapor pressures of $CdBr_2$ and CdI_2 have been measured using the quasi-static method in the temperature range 595–739° and 523–639°, respectively. Values of standard heat of vaporization, boiling point and entropy of vaporization have been calculated. Experimental data are in good agreement with those obtained by the boiling point method.

There are only few papers dealing with the vapor pressure of liquid cadmium bromide and cadmium iodide. Greiner and Jellinek [1] obtained only one value of vapor pressure for $CdBr_2$ at 752° using the transportation technique. Schmidt and Walter[2] examined CdI_2 in the temperature range 390–450° and obtained values for vapor pressure between 0.504 and 2.92 mm Hg, using also the transportation technique. Tolmacheva and Andrinovskaya [3] have measured the vapor pressure of $CdBr_2$ in the range 570–624° and that of CdI_2 in the range 454–652° by the transportation technique but their results do not allow to obtain a reliable dependence of the vapor pressure upon the temperature because of the small amount of experimental points and relatively great error. The only work concerning a wide temperature range (568–725° for $CdBr_2$ and 500–655° for CdI_2) and a sufficient amount of experimental points is that of Bloom, Bockris, Richards and Taylor [4] performed by the boiling point technique.

EXPERIMENTAL

Vapor pressures of molten $CdBr_2$ and CdI_2 have been determined by the quasi-static Rodebush-Dixon method. The details of experimental equipment and procedure have been reported previously.[5] The cell used in the present work was made of quartz, with cylindrical part of 25 mm in diameter and 25 mm in height. The arms had the inner diameter of about 3 mm. The salts used were Merck's reagent grade materials. Cadmium bromide was dehydrated, distilled and stored in a closed vial. After filling with $CdBr_2$ powder, the cell was slowly heated and a stream of anhydrous HBr was passed over the solid, and after melting, over the liquid $CdBr_2$. After 1 hour the HBr stream was stopped and dry argon was passed to remove the HBr left. CdI_2 was dehydrated by heating in vacuum to about 100° below the melting point, using one trap with liquid nitrogen, and then was melted in dry pure argon. The method[6] of CdI_2 dehydration by passing HI over the solid and liquid CdI_2 did not give, in our case, satisfactory results due to the partial decomposition of HI and to the impossibility to remove completely the condensed iodine and the residual HI by the stream of inert gas, facts that hindered the measurements.

---

*) Present address : Institute of Metallurgy, Polish Academy of Sciences, Reymonta 25, Cracow, Poland.

[1] B. Greiner and C. Jellinek, *Z. Phys. Chem.*, **A165**, 97 (1933).

[2] G. C. Schmidt and R. Walter, *Ann. Physik*, **72**, 565 (1923).

[3] A. T. Tolmacheva and T. L. Andrinovskaya, *Vestnik Leningrad. Univ., Ser. Fiz. Khim.*, **15** (10), 131 (1960).

[4] H. Bloom, J. O'M. Bockris, N. E. Richards and A. Taylor, *J. Amer. Chem. Soc.*, **80**, 2044 (1958).

[5] I. G. Murgulescu and L. Topor, *Rev. Roumaine Chim.*, **11**, 1353 (1966).

During the measurements only a very slight decomposition of CdI_2 occurred (indicated by traces of condensing iodine). The possible error due to decomposition is not greater than the precision of the method, and the control measurements made at the end of the series showed excellent agreement with those made at the beginning.

The values of vapor pressures were measured with the mercury manometer, using a cathetometer, with a precision of 0.1 mm. The temperature was measured with a PtRh-Pt thermocouple and maintained constant with a ±1° accuracy by means of a regulating system based on a galvanometer with photocell.

RESULTS AND DISCUSSION

For $CdBr_2$, 32 measurements in the temperature range 595–739° have been made, while for CdI_2, 40 measurements in the temperature range 523–639°. Experimental results have been used to evaluate equations for vapor pressure as a function of temperature. Two types of equations p = f(T) have been used for each salt. When the difference between the heat capacities for the gas and the liquid phase ΔC_p is assumed constant, the following equation can be used :

$$\lg p = -\Delta H_0/4.575T + \Delta C_p \lg T/1.986 + I \qquad (1)$$

where p is the vapor pressure of substance, ΔH_0 is the standard heat of vaporization at 0°K and I is a constant.

The values of ΔC_p have been obtained as a difference between the classical thermodynamic value of C_p (15 cal. mol^{-1} deg^{-1}) for triatomic linear molecules and C_p for liquid $CdBr_2$ and CdI_2 (24.3 cal. mol^{-1} deg^{-1} and 24.4 cal. mol^{-1} deg^{-1} respectively).[7] By means of these ΔC_p values and of the experimental values of p, the constants ΔH_0 and I in equation (1) have been calculated using the Σ method.[8] A simple equation was used when ΔC_p was assumed to be zero or negligible :

$$\lg p = -\Delta H/4.575T + \Delta S/4.575 \qquad (2)$$

where ΔH and ΔS denote the heat and entropy of vaporization respectively at the midtemperature of the experimental range. Constants ΔH

---

[6] J. O'M. Bockris, A. Pilla and J. L. Barton, *Rev. Roumaine Chim.*, **7**, 59 (1962)

[7] L. E. Topol and L. D. Ransom, *J. Phys. Chem.*, **64**, 1339 (1960).

[8] K. K. Kelley, Bulletin 383, Bureau of Mines, Washington, 1935.

and ΔS have been evaluated using experimental values of vapor pressure. Calculations for both equations have been performed by means of the least squares method, using an IBM computer. Also the standard deviations for p have been calculated. The most important results for equation (1) are presented in table 1.

Table 1

Constants for eq. (1) and standard deviation for p

Substance	$CdBr_2$	CdI_2
Temperature range	595–739	523–639
ΔC_p, cal. mol.$^{-1}$ deg^{-1}	-9.3	-9.4
ΔH_0, cal. mol^{-1}	36376 ± 119	33400 ± 84
I, cal. mol.$^{-1}$ deg^{-1}	24.168 ± 0.027	24.188 ± 0.022
Standard deviation for p, %	1.57	1.34

For equation (2) we have obtained :

$\lg p$ (mm Hg) $= (8.230 \pm 0.018) - (6056.0 \pm 17.7)/T$ for cadmium bromide and

$\lg p$ (mm Hg) $= (8.299 \pm 0.025) - (5581.7 \pm 21.3)/T$ for cadmium iodide.

Experimental results as a plot of $\lg p$ *versus* $1/T$ for $CdBr_2$ and CdI_2 are presented in figs 1 and 2 respectively, compared with those of other authors. We can state, that the agreement between our results and those of Bloom et al[4] is very good. Results of Tolmacheva and Andrinovskaya[5] are of poor agreement with those of Bloom et al[5] and our work ; besides they indicate great deviations from a straight line. A comparison of ΔH_{298} presented by Brewer, Somayajulu and Brackett,[9] with ΔH_{298} values obtained from the third law procedure using Brewer's free energy functions for 1000°K and our vapor pressure data, is presented in table 2.

Table 2

Standard heats of vaporization

Substance	Standard heat of vaporization ΔH_{298}, kcal. mol^{-1}	
	Brewer et al [9]	Third law
$CdBr_2$	39.0	33.1
CdI_2	35.0	33.1

---

[9] L. Brewer, G. Somayajulu and E. Brackett, *Chem. Rev.*, **63**, 111 (1963).

From eq. (2) we have calculated boiling points of both salts. Our values are 1132 ± 7°K for $CdBr_2$ and 1030 ± 8°K for CdI_2, while those of Bloom et al [4] are 1120 ± 3°K and 1014 ± 2°K, respectively.

The values of entropy of vaporization have been also calculated from eq. (2) for the midtemperature of experimental range for each salt. Corresponding values are 24.5 e.u. at 667° for $CdBr_2$ and 24.8 e.u. at 581° for CdI_2.

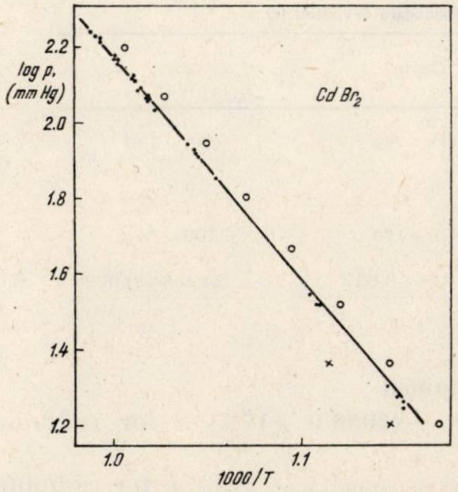

Fig. 1. — Vapor pressure data for $CdBr_2$. Crosses — results of Tolmacheva and Andrinovskaya.[5] Open circles — results of Bloom et al,[4] calculated from equation : log p (mm Hg) = 8.252 − 6011.3/T. Full circles and line — this work.

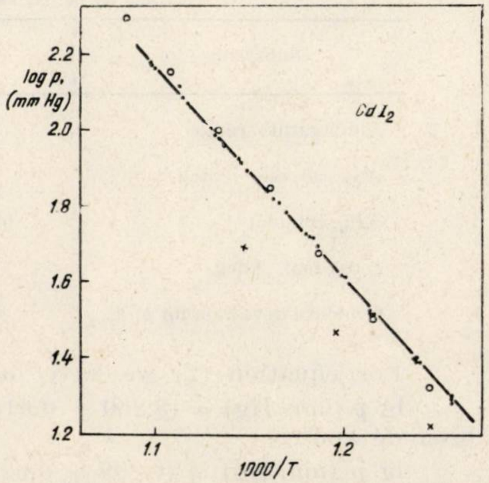

Fig. 2. — Vapor pressure data for CdI_2. Crosses — results of Tolmacheva and Andrinovskaya. [5] Open circles — results of Bloom et al,[4] calculated from equation : log p (mm Hg) = 8.812 − 6012.4/T. Full circles and line — this work.

The quasi-static Rodebush-Dixon method has been used for the first time by us to determine the vapor pressure of molten $CdBr_2$ and CdI_2. To calculate the vapor pressure by the transportation method, the molecular weight of the vapor species must be known and therefore the knowledge of the vapor composition is essential. A poor agreement between the transportation method and a direct method is due either to the experimental errors or to the presence of polymeric species in vapor. In the later case the transportation vapor pressure values, calculated assuming only the monomer in the vapor phase, must be higher than those obtained by a direct method. Vapor pressure measurements of the molten $CdBr_2$ and CdI_2 cannot be used to obtain the composition of the vapor phase because the only available transportation data are lower than those obtained by the boiling point or by the quasi-static methods (fig. 1 and fig. 2).

Revue Roumaine de Chimie, 17, 5, 835–840 (1972)

ÉTUDE PAR CHROMATOGRAPHIE PYROLYTIQUE DE QUELQUES POLYMÈRES VINYLIQUES*

C. N. CAŞCAVAL et I. A. SCHNEIDER

Institut de Chimie Macromoléculaire « P. Poni », Jassy, 41 A, Aleea Gr. Ghica Vodă

Reçu le 22 novembre 1971

Le travail étudie comparativement la pyrolyse chromatographique du polychlorure de vinyle (PVC), du polyacétate de vinyle (PA_cV) et de l'alcool polyvinylique (APV). Par l'étude de l'influence de la quantité d'échantillon et de la température on établit les conditions expérimentales qui assurent la caractérisation reproductible des polymères étudiés.

INTRODUCTION

La technique de la pyrolyse employée surtout avec la chromatographie en phase gazeuse présente un grand intérêt comme méthode expérimentale d'une part pour l'élucidation de la structure des macromolécules [1,2] et d'autre part pour la caractérisation qualitative[3-5] et quantitative[6,7] des polymères. L'étude quantitative de la décomposition thermique des polymères peut être réalisée par l'utilisation d'un pyrolyseur en spirale [8,9], ou d'un microréacteur. [10,11]

Une méthode originale de la pyrolyse des polymères a été proposée par Simon et Giacobbo,[12] qui ont utilisé un pyrolyseur au chauffage par induction de haute fréquence, dont l'application pour l'analyse qualitative progresse de plus en plus, tenant compte des nombreux avantages, parmi lesquels :

1. la connaissance exacte de la température de la pyrolyse ;
2. la réalisation rapide de la température de la pyrolyse ;
3. l'utilisation comme échantillon de quantités extrêmement réduites ;
4. la haute reproductibilité des chromatogrammes.

---

* Travail communiqué au 39ᵉ Congrès International de Chimie Industrielle, 7–11 septembre 1970, Bucarest.

[1] S. G. Perry, *J. Gas Chromatog.*, **5**, 77 (1967).

[2] M. Vacherot, *J. Gas Chromatog.*, **5**, 155 (1967).

[3] B. Groten, *Analyt. Chem.*, **36**, 1206 (1964).

[4] B. C. Cox et B. Ellis, *Analyt. Chem.*, **36**, 90 (1964).

[5] G. C. Hewitt et B. T. Whitham, *Analyst*, **86**, 643 (1961).

[6] K. Etrre et P. F. Varadi, *Analyt. Chem.*, **34**, 752 (1962).

[7] F. A. Lehmann et G. M. Brauer, *Analyt. Chem.*, **33**, 673 (1961).

[8] N. McCormick, *J. Chromatog.*, **40**, 1 (1969).

[9] C. E. R. Jones et G. E. J. Reynolds, *S. C. I. Monograph.*, **26**, 260 (1967).

[10] C. E. Legate et H. D. Burnham, *Analyt. Chem.*, **32**, 1042 (1960).

[11] K. Ettre et P. F. Varadi, *Analyt. Chem.*, **35**, 69 (1963).

[12] W. Simon et N. Giacobbo, *Chem. Ing. Techn.*, **37**, 709 (1965).

Tenant compte des avantages de ce type de pyrolyseur nous sommes arrivés à l'idée de l'utiliser à l'étude quantitative de la pyrolyse séquentielle des polymères. Dans ce but, nous avons pyrolysé trois polymères vinyliques ayant des structures semblables et nous avons réussi à réaliser une bonne séparation des produits caractéristiques de scission, ainsi qu'une détermination quantitative de ces produits, en fonction de la température de la pyrolyse.

PARTIE EXPÉRIMENTALE

L'étude pyrolytique a été appliquée sur trois sortes de polymères vinyliques : PVC avec $\overline{M}_w = 52\,000$, PA_cV ayant $\overline{M}_w = 170\,000$ et APV avec $\overline{M}_w = 178\,000$.

Pour l'analyse chromatographique des produits de la pyrolyse on a utilisé un chromatographe de gaz en phase de vapeurs du type Siemens L-400 avec un détecteur à ionisation de flamme, possédant un pyrolyseur Phillips (à la base du point Curie), placé devant la chambre de volatilisation du chromatographe.

La séparation chromatographique des produits de la pyrolyse a été réalisée dans les conditions suivantes : la longueur de la colonne chromatographique 1,60 m, le diamètre intérieur 3 mm, le matériau de remplissage 10 % Apiezon L sur Célite 545 traité avec $AgNO_3$ 2 % ; la température de la colonne 110° ; le gaz porteur, argon ; le débit du gaz porteur, 35 ml/mn.

Les échantillons de polymères ont été mis en solution par les solvants convenables aux points d'ébullition basses en obtenant des solutions d'une concentration de 88 μg/μl. Afin d'obtenir une couche de polymère à partir des solutions préparées, on introduit celles-ci dans la bouche formée à l'une des extrémités aplatie du filament ferromagnétique, à l'aide d'une séringue Hamilton. Ainsi le dosage identique des échantillons est parfaitement assuré.

Le solvant est complètement éliminé en maintenant pendant 30 minutes les échantillons déposés sur le filament ferromagnétique dans une étuve à une température un peu supérieure à la température d'évaporation du solvant. Les pyrolyses ont été effectuées à 358°, 480°, 510°, 610° et 778°.

Les conditions de la pyrolyse ont été les mêmes pour tous les polymères, excepté le PVC, où on a utilisé une précolonne remplie de NaOH fondu sur l'asbeste, afin de prévenir l'introduction d'HCl résulté de la décomposition du PVC, dans la colonne chromatographique.

RÉSULTATS ET DISCUSSIONS

Avant de présenter les résultats concernant la pyrolyse chromatographique des trois polymères vinyliques étudiés, il convient de discuter l'influence de la quantité d'échantillons et le problème de la reproductibilité de la méthode. Afin de démontrer la reproductibilité de la méthode, la figure 1 présente deux chromatogrammes obtenus dans des conditions standard.

Les conditions standard pour le PVA_c (figure 1*a*) sont les suivantes : 4μl solution déposée sur le filament, température de la pyrolyse 610° et pour la APV (figure 1b) 4μl solution, température de la pyrolyse 480°.

Pour illustrer l'influence de la quantité d'échantillon étudié, le tableau 1 rassemble les aires correspondant aux pics des produits principaux de la pyrolyse du PVC et aussi la diminution apparente du degré de la transformation, due à la pyrolyse incomplète des grands échantillons, par rapport au rendement de la pyrolyse réalisée sur le plus petit échantillon (4μl solution), considéré comme étant de 100 %.

Compte tenu de l'influence observée de la quantité des échantillons, toutes les déterminations ultérieures ont été réalisées sur des échantillons de 4 μl d'une solution de polymère correspondant à 0,352 mg de polymère pur. Ce choix est justifié par nos données expérimentales, comme l'on peut voir à la figure 2, qui présente la variation du rendement en fonction de la quantité d'échantillon.

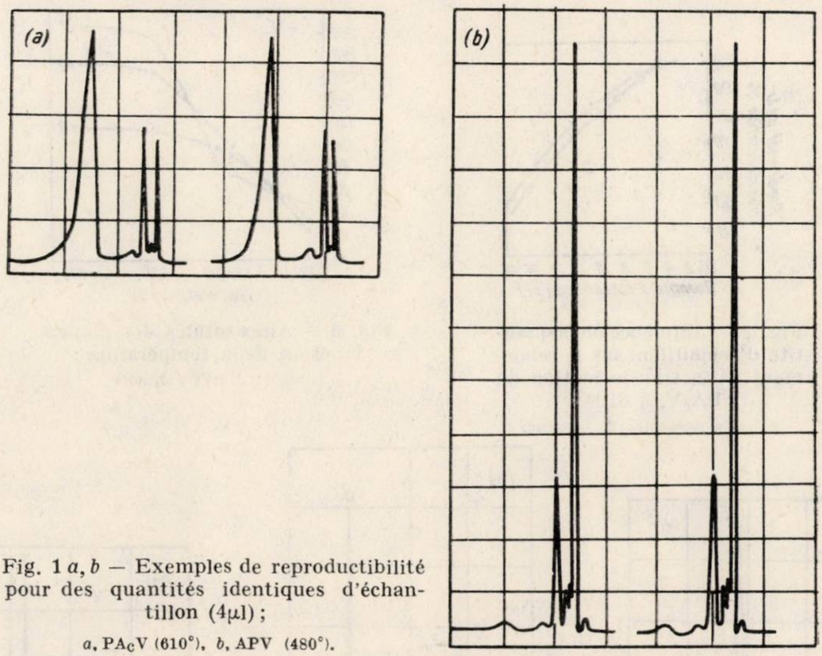

Fig. 1 *a, b* — Exemples de reproductibilité pour des quantités identiques d'échantillon (4μl) ;

a, PA_CV (610°), *b*, APV (480°).

Tableau 1

Influence de la quantité d'échantillon sur le degré de la pyrolyse du $PA_C V$, à 610°

Quantité d'échantillon		Acide acétique		Benzène	
μl	mg	Aire du pic, mm^2	Rendement %	Aire du pic, mm^2	Rendement %
4	0,352	171	100*	9,72	100*
6	0,528	244	95,1	13,76	94,3
8	0,704	314	90,1	17,28	88,8
10	0,88	360	84,3	19,98	82.2
12	1,052	396	77,1	21,86	74,9
16	1,408	423	61,8	22.95	59,0

* L'hypothétique 100%.

La figure 2 montre que l'on obtient des variations identiques du rendement pour les deux produits principaux de la pyrolyse, ce qui confirme encore une fois que la variation observée peut être attribuée à la pyrolyse incomplète des échantillons plus grands.

La figure 3 démontre l'influence de la température sur le degré de transformation par la pyrolyse chromatographique des polymères étudiés, en présentant la variation de la somme des aires des pics chromatographiques en fonction de la température.

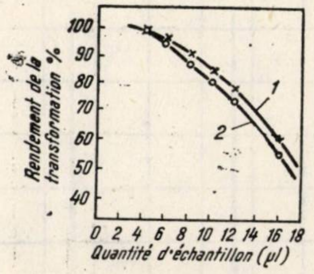

Fig. 2. — Influence de la quantité d'échantillon sur le rendement de la transformation du PA_cV, à 610° ;

1, acide acétique ; *2*, benzène.

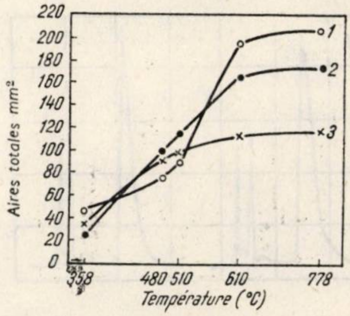

Fig. 3 — Aires totales des pics en fonction de la température : *1*, PA_cV ; *2*, PVC ; *3*, APV.

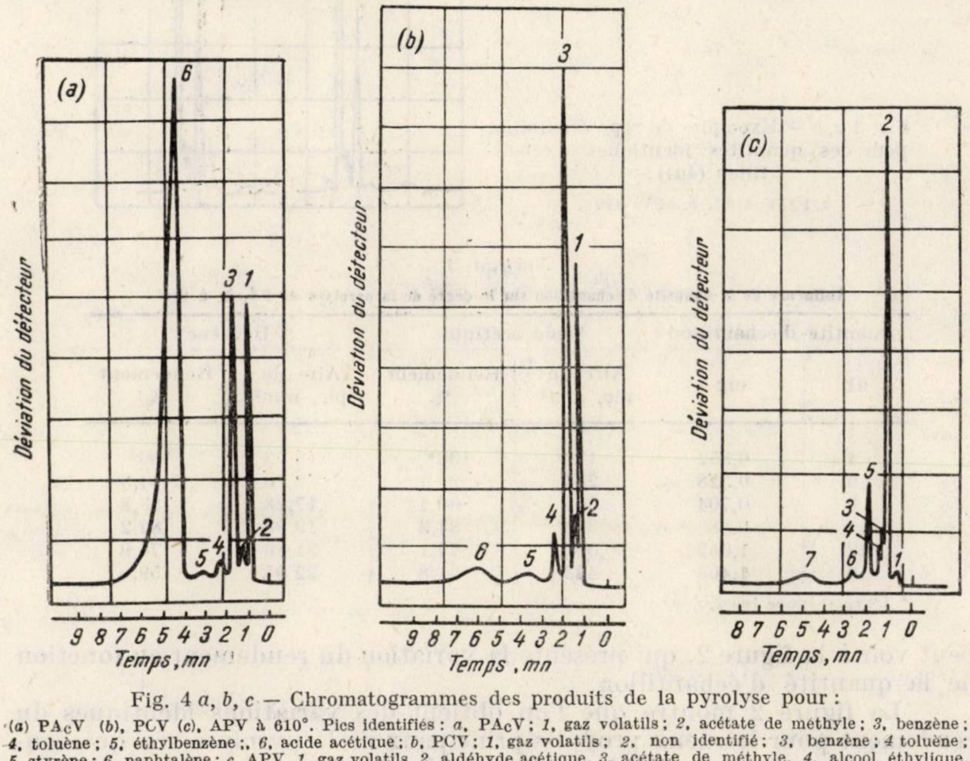

Fig. 4 *a*, *b*, *c* — Chromatogrammes des produits de la pyrolyse pour :
(*a*) PA_cV (*b*), PCV (*c*), APV à 610°. Pics identifiés : *a*, PA_cV ; *1*, gaz volatils ; *2*, acétate de methyle ; *3*, benzène ; *4*, toluène ; *5*, éthylbenzène ;, *6*, acide acétique ; *b*, PCV ; *1*, gaz volatils ; *2*, non identifié ; *3*, benzène ; *4* toluène ; *5*, styrène ; *6*, naphtalène ; *c*, APV, *1*, gaz volatils, *2*, aldéhyde acétique, *3*, acétate de méthyle. *4*, alcool éthylique, *5*, benzène, *6*, toluène, *7*, acide acétique.

L'analyse de la figure 3 indique d'une part un comportement analogue des trois polymères vinyliques étudiés, d'autre part le fait que la pyrolyse peut être considérée complète au-dessus de la température de 610°.

Il convient de remarquer, aussi, que la durée de la pyrolyse déterminée par le moyen de travail utilisé a été dans tous les cas de 2 s. Même,

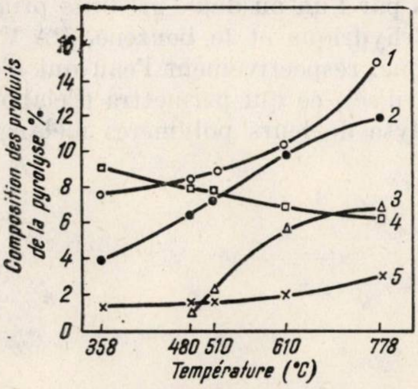

Fig. 5

(PA$_c$V,) *1*, gaz volatils, *2*, benzène, *3*, toluène, *4*, acide acétique ×10, *5*, acétate de méthyle.

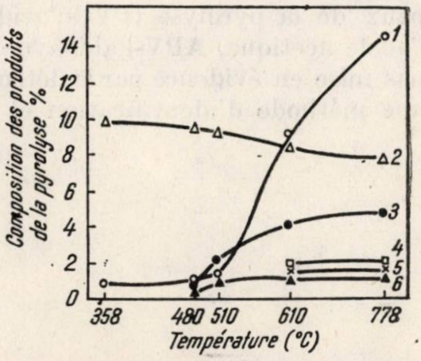

Fig. 6

(PVC), *1*, gaz volatils, *2*, benzène ×10 ; *3*, toluène ; *4*, naphtalène ; *5*, styrène, *6*, non identifié.

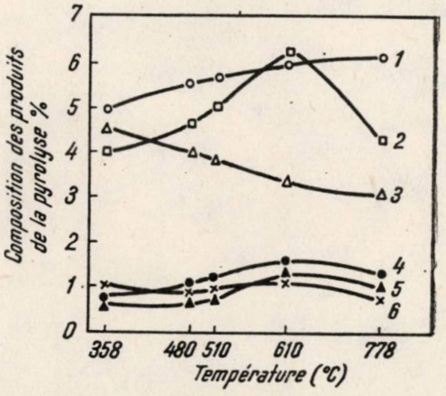

Fig. 7

(APV), *1*, aldéhyde acétique × 10 ; *2*, acide acétique ; *3*, benzène ×10, *4*, toluène ; *5*, alcool éthylique ; *6*, acétate de méthyle.

Fig. 5—7. — Composition des produits de la pyrolyse de PA$_c$V, PVC et APV en fonction de la température.

si apparemment le comportement thermique des polymères étudiés est identique, les chromatogrammes obtenues à 610°, présentés dans la figure 4-*a*, *b*, *c* montrent qu'il y a des différences importantes, ce qui permet leur caractérisation.

Dans ce sens les données des figures 5, 6, et 7 illustrent la variation des produits principaux de la pyrolyse des polymères étudiés par rapport à la température, ce qui témoigne encore une fois en faveur de cette observation.

Les produits de la pyrolyse ont été identifiés par comparaison des durées de rétention par rapport aux substances étalon pures, dans les mêmes conditions. On peut voir sur les figures 5—7, de variations caractéristiques de chaque polymère, ce qui permet leur caractérisation et leur identification.

En tenant compte du fait que dans le cas de PVC, l'acide chlorhydrique a été adsorbé préalablement, on peut admettre que tous les polymères étudiés peuvent être caractérisés par l'un ou deux produits principaux de la pyrolyse (PVC-l'acide chlorhydrique et le benzène, PA_cV — l'acide acétique, APV-l'aldéhyde acétique, respectivement l'eau qui n'est pas mise en évidence par le détecteur utilisé), ce qui permettra d'élaborer une méthode d'identification et d'analyse de leurs polymères mēlangés.

Revue Roumaine de Chimie, 17, 5, 841 – 846 (1972)

KINETICS AND MECHANISM OF BROMINATION OF CROTONIC ACID BY AQUEOUS BROMINE

V. P. KUDESIA

Chemical Laboratories, D. N. College, Meerut, U. P. India

Received November 25, 1971

The kinetics of bromination of crotonic acid with aqueous bromine has been investigated in 70 % (vol/vol) aqueous acetic acid. The reaction is first order with respect to both substrate and bromine. The reactions of bromine with methyl crotonate, ethyl crotonate and propyl crotonate have also been investigated. The molecular bromine has been shown to be the principal oxidizing agent. The various activation parameters have been evaluated and a possible mechanism based on deuterium isotope effect is suggested.

INTRODUCTION

Williams et al[1] while investigating the bromination and iodination of olefins concluded that the molecular bromine is the principal oxidizing agent. They also concluded that the response by neighbouring group was greatest for the most selective electrophilic rearrangement and the intermediates formed during the reaction of series of compounds $CH_2 = CH\cdot(CH_2)_n.\ OH$ with bromine are not necessarily carbonium ions but may be bridged halonium ions. In the present paper the kinetics of addition of bromine to crotonic acid and its esters has been carried out with a view to establish that molecular bromine is the principal oxidising agent and to know the nature of bromine reaction with the substrate.

EXPERIMENTAL

All the chemicals used were of B.D.H. quality or A.R. or purified by usual procedures. Water was purified by passage through an ion exchange column and distilled from potassium permanganate.

Kinetic Measurement. The thermostat was maintained at a constant temperature at 30°. The reaction was started by adding an aqueous solution of bromine to the solution of substrate containing 0.2M lithium bromide and 70 % (vol/vol) aqueous acetic acid at $\mu = 0.2$ (by addition of lithium perchlorate). The reaction vessel was protected from light and aliquots were withdrawn at suitable intervals, usually by an automatic pipette. These aliquots were run into an ice

---

D. L. H. Williams, E. B. Goetz and J. E. Dubois, *J. Chem. Soc.* (*B*), **1969**, 517.

cold solution of potassium iodide and the liberated iodine was titrated with thiosulphate using starch as indicator. Blank runs were also carried out and some correction was made for such decomposition where necessary. The first order rate constants (k) were calculated by using integrated rate equation. The second order rate constant k_2 was obtained by the formula

$$k_2 = \frac{k}{(\text{Substrate})\,(\text{Br}_2)}$$

RESULTS AND DISCUSSION

The hydrolysis of bromine in water is known to proceed through the reaction

$$\text{Br}_2 + \text{H}_2\text{O} \rightleftharpoons \text{HOBr} + \text{H}^+ + \text{Br}^-$$

The bromide ions (Br^-) which are formed during the reaction further react with Br_2 to form Br_3^- ion.

$$\text{Br}_2 + \text{Br}^- \rightleftharpoons \text{Br}_3^-$$

Hence it is clear that bromine water contains three species namely Br_2, Br_3^- and HOBr in the solution. In 70% (vol/vol) aqueous acetic acid and in presence of 0.2 M lithium bromide the only brominating species are Br_2 and Br_3^-.[2,3] The equilibrium constant (K) for tribromide ion formation in the solvent used is 84 at 20°.[4] According to Kudesia's method[2] this value of K is found to be 88.6 in 70% (vol/vol) aqueous acetic acid at 30°.

From equation (a) the value of $k_2\text{obs}\ [1+K\,(\text{Br}^-)]$

$$(\text{Br}_2)\ [1+K\,(\text{Br}^-)] = (\text{Br}_2)^* \ldots \text{(a)}$$

$(\text{Br}_2)^*$ = total (analytical) concentration.

should remain constant if bromine molecule is the principal oxidizing agent.[5] The data in table 1 clearly show that the factor $k_2\text{obs}\ [1 + K\,(\text{Br}^-)]$ remains almost constant with change of (Br^-). Hence it follows that the bromine molecule is the main brominating agent in this reaction.

Table 1

Influence of bromide ion on the reaction rate at 30.°

$(\text{Br}_2) = 2.7 \times 10^{-3}$ M; (Substrate) $= 2.6 \times 10^{-2}$ M; $\mu = 0.2$

(Br^-) M	$10^3 k_2$ obs. l.mole^{-1} sec.$^{-1}$	$10^3\,k_2$ obs. × $[1 + K(\text{Br}^-)]$ l. mole^{-1} sec^{-1}
0.03	49.8	182.3
0.05	33.4	181.2
0.10	18.1	180.2
0.15	12.6	180.0
0.20	9.96	179.7

---

[2] V. P. Kudesia, *Bull. Soc. chim. belges*, **80**, 469 (1971).

[3] J. E. Dubois and J. Aaron, *J. chim. Phys.*, **61**, 1354 (1964).

[4] P. B. D. De la Mare, O.M.H. El Dusouqui, J. G. Tillett and M. Zeltner, *J. Chem. Soc.*, **1964**, 5306.

[5] C. Barnett, D. R. Marshal and L. A. Mulligan, *J. Chem. Soc.* (*B*), **1971**, 1529.

RATE LAW

The rates of bromination of crotonic acid were studied at 30° in presence of 70% (vol/vol) aqueous acetic acid and 0.20 M LiBr at $\mu = 0.2$. The rate constants were constant when calculated on the basis of the rate law

$$\frac{-\mathrm{d}\,(\text{Crotonic acid})}{\mathrm{d}t} = k_2\,(\text{Crotonic acid})\,(\mathrm{Br_2})$$

as described in the experimental section. The value of k_2 was found to be 9.96×10^{-3} l. mole^{-1} sec^{-1}.

Table 2

Dependence of rate constant on bromine concentration at 30°
(Crotonic acid) = 2.6×10^{-2} M; (LiBr) = 0.20M. μ = 0.2

$(\mathrm{Br_2}) \times 10^3$, M	$k \times 10^7$, sec^{-1}	$10^4\,k/(\mathrm{Br_2})$
2.5	6.48	2.59
2.8	7.25	2.59
3.0	7.77	2.59
3.2	8.29	2.59
3.5	9.07	2.59
3.8	9.84	2.59
4.1	10.6	2.58
4.3	11.1	2.59
4.7	12.2	2.59
4.9	12.7	2.59
5.2	13.4	2.58
5.5	14.2	2.58
6.0	15.5	2.59
6.4	16.6	2.59
6.8	17.8	2.62

Table 3

Dependence of rate constant on substrate concentration at 30° $(\mathrm{Br_2}) = 2.7 \times 10^{-3}$ M;
(LiBr) = 0.20M; μ = 0.2

10^2 (Crotonic acid), M	$k \times 10^7$, sec^{-1}	$10^5\,k$(crotonic acid)	$10^3\,k_2$ l. mole^{-1} sec.$^{-1}$
2.6	6.99	2.69	9.96
2.9	7.80	2.69	9.96
3.2	8.61	2.69	9.96
3.7	8.67	2.69	9.96
4.2	11.3	2.69	9.96
4.5	12.1	2.69	9.96
4.9	13.2	2.69	9.96
5.1	13.7	2.69	9.96
5.5	14.8	2.69	9.96
5.9	15.9	2.69	9.96
6.1	16.4	2.69	9.96
6.6	17.7	2.69	9.96
7.2	19.4	2.69	9.96
8.4	22.6	2.69	9.96
10.1	27.2	2.69	9.96

IONIC STRENGTH DEPENDENCE

The influence of ionic strength on the reaction rate has been studied for crotonic acid and Br_2 system. The lack of any significant deviation from second order kinetics, therefore, indicates that the rate is independent of change of ionic strength. Hence it is clear that the neutral species of substrate and oxidising agent are taking part in the reaction because for charged ions it is necessary that a plot of log k_2 versus $\sqrt{\mu}$ would have been linear with a negative slope.

Table 4

Influence of ionic strength on the bromination of crotonic acid at 30°. (Crotonic acid) = 2.6×10^{-2}M ; (Br_2) = 2.7×10^{-3}M ; (LiBr) = 0.20 M

$NaClO_4$ (M)	.10	.15	.20	.25	.30	.35	.40
10^3 k_2 mole^{-1} sec^{-1}	9.81	9.85	9.96	10.1	10.1	10.1	10.1

DEPENDENCE ON SOLVENT DIELECTRIC CONSTANT

The reaction has also been investigated in solvent mixtures of acetic acid and water of varying dielectric constant (table 5). The results have shown that the rate of addition of bromine increases with increase in water content (or polarity) of solvent suggesting that the activated complex is more polar than the reactants.[6,7] It also suggests that the reaction involves dipole – dipole interactions.

Table 5

Effect of change of dielectric constant on the second order rate constant at 30°
(Br_2) = 2.7×10^{-3}M ; (crotonic acid) = 2.6×10^{-2}M ; (LiBr) = 0.20M ; μ = 0.2

% Aq. acetic acid	30	35	40	50	70
$10^2 k_2$, 1 mole^{-1} sec.$^{-1}$	12.2	8.61	5.34	2.15	.996

EFFECT OF VARYING TEMPERATURE

The plots of logarithms of the second order rate constants against the reciprocal of the absolute temperature yield satisfactory straight line from which activation energy is evaluated : slope = $-Ea/2.3RT$. Em-

---

[6] E. D. Hughes, *Trans. Faraday Soc.*, **37**, 603 (1941).

[7] A. A. Frost and R. G. Pearson, "Kinetics and Mechanism", John Wiley and Sons Inc., New York, 1961, p. 140.

ploying this value and the following expressions, activation parameters were calculated and have been included in table : $\Delta H^{\neq} = Ea - RT$,

$$k_r = \left(\frac{kT}{h}\right) \exp\left(-\Delta G^{\neq}\ RT\right),\quad \Delta S^{\neq} = \left(\Delta H^{\neq} - \Delta G^{\neq}\right)/T$$

Table 6

Various activation parameters for the reaction of bromine and crotonic acid
$(Br_2) = 2.7 \times 10^{-3}$M ; (Crotonic acid) $= 2.6 \times 10^{-2}$M ; (LiBr) $= 0.21$ M ; $\mu = 0.2$

Temp.	$10^3 k_2$ l.mole^{-1} sec^{-1}	$\Delta H^{\neq}$ kcal/mole	$\Delta G^{\neq}$ kcal/mole	$\Delta S^{\neq}$ e.u.
298.11	7.65	10.9 ± 0.04	20.19	−31.2
303.22	9.95			
308.24	13.3			
318.28	24.3			

The energy of activation of $\Delta G^{\neq}$ was calculated at 25.11°. The standard deviations, *r.m.* were calculated by the formula

$$r.m. = 4.574 \sqrt{\frac{\Sigma\,(\log k_2 \,|\, k_{\text{int}})^2 \times n}{(n-2)\,[(\Sigma 1/T)^2 - n\,\Sigma 1/T^2]}}$$

where n is the number of experimental points, T is absolute temperature and k_{int} is the intrinsic value of the rate constant calculated by using values of $\Delta Y^{\neq}$ and $\Delta S^{\neq}$. The high negative value of $\Delta S^{\neq}$ clearly indicates that the activated complex is more solvated than the reactants.

DEUTERIUM ISOTOPE EFFECT

A kinetic isotope effect, kH/kD = 0.86 was observed for the addition of bromine to crotonic acid. This value suggests the formation of charged compound at the activated state.

STOICHIOMETRY

The stoichiometry was determined by adding different measured amounts of bromine to a series of solutions each containing the crotonic acid (2.9×10^{-2} M) together with lithium bromide and sodium perchlorate (all 0.1M). Each solution after reaction was analyzed for unchanged crotonic acid by UV spectrophotometry and for excess of bromine by titration with standard thiosulphate. From the results it is clear that reaction consumes one molecule of bromine per molecule of crotonic acid.

PRODUCTS OF THE REACTION

In a typical experiment 50 ml of crotonic acid and 25 ml of 0.006 M bromine solution were mixed at 30°C in 70% aqueous acetic acid. The yield of bromoderivative was found to be 89%. The analysis of the product gave the following data from which it is concluded that the product is dibromocrotonic acid $CH_3CHBrCHBrCOOH$.

Anal. *Calcd.* for $C_4H_6Br_2O_2$: C, 19.5 ; H, 2.4 ; Br. 65.0 ; 0.13.0

Found : C, 19.5 ; H, 2.4 ; Br, 65.0 ; 0.13.0%.

EFFECT OF SUBSTITUENTS

The effect of second order rate constant with change of substituent has also been investigated at 30°C. The results of the table 7 provide an evidence that alkyl groups exhibit a sudden decrease in the reaction rate. This substituent effect has important bearing on the mechanism of the bromination reaction as this sudden decrease in rate clearly shows that the process does not involve the removal of any ion from the substrate. It only suggests the possibility of the addition of bromine to the substrate.

Table 7

Effect of substituents upon second order rate constants at 30°
$(Br_2) = 2.7 \times 10^{-3}M$; $(LiBr) = 0.20M$; $\mu = 0.2$
$(substrate = 2 \cdot 6 \times 10^{-2}$ M)

Substrate	10^3k_2,1 mole^1 sec^{-1}
1. Crotonic acid	9.96
2. Methyl crotonate	2.00
3. Ethyl crotonate	0.523
4. Propyl crotonate	0.310

When looking for the mechanism, it is clear from the above results that one molecule of bromine reacts with one mole of substrate. Hence the probable mechanism on the basis of above results may be represented as

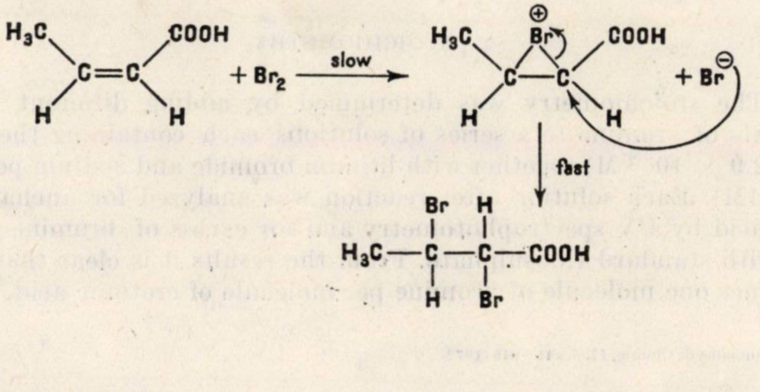

Revue Roumaine de Chimie, 17, 5, 847–853 (1972)

L'OBTENTION DE COMBINAISONS COMPLEXES MIXTES DES Ti(IV) ET Bi(III) AVEC LES ACIDES OXALIQUE ET TARTRIQUE POUR LEUR CONVERSION AUX OXYDES MIXTES CORRESPONDANTS

CONST. GH. MACAROVICI et GH. MORAR
Institut de Chimie, Cluj, 65–103, str. Donáth

Reçu, 31 mai 1971

En vue de la préparation des oxydes mixtes de titane et de bismuth par l'entremise des combinaisons complexes, on donne les conditions de synthèse de quelques oxalotitanates et tartratotitanates de bismuth. Par analyse chimique et spectres en IR on déduit les formules structurales les plus probables.

Vu les multiples applications pratiques des oxydes mixtes (catalyseur, semiconducteur, diélectriques, ferromagnétiques, pigments, matériaux réfractaires, etc.) on se propose d'obtenir des composés à composition stœchiométrique bien définie et reproductible, par des méthodes techniques opératoires aussi simples que possible et une température de réaction aussi basse que possible.

Les méthodes de préparation des oxydes mixtes sont aussi différentes que nombreuses.[1,2] Nous utilisons la décomposition thermique des combinaisons complexes mixtes,[2] c'est-à-dire avec des cations complexes et des anions complexes. Par ce procédé on peut obtenir des oxydes mixtes ou des solutions très réactives grâce à leur obtention à des températures beaucoup plus basses que par la calcination du mélange d'oxydes.

Par la décomposition thermique des combinaisons respectives il se forme un mélange très intime (moléculaire) d'oxydes métalliques qui se trouvent dans un état de réactivité élevée, et entrent directement en réaction.

Parmi les combinaisons complexes utilisées à cette fin, les plus indiquées sont celles du type des oxalates et des tartrates complexes, qui se décomposent à des températures plus basses et selon un mécanisme plus simple.

Dans ce travail, on a obtenu quelques complexes nouveaux d'oxalotitanates ou de tartratotitanates de bismuth, du type suivant :

I. $Bi_2\,[TiO(C_2O_4)_2]_3 \cdot 4H_2O$ III. $(BiO)_2[(TiO)_2(C_4O_6H_4)_3] \cdot 2H_2O$
II. $(BiO)_2\,[TiO(C_4O_6H_4)_2] \cdot 4H_2O$ IV. $Bi_2[(TiO)_3(C_4O_6H_2)_3] \cdot 4H_2O$

---

[1] J. Paris et R. A. Paris, *Bull. Soc. chim. France*, **4**, 1138 (1965).
[2] C. G. Macarovici et M. Străjescu, *Rev. Roumaine Chim.*, **13**, 1601 (1968).

Ceux-ci sont du type des acidocomplexes parce que seul le titanate est capable de former des anions complexes avec les acides oxalique et tartrique, et vu que pour le bismuth on ne connaît pas de cations complexes facilement accessibles. On a étudié les conditions d'obtention de ces types de substances complexes dans lesquelles le rapport de combinaisons Bi : Ti soit différent et coïncide avec celui des oxydes métalliques mixtes que nous nous proposons de préparer.

SYNTHÈSE DES COMPLEXES

I. $Bi_2[TiO(C_2O_4)_2]_3 \cdot 4H_2O$ — On part de l'acide titanyldioxalique connu[3-5] et du nitrate de bismuth, en procédant comme suit : une solution aqueuse de $H_2[TiO(C_2O_4)_2]$ ou le sel de potassium correspondant, $K_2[TiO(C_2O_4)_2]$, est ajoutée à froid à une solution aqueuse de $Bi(NO_3)_3$ acidulée de HNO_3 jusqu'à pH$\sim$1. Le mélange se fait en quantités stœchiométriques. Il se forme instantanément un précipité microcristallin blanc, que l'on filtre, lave à l'eau et sèche à l'air.

Il est préférable d'utiliser l'acide titanyloxalique et non son sel de potassium afin de ne pas impurifier le précipité formé et l'oxyde mixte que l'on désire obtenir, qui résulte de la décomposition thermique du complexe.

Pour obtenir la solution d'acide titanyldioxalique, on commence par préparer le $TiO_2 \cdot xH_2O$ en précipitant par de l'ammoniac une solution aqueuse de $TiCl_4$ et par laver le précipité jusqu'à ce qu'il ne contienne plus d'ions de chlore. On dissout à froid le gel de $TiO_2 \cdot xH_2O$ fraîchement préparé dans une solution aqueuse d'acide oxalique,[6,7] qui contient $2H_2C_2O_4$ pour un $Ti(OH)_4$.

L'absence des ions Cl^- est indispensable parce que, en cas contraire, il se forme du chlorure de bismutyle (BiOCl) très difficilement soluble, qui empêche la formation du complexe de titanyldioxalate de bismuth par l'extraction du bismuth du système. C'est pourquoi le complexe I ne peut être obtenu directement à partir de $TiCl_4$, $H_2C_2O_4$ et $Bi(NO_3)_3$, selon la méthode employée à la préparation de titanyloxalates avec d'autres métaux bivalents ou trivalents.[2,8-10]

II. $(BiO)_2[TiO(C_4O_6H_4)_2] \cdot 4H_2O$ — On a obtenu le titanylbistartrate de bismuthyle en additionnant la solution aqueuse de l'acide titanylbistartrique, $H_2\,[TiO(C_4O_6H_4)_2]$, d'une solution aqueuse de nitrate de bismuth acidulée (pH $\simeq$ 1) avec de l'acide nitrique, en quantités stœchiométriques. On sépare immédiatement le précipité se présentant sous forme d'une poudre dense blanche, on le filtre, on rince à l'eau et on fait sécher à l'air.

L'acide titanylbistartrique a été obtenu tout comme l'acide titanylbisoxalique, par dissolution à chaud du gel de $TiO_2 \, . \, xH_2O$, fraîchement préparé, dans une solution aqueuse d'acide tartrique en quantités de $2H_2C_4O_6H_4$ à 1 $TiO_2 \cdot xX_2O$.[4]

III. $(BiO)_2[(TiO)_2(C_4O_6H_4)_3] \cdot 2H_2O$ — Pour obtenir cette substance, on additionne à froid, sous agitation, à la solution d'acide $H_2[(TiO)_2\,(C_4O_6H_4)_3]$ une solution aqueuse de nitrate de bismuth acidulée (pH $\simeq$ 1). Il précipite instantanément une poudre blanche amorphe que l'on rince à l'eau et on fait sécher à l'air.

---

[3] E. Péchard *Compt. rend.*, **116**, 1513 (1893).

[4] A. Rosenheim et O. Schutte, *Z. anorg. Chem.*, **26**, 238 (1901).

[5] R. Feld et P. L. Cowe, « The Organic Chemistry of Titanium ». Butterworths, Londres, 1965, p. 81—96.

[6] J. Kharkar et L. Patel, *J. Indian Inst. Sci.*, **39A**, 41 (1957) ; *Chem. Abstr.*, **51**, 15317 (1957).

[7] W. S. Clabangh, E. M. Swiggard et R. Gilchrist, *J. Res. Nat. Bur. Stand*, **56**, 289 (1956).

[8] P. P. Bhatnager et T. Banerjee, *J. Sci. Ind. Res., India*, **15B**, 715 (1956).

[9] B. V. Strijkov, A. V. Lapitakii, L. G. Vlasov et A. I. Tvetkov, *Doklady Akad. Nauk S.S.S.R.*, **133**, 1347 (1960).

[10] B. V. Strijkov, A. V. Lapitakii et L. G. Vlasov, *Zhur. priklad. Khim.*, **33**, 2009 (1960) ; **34**, 673 (1961).

Tableau 1

Résultats de l'analyse chimique des complexes synthétisés

Substance analysée	Ti %		Bi %		Oxalique ou tartrique		H_2O %	
	Calculé	Trouvé	Calculé	Trouvé	Calculé	Trouvé	Calculé	Trouvé
I $Bi_2[TiO(C_2O_4)_2]_3.4H_2O$	11,87	11,80 11,98 11,84	34.44	34,47 34,68 34,52	43,65	43,62 43,68 43,41	5,95	6,3
II $(BiO)_2[TiO(C_4O_6H_4)_2].4H_2O$	5,43	5,53 5,41 5,48	47,39	47,52 47,40 47,36	33,56	33,80 33,72 33,60	8,17	8,6
III $(BiO)_2[(TiO)_2(C_4O_6H_4)_3].2H_2O$	9,05	9,07 8,92 9,03	39,53	39,56 39,43 39,49	41,99	41,94 41,67 41,89	3,40	3,65
IV $Bi_2[(TiO)_3(C_4O_6H_2)_3].4H_2O$	12,84	12,60 12,78 12,80	37,32	37,10 37,34 37,28	39,65	39,43 39,93 39,71	6,44	6,99

On obtient de façon analogue l'acide bistitanyl-tristartrique avec les autres acides titanyltartriques, par dissolution à chaud du gel $TiO_2 \cdot xH_2O$, fraîchement préparé, dans une solution aqueuse d'acide tatrique, au rapport de $3H_2C_4O_6H_4$ à $2TiO_2 \cdot xH_2O$.

IV. $Bi_2[(TiO)_3(C_4O_6H_2)_3] \cdot 4H_2O$ — Si l'on additionne une solution aqueuse de nitrate de bismuth, acidulée (pH $\simeq$ 1) avec de l'acide nitrique, sous agitation et goutte à goutte, d'une solution aqueuse d'acide titanylbistartrique, $H_2[TiO(C_4O_6H_4)_2]$, il précipite avec un léger retard une substance blanche amorphe dense. On la rince et fait sécher comme les autres substances. Il est probable qu'à l'addition de l'acide titanylbistartrique à la solution acide de nitrate de bismuth, celui-ci se décompose et ce n'est qu'après que se forme la combinaison IV. Les analyses chimiques sont incluses dans le tableau 1.

Lors de l'analyse chimique, l'acide oxalique et tartrique ont été déterminés par voie permanganométrique après la dissolution des substances dans l'acide sulfurique (1 : 1) ; la vérification a été faite moyennant les données de la microanalyse pour le carbone et l'hydrogène.

Le titane et le bismuth ont été dosés complexométriquement selon une méthode mise au point à cette occasion.[11]

L'eau de cristallisation a été dosée suivant le procédé habituel par échauffement de la substance à 110—120° et vérifiée par des thermogrammes.

Parmi les substances synthétisées seul le titanyldioxalate de bismuth (I) est microcristallin et présente un spectre de diffraction rœntgen ; les autres sont amorphes et ont le spectre de rayons rœntgen très diffus.

Le spectre rœntgen a été obtenu au moyen d'un appareil Tu-2-60 Dresden à cassettes Debye-Scherrer, en utilisant la radiation Kα du cuivre.

Les valeurs des constantes d/n déterminées par voie rœntgénographique pour le $Bi_2[TiO(C_2O_4)_2]_3 \cdot 4H_2O$ sont inscrites au tableau 2.

Tableau 2

Valeurs des constantes d/n déterminées par voie rœntgénographique pour le Bi_2 [TiO $(C_2O_4)_2]_3$.$4H_2O$

d/n Å	I	d/nÅ	I	d/n Å	I
1,238	1	1,717	2	2,851	6
1,272	1	1,820	2	3,001	2
1,353	1	1,841	6	3,705	2
1,395	2	2,028	2	3,235	6
1,434	1	2,072	2	4,052	4
1,460	1	1,158	4	4,546	4
1,505	4	2,285	4	5,235	5
1,571	4	2,367	4	7,314	5
1,616	2	2,454	2	—	
1,658	2	2,563	2	—	

L'intensité minimale de diffraction a été appréciée subjectivement par comparaison avec un spectre étalon gradué en sept unités d'intensité (tti = 10 ; ti = 9 ; i = 7 ; m = 6 ; f = 4 ; tf = 3 ; ttf = 1).

Les spectres d'absorption en infrarouge ont été obtenus à l'aide d'un spectrographe UR-10 — Karl Zeiss Iéna, sur des substances solides incluses dans les disques de KBr. Les bandes d'absorption respectives correspondant aux combinaisons I. . . IV, à l'état hydraté ou à l'état anhydre, sont consignées au tableau 3, pour le domaine 1800—400 cm^{-1}.

---

[11] Const. Gh. Macarovici et Gh. Morar (sous presse).

Tableau 3

Bandes d'absorption en IR dans le domaine 1800–400 cm⁻¹

	$Bi_2[TiO(C_2O_4)_2]_3.4H_2O$		$(BiO)_2, [TiO(C_4O_6H_4)_2]\ 4H_2O$		$(BiO)_2 [(TiO)_2 (C_4O_6H_4)_3]\cdot 2H_2O$ cm^{-1}	$Bi_2 [(TiO)_3 (C_4O_6H_2)_3].4H_2O$ cm^{-1}
	Hydraté cm^{-1}	Anhydre cm^{-1}	Hydraté cm^{-1}	Anhydre cm^{-1}		
	1724 i	1720 ti	—	—	—	—
νC = 0	1700 ti	1 710 – 1 620 ti	1 650 – 1 580 mi	1 630 – 1 570 i	1 640 i (large)	1 620 i (large)
	1 620 i	1 610 u ti	—	—	—	
νC – O	1 420 m	1 460 m	1 408 f	—	—	—
νC – C	—	—	1 392 m	1 390 – 1 360 m	1 390 – 1 360 mi	1 390 – 1 360 m
	—	1 350 – 1 340 m	1 370 m	—	—	—
νC – O	1 310 fm	1 110 m	1 320 – 1 310 t	1 320 t	—	1 320 t
δ (O – C = O)	1 270 f	—	1 235 tf	1 250 – 1 230	1 240 – 1 220 f	—
νOH	—	—	—	1 110 t	1 130 m	1 120 t
	—	—	1 080 fn	1 080 m	1 008 m	1 080 m
ν C – O	—	—	1 005 tf	—	—	– 1 010 – 990 t
δ (O – C = O)	—	930 t	920 f	920 – 890 mf	—	920 – 700 mi
δ (O – C = O)	—	850 t	850 fm	860 – 840 m	860 – 830 m	—
ν – OH	805 mi	800 i	815 m	820 – 800 m	—	—
νM – O	—	—	755	750 m	760 – 740 mi	—
H_2O	—	830 m	655 m	665 m	670 – 665 mi	665 i (large)
νM – O	530 m	530 m	540 m	540 m	540 mi	540 i
νC – C	510 – 480 m	480 m	—	—	—	—
νM – O	410 fm	430 m	—	—	—	—

ti = très intense ; i = intense ; m = moyen ; f = faible ; tf = très faible ; t = trace.

L'examen des spectres en IR permet d'identifier les bandes d'absorption caractéristiques aux différentes liaisons dans les molécules des substances étudiées, telles que : $\nu C = O$, $\nu C - O$, $\nu{-}OH$, $\nu(O-C=O)$, $\nu M-O$. Elles sont en bonne concordance avec les résultats obtenus dans le cas d'autres complexes des acides oxalique ou tartrique.[12-19] Les spectres des substances anhydres sont quelque peu modifiés par rapport aux spectres des substances hydratées, dans le sens que les bandes attribuées aux vibrations d'allongement O—H et de déformation H—O—H de l'eau de cristallisation disparaissent ou diminuent.[19] L'aspect similaire des spectres d'absorption en IR pour toutes les quatre substances apparaît comme une conséquence immédiate de la ressemblance structurale des complexes étudiés.

De l'analyse chimique on a déduit les formules rationnelles I. . .IV, indiquées au début. Mais compte tenu du fait que dans les solutions aqueuses faiblement acides le titane forme des ions octaédrique[20] du type $[Ti(OH)_2(H_2O)_4]^{2+}$, les formules des complexes synthétisés peuvent être écrites de la façon suivante :

$$\text{I}'\ Bi_2[Ti(OH)_2(C_2O_4)_2]_3 \cdot H_2O \qquad \text{III}'\ (BiO_2)[2Ti(OH)_2(C_4O_6H_4)_3]$$

$$\text{II}'\ (BiO)_2[Ti(OH)_2(C_4O_6H_4)_2].3H_2O \qquad \text{IV}'\ Bi_2[Ti(OH)_2(C_4O_6H_2)]_3.H_2O$$

On peut en déduire les formules structurales les plus probables. Par exemple, il est très probable que les substances I' et III' ont les structures suivantes.

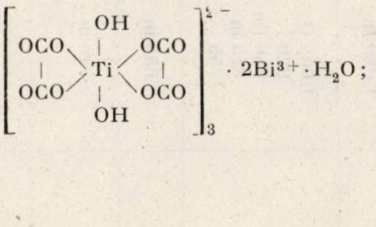

I'

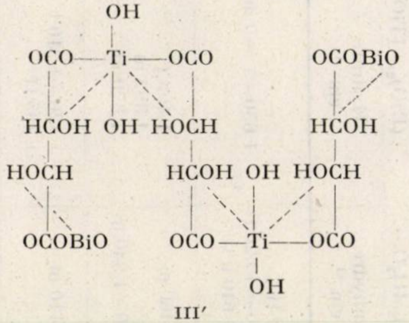

III'

Une formule similaire à III' peut être déduite aussi pour la substance II', tandis que pour la substance IV' on suppose une formule structurale identique à celle du dioxalatetitanate de bismuth I'.

[12] K. Nakamoto, « Infrared Spectra of Inorganic and Coordination Compounds », Inc. New York, Londres, 1963, p. 210—215.

[13] J. Fujita, A. E. Martell et K. Nakamoto, *J. Chem. Phys.*, **36**, 331 (1962).

[14] F. Douvillé, C. Douval et J. Lecompte, *Bull. Soc. chim. France*, **9**, 548 (1942).

[15] J. D. S. Goulden, Spectrochim. *Acta*, **16**, 715 (1960).

[16] M. Girard et J. Lecompte, *Compt. rend.*, **241**, 292 (1955).

[17] S. Krischner et R. Kiesling, *J. Amer Chem. Soc.*, **82**, 4174 (1960).

[18] J. Kuroda et M. Kubo, *J. Phys. Chem.*, **64**, 759 (1960).

[19] P. I. Lucchesi et W. A. Glasson, *J. Amer Chem. Soc.*, **78**, 1347 (1956).

[20] F. A. Cotton et G. Wilkinson, « Advanced Inorganic Chemistry », John Wiley & Sons, New York, Londres, Sydray, 1966, p. 803.

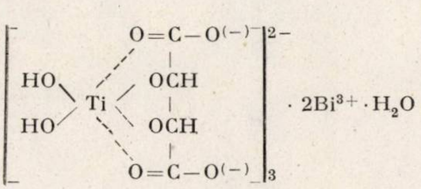

IV′

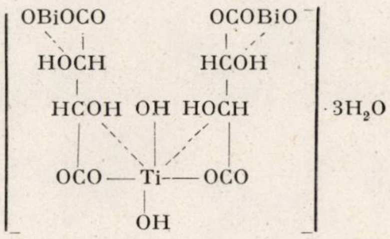

II′

Dans une prochaine note nous communiquerons l'analyse thermique et le mécanisme de la thermolyse de ces combinaisons complexes.

Revue Roumaine de Chimie, 17, 5, 855 – 861 (1972)

STUDY ON THE BEHAVIOUR OF THE NaA TYPE ZEOLITE IN THE PRESENCE OF NITRATES OF SOME BIVALENT CATIONS DISSOLVED IN MOLTEN SODIUM NITRATE

AGNETA BĂTCĂ-CERBU

Department of Inorganic Chemistry, Polytechnic Institute
Str. Polizu 1, Bucharest

Received May 27, 1971

The behaviour of dehydrated NaA type zeolite in the presence of calcium, strontium, barium and lead nitrate, dissolved in molten sodium nitrate has been investigated. It has been found that the equilibrium of ionic exchange which occurs is influenced by the nature of the bivalent cation, its concentration in the melt, the amount of the zeolite to the melt ratio, and that it is not influenced by the presence of the binding agent in the granulated zeolite. The ionic exchange process may be applied to the purification of some molten salts. At low concentration of the bivalent cation, the intensity of the ionic exchange is greater in aqueous solutions than in the medium of molten sodium nitrate.

When the NaA type zeolite contacts the melts of some ionic substances as the molten salts, two phenomena may occur : a sorption phenomenon when the molten salt replaces the water and fills the intracrystalline cavities of the zeolite and brings about inclusion compounds of various compositions and ionic exchange phenomenon, occurring on contacting melts with cations different from those of the zeolite.

The formation of the inclusion compounds as well as the ionic exchange in molten salts have been studied by several authors.[1–5] It is neverthless a field yet new and much less investigated sofar, than the domain of the reactions originating in aqueous solutions.

The present paper deals with phenomena occurring when the dehydrated NaA type synthetic zeolite comes into contact with the binary systems of molten salts : $Ca(NO_3)_2 - NaNO_3$; $Sr(NO_3)_2 - NaNO_3$; $Ba(NO_3)_2 - NaNO_3$ and $Pb(NO_3)_2 - NaNO_3$.

---

[1] R. M. Barrer and W. M. Mayer, *J. Chem. Soc.*, **1958**, 299.

[2] E. C. Freiling, *Thermodynamics Proc. Symp. Vienna*, **1**, 435 (1965). *Chem. Abstr.*, **65**, 8078 g (1966).

[3] M. Liquornic and Y. Marcus, *Israel J. Chem.*, **6**, 11 (1968).

[4] M. Liquornic and Y. Marcus, *J. Phys. Chem.*, **72**, 2885 (1968).

[5] M. Liquornic and Y. Marcus, *J. Phys. Chem.*, **72**, 4704 (1968).

EXPERIMENTAL

Two zeolite samples were used : NaA zeolite powder obtained by hydrothermal synthesis and granulated synthetic Linde NaA zeolite, which has been ground up to 400 mesh.

Both zeolite samples have been kept for 48 hours in a vater vapour atmosphere, at room temperature, then dried in air to constant weight and kept in a close container in order to keep a constant moisture.

The binary salt mixtures have been prepared of chemically pure substances. For the sake of homogenization and in order to remove humidity, the mixtures have been kept for 10 hours in molten state at 350° by periodical stirring. For the calcium nitrate, $Ca(NO_3)_2 . 4H_2O$ has been employed, previously dehydrated by keeping it for several days at 160°.

The zeolite samples were used ranging from 0.1 to 1 g. The volume of the melt was of 4.5 and 9.0 ml. To calculate the volume of the salt mixtures at 350°, working temperature, the mean densities of the mixtures, calculated from the partial molar volumes of the pure salts have been used.

The concentration of bivalent cations in the binary mixtures with sodium nitrate, varied from 5×10^{-3} to 6×10^{-2} mol/mol $NaNO_3$. For the calcium nitrate, determinations were made up to the 0.2 mol/mol $NaNO_3$.

The apparatus used was that described in a previous paper.[6]

The activation of the zeolite and its keeping into contact with the molten mixture occurred as in the above mentioned paper.

The activation time of the zeolite was of 4 h and the contact lasted for 24 h.

Working temperature on activation and during the reaction was of 350 ± 3°.

The separation of the zeolite from the melt has been made by filtering in a Rose crucible filter, at 350°. The mixture had been previously ground for homogenization.

The determination of the cations in the salt mixture and in the filtered melt, occurred by chemical analysis methods. Checking up of the analysis methods was made on standard mixtures of the same composition as the samples.

RESULTS AND DISCUSSION

On calculating the results the sorption of the sodium nitrate in the zeolite's cavities were taken into account, that leads to the formation of an inclusion compound. The zeolite treated in this way has the following formula of the unit cell :

$$Na_{22}[SiO_2 \cdot AlO_2]_{12}(NO_3)_{10} .$$

The foregoing has been mentioned in the literature[5] and checked up by the author of the present paper.

The experimental data represented as isotherms of ionic exchange at 350°, in figure 1 show that the quantity of bivalent cations retained by the NaA type zeolite in the already mentioned working conditions, is not determined only by the size of the cation in the melt, as in the case of alkaline cations,[6] this also depends on their concentration in the molten mixture.

---

[6] S. Sternberg and A. Cerbu, *Rev. Roumaine Chim.*, **14**, 1215 (1969).

Thus, for small values of the molar fraction of the bivalent cation in the melt,up to $X_C = 0.01$, the bivalent cations investigated are practically retained in the same proportion (fig. 1). For greater X_C values there is another proportion of cations retained by the zeolite. For X_C values ranging from 0.02 to 0.035 the quantity of bivalent cation retained by the zeolite decreases in the following order : $Pb^{2+} > Ca^{2+} > Ba^{2+} > Sr^{2+}$ i.e. it decreases with the increase of the ionic radius for alkaline-earth cations. This order is changing for greater concentrations. For a X_C value equal to 0.059 the retention of the cation from the melt occurs as follows : $Pb^{2+} > Sr^{2+} > Ba^{2+} > Ca^{2+}$. This may be explained by the different position of the bivalent cations in the zeolite's cavities. The cations located near the six octagonal rings of the great cavities, hemper the shift of the cations in either sense — the release of sodium and penetration of the bivalent cation. The argument is supported also by the fact that the retention of one mol of bivalent cation in each zeolite mol occurs at the same concentration of the bivalent cation in the melt, for all cations under consideration (see the initial part of the isotherms).

For calcium nitrate, the appearance of a plateau is noticed at 6 mol Ca^{2+}/mol zeolite. This starts at relatively law values of the molar fraction of calcium nitrate in the melt $X_{Ca^{2+}} \approx 0.045$. The explanation of the saturation phenomenon of the zeolite's cavities during the ionic exchange with the calcium nitrate and under working conditions similar to those pointed to by the author of the present paper, has been given by Liquornic and Marcus.[5] They have shown that in solutions of calcium nitrate dissolved in molten sodium nitrate a monovalent $CaNO_3^+$ cation is forming with dimensions close to those of the sodium nitrate and that is retained in zeolite's cavities. In our work we have shown that up to the value of $X_{Ca^{2+}} \approx 0.16$, the NaA zeolite cannot retain more than six mol Ca^{2+}/mol.

For the other bivalent cations, within the above mentioned concentration range, no formation of such a cation in the melt has been noticed, a fact that may be accounted for by the value of their ionic radius, that brings about low values of their fields.[5]

For calcium, the value $\frac{z}{r^2} \approx 2$ is much greater than for sodium, i.e. almost twice. Therefore calcium may coordinate the NO_3^- anion in the presence of a great excess of molten sodium nitrate. As for the other cations, since they have this value much smaller and close to that of sodium, we can suppose that they are not able to bring about the $MeNO_3^+$ cation in the sodium nitrate melts. Consequently, the only process occurring during the contact of the NaA type zeolite charged with sodium nitrate, with the mixture of the above mentioned molten salts, is the ionic exchange, each bivalent cation replacing two sodium ions.

This allows to check up the behaviour of the inclusion compound within the ionic exchange.

In the case of lead and barium ions, the zeolite may retain more than six mols bivalent cation per each mol of zeolite (fig. 1). The replacing of a greater number of sodium ions than that of the initial composition of zeolite — i.e. 12 sodium ions/mol zeolite, will thus take place. Hence, the

NaA type zeolite, treated with molten sodium nitrate, increases its ionic exchange capacity in the melt, being able to participate in the ionic exchange also with the cations included in cavities by the sorption process of molten sodium nitrate.

The total replacement of the 22 sodium ions in the above mentioned working conditions has not been possible owing to the high melting point

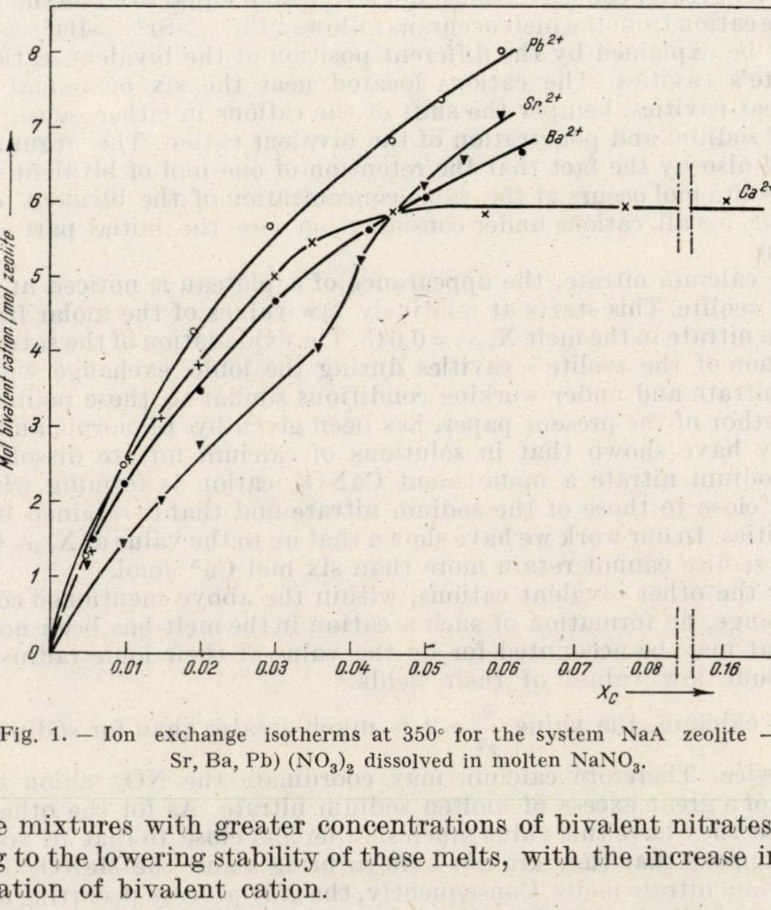

Fig. 1. — Ion exchange isotherms at 350° for the system NaA zeolite — (Ca, Sr, Ba, Pb) $(NO_3)_2$ dissolved in molten $NaNO_3$.

of the mixtures with greater concentrations of bivalent nitrates and also owing to the lowering stability of these melts, with the increase in the concentration of bivalent cation.

The quantity of bivalent cation retained by the zeolite, in the above mentioned working conditions is also influenced by the electronic configuration of the cation in the melt. Experimental data show that lead, placed according to its ionic radius between strontium and barium ions : $r_{Sr^{2+}} < r_{Pb^{2+}} < r_{Ba^{2+}}$, is retained to a greater extent than these, at all concentrations except for low concentrations $-X_{Pb^{2+}} \leqslant 0.01$. The phenomenon may be explained by the electronic configuration of this ion. Lead is different from the other bivalent cations under consideration, by the absence of an inert gas configuration. The presence of free orbitals in the valence core, and especially the presence of the three 6p unoccupied orbitals, enable this cation to coordinate free electron pairs of the oxygen atoms from the aluminosilicate lattice of the zeolite. This fact might possibly increase the force of attraction between the cation and the zeolite and consequently the affinity of the zeolite for the lead cation and it most likely brings about a more close packing of ions in the zeolite's cavities and therefore their possible retention to a greater extent. This explanation is supported by the fact that in presence of the thallium nitrate dissolved in molten natrium nitrate, the NaA type zeolite behaves similarly to the monovalent thallium ion having an electronic structure identical with that of the lead ion.

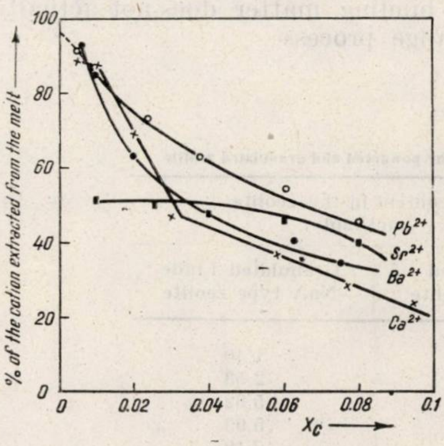

Fig. 2. — Amount of the bivalent cation extracted from the melt.

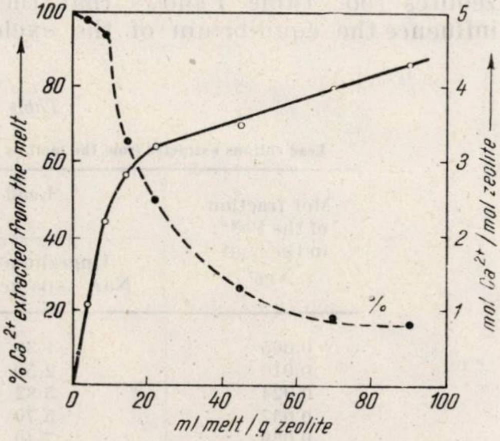

Fig. 3. — Influence of the zeolite weight/melt volume ratio on the amount of calcium retained by the zeolite-mile/mol and that extracted from melt - as a %.

Other experiments have been carried out in view of finding out the possibility to use the ionic exchange zeolite-molten salt as a purification method. To this end determinations were made to determine the extraction yield of the bivalent cation with respect to the concentration of bivalent cation nitrate in the melt. The results are represented in figures 2 and 3.

Figure 2 shows that for small X_C values, the amount of bivalent cation extracted from the melt is great and in general decreases with the increase of the mol fraction of the bivalent cation in the melt.

Figure 3 shows that for the same value of the molar fraction of the calcium in the mixture of molten salt $X_{Ca^{2+}} = 0.005$, the amount of cation extracted from the melt is greater as the ratio of the zeolite amount to the melt volume increases and the quantity of the cation retained by the zeolite is varying inversely.

It results that, as in the case of aqueous solutions, the intensity of the ionic exchange is greater as the amount of bivalent cation in the melt is lower, an extraction close to 100% being reached for some cations.

From the foregoing it results that the ionic exchange in the melt may be used to remove certain impurities in molten salts. In our case, the dehydrated NaA type zeolite may be used to remove traces of bivalent cations from the molten sodium nitrate.

Because only processes using granulated zeolites are of technological significance, determinations were carried out with granulated NaA Linde zeolites too. Table 1 shows that the binding matter does not actually influence the equilibrium of the exchange process.

Table 1

Lead cations extracted from the melt by the powdered and granulated zeolite

Mol fraction of the Pb^{2+} in the melt $X_{Pb^{2+}}$	Lead content in the zeolite mol/mol	
	Ungranulated NaA type zeolite	Granulated Linde NaA type zeolite
0.005	1.30	1.40
0.010	2.50	2.53
0.024	5.82	5.62
0.037	5.70	5.93
0.059	7.40	7.19

Determinations have been also made for the comparison of the ionic exchange in the melt and in the aqueous medium. Table 2 shows that at a small concentration of the calcium nitrate in the melt and in aqueous solution — 0.1 m, the ionic exchange proceeds with varied intensities in the two media. A higher proportion is noticed for the calcium extracted from aqueous solution and this may be accounted for by the fact that in zeolite, the hydrated sodium ion is not so strongly bound to the aluminosilicate lattice and therefore, enjoys greater mobility. At the same time, the presence of a great excess of sodium nitrate in the case of the ionic exchange in the melt in the above mentioned conditions, may exert a negative influence on the replacement of sodium from zeolite by the bivalent cations from the melt, a fact that could not occur in the case of the ionic exchange in aqueous solutions.

Table 2

Intensity of the ionic exchange in aqueous medium and in molten sodium nitrate, in the presence of calcium nitrate

Solvent	Cation concentration mol/1	Zeolite amount g	Liquid volume ml	Amount of cation extracted from the reaction medium as %
Water	0.11	1.0000	75	22.5
Molten sodium nitrate	0.11	1.0000	75	17.5

CONCLUSIONS

On the basis of experimental results, the following conclusions may be drawn. The ionic exchange between zeolite sodium and studied bivalent cations, is influenced by the nature of the cation, its concentration in the melt, the ratio of zeolite amount to the volume of the melt, and it is not influenced by the presence of the binding matter in the granulated zeolite.

The extraction yield increases with the decrease in the cation concentration in the melt; the process may be applied to remove traces of bivalent cations from the molten sodium nitrate.

The intensity of the ionic exchange process is greater in aqueous solution than in molten sodium nitrate, at low concentrations of the bivalent cation in the liquid phase.

Revue Roumaine de Chimie, **17**, 5, 855 – 861 (1972)

Revue Roumaine de Chimie, 17, 5, 863–864 (1972)

AN MO APPROACH TO THE STABILIZATION PROBLEM OF THE COORDINATION CLUSTERS

C. I. LEPĂDATU
Centre of Physical Chemistry, Dumbrava Roșie 23,
Bucharest, Romania

Received January 17, 1972

The stabilization of the coordination clusters is discussed in terms of the LCAOMO theory, introducing the notions of molecular orbital energy and bond stabilization energy.

In an earlier work,[1] a MO approach to the stabilization of the coordination clusters has been presented, in order to get better results than those obtained in the framework of the crystal and ligand field theories. Since the treatment has been done on particular cases, we shall try next to extend the MO treatment and to put the stabilization problem of the coordination clusters on more consistent bases.

Let us consider $\{m\}$, the set of AO's belonging to the central atom which interacts with the set $\{l\}$ of ligand orbitals. The bonding and antibonding molecular energies calculated using the angular overlap model[2] in the LCAOMO alternative, as recently described,[3] are given by the formulas

Antibonding

$$E_i = \alpha'_i + \sum_k \sum_j {}^k\mathcal{D}^2_{ij} \frac{{}^\lambda\beta'^2_{jk}}{E_i - \alpha'_k} + \sum_k \sum_r \sum_j {}^k\mathcal{D}_{ij}\,{}^r\mathcal{D}_{ij} \frac{{}^\lambda\beta'_{jk}\,{}^\lambda\beta'_{rj}\,{}^\lambda\beta'_{kr}}{(E_i-\alpha'_k)(E_i-\alpha'_r)} + \cdots$$

Bonding

$$E_k = \alpha'_k + \sum_i \sum_j {}^k\mathcal{D}^2_{ij} \frac{{}^\lambda\beta'^2_{jk}}{E_k - \alpha'_i} + \sum_{r \neq k} \frac{{}^\lambda\beta'^2_{kr}}{E_k - \alpha'_r} + \cdots$$

where α's are the zero-order energies, β's the resonance integrals, the primes showing that a linear orthogonalization has been performed on the interacting orbitals, ${}^k\mathcal{D}_{ij}$ are the angular matrix elements,[4] the indices (i, j) running over the set $\{m\}$ of central atom orbitals and (k, r) over the set $\{l\}$ of ligand orbitals, λ being the bonding type.

---

[1] P. Spacu and C. I. Lepădatu, *Z. phys. Chem. (Frankfurt)*, **76**, 168 (1971).

[2] C. E. Schäffer and C. K. Jørgensen, *Mol. Phys.*, **9**. 401 (1965).

[3] C. I. Lepădatu, *Z. phys. Chem. (Frankfurt)*, **73**, 249 (1970).

[4] C. E. Schäffer, *Struct. and Bonding*, **5**, 68 (1968).

It is obvious that the molecular system will be stable if the following condition holds

$$\sum_k^{\text{occ}} n_k E_k + \sum_i^{\text{occ}} n_i E_i < \sum_k^{\text{occ}} n_k \alpha'_k + \sum_i^{\text{occ}} n_i \alpha'_i$$

where $n_k(n_i)$ is the electron number of the bonding (antibonding) levels. Assuming that $\alpha'_k \ll \alpha'_i$, $E_k \sim \alpha'_k$, $E_i \sim \alpha'_i$, and neglecting the high order perturbations, the last inequality becomes

$$\sum_k \sum_i \sum_j (n_k - n_i)\, {}^k\mathcal{D}^2_{ij}\, e^k_{\lambda(j)} + R < 0$$

where $e^k_{\lambda(j)} = \dfrac{\lambda \beta'^2_{jk}}{\alpha'_k - \alpha'_i}$ is taken as an energetical parameter transferable with a fairly good degree of accuracy from one cluster to another,[5] and R includes the ligand-ligand interactions (the third term in E_k). It should be mentioned that generally $n_k = 2$. The left-hand side member of the last formula represents a quantity which may be called the molecular orbital stabilization energy (MOSE). For a cluster ML_N, the stabilization energy of one coordination point can be derived dividing the left-hand side member of the last inequelity by the coördination number N. The bond stabilization energy (BSE) obtained, may be used to explain the coördination geometries of the clusters and the pathway followed by the ligand substitution processes.[6]

---

[5] P. Spacu and C. I. Lepădatu, *Z. phys. Chem. (Frankfurt)*, **73**, 255 (1970).

[6] C. I. Lepădatu, *J. Cryst. Mol. Structure*, **1**, 397 (1972).

Revue Roumaine de Chimie, 17, 5, 865 – 881 (1972)

CHEMICAL GRAPHS. XIV.[1]
VALENCE ISOMERS OF [12]ANNULENE

A. T. BALABAN
Institute of Atomic Physics, P.O.B. 35, Bucharest, Romania

Received January 5, 1972

Structures for all possible valence isomers of [12]annulene are given, as trivalent (cubic) planar* multigraphs of order 12. A survey of the literature data for known valence isomers of [4]- to [12]annulene is presented.

INTRODUCTION

In the years which have elapsed since the first exhaustive list of valence isomers of [4]-, [6]-, [8]-, and [10]annulenes was published,[5] many of these were prepared in various laboratories. Subsequently, the graph-theoretical treatment was extended by means of general trivalent graphs to finding out valence isomers of aromatic heterocyclic systems with odd-membered rings,[6] but owing to the rapidly increasing numbers of isomers, the order of graphs was still limited to 10 (i.e. at most 10 points were considered).

In a strict graph-theoretical definition, graphs can only have single edges, but multigraphs can have multiedges (multiple bonds). No geometric or steric isomerism is considered, only the topology of the molecules represented by the trivalent multigraphs is taken into account.

The mathematically complicated problem of finding all trivalent multigraphs of a given order has led to erroneous statements as to the number of valence isomers of annulenes, even after reference 5 was published. Thus in some reviews on valence isomers $(CH)_6$ of benzene,[7-9] bicyclopropenyl was not included, probably owing to the fact that it is the only one which does not have a six-membered ring (Hamiltonian circuit). It was written[10] that there are 16 possible valence isomers $(CH)_8$ of cycloöctatetraene when in fact there are 17 planar trivalent multigraphs of order 8.

---

* Throughout the present paper, the terms "planar" and "non planar", are used in the graph-theoretical sense : a planar graph can (whereas a non-planar graph cannot) be drawn in a plane representation so that no bonds (edges) meet except at a vertex (point).[2-4] In the tables from references 5 and 6, notations of non-planar graphs were enclosed in brackets, while those of planar graphs were without brackets.

[1] Part XIII, A. T. Balaban, *Rev. Roumaine Math. Pures Appl.*, **17**, 3 (1972).

[2] F. Harary, "Graph Theory", Addison-Wesley Publ. Comp., Reading, Mass., 1969, chapter 11.

[3] K. Kuratowski, *Fund. Math.*, **15**, 271 (1930).

[4] J. W. Essam and M. E. Fisher, *Rev. Modern Phys.*, Suppl. **42**, 271 (1970).

[5] A. T. Balaban, *Rev. Roumaine Chim.*, **11**, 1097 (1966); Erratum, *ibid.*, **12**. No. 1, 103 (1967).

[6] A. T. Balaban, *Rev. Roumaine Chim.*, **15**, 463 (1970).

LITERATURE SURVEY FOR VALENCE ISOMERS OF [4]- TO [10]ANNULENE

To summarize developments in valence isomers of annulenes (including substituted, but not benzo, derivatives) which can only have even-membered $(CH)_p$ rings, for $(CH)_4$ both possible valence isomers, tetrahedrane (4—0—0—1)[11,12,*] and cyclobutadiene (4—2—0—1)[13-30] have now been evidenced as reactive molecules. All five planar valence isomers $(CH)_6$ of benzene are now known : benzene (6—3—0—1), Dewarbenzene (6—2—0—2),[7,8,21,31-41] bicyclopropenyl (6—2—0—1),[40-43] benzvalene (6—1—0—1),[38,39,44-49] and prismane, triprismane or benzprismane (6—0—0—1).[32,34,37,50,51] The list of known valence isomers of $(CH)_8$ is continuously increasing totalling out of 17 possible planar multigraphs, 10 known structures : cycloöctatetraene (8—4—0—1),[24,52-55] barrelene (8—3—0—4),[10,56-61] dihydrocalicene (8—3—0—2),[62] bicyclo-

---

* Notations are those of reference 6. The literature survey only includes newer quotations which were not cited in ref. 5 or 6. A few misprints in Tables 4d and 4e of ref. 6 should be corrected : for 8—0—3—1 in table 4d (p. 471) replace two loops joined to the same point by just one loop ; for 10—0—0—16, 10—2—0—24 and 10—0—1—3 in table 4e (p. 472 and 473) join the two vertices of degree 2 by a line ; for 10—2—0—24 and 10—3—1—1 in table 4e (p. 473) delete the point of degree 2. Also, on p. 477 line 35, replace "pictures" by "pictured".

[7] W. Schäfer and H. Hellmann, *Angew. Chem.*, **79**, 566 (1967) ; *Angew. Chem. internat. Edit.*, **6**, 518 (1967).

[8] I. G. Bolesov, *Uspekhi Khim.*, **37**, 1567 (1968).

[9] A. Sementsov, in "Kekulé Centennial", Adv. Chem. Series No 61, Amer. Chem. Soc., Washington, 1966, p. 72.

[10] H. E. Zimmerman, R. W. Binkley, R. S. Givens, G. L. Grunewald and M. A. Sherwin, *J. Amer. Chem. Soc.*, **91**, 3316 (1969).

[11] P. B. Shevlin and A. P. Wolf, *J. Amer. Chem. Soc.*, **92**, 406, 3523. 5291 (1970) ; R. F. Petersen, R. T. K. Baker and R. L. Wolfgang, *Tetrahedron Letters*, **1969**, 4749.

[12] I. J. Miller, *Tetrahedron*, **25**, 1349 (1969).

[13] M. P. Cava and M. J. Mitchell, "Cyclobutadiene and Related Compounds", Academic Press, New York, 1967.

[14] R. Gompper and G. Seybold, *Angew. Chem.*, **80**, 804 (1968) ; *Angew. Chem. internat. Edit.*, **7**, 824 (1968).

[15] M. Neuenschwander and A. Niederhauser, *Chimia (Aarau)*, **22**, 491 (1968).

[16] H. J. Lindner and B. von Gross, *Angew Chem.*, **83**, 489 (1971) ; *Angew. Chem. internat. Edit.*, **10**, 490 (1971).

[17] K. V. Scherer, Jr. and T. J. Meyers, *J. Amer. Chem. Soc.*, **90**, 6253 (1968).

[18] P. Reeves, J. Henery and R. Pettit, *J. Amer. Chem. Soc.*, **91**, 5888 (1969).

[19] P. Reeves, T. Devon and R. Pettit, *J. Amer. Chem. Soc.*, **91**, 5890 (1969).

[20] G. Amiet, K. Nicholas and R. Pettit, *Chem. Commun.*, **1970**, 161.

[21] P. R. Story, W. H. Morrison and J. M. Butler, *J. Amer. Chem. Soc.*, **19**, 2398 (1969).

[22] R. Criegee and R. Huber, *Chem. Ber.*, **103**, 1862 (1970).

[23] G. Maier and U. Mende, *Tetrahedron Letters*, **1969**, 3155 ; *Angew.* Chem., **81**, 114 (1969) ; *Angew. Chem. internat. Edit.*, **8**, 132 (1969).

[24] G. Maier, G. Fritschi and B. Hoppe, *Tetrahedron Letters*, **1971**, 1463 ; *Angew. Chem.*, **82**, 551 (1970) ; *Angew. Chem. internat. Edit.*, **9**, 529 (1970).

[25] H. Ona, H. Yamaguchi and S. Masamune, *J. Amer. Chem. Soc.*, **92**, 7495 (1970).

[23] W. J. R. Tyerman, M. Kato, P. Kebarle, S. Masamune, O. P. Strausz and H. E. Gunning, *Chem. Commun.*, **1967**, 497.

[27] E. Hedaya, R. D. Miller, D. W. Mc Neil, F. D'Angelo and P. Schissel, *J. Amer. Chem. Soc.*, **91**, 1875 (1969).

[28] R. D. Miller and E. Hedaya, *J. Amer. Chem. Soc.*, **91**, 5401 (1969).

[29] M. J. S. Dewar, M. C. Kohn and N. Trinajstić, *J. Amer. Chem. Soc.*, **93**, 3437 (1971).

[30] G. Maier and M. Schneider, *Angew. Chem.* **83**, 885 (1971) ; *Angew. Chem. internat. Edit.* **10**, 809 (1971).

---

[31] W. Schäfer, *Angew. Chem.*, **78**, 716 (1966) ; *Angew. Chem. internat. Edit.*, **5**, 669 (1966).

[32] W. Schäfer, R. Criegee, R. Askani and H. Grüner, *Angew. Chem.*, **79**, 54 (1967) ; *Angew. Chem. internat. Edit.*, **6**, 78 (1967).

[33] H. N. Junker, W. Schäfer and H. Niedenbrück, *Chem. Ber.*, **100**, 2508 (1967).

[34] R. Criegee and H. Grüner, *Angew. Chem.*, **80**, 447 (1968) ; *Angew. Chem. internat. Edit.*, **7**, 467 (1968).

[35] H. Hogeveen and H. C. Volger, *Rec. Trav. chim.*, **86**, 830 (1967).

[36] E. E. van Tamelen and D. Carty, *J. Amer. Chem. Soc.*, **89**, 3932 (1967) ; **93**, 6102 (1971) ; E. E. van Tamelen, S. P. Pappas and K. L. Kirk, *ibid.*, 6092.

[37] J. F. M. Oth, *Angew. Chem.*, **80**, 633 (1968) ; *Angew. Chem. internat. Edit.*, **7**, 646 (1968).

[38] H. R. Ward and J. S. Wishnok, *J. Amer. Chem. Soc.*, **90**, 1085 (1968).

[39] K. E. Wilzbach and L. Kaplan, *J. Amer. Chem. Soc.*, **93**, 2073 (1971).

[40] G. Berthier, A. Y. Meyer and L. Praud, in "The Jerusalem Symposia on Quantum Chemistry and Biochemistry", vol. 3, "Aromaticity, Pseudoaromaticity and Anti-Aromaticity", edited by E. D. Bergmann and B. Pullman, p. 174, Israel Acad. Sci. Humanities, Jerusalem, 1971.

[41] R. Weiss and C. Schlierf, *Angew. Chem.*, **83**, 887 (1971) ; *Angew. Chem. internat. Edit.*, **10**, 811 (1971).

[42] C. De Boer and R. Breslow, *Tetrahedron Letters*, **1967**, 1033.

[43] G. L. Closs, in "Advances in Alicyclic Chemistry", **1**, 53, 90 (1966) edited by H. Hart and G. J. Karabatsos, Academic Press, New York.

[44] T. J. Katz, E. J. Wang and N. Acton, *J. Amer. Chem. Soc.*, **93**, 3782 (1971).

[45] K. R. Jennings, *Z. Naturforsch.*, **22a**, 454 (1967).

[46] I. Horman, A. N. H. Yeo and D. H. Williams, *J. Amer. Chem. Soc.*, **92**, 2131 (1970).

[47] I. E. Den Besten, L. Kaplan and K. E. Wilzbach, *J. Amer. Chem. Soc.*, **90**, 5868 (1968) ; K. E. Wilzbach, J. S. Ritscher and L. Kaplan, *ibid.*, **89**, 1031 (1967) ; K. E. Wilzbach, A. L. Harkness, and L. Kaplan, *ibid.*, **90**, 1116 (1968).

[48] L. Kaplan and K. E. Wilzbach, *J. Amer. Chem. Soc.*, **90**, 3291 (1968).

[49] J. M. Blair and D. Bryce-Smith, *Proc. Chem. Soc.*, **1967**, 287.

[50] R. Criegee, *Angew. Chem.* **80**, 585 (1968) ; *Angew. Chem. internat. Edit.*, **7**, 559 (1968).

[51] H. Hogeveen and H. C. Volger, *Chem. Commun.*, **1967**, 1133.

[52] F. A. L. Anet and L. A. Bock, *J. Amer. Chem. Soc.*, **90**, 7130 (1968).

[53] L. A. Paquette, J. R. Malpass and T. J. Barton, *J. Amer. Chem. Soc.*, **91**, 4714 (1969).

[54] M. Jones Jr. and L. O. Schwab, *J. Amer. Chem. Soc.*, **90**, 6549 (1968).

[55] P. J. Garratt and M. V. Sargent, in "Advances in Organic Chemistry, Methods and Results", edited by E. C. Taylor and H. Wynberg, Interscience, New York, **6**, 1 (1969).

[56] G. L. Grunewald, *Diss. Abstr.*, **27B**, 1087 (1966).

[57] M. A. Sherwin, *Diss. Abstr.*, **30B**, 1053 (1969).

[58] H. E. Zimmerman, R. W. Binkley, R. S. Givens and M. A. Sherwin, *J. Amer. Chem. Soc.*, **89**, 3932 (1967).

[59] H. E. Zimmerman, G. L. Grunewald, R. M. Paufler and M. A. Sherwin, *J. Amer. Chem. Soc.*, **91**, 2330 (1969).

[60] N. L. Allinger, J. Chow-Tai and T. W. Stuart, *Theor. Chim. Acta*, **8**, 101 (1967).

[61] R. S. H. Liu, *J. Amer. Chem. Soc.*, **90**, 215 (1968).

[62] H. Prinzbach, H. Knöfel and E. Woischnik, in "Aromaticity, Peseudo-Aromaticity and Anti-Aromaticity" edited by E. D. Bergmann and B. Pullman, Jerusalem, 1971, p. 269; H. Prinzbach, *Pure Appl. Chem.*, **28**, 281 (1971).

[4.2.0] octa-2, 4, 7-triene (8—3—0—3), [63–66] semibullvalene or tricyclo-$[3.3.0.0^{2,8}]$ octa-3, 6-diene (8—2—0—3) [57,58,61,67–78] which is almost a mesovalent molecule [69] owing to the very rapid degenerate rearrangement, [10] tricyclo $[4.2.0.0^{2,5}]$ octa-3, 7-diene (8—2—0—4), [17,30,64,67,74,79–87,*] tricyclo $[3.3.0.0^{2,6}]$octa-3,7-diene (8—2—0—5), [70,75,88] tetracyclo-$[3.3.0.0^{2,4}.0^{3,6}]$ oct-7-ene (8—1—0—4), [89,90] cubane (8—0—0—4), [12,78,79,91,92] and pentacyclo $[3.3.0.0^{2,4}.0^{3,7}.0^{6,8}]$ octane or cuneane (8—0—0—2). [67,78,93] Still unknown valence isomers $(CH)_8$ of interest are 8—0—0—1, [78] 8—1—0—3, [90] 8—1—0—4 which was discussed in connection with semibullvalene, [10] and 1,2-dicyclopropenyl-ethylene (8—3—0—1), or the vinylogous benzvalene 8—2—0—2 which by a 1,5-carbon shift should present a

---

[*] The *syn-* and *anti-* octamethyl-derivatives are known as Criegee hydrocarbons.[82]

[63] I. W. McCay and R. N. Warrener, *Tetrahedron Letters*, **1970**, 4783.

[64] W. Merk and R. Pettit, *J. Amer. Chem. Soc.*, **89**, 4788 (1967).

[65] L. A. Paquette and J. C. Philips, *Chem. Commun.*, 1969, 680; L. A. Paquette, J. C. Philips and R. E. Wingard Jr., *J. Amer. Chem. Soc.*, **93**, 4516 (1971).

[66] R. Askani, *Chem. Ber.*, **102**, 3304 (1969).

[67] R. Criegee and R. Askani, *Angew. Chem.*, **80**, 531 (1968); *Angew. Chem. internat. Edit.*, **7**, 537 (1968).

[68] H. E. Zimmerman and H. Iwamura, *J. Amer. Chem. Soc.*, **90**, 4763 (1968); **92**, 2015 (1970).

[69] M. J. S. Dewar and W. W. Schoeller, *J. Amer. Chem. Soc.*, **93**, 1481 (1971); M. J.S. Dewar, Z. Náhlovská and B. D. Náhlovský, *Chem. Commun.*, **1971**, 1377.

[70] H. E. Zimmerman, J. D. Robbins and J. Schantl, *J. Amer. Chem. Soc.*, **91**, 5878 (1969); H. Iwamura, K. Morio and T. L. Kunii, *Chem. Commun.*, **1971**, 1408.

[71] R. Askani, *Tetrahedron Letters*, **1970**, 3349.

[72] L. A. Paquette, *J. Amer. Chem. Soc.*, **92**, 5765 (1970).

[73] R. Askani, R. Glerter, E. Heilbronner, V. Hornung and H. Musso, *Tetrahedron Letters*, **1971**, 4461.

[74] J. M. Bollinger and G. A. Olah, *J. Amer. Chem. Soc.*, **91**, 3380 (1969).

[75] J. Meinwald and D. Schmidt, *J. Amer. Chem. Soc.*, **91**, 5877 (1969).

[76] R. W. Binkley, R. S. Givens and M. A. Sherwin, *J. Amer. Chem. Soc.*, **89**, 3932 (1967).

[77] R. M. Moriarty, C. L. Yeh and N. Ishibi, *J. Amer. Chem. Soc.*, **93**, 3085 (1971).

[78] L. Cassar, P. E. Eaton and J. Halpern, *J. Amer. Chem. Soc.*, **92**, 6366 (1070).

[79] L. Cassar, P. E. Eaton and J. Halpern, *J. Amer. Chem. Soc.*, **92**, 3518 (1970).

[80] T. J. Katz and E. W. Turnblom, *J. Amer. Chem. Soc.*, **92**, 6701 (1970).

[81] H. M. Rosenberg and E. C. Eimutis, *Canad. J. Chem.*, **45**, 2263 (1967).

[82] H. Hart and L. R. Lerner, *Tetrahedron*, **25**, 813 (1969).

[83] M. Avram, G. D. Mateescu, M. Renţea, I. G. Dinulescu and C. D. Nenitzescu, *Rev. Roumaine Chim.*, **13**, 1097 (1968).

[84] R. Criegee, W. Eberius and H. A. Brune, *Chem. Ber.*, **101**, 94 (1968).

[85] G. L. Closs and V. N. M. Rao, *J. Amer. Chem. Soc.*, **88**, 4116 (1966).

[86] D. G. Whitten and W. Berngruber, *J. Amer. Chem. Soc.*, **93**, 3204 (1971).

[87] K. Mano, K. Kusuda and A. Fujino, *Bull. Chem. Soc. Japan*, **41**, 1404 (1968).

[88] J. Meinwald and H. Tsuruta, *J. Amer. Chem. Soc.*, **92**, 2579 (1970).

[89] G. W. Klumpp and P. M. Van Dijk, *Rec. Trav. Chim.*, **90**, 381 (1971).

[90] G. V. Klumpp, W. G. Rietman and J. J. Vrielink, *J. Amer.Chem. Soc.*, **92**, 5266 (1970).

[91] H. Preuss and R. Janoschek, *J. Mol. Struct.*, **3**, 438 (1969); N. L. Allinger, M. T. Tribble, M. A. Miller and D. H. Hertz, *J. Amer. Chem. Soc.*, **93**, 2335 (1971).

[92] A. Tzschach and A. Balszuvweit, *Z. Chem.*, **8**, 121 (1968).

[93] L. A. Paquette, *Accounts Chem. Res.*, **4**, 280 (1971).

degenerate rearrangement (I) (only few instances of 1,5-carbon shifts

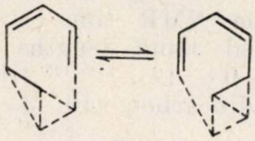

I

are known [94,95]). Several new $(CH)_{10}$ molecules were prepared and evidenced by physical methods, leading to 19 or 20 known valence isomers out of 71 theoretically possible planar trivalent multigraphs of order 10 : [10]annulene (10 − 5 − 0 − 1) where the conflicting results seem to have been resolved,[96–103] *cis*- and *trans*-9,10-dihydronaphthalene (10 − 4 − 0 − 6),[99–100,104–108] 9,10-dihydrofulvalene (10 − 4 − 0 − 4),[109] bicyclo[6.2.0]deca-2,4,6,9-tetraene (10 − 4 − 0 − 5),[100, 110–114] prebullvalene or bicyclo[4.2.2]deca-2,4,7,9-tetraene (10 − 4 − 0 − 7),

---

[94] L. A. Paquette and J. C. Stowell, *Tetrahedron Letters*, **1969**, 4159.

[95] P. Le Perchec, F. Rouessac and J. M. Conia, *Bull. Soc. chim. France*, **1967**, 826 ; J. A. Berson, *Accounts Chem. Res.*, **1**, 152 (1968) ; L. L. Miller, R. Greisinger and R. F. Boyer, *J. Amer. Chem. Soc.*, **91**, 1578 (1969) ; J. M. E. Krekels, J. W. de Haan and H. Kloosterziel, *Tetrahedron Letters*, **1970**, 2751 ; M. A. M. Boersma, J. W. de Haan, H. Kloosterziel and L. J. M. de Ven, *Chem. Commun.*, **1970**, 1168 ; V. A. Mironov, A. D. Fedorovich and A. A. Akhrem, *Izv. Akad. Nauk, Ser. khim.*, **1971**, 2848.

[96] E. E. van Tamelen and T. L. Burkoth, *J. Amer. Chem. Soc.*, **89**, 151 (1967) ; E. E. van Tamelen, T. L. Burkoth and R. H. Greeley, *ibid.*, **93**, 6120 (1971).

[97] T. L. Burkoth, *Diss. Abstr.*, **28B**, 2762 (1968) ; J. R. Irelan, *ibid.*, **29B**, 2808 (1969) ; E. E. van Tamelen and B. C. T. Pappas, *J. Amer. Chem. Soc.*, **93**, 6111 (1971).

[98] T. L. Burkoth and E. E. van Tamelen, in "Nonbenzenoid Aromatics", edited by J. P. Snyder, Academic Press, New York, **1**, 63 (1969).

[99] E. E. van Tamelen and R. H. Greeley, *Chem. Commun.* **1971**, 601.

[100] S. Masamune and R. T. Seidner, *Chem. Comun.* **1969**, 542. S. Masamune, K. Hojo, K. Hojo, G. Bigam and D. L. Rabenstein, *J. Amer. Chem. Soc.* **93**, 4966 (1971).

[101] L. A. Paquette and J. F. Kelly, *Tetrahedron Letters*, **1969**, 4509.

[102] P. H. Nelson and K. G. Untch, *Tetrahedron Letters*, **1969**, 4475 ; E. Vogel, in "Aromaticity", Chem. Soc. Spec. Publ., 21, p. 113, London, 1967.

[103] F. Bär, H. Kuhn and W. Regel, *Z. Naturforsch.*, **22a**, 103 (1967).

[104] M. Banciu, *Studii Cercetări Chim. Acad. R. S. România*, **18**, 657 (1970) ; J. Cizek and J. Paldus, *J. Chem. Phys.*, **47**, 3976 (1967) ; W. E. Doering and J. W. Rosenthal, *Tetrahedron Letters*, **1967**, 349 ; *J. Am. Chem. Soc.*, **89**, 4534 (1967).

[105] M. Jones Jr., S. D. Reich and L. T. Scott, *J. Amer. Chem. Soc.*, **92**, 3118 (1970).

[106] R. T. Seidner, N. Nakatsuka and S. Masamune, *Canad. J. Chem.*, **48**, 187 (1970).

[107] K. w. Shen, *Chem. Commun.*, **1971**, 391 ; *J. Amer. Chem. Soc.* **93**, 3064 (1971).

[108] S. Masamune, R. T. Seidner, H. Zenda, M. Wiesel. N. Nakatsuka and G. Bigam, *J. Amer. Chem. Soc.*, **90**, 5286 (1968).

[109] P. Schissel, D. J. McAdoo, E. Hedaya and D. W. McNeil, *J. Chem. Phys.*, **49**, 5061 (1968) ; E. Hedaya, D. W. McNeil, P. Schissel and D. J. McAdoo, *J. Amer. Chem. Soc.* **90**, 5284 (1968).

[110] G. Schröder and T. Martini, *Angew. Chem.*, **79**, 820 (1967) ; *Angew. Chem. internat. Edit.*, **6**, 806 (1967).

[111] S. Masamune, G. G. Chin, K. Hojo and R. T. Seidner, *J. Amer. Chem. Soc.*, **89**, 4804 (1967).

[112] S. Masamune, *Angew. Chem.*, **80**, 632 (1968) ; *Angew. Chem. internat. Edit.*, **7**, 645 (1968).

[113] M. Jones Jr. and S. D. Reich, *J. Amer. Chem. Soc.*, **89**, 3935 (1967).

[114] M. Jones Jr., S. D. Reich, T. L. Scott and L. E. Sullivan, *Angew. Chem.*, **80**, 631 (1968) ; *Angew. Chem. internat. Edit.*, **7**, 644 (1968).

[105,106,111–121] bullvalene or tricyclo[3.3.2.0 ^{4,6}]deca-2,7,9-triene (10—3—0—10)[104,117,118,120–137] which at slightly elevated temperature is a fluxional molecule in solution on the NMR time scale, but in va-pour or crystalline state has normal bond lengths and does not fluctuate, [138–142] triquinacene (10—3—0— 14), [143–145] tricyclo[4.2.2.0 ^{2,5}]deca-3,7,9-triene or Nenitzescu's hydrocarbon (10—3—0—15), [28,113,117,127,132,146–149]

[115] U. Krüerke, *Angew. Chem.*, **78**, 55 (1967); *Angew. Chem. internat. Edit.*, **6**, 79 (1967); J. S. McConaghy Jr. and J. J. Bloomfield, *Tetrahedron Letters*, **1969**, 1121.

[116] W. Grimme, H. J. Riebel and E. Vogel, *Angew. Chem.*, **80**, 803 (1968); *Angew. Chem. internat. Edit.*, **7**, 823 (1968); M. Jones Jr. and B. Fairless, *Tetrahedron Letters*, **1968**, 4881.

[117] M. Jones Jr. and L. T. Scott, *J. Amer. Chem. Soc.*, **89**, 150 (1967).

[118] H. P. Löffler and G. Schröder, *Angew. Chem.*, **80**, 758 (1968); *Angew. Chem. internat. Edit.*, **7**, 736 (1968).

[119] J. Altman, E. Babad, D. Ginsburg and R. B. Mordecai, *Israel J. Chem.*, **7**, 435 (1969); J. Altman, E. Babad, M. Rubin and D. Ginsburg, *Tetrahedron Letters*, **1969**, 1125.

[120] D. Ginsburg, *Accounts Chem. Res.*, **2**, 121 (1969).

[121] T. J. Katz and J. J. Cheung, *J. Amer. Chem. Soc.*, **91**, 7772 (1969).

[122] G. Schröder and J. F. M. Oth, *Angew. Chem.*, **79**, 458 (1967); *Angew. Chem. internat. Edit.*, **6**, 414 (1967).

[123] G. Schröder (to Union Carbide), U. S. Pat., 3, 288, 869, Nov. 26, 1966; *Chem. Abstr.*, **66**, 115365 (1967).

[124] Union Carbide Corp. (by G. Schröder), Ger. Pat., 1, 244, 772, July 20, 1967; *Chem. Abstr.*, **67**, 90465 (1967).

[125] J. F. M. Oth, E. Machens, H. Röttele and G. Schröder, *Liebigs Ann. Chem.*, **745**, 112 (1971).

[126] H. Röttele, P. Nikoloff, J. F. M. Oth and G. Schröder, *Chem. Ber.*, **102**, 3367 (1969).

[127] W. von E. Doering and J. W. Rosenthal, *J. Amer. Chem. Soc.*, **88**, 2078 (1966).

[128] J. F. M. Oth, R. Meréyni, H. Röttele and G. Schröder, *Chem. Ber.*, **100**, 3538 (1967).

[129] W. von E. Doering, B. M. Ferrier, E. T. Fossel, J. M. Hartenstein, M. Jones Jr., G. Klumpp, R. M. Rubin and M. Saunders, *Tetrahedron*, **23**, 3943 (1967).

[130] M. Banciu, *Studii Cercetări Chim. Acad. R. S. România*, **18**, 347 (1970).

[131] L. A. Paquette, S. Kirschner and J. R. Malpass, *J. Amer. Chem. Soc.*, **91**, 3970 (1969).

[132] M. Jones Jr., *J. Amer. Chem. Soc.*, **89**, 4236 (1967).

[133] S. Masamune, I. A. Zenda, M. Wiesel, N. Nakatsuka and G. Bigam, *J. Amer. Chem. Soc.* **90**, 2727 (1968).

[134] E. Vedejs, *J. Amer. Chem. Soc.*, **90**, 4751 (1968).

[135] H. Gunther, H. Klose and D. Wendisch, *Tetrahedron*, **25**, 1531f(1969).

[136] P. Bischof, R. Gleiter, E. Heilbronner, V. Hornung and G. Schröder, *Helv. Chim. Acta*, **53**, 1645 (1970).

[137] R. Aumann, *Angew. Chem.*, **83**, 583 (1971); *Angew. Chem. internat. Edit.*, **10**, 560 (1971).

[138] J. S. McKechnie, M. G. Newton and I. C. Paul, *J. Amer. Chem. Soc.*, **89**, 4819 (1967).

[139] S. M. Johnson, J. S. McKechnie, B.T.S. Lin and I. C. Paul, *J. Amer. Chem. Soc.* **89**, 7123 (1967).

[140] A. Amit, R. Huber and W. Hoppe, *Acta Crystallogr.*, **B**, 865 (1968).

[141] B. Andersen and A. Marstrander, *Acta Chem. Scand.*, **?1**, 1676 (1967).

[142] J. S. McKechnie and I. C. Paul, *J. Chem. Soc.*, (*B*), **1968**, 1445.

[143] A. de Meijere, D. Kaufmann and O. Schallner, *Angew. Chem.*, **83**,. 404 (1971); *Angew. Chem. internat. Edit.*, **10**, 417 (1971).

[144] R. C. Kelly, *Diss. Abstr.*, **27**B, 1091 (1967).

[145] I. T. Jacobson, *Acta Chem. Scand.*, **21**, 2235 (1967).

[146] E. Vedejs, *Chem. Commun.*, **1971**, 536; *Tetrahedron Letters*, **1970**, 4973.

[147] R. S. H. Liu, *Tetrahedron Letters*, **1969**, 1409.

[148] E. N. Cain, R. Vukov, and S. Masamune, *Chem. Commun.*, **1969**, 98.

[149] H. H. Westberg, E. N. Cain and S. Masamune, *J. Amer. Chem. Soc.*, **91**, 7512 (1969).

isobullvalene or tricyclo [$5.3.0.0^{2,10}$] deca-3,5,8-triene (10 – 3 – 0 – 9),[121,150–154] tricyclo [$4.4.0.0^{2,5}$] deca-3,7,9-triene (10 – 3 – 0 – 12),[107,146–149] tricyclo-[$5.3.0.0^{4,8}$]deca-2,5,9-triene (10 – 3 – 0 – 11),[112,113,121,127,132,133,137,152,153] tetracyclo[$4.4.0.0^{2,10}.0^{5,7}$]deca-3,8-diene (10 – 2 – 0 – 11),[105,106,108,116,117,119,120,127,155,156] tetracyclo[$4.4.0.0^{2,8}.0^{5,7}$]deca-3,9-diene (10 – 2 – 0 – 16),[113,132,157] hypostrophene or tetracyclo [$5.3.0.0^{2,6}.0^{3,10}$]-deca-4,8-diene (10 – 2 – 0 – 19),[158] tetracyclo [$4.4.0.0^{4,10}.0^{5,9}$]deca-2,7-diene (10 – 2 – 0 – 22),[158] pentacyclo [$4.4.0.0^{2,5}.0^{3,8}.0^{4,7}$] dec-9-ene, basketene or 1,1'-bis-homo-cubane (10 – 1 – 0 – 19),[107,148,149,159-162] pentacyclo-[$4.4.0.0.^{2,4}.0^{3,8}.0^{5,7}$] dec-9-ene, bis-homo-barrelene or snoutene (10 – 1 – 0 – 9) obtained by Ag^+-catalyzed isomerization of the latter,[143,160–162] (initially unintentionally [163] leading to an erroneous structure assignment), pentacyclo [$6.2.0.0^{2,4}.0^{3,6}.0^{5,7}$] dec-9-ene (10 – 1 – 0 – 11),[147] and diademane [143] or mitrane,[164] i.e. hexacyclo [$4.4.0.0^{2,4}.0^{3,9}.0^{5,7}.0^{8,10}$]-decane (10 – 0 – 0 – 5). Unsuccessful attempts to prepare pentaprismane (10 – 0 – 0 – 14) were reported.[107,158,165] Other $(CH)_{10}$ isomers which were discussed but not isolated include tricyclo [$6.2.0.0^{4,7}$] deca-5,9-diene (10 – 3 – 0 – 13) which was discussed as an alternative but less plausible structure for 10 – 3 – 0 – 11,[111,113,132] tetracyclo [$4.4.0.0^{2,5}.0^{7,10}$] deca-3,8-diene (10 – 2 – 0 – 20),[166] and also 10 – 1 – 0 – 15,* 10 – 1 – 0 – 2,[105] 10 – 1 – 0 – 8,[105] 10 – 4 – 0 – 2,[105] 10 – 2 – 0 – 10,[105] 10 – 4 – 0 – 3,[160] 10 – 3 – 0 – 4,[160] and 10 – 2 – 0 – 19.[160]

---

* Tentative structure for an unidentified $(CH)_{10}$ valence isomer[105] which would be the twentieth in the list of actually prepared valence isomers.[1,2] In table 4e of ref. 6, the second 10 – 1 – 0 – 14 should de changed into 10 – 1 – 0 – 15.

[150] E. Vedejs, R. A. Shepherd and R. P. Steiner, *J. Amer. Chem. Soc.*, **92**, 2158 (1970).

[151] L. A. Paquette and J. R. Malpass, *J. Amer. Chem. Soc.*, **90**, 7151 (1968).

[152] K. Hojo, R. T. Seidner and S. Masamune, *J. Amer. Chem. Soc.*, **92**, 6641 (1970).

[153] T. J. Katz, J. J. Cheung and N. Acton, *J. Amer. Chem. Soc.*, **92**, 6643 (1970).

[154] R. Aumann, *Angew. Chem.*, **83**, 177 (1971); *Angew. Chem. internat. Edit.*, **10**, 190 (1971).

[155] L. Babad, D. Ginsburg and M. B. Rubin, *Tetrahedron Letters*, **1968**, 2361.

[156] R. Aumann, *Angew. Chem.*, **83**, 176 (1971); *Angew. Chem. internat. Edit.*, **10**, 188 (1971).

[157] C. G. Krespan, M. C. McKusick and T. L. Cairns, *J. Amer. Chem. Soc.*, **82**, 1515 (1960); **83**, 3428 (1961); H. E. Zimmerman, and G. L. Grunewald, *ibid.*, **86**, 1434 (1964).

[158] J. S. McKennis, L. Brener, J. S. Ward and R. Pettit, *J. Amer. Chem. Soc.*, **93** 4957 (1971).

[159] E. LeGoff and S. Oka, *J. Amer. Chem. Soc.*, **91**, 5665 (1969); C. G. Chin, H. W. Cuts and S. Masamune, *Chem. Commun.*, **1966**, 880.

[160] L. A. Paquette and J. C. Stowell, *J. Amer. Chem. Soc.*, **92**, 2584 (1970); **93**, 2459 (1971).

[161] W. G. Dauben, C. H. Schallhorn and D. L. Whalen, *J. Amer. Chem. Soc.* **93**, 737 (1971).

[162] W. G. Dauben, M. G. Buzzolini, C. H. Schallhorn and D. L. Whalen, *Tetrahedron Letters*, **1970**, 787, 1218.

[163] R. Furstoss and J. M. Lehn, *Bull. Soc. Chim. France*, **1966**, 2497.

[164] H. Prinzbach and D. Stusche, *Helv. Chim. Acta*, **54**. 755 (1971).

[165] H. J. Lipp, *Diss. Abstr.*, **30B**, 129 (1969).

[166] S. Masamune, lecture presented at the IUPAC Symposium on Valence Isomerization, 9 – 12 Sept., 1968, Karlsruhe.

A major advance is the isomerization catalyzed by transition metal ions such as Ag(I), [78,93,167] Pd(II), [78] or Rh(I). [78,79] Such rearrangements, as well as thermally allowed (e.g. degenerate Cope rearrangements for semibullvalene, bullvalene or hypostrophene, Diels-Alder and retrodiene intramolecular reactions for 10 — 4 — 0 — 7 and 10 — 1 — 0 — 11, or the snoutene degenerate rearrangement) or photochemical conversions of valence isomers are common in the $(CH)_p$ series. The various valence isomers are visualized as pits connected by valleys on the energy surface of the $(CH)_p$ system [10,105,127] or the $(CH)_pCH_2$ labyrinth.[168]

It seems timely to expand the list of all possible valence isomers to [12] annulene, since a few of these have now been prepared as will be seen in the present paper.

Unlike the previous lists [5,6] which included all cubic (trivalent) multigraphs, both planar and non-planar, in the present treatment only planar graphs will be included because until now no molecule represented by a non-planar graph is known. Also, no loop-graphs will be discussed, therefore we will be concerned only with planar trivalent multigraphs of order 12 in the subsequent discussion.

PLANAR TRIVALENT MULTIGRAPHS OF ORDER 12

The procedure for finding all possible trivalent graphs of order 2k + 2 from those of order 2k was presented earlier.[6] Since manual application of this procedure starts to be impracticable for orders higher than 10, recourse was also had to published papers[169] or reports [170,171] describing part of the trivalent graphs of order 12. Lederberg [171] developed a computer programme for searching non-separable cubic graphs.

Table 1 presents the numbers of various types of trivalent graphs with 2, 4, 6, 8, 10, or 12 points : simple graphs (without loops or multiple

Table 1

Numbers of trivalent graphs

Order	2	4	6	8	10	12
Simple graphs	0	1	2	5	19	85
Simple planar graphs	0	1	1	3	9	32
Multigraphs	1	2	6	20	91	506
Planar multigraphs	1	2	5	17	71	357
General graphs	2	5	17	71	388	—

---

[167] L. A. Paquette, R. S. Beckley and T. McCreadie, *Tetrahedron Letters*, **1971**, 775.

[168] M. R. Willcott III and C. J. Boriack, *J. Amer. Chem. Soc.* **90**, 3287 (1968).

[168] A. T. Balaban, R. A. Davies, F. Harary, A. Hill and R. Westwick, *J. Austral. Math. Soc.* **11**, 207 (1970).

[170] D. W. Grace, Stanford Computation Center Technical Repor CS 15 (1956).

[171] J. Lederberg, "DENDRAL-64. A System for Computer Construction, Enumeration and Notation of Organic Molecules as Tree Structures and Cyclic Graphs. Part II. Topology of Cyclic Graphs", Interim Report to the NASA, CR 68898, Star No. 66—14074 (15 December 1965).

bonds), multigraphs (with single or multiple bonds but without loops), and general graphs (where both loops and multiple bonds are allowed). A mathematical formula for calculating the number of general trivalent graphs was recently found by Read,[172] but requires a computer to be applied for orders higher than 4. The numbers in Table 1 for graphs with 12 points were found in the present work, the remaining ones from Table 1 are based on previous data.[5,6]

The list of simple trivalent graphs of order 12 consists of the 14 planar "polyhedra", of the last 15 "planar unions" and the last 51 "gauche graphs" enumerated by Lederberg,[171] as well as one non-planar non-hamiltonian graph derived by the usual procedure[6] from the Petersen graph of order 10, and four non-hamiltonian "bridge graphs" (one of which is non-planar).

The list of multigraphs of order 12 contains, in addition, the remaiing 167 "planar unions", * 83 "gauche graphs" and 30 planar "non-polygonal graphs" enumerated by Lederberg,[171] as well as one non-planar non-hamitltonian multigraph derived from the Petersen graph, and 140 non-hamiltonian bridge graphs (12 of which are non-planar).

The resulting numbers of various kinds of graphs with 12 vertices are presented in Table 2. In the following we will be concerned only with planar graphs or multigraphs.

Table 2

Trivalent graphs of order 12

Cubic graphs of order 12	Planar			Non-planar		
	With	Without		With	Without	
	Hamiltonian circuit					
	Non-separable		Separable	Non-separable		Separable
Simple graphs	29	—	3	51	1	1
Multigraphs [a]	196	30	131	134	2	13

[a] Multigraphs include simple graphs.

Bridge (or separable) graphs of order 12 are obtained from general graphs[6] of order 10 with one loop by replacing the loop with a cyclopropenyl group, and by joining the four graphs of order 6 with one loop to any of the graphs of order 8 with one loop : the loops are removed and the two remaining fragments are joined by a "bridge-line". Redundancies are then eliminated.

To assist in characterizing graphs for the elimination of redundancies, as well as for their classification and systematical enumeration, two simple indices are the numbers of distinct 3- and 4-circuits.The previously used notation of trivalent multigraphs consisted[5] in three numbers indicating : the order p of the graph, the number β of double bonds, and a serial number s ; for general trivalent graphs, the serial number was preceded by a fourth index, the number λ of loops,[6] leading to the notation : $p-\beta-\lambda-s$. In the present paper we will only be concerned with graphs of order $p = 12$, therefore this number can be omitted. Also, since no loops are present, λ will be omitted too. Instead, four other numbers will be used to characterize each graph : the number β of double bonds (or 2-circuits), the number t of 3-circuits (triangles), the number q of 4-circuits (quadrangles), and a serial number s (this is 1 unless the first three numbers are identical for r graphs where $r > 1$; in this case, s discriminates among these graphs by taking all integer values between 1 and r).

---

* The graph listed[171] as AEGAEA is not planar, therefore it should belong to gauche (non-planar) graphs. Bridge graphs were not considered in Lederberg's report,[171] or in reference 169.

[172] F. Harary and E. M. Palmer, "Graphical Enumeration", chapter 7, Academic Press, New York, (in press).

With the notation consisting of these four numbers β-t-q-s,* planar trivalent graphs of order 12 are presented in figures 1 to 4, arranged according to the increasing order of these numbers. The drawings in figures 1—4 do not represent the actual geometry of the molecules, but emphasize the planarity of the graphs in that no lines cross. No consideration of steric isomerism is included in any of these figures : the actual numbers of isomers are therefore higher than those presented in Tables 1 and 2, e. g. two geometrical isomers of tricyclo [4.2.9.$0^{2,5}$] octa-3,7-diene are known.[173,174] Geometrical isomerism of annulenes (cyclopolyenic valence isomer) was discussed separately.[175] Also, enantiomerism is possible in several cases but is not considered in the Tables and figures.

KNOWN VALENCE ISOMERS OF [12]ANNULENE

[12] Annulene (6 — 0—0—1) for which theoretical calculations are available[103,176–178] was one of the products reported to be formed in the polymerization of acetylene.[179] However, this result was not confirmed by subsequent investigations.[180,181] Only recently was [12] annulene obtained[182–184] and it shows a mobile geometrical isomerization by low temperature NMR. At temperatures higher than — 40° it gives *cis* - 5—0—0—1 by an intramolecular Diels-Alder cyclization.

---

* This is abridged from the full notation : $p-\beta-\lambda-t-q-s$ ($p = 12$, $\lambda = 0$)

[173] M. AVRAM, I. G. DINULESCU, E. MARICA, G. MATEESCU, E. SLIAM and C. D. NENITZESCU, *Chem. Ber.*, **97**, 382 (1974).

[174] R. CRIEGEE, G. SCHRÖDER, G. MAIER and H. G. FISCHER, *Chem. Ber.* **93**, 1553 (1960).

[175] A. T. BALABAN, *Tetrahedron*, **27**, 6115 (1971).

[176] K. FUKUI et al., *Bull. Chem. Soc. Japan*, **33**, 1591 (1960).

[177] W. T. DIXON, *Tetrahedron*, **18**, 875 (1972).

[178] M. J. S. DEWAR and G. J. GLEICHER, *J. Amer. Chem. Soc.*, **87**, 685 (1965).

[179] W. REPPE, *Modern Plastics*, **23**, No. 6, 169, 218, 220 (1946).

[180] R. WOLOWSKI sand F. SONDHEIMER, *J. Amer. Chem. Soc.*, **87**, 5720 (1965).

[181] G. WILKE, *Angew. Chem.* **69**, 397 (1957).

[182] G. SCHRÖDER and W. MARTIN, *Angew. Chem.*, **78**, 117 (1966) ; *Angew. Chem. internat. Edit.* **5**, 130 (1966).

[183] J. F. M. OTH, H. RÖTTELE and G. SCHRÖDER, *Tetrahedron Letters*, **1970**, 61.

[184] J. F. M. OTH, J. M. GILLES and G. SCHRÖDER, *Tetrahedron Letters*, **1970**, 67.

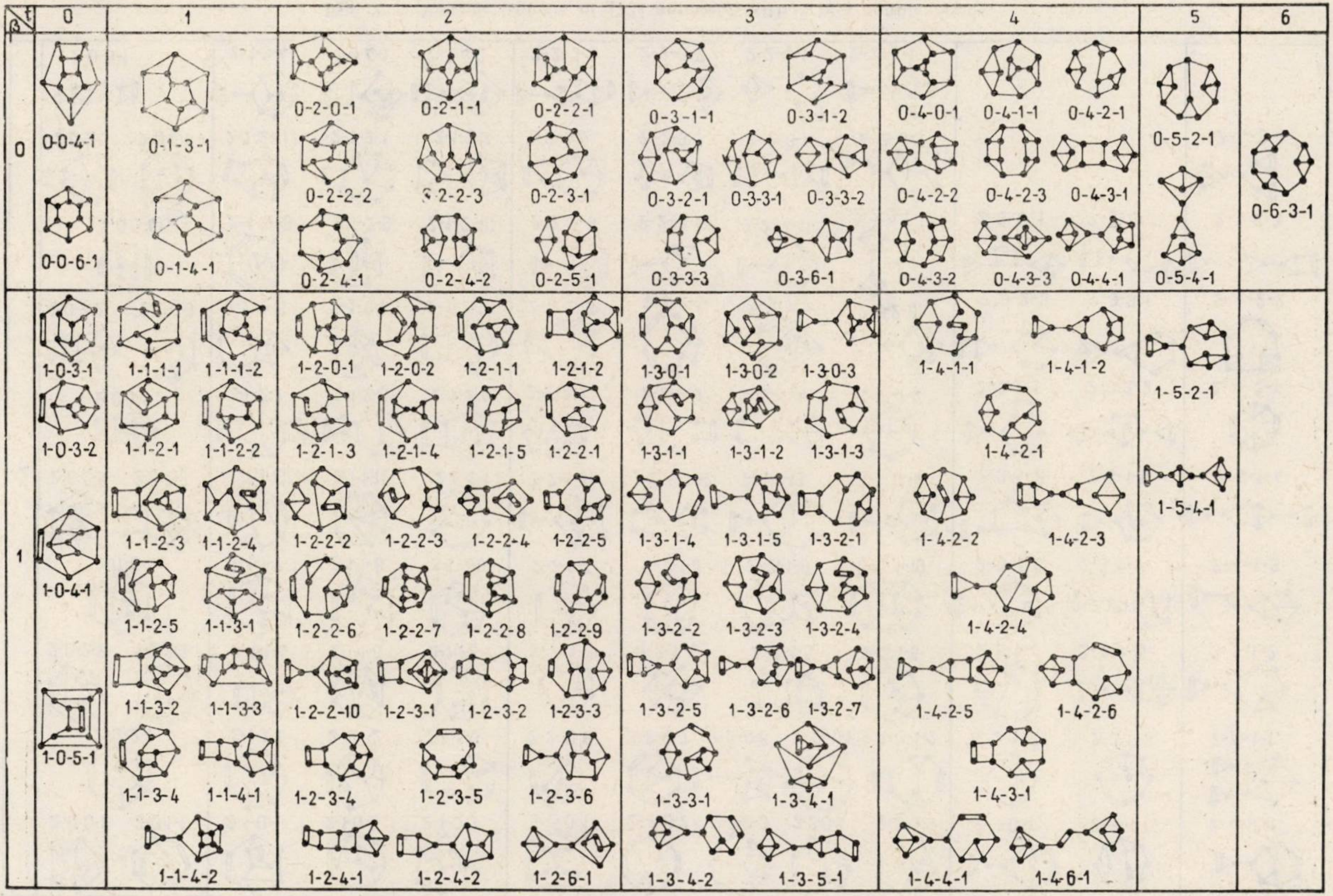
β\f
0
1
2
3
4
5
6
0
0-0-4-1
0-0-6-1
0-1-3-1
0-1-4-1
0-2-0-1
0-2-1-1
0-2-2-1
0-2-2-2
0-2-2-3
0-2-3-1
0-2-4-1
0-2-4-2
0-2-5-1
0-3-1-1
0-3-1-2
0-3-2-1
0-3-3-1
0-3-3-2
0-3-3-3
0-3-6-1
0-4-0-1
0-4-1-1
0-4-2-1
0-4-2-2
0-4-2-3
0-4-3-1
0-4-3-2
0-4-3-3
0-4-4-1
0-5-2-1
0-5-4-1
0-6-3-1
1
1-0-3-1
1-0-3-2
1-0-4-1
1-0-5-1
1-1-1-1
1-1-1-2
1-1-2-1
1-1-2-2
1-1-2-3
1-1-2-4
1-1-2-5
1-1-3-1
1-1-3-2
1-1-3-3
1-1-3-4
1-1-4-1
1-1-4-2
1-2-0-1
1-2-0-2
1-2-1-1
1-2-1-2
1-2-1-3
1-2-1-4
1-2-1-5
1-2-2-1
1-2-2-2
1-2-2-3
1-2-2-4
1-2-2-5
1-2-2-6
1-2-2-7
1-2-2-8
1-2-2-9
1-2-2-10
1-2-3-1
1-2-3-2
1-2-3-3
1-2-3-4
1-2-3-5
1-2-3-6
1-2-4-1
1-2-4-2
1-2-6-1
1-3-0-1
1-3-0-2
1-3-0-3
1-3-1-1
1-3-1-2
1-3-1-3
1-3-1-4
1-3-1-5
1-3-2-1
1-3-2-2
1-3-2-3
1-3-2-4
1-3-2-5
1-3-2-6
1-3-2-7
1-3-3-1
1-3-4-1
1-3-4-2
1-3-5-1
1-4-1-1
1-4-1-2
1-4-2-1
1-4-2-2
1-4-2-3
1-4-2-4
1-4-2-5
1-4-2-6
1-4-3-1
1-4-4-1
1-4-6-1
1-5-2-1
1-5-4-1

Fig. 1. — Valence isomers of [12] annulene with β = 0 or 1 double bonds.

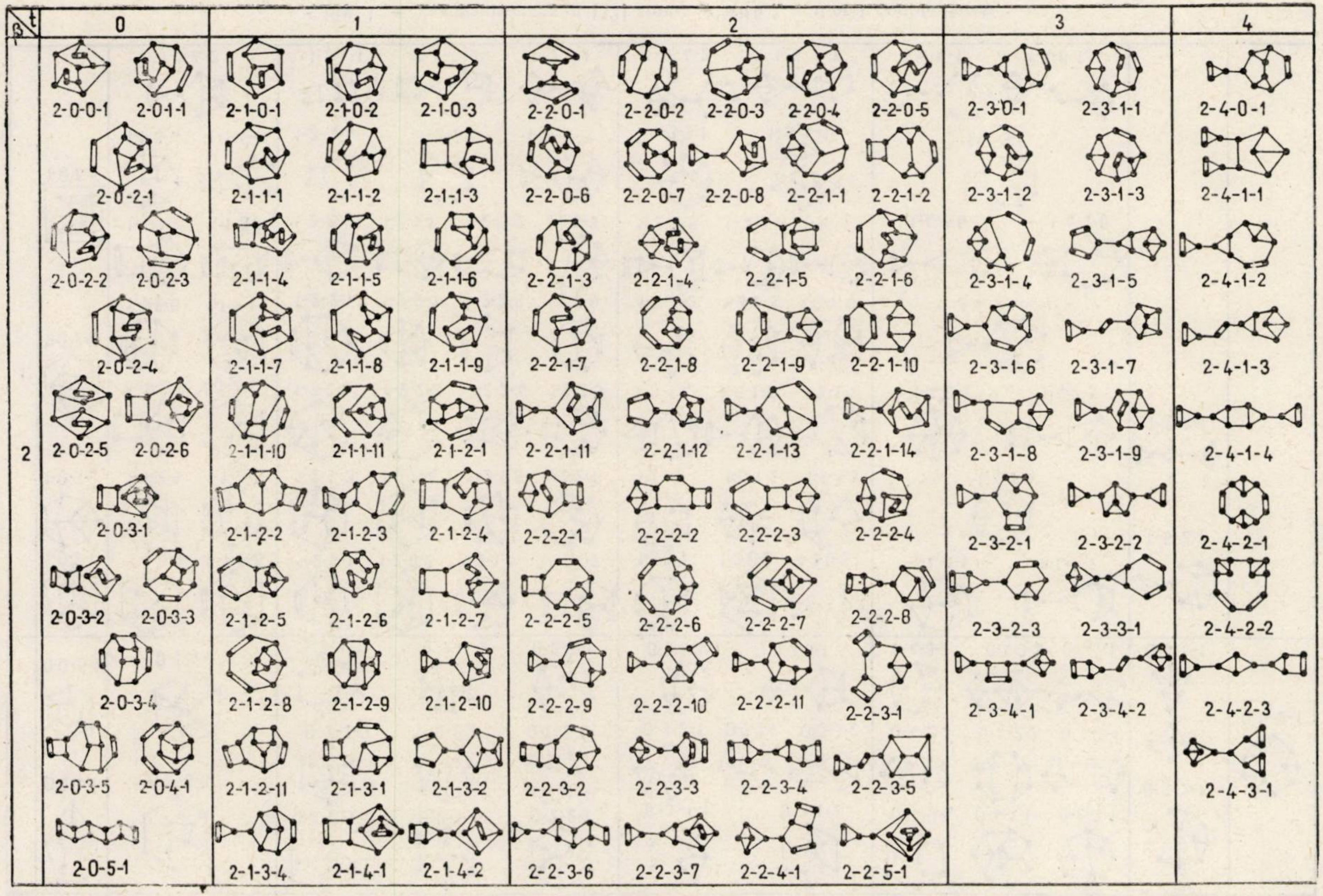
β
t
0
1
2
3
4
2
2-0-0-1
2-0-1-1
2-1-0-1
2-1-0-2
2-1-0-3
2-2-0-1
2-2-0-2
2-2-0-3
2-2-0-4
2-2-0-5
2-3-0-1
2-3-1-1
2-4-0-1
2-0-2-1
2-1-1-1
2-1-1-2
2-1-1-3
2-2-0-6
2-2-0-7
2-2-0-8
2-2-1-1
2-2-1-2
2-3-1-2
2-3-1-3
2-4-1-1
2-0-2-2
2-0-2-3
2-1-1-4
2-1-1-5
2-1-1-6
2-2-1-3
2-2-1-4
2-2-1-5
2-2-1-6
2-3-1-4
2-3-1-5
2-4-1-2
2-0-2-4
2-1-1-7
2-1-1-8
2-1-1-9
2-2-1-7
2-2-1-8
2-2-1-9
2-2-1-10
2-3-1-6
2-3-1-7
2-4-1-3
2-0-2-5
2-0-2-6
2-1-1-10
2-1-1-11
2-1-2-1
2-2-1-11
2-2-1-12
2-2-1-13
2-2-1-14
2-3-1-8
2-3-1-9
2-4-1-4
2-0-3-1
2-1-2-2
2-1-2-3
2-1-2-4
2-2-2-1
2-2-2-2
2-2-2-3
2-2-2-4
2-3-2-1
2-3-2-2
2-4-2-1
2-0-3-2
2-0-3-3
2-1-2-5
2-1-2-6
2-1-2-7
2-2-2-5
2-2-2-6
2-2-2-7
2-2-2-8
2-3-2-3
2-3-3-1
2-4-2-2
2-0-3-4
2-1-2-8
2-1-2-9
2-1-2-10
2-2-2-9
2-2-2-10
2-2-2-11
2-2-3-1
2-3-4-1
2-3-4-2
2-4-2-3
2-0-3-5
2-0-4-1
2-1-2-11
2-1-3-1
2-1-3-2
2-2-3-2
2-2-3-3
2-2-3-4
2-2-3-5
2-4-3-1
2-0-5-1
2-1-3-4
2-1-4-1
2-1-4-2
2-2-3-6
2-2-3-7
2-2-4-1
2-2-5-1

Fig. 2. — Valence isomers of [12] annulene with β = 2 double bonds.

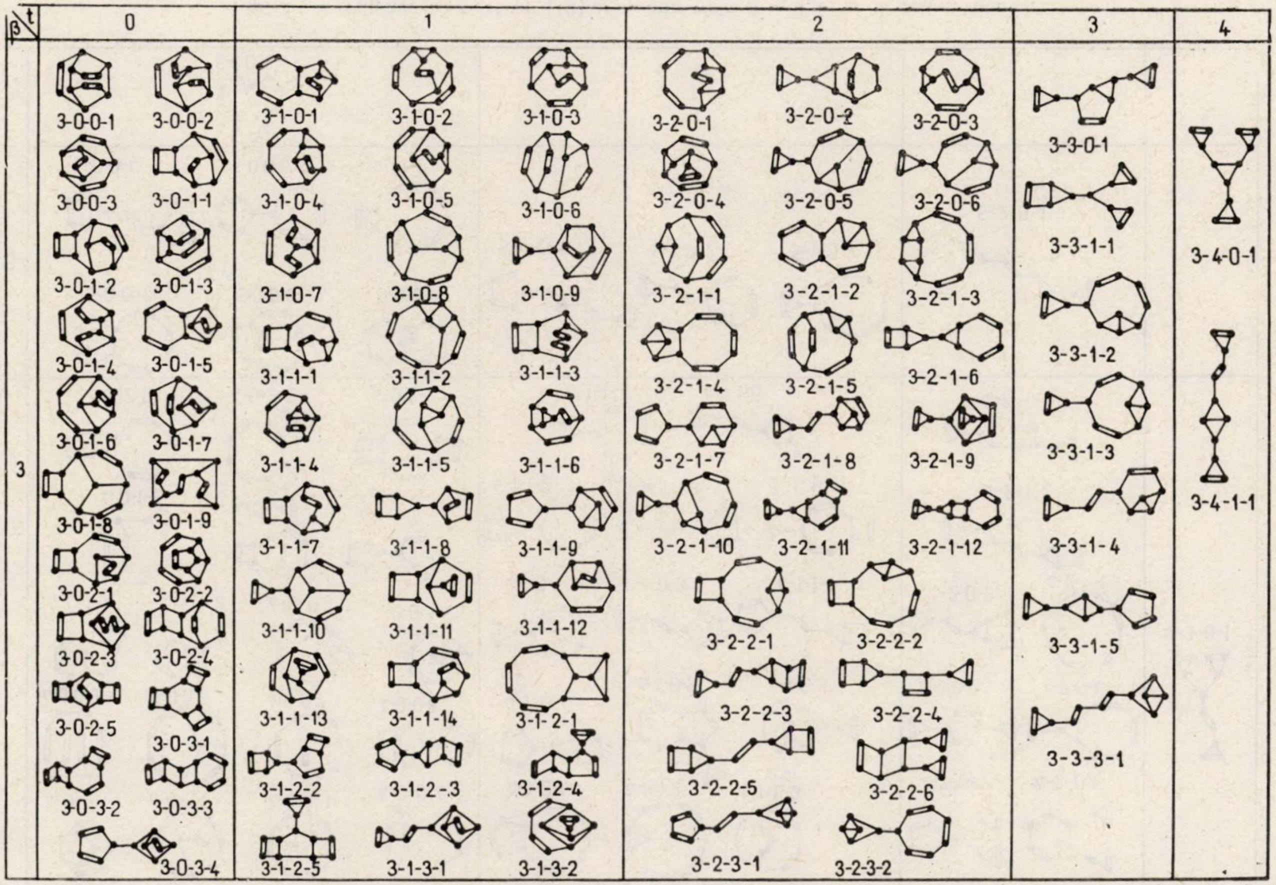
β
t
0
1
2
3
4
3
3-0-0-1
3-0-0-2
3-0-0-3
3-0-1-1
3-0-1-2
3-0-1-3
3-0-1-4
3-0-1-5
3-0-1-6
3-0-1-7
3-0-1-8
3-0-1-9
3-0-2-1
3-0-2-2
3-0-2-3
3-0-2-4
3-0-2-5
3-0-3-1
3-0-3-2
3-0-3-3
3-0-3-4
3-1-0-1
3-1-0-2
3-1-0-3
3-1-0-4
3-1-0-5
3-1-0-6
3-1-0-7
3-1-0-8
3-1-0-9
3-1-1-1
3-1-1-2
3-1-1-3
3-1-1-4
3-1-1-5
3-1-1-6
3-1-1-7
3-1-1-8
3-1-1-9
3-1-1-10
3-1-1-11
3-1-1-12
3-1-1-13
3-1-1-14
3-1-2-1
3-1-2-2
3-1-2-3
3-1-2-4
3-1-2-5
3-1-3-1
3-1-3-2
3-2-0-1
3-2-0-2
3-2-0-3
3-2-0-4
3-2-0-5
3-2-0-6
3-2-1-1
3-2-1-2
3-2-1-3
3-2-1-4
3-2-1-5
3-2-1-6
3-2-1-7
3-2-1-8
3-2-1-9
3-2-1-10
3-2-1-11
3-2-1-12
3-2-2-1
3-2-2-2
3-2-2-3
3-2-2-4
3-2-2-5
3-2-2-6
3-2-3-1
3-2-3-2
3-3-0-1
3-3-1-1
3-3-1-2
3-3-1-3
3-3-1-4
3-3-1-5
3-3-3-1
3-4-0-1
3-4-1-1

Fig. 3. — Valence isomers of [12] annulene with β = 3 double bonds.

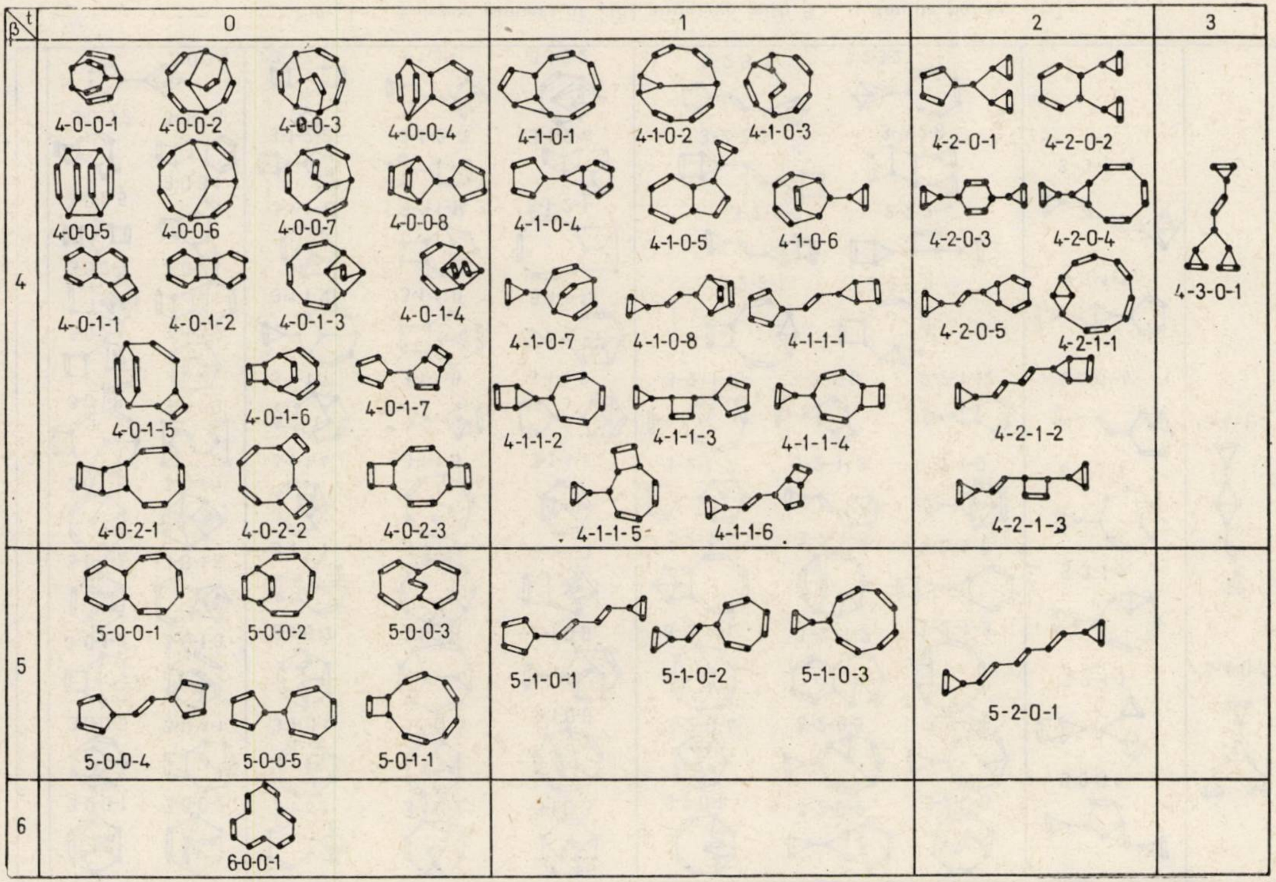
β
t
0
1
2
3
4
5
6
4-0-0-1
4-0-0-2
4-0-0-3
4-0-0-4
4-1-0-1
4-1-0-2
4-1-0-3
4-2-0-1
4-2-0-2
4-0-0-5
4-0-0-6
4-0-0-7
4-0-0-8
4-1-0-4
4-1-0-5
4-1-0-6
4-2-0-3
4-2-0-4
4-3-0-1
4-0-1-1
4-0-1-2
4-0-1-3
4-0-1-4
4-1-0-7
4-1-0-8
4-1-1-1
4-2-0-5
4-2-1-1
4-0-1-5
4-0-1-6
4-0-1-7
4-1-1-2
4-1-1-3
4-1-1-4
4-2-1-2
4-0-2-1
4-0-2-2
4-0-2-3
4-1-1-5
4-1-1-6
4-2-1-3
5-0-0-1
5-0-0-2
5-0-0-3
5-1-0-1
5-1-0-2
5-1-0-3
5-2-0-1
5-0-0-4
5-0-0-5
5-0-1-1
6-0-0-1

Fig. 4. — Valence isomers of [12] annulene with β = 4, 5, or 6 double bonds.

Both *cis*- and *trans*-bicyclo[6.4.0] dodeca-2,4,6,9,11-pentaene (5–0–0–1) afford[12]annulene on irradiation with ultraviolet light.[182–184] At room temperature, *cis*-5–0–0–1 isomerizes to tricyclo[6.4.0.$0^{7,12}$]-dodeca-2,4,8,10-tetraene (4–0–1–2) which results theoretically from a 2 + 2 cycloaddition of benzene.[182,185]

The starting material for these valence isomers is obtained from a dimer of cyclcloöctatetraene with m. p. 53° (II). Its adduct (III) with acetylenedicarboxylic ester affords on heating phthalic ester and tricyclo-[6.4.0.$0^{9,12}$] dodeca-2, 4, 6, 10-tetraene (4–0–2–1),[182] by an Alders-Rickert reaction. By an intramolecular Cope rearrangement, 4–0–2–1 is converted into tricyclo[4.4.2.$0^{2,5}$]dodeca-3,7,9, 11-tetraene (4–0–1–6).[95,182]

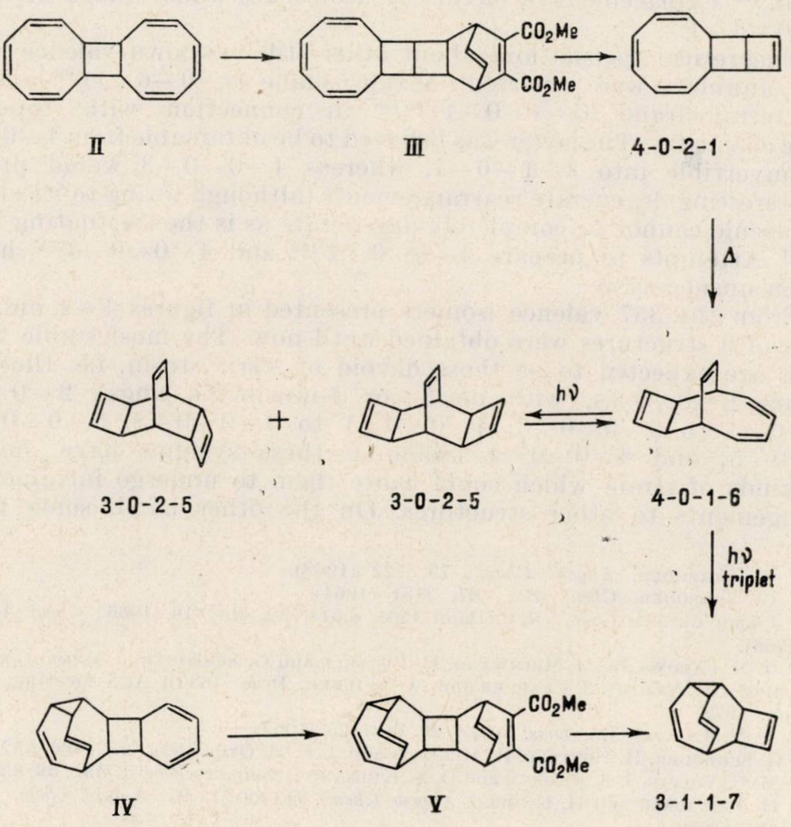

---

[185] G. Schröder, W, Martin and H. Röttele, *Angew. Chem.*, **81**, 33 (1969); *Angew. Chem. internat. Edit.*, **8**, 69 (1969).

A similar Alders-Rickert reaction of the adduct (V) of a different cycloöctatetraene dimer (IV) yields tetracyclo$[5.3.2.0^{2,5}.0^{6,8}]$dodeca-3, 9, 11-triene (3—1—1—7).[186–191]

Thermolysis of the previous compound gives tricyclo$[5.3.2.0^{4,8}]$-dodeca-2, 5, 9, 11-tetraene (4—0—0—7),[189,190] probably *via* a Cope rearrangement of 4—1—0—3 which is intermediately formed by opening of the four-membrered ring of 3—1—1—7.

Two *syn-anti* isomers of 3—0—2—5 were formed by ultraviolet irradiation of 4—0—1—6; they revert thermally into this compound.[94]

Cyclopentadienyl-cycloheptatriene (dihydro-sesquifulvalene) (5—0—0—5) was prepared[192,193] and calculations are available[194] in connection with the aromaticity of sesquifulvalene.

Saturated analogues of 1—0—3—1 were obtained from activated olefins like tetracyanoethylene, and basketene, followed by 2 + 2 cycloaddition.[159] Replacement of olefins by acetylenes would afford derivatives of 1—0—3—1.

Theoretical speculations about other still unknown valence isomers of [12] annulene were reported : hexaprismane (0—0—6—1)[195] and truncated tetrahedrane (0—4—0—1)[195,196] in connection with topological organic chemistry. The latter was believed to be obtainable from 4—0—0—1 and convertible into 3—1—0—7, whereas 4—0—0—3 would probably give interesting degenerate rearrangements (although owing to its chirality the molecule cannot be completely degenerate as is the fluctuating bullvalene).[196] Attempts to prepare 4—0—0—1[189] and 4—0—0—3[197] have so far been unsuccessful.

From the 357 valence isomers presented in figures 1—4 only derivatives of 9 structures were obtained until now. The most stable valence isomers are expected to be those devoid of steric strain, i.e. those with notations β—0—0—s, with no 3- or 4-membered rings: 2—0—0—1, 3—0—0—1 to 3—0—0—3, 4—0—0—1 to 4—0—0—8, 5—0—0—1 to 5—0—0—5, and 6—0—0—1. Some of these systems have, however, other kinds of strain which could cause them to undergo intramolecular rearrangements to other structures. On the other hand, some valence

---

[186] G. Schröder, *Angew. Chem.*, **75**, 722 (1963).

[187] G. Schröder, *Chem. Ber.*, **97**, 3131 (1964).

[188] Union Carbide Corp,. Netherland Pat., 6,514,760, May 16, 1966; *Chem. Abstr.*, **65**, 15240 (1966).

[189] J. N. Labows Jr., J. Meinwald, H. Röttele and G. Schröder, *J. Amer. Chem. Soc.*, **89**, 612 (1967); E. Vedejs, J. Clapper and W. Wilber, Proc. 163 rd ACS Meeting, Boston, 9—14 Apr. 1972.

[190] J. N. Labows Jr., *Diss. Abstr.* **28** B, 1425 (1967).

[191] G. Schröder, H. Röttele, R. Merényi and J. F. M. Oth, *Chem. Ber.*, **100**, 3527 (1967).

[192] M. E. Volpin, I. S. Akhrem and D. N. Kursanov, *Zhur. obschchei Khim.*, **28**, 330 (1958).

[193] H. Prinzbach and H. Knöfel, *Angew. Chem.*, **81**, 900 (1969); *Angew. Chem. internat. Edit.*, **8**, 881 (1969).

[194] J. F. Tinker, *J. Chem. Phys.*, **19**, 981 (1951).

[195] H. P. Schultz, *J. Org. Chem.*, **30**, 1361 (1965).

[196] R. Hoffmann, lecture presented at the IUPAC Symposium on Valence Isomerization, 9—12 Sept. 1968, Karlsruhe, W. Germany; R. B. Woodward and R. Hoffmann, *Angew. Chim.* **81**, 797 (1969); *Angew. Chem. Internat. Edit.*, **4**, 752 (1969).

[197] D. G. Farnum, Petroleum Res. Fund, 15th Annual Report, Amer. Chem. Soc. Washington, 1970, p. 216.

isomers like 0—6—3—1 possess a high ring strain and are therefore expected to be rather unstable. However, most of the structure presented in figures 1—4 are not too unduly strained to prevent the respective compounds from being obtainable by normal chemical reactions. Thus a wealth of synthetic chemistry could be based on valence isomers of [12]annulene.

Many of the valence isomers listed in figures 1—4 could undergo isomerizations or degenerate isomerizations through thermally-allowed processes (e.g. Cope rearrangements, Diels-Alder cycloadditions and other reactions with aromatic transition state[198]) or through thermally forbidden reactions (e.g. photochemically, or using as catalysts transition metal ions). The following paper in this series will analyze degenerate Cope rearrangements presented by valence isomers of annulenes.[199]

---

[198] M. J, S. Dewar, *Angew. Chem.*, **83**, 859 (1971).
[199] A. T. Balaban, following paper.

See also recent papers:

L. T. Scott and M. Jones, Jr., *Chem. Rev.*, **72**, 181 (1972);
F. Sondheimer, *Accounts Chem. Res.*, **5**, 81 (1972);
S. Masamune and N. Darby, *ibid.*, in press;
E. E. van Tamelen, *ibid.*, in press.

Revue Roumaine de Chimie, **17**, 5, 883 – 896 (1972)

CHEMICAL GRAPHS. XV.[1]

DEGENERATE COPE REARRANGEMENTS OF VALENCE ISOMERS OF ANNULENES

ALEXANDRU T. BALABAN

Institute of Atomic Physics, P.O. Box 35, Bucharest, Romania

Received January 18, 1972

A systematic survey of all possible degenerate Cope rearrangements of valence isomers of annulenes is presented on the basis of the tables of general trivalent graphs. This topological treatment gives the necessary but insufficient condition for degenerate rearrangement (automerization), since in addition the individual geometry of the transition state must be considered.

INTRODUCTION

In previous parts of this series, trivalent (cubic) graphs were presented, accounting for valence isomers of [4]-, [6]-, [8]-, and [10]-annulenes,[2] and of [12] annulene[1]; also, on the basis of general trivalent graphs,[3] valence isomers of aromatic heterocycles or of cyclic hydrocarbons possessing odd numbers of carbon atoms were systematically explored.

One of the most interesting features of some of these compounds is their degenerate rearrangement giving rise to "fluxional"[4,5] properties such as proton equivalence in NMR spectra. Homotropylidene,[6] bullvalene[5–8] and barbaralone[5,7] are well-known examples of such systems, and newer ones continue to be discovered.

To proceed with a measurable rate in the practical temperature range around −100° to + 200°, such rearrangements must be thermally allowed.[9,10] One of degenerate thermally-allowed processes with aromatic six-membered transition state[10,11] is the Cope rearrangement.

---

[1] A. T. Balaban, Part XIV, preceding paper.

[2] A. T. Balaban, *Rev. Roumaine Chim.*, **11**, 1097 (1966).

[3] A. T. Balaban, *Rev. Roumaine Chim.*, **15**, 463 (1070).

[4] W. K. Bratton, F. A. Cotton, A. Davison, A. Musco and J. W. Faller, *Proc. Natl. Acad. Sci.*, **58**, 1324 (1967).

[5] W. von E. Doering, B. M. Ferrier, E. T. Fossel, J. H. Hartenstein, M. Jones Jr., G. Klumpp, R. M. Rubin and M. Saunders, *Tetrahedron*, **23**, 3943 (1967).

[6] W. von E. Doering and W. R. Roth, *Angew. Chem.*, **75**, 27 (1963); *Angew. Chem. Internat. Edit.*, **2**, 115 (1963); *Tetrahedron*, **19**, 715 (1963).

[7] M. J. S. Dewar and W. W. Schoeller, *J. Amer. Chem. Soc.*, **93**, 1481 (1971); M. J. S. Dewar, Z. Náhlovská and B. D. Náhlovský, *Chem. Commun.*, **1971**, 1377.

[8] G. Schröder, *Angew. Chem.*, **75**, 772 (1963); *Angew. Chem. Internat. Edit.*, **2**, 481 (1963); G. Schröder, J. F. M. Oth and R. Merényi, *Angew. Chem.*, **77**, 774 (1965); *Angew. Chem. Internat. Edit.*, **4**, 752 (1965).

The present paper makes a systematic enumeration of all valence isomeric structures of annulenes which fulfil the structural (topological) requirements for undergoing intramolecular degenerate Cope rearrangements, and which therefore could present fluxional properties like bullvalene or semibullvalene. Since this enumeration is based on topological rather than geometrical considerations, it represents a necessary but insufficient condition for degenerate rearrangement; we deem, however, that it is of some interest to provide the basis for search of molecules which fulfill, in addition, the geometrical conditions (structure and conformation of the transition state) for rearrangement. This treatment could be extended to systems whose formulas are not represented by trivalent graphs (homotropylidene [6] or barbaralone[5] are examples of such systems), or to other degenerate electrocyclic processes than the Cope rearrangement, such as the 1,5-shift in the yet unknown I (1,5-hydrogen shifts are well documented, but 1,5-carbon shifts are only scarcely known[12–16]), or even to degenerate processes such as II$\rightleftharpoons$IV which proceed rapidly by means of nondegenerate rearrangements, i.e. through intramolecular Diels-Alder reactions II$\rightleftharpoons$III$\rightleftharpoons$IV.[17–21]

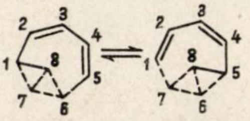

I

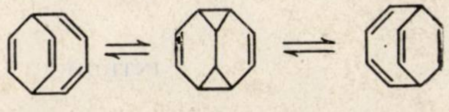

II III IV

---

[9] R. B. Woodward and R. Hoffmann, *Angew. Chem.* **81**, 797 (1969) *Internat. Edit.*, **8**, 787 (1969) R. Hoffmann andW.-D. Stohrer, *J. Amer. Chem. Soc.*, **93**, 6941 (1971).

[10] M. J. S. Dewar, *Angew. Chem.*, **83**, 859 (1971); *Angew. Chem. Internat. Edit.*, **10**, 761 (1971).

[11] A. T. Balaban, *Rev. Roumaine Chim.* **12**, 875 (1967), reprinted in "Recherches sur la philosophie des sciences", Edit. Acad. R. S. Romania, Bucharest, 1971, p. 207.

[12] P. Le Perchec, F. Rouessac and J. M. Conia, *Bull. Soc. Chim. France*, **1967**, 826.

[13] L. A. Paquette and J. C. Stowell, *Tetrahedron Letters*, **1969**, 4159.

[14] J. A. Berson, *Accounts Chem. Res.*, **1**, 152 (1968).

[15] L. L. Miller, R. Greisinger and R. F. Boyer, *J. Amer. Chem. Soc.*, **91**, 1578 (1969).

[16] J. M. E. Krekels, J. W. de Haan and H. Kloosterziel, *Tetrahedron Letters*, **1970**, 2751; M. A. M. Boersma, J. W. de Haan, H. Kloosterziel and L. J. M. van de Ven, *Chem. Commun.*, **1970**, 1168.

[17] J. Altman, E. Babad, D. Ginsburg and R. B. Mordecai, *Israel J. Chem.*, **7**, 435 (1969); J. Altman, E. Babad, M. Rubin and D. Ginsburg, *Tetrahedron Letters*, **1969**, 1125; D. Ginsburg, *Accounts Chem. Res.*, **2**, 121 (1969).

[18] W. Grimme, H, J, Riebel and E. Vogel, *Angew. Chem.*, **80**, 803 (1968); *Angew. Chem. Internat. Edit.*, **7**, 823 (1968); L. A. Paquette and J. C. Stowell, *J. Amer. Chem. Soc.*, **92**, 2584 (1970); **93**, 2459 (1971).

[19] M. Jones Jr. and B. Fairless, *Tetrahedron Letters*, **1968**, 4881; M. Jones Jr. and L. T. Scott, *J. Am. Chem. Soc.* **89**, 150 (1967); M. Jones Jr., *ibid.*, **89**, 4236 (1967).

[20] S. Masamune, I. A. Zenda, W. Wiesel, N. Nakatsuka and G. Bigam, *J. Amer. Chem. Soc.*, **90**, 2727 (1968).

[21] H. P. Löffler and G. Schröder, *Angew. Chem.*, **80**, 758 (1968); *Angew. Chem. Internat. Edit.*, **7**, 736 (1968); J. S. McConaghy Jr. and J. J. Bloomfield, *Tetrahedron Letters*, **1969**, 1121.

NOMENCLATURE AND NOTATIONS

The general nomenclature of degenerate reactions is still under discussion. Various names were proposed: fluxion,[4,5] automerization,[22] narcissism,[23] topomerization,[24,25] reversible bond shift,[26] each with a specific phenomenological, structural, or stereochemical connotation.

In the following discussion, notations of trivalent graphs of orders 6, 8, or 10 will be those adopted in Part VIII[3] of this series by means of four numbers $p-\beta-\lambda-s$: the order p of the graph (i.e. the number p of its points or of the CH groups in the valence isomer), the number β of double bonds, the number λ of loops, and a serial number, s. However, when enumerating graphs of order 12, in order to break down the numbers of isomers into smaller s groups, two further numbers were added to the notation (which thus becomes $p-\beta-t-q-\lambda-s$):[1] the number t of 3-circuits and the number q of 4-circuits. Since this notation was too cumbersome, as long as it was clear that we are dealing with graphs of order 12 with no loops, p and λ could be dropped out and the notation simplified[1] to $\beta-t-q-s$. In the present case, however, care must be taken not mix up the two notations, therefore we will conserve p, and will have for trivalent (cubic) graphs of order smaller than 12 a notation[3] of four numbers $p-\beta-\lambda-s$, and for cubic graphs of order 12 a notation of five numbers $p-\beta-t-q-s$ derived from that used in Part XIV[1] by adding $p = 12$ to each notation, as the first number.

STRUCTURAL (TOPOLOGICAL) REQUIREMENTS FOR DEGENERATE COPE REARRANGEMENTS

Two approaches for finding out theoretically which valence isomers of annulenes could undergo degenerate Cope rearrangements can be followed: (i) a brute-force approach, examination of formulas of all valence isomers; this could be done on the basis of tables contained in references 1–3 but this approach is limited to valence isomers of [4]- to [12] annulenes for which these tables are available; and (ii) a systematic approach, starting from the structural conditions of a degenerate Cope rearrangement, and devising a procedure for obtaining all annulene valence isomers fulfilling these conditions. We will follow the latter approach, since this enables us to transcend the present limits of trivalent graphs for which exhaustive tables exist for orders of at most 12 (without loops) or at most 10 (with loops).

The Cope rearrangement of 1,5-hexadienes $V \rightleftharpoons VII$,[27] proceeding through an aromatic six-membered transition state VI, can only be degenerate (i.e. $V \equiv VII$) when either of the two structural requirements (1) or (2) are fulfilled :

---

[22] A. T. Balaban and D. Fărcaşiu, *J. Amer. Chem. Soc.*, **89**, 1958 (1967).

[23] L. Salem, J. Durup, G. Bergeron, D. Cazes, X. Chapuisat and M. Kagan, *J. Amer. Chem. Soc.*, **92**, 4472 (1970).

[24] G. Binsch, E. L. Eliel and H. Kessler, *Angew. Chem.*, **83**, 618 (1971); *Angew. Chem. Internat. Edit.*, **10**, 570 (1971).

[25] E. L. Eliel, *J. Chem. Educ.*, **48**, 163 (1971).

[26] G. Schröder and J. F. M. Oth, *Tetrahedron Letters*, **1966**, 4083.

[27] S. J. Rhoads, in "Molecular Rearrangements" (edited by P. de Mayo), Interscience, New York, vol. 1, p. 655; K. Mackenzie, in "The Chemistry of Alkenes" (edited by S. Patai), Interscience, London, 1964, p. 387;

M. Banciu, *Studii şi Cercetări Chim. Acad. R. S. România*, **8**, 603 (1967).

$$A \equiv B, C \equiv D \quad (1)$$

$$A \equiv C,\ B \equiv D,\ R \equiv R'. \quad (2)$$

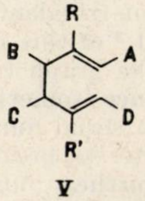

V

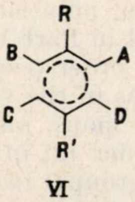

VI

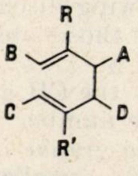

VII

The nature of the R and R′ groups is irrelevant in case (1) because they lie on the symmetry axis of the transition state VI with C_{2v} topological point group;* in case (2) with topological point group C_{2h}, i.e. with a centre of symmetry, R and R′ must be identical. A degenerate Cope rearrangement which can be observed through racemization is shown by VIII.[28]

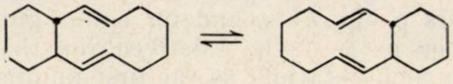

VIII

In order to limit the present discussion to valence isomers of annulenes $(CH)_p$, we will suppose R and R′ to be hydrogen atoms, $R = R' = H$. Case (1) then reduces to :

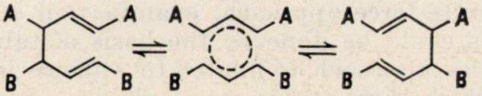

(1)

whereas case (2) reduces to:

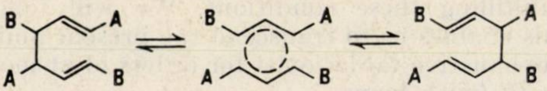

(2)

To explore systematically all structural variations allowed by these conditions, we have to combine the 1,5-hexadienic framework of six carbon atoms with four groups A, A, B, and B. In order to limit the discussion to valence isomers of annulenes, these groups must themselves be trivalent graphs. Therefore we must find trivalent general graphs (which need not be connected) with four loops fulfilling the symmetries of cases (1) or (2) : by removing the loops, the four links to the framework of six carbon atoms are obtained. It is easily seen that the 4-loop graph(s) must have a total of p—2 points so that by removing 4 points (and loops) and adding six points, a trivalent graph of p points is obtained. Thus the partitions of p−2 into at least one and at most four terms must be found, respecting the symmetries of cases (1) and (2). The four possible types, a−d, are presented in table 1. The general graphs must have a C_2 symmetry axis whenever they have 2 or 4 loops; no symmetry restriction is placed on them when they have only one loop.

---

* The actual (geometrical) point group of the chair-shaped transition state is in case (1) C_s, and in case (2) C_i.

[28] R. A. Kretchner, *Diss. Abstr.*, **28 B**, 582 (1967).

Table 1

Partition of p − 2 points among 1 to 4 general cubic graphs

Type	Partition into 1 to 4 graphs	General graphs[a]							
		1		2		3		4	
		Points	Loops	Points	Loops	Points	Loops	Points	Loops
a	1	$p-2$	4	—	—	—	—	—	—
b	2	$p-p'-2$	2	p'	2	—	—	—	—
c	3	$\frac{p-p''-2}{2}$	1	$\frac{p-p''-2}{2}$	1	p''	2	—	—
d	4	$\frac{p}{2}-p'''-1$	1	$\frac{p}{2}-p'''-1$	1	p'''	1	p'''	1

[a] $2 \leqslant p' \leqslant \frac{p-2}{2}$; $2 \leqslant p'' \leqslant \frac{p-2}{3}$; $4 \leqslant p''' \leqslant \frac{p-2}{4}$; all numbers of points, p, p′, p″, and p‴, must be even.

Since so far no molecule is known whose formula is a non-planar graph, we will restrict the discussion to planar graphs; here, "planar graph" is used in the graph-theoretical sense to imply a graph which can be drawn in a plane so that no lines cross except at a vertex (point) of the graph.[29−31]

From the tables of general trivalent graphs,[3] it is apparent that there are no general cubic graphs with 2 points and 1 or 4 loops, or with 4 points and 4 loops; there is exactly one graph each with 2 points and 2 loops, or with 4 points and 1 or 2 loops, or with 6 points and 4 loops. For higher orders up to p = 10, the numbers of general planar cubic graphs which must be considered are presented in table 2: these planar loop-graphs have a binary symmetry axis when they have 2 or 4 loops; in order to lead to

Table 2

Numbers of general trivalent loop-graphs which fulfill the structural requirements for degenerate Cope rearrangements

Order p of graph / Number λ of loops	2	4	6	8	10
1	0	1	4	18	97
2	1	1	4	13	50
4	0	0	1	3	12

---

[29] K. Kuratowski, *Fund. Math.*, **15**, 271 (1930).

[30] F. Harary, "Graph Theory", Addison-Wesley Publ. Co., Reading, Mass., 1969, chapter 11.

[31] J. W. Essam and M. E. Fisher, *Rev. Modern Phys.*, Suppl. April, **42**, 271 (1970).

planar graphs on linking with the 6-point framework, the two or four loops must belong to the same region of the plane delineated by the lines (edges) of the loop-graph. For instance, loop-graphs 8—0—2—5, 10—0—4—7 or 10— 0 — 4 —8, although planar and symmetrical, lead to non-planar graphs, therefore they are not included in table 2.

VALENCE ISOMERS OF [6]-, [8]-, [10]-, AND [12]ANNULENES WHICH FULFILL THE STRUCTURAL REQUIREMENTS FOR DEGENERATE COPE REARRANGEMENTS

Proceeding along the lines presented in the preceding paragraphs, the combinations of trivalent loop-graphs which can lead to degenerate Cope rearrangements are indicated in table 3 for p = 6 to 18. Table 4 presents in more detail the first part of

Table 3

Combinations of cubic loop-graphs which lead to structures fulfilling the requirements for degenerate Cope rearrangement

Total p	Type	General graph								Number of combinations *
		1		2		3		4		
		p	λ	p	λ	p	λ	p	λ	
6	b	2	2	2	2	—	—	—	—	1
8	a	6	4	—	—	—	—	—	—	1
	b	2	2	4	2	—	—	—	—	1
10	a	8	4	—	—	—	—	—	—	3
	b	2	2	6	2	—	—	—	—	4
	b	4	2	4	2	—	—	—	—	1
12	a	10	4	—	—	—	—	—	—	12
	b	2	2	8	2	—	—	—	—	13
	b	4	2	6	2	—	—	—	—	4
	c	4	1	4	1	2	2	—	—	1
14	a	12	4	—	—	—	—	—	—	50
	b	2	2	10	2	—	—	—	—	50
	b	4	2	8	2	—	—	—	—	13
	b	6	2	6	2	—	—	—	—	6
	c	4	1	4	1	4	2	—	—	1
16	a	14	4	—	—	—	—	—	—	**
	b	2	2	12	2	—	—	—	—	**
	b	4	2	10	2	—	—	—	—	50
	b	6	2	8	2	—	—	—	—	52
	c	4	1	4	1	6	2	—	—	4
	c	6	1	6	1	2	2	—	—	6
18	a	16	4	—	—	—	—	—	—	**
	b	2	2	14	2	—	—	—	—	**
	b	4	2	12	2	—	—	—	—	**
	b	6	2	10	2	—	—	—	—	200
	b	8	2	8	2	—	—	—	—	78
	c	4	1	4	1	8	2	—	—	13
	c	6	1	6	1	4	2	—	—	6
	d	4	1	4	1	4	1	4	1	1

* Each of these combinations gives rise to 2—4 graphs.

** Number not yet determined.

table 3, namely for p = 6 to 12. Since the diagrams of the graphs can be found in preceding parts of this series,[1,3] they have not been included in table 4. Some valence isomers appear twice in table 4 : these are 10−3−0−7 (IX), 12−3−0−0−2 (X), 12−4−0−0−2 (XI), 12−4−0−0−3 (XII), 12−4−0−1−7 (XIII), 12−4−0−1−5 (XIV), and 12−4−1−1−3 (XV) which rearrange owing to different pairs of 1,5-double bonds, represented in formulas IX−XV on a hexagonal framework.

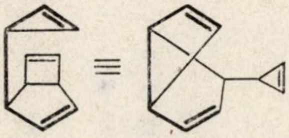

10-3-0-7

IX

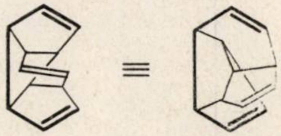

12-3-0-0-2

X

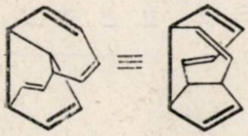

12-4-0-0-2

XI

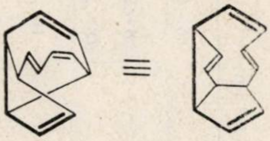

12-4-0-0-3

XII

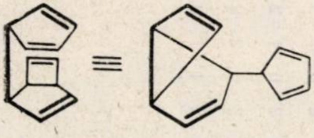

12-4-0-1-7

XIII

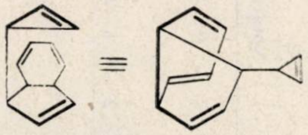

12-4-1-0-5

XIV

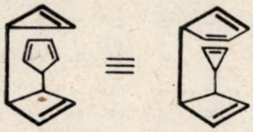

12-4-1-1-3

XV

In table 3, for a given type of partition, the 1, 2, 3, or 4 general loop-graphs are arranged in the order of increasing p and λ values. As

Table 4

Valence isomers of [6]- to [12]annulenes which fulfill the topological requirements for degenerate Cope rearrangement

Total p	Type	General loop-graph									Valence isomer	
		1			2			3				
		p	λ	Notation	p	λ	Notation	p	λ	Notation	Case (1)	Case (2)
6	b	2	2	2–0–2–1	2	2	2–0–2–1	—	—	—	(6–2–0–1)	(6–2–0–2)
8	a	6	4	6–0–4–1	—	—	—	—	—	—	8–2–0–3, 8–2–0–4	8–2–0–5
	b	2	2	2–0–2–1	4	2	4–1–2–1	—	—	—	(8–3–0–2)	(8–3–0–3)
10	a	8	4	8–0–4–1	—	—	—	—	—	—	10–2–0–17	10–2–0–16
	a	8	4	8–1–4–2	—	—	—	—	—	—	10–3–0–13, 10–3–0–10	10–3–0–11
	a	8	4	8–0–4–2	—	—	—	—	—	—	10–2–0–19	10–2–0–22
	b	2	2	2–0–2–1	6	2	6–0–2–1	—	—	—	(10–2–0–2)	(10–2–0–8)
	b	2	2	2–0–2–1	6	2	6–1–2–1	—	—	—	(10–3–0–3)	(10–3–0–7)
	b	2	2	2–0–2–1	6	2	6–1–2–2	—	—	—	(10–3–0–7)	(10–3–0–13)
	b	2	2	2–0–2–1	6	2	6–2–2–1	—	—	—	(10–4–0–3)	(10–4–0–5)
	b	4	2	4–1–2–1	4	2	4–1–2–1	—	—	—	(10–4–0–4)	10–4–0–6
12	a	10	4	10–0–4–1	—	—	—	—	—	—	12–2–2–3–1, 12–2–3–1–1	12–2–2–1–3
	a	10	4	10–0–4–3	—	—	—	—	—	—	12–2–2–0–1, 12–2–2–1–7	12–2–2–0–6
	a	10	4	10–0–4–4	—	—	—	—	—	—	12–2–1–2–4	12–2–1–1–7
	a	10	4	10–0–4–9	—	—	—	—	—	—	12–2–0–2–3, 12–2–0–3–4	12–2–0–2–1, 12–2–0–2–2
	a	10	4	10–1–4–2	—	—	—	—	—	—	12–3–1–1–1	12–3–1–0–2
	a	10	4	10–1–4–5	—	—	—	—	—	—	12–3–1–2–5, 12–3–2–0–4	12–3–1–0–9

$-4-5$, $10-1-4-7$, $10-2-4-1$), two graphs result for case (1) and one graph for case (2); when the 4-loop graph has D_{2h} symmetry and is not a bridge graph (e.g. $10-0-4-9$), two graphs result for each of the two cases (1) and (2). This is illustrated in the Scheme 1.

Until now, in case (1) degenerate isomerizations of singly-bonded cyclopropenyl or cyclopentadienyl groups which change their point of attachment in compounds whose formulas are bridge (separable) graphs, are not known (e. g. XVI – XIX). Neither are degenerate isomerizations known in case (2) for structures where a cyclobutene ring changes places, e. g. XX – XXIII. This is probably due to geometrical constraints which would occur in these cases (see below) since several of the above molecules are known (i.e. XVI–XVIII, XX, XXI) and are not reported to present temperature-dependent NMR spectra with a higher equivalence of their hydrogens at elevated temperatures than required by their formulas. Therefore the notations of such structures are enclosed in brackets in table 4 and will not be further discussed. A degenerate rearrangement of $8-3-0-2$ (bicyclo[4.2.0]octa-2,4,7-triene, XX) does take place, but it proceeds *via* a valence tautomerization to cycloöctatetraene and not *via* a Cope rearrangement; indeed, by preventing the valence isomerization through a propellane structure, the bicyclo[4.2.0]octa-2,4,7-triene becomes stable,[32] XXIV. Structure $12-4-1-0-5$ appears once in brackets in table 4, when its degenerate Cope rearrangement involves the (presumably) unfavourable shift of a cyclopropenyl group, and a second time without brackets when a less strained transition state is involved.

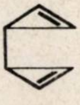
6-2-0-1
XVI

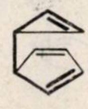
8-3-0-2
XVII

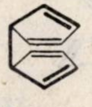
10-4-0-4
XVIII

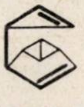
10-2-0-2
XIX

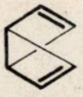
6-2-0-2
XX

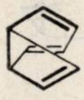
8-3-0-3
XXI

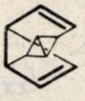
10-2-0-8
XXII

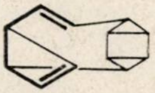
12-2-2-2-5
XXIII

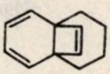
XXIV

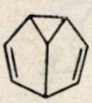
XXV

Remaining structures in table 4 without brackets will now be checked against known valence isomers of annulenes.

From the three non-bracketed $(CH)_8$ valence isomers listed in table 4, $8-2-0-3$, $8-2-0-4$ and $8-2-0-5$, only the first two are known.

---

[32] I. W. McCay and R. N. Warrener, *Tetrahedron Letters*, **1970**, 4783; L. A. Paquette and J. C. Philips, *Chem. Commun.*, **1969**, 680; L. A. Paquette, J. C. Philips and R. E. Wingard Jr., *J. Amer. Chem. Soc.*, **93**, 4516 (1971).

The former, semibullvalene, XXV, presents indeed a very rapid degenerate Cope rearrangement even at the lowest attainable temperature (−110°)[33] and is almost a mesovalent molecule.[7,9] The latter (8−2−0−4, XXVI), cyclobutadiene dimer or tricyclo[4.2.0.0^{2,5}]octa-3,7-diene, occurring in two geometrically isomeric forms, is not reported to behave like a fluxional molecule, whichfact again may be due to geometrical constraints on the transition state.

It was conclusively demonstrated by Doering[6,34] that the transition state of the Cope rearrangement has a favourable geometry when it possesses a chair conformation, and this is borne out by theoretical calculations.[11,35–38] However, the rapidly reversible degenerate Cope rearrangements of semibullvalene and bullvalene must proceed through less favour-

Scheme 2

Geometries of transition states in degenerate Cope rearrangements of annulene valence isomers

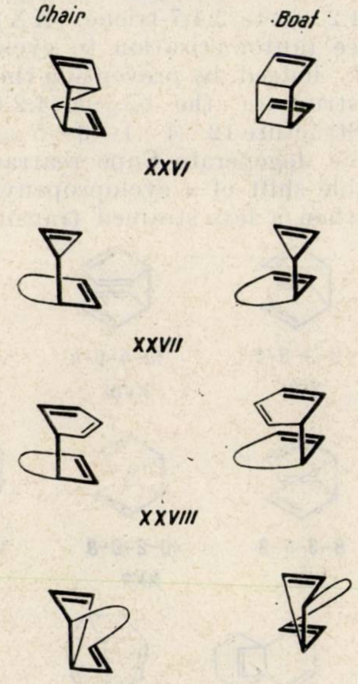

XXVI

XXVII

XXVIII

XXIX

---

[33] H. E. Zimmerman, R. W. Binkley, R. S. Givens, G. L. Grunewald and M. A. Sherwin, *J. Am. Chem. Soc.*, **91**, 3316 (1969); R. W. Binkley, R. S. Givens and M. A. Sherwin, *ibid.*, **89**, 3932 (1967).

[34] W. von E. Doering and W. R. Roth, *Tetrahedron*, **18**, 67 (1962).

[35] M. J. S. Dewar, *Tetrahedron*, Suppl. **8**, 75 (1966).

[36] L. Salem, *Accounts Chem. Res.*, **4**, 322 (1971).

[37] J. Chuche and J. Wiemann, *Bull. Soc. Chim. France*, **1968**, 1491; M. Simonetta, G. Favini, C. Mariani and P. Gramaccioni, *J. Amer. Chem. Soc.*, **90**, 1280 (1968); R. K. Hill and N. W. Gilman, *Chem. Commun.*, **1967**, 619.

[38] E. Vogel, W. Grimme, W. Meckel, H. J. Riebel and J. F. Oth, *Angew. Chem.* **78**, 599 (1966); *Angew. Chem. Internat. Edit.*, **5**, 590 (1966).

able boat-shaped transition states. Both chair- and boat-shaped transition states are sterically twisted in the bracketed cases of table 4, as seen in formulas XXVII—XXIX of Scheme 2, where the initial molecules are represented for this purpose in the geometry of the transition state.

The *syn*-dimer of cyclobutadiene, XXVI, has a strained chair-shaped but a relatively unstrained boat-shaped transition state for degenerate Cope rearrangement (scheme 2). It might therefore be interesting to reinvestigate the high-temperature NMR spectrum of this compound.

From the eight non-bracketed valence isomers of $(CH)_{10}$ in table 4, six are known : structures 10—2—0—16, 10—2—0—22 and 10—3—0—11 are not reported to present degenerate Cope rearrangement, but bullvalene, 10—3—0—10,[5–8,38] and hypostrophene, 10—2—0—19,[39] present degenerate Cope rearrangement ; finally, *cis*-9,10-dihydronaphthalene, 10—4—0—6, has not been reported to be a fluxional molecule, but to rearrange to various other $(CH)_{10}$ valence isomers.[40,41] *trans*-9,10-Dihydronaphthalene[42] cannot, for obvious geometrical reasons, undergo an intramolecular Cope rearrangement. Several papers reported conversions of *cis*-9,10-dicarbomethoxy-9,10-dihydronaphthalene into 2,6-dicarbomethoxynaphthalene derivatives, interpreting this conversion as involving valence isomerization to a cyclodecapentaene followed by intramolecular recyclization and double bond migration or dehydrogenation.[38,40,41,43–46] However, a different interpretation is possible, *via* a direct intramolecular Cope rearrangement, which in this case is no longer degenerate, and whose driving force is alleviation of steric strain. In this case, isotopic labels at positions 9 or 10 in 9,10-dihydronaphthalene should also appear first in positions 2 or β before becoming scrambled also to positions 1 or α.

Only very few of the possible valence isomers of $(CH)_{12}$ have so far been prepared.[1] Compound 12—3—1—1—7 is known [47–50] and presents the expected homotropylidenic degenerate rearrangement. However, this rearrangement is not totally degenerate because of the annelated cyclobutene ring ; similarly, benzoderivatives of bullvalene are less prone to degenerate rearrangements than the parent systems.[48,51] Table 4 presents 36 more non-bracketed $(CH)_{12}$ systems, which are yet to be prepared and checked for the occurence of degenerate rearrangements. Compound 12—4—0—0—3 was already discussed in this respect by Hoffman.[52]

---

[39] J. S. McKennis, L. Brener, J. S. Ward and R. Petit, *J. Amer. Chem. Soc.*, **93**, 4957 (1971).

[40] T. L. Burkoth and E. E. van Tamelen, in "Nonbenzenoid Aromatics", (edited by J. P. Snyder), Academic Press, New York, 1969, vol. 1, p. 63.

[41] E. E. van Tamelen and B. C. T. Pappas, *J. Amer. Chem. Soc.*, **93**, 6111 (1971).

[42] E. E. van Tamelen, T. L. Burkoth and R. H. Greeley, *J. Amer. Chem. Soc.*, **93**, 6120 (1971).

[43] M. Avram, C. D. Nenitzescu and E. Marica, *Chem. Ber.*, **90**, 1857 (1957) ; M. Avram, G. Mateescu and C. D. Nenitzescu, *Liebigs Ann. Chem.*, **636**, 174 (1960).

[44] R. C. Cookson, J. Hudec and J. Marsden, *Chem. Ind.*, **1961**, 21.

[45] E. Vogel, W. Meckel and W. Grimme, *Angew. Chem.*, **76**, 786 (1964) ; *Angew. Chem., Internat. Edit.*, **3**, 643 (1964).

[46] E. Vogel, in "Aromaticity", Chem. Soc. Spec. Publ. Nr. 21, Chem. Soc. London, 1967, p. 113.

[47] G. Schröder, *Angew. Chem.*, **75**, 722 (1963) ; *Chem. Ber.*, **97**, 3131 (1964).

[48] G. Schröder, H. Röttele, R. Merényi and J. F. M. Oth, *Chem. Ber.*, **100**, 3527 (1967).

[49] J. N. Labows Jr., J. Meinwald, H. Röttele and G. Schröder, *J. Amer. Chem. Soc.*, **89**, 612 (1967).

[50] J. N. Labows Jr., *Diss. Abstr.*, **28 B**, 1425 (1967).

From the valence isomers listed in table 4, completely degenerate Cope rearrangements are presented by bullvalene 10—3—0—10 and hypostrophene 10—2—0—19 from the $(CH)_{10}$ series, and should occur with 12—2—0—3—4 and 12—3—0—3—1 from the $(CH)_{12}$ series.

Note added in proof. By using deuterium labelling, Paquette recently evidenced the degenerate thermal rearrangement of *cis*-9,10-dihydronaphthalene 10—4—0—6.[53]

---

[51] P. W. Rabideau, J. B. Hamilton and L. Friedman, *J. Amer. Chem. Soc.*, **90**, 4201 (1968); E. Vedejs, R. A. Shepherd and R. P. Steiner, *ibid.*, **92**, 2158 (1970).

[52] R. Hoffmann, personal communication.

[53] L. A. Paquette, *J. Amer. Chem. Soc.*, **93**, 7110 (1970).

Revue Roumaine de Chimie, **17**, *5*, 897 – 903 (1972)

REDUCTIVE CYCLIZATION OF α- and β-(*o*-NITROPHENYL)-SUBSTITUTED AMIDES

FLAVIAN CUIBAN

Department of Industrial Chemistry, Polytechnic Institute "Traian Vuia",
Timişoara, P.O.B. 103, Romania

Received December 22, 1971

The influence of several constitutive factors on the catalytic reduction of α- and β- (*o*-nitrophenyl)-substituted amides was investigated. Depending on the reaction conditions and on the nature of substituents, the corresponding anilines or cyclic compounds such as lactams or N-hydroxy-lactams are formed in this reaction.

The cyclization tendency of acids substituted in γ- or δ- position with nucleophilic groups is generally preserved by the corresponding functional derivatives of the carboxyl group. Regarding the amides for example, several experimental data support this conclusion.[1-3] Johnson, Panetta and Smith have showed recently[4] that the reduction of *o*-nitrophenyl-substituted penicillines gives 6-amino-penicillanic acid and the corresponding lactams.

However, it is hazardous to consider that it is an unconditional parallelism between the cyclization tendencies of these substituted acids and their functional derivatives. As an illustrative example, N-(*o*-aminophenyl)-glycine which could only be obtained by the catalytic reduction of nitro-phenyl-glycine in its lactam form, [5] although the cleavage of the corresponding amides may be performed only by heating. [1]

In figure 1 are given the reactions which take place in this catalytic reduction of the *o*-nitrophenyl-substituted amides (I). From the figure it may be expected that intramolecular participation of the hydroxylamines (II) and the amines (III) in the amide hydrolysis, depend on the structure of the acid (I) (Y = OH) and on the nature of the substituents (Y). In order to distinguish between these influences, we investigated several simple compounds whose structure was presumed to be suitable for this purpose. As acids (I) (Y = OH) six compounds were studied, given in

---

[1] R. W. Holley and A. D. Holley, *J. Amer. Chem. Soc.*, **74**, 3069 (1952).

[2] W. C. Rhodes and W. D. McElroy, *J. Biol. Chem.*, **233**, 1528 (1958).

[3] P. de la Llosa, M. Justisz and E. Scoffone, *Bull. Soc. chim. France*, **1960**, 1621.

[4] D. A. Johnson, C. A. Panetta and R. R. Smith, *J. Org. Chem.*, **31**, 2560 (1966).

[5] F. Cuiban, M. Ionescu, E. Bălă and M. Sterescu, *Bull. Soc. chim. France*, **1963**, 356.

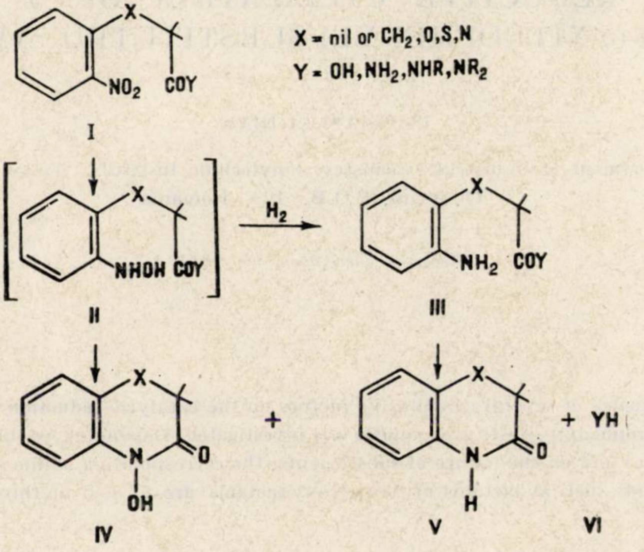

Fig. 1. — Scheme of reductive steps and ring closures of o-nitro-phenyl-substituted acid amides.

table 2. Instead of β-(*o*-nitrophenyl)-propionic acid, *trans*-*o*-nitrocinnamic acid was used since its double bond is easily reduced and gives the same final product as the former acid. As amines, aniline, benzylamine, cyclohexylamine and diethylamine were used in order to appreciate the influence of the substituent of the $-CONH_2$ group on the reactions of lactam formations.

The main characteristics of the amides *1—17* are given in table 1. They were obtained either through the corresponding acyl chlorides, or from *p*-nitrophenyl esters (*o*-nitrophenylacetyl chloride is stable only in solution), or through condensation of the reaction partners by means of N, N′-dicyclohexyl-carbodiimide (DCC). The last method was preferred for preparing *o*-nitro-phenyl-glycine amides because of the unsatisfactory results given by other methods.

The standard conditions used for the catalytic hydrogenation (see the experimental part) were rigorously respected, especially those regarding the amount and the quality of the catalyst, in order to avoid any effects caused by the changes of the catalytic activity. In all cases the reduction occurred normally and the reaction stopped at the amine (III) step. If cyclization reactions occur too, besides the amine (VI), the corresponding lactam (V) and occasionally cyclic hydroxamic acids (IV) were formed (by intramolecular cyclization of the hydroxylamines (II) which appeared as intermediates in the reduction). In the conditions used in our experiments

Table 1

Substituted amides o-$NO_2-C_6H_4-R$ as model substances

Formula R	Analysis calcd./found C	H	N	M.p. °C	Synthesis with:	Yields %	Recrystn. solv.
$-CH_2CONHCH_2C_6H_5$ $C_{15}H_{14}N_2O_3$	66.64	5.22	10.36	144	DCC	56	EtOH
	66.70	5.20	10.50	148	a	>95	EtOH
				148	b	68	EtOH
$-CH_2CONHC_6H_{11}$ $C_{14}H_{18}N_2O_3$	64.10	6.91	10.68	154	a	98	EtOH
(cyclo)	64.00	7.00	11.00				
$-CH_2CONHC_6H_5$ $C_{14}H_{12}N_2O_3$	65.61	4.72	10.93	150	b	82	EtOH
	65.40	4.70	11.10				
$-CH_2CON(C_2H_5)_2$ $C_{12}H_{16}N_2O_3$	61.00	6.82	11.85	oil	b	80	
	61.00	6.70	11.90				
$-CH=CHCONHCH_2C_6H_5$ $C_{16}H_{14}N_2O_3$	68.07	4.99	9.88	182	b	95	EtOH
	68.03	5.14	10.10				
$-CH=CHCONHC_6H_{11}$ $C_{15}H_{18}N_2O_3$	65.67	6.57	10.21	195	b	90	EtOH
(cyclo)	65.40	6.33	10.30				
$-CH=CHCONHC_6H_5$ $C_{15}H_{12}N_2O_3$	67.15	4.50	10.44	194	b	94	EtOH
	67.20	4.50	10.55				
$-CH=CHCON(C_2H_5)_2$ $C_{13}H_{16}N_2O_3$	62.88	6.49	11.28	55	b	87	Ligroin
	63.00	6.60	11.25				
$-OCH_2CONHCH_2C_6H_5$ $C_{15}H_{14}N_2O_4$	62.92	4.92	9.78	117	b	95	EtOH
	62.70	4.90	9.90				
$-OCH_2CONHC_6H_5$ $C_{14}H_{12}N_2O_4$	61.75	4.44	10.28	126	b	82	EtOH
	61.70	4.30	10.25				
$-OCH_2CON(C_2H_5)_2$ $C_{12}H_{16}N_2O_4$	57.13	6.39	11.10	59	b	90	Ligroin
	57.00	6.35	11.00				
$-OC(CH_3)_2CONHCH_2C_6H_5$ $C_{17}H_{18}N_2O_4$	64.95	5.74	8.91	78	b	95	Petroleum ether
	64.80	5.80	9.00				
$-OC(CH_3)_2CONHC_6H_{11}$ $C_{16}H_{22}N_2O_4$	62.72	7.23	9.14	83	b	86	Ligroin
(cyclo)	63.00	7.00	9.15				
$-OC(CH_3)CONHC_6H_5$ $C_{16}H_{16}N_2O_4$	63.98	5.37	9.32	97	b	100	EtOH
	64.20	5.30	9.45				
$-OC(CH_3)_2CON(C_2H_5)_2$ $C_{14}H_{20}N_2O_4$	59.98	7.19	9.99	73	b	82	EtOH
	59.84	7.10	9.98				
$-NHCH_2CONHCH_2C_6H_5$ $C_{15}H_{15}N_3O_3$	63.14	5.30	14.81	153	DCC	77	EtOH
	63.50	5.40	15.00				
$-SCH_2CONHCH_2C_6H_5$ $C_{15}H_{14}N_2O_3S$	59.58	4.66	9.26	130	b	92	EtOH
	59.80	5.00	9.40				

a – Activated ester.
b – Acid chloride.

Revue Roumaine de Chimie, 17, 5, 897–903 (1972)

hydroxamic acids are not reduced catalytically,[6,7] the hydrogen consumed depends only on the reduction stage, and is in good agreement with the relative proportion of the cyclic products (IV and V).

A practically quantitative separation of the various reaction products could be achieved owing to their different properties (acids, bases, amides). By means of sensitive spot test reactions (hydroxamic acids with $FeCl_3$; and aromatic amines with HNO_2 and β-naphthol) it was possible to evidence also compounds which were present only in traces.

The data given by table 2 indicate that for anilides, benzylamides and cyclohexylamides the cyclization occurred almost quantitatively. From the amides of the acids A and D important amounts of hydroxamic acid besides the corresponding lactam resulted, while for acids B, C, E and F only the lactams are formed.

Table 2

Percentage composition *a* **of products resulted after reducing the** *o*-**nitrophenyl-substituted acid amides**

Amine / *o*-Nitro-acid	Benzylamine			Cyclohexylamine			Aniline			Diethylamine		
	III	IV	V	III	IV	V	III	IV	V	III	IV	V
A. Phenylacetic	—	40	60	—	40	60	—	33	66	98	—	tr[a]
B. Cinnamic	—	—	100	—	—	100	—	—	—100	100	—	—
C. Phenoxyacetic	—	tr	95	—	tr	95	—	tr	95	98	—	tr
D. 2-Methyl-2-phenoxy-propionic	—	68	32	—	65	35	—	45	55	—	tr	98
E. N-Phenyl-glycine[c]	—	—	98	—								
F. Phenyl-thioglycolic[c]	—	tr	60[b]									

a – Determined through isolation of the reaction products, or TLC on silicagel, or hydrogen consumption in reduction, or titration of resulted amine (VI); b – Reduction was not complete even after repeated catalyst additions; c – The reduced tendency towards cyclization and synthetic difficulties decided us to discontinue investigations; tr – Trace.

A different behaviour is observed for diethylamides. The reduction occurred normally, yielding the expected anilines (III) (for their isolation, see experimental section). However from the diethylamide of the 2-methyl-2-*o*-nitrophenoxypropionic acid diethyl-amine was eliminated in the reduction and only one cyclization product, the lactam (V), was obtained.

From the given data we may comparatively appreciate the cyclization tendency of the acids (A—F) through two criteria: namely from the lactam/hydroxamic acid ratio (if the acyl elimination took place) as well as from the cyclization tendency of the diethylamides. The increased hydroxamic acid amounts means that in such cases the cyclization reaction became competitive with the reduction of (II) to (III). Although

---

[6] J. D. Dutscher, *J. Biol. Chem.*, **171**, 321 (1947).

[7] J. Smrt, J. Beránek and M. Horák, *Coll. Czech. Chem. Comm.*, **24**, 1672 (1959).

the inductive effect of the amide substituent does not have a determining character, it allows to establish a decreasing order of the cyclization tendency in dependence of the released amines (VI) as it follows : primary aliphatic >primary aromatic >secondary amine.

In the cyclization reactions an important influence is exerted by steric factors. In 2-methyl-2-(*o*-nitro-phenoxy)-propionic acid (D) the two geminal methyl groups cause the significant increase of the cyclization tendency as compared to acid C, compensating also the negative steric effect of the alkyl groups in diethylamine. This behaviour agrees with the reported [8] favorization of the cyclization to 5- and 6-membered rings if the original chain is substituted for alkyl groups. A similar observation was made by the cleavage of the nitropenicillins.[4]

Since from the studied acids of type I (Y = OH), the acids D and C showed the highest cyclization tendency, they were tested as protecting groups in peptide syntheses.[9]

It must be noted that our conclusions are valid for the standard conditions applied by the reduction. If increased catalyst amounts are used only lactams result and no cyclic hydroxamic acids. Similarly, only lactams were obtained if the reduction was performed in strongly acid medium (2—3 moles of mineral acid in excess). Surprisingly, only the aniline (III) resulted in neutral media such as alcohol or dioxan. The anilines cyclyse rapidly on acid treatment. Similar observations have been reported for the reduction of 2-nitrobiphenyl derivatives [10] and for the hydrolytic peptide bond cleveage with intramolecular participation of the benzimidazolinium ion.[11]

Acknowledgement. For the material help in realizing of the experiments, the author expresses his gratitude to the directors of the Institute for Chemical Pharmaceutical Researches, Bucharest, and to Mrs. Cornelia Ioan for the combustion analyses.

EXPERIMENTAL

Preparation of the acids

The *o*-nitrophenyl-acetic acid was prepared according to the method described by Wright and Collins.[12] Acids (C) and (D) were obtained by condensing *o*-nitrophenol with chloroacetic or α-chloroisobutyric acid.[4] The *o*-nitrophenylthioglycolic acid was prepared from mercaptoacetic acid and chloronitrobenzene,[13] while nitrophenylglycine was obtained according to

---

[8] B. Capon, *Quart. Rev.*, **18**, 45 (1964).

[9] F. Cuiban, *Tetrahedron Letters*, **27**, 2471 (1971).

[10] C. W. Muth, J. R. Elkins, M. L. De Matte and S. T. Chiang, *J. Org. Chem.*, **32**, 1106 (1967).

[11] K. L. Kirk and L. A. Cohen, *J. Org. Chem.*, **34**, 390 (1969).

[12] W. B. Wright jr. and K. H. Collins, *J. Amer. Chem. Soc.*, **78**, 221 (1956).

[13] G. M. Badger, D. J. Clark, W. Davies, K. T. H. Farrer and N. P. Kefford, *J. Chem. Soc.*, **1957**, 2624.

Plöchl.[14] The *o*-nitrocinnamic acid was prepared as usually from malonic acid and *o*-nitrobenzaldehyde.[15]

The amides (1—17) in table 1 were obtained by means of the corresponding acyl chlorides without isolating from the solution. The chloride of *o*-nitrophenylacetic acid decomposed suddenly on concentrating its solution even at low temperatures. In the same cases the *p*-nitrophenyl esters of acids have been converted into amides, or the condensation of components was performed by means of N,N'-dicyclohexyl-carbodiimide. The following methods were used:

a) *Through acid chlorides* : To the solutions of 20 mmole acid in 50 ml anhydrous methylene chloride 1—2 drops of dimethylformamide were added and 2.65 ml (30 mmole) $SOCl_2$ in 10 ml CH_2Cl_2 were introduced dropwise with stirring at room temperature. After a 2-hour heating of the mixture on a water bath, the $SOCl_2$ excess and the solvent were subsequently removed in vacuum. The solution of the residue (in 50 ml CH_2Cl_2) was added with stirring on to ice-cooled methylene chloride solution of the amine (50 mmole). After 2 hours' standing at room temperature it was washed in a separatory funnel with 30 ml 2N HCl, water, 2N ammonia solution and water again. The solution was dried over Na_2SO_4, filtered, evaporated and the residue recrystallised as above.

b) *Through p-nitrophenyl esters* : Equimolar amounts of *p*-nitrophenyl ester and amine (10 mmole) are solved in 50 ml $CHCl_3$, stirring from time to time and allowed to stand several hours at room temperature. The chloroformic solution was subsequently washed with 30 ml 2N HCl, water, 2N ammonia solution and water again. Dried with Na_2SO_4, filtered, evaporated and the residue recrystallized as above.

c) *With N, N'-dicyclohexyl-carbodiimide* (*DCC*) : To the solution of 10 mmole acid in dioxan or a mixture of dioxan and CH_2Cl_2, an equimolar amount of amine was added. Under water cooling, 10 mmole DCC solved in 10 ml dioxan was added dropwise. After 2 hours' stay, the dicyclohexylureea was filtered off, the solvent removed, and the residue recrystallized.

The p-nitro-phenyl esters used in amide synthesis were prepared similarly to activation of the amino - acid carboxyl group in peptide syntheses.[16]

a) To the solution of 10 mmole acid in 50 ml ethyl acetate 20 mmole pyridine and 15 mmole *p*-nitrophenyl carbonate were added. After 3 hours' refluxing on water bath, the solvent was removed in vacuum, and the residue washed with saturated $NaHCO_3$ solution, and with water to remove *p*-nitrophenol and pyridine. The filtered and dried product was recrystallized.

b) Another simple way for obtaining the esters used acid chlorides : to the dissolved 10 mmole of acid chloride in 20 ml anhydrous benzene, 1.65 g (10.25 mmole) of anhydrous and finely powdered sodium *p*-nitrophenoxide were added. The mixture was heated under stirring until the precipitate became colourless. After cooling and filtering the resulted sodium chloride, the solvent was removed in vacuum. The crude product was washed with saturated sodium bicarbonate, water and after drying, it was recrystallized.

Data concerning the prepared esters are given in table 3.

Reduction of amides

A suspension of 2g palladized carbon with 5% Pd/as Pd $(OH)_2$/in glacial acetic acid was hydrogenated until the hydrogen absorbtion stopped. To this catalyst 10 mmole amide solved in 30—40 ml glacial acetic acid was added then the hydrogen flow was continued measuring the consumed volumes. The reduction is exothermic and is usually completely in 30—40 min.

---

[14] J. Plöchl, *Ber. dtsch. chem. Ges.*, **6**, 19 (1886).

[15] R. H. Wiley and N. R. Smith, *J. Amer. Chem. Soc.*, **72**, 5198 (1950)

[16] Th. Wieland, B. Heinke, K. Vogeler and H. Morimoto, *Liebigs Ann. Chem.*, **655**, 189 (1962).

Table 3

p-Nitrophenyl esthers

Acid	Molecular formula	Analysis calcd./found			Yield		M.p. °C	Recrystn solvent
		C	H	N	a	b		
o-Nitrophenylacetic (A)	$C_{14}H_{10}N_2O_6$	55.60 55.30	3.31 3.35	9.27 9.30	99	90	108— 109	Me_2CO
o-Nitrocinnamic (B)	$C_{15}H_{10}N_2O_6$	57.32 57.20	3.20 3.30	8.91 9.10	—	90	164.5	Me_2CO
o-Nitrophenoxyacetic (C)	$C_{14}H_{10}N_2O_7$	52.83 52.70	3.16 3.10	8.77 8.10	93	80	168	AcOEt
2-Methyl-2-o-nitro -phenoxypropionic (D)	$C_{16}H_{14}N_2O_7$	55.49 55.60	4.07 4.10	8.08 8.10	98	90	98	Me_2CO

a — With p-nitrophenyl carbonate
b — With acid chloride

With TLC (on silica with $CHCl_3 : CH_3OH = 92 : 8$, and iodine vapour colouring) samples prelevated at various reduction times made it possible to evidence the resulted compounds : the eliminated amines (VI) remained near to the start, lactams have $R_f = 0.8$ above the cyclic hydroxamic acids ($R_f = 0.7$), while anilines (III) are intensely coloured with iodine vapours. Anilines (III) gave on diazotization and coupling with naphthols red dyes. Due to the catalyst poisoning the reduction of o-nitro-phenyl-thioglycolic-benzylamide remains incomplete, even after addition of fresh catalyst.

When the hydrogen absorption was finished, the catalyst was filtered off on a cellite layer, 10 mmole hydrochloric acid were added to the solution which was concentrated in vacuum in order to remove completely the acetic acid. From the residue, by adding of 50 ml benzene, the hydrochloride of amine (VI) or (VIII) are separated ; these can be purified by recrystallization from ethanol-ethyl ether mixtures.

o-Amino-phenylacetic acid diethyl amide hydrochloride, white needles, m.p. 165°, *Calcd.* : $C_{12}H_{19}Cl\ N_2O$, C: 59.37 ; H : 7.47 ; Cl^-: 14.60 ; N: 11.54 ; *Found* : C: 59.40 ; H: 7.50 ; Cl^-: 14.75 ; N : 11.50 %.

o-Amino-phenyl propionic acid diethylamide bis hydrochloride, white needles, m.p. 162—164°, obtained by solving the crude product in water, alkalinised with NaOH, extraction with benzene, dried, precipitated with an ethereal HCl solution in excess : *Calcd.* : $C_{13}H_{22}Cl_2N_2O$, C : 53.3 ; H : 7.55 ; Cl^-: 24.2 ; N :9.56 ; *Found* : C : 53.3 ; H : 7.60 ; Cl^- : 25.3 ; N : 9.60 %. After diazotization and coupling with β-naphthol precipitated a red dye with m.p. 126°.

o-Amino-phenoxyacetic acid diethyl amide hydrochloride, white needles, m.p. 158°. *Calcd* : $C_{12}H_{19}ClN_2O_2$, C : 55.70 ; H : 7.40 ; Cl^- : 13.70 ; N : 10.82. *Found*: C: 55.50 ; H :7.20 ; Cl^- : 13.20 ; N : 10.70 %. After diazotization and coupling with β-naphthol a red dye with m.p. 133° precipitated.

By removing the solvent from the benzene solution a mixture of lactam and cyclic hydroxamic acid remains. In order to separate the lactams from their N-hydroxy-derivatives, the solid mixture is solved in ethanol, treated with an excess of ammonia solution, and the ethanol is removed in vacuum. The filtered precipitate is recrystallized from water or water-alcohol mixtures. By acidifying the filtrate the hydroxamic acid precipitates which is recrystallized from water.

Revue Roumaine de Chimie, **17**, *5*, 905 – 914 (1972)

THE PROTON MAGNETIC RESONANCE SPECTRA OF SULTAMS

S. H. DOSS*

Received August 17, 1971

Proton magnetic resonance chemical shifts and coupling constants for a series of sultam compounds are reported. Detailed interpretations of the spectra of 12 compounds containing the six-membered sultam ring are given ; it is shown that for the methylene group adjacent to nitrogen it appears at 6.68 ppm, and that for the methylene group adjacent to SO_2 at 6.98 ppm, the other two methylene groups appear at 7.7 and 8.2 ppm showing coupling constant $\sim$ 6, 3.5 and 2.5 cps, respectively. Dreiding models show that the nitrogen and sulphur atoms are rigid in the ring exhibiting no rotations ; any substituent for the secondary amine's hydrogen will lay in the plane of the molecule.

INTRODUCTION

It has been stated[1, 2, 3] that some insight into the problems involved in reaching a better understanding of the effects of substitution on chemical shifts and coupling constants in systems might be obtained from investigations with substituted heterocycles since the heteroatom will appreciably perturb the electronic structure of the compound relative to that of the corresponding carbocyclic species.

During our investigation into anticarcinogenic, anticonvulsant drugs a series of 1,4-butanesultams became available to us. We report here the NMR spectra of these compounds.

Generally sultams are cyclic sulfonamides, analogous to the γ-, δ-and ε-lactams and may have a five- or a six-membered ring. They are well crystallized substances, their solubilities in alkalies are due to the formation of metallic salts. The "imino group" has assumed an acid nature owing to the influence of the negative SO_2 group .[4]

---

* Present address : Organisch-chemisches Institut der Universität Bonn, W/Germany

[1] J. B. Merry and J. H. Goldstein, *J. Amer. chem. Soc.*, **88**, 5560 (1966).

[2] M. H. Palmer and B. Semple, *Chem. and Ind.*, **1965**, 1766.

[3] J. T. Gerig and J. D. Reinheimer, *Org. Mag. Reson.*, **7**, 239 (1969).

A. Mustafa, *Chemical Rev.*, **54**, 195 (1954).

EXPERIMENTAL

PMR spectra were recorded on either a Varian A-60 spectrometer operating at 60 MHz or a Bruker HX-90 operated at 90 MHz at ambient temperature using approximate 150 mg/ml concentration of sultam in deutero chloroform. Tetramethylsilane was used as internal reference.

RESULTS AND DISCUSSION

A list of the sultams investigated is given in table 1 ; all N-substituted sultams gave similar spectra, for the protons in the sultam ring, consistent with the rapid inversion of both the six-membered ring and the nitrogen atom.

This is in agreement with the known behaviour of six-membered lactams with respect to ring inversion and with the behaviour of sulphonamides with respect to the inversion of the nitrogen atom. The inversions combined with the system of the unsubstituted sultam ring result in a relatively simple AA'BB'MM'XX' system.

The spectra of all the sultams showed two triplets at low field $\tau C_1 = 6.89$ and $\tau C_4 = 6.62$ which were assigned to the protons on the methylene groups neighbouring the sulphur and nitrogen atoms. In the case of the parent 1,4-butanesultam, the proton at lower field showed considerable broadening, due to the coupling with the proton on nitrogen which was manifest as a broad absorption at $\tau = 5.33$. Shaking with deuterium oxide removed this absorption and sharpened the triplet. In view of this and of the known chemical shift data the lower field of the two triplets was assigned to that neighbouring the nitrogen atom.

Both triplets showed broadened center absorption consistent with XX' or MM' parts of an AA' BB' MM' XX' system in which XX' is coupled to AA' and MM' only to BB'.

The spectra of the outer two peaks was taken to equal the sum of the two averaged coupling constants, *cis* and *trans*, and is shown in table 2.

The methylene protons on carbons 2 and 3 appeared as two multiplets consistent with AA' and BB' parts of an AA'BB'MM'XX' system in which AA' couples with BB' and MM' and BB' couples with AA' and XX'.

By decoupling experiments it was shown that the protons at position 4, next to the nitrogen atom, coupled with higher field multiplet and that the multiplet to lower field, coupled with the protons of the methylene group adjacent to the sulphur atom.

For certain compounds these multiplets appeared as nine line absorptions whose peaks heights were in the ratio 1 : 1 : 2 : 1 : 4 : 1 : 2 : 1 : 1 typical of the A_2 part of an $A_2M_2X_2$ spectrum and could be analysed (first order) to give J_{ax} J_{am} which correspond to the averaged *cis* and *trans* vicinal coupling constants.

Such a first order analysis requires neglection of $J_{AA'}$, and $J_{BB'}$, and the assumption that $J_{AB'} = J_{AM'}$ and $J_{AB} = J_{AM}$, that means the averaged *cis* (and *trans*) vicinal couplings to the neighbouring methylene protons are the same.

Table 1

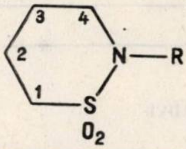

No.	Compound	R	Ref.
I	Butanesultam (1,4)	H	5
II	Bis-1,2-(N)-1,4 n-butanesultamylethane	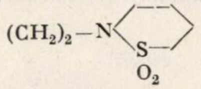	6
III	N-Benzyl-butanesultam (1,4)	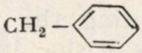	7
IV	Bis-1,3-(N)-1,4-n-butanesultamylpropane	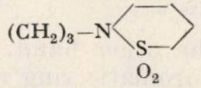	6
V	Bis-1,6-(N)–1,4-n-butanesultamylhexane	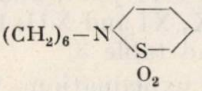	6
VI	Bis-*p*, *p*-(N)-1,4-n-butanesultamyl-dicyclohexylmethane	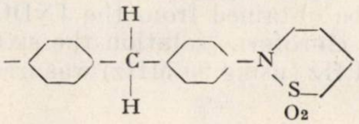	8
VII	N-*p*-Tolyl-butanesultam (1,4)	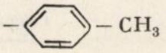	7
VIII	N-(*p*-nitrophenyl) butanesultam (1,4)	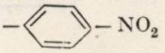	7
IX	N-(4′-aminophenyl)-butanesultam (1,4)	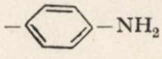	9
X	*p*-1,4-n-butanesultamyl-(N)-N-methyl-N-acetyl-benzylamine	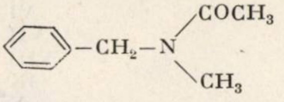	10

---

[5] W. Dirscherl and F. W. Weingarten, *Liebigs Ann. Chem.*, **588**, 200 (1954).

[6] B. Helferich, L. Bettin and S. H. Doss, *Liebigs Ann. Chem.*, **741**, 139, (1970).

[7] B. Helferich, R. D. Lein, K. Geist, H. Junger and D. Wiehle, *Liebigs Ann. Chem.*, **646**, 32 (1961).

[8] S. H. Doss, unpublished results.

[9] B. Helferich and K. G. Kleb, *Liebigs Ann. Chem.*, **635**, 91 (1960).

[10] B. Helferich and S. H. Doss, *Liebigs Ann. Chem.*, **747**, 107 (1971).

Table 1 (continued)

N_o.	Compound	R	Ref.
XI	*p*-1,4-n-Butanesultamyl-(N)-N-methylbenzylamine	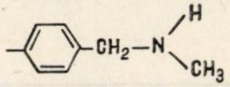	10
XII	Bis-*p*-n-sultamyl-(1,4)-benzyl-methylamine	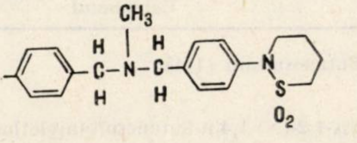	10

Substituting the hydrogen atom neighbouring N with alipathic groups results in shielding of the protons at C_1 and C_4 by a value ~ 0.1 ppm as in II, III, IV, V and VI, which is in agreement with values reported.[11a, 12a b.]

On the other hand, substituting the hydrogen atom neighbouring to N with aromatic ring results in deshielding of the protons at C_1 by a value of ~ 0.14 ppm, and protons at C_4 by a value of ~ 0.4 ppm as in VIII, IX, X, XI and XII: the shielding and deshielding values are shown in figure 1 and table 3.

More explainations for the bands centered at τ 6.62 and τ 6.89 can be obtained from the INDOR type experiments[13]; thus in deuteriorated cloroform solution the sixtet at 269.1 ; 275.6 ; 281.4 ; 283.1 ; 288.8 ; 294.3 Hz (using 90 MHz) was irradiated at 142 Hz and 196 Hz. Irradiation

Table 2

Coupling constants of protons of sultam ring Jcps

Cpd	J 1.2	J 4.3
I	6	5.5
II	5	5
III	5	5
IV	6	5.5
V	6	5
VI	5	5
VII	6	5
VIII	6	5
IX	6	5
X	6	5
XI	6	5
XII	6	5

---

[11] N. S. Bhacca, L. F. Johnson and J. N. Shoolery, "NMR spectra catalog", vol., 1, Varian Associates, Palo Alto, California, 1962 spectra *a* No. 330, *b* No. 31, *c* No. 22.

[12] N. S. Bhacca, D. P. Hollis, L. F. Johnson and E. A. Pier "NMR spectra catalog" vol. 2, Varian Associates, Palo Alto, California, 1963, spectra *a* No. 340, *b* 406.

[13] V. J. de Kowalewski, D. G. de Kowalewski and E. C. Ferra, *J. Mol. Spectroscopy*, **20**, 203 (1966).

at 142 Hz suppressed the coupling of the methylene group at C_4 with the methylene at C_3 reducing the triplet at 294.3, 288.8 and 283.1 to a singlet at 290 Hz – while the coupling of the methylene groups at C_1 with C_2 is still existing at 283, 277 and 271 Hz.

Table 3

Chemical shifts of protons of sultam ring ppm

Cpd	C1	C2	C3	C4
I	6.89	7.80	8.32	6.62
II	6.98	7.78	8.3	6.55
III	6.98	7.82	8.4	6.75
IV	6.98	7.98	8.4	6.70
V	6.98	7.80	8.4	6.68
VI	6.98	7.75	8.35	6.71
VII	6.9	7.8	8.25	6.40
VIII	6.75	7.65	8.08	6.17
IX	6.77	7.75	8.2	6.44
X	6.86	7.72	8.18	6.36
XI	6.83	7.72	8.18	6.30
XII	6.88	7.73	8.2	6.45

Irradiation at 196 Hz suppressed the coupling of the methylene group at C_1 with the methylene at C_2 reducing the triplet at 281.4, 275.6, 269.1 to a singlet at 279 while the coupling of the methylene groups at C_3 with C_4 is still existing (Fig. 2).

The chemical shift for the methylene protons at C_2 is centered at τ 7.8 ± 0.1 ppm which is in good agreement with values reported,[11b]. These protons are coupled with C_1 and C_3 protons giving rise to a multiplet, whereas the protons of C_3 are coupled with that at C_4 and C_2 giving rise to a multiplet centered at 8.2 ± 0.2 ppm.

It was stated,[14] that in systems containing S and N as heteroatoms like thieno [3,2–b] pyrrole and derivatives, exhibit long range coupling between the hydrogen atom neighbouring S and that neighbouring N; but from the data shown here, there is no coupling like that occurring in the sultam ring.

It is known,[15] that spin-spin coupling constants provide information about the structure, bond angles and nature of bonding in molecules. Accepting the warning given by Bhacca and Williams,[16] measuring the dihedral angles by applying Karplus curve,[17] the following dihedral angles are found for the hydrogen at C_1 small (40–45°); C_2 small (~ 50°); C_3 small (40–45°); C_4 small (57–62°).

---

[14] R. J. Tinte, H. R. Snyder, A. L. Porte and H. S. Gutowsky; *J. Phys. Chem.* **65**, 187 (1961).

[15] H. M. Mc Connell, *J. Chem. Phys.*, **23**, 2454 (1955), and **24** 460 (1956).

[16] N. S. Bhacca and D. H. Williams, "Applications of NMR spectroscopy in Organic Chemistry", Holden Day, Inc., 1964, p. 156.

[17] M. Karplus, *J. Chem. Phys.*, **30**, 11 (1959).

Dreiding models show that the six-membered sultam ring can have the following conformations. The N and S atoms are rigid ; substituents for the secondary amine's hydrogen lay in the plane of the molecule.

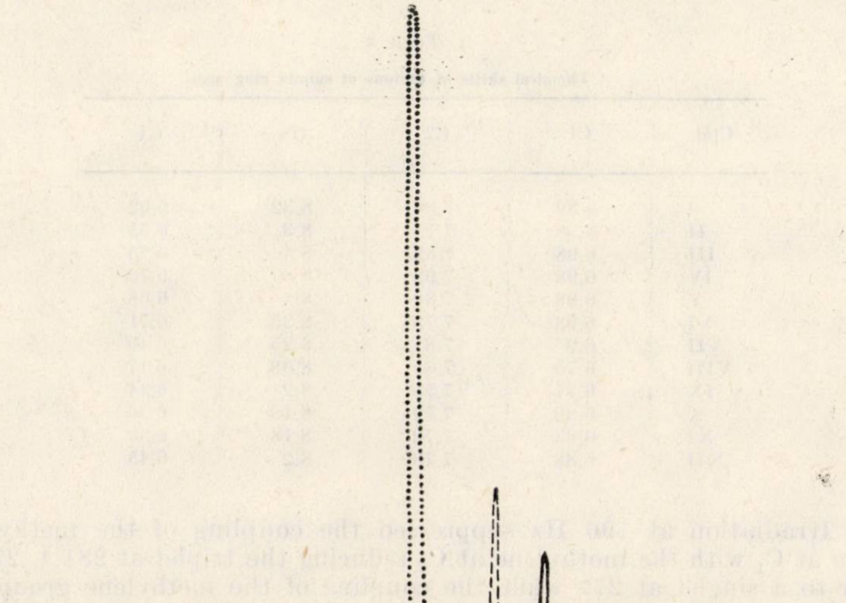

Fig. 1. — NMR spectra of compound I(—), VIII (— — —) and II(. . .)

The values obtained by these approximate calculations are given in table 3. They are in agreement with the expected average vicinal

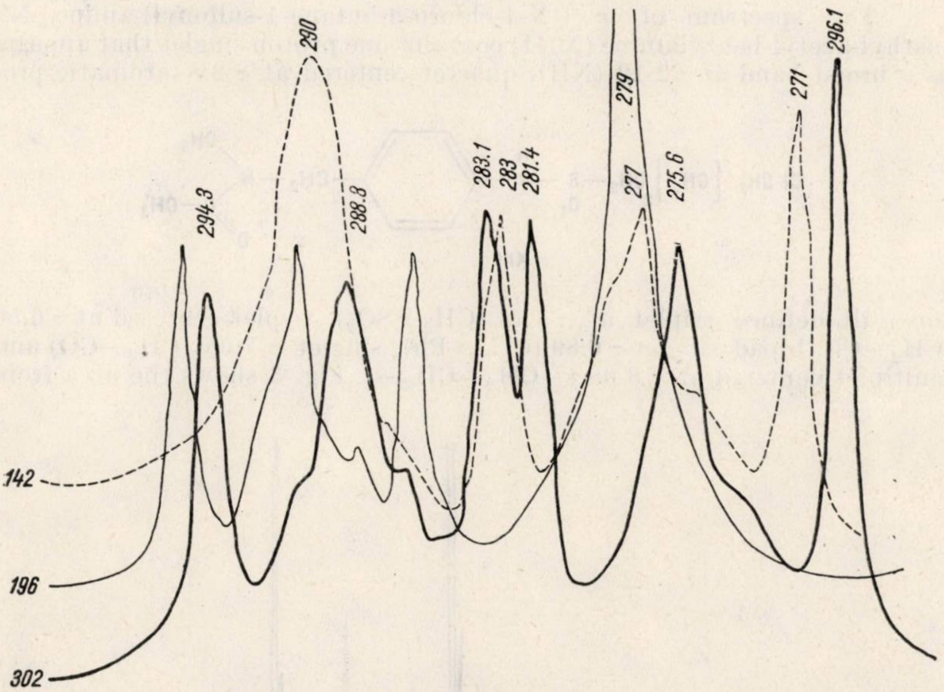

Fig. 2. — Indor type experiments for compound III showing irradiation for the bands centered at τ 6.62 and τ 6.89, respectively.

couplings in the rigid system. In an inverting chair six-membered ring if J_{ax-ax} is taken to be 10 Hz J_{eq-eq} 2–3 Hz, J_{ax-eq} =4–5 Hz

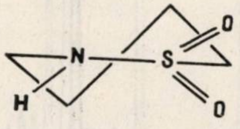

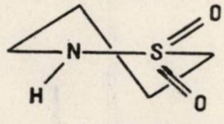

In compound XIII, the intermediate product of sultam X, the four methylene groups form an acyclic system with terminal Cl and SO_2 groups ; the predicted shielded values will be calculated from the following equation.

$$\tau - \text{alkyl} = 9.767 - \sum_{i}{}^{\circ} i \text{ eff}$$

The values calculated for $CH_2 - Cl$ and $CH_2{-}SO_2 -$ are analogous with the observed values and in accordance with values stated in literature.[11c,18]

---

[18] D. H. Williams and I. Fleming., "Spectroscopic Methods in Organic Chemistry", McGraw-Hill, London, 1966, p. 126.

The spectrum of *p* [(N-4-chloro-n-butane-1-sulfonyl)-amino]-N′-methyl-acetyl-benzylamine (XIII) contains one proton singlet that appears as a broad band at τ 2.12 (NH), quartet centered at τ 2.8 (aromatic protons), ill defined triplet at τ 5.48 (CH_2-SO_2), triplet centered at τ 6.50 (CH_2-Cl), broad singlet τ 6.89 (CH_2-Ph), singlet τ 7.05 (CH_3-CO) and multiplet centered at τ 8.08 ($-CH_2-CH_2-$). Fig. 3 shows the area from τ 5–9 for compounds X, XI and XIII. Expansion of the triplet at τ 6.68 and the ill defined triplet at τ 6.98 in compound V on a 90 MHz sweep, revealed five splittings for the triplet at τ 6.98, into sextet, indicating coupling of the methylene group at C_1 with that at C_2, giving rise to triplet, and the methylene group, neighbouring the nitrogen in the hexamethylene chain,

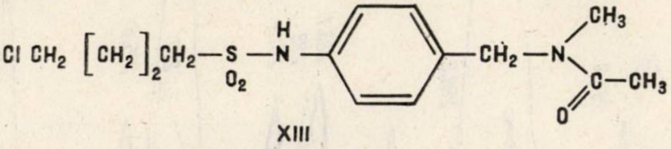

XIII

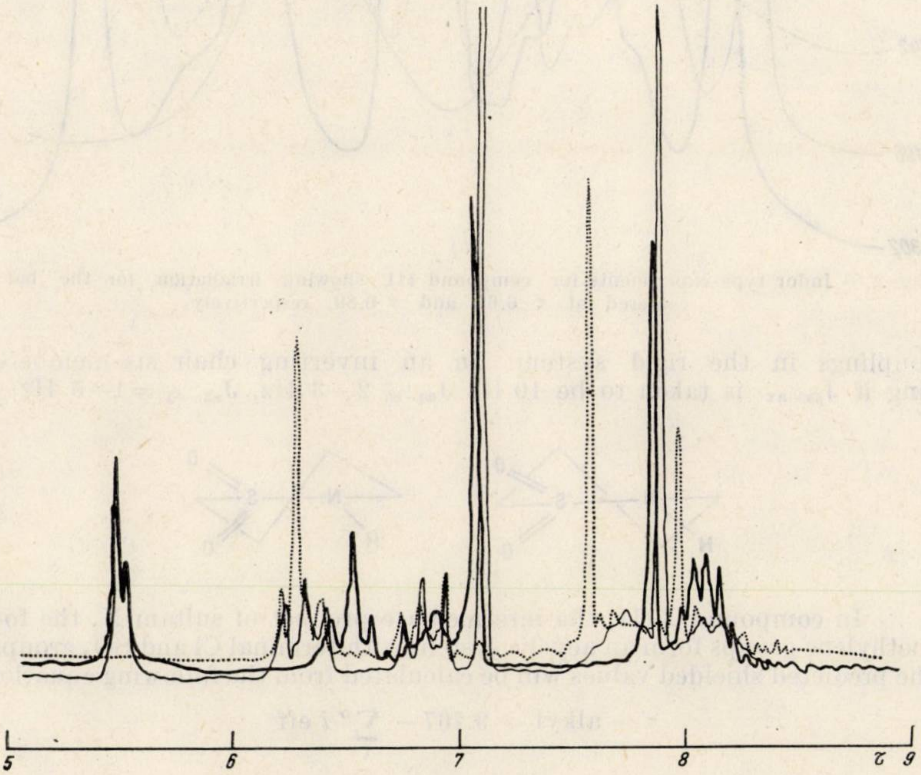

Fig. 3. — NMR spectra of compound X (—), XI (············) and XIII (—).

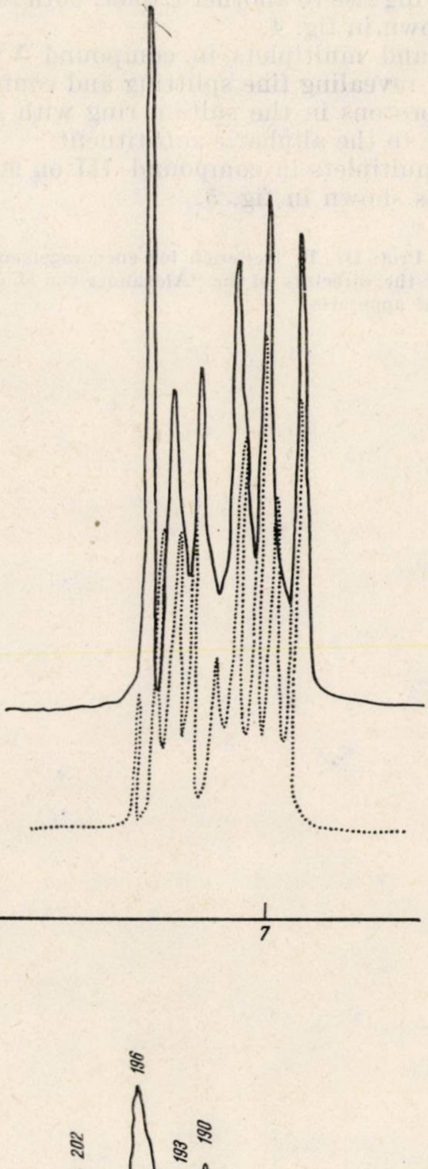

Fig. 4. — NMR spectra of compound V : sweep at 60 Hz (—), sweep at 90 Hz (. . .).

Fig. 5. — NMR spectrum of compound III : Sweep at 90 Hz for the ill defined multiplets.

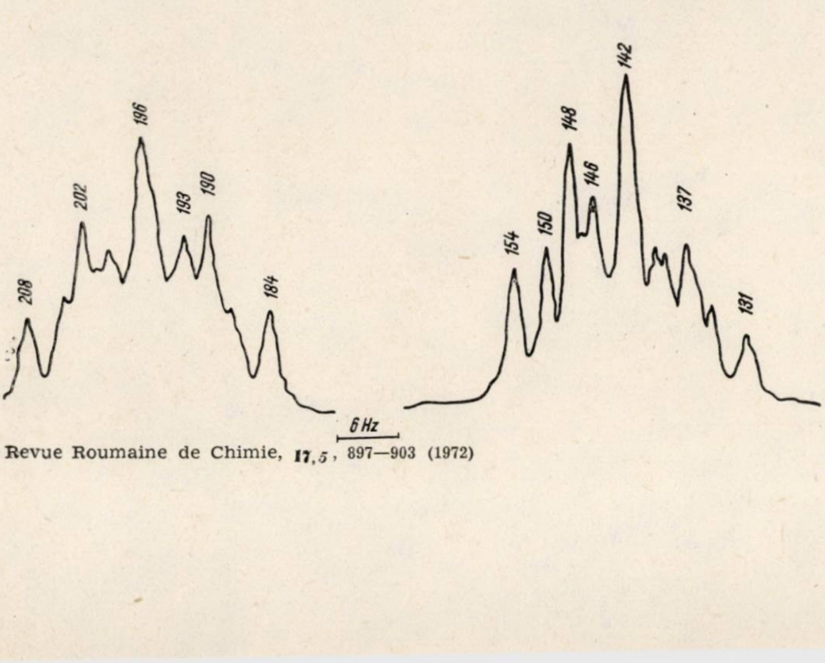

with its neighbouring methylene giving rise to another triplet, both forming the sextet centered at τ 6.98 as shown in fig. 4.

The poorly defined triplets and multiplets in compound VI were also expanded on a 90 MHz sweep, revealing fine splitting and confirming the assignments for the different protons in the sultam ring with special reference to the shielding value due to the aliphatic substituent.

Expansion of the ill defined multiplets in compound III on 90 MHz sweep revealed the fine splitting as shown in fig. 5.

Acknowledgement. The author thanks Prof. Dr. B. Helferich for encouragement, Prof. Dr. G. Snatzke for helpful discussions and the directors of the "Alexander von Humboldt" Stiftung for a scholarship award and gift of apparatus.

Revue Roumaine de Chimie, 17, 5, 915–923 (1972)

SPEKTROPHOTOMETRISCHE DOSIERUNG DES BENZIDINS MIT NATRIUMHYPOCHLORIT UND MIT UNTERCHLORIGER SÄURE

I. FLOREA

vom Polytechnischen Institut, Timişoara, Laboratorium für Allgemeine Chemie, str. Remus, 14

Eingegangen am 16. November 1971

Man verfolgt eine neue spektrophotometrische Methode für die Dosierung des Benzidins a) mit Natriumhypochlorit und b) mit Unterchloriger Säure. Die entstehende orangegelbe Verbindung wird mit Chloroform extrahiert. Die Chloroformlösung hat eine gelbe Farbe und weist zwei Absorptionsmaxima auf, eines bei $\lambda = 417$ nm und eines bei $\lambda = 443$ nm. Die durchgeführten Bestimmungen zeigten, daß Benzidin nach dieser Methode, innerhalb der Grenzen 1,8–36,8 μg mit Natriumhypochlorit und 1,8–55,2 μg mit Unterchloriger Säure nachweisbar ist. Die Dosierung des Benzidins mit Natriumhypochlorit kann man in Gegenwart von Anilin, *o*-, *m*- und *p*-Toluidin, sowie von β-Naphthylamin durchführen. Es wurden gute Ergebnisse verzeichnet, gleichzeitig ist auch die Empfindlichkeit der Methode bemerkenswert.

In der Fachliteratur sind als Bestimmungsmethoden von Benzidin die Ausfällung mit Heteropolysäuren[1] und die Chromatographie [2–9] angegeben.

---

[1] V. V. KOZLOV und V. P. SAGALOVICH, *Izvest. V.U.Z.M.V.O. S.S.S.R., Khim. i khim. Tekhnol.*, **8**, 609 (1965); *Chem. Abstr.*, **65**, 15665 c (1966).

[2] H. J. HECKEMANN und E. BAUMANN, *J. prakt. Chem.*, **36**, 265 (1967); *Chem. Abstr.*, **69**, 83043 q (1968).

[3] I. GEMZOVA und J. GASPARIC, *Coll. Czech. Chem. Comm.*, **31**, 2525 (1966); *Chem. Abstr.*, **65**, 3773 a (1966).

[4] I. GEMZOVA und J. GASPARIC, *Mikrochim. Acta*, **1**, 310 (1966); *Chem. Abstr.*, **65**, 7983 h (1966).

[5] A. CEE, und J. GASPARIC, *Mikrochim. Acta*, **1–2**, 295 (1966); *Chem. Abstr.*, **65**, 7983 (1966).

[6] K. C. KHNEBE und S. P. SRIVASTOVA, *Z. analyt. Chem.*, **210**, 282 (1965); *Chem. Abstr.*, **63**, 3602 b (1965).

[7] P. EHRLICH, *Z. physiol. Chem.*, **41**, 329 (1904); *J. Appl. Chem.*, **6**, 525 (1966); *Chem. Abstr.*, **51**, 7244 i (1957).

[8] W. S. BROWN, *Nature*, 143, 377 (1939); *J. Appl. Chem.*, **6**, 525 (1956); *Chem. Abstr.*, **51**, 7244 i (1957).

[9] D. ADLER und A. CHRZASCZEWA, *Med. Pracy*, **8**, 15 (1957); *Chem. Abstr.*, **53**, 191611 d (1959).

Für die Dosierung des Benzidins stehen folgende Beschreibungen zur Verfügung : die jodometrische,[10] die konduktometrische Methode mit Perchlorsäure in einem Wasser - organischen Lösungsmittel-Gemenge, [11] die polarographische,[12,13] mit Ionenaustauschern,[14] die potentiometrische Methode mit Perchlorsäure in einem organischen Lösungsmittelgemisch,[15] sowie in bestimmten organischen Lösungsmitteln,[16] die photometrische Methode mit Natriumchlorit,[17] weiterhin eine kolorimetrische Methode mit Chloramin T.[18,19]

In vorliegender Arbeit wird eine neue Dosierungsmethode des Benzidins verfolgt, wobei als Reagenzien a) eine Natriumhypochloritlösung und b) eine Unterchlorige Säurelösung verwendet werden. Der Methode liegt die Bildung eines Diphenochinondichlorimins[20] orangegelber Farbe zugrunde, welches infolge der oxidierenden Wirkung des Hypochlorits und der Unterchlorigen Säure auf eine Benzidinlösung entsteht. Die gebildete und mit Chloroform extrahierte Verbindung ermöglicht die spektrophotometrische Dosierung des Benzidins bei $\lambda = 443$ nm. Die Methode empfichlt sich im Falle von Benzidinmengen zwischen 1,8—36,8 g bei Verwendung von Natriumhypochlorit und 1,8—55,2 µg mit Unterchloriger Säure.

Das Benzidin kann mit Natriumhypochlorit und Unterchloriger Säure in den angeführten Mengen dosiert werden, und zwar in a) Wasser, b) in Gegenwart von bis zu 93 µg Anilin, c) in Gegenwart von bis zu 108 µg *o*-, *m*- und *p*-Toluidin.

EXPERIMENTELLES

Geräte

Die spektrophotometrischen Messungen wurden mit einem UNICAM SP 800-Spektrophotometer durchgeführt, wobei Küvetten von 4,2 und 1 cm verwendet wurden.

Den pH-Wert der Lösung nahm man nach Anzeigen eines MULTOSCOP V Apparates an.

---

[10] A. Roesler und D. Glasmann, *Chem.-Ztg.*, **27**, 986. 7/10 ; *Chem. Zentr.*, **2**, 1147 (1903).

[11] T. Jasinski und Z. Pawlak, *Chem. Analyt.*, **10**, 865 (1956) ; *Chem. Abstr.*, **64**, 11845 c (1966).

[12] Yu. I. Beilis, *Ukrain. Res. Inst. Ind. Hyg. and Occupational Diseases, Kharkov*, **10**, 584 (1965) ; *Chem. Abstr.*, **64**, 2742 g (1966).

[13] V. D. Bezuglyi und Yu. I. Beilis, *Zhur. analit. Khim.*, **20**, 1000 (1965) ; *Chem. Abstr.*, **64**, 5756 c (1966).

[14] A. Tomoyuki und Y. Hiroshi, (*Coll. Pharm., Kyoto, Japan*). *Kyoto Yakka Daigaku Gakuho*, **12**, 25 (1965) ; *Chem. Abstr.*, **64**, 1355 c (1967).

[15] T. Jasinski und Z. Szpouar, *Zeszyty Nauk. Mat. Fiz. Chem. Wyzsza Szkola Pedagog Gdansk*, **5**, 59 (1965) ; *Chem. Abstr.*, **65**, 16142 (1966).

[16] A. P. Kreshkov, L. N. Byukova und I. D. Pevznev, *Zhur. analit. Khim.*, **19**, 890 (1964) ; *Chem. Abstr.*, **61**, 12638 (1964).

[17] Gr. Popa, El. Rădulescu-Jercan und F. M. Albert, *Rev. Roumaine Chim.*, **11**, 1449 (1966).

[18] J. M. Glasmann und J. W. Meigs, *Arch. industr. Hyg.*, **4**, 519 (1951) ; *J. Appl. Chem.*, **6**, 525 (1956).

[19] L. T. Butt und N. Stafford, *J. Appl. Chem.*, **6**, 525 (1966) ; *Chem. Abstr.*, **51**, 7244 i (1957).

[20] W. Schlenk, *Liebigs Ann. Chem.*, **365**, 313 (1908) ; *Chem. Zentr.*, **1**, 179 (1909).

Reagenzien

Die Benzidinlösung. a) man löst 0,1841g, durch mehrfaches Umkristallisieren aus Wasser erhaltenes, reines Benzidin in einem 100ml Meßkolben und füllt mit Alkohol bis zur Marke auf. Man erhält auf diese Weise eine 1.10^{-2} m Benzidinlösung. 1ml Lösung enthält 1,841mg Benzidin; b) man verdünnt 20ml der a-Lösung mit Alkohol auf 200ml. 1ml dieser Lösung enthält 184,1µg Benzidin; c) man verdünnt 20ml der b-Lösung mit Alkohol auf 200ml. 1ml Lösung enthält nun 18,41µg Benzidin.

Die Natriumhypochloritlösung wird durch Einblasen von Chlor in eine $\simeq$ 0,1n Natriumhydroxydlösung, bis zur Sättigung, zubereitet.

Die Lösung der Unterchlorigen Säure gewinnt man, indem man Chlor bis zur Sättigung in destilliertes Wasser einbläst.

Die *o*-, *m*- und *p*-Toluidin-, sowie die β-Naphthylaminlösungen (Konzentration 1.10^{-3}m) wurden aus reinen Substanzen, durch Wägen zubereitet. Für die Untersuchungsproben wurden Volumen zwischen 0,1 und 1ml, im Falle des Anilins, *o*-, *m*- und *p*-Toluidins verwendet; bei β-Naphthylamin hingegen nahm man 0,1—0,5ml. 1ml Anilin 1.10^{-3}m enthält 93.06 µg; 1ml *o*-, *m*- und *p*-Toluidin 1.10^{-3}m enthält 107,88 µg und 1ml β-Naphthylamin 1.10^{-3} m enthält 143,08 µg.

Die Natriumhypochloritlösung, sowie die Unterchlorige Säurelösung werden in dunkleu Flaschen aufbewahrt.

Arbeitsweise

Mit einer Mikrobürette werden zwischen 0,1—2ml c-Lösung, welche 1,84—36,8µg Benzidin enthält, in einen Trenntrichter eingegossen. Dann fügt man 10—15ml Wasser, 4ml Natriumhypochloritlösung hinzu und schüttelt eine Minute lang durch. Weiterhin gibt man 6ml Chloroform dazu und schüttelt den Trichter energisch 1—2 Min. lang, während sich die Chloroformschichte gelb färbt; dann gießt man den Inhalt in einen 25ml Meßkolben ab. Der Vorgang wird mit derselben Chloroformmenge zweimal wiederholt, und wenn es erforderlich ist, noch ein- oder zweimal mit je 3ml Chloroform, bis die letzte Chloroformschichte farblos bleibt. Dann füllt man den Kolben mit Chloroform bis zu 25ml auf. Wenn die Lösung etwas trübe ist, fügt man einige Kristalle wasserfreies Kalziumkarbonat hinzu und schüttelt um. Die Lösung klärt sich innerhalb weniger Minuten und man mißt die Extinktion bei λ = 443nm. Als Vergleichsprobe benützt man Chloroform.

Die mit Unterchloriger Säure erfolgte Dosierung des Benzidins wird auf dieselbe Weise durchgeführt, wobei man 0,1—3ml der c-Lösung verwendet, welche 1,84—55,2µg Benzidin enthält; an Stelle von Natriumhypochlorit wird aber dasselbe Volumen Unterchlorige Säure benützt.

ERGEBNISSE UND DISKUSSION

DAS ABSORPTIONSSPEKTRUM

Die Absorptionskurven der durch das Vermengen der Benzidinlösung mit einer Natriumhypochloritlösung bei pH = 10,65 und einer Unterchlorigen Säurelösung bei pH = 4.15 entstandenen Verbindung sind in Abb. 1 ersichtlich und weisen 2 Maxima auf: bei $\lambda = 417$nm und $\lambda = 443$nm.

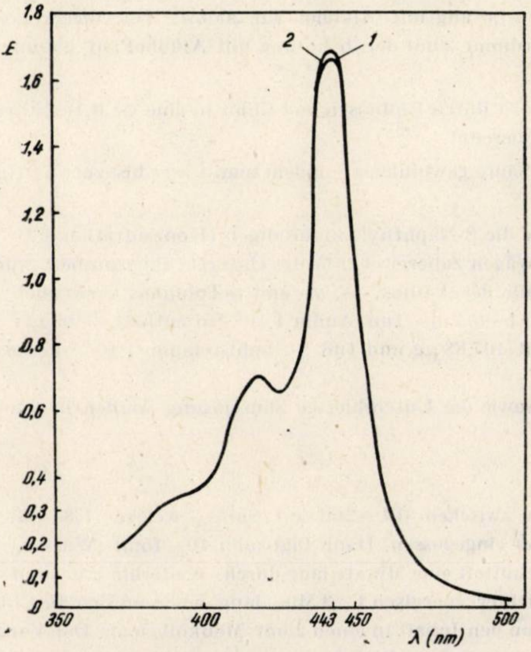

Abb. 1. — Das Absorptionsspektrum der entstandenen Verbindung mit Chloroform extrahiert, bei 4 cm Küvettengröße.

1. 1ml c-Lösung + 10ml destilliertes Wasser + 4ml Natriumhypochlorit; *2,* 1ml c-Lösung + 10 ml destilliertes Wasser + 4ml Unterchlorige Säure.

Aus den bei verschiedenen pH-Werten durchgeführten Bestimmungen geht hervor, daß der pH-Wert der Lösung das Absorptionsspektrum der gebildeten Verbindung nicht beeinflußt. Die Dosierung des Benzidins mit a) Natriumhypochlorit und b) mit Unterchloriger Säure ist auch im Falle eines Gemisches von Aminen zu empfehlen, da die quantitative Bestimmung des Benzidinsja in Gegenwart von Anilin, *o*-, *m*-, *p*-Toluidin und β-Naphthylamin, in den oben angegebenen Mengen, möglich ist. In diesen Fällen nimmt man für jede Probe 8ml Natriumhypochlorit beziehungsweise Unterchlorige Säure. Die Dosierung des Benzidins mit Natriumhypochlorit kann auch in Gegenwart von β-Naphthylamin erfolgen, während diese Dosierung mit Unterchloriger Säure nicht möglich ist.

EINFLUSS DER ZEIT

Die Farbenbeständigkeit der Verbindung die durch Oxidation des Benzidins durch Natriumhypochlorit und Unterchlorige Säure entstanden ist und nachträglich extrahiert wurde, hat man innerhalb 150 Minuten beobachtet, sowohl im Dunkeln, als auch bei Zimmerlicht, wobei gleichzeitig die Extinktion bei λ = 443nm gemessen wurde. Die Ergebnisse sind in Abb. 2 angeführt.

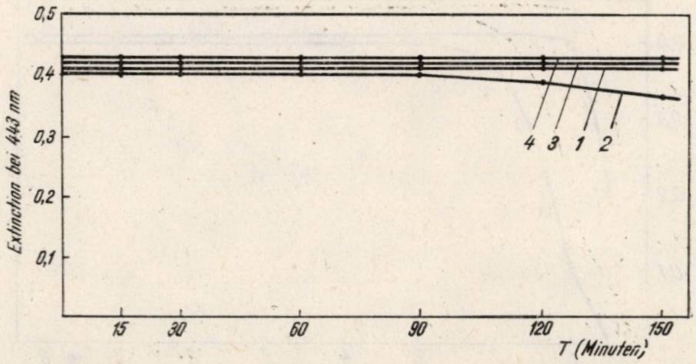

Abb. 2. — Die Farbenbeständigkeit der entstandenen und mit Chloroform extrahierten Verbindung, in Abhängigkeit von der Zeit.

1, 1ml c-Lösung + 10ml destilliertes Wasser + 3ml Natriumhypochlorit, im Dunkeln; *2*. 1ml c-Lösung + 10ml destilliertes Wasser + 3ml Natriumhypochlorit bei Zimmerlicht; *3*, 1ml c-Lösung + 10ml destilliertes Wasser + 4ml Unterchlorige Säure, im Dunkeln; *4*, 1ml c-Lösung + 10ml destilliertes Wasser + 4ml Unterchlorige Säure, bei Zimmerlicht.

Die in alkalischem Mittel gewonnene Verbindung ist 60 Min. lang lichtbeständig. Nach dieser Zeit fallen allmählich die Extinktionswerte. In den anderen drei Fällen (dieselbe Abbildung) bleibt die Extinktion während 150 Min. konstant.

EINFLUSS DER REAGENZIENKONZENTRATION

Die zugeführte Reagensmenge spielt bei den Bestimmungen eine bedeutende Rolle. Bei einer ungenügenden Quantität ist die Farbintensität der Verbindung keineswegs im Verhältnis zur Konzentration der Benzidinlösung. Somit sind die Ergebnisse falsch. In Abb. 3 trägt man die Extinktion der Verbindung bei λ = 443nm in bezug auf die ml-Anzahl der Reagenzien auf. Bei Benzidindosierungen mit a) Natriumhypochlorit ist die minimale Reagenzienquantität 3ml und mit b) Unterchloriger Säure 2ml.

DIE EICHKURVEN

In Abb. 4 sind die Eichkurven bei der Dosierung des Benzidins mit a) Natriumhypochlorit und b) mit Unterchloriger Säure dargestellt. Das Beersche Gesetz wird im Falle von Benzidinmengen zwischen 1,8—36,8 μg mit Natriumhypochlorit (*1*) und 1,8—55,2 μg mit Unterchloriger Säure (*2*) berücksichtigt.

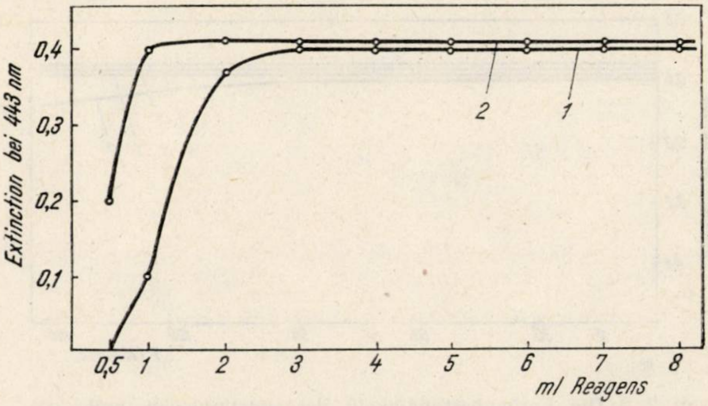

Abb. 3. — Die Extinktion der entstandenen und mit Chloroform extrahierten Verbindung, abhängig von der ml-Anzahl der hinzugefügten Reagenslösung.

1. 1ml c-Lösung + 10ml destilliertes Wasser + 1—8ml Natriumhypochlorit;
2. 1ml c-Lösung + 10ml destilliertes Wasser + 1 — 8ml Unterchlorige Säure.

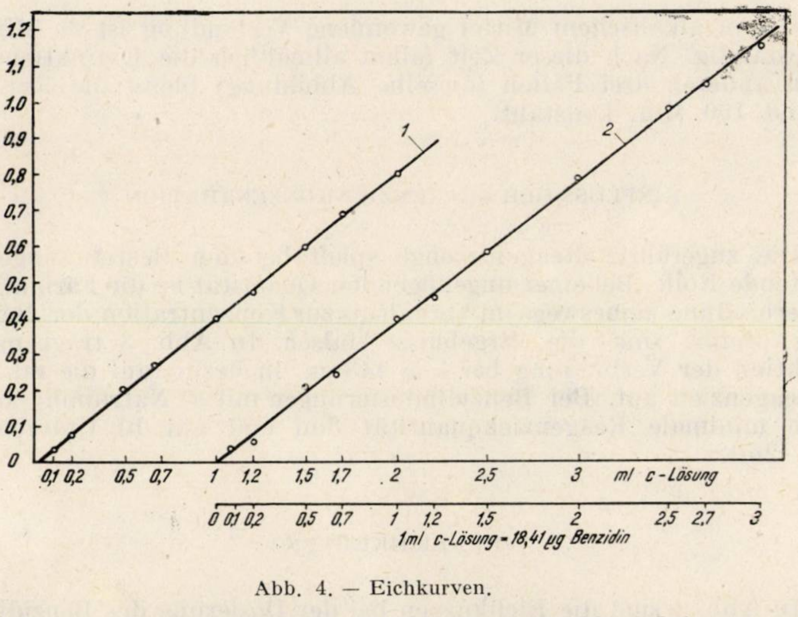

Abb. 4. — Eichkurven.

1. Proben von c-Lösung, jeweils mit 3ml Natriumhypochlorit behandelt; *2*. Proben von c-Lösung, jeweils mit 4ml Unterchloriger Säure behandelt.

Die Versuchsergebnisse sind in Tabelle 1—6 zusammengefaßt. In Tabelle 1 wurde eine wässerige Lösung verwendet, zu der verschiedene

Mengen Benzidin hinzugefügt wurden. In Tabelle 2 wurde Benzidin in Gegenwart von Anilin, in Tabelle 3—5 in Gegenwart von *o*-, *m*- bzw. *p*-Toluidin dosiert. In den Tabellen 1—5, Proben 1—5 wurde die Dosierung des Benzidins mit Natriumhypochlorit und in den Proben 6—10 mit Unterchloriger Säure durchgeführt. In Tabelle 6 wurde Benzidin mit Natriumhypochlorit in Gegenwart von bis zu 71 μg β-Naphthylamin dosiert. Toluidin und Dianisidin behindern die Dosierung.

Unter den in der Fachliteratur angeführten Dosierungsmethoden des Benzidins ist jene mit Chloramin T [18,19] am häufigsten verwendet, besonders aus den Abwässern. Im Verhältnis zu dieser Methode weist die jetzt beschriebene Methode folgende Vorteile auf : a) die bequeme Dosierung des Benzidins mit Natriumhypochlorit und Unterchloriger Säure infolge der relativ hohen Farbenbeständigkeit der Verbindung bei Lichteinwirkung. Die Chloramin T-Methode muß, hinsichtlich der

Tabelle 1

Spektrophotometrische Dosiernung des Benzidins, in einer wässerigen Lösung hinzugefügt

Lfd. Nr.	Verbrauchtes Benzidin c-Lösung in ml	Verbrauchtes Benzidin in μg	Beigefügtes Wasser in ml	E $d = 1$ cm	Gefundenes Benzidin in μg	E%
1	1,90	34,99	20,00	0,74	33,87	−3,20
2	1,40	25,77	25,00	0,55	25,40	−1,44
3	0,90	16,58	24,00	0,35	16,19	−2,35
4	0,40	7,36	21,00	0,16	7,45	+2,40
5	0,20	3,68	23,00	0,08	3,68	0,00
6	2,80	51,56	20,00	1,07	50,82	−1,44
7	2,20	40,52	22,00	0,81	39,57	−2,44
8	1,60	29,45	25,00	0,62	29,82	+1,30
9	0,80	14,72	21,00	0,30	14,35	−2,52
10	0,30	5,25	25,00	0,11	5,34	−3,26

Tabelle 2

Spektrophotometrische Dosierung des Benzidins in Gegenwart von Anilin

Lfd. Nr.	Verbrauchtes Benzidin c-Lösung in ml	Verbrauchtes Benzidin in μg	Verbrauchtes Anilin in μg	Beigefügtes Wasser in ml	E $d=1$ cm	Gefundenes Benzidin in μg	E%
1	2,00	36,84	93,06	25,00	0,78	36,09	−2,04
2	1,70	31,29	65,15	24,00	0,68	31,66	+1,20
3	0,80	14,72	37,22	23,00	0,35	15,09	+2,50
4	0,60	11,04	9,30	22,00	0,23	10,67	−3,35
5	0,10	1,84	74,45	21,00	0,04	1,84	0,00
6	2,90	53,42	18,61	20,00	1,09	52,30	−2,10
7	2,30	42,36	55,84	21,00	0,90	42,92	+1,40
8	1,70	31,29	27,92	22,00	0,63	30,37	−2,94
9	0,70	12,88	46,53	24,00	0,26	12,59	−3,25
10	0,20	3,68	83,75	25,00	0,07	3,50	−4,89

Tabelle 3

Spektrophotometrische Dosierung des Benzidins in Gegenwart von *o*-Toluidin

Lfd. Nr.	Verbrauchtes Benzidin c-Lösung in ml	Verbrauchtes Benzidin in µg	Verbrauchtes *o*-Toluidin in µg	Beigefügtes Wasser in ml	*E* *d* = 1 cm	Gefundenes Benzidin in µg	*E* %
1	2,00	36,84	64,73	20,00	0,78	35,91	−2,32
2	1,50	27,61	86,30	21,00	0,61	28,16	+2,00
3	1,10	20,25	32,34	22,00	0,43	19,88	−1,83
4	0,50	9,20	107,88	23,00	0,18	8,83	−4,11
5	0,30	5,52	10,79	24,00	0,11	5,34	−3,26
6	3,00	55,23	43,15	25,00	1,13	53,97	−2,28
7	2,40	44,20	75,52	24,00	0,94	44,94	+1,70
8	1,80	33,13	97,09	23,00	0,68	32,39	−2,23
9	1,00	18,41	21,58	22,00	0,37	17,87	−4,07
10	0,30	5,52	53,94	20,00	0,11	5,34	−3,26

Tabelle 4

Spektrophotometrische Dosierung des Benzidins in Gegenwart von *m*-Toluidin

Lfd. Nr.	Verbrauchtes Benzidin c-Lösung in ml	Verbrauchtes Benzidin in µg	Verbrauchtes *m*-Toluidin in µg	Beigefügtes Wasser in ml	*E* *d* = 1 cm	Gefundenes Benzidin in µg	*E* %
1	1,70	31,29	32,34	20,00	0,66	30,55	−2,35
2	1,00	18,41	107,88	22,00	0,40	18,59	+2,90
3	0,90	16,58	10,79	24,00	0,35	16,19	−2,35
4	0,60	11,04	43,15	21,00	0,23	10,67	−3,55
5	0,30	5,52	75,52	25,00	0,12	5,69	+3,10
6	2,60	47,88	97,09	23,00	0,98	46,78	−3,30
7	2,10	38,68	21,58	20,00	0,82	39,42	+1,90
8	1,30	23,93	53,94	22,00	0,49	23,56	−1,55
9	0,70	12,88	64,73	23,00	0,26	12,51	−2,87
10	0,40	7,36	86,30	21,00	0,15	7,18	−2,45

Tabelle 5

Spektrophotometrische Dosierung des Benzidins in Gegenwart von *p*-Toluidin

Lfd. Nr.	Verbrauchtes Benzidin c-Lösung in ml	Verbrauchtes Benzidin in µg	Verbrauchtes *p*-Toluidin in µg	Beigefügtes Wasser in ml	*E* *d* = 1 cm	Gefundenes Benzidin in µg	*E* %
1	1,80	33,13	10,79	20,00	0,70	32,55	−1,75
2	1,20	22,09	43,15	21,00	0,47	21,72	−1,68
3	0,80	14,72	75,52	22,00	0,32	14,90	+1,20
4	0,50	9,20	97,09	23,00	0,19	8,33	−4,02
5	0,20	3,68	21,58	24,00	0,075	3,50	−4,89
6	2,70	49,72	53,94	25,00	1,02	48,61	−2,21
7	2,20	40,52	64,73	24,00	0,83	39,78	−1,83
8	1,40	25,77	86,30	23,00	0,53	25,22	−2,13
9	1,10	20,25	32,34	22,00	0,43	20,62	+1,80
10	0,40	7,36	107,88	21,00	0,15	7,18	−2,45

Tabelle 6

Spektrophotometrische Dosierung des Benzidins in Gegenwart von β-Naphthylamin

Lfd. Nr.	Verbrauchtes Benzidin c-Lösung in ml	Verbrauchtes Benzidin in μg	Verbrauchtes β-Naphthylamin in μg	Beigefügtes Wasser in ml	E $d = 1$ cm	Gefundenes Benzidin in μg	E %
1	1,90	34,99	42,92	20,00	0,75	34,79	−0,43
2	1,60	29,45	14,31	22,00	0,63	29,08	−1,26
3	0,90	16,58	71,54	25,00	0,35	16,19	−2,35
4	0,60	11,04	28,62	24,00	0,23	10,67	−3,35
5	0,20	3,68	57,23	21,00	0,075	3,50	−4,89

schwachen Lichtbeständigkeit, in rascher Zeit und bei diffusem, schwachem Licht vorgenommen werden, oder man vergleicht die zu analysierende Probe mit einer Standardlösung von Kaliumdichromat; b) die Dosierung von Benzidin, sowohl in saurem, als auch in basischem Mittel, ohne besondere Vorsichtsmaßnahmen hinsichtlich der pH-Werte, wie im Falle des Chloramins T.

Aus dem Absorptionsspektrum der entstandenen Verbindung folgt, daß das ClO^--Ion das Benzidin zur selben Verbindung oxydiert, sei es in basischem oder in saurem Mittel.

Revue Roumaine de Chimie, **17**, 5, 925 – 930 (1972)

DETERMINATION OF THE PARTITION CONSTANT OF COMPOUNDS USED IN SPECTROPHOTOMETRIC ANALYSIS

V. ARMEANU, STELA OANCEA, STANA RUSENESCU and L. M. BĂLOIU

Department of Chemistry and Physics, Academy of Economic Studies
Bucharest, Romania

Received August 19, 1971

A new method is established for the determination of the partition constant of compounds of (dyestuff)$^+$ $[ML_n]^-$type, used in spectrophotometric analysis. The method allows the determination of the partition constant and of the molar absorbance coefficient of the compound dissolved in the organic solvent. The method consists of two successive extractions, whose absorbances are recorded. If the partition constant is high, several solvents are used, the true value of the partition constant being computed from the slopes of Lambert-Beer diagrams obtained with each solvent.

I. INTRODUCTION

There are several spectrophotometric methods used for the determination of metal ions, based on the extraction of a coloured compound in an organic phase.

The partition constant, defined[1] as :

$$P = \frac{[\text{compound}]_o}{[\text{compound}]_w} \tag{1}$$

is an important parameter of such systems. But, as far as we know, very few methods are applied for its determination.

For the systems consisting of a complex anion $[ML_n]^-$ and an organic basic dyestuff cation, D^+, only two spectrophotometric methods are found in the literature.

One of the methods[2,3] uses "interchange extraction", which consists of several extractions and reextractions by means of two separatory funnels, combined with a special way of mixing aliquots from the two aqueous phases.

---

[1] IUPAC, *Information Bulletin*, **26**, 31 (August 1966).

[2] C. Golumbic and S. Weller, *Anal. Chem.*, **22**, 1418 (1950).

[3] H. Irving and C. F. Bell, *J. Chem. Soc.*, **1952**, 1216.

The method is very laborious and due to the large number of operations requested, susceptible of considerable experimental errors.

The second method consists of several successive extractions, until all the compound is extracted.[4]

The partition constant is :

$$P = \frac{A_1}{A_2 + A_3 + A_4 \ldots + A_n} \tag{2}$$

where A_i is the absorbance of the i-th extraction step. The method supposes correct linearity of the diagram $A = f\,(C'_w)$ at its lower limit, which does not generally happen.

In this paper we are presenting a new method.

II. THE METHOD OF DOUBLE EXTRACTION

We shall assume :

— that the equilibrium :

$$M^{m+} + {}_nL^{p-} \rightleftharpoons [ML_n]^{(m-np)} \tag{a}$$

(supposing that $m-np = -1$), is totally shifted to the right, so that all metal ions are complexed ; this condition is accomplished either by means of a large amount of L^{p-}, or using complexes with high stability constants,

— that only the compound $D\,[ML_n]$ is soluble in the organic phase. Frequently, the free acid, $H_p\,L$ extracts itself also, but this fact does not interfere with our equilibria. We suppose that, extracted in the organic layer, the acid does not absorb light ; if it did, this can be avoided using a blank prepared by extracting H_pL from an aqueous solution of the same pH and containing the same L^{p-} concentration as our samples,

— that the volume of the organic solvent is equal to the volume of water,

— that the partition constant does not depend on the concentration,

— that the equilibrium :

$$[ML_n]^- + D^+ \rightleftharpoons D\,[ML_n] \tag{b}$$

is totally shifted to the right, due to a large excess of dyestuff, and to a suitable value of pH.

According to Lambert-Beer law, the absorbance of the organic phase, after extraction, will be :

$$A_1 = kdC_o = kdRC'_w \tag{3}$$

where k is the molar absorbance coefficient of the compound in the organic phase ; d is the length of the cell ; C_o is the concentration of the compound in the organic phase ; C'_w is the concentration of the compound in the aqueous phase, before extraction ; R is the recovery factor, defined as :

---

[4] V. Armeanu and P. Costinescu, *Talanta*, **14**, 669 (1967).

$$R = \frac{C_o}{C'_w} = \frac{P}{P+1} \tag{4}$$

After the extraction, the concentration of the compound in th aqueous phase is :

$$C_w = C'_w - C_o = C'_w(1 - R) \tag{5}$$

If a new extraction is made, the absorbance of the organic phase will be :

$$A_2 = kdC'_o \tag{6}$$

The partition constants, for the two extractions, are :

$$P_1 = \frac{C_o}{C_w} = \frac{C_o}{C'_w - C_o} \tag{7}$$

$$P_2 = \frac{C'_o}{C_w - C'_o} = \frac{C'_o}{C'_w - C_o - C'_o} \tag{8}$$

Equaling (7) to (8), we obtain :

$$P = \frac{C_o}{C'_w - C_o} = \frac{C'_o}{C'_w - C_o - C'_o} = \frac{C_o - C'_o}{C'_o} \tag{9}$$

Replacing in eq. (9), C_o and C'_o by their expressions from (3) and (6) :

$$P = \frac{A_1 - A_2}{A_2} \tag{10}$$

The partition constant can be determined by measuring the absorbance of two successive extractions. But the value we found is correct only if the Lambert-Beer law is obeyed in the whole concentration range between C'_w and C_w that is larger as P is bigger.

Usually the diagram $A = f(C'_w)$ has not a good linearity for such systems (Fig. 1[5]). The curve is S-like, as the equilibrium (b) is not totally shifted to the right, due to the ionic character of the bond $[ML_n]^- - D^+$, that leads to small stability constants.

---

[5] V. Armeanu, S. Oancea, S. Rusenescu and L. M. Băloiu, unpublished.

Equation (3) can be written as .

$$R = \frac{1}{kd}\frac{A}{C'_w} = \frac{1}{kd}\,\mathrm{tg}\,\alpha \tag{11}$$

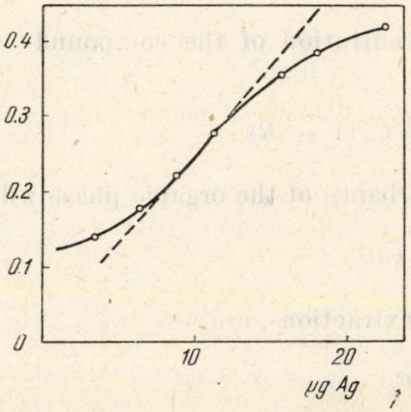

Fig. 1. – Plotting $A = f(C'_w)$ for the system $[Ag(CN)_2]$-Astraviolett 3R.

where α is the angle made by the linear part of the plot $A = f(C'_w)$ with the abscissa.

When several solvents are used ;

$$\frac{R_1}{\mathrm{tg}\,\alpha_1} = \frac{R_2}{\mathrm{tg}\,\alpha_2} \ldots\ldots = \frac{R_n}{\mathrm{tg}\,\alpha_n} = \frac{1}{kd} = \text{constant} \tag{12}$$

for solvents having close polarities, so that the absorbance spectra of the compound dissolved in each solvent are identical, i.e. $k_1 = k_2 = \ldots = k_n$.

The plotting $R = f(\mathrm{tg}\,\alpha)$ will be a straight line, passing through the origin.

If our first solvent is a "too good" extractor, so that the C_w left after the first extraction is no more in the linear part of the plot $A = f(C'_w)$ another solvent has to be used. The new solvent can be obtained by diluting the first with another one, with a close polarity, and that does not extract.

With the new solvent, equation (10) becomes valid. Plotting a diagram $A' = f(C'_w)$, we obtain α' and :

$$R = R'\frac{\mathrm{tg}\,\alpha}{\mathrm{tg}\,\alpha'} \tag{13}$$

Extrapolating the plotting of the diagram $R = f(\mathrm{tg}\alpha)$ to $R = 1$, we find the slope of the diagram $A = F(C'_w)$ for an ideal solvent, which could extract all the compound.

Equation (11) allows also the determination of the molar absorbance coefficient :

$$k_0 = \frac{1}{d} \frac{A}{RC'_w} \tag{14}$$

III. APPLICATION OF THE METHOD

The theoretical approach presented above was verified by the application to a definite system, $[Au(CN)_2]^-$ — Astraviolett 3R. Astraviolett 3R is 1-methyl-2-(*p*-diethylaminostyrene)-3,3′-dimethyl-indole chloride. The dyestuff was purified by recrystallization and its final purity checked with the $TiCl_3$ method.[6] All other reagents were analytical reagent grade.

All measurements were made at (room temperature) 25°.

The system shows no change over a pH range from 2.4—11. All determinations were carried out at pH = 6.

The spectrophotometric method for the determination of gold with Astraviolett uses benzene as solvent.[7] But benzene is too good an extractor for our purposes. The second absorbance is very low. Therefore we used mixtures consisting of benzene and n-hexane or toluene and n-hexane. The spectra of the compound in all solvents are identical (fig. 2); n-hexane itself does not extract the compound.

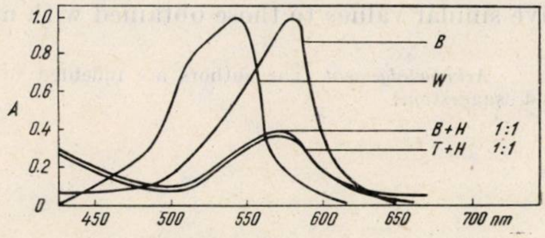

Fig. 2.—Spectra of the compound (Astraviolett 3R) $[Au(CN)_2]$ dissolved in different solvents.

The experimental results are given in Tables 1—3

Table 1

Results of the experimental measurements

Solvent	*P*	*R*	tg α (μg Au/ absorbance)
Benzene	—	—	0.235
B + H (2 : 1)	2.00	0.666	0.160
Toluene	4.15	0.806	0.200
T + H (1 : 1)	0.31	0.236	0.046

---

[6] H. E. Fierz-David and L. Blangley, "Grundlegende Operationen der Farbenchemie", Springer Verlag, Wien, 1952, p. 384.

[7] V. Armeanu and L. M. Băloiu, *Analyt. Chim. Acta*, **44**, 230 (1969).

Table 2

Determination of R_{benzene}

Solvent	R'	$\text{tg}\alpha'$	R
Toluene	0.806	0.200	0.95
$T + H$ (1 : 1)	0.236	0.046	0.99
$B + H$ (2 : 1)	0.666	0.160	0.98
average value			0.97

Table 3

Determination of the molar absorbance coefficient

Solvent	$\frac{A}{\alpha}$	R	k
Benzene	0.46	0.97	4.8×10^4
Toluene	0.39	0.806	4.8×10^4
$B + H$ (2 : 1)	0.32	0.666	4.8×10^4
$T + H$ (1 : 1)	0.09	0.236	3.9×10^4
Average value			4.6×10^4

The value found for k does not correspond to the absorbance maximum of the compound in benzene, but to 528 nm. For our compound, the measurements carried out with the VG — 9 filter of a Lange colorimeter give similar values to those obtained with monochromatic light of 528nm.

Acknowledgement. The authors are indebted to the Referee, for useful observations and suggestions.

Revue Roumaine de Chimie, **17**, 5, 931−936 (1972)

THE SOLVENT EFFECT ON UV SPECTRA OF SOME AMINOPYRIDINE DERIVATIVES

VIORICA PELLONI-TAMAŞ, NORA RĂDULESCU and ROCSANDRA SIMIONOVICI

Chemical and Pharmaceutical-Research Institute
Şos. Vitan 112, Bucharest, Romania

Received August 2, 1971

The UV spectra of certain aminopyridine derivatives have been investigated in different solvents with various solvation power. The solvent shifts observed in the investigated compounds were found to be in good correlation with *Z* value proposed by Kosower for measuring solvent polarity and also with *S* parameter which is a solvent characteristic in Brownstein's equation.

In the absence of certain chemical interactions the changes observed in UV spectra of organic compounds under the solvent influence i.e. solvent shifts and variation of extinctions, are due to solvation. This is the reason why these changes are in good correlation with those properties of the solvent that are able to express its solvation power or with other phenomena brought about by solvation. In this connection correlations have been established between solvent shifts and *Y* parameter in Swain-Winstein's equation,[1] or *S* parameter, a solvent characteristic in Brownstein's equation.[2] The solvent shifts can also be correlated with the reactivity of organic compounds in some reactions influenced by the solvent.[3]

Though some spectral data regarding aminopyridine derivatives did exist before [4] systematic spectral investigations of these compounds have been developed only recently.[5]

In our work UV spectra of 2-aminopyridine, 2-amino-6-methylpyridine, 2-formylamino-6-methylpyridine, and N′-(6-methylpyridyl-2)-N,N-dimethylaminoformamidine have been determined in eight different solvents. The observed solvent shifts have been correlated with the solvent's properties that are able to express its solvation power.

---

[1]a E. M. Kosower, *J. Amer. Chem. Soc.*, **80**, 3261 (1958) ; b. *Idem, J. Amer. Chem. Soc.* **80** 3267 (1958).

[2] S. Brownstein, *Canad. J. Chem.*, **38** 1590 (1960).

[3]a A. J. Parker and D. Brody, *J. Chem. Soc.*, **1963**, 4061 ; b. *Idem, Quart. Rev.*, **16**, 163 (1962).

[4]a P. Grammaticakis, *Bull. Soc. chim. France*, **1959**, 480 ; b.S.F. Mason, *J. Chem. Soc.*, **1960**, 219 ; c. J. Essery and K. Schofield, *J. Chem. Soc.*, **1961**, 3939.

[5] C. W. N. Cumper and A. Singleton, *J. Chem. Soc.* (*B*), **1968**, 649.

EXPERIMENTAL

Aminopyridine derivatives *. 2-Aminopyridine and 2-amino-6-methylpyridine were obtained by amination of pyridine and α-picoline with sodium amide in an inert solvent using a convenient method established in our laboratory. The compounds were fractionated twice and obtained in a high purity grade: 2-aminopyridine b.p. 104–106°/20–22 mm; m.p. 57–58°; t.l.c. on H active kieselgel in acetone : water system 45 : 5, $R_f = 0.7$ identification by iodine vapours – only one spot; 2-amino-6-methylpyridine, b.p. 98–100°/10–11 mm; m.p. 40–41°; t.l.c. on H active kieselgel in ethylacetate : methanol : acetic acid system 65 : 30 : 5, $R_f = 0.20$ identification by iodine vapours – only one spot; 2-formylamino-6-methylpyridine was prepared using a method described in the literature.[6] The compound was fractionated twice, b.p. 158–159°/10 mm; m.p. 78–79°; t.l.c. on H active kieselgel in dioxane : water system 40 : 10, $R_f = 0.7$ identification by iodine vapours – only one spot; N′-(6-methylpyridyl-2)-N,N-dimethylaminoformamidine was prepared by reaction of 2-amino-6-methylpyridine with Vilsmeyer-Haack reactive dimethylformamide $POCl_3$, using a convenient method established in our laboratory. The compound was fractionated twice, b. p. 118–119°/5 mm; t. l. c. on H active kieselgel in acetone :water system 45: 5, $R_f = 0.4$, identification by iodine vapours-only one spot.

Solvents. Benzene (Uvasol Merck) and *n*-hexane (Carlo Erba for spectroscopy) were dried over sodium wire and used without further purification. Absolute ethanol (reactive grade) was dried with magnesium and fractionated. Ethylether (reactive grade) was dried over sodium wire. 1,4-Dioxane and carbon tetrachloride (Uvasol Merck) were used without further purification. Dimethylsulphoxide (U. C. B. for analysis) was fractionated b. p. 84°/16 mm.

Spectroscopic measurements. UV spectra of the investigated compounds were determined using a UVS0 4 spectrophotometer, in quartz absorption cells of 1.00 cm length. The error of the instrument was ± 0.5 nm in the wavelength interval of 250–320 nm. Concentrations of about 10 γ/ml aminoderivatives were used. The Lambert-Beer law was obeyed by the studied compounds in the concentration range used.

DISCUSSION

The characteristic bands of $\pi\rightarrow\pi^*$ transition in monocyclic-aminoazine were interpreted by Mason[4b] using a benzyl anion model. The bands were grouped in three main types : α, p, β (following the increasing value of λ_{max})[7] similar to Clar's classification of aromatic compounds UV spectra.[8]

The present work discusses the α bands of $\pi\rightarrow\pi^*$ transitions in aminopyridines observed in the 250–320 nm region.

Table 1 presents the wavelength (λ_{max}) and extinction coefficient (ε) of the absorption maxima in different solvents for the investigated compounds.

---

* The aminopyridine derivatives were prepared and purified by Veronica Badea, Elena Bădic and Nora Rădulescu.

[6] A. E. Cicibabin, *Ber. dtsch. chem. Ges.*, **64**, 284 (1931).

[7] A. R. Katritzky, "Physical Methods in Heterocyclic Chemistry", vol. II. Acad. Press, New York, 1963, p. 35.

[8] E. Clar, "Aromatische Kohlenwasserstoffe", 2nd ed. Springer, Berlin, 1952.

In 2-aminopyridine, 2-amino-6-methylpyridine and N′-(6-methylpyridyl-2)-N,N-dimethylaminoformamidine, bathochromic shifts were observed in the range of the investigated solvents from water to dimethylsulphoxide.

Table 1

Absorption maxima and molar extinction coefficients

Compound / Solvent	2-Aminopyridine		2-Amino-6-methylpyridine		2-Formylamino-6-methylpyridine		N′-(6-Methylpyridyl-2)-N,N-dimethylaminoformamidine	
	λ max. (nm)	ε	λ max. (nm)	ε	λ max. (nm)	ε	λ max (nm)	ε
Water	287	3800	287	5300	280	7200	285	9200
n-Hexane	290	3600	291	5400	280	7100	300	9850
Benzene	290	3550	291	5300	280	5400	300	10700
Ethanol	295	3950	297	5000	280	5600	305	10000
Ethyl ether	296	3550	297	5300	280	7100	310	12300
1,4-Dioxane	296	3700	297.5	5200	280	7800	313	10700
Carbon tetrachloride	300	3750	298	4800	280	6000	315	7500
Dimetylsulphoxide	300	3800	300	4800	285	9200	315	9500

The different solvation degrees of the ground and excited state determines the differences in transition energy from one solvent to another.

In aminopyridine derivatives Pimentel[9] considered that in the excited state the amino group has a reduced electronic density as compared to the ground state. Thus, in solvents i.e. water, able of hydrogen bonds with aminoderivatives, where nitrogen is the electron donating atom (formula I), the transition energy is larger because the excited state is less solvated than the ground state. In solvents, i.e. 1,4-dioxane, ether, that solvate the aminoderivative through hydrogen bonds where the amino group supplies the hydrogen atom (formula II), the transition energy is smaller because the excited state is more solvated than the ground state.[5]

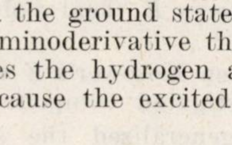

I

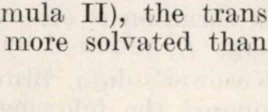

II

---

[9] G. C. Pimentel, *J. Amer. Soc.*, **79**, 3323 (1957).

Solvents having small polarity and unable of hydrogen bonds i.e. n-hexane, benzene, required transition energy of intermediate value.

Aprotic and aprotic dipolar solvents solvated more strongly the excited state, poorer in electrons, than the ground state bringing thus about reduced transition energies, and absorptions at high wavelengths.

These phenomena could explain the increase in λ_{max} values shown in table 1 in the range : water, n-hexane, 1,4-dioxane, dimethylsulphoxide for 2-aminopyridine, 2-amino-6-methylpyridine, and N′-(6-methylpyridyl-2)-N,N-dimethylaminoformamidine.

Table 1 also points out that in 2-formylamino-6-methylpyridine the λ_{max} is very little influenced by the nature of the solvent, (λ_{max} is 280 nm in seven different solvents). This molecule is likely to have a small ability to be solvated because its nonbonding electrons of the nitrogen atom are conjugated with π electrons of the C=0 double bond.

The solvent shifts are due to solvation. They are in good correlation with other solvent properties that would be able to express their solvation power. But such properties are difficultly found because the solvation process is a complex one involving both the solvent and the solute molecule.[10] The dielectric constant and the refractive index cannot be well correlated with solvent shifts because they are a macroscopic measure of the solvent response to an electric field, whereas the solvent shift is the result of the solvent-solute microscopic interaction.

Kosower studied the position of the charge transfer absorption band of 1-alkylpyridinium iodides in different solvents and proposed a new empirical measure for solvent polarity, the Z value calculated from the UV spectra,[1] Z expressed in kcal/mol represents the transition energy required by the charge transfer transition in 1-ethyl-4-carbomethoxipyridinium iodide. It is correlated to the position of the band by the relation $Z = h.\nu$. The solvent polarity expressed by Z is a measure of the solvent-solute interaction at the microscopic level. Kosower[1] established that Z is in good correlation with Winstein's values for Y parameter (a kinetic measure of ionizing power of the solvent[11]) and also with the transition energy E_T of various compounds in the coresponding solvents.

Figure 1 represents Z *vs.* transition energy E_T (kcal/mol) of the investigated aminopyridines.

A linear variation is observed between Kosower's Z value and the transition energy E_T required by the investigated compounds.

Using Kosower's data, Brownstein[2] generalized the solvent influence and proposed the folowing equation, to express the correlation between the modifications caused by the solvent and the properties of the investigated system :

$$\log\left(\frac{k_{\text{solv}}}{k_{\text{EtOH}}}\right) = SR$$

---

[10] N. Rădulescu, *Rev. Chim.* (*București*), **21**, 269 (1970).

[11]a. E. Grunwald and S. Winstein, *J. Amer. Chem. Soc.*, **70**, 846 (1948) ; b. S. Winstein, E. Grunwald and H. W. Jones, *J. Amer. Chem. Soc.* **73** 2700 (1951) ; c. A. H. Fainberg and S. Winstein, *J. Amer. Chem. Soc.*, **78**, 2770 (1956).

where : k may be rate constant, equilibria constant or a function of spectral shifts ;
S is a solvent characteristic constant in correlation to its polarity ;
R is a constant which expresses sensitivity of the system to the change of solvent polarity.

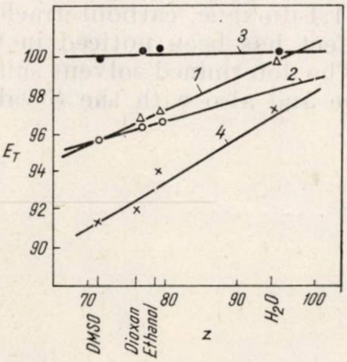

Fig. 1. — Z. values *vs.* transition energy E_T (kcal/mol) for 2-aminopyridine (1), 2-amino-6-methylpyridine (2), 2-formylamino-6-methylpyridine (3), and N′-(6-methylpyridyl-2)-N,N-dimethylaminoformamidine (4).

Using Brownstein's S values for the different solvents and the experimentally determined $\lambda_{\max}$ values (table 1), the R values were calculated for $\pi \rightarrow \pi^*$ transitions in aminopyridines by means of the formula :

$$R = \frac{\tilde{\nu}_{\max\ \mathrm{solv}} - \tilde{\nu}_{\max\ \mathrm{EtOH}}}{S \cdot \tilde{\nu}_{\max\ \mathrm{EtOH}}}$$

where : $\tilde{\nu}_{\max\ \mathrm{EtOH}}$, $\nu_{\max\ \mathrm{solv}}$ are the maximum wave numbers of aminopyridine derivatives in ethanol respectively in any solvent of a known S value.

Table 2 represents the R mean values for $\pi \rightarrow \pi^*$ transitions in the range of the investigated compounds.

Table 2

R values calculated by Brownstein's equation

Compound	R
2-Aminopyridine	0.114
2-Amino-6-methylpyridine	0.0967
2-Formylamino-6-methylpyridine	0.0
N′-(6-Methylpyridyl-2) N,N-dimethylaminoformamidine	0,17

In the investigated compounds the sensitivity of $\pi \rightarrow \pi^*$ transitions to the changes of solvent polarity diminishes as follows : N′-(6-methylpyridyl-2)-N,N-dimethylaminoformamidine > 2-aminopyridine > 2-amino-6-methylpyridine > 2-formyl-amino-6-methylpiridine.

CONCLUSIONS

The position of the characteristic bands of $\pi \rightarrow \pi^*$ transition in aminopyridine derivatives is influenced by the nature of the solvent used.

In the range of solvents : water, n-hexane, benzene, ethanol, ethyl ether, 1,4-dioxane, carbontetrachloride, dimethylsulphoxide, a bathochromic effect has been noticed in the investigated aminopyridines.

The determined solvent shifts are in good correlation with Kosower's Z value and also with the S value in Brownstein's equation.

Revue Roumaine de Chimie, 17, 5, 937–944 (1972)

RECHERCHES SUR L'OBTENTION DU HAFNIUM DE PURETÉ NUCLÉAIRE. I

LUCREȚIA I. POPA et IOANA ARSENIE

Institut de Physique Atomique, B. P. 35, Bucarest, Roumanie

Reçu le 11 mai 1971

Les auteurs exposent les recherches effectuées pour la séparation du hafnium par résine échangeuse d'anions, dans un milieu de sulfate. Le travail est divisé en cinq parties : I. Introduction. II. Données sur l'obtention du hafnium. III. Données expérimentales. IV. Coefficients de partage. V. Discussions. VI.Conclusions.

I. INTRODUCTION

Les recherches pour la séparation du zirconium de son homologue naturel, le hafnium, ont été effectuées jusqu'en 1950 seulement dans des buts scientifiques.[1]

Ce n'est qu'à partir de cette date que l'obtention du zirconium et du hafnium devint une nécessité, imposée par le développement rapide de l'énergétique nucléaire.

L'intérêt suscité par ces métaux (et alliages) s'explique par leurs qualités remarquables telles que : résistance mécanique supérieure, point de fusion élevé, grande résistance à la corrosion, bon transport colorique, etc.

Étant donné le comportement différent de ces métaux envers les neutrons (le zirconium est transparent, $\sigma = 0{,}18 \pm 0{,}05$ barns, tandis que le hafnium est absorbant, $\sigma = 105 \pm 5$ barns), dans le réacteur on emploie le zirconium comme matériau structurel (pour le cœur du réacteur, les gaines de combustible, l'armature etc.), et le hafnium pour les barres de contrôle et réglage.

II. QUELQUES DONNÉES SUR L'OBTENTION DU HAFNIUM DE PURETÉ NUCLÉAIRE

On a obtenu simultanément du zirconium et du hafnium, de pureté nucléaire, par une des méthodes suivantes :

- extraction par solvants organiques,
- distillation fractionnée,
- échange d'ions,
- chromatographie.[2,3]

---

[1] P. Pascale, « Nouveau traité de Chimie Minérale », vol. 9, Masson et Cie, Paris. 1963 p. 771–900.

[2] James S. Fritz et Russell T. Frazee, *Analyt Chem.*, 11, 1358 (1965).

[3] C. Poitrenaud, *Chem. Analyt.*, **1**, 39 (1970).

Les méthodes de l'échange d'ions sont employées avec de bons résultats pour la séparation du zirconium et du hafnium. A ce propos nous mentionnons tant la séparation par cations [4-8] que par anions [9-12], qui permettent d'obtenir une quantité de zirconium et de hafnium, allant de quelques grammes jusqu'à 1 kilogramme.

Le présent travail expose les possibilités d'obtenir le hafnium nucléaire par échange d'ions.

III. DONNÉES EXPÉRIMENTALES

L'obtention du hafnium dans les solutions de sulfate de zirconium par les résines anioniques (type Dovex 3 et la résine roumaine Vionit AT 1) est réalisée par les groupes d'expériences ci-dessous :

— la séparation de la mixture de hafnium spectral et de zirconium nucléaire ;

— l'obtention du hafnium en solutions de sulfate de zirconium (avec différentes concentrations en zirconium) ; les solutions de zirconium résultant du traitement du zircon.

Ce groupe d'expériences a été effectué sur la résine roumaine Vionit AT 1.

Le troisième groupe d'expérience pour l'obtention du hafnium dans un milieu de sulfate a porté sur la résine de type Dowex 3.

III.1. FORME DE LA RÉSINE ET DES SOLUTIONS

La résine anionique Vionit AT 1 (la forme styrène, capacité 0,4—0,6 méquiv/ml, granulation 0,3 mm) comme la résine Dowex (capacité d'échange 2,5 mval/ml, granulation 0,3 mm) ont été amenées à la forme bisulfate, $RHSO_4^-$, par lavages répétés avec de l'acide sulfurique 1,4 N et 5 N. La résine a été préparée au préalable avec une attention toute spéciale (lavages répétées à l'eau déionisée, décantation des portions fines, lavages au sodium hydroxyde 1 N, à l'acide chlorhydrique 1 M et à l'eau pour neutraliser la résine, etc.).

III.2. CONCENTRATION DES SOLUTIONS

On a utilisé des solutions de zirconium (Hf) récemment préparées (pour éviter l'hydratation du zirconium) de concentration : 0,04 M Zr et 0,16 M Zr, marquées, par ^{95}Zr et ^{181}Hf ainsi que du mélange de sulfate de zirconium nucléaire de concentration $2{,}05 \times 10^{-4}$ M ^{95}Zr et de hafnium spectral de concentration $3{,}07 \times 10^{-5}$M^{181} Hf.

L'élution a été réalisée par acide sulfurique : 1,4 N, 5 N et 10 N.

---

[4] K. Street et Jr. G. T. Seaborg, *J. Amer. Chem. Soc.*, **70**., 4268 (1948).

[5] I. E. Newnham, *J. Chem. Amer. Scoc.* **73**, 5899 (1951).

[6] B. A. J. Lister, *J. Chem. Soc.*, **1951** 3123.

[7] J.T. Benedict, W. C. Schumb et Ch. D. Coryell, *J. Amer. Chem. Soc.*, **73**, 2036 (1954).

[8] Moshin Qureshi et Khadim Husain, *Analyt. Chem.*, **3**, 447 (1971).

[9] E. M. Larsen et P. Wang, *J. Amer. Chem. Soc.*, **76**, 6323 (1954.

[10] W. E. Brown et W. Riemann, *J. Amer. Chem. Soc.*, **74**, 1278 (1952).

[11] K. S. Rajan et J. Gupta, *J. Sci. Ind. Res. India*, **16**, 459 (1957).

[12] B. Tremillon, C. Cornet, M. Thiboult et J. Huré, *Bull. Soc. Chim. France*, 286 (1961).

III.3. FIXATION SUR RÉSINE

Le zirconium et le hafnium se trouvent sous forme de complexes, $Zr\,(SO_4)_3^{2-}$ et $Hf(SO_4)_3^{2-}$, formes signalées par Connick et Mc Vey[13]

$$Zr\,(SO_4)_2 + H_2SO_4 \rightleftarrows Zr\,(SO_4)_{3(S)}^{2-} + 2H^+ \quad (K = 1)$$

La solution de sulfate de zirconium $(Zr(SO_4)_{3(S)}^{2-})$ est amenée sur la résine sous forme de bisulfate $(HSO_4^{2-}\ R)$. L'échange d'anions de la résine contre ceux de la solution a lieu sous forme de bisulfate, conformément à équilibre du type :

$$2HSO_{4(R)}^{-} + Zr\,(SO_4)_{3\,(S)}^{2-} \rightleftarrows Zr(SO_4)_3^{2}\,(R) + 2(HSO_4^{-})_{(S)}$$

III.4. ANALYSES

Le contenu global de zirconium et de hafnium a été déterminé chimiquement (gravimétriquement).

La teneur en hafnium (dans les épreuves séparées de zirconium, amenées à l'oxyde) a été déterminée par radioactivation.[14,15] Les mesurages ont été effectués à l'aide d'un analyseur d'amplitude à 4096 canaux, de type MB, à détecteur de Ge (Li). L'activité des épreuves dans l'élution marquées par ^{95}Zr et ^{181}Hf a été mesurée à l'aide du scintillateur avec du NaI(Tl).

III.5. RÉSULTATS EXPÉRIMENTAUX

Les résultats expérimentaux sont présentés dans les figures 1—7 :

IV. ÉVALUATION DES COEFFICIENTS DE PARTAGE

Les coefficients de partage sont déterminés par deux méthodes :

1) la méthode de détermination du volume de rétention sur colonne par la méthode de fixation sur résine ;

2) la méthode de détermination sur la courbe d'élution.

1. DÉTERMINATION DU VOLUME DE RÉTENTION SUR COLONNE

Les coefficients de partage (*Kd*) représentent le rapport de concentration d'un élément dans la résine (C_R) et la concentration (du même

---

[13] R. E. Conniek et W. H. Mc Vey, *J. Amer. Chim. Soc.*, **71**, 3183 (1949).

[14] W. Haerdi, L. Balseine et S. Monnier, *J. Radioanalyt. Chim.*, **1**, 51 (1968).

[15] L. I. Popa, D. Dorcioman, D. Pantelică et A. Popa-Ghițescu, MN-12-1970.

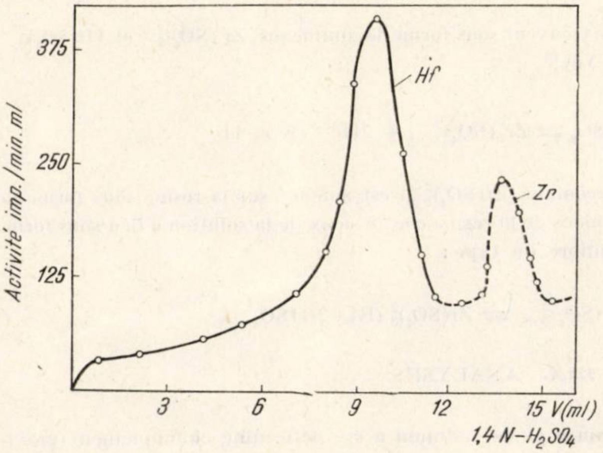

Fig. 1. — Élution du hafnium spectral et du zirconium nucléaire sur la résine Vionit AT 1. Eluant : l'acide sulfurique 1,4 N.

Concentration initiale de la mixture : $2{,}04 \cdot 10^{-4}$ M ^{95}Zr et $3{,}7 \cdot 10$ M^{-5} ^{181}Hf. Débit d'élution 16 ml/h. Résine Vionit AT 1. Colonne de résine : ∅ = 8,3 mm ; h = 600 mm. L'élution du hafnium précède celle du zirconium.

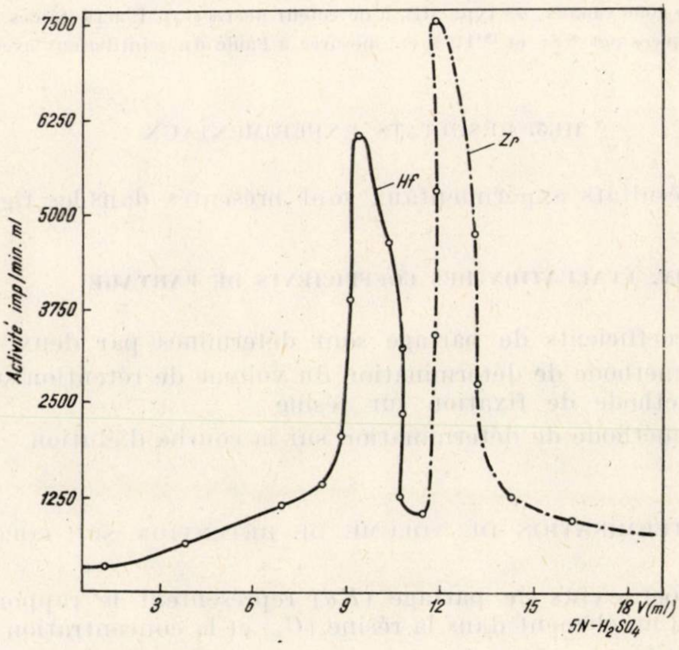

Fig. 2. — Elution du hafnium spectral et du zirconium nucléaire sur la résine Vionit AT 1. Eluant : l'acide sulfurique 5 N.

Concentration initiale de la mixture : $2{,}04 \cdot 10^{-4}$ M Zr et $3{,}7 \cdot 10^{-5}$ M ^{181}Hf. Débit d'élution 16 ml/h. Résine Vionit AT 1. Colonne de résine : ∅ = 8,3 mm ; h = 600 mm. L'élution du hafnium se produit avant celle du zirconium.

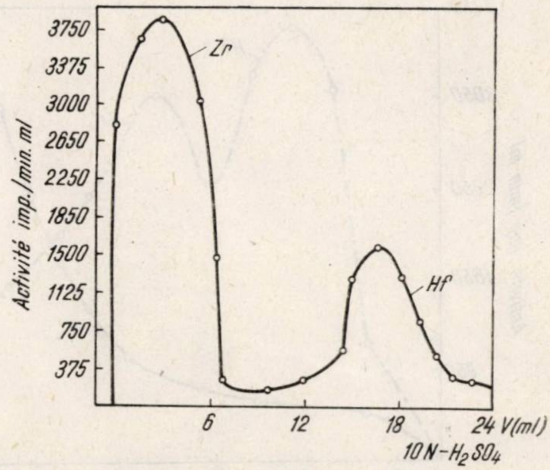

Fig. 3. — Elution du hafnium spectral et du zirconium nucléaire sur la résine Vionit AT 1. Eluant : l'acide sulfurique 10 N.

Concentration initiale de la mixture : 2,04 . 10^{-4} MZr^{95} et 3,7 . 10^{-5} M ^{181}Hf. Colonne de résine : ∅ = 8.3 mm, h = 600 mm. L'élution du zirconium a lieu avant celle du hafnium.

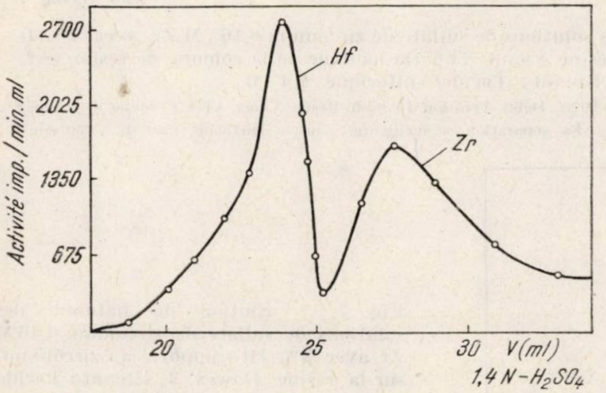

Fig. 4. — Élution du hafnium des solutions de sulfate de zirconium 0,04 M Zr avec 2 %Hf (rapporté au zirconium), sur la résine Vionit AT 1. Eluant : l'acide sulfurique 1,4 N.

La solution a été marquée par ^{95}Zr et ^{181}Hf. Débit d'élution 16 ml/h. Résine VionitAT 1. Colonne de résine ∅ = 8,3 mm ; h = 600 mm.

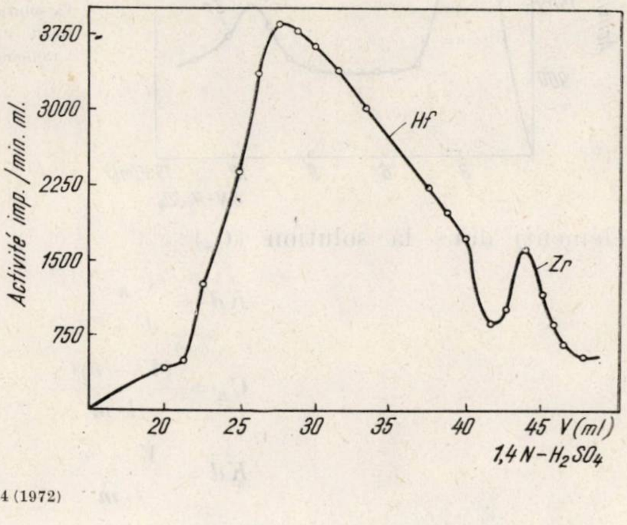

Fig. 5. — Elution du hafnium des solutions de sulfate de zirconium 0,166MZr avec 2 %Hf (rapporté au zirconium) sur la résine Vionit AT 1. Eluant : l'acide sulfurique 1,4 N.

La solution a eté marquée par ^{95}Zr et ^{181}Hf. Débit d'élution 16 ml/h. Résine Vionit AT 1. Colonne de résine ; ∅ = 8,3 mm ; h = 600 mm.

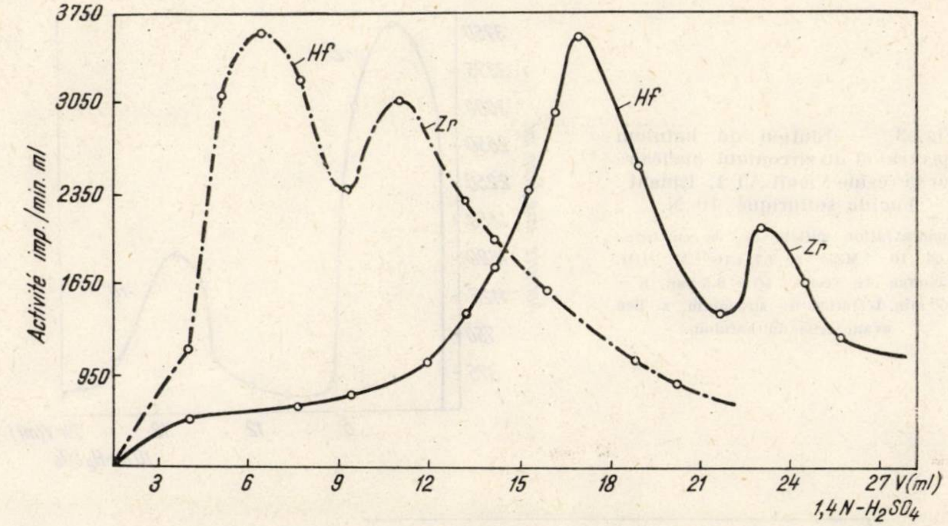

Fig. 6. — Elution du hafnium des solutions de sulfate de zirconium 0,16 M Zr avec 2 %Hf (rapporté au zirconium) sur la résine Vionit AT 1 (la hauteur de la colonne de résine est différente). Eluant ; l'acide sulfurique 1.4 M.

La solution a été marquée par ^{95}Zr et ^{181}Hf. Débit d'élution 16 ml/h. Résine Vionit AT 1. Colonne de résine ; ∅ = 8,3 mm ; h = 600 mm. et 750 mm. La séparation est meilleure dans le deuxième cas (h = 750 mm).

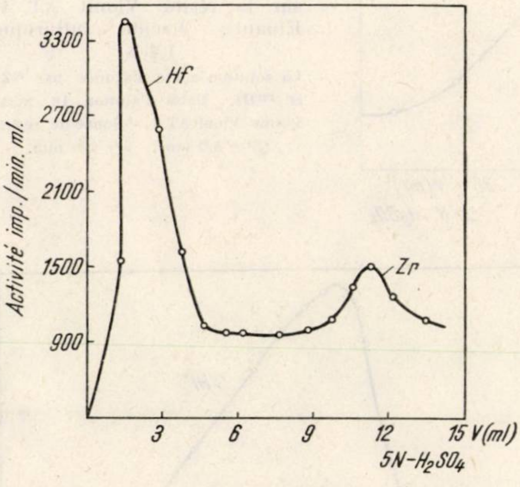

Fig. 7. — Elution du hafnium des solutions de sulfate de zirconium 0,16 M Zr avec 2 % Hf (rapporté au zirconium) sur la résine Dowex 3. Eluant : l'acide sulfurique 1,4 N.

La solution a été marquée par ^{95}Zr et ^{181}Hf. Débit d'élution 16 ml/h. La résine Dowex 3. Colonne de résine : ∅ = 11 mm ; h = 370 mm.

élément) dans la solution (C_S) :

$$Kd = \frac{C_{(R)}}{C_{(S)}}$$

$$C_R = \frac{(V - v)C_S}{l \cdot m}$$

$$Kd = \frac{V - v}{l \cdot m}$$

où :

Kd = coefficient de partage,
V = volume d'éluant récolté à l'extrémité de la colonne,
v = volume interstitiel de la colonne de résine,
l = longueur de la colonne de résine,
m = gramme de résine séchée par unité de longueur.

2. DÉTERMINATION DU COEFFICIENT DE PARTAGE SUR LA COURBE D'ÉLUTION

Selon Mayer et Tompkins le volume d'effluent V, qui marque l'apparition du maximum de la courbe d'élution est égal à :

$$V = v\left(l + Kd\,\frac{l\cdot m}{v}\right)$$

On en déduit :

$$Kd = \frac{V - v}{l\cdot m}$$

où : Kd, V, v, l m ont la même signification que dans la première méthode.

Le zirconium nucléaire et le hafnium spectral ont été élués par acide sulfurique 1,4 N ; 2,5N et 5N sur une colonne anionique Vionit AT 1. Les résultats obtenus sont représentés dans la figure 8.

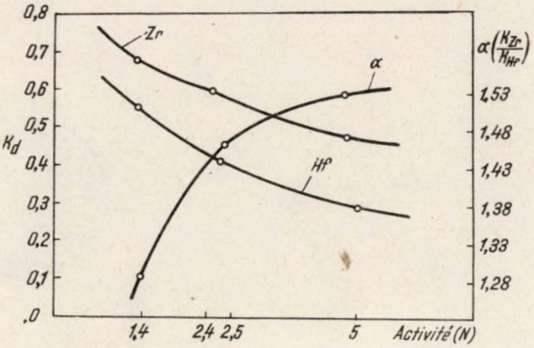

Fig. 8. — Variation des coefficients de partage (Kd) du zirconium et du hafnium et du facteur de séparation $\left(\alpha = \frac{KZr}{KHf}\right)$ en fonction de l'acidité d'éluant. Les expériences ont porté sur la résine Vionit AT 1.

V. DISCUSSIONS

Les données expérimentales permettent d'élucider la séparation du hafnium et du zirconium par résine échangeuse d'anions dans une milieu de sulfate.

Le zirconium forme des complexes stables dans un intervale d'acide sulfurique de 1,4 à 2,5 N ; dans les mêmes conditions d'acidité, le hafnium forme des complexes moins stables, la valeur du Kd(Zr) étant supérieure au Kd(Hf) (20–22%), (fig.. 8).

Les coefficients de partage indiquent une faible décroissance avec l'accroissement de la concentration de l'acide sulfurique (vers 5 N).

Le hafnium est obtenu dans les premières fractions éluées par acide sulfurique 1,5–5N et seulement après le zirconium (fig. 1–6) ; à l'élution par acide sulfurique 10N, c'est le zirconium qui apparaît le premier (dans les premières fractions). le hafnium étant obtenu dans les dernières fractions éluées (fig. 3).

VI. CONCLUSIONS

Les recherches effectuées pour la séparation du zirconium et du hafnium sur la résine anionique permettent d'établir :

– l'ordre d'élution des composants en fonction de l'acidité de l'éluant ;

– les conditions d'élution (des composants) ;

– le bon comportement de la résine lors de la séparation de ces composants.

ORSZÁGOS MŰSZAKI KÖNYVTÁR ÉS * DOKUMENTÁCIÓS KÖZPONT *

NOTE POUR LES AUTEURS

La *Revue Roumaine de Chimie* publie des articles en anglais, français, russe, allemand ou espagnol. Les auteurs sont priés d'envoyer des articles, notes, communications et comptes rendus inédits.

Les manuscrits seront dactylographiés à deux intervalles. Les tableaux seront dactylographiés sur feuilles séparées, de même que la légende des figures. Les diagrammes seront tracés à l'encre de Chine sur papier calque. Les tableaux et les figures seront numérotés par des chiffres arabes, en nombre strictement nécessaire. Prière de ne pas inscrire les mêmes données dans les tableaux et les figures. Les formules chimiques seront incluses dans le texte ; en outre, elles seront transcrites sur des feuilles séparées. Les auteurs sont priés d'indiquer les caractères italiques (en soulignant les lettres au crayon), ainsi que tout autre caractère spécial. L'ordre des références bibliographiques sera celui de leur mention dans le texte ; le nom de l'auteur sera précédé de l'initiale du prénom ; les publications périodiques seront présentées suivant les prescriptions internationales. Les références seront ajoutées à la fin de l'article ; elles paraîtront comme des notes, au bas de la page. Le texte sera précédé d'un résumé, comprenant 15 lignes au maximum.

L'entière responsabilité du contenu des articles appartient aux auteurs. On publie des articles dus aux collaborateurs roumains ou étrangers. Les auteurs recevront 50 tirés à part.

PRINTED IN ROMANIA

1972 AUG 2

TRAVAUX PARUS AUX ÉDITIONS DE L'ACADÉMIE DE LA RÉPUBLIQUE SOCIALISTE DE ROUMANIE

I. ZUGRĂVESCU et L. STOICESCU-CRIVETZ, **Polimerii hetero-ciclici** (Polymères hétérocycliques), 1971, 190 p., 9,50 lei.

CRISTOFOR SIMIONESCU et CLEOPATRA VASILIU-OPREA, **Mecanochimia conmpuşilor macromoleculari** (La mécanochimie des composés macromoléculaires), 1967. 344 p., 23,50 lei.

I. V. MAXIM, **Materiale nucleare** (Matériaux nucléaires), 1969, 444 p., 30 lei.

CORNEL BODEA et collab., **Tratat de biochimie vegetală**, partea I, **Fitochimie** (Traité de biochimie végétale, Ire partie, Phytochimie), 1er vol., 1964, 747 p. + 4 annexes + 2 pl., 41 lei, IIe vol., 1265, 1962 p., 1 pl., 56 lei, IIIe vol., 1967, 773 p., 35 lei.

V. GHEŢIE et V. MICUŞAN, **Analiza imunochimică. Teorie şi practică** (Analyse immunochimique. Théorie et pratique), 1966, 369 p., 28 lei.

R. PORTOCALĂ et L. POPA, **Acizii ribonucleici celulari şi virali** (Les acides ribonucléiques cellulaires et viraux), 1966, 375 p., 8 pl., 26 lei.

D. PURDELA et R. VÎLCEANU, **Chimia compuşilor organici ai fosforului şi ai acizilor lui** (La chimie des composés organiques du phosphore et de ses acides), 1965, 540 p., 37 lei.

SILVIA IONESCU, **Reacţii chimice induse de radiaţiile ionizante** (Réactions chimiques produites par les radiations ionisantes), 1963, 271 p., 15 lei.

MARIETA NICOLAE, **Fizico-chimia proceselor fotografice** (Physico-chimie des processus photographiques), 1964, 426 p. + 4 pl., 35 lei.

CRISTOFOR SIMIONESCU, MARGARETA GRIGORAŞ et AGATA CERNĂTESCU-ASANDEI, **Chimia lemnului din R.P.R.** (La chimie du bois en Roumanie), 1964, 239 p. + 6 pl., 27 lei.

I.P.I. — c. 1256

43 426

Lei 25.—

ORSZÁGOS MŰSZAKI KÖNYVTÁR ÉS DOKUMENTÁCIÓS KÖZPONT 1883

REVUE ROUMAINE DE CHIMIE

Tome 17, N° 6 Juin 1972

Page

P. SPACU and G. D. CISMARU, Behaviour of uranium compounds on heating. Thermal decomposition of ammonium uranates . . . . 947–959 R

DUMITRU TOPOR and ALEXANDRU BÎRHALĂ, Cryolite bath ratio by X-ray diffraction 961–968

P. BALTĂ, New theoretical data on the structural chemical equilibrium in molten glass . . . . 969–975 R

P. SPACU, D. CIOMÂRTAN and MARGARETA TEODORESCU, Roentgenographic studies of [Fe (II) $\text{phen}_2(\text{NCS})_2$] 977–980

RODICA MICU-SEMENIUC et CONST. GH. MACAROVICI, Combinaisons complexes avec dérivés biphényliques. XXVI. Cyanates métalliques simples et complexes avec dérivés diaminobiphényliques 981–992

RODICA MICU-SEMENIUC, CONST. GH. MACAROVICI et D. LUPU, Combinaisons complexes avec dérivés diaminobiphényliques. XXVII. Cyanates complexes du Cu(II) 993–1004

CLARA MAKKAY, FRANCISC MAKKAY and MARIA IONESCU, Polarographic behaviour of some cyclohexanone derivatives . . . . 1005–1011 R

CĂTĂLINA DEMETRESCU, Recherches sur la cyclisation des N_1-acyl-N_4-aryl-thiosemicarbazides. II. Nouveaux *p*-fluorodiphénylsulfonyl-5-arylamino-1,3,4-thiadiazoles et 1,2,4-mercapto-triazoles à intérêt thérapeutique 1013–1031

D. FELDMAN, C. V. UGLEA, VIOLETA NUȚĂ et MIHAELA POPA, Caractérisation du polychlorure de vinyle. Relation viscosité intrinsèque — poids moléculaire 1033–1041

I. NANU and C. ANDREI, Copolymers of conjugated dienes with maleic acid monoesters. VI. Constants *Q* and *e* in the copolymerization of isoprene with maleic acid monoesters 1043–1049

CONST. GH. MACAROVICI et GH. MORAR, Étude de la cinétique de la réaction $Bi_2O_3 + TiO_2$ avec formation de $Bi_4Ti_3O_{12}$ . . . . 1051–1059 R

GH. MORAR et CONST. GH. MACAROVICI, Le dosage complexométrique du mélange bismuth-ti[illegible]ne . . . . 1061–1064 R

L. M. BĂLOIU, Determination of the stability constant of compounds used in spectrophotometric analysis 1065–1069

J. ZSAKÓ und F. MAKKAY, Linearisation der potentiometrischen Titrationskurven. I. Fällungstitrationen 1071–1081

D. NEGOIU and ZAMFIRA TOMA, The determination of osmium as $[\text{Os (thio)}_6]\,[\text{Cr (NH}_3)_2(\text{NCS})_4]_3$. 1083–1086

LUIGI CAMPANELLA and GIORGIO DE ANGELIS, Electrochemical behaviour of isonicotinic acid in aqueous solution 1087–1113

P. NAGY, I. GÖRBE and A. SZURKOS, The polarographic reduction of methyl-substituted N-ethyl pyridinium ions. A HMO treatment 1115–1124

IG. POINESCU, Transformations chimiques du polychlorure de vinyle. III. Synthèses de polyélectrolytes réticulés avec groupes sulfoniques sur la base du polychlorure de vinyle arylé avec des hydrocarbures aromatiques polynucléaires 1125–1136

Rev. Roumaine Chim. 17, *6*, 945 – 1136 (1972) Bucarest

Revue Roumaine de Chimie, 17, 6, 947–959 (1972)

BEHAVIOUR OF URANIUM COMPOUNDS ON HEATING.
THERMAL DECOMPOSITION OF AMMONIUM URANATES

P. SPACU and G. D. CISMARU

Centre of Physical Chemistry, Str. Dumbrava Roşie 23, Bucharest, Romania

Received February 7, 1972

The behaviour of ammonium uranates on heating between 25–1100° has been studied in air, argon and hydrogen. In air and in argon, the weight loss, until the formation of U_3O_8, takes place in 4 stages, while in hydrogen, till the formation of UO_2, it occurs in 5 stages. The influence of the H_2O/UO_3 ratio increase on the thermogram was determined. The most probable formula for ammonium uranates was established as being $[(UO_2)_m(OH)_{2(m-n)}(ONH_4)_{2n} \cdot (H_2O)_{(m-n)}]\,(p-n)\,H_2O$

INTRODUCTION

The thermal decomposition of certain uranium compounds, among which the ammonium uranates, has as practical purpose the obtaining of uranium oxides to be applied to the technology of fuels for secondary nuclear reactors. To obtain the best results, it is necessary to know the chemical composition of the ammonium uranates, as well as their thermal decomposition mechanism, in different gaseous media.

Among the data obtained by various researches, when studying the ammonium uranates,[1–11] disagreements appeared about their composition and structure as a consequence of the fact that they were considered as singular compounds.

---

[1] J. Decrop, M. Delange, J. Holder, H. Huet, J. Sauteron and P. Vartes "Proceedings International Conference Peaceful Uses Atomic Energy II" Genève, **1958**, 15/P/1252.

[2] M. Delange, *CEA* CN 16/9/1963.

[3] D. Jovanović and J. Milosavljević, *Tehnika (Belgrad)*, **21**, 1530 (1966); *Chem. Abstr.*, **68**, 31621 M (1968).

[4] G. Tridot, *Ann. Chim. (France)*, **1950**, 358.

[5] A. M. Deane, *A ERE*, R–3411 (1960).

[6] J. Decrop, J. Holder and J. Sauteron, *CEA* Rap., 1974/61 (1961).

[7] E. V. Garner, *J. Inorg. Nuclear Chem.*, **21**, 380 (1962).

[8] E. H. P. Cordfunke, *J. Inorg. Nuclear Chem.*, **24**, 303 (1962).

[9] Nguyen Quy Dao and H. Brusset, *Compt. rend. Ser. C*, **265**, 1141 (1967).

[10] Nguyen Quy Dao, *Bull. Soc. chim. France*, **1968**, 4751.

[11] N. V. Zubova, V. M. Makarov, V. D. Nikolskii, P. N. Petrov, E. G. Teterin and N. T. Chebotarev, *Zhur. neorg. khim.*, **13**, 329 (1968).

An important contribution to the elucidation of the structure and composition of the ammonium uranates was brought by works based on the studies made by means of X-ray, IR spectra and thermal analysis. Thus, Debets and Loopstra [12] suggested, on the basis of X-ray studies, a sandwich structure consisting of hexagonal and pseudo-hexagonal layers, having the composition $UO_2(O_2)\infty$ with additional oxygen and nitrogen atoms from the molecule of H_2O and NH_3, situated between the layers.

Stuart and Wateley,[13] who made use of the results obtained from IR spectra and thermal analysis, showed that the NH_3 is present in al ammonium uranates as a NH_4^+ ion which produces a displacement of the coordinated water molecules by means of an ion exchange mechanism. Since these exchanges occurred smoothly, it was inferred that a continuous $UO_3-NH_3-H_2O$ system exists.

With regard to the hygroscopicity of the ammonium uranates, Cordfunke [8] shows that they can absorb up to 4 mols of H_2O for 1 mol of UO_3, which means a ratio higher than that of 1.66 previously accepted as maximum.

Fodor and Poko [14] confirm the results obtained by the above mentioned authors [8,12,13] and obtain, on the basis of the IR spectra and TG diagrams, data concerning the appearance in the ammonium uranates, beside the constitutional water, of a part of weakly bound water — the absorbed water — and the possibility of NH_3 to be incorporated instead of a part of the structural water.

As to the researches in the domain of the thermal decomposition of the ammonium uranates, some results are not confirmed by all studies. The disagreements refer, on the one hand, to the appearance of a level corresponding to $UO_{2.9}$ between 500° and 600°, as indicated by Sanchez and Cellini [15] and Landsperski et al.[16] as well as to the appearance of exothermal effects between 475° and 500°, attributed to UO_3 recrystallization by Zubova et al.[11] and, on the other hand, to the temperature range in which decomposition of UO_3 into U_3O_8 occurs.

Concerning this temperature range, Jovanović and Milosavljeić [3] give 570—675°, Zubova et al.[11] 575—625°, Sanchez and Cellini [15] 600—675°, Landsperski et al.[16] 623—640°, Lebeau,[17] Tammann and Rosenthal,[18] and Duval [19] 610—745° and Lister and Richardson [20] 560—650°.

Besides these discrepancies, some other differences appeared in the thermogravimetric studies, in the initial part of the ammonium uranates decomposition, as to the assignment of some stages and thermal effects.

---

[12] P. C. Debets and B. O. Loopstra, *J. Inorg. Nuclear Chem.*, **25**, 945 (1963).

[13] W. I. Stuart and T. L. Wateley, *J. Inorg. Nuclear Chem.*, **31**, 1939 (1969).

[14] M. Fodor and Z. Poko, "Proc. Conf. Appl. Phys.-Chem. Method. Anal. Chem.", Budapest, **1966**, 3, 281.

[15] L. G. Sanchez and R. F. Cellini, *Anales real. Soc. españ. Fis. Quim.*, **54**, 181 (1958).

[16] H. Landsperski, D. Imrisova, L. Sedlacova and Z. Urbanec, *UJV* Rap., 929/63 (1963).

[17] P. Lebeau, *Compt. rend.*, **174**, 388 (1922).

[18] G. Tammann and W. Rosenthal, *Z. anorg. Chem.*, **156**, 20 (1926).

[19] C. Duval, "Inorganic Thermogravimetric Analysis", Ed. Elsevier, Amsterdam, 1963, p. 659—661.

[20] B. A. J. Lister and R. J. Richardson, *AERE* C/R, 2276 (1957).

A particular interest concerning the thermogravimetric studies of the ammonium uranates, is offered by the researches of Wheeler et al.[21] who were studying the thermal decomposition of the various polymorphic forms of UO_3, their appearance as a function of the component from which they are derived as well as the decomposition rate used.

In order to contribute to the establishing of the thermal decomposition mechanism of the ammonium uranates and to their best formulation, as well as to state more clearly some origins of the discrepancies occurring in the studies carried out so far, we considered necessary to undertake new researches on the basis of the thermal analysis of these compounds.

EXPERIMENTAL

Thermogravimetric determinations in air, argon and hydrogen were made on several samples of ammonium uranates prepared by precipitation under various conditions. Thermodifferential determinations were performed only in air. We used five samples of uranates with a UO_3 amount varying from 88% to 79% and an NH_3 amount of 3–6.5%, as indicated by the chemical analysis (see table 1).

In order to obtain curves TG, DTG and DTA in air, we used an L. Erdey, P. Paulik and J. Paulik Derivatograph. For TG curves in argon and hydrogen, we made use of a thermobalance with quartz thread (equipped with a cathetometer) having a sensitivity of 5×10^{-5} g. A sketch of the apparatus is shown in figure 1.

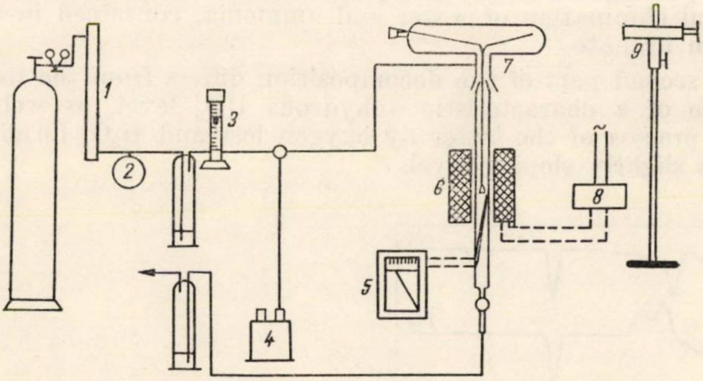

Fig. 1. — Sketch of the thermobalance with quartz thread.
1, Purification column; *2*, Elastic buffer vessel; *3*, Flow gauge; *4*, Vacuum pump; *5*, Temperature recorder; *6*, Furnace; *7*, Thermobalance with quartz thread; *8*, Current feeder with program; *9*, Cathetometer.

The determinations were carried out on amounts of 1 g with the Derivatograph and amounts of 0.050 g with the quartz thermobalance.

---

[21] V. J. Wheeler, R. M. Dell and E. Wait, *J. Inorg. Nuclear Chem.*, **26**, 1829 (1964).

With the Derivatograph, the determinations were made in platinum or Al_2O_3 crucibles. The inert substance used in DTA determinations was Al_2O_3 in powder form calcinated at 1100°. The heating rate was 5°/min. The work was performed in air at normal pressure.

A platinum nacelle was used in the quartz thread thermobalance. The heating rate used in this case was 6°/min. These determinations, as well as those in hydrogen were made with a gas flow of 6 l/h.

In all these cases, the decomposition was observed in the 25—1100° range; in both apparatuses the temperature was measured inside the heating space, at the level of the samples.

On the thermogravimetric curves, the weight loss is given in % on the ordinate, and the temperature in °C on the abscissa.

The X-ray determinations on the oxides obtained by the thermal decomposition, were made by means of the X-ray powder diffraction method, with a TUR-M 60 apparatus, using Cu Kα-radiation.

RESULTS AND DISCUSSION

From the examination of the TG, DTG and DTA curves, obtained on thermal decomposition in air of the ammonium uranates, eight temperature zones should be observed, where the weight losses appear, together with two characteristic levels for the resulting oxides.

In the first part of the decomposition, five successive domains should be observed, where the weight losses are only limited by small inflexions, without clear-cut steps; the appearing products are therefore unstable, passing from one composition to another proportionally to the gradual elimination of water and ammonia, contained in the initial ammonium uranate.

The second part of the decomposition differs from the first by the appearance of a characteristic anhydrous UO_3 level, as well as by a reduction process of the latter by oxygen loss and U_3O_8 formation that presents a slightly sloping level.

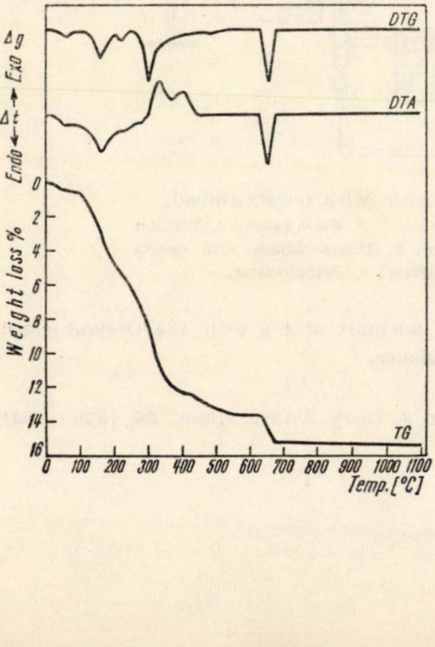

Fig. 2. — TG, DTG and DTA curves of ammonium uranate (II) in air.

By examining the processes occurring during the decomposition, it may be observed that the beginning of the heating is accompanied by the removal of the absorbed water, which continues to diminish till 100 ± 5°, when the loss of the coordination water (a part of the constitution water) and of the last part of the absorbed water begins. In this region the superposition of the last part of the absorbed water, presents an increasing slope of the decomposition curve until total removal of this water, in this case at 170°. From this point, the curve slope diminishes, as a result of the continuous loss of a part of the constitution water, until 275°. From 275° to 335° a more rapid diminishing occurs, due to the elimination of NH_3. After 335°, a UO_3 hydrate appears (probably the $UO_3 . 0.5\ H_2O$ in this case) that losses slowly the water till 400°, when the $UO_3 . (0.2-0.3)\ H_2O$ is formed. Concomitantly with the formation of the latter, an inflexion of the curve occurs at 400–425°, the water elimination of the last hydrate continuing up to 550° when the characteristic level of the anhydrous UO_3 appears. This level is maintained up to 630°, where the decomposition of the UO_3 begins with the formation of U_3O_8 at 675°. At this point a slightly sloping level appears which continues up to 1100°, where the loss of weight does not exceed 0.1 % for100°.

On the DTA curve, a series of endothermic effects appear, with the maximum of the peaks at 165 ± 5° and at 225 ± 5°, which are characteristic of the removal of absorption water and of a part of the constitution water. An exothermic effect appears afterwards with a maximum at 335° corresponding to the removal of NH_3, followed by a diminution corresponding to the elimination of a part of the UO_3 hydration water. At 385° a new exothermic effect appears, with a maximum at 400°, which could be attributed to a UO_3 recrystallization due to a slow dehydration. Following this effect, the curve does no more show any thermic effect until 630°. At this temperature, a marked endothermic effect appears, due to the decomposition of UO_3 into U_3O_8, with a maximum at 650° and its end at 675°. Beyond this temperature, no other thermic effect appeared until 1100°.

As to the differences between the uranate samples under study, it should be remarked that those samples containing a smaller amount of water, offer a greater possibility to distinguish the above mentioned temperature zones, where the thermal decomposition processes take place, than those containing a higher water amount, where the decomposition processes interpenetrate, in the interval corresponding to the H_2O and NH_3 elimination, thus marking the limits within which they occurred.

We remark that as the amount of absorbed water increases, therefore as the H_2O/UO_3 ratio increases, the curve presents a shift of the inflexion point (occurring at 170° for the sample, as seen in Fig. 2) towards higher temperatures, reaching even 275° as shown in Fig. 3.

Beside this shift, in the case of the ammonium uranates containing a large amount of absorbed water or of NH_3, we remark that even the portion preceding the UO_3 formation, presents some changes after the elimination of NH_3, i.e. the $UO_3 . 0.8\ H_2O$ can appear instead of $UO_3 . 0.5\ H_2O$. It results that a larger amount of absorbed water can modify the decomposition curve, since the elimination of the constitution water can take place in another form.

The appearance of these differences, in the first portion of the curves, already observed in other works, is mainly due to the use of ammonium uranates having various H_2O/UO_3 and NH_3/UO_3 ratios.

With respect to the zone of the thermograms, where the UO_3 characteristic level appears, we remark that while Sanchez,[15] and Ladsperski,[22] claim that they have obtained $UO_{2 \cdot 9}$, Lebeau [17] Tammann and Rosenthal,[18] Duval,[19] as well as Lister and Richardson [20] confirmed the appearance of the oxide UO_3 as obtained by our investigations.

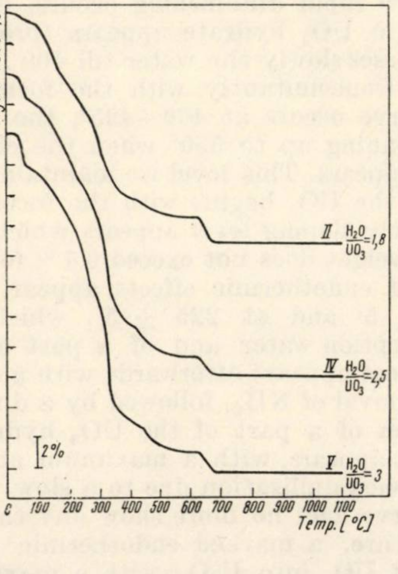

Fig. 3. — Influence of the increase of H_2O/UO_3 ratio in ammonium uranates on the aspect of the thermograms.

As previously shown, when U_3O_8 is formed, a small slope of the level appears, due to the loss of a very small amount of oxygen not exceeding 0.1 % in an interval of 100°. This changes the composition of U_3O_8, from $UO_{2 \cdot 67}$ to $UO_{2 \cdot 645}$ or $UO_{2 \cdot 63}$ at 1100°, as also observed by Kunihiro Goto [23], and by Malinin et al.[24] From the DTA curve, as well as from the Debye-Scherrer X-ray photographs of the U_3O_6 samples, heated at various temperatures, it results that the structure remains unchanged. In the debyegram, obtained for 1100°, only few lines of reverse reflexion show a widening corresponding to the defect appearing in the lattice due to oxygen losses.

On the basis of observations made on the thermal decomposition of ammonium uranates in air, and taking into account the processes which can occur and the possibility of their interpenetration, owing to changes in the composition of the compounds, the following main stages could be considered : I) Elimination of the absorbed water and of a part of the constitution water; II) Elimination of the ammonia; III) Dehydration of the UO_3 hydrates ; IV) Decomposition of the anhydrous UO_3, with formation of U_3O_8 ; V) Loss of atomic oxygen from U_3O_8. These stages can be represented by the following reaction :

---

[22] H. LANDSPERSKI, L. SEDLACOVA and D. JAKES, *UJV* Rap., 990/64 (1964).

[23] KUNIHIRO GOTO, *Nippon Kagaku Zasshi*, **89**, 927 (1968); *Chem. Abstr.*, **70**, 25253 T (1969).

[24] G. V. MALININ, V. B. YADRINTSEV and YU. M. TOLMACEV, *Radiokhimya*, **11**, 438 (1969).

$$[m\,UO_3 .\ 2n\,NH_3 .\ 2\,(m-n)\,H_2O] .\ p\,H_2O \xrightarrow{25-275^\circ}$$

$$\rightarrow m\,UO_3 \cdot 2n\,NH_3 \cdot [2\,(m-n)-r]H_2O + (p+r)\,H_2O$$

$$m\,UO_3 .\ 2n\,NH_3 .\ [2\,(m-n)-r]H_2O \xrightarrow{275-335^\circ}$$

$$\rightarrow m\,UO_3 .\ [2(m-n)-r]\,H_2O + 2n\,NH_3$$

$$m\,UO_3 .\ [2(m-n)-r]\,H_2O \xrightarrow{335-550^\circ} m\,UO_3 + [2\,(m-n)-r]H_2O$$

$$m\,UO_3 \xrightarrow{630-675^\circ} \frac{m}{2}\,U_3O_8 + \frac{m}{6}\,O_2$$

$$\frac{m}{2}\,U_3O_8 \xrightarrow{700-1100^\circ} \frac{m}{2}\,U_3O_{8-x} + \frac{mx}{2}\,O$$

The losses in weight of ammonium uranates samples, obtained from the thermograms, are presented in table 1 so as to allow the observation of the changes appearing in the amounts of the losses function of the H_2O/UO_3 ratio. It can thus be seen that as this ratio increases, the weight losses on the first stage increase, too.

The crude formulas of the uranates under study were deduced from the calculations based on the weight losses during thermal decomposition and on the chemical analysis.

From our results and on the basis of the data referring to structure and composition, published by several authors [8,12–14] we admitted that the most proper formula representing the ammonium uranates, appearing in the continuous system $UO_3-NH_3-H_2O$, is

$$[(UO_2)_m\ (OH)_{2(m-n)}\ (ONH_4)_{2n}\ (H_2O)_{(m-n)}] \cdot (p-n)\,H_2O$$

with the corresponding crude formula

$$[m\,UO_3 .\ 2n\,NH_3 .\ 2\,(m-n)\,H_2O] .\ pH_2O$$

where pH_2O is the absorbed water and n will always be smaller than m.

In the case of the thermal decomposition of the ammonium uranates in argon (Fig. 4), the same zones of temperature and the same stages appear as in the decomposition in air, except that the UO_3 characteristic level is very low, the loss of oxygen occurring at 600°, lower than

Table 1

Composition and the weight losses of ammonium uranates samples

Sample No.	Ammonium uranates (crude formula)	Composition (weight %)			Molar ratio	Weight loss % in the temperature ranges (°C)						
		UO_3	NH_3	H_2O	$\frac{H_2O}{UO_3}$	25–275	275–335	335–550	550–630	630–675	675–700	700–1 100
I	$[5UO_3.3NH_3.7H_2O].0.13H_2O$	87.9	3	9.1	1.6	6.5	3	2.6	—	1.5	—	0.4
II	$[15UO_3.11NH_3.19H_2O].8.5H_2O$	86.3	3.8	9.9	1.8	7.2	3.8	2.7	—	2.2	—	0.3
III	$[29UO_3.35NH_3.23H_2O].33H_2O$	83.8	6	10.2	2	7.5	6	2.7	—	1.65	—	0.3
IV	$[4UO_3.5NH_3.3H_2O].7H_2O$	81.3	6	12.7	2.5	9	6	3.7	—	1.3	—	0.3
V	$[7UO_3.9NH_3.5H_2O].15.5H_2O$	79	6.5	14.5	3	10.5	6.5	4	—	1.4	—	0.4

that in air. In argon, the UO_3 decomposition takes place with a lesser slope than that in air, but the final temperature of the conversion into U_3O_8 is the same as in air, while the weight loss of U_3O_8 does not present any difference.

As to the difference appearing on UO_3 decomposition, we remark that the situation is similar to that described by Wheeler et al.[21] in the decomposition of the various crystalline forms of UO_3 at low oxygen pressure. By taking into account that the argon used does not contain oxygen, the equilibrum could be possibly shifted towards a more rapid decomposition of the UO_3. On the other hand, this more rapid decomposition could also be ascribed to the appearance of the α form of the oxide.

The thermal decomposition of the ammoniun uranate in hydrogen flow, takes place in five stages, with the final formation of UO_2.

In the case of samples with a smaller H_2O/UO_3 ratio, in contrast to those with a higher ratio, we can see much more easily the inflexions of the curve and the delimitations between the temperature zones where the elimination of H_2O and NH_3 occurs. For instance, from the beginning of the sample heating, a weight loss can be observed due to the elimination of the absorbed water. At 120°, the concomitant elimination begins also for part of the constitution water (the coordination water). In the case presented in Fig. 5, an inflexion of the curve is seen at 150°, where the elimination of the absorbed water is completed. Continuing up to 200°, the rest of the first part of the constitution water is eliminated, the second part of it being removed during a new stage from 200 to 250°. At 250°, the elimination of NH_3 begins and continues till 325°, when a UO_3 hidrate ($UO_3 . 0.5\,H_2O$) appears. This is quickly dehydrated until 420°, accompanied by the formation of anhydrous UO_3 that does not possess any stability in hydrogen. The reduction of UO_3 begins immediately, at 420°, in a single stage into UO_2 that presents an invariable horizontal level up to 1100°. The total conversion into UO_2 occurs at 535°.

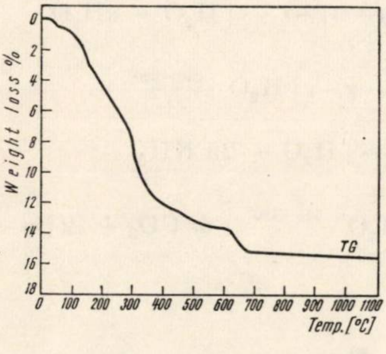

Fig. 4. — TG curve of ammonium uranate (II) in argon.

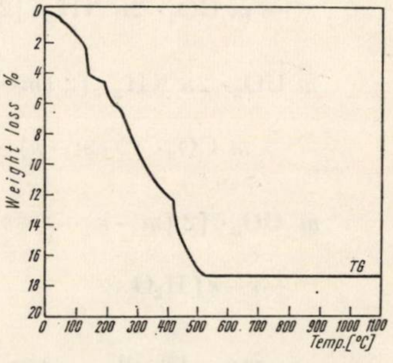

Fig. 5. — TG curve of ammonium uranate (II) in hydrogen.

As it can be observed, the decomposition in hydrogen presents some differences as compared to that in air or in argon. Thus, a second stage appears in the elimination of a part of the constitution water, prior to the NH_3 elimination. The elimination of NH_3 occurs by 25° earlier than in air. The uranium trioxide does not present any level, its appearance in an anhydrous form is only shown by an inflexion. When UO_3 is reduced to UO_2, no stages appear for intermediate oxides.

From the determinations made in hydrogen, it results that the main stages of the decomposition are as follows : I) Elimination of the absorbed water and of a first part of the constitution water ; II) Elimination of the second part of the constitution water ; III) Elimination of the ammonia ; IV) Dehydration of the UO_3 hydrate ; V) Reduction of UO_3 with formation of UO_2.

These stages can be illustrated by the following reactinos :

$$[m\mathrm{UO_3}\cdot 2n\,\mathrm{NH_3}\cdot 2\,(m-n)\,\mathrm{H_2O}]\cdot p\,\mathrm{H_2O} \xrightarrow{25-200^\circ}$$

$$\rightarrow m\,\mathrm{UO_3}\cdot 2n\,\mathrm{NH_3}\cdot [2\,(m-n)-r]\,\mathrm{H_2O} + (p+r)\,\mathrm{H_2O}$$

$$m\,\mathrm{UO_3}\cdot 2n\,\mathrm{NH_3}\cdot [2\,(m-n)-r]\mathrm{H_2O} \xrightarrow{200-250^\circ}$$

$$\rightarrow m\,\mathrm{UO_3}\cdot 2n\,\mathrm{NH_3}\cdot [2\,(m-n)-r-s]\,\mathrm{H_2O} + s\mathrm{H_2O}$$

$$m\,\mathrm{UO_3}\cdot 2n\,\mathrm{NH_3}\cdot [2\,(m-n)-r-s]\,\mathrm{H_2O} \xrightarrow{250-325^\circ}$$

$$\rightarrow m\,\mathrm{UO_3}\cdot [2\,(m-n)-r-s]\,\mathrm{H_2O} + 2n\,\mathrm{NH_3}$$

$$m\,\mathrm{UO_3}\cdot [2\,(m-n)-r-s]\,\mathrm{H_2O} \xrightarrow{325-420^\circ} m\,\mathrm{UO_3} + [2\,(m-n) -$$

$$-r-s]\,\mathrm{H_2O}$$

$$m\,\mathrm{UO_3} \xrightarrow{420-535^\circ} m\,\mathrm{UO_2} + \frac{m}{2}\,\mathrm{O_2}$$

From the standpoint of the water amounts eliminated on the first stage, as resulted from the calculations, no differences appear with regard to the decomposition in air, though on the curve obtained in hydrogen, the elimination of the second part of the constitution water is better emphasized.

From our researches and by taking also into account the technical use of the thermal decomposition of ammonium uranates in view of obtaining uranium oxides, it should be remarked that the large variety of the ammonium uranates is no hindrance to their use to this end since, after the water and the ammonia are eliminated, the decomposition curve is identical, in the same medium, for whatever compound of the UO_3—NH_3—H_2O system. For the choice of a gaseous medium suitable to obtain the oxides, Table 2 can be advantageously used since it contains the temperatures of formation and the temperature intervals for the characteristic levels of the UO_3, U_3O_8 and UO_2 oxides, resulting from the thermogravimetric study.

Table 2

Temperatures of formation and temperatures of the characteristic levels of uranium oxides, on the decomposition of the ammonium uranates in air, argon and hydrogen

Oxide	Temperature of formation (°C)				Temperature interval in which characteristic levels appear (°C)			
	Air	Ar	H_2	Data from literature* (in air)	Air	Ar	H_2	Data from literature * (in air)
UO_3	550	585	420	450^{3} 500^{15} 550^{16} 480^{17-19}	550–630	585–600	–	$450-570^{3}$ $500-600^{15}$ $550-623^{16}$ $480-610^{17-19}$
U_3O_8	675	675	–	$675^{3,15}$ 625^{11} 640^{16} 745^{17-19} 650^{20}	675–700	675–700	–	$600-900^{15}$ $745-946^{17-19}$
UO_2	–	–	535	–	–	–	535–1100	

* The only data to be found in literature refer to the thermal decomposition of ammonium uranates in air.

In order to explain the differences between the results obtained by different researchers in the thermal analysis of the ammonium uranates, we have examined the causes liable to lead to changes in the thermogravimetric curves of these compounds. For example, when interpreting the results, it is necessary to take into account the possibility of a continuous variation in the composition of the uranates from the $UO_3-NH_3-H_2O$ system, as well as their hygroscopicity (the H_2O/UO_3 ratio being able to reach the value of 4), and also the polymorphic modifications of the UO_3 liable to appear, as a function of the decomposition rate, of the compound from which it derives and of the gaseous medium used. As to the water amount of the uranates used, we remarked that as the amount of the absorbed water increases, in the first part of the decomposition, a shift of the inflexion occurs at the end of the elimination of this water, towards 275°, so that, instead of two inflexions, only one appears, corresponding to the beginning of the NH_3 elimination, (see Fig. 3). On the other hand, after the NH_3 elimination, $UO_3 . 0.8\,H_2O$ appears in the case of samples with $H_2O/UO_3 > 2$ or with $NH_3/UO_3 > 1$, while in the case of samples with $H_2O/UO_3 \leqslant 2$ it is the $UO_3 . 0.5\,H_2O$ that appears, which explains why some researchers [16] showed the appearance of the first hydrate, although this is not always formed.

As to the formation of the one or the other of the polymorphic modifications of the UO_3, this could also explain some of the disagreements among the results of some authors [11.15-20.22.25] referring to the decomposition temperature of UO_3 into U_3O_8, as well as to the formation of the $UO_{2\cdot 9}$ oxide.

CONCLUSIONS

1) The mechanism of the ammonium uranates decomposition by heating presents 4 principal stages : I) Elimination of the absorbed water and of a part of the constitution water ; II) Elimination of NH_3 ; III) Dehydration of the UO_3 hydrates ; IV) Decomposition of the UO_3.

The differences observed between the reaction in hydrogen as compared with that in air and argon, appear on the first stage, which is divided into two (since the water elimination takes place in two stage at the beginning), while the decomposition of UO_3 yields UO_2, whereas in air and in argon it yields U_3O_8. Therefore, in hydrogen there are 5 stages till the UO_2 is produced, while in air and in argon there are only 4 stages till the U_3O_8 is obtained.

2) From the determination of the composition, made on the basis of thermograms, considering that the $UO_3-NH_3-H_2O$ system is continuous and taking into account the hygroscopicity of the ammonium uranates, we propose the following general formula :

$$[(UO_2)_m\,(OH)_{2(m-n)}\,(ONH_4)_{2n}\,(H_2O)_{(m-n)}]\,.\,(p-n)\,H_2O$$

the corresponding crude formula being

$$[mUO_3\,.\,2n\,NH_3\,.\,2\,(m-n)\,H_2O]\,.\,pH_2O$$

where n will always be smaller than m, while p can assume values from 0 to $2\,(m+n)$, since the ratio H_2O/UO_3 can reach values up to 4.

3) From the same thermograms, it results that, owing to the variation of the ratios H_2O/UO_3 and NH_3/UO_3, at various compositions of the ammonium uranates, changes appear in the aspect of the thermograms in the first part of the decomposition until the total elimination of the water and of the ammonia (Fig. 3), no differences appearing in the second part when the oxides are formed.

4) As to the influence of the gaseous medium in which the ammonium uranate heating is made, a displacement of the temperature of the UO_3 decomposition towards lower values was remarked when passing from air to argon and then to hydrogen. As a matter of fact, it can be considered that, in hydrogen, the anhydrous UO_3 is unstable since by heating, after it is formed, its reduction to UO_2 begins.

---

[25] H. R. Hoekstra and S. Siegel, "Proceedings International Conference Peaceful Uses Atomic Energy II", Geneve, 1958, 15/P/548.

5) Our results brought a confirmation of the structure and composition proposed by Debets and Loopstra [12] on the one hand, and by Stuart and Wateley [13] on the other hand, as well as of the hygroscopicity of the ammonium uranates, observed by Cordfunke.[8] Moreover, they allowed us to establish some of the causes of the differences appearing in some thermogravimetric studies of the ammonium uranates.

6) The formation temperatures were established for UO_3 and U_3O_8 in air and in argon, and for UO_2 in hydrogen, as well as temperature intervals in which the oxides present characteristic levels, in the already mentioned conditions.

Revue Roumaine de Chimie, 17, 6, 961–968 (1972)

CRYOLITE BATH RATIO BY X-RAY DIFFRACTION*

DUMITRU TOPOR and ALEXANDRU BÎRHALĂ
Centre of Physical Chemistry, P.O.Box 2103, Bucharest

Received January 19, 1972

The improvements in the determination by X-ray diffraction of cryolite ratio of the aluminium cell electrolyte are described. Ammonium nitrate was used as internal standard and the calibration was made with known cryolite and chiolite mixtures. A precision of 1.3 per cent was obtained.

INTRODUCTION

Close control of aluminium production by the Hall-Heroult process is conditioned by the electrolyte cell composition. Among other components (Al_2O_3, CaF_2) the content in NaF and AlF_3 must be controlled as accurately as possible. The ratio sodium fluoride to aluminium fluoride, i.e. the cryolite ratio (CR), can be evaluated by chemical and physico-chemical methods, which were described at large by Fiquet and Armand [1] and Lobos and Black.[2]

The X-ray diffraction method for the determination of a crystalline component concentration in a powder sample is described in some papers or books.[3–9] The method is based on the proportionality between

---

*) This work was supported by ALRO, Aluminium Plant, Slatina, under Contract no. 26–1971.

[1] M. Fiquet and M. Armand, *Alluminio*, **22**, 621(1953).

[2] J. S. Lobos and R. H. Black, in "Extraction Metallurgy of Aluminium", vol. 2, p. 277, 1963.

[3] D. M. Heiker and L. S. Zervin, "Difractometria rontgenovaskyh luchei", Fizmatghiz, Moscow, 1963.

[4] A. Guinier, "X-ray Diffraction", W. Freeman and Co., San Francisco, 1963.

[5] J. B. Cohen, "Diffraction Methods in Material Science", McMillan and Co., N.Y., 1966.

[6] N. A. Krylov, V. Kalashnikov and M. Polischuk, "X-ray Techniques for Reinforced Concrete Quality Control", Stroiizdat, Leningrad, 1966.

[7] H. Klug and L. Alexander, "X-ray Diffraction Procedures", J. Wiley and Sons Inc., N. Y., 1966.

[8] G. Mallet, M. Fay and W. Mueller, "Advances in X-ray Analysis", vol. 9, 1966, Plenum Press, N. Y., p. 544.

[9] J. Hancart, *Meth. Phys. Anal.* (*GAMS*), **5**, 190 (1969).
A. F. Giamei and E. Freise, *Trans. Met. Soc. AIME*, **239**, 1676 (1967).
W. Croft, *Encyclop. Ind. Chem. Analyt*, **3**, 796 (1966).

the intensity I_i of a diffraction line (usually the strongest line) of the i-th component and the quantity in which this component is present in the sample :

$$I_i = k_i f_i / \mu \tag{1}$$

where k_i is a proportionality constant, f_i is the volume fraction of the i-th component and μ is the linear X-ray absorption coefficient of the powder mixture. If f_i is expressed by weight fraction x_i and density ρ_i, and μ by mass absorption coefficient ($\mu = \Sigma x_i \mu_i^x / \Sigma (x_i / \rho_i)$ the equation (1) becomes :

$$I_i = k_i x_i / \rho_i \Sigma \mu_i^x x_i \tag{2}$$

In most quantitative analyses the mixture of compounds is regarded as made up of two components : the component to be analysed for (subscript C) and the sum of the others components which can be designated the matrix (subscript M). Thus, the diffraction intensity follows the relation :

$$I_C = k_C x_C / \rho_C [x_C(\mu_C^x - \mu_M^x) + \mu_M^x] \tag{3}$$

This equation relates the intensity of a selected diffraction line of the C component to its concentration, density and mass absorption coefficient and to mass absorption coefficient of the matrix.

The main crystalline components in the acid electrolyte cell, i.e. with C.R. 1.5, are cryolite (Na_3AlF_6) and chiolite ($Na_5Al_3F_{14}$).

The cryolite ratio can be determined as Fiquet and Armand [1] suggested in 1953 by X-ray diffraction. Only two papers [2,10] in which this method was used are known, and few papers [11-14] applied it to elucidate the composition of molten or solid systems : $NaF + AlF_3$, $NaF + AlF_3 + Al_2O_3$ and $CaF_2 + Al_2O_3$.

Beletzki [10] admitted a simple dependence of CR on diffraction line intensity ratio of chiolite and cryolite. The synthetic samples having CR within the 1.15 and 1.5 range were used for calibration plotting : cryolite ratio — $I_{\text{chiolite}}/I_{\text{cryolite}}$. These standard samples were obtained by melting of powder mixtures of NaF and AlF_3. The lack of specific conditions for high-temperature synthesis of standards represents an important impediment in the application of this method.

Lobos and Black,[2] for a cryolite ratio within the 1.5 and 1.3 range, revealed the difficulties in the determination of chiolite and accounted for the formation of calcium cryolite $3CaF_2 . 2AlF_3$.

The quantitative X-ray diffraction analysis of the actual aluminium cell electrolyte being possible only for its crystalline components we consider first the composition of the solid electrolyte.

---

[10] M. S. Beletzkii, *Tvet. Met.*, **35**, 56 (1962).

[11] E. Zintl and S. Morawietz, *Z. anorg. Chem.*, **240**, 145 (1939).

[12] H. Ginsberg and K. Resch, *Z. Erzberg. Metallhüt.*, **13**, 523 (1960).

[13] L. Holm, Doctoral Thesis, Technical University of Norway, Trondheim, 1963.

[14] D. Buist, *Mineralogical Mag.*, **36**, 281, 676 (1968).

CRYSTALLINE COMPOSITION OF SOLID ELECTROLYTE

The physico-chemical studies of the $NaF + AlF_3 + Al_2O_3 + CaF_2$ system have cleared up the nature of the components in melt as well as the crystalline phases formed by solidification.

In the molten $NaF + AlF_3$ system, by different methods[15-20] (phase diagram, equilibrium vapor composition, Raman spectroscopy etc.) the following compounds have been found : sodium fluoride, cryolite and sodium tetra-fluoro-aluminate correlated by the equilibrium :

$$Na_3AlF_6 \rightleftharpoons NaAlF_4 + 2NaF \qquad (A)$$

An AlF_3 excess leads to the formation of chiolite according to the equilibrium :

$$3Na_5Al_3F_{14} \rightleftharpoons 5Na_3AlF_6 + 4AlF_3 \qquad (B)$$

These equilibriums are completely shifted to the left side only in the solid state at temperatures just below the melting point.

In the AlF_3 + cryolite system, aluminium fluoride cannot exist as such, but only in the bound form, the solidified melt being a cryolite + chiolite mixture.[21-23]

Ginsberg and Resch [23] have first pointed out the importance of the cooling rate for a determined composition of the solidified $NaF + AlF_3$ system. On a sudden cooling ("freezing") of the system in the diffraction spectra the lines of sodium fluoride, cryolite and chiolite can be identified. On a slow or moderate cooling (as it is done with plant sample pick-up) the complete left shifting of the (A) and (B) equilibriums is ensured.

Rolin [24] has studied the $NaF + AlF_3$ system with 10 pc CaF_2 and stated that between CaF_2 and AlF_3 no chemical compound is formed. Beletzki [25] has confirmed, by X-ray diffraction, that a simple binary mixture, without solid solution formation, exists in the cryolite + CaF_2 system. This statement is supported also by the studies of density,[26]

---

[15] K. GRJOTHEIM, Doctoral Thesis, Thechinal University of Norway, Throndheim, 1956.

[16] M. ROLIN and M. REY, *Bull. Soc. chim. France*, **1966**, 2785.

[17] M. ROLIN and J. HOURIEZ, *Bull. Soc. chim. France*, **1964**, 891.
M. ROLIN and G. POUPA, *id.*, **1966**, 3953.

[18] J. HOWARD, *J. Amer. Chem. Soc.*, **76**, 2041 (1954).

[19] L. D. MCCARY, R. PAULE and J. MARGRAVE, *J. Phys. Chem.*, **67**, 1086 (1963).

[20] M. PAUCIROVA, K. MATIASOVSKY and M. MALINOVSKY, *Rev. Roumaine Chim.*, **15**, 201 (1970).

[21] W. FRANK and L. FOSTER, *J. Phys. Chem*, **61**, 1531 (1957).

[22] U. KUXMANN and U. TILLESEN, *Z. Erzberg. Metallhüt.*, **20**, 147 (1967).

[23] H. GINSBERG and K. RESCH., *Z. Erzberg. Metallhüt.*, **13**, 523 (1960).

[24] M. ROLIN, *Bull. Soc. chim. France*, 1351 (1961).

[25] M. S. BELETZKI, in "Teoreticheskie osnovy elektrometalurgyi aluminia" by G. ABRAMOV et al., Metallurgizdat, Moscow, 1953, p. 482.

[26] G. ABRAMOV and P. KOZUNOV, Trudy L.P.I., **1**, 60 (1939).

viscosity,[27a] electroconductivity [28,29] and molecular volumes.[30-33] Calcium cryolite was not synthetized by the melting of CaF_2 and AlF_3 mixture and not evinced in the X-ray diffraction spectra.

In the cryolite + Al_2O_3 system no chemical combinations did appear [13,34-36] after cooling.

We can draw the conclusion that aluminium fluoride and sodium fluoride are bound as cryolite and chiolite for a plant bath with cryolite ratio within the 1.5 and 0.83 range.

CRYOLITE RATIO DETERMINATION BY INTERNAL STANDARD METHOD

In order to overcome the difficulties of obtaining and measuring the diffraction spectra, the internal standard method was used.

From equations (1) and (2) it is seen that if an internal standard (component S) is added to the sample in known amount, then :

$$x_C = k'I_C/(1 - x_S)\, I_S = kI_C/I_S \tag{4}$$

provided x_S – the weight fraction of S, is held constant. Thus, the concentration of the C component is a linear function of the intensity ratio I_C/I_S. In practice, the linear plot is obtained by calibration with some synthetic mixtures.

For the determination of the cryolite ratio it is necessary and sufficiently to know the concentration of cryolite and chiolite in sample, i.e. x_{CR} and x_{CH} respective. This feature enables the preparation of synthetic mixtures of cryolite and chiolite in different proportions (to cover the CR range from 1.5 and 0.83), each being admixed with the same quantity of standard substance. Thus, from a single diffraction record the two constants in eq. (4), one for cryolite and the other for chiolite, may be obtained. To perform an analysis, the following characteristic lines were used : for cryolite $d = 2.74$ Å and for chiolite $d = 2.91$ Å.

EXPERIMENTAL

The substance designed as internal standard must satisfy some conditions, namely : a high purity, possibility to be ground until the crystallite dimensions are below 20 mμ (to produce clear-cut diffraction lines), strong diffraction lines close to the strong lines of the components to be analysed and not to overlap on these. In table 1 six chemical compounds which can be used as internal standard are presented.

[27a] G. Abramov, M. Vetyukov, I. Gupalo, A. Kostyukov and L. Lozhkin, "Teoreticheskie osnovy electrometalurgyi aluminia", Metalurghizdat. Moscow, 1953, p. 515.

[27b] *Ibidem*, p. 461.

[28] T. Pirson and D. Weddington, *Discuss. Faraday Soc.*, **1**, 307 (1947).

[29] A. Vajna, *Alluminio*, **19**, 215 (1950).

[30] A. Vajna, *Alluminio*, **20**, 29 (1951).

[31] V. Mashovetz, "Electrometalurgia aluminia", ONTI, Moscow, 1938.

[32] Reference 27, p. 536.

[33] P. Foster Jr., *J. Chem. Eng. Data*, **9**, 200 (1964).

[34] K. Yoshida, T. Ishihara and M. Yokoi, *T.M.S.—AIME*, **242**, 231 (1968).

[35] P. Foster Jr., *J. Amer. Ceram. Soc.*, **43**, 66 (1960).

[36] K. Grjotheim, L. Holm. C. Khron and J. Thonstad, in "Selected Topics in High Temperature Chemistry", Universitetforlaget, Oslo, 1966, p. 151.

The ammonium bromide line at $d = 2.78$ Å is placed between the characteristic lines of cryolite and chiolite, but in the diffraction records these lines are superposed. The other five compounds do not give any interference.

To ensure the accurate weighing of the components and their efficient mixing, the various mixtures were prepared under fixed experimental conditions. The same proportion, i.e. 10 per cent in weight, of the five substances mentioned in table 1, was mixed with different mixtures of cryolite and chiolite.

Table 1

Chemical compounds proposed as internal standard

Chemical compound	The strongest diffraction line d, Å
NH_4Br	2.87
NH_4NO_3	3.17
$NaNO_3$	3.03
$RbNO_3$	3.09
$CaCO_3$	3.04
$MnSO_4$	2.70

The most convenient chemical compounds are those with small or no X-ray absorption (compounds formed by the elements with small atomic number) and from table 2, we notice that such are the ammonium nitrate and the sodium nitrate.

The inspection of the diffraction spectra covered by the electrolyte lines and those of the two substances, shows a better resolution for ammonium nitrate. Thus, we have used ammonium nitrate as internal standard represented by the line $d = 3.17$ Å.

For calibration of the eq. (4) a few cryolite and chiolite mixtures (from 10 to 90 per cent chiolite content) mixed with 10 per cent ammonium nitrate (in weight) have been prepared.

Table 2

Influence of the additions on I_{CR} and I_{CH}

Sample + addition	I_{CR}	I_{CH}	I_S
	relative units		
Electrolyte (C.R. = 1.26)	82.0	20.5	—
Electrolyte + NH_4NO_3	82.0	20.5	25.5
Electrolyte + $NaNO_3$	68.5	17.5	77.0
Electrolyte + $RbNO_3$	65.5	16.0	59.0
Electrolyte + $CaCO_3$	60.5	15.0	60.0
Electrolyte + $MnSO_4$	58.0	15.0	43.0

Natural cryolite (hand-picked at Arksutfijord, Greenland) and synthetic chiolite were used.

The chiolite was prepared by careful melting of sodium fluoride and aluminium fluoride mixture in stoichiometric proportion. The product was analysed by pyrotitration and a CR of 0.85 was found (compare with theoretical value 0.83).

Cryolita, chiolite and ammonium nitrate have been ground for 15 minutes each in an agate mortar and then mixed by vibration, for 15 minutes, in a GM 9458 M. von Ardenne model vibrator.

The X-ray diffraction records have been obtained by a Geiger-counter X-ray spectrometer type URS-50IM with incorporated GUR-4 goniometer. The instrumental conditions for recording have been as follows:

- Cu Kα radiation (anodic current 10 mA and 35 kV voltage).
- slit set: source slit: 1 mm
  goniometer slit: 2 mm
  counter slit: 0.5 mm
- counter rotation speed: 4°/min.
- time constant for pulse-averaging circuit: 3 s.
- scanning speed of the strip-chart recorder was of 1.6 m/h.

The powder mixtures have been placed in a plastic cell and then in a sample holder to the goniometer.

The chart-records cover the 2θ-spectral area within 26° and 33° where three peaks appear: at 28°9′ for ammonium nitrate, at 30°50′ for chiolite and at 32°26′ for cryolite. The intensity of each line has been measured as the peak height against the background.

RESULTS AND DISSCUSIONS

The diffraction data for five synthetic mixtures are presented in table 3 and plotted in figure 1 to demonstrate the linearity.

The equations of the two straight lines from fig. 1 are:

$$I_{\mathrm{CH}}/I_{\mathrm{S}} = 0.648\, x_{\mathrm{CH}}$$

and

$$I_{\mathrm{CR}}/I_{\mathrm{S}} = 0.0547\, x_{\mathrm{CR}}$$

where x_{CH} and x_{CR} are expressed in per cent in weight.

Table 3

Diffraction intensities of the cryolite + chiolite + NH_4NO_3 mixtures

Chiolite %	I_{CR}	I_{CH}	I_{S}	$I_{\mathrm{CR}}/I_{\mathrm{S}}$	$I_{\mathrm{CH}}/I_{\mathrm{S}}$
	relative units				
11.1	141.5	16.0	30.0	4.71	0.53
22.2	130.0	31.5	30.5	4.26	1.03
44.5	111.5	78.0	36.0	3.10	2.17
66.7	58.0	100.0	31.5	1.84	3.17
88.9	20.5	121.0	28.5	0.72	4.24

If the points on the straight lines are the most probable values of the diffraction intensities, it is possible to draw another graph to exemplify the direct correlation between the $I_{\mathrm{CH}}/I_{\mathrm{CR}}$ ratio and the chiolite concentration (fig. 2).

This graph can be used as calibration curve for the determination of the cryolite ratio of a cell electrolyte. In this way the CR of some electrolyte cell plant samples (from ALRO, Slatina) have been determined. The diffraction results have been compared (table 4) with the pyrotitration results (this method was elaborated after both Abramov et al [27b] procedure and Lobos and Black's [2] improvements). A good agreement between the two sets of values is noticed and the maximum error is of 0.04 units. The average deviation is 1.3 per cent.

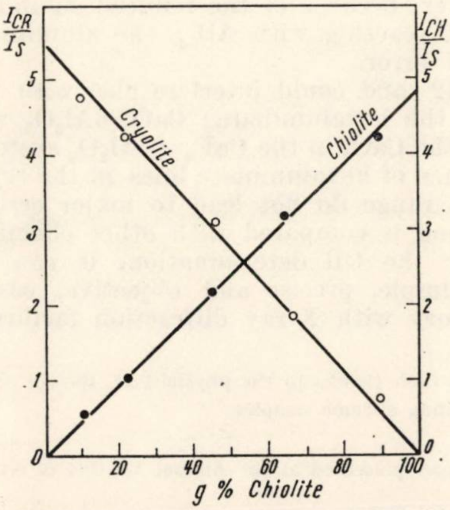

Fig. 1. — Linearity of the relation (4) for cryolite + chiolite + NH_4NO_3 mixtures.

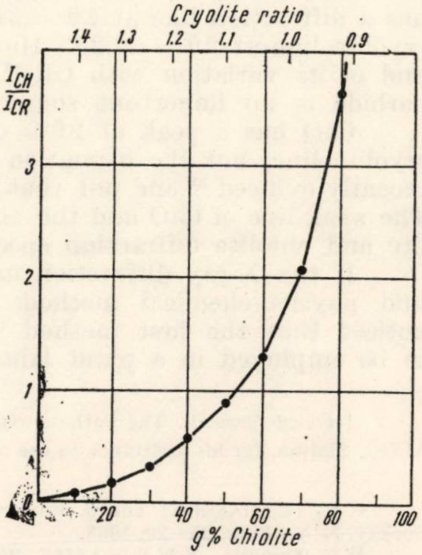

Fig. 2. — Calibration graph for cryolite ratio determination.

Finally, a few error sources which can lead to uncertain results are metioned.

The presence of the impurities with strong absorption elements as iron (in electrolyte bath or accidentally from the rod or the spoon) can

Table 4

Cryolite ratios of some electrolyte samples from ALRO aluminium plant

Electrolyte sample	$\frac{I_{CH}}{I_{CR}}$	Cryolite ratio		ΔRC
		X-ray	Pyrotitration	
H2 —133	0.951	1.09	1.08	+0.01
—136	1.027	1.08	1.07	+0.01
—138	1.613	1.01	0.98	+0.03
—142	0.290	1.17	1.15	+0.02
—161	0.207	1.33	1.31	+0.02
—163	0.431	1.22	1.21	+0.01
—165	0.833	1.11	1.09	+0.02
—167	1.107	1.06	1.10	—0.04
—171	0.247	1.30	1.30	0.0
—175	0.482	1.20	1.20	0.0

induce the decrease of the peak heights. More frequently these impurities are the coal foam and the alumina, but they are not active in the X-ray diffraction spectra.

Sometimes, the anomalous working of the reduction cells, would bring about chemical and electrochemical secondary reactions, the diffraction analysis leading to less accurate results. Thus, from the cathodically polarized carbon pieces in the presence of both molten cryolite and aluminium, the aluminium carbide, Al_4C_3, may be formed.[37] This has a diffraction line at $2\theta = 31°48'$ which would partially overlap the cryolite line at $2\theta = 32°28'$. However, because of the reduced solubility and of its variation with CR,[38] i.e. reacting with AlF_3, the aluminium carbide is no important source of error.

CaO has a peak at $2\theta = 32°12'$ and could interfere also with the cryolite line, but the formation of the hexaluminate : $CaO . 6Al_2O_3$ was recently evinced [39] and not that of the CaO, in the $CaF_2 + Al_2O_3$ system. The weak line of CaO and the absence of hexaluminate lines in the cryolite and chiolite diffraction spectra range do not lead to major errors.

If the X-ray diffraction method is compared with other chemical and physico-chemical methods for the CR determination, it can be noticed that the first method is simple, precise and objective, easily to be employed in a plant laboratory with X-ray diffraction facilities.

Acknowledgements. The authors express their thanks to the physicist D. Bârsan from ALRO, Slatina, for his assistance in the recording of some samples.

---

[37] E. Hollingshead and J. Brown, paper presented at the Annual Meeting of AIME Society, N.Y., Febr. 25–29, 1968.

[38] E. Dewing, *T.M.S.–AIME*, **245**, 2181 (1969).

[39] A. Mitchel and E. Burel, *J. Iron Steel Inst.*, **1970**, 407.

Revue Roumaine de Chimie, 17, 6, 969–975 (1972)

NEW THEORETICAL DATA ON THE STRUCTURAL CHEMICAL EQUILIBRIUM IN MOLTEN GLASS

P. BALTĂ

Polytechnic Institute of Bucharest,
Str. Polizu 1, Bucharest, Romania

Received November 25, 1971

As a sequel to previous works new, theoretically calculated data on the distribution of polymers for some binary and ternary glasses in the system $SiO_2-CaO-Na_2O$ have been put forward. On this basis a model of the structure of molten sodium metasilicate has been worked out. The obtained data are in good agreement with the properties of the melts under study and with the experimental results referring to the influence of the development of the melt on glass properties, published elsewhere.

★

The existence in the melt of a chemical-structural, equilibrium dependent on temperature and on time, has been convincingly proved in recent years, although there are still few works devoted to such a topic. In 1959 McKinnis and Sutton [1] have emphasized the influence of the melting temperature on the mechanical properties of glass fibers, providing also an interesting theoretical explanation and launching the notion of "history of the melt". Rindone [2] and his collaborators have studied the influence of the melting conditions on the properties of some simple glasses and have found important changes accounted for by the chemical-structural equilibrium in the melt.

Bobkova and collab.[3,4] have published some series contributions dealing with the influence of temperature and duration of the melt on the properties of some more complex glasses including industrial glasses.

The experimental results are generally interpreted in terms of the chemical-structural equilibrium, influenced by temperature and time, among the various polymer species existing in the melt. The first theoretical approaches of the chemical-structural equilibrium set in some silicate melts (SiO_2-FeO and SiO_2-CaO) are due to Masson [5, 6] and Pretnar.[7] Making use of their methods the author has obtained, by calculations, some data on the polymer distribution in silico-sodium melts.[8] In the following, new data accumulated in this way are presented.

---

[1] C. L. McKinnis and J. W. Sutton, *J. Amer. Ceram. Soc.*, **42**, 194 (1959), **42**, 250 (1959).

[2] G. E. Rindone, *Glass Ind.*, **1969**, 138.

[3] N. M. Bobkova and V. V. Rudakov, *Steklo i Keramika*, **1967**, 11.

[4] N. M. Bobkova and I. A. Trunets in "Likvatsionye iavlenia v steklakh", Leningrad, Izd. Nauka, 1969, p. 36–39.

DISTRIBUTION OF POLYMER IN SOME GLASSES OF THE $SiO_2 - CaO - Na_2O$ SYSTEM

As already known, in the most general case, a silico-alkaline melt is obtained by the high temperature reaction of silicium dioxide as quartz sand, with the alkaline carbonate. Under industrial conditions, the heating of the mixture to over 1000° occurs very quickly so that, neglecting the solid phase reactions, we may consider from the beginning the solving of the SiO_2 tridimensional lattice in the alkaline melt.

As shown in [8,9] the alkaline cations, weaken the Si—O—Si bridges so that from the tridimensional lattice short chains or bands are loosening which, keep being attacked by the alkaline melt, and break down to simple orthosilicate molecules. Among the appearing various molecule species an equilibrium sets up, that may be expressed by the reaction.

$$Si_xO_{3x+1}\,Na_{2x+2} + SiO_4\,Na_4 \rightleftharpoons Si_{x+1}\,O_{3x+4}\,Na_{2x+4} + Na_2O \tag{1}$$

It therefore results that, in principle, any polymer may appear due to the condensation of an inferior polymer with a monomer. The reaction is controlled by an equilibrium constant according to relation

$$K_{1x} = \frac{N_{Si_{x+1}\,O_{3x+4}\,Na_{2x+4}} \cdot N_{Na_2O}}{N_{SiO_4\,Na_4} \cdot N_{Si_x\,O_{3x+1}\,Na_{2x+2}}} \tag{2}$$

The existence of a correlation such as below has been theoretically and experimentally proved [5].

$$\frac{N_{Si_{x+1}\,O_{3x+4}\,Na_{2x+4}}}{N_{Si_x\,O_{3x+1}\,Na_{2x+2}}} = \frac{K_{1x} \cdot N_{SiO_4\,Na_4}}{N_{Na_2\,O}} = r \tag{3}$$

where N is the molar fraction of the respective species, K_{1x} — the equilibrium constant corresponding to the reaction between a monomer and a polymer with x silicon atoms and r — the rate of the geometrical progression pointing to the ratio of the successive terms of the homologue polymer series. Knowing K_{1x} and the molar fraction of a polymer, by relation (3) we may calculate the polymer distribution for a given composition. Obtaining rate r as indicated by Pretnar,[7−9] the following relation may be used to calculate the distribution

---

[5] C. R. MASSON, *J. Amer. Ceram. Soc.*, **51**, 134 (1968).

[6] C. R. MASSON, I. B. SMITH and S. G. WHITEWAY, *Canad. J. Chem.*, **48**, 1456 (1970).

[7] B. PRETNAR, *Ber. Bunsengesellschaft Phys. Chem.*, **72**, 773 (1968).

[8] P. BALTĂ and E. BALTĂ, *Rev. Roumaine Chim.*, **16**, 1543 (1971).

[9] P. BALTĂ and E. BALTĂ, "Introducere în chimia fizică a stării vitroase", Bucharest, 1971, p. 93—107.

$$n_x = n_{\mathrm{SiO_2}\,(1-r)^2} \cdot r^{x-1} \tag{4}$$

where n stands for the number of moles. The values of the K_{1x} constant for systems which have not been determined experimentally, may be obtained by means of the correlation, emphasized in,[8,9] between $\log K_{1x}$ and the ionization potential of the metallic ion expressed in eV.

Proceeding as above we have calculated the polymer distribution for melts of the sodium metasilicate and calcium metasilicate, using in the former case the value $K_{1x} = 8 \times 10^{-8}$, obtained by the already mentioned correlation, and in the latter case, the value $K_{1x} = 0{,}03$. [6] In calculating the formula of the molecule with x silicon atoms, after Pretnar,[7] we reached the molecular weight and then the products $n_x . M_x$ where M_x stands for the molecular weight of the polymer with x silicon atoms.

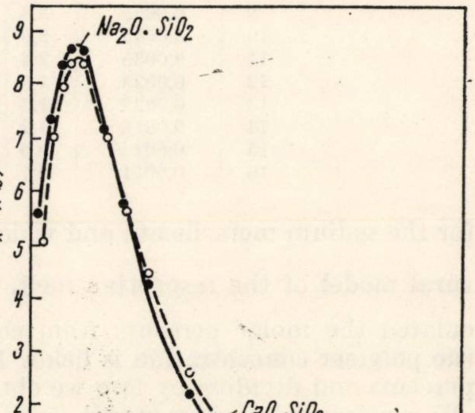

Fig. 1. — Polymer distribution in melts with sodium metasilicate and calcium metasilicate composition.

In this way we could represent in figure 1 the variation of the weight of various polymer species with respect to x, for melts with the composition of the sodium metasilicate and calcium metasilicate.

The diagram points to the special significance, in this melt, of tetramers, and then to the fact that the weight of molecules with over 30 silicon atoms is negligible and also that the monomers (orthosilicate molecules) are present in a great amount. Besides, although the equilibrium constants have very different values, the polymer distribution in both metasilicates is most similar. It may be inferred that with the decrease in the value of the K_{1x} constant below a certain limit, its specific influence also markedly fades.

Table 1 one lists a summary of the data obtained by calculation for the sodium metasilicate and which underlie the elaboration of a structural model of the respective melt. Using as reference $\sum_{x=1}^{40} n_x$ we have calculated the molar percents from column 3, and found that for $x > 16$ the polymer concentration is below 1 % molar. By rounding off the molar percents and dividing by two we obtained the number of molecules (46 in all) represented on the model (5th column). For molecules with concentrations smaller than 2 % molar (from $x = 13$ onward), dividing by two occurred by removing every second molecule species. In this way we have avoided the representation in the model of some molecule halves.

Table 1

Calculated data used for the elaboration of the model of molten $Na_2O.SiO_2$ structure

x	n_x		Formula after[7]	Molecules represented on the model
	Calculated with rel. (4)	% molar		
1	0.0296	19.3	SiO_4Na_4	9
2	0.0239	15.5	$Si_2O_7Na_6$	8
3	0.0194	12.6	$Si_3O_{10}Na_8$	6
4	0.0157	10.2	$Si_4O_{13}Na_{10}$	5
5	0.0127	8.2	$Si_5O_{16}Na_{12}$	4
6	0.0103	6.7	$Si_6O_{18}Na_{12}$	3
7	0.0083	5.4	$Si_7O_{21}Na_{14}$	2
8	0.0068	4.4	$Si_8O_{24}Na_{16}$	2
9	0.0055	3.6	$Si_9O_{26}Na_{16}$	2
10	0.0044	2.9	$Si_{10}O_{28}Na_{16}$	1
11	0.0035	2.3	$Si_{11}O_{31}Na_{18}$	1
12	0.0028	1.8	$Si_{12}O_{33}Na_{18}$	1
13	0.0023	1.5	$Si_{13}O_{36}Na_{20}$	—
14	0.0018	1.2	$Si_{14}O_{38}Na_{20}$	1
15	0.0014	0.9	$Si_{15}O_{41}Na_{22}$	—
16	0.0011	0.7	$Si_{16}O_{43}Na_{22}$	1

Although if Pretnar's [7] calculation, used to obtain the formulae of molecules corresponding to certain values of x, is sensible enough, for metasilicate we appreciated more suitable to consider that, even for values of x exceeding 12, one obtains bidimensional structures, corresponding to the bisilicate, and not tridimensional ones. Another simplifying condition was that, in the melt, there are only cycles with 6 tetrahedra each and not with 5,4 or 3. Thus, the representation of all plotted molecule species has become relatively simple.

The picture (fig. 2) may be considered, with a certain approximation, as a monomolecular cross-section through the sodium metasilicate melt. For the sake of simplification we represented only 3 but of the 4 Si-O- bonds of each tetrahedron and obviously less non-bridged oxygen atoms and sodium atoms.

The model also enhances the structural heterogeneity of the melt, as well as the lubrifying part played by small molecules of monomers, dimers, trimers, surrounding the great bidimensional molecules. It also enables the devising of the ordering process, during the cooling, based on the redistribution of sodium atoms followed by the loosening of the two parallel chains forming the bisilicate bands, by the condensation of small molecules in longer chains and their final ordering by the insertion of $-O^{-}-\ Na^{+}$ dipoles from neighbouring chains.

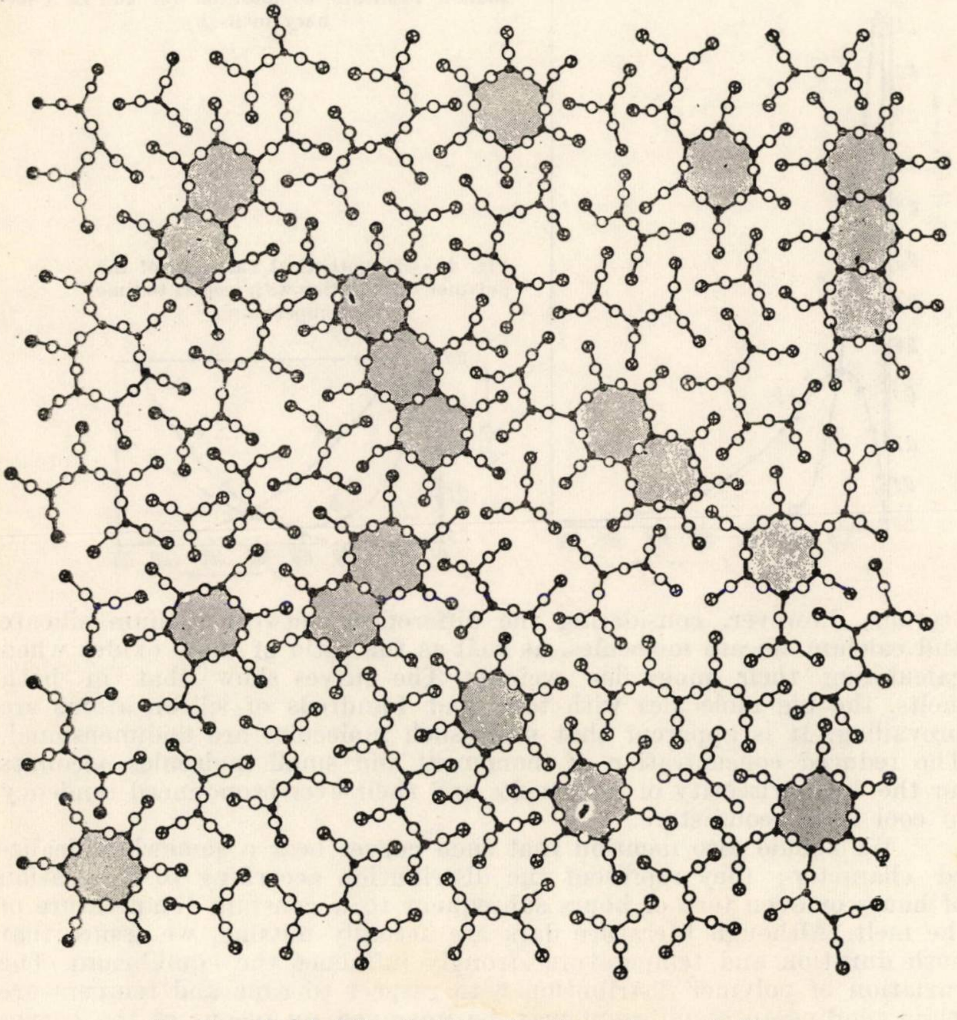

Fig. 2. — Model of the structure of molten sodium metasilicate.

By a similar calculation we obtained the polymer distribution in a melt with sodium bisilicate composition.

The curve is represented in figure 3. The sams diagram also plots the distribution curve for a silico-calcium-sodium ternary glass with component ratio similar to that in common window glass. For this calculation we started from the above statement, namely that belove a certain value, the equilibrium constants do no longer exert any decisive influence on the distribution. As a result, we used only one constant i.e. that of the $CaO-SiO_2$ (0.003) and the sum of the Na_2O and CaO concentrations, however, considering the differences between sodium silicate and calcium silicate molecules, as well as the ratio of these oxides when calculating their molecular weights. The curves show that in both melts, the big molecules with tens and hundreds of silicon atoms are prevailing. It is apparent that most such molecules are tridimensional. The reduced concentration of monomers and small molecules accounts for the high viscosity of such melts and their ever-pronounced tendency to cool in vitreous state.

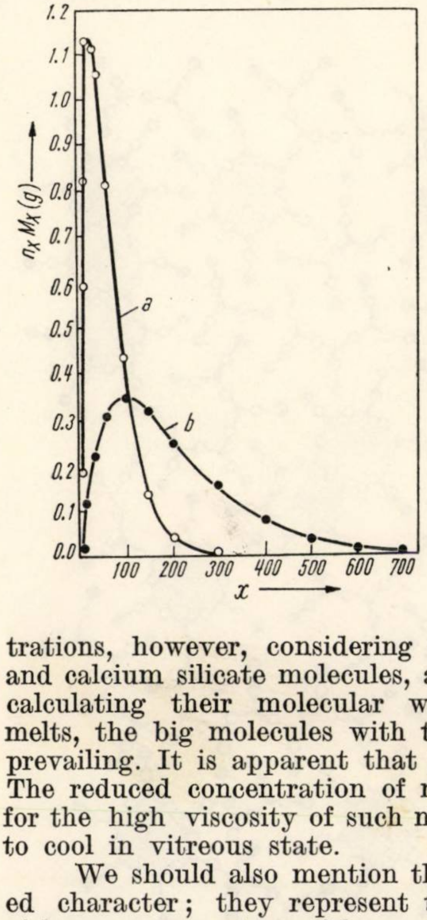

Fig. 3. — Polymer distribution in the melt with sodium bisilicate composition (a) and in a ternary melt (b).

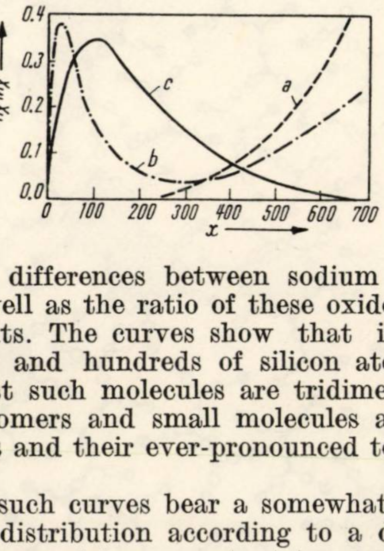

Fig. 4. — Hypothetical variation of the polymer distribution with respect to time and temperature.

We should also mention that such curves bear a somewhat idealized character; they represent the distribution according to a duration of hours or even tens of hours subsequent to a constant temperature of the melt. Although literature data are actually missing, we assure that both duration and temperature strongly influence the equilibrium. The variation of polymer distribution with respect to time and temperature while tending to equilibrium may be imagined by means of the curves in figure 4. Curve a stands for the initial phase. Sand granules may be considered as fragments of tridimensional lattice with hundreds and thousands of silicon atoms. At the other end we have the carbonate resp., sodium oxide, as isolated molecules. After a time interval, subsequent to the solving of surface layers of the granules, a great number of small molecules, and a relatively smaller number of medium-sized molecules are forming while numerous great fragments of tridimensional lattice still remain. Such distribution is represented by curve b. At last, at equilibrium, we reach curve c, which corresponds to the theoretical calculation. It results that the actual distribution of polymers in solid glass depends essentially on the stage the processes developing in the melt are stopped at. It is therefore obvious that the chemical-structural equilibrium in the melt depending on the melt history, ought to influence to a great extent the glass properties obtained by its undercooling. The above assertion is supported by the above quoted works and by our own experimental results published in.[10]

CONCLUSIONS

With Pretnar's calculation method and the values of the equilibrium constants existent in literature or deduced on the basis of the correlation with the ionization potential, we have obtained the polymer distribution for binary and ternary melts in the system $SiO_2-CaO-Na_2O$. The distribution curves allow the concretization of the opinions on the melt structure and are in good agreement with their properties.

On the basis of the calculated distribution, we have worked out the model of the structure of sodium metasilicate melt, which offers a useful intuitive picture and allows to interpret the properties of this melt.

The results are in good agreement with the experimental data referring to the influence of the melt history on the properties both those provided by other authors and ours which have been published elsewhere.

---

[10] P. Baltă and C. Stoicănescu, *Ind. Uşoară*, **1971**, 621.

or small molecules, and a relatively smaller number of medium-sized molecules are formed, while [illegible] gives fragments of the metasilicate [illegible] [illegible] [illegible] is represented by curve b. In [illegible] bath at equilibrium, we reach curve c, which corresponds to the theoretical calculation. It results that the actual distribution of polymers in solid glass depends essentially on the stage the processes developing in the melt are stopped at. It is therefore obvious that the chemical structural equilibrium in the melt depending on the melt history, ought to influence to a great extent the glass properties obtained by its subsequent [illegible]. The above assertion is supported by the above quoted works and by our own experimental results published in[9].

CONCLUSIONS

With Prener's calculation method and the values of the equilibrium constants existent in literature or deduced on the basis of the correlation with the ionisation potential, we have obtained the polymer distribution for binary and ternary melts in the system $SiO_2-CaO-Na_2O$. The distribution curves allow the concentration of the opinions on the melt structure and are in good agreement with their properties.

On the basis of the calculated distribution, we have worked out the model of the structure of sodium metasilicate melt, which offers a useful intuitive picture and allows to interpret the properties of this melt.

The results are in good agreement with the experimental data referring to the influence of the melt history on the properties both those provided by other authors and ours which have been published elsewhere.

---

[9] [illegible] [illegible] [illegible] [illegible] 1971, [illegible].

Revue Roumaine de Chimie, 17, 6, 977–980 (1972)

ROENTGENOGRAPHIC STUDIES OF $[Fe(II)PHEN_2(NCS)_2]$***

P. SPACU,* D. CIOMÂRTAN** and MARGARETA TEODORESCU*

Received January 26, 1972

The mixed ligand complex $[Fe(II)phen_2(NCS)_2]$ obtained using three different preparation ways, has been roentgenographically studied and the parameter of the unit cell and the spatial group reported.

INTRODUCTION

In recent years, the mixed ligand complex $[Fe(II)phen_2(NCS)_2]$, where phen = orthophenantroline, has been intensively studied by many authors, which have shown, that a temperature-dependent spin equilibrium, high spin (quintet) $\rightleftarrows$ low spin (singlet), should take place for this compound. That equilibrium has been proved using physical methods such as measurements of : the paramagnetic susceptibility,[1] IR spectra,[2] as well as γ-resonance spectroscopy and electronic spectra, recorded at different temperatures.[3] It should be mentioned in this context, that an obvious variation of the magnetic moment with the preparation way, has been reported and assigned to a polymorphic change in the crystal package.[3]

Roentgenographic studies performed on the paramagnetic complex $[Fe(II)phen_2(NCS)_2]^1$, prepared using the method (i) (see Experimental) show at a simple comparison of the diffraction lines, that the complex belongs to the same crystallographic system as the *cis*-$[Fe(II)phen_2(CN)_2]$ studied by Hamer and Orgel[4] (IR data). The aim of this note is to present the roentgenographic measurements, performed on powders, at room temperature for the mentioned compound, obtained using three different preparation ways, in order to estimate the parameters of its unit cell and the corresponding crystallographic group.

---

* Faculty of Chemistry, University of Bucharest

** Center of Chemical Physics, Section of Chemical Bond, Bucharest

*** The present paper was presented at the Second National Conference on Pure and Applied Chemical Physics, 1–4 September 1970, Bucharest.

[1] W. A. Baker and H. M. Bobonich, *Inorg. Chem.*, **3**, 1184 (1964).

[2] E. König and K. Madeja, *Spectrochim. Acta*, **23A**, 45 (1967).

[3] E. König and K. Madeja, *Inorg. Chem*, **6**, 48 (1967).

[4] N. K. Hamer and L. E. Orgel, *Nature*, **190**, 439 (1961).

EXPERIMENTAL

The compound has been prepared using three methods:

(i) from [Fe (II) $phen_3$] $(NCS)_2$[1]

(ii) from [Fe (II) py_4 $(NCS)_2$], the yellow form in methanol, the substitution of the pyridine leading under certain conditions earlier reported [5,6] either to the paramagnetic blue-violet species-[Fe (II) $phen_2(NCS)_2$] or to the deep-violet mixed ligand complex [Fe (II)py_2 phen $(NCS)_2$]

(iii) from [Fe (II) $py_4(NCS)_2$] where pyridine is substituted by *ortho*-phenantroline in solution of pyridine.[7]

The diffraction spectra of powders have been obtained with a diffractometer H Z G 1 joined to T U R M 61 equipment, using the radiation $\lambda = 1.93597$ Å of $FeK\alpha_1$ passed through a Mn-filter.

RESULTS AND DISCUSSION

The diffractions spectra recorded for the final products of all the three preparation methods were identical, the results being summarized in the table 1.

The quantities θ° and $[\sin^2\theta]_{exp.}$ have been obtained experimentally, and the relative intensities I/I_1 measured. To obtain the parameters of the unit cell and the assignement of the indices *h*, *k*, *l* for every diffraction line, the procedure earlier described by Zachariasen [8] for the monoclinic system has been adopted. Three orthogonal vectors have been then obtained, the crystallographic system being, for this reason, most probably orthorhombic. The calculated parameters for the unit cell are $a = 13.23 \pm 0.01$ Å; $b = 17.51 \pm 0.02$ Å and $c = 10.18 \pm 0.01$ Å, these values being used in order to index the diffraction lines, in agreement with the results from the table 1. From the extinction rules for *h*, *k* and *l* it may be concluded that [Fe(II)$phen_2(NCS)_2$] belongs to the orthorhombic system and to the spatial group P_{nna} (D_{2h}^6), no 52 in the International Tables.

The experimental density was measured with the pycnometer method in ethyl ether at 20° ($\rho_{exp.} = 1.65 \pm 0.03$ g/cm³) leading to four molecules included in the unit cell. These four molecules could be arranged in the unit cell with central ions placed in the general positions (8e), in agreement with the extinction rules for $P_{nna}(D_{2h}^6)$. It should be therefore concluded that the molecules have the ligands arranged in a *cis*-configuration, in agreement with the assumption advanced elsewhere by Baker [1] and König.[9] The comparison between the parameters of the unit cell for [Fe(II)$phen_2(NCS)_2$] herein reported, and [Fe(II)$dipy_2(NCS)_2$][10] reported elsewhere ($a = 13.17$ Å; $b = 16.50$ Å and $c = 10.08$ Å), shows that the parameter "b" takes a greater value for the first complex. The last compound belongs to a different spatial group, P_{cnb} (D_{2h}^{14}) no 60 in the

---

[5] P. Spacu, M. Teodorescu and C. Lepadatu, *Rev. Roumaine Chim.*, **9**, 1(1964).

[6] P. Spacu, M. Teodorescu and D. Ciomârtan, *Monatsh. Chem.* **103**, 1–8 (1972).

[7] K. Madeja, W. Wilke and S. Schmidt, *Z. Anorg. Chem.*, **346**, 306 (1966).

[8] W. Zachariasen, *Acta Crystallog.*, **16**, 784 (1963).

[9] E. König, K. Madeja and K. J. Watson, *J. Amer. Chem. Soc.*, **90**, 1146 (1968).

[10] E. König and K. Madeja, *Chem. Commun.*, 61 (1966).

Table 1

X-ray data on the complex compound [Fe (phen)$_2$ (NCS)$_2$]

No	θ°	$\sin^2\theta_{exp}$	$\sin^2\theta_{calc}$	d(Å)	*hkl*	I/I_1
1	6.33	0.0122	0.0122	8.78	020	42
2	6.88	0.0144	0.0144	8.08	101	32
3	7.59	0.0174	0.0175	7.33	111	51
4	8.40	0.0214	0.0214	6.63	002	5
5	9.39	0.0266	0.0266	5.93	121	12
6	10.55	0.0335	0.0336	5.29	022	9
7	10.95	0.0361	0.0362	5.10	200	10
8	11.44	0.0394	0.0393	4.88	210	5
9	11.84	0.0421	0.0420	4.72	131	45
10	11.94	0.0428	0.0427	4.68	122	21
11	12.78	0.0489	0.0490	4.38	040	5
			0.0485		220	
12	13.20	0.0521	0.0513	4.24	013	6
13	13.45	0.0539	0.0542	4.16	221	10
14	13.84	0.0572	0.0572	4.05	103	18
			0.0576		202	
15	14.24	0.0605	0.0607	3.94	212	24
			0.0603		113	
16	14.64	0.0639	0.0638	3.83	230	100
17	15.27	0.0694	0.0695	3.68	123	7
			0.0698		222	
18	16.40	0.0797	0.0794	3.43	142	7
19	17.00	0.0855	0.0852	3.31	240	30
			0.0852		232	
			0.0856		004	
20	17.24	0.0878	0.0875	3.27	213	11
21	17.54	0.0908	0.0907	3.21	151	26
22	18.24	0.0984	0.0979	3.09	024	6
			0.0977		114	
23	19.54	0.1119	0.1119	2.89	233	7
24	20.44	0.1220	0.1220	2.77	204	9
			0.1222		134	
25	21.68	0.1365	0.1368	2.62	015	9
			0.1359		341	
26	22.55	0.1471	0.1480	2.52	410	5
27	23.02	0.1529	0.1530	2.48	411	4
28	26.48	0.1981	0.1981	2.17	073	13
			0.1982		254	
29	28.86	0.2330	0.2336	2.00	414	7

International Tables. The difference of about 1 Å between the values of "b" is probably due to the fact that the *ortho*phenantroline has three more "σ" C—C bonds which enlarge the direction on the bisecting line of the angle N(phen) — Fe—N(phen) with 1.4 Å (fig. 1).

Since the complex molecules make a given angle with the axis "b", the projection of this additional elongation must be consequently less than 1.40 Å, in agreement with our results. It should be finally mentioned that the attempt to find again the experimental data for $[Fe(II)phen_2(NCS)_2]$ using the parameters of the unit cell and the spatial group found for $[Fe(II)dipy_2(NCS)_2]$[10] has been unsuccessful and it may be therefore concluded that no isotypism between the mixed ligand complexes could exist.

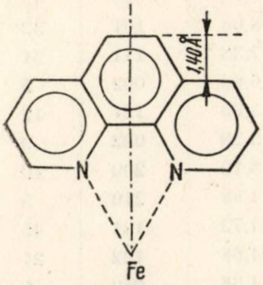

Fig. 1. — Elongation on the bisecting line due to the additional ring of the "phen" against the "dipy".

Revue Roumaine de Chimie, **17**, *6*, 981–992 (1972)

COMBINAISONS COMPLEXES AVEC DÉRIVÉS BIPHÉNYLIQUES. XXVI

CYANATES MÉTALLIQUES SIMPLES ET COMPLEXES AVEC DÉRIVÉS DIAMINOBIPHÉNYLIQUES

RODICA MICU-SEMENIUC et CONST. GH. MACAROVICI

Chaire de Chimie inorganique de l'Université de Cluj, 11, str. Arány Janos

Reçu le 18 août 1971

On a obtenu des cyanates simples et complexes avec les dérivés diaminobiphényliques de cobalt (II) et nickel (II). On a enregistré leurs spectres en IR, de réflexion et de micro-ondes. On a fait des déterminations de susceptibilité magnétique. Sur la base des données expérimentales on suggère que les ions métalliques sont hexacoordinés, les uns étant monomères, les autres, probablement, polymères.

Les ions de la première rangée de métaux transitionnels sont caractérisés par leur capacité de former une large gamme de combinaisons complexe, où le nombre de coordination six domine. Dans le présent ouvrage on étudie les cyanates complexes des ions d^7 et d^8, par dérivés diaminobiphényliques qui n'ont pas encore été étudiés jusqu'à présent.

La littérature de spécialité n'est pas trop riche en études sur les cyanates. On a étudié quelques cyanates simples des éléments alcalins [1–5] et de Ag(I), Tl(I), Cd(II), Hg(II), Pb(II), Si(IV) et Ge(IV). [1,5–8] Les premières études de synthèse sur les cyanates métalliques complexes ont été initiées par Ripan [9] qui obtient deux classes de combinaisons $M(py)_{2\,(4)}(NCO)_2$ où M = Mn(II), Fe(II), Co(II), Ni(II), Cu(II), Zn(II) et py = pyridine et $[M(NCO)_4]^{2-}$ où M = Co(II), Ni(II), Cu(II).

On connaît aussi d'autres cyanates complexes des éléments *3d* avec pyridine, [10–13] méthylpyridine,[12,13] quinoléine et isoquinoléine, [13,14]

---

[1] L. Birçkenbach et H. Kolb, *Ber. dtsch. Chem. Ges.*, **68**, 895 (1935).

[2] F. A. Miller et Ch. H. Wilkins, *Analyt. Chem.*, **24**, 1253 (1952).

[3] W. H. T. Davison, *J. Chem. Soc.*, 1953, 3712.

[4] A. Maki et J. C. Decius, *J. Chem. Phys.*, **28**, 1003 (1958).

[5] T. C. Waddington, *J. Chem. Soc.*, **1959**, 2499.

[6] F. A. Miller et G. L. Carlson, *Spectrochim. Acta*, **17**, 977 (1961).

[7] J. W. Rabalais, J. R. McDonald et S. P. McGlynn, *J. Chem. Phys.*, **51**, 5095 **(1969)**.

[8] J. W. Rabalais, J. R. McDonald et S. P. McGlynn, *J. Chem. Phys.*, **51**, 5103 **(1969)**.

[9] R. Ripan, *Bull. Soc. Sci. Cluj*, II, **1924–25**, 73 ; III, **1926–27**, 176 ; IV, **1928–29**, 499.

[10] S. M. Nelson, *Proc. Chem. Soc.*, **1961**, 372.

[11] H. C. A. King, E. Kőrős et S. M. Nelson, *Nature*, **196**, 572 (1962).

[12] H. C. A. King, E. Kőrős et S. M. Nelson, *J. Chem. Soc.*, **1964**, 5449.

[13] S. M. Nelson et T. M. Shepherd, *Inorg. Chem.*, **4**, 813 (1965).

[14] H. C. A. King, E. Kőrős et S. M. Nelson, *J. Chem. Soc.*, **1964**, 4832.

cyanopyridine[11,15], dipyridyl[14,16] *o*-phénantroline[16] et urotropine,[17] ainsi que des combinaisons du type des acidocomplexes à trois, quatre ou six ions NCO^{-}. [17–23]

Notre but est d'étudier le comportement des cyanates, dans une étude plus ample, comparé au comportement des thiocyanates et sélénocyanates métalliques correspondants.[24]

PARTIE EXPÉRIMENTALE

Les substances nécessaires pour l'obtention de nouvelles combinaisons ont été acquises dans le commerce, à l'exception des dérivés diaminobiphényliques, qui ont été préparés selon les indications de la littérature.[25]

Pour l'obtention des cyanates simples, on dissout les quantités stœchiométriques de $Co(NO_3)_2 \cdot 6H_2O$, $Ni(NO_3)_2 \cdot 6H_2O$ en 50–100 ml d'eau et séparément de KOCN en 30–40 ml d'eau. Les solutions sont chauffées jusqu'à proximité du point d'ébullition et mélangées. On agite et on laisse refroidir, après quoi on filtre le précipité formé et on le lave plusieurs fois à l'eau chaude et froide. On utilise la même méthode de travail pour obtenir les combinaisons avec l'*o, o'*-DABP, à la différence qu'en même temps que le cyanate de potassium on ajoute aux solutions d'azotate de Co (II) et Ni (II) de l'*o, o'*-DABP (la quantité nécessaire pour le rapport 1M : 2 amines) dissous dans un mélange eau-alcool en proportion de 3 : 1, amené au point d'ébullition. Par repos et agitation, des combinaisons correspondantes microcristallines sont précipitées et filtrées, lavées et séchées à l'air. La composition des combinaisons synthétisées résultant de l'analyse élémentaire, ainsi que d'autres propriétés se trouvent incluses dans le tableau 1.

Les essais de synthétiser les cyanantes de ces éléments avec m, *m'*-DABP et *p, p'*-DABP n'ont pas donné de résultats. Dans le premier cas on obtient des cyanates métalliques simples et dans le dernier, les composés obtenus se dégradent pendant le séchage même, en changeant graduellement de couleur. On doit souligner en même temps la difficulté de purification finale des produits, étant donné qu'ils ne sont pas dissous ou se décomposent dans les solvants accessibles.

Les spectres IR ont été enregistrés avec un appareil U.R.-10 Zeiss Jéna dans le domaine 3600–400 cm^{-1}, les substances étant incluses dans des pastilles de KBr. La valeur des bandes d'absorption en IR et les attributions faites ont été marquées dans le tableau 2.

[15] J. Nelson et S. M. Nelson, *J. Chem. Soc.*, **1969** A, 1597.

[16] A. M. Golub, G. V. Tsintsadze et A. M. Mamulashvili, *Zhur. neorg. Khim.*, **14**, 3013 (1969).

[17] G. V. Tsintsadze. A. M. Mamulashvili et L. P. Demchenco, *Zhur. neorg. Khim.*, **15**, 276 (1970).

[18] A. Yu. Tsivadze, G. V. Tsintsadze, Yu. Ya. Kharitonov, A. M. Golub, et A. M. Mamulashvili, *Zhur. neorg. Khim.*, **15**, 1818 (1970).

[19] G. V. Tsintsadze. A. Yu. Tsivadze et Ts. L. Makhatadze, *Soobshch. Akad. Nauk. Gruzz. S.S.R.*, **56**, 301 (1969).

[20] A. R. Chugnatai et R. N. Keller, *J. Inorg. Nucl. Chem.*, **31**, 633 (1969).

[21] F. A. Cotton et M. Goodgame, *J. Amer. Chem. Soc.*, **83**, 1777 (1961).

[22] D. Forster et D. M. L. Goodgame, *J. Chem. Soc.*, **1964**, 2790 ; **1965**, 262 et 1286.

[23] R. A. Bailay et S. L. Kozak, *J. Inorg. Nucl. Chem.*, **31**, 689 (1969).

[24] C. Gh. Macarovici et R. Micu-Semeniuc, *Rev. Roumaine Chim.*, **14**, 257 (1969); XXV Partie, **16**, (1971) (sous presse).

[25] St. Niementowschi, *Ber. dtsch. Chem. Ges.*, **34**, 3327 (1901).

Tableau 1

Composition, analyse des éléments et autres propriétés des cyanates discutés

N° crt.	Substance	Couleur	Stabilité thermique °C	MB	% Métal		% N		% H_2O	
					calculé	trouvé	calculé	trouvé	calculé	trouvé
I	$Co(NCO)_2$	rose violacé	<270	5.49	41,25	42,30	19,58	19,89	—	1,40
II	$Co(o,o'-DABP)_2(NCO)_2$	rose	<250	5,59	11,53	12,58	16,43	16,16	—	—
III	$Ni(NCO)_2 . H_2O$	vert	<320	3,49	36,77	36,55	17,41	18,01	11,18	10,40
IV	$Ni(o,o'-DABP)_2\ (NCO)_2$	vert bleuâtre	~140	3,17	11,22	10,84	16,43	16,78	—	—

Les mesures de susceptibilité magnétique ont été effectuées à la température ambiante avec une balance de type Faraday, calibré par Co $(NCS)_4Hg$. Les moments magnétiques ont été calculés à l'aide de la relation $\mu_{eff} = 2{,}84\sqrt{\chi_{M_c} \cdot T}$, après avoir fait les corrections nécessaires pour le diamagnétisme (tableau 1).

Les spectres électroniques ont été obtenus en utilisant un spectrophotomètre type Beckmann équipé avec un dispositif pour réflexion, sur pastilles pressées des composés étudiés, en prenant le MgO pour référence (tableau 3, fig. 1 et 2).

RÉSULTATS ET DISCUSSIONS

Les cyanates étudiés par nous sont des substances microcristallines prismatiques (II), microgranules sphériques (IV), ou n'ont pas d'aspect cristalin (I et III). Elles sont stables dans l'air, mais ont une stabilité thermique relativement faible (tableau 1). Les cyanates de Co(II) et Ni(II), tenus en étuve à 110—115° pendant 20—22 heures, perdent du poids : $Co(NCO)_2$ approximativement 1,4 % et $Ni(NCO)_2$ — 10,40 %. Cette perte de poids correspondrait à une molécule d'eau pour la combinaison III. En chauffant, la couleur du $Co(NCO)_2$ passe du rose-violet au marron et se décompose au-dessus de 270° et le $Ni(NCO)_2 \cdot H_2O$ perd de l'eau (110°) et devient vert clair ; au-dessus de 320° il se décompose. La combinaison II perd la transparence des cristaux à 130—140° et se décompose au-dessus de 250°, et IV se décompose graduellement à partir de 140°.

On a essayé la solubilité des combinaisons en éthanol, éther éthylique, acétone, benzène, xylène, chloroforme, diméthylformamide (DMF) et pyridine (py). La combinaison II se dissout un peu en éthanol et mieux en acétone et en DMF, en formant des solutions colorées en bleu, coloration due à l'ion complexe $[Co(NCO)_4]^{2-}$ qui donne naissance aux solvants anhydres mentionnés, probablement selon le schéma suivant :

$$2[Co(o,o'\text{—DABP})_2(NCO)_2] \rightarrow [Co(o,o'\text{—DABP})_3][Co(NCO)_4] + o,o'\text{—DABP}$$

ou

$$2[Co(o,o'\text{—DABP})_2(NCO)_2] + 2 \text{ solvants} \rightarrow$$

$$\rightarrow 2\, o,o'\text{—DABP} + [Co(o,o'\text{—DABP})_2(\text{solvants})_2][Co(NCO)_4]$$

La pyridine dissout les combinaisons II et IV et forme des combinaisons complexes mixtes, contenant aussi de la py dans la sphère coordinative. Aucune combinaison ne se dissout dans les autres solvants. Pour cette raison on a fait des études sur des substances solides et non sur des solutions.

L'ion cyanate a été amplement étudié à l'aide de la *technique IR*[1—6,15—20,26—30] et on a pu établir que parmi les 25 niveaux vibrationnels de

---

[26] A. Maki et J. C. Decius, *J. Chem. Phys.*, **31**, 772 (1959).

[27] J. C. Decius, J. L. Jacobson. W. F. Sherman et G, R. Wilkinson, *J. Chem. Phys.*, **43**, 2180 (1965).

[28] A. Sabatini et I. Bertini, *Inorg. Chem.*, **4**, 959 (1965).

[29] J. C. Decius et D. J. Gordon, *J. Chem. Phys.*, **47**, 1286 (1967).

[30] A. H. Norbury et A.I.P. Sinha, *J. Chem. Soc.*, **1968 A**, 1599.

Tableau 2

Spectres IR des cyanates simples et complexes en cm^{-1}

N° crt.	Composé	ν *as* 3430—3320	ν *s* 3320—3250	δ NH_2 1640—1555	ν CN amine 1290—1250	δ_{tw} NH_2 1080	ν CN 2300—2200	ν CO 1400—1200	δ NCO 650—590	Bandes de combinaison
I	$Co(NCO)_2$	—	—	—	—	—	2210 it 2200 ei	1460 f 1360 f	640 ti	1535 f; 1630 f 2400 tf 2855 tf 2925 tf 3385 e, i 3490 e, m 3590; 3612 m
II	Co(*o, o'*—DABP)$_2$ $(NCO)_2$	3351 ti 3329 ti	3290 ti 3250 ti	1620 ti 1600 ti	1285 f-m 1240 f	1080 f	2256 ti 2200 ti 2146 i	* 1210 tf	615 ti 602 i	2522 f; 2618 f 2925 f; 3035 f 3070 m; 3492 i
III	$Ni(NCO)_2.H_2O$	—	—	—	—	—	2262 ti 2200 i	1460 m 1360 m	645 i	1550 t.f 1635 m; 2850 tf 2920 tf; 3485 m 3610 m
IV	Ni(*o, o'*—DABP)$_2$ $(NCO)_2$	3358 i 3322 i	3288 i 3250 i	1623 i 1609 m	1285 tf 1240 tf	1081 tf	2210 fi 2170 m	* 1208 tf	622 m 610 m	2512 tf 2605 tf 2930 tf 3035 f; 3492 m
V	KOCN	—	—	—	—	—	2165	1301 1207	636 628	
VI	$Si(NCO)_4$	—	—	—	—	—	2284	1482	—	—

* = obscur; ti = très intense; i = intense;
m = moyen; f = faible; tf = très faible;
é = épaule.

l'ion,[29] trois seulement sont actifs en IR. On attribue aux vibrations fondamentales : la vibration d'allongement νCN, dans le domaine 2300 – 2000 cm^{-1}, la vibration d'allongement νCO approximativement à 1258 cm^{-1} et la vibration de déformation δNCO dans le domaine 650 – 600 cm^{-1}. Vu que la première harmonique supérieure de la vibration de déformation 2 δNCO, apparaît dans le même domaine que la vibration CO, le phénomène de résonance Fermi a lieu, ce qui détermine l'apparition de deux bandes d'égale intensité, déplacées approximativement à égale distance par rapport à la valeur moyenne (1258 cm^{-1}), dans le domaine 1200 et 1300 cm^{-1}. En dehors de ceux-ci, dans les spectres IR des cyanates, dans des domaines de plus haute fréquence apparaissent des bandes de combinaisons, d'intensité moyenne [18,25,26] qu'on retrouve aussi dans certains de nos spectres.

Le critère d'attribution de la liaison M—NCO n'est pas unique ; dans la littérature on trouve des options pour chacune des trois vibrations fondamentales, comme ayant le rôle décisif dans l'attribution de la liaison : νCN,[31] νCO[18] et δNCO[15]. On attribue ainsi une décroissance de l'intensité de la bande νCN et sa présence pour de plus basses fréquences dans les cyanato-combinaisons et une croissance de l'intensité accompagnée d'un déplacement vers des numéros d'onde supérieurs et d'une bande plus large, quand des isocyanates-complexes [31] se forment. Le déplacement vers des numéros d'onde inférieurs du νCN a lieu en même temps que la croissance du caractère ionique de la liaison. Si pour les isocyanates organiques, où le degré de covalence est appréciable, la vibration νCN se trouve dans le domaine 2280 – 2240 cm^{-1}, [7,31] pour les cyanates des éléments alcalins, elle se trouve dans le domaine 2190 – 2150 cm^{-1}.

La vibration νCO se déplace approximativement de 30 cm^{-1} vers des plus hautes énergies quand la liaison du cyanate a lieu par N, pendant que pour la liaison par 0, on considère une liaison en sens inverse.[18,23,28] Dans le premier cas, le déplacement est accompagné d'une diminution marquée d'intensité.

Pour la vibration δNCO, étant une manière de vibration dégénérée, on attend l'apparition d'une seule bande dans le domaine 600 cm^{-1}, mais pour des combinaisons à l'état solide, celle-ci apparaît souvent scindée. On peut tirer des conclusions sur le mode de liaison du cyanate [15] d'après la dimension du scindement.

La possibilité du thio- et du séléno-cyanate de se coordonner simultanément par les deux atomes N et S (Se), en réalisant la liaison «pont», est bien connue [28,32,33–36] et cela est liée à leur capacité d'accepteur π. Etant donné la capacité diminuée d'accepteur π du cyanate, il préfère une coordination monodentée, généralement par l'azote. On peut réaliser une coordination bifonctionnelle seulement quand les ligands partenaires ont une faible capacité de donneur σ et sont fortement accepteurs π. Sans ce cas la liaison «pont» est réalisée seulement par l'atome N.[15,18,32] On suppose que l'atome 0 participe à la liaison seulement dans le composé $[Co(4-CN\ py)_2\ (NCO)_2]$, où Co(II) apparaît hexacoordiné. [11]

---

[31] T. N. Srivastawa et S. N. Bhattacharya, *J. Inorg. Nucl. Chem.*, **29**, 1873 (1967).

[32] A. Tramer, *J. Chim. phys.*, **59**, 232 (1962).

[33] F. A. Cotton, D. M. L. Goodgame et T. E. Haas, *Inorg. Chem.*, **1**, 565 (1962).

[34] A. Torco, C. Pecile, et M. Nicolini, *Proc. Chem. Soc.*, **1961**, 213 ; *J. Chem. Soc.*, **1962**, 3008.

[35] Yu. Ya. Kharitonov, et M. A. Porai-Koshits, *Doklady Akad. Nauk S.S.S.R.*, **160**, 1354 (1965).

[36] D. Britton et J. D. Dunitz, *Acta Cryst.*, **18**, 424 (1965).

La bande νCN des composés étudiés a une grande intensité et est scindée en trois composantes, dont deux se trouvent d'un côté et l'autre du pic principal, à une distance approximativement égale (II), ou avec des bandes satellites se trouvant à des énergies plus basses (IV). Dans les cyanates simples les vibrations νCN ont des valeurs situées dans le domaine des fréquences plus élevées, et se présentent sous forme de bandes uniques, ayant une épaule située à des numéros d'onde plus petits.

Pour les cyanates simples (I, III), la vibration νCO apparaît à des valeurs supérieures à ceux complexes (II, IV), correspondant aux bandes de 1360 ou 1460 cm^{-1}.

L'absorption de la vibration νCO étant située vers des énergies plus élevées que dans le cas de l'ion libre, on n'observe plus le doublet Fermi dans le domaine de 1300 à 1200 cm^{-1}.

Pour les combinaisons complexes *o*, *o'*—DABP, l'attribution univoque de νCO est plus difficile à cause des vibrations de l'amine apparaissant dans ce domaine. Dans les spectres des combinaisons II et IV une bande d'absorption apparaît à 1210, respectivement à 1208 cm^{-1}, qui ne s'identifie pas dans le spectre de l'amine et qui pourrait être la composante de basse énergie du doublet Fermi attendu. La composante d'énergie plus élevée (1300 cm^{-1}) ne peut plus être mise en évidence.

Le mode de vibration δNCO reste dégénéré pour les cyanates simples, les bandes étant d'une intensité remarquable, pendant que pour les complexes correspondants, la dégénérescence s'élève en subissant une scission de 12—13 cm^{-1} et une légère diminution d'intensité. Cette scission pas trop élevée est caractéristique d'une liaison M—NCO.[15]

La position des bandes d'absorption dans les spectres de vibration suggère la formation d'une liaison M—NCO par les combinaisons II et IV et le caractère plus complexe de celle-ci dans les combinaisons I et III.

En comparant les valeurs des bandes des cyanates de Co(II) et Ni(II) à celles de KOCN et $Si(NCO)_4$ (tableau 2) on observe une ressemblance remarquable avec le dernier, ce qui suggère un caractère covalent appréciable de la liaison M-isocyanate.

En ce qui concerne la coordination de l' *o*,*o'*—DABP on observe dans le spectre des complexes des déplacements significatifs de bandes en comparaison de l'amine libre, déplacements discutés ailleurs.[24] On remarque également dans ces composés l'apparition de quatre bandes dans le domaine de vibration du νNH_2, approximativement à 3250, 3290 et 3329, 3351 cm^{-1} dont la position comparée à l'amine libre confirme le comportement de l'amine à ligand bidentée.

Les propriétés magnétiques des combinaisons de Co(II) et Ni(II) peuvent être expliquées si nous rappelons que dans une configuration octaédrique le terme d'énergie la plus basse de l'ion Co^{2+} est un triplet orbital, tandis que pour l'ion Ni^{2+} le même terme est un singlet orbital. En conséquence, les valeurs expérimentales des moments magnétiques couvrent un domaine assez large, situé entre 4,7 et 5,6 MB pour le Co(II)[37,38] et entre 3,0 et 3,4 MB pour le Ni(II).[12,38]

Les valeurs des moments magnétiques calculées pour nos composés correspondent à des ions à haut spin et sont situées dans le domaine caractéristique d'une configuration hexacoordinée. (tabl. 2).

Les spectres électroniques d'absorption procurent des informations supplémentaires en ce qui concerne la structure des composés et la configuration locale des ions. Pour l'ion Co(II), un champ cristallin de symétrie O_h détermine la succession des termes énergétiques suivants : ${}^4T_{1g}(F)$, ${}^4T_{2g}(F)$, ${}^4A_{2g}(F)$ et ${}^4T_{1g}(P)$ — dans l'ordre montant de l'énergie. Par conséquent, il y a trois transitions électroniques donnant naissance à trois bandes d'absorption dans le domaine visible du spectre :

$$\nu_1 = {}^4T_{1g} \longrightarrow {}^4T_{2g} \qquad \nu_2 = {}^4T_{1g} \longrightarrow {}^4A_{2g}$$

$$\nu_3 = {}^4T_1\mathrm{g} \longrightarrow {}^4T_{1g}(P)$$

Dans de champs de symétrie plus petits les bandes d'absorption ν_1 et ν_3 seront faites chacune de deux composantes ; il s'ensuit que dans la symétrie D_{4h} nous nous attendons à l'apparition de cinq bandes dans un spectre. L'ordre des niveaux énergétiques dépendra de la force du champ créé par le ligand axial.[39]

Les spectres de réflexion des composés de Co(II) sont rendus dans la figure 1, et la valeur des bandes et les attributions faites, dans le tableau 3. La position et le nombre des bandes indique une configuration hexacoordinée pour l'ion Co(II). Dans les spectres des combinaisons I et II, à côté des bandes appartenant aux transitions attendues, apparaissent des épaules faiblement résolues et de petite intensité, situées à 13 000 et 14.300 cm^{-1} pour I, respectivement à 13500 et 15100 cm^{-1} pour II. Ces épaules peuvent être dues soit à certaines transitions interdites de spin, soit à des espèces tétraédriques existentes comme impuretés dans les composés étudiés.[40] Le tableau 3 nous apprend que toutes les bandes appartenant au Co(NCO)$_2$ se trouvent à des énergies plus basses comparées à [Co(*o*, *o'*—DABP)$_2$ (NCO)$_2$]. Dans les deux composés la bande ν_1 apparaît non scindée, pendant que ν_3 apparaît d'une large bande placée à 18870 cm^{-1} pour la combinaison I, ayant deux épaules situées à plus hautes énergies et pour la combinaison II, ν_3 apparaît à 20400 cm^{-1}, avec une épaule située à plus basses énergies. Ceci indique l'existence d'une distorsion tétragonale. La position des composantes de la bande ν_3 pour le Co(NCO)$_2$ suggérerait l'idée que la symétrie locale de l'ion est plus petite qu'en [Co(*o*,*o'*—DABP)$_2$ (NCO)$_2$], probablement D_{2h}, ce qui conduit à l'élévation de l'état de dégénération du niveau ${}^4E_g(F)$ et les transitions ont lieu entre l'état fondemental et les états ${}^4B_{3g}$, ${}^4B_{2g}$, ${}^4B_{1g}$.

---

[37] B. N. Figgis et R. S. Nyholm, *J. Chem. Soc.*, **1954**, *12* ; **1959**, 338.

[38] E. K. Barefield, D. H. Busch et S. M. Nelson, *Quart. Rev.*, **22**, 457 (1968).

[39] B. J. A. Kakazai et G. A, Melson, *Inorg. Chim. Acta*, **4**, 360 (1970).

[40] M. Goodgame, *J. Chem. Soc.*, **1966** A, 63.

Tableau 3

Spectres électroniques des cyanates simples et complexes de Co (II) et Ni (II) en cm^{-1}

N^o crt.	Composé	ν_1		ν_2		ν_3	ν_4	D_q^z	D_t
I	$Co(NCO)_2$	8600	13000 u ; 14300 u	16600 u		18870 19600 21400	—	—	—
II	$Co(o,\ o'-DABP)_2(NCO)_2$	9100	13500 u ; 15100 u	17800 u		19600 20400	—	—	—
III	$Ni(NCO)_2H_2O$	8000		8600	13800	15100	22200 u 23300 u	740	68,5
IV	$Ni(o,\ o'-DABP)_2(NCO)_2$	10000		10700	15600	17000	22300 u 23200 u	930	80

La différence entre les composantes de plus haute et plus basse énergie de ν_3 dépend de la nature des groupes axiaux.[39] Pour d'autres combinaisons avec l'*o,o'*—DABP la différence énergétique entre les composantes de la bande ν_3 suit l'ordre : $NCS^- < NO_3 < Cl^- < Br^- < J^-$. Les valeurs obtenues par nous pour I ($\Delta\nu_3 = 2530\ cm^{-1}$) situent le ligand *trans* à la fin de la série, entre Br^- et J^- ou D_b^z à des valeurs de beaucoup plus petites que D_q^{xy}, donc la distorsion tétragonale présente est plus grande.

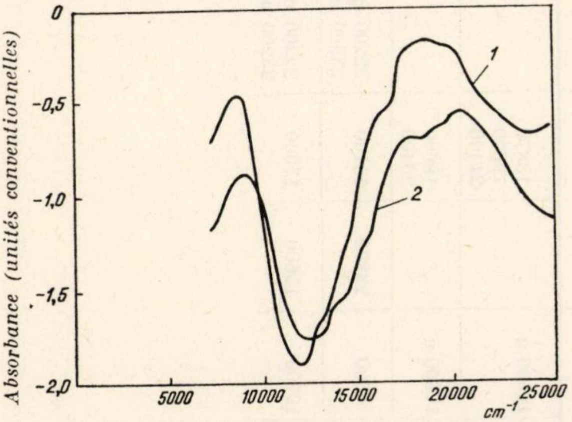

Fig. 1.—Spectres de réflexion de : *1*, $Co(NCO)_2$ et *2*, $[Co(o,o'-DABP)_2(NCO)_2]$.

La couleur rose violacée, la solubilité réduite, la valeur (tableau 1) et la position des bandes des spectres de réflexion suggèrent pour cette combinaison une configuration hexacoordinée autour de l'ion Co(II). Par analogie avec les thiocyanates simples des éléments 3*d*,[41] qui paraissent dans un arrangement tétragonal, nous supposons que l'ion Co(II) a dans le plan 4 atomes N liés en pont, associant des chaînes de forme : 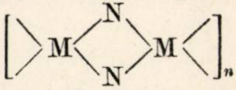 avec deux atomes d'oxygène occupant les positions *trans*. Étant donné les positions des ligands contenant de l'oxygène par rapport à ceux contenant de l'azote, dans la série spectrochimique,[42,43] nous nous attendons à un champ de ligand axial plus faible que celui du plan, ce qui correspond à la valeur ν_3 de la combinaison I.

La séparation $\Delta\nu_3$ pour $[Co(o, o'-DABP)_2(NCO)_2]$ situe l'ion cyanate entre NCS^-, et NO_3^-, à la limite entre la contraction et l'allongement de l'octaèdre,[39] ce qui conduit à une distorsion modérée de la configuration. Le spectre de la combinaison II peut être interprété dans les limites d'une symétrie D_{4h}, avec les termes dégénérés situés à plus basses énergies. Ceci peut être aussi mis en corrélation avec la valeur du champ cristallin de l'isocyanate, légèrement inférieure à celui de l'*o, o'*—DABP. On attribue à la combinaison $[Co(o, o'-DABP)_2(NCO)_2]$ une configuration hexacoordinée, avec deux molécules d'amine liées bidentées dans le plan de la molécule complexe et deux ions NCO^- en *trans*, liés par N.

---

[41] C. D. Flint et M. Goodgame, *J. Chem. Soc.*, **1970** A, 442.

[42] B. N. Figgis, « Introduction to Ligand Fields », Interscience Publ. John Wiley, New York—Londres-Sydney, 1966, p. 243.

[43] F. A. Cotton, O. D. Fant, D. M. L. Goodgame et R. H. Holm, *J. Amer. Chem. Soc.*, **83**, 1780 (1961).

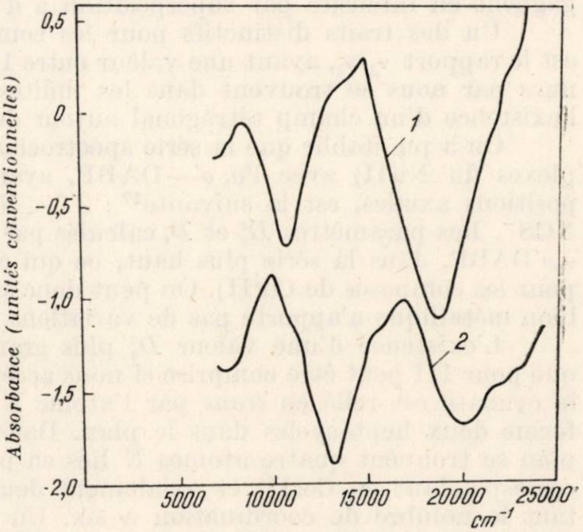

Fig. 2. — Spectres de réflexion de : *1*, $Ni(NCO)_2$ et *2*, $[Ni(o, o'-DABP)_2(NCO)_2]$.

Pour les ions Ni(II) se trouvant dans une configuration octaédrique, l'ordre des niveaux énergétiques est $^3A_{2g}$, $^3T_{2g}$, $^3T_{1g}$ et $^3T_{1g}(P)$. Le spectre d'absorption des ions Ni(II) qui se trouvent dans une configuration d'une symétrie plus petite D_{4h} présentera quatre bandes d'absorption en visible correspondant aux transitions :

$$\nu_1 = {}^3B_{1g} \longrightarrow 3E_g \qquad \nu_2 = {}^3B_{1g} \longrightarrow {}^3B_{2g}.$$

$$\nu_3 = {}^3B_{1g} \longrightarrow {}^3A_{2g} \qquad \nu_3 = {}^3B_{1g} \longrightarrow {}^3E_g$$

(tableau 3 et figure 2). L'ordre des niveaux énergétiques dépend de la force du champ cristallin du plan et axial. Pour $D_q^z < D_q^{xy}$ (comme dans le cas présent) la distorsion tétragonale correspond à un octaèdre allongé à l'état ^3E_g situé à des énergies moindres que $^3B_{2g}$.

La position de la bande ν_1 des spectres donne des informations sur la force du champ cristallin des composés respectifs et est influencée par les distorsions tétragonales présentes, pendant que ν_2 sera indépendante des paramètres caractéristiques de cet état.

En partant des données expérimentales, on a calculé à l'aide des relations données,[44] le paramètre du champ axial D_q^z et le paramètre de la distorsion tétragonale D_t (tableau 3). La valeur et la position des bandes des spectres des combinaisons III et IV correspondent à une configuration hexacoordinée du Ni(II). Comme dans le cas du Co(II), la présence de

[44] G. R. Brubaker et D. H. Busch, *Inorg. Chem.*, 5, 2114 (1966).

l'amine dans le composé IV déplace les bandes du spectre vers des numéros d'onde plus grands en comparaison des bandes du spectre $Ni(NCO)_2$, déplacement accompagné par la croissance de la force du champ cristallin.[45]

Dans les deux spectres, outre les bandes correspondant aux transitions attendues on trouve encore une épaule à 13800 cm^{-1}(III) et 15600 cm^{-1} (IV), que l'on peut attribuer à des transitions interdites par le spin, qui gagnent en intensité par superposition à d'autres transitions permises.[46]

Un des traits distinctifs pour les composés de Ni(II) octaédriques est le rapport ν_3/ν_1, ayant une valeur entre 1,6—1,8.[45] Les grandeurs obtenues par nous se trouvent dans les limites de cette valeur, confirmant l'existence d'un champ tétragonal autour de Ni(II).

On a pu établir que la série spectrochimique pour une série de complexes du Ni(II) avec l'*o*, *o*'—DABP, ayant différents anions dans les positions axiales, est la suivante[47] : $J^- < NO_3^- < Br^- < Cl^- <$ diamine $< NCS^-$. Les paramètres D_q^z et D_t calculés par nous se situent entre Cl^- et *o*,*o*'DABP, dans la série plus haut, ce qui confirme les résultats obtenus pour les composés de Co(II). On peut donc suggérer que le changement de l'ion métallique n'apporte pas de variations significatives dans cette série.

L'existence d'une valeur D_q^z plus grande pour la combinaison IV que pour III peut être comprise si nous acceptons que dans le premier cas le cyanate est relié en *trans* par l'atome N, pendant que l'*o*, *o*'—DABP forme deux heptacycles dans le plan. Dans le cas de $Ni(NCO)_2$ dans le plan se trouvent quatre atomes N liés en pont, comme dans le composé correspondant de Co(II), et axialement deux atomes d'oxygène complétant le nombre de coordination à six. Un des atomes d'oxygène situés en *trans* peut provenir de la molécule d'eau du cyanate de nickel. Ces valeurs de D_q^z correspondent à la position des ligands dans la série spectrochimique mentionnée.[42,43]

Les plus hautes valeurs du paramètre D_t sont corrélées à une certaine croissance du degré de covalence de la combinaison,[46] ce qui est confirmé aussi dans notre cas : la liaison M—N est plus covalente que M—O.

Les résultats obtenus par les déterminations magnétiques et les spectres électroniques pour les composés des ions d^7 et d^8 étudiés ici peuvent être mis en corrélation avec les spectres IR pour les combinaisons II et IV. D'après les déterminations magnétiques et les spectres électroniques pour les combinaisons I et III, nous avons attribué une configuration hexacoordinée, en conséquence l'atome d'azote est lié en « pont ». Une coordination pareille devrait être cependant accompagnée par la disparition de la dégénérescence de la vibration NCO, mais le bande d'absorption correspondante n'est pas scindée. Pour le moment on constate seulement que pour ce type de combinaisons, les spectres électroniques ne peuvent pas nous donner d'une manière univoque la nature de la liaison de l'ion cyanate. D'autres recherches sont nécessaires.

Des résultats similaires ont été obtenus par les cyanates de Cu(II) avec l'*o*, *o*'—DABP, le *m*, *m*'—DABP et le *p*, *p*'—DABP.[48]

---

[45] W. Manch et W. C. Fernelius, *J. Chem. Educ.*, **38**, 192 (1961).

[46] D. M. L. Goodgame, M. Goodgame, M. A. Hitchman et M. F. Weeks, *J. Chem. Soc.*, **1966** A, 1769.

[47] B. J. Kakazai et G. A. Melson, *Inorg. Chim. Acta*, **2**, 186 (1968).

[48] C. Gh. Macarovici, R. Micu-Semeniuc et D. Lupu, résultats non publiés.

Revue Roumaine de Chimie, 17, 6, 993–1004 (1972)

COMBINAISONS COMPLEXES AVEC DÉRIVÉS DIAMINOBIPHÉNYLIQUES. XXVII[1–3]

CYANATES COMPLEXES DU Cu(II)

RODICA MICU-SEMENIUC, CONST. GH. MACAROVICI et D. LUPU

Chaire de Chimie Inorganique de l'Université de Cluj, 11, str. Arany János
Institut de Chimie, Cluj, 65–69, Str. Donáth

Reçu le 18 août 1971

On a synthétisé quelques cyanates complexes du Cu(II), avec des dérivés diaminobiphényliques et on les a étudiés à l'aide des spectres en IR, de micro-ondes et de réflexion diffuse. On a fait des déterminations de susceptibilité magnétique. A l'aide des données expérimentales on a déduit que tous les composés de Cu(II) étudiés dans le travail ont l'état fondamental B_{1g} étant héxacoordinnés et ayant une configuration octaédrique distorse rhombique ou tétragonale.

Les recherches sur le comportement de l'ion cyanate dans les combinaisons complexes des éléments 3*d* avec des dérivés diaminobiphényliques font partie d'une étude plus vaste sur la capacité de complexation de cet ion, en comparaison de celle du thiocyanate et du sélénocyanate dans les mêmes conditions.[1,2]

Dans un ouvrage antérieur[3] on a communiqué les résultats obtenus dans la recherche concernant certains cyanates simples et complexes du Co(II) et Ni(II) et dans le présent ouvrage on discute les résultats relatifs au comportement de quelques cyanates complexes de Cu(II).

Les premières études de synthèse des cyanates de Cu(II) complexes ont été initiées par Ripan,[4] qui a obtenu deux classes de combinaisons : amines du type $[\mathrm{Cu\ py_2\ ;\ 6(NCO)_2}]$ et l'acido-complexe $\mathrm{M^I_2\ [Cu(NCO)_4]}$. L'ion complexe $[\mathrm{Cu(NCO)_4}]^{2-}$ a été étudié ultérieurement par déterminations physico-chimiques appropriées [5,6] et on a constaté qu'il s'agit d'un isocyanatocomplexe avec un arrangement tétraédrique distors des ions $\mathrm{NCO^-}$ autour du Cu(II), mais, qui, en fonction de la température et du type de cation utilisé, peut être réarrangé dans la configuration plan-carrée,

---

[1] C. Gh. Macarovici et R. Micu Semeniuc, *Rev. Roumaine Chim.*, **14**, 35, 357 (1969); **16** (sous presse).

[2] A. Nicule, R. Micu-Semeniuc et C. Gh. Macarovici, *Rev. Roumaine Chim.*, **13**, 1329 (1968).

[3] R. Micu-Semeniuc et C. Gh. Macarovici, sous presse.

[4] R. Ripan, *Bull. Soc. Sci. Cluj*, II, **1924–25**, 73 ; IV, **1928–29**, 499.

[5] D. Forster et D. M. L. Goodgame, *J. Chem. Soc.*, **1964**, 2790 ; **1965**, 262.

[6] A. R. Csughtai et R. N. Keller, *J. Inorg. Nucl. Chem.*, **31**, 633 (1969).

jusqu'à la forme pseudo-octaédrique.[6] Ainsi les cations à grand volume à des températures élévées favorisent la forme tétraédrique, pendant que les petits cations et les basses températures déterminent l'apparition de la forme pseudo-octaédrique. On a également synthétisé et étudié le composé $K[Cu(NCO)_3]$,[7] dans lequel on trouve des groupes isocyanates, ainsi que des ponts du type 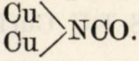 $\begin{matrix}Cu\\Cu\end{matrix}\!\!>NCO$.

Dans le présent ouvrage on étudie les composés du cyanate de Cu(II) avec les trois isomères diaminobiphényliques, ainsi que'avec la pyridine et le 2,7-diaminofluorène, comme ligands.

PARTIE EXPÉRIMENTALE

Les combinaisons mentionnées ont été réalisées en partant de substances acquises dans le commerce [$Cu(NO_3)_2 \cdot 3\,H_2O$, KOCN, pyridine (py) et benzidine (*p*, *p'*-DABP)], les autres étant synthétisées par nous d'après les indications de la littérature [*o*, *o'*-diaminobiphényl (*o*, *o'*-DABP), *m*, *m'*-diaminobiphényl (*m*, *m'*-DABP),[8] et 2,7-diamino-fluorène (2,7-DAF)[9]].

On a essayé la préparation du $Cu(NCO)_2$ en partant de solutions aqueuses concentrées équimolaires d'azotate de cuivre (II) et de cyanate de potassium, qui, par mélange et agitation, donnent un précipité vert, d'aspect non cristallin, d'une composition complexe. On a enregistré les spectres en IR, de réflexion diffuse en RES pour ce composé, mais leur complexité ne nous permet pas de leur attribuer une structure ou une configuration quelconque. Il est néanmoins probable que la substance obtenue contienne aussi des ions Cu (I), probablement dans un arrangement de la forme $Cu^{I}\ [Cu(NCO)_3]$.

Les combinaisons I et II (tableau 1) ont été obtenues en dissolvant 1,2 g d'azotate de cuivre (II) et 1 g de KOCN, chacun dans 70 ml d'eau, et séparément 1,8 g d'*o*, *o'*-DABP, respectivement 0,9 g de *m*, *m'*-DABP en 10—15 ml d'alcool éthylique. Par le mélange des solutions et agitation, il résulte un précipité vert brun (I), respectivement vert foncé (II) d'aspect cristallin.

Le [Cu (p, p'-DABP) (NCO)$_2$] est préparé de la même façon : on dissout 2,4 g de $Cu(NO_3)_2 \cdot 3H_2O$ en 150 ml d'eau, 1,6 g de KOCN en 100 ml d'eau et 1,8 g de benzidine en 150 ml d'eau et 25 ml d'alcool. On amène les solutions au point d'ébullition et on les mélange. Le résultat immédiat est un précipité marron foncé, amorphe, et d'une pureté pas trop élevée. Le produit ne peut même pas être purifié étant insoluble dans les solvants habituels ou se décomposant dans quelques-uns de ceux-ci.

Pour l'obtention du [Cu (2,7-DAF) $(NCO)_2$] on dissout 0,3 g d'azotate de cuivre (II) en 85 ml d'eau, on mélange avec une solution de 0,5 g de KOCN dans 35 ml d'eau, à laquelle on ajoute 0,45 g d'amine dissoute dans 25 ml d'alcool. Le précipité obtenu est de couleur bleu foncé, ayant un aspect amorphe.

Les combinaisons avec de la pyridine ont été synthétisées d'après les indications de la littérature [4] mais elles ne sont pas encore étudiées par spectres ou d'autres déterminations physiques.

La composition des combinaisons synthétisées, le résultat de l'analyse élémentaire et autres propriétés sont inclus dans le tableau 1.

---

[7] A. Iu. Tsivadze, G. V. Tsintsadze, Yu. Ya. Kharitonov, A. M. Golub et A.M. Mamulaşhvili, *Zhur. neorg. Khim.*, **15**, 1818 (1970).

[8] St. Niementowachi, *Ber. dtsch. Chem. Ges.*, **34**, 3327 (1901).

[9] J. Schmidt et W. Hinderer, *Ber. dtsch. Chem. Ges.*, **64**, 1793 (1931).

Tableau 1

Composition, analyse procentuelle et autres propriétés physiques des cyanates complexes Cu (II)

N° crt.	Substance	Couleur	Stabilité thermique °C	μ_{MB}	% Metal		% N	
					Calculé	Trouvé	Calculé	Trouvé
I	$[Cu(o, o'-DABP)_2\ (NCO)_2]$	vert-brun	150	1,87	12,32	12,37	16,28	16,52
II	$[Cu(m, m'-DABP)\ (NCO)_2]$	vert	115–140	1,80	19,17	18,98	16,92	16,64
III	$[Cu(p, p'-DABP)\ (NCO)_2]$	marron foncé	<170	1,92	19,17	20,75	16,92	17,30
IV	$[Cu(2,7-DAF)(NCO)_2]$	bleu foncé	<200	1,64	18,48	17,91	16,29	16,52
V	$[Cu(py)_2(NCO)_2]$	bleu	165–170	1,90	20,80	21,08	–	–
VI	$[Cu(py)_6]\ (NCO)_2$	bleu	<163	1,95	10,22	10,32	–	–

On a enregistré les spectres en IR et de micro-ondes des composés obtenus, on a déterminé la susceptibilité magnétique et pour certains composés on a aussi obtenu les spectres de réflexion (diffuse).

Les spectres en IR ont été enregistrés à l'aide d'un appareil UR-10 Zeiss-Jéna, dans le domaine de 3600 à 400 cm^{-1}, sur des substances incluses dans des pastilles de KBr. La valeur des bandes d'absorption et les attributions faites sont indiquées dans le tableau 2.

Les mesures de susceptibilité magnétique ont été effectuées à la température ambiante à l'aide d'une balance de type Faraday calibrée avec du $CuSO_4 . 5H_2O$. Les moments magnétiques ont été calculés à l'aide de la relation $\mu_{ef} = 2{,}84 \sqrt{\chi M_c} . T$ après avoir effectué les corrections pour le diamagnétisme (tableau 1).

Les spectres électroniques ont été obtenus avec un spectrophotomètre de type Beckmann, muni d'un dispositif de réflexion, sur des pastilles pressées des composés étudiés ayant le MgO comme référence (tableau 3, fig. 1).

Les spectres de micro-ondes ont été enregistrés avec un spectromètre J.E.S.-3B, à la température ambiante.

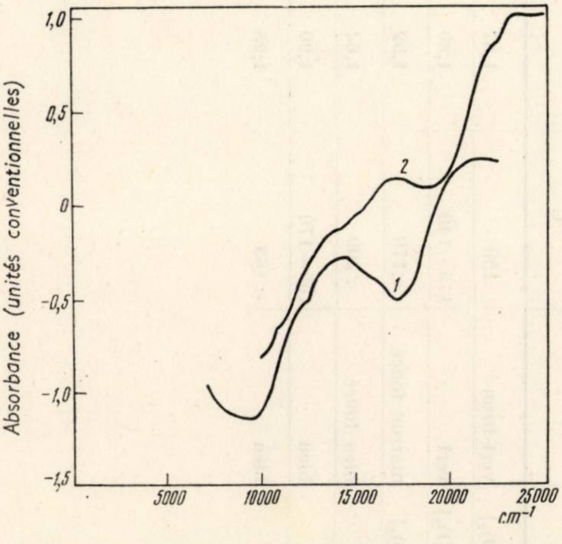

Fig. 1. — Spectres de réflexion : *1*, [Cu (*o*, *o'*-DABP)$_2$ (NCO)$_2$]; *2*, [Cu (*m*, *m'*-DABP)(NCO)$_2$].

RÉSULTATS ET DISCUSSIONS

Le rapport de combinaison pour tous les composés discutés ici est 1 Cu : 2 NCO^-, le rapport Cu : amine varie, 1 Cu : 1 amine (pour le *m*, *m'*-DABP, le *p*, *p'*-DABP et le 2,7-DAF, ainsi qu'on l'a obtenu dans le cas des complexes avec du thiocyanate et du sélénocyanate [1]), 1 Cu : 2 amines (dans le cas de l'*o*, *o'*—DABP et py) et le rapport 1 Cu : 6 py.

Les combinaisons mentionnées sont assez stables dans l'air, mais ont une stabilité thermique assez basse (tableau 1). Ainsi les combinaisons I et II se décomposent en fondant, tandis que le reste des composés se décompose graduellement.

On a essayé la solubilité de ces substances dans une série de solvants habituels et accessibles. La majorité des combinaisons ne sont pas solubles

Tableau 2

Les spectres en I R des cyanates complexes de Cu (II) cm⁻¹

Combinaison	$\nu_{as}NH_2$ 3430–3320	ν_sNH_2 3320–3250	δNH_2 1640–1555	νCN amine 1290–1250	$\delta_{tw}NH_2$ 1080	νCN 2300–2000	νCO 1400–1200	δNCO 650–590	Bandes de combinaisons
$[Cu(o, o'-DABP)_2(NCO)_2$	3362 m 3340 m	3280 m 3250 m	1610 i	1297 m 1282 f 1242 f	1076 f	2217 ti 2168 i	* 1200 f	606 i	2530 tf 2635 tf 2850 tf 2920 tf 3520 m ; 3555 f 3595 f.
$[Cu(m, m'-DABP)(NCO)_2]$	3320 i 3305 é, i	3260 é, i 3245 i	1605 é, i 1655–1675 f	1285 f 1238 f-m	1070 i	2215 ti 2190 é, ti 2160 é, m	*	602 m 615 m	2530 tf 2640 tf 3509 m
$[Cu(p, p'-DABP)(NCO)_2]$	3320 ti	3265 ti	1627 i 1610 m	1278 f 1245 f	1085 ti 1058 ti	2250–27 ti 2200 ti 2170 é, i 2050 é, m	*	598 m,i 610 m-i	2532 tf 2650 tf 2855 tf 3530 m
$[Cu(2,7-DAF)(NCO)_2]$	3330 m	3268 i	1622 m	1275 f	1068 f	2240 ti 2195 i 2171 m	*	597 f 610 f	2858 f 3542 m 3570 m
$[Cu(py)_2(NCO)_2]$	—	—	—	—	—	2215–2200 ti 2185 é, ti	1332 ti 1230m-i	610 ti 624 ti	2482 f 2550 f ; 2610 f 2855 m ; 3515 ti
$[Cu(py)_6](NCO)_2$	—	—	—	—	—	2220–2200 ti 2150 i	1332 m-i 1230 f-m	612 i 625 i	2480 tf ; 2552 tf ; 2650 tf 2858 tf 3515 m

* = masqué; ti = très intense; i = intense;
m = moyen; f = faible; tf = très faible;
é = épaule.

Tableau 3

Spectres éléctroniques de quelques cyanates de Cu (II) cm^{-1}

	Composé								
I	[Cu(o,o'−DABP)$_2$(NCO)$_2$]	solide		1220 u	14300	21700			
		solution			14800			27030	33330
II	[Cu(m, m'−DABP)(NCO)$_2$]	solide	11100 u	14300 u	17200	22800	23600		
		solution	13800		17500			29410 u	32260

dans tous les solvants utilisés. L'acétone, le diméthylformamide (DMF) et la pyridine (py) sont les meilleurs solvants pour les combinaisons de Cu(II) étudiées ici. Les composés III et IV se dissolvent partiellement ou totalement dans tous les solvants, en formant des solutions de couleur différente. Leur basse solubilité dans les solvants qui ne dissolvent pas les autres complexes, ainsi que la couleur des solutions obtenues nous font croire qu'à côté du complexe proprement dit une petite quantité d'amine se trouve sous forme d'un complexe de transfert de charge et que celle-ci se dissout en premier lieu. D'ailleurs la capacité des *p*, *p*'—DABP et DAF de former de pareils composés avec les halogènes ou quelques pseudo-halogènes est bien connue.[10-13] L'existence de complexe avec transfert de charge à côté du complexe Cu(II) explique aussi la couleur intense, foncée, des combinaisons III et IV.

Il est également visible que le DMF et la pyridine modifient la sphère coordinative du Cu(II) par participation à la coordination.

L'étude des spectres en IR nous a permis d'attribuer les bandes caractéristiques à l'ion cyanate par comparaison des données de la littérature.[7,14-18]

Ainsi la vibration d'allongement ν CN apparaît dans le domaine attendu (approx. 2200 cm^{-1}) sous forme de larges bandes, très intenses, accompagnées d'épaules ou bandes satellites situées pour des numéros d'onde plus petits, comme on les rencontre pour tous les cyanates étudiés en état solide. Les valeurs plus élevées de νCN pour les combinaisons III et IV sont corrélées à l'existence du complexe de transfert de charge, dans lequel la liaison doit avoir un degré plus accentué de covalence ce qui détermine l'apparition de la bande pour des énergies plus élevées.[19]

La variation d'allongement symétrique νCO ne peut être attribuée d'une manière univoque étant donné que dans le domaine attendu pour l'apparition du doublet Fermi apparaissent également des bandes d'absorption propres aux amines, ce qui rend l'attribution impossible.

La vibration de déformation δNCO apparaît dans le domaine 600 cm^{-1}, étant dégénérée pour la combinaison I, et ayant des scissions de 12—14 cm^{-1} pour II—VI.

Ces résultats suggèrent la formation de certains isocyanates dans lesquels l'ion NCO^- paraît réaliser une liaison terminale, malgré le fait que d'autres déterminations ne confirment pas cette chose.

Pour l'ion Cu(II) ayant une configuration électronique d^9, l'état fondamental est ^2D qu'on peut scinder de manière différente, en fonction

---

[10] P. Smejtek, J. Honzl et M. Metalova, *Coll. Czech. Chem. Comm.*, **30** 3875 (1965).

[11] C. Nicolau, I. Pascaru et Z. Simon, *Rev. Chim. Acad. R.P.R.*, **7**, 1119 (1962).

[12] P. Spacu, O. Constantinescu, I. Pascaru, C. Gheorghiu et M. Brezeanu, *Rev. Roumaine Chim.*, **11**, 161 (1966).

[13] J. B. Jones, M. Bersolm et G. C. Niece, *Nature*, **209**, 908 (1966).

[14] J. Nelson et S. M. Nelson, *J. Chem. Soc. A*, **1969**, 1597.

[15] A. Maki et J. C. Decius, *J. Chem. Phys.*, **31**, 772 (1959).

[16] J. C. Decius, J. L. Jacobson, N. F. Sherman et G. R. Wilkinson, *J. Chem. Phys.*, **43**, 2180 (1965).

[17] J. C. Decius et D. J. Gordon, *J. Chem. Phys.*, **47**, 1286 (1967).

[18] A. Sabatini et I. Bertini, *Inorg. Chem.*, **4**, 959 (1965).

[19] T. N. Srivastawa et S. N. Bhattacharya, *J. Inorg. Nucl. Chem.*, **29**, 1873.

de la symétrie du champ cristallin. En champ cubique, l'état énergétique le plus bas est ^2E_g, pendant que le seul état excité est $^2T_{2g}$, leur différence énergétique étant 10 D_q. Dans une configuration de moindre symétrie D_{4h}, chacun des deux niveaux est scindé : ^2E_g en $^2B_{1g}$ et $^2A_{1g}$, et $^2T_{2g}$ en $^2B_{2g}$ et ^2E_g.[20,21]

Dans les configurations les plus usuelles du Cu(II) l'état fondamental est non dégénéré, orbital de symétrie B_{1g} (pour l'octaèdre allongé tétragonal ou rhombique, plan-carré ou pyramide carrée), A_{1g} (pour l'octaèdre comprimé rhombique ou tétragonal, bipyramide trigonale) ou l'état B_{2g} (pour tétraèdre distors ou plan-carré). L'état dégénéré est rarement rencontré comme état fondamental et, en général, la dégénérescence s'élève à cause des déformations dues à la géométrie du réseau ou à l'effet Jahn-Teller.[22] Du fait que l'état fondamental pour l'ion de cuivre (II) est dans la majorité des cas un singlet orbital, les propriétés magnétiques des composés donnent peu d'informations sur la stéréochimie de ceux-ci. Il s'ensuit que la contribution orbitale au moment magnétique n'est pas caractéristique ; sa valeur à la température ambiante s'approche de la valeur du spin pur (1,73 MB).[21] Les valeurs pratiques des moments magnétiques pour les composés étudiés par nous se trouvent entre les limites 1,80—1,95 MB, un peu plus élevées que la valeur de spin. Cette croissance est due à une contribution du moment magnétique orbital provenant d'un état énergétique supérieur, à l'état fondamental, par l'intermédiaire du couplage spin-orbite. Cet effet dépend sensiblement de la symétrie et de l'énergie de l'état excité. Le mécanisme a quand même une trop petite contribution au moment magnétique, de sorte qu'on ne peut pas obtenir des informations stéréochimiques des mesures de susceptibilité magnétique.[21,22] Les moments magnétiques obtenus par nous sont caractéristiques pour un état fondamental B_{1g}. La combinaison IV a le moment magnétique 1,64 MB, ce qui suggère l'existence d'un système d'ions Cu(II) non dilués magnétiquement, ou la présence à côté de Cu(II) dans une certaine proportion des ions Cu(I), ce qui conduit implicitement à la diminution de la valeur μ.

Un meilleur critérium pour la détermination de la stéréochimie de Cu(II) est le *spectre électronique* d'absorption, mesuré en solution ou à l'état solide (spectre de réflexion diffuse). Les transitions qui apparaissent peuvent être des types suivants : transitions *d-d*, qui apparaissent sous 20 000 cm^{-1}, transitions internes des ligands, et transitions de transfert de charge qui apparaissent au-dessus de 20 000 cm^{-1}.[22]

Pour un composé de symétrie octaédrique on attend une seule bande, accompagnée souvent par une épaule située à des énergies plus petites. Dans une configuration tétragonale on attend trois transitions, l'ordre des niveaux énergétiques étant déterminé par la nature des ligands coordinés. On fait, en général, les attributions suivantes pour certains composés du Cu(II) avec l'éthylènediamine[23] : transition $^2B_{1g} \rightarrow {}^2E_g$ (la plus intense) dans le domaine 20 000 — 17 900 cm^{-1}, transition $^2B_{1g} \rightarrow {}^2B_{2g}$ dans le

---

[20] C. Balhausen, "Vvedenie v teoriiu polia ligandov", traduit en russe, Ed. Mir, Moscou, 1964, p. 327.

[21] B. J. Hathaway et A. A. J. Tomlinson, *Coord. Chem. Reviews*, 5, 1 (1970).

[22] B. J. Hathaway et D. E. Billing, *Coord. Chem. Review*, 5, 143 (1970).

[23] J. M. Procter, B. J. Hathaway et P. Nicholls, *J. Chem. Soc. A.* **1968**, 1678.

domaine 18 000 — 16 200 cm^{-1}, et $^2B_{1g} \rightarrow {}^2A_{1g}$ dans le domaine 16 800 — 12 200 cm^{-1} ; pour les composés avec l'ammoniaque,[24] les transitions apparaissent dans les domaines 17 500 — 17 000 ; ~ 16 000 et 14 300 — 13 400 cm^{-1}.

Nous avons enregistré les spectres électroniques des combinaisons I et II sur solide, comme spectres de réflexion, et en solution de DMF (tableau 3 et fig. 1).

Dans les spectres de réflexion de la combinaison I on trouve un maximum à 14 300 cm^{-1} accompagné par une épaule à 12 200 cm^{-1} ; et dans le spectre enregistré sur solution de DMF une seule bande apparaît, avec le maximum déplacé à de plus hautes énergies. Ce déplacement est corrélé avec le remplacement des ions NCO^- coordinés à l'état solide, par les molécules du solvant et avec la position de ces ligands dans la série spectrochimique. Le spectre est interprété comme étant celui d'un composé octaédrique légèrement distors d'une manière tétragonale.

Le spectre de la combinaison II a une bande à 17 200 cm^{-1} et deux épaules à des énergies plus petites, pendant que le spectre de la solution a deux épaules situées à des énergies plus grandes en comparaison des valeurs obtenues pour le solide. Ceci suggère de nouveau la coordination de dissolvant du DMF. La position des bandes du spectre discuté permet l'attribution d'une symétrie D_{4h}, mais la symétrie locale peut être encore plus diminuée, à savoir : D_{2h}. Le déplacement des bandes à des numeros d'onde plus élevés en comparaison du spectre de la combinaison I, ainsi que leur intensité réduite peuvent être corrélés à une stéréochimie octaédrique distorse rhombiquement,[25] l'ordre le plus probable des niveaux électroniques étant : $^2B_{1g}$ $^2A_{1g}$ $^2B_{2g}$ ^2E_g. Les valeurs obtenues par nous sont à des énergies moindres en comparaison de celles obtenues pour les combinaisons avec l'éthylendiamine [23] ou le NH_3[24] en concordance avec la position des ligands en série spectrochimique.

Les bandes au-dessus de 20 000 cm^{-1}, tant dans le spectre de réflexion que dans celui d'absorption (sur solutions), sont attribuées à des transitions ligand-ligand, très probablement de caractère $n-\pi$, et celles dans le domaine 32 000 — 33 000 cm^{-1}, de caractère $\pi-\pi^*$.

Les spectres RES ont été enregistrés sur des poudres et en solutions de DMF, à la température ambiante (tableau 4). En général, les spectres indiquent un arrangement tétragonal des ligands autour de l'ion Cu(II), donnant naissance à un signal isotrope et une seule valeur g(I), un signal à deux valeurs g(III et IV) et un spectre de symétrie, rhombique, à trois valeurs g(II et V). Le spectre $[Cu(o,o'\text{-}DABP)_2(NCO)_2]$ enregistré en solution d'acétone résout la structure surfine, mais l'intensité du signal est petite et la ligne large. En solution de DMF le spectre devient anisotrope, avec $g_\perp = 2{,}067$ et $g_\parallel = 2{,}155$ et le signal s'élargit $\Delta H_{1/2} = 176$ gauss.

Les spectres axiaux des combinaisons III et IV sont similaires à ceux des composés correspondants du thiocyanate, et le composé IV donne un spectre anisotrope avec une large bande, laquelle, en même temps que

---

[24] A. A. G. Tomlinson, B. J. Hathaway, D. E. Billing et P. Nicholls, *J. Chem. Soc. A*, **1969**, 65.

[25] A. A. G. Tomlinson et B. J. Hathaway, *J. Chem. Soc. A*, **1968**, 2578.

Tableau 4

Paramètres des spectres RES

N^0 crt.	Combinaison	$\Delta H_{1/2}$ gauss	$I_\parallel / I_\perp$	g	$g_\perp$	$g_\parallel$	g_1	g_2	g_3	G
I	$[Cu(o,o'-DABP)_2(NCO)_2]$	108,7	10/10,7	2,134	—	—	—	—	—	—
II	$[Cu(m,m'-DABP)(NCO)_2]$	151,1	7,1/11,3	—	—	—	2,043	2,09	2,137	—
III	$[Cu(p,p'-DABP)(NCO)_2]$	105,7	4,1/11,1	—	2,06	2,22	—	—	—	3,66
IV	$[Cu(2,7-DAF)(NCO)_2]$	176,2	6,9/11,2	2,104	—	—	—	—	—	—
V	$[Cu(py)_2(NCO)_2]$	152,7	10,8/7,4	—	—	—	2,063	2,13	2,172	—
VI	$[Cu(py)_6]\,(NCO)_2]$	176,2	5,8/12,6	—	2,05	2,21	—	—	—	4,20

la valeur moindre du moment magnétique, indique des interactions d'échange complexes.

Chacun des spectres enregistrés en solution de DMF ont une forme et des paramètres différents de ceux des spectres obtenus sur solide, ce qui suggère le changement de la sphère coordinative du métal, par participation du solvant à la liaison.

Dans le cas des spectres axiaux suggérant une symétrie D_{4h} on a corrélé les valeurs des facteurs g par la relation $\frac{g_{\parallel} - 2}{g_{\perp} - 2} = G^{23}$ suggérant que la valeur numérique du facteur G peut être utilisée comme indice de l'existence ou de l'absence des interactions d'échange entre les ions Cu(II). Ainsi, pour des valeurs de $G < 4$ on suppose l'existence de ce genre d'interactions pour les ions Cu(II) non dilués magnétiquement, et pour $G > 4$ ces interactions n'existent pas ou sont minimales. Etant donné que la majorité des valeurs μ (tableau 1) sont supérieures à la seule valeur spin, les interactions qui apparaissent doivent être plus petites que l'énergie thermique, et donc le phénomène se manifeste seulement par l'élargissement de la ligne de résonance (tableau 4). Les valeurs G (tableau 4) indiquent la présence d'une interaction d'échange pour la combinaison III, probablement par l'intermédiaire du NCO^- lié en pont (malgré les valeurs NCO du spectre IR qui ne supportent pas un telle attribution), et l'absence de celle-ci dans la combinaison VI, dans laquelle les ions Cu(II) paraissent bien séparés des six molécules de pyridine coordinées autour de chacun.

On a constaté[22] que dans le cas des spectres de symétrie rhombique ayant trois valeurs g, lorsque la plus petite valeur du facteur g est supérieure à 2,04 (le cas des combinaisons II et V) la symétrie locale peut être un octaèdre allongé rhombique (ce qui correspond aux résultats déduits du spectre de réflexion) on un plan-carré rhombique, ayant les axes locaux alignés parallèlement à ceux des coordonnés (ce qui correspond aux valeurs δNCO des spectres IR).

Si nous admettons que l'ion Cu(II) est hexacoordiné, les combinaisons étudiées par nous peuvent être interprétées dans les limites de la symétrie D_{4h}, plus ou moins distorse. La combinaison I sera un octaèdre avec les deux molécules d'*o*, *o'*—DABP formant deux heptacycles dans le plan du complexe, et deux ions NCO^- coordonnés en trans. Les combinaisons II et V auront de même une configuration octaédrique mais distorse rhombiquement, ce qui concorde avec les données obtenues des spectres de réflexion RES, ayant probablement la forme :

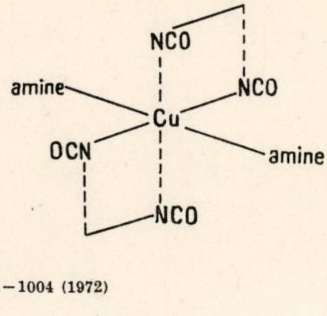

La symétrie locale de la combinaison III peut être interprétée de la même manière, malgré le spectre RES axial obtenu, ayant seulement deux valeurs g, mais ce fait a été aussi rencontré dans le cas d'autres diamines de Cu(II).[25] Les données expérimentales ne sont pas suffisantes pour que l'on puisse attribuer une configuration aussi probable que possible à la combinaison IV. Étant donné la complexité des interactions présentes, de nouvelles recherches sont nécessaires.

Les combinaisons discutées ici ont le Cu(II) dans l'état fondamental B_{1g}, ainsi qu'il résulte de toutes les déterminations expérimentales, et l'ordre des niveaux énergétiques est celui de composés tétragonaux ou rhombiques normalement distors.

Revue Roumaine de Chimie, 17, 6, 1005–1011 (1972)

POLAROGRAPHIC BEHAVIOUR OF SOME CYCLOHEXANONE DERIVATIVES

CLARA MAKKAY, FRANCISC MAKKAY and MARIA IONESCU

Babeş-Bolyai University, Cluj, Romania

Received October 27, 1971

The polarographic behaviour of the cyclohexanone derivatives II–VI on mercury dropping electrode in ethanol was studied, using as basic solution 3 M tetramethylammonium chloride. Well formed waves corresponding to the reduction of the double bonds for compounds II–VI and the reduction of the nitro group for compounds IV–VI, were obtained. The wave corresponding to the reduction of the carbonylic function appears with certainty only for product VI. For the study of the influence of the temperature on the form of the polarograms and the diffusion current polarograms have been registered at various temperatures.

Cyclohexanone, like the saturated aliphatic ketones generally is polarographically reduced in the very negative potential field, for instance in 0.05 N tetraethylamonium-chloride-dioxan 75 % the half-wave potential ($E_{1/2}$) being -2.45 V (S.C.E.).[1] By using another basic solution, such as HCl, LiCl, NH_4Cl, the reduction of the cyclohexanone does not even take place.[2]

The unsaturated aliphatic ketones, in which the double bond is conjugated with the double carbonylic bond, are more easily polarographically reduced and generally give polarograms of two reduction degrees.[3,4] First the reduction of the double bond takes place according to the mechanism 1–4, namely through keto-enolic tautomerization and in acid solution we obtain a diketone, while in alkaline solution a saturated ketone [3]:

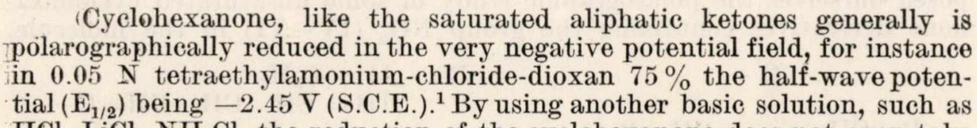

$$\begin{array}{l} R-CH-CH_2-COR \xleftarrow[2H^+]{2e^-} 2R-CH=CH-COR \xrightarrow[2H_2O]{2e^-} 2R-CH_2-CH_2-COR \\ \quad | \\ R-CH-CH_2-COR \end{array}$$

---

[1] M. von Stackelberg and W. Strache, *Z. Elektrochem.*, **53**, 118 (1949); *Chem. Abstr.*, **43**, 4183 (1949).

[2] R. Portillo and G. Varela, *Anales real Soc. españ. Fís. Quím.* **41**, 1429 (1945); *Chem. Abstr.*, **42**, 7199 (1948).

[3] J. Proszt, V. Cieleszky and K. Györbiró, *Polarográfia*, Akadémiai kiadó, Budapest, 1964, p. 382.

[4] H. W. Untermann and Al. Duca, *Chimie Analitică*, **1**, 97 (1971).

The saturated ketone can be further reduced in a more negative potential field.

Owing to the double bond, contained in the 2-cyclohexanone molecule, in the presence of the basic solution 0.1 N ammonium chloride it is more easily reduced than cyclohexanone, having $E_{1/2} = -1.55$ V (S.C.E.).[5]

Santonine, I, a derivative of cyclohexanone, having two bis-conjugated double bonds with carbonylic double bond, is still easier reduced in water-alcohol medium.[6]

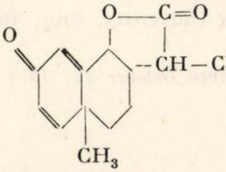

I.

For the santonine in the pH range 4 — 7, there appear two waves. For pH = 7 only a single wave appears, the second wave being blended to the discharge of the hydrogen. The half-wave potential for the first stage at pH = 2.5 is −1.1 V(S.C.E.) and at pH = 5, $E_{1/2} = -1.45$ V.

Taking into account this interesting behaviour of the cyclohexanone derivatives, we attempted the polarographic study of some previously obtained cyclohexanone derivatives.[7–9] We have thus dealt with the polarographic behaviour of some derivatives with double bonds in positions 2 and 6 (II and III).

Knowing that functional groups with negative inductive effect shift the half-wave potential towards more positive values, we have also proposed ourselves the polarographic study of some unsaturated cyclohexanone derivatives containing the group NO_2 (IV—VI) in the molecule.

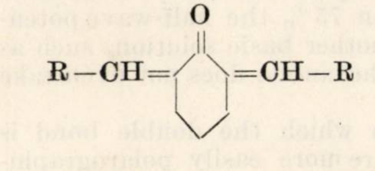

R : II = C_6H_5

III = CH=CH—CH=C—O

IV = $o\ C_7H_4NO_2$

V = $m\ C_6H_4NO_2$

VI = $p\ C_6H_4NO_2$

The study of the polarographic behaviour of these derivatives was also carried out at different temperatures.

EXPERIMENTAL

The polarographic behaviour of the II—VI cyclohexanone derivatives was studied in the ethanol-tetramethyl-ammonium chloride solution by recording the cathodic polarograms in $4.5 \times 10^{-4} - 2.25 \times 10^{-3}$ M concentrations by means of an OH 102 Radelkis recording polarograph, the scanning rate being 4.17 mV/sec. (The concentration differences of the studied compounds were determined by the different solubility of these substances in ethyl alcohol). Before each recording the solution was deaerated with purified methane gas. A mercury dropping electrode with $h_{Hg} = 52$ cm 19 drops per minute, was used as electrode. A 25 ml double-wall cylindric cell was used as electrolytic cell for thermostatic reasons. All the potentials in this paper refer to the mercury electrode in the cell. An aqueous solution of 3 M tetramethylammonium chloride was used as basic solution, of which 1 ml has been added to the solutions studied, the final volume of each sample being 10 ml.

---

[5] I. M. Kolthoff and I. I. Lingane, *Polarography*, vol. 2, Interscience, New York 1952, p. 665.

[6] F. Santavy, *Coll. Czech. Chem. Comm.*, **12**, 422 (1947).

[7] D. Vorländer and K. Kunze, *Ber. dtsch. chem. Ges.*, **59**, 2078 (1926).

[8] M. Ionescu and C. Makkay, *Stud. Univ. Babeş Bolyai Chem.*, **1966**, 115.

[9] M. Ionescu and C. Makkay, *Rev. Roumaine Chim.*, **15**, 265 (1970).

To study the influence of temperature on the form of the polarograms and the diffusion current, respectively on the half-wave potential, the polarograms were recorded at 20, 30, 40, 50, 60 and 70°, maintaining the temperature with a ±0,1° precision.

EXPERIMENTAL DATA

By recording the cathodic polarograms of the cyclohexanone unsaturated derivatives with two double bonds, II and III, we have obtained polarograms of three, respectively of two stages. The polarograms obtained at 20 and 70° are rendered on figures 1 and 2.

In the case of 2,6-bis-benzylidene-cyclohexanone, II, the half-wave potential for the first wave at 20° is – 0.786 V, and for the second wave – 1.060 V. The first two waves always appear and are well formed, while the third, wave with $E_{1/2} = -1.475$ V, does not appear constantly. For 2,6-bis-furfurylidene cyclohexanone, III, only two waves appear with $E_{1/2(1)} = -0.770$ V and $E_{1/2(2)} = -1.060$ V. The first two waves for II as well as for III are probably due to the reduction of the double bonds, and the third wave, in case II, to the reduction of the function C = O.

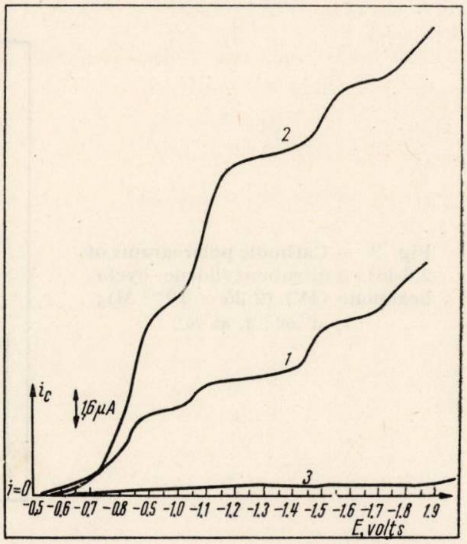

Fig. 1. – Cathodic polarograms of 2,6-bis-benzylidene-cyclohexanone (II) (9×10^{-4} M), respectively of the basic solution 0,3 M:

1, at 20°; *2*, at 70°; *3*, the basic solution at 20°

From the polarograms obtained for II and III, and partially represented in figures 1 and 2, we have been able to notice that through the rise of temperature the values of the diffusion current increase, and the polarograms become better formed.

By watching the polarographic behaviour of the 2,6-bis-*o*-, *m*- and *p*-nitro-benzylidene-cyclohexanone combinations, IV—VI, we have obtained the polarograms partially represented in figure 3—5.

On the polarograms obtained for 2,6-bis-*o*-nitrobenzylidene-cyclohexanone, IV, (fig. 3) two stages appear regularly with the following values for the half-wave potentials at 20° $E_{1/2(1)} = -0.422$ V and $E_{1/2(2)} = -0.865$V. At 20° the third wave appears too poorly formed with a half-wave potential of — 1.170 V, that at higher temperatures is distorted and disappears. At 20° the first wave is also poorly formed (curve 1, fig. 3) but already at 30° it is much better formed, being identical to the polarogram obtained at 70° (curve 2, fig. 3). With the rise in temperatures, besides a better formation of the polarograms, the diffusion current also increases thoroughly.

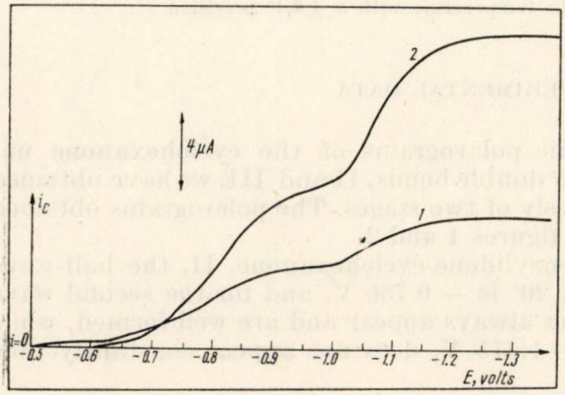

Fig. 2. — Cathodic polarograms of 2,6-bis-furfurylidene-cyclohexanone (III) (10^{-4} M); *1*, at 20°; *2*, at 70°.

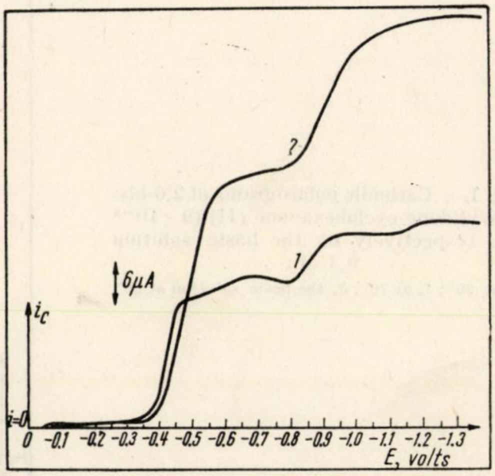

Fig. 3. — Cathodic polarograms of 2,6-bis-*o*-nitrobenzylidene-cyclohexanone (IV) (2.25×10^{-3} M); *1*, at 20°; *2*, at 70°.

The polarograms obtained for 2,6-bis-*m*-nitrobenzylidene-cyclohexanone V, (fig. 4) always occur between − 0.3 and −1.0 V and are made up of two waves having at 20° half-wave potentials of $E_{1/2(1)} = -0.391$ V and $E_{1/2(2)} = -0.735$ V. It is worth noticing that at 0 V we already obtain in each case an appreciable anodic current. The temperature rise, in this case, too, has a strong influence on the formation of the polarograms. Besides the increase of the diffusion current, even the shape of the

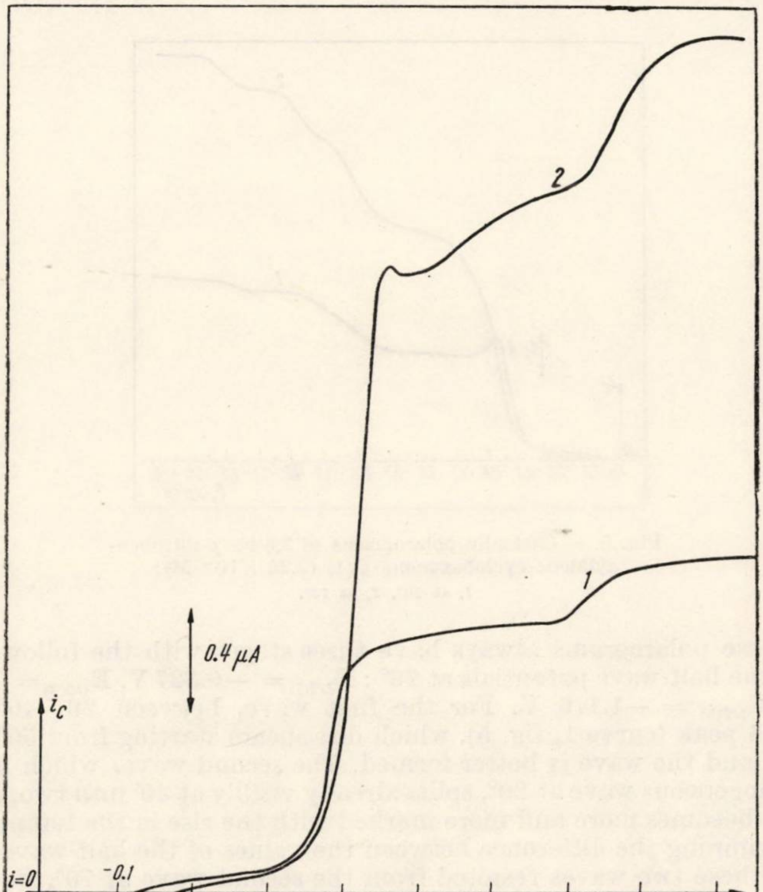

Fig. 4. — Cathodic polarograms of 2,6-bis-*m*-nitrobenzylidene-cyclohexanone (V) (4.5×10^{-4});
1, at 20°; *2*, at 70°.

polarograms changes with the temperature rise. Starting from 40° a peak appears on the polarograms at the first wave (curve 2, fig. 4) and is maintained at higher temperatures.

Among the polarograms obtained for nitroderivatives the most interesting seem to be those obtained in the case of 2,6-bis-*p*-nitro-benzylidene-cyclohexanone, VI (fig. 5).

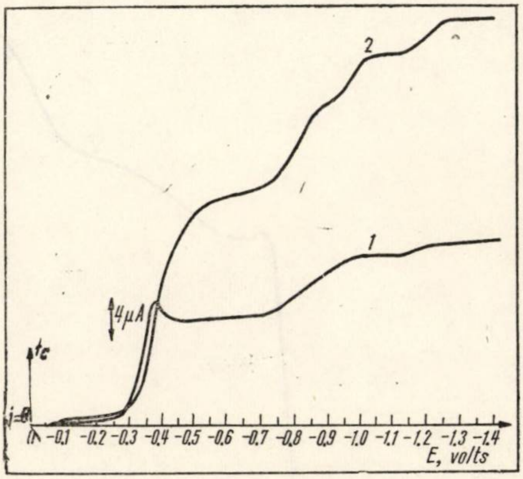

Fig. 5. — Cathodic polarograms of 2,6-bis-*p*-nitrobenzylidene-cyclohexanone (VI) (2.25×10^{-3}M); *1*, at 20°. *2*, at 70°.

These polarograms always have three stages with the following values for the half-wave potentials at 20° : $E_{1/2(1)} = -0.327$ V, $E_{1/2(2)} = -0.850$ V and $E_{1/2(3)} = -1.170$ V. For the first wave, between 20—40°, there appears a peak (curve 1, fig. 5), which disappears starting from 50° (curve 2, fig. 5) and the wave is better formed. The second wave, which appears as a homogeneous wave at 20°, splits already visibly at 40° into two, and the splitting becomes more and more marked with the rise in the temperature. By determining the difference between the values of the half-wave potentials for these two waves resulted from the second wave at 70°, we obtain 180 mV.

The first wave for the polarograms obtained for the three nitroderivatives corresponds to the reduction of the nitro groups, and the second wave to the reduction of the double bonds, however while the reduction of the two nitro groups takes place concomitantly, the reduction of the double bonds may occur successively.

The reduction of the function C=0 takes place at more negative potentials, but the presence of the nitro group in *para*-position facilitates this process, causing the appearance of a well formed wave.

With the rise in temperature from 20 to 70° the diffusion current also increases very much. This increase is generally linear between 20 and 50°, but at higher temperatures there appear deviations from the straight lines ; the values are slightly higher, owing to the concentration possibilities of the solutions (alcoholic solutions) during the recording of the polarograms. To elucidate whether the intensity of the limit current is determined exclusively by the diffusion of the depolarizing agent, or also by the chemical reaction, we have calculated the temperature coefficient[10] between 20 and 50° for the combination under study, obtaining the following values for the global polarogram : 1.70 %/degree at II, 1.57 %/degree at III, 1.53 %/degree at IV, 1.76 %/degree at V and 1.47 %/degree at VI. From these values one may notice that the intensity increase of the limit current with the rise of the temperature is only provided by the diffusion of the studied substance.

The variation of the temperature also influences the values of the half-wave potentials. This shifts towards more negative values while the temperature rises. Thus, for substance II, for the first wave, the half-wave potential shifts from −0.786 V (20°) for − 0.820 V(70°), for the second wave, from −1.060 V to −1.097 V, and for the third wave, from −1.475 V to −1.500 V. For the other combinations the half-wave potentials vary as follows :

for substance III : $E_{1/2\,(1)} = -0.770 - -0.796$ V ; $E_{1/2(2)} =$
$= -1.060 - -1.080$ V
" " IV : $E_{1/2(1)} = -0.422 - -0.487$ V ; $E_{1/2(2)} = -0.865 -$
-0.930 V
" " V : $E_{1/2(1)} = -0.327 - -0.433$ V ; $E_{1/2(2)} = -0.735 -$
-0.780 V
" " VI : $E_{1/2(1)} = -0.327 - -0.385$ V ; $E_{1/2(2)} = -0.850 -$
-0.860 V
and $E_{1/2(3)} = -1.170 - -1.210$ V.

The variations of the half-wave potentials with the temperature are characteristic of the irreversible waves.

CONCLUSIONS

The cyclohexanonic derivatives (2,6-bis-benzylidene-cyclohexanone, II ; 2,6-bis-furfurilydene-cyclohexanone, III ; 2,6-bis-*o*-, *m*-, *p*-nitro-benzylidene-cyclohexanone IV−VI, are easily reduced polarographically on a mercury dropping electrode, in alcoholic solution and in the presence of tetramethylammonium chloride. Well-formed waves appear on the polarograms obtained, corresponding to the reduction of the nitro groups (IV−VI) and to the reduction of the double bonds (II−VI). The wave corresponding to the reduction of the well formed function C=O appears certainly only in the case of 2,6-bis-*p*-nitrobenzylidene-cyclohexanone (VI).

The polarograms obtained may serve not only to the quantitative determination of these combinations, but also for kinetic studies.

They may also be helpful in clearing some structural problems, a study which is actually under way.

---

[10] C. Makkay, Fr. Makkay and M. Ionescu, *Stud. Univ. Babeş Bolyai Chem.*, **1970**, 71.

Revue Roumaine de Chimie, 17 6, 1005−1011 (1972)

Revue Roumaine de Chimie, 17, 6, 1013–1031 (1972)

RECHERCHES SUR LA CYCLISATION DES N_1-ACYL-N_4-ARYL-THIOSEMICARBAZIDES. II.*

NOUVEAUX *p*-FLUORODIPHÉNYLSULFONYL-5-ARYL-AMINO-1,3,4-THIADIAZOLES ET 1,2,4-MERCAPTO-TRIAZOLES À INTÉRÊT THÉRAPEUTIQUE

CĂTĂLINA DEMETRESCU

Laboratoire de Chimie Organique de la Faculté de Pharmacie de Bucarest
19–21, str. Alex. Sahia, Bucarest, Roumanie

Reçu le 29 juin 1971

L'auteur obtient par synthèse une nouvelle classe de N_1-acyl-N_4-aryl-thiosemicarbazides, dérivés de la *p*-fluorodiphénylsulfone qui ont été cyclisés en catalyse acide et basique. On a obtenu ainsi de nouveaux 5-arylamino-1, 3, 4-thiadiazoles et mercapto-1,2, 4-triazoles, qui sont des composés doués d'une potentialité chimico-thérapeutique intéressante. La structure des nouveaux composés obtenus a été confirmée par synthèse inverse, par analyse des éléments (N et S), ainsi que par une étude complète des spectres de vibration en infrarouge.

La synthèse de quelques nouveaux antimétabolites, ayant une structure adéquate pour interférer dans certains processus enzymatiques fondamentaux, est peut-être un des objectifs les plus intéressants des recherches actuelles, qui préoccupent de plus en plus les chimistes contemporains.

Les recherches récemment entreprises dans ce domaine par Buu-Hoï et son école[1,2] et par d'autres chercheurs,[3–7] sur quelques antagonistes fluorés des amino-acides ou des bases puriniques, ainsi que sur les composés organo-fluorés dérivés de la thio-urée, sont dignes d'être mentionnés comme intéressant la thérapie des substances antivirotiques.

De même, les composés du type *p*-fluorophényl-amino-thioformyl-thiosemicarbazides : $p\text{-F}-C_6H_4-NH-CS-NH-NH-CS-NH-R$ ou

---

* Ire partie : C. Demetresco, V. Manu et R. Răcăşanu, *Pharmazie — Berlin*, **25**, 409 (1970).

[1] N. P. Buu-Hoï, T. B. Loc et N. D. Xuong, *Bull. Soc. chim. France*, **1955**, 694 ; **1956**, 363.

[2] N. P. Buu-Hoï, N. D. Xuong et N. H. Nam, *J. Chem. Soc.*, **1956**, 2160.

[3] H. K. Mitchell et C. Niemann, *J. Amer. Chem. Soc.*, **69**, 1232 (1947).

[4] R. Duschinsky, E. Pleven et C. Heidelberger, *J. Amer. Chem. Soc.*, **79**, 4559 (1957).

[5] A. Giner-Sorella et A. Bendich, *J. Amer. Chem. Soc.*, **80**, 5744 (1958).

[6] J. Horovitz et E. Chargaff, *Nature* (*London*), **184**, 1213 (1959).

[7] N. K. Cahudhuri, B. J. Montag et C. Heidelberger, *Cancer Res.*, **18**, 318 (1959).

p-fluorophényl-thiosemicarbazides (Flusone) : *p*-$F-C_6H_4-NH-CS-NHR$ ont été introduits en thérapeutique comme antiseptiques des cavités rhino-pharingiennes.[8]

L'augmentation de l'effet thérapeutique, due au groupe $>C=S$, est mise en évidence par le professeur Lépine de l'Institut Pasteur de Paris, qui a montré l'effet d'inhibition, déterminé par le composé *p*-fluoro-*p'*-chloro-thiocarbanylide : *p*-$F-C_6-H_4-NH-CS-NH-C_6H_4-Cl$-*p'* sur l'évolution de la poliomyélite expérimentale, provoquée chez la souris avec le virus Lansing, pendant que son analogue oxygéné est pratiquement inactif.[8]

Autres dérivés fluorurés de la thio-urée, comme par ex. le *p*-fluoro-*m*-brome-thiocarbanilide, manifestent une action micostatique prononcée.[9]

En étudiant certaines classes de composés à action antivirotique nette, synthétisées antérieurement par différents chercheurs, Buu-Hoï a supposé que, pour obtenir un bon effet antivirotique, il est indiqué que la molécule organique contienne une fonction avec du soufre, dans laquelle l'atome de soufre soit lié à un groupe hydrazinique.

D'autre part, on admet que les substances antituberculeuses du groupe des thiosemicarbazides devraient leur action à la compétition avec certaines enzymes bactériennes, pour la fixation de certains cations métalliques (Cu^{2+}, Co^{2+}, Fe^{3+}, etc.), qui jouent le rôle de coenzymes.

On pourrait considérer les N_1-acyl-N_4-aryl-thiosemicarbazides comme étant constituées par un groupe haptofore (formé par les deux radicaux acyl et aryl, liés aux atomes d'azote N_1 et N_4) et par un autre groupe toxofore, actif, représenté par la fonction thio-urée. Ce dernier groupe est en fait le groupement complexant, grâce à sa possibilité de tautomérisation thion-thiolique : $-NH-CS-NH- \rightleftarrows -NH-C(SH)=N-$.

La valeur de l'effet biologique devient ainsi mesurable par le degré dont les métalloenzymes, essentielles pour la vie du bacille tuberculeux, sont inactivées comme suite de l'action complexante des thiosemicarbazides, dans leur forme thiolique.

Fondés sur ces prémisses, nous nous sommes proposé une étude systématique sur l'addition des hydrazides des acides *p*-*X*-diphénylsulfonyle-*p'*-carboxyliques à certains isothiocyanates aryliques, convenablement substitués en position *para* du noyau benzénique, avec les halogènes brome ou iode, qui exercent des effets mésomères marquants. L'introduction comme radical acyl du groupe *p*-fluoro-diphényl-sulfonyl-*p'*-carboxy ($p-F-C_6H_4-SO_2-C_6H_4-CO-p'$) vérifiée par nous comme particulièrement efficace pour l'action antibactérienne,[3] par l'intermédiaire de l'addition de l'hydrazide de l'acide *p*-fluorodiphénylsulfonyl-*p'*-carboxylique aux isothiocyanates de phényle, respectivement de *p*-bromo-ou de *p*-iodophényle — nous a permis la synthèse de nouvelles N_1-(*p*-fluoro-

---

[8] N. P. Buu-Hoï, «Progress in Drug Research», tome 3., Birkhäuser-Verlag, Basel-Stuttgart, 1961.

[9] Al. Mavrodin, C. Demetresco, C. Chiritza et O. Macovschi, *Rev. Roumaine Chim.*, **15**, 1953 (1970).

V

Gyors, egyszerü módszer higanynyomok meghatározása halak testében neutronaktivációs elemzéssel.

A simple, rapid method for determining trace amounts of mercury in fish via neutron activation analy

73, 13

60 : 9 = 6
6

3×6 = 18
6×7 = 42

V

Gyors, egyszerü módszer higanynyomok meghatározására halak testében neutronaktivációs elemzéssel.

A simple, rapid method for determining trace mercury in fish via neutron activation analysis.

ROTTSCHAFER,J.M;

V

Benzol-karboxilsavak, mono- és bisz-2-hidroxi-etil -észtereik oldékonysága vízben és szerves oldószerekben.

Rozpustnosti benzenkarbonovych kyselin a jejich mono- a bis 2-hydroxyetyl -esteru ve vode a organickych rozpouztedlech.

HRADIL,J; MÁLEK,J.stb.-

Chemicky Prumysl

Chem. Prum.

20 3 7P 117 120

4 21 18 8

Oldékonysági mérések:benzoesav, izoftálsav 1-butanolban 1-B , tereftálsav 2-propanolban 2-P , dimetil-szulfoxidban DMSO , 3,5-dikarboxi-benzol-szulfonát 1-B-ben, 2- hidroxi-etil-benzoát 1- és 2-B-ben, bisz-2-hidroxi-etil-izoftalát vízben, 1- és 2-B-ben,2-hidroxi-etil-terftalát vízben, 1- és 2-B-ben, DMSO-ban, bisz-2-hidroxi-etil-terftalát vízben, metanolban, 1- és 2-B-ben, 2-P-ben, DMSO-ban.

Ádám Magda

OMKDK Ádám Magda

diphénylsulfonyle)-N_4-aryl-thiosemicarbazides, d'après le schéma suivant :

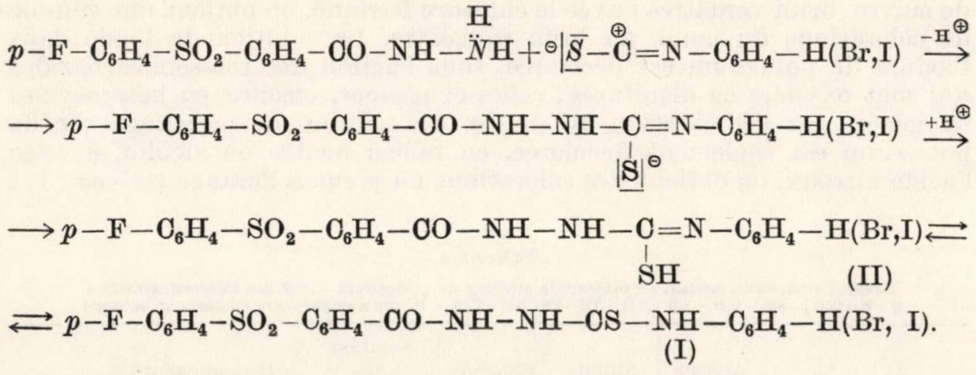

$$p\text{-F-}C_6H_4\text{-}SO_2\text{-}C_6H_4\text{-CO-NH-}\overset{H}{\ddot{N}}H + {}^{\ominus}|\overline{S}\text{-}\overset{\oplus}{C}=N\text{-}C_6H_4\text{-}H(Br,I) \xrightarrow{-H^{\oplus}}$$

$$\longrightarrow p\text{-F-}C_6H_4\text{-}SO_2\text{-}C_6H_4\text{-CO-NH-NH-}\underset{|\underline{S}|^{\ominus}}{C}=N\text{-}C_6H_4\text{-}H(Br,I) \xrightarrow{+H^{\oplus}}$$

$$\longrightarrow p\text{-F-}C_6H_4\text{-}SO_2\text{-}C_6H_4\text{-CO-NH-NH-}\underset{SH}{C}=N\text{-}C_6H_4\text{-}H(Br,I) \rightleftarrows \quad (II)$$

$$\rightleftarrows p\text{-F-}C_6H_4\text{-}SO_2\text{-}C_6H_4\text{-CO-NH-NH-CS-NH-}C_6H_4\text{-}H(Br, I). \quad (I)$$

Dans ces nouvelles molécules, le groupe thiosemicarbazide —NH—NH—CS—NH— joue le rôle d'un centre biologique actif — étant également inclus dans une structure vinylogue (ayant de nombreux systèmes de doubles liaisons polyconjuguées). Ce fait rend possible une diminution de la toxicité, propre aux thiosemicarbazides, ainsi qu'une éventuelle élimination des effets secondaires indésirables comme l'anémie, la leucopénie, l'agranulocitose, l'anorexie, etc. Ce n'est qu'à cause de ces effets, que les composés de cette classe sont restés longtemps inutilisables, bien qu'ils soient du nombre réduit de substances auxquelles les bacilles tuberculeux ne présentent aucune résistence.

Conformément aussi aux études cinétiques, effectuées sur d'autres N_1-acyl-N_4-aryl-thiosemicarbazides par Proinov[10] et à nos conclusions antérieures,[11] se référant à l'addition d'un nombre de 20 nouvelles hydrazides aryliques à l'isothiocyanate de phényle, avec obtention des N_1-acyl-N_4-aryl-thiosemicarbazides correspondantes, nous avons supposé que cette réaction a lieu suivant un mécanisme nucléophile, en deux étapes.

Dans une première phase a lieu l'attaque du réactant nucléophile (l'hydrazide fluorée) sur l'atome de carbone de la molécule de l'isothiocyanate arylique, ayant un déficit de charge électronique, dû aux déplacements électromères, résultant de l'influence réciproque des atomes. L'expulsion d'un proton suit.

Dans la seconde phase de la réaction, a lieu la stabilisation du composé intermédiaire (par l'acceptation d'un proton) et on obtient la forme thiolique de la thiosemicarbazide (II), qui se trouve en équilibre avec sa forme thionique (II).

Les nouvelles thiosemicarbazides (II) synthétisées sont facilement solubles dans des alcalis et dans l'ammoniaque, mettant ainsi en évidence la fonction thiol (—SH), présente dans la molécule. Elles donnent naissance avec l'acétate de plomb aux mercaptides (précipités jaunes), avec le sulfate de cuivre, en solution alcaline, on obtient des précipités de sels de cuivre brun verdâtres ; avec le chlorure ferrique, on obtient une gamme de colorations du jaune au brun rougeâtre. La solution de l'iode dans l'iodure de potassium est décolorée, sous l'action des thiosemicarbazides qui sont oxydées en disulfures ; celles-ci passent, ensuite, en hétérocycles oxygénés, par l'élimination du soufre. La solution de permanganate de potassium est également décolorée, en milieu neutre ou alcalin, et avec l'acide nitreux, on obtient des colorations du jaune à l'orange (tableau 1) :

---

[10] I. Proinov, « Thèse de doctorat », Institut de Médecine et de Pharmacie, Cluj, Juin 1966.

[11] C. Demetresco, C. Chiritza, V. Manu et M. Vanghelovici, « IIIe Conférence Républicaine de Chimie », Timişoara, juin 1966, p. 315.

Tableau 1

Données analytiques mettant en évidence la présence du groupement – SH des thiosemicarbazides $p-F-C_6H_4-SO_2-C_6H_4-CO-NH-NH-CS-NH-C_6H_4-R$ (On a employé des solutions en acétone)

N°	R	Acétate de plomb	Sulfate de cuivre	Chlorure de Fe^{3+}	Solution de l'iode dans l'iodure de potassium	Permanganate de potassium	Acide nitreux
I	H	Précipitée jaune canari intense	Précipité vert-brun	Précipité vert intense	Décoloration rapide	Décoloration rapide	Coloration orange rougeâtre
II	Br–p	Précipité jaune pâle	Précipité vert-olive	Précipité vert brunâtre	Décoloration lente	Décoloration initiale ; puis coloration brune (MnO_2)	Coloration jaune canari intense
III	I–p	Précipité jaune canari	Précipité vert-olive	Précipité jaune verdâtre	Précipité jaune verdâtre	Décoloration initiale ; puis précipité brun de MnO_2	Coloration jaune-orange

LA CYCLISATION DES NOUVELLES N_1-ACYL-N_4-ARYL-THIOSEMICARBAZIDES EN CATALYSE ACIDE OU BASIQUE

Pour obtenir des dérivés des thiosemicarbazides, moins toxiques et ayant une activité sélective, nous nous sommes proposé d'étudier la cyclisation de ceux-ci en catalyse acide et basique. Nous avons supposé qu'on peut modifier par cyclisation la nature des centres biologiques actifs de la molécule et ainsi le type d'activit pharmacodynamique.

Les recherches antérieures, indiquées dans la littérature[12–15] montrent que les hétérocycliques, pouvant être obtenus par cyclisation des

---

[12] F. Mitschet F. Wuppertal, *Angew. Chem.*, **63**, 250 (1951).
[13] R. Neidlein et J. Tauber, *Pharm. Zhalle*, **107**, (6), 430 (1968).
[14] R. Clarkson et J. K. Landquist, *J. Chem. Soc.*, **1967**, 24, 2700.
[15] E. Hoggart, *J. Chem. Soc.*, **1949**, 1160; **1950**, 612.

acyl-aryl-thiosemicarbazides dans des conditions expérimentales différentes, présentent un intérêt thérapeutique remarquable.

Etant donné la possibilité de nos acyl-aryl-thiosemicarbazides (I) d'exister d'une manière permanente sous trois formes tautomères I, II_A et II_B, nous avons supposé qu'elles puissent être cyclisées avec formation de nouveaux 5-arylamino-1,3,4-thiadiazoles (III) ou de nouveaux 2-mercapto-1, 2, 4-triazoles (IV), en suivant les schémas de réaction (a) et (b) et nous avons réalisé ainsi deux types de cyclisations, en catalyse acide et basique

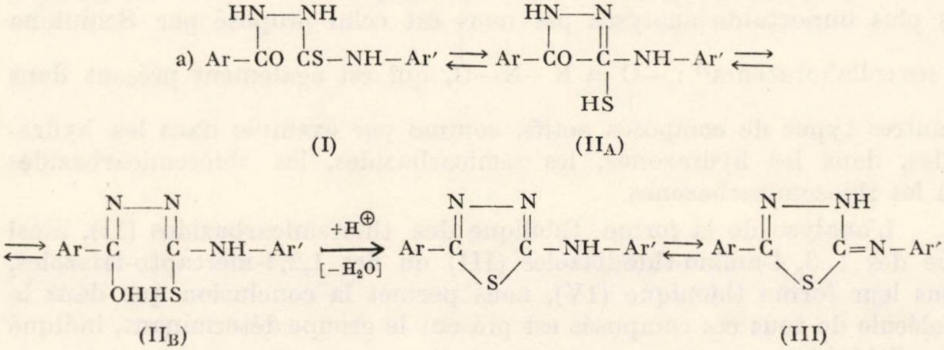

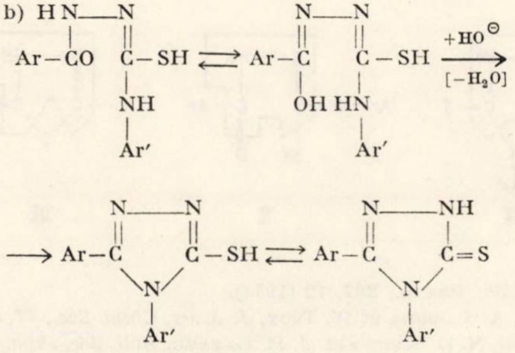

dans laquelle ; $Ar = (p)-F-C_6H_4-SO_2-C_6H_4-$

et $Ar' = -C_6H_5$; $-C_6H_4-Br-(p)$; $-C_6H_4-I-(p)$.

Nous avons ainsi obtenu 6 nouveaux composés hétérocycliques : 1, 3, 4-amino-thiazoles et 1, 2, 4-mercapto-triazoles, dérivés de la *p*-fluorodiphénylsulfone.

Les thiadiazoles et les triazoles, obtenus par cyclisation, ne sont pas mentionnés dans la littérature de spécialité ; ces composés se présentent sous forme de poudres microcristallines, stables, incolores ou faiblement jaunâtres, aux points de fusion nets, élevés.

La littérature récente met en évidence différents effets thérapeutiques aux composés où le groupe 5-arylamino-1, 3, 4-thiadiazole constitue le centre déterminant de l'activité biologique.[16–22] Les mêmes hétérocycles semblent être responsables de certains autres effets intéressants, tels que : l'action analgésique, anti-inflammatoire, antituberculeuse, hypoglycémiante, antivirotique, cytostatique, antipyrétique, etc.

Dans les travaux antérieurs, nous avons montré l'importance de certains groupes ou squelettes fonctionnels, considérés comme déterminants des différents types d'effets biologiques.[23–26] L'un des groupes les plus importants analysés par nous est celui proposé par Schiukina et ses collaborateurs[27] : 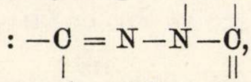 $-\underset{|}{C}=N-\overset{|}{N}-\underset{\|}{\overset{|}{C}}$, qui est également présent dans d'autres types de composés actifs, comme par exemple dans les hydrazides, dans les hydrazones, les semicarbazides, les thiosemicarbazides ou les thiosemicarbazones.

L'analyse de la forme thiolique des thiosemicarbazides (II), ainsi que des 1, 3, 4-amino-thiadiazoles (III) ou des 1,2,4-mercapto-triazoles, sous leur forme thionique (IV), nous permet la conclusion que dans la molécule de tous ces composés est présent le groupe déterminant, indiqué par Schiukina :

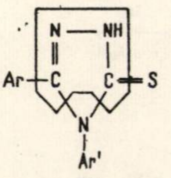

IV

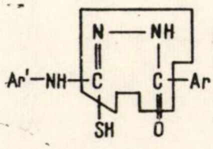

II

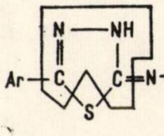

III

---

[16] J. Klosa, *Arhiv. Pharm.*, **287**, 12 (1954).

[17] J. J. Oleson, A. Sloboda et W. Troy, *J. Amer. Chem. Soc.*, **77**, 6713 (1955).

[18] N. P. Buu-Hoï, N. D. Xuong et J. H. Gazave, *Bull. Soc. chim. France*, **5**, 363 (1956).

[19] N. P. Buu-Hoï et N. D. Xuong, *J. Chem. Soc.*, **1955**, 1573 ; Comptes rend. Acad. Sci. Paris, **238**, 295 (1954) ; **235**, 329 (1952).

[20] F. Russo et M. Ghelardoni, *Boll. Chim. Farm.*, **108**, 1281 (1969).

[21] M. T. Shah, J. Mhasalkar, N. A. Varaya, R. A. Bellare et C. V. Deliwala, *Indian J. Chem.*, **5** (8), 391 (1967).

[22] O. Masaki et M. Akira, *J. Pharm. Soc. Japan*, **72**, 373, 1533 (1952).

[23] C. Demetresco, « Thèse », Université de Bucarest, mai, 1962.

[24] C. Demetresco, C. Chiritza, El. Stanciu et Al. Mavrodin, *Pharm. Zhalle*, **106**, (12), 805 (1967).

[25] C. Chiritza, C. Demetresco, D. Trană et Al. Mavrodin, *Chim. Thérap., Paris*, **3** (*1*), 12 (1968).

[26] P. Gheorghiu, V. Stroesco, C. Demetresco et H. Benes, *Compt. rend. Soc. Biol.-Paris*, **159**, (2), 366 (1965).

[27] M. N. Schiukina, T. N. Perşhin, O. O. Makeeva, E. Sazonova, E. S. Nikitskaya, A. D. Yanina et A. N. Jakovleva, *Doklady Akad. Nauk, S.S.S.R.*, **84**, 981 (1952).

Ce fait nous fait escompter — pour nos composés — la potentialité de certains effets thérapeutiques prometteurs.

Nos recherches pharmacodynamiques sur les nouveaux composés sont en cours et feront l'objet d'autres recherches.

LE MÉCANISME DE LA RÉACTION DE CYCLISATION

Pour la cyclisation des nouvelles thiosemicarbazides (I) synthétisées en catalyse acide, nous proposons un mécanisme qui suppose — dans la première phase — une protonisation du groupe thiocarbonyle, sous l'influence du catalyseur acide. Il en résulte la forme thiolique(II_A).

Dans une seconde étape a lieu la protonisation du groupe carbonyle[28] sous l'action du catalyseur acide. Le produit d'addition résultant, ayant une moindre densité électronique à l'atome de carbone carbonylique, devient plus réactif par rapport à l'attaque des réactants nucléophiles. Dans cette seconde étape, on aboutit finalement à la forme énolique-thiolique (II_B) des thiosemicarbazides :

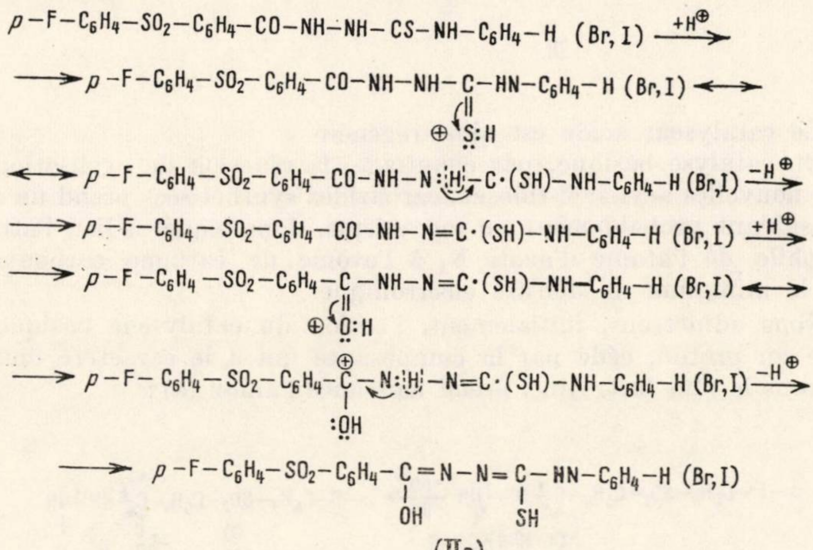

$$p\text{-}F-C_6H_4-SO_2-C_6H_4-CO-NH-NH-CS-NH-C_6H_4-H\ (Br, I) \xrightarrow{+H^{\oplus}}$$

$$\longrightarrow p\text{-}F-C_6H_4-SO_2-C_6H_4-CO-NH-NH-\underset{\oplus\ \ddot{S}:H}{\underset{\|}{C}}-HN-C_6H_4-H\ (Br, I) \longleftrightarrow$$

$$\longleftrightarrow p\text{-}F-C_6H_4-SO_2-C_6H_4-CO-NH-N:H-C\cdot(SH)-NH-C_6H_4-H\ (Br, I) \xrightarrow{-H^{\oplus}}$$

$$\longrightarrow p\text{-}F-C_6H_4-SO_2-C_6H_4-CO-NH-N=C\cdot(SH)-NH-C_6H_4-H\ (Br, I) \xrightarrow{+H^{\oplus}}$$

$$\longrightarrow p\text{-}F-C_6H_4-SO_2-C_6H_4-\underset{\oplus\ \ddot{O}:H}{\underset{\|}{C}}-NH-N=C\cdot(SH)-NH-C_6H_4-H\ (Br, I) \longleftrightarrow$$

$$\longrightarrow p\text{-}F-C_6H_4-SO_2-C_6H_4-\underset{:\ddot{O}H}{\underset{|}{\overset{\oplus}{C}}}-\ddot{N}:H-N=C\cdot(SH)-NH-C_6H_4-H\ (Br, I) \xrightarrow{-H^{\oplus}}$$

$$\longrightarrow p\text{-}F-C_6H_4-SO_2-C_6H_4-\underset{OH}{\underset{|}{C}}=N-N=\underset{SH}{\underset{|}{C}}-HN-C_6H_4-H\ (Br, I)$$

(II_B)

Dans une troisième étape, un proton, cédé par le catalyseur acide, se rattache à l'hydroxyle énolique et une molécule d'eau est éliminée. Il se produit ensuite l'attaque nucléophile du soufre sur l'atome de carbone, où il existe un déficit de charge électrique. L'atome d'hydrogène, lié au soufre, est expulsé simultanément sous forme de proton et on obtient le cycle thiadiazolique :

---

[28] C. D. NENIȚESCO, «Traité de Chimie Organique» VIe Éd., tome I, Ed. didactică şi pedagogică, 1966, p. 667.

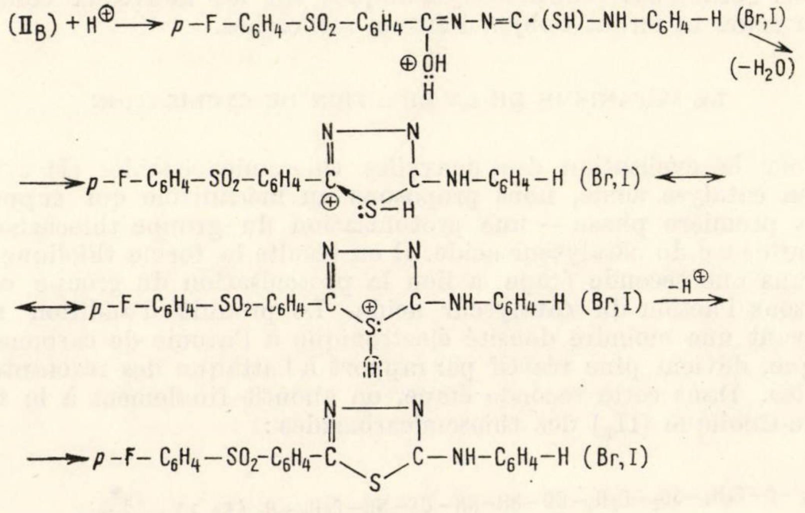
(II_B) + H⊕ ⟶ p-F-C6H4-SO2-C6H4-C=N-N=C·(SH)-NH-C6H4-H (Br,I)
⊕OH
(-H2O)
⟶ p-F-C6H4-SO2-C6H4-C ... C-NH-C6H4-H (Br,I) ⟷
:S-H
⟷ p-F-C6H4-SO2-C6H4-C ... C-NH-C6H4-H (Br,I) ⟶
-H⊕
⟶ p-F-C6H4-SO2-C6H4-C ... C-NH-C6H4-H (Br,I)
N
S

III

Le catalyseur acide est ainsi régénéré.

En catalyse basique, par chauffage, la réaction de cyclisation des mêmes nouvelles acyl-aryl-thiosemicarbazides synthétisées prend un autre cours, suivant probablement un mécanisme, dans lequel a lieu l'attaque nucléophile de l'atome d'azote N_4 à l'atome de carbone carbonylique ayant le minimum de densité électronique.

Nous admettons, initialement, l'action du catalyseur basique qui accepte un proton, cédé par la composante qui a le caractère donneur d'électrons le plus fort. Ainsi prend naissance l'anion (a) :

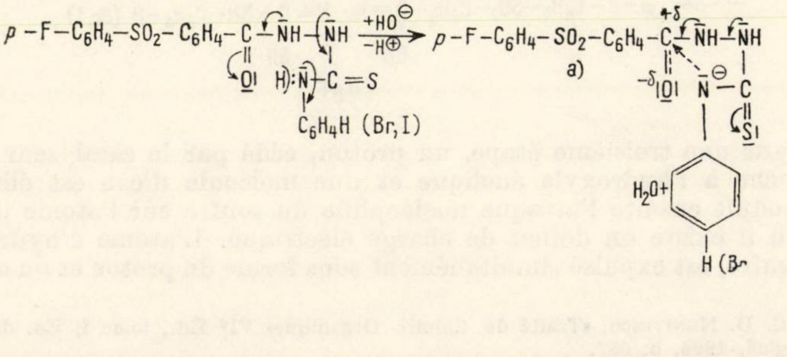
p-F-C6H4-SO2-C6H4-C-NH-NH
O
H):N-C=S
C6H4H (Br,I)
+HO⊖
-H⊕
p-F-C6H4-SO2-C6H4-C-NH-NH
a)
+δ
-δ
O
N⊖-C
S
H2O+
H (Br

Dans une seconde phase de la réaction, l'anion (a) est additionné à la partie de la molécule, contenant la composante carbonylique, et il résulte un nouvel anion (a_1) :

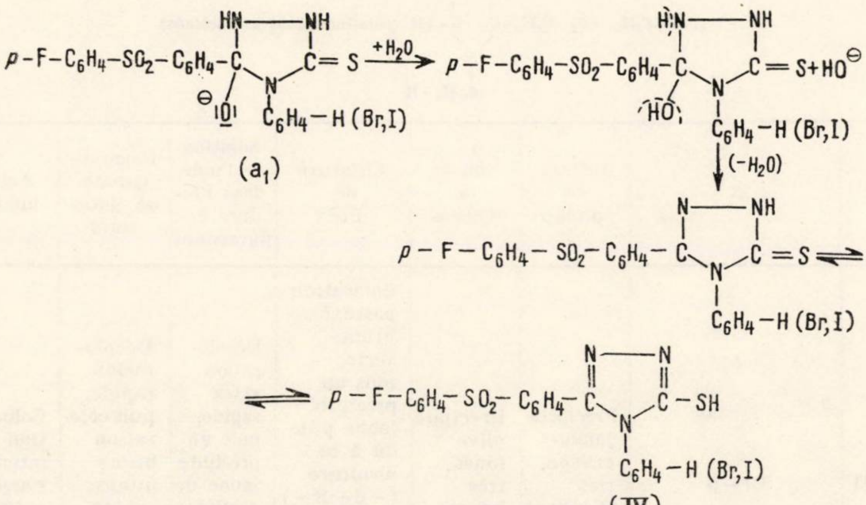

(IV)

Dans une troisième étape, l'anion (a_1) entre en réaction avec l'eau du milieu de réaction, avec laquelle a lieu une échange d'un proton et la base catalysatrice est régénérée. Le produit est finalement stabilisé par l'élimination de l'eau, après le chauffage.

Les nouveaux 5-arylamino-1, 2, 4-mercapto-triazoles synthétisés peuvent exister sous deux formes tautomères, l'une thionique et l'autre thiolyque, se trouvant en équilibre dynamique.

En effet, en présence de certains cations métalliques complexants (Cu^{2+}, Fe^{3+}, Hg^{2+}, Pb^{2+}, Cd^{2+}, etc.) nous avons facilement obtenu des mercaptides, intensément colorées (tableau 2).

Les autres réactions spécifiques du groupe thiol ont été également positives : décoloration de la solution de l'iode dans l'iodure de potassium, du permanganate de potassium en milieu alcalin, la réaction avec l'acide nitreux, etc.

Des études cinétiques en cours nous permettront de mettre en évidence la croissance de la vitesse de cette réaction de cyclisation, proportionnellement à la concentration en ions d'hydroxyle, pour démontrer le mécanisme proposé. Étant donné que les anions (a) et (a_1), résultant au cours de cette réaction, peuvent être stabilisés par effet de conjugaison à l'intérieur de la molécule vinylogue, nous supposons qu'ils peuvent avoir une certaine existence cinétique, en solution. Nous essayons aussi à déduire l'équation globale de vitesse pour la formation des triazoles, par l'application de la méthode de l'état stationnaire. Ainsi, l'étude de la vitesse de cyclisation devient possible, pour chacun des 1,2,4-triazoles et on pourrait établir l'influence du substituant en position *para* (brome ou iode). La nucléophilicité du groupe — NH, exprimée par le degré

Tableau 2

Données analytiques mettant en évidence la forme thyolique des 1,2,4-mércapto-triazoles

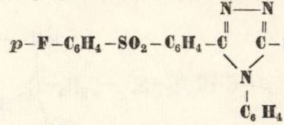

(solutions dans de l'acétone)

N°	R	Acétate de plomb	Sulfate de cuivre	Chlorure de Fe^{3+}	Solution de l'iode dans l'iodure de potassium	Permanganate de potassium	Acide nitreux
VIII	Br—p	Précipité jaune-orange, très abondant	Précipité olive foncé, très intense	Coloration passagère brune-verte, puis un précipité jaune pâle dû à la disulfure (—S—S—) résulté par oxydation du groupe thyole (—SH)	Décoloration assez rapide, puis un précipité jaune de disulfure abondant et intense	Décoloration rapide, puis coloration brune intense et un précipité brun de MnO_2	Coloration intense rouge—brun
IX	I—p	Précipité jaune canari intense	Précipité abondant verdâtre bleu-violet	Coloration temporaire, verdâtre, et après un précipité jaune pâle, dû au disulfure résulté par oxydation de la fonction thyole	Décoloration lente ; précipité abondant jaune pâle, dû au disulfure obtenu par oxydation	Décoloration assez rapide ; précipité abondant de MnO_2 qui se dépose immédiatement	Coloration rouge jaunâtre intense

dont celui-ci prend part (en qualité de composante donneuse d'électrons) à l'attaque nucléophile de l'atome de carbone carbonylique, dépend étroitement des effets mésomères positifs (+M) des halogènes [—Br ou—I].

CONFIRMATION DE LA CONSTITUTION DES NOUVEAUX COMPOSÉS

1) Par des réactions analytiques

— En présence des réactifs spécifiques (sels de Cu^{2+}, Pb^{2+}, Fe^{3+}) pour identifier le groupe thyole (—SH), nous avons réalisé — dans le cas des nouvelles thiosemicarbazides — des réactions analytiques spécifiques, indiquées antérieurement dans le tableau 1.

— Dans le cas des 1,3,4-amino-thiadiazoles nous n'avons pas obtenu des mercaptides insolubles, ce qui dénote l'absence du groupe thyole, et confirme la réaction de cyclisation, effectuée par nous en catalyse acide.

— Dans le cas des 1,2,4-mercapto-triazoles, nous avons réussi à mettre en évidence la présence du groupe thiol (—SH), par les réactions analytiques, indiquées dans le tableau 2.

— Toujours dans le même but de confirmer la structure, nous avons transformé les thiadiazoles obtenus en composés N_1-acétylés, par l'acylation de la fonction amine secondaire, présente dans la molécule, à l'aide de l'anhydride acétique et nous avons obtenu les dérivés acétylés correspondants :

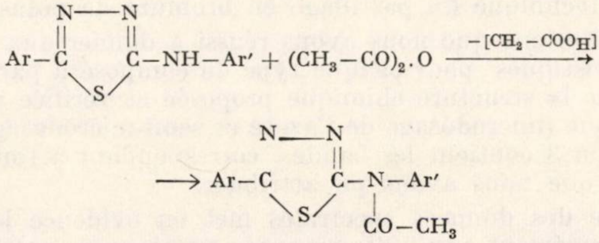
Ar—C
C—NH—Ar′ + (CH₃—CO)₂.O
—[CH₂—COOH]
N—N
S
Ar—C
C—N—Ar′
CO—CH₃

2) *Par synthèse inverse*

Nous avons ensuite effectué une synthèse inverse, en partant de la *p*-F-phénylsulfonyl-benzaldéhyde, synthétisée pour la première fois par nous.[29] Celle-ci a été condensée avec la phényl-thiosemicarbazide et nous avons obtenu la *p*-flurophénylsulfonyl-phényl-thiosemicarbazone (V). Cette thiosemicarbazone (V) a été cyclisée par nous, sous l'action du chlorure ferrique, en appliquant la méthode de R. Stollé [30] :

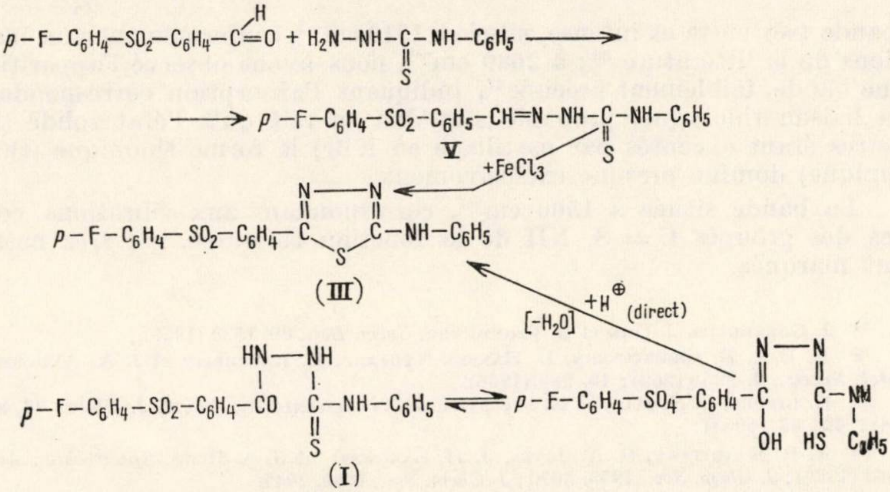
p-F-C₆H₄-SO₂-C₆H₄-C(H)=O + H₂N-NH-C(=S)-NH-C₆H₅
p-F-C₆H₄-SO₂-C₆H₅-CH=N-NH-C(=S)-NH-C₆H₅
V
+FeCl₃
N—N
p-F-C₆H₄-SO₂-C₆H₄-C
C-NH-C₆H₅
S
(III)
+H⊕ (direct)
[-H₂O]
HN—NH
p-F-C₆H₄-SO₂-C₆H₄-CO
C-NH-C₆H₅
S
(I)
p-F-C₆H₄-SO₄-C₆H₄-C
OH
HS
C-NH
C₆H₅

---

[29] C. Demetresco et R. Alexiu-Amariutzei, *Pharmazie-Berlin*, 1971 (sous presse).

[30] R. Stollé et K. Fehrenbach, *J. prakt. chem.*, 2, 122, 289 (1929).

De cette manière nous avons obtenu le même *p*-F-phényl-sulfonyl-5-phénylamino-1,3,4-thiadiazole du type (III), comme celui obtenu de l'acyl-aryl-thiosemicarbazide correspondante (I), par cyclisation en catalyse acide.

3) *Par l'étude des spectres d'absorption en IR*

Nous avons effectué l'étude de tous les spectres d'absorption des nouveaux composés synthétisés. Le domaine spectral étudié a été compris entre 400 et 4000 cm^{-1}. Les déterminations ont été effectuées avec un spectrophotomètre automatique du type U.R.10, à double faisceau, en employant la technique du pastillage en bromure de potassium.

Les attributions que nous avons réussi à donner aux bandes spectrales, caractéristiques pour chaque type de composé à part, confirment avec exactitude la structure chimique proposée et vérifiée par nous, par analyse chimique (microdosage de l'azote et semi-microdosage du soufre). Le tableau 3 contient les bandes, correspondant à tous les groupes actifs en IR, que nous avons pu attribuer.

L'analyse des données spectrales met en évidence les suivantes :

— Conformément aux indications peu nombreuses, mentionnées dans la littérature, concernant les vibrations de l'hétérocycle 1,3,4-thiadiazolique,[31-35] nous avons attribué dans les spectres de nos 1,3,4-thiadiazoles (III), les bandes de basse intensité, situées à 555 cm^{-1} et 1 225 cm^{-1}, correspondant aux vibrations de déformation spécifiques de cet anneau hétérocyclique.

— Dans le spectre des thiosemicarbazides (I), nous avons attribué pour le groupe thiocétone (C = S) du groupe thio-urée :

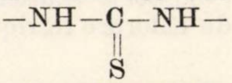

$-NH-\underset{\underset{S}{\|}}{C}-NH-$

la bande très nette et intense, située à 1310 cm^{-1}, conformément aux indications de la littérature [36] ; à 2660 cm^{-1}, nous avons observé l'apparition d'une bande, faiblement précisée[37], indiquant l'absorption correspondant à la liaison thiolyque, probablement due au fait qu'à l'état solide (les spectres étant exécutés par pastillage en KBr) la forme thionique (thiocétonique) domine presque exclusivement.

La bande située à 1500 cm^{-1}, correspondant aux vibrations couplées des groupes C = S, NH de la fonction thio-urée, est très nettement marquée.

---

[31] J. Goerdeler, J. Ohm et O. Tegtmeyer, *Chem. Ber.*, **89**, 1534 (1956).

[32] B. Bak, D. Christensen, L. Hansen-Nygaard, L. Lipschritz et I. A. Andersen, *J. Mol. Spectr.*, **9**, 225 (1962) ; **19**, 283 (1966).

[33] E. Lieber, C. N. Rao, C. N. Pillai et G. Ramachandran, *Canad. J. Chem.*, **36**, 801 (1958) ; **42**, 63 (1964).

[34] A. R. Katritzky, R. A. Jones, J. H. Lagowski et J. A. Berd, *Spectrochim. Acta*, **16**, 964 (1960) ; *J. Chem. Soc.*, **1959**, 3670 ; *J. Chem. Soc.*, **1960**, 2942.

[35] G. Sbrana et M. Ginammeschi, *Spectrochim. Acta*, **22**, 517 (1966).

[36] L. J. Bellamy, «The Infrared Spectra of Organic Sulfur Compounds», dans le traité : N. Kharash « Organic Sulfur Compounds », Pergamon Press, 1961, p. 47.

[37] L. J. Bellamy, «Infrared Spectra of Complex Molecules», Londres, Methuen Co., 1959, p. 351.

Tableau 3

Attributions pour les bandes dûes aux vibrations des groupements actifs (cm^{-1})

II. =
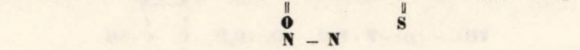

$(p)-F-C_6H_4-SO_2-C_6H_4-\underset{\overset{\|}{O}}{C}-NH-NH-\underset{\overset{\|}{S}}{C}-NH-C_6H_4-Br-p$

V. =
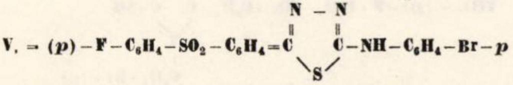

	II.	V.
C−F (1000−1400)	1020 i 1080 i 1115 i 1405 i	1025 i 1090 f 1105 i 1265 inf 1405 t.i.
C−Br	585 i 785 t.i.	585 m 750 t.i.
N−C=S	656 f 690 inf 1310 i 1500 i	—
C−S	640 f 1540 i	640 f 1540 i
N=C−S	1540 i	1480 inf 1540 i
O=C−NH	C=O, Am.I ... 1660 m. (NH δ pl.) Am. II ... 1535 i δ (C = N) Am. III ... {1270 i 1310 i δ (O=C−N) Am. IV ... 755 m Am. V ... 730 m NH v. .... 3300 m	(NH δ pl) Am. II ... 1540 δ (C−N) Am. III ... {1275 i 1305 inf Am. V. ... 710 m NH v. ....3300 t.i.
SH	2600 f.	—
.C_6H_4	ν_4 : (C−H) δ⊥pl. 690 i ν_{14} : (C−H) δ II pl. 1020 i ν_{12} : (C−H) v. ... 3100 inf v_{13} : (C−C) v. ... 1490 m	ν_4 : (C−H) δ⊥pl. 690 inf ν_{14} : (C−H) δ ‖ pl. 1020 i ν_{12} : (C−H) v. ...3100 f ν_{13} : (C−C) v. ...1490 i
Phényle disubstitué	835 t.i.	830 t.i.
SO_2	déf .... 520 i v_1 sym ...... 1155 t.i v_2 asym ...... 1310 inf	déf. .... 510 m v_1 sym ...... 1165 t.i v_2 asym ...... 1305 i
Vibrations couplées C=S, NH	1500 i	—
C=N dans l'anneau hétérocyclique (1490−1530 1500−1614)	1480 inf 1500 t.i	1480 inf 1500 t.i

Tableau 3 (suite)

VIII.

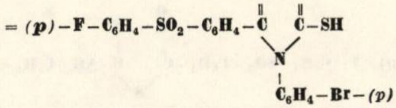

$$= (p)-F-C_6H_4-SO_2-C_6H_4-\overset{\displaystyle N{-}N}{C\quad C}-SH \;\; \underset{\displaystyle C_6H_4-Br-(p)}{N}$$

	VIII.
C–F (1000–1400)	1020 i 1090 inf 1105 i 1260 f 1405 i
C–Br	595 i 755 i
N–C=S	680 f 1500 i
C–S	1540 i
N=C–S	1540 i
O=C–NH	(NH δ pl.) Am. II ... 1535 m δ (C–N) Am. III ... {1305 m 1265 f Am. V. ... 710 f NH v. .... 3300 t.i
SH	2550 f.
C_6H_5	ν_4 : (C–H) δ ⊥ pl. 690 inf ν_{14} : (C–H) δ ∥ pl. 1020 i ν_{12} : (C–H) v. .... 3100 f ν_{13} : (C–C) v. .... 1495 i
Phényle disubstitué	830 t.i.

Tableau 3 (suite)

	VIII.
SO_2	déf. .... 505 m v_1 sym. ....1165 t.i v_2 asym. ....1305 m
Vibrations couplées $C=S$, NH	1500 i 1630 f
$C=N$ dans l'anneau hétérocyclique (1490–1530 1590–1614)	1498 i 1605 t.i

Légende:

i = intense
t.i = très intense
m = intensité moyenne
f = faible
inf = inflexion
Am = amide
pl = plane
v = vibration de valence
déf = vibration de déformation
sym = symétrique
asym = asymétrique

— Dans les spectres des 1,3,4-thiadiazoles (III) apparaît une bande, située à 1535 cm^{-1}, caractéristique de la liaison $C = N$ comprise dans la structure d'un hétérocycle (indiquée dans la littérature comme située dans la région 1490–1530 cm^{-1}) et aucune bande n'apparaît à 1640 cm^{-1}, caractéristique de la liaison $C = N$ exocyclique. Ceci dénote que la forme prédominante dans ces structures est celle thiadiazolique proprement dite, et non pas celle tautomère, qui résulterait de la migration de l'hydrogène du groupe amine secondaire exocyclique à l'atome d'azote voisin.

— Dans les spectres des 1,2,4-mercapto-triazoles, nous avons mis en évidence une bande, située à 1498 cm^{-1}, correspondant à la vibration de valence de la liaison $C = N$ de l'hétérocycle. Une bande qui manque dans les spectres des 1,3,4-thiadiazoles est présente à 1630 cm^{-1}. Cette bande, comme celle de 1500 cm^{-1}, correspond aux vibrations couplées des groupes NH et $C = S$ de la fonction thio-urée, fait qui plaide en faveur de la forme thiocétonique des 1,2,4-mercapto-triazoles synthétisés. Cette forme est prépondérante dans le spectre d'absorption en IR des triazoles, probablement à cause du fait que nous avons effectué les déterminations spectrales à l'état solide.

Les données spectrales confirment exactement la structure chimique des nouveaux composés.

PARTIE EXPÉRIMENTALE

Synthèse des matières premières

L'hydrazide de l'acide p-fluor-diphénylsulfonyl-p'-carboxylique à été synthétisée selon la méthode indiquée par nous dans un travail récent.[9]

L'isocynate de phényle, l'isothiocynate de p-brome- et de p-iode-phenyle ont été synthétisés par nous, par adaptation des méthodes indiquées dans la littérature.[38]

Synthèse des nouvelles thiosemicarbazides

Le N_1-(p-(p'-fluor-phénylsulfonyl)-benzoyle)-N_4-(p-bromephényl)-thiosemicarbazide (II) :

On dissout à chaud 2 g (0,006 moles) d'hydrazide de l'acide *p*-F-diphénylsulfonyl-*p'*-carboxylique en 240 ml (excès) d'éthanol absolu et on ajoute 0,72 (0,003 moles) d'isothiocynante de *p*-bromephényl, en 10 ml d'éthanol absolu ; puis on chauffe à reflux pendant 3 heures. Après 30 minutes, des cristaux aciculaires, incolores se séparent pendant l'ébullition même et à mesure que la réaction s'achève ils deviennent de plus en plus abondants. On essore à chaud, et les cristaux sont lavés 2—3 fois, avec un peu d'éthanol absolu. Recristallisés à l'acétone diluée, ils se présentent sous forme de feuillets incolores, au point de fusion à 2300, difficilement solubles dans de l'éthanol, du méthanol, du propylèneglycol, insolubles dans de la ligroïne, de l'éther du pétrole, du benzène et de l'eau, solubles dans de l'acide acétique, de la pyrydine et du diméthylformamide.

Nous avons obtenu ainsi 1,92 g composé II. Rend = 58,2 %.

$C_{20}H_{15}O_3N_3S_2$ FBr, *calculé* : N, 8, 26 ; S, 12,61 ;

Trouvé : N, 8,31 ; S, 12,34 %.

Synthèse des 5-arylamino-1, 3, 4-thiadiazoles

Le 2-[(p-brome phénylamino)-5-(p-fluor-phénylsulfonyl)-phényl]-1,3,4-*thiadiazole :*

0,5 g de N_1 (p'-fluore-phényl-sulfonyl)-benzoyl-N_4-(*p*-bromphényl)-thiosemicarbazide ont été solubilisés, par agitation continue, en 2,5 ml (excès) d'acide sulfurique concentré (d = 1,84). La solution a pris une couleur orange, devenant de plus en plus rouge à mesure que la réaction de cyclisation s'achève. Après 20 minutes, la dissolution a été complète. Le produit de réaction a été versé sur 30 g de glace pillée. On a obtenu un composé gélatineux et après que la glace a fondu, on a ajouté de l'ammoniaque, jusqu'au pH alcalin ; ensuite, on a essoré et lavé les cristaux à l'eau, jusqu'à la réaction neutre, quand ils ont pris la forme d'une poudre amorphe.

Recristallisés à partir du méthanol, on obtient des cristaux aciculaires d'un jaune pâle, p.f. = 259°, très solubles dans de l'acétone et de l'acide acétique à froid, solubles dans de l'éthanol et dans du propylènglycole, insolubles dans du toluène, de l'éther de pétrole et de l'eau. Nous avons obtenu 0,310 g de composé pur. Rendement : 77,5 %.

$C_{20}H_{13}O_2N_3S_2FBr$, *Calculé* : N, 8,57 ; S, 13,07 %

Trouvé : N, 8,55 ; S, 13,18 %

---

[38] A. Vogel, « Practical Organic Chemistry », 3e Edition, Ed. Longmans, Green and Co. Ltd., Londres, 1959, p. 644.

Synthèse des 2-mercapto-1, 2, 4-triazoles

Le 1-(p)-brome-phényl-2-mercapto-5-[(p-fluor-phényl-sulfonyl)-phényl]-1, 2, 4-triazole :

0,5 g (1 mmoles) de la même thiosemicarbazide, indiquée plus haut, ont été dissous dans 50 ml (excès) d'acétone et on a ajouté 10 ml d'hydroxyde de sodium 2N ; ensuite, on a chauffé 20 mn. et on a refroidi ; on a ajouté 15 ml d'eau. On a acidulé après, avec du H_2SO_4 (jusqu'au pH = 3), quand un précipité abondant, d'une couleur moutarde, très claire, ayant une forte et désagréable odeur de mercaptane, a été obtenu. Recristallisé dans de l'éthanol, celui-ci a un p.f. = 238°.

En présence des cations métalliques : Cu^{2+}, Pb^{2+}, Fe^{3+}, etc. on obtient des mercaptides, intensément colorées (tableau 2).

On a obtenu 0,28 g de produit cristallin pur, très soluble dans du chloroforme et dans de l'acétone à froid, soluble dans de l'éthanol, du méthanol et de l'acide acétique glacial, insoluble dans du benzène, du toluène, du xylène et dans de l'eau. Rend 70 %.

$C_{20}H_{13}O_2N_3S_2FBr$, *Calculé* : N, 8,57 ; S, 13,07

Trouvé : N, 8,61 ; S, 13,02 %.

Les autres composés, synthétisés par des voies analogues, sont indiqués dans le tableau synoptique 4, en même temps que leurs constantes physiques et les données analytiques correspondantes.

CONCLUSIONS

En partant des conclusions de quelques chimistes contemporains remarquables, sur l'importance de l'introduction du groupe thio-urée [NH—CS—NH] dans la molécule organique, on a étudié l'addition nucléophile de l'hydrazide de l'acide *p*-F-diphénylsulfonyl-*p'*-carboxylique aux isothiocyanates de phényle, de *p*-brome et respectivement de *p*-iode-phényle.

Les nouvelles acyl-aryl-thiosemicarbazides, synthétisées par cette voie, ont été ensuite cyclisées, en catalyse acide et basique, en obtenant de nouveaux composés hétérocycliques, de la classe de 5-aryl-amino-1, 3, 4-thiadiazoles et 2 mercapto-1, 2, 4-triazoles, ayant un intérêt thérapeutique.

Les recherches entreprises ont été fondées sur l'idée que l'atome de fluor, grâce à sa constitution spéciale, peut donner naissance à des analogues structurels de certains composés organiques, à effet vérifié. Ceux-ci présentent la particularité spécifique d'avoir un effet tout à fait contraire, par rapport aux métabolites normaux de l'organisme, bien que leur structure soit presque identique à ces derniers, si nous nous référons aux distances interatomiques, à la planarité de la molécule et à la similitude de distribution du nuage électronique.

Tableau synoptique 4

Données analytiques et constantes physiques des nouveaux composés synthétisés
$p-F-C_6H_4-SO_2-C_6H_4-CO-NH-NHCS-NH-Ar$

N°	Ar	Formule	Rend. %	Point de fusion et solvant de cristallisation	N % Calculé Trouvé	S % Calculé Trouvé
I	$-C_6H_5$	$C_{20}H_{16}O_3N_3S_2F$	62,3	233 (acétone dil.)	9,78 9,91	14,93 14,87
II	$-C_6H_4-Br-p$	$C_{20}H_{15}O_3N_3S_2FBr$	58,2	230 (éthanol abs.)	8,26 8,31	12,61 12,34
III	$-C_6H_4-I-p$	$C_{20}H_{15}O_3N_3S_2FI$	48,3	242 (acétone dil.)	7,56 7,59	11,54 11,34

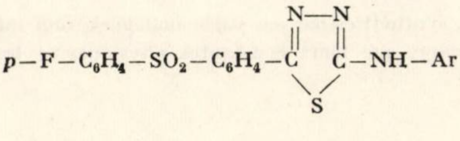

IV	$-C_6H_5$	$C_{20}H_{14}O_2N_3S_2F$	72,2	263 (éthanol)	10,21 10,22	15,56 15,48
V	$-C_6H_4-Br-p$	$C_{20}H_{13}O_2N_3S_2FBr$	77,5	259 (méthanol)	8,57 8,55	13,07 13,18
VI	$-C_6H_4-I-p$	$C_{20}H_{13}O_2N_3S_2FI$	65	276 (éthanol)	7,81 7,87	11,93 11,98

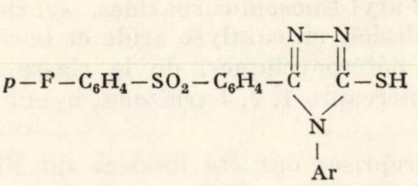

VII	$-C_6H_5$	$C_{20}H_{14}O_2N_3S_2F$	69,9	242-4 (éthanol)	10,29 10,29	15,56 15,46
VIII	$-C_6H_4-Br-p$	$C_{20}H_{13}O_2N_3S_2IBr$	70	238 (éthanol)	8,57 8,64	13,07 13,02
IX	$-C_6H_4-I-p$	$C_{20}H_{13}O_2N_3S_2FI$	77,7	274 (éthanol abs.)	7,81 7,88	11,93 11,90

On discute la structure des composés, à la lumière des théories récentes sur les groupes et les centres, déterminants de l'effet biologique.

On discute les mécanismes de réaction et l'importance de la cyclisation pour l'apparition de nouveaux centres biologiquement actifs, dans les molécules synthétisées.

La structure de tous les composés a été vérifiée avec précision par voie chimique et par spectrographie en IR.

Des recherches pharmacodynamiques multiples sont en cours, ainsi que l'étude de la toxicité des nouveaux composés, obtenus par synthèse.

Revue Roumaine de Chimie, 17, *6*, 1013–1031 (1972)

Revue Roumaine de Chimie, 17, 6, 1033 – 1041 (1972)

CARACTÉRISATION DU POLYCHLORURE DE VINYLE

RELATION VISCOSITÉ INTRINSÈQUE – POIDS MOLÉCULAIRE

D. FELDMAN, C. V. UGLEA, VIOLETA NUȚĂ et MIHAELA POPA

Institut de Chimie Macromoléculaire « P. Poni », 41A, Aleea Gr. Ghica Vodă, Jassy

Reçu le 30 octobre 1970

On a caractérisé par fractionnement les épreuves de polychlorure de vinyle qui diffèrent par la distribution et la moyenne du poids moléculaire. Pour le fractionnement on a utilisé la précipitation successive dans le système solvant/non-solvant cyclohexanone/éthylèneglycol. L'efficacité du fractionnement à été vérifiée par détermination des gel-chromatogrammes pour cinq fractions. À l'aide des données obtenues par la caractérisation des fractions on a déterminé les constantes K_θ par la méthode de Kurata et Stockmayer et aussi les constantes K et a de la relation $[\eta] = KM^a$. On a démontré par les résultats obtenus que la valeur de ces constantes est indépendante de la distribution et de la moyenne du poids moléculaire.

INTRODUCTION

La caractérisation des polymères par détermination de la distribution et de la valeur moyenne du poids moléculaire, de la conformation et des dimensions non perturbées de la chaîne constitue le principal moyen de détermination du comportement des composés macromoléculaires en solution. La détermination de la relation spécifique entre la viscosité intrinsèque et le poids moléculaire, pour le système considéré, nous permet aussi d'éliminer, ultérieurement, les déterminations directes du poids moléculaire et d'obtenir de précieux renseignements concernant la qualité du solvant.

Les valeurs obtenues pour les principaux paramètres moléculaires du polychlorure de vinyle (PVC) se sont intégrées dans un domaine assez grand. C'est ainsi que les valeurs correspondant à l'exposant de la relation $[\eta] = KM^a$, pour les systèmes PVC — cyclohexanone (CH) et PVC — tétrahydrofuranne (THF) se sont groupées autour de 0,5 ou entre 0,8 – 1,00 ; le THF et le CH pourraient donc constituer, à la fois, de bons ou de faibles solvants pour le PVC.[1,2]

Il est connu le fait que les associations moléculaires entre les chaînes de PVC, tant dans le CH que dans le THF, constituent la cause

---

[1] P. V. McKinney, *J. Appl. Polymer Sci.*, 9, 6 (1965).

[2] M. Freman et P. P. Maning, *J. Polymer Sci.*, *A – 1*, 2, 2017 (1964).

déterminante de la distribution des valeurs *a* sur un domaine si grand. De plus, la présence des groupes allyliques et du carbone tertiaire s'ajoute aussi aux causes qui accentuent la complexité des problèmes qui surgissent pendant la caractérisation du PVC.

Le but de notre ouvrage est d'établir l'influence des caractéristiques de l'épreuve non fractionnée (distribution du poids moléculaire, défauts structuraux, procédé de synthèse) sur les paramètres de conformation du PVC, de même que sur les valeurs des constantes de la relation $[\eta] = KM^a$.

PARTIE EXPÉRIMENTALE

a) *Echantillons*

Nous avons analysé 16 épreuves de PVC, produits industriels, parmi lesquelles, 10 obtenues par polymérisation en suspension et 6 par polymérisation en émulsion.

b) *Fractionnement*

Les polymères ont été fractionnés dans le système solvant/non-solvant (S/NS) CH/éthylèneglycol (CH/EG). La séparation a été réalisée par précipitation successive des solutions de PVC en CH, dans une concentration de 1 %. Le fractionnement s'est déroulé dans un récipient cylindrique (de 60 cm en hauteur et de 5 cm en Ø), thermostaté, rempli de 250 ml solution de polymère dont on a fait ajouter du NS en gouttes, sous agitation continue. L'adjonction du NS a continué même après l'apparition d'une opalescence persistante, jusqu'à la précipitation d'une quantité suffisante de polymère qui puisse constituer une fraction.

On interrompt l'adjonction de NS mais on continue encore l'agitation pendant 15 mn ; on laisse alors le système dans un repos d'une heure et demi pour décanter.

On passe ensuite à la séparation du liquide supernatant et la phase concentrée est de nouveau dissoute en CH ; elle est alors collectée dans un flacon où on la fait précipiter, totalement cette fois-ci, avec de l'alcool méthylique (les dernières fractions étant précipitées à l'aide d'une solution aqueuse de chlorure de sodium 10 pour cent).

Le précipité ainsi obtenu est séparé à l'aide d'un filtre en verre G_3 ; il est lavé, à l'eau distillée jusqu'à la disparition de l'ion de chlore ; puis, on le fait sécher, à poids constant, en étuve, à 60°.

L'opération est reprise jusqu'à la disparition totale du polymère de la solution.

Le processus de séparation se déroule à 120°. C'est ainsi que nous avons séparé chaque épreuve en 7—8 fractions.

c) *Caractérisation des fractions*

— *Viscosimétrique.* La viscosité de chaque fraction a été déterminée en CH, à 25°, à l'aide d'un viscosimètre à niveau suspendu, prévu d'une boule de dilution et d'une plaque de filtrage. La valeur de la viscosité intrinsèque a été obtenue graphiquement par extrapolation par quatre points. Les solutions des fractions ont été réchauffées préalablement pendant 30 mn à 120°.[3] La viscosité intrinsèque de quelques fractions seulement à été déterminée à 20°, 25°, 30° et 35°. Le temps d'écoulement du solvant dépassant 200 secondes, les corrections d'énergie cinétique n'ont plus été nécessaires.

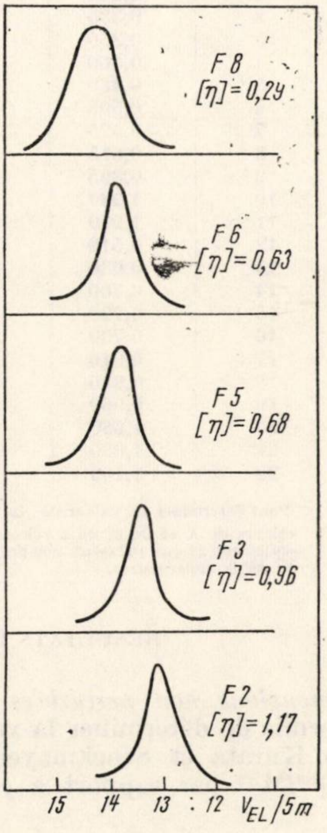

Fig. 1. — Gel-chromatogrammes des fractions séparées par précipitation successive.

— *Osmométrique.* La moyenne en nombre du poids moléculaire des fractions a été déterminée en CH, à 25°, à l'aide d'un osmomètre Pinner-Stabin.

— *Chromatographie sur gel perméable.* L'efficacité du fractionnement a été déterminée par gel-chromatogrammes réalisés pour 5 des fractions (fig. 1). La détermination a été effectuée en CH, à 50°, avec une vitesse d'écoulement de 1 ml/mn. Nous avons utilisé un chromatographe Waters Model 200.

Toutes les caractéristiques des fractions sont présentées dans le tableau 1.

[3] C. Garbuglio, A. Mula et L. Chinellato, *J. Polymer Sci., C,* **16**, 1529 (1967).

Tableau 1

Caractéristique des fractions

Numéro de la fraction*	$[\eta]$ ml/g	M_n	Méthode de synthèse du PVC
1	0,264	8 400	émulsion
2	0,335	11 400	suspension
3	0,350	12 500	émulsion
4	0,360	13 000	suspension
5	0,480	18 000	,,
6	0,500	19 000	,,
7	0,575	22 000	émulsion
8	0,615	24 000	suspension
9	0,865	36 000	,,
10	1,280	57 200	,,
11	1,910	92 000	émulsion
12	0,519	26 000	,,
13	0,630	33 800	,,
14	0,700	39 000	suspension
15	0,720	40 300	émulsion
16	0,730	41 000	suspension
17	0,916	55 000	émulsion
18	0,930	57 000	suspension
19	0,960	58 400	,,
20	1,080	68 000	,,
21	1,080	68 200	,,
22	1,100	69 000	émulsion

* Pour déterminer la valeur de la constante K_θ, de même que pour les valeurs de K et de a, on a sélectionné, du total des fractions séparéess, seulement 22 qui puissent comprendre le domaine le plus vaste possible de poids moléculaires.

RÉSULTATS ET DISCUSSIONS

— *Dimensions non perturbées de la chaîne.* Les données obtenues nous ont permis de déterminer la valeur de constante $K_\theta^{2/3}$ en appliquant la méthode Kurata et Stockmayer (K—S)[4] par la représentation du rapport $[\eta]^{2/3}/M^{1/3}$ par rapport à $g(\alpha)\,M^{2/3}/[\eta]^{1/3}$, conformément à la relation :

$$\frac{[\eta]^{2/3}}{M^{1/3}} = K_\theta^{2/3} + 0{,}363\ \Phi_0 . B . g(\alpha) . \frac{M^{2/3}}{[\eta]^{1/3}} \qquad (1)$$

dans laquelle :

$$K_\theta = 6^{3/2}\Phi_0(<\overline{S}^2>_0/M)^{3/2} \qquad (2)$$

Φ_0 = constante ayant la valeur $2{,}87.10^{21}$;
$<\overline{S}^2>_0$ = la moyenne des carrés du rayon de giration ;

---

[4] M. Kurata et W. H. Stockmayer, *Fortschr. Hochpolym.-Forsch.*, **3**, 196 (1963).

$g(\alpha)$ = fonction caractéristique pour la méthode K–S, égale à

$$\frac{8\alpha^3}{(3\alpha^2+1)^{3/2}} \qquad (3)$$

α = une grandeur qui représente l'effet du volume exclu ;

$B = \dfrac{\beta}{c^2 m^2}$

m = poids moléculaire de l'unité structurale ;

$\dfrac{\beta}{c} = 2{,}6 \pm 1$

On constate (fig. 2) que les points caractéristiques des fractions s'inscrivent sur deux droites tout à fait séparées. Ce comportement nous impose l'investigation détaillée des caractéristiques structurales de ces fractions. Les données à l'aide de la gaz-chromatographie [5] pour les fractions inscrites sur la droite 1 mettent en évidence, pour le rapport benzène/toluène (résultés de la thermodestruction) une valeur supérieure par rapport à la valeur caractéristique aux fractions inscrites sur la droite 2. La quantité du toluène est en liaison avec les défauts structuraux dans la chaîne de PVC. Par conséquent, les caractéristiques du PVC exercent une certaine influence sur les valeurs de la constante K_θ et, par suite, sur les dimensions non perturbées de la chaîne.

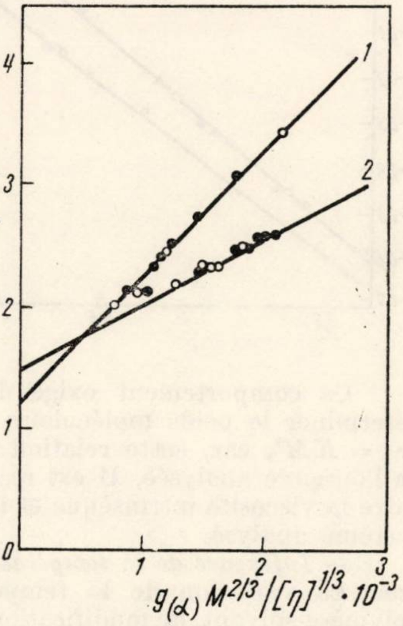

Fig. 2. — Détermination de la valeur pour la constante K_θ par la méthode Kurata—Stockmayer.

Droite 1, $K_\theta = 0{,}00133$; droite 2, $K_\theta = 0{,}00178$) ; –●– suspension ; –○– émulsion

---

[5] A. Schneider, Communication personnelle.

Si on analyse la provenance des fractions reproduites dans la figure 2, on trouve, inscrites sur la droite *1*, 7 fractions de PVC suspension et 4 fractions de PVC émulsion, tandis que sur la droite *2*, 5 fractions de PVC émulsion et 6 fractions de PVC suspension.

On constate aussi que la droite *1* contient 8 fractions dont le poids moléculaire n'atteint pas 26 000, tandis que la droite *2* contient 11 fractions dont le poids moléculaire dépasse 26 000. Les défauts structuraux du PVC sont, en conclusion, particulièrement liés au poids moléculaire ; ce paramètre entraîne donc des modifications dans la valeur des dimensions non perturbées de la chaîne, déterminées par des mesurages viscosimétriques, dans de bons solvants.

— *Relation viscosité intrinsèque—poids moléculaire.* La représentation du log $[\eta]$ par rapport à log M_n (fig. 3) nous a facilité la détermination de la relation $[\eta] = KM^a$. A cette occasion, nous avons enregistré des comportements différents pour les fractions analysées ; nous avons obtenu, par conséquent, aussi des valeurs différentes (tableau 2) pour les deux constantes.

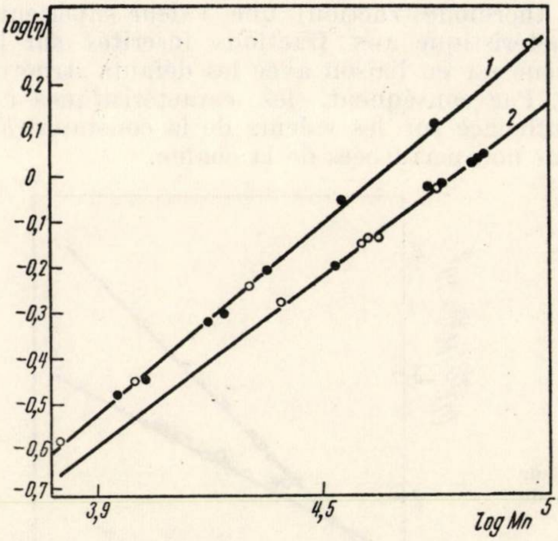

Fig. 3. — Représentation de log. $[\eta]$ par rapport à log. M_n pour les fractions séparées de PVC.

Ce comportement exige des soins particuliers lorsqu'il s'agit de déterminer le poids moléculaire des fractions, en appliquant la relation $[\eta] = KM^a$, car, cette relation dépend des caractéristiques structurales de l'épreuve analysée. Il est recommandable de déterminer une relation entre la viscosité intrinsèque et le poids moléculaire, spécifique de chaque système analysé.

— *Influence de la température sur le comportement du PVC en solution.* La variation de la température entraîne pour chaque système polymère-solvant la modification des interactions des deux composants. Par suite, les principaux paramètres qui définissent la conformation de la chaîne en solution subissent aussi d'importantes modifications. La poursuite de l'évolution de la conformation de la chaîne et de la varia-

Tableau 2

Valeurs des constantes K et a de la relation $[\eta] = KM^a$

Les fractions	$K.10^{+4}$	a
Pour la droite *1*	2,539	0,77
Pour la droite *2*	1,445	0,85

tion de la température, simultanément, est réalisée par la détermination de la viscosité intrinsèque à diverses températures. La nature de la fonction qui exprime l'interdépendance $[\eta] - T$ est déterminée par les caractéristiques structurales de chaque système polymère-solvant. L'interprétation théorique de la dépendance $[\eta] - T$ peut être réalisée aussi bien par voie thermodynamique que par considérations purement énergétiques. Si l'on applique la relation :

$$[\eta] = \Phi_0 \left(\frac{<\bar{r}^2>_0}{M} \right)^{3/2} . M^{1/2} . \alpha^3 \tag{4}$$

où $<\bar{r}^2>_0$ représente la moyenne des carrés de la distance entre les deux extrémités de la chaîne polymérique, on observe que, outre le poids moléculaire, tous les autres facteurs dépendent, plus ou moins, des variations de la température. On peut écrire par suite :

$$\frac{\mathrm{d} \log . [\eta]}{\mathrm{d}T} = \frac{\mathrm{d} \log . \Phi_0}{\mathrm{d}T} + 3/2 \frac{\mathrm{d} \log . \dfrac{<\bar{r}^2>_0}{M}}{\mathrm{d}T} + \frac{\mathrm{d} \log . \alpha^3}{\mathrm{d}T} \tag{5}$$

Comme la constante Φ_0 ne présente qu'une petite variation par rapport à la température, on peut déduire que la modification des valeurs de $[\eta]$ est surtout déterminée par la dépendance des deux autres termes de la température. La figure 4 et le tableau 3 reproduisent la variation de $[\eta]$ par rapport à T, pour 4 fractions seulement. On y observe que la dépendance $[\eta] - T$ varie d'une fraction à l'autre, fait qui nous permet de supposer que la modification de la viscosité intrinsèque résulte de la somme des variations du rapport $<\bar{r}^2>_0/M$ et du volume exclu α par rapport à T et tient du domaine de température et du poids moléculaire des fractions dans lesquelles elle a été étudiée. Et comme α connaît une augmentation, tandis que le rapport $<\bar{r}^2>_0/M$ diminue, lorsque la température augmente, on peut supposer que, pour les poids moléculaires petits, la diminution de la valeur de ce rapport détermine la relation entre $[\eta]$ et T. Dans la même figure 4 on observe qu'à l'exception de la fraction 5 pour tout le domaine de température $[\eta]$ présente une valeur maximale pour laquelle $\mathrm{d}\,[\eta]/\mathrm{d}T = 0$. Ce comportement constitue un état caractéristique pour le système polymère-solvant pour lequel les dimensions de la chaîne ont des valeurs les plus grandes possibles.

Kawai[6] considère cette température tout à fait opposée à la température T_θ pour laquelle la chaîne macromoléculaire présente la conformation la plus restreinte.

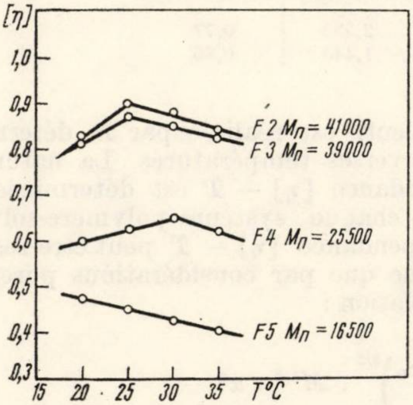

Fig. 4. — Variation de la viscosité intrinsèque avec la température pour les fractions séparées.

Tableau 3

Variation de la viscosité intrinsèque par rapport à la température

Nº de la fraction	T °C	[η] ml/g	M_n
1	20	1,180	—
	25	1,075	51500
	30	1,125	—
	35	1,100	—
2	20	0,825	—
	25	0,900	41000
	30	0,880	—
	35	0,840	—
3	20	0,820	—
	25	0,875	39500
	30	0,850	—
	35	0,825	—
4	20	0,600	—
	25	0,625	25500
	30	0,650	—
	35	0,620	—
5	20	0,480	—
	25	0,450	16500
	30	0,430	—
	35	0,400	—

---

[6] T. Kawai et F. Ueyama, *J. Appl. Polymer Sci.*, 3, 227 (1960).

CONCLUSIONS

Les données présentées permettent de faire des appréciations concernant l'influence des particularités structurales sur le comportement et la caractérisation du PVC en solution.

La détermination des dimensions non perturbées de la chaîne, à l'aide des mesurages viscosimétriques effectués dans de bons solvants, conduit à des résultats reproductibles mais seulement dans les cas où les polymères analysés ne présentent pas de différences dans leur structure chimique. Les défauts structuraux du PVC influencent aussi la relation viscosité intrinsèque — poids moléculaire. Il est recommandable que la séparation selon le poids moléculaire de ce polymère ait lieu dans des conditions telles que l'on puisse éliminer l'influence des associations moléculaires sur les déterminations viscosimétriques et du poids moléculaire.

Revue Roumaine de chimie, 17, 6, 1033–1041 (1972)

Revue Roumaine de Chimie, 17, 6, 1043–1049 (1972)

COPOLYMERS OF CONJUGATED DIENES WITH MALEIC ACID MONOESTERS. VI.

CONSTANTS *Q* AND *e* IN THE COPOLYMERIZATION OF ISOPRENE WITH MALEIC ACID MONOESTERS

I. NANU* and C. ANDREI**

* Chair of Macromolecular Chemistry, Polytechnic Institute, str. Karl Marx 3, Timișoara, Romania

** Research Laboratory, Petrochemical Industrial Group, Ploiești, Brazi, Romania

Received December 25, 1971

Constants *Q* and *e* were calculated for a series of maleic acid monoesters in the copolymerization of isoprene. In general, the alternating tendency in the copolymerization of these systems is explained by the difference of polarity; however, the small differences of polarity between the monoesters were not remarked in the *Q – e* scheme. The increased reactivity of maleic acid monoesters with the greater alkyl groups, can be explained by the increase of the steric effect of the voluminous groups, which leads to the decrease of the termination rate constant (radical-radical reaction). As the viscosities of maleic acid monoesters increase with the number of carbon atoms of the alkyl groups, in the explanation of the results obtained, consideration is given to the role played by the control of diffusion on the termination rate constant. The alternating tendency in copolymerization of the systems under study, can also be attributed to the stabilization of the transition state as a consequence of the electron transfer between the radical and the monomer.

INTRODUCTION

Research work carried out on copolymerization of isoprene with different monoesters of maleic acid [1–5] in the presence of free radicals, showed a marked trend towards alternating copolymers. This is reflected in the values of (r_1 and r_2) reactivity ratios, the systems studied being typical cases of heterocopolymerization. [1,4,5]

The alternating tendency in radical copolymerization is a significant phenomenon (observed usually between the electron donor and electron acceptor monomers) which was explained as being due to the

[1] I. Nanu and C. Andrei, *Rev. Roumaine Chim.*, **15**, 1883 (1970).

[2] I. Nanu and C. Andrei, *Rev. Roumaine Chim.*, **16**, 75 (1971).

[3] I. Nanu and C. Andrei, R.S.R. patent 67, 663, 16th July, 1971.

[4] I. Nanu and C. Andrei, *Makromol. Chem.*, (in print).

[5] I. Nanu and C. Andrei, *Rev. Roumaine Chim.*, **17**, 741 (1972).

following causes : electrostatic interactions between the permanent charges of the radical and the monomer (theory of polar factors)[6-10]; stabilization of the transition state as a result of the electron transfer between the radical and the monomer[11-12]; formation of the charge-transfer complex between the donor and acceptor monomers and its participation in the reaction (theory of initial complex)[13-20] and finally to the steric effects.[21]

It should be remarked that even at present, all the hypotheses proposed for the explanation of the mechanism of alternating copolymerization are still maintained in the interpretation of the different copolymerization systems.

The theory of polar factors (recognized much earlier in the copolymerization reaction) was developed, as is known, by Alfrey and Price,[7] in a semi-quantitative scheme (known also as the $Q - e$ scheme), which endeavours to sum up the effects of the resonance stabilization and polarity on the relative reactivities of the different monomers with different radicals.

An argument in favour of the theory of polar factors was provided by the copolymerization of maleic anhydride with methyl methacrylate, by which a copolymer enriched in methyl methacrylate is obtained and not an alternating equimolecular copolymer.[22,23]

This phenomenon was explained by the fact that methyl methacrylate in also a monomer with an electron-attracting substituent (which compensates the inductive effect of the methyl group) as is maleic anhydride, whereas the difference in polarity is small.

The aim of the present work is to demonstrate the manner in which the copolymerization systems of isoprene with maleic acid monoesters align to the $Q - e$ scheme.

[6] C. C. Price, *J. Polymer Sci.*, **1**, 83 (1946).

[7] T. Alfrey and C. C. Price, *J. Polymer Sci.*, **2**, 101 (1947).

[8] C. C. Price, *J. Polymer Sci.*, **3**, 772 (1948).

[9] C. C. Price and J. W. Walsh, *J. Polymer Sci.*, **6**, 239 (1951).

[10] M. M. Martin and N. P. Jensen, *J. Org. Chem.*, **27**, 1201 (1962).

[11] C. Walling and F. R. Mayo, *J. Polymer Sci.*, **3**, 895 (1948).

[12] C. Walling, E. R. Brigs, K. B. Wolfstirn and F. R. Mayo, *J. Amer. Chem. Soc.*, **70**, 1537 (1948).

[13] W. G. Barb, *J. Polymer Sci.*, **10**, 49 (1953).

[14] S. Iwatsuki and Y. Yamashita, *Makromol. Chem.*, **89**, 205 (1965).

[15] A. Winston and F. L. Hamb, *J. Polymer Sci.*, *Part A*, **3**, 583 (1965).

[16] A. A. El. Saied, S. J. Mirlina and V. A. Kargin, *Doklady Akad. Nauk. S.S.S.R.*, **177**, 380 (1967).

[17] M. Matsuda and K. Abe, *J. Polymer Sci.*, *Part A*—1, **6**, 144 (1968).

[18] T. Kakubo, S. Iwatsuki and Y. Yamashita, *Makromol. Chem.*, **123**, 256 (1969).

[19] N. G. Gaylord, *J. Polymer Sci.*, *Part C.*, **31**, 247 (1970).

[20] E. Tsuchida and T. Tomono, *Makromol. Chem.*, **141**, 265 (1971).

[21] G. E. Ham, "Copolymerization", High Polymer Series, vol. XVIII, Interscience Publishers, J. Wiley, New York, 1964, p. 67—78, p. 845—863.

[22] M. C. Wilde and G. Smets, *J. Polymer Sci.*, **5**, 253 (1950).

[23] D. C. Blackley and H. W. Melville, *Makromol. Chem.*, **18**, 16 (1956).

EXPERIMENTAL

The reactivity ratios which are used for the calculation of Q and e values were determined experimentally. The conditions as well as the methods of determination were presented in previous works.[1,4,5]

RESULTS AND DISCUSSIONS

The values of Q and e for the studied systems were calculated with the following two well-known relations:

$$e_2 = e_1 \pm (-1nr_1r_2)^{1/2}$$

$$Q_2 = Q_1/r_1 \exp. \{-e_1(e_1 - e_2)\}$$

in which:

Q_1, Q_2 — characterizes the reactivity of monomers determined by conjugation stabilization.

e_1, e_2 — polarities of structures correlated with the electron-donor and electron-acceptor character of the substituents at the double bond.

r_1, r_2 — reactivity ratios determined experimentally.

For isoprene $Q_1 = 3.33$ and $e = -1.22$ values were taken, which are known from literature.[21,24] It is necessary to point out that, as for the systems studied $r_2 = 0$, in order to enable the calculation a small finite value was taken (method also used by Young[24]).

The values Q and e obtained from the calculation for monoesters are shown in table 1.

Table 1

Q and e constants in copolymerization of isoprene (M_1) with maleic acid monoesters (M_2)

M_2	Reactivity ratios[1,4,5]		e	Q
	r_1	r_2		
Monomethylmaleate	0.151	0	1.746	0.596
Monoethylmaleate	0.141	0	1.757	0.630
Monopropylmaleate	0.058	0	1.903	1.276
Monobutylmaleate	0.093	0	1.827	0.877
Monoamylmaleate	0.089	0	1.834	0.906
Monoheptylmaleate	0.086	0	1.839	0.938
Monolauroylmaleate	0.083	0	1.845	0.960
Monocetylmaleate	0.083	0	1.845	0.960
Monocyclohexylmaleate	0.121	0	1.783	0.708
Monobenzylmaleate	0.055	0	1.912	1.330

---

[24] L. J. Young, *J. Polymer Sci.*, **54**, 411 (1961).

With the help of these values for monoesters and the values for isoprene, the $Q - e$ scheme was plotted (fig. 1).

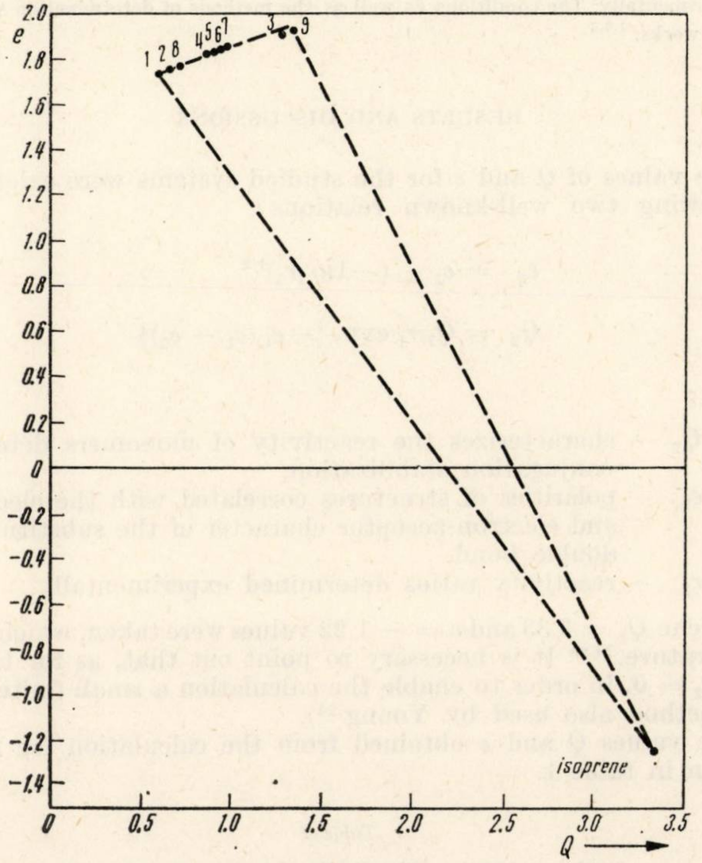

Fig. 1. — $Q - e$ diagram for isoprene (M_1) — maleic acid monoesters (M_2) systems :

1, monomethylmaleate ; *2*, monoethylmaleate ; *3*, monopropylmaleate ; *4*, monobutylmaleate ; *5*, monoamylmaleate ; *6*, monoheptylmaleate ; *7*, monolauroyl and monocetylmaleate ; *8*, monocyclohexylmaleate and *9*, monobenzylmaleate.

A great difference in polarity is noticed in the $Q - e$ scheme between isoprene and maleic acid monoesters, the fact explaining the marked alternating tendency in copolymerization. Following up the "e" values for monoesters, depeding on the length of the alkyl chain in the monoester, small differences are distinguished in polarity. In this case, the $Q-e$ scheme is of no use in the examination of the minor structural modifications. The differences among "e" values should be at least ± 0.2, in order to enable to distinguish two monomers.[25] If we compare the "e" values of maleic monoesters with the "e" values of maleic alhydride [21] ($e = 2.25$), a difference can be observed ("e" values for monoesters being smaller). This is due to the inductive effect of the alkyl groups (effect + I) opposed to the strong electron-attracting effect of the carboxyl groups. The "e" values obtained for monoesters in the system with isoprene are comparable with the values obtained from other systems.

---

[25] T. Alfrey, J. J. Bohrer and H. Mark, "Copolymerization", High Polymer Series, vol. VIII, Interscience Publishers, New York, 1952, p. 94.

Thus, value $e = 1.78$ found for monomethylmaleate copolymerized with other systems,[21] is close to the value calculated by us in the copolymerization with isoprene. The differences among the values of the Q parameter enable us to analyze the influence of the alkyl radical length in the monoester on this parameter.

In fig. 2 the variation of the Q parameter is represented depending on the number of carbon atoms in the monoester alkyl chain.

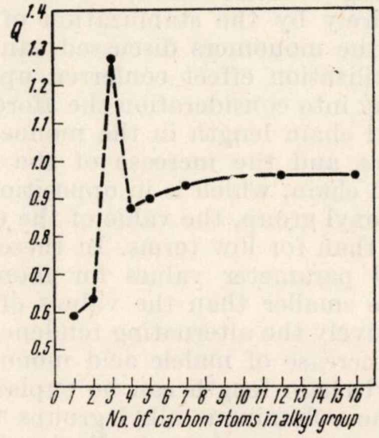

Fig. 2.—Effect of the size of the alkyl group on the Q parameter.

The shape of the curve is similar to that of the $1/r_1$ ratio representation of the same function.[4]

For this homologous series, the Q parameter shows an increase from the low terms towards the high terms, becoming practically constant for monoesters which have more than 6 carbon atoms in the alkyl group. Discontinuity introduced by the maleic acid monoester with n-propyl alcohol is noticed on going over from monoethylmaleate to monobutylmaleate.

As is known, the inductive effect (+I) of the n-alkyl group increases with the length of the alkyl chain faster at the beginning, reaching a maximum close to the hexyl and remaining constant for higher values of the chain length. This fact was reflected in the variation of the acidity constant of monocarboxylic acids, which decreases to a constant boundary value.[26,27]

[26] C. D. Nenițescu, "Chimie Organică", vol. I, 6, Ed. Didactică şi Pedagogică, Bucharest, 1966, p. 730.

[27] G. G. Cameron, D. H. Grant, N. Grassie, J. E. Lamb and I. C. McNeill, J. *Polymer Sci.*, **36**, 173, (1959).

Analogy is remarked between the discontinuity in variation of the acidity constant, observed in the case of butyric acid, and the discontinuity introduced by monopropylmaleate (with the same alkyl group) in the variation of the Q parameter depending on the length of the alkyl group.

Evans and co-workers [28] have come to the conclusion that a high reactivity of the monomer is associated with an increase in resonance from the monomer to the radical and that the Q value can be identified with :

$$Q = \exp\{\alpha (R_A - R_M)/RT\}$$

in which R_A and R_M are the resonance energies of the monomer and the corresponding radical. Thus, the monomer reactivity is determined almost entirely by the stabilization of the resulting radical and the Q values for the monomers discussed can be interpreted as a consequence of the stabilization effect conferred upon by the different substituents.

Taking into consideration the aforesaid and the fact that an increase of the alkyl chain length in the monoesters would lead to an inhibition of resonance and the increase of the inductive effect with the length of the alkyl chain, which is in opposition to the electron-attracting effect of the carboxyl group, the value of the Q parameter for high terms should be smaller than for low terms. In these conditions the question is raised why the Q parameter values for monomethylmaleate and monoethylmaleate are smaller than the values of monoesters with higher alcohols and respectively the alternating tendency is greater for the latter.

The increase of maleic acid monoester reactivity with the increase of the alkyl chain length can be explained by the increase of the steric effect of the voluminous alkyl groups that leads to the decrease of the termination rate constant (radical-radical reaction). However, as the viscosity of maleic acid monoesters increases with the number of carbon atoms in the alkyl groups, it is possible to explain the results obtained also by the fact that the termination reaction is controlled by diffusion.

To support these explanations for our results, works of Burnett and co-workers [29] can be reminded who came to the conclusion that the (k_t) termination rate constant in the polymerization of alkyl methacrylates decreases with the increase of the alkyl group, as a result of the increase of their steric effects.

In another series of works, Benson, North and Reed,[30-32] confirmed experimentally that the termination rate in radical polymerization of some alkyl acrylates and methacrylates is controlled by the diffusion of macroradicals, it being established that the termination rate constant is inversely proportional to the viscosity of the polymerization mixture, even on the initial stage of polymerization.

---

[28] M. G. Evans, J. Gergely and E. C. Seaman, *J. Polymer Sci.*, **3**, 866, (1948).

[29] G. M. Burnett, P. Evans and H. W. Melville, *Trans. Faraday Soc.*, **49**, 1096, 1105 (1953).

[30] S. W. Benson and A. M. North, *J. Amer. Chem. Soc.*, **81**, 1339 (1959) ; **84**, 935 (1962).

[31] A. M. North and G. A. Reed, *Trans. Faraday Soc.*, **57**, 859 (1961).

[32] A. M. North and G. A. Reed, *J. Polymer Sci., Part A*, **1**, 1311 (1963).

Otsu and co-workers,[33] on studying the effects of the alkyl group on the polymerization of alkyl methacrylates, observed that the polymerization rates increase with the increase of the alkyl group length. This increase is explained by the increase diffusion control of the termination rate with the increase in the length of the alkyl groups in methacrylates, distinguished by an inversely proportional ratio between the constants of polymerization rates and viscosities.

The difference between the reactivity of monocyclohexylmaleate and monobenzylmaleate can be explained by the same considerations as above. Although the alternating tendency in copolymerization of isoprene with maleic acid monoesters is explained by the polarity differences of comonomers as a consequence of a coulomb attraction between two dipoles (the small differences of polarity not being distinguished however between the monoesters) according to Alfrey and Price's theory of polar factors,[7] the adoption of the point of view of Mayo and Walling [11,12] is neither excluded, consisting in the explanation of the transition stage by the dipolar structures of resonance, the transition stage being the result of the electron transfer between the radical and the monomer.

[33] T. Otsu, T. Ito and M. Imoto, *J. Polymer Sci., Part A*, **2**, 2901 (1964).

Revue Roumaine de Chimie, **17**, *6*, 1051–1059 (1972)

ÉTUDE DE LA CINÉTIQUE DE LA RÉACTION $Bi_2O_3 + TiO_2$ AVEC FORMATION DE $Bi_4Ti_3O_{12}$

CONST. GH. MACAROVICI et GH. MORAR
Institut de Chimie, Cluj, 65–103, str. Donath

Reçu le 12 mai 1971

On a étudié la cinétique de la réaction des poudres de Bi_2O_3 et TiO_2 avec formation de $Bi_4Ti_3O_{12}$, en partant de mélanges réalisés mécaniquement et par décomposition thermique du coprécipité d'hydroxydes. On a établi que dans le premier cas la réaction a lieu à une température supérieure (850° par rapport à 500°), réclamant une énergie d'activation plus grande (61 kcal/mole par rapport à 46 kcal/mole) et que, dans les deux cas, le processus est dominé par la diffusion.

Le $Bi_4Ti_3O_{12}$ est le représentant le plus important des oxydes mixtes de titane et de bismuth. Cette affirmation est justifiée par ses multiples applications dans l'électronique industrielle amenées par ses propriétés diélectriques remarquables (constante diélectrique et point Curie ferroélectrique très élevés).

Le composé est obtenu de façon classique par suite de la réaction à haute température (1000–1100°) du mélange mécanique des poudres de Bi_2O_3 et TiO_2.[1-4]

Dans un travail précédent [5] nous avons obtenu le même composé à une température moyenne (500–600°) par la décomposition thermique du coprécipité d'hydroxydes de bismuth et de titane. A cette occasion, nous avons fait aussi quelques précisions relatives au mécanisme de la réaction de formation du $Bi_4Ti_3O_{12}$. Ainsi, fondés sur les résultats de l'analyse thermogravimétrique et thermodifférentielle des spectres de diffraction rœntgen et d'absorption en IR, nous avons établi que, en partant du mélange mécanique des poudres de Bi_2O_3 et TiO_2, la formation de l'oxyde mixte commence vers 850°, par suite de la réaction entre le Bi_2O_3, se trouvant à l'état liquide à cette température, et le TiO_2 à l'état solide, conformément à l'équation :

$$2Bi_2O_{3\ \text{liquide}} + 3TiO_{2\ \text{solide}} \rightarrow Bi_4Ti_3O_{12\ \text{solide}} \tag{1}$$

---

[1] B. Aurivillius, *Arkiv. Kemi*, **1**, 463 (1949).
[2] E. C. Subbarao, *J. Chem. Phys.*, **34**, 695 (1961).
[3] G. I. Skanavi et A. I. Demeshina, *Zhur. eksp. teor. Fiz.*, **31**, 656 (1957).
[4] E. I. Speranskaya, I. S. Rez., I. V. Kozlova, V. M. Skoricov et V. I. Slavov, *Izvest. Akad. Nauk, S.S.S.R., Neorg. Materialy* **1**, 232 (1965).
[5] C. Macarovici et Gh. Morar, *Rev. Roumaine Chim.* (sous presse).

En même temps, la formation de l'oxyde mixte par la décomposition thermique du coprécipité d'hydroxydes a lieu à une température inférieure (500°). Cela s'explique par le fait qu'à la suite de la décomposition thermique du coprécipité d'hydroxydes il résulte un mélange d'oxydes ($Bi_2O_3+TiO_2$) à réactivité élevée qui relève de leur état amorphe et à haut degré (moléculaire) de dispersion et d'homogénéité. Schématiquement, le processus est représenté comme suit :

$$Bi_2O_3 . TiO_2 . xH_2O_{\text{coprécipité}} \rightarrow Bi_2O_{3\,\text{amorphe}} + TiO_{2\,\text{amorphe}} \rightarrow$$

$$\rightarrow Bi_4Ti_3O_{12\,\text{cristallin}} \qquad (2)$$

Pour l'élucidation complète du mécanisme de la réaction de formation du $Bi_4Ti_3O_{12}$, nous avons jugé nécessaire d'effectuer une étude de la cinétique de la réaction, en nous plaçant dans les conditions distinctes des deux méthodes susmentionnées.

Selon les connaissances actuelles,[6,7] les réactions chimiques dans les mélanges de substances à l'état solide ne se distinguent pas essentiellement de celles qui ont lieu en phase gazeuse ou liquide, réclamant les mêmes stades : le contact entre les molécules qui réagissent et la réaction proprement dite.

Mais dans la phase solide, la diffusion, soit la prise de contact des molécules, est sensiblement plus difficile, ayant lieu à une vitesse beaucoup plus petite que la réaction proprement dite, laquelle détermine la vitesse globale de la réaction.

Il a été prouvé[6,7] que la vitesse des réactions dans les milieux solides ne peut pas s'exprimer par une seule équation sur toute la durée, mais par des équations différentes et propres à chaque étape cinétique du processus. On distingue généralement trois étapes d'une réaction dans les milieux solides.

Pendant la première étape, les réactants se trouvent en contact et, de ce fait, la réaction découle sans les implications du phénomène de diffusion, pouvant être décrite par les équations cinétiques suivantes :[6–10]

$$kt = Z \qquad (3)$$

$$kt = 1 - (1 - Z)^{1/3} \qquad (4)$$

A l'étape suivante, les réactants étant séparés par le produit de réaction, le processus sera contrôlé par le phénomène de diffusion. Dans ce cas, la constante de la vitesse de réaction peut s'exprimer par une des équations suivantes.

$$1 + (1 - Z)^{2/3} - 2\,(1 - Z)^{1/3} = kt = I_J \qquad (5)$$

---

[6] A. M. Ghinstling et B. I. Brounstein, *Zhur. priklad. Khim.*, **23**, 1949 (1950).

[7] D. Cismaru, *Studii şi Cercetări Fiz.*, **6**, 435 (1955).

[8] A. M. Ghinstling et T. P. Frodkina, *Zhur. priklad, Khim.*, **25**, 1134 (1952).

[9] A. M. Ghinstling et T. P. Frodkina, *Zhur. priklad. Khim.*, **25**, 1268 (1952).

[10] D. Cismaru et V. Nacea, *Rev. Roumaine Chim.*, **13**, 541 (1968).

déduite par Jander[11]

$$1-(1-Z)^{2/3}-2/3\,Z = kt = I_G\,;\; k = k'^2/r^2 \qquad (6)$$

déduite par Ghinstling, Brounstein[6] et Cismaru[7], et

$$(1-Z) = 6/\pi^2 \sum_{n=1}^{\infty} 1/n^2 .\ \exp.(-n^2kt)\,;\quad k = \pi^2 D/r^2 \qquad (7)$$

déduite par Serin et Ellickson.[12]

Dans ces équations, k est la constante de la vitesse de réaction ; Z — le degré de transformation ; t — le temps de réaction ; n — le nombre entier qui peut prendre des valeurs de 1 à ∞. Dans l'expression de la constante de vitesse (k) sont inclus le coefficient de diffusion D, conformément à la loi de Fick, ainsi que le rayon des particules r.

A la dernière étape, la vitesse de réaction diminue beaucoup et ne peut plus être exprimée par les équations 5—7, le processus tendant à devenir stagnant.

PARTIE EXPÉRIMENTALE

Le mélange des deux oxydes a été obtenu d'après les deux variantes susmentionnées. Le mélange mécanique a été réalisé en utilisant un vibrateur électromagnétique à bille. Les oxydes de départ, le Bi_2O_3 et le TiO_2, ont été obtenus par calcination à 700° pendant 2 heures des précipités lavés et séchés de $Bi(OH)_3$, respectivement $TiO_2.xH_2O$.

Dans la seconde variante, le mélange de départ a été réalisé par la conversion thermique du coprécipité d'hydroxydes de bismuth et de titane dans les oxydes correspondants (calcination à 400°C pendant 2 heures). Le coprécipité a été obtenu par la précipitation par du NH_4OH à froid et sous agitation d'une solution aqueuse acidulée avec du HNO_3 (pH = 1), contenant du $Bi(NO_3)_3$ et du $TiO(NO_3)_2$ au rapport molaire de 4 :3, suivie du filtrage, lavage et séchage du précipité à 105°.

Les échantillons sous forme de poudre (tels qu'ils ont été obtenus), placés dans un creuset de platine de taille correspondante, légèrement tassés et pesant environ 1 g, étaient chauffés à différents températures et intervalles de temps (tableaux 1 et 2), dans un four électrique amené au préalable à la température de la réaction, maintenue avec une approximation de $\pm 10°$.

Le degré de transformation était déterminé chimiquement par dosage du Bi_2O_3 qui n'était pas entré en réaction à la fin de la calcination, après avoir fait « geler » l'échantillon à la température ambiante. En agitant le mélange obtenu de cette manière avec une solution aqueuse de HNO_3, 1 M, pendant 30 minutes, il se produit la solubilisation de l'oxyde de bismuth, qui, par filtrage, se sépare du reste des composants (TiO_2 et $Bi_4Ti_3O_{12}$). La solution de Bi^{3+} ainsi obtenue est titrée avec le complexon III solution 0,02 M en présence de xylénolorange comme indicateur.

---

[11] W. Jadner, *Z. anorg. Chem.*, **163**, 30 (1927).

[12] B. Serin et R. T. Ellickson, *J. Chem. Phys.*, **9**, 742 (1941).

RÉSULTATS ET DISCUSSION

En vertu des valeurs expérimentales des quantités de Bi_2O_3 qui n'ont pas réagi à la fin de l'expérience, on a déterminé le degré de transformation Z (tableaux 1, 2 et figures 1 et 2), qui a été utilisé par la suite à l'établissement de l'équation cinétique pour la réaction étudiée.

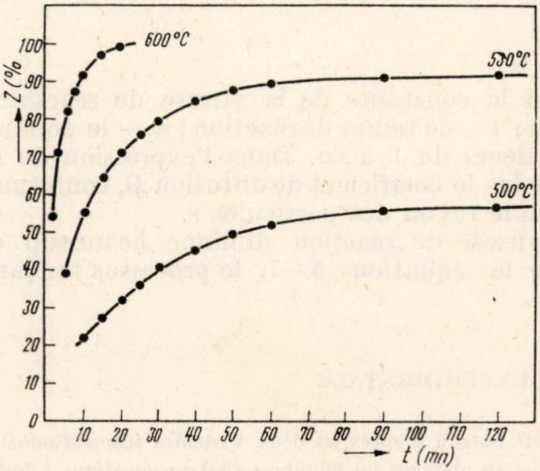

Fig. 1. — Variation du degré de transformation (Z) en fonction du temps, à différentes températures pour le mélange de $2Bi_2O_3 + 3TiO_2$, obtenu par décomposition thermique du coprécipité d'hydroxydes.

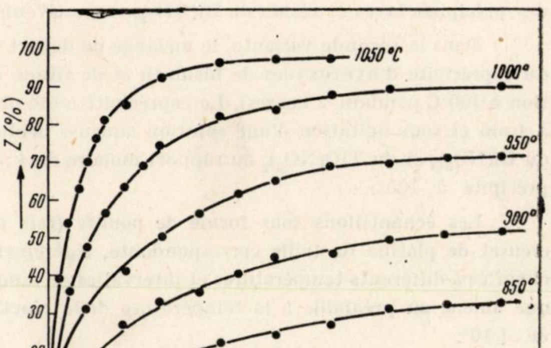

Fig. 2. — Variation du degré de transformation en fonction du temps à différentes températures pour le mélange mécanique.

Les résultats obtenus montrent que la cinétique de la réaction $Bi_2O_3 + TiO_2$ est la mieux rendue par les équations de Ghinstling et Serin-Ellickson, tandis que l'équation de Jander a une applicabilité limitée aux valeurs basses du degré de transformation.

Au moyen des équations 6 et 7 on a rendu linéairement la vitesse de réaction, en déterminant aussi la limite d'applicabilité des équations

Tableau 1

Données cinétiques pour la réaaction $Bi_2O_3 + TiO_2$
(Décomposition thermique du coprécipité d'hydroxydes)

Température (°C)	Temps de réaction (mn)	Z	$I_G.10^3$	$K_G.10^3$	$I_{SE}.10^2$	$K_{SE}.10^2$
500	10	0,210	7,0	0,700	4,2	0,42
	15	0,270	11,0	0,733	7,8	0,52
	20	0,322	14,5	0,725	10,8	0,54
	25	0,360	18,5	0,740	14,0	0,56
	30	0,411	22,2	0,740	19,0	0,63
	40	0,447	29,5	0,738	23,0	0,58
	50	0,504	37,0	0,740	30,2	0,60
	60	0,520	41,5	0,692	32,6	0,54
	90	0,560	48,0	0,533	40,0	0,44
	120	0,571	50,5	0,422	42,1	0,35
550	5	0,392	22	4,40	17,0	3,40
	10	0,545	45	4,50	36,9	3,70
	15	0,638	67	4,47	55,9	3,74
	20	0,712	90	4,50	76,1	3,80
	25	0,755	112	4,48	91,5	3,66
	30	0,785	128	4,27	103,5	3,46
	40	0,845	149	3,73	—	—
	50	0,875	167	3,34	—	—
	60	0,890	177,5	2,96	—	—
	90	0,911	192	2,13	—	—
	120	0,920	201,5	1,68	—	—
600	2	0,540	44,0	22,0	36,0	18,0
	4	0,707	88,1	22,02	74,5	18,6
	6	0,824	132,9	22,2	130,0	21,7
	8	0,870	164,0	20,5	—	—
	10	0,920	202,0	20,2	—	—
	15	0,970	257,5	17,2	—	—
	20	0,990	294,5	14,8	—	—

de Ghinstling et Serin-Ellickson. La constante de la vitesse de réaction a été trouvée par calcul, sur la base des équations 6 et 7 et graphiquement (sa valeur moyenne) de la variation des valeurs I_G et I_{SE} en fonction du temps.

L'allure des courbes des figures 1 et 2 nous indique que la réaction $Bi_2O_3 + TiO_2$ se déroule à une vitesse mesurable au-dessus des températures de 500°, respectivement 850°, au cas où le mélange de réaction a été réalisé respectivement par coprécipitation ou mécaniquement, consignant en même temps une accélération du processus lors de l'augmentation de la température.

L'applicabilité des équations de Ghinstling et Serin-Ellickson avec des résultats similaires confirme le rôle déterminant de la diffusion dans l'évolution du processus chimique.

En raison de la grande vitesse de déroulement de la réaction dans la première phase, quand n'intervient pas le phénomène de diffusion,

Tableau 2

Données cinétiques pour la réaction $Bi_2O_3 + TiO_2$ (mélange mécanique)

Température (°C)	Temps de réaction (mn)	Z	$I_G.10^3$	$K_G.10^4$	$I_{SE}.10^2$	$K_{SE}.10^3$
850	30	0,104	1,24	0,413	1,0	0,138
	60	0,177	3,8	0,633	2,9	0,483
	90	0,219	5,9	0,655	4,6	0,512
	120	0,255	7,8	0,650	6,4	0,533
	150	0,275	9,8	0,652	7,5	0,500
	180	0,301	11,7	0,651	9,3	0,517
	210	0,323	13,6	0,648	10,9	0,519
	240	0,331	14,3	0,596	11,6	0,483
900	20	0,147	4,6	2,30	2,2	1,10
	40	0,2665	9,0	2,25	7,0	1,75
	60	0,323	13,6	2,26	10,9	1,82
	80	0,3665	18,0	2,25	14,6	1,82
	100	0,404	22,5	2,25	18,3	1,83
	120	0,438	27,0	2,25	22,0	1,83
	150	0,483	33,8	2,26	27,3	1,82
	180	0,499	36,4	2,02	29,5	1,84
	210	0,512	38,7	1,84	31,4	1,50
	240	0,521	40,3	1,61	32,7	1,36
950	20	0,314	10,24	5,12	10,2	5,10
	40	0,422	24,8	6,20	20,2	5,05
	60	0,502	37,0	6,17	27,2	4,54
	80	0,56	49,4	6,18	41,7	5,20
	100	0,623	62,8	6,28	52,6	5,26
	120	0,650	69,8	5,82	58,8	4,90
	150	0,689	81,5	5,44	69,0	4,60
	180	0,702	85,9	4,77	73,0	4,06
	210	0,711	89,0	4,23	76,0	3,62
	240	0,719	91,6	3,81	78,5	3,27
1000	10	0,354	16,7	16,7	13,5	13,5
	20	0,4775	32,9	16,85	26	13,3
	30	0,5665	49,5	16,5	41,2	13,7
	40	0,635	65,8	16,4	55,2	13,8
	50	0,692	82,7	16,5	70,0	14,0
	60	0,738	99,0	16,5	85,0	14,1
	90	0,813	131,4	14,6	118,0	9,83
	120	0,848	150,3	12,5	—	—
	150	0,875	166,7	11,1	—	—
	180	0,889	183,0	10,1	—	—
	240	0,901	184,5	7,67	—	—
1050	5	0,390	21,7	43,4	15,0	30,0
	10	0,535	43,1	43,1	35,1	35,1
	15	0,629	64,6	43,1	54,0	36,0
	20	0,703	86,6	43,3	73,2	36,8
	25	0,758	107,5	43,0	85,0	33,2
	30	0,813	131,2	42,7	118,0	39,3
	40	0,851	152,1	38,0	—	—
	60	0,924	194,3	32,4	—	—
	90	0,966	247,8	27,5	—	—
	120	0,970	—	—	—	—
	150	0,978	—	—	—	—

celle-ci n'a pas pu être étudiée par les mêmes moyens, et de ce fait il n'en sera pas fait mention.

On n'a pas non plus déterminé la cinétique de la réaction dans la dernière phase, quand les équations 6 et 7 ne s'appliquent plus (les valeurs expérimentales des expressions I_G et I_{SE} ne varient plus linéairement avec le temps), quand la vitesse de la réaction diminue beaucoup et quand le processus tend à stagner.

En exprimant la variation de la constante de la vitesse moyenne de réaction en fonction de la température (tableaux 3 et 4) par l'équation d'Arhenius :

$$K = A \,.\, \exp. (-E/RT) \tag{8}$$

et en représentant graphiquement son expression logarithmique (figures 3–6)

$$\lg K = -2{,}303\, E/R \,.\, 1/T + \lg A \tag{9}$$

on a pu déterminer l'énergie d'activation (E) de la réaction et de la constante d'Arhenius (A).

Tableau 3

Variation de la constante de la vitesse de réaction avec la température (coprécipité d'hydroxydes)

Température (°C)	$1/T.10^4$	$K_G.10^4$	$\lg K_G + 4$	$K_{SE}.10^3$	$\lg K_{SE} + 3$
500	12,94	7,4	0,869	6,45	0,810
550	12,15	44,5	1,648	39,6	1,597
600	11,45	223,5	2,341	253,0	2,403

Tableau 4

Variation de la constante de la vitesse de réaction avec la température (mélange mécanique)

Température (°C)	$1/T.10^4$	$K_G.10^5$	$\lg K_G + 5$	$K_{SE}.10^4$	$\lg K_{SE} + 4$
850	8,90	6,47	0,810	5,5	0,740
900	8,53	22,4	1,330	19	1,278
950	8,17	62,3	1,794	53	1,724
1000	7,85	164,2	2,215	141	2,149
1050	7,56	429,6	2,633	464	2,666

Voici les valeurs qui ont été trouvées : $E_G = 45$ kcal/mole ; $E_{SE} = 46{,}8$ kcal/mole ; $A_G = 6{,}82.10^9$; $A_{SE} = 1{,}16.10^{11}$ pour le mélange obtenu par la décomposition thermique du coprécipité et $E_G = 60{,}8$ kcal/mole ; $E_{SE} = 61{,}7$ kcal/mole ; $A_G = 4{,}78.10^7$; $A_{SE} = 5{,}63.10^8$ pour le mélange réalisé mécaniquement.

Les résultats obtenus nous autorisent à considérer le mécanisme suivant pour la réaction entre Bi_2O_3 et TiO_2.

Au cas où le mélange de réaction a été obtenu de manière mécanique en partant des poudres de Bi_2O_3 et TiO_2, dans la première phase, lorsque l'énergie d'activation a été atteinte, il se produit la réaction entre les granules de TiO_2 immergés dans le Bi_2O_3. A l'étape suivante, les granules de TiO_2 sont recouverts d'une couche de $Bi_4Ti_3O_{12}$ solide, qui sépare le TiO_2 de Bi_2O_3. Pour que la réaction puisse continuer à se dérouler, il faut que les deux réactants entrent de nouveau en contact, par la diffusion d'au moins un d'entre eux à travers la couche isolante de $Bi_4Ti_3O_{12}$.

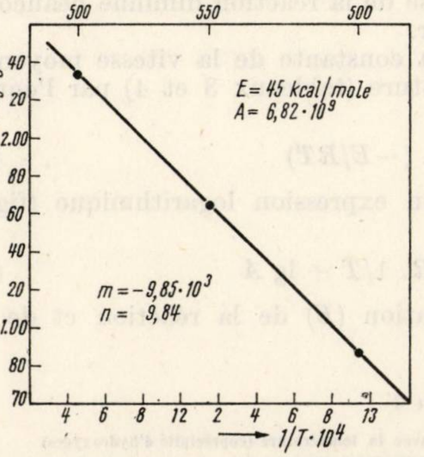

Fig. 3. — Dépendance du lg K_G de $1/T$ pour le mélange obtenu par décomposition thermique du coprécipité d'hydroxydes.

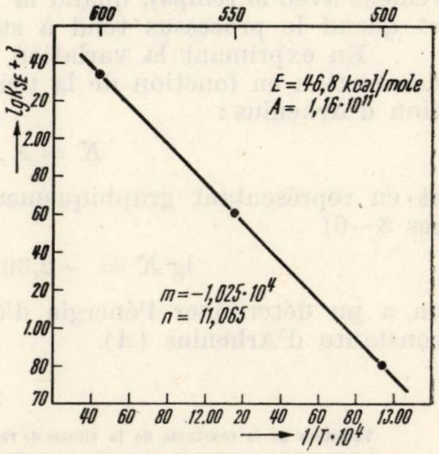

Fig. 4.—Dépendance du lg K_{SE} de $1/T$ pour le mélange obtenu par décomposition thermique du coprécipité d'hydroxydes.

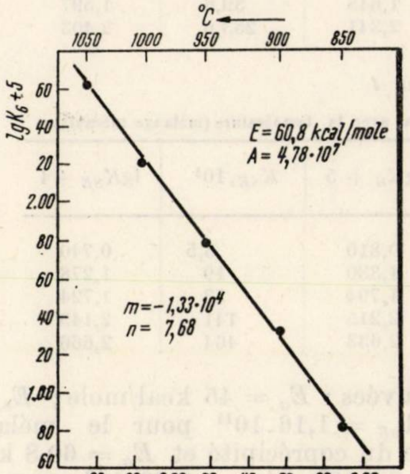

Fig. 5. — Dépendance du lg K_G de $1/T$ pour le mélange mécanique.

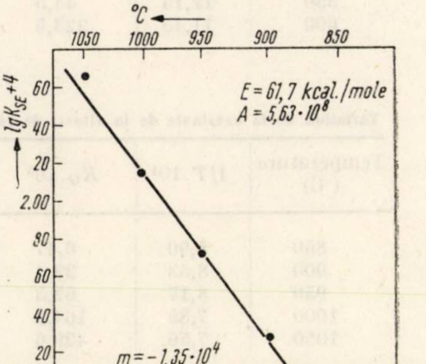

Fig. 6.—Dépendance du lg K_{SE} de $1/T$ pour le mélange mécanique.

Compte tenu de la mobilité plus grande du Bi_2O_3, due à l'état liquide où il se trouve à la température de réaction, et du fait que le $Bi_4Ti_3O_{12}$ forme des solutions solides seulement avec le Bi_2O_3,[4] on peut affirmer qu'il est le partenaire diffusant.

Lorsque le mélange de réaction se réalise par la décomposition thermique du coprécipité d'hydroxydes, le mécanisme est quelque peu différent.

Deux substances solides, cristallisées, qui réagissent entre elles, ont pour phase précédant la combinaison mutuelle proprement dite la destruction du réseau cristallin et la transformation en un produit amorphe ou imparfaitement cristallisé.[13,14] Il est bien entendu que cette phase précédente, de transition, réclame elle aussi une consommation d'énergie. Par conséquent, lorsque les partenaires de la réaction (Bi_2O_3 et TiO_2) se trouvent à l'état cristallin (mélange réalisé mécaniquement), l'énergie d'activation de la réaction a une valeur plus élevée (61 kcal/mole) et se réalise à une température plus haute (850°).

A la décomposition thermique du coprécipité d'hydroxydes, les oxydes métalliques résultent à l'état amorphe, très finement dispersés l'un dans l'autre, et ont une degré moléculaire d'homogénéité.

L'existence des réactants à l'état amorphe écarte la phase de transition, préliminaire à la réaction, et la consommation d'énergie correspondante, de sorte que la réaction réclame une énergie d'activation plus petite (46 kcal/mole), réalisable, à des températures plus basses (500—600°).

La dispersion très fine, presque moléculaire, des réactants et l'homogénéité du mélange résulté confèrent une surface de contact et donc de réaction et de diffusion très grande, ce qui fait que la réaction acquière des taux assez élevés.

Par ailleurs, l'homogénéité parfaite du mélange empêche la cristallisation des deux oxydes, qui restent amorphes à une température supérieure à celle de cristallisation.

CONCLUSIONS

Les résultats expérimentaux obtenus à l'étude de la réaction $Bi_2O_3 + TiO_2$ nous amènent à formuler les conclusions suivantes :

1. Quelle que soit la manière dont se réalise le mélange de réaction, la vitesse du processus est la mieux rendue par les équations de Ghinstling et Serin-Ellickson, confirmant ainsi le rôle prépondérant de la diffusion.

2. Au cas où le mélange des deux oxydes a été obtenu par la décomposition thermique du coprécipité d'hydroxydes, la réaction commence à une température inférieure (500°), réclamant une énergie d'activation plus petite (46 kcal/mole) que dans le cas où le mélange s'est réalisé mécaniquement (850° respectivement 61 kcal/mole).

3. Au point de vue pratique il est recommandable d'utiliser pour l'obtention du $Bi_4Ti_3O_{12}$ la méthode de la décomposition thermique du coprécipité d'hydroxydes de bismuth et de titane.

---

[13] J. R. Portington, « An Advanced Treatise on Physical Chemistry », IIIe vol., Longmans, Londres, 1963, p. 5—8.

[14] K. Hauffe, « Reaktionen in und an festen Stoffen », Springer-Verlag, Berlin, 1955.

Compte tenu de la mobilité plus grande du Bi_2O_3, due à l'état liquide où il se trouve à la température de réaction, et du fait que le $Bi_4Ti_3O_{12}$ formé des solutions solides seulement avec le Bi_2O_3,[4] on peut affirmer qu'il est le partenaire diffusant.

Lorsque le mélange de réaction se réalise par la décomposition thermique du coprécipité d'hydroxydes, le mécanisme est quelque peu différent.

Deux substances solides, cristallisées, qui réagissent entre elles, ont pour phase précédant la combinaison mutuelle proprement dite la destruction du réseau cristallin et la transformation en un produit amorphe ou imparfaitement cristallisé.[23,24] Il est bien entendu que cette phase précédente, de transition, réclame elle aussi une consommation d'énergie. Par conséquent, lorsque les partenaires de la réaction (Bi_2O_3 et TiO_2) se trouvent à l'état cristallin (mélange réalisé mécaniquement), l'énergie d'activation de la réaction a une valeur plus élevée (61 kcal/mole) et se réalise à une température plus haute (850°).

A la décomposition thermique du coprécipité d'hydroxydes, les oxydes métalliques résultent à l'état amorphe, très finement dispersés l'un dans l'autre, et ont une degré moléculaire d'homogénéité.

L'existence des réactants à l'état amorphe écarte la phase de transition, préliminaire à la réaction, et la consommation d'énergie correspondante, de sorte que la réaction réclame une énergie d'activation plus petite (46 kcal/mole), réalisable, à des températures plus basses (500–600°).

La dispersion très fine, presque moléculaire, des réactants et l'homogénéité du mélange résulté confèrent une surface de contact et donc de réaction et de diffusion très grande, ce qui fait que la réaction acquière des taux assez élevés.

Par ailleurs, l'homogénéité parfaite du mélange empêche la cristallisation des deux oxydes, qui restent amorphes à une température supérieure à celle de cristallisation.

CONCLUSIONS

Les résultats expérimentaux obtenus à l'étude de la réaction $Bi_2O_3 + TiO_2$ nous amènent à formuler les conclusions suivantes :

1. Quelle que soit la manière dont se réalise le mélange de réaction, la vitesse du processus est le mieux rendue par les équations de Ginstling et Brounshtein, confirmant ainsi le rôle prépondérant de la diffusion.

2. Au cas où le mélange des deux oxydes a été obtenu par la décomposition thermique du coprécipité d'hydroxydes, la réaction commence à une température inférieure (500°), réclamant une énergie d'activation plus petite (46 kcal/mole) que dans le cas où le mélange s'est réalisé mécaniquement (850° respectivement 61 kcal/mole).

3. Au point de vue pratique il est recommandable d'utiliser pour l'obtention du $Bi_4Ti_3O_{12}$ la méthode de la décomposition thermique du coprécipité d'hydroxydes de bismuth et de titane.

---

[23] J. R. Partington, « An Advanced Treatise on Physical Chemistry », IIIe vol., Longmans, Londres, 1952, p. 1–8.

[24] K. Hauffe, « Reaktionen in und an festen Stoffen », Springer-Verlag, Berlin, 1955.

Revue Roumaine de Chimie, **17**, *6*, 1061–1064 (1972)

LE DOSAGE COMPLEXOMÉTRIQUE DU MÉLANGE BISMUTH-TITANE

GH. MORAR et CONST. GH. MACAROVICI
Institut de Chimie de Cluj
65–103, str. Donath

Reçu le 19 octobre 1971

On donne une méthode d'analyse complexométrique du mélange Bi(III)—Ti(IV) qui consiste dans le dosage du Bi^{3+} par titrage direct avec le complexon III 0,02 m, au pH = 1—2, en présence de xylénolorange comme indicateur, et dans la détermination du TiO^{2+} dans le même échantillon, après oxydation préalable de celui-ci en TiO_2^{2+} avec de l'H_2O_2 30% et élévation du pH à 5, en employant un excès de complexon III, qu'on retitre ensuite par $Bi(NO_3)_3$ 0,02, en présence du même indicateur.

Dans le cadre de nos travaux [1,2] sur la chimie des oxydes mixtes de bismuth et titane, l'élaboration d'une méthode d'analyse chimique du système bismuth-titane s'est imposée dès le début comme une nécessité, et cela d'autant plus que les procédés connus et décrits dans la littérature n'étaient pas satisfaisants à tous points de vue.

Ainsi, le problème du dosage du bismuth et du titane en mélange n'était résolu que dans le sens de la séparation préalable des composants (par précipitation sélective,[3,4] complexation sélective + extraction [5] et sur échangeurs d'ions [3]) et leur dosage ultérieur par un procédé convenable.

L'opération de séparation est laborieuse, complique l'analyse et constitue souvent une source d'erreurs systématiques et aléatoires, raisons qui nous ont déterminées à l'éviter.

Les moyens les plus indiqués pour réaliser ce but étaient ceux presque universels de l'analyse complexométrique, qui d'ailleurs ont été employés jusqu'à présent (dans une série de variantes) seulement pour le dosage des cations simples.

Ainsi, on détermine généralement le Bi^{3+} par titrage direct avec complexon III, en travaillant dans un milieu acide (pH = 0,7—3) et

---

[1] C. G. Macarovici et G. Morar, *Rev. Roumaine Chim.* (sous presse).

[2] C. G. Macarovici et G. Morar, *Rev. Roumaine Chim.* (sous presse).

[3] R. Pribil, «Complexons en chimie analytique», Ed. tehnică, Bucarest, 1958.

[4] A. K. Majumdar et J. B. Roy Chawdhury, *Analyt. Chim. Acta*, **15**, 105 (1966).

[5] I. K. Tselinskii, *Metody. Anal. Khim. Reaktivev Prep.*, **14**, 101 (1967); *Chem. Abstr.*, **70**, 84018 (1969).

en employant une large gamme d'indicateurs tels que : bleu de méthylthymol,[6,7] naphtol violet,[8] galéine,[9] xylénolorange, [10] violet de pyrocatéchine [11], hématoxyline ,[11] thorine, [11] thio-urée [12], brompyrogallol,[13] sanazoxs,[14] Pan,[11] etc.

Le titane est déterminé d'habitude par titrage indirect, au $pH = 4-5$, en employant un excès de complexon III, qui est retitré avec du $ZnCl_2$ ou du $CuSO_4$ en présence de : Eriochrome,[15] violet de pyrocatéchine,[15] bleu de thymol,[16] bleu de méthylène [16] ; avec du $FeCl_3$ en employant le SCN^- comme indicateur, avec du $TlNO_3$[17] ou du $Bi(NO_3)_3$[18] en présence d'H_2O_2 et de xylénolorange.

La méthode élaborée est basée sur la stabilité différente des complexonnés de bismuth et de titane au $pH = 1$ et le changement de la stabilité par oxydation du titane et hausse du pH.

Ainsi pour le $pH \leqslant 2$ le complexonné de bismuth est beaucoup plus stable que celui de titanyl ($K_{BiY^-} = 8{,}71 . 10^{27} > K_{TiOY^{2-}} = 2{,}00 . 10^{17}$), est formé le premier et rend possible le dosage exclusif du bismuth, en employant un indicateur sélectif. En oxydant par H_2O_2 l'ion TiO^{2+} du TiO_2^{2+} et la hausse du pH à 5, la stabilité des complexonnés est inversée (le TiO_2Y^{2-} devient plus stable que le BiY^-) en réalisant ainsi les conditions nécessaires pour le dosage indirect du titanium, par retitrage de l'excès de complexon III par $Bi(NO_3)_3$ et en présence du même indicateur.

Les caractéristiques requises par l'indicateur (fonctionner dans un milieu acide, $pH \leqslant 2$ — pour éviter l'hydrolyse des ions Bi^{3+} et TiO^{2+}, et être spécifique des ions Bi^{3+}) rendent le choix assez difficile. Le xylénolorange possède ces qualités constituant ainsi l'indicateur le plus convenable pour le dosage complexométrique successif du bismuth et du titane en mélange.

PARTIE EXPÉRIMENTALE

Réactifs

Le complexon III 0,02 m a été obtenu très simplement, à partir du $Na_2H_2Y.2H_2O$ (substance standard).

Le $Bi(NO_3)_3$ 0,02 m a été obtenu à partir du $Bi(NO_3)_3.5H_2O$ *p.a.* Le titre de la solution a été établi gravimétriquement (précipité comme $Bi(OH)_3$ et pesé comme Bi_2O_3) et complexométriquement (en présence de xylénolorange).

---

[6] L. Barcza et E. Koros, *Chemyst-Analyst.*, **48**, 94 (1959).

[7] J. Korbl, *Chem. listy.*, **51**, 1061 (1957).

[8] B. Budesinsky, *Chem. Listy*, **51**, 726 (1957).

[9] Peng-Joung Sun, *J. Chinese Chem. Soc.* (*Taiwan*), **8**, 314 (191).

[10] J. Korbl, *Chem. listy*, **50**, 1440 (1956).

[11] G. Gattow et D. Schott, *Z. analyt. chem.*, **188**, 10 (1962).

[12] G. Gattow et D. Schott, *Z. analyt. chem.*, **188**, 81 (1962).

[13] A. Jenicova, *Chem. listy*, **50**, 760 (1956).

[14] G. Guerrin, *Chemyst-Analyst.*, **49**, 36 (1960).

[15] Z. Sir et R. Pribil, *Coll. Czech. Chem. Comm.*, **20**, 871 (1955).

[16] J. Novak et H. Arendo, *Chemyst-Analyst*, **46**, 92 (1957).

[17] J. Kinnunen, *Chemyst-Analyst*, **46**, 92 (1957).

[18] B. Bieber et Z. Vercea, *Coll. Czech. Chem. Comm.*, **26**, 2081 (1961).

Le $TiO(NO_3)_2$ a été obtenu par dissolution par HNO_3 du gel de $TiO_2.xH_2O$ fraîchement préparé et lavé jusqu'à la libération des ions étrangers.

Indicateur — solution aqueuse 0,1 % de xylénolorange (sel tétrasodique) ou mélange solide 1 :100 avec du KNO_3. La solution aqueuse est stable pendant approximativement 30 jours.

Les H_2O_2 30 %, CH_3COOH glacial, CH_3COONa et NH_4OH ont été du degré de pureté : pour l'analyse (*p.a.*)

Procédé proposé

Dosage du bismuth. La solution à analyser qui contient tout au plus 40 mg de Bi est amenée au pH = 1—3 par du $NaHCO_3$ ou du CH_3COONa. On ajoute ensuite l'indicateur (3—4 gouttes de solution aqueuse, ou approximativement 10 mg de mélange solide), à la suite de quoi la solution doit se colorer en rouge. Si celle-ci est trop acide, elle se colorera en orange ou même en jaune — et dans ce cas le pH doit être corrigé (en diluant ou en ajoutant du $NaHCO_3$ ou du CH_3COONa). On titre ensuite avec une solution de complexon III 0,02 m jusqu'à ce que la couleur change en jaune. Le virage est très net.

Dosage du titane. Dans l'échantillon dans lequel on a dosé le bismuth on ajoute 0,5—1ml d'H_2O_2 30 %, pour l'oxydation du TiO^{2+} à TiO_2^{2+}, et un excès de solution de complexon. L'échantillon est ensuite alcalinisé avec du NH_4OH (pH = 9) et après acidulé avec du CH_3COOH glacial, en ajoutant 1—2 ml en excès, réalisant un milieu tampon de pH = 5, constitué par le CH_3COONH_4 et le CH_3COOH. Dans ces conditions le complexonné de peroxytitane se forme et la couleur de la solution tourne au rouge, rouge-orange (spécifique de l'ion TiO_2^{2+}) et jaune pâle (couleur du TiO_2Y^{2-}).

L'excès de complexon III est ensuite titré (sous 20°) avec une solution de $Bi(NO_3)_3$ 0,02 m, en présence du même indicateur, jusqu'à ce que la couleur passe du jaune au rouge.

RÉSULTATS ET DISCUSSIONS

La méthode élaborée a été vérifiée sur des solutions contenant des quantités connues de Bi $(NO_3)_3$ et $TiO(NO_3)_2$.

Tableau 1

Résultats obtenus pour le titrage du mélange de $Bi(NO_3)_3$ et $TiO(NO_3)_2$

N°	Rapport du mélange Bi : Ti	Bismuth			Titane		
		mg pris	mg trouvé	erreur %	mg pris	mg trouvé	erreur %
1	5 :1	21,30	21,34	+0,19	0,97	0,98	+1,16
2	5 :2	21,30	21,36	+0,27	1,94	1,93	−0,52
3	5 :3	21,30	21,28	−0,09	2,91	2,93	+0,69
4	5 :4	21,30	21,37	+0,33	3,88	3,89	−0,26
5	5 :5	21,30	21,26	−0,19	4,86	4,89	+0,63
6	4 :5	17,04	17,00	0,00	4,86	4,82	−0,82
7	3 :5	12,78	12,80	+0,16	4,86	4,86	0,00
8	2 :5	8,52	8,55	+0,35	4,86	4,88	+0,41
9	1 :5	4,26	4,38	+0,47	4,86	4,82	−0,63

Revue Roumaine de Chimie, **17**, *6*, 1061—1064 (1972)

Les résultats obtenus sont présentés dans le tableau 1. Leur précision est satisfaisante, étant comprise dans les limites des erreurs volumétriques $e_{\mathrm{Bi\,max}} = \pm 0{,}47\,\%$ et $e_{\mathrm{Ti\,max}} = \pm 0{,}82\,\%$.

La durée d'une analyse (dosage du bismuth et du titane) ne dépasse pas 10 minutes.

Observations

On a constaté (nous et autres [12]) que si la solution acide (au dosage du Bi^{3+}) est neutralisée par NaOH, NH_4OH ou pyridine jusqu'au commencement de la précipitation et est ensuite clarifiée par HNO_3 (pH = = 2—3), les résultats du titrage sont plus faibles. Dans ce cas, des polycations complexes du type $[Bi_6O_4(OH)_5]^{5+}$ se forment, à la suite de l'hydrolyse, qui ne sont pas décomposés par le complexon III dans les conditions du titrage. L'emploi du bicarbonate de sodium ou de l'acétate de sodium, pour l'ajustage du pH, ne présente pas cet inconvénient.

L'excès de complexon III (pour le dosage du titane) sera ajouté de sorte que son titrage ait lieu avec 5—10 ml de solution de $Bi(NO_3)_3$ 0,02 m.

Les mélanges à analyser seront dilués de manière que l'échantillon sur lequel on travaille ne contienne pas plus de 20 mg Ti/100 ml, dans le cas contraire la coloration jaune-orange du complexonné du peroxytitane sera trop intense et gênera l'observation du virage de l'indicateur.

L'effet des différents ions

On a étudié seulement l'influence des anions, et on a constaté que le titrage peut être effectué en présence des ions : NO_3^-, SO_4^{2-}, ClO_4^-, HCO_3^-, CH_3COO^- et qu'il est empêché par les ions d'halogénure (Cl^-, Br^-, I^-), qui ne permettent pas la réalisation du pH de fonctionnement de l'indicateur (1—3), étant donné qu'à la valeur zéro même de celui-ci ils sortent les ions Bi^{3+} du système, en les précipitant sous forme d'halogénure de bismuthyl, substance beaucoup plus stable que le complexonat de bismuth et qui en conséquence ne se dissout pas quand on ajoute le complexon III (au moment du titrage).

CONCLUSIONS

Une méthode complexométrique simple, rapide et précise de dosage du mélange bismuth-titane a été élaborée, méthode qui facilite considérablement l'abord des combinaisons mixtes de ces éléments. Cette méthode a d'ailleurs été employée pour établir la composition chimique de certaines combinaisons complexes mixtes de Bi (III) et Ti (IV) avec les acides oxalique et tartrique, de certains co-précipités d'hydroxydes de Bi (III) et Ti (IV) et de certaines phases oxydiques du système $Bi_2O_3-TiO_2$.

Revue Roumaine de Chimie. 17, 6, 1065 – 1069 (1972)

DETERMINATION OF THE STABILITY CONSTANT OF COMPOUNDS USED IN SPECTROPHOTOMETRIC ANALYSIS

L. M. BĂLOIU
Department of Chemistry and Physics
Academy of Economic Studies
Bucharest, Romania

Received August 19, 1971

The paper describes a method for the determination of the stability constants of compounds of (Dyestuff)$^+[ML_n]^-$ type, which are used in spectrophotometric determinations of M by extraction in organic solvents. The suggested method is based on the extraction mechanism. The values obtained for K are different from those obtained by means of the methods established for single-phase studies and incorrectly but usually applied in studies where extraction is involved.

I. INTRODUCTION

There are several spectrophotometric methods for the determination of metal ions by extracting the complex ion $[ML_n]^-$, bound to a basic dystuff D^+, in an organic phase and for measuring the absorbance of the extracted compound.

The bond between the complex and the dyestuff is mainly ionic, so that the compound is higly dissociated in aqueous solution.

The value of the stability constant is correlated with the width of the concentration range for which the Lambert-Beer law is obeyed. For small stability constants, large amounts of dyestuff have to be added, until all complex ions are associated as $D[ML_n]$. If the small water solubility of the dyestuff does not allow the addition of the requested amount of dyestuff, the diagram absorbance *vs.* metal concentration is not a straight line but an S-like curve, the compound being useless for analytical purposes.

As far as we know, for the determination of the stability constants of such compounds, the methods established for the spectrophotometric studies without extraction, e.g. Job method,[1] are used. But, as the equilibrium in the aqueous phase is disturbed by extraction, these methods, when applied to extraction systems, lead to incorrect results.

---

[1] P. Job, *Ann. Chim.* (*France*), **9**, 113 (1928).

The aim of this paper is to present a spectrophotometric method for the determination of a stability constant of such compounds, based on their extraction properties. The method is an adaptation of the method for the stability constants of metal complexes determination by extraction.[2]

II. THEORETICAL APPROACH

We shall consider that the conditions are such that the reaction :

$$M^{m+} + {}_nL^{p-} \rightleftharpoons [ML_n]^{m-np} \tag{a}$$

(where $m-np = -1$) is totally shifted to the right. Another condition is that only the compound $D\,[ML_n]$ is extracted. The pH of the aqueous solution has such a value that both equilibria :

$$DOH \rightleftharpoons D^+ + OH^- \tag{b}$$

$$H\,[ML_n] \rightleftharpoons H^+ + [ML_n]^-$$

are totally shifted to the right.

The volumes of organic and aqueous phases are equal to each other.

We shall suppose concentrations equal to activities ; anyway, the differences which would appear neglecting the activities are by far smaller than the experimental errors involved by the method.

We shall denote the concentration of compound $D\,[ML_n]$ by C and the concentration of $[ML_n]^-$ by c.

The extraction coefficient[3] is :

$$E = \frac{[M]_o}{[M]_w} = \frac{C_o}{C_w + c_w} \tag{1}$$

The partition constant is :

$$P = \frac{C_o}{C_w} \tag{2}$$

We are looking for the stability constant :

$$\beta = K = \frac{C_w}{c_w \times [D]_w} \tag{3}$$

---

[2] M. T. Beck, "Chemistry of Complex Equilibria", Akademiai Kiado, Budapest, 1970, p. 113, (English).

[3] * * *IUPAC Information Bulletin, 26, 31 (August 1966).

which can be written as:

$$\frac{c_w}{C_w} = \frac{1}{K \times [D]_w} \tag{4}$$

From equations (1) and (2):

$$E = \frac{P \times C_w}{C_w + c_w} = \frac{P}{1 + \dfrac{c_w}{C_w}} \tag{5}$$

so that:

$$E = \frac{P}{1 + \dfrac{1}{K \times [D]_w}} \tag{6}$$

or:

$$K = \frac{E}{[D]_w \times (P - E)} \tag{7}$$

where E, P and $[D]_w$ can be determined spectrophotometrically.

The determination of the partition constant has been described in a previous paper.[4]

For the determination of the extraction coefficient we start from relation (1) which can be written as:

$$E = \frac{C_o}{C_w + c_w + C_o - C_o} = \frac{C_o}{[M]_t - C_o} \tag{8}$$

where $[M]_t$ (meaning $[M]_{\text{total}}$) is known and

$$C_o = \frac{A}{kd} \tag{9}$$

Here A is the absorbance of the organic phase, d is the length of the cell and k is the molar absorbance coefficient of the compound in the organic phase.[4]

---

[4] V. Armeanu, S. Oancea, S. Rusenescu and L. M. Băloiu, *Rev. Roumaine Chim.*, **17**(5), 925(1972)

The dyestuff concentration can be obtained as follows:

$$[D]_t = [D]_w + C_w + C_o = [D]_w + \frac{C_o}{P} + C_o \qquad (10)$$

or, in our terms:

$$[D]_w = [D]_t - \frac{A}{kd}\,(1 + \frac{1}{P}) \qquad (11)$$

where $[D]_t = [D]_{\text{total}}$.

Finally we obtain:

$$K = \frac{\dfrac{A}{kd}}{\{[D]_t - \dfrac{A}{kd}\,(1 + \dfrac{1}{P})\}\{P\,[M]_t - \dfrac{A}{kd}\,(P + 1)\}} \qquad (12)$$

If the partition constant is high enough, we can approximate $(1 + \frac{1}{P}) = 1$.

III. APPLICATIVE PART

The method presented above is applied to the systems $[Au(CN)_2]^- -$ Astraviolett 3R[5] and $[Au\,(CN)_4]^- -$ Astraviolett 3R[6], where Astraviolett 3R is 1-methyl-2-(*p*-diethylaminostyrene)-3,3′-dimethylindole chloride.

The dyestuff was purified by recrystalization and its purity checked with the $TiCl_3$ method.[7] All other reagents were analytical purity grade.

The systems show no changes over a pH range between 3 and 10.

All determinations were carried out at pH = 6, obtained by mixing the neutral solutions of the reagents and at room temperature, 25°.

The molar absorbance of the compounds in benzene, at 528 nm, corresponding to the VG — 9 filter of a Lange Colorimeter, is $k = 4.6 \times 10^4$. The partition constants are P = 32 for Astra $[Au(CN)_2]$[5] and $P = 49$ for Astra $[Au(CN)_4]$.[6] The excess of dyestuff requested for the total shifting of the equilibria to the right is, for both systems, 100: 1.

[5] V. Armeanu and L. M. Băloiu, *Analyt. Chim. Acta,* **44,** 230 (1969).

[6] V. Armeanu, S. Oancea, S. Rusenescu and L. M. Băloiu, unpublished.

[7] H. E. Fierz-David and L. Blangey, "Grundlegende Operationen der Farbenchemie", Springer-Verlag, Wien, 1952, p. 384.

The Beer law was verified before the measurings in the organic solvent, proving that the dyestuff shows no association phenomena.

We started from solutions containing smaller amounts of dyestuffs than requested.

The values of the stability constants, calculated with the approximation $(1 + \frac{1}{P}) = 1$, are presented in Tables 1 and 2.

Table 1

Experimental data for the system $[Au(CN)_2]^-$ – Astraviolett 3R

A ($d = 1$cm) ($\lambda = 528$ nm)	$\frac{A}{kd} \times 10^6$	$[D]_{total} \times 10^4$	$[M]_{total} \times 10^6$	K
0.25	5.3	1	12.9	2.35×10^2
0.18	3.9	1	8.6	2.78×10^2
0.33	7.0	2	12.9	1.99×10^2
0.26	5.5	2	8.6	3.00×10^2
0.28	6.0	3	8.6	2.65×10^2
0.13	2.8	2	4.3	3.15×10^2
0.14	3.0	3	4.3	2.59×10^2
average value				2.64×10^2

The value $K = 2.64 \times 10^2$ obtained for the first system is very different from the value $K = 2 \times 10^5$ obtained[5] by a single-phase method.[8] In our opinion the value obtained with our method is supported by the large excess of dyestuff requested, as well as by the limited linearity of the plot absorbance *vs.* concentration.[5]

Table 2

Experimental data for the system $[Au(CN)_4]^-$ – Astraviolett 3R

A ($d = 1$ cm) ($\lambda = 528$ nm)	$\frac{A}{kd} \times 10^6$	$[D]_{total} \times 10^4$	$[M]_{total} \times 10^6$	K
0.305	6.5	0.5	15	3.55×10^2
0.445	9.45	1	15	3.99×10^2
0.31	6.6	1	10	4.40×10^2
0.215	4.6	1	7.5	3.70×10^2
0.39	8.3	4	10	2.81×10^2
average value				3.69×10^2

ACKNOWLEDGEMENT. The author is indebted to the Referee for useful observations and suggestions.

---

[8] A. K. Majumdar and C. P. Savariar, *Analyt. Chim. Acta*, **21**, 47 (1959).

Revue Roumaine de Chimie, 17, 6, 1065–1069 (1972)

Revue Roumaine de Chimie, 17, 6, 1071 – 1081 (1972)

LINEARISATION DER POTENTIOMETRISCHEN TITRATIONSKURVEN. I

FÄLLUNGSTITRATIONEN

J. ZSAKÓ und F. MAKKAY

Aus der Chemischen Fakultät der „Babeş-Bolyai"-Universität, str. Arany János 11, Cluj — und dem Zentralinstitut für Fortbildung der Lehrkader, Zweigstelle Cluj, str. Matei Corvin 4.

Eingegangen am 28. Juni 1971

Das Gransche Linearisationsverfahren wird untersucht und man schließt, daß es keine Vorzüge bietet, da es zur Bestimmung des Inflexionspunktes und nicht zu der des Äquivalenzpunktes führt. Das Liteanu-Mioşcu-Verfahren ergibt parabolische Kurven, da es auf einer nur als Grenzfall gültigen Hypothese begründet ist. Trotzdem erlauben die in der Nähe des Äquivalenzpunktes erhaltenen Kurven die quantitative Charakterisierung der Empfindlichkeit der potentiometrischen Titrationen.

In potentiometrischen Titrationen ist der Äquivalenzpunkt im allgemeinen durch Auftragung von E oder pH gegen das Volumen des zugefügten Reagens bestimmt, und zwar nimmt man die Gleichheit des Äquivalenzpunktes mit dem Inflexionspunkt der Titrationskurve an. Da diese zwei Punkte nicht immer identisch sind, wurden einige Linearisationsverfahren vorgeschlagen, die die Ermittlung des Äquivalenzpunktes als Intersektion von zwei Geraden erlaubt. Man nimmt an, daß diese Verfahren pünktlichere Ergebnisse gaben als jene, die auf der Bestimmung des Inflexionspunktes der Titrationskurve begründet sind. Alle diese Linearisationsverfahren sind auf vereinfachende Annahmen begründet, und manchmal erlauben diese Vereinfachungen die Erhöhung der Pünktlichkeit nicht. Um die Rechtmäßigkeit dieser Linearisationsverfahren zu erklären, haben wir das Verfahren von Gran[1] und jenes von Liteanu und Mioşcu, [2] im Fälle der Fällungstitrationen einer theoretischen Analyse unterworfen.

Gran betrachtet folgende Fällungsreaktion :

$$xA + yB = A_xB_y \tag{1}$$

Wenn man V_0 ml einer Lösung des Reagens A, von ursprünglicher Konzentration a, mit einer Lösung des Reagens B, der Konzentration b titriert, gibt Gran die Konzentration [A] vor dem Äquivalenzpunkt, nach der Zufügung von V ml Lösung des Reagens B, mit folgender Gleichung:

---

[1] G. Gran, *Acta Chem. Scand.*, 4, 559 (1950).

[2] C. Liteanu und M. Mioşcu, *Rev. Roumaine Chim.*, 13, 1185 (1968).

$$[A] = \frac{aV_0}{V_0 + V} - \frac{x}{y}\,\frac{bV}{V_0 + V} \tag{2}$$

Ähnlicherweise erhält man für die Konzentration $[B]$ folgenden Ausdruck:

$$[B] = \frac{L^{1/y}}{\left(\dfrac{aV_0}{V_0 + V} - \dfrac{x}{y}\,\dfrac{bV}{V_0 + V}\right)^{x/y}} \tag{3}$$

wo L das Löslichkeitsprodukt der Verbindung $A_x\,B_y$ ist:

$$L = [A]^x\,[B]^y \tag{4}$$

Wie aus Formel (2) leicht ersichtlich ist, nimmt Gran die praktisch vollständige Ausfällung des zugefügten Reagens B an.

Mit einer auf B reversibler Indikatorelektrode, kann man das Elektrodenpotential durch die Gleichung

$$E = e_0 + \frac{RT}{n_B F}\ln[B] = e_0 - \frac{x}{y}\,\frac{RT}{n_B F}\ln[A] \tag{5}$$

angeben. Aus Gleichungen (2) und (5) erhält Gran folgende Beziehung:

$$\frac{\mathrm{d}V}{\mathrm{d}E} = \frac{y}{x}\,\frac{n_B F}{RT}\,\frac{V_0 + V}{V_0 + V_e}\,(V_e - V) \tag{6}$$

wobei V im Äquivalenzpunkt

$$V_e = \frac{y}{x}\,\frac{aV_0}{b} \tag{7}$$

ist.

Nach dem Äquivalenzpunkt wird die Konzentration $[B]$ von der Gleichung

$$[B] = \frac{bV}{V_0 + V} - \frac{y}{x}\,\frac{aV_0}{V_0 + V} \tag{8}$$

gegeben. Mit Hilfe der Beziehung (5) erhält man

$$\frac{\mathrm{d}V}{\mathrm{d}E} = \frac{n_B F}{RT}\,(V - V_e)\,\frac{V_0 + V}{V_0 + V_e} \tag{9}$$

In der Nähe des Äquivalenzpunktes schlägt Gran vor die Gleichungen (6) und (9) mit Hilfe der folgenden Beziehungen zu approximieren :

$$\frac{\mathrm{d}V}{\mathrm{d}E} = \frac{y}{x}\frac{n_B F}{RT}(V_e - V) \text{ bzw. } \frac{\mathrm{d}V}{\mathrm{d}E} = \frac{n_B F}{RT}(V - V_e). \tag{10}$$

Um den Äquivalenzpunkt zu erhalten, muß man die Größe

$$y = \frac{1}{V_0 + V}\frac{RT}{n_B F}\frac{\mathrm{d}V}{\mathrm{d}E} \tag{11}$$

als Funktion von V graphisch darstellen, und die Intersektion der zwei erhaltenen Geraden ergibt den gesuchten Äquivalenzpunkt.

In Wirklichkeit fällt die vor dem Äquivalenzpunkt zugefügte B-Menge nicht vollständig aus, und Gleichungen (2) und (3) können die Konzentrationen, besonders in der Nähe des Äquivalenzpunktes, nicht richtig ergeben. Die von Gran vorgeschlagene Näherung gilt nur als Grenzfall für sehr schwerlösliche Verbindungen. Wir haben deswegen versucht, die genaue Funktion $\mathrm{d}V/\mathrm{d}E = \mathrm{f}(V)$ zu erhalten. Diese Funktion erhält man leicht, wenn $n_A = n_B = n$, das heißt $x = y = 1$. In diesem Falle wird das Löslichkeitsprodukt die Form

$$L = [A]\ [B] \tag{12}$$

haben. Während der Titration sind folgende Beziehungen weiter gültig :

$$[A] = \frac{aV_0 - [AB]}{V + V_0} \text{ und } [B] = \frac{bV - [AB]}{V + V_0} \tag{13}$$

wo $[AB]$ die Menge des ausgefällten Produktes AB bedeutet. Wenn das Volumen V_e des zugefügten Reagens B für das Erreichen des Äquivalenzpunktes nötig ist, so gilt auch die Beziehung :

$$V_e = \frac{aV_0}{b.}\,. \tag{14}$$

Die Gleichung der Titrationskurve erhält man für auf B reversible Elektrode, die Gleichungen (12) und (13) berücksichtigend, in folgender Form :

$$E = e_0 + \frac{RT}{nF}\ln[B] =$$

$$= e_0 + \frac{RT}{nF}\ln\frac{-(bV - aV_0) + \sqrt{(bV - aV_0)^2 + 4L(V + V_0)^2}}{2(V + V_0)} \tag{15}$$

Für dem Äquivalenzpunkt gibt Gleichung (15) folgenden Ausdruck

$$E(V_e) = e_0 + \frac{RT}{nF} \ln \sqrt{L} \tag{16}$$

Durch Ableitung der Gleichung (15) erhält man, auch die Gleichung (14) berücksichtigend

$$y = \frac{1}{V_0 + V} \frac{RT}{nF} \frac{\mathrm{d}V}{\mathrm{d}E} = \frac{1}{V_0 + V_e} \sqrt{(V - V_e)^2 + \frac{4L}{b^2} (V_0 + V)^2} \tag{17}$$

Im Grenzfall, für $L \to 0$, folgen aus Gleichung (17) die Beziehungen:

$$\lim_{L \to 0} y = \frac{V - V_e}{V_0 + V_e} \text{ wenn } V < V_e \text{ und}$$

$$\lim_{L \to 0} y = \frac{V_e - V}{V_0 + V_e} \text{ wenn } V > V_e, \tag{18}$$

die identisch mit den von Gran gegebenen sind. Die Intersektion der zwei Geraden erfolgt bei $V = V_e$ und $y(V_e) = 0$. Anderseits gibt die Gleichung (17) für $V = V_e$ den Wert

$$y\ (V_e) = \frac{2\sqrt{L}}{b} \tag{19}$$

Wenn die Verbindung sehr schwerlöslich ist, ist die Abweichung der Funktion $y = f(V)$ von der Linearität wirklich sehr klein. In der Nähe des Äquivalenzpunktes sind aber die Gleichungen (10) nicht gültig. Eine Reihenentwicklung der Gleichung (17) gibt in der Nachbarschaft des Äquivalenzpunktes eine lineare Beziehung, die aber von (10) verschieden ist, nämlich:

$$y = \frac{2\sqrt{L}}{b} \left(1 + \frac{V_e - V}{V_0 + V_e}\right) \text{ für } V < V_e \text{ bzw.}$$

$$y = \frac{2\sqrt{L}}{b} \left(1 + \frac{V - V_e}{V_0 + V_e}\right) \text{ für } V > V_e \tag{20}$$

Wenn die Indikatorelektrode auf A reversibel ist, wird das Elektrodenpotential durch folgende Gleichung gegeben :

$$E = e_0 + \frac{RT}{nF} \ln [A] =$$

$$= e_0 + \frac{RT}{nF} \ln \frac{aV_0 - bV + \sqrt{(aV_0 - bV)^2 + 4L(V + V_0)^2}}{2(V + V_0)} \tag{21}$$

Anstatt der Gleichung (17) erhält man

$$y = -\frac{1}{V_0 + V_e} \sqrt{(V_e - V)^2 + \frac{4L}{b^2}(V + V_0)^2} \tag{22}$$

welche für den Grenzfall $L \to 0$ folgende Beziehung gibt :

$$\lim_{L \to 0} y = \frac{V - V_e}{V_0 + V_e} \text{ für } V < V_e \text{ bzw. } \lim_{L \to 0} y = \frac{V_e - V}{V_0 + V_e} \text{ für } V > V_e \tag{23}$$

Den Inflexionspunkt kann man aus Gleichung (15) oder (21) durch zweifache Ableitung erhalten :

$$V_i = V_0 \frac{3ab - b^2 - 16L + (a + b)\sqrt{b^2 - 32L}}{4(4L + b^2)} \tag{24}$$

Wie aus Gleichung (24) ersichtlich, ist der Inflexionspunkt nicht mit dem Äquivalenzpunkt identisch ; aber die Abweichung ist in praktischen Fällen vernachlässigbar klein ; denn

$$\lim_{L \to 0} V_i = V_0 \frac{a}{b} = V_e \tag{25}$$

und wenn L sehr klein ist (wie im Falle aller Fällungstitrationen), führt die Reihenentwicklung der Quadratwurzel zu folgendem Ausdruck :

$$V_i = V_e - 8L \frac{a + b}{b\,(b^2 + 4L)} \tag{26}$$

Um die Verwendungsgrenze des Granschen Linearisationsverfahrens zu erklären, haben wir die Funktion $y = f(V)$ auf Grund der Gleichung (17), für verschiedene hypothetische Fälle ausgerechnet. Einige Beispiele sind in Abb. 1 aufgetragen.

Wie aus Abbildung 1 ersichtlich, gibt das Gransche Verfahren eine gute Linearisation in 10^{-2}M Lösungen, nur wenn $L \leqslant 10^{-8}$ ist. Im Falle löslicherer Fällungen ist eine Linearisation unmöglich. Sogar für $L = 10^{-8}$ kann man die experimentellen Punkte, nur wenn $V < 0{,}9\ V_e$ oder $V > 1{,}1\ V_e$, für die Linearisation benutzen.

Die Gleichungen der zwei Geraden wurden mit Hilfe der kleinsten Quadrate aus den berechneten y-Werten erhalten und die Intersektion dieser Geraden auf analytischem Wege ermittelt. Die so erhaltenen

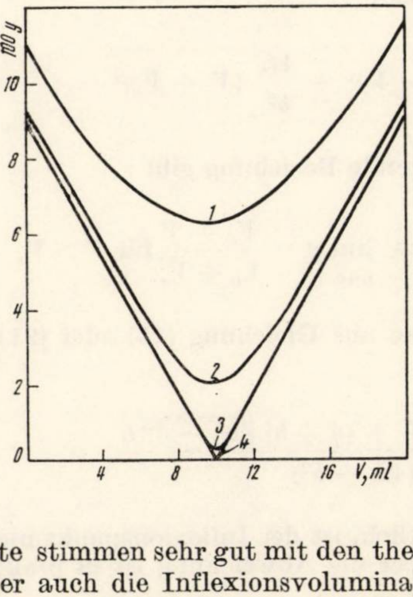

Abb. 1. — Gransche Linearisation für $a = 10^{-2}$ M, $b = 10^{-1}$ M, $V_0 = 100$ ml.
1. $L = 10^{-5}$; 2. $L = 10^{-6}$; 3. $L = 10^{-8}$; 4. $L = 10^{-10}, 10^{-12}, 10^{-14}$...

V_e-Werte stimmen sehr gut mit den theoretischen überein. In diesen Fällen sind aber auch die Inflexionsvolumina praktisch mit V_e gleich, wie aus Tabelle 1 ersichtlich ist. Die Bestimmung der Inflexionsvolumina gibt also ebenso gute Ergebnisse wie das Gransche Linearisationsverfahren.

Tabelle 1

Inflexionsvolumina für $a = 10^{-2}$ M; $b = 10^{-1}$ M; $V_0 = 100$ ml

L	V_i, ml
10^{-8}	9,99912
10^{-10}	9,9999912
10^{-12}	9,999999912
10^{-14}	9,99999999912

Da die graphische Ermittlung von $\mathrm{d}V/\mathrm{d}E$ aus der Neigung der Tangente der Titrationskurve einige Schwierigkeiten darstellt, hat Gran die Benützung des Quotienten $\Delta V / \Delta E$ vorgeschlagen. Wenn der Anfangs-punkt des Intervalles ΔV dem Volumen V entspricht, wird die Abgeleitete $\mathrm{d}V/\mathrm{d}E$ denselben Wert wie $\Delta V/\Delta E$, im Punkte

$$V_c = V + c\frac{1}{2}\ \Delta V \tag{27}$$

haben. Gran behauptet, daß der Koeffizient c eine eindeutige Funktion des Quotienten $\Delta V/(V_e - V)$ sei, und gibt sogar eine Tabelle mit c-Werten als Funktion von $\Delta V/(V_e - V)$, ohne die Herkunft dieser Angaben zu erwähnen. Um die Richtigkeit dieser Tabelle zu prüfen, haben wir theoretische Titrationskurven für verschiedene L-Werte mit Hilfe der Gleichung (15) konstruiert und eine große Zahl von $\Delta V/\Delta E$-Werten bestimmt. In jedem Falle haben wir auf Grund der Gleichung (17) den V-Wert ermittelt, für welchen die Ableitung $\mathrm{d}V/\mathrm{d}E$ denselben Wert hat. Dieses Verfahren erlaubte uns, den Koeffizienten c aus Gleichung (27) zu erhalten. Diese Koeffizienten sind für zwei $\Delta V/(V_e - V)$-Werte vor dem Äquivalenzpunkt, für verschiedene Löslichkeitsprodukte und zugefügte Volumina V in der Tabelle 2 zusammengestellt. Der von Gran gegebene Wert ist $c = 1,1146$ für $\Delta V/(V_e - V) = 0,5$.

Tabelle 2

Koeffizienten c aus Gl. (27) für $a = 10^{-2}$ M; $b = 10^{-1}$ M; V_0 = 100ml

V	$\Delta V/(V_e - V) = 0,5$				$\Delta V/(V_e - V) = 1$			
	L				L			
	10^{-6}	10^{-8}	10^{-10}	10^{-12}	10^{-6}	10^{-8}	10^{-10}	10^{-12}
2	1,060	1,055	1,055	1,053	1,100	1,508	1,675	1,758
6	0,920	1,075	1,088	1,084	0,950	1,450	1,650	1,750
8	0,900	1,066	1,102	1,102	0,900	1,380	1,600	1,720
9,2	0,820	1,050	1,110	1,111	0,800	1,250	1,525	1,700
9,6	0,450	0,950	1,106	1,115	0,500	1,050	1,450	1,700
9,8	–	0,900	1,078	1,115	–	0,980	1,300	1,700

Wie aus Tabelle 2 ersichtlich, hängen die c-Werte von L und V ab. Den von Gran gegebenen Wert erhält man als Grenzfall für sehr schwerlösliche Fällungen und meistens in der Nähe des Äquivalenzpunktes. Die Benutzung der Granschen Koeffizienten c erlaubt die Verbesserung der Ergebnisse nur im Falle sehr schwerlöslicher Verbindungen ; ein andermal kann die gewöhnliche Näherung $c = 1$ sogar bessere Ergebnisse liefern.

Im Falle asymmetrischer Titrationen, wenn $n_A \neq n_B$, d.h. $x \neq y$, kann man die genaue Gleichung der Titrationskurve in expliziter Form nicht angeben, es ist aber möglich diese Kurve graphisch zu konstruieren. Als Beispiel geben wir hier die Titrationskurven und ihre Linearisation nach dem Granschen Verfahren im Falle der Fällungsreaktionen von Type

$$A + 2B = AB_2 \tag{28}$$

Anstatt der Gleichungen (12), (13) und (14) haben wir folgende Beziehungen zur Verfügung:

$$L = [A]\,[B]^2 \tag{29}$$

$$[A] = \frac{aV_0 - [AB_2]}{V_0 + V} \text{ bzw. } [B] = \frac{bV - 2\,[AB_2]}{V_0 + V} \tag{30}$$

$$V_e = \frac{2aV_0}{b} \tag{31}$$

Aus den Gleichungen (29) und (30) erhält man durch Ausschließen von $[A]$ und $[AB_2]$ folgende Gleichung:

$$V = V_0 \frac{[B]^3 + 2a[B]^2 - 2L}{-[B]^3 + b[B]^2 + 2L} \tag{32}$$

welche die Ermittlung von V für verschiedene $[B]$-Werte und so die Auftragung der Titrationskurve, der Gleichung (15) entsprechend, erlaubt. Eine so erhaltene Titrationskurve ist in Abb. 2 dargestellt. Ihre Linearisation nach dem Granschen Verfahren ist in derselben Abbildung gegeben.

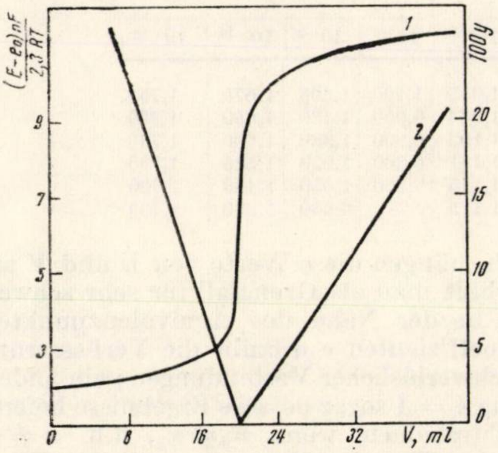

Abb. 2. — Asymmetrische Titration der Type (28), für $a = 10^{-2}$ M, $b = 10^{-1}$M, $V_0 = 100$ ml, $L = 10^{-15}$.

1 – potentiometrische Titrationskurve; 2 – Gransche Linearisation.

Die Linearisation ist gut und erlaubt die Bestimmung des Äquivalenzpunktes nach dem Granschen Verfahren. Die Gleichungen der Geraden nach der Methode des kleinsten Quadrates berechnend, erhält man $V_e = 20{,}020$ ml, weil der theoretische Wert $V_e = 20{,}000$ ml ist. Der auf graphischem Wege bestimmte Inflexionspunkt ist $V_i = 20{,}022$ ml. Dieses Ergebnis zeigt, daß das Gransche Linearisationsverfahren bei asymmetrischen Titrationen den Inflexionspunkt gibt und nicht den Äquivalenzpunkt, wie angenommen.

Die von Liteanu und Mioşcu vorgeschlagene Linearisation ist auf die Behauptung von Gran begründet, betreffend die Eindeutigkeit der Funktion, die die Abhängigkeit des Koeffizienten c aus Gleichung (27) von $\Delta V/(V_e - V)$ ausdrückt. Wie oben gezeigt (Tab. 2), ist Koeffizient c keine eindeutige Funktion des Quotienten $\Delta V/(V_e - V)$, und so kann das Liteanu-Mioşcu-Verfahren keine Gerade liefern. Die obenerwähnten Autoren schlagen die Auftragung von $|V_i - V| \,/\, |E_i - E|$ gegen V vor, wo V_i und E_i die entsprechenden Größen bei dem Inflexionspunkt der Titrationskurve bedeuten. Einige theoretische Titrationskurven, nach dem Liteanu-Mioşcu-Verfahren „linearisiert'', sind in Abb. 3 gegeben.

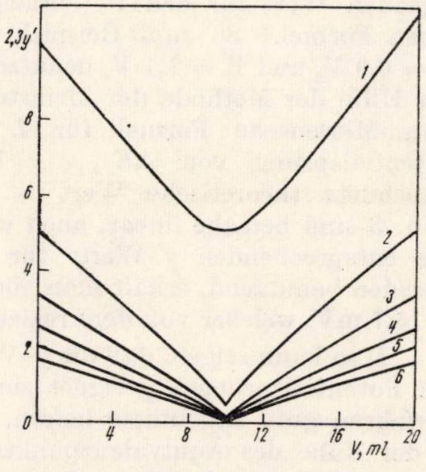

Abb. 3. — Die Liteanu-Mioşcu-Linearisation für $a = 10^{-2}$ M, $b = 10^{-1}$ M, $V_0 = 100$ ml.
1, L = 10^{-6}; 2, L = 10^{-8}; 3, L = 10^{-10}; 4, L = 10^{-12}; 5, L = 10^{-14}; 6, L = 10^{-16}.

Es ist leicht ersichtlich, daß man anstatt Geraden immer parabolische Kurven erhält. Das ist gar nicht überraschend, da aus den Gleichungen (15) und (16), $V_e = V_i$ annehmend, die Beziehung

$$y' = \frac{RT}{nF} \frac{|V_i - V|}{|E_i - E|} =$$

$$= \frac{|V_e - V|}{\ln\sqrt{L}\ \ln - \dfrac{bV - aV_0 + \sqrt{(bV - aV_0)^2 + 4L(V + V_0)^2}}{2(V + V_0)}} \tag{33}$$

erhält. Im Äquivalenzpunkt wird die Größe y' beinahe Null sein. Mit Hilfe der L'Hospitalschen Regel erhält man den Wert

$$\lim_{L \to 0} y' = 2\sqrt{L}\,\frac{V_0 + V_e}{b} \tag{34}$$

welcher im Falle schwerlöslicher Verbindungen praktisch Null ist.

Es ist offenbar, daß y' keine lineare Funktion von V ist. Also kann die von Liteanu und Mioşcu vorgeschlagene Linearisation und hauptsächlich die Verwendung der Statistik der Geraden auf die ganze Kurve keine wertvolle Information liefern.

Die obenerwähnten Autoren haben das bei ihnen vorgeschlagene Verfahren zur Charakterisierung des Potentialsprunges in der Nähe des Äquivalenzpunktes gebraucht. Wie aus Abb. 3 ersichtlich ist, ändert sich die Größe y' in der Nähe des Äquivalenzpunktes beinahe linear. Wenn wir nur diese lineare Portion benutzen, erhalten wir einen befriedigenden Wert für den Potentialsprung mit Hilfe der Liteanu-Mioşcuschen Formel.[2] So zum Beispiel, wenn wir nur die y'-Werte zwischen $V = 0{,}9\ V_e$ und $V = 1{,}1\ V_e$ benutzen und die Parameter der zwei Geraden mit Hilfe der Methode der kleinsten Quadrate berechnen, ergibt die Liteanu-Mioşcusche Formel für $L = 10^{-10}$, $a = 10^{-2}$, $b = 10^{-1}$, einen Potentialsprung von $\Delta E_{\pm 1\%} = 102{,}2$ mV. Der mit der Formel (15) berechnete theoretische Wert ist $\Delta E_{\pm 1\%} = 113{,}7$ mV. Die Kurven in Abb. 3 sind beinahe linear, auch wenn $V < 0{,}6\ V_e$, bzw. $V > 1{,}4\ V_e$ ist. Die entsprechenden y'-Werte für die Bestimmung der Parameter der Geraden benutzend, erhält man aber einen Potentialsprung von $\Delta E_{\pm 1\%} = 15{,}7$ mV, welcher von dem realen Wert ganz verschieden ist.

Man kann zeigen, daß die y'-Werte wirklich für die Charakterisierung des Potentialsprunges geeignet sind, und so kann das Liteanu-Mioşcu-Verfahren gute Ergebnisse liefern, aber nur dann, wenn nur die Punkte in der Nähe des Äquivalenzpunktes in Betracht gezogen sind. Auch in diesem Falle würde eine Näherung der y'-V-Kurven mit Hilfe von Polynomen zweiter Ordnung bessere Ergebnisse liefern. Mit dieser Bedingung könnte der vorgeschlagene $\Delta E_{\pm e}$-Wert die Empfindlichkeit der entsprechenden potentiometrischen Titrationen wirklich gut charakterisieren.

Um die obenerwähnten Schlußfolgerungen auf Experimentaldaten zu prüfen, haben wir einige potentiometrische Titrationen ausgeführt. Als Beispiel ist auf Abb. 4 die Titrationskurve von 100 ml 10^{-2} M NaCl mit 10^{-1} M $AgNO_3$ gegeben. Auf dieselbe Abbildung ist auch die nach Liteanu und Mioşcu linearisierte y'-V-Kurve aufgetragen. Wie aus dieser Abbildung ersichtlich, hat die Kurve y'-V dasselbe parabolische Aussehen wie die theoretischen Kurven auf Abb. 3. Im Falle der von Liteanu und Mioşcu gegebenen Titrationskurven[2] ergeben die experimentellen Punkte ebenfalls parabolische Kurven, aber dieser Charakter der Kurven war von den Autoren nicht berücksichtigt. In der Nachbarschaft des Äquivalenzpunktes sind die y'-V-Kurven beinahe linear, mit Ausnahme der unmittelbaren Nachbarschaft des Äquivalenzpunktes, wo die obenerwähnten Autoren zu wenig experimentelle Punkte aufgenommen haben, um den parabolischen Charakter der Kurven zu erkennen. Obgleich die Benützung der Statistik der Geraden als erste Näherung ganz berechtigt

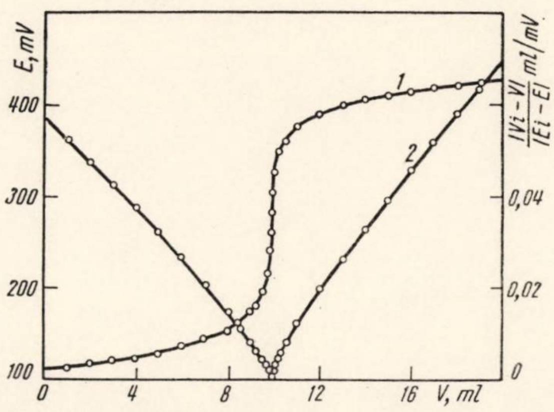

Abb. 4. — Experimentelle potentiometrische Titration von HCl mit $AgNO_3 \cdot a = 10^{-2}$ M, $b = 10^{-1}$M, $V_0 = 100$ ml.

1, potentiometrische Titrationskurve; *2*, Liteanu-Mioşcu Linearisation.

ist, verursacht sie einen gewissen Fehler in der Ausrechnung des Potentialsprunges. Durch die Benützung von Polynomen zweiter Ordnung kann man diesen Fehler leicht vermeiden.

Revue Roumaine de Chimie, 17, 6, 1083–1086 (1972)

THE DETERMINATION OF OSMIUM AS $[Os(thio)_6][Cr(NH_3)_2(NCS)_4]_3$

D. NEGOIU and ZAMFIRA TOMA

Faculty of Chemistry, University of Bucharest Splaiul Independenţei 89
and
Center of Chemical Physics, Dumbrava Roşie 23
Bucharest, Romania

Received December 31, 1971

The present paper deals with the chemical characterization, thermogravimetric data and the X-ray diffraction spectra of the osmium complex formed from the reaction of osmium chloride with thiourea and the Reinecke salt. A new gravimetric method for the direct determination of osmium is proposed.

INTRODUCTION

It is well known that very few gravimetric methods by direct weighing are reported in the literature for the osmium ion.[1-8] Beamish[9-10] in two critical studies concerning the analytical gravimetric methods applied to the platinic metals, showed that, at least in the case of osmium, the reported methods lead to poorer results, probably caused by the incomplete precipitation or by the presence of non-unitary products in the chemical reactions of osmium.

The aim of this note is to characterize some properties of the complex formed by osmium in hydrochloric solutions with a Reinecke salt (ammonium-tetrarhodanide-diammino-chromate (III)) in the presence of thiourea, in order to apply the above reaction to analytical purposes for the quantitative determination of osmium by direct weighing.

---

[1] S. C. Ogburn and L. F. Miller, *J. Amer. Chem. Soc.*, **52**, 42 (1930).

[2] I. Hoffman, J. E. Schweitzer, D. E. Ryan and F. E. Beamish, *Analyt. Chem.*, **25**, 1091 (1953).

[3] R. F. Wilson and L. J. Baye, *Talanta*, **1**, 351 (1958).

[4] P. Spacu and C. Gheorghiu, *Z. analyt. Chem.*, **174**, 341 (1960).

[5] R. Neeb, *Z. analyt. Chem.*, **177**, 20 (1960).

[6] A. I. Busev and V. K. Akimov, *Vestnik. Mosk. Univ. Ser. II, Khim.*, **18**, 43 (1963) from 10.

[7] A. I. Busev and V. K. Akimov, *Talanta*, **11**, 1657 (1964).

[8] Achim Mueller, E. Diemann and F. Bollmann, *Naturwiss.*, **55**, 443 (1968).

[9] F. E. Beamish, *Talanta*, **1**, 3 (1958).

[10] F. E. Beamish, *Talanta*, **13**, 773 (1966).

EXPERIMENTAL

As it has been earlier reported, osmium in hydrochloric solutions forms with thiourea and the Reinecke salt the following compound [11]: $[Os(thio)_6]$ $[Cr(NH_3)_2(NCS)_4]_3$.

The above complex has been obtained using the preparation method of the cited authors. The elemental analyses given: C% contained 13.49, found 13.45, N% contained 26.23, found 26.32, S% contained 36.02, found 35.92, Cr% contained 9.73, found 9.43, Os% contained 11.87, found 11.66, confirmed the above chemical formulation.

The formation of the complex $[Os(thio)_6]$ $[Cr(NH_3)_2(NCS)_4]_3$ is also confirmed by the X-ray diffraction spectra obtained using the Debye-Scherrer powder method on a TUR M–60 equipment.

Its thermal stability and decomposition, function of temperature, were followed on a Stanton balance, Model HT.

RESULTS AND DISCUSSION

The visual examination of the debyegrams showed that the diffraction lines of the final product were different from those corresponding to the initial reacting substances. They are numerous, grouped towards smaller θ angles which would indicate a lower symmetry for the unit cell.

The thermogravimetric study showed that up to 125° no chemical changes occurred, this fact being suitable for a drying of this compound without losses in its weight.

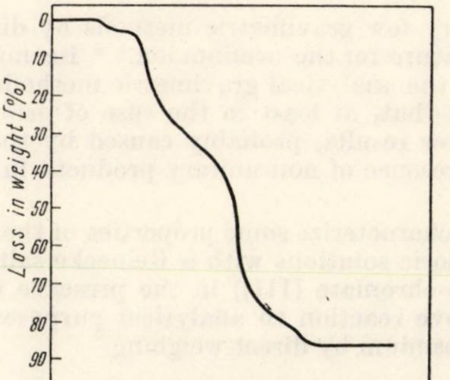

Fig. 1. — TG curve for $[Os(thio)_6][Cr(NH_3)_2(NCS)_4]_3$ in air.

In the range of 125°–200° the thermogravimetric curves showed a slight loss of weight. The changes occurring between 200°–670° cannot be cleared up and assigned to well defined intermediate steps of decomposition; it should be however emphasized that beyond 670° the system

[11] P. Spacu, C. Gheorghiu and L. Zubov, *Studii si Cercetări Chim. Acad. R.S. Romania*, **9**, 493 (1961).

becomes stable, as may be observed with the thermogravimetric curves plotted in figure 1. As shown by X-ray analysis, the oxide Cr_2O_3 (13.6 % found, 14.2 % calcd.) is the single component of the residue (Joint Committee on Powder Diffraction Standards, JCPDS, 6–504).

The good thermal stability up to 105° and the high molecular weight of the complex $[Os(thio)_6][Cr(NH_3)_2(NCS)_4]_3$, stable in acid solutions, practically insoluble in cooled water, make the mentioned compound suitable for the microgravimetric determination of osmium.

The proposed method should be performed as follows :

Samples containing OsO_4 obtained by distillation in hydrochloric acid are treated with an aqueous solution of 10 % thiourea. After 15–20 min the solution, cooled on ice, is precipitated by a fresh solution containing 2.4 % Reinecke salt. The crystalline precipitate thus obtained is filtered in a microcrucible type A_1 or A_2 and then washed by water cooled on ice, and finally dried at 105°.

Table 1

Gravimetric determination of osmium as the complex compound $[Os(thio)_6][Cr(NH_3)_2(NCS)_4]_3$

mg Osmium analysed	mg Osmium found	Difference mg	Error %
0.207	0.209	+0.002	+0.96
0.444	0.437	−0.007	−1.57
	0.443	−0.001	−0.23
0.637	0.635	−0.002	−0.30
	0.621	−0.016	−2.51
0.870	0.857	−0.013	−1.50
0.888	0.891	+0.003	+0.33
	0.883	−0.005	−0.54
1.155	1.147	−0.008	−0.69
	1.144	−0.011	−0.95
1.189	1.192	+0.003	+0.25
	1.203	+0.014	+1.17
1.325	1.317	−0.008	−0.60
	1.341	+0.016	+1.20
1.525	1.493	−0.032	−2.09
	1.496	−0.029	−1.90
1.612	1.616	+0.004	+0.24
1.787	1.746	−0.041	−2.29
	1.755	−0.032	−1.79
1.830	1.831	+0.001	+0.05
	1.808	−0.022	−1.20
2.177	2.173	−0.004	−0.18
2.350	2.364	+0.014	+0.60
2.740	2.730	−0.010	−0.40
3.240	3.250	+0.010	+0.30
	3.225	−0.015	−0.46

The converting factor for osmium was $F = 0.1187$.

The analytical data are summarized in the table 1.

As may be seen from table 1, the results are satisfactory, the error being of ±2.5 %.

It should be mentioned that the results obtained were influenced by the acidity of the solution, the working procedure and the temperature at which the precipitating reaction was performed. Good results have been obtained using ~4M hydrochloric solutions of osmium, stirring continuously during the reaction, in order to get a crystalline precipitate easily filtered, and maintaining a low temperature of the precipitate in the course of its handling.

Revue Roumaine de Chimie, 17, 6 1087–1113 (1972)

ELECTROCHEMICAL BEHAVIOUR OF ISONICOTINIC ACID IN AQUEOUS SOLUTION

LUIGI CAMPANELLA and GIORGIO DE ANGELIS

Institute of Analytical Chemistry of the University, Rome, Italy
Italian C.N.R., Rome, Italy

Received November 9, 1971

The polarographic, oscillopolarographic and chronopotentiometric behaviour of isonicotinic acid was studied in aqueous media, at 25.0±0.5°. Three polarographic waves and the corresponding oscillopolarographic peaks were evidenced. By their analysis (existence field, influence of concentration, pH and addition of surface active agents on the characteriatic values of potential and current) it can be concluded that they are ascribed to the hydrogen discharge catalysed by the cationic protonated species. The variation of $E_{1/2}$ of the first wave with pH gives the possibility of determining the dissociation constants of the acid. The Ilkovich and Randles-Sevcik equations, ensuring the proportionality between current and concentration and giving thus the possibility of quantitatively determining the studied compound by the polarographic techniques, are followed.

The reduction at the mercury dropping electrode of pyridine-mono and di-carboxylic acids can concern the heterocyclic ring[1-3] or its substituents.(1,4) The reduction of the ring is generally observed in the case of nitrogen heterocyclic compounds not containing carboxylic groups yielding dihydroderivatives. Volke (1) has considered this mechanism as the most, probable also in the case of the reduction of cichomeronic, quinolinic and pyridine-2,3,5,5 tetracarboxylic acids, for which the author has not excluded the reduction of the carboxylic groups too, similarly to what was observed by Sorm (2,3) for picolinic and isonicotinic acids and by Volke and Volkova[5] for nicotinic acid.

Moreover the voltammetric behaviour of heterocyclic compounds containing an N atom in their molecule is quite complicated because in addition to normal waves and peaks these compounds can yield also catalytic ones, generally ascribed to the hydrogen discharge. The shape and the height of these waves and peaks are largely varying according to

---

[1] J. Volke, *Coll. Czech. Chem. Comm.*, **22**, 1777 (1957).
[2] F. Sorm, *Chem. Listy*, **37**, 112 (1943).
[3] F. Sorm, *Chem. Obzor*, **17**, 213 (1943).
[4] J. Volke and V. Volkova, *Coll. Czech. Chem. Comm.*, **20**, 908 (1955).
[5] J. Volke and V. Volkova, *Coll. Czech. Chem. Comm.*, **20**, 1332 (1955).

the experimental conditions, particularly those referring to pH, ionic strength, concentration, potential scanning rate, presence and nature of the buffer system.

A research is being performed in our laboratory on the electrochemical behaviour of pyridine carboxylic acids,[6-8] with the aim of getting useful information about the equilibria in solution among the species of the acids and the electrochemical activity of some of these species in comparison with others.

Here we refer to the results concerning isonicotinic (or γ-pyridinecarboxylic) acid. The study was performed by the polarographic, oscillopolarographic, chronopotentiometric, spectrophotometric and electrocapillary measurements. The electrochemical behaviour of isonicotinic acid was already studied by several researchers (8-16) but it can be said that the available results do not always agree and appear randomly distributed for different values of pH and ionic strength, somehow incomplete as to the width of the pH and ionic strength ranges, the correct consideration of all the species of acids and the necessary pointing out of the different waves and peaks. From the general analysis of the published results it can be inferred that isonicotinic acid is reducible in a large range of pH (1—12) yielding only one wave with half wave potentil $E_{1/2}$ increasing from about -0.8 V to about -1.4 V (vs SCE) as pH increases. Some kinetic and catalytic character was assigned to this wave. The Ilkovich equation is obeyed in very particular conditions and in a narrow range of concentration ($10^{-4}-10^{-3}$ M). The reduction is attributed either to the carboxylic group that is thus transformed into an aldheydic one or to the ring that is partially hydrogenated.[17]

We thought of particular interest on the one hand to try to get more consistent and complete information and on the other hand to investigate the influence of the experimental conditions on the electrochemical results.

EXPERIMENTAL

MATERIALS

Isonicotinic acid supplied by Carlo Erba was purified by recrystallization from water and controlled by melting point determination [18] and by potentiometric titration.

---

[6] L. Campanella and G. De Angelis, *Rev. Roumaine Chim.*, **16**, 545 (1971).

[7] L. Campanella and G. De Angelis, to, be presented at the IUPAC International Congress on Analytical Chemistry, Kyoto 3—7 April, 1972.

[8] L. Campanella, E. Chiacchierini and M. Palchetti, *Rev. Roumaine Chim.*, in press.

[9] P. C. Tompkins and C. L. A. Schmidt, *Pub. Physiol.*, **8**, 229 (1944).

[10] P. C. Tompkins and C. L. A. Schmidt, *J. Biol. Chem.*, **143**, 643 (1942).

[11] M. Murayama, *J. Pharm. Soc. Japan*, **72**, 1213 (1952).

[12] H. H. G. Jellinek and J. R. Urwin, *J. Phys. Chem.*, **58**, 168 (1954).

[13] J. Volke and V. Volkova, *Chem. Listy*, **49**, 490 (1955).

[14] Y. Nagata and I. Tachi, *Bull. Chem. Soc. Japan*, **27**, 290 (1954).

[15] H. Lund, *Acta Chem. Scand.*, **17**, 272 (1963).

[16] A. G. Pozdeeva and E. G. Novikan, *Zhur. priklad. Khim.*, **40**, 213 (1967).

[17] F. Sorm, *Coll. Czech. Chem. Comm.*, **12**, 407 (1947).

[18] E. P. Oliveto, "Pyridine and its derivatives", part 3, E. Kingsborg, New York, 1962.

The study was carried out at 25.0±0.5° in aqueous solutions, whose free acidity was varied from very high values (~2M $HClO_4$) up to pH 10, with $NaClO_4$0.5 M as supporting electrolyte and citric buffer as buffering agent. For the experiments at high acidity the ionic strength was buffered at 2.0 M with $NaClO_4$ and $HClO_4$. The solutions were prepared by dissolving in distilled water weighed amounts of isonicotinic acid (dried at 115°) in order to have concentration of about 10^{-3} M. The known equilibrium constants for proton transfer reactions in water of the isonicotinic acid are reported in table 1. As surface active agent Merck gelatin was used. All chemicals used were analytically pure.

Table 1

Successive apparent equilibrium constants of proton transfer reactions in water: $H_2PC^+ + H_2O \rightleftarrows + HPC + H_3O^+$ (1); $HPC + H_2O \rightleftarrows PC^- + H_3O^+$ (2)

pK_{a_1}	pK_{a_2}	Reference	Method
1.88 ± 0.03	4.76±0.03	19	spectrophotometry
1.79 ± 0.02	4.78±0.02	19	spectrophoyometry
1.84 ± 0.04	4.78±0.01	19	spectrophotometry
1.70	4.95	20	spectrophotometry
2.3	4.5	21	potentiometry
1.92	4.68	22	spectrophotometry
1.84	4.86	23	spectrophotometry
1.70	4.89	24	potentiometry

APPARATUS AND PROCEDURE

AMEL (Milan, Italy) polarograph (mod. 461) with pen recording and with a dropping mercury electrode having at open circuit the following characteristics $m = 0.865$ mg sec^{-1}, $t = 3.00$ sec (obtained by a hammer), $r = 0.050$ mm.

Saturated calomel electrode (SCE) was always employed as reference electrode connected to the measurement cell by means of an agar KNO_3 conductivity bridge. Oscillopolarograph AMEL mod 448, dropping time 8 sec, waiting time 6 sec, measurement time 2 sec. pH meter Electroscan Bechman 30 equipped with usual electrodes and agar KNO_3 bridges.

The scanning rate of the potential in the polarographic experiments was 0.2 V/min, in the oscillopolarographic ones it was varied in the range 0.25 V/sec—25.0 V/sec; if not otherwise stated must be considered as 1.0 V/sec.

Chronopotentiometry was performed by means of Electroscan and a stationary working electrode formed by a Hg drop of volume 4 μl (surface = 0.12 cm^2). The solution for the polarographic analysis were deaerated by N_2 and deoxygenated. AMEL Corrograph mod. 561. Spectrophotometer Beckman DU. Spectrophotometer IR Perkin Elmer Infracord. All the reported results are at least the mean of five values. The $E_{1/2}$ values agreed within 2 mV (ohmic drop due to resistance of the cell circuit taken into the proper count, if due).

[19] R. E. Evans, E. F. G. Herington and W. Kynaston, *Trans. Faradaig. Soc.*, **49**, 1284 (1953).

[20] H. H. G. Jellinek and J. R. Urwin, *J. Phys. Chem.*, **58**,548 (1958).

[21] H. H. Jaffè, *J. Amer. Chem. Soc.*, **77**, 4445 (1955).

[22] H. P. Stephenson and H. Sponer, *J. Amer. Chem. Soc.*, **79**, 2050 (1957).

[23] R. W. Green and H. V. Tong, *J. Amer. Chem. Soc.*, **78**, 4896 (1956).

[24] P. O. Lumme, *Suomen khem.*, **30B**, 168 (1957).

RESULTS

POLAROGRAPHIC MEASUREMENTS

1) Behaviour in solution at $\mu = 0.5$ M and pH $= 1.00 - 11.00$

The polarographic curves recorded for solutions of isonicotinic acid buffered with citric buffer 0.02 M yield reduction waves at the dropping mercury electrode in a large range of pH (fig. 1), only at pH > 8 not being evidenced any polarographic step in the explored potential interval. Three waves can be observed. The first, with the most positive $E_{1/2}$, is present in the whole range where the acid is polarographically active. The height of this wave is constant within $\pm 5\,\%$ in the pH range $2.5 - 5.5$, decreases for pH 5.5 and it is always proportional to the concentration of the acid in the range $10^{-4} - 10^{-3}$ M (fig. 2,3); its $E_{1/2}$ is a linear function of pH with two break points at pH 1.4 and 4.3 (fig. 4); the resulting three slopes $\Delta E_{1/2}/\Delta$pH are 0 mV/pH, 56 mV/pH and 112 mV/pH respectively for pH lower than 1,4, included in the range 1.4—4.3 and higher than 4.3.

As the free acidity of the solution increases at pH 2.5 a second wave appears. This wave becomes more evident as the pH decreases and follows the Ilkovich equation, ensuring proportionality between limiting current and acid concentration, in the concentration range $10^{-4} - 10^{-3}$ M (fig. 2,3). Beyond the two described waves a third wave can be recorded, even if not so well formed as the other two. This third wave is grafted on the discharge of the supporting electrolyte, thus not attaining its limiting value and being unamenable to a quantitative study.

2) Behaviour in solutions at $\mu = 2.0$ M and $-\log\,[H^+] = 2.00 + + -0.30$ With the aim of evidencing better the second wave we thought to study the field of the very acid solutions and therefore to buffer the ionic strength at low pH values; thus to the acid solutions of $HClO_4$, $NaClO_4$ was added so that the ionic strength ($HClO_4 + NaClO_4$) resulted 2.00 M. In these conditions $E_{1/2}$ of the first wave is constant in the whole acidity range we explored (fig. 5), the height of the first wave is unchanged while that one of the second increases with increasing $[H^+]$, yielding an inflection point at $-\log\,[H^+] = 0.75$ (fig. 6,7). If $E_{1/2}$ values are plotted vs $-\log[H^+]$ the same behaviour observed for $E_{1/2}$ of the first wave is obtained (fig. 5), with only a shift of about 0.15 V towards more negative potential values.

OSCILLOPOLAROGRAPHIC MEASUREMENTS

The oscillopolarographic behaviour of isonicotinic acid is characterized in acid media by the presence of a well developed peak. The potential of this peak is function of pH and of the scanning rate of potential as shown by figures 8 to 17 and by tables 2, 3 and 4. By the analysis of the plotted and reported values it can be said that the peak potential is shifted to more negative values by increasing pH and scanning rate. The influence of pH, concentration and scanning rate on the height of this peak was also investigated (fig. 14, 18—21, table 2, 3), thus being eviden-

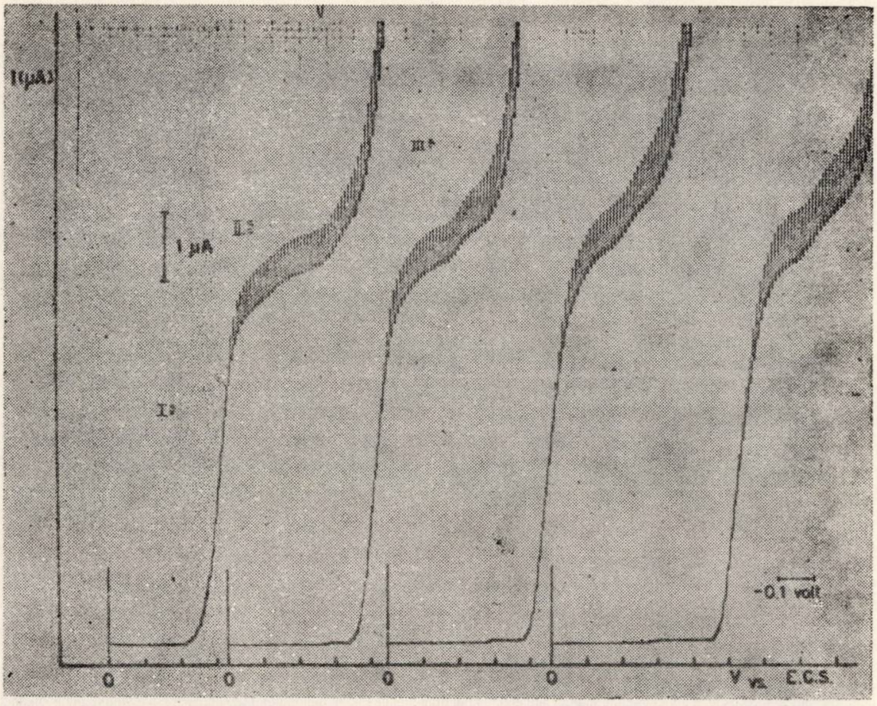

Fig. 1. — Polarographic behaviour of isonicotinic acid at different pH; from left to right pH=1.90, 3.50, 4.20, 5.30.

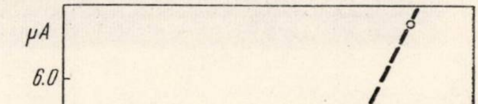

Fig. 2. — Limiting current values of the first (○) and second (●) wave vs isonicotinic acid concentration; pH=2.00.

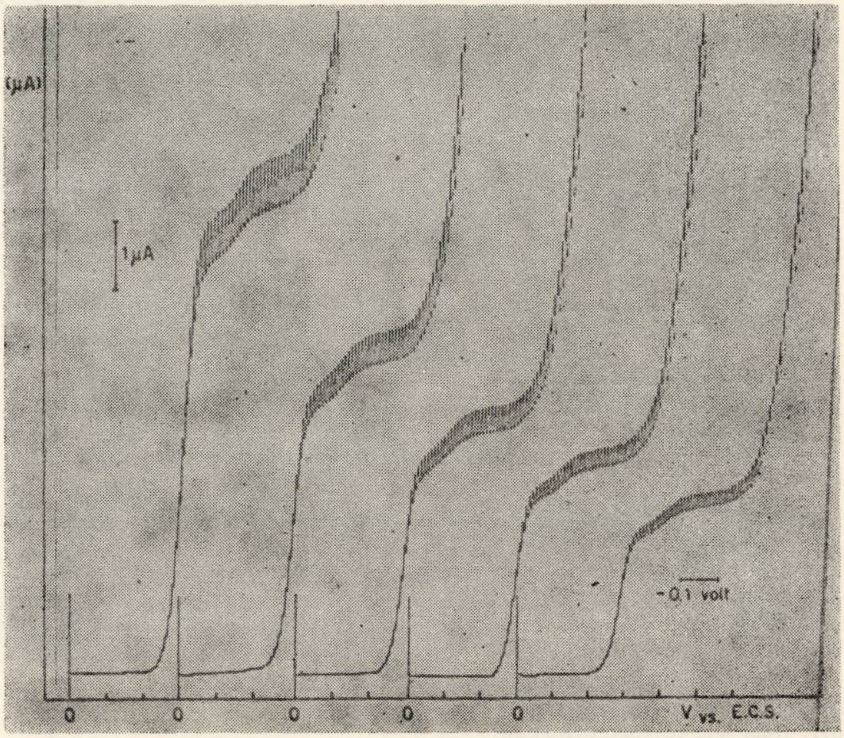

Fig. 3. — Polarographic curves at different concentrations; from left to right 1.67×10^{-3}, 8.33×10^{-4}, 7.14×10^{-4}, 5.56×10^{-4}M.

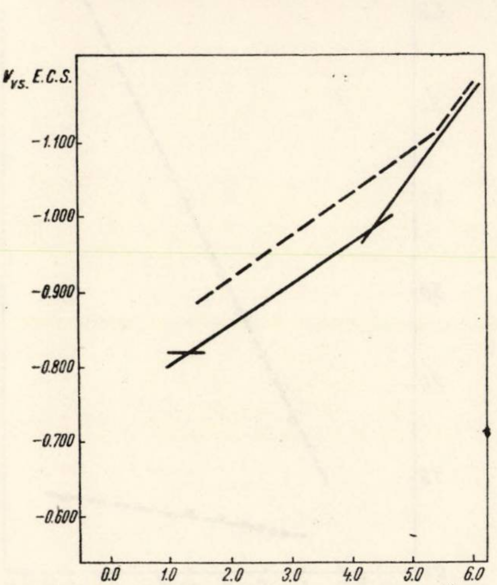

Fig. 4. — $E_{1/2}$ of the first wave as function of pH.

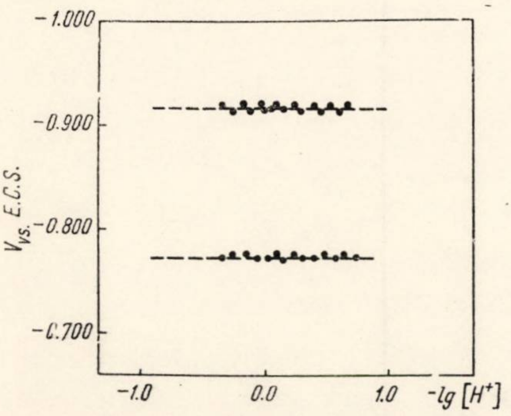

Fig. 5. — $E_{1/2}$ of the first wave as function of $-\log[H^+]$; up $NaClO_4$, 2.0M down $NaClO_4$ 0.5M.

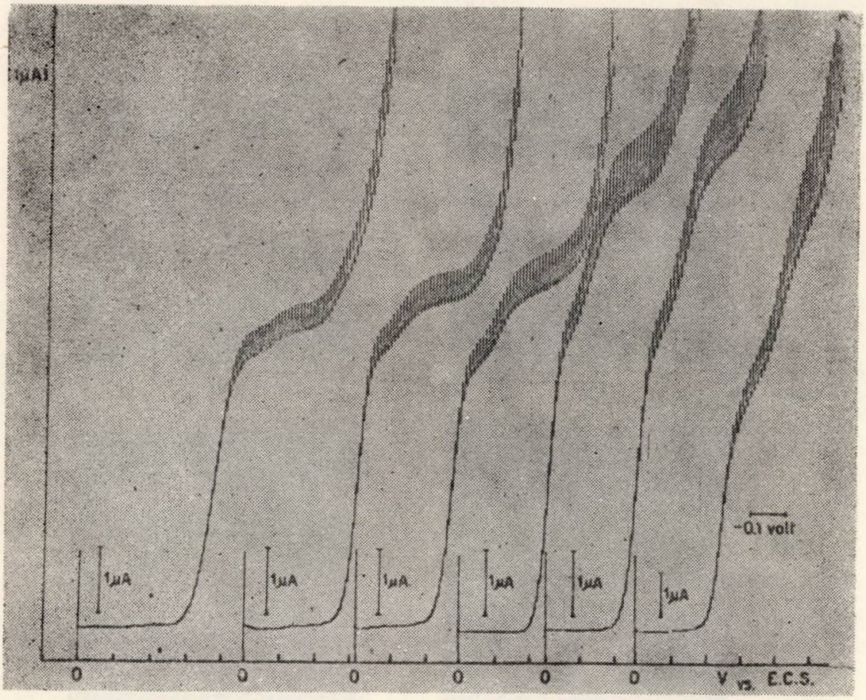

Fig. 6. — Polarographic behaviour of isonicotinic acid vs $-\log[H^+]$; from left to right $-\log[H^+] = 1.71$, 1.18, 0.86, 0.48, 0.26, -0.30. $NaClO_4 = 2M$.

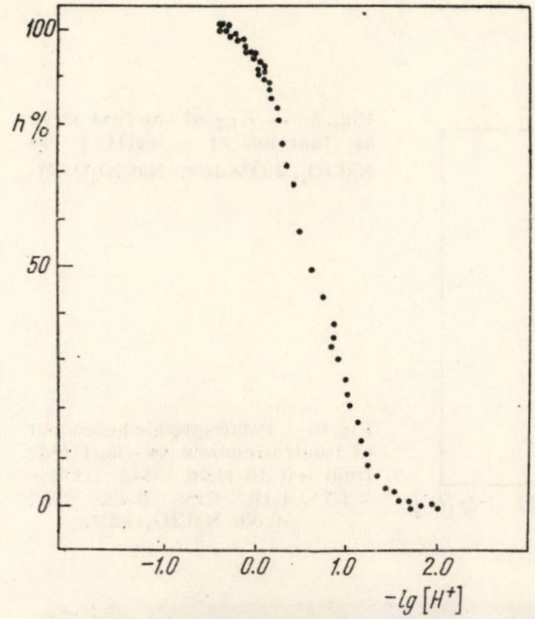

Fig. 7. – Height of the second wave *vs* $-\log [H^+]$; $NaClO_4 = 2M$

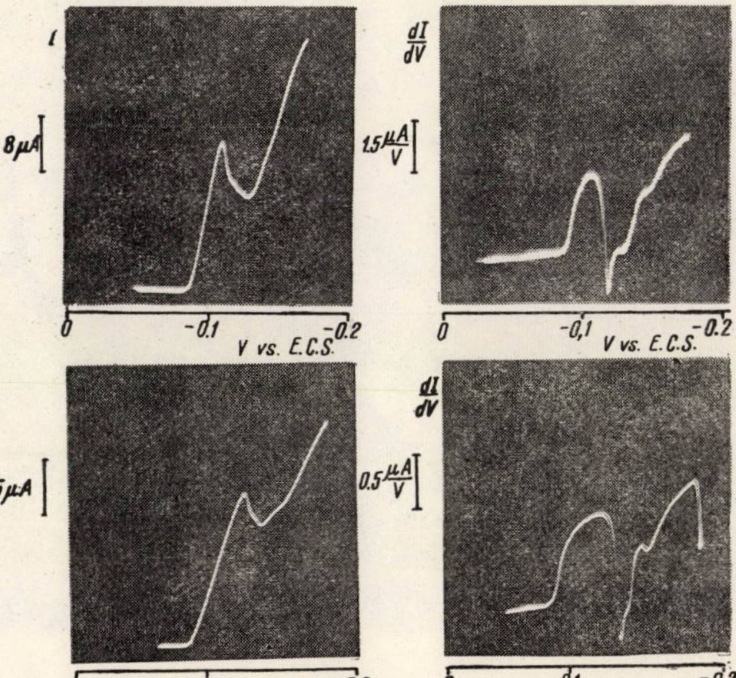

Fig. 8 – Oscillopolarographic direct (a) and derivative (b) curves of isonicotinic acid at different pH; up, pH=1.60 down ,pH=2,25.

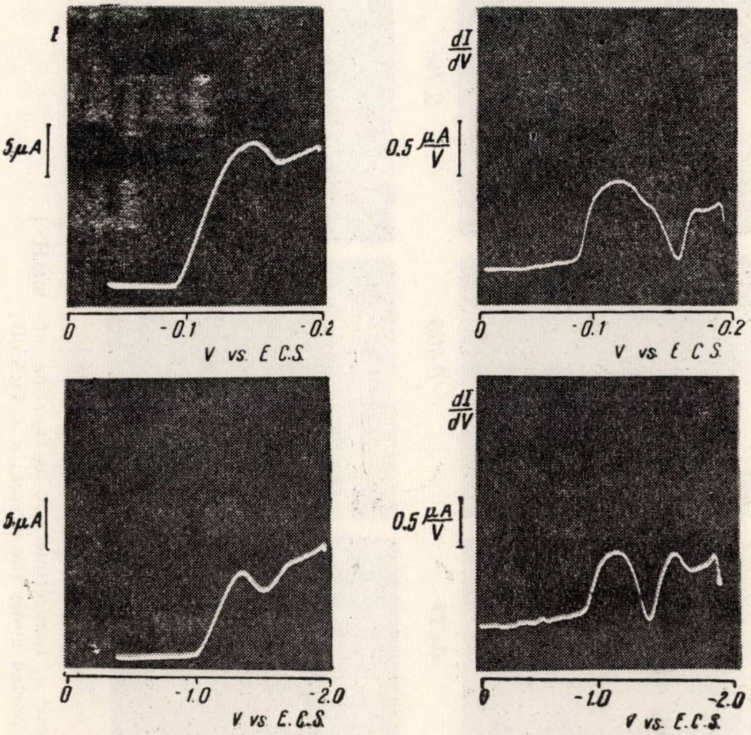

Fig. 9. — Oscillopolarographic direct (a) and derivative (b) curves of isonicotinic acid at different pH; up, pH=3.00 down, pH=3.85.

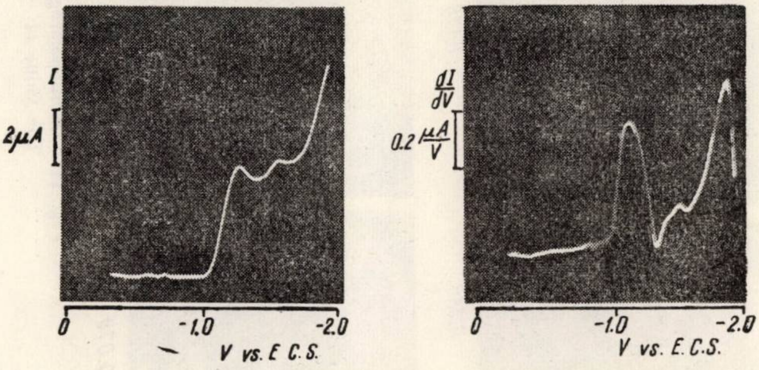

Fig. 10. — Oscillopolarographic direct (a) and derivative (b) curves at pH=5.00.

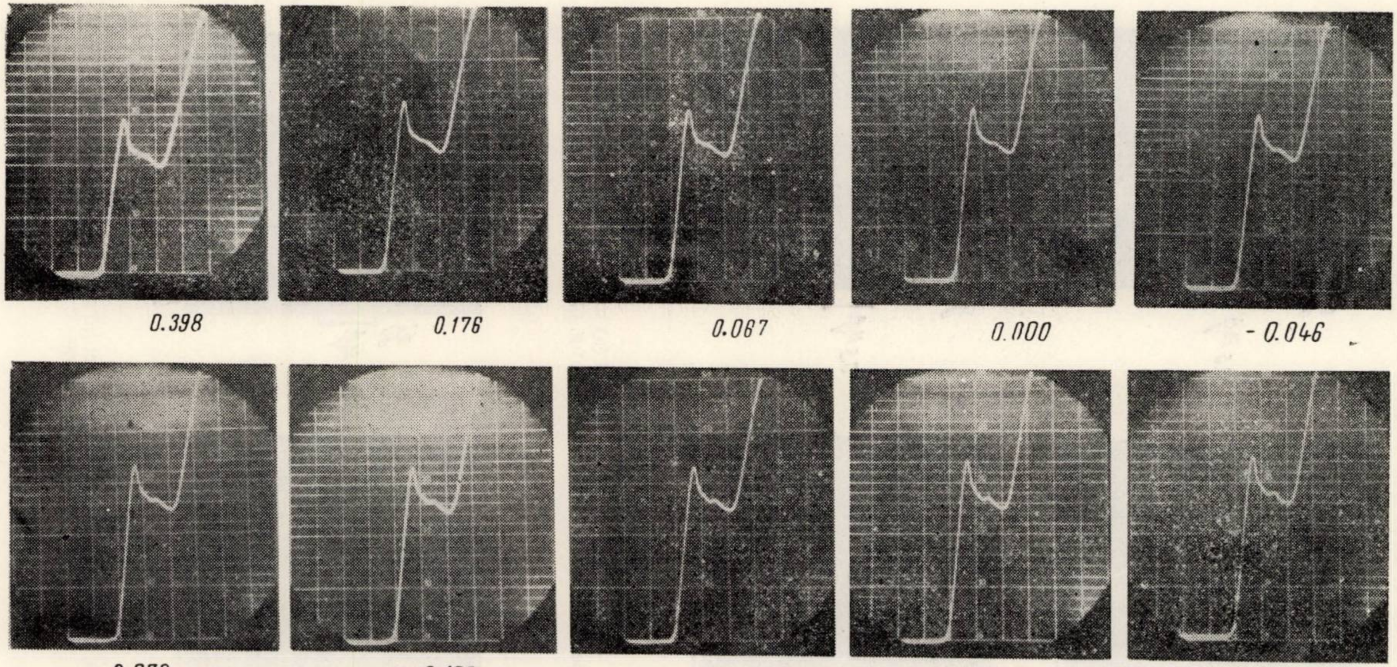

0.398 0.176 0.067 0.000 - 0.046

- 0.079 - 0.105 -0.122 - 0.144 - 0.0155

Fig. 11.—Oscillopolarographic behaviour of isonicotinic acid as function of $-\log[H^+]$.
The value of $-\log[H^+]$ si reported under the curves; $\sigma = 3\ \mu A/div$.

ced that the height of the peak is proportional to concentration and logarithmically proportional to the scanning rate, while the dependence on pH is more complicated, being characterized by the presence of two humps at pH 3 and 1.6, the first of which becomes quite a maximum for the lowest scanning rates.

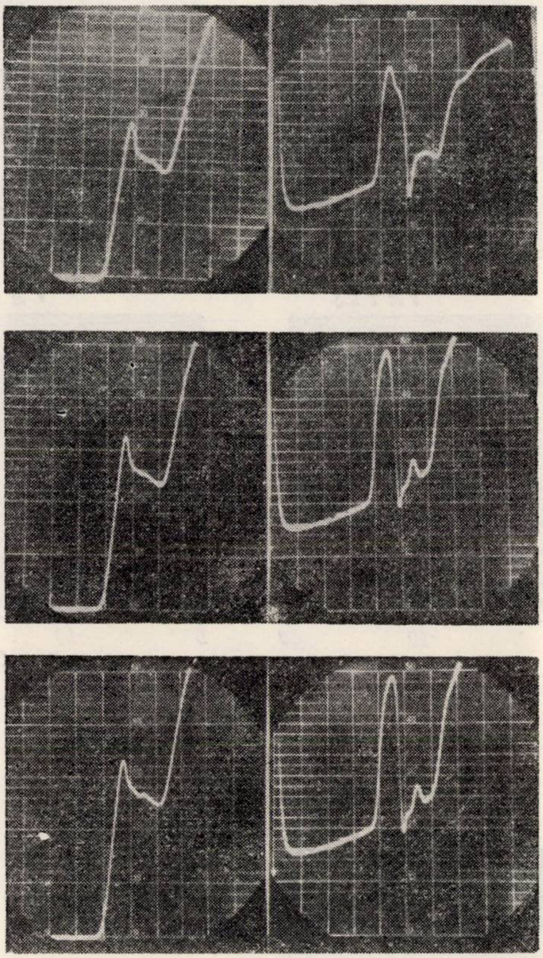

Fig. 12. — Oscillopolarographic direct (a) and derivative (b) behaviour of isonicotinic acid as function of $-\log\,[H^+]$; from up to down $-\log\,[H^+] = 0.40$, 0.067, -0.12, $\sigma = 3\ \mu A/\text{div}$.

Close to the first peak a second one can be recorded in a wide range of pH (fig. 10—13); the dependence of its potential and its height on the scanning rate, pH and concentration was studied (fig. 13, 16, 17, 21).

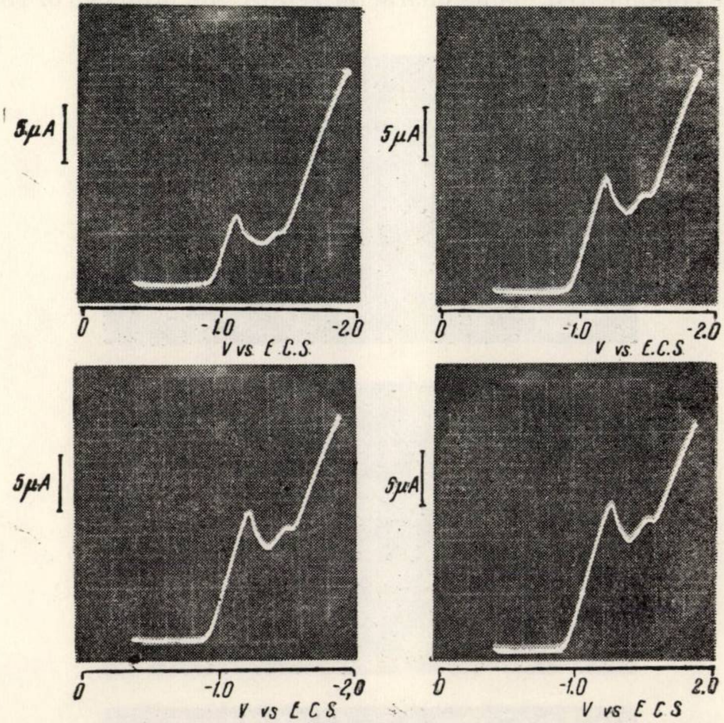

Fig. 13. — Oscillopolarographic behaviour of isonicotinic acid as function of the concentration. From left to right and from up to down c = 4.00 × 10^{-4}, 7.73 × 10^{-4}, 9.28 × 10^{-4}, 11.02 × 10^{-4} M; pH = 2.45.

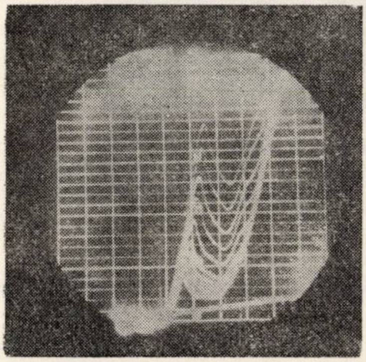

Fig. 14. — Oscillopolarographic behaviour of isonicotinic acid as function of the scanning rate. From down to up v = 0.25, 0.4, 0.6, 1.0, 1.5, 2.5, 4.0, 6.0, 10, 15, 25 V/sec; pH = 1.68.

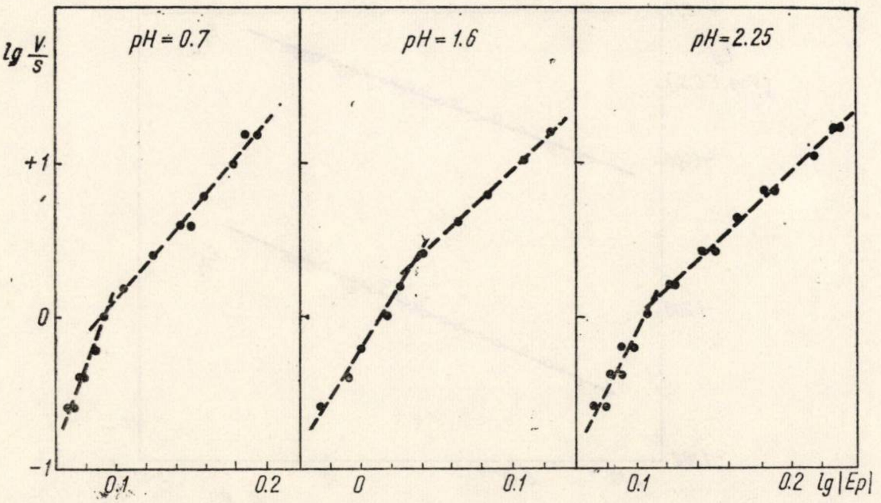

Fig. 15. — Logarithmic dependence of E_p of the first peak on the scanning rate at different pH.

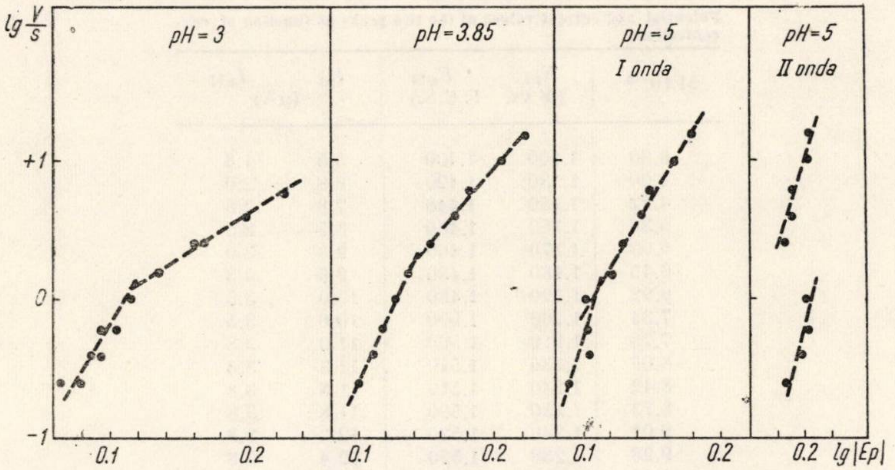

Fig. 16. — Logarithmic dependence of E_p of the first and second peak on the scanning rate at different pH.

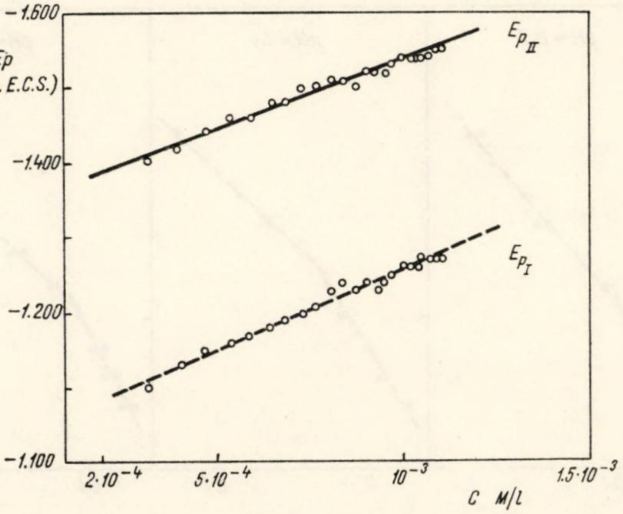

Fig. 17. — E_p of the first and second peak *vs* isonicotinic acid concentration ; pH = 2.45.

Table 2

Potential and current values of the two peaks as function of concentration

M 10^{-4}	$E_{p\text{I}}$ (V vs.	$E_{p\text{II}}$ E.C.S.)	$I_{p\text{I}}$	$I_{p\text{II}}$ (μA)
3.20	1.100	1.400	5.5	1.8
4.00	1.130	1.420	6.8	2.0
4.72	1.150	1.440	7.8	2.5
5.36	1.160	1.460	8.5	2.5
5.93	1.170	1.460	9.3	3.0
6.45	1.180	1.480	9.6	3.3
6.92	1.190	1.480	10.0	3.5
7.34	1.200	1.500	10.6	3.5
7.73	1.210	1.500	11.0	3.8
8.09	1.230	1.510	11.3	3.8
8.42	1.240	1.510	11.8	3.8
8.73	1.230	1.500	11.8	3.8
9.01	1.240	1.520	12.3	3.8
9.28	1.230	1.520	12.4	3.8
9.52	1.240	1.520	12.5	3.9
9.75	1.250	1.530	12.9	4.0
9.97	1.260	1.540	13.1	4.3
10.17	1.260	1.540	13.3	4.3
10.36	1.260	1.540	13.4	4.6
10.54	1.270	1.540	13.6	4.5
10.70	1.270	1.540	13.8	4.8
10.86	1.270	1.550	13.6	4.8
11.02	1.270	1.550	13.6	4.8

Table 3

E_p of the first peak at varying free acidity degrees and potential scanning rates

$-\lg [H^+]$	pH	E_{pI} (− V vs. E.C.S.)										
		V/s										
		0.25	0.40	0.60	1.00	1.50	2.50	4.00	6.00	10.00	15.00	25.00
−1.55		0.920	0.940	0.940	0.960	0.980	1.000	1.020	1.040	1.060	1.080	1.100
	1.68	0.955	0.975	0.985	0.995	1.005	1.045	1.065	1.085	1.095	1.135	1.165
	3.48	1.045	1.065	1.085	1.105	1.135	1.160	1.175	1.205	1.225	1.265	—
	4.75	1.160	1.180	1.200	1.220	1.240	1.260	1.280	1.300	1.320	1.360	1.400

Table 4

I_p of the first peak at varying free acidity dgreees and potential scanning rate

$-\lg [H^+]$	pH	I_{pI}(μA)										
		V/s										
		0.25	0.40	0.60	1.00	1.50	2.50	4.00	6.00	10.00	15.00	25.00
−0.155		75.0	93.7	97.5	105.0	120.0	150.0	180.0	206.2	243.7	288.7	337.5
	1.68	61.4	72.2	83.0	97.5	108.3	137.2	169.7	198.6	238.3	274.4	325.0
	3.48	66.3	71.0	78.7	103.6	116.0	145.0	178.1	203.0	240.3	290.0	—
	4.75	68.5	83.7	95.1	106.5	125.5	152.1	186.4	213.0	254.8	292.8	361.3

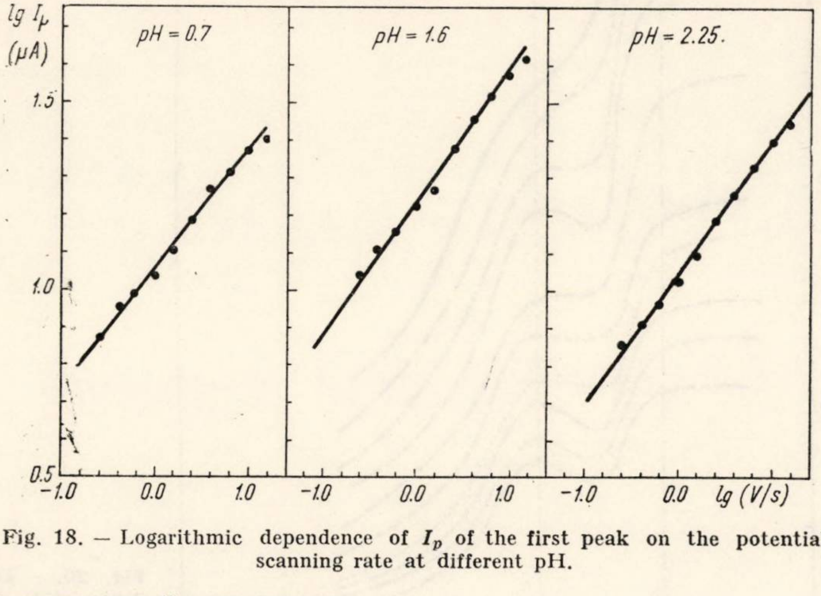

Fig. 18. — Logarithmic dependence of I_p of the first peak on the potential scanning rate at different pH.

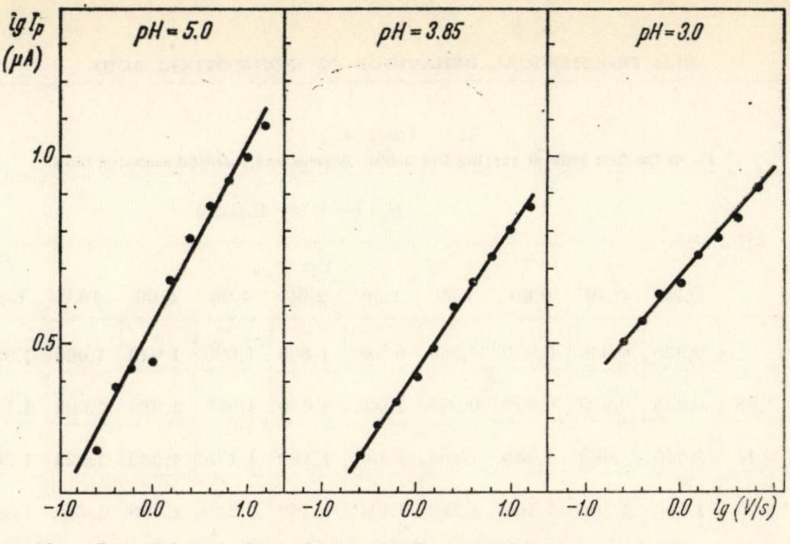

Fig. 19. — Logarithmic dependence of I_p of the first peak on the potential scanning rate at different pH.

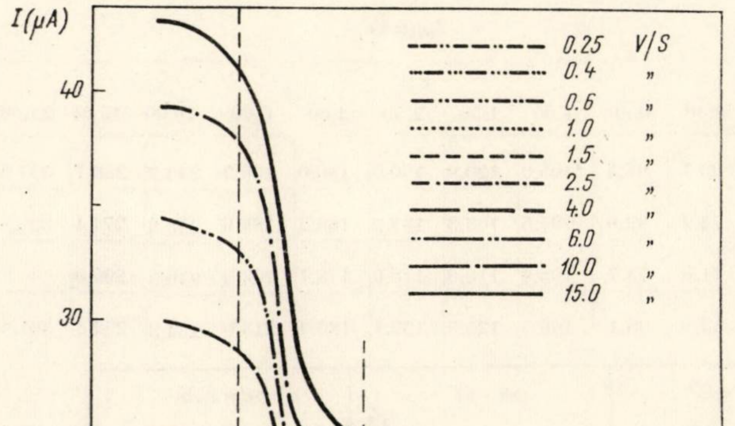

Fig. 20. — Dependence of I_p of the first peak on the pH and on the potential scanning rate.

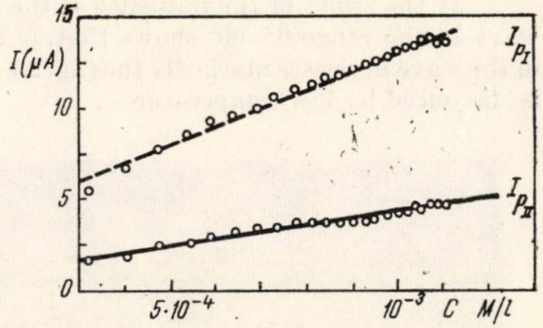

Fig. 21. — Dependence of I_p of the first and second peak on the isonicotinic acid concentration ; pH = 2.45.

DISCUSSION

As the height of the first polarographic wave is not depending on pH, contrary to $E_{1/2}$, while it is depending on concentration of isonicotinic acid it could be supposed that this wave is an adsorption wave for which the controlling factor is not the percentage concentration of a certain species of the acid, but the total concentration of the acid itself in the electrode region and the adsorbing electrode surface area. This hypothesis must be rejected on the basis of the following experiments :

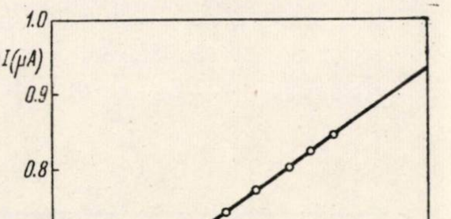

Fig. 22. — Dependence of the height of the first reduction wave on the height of the mercury column.

1) the height of the first wave plotted *vs* the height of the mercury column [25] gives a straight line with slope =0.70 ; this value is different both from 0.5 and from 1.0, respectively corresponding to diffusion-controlled and adsorption waves (fig. 22) ;

---

[25] L. Ya. Kheifets, *Anal. Chem. USSR*, **20**, 355 (1965).

2) the study of the influence of the temperature on the height of the wave in the range 0 — 60° shows that as temperature increases the height of the wave increases markedly too (fig. 23, 24), while adsorption, as known, is favoured by low temperatures;

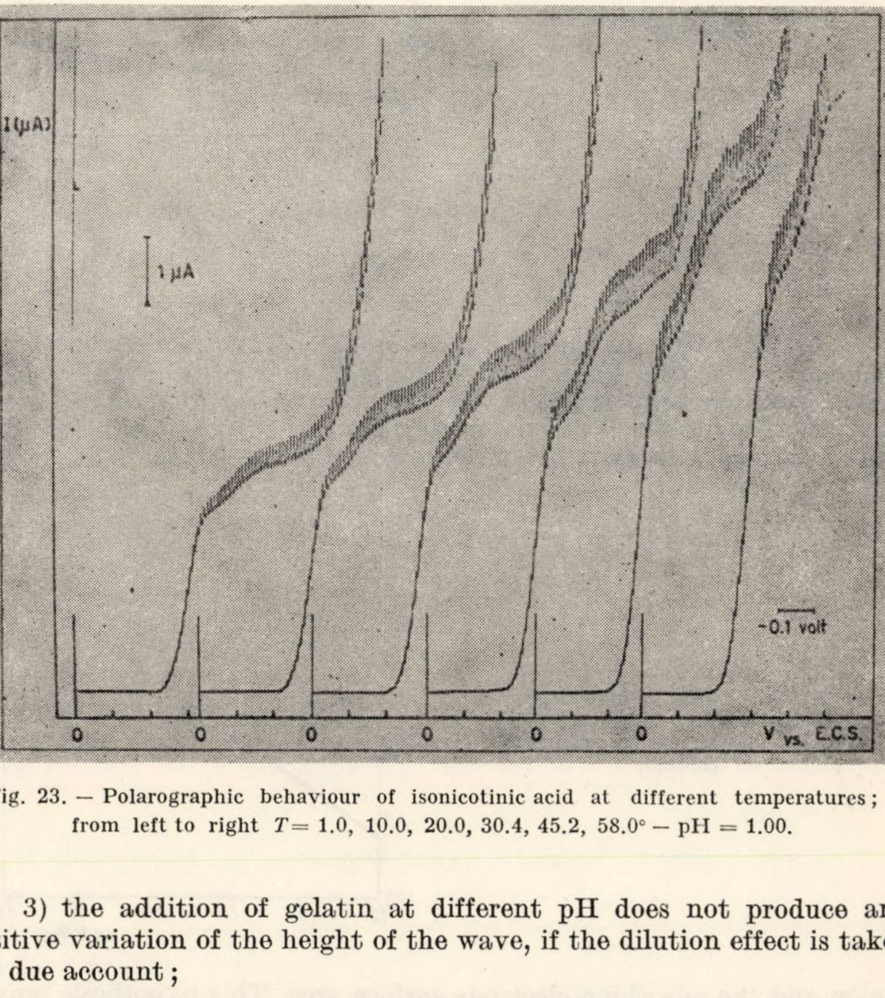

Fig. 23. — Polarographic behaviour of isonicotinic acid at different temperatures; from left to right $T = 1.0, 10.0, 20.0, 30.4, 45.2, 58.0°$ — pH = 1.00.

3) the addition of gelatin at different pH does not produce any sensitive variation of the height of the wave, if the dilution effect is taken into due account;

4) the determination of the electrocapillary curves (fig. 25) carried out in solutions a) of the only supporting electrolyte, b) of the electrolyte + isonicotinic acid, c) of the electrolyte + isonicotinic acid + gelatin, d) as c) + potassium iodide shows that while the adsorption of I^- is clearly evidenced by the variation of the electrocapillary curves, these are unchanged by the presence of isonicotinic acid, both in presence and in the absence of gelatin; further in the presence of gelatin the whole curve is characterized by a shift along the y axis (dropping time) toward lower values.

Fig. 24. — Height of the first (up) and second (down) wave vs temperature; pH = 1.00.

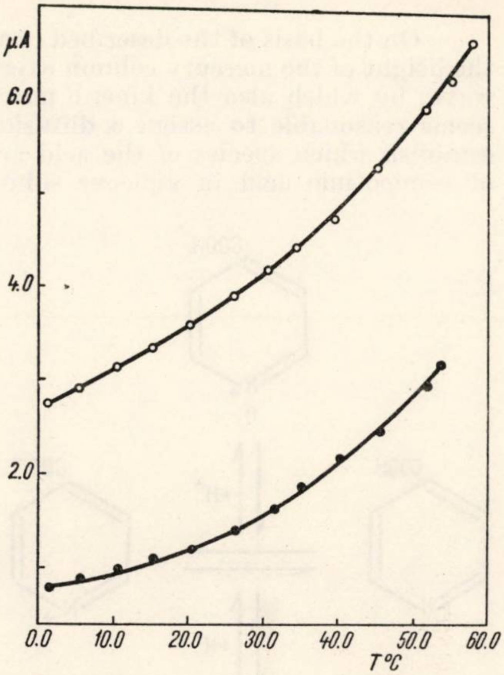

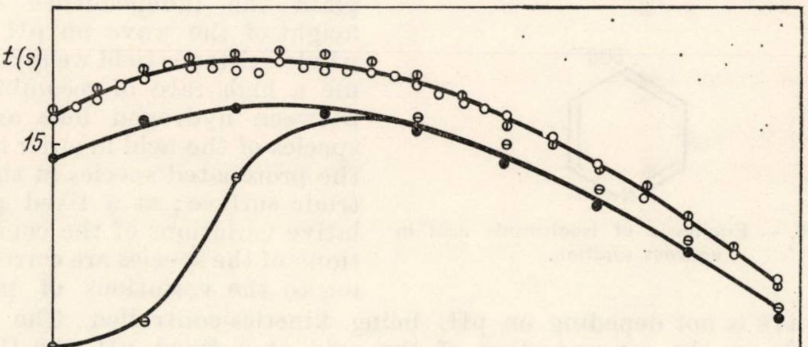

Fig. 25. — Electrocapillary curves in (○) $NaClO_4$ 0.5 M (⦶) $NaClO_4$ 0.5 M + isonicotinic acid (●) $NaClO_4$ 0.5 M + isonicotinic acid + gelatin (⊖) $NaClO_4$ 0.5 M + isonicotinic acid + gelatin + potassium iodide 10^{-1} M.

On the basis of the described results and of the kind of influence that the height of the mercury column exerts on the limiting current of the first wave, by which also the kinetic nature of the wave can be excluded, it seems reasonable to assign a diffusion nature to the wave. In order to establish which species of the acid accounts for the wave, the equilibria of isonicotinic acid in aqueous solutions must be considered (fig. 26). The wave disappears when the polarographic curves are recorded for solutions at pH. 8. This observation makes possible to discard the anion of the acid. On the other hand the variation of $E_{1/2}$ with pH is characterized by a slope $\Delta E_{1/2}/\Delta$ pH varying from 0mV/pH to 56 mV/pH before and 112 mV/pH after, the breaking points corresponding at pH values which are in very good agreement with the pK values of the acid. From these experimental data it seems correct to deduce that the first wave has to be attributed to the protonated cationic species. In order to explain the independence of the height of the wave on pH in the whole existence field we must assume a high rate of recombination between hydrogen ions and the species of the acid in order to form the protonated species at the electrode surface; at a fixed pH relative variations of the concentrations of the species are corresponding to the variations of pH and the wave is not depeding on pH, being kinetics-controlled. The height depends on the concentration of the acid at a fixed pH, the Ilkovich equation being obeyed. The reduction processes can be so represented for this wave, indicating with HPC the acid as such:

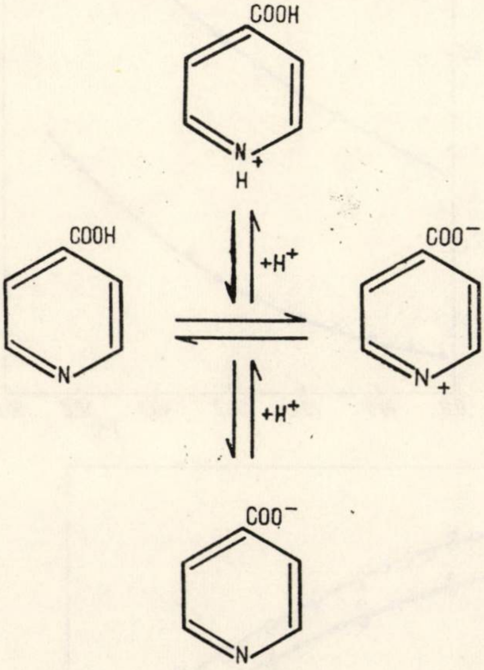

Fig. 26. – Equilibria of isonicotinic acid in aqueous solution.

(1) $$\mathrm{pH} < 1.4 : \{4-\mathrm{H_2PC^+} + e \rightarrow 4-\mathrm{HPC} + 1/2\ \mathrm{H_2}\}_{\mathrm{electrode}}$$

(2) $$1.4 < \mathrm{pH} < 4.3 : \{4-\mathrm{HPC} + \mathrm{H^+}\}_{\mathrm{solution}} \rightarrow$$

$$\rightarrow \{4-\mathrm{H_2PC^+} \overset{e}{\rightarrow} 4-\mathrm{HPC} + 1/2\ \mathrm{H_2}\}_{\mathrm{electrode}}$$

(3) $$4.3 < \mathrm{pH} < 8 : \{4-\mathrm{PC^-} + 2\ \mathrm{H^+}\}_{\mathrm{solution}} \rightarrow$$

$$\rightarrow \{4-\mathrm{H_2CP^+} \overset{e}{\rightarrow} 4 - \mathrm{HPC} + 1/2\ \mathrm{H_2}\}_{\mathrm{electrode}}$$

according to the species which are prevailing in the different intervals of pH where isonicotinic acid is polarographically active.

This assumption is based not only on the value of $\Delta E_{1/2}/\Delta \mathrm{pH}$ but also on the following other experimental data :

1) the UV spectra of a solution of isonicotinic acid before and after the reduction performed in polarographic conditions for prolonged times and at potential values corresponding to the limiting current of the wave show no absorbance variation even though a variation should be foreseen according to the passed charge ;

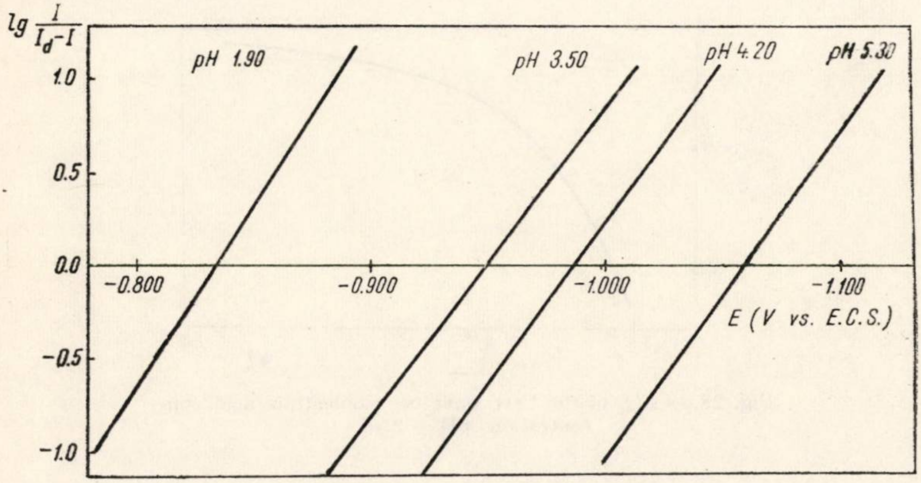

Fig. 27. — Reversibility test for the first reduction wave.

2) also the IR spectra of the crystalline residue obtained by evaporation to dryness of the solution before and after electrolysis are unchanged ;

3) the polarographic curve before and after electrolysis for prolonged times (~ 48 hrs) on mercury cathode pool is just the same ;

4) the number of the electrons taking part in the electrode reaction is 1, as shown by the analysis of the curve (fig. 27).

It must be concluded that the reduction process does not affect the species if isonicotinic acid which can be considered only as catalyzing agent for the reduction of the hydrogen ions. This agrees perfectly with the above reactions which are really catalyzed hydrogen discharge.

The second wave appears at potential values near those of the first one and is characterized by an increasing height as pH decreases and by an $E_{1/2}$ not depending on pH. Moreover by adding gelatin, the height of this wave, corrected for the dilution effect, is unchanged. To this second wave a diffusion nature is attributed, the species interested being H_2PC^+ and the reduction process :

$$4-H_2PC^+ + e \rightarrow 4-HCP + 1/2\ H_2$$

in agreement with the results of the semilogarithmic analysis of the polarographic curve according to which $n = 1$. The proposed mechanism has its weak point in the different $E_{1/2}$ values which result for the same process; however, the nature of the process can account for this; at the potential of the first process gaseous hydrogen is formed on the dropping mercury electrode that becomes polarized so that an excess of tension must be applied in order to maintain the process. This excess is more evident in acid solutions where the half wave potential of the first wave is less negative; moreover it has been experimentally determined as 140 mV.

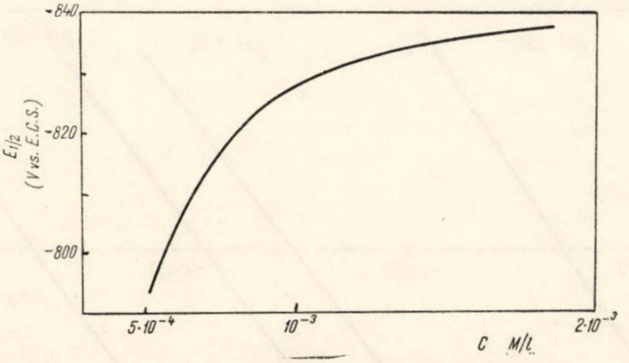

Fig. 28. — $E_1/_2$ of the first wave vs isonicotinic acid concentration; pH = 2.45.

A second objection to the proposed mechanism can also be countered: according to it in experimental conditions for which the second wave is not recorded as the height of the first wave increases by increasing concentration of the acid the doubling of the first wave should be observed at concentrations higher than a certain value, this being due to the polarization of the working electrode because of the gaseous hydrogen. It can be answered that at pH for which the second wave is absent the reduction potentials of the first process are more negative; moreover they become furtherly more negative as the concentration increases (fig. 28), so being unnecessary the above said excess of tension.

A third objection can be advanced concerning the Kheifets slope. For diffusion-kinetics mixed processes this slope should fall in the interval 0—0.5, the limits of which take respectively for only kinetics and only diffusion-controlled processes, while our experimental values are higher than 0.5. This can be due to the increase of the mean electrode surface following the increase of the mercury height. Consequently the diffusion current and the electrode concentration of the reduced species increase too. As according our hypothesis the reducible species can be regenerated by the reduced ones, the recombination rate becomes higher. The kinetics component of the wave currents is so enhanced; this increase must be added to that one of the diffusion current: hence a higher slope of the Kheifets line than expected. The third wave cannot be quantitatively studied but for it two hypotheses can be reasonably advanced: either the third wave is to be related to the second as the second is to the first one, or it is due to the reduction of a species (excepting the anionic one) whose polarographic inactivity must be related to the very low concentration of hydrogen ions in the solution where this species is prevailing. Consequently the catalyzing action and the above written equations (1) (2) (3) cannot be initiated.

An interesting application of the polarographic data is the determination of the kinetic constant of the reaction

$$H_3O^+ + HPC \rightleftarrows H_2PC^+ + H_2O$$

rom the equation : of Brdicka, Wiesner and Koutecky [26–28] :

$$\lg K_r = 2\,pK' + \log 1.31 - \mathrm{pK} - \log t_1$$

where K_r, pK′, pK and t_1 are respectively the rate constant of the reaction› the polarographic pK, the spectrophotometric pK and the dropping time. Here we obtain $K_r = 10^{11}$ a value lower than that found by other authors. [12,13] The difference of the experimental conditions as ionic strength and buffer nature can account for the disagreement ; the importance of the experimental conditions on the polarographic data is also pointed out by the fact that while we found activity up to pH 8, in other conditions waves and peaks can be recorded up to pH 10.[12,13]

The oscillopolarographic measurements gave results in agreement with those of normal polarography. To the first polarographic waves two oscillopolarographic peaks are corresponding : this has its reason in the nature itself of the technique which with its high rate of potential scanning makes possible to discriminate the kinetic process from the diffusion-controlled one. This discrimination is evidenced at $1.78 < \mathrm{pH} < 6.0$ or in very acid media where the concentration of hydrogen ions or of the deprotonated species of isonicotinic acid are such that the recombination rate is small enough to make possible the distinguishing of the kinetics process from the diffusion controlled one and high enough to make possible the recording of the kinetic peaks in the experiment time.

Quantitatively studying the oscillopolarographic curves the following conclusions can be drawn :

1) The peak current is proportional to the concentration, giving thus the possibility of quantitatively determining the studied compounds by polarographic techniques.

2) From the application of the Randles and Sevcik equation to the dependence of the peak current I_p on the scanning rate of potential V

$$I_p = ,\, Kn^{3/2}\, m^{2/3}\, t^{2/3}\, D^{1/2}\, V^x\, C = K'C^x$$

the parameter x results to be about 0.4, a value which in comparison with the theoretical 0.5 shows the kinetics-diffusion control of the process (table 5).

---

[26] R. Brdicka, *Coll. Czech. Chem. Comm.*, **12**, 212 (1947).

[27] K. Wissner, *Analyt. Chem.*, **27**, 1712 (1955).

[28] K. Wiesner, *Analyt. Chem.*, **28**, 75 (1956).

3) The variation of the peak potential E_p with the scanning rate of potential shows the irreversibility of the process; particularly the variation is less marked around pH 5.0, where presumably the kinetic character is poorly felt.

The chronopotentiometric behaviour of isonicotinic acid can be considered as a further proof of the proposed mechanism, based on the recombination reaction between the different species under which the acid can exist in aqueous solution and the hydrogen ions, with formation of the protonated cationic species. The chronopotentiometric curves are varying according to the pH, the applied current and the presence or not the absence of the buffer. In presence of the buffer only one wave is observed (fig. 29, 30), the transition time of which is reported in table 6 as function of pH and electrolysis current. In the case of unbuffered solutions successive multiple waves appear, fig. 31 characterized by a rate of the potential decay (dE/dt) that is proportional to the value of the impressed current.

Table 5

Variation of the coefficient x in the equation: $\log I_p = \log K' + x \log v$ as function of pH

pH	X
0.70	0.31
1.60	0.35
2.25	0.36
3.00	0.30
3.85	0.39
5.00	0.48

Table 6

Transition time in buffered solutions as function of pH and of the value of the electrolysis current

pH	τ Electrolysis current (μA)			
	5.0	2.5	1.0	0.5
2.10	—	1.8	6.3	40.4
3.00	0.9	3.4	17.6	74.0
3.95	1.0	3.6	20.6	—
4.95	1.5	4.5	23.6	—
6.15	—	2.2	9.7	31.4

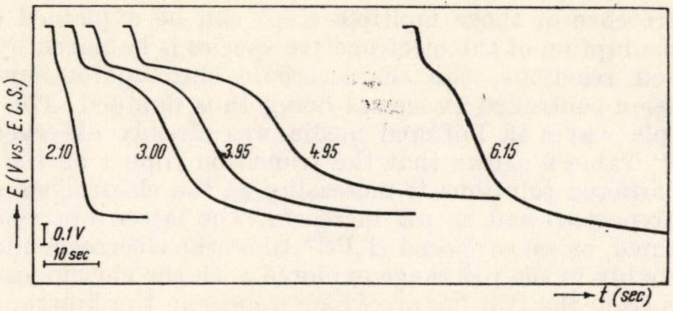

Fig. 29. – Chronopotentiometric curves at different pH; electrolysis current = 1 μA; potential values at zero time + 0.190 (pH = 2.10), +0.190 (pH = 3.00). + 0.180 (pH = 3.95), +0.170 (pH = 4.95), +0.125 (pH = 6.15) V vs SCE.

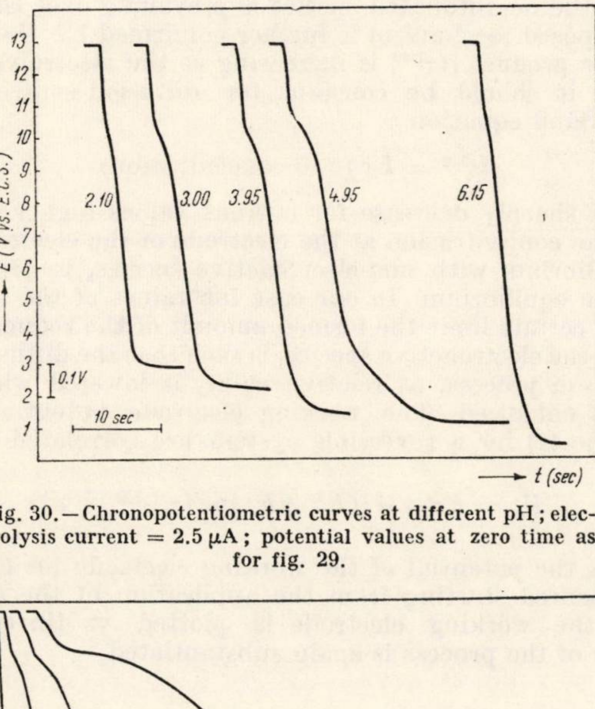

Fig. 30. – Chronopotentiometric curves at different pH; electrolysis current = 2.5 μA; potential values at zero time as for fig. 29.

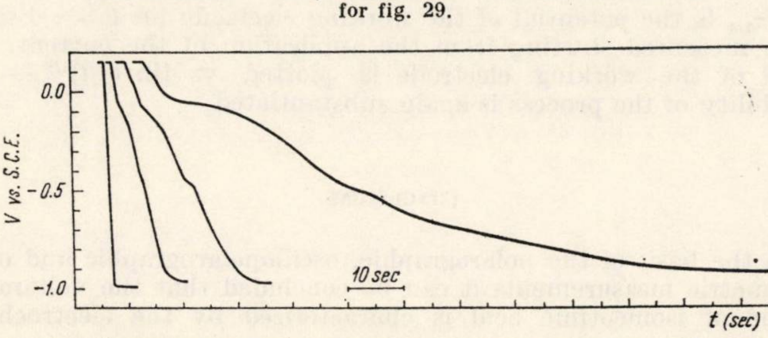

Fig. 31. – Chronopotentiometric curves in unbuffered solutions with different electrolysis current; from left to right 5.0, 1.0, 0.5, 0.25 μA; pH = 3.85.

The presence of these multiple steps can be explained considering that the consumption of the electroactive species is balanced by the above recombination reactions, the characteristic chronopotentiometric jump of the diffusion-controlled processes being thus damped. The absence of these multiple waves in buffered media was already observed by other authors.[29,30] Table 6 shows that the transition time τ of the only wave present in buffered solutions is increasing as the electrolysis current decreases, as expected, and as pH increases. The latter observation is not easily explained, as we supposed H_2PC^+ to be the electrochemically active species. Probably in the pH range explored with the chronopotentiometric experiments from the two factors which appear in the kinetic equation of the recombination reaction

$$V = K\,[H]^x\,[M]^y$$

where M = deprotonated species of the acid, the term concerning the concentration of the deprotonated species is prevailing over the other.

The proposed mechanism is further confirmed by the following observation : the product ($i\tau^{1/2}$) is increasing as the electrolysis current increases while it should be constant for diffusion-controlled processes according to Sand equation

$$i\tau^{1/2} = k\,c \;(c = \text{concentration})$$

and it should sharply decrease for current values higher than a certain limit, when the concentration at the electrode of the electroactive species, being in equilibrium with non-electroactive species, is depending on the kinetics of the equilibrium. In our case for values of the applied current higher than a certain limit the formed amount of the reduced species able to yield again the electroactive species, is such that the diffusion component of the reduction process, as relative value, is lowered while the kinetic component is enhanced. The working electrode potential (E_w) and the transition time (τ) for a reversible system are correlated as it follows :

$$E_w = E\tau_{1/4} + (RT/nF)\ln\,[(\tau/t)^{1/2} - 1]$$

where $E\tau_{1/4}$ is the potential of the working electrode for $t = \tau/4$ and t is the time measured starting from the application of the current. If the potential of the working electrode is plotted vs $[\ln\,(\tau/t)^{1/2} - 1]$ the irreversibility of the process is again substantiated.

CONCLSIONS

On the basis of the polarographic, oscillopolarographic and chronopotentiometric measurements it can be concluded that the voltammetric behaviour of isonicotinic acid is characterized by the electrochemical

---

[29] V. Carunchio and L. Campanella, *Ann. Chim.* (Ital.), 57, 1378 (1967).

[30] R. C. Henney, H. F. Holtzclaw and R. C. Larsen, *J. Electroanalyt. Chem.*, 14, 435 (1967).

activity of the protonated cationic species which is reduced at the dropping mercury electrode either directly or through a kinetic process of equilibrium with the other species that are transformed into the cationic one by recombination with hydrogen ions at the electrode solution interface. The rate of this transformation plays an extremely important role; it is sufficiently high to make it possible for the protonated cationic species to exist in a wider range of pH than expected based on values of the equilibria constants among the species of the acid. When the concentration of hydrogen ion is very low ($\mathrm{pH} \geqslant 8$), this rate is that much decreased that no voltammetric activity can be recorded. All the reduction processes interest one electron, do not involve any consumption of the organic acid and can be assumed as not interesting directly the sort of the acid which must be considered only as catalyzing agents for the hydrogen discharge. The Ilkovich and Randles-Sevcik equations, ensuring the proportionality between current and concentration are followed, giving the possibility to determine quantitatively the isonicotinic acid.

Revue Roumaine de Chimie, **17**, 6, 1115–1124 (1972)

THE POLAROGRAPHIC REDUCTION OF METHYL-SUBSTITUTED N-ETHYL PYRIDINIUM IONS
A HMO TREATMENT

P. NAGY, I. GÖRBE and A. SZURKOS

Chemical Faculty of the Pedagogical Institute, str. Nicolae Iorga 1, Tg.-Mureş

Received August 6, 1971

Polarograms of five methyl-substituted N-ethyl pyridinium ions were recorded in water (Britton-Robinson buffer pH = 11.6) and in methanol (0.1 M CH_3ONa/CH_3OH), at about 22°. The Hückel MO energies were calculated by the inductive and the heteroatom model. It was pointed out, that no correlation exists between $E_{1/2}$ and the electron density on the nitrogen atom. The correlation between the lowest vacant MO energy (ε_{LV}) and $E_{1/2}$ was studied. The effective value of the resonance integral was determined. The substituent and medium effects are discussed as well.

The correlation between the polarographic reduction parameters and MO energies, calculated by different MO methods will be very useful in investigating the structure of the organic compounds. Such a correlation has been found first by Macoll.[1] He showed that the half-wave potentials ($E_{1/2}$) of several unsaturated hydrocarbons are related linearly to their lowest vacant HMO energy. This correlation was confirmed and interpreted by several workers.[2,3] It obeys an equation of the form :

$$E_{1/2} = -b.m_{m+1} + C \tag{1}$$

where

b — parameter expressing the effective value of β,
m_{m+1} is a number proportional to ε_{LV} ($\varepsilon_{LV} = \alpha_0 + m_{m+1} \cdot \beta_0$), C is a constant.

It must be, however, pointed out, that this equation has a correct physical meaning only if several special conditions concerning the reaction mechanism are fulfilled. These conditions were treated by Zahradnik[4],

---

[1] A. Macoll, *Nature*, **163**, 178 (1949).

[2] G. J. Hoijtink and J. van Scooten, *Rec. Trav. chim.*, **71**, 1089 (1952); **72**, 691 (1953).

[3] A. Pullmann, B. Pullmann and G. Berthier, *Bull. Soc. chim. France*, **1950**, 591.

[4] R. Zahradnik and I. Parkany, *Talanta*, **12**, 1289 (1965).

Mark,[5] and recently by Freimanis,[6] and may be formulated as follows :

(i) The complete reduction mechanism should be known.

(ii) The reduction step cannot be preceded or followed by the protonization of the molecules.

(iii) The reduction mechanism must be reversible.

(iv) The mechanism must be the same in the whole reaction series under study.

While condition (iv) is reasonable when we intend to make a comparison in a given reaction series, conditions (i), (ii) and (iii) require some comments : for the polarographic reduction of hydrocarbons Mark[5] has shown that, if a protonation occurs, the measured $E_{1/2}$ may differ to a large extent from that for the couple $RH_2 + e^- \rightleftharpoons R \cdot H_2^-$, needed for theoretical MO calculations. He has also shown, that the formed $R \cdot H_2^-$ can be protonated even under aprotic conditions by side-reactions. However, empirical correlations between $E_{1/2}$ and $\varepsilon_{J.V}$ may be occasionally successful,[5] because the anodic shift, due to protonation, may be of the same magnitude for all the members of the series. The reversible nature of the electrode process is also a necessary condition.[4–6] The quantum mechanically calculated energies are generally those required by the addition of an electron to the lowest unoccupied MO, but the half-wave potential represents this energy difference (between the intial and final state) only if the electrode process is reversible. For the irreversible electrode process $E_{1/2}$ represents the energy difference between the initial and the transition state. The MO calculation for this transition state is, however, very difficult. Empirical correlation have been nevertheless found even for irreversible processes. The success of such empirical correlations may be explained[6] either by the parallel change in the initial and transition state energies, or by the fact, that $E_{1/2}$ is determined by a reversible or quasi-reversible elementary electrode process.

The above discussions emphasize, that it is absolutely necessary to understand completely the whole electrode process before using a polarographic parameter in a theoretical correlation.

The first studies concerning the electrochemical reduction mechanism of N-alkyl-pyridinium ions were carried out by Emmert,[7] and later by Tompkins.[8] They established that the reduction takes place by the acceptance of a single electron, and the resulted radical is stabilized by dimerization. Hence the following reduction scheme was proposed :

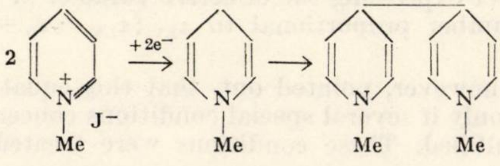

---

[5] H. B. Mark jr., *Rec. Chem. Progr.*, **29**, 219 (1968).

[6] I. F. Freimanis, *Zhur. obsch. Khim.*, **39**, 631 (1969).

[7] B. Emmert, *Ber.*, **42**, 1507 (1909).

[8] P. Tompkins quoted by S. Wawzonek, *Analyt. Chem.*, **21**, 64 (1959).

The reduction of these ions was then carried out (on the dropping mercury electrode) polarographically by Collichman and Donovan.[9] They have observed a diffusion-controlled one-electron wave and have assumed a reversible character for the electrode process, which is followed by a fast dimerization of the primarily formed free radicals.

By a fundamental analysis of the reduction mechanism Mairanovski[10] has established a quasireversible character for this reduction process. This is due to the adsorption of the dimer product at the surface of the dropping mercury electrode. Mairanovski has also shown, that at low depolarizer concentration ($c < 4 \times 10^{-5}$ M/l) the rate of the dimerization is decreased substantially and the process will be controlled kinetically. If the depolarizer concentration is high enough ($c > 4 \times 10^{-5}$ M/l) the electrode process will be diffusion-controlled.

This paper presents a study upon the polarographic reduction of methyl-substituted N-ethyl pyridinium ions. The substituent effects on the half-wave potentials, and on the lowest vacant HMO energies, hence the $\varepsilon_{LV} \sim E_{1/2}$ correlations, are studied on the basis of the reduction mechanism given by Mairanovski. The solvent effect is discussed as well.

EXPERIMENTAL

1. MATERIALS

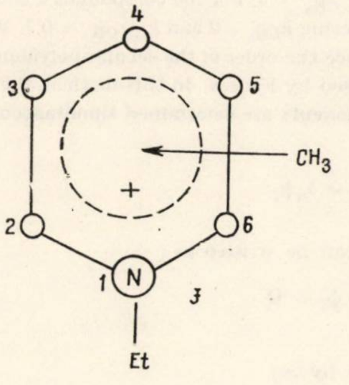

a. none substituted
b. $2-CH_3$
c. $3-CH_3$
d. $4-CH_3$
e. 2,6-di CH_3
f. 2,4,6-tri CH_3

The compounds used were prepared by heating the corresponding free nitrogen bases in equimolecular proportion with ethyl-iodide on a water bath. The precipitates were fitered, washed with acetone, and recrystallized from ethanol.

---

[9] E. Collichmann and P'O. Donovan, *J. Amer. Chem. Soc.*, **76**, 3588 (1954).
[10] S. G. Mairanovski, *Doklady Akad. Nauk S.S.S.R.*, **110**, 593 (1956).

Revue Roumaine de Chimie, 17, 6, 1117–1134 (1972)

2. POLAROGRAPHIC MEASUREMENTS

An LP-60 model polarograph was used to record the polarograms. As the external reference, a saturated calomel electrode SCE was used in a Lingane-Laitinen cell. The capillary of the dropping mercury electrode had the following m and t values at $h = 80$ cm and in 0.1 N KCl: $m = 2.37$ mg/sec and $t = 3.01$ sec. Polarographic measurements were made at 22° with solutions of about 10^{-4} M/l containing accurately weighed samples. Britton-Robinson buffer ($pH = 11.6$) respectively 0.1 M/l CH_3ONa in absolute methanol was used as supporting electrolytes. Dissolved oxygen was removed before each measurement by bubbling with purified methane gase. The observed polarographic maxima in the methanolic solution were removed by adding 1 ml of 0.5% gelatine to the sample solution.

3. HÜCKEL MO CALCULATIONS

Several MO calculation methods have been used concerning the pyridinium ion.[11-13] In order to calculate the MO energies of methyl-substituted N-ethyl pyridinium ions we have chosen the simple Hückel method using the following parameters [11b-14a] : $h_{N+} = 2$ and $k_{C-N+} = 1$. The effect of the ethyl group on the nitrogen atom has been considered as an inductive one, therefore the Coulomb integral of this atom was diminished by $0.2\ \beta_0$.[14a] Hence $\alpha_{N+} = \alpha_0 + 1.8\,\beta_0$ and $\beta_{CN+} = \beta_0$. We have used an AIP (auxiliary inductive parameter) only at the α carbon atom which is attached to the heteroatom (Mataga [13] has done the same for the pyridinium ion) so that the corresponding Coulomb integrals are :

$$\alpha_{C_2} = \alpha_{C_6} = \alpha_0 + \delta\,1.8\,\beta_0, \text{ with } \delta = 1/10$$

The MO energies of the compounds **b**, **c**, **d**, **e**, **f** have been calculated by the inductive model[14b] using the parameters $h_{C-CH_3} = -0.2$ and $k_{C-CH_3} = 0$. For the compounds **d** and **e** calculations have been also made by the heteroatom model using $h_{CH_3} = 2$ and $k_{C-CH_3} = 0.7$. Where possible, the symmetry elements have been used to reduce the order of the secular polynomial.

The calculation method was that proposed by Fadeev. In this method, the coefficients of the secular equation and the eigenvector components are determined simultaneously. The linear transformation

$$H\psi_i = \lambda_i\psi_i \tag{2}$$

which represents the Schrödinger equation, can be written as :

$$|H - \lambda\varepsilon|\,\psi_i = 0 \tag{3}$$

where ε is the unit matrix
λ the eigenvalue (denoted previously by m)
ψ_i the eigenvector
$|H - \lambda\varepsilon|$ the secular square matrix.
According to Fadeev

---

[11] B. Pullmann and A. Pullmann, "Kvantovaya Biokhimia" Izdatelstvo Mir, Moscow, 1965, a) p. 116, b) p. 92.

[12] R. D. Brown and A. Penfold, *Trans. Faraday Soc.*, **53**, 397 (1957).

[13] S. Mataga and N. Mataga, *Z. Phys. Chem. (Frankfurt)*, **19**, 231 (1959).

[14] A. Streitwieser "MO Theory for Organic Chemists", J. Wiley Inc., New York, London, 1962 a.) p. 135, b.) p. 182, c.) p. 181.

$$| \lambda\varepsilon - H | \,.\, B(\lambda) = D(\lambda) . \varepsilon \tag{4}$$

where $D(\lambda)$ is the characteristic polynomial

$$D(\lambda) = \lambda^n - p_1\lambda^{n-1} + p_2\lambda^{n-2} - \dots + (-1)^n p_n \tag{5}$$

and $B(\lambda)$ is a matrix

$$B(\lambda) = \lambda^{n-1} \,.\, \varepsilon + B_1\lambda^{n-2} + \dots + B_{n-1} \tag{6}$$

If $H_1 = H$ the following equalities hold

$$H_i = H . B_{i-1}$$

$$p_i = \frac{(-1)^{i-1}}{i} \mathcal{U}(H_i) \tag{7}$$

$$B_i = H_i + (-1)^i \,.\, p_i$$

where $\mathcal{U}(H_i)$ is the trace of the square matrix (H_i).

If λ_0 is an eigenvalue, respectively a root of the characteristic polynomial $D(\lambda)$, the equation (4) can be rewritten as :

$$|\lambda_0\varepsilon - H| \,.\, B(\lambda_0) = 0 \tag{8}$$

Therefore the elements of a single column-vector from the matrix $B(\lambda_0)$ are the elements of the expected eigenvector. The eigenvector components determined from $B(\lambda_0)$ have been normalized finding in this way the coefficient set of the atomic orbitals in the corresponding MO. The calculation of matricial products, and the determination of the characteristic roots, were carried out with an Olivetti-programma-101 desk computer.

RESULTS AND DISCUSSIONS

1. THE PROBLEM OF THE REACTION CENTER

According to our previous papers,[15–16] the electrochemically active center for this type of compounds is the quaternary nitrogen atom. This assumption had been relied on the fact, that for the compounds of the type I and II

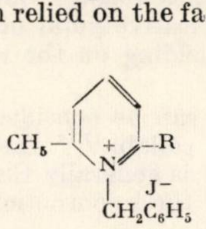

(I)

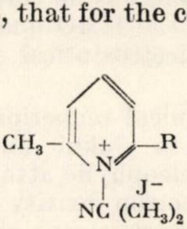

(II)

---

[15] A. Szurkos and P. Nagy, *Rev. Roumaine Chim.*, **15**, 607 (1970).
[16] A. Szurkos, unpublished results.

in which the assumed reaction center is sterically hindered, the polarographic reduction has not been observed.

According to the classical electronic theory of the organic chemistry, the effect of the methyl substitution on the polarographic reduction of the studied N-ethyl pyridinium ions, can be explained as follows : the methyl group having a positive inductive effect (+I) would increase the electron density on the reaction center. Therefore, an electrostatic shielding on the quaternary nitrogen atom occurs, and the reduction process takes place more difficulty. Hence, it can be assumed that a correlation does exist between the electron density on the azoatom (q_{N^+}) and the corresponding half-wave potentials ($E_{1/2}$). This assumption, however, is not supported by the calculations and experimental data, because there is no correlation between $E_{1/2}$ and q_N+ (calculated by the inductive model, see Table 1). It must be pointed out, however, that the inductive model operates only with a delocalization in the α position relative to the methyl substituent and does not involve the effective increase in electron density due to the +I effect of this group. That is why the q_N+ values were calculated for some of the studied compounds, also by the heteroatom model. Table 1 shows, that there is no correlation again. Such experimental facts point out, that from the HMO quantitative point of wiew the traditional explanation of the electrostatical shielding on the reaction center is not correct.

Table 1

Lowest vacant MO energies calculated by: a) – Hückel-inductive and b) – Lyons-Hoijtink approximate method. The electron densities at the nitrogen atom, calculated by the inductive and heteroatom models. The corresponding $E^1/_2$ values in Britton-Robinson buffer (pH = 11.6) and 0.1 molar CH_3ONa/CH_3OH. The polarographic αn values in Britton-Robinson buffer.

+) – for this compound the reduction wave has not been observed.

No	a) m_{m+1}	b) m_{m+1}	q_N+		$E_{1/2}$		αn
			inductive	hetero-atom	buffer	methanol	
a.	−0.4541	−0.4541	1.5523	1.5523	1.564	1.442	1.20
b.	−0.5001	−0.5021	1.5186	—	1.616	1.524	1.20
c.	−0.4569	−0.4580	1.5277	—	1.573	1.486	1.10
d.	−0.5134	−0.5141	1.5417	1.5062	1.687	1.590	—
e.	−0.5488	−0.5501	1.5803	1.6264	1.679	1.599	1.00
f.	−0.6121	−0.6201	1.5723	—	—+)	—+)	—

The electrochemical reduction, can be considered as a nucleophylic reaction. According to Fukui and collab. [17,18] the most active center with respect to a nucleophylic attack is generally that atom from a molecule on which the electron density of the hypothetically added electron is the largest, in the lowest vacant MO.

This quantity is denoted by the symbol $f_N^{(r)}$, and $f_N^{(r)} = c_{fr}^2$ (where c_{fr} is the coefficient of the r-th atomic orbital on the frontier MO). The values

---

[17] K. Fukui, T. Yonezava, C. Nagata and H. Shingu, *J. Chem. Phys.*, 22, 1433 (1954).

[18] K. Fukui, T. Yonezava and H. Shingu, *J. Chem. Phys.*, 20, 722 (1952).

of this reactivity index were calculated by the inductive model. The results are given in the Diagram 1. It can be seen from these results, that according to the HMO calculations, the reaction center is the carbon atom from the γ position. This result obviously contradicts our previous assumption, but it should be accepted with some reserve, because in the reduction processes taking place at the dropping mercury electrode, the orientation and adsorption phenomena may play a considerable role.

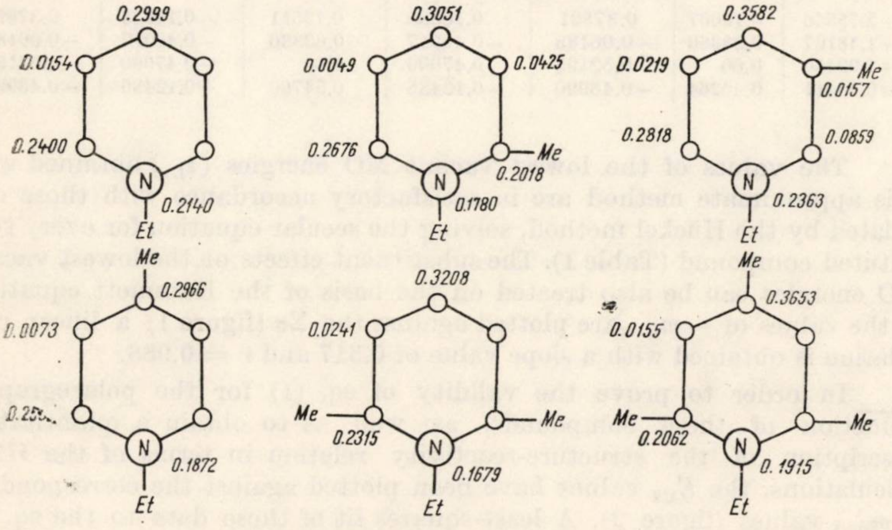
0.2999
0.0154
0.2400
0.2140
N
Et
0.3051
0.0049
0.0425
0.2676
Me
0.2018
0.1780
N
Et
0.3582
0.0219
Me
0.0157
0.2818
0.0859
0.2363
N
Et
Me
0.2966
0.0073
0.25
0.1872
N
Et
0.3208
0.0241
Me
Me
0.2315
0.1679
N
Et
Me
0.3653
0.0155
Me
Me
0.2062
0.1915
N
Et

The values of $f_N^{(-)}$ for the methyl-substituted pyridinium ions calculated by the Hückel inductive method

2. CORRELATIONS BETWEEN $E_{1/2}$ AND ε_{LV}

In any reduction process the molecules are accepting electrons to the lowest vacant MO. Therefore, the quantitative effect of the structural changes, on the reduction process can be evaluated on the basis of these frontier MO energies. In order to obtain the ε_{LV} of the studied compounds, in the first approximation, we have used the method proposed by Lyons [19] and Hoijtink.[2] This method is above all inductive, i.e. the secular determinant must be solved only for the nonsubstituted compound, and the energy differences (δm_j) caused by the introduced methyl groups calculated by the formula :

$$\delta m_j = \sum_r c_{jr}^2 \cdot h \qquad (9)$$

where $h = -0.2^{14b}$ and c_{jr} are the coefficients of the r-th AO in the j-th MO. The summation is extended only to the attached carbon atoms. The necessary coefficient set of the atomic orbitals of the N-ethyl pyridinium ion is given in Table 2.

---

[19] L. E. Lyons, *Research*, **2**, 587 (1949).

Table 2

HMO energies of the pyridinium ion (calculated by the inductive method) and the corresponding c sets of the atomic orbitals

E	c_1	c_2	c_3	c_4	c_5	c_6
+2.75846	0.79067	0.37891	0.18635	0.13511	0.18635	0.37891
+1.48167	0.38860	−0.06185	−0.46917	−0.63330	−0.46917	−0.06185
+1.09450	0.00	0.52193	0.47000	0.00	−0.47000	−0.52193
−0.45411	0.46264	−0.48990	−0.12435	0.54760	−0.12435	−0.48990

The values of the lowest vacant MO energies (ε_{LV}) obtained with this approximate method are in satisfactory accordance with those calculated by the Hückel method, solving the secular equation for every substituted compound (Table 1). The substituent effects on the lowest vacant MO energies can be also treated on the basis of the Hammett equation. If the values of $-m_{m+1}$are plotted against the $\Sigma\sigma$ (figure 1) a linear correlation is obtained with a slope value of 0.317 and $r = 0.988$.

In order to prove the validity of eq. (1) for the polarographic reduction of these compounds, as well as to obtain a quantitative description of the structure-reactivity relation in terms of the HMO calculations, the $E_{1/2}$ values have been plotted against the corresponding $-m_{m+1}$ values (figure 2). A least-squares fit of these data to the eq. (1) gives the results : $b = -1.18$ eV and $r = 0.960$ in the aqueous solution, respectively $b = -1.44$ eV and $r = 0.959$ in the methanolic solution.

Large deviations from the correlation lines may be observed for the compound **d** in both solvents used. These points were not involved in the correlation calculus. In order to clear up the reason of these deviations, the logarithmic analysis of the polarographic waves has been made, i.e. the $\log i/i_a - i$ values have been plotted against the corresponding potential (E). These plots are linear for the compounds **a**, **b**, **c**, and **e** (see e.g. curve 1 figure 3, for the compound **e**) but not linear for the compound **d** (curve 2, figure 3).

From the slope values of these linear plots the values of αn have been calculated (where α is the transfer coefficient and n the electron number in the reduction process) (Table 1). The well grouped αn values for the compounds **a**, **b**, **c**, and **e**, prove that the reduction mechanism for these compounds is nearly the same. The nonlinear $\log i/i_d - i \sim E$ profile of the compound **d** means that in this case the reduction mechanism is altered. This change may be explained as follows : as known,[10] the one-electron reduction is followed by the dimerization of the formed radicals. According to the present HMO calculations (Diagram 1) the most probable reaction centre for this dimerization is the 4-carbon atom from the pyridine ring, but this position in compound **d** is sterically hindered by the presence of the methyl group. The steric effect cannot be, however, taken into account in the HMO calculations, because it is foreign to its nature. On the other hand, if the dimerization occurs at the 2-carbon atom, the reduction mechanism of the compound **d** is obviously changed with respect to the rest of the studied compounds.

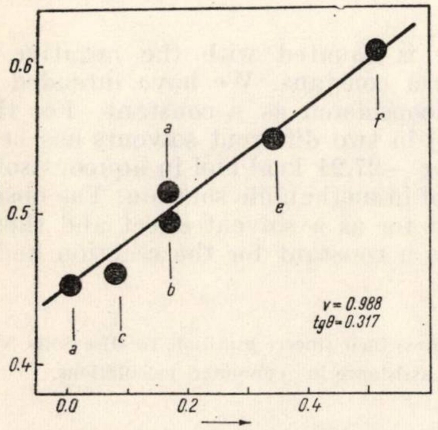

Fig. 1. — Plot of ε_{LV} *versus* $\Sigma\sigma$

$\sigma_{orto} = \sigma_{para} = -0.170$; $\sigma_{meta} = -0.069$

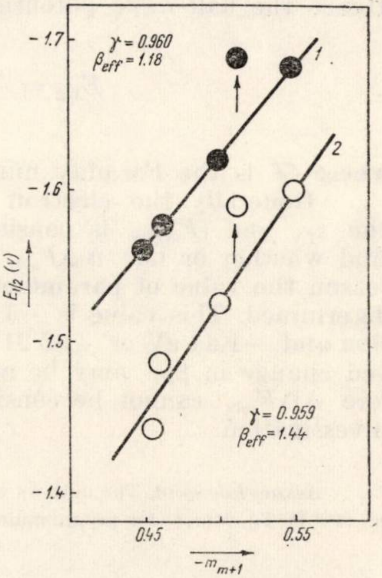

Fig. 2. — Plot of $E_{1}/_{2}$ *versus* ε_{LV}

1, — in Britton-Robinson buffer pH = 11. 6; *2*, — in 0.1 M CH_3ONa/CH_3OH.

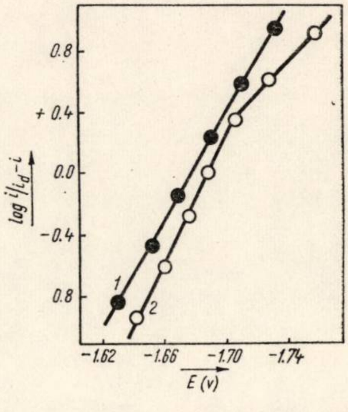

Fig. 3. — Logarithmic analysis of the polarographic waves

1, — the compound **e**; *2*, — the compound **d**.

3. THE SOLVENT EFFECT

The free-energy change represented by the half-wave potential of a reversible one-electron reduction is:

$$\Delta F^{\circ} = A + (F^{0}{}_{el})_{Hg} + \Delta\Delta F^{\circ}{}_{solv} \tag{10}$$

where A is the electron affinity of the molecule,

$(F^{\circ}_{el})_{Hg}$ is the free energy of the electron in the mercury drop,

$\Delta\Delta F^{\circ}_{solv}$ is the difference between the solvatation free energies of the oxidized and reduced species.

Hence the half-wave potential is given by [14] :

$$E_{1/2} = \frac{A + (F^{\circ}_{el})_{Hg} + \Delta\Delta F^{\circ}_{solv}}{\mathcal{F}} \tag{11}$$

where $\mathcal{F}$ is the Faraday number.

Generally the electron affinity is equated with the negative of the ε_{LV} and $(F^{\circ}_{el})_{Hg}$ is considered as a constant. We have intended to find whether or not $\Delta\Delta F^{\circ}_{solv}$ can be considered as a constant. For this reason the value of parameter b (β_{eff}) in two different solvents has been determined. This value is -1.18 eV or -27.21 kcal/mol in aqueous solution and -1.44 eV or -33.21 kcal/mol in methanolic solution. The observed change in β_{eff} may be accounted for as a solvent effect and therefore $\Delta\Delta F^{\circ}_{solv}$ cannot be considered as a constant for the reaction under investigation.

Acknowledgement. The authors wish to express their sincere gratitude to Miss Sofia Neagoi (I.J.P. Tg.-Mureş) for programming and for assistance in computer calculations.

Revue Roumaine de Chimie, 17, 6 1125–1136 (1972)

TRANSFORMATIONS CHIMIQUES DU POLYCHLORURE DE VINYLE. III

SYNTHÈSES DE POLYÉLECTROLYTES RÉTICULÉS AVEC GROUPES SULFONIQUES SUR LA BASE DU POLYCHLORURE DE VINYLE ARYLÉ AVEC DES HYDROCARBURES AROMATIQUES POLYNUCLÉAIRES

IG. POINESCU

Institut de Chimie Macromoléculaire « P. Poni », Jassy, 41 A, Aleea Gr. Ghica Vodă

Reçu le 4 juin 1971

Des synthèses de nouveaux échangeurs d'ions avec des groupes sulfoniques basées sur le polychlorure de vinyle arylé par naphtalène, anthracène ou phénantrène sont présentées.

Dans des ouvrages antérieurs [1,2] on a présenté des synthèses d'échangeurs d'ions, obtenus par substitution du chlore du polychlorure de vinyle par des groupes aryl- ou polyalkylarylsulfoniques.

Dans le présent ouvrage on continue les recherches sur de nouveaux échangeurs de cations sulfoniques, par substitution du chlore du polychlorure de vinyle (P.C.V.) par des hydrocarbures aromatiques polynucléaires et leur sulfonation ultérieure.

L'arylation du P.C.V. par les hydrocarbures aromatiques indiqués a été effectuée par réactions Friedel-Crafts d'après les indications de la littérature [3]. On obtient des polymères arylés dont le degré de substitution dépend des conditions de réaction.

PARTIE EXPÉRIMENTALE

La réaction d'arylation du P.C.V. par naphtalène, anthracène ou phénantrène a été réalisé à O°[3]. On a obtenu des polymères arylés dont le contenu en chlore, après arylation, varie dans différentes conditions entre 9,0 et 49,85 %Cl, ce qui correspond à un degré de substitution calculé d'après le contenu en chlore de 12,08 à 84,13 %.

La sulfonation a été exécutée par H_2SO_4 96 %, ou HSO_3Cl en présence du 1,2-dichloréthane, un solvant qui dissout facilement les polymères obtenus.

---

[1] Ig. Poinescu, *Rev. Roumaine Chim.*, **14** , 375 (1969).

[2] Ig. Poinescu, *Rev. Roumaine Chim.* (sous presse).

[3] Ph. Teyssiè et G. Smets, *J. Polymer Sci.*, **20**, 351 (1956).

L'installation pour la sulfonation et la technique de la sulfonation ont été décrites dans les ouvrages antérieurs [12].

RÉSULTATS ET DISCUSSIONS

Les conditions de synthèse de ces échangeurs de cations sulfoniques ont été établies en premier lieu par l'étude du polychlorure de vinyle arylé par naphtalène (P.C.V.N.), ayant un degré de substitution (S %) convenable (S = 58,19 %) ; Cl = 23,71 %) * qui permette de suivre l'action de l'agent de sulfonation tant sur les unités structurelles vinylnaphtaléniques que sur celles chlorvinyliques restées dans le polymère après arylation du P.C.V. par naphtalène. Les conditions établies à la sulfonation du P.C.V.N. ont été également appliquées au polychlorure de vinyle arylé par anthracène (P.C.V.A.) ou phénantrène (P.C.V.F.), la structure de ces polymères étant analogue à celle du P.C.V.N.

Le degré d'arylation du polychlorure de vinyle par hydrocarbures aromatiques polynucléaires dépend, dans des conditions identiques, de la nature du composé organique substituent.

Selon leur capacité d'arylation (tableau 1), les hydrocarbures aromatiques suivent l'ordre ci-dessus :

Benzène > naphtalène > phénantrène > anthracène.

Le degré d'arylation est influencé par la basicité des hydrocarbures aromatiques et par les facteurs stériques.

Tableau 1

Arylation du polychlorure de vinyle dans les conditions*

N°	Hydrocarbure aromatique	P.C.V.		Quantité d'unités chlorovinyliques (g) pour 100 g de polymère %
		Hydrocarbure aromatique moles	Chlore %	
1	Benzène	1,0/17,6	22,42	50,12
2	Naphtalène	1,0/3,0	38,72	68,29
3	Anthracène	1,0/3,0	51,64	91,07
4	Phénantrène	1,0/3,0	40,00	70,54

* – P.C.V./AlCl$_3$ – 1,0/0,5 moles
– Concentration de la solution de P.C.V. en 12 dichloréthane (g%) – 4,0 %
– Température (°C) – 0°
– Durée – 90 minutes

Le degré de sulfonation du polymère arylé, exprimé en valeurs de capacité d'échanges sulfoniques, est fonction de la nature de l'agent de sulfonation, du rapport des réactants, de la température, de la durée de la réaction de sulfonation et du degré de substitution du chlore du P.C.V. par le naphtalène.

---

* Le P.C.V.N. ayant un contenu en chlore de 23,71 % a été obtenu dans les conditions suivantes ; P.C.V. – 1,5 g ; 1,2-dichloréthane-52,2 ml-naphtalène ; durée de la réaction d'arylation-20 minutes ; température 0° ; P.C.V. 1,2 dichloréthane-52,5 ml ; naphtalène 4,6 g ; AlCl$_3$ – 1,0/0,5 mole.

La nature d'agent de sulfonation influence beaucoup tant les valeurs des capacités d'échange sulfonique que le genre du groupe fonctionnel d'échange introduit. Ainsi, pour la sulfonation par H_2SO_4 (H_2SO_4/ /P.C.V.N. = 3,0) la valeur de la capacité d'échange sulfonique (K_{SO_3H}) est de 0,67 méq/g plus petite que dans le cas de sulfonation par HSO_3Cl (fig. 1 *a* et *b*). On constate que pour une augmentation de la quantité de HSO_3Cl, la capacité d'échange sulfonique décroît de 2,40 à 1,84 méq/g, avec apparition simultanée d'une capacité d'échange d'un autre genre : la capacité d'échange carboxylique (K_{COOH}), (fig. 1 *d*). Pour la sulfonation par acide sulfurique, le K_{COOH} a été mis en évidence seulement pour l'emploi de rapports élevés de H_2SO_4/P.C.V.N. (fig. 1 *c*).

Les groupes carboxyliques sont le résultat de l'action oxydante des agents de sulfonation sur la chaîne macromoléculaire.

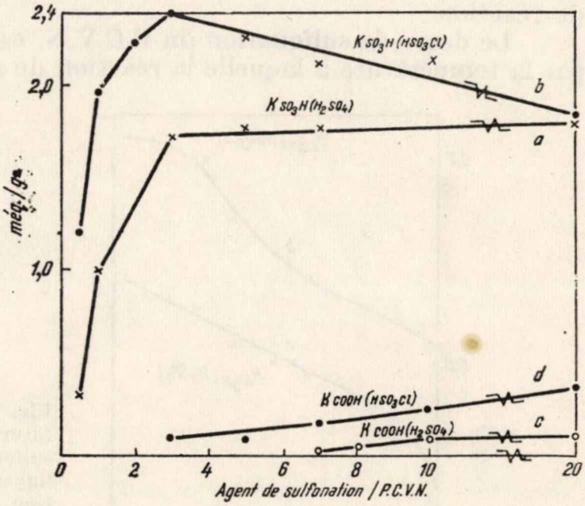

Fig. 1. — Influence de la quantité d'agent de sulfonation sur la capacité d'échanges sulfoniques (K_{SO_3H}) et carboxylyques (K_{COOH}) ; température — 25°, durée 5 heures ;

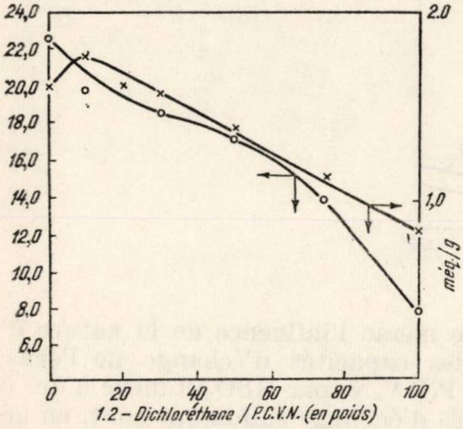

Fig. 2. — Influence de la concentration de la solution de P.C.V.N. sur la capacité d'échanges sulfoniques (K_{SO_3H}), et des pertes en chlore (P %) ; H_2SO_4/P.C.V.N. = 5,0 ; température 25° ; durée 5 heures.

La décroissance de la valeur de la capacité d'échange sulfonique à l'accroissement de la quantité de HSO_3Cl s'explique par la décomposition de certains groupes sulfoniques avec formation de groupes $\rangle SO_2$, qui génèrent des ponts de réticulation. Le soufre de ce groupe est «inactif» du point de vue de l'échange ionique et a été mis en évidence par la différence entre le contenu total de soufre et celui calculé à partir de la capacité d'échange sulfonique.[4]

La dilution du milieu de réaction par la croissance du rapport 1,2-dichloréthane/P.C.V.N. mène à la décroissance de la capacité d'échange sulfonique comme suite de la diminution de la concentration de l'acide sulfurique (fig. 2).

La capacité d'échange sulfonique décroît linéairement en même temps que l'augmentation de la quantité de solvant additionnée au milieu de réaction.

Le degré de sulfonation du P.C.V.N. est influencé en grande mesure par la température à laquelle la réaction de sulfonation a eu lieu (fig. 3).

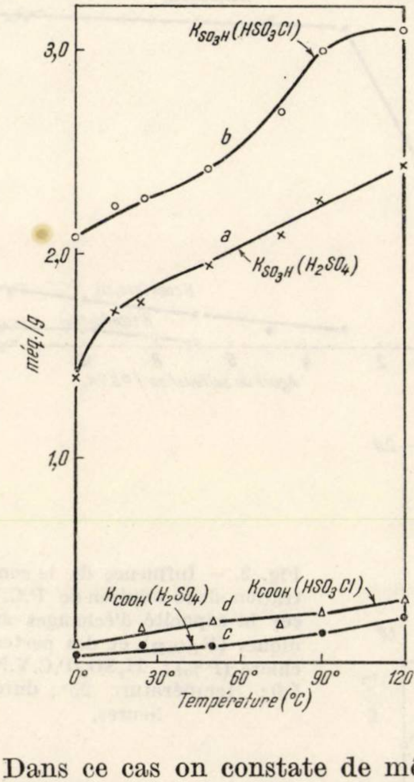

Fig. 3. — Influence de la température sur la capacité d'échanges sulfoniques (K_{SO_3H}) et carboxyliques (K_{COOH}) ; agent de sulfonation /P.C.V.N. — 5,0 ; durée — 5 heures.

Dans ce cas on constate de même l'influence de la nature d'agent de sulfonation sur la valeur des capacités d'échange de l'échangeur d'ions obtenu. La sulfonation du P.C.V.N. par HSO_3Cl mène à des échangeurs de cations dont les capacités d'échange sulfonique sont, en général, de 0,5 méq/g supérieures à celles obtenues pour la sulfonation du polymère par H_2SO_4. Les valeurs des capacités d'échanges carboxyliques diffèrent par approximativement 0,1 méq/g. Les courbes de la dépendance des capacités d'échange de température sont presque parallèles.

---

[4] G. J. MORALLI, *J. Recherches Centre National Recherches Sci.*, **26**, 277 (1954).

La sulfonation du polymère arylé par H_2SO_4 96 % mène à des échangeurs d'ions dont les groupes sulfoniques sont fixés dans le noyau aromatique, indifféremment de la température à laquelle la réaction de sulfonation a eu lieu. Cette remarque est basée sur les résultats expérimentaux des essais de sulfonation du P.C.V. par H_2SO_4 96 % à différentes températures (tableau 2).

Tableau 2

Déhydrochloruration du P.C.V. par $H_2SO_4$96 %*

N°	Température °C	Chlore %		Soufre %
		Initial	Final	
1	0°	56,70	56,70	0,00
2	25°	56,70	56,65	,,
3	50°	56,70	54,50	,,
4	75°	56,70	53,92	,,
5	90°	56,70	53,72	,,
6	120°	56,70	53,12	,,

* – H_2SO_4 96 % – 5,0 moles
– Durée de réaction – 300 minutes
– Concentration de la solution de P.C.V. en 1,2-dichloréthane (g%) – 4,0%

L'acide sulfurique réagit très faiblement avec le P.C.V., donnant lieu seulement à une faible déhydrochloruration du polymère.

En sulfonant le P.C.V.N. par HSO_3Cl à des températures plus élevées que 60°–65° on obtient des échangeurs de cations, qui contiennent des groupes sulfoniques fixés au noyau aromatique, ainsi qu'à la chaîne macromoléculaire aliphatique. Avec l'acide chlorsulfonique, le P.C.V. réagit à partir de 60°–70°, avec introduction de groupes sulfoniques et formation de groupes carboxyliques, comme résultat des réactions d'oxydation.[5]

En sulfonant le P.C.V.N. à différentes durées de réaction on obtient des échangeurs de cations, qui se différencient par le degré de sulfonation. Ceci dépend de la durée et de la température de la réaction de sulfonation (fig. 4).

Par exemple, les échangeurs de cations obtenus à la sulfonation du P.C.V.N. par HSO_3Cl à 25° ont de plus grandes capacités d'échanges sulfoniques, de 0,85 méq/g plus élevées que ceux synthétisés pour la sulfonation du polymère par H_2SO_4 96 % à la même température (fig. 4 *a* et *b*). A 90° l'action du HSO_3Cl est plus énergique, la capacité d'échange sulfonique des échangeurs d'ions augmentant jusqu'à 2,96 méq/g et la capacité totale est de 3,32 méq/g, à la suite de l'apparition de la capacité d'échange carboxylique (fig. 4 *c*).

---

[5] M. Dima, I. Scondac, Ig. Poinescu, A. Carpov et Gh. Cotruț, *Studii si Cercetări Chim., Fil. Iași*, **15**, 233, 255, 265 (1963).

Les durées optimales des réactions de sulfonation sont influencées plutôt par la température à laquelle celles-ci ont lieu que par la nature d'agent de sulfonation. En général, les réactions de sulfonation sont complètes après approximativement 1—3 heures, les courbes de la dépendance des capacités d'échange sulfoniques de la durée des réactions de sulfonation étant très semblables (fig. 4).

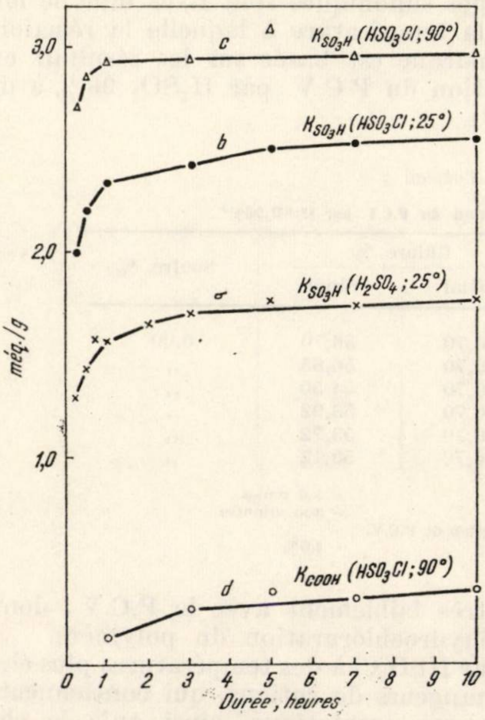

Fig. 4. — Influence de la durée de la réaction de sulfonation sur la capacité d'échanges sulfoniques ($K_{SO_3}H$) et carboxyliques (K_{COOH}); agent de sulfonation/P.C.V.N.—5,0

Les échangeurs de cations obtenus à la sulfonation du P.C.V.N. par HSO_3Cl, à 90°, contiennent du « soufre inactif » (tableau 3) et des groupes carboxyliques (fig. 4 *d*). Leur contenu dépend de la durée de la réaction de sulfonation.

Entre le degré de substitution (S %) du P.C.V.N. et les valeurs de la capacité d'échanges sulfoniques des échangeurs de cations obtenus à la sulfonation du polymère (25°) il existe une relation directe, comme conséquence de la fixation du groupe—SO_3H seulement au noyau naphtalénique (fig. 5). Le fait que les droites *a* et *b* de la figure 5 ont des inclinaisons différentes par rapport à l'abscisse s'explique par la sulfonation très accusée du noyau naphtalénique par le HSO_3Cl.[6]

---

[6] C. D. NENIȚESCU, « Chimie organică », vol. Ier, VIIe Éd., Ed. didactică și pedagogică, Bucarest, 1966, p. 512.

Le contenu de groupes sulfoniques fixés à la chaîne macromoléculaire aliphatique K'_{SO_3H} exprimé en capacité d'échanges sulfoniques est égal à la différence entre la capacité d'échange sulfonique du P.C.V.N.

Tableau 3

Influence de la durée et de la température de la réaction de sulfonation sur le contenu en soufre actif et inactif pour la sulfonation du P. C.V.N. par HSO_3 Cl à 90° (HSO_3 Cl/P.C.V.N. – 5,0)

N°	Durée de sulfonation minutes	Capacité d'échange sulfonique méq/g	Contenu en soufre		
			Total expéri-mental %	Calculé à partir du K_{SO_3H} %	Inactif %
1	30	2,86	11,42	9,15	2,27
2	60	2,93	11,51	9,37	2,14
3	180	2,95	11,81	9,44	2,37
4	300	3,09	12,61	9,88	2,62
5	420	2,96	12,53	9,47	3,06
6	600	2,96	12,08	9,47	2,61

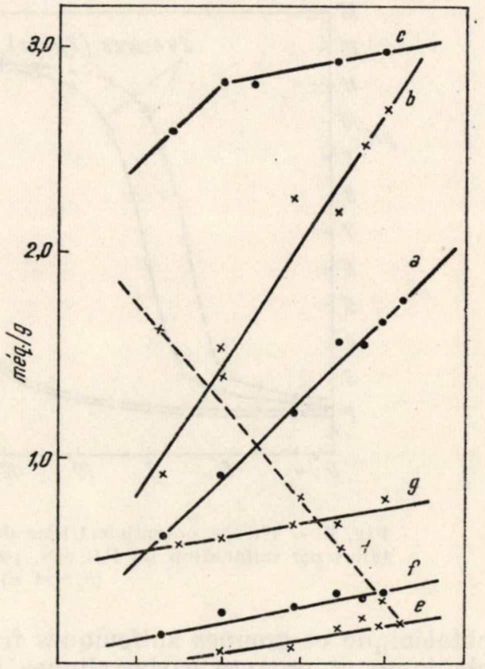

Fig. 5. — Dépendance des capacités d'échanges sulfoniques (K_{SO_3H} ; K_{SO_3H}) et carboxyliques (K_{COOH}) du degré de substitution (S %) du chlore dans le P.C.V.N. par le naphtalène ; agent de sulfonation /P.C.V.N. — 5,0 ; durée—5 heures.

sulfoné par HSO_3Cl à 90° et la capacité d'échanges sulfoniques à 25° (figure 5 ; d (K'_{SO_3H}). La valeur de K'_{SO_3H} décroît en même temps que le degré de substitution du chlore dans le P.V.N. par naphtalène croît.

Il fallait s'attendre à ce comportement, étant donné que par la croissance du degré de substitution le contenu en chlore, c'est-à-dire le nombre des unités chlorvinyliques, décroît, et partout la possibilité de sulfonation de ces unités structurelles est réduite. Pour des degrés de substitutions avancés, la déhydrochloruration intramoléculaire est la réaction dominante avec formation de doubles liaisons. Pratiquement, pour la sulfonation du P.C.V.N. avec des degrés de substitution dépassant 85 % on obtient des polyélectrolytes sulfoniques solubles dans l'eau.

Ces échangeurs de cations, obtenus par la sulfonation du P.C.V.N. par HSO_3Cl, à 90°, contiennent aussi des groupes carboxyliques ce qui leur donne un caractère polyfonctionnel.

La structure polyfonctionnelle de ces échangeurs de cations a été mise en évidence aussi par titrage potentiométrique (fig. 6).

L'allure des courbes de titrage potentiométrique, dans le cas de sulfonation à 25° du P.C.V.N. est semblable, indifféremment de la nature de l'agent de sulfonation (fig. 6 *a* et *b*). En échange, la sulfonation du P.C.V.N. par HSO_3Cl, à 90°, mène à des changements chimiques plus profonds. Les courbes de titrage potentiométrique mettent en évidence deux sortes de groupes sulfoniques (groupes sulfoniques fixés au noyau naphtalénique et groupes sulfoniques fixés à la chaîne macromoléculaire aliphatique) et groupes carboxyliques dans la structure de l'échangeur de cations (fig. 6 *c* et *d*).

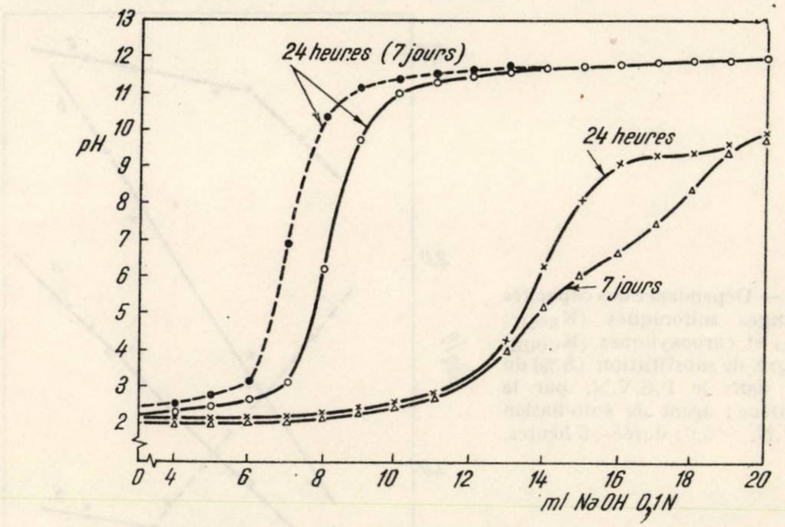

Fig. 6. — Titrage potentiométrique des échangeurs de cations obtenus par sulfonation du P.C.V.N. par H_2SO_4 96 % (*a*) et HSO_3Cl (*b*, *c* et *d*).

Les valeurs des capacités d'échanges sulfoniques et carboxyliques, déterminées potentiométriquement, concordent avec celles déterminées avec des solutions de $CaCl_2$ 2 ‰ et $Ca(CH_3COO)_2$ 2 ‰. Du point de vue théorique les échangeurs de cations sulfoniques basés sur le P.C.V.A. et le P.C.V.F. présentent également de l'intérêt. La sulfonation des polymères arylés a été faite par le HSO_3Cl à 25° et 90°. Le tableau 4 donne

Tableau 4

Sulfonation des polymères P.C.V.A. et P.C.V.F. par HSO_3Cl

P.C.V. arylé par	Température de sulfonation °C	Cl, %		Substitution S %	Pertes en chlore P %	Capacité d'échanges méq/g		
		avant sulfonation	après sulfonation			K_{SO_3H}	K_{COOH}	K_T
Anthracène	25°	13,28	12,95	76,58	2,50	1,76	0,49	2,25
Anthracène	90°	13,28	4,42	76,58	66,78	12,05 %		
					Soufre (soluble dans l'eau)			
Phénantrène	25°	32,19	24,13	43,23	23,48	1,74	0,16	1,90
Phénantrène	90°	32,19	3,68	43,23	88,56	2,94	0,62	3,56

les principales caractéristiques de ces types d'échangeurs de cations, qui, à part la capacité d'échanges sulfoniques, possèdent également une capacité d'échanges carboxyliques dont la valeur est suffisamment élevée. En sulfonant le P.C.V.A. à 90° on obtient des polyélectrolytes sulfoniques de couleur foncée solubles dans de l'eau.

La stabilité chimique de ces échangeurs d'ions est satisfaisante.

La réaction de sulfonation des polymères arylés par des hydrocarbures aromatiques polynucléaire, de même que pour les autres polymères arylés,[1,2] est accompagnée de réactions secondaires (déhydrochloruration des unités chlorvinyliques existentes dans la chaîne macromoléculaire à côté des unités structurellement vinylaromatiques, formation de groupes $>SO_2$, oxydation partielle des macromolécules avec formation de groupes $-COOH$, etc.), qui mènent à une structure plus compliquée des échangeurs de cations. Comme la réaction de déhydrochloruration des unités structurelles chlorvinyliques est la plus importante, puisqu'elle modifie essentiellement la structure des produits finals, elle a été étudiée en observant la dépendance des pertes procentuelles de chlore (P %) de différents facteurs, qui ont été analysés à la réaction de sulfonation. Les résultats obtenus sont donnés dans les figures 2,7–10.

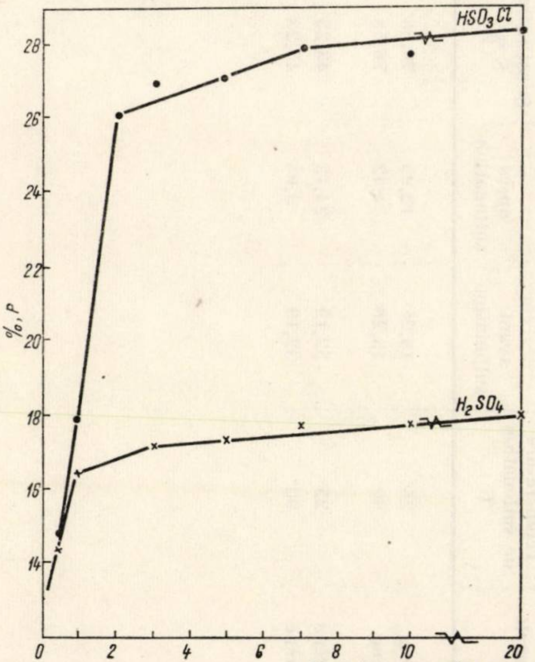

Fig. 7. — Influence de la quantité d'agent de sulfonation sur les pertes en chlore (P %) durée — 5 heures; température 25°.

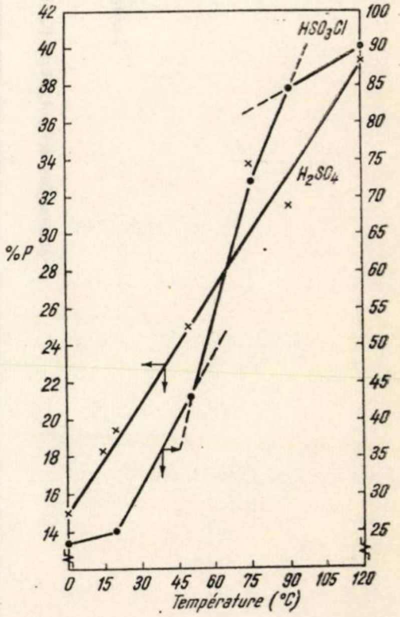

Fig. 8. — Influence de la température sur les pertes en chlore (P %) à la sulfonation de la P.C.V.N. par H_2SO_4 ou HSO_3Cl; agent de sulfonation/P.C.V.N. – 5,0; durée – 5 heures.

L'étude des diagrammes des figures 2,7–10 permet de remarquer :

– La réaction de déhydrochloruration du P.C.V.N. dépend de la nature et de la quantité de l'agent de sulfonation (fig. 7). Pour les mêmes rapports – agent de sulfonation/P.C.V.N. – 20,0 et la même température (25°) les pertes en chlore (P %), pour la sulfonation par HSO_3Cl, sont de 67,0 % plus grandes qu'au cas de sulfonation par H_2SO_4 96 %.

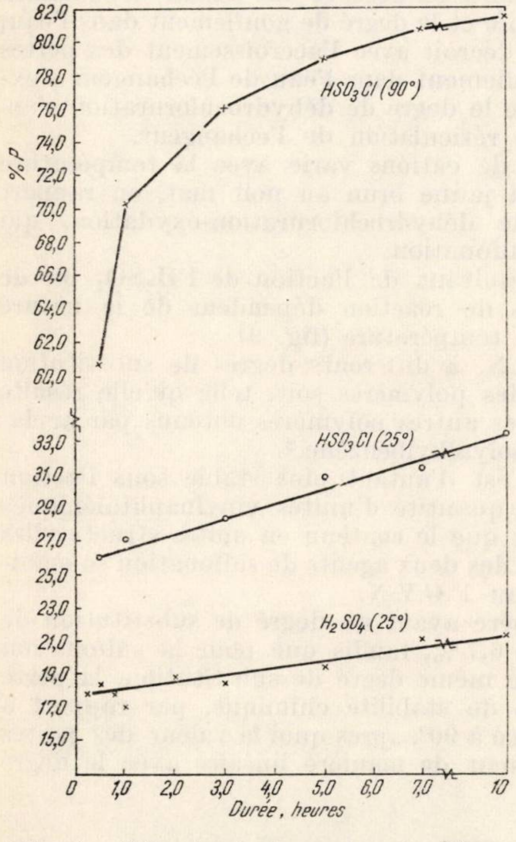

Fig. 9. – Dépendance des pertes en chlore (P %) de la durée de la réaction de sulfonation et de la nature de l'agent de sulfonation ; agent de sulfonation/P.C.V.N. – 5,0.

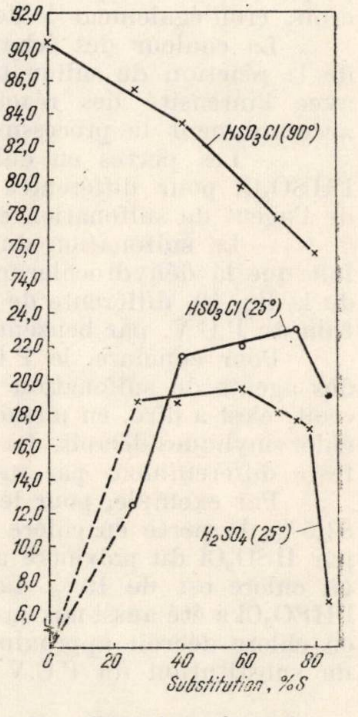

Fig. 10. – Dépendance des pertes en chlore (P %) du degré de substitution du chlore du P.C.V. avec du naphtalène ; agent de sulfonation/P.C.V.N. – 5,0 ; durée – 5 heures.

– Le degré de déhydrochloruration du P.C.V.N. décroît avec l'augmentation de la dilution du système (fig. 2).

– La valeur des pertes de chlore (P %) dépend de la température de la réaction de sulfonation du P.C.V.N. et de la nature de l'agent de sulfonation (fig. 8).

Les pertes en chlore à la sulfonation par H_2SO_4 ou HSO_3Cl augmentent avec la température de sulfonation. On remarque que dans le cas de sulfonation par H_2SO_4 les pertes en chlore dépendent linéairement de la température, ce qui n'a pas lieu à la sulfonation par HSO_3Cl (fig. 8).

L'allure des courbes (fig. 8) indique une différence appréciable entre la réactivité des deux acides.

Aux échangeurs d'ions résultants on observe une étroite dépendance entre les valeurs des pertes en chlore et le degré de gonflement dans l'eau, dans le sens que leur gonflement décroît avec l'accroissement des pertes en chlore. La décroissance du gonflement dans l'eau de l'échangeur s'explique par le fait qu'à mesure que le degré de déhydrochloruration s'accroît, croît également le degré de réticulation de l'échangeur.

La couleur des échangeurs de cations varie avec la température de la réaction de sulfonation, du jaune brun au noir mat, en rapport avec l'intensité des réactions de déhydrochloruration-oxydation, qui accompagnent le processus de sulfonation.

— Les pertes en chlore, résultant de l'action de l'H_2SO_4 ou de l'HSO_3Cl pour différentes durées de réaction dépendent de la nature de l'agent de sulfonation et de la température (fig. 9).

— La sulfonation du P.C.V.N. à différents degrés de substitution fait que la déhydrochloruration des polymères soit, telle qu'elle résulte de la fig. 10, différente de celle des autres polymères obtenus par arylation du P.C.V. par benzène,[1] ou polyalkylbenzène.[2]

Pour conclure, le P.C.V.N. est d'autant plus stable sous l'action des agents de sulfonation que la quantité d'unités vinylnaphtaléniques croît, c'est-à-dire, en même temps que le contenu en unités structurelles chlorvinyliques décroît. La nature des deux agents de sulfonation se manifeste différemment par rapport au P.C.V.N.

Par exemple, pour le polymère ayant un degré de substitution de 84,5 %, la perte en chlore est de 6,7 %, tandis que pour la sulfonation par HSO_3Cl du polymère ayant le même degré de substitution, la perte en chlore est de 19 %. Le degré de stabilité chimique, par rapport à l'HSO_3Cl a été aussi mis en évidence à 90°, après quoi la valeur des pertes en chlore décroît approximativement de manière linéaire avec le degré de substitution du P.C.V.N.

CONCLUSIONS

1. On a obtenu de nouveaux échangeurs de cations par sulfonation du polychlorure de vinyle arylé par hydrocarbures aromatiques polynucléaire.

2. Les échangeurs de cations synthétisés contiennent des groupes sulfoniques, et si la sulfonation a lieu par HSO_3Cl à 90°, des groupes carboxyliques apparaissent en même temps que des groupes sulfoniques.

3. La structure chimique des échangeurs de cations obtenus est fonction des conditions qui ont régi la sulfonation.

ORSZÁGOS MŰSZAKI KÖNYVTÁR ÉS DOKUMENTÁCIÓS KÖZPONT 1883

NOTE POUR LES AUTEURS

La *Revue Roumaine de Chimie* publie des articles en anglais, français, russe, allemand ou espagnol. Les auteurs sont priés d'envoyer des articles, notes, communications et comptes rendus inédits.

Les manuscrits seront dactylographiés à deux intervalles. Les tableaux seront dactylographiés sur feuilles séparées, de même que la légende des figures. Les diagrammes seront tracés à l'encre de Chine sur papier calque. Les tableaux et les figures seront numérotés par des chiffres arabes, en nombre strictement nécessaire. Prière de ne pas inscrire les mêmes données dans les tableaux et les figures. Les formules chimiques seront incluses dans le texte ; en outre, elles seront transcrites sur des feuilles séparées. Les auteurs sont priés d'indiquer les caractères italiques (en soulignant les lettres au crayon), ainsi que tout autre caractère spécial. L'ordre des références bibliographiques sera celui de leur mention dans le texte ; le nom de l'auteur sera précédé de l'initiale du prénom ; les publications périodiques seront présentées suivant les prescriptions internationales. Les références seront ajoutées à la fin de l'article ; elles paraîtront comme des notes, au bas de la page. Le texte sera précédé d'un résumé, comprenant 15 lignes au maximum.

L'entière responsabilité du contenu des articles appartient aux auteurs. On publie des articles dus aux collaborateurs roumains ou étrangers. Les auteurs recevront 50 tirés à part.

PRINTED IN ROMANIA

1972 AUG 1 [illegible]

TRAVAUX PARUS AUX ÉDITIONS DE L'ACADÉMIE DE LA RÉPUBLIQUE SOCIALISTE DE ROUMANIE

I. ZUGRĂVESCU et L. STOICESCU-CRIVETZ, **Polimeri heterociclici** (Polymères hétérocycliques), 1971, 190 p., 9,50 lei.

I. MAXIM, **Materiale nucleare** (Matériaux nucléaires), 1969, 444 p., 30 lei.

CORNEL BODEA et collab., **Tratat de biochimie vegetală**, partea I, **Fitochimie** (Traité de biochimie végétale, Ire partie, Phytochimie), Ier vol., 1964, 747 p. + 4 annexes + 2 pl., 41 lei ; IIe vol., 1965, 1262 p., 1 pl., 56 lei, IIIe vol., 1967, 773 p., 35 lei.

V. GHEŢIE et V. MICUŞAN, **Analiza imunochimică. Teorie şi practică** (Analyse immunochimique. Théorie et pratique), 1966, 369 p., 28 lei.

SILVIA IONESCU, **Reacţii chimice induse de radiaţiile ionizante** (Réactions chimiques produites par les radiations ionisantes), 1963, 271 p., 15 lei.

MARIETA NICOLAE, **Fizico-chimia proceselor fotografice** (Physico-chimie des processus photographiques), 1964, 426 p. + 4 pl., 35 lei.

R. PORTOCALĂ et L. POPA, **Acizii ribonucleici celulari şi virali** (Les acides ribonucléiques cellulaires et viraux), 1966, 375 p., 8 pl., 26 lei.

D. PURDELA et R. VÎLCEANU, **Chimia compuşilor organici ai fosforului şi ai acizilor lui** (La chimie des composés organiques du phosphore et de ses acides), 1965, 540 p., 37 lei.

CRISTOFOR SIMIONESCU, MARGARETA GRIGORAŞ et AGATA CERNĂTESCU-ASANDEI, **Chimia lemnului din R.P.R.** (La chimie du bois en Roumanie), 1964, 239 p. + 6 pl., 27 lei.

CRISTOFOR SIMIONESCU et CLEOPATRA VASILIU-OPREA, **Mecanochimia compuşilor macromoleculari** (La mécanochimie des composés macromoléculaires), 1967, 344 p., 23,50 lei.

I.P.I. c. 1364

43 426

Lei 25.—

F 1103

04-

ENTRALA

REVUE ROUMAINE DE CHIMIE

Tome 17

N° 7

Juillet 1972

RRCHAX, 17, 7, 1137–1284 (1972)

ÉDITIONS DE L'ACADÉMIE DE LA RÉPUBLIQUE SOCIALISTE DE ROUMANIE

Rev. Roumaine Chim.

17, 7, p. 1137–1284 (1972), Bucarest

COMITÉ DE RÉDACTION

Rédacteur en chef :

I. G. MURGULESCU, membre de l'Académie de la République Socialiste de Roumanie

Rédacteurs en chef adjoints :

A. T. BALABAN et V. EM. SAHINI, membres correspondants de l'Académie de la République Socialiste de Roumanie

Collège de rédaction :

C. DRĂGULESCU, RALUCA RIPAN, CR. SIMIONESCU, membres de l'Académie de la République Socialiste de Roumanie; EM. BRATU, ECATERINA CIORĂNESCU-NENITZESCU, P. SPACU, membres correspondants de l'Académie de la République Socialiste de Roumanie; MARGARETA AVRAM, I. D. MARGHIDAN, G. NIAC et D. SĂNDULESCU

La *Revue Roumaine de Chimie* paraît 12 fois par an. Toute commande de l'étranger (fascicules ou abonnements) sera adressée à Întreprinderea Rompresfilatelia, Boîte postale 2001, telex 011631, Bucarest, Roumanie

Les manuscrits, les livres et les revues proposés en échange, ainsi que toute correspondance seront envoyés à la rédaction :

REVUE ROUMAINE DE CHIMIE
23, str. Dumbrava Roşie, Bucarest, Roumanie

ÉDITIONS DE L'ACADÉMIE DE LA RÉPUBLIQUE SOCIALISTE DE ROUMANIE,
3 bis, str. Gutenberg, Bucarest

ORSZÁGOS MŰSZAKI KÖNYVTÁR ÉS DOKUMENTÁCIÓS KÖZPONT
1883

REVUE ROUMAINE DE CHIMIE

Tome 17, N° 7 Juillet 1972

Page

M. CIOPEC and D. I. MARCHIDAN, The use of the digital computer in the phenomenological thermodynamics. I. Termox — program for processing experimental data from the thermodynamical measurements of oxides. . . . . 1139—1146

S. STERNBERG and MARIANA TERZI, Surface tension of the reciprocal molten salt pairs (Na, Ag, Cl, Br) . . . . 1147—1151 R

O. RADOVICI, MARIA MAVRODIN-TĂRĂBÎC, IOANA ONACA et I. SOLACOLU, L'étude de la réduction de l'oxygène sur les électrodes poreuses en argent . . . . 1153—1161 R

VIOLETA ALEVRA, D. CIOMÎRTAN and MARIA IONESCU, Influence of the preparation method on the structure and physical properties of alumina. I. Aluminium hydroxides . . . . 1163—1179 R

C. DRĂGULESCU, ANA NIMARĂ and I. JULEAN, Contributions to the bismuth hydrolysis study. II. Spectrophotometric and polarographic investigations on bismuthyl perchlorate hydrolysis . . . . 1181—1190

MARGARETA TEODORESCU, MARIA BREZEANU and P. SPACU, Cobalt complexes with 2,9-dimethyl-1,10-phenanthroline . . . . 1191—1197

MARIA MAVRODIN, Nouveaux réactifs pour le dosage spectrophotométrique de l'uranium . . . . 1199—1209

I. TEOREANU, Considérations générales sur l'apparition des propriétés liantes 1211—1217

Ş. SOLACOLU und D. TENŢULESCU, Struktur der gezogenen Glasfasern aus dem System $Na_2O-ZnO-SiO_2$ . . . . 1219—1226

A.T.BALABAN and N. NEGOIŢĂ, Factors affecting stability and equilibria of free radicals. VII. Arenesulphonyl-phenyl-nitroxides and 1-arenesulphonyl-2,2-diphenylhydrazyls . . . . 1227—1234

M. MORARU and F. CHIRALEU, Spectra-stereochemistry correlations for bicyclic rigid arylidenecyclohexanones . . . . 1235—1240

EUGENIA BALTĂ, Etude de la réaction d'alkylation du colorant azoïque benzothiazolique à l'aide de l'analyse thermique différentielle . . . . 1241—1252

M. E. LUPEŞ, The mechanism of the benzidine rearrangement. . . . . 1253—1260

M. IOVU, Aromatic bis-ethers. III. Condensation of sodium dimethylphenoxides with dichloromethylated derivatives . . . . 1261—1266 R

A. WOHL, Prinzipielle Betrachtungen über die Wirksamkeit einiger Reinigungsmethoden durch Adsorption. II. Mathematische Modelle . . . . . . 1267—1279

COMPTES RENDUS . . . . 1281—1284

Rev. Roumaine Chim. 17, 7, p. 1137—1284 (1972), Bucarest

Revue Roumaine de Chimie, 17, 7, 1139–1146 (1972)

THE USE OF THE DIGITAL COMPUTER IN THE PHENOMENOLOGICAL THERMODYNAMICS. I

TERMOX – PROGRAM FOR PROCESSING EXPERIMENTAL DATA FROM THE THERMODYNAMICAL MEASUREMENTS OF OXIDES

M. CIOPEC and D. I. MARCHIDAN

Center of Physical Chemistry, str. Galaţi 31,
Bucharest, Romania

Received March 14, 1972

The computation program set forth is written in the FORTRAN IV language and is adapted for use on IBM system 360/30 computer. For sets of 100 pairs of experimental data the computation duration does not exceed 4 minutes. TERMOX helps to process experimental enthalpies with a view of obtaining the analytical relation $H_T - H_{298.15} = f(T)$, by which derivated thermodynamic magnitudes can be deduced. The program provides for the calculation of regression coefficients by the least square method for relations of the following form

$$H_T - H_{298.15} = a + b(T) + c(T^2)$$

$$H_T - H_{298.15} = a + b(T) + c(T^2) + d(T^3)$$

$$H_T - H_{298.15} = a + b\,(T) + c(T^2) + d(T^{-1})$$

$$H_T - H_{298.15} = 2 + b(T) + c(T^2) + d(T^{-2}),$$

as well as for the listing of values of experimental and calculated enthalpies, of absolute, relative and standard calculated deviations. When the percent standard deviations is less than 2%, then the values of enthalpies, of heat capacities, of the increases in entropies and free energies are calculated and listed for the whole working range, every 50 K.

★

Nowadays one of the most important phenomena, with major significances and deep implications in every domain of human activity, lies both in the huge proliferation of digital computers and in their extended use. As a natural consequence of this phenomenon, specialists of the most varied realms should become acquainted with the programming and use of computers, at least in their own research field.

For the research worker the computer can and must be an immediate help in processing the own experimental data, an objective judge of the accuracy of the experiments.

Undoubtedly, not even the most advanced computer will ever enable the improvement of the performances of outdated apparatuses or methods, which does not suit the chosen research field. It can, however, report, with unparalleled impartiality and enviable objectivity, the mistakes and the vulnerable points in the research, it can point to the shortest and most efficient pathway which helps improve the performances.

Thermodynamics, fundamental discipline of the physical chemistry, due to its pronounced experimental character and its manysided theoretical possibilities, may wholly avail itself of the advantages of digital computers.

The thermodynamic studies of the oxides, the measurements of the physico-chemical properties of such systems, mightly asserted themselves the last decades and have stored an appreciable amount of data and scientific knowledge.

The experimental techniques devised for the investigation of the compounds have been improved and diversified, the theoretical concepts have been developed, while the knowledge of the intimate structure and its correlation to the physico-chemical and the thermodynamical properties has been more thoroughly studied.

Concomitantly, the application domains of the oxides have been extended to the manufacturing of semi-conductors, of fireproof and superfireproof materials, to the manufacturing of ceramic nuclear fuel a.s.o.

The research centered around the technological use of the oxides enjoyed a quick progress, since the thermodynamics of such systems is of outmost importance for the economy.

★

Studies carried out on the thermodynamic properties of some compounds in the uranium-oxygen system, [1,2] with the final aim of obtaining the values of entropy, heat capacity, increase in entropy and free energy, have required the processing of experimental data of heat content in the range 300 — 1300 K, by the least squares method, in order to obtain the functional dependence enthalpy-temperature. The problem of checking the various empirical relations of functional dependence has been raised, the selection having as unique criterion the value of the standard deviation. To this end we have resorted to the digital computer.

CALCULATION PROGRAM

To elaborate the TERMOX program (THERModynamics of OXides) we have used an algorithm based on the mathematical treatment of regressional analysis problems by the least squares method. [3-5]

---

[1] D. I. Marchidan and M. Ciopec, *Rev. Roumaine Chim.*, **15**, 1287 (1970).

[2] D. I. Marchidan and M. Ciopec, *Rev. Roumaine Chim.*, **16**, 1145 (1971).

[3] C. J. Brookes, I. G. Betteley and S. M. Loxton, "Mathematics and Statistics for Chemists", J. Wiley & Sons, New York, 1966, p. 346.

[4] A. G. Worthing and J. Geffner, "Treatment of Experimental Data", ed. 7, J. Willey & Sons, New York, 1955, cap. XI.

[5] I. I. Plăcințeanu, "Teoria erorilor de măsurare şi metoda celor mai mici pătrate", Ed. Tehnică, Bucharest, 1957, p. 200.

Denoting by H the experimentally measured enthalpy ($H_T - H_{298.15}$) and by T the absolute temperature, we have to find the dependence $H = f(T)$, that for the systems under consideration may have the following form[6] :

$$H = a + b(T) + c(T^2) \tag{1}$$

$$H = a + b(T) + c(T^2) + d(T^3) \tag{2}$$

$$H = a + b(T) + c(T^2) + d(T^{-1}) \tag{3}$$

$$H = a + b(T) + c(T^2) + d(T^{-2}) \tag{4}$$

To calculate coefficients a, b, c, d, the available experimental data will undergo a regressional analysis by the least squares method. This is tantamount to the condition that the sum of squared deviations should be minimum. For a functional dependence as that in relation (2) this condition is written as

$$S = \sum_{1}^{N} \{H - [a + b(T) + c(T^2) + d(T^3)]\}^2 \tag{5}$$

$$(\partial/\partial a)\, S = 0 ;\ (\partial/\partial b)\, S = 0 ;\ (\partial/\partial c)\, S = 0 ;\ (\partial/\partial d)\, S = 0 \tag{6}$$

i.e.

$$\begin{aligned} &aN + b\Sigma(T) + c\Sigma(T^2) + d\,\Sigma(T^3) = \Sigma(H) \\ &a\,\Sigma(T) + b\,\Sigma(T^2) + c\,\Sigma(T^3) + d\,\Sigma(T^4) = \Sigma(HT) \\ &a\,\Sigma(T^2) + b\Sigma(T^3) + c\,\Sigma(T^4) + d\,\Sigma(T^5) = \Sigma(HT^2) \\ &a\,\Sigma(T^3) + b\,\Sigma\,(T^4) + c\,\Sigma(T^5) + d\,\Sigma(T^6) = \Sigma(HT^3) \end{aligned} \tag{7}$$

Solving system (7) by an usual method (Gauss) we obtain the numerical values of the coefficients a, b, c, d.

The Gauss method of solving such a system may be applied by resorting to one of the subroutines existent in the library of scientifical subroutines of the computer. In the present case we used subroutine GELG i.e. solving by means of the Gauss elimination with complete pivoting. [7]

---

[6] M. N. Rand and O. Kubaschewski, "The Thermochemical Properties of Uranium Compounds", Interscience Publishers, London, 1963.

[7] * * * IBM Application Program H20–0205–3, "System/360 Scientific Subroutine Package. Programmer's Manual", IBM Corporation, New York, 1968, p. 121.

With an analytical relation of type (2) we can calculate the enthalpy values for all T temperatures at which determinations had been carried out, the values of the absolute deviations being

$$\Delta_{abs.} = H_{exp.} - H_{calcd}$$

of the relative (percent) deviations

$$\Delta_{rel} = 100 \times (H_{exp.} - H_{calcd}) / H_{exp}$$

absolute standard error

$$\sigma_{abs} = \sqrt{\left[\sum_{1}^{N} (\Delta_{abs})^2\right] / (N-1)} \tag{8}$$

and relative (percent) standard error

$$\sigma_{rel} = \sqrt{\left[\sum_{1}^{N} (\Delta_{rel})^2\right] / (N-1)} \tag{9}$$

From relation of type (2) we can deduce the relation describing the variation of the heat capacity with temperature

$$C_p = (\partial / \partial T)(H_T - H_{298.15})_p = b + 2c(T) + 3d(T^2) \tag{10}$$

The entropy variation is calculated from relation

$$S_T - S_{298.15} = \int_{298.15}^{T} (C_p/T)\, dT = b \ln (T/298.15) + 2c\,(T - 298.15) +$$

$$+ (3/2)\, d\, [(T^2) - (298.15)^2] \tag{11}$$

while the value of the free energy from

$$(G_T - H_{298.15})/T + S_T = (H_T - H_{298.15})/T = a/(T) + b + c(T) + d(T^2) \tag{12}$$

By means of (2), (10) — (12) we can calculate the functional thermodynamical values at various temperatures, in the working range.

Based on the cited algorithm, we have elaborated the calculation program TERMOX in the FORTRAN IV language (variant FULL FORTRAN) according to the following logical scheme :

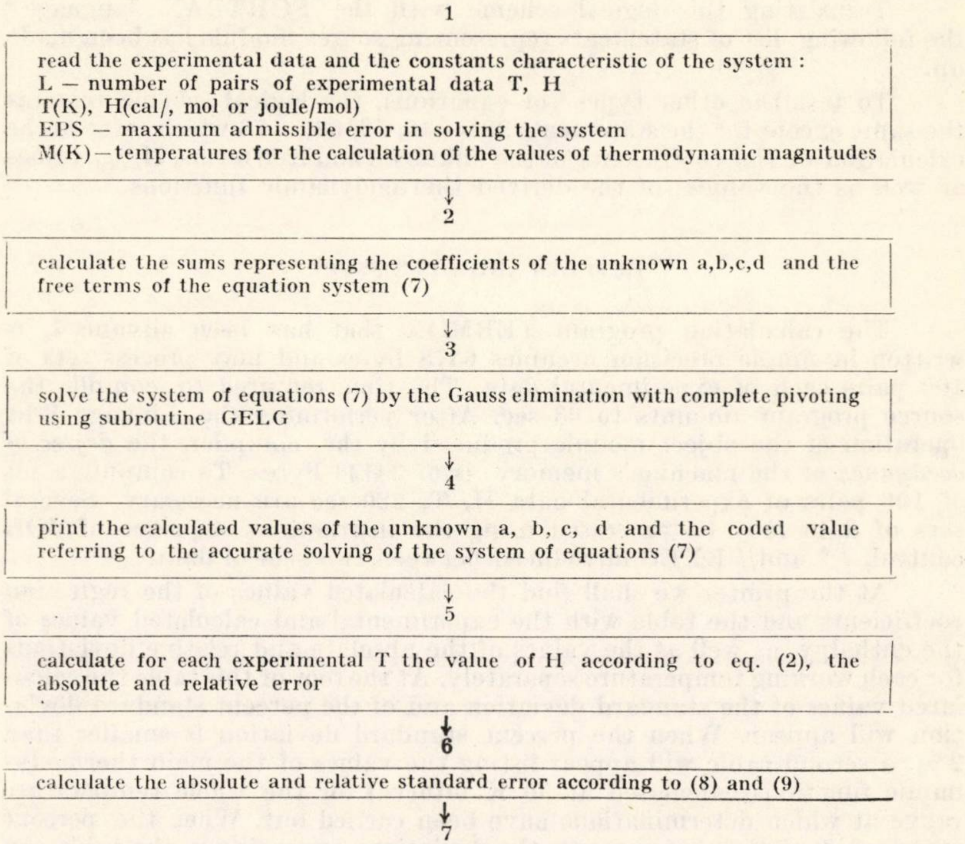

1

read the experimental data and the constants characteristic of the system :
L — number of pairs of experimental data T, H
T(K), H(cal/, mol or joule/mol)
EPS — maximum admissible error in solving the system
M(K) — temperatures for the calculation of the values of thermodynamic magnitudes

2

calculate the sums representing the coefficients of the unknown a,b,c,d and the free terms of the equation system (7)

3

solve the system of equations (7) by the Gauss elimination with complete pivoting using subroutine GELG

4

print the calculated values of the unknown a, b, c, d and the coded value referring to the accurate solving of the system of equations (7)

5

calculate for each experimental T the value of H according to eq. (2), the absolute and relative error

6

calculate the absolute and relative standard error according to (8) and (9)

7

print the table of experimental and calculated data, the absolute and relative errors : T, H_{exp}, H_{calcd}, DEV, PDEV ; type the values of the relative and absolute standard deviation : ABAT, PABAT

8

PABAT − 2 = 0 → YES

NO

9

calculate for the temperatures ranging from 300 to 1300 K, at 50 K intervals the values of the thermodyn amic functions : $H_t - H_{298.15}$, C_p, $S_T - S_{298.15}$, $S_T + (G_T - H_{298.15})/T$ according to rel. (2), (10)–(12)

10

print the table of the values of thermodynamic functions calculated at sequence 9

11

STOP

Translating this logical scheme with the FORTRAN language[8] the following list of statements representing source module has been made up.

To test the other types of equations, the logical scheme remains the same except for the statements 28 — 46, 53, 68 — 73 which refer to the calculation of the coefficients of the unknown and free terms, H_{calcd} values as well as the values of the derived thermodynamic functions.

RESULTS AND DISCUSSION

The calculation program TERMOX that has been advanced, is written in simple precision, occupies 6378 bytes and may process sets of 100 pairs each of experimental data. The time required to compile the source program amounts to 63 sec. After performing the Linkage Edit operation of the object module produced by the compiler, the *degree of occupancy* of the machine's memory is of 34144 bytes. To compute a set of 100 pairs of experimental data H, T, 220 sec are necessary. Several sets of data may be processed using the instructions sequence of JOB control, / * and// EXEC introduced between two sets of data.

At the printer we shall find the calculated values of the regression coefficients and the table with the experimental and calculated values of the enthalpy, as well as the values of the absolute and relative deviations for each working temperature separately. At the foot of this table the calculated values of the standard deviation and of the percent standard deviation will appear. When the percent standard deviation is smaller than 2 % a second table will appear listing the values of the main thermodynamic functions calculated at 50 K interval for the whole temperature range at which determinations have been carried out. When the percent standard deviation is too great, the deviations appearing in the table can be analysed and dropped from the computation of the pairs of the data which generate inadmissibly great deviations, without, however, impairing the significant temperatures at which measurements have been performed. In this way we obtain a relation reflecting more accurately the dependence of the measured magnitude on the temperature.

To exemplify we present in the following the results obtained by processing a set of experimental data stemming from determinations carried out with a drop calorimeter, [2] on a non-stoichiometric oxide of uranium. [9] With the set of 39 pairs of experimental data we have checked the relations of functional dependence of the type (1) — (4) obtaining the results in Table I.

Table 1 shows that the enthalpy dependence on temperature is described with a minimum deviation (Fig. 1) by relation

$$H_T - H_{298.15} = 20155.7 + 63.95(T) + 16.68.10^{-3}(T^2) - 2.38.10^{-6}(T^3) \pm$$
$$\pm\ 269.6 \text{ joule/mol}$$

[8] * * IBM Systems Reference Library Form C28—6515—7, "IBM System/360. Fortran IV language", ed. 8, IBM Corporation, New York, 1968.

[6] D. I. Marchidan and M. Ciopec, *Rev. Roumaine Chim.*, (in press).

Table 1

Final results obtained on checking various types of analitical relations

$H_T - H_{298.15}$ (J/mol)	REGRESSION COEFFICIENTS				Standard deviation (J/mol)
	a	b	c	d	
$a+bT+cT^2$	−21087.11	68.10374	$11.03753(10^{-3})$	–	273.0886
$a+bT+cT^2+dT^3$	−20155.68	63.94986	$16.67863(10^{-3})$	$-2.381161(10^{-6})$	269.5891
$a+bT+cT^2+dT^{-1}$	−23336.30	71.28314	$9.64994(10^{-3})$	$0.4828268(10^{-6})$	271.9629
$a+bT+cT^2+dT^{-2}$	−21905.62	69.62456	$10.29934(10^{-3})$	$52.90678(10^{6})$	272.5212

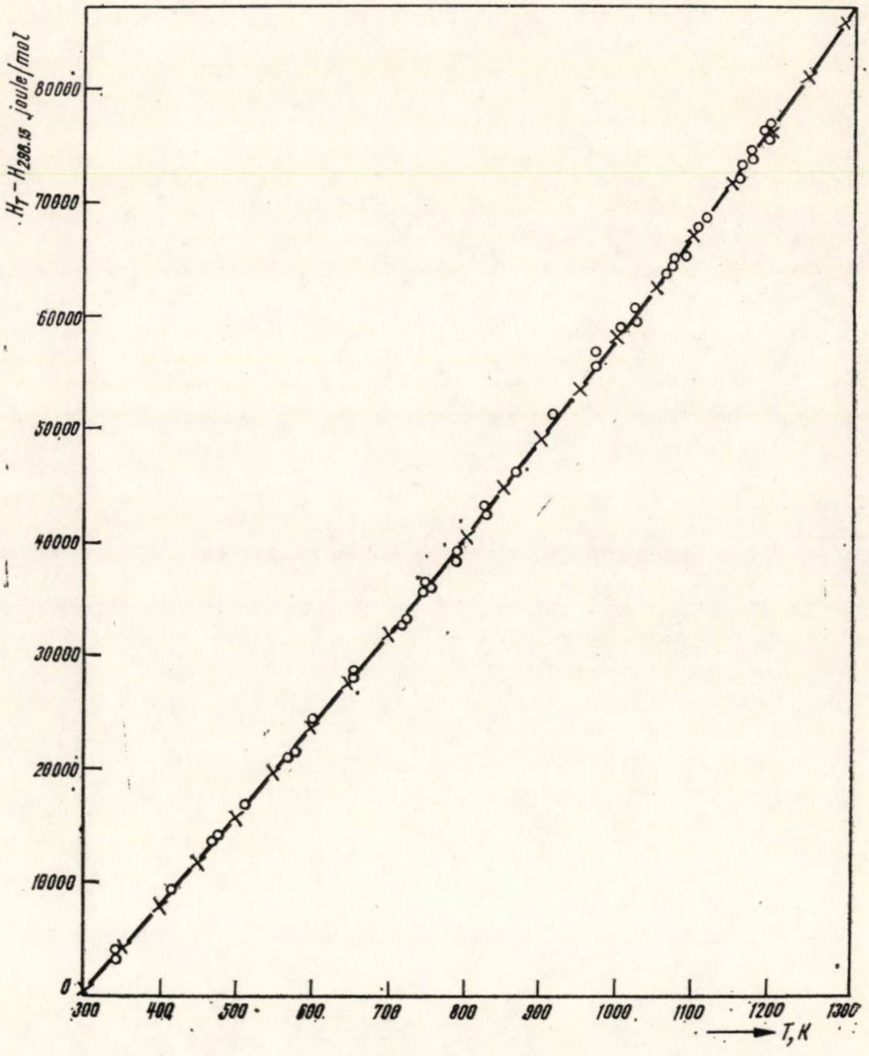

Fig. 1. — Deviation of experimental data from the calculated curve ;
0 = experimental point ; X = calculated point.

For this type of relation, using the source program previously presented, the results in table 2 will appear on the print paper.

The TERMOX program has a prononunced working tool character. It has been checked according to sets of experimental data resulted from various measurements.

The details (seemingly unsignificant) provided by the present contribution, may facilitate the use of this program as such, also by personnel less acquainted with the usage of digital computer.

Revue Roumaine de Chimie, **17**, 7, 1147 – 1151 (1972)

SURFACE TENSION OF THE RECIPROCAL MOLTEN SALT PAIRS (Na, Ag, Cl, Br)

S. STERNBERG and MARIANA TERZI
Institute of Physical Chemistry
Str. Galaţi 31, Bucharest, Romania

Received March 3, 1972

The surface tension of the molten $NaCl + AgBr$, $NaBr + AgCl$ and $NaBr + AgBr$ mixtures as well as pure molten NaBr and AgBr was measured. The surface tension dependence on temperature and composition was studied. A method of detachment of a platinum pin from the melt surface was used. The surface tension isotherms for the $NaCl + AgBr$, $NaBr + AgCl$ and $NaBr + AgBr$ systems show large negative deviations from linearity. The surface tension was calculated according to Eberhart's equation.

There are only a few surface tension data in the literature for the reciprocal systems of molten salts.[1-3] In the present paper, our results obtained from the surface tension measurements of molten $NaCl + AgBr$, $NaBr + AgCl$ and $NaBr + AgBr$ mixtures are presented. The surface tension data of molten binary mixtures $NaCl + AgCl$,[4] $NaCl + NaBr$[5] and $AgCl + AgBr$[6] were previously reported.

EXPERIMENTAL

The measurements of surface tension were carried out by a detachment method, adapted by Janz and Lorenz [7] for molten salts. This consists of measuring the force necessary to detach a platinum pin from the melt surface. Details of the device used were reported in our previous paper. [4] Use was made of a platinum pin the dimensions of which were calibrated at 20° in distilled water and different organic liquids with surface tensions accurately known, such as benzene, carbon tetrachloride, toluene, and acetone. A quartz vessel was used for the melts.

The surface tension σ was calculated from the equation:

$$\sigma = AG/(1 + \alpha \Delta T) \qquad (1)$$

---

[1] V. K. Semencenko and L. P. Shikobalova, *Zhur. fiz. Khim.*, **21**, 707 (1947).
[2] I. D. Sokolova and N. K. Voskresenskaia, *Zhur fiz. Khim.*, **36**, 955 (1962).
[3] R. B. Ellis and A. C. Freeman, *J. Phys. Chem.*, **69**, 1443 (1965).
[4] S. Sternberg and M. Terzi, *Rev Roumaine Chim.*, **15**, 527 (1970).
[5] G. Bertozzi, *J. Phys. Chem.*, **69**, 2606 (1965).
[6] N. K. Boardman, A. R. Palmer and E. Heymann, *Trans. Faraday Soc.*, **51**, 277 (1955).
[7] G. I. Janz and M. R. Lorenz, *Rev. Sci. Instr.*, **31**, 18 (1960).

where A is a constant specific to the pin dimensions and equal to $g/2\pi r_0$, g being the acceleration of free fall and r_0 the pin radius at calibration temperature, α is the linear expansivity of platinum, equal to 8.86810^{-6} degree^{-1}, ΔT is the difference between the measurement and calibration temperatures and G is the difference between the mass of the pin when the liquid film which adheres to the pin surface has a maximum pull (which is indicated by a sudden increase of the pin mass observed at the analytical balance) and the mass of the pin after the detachment. The value obtained for A is 2492 s^{-2}.

The temperature was maintained constant, within ± 0.5°, by means of a thermostating device with a photocell, and was measured directly in the melt, 2 mm under the melt level, with a Pt-PtRh 10 % thermocouple. Chemically pure NaCl and NaBr, recrystallized and melted in dried gaseous HCl and HBr to remove the traces of mixture, were used. The gaseous halogenated acids were obtained from their solutions by dehydration with concentrated H_2SO_4. AgCl and AgBr were prepared from chemically pure $AgNO_3$ and HCl, respectively HBr, and then pre-melted.

For each composition, 8 to 10 surface tension measurements were carried out over a temperature range of 200°. The experimental results were reproducible within 1 per cent.

RESULTS AND DISCUSSION

The surface tensions for the pure NaBr and pure AgBr as well as for the reciprocal salt pairs (Na, Ag, Cl, Br) were measured as a function of temperature and composition. A linear dependence of surface tension σ on temperature t holds within a temperature range of 200° above the melting temperature for all the simple salts and mixtures studied:

$$\sigma = a - bt \qquad (2)$$

Table 1

Temperature variation of surface tension for reciprocal molten NaCl+AgBr and NaBr+AgCl mixtures at mole fraction x(AgX) of silver halide

NaCl+AgBr mixture

x(AgX)	a dyne cm^{-1}	b.10^3 dyne cm^{-1} degree^{-1}	Av. Std. Dev. for σ, dyne cm^{-1}	Temperature range °C
1.0	177.998 ± 0.681	−39.969 ± 1.112	±0.426	467 − 728
0.9	191.820 ± 2.992	−73.619 ± 4.269	±0.314	650 − 750
0.8	186.592 ± 1.868	−75.435 ± 2.715	±0.271	625 − 748
0.7	183.690 ± 1.531	−75.125 ± 2.094	±0.279	650 − 812
0.5	171.518 ± 0.639	−66.856 ± 0.835	±0.104	691 − 841
0.3	170.860 ± 0.989	−71.089 ± 1.213	± 0.150	728 − 881
0.2	187.347 ± 1.675	−90.857 ± 1.992	±0.187	780 − 899
0.1	182.875 ± 1.035	−86.371 ± 1.213	± 0.170	783 − 915
0.0	186.912 ± 0.968	−90.033 ± 2.083	± 0.405	811 − 942
		NaBr + AgCl mixture		
1.0	209.189 ± 0.752	−56.412 ± 2.531	± 0.109	460 − 706
0.9	197.187 ± 1.169	−59.036 ± 1.893	± 0.293	506 − 703
0.8	188.237 ± 1.686	−60.369 ± 2.366	± 0.349	602 − 793
0.7	188.758 ± 0.875	−73.490 ± 1.228	± 0.162	633 − 791
0.5	181.645 ± 2.024	−79.272 ± 2.501	± 0.275	746 − 888
0.3	163.253 ± 1.762	−68.341 ± 2.118	± 0.246	757 − 901
0.1	163.862 ± 1.904	−76.632 ± 2.297	± 0.267	751 − 902
0.0	154.841 ± 1.207	−68.195 ± 1.409	± 0.256	773 − 920

The values of constants *a* and *b* together to the standard average deviation for σ derived by the least squares method for the three mixtures are given in Tables 1 and 2.

Table 2

Temperature variation of surface tension for binary molten NaBr + AgBr mixture at mole fraction of silver bromide x (AgBr)

x(AgBr)	a dyne cm^{-1}	b.10^3 dyne cm^{-1} degree^{-1}	Av. Std. Dev. for σ dyne cm^{-1}	Temperature range °C
1.0	177.998 ± 0.681	−39.969 ± 1.112	± 0.426	467 – 727
0.9	173.680 ± 0.216	−48.467 ± 0.344	± 0.063	502 – 731
0.8	174.244 ± 0.367	−60.253 ± 0.567	± 0.079	557 – 730
0.7	164.996 ± 0.773	−55.568 ± 1.171	± 0.189	551 – 753
0.5	161.309 ± 1.151	−61.527 ± 1.522	± 0.220	667 – 850
0.3	164.115 ± 1.420	−72.324 ± 1.832	± 0.237	689 – 854
0.1	165.110 ± 1.328	−78.221 ± 1.575	± 0.192	764 – 918
0.0	154.841 ± 1.207	−68.195 ± 1.409	± 0.256	773 – 920

Our values of surface tension for NaBr are the same as those of Bertozzi,[5] obtained by the Wilhelmy plate method, but are by 4 % lower than those of Jaeger,[8] and by 4 % higher than the results of Bloom,[9] who used the maximum bulble pressure method. Our results for AgBr are by 4 % higher than those of Boardman et al.,[6] obtained by the maximum bulble pressure method.

The surface tension isotherms *versus* the mole fraction of silver halide for the reciprocal NaCl + AgBr and NaBr + AgCl mixtures, at 800°, are plotted in Figure 1. In Figure 2, the surface tension isotherm for the binary NaBr + AgBr system, at 800°, is represented. The large negative deviations from linearity are visible for all the three systems.

In Figures 1 and 2, together with the experimental points for all mixtures (full lines) the surface tensions calculated according to Eberhart[10] equation (dashed lines) are represented also :

$$\sigma = x_A^\sigma \sigma_A + x_B^\sigma \sigma_B = (s x_A \sigma_A + x_B \sigma_B)/(s x_A + x_B), \tag{3}$$

where x_A and x_B are the mole fractions in the bulk liquid, x_A^σ and x_B^σ are the mole fractions in the surface layer of the liquid, σ_A and σ_B are the surface tension values for the pure salts, and s is a factor of enrichment of the surface layer in the component with the smaller surface tension. This is defined, according to Eberhart,[10] by the equation :

$$s = x_A^\sigma x_B / x_B^\sigma x_A \tag{4}$$

The values of s were determined by the Eberhart[10] method in which ξ is plotted against ξ/r. A straight line was obtained having the slope s according to the equation :

$$\xi = -s(\xi/r) + 1 \tag{5}$$

---

[8] F. M. Jaeger, *Z. anorg. Chem.*, **1**, 101 (1917).

[9] H. Bloom, F. G. Davis and D. W. James, *Trans. Faraday Soc.*, **56**, 1179 (1960).

[10] J. G. Eberhart, *J. Phys. Chem.*, **70**, 1183 (1966).

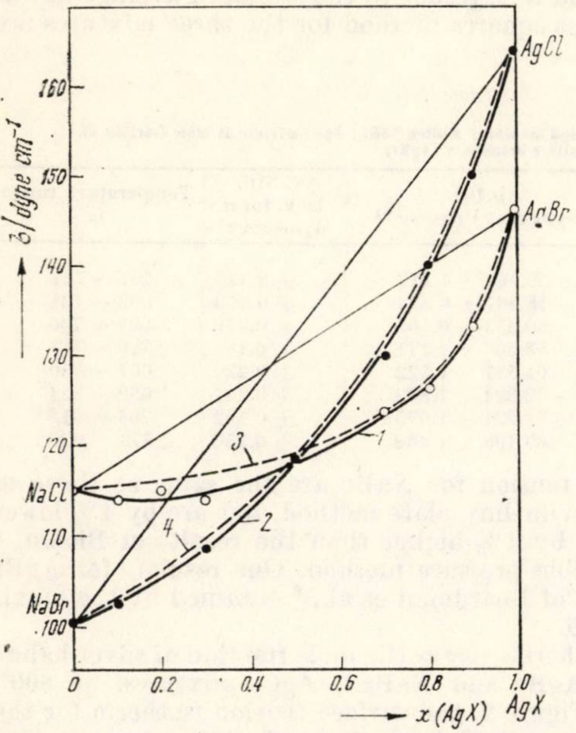

Fig. 1. – Surface tension isotherms at 800° for the reciprocal NaCl + AgBr and NaBr + AgCl mixtures :

1, experimental curve for NaCl + AgBr mixture ; *2*, experimental curve for NaBr + AgCl mixture ; *3* and *4*, calculated curves (eq 3).

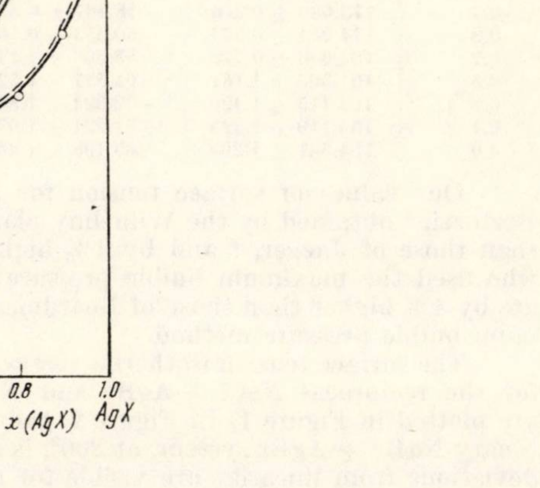

Fig. 2. – Surface tension isotherm at 800° for the NaBr + AgBr mixture :

1, experimental curve ; *2*, calculated curve (equation 3).

where ξ and r are given by the relations :

$$\xi = (\sigma - \sigma_A)/(\sigma_B - \sigma_A)\,;\; r = x_B/x_A \tag{6}$$

The following values of s were obtained : 6.53 for NaCl + AgBr mixture, 2.65 for NaBr + AgCl mixture, and 2.96 for NaBr + AgBr mixture, at 800°. These values were used in eq. (3) to represent the dashed lines in Figures 1 and 2. A very good agreement is found between the experimental curve and that calculated according to Eberhart equation for the NaBr + AgCl and NaBr + AgBr systems. For the NaCl + AgBr mixture there is a small deviation from the experimental curve (within experimental errors) at high NaCl concentrations.

Revue Roumaine de Chimie, 17, 7, 1153 – 1161 (1972)

L'ÉTUDE DE LA RÉDUCTION DE L'OXYGÈNE SUR LES ÉLECTRODES POREUSES EN ARGENT

O. RADOVICI, MARIA MAVRODIN-TĂRĂBÎC, IOANA ONACA
et I. SOLACOLU
Centre de Chimie Physique, Bucarest, 31, str. Galaţi

Reçu le 24 février 1972

On a réalisé une série d'électrodes à gaz en argent du type MSK(«Monoskelet Katalyst») à petits pores, du type MSK à grands pores et du type DSK («Doppelskelet Katalyst»), caractérisées par des porosités comprises entre 20 et 60%. Les électrodes ont été caractérisées au point de vue structural, en déterminant les dimensions et la répartition des pores, la porosité totale et la surface spécifique intérieure. La réaction de réduction de l'oxygène sur les électrodes poreuses en argent a été étudiée en solution de potasse 5N, à 25°, en utilisant la technique potentiostatique. On a calculé, pour chaque type d'électrode et à de différentes surpressions de l'oxygène, comprises entre 25 et 400 mm Hg, les constantes Tafel et on a tiré des conclusions concernant la réaction de réduction de l'oxygène sur les électrodes poreuses en argent. La corrélation entre la structure et l'efficacité électrochimique des électrodes a démontré que la structure la plus favorable pour la réaction de réduction de l'oxygène est la structure du type DSK.

Étant donné les domaines variés dans lesquels les électrodes à gaz peuvent être utilisées avec grande efficacité électrochimique et surtout leur emploi dans les piles à combustible et les piles zinc-air, les études théoriques et à application pratique concernant ces électrodes sont très actuelles.

La grande importance de l'étude des électrodes poreuses en argent est illustrée par le grand nombre de travaux qui étudient l'activité catalytique de l'argent sur le processus de la réduction de l'oxygène,[1–4] les phénomènes qui accompagnent cette réaction,[5–8] les différents paramètres

---

[1] J. JAUSTA, *Coll. Czech. Chem. Comm.*, **33**, 160 (1968).
[2] I. LINDHOLM, *J. Electrochem. Soc.* **116**, 1150 (1969).
[3] LING-YING KU et V. S. BAGOTSKII, *Electrokhimiya*, **3**, 1279 (1967).
[4] J. MRHA et J. JINDRA, *Coll. Czech. Chem. Comm*, **34**, 2465 (1969).
[5] I. S. PAVLENKO, *Dopovidi Akad. Nauk. Ukr. S.S.R.*, **1**, 49 (1958).
[6] S. PALOUS et R. BUVET, *Bull. Soc. chim. France*, **1962**, 1602.
[7] MASAO KUBOKAWA, *Denki Kagaku*, **36**, 64 (1968); *Chem. Abstr.*, **69**, 23972g (1968).
[8] J. JAUSTA et K. MICKA, *Coll. Czech. Chem. Comm.*, **35**, 1650 (1970).

qui influencent ce processus,[9–11] la base théorique du mécanisme de la réduction de l'oxygène,[12–14] etc.

Dans les solutions alcalines concentrées, à des températures comprises entre 25 et 60°, la réaction de la réduction de l'oxygène sur une électrode poreuse en argent ou activée avec de l'argent est la suivante :

$$O_2 + H_2O + 4\,e^- \rightarrow 4\,OH^-$$

Des études récentes[15–23] ont montré que l'argent, à la différence de certains autres catalyseurs (Au, Pt, Pd), n'ayant pas une adsorption dissociative de l'oxygène ($O_{2(gaz)} \rightarrow 2O_{(ads)}$), qui puisse favoriser la réduction directe, dans une seule étape, de l'oxygène, à des ions OH^-, cette réaction a lieu par un processus intermédiaire à deux électrons faisant apparaître des ions peroxyde HO_2^- :

$$O_2 + H_2O + 2e^- \rightarrow HO_2^- + OH^-$$

Hoar[24] propose, en milieu alcalin, la chaîne réactionnelle :

1. $O_2 + 2\,M \rightarrow M_2O_2$
2. $M_2O_2 + e^- \rightarrow M_2O_2^-$
3. $M_2O_2^- + H_2O \rightarrow M_2O_2H + OH^-$
4. $M_2O_2H + e^- \rightarrow M_2O_2\,H^-$
5. $M_2O_2H^- + H_2O \rightarrow M_2O_2H_2 + OH^-$
6. $M_2O_2H_2 + e^- \rightarrow MOH + M + OH^-$
7. $MOH + e^- \rightarrow M + OH^-$

---

[9] A. Hartner, *Adv. Chem. Ser.*, **47**, 141 (1965).
[10] S. Szpak et E. A. Greus, *J. Electrochem.* Soc., **112**, 1166 (1965).
[11] J. Marcos, *J. Electroanalyt. Chem.*, **20**, 479 (1969).
[12] M. Bonnemay, *Compt. rend.*, **257**, 3394 (1963).
[13] K. Micka et I. Rousar, *Coll. Czech. Chem. Comm.*, **39**, 3197 (1969).
[14] K. Micka, *Electrochim. Acta*, **12**, 1273 (1967).
[15] W. Vielstich, *Z. physik. Chem.*, **15**, 409 (1958).
[16] G. Bianchi, *Electrochim. Acta*, **4**, 232 (1961).
[17] T. Hurlen et I. L. Sandler, *Electrochim Acta*, **11**, 1473 (1966).
[18] S. Beer, *J. Electrochem. Soc.*, **112**, 1133 (1965).
[19] Yu. A. Mazitov, *Zhur. fiz. Khim.*, **38**, 449 (1964).
[20] S. Palous, *Bull. Soc. chim. France*, **1963**, 2490.
[21] U. Evans, *Nature*, 602 (**1968**).
[22] M. R. Tarasevich et R. Rh. Burshtein, *Adv. Chem. Ser.*, **90**, 81, (1969).
[23] S. Kondo, *Denki Kagaku*, **37**, 212 (1969) ; *Chem. Abstr.*, **71**, 44945g (1969).
[24] T. P. Hoar, Proc. Eightieth Meeting of C.I.T.C.E. Butterworths, 439 (1956).

Conformément à ce mécanisme, le processus de réduction de l'oxygène implique le transfert de deux électrons pour chaque molécule d'oxygène, le transfert des charges ayant lieu dans des étapes qui ne contrôlent pas, au moins dans les solutions alcalines, la vitesse de réaction.

L'étape déterminante de vitesse est un réarrangement de la surface ($HO_2^- \rightarrow OH^- + \frac{1}{2}O_2$), qui est précédé et suivi par deux étapes de transfert des charges (la réaction 5 de la chaîne réactionnelle proposé par Hoar).

Berl [25] propose, pour la première étape, la réaction d'équilibre :

$$O_2 + H_2O + 2e^- \rightarrow OH^- + O_2H^-$$

qui a été établie par des études effectuées sur des électrodes de charbon et vérifiée par Beaton [26] sur des électrodes de platine et d'argent. On a suggéré que l'adsorption — désorption de l'eau oxygénée à l'électrode est plus rapide que sa décomposition (la réaction 6 du schéma de Hoar). La décomposition de l'eau oxygénée, dans des solutions alcalines, peut avoir lieu par une des réactions :

$$H_2O_2 + 2e^- \rightarrow 2OH^- \text{ ou}$$

$$H_2O_2 + 2\,OH^- \rightarrow O_2 + H_2O + 2e^-$$

La décomposition de l'eau oxygénée a lieu conformément à la réaction d'équilibre :

$$O_2H^- \rightleftarrows OH^- + \tfrac{1}{2}O_2,$$

la valeur de la constante d'équilibre , d'après Latimer, [27] étant, à 25°, égale à 8.10^{14}.

Le potentiel de l'électrode, calculé pour cette réaction à l'aide de la relation :

$$E = 0{,}75 + 0{,}03 \log C_{OH^-}/C_{O_2H^-},$$

est égal, à 25° C et $P_{O_2} = 1$ atm, à 1,23 V («le potentiel idéal» de l'électrode à oxygène).

La valeur de ce potentiel, variant en fonction du rapport des concentrations des espèces ioniques OH^- et O_2H^- qui se trouvent dans la zone de réaction, l'augmentation de la concentration des ions O_2H^- conduit au décroissement du potentiel de l'électrode, c'est-à-dire à l'apparition d'une surtension qui peut atteindre la valeur maximale théorique de 0,49 V.

---

[25] W. S. Berl, *Trans. Electrochem. Soc.*, **83**, 253 (1943).

[26] E. S. Beaton, Thèse Univ. Glasgow, 1960.

[27] W. P. Latimer, «The Oxydation Potentials», Prantice-Hall Inc., 1954.

Cette grande perte de potentiel — provoquée par l'accumulation de l'eau oxygénée dans les électrodes poreuses — explique le mauvais fonctionnement qui caractérise parfois les électrodes à oxygène dans les piles à combustible.

Pour l'abaissement de la surtension on a fait des expériences sur une série de catalyseurs qui facilitent la réaction de décomposition de l'eau oxygénée ; les études effectuées avec différents métaux (Co, Ni, métaux platiniques, Ag, Cu, Au, etc.) ont démontré la grande efficacité du catalyseur d'argent qui décompose l'eau oxygénée dans la zone de réaction. En utilisant comme catalyseur l'argent, on peut aboutir — à des courants d'environ 100 mA/cm^2, en solutions concentrées et à 25° — à une surtension de 0,3 V[28].

Un autre facteur qui influence le processus de réduction de l'oxygène est la structure de l'électrode poreuse. La structure DSK — électrodes à gaz caractérisées par la présence des grands pores, dans lesquels a lieu la réaction, et des petits pores qui ont le rôle d'alimenter la zone triphasique de réaction avec de l'électrolyte et en même temps d'éliminer les produits de réaction — favorise la réaction de réduction de l'oxygène, en maintenant, dans la zone de réaction, un rapport élevé entre les concentrations des espèces ioniques OH^- et O_2H^-. Ainsi, une électrode DSK en argent a présenté, en solution alcaline, à 25° et à des courants d'environ 100 mA/cm^2, une surtension de 0,1 V, à cause des effets favorables du catalyseur et de la structure [29].

★

Dans ce travail nous nous sommes proposé d'étudier la réaction de réduction de l'oxygène sur une série d'électrodes à gaz en argent, différentes en ce qui concerne leur structure et leur porosité et de déterminer la corrélation entre les performances électrochimiques et la structure des électrodes. Dans ce but on a réalisé :

— des électrodes poreuses en argent du type MSK (Mono Skelet Katalyst — électrodes dont les diamètres des pores sont très peu différents) à petits pores, caractérisés par un diamètre moyen inférieur à 5 microns ;

— des électrodes du type MSK à grands pores (diamètre moyen d'environ 50 microns), et

— des électrodes du type DSK («Doppel Skelet Katalyst» — avec deux sortes de pores : de grands pores dont le diamètre est d'environ 50 microns et de petits pores à un diamètre inférieur à 5 microns), de porosité totale variée.

PARTIE EXPÉRIMENTALE

1. ÉLECTRODES

On a préparé les électrodes en utilisant deux substances génératrices de pores : du carbonate d'argent (diamètre des grains inférieur à 5 microns) et du bicarbonate d'ammonium (grains d'environ 50 microns). Ces deux substances dégagent, par décomposition thermique, du bioxyde de carbone et, respectivement, du bioxyde de carbone, de l'ammoniac et de l'eau. Il en résulte, à l'intérieur du matériel de l'électrode, des espaces libres (des pores) caractérisés par des dimensions qui correspondent à la granulation des substances initiales ; en variant le rapport entre le carbonate d'argent et le bicarbonate d'ammonium on a obtenu des électrodes en argent de porosité variée.

---

[28] A. B. Hart et G. J. Womack «Fuel Cells : Theory and Application», Chapman and Hall Ltd., 1967, p. 97.

[29] E. Justi et A. Winsel, *Naturwiss.*, **47**, 289 (1960).

a. *Préparation des substances nécessaires à la réalisation des électrodes*

Le carbonate d'argent a été obtenu en mélangeant, sous agitation et dans l'obscurité, une solution de bicarbonate de sodium avec une solution d'azotate d'argent. Le carbonate d'argent précipité, après filtration et lavage, a été séché, à température ordinaire et dans l'obscurité.

L'oxyde d'argent a été obtenu en mélangeant, sous agitation et dans l'obscurité, une solution d'hydroxyde de sodium avec une solution d'azotate d'argent. L'oxyde d'argent précipité, après filtration et lavage, a été séché sous vide, à la température ordinaire et dans l'obscurité.

Le bicarbonate d'ammonium de granulation d'environ 50 microns a été obtenu par mouture et triage, en retenant la fraction comprise entre les sas caractérisés par 10 000 et 20 000 mailles/cm^2.

b. *Préparation des électrodes*

Pour réaliser des électrodes à gaz de porosité variée, on a préparé six mélanges (contenant du carbonate d'argent et du bicarbonate d'ammonium), dont la composition est présentée dans le tableau 1. Ces mélanges ont été homogénéisés pendant deux heures et comprimés à l'intérieur d'une matrice sous une pression de 4000 kg/cm^2 ; on a obtenu ainsi des électrodes cylindriques caractérisés par un diamètre de 10 mm et une épaisseur de 3 mm.

Pour obtenir la structure poreuse désirée, en éliminant les substances volatiles, les électrodes ont été chauffées pendant 3 heures à 140°. (A mentionner que les électrodes caractérisées par une porosité supérieure à 55 % — les électrodes 3.4 — n'ont pas une bonne résistance mécanique.)

Après avoir fixé les contacts électriques, on a fait le montage des électrodes dans des supports de verre et on les y a collées avec de la résine époxidique.

c. *Activation des électrodes*

Pour l'activation (réduction de l'oxyde d'argent, résultée de la décomposition thermique du carbonate d'argent à l'argent métallique actif au point de vue catalytique), le matériel des électrodes a été réduit, par voie électrochimique, dans une solution de potasse 1N, la densité de courant étant égale à 10 mA/cm^2.

2. CARACTÉRISATION DES ÉLECTRODES

Pour la caractérisation des électrodes au point de vue structural on a effectué :

— l'étude de la répartition des pores par examen microscopique effectué à l'aide d'un microscope métallographique du type MIM — 7 ;

— des déterminations de la porosité totale (par des méthodes ASTM), et

— des déterminations de la surface spécifique intérieure (par la méthode BET[30,31]), réalisées à l'aide d'un appareil prototype ICPE 6/1969.

---

[30] S. Brunauer, P. H. Emmett et E. Teller, *J. Amer. Chem. Soc.*, **60**, 309 (1938).

[31] P. H. Emmett et S. Brunauer, *J. Amer. Chem. Soc.*, **59**, 1553 (1937).

L'étude de la cinétique de la réduction de l'oxygène a été effectuée par la technique potentiostatique à l'aide du montage représenté dans la figure 1, en utilisant : un potentiostat du type CCF (précision $\simeq \pm 1$ mV), un millivoltmètre électronique Radiometer 22 (précision ± 1 mV,), un milliampèremètre(classe de précision 0,5), une électrode de référence (calomel saturé). La cellule de travail (dimensions 120 × 72 × 56 mm) a été confectionnée en polystyrène ; comme électrode auxiliaire on a utilisé une spirale de nickel de grande pureté.

L'alimentation des électrodes avec de l'oxygène, à pression constante, a été réalisée à l'aide de l'installation représentée dans la figure 2.

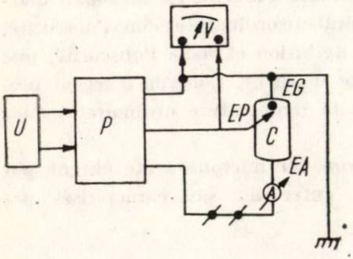

Fig. 1. — Schéma du montage potentiostatique en vue de l'étude de la cinétique des réactions sur une électrode à gaz.

V tension pilote ; *P*, potentiostat ; *C*, cellule ; *EG*, électrode à gaz ; *EA*, électrode auxiliare ; *ER*, électrode de référence ; *V*, Millivoltmètre électronique ; *A*, milliampèremètre.

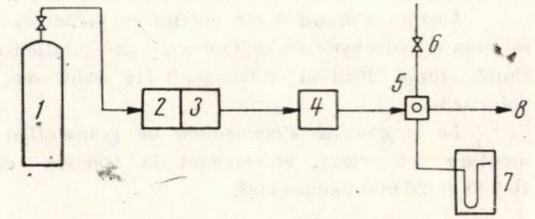

Fig. — 2. Schéma de l'installation de l'alimentation de l'électrode avec de l'oxygène, à surpression constante.

1, bouteille à gaz ; *2*, *3*, réducteurs ; *4*, valve de réglage fin ; *5*, distributeur ; *6*, soupape de surpression ; *7*, manomètre à mercure ; *8*, vers l'électrode.

On a déterminé les courbes de polarisation $\eta - I$, obtenues à différentes surpressions de l'oxygène comprises entre 25 et 400 mm Hg. Les déterminations ont été effectuées à la température ordinaire, en utilisant comme électrolyte une solution de potasse 5N. On a utilisé pour la préparation des solutions des substances très pures (*p.a.*).

RÉSULTATS ET DISCUSSIONS

1. CARACTÉRISATION DES ÉLECTRODES AU POINT DE VUE STRUCTURAL

L'examen microscopique a démontré, tel qu'on le voit dans les microphotographies (fig. 3 — 5), que les pores, petits et grands, sont uniformément répartis dans la masse de l'électrode.

Les résultats des déterminations de la porosité totale (effectuées par la méthode ASTM, en toluène) et des surfaces intérieures des électrodes (effectuées par la méthode BET) sont présentés dans le tableau 1 (les données du tableau 1 représentent la valeur moyenne obtenue à la suite de cinq déterminations).

Des résultats présentés dans le tableau 1, on constate que l'augmentation de la quantité de bicarbonate d'ammonium (qui forme les pores à grand diamètre) conduit au décroissement appréciable de la surface spécifique intérieure des électrodes à gaz ; mais l'efficacité électrochimique des électrodes ne diminue pas, parce que la zone triphasique de réaction

Fig. 3. — Electrode 1 du type MSK à petits pores. Microphotographie, 240 ×.

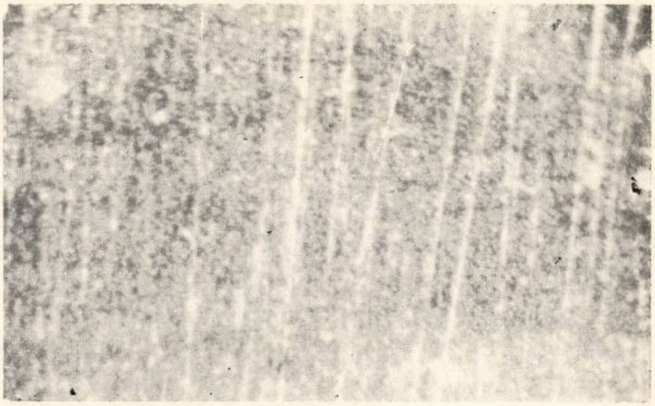

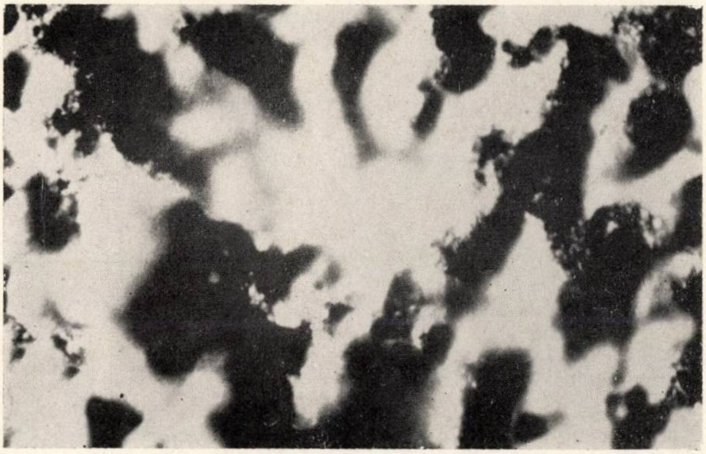

Fig. 4. — Electrode 2 du type MSK à grands pores. Microphotographie, 196 ×.

Fig. 5. — Electrode 3.3 du type DSK. Microphotographie, 196 ×.

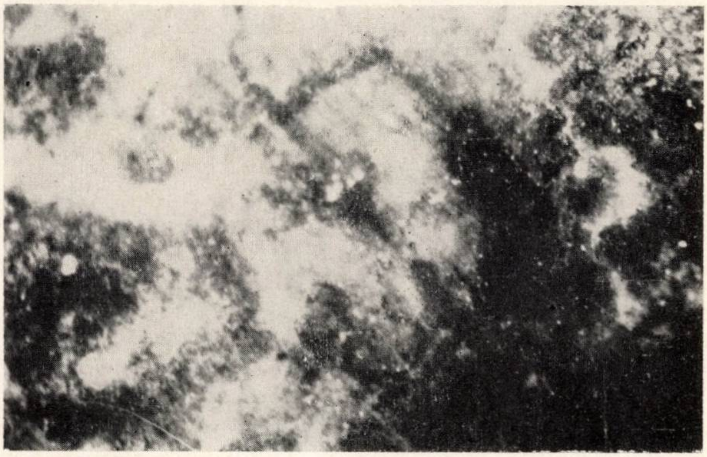

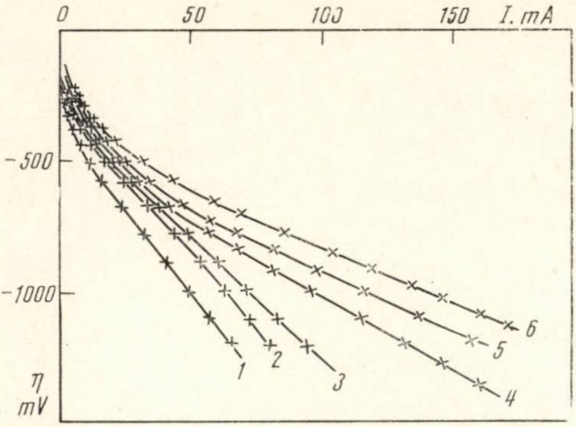

Fig. 6. — Courbes de polarisation η — I, pour l'électrode 1.

1, ΔP_{O_2} = 100 mm Hg, 2, ΔP_{O_2} = 150 mm Hg, 3, ΔP_{O_2} = 200 mm Hg, 4, ΔP_{O_2} = 250 mm Hg, 5, ΔP_{O_2} = 300 mm Hg, 6, ΔP_{O_2} = 400 mm Hg.

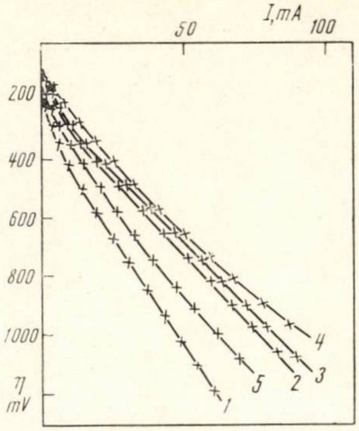

Fig. 7.—Courbes de polarisation η—I pour l'électrode 2.

1 – ΔP_{O_2} = 100 mm Hg, 2 – ΔP_{O_2} = 200 mm Hg, 3 – ΔP_{O_2} = 250 mm Hg, 4 – ΔP_{O_2} = 300 mm Hg, 5 – ΔP_{O_2} = 350 mm Hg.

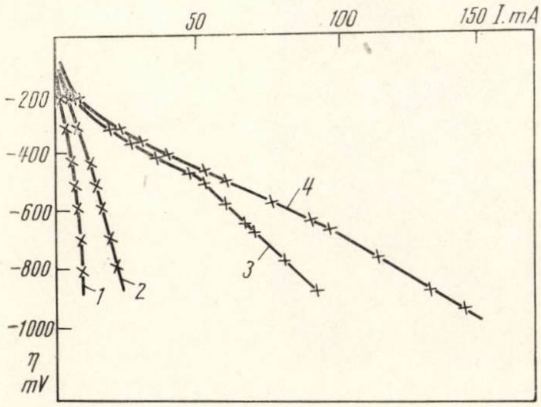

Fig. 8.—Courbes de polarisation η — I pour l'électrode 3.1.

1 – ΔP_{O_2} = 100 mm Hg, 2 – ΔP_{O_2} = 200 mm Hg, 3 – ΔP_{O_2} = =300 mm Hg, 4 – ΔP_{O_2} = 400 mmHg.

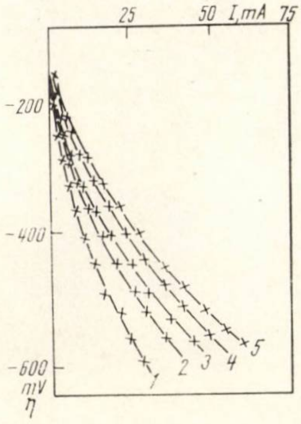

Fig. 9.—Courbes de polarisation η — I pour l'électrode 3.2.

1 – ΔP_{O_2} = 50 mm Hg, 2 – ΔP_{O_2} = =100 mm Hg, 3 = ΔP_{O_2} = 300 mm Hg, 4 – ΔP_{O_2} = 350 mm Hg, 5 – ΔP_{O_2} = =400 mm Hg.

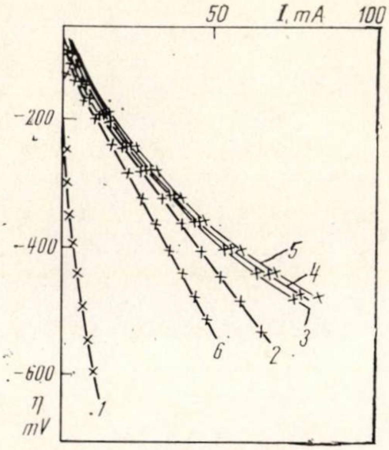

Fig. 10. — Courbes de polarisation η — I pour l'électrode 3.3

1 – ΔP_{O_2} = 25 mm Hg; 2 – ΔP_{O_2} = 50 mm Hg; 3 – ΔP_{O_2} = 100 mm Hg; 4 – ΔP_{O_2} = 200 mm Hg; 5 – ΔP_{O_2} = 300 mm Hg; 6 – ΔP_{O_2} = 400 mm Hg.

Tableau 1

Composition, caractéristique structurale, porosité totale et surface spécifique intérieure des électrodes

Electrode	Composition			Type d'électrode	Porosité totale	Surface spécifique
	Ag_2CO_3	NH_4HCO_3	Ag_2O			
	%	%	%	—	%	cm^2/cm^3
1	100	—	—	MSK avec de petits pores	8,35	24 900
2	—	25	75	MSK avec de grands pores	50,01	10 200
3,1	93,75	6,25	—	DSK avec de petits et de grands pores	21,13	22 900
3,2	87,50	12,50	—	idem	33,05	17 900
3,3	81,25	18,75	—	idem	43,45	14 100
3,4	75	25	—	idem	58,69	12 600

(gaz — électrolyte — catalyseur) est localisée dans les pores à grand diamètre formés par la décomposition du bicarbonate d'ammonium, les petits pores ayant le rôle d'alimenter la zone de réaction avec de l'électrolyte et d'éliminer les produits de réaction.

2. DÉTERMINATIONS ÉLECTROCHIMIQUES

En vue d'établir une corrélation entre la structure des électrodes et leur comportement dans la réaction de réduction de l'oxygène, on a fait des études, par la technique potentiostatique, à des surpressions de l'oxygène comprises entre 25 et 400 mm Hg ; les courbes $\eta - I$ déterminées sont représentées dans les figures 6 — 10.

On constate que l'augmentation de la pression de l'oxygène a un effet favorable sur la réaction, diminuant la tension de polarisation. Il y a une surpression optimale, à laquelle la surtension atteint sa moindre valeur. Dans le cas de l'électrode 3.3, cette surpression est de 300 mm Hg (fig. 10). La surpression optimale est située entre la surpression de « bullage » (400 mm Hg) et la surpression de « noyage » (25 mm Hg). Ce sont les deux cas extrêmes dans lesquels la réaction n'a plus lieu à l'intérieur des pores, mais sur la surface extérieure de l'électrode. Les résultats obtenus indiquent l'effet favorable de la structure du type DSK sur la réaction de réduction de l'oxygène ; ainsi, à une surpression de l'oxygène de 300 mm Hg et à un courant de 50 mA/cm², la surtension a une valeur de — 370 mV, dans le cas de l'électrode 3.3 (du type DSK), par rapport aux valeurs de — 700 mV et de — 650 mV, caractéristiques pour les électrodes du type MSK avec de petits et, respectivement, de grands pores (électrodes 1 et 2).

Les courbes de polarisation $\eta - \log I$ indiquent l'applicabilité de la relation de Tafel : $\eta = a + b \log I$ (dans laquelle $b = \frac{RT}{\alpha F}$

représente la pente des courbes de polarisation). Les valeurs calculées pour les constantes Tafel (*b*) sont représentées dans le tableau 2.

Tableau 2

Valeurs de la constante Tafel (b) pour les différents types d'électrodes réalisées

Electrode	Surpression de l'oxygène Δ PO_2	Valeur de la constante Tafel (*b*)	Electrode	Surpression de l'oxygène Δ PO_2	Valeur de la constante Tafel
	mm Hg	V		mmHg	V
1	100	0,20	3,1	100	0,19
	150	0,20		200	0,17
	200	0,20		300	0,16
	250	0,20		400	0,16
	300	0,20			
	400	0,20	3,2	50	0,20
				100	0,17
2	100	0,17		300	0,17
	200	0,17		350	0,16
	250	0,17		400	0,16
	300	0,17			
	350	0,17	3,3	25	—
				50	0,15
				100	0,15
				200	0,15
				300	0,15
				400	0,16

Dans une électrode poreuse, la vitesse du processus de réduction de l'oxygène est contrôlée non seulement par la réaction déterminante de vitesse $O_2H^- \rightarrow OH^- + \frac{1}{2}O_2$, mais aussi par l'étape de diffusion.

Le courant total produit par un pore peut être déterminé en utilisant la relation[32] :

$$I = (n\,F\,D\,A\,c_0 i_0 S)^{\frac{1}{2}} \exp\left(\frac{\alpha n \eta F}{2\,RT}\right)$$

dans laquelle I représente le courant produit par un pore, D — le coefficient de diffusion (cm^2/s), A — la surface du pore (cm^2), c_0 — la concentration de l'espèce ionique (moles /cm^3), i_0 — la densité du courant de change (A/cm^2), S — la surface du pore, rapportée à l'unité de longueur du pore (cm^2/cm), α — le coefficient de transfert, n — le nombre d'équivalents per mole, η — la surtension (V), F — la constante de Faraday·

De cette équation il résulte clairement que la cinétique de l'électrode poreuse à gaz est nettement différente de celle de l'électrode non poreuse : une électrode poreuse à gaz peut présenter une tension de polarisation deux fois plus grande qu'une électrode non poreuse, la constante Tafel (*b*) ayant la valeur de 0,24 V. Il en résulte que les performances des électrodes à gaz sont dues à la réalisation d'une zone de réaction très étendue et non à l'accélération du processus électrochimique.

---

[32] W. MITCHELL, «Fuel Cells», vol. i, Academic Press, New York—Londres, 1963, p. 98.

Des données obtenues pour les constantes Tafel (*b*) (tableau 2) il résulte que ces valeurs varient entre 0,15 et 0,2 V, ce qui correspond à des coefficients de transfert $\alpha = 0,3 \cdots 0,4$ (les valeurs limites sont $\alpha = 0,25 \ldots 0,65$[32]).

La valeur $b = 0,2$ V calculée pour les électrodes MSK caractérisées par de petits pores (l'électrode 1) indique que, dans le cas de ces électrodes, la vitesse du processus de réduction de l'oxygène est contrôlée surtout par l'étape de diffusion. Dans le cas des électrodes MSK à grands pores (l'électrode 2), la valeur de la constante Tafel ($b = 0,17$ V) démontre que la diffusion est facilitée par l'existence des pores à grand diamètre où se trouve localisée la zone triphasique de réaction. La valeur moindre obtenue pour la constante Tafel ($b = 0,15$ V) dans le cas des électrodes du type DSK (l'électrode 3.3) indique que la surtension de diffusion est petite, l'étape de transfert de charge étant déterminante pour la vitesse de la réaction de réduction de l'oxygène.

Les performances supérieures des électrodes DSK sont dues à la présence, dans l'électrode, des grands pores où est localisé la zone triphasique de réaction et des petits pores qui assurent l'alimentation de la zone de réaction avec de l'électrolyte et l'élimination des produits de réaction, en facilitant la diffusion des espèces ioniques formées dans la zone de réaction vers l'intérieur de l'électrolyte.

CONCLUSIONS

1. On a réalisé, par une méthode originale, une série d'électrodes à gaz, en argent, du type MSK et DSK, caractérisées par des porosités comprises entre 20 et 60 % et des surfaces spécifiques intérieures de 10 000. . . . . .25.000 cm^2/cm^3.

2. La réaction de réduction de l'oxygène sur ce type d'électrode est favorisée par l'augmentation de la surpression ; il y a une surpression optimale — à laquelle la surtension est minimale — située entre la surpression de « bullage » et la surpression de « noyage ».

3. La structure la plus favorable pour la réaction de réduction de l'oxygène est la structure DSK ; les performances supérieures de ces électrodes sont dues à la présence, dans l'électrode, des pores à grand diamètre (environ 50 microns) où est localisée la zone triphasique de réaction et des pores à petit diamètre (< 5 microns) qui assurent l'alimentation de la zone de réaction avec de l'électrolyte et l'élimination des produits de réaction.

4. Les électrodes poreuses en argent du type DSK, réalisées et caractérisées dans ce travail, présentant une efficacité supérieure dans la réaction de réduction de l'oxygène, peuvent être utilisées avec de bons résultats comme cathodes dans les piles à combustible et dans les sources chimiques de courant du type zinc-air.

★

Nous exprimons nos remerciements au collectif du laboratoire pour la Protection contre la Corrosion de l'INCERC pour l'aide qu'il nous a accordée à la réalisation des électrodes à gaz et à Monsieur M. Macovschi pour ses précieux conseils techniques.

Revue Roumaine de Chimie, 17, 7, 1163 – 1179 (1972)

INFLUENCE OF THE PREPARATION METHOD ON THE STRUCTURE AND PHYSICAL PROPERTIES OF ALUMINA. I.

ALUMINIUM HYDROXIDES

VIOLETA ALEVRA, DAN CIOMÎRTAN and MARIA IONESCU
Centre of Physical Chemistry, str. Dumbrava Roşie 23, Bucharest, Romania

Received February 15, 1972

The present contribution deals with some modifications of aluminium hydroxide obtained by the hydrolysis of aluminium isopropylate or by ammonia precipitation of the sol from the hydrolysis of aluminium amalgamated in acidified water. The development of aluminium hydroxide from wholly amorphous gel to well crystallized bayerite is followed by various physical methods: X-ray diffraction, IR spectroscopy, textural determinations. A correlation is established between the obtention conditions of aluminium hydroxides and their structural-physical properties.

1. INTRODUCTION

The study of aluminium oxide acquired considerable significance these last decades, due to its manysided uses such as : medicinals, ceramics, abrasives, adsorbents, carriers and catalysts. The possibility to obtain aluminium oxide in a great variety of structural modifications with very different physico-chemical properties underlies its application in the most various domains. The use on an even wider scale of modern investigation methods: X-ray diffraction, IR spectroscopy, thermal analysis, electron spectroscopy and others, has contributed to the identification of several crystalline forms in the so-called,in the past, "active alumina" and has explained to a great extent the formation mechanism of such forms. Nowaday the problem of nomenclature seems also to be solved ; we shall therefore use the terminology recommended by the International Symposium in Münster. [1]

---

[1] H. GINSBERG, W. HUTTIG and G. STRUNK-LICHTENBEERG, *Z. anorg. Chem.*, **293**, 204 (1957).

The relatively well known aluminium hydroxides may be divided into several categories

a) *trihydroxides or crystalline trihydrates* with composition formula $Al(OH)_3$ or $Al_2O_3 \cdot 3H_2O$ may exist as 3 crystalline forms : gibbsite, bayerite, nordstrandite.

b) *oxihydroxides or crystalline monohydrates* with the composition formula $AlO(OH)$ or $Al_2O_3.H_2O$ with 2 crystalline modifications : diaspore and boehmite.

c) *hydroxides as amorphous or pseudoamorphous gels*, with the composition $Al_2O_3 \cdot xH_2O$ have different physico-chemical properties in terms of the preparation method. We include here both wholly amorphous gels and those hardly organized which build up the transition to crystalline forms. The best studied and known is pseudoboehmite.

New crystalline phases of aluminium hydroxide have been found in recent years. E. g. *tucanite*, with the composition $Al_2O_3 \cdot 31/2\ H_2O$ has been found in nature and synthetically prepared.[2] Another aluminium hydrate, *tohdite*, has assumedly [3] the composition $5\ Al_2O_3.H_2O$ and has been subsequently proved to be actually a form of aluminium oxide with 0.13 – 0.20 mol of adsorbed water. [4] Other phases of aluminium trihydroxyoxide seem also to exist.[5]

Numerous authors have proved the close relationship between the preparation method of initial aluminium hydroxides and the physico-chemical properties of their products of thermal decomposition.

The obtention of chemically pure and especially crystallographically pure aluminium hydroxides is still a difficult problem. Very often phase mixtures with different crystallinity degree are obtained, whose composition is particularly sensitive to minor variations of the preparation method. Although important progress has been made toward the knowledge of the physico-chemical factors determining such processes, the problem of the concomitant influence of all parameters which may vary during preparation is far from being elucidated. The extremely high number of works on this subject—among which we mention some which are more recent [6–15]

---

[2] M. Karsulin, "Symposium bauxites, oxydes, hydroxides aluminium", vol. II, Zagreb, 1963, paper 37.

[3] G. Yamagucki, H. Yonogida and S. Ono, *Bull. Chem. Soc. Japan*, **37**, 752 (1964).

[4] K. Torkar and H. Krischner, *Bull. Chem. Soc. Japan*, **39**, 1356 (1966).

[5] Y. Schimizu, N. Mitsui and K. Funaki, *Kogyo Kagaku Zashi*, **67**, 1190, (1964). from *Ceramic abstracts*, **63**, 1470 (1956).

[6] E. Calvet, P. Boivinet, M. Noel, H. Thibon, A. Maillard and R. Tertian, *Bull. Soc. chim. France*, **1953**, 99.

[7] B. Imelik, M. V. Mathieu, M. Prettre and S. Teichner, *J. Chim. phys.*, **51**, 651 (1954).

[8] M. V. Mathieu, Thèse, Lyon, 1956.

[9] R. Tertian and D. Papée, *J. Chim. phys.*, **55**, 341 (1958).

[10a] D. Papée, R. Tertian and R. Biais, *Bull. Soc. chim. France*, **1955**, 983.

[10b] D. Papée, R. Tertian and R. Biais, *Bull. Soc. chim. France*, **1958**, 1301.

[11] B. C. Lippens, Thesis, Delft, 1961.

[12] B. C. Lippens and J. H. de Boer, *J. Catalysis*, **3**, 44 (1964) ; **4**, 319 (1965).

[13] B. C. Lippens and J. H. de Boer, *Acta Cryst.*, **17**, 1312 (1964).

[14] B. C. Lippens, *Chem. Weekbl.*, **62**, 336 (1966).

[15] B. C. Lippens and J. J. Stegerda, in "Physical and Chemical Aspects of Adsorbents and Catalysts", Ed. B. G. Linsen, Academic Press, London-New York, 1970, p. 171.

— is justified by the multitude of these parameters : nature, purity and form under which the raw material is used, the precipitation conditions of gels : medium, pH, rate and addition order of reagents, temperature, character of strirring, washing and drying conditions such as : temperature, pressure, atmosphere and grain size of products. The reproductibility of the products is sometimes poor, due to scarce details of the preparation method in most works. Thus, the obtainment of aluminium oxides with well defined properties, suitable to well determined practical purposes, e.g. catalysts, is still a matter of investigation.

The present paper aims at studying some of the above problems, in the particular case of the hydrolysis method of amalgamated aluminium, since we are convinced,[16] that varieties of aluminium oxide with interesting catalytic properties related to the genesis of initial aluminium hydroxides may be thus obtained.

2. EXPERIMENTAL

2.1. SAMPLE PREPARATION

To obtain aluminium hydroxide precipitates we have used : a) the sol resulted from the hydrolysis of amalgamated aluminium and b) aluminium isopropylate.

a) Metallic aluminium (Slatina, 99.6 %) as chips, has been amalgamated at room temperature with aqueous mercury chloride solution of a 0.12 % concentration for 5 min. After removal of the amalgamation solution and washing with distilled water, the activated aluminium has been introduced into a weakly acid solution (HCl 1 % + acetic acid 2 %) at 65° in a polyethylene vessel. After completion of the violent hydrolysis reaction the sol has been separated by settling and filtering off. The Al hydroxide has been obtained by precipitation with 10 % ammonia of the sol with a concentration of 3.5 – 4 % Al_2O_3, at room temperature.

Precipitations occurred at constant pH($\pm$0.2 pH units) by stepwise, concomitant introduction with adequate rates, of the reagents into a determined amount of aqueous ammonia solution with desired pH, under vigorous stirring. The suspensions obtained are at once centrifuged, washed and dried or are first brought to various aging conditions. Washing occurred by repeated reduction to the initial state in water and filtering off up to the disappearance of the chloride ion. Drying of suspensions with a water content of 85 – 90 % occurred in a drying chamber with reduced air circulation, at 115° – 120°. The resulted samples (H I, H III – H VIII) are characterized in Table 1.

b) Since the purity of metallic aluminium used in the above preparation was not satisfactory, for the sake of comparison we have prepared a pure aluminium hydroxide, starting from distilled aluminium isopropoxide (Carlo Erba). The hydrolysis reaction occurred by the gradual introduction, under stirring, of the molten aluminium isopropoxide in distilled water at 85 – 92° ; the suspension has been left for other 5 hours in the same conditions. Filtering, washing and drying proceeded as above. The resulted sample, H II, is characterized in Table 1.

---

[16] I. V. NICOLESCU and V. DUMITRESCU, *Ind. chim. belge*, **32**, (spc. no.) Pt (2) 712 (1967).

2.2. PHYSICAL DETERMINATIONS

a) *Measurement of the surface area and of the pore distribution.* The specific surface BET has been measured by nitrogen adsorption at − 196°, in a simplified BET installation made in the laboratory. The total porosity has been deduced from the values of the real and apparent density : total pore volume $V_t(\text{cm}^3/\text{g}) = d_r - d_{ap}/d_r \cdot d_{ap}$.

The real density has been determined by the picnometric method, while apparent density by mercury immersion. The distribution of the pore size has been calculated from the diagrams obtained with the mercury porosimeter, type Carlo Erba (1 − 2000 at), using the value of the total pore volume calculated as above.

b) *IR spectroscopic determinations.* IR absorption spectra have been recorded with a Karl Zeiss, Jena, spectrophotometer, type UR-10, using the technique of potassium bromide pellets (1 mg sample + 300 mg potassium bromide) at a pressure of about 50 kgf/cm².

c) *Roentgenographic determinations.* X-ray diffraction patterns were obtained by Debye-Scherrer powder technique by means of a HZG-1 diffractometer connected to the X-ray source TURM-61 (GDR). We used the radiation CuK_α ; $\lambda = 1.5418$ Å filtered on nickel at 30 kV and 22 mA ; recording range : 5 − 45° Bragg.

The average size of crystallites has been determined by applying Scherrer formula

$$D = \frac{K\lambda}{\beta_{\cos\theta}}$$

where : D = crystallite size in Å, K (constant related to the crystallite shape) = 0.90 for the almost spherical shape ; β(integral diffraction width) = $B - b$, where B = experimental diffraction width and b = width of the control ; θ = angle of the diffraction line under consideration, in this case = 24.38° Bragg.

3. RESULTS AND DISCUSSIONS

Table 1 lists the general physico-structural characteristics of the main varieties of aluminium hydroxide obtained, together with these details of the preparation method, which were not quoted in the experimental part. For the sake of comparison we have also included a commercially available aluminium oxide of known origin and characteristics : prevailingly γ-aluminium-hydroxide-Merck.

3.1. IDENTIFICATION OF $AL_2O_3 \cdot xH_2O$ PHASES IN X-RAY DIFFRACTION SPECTRA

X-ray diffraction spectrum of the sample H I is characterized by the absence of diffraction maxima, which proves the existence of a disordered structure. The fact that not even the weakly scattered bands characteristic of the classical amorphous solid substances — glasses, organic resins — or of the fluids appear, proves that the structure of this sample lacks any ordering, even the long-range order ; we can therefore consider

Table 1

Preparation and physical properties of aluminium hydrates

Name	Preparation method	Aspects	Crystal Structure	Density (cmc/g)		Volume of pores (cmc/g)			Surface m²/g
				D_r	D_{app}	TOTAL	$R_p < 75$ (Å)	$R_p = 75 - 75 \times 10^3$	
H I	Precipitation at pH = 7	Glass-like	Amophous	2.48	2.46	no pores			4.0
H II	Aluminium isopropoxyde aqueous hydrolisis	Opalescent	Pseudoboehmite	2.88	1.63	0.270	0.258	0.012	254
H III	Precipitation pH = 9.5	Opalescent	Pseudoboehmite	2.88	1.70	0.250	0.246	0.004	216
H IV	Precipitation pH= =9.0 in water aging 24 h	Opalescent	Pseudoboehmite +traces(?) of bayerite	2.61	1.65	0.220	0.216	0.004	209
H V	Precipitation pH=10 in water aging 24h	Less opalescent	Pseudoboehmite+ aprox.25 %bayerite	2.77	1.67	0.230	0.164	0.066	167
H VI	Precipitation pH = =11.5 in water aging 24 h	Milk-white	Pseudoboehmite+ bayerite	2.64	1.56	0.262	0.180	0.082	130
H VII	Precipitation pH = =9.5 in aqueous ethanolamine(0,5 %) aging 24 h	Milk-white	Bayerite+traces of pseudoboehmite	2.60	1.11	0.510	0.040	0.470	100
H VIII	Precipitation pH = =10 in mother liquor aging 24 h	Milk-white	Bayerite	2.50	1.17	0.455	0.070	0.384	58
H IX	Preponderent- γ Aluminium hydroxide (Merck)	White-powder	Gibbsite	2.42	— —	no pores			1.5

that we have in this case an ideally disordered or wholly amorphous structure.

The other hydroxide samples (H II – H IX) are characterized by the presence in the X-ray diffraction spectrum of several diffraction bands, of variable intensity and width which enable the accurate identification of their structure. In table 2 we give comparative data obtained by us and by other authors [10b,15] as regards the position and the intensity of diffraction maxima corresponding to various sample groups.

To the first category belong the samples with pseudoboehmite structure (H II – H V). In the spectrum of these samples intense bands appear, which are however broad (scattered), whose maxima coincide fairly well as to their position with the most intense lines of the well crystallized mite however, in comparison with the position of the most intense boeh-boehmite line ($d = 6.11$ Å) the maxima corresponding to the first interference are shifted, in our samples, with a variable value, depending on the actual preparation method of the samples. The values of these shifts, together with other data on the composition and specific surface, are given in table 3.

The broadering of the lines of the well crystallized boehmite or, in other words, the conversion of these lines into broad diffraction maxima, as well as the slight shift in the position of some of them – among which the most important is that corresponding to the first interference – are considered as evidences of the existence of gelatinous boehmite [10–15] or, using the more suitable term of Tartian and collab.[6] – pseudoboehmite. The fact that no weakening in the band intensity at great angles – which occurs in perturbed crystalline lattices – is noticed, also pleads for an organized structure of the boehmite type.[10b]

The pseudoboehmite structure, recently discussed by Lippens,[15] is differing from that of the well crystallized boehmite, by that an excess of water appears, as compared to the stoichiometrical composition, in its complex stratified structure (octohedral chains AlO_6– distorted or polymers of dimer units – $(AlOOH)_2$). This excess water reaching up to values beyond 2 mol/mol aluminium oxide, is implied in strong hydrogen bonds. [17,18]

The excess water is an important structural factor since it locates in the interlamellar holes of the boehmite structure and leads to the lattice distortion, bringing about the increase in the c axis. The products corresponding to the various compositions intermediary between the well-crystallized boehmite the stoichiometric and the non-stoichiometric one pseudoboehmite are characterized by a certain relationship between the excess water and some textural properties e. g. specific surface. [10b] Thus, the farther away the pseudoboehmite moves from the stoichiometric composition of the crystalline boehmite, the greater becomes its surface. Studying the crystallization process of boehmite, Lippens [11,14] finds a large scale of pseudoboehmite products, for which he establishes a linear correlation between the content of interlamellar water and the value of the c axis of

---

[17] B. Imelik, M. Petitjean and M. Prettre, *Compt. rend.*, **238**, 900 (1954).

[18] O. Glemser and G. Rieck, *Angew. Chem.*, **67**, 652 (1955); **68**, 182 (1966).

Table 2

X-Ray data for aluminium-hydrate structures

BOEHMITE					PSEUDOBOEHMITE				BAYERITE						
ASTM(5 – 190)			Lippens [15]		Tertian-Papée [10b]		this work		ASTM(12 – 457)			Lippens [15]		this work	
hkl	I/I_0	*d*	*d*	*I*	*I*	*d*	*d*	I/I_0	hkl	I/I_0	*d*	*d*	*I*	*d*	I/I_0
020*	100	6.110	6.112	100	100	6.58–6.70	6.13–6.54	100	001	100	4.72	4.716	100	4.69	100
021	65	3.164	3.160	53	68	3.18–3.20	3.13	50	100	70	4.36	4.370	110	4.33	80
041	53	2.346	2.343	50	51	2.34	2.32	42	101	25	3.19	3.207	40	3.18	40
131	6	1.980	1.979	6	—	—	—	—	Ni	2	3.08	—	—	3.10	13
150	32	1.860	1.857	24	73	1.86	1.84	61	Ni	4	2.69	2.708	5	—	—
002	27	1.850	1.847	17	—	—	—	—	110	4	2.45	2.468	3	2.47	11
022	6	1.770	1.768	8	—	—	—	—	002	6	2.34	2.361	7	2.35	21
151	13	1.662	1.661	14	7	1.65	1.66	10	Ni	4	2.28	—	—	2.28	15
080	6	1.527	1.526	9	—	—	1.52	7	111	65	2.21	2.224	140	2.21	98
132	16	1.453	1.452	14	40	1.44	—	—	200	4	2.14	2.160	3	2.16	21
200	9	1.434	1.435	7	—	—	1.43	34	102	2	2.06	2.078	3	2.09	7
—	—	—	1.430	7	—	—	—	—	—	—	—	1.986	4	1.99	11
081	1	1.412	1.410	1	—	—	—	—	201	4	1.97	1.974	2	1.97	11
220	2	1.396	1.402	3	10	1.41	—	—	Ni	2	1.91	1.918	1.5	1.92	8
171	6	1.383	1.382	9	—	—	—	—	Ni	2	1.83	1.841	2	1.84	8
062	2	1.369	—	—	—	—	—	—	—	—	—	1.830	0.2	—	—
152	15	1.312	—	—	20	1.31	1.33	25	—	—	—	1.770	0.5	—	—
221	3	1.303	—	—	—	—	—	—	112	25	1.71	1.723	30	1.72	40

*–002 by Lippens. [15]

Table 3

Corelation between structure and properties of pseudoboehmite

Name	Spacing (002) refl. (Å)	Moles H_2O per mole Al_2O_3		Area surf. (m^2/g)	Structure
		Lippens' diagram	chemical analysis		
H II	6.18	1.15	1.16	254	Pseudoboehmite
H III	6.52–6.54	1.52–1.56	1.60	216	Pseudoboehmite
H IV	6.23–6.52	1.24–1.52	1.67	209	Pseudoboehmite and possible traces of bayerite (undetectable by X ray)
HV	6.13	1.03	1.50	167	Pseudoboehmite and about 25 % bayerite

the boehmite structure, i.e. for each mol of excess water the value of the c axis increases by about 1.2 Å [15].

For our pseudoboehmite samples, the diffraction maximum corresponding to the first interference (002 according to Lippens and 020 – ASTM) is located between 6.13 – 6.54 Å (table 3). The sample closest to the structure of stoichiometric boehmite is H II ; at this hydroxide the sharpest diffraction maxima appear while the value of the investigated shift is minimum (6.18 as compared to 6.11 Å). The content in composition water calculated after Lippens (c axis deduced = 12.34 – 12.35 Å) is of about 1.15 mol, which is in good agreement with the value found by chemical analysis (prolonged discharge at 100°). However, at room temperature, the non-discharged sample has the following composition : 2.3 H_2O. Al_2O_3. The difference of about 1.15 mol represents physically adsorbed water at the sample surface, due to the microporosity and to its great surface (Table 1 – fig. 2). H II may be considered as microcrystalline boehmite.

Among the samples prepared by the hydrolysis of amalgamated aluminium, H III is the purest pseudoboehmite, with diffraction maxima somewhat broader than those of H II. The agreement between the values of the composition water deduced by the above methods is satisfactory. For the next sample, H IV, the diffraction maxima become even wider and the agreement referring to the composition water is somewhat poorer. In the X-ray spectrum of these three sample (H II – H IV) no other crystalline structure could be identified. For sample H V, although showing much clearer diffraction maxima, similar to H II, while the position of the first interference is even closer to that of crystalline boehmite, the actual content in composition water is much greater, due to the appearance of the bayerite structure of about 25 %. The decrease in the value of the specific surface also proves the gel evolution toward more organized forms.

The fact that in the H II – H IV series, the diffraction maxima become wider and wider, shows that the crystallite size is decreasing in the same direction. Indeed, if we calculated the average size of crystallites (table 4) we would notice their slight decrease.

For sample H V, although more difficultly to be measured, the crystallite size is somewhat greater. Of course, the most accurate value for the crystallite size has been obtained in the case of H II, because the content of excess water being very low, hence the distorsion of the c axis very small, the particles come much closer to the spherical shape assumed in the formula ($K = 0.90$).

Table 4

Average size of crystalites for pseudoboehmite

Name	$B°$	$b°$	b/B	β/B	$\beta°$	D(Å)
H II	1.25	0.45	0.36	0.935	1.18	74
H III	1.60	0.45	0.28	0.963	1.54	57
H IV	2.00	0.45	0.23	0.973	1.95	44

Sample H IV contains a mixture of pseudoboehmite and bayerite in approximately aquivalent amounts ; it represents the next transition phase in the evolutive process of amorphous gel toward structurally more organized species.

The last category of samples, H VII and H VIII, have their diffraction spectra characteristic of the well crystallized bayerite. Since the half wave width of diffraction lines is identical to that of the controls, NaCl or Al, we conclude that the average size of crystallites lies in the range 5 — — 15 μ. We also mention that no other structures could be found in the spectrum of these samples. Sample H IX proved to be practically pure gibbsite.

3.2. ANALYSIS OF IR SPECTRA

The IR spectroscopic measurements of the hydroxides obtained by us were carried out merely in order to supplement the information on their structure obtained by other methods.

Figure 1 shows the IR spectra corresponding to the samples characterized in table 1, i.e. the domains where strong absorptions have appeared : 3600 — 2700 $\mathrm{cm^{-1}}$ and 1800—400 $\mathrm{cm^{-1}}$. In the 2 300—1 900 $\mathrm{cm^{-1}}$ domain there are but very weak absorption bands which could not be assigned. We mention however, that the literature [19] notices some weak bands in this range, characteristic, especially, of the crystalline aluminium trihydroxides.

---

[19] U. Hauschild, *Z. anorg. Chem.*, **324**, 15 (1963).

As already known [20-22] the absorption bands significant for the structure of the Al oxide hydrates appear in the 1200—400 cm^{-1} range. For all our samples, some strong bands appear in the 800—400 cm^{-1} range, characteristic of the interatomic bonds in the lattice of aluminium hydroxides ; thus, the ground vibrational modes of Al octahedra (ν_3 and ν_4) appear at about 600 — 750 and 520 — 525 cm^{-1} and here, too, appears the band corresponding to the vibration of the Al-O bond.

The IR spectrum of gibbsite — Merck, included for the sake of comparison and checking, is practically identic to that found by various authors for this structure, [20-22] as regards number, position and relative intensity of the characteristic bands (Fig. 1)

The presence even of weak bands at 3378 cm^{-1} and 3260 cm^{-1}, which are known [22] to decrease in intensity and slightly shifting due to the compression (pelleting) effect, made sure that we are in reasonable conditions suitable for structural identifications.

To identify the various forms of the Al hydroxide we have used the narrow range 1200—980 cm^{-1} where strong bands appear, which are generally well resolved and whose position and relative intensity are assigned with fair accuracy.

Thus the strong absorption maximum, centered at 1075—1080 cm^{-1}, accompanied by a weaker one at about 1150—1160 cm^{-1}, which appears in the spectrum of our samples H II — HV, is due to the distortion vibration (δ_{OH}) of the hydroxyl in a boehmite structure.

Hence, we deduce the prevailing boehmite structure of such samples, H II having the spectrum closest to that of well crystallized boehmite. As we advance in series H II — HV, this band becomes more and more scattered and decreases in intensity, while in a domain in close neighbourhood the absorption grows progressively to about 1000 cm^{-1}, i.e. characteristic of crystalline trihydrates, indeed, in the next category of samples, H V — H VIII, as the band at about 1075 cm^{-1} fades more and more, the absorption in the 1000 cm^{-1} range, progressively grows, becoming the doublet characteristic of the vibrational distortion of the bayeritic hydroxyl for sample H VI while for H VII and mainly for H VIII, it remains the only detectable absorption in this region.

We, therefore, have for samples H II—H VIII, an almost continuous transition between the boehmite and the bayerite structure, in terms of working conditions—a conclusion confirming the deductions made by X-ray analysis.

The X-ray spectrum of the amorphous sample H I, shows, as expected, two strong, actually unresolved bands at 800 —400 cm^{-1} and 900 — 100 cm^{-1} including, we may say, the absorption maxima characteristic of all known structures.

If we refer now to the 4000 — 2600 cm^{-1} region, we shall find that the conclusions so far reached at, are wholly valid.

[20] H. Ginsberg, W. Huttig and H. Stiel, *Z. anorg. Chem.*, **318**, 238 (1962).

[21] A. J. Leonard, F. Van Cauwelaert and J. J. Fripiat, *J. Phys. Chem.*, **71**, 695 (1967).

[22] J. Rouquerol, J. Faissard, M. V. Mathieu, J. Elston and B. Imelik, *Bull. Soc. chim. France*, **1970**, 4233.

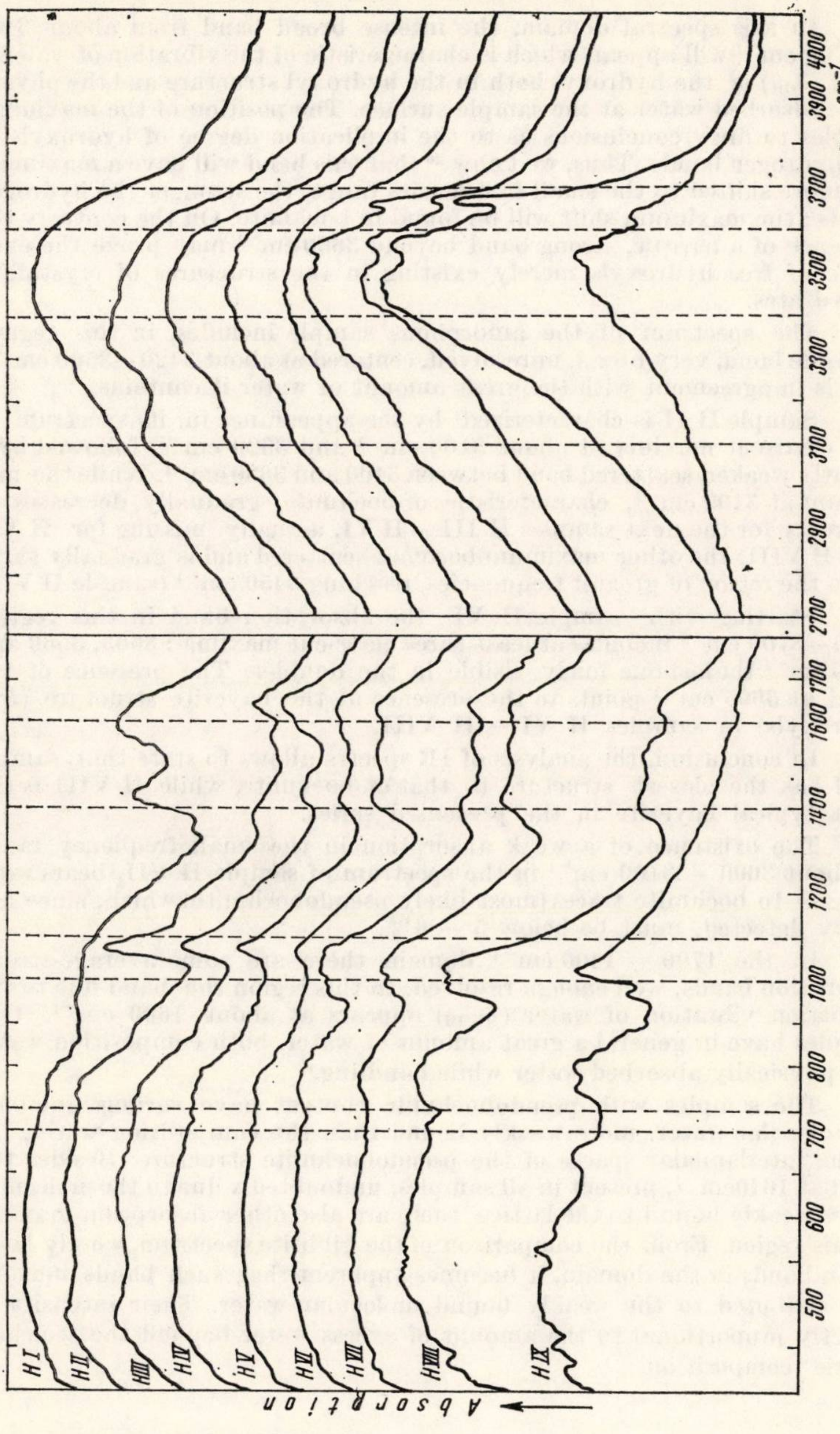

Fig. 1. — IR spectra of Al hydroxides.

In this spectral domain, the intense broad band from about 3100 -3700 cm^{-1} will appeal, which is characteristic of the vibration of valence bond (δ_{OH}) of the hydroxyl both in the hydroxyl structure and the physically adsorbed water at the sample surface. The position of the maximum enables to draw conclusions as to the implication degree of hydroxyls in the hydrogen bonds. Thus, we know [20] that this band will have a maximum the more shifted to the small frequencies range, the stronger the hydrogen bonds ; the maximum shift will be found in boehmite. On the contrary the presence of a narrow, strong band beyond 3600 cm^{-1} may prove the existence of free hydroxyls merely existing in the structures of crystalline trihydrates.

The spectrum of the amorphous sample includes, in this region, a simple bond, very broad, unresolved, centered at about 3420$-$3500 cm^{-1}; this is in agreement with the great amount of water it contains.

Sample H II is characterized by the appearance in its spectrum of two clear-cut maxima at about 3100 cm^{-1} and 3320 cm^{-1}, followed by a slightly weaker, scattered band between 3400 and 3630 cm^{-1}. While the maximum at 3100 cm^{-1}, characteristic of boehmite, gradually decreases in intensity for the next samples H III $-$ H VI, actually missing for H VII and H VIII, the other maximum becomes scattered and is gradually shifted to the region of greater frequencies, reaching 3450 cm^{-1} (sample H V).

Starting with sample H VI the absorption band in this region, 3400$-$3700 cm^{-1} includes at least three clear-cut maxima : 3665, 3560 and 3480 cm^{-1} the last one fairly visible in the doublet. The presence of the band at 3665 cm^{-1} points to the presence of the bayerite structure (free hydroxyls) in samples H VI $-$ H VIII.

In conclusion, the analysis of IR spectra allows to state that sample H II has the closest structure to that of boehmite, while H VIII is the most typical bayerite in the presented series.

The existence of a weak absorption in the small frequency range at about 3000 $-$ 3100 cm^{-1} in the spectrum of sample H VII, bears wittness as to boehmite traces (most likely pseudoboehmite) which, since not X-ray detected, must be below 5 $-$ 6 %.

In the 1700 $-$ 1400 cm^{-1} domain there are some average-strong absorption bands, well enough resolved. In this region the band due to the distortion vibration of water (δ_{HOH}) appears at about 1600 cm^{-1}. Our samples have in general a great amount of water, both composition water and physically absorbed water while handling.

The samples with pseudoboehmite content have various amounts of molecular water, more weakly bound than the composition water, i.e. in the interlamellar spaces of the pseudoboehmite structure. Besides the band at 1640cm^{-1}, present in all samples, undoubtedly due to the molecular water weakly bound to the lattice, there are also other absorption maxima in this region. From the comparison of the gibbsite spectrum, wholly lacking in bands in the domain, it becomes apparent that such bands may be also atributed to the weakly bound molecular water. Their intensity is directly proportional to the amount of excess water beyond the stoichiometric composition.

3.3. TEXTURAL PROPERTIES

Textural characteristics of the aluminium hydroxides obtained are presented in table 1 and figure 2, where we have plotted the distribution of the pore volume with respect to their radius.

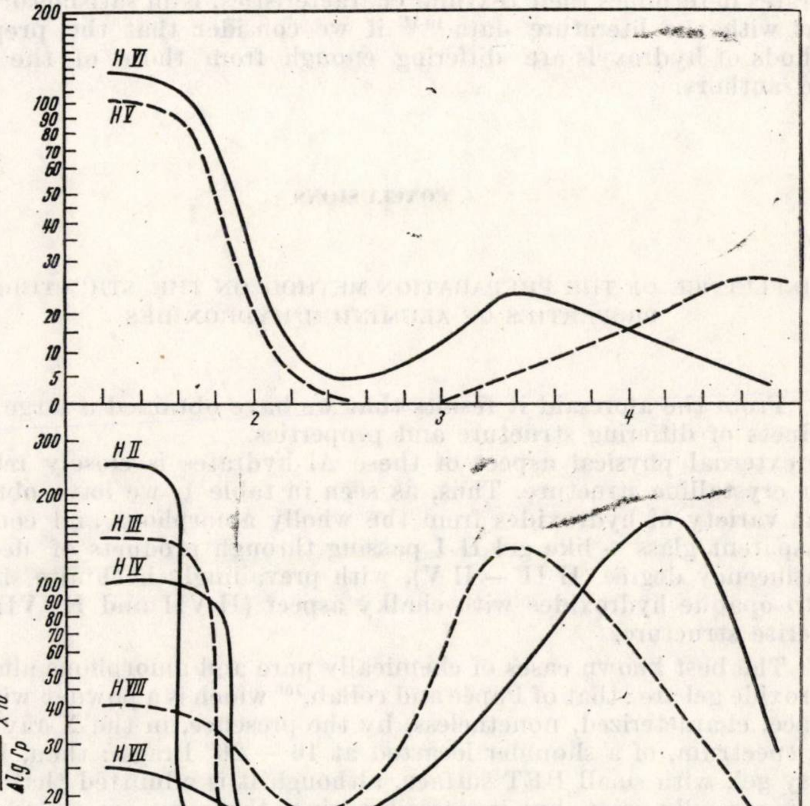

Fig. 2. — Pore-radius dependence of pore volume.

The data on the specific surface and the porosity of the samples wholly confirm the conclusions on their crystalline structure. Thus, prevailingly pseudoboehmite samples have a great surface given by a porosity made up of over 90 % micropores, while the prevailingly bayerite samples are characterized by much smaller surfaces and by the practically total absence of micropores. The intermediate samples have a larger pore distribution and surface with intermediate values.

The somewhat greater value of the surface of sample H VII, as well as the relatively high percent of micropores for a bayerite sample on X-ray, confirm the conclusion drawn subsequent to the interpretation of its IR spectrum, i.e. that here too, pseudoboehmite traces are likely to exist. Our conclusions on the way in which the crystalline structure of aluminium hydrates determines their textural characteristics, is in satisfactory agreement with the literature data [10,15] if we consider that the preparation methods of hydroxyls are differing enough from those of the already cited authors.

4. CONCLUSIONS

4.1. INFLUENCE OF THE PREPARATION METHOD ON THE STRUCTURE AND PROPERTIES OF ALUMINIUM HYDROXIDES

From the aforesaid it results that we have obtained a large scale of products of differing structure and properties.

The external physical aspect of these Al hydrates is closely related to their crystalline structure. Thus, as seen in table 1, we have obtained a great variety of hydroxides from the wholly amorphous and completely transparent glass — like gel H I passing through products of decreasing translucency degree (H II — H V), with prevailingly boehmite structure, up to opaque hydroxides with chalky aspect (H VII and H VIII) with bayerite structure.

The best known cases of chemically pure and amorphous aluminium hydroxide gel are : that of Papée and collab.[10b] which is a powder with great surface, characterized, nonetheless, by the presence, in the X-ray diffraction spectrum, of a shoulder locatted at 16 — 26° Bragg : then, Lippens' glassy gel, with small BET surface, although it is admitted that the surface is actually great, but inaccessible, since the pores are closed. [11]

Our gel H I is perfectly amorphous and transparent, with small BET surface. Its transparency and the fact that it may be obtained in a preestablished geometrical shape, makes it very useful for physical studies.

The relatively high level of impurities in the initial aluminium might be, of course, a stabilizing factor of the amorphous character, which also accounts for its great stability during prolonged washing. We should however mention, that the assumedly well washed gels still contain small amounts of anions (chlorine and acetate).

The peculiar catalytic and adsorptive properties [16] of aluminium oxides stemming from prevailingly pseudoboehmite gels induced us to check the part played by the metallic impurities present in our samples. To this end we have prepared sample H II starting from the distilled aluminium isopropylate with structure and textural properties sensibly similar to those of other samples, and that we have used as comparison in catalytic studies.

The preparation of aluminium hydroxide by the hydrolysis of amalgamated aluminium has been known for a long time. [23] If hydrolysis is carried through in conductometric water, then crystallographic pure bayerite may be obtained [24] at room temperature, or by aging in aqueous medium devoid of carbon dioxide, while at higher temperature (80°) we obtain boehmite; at intermediate temperatures we obtain boehmite-bayerite mixtures. [24,25] On lowering the suspension's pH by bubbling of carbon dioxide, we obtain pure pseudoboehmite at room temperature. [26]

The case investigated by us is different, in that all samples have been obtained by the precipitation at room temperature with ammonia of a sol from the acid hydrolysis of amalgamated aluminium. Therefore the physico-chemical factors which bring about the properties of aluminium hydroxides may be different, although, on the whole, they observe the already known laws.

The kinetics of the hydrolysis reaction of the amalgamated aluminium, followed by the measurement of the hydrogen amount evolved during the reaction, [16] has shown that, considering the strictness of amalgamation conditions : temperature, time and concentration of the amalgamation solution, sols of various concentrations may be obtained.

In the present contribution we have started from the sol of a concentration of 3.5 — 4 % Al_2O_3 in order to remove the influence of the variation in the concentration of the initial sol. The factors whose influence we have followed up so far, have been the precipitation pH and the nature of aging, the other conditions regarding : precipitation, washing, drying being identical for all samples.

We can generally say that the well known rule is observed [10−15] i.e. the lower the final precipitation pH (acid), the greater the possibility to obtain structurally more weakly organized gels, and the higher the pH (alkaline), the more ordered structures are obtained, which tend, in time, to the structure of crystalline trihydrates.

However, in our case, for gels with no aging, the complete transition to crystalline trihydrates is neither achieved even at pH 11.5 — 12.0 ; subsequent to washing and drying pseudoboehmite-bayerite mixtures are obtained. The explanation lies undoubtedly in the presence of carbon dioxide in the air and in the washing water, that hinders the evolutive process of structural organization as well as the aging process of gels. [27] The great stability of the amorphous phase obtained at about pH = 7, which enables prolonged washings, is in contradiction with the extremely great instability of amorphous gels obtained by other methods, e.g. from solutions of alkaline aluminate, which rapidly develop into crystalline forms.

Therefore, the presence, in small amounts, in all our samples, of an amorphous, hardly detectable fraction or of a pseudoboehmite fraction in amounts which could not be X-ray detected, is not excluded.

---

[23] I. Wislicenius, *Kolloid* Z., **2**, 11 (1908).

[24] R. Fricke and K. Jockers, *Z. anorg. Chem.*, **262**, 3 (1950).

[25] A. Simon, H. Scheibe, K. Pohl and E. Lichter, *Z. anorg. Chem.*, **314**, 61 (1962).

[26] J. J. Stegerda, Thesis, Delft, 1955.

[27] H. Havestadt and R. Fricke, *Z. anorg. Chem.*, **188**, 379 (1930).

Table 5

Precipitation pH dependence of crystalline structure

Precipitation pH	7		8		9		10		11		12
No aging	Amorphous product →					Pure pseudoboehmite →				Preponderent pseudoboehmite and some bayerite	
In water aging	Amorphous product →				Pseudoboehmite and traces of bayerite →		Pseudoboehmite and about 25 % bayerite →			Bayerite and about 25 % pseudoboehmite	
In mother liquors aging	Pseudoamorphous products →			Pseudoboehmite + bayerite →			Pure bayerite →			Pure bayerite	

The factor speeding up the crystallization action of aluminium hydroxide gels is aging. While aging through bringing to the initial state in water of the freshly precipitated and filtered gel, has no effect even for 24 hrs in the case of precipitation at pH = 7, or it has a slight effect at a higher pH, in the presence of ammonia salts or of other substances, it has a more pronounced effect. Thus, during the same maturation time (24hrs), even at smaller pH (9.5 – 10.0) more organized species are obtained, if the maturation occurs in mother liquor (H VIII) or in ethanolammine solution (H VII).

The samples presented in table 1 are chosen to illustrate the possible obtainment of a large scale of products in terms of preparation conditions. For simplicity we have merely included the most representative series among the numerous ones obtained by modifying also other working parameters. Based on data obtained while studying the preparation of a aluminium hydroxide by the hydrolysis of amalgamated aluminium, we have give Table 5 which expresses but a qualitative relationship between the preparation method and the crystalline structure of the aluminium hydroxide.

Revue Roumaine de Chimie, 7, 7, 1181 – 1190 (1972)

CONTRIBUTIONS TO THE BISMUTH HYDROLYSIS STUDY. II*

SPECTROPHOTOMETRIC AND POLAROGRAPHIC INVESTIGATIONS ON BISMUTHYL PERCHLORATE HYDROLYSIS

C. DRĂGULESCU, ANA NIMARĂ and I. JULEAN

Chemical Research Center, Bd. Mihai Viteazul 24, Timişoara,
Romania

Received January 1972

The spectrophotometric, polarographic and cyclic-voltammetric investigations on the hydrolysis of bismuthyl perchlorate with a hexacondensed ion $Bi_6(OH)_{12}^{6+}$ have confirmed the hydrolysis mechanism suggested by Olin, with the formation of products with a higher condensation degree, having the following spectrophotometrically obtained stability constants:

$$1.5\ Bi_6(OH)_{12}^{6+} + 2H_2O \rightleftharpoons Bi_9(OH)_{20}^{+} + 2H^+;\ \log K_h = -3.9 \pm 0.2$$

$$Bi_9(OH)_{20}^{7+} + H_2O \rightleftharpoons Bi_9(OH)_{21}^{6+} + H^+;\ \log K_1 = -3.2 \pm 0.38$$

$$Bi_9(OH)_{21}^{6+} + H_2O \rightleftharpoons Bi_9(OH)_{22}^{5+} + H^+;\ \log K_2 = -2.8 \pm 0.1$$

Taking into account that the bismuthyl perchlorate solutions, with the analytical structure $BiOClO_4 \cdot H_2O$, have an acid character, Holmquist [1] came to the conclusion that the bismuth hydrolysis does not stop at the bismuthyl stage which according to his results would be a dimer, $Bi_2(OH)_4^{2+}$ but goes on with formation of the basic product, $Bi_2(OH)_5^{+}$. At the same time, Prytz and Nagel [2] came to the conclusion that the basic product resulted from the bismuthyl perchlorate hydrolysis had the formula $Bi_4O_3(OH)_4^{2+}$.

Starting from the results obtained by Souchay and Peshansky a who assume the existence of a tetracondensed product, $Bi_4O_4^{4+}$, Faucherre[4] shows that, by hydrolysis, the latter leads to a more basic product: $Bi_8O_{10}^{4+}$.

---

* Part I, ref. 14.

[1] A. Holmquist, *Svensk Kem. Tidskr.*, **48**, 106 (1936).

[2] M. Prytz and P. Nagel, *Z. anorg. Chem.*, **227**, 65 (1936).

[3] P. Souchay and D. Peshanski, *Bull. Soc. chim. France*, **1948**, 439.

[4] Y. Faucherre, *Bull. Soc. chim. France*, **1954**, 253.

The latest investigations on the bismuth hydrolysis have as a starting point the hexacondensed bismuthyl polycation

$(Bi_6(OH)_{12}^{6+}$;[5] $Bi_6O_6^{6+}$;[6] $Bi_6O_6(ClO_4)_2^{4+}$.[7]

The further hydrolysis mechanism of this cation is still questionable.

After Olin,[8] the hydrolysis takes place with the condensation degree increasing from 6 to 9 and the following series of compound formation :

$$1.5.\quad Bi_6(OH)_{12}^{7+} + 2H_2O \rightleftharpoons Bi_9(OH)_{20}^{7+} + 2H^+ \quad \log.K = -3.5 \pm 0.1$$

$$Bi_9(OH)_{20}^{7+} + H_2O \rightleftharpoons Bi_9(OH)_{21}^{6+} + H^+ \quad \log.K_1 = -3.2 \pm 0.2$$

$$Bi_9(OH)_{21}^{6+} + H_2O \rightleftharpoons Bi_9(OH)_{22}^{5+} + H^+ \quad \log.K_2 = -2.6 \pm 0.2$$

Tobias[6] considers that the hydrolysis takes place with the condensation degree being maintained at six but with formation of more basic products of the following type :

$$Bi_6O_6^{6+} + {}_3H_2O \rightleftharpoons Bi_6O_6(OH)_3^{3+} + 3H^+ \quad \log \beta_{6.15} = -8.1.$$

The mechanism suggested by Olin[8] is derived from the z(log h) curves (average number, z, of protons split off by one Bi(III) as a function of log h) which depend on the bismuth concentration, as well as from the fact that the equivalence point marking the end of hydrolysis and the precipitation of a basic perchlorate corresponds to the 9/5 ratio$(Bi^{3+})ClO_4^-)$.

The mechanism suggested by Tobias[6] is confirmed by the existence of basic salts with the bismuth/anion combination ratio of 6/5, 6/4, 6/3 and $6/2^{9-12}$.

Both mechanisms being possible, we have tried to bring in the present paper additional data by using spectrophotometric, polarographic and cyclic voltammetric methods in order to back up one or the other mechanism.

EXPERIMENTAL

Bismuthyl Perchlorate – $BiOClO_4.H_2O$ – was prepared by dissolvin gknown amounts of Bi_2O_3p.a. (USSR) in HCl_4 and heating to boiling and finally crystallizing. The bismuth content in solutions obtained by dissolving these crystals was determined complexometrically with EDTA.[13]

---

[5] A. Olin, *Acta Chem. Scand.*, **11**, 1445 (1957).

[6] R. S. Tobias, *J. Amer. Chem. Soc.*, **82**, 1070 (1960).

[7] R. W. Holmberg, K. A. Kraus and J. S. Johnson, *J. Amer. Chem. Soc.*, **78**, 5506 (1956).

[8] A. Olin, *Acta Chem. Scand.*, **13**, 1791 (1959).

[9] G. Gattow and D. Schott, *Z. anorg. Chem.*, **324**, 31 (1963).

[10] C. Drăgulescu, I. Julean and A. Nimară, *Rev. Roumaine Chim.*, **14**, 189 (1969).

[11] F. Fichter and E. Jenny, *Helv. Chim. Acta*, **6**, 225 (1923).

[12] F. Hein and H. Holzapfel, *Z. anorg. Chem.*, **248**, 77 (1941).

[13] H. A. Flaschka, "E.D.T.A. Titration" and ed. Pergamon Press, London, 1964.

Perchloric acid solutions (70% – Carlo Erba, Italy) were checked by NaOH standard. *Sodium perchlorate* solutions were prepared from a Merck p.a.$NaClO_4$ product.

The absorption spectra were recorded by a "UNICAM SP 800" spectrophotometer. For 10^{-3}M, 5×10^{-3}M and 10^{-2} M Bi^{3+} concentrations, cells of 0.2 and 0.1 cm respectively were used. For 10^{-2}M Bi^{3+}, concentration, cells with 0.01 – 1 mm were used. Distilled water was used as reference.

Measurements were carried out on a "Radiometer" pH-meter with a G-202 C glass electrode. Scale extension allowed a reading accuracy within 0.005 pH units.

Polarograms have been recorded on a "PO4 Radiometer" polarograph. Saturated calomel electrode connected by a $NaClO_4$ – agar bridge to the polarographic cell was used as reference. The capillary had following characteristics : h = 58 cm ; t = 3.5 s ; m = 2.09 mgs^{-1} in $HClO_4$ + $NaClO_4$ 0.1 M solution, open circuit.

The cyclic voltammograms were recorded on the same polarograph using a hanging dropping mercury electrode Kemulla type, E – 69B.

A slow cyclic polarization technique was applied, using a 0.4 – 0.8 v.p.m. potential change rate.

N_2, purified in washing bottles containing the alkaline solution of pyrogallol was bubbled to remove the oxygen from the solutions.

The experimental investigations were carried out with several bismuth concentrations (10^{-3} M, 5×10^{-3} M, 10^{-2} M) and for each of them, with different perchloric acid concentrations, at pH = 2–3.5.

The ionic strength has been maintained constant with sodium perchlorate. The absorption spectra of these solutions, their polarograms and cyclic voltammograms have been recorded.

RESULTS

a) – SPECTROPHOTOMETRIC DATA

The absorption spectra obtained for a10^{-3} M Bi^{3+}. For simplification, concentration is expressed in Bi^{3+} instead of $Bi_6\ (OH)_{12}^{6+}$ concentration in 0.1 M $NaClO_4$ as pH function are shown in fig. 1.

As shown in a previous work,[14] the absorbance keeps decreasing with the pH increase. More precisely, the absorbance decreases at λ 232 nm and it increases at λ 200 and 250 nm. At the same time, a bathochromic effect of the absorption peak is noticed.

The same curves recorded by means of a scale extension design evince the existence of some isosbestic points pairs which show that some equilibria take place in solutions.

Curve families, for pairs of isosbestic points, are presented in table 1.

In order to try to explain the nature of the species that take part in the equilibria corresponding to these isosbestic points, the inverse value of molar absorptivity was plotted at λ 223 nm *versus* pH, for these bismuth concentrations in 0.1 M $NaClO_4$ (fig. 2).

---

[14] C. Drăgulescu, A. Nimară and I. Julean, *Chem. Anal.* (in press).

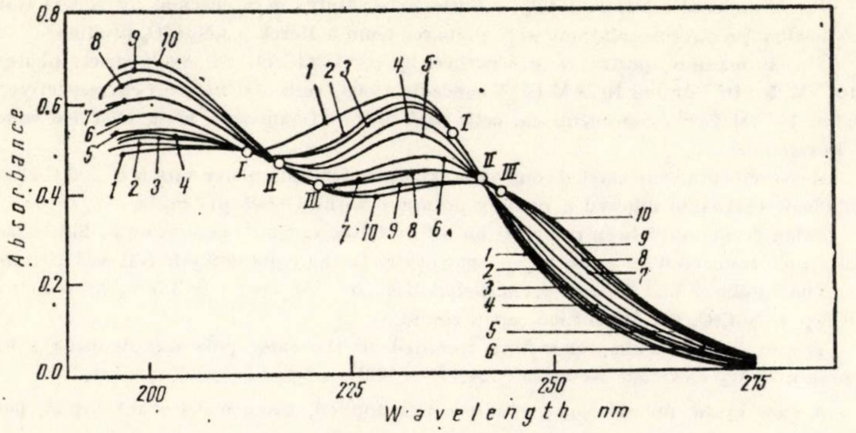

Fig. 1. — Absorption spectra as a pH function;
Bi^{3+} conc. 10^{-3} M, constant for all the curves pH: 1.95 (curve *1*); 2.05 (*2*); 2.18 (*3*); 2.38(*4*); 2.5(*5*); 2.70(*6*); 2.78 (*7*); 2. 87(*8*); 2.99(*9*); 3.15 (*10*).

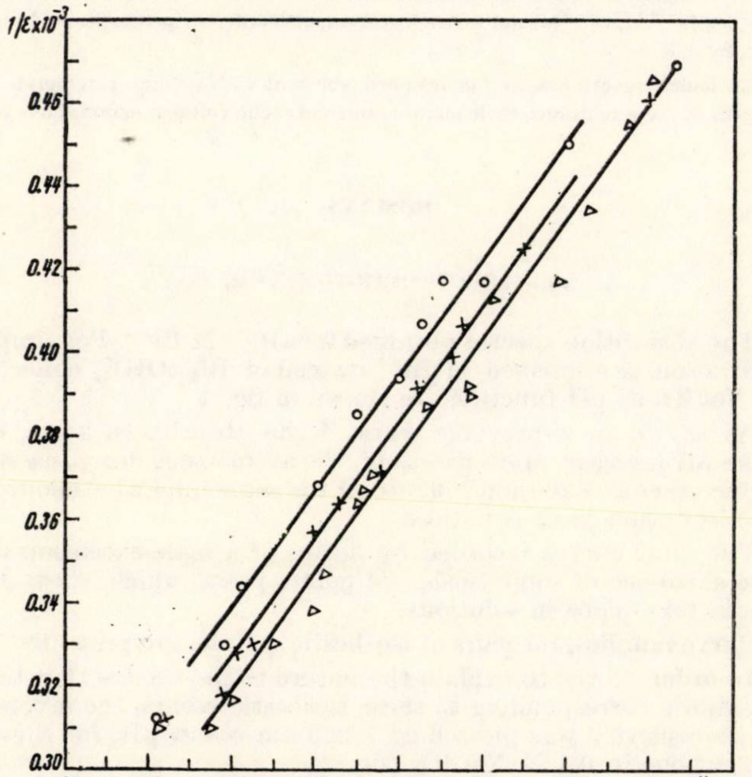

Fig. 2. — Plot of experimental values of 1/ε against pH; vawe-length 232 nm; 0.1 M(N, Na)ClO_4;
Bi^{3+}conc. 10^{-3}M (Δ); 5 x 10^{-3}M (x); 10^{-2} M (0).

Table 1

Number of curves passing through pairs of isosbestic points in a certain pH range

Isosbestic point	Curve number	pH range	$\lambda_{\text{isosb.}}$ nm	λ_{isosb} nm
I	1–3	1.95–2.18	213.4	237.8
II	4 – 6	2.18–2.70	215.6	241.8
III	7–10	2.78–3.4	220.3	242.5

As seen from figure 2 the absorbance does not depend only on pH but also on bismuth concentration ; thus the conclusion can be drawn that hydrolysis goes on with polynuclear species formation.

In fig. 3 $\lambda_{\max} = f$ (pH) is plotted.

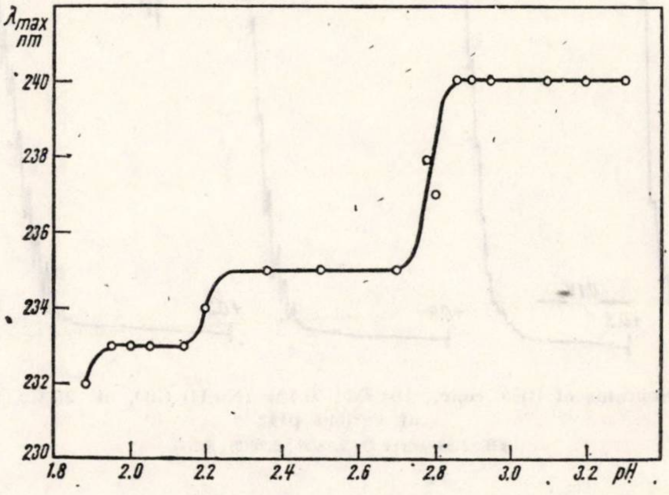

Fig. 3. – Plot of $\lambda_{\max}$ against pH ; Bi^{3+} conc. 10^{-3} M ; 0.1 M (Na,H) ClO_4.

The three levels obtained show the possibility of three products existing in equilibrium.

b) – POLAROGRAPHIC AND CYCLIC VOLTAMMETRIC DATA

The polarographic curves obtained with the same solutions used for the spectrophotometric determinations are not that conclusive; they present well-parked maxima due to some adsorption processes. By adding 0.1 % gelatine these (maxima) are eliminated but this leads to the wave height decreasing.

Besides reduction peaks, the voltammograms also show, peaks due to the adsorption processes.

The polarograms and voltammograms are shown in figures 4 and 5.

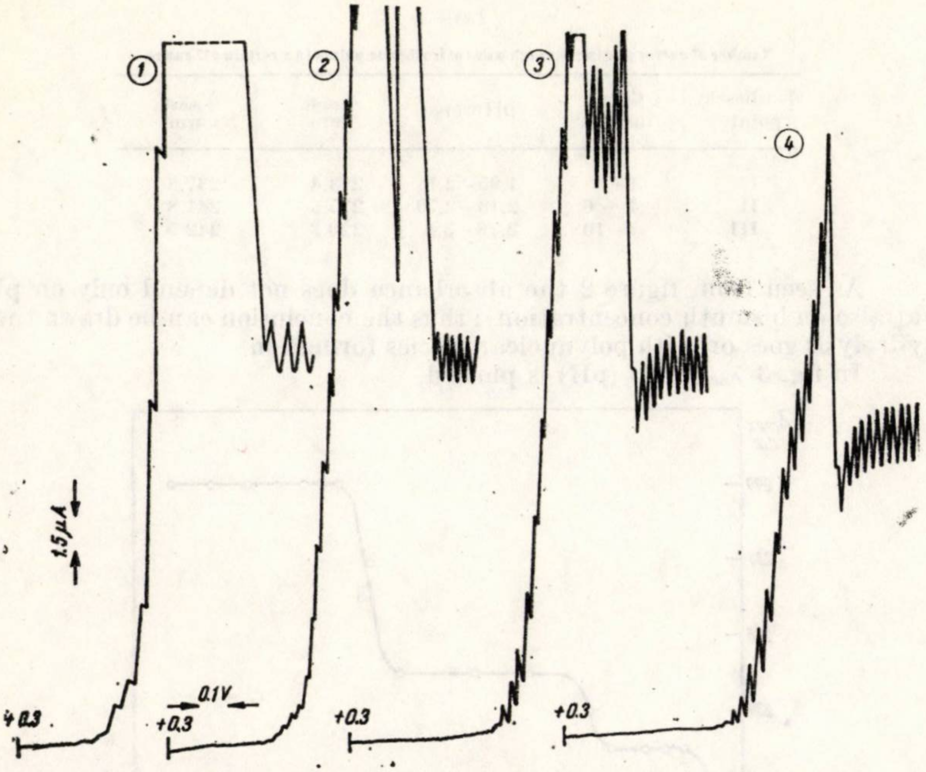

Fig. 4. — Polarograms of Bi^{3+} conc. $10^{-3}M$; 0.1M (Na,H) ClO_4 at 25°C; $v = 0.8$ V/min at various pH;

pH : 1.88 (curve *1*) ; 2.18(*2*) ; 2.70(*3*) ; 3.3(*4*).

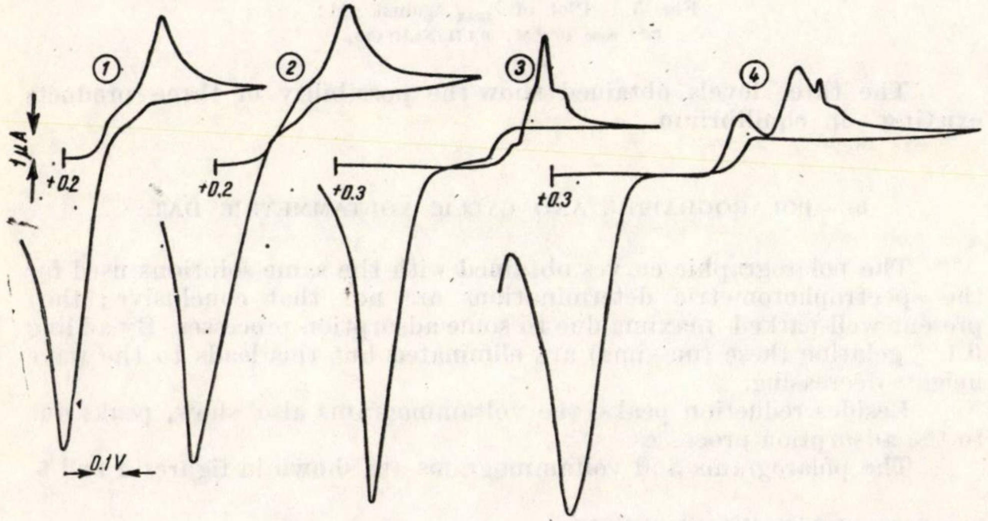

Fig. 5. — Voltammograms of Bi^{3+} conc. 10^{-3} M ; 0.1M (H, Na) $3ClO_4$ az 25° ; $v = 0.80$ V/min at various pH ;

pH : 1.88 (curve 1); 2.18(2); 2.70(3); 3.3(4).

In a previous paper,[14] we showed that the half-wave potential, characteristic of the bismuthyl ion, is of $-0.12-0.14$ V (SCE) at $\text{pH} = 1.60 - 1.88$. The reduction process is reversible, as it results from the voltammograms.

From figs 4 and 5 it can be seen that at $\text{pH} = 2$ the half-wave potential, respectively the potential peak shifts towards more negative values, which is characteristic of complex formation.

The results are illustrated in table 2.

Table 2

Variation of $E_{1/2}$ and $E_{\max}$ versus pH

pH	$E_{1/2}$ (SCE)	E_p (SCE)	ΔE (SCE)
1.88	-0.12	-0.12	
2.18	-0.22	-0.22	-0.10
2.70	-0.32	-0.32	-0.20
3.3	-0.42	-0.42	-0.30

The shifting of the half-wave potential, as well as of the peak potential of 100 mV/0.3. pH unit (tab. 2) for the first equilibrium, respectively of 100 mV/0.6 pH unit for the following two, shows that the hydrogen ion number in the first equilibrium is twice their number in the last two.

DISCUSSIONS

The experimental results show that at $\text{pH} > 1.88$ the $Bi_6(OH)_{12}^{6+}$ ion hydrolysis takes place with three compounds formation. These compounds are polynuclear as it results from fig. 2. As for their condensation degree, this is rather difficult to be definitely expressed. Only some indirect calculations allowed us to be in favour rather of one of the two still controversial mechanisms.

By comparing the hydrogen ion quantity (in Mol/1), measured experimentally on attaining equilibrium, with the calculated value necessary for hydrolysis regression – that is the conversion of the most basic product into $Bi_6(OH)_{12}^{6+}$ – the number of hydrogen ions involved in different hydrolysis phases can be calculated.

The number of hydrogen ions are in agreement with the obtained spectrophotometric results. Within the 3.3 – 2.90 pH range the spectrum varies very little and corresponds to the last hydrolysis product, the obtained hydrogen concentration being almost 0.

At pH 2.65 one H ion is used: the product III is converted into product II. At pH 2.18 and 2.08 two H ions are consumed, product II being converted into product I. Finally, at pH 1.80 four H ions are consumed corresponding to isosbestic point I, product I is converted into the hexabismuthylic polycation ($Bi_6(OH)_{12}^{6+}$).

This fact, as well as the conclusions drawn from polarographic determinations, made us to accept the hydrolysis mechanism suggested by Olin,[8] with successive complex formation :

$$1.5\ Bi_6(OH)_{12}^{6+} + 2H_2O \rightleftharpoons Bi_9(OH)_{20}^{7+} + 2H^+ \qquad (I)$$

$$Bi_9(OH)_{20}^{7+} + H_2O \rightleftharpoons Bi_9(OH)_{21}^{6+} + H^+ \qquad (II)$$

$$Bi_9(OH)_{21}^{6+} + H_2O \rightleftharpoons Bi_6(OH)_{22}^{5+} + H^+ \qquad (III)$$

which would determine the use of four H ions, in a good agreement with the experimentally obtained results, rather than the one suggested by Tobias[6] which would determine the use of three hydrogen ions only.

$$Bi_6(OH)_{12}^{6+} + H_2O \rightleftharpoons Bi_6(OH)_{13}^{5+} + H^+$$

$$Bi_6(OH)_{13}^{5+} + H_2O \rightleftharpoons Bi_6(OH)_{14}^{4+} + H^+$$

$$Bi_6(OH)_{14}^{4+} + H_2O \rightleftharpoons Bi_6(OH)_{15}^{3+} + H^+$$

The absorbance increase at λ = 180 − 200 nm, characteristic band for OH^-, proves the addition of OH^- groups, respectively the increase in the condensation degree.

DETERMINATION OF SUCCESSIVE FORMATION CONSTANTS BY SPECTROPHOTOMETRY

The stability constants for equilibria I, II and III are :

$$K_h = \frac{[Bi_9(OH)_{20}^{7+}]\,[H^+]^2}{[Bi_6(OH)_{12}^{6+}]\,1.5}$$

$$K_1 = \frac{[Bi_9\,(OH)_{21}^{6+}]\ [H^+]}{[Bi_9(OH)_{20}^{7+}]}$$

$$K_2 = \frac{[Bi_9\,(OH)_{22}^{5+}]\ [H^+]}{[Bi_9(OH)_{21}^{6+}]}$$

They were calculated according Newman and Hume's equations [15] by use of values included between two isosbestic points, considering that 2 species, 2 absorbers are present.

For equilibrium I we have the following relation :

$$A = \frac{1}{K}\,(A_0 - A)\ [H^+]^2 + \varepsilon\,M_t$$

For equilibria II and III

$$A = \frac{1}{K}\,(A_0 - A)\ [H^+] + \varepsilon\,M_t$$

---

[15] L. Newman and D. N. Hume, *J. Amer. Chem. Soc.*, **79**, 4571 (1957).

where :

A — absorbance for 1 cm cell
A_0 — absorbance when only one species is present
ε — molar absorptivity of the following species
M_t — total concentration of metallic ion
$[H^+]$ — hydrogen concentration as resulted from hydrolysis

The results for the 3 equilibria are plotted in figs 6, 7, 8.

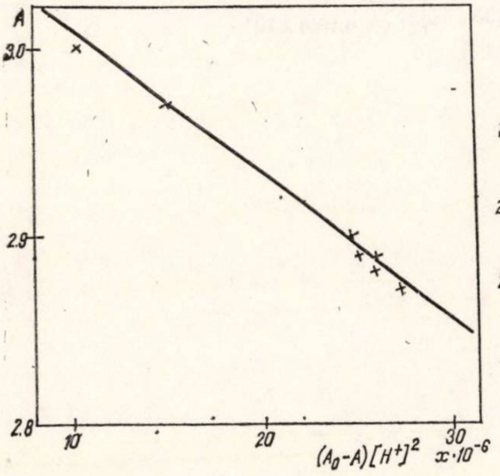

Fig. 6. — Determination of stepwise formation of $Bi_9(PH)_{20}^{7+}$ complex ion ; two species present, both absorbing at λ 232 nm ;
10^{-3} M Bi^{3+} conc. 0.1 M (H, Na)ClO_4 ; 25°C.

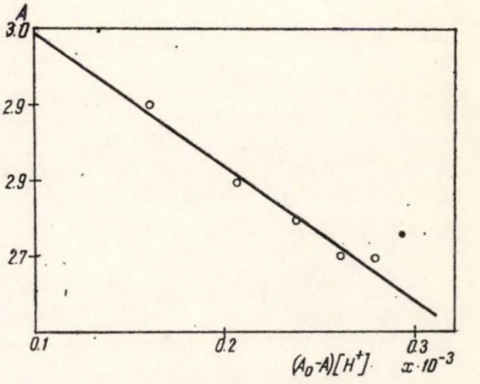

Fig. 7. — Determination of stepwise formation of $Bi_9(OH)_{21}^{6+}$ complexion. Two species present, both absorbing at λ_{232} nm ;
10^{-3} M Bi^{3+} ; 0.1 M (H, Na) ClO_4 ; 25°C.

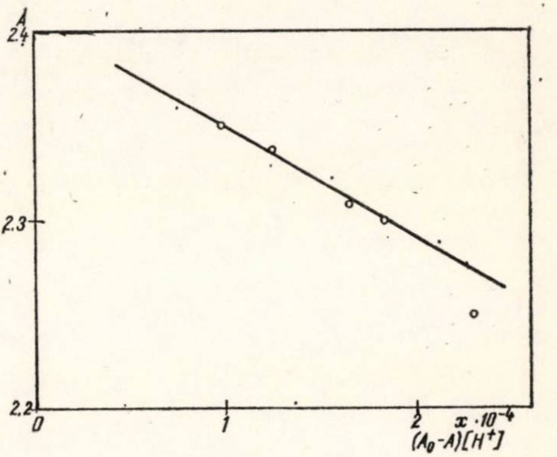

Fig. 8. — Determination of stepwise formation of $Bi_9(OH)_{22}^{5+}$ + complex ion. Two species present, both absorbing at λ_{232} nm ;
10^{-3} M Bi^{3+} ; 0.1 M (H, Na)ClO_4 ; 25°C.

The values of stability constants and of molar absorptivities are illustrated in Table 3.

Table 3

Calculated stability constants and molar absorptivities

Product	log K	ε
$Bi_9(OH)_{20}^{7+}$	-3.9 ± 0.2	$(28.6 \pm 0.280) \times 10^3$
$Bi_9(OH)_{21}^{6+}$	-3.2 ± 0.38	$(28.0 \pm 0.340) \times 10^3$
$Bi_9(OH)_{22}^{5+}$	-2.8 ± 0.1	$(21.6 \pm 0.100) \times 10^3$

Revue Roumaine de Chimie, **17**, 7, 1191 – 1197 (1972)

COBALT COMPLEXES WITH 2,9-DIMETHYL-1,10-PHENANTHROLINE

MARGARETA TEODORESCU, MARIA BREZEANU and P. SPACU

Faculty of Chemistry, University of Bucharest,
Spl. Independenţei 89, Bucharest, Romania

Received February 15, 1972

Three new cobalt complexes with 2,9-dimethyl-1,10-phenanthroline (dmphen) were prepared. Chemical data, electronic spectra and magnetic measurements showed that depending on the preparation method used, two tetrahedral Co(II) complexes (the blue form $[Co(II)LX_2]$ and the green one $[Co(II)_2 L_2X_2] X_2.4HCl$) as well as the pink octahedral $[Co(III)L_2X_2]X$ where L = 2,9-dimethyl-phenanthroline and $X = Cl^-$, were obtained. Attempts to synthetize hexammines $[CoL_3]^{2+}$ or $[CoL_3]^{3+}$ were unsuccessful. The most stable species prepared was the diammine $[Co(II)LX_2]$.

1,10-Phenanthroline, like dipyridyl, acts as a bidentate heterocyclic ligand forming with almost all transition-metal ions complexes having high thermal stabilities. One of the reasons would be the strong field produced by this ligand. The formation constants of the similar compounds containing ethylenediammine or ammonia take high values.[1]

The σ and π bonding M-N(phen) strengths are strongly influenced by the introduction of substituents on the aromatic rings, especially on those positions close to the heterocyclic donor nitrogen. The introduction of two methyl groups in positions 2 and 9 on the aromatic rings causes an increase of the steric effects, and consequently a lowering of stability of the corresponding compounds. In this case, a lowering in the value of Δ (orbital splitting parameter) due to the lowering of the ligand field strength should be expected. The lowering of the ligand field strength facilitates the high spin electron distributions in the octahedral $3d^6$ and $3d^7$ configurations, the orbital splitting parameter Δ being lower than the corresponding spin-pairing energy, or the appearance of a spin equilibrium in that case where Δ takes a value close to that of the spin-pairing energy. As an example, $[Fe(II)phen_3]^{2+}$ is diamagnetic, but $[Fe(II)mephen_3]^{2+}$, where mephen = 2 methylphenanthroline,[2] is a high spin complex at room temperature. As the temperature decreases, the magnetic moment suddenly drops to a critical temperature, followed by the rearrangement of the electrons into a low spin ground state.

[1] C. K. Jørgensen, "Inorganic Complexes" Acad. Press London, 1963.

[2] H. A. Goodwin and R. N. Sylva, *Austr. J. Chem.*, **21**, 83 (1968).

Other complexes of phenanthroline derivatives, especially with iron, have been reported in the literature.[3,4]

The present note deals with the behaviour of 2,9-dimethyl-1,10-phenanthroline (2,9 dmphen) and cobalt ion, trying to prepare complexes of di-, tetra- and hexammine type. As may be seen in the following, the last type is unstable and cannot be prepared, proving the existence of strong steric repulsions in this system

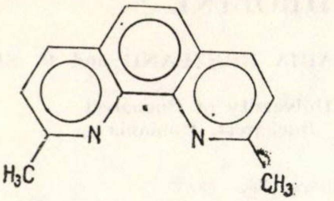

Fig. 1. — 2,9-Dimethylphenanthroline.

EXPERIMENTAL

1. $[CO(II)_2\ dmphen_2CL_2]CL_2.4HCL$, GREEN FORM

Solid 2,9-dimethyl-1,10-phenanthroline (0.32 gr) is added to a concentrated aqueous solution of cobalt chloride (0.20 gr) at the molar ratio 1 :2, and then 1 ml concentrated hydrochloric acid and 1 ml cool hydrogen peroxide. The solution is heated and dried on water bath, and then the precipitate is washed in acetone, a green compound being thereby separated. The same compound is obtained working at the molar ratio 1 :1 or 1 :3 ($CoCl_2$ — base). The compound was separated working in the same way but without hydrogen peroxide. Anal. *Calcd.* for $[Co(II)_2L_2Cl_2]Cl_2.4HCl$: C, 40.87 ; H, 3.40 ; N, 6.81 ; Cl, 34.50 ; Co, 14.30. *Found* : C, 40.07 ; H,3.13 ; N, 7.01 ; Cl, 34.77 ; Co, 14.00.

2. $[CO(II)dmphen\ CL_2]$ BLUE FORM

The same preparation method as for the green form is used, solving the green residium in methanol, ethanol or DMF. A blue compound is thus obtained. The same blue form may be obtained by heating the green compound. *Anal.* : *Calcd.* for $[Co(II)LX_2]$: C, 49.60 ; H, 3.55 ; N, 8.28 ; Cl, 20.97 ; Co, 17.40. *Found* : C, 49.90 ; H, 3.25 ; N, 8.75 ; Cl, 20,63 ; Co, 16.66.

3. $[CO(III)dmphen_2CL_2]CL$, PINK FORM

Solid 2,9-dmphen (0.32 gr) is added to a concentrated aqueous solution of $CoCl_2.6H_2O$(0.20 gr.) at the molar ratio 1 :2, and then 0.1 $NaClO_2$. The cooled mixture was left to interact, and then heated and dried on water bath. The pink compound was extracted from the residium

---

[3] E. König, *Coord. Chem. Rev.*, **3**, 471 (1968).

[4] R. L. Collins, R. Pettit and W. A. Baker, *J. Inorg. Nuclear Chem.*, **28**, 1001 (1966).

with water, and then washed with alcohol. Anal. *Calcd.* for $[Co(III)L_2Cl_2]$ Cl :Co, 10.10 ; N, 9.63 ;-Cl, 18.28 ; *Found* : Co, 9.89 ; N, 9.49 ; Cl, 18.53.

The magnetic moments were determined by means of Faraday method, using the formula $\mu = 2.84\ (\chi'_m T)^{1/2}$ where $\chi'_m = \chi_m^* - \chi_{dia}$ ($\chi_{dia\ 2,9\ dmphen} = -143.3.10^{-6}$ and $\chi_{dia\ Cl^-} = = -40.2.10^{-6}$).[5] The electronic spectra were recorded for the solid state using a spectrophotometer Zeiss VSU_1 equipped with a reflectance device, and MgO as standards. The electronic spectra cannot be recorded in solutions for compound 1 and 3, because they were rapidly converted into the blue form 2. The melting point and the molecular weights cannot be also determined, since molecular transpositions took place (green form passes into the blue one) or the complexes decompose (pink form) before their melting.

RESULTS AND DISCUSSIONS

As results from the elemental analysis, some chemical formulations could be ascribed to the green compound : $[Co(II)LCl_2].2HCl$, $[CoCl_4][CoL_2].4HCl$ and $[Co(II)_2L_2Cl_2]\ Cl_2.4HCl$. As may be seen below, the last formulation is better supported by the chemical and physical behaviour.

The green compound is unsoluble in acetone, the single solvent in which is stable, passing into the blue form in other solvents. The same process takes place faster by heating or slower by staying at the room temperature. The conversion green form ⇌ blue form is irreversible, the last form being the most stable. The green compound gradually eliminates hydrochloric acid detected with silver nitrate, allowing therefore its chemical formulation as a chlorohydrate. The hydrochloric acid probably promotes the Co --- Cl --- Co bridge breaking and thereby facilitates the conversion into the blue form. It should be mentioned that all syntheses carried out in the presence or the absence of hydrogen peroxide, have led to the same green and blue forms, which would indicate the oxidation state +2 for the central atom in both complexes.

The pink form 3 is soluble enough in water as well as in organic solvents, in the last case pssing gradually into the same blue forms as the green compound. The electronic spectra in DMF solution confirmed the above conclusion (fig. 3).

The magnetic moments are listed in table 1.

Table 1

Magnetic moments oft cobalt complexes wtih 2,9-dimethylphenonantholine

Compound	Colour	μ_{eff}(BM)
$[Co(II)_2L_2Cl_2]Cl_24HCl$	green	4.84
$[Co(II)LCl_2]$	blue	4.74
$[Co(III)L_2Cl_2]Cl$	pink	3.88

---

[5] B. N. Figgis and J. Lewis in „Modern Coordination Chemistry" K. Lewis and R. G. Wilkins, Ed. Interscience Publ., Inc. N. Y., 1960.

The green form, considered as a chlorohydrate $[Co(II)LCl_2].2.HCl$ (molecular weight = 411.00) would have a magnetic moment $\mu = 3.34$ BM, but the chemical formulations as double salts $[Co(II)_2L_2Cl_2]\ Cl_2.4HCl$ or $[Co(II)Cl_4][Co(II)L_2].4HCl$ lead to $\mu = 4.84$ BM, the value of the magnetic moment corresponding to the high spin $Co(d^7)$ tetrahedral complexes.[6]

The electronic spectra of compounds 1—3 recorded for the solid state are plotted in figure 2 and 4. The absorption spectra of the blue form in DMF were plotted in fig. 3, in order to see which species is the most stable in solution.

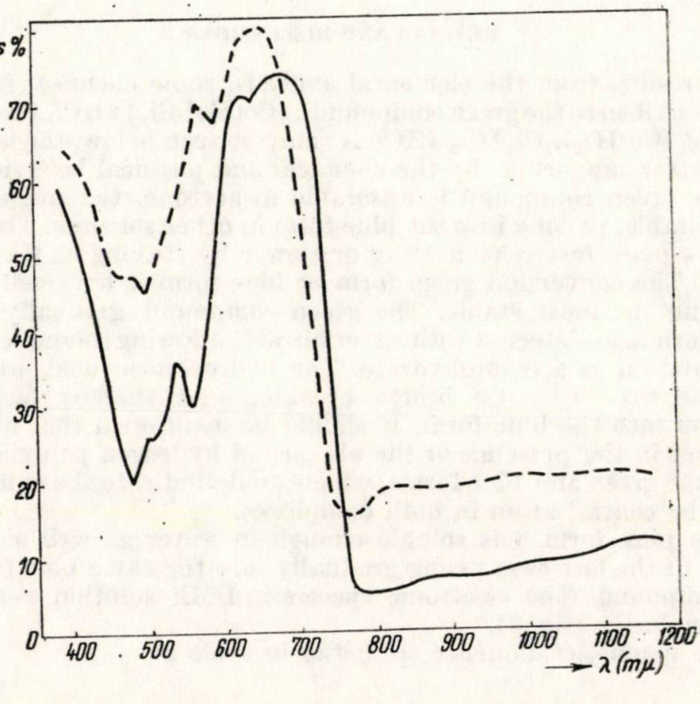

Fig. 2. — Electronic spectra of tetrahedral compounds : $Co(II)LX_2$ blue form (dashed line) and $CO(II)_2L_2Cl_2\ Cl_2.4HCl$ green form (full line) recorded for the solid state.

As may be seen, the electronic spectra of the first two compounds (fig. 2) similar to $[Co(II)Cl_4]^{2-}$ are characteristic of a $3d^7$ high spin configuration in a tetrahedral arrangement of the ligands .[7]

For T_d $Co(d^7)$ the characteristic absorption band occurs at ~ 600mμ, intense and split by the spin-orbit interaction. The following spin-allowed d-d transitions were calculated for the tetrahedral high spin d^7 configuration in the weak coupling scheme [8]:

---

[6] B. N. Figgis, "Introduction to Ligand Fields", Interscience Publ., N. Y., 1967.

[7] F. A. Cotton, D.M.L. Goodgame and M. J. Goodgame, *J. Amer. Chem. Soc.*, **83**, 4690 (1961).

$$^4A_2 \rightarrow {}^4T_2 \quad (\nu_1)$$

$$^4A_2 \rightarrow {}^4T_1(F) \; (\nu_2)$$

$$^4A_2 \rightarrow {}^4T_1(P) \; (\nu_3)$$

Cotton et. al.[7] have ascribed the intense absorption band at 15–17.000cm^{-1} occurring in $[Co(II)Cl_4]^{2-}$ (blue) to the ν_3 transition. This band is split or broadened by the spin-orbit coupling acting on the excited $^4T_1(P)$ term. The ν_3 transition occurs in the blue complex $[Co(II)\ LX_2]$ at 15.380 – –17.540 cm^{-1} and at 14.490–16.000 cm^{-1} in the green species. The striking similarity between the spectra of $[CoCl_4]^{2-}$ and of the blue compound containing 2,9-dimethylphenanthroline confirms the formulation made on the elemental analysis data and chemical properties, namely, the blue form is [Co(II) dmphen Cl_2] tetrahedrally coordinated, stable in organic solvents (fig. 3) too. The corresponding magnetic moment $\mu = 4.74$ BM

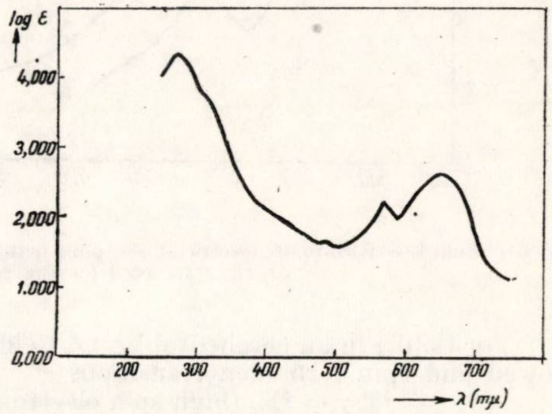

Fig. 3. — Electronic spectra of blue form in DMF solution obtained from the compounds 1,2,3.

is typical for a tetrahedral high spin Co(d^7). The most probable formulation for the green species is 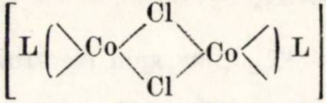 $\left[\mathrm{L}\left(\,\right)\mathrm{Co}\overset{\mathrm{Cl}}{\underset{\mathrm{Cl}}{\langle\,\rangle}}\mathrm{Co}\left(\,\right)\mathrm{L}\right]\mathrm{Cl_2\cdot 4\,HCl}$ and not $[CoCl_4][CoL_2].4HCl$, the transition $^4A_2 \rightarrow {}^4T_1(P)$ being shifted towards smaller wavenumbers than the same transition in $[CoCl_4]^{2-}$ or $[CoLX_2]$. This means that the inner coordination sphere of this species contains weaker Co -- N(L) or Co -- Cl bonds than in the normal compounds

---

[8] Y. Tanabe and S. Sugano, *J. Phys. Soc. Japan*, **9**, 753 (1954).

[Co(II) dmphen Cl_2] or $[Co(II)Cl_4]^{2-}$. The most plausible explanation should be the existence of bridges Co(II)...Cl...Co(II) in the green species. These bridges can be easily broken up, each of the two radicals $[Co(II)LCl]^+$ accepting a chloride ion from the outer sphere, going into the blue form $[Co(II)LCl_2]$. The above assumption agrees with the chemical behaviour, the green species passing irreversibly into the blue one $[Co(II)LCl_2]$.

The weak and narrow absorption bands occurring at 20–21.000 cm^{-1} should be assigned to a spin forbidden transition up to a doublet excited term ^2E, split by the spin-orbit coupling. These transitions are better resolved in the green species, being masked by the intense spin allowed d-d band ν_3 in the blue compound.

The spectrum of octahedral pink form $[Co(III)\ L_2Cl_2]Cl$ is plotted in figure 4.

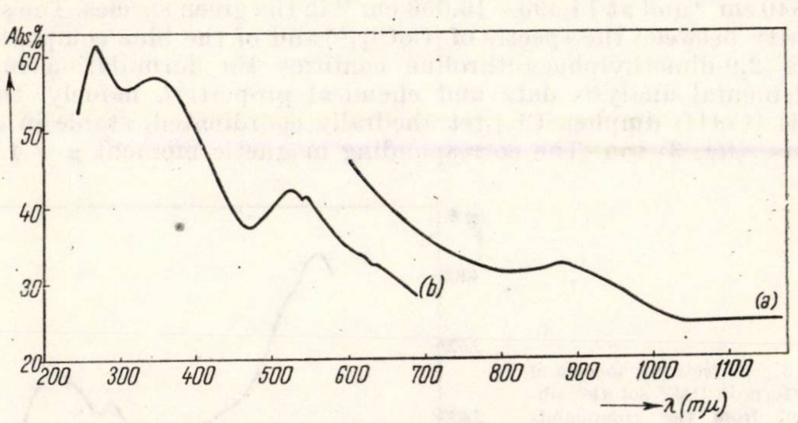

Fig. 4. – Electronic spectra of the pink octahedral compound $Co(II)L_2Cl_2$ $Cl_2.4HCl$ recorded for the solid state.

For $Co(d^6)$ in an octahedral ligand field, there are the following spin allowed and spin forbidden transitions .[9]

$^5T_{2g} \rightarrow {}^5E_g$ (high spin electron distribution)

and :

$^1A_{1g} \rightarrow {}^1T_{1g}$

$^1A_{1g} \rightarrow {}^1T_{2g}$ (low spin electron distribution)

$^1A_{1g} \rightarrow {}^3T_{1g}$

The single d-d transition occurring in the absorption spectrum of [Co(III) dmphen$_2$Cl$_2$] Cl is most probably the spin forbidden transition $^1A_{1g} \rightarrow {}^3T_{1g}$ as in the similar low spin $3d^6$ compound, such as $[Fe(II)\ phen_3]^{2+}$, the other two possible spin allowed transitions being masked by the more intense charge transfer bands at 525 – 545 mμ and 350 mμ. The assignment of the absorption bands is strongly supported by intensity arguments (fig. 4).

---

[9] J. S. Griffith, "The Theory of Transition-Metal Ions", London, Cambridge Univ. Press, 1961.

The magnetic measurements carried out at room temperature lead to the magnetic moment $\mu_{eff} = 3.88$BM, an intermediate value between the values typical for $3d^6$ with high spin and low spin states. The introduction of two methyl groups on the heterocyclic rings close to the metal-ligand bonds determines the weakening of these bonds, and hence the lowering of Δ parameter. The value in [Co(III) dmphen$_2$Cl$_2$] Cl lower than that in the diamagnetic compound [Co(IIII) phen$_2$Cl$_2$] Cl can lead to the stabilization of the high spin ground state or to a high spin — low spin mixture which is more probable than the intermediate spin state ($S = 2$) ascribed by König and Madeja [10] to the complexes [Fe(II)phen$_2$oxal$_2$] and [Fe(II) phen$_2$mal$_2$].

The paramagnetism of 3.88 B M observed with [Co(III)2,9 —dmphen$_2$Cl$_2$] Cl could most probably result from the electron distribution on the two possible ground states, high spin and low spin, according to the Maxwell-Boltzmann equilibrium statistics in a given ratio at the room temperature. The above assumption will be checked up in a forthcoming note concerning the paramagnetic behaviour dependent on temperature for this compound.

Ackonwledgment. The authors are indebted to V. Mincu for the kind help in performing the magnetic measurements.

---

[10] E. KÖNIG and K. MADEJA, *J. Amer. Chem. Soc.*, **19**, 4528 (1966).

other two possible spin-allowed transitions being masked by the more intense charge transfer bands at [illegible] cm⁻¹ and [illegible] cm⁻¹. The assignment of the absorption bands is strongly supported by intensity arguments (Fig. 11).

The magnetic measurements carried out at room temperature lead to the magnetic moment value 3.83 B.M., an intermediate value between the values typical for 3d⁶ with high spin and low spin states. The introduction of two methyl groups on the heterocyclic rings close to the metal-ligand bonds determines the weakening of these bonds, and hence the lowering of Δ parameter. The value of [illegible] that is [illegible] compound [illegible] can lead to the stabilization of the high spin ground state or to a high spin – low spin mixture which is more probable than the intermediate spin state (S = 1) ascribed by König and Madeja* to the complexes [illegible] and [illegible].

The paramagnetism of 3.83 B.M. observed with [illegible] could most probably result from the electron distribution on the two possible ground states, high spin and low spin, according to the Maxwell-Boltzmann equilibrium at a given ratio at the room temperature. The above assumption will be checked up in a forthcoming note concerning the paramagnetic behaviour dependent on temperature for this compound.

Acknowledgement. The authors thank [illegible] V. [illegible] for the help in performing the magnetic measurements.

---

* E. König and K. Madeja, Inorg. Chem., [illegible] (196[illegible]).

Revue Roumaine de Chimie, 17, 7, 1199 – 1209 (1972)

NOUVEAUX RÉACTIFS POUR LE DOSAGE SPECTROPHOTOMÉTRIQUE DE L'URANIUM

MARIA MAVRODIN

Centre de Chimie Physique, Bucarest, 31, str. Galaţi

Reçu le 11 mai 1971

On propose trois nouveaux réactifs de dosage spectrophotométrique de l'uranium : l'acide Calcon Carboxylique, l'Eriocrom Blue S.E. et le Diamant Blue-Black E.B. Pour éliminer les interférences, on recommande une séparation préalable de l'uranium à l'aide des échangeurs d'anions. La base théorique des méthodes proposées a été établie par l'étude quantitative des systèmes UO_2^{2+} : R, effectuée en utilisant des méthodes spectrophotométriques.

L'étude quantitative des réactions de l'azotate d'uranyle avec les acides : 1-(2-hydroxy- 4-sulfo- 1-naphtyl-azo)- 2-hydroxy- 3-naphtoïque (Calcon Carboxylique), 3-(5-chloro-2-hydroxy-phényle-azo)-4-5-dihydroxy-naphtaline-2,7-disulfonique (Eriocrom Blue S.E.) et 1-(2′-hydroxynaphtyl azo)-2-naphtol-4-sulfonique (Diamant Blue-Black E.B) nous a suggéré la possibilité de leur utilisation comme réactifs de dosage spectrophotométrique de l'ion U^{6+}.

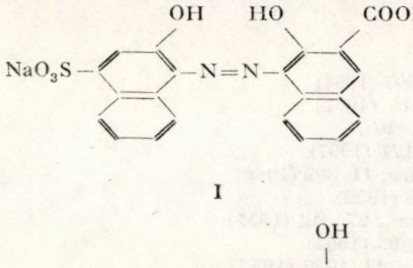

I

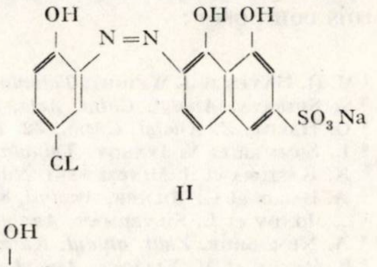

II

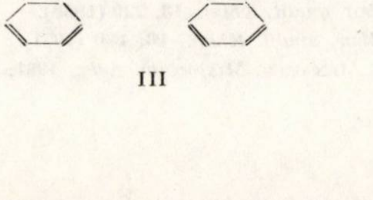

III

À mentionner que la littérature de spécialité met en évidence les réactifs «azo» (PAN,[1,2] PAR,[3] TAR,[4] TAM,[5] Arsenazo III,[6-9] Thoron,[10] Arsenazo IV, [11] Clorofosfonazo III, [12] Solocrom Black 6 BN [13]) pour la grande sensibilité de leur réaction avec l'ion UO_2^{2+}.

La base théorique des méthodes proposées a été établie par l'étude des systèmes :

— azotate d'uranyle — Acide Calcon Carboxylique (I) ;
— azotate d'uranyle — Eriocrom Blue S.E. (II) ;
— azotate d'uranyle — Diamant Blue-Black E.B (III).

Par cette étude on a mis en évidence (on a utilisé les méthodes des variations continues, du rapport molaire, des pentes, logarithmique et du point isobesthique) la formation de quelques complexes solubles, colorés, pour lesquels on a déterminé les rapports de formation et les constantes de stabilité.

PARTIE EXPÉRIMENTALE

Appareils. Spectrophotomètre Karl-Zeiss-Jena V.S.U. 1, avec prisme et cuvettes de verre au diamètre 0,5 et 1 cm.

Réactifs. Solutions d'azotate d'uranyle ($1,25.10^{-4}$ M pour les systèmes I et III et 2.10^{-4} M pour le système II), préparées en dissolvant dans de l'eau les quantités correspondantes de $UO_2(NO_3)_2.6\ H_2O$ (*p.a.* Chemapol).

La concentration a été déterminée par évaporation et calcination directe à U_3O_8.

Les solutions d'acide Calcon Carboxylique ($1,25.10^{-4}$ M), d'Eriocrom Blue S.E ($2,0.10^{-4}$M) et de Diamant Blue-Black E.B. ($1.25.10^{-4}$M) ont été préparées en dissolvant, dans de l'eau, les quantités correspondantes de réactifs (*p.a.* Lachema).

Pour séparer l'uranium on a utilisé des échangeurs d'anions tels que : Amberlite IR-400, Amberlite IR-410, Dowex 1 et Dowex 2.

RÉSULTATS ET DISCUSSIONS

Par l'étude spectrophotométrique on a déterminé, pour chacun de ces trois composés :

---

[1] M. R. Hayes et J. Wright, *Talanta*, **11**, 607 (1964).

[2] S. Shibata, *Analyt. Chim. Acta*, **25**, 348 (1961).

[3] O. Hackl, *Z. Analyt. Chem.*, **32**, 119 (1940).

[4] L. Sommer et V. Ivanov, *Talanta*, **14**, 171 (1967).

[5] K. Kasiura et J. Minczewski, *Nukleonica*, **11**, 399 (1966).

[6] A. Bacon et G. Milner, *Analyst*, **81**, 456 (1956).

[7] L. Mondy et L. Silverman, *Analyt. Chem.*, **27**, 312 (1955).

[8] A. Nemodruk, *Zhur. analyt. Khim.*, **18**, 93 (1963).

[9] B. Payge et M. Elliott, *Analyt. Chem.*, **29**, 1029 (1957).

[10] E. A. Arnold et A. R. Pray, *Analyt. Chem.*, **15**, 294 (1943).

[11] T. Kuznețsov, *Zhur. analit. Khim.*, **13**, 220 (1958).

[12] A. Nemodruk, *Zhur. analit. Khim.*, **16**, 180 (1961).

[13] J. Korkisch et G. Jenauer, *Mikrochim. Acta.*, **1961**, 537.

— la variation de l'absorption des réactifs, en fonction de la longueur d'onde λ, dans le but d'établir les conditions optimales pour l'étude quantitative des systèmes ;

— la variation de l'absorption du mélange des réactifs en fonction de la longueur d'onde, dans le but de mettre en évidence les phénomènes de complexation ;

— le rapport de formation des composés qui prennent naissance dans les réactions ;

— les constantes de dissociation des complexes ;

— la stabilité des composés formés en fonction du temps ;

— l'applicabilité de la loi de Lambert — Beer et les coefficients molaires d'extinction.

Pour caractériser les composés formés dans les réactions, les données obtenues par l'étude spectrophotométrique ont été complétées par l'étude effectuée à l'aide des échangeurs d'ions. On a travaillé avec des échangeurs de cations et d'anions, en utilisant des méthodes statiques et dynamiques.

Les courbes d'absorption des réactifs. Tel que l'on voit dans les figures 1 — 3, les maxima d'absorption des réactifs sont situés à $\lambda = 550$ nm (pour l'acide Calcon Carboxylique), à $\lambda = 530$ nm (pour l'Eriocrom Blue S.E.) et à $\lambda = 510$ nm (pour le Diamant Blue-Black E.B).

La solution de l'azotate d'uranyle, de concentration 2.10^{-4} M, se caractérise par une absorption négligeable.

La variation de l'absorption du mélange des réactifs en fonction de λ (fig. 1 — 3) indique nettement la formation, dans chaque système étudié, d'un nouveau composé, les courbes d'absorption des mélanges présentant des maxima déplacés à $\lambda = 570$ nm (pour le système I) à $\lambda =$ $= 550$ nm (pour le système II) et à $\lambda = 540$ nm (pour le système III).

L'étude quantitative des systèmes a été effectuée dans le but de déterminer les rapports de formation et les constantes de dissociation des composés qui prennent naissance dans ces réactions. Les méthodes utilisées ont été les suivantes : la méthode du point isobesthique,[14] la méthode des variations continues, [15] la méthode du rapport molaire,[16] la méthode des pentes [17] et la méthode logarithmique. [18]

L'étude des réactions par la méthode du point isobesthique a été effectuée en traçant les courbes d'absorption pour dix preuves, mélanges des réactifs, caractérisées par les rapports : azotate d'uranyle : R = 1 : 9 (courbe *1*) ; 2 : 8 (courbe *2*) ; 3 : 7 (courbe *3*) ; 3,33 : 6,66 (courbe *4*) ; 4 : 6 (courbe *5*) ; 5 : 5 (courbe *6*) ; 6 : 4 (courbe *7*) ; 7 : 3 (courbe *8*) ; 8 : 2 (courbe *9*) ; 9 : 1 (courbe *10*). Tel qu'on le voit dans les figures 4, 5, 6, les courbes obtenues pour les preuves 1, 2 et 3, qui contiennent, par rapport à la preuve UO_2^{2+} : R = 1 : 2, un excès de réactifs, se rencontrent dans le même point, le point isobesthique, avec la courbe d'absorption du réactif (courbe 1') et avec la courbe d'absorption qui caractérise la preuve UO_2^{2+} : R = 1 :2 (courbe *4*). La position du maximum obtenu pour chaque courbe d'absorption se déplace graduellement pour les preuves 1, 2 et 3, qui contiennent, par rapport à la preuve UO_2^{2+} : R = 1 : 2, un excès de réactif, de la longueur d'onde qui caractérise le réactif vers la longueur d'onde qui caractérise le composé. Pour toutes les preuves caractérisées par un rapport R : $UO_2^{2+} < 2$, le maximum est situé à la longueur d'onde qui caractérise le complexe, l'extinction décroissant vers la preuve 10, à mesure que la quantité de complexe décroît. Les considérations ci-dessus conduisent à la conclusion que, dans les systèmes I, II et III, se forment des composés caractérisés par le rapport UO_2^{2+} : réactif = 1 : 2.

---

[14] E. Asmus, *Z. analyt. Chem.*, **193**, 81 (1963).

[15] P. Job, *Ann. Chim (France)*, **9**, 113 (1928).

[16] J. H. Yoe et A. E. Harvay, *J. Amer. Chem. Soc.*, **70**, 648 (1948).

[17] A. E. Harvay et D. L. Manning *J. Amer. Chem. Soc.*, **72**, 4488 (1950).

[18] W. Kingery et N. Hume, *J. Amer. Chem.* Soc., **71**.

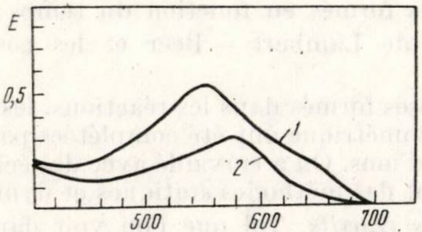

Fig. 1. — Courbe d'absorption de l'acide Calcon Carboxylique (1) et du complexe formé dans le système azotate d'uranyle — acide Calcon Carboxylique (2).

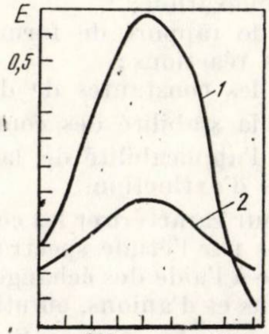

Fig. 2. — Courbe d'absorption de la solution d'Eriocrom Blue S.E. (1) et du complexe formé dans le système azotate d'uranyle — Eriocrom Blue S.E. (2).

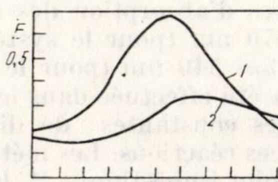

Fig. 3. — Courbe d'absorption de la solution de Diamant Blue-Black E.B. (1) et du complexe formé dans le système azotate d'uranyle — Diamant Blue-Black E.B. (2).

L'étude des systèmes par *la méthode des variations continues* (Job) a été effectuée en travaillant avec des solutions équimolaires, de concentration $1,25.10^{-4}$M (systèmes I et III) et 2.10^{-4} M (système II).

Dans le cas des preuves caractérisées par des rapports R : $UO_2^{2+} < 2$, l'extinction a été lue en utilisant des preuves-témoin qui contiennent une quantité de réactif égale à l'excès.

La conclusion qu'on tire des données expérimentales représentées dans les figures 7 — 9 du fait qu'on obtient un maximum très accentué pour les preuves qui contiennent 3,33 cm³ solution d'azotate d'uranyle

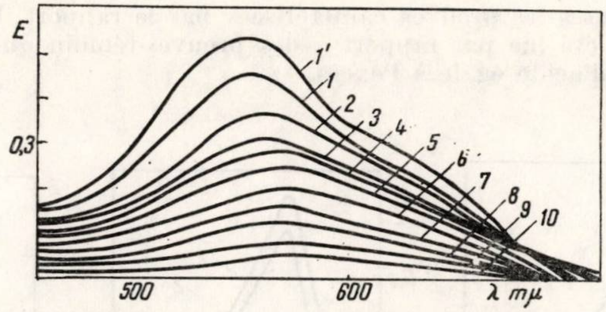

Fig. 4. — Etude du système azotate d'uranyle — Calcon Carboxylique, par la méthode du point isobesthique.

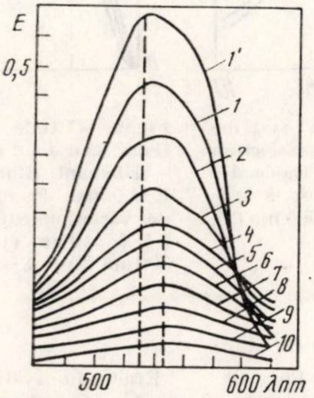

Fig. 5. — Etude du système azotate d'uranyle — Eriocrom Blue S.E, par la méthode du point isobesthique.

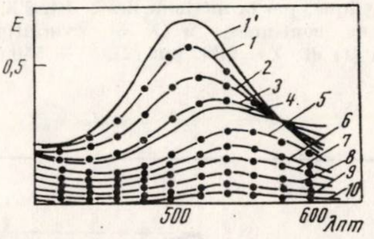

Fig. 6. — Etude du système azotate d'uranyle — Diamant Blue-Black E.B., par la méthode du point isobesthique.

et 6,66 cm³ solution d'acide est que, dans les systèmes I, II et III, se forme un composé caractérisé par le rapport de formation UO_2^{2+} : R = 1 :2.

L'étude des systèmes par *la méthode du rapport molaire* a été effectuée en travaillant avec des solutions équimolaires, dans des cuvettes à 1 cm de diamètre (fig. 10).

Conformément à la méthode, on a effectué deux séries de déterminations : dans une première série on a maintenu constante la quantité de réactif (chaque preuve contient 2 cm³) et on a varié graduellement la quantité d'azotate d'uranyle ; dans la deuxième série, on a maintenu constante la quantité d'azotate d'uranyle (chaque preuve contient aussi 2 cm³ d'azotate) et on a varié, toujours graduellement, la quantité d'acide.

Les résultats obtenus lorsqu'on a mesuré la variation de l'extinction en fonction de la quantité d'azotate d'uranyle (1) et en fonction de la quantité d'acide (2) confirment le rapport de formation UO_2^{2+} : R = 1 : 2.

Pour toutes les preuves caractérisées par le rapport $R : UO_2^{2+} < 2$, l'extinction a été lue par rapport à des preuves-témoin qui contiennent une quantité d'acide égale à l'excès.

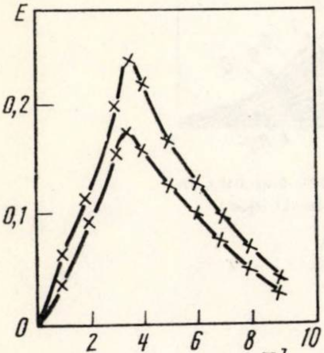

Fig. 7. — Etude du système azotate d'uranyle — acide Calcon Carboxylique, par la méthode des variations continues, à λ = 570 nm (1) et λ = 530 nm (2).

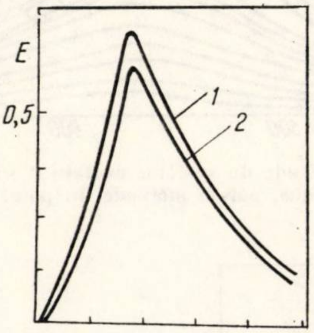

Fig. 8. — Etude du système azotate d'uranyle — Eriocrom Blue S.E. par la méthode des variations continues, à λ = = 550 nm (1) et λ=500 nm (2).

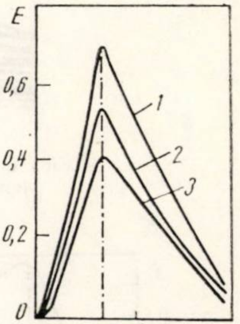

Fig. 9. — Etude du système azotate d'uranyle — Diamant Blue-Black E.B., par la méthode des variations continues, à λ = 540 nm (1) ; λ = 500 nm (2) et λ=600 nm (3).

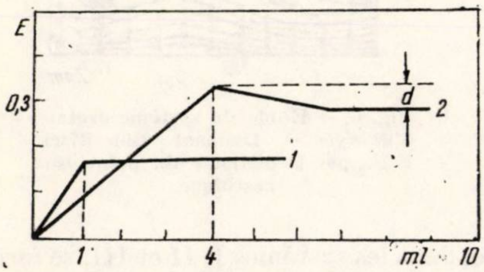

Fig. 10. — Etude du système azotate d'uranyle — Calcon Carboxylique, par la méthode du rapport molaire (Dans les mêmes conditions de travail, on a obtenu, pour les systèmes II et III, des résultats similaires).

La formation de ces composés a été vérifiée aussi par *la méthode des pentes* (fig. 11), en travaillant avec des solutions équimolaires $1{,}25.10^{-4}$ M (les systèmes I et III) et 2.10^{-4} M (le système II). L'extinction des preuves caractérisées par le rapport $R : UO_2^{2+} > 2$ a été lue par rapport à des preuves-témoin qui contiennent une quantité de réactif égale à l'excès. Le fait que le rapport des tangentes des angles α_1 et α_2, que les droites 1 et 2 forment par rapport à l'axe 0 — X, est approximativement égal à 2, confirme, encore une fois, que le rapport de formation des composés qui résultent dans les systèmes I, II et III est $UO_2^{2+} : R = 1 : 2$.

L'étude des systèmes I, II et III par la *méthode logarithmique* (fig. 12) a été effectuée en transformant, par calculs, les données obtenues dans l'étude des systèmes par la méthode des pentes. En logarithmant l'expression de la constante de formation et en représentant, sur l'axe *O — Y*, log [complexe]/[métal] et, sur l'axe $O-X$, log [ligand], on obtient pour les systèmes étudiés, une ligne droite, caractérisée par un angle d'inclinaison par rapport à l'axe $O-X$, α, dont la tangente a la valeur $\simeq 2$, ce qui confirme que le rapport de formation $UO_2^{2+} : R = 1 : 2$.

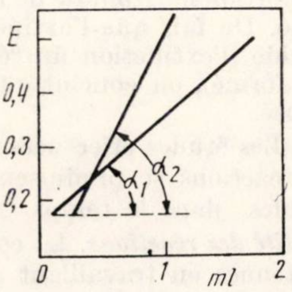

Fig. 11. — Etude du système azotate d'uranyle — Calcon Carboxylique, par la méthode des pentes (dans les mêmes conditions de travail, on a obtenu, pour les systèmes II et III, des résultats similaires).

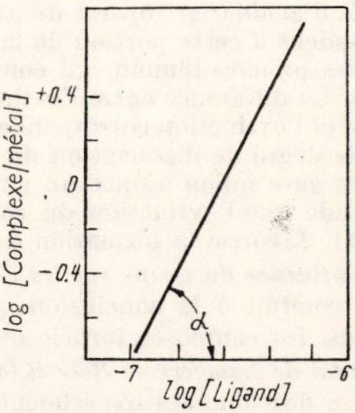

Fig. 12. — Etude du système azotate d'uranyle — Calcon Carboxylique par la méthode logarithmique (dans les mêmes conditions de travail, on a obtenu, pour les systèmes II et III, des résultats similaires).

Les degrés et les constantes de dissociation ont été déterminés par la méthode de Harvey et Manning [19] en utilisant les formules :

$$\alpha = \frac{E_1 - E_2}{E_1} \quad \text{et} \quad K = \frac{(\alpha C)\,(n\alpha C)^n}{C(1-\alpha)}$$

où

α = le degré de dissociation ;
K = la constante de dissociation ;
E_1 = le maximum de l'extinction, après le rapport de formation ;
E_2 = l'extinction qui correspond à la portion horizontale de la courbe ;
C = la concentration totale du complexe mole/l ;
n = le nombre des molécules du ligand dans le complexe.

Conformément aux formules ci-dessus, les degrés et les constantes de dissociation sont :

$\alpha_{I} = 0{,}16$, $K_{I} = 1{,}2 . 10^{-11}$ (pour le complexe formé dans le système : azotate d'uranyle — Calcon Carboxylique) ;

$\alpha_{II} = 0{,}21$, $K_{II} = 7{,}4 . 10^{-12}$ (pour le complexe formé dans le système azotate d'uranyle — Eriocrom Blue S.E) et

---

[19] A. E. Harvay et D. L. Manning, *J. Amer. Chem. Soc.*, **74**, 4744 (1952).

$\alpha_{III} = 0{,}19$, $K_{III} = 1{,}88.10^{-11}$ (pour le complexe formé dans le système azotate d'uranyle — Diamant Blue-Black E.B).

Le décroissement de l'extinction après le point qui marque le rapport de formation des composés, dans le cas des déterminations faites en maintenant constante la quantité d'azotate d'uranyle et en variant les quantités d'acide (fig. 10), est dû au fait que, pour toutes les preuves qui correspondent à cette portion de la courbe, l'extinction a été lue par rapport à des preuves-témoin qui contiennent une quantité de réactif égale à l'excès. La différence entre l'extinction correspondant au point stœchiométrique et l'extinction correspondant à la portion horizontale de la courbe mesure le degré de dissociation du composé. Du fait que l'extinction décroît à mesure qu'on ajoute un excès d'acide (l'extinction du réactif est plus grande que l'extinction du complexe formé), on conclut que l'excès de réactif favorise la formation du composé.

L'influence du temps sur les réactions. Les études effectuées dans ce but ont conduit à la conclusion que ces réactions se produisent immédiatement, les composés formés étant stables dans le temps.

La loi de Lambert — Beer et la sensibilité des réactions. La conclusion qu'on tire des données expérimentales obtenues en travaillant avec des solutions $1{,}25.10^{-4}$ M (les systèmes I et III) et 2.10^{-4} M (le système II) (fig. 13) est que les composés formés respectent rigoureusement la loi de Lambert-Beer, les coefficients molaires d'extinction étant :

$$\varepsilon_{I} = 13602 \text{ (à } \lambda = 570 \text{ nm)};$$

$$\varepsilon_{II} = 19059 \text{ (à } \lambda = 550 \text{ nm) et}$$

$$\varepsilon_{III} = 18700 \text{ (à } \lambda = 540 \text{ nm)}.$$

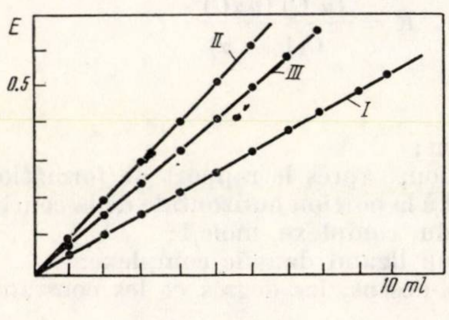

Fig. 13. — Applicabilité de la loi de Lambert-Beer, dans le cas des complexes formés par l'azotate d'uranyle avec les réactifs : Calcon Carboxylique (I) ; Eriocrom Blue S.E (II) et Diamant Blue-Black EB (III).

MÉTHODES DE DOSAGE DE L'URANIUM

L'étude quantitative des systèmes I, II et III nous a suggéré la possibilité de l'utilisation de l'acide Calcon Carboxylique, de l'Eriocrom Blue S. E et du Diamant Blue-Black EB comme réactifs pour le dosage spectrophotométrique de l'ion UO_2^{2+}.

Étant donné que ces réactifs réagissent avec beaucoup d'ions Fe^{3+}, Co^{3+}, Ni^{3+}, La^{3+} Sm^{3+}, Th^{4+} Y^{3+}, Zn^{2+} etc.), on recommande, pour éliminer les interférences, une séparation préalable de l'uranium.

Très efficace — surtout lorsqu'on veut doser l'uranium des minerais — est la séparation de l'uranium, de ses solutions sulfuriques, à l'aide des échangeurs d'anions basiques du type Amberlite IR-400, Amberlite IR-410, Dowex 1, Dowex 2, D-Acidit FF, etc. Dans ce cas, l'uranium est retenu quantitativement sous la forme d'un anion complexe formé avec l'acide sulfurique, pendant que tous les autres ions métalliques traversent la colonne sans être retenus. La solution sulfurique qui va traverser l'échangeur d'anions doit être menée au pH = 1,5 — 2,1. La récupération de l'uranium retenu par l'échangeur se fait à l'aide d'un acide fort, tels que $HClO_4$, HNO_3 ou HCl (concentration 0,5 — 1 N). Les déterminations que nous avons effectuées ont utilisé des solutions 0,01 N H_2SO_4 qui contenaient, en dehors de $2{,}5.10^{-2}$gU/ml, Fe^{3+}, Co^{3+}, Ni^{3+}, La^{3+}, Sm^{3+}, Th^{4+}, Y^{3+}. Après le passage de la solution (pH = 2) à travers la colonne et le lavage de l'échangeur avec un volume de H_2SO_4 0,01 N, environ trois fois plus grand que le volume de l'échangeur, on a procédé à la récupération de l'uranium avec du HNO_3 0,5 N. Le contrôle de la séparation a été fait par dosage gravimétrique, sous forme de U_3O_8, de l'uranium ; les résultats ont été comparés à ceux obtenus à l'aide des méthodes spectrophotométriques proposées.

DÉTERMINATION DE LA DROITE D'ÉTALONNAGE

Après la séparation, le dosage de l'uranium a été fait à l'aide de la droite d'étalonnage, en mesurant l'absorption à $\lambda = 570$ nm (lorsqu'on utilise comme réactif l'acide Calcon Carboxylique), à $\lambda = 550$ nm (réactif — l'Eriocrom Blue S.E) et à $\lambda = 540$ nm (réactif — le Diamant Blue-Black E.B).

En considérant que les réactions sont pratiquement totales — (les constantes de dissociation K sont très petites pour tous ces trois complexes) — si, dans une série de preuves synthétiques avec un contenu variable et connu en uranium, on ajoute une quantité constante et en excès de réactif, l'extinction de chaque preuve se compose de l'extinction due au complexe formé, E_{RM}, et de l'extinction due à l'excès de réactif, E_R :

$$E = E_{RM} + E_R \tag{1}$$

Étant donné que l'excès de réactif

$$R = C_R^0 - C_{RM} \tag{2}$$

(C_R^0 = la quantité totale, constante, de réactif, ajoutée dans la preuve et C_{RM} = la quantité de réactif liée dans le complexe) et que le réactif, ainsi que le complexe formé avec l'ion UO_2^{2+} respectent rigoureusement la loi de Lambert – Beer, on peut écrire :

$$E = E_R + E_{RM} = \varepsilon_\lambda\, l\, (C_R^0 - C_{RM}) + \varepsilon_\lambda'\, l\, C_{RM} \qquad (3)$$

$$E = \varepsilon_\lambda\, l\, C_R^0 + l\,(\varepsilon_\lambda' C_{RM} - \varepsilon_\lambda C_{RM}) = \varepsilon_\lambda\, l C_R^0 + l(\varepsilon_\lambda' - \varepsilon_\lambda)\, C_{RM} \qquad (4)$$

En représentant E en fonction de C_{RM}, on obtient une droite — — la droite d'étalonnage — qui, conformément à l'équation (4), se caractérise par la pente $\mathrm{tg}\,\alpha = l(\varepsilon_\lambda' - \varepsilon_\lambda)$ et entrecoupe l'axe $O - Y$ à $\varepsilon_\lambda\, l\, C_R^0$.

RÉSULTATS

Quelques-uns des résultats obtenus sont représentés dans le tableau 1.

Tableau 1

Dosage spectrophotométrique de l'uranium

Réactif	Concentration en uranium 10^{-3} mole/l	
	Calculée	Trouvée
Acide Calcon	0,0756	0,0750
Carboxylique	0,1512	0,1510
	0,1890	0,1870
	0,1761	0,1750
	0,2548	0,2560
Eriocrom	0,0587	0,0560
Blue S.E	0,1174	0,1155
	0,1467	0,1450
	0,1761	0,1730
	0,2548	0,2330
Diamant	0,0756	0,0755
Blue-Black EB	0,1512	0,1520
	0,1890	0,1880
	0,1761	0,1765
	0,2548	0,2540

CONCLUSIONS

On propose quelques nouveaux réactifs pour le dosage spectrophotométrique de l'uranium, caractérisés par la fonction «azo» : l'acide Calcon Carboxylique, l'Eriocrom Blue S. E. et le Diamant Blue-Black E. B. Pour éliminer les interférences on recommande une séparation préalable de l'uranium à l'aide des échangeurs d'anions.

La base théorique des méthodes proposées a été établie par l'étude quantitative des systèmes azotate d'uranyle : ***R*** qui a mis en évidence la formation de quelques anions complexes colorés, caractérisés par le rapport UO_2^{2+} : R=1 :2, les constantes de dissociation $K_I = 1{,}2.10^{-11}$, $K_{II} = 7{,}4.10^{-12}$, $K_{III} = 1{,}88.\ 10^{-11}$ et les coefficients molaires d'extinction $\varepsilon_I = 13602$ (à $\lambda = 570$ nm, pour le complexe formé avec l'acide Calcon Carboxylique), $\varepsilon_{II} = 19059$ (à $\lambda = 550$ nm, pour le complexe formé avec l'Eriocrom Blue S.E) et $\varepsilon_{III} = 18700$ (à $\lambda = 540$ nm, pour le complexe formé avec le Diamant Blue-Black EB).

Revue Roumaine de Chimie, 17, 7, 1199 - 1209 (1972)

Revue Roumaine de Chimie, 17, 7, 1211–1217 (1972)

CONSIDÉRATIONS GÉNÉRALES SUR L'APPARITION DES PROPRIÉTÉS LIANTES

I. TEOREANU

Institut Polytechnique Bucarest, 1, str. Polizu

Reçu le 9 février 1972

Les propriétés liantes apparaissent dans un nombre impressionnant de systèmes, comme résultat d'une gamme variés de réactions chimiques. L'apparition des propriétés liantes est soumise à certaines règles, leur étude faisant l'objet du présent travail.

1. Les études entreprises ce dernier temps permettent de conclure que l'apparition des propriétés liantes est gouvernée par certaines règles, qu'elles existent pour un nombre impresionnant de système, que le durcissement des liants est le résultat d'une gamme variée de réactions chimiques.

L'analyse de la variété des réactions chimiques déterminant le durcissement des liants connus — partant de la chaux et du plâtre, du ciment Portland et du ciment alumineux et finissant par des ciments magnésiens et dentaires et par les mastics litharge-glycérine — révèle qu'elles supposent la participation à côté des radicaux acides et des cations métalliques, des grouppements hydroxyle et des protons.

Ces réactions pourraient être rapportées aux types de systèmes suivants :

a) sel (minéral, oxyde métallique)-eau ;
b) oxyde basique — oxyde acide — eau (vapeur saturée) ;
c) oxyde métallique (hydroxyde) — sel — eau ;
d) oxyde métallique(hydroxyde) — acide ;
e) oxyde métallique (hydroxyde) — composés organiques à caractère acide.

Les deux premiers types se rapportent aux réactions servant de base au durcissement de la plupart des liants usuels : la chaux, le plâtre, les ciments Portland et alumineux, avec toutes leurs variantes, les ciments de scorie, les ciments pouzzolaniques. En ce cas les réactions d'hydratation-hydrolyse ont un rôle primordial. Le troisième type de systèmes est caractéristique des ciments magnésiens (Sorel) où, à côté du processus de l'hydratation MgO, il faut tenir compte de la formation des hydroxysels, — spécialement l'hydroxy chlorure ou l'hydroxysulfate de mganésium comme suite de la réaction MgO-$MgCl_2$ ($MgSO_4$), en présence et avec la participation de l'eau. Les deux dernières catégories durcissent sur la base de réactions de type base-acide, caractéristiques — parmi les liants les plus connus — des liants phosphatiques et des mastics à base d'oxyde de plomb et glycérine. On observe la position intermédiaire, de transition, des liants magnésiens.

Bien qu'à présent on utilise un nombre assez restreint de liants, correspondant à chaque catégorie de systèmes présentés plus haut, l'aire des composés étudiés et qui font preuve de propriétés liantes se développe. La connaissance des lois qui gouvernent l'apparition des propriétés liantes présente un immense intérêt.

2. Analysant les données expérimentales de la littérature [1,2] concernant les composés ressemblant à ceux qui existent dans le ciment Portland ou dans le ciment alumineux et qui donnent des masses durcies à la suite des réactions dans les systèmes du type (a) ou du type (b), on obtient — en employant une systématisation utilisée encore par Juravlev — l'image présentée dans le tableau 1. On constate une certaine régularité et une certaine corrélation avec le système périodique des éléments.

Tableau 1

La régularité de l'apparition des propriétés liantes

Oxydes des éléments du gr. II	Oxydes acides								
	Al_2O_3	SiO_2	GeO_2	TiO_2	SnO_2	PbO_2	Cr_2O_3	Mn_2O_3	Fe_2O_3
BeO	⊗	⊗	○	○	○	○	○	○	○
MgO	⊗	⊗	○	○	⊗	○	○	○	⊗
CaO	⨹	⨹	⨹	⨹	⨹	⨹	⨹	⨹	⨹
ZnO	⊗	⊗	○	○	○	○	⊗	○	⊗
SrO	⨹	⨹	△	⨹	⨹	⨹	△	△	⨹
CdO	⊗	⊗	○	○	○	○	○	○	○
BaO	⨹	⨹	△	⨹	⨹	⨹	⨹	⨹	⨹

Propriétés liantes	Sans propriétés liantes
⨹ étudiés	⊗ étudiés
△ non étudiés	○ non étudiés

Les résultats qui ont servi de base pour concevoir le tableau 1 ont été obtenus pour le durcissement dans des conditions normales de température. Comme prévu, le traitement par autoclave influence négativement sur les propriétés de résistance de ces composés qui ont une grande vitesse d'hydratation à température et pression normales ; on constate, par contre, la possibilité d'accélerer le durcissement par traitement par autoclave de certains minéraux qui, d'habitude, ne durcissent pas ou donnent des résistances mécaniques relativement réduites, obtenant des systèmes durcis avec de bonnes propriétés de résistance. Il faut remarquer dans ce sens le

---

[1] F. V. Joravliev, « Chimia lianţilor » (traduit du russe), chap. VIII, Ed. construcţiilor şi materialelor de construcţii, Bucarest, 1953.

[2] N. F. Fedorov, *Epitöanyag*, **21**, 217 (1969).

durcissement par traitement par autoclave des composés $2CdO.ZrO_2$, $MgO.SnO_2$ et $2MgO.SnO_2$. Dans le cas de $2CdO.ZrO_2$ on obtient, par traitement par autoclave à 8 atm. (2 — 8 — 2 heures), des résistances mécaniques plus grandes que celles obtenues par durcissement normal d'un ciment P500.

Analysant les résultats obtenus par durcissement dans des conditions normales, Juravlev[1] constate que parmi les composés englobant les éléments du IIe groupe du système périodique, ce sont seulement ceux où ces éléments ont le rayon ionique égal ou plus grand que 1,06Å qui possèdent des propriétés liantes (tableau 2).

Tableau 2

Corrélation entre l'apparition des propriétés liantes et le rayon ionique du cation métallique

Elément	Rayon ionique R_i(Å)	Propriétés liantes
Be	0,34	Non
Mg	0,78	Non
Zn	0,83	Non
Cd	1,03	Non
Ca	1,06	Oui
Sr	1,27	Oui
Ba	1,43	Oui

A première vue, du tableau 2 il pourrait résulter que les propriétés liantes, considérées à travers les résistances mécaniques du composé durci, s'intensifient des composés à calcium aux composés à baryum. Mais cet ordre n'est pas toujours respecté. Par exemple, si l'on respecte cette règle dans le cas des titanates de calcium, strontium ou baryum, les choses se passent inversement pour les stannates et plombates bibasiques ($2CaO.SnO_2 < 2SrO.SnO_2 < 2BaO.SnO_2$), bien que pour les composés monobasiques correspondants la règle soit respectée. Il faut considérer les facteurs cinétiques du processus chimique mis en corrélation directe avec le processus de cristallisation et de développement de la structure de résistance du liant durci. Les vitesses réduites de la réaction chimique déterminent des résistances sans importance ou nulles du système durci. Donc, elles doivent être accélérées, le traitement par autoclave remplissant ce rôle. Les vitesses très grandes de la réaction chimique peuvent déterminer un tel développement de la structure cristalline que celle-ci se caractérise par de grandes tensions internes, à conséquences négatives sur les résistances mécaniques. Il existe donc, à ce point de vue, une valeur optimale de la vitesse d'interréaction avec l'eau et ainsi du développement de la structure de résistance.

Il faut remarquer que pour le durcissement des constituants minéralogiques du ciment Portland ou alumineux et de leurs analogues, les processus de l'interréaction avec l'eau sont des processus d'hydrolyse. On sait que les processus d'hydrolyse sont caractéristiques des sels résultants d'une base forte et d'un acide faible. d'une base faible et d'un acide fort, ou, enfin, d'une base faible et d'un acide faible. Autant la base est plus forte et l'acide plus faible, et vice versa, autant l'hydrolyse est plus forte. Pour le cas des liants auxquels nous nous rapportons, on obtiendra des sels d'autant plus hydrolysables que les acides correspondant à leurs anions (radicaux acides) sont plus faibles et les bases correspondant aux cations métalliques composants sont plus fortes. Une mesure dans ce sens pourrait être soit l'électronégativités des cations, soit leur potentiel ionique. Conformément à ce qu'on a montré ci-dessus, il résulterait que la vitesse d'hydrolyse est d'autant plus grande que le potentiel ionique des deux cations est plus petit. Ceci explique, par exemple, pourquoi les aluminates de calcium interactionnent avec l'eau plus vite que les silicates de calcium ou bien pourquoi la vitesse du même processus est plus grande pour les silicates de baryum que pour les silicates de magnésium correspondants. D'après ce critère, en gardant le même anion (radical acide), la vitesse d'interréaction avec l'eau devrait s'accroître — par exemple — dans la série* :

Cation métallique	Mg^{2+}	Fe^{2+}	Zn^{2+}	Mn^{2+}	Cd^{2+}	Ca^{2+}	Sr^{2+}	Ba^{2+}
Potentiel ionique	2,57	2,50	2,41	2,20	1,94	1,88	1,57	1,40

Dans le cas du même cation métallique on devrait obtenir — par exemple — une croissance de l'interaction avec l'eau dans la série :

Cation des radicaux acides	Si^{4+}	Ge^{4+}	Ti^{4+}	Al^{3+}	Cr^{3+}	Zr^{4+}	Fe^{3+}
Potentiel ionique	10,25	9,10	6,25	5,26	4,68	4,61	4,48

Les résultats expérimentaux obtenus mettent en évidence le fait qu'une pareille règle est respectée dans la comparaison des composés ayant des cations à configuration électroniques ressemblante [5]. Pour illustrer cela, dans les figures 1 – 3 sont représentées les variations dans le temps de la résistivité électrique des différentes suspensions – comme mesure de la vitesse et de la capacité d'hydrolyse des composés examinés*.

---

* La série est donnée pour les composés ayant le même rapport $\frac{\text{oxyde basique}}{\text{oxyde acide}}$; l'accroissement du rapport mentionné détermine une croissance de la vitesse de l'interaction avec l'eau [3,4]

[3] S. Solacolu, P. Baltă et C. Hofman, *Rev. Roumaine Chim.*, **11**, 481 (1966).

[4] I. Teoreanu, « L'Action du chlorure de calcium sur les processus de durcissement d'une catégorie de liants », 39e Congrès international de Chimie Industrielle, vol. 3, Bucarest, 1970, p. 11/61.

[5] I. Teoreanu et A. Puri, « Considérations sur l'activité hydraulique des scories », ouvrage communiqué à la Session scientifiques des cadres didactiques de l'Institut Polytechnique, Bucarest, 1971.

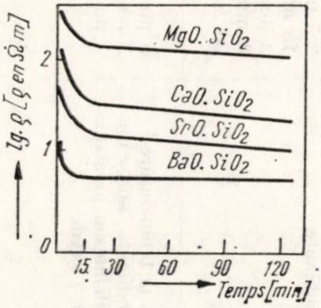

Fig. 1. – Variation de la résistivité des suspensions aqueuses des métasilicates alcalino-terreux.

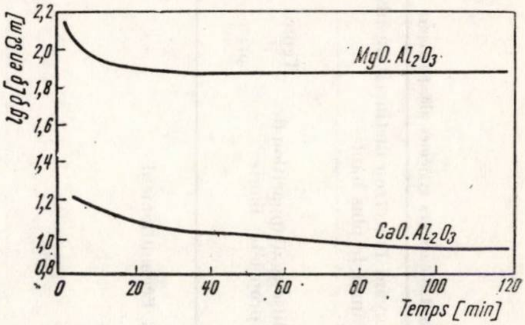

Fig. 2. – Variation de la résistivité des suspensions aqueuses de $MgO.Al_2O_3$ et de $CaO.Al_2O_3$.

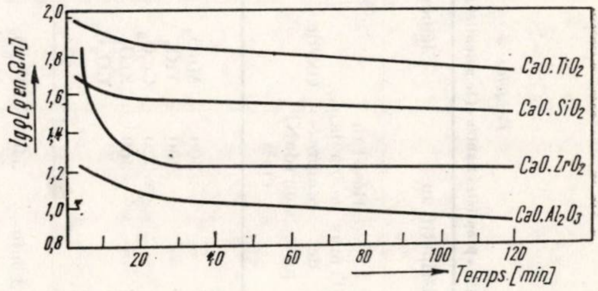

Fig. 3. – Variation de la résistivité des suspensions aqueuses de quelques composés avec du calcium.

3. L'apparition des propriétés liantes dans des systèmes pareils au ciment Sorel présente aussi une certaine régularité, reflétant la position du cation métallique composant dans le système périodique des éléments. L'étude des propriétés de durcissement (dans des conditions normales de température et de pression) dans le système $MeO\text{-}MeCl_2\text{-}H_2O$, mène à la conclusion que les résistances mécaniques diminuent de façon continue en fonction de la nature du cation métallique Me^{2+}, dans la série :

$$Mg^{2+} \rightarrow Ca^{2+} \rightarrow Sr^{2+} \rightarrow Ba^{2+}$$

Si l'on considère le potentiel ionique des cations mentionnés, on constate sa baisse dans le même sens. Le parallélisme entre la résistance mécanique et le potentiel ionique des cations s'explique par une telle

---

* Sans doute, une comparaison plus rigoureuse doit prendre en considération les composés ayant une structure cristallochimique similaire.

Tableau 3

Corrélation entre les conditions de l'apparition des propriétés liantes et le potentiel ionique de cations métalliques des systèmes phosphatiques

Eléments cationiques ayant l'électron distinctif au niveau le plus haut					Eléments cationiques ayant l'électron distinctif au niveau II, après le plus haut				
Oxyde	Potentiel ionique	Conditions d'apparition des propriétés liantes	Temps de prise	Résistance à la compression (daN/cm^2)	Oxyde	Potentiel ionique	Conditions d'apparition des propriétés liantes	Temps de prise	Résistance à la compression (daN/cm^2)
SiO_2	10,25	A l'échauffement	—	300	MnO_2	7,70	A l'échauffement	—	80
SnO_2	5,42		—	260	TiO_2	6,25		—	600
Al_2O_3	5,26		—	320	Cr_2O_3	4,68		—	330
PbO_2	4.75		—	360	ZrO_2	4,61		—	225
					CO_2O_3	4,55		—	130
MgO	2,57	A la température ambiante, après une calcination préalable de l'oxyde	3 min	540	Fe_2O_3	4,48	A la température ambiante	48 h	50
					Mn_2O_3	4,29		2,5 h	30
					Y_2O_3	2,90		15 mn	80
					NiO	2,57		3 mn	250
					FeO	2,50		2 mn	500
					CuO	2,50		30 mn	630
CaO	1,88	La réaction a lieu avec violence au froid ; la formation de la structure de durcissement n'est pas possible	—	—	La_2O_3	2,45	A la température ambiante, après une calcination préalable de l'oxyde	5 mn	45
SrO	1,57		—	—	ZnO	2,41		3 mn	330
BaO	1,40		—	—	CdO	1,94		2 mn	90

intensification de la réaction d'hydratation et de la réaction oxyde — sel — en même temps que la croissance de la basicité du cation (la baisse de son potentiel ionique) — qu'une croissance importante des tensions internes dans la structure de durcissement a lieu avec des conséquences négatives sur ses résistances mécaniques.

4. Les systèmes phosphatiques (Me_xO_y — H_3PO_4) sont typiques du durcissement basé sur des réactions base-acide. Le caractère chimique du cation métallique (Me^{n+}) est essentiel pour la manifestation des propriétés liantes. L'électronégativité, la valeur du rayon ionique, la charge, la configuration électronique du cation sont déterminantes pour le caractère chimique d'un ion. Vu qu'à la comparaison des combinaisons analogues des éléments des différents groupes, les charges et les rayons ioniques ne peuvent être pris en considération, et que l'emploi de la valeur de l'électronégativité n'est pas toujours possible, on peut utiliser, comme avant, en tant que grandeur caractéristique pour les cations métalliques des systèmes phosphatiques leur potentiel ionique. Sychev et ses coll.[6] pour mettre en évidence les manifestations de la régularité de l'apparition des propriétés liantes dans les systèmes phosphatiques ont comparé la modification du caractère et les conditions de l'apparition des propriétés liantes d'un côté, et la variation des potentiels ioniques de cations métalliques composants, de l'autre côté. Dans le tableau 3 on observe qu'à des potentiels ioniques en baisse, pour des systèmes contenant des éléments cationiques à configuration électronique pareille, la réaction oxyde-acide phosphorique est accélérée, les potentiels ioniques caractérisant la basicité des cations (celle-ci est d'autant plus grande que le potentiel ionique du cation est plus petit)*. Ainsi que dans le cas des liants dont le durcissement est basé sur l'hydrolyse. quand la vitesse de la réaction oxyde-acide phosphorique est trop grande, comme suite des tensions grandes qui apparaissent dans le développement du réseau de cristallisation, la formation de la structure de durcissement n'est pas possible (exemple le système BaO-H_3PO_4) ; lorsque la vitesse de réaction oxyde-acide phosphorique est trop petite — dans le cas de pression et temperature normales — le durcissement de même n'a pas lieu dans ces conditions (par exemple le système $ZrO_2—H_3PO_4$). Par freinage ou par accélération de la réaction, le processus de durcissement peut être réglé afin d'obtenir une résistance mécanique convenable.

5. Il résulte clairement, la régularité de l'apparition des propriétés liantes, la liaison de ce phénomène avec le système périodique des éléments ; elle représente une caractéristique commune des systèmes variés de substances, mettant en évidence les lois générales gouvernant l'apparition des propriétés liantes.

---

* Le tableau 3 est modifié par rapport à celui présenté dans le travail [6] pour un groupement en fonction de la nature des éléments cationiques composants des oxydes. En même temps, pour une bonne concordance avec les données présentées ci-dessus, on a utilisé la même source pour les valeurs des rayons ioniques.

[6] S. L. Golyko-Volfson, M. M. Sychev, L. G. Sudakas et L. I. Skoblo, « Khimicheskie osnovy tehnologuii i primenenia fosfatnykh sviazok i pokrytii », Izd. Khimia, Moscou, 1968, gl. III.

Revue Roumaine de Chimie, 17, 7, 1219 – 1226 (1972)

STRUKTUR DER GEZOGENEN GLASFASERN AUS DEM SYSTEM $Na_2O-ZnO-SiO_2$

Ş. SOLACOLU und D. TENȚULESCU

vom Lehrstuhl für Physikalische Chemie der Silikate und der oxydischen Komponenten der Technischen Hochschule Bukarest

Eingegangen am 25. August 1971

Die Struktur der Glasfasern aus $[SiO_4)^{-4}$ und $[ZnO_4]^{6-}$-Tetraedern besitzt, im Vergleich zu granuliertem Glas gleicher Zudammensetzung, eine bessere Beständigkeit gegen Wassereinwirkung, obwohl die Natriumionen durch Austausch mit Hydroniumionen gegenseitig leichter diffundieren. Das Verhalten bei der Hydrolyse, die Thermogramme und die Elektronogramme sind vom Molverhältnis $Na_2O/ZnO \geqslant 1$ bedingt und als Folge können diese in $[ZnO_4]$ und $[ZnO_6]$ koordinieren.

EINLEITUNG

In den letzten zehn Jahren sind Arbeiten erschienen, welche die Frage der Glasfaserstruktur erörtern. In Folge der Entstehungsbedingungen[1] ist diese Struktur von derjenigen des granulierten Glases, dessen Zusammensetzung dieselbe ist, verschieden.

— Einige Glasfasern, zum Beispiel $Na_2O.MgO.3SiO_2$, weisen bei der Röntgenuntersuchung unter kleinem Winkel eine veränderliche Elektronenverteilung auf, deren Periodizität von der Kühlungsgeschwindigkeit abhängt.[2]

— Die Glasfasern der Systeme $Na_2O-CaO-SiO_2$, Na_2O-SiO_2 und K_2O-SiO_2 zeigen im Elektronenmikroskop eine „Myzellenstruktur" mit schuppigem Aussehen, welche unter der Einwirkung der Luftfeuchtigkeit, die in die Säule des Mikroskops dringt, den schrittweisen Schwund des myzelligen Anfangsbildes verursacht, je mehr die hydrolytische Wirkung des Wassers fortschreitet.[3]

— Wenn die Glasfasern des Systems $CaO-Al_2O_3-B_2O_3-SiO_2$ Wasser, Säuren und Alkalien ausgesetzt sind, führen sie, bei elektronenmikroskopischer Untersuchung zur Schlußfolgerung, daß die Struktur der Oberflächenschicht von der des zentral gelegenen Teiles der Fasern, verschieden ist. Die an der Oberfläche gelegene Schicht reagiert mit Wasser sehr intensiv, wodurch eine an der Oberfläche gelegene Korrosionsschicht nach den bekannten Angriffsmechanismen entsteht.[4]

---

[1] G. Manfre, *Glass Technol.*, **10**, 99 (1969).

[2] W. Stattion und L. Hoffman, *J. Appl. Phys.*, **31**, 404 (1960).

[3] J. Zarzycki und R. Mezard, *Phys. and Chem. Glasses*, 3, 163 (1962).

— Wenn Glasfasern der Systeme $Na_2O - CaO - SiO_2$ und $Na_2O - CaO - B_2O_3 - SiO_2$ der thermischen Behandlung bei 300° ausgesetzt sind weisen sie bei etwa 190° nicht diejenige thermischen Effekte auf, welche sonst die Fasern ohne thermische Behandlung aufweisen.[5]

1. EXPERIMENTELLES

1.1. ARBEITSWEISE

Die untersuchten 24 Glasfasern befanden sich im sauren Teil des ternären Systems $Na_2O - ZnO - SiO_2$. Die für die Aufbereitung der Glasproben verwendeten Rohstoffe waren chemisch rein. Das Schmelzen wurde in Platintiegeln im Elektroofen etwa 250 bis 300° über der Liquidustemperatur durchgeführt und wurden durch Wiederschmelzen homogenisiert. Das Ziehen der Glasfaser, dünner als 10 μ wurde durch Wiederschmelzen der Glasproben im Düsen-Platintiegel mit Hilfe des Joule-Effektes erreicht.

Zur Festlegung der Struktur, wurde die Glasfaser folgenden Bestimmungen unterworfen :

— Die Analyse der hydrolytischen Beständigkeit gegen Wasser bei 98,4° wurde in einem besonderen von den Verfassern verbesserten Extraktionsapparat[6] durchgeführt.

— Die differential-thermische Analyse der hydrolytisch unbehandelten Proben wurde mit einem SETARAM-Gerät durchgeführt.

— Die elektronenmikroskopische Analyse auf Au-Ni-C Replik wurde mit einem JEM-7A Apparat durchgeführt.

— Die Feststellung der Protonenmenge in den Glasfasern, vor und nach dem hydrolytischen Angriff, wurde mit Hilfe der magnetischen Kernresonanz mit dem JNM-3H-Gerät durchgeführt.

Von allen untersuchten Proben, die in Abb. 1 makriert sind, seien nur einige repräsentativere angegeben, welche in Tabelle 1 zusammengefaßt sind.

2. DIE EXPERIMENTELLEN ERGEBNISSE UND DEREN ERÖRTERUNG

2.1. DIE PHASEN THERMISCHEN GLEICHGEWICHTS DES SYSTEMS Na_2O-ZnO-SiO_2

Unsere Forschungen[7] haben ergeben, daß der saure Teil des Systems $Na_2O - ZnO - SiO_2$ (Abb.1) sich in drei Untersysteme teilen läßt und zwar :

---

[4] A. J. Barker und R. T. Bott, *Trans. Inst. Chem. Engineers*, **47**, 212 (1969).

[5] G. Dusollier und J. Robreda, *Verres et refractaires*, **24**, 63 (1970).

[6] M. A. Rana und R. W. Douglas, *Phys. and. Chem. Glasses*, **9**, 179 (1961).

[7] D. Tenţulescu, Dissertation Inst. Politehnic, Bucureşti, 1971.

— Untersystem I : $SiO_2 - 2ZnO.SiO_2 - Na_2O.2SiO_2$ in welchem die Proben 1 – 16 enthalten sind ;

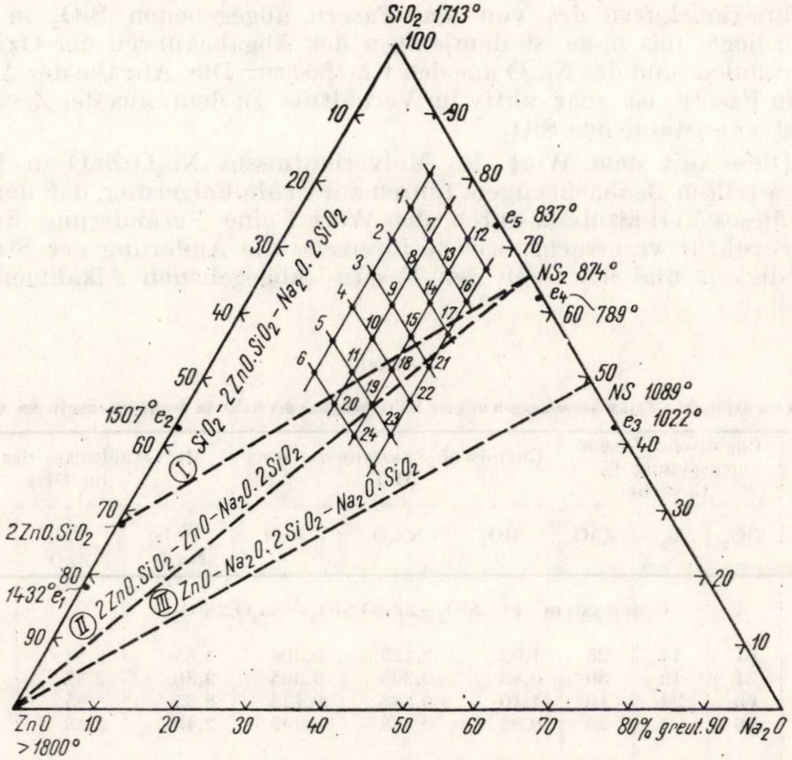
SiO2 1713°
100
10
90
20
80
e5 837°
30
70
NS2 874°
e4
40
60 789°
50
50
NS 1089°
1507° e2
e3 1022°
60
40
70
30
2ZnO.SiO2
80
20
1432° e1
90
10
ZnO
>1800°
10
20
30
40
50
60
70
80% greut. 90
Na2O
SiO2 – 2ZnO.SiO2 – Na2O.2SiO2
2ZnO.SiO2 – ZnO – Na2O.2SiO2
ZnO – Na2O.2SiO2 – Na2O.SiO2
I
II
III
1
2
3
4
5
6
7
8
9
10
11
12
13
14
15
16
17
18
19
20
21
22
23
24

Abb. 1.— System : $Na_2O-ZnO-SiO_2$; die untersuchten Zusammensetzungen 1–24 N = Na_2O ; S = SiO_2.

— Untersystem II : $2ZnO.SiO_2-ZnO-Na_2O.2SiO_2$ in welchem die Proben 17 – 20 enthalten sind ;

— Untersystem III : $ZnO-Na_2O.2SiO_2-Na_2O.SiO_2$ in welchem die Proben 21 – 24 enthalten sind.

2.2. DIE ANALYSE DER HYDROLYTISCHEN BESTÄNDIGKEIT DER GLASFASERN UND GLASGRANALIEN

Die hydrolytische Beständigkeit wird für die Oberfläche, welche dem Wasser ausgesetzt ist, sowohl für die Glasfasern als auch für die Glasgranalien, in Mol SiO_2 und in Mol $Na_2O/qm \times 10^3$ ausgedrückt.

In Abb. 2 sind die Schwankungen der Oxidmengen im Extrakt in Abhängigkeit von der hydrolytischen Angriffsdauer angegeben. Aus den Diagrammen geht hervor, daß, bei den Proben 4 bis 11, welche in der Zusammensetzung ein Molverhältnis $Na_2O/ZnO < 1$ aufweisen, die Variationskurve des von den Fasern abgegebenen SiO_2 in einem Niveau liegt das nahe ist demjenigen der Abgabekurven der Oxide aus den Granulen und des Na_2O aus den Glasfasern. Die Abgabe der Alkalien aus den Fasern ist sehr aktiv im Verhältnis zu dem aus der Zerstörung des Netzes enstandenen SiO_2.

Diese mit dem Wert des Molverhältnisses Na_2O/ZnO in Verbindung gestellten Beobachtungen, führen zur Schlußfolgerung, daß der Übergang dieses Verhältnisses durch den Wert 1 eine Veränderung der glasigen Struktur verursacht, welche ihrerseits die Änderung der Strukturbeständigkeit und der von den Fasern abgegebenen Alkalimenge zur Folge hat.

Tabelle 1

Die chemisch oxydischen Zusammensetzungen und die Molverhältnisse der Oxide in den repräsentativeren Glasproben

	Chemische Zusammensetzung % Gewicht			Chemische Zusammensetzung Mol			Molverhältnisse der Oxide im Glas		
	SiO_2	Na_2O	ZnO	SiO_2	Na_2O	ZnO	$\frac{SiO_2}{Na_2O}$	$\frac{SiO_2}{ZnO}$	$\frac{Na_2O}{ZnO}$
	Untersystem I: $SiO_2-2ZnO.SiO_2-Na_2O.2SiO_2$								
4	61	14	25	1,02	0,225	0,306	4,55	3,34	0,75
11	51	19	30	0,85	0,305	0,365	2,80	2,32	0,84
13	66	24	10	1,10	0,388	0,123	2,85	8,95	3,15
15	56	24	20	0,94	0,388	0,245	2,43	3,85	1,58
	Untersystem III: $ZnO-Na_2O.2SiO_2-Na_2O.SiO_2$								
21	51	29	20	0,85	0,47	0,245	1,80	3,45	1,90

Diese entspricht der Umänderung der Koordination des Zinks, welches je nach dem Molverhältnis $Na_2O/ZnO \gtreqless 1$[8.9.10] in $[ZnO_4]$ und in $[ZnO_6]$ koordinieren kann. Ist das Molverhältnis $Na_2O/ZnO > 1$, dann koordiniert Zink als $[ZnO_4]$ und wirkt als Strukturbildner. Bei $Na_2O/ZnO < 1$ koordiniert Zink auch als $[ZnO_6]$ und wirkt sowohl als Strukturbildner als auch als Strukturwandler. [11.12]

---

[8] J. Hurt und W. Phillips, *J. Amer. Cer. Soc.*, 5, 126 (1970).

[9] V. Vargin, G. Dzhavaktyan und P. Tarlakov, *Armyanskii Khim.*, **22**, 765 (1969); In: *Phys. and Chem. Glasses*, **2**, N3 (1970).

[10] M. Hänert und W. Hintz, *Silikat Tehn.*, **1**, 8 (1969).

[11] D. Tenţulescu und E. Popovici, *Bul. I.S.C.A.S.*, **2**, 157 (1962).

[12] T. Tenţulescu und E. Popovici, *Rev. Industria Uşoară*, **2**, (1960).

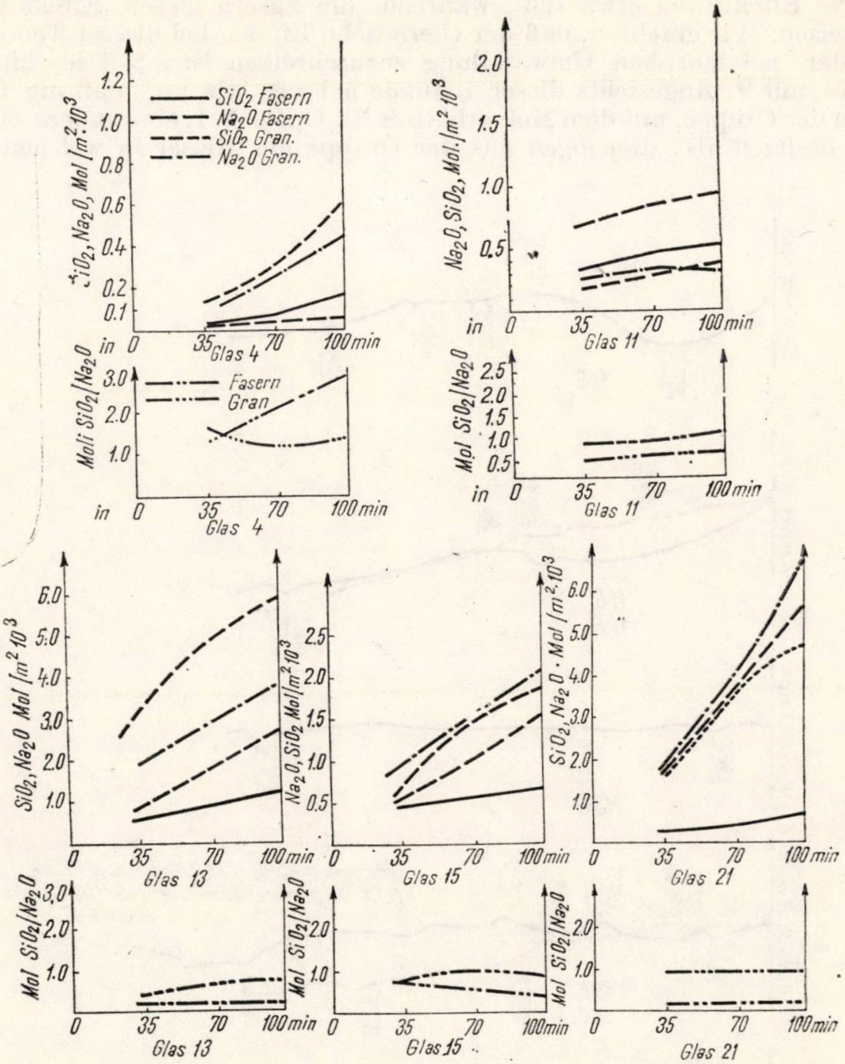

Abb. 2. – Die zeitbedingte Veränderung des Na_2O- und SiO_2 -Gehaltes und das Verhältnis SiO_2/Na_2O im Wasserextrakt nach der Hydrolyse der Faser und Granalien, der Gläser 4, 11, 13, 15, 21 der Untersysteme I und III.

2.3. DIFFERENTIAL-THERMISCHE ANALYSE DER GLASFASERN UND GLASGRANALIEN

Aus der Analyse der DTA-Thermogramme (Abb. 3), der Fasern und Granalien derselben Gläser, wird ein verschiedenartiges Verhalten festgestellt u.zw. : die Granalienproben 13, 15 und 21 zeigen endothermische Effekte bei etwa 120°, während die Fasern diesen Effekt nicht aufweisen. Wir erachten, daß der thermische Effekt bei diseser Temperatur der polymorphen Umwandlung zuzuschreiben ist : β Tridymit $\rightleftarrows$ γ Tridymit [13]. Angesichts dieser Befunde nehmen wir an, daß die Glasfäden der Gruppe, mit dem Molverhältnis $Na_2O/ZnO > 1$, eine andere Struktur besitzen als diejenigen aus der Gruppe der Gläser in welchen das

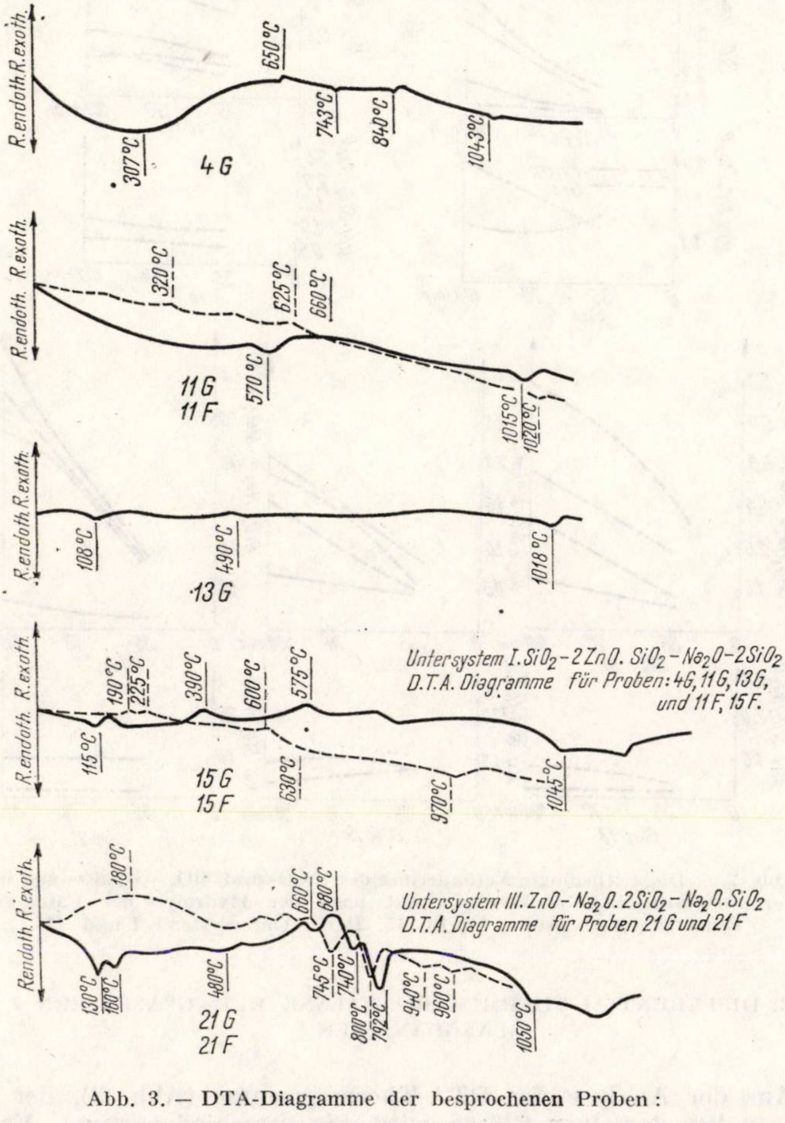

Abb. 3. — DTA-Diagramme der besprochenen Proben :

——— G — Glasgranalien ; – – – F — Glasfasern.

---

[13] S. Solacolu, ,,Chimia fizică a silicaţilor tehnici''. Ed. Tehnică, Bucureşti, 1968, S. 307.

Molverhältnis $Na_2O/ZnO < 1$ ist. Die Faserstruktur ist verschieden, weil die beobachteten thermischen Effekte bei anderen Temperaturen entstanden sind.

2.4. ELEKTRONENMIKROSKOPISCHE ANALYSE

Aus den Eektronogrammen der hydrolytisch, unbehandelten Proben von Glasfasern und Granalien Nr. 4, 11, 15 und 21 (Abb. 4) läßt sich eine zwischen den Proben (4 F und 11 F), welche der Gruppe des Molverhältnisses $Na_2O/ZnO < 1$ und den Proben (13 F, 15 F und 21 F), welche der Gruppe des Molverhältnisses $Na_2O/ZnO > 1$ angehören eindeutige Verschiedenheit feststellen. Das Aussehen der Elektronogramme der ersten Gruppe ist schuppig, myzellig, mit Myzellen zwischen 300 Å und 2000 Å. Dieses schuppige Aussehen, die verhältnismäßige Orientierung im allgemeinen entlang der Faser, schließt den heterogenen Charakter der untersuchten glasigen Struktur, der auf allen Elektronenmikronenmikrogrammen erscheint nicht aus; die Mikrophasen der Granaliengläser besitzen interessante morphologische Aspekte, die bei den Proben 11, 13 und 21 klar umrissen sind.

Die Koordinierung des Zinkes in $[ZnO_4]$ oder $[ZnO_6]$, wenn das Molverhältnis $Na_2O/ZnO \gtreqless 1$ ist, trägt zur Bildung einiger glasiger gänzlich verschiedener Strukturen bei.

2.5. STRUKTURANALYSE DER HYDRIERTEN GLASFASERN MIT HILFE DER MAGENTISCHEN KERNRESONANZ

Der Protonengehalt in den Glasfasern wurde mit der magnetischen Kernresonanz vor und nach deren Aussetzung zum hydrolytischen Angriff festgelegt.

Es wurde festgestellt, daß die Anzahl der bestimmten Protonen, etwa dreimal größer ist als diejenige, welche durch Ionenaustausch die Stelle der Natriumionen im Interdiffusionsprozeß, angenommen hätten. Dieses ist auf die Tatsache zurückzuführen, daß die Interdiffusion zwischen Na^+ und H_3O^+ stattfindet. In der Struktur nimmt das Proton praktisch keinen Raum ein, da es die elektronische Hülle des O^{2-} durchdringt und hiermit die vom Na^+ freigelassene Stelle vom Wassermolekül besetzt wird. Das Wassermolekül wird seinerseits durch die Ausscheidung des Protons aus dem sehr unbeständigen Hydroniumion frei.

In Abb. 5 sind die Absorptionskurven der magnetischen Kernresonanz für die Faser der Probe 13 F vor und nach der Hydrolyse angegeben.

Bezüglich der Anlagerungsart des Wassers in der Struktur des hydrolysierten Glases, machen wir wie folgt einige Betrachtungen. Das Vorhandensein einer schmalen und scharfen Komponente rings umdas Resonanzfeld H_0 herum, deuten wir durch eine hochgradige Bewehungsfreiheit des Protons; die breite Komponente wird auf die in der Struktur stark gebundenen Protone zurückgeführt.

Das Verhältnis zwischen den beiden Bestandteilen kann nur qualitativ geschätzt werden.

SCHLUSSFOLGERUNGEN

Im Vergleich zu den Glasgranalien weisen die untersuchten Glasfasern vom Gesichtspunkt der Strukturen Unterschiede auf.

1. Es wurden die Phasen der thermischen Gleichgewichtverhältnisse des sauren Teiles des ternären Systems $Na_2O - ZnO - SiO_2$ festgestellt.

2. Die hydrolytische Beständigkeit zeigt, daß die Struktur der Fasern, die aus $[SiO_4]^{4-}$ -und $[ZnO_4]^{6-}$ -Tetraederen bestehen, einen besseren Widerstand gegen Wassereinwirkung besitzt, während die Na^+ -Ionen, durch Austausch mit dem H_3O^+ -Ion, im Vergleich zum granulierten Glas, leicht diffundieren.

3. Vom Molverhältnis der Oxide $Na_2O/ZnO \gtrless 1$ aus der Zusammensetzung der Gläser bedingt, ist deren Verhalten bei der Hydrolyse ganz verschieden. Das ist auf die Veränderung der Zinkkoordination von $[ZnO_4]$ auf $[ZnO_6]$ zurückzuführen, wenn das obenerwähnte Verhältnis durch den Wert 1 geht.

4. Die Thermogramme zeigen endothermischen Effekt bei etwa 120° nur für die Proben der Glasgranalien und nämlich für diejenigen deren Verhältnis $Na_2O/ZnO > 1$ ist.

5. Das schuppige, myzellige Aussehen erscheint elektronographisch nur auf den Elektronogrammen der Glasproben deren Verhältnis $Na_2O/$ $/ZnO < 1$ ist.

Die Verfasser danken Dipl.-Ing. N.Butucescu und Dipl.-Chem.A.Popescu vom Forschungsinstitut für Baustoffe Bukarest für deren Mitarbeit bei den physikalischen Analysen der Proben, sowie Dipl.-Phys. S. Mandache vom Institut für Physik Bukarest, für die Mitarbeit bezüglich magnetischer Kernresonanz.

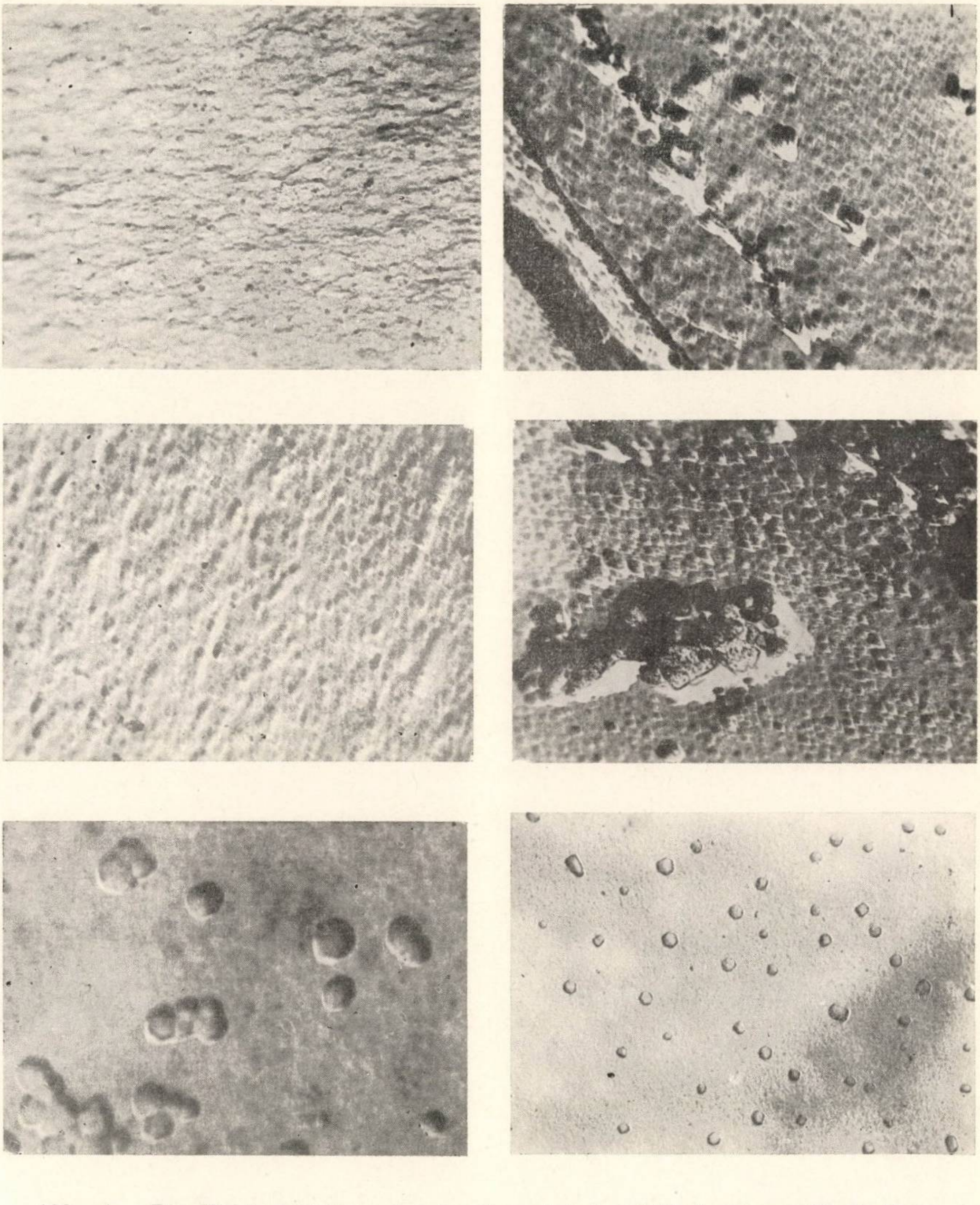

Abb. 4. — Die Elektronogramme der in dieser Arbeit auf Glasfasern und Glas in Granalienform analysierten Proben, vor der hydrolytischen Behandlung.

Pr. 4 — weist einen Trennungsbeginn von Mikrophasen auf × 60 000; Pr. 4 — F myzelliges Aussehen × 32 000; Pr. 11 — Phasentrennungen von etwa 600 Å × 15 000; Pr. 11 — F myzelliges Aussehen × 32 000; Pr. 13 — tropfenförmiges Glas × 40 000; Pr. 13 — F — verschiedene Tropfen × 10 000; Pr. 15 — nadelförmiges Aussehen × 10 000; Pr. 15 — F — schwach definiertes Aussehen × 40 000; Pr. 21 — weist Phasentrennungen auf; Pr. 21 — F — punktförmige Tropfen

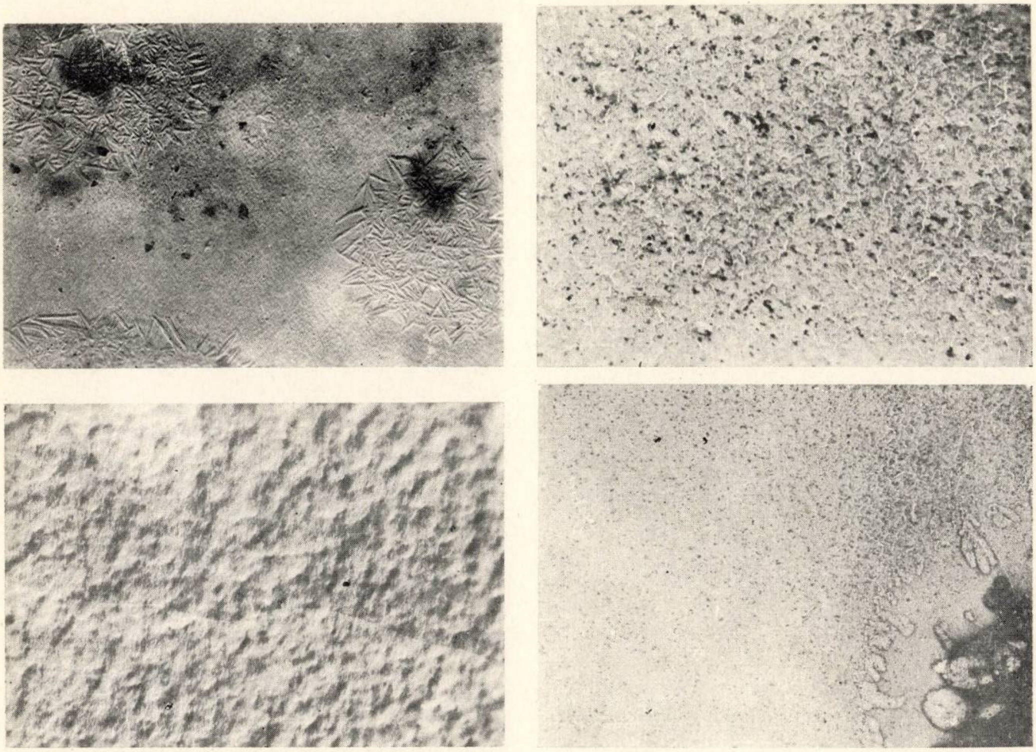

Abb. 4

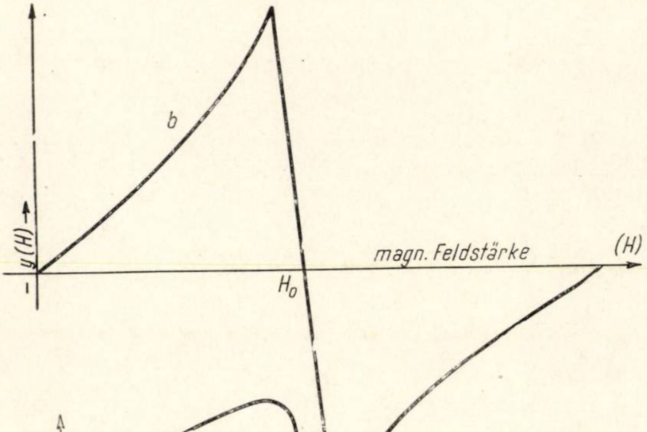

Abb. 5. — Die Absorptionskurven der magnetischen Kernresonanz der Fasern aus der chemischen Zusammensetzung 13 — F.
a) vor der Hydrolyse; *b*) nach der Hydrolyse.

Revue Roumaine de Chimie, **17**, 7, 1227 – 1234 (1972)

FACTORS AFFECTING STABILITY AND EQUILIBRIA OF FREE RADICALS. VII*

ARENESULPHONYL-PHENYL-NITROXIDES AND 1-ARENESULPHONYL-2,2-DIPHENYLHYDRAZYLS

A. T. BALABAN and N. NEGOIȚĂ
Institute of Atomic Physics, P.O. Box 35, Bucharest, Romania

Received March 20, 1972

Oxidation of N-hydroxy-arenesulphonylanilides I affords arenesulphonyl-phenyl-nitroxides II, which decompose slowly affording N-nitroso-phenyl-nitroxide III. ESR spectra of II are discussed : the arenesulphonic group does not couple with the unpaired electron. 1-Benzenesulphonyl-2,2-diphenylhydrazine and related compounds (*p*-toluenesulphonyl- and *p*-bromobenzenesulphonyl-analogues) were synthetized. Infrared, ultraviolet and NMR spectra are reported. Oxidation affords hydrazyls which can be conserved in solution ; their ESR spectra are recorded and interpreted in terms of couplings with the 2,2-diphenylhydrazine moiety only, since the arenesulphonic group does not present any direct coupling.

ARENESULPHONYL-PHENYL-NITROXIDES

Within the framework of a systematic survey of stable nitrogen free radicals, it was inferred [1] that arenesulphonyl-aryl-nitroxides fulfil the conditions for being observable in static systems. This prediction was now verified.

$$p\text{-R}-C_6H_4-SO_2-NPh-OH \qquad p\text{-R}-C_6H_4-SO_2-NPh-O\cdot$$

$$\text{I} \qquad\qquad\qquad\qquad \text{II}$$

a, R = H ; b, R = Me ; c, R = Br.

Oxidation by lead tetraacetate of N-hydroxy-benzenesulphonanilide[2–4] (Ia) in degassed dioxan afforded a paramagnetic solution showing a well-resolved ESR spectrum with $g = 2.0059$. The spectrum is due to benzenesulphonyl-phenyl-nitroxide (IIa) and is easily interpreted in terms of the following approximate coupling constants:

---

* Part VI, A. T. Balaban, N. Negoiță and I. Pascaru, *J. Magnetic Resonance* (in press).

[1] A. T. Balaban, *Rev. Roumaine Chim.*, **16**, 725 (1971).

[2] O. Piloty, *Ber. dtsch. chem. Ges.*, **29**, 1559 (1896).

[3] I. Exner, *Coll. Czech. Chem. Comm.*, **30**, 4078 (1965).

[4] R. Adams, E. J. Agnello and R. S. Colgrove, *J. Amer. Chem. Soc.*, **77**, 5617 (1955).

$$a_N = 11.5 \text{ gauss}; \quad a_{o,p-H} = 1.75 \text{ gauss}; \quad a_{m-H} = 0.74 \text{ gauss}.$$

During ca. 10 minutes at room temperature this ESR spectrum decreases and disappears, being replaced by a progressively increasing different ESR spectrum which reaches its maximum intensity after ca. 5 hours. Its coupling constants are: $a_N = 10.34$, $a_{N=O} = 3.78$, $a_{o,p-H} = 2.80$, $a_{m-H} = 0.95$ Gauss. This is identical with the ESR spectrum of the π-radical III, N-nitroso-N-phenyl-nitroxide,[5] obtained on chemical oxidation (lead tetraacetate in dioxan) of cupferron or of N-nitroso-N-phenylhydroxylamine*.

One can speculate about the mechanism of this conversion. It is known that alkalies cause the ready decomposition of I into arenesulphonic acids and nitrosobenzene. [2] A similar decomposition can occur with IIa affording nitrosobenzene and $PhSO_2$. This radical (or Ph· formed

$$PhSO_2 - NPh - O\cdot \rightarrow PhSO_2\cdot + PhNO \rightarrow PhSO_2Ph + NO$$

IIa

$$PhSO_2\cdot \rightarrow Ph\cdot + SO_2$$

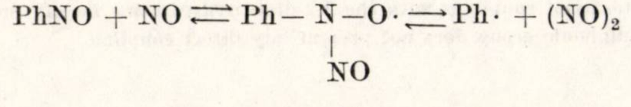

$$PhNO + NO \rightleftharpoons Ph-\underset{\displaystyle NO}{\underset{|}{N}}-O\cdot \rightleftharpoons Ph\cdot + (NO)_2$$

III

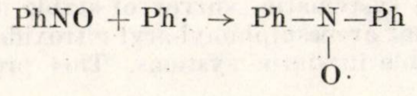

$$PhNO + Ph\cdot \rightarrow Ph-\underset{\displaystyle O\cdot}{\underset{|}{N}}-Ph$$

IV

by loss of SO_2) could split nitrosobenzene forming NO. The reversible reaction between nitrosobenzene and nitric oxide[6-8] then affords III. Indeed, the same ESR spectrum is obtained on introducing NO into a dioxan solution of PhNO. [5] As mentioned earlier,[5] in concentrated solutions or on prolonged conservation, N-nitroso-phenyl-nitroxide decomposes affording diphenylnitroxide IV with its known ESR spectrum.

---

* An alternative structure of III, namely 2-phenyl-oxadiaziridine-3-oxyl, formed by intramolecular closure of a 3-membered ring with three heteroatoms, could also be considered.

[5] A. T. Balaban, N. Negoiță and I. Pascaru, *Rev. Roumaine Chim.*, **16**, 721 (1971).

[6] E. Bamberger *Ber. dtsch. chem. Ges.*, **51**, 634 (1918);

[7] A. N. Nesmeyanov and S. T. Ioffe, *Zhur. obschei, Khim.*, **11**, 392 (1941).

[8] J. G. Lawless and M. D. Hawley, *Analyt. Chem.*, **40** 948 (1968).

After completion of this work, a paper [9] came to our attention, where the same free radicals II had been obtained, with closely similar coupling constants. No mention of their decomposition is made, however. The Dutch authors [9,10] also investigated aryl-sulphonyl-alkyl-nitroxides, as well as *p*-nitro- and *p*-methoxy-benzenesulphonyl-phenyl-nitroxides,[9] but not the following two nitroxides.

Similar oxidation of N-hydroxy-*p*-toluenesulphonanilide [11–13] (Ib) and of N-hydroxy-*p*-bromobenzenesulphonanilide (Ic), m.p. 136°, afforded closely similar free radicals II, $R = CH_3$ and Br, whose ESR spectra are practically identical with that of II, R = H, and which undergo a similar conversion into III.

1-ARENESULPHONYL-2,2-DIPHENYLHYDRAZYLS

It was pointed out earlier[1] that the still unknown 1-arenesulphonyl-2,2-diphenylhydrazyls (V) fulfil the conditions for being chemically stable compounds. In order to test this assumption, and to compare such compounds with the known 1-acyl-2,2-diphenylhydrazyls (VI),[14–22] 1-benzenesulphonyl-2,2-diphenylhydrazine (VII a) and two *p*-substituted derivatives (VII b and VIIc) were prepared and investigated.

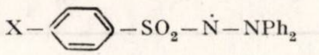

V

$R-CO-\dot{N}-NPh_2$

VI

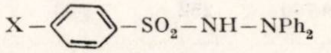

VII

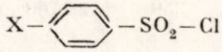

VIII

a, X=H; *b*, X= CH_3; *c*, X=Br

---

[9] T. A. J. W. Wajer, H. W. Geluk, J.B.F.N. Engberts and T. J. De Boer, *Rec. Trav. Chim.* **89**, 696 (1970).

[10] G. Rawson and J.B.F.N. Engberts, *Tetrahedron*, **26**, 5653 (1970).

[11] E. Bamberger and A. Rising, *Ber. dtsch. chem. Ges.*, **34**, 228, 241 (1901).

[12] E. Bamberger, H. Büsdorf and B. Szolayski, *ibid.*, **32**, 210 (1899).

[13] W. Bretschneider, *J. prakt. Chem.*, (2), **55**, 285 (1897).

[14] S. Goldschmidt, A. Wolf, E. Wolffhardt, I. Drimmer and S. Nathan, *Liebigs Ann. Chem.* **437**, 194 (1924).

[15] W. K. Wilmarth and N. Schwartz, *J. Amer. Chem. Soc.*, **77**, 4543, 4551 (1955).

[16] I. S. Ciccarello, T. Garofano and M. Santangelo, *Nuovo Cimento*, **17**, 881 (1960).

[17] B. H. Bielski and J.M. Gebicki, "Atlas of ESR Spectra", Academic Press, New York, 1967, p. 289.

[18] Yu. M. Ryzhmanov, Yu. V. Yablokov, B. M. Kozyrev, L. I. Stashkov and R. O. Matevosyan, *Doklady Akad. Nauk S.S.S.R.* **162**, 116 (1965) and further references therein.

[19] A. E. Arbuzov and F. G. Valitova, *ibid.*, **147**, 99 (1962).

[20] A. E. Arbuzov, S. Yu. Baigildina, F. G. Valitova, Yu. M. Ryzhmanov and Yu. V. Yablokov, *Izvest. Akad. Nauk S.S.S.R.* **1966**, 1547.

[21] D. Braun, G. Peschk and E. Hechler, *Chem. Ztg.* **94**, 703 (1970).

[22] A. R. Forrester, J. M. Hay and R. T. Thomson, "Organic Chemistry of Stable Free Radicals", Academic Press, London, 1968.

Arenesulphonyl chlorides (VIIIa—c) react smoothly with 1,1-diphenylhydrazine affording the corresponding sulphonyl-hydrazines VII. These had to be purified by preparative TLC from traces of diphenylhydrazine hydrochloride, in order to give correct elemental analyses (samples which had been purified by recrystallization only were, however, pure enough for most other purposes).

Infrared absorption spectra of VII, determined in potasium bromide pellets reveal intense ν NH bands at 3215 — 3220 cm^{-1} (an additional band at 3240 cm^{-1} is observable in VII c), and νSO_2 bands [23] at 1338 and 1165—1175 cm^{-1} (the former band appears at 1350 cm^{-1} in VIIc), in addition to the bands due to the aromatic rings. This is in agreement with the structure.

Ultraviolet absorption spectra of VII are indicated in table 1, both in neutral and in alkaline ethanolic solution.

Table 1

Ultraviolet and visible absorption (in nm)

Compound	VIIa-c						Va-c
Solvent	Ethanol				0.1 N NaOH in EtOH		C_6H_6
Absorption data	λ	ε	λ	ε	λ	λ	λ
a	224	16 300	272	7 700	252	305	492
b	230	24 700	273	9 700	252	303	494
c	238	20 600	274	7 200	255	301	496.5

Nuclear magnetic resonance spectra of VII, determined in acetonitrile or in deuterochloroform, reveal the aryl multiplet at 2.3 and 3.2 τ, while the NH proton appears at $1.8 - 1.9\tau$ (in CH_3CN) or $- 0.2\tau$ (in $CDCl_3$), confirming thus the structure.

Oxidation of arenesulphonylhydrazines VII in benzene solution with lead dioxide affords violet paramagnetic solutions of free radicals V with absorption maxima in the visible range (table 1).

First derivative ESR spectra were recorded in dioxan solutions of sulphonylhydrazyls Va—c obtained by oxidation of VII a—c with lead tetraacetate or lead dioxide. As seen from figures 1—3 the fine structure which is apparent in these ESR spectra and which is better resolved then in 1-acyl-2,2-diphenylhydrazyls reveals a closely related spin distribution in all three radicals. In fact, the ESR spectra of Va and Vb presenting each 50 lines are practically identical; that of Vc has 53 lines and differs mainly in the central part of the spectrum from the other two spectra.

Since only minor differences occur in the ESR spectra of Va — Vc, it results that little coupling of the unpaired electron with any nucleus of the arenesulphonyl group takes place and that the slight modifications of the spectra occur owing to indirect effects on couplings with nuclei of the 2,2-diphenylhydrazine moiety.

---

[23] E. A. Robinson, *Canad. J. Chem.*, **39**, 247 (1961).

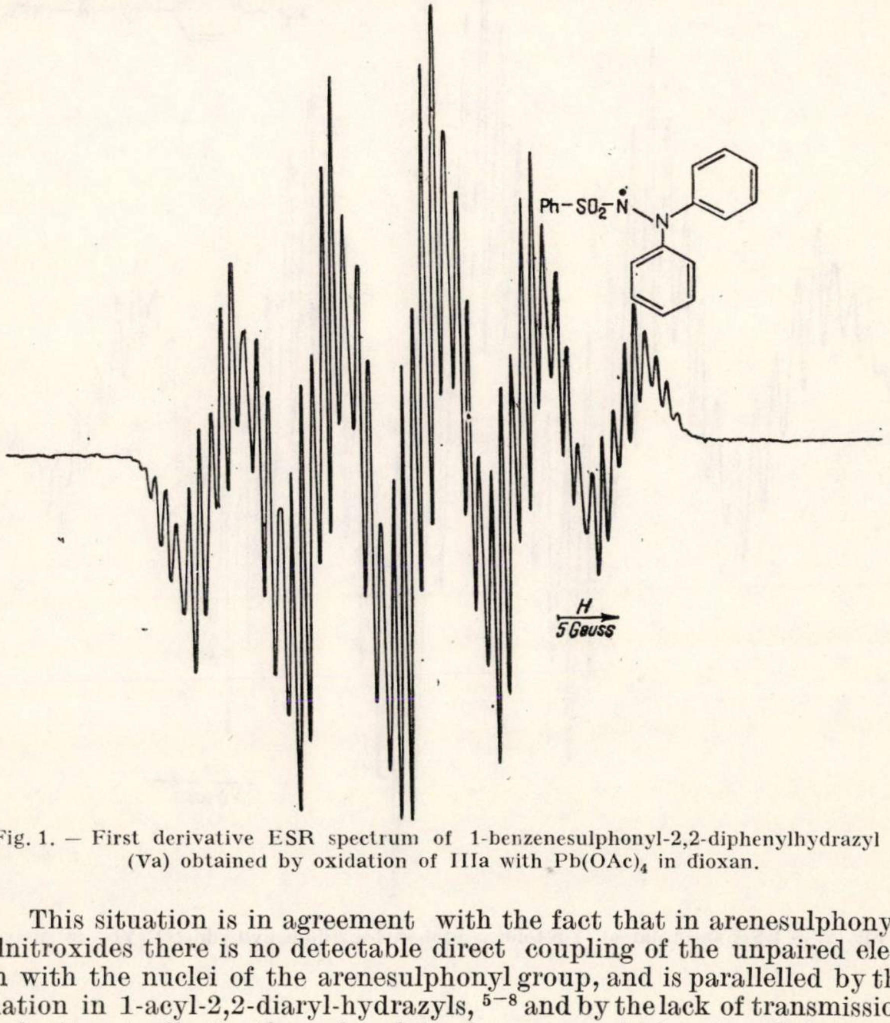

Fig. 1. — First derivative ESR spectrum of 1-benzenesulphonyl-2,2-diphenylhydrazyl (Va) obtained by oxidation of IIIa with $Pb(OAc)_4$ in dioxan.

This situation is in agreement with the fact that in arenesulphonylarylnitroxides there is no detectable direct coupling of the unpaired electron with the nuclei of the arenesulphonyl group, and is parallelled by the situation in 1-acyl-2,2-diaryl-hydrazyls, [5–8] and by the lack of transmission of substituent effects through sulphonic groups which act as "electronic insulator groups". [24–26]

Table 2 presents the g factors and the approximate coupling constants of the hydrazyls Va-c.* The g factors, which are lower than 2.0035,

---

* The analysis of the ESR spectrum of Va was discussed in detail in ref. 27.

[24] J. B. Hyne, *Organic Reactivity*, **5**, 886 (1968).

[25] R. W. Wisghert and I. E. Kachanko, *ibid*. 9.

[26] L. M. Litvinenko and N. F. Levchenko, *Zhur. obschei Khim.*, **30**, 1673 (1960).

[27] A. T. Balaban, *Rev. Roumaine Chim.*, **17**, 9 (1972).

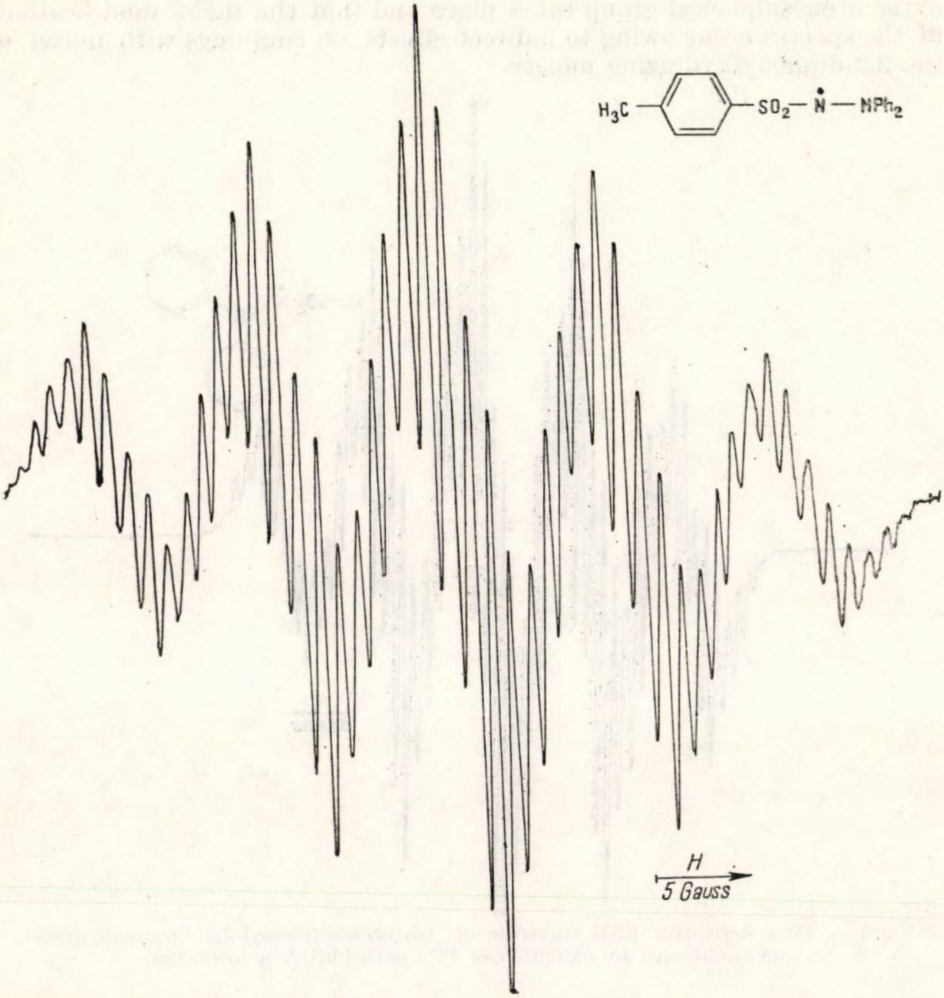

Fig. 2. — ESR spectrum of 1-*p*-toluenesulphonyl-2,2-diphenylhydrazyl (Vb) in dioxan.

Table 2

ESR spectral data

Radical	g factor	Coupling constants (Gauss)						
		a_N	a_N	a_H Phenyl			a_H Phenyl	
				o	m	p	o	p
Va, Vb	2.0033	9.4	9.4	2.1	1.0	4.2	1.0	1.0
Vc	2.0034	10.5	9.4	2.1	1.0	4.2	1.0	1.0

clearly confirm the hydrazylic structure. Interestingly, the coupling constants seem to indicate that the two phenyl groups of the 1,1-diphenylhydrazine moiety are magnetically non-equivalent ; further experimental testing of this conjecture is in progress.

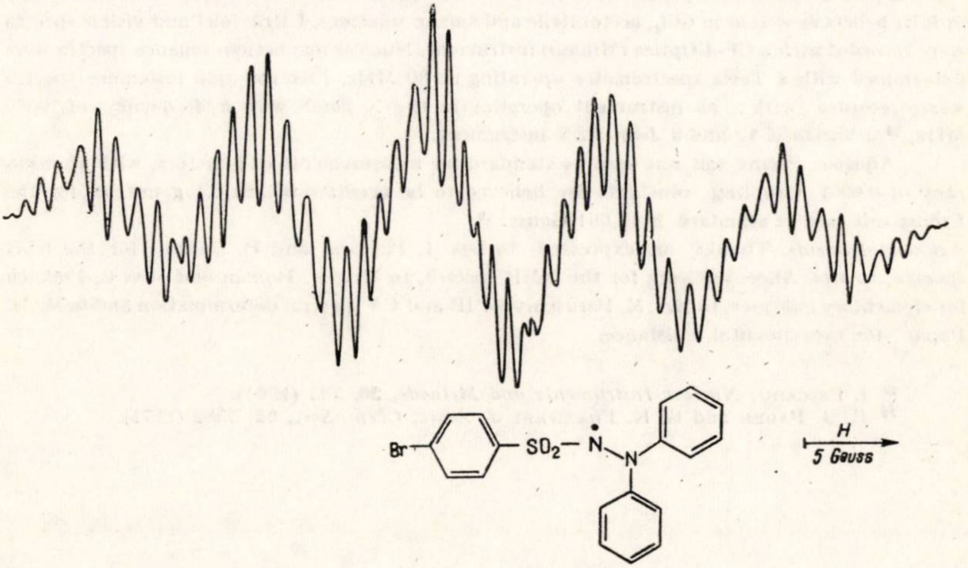

Fig. 3. — ESR spectrum of 1-*p*-bromobenzenesulphonyl-2,2-diphenylhydrazyl (Vc) in dioxan.

For each of the radicals Va and Vb, the two nitrogen coupling constants are found to be approximately identical.

EXPERIMENTAL

Arenesulphonanilides were prepared [2] from one mole of arenesulphonyl chloride and two moles of N-phenylhydroxylamine in absolute ethanol at room temperature. After one hour the mixture was diluted with water and the crystalline material was recrystallized from benzene-petroleum ether of from methanol-water. Melting points for Ia and Ib agreed with literature data. Compound Ic melts at 136° (*found* : C,44.24 ; H,3.34 ; N,4.62. $C_{12}H_{10}BrNO_3S$ *requires* : C, 43.91 ; H, 3.07, N, 4.27 %).

1-Benzenesulphonyl-2,2-diphenylhydrazine (VIIa). Two moles of 1,1-diphenylhydrazine were left at room temperature with one mole of benzenesulphonyl chloride in benzene solution for 24 hrs. The precipitated diphenylhydrazine hydrochloride was filtered off, the filtrate evaporated and recrystallized from dil. ethanol, m.p.159°. For analysis, a TLC separation on silica-gel from benzene-methanol (3 :1) was necessary : the spot of VIIa becomes violet when exposed to iodine vapors. Analysis : *found* C,66.23 ; H,4.69 ; N, 8.87.$C_{18}H_{16}N_2O_2S$ requires C,66.64 ;H,4.97 ; N, 8.64 %.

1-p-Toluenesulphonyl-2,2-diphenylhydrazine (*VIIb*) was prepared similarly and had m.p. 144 – 145°. Found C, 67.87 ; H, 5.50 ; N, 8.32. $C_{19}H_{18}N_2O_2S$ requires C, 67.43 ; H, 5.36 ; N, 8.28 %.
1-p-Bromobenzenesulphonyl-2,2-diphenylhydrazine (*VIIc*) was prepared by the same procedure and had m.p. 166 – 167°.
Found ; C,53.94 ; H, 3.74 ; N, 7,36.$C_{18}H_{15}BrN_2O_2S$ *requires* C, 53.61 ; H, 3.92 ; N, 6.94 %.

Spectra. Infrared spectra were recorded with a Jena UR-10 double-beam instrument in KBr pellets as well as in CCl_4, acetonitrile and dioxan solutions. Ultraviolet and visible spectra were recorded with a CF-4 Optica (Milano) instrument. Nuclear magnetic resonance spectra were determined with a Tesla spectrometer operating at 80 MHz. Electron spin resonance spectra were recorded with : an instrument operating in the X band with a frequency of 9060 MHz, [28] a Varian-E 12 and a Jeol -M3X instrument.

Aqueous Frémy salt was used as standard for measurements of g-factors, with an accuracy of 0.0001. Coupling constants are believed to be accurate within 0.1 gauss ; a_N for the Frémy salt used as standard is 13.091 Gauss. [29]

Acknowledgements. Thanks are expressed to Drs. I. Pascaru and R. Baican for the ESR spectra, to Mrs. Alice Vasilescu for the NMR spectra, to Mrs. M. Roman and Miss C. Popescu for elementary analyses, to Mrs. M. Paraschiv for IR and UV spectral determination and to Mr.D. Papae for experimental assistance.

[28] I. Pascaru, *Nuclear Instruments and Methods*, **26**, 333 (1964).
[29] R. J. Faber and G. K. Fraenkel *J. Amer. Chem. Soc.*, **92**, 5582 (1971).

Revue Roumaine de Chimie, **17**, 7, 1235 – 1240 (1972)

SPECTRA-STEREOCHEMISTRY CORRELATIONS FOR BICYCLIC RIGID ARYLIDENECYCLOHEXANONES

M. MORARU and F. CHIRALEU
Department of Organic Chemistry, University,
Spl. Independenţei 89, Bucharest, Romania
and
Institute of Organic Chemistry,
Spl. Independenţei 202 B, Bucharest, Romania

Received January 28, 1972

NMR and IR data, show that rigid bicyclic arylidenecyclohexanones have a *trans* stereochemistry and that the six-membered ring assumes a "chair-like" conformation.

INTRODUCTION

The arylidenecyclohexanones, which are α, β-unsaturated ketones with a fixed *s-cis* conformation, may exhibit a *cis-trans* isomerism.

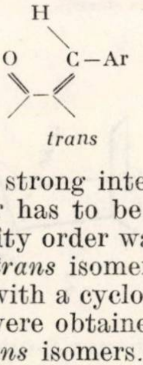

trans

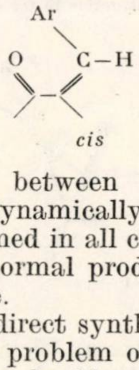

cis

Because of the strong interference between Ar and the carbonyl group, the *cis* isomer has to be thermodynamically less stable than the *trans* one. This stability order was confirmed in all cases when both forms were known.[1–4] The *trans* isomer is the normal product of reaction of an aromatic aldehyde with a cyclohexanone.

The *cis* forms were obtained by indirect synthesis[4] or by photoisomerization of the *trans* isomers.[1–3] The problem of ascribing to a new compound one or another form is generally solved by spectroscopic measurements.

Another point of interest is the actual conformation of the six-membered. ring for this kind of compounds. Some recent reports on this problem are rather contradictory and need serious criticism.[5,6]

---

[1] D.H.R. Barton, A. J. Head and P. J. May, *J. Chem. Soc.*, **1957**, 935.

[2] D. N. Kevill, E. D. Weiler, and N. H. Cromwell, *J. Org. Chem.*, **29**, 1276 (1964).

[3] A. Hassner and T. C. Mead, *Tetrahedron*, **20**, 2201 (1964).

[4] J. Kossanyi, B. Furth and J. P. Morizur, *Tetrahedron*, **26**, 395 (1970).

[5] H. J. Köhler, M. Scholz and M. Mühlstadt, *J. prakt. Chem.*, **313**, 17 (1971).

[6] M. Mühlstädt, H. J. Köhler, D. Porzig and M. Scholz, *J. prakt. Chem.*, **312**, 292 (1970).

As a part of a continuing investigation program of the stereochemical aspects of bycyclic compounds, we report here some results concerning bicyclic arylidenecyclohexanones.

RESULTS AND DISCUSSION

The arylidenecyclohexanones were prepared by the reaction of benzaldehyde and furfural with a series of bicyclo[3.3.1]nonan-2-ones and bicyclo[3.2.1]octan-2-ones. The resulting compounds **1** and **2** respectively (where R = H or Ph) are listed in Table 1; excepting **1a** and **2a**, they are new compounds.

Table 1

Arylidenecyclohexanones

Compound			m.p °C	Compound			m.p. °C
1a	R=H	Ar=C_6H_5	119–120*	2a	R=H	Ar=C_6H_5	73–74**
1b	R=H	Ar=Furyl	56–57	2b	R=H	Ar=Furyl	58–59
1c	R=βC_6H_5***	Ar=C_6H_5	86–87	2c	R=βC_6H_5	Ar=C_6H_5	124–125
1d	R=βC_6H_5	Ar=Furyl	124–125	2d	R=βC_6H_5	Ar=Furyl	150–150,5
1e	R=αC_6H_5	Ar=C_6H_5	118–121	2e	R=αC_6H_5	Ar=C_6H_5	108–109
1f	R=αC_6H_5	Ar=Furyl	180–181	2f	R=αC_6H_5	Ar=Furyl	122–123

* 120–121°C A. C. COPE and others, *J. Amer. Chem. Soc.*, **87**, 3130 (1965).
** 71°C, K. ALDER and R. REUBKE, *Chem. Ber.*, **91**, 1525 (1958).
*** β and α designate configuration in the same sense as in steroids.

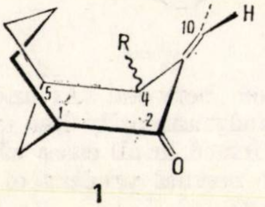

1

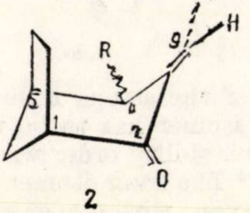

2

The parent ketones, bicyclo[3.3.1]nonan-2-one and bicyclo[3.2.1]octan-2-one, were synthesized by known methods. [7,8] 4β – and 4α – Phenylbicyclo[3.2.1]octan-2-ones are compounds previously obtained[9]; their stereochemistry at C-4 was fully established by means of chemical and spectroscopic data.

The same thing is true for 4β – and 4α – phenylbicyclo[3.3.1]nonan-2-ones; for these ketones the C_4 stereochemistry was previously determined by German authors [10] and confirmed independently by us.

---

[7] W. KRAUS, *Liebigs Ann. Chem.*, **683**, 97 (1965).

[8] M. HARTMAN, *Z. Chem.*, **6**, 182 (1966).

[9] N. BĂRBULESCU and M. MORARU, to be published.

[10] V. DRESSLER and K. BODENDORF, *Liebigs Ann, Chem.*, **720**, 71 (1968).

The NMR and IR data (see Table 2) strongly support the *trans* stereochemistry of all arylidene derivatives (**1** and **2**) under study.

NMR-Spectroscopy was extensively used in order to assign the conformation of α, β — unsaturated ketones. [6,11–13] The magnetically anisotropic carbonyl group exercises a strong deshielding effect on *cis*-β protons in *s-cis* compounds. For methylenecyclohexanones with a fixed *s-cis* conformation, the chemical shifts of the *cis*-protons are invariably downfield from the corresponding *trans* protons. [14]

Table 2

NMR and IR data

Chemical shift(δ)						Coupling constant (Hz)			IR — frequency (cm^{-1})		
	H—5	H—4β	H—4α	H—1	H—10	$J_{4,5}$	$J_{4\beta,10}$	$J_{4\alpha,10}$	ν(C=O)	ν(C=C)	Δν
1a	2.23	2.93	2,90	2.57	7.4	ΣJ=6.0	ΣJ=4.8		1682	1596	86
1b	2.30	2.99	2.93	2.57	7.44	ΣJ=5.7	ΣJ=5.0		1681	1597	84
1c	2.18	—	4.27	2.68	7.51	1.0	—	0.9	1682	1598	84
1d	2.21	—	4.44	2.72	7.53	0.8	—	1.3	1680	1597	83
1e	2.63	4.68	—	2.63	7.60	6.9	2.6	—	1683	1595	88
1f	2.58	4.59	—	2.58	7.62	8.1	2.4	—	1680	1593	87
	H—5	H—4β	H—4α	H—1	H—9	$J_{4,5}$	$J_{4\beta,9}$	$J_{4\alpha,9}$	ν(C=0)	ν(C=C)	△ν
2a	2.53	2.7—2.85			7.47			ΣJ=4.9	1692	1601	91
2b	2.57	2.7—2.85			7.35			ΣJ=4.6	1692	1603	89
2c	2.55	—	4.13	2.83	7.49	1.8	—	1.3	1693	1605	88
2d	2.59	—	4.32	2.95	7.57	1.0	—	1.4	1690	1603	87
2e	2.65	4.47	—	2.83	7.69	6.7	2.4	—	1690	1594	96
2f	2.7—2.8	4.43	—	2.7—2.8	7.60	6.6	2.2	—	1690	1597	93

Methyl groups at the β — carbon atom, *cis* to the carbonyl, also resonate downfield from their *trans* counterparts. [15]

In benzylidenecyclohexanones the vinylic proton resonates downfield for the *trans* isomers (7.28 ppm for *trans* 2-benzylidenecyclohexanone) and upfield for the *cis* isomers (6.18 ppm for *cis*-2-benzylidenecyclohexanone). [2,3,4,16]

The chemical shifts of vinylic protons (H-10 respectively H-9) in (**1**) and (**2**) are in the range 7.35 — 7.69 ppm, without a significant difference between Ar = Ph and Ar = furyl. These values are consistent with the *trans* stereochemistry and this is true even for compounds bearing a 4-phenyl substituent. In this case the *cis* isomer could be equally if not more stable than *trans*, because of the steric hindrance between the two aryl groups.

---

[11] D. D. Faulk and A. Fry, *J. Org. Chem.*, **35**, 364 (1970).

[12] J. Kossanyi, *Bull. Soc. chim. France*, **1965**, 704.

[13] F. H. Cottee and C. J. Timmons, *J. Chem. Soc(B)* **1968**, 326.

[14] R. Kaiser and D. L. Hopper, *Mol. Phys.*, **8**, 403 (1964).

[15] L. M. Jackman and S. Sternhell, "Applications of NMR Spectroscopy in Organic Chemistry," 2nd edition, Pergamon Press, 1969, p. 22.

[16] J. H. Brewster and J. E. Privett, *J. Amer. Chem. Soc.*, **88**, 1419 (1966).

The *trans*-stereochemistry is confirmed by the more reliable IR data. Unlike electronic spectra, which are somewhat insensitive to small changes of conformation, the vibrational spectra reflect well every change of the interplanar angle between C = O and C = C double bonds.

The ratio of the band intensifies of the C = O and C = C stretching vibrations is useful for the assignement of *s-cis* or *s-trans* conformation at α, β — unsaturated ketones.[17] The same ratio is characteristic of arylidenecyclohexanones ; it is 1 for *trans* or 0.2 for *cis* isomers.[2,3]

The frequency separation $\Delta\nu = \nu_{C=O} - \nu_{C=C}$ affords another criterion to distinguish between various conformations ; *trans*-benzylidenecyclohexanones have Δν values between 75 and 90 cm^{-1}, while *cis* isomers have $\Delta\nu = 60-65$ cm^{-1}.[2,3]

All compounds of type (**1**) and (**2**) show a narrow range of Δν values (83 — 96 cm^{-1}) (Table 2, last column) ; moreover, the ratio of integrated band intensities is approximately 1.[18]

There is a scarcity of information with regard to the conformation of the six-membered ring in arylidenecyclohexanones. From ORD-data at 2 -arylidene-5-methyl cyclohexanones of known configuration Brewster and Privett[16] came to the conclusion that a "twist-like" conformation (Figure 1a) is more favorable than a "chair-like" one (Figure 1b).

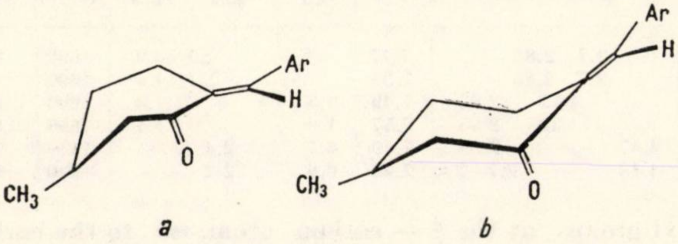

Figure 1

R(-) 2-benzylidene-5-methyl cyclohexanone shows a negative Cotton effect, due to the chromophore C = C — C = O ; the large amplitude of this effect clearly indicates the twisting around C—C single bond. In the view of the above mentioned authors, only a "twist-like" conformation could accommodate a distorsion like this.

There are also NMR data[6] indicating a remarkable twisting around C—C bond ; but extended HMO calculations fail to account for such a twisting.[5]

Because of their rigidity, the bycyclic arylidenecyclohexanones (**1**) and (**2**). can be taken as models for the study of conformation in connection with spectral data.

The values of $J_{4,5}$ for (**1**) and (**2**) follow the general pattern of couplings in the chair conformation of cyclohexane. For β-protons at C_4, $J_{4,5}$ is somewhat greater than that corresponding to a pure axial-equatorial coupling ; the situation is reversed for α-protons were $J_{4,5}$ is less than an equatorial-equatorial coupling. The examination of the dihedral angle $H_{\beta}-C_4-C_5-H$ and $H_{\alpha}-C_4-C_5-H$ (Figure 2) in the extreme conformations, namely chair (a) and boat (b), gives values of 40° and 80° for (a), respectively 15° and 135° for (b).

---

[17] R. L. Erskine and E. S. Waight, *J. Chem. Soc.*, **1960**, 3425.

[18] These values are less accurate, therefore not listed.

$J_{4,5}$ calculated by means of a Karplus equation, is in a better agreement with the experimental J for the chair conformation than for the other one.

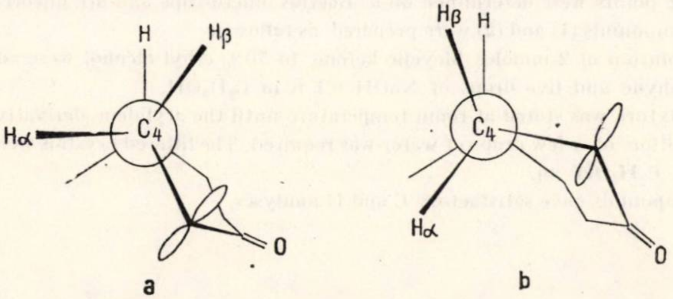

Figure 2

The allylic coupling $J_{4,10}$ for (**1**) respectively $J_{4,9}$ for bicyclo[3.2.1] octanes (**2**), supports the same conclusion. It is well known that allylic coupling involves a mechanism related to $\sigma - \pi$ orbital overlap, so that it is negative in sign and shows a $\cos^2\theta$ dependence.

For transoid allylic coupling this dependence is well documented. [19]

Keeping this in mind, the following prediction can be made: in a chair conformation $J_{4\beta,10}$ and $J_{4\beta,9}$ must be greater than $J_{4\alpha,10}$ and $J_{4\alpha,9}$. The situation would be reversed in a pure boat or a twist conformation (In 2-benzylidene bicyclo[2.2.1]heptane derivatives, where the six-membered ring is constrained in a pure boat conformation, the allylic coupling is 2.5 – 2.6 Hz for 3-exo protons and 2 – 2.1 Hz for 3-endo protons [4]) Our data for allylic couplings correspond to the first situation with some differences between bicyclo[3.3.1]nonane and bicyclo [3.2.1]octane series.

The allylic coupling constants for 4β-protons- are smaller for bicyclooctanes and conversely, they are larger for 4α protons.

This fact seems to indicate that the six-membered ring is more flattened in arylidene bicyclo[3.2.1]octanes than in the corresponding bicyclo[3.3.1]nonanes.

There are some other differences between the two series, which must be pointed out. Between the chemical shifts of H-1 and H-5 in bycyclo [3.2.1] octanes and in bicyclo[3.3.1]nonanes the differences are significant and indicate an important deshielding of bridgehead protons in the first series. On the other hand H-4 protons are more shielded in bicyclo [3.3.1]nonanes.

Unfortunately, because of the lack of more exact data about the conformation and hybridization in the two series of compounds, all those changes cannot be unambiguously considered.

---

[19] M. Bartfield and B. Chakrabarti, *Chem. Rev.*, **69**, 757 (1969).

EXPERIMENTAL

NMR spectra were recorded on a Varian A-60 A Spectrometer with TMS as an internal standard. Coupling constants were determined by spin decoupling experiments at a sweep width of 250 Hz.

Infrared spectra were taken with a UR-20 spectrophotometer in CCl_4 solution.

Melting points were determined on a Boetius microscope and are uncorrected.

The compounds (**1**) and (**2**) were prepared as follows :

In a solution of 2 mmoles bicyclic ketone in 70% ethyl alcohol were added 4 mmoles aromatic eldehyde and five drops of NaOH 0.1 n in C_2H_5OH.

The mixture was stored at room temperature until the arylidene derivative crystallized ; somtimes addition of a few drops of water was required. The filtered crystals were twice recrystallized from C_2H_5OH aq.

All compounds gave satisfactory C and H analyses.

Revue Roumaine de Chimie, **17**, 7, 1241 – 1252 (1972)

ÉTUDE DE LA RÉACTION D'ALKYLATION DU COLORANT AZOÏQUE BENZOTHIAZOLIQUE À L'AIDE DE L'ANALYSE THERMIQUE DIFFÉRENTIELLE

EUGENIA BALTĂ

Institut Polytechnique de Bucarest, 1, str. Polizu

Reçu le 15 octobre 1971

On présente l'utilité particulière de l'analyse thermique différentielle employée pour la première fois dans l'étude d'une réaction complexe d'alkylation dans un système hétérogène. A l'aide de cette méthode, on peut démontrer le mécanisme de l'alkylation du colorant azoïque benzothiazolique. On a mis en évidence l'influence spécifique des différents composants sur la quantité de colorant résultant de la réaction.

★

La réaction d'alkylation des composants organiques, qui contiennent dans leur molécule des atomes d'azote, constitue l'une des réactions les plus complexes et les plus controversées de ce domaine de la chimie. Si dans le cas des amines aliphatiques et aromatiques, le mécanisme de cette réaction, étant du type SN_2, est généralement élucidé, on ne peut affirmer la même chose dans le cas des polyamides et particulièrement lorsqu'il s'agit d'hétérocycles à atomes d'azote.

On rencontre et on utilise l'alkylation, ces dernières années, dans de nombreux domaines de la chimie organique, l'un des plus importants étant le domaine des colorants azoïques cationiques hétérocycliques pour la peinture des fibres polyacryle-nitriliques (PAN). La littérature de spécialité donne des indications sur la manière d'obtenir une série de tels colorants hétérocycliques : benzothiazoliques, [1–4] triazoliques, [5–8] thiadiazoliques,[6] etc. Les données de la littérature se réfèrent particuliè-

---

[1] Brevet suisse, Ciba Ltd. Swiss 341247 (1959) ; *Chem. Abstr.*, **55**, 1004 e (1961).

[2] Brevet allemand IG Geygy Akt. Ges. - Ger. 1050940 (1959) ; *Chem. Abstr.*, **55**, 9886 h (1961).

[3] Brevet allemand IG Geygy Akt. Ges.-Ger. 1056757 (1959) ; *Chem. Abstr.*, **55**, 11870 d (1961).

[4] Brevet français, Compagnie française des matières colorantes, Fr. 1217248 (1960) ; *Chem. Abstr.*, **55**, 22840e (1961).

[5] W. Bossard, US 2883373 (1959) ; *Chem. Abstr.*, **54**, 3970 (a (1960).

[6] I. R. Geygy Akt. Ges. - Brit. 791932 (1958) ; *Chem. Abstr.*, **53**, 1734 b (1959).

[7] Robbins Woodrow W, US 3438963 (1969) ; *Chem. Abstr.*, **71**, 14170 h (1969).

[8] A. Spiliadis, Thèse de doctorat, 1970.

rement aux synthèses de ces colorants, sans élucider le mécanisme de ces réactions spéciales d'alkylation.

Parmi les colorants à propriétés tinctoriales supérieures on trouve en premier lieu les colorants bleu vif à benzothiazolique. Les indications de la littérature sur ce type de colorants sont très peu nombreuses et indiquent des rendements réduits.

Dans la présente étude l'auteur s'est proposé d'éclaircir certains problèmes liés à la réaction d'alkylation, dans le cas d'un colorant benzothiazolique, à savoir le 2-amino-6-méthoxy-benzothiazole, diazoté et couplé à la diméthylaniline :

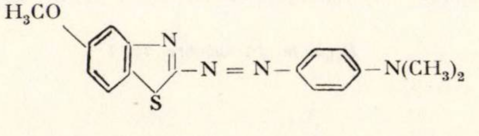

(I)

La substance de formule 1, dénommée dans le présent ouvrage « pigment », a la couleur rouge foncé ; son obtention a été présentée par l'auteur dans un article antérieur[9].

Par l'alkylation du pigment I avec diméthylesulfate, on obtient, conformément à la réaction globale indiquée ci-dessous, le colorant bleu benzothiazolique (II) :

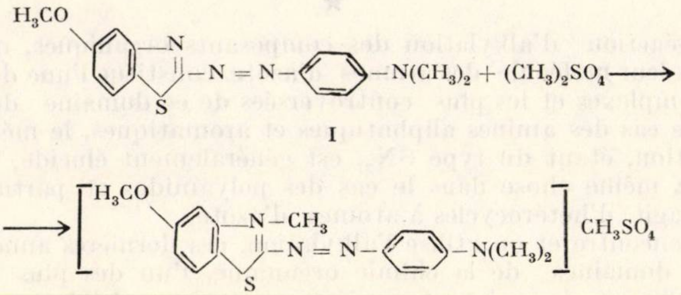

(1)

Dans le cadre d'une étude effectuée par l'auteur, sur les rendements convenables au point de vue technologique, [10] on a remarqué la présence de certains effets thermiques concrétisés par l'apparition de différences de température, entre la cuve d'échauffement (T_1) et le ballon d'alkylation (T_2) ($T_2 < T_1$).

Basés sur cette observation, aussi bien que sur le fait que dans d'autres domaines de la chimie, l'analyse thermique différentielle (ATD) met en évidence des aspects extrêmement intéressants du domaine étudié, afin d'élucider le mécanisme de cette réaction, l'auteur a essayé d'utiliser cette méthode moderne adaptée aux conditions spécifiques dans lesquelles la réaction d'alkylation du colorant benzothiazolique (I) se déroule.

---

[9] A. Spiliadis, M. Hilsenrath, V. Cornea, E. Baltă, G. Molău, E. Teodorescu, et L. Predescu, *Rev. Chim.* (*București*), **17**, 271 (1967).

[10] A. Spiliadis, V. Cornea et E. Baltă, *Teintex*, **31**, 430 (1966).

PRINCIPE DE LA MÉTHODE ET MODE DE TRAVAIL

Il est bien connu que le principe de la méthode ATD consiste à mesurer, à l'aide de deux thermocouples connexés en série (en opposition), les différences de température entre une substance inerte de référence et la substance étudiée, les deux étant échauffées à vitesse constante. Dans le cas de la présente étude vu les conditions particulières où les réactions se déroulent, un appareillage spécial a été utilisé, adéquat aux réactions qui ont lieu dans une suspension ou une solution.

La construction de l'appareil qui remplit ces conditions est sur le point d'être breveté. L'enregistrement des effets thermiques et de la température se fait automatiquement, sur une bande de papier à deux plumes.

Le mode de travail pour une analyse thermique différentielle consiste à peser une certaine quantité du colorant I (dénommé pigment), à ajouter ensuite le solvant et, après avoir réalisé une homogénéité parfaite, à introduire dans le récipient de réaction, l'agent d'alkylation. Après avoir introduit les substances réagissantes, on effectue l'analyse thermique différentielle. La vitesse d'échauffement (le gradient de température) est de 2° par minute, le temps de réaction — constitué par la durée d'échauffement à partir de la température ambiante jusqu'à 100° — étant de 40 minutes.

Dans le présent ouvrage, pour des raisons qui seront exposées par la suite, nous avons utilisé comme solvant l'eau distillée et comme agent d'alkylation le diméthyl-sulfate distillé.

Pour la corrélation des données offertes par l'analyse thermique différentielle avec les différents phénomènes ou aspects de la réaction d'alkylation, certaines analyses thermiques ont été suivies par un travail de la masse de réaction résultée. Le mode de travail utilisé par la suite a été déterminé par les aspects suivants :

Le colorant résulté de la réaction présente une solubilité réduite dans l'eau, par conséquent la dilution de la masse de réaction est nécessaire. Afin d'accélérer ce phénomène la solution est réchauffée jusqu'à 70°, température qui ne peut être dépassée car c'est seulement jusqu'à 85° que le colorant présente une bonne stabilité [11] L'isolation de la solution du colorant alkylé est basée sur sa propriété de former des complexes avec le NaCl et le $ZnCl_2$, ayant la forme :

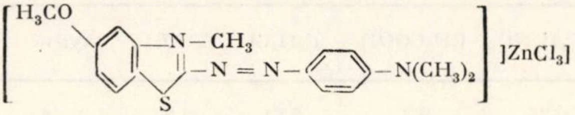

En ce qui concerne l'isolation du colorant non alkylé (le pigment), ce processus présente certaines difficultés. A la suite de l'hydrolyse du diméthylsulfate, de l'alcool méthylique et de l'acide sulfurique sont mis en liberté, conformément aux réactions suivantes :

$$\begin{aligned} (CH_3)_2SO_4 + H_2O &= CH_3OH + CH_3HSO_4 \\ CH_3HSO_4 + H_2O &= CH_3OH + H_2SO_4 \end{aligned} \qquad (2)$$

---

[11] A. Spiliadis, V. Cornea et E. Baltă, *Bull. Soc. chim. France*, **1966**, 921.

Le pigment non alkylé sera partiellement dissous par l'acide sulfurique résulté des réactions ci-dessus, fait vérifié par chromatographie sur papier (papier chromatographique MN214 et éluant CH_3COOH : H_2O 1 :1). Afin de récupérer intégralement le pigment non alkylé, la solution est neutralisée par une substance à caractère légèrement basique ; cette dernière précaution est nécessaire, étant donné la réaction de dégradation du colorant alkylé en présence d'une substance fortement alcaline. Le pH pouvant être utilisé ne dépasse pas 4,6...4,8 pour la même raison : la stabilité du colorant.

Compte tenu de ce qui précède, on a mis au point le procédé suivant, utilisé pour travailler la masse de réaction résultée de l'analyse thermique différentielle et dans le but d'isoler le colorant et récupérer le pigment non alkylé : la masse de réaction est diluée avec 500 cm³ d'eau distillée (jusqu'à la concentration de 1 % colorant) et réchauffée ensuite à 70°, pendant 30 minutes, pour la dissolution complète du colorant alkylé. On neutralise ensuite l'acide sulfurique résulté de l'hydrolyse du diméthylsulfate par du MgO (magnésia usta) jusqu'à un pH de 4,6...4,8,à 60°, température nécessaire pour faciliter la réaction de neutralisation, vu la bien connue insolubilité du MgO à froid et l'amélioration de cette solubilité quand la température augmente. La masse est ensuite lentement refroidie jusqu'à la température ambiante et filtrée sous vide, pour la séparation du pigment non alkylé du colorant. Cette opération est suivie par le réchauffement de la solution du colorant à 60° et sa précipitation au NaCl solution 20 % par rapport au volume et 1 % de $ZnCl_2$. On refroidit lentement à la température ambiante, on filtre le colorant précipité en chlorozincate et on le sèche sous poids constant, en étuve à 60°.

La pureté du colorant et sa concentration ont été établiès par des méthodes de séparation chromatographiques [12] et des méthodes pour la détermination du colorant au reineckate d'ammonium mises au point par l'auteur.

RÉSULTATS EXPÉRIMENTAUX

Dans le présent ouvrage des analyses thermiques différentielles ont été effectuées sur un système ternaire constitué de solvant — pigment agent d'alkylation. Il est connu, des travaux de Menchutkine [13] que la vitesse de réaction d'alkylation de la pyridine avec de l'iodure de méthyle est d'autant plus grande que le solvant utilisé a une constante diélectrique plus grande. On donne dans le tableau ci-dessus la valeur de la constante diélectrique pour une série de solvants usuels :

solvant	H_2O	$C_6H_5NO_2$	CH_3COOH	C_6H_5Cl	$C_2H_2CL_4$	xylène	$C_6H_5CH_3$	C_6H_6
ε	88	35	9,7	5,61	2.5	2,38	2,37	2,28

Sur la base de ces données, on a choisi, pour le présent ouvrage, l'eau ; d'autres solvants seront essayés dans les futures recherches.

Le choix du diméthylsulfate comme agent d'alkylation est justifié par des considérations tant théoriques que pratiques dont il faut mentionner la réactivité plus grande du diméthylsulfate parmi les agents d'alkylation les plus connus [14].

---

[12] E. Baltă, Communication à la troisième Conf. Rép. de Chimie analytique, Braşov sept. 1971 ; publiée dans les matériaux de la Conférence, vol., III-ème, p, 150.

[13] «Noţiuni de cinetică chimică», Ed. tehnică, 1963, p. 157.

[14] A. I. Kiprianov et P. A. Mihailenco, *Zhur. obshchei Khim.*, **33**, 1415 (1963).

L'aspect d'un thermogramme, effectué dans les conditions et selon le mode de travail ci-dessus exposés, est présenté figure 1*a*. Les caractéristiques de la réaction où le thermogramme a été effectué sont : eau 50 %, pigment 10 %, diméthylsulfate 40 %.

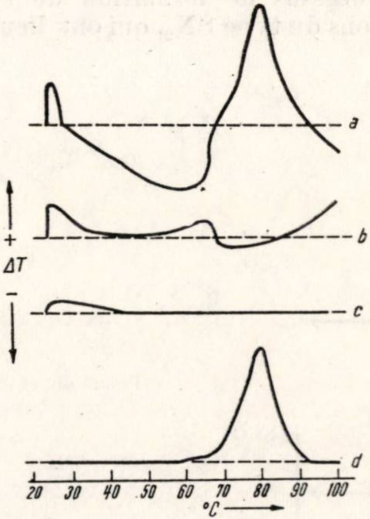

Fig. 1. — Aspect d'un thermogramme effectué dans les conditions : 50 % d'eau, 10 % de pigment, 40 % de diméthylsulfate.

On remarque avec certitude la présence de trois effets thermiques prononcés, à savoir : un effet exothermique entre 24 et 26,5°, un effet endothermique entre 26,5 et 66° et un second effet exothermique entre 66 et 85,5°. Les trois effets thermiques bien différenciés nous font supposer que, pendant la réaction d'alkylation, plusieurs étapes intermédiaires ont lieu, qui conduisent finalement à l'obtention du colorant alkylé.

Ainsi, par exemple, le premier effet exothermique peut être déterminé par l'humectage du pigment soit avec de l'eau, soit avec du diméthylsulfate ou avec les deux simultanément. A l'appui de cette affirmation sont également présentés les thermogrammes : 1*b* correspondant à une mixture formée de 10 % de pigment et 90 % de diméthylsulfate, 1*c*, correspondant au mélange formé de 10 % de pigment et 90 % d'eau. On remarque l'effet exothermique en discussion, dans ce domaine de température, sur tous ces diagrammes (1*a*, 1*b* et 1 *c*). Ce phénomène peut être expliqué par la présence dans la molécule du pigment de nombreux couples d'électrons non participants, tel que l'on peut remarquer dans la formule ci-dessous :

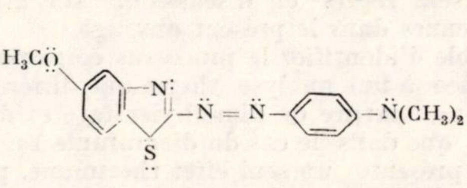

et qui peuvent déterminer l'apparition de liaisons d'hydrogène entre les molécules du pigment et l'eau ou le diméthylsulfate. La mise en corrélation de ce premier effet thermique avec l'humectage est également basée sur le fait que, généralement, ces phénomènes sont accompagnés par un dégagement de chaleur.

Le second effet thermique, l'effet endothermique, peut être attribué au processus de formation de l'état intermédiaire, rencontré dans les réactions du type SN_2, qui ont lieu par le mécanisme de l'état de transition :

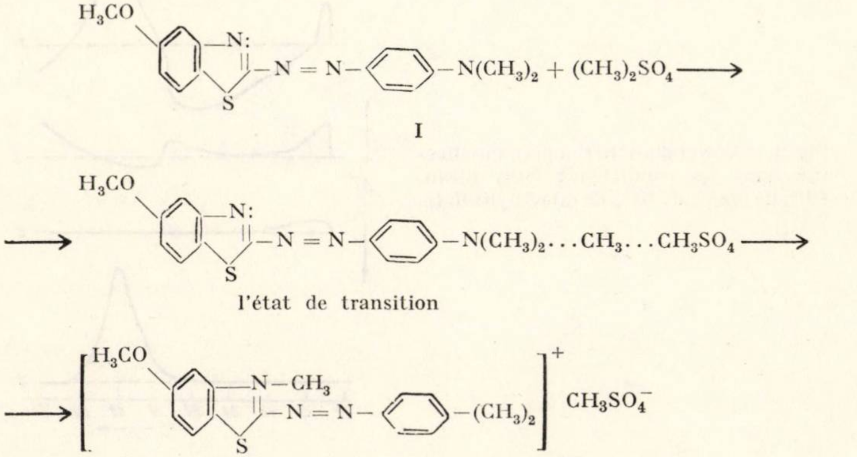

(3)

ou d'une réaction d'ionisation du diméthylsulfate, étape lente déterminante de vitesse, caractéristique de la réaction du type SN_1 :
$(CH_3)_2SO_4 \rightarrow CH_3^+ + CH_3SO_4^-$ réaction lente, déterminante de vitesse

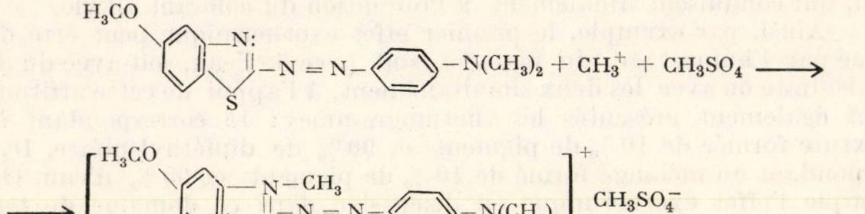

(4)

Ce problème sera repris en discussion, sur la base des données expérimentales obtenues dans le présent ouvrage.

Il a été possible d'identifier le processus correspondant au troisième effet thermique, grâce à une analyse thermique différentielle supplémentaire effectué sur une mixture de diméthylsulfate et d'eau, pris dans les mêmes proportions que dans le cas du diagramme 1*a*. Le thermogramme correspondant (1d) présente un seul effet thermique, pratiquement identique, à tous les points de vue, au troisième effet marqué sur le thermogramme 1*a*. Il en résulte que cet effet est dû exclusivement au diméthyl sulfate, à savoir au processus d'hydrolyse, qui — conformément aux indications de la littérature [14] — a lieu dans ce domaine de température.

Pendant l'analyse thermique, on a remarqué que la formation du colorant commence à des températures rapprochées de la température où le deuxième effet exothermique commence. Le fait que le colorant n'apparaît pas dans le système jusqu'à cette température peut être constaté visuellement (la couleur bleu correspondante ne se montre pas), aussi bien que par chromatographie sur papier et séparation du colorant conformément au mode de travail montré ci-dessus. L'égalité des effets exothermiques montrés sur les thermogrammes 1 *a* et 1*d* conduisent à l'idée que la formation du colorant n'est pas accompagnée par un effet thermique que l'on puisse observer, quoiqu'elle ait lieu en même temps que la décomposition du diméthylsulfate.

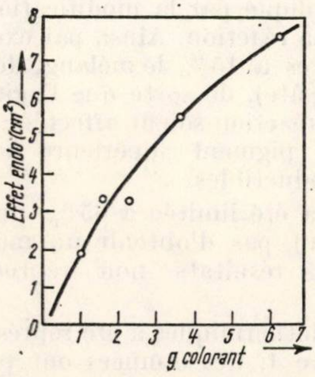

Fig. 2. — Corrélation entre l'aire des effets endothermiques et la quantité de colorant, exprimée en grammes.

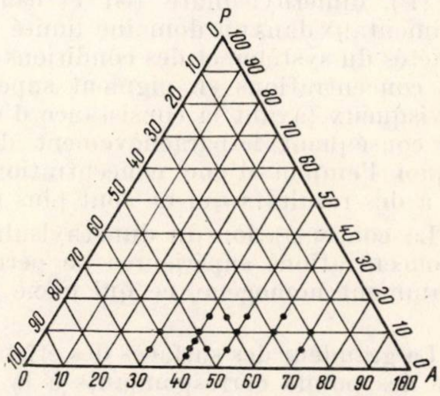

Fig. 3. — Le triangle de Gibbs, dont les sommets sont constitués par les trois composants : eau (A), pigment (P), diméthylsulfate (S).

Compte tenu que la zone de l'effet endothermique paraît être la seule dans laquelle se déroule le processus de formation du colorant on a continué d'étudier la corrélation de cet effet avec la quantité de colorant effectivement obtenu. A cette fin, une série de compositions soumises à l'analyse thermique différentielle ont été travaillées de suite, pour que la quantité de colorant soit séparée et déterminée. A la figure 2 on a essayé de mettre en corrélation l'aire de l'effet endothermique avec la quantité en grammes du colorant dosé dans la mixture respective. On a constaté que les points expérimentaux sont situés, avec une précision suffisante, le long d'une courbe qui indique l'existence d'une proportionnalité entre l'aire de l'effet endothermique et la quantité de colorant. L'équation correspondant à cette courbe est :

$$y = 0{,}074\,x^2 + 0{,}22\,x + 0{,}17$$

de sorte qu'il est possible de calculer la quantité de colorant formé dans le système, (y), en fonction de l'aire de l'effet endothermique mesuré sur le thermogramme (x).

Sur la base de cette observation, on utilise par la suite les analyses thermiques différentielles, respectivement l'aire de l'effet endothermique, pour obtenir des informations sur la composition des mixtures permettant d'obtenir les plus grandes quantités de colorants. A cet effet, on a effectué des analyses thermiques différentielles sur quelques mixtures représentées figure 3, sous la forme de points à l'intérieur d'un triangle Gibbs, dont les sommets sont constitués par les trois composants : pigment (P), diméthylsulfate (S) et eau (A). Le groupement des points expérimentaux dans un domaine limité s'explique par la modification des propriétés du système et des conditions de la réaction. Ainsi, par exemple à des concentrations en pigment supérieures à 15 % le mélange devient trop visqueux (ayant la consistance d'une pâte), de sorte que l'agitation et par conséquent le parachèvement de la réaction soient affectées. C'est pourquoi l'emploi d'une concentration en pigment supérieure à 15 % mène à des résultats qui ne sont plus reproductibles.

La concentration du diméthylsulfate a été limitée à 65 %, puisque des concentrations supérieures ne permetent pas d'obtenir un mélange suffisamment homogène, ce qui mène à des résultats non reproductibles.

La grandeur des surfaces des effets endothermiques a été représentée à côté des points correspondants à la figure 4. Ces données ont permis d'apprécier l'allure des courbes représentant des surfaces égales de l'effet endothermique, correspondant donc à des quantités égales de colorant résulté de la réaction. Malgré le caractère approximatif de ces courbes, on peut remarquer l'existence d'une zone où l'on obtient des quantités maximales de colorant. Cette zone est placée dans la région centrale de la portion étudiée, de notre système ternaire, un peu plus rapprochée du sommet A. La quantité de colorant formé augmente quand la teneur en pigment croît et diminue vers les sommets A et S. Il en résulte un rapport optimal entre les quantités de diméthylsulfate et d'eau, la valeur de ce rapport gravimétrique optimal étant d'environ 1/1. Les résultats obtenus démontrent que, au point de vue de la quantité de colorant obtenu dans le système aussi, la limitation de la zone explorée est raisonnable.

Des informations supplémentaires ont été obtenues en étudiant la corrélation entre les aires des effets endothermiques et la concentration de certains composants, sur des diagrammes plus simples.

Sur la figure 5 on représente la variation de l'aire de l'effet endothermique, en fonction de la quantité de pigment exprimée en %. Les courbes correspondent à une teneur constante en eau. Il en résulte clairement que pour des teneurs en eau de 40 à 50 % on obtient les plus grandes quantités de colorant ; pour des taux d'eau supérieurs le contenu de colorant diminue. L'allure des courbes indique aussi que le rendement en colorant diminue quand la quantité de pigment augmente. Ce fait inattendu a probablement des causes multiples. Ainsi, par exemple, à un contenu d'eau constant quand la quantité de pigment augmente, le rapport diméthylsulfate /pigment diminue. Dans le cas des masses de réaction avec 70 % d'eau, ce rapport diminue de 5/1 pour une mixture à 5 % de pigment, à 1/1 pour une mixture à 15 % de pigment ; aux mixtures à 40 % d'eau, ce rapport varie, pour les mêmes concentrations de pigment de 11/1 à 3/1.

Mais, en même temps, avec la diminution du rapport gravimétrique diméthylsulfate/pigment, la diminution de la quantité de diméthylsulfate par l'hydrolyse se fait de plus en plus sentir grâce à l'augmentation du rapport eau/diméthylsulfate.

La situation peut aussi devenir encore plus compliquée du fait que, à la suite de l'hydrolyse de diméthylsulfate, du méthanol et de l'acide sulfurique font leur apparition dans le système. Il est donc possible qu'une partie du pigment soit consommée dans une réaction secondaire de fixation de protons (protonations) de la forme :

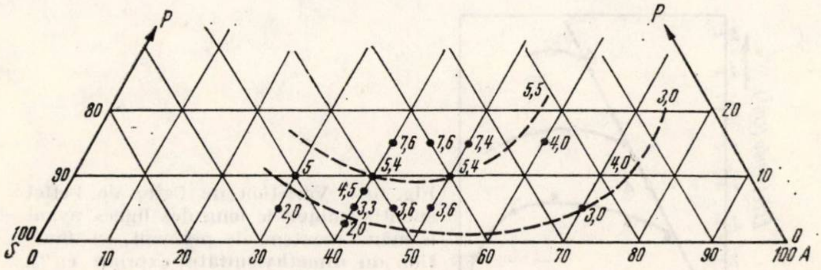

Fig. 4. — Courbes d'égale valeur de l'aire de l'effet endothermique.

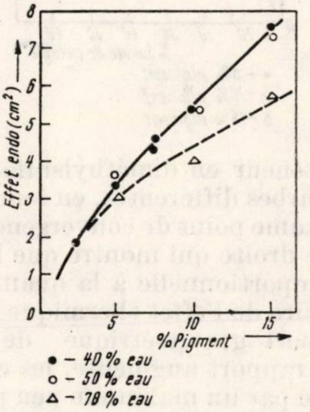

Fig. 5. — Variation de l'aire de l'effet endothermique en fonction de la quantité de pigment exprimé en %.

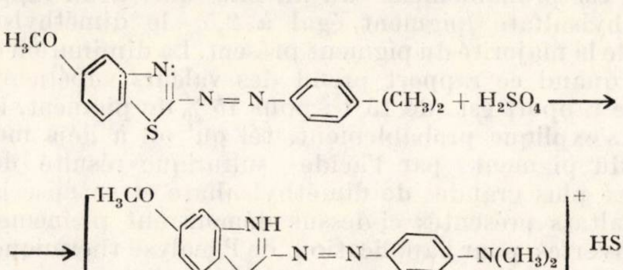

$$\text{H}_3\text{CO}-\text{C}_6\text{H}_3\text{(N=C(S))}-\text{N}=\text{N}-\text{C}_6\text{H}_4-(\text{CH}_3)_2 + \text{H}_2\text{SO}_4 \longrightarrow \tag{5}$$

$$\longrightarrow \left[\text{H}_3\text{CO}-\text{C}_6\text{H}_3\text{(NH=C(S))}-\text{N}=\text{N}-\text{C}_6\text{H}_4-\text{N}(\text{CH}_3)_2\right]^{+} \text{HSO}_4^-$$

Le produit protoné, conformément à la réaction ci-dessus, ne participe plus à la réaction d'alkylation.

Ce qui précède met en évidence la manière complexe dont les composants agissent mutuellement en fonction de leur concentration relative dans le système.

On représente à la figure 6 la variation de l'aire de l'effet endothermique le long des lignes d'égal contenu de pigment, c'est-à-dire en fonction de la teneur en diméthylsulfate. Les points expérimentaux se groupent sur des courbes différentes, en fonction de leur contenu de pigment, courbes qui ont comme point de convergence l'origine. Leurs portions initiales constituent une droite qui montre que la quantité de diméthylsulfate est directement proportionnelle à la quantité de pigment. Les mixtures pour lesquelles l'aire de l'effet thermique est placée sur cette droite correspondent à un rapport gravimétrique de 2,5 entre diméthylsulfate et pigment. Quand ce rapport augmente, les courbes se séparent de la droite et, après avoir passé par un maximum peu prononcé, elles indiquent une diminution de la quantité de colorant. Il en résulte que l'augmentation du rapport gravimétrique au-delà de 2,5 est généralement peu efficace ; à des valeurs plus grandes de ce rapport, on obtient une diminution de la quantité de colorant obtenue. Ce résultat particulièrement intéressant au point de vue pratique est probablement dû au fait que. à un rapport gravimétrique diméthylsulfate /pigment égal à 2,5, le diméthylsulfate assure l'alkylation de la majorité du pigment présent. La diminution de la quantité de colorant, quand ce rapport prend des valeurs supérieures (pour 5 % de pigment le rapport est de 13/1 : pour 15 % de pigment, le rapport est à peine 6/1) s'explique probablement, tel qu' on à déjà montré, par la protonation du pigment par l'acide sulfurique résulté de l'hydrolyse d'une quantité plus grande de diméthylsulfate et sa mise hors réaction.

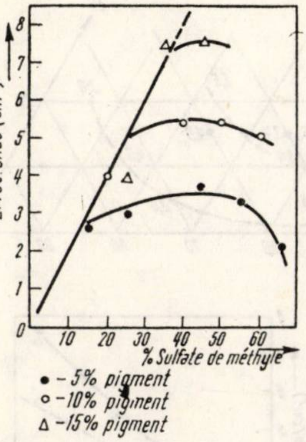

Fig. 6. — Variation de l'aire de l'effet endothermique le long des lignes ayant le même contenu de pigment, en fonction du diméthylsulfate exprimé en %.

Les résultats présentés ci-dessus démontrent pleinement les larges possibilités ouvertes pour l'application de l'analyse thermique différentielle, même dans le cas d'un système complexe où sept composants (pigment, diméthylsulfate, colorant alkylé, méthanol, acide sulfurique, eau, pigment protoné) sont présents, dans des conditions déterminées.

Le troisième effet thermique, dû, tel que nous l'avons montré, à l'hydrolyse du diméthylsulfate, peut fournir des informations sur le comportement de ce dernier, en différentes mixtures. Nous présentons, à la figure 7, la variation de l'aire de l'effet exothermique 2 en fonction du contenu en diméthylsulfate, exprimé en % du poids. On constate que tous les points expérimentaux se placent à une approximation satisfaisante, le long d'une droite intersectant l'abscisse à environ 10 %. A une analyse plus approfondie, on peut constater de légères différences en fonction des teneurs en pigment dans les mixtures respectives.

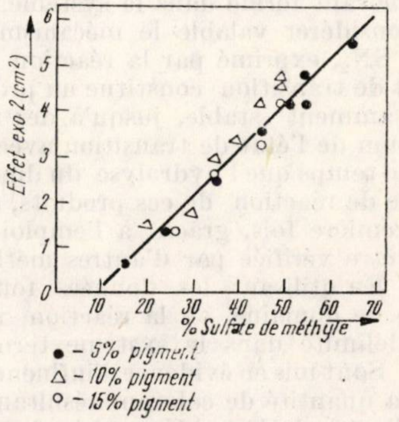

Fig. 7. — Variation de l'aire de l'effet exothermique 2, en fonction de la teneur en diméthylsulfate, exprimée en %.

Le fait que les effets thermiques peuvent être mesurés quand la concentration du diméthylsulfate dépasse 10 % seulement, montre que jusqu'à la température où commence l'hydrolyse, respectivement l'effet exothermique, environ 10 % du diméthylsulfate est consommé dans d'autres réactions. On peut constater, par voie stœchiométrique, que cette quantité de diméthylsulfate est 1,7 fois plus grande que celle nécessaire pour alkylation dans le cas de la mixture à 15 % de pigment, 2,5 fois plus grande que dans le cas de la mixture à 10 % de pigment et 5 fois plus grande que celle nécessaire dans le cas de la mixture à 5 % de pigment. Il résulte de la figure 6 que, pour les points placés sur la droite indiquant une proportionnalité directe, on a besoin d'une quantité de diméthylsulfate 6 fois plus grande que la quantité stœchiométrique. Cette consommation plus élevée de diméthylsulfate pourrait être due à certaines réactions secondaires. La possibilité du déroulement de telles réactions secondaires et leur nature seront établies et étudiées dans l'avenir, d'autres méthodes d'investigations étant aussi utilisées. A la figure 7 on remarque également que la plus grande partie du diméthyl sulfate, introduit dans la masse de réaction, est inutilement perdu, par l'hydrolyse à des températures supérieures à 60°. Il en résulte la nécessité évidente de certaines études qui puissent permettre, dans la pratique industrielle, d'utiliser d'une manière plus raisonnable le diméthylsulfate (qui est très toxique).

CONCLUSIONS

Les résultats présentés démontrent l'utilité particulière de l'analyse thermique différentielle, utilisée pour la premiere fois dans l'étude d'une réaction complexe d'alkylation, dans un système hétérogène. A l'aide de cette méthode on peut metre en évidence un processus intermédiaire à caractère endotherme. L'effet thermique est proportionnel à la quantité de colorant formé dans le système. Sur cette base il paraît vraisemblable de considérer valable le mécanisme de substitution nucléophile bimoléculaire SN_2, exprimé par la réaction (3). Il est connu que la formation de l'état de transition constitue un processus endotherme et que cet état est suffisamment stable, jusqu'à des températures assez élevées. La décomposition de l'état de transition avec formation du produit alkylé a lieu en même temps que l'hydrolyse du diméthylsulfate. L'hypothèse sur le mécanisme de réaction de ces produits, dont l'énoncé est devenu possible pour la première fois, grâce à l'emploi de l'analyse thermique différentielle, doit être vérifiée par d'autres méthodes.

En utilisant les données fournies par l'analyse thermique différentielle, le domaine, où la réaction se déroule au rendement maximum, a été délimité dans le système ternaire pigment — eau — diméthylsulfate.

Sont mis en évidence l'influence spécifique des différents composants sur la quantité de colorant résultant de la réaction, aussi bien que le rôle du diméthylsulfate. Une série de constatations occasionnées par les résultats obtenus présentent un intérêt particulier, au point de vue pratique, pour la production industrielle du colorant.

Revue Roumaine de Chimie, **17**, 7, 1253 – 1260 (1972)

THE MECHANISM OF THE BENZIDINE REARRANGEMENT

MIRCEA E. LUPEŞ

Aleea Stanila 4, Bucharest 57, Romania

Received February 3, 1972

This paper presents a new hypothesis concerning the mechanism of the benzidine rearrangement, which is an alternative to the more important theories known up to the present and which is based on a new type of reaction intermediate (III). This intermediate is formed by "adjacent electron localization" in the benzene ring and leads, without any sort of special chemical bond, to the formation of all the rearrangement products, including that of *p*-semidine, by intramolecular electrophilic substitution within intermediates (III). The mechanism of the diprotonated, monoprotonated and nonprotonated benzidine rearrangement is discussed in terms of this theory and in connexion with experimental data described in literature.

The term "benzidine rearrangement" as usually understood means the reaction of hydrazo-compounds leading to benzidines, diphenylines and semidines.

I. APPROACHING

The mechanism of the benzidine rearrangement, whose elucidation was attempted as far back as at the beginning of this century, continues to be an unsatisfactorily solved problem. There are three more important theories which account for this mechanism, each of them trying to get over the uncommon stereochemical difficulties of this reaction: "caged-dissociation" [1], "π-complex" [2], and "polar-transition-state" [3]. In agreement with Ingold's opinion [3e] we think that the first two of them are not consistent satisfactorily with experimental data. At the same time we do not agree with the "polar-transition-state" theory either, as this one is based on Hammond and Shine's suggestion [4] that the intermediate in the diprotonated benzidine rearrangement is the doubly charged cation with the two positive charges at the two neighbouring nitrogen atoms. Obviously the existence of a whole positive charge at a neighbouring atom produces a strong electrostatic repulsion of the second proton to be added. On the other hand, this theory adopts a special sort of chemical bond — an electrovalent one — between the two hydrazo-compound moieties, though it is difficult to understand the heterolysis itself which produces it in the case of perfectly symmetrical molecules. Finally, the polar-transition-state theory cannot explain satisfactorily either the *p*-semidine formation or the nonprotonated benzidine rearrangement in aprotic solvents.

---

[1] M. Vecera, L. Synek and V. Sterba, *Coll. Czech. Chem. Comm.*, **25**, 1992 (1960).

[2] M. J. S. Dewar, (a) *Nature*, **176**, 784 (1945); (b) *J. Chem. Soc.*, **1946**, 406; (c) *ibid.*, **1946**, 777; (d) "Electronic Theory of Organic Chemistry", Clarendon Press, Oxford, 1949, p. 233; (e) *Bull. Soc. chim. France*, **1951**, 71 C; (f) *Ann. Reports*, **48**, 126 (1951); (g) "Theoretical Organic Chemistry", Kekulé Symposium, Butterworths, London, 1959, p. 195.

[3] (a) E. D. Hughes and C. K. Ingold, *J. Chem. Soc.*, **1941**, 608; (b) E. D. Hughes and C.K. Ingold, *ibid.*, **1950**, 1638; (c) D. V. Banthorpe, E. D. Hughes and C. K. Ingold, *ibid.*, **1964**, 2864; (d) C. K. Ingold, *Proc. Israel Acad. Science &Humanities*, Section of Science, No. 10, Jerusalem, 1968; (e) C. K. Ingold, "The Transition State", *Chem. Soc. Special Publ.*, **16**, 118 (1962).

As an alternative to these three theories we have previously proposed a different mechanism, [5] whose main idea was the fact that in the case of the diprotonated benzidine rearrangement the second proton is added to that carbon atom of the benzene ring adjacent to the NH_2^+ group previously formed. The mechanism proposed here is only an improved development of our first one.

II. "ADJACENT ELECTRON LOCALIZATION" THEORY

a) DIPROTONATED BENZIDINE REARRANGEMENT

According to our proposed mechanism, in the first step of the rearrangement giving a pure kinetic order of two with respect to hydrogen ions, the hydrazo-compounds add a proton to a nitrogen atom giving the monocation (II_2). In unsymmetrical hydrazo-compounds this addition takes place at the more basic nitrogen atom, the basicity being dictated by the nature and the position of the substituents. However, the second proton is added to the carbon atom of the benzene ring adjacent to the NH_2^+ group initially formed giving the dication (III_2) which is the key intermediate of the diprotonated benzidine rearrangement.

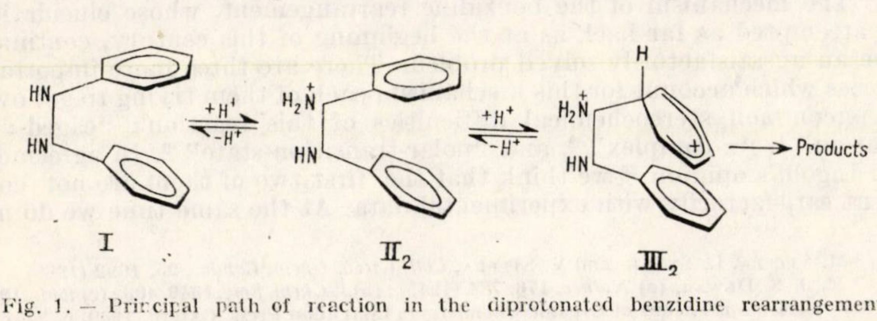

I $\qquad$ II_2 $\qquad$ III_2

Fig. 1. — Principal path of reaction in the diprotonated benzidine rearrangement.

This intermediate must be more stable than that suggested by Hammond and Shine [4] as now the two positive charges have a greater distance between them. At the same time the protonated nucleus adopts a position closer to the nonprotonated one (see Fig. 1), which allows a direct reaction between different positions in the molecule. Thus, the difficult stereochemical problem of this reaction is easily overcome without implying any special kind of chemical bond between the two moieties of the hydrazo-compound molecule. We must also say that this second proton may be added to the other positions of the benzene rings but the compounds thus formed probably do not undergo the benzidine rearrangement but give, by a reversible reaction, the dication(III_2). This one rearranges by a cyclic transition state.

---

[4] G. S. Hammond and H. J. Shine, *J. Amer. Chem. Soc.*, **72**, 220 (1950).

[5] M. E. Lupeş, unpublished work (1969).

All known cases of the diprotonated benzidine rearrangement are consistent with this schema. Thus, hydrazobenzene,[4] *p*, *p*′-hydrazotoluene,[3c] 4,4′-dichlorohydrazobenzene,[6e] 4,4′-dibromohydrazobenzene,[6f] 4,4′-diiodohydrazobenzene, [6g] *p*,*p*′-hydrazobiphenyl,[7] 2,2′-difluorohydrazobenzene,[6d] and 2,2′-dichlorohydrazobenzene [6e] have all of them an order of two with respect to hydrogen ions because their nitrogen atoms are the most basic positions in the molecule. This compels the first proton to be added to the nitrogen atom, which is however insufficient for the rearrangement to take place. A second proton must be added to the adjacent position of the benzene ring in order to bring the molecule in such a geometrical shape as to allow it to rearrange. The reaction rate is ordered by the substituents, i.e. the electron-releasing ones increase it by increasing the basicity of both the nitrogen atom and the adjacent position, whilst electron-attracting ones decrease it by decreasing the basicity of the same positions.

b) MONOPROTONATED BENZIDINE REARRANGEMENT

A series of benzidine rearrangements are now known which have a pure kinetic order of one with respect to hydrogen ions. The hydrazo-compounds that react in this way have a much greater basicity at the adjacent position of the benzene ring than that of the nitrogen atom. For this reason they add a proton directly to the adjacent position giving the monocation (III_1) capable of reaction (Fig. 2). Here again the possibility of pro-

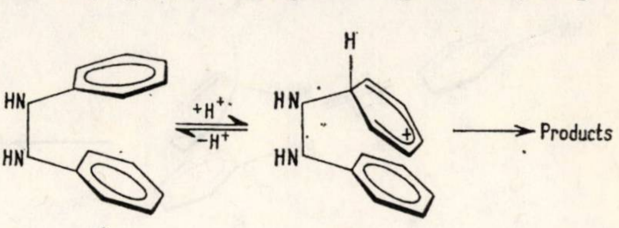

I

III_1

Fig. 2. — Principal path of reaction in the monoprotonated benzidine rearrangement.

---

[6] (a) D. V. Banthorpe, C. K. Ingold and J. Roy, *J. Chem. Soc.*, **1968**, 64 ; (b) D. V. Banthorpe and A. Cooper, *ibid.*, **1968**, 605 ; (c) D. V. Banthorpe, A. Cooper and C. K. Ingold, *ibid.*, **1968**, 609 ; (d) D. V. Banthorpe and M.O'Sullivan, *ibid.*, **1968**, 615 ; (e) D. V. Banthorpe and A. Cooper, *ibid.*, **1968**, 618 ; (f) D. V. Banthorpe, C. K. Ingold and M. O'Sullivan, *ibid.*, **1968**, 624 ; (g) D. V. Banthorpe and M. O'Sullivan, *ibid.*, **1968**, 627.

[7] H. J. Shine and J. P. Stanley, *Chem. Comm.*, **1965**, 294.

ton addition to the other positions in the benzene rings exists, but the compounds that are formed are also inactive in this reaction as they do not have the required geometrical shape. The monocation (III_1) gives the rearrangement products by a cyclic transition state, too.

The known cases of such a rearrangement are also consistent with this theory. Thus, 2,2′-dimethoxyhydrazobenzene,[6b] 2,2′-diiodohydrazobenzene,[6g] 2,2′-hydrazobenzene-dicarboxilic acid,[8] 1,1′-hydrazonaphthalene,[9a] and 1,2′-hydrazonaphthalene [9b] all show kinetics of a first order with respect to hydrogen ions. The necessary condition for the reaction to follow this mechanism is a greater basicity of the adjacent position than that of the nitrogen atom. This is chiefly managed by the steric hindrance caused by the bulky substituents in the *ortho* positions. When these ones are electron-releasing they increase the reaction rate by increasing the basicity of the adjacent positions. On the contrary, when they are electron-attracting the reaction rate is decreased.

c) INTERMEDIARY-PROTONATED BENZIDINE REARRANGEMENT

Carlin and Odioso [10] were the first to discover such a reaction. They found an order of 1.6 with respect to hydrogen ions. Afterwards other similar cases were recorded. Our viewpoint is in fully agreement with Ingold's opinion [3c,d] who assumes that there are here two independent rearrangements: the former following the two-proton mechanism and the latter the one-proton one, both of them competing (Fig. 3). This is accounted for by the fact that substituents in the molecule increase the basicity of

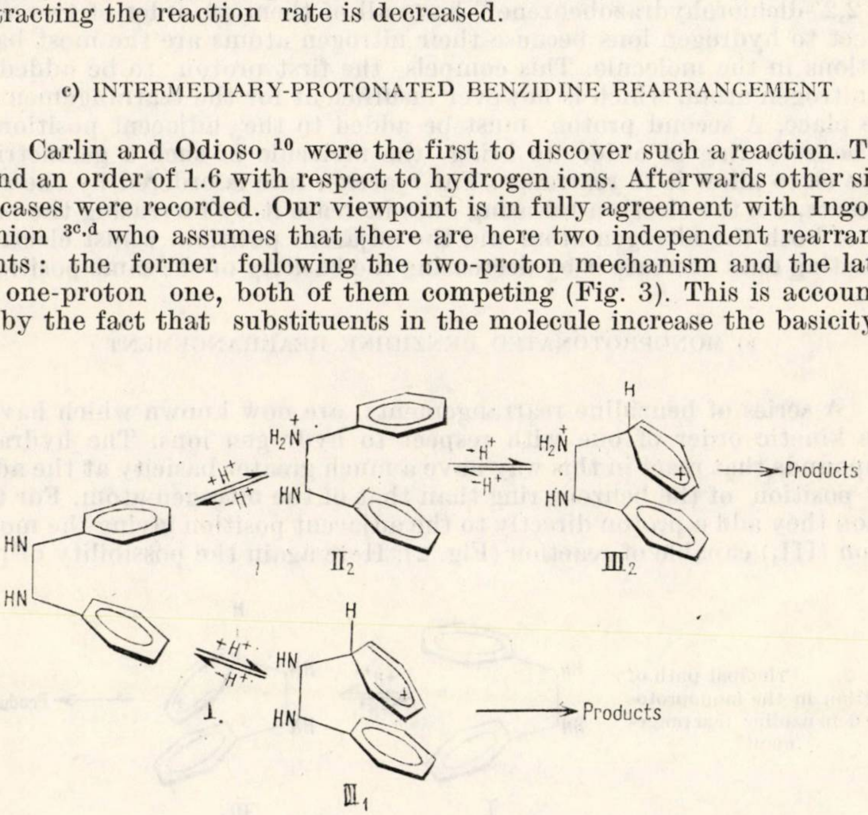

Fig. 3. — Principal path of reaction in the intermediary-protonated benzidine rearrangement.

---

[8] M. Kurihara and N. Yoda, *Bull. Soc. Chem. Japan*, **40**, 2429 (1967).

[9] (a) D. V. Banthorpe, E. D. Hughes and C. K. Ingold, *J. Chem. Soc.*, **1962**, 2386; (b) D. V. Banthorpe and E. D. Hughes, *ibid.*, **1962**, 2402; (c) D. V. Banthorpe, *ibid.*, **1962**, 2407; (d) D. V. Banthorpe, C. K. Ingold, J. Roy and S. M. Somerville, *ibid.*, **1962**, 2436.

[10] R. B. Carlin and R. C. Odioso, *J. Amer. Chem. Soc.*, **75**, 100 (1953).

the nitrogen atom to a smaller extent and, as a result, the basicity of the two positions (both nitrogen atom and adjacent carbon atom) come closer to each other. As in the rate equation of the diprotonated rearrangement the acidity is of second order, the share of this mechanism in the total rate equation will increase with increasing acidity in the medium and thus the total order with respect to hydrogen ions will increase too. Thus, 2,2′-dibromohydrazobenzene [6f] has an order of 1.2 — 1.9 and 2,2′-hydrazonaphthalene[9c] of 1.0 — 1.2. Even the case of *o,o′*-hydrazotoluene, discovered by Carlin and Odioso, was reinvestigated over a larger range of acidities giving an order of 1.3 – 2.0.[9d]

One can see that we have discussed here only the symmetrical hydrazo-compounds which have the two nitrogen atoms and the two "adjacent positions" equivalent, respectively. The same is true for the other types of benzidine rearrangements described here. The reason is that unsymmetrical hydrazo-compounds have four different positions to be considered, not only two. That is why it is more difficult to find out which of all these positions is more basic. We thus think that reliable information might be obtained by quantum chemical calculation only. As to the influence of substituents on the reaction rate this is the same as shown above.

d) NONPROTONATED (THERMAL) BENZIDINE REARRANGEMENT

The above proposed scheme for the protonated rearrangement also embraces the nonprotonated one. Thus, in the case of the reaction carried out in aprotic solvents or without any solvent the relatively high temperature required by the reaction allows the transition of the molecule in an "excited" state characterized by a localization of a π-electron pair to the adjacent carbon atom of the benzene ring (which becomes now negatively charged), whilst the other two π-electron pairs remain in a pentadienyl cation form. The change of the hybridization of the adjacent carbon atom from sp^2 to sp^3 brings the benzene ring in a favourable situation (III_0) similar to that of the protonated rearrangements (III_2 and III_0) (Fig. 4).

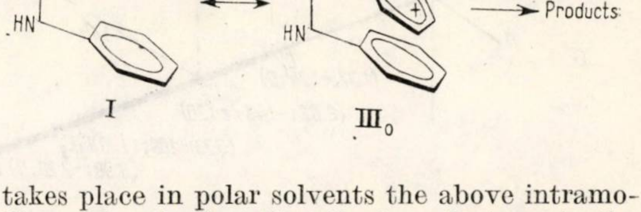

Fig. 4. — Principal path of reaction in the nonprotonated benzidine rearrangement.

When the reaction takes place in polar solvents the above intramolecular polarization is facilitated by the fact that the two electrons in the sp^3 orbital of the adjacent carbon atom form a hydrogen bond with the solvent molecules, which thus has a rôle similar to that of protons in the monoprotonated rearrangement. Moreover, it is known now that by adding bases (pyridine) to 2,2′-hydrazonaphthalene in ethanol the reaction rate of the thermal rearrangement decreases.[11]

III. INTERMEDIATES IN THE BENZIDINE REARRANGEMENT

To illustrate the way in which the new type of intermediate (III) facilitates the direct reaction between different positions in hydrazo-compounds without necessarily adopting any special sort of chemical bond, we have devised, based on known bond angles and distances, a model (Fig. 5) whose geometry, though it might not correspond to reality in all its details, exemplifies concretely this possibility. Thus it results that the *p-p′* distance becomes 1.76 Å (given the same distance in hydrazobenzene is 4.40 Å). Similarly, the other distances are decreased to 2.37Å, 2.23Å and 3.12 Å for *p-o′*, *o-o′* and *o-N′* ones, respectively (given the same distances in hydrazobenzene which are 4.34 Å, 2.96 Å, 3.23 Å, respectively). Only the *p-N′* distance is rather greater in this model (3.79 Å), but we do think that for the *p*-semidine formation the benzene ring adopts a boat shape decreasing this distance to 2.61 Å (Fig. 6). In this way, the *p*-semidine formation has a simple explanation, expected since

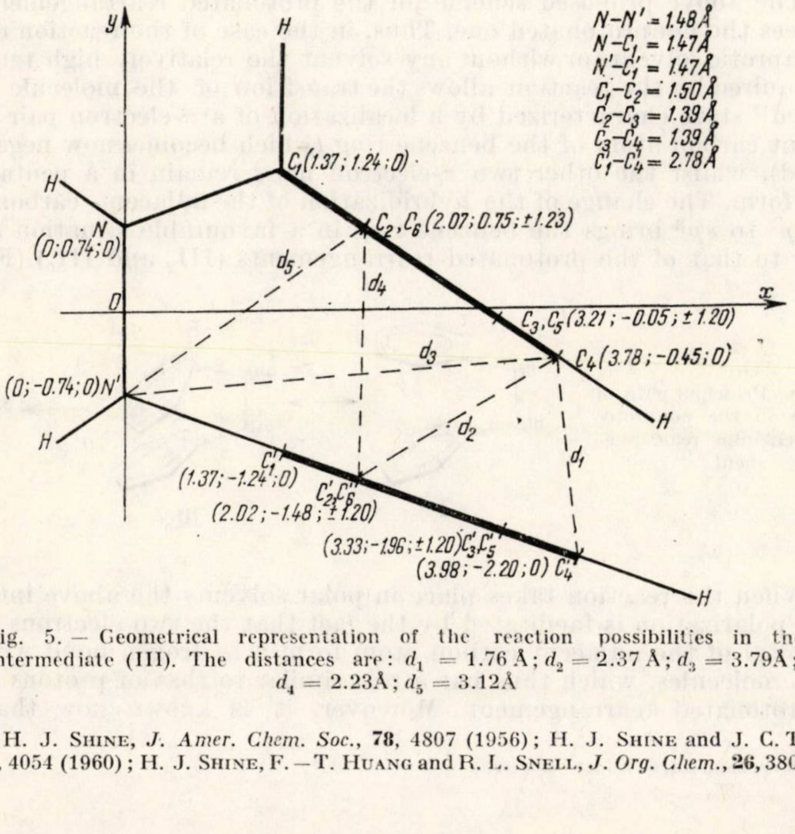
y
H
N−N′ = 1.48Å
N−C₁ = 1.47Å
N′−C′₁ = 1.47Å
C₁−C₂ = 1.50Å
C₂−C₃ = 1.39Å
C₃−C₄ = 1.39Å
C′₁−C′₄ = 2.78Å
C₁(1.37; 1.24; 0)
H
N
(0; 0.74; 0)
C₂, C₆ (2.07; 0.75; ±1.23)
d₅
d₄
0
x
C₃, C₅ (3.21; −0.05; ±1.20)
d₃
C₄ (3.78; −0.45; 0)
(0; −0.74; 0) N′
H
d₂
H
d₁
C′₁
(1.37; −1.24; 0)
C′₂, C′₆
(2.02; −1.48; ±1.20)
(3.33; −1.96; ±1.20) C′₃, C′₅
(3.98; −2.20; 0) C′₄
H

Fig. 5. — Geometrical representation of the reaction possibilities in the intermediate (III). The distances are: $d_1 = 1.76$ Å; $d_2 = 2.37$ Å; $d_3 = 3.79$Å; $d_4 = 2.23$Å; $d_5 = 3.12$Å

---

[11] H. J. Shine, *J. Amer. Chem. Soc.*, **78**, 4807 (1956); H. J. Shine and J. C. Trisler, *ibid.*, **82**, 4054 (1960); H. J. Shine, F. — T. Huang and R. L. Snell, *J. Org. Chem.*, **26**, 380 (1961).

Hammick and Munro's opinion,[12] according to which the presence of metal ions is decisive for its formation, has been invalidated by later works.[6c,6e,13] In fact we have analyzed more precisely only the stereochemical possibility of the *p-p'* and *p-N'* reaction, respectively. For the other possibilities of reaction (*p-o'*, *o-o'* and *o-N'*) a correct analysis can be made only on the basis of molecular models as in this case a rocking of one or both benzene rings may occur around the C-N bond bringing the reactive positions in a more favourable stereochemical situation.

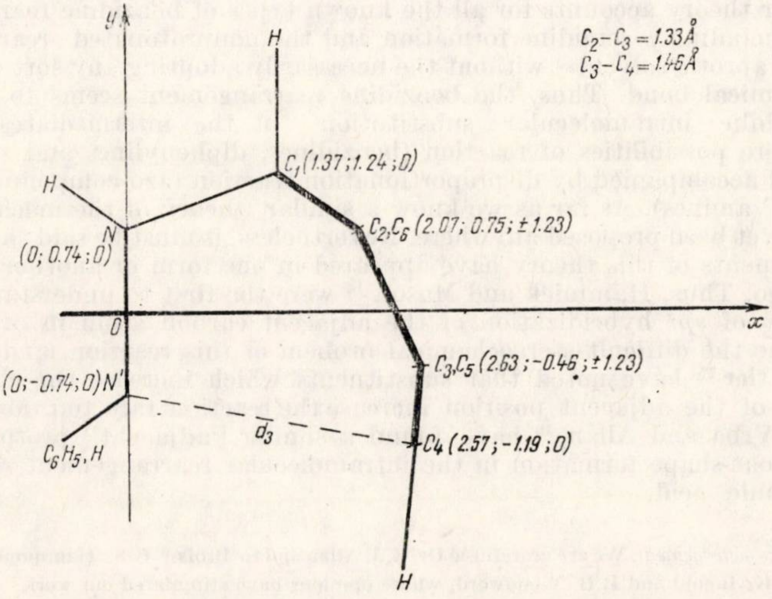

Fig. 6. — Geometrical representation of the reaction possibilities in the boat-shape of the intermediate (III). The *p-N'* distance is : $d_3 = 2.61$ Å.

IV. CONCLUSIONS

One can see that all the types of benzidine rearrangement are consistent with the above described scheme of mechanism whose key elements are the intermediates (III). They are characterized by the fact that the carbon atom of the benzene ring adjacent to the N atom has sp^3 hybridization by means of an "adjacent localization" of a π-electron pair. This localization is supported by a proton addition (in di-and monoprotonated rearrangements), by formation of a hydrogen bonding with solvent molecules (in the nonprotonated rearrangement in polar solvents), or by thermal excitation only (in the nonprotonated rearrangement in aprotic solvents). Obviously, each of this cases has a different distribution of products though the intermediate geometry is the same, depending on the electronic effects of substituents and on the reaction medium. In this way, our theory accounts for all the known types of benzidine rearrangement (including *p*-semidine formation and the nonprotonated rearrangement in aprotic solvents) without the necessarily adopting any sort of special chemical bond. Thus, the benzidine rearrangement seems to be an electrophilic intramolecular substitution of the intermediates (III) with more possibilities of reaction (benzidines, diphenylines and semidines) and accompanied by disproportionation reaction (azo-compounds and "fission" amines). As far as we know a similar theory of the mechanism has not yet been proposed anywhere. Nevertheless, it must be said that certain elements of this theory have appeared in one form or another many years ago. Thus, Hammick and Mason [14] were the first to understand the necessity of sp^3 hybridization of the adjacent carbon atom in order to overcome the difficult stereochemical probem of this reaction, and Croce and Gettler [15] have noted that substituents which increase the electron density of the adjacent position increase the reaction rate too. More recently, Vrba and Allan [16] have found a similar "adjacent" protonation and a boat-shape formation in the intramolecular rearrangement of phenylsulfamic acid.

---

[12] D. L. Hammick and D. C. Munro, *J. Chem. Soc.*, **1950**, 2049.

[13] M. Vecera and J. Petranek, *Coll. Czech. Chem. Comm.*, **25**, 2005 (1960) ; H. J. Shine, C. M. Baldwin and J. H. Harris, *Tetrahedron Letters*, **1968**, 977.

Acknowledgement. We are grateful to Dr. Z.J. Allan and to Profs. G.S. Hammond, H.J. Shine, C. K. Ingold and R.B. Woodward, whose opinions have stimulated our work.

[14] D. L. Hammick and S. F. Mason, *J. Chem. Soc.*, **1946**, 638.

[15] L. J. Croce and J. D. Gettler, *J. Amer. Chem. Soc.*, **75**, 874 (1953).

[16] Z. Vrba and Z. J. Allan, *Tetrahedron Letters*, **1968**, 4507.

Revue Roumaine de Chimie, **17**, 7, 1261 – 1266 (1972)

AROMATIC BIS-ETHERS. III[1,2]
CONDENSATION OF SODIUM DIMETHYLPHENOXIDES WITH DICHLOROMETHYLATED DERIVATIVES

M. IOVU

University of Bucharest, Department of Chemistry
Şoseaua Panduri 90, Bucharest, Romania

Received February 22, 1972

Using the method described in a previous paper [1] we have obtained sodium dimethylphenoxides, from xylenol and sodium hydroxide by azeotropic distillation of the water resulting of the reaction, and anhydrous sodium dimethylphenoxides with dichloro-methylated derivatives were condensed in an ethanol and benzene medium. Aromatic bis-ethers of a new class were synthetized. These correspond to the general formula $Ar-O-CH_2-Ar-CH_2-O-Ar$ in which the two aromatic nuclei directly bound to oxygen are replaced by two methyl radicals.

In a previous paper [1] we have presented the synthesis of some bis-ethers with the general formula $Ar-O-CH_2-Ar-CH_2-O-Ar$ in which the oxygen is bound through a valency directly to an aromatic nucleus (common to both ether functions) and through a second valency by an intermediate methylene bridge.

Starting from phenol or cresols, the bis-ethers (described in the first article[1]), have aromatic nuclei directly bound to oxygen of the ether function, replaced or not by a methyl radical. Using xylenols as starting material, bis-ethers have resulted in which the same aromatic nuclei are replaced by two methyl radicals.

In the present paper we present the results of the bis-ether synthesis produced by condensation of the sodium salts of 2,3-xylenol, 3,4-xylenol, 2,6-xyelenol and 3,5-xylenol with 1,4-di(chloromethyl)-benzene,1,4-di(chloromethyl)-2,5-dimethylbenzene and with 1,3-di(chloromethyl)-4,6-dimethylbenzene.

The bis-ethers, in which the benzenic nuclei directly bound to oxygen, are replaced by two methyl radicals, have not either been described so far, but xylenyl benzyl ethers, such as 3,5-dimethylphenoxytoluene are known.[3]

---

[1] M. Iovu, *Rev. Roumaine Chim.*, **16**, 1223 (1971).

[2] M. Iovu and N. Nicolau, *Rev. Roumaine Chim.*, **16**, 1919 (1971).

[3] E. A. Depp and M. B. Neuworth *Brennstoff- Chem.*, **39**, 90 (1958).

For the synthesis of the new bis-ethers we used the method described for the first time in the first paper of this series and which can be presented schematically as follows.

The xylenol dissolved in an alcohol and benzene mixture is treated with sodium hydroxide yielding sodium dimethylphenoxide plus water :

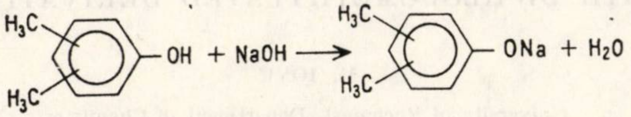

The reaction water is removed through distillation as a benzene-ethanol-water ternary azeotropic mixture. The dichloromethylated derivative was added to the dimethylphenoxide partially dissolved in the benzene and alcohol mixture, when the nucleophilic attack of the phenoxidic ion on the dichloromethylated derivative takes place, such as :

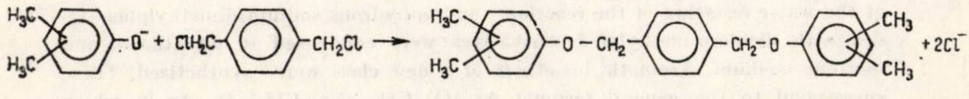

The resulting bis-ether, which crystallizes from the benzene and alcohol solution, is separated by filtration and washed with water to remove the sodium chloride and the unreacted xylenol traces.

The new method has allowed the easy synthetization of 12 new aromatic bis-ethers.

RESULTS AND DISCUSSIONS

The formulae of the 12 synthetized bis-ethers, starting from the same xylenol, with each of the three chloromethylated derivatives are given in table 1, which also shows the melting temperatures, yields and results of the semimicro-analysis of carbon and hydrogen.

By studying the table one notices that the bis-ethers are solid and generally crystallized. The 4,6-bis(2,6-dimethylphenoxymethyl)-*m*-xylene, is an exception because it cannot be obtained in a crystallized form. The presence of the second methyl radical on the phenoxidic nucleus, in comparison with the results presented in the first paper, [1] only very slightly raises the melting temperatures.

The bis-ethers obtained from xylenols, as those obtained from phenols and cresols by condensation with 1,3-di(chloromethyl)-4,6-dimethylbenzene, have much lower melting temperatures than those obtained from 1,4-dichloromethylbenzene and 1,4-diachloromethyl)-2,5-dimethylbenzene.

The IR spectral analysis points out the presence of the ether function. Figure 1 gives the absorption spectra of only 4 representatives of

Table 1

New bis-ether

Ether	Formula	C % calculated / found	H % calculated / found	Melting point °C	Yield %
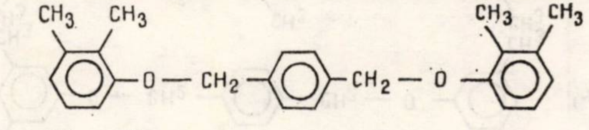	$C_{24}H_{26}O_2$	83.20 / 83.48	7.56 / 7.52	130.5 – 131	67.7
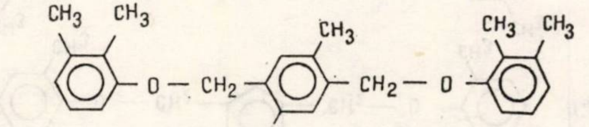	$C_{26}H_{30}O_2$	83.38 / 83.36	8.07 / 8.15	148 – 148.5	89.3
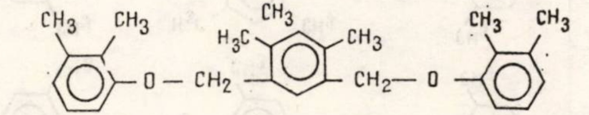	$C_{26}H_{30}O_2$	83.38 / 83.75	8.07 / 7.82	99.5 – 100.5	31.4
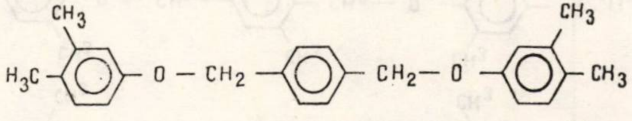	$C_{24}H_{26}O_2$	83.20 / 83.21	7.56 / 7.26	114 – 115.5	71.9
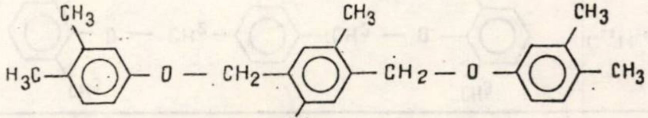	$C_{26}H_{30}O_2$	83.38 / 83.70	8.07 / 8.14	133 – 134.5	67.5
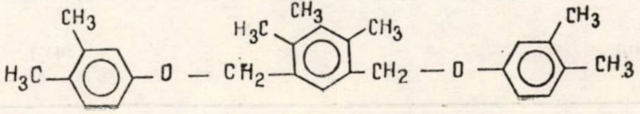	$C_{26}H_{30}O_2$	83.38 / 83.78	8.07 / 8.27	106 – 107.5	23.4

(contin

Ether	Formula	C% calculated / found	H% calculated / found	Melting point °C	Yield
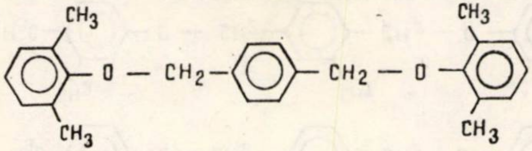	$C_{24}H_{26}P_2$	83.20 / 82.88	7.56 / 7.88	127–128	61.9
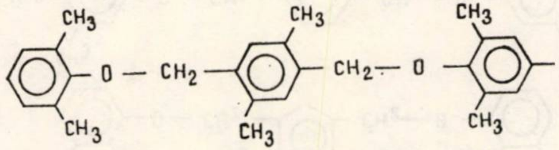	$C_{26}H_{30}O_2$	83.38 / 82.82	8.07 / 8.03	103.5–105	71.4
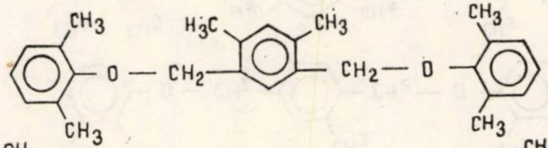	$C_{26}H_{30}O_2$	83.38 / 83.39	8.07 / 8.23	61–62	32.3
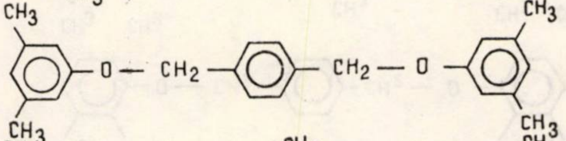	$C_{24}H_{26}O_2$	83.20 / 82.88	7.56 / 7.40	91–92	64.6
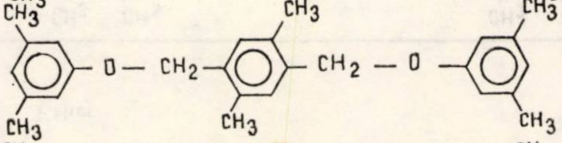	$C_{26}H_{30}O_2$	83.39 / 83.77	8.07 / 8.31	169–169.5	65.3
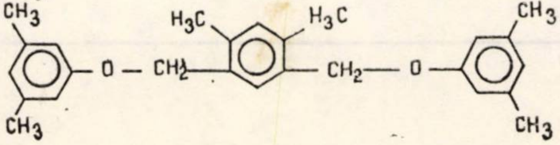	$C_{26}H_{30}O_2$	83.38 / 83.34	8.07 / 8.12	176–178	36.6

this bis-ethers series in the 1300 – 950 cm^{-1} (7.69 – 10.53μ) region, in which the bands due to the ether function are found.

All ethers mentioned in the table are characterized by an intensive band at 1250 – 1270 cm^{-1} owing to the asymmetric valence vibration C–O–C. The position of the substitutes of the phenoxidic nucleus brings about certain shifts of the absorption maxima. Thus, the bis-ethers represented in filgure 1 have their absorption maxima as follows : 1,4-bis (2,3-dimethylphenoxymethyl)-benzene 1259cm^{-1}, 2,5-bis (2,3-dimethylphenoxymethyl)-*p*-xylene 1256 cm^{-1}, 1,4-bis(3,4-dimethylphenoxymethyl)-benzene 1252 cm^{-1} and 2,5-bis (2,5 - dimethylphenoxymethyl) - *p*-xylene 1266 cm^{-1}.

The second band due to symmetrical valence vibration C–O–C is very weak, and is hardly detectable in the 1005 ± 10 cm^{-1} region, in which absorptions take place also due to the plane vibrations of the C–H bonds in the aromatic nucleus and the ring vibrations.

The differential thermogravimetric analysis shows that the thermal stability of the bis-ethers of this group is the same up to 240 – 260° when it undergoes a transposition, in which the weight loss of the analysed product depends on the position of the substitutes in the phenoxidic nucleus.

EXPERIMENTAL

The 1,4-dichloromethylbenzene, 1,4-di(chloromethyl)-2,5-dimethylbenzene and 1,3-di(chloromethyl)-4,6-dimethylbenzene were obtained as we mentioned in our first paper. [1]

The 2,3-and 2,5-xylenol were BDH products.

The 3,4-xylenol was a UCB product and the 3,5-xylenol, a Loba Chemie — Wien product.

The IR spectra were obtained in KBr pellet with a Leitz Vetzlar apparatus.

The thermogravimetric analysis carried out with Paulik type derivatographe.

Synthesis of 1, 4-bis (2, 3-dimethylphenoxymethyl)-benzene

In a 75 ml double-necked flask equipped with a reflux refrigerator and thermometer, we introduced 2.443 g (1/50 mol) 2,3-dimethyl-phenol, 0.808 g NaOH

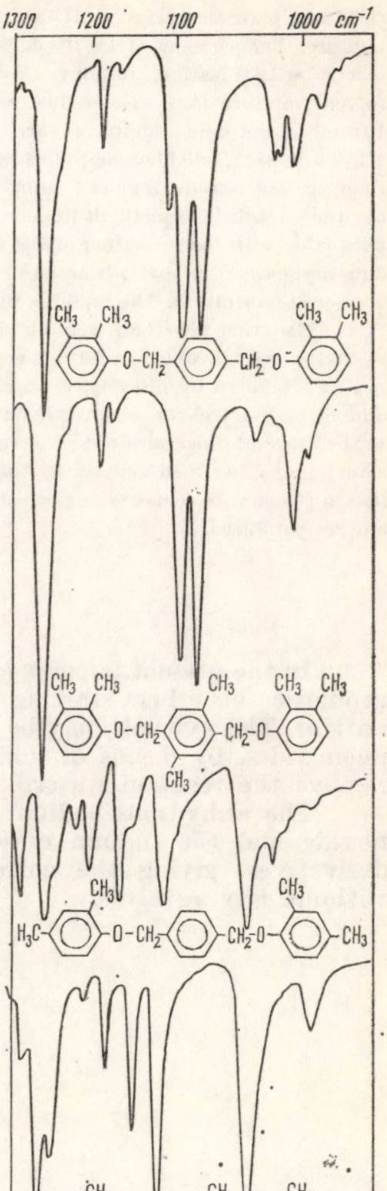

Fig. 1. — IR spectra of : 1,4-bis (2,3-dimethylphenoxymethyl)-benzene, 2,5-bis (2,3-dimethylphenoxymethyl)-*p*-xylene, 1,4-bis(3.4-dimethylphenoxymethyl) - benzene and 2,5-bis(2,5-dimethylphenoxymethyl)-*p*-xylene.

(1/50 mol plus an excess of 1/5000 mol) and 20 ml ethanol and a benzene (1 :1 in volume) mixture. The content of the flask is heated to boiling (65°) till the 2,3-dimethylphenol reacts with NaOH forming sodium 2,3-dimethylphenoxide, partially soluble in the solvent mixture (1h). The reflux refrigerator is then changed for a descending one and 10 ml azeotropic mixtures are distilled to remove the reaction water; 1.751 g(1/100 mol) 1,4-dichloromethylbenzene is then added, the descending refrigerator is again changed for a refluxing one and heated for 4 hours to 65 – 67°. The dissolution of the 1,4-dichloromethylbenzene and also its reaction with sodium-2,3-dimethylphenoxide with the formation of the sodium chloride precipitate takes place. The 1,4-bis (2,3-dimethylphenoxymethyl-*p*-benzene then precipitates, after the cooling of the reaction recipient at room temperature. The liquid is filtered to separate the bis-ether and the sodium chloride.

The other bis-ethers were obtained in a similar way. The 4,6-bis(2,6-dimethylphenoxymethyl)-*m*-xylene which could not crystallize from the reaction medium and therefore could not be separated by filtering, is an exception. For its separation, the reaction products were diluted with petroleum ether, ethylic ether and benzene in a volumetric ratio of 1 : 1 : 1 and washed several times with water to remove the sodium chloride. The organic layer in the separatory funnel has then underwent simple distillation to remove the solvents and vacuum distillation (12 mm) to remove the raw materials. The product thus purified could be solidified but not recrystallized.

CONCLUSIONS

In the present paper we have shown the possible obtaining of certain aromatic bis-ethers starting from xylenols and dichloromethylated derivatives. The xylenols may be converted into anhydrous sodium dimethylphenoxides, by means of sodium hydroxide and azeotropic distillation to remove the reaction water.

The anhydrous sodium dimetethylphenoxides as well as the phenoxide and the sodium cresoxides react with the dichloro-methylated derivatives, giving the corresponding bis-ethers and sodium chloride without any catalyst.

Revue Roumaine de Chimie, 17, 7, 1267–1279 (1972)

PRINZIPIELLE BETRACHTUNGEN ÜBER DIE WIRKSAMKEIT EINIGER REINIGUNGSMETHODEN DURCH ADSORPTION. II

MATHEMATISCHE MODELLE

ANDREI WOHL

von der Abteilung Rein- und Edelmetalle des Projektions- und Forschungsinstituts für Bunt- und Edelmetalle

Eingegangen am 12. Juni 1971

Für die „einfache" Methode, für die der „Adsorptionsmittelaufteilung", der „Lösungaufteilung" und für die dynamische Methode auf einer Säule, welche zur Reinigung einer Lösung (eines Gases) mit Hilfe eines festen Adsorptionsmittels dienen, werden mathematische Modelle abgeleitet, zwecks deren Veranschaulichung einige numerische Beispiele gegeben und besprochen sind.

Aus den Darlegungen, die im ersten Teil dieser Arbeit [1] veröffentlicht wurden, ergibt sich, daß der sicherste Weg für die Erreichung eines erhöhten Wirkungsgrades der Reinigung, im Vergleich zu der „einfachen" Methode, die Verwendung der Methode der „Adsorptionsmittelaufteilung" in dem Bereich, in welchem die scheinbare spezifische Adsorption positiv und zunehmend in Abhängigkeit von der Gleichgewichtskonzentration der Verunreinigung der Lösung ist. Dieser Bereich befindet sich in allen Systemen in dem Gebiet der kleinen Konzentrationen. Oftmals, insbesondere bei sehr kleinen Konzentrationen, ist die Variation der scheinbaren spezifischen Adsorption linear and kann durch die Beziehung

$$a = k.c \tag{22}$$

ausgedrückt werden, was die mathematische Behandlung des Problems äußerst erleichtert. Zum Beispiel folgt aus Formel (2)[1*] sofort, daß die Endkonzentration, c_s, der Verunreinigung im Fall der „einfachen" Methode:

$$c_s = \frac{c_0}{1 + kr} \tag{2'}$$

sein wird.

---

[1] S. Tilenschi und A. Wohl, *Rev. Roumaine Chim.*, 15, 1017 (1970).

* $c_s = c_0 - r \cdot a_s$

Wenn man annimmt, daß die Fraktionen des Adsorptionsmittels alle gleich dem n-ten Teil der gesamten Menge des Adsorptionsmittels sind* (in g Adsorptionsmittel /100 g Lösung), erhält man folgenden Ausdruck der prozentualen Konzentration der Endlösung:

$$c_n = \frac{c_0}{\left(1 + k\frac{r}{n}\right)^n} \tag{23}$$

Die Funktion $c_0/c_n = (1 + kr/n)^n$ hat ein Maximum für den Wert von n, der ihre Derivierte in bezug auf n annulliert. Diese Derivierte ist:

$$\frac{d}{d_n}\left(\frac{c_0}{c_n}\right) = (1 + kr/n)^n\left[\ln(1 + kr/n) - kr/(kr+n)\right] \tag{24}$$

Es bedeutet, daß, falls man die Menge des Adsorptionsmittels (pro 100 g Lösung) in n gleiche Teile derart fraktioniert, daß der Wert von n die Gleichung

$$\ln(1 + kr/n) = kr/(kr + n) \tag{24'}$$

befriedigt, man einen maximalen Wirkungsgrad für dieselbe Anfangskonzentration, c_0, dasselbe Adsorptionsmittel und — natürlich — dieselbe Lösung und Temperatur erhält.

Ist n sehr groß, aber endlich, so wird der Nenner des Bruchs von der rechten Seite der Gleichung (23) gleich $(1 + kr)$, d.h. man erhält eine Lösung mit derselben Konzentration wie durch die Anwendung der „einfachen" Methode.

Wenn n nach Unendlich strebt, so ist $c_0/c_n = 1$, also man erreicht keine Reinigung mehr.

Man hat gezeigt,[1] daß wenn das Lösungsmittel von dem Adsorptionsmittel nicht zurückgehalten wird, und in sehr verdünnten Lösungen, die scheinbare spezifische Adsorption mit der realen zu verwechseln ist. Wenn sich dieses mit der Konzentration im Sinne der Gleichung (22) linear ändert, so kann man ein relativ einfaches mathematisches Modell des Verlaufes der adsorptiven Reinigung durch die Methode der „Lösungaufteilung" aufstellen und zwar:

Wird die Lösung in m gleiche Fraktionen aufgeteilt, die sukzessiv mit der gesamten Menge des Adsorptionsmittels (r Gramm Adsorptionsmittel auf 100 Gramm Lösung) in Kontakt kommen, so daß jedesmal das Adsorptionsgleichgewicht erreicht wird, so erhält man folgende Verunreinigungsbilanzen:

$\frac{c_0}{m} - \frac{c_1}{m} = k.r.c_1$ — da die Menge der von je 1g Adsorptionsmittel zurückgehaltene Verunreinigung von 0 auf $k.c_1$ zugenommen hat;

---

* Man kann beweisen, daß in diesem Fall der Wirkungsgrad der Adsorptionsmittel-Fraktionierung der höchste ist.

$\frac{c_0}{m} - \frac{c_2}{m} = k.r(c_2 - c_1)$ – da die Menge der von je 1 g Adsorptionsmittel zurückgehaltene Verunreinigung von $k.c_1$ auf $k.c_2$ zugenommen hat ;

$\frac{c_0}{m} - \frac{c_3}{m} = k.r(c_3 - c_2)$ – da die Menge der von je 1 g Adsorptionsmittel zurückgehaltene Verunreinigung von $k.c_2$ auf $k.c_3$ zugenommen hat ;

und so weiter...

Man berechnet daraus, daß, nach dem Kontakt mit dem Adsorptionsmittel, die Konzentrationen der sukzessiven Lösungsfraktionen folgende sein werden :

$$c_1 = c_0 \frac{1}{1 + mkr} ;$$

$$c_2 = c_0 \frac{(1 + 2mkr)}{(1 + mkr)^2}$$

$$c_3 = c_0 \frac{1 + 3mkr + 3(mkr)^2}{(1 + mkr)^2} \cdots\cdots$$

$$\vdots$$

$$c_j = c_0 \frac{1 + C_j^1 (mkr) + C_j^2 (mkr)^2 + \ldots + C_j^{j-1} (mkr)^{j-1}}{(1 + mkr)^j} \qquad (25)$$

wo C_j^v die Zahl der Kombinationen von j Elementen zu je v bedeutet ($v = 1, 2, \ldots j - 1$).

Die Konzentration $\bar{c}_m$ der Lösung, die sich durch Zusammenschütten der einzelnen Fraktionen ergibt, wird das arithmetische Mittel deren Konzentrationen sein :

$$\bar{c}_m = \frac{1}{m} (c_1 + c_2 + \ldots + c_m) \qquad (26)$$

DIE DYNAMISCHE ADSORPTION AUF EINER SÄULE

Im Falle der Adsorption auf einer Säule, wenn sukzessive Anteile der Lösung mit sukzessiven Schichten des Adsorptionsmittels von der Säule in Kontakt kommen, findet eigentlich eine „Aufteilung des Adsorptionsmittels", gleichzeitig mit einer „Aufteilung der Lösung" statt. Aus den Schlüssen des ersten Teils dieser Arbeit folgt, daß von einem auf das Verbinden der zwei obigen Methoden beruhenden Reinigungsprozeß nicht behauptet werden kann, daß er in allen Fällen wirksamer wäre, als die statische („einfache") Methode. Bleiben wir aber in dem Gebiet der sehr kleinen Gleichgewichtskonzentrationen und befinden wir uns auf dem aufsteigenden Zweig der *a-c* Kurve, so können wir sicher sein, daß die „Adsorptionsmittelaufteilung" den Wirkungsgrad der Reinigung durch Adsorption erhöhen wird. Man sah auch, daß um sicher zu sein, daß die „Lösungaufteilung" ein wirksamerer Reinigungsweg als die „einfache Methode" sein wird, außer der großen Verdünnung der Lösung (geringe Konzentration der Verunreinigung), auch die Bedingung des Nichtfesthaltens des Lösungsmittels von dem Adsorptionsmittel erfüllt werden muß. Bei sehr kleinen Konzentrationen und wenn die reale spezifische Adsorption nach einer Beziehung $A_i = K^+ . c_1$ linear mit der Konzentration wächst, so kann man nach Gleichung (13) annehmen, daß die von 1 g Adsorptionsmittel festgehaltene Menge B des Lösungsmittels konstant bleibt. In diesem Fall nimmt Gleichung (13) folgende Form an :

$$a_i = c_i \; (K' - B/100 - K'c_i/100) \qquad (13')$$

Bei geringen Konzentrationen kann man (wenigstens) das letzte Glied der Klammer vernachlässigen, so daß der Ausdruck der scheinbaren spezifischen Adsorption sich folgenderweise vereinfacht :

$$a_i = c_i \, (K' - B/100) = k' . c_i \qquad (13'')$$

Es folgt daraus, daß falls $c_i \rightarrow 0$ und $B =$ konst., die scheinbare,wie auch die reale spezifische Adsorption sich linear mit der Konzentration (c_i) ändern und sich für $c_i = 0$ annullieren.

Aber das Konstantbleiben von B deutet die Sättigung mit Lösungsmittel des Adsorptionsmittels in der Säule, nach seinem ersten Kontakt mit der Lösung, so daß die folgenden Fraktionen des Lösungsmittels die (mit Lösungsmittel gesättigten) Schichten des Adsorptionsmittels ohne bedeutsame Verluste durchgehen, was die Gleichheit der sukzessiven Lösungsfraktionen bedeutet.

Man nimmt noch folgendes an :

— die Adsorptionsmittelmengen in der Säule, welche mit der Lösung in Adsorptionsgleichgewicht gelangen, sind gleich ;

— das Verhältnis Adsorptionsmittel : Lösung ist in der ganzen Säule dasselbe (was auch die Gleichheit der mit den Adsorptionsmittelfraktionen im Gleichgewicht stehenden Lösungsfraktionen miteinbezieht)

— der Adsorptionsprozeß verläuft isotherm, isobar und isochor.

So kann man die eingeführten, vereinfachenden Bedingungen folgenderweise zusammenfassen :

a) In der zu entfernenden Verunreinigung sehr verdünnte Lösungen.

b) Konstante Proportionalität zwischen der spezifischen (scheinbaren und realen) Adsorption und der Gleichgewichtskonzentration.

c) Die Abwesenheit eines bedeutsamen Festhaltens der Lösung von dem Adsorptionsmittel, d.h. die Gleichheit der Mengen der Lösungsfraktionen vor und nach ihrem Kontakt mit dem Adsorptionsmittel. (Findet anfangs ein Festhalten des Lösungsmittelss tatt, welches aber von der Konzentration unabhängig ist, so ist die erwähnte Bedingung nach der Sättigung des Adsorptionsmittels mit dem Lösungsmittel erfüllt, also nach dem Erscheinen der Lösung unter den Adsorptionsmittelschichten).

d) Eine gleichmäßige Verteilung auf der Säule des Adsorptionsmittels, wie auch der Lösung.

e) Die Abwesenheit einer Diffusion zwischen den auf die Säule sukzessive aufgebrachten Lösungsmittelfraktionen.

Unter diesen Bedingungen ist das untere mathematische Modell gültig, das den Verlauf der Beseitigung einer Verunreinigung aus einer Lösung wiedergibt, die durch eine Adsorptionssäule geht.

Im folgenden sei als (theoretischer) Teller eine Portion der Säule benannt, in welcher das Adsorptionsgleichgewicht zwischen dem Adsorptionsmittel und der in der Lösung verbliebenen Verunreinigung erreicht ist *.

Für den ersten Teller (beim Eintritt der Lösung in die Säule) kann man folgende Verunreinigungsbilanz aufschreiben :

$$l.p_0 = l.p_1^{\mathrm{I}} + s.a_1^{\mathrm{I}} \tag{27}$$

wo: l = die Menge der Lösung in einem Teller, [g];
s = die Menge des Adsorptionsmittels in einem Teller, [g];
p = die Konzentration der Verunreinigung in der Lösung, [g/g]; der untere Index betrifft die Ordnung des Tellers von oben herab (vom Eintritt der Lösung in die Kolonne), und der obere Index die Zahl der Auffüllungen des Tellers mit Lösung; p_0 bedeutet also die Anfangskonzentration der Lösung und p_1^{I} die Konzentration der Lösung, die den ersten Teller der Säule verläßt;
a = die scheinbare spezifische Adsorption; die unteren und die oberen Indexe haben die obigen Bedeutungen, so daß a_1^{I} die spezifische Adsorption beim Gleichgewicht des Adsorptionsmittels vom ersten Teller, nach dessen ersten Auffüllung mit Lösung bezeichnet.

Im Sinne der festgestellten Grundbedingungen ergibt sich $a_1^{\mathrm{I}} = q.p_1^{\mathrm{I}}$, wenn man den Wert der Proportionalitätskonstante k aus Gleichung (22) jetzt mit q bezeichnet, da in vorliegendem Fall die Konzentrationen in g/g (und nicht in % wie vorher) ausgedrückt werden; also $q = 100\ k$.

Dann schreibt man die Gleichung (27) :

$$l.p_0 = l.p_1^{\mathrm{I}} + s.q.p_1^{\mathrm{I}} \tag{27'}$$

woraus folgt :

$$p_1^{\mathrm{I}} = l.p_0 /(l + s.q) \tag{27''}$$

---

* Es wäre eigentlich richtiger von der äquivalenten Länge eines theoretischen Tellers (HETP—in der angelsächsischen Literatur) zu sprechen. Wir haben aber die Bezeichnung „Teller" bewahrt, einerseits wegen der Geläufigkeit des Ausdrucks, und anderseits weil die folgenden Überlegungen sich nicht unbedingt auf Portionen der Länge (=der Höhe) der Säule beziehen.

Für den zweiten Teller gilt:

$$l.p_1^{\mathrm{I}} = l.p_2^{\mathrm{I}} + s\cdot q\cdot p_2^{\mathrm{I}} \tag{28}$$

und daraus:

$$p_2^{\mathrm{I}} = p_0 . l^2/(l + s\cdot q)^2 \tag{28'}$$

Man notiert das Verhältnis s/l mit G; dann wird die letzte Gleichung zu:

$$p_2^{\mathrm{I}} = p_0/(1 + G\cdot q)^{2*} \tag{28''}$$

und Gleichung (27″) nimmt folgende Form an:

$$p_1^{\mathrm{I}} = p_0^{\mathrm{I}}/(1 + G\cdot q) \tag{27'''}$$

Im Falle des dritten Tellers kann man schreiben:

$$l\cdot p_3^{\mathrm{I}} = l\cdot p_3^{\mathrm{I}} + s\cdot q\cdot p_3^{\mathrm{I}} \tag{29}$$

woraus mit den neuen Notationen und mit dem Wert von p_2^{I} aus (28″) folgt:

$$p_3^{\mathrm{I}} = p_0/(1 + G\cdot q)^3 \tag{29'}$$

usw.

Für den letzten, den N-ten Teller (der vom Austritt der Lösung aus der Kolonne) gilt:

$$p_N^{\mathrm{I}} = p_0/(1 + G\cdot q)^N \tag{30}$$

Nach der zweiten Auffüllung des ersten Tellers mit Lösung, gelten folgende Beziehungen:

$$l\cdot p_0 = l\cdot p_1^{\mathrm{II}} + s(a_1^{\mathrm{II}} - a_1^{\mathrm{I}}) \tag{31}$$

oder

$$l\cdot p_0 = l\cdot p_1^{\mathrm{II}} + s\cdot q\,(p_1^{\mathrm{II}} - p_1^{\mathrm{I}}) \tag{31'}$$

Führt man den Wert von p_1^{I} aus (27‴) und die Notierung $s/l = G$ ein, erhält man

$$p_1^{\mathrm{II}} = p_0(1 + 2\,Gq)\,/(1 + Gq)^2 \tag{31''}$$

Für den zweiten, zum zweiten Mal aufgefüllten Teller, schreibt man:

$$l\cdot p_1^{\mathrm{II}} = l\cdot p_2^{\mathrm{II}} + s\cdot q(p_2^{\mathrm{II}} - p_2^{\mathrm{I}}) \tag{32}$$

---

* Man bemerkt, daß $Gq = kr$.

Bedient man sich des Wertes von p_2^{I} aus (28″) und dessen von p_1^{II} aus (31″), ergibt sich:

$$p_2^{\mathrm{II}} = p_0(1 + 3\,Gq)/(1 + Gq)^3 \tag{32'}$$

Für den dritten Teller erhält man nach seiner zweiten Auffüllung:

$$l \cdot p_2^{\mathrm{II}} = l \cdot p_3^{\mathrm{II}} + s \cdot q(p_3^{\mathrm{II}} - p_3^{\mathrm{I}}) \tag{33}$$

Benützt man die bekannten Werte von p_2^{II} aus (32′) und von p_3^{I} aus (29′), ergibt sich:

$$p_3^{\mathrm{II}} = p_0(1 + 4Gq)/(1 + Gq)^4 \tag{33'}$$

Für den N-ten Teller (den letzten), erhält man:

$$p_N^{\mathrm{II}} = p_0\,(1 + N\,Gq)/(1 + Gq)^{N+1} \tag{34}$$

Bei der dritten Auffüllung des ersten Tellers hat man:

$$l \cdot p_0 = l \cdot p_1^{\mathrm{III}} + s \cdot q\,(p_1^{\mathrm{III}} - p_1^{\mathrm{II}}) \tag{35}$$

woraus mit Hilfe der Beziehung (31″) sich

$$p^{\mathrm{III}} = p_0\,[1 + 3Gq + 3\,(Gq)^2]/(1 + Gq)^3 \tag{35'}$$

ergibt.

Für den zweiten Teller erhält man nach der dritten Auffüllung:

$$l \cdot p_1^{\mathrm{III}} = l \cdot p_2^{\mathrm{III}} + s \cdot q\,(p_2^{\mathrm{III}} - p_2^{\mathrm{II}}) \tag{36}$$

Benützt man die Beziehungen (35′) und (32′), so folgt:

$$p_2^{\mathrm{III}} = p_0[1 + 4Gq + 6(Gq)^2]/(1 + Gq)^4 \tag{36'}$$

Wenn man diese Beweisführungen fortsetzt, gelangt man zur folgenden Beziehung:

$$p_N^M = p_0 \left\{ \frac{1 + C_{N+M-1}^1 \cdot G.q + C_{N+M-1}^2\,(Gq)^2 + \ldots}{(1 + Gq)^{N+M-1}} \right.$$

$$\left. \frac{\ldots + C_{N+M-1}^{M-1} \cdot (Gq)^{M-1}}{(1 + Gq)^{N+M-1}} \right\} \tag{37}$$

Drückt man die Konzentrationen in g/100 g Lösung aus, ändern sich in der obigen Gleichung nur die Notationen, so daß sie auch in der Form:

$$c_N^M = c_0 \left\{ \frac{1 + C_{N+M-1}^1 \cdot r \cdot k + C_{N+M-1}^2 (rk)^2 + \ldots}{(1 + rk)^{N+M-1}} \right.$$

$$\left. \frac{\ldots + C_{N+M-1}^{M-1} (r \cdot k)^{M-1}}{(1 + rk)^{N+M-1}} \right\} \tag{37'}$$

gültig bleibt.

Die Konzentration der Verunreinigung in der nach M Auffüllungen der Säule (=jeden einzelnen Tellers) gesammelten Lösung, entspricht dem arithmetischen Mittel der Konzentrationen nach I, II, III, ... M Auffüllungen der Säule, also:

$$p^{-}{}_N^M = \frac{1}{M} (p_N^{\mathrm{I}} + p_N^{\mathrm{II}} + p_N^{\mathrm{III}} + \ldots p_N^M), \ [\mathrm{g/g}] \tag{38}$$

oder

$$c^{-}{}_N^M = \frac{1}{M} (c_N^{\mathrm{I}} + c_N^{\mathrm{II}} + c_N^{\mathrm{III}} + \ldots c_N^M), \ [\mathrm{g/100\ g}] \tag{38'}$$

BEMERKUNGEN

1) Bei der Adsorption auf einer Säule, muß man unterscheiden zwischen dem Verhältnis Adsorptionsmittel: Lösung in einem Teller und dem Verhältnis der gesamten Mengen des Adsorptionsmittels und der gereinigten (durch die Säule durchgeflossenen) Lösung. Das letzte Verhältnis haben wir mit R notiert, wenn es in g Adsorptionsmittel/g Lösung, bzw. mit R', wenn es in g Adsorptionsmittel /100 g Lösung ausgedrückt ist. So erhält man die Beziehungen:

$$R = G \frac{N}{M} \tag{39}$$

bzw.

$$R' = r \frac{N}{M} \tag{39'}$$

(Offenbar ist $R = 100\ R'$).

M bezieht sich auf die letzte Auffüllung der Säule.

2) Zwischen den in g ausgedrückten Mengen:

– der der Säule zugeführten Lösung (P);

– des Adsorptionsmittels aus der Säule (Ad);

– der zur Auffüllung aller Teller notwendigen Lösung (So);

– der gereinigten, die Säule verlassenden Lösung (Sp) einerseits und

M, N, G andererseits, bestehen folgende Beziehungen:

$$\begin{gathered} P - So = Sp \\ Ad/So = G \qquad (40) \\ P.N/Sp = M \end{gathered}$$

NUMERISCHE BEISPIELE

In Tabelle 1, bzw. in Abbildung 1, hat man die Änderung des Verhältnisses $p_0/p_N^M (= c_0/c_N^M)$ (d. h. des Verhältnisses zwischen den Konzentrationen der Verunreinigung in der Anfangslösung und in dem ersten Tropfen der Lösung, die den N-ten Teller nach dessen M-ter Auffüllung verläßt), bzw. die Variation des Logarithmus dieses Verhältnisses, in Abhängigkeit von der Zahl der Auffüllungen (M) der Teller, für verschiedene Tellerzahlen (N) wiedergegeben.

Tabelle 1

M \ N	5	6	7	8	9	10
I	32	64	128	256	512	1024
II	9,14	16	28,44	51,2	93,09	170,7
III	4,41	6,92	11,13	18,29	30,57	51,85
IV	2,75	3,94	5,818	8,828	13,70	21,67
V	2,00	2,65	3,644	5,505	7,495	11,14
VI	1,605	2,00	2,667	3,442	4,718	6,628
VII	1,378	1,665	2,000	2,530	3,294	4,400
VIII	1,260	1,409	1,654	2,000	2,862	3,179

Es folgt, daß der durch das Verhältnis p_0/p_N^M $(= c_0/c_N^M)$ ausgedrückte Wirkungsgrad der Säule mit dem Zunehmen der Zahl der Auffüllungen der Teller äußerst schnell abnimmt.

In Tabelle 2 sind die durch das Verhältnis zwischen Anfangs- und End-(Mittel)Konzentration der Verunreinigung in der der adsorptiven Reinigung durch eine der vier Methoden ausgesetzten Lösung ausgedrückten Reinigungswirkungsgrade E gegeben. Es sei daran erinnert, daß diese mittleren Endkonzentrationen im Fall der Lösungsaufteilungsmethode nach der Gleichung (26) und im Fall der Reinigung auf einer Säule nach der Gleichung (36) ausgerechnet wurden.

Untersucht man die Werte aus Tabelle 2 und bezieht man sich auf dasselbe R (d.h. auf dasselbe Gesamtverhältnis Adsorptionsmittel : Lösung), so kann man folgende Feststellungen machen:

— Die Reinigung auf einer Säule ist die wirksamste der in Betracht gezogenen Methoden, wenn N (die Tellerzahl) und n (die Zahl der Fraktionen, in denen das Adsorptionsmittel aufgeteilt wurde) bzw. m (die Zahl der Fraktionen, in denen die Lösung aufgeteilt wurde) gleich sind.

– Die „einfache" (statische) Methode ist die wirkungsloseste Weise der Anwendung der Adsorption für Reinigung.

– Wenn kr ($=Gq$) $= 1$, ist die Wirksamkeit der Adsorptionsmittelaufteilungsmethode der der Lösungaufteilungsmethode identisch.

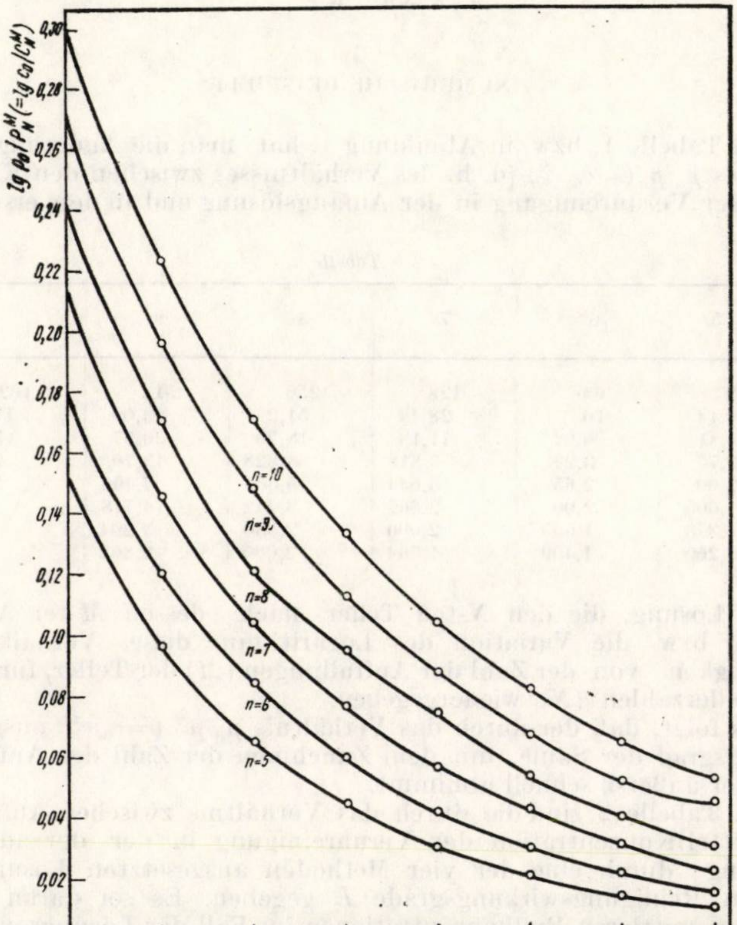

Abb. 1. – Die Änderung des Logarithmus des Verhältnisses p_0/p_N^M ($=c_0/c_N^M$), in Abhängigkeit von der Zahl der theoretischen Teller (N) und deren Auffüllungen (M). $Gq(=kr)$ in den Tellern$=1$

– Wenn $n = m$, ist die „Lösungaufteilung" wirksamer als die „Adsorptionsmittelaufteilung" für $kr < 1$ und umgekehrt für $kr > 1$.

Alle numerischen Beispiele wurden für denselben Wert k der Proportionalitätskonstante von dem Ausdruck (22) der spezifischen scheinbaren Adsorption aus berechnet.

Tabelle 2

Die Wirksamkeit *E* ausgedrückt in den Werten des Verhältnisses zwischen der Konzentration der Verunreinigung in der Anfangslösung und in der Lösung nach der Reinigung durch Adsorption, bei verschiedenen Methoden der Anwendung des Adsorptionsmittels

Reinigungsmethode	$kr=Gq$	R	n	m	N	M	E
Die „einfache"(statische) Methode[a]	5/8	5/8k	1	1	—	—	1,625
	6/8	6/8k	1	1	—	—	1,750
	1	1/k	1	1	—	—	2,000
	2	2/k	1	1	—	—	3,000
	3	3/k	1	1	—	—	4,000
Die Methode der „Adsorptionsmittelaufteilung"[b]	5/8	5/8k	5	1	—	—	1,801
	6/8	6/8k	6	1	—	—	2,027
	1	1/k	2	1	—	—	2,250
	1	1/k	3	1	—	—	2,370
	1	1/k	4	1	—	—	2,441
	1	1/k	5	1	—	—	2,480
	1	1/k	6	1	—	—	2,527
	1	1/k	7	1	—	—	2,547
	1	1/k	8	1	—	—	2,570
	2	2/k	2	1	—	—	4,000
	2	2/k	3	1	—	—	4,631
	3	3/k	2	1	—	—	6,250
	3	3/k	3	1	—	—	8,000
Die Methode der „Lösungaufteilung"[c]	5/8	5/8k	1	5	—	—	1,887
	6/8	6/8k	1	6	—	—	2,105
	1	1/k	1	2	—	—	2,250
	1	1/k	1	3	—	—	2,370
	1	1/k	1	4	—	—	2,441
	1	1/k	1	5	—	—	2,480
	1	1/k	1	6	—	—	2,527
	1	1/k	1	7	—	—	2,547
	1	1/k	1	8	—	—	2,570
	2	2/k	1	2	—	—	3,571
	2	2/k	1	3	—	—	3,853
	3	3/k	1	2	—	—	4,900
	3	3/k	1	3	—	—	5,348
Die dynamische Methode, auf einer Säule[d]	1	1/k	—	—	5	5	4,062
	1	1/k	—	—	6	6	4,433
	1	1/k	—	—	7	7	4,815
	1	1/k	—	—	8	8	5,131
	1	5/k	—	—	5	8	2,371
	1	6/8k	—	—	6	8	3,003
	2	2/k	—	—	2	2	5,400
	2	2/k	—	—	3	3	14,878
	3	3/k	—	—	3	3	27,000

[a] Berechnet nach Gl. (2′)
[b] Berechnet nach Gl. (23)
[c] Berechnet nach Gl. (25) – (26)
[d] Berechnet nach Gl. (37) – 39)

SCHLUSSFOLGERUNGEN

Wenn die spezifische Adsorption ideal ist, also mit der Konzentration linear wächst, kann man verhältnismäßig einfache Formeln für die Berechnung der Gleichgewichtskonzentration der Verunreinigung in einer Lösung ableiten, die der Reinigung durch die in dem ersten Teil dieses Beitrags [1] dargestellten Methoden (,,einfache”, der ,,Adsorptionsmittelaufteilung” und der ,,Lösungaufteilung”) ausgesetzt wurde.

Man erweist, daß die dynamische Adsorption auf einer homogenen Säule, in welcher kein Vermischen der allmählich zugeführten Lösungsfraktionen stattfindet, als eine Kombination zwischen der durch Adsorptionsmittelaufteilung und der durch Lösungsaufteilung hervorgerufenen Adsorption betrachtet werden kann, man leitet ein mathematisches Modell der Reinigung durch ideale Adsorption auf eine derartige Säule, in gewissen vereinfachenden Bedingungen ab.

Man vergleicht die Wirksamkeitsgrade der in Betracht gezogenen Adsorptionsmethoden anhand einiger rechnerischer Beispiele und man gelangt zur Folgerung, daß in den gewählten Fällen, die Reinigung auf Säule die wirksamste ist.

Es ist empfehlenswert, die experimentelle Bestätigung dieser Modelle auf solchen Adsorptionsmitteln vorzunehmen, die mit dem für die betreffende Lösung angewendeten Lösungsmittel gesättigt sind und daß die Lösungen die Verunreinigung in einer möglichst geringen, aber noch genau bestimmbaren Konzentration enthalten.

BEZEICHNUNGEN

a = spezifische scheinbare Adsorption, (g Verunreinigung die von 1 g Adsorptionsmittel zurückgehalten sind);

c bzw. p = Konzentration der Verunreinigung in der Lösung, [%] bzw. [g/g];

$k(k')$ bzw. q = Proportionalitätskonstante zwischen c bzw. p und a;

G bzw. r = g Adsorptionsmittel/g Lösung, bzw. g Adsorptionsmittel/100 g Lösung; im Falle der Adsorption auf einer Säule, r und G beziehen sich nur auf das Verhältnis Adsorptionsmittel : Lösung in den Tellern;
$kr = Gq$

l bzw. s = Menge der Lösung bzw. des Adsorptionsmittels in den Säulentellern, [g];
$s/l = G$;

R bzw. R' = Verhältnis zwischen den gebrauchten Gesamtmengen des Adsorptionsmittels und der Lösung, [g/g] bzw. [g/100 g];

A = spezifische reale Adsorption, [g/g];

K' = Proportionalitätskonstante zwischen c und A;

B = g Lösung die von 1 g Adsorptionsmittel zurückgehalten sind;

n bzw. m = Zahl der Fraktionen, in denen die gesamte Menge des Adsorptionsmittels, bzw. der Lösung, aufgeteilt wurde;

N = Zahl der (theoretischen) Teller der Säule;

M = Zahl der Auffüllungen der Teller der Säule.

Indizes

0 = Anfangswert (vor der Reinigung);

n = Gleichgewichtswert nach Zusatz der n-ten Fraktion des Adsorptionsmittels;

$1, 2, 3 \ldots i\ (j)$ = Gleichgewichtswert in der $1,2,3,\ldots i(j)$-ten Fraktion der Lösung oder im 1.,2.,3.-ten Teller der Säule;

m = Gleichgewichtswert nach Zusatz der m-ten Fraktion der Lösung;

N = Gleichgewichtswert in dem N-ten Teller der Kolonne.

$\mathrm{I}, \mathrm{II}, \mathrm{III} \ldots M$ = Zahl der Auffüllungen eines Tellers oder der Kolonne;

C_u^v = Kombination von u Elementen je v (statt u und v kann irgend ein anderes Zeichen stehen);

$\bar{c}_m$ = Mittelkonzentration der Verunreinigung in den m, nach der Adsorption zusammengeschütteten Lösungsfraktionen;

$\bar{p}_N^M$ bzw. $\bar{c}_N^M$ = Konzentration der Verunreinigung in der Lösung die aus einer Säule mit N Tellern fließt, nach M Auffüllungen der Säule (d.h. jeden Tellers), [g/g], bzw. [%].

D. L. DOUGLASS, *The metallurgy of zirconium*, edited by the International Atomic Agency, Vienna 1971 (Atomic Energy Review, Supplement, 1971).

D. L. Douglass' monograph "The metallurgy of zirconium" is a comprehensive synthesis of the research results, performed all over the world in the last two decades, in the field of the physical metallurgy of zirconium. The vast volume of researches in this field directed toward the determination of the technological as well as of the physical, chemical and mechanical properties of zirconium, was focussed on the chief use of this material, namely the construction of nuclear reactor.

D. L.Douglass is himself a researcher in the field of the physical metallurgy of zirconium, as one can see from the large number of papers cited in the monograph's references, and which deal with the heat treatment and the structural transformations in zirconium alloys, with the mechanical strength and creep behaviour of zirconium and its alloys, with the corrosion and oxidation of zirconium and with the associated diffusion phenomena. His competence enables the author to analyse clearly, concisely and critically the informational material contained in the 719 references of the monograph, covering the whole amount of original researches concerning this subject and published all over the world since 1953 up to 1970 (papers, reports and symposium proceedings).

"The metallurgy of zirconium" is an amplification and updating of a previous work of D.L. Douglass, namely "The physical metallurgy of zirconium" published in the Atomic Energy Review (*1*, 4, 1963, 71). This amplification was required by the vast number of researches performed in the meantime, researches aimed at the thorough understanding of the behaviour of zirconium and its alloys in their chief application : pressure tubes and fuel cladding in nuclear reactors. This major practical problem guides the author in selecting the material—(from this standpoint the title of the monograph is somewhat misleading, because it contains exclusively the physical metallurgy of zirconium and does not deal with the extractive metallurgy of this metal)—, in organizing the material and in deciding on the length of each chapter.

"The metallurgy of zirconium" extends on 466 pages and comprises 12 chapters : 1. Crystallography, 2.Deformation and textures, 3. Physical properties, 4. Recovery, recrystallization and grain growth, 5. Theory of alloying, 6. Phase equilibria, 7. Phase transformations and precipitation in alloys, 8. Mechanical properties, 9. Diffusion, 10. Irradiation effects, 11. Corrosion, 12. Oxidation.

Each chapter is treated as a comprehensive synthesis of all available data on the respective subject, the data being exposed concisely in the text discussion as well as in 360 figures (diagrams and micrographs) selected by the author from the original papers, in 140 mathematical relations and in 33 tables. The discussion of the data is quite sober, in most cases the interpretations of the original authors being used ; in controversial cases the author makes a critical analysis and draws his own conclusions.

In the first chapter, "Crystallography", the author deals with the allotropic transformation of zirconium, gives quantitative data on the influence of temperature and of alloying elements on the lattice parameters, presents the phases resulting from different kinds of solid state transformations in zirconium alloys (omega transition, martensitic transformation, Widmanstätten precipitation). Since the number one problem in the use of zirconium is that of hydrogen pick-up (zirconium being a strong hydride former and hydrogen being generated as one of the products of corrosion of zirconium with water) and because of the interest in the moderating properties of zirconium hydrides for nuclear reactors, the author gives a special emphasis to the structure, transformations and orientation in the matrix of the zirconium hydrides.

In the second chapter, "Deformation and textures", the author analyses the slip and especially the twinning mechanism of zirconium. The deformation textures and the influence of the technological processing in producing the best textures are considered in detail.

In chapter 3, "Physical properties", the author presents the existing data on the following properties of zirconium and its alloys : elastic properties, inelastic properties (internal friction and elastic after-effect), thermal properties (specific heat, heat content, heat of transformation, dilatational properties), electrical properties (resistivity, superconductivity), magnetic properties (Hall effect magnetoresistivity), vapour pressure and surface tension.

In chapter 4, "Recovery, recrystallization and grain growth" the author presents the basical problems of the annealing heat treatments of zirconium and its alloys.

In chapter 5, "Theory of alloying", the author presents information about the factors governing the phase formation in zirconium alloys. The problems considered are : the allotropic transformation of zirconium, the electronic structure of zirconium, the structure of Brillouin zones in different types of phases in zirconium alloys (alpha zirconium, omega transition phase, Laves type phase).

Chapter 6, "Phase equilibra" is very important for the understanding of the structures and transformations in zirconium alloys. It contains all the phase diagrams of the ternary and quarternary zirconium alloys determined up-to-day, as no compendium of such diagrams exists. As far as the binary diagrams are concerned, the author has decided to present only those zirconium phase diagrams not included yet in the general compendiums (Hansen 1961, Elliot 1965). The reader is thus provided with a complete compilation of the phase diagrams of zirconium systems. A special emphasis is laid on the Zr — H phase diagram, owing to the importance of the problem of zirconium hydrides in the practical uses of zirconium.

The understanding of the structure of zirconium alloys is completed in chapter 7, "Phase transformations and precipitation in alloys". The author gives here the TTT curves for the isothermal transformations in numerous binary zirconium alloys ; he presents the kinetics of the precipitation and dissolution of zirconium hydrides and discusses the quantitative features of the athermal transformations in zirconium alloys (omega and martensitic transformations).

Chapter 8, "Mechanical properties" deals with the quantitative effects in zirconium alloys of the chief hardening mechanisms (solid solution hardening, dispersion strengthening, martensitic hardening). The yield point of zirconium is discussed in connection with the controlling factors. Of real practical interest is subchapter 8.5 which analyses the influence of the orientation of the precipitated hydrides on the mechanical properties of zirconium and its alloys, the influence of the textures induced by mechanical processing on hydrides orientation in the matrix ; the importance of the choice of the mechanical processing schedules in producing the most convenient textures is discussed. In subchapter 8.6 the author analyses the fatigue behaviour and the fatigue mechanism in zirconium-base materials. Subchapter 8.7 deals with zirconium and zirconium alloys fracture ; oxygen and especially hydrogen embrittlement is discussed. The last subchapter, 8.8 analyses the creep behaviour of zirconium and its alloys, and discusses the methods of improving creep resistance by choice of composition and metallographic structure of zirconium-base materials.

Chapter 9, "Diffusion", is a very useful compilation of data on the self-diffusion and on the diffusion of the alloying elements in the two allotropic modifications of zirconium (α and β). The diffusional growth of intermediate phases in zirconium alloys is considered in detail.

Chapter 10 deals with a problem specific to the use of zirconium and its alloys in the nuclear reactor equipment, namely the irradiation efects. The author analyses the irradiation effects on the volume swelling of the metal and also the irradiation effects on the mechanical properties of zirconium and its alloys (tensile properties, impact, creep and fracture).

The last two chapters deal with the chemical interaction of zirconium-base materials with the environment.

Chapter 11, "Corrosion" analyses the corrosion of zirconium and its alloys in steam and water, emphasizing the role played by the environmental impurities, which can act as corrosion inhibitors or, on the contrary, as corrosion accelerators. The specific problem of zirconium— the hydrogen pick-up when corroding in aqueous media — is considered in detail and emphasis is laid on the deleterious effects of the hydrides precipitates on the mechanical properties. The author also presents the available data on the corrosion of zirconium and its alloys in other media, specific to the uses of theses materials in nuclear energetics and in chemical industry equipment (corrosion in liquid sodium, corrosion in acids, oxidation in fused salts). The properties of the corrosion films formed on zirconium are presented. Finally the effect of irradiation on corrosion is discussed.

The last chapter, chapter 12"Oxidation", analyses : the oxidation kinetics of zirconium in different media ; the mechanism of the oxigen diffusional penetration through the oxide film in the metallic matrix : the structural peculiarities of the oxide films ; the epitaxial relationship of oxide to metal ; the electrochemical aspects of zirconium oxidation. At last, the author gives the available data about the nitrogen penetration from the environment in the metallic zirconium by dissolution and nitrides formation.

In conclusion, "The metallurgy of zirconium" treats the physical metallurgy of zirconium and of its alloys, and gives a comprehensive review of the mechanical and physico-chemical properties, essential for the practical uses of these materials. The monograph is a quite valuable work, which distinguishes itself by the multitude of the quantitative data, by the scientific sober way of presenting and interpreting them, and by the vast number of references.

Maria Petrescu

P. BALTĂ and E. BALTĂ. *Introduction to the Physical Chemistry of the Vitreous State* (in Romanian). Introducere în chimia fizică a stării vitroase. Editura Academiei Republicii Socialiste România. Bucharest 1971 ; 237 p. ; 164 figures ; 12 tables ; 253 lit. ind. ; price 15.5 lei.

From the numerous problems of the vitreous state, highlighted by specialists, the authors of the present work have selected only a few, which, deriving a substantial advantage from the latest research, have led to the clarification of some ideas and to the opening of interesting prospects for theory and practice.

The first chapter deals with the non-crystalline solid. After presenting some of the methods which enable the obtaining of solids with non-crystalline structure, the content of the notions "amorphous" and "vitreous", frequently used by specialists, is discussed.

Chapter 2 is concerned with the nature of chemical bonds in glasses. A succint report on several research workers who attempted to correlate the various aspects of the chemical bonds tending to form glasses by melts undercooling, is followed by the present-day of tackling the nature of chemical bonds in glass-forming substances; the resulting structural peculiarities as well as their influence on some properties are emphasized. The authors also point out the role of the chemical bonds in obtaining the vitreous state: that of σ bonds, of bridges made up of two such bonds and of donor-acceptor bonds. The conclusion, strongly resulting from this chapter, is that the nature of glass-forming substances determines their polymer structure. The polymer structure accounts for the existence of the formation trend of the vitreous state by melts undercooling.

Based on this highly significant statement, chapter 3 tackles processes leading to the formation of the vitreous state. Some of these are: structural disordering, structure of the melts inclusively the variation in polymer distribution with respect to various factors, structural chemical equilibriun established within melts, the influence of this equilibrium, i.e. of the history of melting on the properties, the changes occurring on melts cooling up to the temperature Tg. a.s.o. The new pathways are stressed which were opened to research and technology by tackling the problems of the vitreous state starting from the polymer structure and making use of the chemistry of organic polymers for glass.

Chapter 4 deals with the most interesting phenomenon of the separation of vitreous microphases into glasses. After a short presentation of the thermodynamical theory of the phenomenon, the opinions of various researches on the causes which bring about separation are reviewed and the role of the chemical bonds and of the polymer structure is once again emphasized. The mechanism and the kinetics of the process are also presented on the basis of latest research. By means of existing concrete data, it is also pointed to the practical significance of the separation microphases into glasses.

Chapter 5 is devoted to optical processes occurring within the vitreous solid. After-an overall presentation of the interaction of the radiations with the vitreous state, the authors discuss the mechanism of light absorption in glasses based on the theory field and of the charge transfer. The redox equilibria in glasses are discussed in connection with light absorption. The mechanism of processes which take place in photosensitive glasses, as well as the stimulated light emission in glasses are presented. It thus results the uncommonly interesting view on the applicability of the knowledge proper to the chemistry of complex compounds, to the understanding and interpretation of some optical phenomena in glasses.

Chapter 6 points to the results obtained by studying structural glass changes by means of the thermal differential analyses and the measurements, depending on temperature, of some electrical properties. The efficiency of such relatively simple methods in the study of vitreous state becomes obvious.

By the present work the authors attempt to achieve a unitary treatment of the problems of the vitreous state on the basis of present-day knowledge stored in chemistry and physics. The tackling of these issues in the light of chemical bonds leads to the most general scientifical foundation needed for the understanding and interpretation of the problems of vitreous state.

Besides their genuine conception each chapter of this work puts forward numerous results and original ideas of the authors, most of them not yet published elsewhere.

By its content and high standard, the work will be very useful for chemists, chemical engineers and physicists interested in some general or particular aspects of the vitreous state. It is mainly devoted to the glass specialists, active in research and industry as well as to the students specializing in this field.

D. I. Marchidan

ORSZÁGOS MŰSZAKI KÖNYVTÁR ÉS DOKUMENTÁCIÓS KÖZPONT

NOTE POUR LES AUTEURS

La *Revue Roumaine de Chimie* publie des articles en anglais, français, russe, allemand ou espagnol. Les auteurs sont priés d'envoyer des articles, notes, communications et comptes rendus inédits.

Les manuscrits seront dactylographiés à deux intervalles. Les tableaux seront dactylographiés sur feuilles séparées, de même que la légende des figures. Les diagrammes seront tracés à l'encre de Chine sur papier calque. Les tableaux et les figures seront numérotés par des chiffres arabes, en nombre strictement nécessaire. Prière de ne pas inscrire les mêmes données dans les tableaux et les figures. Les formules chimiques seront incluses dans le texte : en outre, elles seront transcrites sur des feuilles séparées. Les auteurs sont priés d'indiquer les caractères italiques (en soulignant les lettres au crayon), ainsi que tout autre caractère spécial. L'ordre des références bibliographiques sera celui de leur mention dans le texte ; le nom de l'auteur sera précédé de l'initiale du prénom ; les publications périodiques seront présentées suivant les prescriptions internationales. Les références seront ajoutées à la fin de l'article ; elles paraîtront comme des notes, au bas de la page. Le texte sera précédé d'un résumé comprenant 15 lignes au maximum.

L'entière responsabilité du contenu des articles appartient aux auteurs. On publie des articles dus aux collaborateurs roumains ou étrangers. Les auteurs recevront 50 tirés à part.

PRINTED IN ROMANIA

TRAVAUX PARUS AUX ÉDITIONS DE L'ACADÉMIE DE LA RÉPUBLIQUE SOCIALISTE DE ROUMANIE

I. ZUGRĂVESCU et L. STOICESCU-CRIVETZ, **Polimeri heterociclici** (Polymères hétérocycliques), 1971, 190 p., 9,50 lei.

CORNEL BODEA et collab., **Tratat de biochimie vegetală**, partea I, **Fitochimie** (Traité de biochimie végétale, Ire partie, Phytochimie), Ier vol., 1964, 747 p.+ 4 annexes + 2 pl., 41 lei; IIe vol., 1965, 1262 p., 1 pl., 56 lei, IIIe vol., 1967, 773 p., 35 lei.

V. GHEȚIE et V. MICUȘAN, **Analiza imunochimică. Teorie și practică** (Analyse immunochimique. Théorie et pratique), 1966, 369 p., 28 lei.

SILVIA IONESCU, **Reacții chimice induse de radiațiile ionizante** (Réactions chimiques produites par les radiations ionisantes), 1963, 271 p., 15 lei.

MARIETA NICOLAE, **Fizico-chimia proceselor fotografice** (Physico-chimie des processus photographiques), 1964, 426 p. + 4 pl., 35 lei.

R. PORTOCALĂ et L. POPA **Acizii ribonucleici celulari și virali** (Les acides ribonucléiques cellulaires et viraux), 1966, 375 p., 8 pl., 26 lei.

D. PURDELA et R. VÎLCEANU, **Chimia compușilor organici ai fosforului și ai acizilor lui** (La chimie des composés organiques du phosphore et de ses acides), 1965, 540 p., 37 lei.

CRISTOFOR SIMIONESCU, MARGARETA GRIGORAȘ et AGATA CERNĂTESCU-ASANDEI, **Chimia lemnului din R.P.R.** (La chimie du bois en Roumanie), 1964, 239 p. + 3 pl., 27 lei.

CRISTOFOR SIMIONESCU et CLEOPATRA VASILIU-OPREA, **Mecanochimia compușilor macromoleculari** (La mécanochimie des composés macromoléculaires), 1967, 344 p., 23,50 lei.

I. MAXIM, **Materiale nucleare** (Matériaux nucléaires), 1969, 444 p., 30 lei.

1972 SEP 22

I.P.I. c. 1445

43 426

LEI 25.—

F 1103

REVUE ROUMAINE DE CHIMIE

TOME 17
Nº 8
Août 1972

RRCHAX, 17, 8, 1285–1484 (1972)

EDITIONS DE L'ACADÉMIE DE LA RÉPUBLIQUE SOCIALISTE DE ROUMANIE

Rev. Roumaine Chim. 17, 8, 1285 – 1484 (1972) Bucarest

COMITÉ DE RÉDACTION

Rédacteur en chef:

I. G. MURGULESCU, membre de l'Académie de la République Socialiste de Roumanie

Rédacteurs en chef adjoints:

A. T. BALABAN et V. EM. SAHINI, membres correspondants de l'Académie de la République Socialiste de Roumanie

Collège de rédaction:

C. DRĂGULESCU, RALUCA RIPAN, CR. SIMIONESCU, membres de l'Académie de la République Socialiste de Roumanie; EM. BRATU, ECATERINA CIORĂNESCU-NENITZESCU, P. SPACU, membres correspondants de l'Académie de la République Socialiste de Roumanie; MARGARETA AVRAM, D. I. MARGHIDAN, G. NIAC et D. SĂNDULESCU

La Revue Roumaine de Chimie paraît 12 fois par an. Toute commande de l'étranger (fascicules ou abonnements) sera adressée à Întreprinderea — Rompresfilatelia Boîte Postale 2001, telex 011631, Bucarest, Roumanie

Les manuscrits, les livres et les revues proposés en échange, ainsi que toute correspondance seront envoyés à la rédaction :

REVUE ROUMAINE DE CHIMIE

23, str. Dumbrava Roşie, Bucarest, Roumanie

ÉDITIONS DE L'ACADÉMIE DE LA RÉPUBLIQUE SOCIALISTE DE ROUMANIE
3 bis, str. Gutenberg, Bucarest, Roumanie

REVUE ROUMAINE DE CHIMIE

Tome 17, N° 8 Août 1972

MŰSZAKI KÖNYVTÁR
83333

Page

I. G. MURGULESCU and LUDMILA POPESCU, Thermodynamic properties from electromotive force measurements with formation cells in molten salts. AgBr + CsBr mixture 1287–1292

KEITH D. WARREN, Strong field spin-orbit matrices for d^3 configurations in tetragonal symmetry 1293–1312

M. CIOPEC and D. I. MARCHIDAN, The use of the digital computer in phenomenological thermodynamics. II 1313–1326

D. I. MARCHIDAN and LIANA PANDELE, Thermal properties of ALUROM aluminium heat content at high temperatures 1327–1330

G. COSTEANU et ORTANSA LANDAUER, L'influence du solvant sur la vitesse de réaction. L'hydrolyse acide du formiate, de l'acétate et du propionate de *n*-butyle dans le solvant mixte eau-alcool éthylique 1331–1337

G. COSTEANU et ORTANSA LANDAUER, L'influence du solvant sur la vitesse de réaction. L'hydrolyse acide du formiate, de l'acétate et du propionate de *n*-butyle dans le solvant mixte eau-acétone 1339–1345

G. COSTEANU et ORTANSA LANDAUER, L'influence du solvant sur la vitesse de réaction. L'hydrolyse acide du formiate, de l'acétate et du propionate de *n*-butyle dans le solvant mixte eau-dimétylsulfoxyde 1347–1352

G. COSTEANU et CORNELIA MATEESCU, L'influence du solvant sur la vitesse de réaction. L'hydrolyse alcaline de l'acétate, du propionate et du butyrate de *n*-butyle dans le solvant mixte eau-tétrahydrofuranne 1353–1360

IUDITA ADORIAN and S. STERNBERG. Thermodynamic excess functions in molten mixtures of potassium chloride with alkaline-earth chloride 1361–1366

IOAN RĂDOI, Die Anordnung der Grenzschicht an zylindrischen Elektroden bei erzwungener Konvektion 1367–1374

I. JANACHKOVA und M. STAEVSKI, Derivatographische Untersuchung eines Dreikomponenten-Oxydsystems $MnO_2-CO_2O_3-Ni_2O_3$ 1375–1378

VIOLETA ALEVRA, DAN CIOMÎRTAN and MARIA IONESCU, Influence of the preparation method on the structure and physical properties of alumina. II. Aluminium oxides . . . . 1379–1391 R

M. BANCIU, P. BUCK, ECATERINA CIORĂNESCU and C. D. NENITZESCU, Solvolysis of Δ^2-cyclobutenylethyl-β-tosylate and Δ^2-cyclobutenylpropyl-γ-tosylate 1393–1407

Rev. Roumaine Chim. 17, 8, 1285–1484 (1972), Bucarest

R IOSIF DRIMUŞ et ANGELA LUPU, Oxydation du *n*-dodécane en phase liquide par l'oxygène moléculaire en présence des catalyseurs métalliques pseudo-homogènes. I. L'effet des naphténates des métaux alcalins et alcalino-terreux 1409–1416

M. IOVU, N. MICLOVICI and STELIANA CREŢU, Aromatic bis-ethers. IV. Condensation of sodium cyclohexylphenoxides with dichloromethylated derivatives 1417–1421

I. PANEA, ILEANA GOIA and MARIA IONESCU. Acridone. XLI. The proton magnetic resonance spectrum of thioacridone 1423–1435

R STELIANA MAXIM, IG. POINESCU, STELA DRĂGAN and M. DIMA, Chloromethylation of ternary macroporous copolymers 1437–1445

STELIANA MAXIM, IG. POINESCU, STELA DRĂGAN and M. DIMA, Syntheses of anion exchangers based on macroporous ternary copolymers 1447–1456

I. FLOREA, Über das 2-Äthoxy-6,9-Diaminoakridin-Molybdatophosphat . . 1457–1463

C. LITEANU und AGNES BLAZSEK-BODÓ, Die Verwendung des Salzeffektes in nichtwäßrigen Lösungen bei acido-basischen Titrationen. II. Studium über das analytische Verhalten einiger Dicarbonsäuren und Hydroxysäuren in methanolischen Lösungen in Gegenwart von $Ca(NO_3)_2$ 1465–1474

GRIGORE TEODORESCU, Determination of codeine phosphate. Visible and IR spectra of the compound obtained by the combination with ammonium reineckate 1475–1481

Comptes rendus 1483–1484

Revue Roumaine de Chimie, **17**, *8*, 1287–1292 (1972)

THERMODYNAMIC PROPERTIES FROM ELECTROMOTIVE FORCE MEASUREMENTS WITH FORMATION CELLS IN MOLTEN SALTS. AgBr+ CsBr MIXTURE

I. G. MURGULESCU and LUDMILA POPESCU
Centre of Physical Chemistry
Str. Galaţi 31, Bucharest, Romania

Received March 30, 1972

The electromotive force of the formation cells: $Ag(s)|AgBr(l)|C, Br_2$ (g, 1 (at) and $Ag(s)|AgBr(l)+CsBr$ (l) |C, Br_2 (g, 1 at) was measured as a function of the temperature (500°–600°) and molar fraction ($x_{AgBr} = 0.3-0.9$). From e.m.f. measurements the thermodynamic partial molar and excess functions of AgBr in the AgBr + CsBr mixture were computed.

The study of the thermodynamic properties of the mixtures of silver halides and alkali halides was carried out by various methods, such as formation cells, concentration cells and melting diagrams.

So far, all mixtures of the type AgX + MeX (where Me = Li, Na, K, Rb, Cs and X = Cl, Br, I) except AgBr + CsBr mixture, were studied by the formation cell method.[1–14]

Therefore, it has been proved expedient to measure the e.m.f. of the following cells:

$$Ag(s)|AgBr(l)|C, Br_2(g, 1\ at) \text{ and } Ag(s)|AgBr(l)+CsBr(l)|C, Br_2(g, 1at).$$

---

[1] E. J. Salstrom and H. J. Hildebrand, *J. Amer. Chem. Soc.*, **52**, 4650 (1930); **54**, 4257 (1932).

[2] E. J. Salstrom, *J. Amer. Chem. Soc.*, **53**, 1794, 3385 (1931); **54**, 4252 (1932).

[3] E. J. Salstrom, T. J. Kew and T. M. Powell, *J. Amer. Chem. Soc.*, **58**, 1848 (1936).

[4] K. H. Stern, *J. Phys. Chem.*, **60**, 679 (1956).

[5] I. G. Murgulescu and S. Sternberg, *Rev. Chim. Acad. R.P.R.*, **2**, 251 (1957).

[6] K. H. Stern, *J. Phys. Chem.*, **62**, 385 (1958).

[7] I. G. Murgulescu and D. I. Marchidan, *Rev. Chim. Acad. R.P.R.*, **3**, 1 (1958).

[8] M. B. Panish, F. F. Blankenship, W. R. Grimes and R. F. Newton, *J. Phys. Chem.*, **62**, 1325 (1958).

[9] M. B. Panish, R. F. Wewton, W. R. Grimes and F. F. Blankenship, *J. Phys. Chem.*, **63**, 668 (1959).

[10] S. Sternberg and S. Gheorghiu, *Studii şi cercetări Chim. Acad. R.P.R.*, **7**, 107 (1959).

[11] S. Sternberg, I. Adorian and I. Galasiu, *Electrochim. Acta*, **11**, 385 (1966).

[12] J. Guion, M. Blander, D. Hengstenberg and K. Hagemark, *J. Phys. Chem.*, **72**, 2086 (1968).

[13] S. Sternberg and I. Adorian, *Electrochim. Acta.*, **13**, 1647 (1968).

[14] A. D. Pelton and S. N. Flengas, *J. Electrochem. Soc.*, **117**, 1130 (1970).

EXPERIMENTAL

The experimental cell, entirely made of quartz, is shown in Fig. 1. It consists of a tube *A* (Ø 30 mm, length 160 mm) which contains the studied molten salt and the two working electrodes : the graphite electrode and the silver electrode.

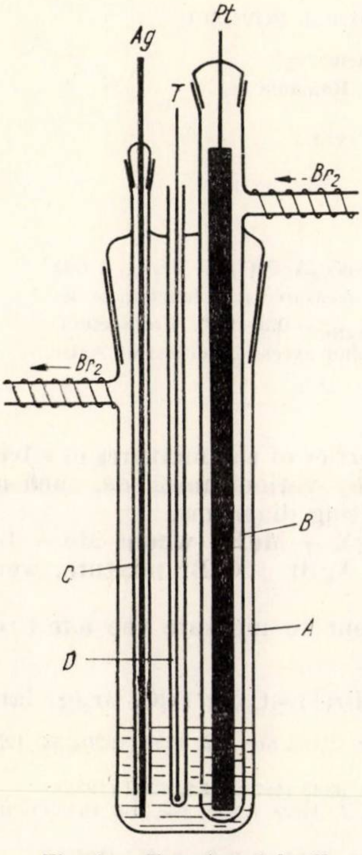

Fig. 1. — Experimental cell.

The graphite electrode, made of spectrally pure graphite, was entirely enclosed in a protection tube B (Ø 15 mm) provided with a hole in order to assure the gase flow through the melts in the tube *A*. The graphite electrode was connected to the measuring device by a platinum wire.

The silver electrode, made of 99,9% purity silver wire (Ø 2 mm), was protected by a thin silica tube *C*, dipping into the melts so as to form at its bottom a hydraulic closure. The silver electrode was directly connected to the measuring device.

The open end of the cell was closed by means of a ground joint. The experimental cell was placed in a vertical Kanthal resistance furnace. With the view to get a better thermostating, two metallic sheats, surrounding the cell, were placed inside the furnace. A constant temperature of the furnace, within ± 1° was maintained. The temperature has been measured by means of a calibrated Pt/Pt 13% Rh thermocouple *D*, immersed directly in the studied molten salt.

The main difficulty encountered with, when carrying out such experiment, is the achievement of a reversible bromine electrode.

It is necessary first, to maintain the bromine in a gaseous state and at a constant flow all over its way and secondly to saturate the graphite electrode with bromine.

The first condition was fulfilled by electrically heating all connection tubes for bromine (by means of an electrical resistance).

In order to saturate the graphite electrode with bromine, this was kept, in the beginning, in pure melted silver bromide at 600° bubbling for a couple of days bromine gas through the melts. It was thus possible to obtain the reversible bromine electrode without any preliminary treatment, by electrolysis provided that the graphite stick be introduced in a separate enclosure, *B* filled up with bromine gas, as it is shown in Fig. 1.

The reversible potential value was reached within a very short time, about 15 minutes, after the constant bromine flow was settled and the constant temperature reached.

The gaseous bromine was obtained by heating the liquid bromine to the boiling point. After its bubbling through the graphite electrode tube *B* and through the melts, the gaseous bromine was condensed in an outer glass reservoir, kept at 0°.

It is worth noting that some experiments were performed in a different type of cell, where the graphite electrode was placed directly into the molten salts without being protected by any enclosure and where its upper end emerged from the cell, contacting the atmosphere. In this case the obtained e.m.f. value, E_0 was by 10 mV lower than the reversible e.m.f. given by Salstrom,[1,2] even if a preliminary electrolysis was carried out and a bromine gas was bubbled through the melts for long time.

The cell e.m.f.'s were measured with an electronic digital voltmeter "Solartron", L.M. 1440.2 type, with a large inner resistance (2×10^{10} Ω) and an accuracy of 0.1 mV.

The reproducibility of the e.m.f. was maintained within 1 – 2 mV limits.

We note that the experimentally obtained value of E_0 had to be corrected for the voltage of the Ag – C(Pt) couple contribution. In order to measure it, the connection between graphite electrode and silver electrode was made by a silver wire instead of molten electrolyte. The value thus obtained was of 3 – 5 mV in the temperature range of 500 – 600° and was always subtracted from the E_0 value.

Chemicals

Silver bromide was prepared by precipitation with dilute *p.a.* HBr from a dilute solution of *p.a.* reagent silver nitrate. After drying and melting, it was scrubbed by electrolysis.

Cesium bromide was BDH *p.a.* degree reagent. It was purified by single recrystallization from distilled water, dried for 24 h at 150° and melted. In order to remove any trace of humidity, a dry HBr gas was bubbled through the melts. All salts were stored in a dessicator.

RESULTS

In Table 1, the experimental values of e.m.f. of the silver bromide, E_0, obtained in this work, are compared to Salstrom's[1,2] data and to Murgulescu and Marchidan's data .[7]

Table 1

Electromotive force, E_0 of the formation cell in the pure salt, AgBr

	Salstrom	Murgulescu, Marchidan	Our data
t°C	E_0(V)	E_0(V)	E_0(V)
500°	0.7865	0.7845	0.7870
600°	0.7577	0.7557	0.7570

It is evident that within the experimental errors there is a good agreement between the different authors.

Table 2 gives the e.m.f. values of the pure AgBr salt and of AgBr + + CsBr mixtures, at different temperatures and molar fractions together with the activity a_1, the activity coefficient γ_1 and the temperature coefficient of electromotive force, $d\mathrm{E}/dt$.

This table contains also the thermodynamic functions : the mixing free enthalpies ΔG_1^0, ΔG_1, the mixing entropies ΔS_1^0, ΔS_1, the mixing enthalpies ΔH_1^0, ΔH_1 and also the partial molar values $\overline{G}_1 - G_1^0$, $\overline{S}_1 - S_1^0$, $\overline{H}_1 - H_1^0$ and the partial molar excess functions : $\overline{G}_1^E$, $\overline{S}_1^E$, $\overline{H}_1^E$.

Table 2

Thermodynamic functions of AgBr in the AgBr + CsBr mixture*

xAgBr	1.0	0.9	0.8	0.7	0.6	0.5	0.4	0.3
E(V) — 500°C	0.787	0.797	0.809	0.824	0.844	0.870	0.892	0.936
$\mathrm{d}E/\mathrm{d}T \times 10^{-4}$(V/grad)	−3.00	−2.90	−2.90	−2.80	−2.70	−2.60	−2.40	−2.10
a_1	1	0.861	0.719	0.573	0.425	0.288	0.207	0.109
γ_1	1	0.956	0.898	0.818	0.709	0.576	0.517	0.365
ΔS_1 (cal/grad/mol)	−6.918	−6.687	−6.687	−6.457	−6.226	−5.995	−5.534	−4.843
$\overline{S}_1 - S_1^0$(cal/grad/mol)	0	+0.231	+0.231	+0.461	+0.692	+0.922	+1.384	+2.075
$\overline{S}_1^{i} - S_1^0$(cal/grad/mol)	0	+0.209	+0.443	+0.708	+1.015	+1.378	+1.821	+2.393
$\overline{S}_1^E$(cal/grad/mol)	0	+0.021	−0.213	−0.247	−0.323	−0.455	−0.437	−0.317
ΔG_1 (cal/mol)	− 18148	− 18379	− 18655	− 19001	− 19462	−20062	−20569	−21584
$\overline{G}_1 - G_1^0$(cal/mol)	0	−231	−507	−853	−1314	−1914	−2421	−3436
$\overline{G}_1^{i} - G_1^0$ (cal/mol)	0	−162	−343	−548	−785	−1065	−1407	−1849
$\overline{G}_1^E$ (cal/mol)	0	−68	−164	−308	−529	−848	−1012	−1550
ΔH_1 (cal/mol)	− 23496	− 23549	−25327	− 24847	− 24697	−24275	−23991	−23823
$\overline{H}_1^E$ (cal/mol)	0	−52	−328	−499	−779	−1200	−1350	−1795
E(V) — 600°C	0.757	0.768	0.780	0.796	0.817	0.844	0.868	0.915
a_1	1	0.864	0.737	0.594	0.451	0.315	0.229	0.123
γ_1	1	0.960	0.921	0.849	0.751	0.630	0.572	0.409
ΔG_1 (cal/mol)	− 17456	− 17710	− 17987	− 18356	−18840	−19462	−20016	−21099
$\overline{G}_1 - G_1$ (cal/mol)	0	−253	−530	−899	− 1383	−2006	−2560	−3643
$\overline{G}_1^{i} - G_1$ (cal/mol)	0	−183	−387	−618	−886	−1203	−1590	−2089
$\overline{G}_1^E$ (cal/mol)	0	−62	−143	−284	−494	−803	−967	−1552

* R = 8,3143 J/K mol = 1,98716 cal/grad/mol; F = 96 487 Coulomb/mol

The thermodynamic functions of AgBr in the AgBr + CsBr mixture were computed from the electromotive forces and corresponding temperature coefficients, using the common formulas :

$$\overline{G}_1^E = RT \ln \gamma_1$$

$$\overline{S}_1^E = 0.239\, F\left(\frac{dE_1}{dT} - \frac{dE_0}{dT}\right) + R \ln x_1$$

$$\overline{H}_1^E = \overline{G}_1^E + T\overline{S}_1^E$$

From the data listed in Table 2, it can be seen that the molten AgBr + CsBr mixture shows negative deviations from the ideal solutions behaviour. The activity a_1 is always smaller than the molar fraction x_{AgBr} and the activity coefficient γ_1, is subunitary.

As the molar fraction decreases, the negative deviation increases. Since $\overline{G}_1^E$ and $\overline{H}_1^E$ are negative, it results that the mixing of AgBr and CsBr takes place by heat releasing.

As one can see from Fig. 2, the AgBr + CsBr mixture behaves in its molten state as a regular system.

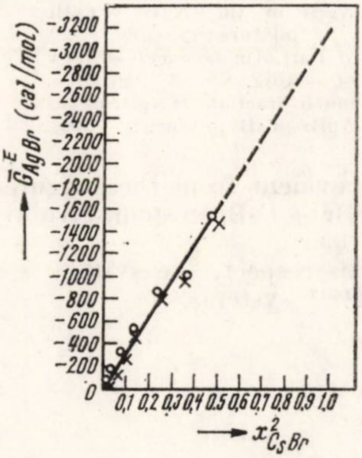

Fig. 2. – Partial molar excess free enthalpy of mixing, $\overline{G}^E$ of AgBr *vs.* molar fraction of CsBr in the AgBr + CsBr mixture ; ○ – 500° ; x – 600°.

Indeed, the partial molar entropy $(\overline{S}_1 - S_1^0)$, experimentally determined, is practically equal to the ideal entropy $(\overline{S}_1^i - S_1^0)$, and the partial molar excess entropy $\overline{S}_1^E$ reaches small values. At the same time, the variation of the activity coefficient γ_1 of AgBr as a function of the molar fraction of CsBr is expressed by the well know relation :

$$2.303\, RT \log \gamma_{\mathrm{AgBr}} = Bx^2_{\mathrm{CsBr}}$$

The numerical values of B, graphically obtained from Fig. 2, is equal to 3200 cal/mol.

Figures 3 and 4 represent the variation of the partial molar excess functions $\overline{G}_1^E$, $\overline{S}_1^E$, $\overline{H}_1^E$ as a function of molar fraction x_{AgBr} at 500°.

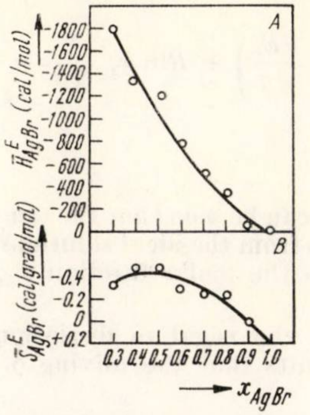

Fig. 3. — A, Partial molar excess enthalpy of mixing, $\overline{H}^E$ of AgBr *vs.* molar fraction of AgBr in the AgBr + CsBr mixture ; ○ — 500°.
B, Partial molar excess entropy of mixing, $\overline{S}^E$ of AgBr *vs.* molar fraction of AgBr in the AgBr + CsBr mixture ; ○ — 500°.

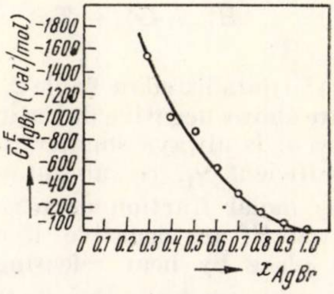

Fig. 4. — Partial molar excess free enthalpy, $\overline{G}^E$ of AgBr *vs.* molar fraction of AgBr in the AgBr + CsBr mixture ; ○ — 500°.

It is evident from these figures, that the partial excess functions for the AgBr + CsBr system, give always negative deviations from ideality.

In this respect, the system is similar to the AgCl + CsCl[12,14] and AgI + CsI[11,13] systems.

Revue Roumaine de Chimie, **17**, *8*, 1293–1312 (1972)

STRONG FIELD SPIN-ORBIT MATRICES FOR d^3 CONFIGURATIONS IN TETRAGONAL SYMMETRY

KEITH D. WARREN
Department of Chemistry, University College, Cardiff, Wales, United Kingdom

Received February 19, 1972

The spin-orbit matrices for the d^3 configuration have been calculated in the strong field scheme for systems of tetragonal (D_4^*) symmetry. These results are tabulated together with the appropriate space-spin symmetry adapted determinental functions for the double group irreducible representations Γ_6 and Γ_7.

Although the optical behaviour of d^n configurations in systems of octahedral symmetry is now well understood, few attempts have, until recently, been made to treat systems of lower than cubic symmetry in a quantitative fashion. Of these the numerous complexes of tetragonal symmetry are of particular importance since the electronic spectra of both MX_5Y (C_{4v}) and of *trans*-MX_4Y_2 (D_{4h}) species may be interpreted by use of the tetragonal crystal field parameters, whilst Ballhausen[1] has shown that the spectra of *cis*-MX_4Y_2 complexes (formally of the lower C_{2v} symmetry) may also be understood in terms of these quantities.

The tetragonal d^3 system was treated by Perumareddi[2] by considering the axial (non-cubic) field as a perturbation of the strong field O_h scheme, but Ōtsuka [3] has given the more familiar strong field matrices for all the d^n configurations in D_4 symmetry. Here the cubic and tetragonal field contributions are diagonal, and the electron repulsion terms act as off-diagonal perturbations. Similar strong field electrostatic matrices for d^2 and d^3 systems have also been calculated by the author,[4] and used in a corrigendum by Brezuleanu and Ivanov,[5] as well as for the interpretation of the electronic spectrum of the tetragonally distorted d^7 NiF_6^{3-} anion.[6]

However, all these treatments neglect the effects of spin-orbit coupling, which , although not large in the 3d series, can produce significant modifications in the interpretation of the optical spectra, and must necessarily be included for any treatment of magnetic susceptibility or of magnetic resonance phenomena. The spin-orbit matrices have already been given for tetragonal d^2 systems in both the weak and the strong field forms,[7] and in the weak field form for the d^3 configuration, [8] but for tetragonal d^3 Cr (III) and low-spin d^7 Co (II) complexes the strong field approach is considerably the more convenient, and the results of the complete spin-orbit calculations in this basis are now therefore presented.

---

[1] C. J. Ballhausen, "Introduction to Ligand Field Theory", McGraw-Hill Book Co. Inc., New York, 1962, pp. 99–112.

[2] J. R. Perumareddi, *J. Phys. Chem.*, **71**, 3144 (1967).

[3] Ōtsuka, *J. Phys. Soc. Japan*, **21**, 596 (1966).

[4] K. D. Warren, unpublished results (communicated to the Editor of *Rev. Roumaine Chim.*, Dec. (1968).

[5] V. Brezuleanu and A. Ivanov, *Rev. Roumaine Chim.*, **14**, 1633 (1969).

[6] G. C. Allen and K. D. Warren, *Inorg. Chem.*, **8**, 1895 (1969).

In the absence of spin-orbit coupling the electrostatic repulsion matrices for the d^3 configuration in tetragonal (D_4) symmetry belong to the following orbital representations, their dimensions being indicated in parentheses : ${}^2A_1$ (5), ${}^2A_2$ (5), ${}^2B_1$ (5), ${}^2B_2$(5), ${}^2E$ (10), ${}^4A_2$(2), ${}^4B_1$ (1), ${}^4B_2$ (1), and ${}^4E$ (3). When spin-orbit coupling is included symmetry adapted linear combinations of Slater determinental functions must be constructed[9] whose complete space-spin transformation properties are appropriate for the Γ_6 and Γ_7 irreducible representations of the double group D_4^*, this yielding two 30 square matrices representing the 60 Kramers' doublets of the d^3 configuration.

The symmetry adapted combinations are expressed in terms of the usual functions d_{z^2}, $d_{x^2-y^2}$, d_{xy}, d_{xz}, and d_{yz}, denoted respectively by a_1, b_1, b_2, e_a, and e_b, that is according to their transformation properties in the point group D_4. The Γ_6 and Γ_7 functions are listed in Table 1 and are labelled according to their one-electron configurations, as well as in terms of their orbital symmetry. Thus Γ_6 spans the orbital representations ${}^2A_1$, ${}^2A_2$, ${}^2E$, ${}^4A_2$, ${}^4B_1$, ${}^4B_2$, and $2{}^4E$, whilst Γ_7 spans ${}^2B_1$, ${}^2B_2$, ${}^2E$, ${}^4A_2$, ${}^4B_1$, ${}^4B_2$ and $2{}^4E$. In both cases the repeated representations of ${}^4E$ are distinguished by primes (′) and double primes (″). The two components of each Kramers' doublet are phased so as to yield identical spin-orbit matrices and are therefore appropriate for use with operators such as the magnetic moment operator which lift the time-reversal degeneracy. The first component of each doublet transforms as either $(2)^{-\frac{1}{2}}(1+i)$, (Γ_6), or $-(2)^{-\frac{1}{2}}(1+i)$, (Γ_7), under $\widehat{C}_4$, defining the operation according to Griffith. [10]

In Table 2 are listed the non-zero elements of the Γ_6 and Γ_7 spin-orbit matrices, in units of the spin-orbit coupling constant, ξ. Only the elements of the upper triangle are given since the matrices are Hermitian. They have been checked by numerical diagonalisation when both yield 15 eigenvalues of $+1/2$, 9 of -2, 5 of $+3$, and 1 of $-9/2$; this is as required for the *jj* limit of the d^3 configuration, and by descent in symmetry from the O_h results. The functions of Table 1 are phased so that the elements of Table 2 are consistent with the electrostatic repulsion matrices previously given, [4,5] and the combined repulsion + spin-orbit matrices have been checked by diagonalisation in the weak field limit. The one-electron contributions to the diagonal matrix elements are easily evaluated in terms of the parameters Dq, Ds, and Dt, as defined by Ballhausen,[1] whilst the matrix elements of the d^7 configuration are obtained from those of the d^3 situation by changing the signs of Dq, Ds, Dt, and ξ, leaving those of B and C unaltered.

---

[7] R. F. Fenske, D. S. Martin Jr., and K. Ruedenberg, *Inorg. Chem.*, **1**, 441 (1962); D. S. Martin Jr., M. A. Tucker, and A. J. Kassman, *Inorg. Chem.*, **5**, 1298 (1966).

[8] J. P. Jesson, *J. Chem. Phys.*, **48**, 161 (1968).

[9] Ref. 1, pp. 120–124.

[10] J. S. Griffith, "The Theory of Transition Metal Ions", Cambridge University Press, London, 1961, p. 147.

Table 1

Symmetry adapted strong field determinental functions, d^3, D_4^*

Representation Γ_6

$|1\rangle$ $^2A_1(a_1b_1^2)$ $\left\{\left|\overset{-}{a_1}\overset{-}{b_1}\overset{+}{b_1}\right|\right\}\ ;\ \left\{\left|\overset{+}{a_1}\overset{+}{b_1}\overset{-}{b_1}\right|\right\}$

$|2\rangle$ $^2A_1(a_1b_2^2)$ $\left\{\left|\overset{-}{a_1}\overset{-}{b_2}\overset{+}{b_2}\right|\right\}\ ;\ \left\{\left|\overset{+}{a_1}\overset{+}{b_2}\overset{-}{b_2}\right|\right\}$

$|3\rangle$ $^2A_1(a_1e^2)$ $(2)^{-\frac{1}{2}}\left\{\left|\overset{-}{a_1}\overset{-}{e_a}\overset{+}{e_a}\right| + \left|\overset{-}{a_1}\overset{-}{e_b}\overset{+}{e_b}\right|\right\}\ ;\ (2)^{-\frac{1}{2}}\left\{\left|\overset{+}{a_1}\overset{+}{e_a}\overset{-}{e_a}\right| + \left|\overset{+}{a_1}\overset{+}{e_b}\overset{-}{e_b}\right|\right\}$

$|4\rangle$ $^2A_1(b_1e^2)$ $(2)^{-\frac{1}{2}}\left\{\left|\overset{-}{b_1}\overset{-}{e_a}\overset{+}{e_a}\right| - \left|\overset{-}{b_1}\overset{-}{e_b}\overset{+}{e_b}\right|\right\}\ ;\ (2)^{-\frac{1}{2}}\left\{\left|\overset{+}{b_1}\overset{+}{e_a}\overset{-}{e_a}\right| - \left|\overset{+}{b_1}\overset{+}{e_b}\overset{-}{e_b}\right|\right\}$

$|5\rangle$ $^2A_1(b_2e^2)$ $(2)^{-\frac{1}{2}}\left\{\left|\overset{-}{b_2}\overset{-}{e_a}\overset{+}{e_b}\right| - \left|\overset{-}{b_2}\overset{+}{e_a}\overset{-}{e_b}\right|\right\}\ ;\ (2)^{-\frac{1}{2}}\left\{\left|\overset{+}{b_2}\overset{+}{e_a}\overset{-}{e_b}\right| - \left|\overset{+}{b_2}\overset{-}{e_a}\overset{+}{e_b}\right|\right\}$

$|6\rangle$ $^2A_2(a_1b_1b_2)$(i) $(2)^{-\frac{1}{2}}\left\{\left|\overset{-}{a_1}\overset{-}{b_1}\overset{+}{b_2}\right| - \left|\overset{-}{a_1}\overset{+}{b_1}\overset{-}{b_2}\right|\right\}\ ;\ -(2)^{-\frac{1}{2}}\left\{\left|\overset{+}{a_1}\overset{+}{b_1}\overset{-}{b_2}\right| - \left|\overset{+}{a_1}\overset{-}{b_1}\overset{+}{b_2}\right|\right\}$

$|7\rangle$ $^2A_2(a_1b_1b_2)$(ii) $(6)^{-\frac{1}{2}}\left\{2\left|\overset{+}{a_1}\overset{-}{b_1}\overset{-}{b_2}\right| - \left|\overset{-}{a_1}\overset{-}{b_1}\overset{+}{b_2}\right| - \left|\overset{-}{a_1}\overset{+}{b_1}\overset{-}{b_2}\right|\right\}\ ;\ -(6)^{-\frac{1}{2}}\left\{2\left|\overset{-}{a_1}\overset{+}{b_1}\overset{+}{b_2}\right| -\right.$

$\left. - \left|\overset{+}{a_1}\overset{+}{b_1}\overset{-}{b_2}\right| - \left|\overset{+}{a_1}\overset{-}{b_1}\overset{+}{b_2}\right|\right\}$

$|8\rangle$ $^2A_2(a_1e^2)$ $(6)^{-\frac{1}{2}}\left\{2\left|\overset{+}{a_1}\overset{-}{e_a}\overset{-}{e_b}\right| - \left|\overset{-}{a_1}\overset{-}{e_a}\overset{+}{e_b}\right| - \left|\overset{-}{a_1}\overset{+}{e_a}\overset{-}{e_b}\right|\right\}\ ;\ -(6)^{-\frac{1}{2}}\left\{2\left|\overset{-}{a_1}\overset{+}{e_a}\overset{+}{e_b}\right| -\right.$

$\left. - \left|\overset{+}{a_1}\overset{+}{e_a}\overset{-}{e_b}\right| - \left|\overset{+}{a_1}\overset{-}{e_a}\overset{+}{e_b}\right|\right\}$

$|9\rangle$ $^2A_2(b_1e^2)$ $(2)^{-\frac{1}{2}}\left\{\left|\overset{-}{b_1}\overset{-}{e_a}\overset{+}{e_b}\right| - \left|\overset{-}{b_1}\overset{+}{e_a}\overset{-}{e_b}\right|\right\}\ ;\ -(2)^{-\frac{1}{2}}\left\{\left|\overset{+}{b_1}\overset{+}{e_a}\overset{-}{e_b}\right| - \left|\overset{+}{b_1}\overset{-}{e_a}\overset{+}{e_b}\right|\right\}$

$|10\rangle$ $^2A_2(b_2e^2)$ $(2)^{-\frac{1}{2}}\left\{\left|\overset{-}{b_2}\overset{-}{e_a}\overset{+}{e_a}\right| - \left|\overset{-}{b_2}\overset{-}{e_b}\overset{+}{e_b}\right|\right\}\ ;\ -(2)^{-\frac{1}{2}}\left\{\left|\overset{+}{b_2}\overset{+}{e_a}\overset{-}{e_a}\right| - \left|\overset{+}{b_2}\overset{+}{e_b}\overset{-}{e_b}\right|\right\}$

$|11\rangle$ $^2E(a_1e^2)$ $(2)^{-\frac{1}{2}}\left\{i\left|\overset{-}{a_1}\overset{+}{a_1}\overset{+}{e_b}\right| - \left|\overset{-}{a_1}\overset{+}{a_1}\overset{+}{e_a}\right|\right\}\ ;$

Representation Γ_6

$$(2)^{-\frac{1}{2}}\{i|\overset{+}{a}_1\overset{-}{a}_1\overset{-}{e}_b|+|\overset{+}{a}_1\overset{-}{a}_1\overset{-}{e}_a|\}$$

$|12\rangle$ $^2E(b_1e^2)$ $$(2)^{-\frac{1}{2}}\{i|\overset{-}{b}_1\overset{+}{b}_1\overset{+}{e}_b|-|\overset{-}{b}_1\overset{+}{b}_1\overset{+}{e}_a|\}\ ;$$

$$(2)^{-\frac{1}{2}}\{i|\overset{+}{b}_1\overset{-}{b}_1\overset{-}{e}_b|+|\overset{+}{b}_1\overset{-}{b}_1\overset{-}{e}_a|\}$$

$|13\rangle$ $^2E(b_2e^2)$ $$(2)^{-\frac{1}{2}}\{i|\overset{-}{b}_2\overset{+}{b}_2\overset{+}{e}_b|-|\overset{-}{b}_2\overset{+}{b}_2\overset{+}{e}_a|\}\ ;$$

$$(2)^{-\frac{1}{2}}\{i|\overset{+}{b}_2\overset{-}{b}_2\overset{-}{e}_b|+|\overset{+}{b}_2\overset{-}{b}_2\overset{-}{e}_a|\}$$

$|14\rangle$ $^2E(a_1b_1e)(i)$ $$\tfrac{1}{2}\{[|\overset{+}{a}_1\overset{+}{b}_1\overset{-}{e}_a|-|\overset{+}{a}_1\overset{-}{b}_1\overset{+}{e}_a|]+i[|\overset{+}{a}_1\overset{+}{b}_1\overset{-}{e}_b|-|\overset{+}{a}_1\overset{-}{b}_1\overset{+}{e}_b|]\}\ ;$$

$$-\tfrac{1}{2}\{[|\overset{-}{a}_1\overset{-}{b}_1\overset{+}{e}_a|-|\overset{-}{a}_1\overset{+}{b}_1\overset{-}{e}_a|]-i[|\overset{-}{a}_1\overset{-}{b}_1\overset{+}{e}_b|-|\overset{-}{a}_1\overset{+}{b}_1\overset{-}{e}_b|]\}$$

$|15\rangle$ $^2E(a_1b_1e)(ii)$ $$(12)^{-\frac{1}{2}}\{[2|\overset{-}{a}_1\overset{+}{b}_1\overset{+}{e}_a|-|\overset{+}{a}_1\overset{+}{b}_1\overset{-}{e}_a|-|\overset{+}{a}_1\overset{-}{b}_1\overset{+}{e}_a|]+i[2|\overset{-}{a}_1\overset{+}{b}_1\overset{+}{e}_b|-|\overset{+}{a}_1\overset{+}{b}_1\overset{-}{e}_b|$$

$$-|\overset{+}{a}_1\overset{-}{b}_1\overset{+}{e}_b|]\}\ ;\ -(12)^{-\frac{1}{2}}\{[2|\overset{+}{a}_1\overset{-}{b}_1\overset{-}{e}_a|-|\overset{-}{a}_1\overset{-}{b}_1\overset{+}{e}_a|-|\overset{-}{a}_1\overset{+}{b}_1\overset{-}{e}_a|]$$

$$-i[2|\overset{+}{a}_1\overset{-}{b}_1\overset{-}{e}_b|-|\overset{-}{a}_1\overset{-}{b}_1\overset{+}{e}_b|-|\overset{-}{a}_1\overset{+}{b}_1\overset{-}{e}_b|]\}$$

$|16\rangle$ $^2E(a_1b_2e)(i)$ $$\tfrac{1}{2}\{[|\overset{+}{a}_1\overset{+}{b}_2\overset{-}{e}_b|-|\overset{+}{a}_1\overset{-}{b}_2\overset{+}{e}_b|]-i[|\overset{+}{a}_1\overset{+}{b}_2\overset{-}{e}_a|-|\overset{+}{a}_1\overset{-}{b}_2\overset{+}{e}_a|]\}\ ;$$

$$-\tfrac{1}{2}\{[|\overset{-}{a}_1\overset{-}{b}_2\overset{+}{e}_b|-|\overset{-}{a}_1\overset{+}{b}_2\overset{-}{e}_b|]+i[|\overset{-}{a}_1\overset{-}{b}_2\overset{+}{e}_a|-|\overset{-}{a}_1\overset{+}{b}_2\overset{-}{e}_a|]\}$$

$|17\rangle$ $^2E(a_1b_2e)(ii)$ $$(12)^{-\frac{1}{2}}\{[2|\overset{-}{a}_1\overset{+}{b}_2\overset{+}{e}_b|-|\overset{+}{a}_1\overset{+}{b}_2\overset{-}{e}_b|-|\overset{+}{a}_1\overset{-}{b}_2\overset{+}{e}_b|]-i[2|\overset{-}{a}_1\overset{+}{b}_2\overset{+}{e}_a|$$

$$-|\overset{+}{a}_1\overset{+}{b}_2\overset{-}{e}_a|-|\overset{+}{a}_1\overset{-}{b}_2\overset{+}{e}_a|]\}\ ;\ -(12)^{-\frac{1}{2}}\{[2|\overset{+}{a}_1\overset{-}{b}_2\overset{-}{e}_b|-|\overset{-}{a}_1\overset{-}{b}_2\overset{+}{e}_b|$$

$$-|\overset{-}{a}_1\overset{+}{b}_2\overset{-}{e}_b|]+i[2|\overset{+}{a}_1\overset{-}{b}_2\overset{-}{e}_a|-|\overset{-}{a}_1\overset{-}{b}_2\overset{+}{e}_a|-|\overset{-}{a}_1\overset{+}{b}_2\overset{-}{e}_a|]\}$$

$18\rangle$ $^2E(b_1b_2e)(i)$ $$\tfrac{1}{2}\{[|\overset{+}{b}_1\overset{+}{b}_2\overset{-}{e}_b|-|\overset{+}{b}_1\overset{-}{b}_2\overset{+}{e}_b|]+i[|\overset{+}{b}_1\overset{+}{b}_2\overset{-}{e}_a|-|\overset{+}{b}_1\overset{-}{b}_2\overset{+}{e}_a|]\}\ ;$$

$$-\tfrac{1}{2}\{[|\overset{-}{b}_1\overset{-}{b}_2\overset{+}{e}_b|-|\overset{-}{b}_1\overset{+}{b}_2\overset{-}{e}_b|]-i[|\overset{-}{b}_1\overset{-}{b}_2\overset{+}{e}_a|-|\overset{-}{b}_1\overset{+}{b}_2\overset{-}{e}_a|]\}$$

Representation Γ_6

$|19\rangle$ $^{2}E(b_1b_2e)(ii)$

$$\begin{aligned}&(12)^{-\frac{1}{2}}\Big\{\Big[2\left|\overset{-++}{b_1b_2e_b}\right| - \left|\overset{++-}{b_1b_2e_b}\right| - \left|\overset{+-+}{b_1b_2e_b}\right|\Big] + i\Big[2\left|\overset{-++}{b_1b_2e_a}\right|\\ &- \left|\overset{++-}{b_1b_2e_a}\right| - \left|\overset{+-+}{b_1b_2e_a}\right|\Big]\Big\}\ ;\ -(12)^{-\frac{1}{2}}\Big\{\Big[2\left|\overset{+--}{b_1b_2e_b}\right| - \left|\overset{--+}{b_1b_2e_b}\right|\\ &- \left|\overset{-+-}{b_1b_2e_b}\right|\Big] - i\Big[2\left|\overset{+--}{b_1b_2e_a}\right| - \left|\overset{--+}{b_1b_2e_a}\right| - \left|\overset{-+-}{b_1b_2e_a}\right|\Big]\Big\}\end{aligned}$$

$|20\rangle$ $^{2}E(e^3)$

$$(2)^{-\frac{1}{2}}\left\{i\left|\overset{-++}{e_ae_ae_b}\right| - \left|\overset{-++}{e_be_be_a}\right|\right\}\ ;$$

$$(2)^{-\frac{1}{2}}\left\{i\left|\overset{+--}{e_ae_ae_b}\right| + \left|\overset{+--}{e_be_be_a}\right|\right\}$$

$|21\rangle$ $^{4}A_2(a_1b_1b_2)$

$$(3)^{-\frac{1}{2}}\left\{\left|\overset{--+}{a_1b_1b_2}\right| + \left|\overset{-+-}{a_1b_1b_2}\right| + \left|\overset{+--}{a_1b_1b_2}\right|\right\}\ ;$$

$$-(3)^{-\frac{1}{2}}\left\{\left|\overset{++-}{a_1b_1b_2}\right| + \left|\overset{+-+}{a_1b_1b_2}\right| + \left|\overset{-++}{a_1b_1b_2}\right|\right\}$$

$22\rangle$ $^{4}A_2(a_1e^2)$

$$(3)^{-\frac{1}{2}}\left\{\left|\overset{--+}{a_1e_ae_b}\right| + \left|\overset{-+-}{a_1e_ae_b}\right| + \left|\overset{+--}{a_1e_ae_b}\right|\right\}\ ;$$

$$-(3)^{-\frac{1}{2}}\left\{\left|\overset{++-}{a_1e_ae_b}\right| + \left|\overset{+-+}{a_1e_ae_b}\right| + \left|\overset{-++}{a_1e_ae_b}\right|\right\}$$

$|23\rangle$ $^{4}B_1(b_2e^2)$

$$\left\{\left|\overset{+++}{b_2e_ae_b}\right|\right\}\ ;\ \left\{\left|\overset{---}{b_2e_ae_b}\right|\right\}$$

$|24\rangle$ $^{4}B_2(b_1e^2)$

$$\left\{\left|\overset{+++}{b_1e_ae_b}\right|\right\}\ ;\ \left\{-\left|\overset{---}{b_1e_ae_b}\right|\right\}$$

$|25\rangle$ $^{4}E'(a_1b_1e)$

$$(2)^{-\frac{1}{2}}\left\{\left|\overset{---}{a_1b_1e_a}\right| - i\left|\overset{---}{a_1b_1e_b}\right|\right\};$$

$$-(2)^{-\frac{1}{2}}\left\{\left|\overset{+++}{a_1b_1e_a}\right| + i\left|\overset{+++}{a_1b_1e_b}\right|\right\}$$

$|26\rangle$ $^{4}E'(a_1b_2e)$

$$(2)^{-\frac{1}{2}}\left\{\left|\overset{---}{a_1b_2e_b}\right| + i\left|\overset{---}{a_1b_2e_a}\right|\right\};$$

$$-(2)^{-\frac{1}{2}}\left\{\left|\overset{+++}{a_1b_2e_b}\right| - i\left|\overset{+++}{a_1b_2e_a}\right|\right\}$$

$|27\rangle$ $^{4}E'(b_1b_2e)$

$$(2)^{-\frac{1}{2}}\left\{\left|\overset{---}{b_1b_2e_b}\right| - i\left|\overset{---}{b_1b_2e_a}\right|\right\};$$

$$-(2)^{-\frac{1}{2}}\left\{\left|\overset{+++}{b_1b_2e_b}\right| + i\left|\overset{+++}{b_1b_2e_a}\right|\right\}$$

Representation Γ_6

$|28\rangle$ $^4E''(a_1b_1e)$

$$\begin{aligned}
&(6)^{-\frac{1}{2}}\Big\{i\Big[\Big|\overset{++-}{a_1b_1e_a}\Big| + \Big|\overset{+-+}{a_1b_1e_a}\Big| + \Big|\overset{-++}{a_1b_1e_a}\Big|\Big] - \Big[\Big|\overset{++-}{a_1b_1e_b}\Big| + \Big|\overset{+-+}{a_1b_1e_b}\Big|\\
&+ \Big|\overset{-++}{a_1b_1e_b}\Big|\Big]\Big\};\ -(6)^{-\frac{1}{2}}\Big\{i\Big[\Big|\overset{--+}{a_1b_1e_a}\Big| + \Big|\overset{-+-}{a_1b_1e_a}\Big| + \Big|\overset{+--}{a_1b_1e_a}\Big|\\
&+ \Big[\Big|\overset{--+}{a_1b_1e_b}\Big| + \Big|\overset{-+-}{a_1b_1e_b}\Big| + \Big|\overset{+--}{a_1b_1e_b}\Big|\Big]\Big\}
\end{aligned}$$

$|29\rangle$ $^4E''(a_1b_2e)$

$$\begin{aligned}
&(6)^{-\frac{1}{2}}\Big\{\Big[\Big|\overset{++-}{a_1b_2e_a}\Big| + \Big|\overset{+-+}{a_1b_2e_a}\Big| + \Big|\overset{-++}{a_1b_2e_a}\Big|\Big] + i\Big[\Big|\overset{++-}{a_1b_2e_b}\Big|\\
&+ \Big|\overset{+-+}{a_1b_2e_b}\Big| + \Big|\overset{-++}{a_1b_2e_b}\Big|\Big]\Big\};\ -(6)^{-\frac{1}{2}}\Big\{-\Big[\Big|\overset{--+}{a_1b_2e_a}\Big| + \Big|\overset{-+-}{a_1b_2e_a}\Big|\\
&+ \Big|\overset{+--}{a_1b_2e_a}\Big|\Big] + i\Big[\Big|\overset{--+}{a_1b_2e_b}\Big| + \Big|\overset{-+-}{a_1b_2e_b}\Big| + \Big|\overset{+--}{a_1b_2e_b}\Big|\Big]\Big\}
\end{aligned}$$

$|30\rangle$ $^4E''(b_1b_2e)$

$$\begin{aligned}
&(6)^{-\frac{1}{2}}\Big\{i\Big[\Big|\overset{++-}{b_1b_2e_b}\Big| + \Big|\overset{+-+}{b_1b_2e_b}\Big| + \Big|\overset{-++}{b_1b_2e_b}\Big|\Big] - \Big[\Big|\overset{++-}{b_1b_2e_a}\Big|\\
&+ \Big|\overset{+-+}{b_1b_2e_a}\Big| + \Big|\overset{-++}{b_1b_2e_a}\Big|\Big]\Big\};\ -(6)^{-\frac{1}{2}}\Big\{i\Big[\Big|\overset{--+}{b_1b_2e_b}\Big| + \Big|\overset{-+-}{b_1b_2e_b}\Big|\\
&+ \Big|\overset{+--}{b_1b_2e_b}\Big|\Big] + \Big[\Big|\overset{--+}{b_1b_2e_a}\Big| + \Big|\overset{-+-}{b_1b_2e_a}\Big| + \Big|\overset{+--}{b_1b_2e_a}\Big|\Big]\Big\}
\end{aligned}$$

Representation Γ_7

$|1\rangle$ $^2B_1(a_1{}^2b_1)$ $\quad \Big\{\Big|\overset{-+-}{a_1a_1b_1}\Big|\Big\};\ \Big\{\Big|\overset{+-+}{a_1a_1b_1}\Big|\Big\}$

$|2\rangle$ $^2B_1(b_1b_2^2)$ $\quad \Big\{\Big|\overset{--+}{b_1b_2b_2}\Big|\Big\};\ \Big\{\Big|\overset{++-}{b_1b_2b_2}\Big|\Big\}$

$|3\rangle$ $^2B_1(a_1e^2)$ $\quad (2)^{-\frac{1}{2}}\Big\{\Big|\overset{--+}{a_1e_ae_a}\Big| - \Big|\overset{--+}{a_1e_be_b}\Big|\Big\};\ (2)^{-\frac{1}{2}}\Big\{\Big|\overset{++-}{a_1e_ae_a}\Big| - \Big|\overset{++-}{a_1e_be_b}\Big|\Big\}$

$|4\rangle$ $^2B_1(b_1e^2)$ $\quad (2)^{-\frac{1}{2}}\Big\{\Big|\overset{--+}{b_1e_ae_a}\Big| + \Big|\overset{--+}{b_1e_be_b}\Big|\Big\};\ (2)^{-\frac{1}{2}}\Big\{\Big|\overset{++-}{b_1e_ae_a}\Big| + \Big|\overset{++-}{b_1e_be_b}\Big|\Big\}$

$|5\rangle$ $^2B_1(b_2e^2)$

$$\begin{aligned}
&(6)^{-\frac{1}{2}}\Big\{2\Big|\overset{+--}{b_2e_ae_b}\Big| - \Big|\overset{--+}{b_2e_ae_b}\Big| - \Big|\overset{-+-}{b_2e_ae_b}\Big|\Big\};\ (6)^{-\frac{1}{2}}\Big\{2\Big|\overset{-++}{b_2e_ae_b}\Big| -\\
&- \Big|\overset{++-}{b_2e_ae_b}\Big| - \Big|\overset{+-+}{b_2e_ae_b}\Big|\Big\}
\end{aligned}$$

$|6\rangle$ $^2B_2(a_1b_2^2)$ $\quad \Big\{\Big|\overset{-+-}{a_1a_1b_2}\Big|\Big\};\ \Big\{-\Big|\overset{+-+}{a_1a_1b_2}\Big|\Big\}$

$|7\rangle$ $^2B_2(b_1b_2)$ $\quad \Big\{\Big|\overset{-+-}{b_1b_1b_2}\Big|\Big\};\ \Big\{-\Big|\overset{+-+}{b_1b_2b_1}\Big|\Big\}$

Representation Γ_7

$|8\rangle$ $^2B_2(a_1e^2)$

$$(2)^{-\frac{1}{2}}\left\{\left|\overset{--+}{a_1e_ae_b}\right|-\left|\overset{-+-}{a_1e_ae_b}\right|\right\};\ -(2)^{-\frac{1}{2}}\left\{\left|\overset{++-}{a_1e_ae_b}\right|-\left|\overset{+-+}{a_1e_ae_b}\right|\right\}$$

$|9\rangle$ $^2B_2(b_1e^2)$

$$(6)^{-\frac{1}{2}}\left\{2\left|\overset{+--}{b_1e_ae_b}\right|-\left|\overset{--+}{b_1e_ae_b}\right|-\left|\overset{-+-}{b_1e_ae_b}\right|\right\};\ -(6)^{-\frac{1}{2}}\left\{2\left|\overset{-++}{b_1e_ae_b}\right|-\right.$$

$$\left.-\left|\overset{++-}{b_1e_ae_b}\right|-\left|\overset{+-+}{b_1e_ae_b}\right|\right\}$$

$|10\rangle$ $^2B_2(b_2e^2)$

$$(2)^{-\frac{1}{2}}\left\{\left|\overset{--+}{b_2e_ae_a}\right|+\left|\overset{--+}{b_2e_be_b}\right|\right\};\ -(2)^{-\frac{1}{2}}\left\{\left|\overset{++-}{b_2e_ae_a}\right|+\left|\overset{++-}{b_2e_be_b}\right|\right\}$$

$|11\rangle$ $^2E(a_1e^2)$

$$(2)^{-\frac{1}{2}}\left\{\left|\overset{+-+}{a_1a_1e_b}\right|-i\left|\overset{+-+}{a_1a_1e_a}\right|\right\};$$

$$(2)^{-\frac{1}{2}}\left\{\left|\overset{-+-}{a_1a_1e_b}\right|+i\left|\overset{-+-}{a_1a_1e_a}\right|\right\}$$

$|12\rangle$ $^2E(b_1e^2)$

$$(2)^{-\frac{1}{2}}\left\{\left|\overset{+-+}{b_1b_1e_b}\right|-i\left|\overset{+-+}{b_1b_1e_a}\right|\right\};$$

$$(2)^{-\frac{1}{2}}\left\{\left|\overset{-+-}{b_1b_1e_b}\right|+i\left|\overset{-+-}{b_1b_1e_a}\right|\right\}$$

$|13\rangle$ $^2E(b_2e^2)$

$$(2)^{-\frac{1}{2}}\left\{\left|\overset{+-+}{b_2b_2e_b}\right|-i\left|\overset{+-+}{b_2b_2e_a}\right|\right\};$$

$$(2)^{-\frac{1}{2}}\left\{\left|\overset{-+-}{b_2b_2e_b}\right|+i\left|\overset{-+-}{b_2b_2e_a}\right|\right\}$$

$|14\rangle$ $^2E(a_1b_1e)(i)$

$$-\tfrac{1}{2}\left\{i\left[\left|\overset{++-}{a_1b_1e_a}\right|-\left|\overset{+-+}{a_1b_1e_a}\right|\right]+\left[\left|\overset{++-}{a_1b_1e_b}\right|-\left|\overset{+-+}{a_1b_1e_b}\right|\right]\right\};$$

$$\tfrac{1}{2}\left\{i\left[\left|\overset{--+}{a_1b_1e_a}\right|-\left|\overset{-+-}{a_1b_1e_a}\right|\right]-\left[\left|\overset{--+}{a_1b_1e_b}\right|-\left|\overset{-+-}{a_1b_1e_b}\right|\right]\right\}$$

$|15\rangle$ $^2E(a_1b_1e)(ii)$

$$-(12)^{-\frac{1}{2}}\left\{i\left[2\left|\overset{-++}{a_1b_1e_a}\right|-\left|\overset{++-}{a_1b_1e_a}\right|-\left|\overset{+-+}{a_1b_1e_a}\right|\right]\right.$$

$$\left.+\left[2\left|\overset{-++}{a_1b_1e_b}\right|-\left|\overset{++-}{a_1b_1e_b}\right|-\left|\overset{+-+}{a_1b_1e_b}\right|\right]\right\};\ (12)^{-\frac{1}{2}}\left\{i\left[2\left|\overset{+--}{a_1b_1e_a}\right|\right.\right.$$

$$\left.\left.-\left|\overset{--+}{a_1b_1e_a}\right|-\left|\overset{-+-}{a_1b_1e_a}\right|\right]-\left[2\left|\overset{+--}{a_1b_1e_b}\right|-\left|\overset{--+}{a_1b_1e_b}\right|-\left|\overset{-+-}{a_1b_1e_b}\right|\right]\right\}$$

$|16\rangle$ $^2E(a_1b_2e)(i)$

$$\tfrac{1}{2}\left\{\left[\left|\overset{++-}{a_1b_2e_a}\right|-\left|\overset{+-+}{a_1b_2e_a}\right|\right]-i\left[\left|\overset{++-}{a_1b_2e_b}\right|-\left|\overset{+-+}{a_1b_2e_b}\right|\right]\right\};$$

$$\tfrac{1}{2}\left\{\left[\left|\overset{--+}{a_1b_2e_a}\right|-\left|\overset{-+-}{a_1b_2e_a}\right|\right]+i\left[\left|\overset{--+}{a_1b_2e_b}\right|-\left|\overset{-+-}{a_1b_2e_b}\right|\right]\right\}$$

Representation Γ_7

$|17\rangle$ $^2E(a_1b_2e)(ii)$

$$(12)^{-\frac{1}{2}}\Big\{\Big[2\,|\overset{-}{a_1}\overset{+}{b_2}\overset{+}{e_a}| - |\overset{+}{a_1}\overset{+}{b_2}\overset{-}{e_a}| - |\overset{+}{a_1}\overset{-}{b_2}\overset{+}{e_a}|\Big] - i\Big[2\,|\overset{-}{a_1}\overset{+}{b_2}\overset{+}{e_b}|$$

$$- |\overset{+}{a_1}\overset{+}{b_2}\overset{-}{e_b}| - |\overset{+}{a_1}\overset{-}{b_2}\overset{+}{e_b}|\Big]\Big\};\ (12)^{-\frac{1}{2}}\Big\{\Big[2\,|\overset{+}{a_1}\overset{-}{b_2}\overset{-}{e_a}| - |\overset{-}{a_1}\overset{-}{b_2}\overset{+}{e_a}|$$

$$- |\overset{-}{a_1}\overset{+}{b_2}\overset{-}{e_a}|\Big] + i\Big[2\,|\overset{+}{a_1}\overset{-}{b_2}\overset{-}{e_b}| - |\overset{-}{a_1}\overset{-}{b_2}\overset{+}{e_b}| - |\overset{-}{a_1}\overset{+}{b_2}\overset{-}{e_b}|\Big]\Big\}$$

$|18\rangle$ $^2E(b_1b_2e)(ii)$

$$-\tfrac{1}{2}\Big\{i\Big[|\overset{+}{b_1}\overset{+}{b_2}\overset{-}{e_b}| - |\overset{+}{b_1}\overset{-}{b_2}\overset{+}{e_b}|\Big] + \Big[|\overset{+}{b_1}\overset{+}{b_2}\overset{-}{e_a}| - |\overset{+}{b_1}\overset{-}{b_2}\overset{+}{e_a}|\Big]\Big\};$$

$$\tfrac{1}{2}\Big\{i\Big[|\overset{-}{b_1}\overset{-}{b_2}\overset{+}{e_b}| - |\overset{-}{b_1}\overset{+}{b_2}\overset{-}{e_b}|\Big] - \Big[|\overset{-}{b_1}\overset{-}{b_2}\overset{+}{e_a}| - |\overset{-}{b_1}\overset{+}{b_2}\overset{-}{e_a}|\Big]\Big\}$$

$|19\rangle$ $^2E(b_1b_2e)(ii)$

$$-(12)^{-\frac{1}{2}}\Big\{i\Big[2\,|\overset{-}{b_1}\overset{+}{b_2}\overset{-}{e_b}| - |\overset{+}{b_1}\overset{+}{b_2}\overset{-}{e_b}| - |\overset{+}{b_1}\overset{-}{b_2}\overset{+}{e_b}|\Big] + \Big[2\,|\overset{-}{b_1}\overset{+}{b_2}\overset{+}{e_a}|$$

$$- |\overset{+}{b_1}\overset{+}{b_2}\overset{-}{e_a}| - |\overset{+}{b_1}\overset{-}{b_2}\overset{+}{e_a}|\Big]\Big\};\ (12)^{-\frac{1}{2}}\Big\{i\Big[2\,|\overset{+}{b_1}\overset{-}{b_2}\overset{-}{e_b}|$$

$$- |\overset{-}{b_1}\overset{-}{b_2}\overset{+}{e_b}| - |\overset{-}{b_1}\overset{+}{b_2}\overset{-}{e_b}|\Big] - \Big[2\,|\overset{+}{b_1}\overset{-}{b_2}\overset{-}{e_a}| - |\overset{-}{b_1}\overset{-}{b_2}\overset{+}{e_a}| - |\overset{-}{b_1}\overset{+}{b_2}\overset{-}{e_a}|\Big]\Big\}$$

$|20\rangle$ $^2E(e^3)$

$$(2)^{-\frac{1}{2}}\Big\{|\overset{+}{e_a}\overset{-}{e_a}\overset{+}{e_b}| - i\,|\overset{+}{e_b}\overset{-}{e_b}\overset{+}{e_a}|\Big\};$$

$$(2)^{-\frac{1}{2}}\Big\{|\overset{-}{e_a}\overset{+}{e_a}\overset{-}{e_b}| + i\,|\overset{-}{e_b}\overset{+}{e_b}\overset{-}{e_a}|\Big\}$$

$|21\rangle$ $^4A_2(a_1b_1b_2)$

$$\Big\{|\overset{+}{a_1}\overset{+}{b_1}\overset{+}{b_2}|\Big\};\ \Big\{-|\overset{-}{a_1}\overset{-}{b_1}\overset{-}{b_2}|\Big\}$$

$|22\rangle$ $^4A_2(a_1e^2)$

$$\Big\{|\overset{+}{a_1}\overset{+}{e_a}\overset{+}{e_b}|\Big\};\ \Big\{-|\overset{-}{a_1}\overset{-}{e_a}\overset{-}{e_b}|\Big\}$$

$23\rangle$ $^4B_1(b_2e^2)$

$$(3)^{-\frac{1}{2}}\Big\{|\overset{-}{b_2}\overset{-}{e_a}\overset{+}{e_b}| + |\overset{-}{b_2}\overset{+}{e_a}\overset{-}{e_b}| + |\overset{+}{b_2}\overset{-}{e_a}\overset{-}{e_b}|\Big\};$$

$$(3)^{-\frac{1}{2}}\Big\{|\overset{+}{b_2}\overset{+}{e_a}\overset{-}{e_b}| + |\overset{+}{b_2}\overset{-}{e_a}\overset{+}{e_b}| + |\overset{-}{b_2}\overset{+}{e_a}\overset{+}{e_b}|\Big\}$$

$|\ \rangle$ $^4B_2(b_1e^2)$

$$(3)^{-\frac{1}{2}}\Big\{|\overset{-}{b_1}\overset{-}{e_a}\overset{+}{e_b}| + |\overset{-}{b_1}\overset{+}{e_a}\overset{-}{e_b}| + |\overset{+}{b_1}\overset{-}{e_a}\overset{-}{e_b}|\Big\};$$

$$-(3)^{-\frac{1}{2}}\Big\{|\overset{+}{b_1}\overset{+}{e_a}\overset{-}{e_b}| + |\overset{+}{b_1}\overset{-}{e_a}\overset{+}{e_b}| + |\overset{-}{b_1}\overset{+}{e_a}\overset{+}{e_b}|\Big\}$$

Representation Γ_7

$|25\rangle$ $^4E'(a_1b_1e)$

$$(2)^{-\frac{1}{2}}\Bigl\{i\left|\overset{-}{a}_1\overset{-}{b}_1\overset{-}{e}_a\right| - \left|\overset{-}{a}_1\overset{-}{b}_1\overset{-}{e}_b\right|\Bigr\};$$

$$-(2)^{-\frac{1}{2}}\Bigl\{i\left|\overset{+}{a}_1\overset{+}{b}_1\overset{+}{e}_a\right| + \left|\overset{+}{a}_1\overset{+}{b}_1\overset{+}{e}_b\right|\Bigr\}$$

$|26\rangle$ $^4E'(a_1b_2e)$

$$(2)^{-\frac{1}{2}}\Bigl\{\left|\overset{-}{a}_1\overset{-}{b}_2\overset{-}{e}_a\right| + i\left|\overset{-}{a}_1\overset{-}{b}_2\overset{-}{e}_b\right|\Bigr\};$$

$$(2)^{-\frac{1}{2}}\Bigl\{\left|\overset{+}{a}_1\overset{+}{b}_2\overset{+}{e}_a\right| - i\left|\overset{+}{a}_1\overset{+}{b}_2\overset{+}{e}_b\right|\Bigr\}$$

$|27\rangle$ $^4E'(b_1b_2e)$

$$(2)^{-\frac{1}{2}}\Bigl\{i\left|\overset{-}{b}_1\overset{-}{b}_2\overset{-}{e}_b\right| - \left|\overset{-}{b}_1\overset{-}{b}_2\overset{-}{e}_a\right|\Bigr\};$$

$$-(2)^{-\frac{1}{2}}\Bigl\{i\left|\overset{+}{b}_1\overset{+}{b}_2\overset{+}{e}_b\right| + \left|\overset{+}{b}_1\overset{+}{b}_2\overset{+}{e}_a\right|\Bigr\}$$

$|28\rangle$ $^4E''(a_1b_1e)$

$$(6)^{-\frac{1}{2}}\Bigl\{\Bigl[\left|\overset{+}{a}_1\overset{-}{b}_1\overset{-}{e}_a\right| + \left|\overset{+}{a}_1\overset{-}{b}_1\overset{+}{e}_a\right| + \left|\overset{-}{a}_1\overset{+}{b}_1\overset{+}{e}_a\right|\Bigr] - i\Bigl[\left|\overset{+}{a}_1\overset{-}{b}_1\overset{-}{e}_b\right|$$

$$+ \left|\overset{+}{a}_1\overset{-}{b}_1\overset{+}{e}_b\right| + \left|\overset{-}{a}_1\overset{+}{b}_1\overset{+}{e}_b\right|\Bigr]\Bigr\};\ -(6)^{-\frac{1}{2}}\Bigl\{\Bigl[\left|\overset{-}{a}_1\overset{-}{b}_1\overset{+}{e}_a\right|$$

$$+ \left|\overset{-}{a}_1\overset{+}{b}_1\overset{-}{e}_a\right| + \left|\overset{+}{a}_1\overset{-}{b}_1\overset{-}{e}_a\right|\Bigr] + i\Bigl[\left|\overset{-}{a}_1\overset{-}{b}_1\overset{+}{e}_b\right| + \left|\overset{-}{a}_1\overset{+}{b}_1\overset{-}{e}_b\right| + \left|\overset{+}{a}_1\overset{-}{b}_1\overset{-}{e}_b\right|\Bigr]\Bigr\}$$

$|29\rangle$ $^4E''(a_1b_2e)$

$$(6)^{-\frac{1}{2}}\Bigl\{i\Bigl[\left|\overset{+}{a}_1\overset{+}{b}_2\overset{-}{e}_a\right| + \left|\overset{+}{a}_1\overset{-}{b}_2\overset{+}{e}_a\right| + \left|\overset{-}{a}_1\overset{+}{b}_2\overset{+}{e}_a\right|\Bigr] + \Bigl[\left|\overset{+}{a}_1\overset{+}{b}_2\overset{-}{e}_b\right|$$

$$+ \left|\overset{+}{a}_1\overset{-}{b}_2\overset{+}{e}_b\right| + \left|\overset{-}{a}_1\overset{+}{b}_2\overset{+}{e}_b\right|\Bigr]\Bigr\};\ (6)^{-\frac{1}{2}}\Bigl\{i\Bigl[\left|\overset{-}{a}_1\overset{-}{b}_2\overset{+}{e}_a\right| + \left|\overset{-}{a}_1\overset{+}{b}_2\overset{-}{e}_a\right|$$

$$+ \left|\overset{+}{a}_1\overset{-}{b}_2\overset{-}{e}_a\right|\Bigr] - \Bigl[\left|\overset{-}{a}_1\overset{-}{b}_1\overset{+}{e}_b\right| + \left|\overset{-}{a}_1\overset{+}{b}_2\overset{-}{e}_b\right| + \left|\overset{+}{a}_1\overset{-}{b}_2\overset{-}{e}_b\right|\Bigr]\Bigr\}$$

$|30\rangle$ $^4E''(b_1b_2e)$

$$(6)^{-\frac{1}{2}}\Bigl\{\Bigl[\left|\overset{+}{b}_1\overset{+}{b}_2\overset{-}{e}_b\right| + \left|\overset{+}{b}_1\overset{-}{b}_2\overset{+}{e}_b\right| + \left|\overset{-}{b}_1\overset{+}{b}_2\overset{+}{e}_b\right|\Bigr] - i\Bigl[\left|\overset{+}{b}_1\overset{+}{b}_2\overset{-}{e}_a\right|$$

$$+ \left|\overset{+}{b}_1\overset{-}{b}_2\overset{+}{e}_a\right| + \left|\overset{-}{b}_1\overset{+}{b}_2\overset{+}{e}_a\right|\Bigr]\Bigr\};\ -(6)^{-\frac{1}{2}}\Bigl\{\Bigl[\left|\overset{-}{b}_1\overset{-}{b}_2\overset{+}{e}_b\right| + \left|\overset{-}{b}_1\overset{+}{b}_2\overset{-}{e}_b\right|$$

$$+ \left|\overset{+}{b}_1\overset{-}{b}_2\overset{-}{e}_b\right|\Bigr] + i\Bigl[\left|\overset{-}{b}_1\overset{-}{b}_2\overset{+}{e}_a\right| + \left|\overset{-}{b}_1\overset{+}{b}_2\overset{-}{e}_a\right| + \left|\overset{+}{b}_1\overset{-}{b}_2\overset{-}{e}_a\right|\Bigr]\Bigr\}$$

Table 2

Non-Zero strong field matrix elements of spin-orbit coupling, d^3, D_4^*

Representation Γ_6

Matrix Element	Value	Matrix Element	Value
$\langle 1^* \mid 7 \rangle$	$\frac{1}{3}\sqrt{6}\ i$	$\langle 3^* \mid 8 \rangle$	$\frac{1}{3}\sqrt{3}\ i$
$\langle 1^* \mid 12 \rangle$	$-\frac{1}{2}\sqrt{6}$	$\langle 3^* \mid 11 \rangle$	$\frac{1}{2}\sqrt{3}$
$\langle 1^* \mid 15 \rangle$	$\frac{1}{3}\sqrt{3}$	$\langle 3^* \mid 15 \rangle$	$\frac{1}{6}\sqrt{6}$
$\langle 1^* \mid 21 \rangle$	$-\frac{2}{3}\sqrt{3}\ i$	$\langle 3^* \mid 17 \rangle$	$\frac{1}{6}\sqrt{6}$
$\langle 1^* \mid 25 \rangle$	$\frac{1}{2}\sqrt{2}$	$\langle 3^* \mid 20 \rangle$	$-\frac{1}{2}\sqrt{3}$
$\langle 1^* \mid 28 \rangle$	$\frac{1}{6}\sqrt{6}\ i$	$\langle 3^* \mid 22 \rangle$	$-\frac{1}{3}\sqrt{6}\ i$
$\langle 2^* \mid 7 \rangle$	$\frac{1}{3}\sqrt{6}\ i$	$\langle 3^* \mid 25 \rangle$	$\frac{1}{2}$
$\langle 2^* \mid 13 \rangle$	$-\frac{1}{2}\sqrt{6}$	$\langle 3^* \mid 26 \rangle$	$\frac{1}{2}$
$\langle 2^* \mid 17 \rangle$	$\frac{1}{3}\sqrt{3}$	$\langle 3^* \mid 28 \rangle$	$\frac{1}{6}\sqrt{3}\ i$
$\langle 2^* \mid 21 \rangle$	$-\frac{2}{3}\sqrt{3}\ i$	$\langle 3^* \mid 29 \rangle$	$\frac{1}{6}\sqrt{3}$
$\langle 2^* \mid 26 \rangle$	$\frac{1}{2}\sqrt{2}$	$\langle 4^* \mid 10 \rangle$	i
$\langle 2^* \mid 29 \rangle$	$\frac{1}{6}\sqrt{6}\ i$	$\langle 4^* \mid 12 \rangle$	$-\frac{1}{2}$
$\langle 4^* \mid 14 \rangle$	$-\frac{1}{4}\sqrt{6}$	$\langle 5^* \mid 26 \rangle$	$\frac{1}{2}\sqrt{3}$
$\langle 4^* \mid 15 \rangle$	$-\frac{1}{4}\sqrt{2}$	$\langle 5^* \mid 27 \rangle$	$-\frac{1}{2}$
$\langle 4^* \mid 19 \rangle$	$-\frac{1}{6}\sqrt{6}$	$\langle 5^* \mid 29 \rangle$	$\frac{1}{2}i$

continued

Matrix Element	Value	Matrix Element	Value
$\langle 4^* \mid 20\rangle$	$-\frac{1}{2}$	$\langle 5^* \mid 30\rangle$	$-\frac{1}{6}\sqrt{3}\ i$
$\langle 4^* \mid 25\rangle$	$\frac{1}{2}\sqrt{3}$	$\langle 6^* \mid 15\rangle$	$\frac{1}{6}\sqrt{6}\ i$
$\langle 4^* \mid 27\rangle$	$-\frac{1}{2}$	$\langle 6^* \mid 17\rangle$	$-\frac{1}{6}\sqrt{6}\ i$
$\langle 4^* \mid 28\rangle$	$\frac{1}{2}\ i$	$\langle 6^* \mid 18\rangle$	$\frac{1}{4}\sqrt{6}\ i$
$\langle 4^* \mid 30\rangle$	$-\frac{1}{6}\sqrt{3}\ i$	$\langle 6^* \mid 19\rangle$	$\frac{3}{4}\sqrt{2}\ i$
$\langle 5^* \mid 9\ \rangle$	$-i$	$\langle 6^* \mid 25\rangle$	$-\frac{1}{2}i$
$\langle 5^* \mid 13\rangle$	$-\frac{1}{2}$	$\langle 6^* \mid 26\rangle$	$\frac{1}{2}i$
$\langle 5^* \mid 16\rangle$	$-\frac{1}{4}\sqrt{6}$	$\langle 6^* \mid 28\rangle$	$-\frac{1}{6}\sqrt{3}$
$\langle 5^* \mid 17\rangle$	$-\frac{1}{4}\sqrt{2}$	$\langle 6^* \mid 29\rangle$	$\frac{1}{6}\sqrt{3}$
$\langle 5^* \mid 18\rangle$	$\frac{1}{4}\sqrt{2}$	$\langle 7^* \mid 14\rangle$	$\frac{1}{6}\sqrt{6}\ i$
$\langle 5^* \mid 19\rangle$	$\frac{1}{12}\sqrt{6}$	$\langle 7^* \mid 15\rangle$	$\frac{1}{3}\sqrt{2}\ i$
$\langle 5^* \mid 20\rangle$	$-\frac{1}{2}$	$\langle 7^* \mid 16\rangle$	$\frac{1}{6}\sqrt{6}\ i$
$\langle 7^* \mid 17\rangle$	$\frac{1}{3}\sqrt{2}\ i$	$\langle 8^* \mid 25\rangle$	$-\frac{1}{6}\sqrt{3}\ i$
$\langle 7^* \mid 18\rangle$	$\frac{1}{4}\sqrt{2}\ i$	$\langle 8^* \mid 26\rangle$	$-\frac{1}{6}\sqrt{3}\ i$
$\langle 7^* \mid 19\rangle$	$-\frac{1}{12}\sqrt{6}\ i$	$\langle 8^* \mid 28\rangle$	$-\frac{1}{6}$
$\langle 7^* \mid 25\rangle$	$\frac{1}{6}\sqrt{3}\ i$	$\langle 8^* \mid 29\rangle$	$-\frac{1}{6}$

continued

Matrix Element	Value	Matrix Element	Value
$\langle 7^* \mid 26 \rangle$	$\frac{1}{6}\sqrt{3}\,i$	$\langle 9^* \mid 12 \rangle$	$\frac{1}{2}i$
$\langle 7^* \mid 27 \rangle$	i	$\langle 9^* \mid 14 \rangle$	$-\frac{1}{4}\sqrt{6}\,i$
$\langle 7^* \mid 28 \rangle$	$\frac{1}{6}$	$\langle 9^* \mid 15 \rangle$	$-\frac{1}{4}\sqrt{2}\,i$
$\langle 7^* \mid 29 \rangle$	$\frac{1}{6}$	$\langle 9^* \mid 19 \rangle$	$\frac{1}{6}\sqrt{6}\,i$
$\langle 7^* \mid 30 \rangle$	$\frac{1}{3}\sqrt{3}$	$\langle 9^* \mid 20 \rangle$	$\frac{1}{2}i$
$\langle 8^* \mid 11 \rangle$	$\frac{1}{2}i$	$\langle 9^* \mid 25 \rangle$	$-\frac{1}{2}\sqrt{3}\,i$
$\langle 8^* \mid 14 \rangle$	$\frac{1}{6}\sqrt{6}\,i$	$\langle 9^* \mid 27 \rangle$	$-\frac{1}{2}i$
$\langle 8^* \mid 15 \rangle$	$-\frac{1}{3}\sqrt{2}\,i$	$\langle 9^* \mid 28 \rangle$	$-\frac{1}{2}$
$\langle 8^* \mid 16 \rangle$	$\frac{1}{6}\sqrt{6}\,i$	$\langle 9^* \mid 30 \rangle$	$-\frac{1}{6}\sqrt{3}$
$\langle 8^* \mid 17 \rangle$	$-\frac{1}{3}\sqrt{2}\,i$	$\langle 10^* \mid 13 \rangle$	$-\frac{1}{2}i$
$\langle 8^* \mid 20 \rangle$	$\frac{1}{2}i$	$\langle 10^* \mid 16 \rangle$	$\frac{1}{4}\sqrt{6}\,i$
$\langle 10^* \mid 17 \rangle$	$\frac{1}{4}\sqrt{2}\,i$	$\langle 13^* \mid 18 \rangle$	$\frac{1}{2}\sqrt{2}$
$\langle 10^* \mid 18 \rangle$	$\frac{1}{4}\sqrt{2}\,i$	$\langle 13^* \mid 19 \rangle$	$-\frac{1}{6}\sqrt{6}$
$\langle 10^* \mid 19 \rangle$	$\frac{1}{12}\sqrt{6}\,i$	$\langle 13^* \mid 23 \rangle$	$\frac{1}{2}\sqrt{2}$
$\langle 10^* \mid 20 \rangle$	$-\frac{1}{2}i$	$\langle 13^* \mid 30 \rangle$	$-\frac{2}{3}\sqrt{3}\,i$
$\langle 10^* \mid 26 \rangle$	$\frac{1}{2}\sqrt{3}\,i$	$\langle 14^* \mid 15 \rangle$	$\frac{1}{6}\sqrt{3}$
$\langle 10^* \mid 27 \rangle$	$\frac{1}{2}i$	$\langle 14^* \mid 17 \rangle$	$\frac{1}{3}\sqrt{3}$

continued

Matrix Element	Value	Matrix Element	Value
$\langle 10^* \mid 29 \rangle$	$\frac{1}{2}$	$\langle 14^* \mid 21 \rangle$	$-\frac{1}{6}\sqrt{3}\,i$
$\langle 10^* \mid 30 \rangle$	$\frac{1}{6}\sqrt{3}$	$\langle 14^* \mid 22 \rangle$	$-\frac{1}{6}\sqrt{3}\,i$
$\langle 11^* \mid 11 \rangle$	$-\frac{1}{2}$	$\langle 14^* \mid 28 \rangle$	$-\frac{1}{6}\sqrt{6}\,i$
$\langle 11^* \mid 22 \rangle$	$\frac{1}{2}\sqrt{2}\,i$	$\langle 14^* \mid 29 \rangle$	$-\frac{1}{3}\sqrt{6}\,i$
$\langle 12^* \mid 12 \rangle$	$-\frac{1}{2}$	$\langle 15^* \mid 15 \rangle$	$\frac{1}{3}$
$\langle 12^* \mid 18 \rangle$	$\frac{1}{2}\sqrt{2}$	$\langle 15^* \mid 16 \rangle$	$\frac{1}{3}\sqrt{3}$
$\langle 12^* \mid 19 \rangle$	$-\frac{1}{6}\sqrt{6}$	$\langle 15^* \mid 17 \rangle$	$-\frac{2}{3}$
$\langle 12^* \mid 24 \rangle$	$-\frac{1}{2}\sqrt{2}\,i$	$\langle 15^* \mid 21 \rangle$	$\frac{1}{6}\,i$
$\langle 12^* \mid 30 \rangle$	$-\frac{2}{3}\sqrt{3}\,i$	$\langle 15^* \mid 22 \rangle$	$-\frac{1}{6}\,i$
$\langle 13^* \mid 13 \rangle$	$-\frac{1}{2}$	$\langle 15^* \mid 24 \rangle$	i
$\langle 15^* \mid 28 \rangle$	$\frac{1}{6}\sqrt{2}\,i$	$\langle 18^* \mid 21 \rangle$	$\frac{1}{2}\,i$
$\langle 15^* \mid 29 \rangle$	$-\frac{1}{3}\sqrt{2}\,i$	$\langle 18^* \mid 24 \rangle$	$\frac{1}{2}\,i$
$\langle 16^* \mid 17 \rangle$	$\frac{1}{6}\sqrt{3}$	$\langle 18^* \mid 30 \rangle$	$\frac{1}{6}\sqrt{6}\,i$
$\langle 16^* \mid 21 \rangle$	$-\frac{1}{6}\sqrt{3}\,i$	$\langle 19^* \mid 19 \rangle$	$-\frac{1}{3}$
$\langle 16^* \mid 22 \rangle$	$-\frac{1}{6}\sqrt{3}\,i$	$\langle 19^* \mid 21 \rangle$	$-\frac{1}{6}\sqrt{3}\,i$
$\langle 16^* \mid 28 \rangle$	$-\frac{1}{3}\sqrt{6}\,i$	$\langle 19^* \mid 23 \rangle$	$\frac{1}{3}\sqrt{3}$

continued

Matrix Element	Value	Matrix Element	Value
$\langle 16^* \mid 29 \rangle$	$-\frac{1}{6}\sqrt{6}\, i$	$\langle 19^* \mid 24 \rangle$	$\frac{1}{6}\sqrt{3}\, i$
$\langle 17^* \mid 17 \rangle$	$\frac{1}{3}$	$\langle 19^* \mid 30 \rangle$	$-\frac{1}{6}\sqrt{2}\, i$
$\langle 17^* \mid 21 \rangle$	$\frac{1}{6}\, i$	$\langle 20^* \mid 20 \rangle$	$\frac{1}{2}$
$\langle 17^* \mid 22 \rangle$	$-\frac{1}{6}\, i$	$\langle 20^* \mid 22 \rangle$	$\frac{1}{2}\sqrt{2}\, i$
$\langle 17^* \mid 23 \rangle$	-1	$\langle 20^* \mid 23 \rangle$	$\frac{1}{2}\sqrt{2}$
$\langle 17^* \mid 28 \rangle$	$-\frac{1}{3}\sqrt{2}\, i$	$\langle 20^* \mid 24 \rangle$	$-\frac{1}{2}\sqrt{2}\, i$
$\langle 17^* \mid 29 \rangle$	$\frac{1}{6}\sqrt{2}\, i$	$\langle 21^* \mid 25 \rangle$	$-\frac{1}{6}\sqrt{6}\, i$
$\langle 18^* \mid 19 \rangle$	$-\frac{1}{6}\sqrt{3}$	$\langle 21^* \mid 26 \rangle$	$-\frac{1}{6}\sqrt{6}\, i$
$\langle 21^* \mid 27 \rangle$	$\frac{1}{2}\sqrt{2}\, i$	$\langle 25^* \mid 26 \rangle$	-1
$\langle 21^* \mid 28 \rangle$	$\frac{1}{3}\sqrt{2}$	$\langle 26^* \mid 26 \rangle$	$\frac{1}{2}$
$\langle 21^* \mid 29 \rangle$	$\frac{1}{3}\sqrt{2}$	$\langle 27^* \mid 27 \rangle$	$-\frac{1}{2}$
$\langle 21^* \mid 30 \rangle$	$-\frac{1}{3}\sqrt{6}$	$\langle 28^* \mid 28 \rangle$	$\frac{1}{6}$
$\langle 22^* \mid 25 \rangle$	$\frac{1}{6}\sqrt{6}\, i$	$\langle 28^* \mid 29 \rangle$	$-\frac{1}{3}$
$\langle 22^* \mid 26 \rangle$	$\frac{1}{6}\sqrt{6}\, i$	$\langle 29^* \mid 29 \rangle$	$\frac{1}{6}$
$\langle 22^* \mid 28 \rangle$	$-\frac{1}{3}\sqrt{2}$	$\langle 30^* \mid 30 \rangle$	$-\frac{1}{6}$
$\langle 22^* \mid 29 \rangle$	$-\frac{1}{3}\sqrt{2}$		
$\langle 23^* \mid 24 \rangle$	1		

continued

Matrix Element	Value	Matrix Element	Value
$\langle 23^* \mid 29 \rangle$	$-\frac{1}{2}\sqrt{2}\ i$		
$\langle 23^* \mid 30 \rangle$	$\frac{1}{6}\sqrt{6}\ i$		
$\langle 24^* \mid 28 \rangle$	$\frac{1}{2}\sqrt{2}$		
$\langle 24^* \mid 30 \rangle$	$-\frac{1}{6}\sqrt{6}$		
$\langle 25^* \mid 25 \rangle$	$\frac{1}{2}$		

Representation Γ_7

Matrix Element	Value	Matrix Element	Value
$\langle 1^* \mid 6 \rangle$	i	$\langle 3^* \mid 17 \rangle$	$\frac{1}{6}\sqrt{6}\ i$
$\langle 1^* \mid 11 \rangle$	$-\frac{1}{2}\sqrt{2}\ i$	$\langle 3^* \mid 20 \rangle$	$-\frac{1}{2}\sqrt{3}\ i$
$\langle 1^* \mid 14 \rangle$	$\frac{1}{2}\sqrt{3}\ i$	$\langle 3^* \mid 25 \rangle$	$\frac{1}{2}i$
$\langle 1^* \mid 15 \rangle$	$\frac{1}{2}\ i$	$\langle 3^* \mid 26 \rangle$	$-\frac{1}{2}i$
$\langle 1^* \mid 25 \rangle$	$\frac{1}{2}\sqrt{6}\ i$	$\langle 3^* \mid 28 \rangle$	$\frac{1}{6}\sqrt{3}$
$\langle 1^* \mid 28 \rangle$	$\frac{1}{2}\sqrt{2}$	$\langle 3^* \mid 29 \rangle$	$-\frac{1}{6}\sqrt{3}$
$\langle 2^* \mid 7 \rangle$	$-i$	$\langle 4^* \mid 9 \rangle$	$\frac{1}{3}\sqrt{3}\ i$
$\langle 2^* \mid 13 \rangle$	$-\frac{1}{2}\sqrt{2}\ i$	$\langle 4^* \mid 10 \rangle$	i
$\langle 2^* \mid 19 \rangle$	$-\frac{1}{3}\sqrt{3}\ i$	$\langle 4^* \mid 12 \rangle$	$\frac{1}{2}i$

continued

Matrix Element	Value	Matrix Element	Value
$\langle 2^* \mid 27\rangle$	$\frac{1}{2}\sqrt{2}\ i$	$\langle 4^* \mid 14\rangle$	$\frac{1}{4}\sqrt{6}\ i$
$\langle 2^* \mid 30\rangle$	$\frac{1}{6}\sqrt{6}$	$\langle 4^* \mid 15\rangle$	$\frac{1}{4}\sqrt{2}\ i$
$\langle 3^* \mid 11\rangle$	$-\frac{1}{2}\sqrt{3}\ i$	$\langle 4^* \mid 19\rangle$	$-\frac{1}{6}\sqrt{6}\ i$
$\langle 3^* \mid 15\rangle$	$-\frac{1}{6}\sqrt{6}\ i$	$\langle 4^* \mid 20\rangle$	$-\frac{1}{2}i$
$\langle 4^* \mid 24\rangle$	$-\frac{1}{3}\sqrt{6}\ i$	$\langle 5^* \mid 27\rangle$	$-\frac{1}{6}\sqrt{3}\ i$
$\langle 4^* \mid 25\rangle$	$\frac{1}{2}\sqrt{3}\ i$	$\langle 5^* \mid 29\rangle$	$\frac{1}{6}\sqrt{3}$
$\langle 4^* \mid 27\rangle$	$\frac{1}{2}i$	$\langle 5^* \mid 30\rangle$	$-\frac{1}{6}$
$\langle 4^* \mid 28\rangle$	$\frac{1}{2}$	$\langle 6^* \mid 11\rangle$	$\frac{1}{2}\sqrt{2}$
$\langle 4^* \mid 30\rangle$	$\frac{1}{6}\sqrt{3}$	$\langle 6^* \mid 16\rangle$	$-\frac{1}{2}\sqrt{3}$
$\langle 5^* \mid 9\rangle$	$\frac{1}{3}i$	$\langle 6^* \mid 17\rangle$	$-\frac{1}{2}$
$\langle 5^* \mid 10\rangle$	$-\frac{1}{3}\sqrt{3}\ i$	$\langle 6^* \mid 26\rangle$	$\frac{1}{2}\sqrt{6}$
$\langle 5^* \mid 13\rangle$	$\frac{1}{6}\sqrt{3}\ i$	$\langle 6^* \mid 29\rangle$	$\frac{1}{2}\sqrt{2}\ i$
$\langle 5^* \mid 16\rangle$	$-\frac{3}{4}\sqrt{2}\ i$	$\langle 7^* \mid 12\rangle$	$\frac{1}{2}\sqrt{2}$
$\langle 5^* \mid 17\rangle$	$\frac{1}{12}\sqrt{6}\ i$	$\langle 7^* \mid 18\rangle$	$-\frac{1}{2}$
$\langle 5^* \mid 18\rangle$	$\frac{1}{4}\sqrt{6}\ i$	$\langle 7^* \mid 19\rangle$	$-\frac{1}{6}\sqrt{3}$
$\langle 5^* \mid 19\rangle$	$-\frac{1}{12}\sqrt{2}\ i$	$\langle 7^* \mid 27\rangle$	$\frac{1}{2}\sqrt{2}$
$\langle 5^* \mid 20\rangle$	$\frac{1}{6}\sqrt{3}\ i$	$\langle 7^* \mid 30\rangle$	$\frac{1}{6}\sqrt{6}\ i$

continued

Matrix Element	Value	Matrix Element	Value
$\langle 5^* \mid 24\rangle$	$\frac{2}{3}\sqrt{2}\ i$	$\langle 8^* \mid 11\rangle$	$\frac{1}{2}\sqrt{3}$
$\langle 5^* \mid 26\rangle$	$\frac{1}{2}\ i$	$\langle 8^* \mid 15\rangle$	$-\frac{1}{6}\sqrt{6}$
$\langle 8^* \mid 17\rangle$	$\frac{1}{6}\sqrt{6}$	$\langle 9^* \mid 27\rangle$	$\frac{1}{6}\sqrt{3}$
$\langle 8^* \mid 20\rangle$	$\frac{1}{2}\sqrt{3}$	$\langle 9^* \mid 28\rangle$	$-\frac{1}{6}\sqrt{3}\ i$
$\langle 8^* \mid 25\rangle$	$-\frac{1}{2}$	$\langle 9^* \mid 30\rangle$	$\frac{1}{6}\ i$
$\langle 8^* \mid 26\rangle$	$\frac{1}{2}$	$\langle 10^* \mid 13\rangle$	$-\frac{1}{2}$
$\langle 8^* \mid 28\rangle$	$-\frac{1}{6}\sqrt{3}\ i$	$\langle 10^* \mid 16\rangle$	$-\frac{1}{4}\sqrt{6}$
$\langle 8^* \mid 29\rangle$	$\frac{1}{6}\sqrt{3}\ i$	$\langle 10^* \mid 17\rangle$	$-\frac{1}{4}\sqrt{2}$
$\langle 9^* \mid 12\rangle$	$\frac{1}{6}\sqrt{3}$	$\langle 10^* \mid 18\rangle$	$-\frac{1}{4}\sqrt{2}$
$\langle 9^* \mid 14\rangle$	$-\frac{3}{4}\sqrt{2}$	$\langle 10^* \mid 19\rangle$	$-\frac{1}{12}\sqrt{6}$
$\langle 9^* \mid 15\rangle$	$\frac{1}{12}\sqrt{6}$	$\langle 10^* \mid 20\rangle$	$\frac{1}{2}$
$\langle 9^* \mid 18\rangle$	$\frac{1}{6}\sqrt{6}$	$\langle 10^* \mid 23\rangle$	$-\frac{1}{3}\sqrt{6}$
$\langle 9^* \mid 19\rangle$	$-\frac{1}{3}\sqrt{2}$	$\langle 10^* \mid 26\rangle$	$\frac{1}{2}\sqrt{3}$
$\langle 9^* \mid 20\rangle$	$\frac{1}{6}\sqrt{3}$	$\langle 10^* \mid 27\rangle$	$\frac{1}{2}$
$\langle 9^* \mid 23\rangle$	$-\frac{2}{3}\sqrt{2}\ i$	$\langle 10^* \mid 29\rangle$	$\frac{1}{2}\ i$
$\langle 9^* \mid 25\rangle$	$-\frac{1}{2}$	$\langle 10^* \mid 30\rangle$	$\frac{1}{6}\sqrt{3}\ i$

continued

Matrix Element	Value	Matrix Element	Value
$\langle 11^* \mid 11\rangle$	$\frac{1}{2}$	$\langle 14^* \mid 22\rangle$	$-\frac{1}{2}$
$\langle 11^* \mid 22\rangle$	$\frac{1}{2}\sqrt{6}$	$\langle 14^* \mid 28\rangle$	$\frac{1}{6}\sqrt{6}\ i$
$\langle 12^* \mid 12\rangle$	$\frac{1}{2}$	$\langle 14^* \mid 29\rangle$	$\frac{1}{3}\sqrt{6}\ i$
$\langle 12^* \mid 18\rangle$	$-\frac{1}{2}\sqrt{2}$	$\langle 15^* \mid 15\rangle$	$-\frac{1}{3}$
$\langle 12^* \mid 19\rangle$	$\frac{1}{6}\sqrt{6}$	$\langle 15^* \mid 16\rangle$	$-\frac{1}{3}\sqrt{3}$
$\langle 12^* \mid 24\rangle$	$-\frac{1}{6}\sqrt{6}$	$\langle 15^* \mid 17\rangle$	$\frac{2}{3}$
$\langle 12^* \mid 30\rangle$	$\frac{2}{3}\sqrt{3}\ i$	$\langle 15^* \mid 21\rangle$	$\frac{1}{6}\sqrt{3}$
$\langle 13^* \mid 13\rangle$	$\frac{1}{2}$	$\langle 15^* \mid 22\rangle$	$-\frac{1}{6}\sqrt{3}$
$\langle 13^* \mid 18\rangle$	$-\frac{1}{2}\sqrt{2}$	$\langle 15^* \mid 24\rangle$	$\frac{1}{3}\sqrt{3}$
$\langle 13^* \mid 19\rangle$	$\frac{1}{6}\sqrt{6}$	$\langle 15^* \mid 28\rangle$	$-\frac{1}{6}\sqrt{2}\ i$
$\langle 13^* \mid 23\rangle$	$\frac{1}{6}\sqrt{6}\ i$	$\langle 15^* \mid 29\rangle$	$\frac{1}{3}\sqrt{2}\ i$
$\langle 13^* \mid 30\rangle$	$\frac{2}{3}\sqrt{3}\ i$	$\langle 16^* \mid 17\rangle$	$-\frac{1}{6}\sqrt{3}$
$\langle 14^* \mid 15\rangle$	$-\frac{1}{6}\sqrt{3}$	$\langle 16^* \mid 21\rangle$	$-\frac{1}{2}$
$\langle 14^* \mid 17\rangle$	$-\frac{1}{3}\sqrt{3}$	$\langle 16^* \mid 22\rangle$	$-\frac{1}{2}$
$\langle 14^* \mid 21\rangle$	$-\frac{1}{2}$	$\langle 16^* \mid 28\rangle$	$\frac{1}{3}\sqrt{6}\ i$
$\langle 16^* \mid 29\rangle$	$\frac{1}{6}\sqrt{6}\ i$	$\langle 19^* \mid 24\rangle$	$\frac{1}{6}$
$\langle 17^* \mid 17\rangle$	$-\frac{1}{3}$	$\langle 19^* \mid 30\rangle$	$\frac{1}{6}\sqrt{2}\ i$

continued

Matrix Element	Value	Matrix Element	Value
$\langle 17^* \mid 21\rangle$	$\frac{1}{6}\sqrt{3}$	$\langle 20^* \mid 20\rangle$	$-\frac{1}{2}$
$\langle 17^* \mid 22\rangle$	$-\frac{1}{6}\sqrt{3}$	$\langle 20^* \mid 22\rangle$	$\frac{1}{2}\sqrt{6}$
$\langle 17^* \mid 23\rangle$	$-\frac{1}{3}\sqrt{3}\ i$	$\langle 20^* \mid 23\rangle$	$\frac{1}{6}\sqrt{6}\ i$
$\langle 17^* \mid 28\rangle$	$\frac{1}{3}\sqrt{2}\ i$	$\langle 20^* \mid 24\rangle$	$-\frac{1}{6}\sqrt{6}$
$\langle 17^* \mid 29\rangle$	$-\frac{1}{6}\sqrt{2}\ i$	$\langle 21^* \mid 28\rangle$	$-\frac{1}{6}\sqrt{6}\ i$
$\langle 18^* \mid 19\rangle$	$\frac{1}{6}\sqrt{3}$	$\langle 21^* \mid 29\rangle$	$-\frac{1}{6}\sqrt{6}\ i$
$\langle 18^* \mid 21\rangle$	$\frac{1}{2}\sqrt{3}$	$\langle 21^* \mid 30\rangle$	$\frac{1}{2}\sqrt{2}\ i$
$\langle 18^* \mid 24\rangle$	$\frac{1}{6}\sqrt{3}$	$\langle 22^* \mid 28\rangle$	$\frac{1}{6}\sqrt{6}\ i$
$\langle 18^* \mid 30\rangle$	$-\frac{1}{6}\sqrt{6}\ i$	$\langle 22^* \mid 29\rangle$	$\frac{1}{6}\sqrt{6}\ i$
$\langle 19^* \mid 19\rangle$	$\frac{1}{3}$	$\langle 23^* \mid 24\rangle$	$-\frac{1}{3}\,i$
$\langle 19^* \mid 21\rangle$	$-\frac{1}{2}$	$\langle 23^* \mid 26\rangle$	$-\frac{1}{2}\sqrt{2}\ i$
$\langle 19^* \mid 23\rangle$	$\frac{1}{3}\,i$	$\langle 23^* \mid 27\rangle$	$\frac{1}{6}\sqrt{6}$
$\langle 23^* \mid 29\rangle$	$\frac{1}{3}\sqrt{6}$		
$\langle 23^* \mid 30\rangle$	$-\frac{1}{3}\sqrt{2}$		
$\langle 24^* \mid 25\rangle$	$\frac{1}{2}\sqrt{2}$		
$\langle 24^* \mid 27\rangle$	$-\frac{1}{6}\sqrt{6}$		

continued

Matrix Element	Value	Matrix Element	Value
$\langle 24^* \mid 28 \rangle$	$-\frac{1}{3}\sqrt{6}\ i$		
$\langle 24^* \mid 30 \rangle$	$\frac{1}{3}\sqrt{2}\ i$		
$\langle 25^* \mid 25 \rangle$	$-\frac{1}{2}$		
$\langle 25^* \mid 26 \rangle$	1		
$\langle 26^* \mid 26 \rangle$	$-\frac{1}{2}$		
$\langle 27^* \mid 27 \rangle$	$\frac{1}{2}$		
$\langle 28^* \mid 28 \rangle$	$-\frac{1}{6}$		
$\langle 28^* \mid 29 \rangle$	$\frac{1}{3}$		
$\langle 29^* \mid 29 \rangle$	$-\frac{1}{6}$		
$\langle 30^* \mid 30 \rangle$	$\frac{1}{6}$		

Revue Roumaine de Chimie, 17, 8, 1313 – 1326 (1972)

THE USE OF THE DIGITAL COMPUTER IN PHENOMENOLOGICAL THERMODYNAMICS. II*

RELTET – computation program for the application of linear regressions to the thermodynamics of molten electrolytes

M. CIOPEC and D. I. MARCHIDAN
Centre of Physical Chemistry, str. Galaţi 31
Bucharest, Romania

Received March 14, 1972

The computation program advanced by us is written in the FORTRAN language and is adapted for IBM-system 300/30 computers. For sets of 100 pairs of experimental data the computation duration does not exceed 2 minutes. RELTET enables the processing of physico-chemical and thermodynamic magnitudes varying according to an exponential, logarithmical or linear law. The program provides for the listing of all experimental and calculated data as well as of absolute, relative and standard errors.

★

The thermodynamic studies of molten salts, the measurements of the physical and chemical properties of these systems, laying at the limit between the liquid and the solid state, gained more and more ground in the last decades[1,2] so that a considerable amount of data and scientific knowledge has been accumulated.

The experimental techniques used to investigate such systems have been improved and diversified, the theoretical concepts evolved while the phenomena occurring in molten salts have been thoroughly studied.

Simultaneously, the application domains of molten salts have been extended up to, e.g. the metallurgy of light and non-ferrous metals, chemical technology, nuclear energetics a.s.o. The research developed around the technological use of molten salts enjoyed a rapid progress, the thermodynamics of such systems acquiring ever growing significance.

One of the teams specialized in the theoretical and experimental research of molten salts (ionic liquids) works within the Centre of Physical Chemistry, where measurements of the various physico-chemical and thermodynamical properties of molten salts, both separately and in mixtures, are being carried through.

To process the experimental data, a result of the work of the above team, obtained by various experimental techniques, we set forth a computational program written in the FORTRAN language, able to carry out the regressional analysis by the least squares methods, with possible applications to other experimental data referring to properties with variation laws similar to those met in the case of molten salts.

---

* Previous part, M. Ciopec and D. I. Marchidan, *Rev. Roumaine Chim.*, **17**, 1137 (1972).

[1] I. G. Murgulescu, in "Thermodynamics of nuclear materials, 1967", International Atomic Energy Agency, Vienna, 1968, p. 91.

[2] I. G. Murgulescu, *Rev. Roumaine de Chim.*, **14**, 965 (1969).

PHYSICO-CHEMICAL AND THERMODYNAMIC PROPERTIES OF MOLTEN SALTS CONSIDERED IN THE ELABORATION OF THE PROGRAM

The systems of molten salts investigated by various experimental techniques, possess physico-chemical and thermodynamical properties which mainly depend on the temperature according to laws of the following type.

VAPOUR PRESSURE OF SIMPLE MOLTEN SALTS

The change in the vapour pressure of a liquid with temperature may be obtained by the integration of the Clapeyron equation

$$d \ln P/d\ (1/T) = -\Delta H_{\mathrm{vap}}/R \tag{1}$$

When the vaporization heat is considered as temperature-independent, an equation is obtained, of the form

$$\log P = A + B/T \tag{2}$$

For large temperature ranges

$$(\partial/\partial T)H_{\mathrm{vap}} = \Delta C_{\mathrm{p}} \tag{3}$$

while the equation of the vapour pressure becomes

$$\log P = -(\Delta H_0/2.303\ RT) + (\Delta C_{\mathrm{p}}/R) \log T + I \tag{4}$$

i.e. an equation of the form

$$\log P = A + (B/T) + C \log T \tag{5}$$

where $C = \Delta C_{\mathrm{p}}/R$, a constant characteristic of given species.

Eqs. (2), (4), (5) are the most frequently used in the literature for the calculation of the dependence of vapour pressure of molten salts on the temperature. [3-5]

---

[3] L. Marta, *Studii şi Cercetări Chim. Acad. R.P.R.*, **14**, 729 (1966).

[4] I. G. Murgulescu and L. Topor, *Rev. Roumaine de Chim.*, **11**, 457 (1966).

[5] I. G. Murgulescu and L. Marta, in "Thermodynamics", vol. 1, Proc. Conf. Viena 1965, I.A.E.A. Vienna, 1966, p. 345.

VISCOSITY OF MOLTEN SALTS

The systematic study of the viscosity of alkaline halides [6,7] showed that the variation of viscosity with temperature is faithfully expressed by an Arrhenius type relation

$$\eta = A\exp\,(E_{\text{visc}}/RT) \tag{6}$$

where E_{visc} is the activation energy for the viscous flow.

It has been found that also the viscosity of binary mixtures of molten salts is varying with the temperature according to an experimental relation of the Arrhenius type.[8]

$$\eta_m = A_m \exp\,(E_{\text{visc}}/RT) \tag{7}$$

Both the activation energy, E_{visc}, and pre-exponential constant A_m depend on the mixture composition.

The pre-exponential factor A has a well defined kinetical molecular significance.

DENSITY AND CONDUCTIVITY OF MOLTEN SALTS

The study of individual molten salts and of their mixtures shows that for temperatures greater than the melting point, the experimental results on the density and the electrical conductivity may be accurately represented by the following equations [9]:

$$d = A - BT \tag{8}$$

$$\lambda = A\exp\,(-E/RT) \tag{9}$$

where d = density, λ = equivalent conductivity, E – the activation energy of the conductivity, A, B = constants characteristic of each system under consideration.

E.M.F. OF FORMATION CELLS WITH BINARY OR RECIPROCAL MIXTURES OF MOLTEN SALTS

The e.m.f. yielded by the formation cells of the type

$A(s) \mid AX\,(l),\ BX\,(l) \mid X_2\,(g, 1\ \text{At})$ graphit or

$A(s) \mid AX\,(l),\ BY\,(l) \mid X_2\,(g, 1\ \text{At})$ graphit

---

[6] St. Zuca, Dissertation, Universitatea București, 1964.

[7] I. G. Murgulescu and St. Zuca, in "Chimia fizică a electroliţilor topiţi", Acad. R.P.R., Institutul de studii Româno-Sovietic, București 1963, p. 209.

[8] I. Galasiu, *Studii și Cercetări Chim. Acad. R.P.R.*, **18**, (1970), p. 293.

[9] St. Zuca and M. Olteanu, *Rev. Roumaine de Chim.*, **13**, (1968), p. 1567.

depend on temperature and on the molar fractions of the components. For a certain molar fraction

$$E = f(T) = a + b\,T \tag{10}$$

Studying this dependence for various molar fractions valuable information may be obtained on the thermodynamic partially molar magnitudes of the components in the melt and on the excess magnitudes in binary or reciprocal mixtures of the molten salts. The excess magnitudes thus obtained may be compared with theoretically estimated magnitudes, the validity of the various theories being thus checked.[10]

THE (INTER) DIFFUSION COEFFICIENT IN MOLTEN SALTS

The application of the chromopotentiometric method to the determination of the interdiffusion coefficient of a metallic ion in molten salts provides valuable information on the structure of the melt.[11] This kinetic-molecular characteristic is varying with the temperature according to a law of the type

$$D = D_0 \exp\ (-E/RT) \tag{11}$$

ELABORATION OF THE COMPUTATION PROGRAM

In the elaboration of the RELTET program account has been taken of the fact that an analysis of the rel. (6), (7), (9), (11) points to a similar dependence on temperature of the measured physico-chemical properties.

By denoting the experimentally measured magnitude by the general symbol F (function), the above variation laws may be written as follows

$$F = A_0 \exp\ (E/T) \tag{12}$$

or by means of logarithms

$$\ln F = \ln A_0 + (E/T) \tag{13}$$

passing from the logarithm in base 10

$$\log F = \log A_0 + (E/2.303)\ T \tag{14}$$

Introducing notations

$$\log A_0 = A \quad \text{and} \quad E/2.303 = B$$

rel. (14) becomes

---

[10] S. Sternberg and L. Bejan, *Rev. Roumaine de Chim.*, **14**, 303 (1969).

[11] S. Sternberg and C. Herdlicka, *Rev. Roumaine de Chim.*, **14**, 991 (1969).

$$\log F = A + (B/T) \tag{15}$$

The variation law (15) is also characteristic of the vapour pressure (rel. 2). Rel. (5) becomes identical with rels. (2) and (15) when $C = 0$, so that the general relation for which the computation program is to be elaborated, will be

$$\log F = A + (B/T) + U \log T \tag{16}$$

where U = a pre-calculated numerical constant characteristic of each system separately. Constant U differs from 0 for vapour pressures and is equal to zero for the rest of the measured magnitudes.

By separating the terms affected by coefficients A and B from the other terms and carrying out the substitutions, we get

$$\log F - U \log T = Y$$

$$1/T = X$$

in this case eq. (16) becomes

$$Y = A + BX \tag{17}$$

where Y is the function, X the argument and A, B, the regression coefficients which should be deduced by processing the experimental results by the method of the least squares.

As noticed, both density and e.m.f. (rels. (8), (10)) vary according to a relation of the type (17).

The deduction of coefficients A and B occurs provided that the sum of the squares of deviations

$$S = \sum_{1}^{N} [Y - (A + B X)]^2 \tag{18}$$

should be minimum:

$$(\partial/\partial A)S = 0 \qquad \text{and} \qquad (\partial/\partial B)S = 0$$

which is tantamount to the solving of a system of two equations with two unknowns (A and B). To this end we can make use of Kramer's law.

Subsequent to the deduction of regression coefficients and the establishing of the form of eq. (17), the calculation of the deviations of the experimental data as compared to those calculated becomes necessary. From these deviations the standard deviation is then calculated

$$\sigma = \pm\sqrt{S/(N-1)} \tag{19}$$

where N = the number of determinations.

The calculational errors for the regression coefficients are given by formula [12]:

$$\Delta A = \pm\sigma \sqrt{(\Sigma X^2)/[N\,\Sigma X^2-(\Sigma X)^2]} \tag{20}$$

$$\Delta B = \pm\sigma \sqrt{N^2/[N\,\Sigma X^2-(\Sigma X)^2]} \tag{21}$$

For transport phenomena the activation energy $E = R.B$ and the magnitude

$$\Delta E = R.\ \Delta B \tag{22}$$

should be necessarily known since they enable the estimation of the determination accuracy of this characteristic.

Since the data which underwent regression have been ($\log F - U \log T$) and $1/T$, the standard error does not refer to the experimentally measured F magnitude. To calculate the standard deviation of experimental F from the calculated F the following formula is used, in order to determine F based on eq. (17), by considering the calculated regression coefficients A and B

$$F_{\text{calc}} = \text{exp. } 10\ (Y_{\text{calc}} + U \log T) \tag{23}$$

The standard deviation

$$\sigma' = \pm \sqrt{[\Sigma\,(F_{\text{exp}} - F_{\text{calc}})^2]/\,(N-1)} \tag{24}$$

is calculated from the deviations ($F_{\text{exp}} - F_{\text{calc}}$), which strictly refers to the experimentally measured magnitude. The present standard deviation is similarly calculated.

By means of formulae (17)–(24), the computation program RELTET has been written in the FORTRAN language (variant FULL FORTRAN) according to the next logical scheme

1

Read the experimental data and the constants characteristic of the system : $N\,F$, T (in °C), U, R

↓

2

$Y = \log F - U \log (T + 273.15)$

$X = 1/(T + 273.15)$

↓

3

$A_{11} = N$

$A_{12} = \Sigma X \quad B_1 = \Sigma Y$

$A_{21} = A_{12} \quad B_2 = \Sigma\,(X\,.\,Y)$

$A_{22} = \Sigma\,(X)^2$

$\text{DET} = A_{11}\,.\,A_{22} - A_{12}\,.\,A_{21}$

↓

4

---

[12] J. Carré, Thèse, No. 559, 1969, Lyon.

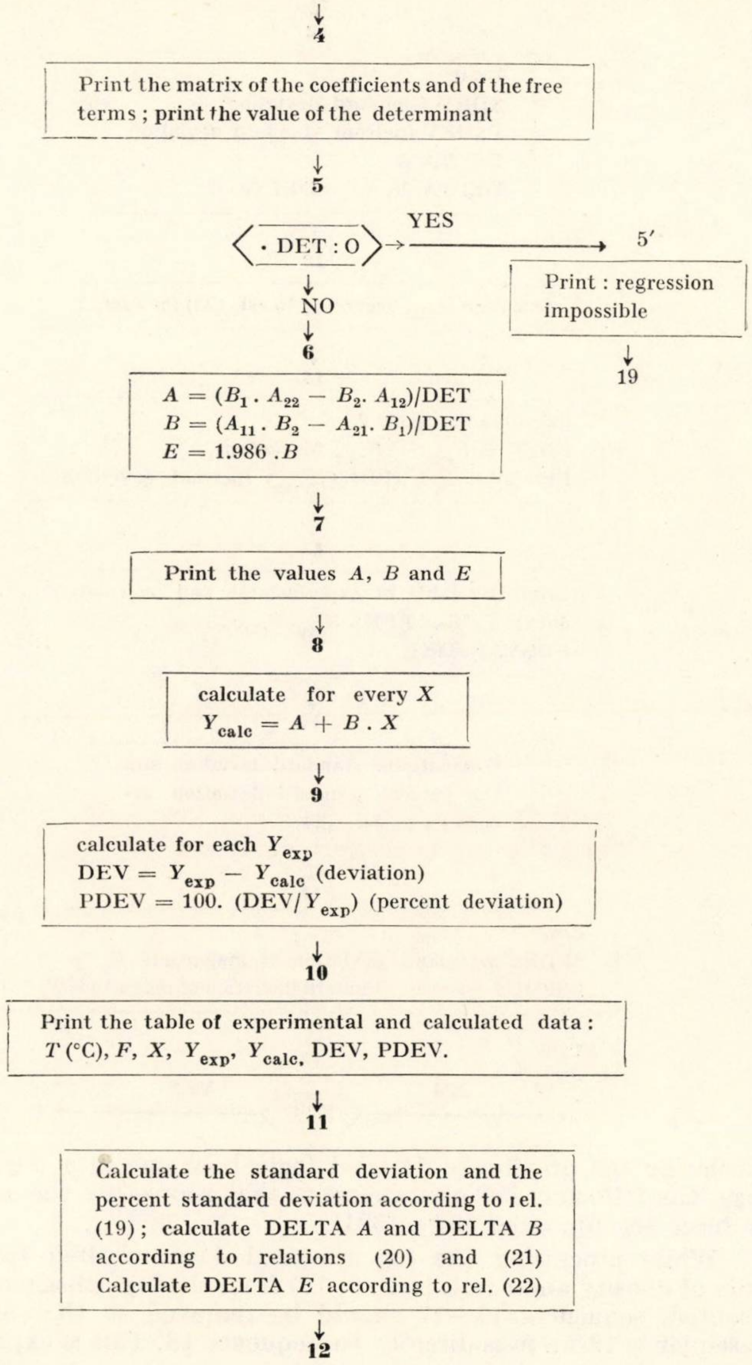

Print the matrix of the coefficients and of the free terms ; print the value of the determinant

DET : 0

Print : regression impossible

$A = (B_1 . A_{22} - B_2 . A_{12})/\mathrm{DET}$
$B = (A_{11} . B_2 - A_{21} . B_1)/\mathrm{DET}$
$E = 1.986 . B$

Print the values A, B and E

calculate for every X
$Y_{\mathrm{calc}} = A + B . X$

calculate for each Y_{exp}
$\mathrm{DEV} = Y_{\mathrm{exp}} - Y_{\mathrm{calc}}$ (deviation)
$\mathrm{PDEV} = 100. (\mathrm{DEV}/Y_{\mathrm{exp}})$ (percent deviation)

Print the table of experimental and calculated data : T (°C), F, X, Y_{exp}, $Y_{\mathrm{calc.}}$ DEV, PDEV.

Calculate the standard deviation and the percent standard deviation according to rel. (19) ; calculate DELTA A and DELTA B according to relations (20) and (21) Calculate DELTA E according to rel. (22)

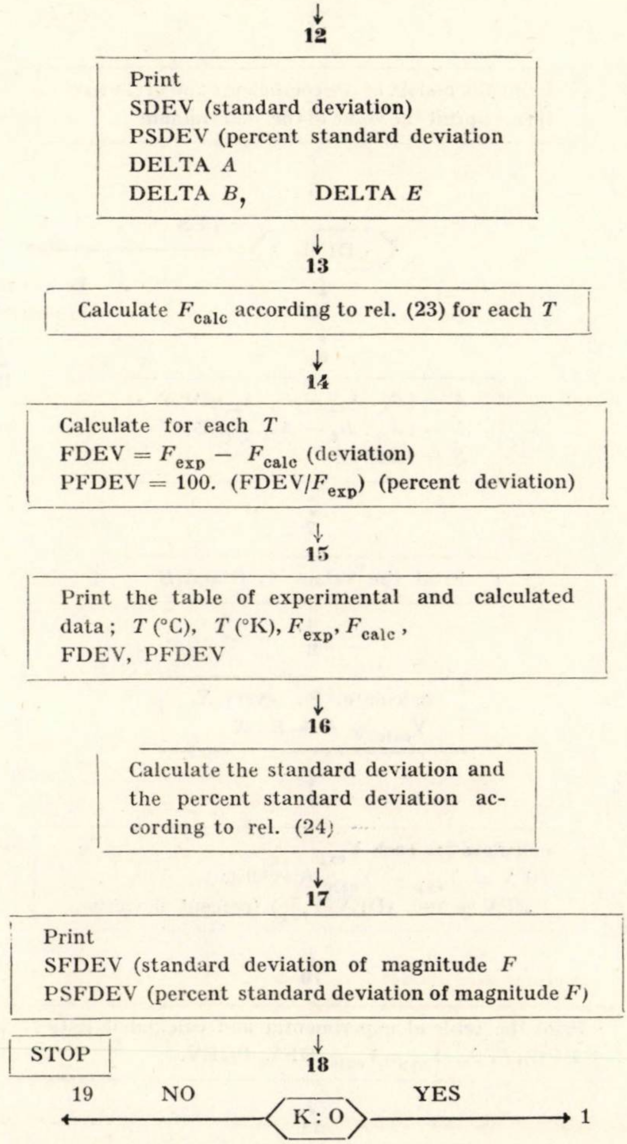
12
Print
SDEV (standard deviation)
PSDEV (percent standard deviation
DELTA A
DELTA B, DELTA E
13
Calculate F_{calc} according to rel. (23) for each T
14
Calculate for each T
FDEV = F_{exp} − F_{calc} (deviation)
PFDEV = 100. (FDEV/F_{exp}) (percent deviation)
15
Print the table of experimental and calculated data ; T (°C), T (°K), F_{exp}, F_{calc},
FDEV, PFDEV
16
Calculate the standard deviation and the percent standard deviation according to rel. (24)
17
Print
SFDEV (standard deviation of magnitude F
PSFDEV (percent standard deviation of magnitude F)
STOP
18
19
NO
K : O
YES
1

Translating the previously detailed logical scheme into FORTRAN language, the following list of statements that represents the source module has been set up. (See page 1321).

While processing the experimental data resulted from measurements of density and e.m.f. (rels. 8, 10) from the logical scheme previously presented, sequences 13—17 should be removed so that after carrying out sequence 12 we pass directly to sequence 18. This is expressed by the following changes of the source program

— statements 3, 12, 15 — 19, 23, 27, 69 — 83 are omitted

SOURCE MODULE

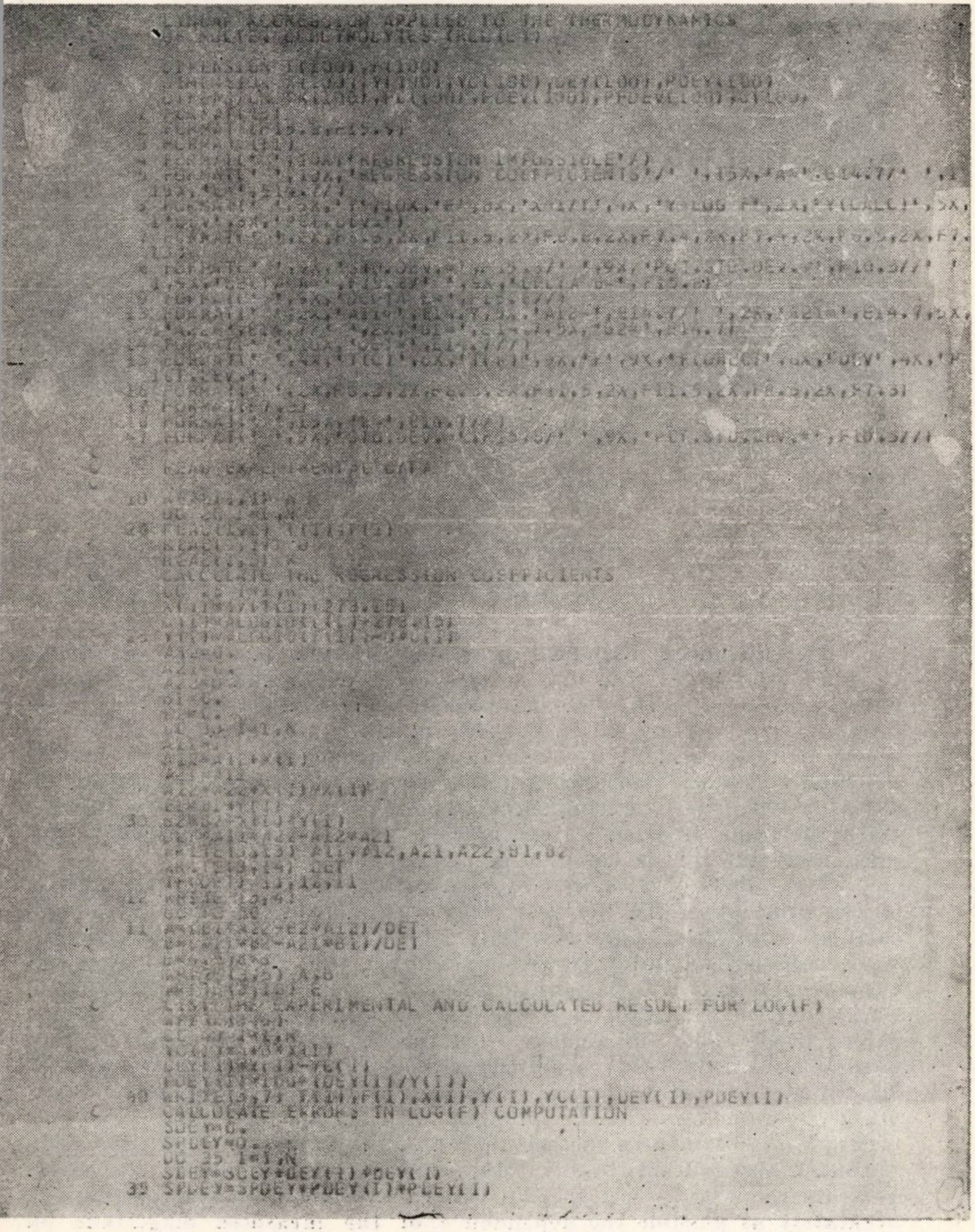

```
C     LINEAR REGRESSION APPLIED TO THE THERMODYNAMICS
C     OF MOLTEN ELECTROLYTES [illegible]
      DIMENSION T(100),F(100)
      DIMENSION X(100),Y(100),YC(100),DEY(100),PDEY(100)
      DIMENSION [illegible],FC(100),FDEV(100),PFDEV(100),[illegible]
    1 FORMAT(I3)
    2 FORMAT(F15.5,F15.5)
    3 FORMAT(I1)
    4 FORMAT(' ',10X,'REGRESSION IMPOSSIBLE'/)
    5 FORMAT(' ',10X,'REGRESSION COEFFICIENTS'/' ',15X,'A=',E14.7/' ',1
     15X,'B=',E14.7/)
    6 FORMAT(' ',5X,'T',10X,'F',8X,'X=1/T',4X,'Y=LOG F',2X,'Y(CALC)',5X,
     1'DEV',5X,'PCT.DEV.')
    7 FORMAT(' ',2X,F6.2,2X,F11.5,2X,F8.6,2X,F7.4,2X,F7.4,2X,F8.5,2X,F7.
     1[illegible])
    8 FORMAT(' ',9X,'STD.DEV.=',F15.5//' ',9X,'PCT.STD.DEV.=',F10.5//' '
     1,5X,'DELTA H=',F15.2//' ',5X,'DELTA S=',F15.5)
    9 FORMAT(' ',5X,'DELTA G=',F15.5//)
   13 FORMAT(' ',2X,'A11=',E14.7,3X,'A12=',E14.7/' ',2X,'A21=',E14.7,5X,
     1'A22=',E14.7/' ',2X,'B1=',E14.7,5X,'B2=',E14.7)
   14 FORMAT(' ',10X,'DET=',E14.7//)
   15 FORMAT(' ',4X,'T(C)',6X,'F(C)',8X,'F',9X,'F(CALC)',6X,'DEV',4X,'P
     1CT.DEV.')
   16 FORMAT(' ',2X,F6.2,2X,F8.5,2X,F11.5,2X,F11.5,2X,F8.5,2X,F7.3)
   17 FORMAT(F7.2)
   18 FORMAT(' ',15X,'G=',E15.7//)
   21 FORMAT(' ',9X,'STD.DEV.=',F15.5//' ',9X,'PCT.STD.DEV.=',F10.5//)
C     READ EXPERIMENTAL DATA
   10 READ(1,1) N
      DO 20 I=1,N
   20 READ(1,2) T(I),F(I)
      READ(1,17) G
      READ(1,3) K
C     CALCULATE THE REGRESSION COEFFICIENTS
      DO 25 I=1,N
      X(I)=1/(T(I)+273.15)
      [illegible]=ALOG10([illegible]+273.15)
   25 Y(I)=ALOG10(F(I))-[illegible]
      A11=0.
      A12=0.
      A21=0.
      A22=0.
      B1=0.
      B2=0.
      DO 30 I=1,N
      A11=A11+1.
      A12=A12+X(I)
      A21=A12
      A22=A22+X(I)*X(I)
      B1=B1+Y(I)
   30 B2=B2+X(I)*Y(I)
      DET=A11*A22-A12*A21
      WRITE(3,13) A11,A12,A21,A22,B1,B2
      WRITE(3,14) DET
      IF(DET) 11,12,11
   12 WRITE(3,4)
      GO TO 50
   11 A=(B1*A22-B2*A12)/DET
      B=(A11*B2-A21*B1)/DET
      [illegible]
      WRITE(3,5) A,B
      WRITE(3,18) G
C     LIST THE EXPERIMENTAL AND CALCULATED RESULT FOR LOG(F)
      WRITE(3,6)
      DO 40 I=1,N
      YC(I)=A+B*X(I)
      DEY(I)=Y(I)-YC(I)
      PDEY(I)=100*(DEY(I)/Y(I))
   40 WRITE(3,7) T(I),F(I),X(I),Y(I),YC(I),DEY(I),PDEY(I)
C     CALCULATE ERRORS IN LOG(F) COMPUTATION
      SDEY=0.
      SPDEY=0.
      DO 35 I=1,N
      SDEY=SDEY+DEY(I)*DEY(I)
   35 SPDEY=SPDEY+PDEY(I)*PDEY(I)
```

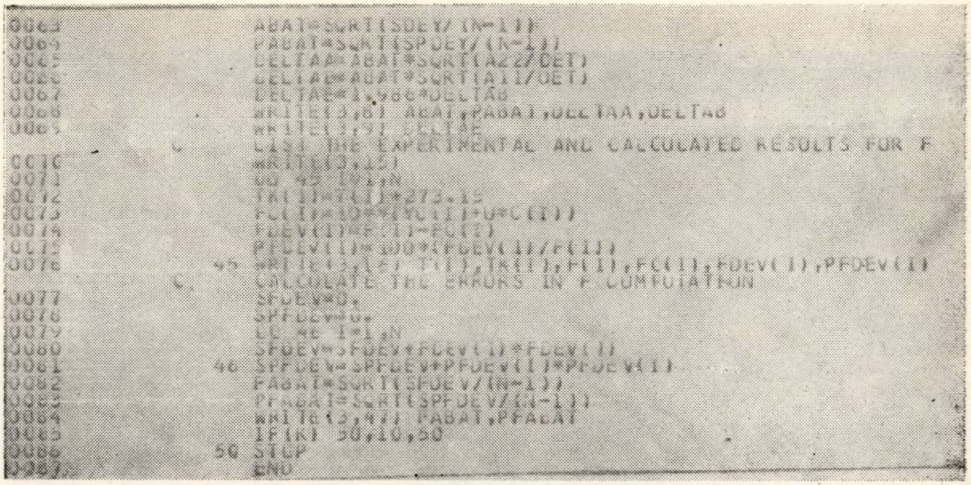

```
0063          ABAT=SQRT(SDEV/(N-1))
0064          PABAT=SQRT(SPDEV/(N-1))
0065          DELTAA=ABAT*SQRT(A22/DET)
0066          DELTAB=ABAT*SQRT(A11/DET)
0067          DELTAE=1.986*DELTAB
0068          WRITE(3,8) ABAT,PABAT,DELTAA,DELTAB
0069          WRITE(3,9) DELTAE
        C     LIST THE EXPERIMENTAL AND CALCULATED RESULTS FOR F
0070          WRITE(3,15)
0071          DO 45 I=1,N
0072          TK(I)=T(I)+273.15
0073          FC(I)=10**(YC(I)+U*C(I))
0074          FDEV(I)=F(I)-FC(I)
0075          PFDEV(I)=100*(FDEV(I)/F(I))
0076       45 WRITE(3,16) T(I),TK(I),F(I),FC(I),FDEV(I),PFDEV(I)
        C     CALCULATE THE ERRORS IN F COMPUTATION
0077          SFDEV=0.
0078          SPFDEV=0.
0079          DO 46 I=1,N
0080          SFDEV=SFDEV+FDEV(I)*FDEV(I)
0081       46 SPFDEV=SPFDEV+PFDEV(I)*PFDEV(I)
0082          FABAT=SQRT(SFDEV/(N-1))
0083          PFABAT=SQRT(SPFDEV/(N-1))
0084          WRITE(3,47) FABAT,PFABAT
0085          IF(K) 50,10,50
0086       50 STOP
0087          END
```

— statements 26 and 28 are replaced by statements the other program is left unchanged.

$$X(\mathrm{I}) = T(\mathrm{I}) \quad + 273.15$$

$$25 \; Y(\mathrm{I}) = F(\mathrm{I}),$$

RESULTS AND DISCUSSIONS

The advanced RELTET program, written in simple precision, occupies 4818 bytes and may process sets of maximum 100 pairs of experimental data. The time necessary to the compilation of the source program is of 55 sec. After the performance of the Linkage Edit of the object module produced by the compiler, the occupational degree of the machine's memory is of 25112 bytes. To carry through calculation on a set of 100 pairs of experimental data *F*, *T*, 100 sec are necessary. With the same program we can process several sets of data (practically unlimited) due to the use of a K counter.

Two tables of data, as seen from data in the appendix, will appear at the print paper. In the first table we can read the accuracy in the calculation of the *Y* value as well as the calculation accuracy of the regression coefficients *A* and *B*. The second table lists the standard deviation and the percent standard deviation calculating *F* values. When the PERCENT STANDARD DEVIATION is too great, we may analyse the deviations shown in the table and remove from the calculation the pairs of data generating inadmissibly great deviations. This operation is greatly simplified since every pair of experimental data is written on a card. On a subsequent run of the program with the selected data, a better accuracy is obtained in the calculation of the values of function *F*. The appendix also contains results obtained after choosing pairs of data which generate the least deviations. We can thus obtain a relation reflecting as accurately as possible the dependence of the measured magnitude on temperature.

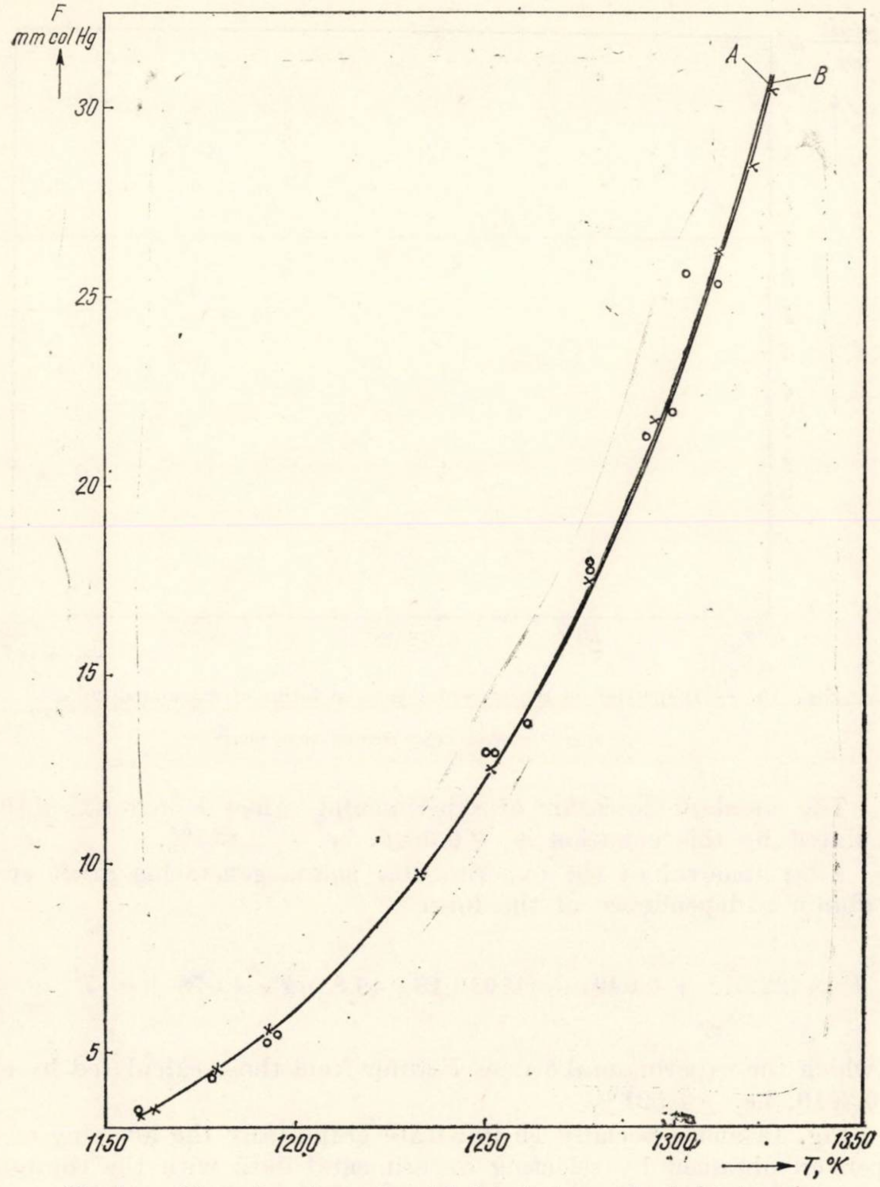

Fig. 1a. — Dispersion of experimental data in terms of calculated curve : A = according to a relation of the type (23) from rel. (25). B = according to a relation of the type (23), from rel. (26). For A the experimental points x and o underwent regression while for B only point x

Analysing the results on the print paper we find that after the first run, the regression equation

$$\log F = (22.588 \pm 0.052) - (11095.38 \pm 64.62)/T - 4.078 \log T \quad (25)$$

is obtained.

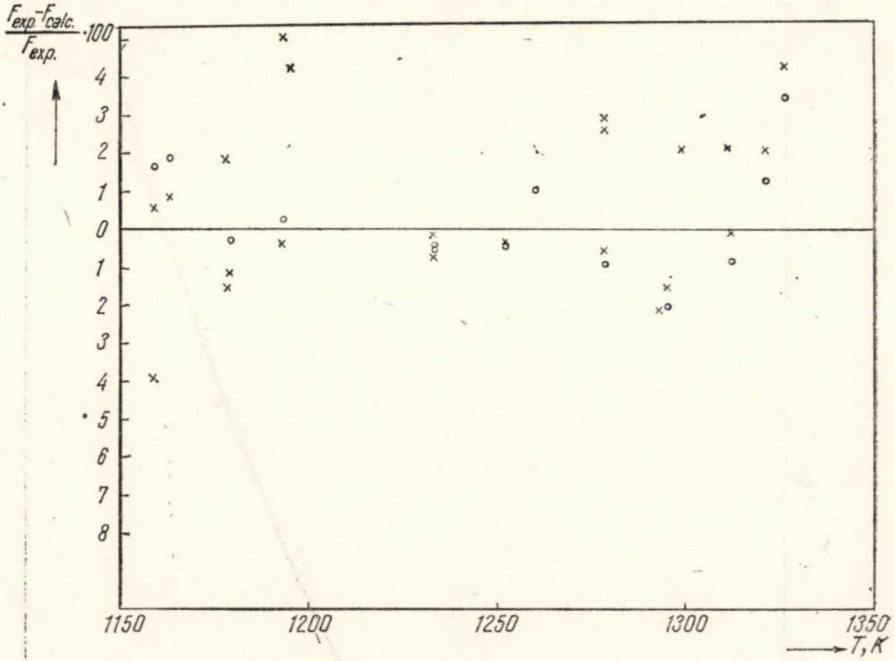

Fig. 1b. — Dispersion of experimental data in terms of calculated curve:

× = after the first run; ○ = after the second run.

The standard deviation of experimental values F in terms of those calculated by this equation is $\pm$ 0.5546, i.e. $\pm$ 2.885%.

After removal of the experimental points generating great errors we obtain a dependence of the form

$$\log F = (22.572 \pm 0.040) - (11019.18 \pm 49.83)/T - 4.078 \log T \qquad (26)$$

for which the experimental values F differ from those calculated by only $\pm$ 0.3619, i.e. $\pm$ 1.521%.

Fig. 1a and especially 1b illustrate graphically the lowering of the dispersion obtained by selecting experimental data with the computer.

Curves A and B in fig. 1a confirm that the shape of the dependence is very slightly modified by eliminating the data which generate errors.

This program RELTET(Linear Regression applied in Thermodynamics of Molten Electrolytes) proves to be a useful tool in processing experimental data. The computation program has been checked and then used for the processing of data resulted from measurements of vapour pressures, conductivity, e.m.f., diffusion coefficients.

Table 1

Results appeared on the print paper on the first running the RELTET program

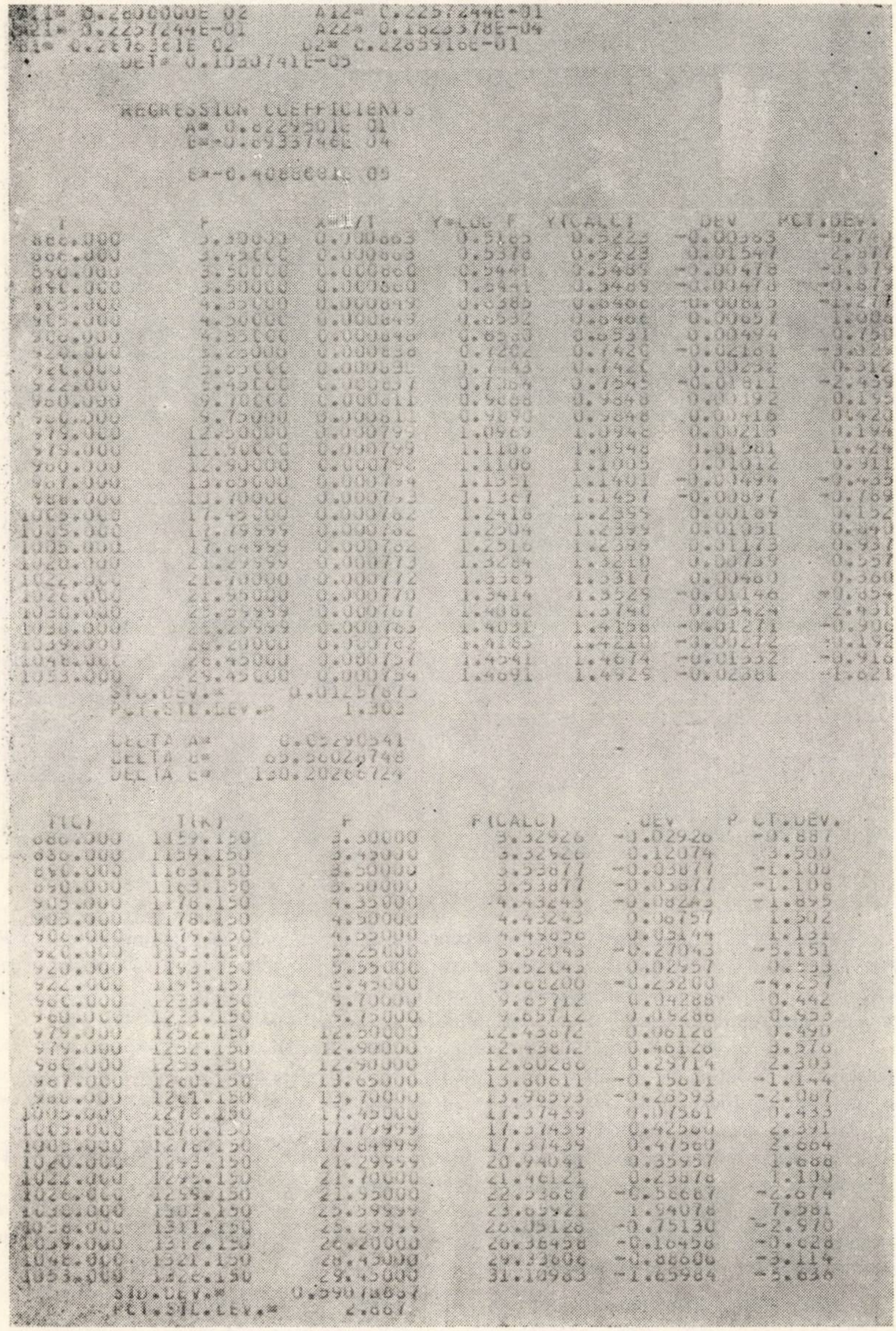

```
A11= 0.28000000E 02        A12= 0.22572446E-01
A21= 0.22572446E-01        A22= 0.18233378E-04
B1= 0.28763818E 02       B2= 0.22859168E-01
          DET= 0.10507418E-05


        REGRESSION COEFFICIENTS
             A= 0.82295016E 01
             B=-0.69337468E 04

             C=-0.40888816E 05

    T             F        X=1/T     Y=LOG F   Y(CALC)      DEV     PCT.DEV.
  886.000      3.30000  0.000863    0.5185    0.5223   -0.00383    -0.739
  886.000      3.45000  0.000863    0.5378    0.5223    0.01547     2.877
  890.000      3.50000  0.000860    0.5441    0.5489   -0.00478    -0.879
  890.000      3.50000  0.000860    0.5441    0.5489   -0.00478    -0.879
  905.000      4.35000  0.000849    0.6385    0.6466   -0.00815    -1.277
  905.000      4.50000  0.000849    0.6532    0.6466    0.00657     1.006
  906.000      4.55000  0.000848    0.6580    0.6531    0.00494     0.750
  920.000      5.25000  0.000838    0.7202    0.7420   -0.02181    -3.028
  920.000      5.55000  0.000838    0.7443    0.7420    0.00232     0.312
  922.000      5.45000  0.000837    0.7364    0.7545   -0.01811    -2.459
  960.000      9.70000  0.000811    0.9868    0.9848    0.00192     0.195
  960.000      9.75000  0.000811    0.9890    0.9848    0.00418     0.420
  979.000     12.50000  0.000799    1.0969    1.0948    0.00213     0.194
  979.000     12.90000  0.000799    1.1106    1.0948    0.01581     1.424
  980.000     12.90000  0.000798    1.1106    1.1005    0.01012     0.911
  987.000     13.65000  0.000794    1.1351    1.1401   -0.00494    -0.435
  988.000     13.70000  0.000793    1.1367    1.1457   -0.00897    -0.789
 1005.000     17.45000  0.000782    1.2418    1.2399    0.00189     0.152
 1005.000     17.79999  0.000782    1.2504    1.2399    0.01051     0.840
 1005.000     17.84999  0.000782    1.2516    1.2399    0.01173     0.937
 1020.000     21.29999  0.000773    1.3284    1.3210    0.00739     0.557
 1022.000     21.70000  0.000772    1.3365    1.3317    0.00480     0.360
 1026.000     21.95000  0.000770    1.3414    1.3529   -0.01146    -0.854
 1030.000     25.59999  0.000767    1.4082    1.3740    0.03424     2.431
 1038.000     25.29999  0.000763    1.4031    1.4158   -0.01271    -0.906
 1039.000     26.20000  0.000762    1.4183    1.4210   -0.00272    -0.192
 1048.000     28.45000  0.000757    1.4541    1.4674   -0.01332    -0.916
 1053.000     29.45000  0.000754    1.4691    1.4929   -0.02381    -1.621
          STD.DEV.=      0.01257875
          PCT.STD.DEV.=      1.303

          DELTA A=       0.05290541
          DELTA B=      65.56026748
          DELTA C=     130.20266724


   T(C)       T(K)            F             F(CALC)        DEV      P CT.DEV.
  886.000   1159.150       3.30000         3.32926     -0.02926     -0.887
  886.000   1159.150       3.45000         3.32926      0.12074      3.500
  890.000   1163.150       3.50000         3.53877     -0.03877     -1.108
  890.000   1163.150       3.50000         3.53877     -0.03877     -1.108
  905.000   1178.150       4.35000         4.43243     -0.08243     -1.895
  905.000   1178.150       4.50000         4.43243      0.06757      1.502
  906.000   1179.150       4.55000         4.49856      0.05144      1.131
  920.000   1193.150       5.25000         5.52043     -0.27043     -5.151
  920.000   1193.150       5.55000         5.52043      0.02957      0.533
  922.000   1195.150       5.45000         5.68200     -0.23200     -4.257
  960.000   1233.150       9.70000         9.65712      0.04288      0.442
  960.000   1233.150       9.75000         9.65712      0.09288      0.953
  979.000   1252.150      12.50000        12.43872      0.06128      0.490
  979.000   1252.150      12.90000        12.43872      0.46128      3.576
  980.000   1253.150      12.90000        12.60286      0.29714      2.303
  987.000   1260.150      13.65000        13.80611     -0.15611     -1.144
  988.000   1261.150      13.70000        13.98593     -0.28593     -2.087
 1005.000   1278.150      17.45000        17.37439      0.07561      0.433
 1005.000   1278.150      17.79999        17.37439      0.42560      2.391
 1005.000   1278.150      17.84999        17.37439      0.47560      2.664
 1020.000   1293.150      21.29999        20.94041      0.35957      1.688
 1022.000   1295.150      21.70000        21.46121      0.23878      1.100
 1026.000   1299.150      21.95000        22.53687     -0.58687     -2.674
 1030.000   1303.150      25.59999        23.65921      1.94078      7.581
 1038.000   1311.150      25.29999        26.05128     -0.75130     -2.970
 1039.000   1312.150      26.20000        26.36458     -0.16458     -0.628
 1048.000   1321.150      28.45000        29.33606     -0.88606     -3.114
 1053.000   1326.150      29.45000        31.10983     -1.65984     -5.636
          STD.DEV.=       0.59078657
          PCT.STD.DEV.=       2.867
```

Table 2

Results appeared on the print paper on the second running of the RELTET program

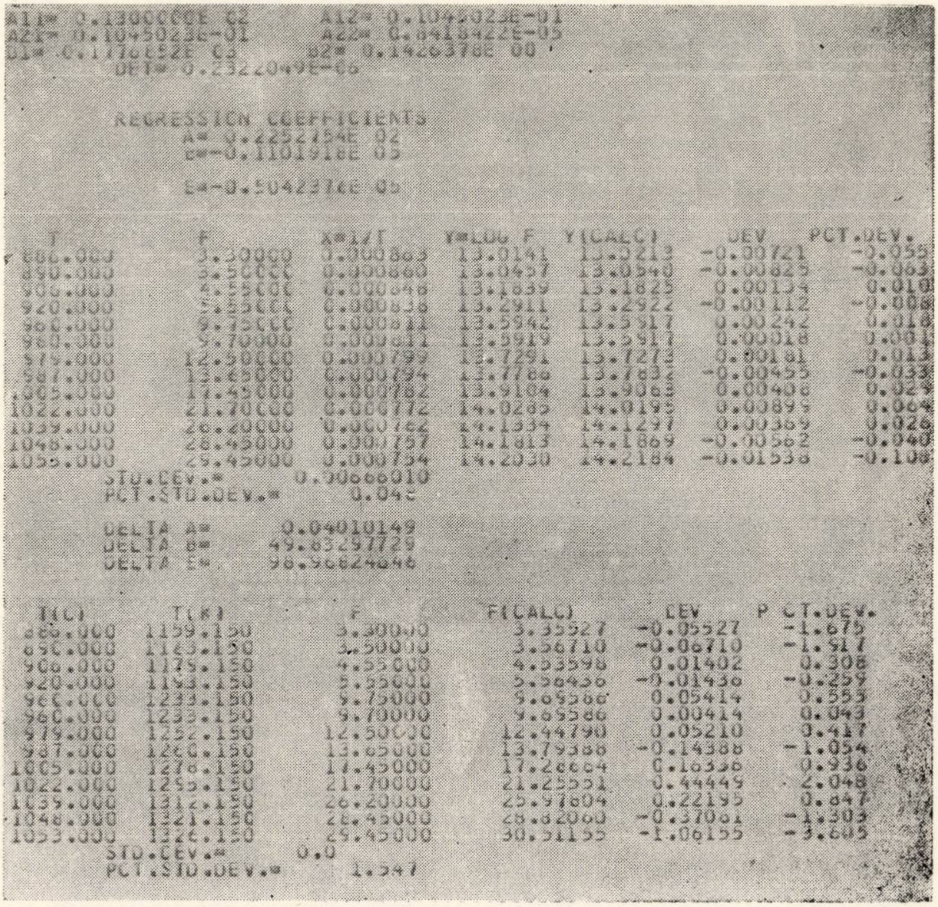

```
A11= 0.13000000E 02      A12= 0.10450236E-01
A21= 0.10450236E-01      A22= 0.84184226E-05
B1= 0.17768852E 03       B2= 0.14263788E 00
     DET= 0.23220499E-06

      REGRESSION COEFFICIENTS
           A= 0.22527154E 02
           B=-0.11019188E 05

           E=-0.50423766E 05

    T            F        X=1/T     Y=LOG F   Y(CALC)      DEV     PCT.DEV.
 886.000      3.30000   0.000863   13.0141   13.0213   -0.00721    -0.055
 890.000      3.50000   0.000860   13.0457   13.0540   -0.00825    -0.063
 906.000      4.55000   0.000848   13.1839   13.1825    0.00134     0.010
 920.000      5.55000   0.000838   13.2911   13.2922   -0.00112    -0.008
 960.000      9.75000   0.000811   13.5942   13.5917    0.00242     0.018
 960.000      9.70000   0.000811   13.5919   13.5917    0.00018     0.001
 979.000     12.50000   0.000799   13.7291   13.7273    0.00181     0.013
 987.000     13.65000   0.000794   13.7786   13.7832   -0.00455    -0.033
1005.000     17.45000   0.000782   13.9104   13.9063    0.00408     0.029
1022.000     21.70000   0.000772   14.0285   14.0195    0.00899     0.064
1039.000     26.20000   0.000762   14.1334   14.1297    0.00369     0.026
1048.000     28.45000   0.000757   14.1813   14.1869   -0.00562    -0.040
1055.000     29.45000   0.000754   14.2030   14.2184   -0.01538    -0.108
      STD.DEV.=          0.00666010
      PCT.STD.DEV.=         0.048

      DELTA A=       0.04010149
      DELTA B=      49.83297729
      DELTA E=      98.96824846

   T(C)         T(K)             F               F(CALC)        DEV      P CT.DEV.
 886.000    1159.150         3.30000            3.35527    -0.05527      -1.675
 890.000    1163.150         3.50000            3.56710    -0.06710      -1.917
 906.000    1179.150         4.55000            4.53598     0.01402       0.308
 920.000    1193.150         5.55000            5.56436    -0.01436      -0.259
 960.000    1233.150         9.75000            9.69586     0.05414       0.555
 960.000    1233.150         9.70000            9.69586     0.00414       0.043
 979.000    1252.150        12.50000           12.44790     0.05210       0.417
 987.000    1260.150        13.65000           13.79386    -0.14386      -1.054
1005.000    1278.150        17.45000           17.28664     0.16336       0.936
1022.000    1295.150        21.70000           21.25551     0.44449       2.048
1039.000    1312.150        26.20000           25.97804     0.22195       0.847
1048.000    1321.150        28.45000           28.82060    -0.37061      -1.303
1055.000    1328.150        29.45000           30.51155    -1.06155      -3.605
      STD.DEV.=        0.0
      PCT.STD.DEV.=       1.547
```

APPENDIX

The RELTET program has been checked on a set of 28 pairs of experimental data F, T resulted from measurements of vapour pressures carried out on a molten salt of the type AX_2 by the Rodebush-Dixon method.[13] For the system under study $U = -4.078$ while $N = 28$. The following results have been obtained at the printer. (See Table 1)

A series of pairs of experimental points contributes with deviations exceeding 2% to the standard deviation of ±0.55457795 (±2.885 %). Removing these values from the calculation so that the significant temperatures of the measurements should not be impaired, another regression equation is obtained with much smaller deviations.

In the following we give the results obtained on the print paper by the removal of 15 pairs of experimental data generating errors greater than 2%. (See Table 2)

After selecting the data a much smaller error is obtained, the coefficients A and B remain practically unchanged. The calculational accuracy of regression coefficients is also apparently improved to a great extent.

---

[13] L. Topor, *Rev. Roumaine de Chim.* (in print).

Revue Roumaine de Chimie, 17, 8, 1327–1330 (1972)

THERMAL PROPERTIES OF ALUROM ALUMINIUM HEAT CONTENT AT HIGH TEMPERATURES

D. I. MARCHIDAN and LIANA PANDELE

Centre of Physical Chemistry
str. Galaţi 31, Bucharest, Romania

Received March 22, 1972

The heat content of ALUROM aluminium has been determined in the temperature range 385–850 K by means of the dropping calorimeter. The data are listed which have been obtained for the heat content, heat capacity, free energy and entropy.

★

The thermochemical properties of the metals are necessarily and largely used for the manufacturing, processing and usage of metals for various purposes. Aluminium and its alloys are used on an even larger scale all over the world.

The thermochemical properties of pure aluminium are mentioned by McDonald,[1] Broocks[2] and Marchidan [3] in their works.

The present paper presents the experimental results on the specific heat of ALUROM aluminium (electrolytically obtained by the Aluminium Works – SLATINA) in the temperature range 385–850 K by using a dropping calorimeter.

EXPERIMENTAL

The main parts of the installation are the furnace, with an inoxiterm steel core and the calorimetric unit made of electrolytic copper. The accuracy of the measurements is of ± 0.4 %. The temperature of the furnace is kept constant with a ± 0.5° accuracy by means of a proportional thermoregulating device. To check the temperature of the furnace we used a thermocouple Pt-Pt Rh (10 %).

The ALUROM sample is suspended in the furnace and kept at constant temperature for 1 hr, until it reaches a thermal equilibrium, then it is dropped into the calorimetric unit where the heat quantity released by its cooling to 298 K, is measured.

[1] R. A. McDonald, *J. Chem. and Eng. Data.*, **12**, 115 (1967).

[2] C. R. Brooks and R. E. Bingham, *J. Phys. Chem. Solids.*, **29**, 1553 (1968).

[3] D. I. Marchidan and M. Ciopec, *Rev. Roumaine Chim.*, **15**, 1005 (1970).

The temperature variation of the calorimetric unit has been measured by a thermistor (CICE – France) whose resistance at 298 K is of 25 000Ω. The variation of the thermistor resistance in terms of temperature is determined with a Wheatstone bridge whose null instrument is a galvanometer of the MG 2 type. The variation in the temperature of the calorimetric unit, of 0.001° leads to the variation of 1Ω of the thermistor resistance.

The electrical calibration of the calorimetric unit has been carried out within the same temperature range as for the experimental determinations.[4]

For the experiments we have used a sample of ALUROM aluminium weighing 11.2470 g. Prior to the measurements, the sample has been brought to constant weight by heating in air to 823 K for 10 hr. The composition of the ALUROM aluminium is given in table 1.

Table 1

Composition of the ALUROM aluminium

Element	Percent (%)	Element	Percent (%)
Aluminium	99.619	Vanadium	0.002
Iron	0.22	Mangan	0.004
Silica	0.136	Chromium	0.001
Titanium	0.001	Magnesium	0.0033
Copper	0.003		

RESULTS AND DISCUSSION

The results of experimental measurements are listed in table 2.

Table 2

Variation with temperature of the heat content of ALUROM aluminium

T (K)	$H_T - H_{298.15}$ (cal/mol)	T (K)	$H_T - H_{298.15}$ (cal/mol)
385	511.5	649	2263
444.85	916.98	669	2389.48
479	1144.98	722	2742.26
523	1403.37	753.55	2997.7
568	1698.8	809	3379
606	1929.75	850	3673.5

By processing these data by the least squares method we obtain the following equation

$$H_T - H_{298.15} = -1640 + 5.01\,T + 1.5 \times 10^{-3} T^2 \tag{1}$$

The values obtained by means of this equation, are compared to the experimental results in table 3.

---

[4] D. I. Marchidan and M. Ciopec, *Studii și Cercetări Chim. Acad. R.S.R.*, **17**, 737 (1969).

Table 3

Comparison between the experimental values and those calculated according to eq. (1) for the heat content of the ALUROM aluminium

T K	$H_T - H_{298.15}$ cal/mol		Deviation	
	Exp.	Calc. eq. (1)	Cal/mol	%
523	1403.37	1390	+13.37	+0.96
568	1698.8	1689	+ 9.8	+0.53
606	1929.75	1947.75	−18	−0.93
649	2263	2243	+20	+0.88
669	2389.48	2382	+ 7.48	+0.29
722	2742.26	2759.2	−16.94	−0.62
753.55	2997.7	2983.7	+14	+0.46
809	3379	3394.7	−15.7	−0.44
850	3673.5	3702	−28.5	−0.77

Table 4 gives the experimental results as compared to those in the J.A.N.A.F. tables. The latter verify an equation [5] of the form :

$$H_T - H_{298.15} = -1598 + 4.915\ T + 1.5 \times 10^{-3} T^2 \qquad (2)$$

while Wicks'[6] data for aluminium verify an equation of the form :

$$H_T - H_{298.15} = -1605 + 4.94\ T + 1.48 \times 10^{-3} T^2 \qquad (3)$$

Table 4

Comparison between experimental data and those calculated according to eq. (2)

T K	$H_T - H_{298.15}$ cal/mol		Deviation	
	Exp.	J.A.N.A.F. eq. (2)	cal/mol	(%)
523	1 403.37	1 382	+21.37	+1.5
568	1 698.8	1 683.8	+15	+0.98
606	1 929.75	1 933	− 3.25	−0.16
649	2 263	2 224	+39	+1.75
669	2 389.48	2 368	+21.48	+0.90
722	2 742.26	2 735.5	+ 6.76	+0.28
753.5	2 997.7	2 959.6	+38.1	+1.26
809	3 379	3 360	+19	+0.56
850	3 673.5	3 669	+ 4.5	+0.12

By deriving eq. (1) with respect to absolute temperature we obtain, for variation of the heat capacity in terms of temperature, an expression of the form

---

[5] "J.A.N.A.F. Thermochemical Tables" (ed. D. R. STULL), Dow Chemical Company, Midland, Mich. Aug. 1965, No. PB 168−370.

[6] C. E. WICKS and F. E. BLOCK, "Thermodynamic Properties of 65 Elements. Their Oxides, Halides, Carbides and Nitrides", Bulletin 605, Bureau of Mines, Washington, 1963, p. 91.

$$C_p = 5.01 + 3 \times 10^{-3}\, T \tag{4}$$

Table 5 gives the calculated values of the heat capacity, of free energy, enthalpy and entropy of ALUROM aluminium, in the temperature range 523—850 K.

Table 5

Thermodynamical functions of ALUROM aluminium

T K	C_p (cal/mol.grad)	$H_T - H_{298.15}$	S_T u.e. (cal/mol.grad)	$\frac{G_T - H_{298.15}}{\mathrm{T}}$ u.e.
523	6.57	1 385	10.261	7.610
568	6.71	1 689	10.810	7.836
606	6.83	1 947.75	11.250	8.035
649	9.96	2 243	11.713	8.256
669	7.02	2 382	11.933	8.372
722	7.18	2 759.2	12.471	8.649
753.55	7.30	2 983.7	12.778	8.818
809	7.44	3 394.7	13.300	9.103
850	7.56	3 709	13.680	9.324

To calculate the free energy we have used relation

$$\frac{G_T - H_{298.15}}{T} = -S_T + \frac{H_T - H_{298.15}}{T} \tag{5}$$

where

$$S_T = \int_{298.15}^{T} (C_p/T)\,\mathrm{d}T + S_{298.15} \tag{6}$$

where $S_{298.15} = 6.77$ u.e. (cal/mol.grad).

By introducing this value in eq. (6), we obtain relation

$$S_T = 5.01 \ln (T/298.15) + 3 \times 10^{-3}\ (T - 298.15) + 6.77 \tag{7}$$

ACKNOWLEDGEMENT. The authors gratefully acknowledge the interest shown by Professor I. G. Murgulescu in their work. They are also indebted to I. Liţescu and C. Volcovici for their skilled help.

Revue Roumaine de Chimie, 17, 8, 1331–1337 (1972)

L'INFLUENCE DU SOLVANT SUR LA VITESSE DE RÉACTION

L'HYDROLYSE ACIDE DU FORMIATE, DE L'ACÉTATE ET DU PROPIONATE DE *n*-BUTYLE DANS LE SOLVANT MIXTE EAU-ALCOOL ÉTHYLIQUE

G. COSTEANU et ORTANSA LANDAUER

Chaire de Chimie Physique et d'Électrochimie
Institut Polytechnique, 132, str. Griviţei, Bucarest

Reçu le 18 septembre 1971

La cinétique chimique de l'hydrolyse acide du formiate, de l'acétate et du propionate de *n*-butyle dans le solvant mixte eau-alcool éthylique permet d'admettre l'existence d'une certaine structure du système eau-alcool éthylique à la concentration de 0,2, en fraction molaire.

Nous avons étudié, dans ce travail, l'hydrolyse acide du formiate de l'acétate et du propionate de *n*-butyle dans le solvant mixte eau-alcool éthylique de différentes concentrations.

PARTIE EXPÉRIMENTALE

Les esters étudiés par nous ont été préparés et purifiés suivant les indications de la littérature[1]. L'eau et l'alcool éthylique ont été aussi bien purifiés au préalable.

La concentration initiale des solutions des trois esters, déterminée par saponification totale, était approximativement de 0,1 M, et celle de l'acide chlorhydrique de 0,05 N.

La cinétique de la réaction a été étudiée à 30, 40, 50 et 60°, en utilisant le méthode déjà publiée dans un travail antérieur.[2]

La réaction vérifie l'équation cinétique du type $k_2 = \frac{2,303}{b.t} \log \frac{a}{a - x}$; où b est la concentration initiale de l'eau.

---

[1] A. I. Vogel, « A Text Book of Practical Organic Chemistry », IIIe vol., Longman, Green and Co., London, New York (1956), 97.

[2] G. Costeanu, O. Landauer et C. Mateescu, *Rev. Roumaine Chim.*, **13**, 155 (1968).

RÉSULTATS EXPÉRIMENTAUX

Les constantes de vitesse, exprimées en mole^{-1} cm^3 s^{-1}, sont réunies dans les tableaux 1, 2 et 3.

Tableau 1

Constantes de vitesse de l'hydrolyse acide du formiate de *n*-butyle dans l'eau-alcool éthylique en cm^3 mole^{-1}s^{-1}

X_{EtOH}	10^2b molesH$_2$O/cm^3	10^3k_2 30°	10^3k_2 40°	10^3k_2 50°	10^3k_2 60°
0,070	4,650	3,59	8,36	14,34	27,84
0,113	4,191	3,17	5,68	11,72	20,98
0,163	3,702	2,80	5,75	9,69	17,11
0,224	3,199	2,88	5,52	8,76	16,60
0,289	2,661	2,18	4,90	8,96	17,74
0,393	2,092	1,86	5,23	9,50	19,06
0,520	1,473	2,34	4,82	11,34	24,12
0,700	0,796	3,78	7,01	17,39	35,63

Tableau 2

Constantes de vitesse de l'hydrolyse acide de l'acétate de *n*-butyle dans l'eau-alcool éthylique en cm^3 mole^{-1} s^{-1}

X_{EtOH}	10^2b molesH$_2$O/cm^3	10^3k_2 30°	10^3k_2 40°	10^3k_2 50°	10^3k_2 60°
0,112	4,190	0,28	0,51	1,23	2,63
0,163	3,707	0,25	0,49	1,05	2,13
0,223	3,200	0,22	0,50	0,94	1,85
0,298	2,661	0,23	0,48	1,03	2,07
0,393	2,090	0,26	0,54	1,25	2,51
0,518	1,482	0,35	0,70	1,58	3,14
0,702	0,791	0,59	1,18	2,53	5,06

Tableau 3

Constantes de vitesse de l'hydrolyse acide du propionate de *n*-butyle dans l'eau-alcool éthylique en cm^3 mole^{-1} s^{-1}

X_{EtOH}	10^2b molesH$_2$O/cm^3	10^4k_2 30°	10^4k_2 40°	10^4k_2 40°	10^4k_2 60°
0,163	3,706	1,19	2,27	5,20	8,50
0,224	3,192	1,06	1,92	4,18	8,00
0,299	2,657	0,92	2,02	3,99	8,06
0,394	2,085	0,96	2,06	3,97	8,00
0,522	1,466	1,13	2,30	4,18	8,05
0,704	0,784	1,76	3,34	6,27	11,37

On a représenté aussi graphiquement (fig. 1) la variation de la constante de vitesse du formiate de *n*-butyle en fonction de la teneur en alcool du solvant mixte.

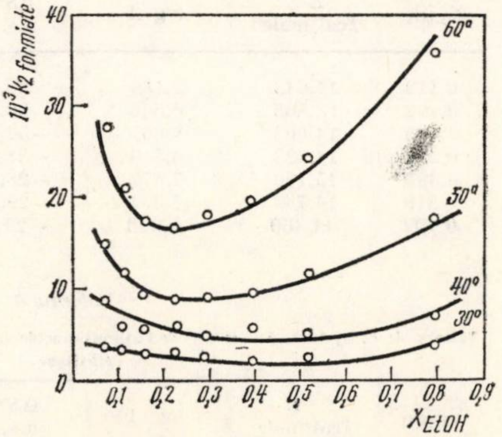

Fig. 1. — Variation de la constante de vitesse de l'hydrolyse acide du formiate de *n*-butyle avec la concentration en alcool éthylique du solvant mixte.

On observe sur les courbes un minimum à toutes les températures. Ce minimum, bien plus accentué à 50° et 60°, correspond, à cette dernière température, à la fraction molaire de X = 0,2.

Le minimum de la constante de vitesse des autres esters se situe presque à la même concentration.

Les données expérimentales nous ont permis de calculer les énergies d'activation *E*, les facteurs préexponentiels *A*, les entropies d'activation ΔS^*, les enthalpies d'activation ΔH^*, et les enthalpies libres d'activation ΔG^* ; dont les valeurs sont réunies dans les tableaux 4,5 et 6.

On remarque que les énergies d'activation des trois esters ont des valeurs extrêmes suivant la composition du solvant mixte.

En représentant graphiquement la variation de *E* en fonction de la fraction molaire du solvant, on voit que le minimum de l'énergie d'activation se situe, dans le cas du formiate, à la concentration de $X = 0,2$, et à une concentration légèrement plus petite pour l'acétate. Dans ce

Tableau 4

Valeurs de E, A, ΔH^*, ΔS^* et ΔG^* de l'hydrolyse acide du formiate de *n*-butyle dans l'eau-alcool éthylique

X_{EtOH}	*E* *k*cal/mole	log *A*	ΔS^* u.e.	ΔH^* *k*cal/mole	ΔG^* *k*cal/mole
0,070	13,728	7,620	−28,25	13,136	21,554
0,113	12,629	6,760	−32,18	12,037	21,626
0,162	12,172	6,371	−33,96	11,580	21,700
0,224	11,898	6,182	−34,83	11,300	21,679
0,289	13,185	7,005	−31,06	12,593	21,849
0,393	16,553	9,409	−20,06	15,961	21,939
0,520	16,748	9,648	−18,77	16,156	21,809
0,700	15,100	8,647	−23,55	14,508	21,526

Tableau 5

Valeurs de E, A, ΔH^*, ΔS^* et ΔG^* de l'hydrolyse acide de l'acétate de *n*-butyle dans l'eau-alcool éthylique

X_{EtOH}	E *k*cal/mole	log A	ΔS^* u.e.	ΔH^* *k*cal/mole	ΔG^* *k*cal/mole
0,112	14,643	7,186	−30,23	14,051	23,060
0,162	13,865	6,566	−33,07	13,273	23,128
0,223	14,003	6,607	−32,88	13,411	23,209
0,298	14,323	6,866	−31,70	13,731	23,178
0,393	15,100	7,477	−28,90	14,508	23,120
0,518	14,780	7,399	−29,35	14,188	22,934
0,702	14,460	7,373	−29,38	13,868	22,623

Tableau 6

Valeurs de E, A, ΔH^*, ΔS^* et ΔG^* de l'hydrolyse acide du propionate de *n*-butyle dans l'eau-alcool éthylique

X_{EtOH}	E *k*cal/mole	log A	ΔS^* u.e.	ΔH^* *k*cal/mole	ΔG^* *k*cal/mole
0,163	13,087	5.672	−37,16	12,495	24,019
0,224	13,545	5,956	−35,86	12,953	23,639
0,299	14,420	6,537	−33,20	13,828	23,722
0,394	14,323	6,483	−33,72	13,731	23,783
0,522	13,087	5,646	−37,28	12,495	23,604
0,704	12,492	5,383	−39,40	11,900	23,641

domaine de concentrations la courbe du propionate de *n*-butyle ne passe pas par un minimum (fig. 2).

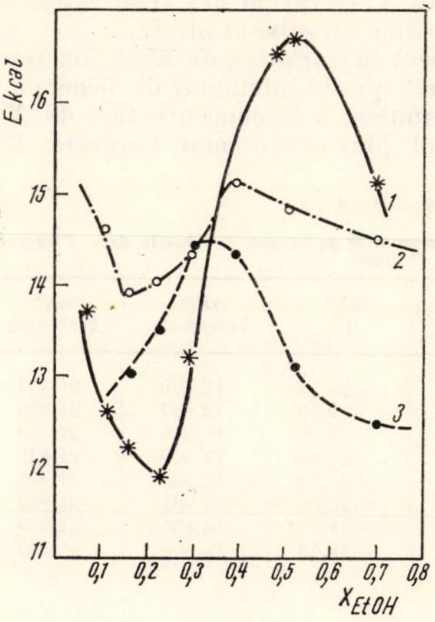

Fig. 2. — Variation de l'énergie d'activation de l'hydrolyse acide du formiate *1*, de l'acétate *2*, et du propionate de *n*-butyle *3*, avec la teneur en alcool éthylique du solvant mixte.

Aux mêmes concentrations du minimum et du maximum de l'énergie d'activation correspondent des valeurs minimales et maximales de l'entropie d'activation.

La corrélation entre les constantes de vitesse et le facteur électrostatique du milieu devrait se traduire soit par l'équation d'Amis [3]

$$\ln k_D = \ln k_{D\infty} - \frac{2\,\mu_1\mu_2}{kTr^3D}$$

où μ_1 et μ_2 sont les moments dipolaires de l'ester et de l'eau ; soit par la relation de Laidler-Eyring : [4]

$$\ln k = \ln\left(x\frac{kT}{h}K^*\right) - \frac{1}{kT}\left[\frac{D-1}{2D+1}\right]\left[\frac{\mu_A^2}{a_A^3} + \frac{\mu_B^2}{a_B^3} - \frac{\mu_{M*}^2}{a_{M*}^3}\right] + \frac{\text{Ø}_A + \text{Ø}_B + \text{Ø}_{M*}}{kT}$$

où Ø est le facteur énergétique de nature non électrostatique.

Les constantes diélectriques du système eau-alcool éthylique ont été interpolées à partir des données de Akerlöf. [5]

On voit, que suivant l'équation d'Amis, le log k varie linéairement avec $\frac{1}{D}$ dans les milieux dont la constante diélectrique est supérieure à 40. La figure 3 représente la variation de log k en fonction de $\frac{1}{D}$ de l'hydrolyse acide du formiate de n-butyle. Les courbes des autres esters, étudiés par nous, ont la même allure.

Suivant l'équation de Laidler-Eyring on obtient une variation linéaire en fonction de $\frac{D-1}{2D+1}$ dans les milieux également de grandes constantes diélectriques.

Cependant aux petites constantes diélectriques l'allure de la courbe doit être influencée par le facteur non électrostatique (fig. 4).

Les pentes (m) des droites, log k en fonction de $\frac{D-1}{2D+1}$ obtenues pour le formiate de n-butyle sont réunies dans le tableau 7.

Elles sont pratiquement constantes pour les trois esters.

Les valeurs de ces pentes varient assez peu avec la température si on les compare avec les pentes trouvées en étudiant l'hydrolyse acide de trois esters dans d'autres solvants mixtes, tels que l'eau-acétone.

Nous avons vu plus haut que l'énergie d'activation présente des valeurs extrêmes qu'on attribue au phénomène de solvatation. Au minimum de l'énergie d'activation le complexe activé doit être plus solvaté que les molécules du réactif.

---

[3] E. S. Amis, *J. Chem. Educ.*, **30**, 351 (1954).

[4] K. J. Laidler et H. Eyring, *Ann. New York Acad. Sci.*, **39**, 303 (1940).

[5] G. Akerlöf, *J. Amer. Chem. Soc.*, **54**, 4125 (1932).

On admet que la solvatation est accompagnée d'un arrangement régulier des molécules du solvant autour du complexe activé. C'est à cette distribution régulière des molécules du solvant qu'on attribue la diminution de l'entropie d'activation de la réaction (tableau 4 et 5). D'après les résultats obtenus par nous on pourrait supposer que le système eau-alcool éthylique présente une certaine structure à la concentration correspondant à la valeur la plus petite de l'énergie d'activation ($X = 0,2$). On sait, d'autre part, que d'après les chaleurs de mélange du même système, on admet un composé du type $C_2H_5OH.3H_2O$, à la même concentration.[6,7] Toujours aux environs de cette concentration on a trouvé une

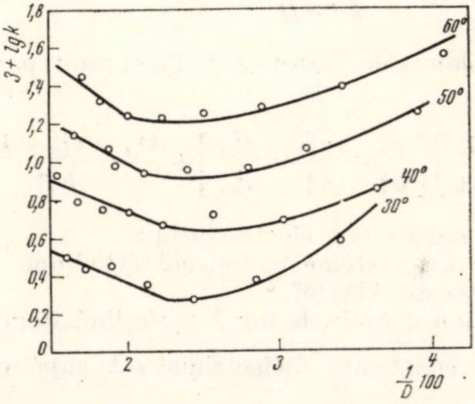

Fig. 3. — Variation de log k en fonction de $\frac{1}{D}$ de l'hydrolyse acide du formiate de *n*-butyle dans l'eau-alcool éthylique.

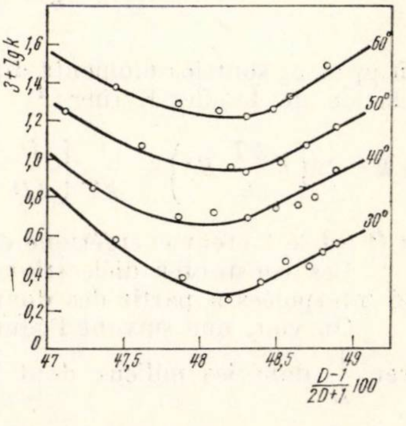

Fig. 4. — Variation de log k en fonction de $\frac{D-1}{2D+1}$ de l'hydrolyse acide du formiate de *n*-butyle dans l'eau-alcool éthylique.

Tableau 7

Les pentes (m) des droites de log k en fonction de $\frac{D-1}{2D+1}$ de l'hydrolyse acide du formiate de *n*-butyle dans l'eau-alcool éthylique

Formiate de *n*-butyle				
t°C	30°	40°	50°	60°
m	42	42	44	32

---

[6] S. V. Zelter, *Ferment. Spirtov. Prom.*, **32**, 11 (1966).

[7] S. V. Zelter, *Pishchevaia Tehnologia*, **62**, 60 (1968).

absorption très forte des ultrasons, qu'on attribue à un arrangement ordonné des molécules.[8] Les spectres RPM et la viscosité confirment aussi ces résultats. [9]

On peut donc conclure que, la cinétique chimique de l'hydrolyse acide des esters étudiés par nous laisse prévoir une certaine structure du solvant eau-alcool éthylique à la concentration de $X = 0{,}2$ (45%). Dans cet état le solvant mixte est capable de mieux solvater le complexe activé qu'à d'autres concentrations.

---

[8] K. G. Akhmentzyanov, *Primen Ultraakust. Issled. Veshestvo*, **21**, 90 (1965).

[9] J. V. Matyash et V. I. Yashkichev, *Zhur. strukt. Khim.*, **5**, 13 (1964).

Revue Roumaine de Chimie, 17, 8, 1339–1345 (1972)

L'INFLUENCE DU SOLVANT SUR LA VITESSE DE RÉACTION

L'HYDROLYSE ACIDE DU FORMIATE, DE L'ACÉTATE[1] ET DU PROPIONATE DE *n*-BUTYLE DANS LE SOLVANT MIXTE EAU-ACÉTONE

G. COSTEANU et ORTANSA LANDAUER

Chaire de Chimie Physique
Institut Polytechnique, 132, Str. Griviței
Bucarest, Roumanie

Reçu le 29 novembre 1971

La cinétique chimique de l'hydrolyse acide du formiate, de l'acétate et du propionate de *n*-butyle dans le solvant mixte montre que le phénomène de solvatation du complexe activé et des molécules du réactif est influencé non seulement par le facteur électrostatique du milieu, mais aussi par les facteurs non électrostatiques.

L'influence de la nature du solvant sur l'hydrolyse acide des esters, déjà mentionnés, a été étudiée dans un mélange de deux solvants, eau-acétone, de constantes diélectriques différentes, en proportions variables. D'autres esters ont été aussi étudiés dans le même solvant.[2,3]

PARTIE EXPÉRIMENTALE

Les esters étudiés par nous ont été préparés et soigneusement purifiés suivant les indications trouvées dans la littérature.[4]

L'acétone aussi a été bien purifiée préalablement.

La concentration initiale des solutions des trois esters, déterminée par saponification totale, était approximativement de 0,1 M et celle de l'acide chlorhydrique de 0,05 N.

La cinétique des réactions a été suivie à 30, 40, 50 et 60° selon la méthode déjà mentionnée dans un travail antérieur.[2]

---

[1] G. Costeanu, O. Landauer et C. Mateescu, *Rev. Roumaine Chim.*, **14**, 845 (1969).

[2] A. G. Kerlöf, *J. Amer. Chem. Soc.*, **54**, 4125 (1932).

[3] H. S. Harned et A. M. Ross, *J. Amer. Chem. Soc.*, **63**, 1928 (1941).

[4] A. I. Vogel, « A Text Book of Practical Organic Chemistry », III, Longman, Green and Co. New York, **97** (1956).

RÉSULTATS EXPÉRIMENTAUX

La réaction est caractérisée par la loi cinétique suivante : $k_2 = \frac{2{,}303}{bt} \ln \frac{a}{a - x}$, où b est la concentration initiale de l'eau.

Les constantes de vitesse sont réunies dans les tableaux 1, 2 et 3. La variation de la constante de vitesse du formiate de n-butyle en fonction

Tableau 1

Constantes de vitesse de l'hydrolyse acide du formiate de n-butyle dans l'eau-acétone en $cm^3 mole^{-1}s^{-1}$

$X_{acétone}$	10^2 moles H_2O/cm^3	10^3k_2 30°	10^3k_2 40°	10^3k_2 50°	10^3k_2 60°
0,055	4,669	4,83	8,90	17,27	31,82
0,091	4,212	3,98	7,52	16,45	30,86
0,130	3,744	4,10	7,48	16,13	30,88
0,179	3,258	3,54	6,88	15,08	31,06
0,239	7,757	3,02	5,92	14,87	28,30
0,317	2,220	2,96	6,31	15,55	33,13
0,424	1,647	4,18	9,09	19,28	40,28
0,578	1,020	8,24	18,81	38,86	81,91
0,648	0,800	14,21	29,27	63,29	132,37

Tableau 2

Constantes de vitesse de l'hydrolyse acide de l'acétate de n-butyle dans l'eau-acétone en cm^3 $mole^{-1}s^{-1}$ [6]

$X_{acétone}$	10^2b moles H_2O/cm^3	10^4k_2 30°	10^4k_2 40°	10^4k_2 50°	10^4k_2 60°
0,041	4,871	2,60	4,31	7,32	12,73
0,076	4,392	2,18	3,69	7,44	12,42
0,112	3,950	2,33	4,03	7,38	12,20
0,168	3,371	2,48	4,47	7,52	13,55
0,232	2,821	2,25	4,27	6,98	12,08
0,295	2,370	1,62	3,17	6,53	12,87
0,400	1,773	1,49	3,46	7,44	15,03
0,551	1,221	2,86	5,74	10,48	20,77
0,796	0,410	13,82	26,75	35,95	54,39

Tableau 3

Constantes de vitesse de l'hydrolyse acide du propionate de n-butyle dans l'eau-acétone en cm^3 $mole^{-1}s^{-1}$

$X_{acétone}$	10^2b moles H_2O/cm^3	10^4k_2 30°	10^4k_2 40°	10^4k_2 50°	10^4k_2 60°
0,157	3,469	1,59	3,09	5,54	11,09
0,214	2,951	1,47	2,77	5,38	9,88
0,289	2,401	1,64	3,07	5,36	9,69
0,390	1,814	2,04	3,72	5,63	9,59
0,532	1,187	2,51	5,26	9,00	15,73
0,763	0,488	9,66	17,23	37,34	66,86

de la teneur en acétone du solvant mixte est représentée graphiquement par la figure 1.

Pour l'acétate et le propionate de *n*-butyle on obtient des courbes semblables. Toutes ces courbes ont une allure parabolique dont le minimum se déplace, avec la température, vers les petites concentrations en acétone, du solvant mixte.

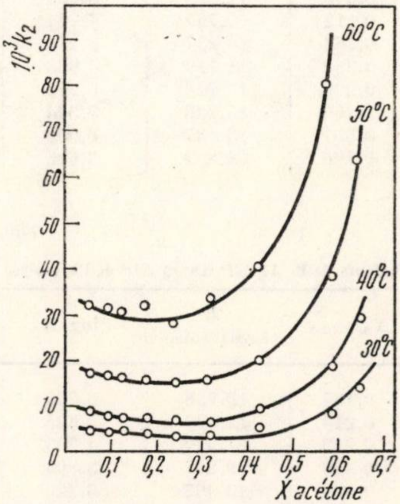

Fig. 1. — Variation de la constante de vitesse de l'hydrolyse acide du formiate de *n*-butyle avec la concentration en acétone du solvant mixte.

On attribue l'allure de ces courbes à la variation du phénomène de solvatation avec la teneur en acétone du solvant et avec la température.

L'ensemble de nos résultats nous ont permis de calculer les fonctions thermodynamiques d'activation ainsi que les facteurs préexponentiels. Tableaux 4, 5 et 6.

La figure 2 représente la variation de l'énergie d'activation en fonction de la concentration en acétone.

Tableau 4

Valeurs de E, A. ΔH^*. ΔS^* et ΔG^* de l'hydrolyse acide du formiate de *n*-butyle dans l'eau-acétone

$X_{acétone}$	E kcal/mole	log A	ΔH^* kcal/mole	ΔS^* u.e.	ΔG^* kcal/mole
0,055	12,630	6,943	12,038	−31,35	21,380
0,091	13,208	7,430	12,816	−29,12	21,493
0,130	13,270	7,342	12,678	−29,52	21,475
0,179	13,407	7,378	12,815	−29,36	21,564
0,239	15,100	8,550	14,508	−23,99	21,657
0,317	16,153	9,314	15,561	−20,50	21,670
0,424	14,100	8,692	14,508	−23,34	21,463
0,578	15,375	9,188	14,783	−21,07	21,062
0,648	15,100	9,223	14,508	−20,90	20,739

Tableau 5

Valeurs de E, A, ΔH^*, ΔS^* et ΔG^* de l'hydrolyse acide de l'acétate de *n*-butyle dans l'eau-acétone

$X_{\text{acétone}}$	E kcal/mole	log A	ΔH^* kcal/mole	ΔS^* u.e.	ΔG^* kcal/mole
0,041	10,525	4,131	10,033	−44,21	23,208
0,076	11,898	5,060	11,306	−39,96	23,214
0,112	10,799	4,284	10,207	−43,51	23,173
0,168	10,257	3,914	9,660	−45,21	23,133
0,232	11,119	4,503	10,527	−42,51	23,195
0,295	13,728	6,273	13,136	−34,41	23,390
0,400	15,238	7,344	14,646	−29,51	23,440
0,551	13,087	6,050	12,495	−35,43	23,053
0,796	8,832	3,616	8,240	−46,57	22,118

Tableau 6

Valeurs de E, A, ΔH^* ΔS^* et ΔG^* de l'hydrolyse acide du propionate de *n*-butyle dans l'eau-acétone

$X_{\text{acétone}}$	E kcal/mole	log A	ΔH^* kcal/mole	ΔS^* u.e.	ΔG^* kcal/mole
0,157	13,728	6,209	13,136	−34,70	23,476
0,214	12,629	5,425	12,037	−38,29	23,447
0,289	11,577	4,703	10,985	−41,60	23,382
0,390	9,247	3,903	8,655	−48,98	23,251
0,532	13,407	6,220	12,815	−34,65	23,014
0,763	12,492	6,143	11,900	−35,00	22,331

Les valeurs de l'énergie d'activation se situent sur des courbes présentant des minimums et des maximums à des concentrations du solvant mixte, différentes d'un ester à un autre.

On remarque que les minimums deviennent, plus accentués, en passant du formiate au propionate de *n*-butyle, à mesure que la teneur en

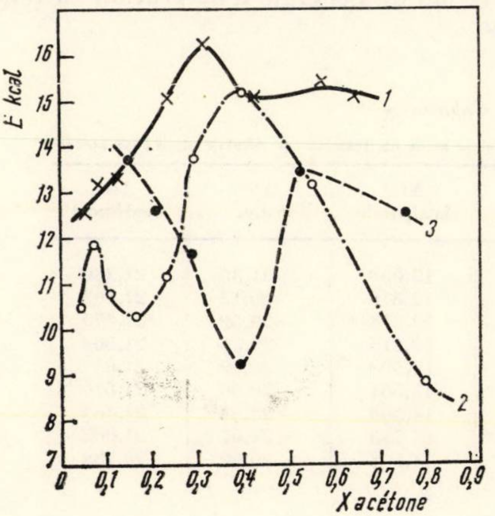

Fig. 2. — Variation de l'énergie d'activation de l'hydrolyse acide du formiate (1), de l'acétate (2) et du propionate de *n*-butyle (3), avec la teneur an acétone du solvant mixte.

acétone augmente, alors que les maximums diminuent dans le même sens. C'est dans le même sens que décroît aussi la solubilité des esters. Celle-ci dépend certainement de la longueur de la chaîne du radical acide.

Les minimums et les maximums de l'énergie d'activation sont attribués à de degrès différents de solvatation du complexe activé et des molécules réagissantes.[6]

Un examen de nos résultats montre qu'au minimum et au maximum de l'énergie d'activation correspondent des valeurs minimales et maximales de l'entropie d'activation.

Il en est de même de l'enthalpie d'activation. D'autre part il semblerait que l'influence du solvant est plus complexe et que la relative simplicité des valeurs de l'enthalpie libre d'activation résulte d'un effet de compensation entre les effets du solvant sur l'enthalpie d'activation et sur l'entropie d'activation.

Nous avons aussi été amené à envisager l'influence du facteur électrostatique sur la vitesse de réaction.

On sait que la constante de vitesse est reliée à la constante diélectrique par la relation d'Amis [7] ou par la relation de Laidler-Eyring [8] en admettant que la réaction est du type dipôle-dipôle.

$$\ln k_D = \ln k_{D\infty} - \frac{2\mu_1 \mu_2}{kTDr^3}$$

où μ_1 et μ_2 sont les moments dipolaires de l'eau et de l'ester.

$$\ln k = \ln\left(x\frac{kT}{h}K^*\right) - \frac{1}{kT}\left[\frac{D-1}{2D+1}\right]\left[\frac{\mu_A^2}{a_A^3} + \frac{\mu_B^2}{a_B^3} - \frac{\mu_{M*}^2}{a_{M*}^3}\right] + \frac{\text{Ø}_A + \text{Ø}_B - \text{Ø}_{M*}}{kT}$$

Ø est le facteur non électrostatique.

Les constantes diélectriques du système eau-acétone ont été interpolées à partir des données de Akerlöf. [9]

La seconde équation contient un terme qui exprime l'influence des facteurs non électrostatiques.

Les deux équations laissent prévoir une variation linéaire de log k en fonction de $\frac{1}{D}$ et de $\frac{D-1}{2D+1}$ (fig. 3 et 4).

Les courbes de la figure 3 représentent la variation de log k en fonction de $\frac{1}{D}$ pour le formiate de n-butyle. La variation est linéaire dans le domaine des grandes constantes diélectriques du solvant.

On voit que les pentes des droites ont des valeurs négatives en accord avec l'équation d'Amis. Dans les milieux de constantes diélectri-

---

[5] G. Costeanu, O. Landauer et C. Mateescu, *Rev. Roumaine Chim.*, **13**, 155 (1968).

[6] E. Tommila, *Ann. Acad. Sci. Fennicae A. II*, **53**, 3 (1954).

[7] E. S. Amis, *J. Chem. Educ.*, **30**, 351, (1953).

[8] K. J. Laibler et H. Eyering, *Ann. New-York Acad. Sci.* **39**, 303 (1940).

[9] G. Akerlöf, *J. Amer. Chem. Soc.*, **54**, 4125 (1932).

ques inférieures à 40 le log k augmente et les courbes passent par un minimum. Quand la température s'élève le minimum se déplace vers les petites valeurs de D.

On attribue ce déplacement à la variation du phénomène de solvatation avec la température.

Les autres esters donnent des courbes similaires.

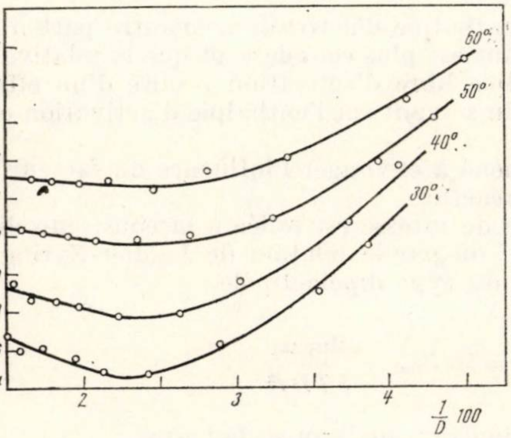

Fig. 3. — Variation de log k en fonction de $\frac{1}{D}$ de l'hydrolyse acide du formiate de n-butyle dans l'eau-acétone.

Fig. 4. — Variation de log k en fonction de $\frac{1}{D}$ de l'hydrolyse acide du formiate de n-butyle dans l'eau-acétone.

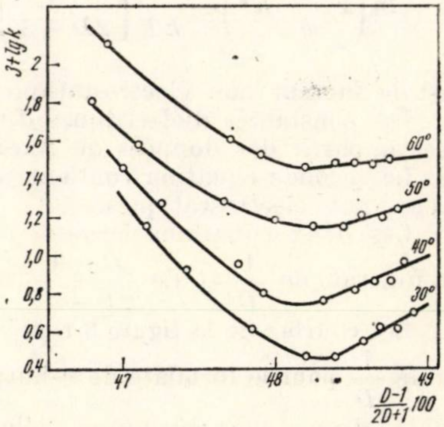

La figure 4 représente la variation de log k en fonction de $\frac{D-1}{2D+1}$ du formiate de n-butyle. On obtient des courbes similaires pour les autres esters. Dans le domaine de grandes constantes diélectriques du solvant la variation est linéaire. En calculant, dans ce cas, les pentes des droites pour les trois esters, nous avons trouvé des valeurs (tableau 7) qui varient sensiblement avec la température et d'une façon très régulière.

Tableau 7

Les pentes des droites de log $k=f\left(\frac{D-1}{2D+1}\right)$ de l'hydrolyse acide du formiate, de l'acétate et du propionate de *n*-butyle dans l'eau-acétone

Ester	Formiate de *n*-butyle				Acétate de *n*-butyle				Propionate de *n*-butyle			
t°C	30°	40°	50°	60°	30°	40°	50°	60°	30°	40°	50°	60°
m	48	32	24	12	38	32	16	8	28	10	8	6

A ce point de vue il y a une grande différence entre le comportement du solvant mixte eau-acétone et eau-alcool éthylique.[10] Dans ce dernier nous avons trouvé, en étudiant l'hydrolyse acide des mêmes esters, que les pentes des droites, log $k=f\left(\frac{D-1}{2D+1}\right)$, ont des valeurs pratiquement constantes à toutes les températures considérées, pour les trois esters.

Dans le domaine de concentration du solvant, où la variation de log $k=f\left(\frac{D-1}{2D+1}\right)$ n'est pas linéaire, c'est-à-dire aux petites constantes diélectriques, on admet que les forces non électrostatiques du milieu prennent une part importante au phénomène de solvatation.

[10] G. Costeanu et O. Landauer, *Rev. Roumaine Chim.*, 17, 1331 (1972).

Revue Roumaine de Chimie, 17, 8, 1347–1352 (1972)

L'INFLUENCE DU SOLVANT SUR LA VITESSE DE RÉACTION

L'HYDROLYSE ACIDE DU FORMIATE, DE L'ACÉTATE ET DU PROPIONATE DE *n*-BUTYLE DANS LE SOLVANT MIXTE EAU-DIMÉTYLSULFOXYDE

G. COSTEANU et ORTANSA LANDAUER

Chaire de Chimie Physique,
Institut Polytechnique, 132,
str. Griviţei, Bucarest, Roumanie

Reçu le 8 janvier 1972

Les auteurs montrent que la cinétique chimique de l'hydrolyse acide du formiate, de l'acétate et du propionate de *n*-butyle dans le solvant mixte eau-DMSO permet d'admettre l'existence d'un groupement moléculaire, DMSO $(H_2O)_2$ à la concentration du solvant de $X_{DMSO} = 0{,}35$.

En poursuivant nos recherches sur l'influence du solvant sur la vitesse de réaction nous avons étudié l'hydrolyse acide du formiate, de l'acétate et du propionate de *n*-butyle dans le solvant eau-dimétylsulfoxyde. Le dimétylsulfoxyde a une constante diélectrique assez grande, $D = 45$, une basicité proche de celle de l'eau, et un moment dipolaire élevé, $\mu = 4{,}3$ D.

PARTIE EXPÉRIMENTALE

Les esters étudiés dans ce travail ont été préparés et purifiés par les méthodes données dans la littérature.[1]

Le diméthylsulfoxyde a été purifié d'abord par distillation à pression réduite et ensuite par cristallisation fractionnée. Le produit final a le point de fusion $P_f = 18{,}52°$ et $n_D^{20} = 1{,}4773$.[2]

La concentration initiale de l'ester, déterminée par saponification totale était approximativement de 0,1M et celle de l'acide chlorhydrique, constante dans tous les cas était de 0,05 N.

La méthode expérimentale a été décrite dans un travail antérieur.[3]

Les réactions ont été étudiées dans des solutions eau-diméthylsulfoxyde contenant de 20 à 90% DMSO, aux températures suivantes : 25, 40, 50 et 60°.

---

[1] A. I. Vogel, « A Text Book of Practical Organic Chemistry », IIIe vol. Longsman, Green and Co. London, New York, 1956, p. 97.

[2] J. Kenttämaa et J. J. Lindberg, *Suomen Kemistilekhti B*, **33** 32 (1960).

[3] G. Costeanu, O. Landauer et C. Mateescu, *Rev. Roumaine Chim.*, **13**, 155 (1968).

Au-dessous de 20% DMSO les esters ne sont plus solubles dans les solvants mixtes et au-dessus de 90% DMSO le solvant ne contient pas assez d'eau pour obtenir la solution d'acide chlorhydrique de 0,05 N.

La réaction vérifie l'équation cinétique suivante : $k_2 = \frac{2,303}{bt} \log \frac{a}{a - x}$, où b est la concentration de l'eau du solvant mixte.

RÉSULTATS EXPÉRIMENTAUX

Les constantes de vitesse de l'hydrolyse acide des trois esters, exprimées, en $\text{mole}^{-1}\ \text{cm}^3\ \text{s}^{-1}$, sont réunies dans les tableaux 1, 2 et 3.

Tableau 1

Constantes de vitesse de l'hydrolyse acide du formiate de *n*-butyle dans l'eau-DMSO en $\text{cm}^3\ \text{mole}^{-1}\text{s}^{-1}$

X_{DMSO}	10^2b moles H_2O/cm^3	$10^3 k_2$ 25°	$10^3 k_2$ 40°	$10^3 k_2$ 50°	$10^3 k_2$ 60°
0,052	4,369	4,39	18,87	41,89	83,50
0,096	3,802	4,51	18,17	37,13	80,74
0,140	3,252	4,92	17,68	38,59	74,46
0,194	2,714	5,69	17,67	40,02	70,99
0,262	2,183	6,73	17,01	38,10	67,61
0,353	1,651	7,71	18,13	35,74	65,76
0,479	1,114	8,92	20,29	40,46	69,10
0,672	0,562	9,85	29,51	46,94	78,35

Tableau 2

Constantes de vitesse de l'hydrolyse acide de l'acétate de *n*-butyle dans l'eau-DMSO en $\text{cm}^3\ \text{mole}^{-1}\text{s}^{-1}$.

X_{DMSO}	10^2b moles H_2O/cm^3	$10^4 k_2$ 25°	$10^4 k_2$ 40°	$10^4 k_2$ 50°	$10^4 k_2$ 60°
0,141	3,247	2,38	8,26	17,61	37,16
0,195	2,711	2,42	8,15	16,84	36,81
0,263	2,178	2,63	8,63	18,40	37,01
0,353	1,648	3,09	9,15	18,02	37,22
0,481	1,104	3,35	10,62	22,60	43,25
0,674	0,556	3,00	13,52	24,60	57,25

Tableau 3

Constantes de vitesse de l'hydrolyse acide du propionate de *n*-butyle dans l'eau-DMSO en $\text{cm}^3\text{mole}^{-1}\text{s}^{-1}$

X_{DMSO}	10^2b moles H_2O/cm^3	$10^4 k_2$ 25°	$10^4 k_2$ 40°	$10^4 k_2$ 50°	$10^4 k_2$ 60°
0,150	3,253	2,64	8,02	16,81	31,87
0,193	2,722	2,77	8,18	17,08	32,43
0,261	2,191	3,07	8,75	16,64	32,11
0,351	1,659	2,98	9,02	16,77	33,75
0,477	1,128	3,30	10,21	17,86	39,45
0,670	0,565	4,16	12,92	28,05	56,34

On remarque que pour certaines concentrations du solvant les constantes de vitesse de l'hydrolyse acide du formiate de *n*-butyle passent par un minimum assez net, surtout aux températures élevées. Ce minimum est presque inexistant dans le cas de l'acétate et du propionate de *n*-butyle à cause de l'effet inductif positif du radical acide dont l'action croît du formiate au propionate de *n*-butyle.

Des résultats semblables ont été trouvés aussi dans d'autres cas [4-7].

A partir des données expérimentales nous avons calculé les énergies d'activation, ainsi que les fonctions thermodynamiques d'activation. Tableaux 4, 5 et 6.

Tableau 4

Valeurs de E, A, ΔH^*, ΔS^* et ΔG^* de l'hydrolyse acide du formiate de *n*-butyle dans l'eau-DMSO

X_{DMSO}	E kcal/mole	log A	ΔH^* kcal/mole	ΔS^* u.e.	ΔG^* kcal/mole
0,052	14,460	8,243	13,868	−25,70	21,437
0,096	16,290	9,597	15,698	−19,20	21,420
0,140	15,558	9,098	14,966	−21,48	21,367
0,194	14,186	8,156	13,594	−25,79	21,279
0,262	13,270	7,056	12,678	−30,83	21,865
0,353	12,172	6,811	11,580	−31,95	21,101
0,479	12,900	7,408	12,308	−29,92	21,016
0,672	13,898	8,182	13,306	−25,68	20,959

Tableau 5

Valeurs de E, A, ΔH^*, ΔS^* et ΔG^* de l'hydrolyse acide de l'acétate de *n*-butyle dans l'eau-DMSO

X_{DMSO}	E kcal/mole	log A	ΔH^* kcal/mole	ΔS^* u.e.	ΔG^* kcal/mole
0,141	15,833	7,958	15,241	−26,70	23,198
0,195	14,918	7,321	14,326	−29,62	23,153
0,263	14,643	7,161	14,051	−30,35	23,095
0,353	13,865	6,655	13,273	−32,66	23,006
0,481	14,323	7,026	13,731	−30,97	22,960
0,674	14,643	7,212	14,051	−30,11	23,023

Tableau 6

Valeurs de E, A, ΔH^*, ΔS^* et ΔG^* de l'hydrolyse acide du propionate de *n*-butyle dans l'eau-DMSO

X_{DMSO}	E kcal/mole	log A	ΔH^* kcal/mole	ΔS^* u.e.	ΔG^* kcal/mole
0,140	14,002	6,687	13,410	−32,52	23,101
0,193	13,865	6,608	13,273	−32,88	23,071
0,261	13,087	6,082	12,495	−35,27	23,005
0,351	13,528	6,323	12,936	−33,86	23,026
0,477	14,186	6,919	13,594	−31,46	22,969
0,670	15,238	7,790	14,646	−27,47	22,832

---

[4] G. Costeanu et O. Landauer, *Rev. Roumaine Chim.*, 17, 1331 (1972)

[5] E. Tommila et A. Helle, *Ann. Acad. Sci. Fennicae A II*, **53**, 3 (1954).

[6] H. Sadek, M. S. Abu Elamayem et M. Abu Elgheit, *Suomen Kemistilehti B*, **37**, 31 (1964).

[7] R. K. Wolford, *J. Phys. Chem.*, **67**, 632 (1963).

On voit que l'énergie d'activation de l'hydrolyse acide du formiate et de l'acétate de *n*-butyle passe par un minimum à la concentration en DMSO du solvant mixte de $X=0,353$, et celle du propionate de *n*-butyle à $X = 0,261$. Tels résultats ont été remarqués aussi dans d'autres cas.[8,9]

La variation de l'énergie d'activation des trois esters avec la teneur en DMSO du solvant est représentée par la figure 1.

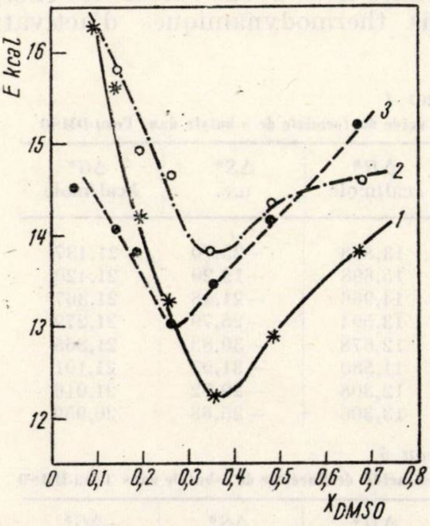

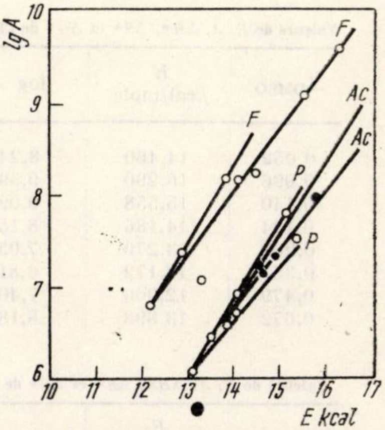

Fig. 1. — Variation de l'énergie d'activation de l'hydrolyse acide du formiate, (*1*), de l'acétate (*2*) et du propionate de *n*-butyle (*3*), avec la teneur en DMSO du solvant mixte.

Fig. 2. — Variation de log *A* en fonction de *E* de l'hydrolyse acide du formiate de l'acétate et du propionate de *n*-butyle dans l'eau-DMSO.

Le minimum de l'énergie d'activation est attribué à une solvatation différente du complexe activé et des molécules du réactif.

La solvatation du complexe activé étant plus forte que celle des molécules du réactif, elle est accompagnée d'une certaine distribution ordonnée des molécules du solvant autour du complexe activé.

C'est à cette structure régulière du système, complexe activé- solvant, qu'on attribue les valeurs minimales de l'entropie d'activation. Voir les tableaux 4, 5 et 6.

En représentant graphiquement la variation de log A en fonction de E on obtient pour chaque ester des droites, ayant des pentes différentes, et dont l'intersection se situe à la valeur minimale de l'énergie d'activation (fig. 2).

La solvatation la plus élevée du complexe activé a lieu, suivant les esters, dans l'intervalle de concentration du solvant mixte de $X_{\mathrm{DMSO}} = 0,26$ à $X_{\mathrm{DMSO}} = 0,25$.

---

[8] G. Costeanu, O. Landauer et C. Mateescu, *Rev. Roumaine Chim.*, **14**, 845 (1969).

[9] H. S. Harnrd et A. M. Ross, *J. Amer. Chem. Soc.*, **63**, 1993 (1941).

On admet que, dans ces conditions, un groupement moléculaire prend naissance, auquel on attribue la formule suivante : DMSO. $(H_2O)_2$.

Ce groupement moléculaire ayant une structure privilégiée est susceptible de solvater le complexe activé bien plus fortement que le solvant à toute autre concentration.

La formation d'un groupement moléculaire à la concentration du solvant de $X_{DMSO} = 0{,}35$, de formule DMSO. $(H_2O)_2$, a été mise en évidence anssi par des méthodes physiques, telles que la densité d'excès, la viscosité, l'indice de réfraction et les fonctions thermodynamiques d'excès du système DMSO$-H_2O$.[10–12]

L'influence du facteur électrostatique sur la vitesse de réaction s'exprime par l'équation d'Amis[13] :

$$\ln k_D = \ln k_{D\infty} - \frac{2\mu_1\mu_2}{kTDr^3}$$

où μ est le moment dipolaire et par l'équation de Laidler-Eyring,[14]

$$\ln k = \ln\left(x\frac{kT}{h}K^+\right) - \frac{1}{kT}\left[\frac{D-1}{2D+1}\right]\left[\frac{\mu_A^2}{a_A^3} + \frac{\mu_B^2}{a_B^3} + \frac{\mu_{M*}^2}{a_{M*}^3}\right] + \frac{Ø_A + Ø_B + Ø_{M*}}{kT}$$

où Ø est le facteur non électrostatique.

Suivant l'équation d'Amis en représentant graphiquement la variation de log k en fonction de $\frac{1}{D}$ on obtient, pour les trois esters, une variation linéaire, toujours positive. On voit que les droites changent de pentes à la constante diélectrique d'environ 72. La valeur des pentes dépend de la nature du milieu de réaction, de la structure de l'ester, ainsi que de la temperature (fig. 3).

D'après l'équation de Laidler-Eyring la variation de $\ln k = f\left(\frac{D-1}{2D+1}\right)$ est linéaire dans le domaine de constantes diélectriques $56 < D < 77$ (fig. 4).

Dans cet intervalle de constantes diélectriques le terme non électrostatique Ø est pratiquement négligéable.

On remarque sur le graphique que chaque ester présente une variation linéaire de log k en fonction de $\frac{D-1}{2D+1}$, à deux pentes différentes.

---

[10] J. J. Lindberg et J. Kenttämaa, *Suomen Kemistilehti B*, **33**, 104 (1960).

[11] J. M. G. Gowie et P. M. Toporowski, *Canad. J. Chem.*, **39**, 2240 (1961).

[12] M. R. Reynaud, *Compt. rend. B.*, **266**, 489 (1968).

[13] E. S. Amis, *J. Chem. Educ.*, **30**, 351 (1953).

[14] K. J. Laidler et H. Eyring, *Ann. New York Acad. Sci.*, **39**, 303 (1940).

Revue Roumaine de Chimie, 17, 8, 1347–1352 (1972)

Il faut donc admettre deux solvatations différentes du complexe activé. En effet, l'hydrolyse est plus rapide quand la pente de la droite a une valeur plus grande, et alors le complexe activé est plus solvaté que les molécules du réactif. Par contre, si la pente de la droite a une valeur plus petite l'hydrolyse est plus lente et le complexe activé est moins solvaté que dans le cas précédent, mais toujours plus solvaté que le réactif.

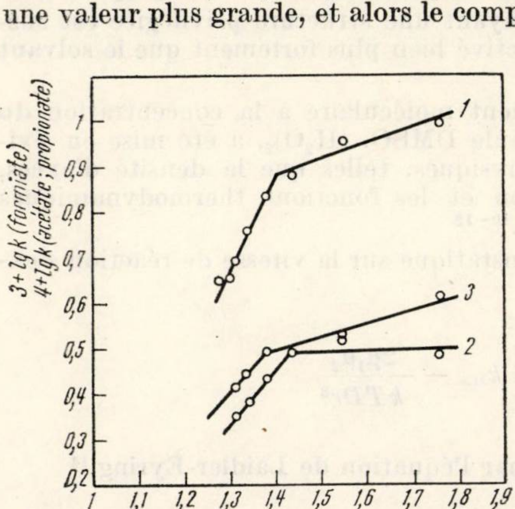

Fig. 3. — Variation de log k en fonction de $\frac{1}{D}$ de l'hydrolyse acide du formiate (1), de l'acétate (2) et du propionate de n-butyle (3), dans l'eau-DMSO.

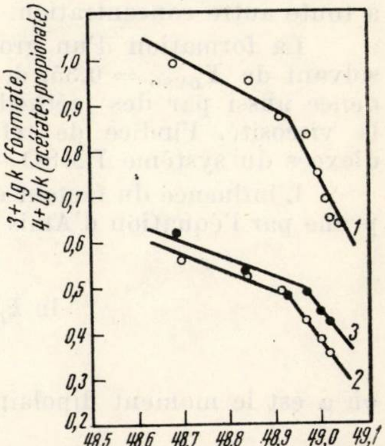

Fig. 4. — Variation de log k en fonction de $\frac{D-1}{2D+1}$ de l'hydrolyse acide du formiate (1), de l'acétate (2) et du propionate de n-butyle (3), dans l'eau-DMSO.

Le changement des valeurs des pentes a lieu à la même concentration du solvant, $X = 0{,}35$, à laquelle on admet l'existence du groupement moléculaire DMSO. $(H_2O)_2$.

On a remarqué le même phénomène pendant la solvolyse du chlorure de benzyle.[15]

---

[15] E. Tommila et O. Virtanen, *Suomen Kemistilekhti B*, 34, 139 (1961).

Revue Roumaine de Chimie, 17, 8, 1353–1360 (1972)

L'INFLUENCE DU SOLVANT SUR LA VITESSE DE RÉACTION.

L'HYDROLYSE ALCALINE DE L'ACÉTATE, DU PROPIONATE ET DU BUTYRATE DE *n*-BUTYLE DANS LE SOLVANT MIXTE EAU-TÉTRAHYDROFURANNE

G. COSTEANU et CORNELIA MATEESCU
Chaire de Chimie-Physique
Institut Polytechnique, 132, str. Griviţei, Bucarest, Roumanie

Reçu le 31 mars 1972

Les auteurs ont étudié l'hydrolyse alcaline de l'acétate, du propionate et du butyrate de *n*-butyle dans le solvant mixte eau-THF à 20, 30, 40 et 50°. Les résultats obtenus sont mis en corrélation avec la constante diélectrique du solvant. On attribue la variation de la constante de vitesse avec la teneur en THF, ainsi que la variation des fonctions thermodynamiques d'activation au phénomène de solvatation. On constate aussi que le THF manifeste une aptitude plus grande à former des liaisons hydrogène que le dioxanne et l'acétone.

Il est connu que l'interaction du solvant et des corps dissous, capables de réagir, a, dans bien des cas, une influence prépondérante sur la vitesse de réaction. L'influence du solvant dépend de la constante diélectrique du milieu de réaction et aussi des forces non électrostatiques. Bien souvent on ne peut faire une distinction nette entre les deux.

En poursuivant nos recherches concernant l'influence du solvant sur la vitesse de réaction, nous avons étudié l'hydrolyse alcaline de l'acétate, du propionate et du butyrate de *n*-butyle dans le solvant mixte eau-THF.

Le tétrahydrofuranne, dont l'atome d'oxygène se trouve dans un cycle de 5 atomes de carbone, confère au solvant mixte des propriétés assez différentes par rapport aux autres solvants, eau-dioxanne [1,2] et eau-acétone [3] que nous avons déjà étudiés.

PARTIE EXPÉRIMENTALE

Les esters ont été préparés et purifiés d'après les méthodes déjà connues [4].

Le tétrahydrofuranne, bien purifié, desséché et distillé doit avoir le $P_e = 65 \pm 0,1°C$.[5]

---

[1] G. Costeanu, O. Landauer et C. Mateescu, *Rev. Roumaine Chim.*, **15**, 27 (1970)

[2] G. Costeanu et C. Mateescu, *Rev. Roumaine Chim.*, **16**, 1803 (1971).

[3] G. Costeanu C. et C. Mateescu, *Rev. Roumaine Chim.*, **17**, 95 (1972).

[4] A. I. Vogel, « A Text Book of Practical Organic Chemistry », IIIe, vol. IIIe éd., Longmans, Green and Co London, New York, 1956, p. 382.

[5] M. Brodon, M. Tamees et S. Scott jr., *J. Amer. Chem. Soc.*, **82**, 2129 (1960).

La concentration de l'ester, approximativement égale a 0,01 M, est déterminée par saponification totale. La concentration de l'hydroxyde de sodium, constante dans tous les essais est égale à 0,01 N.

La méthode utilisée par nous a déjà été publiée dans un travail antérieur.[6]

Les déterminations ont été effectuées à 20, 30, 40 et 50°.

RÉSULTATS EXPÉRIMENTAUX

Les tableaux 1, 2 et 3 ci-joints, réunissent les constantes de vitesse de l'hydrolyse alcaline des trois esters, exprimées en $1\ \text{mole}^{-1}\ \text{s}^{-1}$, calculées au moyen de l'équation cinétique des réactions du second ordre.

Sur les mêmes tableaux figurent aussi les énergies d'activation, E, les facteurs préexponentiels (A), les enthalpies d'activation ΔH^*, les entropies d'activation ΔS^* et les enthalpies libres d'activation ΔG^*, calculées pour différents mélanges eau-THF.

On voit dans tous les cas que les constantes de vitesse diminuent avec la teneur en THF, c'est-à-dire avec la diminution de la constante diélectrique du solvant.

La diminution des constantes de vitesse est attribuée soit aux interactions des molécules du solvant mixte,[7] soit à l'affaiblissement du pouvoir ionisant du milieu de réaction.[8]

On remarque, d'autre part, une diminution de Δk, dans l'intervalle de concentrations considéré $0{,}084 < X_{\text{THF}} < 0{,}377$, de l'acétate au butyrate de n-butyle, à toutes les températures et pour tous les esters.

Δk décroît dans le sens $\Delta k_a > \Delta k_p > \Delta k_b$, c'est-à-dire dans le même sens que les moments dipolaires des trois esters.

La diminution de Δk de l'acétate au butyrate de n-butyle est attribuée à l'effet inductif-positif[9] du groupement alkyle dont l'action augmente dans le même sens.

Nous avons remarqué la même chose en étudiant l'hydrolyse alcaline des trois esters dans l'eau-dioxanne[1,2] et dans l'eau-acétone.[3]

En faisant, d'autre part, les rapports $\frac{\Delta k_i}{\Delta k_j}$ (où i et j sont les symboles des esters considérés) on a trouvé que ces rapports ne tendent pas vers l'unité comme nous l'avons déjà constaté dans les solvants eau-dioxanne et eau-acétone.

On doit donc admettre que le THF a une aptitude plus grande à former des liaisons hydrogène que le dioxanne et l'acétone et par conséquent sa capacité de solvatation est bien plus élevée.[10]

La variation de la constante de vitesse avec la constante diélectrique du solvant s'exprime soit par la relation d'Amis, $\ln k = \ln k_0 + \frac{Ze\mu^{11}}{k\text{T}r^2 D}$ si l'on

---

[6] G. Costeanu, O. Landauer et C. Mateescu, *Rev. Roumaine Chim.*, **13**, 155 (1968).

[7] E. H. Hughes et G. K. Ingold, *J. Chem. Soc.*, **1935**, 244.

[8] E. Tommila, *Suomen Kemistlehti B*, **37,** 119 (1964).

[9] D. E. Evans et J. J. Gordon, *J. Chem. Soc.*, **1938** 1434.

[10] W. Khöler et L. Neuheiser, *Z. Chem. B*, **11**, 425 (1968).

[11] E. S. Amis, *J. Chem. Educ.*, **30**, 351 (1953).

Tableau 1

Constantes de vitesse de l'hydrolyse alcaline de l'acétate de *n*-butyle en l $mole^{-1}$, s^{-1}, et valeurs de E, log A, ΔH^*, ΔS^* et ΔG^*

X THF	10^3k 20°	10^3k 30°	10^3k 40°	10^3k 50°	E *k*cal/mole	log A	ΔS^* u.e.	ΔH^* *k*cal/mole	ΔG^* *k*cal/mole
0,084	31,85	47,31	63,40	94,02	6,983	3,7355	−45,99	6,391	20,333
0,124	26,79	38,23	51,28	75,00	6,146	3,0284	−49,24	5,554	20,481
0,174	23,19	31,47	41,73	54,25	5,262	2,3044	−52,53	4,670	20,594
0,238	18,20	25,08	32,50	43,81	5,551	2,4149	−52,03	4,959	20,731
0,320	12,98	19,10	26,33	35,49	6,054	2,7121	−50,66	5,462	20,820
0,377	12,17	17,18	23,58	31,99	6,177	2,7034	−50,75	5,585	20,970

Tableau 2

Constantes de vitesse de l'hydrolyse alcaline du propionate de *n*-butyle en l mole^{-1} s^{-1} et valeurs de E, log *A*, ΔH*, ΔS* et ΔG*

X THF	10^3k 20°	10^3k 30°	10^3k 40°	10^3k 50°	*E* *k*cal/mole	log *A*	Δ*S** u.e.	Δ*H** *k*cal/mole	Δ*G** *k*cal/mole
0,084	10,36	18,51	31,45	53,12	10,355	6,7582	−36,75	9,763	20,904
0,124	8,84	14,46	24,44	38,29	9,381	4,9280	−40,54	8,789	21,079
0,174	6,16	9,79	15,50	23,72	8,465	4,0888	−44,39	7,873	21,329
0,238	3,58	6,27	12,00	18,63	10,598	5,4638	−38,07	10,006	21,547
0,320	2,52	4,98	8,32	16,02	11,499	6,0155	−35,56	10,907	21,687
0,377	2,35	4,50	7,86	15,00	11,714	6,1271	−35,05	11,122	21,747

Tableau 3

Constantes de vitesse de l'hydrolyse alcaline du butyrate de *n*-butyle en l mole^{-1}. s^{-1}, et valeurs de *E*, log *A*, ΔH^*, ΔS^* et ΔG^*

X THF	10^3k 20°	10^3k 30°	10^3k 40°	10^3k 50°	*E* *k*cal/mole	log *A*	ΔS^* u.e.	ΔH^* *k*cal/mole	ΔG^* *k*cal/mole
0,084	6,73	11,25	15,83	22,01	7,473	3,4571	−47,27	6,881	21,211
0,124	5,89	8,61	12,36	17,95	7,047	3,0329	−49,24	6,455	21,382
0,174	4,96	7,33	10,72	15,00	6,772	2,7638	−50,47	6,180	21,480
0,238	3,30	5,05	7,82	11,52	7,852	3,3834	−47,36	7,260	21,214
0,320	2,29	3,73	5,92	9,08	8,511	3,7288	−46,03	7,919	21,872
0,377	1,92	3,10	5,06	8,00	8,936	3,9556	−44,98	8,344	21,980

Tableau 4

Différences entre les constantes de vitesse (Δk) et les rapports de ces différences pour les trois esters

T °C	Δk acétate	Δk propionate	Δk butyrate	$\frac{\Delta k_a}{\Delta k_b}$	$\frac{\Delta k_a}{\Delta k_p}$	$\frac{\Delta k_p}{\Delta k_b}$
20	1,47	0,64	0,40	3,68	2,30	1,60
30	2,10	1,00	0,55	3,82	2,10	1,82
40	2,77	1,65	0,73	3,79	1,67	2,26
50	4,30	2,33	0,99	4,34	1,84	2,35

admet que la réaction est du type ion- molécule dipolaire, soit par la relation de Laidler-Eyring :

$$\ln k = \ln k_0 - \frac{1}{kT}\left(\frac{D-1}{2D+1}\right)\left[\frac{\mu_A^2}{r_A^3} + \frac{\mu_B^2}{r_B^3} - \frac{\mu_{AB}^2}{r_{AB}^3}\right]$$ [12]

en supposant que la réaction a lieu entre la molécule de l'ester et la molécule de l'eau, réaction du type dipôle-dipôle.

Les constantes diélectriques du solvant mixte ont été déduites par interpolation des données trouvées dans la littérature. [13]

Nous avons trouvé que la variation de log k en fonction de $\frac{1}{D}$ et de $\frac{D-1}{2D+1}$ n'est linéaire que dans les mélanges à grandes constantes diélectriques. Fig. 1 et 2.

On doit, par conséquent, admettre que la constante de vitesse est influencée non seulement par la constante diélectrique, mais aussi par d'autres facteurs du milieu de réaction [14,15]

Les deux équations n'expriment donc que partiellement les interactions entre les molécules réagissantes et le solvant.

On obtient, par contre, une variation linéaire de log k en fonction de D (fig. 3).

En représentant graphiquement la variation de E en fonction de X_{THF} on trouve que l'énergie d'activation passe par un minimum aux environs de X_{THF} 0,175, pour les trois esters (fig. 4).

A cette concentration du solvant mixte, le complexe activé, agrégat moléculaire très polaire, est bien plus solvaté que les molécules réagissantes.

---

[12] K. J. Laidler et H. Eyring, *Ann. New York Acad. Sci.*, **39**, 303 (1940).

[13] H. Heydtmann et H. Stieger, *Ber. Bunsengesellschaft Phys. Chem.*, **70**, 1095 (1966).

[14] E. Tommila et S. Maltamo, *Acta Chem. Scand.*, **8**, 1152 (1954).

[15] E. Tommila, A. Koivisto, J. P. Lyyra, K. Antell et S. Heimo, *Ann. Acad. Sci. Fennicae, A*, **47**, 1 (1952).

Le champ électrique du complexe activé entraîne une orientation des molécules du solvant autour de lui et fait diminuer leur liberté de mouvement.

Ceci se manifeste par une diminution de l'entropie d'activation qu'on constate expérimentalement.

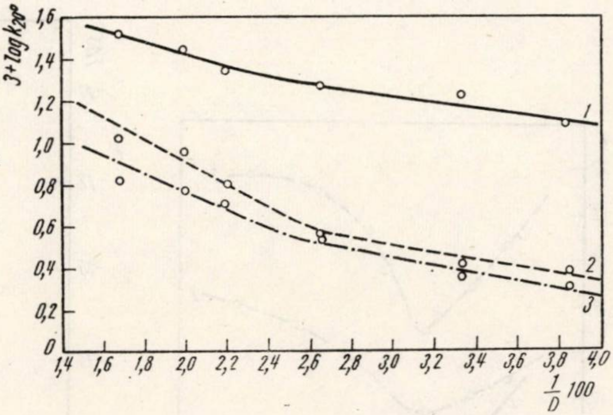

Fig. 1. — Variation de log k en fonction de $\frac{1}{D}$.

1, acétate; 2, propionate; 3, butyrate.

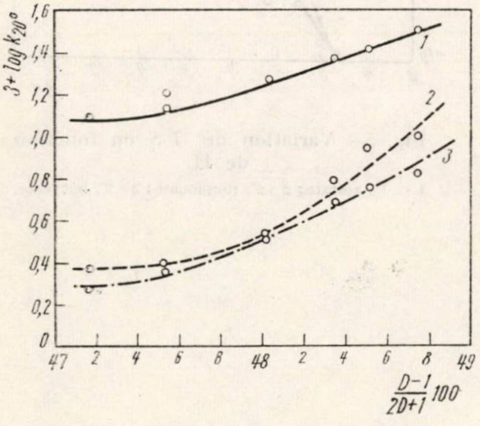

Fig. 2. — Variation de log k en fonction de $\frac{D-1}{2D-1}$.

1, acétate; 2, propionate; 3, butyrate.

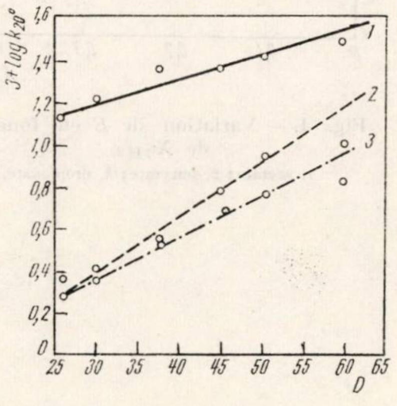

Fig. 3. — Variation de log k en fonction de D.

1, acétate; 2, propionate; 3, butyrate.

En représentant graphiquement, le $T\,\Delta S^*$ en fonction de ΔH^* on obtient deux droites dont le point de rencontre correspond au minimum de l'énergie d'activation (fig. 5).

Ces droites vérifient l'équation : $T\Delta S^* = \alpha\,\Delta H^* + \beta$.

Les valeurs moyennes de α correspondent à 1,19 dans le domaine riche en eau du solvant mixte et à 0,80 dans le domaine riche en THF.

On considère que les valeurs minimales de l'énergie d'activation et de l'entropie d'activation, ainsi que la valeur supérieure à l'unité de la pente $T\Delta S^* = f(\Delta H^*)$ dans les mélanges riches en eau doivent être attribuées à la grande capacité de solvatation du complexe activé.

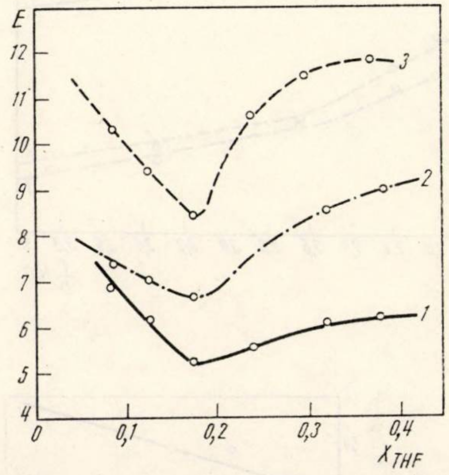

Fig. 4. — Variation de E en fonction de X_{THF}.
1, acétate ; 2, butyrate ; 3, propionate.

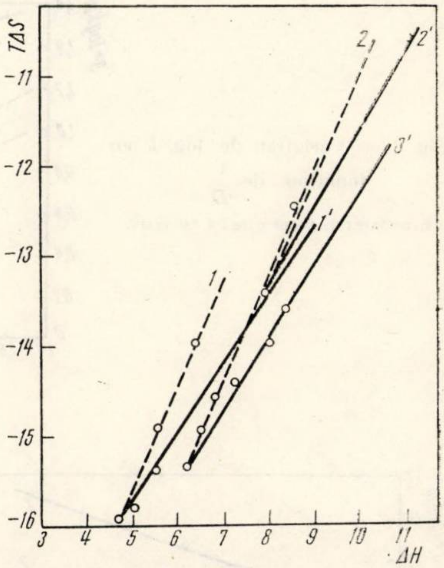

Fig. 5 — Variation de T S en fonction de H.
1 = 1', acétate ; 2 – 2', propionate ; 3 – 3', butyrate.

Revue Roumaine de Chimie, 17, 8, 1361–1366 (1972)

THERMODYNAMIC EXCESS FUNCTIONS IN MOLTEN MIXTURES OF POTASSIUM CHLORIDE WITH ALKALINE-EARTH CHLORIDE

IUDITA ADORIAN and S. STERNBERG

Polytechnic Institute
str. Polizu nr. 1, Bucureşti

Received March 3, 1972

Thermodynamic activities of potassium chloride in molten mixtures with alkaline-earth chlorides are determined by means of the cryoscopic method. Negative excess free enthalpies are obtained which decrease as the radius of the alkaline-earth ion increases. Comparison with the thermodynamic properties of the NaCl + $Me_{II}Cl_2$ mixtures is made.

In the present paper partial molar excess free enthalpies of potassium chloride in KCl + $Me_{II}Cl_2$ mixtures are determined by means of the cryoscopic method, Me_{II} being an alkaline-earth metal.

Utilization of this method in studying the thermodynamic properties of molten salt mixtures is justified by the agreement between data obtained by the said method and those obtained by means of electrochemical equilibrium cells.[1–3]

The activity a_1 of the "solvent" at temperature T can be deduced by the Schroeder – van Laar equation as:

$$\ln a_1 = \frac{\Delta H_{T_0}}{R}\left[\frac{1}{T} - \frac{1}{T_0}\right] + \frac{\Delta C_p}{T}\left[\ln\frac{T_0}{T} - \frac{T_0 - T}{T}\right] \tag{1}$$

ΔH_{T_0} is the molar heat of solidification of the pure solvent at its melting point T_0, T the temperature of first separation of solvent on cooling the solution, and $\Delta C_p = C_p(s) - C_p(l)$ is the difference, regarded as constant, between the molar heat capacities of the solvent in solid and liquid state respectively.

The use of phase diagrams for determining thermodynamic activities based on equation (1) suppose a precise establishment of liquidus curves and the use of most reliable thermochemical data.

---

[1] I. G. Murgulescu and S. Sternberg, *Rev. Chim. Acad. R.P. Roumaine*, **2**, 251 (1957).
[2] I. G. Murgulescu and S. Sternberg, *Discuss. Faraday Soc.*, **32**, 107 (1962).
[3] S. Sternberg and I. Adorian, *Studii și Cercetări Chim. Acad. R.P.R.* **11**, 315 (1963)

EXPERIMENTAL

Temperatures of crystalization of potassium chloride in KCl + $CaCl_2$, KCl+$SrCl_2$ and KCl + $BaCl_2$ mixtures have been determined by the method of cooling curves. The application of this method to ionic liquids is conditioned by certain precautions concerning materials involved — because of the corrosive action of the salts—and by securing an inert gas atmosphere to avoid oxidation.

The phase diagrams of the KCl + $Me_{II}Cl_2$ mixtures exhibit the formation of definite compounds : KCl. $CaCl_2$; 2KCl . $SrCl_2$; 2KCl. $BaCl_2$; KCl.3$BaCl_2$. There are some relatively recent data for the phase diagram of the KCl + Cl_2 system,[4] whereas for the KCl+$SrCl_2$ and the KCl + $BaCl_2$ systems, the available data are obsolete and contain but two temperatures for each of the branches of crystalization of potassium chloride.[5-7]

Therefore, in order to carry out thermodynamic calculations, we considered necessary to establish more accurately the freezing point depressions of the potassium chloride in the respective mixtures. Crystallization temperatures of the potassium chloride have been established with a Pt. Rh-Pt thermocuple, the electromotive force of which was measured by the compensation method. The accuracy of temperature measurements was of ± 0.5° and their reproducibility of ± 1°. The experimental device, the method applied and the preparation of the salts used, have been described in detail in a previous paper.[8]

RESULTS

Temperatures indicating the initial solidification of KCl in the mixtures, as well as the temperature of the first eutectic point, are presented in Table 1. Branches of the crystallization of potassium chloride in the three mixtures in comparison with an ideal solution in KCl are presented in Fig. 1.

Table 1

Temperatures of first separation of KCl in KCl + $Me_{II}Cl_2$ mixtures

x_{KCl}	T °K in KCl + $Me_{II}Cl_2$ mixture		
	KCl + $CaCl_2$	KCl + $SrCl_2$	KCl + $BaCl_2$
1	1044	1044	1044
0.95	—	1016	1023
0.90	993	997	1001
0.85	958	964	977
0.80	915	931	954
0.76	879	—	—
0.75	—	902	929
0.70	—	865	—

---

[4] I. P. Dergunov and A. G. Bergmann, *Doklady Akad. Nauk. S.S.S.R.*, **75,** 815 (1950).

[5] E. Vortisch, *N. Jahrb. Min. Geol. Poläeont. B.B.*, **38,** 185, 301 (1915).

[6] H. Gemsky, *N. Jahrb. Min. Geol. Poläeont. B.B.*, **36,** 513 (1913).

[7] E. H. Gen, *J. Chem. Soc.*, **106,** 51 (1913).

[8] S. Sternberg and I. Adorian, *Rev. Chim. Acad. R.P. Roumaine*, **7,** 1317 (1962).

By means of equation (1) and using thermochemical data indicated by Kubashewski and Evans[9] and presented in Table 2, the following equation for the thermodynamic activity of potassium chloride is obtained :

$$\log\ a_1 = -1249.05\,T^{-1} + 0.3069\ \log\ T + 0.2701 \tag{2}$$

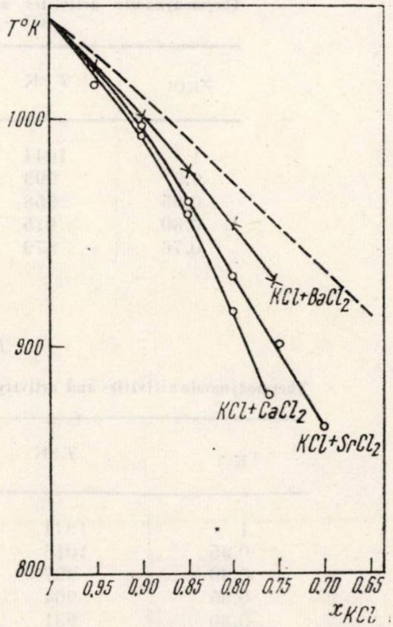

Fig. 1. — Branches of crystallization of potassium chloride in KCl—$Me_{II}Cl_2$ mixtures (Dotted line : ideal mixture).

Thermodynamic activities a_1 and activity coefficients γ_1 of the KCl in the three mixtures, calculated by means of equation (2), are presented in Tables 3—5. Partial molar excess free enthalpies of the potassium

Table 2

Thermochemical data

Compound	ΔH_{T_0} kcal/mole	T_0 K	C_p(s) cal/mole degree	C_p(l) cal/mole degree
KCl	$-6.35 + -0.1$ [10]	1044	$9.89 + 5.20.10^{-3}T + 0.77.10^{5}T^{-2}$ [11]	16[11]

---

[9] O. Kubashewski, E. L. L. Evans and C. B. Alcock, "Metallurgical Thermochemistry" Pergamon Press, Oxford—London, 1967.

[10] A. S. Dworkin and M. A. Bredig, *J. Phys. Chem.*, **64**, 269 (1960) ; **67**, 697, 2499 (1963).

[11] K. K. Kelley, U.S. Dept. Mines. Bul., **1949**, 476.

chloride have been calculated as $\overline{G}_1^E = RT \ln \gamma_1$. Dependence of $\overline{G}_1^E$ on the mole fraction x_2 of $\mathrm{Me_{II}Cl_2}$ in the investigated concentration range is represented in Fig. 2.

Table 3

Thermodynamic activities and activity coefficient of KCl in KCl + $CaCl_2$ mixtures

x_{KCl}	T °K	a_{KCl}	γ_{KCl}
1	1044	1	1
0.9	993	0.855	0.950
0.85	958	0.761	0.895
0.80	915	0.652	0.814
0.76	879	0.569	0.744

Table 4

Thermodynamic activities and activity coefficients of KCl in KCl + $SrCl_2$ mixtures

x_{KCl}	T °K	a_{KCl}	γ_{KCl}
1	1044	1	1
0.95	1016	0.920	0.968
0.90	997	0.866	0.962
0.85	964	0.777	0.914
0.80	931	0.691	0.864
0.75	902	0.620	0.826
0.70	865	0.543	0.763

Table 5

Thermodynamic activities and activity coefficients of KCl in KCl + $BaCl_2$ mixtures

x_{KCl}	T °K	a_{KCl}	γ_{KCl}
1	1044	1	1
0.95	1023	0.940	0.989
0.90	1001	0.877	0.975
0.85	977	0.811	0.955
0.80	954	0.750	0.938
0.75	929	0.686	0.915

In a previous paper[8] the authors determined partial molar excess free enthalpies of sodium chloride in mixtures with alkaline-earth chlorides, the thermodynamic properties of such mixtures having not been studied

by any other method before. Subsequently these mixtures were studied by Østvold and Førland [12] by means of galvanic cells with cation selective glass membranes :
C (graphite) | Cl_2 | NaCl (l) | | glass Na^+ | | NaCl, Me_{II} Cl_2 (l) | Cl_2 | C (graphite).
By the same method the above authors, studied the mixtures KCl + $MeCl_2$, too.[13] In tables 6 and 7 the values of the partial molar excess free enthalpies of the alkaline chloride components /MeCl/ are presented in a comparative way for both series of mixtures. The $\overline{G}^E_{MeCl}$ values in columns (I) are those determined cryoscopically in the present work, while those in columns (II) have been calculated by us according to equations of the type : $\overline{G}^E_1 = Bx_2^2 + Cx_2^3$, indicated by the authors of the electrochemical method. Although the KCl + Me_{II} Cl mixtures do not behave as

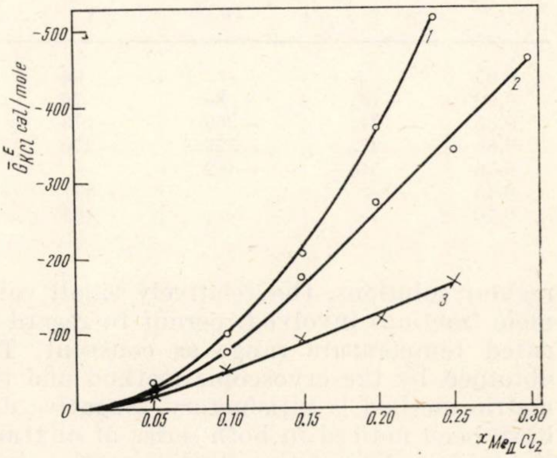

Fig. 2. — Partial molar excess free enthalpy of potassium chloride in KCl + Me_{II} Cl_2 mixtures.
1. KCl + $CaCl_2$; 2. KCl + $SrCl_2$; 3. KCl + $BaCl_2$.

Table 6

Partial molar excess free enthalpies of NaCl in molten NaCl + Me_{II} Cl_2 mixtures

x_{NaCl}	NaCl + $CaCl_2$		NaCl + $SrCl_2$		NaCl + $BaCl_2$	
	$\overline{G}^E_{NaCl}$ cal/mole		$\overline{G}^E_{NaCl}$ cal/mole		$\overline{G}^E_{NaCl}$ cal/mole	
	I	II	I	II	I	II
0.90	0	− 57	− 6	− 14	0	− 4
0.80	− 81	−194	− 62	− 54	−27	−20
0.75	—	—	—	—	−35	−31
0.70	−209	−356	−134	−113	−45	−45
0.65	—	—	—	—	−57	−61
0.60	−427	−493	−229	−189		
0.50	−682	−550	−299	−275		

---

[12] T. Østvold, *Acta Chem. Scand.*, **20**, 2320 (1966).

[13] G. D. Robbins, T. Forland and T. Østvold, *Acta Chem. Scand.*, **22**, 3002 (1968).

Table 7

Partial molar excess free enthalpies of KCl in molten KCl + $Me_{II}Cl_2$ mixtures

x_{KCl}	$KCl + CaCl_2$		$KCl + SrCl_2$		$KCl + BaCl_2$	
	$\overline{G}^E_{KCl}$ cal/mole		$\overline{G}^E_{KCl}$ cal/mole		$\overline{G}^E_{KCl}$ cal/mole	
	I	II	I	II	I	II
0.95	—	—	− 66	− 14	− 22	− 7
0.90	−101	− 86	− 76	− 51	− 51	− 25
0.85	−211	−209	−173	−101	− 90	− 56
0.80	−373	−328	−270	−190	−122	− 95
0.76	−515	−462	—	—	—	—
0.75	—	—	−341	−285	−164	−144
0.70	—	—	−465	−393	—	—

regular solutions, the relatively small values of the Cx_2^3 terms for the mole fractions involved, permit to regard the $\overline{G}^E_{MeCl}$ values in the investigated temperature range as constant. The agreement between results obtained by the cryoscopic method and those obtained by the potentiometric method is satisfactory. Negative departures from ideal behaviour have been noticed in both series of mixtures, departures that decrease as the ionic radius of the alkaline-earth cation increases. The larger excess values in the $KCl + Me_{II}Cl_2$ mixtures as compared with the corresponding $NaCl + Me_{II}Cl_2$ mixtures agree with the difference between the phase diagrams of the two series of mixtures. The phase diagrams of the $NaCl + Me_{II}Cl_2$ mixtures does not show any formation of stable solid compounds and present simple eutectic points, while in the $KCl + Me_{II}\,Cl_2$ mixtures, compounds of definite composition are formed, marked by maxima in the phase diagrams.

Revue Roumaine de Chimie, 17, 8, 1367–1374 (1972)

DIE ANORDNUNG DER GRENZSCHICHT AN ZYLINDRISCHEN ELEKTRODEN BEI ERZWUNGENER KONVEKTION

IOAN RĂDOI

aus dem Laboratorium für Elektrochemie der Polytechnischen
Hochschule Timişoara, Str. Bocşei, 6

Eingegangen am 18. Januar 1972

In den Arbeiten, die die Substanzübertragung an den Elektroden im Falle erzwungener Konvektion betreffen, wird die Stromdichte an der Elektrodenoberfläche als gleichförmig verteilt angenommen. Von hydrodynamischen Untersuchungen oder solchen, die die Wärmeübertragung betreffen, ausgehend, in denen gezeigt wird, daß der Druck beziehungsweise die Intensität der Wärmeübertragung an einem Zylinder im Falle erzwungener Konvektion auf dessen Oberfläche ungleichförmig verteilt sind, können entsprechende Annahmen auch für die Stoffübertragung an Elektroden bei erzwungener Konvektion gemacht werden. Eine experimentelle Methode zur Bestimmung der Stromdichte an verschiedenen Punkten der Elektrodenoberfläche im Falle erzwungener Konvektion wird beschrieben.

Die Anordnung der Grenzschicht im Falle der senkrecht auf die Achse eines Zylinders strömenden Flüssigkeit wurde in der Hydrodynamik, zur Bestimmung des Druckes auf der Oberfläche des Zylinders, und im Zusammenhang mit der Wärmeübertragung behandelt.[1]

Es sei ein Zylinder von unendlicher Länge angenommen, welcher in eine Flüssigkeit mit der Achse senkrecht zur Strömungsrichtung eingetaucht ist. Sobald die Reynoldszahl hinter dem Zylinder die Einheit überschreitet, entstehen zylindrische Turbulenzelemente deren Achsen parallel zur Achse des Zylinders sind. Mit steigendem *Re* nehmen die Turbulenzelemente ein größeres Volumen ein und wachsen auch in der Länge.[2] Für Werte von $Re = 10$ ist praktisch die gesamte hintere Seite des Zylinders mit ihnen bedeckt (Abb.1.a).

[1] L. Rosenhead, „Laminer Boundary Layers", Oxford at the Clarendon Press, 1963, S. 365–370.

[2] E. A. Brun, A. Martinot-Lagarde und J. Mathieu, „Mecanique des Fluides", 3.Bd., Dunod, Paris, 1970, S. 333–345.

Beginnend mit Werten der Reynoldszahl von ungefähr 50 lösen sich die Turbulenzelemente abwechselnd von der einen oder anderen Seite des Zylinders (Abb. 1.b). Es findet so ein Übergang vom stationären Zustand (haftende Turbulenzelemente) zu einem nichtstationären, aber periodischen Zustand (losgelöste Turbulenzelemente) statt. Die losgelösten Turbulenzelemente wurden insbesonders von Kármán erforscht. Er fand, daß diese Turbulenzelemente bei $Re = 32$ sichtbar werden-bei $Re = 50$ einen turbulenten Charakter erhalten und erst bei $\mathrm{Re} > 60$ einen ausgeprägt alternativen Charakter haben. [3]

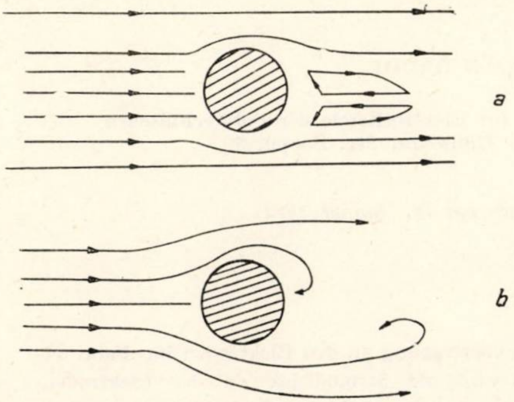

Abb. 1. – Bildungsschema der Turbulenzelemente.

Wenn der Zylinder in einer solchen Lage eine Elektrode ist und wenn der Druck auf seiner Oberfläche ungleichmäßig ist (siehe, [1] S. 375) so ist mit Sicherheit auch die Schichtdicke, in welcher die Stoffübertragung stattfindet, ungleichmäßig. Folglich ist dieses Problem von großem Interesse bei der Stoffübertragung in der Elektrochemie.

Das Interesse läßt sich einerseits dadurch erklären, daß man die Faktoren, die eine Intensivierung der Stoffübertragung ermöglichen, ableiten könnte, und andererseits könnte man die Selektivität der Elektrodenprozesse verbessern. Bei ungleichen Übertragungsbedingungen zur Oberfläche ein und derselben Elektrode sind auch die Polarisationen verschieden, und folglich ist der gleichzeitige Ablauf von mehreren Elektrodenprozessen möglich.

In dieser Lage, im Falle der relativen Bewegung zylindrische Elektrode-Elektrolyt (senkrecht zur Zylinderachse) ist die mittlere Stromdichte kein genügend aufschlußreicher Parameter.

Alle bisher veröffentlichen Arbeiten befassen sich mit der Beziehung zwischen dem gesamten Grenzstrom, ausgedrückt als mittlere Stromdichte, und verschiedenen, mehr oder weniger umfassenden Bewegungsgrößen.[4–14].

---

[3] B. Eck, ,,Technische Strömungslehre'', 5. Aufl, Springer Verlag, Berlin, 1957, S. 238–242.

Um Beziehungen zwischen der Massenübertragung bei Elektroden und den Parametern der relativen Bewegung Elektrode-Elektrolyt aufzustellen, geht man meistens von der Analogie zwischen der Massenübertragung und Wärmeübertragung aus[11] und verwendet eine Gleichung der Form :

$$Sh = f\,(Re,\ Sc) \tag{1}$$

(Sh – Sherwoodzahl, Re – Reynoldszahl, Sc – Schmidtzahl).

Zieht man die Verteilung der Grenzstromdichte auf der Oberfläche der Elektrode in Betracht, dann wird die unklare Situation, bezüglich der verschiedenen Glieder aus Gleichung (1) erklärlich.

In den meisten Arbeiten gelangt man für den Fall der turbulenten Strömung zu einer Gleichung der Form [11] :

$$I_{\mathrm{Gr}} = \text{const.}\ \ C.v^{0,5} \tag{2}$$

wobei mit C die Konzentration des elektroaktiven Stoffes und mit v die relative Geschwindigkeit Elektrode-Elektrolyt bezeichnet wird. Der Exponent der Geschwindigkeit wird häufig auch verschieden von 0,5 angegeben.

Werden in Beziehung (1) die Reynoldszahl und Schmidtzahl durch ihre Ausdrücke ersetzt erhält man für die Massenübertragung :

$$Sh = f\left(\frac{v.1}{\nu} \cdot \frac{\nu}{D}\right) \tag{3}$$

Die Sherwoodzahl für Massenübertragung (gleich der Nusseltzahl) kann noch wie folgt geschrieben werden :

$$Sh = \frac{I.1}{zFD(C - C_0)} \tag{4}$$

---

[4] A. A. Wragg, *Electrochim. Acta*, **13**, 2159 (1968).

[5] J. C. Bazan und A. J. Ariva. *Electrochim. Acta*, **10**, 1025 (1965).

[6] R. E. Sioda, *Electrochim. Acta*, **13**, 375 (1968).

[7] W. J. Blaedel, C. L. Olson und L. R. Sharma, *Analyt. Chem.*, **35**, 2100 (1963).

[8] J. Jordan, R. A. Javick und W. E. Ranz, *J. Amer. Chem. Soc.*, **80**, 3846 (1958).

[9] C. W. Tobias, ,,Advances in Electrochemistry and Electrochemical Engineering'', 2.Bd., Interscience Publishers, New York–London, 1962. S. 79–94.

[10] Rao K. Sudhakara, Raju, G. J. V. Jagannadha und Rao C. Venkata, *Indian J. Technol*, **6**, 46 (1968) aus : *Chem. Abstr.*, **69**, 7848 r (1968).

[11] I. Rădoi, *Rev. Roumaine Chim.*, **11**, 909 (1966).

[12] I. Rădoi, *Bul. Inst. Polit. Timişoara*, **15**, 85 (1970).

[13] I. Rădoi, *Rev. Roumaine Chim.*, **16**, 3. (1971).

[14] Rainer Wilhelm, *VDI. Forschungsheft*, 531, **35** (1969).

Nach Einsetzen der Beziehung (4) in (3) und Umgruppierung der Glieder, erhält man :

$$I_{\mathrm{GR}} = \frac{zFD}{1} C.f\left(\frac{\mathrm{v}.1}{\nu} \cdot \frac{\nu}{D}\right) \tag{5}$$

wenn man in Betracht zieht, daß bei Erreichen des Grenzstromes $C - C_0 \cong C$. In diesem Ausdruck haben die enthaltenen Größen folgende Bedeutung :

I_{GR} = Grenzstromdichte in A/cm²
zF = Coulomb/Mol
D = Diffusionskoeffizient der elektroaktiven Teilchen, cm²/Sek
C = Konzentration der elektroaktiven Teilchen, Mol/cm³
v = relative Geschwindigkeit Elektrode-Elektrolyt, cm/Sek
ν = kinematische Viskosität der Lösung, cm²/Sek
l = charakteristische Länge, cm

Wenn die Viskosität der Lösung, der Diffusionskoeffizient des elektroaktiven Stoffes und die ckarakteristische Länge konstant sind, verwandelt sich Beziehung (5) in die Gleichung :

$$I_{\mathrm{GR}} = \mathrm{Const.}\ v^n \tag{6}$$

Da, wie in der Hydrodynamik bewiesen, die relative Geschwindigkeit des Elektrolyten auf den verschiedenen Punkten der Oberfläche verschieden ist, muß auch die Grenzstromdichte verschieden sein. Diese Unterschiede sind von der relativen Bewegung Elektrode-Elektrolyt abhängig wie aus Gleichung (6) ersichtlich ist. Dies erklärt, weshalb verschiedene Autoren von 0,5 abweichende Exponenten der Geschwindigkeit in der Beziehung (2) erhielten. Andererseits kann behauptet werden, daß es prinzipiell nicht möglich ist, eine Beziehung zwischen dem Grenzstrom und der Gesamtgeschwindigkeit Elektrode-Elektrolyt aufzustellen, da letztere nicht nur auf den verschiedenen Punkten der Elektrodenoberfläche verschieden ist, sondern auch die Art der Änderung von den Geschwindigkeitsparametern abhängig ist (siehe Abb. 5). In dieser Lage ist das Aufstellen einer allgemeinen Beziehung für die Substanzübertragung im Falle der auf die Zylinderachse senkrecht fließenden Strömung von der genauen Kenntnis aller hydrodynamischen Parameter abhängig.

Die Bestimmung der Schichtdicke, in welcher die Massenübertragung auf zylindrischen Elektroden im Falle der relativen Bewegung Elektrode-Elektrolyt stattfindet, aus den in der Hydrodynamik oder den bei der Wärmeübertragung bekannten Parametern, ist sehr kompliziert.

In dieser Lage betrachten wir das Aufstellen einer Methode, welche die Bestimmung einiger Parameter der Übertragung auf der Oberfläche einer zylindrischen Elektrode im Falle einer auf die Elektrodenachse senkrecht fließenden Strömung unmittelbar erlaubt, als sehr nützlich.

GERÄTE UND ARBEITSWEISE

Die Konstruktion der Elektrode geht von der Idee aus, Teile der Elektrodenoberfläche zu begrenzen und den Grenzstrom auf diesen Teilen zu bestimmen. Wenn die entsprechenden von einander isolierten Oberflächenteile genügend nahe zueinander liegen und genügend klein sind, können die verschiedenen Werte den Verlauf des Grenzstromes entlang der Oberfläche in Abhängigkeit von der Lage des entsprechenden Teiles auf der Oberfläche, darstellen. Eine solche Methode ist nicht nur auf zylindrische Elektroden, dem hier diskutierten Fall, beschränkt.

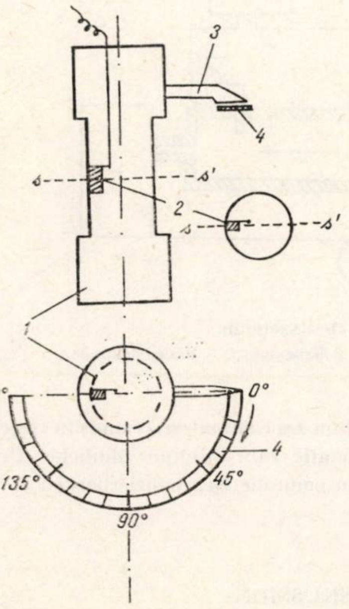

Abb. 2. – Aufbau der Elektrode.
1, **Isolationsmaterial**, *2*, **dünnes Platinplättchen (eigentliche Elektrode)**, *3*, **fester Zeiger in der Ebene der Elektrode**, *4*, **gradierter Halbkreis.**

Abb. 3. – Anordnung der Elektrode in der Röhre durch welche die Elektrolytlösung fließt.
1, **Elektrodenkörper aus Isolationsmaterial**, *2*, **Platinelektrode**, *3*, **Zeiger**, *4*, **gradierter Halbkreis**, *5*, **Dichtung**, *6*, **Kanalwände.**

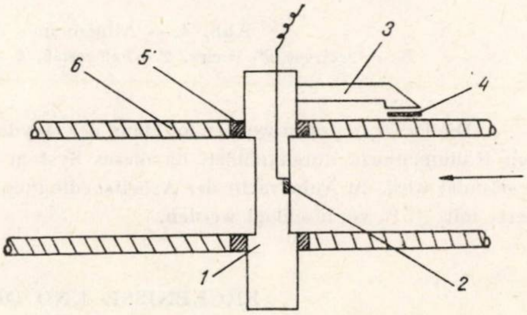

Der Aufbau der Elektrode ist aus Abb. 2 ersichtlich. Die Arbeitselektrode (*2*) aus Pt-Plättchen von verschiendener Stärke (0,06–0,15 mm) wurde in ein Isoliermaterial eingebettet. Als aktive Elektrodenoberfläche arbeitete nur die Seitenkante des Plättchens, mit einer Höhe von 2–3 mm. Durch Drehung des isolierenden Trägers (*1*) um seine Achse konnten mit Hilfe des Zeigers (*3*) und einer halbkreisförmigen Skala, die verschiedenen Winkel zwischen dem Richtungsvektor der Platinplättchen und der Strömungsrichtung der Elektrolytlösung verändert werden.

In Abb. 3 ist die Anordnung der Elektrode in der Röhre mit rechteckigem Querschnitt, durch welche die Elektrolytlösung fließt, wiedergegeben.

Der Träger aus nichtleitendem Material (*1*) ist mittels entsprechenden Dichtungen (*5*) in einer Röhre mit rechteckigem Querschnitt (*6*), durch welchen die Elektrolytlösung mit verschiedener Geschwindigkeit fließt, befestigt.

In Abhängigkeit von der Lage der Platinelektrode bezüglich der Strömungsrichtung der Lösung kann auf diese Art der Grenzstrom auf den verschiedenen Punkten einer Elektrodenoberfläche welche den Durchmesser gleich mit dem Durchmesser des Isoliermaterials in der Schnittfläche $s-s'$ hat bestimmt werden (Abb. 2).

Die Abmessungen der Elektrode und das Verhältnis zu den Abmessungen der Röhre wurden so gewählt, daß der Einfluß der Wände möglichst klein sei. Deshalb nimmt die Platinelektrode nur eine Höhe von 2–3 mm (Abb. 2, 3), und nicht die gesamete Höhe der Röhre, ein.

Der Elektrolyt wurde mittels einer Pumpe senkrecht zur Achse des Elektrodenträgers mit einer kontrollierten Geschwindigkeit bewegt. Der Grenzstrom wurde polarographisch aufgezeichnet. Die Anordnung der gesamten Geräte ist aus Abb. 4 ersichtlich.

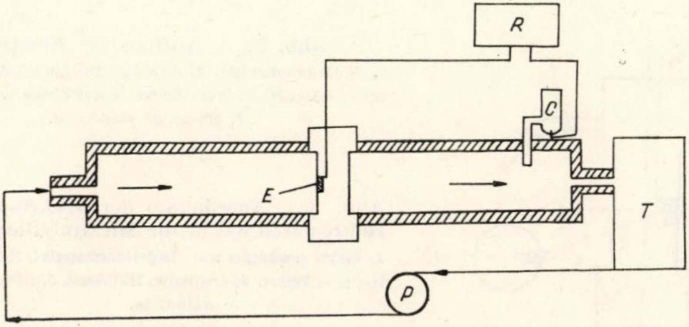

Abb. 4. — Allgemeines Arbeitsschema.
E = Elektrode, P=Pumpe, T = Puffergefäß, R = Polarograph, C = Bezugselektrode.

Die Bestimmungen wurden an Hand der Oxydation des Kaliumferrizyanids in Gegenwart von Kaliumchlorid durchgeführt, da dieses System häufig zum Studium ähnlicher Prozesse verwendet wird. In Anbetracht der Arbeitsbedingungen kann die Reproduzierbarkeit der Meßwerte mit ±5 % veranschlagt werden.

ERGEBNISSE UND DISKUSSION

Die Verteilung der Grenzstromdichte auf der Oberfläche der Elektrode, als Funktion des Winkels α zwischen Strömungsrichtung der Flüssigkeit und Richtungsvektor der Elektrode ist in Abbildung 5 wiedergegeben.

Die maximale Grenzstromdichte ist bei einem Winkel von 50–60° vorzufinden. Bei einem Winkel von 100–120° weist die Grenzstromdichte ein ausgeprägtes Minimum auf. Für größere Werte der Reynoldszahl verschiebt sich das Minimum zu Winkeln von 80–100°.

Durch graphische oder gravimetrische Integration der Kurven aus Abb. 5 kann die mittlere Grenzstromdichte und sodann die lokale Abweichung von dieser in Punkten mit verschiedenem Winkel α bestimmt werden. Es ist leicht ersichtlich, daß bei Winkelwerten α under 100° positive Abweichungen der lokalen Stromdichten auftreten, die bei 50°–60° besonders groß sind. Dem gegenüber liegen die Stromdichten bei Richtungswinkel über 100° zum Teil wesentlich unter dem Mittelwert (Abb. 6).

Folglich können bei ein und derselben mittleren Stromdichte, einer Größe mit welcher sehr häufig gearbeitet wird, auf den verschiedenen Punkten der Elektrodenoberfläche gleichzeitig halb oder doppelt so große Stromdichten vorgefunden werden. Demzufolge ist der Verlauf

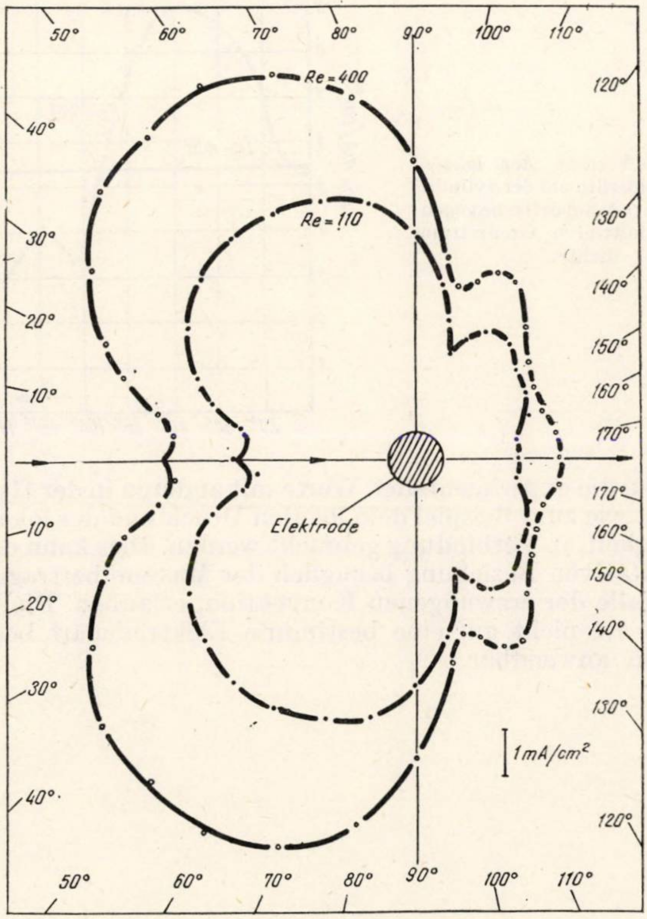

Abb. 5. — Die Anordnung der Grenzstromdichte auf einer zylindrischen Elektrode beim Fließen des Elektrolyts senkrecht zur Achse des Zylinders.

einer Elektrodenreaktion, im Falle einer relativen Bewegung Elektrode-Elektrolyt senkrecht auf die Achse der Elektrode, nur schwer kontrollierbar. Außerdem wird das Auffinden einer allgemeinen Beziehung für die Massenübertragung bei solchartigen Elektroden selbstverständlich problematisch und es ist daher verständlich, daß verschiedene Autoren in den

Gleichungen 1 und 2 bzw. 6, zum Teil sehr unterschiedliche Werte der vorkommenden Exponenten angeben.

Als Schlußfolgerung ist hervorzuheben, daß die beschriebene Methode die Bestimmung des Grenzstromes in jedem Punkt einer Elektrode, im Falle einer relativen Bewegung Elektrode-Elektrolyt erlaubt. Auf diese Weise können die experimentellen Werte mit anderen in der Hydrodynamik berechneten, wie zum Beispiel dem lokalen Druck und der lokalen relativen Geschwindigkeit, in Verbindung gebracht werden. Dies kann das Aufstellen einer quantitativen Beziehung bezüglich der Massenübertragung an Elektroden im Falle der erzwungenen Konvektion, erlauben. Die beschriebene Arbeitsweise ist nicht auf eine bestimmte Elektrodenart beschränkt, sie ist allgemein anwendbar.

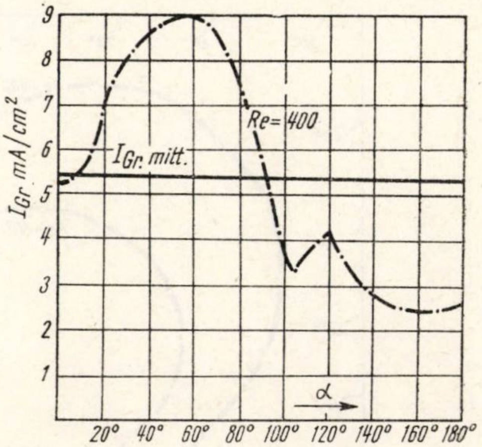

Abb. 6. — Verlauf der lokalen Grenzstromdichte auf der zylindrischen Elektrodenoberfläche gegenüber der mittleren Grenzstromdichte.

Revue Roumaine de Chimie, **17**, *8*, 1375–1378 (1972)

DERIVATOGRAPHISCHE UNTERSUCHUNG EINES DREIKOMPONENTEN-OXYDSYSTEMS $MnO_2-Co_2O_3-Ni_2O_3$

I. JANACHKOVA und M. STAEVSKI

Aus der Hochschule für Maschinenbau und Elektrotechnik, Lehrstuhl für Physik und Chemie
und Forschungsinstitut für Baumaterialien, Sofia 56 / Bulgarien

Eingegangen am 27. Oktober 1971

Untersucht wurde die Thermostabilität der Einzeloxyde, des β-MnO_2, Co_2O_3 und Ni_2O_3 sowie des Oxydsystems $MnO_2-Co_2O_3-Ni_2O_3$ nach Methoden der thermischen, thermogravimetrischen und röntgenologischen Analyse. Die Zersetzung der Oxyde sowie des Gemisches erfolgte nach analogem Mechanismus. Das β-MnO_2 zersetzt sich ursprünglich zu aktivem MnO, das teilweise zu MnO_2 oxydiert. Infolge der Wechselwirkung zwischen MnO und MnO_2 in der festen Phase ergibt sich Mn_2O_3. Bei 1000° werden die Phasen γ-MnO, CoO und NiO nachgewiesen. Durch die Wechselwirkung dieser Oxyde mit dem Sauerstoff der Luft entsteht bei 1150° ein kubisches Spinell der Zusammensetzung

$$\mathrm{Co}^{2+}_{1.14}\,\mathrm{Mn}^{3+}_{6,86}\left[\mathrm{Ni}^{2+}_{0,62}\,\mathrm{Mn}^{3+}_{14,38}\right]\mathrm{O}^{2+}_{32},$$

welches die Eigenschaften eines Halbleiters aufweist.

Einzeloxyde und Gemische aus obigem System besitzen Halbleitereigenschaften und werden verschiedenartigen Untersuchungen,[1-7] unterzogen. Die durchgeführten röntgenstrukturellen Untersuchungen von Heißleitern der Zusammensetzung $MnO_2-Co_2O_3-Ni_2O_3$[2] haben gezeigt, daß die Erhitzung des Gemisches bis auf 1150° eine chemische Wechselwirkung zwischen den Oxyden hervorruft, infolgedessen neue chemische Verbindungen vom Typ der Spinelle entstehen. Es wäre von Bedeutung

---

[1] S. Iwanov, D. Dzhoglev, D. Stefanov, I. Danchev, P. Petrov, I. Jamachkova und L. Bizheva, Comp. rend. Acad. bulg. Sci., **18**, 525 (1965).

[2] D. Stefanov, I. Danchev, I. Jamachkova, P. Petrv, S. Ivanov, D. Dzhoglev und L. Bizheva, *Bulg. Acad. of Sci., Sci., Phys. Inst.*, **13**, 185 (1965).

[3] M. J. Kushnerew, W. R. Linde und S. Roginsky, *Fiz. tverd. tela*, **3**, 384 (1961).

[4] I. T. Sheftel, A. T. Zaslavski, E. V. Kurlina und G. N. Tekster-Proskuryakova, *Fiz. tverd. tela*, **3**, 2712 (1961).

[5] I. Aoki, *J. Coll. Arts and Sci.*, **1**, 133 (1953).

[6] I. Aoki, *J. Coll. Arts and Sci.*, **1**, 150 (1954).

[7] G. W. Malinin und Ju. M. Tolmachev, *Zhur. fiz. Khim.*, **43**, 2012 (1969).

zu erfahren, welchen Phasenveränderungen in den Ausgangsoxyden zufolge dieser Verbindungen entstehen, die Halbleitereigenschaften aufweisen. In der vorliegenden Arbeit geben wir die Ergebnisse über Thermostabilität und Phasenveränderungen im Oxydsystem $MnO_2-Co_2O_3-Ni_2O_3$ an.

Die Ausgangsoxyde stellen β-MnO_2-tetragonale Syngonie, Co_2O_3 — kubische und Ni_2O_3 wieder kubische Singonie dar.[2] Die Thermostabilität der Einzeloxyde und die des Ausgangsoxydgemisches zur Gewinnung von Heißleitern der Zusammensetzung $MnO_2-Co_2O_3-Ni_2O_3$ (43,6 at. % Mn, 14,3 at % Co und 7,7 at % Ni) wurden mit Hilfe eines Derivatographen vom Typ OD-102 untersucht.[8,9] Zu diesem Zwecke wurde ein offener Platintiegel benutzt, mit 0,3—0,5 g des Stoffes beschickt und in einen Ofen mit Aufheizgeschwindigkeit von 5°C/min und 10°/min gebracht. Die Röntgenogramme der neugebildeten Phasen wurden durch Röntgenrefraktion in einer RKD-Kammer, $d = 57{,}3$ mm eines Refraktometers URS-50 IM, Cu/K_α — Strahlung, $\lambda = 1{,}54$ Å gewonnen.

Die Erhitzungskurven von MnO_2 (Abb. 1) lassen erkennen, daß die Zersetzung mit einem Gesamtgewichtsverlust von 22,0% bei 1000° verläuft. Die DTA-Kurve gibt einen exothermen Effekt bei etwa 50° zu erkennen, der voraussichtlich auf Umwandlungen im Kristallgitter zurückzuführen ist. Der endotherme Effekt bei etwa 100°, in Begleitung von Gewichtsverlust, bringt die Zersetzung des MnO_2 zu MnO zum Ausdruck. Der nächste, ausgeschweifte exotherme Effekt mit einem bei etwa 490° ausgeprägten Maximalwert drückt eine teilweise Oxydation des MnO zu MnO_2 aus. Das so erhaltene MnO_2 tritt rasch in Wechselwirkung mit dem MnO in festphasige Reaktion ein, und es ergibt sich Mn_2O_3, das sich in Mn_3O_4 verwandelt. Der endotherme Effekt mit seinem Maximum bei etwa 920° kommt durch die Zersetzung des Mn_3O_4 zustande. Die Thermoanalyse von Co_2O_3 (Abb. 2) veranschaulicht einen breiten exothermen Effekt mit einem Maximum bei etwa 225° und dann einen weiteren endothermen Effekt bei etwa 950° in Begleitung von Gewichtsverlust auf der TG-Kurve — Zersetzung des Co_3O_4 zu CoO. Der Gesamtgewichtsverlust beträgt bei 1000° 7,5%. Das Nickeloxyd (Abb. 3) gibt schwache Effekte auf dem Derivatogramm mit einem Gesamtverlust von etwa 3,0 Gewichtsprozenten zu erkennen. Man kann annehmen, daß das Ni_2O zu NiO zerfällt, welches eine schadhafte Struktur aufweist und den diffundierten Sauerstoff der Luft absorbiert. Die thermische sowie die thermogravimetrische Analyse des Oxydsystems (eines Gemisches): $MnO_2-Co_2O_3-Ni_2O_3$ weist auf einen Gesamtgewichtsverlust von 5,6% bei 1000° hin (Abb. 4). Die endotherme Spitze bei etwa 110° deutet eine Zersetzung des MnO_2 zu MnO. Die breite endotherme Spitze mit dem Maximum bei etwa 230° bringt den gesamten Oxydationsprozeß im Oxydsystem zum Ausdruck. Die Umwandlung von Mn_2O_3 zu Mn_3O_4 kommt durch die endotherme Spitze bei 575° zu Tage. Die endothermen Effekte bei 875 und 945° sind entsprechend auf die Zersetzung von Mn_3O_4 bzw. Co_3O_4 zurückzuführen.

---

[8] J. Paulik, F. Paulik und L. Erdey, *Talanta*, **13**, 1405 (1966).

[9] J. A. Hegedus und C. Martin, *Magyar Kem. Folyóirat*, **72**, 404 (1966).

Die Röntgen-Phasenanalyse hat gezeigt, daß beim Erhitzen von MnO_2 innerhalb von 3 Stunden bei 1000° das Vorhandensein von Mn_3O_4, $d = 2{,}48$ Å (100), und $\gamma - MnO$, $d = 3{,}52$ Å (100), zu beobachten ist. Unter denselben Bedingungen wandelt sich das Kobaltoxyd in CoO, $d = 2{,}12$ Å (100), und $Co_3O_4 - d = 2{,}42$ Å (100)[10,11] übergeht. Gleichzeitig geben die TG-Kurven von Co_2O_3 und Ni_2O_3 einen niedrigeren

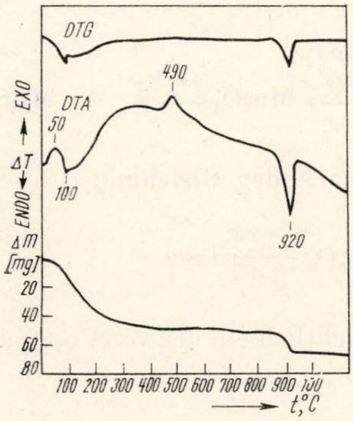

Abb. 1

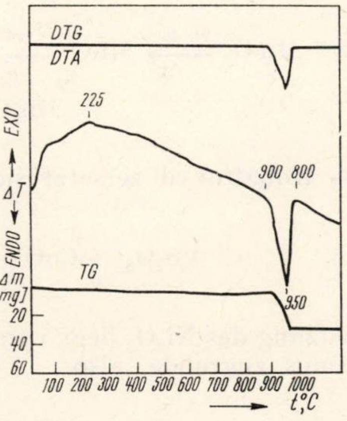

Abb. 2

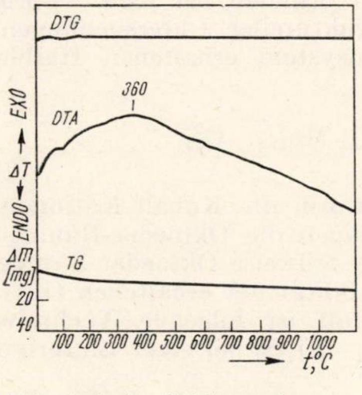

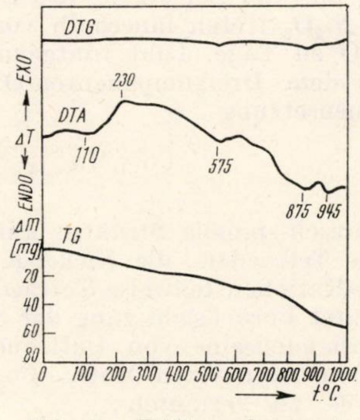

Abb. 1, 2, 3.—Erhitzungskurven von β-MnO_2, Co_2O_3, Ni_2O_3.
1) β-MnO_2; $m = 0{,}3$ g; $v = 5°$/min
2) Co_2O_3; $m = 0{,}4$ g; $v = 5°$/min.
3) Ni_2O_3; $m = 0{,}4$ g; $v = 5°$/min.

Abb. 4. — Erhitzungskurven des Dreikomponenten-Oxydsystems $MnO_2 - Co_2O_3 - Ni_2O_3$.
$m = 0{,}5$g; $v = 10°$/min.

---

[10] L. I. Mirkin „Handbuch für röntgenostrukturelle Analyse", Staatl. Ausgabe. Physik und Mathematik, Moskau, 1961, S. 485–520.

[11] K. Narita, „Kristallstruktur nichtmetallischer Einschlüsse im Stahl", Metallurgie-Ausgabe, 1969, 77–78, 120–140.

Verlust zu erkennen als der theoretische. Dieser Sachverhalt ist durch eine Diffusion des Sauerstoffs der Luft zu erklären : letztere füllt die Anionenmängel der ursprünglich erhaltenen CoO [12] und NiO aus.

Die durchgeführten Untersuchungen haben gezeigt, daß das Dreikomponenten-Oxydsystem $MnO_2-Co_2O_3-Ni_2O_3$ eine Thermostabilität aufweist, die analog zu der der Einzeloxyde ist. MnO_2 zersetzt sich stufenweise nach folgendem Schema

$$\begin{tikzcd}
\beta-MnO_2 \arrow[r, "40-400^\circ", "-O"'] & MnO \arrow[dr] \arrow[rr, "490^\circ"] & & MnO_2 \arrow[dl, "+O"'] & \\
& & Mn_2O_3 \arrow[r, "575^\circ", "-O"'] & Mn_3O_4 \arrow[r, "\text{über } 920^\circ", "-O"'] & \gamma-MnO
\end{tikzcd}$$

Das Kobaltoxyd zersetzt sich nach der Gleichung

$$Co_2O_3 \underset{-O}{\rightarrow} CoO \underset{+O}{\rightarrow} Co_3O_4 \xrightarrow[-O]{\text{über } 950^\circ} CoO$$

Der Zersetzung des Ni_2O_3 liegt voraussichtlich ein der von Co_2O_3 ähnlicher Mechanismus zugrunde, also

$$Ni_2O_3 \underset{-O}{\rightarrow} NiO.$$

Als Ergebnis der Zersetzung des Dreikomponenten-Oxydsystems $MnO_2-Co_2O_3-Ni_2O_3$ treten innerhalb von 3 Stunden bei 1000° γ-MnO, CoO und NiO zu Tage. Laut röntgenostruktureller Untersuchungen[2] weisen die aus dem Dreikomponenten-Oxydsystem erhaltenen Halbleiter der Zusammensetzung

$$Co^{2+}_{1,14}Mn^{3+}_{6,86}\left[Ni^{2+}_{0,62}\;Mn^{3+}_{14,38}\right]O^{2-}_{32}$$

eine kubisch-spinelle Struktur auf, worin die Kobalt-Kationen vorwiegend die Tetraeder-, die Nickel-Kationen die Oktaeder-Räume und die Mangan-Kationen teilweise Tetraeder- teilweise Oktaeder-Räume einnehmen. Unter Berücksichtigung der Stabilität der erhaltenen Oxyde sowie des Vorhandenseins von Luftsauerstoff ist folgende Wechselwirkungsreaktion im Oxydsystem $MnO_2-Co_2O_3-Ni_2O_3$ bei einer Sintertemperatur von 1150° zu vermuten :

$$CoO + NiO + \beta-MnO + O_2 \rightarrow Co^{2+}_{1.14}\,Mn^{2+}_{6.86}\,Ni^{2+}_{0.62}\,Mn^{3+}_{14.38}\,O^{2-}_{32}.$$

Die derart erhaltene Verbindungn spineller Struktur weist Halbleitereigenschaften auf.

---

[12] Hang Nam Ok and James G. Millen, *Phys. Rev.*, **168**, 550 (1968).

Revue Roumaine de Chimie, **17**, *8*, 1379–1391 (1972)

INFLUENCE OF THE PREPARATION METHOD ON THE STRUCTURE AND PHYSICAL PROPERTIES OF ALUMINA. II[1]

ALUMINIUM OXIDES

VIOLETA ALEVRA, DAN CIOMÎRTAN and MARIA IONESCU

Centre of Physical Chemistry, Str. Dumbrava Roşie 23, Bucharest, Romania

Received February 15, 1972

The paper deals with some modifications of aluminium oxides obtained by air annealling of the aluminium hydroxides previously prepared. The thermal dehydration process of different forms of aluminium hydroxides (amorphous, microcrystalline boehmite, pseudoboehmite, bayerite and mixtures) into the corresponding oxides is studied by means of the DTA, DTG, X-ray diffraction and textural techniques.

1. INTRODUCTION

In the field of heterogenous catalysis, there has been enough evidence on the importance of establishing some correlations between the activity and the selectivity of solid catalysts on the one hand their physical-chemical characteristics, on the other hand.

In the category of metallic oxides, the oxide of aluminium is an example in this respect. The active alumina, both single and in combination with other metallic oxides is used as a catalyst for certain groups of reactions : dehydration, isomerization, polymerization, cracking. The differences in quality and in quantity found by different authors in apparently similar aluminas prove that there actually are different distributions of active centers on the surface of these aluminas.

The occurrence of such various superficial atomic structures is most frequently ascribed to the crystalline structure of the solids in question, although even the amorphous oxides may also be active in catalysis.

The investigations on the influence of the crystalline structure on the catalytic activity of these aluminas are rather complicated because of the great difficulties in identifying its numerous possible crystalline forms ; this is particularly true for mixtures of modifications, which is the most frequent case found in practice. The more attention is paid to the formation process of the given catalyst or, in other words, to its "biography", the more chances there are of making accurate approximations in this case.

---

[1] V. Alevra, D. Ciomîrtan and M. Ionescu, *Rev. Roumaine de Chim.*, **17**, (1972).

The present paper is a continuation of a study in process[1], its purpose being the characterization of aluminium oxides obtained by the annealing in air of the previously prepared hydroxides. In order to discuss the forms of the aluminium oxides investigated in this paper, we shall group them according to the temperatures at which aluminas were obtained from their hydroxides.

a) *Low temperature aluminas* called γ-group are obtained by the heat decomposition of the hydroxides at a temperature of maximum 600° ; the constitution formula is $Al_2O_3 \cdot xH_2O$, where $0.6 > x > 0$. To this group belong the following modifications : ρ, ϰ, γ, η.

b) *High-temperature aluminas*, called δ-group are obtained by the decomposition of hydroxydes at temperatures as high as 900—1000° ; they are almost anhydrous and they include the forms : k, θ, δ.

2. EXPERIMENTAL

2.1. PREPARATION OF SAMPLES

The oxides of aluminium, noted A (I, —VI, VIII) were formed by thermal dehydration in air of the previously [1] prepared aluminium hydroxides in an electric oven.

The annealling program was the following : two hours at each of the temperatures of 300°, 400, 500, 600, 700, 800 and 900° ; the index t° represents the final calcination temperature.

The granule size of hydroxides during calcination was that resulting from their preparation : 0.1—1 mm average diameter.

2.2. THERMOGRAPHIC ANALYSIS

The TG, DTG, DTA curves were recorded by a Paulik-Paulik Erday, OD-102 type derivarograph in atmospheric air ; the granulation of the powdered hydroxides involved, presented a diameter smaller than 0.06 mm ; the heating rate was 10°/min ; the reference test was α-Al_2O_3.

2.3. ROENTGENOGRAPHIC DETERMINATIONS

The X-ray diffraction spectra were obtained by the powder technique using a HZG-1 diffractometer attached to the X-ray source TURM-61 (GDR). The procedure involved the radiation CuK_α, $\lambda = 1.5418$ Å filtered on Ni at 30 KV and 22 mA ; the recording range was 5—45° Bragg.

The average size of crystallites was obtained by Scherrer's formula :

$$D = \frac{K\ \lambda}{\beta \cos \theta} \quad \text{where :}$$

D = the average size of crystallites ; K (the constant related to the form of the crystallites) = = 0.90 for the spherical form ; β (the integral diffraction width) = $B - b$; B = the experi-

---

[2] S. K. Bhattacharyya, and V. S. Ramchandra, *J. Sci. Industr. Res.*, **12**, 550 (1952) ; **B 12**, 279 (1953).

Table 1

Structure and Physical Properties of Aluminium Oxides

Oxide	Structure of initial hydroxide	Characteristic ratio (H_{350}/H_{500}) from DTG curve (for fine powdered samples)	Structure of oxide (as macrogranules)	Average size of crystallites (Å)	Surface area (m^2/g)	Pore volume (cm^3/g)	
						Total	Pore radius $> 37,5$ Å
A I_{600}	Amorphous	about 3	Amorphous	—	98	0.17	0.0
A II_{600}	Microcrystalline boehmite	0.50	$\gamma + \delta$ traces	94	200	0.38	0.08
A III_{600}	Pseudoboehmite	0.60	η	86	196	0.40	0.05
A IV_{600}	Pseudoboehmite and traces of bayerite	0.85	η	86	190	0.40	0.05
A V_{600}	Pseudoboehmite and about 25% bayerite	1.50	$\eta + \nu$	100	157	0.43	0.15
A VI_{600}	Bayerite and about 25% pseudoboehmite	5.50	ν	135	154	0.45	0.25
A $VIII_{(600)}$	Bayerite and traces of pseudoboehmite	11.00	γ	157	157	0.48	0.35

mental diffraction width ; b = the standard width ; θ = the angle of the considered diffraction line, in this case $\cong 23°$ Bragg.

2.4. TEXTURAL MEASUREMENTS

The specific surface BET was indentified through nitrogen adsorption at a temperature of −196°. The total porosity resulted from the values of the actual and of the apparent density, identified by means of the picnometric method, or the mercury method. The volume of the pores of the rays between 37.5—75,000 Å was calculated from the curves recorded by the Carlo-Erba type mercury porosimeter, between 1—2000 atmospheres.

3. RESULTS AND DISCUSSIONS

Tables 1 — 2 and figures 1 — 3 present the main results concerning the preparation of the aluminium oxides and their structural and textural characterization.

Table 2

Temperature dependence of structure and textural properties of A II oxide

Anealling temperature	600	700	800	900
Crystalline structure	$\gamma + \delta$-traces	$\gamma + \delta$	$\delta + \theta$	$\delta + \theta$
Surface area (m^2/g)	200	180	172	150
Total volume of pores (cm^3/g)	0.386	0.420	0.330	0.300
Volume of pores of radius >37.5 Å (cm^3/g)	0.086	0.092	0.146	0.290

3.1. STUDY OF THERMAL DEHYDRATION PROCESS BY THERMOGRAPHIC METHODS

The thermographic methods applied in studying the transformation of the metallic hydroxides into their oxides was proved to be a valuable auxiliary to the method of X-ray diffraction, giving important indications on their structure, composition and purity. The behaviour of the aluminium hydroxides during dehydration was correlated to the method of preparation, the purity, the crystallinity, the nature of the constitution water, a.s.o.[2-9]

Our aim in applying the DTA and DTG methods to our samples was both to confirm the data resulting from the X-ray diffraction and to identify the chemical impurities, particularly the crystallographic impurities found in the hydroxides ; we also wanted to reveal certain disparities

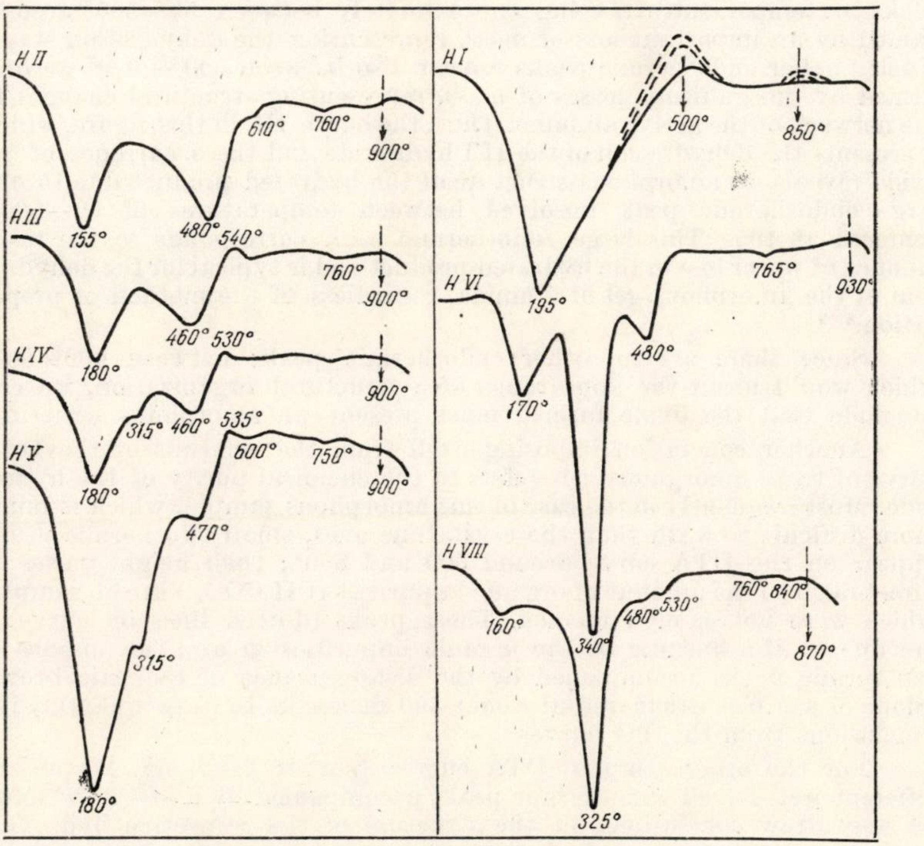

Fig. 1. — DTA curves of aluminium hydroxides.

---

[3] S. K. Bhattacharyya and N. D. Ganguly, *Proc. Nat. Instr. Sci. India*, **27** A, 588 (1961).

[4] S. K. Bhattacharyya and N. C. Datta, *J. Thermal Analysis*, **1**, 75 (1969).

[5] A. Bielonski and A. Sedzimir in ,,Reactivity of Solids'', Ed. Elsevier Publishing Comp., Amsterdam 1961, p. 301.

[6] L. Abrams and M. J. D. Law, IEC. *Prod. Res. Develop.*, **8**, 38 (1969).

[7] S. Yamagucki and H. Jandgida, *Bull. Chem. Soc. Japan*, **35**, 1896 (1962) ; **37**, 1229 (1964) : **38**, 2194 (1965) ; **44**, 418 (1971).

[8] I. Erdey, F. Paulik and J. Paulik, *Acta Chim. Acad. Sci. Hung.*, **10**, 61 (1956).

[9] I. Erdey and F. Paulik, *Acta Chim. Acad. Sci. Hung.*, **7**, 45 (1955).

between the different samples in the amount and the nature of their water content. In the case of mixtures of phases, these disparities were hard to identify by the X-ray diffraction technique.

Figure 1 reproduces the DTA curves for the hydroxide samples which were previously obtained and characterized.[1]

Their analysis confirms in general the conclusions based on the X-ray spectra of these hydroxides ; all the DTA curves show strong endothermic peaks at temperatures ranging approximately between 50—500° accompanied by an important loss of mass, representing the dehydration stage. Much smaller endothermic peaks appear also between 500 — 900° accompanied by unsignificant losses of mass, representing structural changes in the network of the active alumina. Thus, the curve HI in this figure, which represents the dehydration of the H I hydroxide and the occurrence of AI oxide reveals an amorphous structure of the hydrated product due to one large endothermic peak unsolved between temperatures of 50—500°, centered at 195°. This large endothermic peak corresponds to the main amount of water loss in the hydrated product and is typical for the dehydration of the amorphous gel of alumina, regardless of the method of preparation.[8-9]

Since there are no other endothermic peaks between 600—900° which would mean the appearance of a structural organization, we can conclude that the oxide formed must present an amorphous structure.

Another conclusion imposing itself from the analysis of the DTA curve of these amorphous gels refers to the chemical purity of the hydroxide. Most frequently in the case of this amorphous sample, which is much more difficult to wash than the crystalline ones, small exothermic peaks appear on the DTA curve around 500 and 850° ; their height varies in direct ratio to the amount of organic impurities ($CH_3COO_2^-$) in the samples which were not enough washed. These peaks (dotted lines on curve 1) are due to the burning of the organic impurities in air ; the absence of exothermic peaks accompanied by the disappearance of the pale brown colour of samples calcinated at about 500 makes us to draw quantitative conclusions from the TG curves.

For the other samples, DTA curves (curves 2—7, fig. 1) present different well-solved endothermic peaks accompanied by a loss in weight ; we may draw conclusions on the structure of the respective hydroxide from the temperature at which they occur and from their relative height. Thus , it has been established [2-9] that the decomposition of the trihydrates takes place at lower temperatures (approx. 300°) than the decomposition of the alumina monohydrates, which takes place at about 450—480°, depending on crystallinity, granulation, and working conditions. Therefore we consider that the first endothermic peak at 155—180° found in our samples corresponds to the loss of slighter bound water, physically absorbed and/or present in the interlammellar spaces of the pseudoboehmite structure.

The heating rate being rather high (10°/min) there is a practically continuous loss and it is impossible to determine the moment when the water physically absorbed has been lost and when the loss of the excess water from the pseudoboehmite has started (if we make the logical assumption that there must be a difference in the binding strength of the water in the two cases). The endothermic peak at 460 — 480° present, to a very different extent in all the samples, represents the decomposition of the stoichiometric boehmite found or possibly formed in the hydrothermal decomposition of samples with large crystallites.

The endothermic peak at approx. 315—340° found in the samples H (IV—VIII) has a variable height, obviously directly proportional to the amount of trihydrate in the sample. Its presence in the pseudoboehmite sample H IV clearly indicates traces of trihydrate, undetectable by X-ray diffraction — as we saw[1] and the presence of a very slight endo peak at approx. 480° in the bayerite sample H VIII indicates traces of boehmite also undetectable by X rays. The samples H V and VI which are different boehmite-bayerite mixtures (according to the previous interpretation of the X-ray diffraction spectra) gave DTA curves containing both categories of characteristics endothermic peaks ; their relative intensities lead to conclusions regarding the preponderant crystalline structure of the mixtures (table 1).

Between approx. 500 and 940°, curves DTA of the samples H II—VIII reveal much slighter endo-peaks which we can ascribe to the structural changes of the oxide of aluminium from η-respectively γ-Al_2O_3, passing through θ or δ and forming α-Al_2O_3 at a temperature of over 940—960°. These endo-peaks can be seen in fig. 1 at temperatures around 600 and 750°.

After making sure that our hydrated samples have a reasonable purity (in the absence of exothermic peaks) we tried to find in TG and DTG curves (figs. 2 and 3) some criteria which should help us to make special considerations on the hydrate mixtures where the interpretations of the X-ray spectra are more difficult.

Thus, the curves presented in figure 2 (calculated from the TG curves recorded by the derivatograph) show the variation in the number of water mols in the formula $Al_2O_3 . xH_2O$ depending on the dehydration temperature and figure 3 shows the respective differential curves (deducted graphically) since curves DTG recorded by the device were unsatisfactory. We notice that the maximum weight losses take place approximately at the same temperatures at which the endothermic peaks occur on the DTA curves. We shall however take into account only the water loss maxima, which are found at temperatures of over 200° at which the water physically adsorbed has been lost as well as the water in excess to stoichiometric composition (the evacuation of samples 1h at 10^{-1} mm Hg at 100—110° causes a loss which equals that deducted from the TG curve at about 200°).

Since in most cases, the DTG curves present both the characteristic maximum of the bayerite (about 350°) and that of the boehmite (about 500°) the predominant nature of a crystalline structure will be revealed only by the ratio of the heights of the two characteristics maxima (denoted in table 1 by H 350/H 500).

In principle, the same ratio may also be considered for the endopeaks on the DTA curves ; however, these are less sharp (it would be more correct, however more difficult, to establish the ratio of the respective surfaces).

The values of this ratio range from 0.5 to 11.0, corresponding to the extremes of the field between microcrystallines boehmite and bayerite (over 90–95%) and are consistent with the previous conclusions with respect to the structures of these hydroxides.

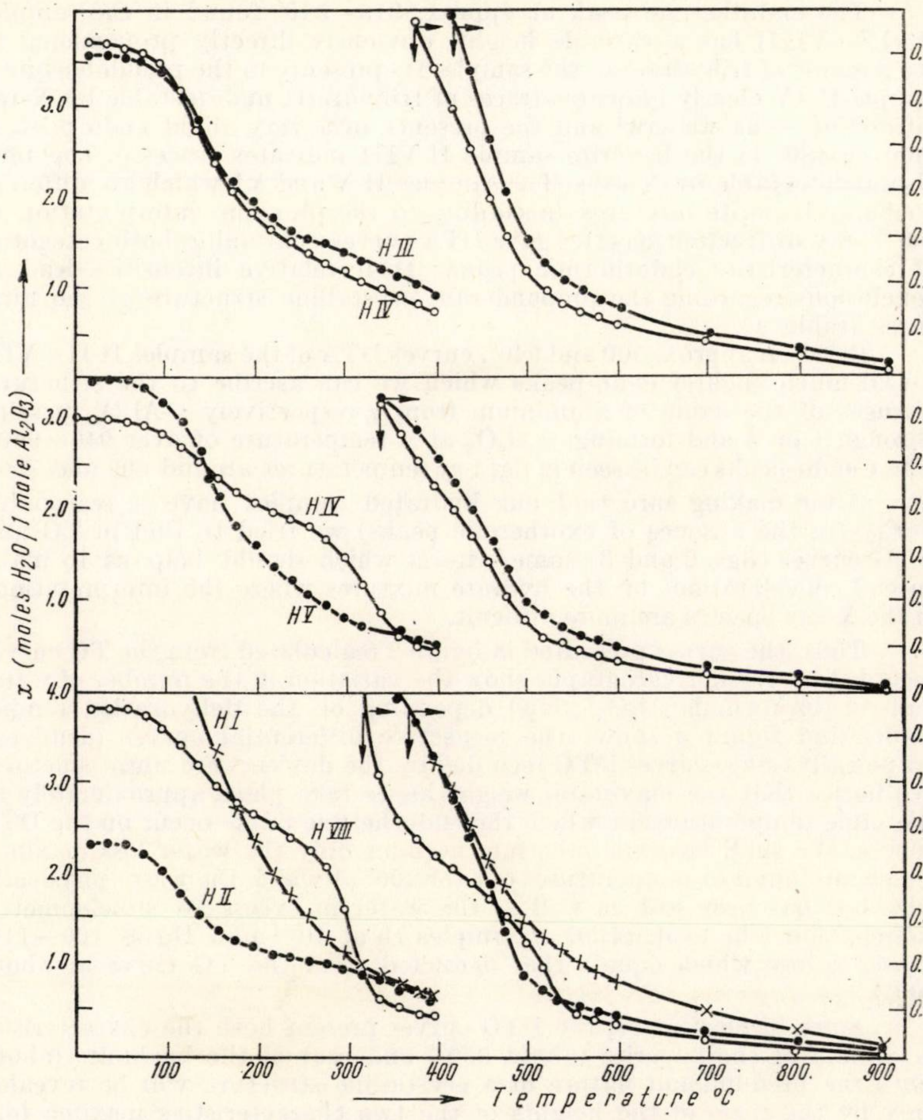

Fig. 2. — Temperature dependence of water content in alumina.

Between the structure of η- and γ-alumina, almost impossible to distinguish in a mixture,[10] some differences are supposed to exist concerning the nature of the constitution water. Thus, in γ-Al_2O_3 there may exist a kind of stronger bound water called "lattice water" while in η-Al_2O_3 the water is slightlier bound, "non-lattice water".[7] These differences are apparent if we examine the behaviour of aluminium hydrates in dehydration, at temperatures corresponding to the formation of these alumina, that is about 350–550°. The samples with the purest structures of micro-

---

[10] B. C. Lippens and Y. Y. Steggerda in: "Physical and Chemical Aspects of Adsorbents and Catalysts", Ed. B. G. Linsen, Academic Press, London–New York, 1970, p. 171.

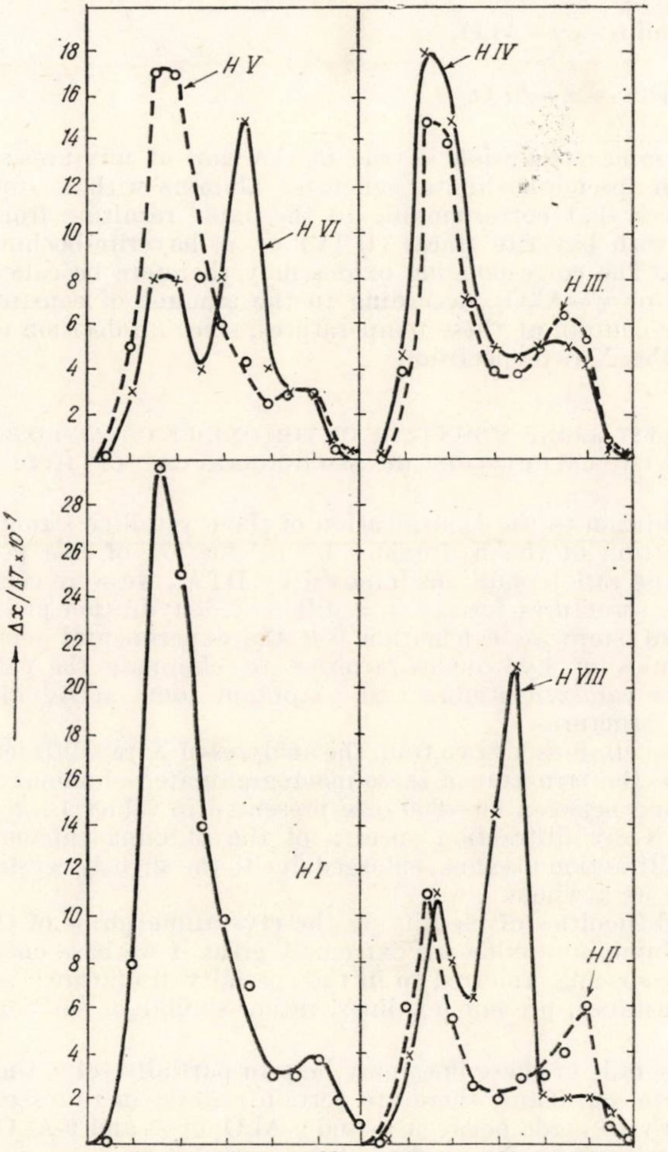

Fig. 3. — TDG curves of aluminium hydroxides.

crystalline boehmite (H II) and bayerite (H VIII) show clearly that in fact at these temperatures, the alumina resulting from the monohydrate contains more water and loses it more difficultly than the corresponding one in the trihydrate (fig. 2 — curves H II, respectively H VIII). This could correspond to a normal dehydration process, namely :

boehmite → $\gamma-Al_2O_3$

bayerite → $\eta-Al_2O_3$

The same conclusion is true in the case of mixtures : the sample H III (pure pseudoboehmite) generates alumina with a superior water content than that corresponding to the oxide resulting from a pseudoboehmite with bayerite traces (H IV) or a bayerite-boehmite mixture (H V—VI). The corresponding oxides may therefore be called preponderantly $\gamma-$ or $\eta-Al_2O_3$, according to the amount of constitution water which they contain at these temperatures, since no decision can be made based on the X-ray spectrum.

3.2. THE CRYSTALLINE STRUCTURE OF THE OXIDES OBTAINED BY SLOW AND STEPWISE CALCINATION OF MACROGRANULES OF HYDROXIDES

In addition to the identification of the crystalline structures formed by dehydration of the hydroxides by calcination of fine powders at a rapid heating rate (conditions imposed by DTA), we were concerned with the kind of structures formed in a different dehydration process, namely in slow and stepwise calcination (see the experimental section) of the macrogranules of hydroxides in order to eliminate the pellet forming effect in the catalytic studies and to obtain some active alumina with stabilized structures.

The conclusions, drawn from the analyses of X-ray diffraction spectra, referring to the structure of these macrogranulated aluminas at temperatures ranging between 60—900° are presented in tables 1—2.

The X-ray diffraction spectra of the alumina calcinated at 600° show few diffraction maxima, enlarged due to the slightly crystalline nature of alumina as a whole.

The difficulties of identifying the crystalline forms of the low temperature aluminium oxide are extremely great if we base only on the list of reticular spacings referred to in the specialty literature ; η- and γ-alumina for instance, present few lines, rather similar in position and intensity.

The profile of these lines may help to partially solve the difficulties of interpretation. Thus, there are certain criteria in terms of which distinction may be made between η- and γ-Al_2O_3 or δ- and θ-Al_2O_3 in the case of the alumina formed at a high temperature.[10]

Our working conditions have permitted us to use in the case of the low temperature alumina only the profile-based criterium namely the splitting of the diffraction maxima at about 1.98 Å (the existence of a symmetrical profile with splitting tendencies is ascribed to the γ-alumina while a clearly asymmetrical profile may be ascribed to η-Al_2O_3). Compared to the most common dehydration process of the bayerite, our results may seem unusual : H VIII (bayerite) $\xrightarrow{600^\circ}$ γ-Al_2O_3. We obtained the same result for the preponderantly bayeritic H VII sample [1] (not included in table 1). This unusual behaviour may be explained if we take into account the fact that the size of the crystallites of preponderantly bayeritic hydroxides is approx. 10 times as large as that of the other hydroxides prepared [1] and that in our conditions of a slow calcination of macrogranules reaching a diameter of few mm, it is very likely to assume that an intragranular hydrothermal decomposition has taken place, so that the actual dehydration process is :

$$\text{Bayerite} \xrightarrow{300-400^\circ} \text{Boehmite} \xrightarrow{500-600^\circ} \gamma\text{-}Al_2O_3$$

Another argument is the fact that the formation of the intermediate boehmite is a well-known phenomenon in the gibbsite which usually has larger sizes of crystallites (compared with the size of samples H VII – VIII).[1]

The same γ-alumina occurs through the dehydration of sample H II (microcrystalline boehmite very similar to the stoichiometric boehmite) at 500° ; the lines of δ-alumina appear already at 600°.

The X-ray spectra of samples H III – IV may be ascribed to the η-alumina (the maximum diffraction at 1.98 Å is enlarged and strongly asymmetrical).

The X-ray spectrum of the samples H V is very difficult to interpret. The profile of the line $d = 1.98$ Å is rather uncertain ; since allowance should be made both for the splitting tendency and for its asymmetry, we assume that this is very likely an η- + γ-Al_2O_3 mixture.

The spectrum of the sample A I is perfectly similar to that of the hydroxide from which it occurs ; it has absolutely no diffraction maxima ; hence we assume the existence of an amorphous state.

We followed the evolution of the crystalline structure at temperatures over 600° only for the purest crystallographic and chemical sample (obtained from aluminium isopropoxide) namely A II. The differences between δ- and θ-Al_2O_3 [10] are :

a) the different ratios of the intensities of lines between 2.73 Å and 2.00 Å (higher at θ than at δ) and,

b) the splitting of the line group from 2.00 Å is double (2.03 and 1.91 Å) at θ-Al_2O_3 and threefold (1.99, 1.95 and 1.91 Å) at δ-Al_2O_3. The identification of samples A $II_{600-900}$ on this ground (table 2) leads to the conclusion that the area of existence of δ-Al_2O_3 is very large and the pure structural forms could not be obtained in the given conditions.

3.3. TEXTURAL PROPERTIES

A rough textural characterization of the oxide samples was made by determining the surface area and the volume of pores (table 1).

It has been noticed that the oxides calcinated in air in large granules have relatively large specific surfaces ranging within the same magnitudes (98—200 m^2/g) resulting however from different pore distributions. The amorphous oxide A I is an airogel with very narrow pores (the average radius is much less than 37.5 Å).

The other samples, similar in the total porosity — which is larger than that of the airogel A I — have different pore distributions; while samples γ- or η-alumina formed from preponderantly boehmite or pseudoboehmite structures of hydroxides have mostly micropores, the oxide products resulting from bayerite structures have a larger distribution of pores. We see therefore that two rather similar *) crystalline structures may give quite different textures.

As the calcination temperature is increasing (A $II_{600-900}$) the specific surface of the alumina is decreasing and the pore distribution changes: there is a significant increase in the contribution of macropores (table 2).

4. CONCLUSIONS

The physico-chemical properties and the catalytic activity of the oxides depend both on the crystalline structure and on their texture. Although it is still very difficult to follow the relation: forming conditions ("biography") — properties in the case of oxides of aluminium, we can make some general remarks.

The influence of the conditions of preparation on the formation of certain structural modifications of aluminium hydroxides is, as we have seen, easier to follow.[1]

The structure of the oxides of aluminium formed between 500°—900° reveals that their nature, purity and area of occurrence are highly dependent in our case on the calcination rate, on the granulation and on the content of chemical impurities in the sample.

Thus while δ-Al_2O_3 starts forming at a temperature as low as 600° by slow calcination in the purest oxide — A II, δ-Al_2O_3 it does not occur in the other samples, due to the lower crystallinity and to the slightly higher concentration of chemical impurities.

The series of samples obtained from the hydrolysis of the amalgamated aluminium reveal very clearly the influence of maturation as a factor favoring more orderly structures. The most unorderly hydrate structures (amorphous-pseudoboehmite) which resulted by calcination in the most deformed structures (amorphous-η-Al_2O_3) were obtained in conditions of non-maturation or a slight maturation and at reduced pH-values.

---

*) According to our present possibilities of X-ray characterization.

In general, for practical purposes the fine powders of alumina obtained by various procedures are developed to an appropriate granulation in order to be used as catalysts or supports through tablet forming or agglomeration with aqueous solutions of strong acids. In both cases the superficial properties, and sometimes the structural ones can undergo important modifications and so, the problem regarding the influence of the preparation method on the properties of the final products will become very difficult.

Our samples are porous solid granules having variable sizes and geometrical forms and can therefore be obtained as such by extrusion of the moist hydroxides, without binding agents or through other simple procedures. The drying and calcination of the hydroxides do not actually modify their size and their geometrical form.

The resistance to mechanical shocks or to friction is directly related to their crystalline structure.

Thus the glassy oxide (amorphous) is very crisp and the chalky oxides (obtained from preponderantly bayerite hydroxides) are the least friction-resistant. The intermediate products, namely the oxides originating from mixtures (bayerite + pseudoboehmite) are the most appropriate from this standpoint.

The appropriate supports from the point of view of structural and textural properties, and of mechanical resistance may be selected according to the purpose to be achieved.

Revue Roumaine de Chimie, 17, 8, 1379–1391 (1972)

7

Revue Roumaine de Chimie, **17**, *8*, 1393–1407 (1972)

SOLVOLYSIS OF Δ^2-CYCLOBUTENYLETHYL-β-TOSYLATE AND Δ^2-CYCLOBUTENYLPROPYL-γ-TOSYLATE

M. BANCIU, P. BUCK *), ECATERINA CIORĂNESCU and C. D. NENITZESCU**)

Laboratory of Organic Chemistry, Polytechnic Institute, str. Polizu 1, Bucharest, Romania

Received March 1, 1972

In order to investigate the possibility of remote nucleophylic participation of a double bond in a cyclobutene ring, the Δ^2-cyclobutenylethyl-β-tosylate (**6***b*) and Δ^2-cyclobutenylpropyl-γ-tosylate (**7***b*) were synthesized and solvolized. The double bond participation could not be evidenced either by comparing their reaction rate with that of the saturated tosylate **9***e* or by product analysis. The major reaction products of the buffered-acetolyses of **6***b* (or **7***b*) were (after $LiAlH_4$-reduction) : the unrearranged alcohol **6***a* (or **7***a*) and a ring opening product, namely 3.5-hexadiene-1-ole (or 4.6-heptadiene-1-ole). No double bond assistance could be demonstrated for the buffered solvolysis of **6***b* in formic acid or in trifluoroacetic acid. From the kinetic data and the comparative analysis of $\Delta H^{\neq}$ and $\Delta S^{\neq}$ as well as from product analysis it was concluded that the same mechanism (solvent assisted solvolysis) was operating in the case of the tosylates **6***b*, **7***b* and **9***e*.

INTRODUCTION

The recent report by McDonald and Lyznicki [1] concerning the buffered acetolysis of Δ^2-cyclobutenylethyl-β-tosylate prompted us to publish our own results.

The participation in solvolytic reactions of a remote carbon-carbon double bond ("π-route") was intensively investigated in different systems such as **1** (n = 1 [2]; n = 2 [3]), **2** (n = 2 [4]; n = 3 [5]), **3** [6], etc.

---

*) Dr. Peter Buck, Institut für Organische Chemie der Universität Heidelberg, postdoctoral fellowship, 1967–1968.

**) Deceased July, 28, 1970.

[1] R. N. McDonald and E. P. Lyznicki, *J. Amer. Chem. Soc.*, **93**, 5920 (1971).

[2] R. G. Lawton, *J. Amer. Chem. Soc.*, **83**, 2399 (1961) ; P. D. Bartlett and S. Bank, *J. Amer. Chem. Soc.*, **83**, 2591 (1961).

[3] S. Winstein and P. Carter, *J. Amer. Chem. Soc.*, **83**, 4485 (1961).

[4] a) G. Le-Ny, *Compt. rend.*, **251**, 1526 (1960) ; b) H. Felkin, G. Le-Ny, C. Lion, W. D. K. Macrosson, J. Martin and W. Parker, *Tetrahedron Letters*, **1966**, 157 ; c) E. Ciorănescu, A. Bucur, F. Badea, M. Rentzea and C. D. Nenitzescu, *Tetrahedron Letters* **1969**, 1867.

[5] M. Hanack and W. Kaiser, *Angew. Chem.*, **76**, 572 (1964) ; A. C. Cope, D. L. Nealy, P. Scheiner and G. Wood, *J. Amer. Chem. Soc.*, **87**, 3130 (1965) ; K. H. Baggaley, J. R. Dixon, J. M. Evans and S. H. Graham, *Tetrahedron*, **23**, 299 (1967) ; W. Kraus, W. Rothenwörher, W. Kaiser and M. Hanack, *Tetrahedron Letters*, **1966**, 1705 ; M. Hanack, W. Kraus and W. Rothenwöhrer, *Liebigs Ann. Chem.*, **703**, 44 (1967).

[6] a) G. D. Sargent, *Tetrahedron Letters*, **1970**, 4359 ; b) E. Ciorănescu, M. Banciu, R. Jelescu, M. Rentzea, M. Elian and C. D. Nenitzescu, *Tetrahedron Letters*, **1969**, 1871 ; *Rev. Roumaine Chim.*, **14**, 911 (1969).

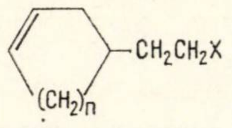

1

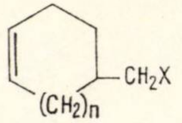

2

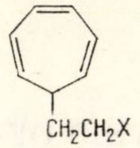

3

In all these cases the reaction rates were found to be greatly enhanced over the rates of the corresponding saturated derivatives and the formation of bicyclic products was explained by intermediate appearance of non-classical carbonium ions.

Conversely, in the solvolyses of Δ^2-cyclobutenylmethyl-tosylate (**4**; n = 1; X = OTs)[7] or Δ^1-cyclobutenylethyl-β-tosylate (**5**; n = 2; X = OTs)[8] no bicyclic product could be isolated.

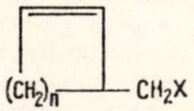

4

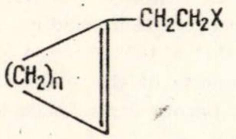

5

Moreover, it seems that in homoallylic systems (like **4**) the usual rearrangement: homoallyl$\rightleftarrows$cyclopropylmethyl$\rightleftarrows$cyclobutyl[9] is prevented when the double bond) is included in the strained four-membered ring.[9] However, homoallylic rearrangements are known for compounds of type **4** and **5**, if n is large enough: (**4**, n = 2)[10]; (**5**, n = 3)[11]; (**5**, n = 4).[12] Participation of a double bond in a small ring could possibly occur in

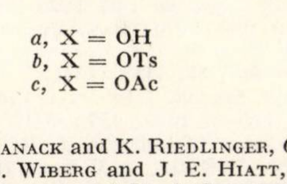

6

a, X = OH
b, X = OTs
c, X = OAc

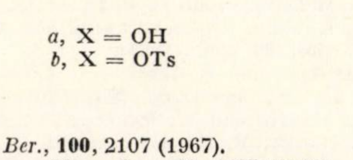

7

a, X = OH
b, X = OTs

---

[7] M. Hanack and K. Riedlinger, *Chem. Ber.*, **100**, 2107 (1967).

[8] K. B. Wiberg and J. E. Hiatt, *J. Amer. Chem. Soc.*, **90**, 6495 (1968).

[9] M. Hanack and H. J. Schneider, *Angew. Chem.*, **79**, 709 (1967).

[10] M. Hanack and H. J. Schneider, *Tetrahedron*, **20**, 1863 (1964).

[11] W. D. Closson and G. T. Kwiatkowski, *Tetrahedron*, **21**, 2779 (1965); W. D. Closson, S. A. Roman, G. T. Kwiatkowski and D. A. Corvin, *Tetrahedron Letters*, **1966**, 2271.

[12] M. Hanack and H. J. Schneider, *Liebigs Ann. Chem.*, **686**, 8 (1965).

the case of the Δ^2-cyclobutenyl-β-ethyl-system, **6**. Such compounds may be regarded as deriving from system **1**, with $n = 0$; at the same time they resemble compounds **4**, with $n = 1$.

In the present paper the solvolytic behaviour of Δ^2-cyclobutenyl-ethyl-β-tosylate (**6***b*) and of the homologous, Δ^2-cyclobutenylpropyl-γ-tosylate (**7***b*) are described).

RESULTS

Synthesis. The Δ^2-cyclobutenyl-β-ethanol (**6***a*) was obtained by a five-step synthesis starting with the known [13] 3-chlorocyclobutylcarboxylic acid (**8***a*) *).

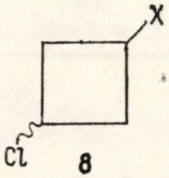

8

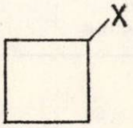

9

a, X = COOH
b, X = COCl
c, X = $COCHN_2$
d, X = $CH_2COOC_2H_5$
e, X = CH_2CH_2OH

f, X = CH_2COOH
g, X = CH_2COCl
h, X = CH_2COCHN_2
i, X = $CH_2CH_2COOC_2H_5$
j, X = $CH_2CH_2CH_2OH$

a, X = COCl
b, X = $COCHN_2$
c, X = $CH_2COOC_2H_5$
d, X = CH_2CH_2OH
e, X = CH_2CH_2OTs

The acid chloride **8***b* was transformed, on treatment with CH_2N_2 into the oily diazomethylketone **8***c* which, without being purified, was subjected to Wolff rearrangement. The 3-chlorocyclobutylethyl acetate (**8***d*) thus obtained was reduced with $LiAlH_4$, affording 3-chlorocyclobutyl-β-ethanol (**8***e*). The last step of the synthesis, namely the dehydrochlorination of **8***e*, was carried out by treatment with *t*-BuOK in anhydrous dimethylsulphoxide at 50°, using the technique of Hanack and Riedlinger.[7] The occurrence of compounds **8***a*—**8***e* as mixtures of *cis*-and *trans*-isomers is unimportant in this case, both isomers of **8***e* giving rise to the unique Δ^2-cyclobutenyl-β-ethanol (**6***a*).

The Δ^2-cyclobutenyl-β-ethanol (**6***a*) b.p.$_{10}$ 54.5—55° was converted into the oily tosylate by standard procedure.

*) The same reaction sequence was presented, without experimental details, by McDonald and Lyznicki.[1]

[13] W. A. Nevill, D. S. Frank and R. D. Trepka, *J. Org. Chem.*, **27**, 422 (1962).

The Δ^2-cyclobutenyl-γ-propanol (**7***a*) was prepared through a similar reaction sequence starting with 3-chlorocyclobutylacetic acid (**8***f*); the subsequent conversions into **8***g*, **8***h*, **8***i* and **8***j* afforded the desired unsaturated alcohol **7***a*, b.p.$_{15}$ 70 – 71° from which the tosylate **7***b* was obtained.

The saturated analogue of **6***b*, namely cyclobutylethyl-β-tosylate (**9***e*), was also synthesized for comparing purposes. Cyclobutyl-β-ethanol (**9***d*), b.p. 60 93°, was prepared using the same reaction scheme, starting from the known [13,14] cyclobutanecarboxylic acid chloride (**9***a*).

Solvolysis. The first-order rate constants for the NaOAc-buffered acetolysis of the tosylates **6***b*, **7***b* and **9***e* and the corresponding activation parameters are presented in Table 1.

Table 1

Rate data for buffered acetolysis[a)] of the tosylates 6*b*, 7*b* and 9*e*

Compound	Temp. °C	$k\,\mathrm{sec}^{-1}$	$\frac{k_{\mathrm{unsat}}}{k_{\mathrm{sat}}}$	$\Delta H\neq$ kcal/mol	$\Delta S\neq$ u.e.
6*b*	75	2.42×10^{-6}	3.25	21.2 (27.4[b)])	−23.1 (−7.9[b)])
	100	1.36×10^{-5} [b)]	2.8		
	110	4.39×10^{-5}	3.28		
	120	9.70×10^{-5} [b)]			
7*b*	75	1.48×10^{-6}	1.85 [c)]	21.8	−22.6
	110	2.9×10^{-5}	2.17 [c)]		
9*e*	75	0.8×10^{-6}	—	20.6 (23.4[b)])	−27.2 −(20.5[b)])
	110	1.34×10^{-5}	—		
	120	2.57×10^{-5} [b)]	—		

a) $[\mathrm{R-OTs}] = 10^{-2}\,M$; $[\mathrm{AcONa}] = 3.3.10^{-2}\,M$
b) Data from ref.[1]; c) comparative with **9***e*

The unbuffered acetolysis of **6***b* indicated a great extent of decomposition.

The composition of the reaction mixture from the AcONa-buffered acetolysis of **6***b*, at 75°, after approximately 7 half-lives, was determined by v.p.c.-analysis after $LiAlH_4$-reduction (Table 2). An important quantity (43%) of unrearranged alcohol **6***a* was v.p.c.-detected and identified by retention time and mixed samples. Another major component (36%) of the acetolysis mixture, with a greater retention time, was 3.5-hexadiene-1-ol (**10**) which was separated by means of preparative v.p.c. Its IR spectrum agrees well with the reported one.[15] The structure was also proved by means of NMR of alcohol and its acetate (see Experimental).

$$\mathrm{H_2^AC{=}CH^B{-}CH^C{=}CH^D{-}CH_2^E{-}CH_2{}^FOH} \qquad \mathrm{H_2^AC{=}CH^B{-}CH^C{=}CH^D{-}CH_2^E{-}CH_2^F{-}CH_2^GOH}$$

10 **11**

The alcohol **10** polymerizes at room temperature when kept for 1 – 2 days.

---

[14] C. G. Overberger, H. Kaye and G. Walsh, *J. Polym. Sci.*, **2**, 755 (1964).

[15] J. Meinwald and S. Nozaki, *J. Amer. Chem. Soc.*, **80**, 3132 (1958).

Beside these compounds, the reaction afforded other alcoholic components in 2.5 and 6% yield *) (shorter retention time) and 5 minor components in a 12.5% average yield **). No attempt was made to separate and identify these products.

Table 2

Product distribution[a)] for the buffered acetolysis of 6*b*

Temp. °C	Time h	Products %		
		6*a*	**10**	Other products [b)]
75	542	43	36	21
110	24	15	50	35

a) v.p.c.-analysis after $LiAlH_4$-reduction;
b) not further studied in this work; see note *

In the unbuffered acetolysis of **6*b*** a brown polymer (m.p. $> 310°$) was formed.

In the HCOONa-buffered formolysis of **6*b*** (356 hrs at 75°) the same products as in the buffered acetolysis could be detected: 58% (**6*a***), 12% (**10**). In the trifluoroacetolysis of **6*b*** at 75° (buffered with F_3C--COONa), only 3% of unrearranged alcohol **6*a*** could be detected in addition to large amounts of polymer.

The solvolysis of Δ^2-cyclobutenylpropyl-γ-tosylate (**7*b***), a compound for which Dreiding models indicated better conditions for double bond participation, was performed in AcONa-buffered acetic acid, at 110°, during 35 hrs. V.p.c.-analysis, (after $LiAlH_4$-reduction) of the reaction mixture indicated the presence of two major components (77%) and six minor components. The first major component (33%) was the unrearranged alcohol **7*a*** identified by its retention time and mixed v.p.c.-samples. The second major component (44%), with a longer retention time than **7*a***, was separated by preparative v.p.c. The structure of 4.6-heptadiene-1-ol (**11**) was attributed to this component, in view of the favourable comparison of its IR and NMR spectra with those reported in the literature.[16] Similarly to the compound **10**, the alcohol **11** polymerises easily at room temperature.

The buffered acetolysis of the satutated tosylate **9*e*** gave rise, after $LiAlH_4$-reduction, only to the starting alcohol **9*d***, in practically quantitative yield.

---

*) The structures of these minor alcoholic components were presented in McDonald and Lyznicki's paper [1] — see **).

) McDonald and Lyznicki [1] have found the following product composition for the acetolysis of **6*b* *at* **100**° (10 half-lives): 92% **10** OAc; 6% **6*c***, 1% *trans*-3-cyclopropyl allyl acetate, 1% 1-cyclopropylallyl acetate and traces of unidentified materials.

[16] J. G. Berger, E. L. Stogrin and A. A. Zimmerman, *J. Org. Chem.* **29**, 950 (1964).

DISCUSSION

Previous investigations carried out in this laboratory [4c,6b] showed that the lengthening of the side chain in tosylate **12** has a dramatic effect upon double bond participation in acetolysis; the π-route represents only 6–8% of the overall reaction of **12*a*** [4c] and increases to more than 90% for **12*b***.[6b]

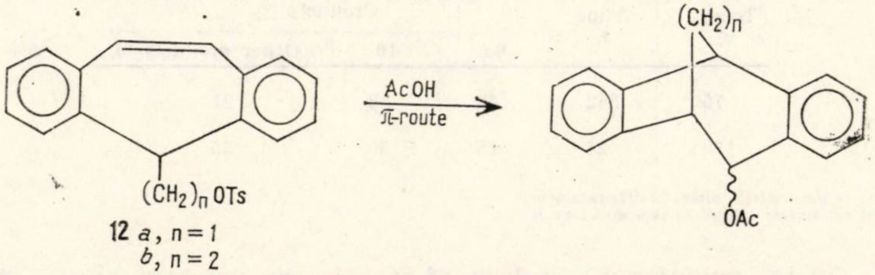

These results determined us to find other examples in which an unfavourable π-route reaction could gain a more significant weight in the overall process, by lengthening the side chain.

Compounds **6*b*** and **7*b***, both related to **4** (n = 1), seemed to be promising in this respect. The nonclassical ion **13*a***, generated by σ-route was admitted as intermediate in the solvolysis of bicyclo [2.2.0] hexyl-tosylate (**14**)[17]; we hoped therefore that π-route ionization of **6*b*** would give rise to the same ion **13*a***.

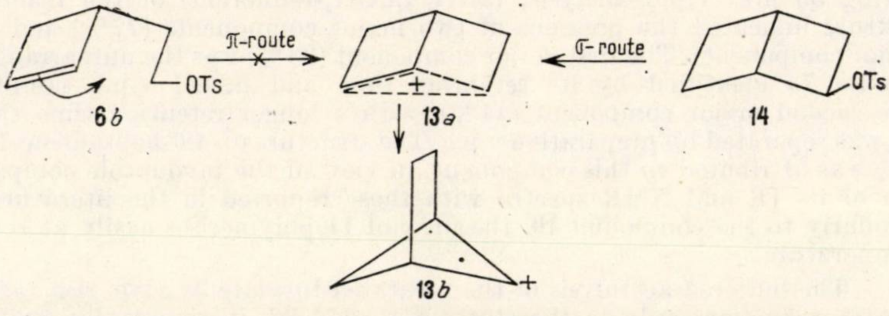

However, in agreement with the recent report of McDonald and Lyznicki,[1] we observed, at 110°, that tosylate **6*b*** prefer to open its ring to the diene **10** *) through a thermally allowed electrocyclic process [18] (see Table 2).

---

*) A similar ring opening was described by Hanack and Riedlinger[7] who indicated that Δ^2-cyclobutenylmethanol (**4**, n = 1, X = OH) is stable under 120°, but is quantitatively isomerised to 2.4-pentadiene-1-ole at 160°.

[17] R. N. McDonald and C. E. Reinecke, *J. Org. Chem.*, **32**, 1878 (1967).
[18] R. B. Woodward and R. Hoffmann, *Angew. Chem.*, **81**, 797 (1969).

Nevertheless, we tried to find conditions (lower temperatures, less nucleophylic solvents) which would favour double bond participation. Thus we hoped that the decrease of temperature of the acetolysis would affect the electrocyclic process to a greater extent than the process of ionisation of **6***b*. However, when the solvolysis was carried out at 75°, the reaction products (Table 2) and the kinetic data (Table 1) did not indicate any amount of π-route. Although the electrocyclic process is significantly diminished, the major reaction product **6***a* is formed by solvent-assisted solvolysis. Table 1 shows that the ratio k_u/k_{sat} is the same at 75° and 110°. Taking into account the fact that the activation energies of solvent-assisted reactions are usually lower than those of π-route reactions (if the resulted nonclassical ion is not specially stabilised [19]) it can be assumed that a further decrease in temperature would have no favourable effect.

The replacement of acetic acid by less nucleophylic solvents like formic acid and trifluoroacetic acid, led to the conclusion that π-route ionization cannot compete with the normal solvent-assisted solvolysis.

The lack of double bond participation in the solvolysis of **6***b* is probably explained by the unfavourable geometric conditions (distances and angles) for overlap between the vacant orbital of the reaction site and π-orbitals of the double bond (**15**).

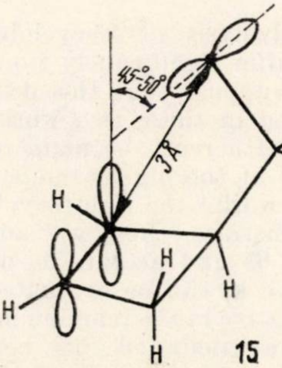

15

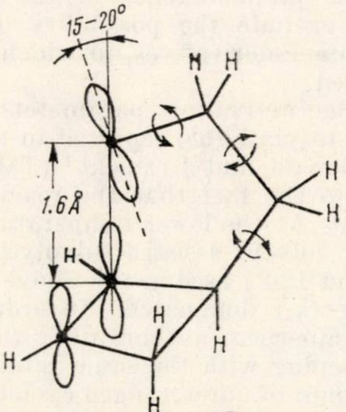

16

In another attempt to achieve participation of a double bond in a four-membered ring, the acetolysis of **7***b* was investigated.

Inspection of Dreiding models reveals that a favourable conformation (**16**) for double bond participation could be attained in the case of this system. Nevertheless, the solvolysis products of **7***b* indicate also a thermal ring-opening reaction beside the clean SN_2-type reaction yielding

---

[19] P. D. Bartlett, W. S. Trahanowski, D. A. Bolon and G. H. Schmid, *J. Amer. Soc.*, **87**, 1314 (1965).

7a. On the other hand the lack of double bond participation is shown by the rate constant of the buffered acetolysis of **7b**, which is only 1.85 — (at 75°) and 2.17 — (at 110°) — times greater than the rate of saturated compound **9e**.

A possible explanation of this behaviour lies in the existence of a very great number of conformers of the three-carbon side-chain, which lowers the enthropy of activation. Similar results were obtained by Bartlett *et al.*[19] for the acetolysis of Δ^3-cyclopentenylpropyl-γ-*p*-nitrobenzensulphonate (*vide infra*).

Another explanation for the absence of π-route reaction in the solvolysis of **7b** (and also of **6b**) could be the interference of the electrocyclic process with the solvolytic process. Our own experience in this field [4c,6b] indicated than when solvent assistance competes well with neighbouring group participation, the raising of the temperature has an overwhelming effect in deciding the final outcome, namely by favouring the π-route. However, in the case of cyclobutene-derivatives, as it has already been shown, the raising of temperature facilitates the electrocyclic process, shadowing thus the π-route reaction. The enthalpy of activation of such ring opening must be higher than that of the solvolysis (but not very different from that of the π-route); the entropy of activation, in its turn, must be higher than the corresponding entropies of activation of the π-route reactions of **6b** and **7b**. The activation parameteres explain thus the preponderence of the electrocyclic process. Nevertheless, we cannot exclude the possibility of double bond participation for other cyclobutene-derivatives, in which the ring opening could be somehow supressed.

The activation parameters of the solvolysis of Δ^2-cyclobutenyl-ethyl-β-tosylate (**6b**) reported in this paper differ significantly from those of McDonald and Lyznicki[1] (Table 1). We suppose that this difference is due to the fact that the reactions followed in these two works were different. At the lower temperatures (75°) used herein, the main reaction was the solvent assisted solvolysis (k_s), while at the higher temperatures (100° and 120°) used in the above mentioned work[1] the electrocyclic ring opening (k_r) dominated. In order to demonstrate this, we admitted as the american authors did,[1] that tosylate **6b** and acetate **6c** undergo ring opening with the same rate. In that case k_r can be evaluated from the amount of unrearranged cyclobutene derivative in the reaction mixture. Considering our product data (Table 2), the calculated rate constants at the two temperatures were: $k_r^{75} = 4.35 \times 10^{-7}$ sec^{-1} and $k_r^{110} = 2.17 \times 10^{-5}$ sec^{-1}, respectively. The resulted enthalpy of activation, 28.9 Kcal/mol, is comparable with the cited[1] enthalpy of 29.1 kcal/mol for the rearrangement of the acetate **6c**.

Additional support for our assumption was provided by the analysis of the activation parameters.

The rates and activation parameters for **6b**, **7b** and **9e** were calculated at 60°. They are presented in the Table 3, along with data for related compounds with five-membered ring, studied by Bartlett and co-workers.[19,20]

---

[20] P. D. Bartlett and G. D. Sargent, *J. Amer. Chem. Soc.*, **87**, 1297 (1965).

Table 3

Activation parameters for buffered acetolysis of 6b, 7b, 9e in comparison with related compounds

Sulphonate	k sec^{-1} 60°	$\Delta H^{\neq}$ kcal/mol	$\Delta S^{\neq}$ e.u.
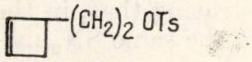 **6b** *a*	$8.52.10^{-7}$ d)	21.2	−22.5
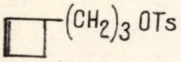 **7b** *a*	$4.27.10^{-7}$ d)	21.7	−22.1
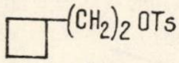 **9e** *a*	$2.5.10^{-7}$ d)	20.6	−26.5
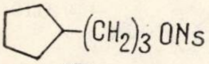 **17** *b*	$2.1.10^{-6}$	22.6	−16.9
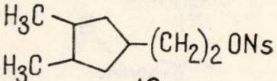 **18** *c*	$1.27.10^{-6}$	23.2	−16.7
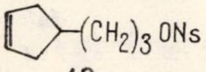 **19** *b*	$1.6.10^{-6}$	23.8	−14.2
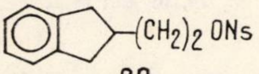 **20** *c*	$7.47.10^{-7}$	25.2	−11.1
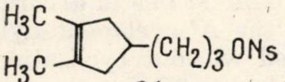 **21** *b*	$8.8.10^{-6}$	23.5	−11.9
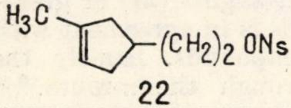 **22** *c*	$7.69.10^{-4}$	21.2	− 9
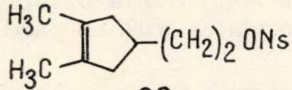 **23** *b*	$4.29.10^{-3}$	20.6	−7.8

a) this work; b) reference[19]; c) reference[20]; d) extrapolated from data of Table 1
Ts = p-CH_3-C_6H_4-SO_2-; Ns p-O_2N-C_6H_4-SO_2-

Graphical representation of $\Delta H^{\neq}$ vs $\Delta S^{\neq}$ (fig. 1) shows that the points corresponding to the saturated compounds **9*e*, 17, 18** and **20** lie practically on the same "isokinetic line", [21] indicating that in the buffered acetolysis of these compounds a single mechanism is operating, which is certainly a SN_2-type one.

The points for both unsaturated tosylates with four-membered ring (**6*b*** and **7*b***) lie on the same isokinetic line demonstrating that, in the given conditions, the compounds react also according to the same SN_2-mechanism.

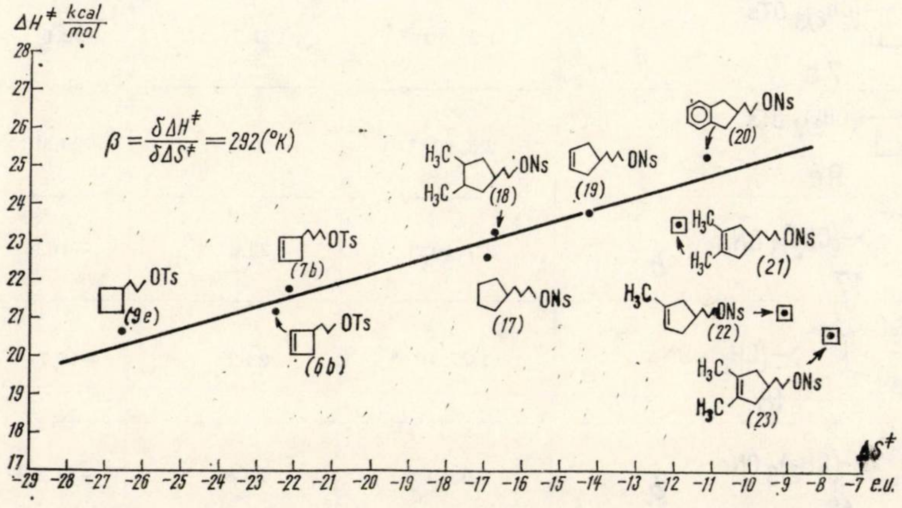

Fig. 1. — $\Delta H^{\neq}$ *vs* $\Delta S^{\neq}$ relationships for buffered acetolysis of **6*b*, 7*b*, 9*e*** and related compounds

In the series of cyclopentene-derivatives, the point for sulphonate **19**, which resembles the tosylate **7*b***, lies on the same isokinetic line in accordance with the experimental results of Bartlett [19] : "the Δ^3-cyclopentenyl-propyl-γ-*p*-nitrobenzenesulphonate (**19**) is acetolysed without cyclisation and without appreciable acceleration by the double bond".

The other five-membered sulphonates present slight- (**21**) or great- (**22** and **23**) deviations from this isokinetic line. This is in agreement with the changes in mechanism exhibited by these compounds, namely the gradual passing to double bond participation through the π-route.[19,20]

The slope of $\beta = 292$ (°K) of the isokinetic line compares favourably with the value of $\beta = 310$ (°K) for acetolysis of brosylates with no participating neighbouring groups.[21,22]

It can be seen, from Table 3, that both tosylates with four-membered ring **6*b*** and **7*b*** have greater activation enthalpies than the saturated compound **9***e*. Bartlett[19] reported a similar behaviour for the derivatives with five-membered ring in the cases when the double bond does not assist the solvolysis (see also Table 3).

---

[21] J. E. LEFFLER and E. GRUNWALD, *Rates and Equilibria of Organic Reactions*, J. WILEY and Sons, Inc. New York, London, **1963**, p. 315.

[22] S. WINSTEIN and H. MARSHALL, *J. Amer. Chem. Soc.*, **74**, 1120 (1952).

From the present work it can be concluded that the participation of a remote double bond (π-route) does not appear either in cyclobutenic rings like **6** (**1**, n = 0) * or in the **7**-type ones, in striking difference from similar compounds with cyclopentene (**1**, n = 1)[2] or cyclohexene- (**1**, n = 2)[3] rings, where such participation was experimentally demonstrated.

These results along with those of Hanack[7,8] and Wiberg[8] illustrate the special behaviour in solvolysis of the cyclobutenic systems.

EXPERIMENTAL

IR-spectra were recorded with a C. Zeiss-Jena-UR-20 spectrophotometer. *NMR-spectra* were obtained on a Varian A-60A spectrometer (TMS-internal standard). The *v.p.c.-analyses* were performed on a Carlo Erba model D gas chromatograph using Carbowax 20M columns (10% on Chromosorb W) 3 m/2 mm diam. Temp. 110° (isotherm), then 110–130° programed with 3°/min, using nitrogen rate flow 30 ml/min. The *v.p.c. separations* were achieved using Carbowax 20M columns (20% on silanisated Chromosorb W), 2.5 m/5 mm diam. at 110° (for alcohols) and 75° (for acetates).

3-Chlorocyclobutylcarboxylic acid (**8***a*) was prepared according to Nevill, Frank and Trepka[13] by chlorination of cyclobutyl-1,1-dicarboxylic acid and subsequent decarboxylation.

3-Chlorocyclobutylcarboxylic acid chloride (**8***b*). Thionyl chloride (126 g ; 77 ml, 106 mmoles) was added dropwise with stirring, during 1 hr, to 3-chlorocyclobutylcarboxylic acid (30 g ; 225 mmoles). The reaction mixture was refluxed for 3 hrs then the excess of thionyl chloride was distilled off at atmospheric pressure. The residue was distilled *in vacuo* affording *3-chlorocyclobutylcarboxylic acid chloride* (**8***b*) 21.5 g (63%) b.p.$_{23-24}$ = 85–90°.

IR-spectrum (CCl_4, cm^{-1}) : 1809 vs, 2879 w, 2966 w, 3011 w.

3-Chlorocyclobutylethyl acetate (**8***d*). a) *3-Chlorocyclobutyl diazomethyl ketone* (**8** *c*). To a cooled ethereal solution of diazomethane (450 ml, containing 0.0189 g CH_2N_2/ml) a solution of 3-chlorocyclobutylcarboxylic acid chloride (15 g, 98,5 mmoles) in anhydrous ether (15 ml) was added dropwise with stirring during 1 hr. The stirring was then continued for 4–5 hrs (the evolution of N_2 ceased) and left overnight. The ether was removed *in vacuo*, without heating, affording the crude *3-chlorocyclobutyl diazomethyl ketone* (**8***c*), a yellow-red oil (15 g, 93%), which was utilised in the next step without other purification.

IR spectrum (CCl_4, cm^{-1}) : 1148 s, 1320 s, 1389 vs, 1660 vs, 2111 vs, 2872 w, 2956 m, 2991 m, 3121 w.

b) *Wolff rearrangement.* Into a stirred solution of 3-chlorocyclobutyl diazomethyl ketone (15 g, 94.5 mmoles) in anhydrous ethanol (200 ml), warmed at 50–60°, Ag_2O (freshly prepared and dried) was added in small portions. The addition of Ag_2O was continued until no evolution of gases was observed when a small portion from the reaction mixture was treated with conc. HCl. The reaction was carried out to completion by refluxing for 1hr. The reaction mixture was filtered, the solvent was removed *in vacuo* and the residue was distilled through a 30 cm column affording 3-chlorocyclobutylethyl acetate (**8***d*) 12 g (68%) b.p.$_9$ = 82–83°. (*Found* : C, 53.86 ; H, 7.45 ; Cl, 19,93. $C_8H_{13}O_2Cl$ requires C, 54.36 ; H, 7.42 ; Cl, 20.08%).

---

* See also ref.[1]

IR spectrum (CS_2, CCl_4, cm^{-1}) : 1185 s, 1741 vs, 2871 w, 2911 w, 2943 m, 2989 s.

3-Chlorocyclobutyl-β-ethanol (**8***e*). To a suspension of $LiAlH_4$ (5g, 132 mmoles) in anhydrous ether (50 ml) a solution of 3-chlorocyclobutylethyl acetate (17.5 g, 100 mmoles) in anhydrous ether (100 ml) was added dropwise with stirring during 2 hrs, maintaining the temperature at 0°. The reaction mixture was then stirred for 2 hrs at room temperature and finally for 2 hrs at reflux. After the usual work-up an oily residue was obtained which was distilled through a 30 cm-column, affording *3-chlorocyclobutyl-β-ethanol* (**8***e*) 9.7 g (73 %) b.p.$_{11}$=96−97° (Found : C, 52,87 ; H, 8.24 ; Cl, 27.30. $C_6H_{11}OCl$ requires C, 53.45 ; H, 8.20 ; Cl, 26.48 %).

IR spectrum (CCl_4 ; cm^{-1}) ; 1042 ws, 1279 s, 1432 m, 2878 s, 2936 vs, 2986 s, 3200−3600 s, 3638 m.

Δ^2-Cyclobutenyl-β-ethanol (**6***a*). To a suspension of freshly prepared potassium *tert.* butoxide (20 g, 207 mmoles) in anhydrous dimethylsulphoxide (120 ml), a solution of 3-chlorocyclobutyl-β-ethanol (13 g, 97 mmoles) in anhydrous dimethylsulphoxide (30 ml) was added dropwise with stirring, during 2 hrs, maintaining the temperature below 30°. The reaction mixture was then stirred for 20 hrs. at 50°, cooled and decomposed with ice (100 g). After neutralization (pH = = 7.0) with HCl and saturation with NaCl, the reaction mixture was ether-extracted. The combined ethereal layers were washed with water (20 ml), dried over anhydrous $MgSO_4$ and evaporated *in vacuo* using a short column. The residue was distilled through a 30 cm column affording *Δ^2-cyclobutenyl-β-ethanol* (**6***a*) 4.3 g (45 %) b.p.$_{10}$ = 54.5−55°. The v.p.c. analysis indicated nearly 90 % purity. Attempts to purify it further by distillation or by column chromatography on Al_2O_3 or SiO_2 failed. The Δ^2-cyclobutenyl-β-ethanol was purified by preparative v.p.c., reaching thus 97 % purity. (*Found* : C, 71.88 ; H, 10.44. $C_6H_{10}O$ requires : C, 73.42 ; H, 10.27 %).

IR spectrum (CCl_4, cm^{-1}) : 1046 s, 1385 w, 1430 w, 2842 m, 2880 s, 2924 vs, 3048 m, 3200−3600 w, 3636 m.

NMR spectrum (CCl_4, δ ppm) 6.1 and 6.0 (2H, AB-system, J=2.8 Hz, H^A) ; 3.58 (2H, triplet, J = 7 Hz, H^E) ; 2.91 (1 H, unresolved multiplet, H^C) ; 2.7 (1 H, quartet, J=12.5 Hz, 4 Hz, H^B-*cis* with H^C) ; 2.1 (1H, doublet, J= 12.5 Hz, H^B-*trans* with H^C) ; 1.69 (2H, quartet, J = 7 Hz, H^D) ; 3.8 (1H, large singlet, OH).

Δ^2-Cyclobutenylethyl-β-tosylate (**6***b*). To a cooled solution of Δ^2-cyclobutenylethyl-β-ethanol (2 g, 20.4 mmoles) in anhydrous pyridine (25 ml) *p*-toluenesulphonyl chloride (4.1 g, 21.5 mmoles) was added in small portions. The reaction mixture was kept in a refrigerator for 48 hrs, then decomposed in ice-cooled water (50 ml). The liquid tosylate was extracted with CH_2Cl_2 (4 portions of 25 ml), and the organic extract was washed successively with : water, dil. HCl, 10 % $NaHCO_3$ and water. After evaporation of the solvent *in vacuo*, without heating, the oily *Δ^2-cyclobutenylethyl-β-tosylate* (**6***b*) was obtained (3.65 g, 72 %) (*Found* : C, 61.80 ; H, 6.63 ; S, 12.37. $C_{13}H_{16}O_3S$ requires : C, 61.89 ; H, 6.35 ; S, 12.70 %).

IR spectrum (CS_2, CCl_4, cm^{-1}) : 1179 vs, 1371 vs, 1602 w, 2842 w, 2922 m, 2948 m, 3051 m, 3131 w.

NMR spectrum (CCl_4, δ ppm) 7.75 and 7.3 (4 H, A_2B_2-system, aromatic H) ; 6.0 (2H, singlet, H^A) ; 4.0 (2 H, triplet, J=6.5 Hz, H^E) ; 2.85 (1 H, unresolved multiplet, H^C) ; 2.66 (1 H, quartet, J=13.5 Hz, 4 Hz, H^B-*cis* with H^C) ; 2.46 (3 H, singlet, CH_3) ; 2.05 (1 H, doublet, J = 13.5 Hz, H^B-*trans* with H^C) ; 1.8 (2 H, quartet, J = 6.5 Hz, H^D).

3-Chlorocyclobutylacetic acid (**8** *f*) was obtained by alkaline hydrolysis (10 % ethanolic KOH ; 2.5 hrs reflux) of the corresponding ester **8***d*, in 68 % yield, b.p.$_1$ = 135−140° (*Found* : C, 47.67 ; H, 5.96 ; Cl, 22.47. $C_6H_9O_2Cl$ requires : C, 48.50 ; H, 6.11 ; Cl. 23.86 %).

IR spectrum (CCl_4, cm^{-1}) : 1230 s, 1280 s, 1418 s, 1708 vs, 2400−3400 m, 2950 s, 2990 s.

3-Chlorocyclobutylacetic acid chloride (**8***g*) was prepared by treatment of the acid **8***f* with $SOCl_2$, as described for the lower homologue **8***b*, 85 % yield, b.p.$_{30}$ = 115−120°.

IR spectrum (CCl_4, cm^{-1}) ; 968 s, 1279 m, 1402 m, 1801 vs. 2860 w, 2944 m, 2992 m.

3-(Chlorocyclobutylmethyl) diazomethyl ketone (**8*h***) was obtained by treatment of the acid chloride **8*g*** with ethereal CH_2N_2, as described for diazoketone **8*c***, in 95% yield, as a yellow oil which was used in the next step without purification.

IR spectrum (CCl_4, cm^{-1}) : 1139 m, 1349 s, 1660 s, 2111 vs, 2885 w, 2942 m, 2990 m, 3118 w.

3-Chlorocyclobutylethyl propionate (**8*i***) was obtained by Wolff rearrangement of the diazoketone **8*h*** in anhydrous ethanol using the procedure described for ester **8*d***; 72% yield, b.p.$_{14}$= 86–91° (Found : C, 56.04 ; H, 7.87 ; Cl, 17.80 $C_9H_{15}O_2Cl$ requires : C, 56.67 ; H, 7.93 : Cl, 18.60%).

IR spectrum (CCl_4, cm^{-1}) : 1180 m. 1735 vs, 2861 w, 2940 m, 2985 m.

3-Chlorocyclobutyl-γ-propanol (**8*j***) was prepared by $LiAlH_4$ reduction of the 3-chlorocyclobutylethyl propionate, as described for the alcohol **8*e***; 90% yield, b.p.$_{11}$ = 97–103° (Found: C, 56.21 ; H, 9.12 ; Cl, 23.15 . $C_7H_{13}OCl$ requires : C, 56.55 ; H, 8.82 ; Cl. 23.87%).

IR spectrum (CCl_4, cm^{-1}) : 1053 s, 1276 s, 1378 m, 1430 m, 1451 m, 2870 s, 2938 vs, 2984 vs, 3200–3550 m, 3632 m.

Δ^2-Cyclobutenyl-γ-propanol (**7*a***) was obtained by *t*-BuOK-dimethylsulphoxide-dehydrochlorination of the above alcohol **8*j*** using the procedure described for the lower homologue **6*a***; 58% yield, b.p.$_{15}$ = 70–71° (Found : C, 73.22 ; H, 10.72. $C_7H_{12}O$ requires : C, 74.94 ; H, 10.79%). The v.p.c.-analysis indicates 90% purity. Due to the difficulties of the purification, the impure alcohol **7*a*** was used as such in the next step.

IR spectrum (CCl_4, cm^{-1}) : 1058 s, 1284 w, 1388 w, 1432 w, 1452 w, 2850 s, 2885 s (shoulder), 2930 vs, 3048 m, 3123 w, 3250–3500 w, 3636 m.

NMR spectrum (CCl_4, δ ppm) 6.1 and 6.0 (2H, AB-system, J = 2.8 Hz, H^A) ; 3.55 (2 H, multiplet, H^F) ; 2.84 (1 H, unresolved multiplet, H^C) ; 2,65 (1 H, quartet, J=12 Hz, 4 Hz, H^B-*cis* with H^C) ; 2.05 (1 H, doublet, J=12 Hz, H^B-*trans* with H^C) ; 1.55 (4 H, multiplet, H^D+ + H^E) ; 2.86 (1 H, singlet, OH).

Δ^2-Cyclobutenylpropyl-γ-tosylate (**7*b***) was prepared from the unsaturated alcohol **7*a*** and *p*-toluenesulphonyl chloride in pyridine, as described for synthesis of **6*b***; 70% yield ; viscous oil (*Found* : C, 62.80 ; H, 6.92 ; S, 11.58. $C_{14}H_{18}SO_3$ requires : C, 63.12 ; H, 6.81 ; S, 12.04%).

IR spectrum (CS_2, CCl_4, cm^{-1}) : 1179 vs, 1189 vs, 1370 vs, 1600 w, 2851 w, 2921 m, 2940 m, 3045 m, 3130 w.

NMR spectrum (CCl_4, δ ppm) : 7.76 and 7.3 (4 H, A_2B_2-system, aromatic H) ; 6.0 (2H, singlet, H^A) ; 4.0 (2H, multiplet, H^F) ; 2.75 (1 H, unresolved multiplet, H^C) ; 2,61 (1H, quartet, J = 12 Hz, 4 Hz, H^B-*cis* with H^C) ; 2.45 (3 H, singlet, CH_3) ; 2.0 (1H, doublet, J=12 Hz, H^B-*trans* with H^C) ; 1.3–1.7 (4 H, unresolved multiplet, H^D+H^E).

Cyclobutylethyl acetate (**9*c***). a) *Cyclobutyl diazomethyl ketone* (**9*b***) was prepared from cyclobutanecarboxylic acid chloride (**9*a***)[13,14] and diazomethane in the manner described for 3-chlorocyclobutyl diazomethyl ketone (**8*c***) ; 96% yield of a yellow viscous oil which was utilised in the next step without purification.

IR spectrum (CCl_4, cm^{-1}) : 1150 s, 1318 s, 1368 vs, 1657 vs, 2090 vs (shoulder), 2110 vs, 2870 w, 2950 m, 2980 m, 3120 w.

b) *Wolff rearrangement* was obtained as previously described for 3-chlorocyclobutylethyl acetate (**8*b***). *Cyclobutylethyl acetate* (**9*c***), 45% yield, b.p.$_{40}$ = 82–83° (lit.[23] b.p.$_2$ = 100°) (*Found* : C, 67.25 ; H, 10.18. $C_8H_{14}O_2$ requires C, 67.56 ; H, 9.93%).

IR spectrum (CCl_4, cm^{-1}) : 1030 m, 1175 s, 1740 vs, 2880 m, 2938 s, 2980 s.

[23] C. D. Nenitzescu, A. M. Glatz, M. Gavăt and I. Pogany, *Izvest. Akad. Nauk S.S.S.R.*, **1963**, 332.

Cyclobutylacetic acid was obtained by alkaline hydrolysis of cyclobutylethyl acetate (**9***c*). The pure acid b.p.$_{10}$ = 87° (lit.[12] b.p.$_2$ = 78°; lit.[23] b..p.$_{60}$ = 145°) (*Found*: C, 62.50; H, 8.86. $C_6H_{10}O_2$ requires: C, 63.13; H, 8.83%).

IR spectrum (CCl_4, cm^{-1}): 943 m, 1230–1305 m, 1415 m, 1713 vs, 2300–2800... 3200 m, 2868 s, 2980 vs.

Cyclobutyl-β-ethanol (**9***d*) was prepared by $LiAlH_4$ reduction of cyclobutylethyl acetate (**9***c*) as described for the 3-chloroderivative **8***e*; 80% yield, b.p.$_{60}$ = 93° (*Found*: C, 71.19; H, 12.14. $C_6H_{12}O$ requires: C, 71.93; H, 12.08%).

IR spectrum (CCl_4, cm^{-1}): 1032 s, 1384 w, 1450 w, 2869 s, 2930 vs, 2968 vs, 2974 vs, 3300–3580 w, 3636 m.

Cyclobutylethyl-β-tosylate (**9***e*) was prepared from cyclobutyl-β-ethanol (**9***d*) with *p*-toluenesulphonyl chloride in pyridine, as described for the unsaturated tosylate (**6***b*); 52% yield, viscous oil (*Found*: C, 61.36; H, 7.34; S, 12.15. $C_{13}H_{18}O_3S$ requires: C, 61.37; H, 7.14; S, 12.61%).

IR spectrum (CS_2, CCl_4, cm^{-1}); 961 s, 1178 vs, 1188 vs, 1382 vs, 1600 w, 2862 m, 2897 m, 2932 s, 2980 s, 3038 w, 3942 w, 3072 w.

NMR spectrum (CCl_4, δ ppm) 7.7 and 7.3 (4 H, A_2B_2-system, aromatic H); 3.9 (2H, triplet, J = 6.5 Hz, $-CH_2$-OTs); 2.45 (3 H, singlet, CH_3); 2.4–1.25 (9 H, unresolved multiplet, 7 cyclobutanic H and CH_2).

Acetolysis of Δ^2-cyclobutenylethyl-β-tosylate (**6***b*): A solution of tosylate **6***b* (3.6 g, 14.3 mmoles) and anhydrous sodium acetate (3.52 g, 42.8 mmoles) in 100 ml anhydrous acetic acid was heated at 75° for 542 hrs (approximately 7 half-lives). The reaction mixture was poured in ice-cold water (150 ml) then extracted with petroleum ether (boiling range 30–40°; 4 × 50 ml) and finally with ether (50 ml). The combined organic layers were washed with Na_2CO_3-solution, then with water, dried and evaporated *in vacuo* using a fractionating column. The oily residue (1.5 g, 75%) was dissolved in anhydrous ether (50 ml) and reduced with $LiAlH_4$ (0.4 g). After the usual work-up a pale-yellow oily product was obtained (0.8 g; 78% calcd. on acetates). On treatment with methanol (7 ml) a small quantity of insoluble polymer was formed. After filtration the methanolic solution was v.p.c.-analysed. Two major components were identified: the first (43%) was the starting alcohol **6***a* (retention time and mixed samples at v.p.c.) while the second (36%) separated by preparative v.p.c. was 3.5-hexadiene-1-ole (**10**).

IR spectrum (CCl_4, cm^{-1}: 902 vs, 1610 w, 1660 w, 2879 s, 2937 vs, 3011 s, 3030 m, 3092 m, 3200–3600 s, 3608 m, 3634 m.

NMR spectrum (CCl_4, δ ppm) 6.6–4.8 (5H, complex multiplet, $H^{A,B,C,D}$); 3.6 (2H, triplet, J = 6.5 Hz, H^F); 2.3 (2H, quartet, J = 6.5 Hz, H^E); 2.7 (1 H, singlet, OH).

In another experiment, from the reaction product, before $LiAlH_4$-reduction, the major components were separated as acetates by preparative v.p.c.:

6*c-IR-spectrum* (CCl_4, cm^{-1}): 1040 s, 1248 vs, 1744 vs, 2843 w, 2921 m, 2957 s, 3052 w, 3131 w.

NMR spectrum (CCl_4, δ ppm) 6.08 (2H, large singlet, H^A); 4.05 (2 H, triplet, J = 7 Hz, H^E); 2.88 (1 H, multiplet, H^C); 2.71 (1 H, quartet, J = 12.5 Hz, 4 Hz, H^B-*cis* with H^C); 2.1 (1 H, doublet, J = 12.5 Hz, H^B-*trans* with H^C); 1.98 (3 H, singlet, CH_3); 1.78 (2 H, quartet, J = 7 Hz, H^D).

10-*OAc-IR-spectrum* (CCl_4, cm^{-1}) 902 m, 1242 vs, 1745 vs, 2860 vs, 2901 w, 1960 m, 3018 w, 3042 w, 3090 w.

NMR spectrum (CCl_4, δ ppm) 6.6–4.8 (5 H, complex multiplet, $H^{A,B,C,D}$); 4.05 (2H, triplet, J = 7 Hz, H^F); 2.38 (2 H, quartet, J = 7 Hz, H^E); 1.96 (3 H, singlet, CH_3).

Acetolysis of Δ^2-cyclobutenylpropyl-γ-tosylate (**7***b*). A solution of tosylate **7***b* (0.7 g; 2.65 mmoles) and anhydrous sodium acetate (0.7 g; 8.5 mmoles) in 25 ml anhydrous acetic acid was heated for 35 hrs at 110°. The reaction mixture wsa then worked-up and reduced by $LiAlH_4$ as described for the acetolysis of **6***b*. The oily product (0.25 g; 85%) was then v.p.c.-analysed.

Two important components were identified; the first (33%) was Δ^2cyclobutenyl-γ-propanol (*7a*) (retention time and mixed samples in v.p.c.) the second (44%) was 4.6-heptadiene-1-ole (**11**) (separated by preparative v.p.c.) (*Found* for **11**; *C*, 75.46; H, 10.92. $C_7H_{12}O$ requires: C, 74.94; H, 10.79).

IR spectrum (**11**) (CCl_4), cm^{-1}): 908 vs, 1010–1060 vs, 2879 vs, 2940 vs, 3010 s, 3040 m, 3090 m, 3200–3600 s, 3635 s.

NMR spectrum (**11**) (CCl_4, δ ppm) 6.8–5.0 (5 H, complex multiplet, $H^{A,B,C,D}$); 3.71 (2 H, triplet, J = 6.5 Hz, H^G); 2.25 (2 H, quartet, J = 6.5 Hz, H^E); 1.68 (2 H, quintet, J = 6.5 Hz, H^F); 2.56 (1 H, singlet, OH).

Acetolysis of cyclobutylethyl-β-tosylate (**9***e*). A solution of saturated tosylate **9***e* (0.5 g; 1.96 mmoles) and anhydrous sodium acetate (0.49 g; 6 mmoles) was heated at 110° for 92 hrs. After working-up, following the procedure used for tosylate **6***b*, and reduction with $LiAlH_4$ (0.1 g), the product (0.17 g; 85%) was found to have the same IR-spectrum as the alcohol **9***d*. The v.p.c.-analysis of this product indicated 92% **9***d* beside 12 minor components.

Kinetic procedure. The acetic acid used in kinetic determinations was obtained by refluxing commercial acetic acid with acetic anhydride, followed by distillation on an efficient column (freezing point 16.4°). Sodium acetate solutions were obtained by dissolving anhydrous sodium acetate in acetic acid. The concentration of the solution was determined by titration with a 0.05 M solution of perchloric acid in acetic acid. For kinetic measurements the ampoule technique was used. The liberated *p*-toluenesulphonic acid was indirectly titrated with 0.05 M sodium acetate solutions (in AcOH) after addition of an excess of 0.05 M perchloric acid in acetic acid. A Metrohm potentiograph, Model E 336, with platinum electrode and graphite capillary electrode designed after Zeidler[24] was used for titrations.

Acknowledgements. We wish to thank Miss Elvira Sliam and Mrs. Violeta Daniel for performing the elemental analyses, Miss Ligia Stănescu, Doina Georgescu and Mrs Ana Haneş for v.p.c.-analyses and separations, Dr. F. Chiraleu for NMR-spectra and Dr. F. Badea, Dr. M. Voicu and Dr. M. Elian for helpful discussions.

---

[24] H. Zeidler, *Z. Analyt. Chem.*, **146**, 271 (1955).

Revue Roumaine de Chimie, **17**, *8*, 1393–1407 (1972)

Revue Roumaine de Chimie, **17**, *8*, 1409–1416 (1972)

OXYDATION DU *n*-DODÉCANE EN PHASE LIQUIDE PAR L'OXYGÈNE MOLÉCULAIRE EN PRÉSENCE DES CATALYSEURS MÉTALLIQUES PSEUDO-HOMOGÈNES. I.

L'EFFET DES NAPHTÉNATES DES MÉTAUX ALCALINS ET ALCALINO-TERREUX

IOSIF DRIMUŞ et ANGELA LUPU

Faculté de Chimie Industrielle de l'Institut Polytechnique de Bucarest, Chaire de Technologie Chimique Organique, 149, Calea Victoriei, Bucarest

Reçu le 2 mars 1972

On étudie l'influence des naphténates de Li, Na, K, Rb, Cs, Be, Mg, Ca, Sr et Ba sur l'oxydation du *n*-dodécane en phase liquide par l'oxygène moléculaire et l'influence de ces catalyseurs pseudo-homogènes sur l'initiation de la réaction, l'accumulation de peroxydes et d'acides.

INTRODUCTION

L'oxydation des *n*-alcanes par l'oxygène moléculaire est une réaction avec des implications dans la synthèse des acides gras,[1] des alcools gras secondaires,[2] des peroxydes [3] et des acides dicarboxyliques.[4,5]

Si l'on fait barboter de l'oxygène dans le *n*-dodécane à 155° on obtient de nombreuses réactions consécutives, parallèles, induites, etc. et au fur et à mesure que les réactions avancent, le produit oxydé contient un nombre toujours plus grand de peroxydes, acides, esters, alcools, cétones, etc.

A cause de l'attaque par oxygène de la chaîne d'atomes de carbone du *n*-dodécane en différents points, des dégradations, etc., il se forme de nombreux isomères et de nombreux homologues.

On a étudié l'influence des métaux alcalins et alcalino-terreux (sous forme de naphténates solubles) sur l'oxydation du *n*-dodécane par l'oxygène moléculaire en observant spécialement l'accumulation de peroxydes et d'acides dans la masse de réaction.

[1] I. Drimuş, *Rev. Chim.* (*Bucureşti*), **1952**, 27.

[2] I. Drimuş et F. Scheuermann, *Bul. Inst. Politeh. Bucureşti*, **20**, 129 (1958).

[3] I. Drimuş, *Studii şi Cercetări Chim. Acad. R.P.R.*, **7**, 79 (1959).

[4] I. Drimuş et I. Manase, *Ind Chim. belge*, **1960**, 151.

[5] I. Drimuş, A. Măcelaru, Th. Spindler, I. Ionescu et V. Poleacov, *Bul. Inst. Politehn. Bucureşti*, **29**, 49 (1967).

CATALYSEURS PSEUDO-HOMOGÈNES D'OXYDATION

Les sels de certains acides organiques avec certains métaux donnent en hydrocarbures des solutions colloïdales. Ces catalyseurs ne font partie ni de la catégorie des catalyseurs homogènes, ni de la catégorie des hétérogènes, mais ils occupent bien une position intermédiaire, raison pour laquelle ils ont reçu le nom de pseudo-homogènes (pseudo-hétérogènes).[6] Il faut retenir le fait que dans ces solutions le métal ne se trouve pas sous forme d'ions. E. T. Denisov avait montré qu'une solution benzénique de naphténate de cobalt a une conductibilité électrique pratiquement identique à celle du benzène pur.[6]

Le choix de l'acide organique pour la préparation des sels métalliques pose certains problèmes. Les acides gras saturés (C_{10} — C_{20}) donnent d'habitude des sels métalliques difficilement solubles en hydrocarbures. Par exemple, le stéarate de lithium (1%) se dissout dans la paraffine (p.t. = 52°) seulement à 200° et par refroidissement à 175° donne un gel par lequel la circulation de l'oxygène nécessaire à l'oxydation se fait avec beaucoup de difficulté. D'une manière semblable se comporte le stéarate de strontium. En échange, les stéarates de fer ou de magnésium donnent des solutions fluides aussi à 100°.

Le raccourcissement de la chaîne d'atomes de l'acide gras (C_6—C_9) conduit en général toujours à des produits difficilement solubles.

De meilleurs résultats sont obtenus par les sels des acides non saturés (oléates et linoléates) ou avec les sels de certains acides qui contiennent des cycles en molécule (résinés et surtout naphténates).

Dans cet ouvrage on a utilisé des acides naphténiques de provenance roumaine déshuilés (3%), desphénolés et doublement distillés (voir la partie expérimentale).

Il faut mentionner le fait que lors du processus d'oxydation, la solution de naphténate métallique en hydrocarbure claire au commencement, se trouble et parfois elle forme un léger précipité, bien sûr à la suite de certains processus de décomposition des naphténates, de la formation de sels des acides dicarboxyliques, des oxyacides, etc.

La majeure partie des oxydations dont cet ouvrage fait mention ont été exécutées dans des solutions où, pour chaque 100 molécules de *n*-dodécane il y avait une molécule de naphténate métallique (respectivement un atome de métal). Les caractéristiques de ces solutions sont données dans le tableau 1.

La littérature concernant l'effet catalytique des sels solubles des métaux alcalins ou alcalino-terreux sur l'oxydation des *n*-alcanes en phase liquide, par l'oxygène moléculaire est limitée. Parmi les auteurs qui s'occupent de ce domaine nous mentionnons :

Tyscovski qui a étudié le mécanisme de l'action d'initiation du naphténate de potassium sur l'oxydation des hydrocarbures paraffiniques.[7]

---

[6] E. T. Denisov et I. M. Emanuel, *Uspekhi Khim.*, **29**, 1409 (1960).

[7] V. K. Tyskovski, B. G. Fredin et E. K. Prokofiev, *Zhur. priklad. Khim.*, **34**, 2586 (1961).

Zenailov étudie d'une manière comparative l'oxydation de *n*-hexadécane en diverses conditions : thermiques, en présence du naphténate de magnésium, du naphténate de calcium et de leur mélange.[8]

L'influence catalytique des mélanges, spécialement de magnésium et de potassium a fait l'objet de nombreuses études.[9–12]

Tableau 1

Caractéristiques des solutions de naphténates en *n*-dodécane

Naphténate de	Masse moléculaire du naphténate	% poids du naphténate dans la solution	% poids du métal dans la solution
$R{-}COOH$	217	1,26	0,000
$R{-}COOLi$	223	1,30	0,041
$R{-}COONa$	239	1,38	0,138
$R{-}COOK$	255	1,47	0,225
$R{-}COORb$	302	1,75	0,491
$R{-}COOCs$	349	2,01	0,771
$(R{-}COO)_{2}Be$	441	2,53	0,052
$(R{-}COO)_{2}Mg$	456	2,61	0,137
$(R{-}COO)_{2}Ca$	472	2,70	0,228
$(R{-}COO)_{2}Sr$	520	2,96	0,503
$(R{-}COO)_{2}Ba$	569	3,22	0,775

PARTIE EXPÉRIMENTALE

Préparation des naphténates. Les acides naphténiques utilisés avaient le poids moléculaire moyen 217 (correspondant à un indice d'acidité de 258 mg KOH. g^{-1}), et contenaient 3 % de non saponificables. Ils étaient de fabrication roumaine et avaient une couleur jaune clair.

Les naphténates des métaux alcalins ont été préparés par la neutralisation des acides naphténiques avec une solution aqueuse de l'hydroxyde respectif, l'évaporation sur bain d'eau de la solution de savon alcalin et le séchage du résidu en couche mince à 105°.

Les naphténates des métaux alcalino-terreux ont été obtenus par des réactions de double échange :

$$2\ \mathrm{R\,COONa} + \mathrm{Me}^{2+} \rightarrow (\mathrm{RCOO})_2\,\mathrm{Me} + 2\ \mathrm{Na}^{+}$$

Dans tous les cas une solution aqueuse de naphténate de sodium a été traitée avec une solution (sulfate ou chlorure) de métal alcalino-terreux, le précipité formé à été lavé à plusieurs reprises à l'eau chaude et séché en couche mince à 105°.

---

[8] ,,Okislenie uglevadarov v jitkoi faze'', Izdatelistvo Akademii Nauk S.S.R. Moskva, 1959, p. 168–182.

[9] N. K. Diaconova, *Neftekhim.*, **9**, 286 (1969).

[10] V. M. Goldberg, L. K. Obuhova et N. M. Emanuel, *Neftekhim.*, **2**, 229 (1962).

[11] A. A. Perchenko, *Maslob. Jirov. Prom.*, **26**, (5), 26 (1960).

[12] B. N. Tiutiunicov, *Maslob. Jirov. Prom.*, **26**, (3), 23 (1960).

Les naphténates des métaux alcalins ou alcalino-terreux sont des substances solides, ils ont un aspect cireux-résineux et ont une couleur d'un blanc-jaune. Leurs rendements sont pratiquement quantitatifs.

La solubilisation en *n*-dodécane se fait par chauffage à 200°. Par refroidissement de la solution à 155° (température d'oxydation) les solutions 0,1 molaires restent fluides.

Réalisation de l'oxydation. Dans un appareil en verre à chemise chauffante, on introduit 100 g de *n*-dodécane. Par une plaque poreuse en verre (G_3) 20 litres d'oxygène sont barbotés par heure. La thermorégulation de l'appareil se fait à 155°.

On fait des épreuves toutes les 30 minutes et on détermine l'indice d'acidité et l'indice de peroxyde (iodométriquement).

Les naphténates métalliques se dissolvent en quantités correspondantes (voir le tableau 1), de sorte que la solution obtenue contienne pour 100 molécules de *n*-dodécane une molécule de naphténate métallique.

INITIATION DE LA RÉACTION D'OXYDATION ET L'ACCUMULATION DE PEROXYDES

En barbotant de l'oxygène dans le *n*-dodécane de haute pureté (donc en l'absence des traces de promoteurs ou de catalyseurs) on n'observe aucune réaction. Même 5 à 10 heures de barbotage après, les indices de peroxyde et d'acidité continuent d'être nuls.

Le cas où le *n*-dodécane est traité ensemencé, au préalable ou sur le parcours de 100 ppm et peroxydes organiques (par exemple peroxyde de lauroile), la réaction commence immédiatement.[13]

En observant la variation de l'indice de peroxyde du produit oxydé, on constate une augmentation de celui-ci jusqu'à la minute 90—95, après quoi une diminution progressive commence, bien sûr, à la suite des réactions consécutives.

L'indice d'acidité apparaît dans la masse de réaction 10—20 minutes après l'apparition des peroxydes et augmente constamment, à vitesse accélérée (fig. 4).

La présence de 0,01 molaire d'acides naphténiques dans le *n*-dodécane n'influe pas sur la courbe des peroxydes ou des acides, en comparaison de l'oxydé de *n*-dodécane pur (mais ensemencé de peroxydes).

La présence de 0,01 molaire de naphténate de lithium, natrium, béryllium, magnésium, calcium, strontium ou baryum permet que l'oxydation de *n*-dodécane commence tout de suite (sans période d'induction) même si on n'a pas exécuté un ensemencement préalable de peroxydes. Donc les naphténates énumérés ci-dessus sont des initiateurs de réaction (fig. 1 et 3).

Par contre, dans des conditions similaires, les naphténates de potassium, rubidium et césium n'initient pas la réaction. Pour obtenir des oxydations en présence de ces naphténates, il est nécessaire d'exécuter un ensemencement préalable de peroxydes (fig. 2.).

Trois expériences en présence de 0,01 molaire naphténate de potassium démontrent ce que nous venons d'affirmer.

Dans la figure 1 on observe qu'en l'absence des promoteurs, après trois heures d'oxydation on n'enregistre aucune accumulation de pero-

---

[13] I. Drimuș et C. Florescu, *Bul. Inst. Politehn București*, (1972). (sous presse)

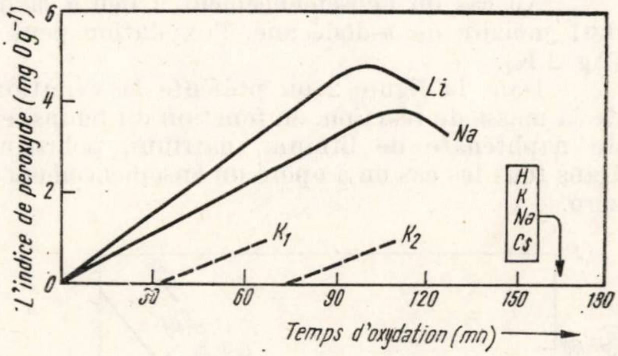

Fig. 1. — L'oxydation des n-dodécane avec de l'oxygène moléculaire à 155°. La dynamique de l'indice de peroxyde.

Li ... en présence de 0,01 molaire naphténate de lithium, sans ajoutage de promoteur peroxydique

Na ... idem naphténate de sodium

K ... idem naphténate de potassium

Rb ... idem naphténate de rubidium

Cs ... idem maphténate de césium

M ... en absence des naphténates métalliques, sans ajoutage de promoteur peroxidique

K_1 ... en présence de 0,01 molaire naphténate de potassium, ensemencé à la minute 30 après le commencement de l'oxydation

K_3 ... idem ensemencé à la minute 75 après le commencement de l'oxydation.

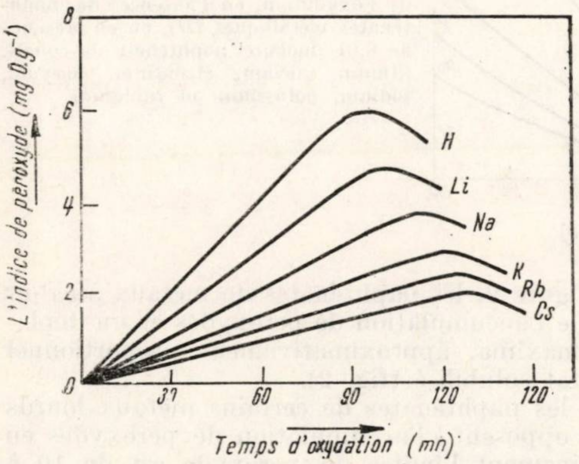

Fig. 2. — L'oxydation du n-dodécane avec de l'oxygène moléculaire à 155°. La dynamique de l'indice de peroxyde avec ensemencement à la minute zéro de l'oxydation, en l'absence desnaphténates métalliques (*H*) ou en présence de 0,01 molaire naphténate de lithium, sodium, potassium, rubidium ou césium.

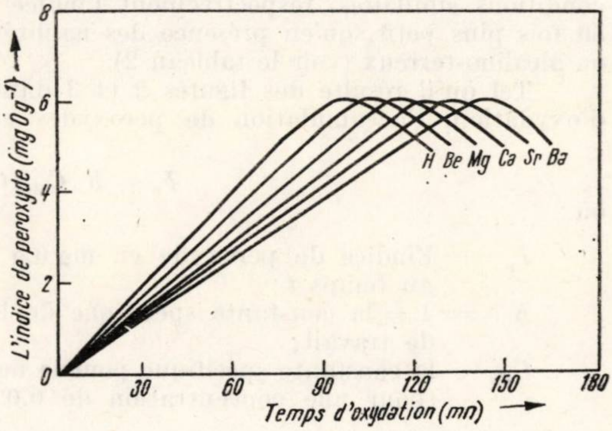

Fig. 3. — Oxydation de n-dodécane avec de l'oxygène moléculaire à 155°. La dynamique de l'indice de peroxyde avec ensemencement au moment zéro de l'oxydation, en l'absence des naphténates métalliques (H) ou en présence de 0,01 molaire naphténate de bérylium, magnésium, calcium, strontium ou baryum.

xydes (K_1). Mais si après 30 minutes de barbotage de l'oxygène on ajoute des peroxydes, l'oxydation commence tout de suite (K_1). La même chose dans le cas de l'ensemencement à la minute 75 (K_2).

Au cas où l'ensemencement a lieu à la minute zéro de la solution 0,01 molaire de *n*-dodécane, l'oxydation peut commencer tout de suite (fig. 2.K).

Dans la figure 2 on présente la variation de l'indice de peroxyde de la masse de réaction, en fonction du temps, en présence de 0,01 molaire de naphténate de lithium, natrium, potassium, rubidium ou césium. Dans tous les cas on à opéré un ensemencement de peroxydes, à la minute zéro.

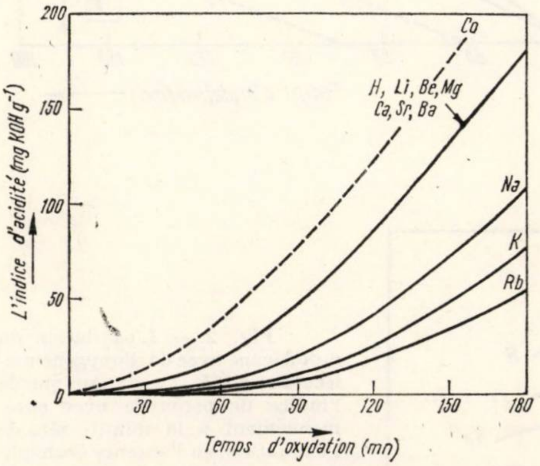

Fig. 4. — Oxydation de *n*-dodécane avec de l'oxygène moléculaire à 155°. La dynamique de l'indice d'acidité avec ensemencement à la minute zéro de l'oxydation, en l'absence de naphténates métalliques (*H*), ou en présence de 0,01 molaire naphténate de cobalt, lithium, calcium, strontium, baryum, sodium, potassium ou rubidium.

Tel qu'il résulte de la figure 2, les naphténates de métaux alcalins déterminent une diminution de l'accumulation de peroxydes et un déplacement vers la droite des maxima, approximativement proportionnel à la masse atomique du métal solubilisé (fig. 2).

Il faut mentionner que les naphténates de certains métaux lourds (cobalt, magnésium, nickel) s'opposent à l'accumulation de peroxydes en conditions similaires, respectivement l'indice de peroxyde est de 10 à 50 fois plus petit, qu'en présence des naphténates des métaux alcalins, ou alcalino-terreux (voir le tableau 2).

Tel qu'il résulte des figures 2 et 3 dans les 80 premières minutes d'oxydation, l'accumulation de peroxydes est donnée par la formule

$$I_p = K . C_{\mathrm{Me}} . t$$

où :

I_p = l'indice de peroxyde en $\mathrm{mg.0.g^{-1}}$ de la masse de réaction au temps t ;
K = 1 = la constante spécifique de l'appareil et des conditions de travail ;
C_{Me} = la constante spécifique pour le naphténate métallique utilisé (pour une concentration de 0,01 molaire).

Dans le tableau 2 il y a les valeurs de C_{Me} pour les naphténates des métaux alcalins et alcalino-terreux.

Tableau 2

Valeurs du C **pour les naphténates des métaux alcalins et alcalino-terreux**

Métal	C_{Me}	Métal	C_{Me}
Témoin	0,687	Témoin	0,687
Li	0,493	Be	0,611
Na	0,353	Mg	0,558
K	0,254	Ca	0,498
Rb	0,200	Sr	0,463
Cs	0,153	Ba	0,434
	Co	0,011	

ACCUMULATION D'ACIDES

En présence des naphténates des métaux alcalins, la vitesse de formation des acides est presque en raison inverse proportionnelle à la masse atomique du métal ajouté (fig. 4).

En présence des naphténates des métaux alcalino-terreux, la courbe de l'accumulation des acides ne diffère ni du témoin (que dans la limite des erreurs expérimentales) (fig. 4), ni de la courbe de l'accumulation d'acides dans le cas de l'oxydation effectuée en l'absence des catalyseurs.

Il faut remarquer le fait que le naphténate de cobalt accélère beaucoup les réactions de formation d'acides.

INFLUENCE DE LA CONCENTRATION DE CERTAINS NAPHTÉNATES MÉTALLIQUES SUR L'ACCUMULATION DE PEROXYDES ET ACIDES

En présence du naphténate de potassium en concentration de 1.10^{-2} ; $0{,}5.10^{-2}$ ou $0{,}25^{-2}$ molaire, on observe une accumulation de peroxydes correspondant à des valeurs intermédiaires entre les courbes *K* et *H* de la figure 2.

En ce qui concerne l'accumulation d'acides on constate la même chose (respectivement la fig. 4).

En présence du naphténate de magnésium en concentration de 2.10^{-2} ; 1.10^{-2} ; $0{,}5.10^{-2}$ et $0{,}25.10^{-2}$ molaire, on n'observe que de variations négligeables dans la courbe de l'accumulation d'acides ou peroxydes.

CONCLUSIONS

Dans le cas de l'oxydation du *n*-dodécane par l'oxygène moléculaire à 155°, en présence des naphténates des métaux du groupe I A et II A on observe que :

1. Les naphténates de potassium, rubidium et césium s'opposent à l'initiation de la réaction, un traitement préalable de *n*-dodécane avec 100 ppm peroxydes étant nécessaire, alors que les naphténates de lithium, natrium, bérylium magnésium, calcium, strontium et baryum ne s'opposent pas à l'initiation de la réaction.

2. Les naphténates des métaux alcalins sont des catalyseurs négatifs pour l'accumulation de peroxydes et d'acides dans la masse de réaction. Cet effet est presque proportionnel à la masse atomique du métal respectif.

3. Les naphténates des métaux alcalino-terreux n'influent d'une manière sensible ni sur l'accumulation de peroxydes, ni sur celle d'acides.

Revue Roumaine de Chimie, 17, 8, 1417–1421 (1972)

AROMATIC BIS-ETHERS. IV[1–3]

CONDENSATION OF SODIUM CYCLOHEXYLPHENOXIDES WITH DICHLOROMETHYLATED DERIVATIVES

M. IOVU, N. MICLOVICI and STELIANA CREŢU

University of Bucharest, Department of Physics, Chair of Chemistry, Şos. Panduri, 90, Bucharest, Romania

Received February 22, 1972

We report the synthesis of 12 new aromatic bis-ethers in which the oxygen, in the ether function, is directly bound through a valency to an aromatic nucleus, substituted for a cyclohexyl radical, and in some cases by a methyl radical as well, and through the second valency to an aromatic nucleus, common to both ether functions, whether substitued or not by a methyl radical, by an intermediate methylene bi-radical. The bis-ethers were obtained by condensing sodium cyclohexylphenoxides with dichloromethylated derivatives under conditions similar to those reported in the first note.

In the preceding note[1] we reported a new synthesis method for bis-ethers of a new class, with the general formula $Ar'-O-CH_2-Ar-CH_2-O-Ar'$, in which the aromatic nucleus, Ar,is a *p*-phenylene group. The aromatic nucleus directly bound to oxygen, Ar′, was substituted for a methyl radical,[1] for a nitro-grouping,[2] or for two methyl radicals.[3]

We now report the synthesis of bis-ethers of the same class, in which the aromatic nuclei are substituted for one cyclohexyl radical or for a cyclohexyl and a methyl radical. Bis-ethers of this group have not yet been reported.

The monoethers like *o*- and *p*-cyclohexylphenoxytoluene are well known.[4–6] Bodroux and Thomassin[4] obtained cyclohexylphenoxytoluenes by making use of the reaction of potassium cyclohexylphenoxide with the benzylchloride in alcohol. The authors mention that such reactions occur better in an anhydrous medium; therefore they prepared the potassium cyclohexylphenoxides through the reaction of potassium alcooxide with cyclohexylphenol.

---

[1] M. Iovu, *Rev. Roumaine Chim.*, **16**, 1223 (1971).

[2] M. Iovu and N. Nicolau, *Rev. Roumaine Chim.*, **16**, 1919 (1971).

[3] M. Iovu, *Rev. Roumaine Chim.*, **17**, 1261 (1972).

[4] D. Bodroux and R. Thomassin, *Compt. rend.*, **208**, 1314 (1939).

[5] S. L. Baas and E. M. Van Duzee (to Dow Chemical Co.), U.S.A. Pat., 2 109 457, March. 1, 1938; *Chem. Abstr.*, **32**, 3051 (1938).

[6] E. M. Van Duzee and S. L. Baas (to Dow Chemical Co,), U.S.A. Pat., 2 109 514, March 1, 1938; *Chem. Abstr.*, **32**, 3051 (1938).

In this note we present the results of the condensation of 2 - and 4-cyclohexylphenoxide, 2-methyl-4-cyclohexylphenoxide and sodium-2-cyclohexyl-4-methylphenoxide separated with 1,4-dichloromethylbenzene, 1,4-di (chloromethyl)-2,5-dimethylbenzene and 1,3-di (chlorometyl)-4,6-dimethylbenzene.

For the condensation we used the same method reported in the first paper of this series [1], which consists in obtaining anhydrous sodium cyclohexylphenoxides through the reaction of cycloalkylphenols with sodium hydroxide in a mixture, (1 : 1 in volumes) of alcohol and benzene; this mixture permits the removal of water, derived from the reaction, through the distillation of the azeotropic mixture of alcohol, benzene and water. This mixture of solvents also permits the condensation of the cyclohexylphenoxide obtained, with the dihalogenated derivative subsequently added.

The reaction takes place due to the nucleophilic attack of the phenoxidic ion on the dihalogenated derivative.

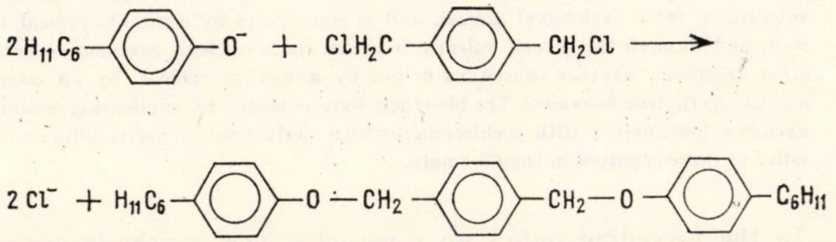

The increase of the substituent on the phenol nucleus from methyl to cyclohexyl, does not prevent the reaction in the mixture of benzene and alcohol solvents (1 : 1 in volumes) and even permits a better separation of the reaction product; the yields have values similar to those obtained earlier [1-3] starting from cresols or xylenols.

RESULTS AND DISCUSSION

In Table 1 we present the formula of the 12-bis-ethers, their melting points as well as the calculated and experimentally found percentage contents in carbon and hydrogen. We show in the respective order bis-ethers obtained from 2-cyclohexylphenol, 4-cyclohexylphenol, 2-methyl-4-cyclohexylphenol to 4-methyl-2-cyclohexylphenol with the three dichloromethylated derivatives.

Table 1 shows that all the bis-ethers are solids. Their melting temperatures were determined after 2 or 3 recrystallizations from the alcohol and benzene mixture (in equal volumes). Bis-ethers obtained from 1,3-di(chloromethyl)-4,6-dimethylbenzene have, in most cases, lower melting temperatures, crystallize more difficultly and result in smaller yields, in comparison to those obtained from 1 : 4-dichloromethylbenzene and 1,4-di(chloromethyl)-2,5-dimethylbenzene using the same phenol.

Table 1

New bis-Ether

Ether	Formula	C% calculaled / found		H% calculated / found		Melting point °C
		calculaled	found	calculated	found	
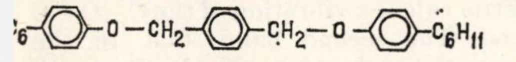	$C_{32}H_{38}O_2$	84.53	84.42	8.42	8.13	210–211
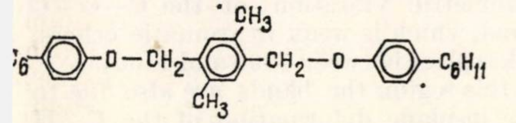	$C_{34}H_{42}O_2$	84.60	84.81	8.77	8.48	181
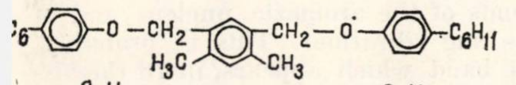	$C_{34}H_{42}O_2$	84,60	84.38	8.77	8.52	118–118.5
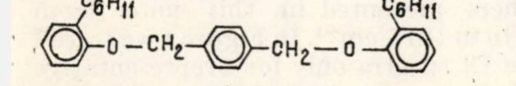	$C_{32}H_{38}O_2$	84.53	84.61	8.42	8.48	111.5–112
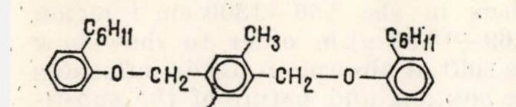	$C_{34}H_{42}O_2$	84.60	84.29	8.77	9.07	156–156.5
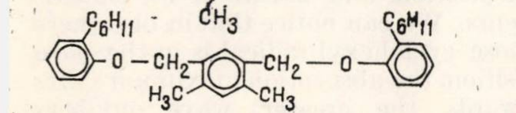	$C_{34}H_{42}O_2$	84.60	84.88	8.77	8.81	134–134.5
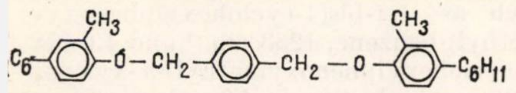	$C_{36}H_{42}O_2$	84.60	85.03	8.77	8.52	145–145.5
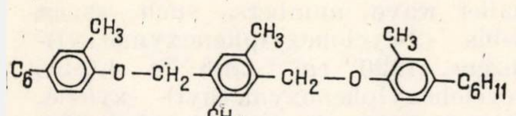	$C_{36}H_{44}O_2$	84.99	84.61	8.71	9.00	173.5–175.5
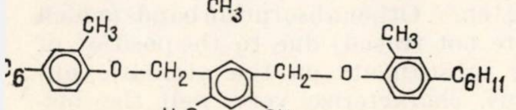	$C_{36}H_{44}O_2$	84.99	85.10	8.71	8.54	87.5–88
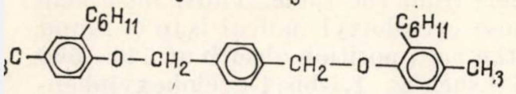	$C_{36}H_{42}O_2$	84.60	84.13	8.77	9.26	172–172.5
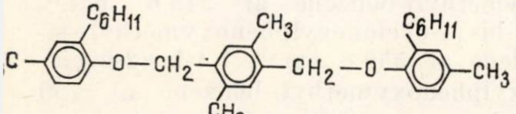	$C_{36}H_{44}O_2$	84.99	84.40	8.71	9.14	174.5–175.5
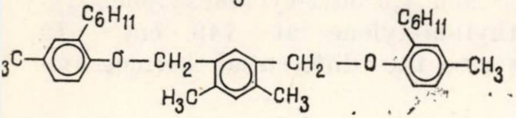	$C_{36}H_{44}O_2$	84.99	84.68	8.71	8.49	150–151.5

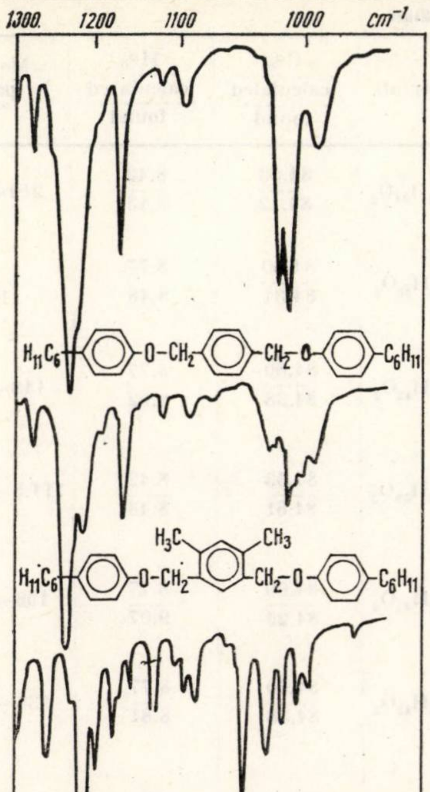

Fig. 1. — IR spectra of 1,4-bis(4-cyclohexylphenoxymethyl) - benzene, 4,6-bis (4cyclo hexylphenoxymethyl)-*m*-xylene, 1,4-bis (2-cyclohexylphenoxy-methyl)-benzene and 4,6-bis)2-cyclohexylphenoxymethyl)-*m*-xylene.

The IR analysis of the new bis-ethers points out the existence of an intensive absorption band between 1220 and 1240 cm^{-1} ascribed to the asymmetric valency vibration of the C—O—C bond. The second band due to the symmetric vibration of the C—O—C bond, which is weak in aromatic ethers, takes place between 1000 and 1100 cm^{-1}; in this region the bands are also due to the in-plane deformation of the C—H bonds of the aromatic nucleus and of the ring vibrations. This is probably, the band which appears, in all the bis-ethers presented in this note, from 1010 to 1018 cm^{-1}. In Figure 1 we traced the IR spectra only for 4 representative ethers in the 950—1300 cm^{-1} region (7.69—10.53 μ) in order to show how the shift of absorption bands influences the position and nature of the substituents. We can notice that in bis-ethers whose cyclohexyl radical is in the *para* position, the absorption maximum shifts towards the greater wave numbers such as 1,4-bis(4-cyclohexylphenoxymethyl)-benzene, 1233 cm^{-1} and 4,6-bis (4-cyclohexylphenoxymethyl)-*m*-xylene, 1239 cm^{-1} whereas in bis-ethers whose cyclohexyl radical is in the *ortho* position, the absorption maximum shifts towards smaller wave numbers, such as in 1,4-bis (2-cyclohexylphenoxymethyl)-benzene, 1220 cm^{-1} and in 4,6-bis (2-cyclohexylphenoxymethyl)- -xylene, 1221 cm^{-1}. Other absorption bands (which were not traced) due to the position of the substituents on the aromatic nucleus, characterize very well the bis-ethers from the table. Thus, bis-ethers whose cyclohexyl radical is to be found in the *para* position absorb at 540—560 cm^{-1} such as 1,4-bis(4-cyclohexylphenoxymethyl)-benzene at 545.6 cm^{-1}, 4,6-bis (4-cyclohexylphenoxymethyl)-*m*-xylene at 559.6 cm^{-1}, 1,4-bis(2-cyclohexylphenoxymethyl)-benzene at 750 cm^{-1} and 4,6-bis(2-cyclohexylphenoxymethyl)-*m*-xylene at 749 cm^{-1}. In this case the differential thermogravimetric analysis also points out the stability of bis-ethers up to 240–260°.

EXPERIMENTAL

The phenol used was a product of „Reactivul". The *o*-cresol was a "Laborchemie, Apolda" product, and the *p*-cresol was a "Schuhardt" product. The dichloromethylated derivatives were obtained in the conditions mentioned in the first note.[1] The cyclohexane was obtained through the dehydration of cyclohexanol on H_3PO_4 and its purity was chromatographically tested. The cyclohexylation of phenol and cresol was achieved with cyclohexene in the presence of $ZnCl_2$ as a catalyst, using the working model described by some of us in an earlier paper.[7] The IR spectra were obtained in KBr pellets with a "Leitz Vetzlar" apparatus. The thermogravimetric analysis was made on a Pauling type derivatograph.

The 2,5-bis (4-cyclohexylphenoxymethyl)-p-xylene synthesis

In a two-necked 50 ml flask, provided with a thermometer and a reflux refrigerator connected with a calcium chloride tube we introduced 3.528 g (1/50 mol) of *p*-cyclohexylphenol and 0.8 g (1/50 mol) of NaOH and 30 ml of benzene alcohol mixture (1 : 1 in volumes). It was heated to 67° for 4 hours till *p*-cyclohexylphenol reacted completely with NaOH forming sodium *p*-cyclohexylphenoxide. Then we exchanged for a distillation refrigerator, and we distilled 10 ml of azeotropic mixtures so as to remove water.

Over the sodium phenoxide in 20 ml of benzene alcohol mixture 2031 g (1/100 mol), 1,4-di (chloromethyl)-2,5-dimethylbenzene was added and the reaction vessel was kept in reflux (cca 67°) for 4 hours. After cooling, the reaction product was filtered so as to remove the solvent and the dissolved reactants which had not reacted. The precipitate was washed with water to remore sodium chloride, till the filtered substance underwent no reactions characteristic of Cl^- ion. The precipitate was then washed with 2 ml of ethyl alcohol and dried in vacuum. This resulted in 4.124 g of product. Yield, 71.6%. After two recrystallizations from alcohol-benzene mixture (1 : 1 in volumes) the product had m.t. = 181°. The other products were synthesized in similar conditions.

CONCLUSIONS

The sodium cyclohexylphenoxides react with the dichloromethyl derivatives forming bis-ethers in the same conditions as with the sodium phenoxide and sodium metylphenoxides. The replacement of the methyl radical by cyclohexyl does not hinder the reaction in the mixture of benzene-alcohol (1 : 1 in volume), and even allows a better separation of the reaction product. The yields in bis-ethers have similar values with those obtained previously [1–3] starting form phenols, cresols or xylenols. The new bis-ethers are characterized by a strong IR absorption from 1220 to 1240 cm^{-1}, which was ascribed to the asymmetric valency vibration of the C–O–C bond.

Revue Roumaine de Chimie, 17, 8, 1417–1421 (1972)

Revue Roumaine de Chimie, **17**, *8*, 1423–1435 (1972)

ACRIDONE. XLI
THE PROTON MAGNETIC RESONANCE SPECTRUM OF THIOACRIDONE

I. PANEA, ILEANA GOIA and MARIA IONESCU

Chair of Organic Chemistry, Department of Chemistry, str. Arany Janos 11, Cluj, Romania

Received September 13, 1971

Continuing the research on acridone, * the NMR (^{1}H) spectrum of the thioacridone (I) is recorded and interpreted. These data, along with other physico-chemical data, converge towards the acceptance of an increased contribution of the betainic structure II to the real structure of the thioacridone molecule. This contribution explains more adequately the chemical and physico-chemical behaviour of thioacridone. The unshielding effect of the cyclic $>C=X$ group (where $X = H_2C$, HN, O, S) on the protons in *ortho* is correlated to the polarization degree of the $>C=X$ group.

In previous papers[1–8] on acridones we have also investigated thioacridone (I) and some of its derivatives. We have thus noted that, certain properties of thioacridone, such as : an increased acidity as compared to acridone,[1,8–10] the marked oxidative splitting capability of the sulphur,[1,5,8–11] the impossibility of directly obtaining electrophilic substitution products,[1,4,6,8,9] the disappearance of fluorescence,[1,8,9] certain aspects revealed

---

[1] M. Ionescu, H. Mantsch and I. Goia, *Studii și Cercetări Chim. Fil. Cluj*, **12**, 135 (1961)

[2] M. Ionescu, I. Goia and H. Mantsch, *Studii și Cercetări Chim. Fil. Cluj*, **13**, 95 (1962) ; H. Mantsch, I. Goia and M. Ionescu, idem, **14**, 281, 283 (1963) ; M. Ionescu, A. R. Katritzky and B. Ternai, *Tetrahedron*, **22**, 3227 (1966) ; M. Ionescu and M. Vlassa, *Rev. Roumaine Chim.*, **16**, 743 (1971).

[3] H. Mantsch, I. Goia and M. Ionescu, "Omagiu R. Ripan", Edit. Acad., București 1966, p. 353 ; *Chem. Abstr.*, **67**, 73.010 (1967).

[4] M. Ionescu and D. Postescu, *Stud. Univ. Babeș-Bolyai, Chem.*, **11**, fasc. 1, 73 (1966).

[5] I. Goia, H. H. Mantsch and M. Ionescu, *Rev. Roumaine Chim.*, **13**, 1511 (1968).

[6] I. Goia and M. Ionescu, *Rev. Roumaine Chim.*, **15**, 1233 (1970).

[7] M. Ionescu, I. Goia and M. Vlassa, *Rev. Roumaine Chim.*, **15**, 1785 (1970).

[8] I. Goia, "Doctoral thesis", Institutul de Chimie al Min. Inv., Cluj, 1969, p. 52–55, 110–137.

[9] H. Mantsch, "Doctoral thesis", Institutul de Chimie al Min. Inv. Cluj, 1963, p. 5 – 34, 98–124.

[10] A. Edinger, *Ber. dtsch. chem. Ges.*, **33**, 3769 (1900) ; A. Edinger and W. Arnold, *J. prakt. Chem.*, **64**, 182, 471 (1901).

[11] A. Albert "The Acridines", 2nd ed., E. Arnold (Publishers) Ltd., Londra, 1966, p. 28 ; 386–387 ; 372–373 ; 174 ; 381–383 ; 50, 51.

* Part XL : M. Ionescu and M. Vlassa, *Rev. Roumaine chim.*, **16**, 743 (1971).

by the IR spectrum,[3,7-9] etc. could not be explained completely. As these properties are correlated to the electronic density and the chemical shift is a reasonable good measure of this density,[12-14] we considered the study of the NMR (^1H) spectrum of thioacridone as a useful contribution to fuller understanding of the structure and properties of thioacridone.

RESULTS AND DISCUSSIONS

In thioacridone, the two benzene rings are considered independent of one another, its NMR (^1H) spectrum, resembling that of acridone (III),[12] can be analysed as a four-spin system, ABCD, to which interrings couplings between the $H-N(H_{10})$ proton and $H_{1,2,3,4}$ were applied as first-order perturbations. This spectrum, as well as the corresponding splitting diagrams, are given in figure 1. Such splitting diagrams may be applied since all spectra examined here are quasi-first order spectra (see [12,14]).

The spectra of acridone and of some nitroacridones [15] were analysed similarly, while for the analysis of the acridine and acridine-N-oxide spectra we have taken into account the fact that the interring couplings appear between the proton H_9 and H_{1and4}.[12,14] These analyses were necessary for a comparative study, and their results are presented in table 1.

The NMR peaks were assigned to individual protons based on : the comparison with the results of earlier interpretations of the spectra of acridine compounds,[12,14] the coupling constants (J), the intensities of the peaks, the modifications produced by the introduction of the substituent ($-NO_2$) in different positions and the strong unshielding exerted by the carbonyl or thiocarbonyl group on the neighbouring protons.[16-18]

The chemical shifts (δ values, in cps and p.p.m.) were obtained directly from the experimental spectra, and are shown in increasing order with decreasing field as compared to tetramethylsilane (TMS), for which $\delta = 0$.

In the case of thioacridone, for which recordings were carried out at different concentrations, we could observe a strong shift of resonance signals towards low values of the field, with increasing concentrations.

---

[12] J. P. Kokko and J. H. Goldstein, *Spectrochim. Acta*, **19**, 1119 (1963).

[13] J. Kuthan and V. Skála, *Z. Chem.*, **6**, 422 (1966); P. J. Black, R. D. Brown and M. L. Heffernan, *Austral. J. Chem.*, **20**, 1305 (1967).

[14] H. H. Mantsch, W. Seiffert and V. Zanker, *Rev. Roumaine Chim.*, **12**, 1137 (1967).

[15] M. Ionescu and I. Panea, To be published.

[16] S. Goodwin, J. N. Schoolery and L. F. Johnson, *J. Amer. Chem. Soc.*, **81**, 3065 (1959) : S. C. Pakrashi, J. Bhattacharyya, L. F. Johnson and H. Budzikiewicz, *Tetrahedron*, **19**, 1011 (1963) : J. A. Diment, E. Ritchie and W. C. Taylor, *Austral. J. Chem.*, **20**, 1719 (1967) : R. H. Prager and H. H. Thredgold, idem, **22**, 1503 (1969).

[17] R. H. Martin, N. Defay, F. Geerts-Evrard, P. H. Given, J. R. Jones and R. W. Wedel, *Tetrahedron*, **21**, 1833 (1965).

[18] A. Schönberg and K. Junghans, *Chem. Ber.*, **99**, 1015 (1966).

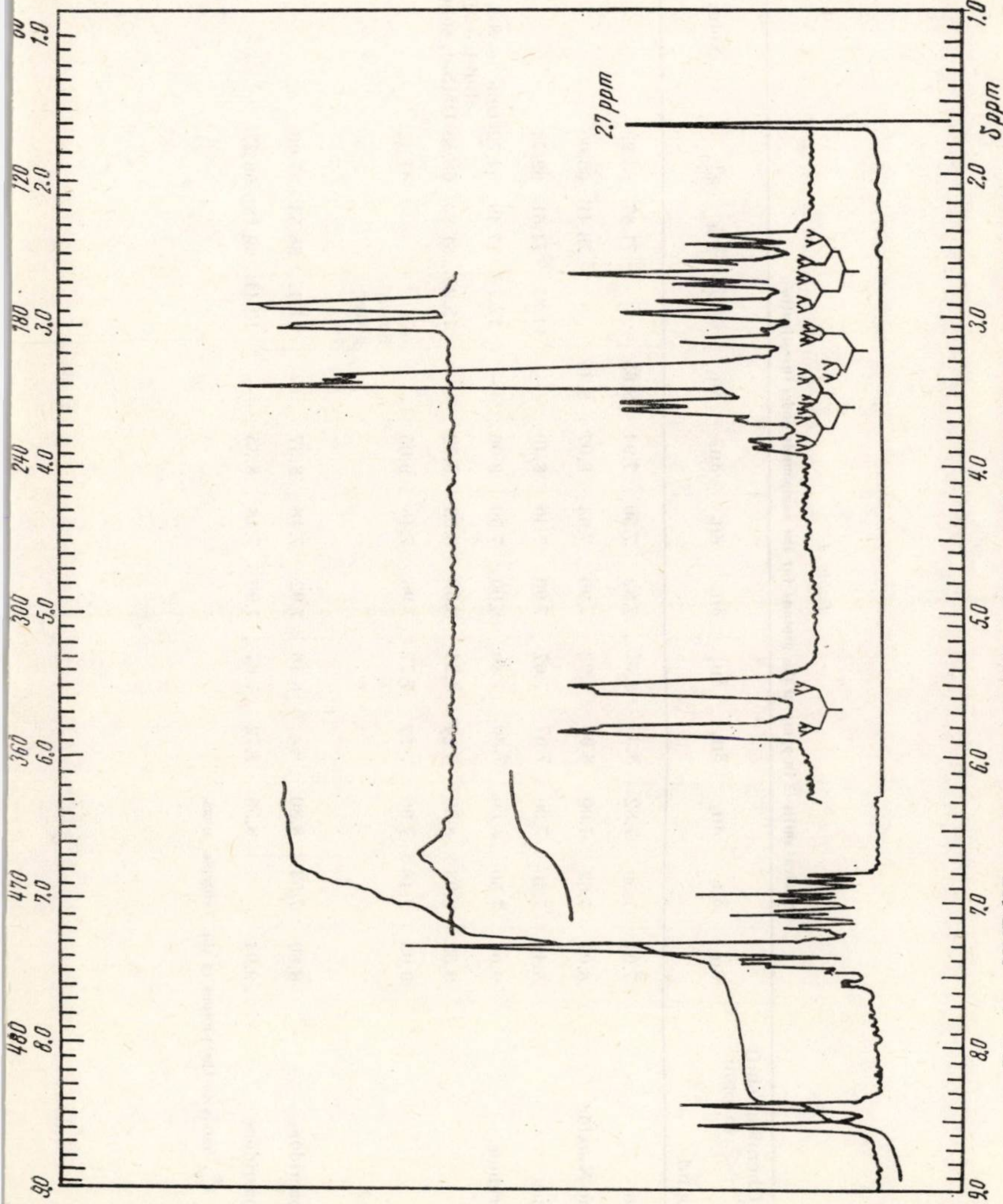

Fig. 1. – NMR(^{1}H) spectrum and splitting diagram of thioacridone, a saturated solution in DMS with TMS as external standard.

Table 1

Chemical shifts (δ in ppm) of the protons for the compounds under investigation

Chemical shift in ppm / Compound	δ_{H_1}	δ_{H_2}	δ_{H_3}	δ_{H_4}	δ_{H_5}	δ_{H_6}	δ_{H_7}	δ_{H_8}	δ_{H_9}	$\delta_{H_{10}}$	δ_{tot}	δ^*_{tot}	Notes
Acridine	7.94	7.50	7.82	8.35	8.35	7.82	7.50	7.94	8.65	—	71.87	63.22	
Acridine-N-oxide	8.07	7.63	7.90	8.93	8.93	7.90	7.63	8.07	8.35	—	73.41	65.06	
Acridone	8.40	7.40	7.90	7.67	7.67	7.90	7.40	8.40	—	11.87	74.61	62.74	
Thioacridone	9.06	7.50	8.00	7.80	7.80	8.00	7.50	9.06	—	12.77	77.49	64.72	conc. ~ 8 %
,,	9.52	8.03	8.50	8.24	8.24	8.50	8.03	9.52	—	13.25	81.83	68.58	saturated solution DMS-d_6 solution
,,	9.05	7.48	7.96	7.77	7.77	7.96	7.48	9.05	—	was not registered	—	64.52	
4-Nitroacridone	8.80	7.53	8.80	—	8.16	7.92	7.48	8.37	—	11.47	68.53	57.06	
2-Nitroacridone	9.04	—	8.55	7.72	7.67	7.96	7.48	8.35	—	12.41	69.18	56.77	

δ^*_{tot} refers to the protons of the benzenic rings.

A. STRUCTURAL AND REACTIVITY INFORMATION BASED ON NMR AND OTHER PHYSICO-CHEMICAL DATA

The chemical shift (δ) of all the protons of the thioacridone have higher values than the shift of the corresponding acridone protons. Hence, on going from acridone to thioacridone the resonances of the protons are shifted towards lower fields. We consider that this shift can be explained by an increased contribution of the betaine structure II, with a possible participation of the mesomeric structures IV and V along with a reduced contribution of the mesomeric forms VI–VII, which leads to a general unshielding of the protons of the thioacridone molecule. This explanation is supported by the vinylogous thioamide character of thioacridone,[5,8,11] since it is well known [19–21] that thioamides have a higher proportion of the betaine form VIIIa than the corresponding amides (see also [22]); for acridone such a structure (IX) was discussed by a number of authors.[8,9,11,23–26]

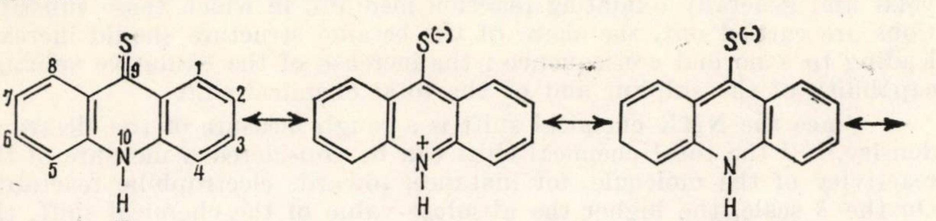

I II IV

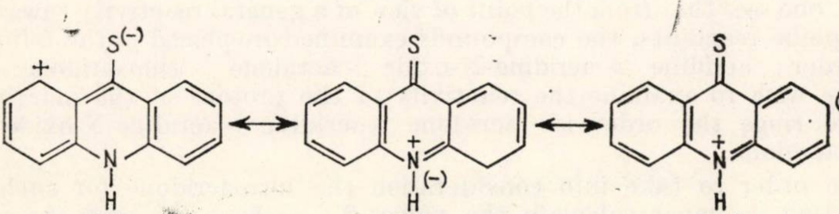

V VI VII

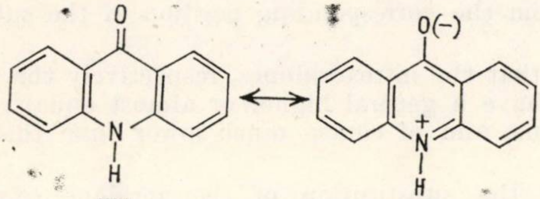

III IX

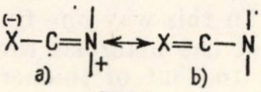

VIII

---

[19] W. Walter and G. Maerten, *Liebigs. Ann. Chem.*, **669**, 66 (1963).

[20] A. Loewenstein and T. M. Connor, *Z. Elektrochem.*, **67**, 280 (1963).

[21] A. Loewenstein, A. Melera, P. Rigni and W. Walter, *J, Phys. Chem.*, **68**, 1597 (1964).

[22] C. M. Lee and W. D. Kumler, *J. Org. Chem.*, **27**, 2052 (1962).

[23] K. Lehmstedt, *Ber. dtsch. chem. Ges.*, **68**, 1455 (1935).

[24] A. W. Karjakin and A. W. Schablja, *Doklady Akad. Nauk S.S.S.R.*, **116**, 969 (1957).

[25] H. Kokuban, *Z. Elektrochem.*, **62**, 599 (1958).

[26] V. Zanker and A. Reichel, *Z. Elektrochem.*, **64**, 431 (1960).

Another argument in favour of an increased contribution of the betaine structure to the real structure of thioacridone as compared to acridone, is revealed by the much higher value of the dipole moment of N-methylthioacridone (5.2 D) as compared to that of N-methylacridone (3.5 D) [11] (see also [22]).

The increased contribution of a betaine structure (II) is supported by the fact that it explains a series of unusual properties of thioacridone, such as its higher acidity compared to acridone — as a result of an increased positive charge at the nitrogen (see [27,28]) — the formation of the S-salts [1,8,9] and the marked oxidative splitting capability of sulphur, resulting from an increased negative charge at the sulphur (see II), a.s.o.

On the other hand, the mentioned oxidative splitting capability of sulphur, added to the very high total chemical shift of thioacridone (see table 1) explains why direct electrophilic substitution products of this (see [1,4,8,9]) could not be obtained so far ; one may expect that in a very polar and generally oxidating reaction medium, in which these substitutions are carried out, the share of the betaine structure should increase leading to a normal consequence : the increase of the oxidative splitting capability of the sulphur and of the total chemical shift.

Since the NMR chemical shift is a rough measure of the electronic density,[12–14] the total chemical shift can be considered a measure of the reactivity of the molecule, for instance, towards electrophilic reactants. On the δ scale, the higher the absolute value of the chemical shift, the smaller the reactivity towards the electrophilic reactants. By examining table 1, one sees that from the point of view of a general reactivity towards electrophilic reactants, the compounds examined are placed in the following order : acridine $>$ acridine-N-oxide $>$ acridone $>$ thioacridone. If we only wish to examine the reactivity of the protons of the marginal benzene rings the order is : acridone $>$ acridine $>$ acridine-N-oxide $>$ $>$ thioacridone.

In order to take into consideration the nitroacridone for such a comparison we must calculate the values $\delta_{tot} - \delta_X = \delta'_{tot}$ for the unsubstituted products, were δ_X is the chemical shift of the proton in the unsubstituted compound from the corresponding position of the substituent in the nitroacridone.

In this way one finds that the nitroacridones, respectively the protons of the marginal rings have a general higher or almost equal reactivity to that of thioacridone, and of course much lower than that of acridone (see table 2).

Expressed differently, the substitution of the acridone oxygen by sulphur, desactivates the molecules towards electrophilic reactants corresponding to the introduction into the ring of a nitro group.

If an electrophilic substitution would still be possible, the reactivity order of the positions in thioacridone would be similar to that in acridone $(2 > 4 > 3 > 1)$ based on the analogous order of the chemical shifts (see table 1).

---

[27] W. Walter and R. F. Becker, *Liebigs. Ann. Chem.*, **727**, 71 (1969).

[28] J. P. Kokko, J. H. Goldstein and L. Mandell, *J. Amer. Chem. Soc.*, **83**, 2909 (1961).

Table 2

Total comparable chemical shifts for acridone, thioacriodone and nitroacridone, in ppm.

Total comparable chemical shift in ppm / Compound	$\delta_{tot} - \delta_{H_2}$	$\delta^*_{tot} - \delta_{H_2}$	$\delta_{tot} - \delta_{H_4}$	$\delta^*_{tot} - \delta_{H_4}$	Notes
Acridone	67.21	55.34	66.94	55.06	
Thioacridone	69.97	57.20	69.68	56.90	concentration ~8 %
2-Nitroacridone	69.17	56.76	—	—	
3-Nitroacridone	—	—	68.53	57.06	

δ^*_{tot} – same significance as in table 1.

Since both introductions of nitro groups in the acridone ring system and the replacement of the acridone oxygen by sulphur result in the disappearance of fluorescence, it appears possible that this disappearance connected to the above mentioned desactivating process.

Starting from the same increased contribution of II to the real structure of the thioacridone molecule, we may estimate again the problem of molecular associations in the solid state and in solution. Based on the data available up to now, we consider that this association takes place in the case of thioacridone, in the first place as a consequence of the polar (betaine) structure of the molecule, the contribution of the hydrogen bond being very small — a fact otherwise easily to be explained through the very reduced tendency to form hydrogen bonds with the participation of sulphur as electrons donor.[29-32] The association would take place by the coplanar disposition of the dipolar molecules of thioacridone (and acridone) according to the following scheme (X) :

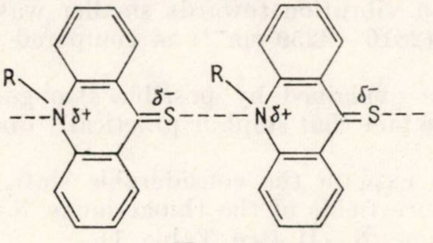

X, R=H, CH_3, C_2H_5, etc.

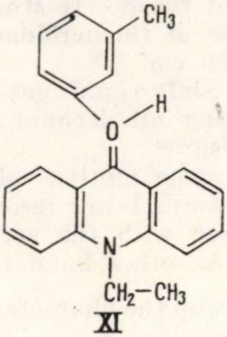

XI

---

[29] W. S. Fyfe, *J. Chem. Phys.*, **21**, 2 (1953); G. C. Pimentel and A. L. McClellan "The Hydrogen Bond", W. H. Freeman and Company, San Francisco and London, 1960, p. 5, 201, 240, 291.

[30] C. G. Cannon, *Mikrochim. Acta*, **1955**, 555; *Spectrochim. Acta*, **10**, 341 (1958).

[31] L. J. Bellamy, "The Infrared Spectra of Complex Molecules", 2nd ed. Methuen and Co. Ltd., London, 1964, p. 351–357; 384, etc.

[32] C.N.R. Rao, "Chemical Applications of Infrared Spectroscopy", Academic Press, New York and London, 1963, p. 185, 186, 296–307, etc.

This association is also rendered probable by the strong shift towards low fields of the resonance of all thioacridone protons for an increasing concentration (Table 1). As known [33] the concentration dependence of the chemical shift can be used to prove the orientation of the rings participating in such associations. For a coplanar orientation of the rings in the aggregate, a shift towards low fields with an increasing concentration [33] takes place, a fact also encountered with thioacridone.

The absence of a strong decrease of the melting point (m.p.) on going from thioacridone (m.p. = 272°) to N-methylthioacridone (m.p. = = 263°)[9,11] is another argument against the association through hydrogen bonds, when a considerable decrease of the m.p. would have been expected, and is an argument in favour of the association suggested in the present paper. The lowering of the m.p. from N-methylthioacridone to N-ethylthioacridone (m.p. = 218°) [11] is in favour of the same association, being the consequence of an increased steric hindrance for such associations by the replacement of methyl with ethyl. As a similar decrease takes also place from N-methylacridone (m.p. = 203°) to N-ethylacridone (m.p. = = 159°),[11] we consider that besides the association by hydrogen bonds, in the case of acridone, there also participates to a certain degree, the associations through dipolar interactions. Actually, the participation of such interactions at the association of amides was already mentioned. [30,31]

The approximately constant value (~ 30 cps) of the shift of the resonance of all thioacridone protons, in dimethylsulphoxide (DMS) solution, towards lower fields, with increasing concentration, induces us to believe that the coplanar aggregates associate among themselves yielding a tridimensional aggregate. This is consistent with the relatively uniform influence of all protons (see also [34]).

Based on the increased contribution of the betaine structure II and on the association through dipolar interactions of thioacridone, which lead to a considerable weakening of the N—H bond, we also understand the shift of the N—H stretch vibration towards smaller wave numbers in the case of thioacridone (2810—3250 cm^{-1}) as compared to acridone (2850—3280 cm^{-1}).*

This shift could not be explained by possible stronger hydrogen bonds, taking into account the fact that sulphur practically does not form such bonds.[29,30]

The same motives also explain the considerable shift, by nearly 1 ppm, towards lower resonance fields of the thioacridone N—H proton as compared with the acridone N—H (see Table 1).

On the other hand the above reasons lead us to assume for the $\rangle C = S$ group the character of a simple bond, in the case of thioacridone. This character cannot be explained by the IR absorption region, 1025——1225 cm^{-1}, accepted lately [31,32,35] for the stretching vibration of this group, taking into account that thioacridone has $\nu_{C=S} = 1215$ cm^{-1}.[3,8,9]

---

* IR spectra were especially recorded for this paper with a double beam spectrophotometer, model U.R-10 (Zeiss-Jena) in the solid state (~ 1 mg) as KBr pellets (~ 300 mg) (see also [8,9]).

[33] D. J. Blears and S. S. Danyluk, *J. Amer. Chem. Soc.*, **89**, 21 (1967).

[34] H. Kessler and A. Rieker, *Liebigs. Ann. Chem.*, **708**, 57 (1967).

Since the absorption at 1215 cm^{-1} in the spectrum of thioacridone corresponds to the stretching vibration of the $>C=S$ group, which has a simple bond character, the absorption of the $>C=S$ stretching vibration with no simple bond character must be found at higher wave lengths. We therefore believe that the initial assignement of the 1400–1300 cm^{-1} region[36] to the IR absorption of the $>C=S$ group was right. The fact that many compounds containing this group do not absorb in this region, does not refute the mentioned assignement,[36] but is only an indication that in these compounds the $>C=S$ group does not have a 100% double bond character. We must anyhow underline here that the problem of the position of the $>C=S$, and the $-\overset{|}{\underset{|}{C}}-S$ respectively, stretching vibration in the IR spectrum has given occasion to numerous discussions.[31,32,37–44] We consider that a series of data, apparently contradictory, may be explained if we take into account the fact that the $>C=S$ bond as the $>S=O$ bond,[45] is partially polarized[22] — as a result of the reduced tendency of sulphur to form double bonds[19–22,35–40] — resulting in the reduction of the double bond character in the $>C=S$ group; the $-\overset{|}{\underset{|}{C}}-S$ bond, on the other hand, can participate in different conjugation effects, leading to the appearance of a double bond character.[38,43]

---

[35] K. Nakanishi, "Infrared Absorption Spectroscopy. Practical". Holden-Day, Inc., San Francisco, 1962, p. 54, etc.

[36] N. B. Colthup, *J. Opt. Soc. Amer.*, **40**, 397 (1950); H. W. Thompson, D. L. Nicholson and L. N. Short, *Discuss. Faraday Soc.*, 9, 222 (1950), in 31, p. 355.

[37] E. Spinner, *J. Chem. Soc.*, **1960**, 1237.

[38] N. Marziano, G. Montaudo and R. Passerini, *Ann. Chim.* (*Ital.*), **52**, 121 (1962); M. Ionescu and I. Panea, *Stud. Univ. Babeș-Bolyai, Chem.*, **12**, fasc. 1, 11 (1967); M. R. Hunt, A. G. Krüger, L. Smith and G. Winter, *Austral. J. Chem.*, **24**, 53 (1971).

[39] M. Avram and Gh. D. Mateescu "Spectroscopia în infraroșu. Aplicații în chimia organică", Edit. Tehnică, București, 1966, p. 353–364, etc.

[40] L. J. Bellamy in N. Kharasch (editor), "Organic Sulphur Compounds", Pergamon Press, 1961, p. 47–55.

[41] C. N. R. Rao, R. Venkataraghavan and T. R. Kasturi, *Canad. J. Chem.*, **42**, 36 (1964).

[42] D. Z. Robinson, *J. Chem. Phys.*, **19**, 881 (1951); E. C. Gregg, jr., *J. Amer. Chem. Soc.*, **74**, 3691 (1952); E. D. Bergmann, idem, **77**, 1549 (1955); R. N. Haszeldine and J. M. Kidd, *J. Chem. Soc.*, **1955**, 3871; N. Lozach and G. Guillouzo, *Bull. Soc. chim. France*, **1957**, 1221; C. N. R. Roo and R. Venkataraghavan, *Spectrochim Acta*, **18**, 541 (1962).

[43] A. W. Baker and G. H. Harris, *J. Amer. Chem. Soc.*, **82**, 1923 (1960).

[44] J. I. Jones, W. Kynaston and J. L. Hales, *J. Chem. Soc.*, **1957**, 614.

[45] R. J. Gillespie and E. A. Robinson, *Canad. J. Chem.*, **41**, 2074 (1963).

Taking into consideration all the data referring to the absorptions of the $>C=S$ and $-\overset{|}{\underset{|}{C}}-S$ groups [31,32,37–41] and all simple and multiple bonds,[31,32,35,39] we appreciate that the vibration of the $>C=S$ bond, with a 100% double bond character, will absorb around 1350 cm^{-1} (see also [36,44]) and the $-\overset{|}{\underset{|}{C}}-S$ bond, without double bond character, around 800 cm^{-1} (see also [35,41,43]). Considering that the stretch frequencies of the bonds are correlated to the order of the bond, we deduce a ~ 24% simple bond character of the $>C=S$ group in thioacridone, which is in agreement with a ~ 14% of simple bond character of the $>C=O$ group in acridone,* data also in agreement with the structural studies on thioamides and amides. [8,9,11,19–26,30,40,46,47]

B. EFFECT OF THE CYCLIC $>C=X$ GROUP ON PROTONS IN *ORTHO* POSITION

As far as we know the cause of the variation of the strongly unscreening effect of the cyclic $>C=X$ groups (where $X = HN, O, S$) on the protons in *ortho*, in the PMR spectra,[16,18] has not yet been cleared and we hope that our data will bring a useful contribution. As a measure of this effect, for the compounds examined, we indicate the difference $(\delta_{H1,8} - \delta_{H2,7})_{C=X}$. As seen in table 3 the deshielding effect increases in the series $HN < O < S$. If we take into account the work of Sisido et al.,[48] giving only the average value of the chemical shift for the aromatic protons of 10-ethyl-9(O-methyl-benzyl)9,10-dihydroacridine (XI, m.p. = 115–117°) at $\delta = 6.95$ ppm, a compound also containing the $>C=X$ group as $X = C\langle^{R}_{H}$, we may extend the above series in the form: $RHC < HN < O < S$. This series corresponds exactly to the variation to the polarization degree of the $>C=X$ bonds, which for the first three elements is expected for electronegativity reasons,

---

* $\nu_{C=O} = 1638$ cm^{-1}. The simple bond character of the acridonic $>C=O$ group results from the contribution of the betaine structure IX and from hydrogen bonds.[3,8,9]

[46] W. Walter and E. Schaumann, *Chem. Ber.*, **104**, 4 (1971): *Liebigs. Ann. Chem.*, **743**, 154 (1971); W. Walter and K. P. Ruess, idem, **743**, 167 (1971); W. Walter and H. Weiss, *Angew. Chem.*, **81**, 1050 (1969); W. Walter and J. Voss in S. Patai "The Chemistry of the Amide Group", J. Wiley and Sons, London, 1970, Chap. 8. p. 383.

[47] W. D. Phillips, *J. Chem. Phys.*, **23**, 1363 (1955); C. M. Lee and W. D. Kumler, *J. Org. Chem.*, **27**, 2055 (1962); J. Sandström, *Acta Chem. Scand.*, **16**, 1616 (1962); L. A. La Planche and M. T. Rogers, *J. Amer. Chem. Soc.*, **85**, 3728 (1963); R. C. Neuman, jr. and L. B. Young, *J. Phys. Chem.*, **69**, 1777 (1965); H. Paulsen and K. Todt, *Chem. Ber.*, **100**, 3385, 3397 (1967).

Table 3

Deshielding effect of cyclic groups $\rangle C=E$ on the protons in ortho position ($H_{1,8}$)

Compound	Formula	$\delta_{H_{1,8}}$ in ppm	Deshielding effect	m.p. (°C)
N-methyl-acridonimine	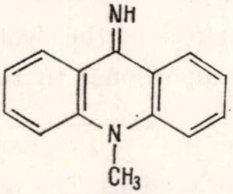 XII	8.25	for X = NH 49.2 cps (= 0.82 ppm) [a]	140
N-methyl acridone	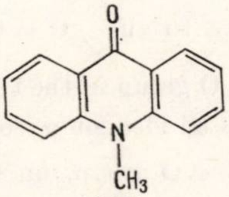 XIII	8.50	for X = O 63 cps (= 1.05 ppm) [b]	203
N-methyl-thio-acridone	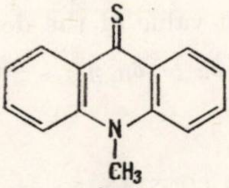 XIV	9.00	for X = S 93 cps (= 1.55 ppm) [c]	263

a) According to [18]

b) According to [18] and to recordings carried out by the present authors in undeuterated DMS at 80°, with TMS as external standard, when $\delta_{H_{1,8}} = 8.50$ ppm, respectively $\delta_{H_{2,7}} = 7.45$ ppm.

c) Approximated value based on the corresponding value in thioacridone taking into account that for acridone, N-methylacridone $(\delta_{H_{1,8}} - \delta_{H_{2,7}})_{C=0}$ is practically the same i.e. ~ 60 cps.

while the double bond $\rangle C = S$ has an inherent higher polarization than the $\rangle C = O$ bond, because of the reduced tendency of the sulphur to form double bonds.[19,22]

On the other hand, the series established by us for the variation of the unshielding effect of the cyclic $\rangle C = X$ group on the protons

---

[48] K. Sisido, K. Toni and H. Nozaki, *Tetrahedron*, **19**, 1323 (1963).

in *ortho*, is identical with the series established by Ferguson[49] for the values of the wave lengths (λ_{max}) for the UV transitions of the $>C = X$ groups ($X = C, N, O, S$). The λ_{max} is higher as the energy of the bond π is smaller, respectively the polarization degree and the simple bond character are greater. This variation order of the polarization degree is also supported by the melting points of the compounds examined (Table 3).

It results that the deshielding effect of the cyclic $>C = X$ group on the protons in *ortho* is directly proportional to the inherent polarization degree of the double bond : $>C = S \leftrightarrow -\underset{(+)|}{\overset{|}{C}}-\underset{(-)}{X}$, respectively to the simple bond character of the $>C = X$ group. The results from Martin and co-workers[17] which show that in the compounds in which the chemical shift (δ) of the protons in *ortho* relative to the $>C = O$ group is greater, the stretching frequency of the $>C = O$ group in the IR spectra ($\bar{\nu}$, cm^{-1}) is smaller, support the above expressed idea of a correlation between the deshielding effect of the cyclic $>C = O$ group, on the *ortho*-protons, with the simple bond character of the $>C = O$ group.

We also underline the very high value of the deshielding effect of $>C = S$ group referring to $>C=O$ $[(\delta_{H_{1,8}} - \delta_{H_{2,7}})_{C=S} - (\delta_{H_{1,8}} - \delta_{H_{2,7}})_{C=O} = 30$ cps].

C. COUPLING CONSTANTS

The coupling constants of the protons ($J_{H_xH_y}$) in thioacridone — as well as in acridone — (table 4) are reasonable values for aromatic compounds, being in agreement with previous results on acridine compounds.[12,14,33,50] They were obtained directly from the experimental spectra.

Based on the large half-band width of the signals and the presence of shoulders on these, we assume the existence of additional long range couplings as referred to those shown by Kokko and Goldstein[12] for acridone (see $J_{1,10}$).

These couplings (see $J_{i,10}$; $i = 2, 3, 4$) are very small and can be only roughly approximated. Such couplings were described and theoretically substantiated in the series of polycyclic aromatic hydrocarbons.[51]

---

[49] L. N. Ferguson "Electron Structures of Organic Molecules", Prentice Hall, New York, 1952, p. 276, see 22.

[50] B. Clin and B. Lemanceau, *Compt. rend.*, **270**, 598 (1970).

[51] M. A. Cooper and S. L. Manatt, *J. Amer. Chem. Soc.*, **91**, 6325 (1969); M. W. Jarvis and A. G. Moritz, *Austral. J. Chem.*, **24**, 891 (1971).

Table 4

Coupling constants (J) of the protons in acridone and thioacridone in cps

Coupling constant in cps / Compound	$J_{1,2} = J_{8,7}$	$J_{1,3} = J_{8,6}$	$J_{1,4} = J_{8,5}$	$J_{1,10} = J_{8,10}$	$J_{2,3} = J_{7,6}$	$J_{2,4} = J_{7,5}$	* $J_{2,10} = J_{7,10}$	$J_{3,4} = J_{6,5}$	* $J_{3,10} = J_{6,10}$	* $J_{4,10} = J_{5,10}$	Notes
Acridone	8.0	1.6	0.4	0.4	6.2	1.6	0.3	8.3	0.3	0.4	saturated solution
Thioacridone	8.6	1.6	0.4	0.4	5.9	1.9	0.3	8.1	0.3	0.4	concentration ~8 %
Thioacridone	8.6	1.6	0.4	0.4	5.9	1.9	0.3	8.1	0.3	0.4	recorded in DMS -d_6
Thioacridone	8.3	1.6	0.4	0.4	5.6	2.0	0.3	8.0	0.3	0.4	saturated solution

* Approximate values (see section C)

EXPERIMENTAL

The NMR (^1H) spectra were recorded with a Jeol NMC-60 HL apparatus of 60 Mc/s.* For acridone compounds, including thioacridone, we used undeuterated DMS as solvent and TMS as external standard, using saturated solutions. In the case of thioacridone we also used a more diluted solution of ~ 8 % and also had at our disposal a spectrum recorded by a Varian A-60 apparatus in hexadeuterated DMS, with TMS as internal standard. We underline the fact that the NMR spectra of the thioacridone as ~ 8 % solutions in DMS with TMS as external standard and in DMS-d_6 with TMS as internal standard are in practice identical (see Table 1).

For acridine and acridine-N-oxide, the solvent was $CDCl_3$ with TMS as internal standard, the concentration being of about 8 %.

The working temperature was 20°, excepting 4-nitroacridone, the spectrum of which was recorded at 60°.

Thioacridone, [10] acridone, [11] nitroacridones [11,52] and acridine-N-oxide, [53] were prepared according to the literature, and commercial acridine was recrystallized three times.

---

* The authors bring hereby their thanks for this possibility to Prof. Dr. I. Zugrăvescu, I. Druţă and I. Bărboi.

[52] K. Lehmstedt, *Ber. dtsch. chem. Ges.*, **64**, 2381 (1931); A. Kliegl and A. Brösamle idem, **69**, 197 (1936).

[53] R. M. Acheson, B. Adcock, G. M. Glover and L. E. Sutton, *J. Chem. Soc.*, **1960**, 3367.

Revue Roumaine de Chimie, **17**, *8*, 1435–1435 (1972)

Revue Roumaine de Chimie, **17**, *8*, 1437 – 1445 (1972)

CHLOROMETHYLATION OF TERNARY MACROPOROUS COPOLYMERS

STELIANA MAXIM, IG. POINESCU, STELA DRĂGAN and M. DIMA
Institute of Macromolecular Chemistry "Petru Pony",
Aleea Grigore Ghica Vodă no. 41 A, Jassy, Romania

Received July 20, 1971

The chloromethylation of ternary styrene-acrylonitrile (alkyl methacrylates)-divinylbenzene copolymers is studied in view of finding the influence of the nature and content of the third comonomer on the transformation degree and mechanical resistance of the copolymer pearls in the process of chloromethylation.

The chloromethylation reaction of the "gel type" styrene-divinylbenzene was studied in detail, and rich literature exists in this field.[1-4]

New types of ion exchangers, qualitatively superior to those of the gel-type have lately appeared.[5-7] These were called "macroporous ion exchangers", owing to the existence of macropores in the structure o the copolymer pearls.[8]

The chloromethylation of the macroporous copolymers is much less studied than that of the gel type copolymers. Svetlov and coworkers [9] have studied the behaviour of the styrene-divinylbenzene macroporous copolymers during the chloromethylation reaction. Bortel [10] has synthetized macroporous anionites based on styrene-divinylbenzene copolymers.

[1] J. Mikes and J. Szanto (to Muanyagipari Kutato Intezet), Hung. Pat. 156 908 22 Dec. 1969; *Chem. Abstr.*, **72**, 91164 g (1970).

[2] A. K. Svetlov ,Z. K. Esipov, T. N. Demenkova, Z. V. Grigoreva, K. L. Poplovskii and L. I. Khomutov, *Vysokomol. Soedinenyia* A, **11**, 2793 (1969).

[3] M. P. Kovaleva, ,,Khim. Aktiv. Polim. ikh Primenenie" Edited by K. M. Saldadze, Ed. Khimiya, Leningrad, U.S.S.R., 1969, p. 39.

[4] G. Z. Esipov, L. A. Derevyanko, V. P. Makridin, R. G. Rakhuda and K. L. Poplovskii, *Vysokomol. Soedineniya* B, **12**, 274 (1970).

[5] W. Busse and E. Schmidt (to Permutit A.-G.), Ger. Pat. 1 569 285, 06 May 1970; *Chem. Abstr.*, **73**, 26244 (1970).

[6] S. N. Il'ichev, M. P. Kovaleva, Z. F. Konstantinova and A. M. Soldatenko, U.S.S.R. Pat., 267 890, 02 Apr. 1970; *Chem. Abstr.*, **73**, 67254 m (1970).

[7] M. P. Kovaleva and G. K. Petrova, ,,Sintez i Svoistva Ionnoobmenih Materialov", Ed. Nauka, Moscow, 1968, p. 38.

[8] J. Seidl and J. Malinský, *Fortschr. Hochpolym.-Forsch.*, **5**, 113 (1967).

[9] A. K. Svetlov, T. W. Semenkova and L. I. Khomutov, *Vysokomol. Soedineniya* A, **11**, 606 (1969).

[10] E. Bortel, *Przemysl Chem.*, **47**, 557 (1968).

Dima and coworkers [11] have made a comparative study of the behaviour of gel type and macroporous styrene-divinylbenzene copolymers during the chloromethylation reaction.

In the present paper the results of the study of the methylation reaction of the macroporous ternary copolymers, synthetized in the course of this research are presented. Special attention is given to the influence of the nature and content in copolymer of the third comonomer on the chloromethylation reaction. The third comonomer is the acrylonitrile or the alkyl methacrylates, in this case the methyl-, ethyl- or n-butyl-methacrylate taking part in a quantity alternating between 1 and 20 g to 100 g copolymer.

We mention the fact that the extisting studies on the chloromethylation reaction of macroporous copolymers were carried out only on binary copolymers, that is to say styrene-divinylbenzene.

EXPERIMENTAL

For all chloromethylation reactions we have used macroporous ternary copolymers in pearl shape and with a diameter between 0.4 and 0.8 mm based on styrene-acrylonitrile(methyl-ethyl- or n-butyl-methacrylate)-divinylbenzene obtained through copolymerization in suspension.[12] The copolymerization of the monomers was carried through in an inert polystyrene (M = 75.000) or benzine (b.p. 125 – 140°) medium.

The chloromethylation agent was monochlordimethylether (M.C.D.E.) (b.p. 56 – 60°) and the catalyst freshly sublimated, $AlCl_3$.

The chloromethylation reaction is carried out in a three-necked flask, provided with a stirer, refrigerator and thermometer, set in an oil bath. We introduced into the flask : 1 mol copolymer, 0.77 mol dichlormehthane- 7 mol monochlordimethyleter and 0.7 mol $AlCl_3$, after which the reaction mixture is stirred for three hours at 40°. After the chloromethylation reaction is over, the chloromethylated copolymer separates from the liquid phase by filtering, then the pearls are treated with methyl alcohol, to desactivate the monochlordimethyl-ether – $AlCl_3$ complex, and washed with distilled water till the free acidity is completely removed.

The nitrogen analyses of the initial copolymer were carried out through the Kjeldahl method. [13] The alkyl methacrylate content of the copolymer was supposed to be not far from that of the initial monomer mixture. This hypothesis was checked by calculating the structure of macroporous anionites, obtained from these copolymers.[14,15]

The chloride was determined by the modified Schöninger method.[16]

RESULTS AND DISCUSSION

In the series of the styrene-acrylonitrile-divinylbenzene copolymers we have studied the influence of the acrylonitrile percentage in the copolymer, on the transformation degree (α) and on the number of styrene units left unchlormethylated (X) (figure 1 and 2, table 1).

The nitrile group, existing in the structure of the ternary macroporous copolymer, should, owing to its electron-attracting effect,have a negative influence on the chloromethylation reaction, through the decrease of the electron density in the *ortho-* and *para*-positions of the benzene nucleus.[17] This effect renders the formation of the transition stage between the reactive electrophilic species more difficult (forming between the monochlordimethylether and the catalyst) and the *para*-position of the benzene nucleus. It is therefore to be expected that the transformation degree should decrease with the increase of the copolymer's acrylonitrile content (only in the domain of small conversion degrees). In fig. 1 (curves 1–4) the dependence of the transformation degree is shown *versus* the acrylonitrile percentage in the copolymer. Curves, *a*, *b*, *c* and *d* represent the theoretical values of the conversion degree, against the acrylonitrile content of the copolymer.

---

[11] M. Dima, A. Carpov, S. Maxim and I. Petrariu, *Mat. Plast.*, **8** 15 (1970).

[12] Ig. Poinescu, Stela Drăgan, Steliana Maxim and M. Dima, Rev. Roumaine Chim. (in press).

[13] T. S. Ma and G. Zuazaga, *Ind. Eng. Chem. Analyst*, **14**, 280 (1942).

[14] H. S. Pinner and T. Alfrey Jr., *J. Polymer Sci.*, **23**, 533 (1957).

[15] I. Scondac and M. Dima, *Studii și Cercetări Sti., Chim. Fil. Iași*, **13**, 217 (1962).

[16] J. Haslam, J. B. Hamilton and D. C. M. Squirell, *Analyst.* **85** 556 (1960).

We notice that if up to an approximate 5% (N % = 1.30 acrylonitrile content the transformation degree decreases slowly, for higher values of the latter, 5.0–17.5% (N % = 1.30–4.67), its decrease is more accentuated, as compared to the theoretical values, thus marking the negative influence of the nitrile group on the chloromethylation reaction. For small percentages of acrylonitrile the influence of the –CN group cannot be detected, probably owing to the partial acid hydrolysis of the acrylonitrile by the HCl existing in the reaction medium.[18]

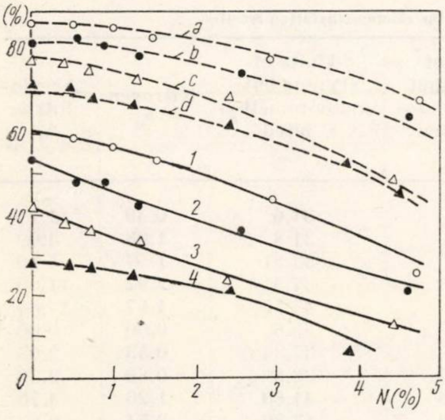

Fig. 1. — Dependence of transformation degree α on the reticulation degree and percent acrylonitrile content of styrene- acrylonitrile-divinylbenzene macroporous ternary copolymers Molar ratio : copolymer/M.C.D.E./AlCl$_3$ = 1/7/0,7 ; 40° ; 3 hours. *1*, 8% D.V.B. ; *2*, 12% D.V.B. ; *3*, 18% D.V.B. ; *4*, 25% D.V.B. *a*, *b*, *c* and *d* represent theoretical data of the variation of the transformation degree α, for reticulation degrees of 8, 12, 18 and 25% D.V.B.

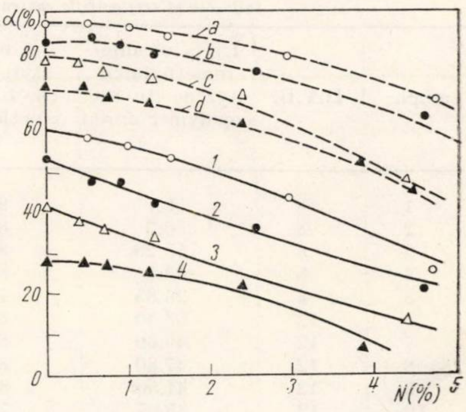

Fig. 2. — Dependence of the number of unchloromethylated (X) styrene units on the reticulation degree and the acrylonitrile quantity of the macroporous ternary copolymers Curves *1*, *2*, *3* and *4* represent 8, 12, 18 and 25% D.V.B.

---

[17] H. Morawetz, ,,Chemical Reactions of Polymers'', Edit. E. M. Fettes, Ed. Interscience Publishers, New York, 1964, pag. 10.

[18] E. A. Sokolova, G. I. Vasilieva, A. A. Kudreațev and P. V. Strepiheev, *Zhur. priklad. Khim.*, **31**, 1 (1958).

The curves representing the experimental values (1—4) are placed under the theoretical ones (a—d); since we have not tried to obtain a maximum transformation degree, we have worked under mild conditions, avoiding an additional reticulation.[11]

The deviation from the theoretical curve is so much more marked as the acrylonitrile content increases. For istance, for the copolymer with 8% D.V.B. and an acrylonitrile content between 1.0 and 5.0%, the difference between the value of the theoretical curves and the experimental ones is of 23.0%, while for the copolymer with a 17.5% acrylonitrile content (8% D.V.B.-divinylbenzene), this difference rises to 42.0% as a result of the negative effect of the group —CN on the chloromethylation reaction, as shown above.

The results in figure 2 show the number of unchloromethylated styrene structural units (X) rises proportionally to the increase of the percent acrylonitrile content in the copolymer, once more confirming the negative influence of group —CN on the chloroethylation reaction for the copolymers with a reticulation degree of 8.12 and 18% D.V.B. (Table 1). For copolymers with a reticulation degree of 25%, the shape of the curve is entirely different, probably owing to the high rigidity of the tridimensional lattice.

Table 1

Influence of acrylonitrile content on the chloromethylation reaction

Sample	D.V.B.	Units of chloromethylated styrene (to 100 copolymer units) %	Units of styrene that can be chloromethylated %	Units of styrene left unchloromethylated %	Nitrogen %	Acrylonitrile %
1	8	58.7	90.3	31.6	0.49	1.7
2	8	56.7	87.9	31.8	1.08	4.09
3	8	53.29	86.1	32.81	1.57	5.90
4	8	43.5	81.0	37.5	2.92	11.00
5	8	26.85	74.7	47.15	4.67	17.60
6	12	53.40	88.0	33.6	0.00	0.00
7	12	49.66	87.0	37.34	0.53	2.00
8	12	47.80	85.60	38.8	0.86	2.36
9	12	41.50	83.30	41.80	1.26	4.70
10	12	35.07	78.40	43.30	2.54	9.6
11	12	22.3	70.90	48.60	4.52	17.10
12	18	42.43	82.00	39.57	0.00	0.00
13	18	38.30	81.60	43.30	0.37	1.40
14	18	37.7	80.40	42.70	0.72	2.60
15	18	35.80	77.00	41.20	1.30	4.90
16	18	24.72	72.90	48.30	2.38	9.10
17	18	10.30	66.60	54.30	4.33	16.40
18	25	28.27	75.00	46.73	0.00	0.00
19	25	27.80	73.00	45.20	0.37	1.40
20	25	27.00	72.7	45.7	0.63	2.30
21	25	26.40	71.00	44.60	1.05	4.00
22	25	22.40	68.30	46.40	2.00	7.50
23	25	5.70	58.80	53.1	4.28	16.20

In this case the influence of the third component can no longer be rendered evident.

From the study of figures 1 and 2 we also notice the influence of the reticulation degree on the chloromethylation reaction, meaning that the value of α decreases with its increase, as a consequence of the decrease of the number of structural styrene units.

At the chloromethylation of the macroporous ternary styrene-alkyl methacrylates-divinylbenzene copolymers, the third comonomer has a positive effect. This is explained by the fact that the alkyl radical of the ester group balances the electronattracting effect of the carbonyl group and, according to the character of the radical, the whole ester group will have a positive influence on the chloromethylation reaction. The positive effect of the alkyl methacrylates used shows in the following order : methyl methacrylate < ethyl methacrylate < n-butyl methacrylate.

To conclude, for a series of copolymers with same reticulation degree, the chloromethylation reaction will be so much more favoured as the content and the volume of the esteric radical of the alkyl methacrylate of the respective copolymer increases.

In figure 3, we give the dependence of the transformation degree (expressed by Cl %), *versus* the duration, for copolymers with 18% D.V.B.

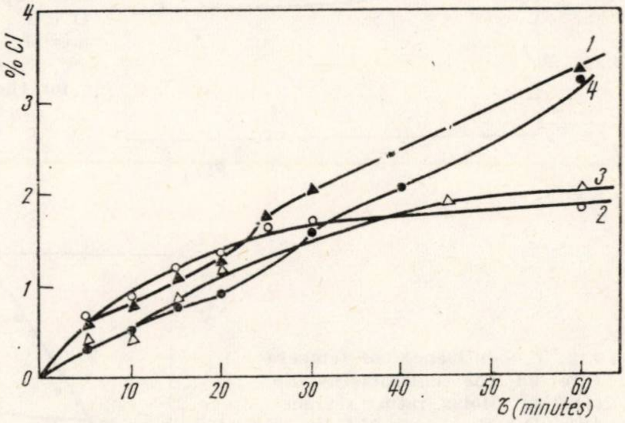

Fig. 3. — Influence of duration on the chloromethylation reaction of styrene-alkyl metacrylates-divinylbenzene macroporous ternary copolymers. Molar ratio copolymer/M.C.D.E./$AlCl_3$ = 1/7/0,7 ; 40°. *1*, styrene — 18% D.V.B. — 20% M.C.Me. copolymer (sample 106) ; *2*, styrene—18% D.V.B — 3% M.C.Me. copolymer (sample 103) ; *3*, styrene — 18% D.V.B. — 3% M.C.Et. copolymer (sample 133) ; *4*, styrene — 18% D.V.B. — 10% M.C.Et. copolymer (sample 134).

and different quantities of methyl and ethyl methacrilate (Table 2).

Table 2

Macroporous ternary styrene-methyl (ethyl)-methacrylate divinylbenzene) copolymers

Sample	D.V.B. %	Methacrylate of		Coefficient of		Apparent density
		methyl %	ethyl %	methanol g/g	toluene g/g	
103	18	3.0	—	0.258	0.939	0.8804
106	18	10.0	—	0.645	1.287	0.719
133	18	—	3.0	0.352	0.607	0.788
134	18	—	10.0	0.391	0.540	0.81

If we compare curves 1 with 2, and 3 with 4, we notice that higher transformation degrees are obtained for the copolymers with a higher methyl and ethyl methacrylate content for relatively small transformation degrees.

The inversion in the location of curves 2 and 3 above curves 1 and 4 for reaction durations up to 25 minutes is probably due to the difference in porosity between the copolymers (table 2).

An additional evidence supporting the hypothesis that alkyl methacrylates favour the chloromethylation reaction is brought by the experimental results shown in figure 4.

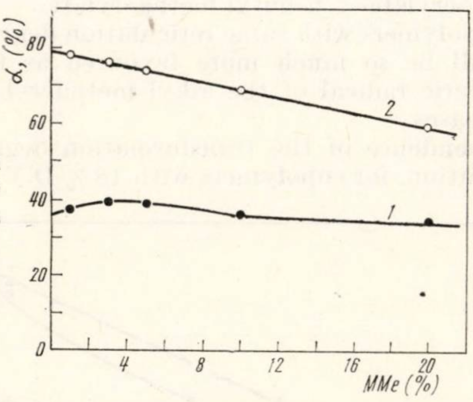

Fig. 4. — Dependence of the transformation degree α on the procentual methyl methacrylate content of the macroporous copolymer. *1*, molar ratio : 18% D.V.B. — (1 — 17.1%) M.C.Me. copolymer/M.C.D.E./$AlCl_3$ = 1/7/0.7 = 3 hours ; 40°. *2*, represents the theoretical data for the same series of copolymers.

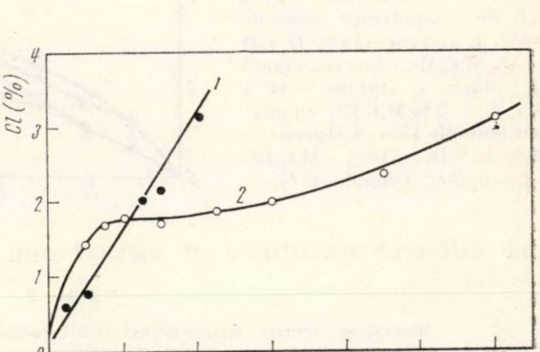

Fig. 5. — Influence of temperature on the chloromethylation reaction. Molar ratio : styrene — 18% D.V.B. — 20% M.C.Me. copolymer/M.C.D.E./$AlCl_3$ = 1/7/0.7 ; 3 hours. *1*, — 40° ; *2*, 50°.

The diagrams in figure 4 show that the curve of experimental results presents a maximum for a methyl methacrylate content of approx. 3.0%, after which the decrease of the transformation degree α, as function of the alkyl methacrylate content is very slow. This means that the chloromethylation reaction is favoured only within a certain range of the methyl metacrylate content.

For a high content of methyl methacrylate (10.0 — 20.0%) α is only slightly smaller than for the copolymers with a small quantity of methyl methacrylate (1.0 — 5.0%). This remark stands good only in the field of small transformation degrees, because for the same reaction time, the styrene structural units will be more easily chloromethylated if neighbouring with alkyl methacrylate structural units, but if we aim at a higher transformation degree, we must take into account the fact that for a copolymer with a higher content of methyl methacrylate, the number of units able to chloromethylate is smaller and consequently the degree of chloromethylation will also be smaller.

The temperature also influences the chloromethylation reaction (figure 5).

Curves 1 and 2 represent the dependence of the copolymers transformation degree (expressed in Cl%) on the duration of the chloroethylation reaction, at 40° and 50°.

Up to a 20 minutes reaction time, curve 2 is placed above curve 1, this being explained by the fact that in the initial moments of the reaction, when the concentration of the monochlordimethylether is the nearest to the initial one, a higher temperature makes the diffusion of the active species in the interior of the pearls easier. The ratio of the reactants changes in time because a quantity of monochlordimethylether has been consumed (the concentration of the active species decreases), and the vapour tension of the monochlordimethylether at 50° is high, which makes the reaction at this temperature unfavourable, as a consequence of the decrease of monochlordimethylether concentration in the liquid phase. For instance, after 60 minutes from the beginning of the reaction, the difference between the quantity of chlorine incorporated into the copolymer at 40° and 50° is considerable.

The insertion of the third comonomer improves the mechanical qualities of the macroporous ternary copolymer pearls. The chloromethylation reaction is by its nature an energetic reaction. Therefore when the reticulation of the binary copolymers (styrene-divinylbenzene) is small, they have a low mechanical resistance, and the pearls split during the chloromethylation reaction. This can be noticed by a microscopic study of the copolymer pearls.

When acrylonitrile is used as a third comonomer, for samples with the same reticulation degree, the mechanical resistance of the pearls changes with the acrylonitrile content (table 3).

In the case of samples containing 8% D.V.B., for a small acrylonitrile content, the pearls do not resist during the chloromethylation reaction, because the structure of the ternary copolymer is very close to that of a binary copolymer (styrene-divinylbenzene) for which the degree of reticulation as well as the mechanical resistance are low. By increasing the quantity of acrylonitrile (3.0—10.0%), we obtain resistant copolymer pearls, because the acrylonitrile promotes the increase of the macromolecular skeleton's elasticity and therefore the increase of the resistance on the chloromethylation of the pearls. For a high acrylonitrile content (approx. 20%) the tridimensional lattice again looses its resistance and the copolymer pearls split during the chloromethylation reaction.

Table 3

Microscopic study of chloromethylated macroporous ternary copolymers

D.V.B. %	Acrylonitrile N %	Microscopic aspect	D.V.B. N %	Methacrylate of			Microscopic aspect
				methyl %	ethyl %	butyl %	
8	0.49	+	8	3	—	—	+++
8	1.08	—	8	10	—	—	++
8	1.57	—	8	—	3	—	+++
8	2.92	—	8	—	10	—	++
8	4.67	+++	8	—	—	3	—
12	0.0	—	12	3	—	—	—
12	0.53	—	12	10	—	—	—
12	0.86	—	12	—	3	—	—
12	0.96	—	12	—	10	—	—
12	2.54	—	18	1	—	—	—
12	4.52	—	18	3	—	—	—
18	0.0	—	18	5	—	—	—
18	0.37	—	18	10	—	—	—
18	0.72	—	18	20	—	—	+++
18	1.30	—	18	—	3	—	+++
18	2.38	—	18	—	10	—	+++
18	4.33	—	25	1	—	—	+++
			25	3	—	—	+++
			25	5	—	—	+++
			25	10	—	—	+++
			25	20	—	—	+++
			25	—	3	—	—
			25	—	10	—	+++
			25	—	—	3	—
			25	—	—	10	—

— intact pearls
+ fissured pearls
++ slightly cleaved pearls
+++ cleaved pearls

The presence of the acrylonitrile in the structure of the copolymer with a higher reticulation degree (12—18% D.V.B.) possessing thus already a fair mechanical resistance, still improves the resistance of the ternary copolymer during chloromethylation.

The influence of alkyl methacrylates on the mechanical resistance of macroporous ternary copolymers pearls is totally different from that of acrylonitrile. If acrylonitrile improves the mechanical resistance by increasing the elasticity of the tridimensional lattice up to certain limits, alkyl methacrylate, besides the plasticizing effect due to the hydrophobic bonds [19,20] between the hydrocarbonate radical of the ester and the main macromolecular chain, also produces a stiffening due to the methyl substituent. This stiffening is accentuated for methyl methacrylate and decreases with the increase of the carbon atom number of the ester radical.

The copolymer with 8% D.V.B. and a variable methyl or ethyl methacrylate content, between 0.0 and 20%, splits during the chloro-

---

[19] I. Sakurada, Yu. Sakaguchi, T. Ono and S. T. Ueda, *Kobunshi* Kagaku, 22, 696 (1965); *Chem. Abstr.*, **64**, 12828 (1966).

[20] S. Yashikawa, and O. Khim, *Bull. Chem. Soc. Japan*, **39**, 1515 (1966).

methylation reaction. Copolymers with an average divinylbenzene content (12% D.V.B.), and variable quantities of methyl- or ethyl methacrylates (0–20%) show a fair mechanical resistance (table 3). For a higher reticulation (18–25% D.V.B.), the resistance of the pearls is good up to approx. 10% methyl or ethyl methacrylate.

For higher alkyl methacrylate contents (20%) and divinylbenzene (25%), we obtain very rigid pearls which do not resist to the chloromethylation reaction.

When butyl methacrylate is used as a third comonomer, we obtain pearls resisting to chloromethylation, for small reticulation degrees (8% D.V.B.) as well as for a high divinylbenzene content (25% D.V.B.).

This is explained through the plasticizing effect of the hydrocarbonated chain of the esther radical exerted on the tridimensional lattice of the macroporous ternary copolymers.

CONCLUSIONS

1. We have studied the influence of the character and quantity of the third comonomer of macroporous ternary copolymers on the chloromethylation reaction.
2. We have studied the plasticizing effect of acrylonitrile and alkyl methacrylates on the mechanical resistance of copolymer pearls during the chloromethylation reaction.
3. We have studied the influence of temperature on the transformation degree of macroporous ternary compolymers.

Revue Roumaine de Chimie, 17, 8, 1437–1445 (1972)

11 – c. 1536

Revue Roumaine de Chimie, 17, 8, 1447–1456 (1972)

SYNTHESES OF ANION EXCHANGERS BASED ON MACROPOROUS TERNARY COPOLYMERS

STELIANA MAXIM, IG. POINESCU, STELA DRĂGAN and M. DIMA

Institute of Macromolecular Chemistry "Petru Poni"
Aleea Grigore Ghica Vodă 41A, Jassy, Romania

Received July 20, 1971

Results of the synthesis of type I, highly alkaline, macroporous anion exchangers based on macroporous ternary copolymers are submitted. The influence of the structure and porosity of copolymers on their amination reaction by trimethylamine has also been considered.

Owing to their higher qualities as compared to those of the gel type (standard), anion exchangers, macroporous anion exchangers have lately been more in use.

A series of works on the synthesis and study of macroporous anion exchangers[1–4] based on styrene-divinylbenzene copolymers has appeared in recent years.

In the present paper a study of the synthesis of type I, highly alkaline macroporous anion exchangers is advanced based on styrene-acrylonitrile-divinylbenzene or styrene-alkyl methacrylates-divinylbenzene copolymers, and the influence of the character and quantity of the third comonomer, as well as of the porosity of the macroporous ternary copolymer on the amination reaction of chloromethylated copolymers is studied.

EXPERIMENTAL

We have used chloromethylated macroporous ternary copolymers[5,6] the third comonomer of which is acrylonitrile or alkyl methacrylates (methyl, ethyl or n-butyl).

The amination of chloromethylated copolymers was carried through by trimethylamine, in 26.0% aqueous solution, at 25° for 6 hours.

---

[1] W. Busse and E. Schmidt (to Permutit A.-G.), Ger. Pat. 1, 569, 285, 06 May 1970; *Chem. Abstr.*, **73**, 26244q (1970).

[2] S. N. Il'ichev, A. P. Kovaleva, Z. F. Konstantinova and A. M. Saidadze, U.S.S.R. Pat., 267, 890, 02 Apr. 1970; *Chem. Abstr.*, **73**, 67254 m (1970).

[3] M. P. Kovaleva and G. K. Petrova, ,,Sintez i Svoistva Ionoobmennýe Materialov", Ed. Nauka, Moscow, 1968, p. 38.

[4] K. Kun and R. Kunin, *J. Polymer Sci.*, C, **16**, 1457 (1967).

[5] Ig. Poinescu, S. Drăgan, S. Maxim and M. Dima, *Rev. Roumaine Chim.* (in press).

[6] S. Ig. Poinescu, S. Drăgan and M. Dima, *Rev. Roumaine Chim.* (in press).

The study of the amination reaction was carried out on a series of chloromethylated copolymers with the same divinylbenzene (D.V.B.) content, but with different quantities of the third comonomer.

The influence of the copolymer reticulation degree was outlined by using chloromethylated copolymers with variable D.V.B. content in the amination reaction. In this way we followed the influence of the character and quantity of the third comonomer and of the reticulation degree on the transformation degree, respectively on the amination with trimethylamine of the chloromethylated macroporous ternary copolymers.

To study the influence of the copolymer porosity on the amination reaction, we have used copolymers with the same reticulation degree and the same content in the third component, but with different porosities, obtained by copolymerization of the monomers in the presence of polystyrene or benzine.

The porosity of macroporous ternary copolymers was calculated by means of the formula[7] :

$$P = (1 - \left(\frac{\rho a}{\rho r}\right) . 100$$

Table 1

Chief characteristics of chloromethylation styrene-acrylonitrile-D.V.B macroporous ternary copolymers

Sample	D.V.B. %	Macroporous ternary copolymer Nitrogen %	Acrylonitrile %	Chlorine %	Porosity %
1	8.0	0.49	1.70	15.32	4.49
2	8.0	1.08	4.09	15.10	17.75
3	8.0	1.57	5.90	14.99	23.67
4	8.0	2.92	11.00	13.10	32.37
5	8.0	4.67	17.60	9.05	34.04
6	12.0	0.0	0.0	14.60	13.97
7	12.0	0.53	2.00	13.80	16.16
8	12.0	0.86	2.36	13.50	19.40
9	12.0	1.26	4.70	12.20	19.33
10	12.0	2.54	9.60	10.80	33.68
11	12.0	4.52	17.10	8.60	29.84
12	18.0	0.0	0.0	12.00	24.86
13	18.0	0.37	1.40	11.01	26.35
14	18.0	0.72	2.60	10.64	21.20
15	18.0	1.30	4.90	10.45	25.01
16	18.0	2.38	9.01	8.10	21.47
17	18.0	4.33	16.40	5.50	26.76
57	25.0	0.0	0.0	8.31	28.29
58	25.0	0.37	1.40	8.25	49.71
59	25.0	0.63	2.30	8.20	52.52
60	25.0	1.05	4.00	8.04	61.58
61	25.0	2.00	7.50	7.10	61.40
62	25.0	4.28	16.20	1.94	—

---

[7] R. Kunin, F. E. Meitzner, A. J. Oline, S. Fischer and N. Frisch, *Ind. Eng. Chem. Res. Develop.*, **1**, 140 (1967).

where :

P — porosity of the copolymer,

ρ_a = apparent density,

ρ_r — real density.

The macroporous anion exchangers were characterized by determinations of the exchange capacity and by nitrogen analyses.[8] Between the experimentally determined and the calculated nitrogen quantity there exists a good agreement [9] (table 4). For ternary copolymers with acrylonitrile we have taken into account the nitrogen content of the chloromethylated copolymer.

The amination degree of the chloromethylated macroporous ternary copolymer was expressed by its exchange capacity. The main characteristics of the styrene-acrylonitrile-D.V.B. ternary copolymers are given in table 1.

RESULTS AND DISCUSSIONS

The exchange capacity of anion exchangers, synthetized from ternary copolymers,[5] decreases with the increase of the reticulation degree [10] and of the number of acrylic units incorporated in the copolymer, respectively with the increase of the nitrogen content of the copolymer.

In figure 1 the variation of the exchange capacity *versus* the acrylonitrile content expressed in nitrogen is given for styrene-acrylonitrile-DVB macroporous ternary copolymers.

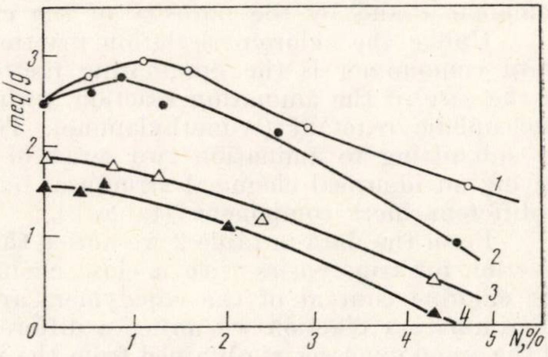

Fig. 1. — Dependence of the exchange capacity of the macroporous anion exchangers on the chemical structure of styrene-acrylonitrile-D.V.B. copolymers with 8.0%(*1*); 12.0%(*2*); 18.0% (*3*) and 25.0% (*4*) D.V.B. Chloromethylated copolymer/$N(CH_3)_3$—1/2 mol

For relatively small reticulation degrees (fig. 1; curves 1 and 2) we notice a maximum shifting towards the ordinate when the D.V.B. content increases. This maximum may be explained by the relatively small increase of the number of aminated structural units for 100 g ternary copolymer, against the binary copolymer (styrene-D.V.B.).

This fact may also be explained if one admits that the structure of a ternary copolymer, containing at the utmost 5.0% acrylonitrile is very similar to that of the binary copolymer, for the same reticulation degree, and therefore the theoretical number of chloromethylated styrene units of the ternary copolymers may be considered fairly near to that of the binary copolymer (table 1).

---

[8] T. S. Ma and G. Zuazaga, *Ind. Eng. Chem. Analyst*, **14**, 280 (1942).

[9] T. G. Moralli, *J.C.N.S.*, **26**, 265 (1954).

[10] E. Bortel, *Chem. Przemysl.*, **47**, 557 (1968).

To conclude, if we compare the binary copolymers to copolymers containing up to approx. 5.0% acrylonitrile, for the same degree of reticulation and having a roughly similar chemical structure, we notice that the amination reaction is favoured in the case of ternary copolymers. This effect is the result of two factors. The former is related to the electron-attracting effect of the group —CN, which probably shows itself favorably directly in the transition stage of the amination reaction of a neighbour chloromethylated group.[11] The latter factor is the plasticizing[12,13] of the copolymer due to the presence of the acrylonitrile in the tridimensional lattice, increasing its elasticity [12,13] and implicitely increasing the number of chloromethylated groups taking part in the amination reaction.

Concurrently with the increase in the content of the third comonomer, the exchange capacity of the anion exchanger decreases, owing to the marked decrease of the number of chloromethylated styrene units that can be aminated.

The absence of a maximum for curves 3 and 4 (fig. 1) may be explained in the following way : for a 18.0 and 25.0 D.V.B. content, the plasticizing effect does not show (or shows very slightly) owing to the increase in the rigidity of the tridimensional lattice.

The amination reaction is influenced by the presence of the third comonomer and by the porosity of the copolymer pearls.

Unlike the chloromethylation reaction, where the influence of the third comonomer is the dominating factor,[6] the situation is different in the case of the amination reaction, owing to the great volume of the nucleophilic reactant (trimethylamine). This may be rendered evident by submitting to amination two series of chloromethylated copolymers having an identical chemical structure, but obtained in the presence of a different inert component (table 2).

From the data in table 2 we notice that after the chloromethylation reaction for copolymers with a close chemical structure, the values of the chlorine content of the copolymers are practically the same. After the amination reaction we notice a difference in the exchange capacity of the anion exchangers obtained from the two series of chloromethylated copolymers, a fact probably due to the different porosities of the two series of copolymers.

Because the content of the third comonomer, as well as the reticulation degree, influence the porosity,[5] the dependence of the amination degree on the value of the porosity of the ternary copolymer is by far more complex.

Figure 2 presents the dependence of the exchange capacity of the anion exchangers on the acrylonitrile content (expressed in nitrogen),

---

[11] H. Morawetz, ,,Chemical Reactions of Polymers'', Edit. E. M. Fettes, Interscience Publishers, New York, 1964, p. 10.

[12] I. Sakurada, Yu. Sakaguchi, T. Ono and T. Ueda, Kobunshi Kagaku, 22, 696 (1965); *Chem. Abstr.*, **64**, 12828 (1966).

[13] S. Yoshikawa and O. Kim, *Bull Chem. Soc. Japan*, **39**, 1515 (1966).

Table 2

Comparative data of elementary analysis of two series of anion exchangers, obtained from macroporous ternary copolymers having an identical chemical structure; styrene-acrylonitrile – D.V.B.

Sample	D.V.B. %	Chloromethylated ternary copolymer			Diluting medium	Porosity %	Exchange capacity meq/g
		Nitrogen %	Acrylo nitrile %	Chlorine %			
12	18.0	0.0	0.0	12.0	Polystyrene	24.86	1.96
13	18.0	0.37	1.40	11.01	,,	26.35	1.87
14	18.0	0.72	2.60	10.64	,,	21.20	1.73
15	18.0	1.30	4.90	10.45	,,	25.01	1.65
16	18.0	2.38	9.01	8.10	,,	21.47	1.20
17	18.0	4.33	16.40	5.50	,,	26.76	0.50
51	18.0	0.0	0.0	11.90	Benzine	7.60	2.05
52	18.0	0.38	1.51	11.01	,,	6.90	2.06
53	18.0	0.78	2.95	10.80	,,	33.39	2.18
54	18.0	1.10	4.01	10.50	,,	43.52	1.80
55	18.0	2.29	9.00	9.00	,,	64.58	1.63
56	18.0	4.10	15.30	5.00	,,	60.45	0.94

and implicitely on their porosity,[5] for two series of macroporous ternary copolymers, differing only by the nature of the dilution medium used in the copolymerization process of the monomers (fig. 2, curves 1 and 2).

If we compare the values of the exchange capacities of the two series of chloromethylated and then aminated copolymers, we notice that in the case of copolymers with an increased porosity (copolymerization in the presence of benzine; fig. 2; curve 2), the curve of analytical data for the whole series is placed above the curve of analytical data of the series of copolymers obtained in the presence of polystyrene, though the number of chloromethylated styrene structural units for copolymers of different series but having an identical chemical structure is very close (table 2). This difference between the exchange capacities of the anion exchangers of the two series may be assigned to porosity (table 2).

The influence of porosity on the amination reaction of styrene-alkyl methacrylates-divinylbenzene macroporous ternary copolymers may be noticed especially for small reaction times, as may be seen from the data presented in figure 3.

The chief characteristics of styrene-alkyl methacrylate-divinylbenzene macroporous ternary copolymers used in the study of the amination reaction are given on table 3.

If we compare sample 103 with 105 (table 3), respectively curve 1 with 2 (fig. 3), owing to the fact that their composition is not very different, the third comonomer does not bring a significant change in the exchange capacity of the obtained anionites, this reaching after 4 hours 2.0 meq/g for sample 105 and 2.15 meq/g for sample 103. The shape of the curves of analytical data for the two copolymers is identical and a small difference remains the whole way (fig. 3; curves 1 and 2).

Though the copolymer with a higher porosity, for which the dynamics of the amination reaction is given by curve 2 (fig. 3), has a smaller theoretical number of chemical active units than copolymer 103, the amination reaction of which is given by curve 1 (fig. 3) their exchange capacity comes nevertheless fairly near, owing to the higher porosity of sample 105.

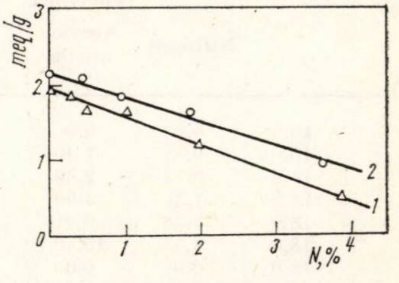

Fig. 2. — Dependence of the exchange capacity of macroporous anion exchangers on the acrylonitrile content and porosity of macroporous ternary copolymers. Chloromethylated copolymer/ $N(CH_3)_3$ — 1/2 mol; D.V.B. — 18.0% *1* — the copolymers were obtained in a diluting polystyrene medium; *2* — the copolymers were obtained in a diluting benzine medium (b.p. — 125 — 140°).

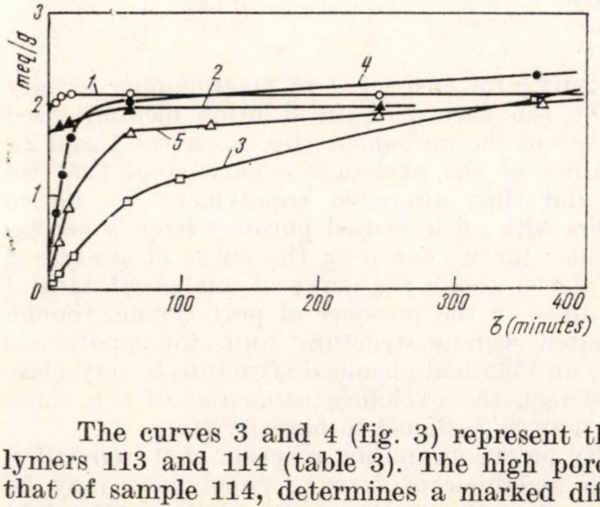

Fig. 3. — Influence of reaction time and of the third comonomer on the amination reaction of styrene alkylmethacrylates-D.V.B· copolymers. Chloromethylated copolymer/ /$N(CH_3)_3$ — 1/2 mol. *1* (sample 103) — copolymer with 3.0% methyl methacrylate and 18.0% D.V.B. *2* (sample 105) — copolymer with 10.0% methyl methacrylate and 18.0% D.V.B.; *3* (sample 114) — copolymer with 10.0% ethyl methacrylate and 18.0% D.V.B.; *4* (sample 113) — copolymer with 3.0% ethyl methacrylate and 18.0% D.V.B.; Curve 5 (sample 134) — Copolymer with 10.0% butyl methacrylate and 18.0% D.V.B.

The curves 3 and 4 (fig. 3) represent the analytical data for copolymers 113 and 114 (table 3). The high porosity of sample 113 against that of sample 114, determines a marked difference in the shape of the curves of analytical data representing the dynamics of the amination reaction for the two samples (fig. 3; curves 3 and 4).

Table 3

Chief characteristics of styrene alkylmethacrylates-divinylbenzene macroporous ternary copolymers

Sample	D.V.B. %	III^d component %	Apparent density	Porosity %
103	18.0	3.0 MCMe	0.8804	18.66
105	18.0	10.0 MCMe	0.7880	30.60
113	18.0	3.0 MCEt	0.8949	12.91
114	18.0	10.0 MCEt	0.9847	—
134	18.0	10.0 MCEt	0.8118	18.56

MCMe — methyl methacrylate
MCEEt — ethyl methacrylate

The copolymer with a high porosity reaches a maximum possible amination degree in given conditions, after a reaction of approximately one hour after which the increase of the exchange capacity is insignificant (fig. 3, curve 4). This is due to the fact that a high porosity favours the amination reaction, as the diffussion of the reactant inside and towards the outside of the pearl does not control the global rate of the amination process.[14]

For the copolymer with a small porosity (table 3, sample 114) the global rate of the amination reaction is, probably, controlled by the diffusion process, therefore the amination reaction takes place slowly, and the curve of the analytical data shows a continuous rise, reaching after 6 hours an exchange capacity of 2.15 meq/g (fig. 3 ; curve 3).

If we compare curves 3 to 5 (fig. 3), which represent the amination reaction for two copolymers of a practically identical chemical composition (table 3, samples 114 and 134), but with different porosity, owing to the use of different inert media for the copolymerization of the monomers, we notice a great difference in the experimental curves. For copolymer 134 with high porosity, the curve increases more rapidly during the first hour of the amination reaction, after which a very slow increase of the exchange capacity follows (2.1 meq/g). For the less porous copolymer (114) the curve presents a slow increase on its whole length ; thus after 6 hours of amination we obtain a macroporous anion exchanger having an exchange capacity of 2.15 meq/g (fig. 3, curve 3). The fact that after 6 hours the values of the exchange capacities are practically equal, demonstrated that the differences appearing in the shape of the curves during the amination process are due to the different porosities of the two copolymers.

From the analytical data given in figure 3 and table 3 we notice that for short reaction times, relatively small contents of the third comonomer of the styrene-alkyl methacrylates-divinylbenzene macroporous ternary copolymers influence to a small extent the course of the amination reaction, when porosity is the prevailing factor.

The influence of the third comonomer on the amination reaction was nevertheless followed on series of styrene-alkyl methacrylates-divinylbenzene macroporous ternary copolymers, having reticulation degrees of 18.0 and 25.0% D.V.B. (fig. 4 ; curves 1 and 2), for which the methylmethacrylate content varies between 0.0 and 20.0% (table 4).

From the data presented in figure 4 (curve 1) we observe an increase in the exchange capacity for copolymers with a 18.0% D.V.B. reticulation degree and a small content of methyl-methacrylate (3.0%), compared to the binary copolymer, a fact that may be explained, as for acrylonitrile, by the positive influence which methylmethacrylate units existing in the copolymer, have on the transition stage [11] of the amination of chloromethylated styrenic groups.

For copolymers with 25.0% D.V.B., the maximum of the curve nearly disappears and the decrease of the value of the exchange capacity

---

[14] A. K. Svetlov, G. Z. Esipov, T. M. Demenkova, Z. V. Grigorieva, K. L. Poplowski and L. I. Khomutov, *Vysokomol. Soedineniya*, A, **11**, 2793 (1969).

versus the third component is more marked (fig. 4 ; curve 2). If we compare the values of the exchange capacities obtained experimentally and through calculation, we notice a good agreement between these data (table 4).

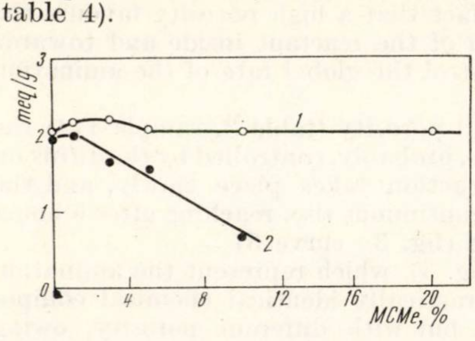

Fig. 4. — Dependence of the exchange capacity on the content of methyl methacrylate and the reticulation degree of the macroporous styrene-methyl methacrylate ternary copolymer (diluting medium, benzine with b.p. 125—140°). D.V.B. 18.0% (curve 1) and 25.0%. (curve 2).

The composition of the copolymers was calculated according to methods known in literature.[15,16]

For sample 111 (table 4) we notice a great difference between the theoretical and the practical value of the exchange capacity. This is explained by the fact that for a high methyl-methacrylates and D.V.B. content, the tridimensional lattice of the copolymers becomes very rigid, and the amination reaction is not complete in 6 hours, as in the case of other copolymers.

Table 4

Chemical composition of anion exchangers obtained from macroporous ternary copolymers, calculated according to the chlorine content of the copolymer after chloromethylation and nitrogen content after amination. Reaction conditions, copolymer/$N(CH_3)_3$ – 1/2 mol 25°, 6 hours

Sample	D.V.B. mol. %	Methyl methacrylate mol %	Unreacted styrene mol %	Chloromethylated styrene mol %	Aminated styrene mol %	Exchange capacity	
						Calculated meq/g	Experimental meq/g
51	13.84	0.0	56.66	29.50	29.50	2.11	2.05
102	13.84	1.0	48.16	37.00	37.00	2.50	2.25
103	13.84	3.0	34.50	39.10	39.10	2.55	2.32
104	13.84	5.0	38.30	38.70	38.70	2.45	2.20
105	13.84	10.0	36.40	35.60	35.60	2.40	2.10
106	13.84	20.0	27.70	34.30	34.30	2.30	2.05
57	19.20	0.0	52.53	28.27	28.27	2.20	2.00
108	19.20	1.0	46.70	33.10	33.10	2.20	2.02
109	19.20	3.0	51.70	26.10	26.10	1.83	1.60
110	19.20	5.0	51.90	23.90	23.90	1.60	1.54
111	19.20	10.0	51.50	19.30	19.30	1.40	0.70

We have also studied the influence of the chemical character of the third comonomer on the exchange capacity.

---

[15] T. Alfrey Jr., and H. S. Pinner, *J. Polymer Sci.*, **23**, 533 (1957).

[16] I. Scondac and M. Dima, *Studii și Cercet. Sti., Chim. Fil. Iași*, **13**, 218 (1962).

If we examine curves 1 and 4 (fig. 3), representing the experimental results for two copolymers with very close apparent densities (table 3 ; samples 103 and 113) having the same reticulation degree, copolymerized in an inert medium, (benzine), with the same content of the third comonomer, but of a different nature, the exchange capacity of the anion exchanger containing ethyl-methacrylates has been found of 2.4 meq/g against 2.2 meq/g methyl-methacrylate content of the anion exchangers.

This difference may be explained by the plastifying effect, which is more marked for ethyl-methacrylate, increasing the elasticity of the tridimensional lattice, and implicitly the number of chloromethylated groups which can be aminated.[12]

The influence of the nature of the third comonomer is also illustrated in table 5.

Table 5

Influence of the character of the third comonomer on the exchange capacity

Sample	D.V.B. %	Third comonomer %	Nitrogen %	Inert component %	Exchange capacity meq/g
129	8.0	3.0 MCEt	3.63	Polystyrene	2.59
135	8.0	3.0 MCBu	3.92	Polystyrene	2.80
125	12.0	3.0 MCMe	3.44	Polystyrene	2.46
131	12.0	3.0 MCEt	3.43	Polystyrene	2.45
137	12.0	3.0 MCBu	3.82	Polystyrene	2.75
103	18.0	3.0 MCMe	3.11	Benzine	2.22
139	18.0	3.0 MCBu	3.32	Polystyrene	2.37
109	25.0	3.0 MCMe	2.25	Benzine	1.60
115	25.0	3.0 MCEt	2.64	Benzine	1.90
121	25.0	3.0 MCBu	2.42	Benzine	1.72
124	8.0	10.0 MCMe	3.43	Polystyrene	2.45
130	8.0	10.0 MCEt	3.77	Polystyrene	2.69
136	8.0	10.0 MCBu	3.80	Polystyrene	2.71
126	12.0	10.0 MCMe	3.37	Polystyrene	2.40
132	12.0	10.0 MCEt	3.37	Polystyrene	2.40
138	12.0	10.0 MCBu	3.70	Polystyrene	2.70
114	18.0	10.0 MCMe	3.01	Benzine	2.15
134	18.0	10.0 MCEt	3.00	Polystyrene	2.14
120	18.0	10.0 MCBu	3.40	Benzine	2.42

MCMe – methyl methacrylate
MCEt – ethyl methacrylate
MCBu – butyl methacrylate

For copolymers with the same content of divinylbenzene and alkylmethacrylate, we notice a slight increase in the exchange capacity in the series Me $<$ Et $<$ Bu. This is the result of the plasticizing effect, which increases with the increase of the hydrocarbonated radical of the methacrylic esthers [12,13] and is due to the hydrophobic bonds between the alkylic radical of the methacrylic esther and the main macromolecular chain.

CONCLUSIONS

1. We have studied the influence of the character and quantity of the third comonomer on the amination reaction of chloromethylated macroporous ternary copolymers.

2. The influence of the porosity of macroporous ternary copolymers on the amination reaction has been followed.

3. We have studied the influence of the plasticizing effect of the third comonomer (acrylonitrile, alkyl-methacrylates) present in the tridimensional structure of macroporous ternary copolymers, on the amination reaction.

Revue Roumaine de Chimie, **17**, *8*, 1457 – 1463 (1972)

ÜBER DAS 2-ÄTHOXY -6,9-DIAMINOAKRIDIN-MOLYBDATOPHOSPHAT

I. FLOREA

Vom Laboratorium für Allgemeine Chemie der Technischen Hochschule „Traian Vuia", Timişoara, Str. Remus 14

Eingegangen am 24. Januar 1972

Es wurde die Reaktion zwischen Natriummolybdatophosphat und dem Lactat des 2-Äthoxy-6,9-diaminoakridins (Rivanol)-BHL konduktometrisch verfolgt. Die während der konduktometrischen Titration entstandene Verbindung wurde isoliert, analysiert, thermogravimetrisch untersucht und außerdem wurde ihre Löslichkeit in Wasser bei 20° bestimmt. Auf Grund der erhaltenen Ergebnisse wurde die chemische Formel $(BH)_3[P(Mo_{12}O_{40})]$ festgelegt. 2-Äthoxy-6,9,diamino-akridinmolybdatophosphat kann zur indirekten photometrischen Dosierung des Molybdatophosphorsäureions dienen. Die Dosierung kann in Gegenwart der Anionen CrO_4^{2} und WO_4^{2-} durchgeführt werden.

In der vorliegenden Arbeit wurde verfolgt, ob das Molybdatophosphorsäure-Anion so wie andere, vorher studierte Anione,[1–8] gleichfalls eine chemische Verbindung mit dem Lactat des 2-Äthoxy-6,9-diaminoakridins (Rivanol)-BHL ergibt, und weitherhin, ob diese Verbindung für analytische Zwecke geeignet ist.

Durch Versetzen einer Natriummolybdatophosphatlösung mit einer BHL-Lösung erhielt man einen schwerlöslichen gelbgrünen Niederschlag. Die chemische Verbindung welche durch Vermischen der obigen Lösungen entsteht, wurde konduktometrisch untersucht, indem die Natriummolybdatophosphatlösungen mit BHL-Lösungen titriert wurden.

---

[1] C. Drăgulescu und I. Florea, *Studii și Cercetări Sti., Chim. Baza Cercetări Sti., Timișoara*, **9**, 222(1962).

[2] C. Drăgulescu und I. Florea, *Studii și Cercetări Sti., Chim. Baza Cerce lări Sti., Timișoara*, **9**, 227(1962).

[3] C. Drăgulescu und I. Florea, *Studii și Cercetări Sti., Chim. Baza Cercetări Sti., Timișoara*, **9**, 247(1962).

[4] C. Drăgulescu und I. Florea, *Studii și Cercetări Sti., Chim. Baza Cercetări Sti., Timișoara*, **10**, 31(1963).

[5] I. Florea, *Bul. Ştiinţific și Tehnic I.P.T.*, **10**, 51(1965).

[6] I. Florea, *Bul. Ştiinţific și Tehnic I.P.T.*, **12**,(1967).

[7] I. Florea, *Rev. Roumaine Chim.*, **14**, 365(1969).

[8] I. Florea, *Rev. Roumaine Chim.*, **14**, 745(1969).

EXPERIMENTELLES

Geräte.

Bei den Titrationen wurde für die Bestimmung der Konduktivität die gebräuchliche Schaltung einer Widerstandsmeßbrücke mit Telephon als Nullinstrument und eine Kolthoffsche Titrationsvorrichtung verwendet. Die Extinktionsmessungen wurden an einem Pulfrichschen Photometer, mit dem grünen Filter bei $\lambda = 530$ mm, vorgenommen. Es wurden noch verwendet; ein Wöbser-Thermostat und eine Thermowaage.

Reagenzien

a) Eine 1.10^{-2} molare Natriummolybdatophosphatlösung der Firma Riedel de Haën A. G. Der Titer der Lösung wurde gravimetrisch mit Oxim bestimmt.

b) Eine 1.10^{-2} molare BHL-Lösung, durch Umkristallisieren des pharmazeutischen Handelsproduktes gewonnen.

c) Eine 1.10^{-3} molare Natriummolybdatophosphatolösung, erhalten durch Verdünnen von 20 ml der Lösung *a* auf 200 ml mit Wasser, mit einem $[P(Mo_{12}O_{40})]^{3-}$-Gehalt von 1,822 mg/ml.

KONDUKTOMETRISCHE TITRATIONEN

In den Abbildungen 1 und 2 sind die behandelten konduktometrischen Titrationen dargestellt.

Abbildung 1 stellt die konduktometrische Titration des Natriummolybdatophosphates mit BHL dar. Bis zum Äquivalenzpunkt stellt man einen Abfall der Konduktivität der Lösung fest, wegen der Ersetzung der Anionen $[P(Mo_{12}O_{40})]^{3-}$ mit L^--Anionen; $\Lambda_L < 1/3[P(Mo_{12}O_{40})]^{3-}$. Nach der Äquivalenz bleibt die Konduktivität durch Zugabe eines Reagenzüberschusses konstant.

Abbildung 2 stellt die umgekehrte konduktometrische Titration der BHL-Lösung mit einer Natriummolybdatophosphatlösung dar. Bis zum Äquivalenzpunkt findet eine Steigerung der Konduktivität der Lösung statt, in Folge der Ersetzung der BH -Ionen mit den H^+-Ionen. Nach der Äquivalenz wächst die Konduktivität wegen dem Zusatz des Reagenzüberschusses.

HERSTELLUNG UND ANALYSE DER ENTSTANDENEN VERBINDUNG

Durch Vermengen der Reagenzien in den Äquivalenzverhältnissen der konduktometrischen Titrationen erhielt man die Verbindung $(BH)_3 [P(Mo_{12}O_{40})]$, in der Form eines Niederschlages, welcher mit destilliertem Wasser gewaschen und im Trockenschrank bei 110° bis zum konstanten Gewicht getrocknet wurde. Die Zusammensetzung der Verbindung wurde durch gravimetrische Dosierung bestimmt: P als $MgNH_4PO_4$ und Mo als MoS_3. Das BH^+-Ion wurde photometrisch bestimmt. [9–11]

Chemische Analyse: *gefunden*: $P = 0{,}98$; $Mo = 44{,}82$; $BH^+ = 30{,}07\,\%$; *Berechnet*: $P = 1{,}20$; $Mo = 44{,}53$; $BH^+ = 29{,}52\,\%$.

---

[9] J. Schulte, *Pharm. Weekblad*, **67**, 601(1930); *Chem. Zentr.*, **2**, 2020(1930).

[10] J. Ssolz, *Farmacia*, **11**, 20(1940); *Chem. Zentr.*, **2**, 23(1941).

[11] J. Maizelis und A. Miasuicova, *Farmatsija*, **4**, 617(1941); *Chem. Abstr.*, **38**, 2435 (1944).

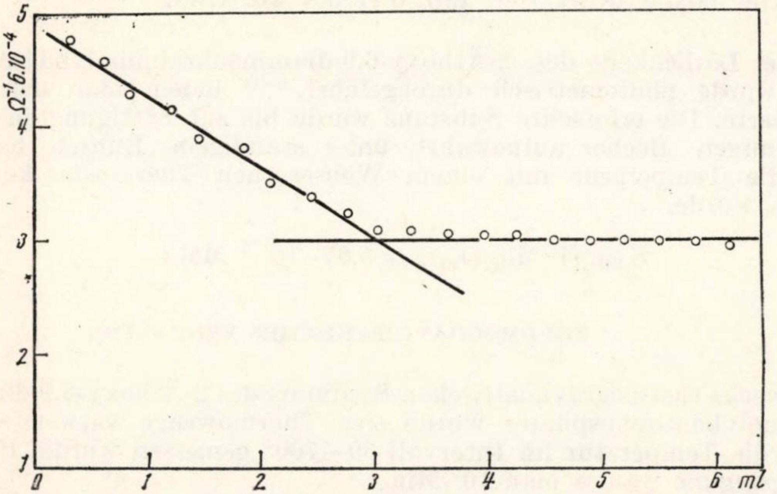

Abb. 1. – 1 ml $Na_3[P(Mo_{12}O_{40})]$ 1.10^{-2} m + 59 ml Wasser titriert man mit BHL1.10^{-2}m.

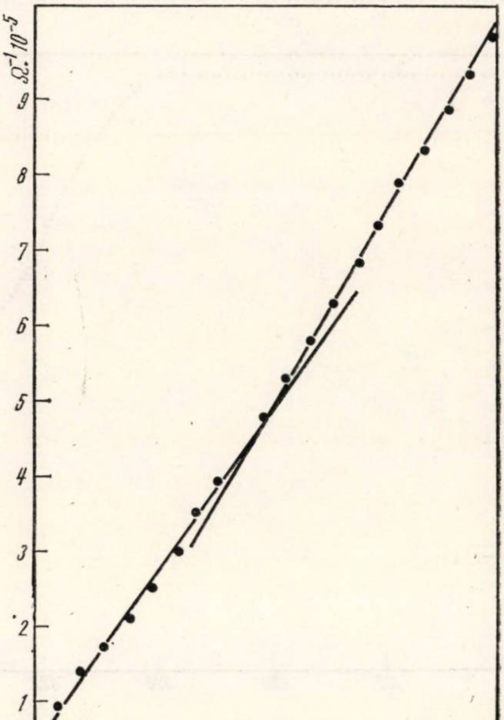

Abb. 2. – 3 ml BHL 1.10^{-2}m + + 14ml Wasser titriert man mit $Na_3[P(Mo_{12}O_{40})]$ 1.10^{-2} m.

DIE LÖSLICHKEIT DER ERHALTENEN SUBSTANZ

Die Löslichkeit des 2-Äthoxy-6,9-diaminoakridinmolybdato-phosphates wurde photometrisch durchgeführt,[9-11] indem man das BH^+-Ion dosierte. Die erforschte Substanz wurde bis zur Sättigung in einem kegelförmigen Becher aufbewahrt, unter ständigem Rühren bei 20°, wobei die Temperatur mit einem Wöbserschen Thermostat konstant gehalten wurde.

$$S_{(BH)_3}[P(Mo_{12}O_{40})] = 5{,}07 \cdot 10^{-8}\ \mathrm{Mol/l}.$$

THERMOGRAVIMETRISCHES VERHALTEN

Zwecks thermogravimetrischen Studiums des 2-Äthoxy-6,9-diaminoakridinmolybdatophosphates wurde eine Thermowaage verwendet, mit welcher die Temperatur im Intervall 30–700° gemessen wurde. Für das Heizungsregime wählte man 10°/Min.

Abbildung 3 stellt das thermogravimetrische Verhalten des 2-Äthoxy-6,9-diaminoakridinmolybdatophosphates dar.

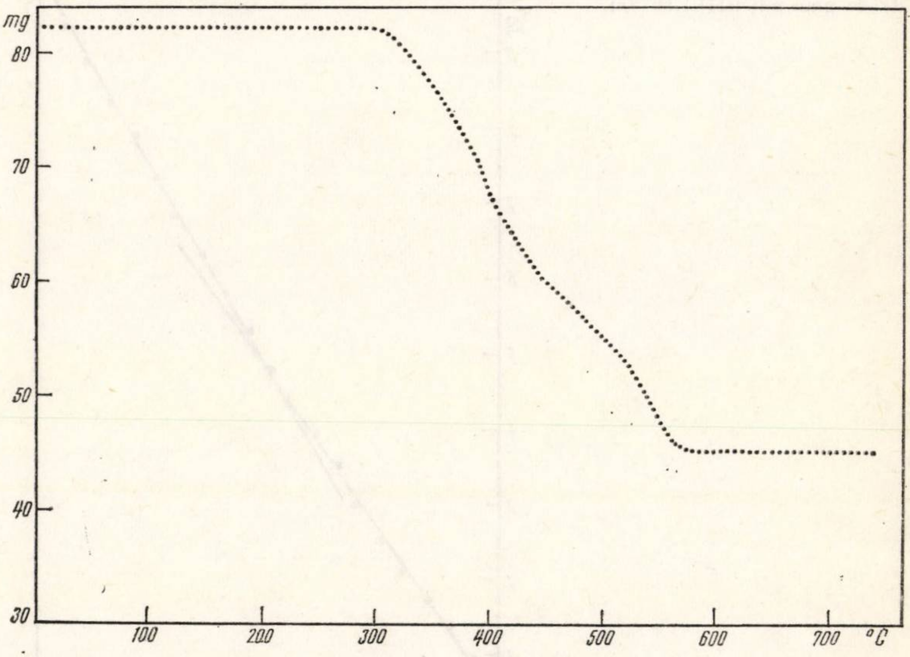

Abb. 3. – Thermolyse von $(BH)_3[P(Mo_{12}O_{40})]$.

Der Rückstand ist aus $MoO_3 + P_2O_5$ gebildet. Die Substanz ist bis zu 230° beständig. Über diese Temperatur hinaus findet die Zersetzung des organischen Teils statt, die bei 560° abschließt. Der Rückstand wiegt

34,7 mg. Aus der verbrauchten Substanzmenge errechnet man 34,2 mg. Die Abweichung bei der thermogravimetrischen Bestimmung beträgt + 1,52 %.

INDIREKTE PHOTOMETRISCHE DOSIERUNG DES MOLYBDATOPHOSPHORSÄUREIONS

Für die indirekte photometrische Bestimmung des Molybdatophosphorsäureions wird dessen Verbindung mit BHL, $(BH)_3[P(Mo_{12}O_{40})]$ verwendet. Das Molybdatophosphosäureion kann in Form dieser Verbindung quantitativ mitwirken, wenn man in die Lösung, die es enthält, einen BHL-Überschuß zuführt. Nach der Trennung löst man die entstandene Verbindung unter Kochen in einigen Milliliter verdünntem Ammoniak auf. Die gelöste Substanz versetzt man mit einer chlorwasserstoffsauren Natriumnitritlösung, wobei sich eine rötlichviolette Verbindung bildet, die man kolorimetriert. Auf einer Eichkurve kann man dann direkt auf der Abszisse den BH^+ -Gehalt ablesen und nachher den Betrag in $[P(Mo_{12}O_{40})]^{3-}$ aus der untersuchten Probe berechnen.

ARBEITSWEISE

Die Probe, mit einem Gehalt an $[P(Mo_{12}O_{40})]^{3-}$ von 0,73–8,93 mg, führt man in einen Zentrifugenbehälter ein, wo sie in 4–5 ml Wasser gelöst wird; nachher fügt man tropfenweise einen Überschuß von 1.10^{-2} molarer BHL-Lösung under Rühren hinzu. Das Ende der Niederschlagsbildung ist durch das Auftreten einer gelblichen Fluoreszenz gekennzeichnet.

Nachdem sich durch Zentrifugieren der gelbgrüne Niederschlag von $(BH)_3$ $[P(Mo_{12}O_{40})]$ gesetzt hat, schüttet man die darüberschwebende Lösung ab und gießt 3–4 ml Wasser dazu. Man rührt mit einem Glasstab gut um, um den BHL-Überschuß wegzuwaschen und zentrifugiert nochmals; der Glasstab wird ebenfalls gut mit Wasser abgespült. Diese Operation wiederholt man 2–3 mal mit 2–4 ml Wasser, anschließend 2–3 mal mit 3–4 ml Äther-Alkohol-Gemisch im Verhältnis 5 : 1, bis im Überstand das BH^+-Ion nicht mehr mit Kaliumeisen (II)-cyanid nachweisbar ist. Nach Entfernen der Lösung versetzt man den Niederschlag mit 3–4 ml 5 %igem Ammoniak, führt den Behälter in ein mit Wasser gefülltes Glas ein und erwärmt bis zum Sieden, Falls der Niederschlag sich nicht völlig löst, fügt man dieselbe ml-Anzahl Eisessig hinzu. Nach dem Abkühlen der Lösung gibt man je 4 ml 0,5 molare Natriumnitritlösung bzw. verdünnte Salzsäure dazu und es entsteht eine rötlichviolette Färbung. Nun überführt man die Lösung quantitativ in einen 100 ml Meßkolben, füllt bis zur Marke an und homogenisiert. Aus dieser Lösung nimmt man Proben für die Kolorimetrierung. Man mißt die Extinktionen an einem Pulfrichschen Photometer mit dem grünen Filter bei $\lambda = 530$ mm.

Man trägt eine Eichkurve auf, Extinktion in bezug auf die Konzentration (Abb. 4). An der Eichkurve kann man auf Grund der gemessenen Extinktionen die BH^+-Konzentration ablesen und nachher den Gehalt an $[P(Mo_{12}O_{40})]^{3-}$in den der Untersuchung unterzogenen Proben errechnen.

In Tabelle 1 sind die anhand der verschiedenen Bestimmungen erhaltenen Werte angeführt, bei Konzentrationen, die zwischen den angegebenen Grenzen schwanken. Aus den Bestimmungen [9–11] geht hervor, daß das Molybdatophosphorsäureion in Gegenwart von CrO_4^{2-}, aus den Bestimmungen jedoch WO_4^{2-} dosiert werden kann, u. zw.

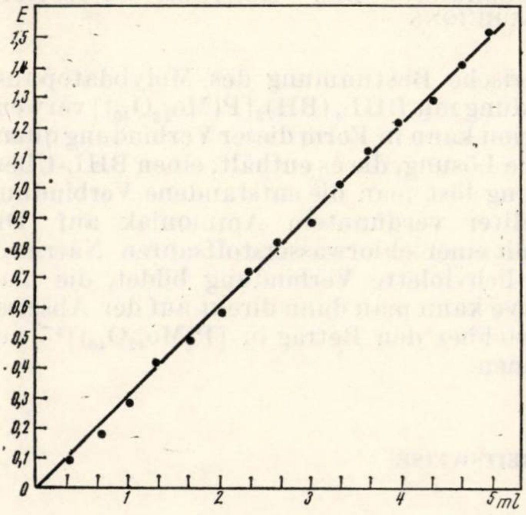

Abb. 4. — $E = f(c)$: 1 ml = $= 2{,}543 \cdot 10^{-4}$ g BH^+. 1 ml $[P(Mo_{12}O_{40})]^{3-} = 1{,}822$ mg.

in doppelt so großen Mengen als man zu den Untersuchungen verwendet hat. Die Abweichung bei den Bestimmungen überschreitet nie ± 2%.

Tabelle 1

Über das 2-Äthoxy-6,9-Diaminoakridin-Molybdatophosphat

Lfd. Zahl	mg* $[P(Mo_{12}O_{40})]^{3-}$ Verbraucht	mg CrO_4^{2-} Verbraucht	mg WO_4^{2-} Verbraucht	E	$[P(Mo_{12}O_{40})]^{3-}$	E %
1	0,73	—	—	0,12	0,72	−1,27
2	1,46	—	—	0,24	1,44	−1,36
3	2,19	—	—	0,36	2,20	+0,40
4	3,10	—	—	0,51	3,08	−0,65
5	4,00	—	—	0,66	4,02	+0,50
6	5,10	—	—	0,84	5,02	−1,57
7	5,83	—	—	0,94	5,83	0,00
8	6,92	—	—	1,14	6,85	−1,82
9	8,02	6,00	—	1,32	7,94	−1,00
10	8,93	12,00	—	1,47	8,83	−1,12
11	4,55	18,00	—	0,75	4,59	+0,90
12	7,65	—	6,00	1,26	7,52	−1,70
13	2,55	—	12,00	0,42	2,51	−1,57
14	8,46	—	18,00	1,41	8,35	−1,30

*1 ml = 1,822 mg $[P(M_{12}O_{40})]^{3-}$

SCHLUSSFOLGERUNGEN

Durch Behandlung von Natriummolybdatophosphat mit 2-Äthoxy-6,9-diaminoakridin-lactat bildet sich ein unlöslicher Niederschlag grünlichgelber Farbe von 2-Äthoxy-6,9-diaminoakridinmolybdatophosphat. Diese Substanz kann zur indirekten photometrischen Dosierung des Molybdatophosphorsäureions dienen. Die Dosierung ist in Gegenwart der Anionen CrO_4^{2-} und WO_4^{2-} möglich. Die Abweichung der Bestimmungen überschreitet nicht ± 2%. Die während der konduktometrischen Titration entstehende Substanz wurde abgetrennt und analysiert. Auf Grund der erhaltenen Ergebnisse wurde ihr die chemische Formel $(BH)_3[P(Mo_{12}O_{40})]$ zugeschrieben. Außerdem wurde die Löslichkeit bei 20° bestimmt, sowie das thermogravimetrische Vorhalten.

Revue Roumaine de Chimie, **17**, *8*, 1465–1474 (1972)

DIE VERWENDUNG DES SALZEFFEKTES IN NICHTWÄSSRIGEN LÖSUNGEN BEI ACIDO-BASISCHEN TITRATIONEN. II [*]

STUDIUM ÜBER DAS ANALYTISCHE VERHALTEN EINIGER DICARBONSÄUREN UND HYDROXYSÄUREN IN METHANOLISCHEN LÖSUNGEN IN GEGENWART VON $Ca(NO_3)_2$[**]

C. LITEANU und AGNES BLAZSEK-BODÓ

von der ,,Babeş-Bolyai'' Universität, Cluj, str. Arany János 11 und der Pharmazeutischen Fakultät Tirgu Mureş, Str. Gh. Marinescu 38

Eingegangen am 29. Februar 1972

Es wird das Verhalten der Dicarbonsäuren und Hydroxysäuren in Methanol, bei hoher Ionenstärke, in Gegenwart von $Ca(NO_3)_2$ untersucht. Es werden die Werte der pK_1 und pK_2 der Oxalsäure, Malonsäure, *o*-Phthalsäure und Bernsteinsäure in Methanol bei $I = 0$ berechnet. In Gegenwart von $Ca(NO_3)_2$ wurde die Nivellierung der beiden Protonen der Dicarbonsäure und das bedeutende Anwachsen der relativen Acidität der untersuchten Säuren ($\Delta pK_{(I_0 - I_{4,37})} < 3{,}0$) festgestellt, welche im Falle der Hydroxysäuren ausgeprägter ist ($\Delta pK_{(I_0 - I_{4,37})} = 3{,}0-4{,}0$). Parallel mit dem Anwachsen der Acidität wird auch das Anwachsen des Potentialsprunges im Raume des Äquivalenzpunktes festgestellt, wobei erhöhte Werte für Oxalsäure, Milchsäure, Zitronensäure, Weinsäure, Apfelsäure und Glykolsäure gewonnen wurden (bei $I = 4{,}37$, $\Delta E_{\pm 1\%} = 80-123$ mV).

Die differenzierte Titration von Gemischen starker, schwacher und sehr schwacher Säuren sowie von Dicarbonsäuren wird unter Verwendung von Ketonen, Nitrilen oder Kohlenwasserstoffen in Mischung mit Ketonen und Nitrilen als Lösungsmittel durchgeführt. Aus der Gruppe der Alkohole erwähnen wir noch die differenzierende Wirkung des Isopropyl- und tertiären Butylalkohols. Der Methyl- und Äthylalkohol wird hauptsächlich zur differenzierten Bestimmung von Gemischen starker Säuren verwendet.[1-9]

---

[*] I Mitt: C. LITEANU und A. BLAZSEK, *Rev. Roumaine Chim.*, **16**, 835 (1971).

[**] Teile vorliegender Arbeit wurden im Verlaufe der 3. Landeskonferenz für Analytische Chemie, Braşov, 1971 vorgetragen.

Bekanntlich[10-12] dissoziieren die Säuren in Methanol schwächer als in Wasser, was in erster Reihe im Falle von acido-basischen Paaren des Types HA/A^- (z.B. Essigsäure, Benzoesäure, $(pK_a)_{H_2O} - (pK_a)_{CH_3OH} = 4{,}9^{+} - 0{,}3$) untersucht wurde. Für den zweiten. Dissoziationsgrad von Dicarbonsäuren ist diese Wirkung ausgesprochener,[13] im Falle von acido-basischen Paaren des Types HA^-/A^{2-} ist daher dieser Wert $(pK_a)_{H_2O} - (pK_a)_{CH_3OH} = 5{,}7 - 0{,}2$. Die differenzierende Wirkung des Methanols wird nur im Falle von Dicarbonsäuren mit kürzerer Kette festgestellt, wenn $pK_2 \leqslant 10{,}0$ und wenn die Differenz $pK_2 - pK_1 \geqslant 3{,}0$ ist.

Eine ausgesprochene differenzierende Wirkung konnten wir im Falle von Oxal- und Malonsäure feststellen. Die zwei dissoziierenden Protone der Bernsteinsäure können nicht mehr unter den günstigsten Bedingungen differenziert titriert werden. Die Gegenwart einer Hydroxylgruppe im Molekül (z.B. im Falle von Apfelsäure) begünstigt in gewissem Maße die Säuretitration der beiden Protonen. Für praktische Zwecke ist es in diesem Falle trotzdem angezeigter, sich differenzierender Lösungsmittel zu bedienen (z.B. Aceton, Methyl-äthylketon, Methyl-i-butylketon, Acetonitril usw.).

In unseren vorhergehenden Forschungen,[14] bei der Untersuchung der Bestimmungsmöglichkeiten von aliphatischen Säuren, konnten wir feststellen, daß in methanolischen Lösungen mit hoher Ionenstärke die relative Acidität der untersuchten Substanzen sich erhöht, die potentiometrischen Titrationsbedingungen sich verbessern, der Potentialsprung beim Äquivalenzpunkt $(\Delta E)_{\pm 1\%}$ sich bedeutend erhöht.

Die Forschung des Salzeffektes bei potentiometrischen Titrationen fortsetzend, verfolgten wir die Änderung des acidobasischen Verhaltens der gesättigten, ungesättigten, aromatischen Dikarbonsäuren und der Hydroxysäuren in methanolischen Lösungen.

Die Beschreibung der für die potentiometrischen Titrationen verwendeten Apparate, sowie die Berechnungsweise der pK_a - Werte haben wir in unserer vorangehenden Arbeit beschrieben.[14]

---

[1] A. P. Kreshkov, L. N. Bykowa und W. T. Smolova, *Zhur. analit. Khim.*, **19**, 156 (1964).

[2] A. P. Kreshkow, L. N. Bykowa und Z. G. Blagodatskaia, *Plast. Massy*, **6**, 58(1968).

[3] A. P. Kreshkow, L. N. Bykowa und N. A. Kazarian, ,,Titrarea în mediu neapos'', Ed. Tehnică, Bucureşti, 1969. S. 36.

[4] G. Bonhomme und M. L. Dondon, *Compt. rend.*, **263**, 1097 (1966).

[5] A. P. Kreshkow, N. A. Kazarian und K. N. Shulunowa, *Zhur. analit. Khim.*, **23**, 1199 (1968).

[6] A. P. Kreshkow und S. P. Swiatunowa, *Zhur. analit. Khim.*, **24**, 321 (1966).

[7] A. P. Kreshkow, N. S. Aldarowa, N. T. Smolowa und M. W. Slawgorodskaia, *Zhur. analit. Khim.*, **24**, 321 (1969).

[8] F. C. Trussel und R. E. Lewis, *Analyt. Chim. Acta.*, **34**, 243 (1966).

[9] N. van Meurs und E. A. F. M. Dahmen, *Analyt. Chim. Acta*, **19**, 64 (1958).

[10] L. Meites, ,,Handbook of Analytical Chemistry'', McGraw-Hill, New York,1963.

[11] A. P. Kreshkow, N. S. Aldarowa und N. T. Smolowa, *Zhur. obshchei Khim.*,, **39**, 1390 (1969).

[12] G. Charlot, ,,Les méthodes de la chimie analytique. Analyse quantiative'', Masson et Cie, Paris, 1966, S. 489.

[13]. G. Charlot und B. Trémillon, ,,Lés réactions chimiques dans les solvants et les sels fondus'', Ed. Gauthier-Villars, Paris, 1963, S. 52.

[14] C. Liteanu und A. Blazsek, *Rev. Roumaine Chim.*, **16**, 835 (1971).

Zur Berechnung beider Dissoziationsgrade der Dicarbonsäuren verwendeten wir die von Birjukow und Ganelina[15] vorgeschlagene Methode, welche die Bestimmung der Dissoziationskonstanten ermöglicht, auch in jenen Fällen, in denen kein ausgesprochener Potentialsprung für den ersten Dissoziationsgrad festgestellt werden kann.

Die graphische Darstellung der Protonenanzahl in Abhängigkeit des pH-Wertes gibt die potentiometrische Kurve, aus der die pK_1 und pK_2 Werte berechnet werden können. Die Anzahl der titrierten Protonen kann durch das Verhältnis z/B angenähert werden, wobei z die Menge der in der hinzugefügten Maßlösung enthaltenen und in mol/l ausgedrückte Substanz ist, und B die in mol/l ausgedrückte Säurekonzentration ist. Im Falle von in Methanol ausgeführten Titrationen stellten wir das Verhältnis zwischen z/B-Werten und der Änderung des im Laufe der Titration gemessenen Potentials graphisch dar. Aus dem graphisch bestimmten Potential, welches dem Verhältnis $z/B = 0,5$ entspricht kann der pK_1 Wert, und aus dem, dem Verhältnis $z/B = 1,5$ entsprechenden Potential, mit Hilfe der Gleichung $pK_a = pH_{1/2} = \frac{E_{1/2} - E_j}{0,059}$, der pK_2 Wert berechnet werden, wobei $E_{1/2}$ das Halbneutralisationspotential, und E_j das Diffusionspotential ist, das mit Hilfe einer Standardsubstanz bestimmt wurde.[14]

Mit Hilfe der oben beschriebenen Methode, haben wir die pK_1- und pK_2- Werte der Oxalsäure, Malonsäure, o-Phthalsäure und Bernsteinsäure

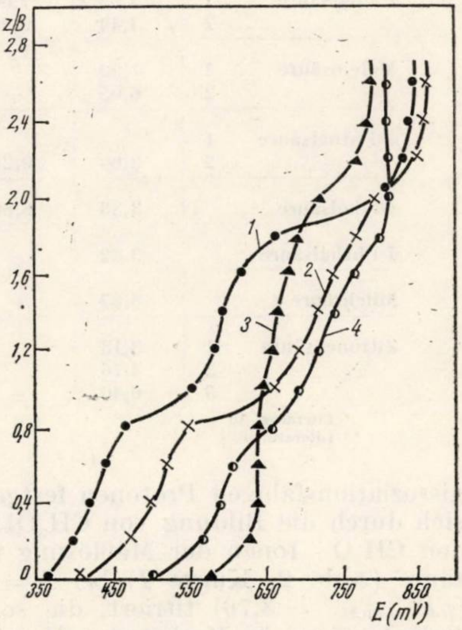

Abb. 1. — Das Verhältnis zwischen den Werten z/B und des im Laufe der Titration gemessenen Potentials.
1, Oxalsäure, *2*, Malonsäure, *3*, Bernsteinsäure, *4*, c-Phthalsäure.

---

[15] W. P. Biriukow und K. S. Ganelina, *Zhur. analit. Khim.*, **25**, 1037 (1970).

(Abb. 1) in Methanol berechnet. Die berechneten pK_a - Werte der untersuchten Säuren sind in der Tabelle 1 zusammengefaßt und mit den $pK_{a(H_2O)}$- und $pK_{a(CH_3OH)}$- Werten der Fachliteratur [13,16] verglichen.

Bei Hinzufügung einer Methanollösung von $Ca(NO_3)_2$, sogar mit einer geringeren Ionenstärke ($I = 0,18$), kann einerseits ein plötzliches Ansteigen der relativen Acidität, und andererseits eine Nivellierung der dissoziationsfähigen Protonen festgestellt werden. Diese Wirkung erklärt sich durch die Bildung von $CH_3OH_2^+$, welche im Laufe der Titration mit den CH_3O^- Ionen der Meßlösung reagieren. Demzufolge wird die Oxalsäure (Abb. 2, Kurve *I*) bei $I = 0,18$ wie eine monobasische Säure ($pK_{a(I=0,18)} = 3,76$) titriert, die so erhaltene Acidität kann mit der, der Salpetersäure in Methanol ($pK_a = 3,21$)[13] verglichen werden.

Tabelle 1

Variationen der pK_a-Werte im Verhältnis zu der Ionenstärke

Die studierte Substanz		$pK^*_{(H_2O)}$	$pK^{**}_{(CH_3OH)}$		$\Delta pK_{I_0-I_{0,95}}$	$\Delta pK_{(I_0-I_{4,37})}$
			Lit.	Ber.		
Oxalsäure	1	1,23	5,85	5,34		
	2	4,26		8,27	4,27	4,31
Malonsäure	1	3,42	—	7,66		
	2	5,11		10,64	2,41	3,16
Bernsteinsäure	1	4,19	8,85	9,32		
	2	5,57	11,40	11,19	2,07	3,22
Apfelsäure		3,65	—	9,18	3,27	3,29
Weinsäure	1	2,93	7,50			
	2	4,74	9,90	8,12	3,15	3,67
Fumarsäure	1	3,03	7,60			
	2	4,44	9,90	9,78	2,02	2,98
Maleinsäure	1	1,92				
	2	6,05	—	8,72	1,73	2,63
o-Phthalsäure	1			7,28		
	2	3,00	9,25	9,79	2,01	3,10
Glykolsäure		3,83	8,80	8,56	2,19	3,32
I-Phthalsäure		3,62	—	9,91	1,59	2,66
Milchsäure		3,87	—	6,78	2,85	3,34
Zitronensäure	1	3,13				
	2	4,76				
	3	6,40	—	9,40	3,33	3,44

* Literatur 16
** Literatur 13

---

[16] I. M. Kolthoff und V. A. Stenger, ,,Volumetric Analysis'' Intersc. Publ., New York, 1954.

Die vorhergehenden Feststellungen[17] bezüglich der potentiometrischen Titration von starken Säuren in Gegenwart neutraler Salze sind für das Verhalten der Oxalsäure auch bei Ionenstärke $I = 0{,}18$ gültig.

Aus den Kurven der bei verschiedener Ionenstärke durchgeführten Titrationen ist klar ersichtlich, daß das Ansteigen der Ionenstärke die relative Acidität dieser Säure nicht mehr beeinflußt. In diesem Falle kann sogar bei einer geringeren Ionenstärke ($I = 0{,}18$), eine Verschiebung der in der Lösung vorhandenen Gleichgewichte, in die Richtung der Bildung des $Ca(COO)_2$ Niederschlages, welcher in Methanol eine niedrigere Löslichkeit besitzt, vorausgesetzt werden. Auf Grund des oben Ausgeführten:

$$(COOH)_2 + Ca(NO_3)_2 \rightleftharpoons Ca(COO)_2 + 2H^+ + 2NO_3^- \qquad (1)$$

und die dissoziierten Protonen sind in Form von $CH_3OH_2^+$ Ionen vorhanden :

$$CH_3OH + H^+ \rightleftharpoons CH_3OH_2^+ \qquad (2)$$

Infolgedessen erklärt es sich, weshalb das Ansteigen der Ionenstärke auf die Beweglichkeit der dissoziierten Protonen keinen Einfluß besitzt. Diese Voraussetzung wird durch die Angaben bezüglich der Titration von aliphatischen Säuren in Acetonitril in Gegenwart von LiCl bestätigt.[17] Whitney-Wharton[18] erklärt die Verbesserung der Titrationen dieser Säuren, und das Ansteigen der relativen Acidität eben durch die Bildung von HCl. Diese Erklärung ist nur in jenen Fällen gültig, wenn die erhaltene relative Acidität in Folge der Zugabe von $Ca(NO_3)_2$-Lösung niedrige Werte des $p\mathrm{K}_a$ erreicht, und tatsächlich eine Möglichkeit der Verschiebung des Gleichgewichtes (1) nach rechts vorhanden ist.

Die aromatischen Dicarbonsäuren zeigen von der Lage der beiden —COOH Gruppen im aromatischen Ring verschiedene Acidität, sowohl in Methanol bei $I = O$, als auch bei verschiedenen Ionenstärken. Das vorher erörterte, kann durch Titration von Phthalsäure in Methanol bei verschiedener Ionenstärke bewiesen werden. In Methanol kann die *o*-Phthalsäure wie eine zweibasische Säure titriert werden (Abb. 3, Kurve *I*) ; im Falle von i-Phthalsäure kann nur die Gesamtacidität des Moleküls bestimmt werden (Abb. 3, Kurve *II*).

Bei hoher Ionenstärke nivelliert sich die Acidität der zwei Protonen, wobei in beiden Fällen ein Anwachsen der relativen Acidität festgestellt werden kann.

Wie auch in wässerigen Lösungen, so ist auch in Methanol die Acidität der *o*-Derivate ausgeprägter. Infolge der schwachen Löslichkeit der Terephthalsäure in Methanol, hatten wir bei den Versuchsbedingungen nicht die Möglichkeit zur Untersuchung dieser Säure. Aus den Werten der Tabelle 1 folgt, daß bei hoher Ionenstärke die Änderung der relativen Acidität niedriger ist im Falle von Fumarsäure, Maleinsäure und i-Phthalsäure $\Delta p\mathrm{K}_{(I_0 - I_{4,37})} < 3.0$.

---

[17] S. Kilpi, *Z. phys. Chem.* (*Leipzig*), **173**, 441 (1945).

[18] A. Whitney,-Wharton, *Analyt. Chem.*, **37**, 730 (1965).

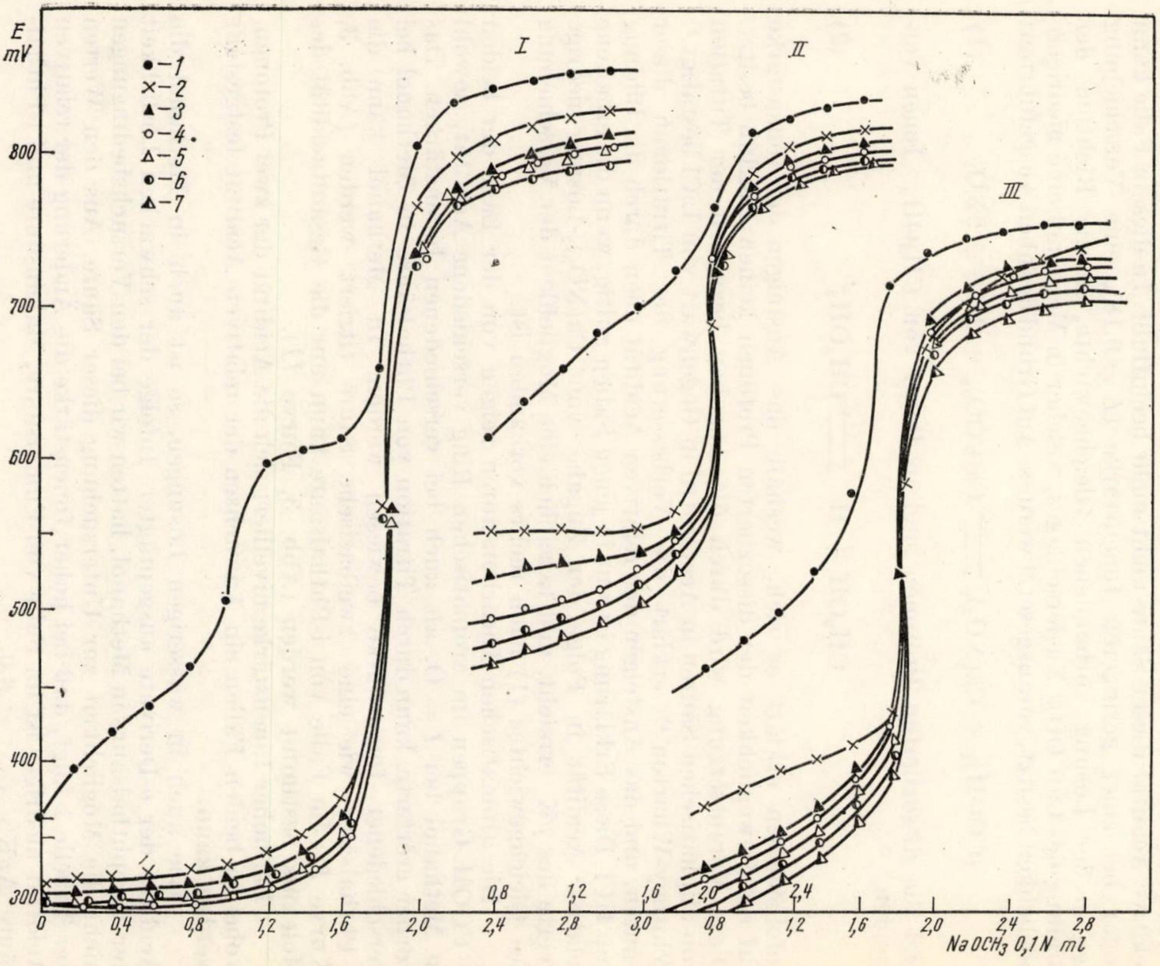

Abb. 2. — Die Titrationskurven bei verschiedener Ionenstärke.

I, – Oxalsäure, *II*. – Bernsteinsäure und *III*. – Milchsäure in 0,1 N Konzentration titriert mit $NaOCH_3$ 0,1 N

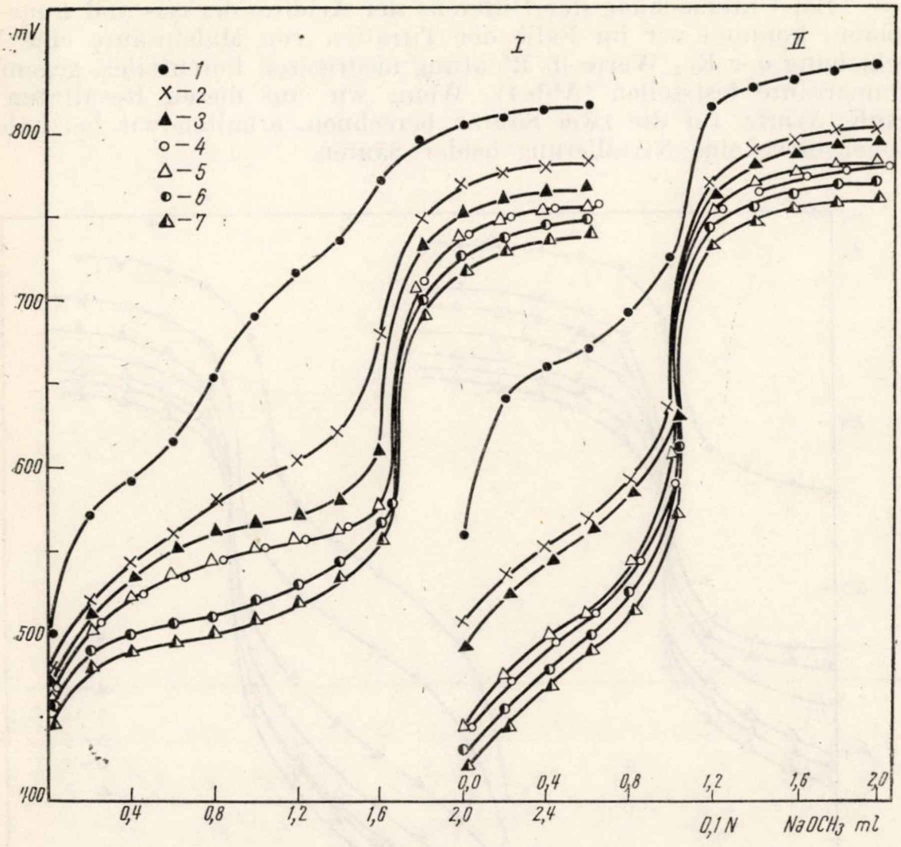

Abb. 3. – Die Titrationskurven der *I. o*-Phthalsäure und *II. i*-Phthalsäure bei verschiedener Ionenstärke, titriert in 0,1N Konzentration, mit $NaOCH_3$, 0,1 N.
1,I = 0,0; *2*,I = 0,18; *3*,I = 0,95; *4*,I = 1,90; *5*,I = 2,85; *6*,I = 3,80; *7*,I = 4,37;

Die Änderung der relativen Acidität der Hydroxysäuren ist ausgeprägter, $\Delta pK_{(I_0-I_{4,37})} = 3{,}0-4{,}0$. Es kann vorausgesetzt werden, daß zwischen $Ca(NO_3)_2$ und α-Hydroxysäuren die Bildung von Komplexen mit stärkerer Dissoziation stattfindet, z.B. :

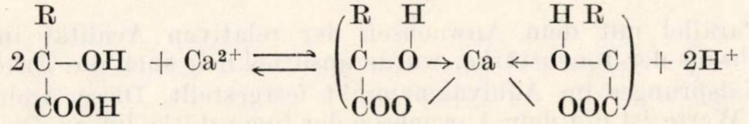

$$2\,\underset{\text{COOH}}{\overset{\text{R}}{\text{C}}}-\text{OH} + \text{Ca}^{2+} \rightleftharpoons \left(\underset{\text{COO}}{\overset{\text{R}}{\text{C}}}-\overset{\text{H}}{\text{O}} \rightarrow \text{Ca} \leftarrow \overset{\text{H}}{\text{O}}-\underset{\text{OOC}}{\overset{\text{R}}{\text{C}}} \right) + 2\text{H}^+$$

Die Feststellungen bezüglich des Verhaltens von α-Hydroxysäuren sind durch die Titrationskurven bei verschiedener Ionenstärke der Milschsäure (Abb. 2, Kurve *III*) veranschaulicht.

Bei Untersuchung der Differenz der Acidität der *cis*- und *trans*-Isomeren, konnten wir im Falle der Titration von Maleinsäure eine Verschiebung der $E_{1/2}$ Werte in Richtung niedrigeren Potentiales, gegenüber Fumarsäure feststellen (Abb.4). Wenn wir aus diesen Resultaten die $\Delta p K_a$ Werte für die zwei Säuren berechnen, erhalten wir bei höherer Ionenstärke eine Nivellierung beider Säuren.

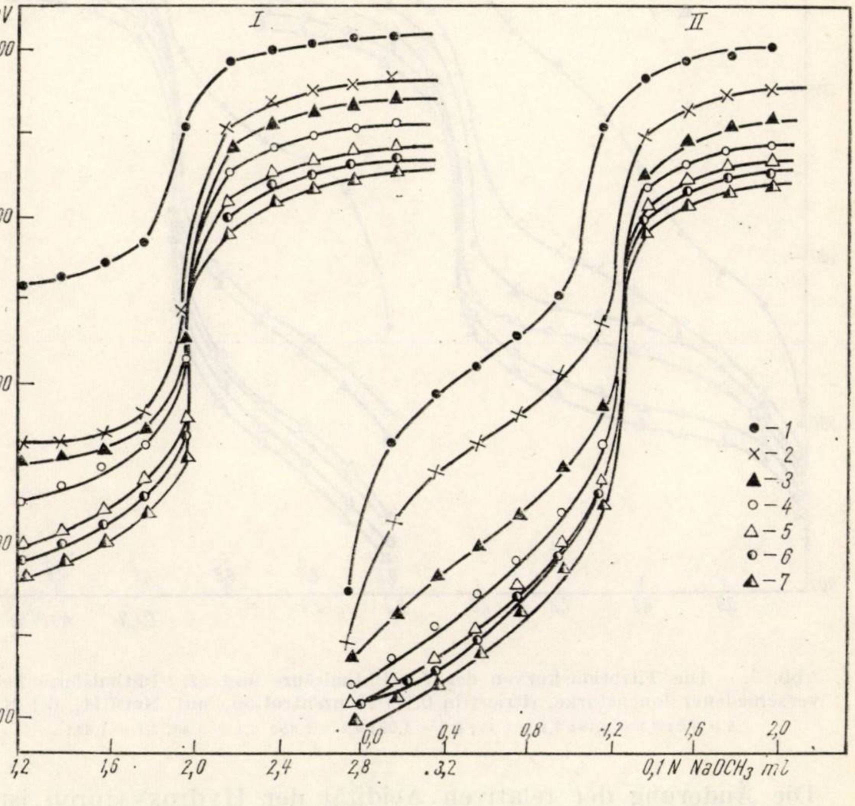

Abb. 4. — Potentiometrische Titrationskurven der I. Fumarsäure und II. Maleinsäure, titriert bei verschiedener Ionenstärke in 0,1 N Konzentration mit $NaOCH_3$ 0,1 N.

1,I = 0,0; *2*,I = 0,18; *3*,I = 0,95; *4*,I = 1,90; *5*,I = 2,85; *6*,I = 3,80; *7*,I = 4,37;

Parallel mit dem Anwachsen der relativen Acidität infolge de Anwachsens der Ionenstärke, wurde ausdrücklich auch die Erhöhung de Potentialsprunges im Äquivalenzpunkt festgestellt. Diese Änderung der $\Delta E_{\pm 1\%}$ Werte ist mit dem Anwachsen der Ionenstärke linear. Die Wirkung der $Ca(NO_3)_2$ erreicht ein Maximum bereits bei $I = 0{,}95$, die bei höherer Ionenstärke eingetretenen Änderungen sind nicht kennzeichnend. Aus den im Verhältniss der Ionenstärke (Abb. 5) dargestellten $\Delta E_{\pm 1\%}$ erfolgt eine Verbesserung der Titrationsbedingungen im Falle jeder untersuchten Säure. Der Potentialsprung erreicht hohe Werte bei $I = 4{,}37$ im Falle der Titration von Oxalsäure ($\Delta E_{\pm 1\%}$) = 123 mV) Milchsäure ($\Delta E_{\pm 1\%}$ = = 108mV), Zitronensäure ($\Delta E_{\pm 1\%}$ = 105 mV), Weinsäure ($\Delta E_{\pm 1\%}$ = 100 mV) Apfelsäure ($\Delta E_{\pm 1\%}$ = 100 mV), Glykolsäure ($\Delta E_{\pm 1\%}$ = 89 mV).

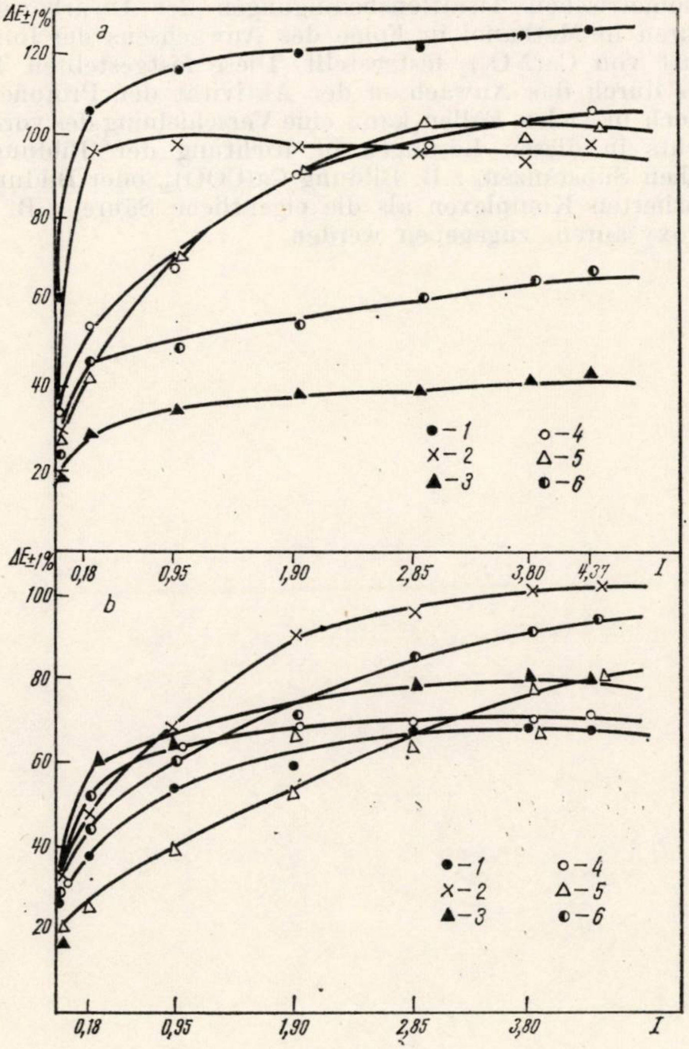

Abb. 5. – Veränderung der $\Delta E_{\pm 1\%}$-Werte im Verhältnis zum Anwachsen der Ionenstärke.

a) *1*, Oxalsäure, *2*, Malonsäure, *3*, Bernsteinsäure, *4*, Apfelsäure, *5*, Weinsäure, *6*, Zitronensäure.

b) *1*, Fumarsäure, *2*, Maleinsäure, *3*, *o*,-Phthalsäure, *4*,*i* - Phthalsäure, *5*, Glykolsäure, *6*, Milchsäure.

Revue Roumaine de Chimie, **17**, *8*, 1455–1474 (1972)

SCHLUSSFOLGERUNGEN

Als Ergebnis der durchgeführten Untersuchungen wurde ein bedeutsames Anwachsen der relativen Acidität, sowie eine Verbesserung der potentiometrischen Titrationsbedingungen der Dicarbonsäure und Hydroxysäuren in Methanol in Folge des Anwachsens der Ionenstärke, in Gegenwart von $Ca(NO_3)_2$ festgestellt. Diese festgestellten Tatsachen können teils durch das Anwachsen der Aktivität der Protonen erklärt werden, jedoch in vielen Fällen kann eine Verschiebung des vorhandenen Gleichgewichts in diesen Lösungen in Richtung der Bildung einiger schwerlöslichen Substanzen, z.B. Bildung $Ca(COO)_2$, oder Bildung einiger besser dissoziierten Komplexen als die eigentliche Säure, z.B. im Falle der α-Hydroxysäuren, zugegeben werden.

Revue Roumaine de Chimie, 17, 8, 1475–1481 (1972)

DETERMINATION OF CODEINE PHOSPHATE
VISIBLE AND IR SPECTRA OF THE COMPOUND OBTAINED BY THE COMBINATION WITH AMMONIUM REINECKATE

GRIGORE TEODORESCU

Polytechnic Institute Bucharest
Department of Inorganic and Analytic Chemistry
Str. Polizu 1, Bucharest, Romania

Received December 20, 1971

The present paper presents a method of determining codeine as free base, hydrochloride or phosphate, based upon its combination with ammonium reineckate, the dissolving of the obtained compound into acetone, followed by the precipitation of the reineckate anion as silver reineckate and the titration of the silver nitrate excess with ammonium thiocyanate. Because the complex compound of codeine is soluble in acetone, forming a red solution, it can be determined colorimetrically. The method can be applied to impure substances, too. The structure of the complex resulted from the combination of codeine and reineckate has been specified by calculating its molecular mass using the visible spectrum of the ammonium and codeine reineckate. For the structural characterization of the codeine reineckate, the IR spectrum of the codeine and its complex has also been analysed.

Codeine (the methylic ether of morphine) is an alkaloid of the opium, which can be used as drug (against cough) because, on the one hand, it lacks the narcotic properties of morphine (which can lead to coma) and on the other hand has its analgesic properties (insensitivity to pain) much diminished.

The codeine contains, like the morphine, an OH group of a secondary alcohol, an ethereal bridge, a methylic group connected to the secondary aminic nitrogen, a benzene and cyclohexene nuclei. The difference consists in the fact that the phenolic group of the morphine is methylated to the codeine.

The codeine is commercialized as base, hydrochlorate or phosphate. In the following, the method for determining the codeine-phosphate will be exposed.

The usual determination method for codeine-phosphate is based upon its conversion into the base, its extraction by means of chloroform, its evaporation to dryness and titrating the group CH_3-NHR with HCl 0.1 n (at methyl red).[1]

---

[1] D. Horn, *Pharm.*, 6, 332 (1951).

As this method requires too long a time, it has been considered necessary to find a new method for the determination of codeine phosphate (CP), by combining the 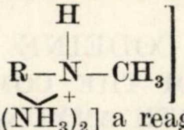 $\left.R{-}\overset{H}{\underset{+}{N}}{-}CH_3\right|H_2PO_4$ ion with the ammonium reineckate $NH_4^+[Cr(NCS)_4(NH_3)_2]$ a reagent which we used for the determination of other substances, too.[2-11] (abbridged $Rc^-NH_4^+$).

The method is feasible especially because the complex resulting from the combination between the $Rc^-NH_4^+$ and the CP is practically insoluble in water and easily soluble in acetone.

THE PRINCIPLE OF THE METHOD

The combination reaction of the CP takes place in an aqueous, slightly acidulated solution, with 1 mole $Rc^-NH_4^+$ and develops according to the following scheme (R = molecular rest of codeine)

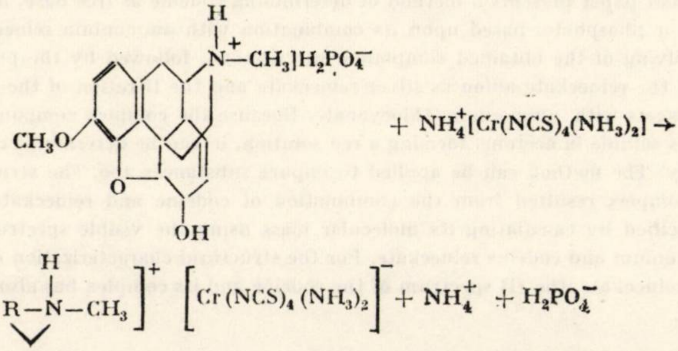

This combination reaction has been used for the determination of codeine in volumetrical, colorimetric and spectral methods.

1. THE VOLUMETRIC METHOD

The aqueous solution of codeine has been acidulated with sulphuric acid 2% and precipitated with $Rc^-NH_4^+$ 2%. The obtained precipitate has been filtered, water-washed and dissolved in acetone. From the solution the silver reineckate precipitates in an excess of nitric acid, according to the equation :

$$[Cr(NCS)_4(NH_3)_2] + Ag^+ \longrightarrow Ag[Cr(NCS)_4(NH_3)_2]$$

[2] P. Spacu and Gr. Teodorescu, *Rev. Chim.*, București, **8**, (1), 41 (1957).

[3] Gr. Teodorescu, *Bul. Inst. Politeh. București*, **29**, (5), 83 (1967).

[4] Gr. Teodorescu and Il. Niculescu, *Bul. Inst. Politeh. București*, **30**, (1), 17 (1968).

[5] Gr. Teodorescu, *Bul. Inst. Politeh. București*, **31**, (3), 51 (1969).

[6] Gr. Teodorescu, *Bul. Inst. Politeh. București*, **31**, (4), 45 (1969).

[7] Gr. Teodorescu, *Bul. Inst. Politeh. București*, **31**, (5), 61 (1969).

[8] Gr. Teodorescu, *Bul. Inst. Politeh. București*, **32**, (1), 43 (1970).

[9] Gr. Teodorescu, *Bul. Inst. Politeh. București*, **32**, (2), 39 (1970).

[10] Gr. Teodorescu, *Bul. Inst. Politeh. București*, **32**, (4), 79 (1970).

[11] Gr. Teodorescu, *Bul. Inst. Politeh. București*, **33**, (1), 67 (1971).

The precipitated silver reineckate has been filtered and washed and the excess of nitric acid titrated in the filtrate by means of ammonium thiocyanate 0.1 n in the presence of iron (III) alumen and ammonium as an indicator.

The calculation (as well as the equations) have been made without taking into account the crystallization water of the CP.

The method is, by all means, applicable to the codeine hydrochlorate (in an aqueous or slightly acidulated medium) or to the base (in acidulated aqueous medium).

1.1. *Experimental*

1.9150 g codeine phosphate (whire crystalline powder) pharmaceutical product are weighed and quantitatively brought in a standard flask of 250 ml with distilled water. After dissolving the substance, the solution is filled up to the mark with distilled water until a concentration of 0.00766 g/ml is obtained.

Tastes of 2–10 ml are taken out of this solution, an equal volume of sulphuric acid 2% is added and is precipitated with a freshly prepared solution of $Rc^- NH_4^+$ 2% (5–15 ml), by gradual addition and continuous stirring until the solution above the precipitate becomes intensely violet-red. A 5 minutes rest is required before dilution in 15–20 ml of water (thus the precipitate being more easily agglomerated). The product obtained is filtred on a G_3 filtrating crucible and drawn with ether after the depositing.

The direct compound is dissolved on the filtrating crucible in 10–20 ml acetone and the crucible is washed in 15–20 ml distiled water, all substances being collected in a 250 ml glass. The product is diluted in 100 ml distilled water, and 10 ml silver nitrate 0.1 n and 3–4 drops of nitric acid 2 n are added. The silver reineckate precipitates. This is filtred, washed by settling in distilled water and the filtrate is collected together with the washing water in a 750 ml titrating decanter. In the same decanter 0.5–1 ml nitric acid 2n, 1 ml saturated solution (about 40%) of iron (III) alumen and ammonium are added and the excess of silver nitrate is titrated by means of ammonium thiocyanate 0.1 n of known factor.

To 1 ml $AgNO_3$ 0.1 n correspond 0.03974 g codeine phosphate.

The results are given in table 1.

Table 1

Results of the CP determination by the volumetric method

CP taken in tastes by acidimetric titration	$AgNO_3$ before precipitation	NH_4SCN $F_{0.1n} = 1.0526$	$AgNO_3$ reacted	CP 100% determined by means of $Rc^-NH_4^+$	CP 100% determined by means of $Rc^-NH_4^+$
g	ml	ml	ml	g	%
0.01532	10	9.62	0.38	0.01510	98.75
0.02298	10	9.44	0.56	0.02254	98.01
0.03064	10	9.24	0.76	0.03020	97.57
0.03830	10	9.05	0.95	0.03775	98.56
0.04596	10	8.86	1.14	0.04530	98.57
0.05362	10	8.66	1.34	0.05325	99.00
0.06128	10	8.49	1.51	0.06000	97.92
0.06894	10	8.30	1.70	0.06756	97.99
0.07660	10	8.10	1.90	0.07551	98.44

Revue Roumaine de Chimie, **17**, *8*, 1475–1481 (1972)

2. COLORIMETRIC METHOD

2.1. *The Principle*

The CP and $Rc^-NH_4^+$ react the same way as in the volumetrical method, in a molar ratio of 1 : 1. As the product is soluble in acetone, forming a red solution, the CP can be colorimetrically determined too.

2.2. *Working Scheme*

The method of standard curves has been used. Corresponding volumes of a required solution of $Rc^-NH_4^+$, with T=0.014 g/ml, were taken in standard flasks of 100 ml and diluted in 50 ml of acetone. They were filled up to the mark with distilled water. Solution of concentrations T = 0.000147 ; 0.000294 ; 0.000441 ; 0.000588 were obtained.

The reading occurred with a B. Lange photocolorimeter, using green filters (λ = 533 nm) and the standard was drawn. Tastes of 0.01915–0.03447 were taken out of the CP solution of T = 0.00766 g/ml and precipitated with $Rc^-NH_4^+$ as in the volumetric method.

After the precipitation, filtration and washing, the tastes were quantitatively dissolved in acetone, the solution being collected in 100 ml standard falsks and filled up to the mark with distilled water. After homogenization they were colorimetered and the obtained results given in table 2.

Table 2

Results of the colorimetration of C.P. reineckate

CP in gram-tastes	Determined CP in grams	Error %
0.0001915	0.0001895	–1.05
0.0002298	0.0002258	–1.74
0.0002681	0.0002650	–1.54
0.0003064	0.0003006	–1.92
0.0003447	0.0003400	–1.39

3. SPECTRAL STUDY

3.1. *Characterization of the visible spectrum of the Codeine Reineckate*

The structure of the compound, whose preparation of CP and $Rc^-NH_4^+$ we mentioned above, can be specified by determining its molecular mass, according to the absorbance (A) and the absorptivity (K) of the visible spectrum.

A common feature of the visible spectrum for $Rc^-NH_4^+$ and for the CP reineckate is that the absorption maximum (λ_{max}) is nearly the same : for $Rc^-NH_4^+$ (in 95% ethanol) λ_{max} = 520–525 nm (1-st diagram) and for CP reineckate (in 95% ethanol) λ_{max} = 520–530 nm (2-nd diagram).

The determination of the absorptivity (K) was made according to the following relation, with $Rc^-NH_4^+$ in 95% ethanol at a concentration $c = 0.00297$ gram-mole $Rc^-NH_4^+$ in a 0.5 cm long tube and for an absorbance $A = 0.154$ read on the 1-st diagram and corresponding to the value : $\lambda_{max} = 520-525$ nm.

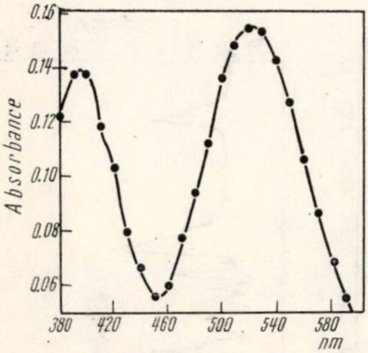

Fig. 1. – Diagram of the visible absorbancy for ammonium reineckate $g_1 = 0.1\%$; $l = 0.5$ cm ; solvent = ethanol 95%.

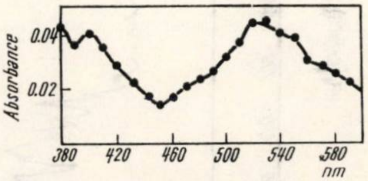

Fig. 2. – Diagram of the visible absorbancy for codeine reineckate $g_1 = 0.1\%$; $l = 0.5$ cm ; solvent = ethanol 95%.

Because the determinations were made with $l=0.5$ cm the value A will be doubled for $l = 1$ cm.

$$K_{ethanol} = 2 \times 0.154/0.00297 = 103.7$$

The value K, determined for $Rc^{-}NH_4^{+}$ can be considered within the limits of admissible errors, as being also available for the CP reineckate, as λ_{max} for the CP reineckate is equal (or nearly so) to λ_{max} for $Rc^{-}NH_4^{+}$ (1-st and 2-nd diagrams).

In order to determine the molecular mass (M_d), the following relation will be used :

$$M_d = g_1/100 . K/A . l . 100 \tag{1}$$

In case $g_1 = 0.1$ g of CP reineckate per 100 ml of solution and $l = 1$ cm, the relation (1) becomes :

$$M_d = K/A \tag{2}$$

Practically, the determination of the visible absorption of the CP reineckate in 95% ethanol is made. The absorbance is 0.042 for $\lambda_{max} = 520-530$ nm in a concentration of 0.05% and in a 0.5 cm long tube, in the above mentioned working conditions.

Applying relation (2) for $l = 1$ cm, the result is :

$$M_d = 103.7/4 \times 0.042 = 617.26$$

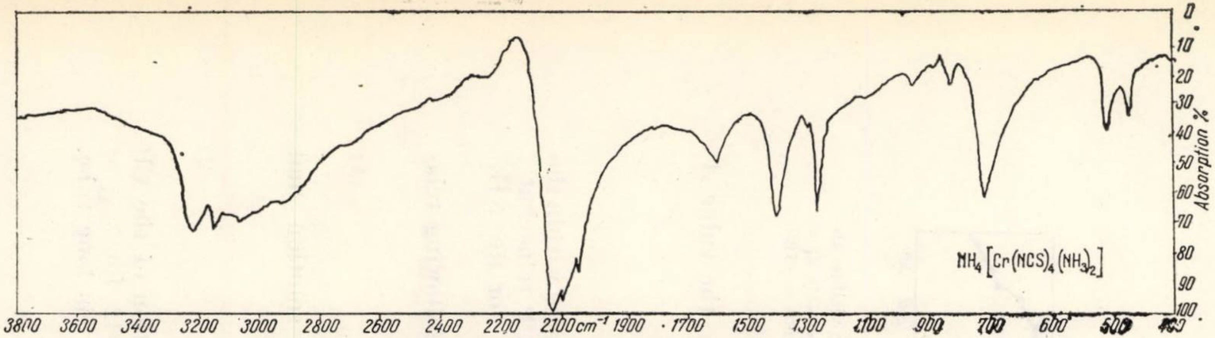

Fig. 3. — IR of ammonium reineckate.

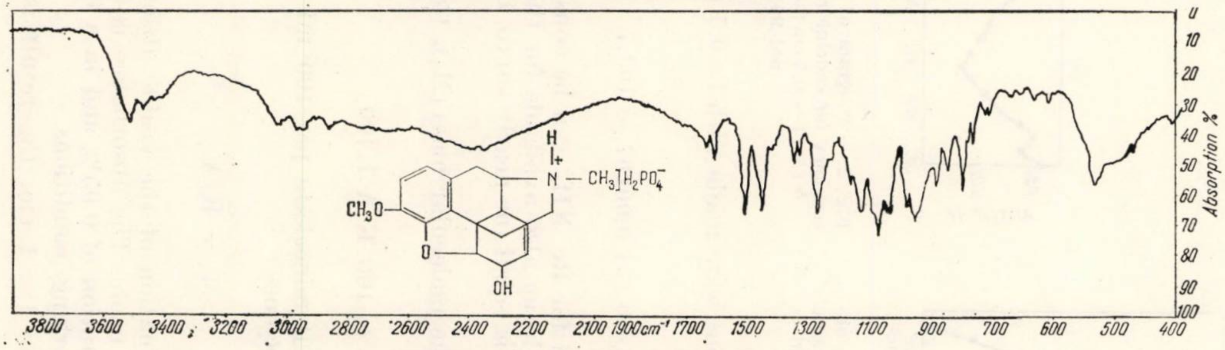

Fig. 4. — IR of codeine phosphate.

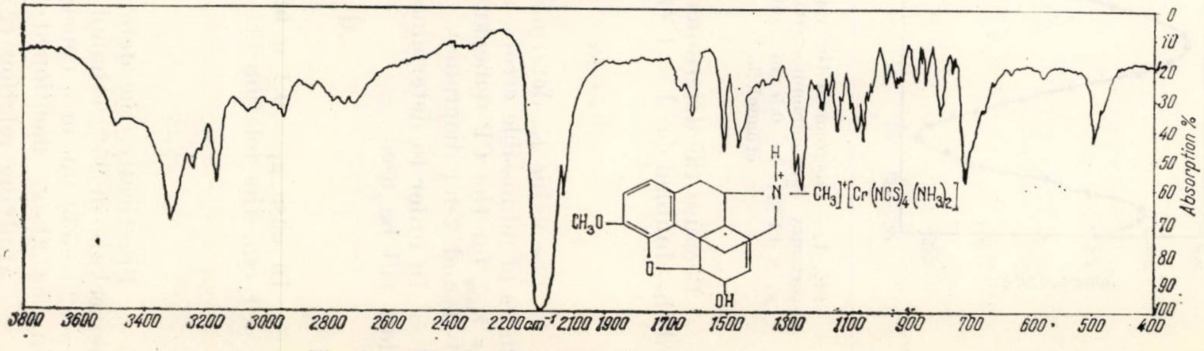

Fig. 5. — IR of codeine reineckate.

Comparing this value with the calculated molecular mass ($M_c = 617.73$), the conclusion that the structure of the compound is one of the monoreineckate type, can be drawn.

3.2. *The IR characterization of the codeine reineckate*

The IR spectrum of the codeine as such and of its complex, has also been carried out in order to structurally characterize the codeine reineckate.

The IR spectrum of the codeine reineckate has been interpreted by comparing it with the $Rc^-NH_4^+$ and the CP spectrum (see figures 3, 4 and 5)

The IR spectrum of the complex shows bands found in the IR spectrum of ammonium reineckate, which can be assigned to the NH_3 and NCS groups in the reineckate anion of the compound. They appear at 498 cm^{-1} (δ_{NCS}), 1257 cm^{-1} (δ^{sym}_{N-H} NH_3), 2095 cm^{-1} (ν_{C-N}) 3165 – –3315 cm^{-1} (ν^{sym}_{N-H} NH_3).

It also shows the band corresponding to the organic base (fig. 5). These bands existing at 795 cm^{-1}, 1075 cm^{-1}, 1140 cm^{-1}, 1469 cm^{-1}, 1512 cm^{-1} are very slightly changed as to their position and intensity in the IR spectrum of the combination under study, this being another proof supporting the scheme given in the principle of the determination method.

J. TÖLGYESSY, T. BRAUN, M. KYRŠ, *Isotope Dilution Analysis.* Akadémiai Kiadó, Budapest, 1972, 194 p.

Although elaborated since 1932 by Hevesy and Hobbie, a development of isotope dilution analysis and remarkable applications of this method have been recorded only in the last 15 years. Without reaching the proportion and development of the activation analysis, the isotope dilution analysis distinguishes itself by a high sensitivity in the microquantities of inorganic ions or organic compounds determination in the presence of great quantities of other ions or substances having tightly related chemical properties.

In principle, the isotope dilution consists in the addition to the original mixture of a radioactive isotope of the interested component having a known specific activity and, after homogenization, the pursued component is separated by an adequate method, purified and the specific activity is measured. The change in the specific activity of the radioactive substances allows the calculation of the respective element concentration. The great advantage of the method consists in the fact that the isolation of the whole quantity of the element to be determined and the knowledge of the losses occurred during the separation are not required. There are several variants of the method.

The about 800 papers published in this rich field are for the first time discussed in a monograph by J. Tölgyessy, Professor at the Slovak Technical University, Bratislava, Dr. T. Braun of the Institute of Inorganic and Analytical Chemistry of the Eötvös Loránd University, Budapest, Hungary and Dr. M. Kyrš of the Nuclear Reasearch Institute, Czechoslovak Academy of Sciences, Czechoslovakia.

After setting forth the general principles of the isotope dilution variants, the place of the method in the frame of the nuclear analysis proceedings is indicated, the theoretical basis of each variant and the mathematical relations for the concentration calculation are given, as well as the accuracy and sensitivity of the isotope dilution analysis.

A particular attention was given to the substoichiometric isotope dilution. Advantages, drawbacks and trends of this method are also discussed.

In the following chapter the authors show the experimental techniques. The chemical purity of analytical reagens and tracers, the separation and purification proceedings of the component to be determined and the proceedings used in the determination of the masses of the separated fractions are also given.

The third chapter deals with the inorganic applications. The element determined,the matrix, the tracer, the amount determined, the separation process, the mass determination and references are given in tables. Such a synoptic table facilitates the rapid choice of the desired variant and is at the same time useful for the researcher looking for new variants or improvements of existent methods. Further on, five representative proceedings are selected and described in detail. According to the opinion of the author of this review, several such examples should be desirable.

The isotope dilution applications to the analysis or organic compunds are described in the following chapter. The successes of the method are briefly commented upon compounds classes.

Chapter five is treating the isotope dilution analysis with stable isotopes. In this case, instead of specific activity measurement, the natural isotope ratio change is established by mass spectrometry. The method is used in the analysis of about 80 % of elements.

The last chapter includes the special applications of isotope dilution. The possibilities to use the method in the determination of water in the human body, of the extracellular fluid, of the volume of erythrocytes, plasma and blood etc. and of some important constants and values in the analytical and physical chemistry are shown. The possibility to determine the solubility of the precipitates of dissociation constants, of the capacity of ion exchangers, on determining the radioactive contaminants, of the coefficient of seld-absorption and the specific activty are also stated.

Written in a concise manner, but perfectly clear, the present monograph is of a great practical utility for the radiochemists as well as for the scientific researchers in various branches of chemistry, interessed in these methods.

For a further edition, we would suggest a greater emphasis laid also on the saturation analysis, a new variant of the isotope, with efficient application in biochemistry.

Dr. Tiberiu Năşcuţiu

ORSZÁGOS MŰSZAKI KÖNYVTÁR ÉS DOK. KÖZPONT

NOTE POUR LES AUTEURS

La *Revue Roumaine de Chimie* publie des articles en anglais, français, russe, allemand ou espagnol. Les auteurs sont priés d'envoyer des articles, notes, communications et comptes rendus inédits.

Les manuscrits seront dactylographiés à deux intervalles. Les tableaux seront dactylographiés sur feuilles séparées, de même que la légende des figures. Les diagrammes seront tracés à l'encre de Chine sur papier calque. Les tableaux et les figures seront numérotés par des chiffres arabes, en nombre strictement nécessaire. Prière de ne pas inscrire les mêmes données dans les tableaux et les figures. Les formules chimiques seront incluses dans le texte ; en outre, elles seront transcrites sur des feuilles séparées. Les auteurs sont priés d'indiquer les caractères italiques (en soulignant les lettres au crayon), ainsi que tout autre caractère spécial. L'ordre des références bibliographiques sera celui de leur mention dans le texte ; le nom de l'auteur sera précédé de l'initiale du prénom ; les publications périodiques seront présentées suivant les prescriptions internationales. Les références seront ajoutées à la fin de l'article ; elles paraîtront comme des notes, au bas de la page. Le texte sera précédé d'un résumé, comprenant 15 lignes au maximum.

L'entière responsabilité du contenu des articles appartient aux auteurs. On publie des articles dus aux collaborateurs roumains ou étrangers. Les auteurs recevront 50 tirés à part.

PRINTED IN ROMANIA

1972 OKT 1 8

TRAVAUX PARUS AUX ÉDITIONS DE L'ACADÉMIE DE LA RÉPUBLIQUE SOCIALISTE DE ROUMANIE

I. ZUGRĂVESCU et L. STOICESCU-CRIVETZ, **Polimeri heterociclici** (Polymères hétérocycliques), 1971, 190 p., 9,50 lei.

CORNEL BODEA et collab., **Tratat de biochimie vegetală**, partea I, **Fitochimie** (Traité de biochimie végétale, Ire partie, Phytochimie), Ier vol., 1964, 747 p. + 4 annexes + 2 pl., 41 lei; IIe vol., 1965, 1262 p., 1 pl., 56 lei, IIIe vol., 1967, 773 p., 35 lei.

V. GHEȚIE et V. MICUȘAN, **Analiza imunochimică. Teorie și practică** (Analyse immunochimique. Théorie et pratique), 1966, 369 p., 28 lei.

SILVIA IONESCU, **Reacții chimice induse de radiațiile ionizante** (Réactions chimiques produites par les radiations ionisantes), 1963, 271 p., 15 lei.

MARIETA NICOLAE, **Fizico-chimia proceselor fotografice** (Physico-chimie des processus photographiques), 1964, 426 p. + 4 pl., 35 lei.

R. PORTOCALĂ et L. POPA, **Acizii ribonucleici celulari și virali** (Les acides ribonucléiques cellulaires et viraux), 1966, 375 p., 8 pl., 26 lei.

D. PURDELA et R. VÎLCEANU, **Chimia compușilor organici ai fosforului și ai acizilor lui** (La chimie des composés organiques du phosphore et de ses acides), 1965, 540 p., 37 lei.

CRISTOFOR SIMIONESCU, MARGARETA GRIGORAȘ et AGATA CERNĂTESCU-ASANDEI, **Chimia lemnului din R.P.R.** (La chimie du bois en Roumanie), 1964, 239 p. + 6 pl., 27 lei.

CRISTOFOR SIMIONESCU et CLEOPATRA VASILIU-OPREA, **Mecanochimia compușilor macromoleculari** (La mécanochimie des composés macromoléculaires), 1967, 344 p., 23,50 lei.

I. MAXIM, **Materiale nucleare** (Matériaux nucléaires), 1969, 444 p., 30 lei.

I P.I. c. 1526

43 426

Lei 25.—

F 1103 04-001

REZERVA

REVUE ROUMAINE DE CHIMIE

Tome 17

N° 9

Septembre 1972

RRCHAX, 17, (9), 1485–1634 (1972)

ÉDITIONS DE L'ACADÉMIE DE LA RÉPUBLIQUE SOCIALISTE DE ROUMANIE

Rev. Roumaine Chim. 17, 9, p. 1485–1634 (1972) Bucarest

COMITÉ DE RÉDACTION

Rédacteur en chef:

I. G. MURGULESCU, membre de l'Académie de la République Socialiste de Roumanie

Rédacteurs en chef adjoints:

A. T. BALABAN et V. E. SAHINI, membres correspondants de l'Académie de la République Socialiste de Roumanie

Collège de rédaction:

C. DRĂGULESCU, RALUCA RIPAN, CR. SIMIONESCU, membres de l'Académie de la République Socialiste de Roumanie ; EM. BRATU, ECATERINA CIORĂNESCU-NENITZESCU, P. SPACU, membres correspondants de l'Académie de la République Socialiste de Roumanie ; MARGARETA AVRAM, D. I. MARCHIDAN, G. NIAC et D. SĂNDULESCU

La Revue Roumaine de Chimie paraît 12 fois par an. Toute commande de l'étranger (fascicules ou abonnements) sera adressée à Întreprinderea Rompresfilatelia B. P. 2001, telex 011631, Boîte Postale 134—135, Bucarest, Roumanie

Les manuscrits, les livres et les revues proposés en échange, ainsi que toute correspondance seront envoyés à la rédaction :

REVUE ROUMAINE DE CHIMIE
23, str. Dumbrava Roşie, Bucarest, Roumanie

ÉDITIONS DE L'ACADÉMIE DE LA RÉPUBLIQUE SOCIALISTE DE ROUMANIE
3 bis, str. Gutenberg, Bucarest, Roumanie

ORSZÁGOS MŰSZAKI KÖNYVTÁR ÉS DOKUMENTÁCIÓS KÖZPONT

REVUE ROUMAINE DE CHIMIE

Tome 17, Nº 9 Septembre 1972

Page

D. I. MARCHIDAN and SPERANȚA MATEI, Thermodynamic data for some uranium oxides with nonstoichiometric compositions 1487–1491

D. I. MARCHIDAN, LIANA PANDELE and ALA NICOLESCU, Thermal properties of alumina TA 600. Heat content at high temperature 1493–1496

ȘTEFANIA ZUCA, I. D. SOKOLOVA, D. GĂGESCU and M. OLTEANU, Density and electrical conductivity of melted metaphosphates 1497–1502

LETIȚIA TOPOR, Vapour pressures of molten magnesium, cadmium and zinc chlorides 1503–1508

T. CHIRULESCU, CORNELIA CIOBANU and GH. ȘERBAN, Reduction studies on nickel oxide catalysts 1509–1516

C. DRĂGULESCU, P. TRIBUNESCU und OLGA GOGU, Lösungsgleichgewicht von MgO aus Serpentinen durch Einwirkung von CO_2 und Wasser 1517–1524

MIHAELA OLTEANU and MARTA STAN, Conductometric study of some mercuric complexes 1525–1530

A. T. BALABAN, Chemical graphs. XVII. (Aromaticity. X) *cata*-condensed polycyclic hydrocarbons which fulfill the Hückel rule but lack closed electronic shells 1531–1543

MARIA NUȚIU, FR. MARX and G. OSTROGOVICH, Studies of the biuret reaction. VII. Crystalline structure of the natrium-copper(II)-tetracyanurate hexahydrate and of its two anhydrous states 1545–1549

M. VOICU and F. BADEA, Kinetics of solvolytic reactions. II. Acetolysis of 5H-dibenzo[a, d]cycloheptene-5-yl-methyl tosylate under thermodynamic control 1551–1562

M. VOICU, F. BADEA and AURORA BUCUR, Kinetics of solvolytic reactions. III. Intermediates involved in the acetolysis of 5*H*-dibenzo[a, d] cycloheptene-5-yl-methyl tosylate and 9,10-bis(hydroxymethyl)-9,10-dihydroanthracene ditosylate 1563–1577

M. ARSHAD A. BEG and IRSHAD A. KHAN, Correlation of the physical properties of organosilicon compounds. I. Boiling point and density of substituted silanes and siloxanes and the additivity of density 1579–1598

M. ARSHAD A. BEG and IRSHAD A. KHAN, Correlation of the physical properties of organosilicon compounds. II. Boiling point, refractivity and density of silanes and siloxanes 1599–1609

Rev. Roumaine Chim. **17**, *9*, 1485 – 1634 (1972), Bucarest

S. H. DOSS, More proofs for a characteristic band in the infrared spectrum of sultams 1611–1614

C. LITEANU, I. C. POPESCU and H. NAŞCU, On the possibility of using Ag_2S ceramic-membrane electrode for the determination of the concentration of solutions in flow conditions. Chromatographic detector . . . 1615–1619

GR. TEODORESCU, Méthodes de détermination de la vitamine B_1 (chlorhydrate de thiamine ou aneurine). Caractéristiques spectrales en visible et infrarouge du produit obtenu 1621–1627

I. C. POPESCU and C. LITEANU, Characterization of ceramic ion-selective membrane electrodes. II. Redox behaviour of the Ag_2S membrane electrode 1629–1633

Revue Roumaine de Chimie, **17**, *9*, 1487–1491 (1972)

THERMODYNAMIC DATA FOR SOME URANIUM OXIDES WITH NONSTOICHIOMETRIC COMPOSITIONS

D. I. MARCHIDAN and SPERANȚA MATEI

Centre of Physical Chemistry
Str. Galați 31, Bucharest, Romania

Received March 22, 1972

Electromotive force measurements on high-temperature galvanic cells containing solid electrolyte have been made in order to obtain thermodynamic data for some uranium oxides which within certain temperature ranges are found disproportionated in two phases. Partial molar free energies, enthalpies and entropies of solution of oxygen in uranium oxides and the corresponding relative integral quantities as a function of the temperature, as well as the equilibrium pressures of oxygen over the two oxides have been calculated.

Owing to the existence of the different phases in certain homogeneity ranges, the composition of which depends upon the temperature, the thermodynamics of the uranium-oxygen system is necessarily complicated.

Although many of the high temperature thermodynamic data for uranium compounds in the $UO_2-U_4O_9-U_3O_{8-y}$ regions are now reliable and well established, a number of inconsistencies still remain and there are some thermodynamic data still lacking for uranium compounds. More data are required on the limits of the UO_{2+x}, U_4O_9, U_3O_{8-y} phases as a function of the temperature, because there are still some doubts concerning the precise position of the phase boundaries.

The measurements of electromotive force on galvanic cells with solid electrolyte proved to be an efficient method in the study of the thermodynamic properties of uranium oxides.[1-4]

In previous papers [4,5] we have related the values of the thermodynamic properties for some uranium oxides having different nonstoichiometric compositions obtained by the EMF method with solid electrolyte cells. Carrying on these studies, determinations were effected about some oxides which within certain temperature ranges are found dispro-

---

[1] S. Aronson and J. Belle, *J. Chem. Phys.*, **29**, 151 (1958).

[2] K. Kiukkola, *Acta Chem. Scand.*, **16**, 327 (1962).

[3] T. L. Markin, L. E. J. Roberts and A. Walter, "Thermodynamics of Nuclear Materials", Ed. IAEA, Vienna, 1962, p. 693.

[4] D. I. Marchidan and S. Matei, *Rev. Roumaine Chim.*, **15**, 1491 (1970).

[5] D. I. Marchidan and S. Matei, *Rev. Roumaine Chim.*, **17**, 195 (1972).

portionated in two phases. To this purpose EMF measurements were effected on cells with solid electrolyte of the type:

$$\text{Fe, wüstite} \mid (0.85\ ZrO_2 + 0.15\ CaO) \mid UO_{2+x}$$

EXPERIMENTAL

The cell assembly consisting of the electrolyte tablet between the two electrode tablets was inserted into a quartz cell, the form and construction of which have been previously shown.[4,6]

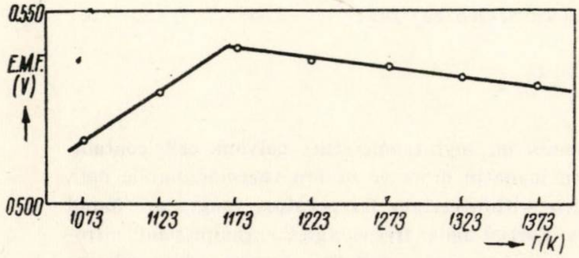

Fig. 1. — Variation of EMF with the temperature for $UO_{2.18}$.

The EMF measurements were carried out in a vacuum installation at the residual gas pressure of about $133 \times 10^{-6}\ N.m^{-2}$. The apparatus, the experimental procedure and the techniques of preparing the tablets were also minutely described in the above mentioned papers.[4,6]

RESULTS AND DISCUSSION

The EMF measurements were effected within the temperature range of 1073–1373 K.

For the oxide having the atomic ratio 2.18 we obtained for EMF a dependence on the temperature having the form shown in Figure 1. We can observe a definite break in the EMF *vs.* temperature curve at about 1160 K. This break indicates a phase transformation at this temperature; the homogeneous phase UO_{2+x} prevails above this temperature, while below it the phases $UO_{2+x} + U_4O_{9-y}$ coexist.

The values of the partial molar free energy of oxygen in equilibrium with the uranium oxides for temperatures comprised between 1073—1373 K are shown in Table 1. The dependence on the temperature of $\Delta\overline{G}_{O_2}$ must be separately calculated for temperature ranges situated on each side of the transformation point, that is for temperature ranges in which phase transformations do not take place.

Thus, for the temperature range in which there is a single phase UO_{2+x} we determined the relationship:

$$\Delta\overline{G}_{O_2}\ (\text{KJ.mol}^{-1}) = -\ 299.043 + 0.112\ T \qquad (1)$$

---

[6] D. I. Marchidan and S. Matei, *Studii şi Cercetări Chim., Acad. R.S.R.*, **18**, 617 (1970).

Table 1

Thermodynamic data for $UO_{2.18}$

Temp. K	$-\Delta\bar{G}_{O_2}$ (KJ.mol^{-1})	$-\Delta G$ (KJ.mol^{-1})	$-\Delta G/n_{UO_2}$ (KJ/g.atom uranium)	$-\log p_{O_2}$ (N.m^{-2})	$-\Delta\bar{H}_{O_2}$ (KJ.mol^{-1})	$-\Delta H$ (KJ.mol^{-1})	$-\Delta H/n_{UO_2}$ (KJ/g. atom uranium)	$-\Delta\bar{S}_{O_2}$ (KJ.K^{-1}.mol^{-1})	$-\Delta S$ (KJ.K^{-1}.mol^{-1})	$-\Delta S/n_{UO_2}$ (KJ.K^{-1}/g.atom uranium)
1073	188.869	15.623	17.033	4.225	435.428	35.919	39.174	0.229	0.019	0.021
1123	176.853	14.698	16.021	3.293	435.428	35.919	39.174	0.229	0.019	0.021
1173	166.958	13.773	15.012	2.440	299.043	24.668	26.903	0.112	0.009	0.010
1223	161.523	13.326	14.522	1.904	299.043	24.668	26.903	0.112	0.009	0.010
1273	155.703	12.844	13.999	1.394	299.043	24.668	26.903	0.112	0.009	0.010
1323	150.272	12.397	13.510	0.938	299.043	24.668	26.903	0.112	0.009	0.010
1373	144.448	11.916	12.987	0.500	299.043	24.668	26.903	0.112	0.009	0.010

and for the temperature range in which UO_{2+x} is found disproportionated in $UO_{2+x} + U_4O_{9-y}$ it has been stated that:

$$\Delta\overline{G}_{O_2}\ (\text{KJ.mol}^{-1}) = -435.428 + 0.229\ T \tag{2}$$

In a previous paper[5] thermodynamic data for uranium oxides with atomic ratio of 2.19 and 2.21 were related. For these compositions we also obtained a definite break at certain temperatures of the curves EMF as a function of the temperature, which shows a phase transformation. The equations which give the dependence on the temperature of $\Delta\overline{G}_{O_2}$ for these compositions in the single-phase UO_{2+x} and in the two-phase regions respectively, were the following:

Fig. 2. – Variation of EMF with the temperature for the two-phase region $U_4O_9 + U_3O_{8-y}$.

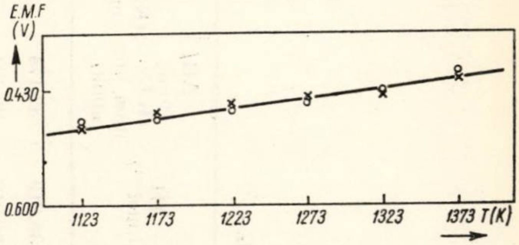

$$UO_{2.19}\ \ \Delta\overline{G}_{O_2}(\text{KJ.mol}^{-1}) = -306.268 + 0.128\ T \tag{3}$$

$$UO_{2.21}\ \ \Delta\overline{G}_{O_2}(\text{KJ.mol}^{-1}) = -296.695 + 0.131\ T \tag{4}$$

and

$$UO_{2.19}\ \ \Delta\overline{G}_{O_2}(\text{KJ.mol}^{-1}) = -435.972 + 0.230\ T \tag{5}$$

$$UO_{2.21}\ \ \Delta\overline{G}_{O_2}(\text{KJ.mol}^{-1}) = -435.930 + 0.229\ T \tag{6}$$

From the values obtained for $UO_{2.18}$, $UO_{2.19}$ and $UO_{2.21}$ one can observe that in the two-phase region $UO_{2+x} + U_4O_9$, $\Delta\overline{G}_{O_2}$ does not practically change with the composition.

Table 1 includes a list of thermodynamic data for $UO_{2.18}$. As we observed for $UO_{2.19}$ and $UO_{2.21}$, for $UO_{2.18}$ as well the passage from the single-phase to the two-phase region is accompanied by a strong decrease in the relative partial molar heat of solution of oxygen in uranium oxide due to the increase of the order in the oxygen lattice with the dissolution of oxygen in the UO_{2+x} phase.

The nonstoichiometric oxides $UO_{2.371}$ and $UO_{2.53}$ were studied in the temperature range of 1123–1373 K. The EMF values for these compositions are practically identical (Fig. 2) indicating the presence of a two-phase region. Actually, as the phase diagram shows it,[7-9] it is the two-phase region $U_4O_9 + U_3O_{8-y}$.

---

[7] L. E. J. Roberts and A. Walter, *J. Inorg. Nucl. Chem.*, **22**, 213 (1961).

[8] M. H. Rand and O. Kubaschewski, "The Thermochemical Properties of Uranium Compounds", Oliver and Boyd, Edinburgh, 1963, p. 26.

[9] * * * "Thermodynamic and Transport Properties of Uranium Dioxide and Related Phases", Technical Report Series No. 39, Ed. IAEA, Vienna, 1965, p. 3.

As well as in the two-phase region $UO_{2+x} + U_4O_9$, the values of partial molar free energy does not change with the composition. In the Table 2 the thermodynamic data referring to the two-phase region $U_4O_9 + U_3O_{8-y}$ are presented. While for the two-phase region $UO_{2+x} + U_4O_9$ a large fall in $\Delta\bar{H}_{O_2}$ is observed, for the second two-phase region $U_4O_9 + U_3O_{8-y}$ the partial molar heat of solution of oxygen in uranium oxide is larger again.

Table 2

Thermodynamic data for the two-phase region $U_4O_9 + U_3O_{8-y}$

Temp. K	$-\Delta\bar{G}_{O_2}$ (KJ.mol^{-1})	$-\Delta G$ (KJ.mol^{-1})	$-\Delta G/n_{UO_2}$ (KJ/g. atom uranium)	log p_{O_2} (N.m^{-2})
1123	142.674	21.970	25.999	1.641
1173	134.724	20.744	24.551	1.004
1223	127.193	19.585	23.179	0.438
1273	119.997	18.476	21.865	−1.929
1323	112.968	17.397	20.585	−1.465
1373	104.809	16.137	19.099	−2.993

$-\Delta\bar{H}_{O_2}$ (KJ.mol^{-1}) = 308.934
$-\Delta H$(KJ.mol^{-1}) = 47.576
$-\Delta H/n_{UO_2}$(KJ.mol^{-1}) = 56.299

$-\Delta\bar{S}_{O_2}$(KJ.mol^{-1}) = 0.148
$-\Delta S$ (KJ.mol^{-1}) = 0.023
$-\Delta S/n_{UO_2}$(KJ.mol^{-1}) = = 0.027

As Roberts and Walter [4] shown, the U_4O_9 phase dissociates at about 1396°K; at higher temperatures a limiting UO_{2+x} phase is in equilibrium with U_3O_{8-y}.

Acknowledgements. This work was performed under contract No. 695/RI/RII/RB with the International Atomic Energy Agency. The authors are grateful to the IAEA for permission to publish this paper. We wish to express our deep gratitude to Professor I. G. Murgulescu for his interest in our work. We also wish to express our thanks to the Laboratory of Nuclear Materials, Institute of Atomic Physics, Bucharest.

Revue Roumaine de Chimie, 17, 9, 1493–1496 (1972)

THERMAL PROPERTIES OF ALUMINA TA 600.*) HEAT CONTENT AT HIGH TEMPERATURE

D. I. MARCHIDAN, LIANA PANDELE and ALA NICOLESCU

Centre of Physical Chemistry
P. O. Box 2103, Bucharest, Romania

Received March 22, 1972

Measurements of the heat content have been carried out in the 573–1177 K range for alumina of the type TA-600 by using the dropping calorimetry. The existence of a crystalline transition from phase η to phase δ has been pointed out around 993°K, graphically represented by the appearance of a discontinuity of heat capacity variation curve with temperature. Also the variation curve of the enthalpy with temperature presents an inflection point.

★

Aluminas obtained in the laboratory and roasted at low temperatures, are characterized by an extended internal surface and are used as adsorbents and carriers for catalysts. The factor determining the change of their properties, both structural and textural, is the thermal treatment.

Therefore, the study of the thermal properties will largely contribute to the deeper knowledge of the phase changes occurring in the evolution of alumina species, in their ordering toward the most stable form, corundum. At the same time the heat transfer (one of the basic factors in the power balance of a technological process) is directly proportional to the thermal properties of the corresponding solid.

EXPERIMENTAL

In a platinum container we have introduced 2.20 g alumina TA 600. The container suspended in the furnace is kept for 1 hr at constant temperature until a thermal equilibrium is reached. The installation and the working technique have been previously described.[1] The container is dropped then into a calorimetric copper unit where the heat content of the respective substance and of the container is determined by cooling up to 298 K.

In order to determine the quantity from the whole heat content, due to empty container, as well as the amount of heat lost on dropping, blank measurements are carried out with the empty container in the same conditions of temperature. The difference between the two determined values is a measure of the enthalpy variation of the substances from 298 K to the temperature of the fuel container.

---

*) Romanian Patent nr. 66608/1972

[1] D. I. Marchidan and M. Ciopec, *St. Cercet. Chim., Acad. R.S.R.*, **17**, 737 (1969.)

RESULTS AND DISCUSSIONS

Previous studies have shown that the aluminium oxide presents itself under a great variety of forms such as : α, γ, η, δ among which the most thermodynamically stable is only form α. The other forms are metastable and tend to pass into modification α at high temperatures. [2]

The physico-chemical conditions governing the formation of the various structural changes of alumina are not yet well known.

They are generally brought about by heating aluminium compounds. The possible appearance of a certain phase depends on a complex of factors such as : temperature, impurities, particle size a.s.o. It should be mentioned that the conversion of one modification into another one usually occurs within a narrow temperature range in terms of the starting material that is used.

TA 600 alumina used by us shows under the η form and has a cubic-spinel structure. On heating, alumina η is converted into alumina δ characterized by a tetragonal structure that is slightly monoclinically distorted.

The results of the experimental measurement on the heat content of TA 600 alumina are given in table 1 in comparison with calculational values obtained by the method of the least squares.

Table 1

Enthalpy variation of TA600 alumina in terms of temperature. Deviation of experimental data from the calculated curve

T K	$H_T - H_{298.15}$ exp. (cal/mol)	$H_T - H_{298.15}$ calc (cal/mol)	Deviation	
			(cal/mol)	%
573	7 284	7 301.11	−17.1	−0.23
620.50	8 706	8 700.60	+ 5.4	+0.06
767.30	12 900	12 896.01	+ 3.99	+0.03
875.30	15 880	15 898.30	−18.30	−0.11
963.15	18 311	18 306.02	+ 4.98	+0.02
974.35	18 581	18 611.36	−30.36	−0.16
991.15	19 074	19 068	+ 6	+0.03
1003	19 584	19 592.47	+ 8.47	+0.04
1014.35	19 990	19 971.24	−18.76	−0.09
1075.55	21 925	21 946.36	+21.35	+0.09
1133	23 740	23 726.74	−13.26	−0.05
1177.15	25 036	25 038.19	+ 2.19	+0.01

For the temperature values below the transition temperature, the experimental results verify an equation of the form

$$H_T - H_{298.15} = -35\ 076.9 + 19.91\ T + 1.23 \times 10^{-3}\ T^2 + 11082.2\ \log\ T \qquad (1)$$

---

[2] O. J. Kleppa, *J. Phys. Chem.*, **68**, 3246 (1964).

Table 2

Heat capacity variation of TA 600 alumina with temperature

T K	C_p (cal/mol. grad)	T K	C_p (cal/mol. grad)
573	29.70	991.15	27.20
620.50	29.18	1003	33.71
767.30	28.04	1014.35	33.35
875.30	27.55	1075.55	31.64
963.15	27.27	1133	30.44
974.35	27.24	1177.15	29.76

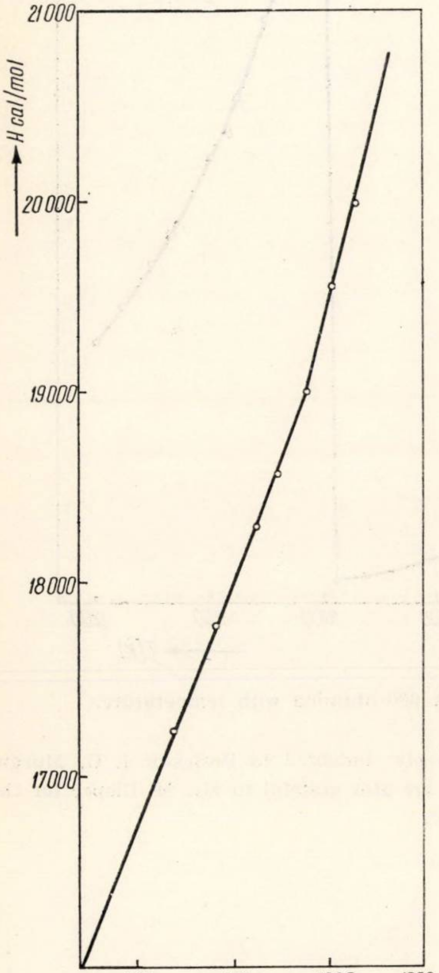

Fig. 1. — Heat content variation of TA 600 alumina in terms of temperature.

By deriving eq. (1) in terms of absolute temperature, for the heat capacity of TA 600 alumina, we obtain expressions of the form

$$C_p = 19.91 + 2.46 \times 10^{-3}\, T + 11082.2/2.303\ T \qquad (2)$$

Analogously processing, by the least squares method, the experimental results obtained at temperatures beyond the transition temperature, we obtain an equation of the form

$$H_T - H_{298.15} = 13298.3 + 8.826\, T + 4.984 \times 10^{-3}\, T^2 - 7\,527 \times 10^6\, T^{-2} \qquad (3)$$

Deriving eq. (3) in terms of absolute temperature we obtain for TA 600 alumina, an expression of the form

$$C_p = 8.826 + 9.968 \times 10^{-3}\ T + 15\,054 \times 10^6\ T^{-3} \qquad (4)$$

By means of eqs. (2), (4) we may calculate the variations of the heat capacity in terms of temperature for the TA 600 alumina. The results are listed in table 2 and plotted in fig. 2.

As seen from figure 2, the transition occurs within a narrow temperature range and the heat capacity shows a pronounced discontinuity in this domain.

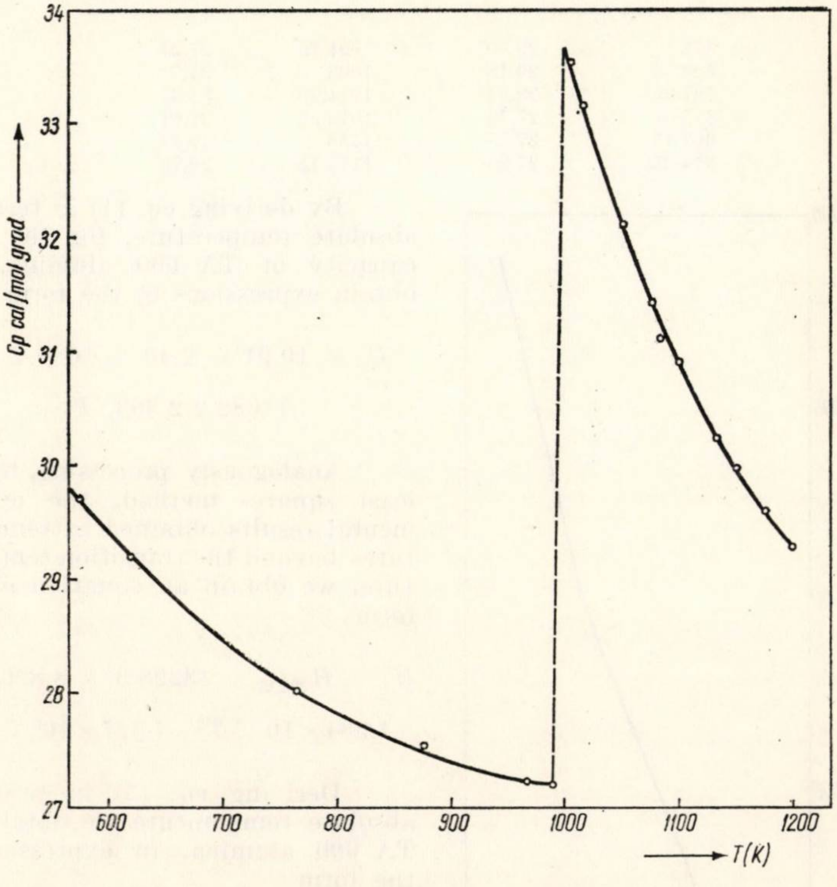

Fig. 2. – Heat capacity variation of TA 600 alumina with temperature.

Acknowledgement. The authors are deeply indebted to Professor I. G. Murgulescu for his interest in the present work. They are also grateful to Mr. M. Ciopec for the programming on the IBM, System/360 computer.

Revue Roumaine de Chimie, 17, 9, 1497–1502 (1972)

ORSZÁGOS MŰSZAKI KÖNYVTÁR ÉS DOKUMENTÁCIÓS KÖZPONT 1883

DENSITY AND ELECTRICAL CONDUCTIVITY OF MELTED METAPHOSPHATES

ŞTEFANIA ZUCA, I. D. SOKOLOVA*, D. GĂGESCU and M. OLTEANU

Institute of Physical Chemistry
Str. Galaţi 31, Bucharest, Romania

Received April 19, 1972

The density of $LiPO_3$, $Ba(PO_3)_2$, $Cd(PO_3)_2$ melts and conductivity of $LiPO_3$, $NaPO_3$, KPO_3, $Ba(PO_3)_2$, $Zn(PO_3)_2$ melts have been determined. It has been established that conductivities in $LiPO_3$, $NaPO_3$, KPO_3 melts are of the order of 1–1.5 $ohm^{-1} cm^{-1}$, and those of $Ba(PO_3)_2$, $Zn(PO_3)_2$ melts of the order of 0.05 $ohm^{-1} cm^{-1}$. The activation energy of electrical conductivity $E_{\lambda \mathrm{LiPO_3}} > E_{\lambda \mathrm{NaPO_3}} \geqslant E_{\lambda \mathrm{KPO_3}}$ is equal to 6.5–5.6 cal/g–eq respectively while E_λ for $Ba(PO_3)_2$, $Zn(PO_3)_2$ is close to 25 cal/g–eq. The sharp difference in conductivities and activation energies of metaphosphates of mono- and divalent cations arises from the complexity of the anion framework in the presence of a polyvalent cation in the melt. It involves the existence of a three-dimensional lattice due to the bonding of the linear polymeric chains.

Melted condensed phosphates found a rather wide application in different branches of industry such as fertilizer technology, electrometallurgy, etc.

A study of melted polyphosphates is of increasing interest all the more as data on their physical properties are scarce.[1] The few available data, especially on electrical conductivity of MPO_3 melts[2,3] may be hardly considered reliable. Therefore, we thought that a new set of data on the density and electrical conductivity of metaphosphates melts (having both mono- and polyvalent cations) should yield useful information about the structure and behaviour of these high-melting and high-polymerical liquids.

EXPERIMENTAL

Density (d) was measured by the platinum-sinker method, previously described,[4] with an accuracy of 0.2–0.3%.

---

* Permanent address: Institute of General and Inorganic Chemistry of the Academy of Sciences of the Soviet Union, Moscow.

[1] N. K. Voskresenskaya and I. D. Sokolova, *Uspekhi Khim.*, **38**, 1894 (1969).

[2] K. Arndt and A. Gessler, *Z. Elektrochem.*, **14**, 662 (1908).

[3] K. P. Müller, *Glastechn. Ber.*, **42**, 1, 44 (1969).

[4] I. G. Murgulescu and S. Zuca, *Rev. Roumaine Chim.*, **4**, 227 (1959).

Due to the high corrosivity of melted metaphosphates it is not possible to measure their electrical conductivity in the usual, high-constant, U-shaped, silica cell, and the use of an all-metal platinum cell is required. The use of an all-metal, low-constant cell is generally connected with increased polarization effects on the electrodes, as well as with a certain dependence of the conductivity itself on the applied frequency. Detailed consideration of these phenomena is given in.[5-7] Both of them lose importance if the frequency increases over 50 Kc.

The conductivity measurements were carried out in a device which was similar in many points to that already described.[7] The bridge was a RLC Wayne-Kerr B 601 bridge provided with Z 601 low impedance adapter, allowing operation within the frequency range from 15 Kc to 5 Mc. A variable frequency RC oscillator Tesla BM—344 fed the bridge with a 100 Kc signal. The bridge balance detector consisted of a tunned amplifier and a Soviet SI—5 oscillosynchroscope.

The bridge accuracy is supposed to be better than $\pm 3\%$ but the agreement between determinations was better than $\pm 2\%$.

The cell consisted of two square platinum electrodes of 5×5 mm size immersed into the melt, contained in a platinum crucible of $\varnothing \approx 35$ mm. A special device was provided to allow x—y—z displacements of the electrodes, resulting in precise positioning of the electrodes relative to the melt level and crucible axis. The temperature was measured by means of a Pt/Pt—Rh thermocouple, the hot junction being located between the electrodes.

The cell constant C, was found by calibration with "Greenland natural cryolite"[6] in a temperature range from 1020 to 1080°, its numerical value being 0.616 cm^{-1}. Because of the cell low resistance, the leads resistance represented 10 to 40% contribution from the total measured resistance. Therefore, prior to any determination, a plot of leads resistance *versus* temperature was performed by shortening the electrodes, and the resistance value, R_c, corrected for leads resistance was finally used to calculate the electrical conductivity $\varkappa = C/R_c$.

The density and conductivity determinations were carried out on metaphosphates prepared by dehydration of either commercially available or synthesized on this purpose, monosubstituted orthophosphates. According to the data of the differential-thermal analysis (heating curves recorded on "NTR—64 Pyrometer") the substances had the following melting points : $LiPO_3$: 670 ± 5°; $NaPO_3$: 622 ± 5°; KPO_3 : 810±3°; $Ba(PO_3)_2$: 863±5°; $Zn(PO_3)_2$: 860 ± 5°; $Cd(PO_3)_2$: 892 ± 5° which are in good agreement with earlier data.[8-10]

The melts were submitted to measurements on cooling, after a previous heating (for 1—2 hours at temperatures exceeding by 200—300° the melting point) and an intense stirring.

The coefficients of the equations representing the density-temperature and conductivity-temperature plots were computed by the least squares method partly on a IBM 360/3 and partly on a Soviet "Nairi" computer.

---

[5] G. D. Robbins and J. Braunstein. "Electrical Conductivity Measurements" in G. Mamantov, "Molten salts" Marcel Dekker, New York, 1969, p. 443.

[6] K. Matiasovsky, M. Malinovsky and V. Danek, *Electrochim. Acta*, **15**, 25 (1970).

[7] K. Matiasovsky, B. Lillenbuen and V. Danek, *Rev. Roumaine Chim.*, **16**, 163 (1971).

[8] I. D. Sokolova, E. L. Krivovyazov and N. K. Voskresenskaya, *Zhur neorg. Khim.*, **8**, 2526 (1963).

[9] E. L. Krivovyazov, N. K. Voskresenskaya and I. D. Sokolova, Coll. "Poverknostnye yavleniya v rasplavakh i voznikayushchikh iz nikh tverdykh fazakh", Nal'chik, 1965, p. 479.

[10] I. D. Sokolova, *Neorg. materialy*, **8**, 187 (1972).

RESULTS AND DISCUSSIONS

The results obtained for the density of $LiPO_3$, $Ba(PO_3)_2$ and $Cd(PO_3)_2$ are summarized in the form of linear function of temperature in Table 1. As regards the density of $NaPO_3$, KPO_3 and $Zn(PO_3)_2$ melts, there is a good agreement between our data and literature data[11–13] and the differences do not exceed ± 0.5%. Therefore for these salts, we have used in the computation of equivalent volume, the literature data as given by.[11]

Table 1

Coefficients of temperature-density relationship; $d = a + bT$ (°K)

Compound	a	$b.10^3$	Standard deviation %	Temperature range T°K	No. of experim. points
$LiPO_3$	2.575_5	-0.527_3	0.1	1097–1193	10
$Ba(PO_3)_2$	3.736_6	-0.492_1	0.2	1163–1246	14
$Cd(PO_3)_2$	3.497_4	-0.186_5	0.1	1197–1262	10

The specific conductivity for presently studied molten metaphosphates are illustrated in Fig. 1 together with the other data quoted in literature.[2,3] As seen in Fig. 1, there is a considerable disagreement among various authors. Generally the present data indicate a somewhat lower temperature dependence and are lower by 5% and 20% than the values given by Arndt[2] and respectively Müller.[3] The equations of the straight lines, in Fig. 1, as determined by the least squares method are given in Table 2. The data in Tables 1 and 2 were used for subsequent calculations of equivalent volumes ($V_{eq} = M_{eq}/d$) and equivalent electrical conductivity ($\lambda = V_{eq} \cdot \chi$).

The plot of log. λ vs. $1/T$ (°K) is linear for all studied metaphosphates (Fig. 2), attesting thus the validity of the Arrhenius equation: $\lambda = Ae^{-E_\lambda/RT}$ for these substances. Table 3 gives numerical values of the pre-exponential constant, A, and the activation energy of electrical conductivity, E_λ, as well as the equations of equivalent conductivity-temperature dependence.

It is worth noting that the specific electrical conductivity, $\varkappa$, of $LiPO_3$, $NaPO_3$ and KPO_3 melts, (about 1–1.5 ohm^{-1} cm^{-1}) are of the same order of magnitude as those of the alkali metal halides, nitrates and sulphates.[11] Certainly, in spite of the high polymerization of the linear $(PO_3)_n$ anion, the degree of electrolytical dissociation is high enough to supply cations for a good electrical conduction. However, the activation energies of electrical conductivity in the named alkali metaphos-

---

[11] A. C. MORACHEVSKY, editor, "Spravochnik po rasplavlennym solyam", vol. 1. "Khimiya", L., 1971.

[12] C. F. CALLIS, J. R. VAN WAZER and J. S. METCALF., *J. Amer. Chem. Soc.*, **77**, 1468 (1959).

[13] A. J. G. BOYER, B. J. FRAY and T. R. MEADOWCROFT, *J. Phys. Chem.*, **71**, 1442 (1967).

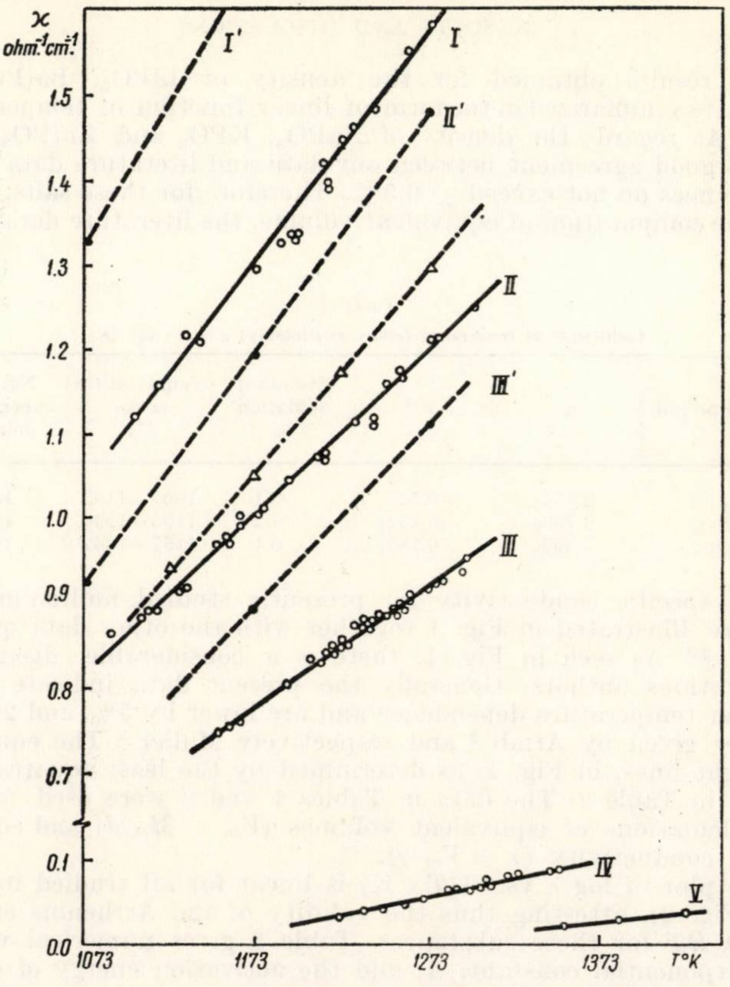

Fig. 1. — Specific conductivity of melted metaphosphates :

·—·—·-Δ-·—·—·— data[2] for $NaPO_3$

— — — —●— — — — data[3] for $LiPO_3$ (I'), $NaPO_3$(II') and KPO_3(III').

———○——— our data for $LiPO_3$(I), $NaPO_3$(II), KPO_3(III), $Ba(PO_3)_2$(IV), $Zn(PO_3)_2$(V).

Table 2

Coefficients of temperature-conductivity relationship $\varkappa = A_I + B_I T$ (°K)

Compound	A_I	$B_I \cdot 10^3$	Standard deviation %	Temperat. range T°K	No. of exper. points
$LiPO_3$	-1.8978 ± 0.0885	$2.7249 \pm 0.04737_9$	1.1	1106−1275	19
$NaPO_3$	-1.2176 ± 0.0354	$1.8953 \pm 0.04298_8$	0.91	1092−1302	31
KPO_3	-0.8738 ± 0.0420	$1.4094 \pm 0.04340_1$	0.78	1155−1226	35
$Ba(PO_3)_2$	-0.4917 ± 0.0193	$0.4308 \pm 0.04149_0$	3.97	1223−1349	18
$Zn(PO_3)_2$	-0.238	0.194		1362−1423	3

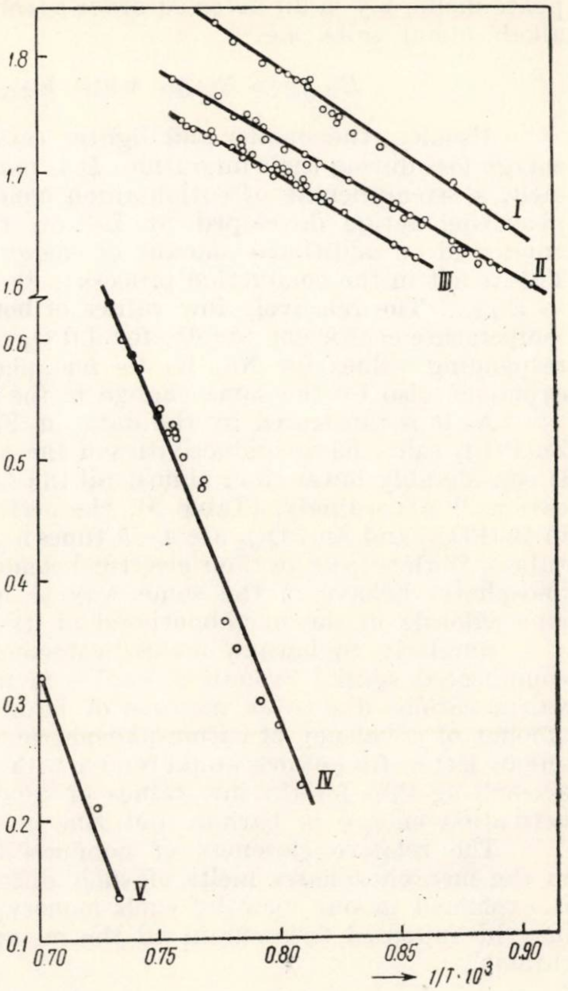

Fig. 2. – Log λ plotted against 1/T (°K) for melted metaphosphates $LiPO_3$(I), $NaPO_3$(II), KPO_3(III), $Ba(PO_3)_2$(IV) and $Zn(PO_3)_2$ (V).

Table 3

Coefficient of temperature-equivalent conductivity relationship log $\lambda = A_2 + B_2/T(°K)$; $\lambda = A.e^{-E_\lambda/RT}$

Compound	A_2	B_2	A	$E\lambda$ Cal/g.eq.	$100\frac{\lambda_c - \lambda_{exp}}{\lambda_c}$
$LiPO_3$	2.9084 ± 0.0281	-1388.51 ± 33.58	809.8	6.35 ± 0.15	1.1
$NaPO_3$	2.7231 ± 0.0148	-1228.20 ± 17.52	528.6	5.62 ± 0.08	0.91
KPO_3	2.6745 ± 0.0200	-1204.06 ± 25.21	472.6	5.51 ± 0.12	0.76
$Ba(PO_3)_2$	4.8395 ± 0.1644	-5268.44 ± 212.75	34 550.0	24.11 ± 0.97	4.42
$Zn(PO_3)_2$	4.289	-5642	19 450	26 ± 4	

phate melts, lay in an inversed order as compared to the majority of other alkali metal salts, i.e.

$$E_{\lambda \mathrm{LiPO}_3} > E_{\lambda \mathrm{NaPO}_3} \text{ while } E_{\lambda \mathrm{LiX}} < E_{\lambda \mathrm{NaX}}, \text{ etc.}$$

Usually, the smaller and lighter cations are, the less will be the energy loss during their migration. It is most probably that in the $LiPO_3$ melt, a strengthening of cation-anion bond occurs as a result of strong polarizing action developed by Li^+ on the large PO_3 – tetrahedron anion and an additional amount of energy is needed to break this bond. This is felt in the conduction process in the form of a noticeable increase in $E_{\lambda \mathrm{LiPO}_3}$. The relatively low values of both surface tension (σ) and its temperature coefficient ($d\sigma/dt$) for $LiPO_3$ melt, as compared to the corresponding values for Na, K, Cs metaphosphates [8-10] melts should be explained also by the same change in the anion – cation bond.

As it is illustrated by the data in Fig. 1, melted $Ba(PO_3)_2$ and $Zn(PO_3)_2$ salts, have conductivities of the order of 0.05 $\mathrm{ohm}^{-1}\,\mathrm{cm}^{-1}$, that is considerably lower than almost all the salts of mono- and polyvalent cations.[11] Accordingly, (Table 3), the activation energy of conductivity in $Ba(PO_3)_2$ and $Zn(PO_3)_2$ are 4–5 times higher than the usually observed values. With respect to their electrical conductivity, the two named metaphosphates behave in the same way as melted barium silicate [14] and zinc chloride in the neighbourhood of its melting point.[11]

Similarly to barium metasilicate and zinc chloride melts, rather complicated spatial structures evolve in metaphosphate melts of polyvalent cations due to an increase of both the cation valency and the amount of covalency of cation-phosphoric tetrahedron oxygen bond. This anion lattice framework would render with difficulty the cation motion, accounting thus for the low values of conductivity and high values of activation energy in barium and zinc metaphosphate melts.

The relative closeness of conductivities and activation energies in the metaphosphates melts of such different cations as Ba^+ and Zn^+ is explained in our view by such monotypic anion frameworks, which may be supposed to occur in all the metaphosphate melts of polyvalent cations.

Acknowledgement. The authors are grateful to Mr. M. Ciopec from the Institute of Physical-Chemistry (Bucharest) and to Dr. V. A. Sokolov from the Institute of General and Inorganic Chemistry (Moscow) for assistance in calculations.

---

[14] J. O'M. Bockris, J. A. Kitschener, S. Ignatowicz and J. W. Tomlinson, *Trans. Faraday Soc.*, **48**, 75 (1952).

Revue Roumaine de Chimie **17**, *9*, 1503–1508 (1972)

VAPOUR PRESSURES OF MOLTEN MAGNESIUM, CADMIUM AND ZINC CHLORIDES

LETIȚIA TOPOR

Institute of Physical Chemistry
str. Galaţi, 31, Bucharest, Romania

Received April 11, 1972

The vapour pressures of molten $MgCl_2$, $CdCl_2$ and $ZnCl_2$ have been measured by the Rodebusch-Dixon method. The heats and entropies of vaporization and the entropies of these gaseous halides have been calculated.

INTRODUCTION

Because of the considerable difficulty in the vapour pressure measurements of molten electrolytes, the experimental results for many individual substances are rather different.

The vapour pressure of molten $MgCl_2$ has been measured by static [1] and boiling point [2] methods.

For molten $ZnCl_2$ the vapour pressure measurements have been carried out by static[1] transportation,[3-7] boiling point[8] and quasi-static Rodebush-Dixon[9] methods.

The vapour pressure of molten $CdCl_2$ has been determined by static [1], transportation, [3,4,6,10] boiling point [11] and Rodebush-Dixon methods. [12] Different authors have combined these vapour pressure values, to gain information about the vapours composition in equilibrium with the liquid phase. The conclusions regarding the amount of dimer and its variation with the temperature depend on the experimental data utilized. [3,4,9,12]

---

[1] C. G. Maier, U.S. Bur. Mines Technical Paper, 360 (1929).

[2] E. Schrier and H. M. Clark, *J. Phys. Chem.*, **67**, 1259 (1963).

[3] H. Bloom and B. J. Welch, *J. Phys. Chem.*, **62**, 1594 (1958).

[4] H. I. Moss, Thesis, Indiana University, 1960, reported by R. L. Seifert in U.S. Atomic Energy Com. Tech. Rept. TID–6289 (1960).

[5] K. Jellinek and R. Koop, *Z. phys. Chem.*, **A 145**, 305 (1929).

[6] D. N. Tarasenkov and G. V. Skulkova, *Zhur obshchei Kkim.*, **7**, 1721 (1937).

[7] D. N. Tarasenkov and A. V. Babaeva, *Zhur. obshchei Kkim.*, **6**, 311 (1936).

[8] H. Bloom, J.O'M. Bockris, N. E. Richards and R. G. Taylor, *J. Amer. Chem. Soc.*, **80**, 2044 (1958).

[9] F. J. Keneshea and D. Cubicciotti, *J. Chem. Phys.*, **40**, 191 (1964).

[10] B. Greiner and K. Jellinek, *Z. phys. Chem.*, **A 165**, 97 (1933).

[11] J. L. Barton and H. Bloom, *J. Phys. Chem.*, **60**, 1413 (1956).

[12] F. J. Keneshea and D. D. Cubicciotti, *J. Chem. Phys.*, **40**, 1778 (1964).

A convenient procedure for determining the saturated vapour composition is to combine the results of vapour pressure measurements from a direct method, i.e. the quasi-static Rodebush-Dixon method, with those of a nonabsolute one, i.e. the transportation method. Both methods have been utilized, but here only the quasi-static Rodebush-Dixon determinations of vapour pressures for $MgCl_2$, $ZnCl_2$ and $CdCl_2$ are reported. The transportation data and the information regarding the saturated vapour composition for these systems will be published elsewhere.

EXPERIMENTAL

The quasi-static Rodebush-Dixon apparatus and the required procedure have been described previously.[13] The cylindrical part of the quartz cell has an inner diameter and a height of 25 mm and two legs of 3 mm inner diameter. The temperature was measured with Pt—PtRh thermocouple and maintained constant with ±1° by means of a photo-cell regulator. The pressure was measured with a mercury manometer using a cathetometer with precision of 0.05 mm.

$CdCl_2$ reagent grade was recrystallized, dried at 110°, distilled under argon atmosphere and stored in sealed vials. After the filling with the required quantity of salt the cell was slowly heated and a stream of anhydrous HCl was passed for about an hour over the solid and after melting over the liquid $CdCl_2$. The residual HCl was removed from the cell by bubbling dry argon.

Anhydrous $MgCl_2$ was prepared [14] from $NH_4Cl.MgCl_2.6H_2O$ and to reduce the amount of by-products the following procedure was used : the salt was dried at 200° under vacuum and dry HCl gas was passed for one hour at 400°. The salt was slowly heated to 800° in the dry HCl gas and the acid bubbled for another half hour, after melting. The dry argon gas was thenpassed for half an hour at 800° to remove the residual HCl and to ensure that after turning of the heater the solidification of the salt will take place without any alteration. The cell was filled with the salt in a dry-box and for melting the same procedure with dry HCl and argon was employed.

$ZnCl_2$ reagent grade was dried under vacuum, melted in a dry stream of HCl and distilled in dry argon. After the filling of the cell in a dry-box the same procedure as for $CdCl_2$ was used.

RESULTS AND DISCUSSION

For $MgCl_2$ 28 measurements in the temperature range 886—1048° have been made; for $CdCl_2$, 25 measurements between 886 and 1048° and for $ZnCl_2$, 26 measurements in the temperature range 533—612°. Two types of equations have been used to represent the vapour pressures as a function of temperature. When the difference between the heat capacities for gas and liquid phase, ΔC_p, is assumed constant :

$$\log P = -\frac{\Delta H_0}{4.574\ T} + \frac{\Delta C_p \log T}{1.986} + I \qquad (1)$$

---

[13] I. G. Murgulescu and L. Topor, *Rev. Roumaine Chim.*, **11**, 1353 (1966).

[14] G. Brauer, "Handbook of Preparative Inorganic Chemistry", Vol. 1, Acad. Press, New York, 1963, p. 905.

and when ΔC_p is assumed zero or negligible :

$$\log P = -\frac{\Delta H}{4.574\,T} + C \tag{2}$$

ΔH_0 is the standard heat of vaporization at 0°K ; ΔH the standard heat of vaporization at the midtemperature of the experimental range; I and C are two constants. ΔC_p values have been taken -8.1 cal mol^{-1} deg^{-1} for $MgCl_2$[2] ; -11.5 cal mol^{-1} deg^{-1} for $CdCl_2$[12] and -10 cal mol^{-1} deg^{-1} for $ZnCl_2$.[15] To obtain (1) type equation the experimental pressures were fitted by the Σ-plot method.[15] The calculations have been performed using the least squares treatment and an IBM computer. The heats of vaporization ΔH_T and the constants I for $MgCl_2$ and $CdCl_2$ obtained from (1) type equations by different authors are given in Tables 1 and 2.

Table 1

Heats of vaporization at temperature T and the constants I for $MgCl_2$

ΔH_T kcal mol^{-1}	I	References
$(50.4 - 8.1 \times 10^{-3}T) \pm 0.2$	22.53 ± 0.04	present data
$(53.7 - 8.1 \times 10^{-3}T) \pm 0.2$	23.15	2
$49.6 - 10\ T$	19.76	1

Table 2

Heats of vaporization at temperature T and the constants I for $CdCl_2$

ΔH_T kcal mol^{-1}	I	References
$(42.1 - 11.5 \times 10^{-3}T) \pm 0.1$	28.21 ± 0.02	present data
$(42.7 - 11.5 \times 10^{-3}T) \pm 0.013$	28.333 ± 0.0013	12
$(42.0 - 10 \times 10^{-3}T) \pm 0.2$	25.907	11

For $CdCl_2$ and $ZnCl_2$ are given in Tables 3 and 4 the heats of vaporization and the constants C obtained from (2) type equations.

Table 3

Heats of vaporization at midtemperature of experimental range and the constants C for $CdCl_2$

ΔH kcal mol^{-1}	C	Temperature range °C	References
30.9 ± 0.1	8.384 ± 0.023	630.0–797.0	present data
31.7	8.53	602.3–753.1	3
32.25 ± 0.08	8.69 ± 0.02	452.5–625.5	4

---

[15] K. K. Kelley, U.S. Bur. Mines Bull., 601 (1962).

Table 4

Heats of vaporization at midtemperature of experimental range and the constants C for $ZnCl_2$

ΔH kcal mol^{-1}	C	Temperature range °C	References
28.9 ±0.2	9.160±0.053	533.0–612.0	present data
30.2 ±0.09	9.550±0.085	420.1–610.0	9
30.2	9.5286	470.5–690.0	8
32.15	10.1233	422.4–552.8	3
29.18±0.03	9.301±0.008	452.5–625.5	4

The standard deviations of the vapour pressure values for $MgCl_2$, $CdCl_2$ and $ZnCl_2$ are 1.5 ; 1.6 and 1.7.

The equations of the vapour pressures as a function of temperature are :

$$\text{for } MgCl_2, \log P(\text{mm}) = -\frac{11019 \pm 49}{T} - 4.078 \log T + 22.527 \pm 0.040 \quad (3)$$

$$\text{for } CdCl_2, \log P(\text{mm}) = -\frac{9209 \pm 24}{T} - 5.790 \log T + 28.212 \pm 0.024 \quad (4)$$

$$\text{for } ZnCl_2, \log P(\text{mm}) = -\frac{8122 \pm 46}{T} - 5.035 \log T + 26.047 \pm 0.054 \quad (5)$$

The heats of sublimation at 298°K, ΔH_{298}, have been deduced from a second-and third-law treatment of the vapour pressure data and are compared with other ΔH_{298} available values.

Using the heat contents for condensed phase,[16] for gas [17] and the heat of vaporization from Table 1, all at 1000°K, the second-law value of ΔH_{298} for $MgCl_2$ has been calculated. To obtain the third-law value the free energy functions [18] and vapour pressures (in atmosphere) from equation (3) have been utilized (all at 1000° K). These ΔH_{298} values for $MgCl_2$ are compared with other available values.[2,19]

Second-law value of ΔH_{298} for $CdCl_2$ has been deduced using the heat contents for the condensed phase,[16,21] for gas [12] and the heat of

---

[16] K. K. Kelley, U.S. Bur. Mines Bull., 584 (1960).

[17] "JANAF Thermochemical Tables", Dow Chemical Company, Midland, Michigan, September 1962.

[18] L. Brewer, G. R. Somayajulu and E. Brackett, *Chem. Rev.*, **63**, 111 (1963).

[19] D. L. Hildenbrand, W. F. Hall, F. Ju and N. D. Porter, *J. Chem. Phys.*, **40**, 2882 (1964).

[20] D. D. Cubicciotti and H. Eding, *J. Chem. Phys.*, **40**, 978 (1964).

[21] J. O'M. Bockris, A. Pilla and J. L. Barton, *Rev. Roumaine Chim.*, **7**, 59 (1962).

Table 5

ΔH_{298} values from second and third law method

ΔH_{298}(kcal mol^{-1}) from second law	ΔH_{298} (kcal mol^{-1}) from third law	References
	$MgCl_2$	
56.0	54.0	present data
59.2	—	2
61.1	54.5	19
	$CdCl_2$	
39.6	41.0	present data
43.3	43.2	12
	$ZnCl_2$	
33.7	35.7	present data
35.7	35.8	20

vaporization from Table 2 (all at 1000°K). For third-law value, the free energy functions [18] and vapour pressures (in atmosphere) from equation (4) have been used. Using the heat contents for condensed phase, for gas and the free energy functions given by Cubicciotti and Eding,[20] the heat of vaporization and vapour pressures from this paper (all at 777°K) the second- and third-law values of ΔH_{298} for $ZnCl_2$ are obtained.

The values of ΔH_{298} presented by Brewer et al.[18] for $MgCl_2$, $CdCl_2$ and $ZnCl_2$ are 53 kcal mol^{-1}, 43 kcal mol^{-1} and 31.5 kcal mol^{-1}. Table 5 shows that there are differences between the values calculated by the two methods. Since each method for evaluating the ΔH_{298} requires the use of thermal and molecular constant data, an error in these data will be reflected in both methods of calculation. A great error in the gas free energy function and heat content values is due to the vibration frequencies, especially the doubly degenerate bending frequencies. To estimate the bending frequencies and the absolute entropies of gases, Brewer et al.[18] use the thermal data and a second-law heat of vaporization. Using this procedure the good agreement between the second- and third-law values of ΔH_{298} is a consequence of the fact that free-energy functions were obtained from the second-law heats of vaporization (Table 5 the values of $CdCl_2$[12] and $ZnCl_2$ [20]).

The entropies of vaporization at midtemperature of experimental range have been calculated from (2) type equations. Using these entropies and the absolute entropies of liquid, the absolute entropies of gas have been obtained at the same temperature. Table 6 presents the entropies of vaporization and the absolute entropies of gas.

The absolute entropy of $MgCl_2$ liquid has been taken from JANAF [17]; for $CdCl_2$ liquid has been calculated from S_{298}, the absolute entropy of solid, the heat and temperature of fusion [16] and the heat capacity data [21]; the absolute entropy of $ZnCl_2$ liquid was obtained from free-energy functions and heat contents for liquid.[20]

Table 6

The entropies of vaporization ΔS_{vap} and the absolute entropies S_{gas} of gaseous $MgCl_2$, $CdCl_2$ and $ZnCl_2$

Salt	$T_{(K)}$	ΔS_{vap} e. u.	S_{gas} e. u.	References
$MgCl_2$	1 240	24.1 ± 0.2	83.6	present data
$CdCl_2$	986	25.2 ± 0.1	86.4	present data
	935	26.4	85.7	12
$ZnCl_2$	845	28.7 ± 0.2	79.6	present data
	777	31.2 ± 0.5	—	20
	750	—	79.4	20

Our entropies of vaporization and absolute entropies of gas results, are in good agreement with the available data from the literature (Table 6).

Revue Roumaine de Chimie, 17, 9, 1509–1516 (1972)

REDUCTION STUDIES ON NICKEL OXIDE CATALYSTS

T. CHIRULESCU, CORNELIA CIOBANU and GH. ŞERBAN

Institute of Physical Chemistry, str. Dumbrava Roşie, 23, Bucharest and
Petrochemical Institute, Ploieşti, Romania

Received February 2, 1972

A magnetic procedure is described for determining the reduction degree of nickel oxide and the activation energy of the reduction. The method involves an open circulation hydrogen system and an a.c. permeameter for measuring the magnetization of the catalysts. Reductions were conducted at a definite temperature ranging from 517 to 607°K, and a gas flow rate of 117.5 $cm^3 min^{-1}$. The increase of the magnetization of the sample (proportional to the increment of metallic nickel amount in the system) was plotted *versus* time. Thus, some reduction magnetic isotherms were obtained. From the logarithmic plotting of these isotherms an expression for the reduction degree of nickel oxide was derived: $\ln f = n \ln t - B/T$ where f is the reduction degree, t – reduction time, T – reduction temperature, and n and B are two constants depending on catalyst. From the reduction time, corresponding to the complete reduction of nickel oxide, the activation energy was determined. The procedure was used for studying the reduction of three different nickel oxide-kiselguhr catalysts. The results showed that the nickel oxide in these catalysts can be easily reduced.

The information regarding the reductibility of the metal oxides are very important in the catalytic research. Such information can be useful in the understanding of various problems related to the preparation and the properties of catalysts: state of the metal oxide (or metal) on the surface, interactions between active metal and support surface, and apparent valence of the metal as determined by the nature of the support. These factors can largely vary with the method of catalyst preparation, and play a very important part in determining the catalytic activity of the metal oxide-support system. Great interest in the reducibility of metal oxide catalysts is demonstrated by many papers on this subject, appeared recently[1-9].

---

[1] G. S. Levinson, *Amer. Chem. Soc. Petroleum Div. Prep. Gen. Papers*, **12**, 47 (1967).
[2] E. J. Bicek and C. J. Kelly, *ibid.*, **12**, 57 (1967).
[3] H. H. Voge and A. T. Atkins, *J. Catalysis*, **1**, 171 (1962).
[4] Y. Yila and E. Shimada, *Bull. Chem. Soc. Japan*, **33**, 8 (1960).
[5] J. J. de Lange and G. H. Visser, *Ingenieur*, **58**, 24 (1946).
[6] J. J. B. van Eijk van Voorthuijsen and P. Franzen, *Rec. Trav. chim.*, **70**, 793 (1951).
[7] P. N. Hill and P. W. Selwood, *J. Amer. Chem. Soc.*, **71**, 2522 (1949).
[8] D. Reinen and P. W. Selwood, *J. Catalysis*, **2**, 109 (1963).
[9] W. C. F. Holm, G. C. Bailey and A. Clark, *Ind. Eng. Chem.*, **49**, 250 (1957), *J. Catalysis*, **11**, 105 (1968).

However, magnetic studies on the reduction of supported nickel oxide catalysts are not too numerous. Heukelom and co-workers [10] observed that the reduction degree and the size of nickel particles were dependent on the reduction time. Partial reduction of a nickel oxide-kieselguhr catalyst was investigated by Umemura.[11] Reduction temperature was between 260 and 470°, and the reduction time ranged from 0.5 to 8 hrs. He obtained an analytic expression for the reduction degree, as function of the reduction time and temperature. Also, the values of activation energy for reduction (18 kcal mol^{-1}), and nickel particles development (30 kcal mol^{-1}) were derived. More recently, Barb and co-workers [12] found that the activation energy of reduction depends on the metal/support ratio. Thus, they reported that in the case of a nickel oxide-chromia catalyst, the activation energy increases from 16.1 to 38.7 kcal mol^{-1}, while the nickel concentration decreases from 100 to 80 per cent.

This report concerns a kinetic study of the reduction of three nickel oxide-kieselguhr catalysts, in a hydrogen flow. The three catalysts samples were labelled as follows : standard sample, sample 26, and used sample, respectively. Metallic nickel concentration in all samples was 55 per cent. In the present study the reducibility of each sample was investigated. Also, the reduction degree as a function of reduction time and temperature was derived, and, ultimately, the values of activation energy were obtained. A test of the effect of the value of hydrogen flow rate upon the reduction kinetics was performed. Also, the magnetic behaviour of nickel particles in standard sample was studied.

EXPERIMENTAL

Materials. The catalysts were prepared by co-precipitation of nickel nitrates with the support, in a 1–4 *M* alkaline solution. The precipitate was separated and washed off until a washing water having pH = 7 was obtained; the separated precipitate was then dried up at 110° for 3 hrs. The resulting powder was pelleted with active carbon as binder. The catalyst pellets had a 5 × 5 mm size. Decomposition of the pellets was conducted in a tubular furnace at 400–450°, for 6–7 hrs, in pure nitrogen flow. It is known that this temperature is high enough to decompose completely the compound formed as a result of co-precipitation. After this, the samples were ground and the 0.2–0.3 mm fraction was retained.

Apparatus and procedure. The gas circulation open system consisted of two gas cylinders (with hydrogen and nitrogen), a two-way stopcock, RDC, a silicon oil flowmeter, D, a silica gel drying vessel, VS, and a working cell, CL.

Magnetic measurements were performed by means of an a.c. permeameter described elsewhere.[13]

Samples weighing from 3 to 5 g were used in various runs, but for a better reproducibility of the experimental data in the case of one sample, the same quantity of catalyst was used. To avoid diffusion processes, samples were used in a powdered form with an average granulation of 0.2–0.3 mm.

---

[10] W. Heukelom, J. J., Broeder and L. L. van Reijen, *J. Phys. Chim.*, **51**, 474 (1954).

[11] K. Umemura, *Nippon Kogaku Zasshi*, **81**, 991 (1960).

[12] D. Barb, M. Morariu, M. Răsvanţă and E. Weissmann, *Rev. Roumaine Phys.*, **10**, 927 (1965).

[13] T. Chirulescu, *Rev. Roumaine Chim.*, **16**, 507 (1971).

All reductions were performed at a temperature ranging from 517 to 607 K, and a hydrogen flow rate of 117.5 $cm^3 \ min^{-1}$.

A current run was conducted as follows : after insertion of the sample into the working cell, this was connected to the experimental device and introduced into the a.c. permeameter ; then the temperature of the working cell was raised up to the working temperature while passing a nitrogen flow over the sample. When a temperature steady state was reached, the two-way stopcock was commuted from nitrogen to hydrogen, and the reduction began.

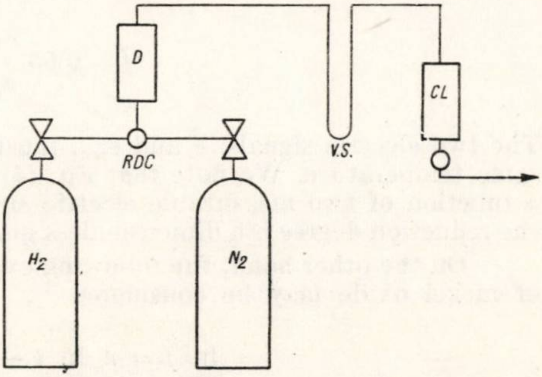

Fig. 1. — Block diagram of gas circulating open system.

RESULTS AND DISCUSSION

The main aim of this study was to obtain the reduction degree of nickel oxide as a function of reduction time and temperature, then some comparative observations on the reducibility of the three samples were made.

To define the reduction degree of nickel oxide, we have considered the two following relations :

$$\frac{m_{Ni} + m_{NiO}}{m_{Ni} + m_{NiO} + m_s} = 0.55 \qquad (1) \ (\text{known } a\ priori)$$

$$f = \frac{m_{Ni}}{m_{Ni} + m_{NiO} + m_s} \qquad (2)$$

where m_{Ni} is the mass of nickel in catalyst, m_{NiO} — the mass of nickel oxide, and m_s the mass of support. Eq. (2) represents just the definition of the reduction degree of nickel oxide. From Eq. (1) and Eq. (2), the following expression for the reduction degree may be obtained :

$$f = 0.55 \frac{m_{Ni}}{m_{Ni} + m_{NiO}} \qquad (3)$$

From Eq. (3) we can see that the reduction degree of nickel oxide varies from 0 to 0.55.

If e and e_{red} are the electric signals corresponding to a partial, and complet reduction state of nickel oxide, respectively, then we can write the following expression for the reduction degree :

$$f = 0.55 \frac{e}{e_{red}} \tag{4}$$

The two electric signals, e and e_{red}, must be measured obviously at the same temperature. We note that Eq. (4) defines the reduction degree as a function of two measurable electric signals. Also, we can remark that the reduction degree is a dimensionless quantity (see also Eqs. (2) and (3)).

On the other hand, the following expression for the reduction degree of nickel oxide may be considered [11] :

$$\ln f = n \ln t - B/T \tag{5}$$

where t, and T represent time, and temperature, respectively, and n and B are two constants. To know the reduction degree as a function of t and T, the values of the two constants, n and B, must be determined from experimental data.

In Figure 2 we have given the logarithmic form of reduction magnetic isotherms in the case of standard sample. We can observe that these isotherms are some parallel straight lines. Therefore, Eq. (5) is satisfied. The slope of these isotherms is just equal to the value of constant n, and from the free terms of these lines, we can obtain the value of constant B. Similar magnetic reduction isotherms were obtained for sample 26 and for the used sample, respectively (Figs. 3 and 4).

The average values of n and B, derived from Figs. 2, 3, and 4, are collected in Table 1.

Table 1

Values of $\overline{n}$ and $\overline{B}$ corresponding to the three catalysts samples.

Sample	$\overline{n}$	$\overline{B}$ (K)
standard	0.38 ± 0.01	971 ± 7.5
26	0.38 ± 0.01	850 ± 14.4
used	0.27 ± 0.01	758 ± 7.3

The examination of Table 1 leads to the following remarks :

1° The very good accuracy in the determination of $\overline{n}$ and $\overline{B}$ should be noted. Thus, the relative error is 2.5 per cent for $\overline{n}$, and 1.7 per cent for $\overline{B}$.

2° We can observe that $\overline{n}$ has the same value for samples standard and 26, while the values of $\overline{B}$ are slightly different. Therefore, we can state that these two samples have a somewhat similar behaviour with respect to the reduction of nickel oxide.

3° Behaviour of the used sample is quite different from that of the other samples.

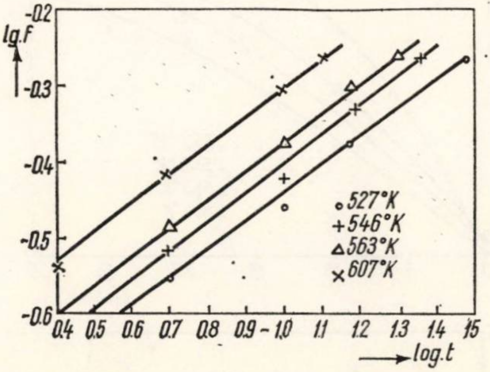

Fig. 2. – Logarithmic form of reduction magnetic isotherms in the case of the standard sample.

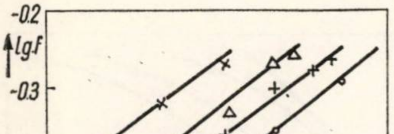

Fig. 3. – Logarithmic form of reduction magnetic isotherms in the case of sample 26.

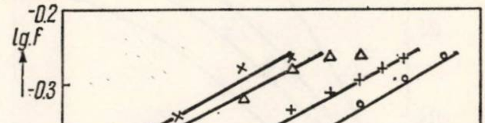

Fig. 4. – Logarithmic form of reduction magnetic isotherms in the case of used sample.

4° From Figs. 2, 3, and 4 we can see that the values of $\overline{n}$ and $\overline{B}$ are not affected by the initial state of the samples, which corresponds to a partial reduction state of nickel oxide.

5° Finally, we can point out that the value of $\overline{B}$ is, in all cases, smaller than the 1290 value, obtained by Umemura in a similar case.[11]

Figure 5 represents the direct plotting of the reduction isotherms corresponding to the standard sample. Similar reduction isotherms for sample 26, and the used sample, are given in Figures 6, and 7.

Examining these reduction isotherms we may observe that when $t = 0$, the reduction degree is different from zero; this fact shows the initial partial reduction state of the samples. The failure of convergency of the reduction isotherms at $t \to 0$, in the case of the used sample, points out an inhomogeneity of this sample, presumably due to its being worn out.

To check up the validity of Eq. (5), we have compared the experimental and calculated values of the time corresponding to the complete reduction state of nickel oxide (Table 2).

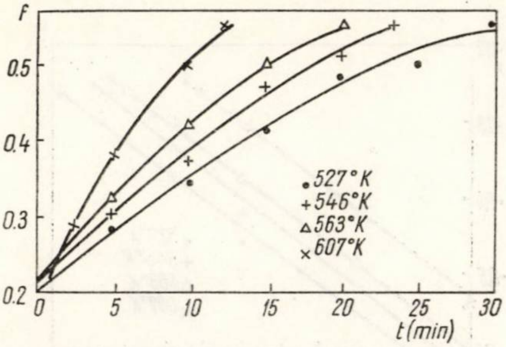

Fig. 5. — Direct plotting of reduction isotherms in the case of standard sample.

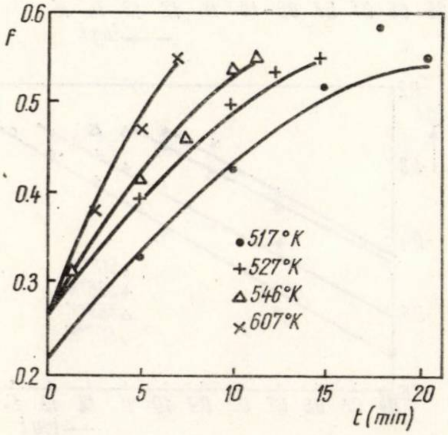

Fig. 6. — Direct plotting of reduction isotherms in the case of sample 26.

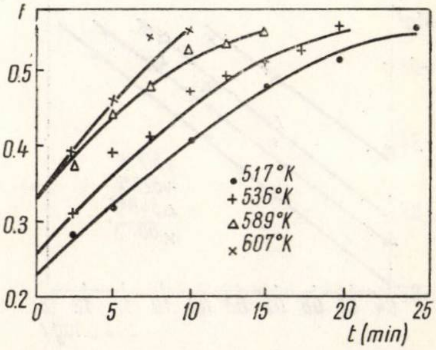

Fig. 7. — Direct plotting of reduction isotherms in the case of used sample.

Table 2

Experimental and calculated values of the time corresponding to the complete reduction state of nickel oxide.

Sample	Temperature of reduction (K)	Time of reduction (min)	
		Experimental	Calculated
Standard	527	30.00	28.25
	546	23.50	25.00
	563	20.00	21.00
	607	12.50	14.50
26	517	21.50	16.20
	527	14.10	14.40
	546	11.20	12.90
	607	7.30	8.90
Used	517	25.00	27.50
	536	20.00	22.50
	589	15.00	14.20
	607	10.00	12.00

The calculated values were obtained by employing Eq. (5), and values of $\overline{n}$ and $\overline{B}$ from Table 1. Some general remarks may be formulated :

1° There is agreement between the experimental and calculated values ;

2° In most instances, the calculated values of the reduction time are higher than the experimental values. This remark is in agreement with the initial partial state of the catalyst samples.

The activation energy corresponding to the reduction of nickel oxide may be estimated by means of the following relation[12] :

$$E = R \frac{\ln t_1/t_2}{\frac{1}{T_1} - \frac{1}{T_2}} \tag{6}$$

where E is the activation energy, $R = 1.98$ cal mol^{-1}K^{-1}, the constant of gases, and t_1 and t_2 are the times corresponding to complete reduction at temperature T_1, and T_2, respectively.

The average values of the activation energy are given in Table 3.

Table 3

Values of the activation energy corresponding to reduction of nickel oxide.

Sample	$\overline{E}$(kcal mol^{-1})
Standard	7.3 ± 0.2
26	6.4 ± 0.8
Used	5.3 ± 0.7

Examination of this Table leads to the following observations :

a) The values of the activation energy are very close.

b) We may see that the used sample is more easily reduced than the other samples.

All previous results were obtained at a hydrogen flow rate of 117.5 cm^3 min^{-1}. To check up the effect of the flow rate upon the kinetics of reduction of nickel oxide, we repeated some runs for each sample at a hydrogen flow rate of 200 cm^{3}min^{-1}. On this occasion no change in the kinetics of reduction was observed. Therefore, we may state that the reduction of nickel oxide is not affected by a flow rate ranging from 117.5 to 200 cm^{3}min^{-1}.

Figure 8 is the magnetization-versus-H/T plot for the standard sample, completely reduced. Here H is the magnetic field strength, and T the absolute temperature. As it appears from Figure 8, at 293°K, the experimental points coincide with the points measured at 461°K for the same H/T, but magnetization at 536°K falls below. Thus, the magnetic behaviour of catalyst standard sample at a temperature between 293° and 461°K, corresponds to a collective paramagnetism of the nickel particles.[14,15]

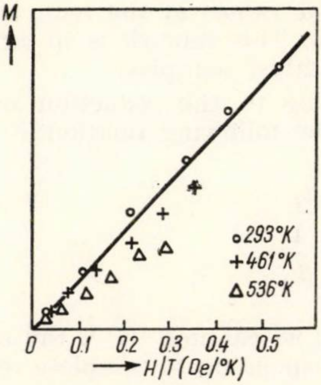

Fig. 8. —Magnetization-*versus*-H/T plot for standard sample complete reduced.

CONCLUSIONS

The results presented herein illustrate the application of a simple and convenient procedure for studying the reducibility of nickel oxide-support catalysts. The magnetic method allows to obtain several important data concerning the reduction kinetics. The experimental equipment is not too expensive, and the operation is very simple.

---

[14] P. W. Selwood, "Adsorption and Collective Paramagnetism", Academic Press, New York, London, 1962, chapter III.

[15] T. Chirulescu, Doctoral Dissertation, Bucharest, 1970.

Revue Roumaine de Chimie, 17, 9, 1517 – 1524 (1972)

LÖSUNGSGLEICHGEWICHT VON MgO AUS SERPENTINEN DURCH EINWIRKUNG VON CO_2 UND WASSER

C. DRĂGULESCU, P. TRIBUNESCU und OLGA GOGU

von der Fakultät für Angewandte Chemie an der Technischen Hochschule, Timişoara,
str. Boçşa, 6

Eingegangen am 22. April 1972

In der Arbeit werden die Möglichkeiten zur Extraktion von Magnesium aus Serpentinen durch Auflösen in einer mit CO_2 gesättigten wäßrigen Lösung untersucht. Vorerst werden an dem verwendeten Serpentin thermische und röntgenographische Untersuchungen vorgenommen, um den Temperaturbereich festzusetzen, innerhalb dessen Phasenumwandlungen stattfinden, die zur Zerstörung des ursprünglichen Gitters führen. Bei 2stündigem Durchperlen von CO_2 durch eine wäßrige Suspension, die 10 g/l Serpentin enthält, welcher 3 Stunden bei 550° geglüht wurde, löst sich 60,5 % des im Serpentin vorhandenen MgO. Durch Glühen bei höheren oder niedrigeren Temperaturen sowie durch Verminderung des Streungsgrades der Partikel wird die Lösungsausbeute ungünstig beeinflußt.

In einigen früheren Arbeiten über die chemische Verwertung verschiedener Komponenten der Serpentine, haben wir deren Behandlung mit anorganischen Säuren sowie die Gewinnung von Salzen bzw. MgO in verschiedenen Varianten verfolgt.[1] Wie aus dem Fachschrifttum ersichtlich, werden die Serpentine durch Glühen bis zu einer bestimmten Temperatur, infolge Verlust von gebundenem Wasser, in eine aktive Form übergeführt, in welcher Magnesiumoxid im Kristallgitter schwächer gebunden ist und infolgedessen fähig ist mit einer gesättigten wäßrigen Lösung von CO_2 zu reagieren.[2,3] Andere Untersuchungen haben gezeigt, daß unter bestimmten Bedingungen, beim Durchperlen von CO_2 durch eine wäßrige Suspension von MgO, metastabile übersättigte Lösungen erhalten werden können, in denen $Mg(HCO_3)_2$ in einer fast doppelten Menge wie bei Gleichgewichtszustand enthalten ist.[4,5]

---

[1] C. Drăgulescu, P. Tribunescu und O. Gogu, *Bul. Sti. Tehn. Inst. Polit. Timişoara* **9 (23)**, 29 (1964); **11 (25)**, 61 (1966); **11 (25)**, 437 (1966); **15 (29)**, 15 (1970).

[2] P. P. Mchedlov-Petrosian, *Doklady Akad. Nauk S.S.S.R.*, **78**, 557 (1951); **87**, 449 (1952).

[3] P. P. Mchedlov-Petrosian und J. L. Vorobiov, *Silikattekhnyie*, **8**, 466 (1960).

[4] R. L. Evans und H. W. St. Clair, *Ind. Eng. Chem.*, **41**, 2814 (1949).

[5] W. Kline, *J. Amer. Chem. Soc.*, **51**, 2093 (1929).

Aufgrund dieser Beobachtungen haben wir in vorliegender Arbeit die Möglichkeiten und Bedingungen untersucht, unter welchen Magnesiumoxid aus banater Serpentinen nach vorherigem Glühen und Durchperlen von CO_2 durch ihre wäßrige Suspension extrahiert werden kann.

Zu diesem Zweck wurden im ersten Teil der Arbeit thermogravimetrische und differentialthermoanalytische Untersuchungen an einigen Serpentinproben durchgeführt und die Temperaturen festgesetzt, bei denen Phasenumwandlungen der rumänischen Serpentine stattfinden. Die thermischen Daten sind durch röntgenographische Untersuchungen der bei verschiedenen Temperaturen geglühten Proben ergänzt worden.

Im zweiten Teil der Arbeit sind die Ergebnisse angeführt, die bei der Wechselwirkung von CO_2 mit wäßrigen Suspensionen der geglühten Serpentine erhalten wurden.

Die thermischen Daten wurden mit einem Derivatographen MOM-Budapest, Typ Erdey — Paulik — Paulik erhalten. In Abbildung 1 sind die ATG- und ATD-Kurven dargestellt.

Beide sind für Serpentine charakteristische ATG- und ATD-Kurven. An der ersten Kurve ist zwischen 60 und 500° ein fast kontinuierlicher Gewichtsverlust zu beobachten; in diesem Bereich entweicht vor allen adsorbiertes Wasser. Dann ist zwischen 500 und 580°, infolge Zersetzung von $MgCO_3$, ein plötzlicher Gewichtsverlust festzustellen; darauf folgt ein größerer, gleichfalls plötzlicher Gewichtsverlust zwischen 600 und 720°, infolge Entfernung des im Serpentingitter gebundenen Wassers.

Die ATD-Kurve weist anfangs einige endotherme Minima auf, danach folgt bei 570° ein Minimum, das der Zersetzung von $MgCO_3$ entspricht, und dann bei 675° ein anderes Minimum, das am meisten ausgeprägt und für die Dehydratation der Serpentine charakteristisch ist. Obwohl die ATG-Kurve, über 720°, einen horizontalen Teil aufweist, ist an der ADT-Kurve bei 800°, ein betontes exothermes Maximum zu beobachten, das infolge der Umgestaltung des Kristallgitters beim Übergang des Serpentins in Forsterit entsteht.

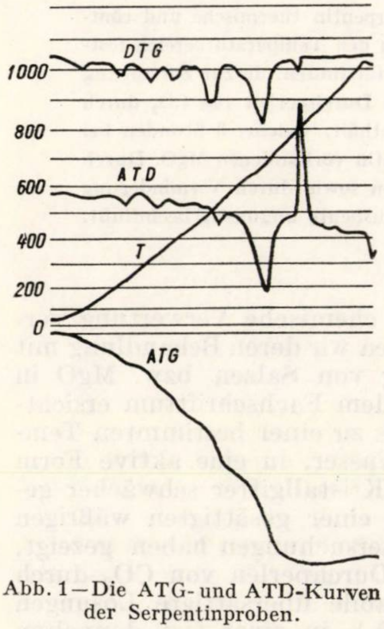

Abb. 1 — Die ATG- und ATD-Kurven der Serpentinproben.

Die aufeinanderfolgenden Umwandlungen und die entstehenden Phasen können in Abbildung 2 verfolgt werden, wo die Ergebnisse der röntgenographischen Bestimmungen dargestellt sind, die mit nichtgeglühten und zwischen 550—800° geglühten Serpentinproben vorgenommen wurden.

Die röntgenographischen Bestimmungen wurden mit Hilfe der Pulvermethode, unter Verwendung einer zylinderförmigen Kammer — ∅ = = 57,5 mm — durchgeführt. Für die Bestimmungen wurde ein TUR-M-

-61-Gerät, mit horizontalem Goniometer HZG-1, und linearem Impulsschreiber VAD-53 verwendet.

Das Röntgenogramm enthält die charakteristischen Linien des nichtgeglühten Serpentins, sowie die Linien, die dem in Serpentin enthaltenen Magnesit entsprechen.

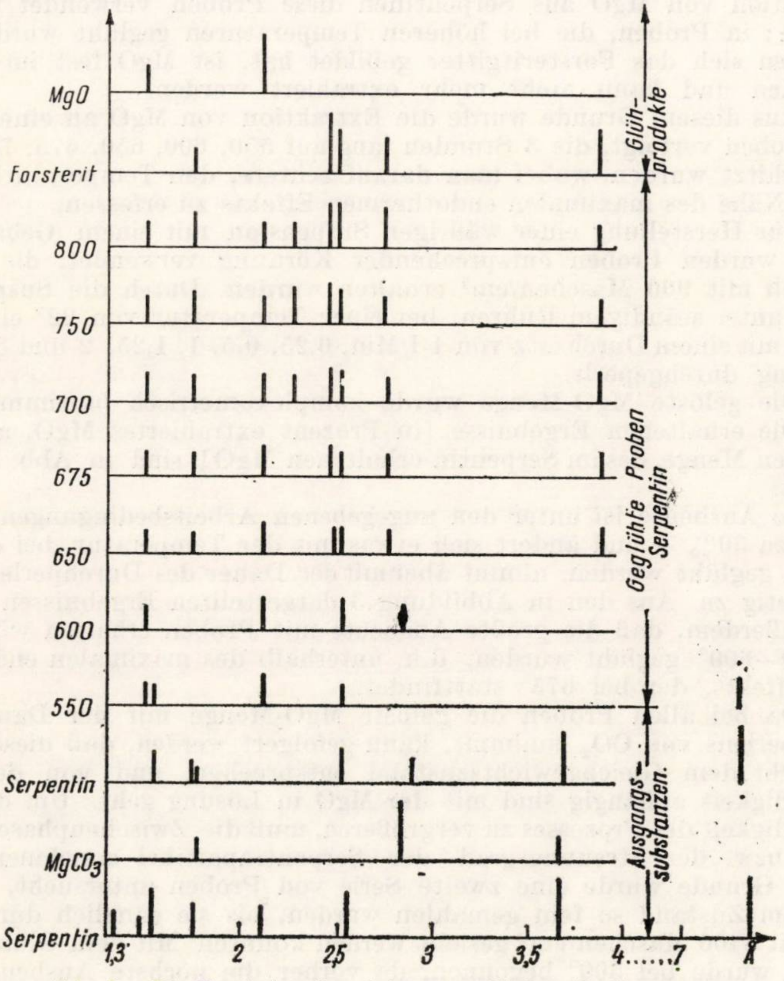

Abb. 2 — Die Ergebnisse der röntgenographischen Bestimmungen.

Aus Abbildung 2 ist ersichtlich, daß die Linien der bei 550° geglühten Proben, auch noch weniger intensive Linien der ursprünglichen Probe enthalten. Über 600° tritt an Stelle von Magnesit jedoch MgO (die Linien 2,10 und 1,485 Å), und gleichzeitig beginnen die dem Serpentin entsprechenden Linien zu verschwinden; ab 650° sind die Linien des Forsterits gut ausgeprägt (die Linien 2,46, 3,88, 2,51 und 1,75 Å).

Eine bezeichnende Eigenschaft der untersuchten Proben besteht in der Tatsache, daß diese zwischen 550 und 650° überwiegend amorph sind; in diesem Temperaturbereich wird das ursprüngliche Kristallgitter zerstört, während die Zersetzungsprodukte noch kein neues gebildet haben, da die Neugestaltung des Kristallgitters erst über 700° stattfindet.

Diese Sachlage ist von besonderer Bedeutung, da zur selektiven Extraktion von MgO aus Serpentinen diese Proben verwendet werden müssen; in Proben, die bei höheren Temperaturen geglüht wurden und in denen sich das Forsteritgitter gebildet hat, ist MgO fest im Gitter gebunden und kann nicht mehr extrahiert werden.

Aus diesem Grunde wurde die Extraktion von MgO an einer Serie von Proben verfolgt, die 3 Stunden lang auf 550, 600, 650, 675, 700 und 725° erhitzt wurden, wobei man darauf achtete, den Temperaturbereich in der Nähe des maximalen endothermen Effekts zu erfassen.

Zur Herstellung einer wäßrigen Suspension mit einem Gehalt von 10 g/l wurden Proben entsprechender Körnung verwendet, die durch ein Sieb mit 900 Maschen/cm^2 erhalten wurden. Durch die Suspension wurde unter ständigem Rühren, bei einer Temperatur von 22° ein CO_2-Strom, mit einem Durchsatz von 1 l/Min, 0,25, 0,5, 1, 1,25, 2 und 3 Stunden lang durchgeperlt.

Die gelöste MgO-Menge wurde komplexometrisch bestimmt.[6]

Die erhaltenen Ergebnisse [in Prozent extrahiertes MgO, aus der gesamten Menge, des im Serpentin erhaltenen MgO], sind in Abb. 3 dargestellt.

Die Ausbeute ist unter den angegebenen Arbeitsbedingungen gering — bis zu 30% — und ändert sich etwas mit der Temperatur, bei der die Proben geglüht wurden, nimmt aber mit der Dauer des Durchperlens von CO_2 stetig zu. Aus den in Abbildung 3 dargestellten Ergebnissen ergibt sich außerdem, daß die größte Ausbeute mit Proben erhalten wird, die bei 550—600° geglüht wurden, d.h. unterhalb des maximalen endothermen Effekts, der bei 675° stattfindet.

Da bei allen Proben die gelöste MgO-Menge mit der Dauer des Durchperlens von CO_2 zunimmt, kann gefolgert werden, daß diese Mengen nicht dem Gleichgewichtszustand entsprechen, und von der Geschwindigkeit abhängig sind mit der MgO in Lösung geht. Um die Geschwindigkeit des Prozesses zu vergrößeren, muß die Zwischenphasenoberfläche bzw. der Streuungsgrad der Serpentinpartikel zunehmen. Aus diesem Grunde wurde eine zweite Serie von Proben untersucht, die in feuchtem Zustand so fein gemahlen wurden, bis sie gänzlich durch ein Sieb mit 6400 Maschen/cm^2 gesiebt werden konnten. Mit dem Glühen der Proben wurde bei 500° begonnen, da vorher die höchste Ausbeute mit Proben erreicht werden konnte, die bei 550° geglüht wurden. Alle anderen Versuche wurden genau wie bei den anderen Proben ausgeführt. Die bei der Extraktion erhaltenen Werte sind in Abbildung 4 dargestellt.

Zum Unterschied von den vorherigen Proben ändert sich bei den in Abbildung 4 dargestellten Proben die extrahierte MgO-Menge sehr stark mit der Temperatur, bei der diese geglüht wurden. Dies ist für Proben gültig, die zwischen 500 und 675° geglüht wurden; über dieser Temperatur,

---

[6] G. Schwarzenbach und H. Ackermann, *Helv. Chim. Acta*, **30**, 1798 (1947).

Abb. 3 – Die gelöste Mg-Menge bei Grobmahlung.

1 – 15 Min.; *2* – 30 Min.;
3 – 45 Min.; *4* – 60 Min.;
5 – 75 Min.; *6* – 120 Min.;
7 – 180 Min.

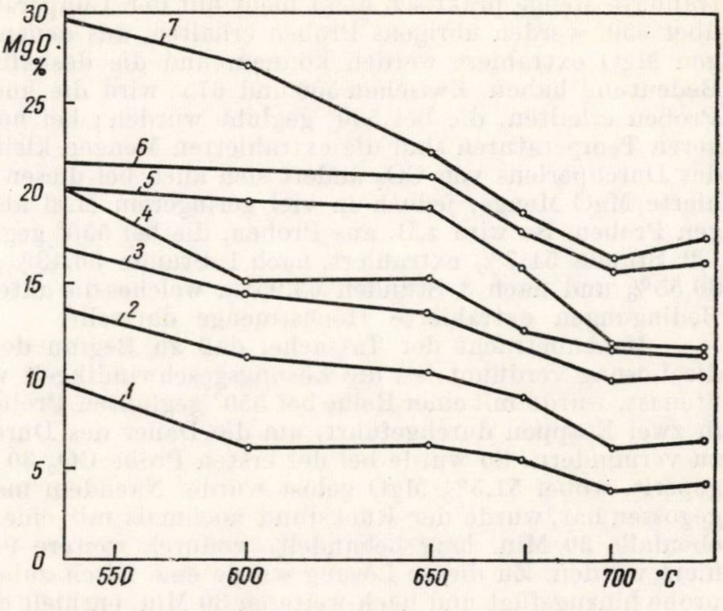

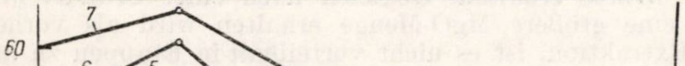

Abb. 4 – Die gelöste Mg-Menge bei Feinvermahlung

1 – 15 Min.; *2* – 30 Min.;
3 – 45 Min.; *4* – 60 Min.;
5 – 75 Min. *6* – 120 Min.;
7 – 180 Min.

die dem maximalen endothermen Effekt entspricht, ändert sich die extrahierte Menge praktisch nicht mehr mit der Temperatur. Durch Glühen über 650° werden übrigens Proben erhalten, aus denen nur geringe Mengen MgO extrahiert werden können, und die deshalb keine praktische Bedeutung haben. Zwischen 500 und 675° wird die höchste Ausbeute für Proben erhalten, die bei 550° geglüht wurden; bei höheren oder niedrigeren Temperaturen sind die extrahierten Mengen kleiner. Mit der Dauer des Durchperlens von CO_2 ändert sich auch bei diesen Proben die extrahierte MgO-Menge, jedoch in viel geringerem Maß als bei den vorherigen Proben. So wird z.B. aus Proben, die bei 550° geglüht wurden, nach 1/2 Stunde 51,7% extrahiert, nach 1 Stunde 56,43%, nach 2 Stunden 60,55% und nach 3 Stunden 63,95%, welches die unter den angegebenen Bedingungen extrahierte Höchstmenge darstellt.

In Anbetracht der Tatsache, daß zu Beginn des Prozesses, wenn die Lösung verdünnt ist, die Lösungsgeschwindikgeit von MgO am größten ist, wurde mit einer Reihe bei 550° geglühten Proben, die Extraktion in zwei Etappen durchgeführt, um die Dauer des Durchperlens von CO_2 zu vermindern. So wurde bei der ersten Probe CO_2 30 Min. lang durchgeperlt, wobei 51,5% MgO gelöst wurde. Nachdem man die Lösung abgegossen hat, wurde der Rückstand nochmals mit einer frischen Lösung, ebenfalls 30 Min. lang behandelt, wodurch weitere 9,82% MgO extrahiert wurden. Zu dieser Lösung wurde eine frisch zubereitete Serpentinprobe hinzugefügt und nach weiteren 30 Min. enthielt die Lösung 61,32% MgO, woraus folgt, daß noch 51,5% in der letzten Serpentinprobe enthaltenes MgO extrahiert werden. Mit mehreren Serien von Proben wurden gut reproduzierbare Werte erhalten. Obgleich nach einer Stunde, mit zwei Extraktionen eine größere MgO-Menge erhalten wird als vorher mit einer einzigen Extraktion, ist es nicht vorteilhalt in Etappen zu arbeiten, da die zusätzlichen Operationen durch den erhaltenen Unterschied nicht gerechtfertigt sind.

Aus diesen Tatsachen ergibt sich, daß das an der Oberfläche der Serpentinkörnchen befindliche MgO verhältnismäßig schnell gelöst wird, gleich ob in der Lösung noch gelöstes MgO vorhanden ist oder nicht. Hieraus folgt, daß die Lösung, selbst bei einer Ausbeute die nach 3stündigem Durchperlen von CO_2 erhalten wird, nicht mit MgO gesättigt ist.

In Abbildung 5 wird die Zunahme der extrahierten MgO-Menge aus dem Serpentin in Abhängigkeit von der Zeit, für Proben, die bei 550° geglüht wurden, graphisch dargestellt (*1* — grob gemahlene Probe; *2* — fein gemahlene Probe). Daraus ist ersichtlich, daß in den ersten Phasen der Extraktion die größte Menge MgO gelöst wird und eine Verlängerung der Extraktionsdauer in allen Fällen zu einer langsameren Zunahme des Magnesiumgehalts der Lösung führt, da nach der Auflösung des an der Oberfläche befindlichen Magnesiumoxids, die Konzentrationszunahme der Lösung auf Kosten des aus den inneren Schichten der Partikel diffundierenden Magnesiums stattfindet und die Diffusionsgeschwindigkeit durch feste Phasen im allgemeinen klein ist. Diese Tatsache erklärt auch die großen Unterschiede, die bei der Extraktion der beiden Proben mit verschiedener Korngröße festgestellt wurden.

Die Feststellung, daß die erhaltenen Lösungen nicht mit MgO gesättigt sind, stimmt mit den Literaturangaben überein, aus denen ersichtlich ist, daß mit CO_2 gesättigte Lösungen, bei 20–25° und Atmosphärendruck, 9–10gMgO/l enthalten,[4] während in den vorliegenden Lösungen im günstingsten Falle ein Gehalt von 2,8 g, MgO/l nicht überschritten wird.

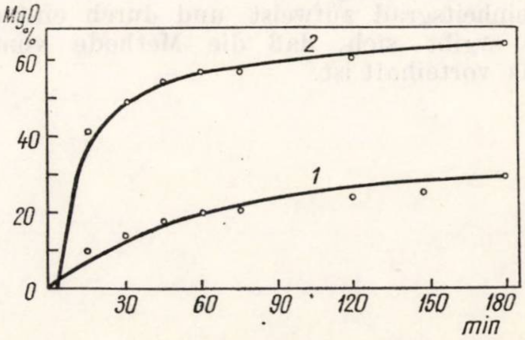

Abb. 5 – Die gelöste Mg-Menge bei Stufenextraktion

1 – grob gemahlene Probe; *2* – fein gemahlene Probe.

Aus den mit CO_2 gesättigten Lösungen, die Magnesium unter der Form von $Mg(HCO_3)_2$ enthalten, wird durch 2–3stündiges leichtes Erwärmen zwischen 25–30°, der CO_2 Überschuß entfernt und Magnesiumbicarbonat geht in Magnesiumcarbonat 3-Hydrat über, das sofort infolge Einstellung des Gleichgewichts zwischen Lösung und 3-Hydrat gefällt wird. Nach der Abtrennung der Kristalle von der Mutterlauge, die entsprechend der Löslichkeit des 3-Hydrat noch 0,12 g MgO/l enthält, wird diese wieder in den Extraktionskreislauf aufgenommen.

Die Serpentinmenge von 10 g/l Lösung wurde willkürlich genommen; es wurde darauf geachtet, daß die gelöste MgO-Menge unter der vorliegenden Arbeitsbedingungen die entsprechende Konzentrationsgrenze von 9–10 g MgO/l nicht überschreite (wobei in Betracht gezogen wurde, daß der geglühte Serpentin ungefähr 44% MgO enthält). Um die Konzentrationsgrenzen der Suspension zu untersuchen, innerhalb deren die extrahierte MgO-Menge konstant bleibt, wurde eine Reihe von Extraktionen mit Proben vorgenommen, die bei 550° geglüht und denen CO_2 30 Min. durchgeperlt wurde, wobei nur die Serpentinmengen verschieden waren. So wurden Proben verwendet, die zwischen 2,50 und 50 g Serpentin/l Lösung enthielten. Aus den Versuchergebnissen ergibt sich, daß zwischen 10 und 30 g/l praktisch eine konstante Extraktionsausbeute erhalten wird – 51,7% – unter 10 g/l werden um 2–3 Einheiten höhere Werte erhalten, während über 30 g/l die Werte stetig fallen, so daß bei 50 g/l nur noch 37,91% extrahiert wird. Es ist offensichtlich, daß bei Suspensionen die 30 g/l überschreiten, die $Mg(HCO_3)_2$-Lösungen gesättigt sind, so daß die Verminderung der Extraktionsausbeute durch die Löslichkeitsgrenze des Bikarbonats verursacht wird.

Aus den Ausführungen ergibt sich, daß durch die Einwirkung einer wäßrigen CO_2-Lösung auf fein gemahlene Serpentinproben, die 3 Stunden bei 550° geglüht und durch die 2 Stunden CO_2 durchgeperlt wurde, 60% des enthaltenen Magnesium extrahiert wird. Berüchsichtigt man, daß die Arbeitsvorgänge einfach sind, keine teuren oder ätzende Reagentien benötigt werden, daß das erhaltene Produkt einen großen Reinheitsgrad aufweist und durch einfaches Glühen in MgO übergeht, so ergibt sich, daß die Methode vom wirtschaftlichen Standpunkt aus vorteihaft ist.

Revue Roumaine de Chimie, **17**, *9*, 1525 – 1530 (1972)

CONDUCTOMETRIC STUDY OF SOME MERCURIC COMPLEXES

MIHAELA OLTEANU and MARTA STAN
Department of Chemistry, Bucharest University, Bd. Republicii 13
Bucharest, Romania

Received January 26, 1972

The equivalent conductances in ethyl alcohol of the compound of the RX, $R[HgX_3]$ and $R_2[HgX_4]$ type were determined ($X = Cl$, Br and R = N-cetyl-γ-picolinium or N-octadecyl-γ-picolinium). There has been found that in alcoholic solution the HgX_4^{2-} ion is absent. The $R_2[HgX_4]$ compounds in fact are mixtures of $R[HgX_3]$ and RX.

INTRODUCTION

The studies undertaken on some simple and mixed N-alkyl-picolinium halogenomercurates (II) led us to the conclusion that the nature of the complex formed is affected to a large extent by the medium of reaction than by the molar ratio between mercuric halide and the alkyl-picolinium halide used for synthesis.

The formation of trihalogenomercurates (II) mainly occurs in ethyl alcohol, while the formation of tetrahalogenomercurates (II) is favoured by the aqueous or acetonitrilic medium.[1–4]

It was pointed out that by recrystallization from ethyl alcohol a transformation of tetrahalogenomercurates (II) into trihalogenomercuric compounds takes place. By increasing the atomic weight of halogen and decreasing the solubility in ethyl alcohol, the transformation tendency decreases in the following order : tetrachloro-, tetrabromo- and tetraiodo-compounds.[1,2]

We could therefore expect that tetrahalogenomercuric compounds, characterized by the presence of one organic cation with high molecular weight, undergo, in alcoholic solution, the following reaction :

$$R_2[HgX_4] \rightarrow R[HgX_3] + RX \qquad (1)$$

---

[1] M. Stan and R. Zeilingher, *Anal. Univ. Buc.*, **2**, 47 (1964).
[2] M. Stan and D. Văcărescu, *Anal. Univ. Buc.*, **2**, 101 (1967).
[3] M. Stan and F. Zălaru, *Anal. Univ. Buc.*, **2**, 55 (1970).
[4] M. Stan and F. Zălaru, *Anal. Univ. Buc.*, in press.

where R = N-cetyl- α (β, γ)-picolinium or N-octadecyl- α (β, γ) -picolinium and X = Cl, Br.

A way of confirming the above reaction (obtained by chemical analysis) can be given by the conductometric data, e.g., by the conductometric behaviour of the complex salts of $R_2[HgX_4]$ type, in ethyl alcohol. If this compound really existed in ethyl alcohol, no matter of the association degree of the salt in the solvent with low dielectric constant,[5] then the solution ought to behave like a typical bi-univalent electrolyte solution. If tetrahalogenomercuric compounds underwent transformation (1), then the solution ought to behave like equimoleculare mixture of two uni-univalent electrolytes.

In order to verify this hypothesis, the variation of electrical conductance as a function of concentration at 25° in ethyl alcohol was carried out for 12 compounds of the RX, $R[HgX_3]$ and $R_2[HgX_4]$ type.

The iodides could not be studied because of their very low solubility in ethyl alcohol.

EXPERIMENTAL

The synthesis of the materials which were used was previously described.[1–4]

The ethyl alcohol was distilled after refluxing for 6 hours on organo-magnesium compounds (0.5 iodine, 5 g magnesium span to 1 l dry ethyl alcohol) and then immediately used. The measurements of electrical conductances were made with "Radelkisz Conductometer" OK 102, with the lower limit at 5×10^{-8} ohm^{-1}. We used a sinking cell with circular, coated platinum electrodes and the constant of 0.977 cm^{-1}. The cell constant was determined in KCl standard solution. All measurements were made at 25±0.1°. The specific conductance of ethyl alcohol was found under the sensibility limit of the device used. For each salt two series of concentrations by dilutions were prepared.

RESULTS AND DISCUSSION

The values of equivalent conductances (Λ), for different molar concentrations of N-cetyl- and N-octadecyl picolinium halides are given in Tables 1 and 2.

From foreogrames (Λ vs. $\sqrt{c}$) the values of equivalent conductances at infinite dilution (Λ_0), for all salts studied, were appreciated. The shape of foreogrames, having the slopes more abrupt than theoretical Onsager slopes, slightly concave with increasing concentration, shows that the salts are not completely dissociated in ethyl alcohol, having a strong tendency towards ion pairing formation.

This behaviour is justified because ethyl alcohol is a smenogenic solvent,[6] having dielectric constant $D_{25^\circ} = 24.3$, small enough to determine the interaction electrostatic potential of counterions to be higher

---

[5] R. M. Fuoss and C. A. Krauss, *J. Amer. Chem. Soc.*, **55**, 1019 (1933); *ibidem* **55**, 2387 (1933).

[6] R. M. Fuoss, *J. Chem. Educ.*, **32**, 527 (1955).

Table 1

Equivalent conductance in ethyl alcohol at 25° of N-acetyl-γ-picolinium compounds

$[C_{16}H_{33}NC_6H_7]$ Cl		$[C_{16}H_{33}NC_6H_7]$ $HgCl_3$		$[C_{16}H_{33}NC_6H_7]_2HgCl_4$	
conc. × 10^4 (m/l)	Δ ($\Omega^{-1}cm^2$)	conc. × 10^4 (m/l)	Δ ($\Omega^{-1}cm^2$)	conc. × 10^4 (m/l)	Δ (Ω^{-1} cm^2)
5	34.38	0.5	49.24	0.5	91.84
10	31.45	2.5	42.20	2.5	78.16
25	28.13	5	38.88	5	70.53
50	25.20	10	35.27	10	65.45
100	21.78	25	30.87	25	53.53
250	18.36	50	25.59	50	43.37
$[C_{16}H_{33}NC_6H_7]$ Br		$[C_{16}H_{33}NC_6H_7]$ $HgBr_3$		$[C_{16}H_{33}NC_6H_7]_2$ $HgBr_4$	
2.5	44.80	1	47.40	1	87.90
5	41.80	2.5	41.60	2.5	82.00
10	38.00	5	40.00	5	73.00
25	33.60	10	35.20	10	65.50
50	28.52	25	31.20	25	50.40
100	25.21				

Table 2

Equivalent conductance in ethyl alcohol at 25° of N-octadecyl-γ-picolinium compounds

$[C_{18}H_{37}NC_6H_7]$ Cl		$[C_{18}H_{37}NC_6H_7]$ $HgCl_3$		$[C_{18}H_{37}NC_6H_7]_2HgCl_4$	
conc. × 10^4 (m/l)	Δ ($\Omega^{-1}cm^2$)	conc. × 10^4 (m/l)	Δ (Ω^{-1} cm^2)	conc. × 10^4 (m/l)	Δ ($\Omega^{-1}cm^2$)
2.5	34.04	2.5	39.60	2.5	74.00
5	31.80	5	38.00	5	68.00
10	29.10	10	34.40	10	64.50
25	26.16	25	30.08	25	74.00
50	22.86				
100	19.93				
$[C_{18}H_{37}NC_6H_7]$ Br		$[C_{18}H_{37}NC_6H_7]$ $HgBr_3$		$[C_{18}H_{37}NC_6H_7]_2$ $HgBr_4$	
2.5	38.80	1	43.00	1	83.04
5	36.60	2.5	41.80	2.5	78.00
10	33.50	5	39.00	5	69.94
25	30.48	10	35.60	10	62.52
50	25.40				

than kT, so that the association process being favoured (association degree is dependent on the dielectric constant of the solvent and on the electrolyte concentrations for a certain temperature).

In this case, to determine the Λ_0 values, the method of Fuoss[7,8] is applied, which solves the equation:

$$\Lambda = r\,(\Lambda_0 - A\sqrt{c \cdot r}) \qquad (2)$$

---

[7] R. M. Fuoss, *J. Amer. Chem. Soc.*, **57**, 488 (1935).

[8] R. M. Fuoss and T. Shedlovsky, *J. Amer. Chem. Soc.*, **71**, 1496 (1949).

under the form of :

$$F(z)/\Lambda = (c\Lambda f^2/F(z))\,(1/k\,\Lambda_0^2) + 1/\Lambda_0 \tag{3}$$

where

A is Onsager coefficient from Onsager's limiting law (for ethyl alcohol at 25^0 $A=89.7+1.33\ \Lambda_0$),

γ — ratio of free ions,

f — mean activity coefficient,

K — dissociation constant,

$F(z)$—a complex function of A, Λ, Λ_0 and c see tables for z from 0 to 0.209).

The mean activity coefficient can be calculated from Debye-Hückel limiting equation :

$$\log f_{\pm} = -\,\alpha z_1 z_2 \sqrt{\sum c_i z_i^2} \tag{4}$$

(for ethyl alcohol $\alpha = 2.962$).

From a plot of $F(z)/\Lambda$ vs. $\Lambda c f^2/F(z)$ we obtain straight lines. The ordinate $1/\Lambda_0$ gives a more precise value for Λ_0, and the slope $1/K\ \Lambda_0$ gives K. The graphic values obtained are given in Table 3.

In the estimation of Λ_0 and K for the compounds of the $R_2[HgX_4]$ type both dissociation possibilities of these salts denoted by "a" and "b" in Table 3 have been considered.

The experimental data show that all equivalent conductances at infinite dilution, Λ_0, for RX and R $[HgX_3]$, which are surely uni-univalent, are very close in value and comparable with the values obtained by other authors[9] for uni-univalent simple salts in the same conditions (Table 4).

For bromine containing compounds, Λ_0 values were found to be slightly higher than those for chlorine and the change of cetyl chain with the longer octadecyl, decreases the values of Λ_0. These results are in good agreement with the literature data.[10]

The Λ_0 values for $R_2[HgX_4]$ were found to be higher than we expected if these compounds would exist as bi-univalent salts in alcoholic solution.

The modifications in volume of anions, would not affect considerably the values of Λ_0, e.g., the ammonium salts NH_4CCl_3COO ; NH_4Cl, ammonium picrate have the following Λ_0 values in ethyl alcohol at 25° : 37 ; 39.7 ; 40.8.[11] This fact is illustrated by our data for the salts containing X^- and HgX_3^- anions (Table 3).

The variation of Λ_0, even by the replacing a uni-univalent electrolyte by one bi-univalent, is not too large. The Λ_0 values for 2,1-valent electrolytes having very big ions, in ethyl alcohol, are spread between

---

[9] J. R. GRAHAM, G. S. KELL and A. R. GORDON, *J. Amer. Chem. Soc.*, **79**, 2352 (1957).

[10] G. J. JANZ, F. J. KELLY and H. V. VENKATASETTY, "A Survey of Nonaqueous Conductance Data", Rensselaer Polytechnic Institute, Troy, New-York, 1962.

[11] R. PARSONS, "Handbook of Electrochemical Constants", Butterworth Publ., 1959, p. 93 (table 78).

42.6 and 57.2 dependent on the size of the component ions.[12] An unimportant variation was observed by replacing the uni-univalent electrolyte by a bi-univalent one in methyl alcohol,[13] e.g., Λ_0 is 103.2 for $[HO(CH_2)_2N^+Me_2(CH_2)_2OH]Br^-$ and 121.3 for $Br^-[Me_3N^+(CH_2)_2CO_2(CH_2)_2CO_2(CH_2)_2N^+Me_3]Br^-$. The latter compound has $\Lambda_0 = 56.3$ in ethyl alcohol.

Table 3

Equivalent conductance Δ_0 and dissociation constants K in ethyl alcohol at 25°

Compounds	Δ_0 (Ω^{-1} cm^2)	K × 10^3
$[C_{16}H_{33}NC_6H_7]Cl$	43.47	1.76
$[C_{16}H_{33}NC_6H_7]HgCl_3$	52.63	1.11
$[C_{16}H_{33}NC_6H_7]_2[HgCl_4]^a$	100.00	0.454
$[C_{16}H_{33}NC_6H_7]_2[HgCl_4]^b$	97.56	0.809
$[C_{16}H_{33}NC_6H_7]Br$	49.75	2.88
$[C_{16}H_{33}NC_6H_7]HgBr_3$	52.63	1.20
$[C_{16}H_{33}NC_6H_7]_2[HgBr_4]^a$	103.50	0.428
$[C_{16}H_{33}NC_6H_7]_2[HgBr_4]^b$	100.00	0.909
$[C_{18}H_{37}NC_6H_7]Cl$	38.16	3.12
$[C_{18}H_{37}NC_6H_7]HgCl_3$	44.05	5.72
$[C_{18}H_{37}NC_6H_7]_2[HgCl_4]^a$	86.95	0.77
$[C_{18}H_{37}NC_6H_7]_2[HgCl_4]^b$	83.66	2.00
$[C_{18}H_{37}NC_6H_7]Br$	43.47	5.29
$[C_{18}H_{37}NC_6H_7][HgBr_3]$	45.87	4.00
$[C_{18}H_{37}NC_6H_7]_2[HgBr_4]^a$	95.23	0.55
$[C_{18}H_{37}NC_6H_7]_2[HgBr_4]^b$	92.16	1.17

The sign "a" indicates that for K calculation was considered the following dissociation mechanism :

$$R_2[HgX_4] \rightleftharpoons 2R^+ + HgX_4^{2-}$$

The sign "b" indicates that for K calculation was considered the following dissociation mechanism :

$$R_2[HgX_4] \rightleftharpoons 2R^+ + HgX_3^- + X^-$$

Table 4

Equivalent conductance at infinite dilution in ethyl alcohol at 25° for alkaline halides

Alkaline halide	Δ_0, Ω^{-1}.cm^2
LiCl	38.90
NaCl	42.16
KCl	45.40

---

[12] O. N. Brody and R. M. Fuoss, *J. Phys. Chem.*, **60**, 156 (1956).
[13] D. Edelson and R. M. Fuoss, *J. Amer. Chem. Soc.*, **73**, 269 (1951).

Close values for equivalent conductance at infinite dilution, λ_0, of single univalent and bivalent ions are pointed out in different solvents.[11]

From the analysis of experimental data (Λ_0), we can conclude that the compounds $R_2[HgX_4]$ are not present in ethyl alcohol solution as biunivalent electrolyte, but only as an equimolecular mixture of univalent electrolytes RX and $R[HgX_3]$. If we sum up the Λ_0 values for RX and $R[HgX_3]$ we find the Λ_0 values of $R_2[HgX_4]^b$.

To support the above conclusion we can quote the K values (the meaning of K is very complex [14,15]).

Krauss and co-workers [16] studying the electrical conductance of some quaternary ammonium compounds in dichlorethylene with big negative counterions, reached the conclusion that together with the increase of ionic volume, the dissociation constants K also increase (about 10 times). Or, from K values given in Table 3, for $R_2[HgX_4]^a$ compounds, the contrary is observed i.e. smaller K values than for $R_2[HgX_4]^b$ compounds.

---

[14] H. Sadek and R. M. Fuoss, *J. Amer. Chem. Soc.*, **76**, 5902 (1954); *ibidem*, **76**, 5905 (1954).

[15] J. C. Nichol and R. M. Fuoss, *J. Amer. Chem. Soc.*, **77**, 198 (1955).

[16] D. L. Fowler and C. A. Krauss, *J. Amer. Chem. Soc.*, **62**, 2237 (1940).

Revue Roumaine de Chimie, 17, 9, 1531 – 1543 (1972)

CHEMICAL GRAPHS. XVII.[1] (AROMATICITY. X[2]) *CATA*-CONDENSED POLYCYCLIC HYDROCARBONS WHICH FULFILL THE HÜCKEL RULE BUT LACK CLOSED ELECTRONIC SHELLS*

A. T. BALABAN
Institute of Atomic Physics, P.O. B. 35, Bucharest, Romania

Received May 15, 1972

The extension of the Hückel 4n + 2 pi-electron rule to *cata*-condensed polycyclic systems is not justified. Counter-examples are given of non-branched *cata*-condensed polycyclic systems which do not have closed electronic shells, both in the case of alternant and of non-alternant compounds. Branched systems are briefly discussed.

The Hückel rule[3-5] states that fully conjugated monocyclic systems possess closed electronic shells (i.e. have all bonding MO's filled, all antibonding MO's emtpy, and no non-bonding MO's) when they possess w = 4n + 2 pi-electrons.

Since the Hückel rule is modulo 4, it will be convenient to define the four possible classes of integers : u ≡ 0(mod 4), v ≡ 1(mod 4), w ≡ ≡ 2(mod 4) and z ≡ 3(mod 4)**. Aromaticity (stability, electronic delocalization, equalized bond lengths, characteristic chemical reactivity and diamagnetic ring current) is associated with closed electronic shells.[6]

---

* Presented in part at the 6th Symposium on Theoretical Chemistry, Bad Ischl (Austria), 6–10 April 1970.

** Throughout this paper, n, u, v, w, z, i, j and k will indicate non-negative integers.

[1] Chemical Graphs, Part XVI, A. T. Balaban, in press.

[2] Aromaticity, Part IX, A. T. Balaban, *Rev. Roumaine Chim.*, **15**, 1251 (1970).

[3] E. Hückel, *Z. Elektrochem.*, **43**, 752, 827 (1937) ; *Z. Physik*, **70**, 204 (1931) : **76**, 628 (1932) ; "Grundzüge der Theorie ungesättigter und aromatischer Verbindungen", Verlag Chemie, Berlin, 1938.

[4] A. Streitwieser Jr., "Molecular Orbital Theory for Organic Chemists", Wiley, New York, 1961.

[5] M. J. S. Dewar, "The Molecular Orbital Theory of Organic Chemistry", Mc Graw-Hill, New York, 1969.

[6] D. P. Craig, in "Theoretical Organic Chemistry" (Kekulé Symposium) Butterworths, London, 1959, p. 20 ; E. D. Bergmann and I. Agranat, in "Aromaticity, Pseudo-Aromaticity, Anti-Aromaticity", (ed. E. D. Bergmann and B. Pullman) Jerusalem, 1971, p. 9 ; "Aromaticity" (Chem. Soc. Spec. Publ. No. 21), London, 1967 ; D. M. G. Lloyd, "Carbocyclic Non-Benzenoid Aromatic Compounds", Elsevier, Amsterdam, 1966 ; D. Ginsburg (editor), "Non-Benzenoid Aromatic Compounds", Interscience, New York, 1959 ; J. F. Labarre and F. Crasnier, *Fortsch. Cehm. Forsch.*, **24**, 33 (1971) ; G. M. Badger, "Aromatic Character and Aromaticity", Cambridge Univ. Press, 1969.

Taking into account the atom types which can form aromatic rings and their electronegativities, all possible monocyclic aromatic systems can be predicted.[7]

It was assumed [5,8,9] that *cata*-condensed fully conjugated polycyclic compounds (the modified definition of branched and non-branched *cata*-condensation is given in ref.[10]) could be considered as bridged monocyclic annulenes, the bridge being a single bond. Truly bridged annulenes are known owing to Vogel, who obtained [10]-, [14]-, and [18]annulenes with -CH_2-, -O-, -NR-, or -CH_2CH_2- bridges.[11] The assumption that naphthalene and azulene could be regarded as bridged [10]annulenes with the bridge being a single bond rested on the fact that their central bonds are long and that in azulene this bond connects atoms of like parity thus causing little perturbation of the [10]annulene periphery. However, *cata*-condensed 4-membered rings fit difficultly into this scheme for electronic and steric reasons, as shown by the instability of the third possible "bridged" [10]annulene, bicyclo[6.2.0]decane.[2,12]

The present paper brings theoretical evidence against this extension of the validity of the Hückel rule to *cata*-condensed polycyclic systems, which therefore should not be considered as bridged annulenes. For convenience the *cata*-condensed systems are grouped into two separate classes, namely alternant and non-alternant systems according to Coulson, Longuet-Higgins and Rushbrooke.[13,14]

ALTERNANT NON-BRANCHED CATA-CONDENSED POLYCYCLIC HYDROCARBONS

In alternant systems, all condensed rings are even-membered [15] and the atoms can be divided into sets of different parity (starred and unstarred set) so that atoms of one set are adjacent only to atoms of the other set. In terms of the graph theory, the molecule is represented by a bipartite or bicolorable graph.[16]

---

[7] A. T. Balaban, *Rev. Roumaine Chim.*, **10**, 1059 (1965); A. T. Balaban and F. Harary *ibid.*, **12**, 1511 (1967).

[8] J. R. Platt, *J. Chem. Phys.*, **17**, 484 (1949); **22**, 1448 (1954); W. Moffitt; *ibid.*, **22**, 320 (1954); M. J. S. Dewar and R. Pettit, *J. Chem. Soc.*, **1954**, 1617, D. Peters, *ibid.* 1023, 1028, 1039, 3763, 3771 (1598); M. E. Volpin, *Usp. Khim.*, **29**, 298 (1960): *Russian Chem. Rev.* **29**, 129 (1960); J. W. Sidman, *J. Amer. Chem. Soc.*, **78**, 4217 (1956).

[9] M. J. S. Dewar, *J. Amer. Chem. Soc.*, **74**, 3341, 3345, 3350, 3353, 3357 (1952).
M. J. S. Dewar, in "Aromaticity", Chem. Soc. Spec. Publ. No. 21, London, 1967, p. 177.

[10] A. T. Balaban and F. Harary, *Tetrahedron*, **24**, 2505 (1968); A. T. Balaban, *ibid.*, **25**, 2949 (1969).

[11] E. Vogel, in ,,Aromaticity", Chem. Soc. Spec. Publ. No. 21, p. 113, London, 1967.

[12] G. Schröder and H. Röttele, *Angew. Chem.*, **80**, 665 (1968).

[13] C. A. Coulson and H. C. Longuet-Higgins, *Proc. Roy. Soc.* (A), **192**, 16 (1947).

[14] C. A. Coulson and G. S. Rushbrooke, *Proc. Camb. Phil. Soc.*, **36**, 193 (1940).

[15] D. König, "Theorie der endlichen und unendlichen Graphen", Leipzig, 1936, p. 170; reprinted Chelsea, New York, 1950.

[16] F. Harary, "Graph Theory", Addison-Wesley, Reading, Mass., 1969 p. 17, 127.

According to the pairing theorem,[14] for alternant systems the eigenvalues of the Hückel matrix occur in pairs of opposite signs. Since, as was demonstrated,[17] the eigenvalues of the Hückel matrix are the same as those of the adjacency matrix of the graph representing the molecule, the energy levels are dictated by the topology of the system and not by the solution of the Schrödinger equation. In an even alternant system (graph) devoid of side-chains, the two sets of points (atoms) include equal numbers of points. If such a system is *cata*-condensed and fulfills the Hückel rule, it was thought to have no eigenvalue equal to zero (non-bonding MO or level).* Actually a number of counter-examples are given below. All molecules are assumed to have D_{nh} symmetry.

A simplified procedure for testing whether a non-branched *cata*-condensed alternant (bipartite) graph presents non-bonding levels is the following. It is derived from the procedure for calculating the coefficients of the non-bonding level.[5,9,18] A non-branched alternant *cata*-condensed system consists of a string of even-membered condensed m_i-membered rings, where $m_i \geqslant 6$.**

From an arbitrary starting place on a marginal ring, two adjacent points which are not bridgehead positions are labelled x and y, respectively. Then all other points are progressively labelled so that the sum of labels of all points adjacent to each point in turn be equal to zero. If a consistent labelling is possible for the whole system (graph) irrespective of the values of x and y, then the adjacency matrix possesses non-bonding levels. If, on the other hand, a consistent labelling requires x and/ or y to be equal to zero, no non-bonding level exists. It can be shown that benzenoid *cata*-condensed polycyclic systems (i.e. graphs consisting only of *cata*-condensed 6-membered rings) do not have nonbonding levels.[19]

On the other hand, there exist non-bonding levels in several cases of non-branched *cata*-condensed alternant polycyclic systems fulfilling the Hückel rule.

Similarly with the procedure of starring alternative atoms in alternant polycyclics, a "dotting" procedure*** can be developed in order to find out which non-branched *cata*-condensed alternant systems have NBMO's. We need the following auxiliary conventions.

If the bonds of each even-membered condensed ring, are alternately labelled with two symbols (in the following formulas these symbols will be single and double bonds), the condensation can occur in two ways. If both bonds (junctions or bridges) common to two rings in a ring forming part of a *cata*-condensed system can be labelled with the same symbol, the condensation is called *even*; an *odd condensation* is characterized by the fact that a junction is labelled with one symbol and the second junction with the other symbol. Primed ring sizes will be used to denote odd condensation (of course, in a string of *cata*-condensed rings, only the inner rings, and not the two marginal ones, can present odd or even condensation).

---

* Abridged NBMO.

** The case of 4-membered rings will be discussed later.

*** Dotted atoms have zero coefficients of the NBMO.

[17] H. H. Gunthard and H. Primas, *Helv. Chim. Acta*, **39**, 1645 (1956) ; K. Ruedenberg, *J. Chem. Phys.*, **34**, 1884 (1961).

[18] H. C. Longuet-Higgins, *J. Chem. Phys.*, **18**, 265, 275, 283 (1950).

[19] D. A. Bochvar and I. V. Stankevich, *Zhur. strukt. Khim.*, **12**, 142 (1971).

As examples of $(4n + 2)$- and $4n$-membered rings we will adopt 6- and 8-membered rings respectively; 4-membered rings have a special situation and will be discussed later.

Discussing now all possibilities of "dotting" an even-membered ring to indicate zeroes resulted by the previously indicated x, y-labelling, the following possibilities emerge:

(i) $4n$-membered rings can be either marginal or inner rings in a string of *cata*-condensed rings. When marginal, the adjacent positions to the junction have zero coefficients (are "dotted").

u_1 will indicate a ring with no zero coefficient. This ring may by either a marginal or an inner ring of the string; in the latter case, u_1 and u_1' will discriminate among even or odd condensation, respectively.

u_2' will indicate inner rings which may be condensed to two u_1-type rings because they have at least four dotted positions next to the two junctions; such rings can only have odd condensation, hence the prime.

u_3' will indicate inner rings which have at least four dotted positions at the two junctions; such rings can only have odd condensation.

$\vec{u}_4$ will indicate inner rings which have the two atoms next to one junction and the two atoms of the other junction dotted; the two orientations of the arrow indicate which junction comes first; such rings can only have even condensation.

(ii) $(4n + 2)$-membered rings can only be inner rings (one exception will be presented later).

w_2' will indicate rings which may be adjacent to two u_1-type rings, because they have dotted positions next to the two junctions; such rings can only have odd condensation.

w_3' will indicate rings which have the four positions at the two junctions dotted; such rings can only have odd condensation.

$\vec{w}_4$ will indicate rings which have the two atoms of one junction dotted, and the positions next to the other junction dotted; the two orientations of the arrow indicate which junction comes first; such rings can only have even condensation.

All these possibilities are indicated in Scheme 1.

Possible ways of combining the above rings are indicated by the directed graph presented in scheme 2.

The graph can end at the final u_1 or can continue in the same fashion replacing the final u_1 or u_1' by the initial u_1.

In the following only those non-branched *cata*-condensed alternant systems will be considered which possess NBMO's and which obey the Hückel rule. With U u-membered and W w-membered rings in a *cata*-condensed string, the total number of atoms is $U(u - 2) + W(w - 2) + 2$. In order that this number be of the form $4n + 2$, it is necessary that U

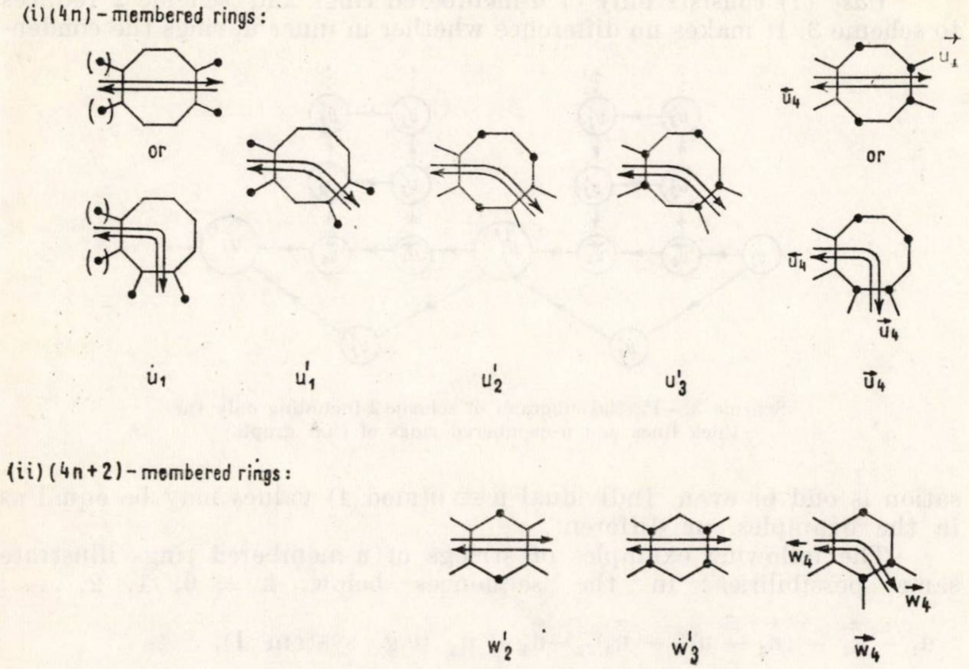
(i) (4n) - membered rings :
or
or
u4
u4
u4
u1
u'1
u'2
u'3
u4
(ii) (4n + 2) - membered rings :
w4
w4
w'2
w'3
w4

Scheme 1. – Dotting possibilities of even-membered rings

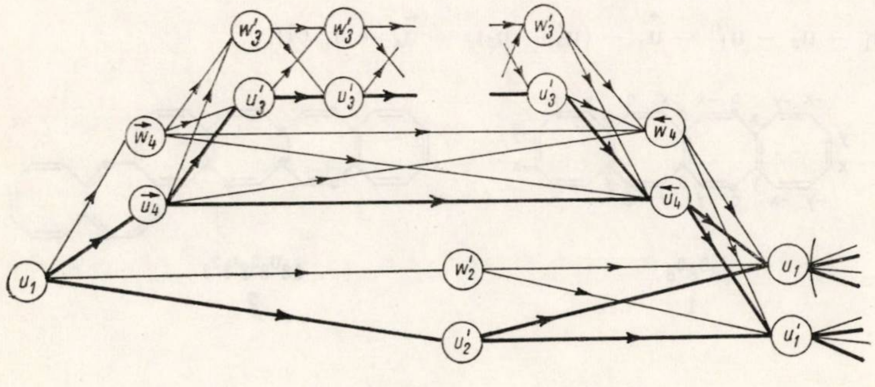
w'3
w'3
w'3
u'3
u'3
u'3
w4
w4
u4
u4
u1
w'2
u1
u'2
u'1

Scheme 2. – Complete graph of *cata*-condensed systems with NBMO's formed from dotted alternant rings

be an even number with no restriction placed on W, since $u \equiv 0 (\text{mod } 4)$ and $w \equiv 2 (\text{mod } 4)$.

On the basis of this condition that the number of u-membered rings be even and of schemes 1 and 2, the following two cases of non-branched *cata*-condensed alternant systems have NBMO's although they satisfy the Hückel rule.

Case (*1*) consists only of u-membered rings and scheme 2 reduces to scheme 3. It makes no difference whether in inner u_1 rings the condensation is odd or even. Individual $u \equiv 0 \pmod 4$ values may be equal as in the examples, or different.

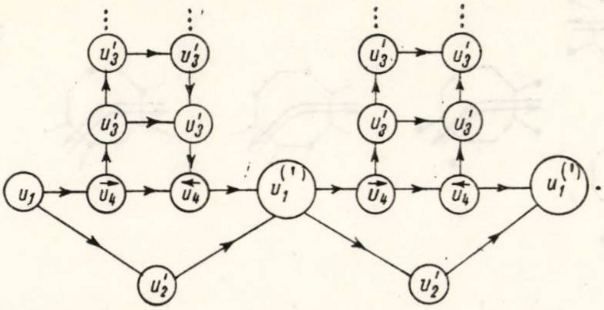

Scheme 3.—Partial subgraph of scheme 2 including only the thick lines and u-membered rings of that graph

The following examples of strings of u-membered rings illustrate same possibilities: in the sequences below, $k = 0, 1, 2, \ldots$:

$u_1 - \overrightarrow{u}_4 - (\overleftarrow{u}_4 - u_1^{(\prime)} - \overrightarrow{u}_4)_{2k} - \overleftarrow{u}_4 - u_1$ (e.g. system **1**),

$u_1 - \overrightarrow{u}_4 - \overleftarrow{u}_4 - (u_1^{(\prime)} - u_2')_{k+1} - u_1$ (e.g. **2**), $u_1 - \overrightarrow{u}_4 - (u_3' - u_3')_{k+1} - \overleftarrow{u}_4 - u_1$ (**3**),

$u_1 - u_2' - u_1^{(\prime)} - \overrightarrow{u}_4 - (u_3' - u_3')_k - \overleftarrow{u}_4 - u_1$ (**4**).

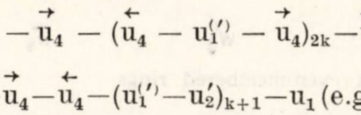

$88^0 8^0 8$

1

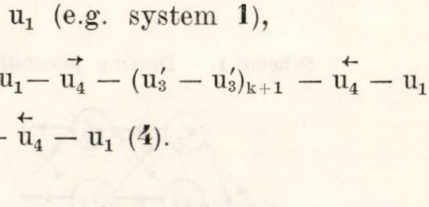

$88^0 8^0 8^1 8^2 8$

2

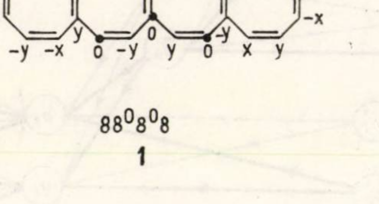

$88^3 8^1 8^1 8^4 8$

3

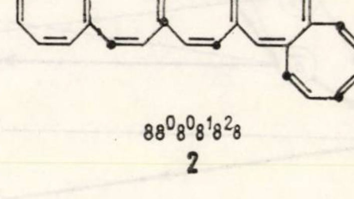

$88^1 8^2 8^4 8^3 8$

4

Case (*2*) includes the whole scheme 2 and includes u- and w-membered rings. Some possibilities are presented in the sequences below where

$k = 0, 1, 2, \dots :$

$u_1 - (w_2' - u_1^{(\prime)})_{2k} - w_2' - u_1$ (e.g. **5**, **6**),

$u_1 - u_2' - (u_1^{(\prime)} - w_2')_{2k+1} - u_1$ (**7**), $u_1 - (u_2' - u_1^{(\prime)})_k - w_2' - u_1$,

$u_1 - [\vec{w}_4 - (w_3')_k - \overset{\leftarrow}{w}_4]_{k'} - u_1$ (**8**, **9**), $u_1 - \vec{u}_4 - (w_3')_k - \overset{\leftarrow}{u}_4 - u_1$ (**10**),

$u_1 - \vec{w}_4 - (u_3' - u_3')_k - (w_3')_k - u_1$ (**11**), $u_1 - \vec{u}_4 - (w_3')_k - u_3' - \overset{\leftarrow}{w}_4 - u_1$ (**12**).

The one exception with marginal w-membered rings is system **13**.

In addition, all systems presented above can act as marginal u_1-type rings leading to more complex systems. Thus **1** is $u_1 - \vec{u}_4 - \overset{\leftarrow}{u}_4 - u_1$; ten linearly condensed 8-membered rings can be considered as deriving from the same type, with **1** replacing the u_1 marginal rings, i.e. **1** $- \vec{u}_4 - \overset{\leftarrow}{u}_4 -$ **1**.

cata-Condensed ring systems can play not only the role of marginal u_1-type rings but also of marginal w-type rings. In this case they must have an odd number of u-membered rings, hence an even number of double bonds, e.g. $68^{1}6$, $88^{1}8$, $86^{1}8^{0}8$, $88^{0}8^{1}8^{0}8$, $86^{0}8^{0}6^{0}8^{0}8^{1}8$, $88^{0}8^{0}8^{0}8^{0}8^{0}8$. Thus, in addition to **13**, many more examples exist for alternant *cata*-condensed non-branched systems satisfying the Hückel rule but possessing NBMO's and marginal w-membered rings, e.g. $68^{0}8^{0}6^{0}8^{1}8$, $68^{0}8^{0}6^{1}8^{2}8$, $68^{1}6^{2}8^{0}8^{0}6^{2}8^{1}6$, $68^{0}8^{3}6^{0}8^{0}8^{4}6^{2}8^{3}8^{0}6$.

The above discussion of alternant systems possessing NBMO's includes as particular cases such systems discussed earlier in the literature.[20,21]

Four-membered rings raise a special problem. Since they can only give even condensations acting as u_1 or u_4-type rings, they impose restrictions in scheme 2. Also, owing to reasons given in the introduction, 4-membered rings are less prone than other even-membered rings for continuous conjugation. Therefore they are not included into the present discussion.

The notation [2] of the *cata*-condensed system which is written under each formula includes the ring sizes of the condensed rings, while the exponents express the geometry of the condensation by selecting among allowed angles of the characteristic graph (exponent zero indicates linear condensation ; the higher the exponent, the more bent is the condensation or the characteristic graph ; even and odd exponents indicate bending in alternative directions).

---

[20] J. D. Roberts, A. Streitwieser Jr. and C. M. Regan, *J. Amer. Chem. Soc.*, **74**, 4579 (1952).

[21] C. F. Wilcox Jr., *Tetrahedron Letters*, **1968**, 795.

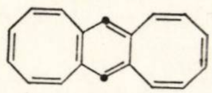

$86^0 8$

5

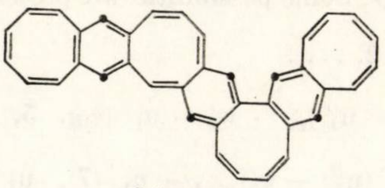

$86^0 8^1 6^0 8^4 6^0 8$

6

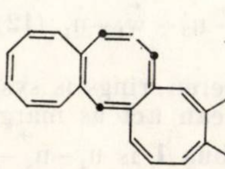

$6^0 8^1 8^2$

7

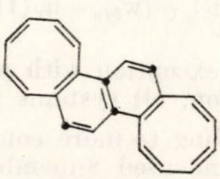

$86^1 6^2 8$

8

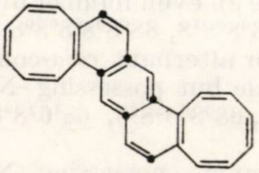

$86^1 6^0 6^2 8$

9

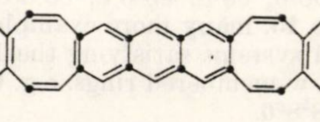

$88^0 6^0 6^0 6^0 8^0 8$

10

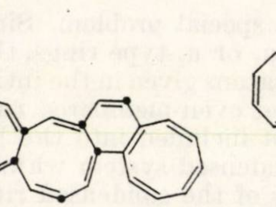

$86^1 8^2 8^2 6^1 8$

11

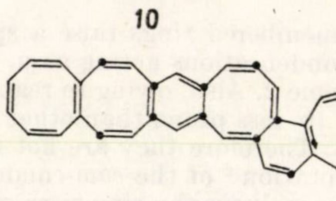

$86^1 8^2 6^0 8^0 8$

12

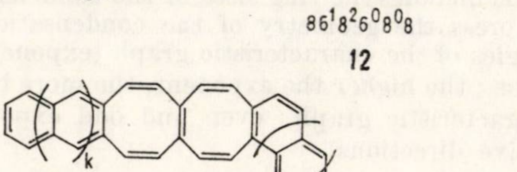

$6(6^0)_k 8^0 8^0 6^1 (6^0)_{k-1} 6$

13

With alternant systems, the bridge always connects atoms of different parity, causing therefore an important perturbation.

NON-ALTERNANT NON-BRANCHED CATA-CONDENSED POLYCYCLIC HYDROCARBONS

When odd-membered rings are also present, to find the eigenvalues of the adjacency matrix a computer programme was employed.

The first counter-example of a non-alternant non-branched *cata*-condensed polycyclic hydrocarbon (**14**) which fulfills the Hückel rule and yet does not have a closed electronic shell was reported by Bochvar *et al.*[22] Subsequently several such systems were described.[2]

There are three cases, (3)—(5), of such systems, all presenting a similar symmetry, namely a centre of inversion.

Case (*3*). An excess of positive over negative eigenvalues (i.e. vacant bonding orbitals) exists when 2i pairs of v_i-membered and any number (including zero) of w_i-membered or of pairs of u_i-membered rings are condensed so that the graph has a centre of symmetry, where $v_i \equiv 1$ (mod 4), $u_i \equiv 0$(mod 4) and $w_i \equiv 2$(mod 4), e.g. **14**—**28**.

To express the above formulae more succinctly the notation proposed in ref.[2] and [10] is indicated under each formula : case (3) is characterized by the presence of classes with 2i pairs of v_i-membered rings ; w_i-membered rings or pairs of u_i-membered rings may also be present. The subclass must have a symmetrical arrangement of ring sizes and the condensation pattern must provide a symmetry centre (classes and subclasses are defined in ref.[2]).

Case (*4*) An excess of negative over positive eigenvalues (i.e. occupied antibonding orbitals) exists when 2i pairs of z_i-membered and any number (including zero) of w_i-membered or of pairs of u_i-membered rings are condensed so that a symmetry centre results, e.g. **29**—**34**.

Case (*5*). There may be non-bonding levels and/or excess of eigenvalues of one sign when pairs of v_i-membered are condensed with pairs of z_i-membered rings (in addition w_i-membered or pairs of u_i-membered rings may be present) so that a centre of symmetry results.

Thus the following systems have non-bonding MO's :
$55^15^27^37^45^15^25$ (**35**), $55^17^45^15^27^35^25$ (**36**), $55^17^47^37^47^35^25$;
the following ones have occupied anti-bonding MO's :
$75^17^25^15^27^15^27$ (**37**), $75^17^27^17^27^15^27$, $77^15^27^17^25^17^27$, $77^17^45^15^27^37^27$ (**38**) ;
and the following ones have vacant bonding MO's :
$55^17^15^25^17^25^25$ (**39**), $55^17^45^15^27^35^25$, $57^35^25^15^25^17^45$, $57^15^25^15^25^17^25$, $55^17^2 - 7^17^27^15^25$, $57^15^27^17^25^17^25$ (**40**).

However, closely related systems like: $55^15^27^17^25^15^25$, $75^15^25^15^25^15^27$, $57^35^27^37^45^17^45$, $57^17^15^25^17^27^25$, $75^17^15^25^17^25^27$, $75^17^45^15^27^35^27$, $77^15^25^15^25^17^27$, $75^15^17^27^15^25^27$, $57^17^27^17^27^17^25$ have closed shells.

---

[22] D. A. Bochvar, I. V. Stankevich and A. V. Tutkevich, *Izvest. Akad. Nauk, S.S.S.R., Otdel. Khim. Nauk*, **1969**, 1185.

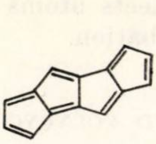

55^15^25

14

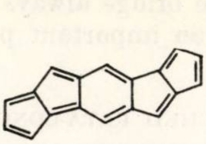

$55^16^05^25$

15

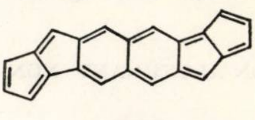

$55^16^06^05^25$

16

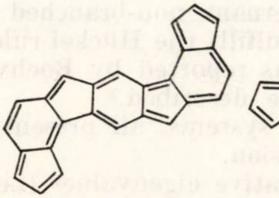

$56^15^16^05^26^25$

17

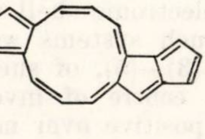

$55^110^05^25$

18

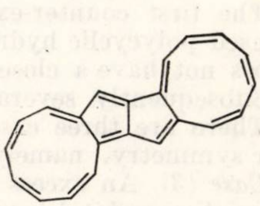

95^15^29

19

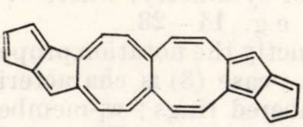

$55^18^08^05^25$

20

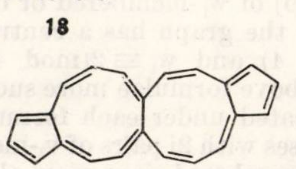

59^19^25

21

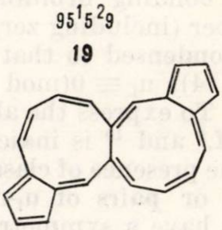

59^39^45

22

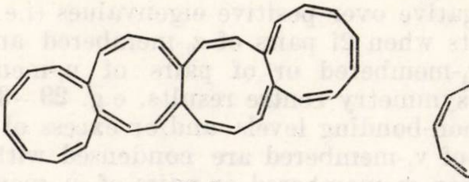

99^19^29

23

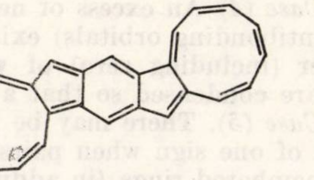

$95^16^05^29$

24

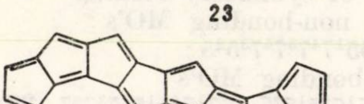

$55^15^15^25^15^25^25$

25

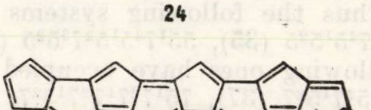

$55^15^25^15^25^15^25$

26

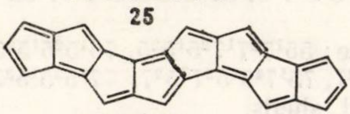

$55^15^25^25^15^15$

27

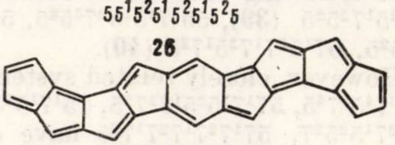

$55^15^15^26^05^15^25^25$

28

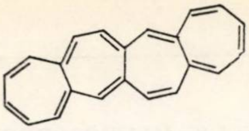

$77^{1}7^{2}7$

29

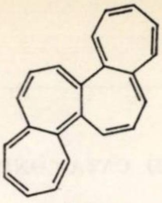

$77^{3}7^{4}7$

30

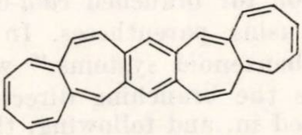

$77^{1}6^{0}7^{2}7$

31

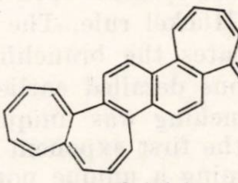

$77^{3}6^{2}6^{1}7^{4}7$

32

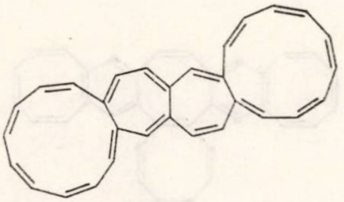

$11\,7^{1}\,7^{2}\,11$

33

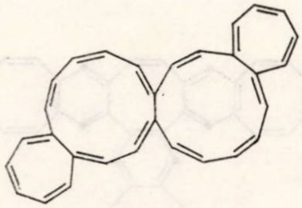

$7\,11^{3}\,11^{4}\,7$

34

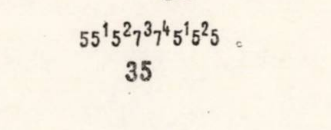

$55^{1}5^{2}7^{3}7^{4}5^{1}5^{2}5$

35

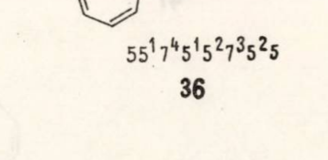

$55^{1}7^{4}5^{1}5^{2}7^{3}5^{2}5$

36

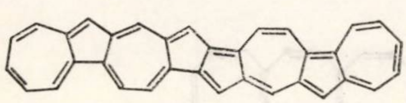

$75^{1}7^{2}5^{1}5^{2}7^{1}5^{2}7$

37

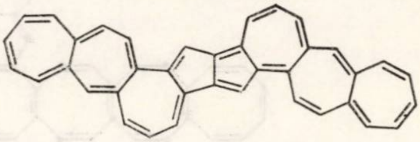

$77^{1}7^{4}5^{1}5^{2}7^{3}7^{2}7$

38

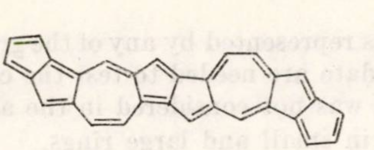

$55^{1}7^{1}5^{2}5^{1}7^{2}5^{2}5$

39

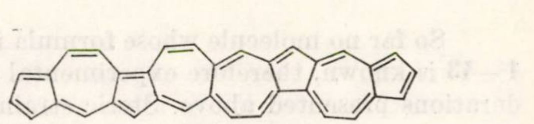

$57^{1}5^{2}7^{1}7^{2}5^{1}7^{2}5$

40

BRANCHED CATA-CONDENSED POLYCYCLIC HYDROCARBONS

The "dotting" procedure outlined for alternant systems leads to the prediction that systems such as **41**—**43** will have NBMO's although they fulfill the Hückel rule. The notation for branched *cata*-condensed polycyclics indicates the branching by using parentheses. In addition to the conventions detailed earlier for benzenoid systems,[10] where the direction of branching was unique, here the branching direction must be specified by the first exponent included in, and following, the parenthesis. For assigning a unique notation to the branched *cata*-condensed system, one takes into account as the primary criterion the smallest number formed by the longest string of ring sizes, and as the secondary criterion the smallest number formed by the exponents.

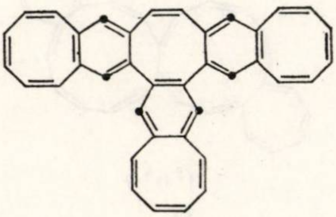

$86^08^0(^36^08)6^08$

41

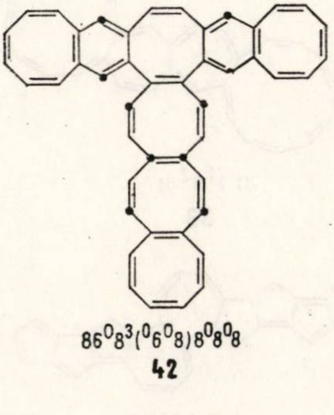

$86^08^3(^06^08)8^08^08$

42

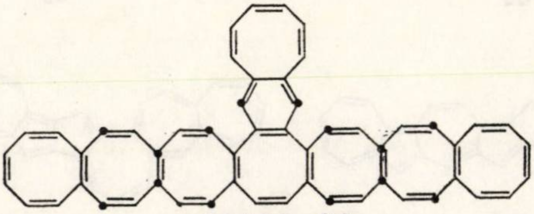

$88^08^08^0(^36^08)8^08^08$

43

So far no molecule whose formula is represented by any of the graphs 1—43 is known, therefore experimental data are needed to test the considerations presented above. Steric strain was not considered in the above discussion even though it is important in small and large rings.

In conclusion, examples were given of *cata*-condensed polycyclic hydrocarbons, both alternant and non-alternant, which although fulfilling the Hückel rule, do not possess a closed electronic shell. These examples invalidate the assumptions that the Hückel rule can be extended to such systems and that such systems could be regarded as bridged annulenes. Truly bridged annulenes have bridges with more than one single bond.

For non-alternant branched *cata*-condensed polycyclic systems results will be reported separately.

Acknowledgement. The kind assistance of Mrs. K. Göttler for computer calculations of eigenvalues is gratefully acknowledged.

Revue Roumaine de Chimie, **17**, *9*, 1545–1549 (1972)

STUDIES OF THE BIURET REACTION. VII[1]

CRYSTALLINE STRUCTURE OF THE NATRIUM-COPPER (II)-TETRACYANURATE HEXAHYDRATE AND OF ITS TWO ANHYDROUS STATES

MARIA NUŢIU, FR. MARX and G. OSTROGOVICH
Department of Organic Chemistry, Polytechnic Institute "Traian Vuia", str. Bocşa 6,
Timişoara, Romania

Received February 29, 1972

The paper presents crystallographic data obtained by powder roentgenograms for the hydrated natrium-copper(II)-tetracyanurate hexahydrate, $[Cu(C_3O_3N_3H_2)_4]Na_2.6H_2O$, (I), and for its two anhydrous states : α, (II), and β, (III). All three compounds were indexed as orthorhombic and the following characteristics were established : for (I) the fundamental parameters are $a_0 = 12.40$ Å, $b_0 = 13.85$ Å, $c_0 = 25.88$ Å, spatial group $P_{mc}2_1$, and the number of molecules per elementary cell $N = 7$; for (II) $a_0 = 19.78$ Å, $b_0 = 15.32$ Å, $c_0 = 11.61$ Å, spatial group $P_{mm}2_1$, and $N = 7$; for (III) $a_0 = 10.82$ Å, $b_0 = 11.70$ Å, $c_0 = 12.57$ Å, spatial group $P_{mm}2_1$ and $N = 2$. The transformation kinetics of the metastable state β in the stable state α was also studied. An activation energy of $E = 25.7$ kcal/mol, and a preexponential coefficient of $A = 3.99 \times 10^{10}\ s^{-1}$ were established for this process.

★

The natrium-copper(II)-tetracyanurate hexahydrate $[Cu(C_3O_3N_3H_2)_4]Na_2.6H_2O$, (I), was obtained in 1913 by Ley and Werner,[2] while the two anhydrous states, α stable, (II), and β metastable, (III), were obtained in 1935 by A. Ostrogovich and G. Ostrogovich.[3]

The study of these compounds is part of our interest concerning the ability of cyanuric acid and of other amidic compounds to give the biuret reaction. As the two anhydrous forms have different colours — α is reddish-violet, and β steel-blue — it is interesting to find out the reasons of this difference. The dehydration of compound (I) directly to the α-state was studied thermogravimetrically [4] ; it takes place as a single step with an activation energy of 52.0 kcal/mol. ESR studies [1] demonstrated a planar tetragonal structure for these three compounds as well as a high degree of covalency for the copper(II)-ligand bonds.

[1] Z. Simon, M. Nuţiu and G. Ostrovich, *Rev. Roumaine Chim.*, **17**, 573 (1972).

[2] H. Ley and G. Werner, *Ber. dtsch. chem. Ges.*, **46**, 4040 (1913).

[3] A. Ostrogovich and G. Ostrogovich, "Atti del Congresso Nazionale di Chimica Pura ed Applicata", Sardegna, Maggio e Giugno, **1935** ; *Chem. Zentr.*, **1937**, I, 2146.

[4] G. Ostrogovich and M. Nuţiu, *Rev. Roumaine Chim.*, **16**, 1473 (1971).

EXPERIMENTAL

The compounds were obtained following the indications given in literature.[3] The structural analysis was performed by the powder method with an X-ray apparatus, model TuR-M61, with horizontal goniometer and a Geiger-Müller counter. Planar pulverulent preparates were used with granule-sizes below 40 mμ. For each complex the diffraction spectra were recorded at two different angular velocities. The CuKa radiation used, produced in each case the dispersion of diffraction lines in the angle range $4° < \theta < 35°$. The line indexation was realized by the graphical method indicated by Gattow and Piotter.[5]

The $\beta \rightarrow \alpha$ transformation kinetics was investigated by the isotherm method. The rate constants were calculated by the equation : $k = 1/t\, 2.303 \log c_0/c$, where t is the time interval, c_0 and c are the concentrations of the β state at moments $t = 0$ and $t = t_1$ respectively.

RESULTS AND DISCUSSIONS

The fundamental parameters of the three compounds, indexed orthorhombically, were :

$$(I) : a_0 = 12.40 \text{ Å} ; b_0 = 13.85 \text{ Å} ; c_0 = 25.88 \text{ Å} \ (\pm 0.1 \text{ Å})$$

$$(II) : a_0 = 19.78 \text{ Å} ; b_0 = 15.32 \text{ Å} ; c_0 = 11.61 \text{ Å} \ (\pm 0.1 \text{ Å})$$

$$(III) : a_0 = 10.82 \text{ Å} ; b_0 = 11.70 \text{ Å} ; c_0 = 12.57 \text{ Å} \ (\pm 0.1 \text{ Å})$$

Tables 1—3 present the diffraction lines, d_{exp}, their relative intensities, the established indexes and the recalculated values, d_{calc}. The differences between d_{exp} and d_{calc} are below 1%, except the range of small θ angles.

The extinction laws permitted to conclude that the network is primitive. For the hydrate, the $P_{mc}2_1$ spatial group was assigned, while for both anhydrous states, the spatial group $P_{mm}2_1$. The number of molecules per elementary cell was calculated for each complex by means of the roentgenographically determined cell volume and of the picnometric densities : $d_4^{25} = 1.938$ for (I), $d_4^{25} = 2.086$ for (II), and $d_4^{25} = 1.974$ for (III). The values obtained are $N_{(I)} = 7.1$, $N_{(II)} = 7.0$, and $N_{(III)} = 2.0$. We thus finally consider the number of molecules per elementary cell 7, 7 and 2, respectively.

Thus, compounds (I) and (II) have similar structures from the crystalline motive point of view (aboth have $N = 7$), while compounds (II) and (III), although similar regarding the reticular symmetry, have different reticular parameters. The existence of the two anhydrous states is thus due to a crystalline dimorphism.

The diffraction spectra of the two anhydrous compounds permit their quantitative determination in mixture so that a kinetic study of the $\beta \rightarrow \alpha$ transformation process was performed using the isotherms method.

---

[5] G. Gattow and H. Piotter, *Z. anorg. Chem.*, **336**, 1 (1965).

Table 1

Indexed diffraction lines for $[(Cu(C_3O_3N_3H_2)]Na_2\ 6\ H_2O$

No of spectrum-line	d_{hkl} exp.	$I/I_{max}\cdot 100$	*hkl*	d_{hkl} calc.	d %
1	9.46	4	012	9.458	0.0
2	9.00	4	102	8.953	0.5
3	6.47	3	004	6.471	0.0
4	6.20	10	200	6.199	0.0
5	5.43	17	122	5.579	0.9
6	5.31	18	114	5.300	0.1
7	4.64	3	220 (030)	4.620 (4.619)	0.4
8	4.33	6	130 (003)	4.328 (4.314)	0.0
9	3.85	3	116	3.910	1.5
10	3.811	3	312	3.788	0.6
11	3.236	7	008	3.236	0.0
12	3.144	8	108	3.131	0.4
13	3.099	100	400	3.100	0.0
14	3.043	33	410	3.025	0.6
15	2.960	5	144	2.966	0.2
16	2.921	15	316	2.917	0.1
17	2.767	25	422 (050)	2.764 (2.771)	0.1
18	2.595	3	424	2.592	0.1
19	2.514	4	406	2.517	0.1
20	2.479	6	500	2.480	0.0
21	2.151	3	506	2.150	0.0
22	2.066	3	600 (450)	2.066 (2.066)	0.0
23	2.036	3	066	2.036	0.0
24	2.002	4	258	1.993	0.4
25	1.966	4	2, 4, 10	1.966	0.0
26	1.912	4	3, 0, 12	1.912	0.0
27	1.865	3	606	1.864	0.0

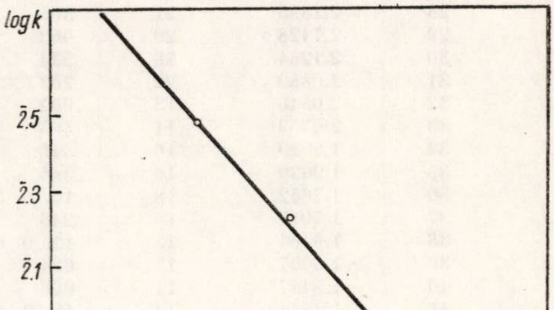

Fig. 1. — Kinetics data of β → α transformation.

Table 2

Indexed diffraction lines for α-$[(CuC_3O_3N_3H_2)_4]Na_2$.

No of spectrum-line	d_{hkl} exp.	$I/I_{max}.100$	$k\,h\,l$	d_{hkl} calc.	d %
1	10.30	13	101	10.001	3.0
2	7.626	18	020	7.660	0.5
3	7.131	19	120	7.143	0.17
4	7.019	27	211	6.756	3.6
5	6.605	24	300	6.593	0.16
6	5.819	22	002	5.804	0.17
7	5.565	100	012	5.428	2.3
8	4.389	11	302 (411)	4.357 (4.361)	0.7 (0.6)
9	4.191	55	420	4.154	0.88
10	3.9516	47	500	3.955	0.0
11	3.8704	16	003	3.870	0.0
12	3.7357	12	113	3.686	1.3
13	3.5928	14	141	3.578	0.42
14	3.4502	25	241	3.413	1.1
15	3.3211	22	332	3.315	0.2
16	3.2969	20	600	3.297	0.0
17	3.2732	28	223	3.261	0.3
18	3.0534	23	133 (050)	3.047 (3.064)	0.2
19	2.9355	55	250	2.927	0.3
20	2.8945	58	004	2.902	0.3
21	2.8145	44	333	2.794	0.7
22	2.7720	41	630	2.769	0.1
23	2.7227	37	052	2.710	0.4
24	2.5496	37	060	2.553	0.15
25	2.4294	17	261	2.418	0.45
26	2.3882	14	360 (424)	2.381 (2.380)	0.3
27	2.2832	16	802	2.275	0.35
28	2.1895	21	305	2.190	0.05
29	2.1428	20	063	2.131	0.6
30	2.1264	28	534	2.127	0.03
31	2.0889	22	263 (803)	2.084 (2.083)	0.2
32	2.0546	13	902	2.055	0.02
33	2.0353	11	363	2.028	0.35
34	1.9020	16	345	1.901	0.05
35	1.9020	16	345	1.901	0.05
36	1.7652	18	10, 0, 3	1.761	0.17
37	1.7017	15	246	1.699	0.0
38	1.6464	13	12, 0, 0	1.648	0.01
39	1.6007	13	084	1.598	0.07
40	1.5487	11	066	1.542	0.45
41	1.4944	13	13, 2, 0	1.492	0.16
42	1.4606	11	057	1.459	0.07
43	1.4372	13	208	1.436	0.07

In figure 1 the plots of log *k vs.* $1/T$ are given. The activation energy of $E = 25.7$ kcal/mol was calculated out of the slope of the linear plot, thus obtained. The preexponential factor $A = 3.99 \times 10^{10}\ s^{-1}$ was also calculated from the Arrhenius equation.

The difference in colour, as well as the infrared spectra,[6] suggest that the anhydrous β state is possibly existing in an associated form, while the hexahydrate and the anhydrous α state are unassociated.

---

[6] G. Ostrogovich and M. Nuțiu, unpublished data.

Table 3

Indexed diffraction lines for β-[(Cu($C_3O_3N_3H_2$)$_4$)]Na_2

No of spectrum-line	d_{hkl} exp.	$I/I_{max}.100$	$h\,k\,l$	d_{hkl} calc.	d %
1	10.80	43	100	10.82	0.2
2	6.505	40	111	6.715	3.4
3	5.869	100	020	5.850	0.3
4	4.2234	69	003	4.190	0.8
5	3.3456	46	222	3.358	0.3
6	3.11725	46	213	3.184	2.0
7	3.0230	34	104	3.018	0.1
8	2.9168	90	040	2.925	0.3
9	2.8875	89	223	2.883	0.0
10	2.8513	62	033	2.855	0.1
11	2.5191	71	005	2.514	0.2
12	2.4130	46	421	2.410	0.1
13	2.2732	46	403	2.273	0.0
14	2.2122	50	324	2.196	0.8
15	2.1674	71	500	2.164	0.1
16	2.1477	53	044	2.141	0.2
17	2.0370	31	252	2.032	0.2
18	2.0028	46	521	2.004	0.6
19	1.9232	28	503	1.923	0.0
20	1.8631	34	062	1.862	0.0
21	1.8419	46	405	1.841	0.0
22	1.7464	34	163	1.745	0.0
23	1.6240	53	534	1.621	0.2
24	1.6182	53	072	1.615	0.2
25	1.5855	46	264	1.584	0.0
26	1.5679	40	008	1.571	0.2
27	1.3368	28	084	1.326	0.6

Revue Roumaine de Chimie, **17**, *9*, 1551–1562 (1972)

KINETICS OF SOLVOLYTIC REACTIONS. II.[1]

ACETOLYSIS OF 5H-DIBENZO [a,d] CYCLOHEPTENE-5-YL-METHYL TOSYLATE UNDER THERMODYNAMIC CONTROL

M. VOICU and F. BADEA

Laboratory of Organic Chemistry, Polytechnic Institute, str. Polizu 1, Bucharest, Romania

Received May 8, 1972

The acetolysis of title compound (**1**–OTs) was studied in the absence and in the presence of sodium acetate, at ratios [NaOAc]/[**1**–OTs] <1. Only in the presence of sodium acetate, a zero order reaction was found to be involved after the disappearance of sodium acetate. In the absence of sodium acetate, the acetolysis of tosylate **1**–OTs follows a good first order kinetics, if sufficient *p*-toluenesulphonic acid is present. The interpretation of these results stresses the equilibration of intermediates with reaction products and reactant, and the importance of internal return.

1. INTRODUCTION

The acetolysis of 5H-dibenzo [a, d] cycloheptene-5-yl-methyl tosylate, **1**–OTs, in unbuffered solutions gives, as principal product, the unrearranged acetate **1**–OAc, beside small amounts of a bridged compound, **3**–OAc. In buffered solutions with sodium acetate, the 5,6-dihydro-di-

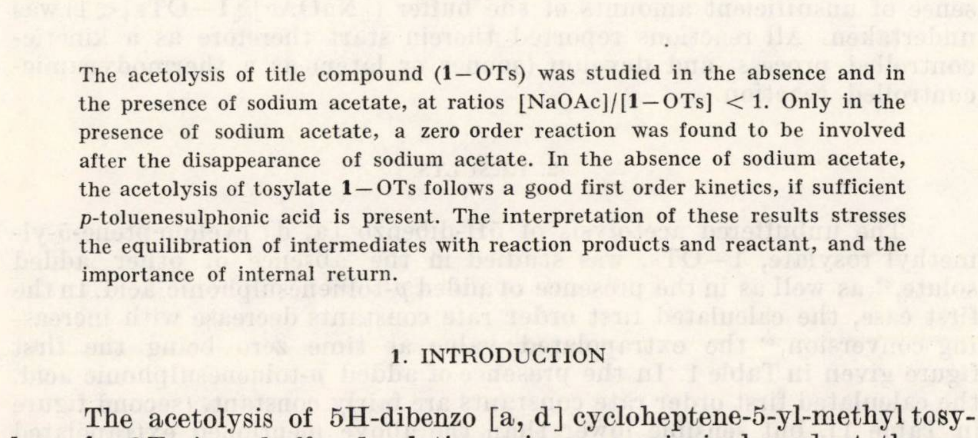

(1)

---

[1] The paper by M. Voicu and F. Badea, *Rev. Roumaine Chim.*, **14**, 929 (1969) is paper I in this series.

benzo [a, e] cyclooctene-5-yl acetate, **2**—OAc is formed in good yields, together with another bridged compound, **4**—OAC.[2]

Two independent ionization steps have been proposed,[2b] in the solvolysis of **1**—OTs. One of these, leading to the major reaction products (90% of the overall reaction), was considered to be assisted by the β-aryl groups (phenonium route, k_{Ph}). The other one, leading to the bridged products (6—8% of the overall reaction), was supposed to involve the participation of the double bond (π-route, k_π).

The composition of the reaction mixtures in buffered and unbuffered solutions suggests that a kinetic *vs* thermodynamic control is responsible for the observed differences in product formation. To get a better insight of the mechanism of the solvolyses of **1**—OTs, the kinetics of its acetolyses in the absence of sodium acetate, as well as in the presence of unsufficient amounts of the buffer ([NaOAc]/[**1**—OTs] < 1) was undertaken. All reactions reported therein start therefore as a kinetic-controlled process, and develop (sooner or later) as a thermodynamic-controlled reaction.

2. RESULTS

The unbuffered acetolysis of 5H-dibenzo [a, d] cycloheptene-5-ylmethyl tosylate, 1—OTs, was studied in the absence of other added solute,[2a] as well as in the presence of added *p*-toluenesulphonic acid. In the first case, the calculated first order rate constants decrease with increasing conversion,[2a] the extrapolated value at time zero being the first figure given in Table 1. In the presence of added *p*-toluenesulphonic acid, the calculated first order rate constants are fairly constant, (second figure in Table 1), but sensible lower than the above mentioned extrapolated rate constant. These rate constants are compared in Table 1 with the rate constants of other structurally similar tosylates.

Using Guggenheim's method,[4] we demonstrated the relationship :

$$\Delta \log k = -\Delta \log t \qquad (2)$$

where t is the time necessary to reach the same conversion, x/a, at different temperatures ; at 20%, 35%, 50% and 65% conversions, the plots $\log t = f(1/T)$ have the slopes 5730, 3800, 6000 and 6200, respectively. The activation parameters for tosylate **1**—OTs in Table 1 were calculated from the extrapolated slope at zero conversion, 5700.

The acetolysis of **1**—OTs in the presence of sodium acetate, ([NaOAc]/[**1**—OTs] < 1), follows a first order reaction in the buffered part of the solvolysis (the lines 2, 3 and 4 in Table 2). The observed rate constant for this part of the reaction corresponds to the extrapolated rate constant

---

[2] a) E. Ciorănescu, A. Bucur, M. Elian, M. Banciu, M. Voicu and C. D. Nenitzescu, *Tetrahedron Letters*, **1964**, 3835 ; *Rev. Roumaine Chim.*, **10**, 161 (1965) ; b) E. Ciorănescu, A. Bucur, F. Badea, M. Rentzea and C. D. Nenitzescu, *Tetrahedron Letters*, **1969**, 1867.

[3] S. Winstein, B. K. Morse, E. Grunwald, K. C. Schreiber and J. Corse, *J. Amer. Chem. Soc.*, **74**, 1113 (1952).

[4] E. A. Guggenheim, *Phil. Mag.*, **2**, 538 (1926).

Table 1

Rate constants and activation parameters for the acetolysis, at 110°, of some primary tosylates, structurally related to β,β-diphenylethyl tosylate

Compound	$10^5 \cdot k$ sec^{-1}	$\Delta H^{\neq 383}$ kcal/mole	$\Delta S^{\neq 383}$ e.u.
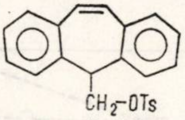 1−OTs	3.18 a) 1.56 b)	25.4	−13.4
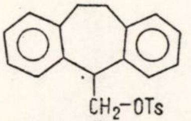 **5**	11.10 a)	26.0	− 9.5
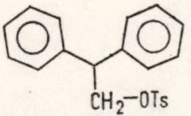 **6**	10.50 c)	27.2	− 6.4

a) Mean value obtained from several runs,[2a] through extrapolation at zero time; b) 4.16 × 10^{-3} moles/l *p*-toluenesulphonic acid was introduced at the beginning of the reaction ($[TsOH]_0/[1-OTs]_0 = 0.384$); c) From ref. 3.

Table 2

Calculated first, and zero order rate constants for the acetolysis of 1−OTs, at 110°, in presence of an unsufficient amount of buffer a)

	Time sec	10^3. [TsOH] moles/l	Conversion %	$10^5 \cdot k_1$ sec^{-1} b)	$10^8 \cdot k_0$ mole$\cdot$l$\cdot^{-1}$sec c.d)
1.	0	0	0	—	
2.	1,800	0.75	5.0	2.95	—
3.	5,400	2.40	15.9	3.24	—
4.	10,800	4.46	29.6	3.24	—
5.	21,600	7.72	51.0	3.31	...
6.	39,300	8.29	55.0	2.02	3.22
7.	73,800	9.52	63.0	1.35	3.43
8.	111,900	10.03	73.0	1.18	3.68
9.	165,600	12.62	83.5	1.09	3.40
10.	260,100	14.00	92.7	1.00	2.68

a) The ratio $[NaOAc]/[1-OTs] = 0.36$; b) $[1-OTs]_0 = 15.12 \times 10^{-3}$ M; c) The initial conditions in zero order process were taken those in line 5: $[1-OTs] = 7.40$ M; d) The mean value is $k_0 = (3.28 \pm 0.3)\cdot 10^{-8}$ mole$\cdot$ l$^{-1}\cdot$sec^{-1}.

in Table 1 (the figures are slightly higher due to the salt effect of sodium acetate).

In the later steps of the acetolysis, after sodium acetate has been consumed, the calculated first order rate constants present a downward drift, as in the unbuffered reaction. From the plots of *p*-toluenesulphonic acid concentration *vs* time (Figure 1) it seems that a zero order reaction settles in.

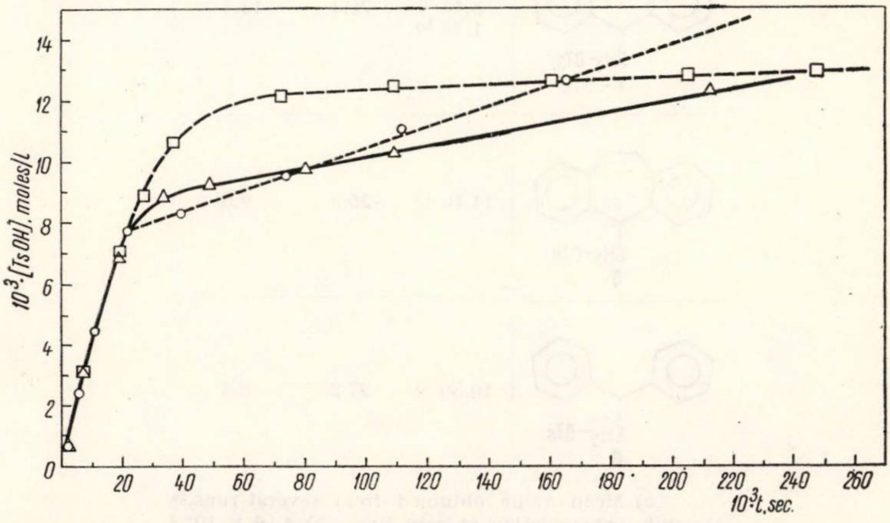

Fig. 1. — Concentration of *p*-toluenesulphonic acid *vs* time, for acetolysis of **1**$-$OTs on condition of the ratio : $[NaOAc]_0/[\mathbf{1}-OTs]_0 < 1$, at 110°. The symbols are : ○ for $[\mathbf{1}-OTs]_0 = 15.12\times10^{-3}$ moles/1, $[NaOAc]_0/[\mathbf{1}-OTs]_0 = 0.36$; Δ for $[\mathbf{1}-OTs]_0 = 14.92\times10^{-3}$ moles/1, $[NaOAc]_0/[\mathbf{1}-OTs]_0 = 0.53$; □ for $[\mathbf{1}-OTs]_0 = 15.15\times10^{-3}$ moles/1, $[NaOAc]_0/[\mathbf{1}-OTs]_0 = 0.77$.

The zero order reaction is better illustrated by the data of Table 2 (the values k_0), in which the time zero was taken from the plots of Figure 1. Of course, zero order rate constants decrease with increasing concentration of sodium acetate ; at ratios : $[NaOAc]/[\mathbf{1}-OTs]$ of 0.36, 0.53 and 0.7,7 the mean values of the zero order rate constants were 3.28×10^{-8}, $1.99\times\times10^{-8}$ and 0.48×10^{-8} mol l^{-8} sec^{-1}, respectively.

A similar behaviour was not observed in the unbuffered acetolysis. A plausible explanation for the observed differences between the unbuffered, and the buffered with unsufficient amounts of sodium acetate reactions is that the initially formed **2**$-$OAc (kinetic-controlled product), as soon as some *p*-toluenesulphonic acid is accumulated in the system, regenerates **1**$-$OTs :

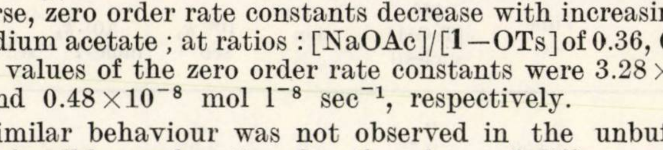

(3)

The reaction (3) was followed spectrophotometrically, the observed first order rate constant, at 110° and 3.76×10^{-3} moles/l *p*-toluenesulphonic acid concentration being $k_i = 1 \times 10^{-4}\ \mathrm{sec}^{-1}$, which gives $k_{ii} = 2.70 \times 10^{-2}\ \mathrm{l \cdot mol^{-1} \cdot sec^{-1}}$, for the second order rate constant.

3. DISCUSSIONS

3.1. *The kinetics of the unbuffered acetolysis of* **1**–*OTs*

Even in the absence of sodium acetate, the acetolysis of **1**–OTs must begin as a kinetic-controlled process ([TsOH] = 0), producing the acetate **2**–OAc. This affirmation is sustained by the fact that the extrapolated rate constant in the unbuffered acetolysis is identical with the rate constant in the buffered reaction.[2a]

As the reaction proceeds, and more *p*-toluenesulphonic acid is formed, equilibrium between all the products and intermediates may be attained. In the following discussion, considering that phenonium-route accounts for more than 90% of the overall reaction, we make abstraction of the π-route. In this case, a simplified description of the reaction, in unbuffered conditions, will be given by Scheme 1, in which the rearranged tosylate **2**–OTs is considered too, because it may be formed by internal return. The conclusions will not be altered, if in the place of one intermediate, *I*, more equilibrating intermediates are involved.

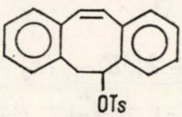

2-OTs

Scheme I

$$\begin{tikzcd}
 & 2\text{–OAc} + \text{TsOH} \arrow[d, shift right, "k'_2"'] & \\
1\text{–OTs} \arrow[r, shift left, "k_1"] & I \arrow[l, shift left, "k_{-1}"] \arrow[u, shift right, "k'_{-2}"'] \arrow[r, shift right, "k'_{-1}"'] \arrow[d, shift left, "k_{-2}"] & 2\text{–OTs} \arrow[l, shift right, "k'_1"'] \\
 & 1\text{–OAc} + \text{TsOH} \arrow[u, shift left, "k_2"] &
\end{tikzcd}$$

Using a steady state treatment, the concentration of the intermediate will be given by the expresion:

$$[I] = \frac{k_1[\mathbf{1}\text{–OTs}] + k'_1[\mathbf{2}\text{–OTs}] + k_2[\mathbf{1}\text{–OAc}] \cdot [\text{TsOH}] + k'_2[\mathbf{2}\text{–OAc}] \cdot [\text{TsOH}]}{k_{-1} + k'_{-1} + k_{-2} + k'_{-2}} \tag{4}$$

If equilibrium is attained in the reaction, the following equilibrium constants may be defined:

$$K = \frac{[1\text{—OTs}]}{[2\text{—OTs}]} \approx \frac{[1\text{—OAc}]}{[2\text{—OAc}]} \tag{5}$$

$$K' = \frac{[1\text{—OAc}][\text{TsOH}]}{[1\text{—OTs}]} \tag{6}$$

Considering the equations (5) and (6), the expression (4) becomes:

$$[I] = \frac{k_1 + k_1'/K + (k_2 + k_2'/K)K'}{k_{-1} + k'_{-1} + k_{-2} + k'_{-2}}\,[1\text{—OTs}] \tag{7}$$

The formation of *p*-toluenesulphonic acid has the equation rate:

$$\text{rate} = (k_{-2} + k'_{-2})\cdot[I] \tag{8}$$

or, considering the equation (7):

$$\text{rate} = (k_{-2} + k'_{-2})\cdot\frac{k_1 + k_1'/K + (k_2 + k_2'/K)\,K'}{k_{-1} + k'_{-1} + k_{-2} + k'_{-2}}\cdot[1\text{—OTs}] \tag{9}$$

The equation (9) shows that if equilibrium is attained, the formation of *p*-toluenesulphonic acid must be of a first order reaction. Obviously, equilibrium occurs only in the presence of *p*-toluenensulphonic acid. This was demonstrated by the experience in which *p*-toluenesulphonic acid was initially added in the reaction mixture. Clean first order reaction was observed ($k_{\text{obs,T}} = 1.56\times10^{-5}\ \text{sec}^{-1}$). This value is about a half of the extrapolated value ($k_{\text{extr}} = 3.18\times10^{-5}\ \text{sec}^{-1}$, the rate constant under kinetic control). The expression for this last one will be:

$$k_{\text{extr}} = \frac{k_1 k'_{-2}}{k_{-1} + k'_{-2}} \tag{10}$$

Comparing this equation with the expresion for the rate constant under thermodynamic control, resulted from (9):

$$k_{\text{obs, T}} = \frac{k_1 k'_{-2} + k_1 k_{-2} + (k_{-2} + k'_{-2})\cdot[k_1'/K + (k_2 + k_2'/K)\,K']}{k_{-1} + k'_{-2} + k'_{-1} + k_{-2}} \tag{11}$$

we see that the numerator must be larger in (11) than in (10). It follows that the denominator in (11) must be also much larger than in (10). As k_{-2} must be much smaller than k'_{-2} (the kinetic controlled product is

2—OAc), it follows that $k'_{-1} \gg 2(k_{-1} + k_{-2})$, because $k_{\mathrm{extr}}/k_{\mathrm{obs,\,T}} \approx 2$. That means that the secondary tosylate, **2**—OTs, is formed in the acetolysis, even if it was not possible to isolate it, or to prepare it, in the usual manner.

Thus, the kinetics of the acetolysis of 5H-dibenzo [a, d] cycloheptene-5-yl-methyl tosylate, **1**—OTs, in unbuffered solution, confirms the formation of equilibrating intermediate (s) with reactants and products. In comparing relations (10) and (11), the results also indicate the return from the initially formed ion pairs (*I*) to covalent tosylate, **2**—OTs.

3.2. *Regeneration of* **1**—*OTs from* **2**—*OAc. Zero order reactions*

The tosylate **1**—OTs is formed from **2**—OAc and *p*-toluenesulphonic acid, as the equation (3) shows. The kinetics of this reaction corresponds to a pseudounimolecular reaction, with a second order rate constant $k_{\mathrm{ii}} = 2.70 \times 10^{-2} \cdot 1 \cdot \mathrm{mol}^{-1} \cdot \mathrm{sec}^{-1}$. Scheme II gives a good account of these facts.

Scheme II

$$\begin{tikzcd} \mathbf{1}-\mathrm{OTs} \arrow[r, shift left, "k_1"] & I \arrow[l, shift left, "k_{-1}"] \arrow[r, shift left, "k_{-3}"] \arrow[d, "k_{-2}"] & \mathbf{2}-\mathrm{OAc} + \mathrm{TsOH} \arrow[l, shift left, "k_3"] \\ & \mathbf{1}-\mathrm{OAc} + \mathrm{TsOH} & \end{tikzcd}$$

In Scheme II, k_1, k_{-1} and k_{-2} have the same meanings as in Scheme I. The rate constants k_3 and k_{-3} differ from the rate constants k'_2 and k'_{-2} from Scheme I; they include the disappearance and formation of the secondary tosylate, **2**—OTs. As that system is far from the equilibrium depicted in Scheme I, the formation of intermediate *I* from **1**—OAc, may be neglected. If no **1**—OTs is present initially in the reaction mixture (3), k_1 may be also neglected. In that case, the second order rate constant k_{ii} will be given by the equation :

$$k_{\mathrm{ii}} = \frac{k_3(k_{-1} + k_{-2})}{k_{-1} + k_{-2} + k_{-3}} \tag{12}$$

The term k_{-2} is also included in this relation, because the used spectrophotometrical method in the determinations cannot discern between **1**—OTs and **1**—OAc (see Experimental part).

If both **1**—OTs and **2**—OAc are present together with TsOH in the reaction mixture, and the reaction is followed by measuring the increase in TsOH concentration, Scheme II will still give a better account for the kinetics, than Scheme I (the system cannot reach equilibrium, due to the presence of **2**—OAc in a great amount). This situation corresponds to the experiments in which sodium acetate was initially added in the reaction mixture ([NaOAc]/[**1**—OTs] < 1). In the first steps of the reaction, until NaOAc is consumed, the kinetic-controlled product, **2**—OAc, will be formed. In the later steps, as some TsOH has been produced, **2**—OAc will regenerate **1**—OTs, together with further acetolysis of **1**—OTs. The observed rate will be given by :

$$\text{rate} = \frac{\mathrm{d}[\mathrm{TsOH}]}{\mathrm{d}t} = (k_{-2} + k_{-3})\cdot[I] - k_3\cdot[\mathbf{2}\text{—OAc}]\cdot[\mathrm{TsOH}] \quad (13)$$

or, considering a stationary state treatment :

$$\frac{\mathrm{d}[\mathrm{TsOH}]}{\mathrm{d}t} = \frac{k_{-2} + k_{-3}}{k_{-1} + k_{-2} + k_{-3}}\cdot k_1\cdot[\mathbf{1}\text{—OTs}] - \frac{k_3\cdot k_{-1}}{k_{-1} + k_{-2} + k_{-3}}\cdot[\mathbf{2}\text{—OAc}]\cdot[\mathrm{TsOH}] \quad (14)$$

The first coefficient in the equation (14) must be of the same order of magnitude as $k_{\mathrm{obs.\,T}}$ (compare with (11)), and probably smaller. The second coefficient must not be very different from k_{ii} (compare with (12), as k_{-2} must be smaller than k_{-1}; actually, only **1**—OTs was isolated on treatment of **2**—OAc with TsOH,[2a] and the comparison of equations (10) and (11) shows also that the return in this reaction must play an important part in the overall reaction).

The ratio of the two coefficients must therefore be of the order of magnitude :

$$k_{\mathrm{obs.\,T}}/k_{\mathrm{ii}} \approx 6\times10^{-4} \quad (15)$$

If **1**—OTs and **2**—OAc have about the same concentration, even at 10^{-3} moles/l TsOH, this last one must be consumed (negative rate), which is not in agreement with the data of Table 2. It can be therefore concluded that Scheme II is not complete ; **1**—OTs must be also involved in another solvolysis producing *p*-toluenesulphonic acid. This reaction is the minor path, leading to the bridged compounds. The π-route can be thus observed due the suppressing of the main reaction path, with the help of **2**—OAc. It therefore means that the zero order reaction represents the π-route, or :

$$\frac{\mathrm{d}[\mathrm{TsOH}]}{\mathrm{d}t} \approx k_\pi(a + x - y) \quad (16)$$

in which a is the initial concentration of **1**—OTs, x is the concentration of **1**—OTs formed from **2**—OAc, and y is the concentration of the bridged compounds. The term $x-y$ will be small as compared to a; therefore, the reaction will appear as a zero order reaction. In the first steps of the reaction, $x-y$ will be positive, and k_0 will increase with time ; in the latter steps, $x-y$ will become negative, and k_0 will decrease. These predictions are in good agreement with the data of Table 2. The unimolecular rate constant, k_π will be :

$$k_\pi = k_0/a' \quad (17)$$

where $a' = a + x_m$, in which x_m is the value of x, when k_0 attains a maximum. Considering the data of Table 2 :

$$k_\pi = \frac{3.28\times10^{-8}}{(7.40+3.31)\times10^{-3}} = 3.05\times10^{-6}\ \text{sec}^{-1} \tag{18}$$

in excellent agreement with the product analysis :

$$\frac{\text{unbridged products}}{\text{bridged products}} \approx 11.5 \approx \frac{3.18\times10^{-5}}{3.05\times10^{-6}} \approx 10.4 \tag{19}$$

3.3. The phenonium and π-route in solvolysis of **1**—*OTs*

From the product analysis and zero order kinetic data, mean values of the two rate constants, k_{Ph} and k_π, corresponding to the two different routes in ionization of tosylate **1**—OTs, may be calculated :

$$k_{\text{Ph}} = 2.95\times10^{-5}\ \text{sec}^{-1} \tag{20a}$$

$$k_\pi = 0.25\times10^{-5}\ \text{sec}^{-1} \tag{20b}$$

It is well known that in π-route reactions, the unsaturated derivative reacts faster than the saturated analog. For example, the ratio k_U/k_S is about 30 for tosylates **7** and **8**.[5]

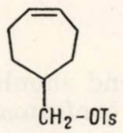

7

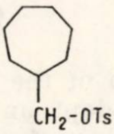

8

The tosylates **1**—OTs and **5**, studied in this work, are similar in their structure with **7** and **8**. However, the ratio k_π/k_5 is only 0.027, the unsaturated tosylate reacting much slower than the saturated derivative. The reason of the observed order of reactivity in this case is that k_U/k_S does not measure the assistance of the double bond as compared to the solvent assistance in ionization, as it usually does. Tosylate **5** ionizes through a phenonium route, and therefore, k_π/k_5 indicates the same thing as k_π/k_{Ph} ; the aryl groups are more effective in assisting the ionization, than the double bond. This needs an explanation, since from the known facts, the opposite should have been expected.

---

[5] G. Le Ny, *Compt. rend.*, **251**, 1526 (1960).

The 5H-dibenzo [a, d] cycloheptene has a stable boat conformation.[6] Tosylate **1**—OTs may therefore exist in an axial conformation, **1**—*a*, and an equatorial one, **1**—*e*, respectively.

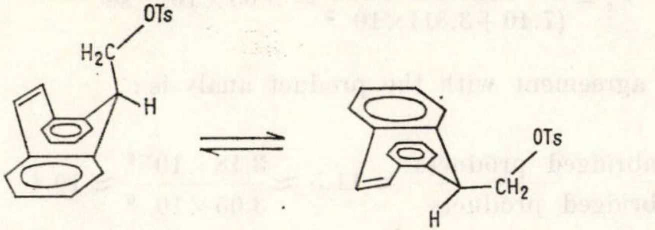

1-a 1-e (21)

In both phenonium, and π-routes, ionization must occur from the axial conformation.[7]

The participation of the aromatic rings should be possible from the two rotamers, **1**—*a*—*s* and **1**—*a*—*s'*, corresponding to the staggered conformation of β, β-diphenylethyl tosylate, **6**, which are stable conformations :

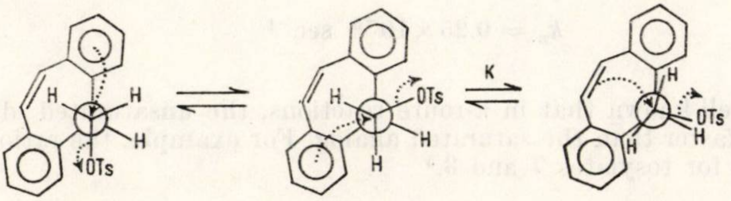

1-a-s 1-a-s' 1-a-ec (22)

The participation of the double bond should be only effective, if the molecule would adopt an eclipsed conformation, **1**—*a*—*ec*, which must be less stable than the other two.

In comparing the activity of the aromatic rings, and the reactivity of the double bond, we must therefore consider equilibrium (22). If we assume that only rotamer **1**—*a*—*ec* is responsible for the π-route, the staggered conformations producing the phenonium ion, then the observed rate constants given in (20a) and (20b) will be :

$$k_{\mathrm{Ph}} = k'_{\mathrm{Ph}} \tag{23}$$

$$k_{\pi} = \frac{K}{K+1} k'_{\pi} \tag{24}$$

---

[6] E. Traetteberg, *J. Amer. Chem. Soc.*, **86**, 4265 (1964) ; E. Ebnöther, E. Jucker and A. Stoll, *Helv. Chim. Acta*, **48**, 1237 (1965) ; R. E. Davis and A. Tulinsky, *J. Amer. Chem. Soc.*, **88**, 4583 (1966) ; H. Schimanouchi, T. Hata and Y. Sasada, *Tetrahedron Letters*, **1968**, 3573 ; W. E. Neyd and C. A. Papas, *J. Amer. Chem. Soc.*, **93**, 6086 (1971).

[7] R. Huisgen and G. Seidl, *Angew. Chem.*, **69**, 341, 390 (1957).

in which k'_{Ph} and k'_{π} are the specific rate constants of the pure conformer in which the assistance is produced, K is the equilibrium constant, $K = [\mathbf{1}-a-ec]/[\mathbf{1}-a-s]$.

The eclipsed conformation in ethane, at room temperature, is about 2.75 kcal/mole less stable than the staggered conformer. Assuming at 100° a difference of about 3 kcal/mole (which is probable larger) between **1**$-a-s$ and **1**$-a-ec$, the actual ratio $k'_{\pi}/k'_{\mathrm{Ph}}$ would be about 10, which seems to be reasonable.

The small value of k_{Ph} given in (20a), as compared with other values summarized in Table 1, may reflect equilibrium (21), in which the axial conformer is unstable.

A similar equilibrium, (25), between an axial and an equatorial conformer, must occur in tosylate **5** as well. Models show that the axial conformation of **5** must be less stable than the axial conformation of **1**—OTs, due to the repulsions between the axial hydrogens H_a of the bridge, with the hydrogen atoms of the CH_2—OTs group.

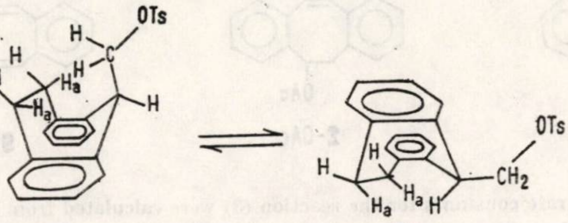

5-a **5-e** (25)

However, tosylate **5** solvolyses with about the same rate as the acyclic tosylate **6**, indicating that in comparing the two rates, equilibrium (25) plays not a significant role.

The same should then be true for tosylate **1**—OTs, in which such axial repulsions are not to be expected. That being so, the small value of k_{Ph} reflects a polar effect, the inductive effect of the double bond in **1**—OTs.

4. EXPERIMENTAL

Acetic acid was prepared as previously noted,[1] and contains a small amount of acetic anhydride.

Sodium acetate solutions were obtained as is previously described.[1]

5H-Dibenzo [a, d] cycloheptene-5-yl-methyl tosylate (**1**—OTs), mp. 140—141° (lit.[8] 140—141°), was prepared by the method reported in the literature.[8]

5,6-Dihydro-dibenzo [a, e] cyclooctene-5-yl acetate (**2**—OAc), was prepared and described previously.[9]

---

[8] E. Ciorănescu, A. Bucur, M. Elian and C. D. Nenitzescu, *Rev. Roumaine Chim.*, **10**, 149 (1965).

[9] E. Ciorănescu, A. Bucur, M. Banciu and C. D. Nenitzescu, *Rev. Roumaine Chim.*, **10**, 141 (1965).

Kinetic measurements

a) *Unbuffered acetolysis* was followed :

— *Titrimetrically.* Acetolyses were performed using the ampoule technique: 5 ml samples of **1**—OTs in acetic acid were thermostated, then chilled at room temperature (in these conditions the reaction is practically quenched), and *p*-toluenesulphonic acid was titrated with a 0.04 M sodium acetate in acetic acid, using a Metrohm potentiograph, Model E336, with a platinium electrode and a graphite capilar electrode, designed after Zeidler.[10] The rate constants were calculated as mentioned before.[1]

— *Spectrophotometrically.* At 300 $m\mu$, the stilbene system in **1** (**1**—OTs and **1**—OAc) has an identical extinction coefficient, $\varepsilon_1 = 11{,}800$, and verifies Lambert-Beer's law. The other reaction products have negligible absorbtions ($\varepsilon_{2-\mathrm{OAc}} = 115$, $\varepsilon_9 = 130$), or do not absorb in this region (**3**—OAc and **4**—OAc). By preliminary attempts, it was found that the amount of **1**—OTs and **1**—OAc may be calculated from the observed extinction ; the extinctions for **2**—OAc and **9** are less than 1 %.

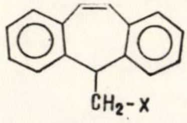

1-X

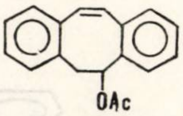

2-OAc

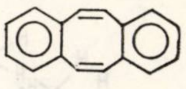

9

The first order rate constants for the reaction (3) were calculated from the usual equation, assuming $a \sim E_\infty$ and $x \sim E$:

$$k = \frac{2.303}{t} \log \frac{E_\infty}{E_\infty - E} \tag{26}$$

b) *Buffered acetolysis*, or buffered part of solvolytic reaction, on condition $[\mathrm{NaOAc}]_0/[\mathbf{1}-\mathrm{OTs}]_0 < 1$, were followed kinetically only by titrimetric method. The samples containing an excess of sodium acetate were acidulated with a measured amount of 0.05 M perchloric acid in acetic acid, and were potentiographically back-titrated with standard sodium acetate, as mentioned above.

---

[10] H. Zeidger, *Z. analyt. Chem.*, **146**, 271 (1955).

Revue Roumaine de Chimie, 17, 9, 1563 – 1577 (1972)

KINETICS OF SOLVOLYTIC REACTIONS. III[1]
INTERMEDIATES INVOLVED IN THE ACETOLYSIS OF 5*H*-DIBENZO [a, d] CYCLOHEPTENE-5-YL-METHYL TOSYLATE AND 9,10-BIS (HYDROXYMETHYL)-9,10-DIHYDROANTHRACENE DITOSYLATE

M. VOICU and F. BADEA

Organic Chemistry Laboratory,
Polytechnic Institute, str. Polizu 1, Bucharest, Romania
and
AURORA BUCUR
Centre of Organic Chemistry, Bucharest, Romania

Received May 8, 1972

The mechanism of the solvolysis of 5*H*-dibenzo [a, d] cycloheptene-5-yl-methyl derivatives, proposed in the previous paper of this series [1] has been supported by the kinetics of the acetolysis of the *cis*-9, 10-*bis* (hydroxymethyl)—9, 10-dihydroanthracene ditosylate, **7**; the kinetic treatment of the obtained data has permitted to evaluate both rate constants of the two consecutive solvolyses, in both buffered and unbuffered solutions. New evidence regarding the number of the intermediates involved in the phenonium route of the first title compound has been obtained from the solvolyses of that compound in kinetically-controlled conditions, with or without added solutes. The reactivity of the 5,6-dihydrodibenzo [a, e] cyclooctene-5-yl bromide, (**2**—Br), and of the corresponding saturated analogue (5, 6, 11, 12-tetrahydro-dibenzo [a, e] cyclooctene-5-yl bromide, **6**—Br) support in their turn the proposed mechanism.

1. INTRODUCTION

In the previous paper of this series,[1] the kinetics of the acetolysis of 5H-dibenzo [a, d] cycloheptene-5-yl-methyl tosylate, **1**—OTs, in thermodynamic conditions has been studied. Evidence has been obtained therein, for two independent routes in the ionization of **1**—OTs, labelled as phenonium route and π-route, respectively. No hint regarding the number of intermediates in each of these routes resulted from the analysis of the kinetic data.

---

[1] Part II., M. Voicu and F. Badea, *Rev. Roumaine Chim.*, **17**, 1551 (1972)

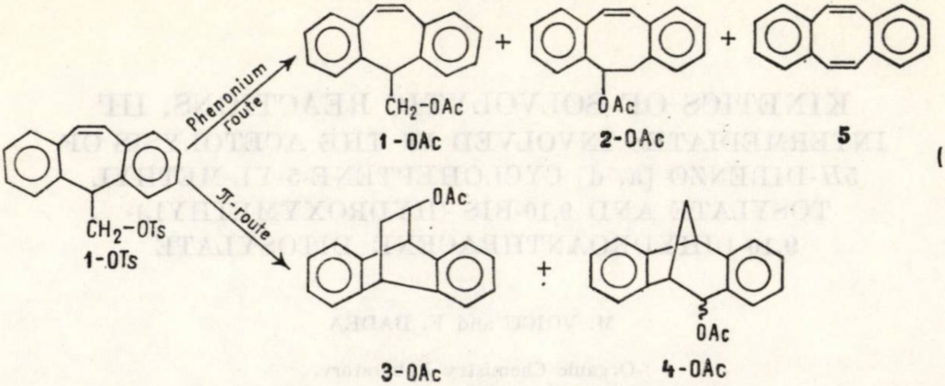

(1)

The present work is especially interested in the number of intermediates involved in the phenonium route. For this purpose, the reactions of the unsaturated bromides **1**—Br, **2**—Br and the saturated bromide **6**—Br have been investigated. Preliminary results have been already published.[2]

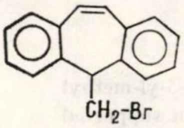

1-Br

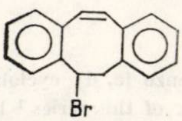

2-Br

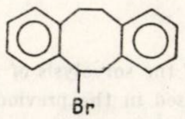

6-Br

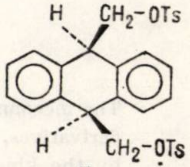

7

The acetolysis of the bromides in studying the phenonium route for the 5H-dibenzo [a, d] cycloheptene-5-yl-methyl system (**1**) and 5,6-dihydro-dibenzo [a, e] cyclooctene-5-yl system (**2**) has the advantage over the acetolysis of the corresponding tosylates *), because the reaction can be followed from either direction of the equilibrium between **1**—X and **2**—X derivatives.

Other indications regarding the number of intermediates in the phenonium route in the acetolysis of **1**—OTs have been also obtained from the observed salt effects of NaOAc, $NaClO_4$ and $LiClO_4$.

The mechanism proposed in this and the preceding paper[1] is also upheld by the acetolysis of the *cis*-ditosylate **7**.

2. RESULTS

2.1. *Preparation of the bromides*

5,6-Dihydro-dibenzo [a, e] cyclooctene-5-yl bromide, **2**—Br (mp. 84—86°) was prepared according to the procedure described by Cope and Smith,[3] from 5,6-dihydro-dibenzo [a, e] cyclooctene with N-bromosuccinimide. At room temperature, **2**—Br can be conserved only few days, but it is stable at lower temperatures (0—5°).

---

*) The secondary benzylic tosylate, **2**—OTs was not prepared; we have not succeeded in obtaining it, even if the kinetic data have demonstrated its formation.[1]

[2] E. Cioränescu, A. Bucur, F. Badea, M. Rentzea and C. D. Nenitzescu, *Tetrahedron Letters*, **1969**, 1867.

5,6,11,12-Tetrahydro-dibenzo[a, e]cyclooctene-5-yl bromide, **6**—Br was obtained from the corresponding alcohol, **6**—OH, with hydrogen bromide, in benzene.[3]

5H-Dibenzo [a, d] cycloheptene-5-yl-methyl bromide, **1**—Br (mp. 64—65°) was obtained either from ditosylate **7**, or from the alcohol **2**—OH, on refluxing with a 10% hydrogen bromide solution in acetic acid.

2.2. Solvolysis of the bromides

In aqueous acetone (75/25, v/v), the bromide **2**—Br is transformed within two minutes at room temperature, into the corresponding alcohol, **2**—OH. The reaction in this solvent could be kinetically followed only at 0°. In similar conditions, the corresponding saturated bromide, **6**—Br is about 10^5 times less reactive than **2**—Br (Table 1). The methanolysis of **2**—Br, at room temperature, occurs also without rearrangement, ether **2**—OCH$_3$ being thus formed. Conversely, in acetic acid, at 0° within 3 hr, the rearranged bromide, **1**—Br is formed quantitatively.

Table 1

Rate constants for hydrolysis of the bromides 2—Br and 6—Br, in aqueous acetone (75/25, v/v).

Compound	Temperature °C	k a) sec^{-1}
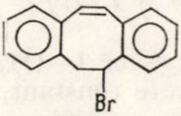 **2-Br**	0.0	6.10^{-2}
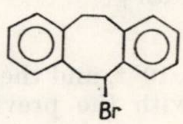 **6-Br**	0.0	6.88.10^{-7} b)
	24.8	1.42.10^{-5}
	40.0	7.30.10^{-5}

a) Conductometric measurements, with 0.005 moles/l bromide; b) Extrapolated value.

The primary bromide **1**—Br is strikingly less reactive than **2**—Br (Table 2); it is recovered unchanged after refluxing for 52 hr in aqueous acetone and is transformed only in 20% yield in the rearranged acetate **2**—OAc, after 264 hr on refluxing in acetic acid. From the data of Table 2, it can be appreciated that the eight-membered ring bromide, **2**—Br is about 10^5—10^6 times more reactive in acetic acid than the seven-membered ring bromide, **1**—Br. In aqueous acetone, the difference must be still larger ($> 10^8$)*).

---

[3] A. C. Cope and R. D. Smith, *J. Amer. Chem. Soc.*, **77**, 4596 (1955).

Table 2

Solvolytic data for 5H-dibenzo [a, d] cycloheptene-5-methyl bromide (1—Br), at reflux [a]**.**

Solvent	Time hr	[**1**—Br] %	[**2**—OAc] %
Aqueous acetone, 75%	52	100	0
Acetic acid	24	95[b]	5
Acetic acid	144	84	16
Acetic acid	264	80	20
Acetic acid (+ NaOAc)	24	95[b]	5
Acetic acid (+ NaOAc)	144	58	42
Acetic acid (+ AgOAc)	6	0	100

a) The amounts of **1**—Br and **2**—OAc were established by combustion analysis of the reaction mixture; b) Estimated data from IR spectra of the reaction mixture.

The low reactivity of bromide **1**—Br, as compared to the reactivity of tosylate **1**—OTs, is a proof that the unimolecular mechanism does not change in passing from the tosylate to the bromide **).

2.3. Buffered acetolysis of **1**—*OTs*

The kinetics of the buffered acetolysis of **1**—OTs is a clean first order reaction. The observed first order rate constant, k, increase with increasing concentration of sodium acetate, satisfying a linear relationship [4] (Figure 1).

$$k = k^0_{\mathrm{extr}}(1 + b\cdot[\mathrm{salt}], \tag{2}$$

The slope of the straight line is 20.4×10^{-5}, and the intercept $k^0_{\mathrm{extr}} = 3.1 \times 10^{-5}\ \mathrm{sec}^{-1}$, in good accordance with the previously mentioned value,[1] $3.18 \times 10^{-5}\ \mathrm{sec}^{-1}$.

---

*) Considering the data of Table 2, a rate constant of about $2.1 \times 10^{-7}\ \mathrm{sec}^{-1}$ for **1**—Br at 118° can be calculated. The quantitative transformation of **2**—Br in **1**—Br, at 80°, in 2.5—3 hr, gives a rate constant of about $7 \times 10^{-4}\ \mathrm{sec}^{-1}$. Considering from the known data [4] that phenonium ion reactions have the differences in the activation energy between a tosylate and a bromide of about 2 kcal/mole, it results the rate constant for **1**—Br, $(2\ldots4) \times 10^{-9}\ \mathrm{sec}^{-1}$ at 80°. The rate in aqueous acetone was appreciated similarly, considering that after 54 hr, a 1% transformation (undetected) has occured.

**) The great value of the ratio $k_{\mathbf{1}-\mathrm{OTs}}/k_{\mathbf{1}-\mathrm{Br}}$ was considered as a proof for a unimolecular mechanism [5] (Hoffmann's criterion [6]).

[4] A. H. Fainberg and S. Winstein, *J. Amer. Chem. Soc.*, **78**, 3763 (1956).

The normal salt effect, $b = \text{slope}/k^0_{\text{extr}}$, has a considerable greater value ($b_{\text{NaOAc}} = 6.6$), than other known values, but significant less than the salt effect of lithium perchlorate [4,7] ($b_{\text{LiClO}_4} = 15$). No special salt effect was observed with sodium acetate.

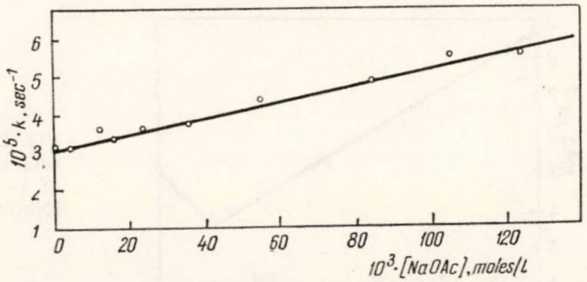

Fig. 1. — Effect of sodium acetate on the rate constants for the acetolysis of **1**—OTs, at 110°.

The salt effects of $LiClO_4$ in the acetolysis of **1**—OTs were determined in absence, as well in presence of sodium acetate (Table 3).

Table 3

Effect of lithium perchlorate on the rate of acetolysis of tosylate 1—OTs, at 110°

$10^3 \cdot [1-\text{OTs}]$ moles/l	$10^3 \cdot [\text{NaOAc}]$ moles/l	$10^3 \cdot [\text{LiClO}_4]$ moles/l	$10^5 \cdot k$ sec^{-1}
....	—	0	3.45[a)]
14.76	—	10	3.90
14.61	—	30	4.80
14.66	—	50	5.70
....	0	0	4.30[a)]
15.18	15.1	10	4.49
15.22	15.1	30	4.71
15.38	15.1	50	5.12

a) Extrapolated values.

Small but definite special salt effects have been observed in each case, the extrapolated rate constant being $k^0_{\text{extr}} = 3.45 \times 10^{-5}$ sec^{-1} in the absence of NaOAc, and 4.30×10^{-5} sec^{-1} in the presence of 0.015 M NaOAc.

The special salt effect of $NaClO_4$ in the presence of NaOAc at constant ionic strength is better represented in Figure 2.
From the relation (2), if S_1 and S_2 are the two concentrations of the added salts, and $S_1 + S_2 = \text{const.}$, it follows:

$$\Delta k = k^0_{\text{extr}}(b_2 - b_1) \cdot \Delta S_2 = k^0_{\text{extr}}(b_1 - b_2) \cdot \Delta S_1 \qquad (3)$$

---

[5] M. Voicu, *Studii şi Cercetări Chim. Acad. R.S.R.*, **18**, 457 (1970).
[6] H. M. R. Hoffmann, *J. Chem. Soc.*, **1965**, 6753.
[7] A. H. Fainberg and S. Winstein, *J. Amer. Chem. Soc.*, **78**, 2767 (1956).

Plotting the observed rate constants *vs* the concentration of the one of added salts, a straight line would be expected. This linear relationship holds only at high $NaClO_4$ concentrations, and breaks down at small concentrations of $NaClO_4$, demonstrating thus a special salt effect.

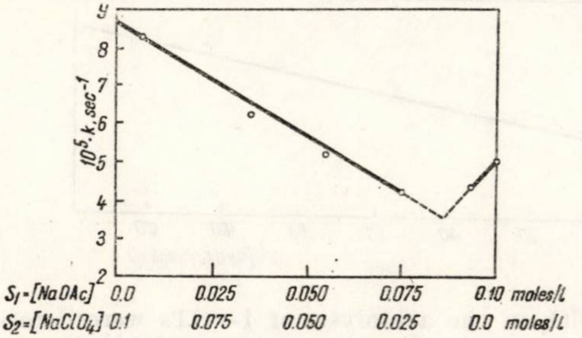

Fig. 2. — Effect of salts on the rate constants for the acetolysis of **1**—OTs, at 110°, on condition: $[NaOAc]_0+[NaClO_4]=0.1$ moles/1.

2.4. *Acetolysis of cis-ditosylate* 7

The preparation of the *cis*-ditosylate **7** has been described elsewhere.[8] Using the time ratio method [9] in the kinetic treatment the necessary times to attain conversions of 15%, 35% and 70% have been determined in both unbuffered and buffered conditions. From these values and diagrams corresponding to this method,[9b] the rate constants k_1 and k_2 for the two steps involved in the acetolysis of the *cis*-ditosylate **7** were calculated (Table 4).

Table 4

Rate constants[a]) and relative concentrations of the monosolvolytic product, in the acetolysis of *cis*-ditosylate 7, at 110°

Reaction parameters	$10^5.k_1$ sec^{-1}	$10^5.k_2$ sec^{-1}	K[d]) —	β_{max} %	β'_{max}[b]) %
Thermodynamic Control	2.87	1.58	0.55	48	45
Kinetic Control c)	2.77	2.36	0.85	40	15

a) The rate constants were obtained by use of the time ratio method[9]; b) Relative concentration of tosylate **1**—OTs; spectrophotometric measurements of the stilbenic system in **1**—OTs and **1**—OAc were corrected with the relative concentration of acetate **1**—OAc; c) $[NaOAc]_0=0.0426$ moles/1; $[NaOAc]_0/[\mathbf{7}]_0=3.55$; d) $K=k_2/k_1$

---

[8] a) E. Bergmann and M. Rabinowitz, *Bull. Res. Council of Israel*, **8A**, 172 (1959); *Chem. Abstr.*, **55**, 3535 (1961); b) E. Ciorănescu, A. Bucur, M. Banciu and C. D. Nenitzescu, *Rev. Roumaine Chim.*, **10**, 141 (1965).

[9] a) C. G. Swain, *J. Amer. Chem. Soc.*, **66**, 1696 (1944); b) A. A. Frost and R. G. Pearson, "Kinetics and Mechanism", 4th ed. John Wiley and Sons, Inc. New York, 1965, p. 161.

3. DISCUSSION

3.1. Reactivity of the **1**–*X and* **2**–*X derivatives*

We have shown previously [1] that the low rate constant in the phenonium route ($k_{\mathrm{Ph}} = 2.95 \times 10^{-5}$ sec^{-1}, at 110°) of **1**–OTs, as compared to the phenonium route of the corresponding saturated tosylate, **8**–OTs ($k_{8-\mathrm{OTs}} = 11.10 \times 10^{-5}$ sec^{-1}, at 110°) is determined by the inductive effect of the double bond in **1**–OTs.

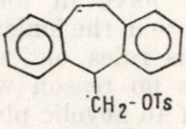

8-OTs

If the ionization of **2**–X derivatives produces the same intermediate as that formed from **1**–X, the same trend in the variation of the rate constants must be observed in passing from the saturated eight-membered ring derivative, **6**–Br, to the unsaturated compound, **2**–Br. Table 1 shows that this is not the case, the unsaturated bromide, **2**–Br, reacting 10^5 times faster than **6**–Br. The different effect of the double bond in **1**–X and **2**–X means that different intermediates must be formed in the ionization of the primary **1**–X, and secondary **2**–X derivatives; otherwise stated, at least two intermediates must be involved in the transformation **1**–X $\rightleftharpoons$ **2**–X. However, the two reactions were not measured at the same temperature, and in the same solvent; the results mentioned in Table 1 might be therefore misleading. Nevertheless, the involvement of more intermediates in this equilibrium, is upheld by other results reported in this and previous work, and namely :

a) If both derivatives, **1**–X and **2**–X ionize through a similar mechanism, the secondary derivative, **2**–X should react only 2–10 times faster than the primary derivative **1**–X*). Table 2 shows that in comparable conditions, the ratio of the two rate constants is much higher than this.

b) Unsaturated tosylate, **1**–OTs have to be comparable in acetolysis with acyclic β, β-diphenylethyl tosylate [11], **9**–OTs, or cyclic derivative, **8**–OTs; all of them are β, β-diarylethyl tosylates. Presently there exist no doubt that in the ionization of β-aryl derivatives, phenonium ions are formed.[12] Due to the similarity of the reaction products (α, β-diarylethyl acetates, **11**—X), and of the observed kinetics, a phenonium ion must be formed in the ionization of **1**—X, too. However, there exists a striking difference between the solvolysis of the unsaturated cyclic derivatives, **1**—X, on the one hand, and the solvolyses of the saturated compounds **8**—X and **9**—X, on the other hand; while the transformation of **1**—X is reversible ($\mathbf{1}-X \rightleftharpoons \mathbf{2}-X$), as we have shown, the corresponding transformation of a saturated α, β-diarylethyl derivative in a β, β-diarylethyl derivative ($\mathbf{11}-X \nrightarrow \mathbf{9}-X$) has never been observed.[12] That means that the ionization of the cyclic unsaturated α, β-diarylethyl derivative, **2**—X, must have in ionization another route than the commonly encountered route in the ionization of the simple α, β-diarylethyl derivatives, **11**—X. This rules out the phenonium route in the ionization of **11**—X (there is no reason why a cyclic phenonium ion, **10** should be more stable than an acyclic phenonium ion, **12**, in the reactions (4) and (5)):

---

*) This ratio between the reactivity of the two derivatives can be approximated from a $\rho^* - \Sigma\sigma^*$-Taft relation, in which [10] $\rho^* = -2$. The $\Delta\sigma^*$ in the acyclic series is about -0.15 (which gives a rate ratio of about 2), and can be a little higher for the substituted aryl rings in **1**–X.

[10] C. J. Lancelot and P. von R. Schleyer, *J. Amer. Chem. Soc.*, **91**, 4291, 4296 (1969); C. J. Lancelot, J. J. Harper and P. von R. Schleyer, *J. Amer. Chem. Soc.*, **91**, 4294 (1969); P. von R. Schleyer and C. J. Lancelot, *J. Amer. Chem. Soc.*, **91**, 4297 (1969).

[11] S. Winstein, B. K. Morse, E. Grunwald, K. C. Schreiber and J. Corse, *J. Amer. Chem. Soc.*, **74**, 1113 (1952).

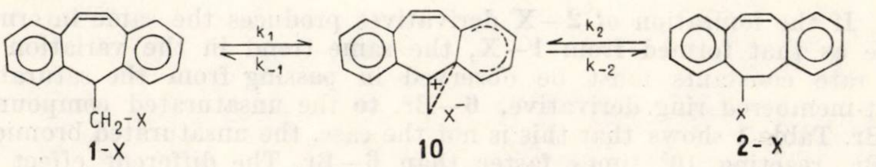

(4)

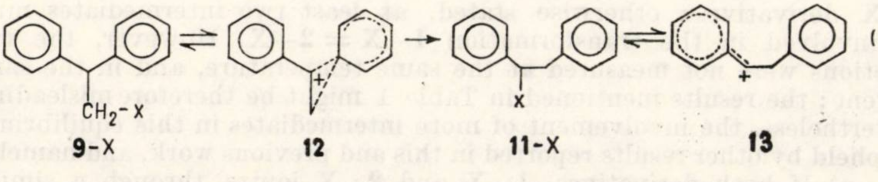

(5)

c) The occurrence of another intermediate, beside the already mentioned phenonium ion, is clearly demonstrated by the combined product and kinetic data. Indeed, if the mechanism, depicted in (4) would be correct, the equilibrium constant K would be given by the product of a partition factor and a reactivity factor[13]:

$$K = \frac{k_2}{k_{-2}} \cdot \frac{k_{-1}}{k_1} = \frac{k_2}{k_1} \cdot \frac{k_{-1}}{k_{-2}} = R \cdot P \tag{6}$$

The equilibrium between the seven- and eight-membered ring derivatives (**1**—X and **2**—X, respectively) can be observed only in those conditions in which α, β-diarylethyl derivatives pass over in the corresponding stilbene derivatives (acid medium). Therefore, in the reversible transformation of **2**$-$X derivatives, we have only observed beside **1**$-$X, dibenzo [a, e] cyclooctene, **5**. However, if we admit that the real equilibrium constant, K is not very different from an equilibrium constant, K' :

---

[12] a) D. J. Raber, J. M. Harris and P. von R. Schleyer, *J. Amer. Chem. Soc.*, **93**, 4829 (1971); b) J. A. Thompson and D. J. Cram, *J. Amer. Chem. Soc.*, **91**, 1778 (1969); c) F. Badea, "Mecanisme de Reacţie în Chimia Organică", Ed. Ştiinţifică, Bucharest, 1971, p. 243.

[13] S. Winstein and E. M. Kosower, *J. Amer. Chem. Soc.*, **81**, 4399 (1959); A. Diaz, M. Brookhart and S. Winstein, *J. Amer. Chem. Soc.*, **88**, 3133 (1966).

$$K' = \frac{[\mathbf{1}-\mathrm{X} + \text{corresponding alkene}]}{[\mathbf{2}-\mathrm{X} + \text{corresponding alkene}]} \approx K = \frac{[\mathbf{1}-\mathrm{X}]}{[\mathbf{2}-\mathrm{X}]} \qquad (7)$$

then, from the already published data,[2] K should have a value of about 15$-$20. On the other hand, the reactivity factor, k_2/k_1 is of about 10^5-10^6 (section 2.2). This high reactivity factor must be therefore compensated by a relative low partition factor, of about $10^{-3}-10^{-4}$. This cannot be true, because in kinetic-controlled conditions, beside **2**$-$OAc, about 9% of **1**$-$OAc is also formed. The experimental results are therefore inconsistent with equation (4).

d) The occurrence of a more stable ion that the phenonium ion in the acetolysis of **1**$-$OTs is infered from the salt effects. Special salt effects have not been observed in the acetolyses of simple β-phenylethyl derivatives, [3,14] as **9**$-$X is. If the phenonium ion is extra-stabilized by an electron-repelling group in the aromatic ring, in *ortho* or *para*, a special salt effect, doubled with a rate enhancement are observable.[12a, 14b, 15] As we have shown, the double bond in **1**$-$OTs acts as an electron-attracting group, and therefore no special salt effect would be predicted. Occurrence of a small, but definite special salt effect in the unbuffered and buffered acetolysis of **1**$-$OTs demonstrates that the phenonium ion **10** passes over in a more stable intermediate. Moreover, as the special salt effect is $W^0_{\mathrm{LiClO_4}} = k^0_{\mathrm{extr}}/k^0 = 1.09$ in the unbuffered conditions, and $W^{\mathrm{NaOAc}}_{\mathrm{LiClO_4}} = k^0_{\mathrm{extr}}/k^0_{\mathrm{NaOAc}} = 1.26$ in the presence of sodium acetate as a buffer, it must be concluded that this second intermediate is more important in the conditions generating the eight-membered ring acetate, **2**$-$OAc, than it is in the formation of **1**$-$OAc.

e) Some mentioned facts could be explained through a benzylic ionization of α, β-diarylethyl derivatives. In the saturated series (cyclic **6**$-$X, or acyclic **11**$-$X), the benzylic route must be favoured over the phenonium route ; a benzylic ion **13** should be more stable than a phenonium ion **10**, and there would be no tendency that a benzylic ion should give a phenonium ion. This explains why simple α, β-diarylethyl derivatives have never converted into the corresponding β, β-diarylethyl derivatives. In the case of benzylic ion **14** (A), derived from **2**$-$X, the

---

[14] a) A. H. Fainberg and S. Winstein, *J. Amer. Chem. Soc.*, **78**, 2780 (1956) ; b) A. H. Fainberg, R. G. Robinson and S. Winstein, *J. Amer. Chem. Soc.*, **78**, 2777 (1956).

[15] S. Winstein and A. H. Fainberg, *J. Amer. Chem. Soc.*, **80**, 959 (1958).

transformation into phenonium ion **10** (C) could be possible through a thermally allowed electrocyclic ring closure (8).

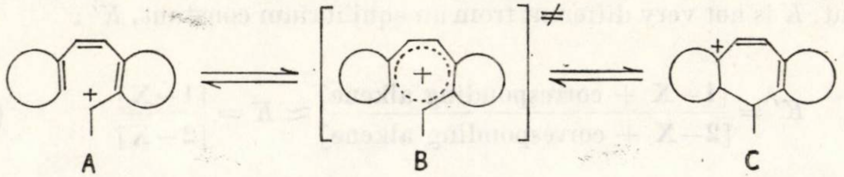

(8)

However, this possibility is excluded in its turn by the data of Table 1. If the benzylic ion is formed in the initial step, the constant rate of **2**—Br should again be not very different from the rate constant of **6**—Br, which must react through the same type of intermediate. Even if we consider the electrocyclic process, the observed ratio between the two derivatives ($\sim 10^5$) cannot be explained (phenonium ion is less stable than benzylic ion).

f) The nature of the first intermediate formed in the ionization of **2**—X results from the foregoing discussion. This intermediate cannot be a phenonium ion, or a benzylic ion; in its formation, the double bond must be involved in a high extent, in order to account for the high reaction rate of **2**—X. The single imaginable intermediate, which would satisfy these claims is an intermediate of the type **B**, depicted in (8). That means that in an energy-potential diagram (Figure 3), the point suitable for the structure **B** should be represented neither by Figure 3-a (**B**-transition state), nor by Figure 3-b (unstable intermediate), but rather by Figure 3-c (a more stable intermediate than phenonium ion and benzylic ion, respectively). As **B** is a homotropylium ion, **15**, this seems to be quite reasonable.

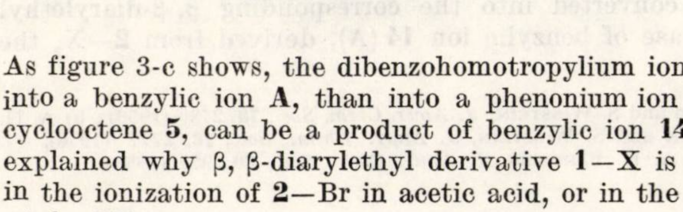

Fig. 3. — Possible potential-energy diagrams, for the reaction (8); (see text).

As figure 3-c shows, the dibenzohomotropylium ion can more easily pass into a benzylic ion **A**, than into a phenonium ion **C**. The dibenzo [a, e] cyclooctene **5**, can be a product of benzylic ion **14**. It must be further explained why β, β-diarylethyl derivative **1**—X is preferentially formed in the ionization of **2**—Br in acetic acid, or in the unbuffered acetolysis of **1**—OTs.

g) The argument used to discard the sequence (4) can now be used to confirm Scheme I, resulted from the above mentioned facts.

Scheme I

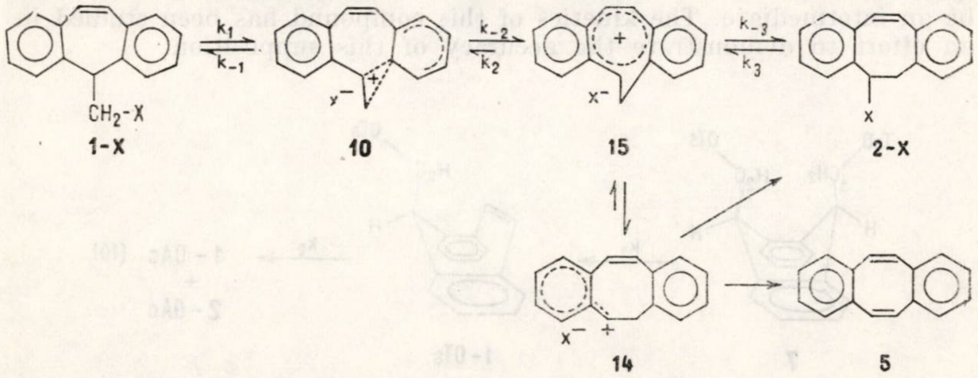

$$K = \frac{k_{-1}}{k_1} \cdot \frac{k_2}{k_{-2}} \cdot \frac{k_3}{k_{-3}} = \frac{k_3}{k_1} \cdot \frac{k_2}{k_{-2}} \cdot \frac{k_{-1}}{k_{-3}} \tag{9}$$

The high reactivity factor, k_3/k_1, would be now compensated by the stability factor, k_2/k_{-2}, measuring the stability of the phenonium ion, as compared with that of the dibenzohomotropylium ion. As we have already shown, dibenzohomotropylium ion must be the most stable intermediate involved in these transformations; k_2/k_{-2} must be therefore low. That statement is also borne out by the work of Mateescu, Nenitzescu and Olah,[16] who have observed, in super-acids, only dibenzohomotropylium ion **15**, starting from either **1**–X or **2**–X derivatives. The high stability of an isomer of the dibenzohomotropylium ion **15** has been also mentioned.[17]

As regards the partition factor, k_{-1}/k_{-3}, this term should be in its turn small, if the phenonium ion **10** is more easily converted into the more stable ion **15**, than it is trapped by a nucleophyle. However, in the presence of a stronger nucleophyle, such as AcO^-, phenonium ion can be trapped, but even in that case, the partition factor must be small too, as is suggested by the works of Schleyer et al.[10] This explains the low salt effects. Despite the instability of phenonium ion, as compared to other intermediates, **1**–X is preferentially formed in thermodynamic control, as a result of the large reactivity gap between **1**–X and **2**–X.

Scheme I is therefore in good agreement with all observed facts cited herein.

The above discussion demonstrates also the utility of considering the partition and reactivity factors [13] in appreciating the mechanism of the thermodynamically and kinetically controlled processes.

Other arguments will be advanced in the following section.

3.2. *Acetolysis of cis-ditosylate* **7**

From the formed products identified in the acetolysis of *cis*-ditosylate **7**, it has been assumed [8b, 18] that the monotosylate **1**—OTs must be an intermediate. The kinetics of this compound has been studied in an effort to demonstrate the accuracy of this supposition.

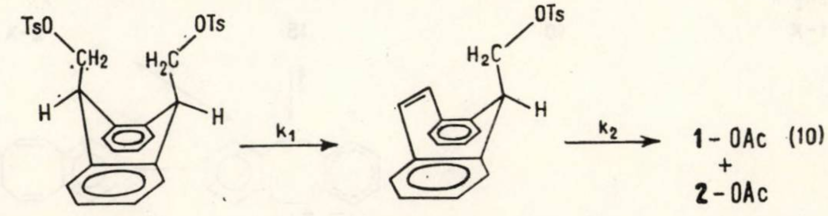

7 **1-OTs**

The models show that the di-axial conformer of **7**, necessary for the phenonium route must not be very different in stability from the axial conformer of **1**—OTs. It follows that the two rate constants, k_1 and k_2 must have comparable values, which would permit a consecutive reaction theory treatment.[9] This assumption has been confirmed (see section 2.4). The data of Table 4 need some complementary comments.

a) In the unbuffered acetolysis of **7** (thermodynamic control), the second step of the solvolysis (k_2), would begin after some **1**—OTs (and TsOH, respectively) have accumulated in the system. This condition corresponds to the unbuffered acetolysis of **1**—OTs with initially added *p*-toluenesulphonic acid [1] ($k_{\text{obs, T}}$). In excellent agreement, the calculated through time ratio method[9] rate constant, k_2, matches with the observed rate constant of **1**—OTs in similar conditions ($k_2 = k_{\text{obs, T}} = 1.58 \times \times 10^{-5}$ sec^{-1}). Moreover, the maximum relative concentration of **1**—OTs ($\beta_{\max}$ in Table 4), calculated theoretically, is in agreement with the spectrophotometrical observed value ($\beta'_{\max}$). Thus, the formation of **1**—OTs as an intermediate in the unbuffered solvolysis of **7** is undoubtedly confirmed.

b) In the buffered acetolysis of **7**, the rate constant k_2 has a higher value (as it should be) than in the unbuffered acetolysis, but significantly less than the corresponding $k_{\text{Ph}} = 2.95 \times 10^{-5}$ sec^{-1} value [1] for tosylate **1**—OTs. Beside the normal product of acetolysis of **1**—OTs, analysis has revealed the presence of 15% diacetate **16** (Scheme II). Its formation results also from the inequality of the $\beta_{\max}$ and $\beta'_{\max}$ values (Table 4), in the buffered conditions.

[16] G. Mateescu, C. D. Nenitzescu and G. Olah, *J. Amer. Chem. Soc.*, **90**, 6235 (1968).

[17] R. F. Childs and S. Winstein, *J. Amer. Chem. Soc.*, **89**, 6348 (1967).

[18] E. Ciorănescu, A. Bucur, M. Elian and C. D. Nenitzescu, *Rev. Roumaine Chim.*, **10**, 149 (1965).

The initial formed phenonium ion, **17**, can either collapse in tosylate **1**–OTs, or in acetoxy-tosylate **18**.

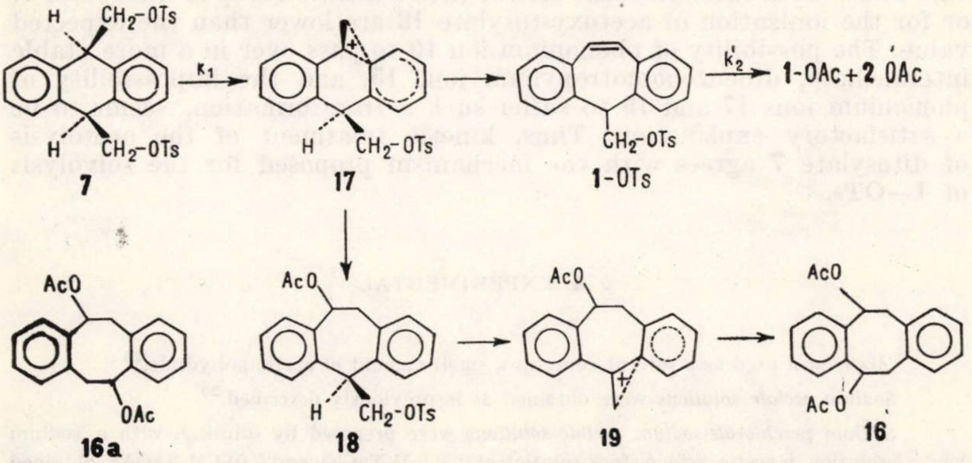

In the acid medium, diacetate **16** was not observed; its precursor, acetoxy-tosylate **18**, even it is formed, would be rapidly converted by *p*-toluenesulphonic acid in its stilbenic correspondent.

In the buffered conditions, the absence of the isomeric diacetate, **16a**, indicates that only phenonium ion **19** is formed from **18**, and that ring *A* does not participate in the ionization of **18**. The low value of k_2 under kinetic-controlled acetolysis of **7** is thus a result of the contribution of tosylate **18** to the overall process. Considering that this compound is formed in about the same amount as diacetate **16** (15%), the calculated rate constant for **18** ($k_2'' = 3.5 \times 10^{-6}$ sec^{-1}), is about ten times less than the corresponding rate constant of **1**–OTs, and 35 times lower than the rate constant of the analogous compound, **8**–OTs [1]($k_{8-\mathrm{OTs}} = 11.10 \times 10^{-5}$ sec^{-1}). However, the reactivity of **18** should differ from that of **8**–OTs through the statistical factor (only one ring participates in the ionization of **18**), and a remote β–OAc group. From the σ_x^H values [19], it can be anticipated that a β–OAc group has a smaller effect than a double bond conjugated to the aromatic ring. The reactivity of **18** should therefore be not very different from that of **1**–OTs. The smaller observed reactivity needs some explanations which confirms in their turn the mechanism of acetolysis of **1**–OTs, proposed in Scheme I.

c) The rate constants for the first ionization step (k_1) are fairly constant in both kinetic and thermodynamic control. Again, from σ_x^H values, a CH (Ar)–CH$_2$–OTs group must have a slighter less inductive effect than a CH = CH–Ar group.[19] The statistical factor is also more favourable for ditosylate **7** than for monotosylate **1**–OTs, or **8**–OTs. The rate constant, k_1 for **7** should therefore not differ very much from the rate constant of **8**—OTs, and should be higher than the corresponding rate constant for **1**—OTs. A small, but definite decrease is however observed. Thus, both rate constants for the first ionization step of ditosylate **7**, or for the ionization of acetoxy-tosylate **18** are lower than the expected value. The possibility of phenonium ion **10** to pass over in a more stable intermediate, dibenzohomotropylium ion, **15**, and the impossibility of phenonium ions **17** and **19** to suffer such a transformation, seems to be a satisfactory explanation. Thus, kinetic treatment of the acetolysis of ditosylate **7** agrees with the mechanism proposed for the solvolysis of **1**—OTs.

---

[19] G. Thirot, *Bull. Soc. chim. France*, **1967**, 739.

4. EXPERIMENTAL

Acetic acid used as a solvent contains a small amount of acetic anhydride.[20]

Sodium acetate solutions were obtained as is previously described.[20]

Sodium perchlorate-sodium acetate solutions were prepared by diluting, with a sodium acetate solution in acetic acid, a stock solution of 0.200 M $NaClO_4$ and 0.014 M NaOAc, obtained in its turn from solutions of perchloric acid, and sodium acetate, in acetic acid.

Lithium perchlorate solutions were obtained from a stock 0.200 M $LiClO_4$ solution, prepared dissolving anhydrous $LiClO_4$,[21] in acetic acid.

Aqueous acetone was obtained by mixing purified anhydrous acetone, with distilled water, in a volume ratio 3/1.

5H-Dibenzo [a, d] cyclohepten-5-yl-methyl tosylate (**1**—OTs), mp. 140—141° (lit.[18] 140—141) was prepared by the method reported in the literature.[18]

cis-9,10-bis (Hydroxymethyl)-9,10-dihydroanthracene ditosylate (**7**), mp. 184—186° (lit.[8b] 183—184°, or[8a] 185—187°) was prepared by the reported method.[8b]

Bromides **1**—*Br*, **2**—*Br* and **6**—*Br* were described in section 2.1.

Kinetic measurements

a) *Conductometric measurements* were used for the solvolyses of bromides. They were performed using a conductivity cell with platinium electrodes. Linear function of the concentration *vs* electrical conductance (*C*), over the used range of concentration of generated bromhydric acid, was verified. The first order rate constants were calculated from the equation :

$$k = \frac{2.303}{t} \cdot \log \frac{C_\infty - C_0}{C_\infty - C} \qquad (11)$$

b) *Titrimetric measurements* were perfomed potentiographically.[20,1]

The stepwise process (10) was followed also titrimetrically. The extents of the reaction ($\delta = x/a$) were plotted *vs* time ; from this graph, were interpolated the time values corresponding to the extent of the reaction of 15 %, 35 % and 70 % (δ = 0.30 ; 0.70 and 1.40, respec-

---

[20] M. Voicu and F. Badea, *Rev. Roumaine Chem.*, **14**, 929 (1969).

[21] T. W. Richards and H. H. Willard, *J. Amer. Chim. Soc.*, **32**, 14 (1910) ; U. Berglung and L. G. Sillen, *Acta Chem. Scand.*, **2**, 116 (1948) ; *Chem. Abstr.*, **43**, 2075 (1949).

Table 5

Calculations of the rate constants for the acetolysis of *cis*-ditosylate 7, at 110° a)

δ	Time sec	$\log \frac{t_{ii}}{t_i}$	τ_i			$10^5 . k_1$ b) sec^{-1}			K	$10^5 . k_2$ c) sec^{-1}
			τ_{15}	τ_{35}	τ_{70}	τ_{15}/t_{15}	τ_{35}/t_{35}	τ_{70}/t_{70}		
0.3	11,200	$\log \frac{t_{35}}{t_{15}} = 0.401$	0.310	0.780	1.98	2.77	2.77	2.79	0.81	2.25
0.7	28,200	$\log \frac{t_{70}}{t_{15}} = 0.802$	0.310	0.780	1.96	2.77	2.77	2.76	0.85	2.38
1.4	71,000	$\log \frac{t_{70}}{t_{35}} = 0.401$	0.308	0.766	1.93	2.75	2.72	2.72	0.88	2.40

a) $[NaOAc]_0 = 42.6 . 10^{-3}$ moles/1; b) Mean value is $k_1 = 2.77 . 10^{-5}$ sec^{-1}; c) Mean value is $k_2 = 2.36 . 10^{-5} sec^{-1}$.

tively). The values log (t_{ii}/t_i) were calculated, and from graphs depicting Swain's time-percentage reaction relations,[9b] the values K and $\tau_i = k_1 . t_i$ were obtained. An example is presented in Table 5.

Revue Roumaine de Chimie, 17, 9, 1579–1598 (1972)

CORRELATION OF THE PHYSICAL PROPERTIES OF ORGANOSILICON COMPOUNDS. I.

BOILING POINT AND DENSITY OF SUBSTITUTED SILANES AND SILOXANES AND THE ADDITIVITY OF DENSITY

M. ARSHAD A. BEG

P.C.S.I.R. Laboratories, Karachi-39, Pakistan
and
IRSHAD A. KHAN

Department of Chemistry, University of Karachi, Karachi-32

Received June 7, 1971

The boiling point and density of alkyl silanes, haloalkyl and alkyl halosilanes, alkoxy, isocyanato and isothiocyanato silanes silazanes and siloxanes have been correlated with the parameter Me^2. This parameter is noted to be additive. The correlation factors have been derived in terms of the slopes of the lines representing each class. The values of Me^2 for different Si-X bonds have been derived and have been used to calculate those for the molecules. The deviations have been discussed in terms of association.

In our previous publications we have tried to establish the parameters Me^2 and $\sqrt{M}/n_D$ both being related to the boiling point of phosphines.[1,2] We have also recently extended these to the sulphides and mercaptans.[3] Phosphines and sulphides are related to one another both having lone pair electrons on the central atom. Silicon has no unshared pair but it utilizes the vacant 3d orbitals whose energy is not much higher than the *p*-orbitals already in use. The non-basic properties of trisilylamine is considered as an indication of the interaction of the nitrogen lone pair with the silicon *d*-orbitals. The molecule, however, is planar and the geometry should also be responsible for the observed properties of the silylamine. From the NMR data, considerable doubt has been expressed[4] regarding the existence of $(p-d)_\pi$ bonding between silicon and the electronegative atoms or groups since anomalies found in the silicon compounds have also been noted in the corresponding derivatives of carbon.

---

[1] M. A. A. Beg, *Bull. Chem. Soc. Japan*, **40**, 15 (1967).

[2] M. A. A. Beg, *Rev. Roumaine de Chim.*, **14**, 503 (1969).

[3] M. A. A. Beg and M. A. Hashmi, under publication.

[4] E. A. V. Ebsworth and S. G. Frankiss, *J. Amer. Chem. Soc.*, **85**, 3516, (1963).

Table 1

Boiling points, density and refractivity parameters for tetra alkyl aryl silanes

S. No.	Compounds	T_b	e	Me^2		n_D	Mn_D		$\sqrt{M/n_D}$	K_n	K_D
1	2	3	4	Observed I	5 Calculated II	6	7 Observed I	Calculated II	8	9	10
1	$(CH_3)_4Si$	299.5	0.6460	36.76	36.76	—	—	119.58	—	—	—
2	$(CH_3)_3SiC_2H_5$	335.0	0.6849	47.89	48.72	1.3820	141.08	141.08	7.32	45.82	6.55
3	$(CH_3)_3SiC_3H_5$	357.9	0.7193	59.03	—	1.4074	160.57	—	7.58	47.13	7.77
4	$(CH_3)_3Si(n-C_3H_7)$	363	0.7020	57.21	58.65	1.3929	161.70	161.71	7.73	46.92	7.39
5	$(CH_3)_3Si(n-C_4H_9)$	388	0.7181	67.08	68.63	1.4030	182.51	182.29	8.12	47.72	8.25
6	$(CH_3)_3Si(i-C_4H_9)$	381	0.7322	69.74	—	—	—	—	—	—	—
7	$(CH_3)_3Si(n-C_5H_{11})$	412	0.7313	77.06	79.42	1.4096	203.10	202.90	8.51	48.37	9.04
8	$(CH_3)_3Si(i-C_5H_{11})$	404.5	0.7322	77.26	—	—	—	—	—	—	—
9	$(CH_3)_3Si(n-C_6H_{13})$	436	0.7422	87.09	89.42	1.4154	223.76	223.40	8.88	49.07	9.80
10	$(CH_3)_3Si(n-C_7H_{15})$	457	0.7506	96.95	99.42	1.4201	244.38	243.90	9.23	49.47	10.49
11	$(CH_3)_3Si(n-C_8H_{17})$	475	0.7581	107.01	109.42	1.4242	265.04	264.40	9.57	49.59	11.16
12	$(CH_3)_3Si(n-C_{10}H_{21})$	513	0.7705	127.10	129.42	1.4310	306.36	305.40	10.22	50.17	12.43
13	$(CH_3)_3Si(n-C_{12}H_{25})$	546	0.7800	147.28	149.42	1.4358	347.59	346.40	10.83	50.38	13.59
14	$(CH_3)_3Si(n-C_{14}H_{29})$	573	0.7911	159.02	169.42	1.4410	389.20	387.40	11.40	50.24	14.82
15	$(CH_3)_3SiC_6H_5$	444.6	0.8730	114.38	114.38	—	—	227.61	—	—	—
16	$(CH_3)_3SiCH_2C_6H_5$	464	0.8720	124.26	124.38	—	—	248.11	—	—	—
17	$(CH_3)_2Si(C_2H_5)_2$	368.8	0.7214	60.41	60.67	—	—	162.58	—	—	—
18	$(CH_3)_2Si(C_2H_5)-(n-C_3H_7)$	394	0.7347	70.22	70.61	—	—	183.20			
19	$(CH_3)_2Si(C_2H_5)-(i-C_4H_9)$	411	0.7463	80.25	—	—	—	—	—	—	—

20	$(CH_3)_2Si(n-C_3H_7)_2$	414.5	0.7414	79.20	80.54	—	—	203.81	—	—	—
21	$(CH_3)_2Si(CH_2)_5$	406.5	0.8039	82.78	—	1.4394	184.37	—	7.86	51.69	10.52
22	$(CH_3)_2Si(C_2H_5)(C_6H_5)$	417	0.8810	127.36	126.33	—	—	249.11	—	—	—
23	$(C_2H_5)_3Si(CH_3)$	400	0.7437	71.95	72.63	1.4160	184.20	184.08	8.05	49.65	8.93
24	$(C_2H_5)_3Si(C_2H_5)$	426	0.7662	84.59	84.59	1.4268	205.58	205.58	8.41	50.63	10.05
25	$(C_2H_5)_3Si(n-C_3H_7)$	446	0.7724	94.31	94.53	1.4308	226.19	226.20	7.78	50.75	10.73
26	$(C_2H_5)_3Si(n-C_4H_9)$	465	0.7786	104.32	104.50	1.4348	246.91	246.79	9.14	50.85	11.41
27	$(C_2H_5)_3Si(i-C_4H_9)$	460	0.7840	105.78	—	—	—	—	—	—	—
28	$(C_2H_5)_3Si(n-C_5H_{11})$	484	0.7835	114.24	115.30	1.4377	267.54	267.40	9.48	51.01	12.04
29	$(C_2H_5)_3Si(i-C_5H_{11})$	478	0.7850	114.66	—	—	—	—	—	—	—
30	$(C_2H_5)_3Si(n-C_6H_{13})$	503	0.7880	124.23	124.30	1.4400	288.12	287.93	9.82	51.20	1264.
31	$(C_2H_5)_3Si(n-C_7H_{15})$	520	0.7907	133.84	135.30	1.4422	308.76	308.43	10.14	51.25	13.19
32	$(C_2H_5)_3Si(n-C_8H_{17})$	535	0.7971	144.92	145.30	1.4438	329.31	328.93	10.46	51.14	13.85
33	$(C_2H_5)_3Si(n-C_{10}H_{21})$	566	0.8036	165.38	165.30	1.4472	370.61	369.93	11.05	51.18	14.95
34	$(C_2H_5)_3Si(C_6H_5)$	512	0.9060	157.66	150.25	—	—	292.11	—	—	—
35	$P-(C_2H_5)_3Si-(C_6H_4OCH_3)$	103— (0.2 mm)	0.9487	199.88	—	1.5130	336.02	—	9.85	—	20.29
36	$(n-C_3H_7)_4Si$	485	0.7883	124.33	124.33	—	288.03	288.03	—	—	—
37	$(n-C_4H_9)_4Si$	157— (22 mm)	0.8008	164.23	164.23	1.4465	370.43	370.43	11.06	—	14.84
38	$(n-C_5H_{11})_4Si$	591	0.8252	207.41	207.41	1.4510	452.84	452.84	12.17	48.54	17.03

It is generally true that with the increasing number of electronegative groups on silicon, the C—Si distances are shortened. This decrease in the bond distance would eventually reduce the molar volume. Since the properties with which we are concerned are colligative and the related parameters are different forms of molar volume, any variation in the latter would be a direct consequence of the change in the overall electronegativity of the molecule. The different physical properties are, therefore, expected to change with a variation in the substituent. With such trends in mind we have extended the parameters to the study of the properties of a series of organosilicon compounds. The subject matter has been divided into two parts. The first part deals with the density and boiling points of the tetraalkyl silanes, the alkyl halo-silanes, the chlorosilanes, alkoxy silanes, the silazanes, and the siloxanes. The second part deals with the refractivity of the compounds and also attempts to correlate the density with their refractivity.

RESULTS AND DISCUSSION

The values for these compounds have been taken from the compilation by Rochow [5] and have been further supplemented with data available in the literature.[6,7] These have been listed along with the values of the parameters in Tables 1—7.

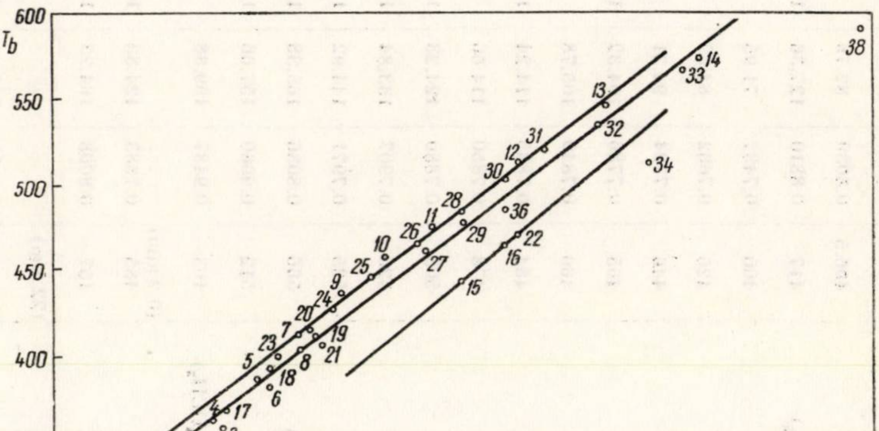

Fig. 1. — Correlation of boiling point and density (numbers refer to compounds listed in table 1).

---

[5] E. G. Rochow, "An Introduction to the Chemistry of the Silicones", John Wiley & Sons, Inc., NY, 1951.

[6] E. G. Rochow in "Encyclopaedia of Chemical Technology" edited by R. E. Kirk and D. F. Other, Vol. 12, p. 372.

[7] G. S. Forbes and H. H. Anderson, *J. Amer. Chem. Soc.*, **70**, 1043, 1222 (1948).

Table 2

Boiling points, density and refractivity parameters for haloalkyl silanes

S No.	Compounds	T_b	e	Me^2		n_D	Mn_D		$\sqrt{M}/n_D$	K_n	K_D
1	2	3	4	5		6	7		8	9	10
				I	II		I	II			
1	$(CH_3)_3SiCH_2Cl$	370.1	0.8791	94.70		1.4180	173.76	173.7660	7.80	47.44	12.12
2	$(CH_3)_3SiCHCl_2$	406	1.0395	169.65	—	1.4430	226.54	—	8.68	46.76	19.53
3	$(CH_3)_3SiCH_2I$	412.5	1.4431	445.63	—	1.4917	319.20	—	9.81	42.06	45.44
4	$(CH_3)_3SiCHClCH_3$	390.8	—	—	—	1.4242	194.46	—	8.21	47.64	—
5	$(CH_3)_3SiCH_2COOC_2H_5$	430	0.8762	122.90	—	1.4149	226.51	—	8.94	48.42	13.74
6	$(CH_3)_3SiC_4H_3S$	433	0.9450	139.44	—	1.4966	233.70	—	8.34	51.87	16.69
7	$(CH_3)_3SiC_4H_3O$	398	0.8800	108.48	—	1.4470	202.71	—	8.18	48.65	13.26
8	$(CH_3)_3SiCH_2[Si(CH_3)_2-$ $-CH_2]_2Si(CH_3)_3$	532	0.8245	206.90	—	1.4552	442.90	—	11.98	44.37	17.25
9	$(CH_3)_3SiCH[Si(CH_3)_2(CH_2)_3-$ $-Si(CH_3)_3$	582	0.8408	265.40	—	1.4640	549.65	—	13.23	43.97	20.05
10	$(CH_3)_2CH_2ClSiCH_2Si(CH_3)_3$	459	0.8950	155.90	—	1.4480	281.82	—	9.63	47.64	16.17
11	$(CH_3)_2CH_2ClSiCH_2Si(CH_3)_2-$ $-CH_2-Si(CH_3)_3$	519	0.9000	216.04	—	1.4630	390.21	—	11.16	46.49	19.35
12	$(CH_3)_2CH_2ClSiCH_2[Si(CH_3)_2-$ $-CH_2]_2Si(CH_3)_3$	570	0.9029	276.20	—	1.4706	498.25	—	12.51	45.54	22.06
13	$(CH_3)_2FSiCH_2Si(CH_3)_2F$	388	0.9200	142.34	—	1.3870	233.26	—	9.35	41.49	15.22
14	$[(CH_3)_2FSiCH_2]_2Si(CH_3)_2$	460	0.9260	206.03	—	1.4150	339.98	—	10.95	41.99	18.80
15	$(C_2H_5)_3SiF$	382	0.8354	93.58	93.58	1.3900	186.38	186.38	8.33	45.85	11.23
16	$(n-C_3H_7)_3SiF$	448	0.8339	122.45	123.38	1.4107	248.41	248.22	9.40	47.61	13.02
17	$(n-C_4H_9)SiF_3$	325.4	1.0060	143.79	131.46	—	—	189.19	—	—	—
18	$(n-C_4H_9)_2SiF_2$	427	0.9048	147.44	142.38	—	—	249.60	—	—	—
19	$(n-C_4H_9)_3SiF$	497	0.8372	152.85	153.30	1.4250	310.77	310.22	10.36	47.95	14.75
20	$(n-C_5H_{11})SiF_3$	350	0.9923	153.70	143.53	—	—	209.79	—	—	—
21	$(n-C_5H_{11})_2SiF_2$	466	0.8972	167.51	166.53	—	—	290.81	—	—	—
22	$(n-C_5H_{11})_3SiF$	540	0.8389	183.05	189.53	1.4305	372.05	372.45	11.27	47.89	16.23
23	$(C_6H_5)SiF_3$	375	1.2010	233.79	184.80	—	—	234.50	—	—	—
24	$(C_6H_5)_2SiF_2$	520	1.1550	293.60	238.94	—	—	340.23	—	—	—

Table 3

Boiling points, density and refractivity parameters for alkyl-halosilanes

1.	Compounds	T_b	e	Me^2		N_D	Mn_D		$\sqrt{M}/n_D$	K_n	K_D
				I	II		I	II			
1	$(CH_3)SiHCl_2$	314	1.1050	140.41	139.45	—	—	161.35	—	—	—
2	$(CH_3)_2SiCl_2$	343	1.060	144.94	144.94	—	—	151.68	—	—	—
3	$(CH_3)_3SiCl$	330.3	0.8536	79.08	90.85	—	—	150.63	—	—	—
4	$(CH_3)(CH_2 = CH)\ SiCl_2$	366	1.085	165.98	174.61	—	—	—	—	—	—
5	$(CH_3)_2(CH_2 = CH.CH_2).SiCl$	386	0.922	114.36	114.36	—	—	187.75	—	—	—
6	$(CH_3)\ (CH_2 = CH.CH_2)SiCl_2$	393	1.057	173.16	180.04	—	—	218.80	—	—	—
7	$Cl[(CH_3)_2SiO]Si(CH_3)_2Cl$	411	1.038	218.81	—	—	—	—	—	—	—
8	$Cl[(CH_3)_2SiO]_2Si(CH_3)_2Cl$	457	1.018	287.23	—	—	—	—	—	—	—
9	$Cl[(CH_3)_2SiO]_3Si(CH_3)_2Cl$	495	1.011	359.02	—	—	—	—	—	—	—
10	$(CH_3)\ (C_6H_5)SiCl_2$	355.5	1.1876	269.38	245.74	—	—	289.70	—	—	—
11	$(C_2H_5)SiCl_3$	370.9	1.2388	250.82	210.98	—	—	234.22	—	—	—
12	$(C_2H_5)_2SiHCl$	372.7	0.8895	96.95	109.28	—	—	173.30	—	—	—
13	$(C_2H_5)_2SiCl_2$	402	1.106	192.03	168.85	—	—	224.68	—	—	—
14	$(C_2H_5)_3SiCl$	416.5	0.9249	128.77	126.72	—	—	215.13	—	—	—
15	$(C_2H_5)\ (n-C_3H_7)_2SiCl_2$	416	1.0420	185.66	178.79	—	—	245.29	—	—	—
16	$(C_2H_5)\ (n-C_4H_9)SiCl_2$	442	1.0235	193.80	188.76	—	—	265.89	—	—	—
17	$(C_2H_5)\ (C_6H_5)SiCl_2$	503	1.159	275.37	234.51	—	—	311.20	—	—	—
18	$CH_2 = CHSiCl_3$	365	1.264	257.94	240.29	—	—	—	—	—	—
19	$(CHCl = CCl)\ SiCl_3$	432	—	—	—	1.4942	344.19	—	10.15	42.53	—
20	$(CH_2 = CH)_2SiCl_2$	392	1.088	181.10	181.10	—	—	—	—	—	—
21	$(n-C_3H_7)SiCl_3$	395.7	1.1967	253.99	255.69	—	—	254.84	—	—	—
22	$(n-C_3H_7)_2SiCl_2$	448	1.035	198.16	188.16	—	—	265.90	—	—	—
23	$(CH_2 = CH.CH_2)SiCl_3$	390.5	1.211	257.29	245.72	—	—	249.84	—	—	—
24	$(CH_2 = CH.CH_2)_2HSiCl_2$	370	1.086	166.29	174.56	—	—	198.47	—	—	—
25	$(n-C_4H_9)SiHCl_2$	397	1.0466	171.97	171.32	1.4272	224.06	224.06	8.77	45.22	19.58
26	$(n-C_4H_9)SiCl_3$	421.9	1.1632	258.64	265.66	—	—	275.44	—	—	—
27	$(i-C_4H_9)SiCl_3$	414	1.154	254.95	—	—	—	—	—	—	—
28	$(t-C_4H_9)_2SiCl_2$	463	1.009	216.85	—	—	—	—	—	—	—
29	$(CH_2)_5SiCl_2$	443	1.156	225.82	—	1.4697	248.37	—	8.84	50.08	25.53
30	$(C_6H_5)SiCl_3$	474.5	1.3256	371.55	311.42	—	—	320.75	—	—	—
31	$(C_6H_5.CH_2)SiCl_3$	489	1.2889	374.53	321.42	—	—	344.22	—	—	—
32	$(CH_3)_3SiBr$	353	1.189	216.29	—	—	—	—	—	—	—

Table 4

Boiling, points, density and refractivity parameters for alkoxy silanes

No	COMPOUNDS	T_b	e	Me²		N_D	Mn_D		$\sqrt{M/n_D}$	K_n	K_D
				I	II		I	II			
1	$(CH_3)_3SiOCH_3$	330.2	—	—	68.04	1.3679	142.38	142.38	7.45	44.27	—
2	$(CH_3)_3SiOC_2H_5$	348	0.7573	67.72	77.00	1.3741	162.26	162.26	7.90	44.00	8.56
3	$(CH_3)_3SiOC_2H_4Cl$	407.3	0.9443	136.02	—	1.4140	215.69	—	8.73	46.63	15.56
4	$(CH_3)_3SiOC_4H_9(n)$	397.6	0.7774	88.29	90.96	1.3925	203.43	203.43	8.68	45.80	10.17
5	$(CH_3)_3SiOC_2H_4OCH_3$	401	0.8492	106.78	115.52	1.3952	206.61	206.61	8.72	45.97	12.24
6	$(CH_3)_2Si(OC_2H_5)_2$	384	0.8900	117.30	117.30	1.3839	204.94	204.94	8.79	43.66	13.33
7	$(CH_3)_2Si(OC_2H_4Cl)_2$	486	1.1350	279.53	279.53	1.4420	312.90	—	10.21	47.57	27.36
8	$(CH_3)_2Si(OC_2H_4OCH_3)_2$	476	0.9663	194.29	194.29	1.4114	293.69	293.64	10.22	46.57	19.11
9	$(CH_3)_2Si(OC_4H_9(n))_2$	460	0.8434	145.16	145.16	1.4058	286.90	287.27	10.16	45.26	14.28
10	$(CH_3)_2Si(Odl.\ SecC_4H_9)_2$	446.6	0.8339	141.92	—	1.4014	286.01	—	10.19	43.80	13.92
11	$(CH_3)_2Si(Odl.\ ScC_4H_9)_2$	447	0.8332	141.67	—	1.4014	286.01	—	10.19	43.84	13.89
12	$(CH_3)_2Si(OCH_5)(OC_4H_9)$	428	0.8426	125.02	128.60	1.3949	245.62	246.10	9.51	44.99	13.14
13	$(CH_3)_2Si(OC_2H_5)(Od.Sec.C_4H_9)$	417.6	0.8328	122.13	—	1.3930	245.29	—	9.52	43.83	12.82
14	$(CH_3)_2Si(OC_2H_5)(Odl.SecC_4H_9)$	417.6	0.8432	125.19	—	1.3932	245.32	—	9.52	43.84	13.14
15	$CH_3Si(OC_2H_5)_3$	416	0.8928	141.79	157.70	1.3835	246.38	247.62	9.64	43.12	14.69
16	$[n-C_4H_9OSi(CH_3)_2]_2O$	498	0.8733	212.16	207.52	1.4051	390.87	390.76	11.80	41.95	17.87
17	$(C_2H_5)_3Si(OC_2H_5)$	426	0.8414	113.34	112.94	—	—	226.76	—	—	—
18	$(C_2H_5)_2Si(OC_2H_5)_2$	428	0.8752	134.88	141.29	—	—	247.94	—	—	—
19	$(C_2H_5)Si(OCH_3)_3$	499	0.9747	142.58	142.58	—	—	269.12	—	—	—
20	$(C_2H_5)Si(OC_2H_5)_3$	432	0.9207	162.83	169.64	1.3853	266.10	269.12	10.01	43.17	16.27
21	$(C_2H_5)Si(OC_3H_7(n))_3$	476	—	—	—	1.4017	328.12	331.12	10.91	43.61	—
22	$(C_2H_5)Si(OC_4H_9(n))_3$	510	—	—	211.33	1.4128	390.06	392.61	11.76	43.36	—

Tabel 4 (continued)

No	COMPOUNDS	T_b	e	Me^2		N_D	Mn_D		$\sqrt{M/n_D}$	K_n	K_D
				I	II		I	II			
23	$(C_2H_5)Si(OC_5H_{11}(n))_3$	558	0.8910	252.53	—	1.4210	452.01	458.61	12.55	44.45	20.11
24	$n-C_3H_7Si(OC_2H_5)_3$	453	0.8520	149.60	179.58	1.4076	290.09	289.73	10.19	44.41	14.66
25	$i-C_3H_7Si(OC_2H_5)_3$	451	0.9194	174.20	—	—	—	—	—	—	—
26	$CH_2 = CH.CH_2Si(OC_2H_5)_3$	448	0.9229	173.82	169.61	1.3952	284.74	284.74	10.23	43.75	16.97
27	$n-C_4H_9Si(OC_2H_5)_3$	464	0.8950	176.29	189.55	1.3976	307.59	310.33	10.61	43.71	16.60
28	$i-C_4H_9Si(OC_2H_5)_3$	459	0.9105	182.45	—	1.3908	306.10	—	10.66	43.03	17.10
29	$i-C_5H_{11}Si(OC_2H_5)_3$	471	0.8955	187.74	—	1.3982	327.30	—	10.94	43.04	17.15
30	$n-C_6H_{13}Si(OC_2H_5)_3$	483	0.8938	198.19	210.35	1.4167	351.46	350.93	11.12	43.44	17.82
31	$C_6H_5Si(OC_2H_5)_3$	506	1.0133	246.52	235.31	—	—	355.65	—	—	—
32	$C_6H_5CH_2Si(OC_2H_5)_3$	521	0.9864	247.23	245.31	—	—	376.15	—	—	—
33	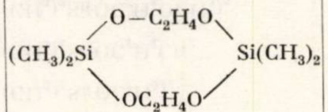	451	1.0585	264.61	—	1.4388	339.81	—	10.68	42.22	24.77
34	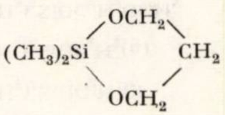	394.7	0.9703	124.36		1.4120	186.51	—	8.13	48.49	15.27
35	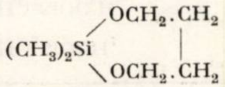	415.0	—	—		1.4218	207.71	—	8.50	48.81	—
36	$(CH_3)_3SiOH$	373	0.8112	59.27	62.88	1.3880	125.04	121.99	6.83	54.54	8.66
37	$(C_2H_5)_3SiOH$	426.5	0.8647	98.76	98.76	—	—	186.49	—	—	—
38	$(C_2H_5)_3Si(OCOCH_3)$	441	0.9039	142.23	142.23	—	—	247.15	—	—	—
39	$(C_2H_5)Si(OC_2H_5)_2(OCOCH_3)$	464.5	1.0200	214.41	198.93	1.4048	289.51	289.51	10.22	45.45	1.46

Table 5

Boiling points, density and refractivity parameters for silazanes

	COMPOUNDS	T_b	e	Me^2		N_D	Mn_D		$\sqrt{M/n_D}$	K_n	K_D
				I	II		I	II			
1	$(CH_3)_3SiNHCH_3$	344.0	0.7395	56.38	—	1.3905	143.34	—	7.30	47.11	7.72
2	$(CH_3)_3SiNHC_2H_5$	363.5	—	—	—	1.3912	162.89	—	7.77	46.73	—
3	$(CH_3)_3SiN(C_2H_5)_2$	399.3	—	—	—	1.4112	204.75	—	8.53	46.78	—
4	$[(CH_3)_3Si]_2NH$	399.2	0.7741	96.57	98.57	1.4078	226.90	225.42	9.01	44.26	10.70
5	$(C_2H_5)_3SiNH_2$	410.3	—	—	—	1.4259	186.92	186.92	8.02	51.10	—
6	$(n-C_3H_7)_3SiNH_2$	462	—	—	—	1.4359	248.53	248.76	9.16	50.42	—
7	$[(CH_3)_2SiNH]_3$	461	0.9196	185.43	185.43	1.4480	317.50	317.50	10.22	45.07	18.13
8	$[(C_2H_5)(CH_3)_2Si]_2NH$	448	0.8079	123.47	122.48	1.4212	268.86	268.42	9.67	46.29	12.75
9	$[(CH_3)_3SiNH]_2Si(CH_3)_2$	466	0.8366	163.96	160.38	1.4281	334.56	331.25	10.71	43.47	15.29
10	$[(C_2H_5)_2SiNH]_3$	423	0.9287	261.57	257.18	1.4670	444.89	446.50	11.87	35.63	22.03
11	$[(C_2H_5)_2SiNH]_4$	464	0.9521	366.55	342.91	1.4769	597.19	595.33	13.61	34.07	26.92

Table 6

Boiling points, density and refractivity parameters for iso-cyanato and iso-thio cyanato silanes

	COMPOUNDS	T_b	e	Me^2 I	Me^2 II	N_D	Mn_D I	Mn_D II	$\sqrt{M/n_D}$	K_n	K_D
1	$Si(OCN)_4$	520.2	1.414	392.06	—	1.4646	287.19	287.19	9.56	54.40	41.00
2	$Si(NCO)_4$	458.6	1.434	403.22	403.22	1.4610	286.49	282.50	9.58	47.84	42.07
3	$SiF(NCO)_3$	407.3	1.456	366.93	335.08	1.4161	245.11	244.07	9.29	43.84	39.49
4	$SiF_2(NCO)_2$	341.6	1.437	309.92	266.93	1.3536	203.16	205.64	9.05	37.74	34.24
5	$SiCl(NCO)_3$	425.0	1.437	391.38	377.28	1.4507	274.96	272.82	9.49	44.79	41.23
6	$SiCl_2(NCO)_2$	390.8	1.437	377.85	351.35	1.4380	263.14	263.14	9.41	41.54	40.17
7	$SiCl_3(NCO)$	359.8	1.445	367.49	325.41	1.4262	251.65	253.46	9.31	38.63	39.55
8	$Si(OCH_3)(NCO)_3$	441.4	1.313	319.07	342.89	1.4287	264.44	264.57	9.52	46.35	33.51
9	$Si(OCH_3)_2(NCO)_2$	425.1	1.208	254.03	282.56	1.4028	244.21	246.64	9.40	45.19	27.01
10	$Si(OCH_3)_3(NCO)$	410.6	1.123	205.67	222.24	1.3839	225.70	228.70	9.23	44.49	22.29
11	$Si(OC_2H_5)(NCO)_3$	452.6	1.236	304.15	351.91	1.4251	283.72	284.45	9.90	49.00	30.72
12	$Si(OC_2H_5)_2(NCO)_2$	448.4	1.108	248.08	245.13	1.4046	283.85	286.40	10.12	44.30	24.51
13	$Si(OC_2H_5)_3(NCO)$	445.9	1.015	211.28	221.56	1.3922	285.52	288.35	10.28	43.34	20.54
14	$Si(CH_3)(NCO)_3$	443.8	1.267	271.44	228.39	1.4430	243.99	241.77	9.01	49.25	30.12
15	$Si(CH_3)_2(NCO)_2$	412.2	1.076	164.51	164.51	1.4221	202.07	201.04	8.38	49.17	19.63
16	$Si(CH_3)_3(NCO)$	364.0	0.867	86.51	100.63	1.3960	160.66	160.32	7.68	47.36	11.26
17	$Si(C_2H_5)(NCO)_3$	456.5	1.2191	272.11	240.34	1.4468	264.89	263.27	9.35	48.81	29.09
18	$Si(C_2H_5)_2(NCO)_2$	449.7	1.0223	177.76	188.43	1.4348	244.04	244.04	9.10	49.47	19.56

19	$Si(C_2H_5)_3(NCO)$	438.1	0.8895	124.29	136.51	1.4295	224.56	224.81	8.77	49.96	14.17
20	$Si(n-C_3H_7)(NCO)_3$	471.2	1.1726	270.99	250.28	1.4462	285.03	283.89	9.71	48.54	27.92
21	$Si(i-C_3H_7)(NCO)_3$	465.0	1.1626	266.38	—	1.4444	284.68	—	9.72	47.84	27.41
22	$Si(n-C_4H_9)(NCO)_3$	488.5	1.141	274.82	260.25	1.4479	305.64	304.48	10.03	48.68	27.39
23	$Si(C_6H_5)(NCO)_3$	524.9	1.273	374.48	389.22	1.5210	351.49	349.80	9.99	52.52	37.47
24	$Si(C_6H_5)_2(NCO)_2$	592.6	1.188	375.53	375.23	1.5675	417,09	417.09	10.40	56.94	36.08
25	$Si(C_6H_5CH_2)(NCO)_3$	538.0	1.225	367.78	399.72	1.5230	373.27	373.27	10.28	52.38	35.78
26	$Si(NCS)_4$	586.0	1.407	515.37	417.64	—	—	422.91	—	—	—
27	$SiCl_3(NCS)$	402.5	1.461	410.91	329.02	1.5091	290.52	288.56	9.19	43.78	44.69
28	$Si(OCH_3)_3(NCS)$	443.5	1.134	230.39	225.85	1.4426	258.44	263.89	9.28	47.81	24.83
29	$Si(OC_2H_5)_3(NCS)$	478.8	1.036	237.36	252.91	1.4431	319.14	323.81	10.30	46.47	23.03
30	$Si(CH_3)(NCS)_3$	539.8	1.304	606.82	322.42	—	—	—	—	—	—
31	$Si(CH_3)_2(NCS)_2$	490.3	1.142	227.20	227.20	1.5677	273.12	271.25	8.42	58.24	26.98
32	$Si(CH_3)_3(NCS)$	416.1	0.931	113.67	131.98	1.4820	194.36	195.42	7.72	53.85	14.70
33	$Si(C_2H_5)(NCS)_3$	549.0	1.264	369.51	334.38	1.6195	374.56	368.58	9.39	58.46	39.35
34	$Si(C_2H_5)_2(NCS)_2$	518.5	1.089	239.81	251.12	1.5540	314.25	314.25	9.15	56.66	26.20
35	$Si(C_2H_5)_3(NCS)$	483.5	0.934	151.04	167.85	1.4944	258.75	259.92	8.80	54.92	17.15
36	$Si(n-C_3H_7)(NCS)_3$	562.5	1.224	367.94	344.31	1.6014	392.79	389.19	9.78	57.51	37.62
37	$Si(i-C_3H_7(NCS)_3$	552.0	1.2177	363.70	—	1.6066	394.07	—	9.75	56.60	37.31
38	$Si(n-C_4H_9)(NCS)_3$	573.6	1·189	366.54	354.28	1.5928	412.98	409.79	10.11	56.74	36.26
39	$Si(C_6H_5)(NCS)_3$	612.6	1.291	465.47	400.04	—	—	455.11	—	—	—
40	$Si(C_6H_5)_2(NCS)_2$	649.0	1.188	420.80	382.44	—	—	487.30	—	—	—
41	$Si(C_6H_5CH_2)(NCS)_3$	621.9	1.275	476.75	410.54	—	—	478.58	—	—	—

Table 7

Boiling points, density and refractivity parameters for siloxanes.

	COMPOUNDS	T_b	e	Me^2		N_D	Mn_D		$\sqrt{M_l n_D}$	K_n	K_D
				I	II		I	II			
1	$(CH_3HSiO)_3$	366.8	0.9677	168.80	168.81	1.3700	248.23	248.23	9.75	37.61	17.31
2	$(CH_3HSIO)_4$	407.5	0.9912	236.15	225.08	1.3870	333.37	330.97	11.17	36.45	21.12
3	$(CH_3HSiO)_5$	441.7	0.9985	299.54	281.35	1.3912	417.98	413.74	12.45	35.45	24.04
4	$(CH_3HSiO)_6$	465.8	1.0060	364.86	337.61	1.3944	502.73	496.72	13.61	26.86	26.79
5	$(CH_3)_3SiOSi(CH_3)_3$	373.5	0.7619	94.14	98.51	1.3774	223.38	223.07	9.24	40.39	10.18
6	$CH_3[(CH_3)_2SiO]_2Si(CH_3)_3$	426	0.8200	158.86	160.26	1.3848	327.18	326.56	11.11	38.37	14.31
7	$CH_3[(CH_3)_2SiO]_4Si(CH_3)_3$	467	0.8563	281.87	283.76	1.3895	543.19	533.54	14.11	33.09	19.97
8	$CH_3[(CH_3)_2SiO]_5Si(CH_3)_3$	515	0.8912	364.17	345.51	1.3948	639.57	637.03	15.35	27.03	23.71
9	$[(ClCH_2)(CH_3)_2SiO]_2O$	477.5	1.0450	287.29	—	1.4390	378.58	—	11.27	42.36	25.48
10	$(ClCH_2)(CH_3)_2SiOSi(CH_3)_3$	424.7	0.9105	163.01	—	1.4106	277.37	—	9.93	42.72	16.39
11	$(CH_3)_3SiOSi(CH_3)_2CH_2OCOCH_3$	453	0.9020	179.13	—	1.4040	309.13	—	10.56	42.86	16.95
12	$[(CH_3)_2CH_2OCOCH_3Si]_2O$	523	0.9930	215.12	—	1.4215	310.14	—	10.39	50.33	20.70
13	$[(CH_3)_3SiO]_3SiCH_3$	463	0.8497	224.18	240.38	1.3880	430.77	430.05	12.69	36.47	17.65
14	$[(CH_3)_2SiO]_4$	448	0.9558	270.75	270.75	1.3968	413.95	413.95	12.32	36.34	21.96
15	$[(CH_3)_2SiO]_5$	483	0.9593	340.92	338.44	1.3982	517.96	517.44	13.76	35.08	24.76
16	$[(CH_3)_2SiO]_6$	518	0.9672	415.86	406.13	1.4015	623.02	620.93	15.04	34.43	27.64
17	$[(CH_3)_2SiO]_7$	427	0.9730	490.98	473.81	1.4040	728.15	724.42	16.22	26.32	30.26
18	$[(CH_3)_2SiO]_8$	448	—	—	541.50	1.4060	833.23	827.91	17.09	25.87	—

19	$[(CH_3)_2SiO]_9$	461	—	—	609.19	1.4070	938.21	931.40	18.28	25.21	—
20	$[(CH_3)_2SiO]_3(ClCH_2)(CH_3)SiO$	487	1.0444	360.85	—	1.4158	468.36	468.13	12.84	37.92	28.07
21	$(CH_3)_{12}Si_7O_8$	527	1.0352	540.76	—	1.4031	708.04	—	16.01	32.91	33.77
22	$(CH_3)_{12}Si_5O_4$	493	0.8677	289.45	—	1.3895	534.19	—	14.11	34.92	20.51
23	$C_2H_5O[(CH_3)_2SiO]C_2H_5$	387	0.8395	104.37	123.05	1.3805	204.43	227.46	8.81	43.90	11.83
24	$C_2H_5O[(CH_3)_2SiO]_2C_2H_5$	434	0.8788.	171.58	184.80	1.3880	308.38	330.95	10.73	40.41	15.97
25	$C_2H_5O[(CH_3)_2SiO]_3C_2H_5$	469	0.9024	241.25	246.54	1.3922	412.46	434.43	12.36	37.93	19.51
26	$C_2H_5O[(CH_3)_2SiO]_4C_2H_5$	500	0.9157	310.54	308.29	1.3950	516.65	537.92	13.79	36.24	22.51
27	$C_2H_5O[(CH_3)_2SiO]_5C_2H_5$	526	0.9207	376.76	370.04	1.3964	620.62	641.41	15.09	34.83	24.95
28	$C_2H_5O[(CH_3)_2SiO]_6C_2H_5$	547	0.9317	450.14	431.79	1.3980	724.91	744.90	16.28	33.58	27.63
29	$C_2H_5O[(CH_3)_2SiO]_7C_2H_5$	565	0.9364	519.61	493.54	1.3990	829.08	848.39	17.40	32.47	29.85
30	$C_2H_5O[(CH_3)_2SiO]_8C_2H_5$	584	0.9409	590.24	555.29	1.3996	933.14	951.88	18.44	31.65	31.99
31	$[(C_2H_5)_2SiO]_3$	390	0.9555	279.62	274.81	1.4308	438.21	439.46	12.23	31.88	22.86
32	$[(C_2H_5)_2SiO]_4$	432	0.9594	375.89	366.42	1.4340	585.95	585.95	14.56	29.65	27.57

Tetraalkyl and trialkylaryl silanes. It might be seen from Table 1 and Fig. 1 that the density of the tetraalkyl silanes goes on increasing with the molecular weight. The branched chain alkyl silanes have a higher density although their boiling point is lower than their normal chain analogues. This increase is not noted either in the hydrocarbons or the sulphides. Since density is governed by the cohesive forces and depends on the packing of the molecules in the liquid shell, it should indicate the participation of the inter- and intra-molecular forces. In Fig. 1, it may be found that the tetraalkyl silanes are divided into three groups governed by equations (1), (2) and (3) and consist of (1) normal chain compounds, (2) branched chain compounds and (3) arylalkyl or alkenyl-alkyl compounds.

$$T_b = 1.90\ \mathrm{Me}^2 + 266.8 \tag{1}$$

$$T_b = 1.92\ \mathrm{Me}^2 + 255.5 \tag{2}$$

$$T_b = 2.03\ \mathrm{Me}^2 + 212.0 \tag{3}$$

The last two groups deviate from the normal. Because of the presence of unsaturated groups an intramolecular interaction is possible and hence the deviation should be due to association in the sense discussed previously. [1]

Haloalkyl and Alkyl Halosilanes. In Table 2 and fig. 2 the haloalkyl and alkylhalosilanes may be seen to fit in nicely on the straight line given by equation (4) :

$$T_b = 1.17\ \mathrm{Me}^2 + 270.8 \ldots \tag{4}$$

Out of these compounds 2, 12, 13 and 14 in Table 2 have more polarizable groups in the molecules. Here again higher cohesive forces set in due to increasing inter-molecular interactions and higher density might be expected. Among the organofluorosilanes, it might be difficult to generalize with the available data, but from fig. 3 it appears that the monofluorides, the di- and trifluorides and the aryl fluorides all form separate groups given by equation (5) and (6).

$$T_b = 1.76\ \mathrm{Me}^2 + 216.7 \ \ldots \tag{5}$$

$$T_b = 2.48\ \mathrm{Me}^2 - 31.6 \ \ldots \tag{6}$$

This would be expected since the degree of inter- and intra-molecular interaction would be different in each case. Among the alkyl chlorosilanes in Table 3 and Fig. 4 the mono-chlorides are similar to the fluorosilanes, and their relation with the boiling point follows a straight line with approximately the same slope as the monofluorides :

$$T_b = 1.73\ \mathrm{Me}^2 + 193.1 \ \ldots \tag{7}$$

The dichlorides are governed by equation (8)

$$T_b = 2.03\ \mathrm{Me}^2 + 28.5 \ldots \tag{8}$$

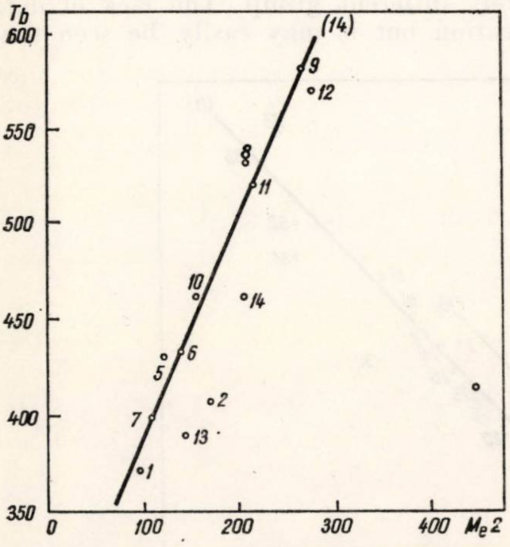

Fig. 2. — Correlation of boiling point and density (numbers refer to compounds listed in table 2).

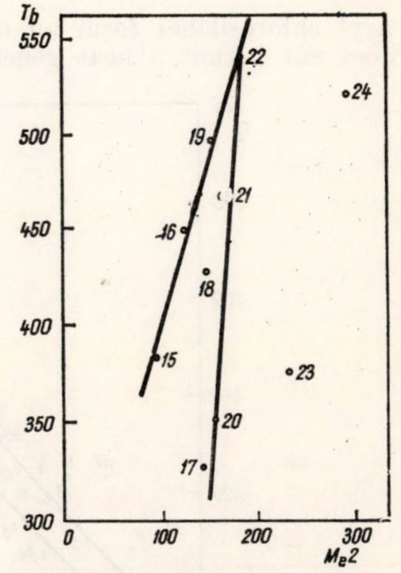

Fig. 3. — Correlation of boiling point and density (numbers refer to compounds listed in table 2).

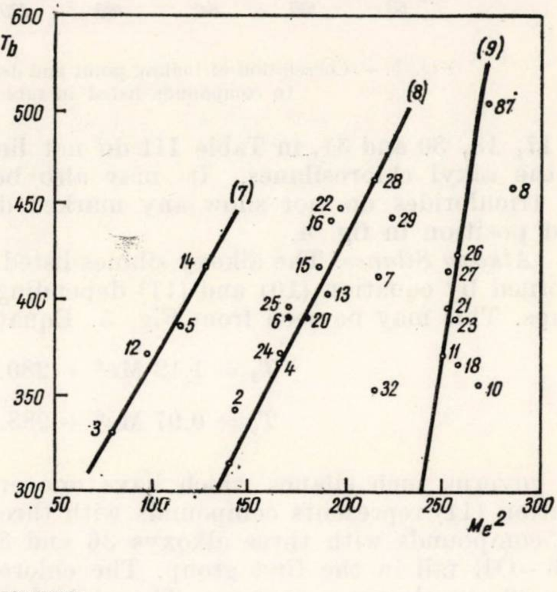

Fig. 4. — Correlation of boiling point and density (numbers refer to compounds listed in table 3).

which is similar in slope to the aryl-alkyl silanes, equation (3). The trichlorides follow the equation

$$T_b = 6.52\ \mathrm{Me}^2 - 1265.1 \ldots \qquad (9)$$

Aryl chlorosilanes form an entirely different group. The lack of data does not permit a neat generalization but it may easily be seen that 10, 17, 18, 30 and 31, in Table III do not lie at the positions predicted by the alkyl chlorosilanes. It may also be noted that the alkyl di- and trichlorides do not show any marked deviations from the calculated position in fig. 4.

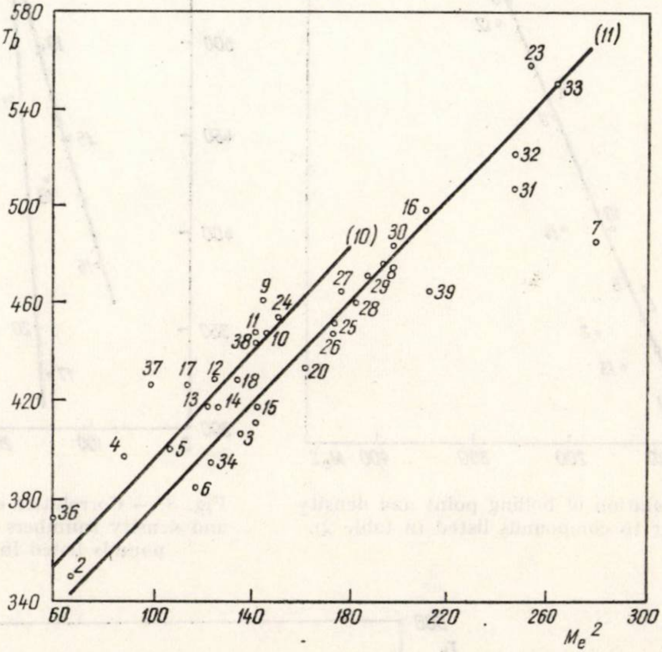

Fig. 5. — Correlation of boiling point and density (numbers refer to compounds listed in table 4).

Alkoxy Silanes. The alkoxy silanes listed in Table 4 fall into groups governed by equation (10) and (11) depending on the number of alkoxy groups. This may be seen from Fig. 5. Equation

$$T_b = 1.12\ \mathrm{Me}^2 + 280.5 \qquad (10)$$

$$T_b = 0.97\ \mathrm{Me}^2 + 283.0 \qquad (11)$$

(10) governs such silanes which have one or two alkoxy groups while equation (11) represents compounds with three alkoxys. It is significant that compounds with three alkoxys 36 and 37 having Si—OH instead of Si—OR fall in the first group. The chloro alkoxy 3 and 7 and the ether 39 are clearly exceptions. The phenyl and alkenyl tri-ethoxy sila-

nes 26,31 and 32 as also compounds like 33 and 34 belong to the second group. The replacement of an alkyl by an alkoxy group gives a much higher intermolecular attraction. This results in higher cohesive energy than would be expected from the rise in molecular weight. The boiling points and the density of the silanes with three alkoxy groups would, therefore, all be high.

The silazanes in Table 5 are seen to be governed by equation (12) which is quite similar to equation (6). This shows that the molecular forces in the alkoxy silanes and the silazanes

$$T_b = 1.55\,\mathrm{Me}^2 + 256.6 \ldots \qquad (12)$$

are almost the same which is in accord with the concept of interpenetration.

Isocyanato and Isothiocyanato Silanes. Among the silyl isocyanates and isothiocyanates in Table 6 a linear relationship is obtained as is depicted by Fig. 6 for the two groups. The isothiocyanates follow equation (13).

$$T_b = 0.52\,\mathrm{Me}^2 + 318.8 \rightarrow \frac{T_b = 0.51\,\mathrm{Me}^2 + 374.7 \ldots (13)}{T_b = 1.19\,\mathrm{Me}^2 + 27.2 \ldots (15)} \qquad (14)$$

It is found that the tetra isocyanato and tetra isothiocyanato silanes fall on the same straight line which represent the isocyanato-halosilanes and is given by equation (15). The alkyl or aryl isocyanato compounds are closely related to equation (14). It is worth noting that the halo-isocyanato-silanes have a slope similar to that for mono or dialkoxy silanes while the alkyl isocyanato and isothiocyanato silanes are governed by straight lines parallel to one another and have slopes similar to the siloxanes. This can be related to the same type of molecular forces in each case.

The predominance of the interaction of the d_π-electrons of silicon should mainly be responsible for the correlation of the properties of the alkyl and aryl silanes at the same time. This is supported by the calculated Me^2 values which indicate deviations particularly for such compounds which according to our definition are associated. This is further substantiated by the high value of Trouton's constant for these compounds as noted by Forbes and Anderson.[7]

The Siloxanes. The siloxanes listed in Table 7 form a set of four groups as may be seen from fig. 7. It would appear that the higher polymers and the ring like systems belong to group II, III and IV and are represented by equations 17, 18 and 19 while the lower siloxanes belong to group I. The slopes of these lines are similar to the isocyanates and isothiocyanates as might be seen from the following equations which govern their T_b and Me^2 values and hence these molecules are also classified as associated.

$$T_b = 0.47\ \mathrm{Me}^2 + 352.5 \tag{16}$$

$$T_b = 0.27\ \mathrm{Me}^2 + 423.7 \tag{17}$$

$$T_b = 0.48\ \mathrm{Me}^2 + 317.4 \tag{18}$$

$$T_b = 0.57\ \mathrm{Me}^2 + 270.1 \tag{19}$$

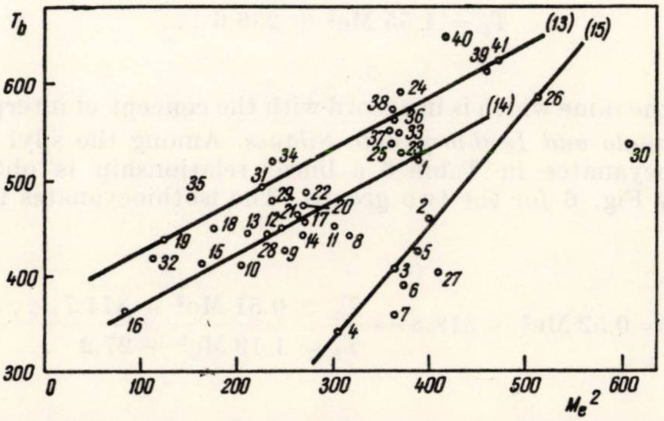

Fig. 6. — Correlation of boiling point and density (numbers refer to compounds listed in table 6).

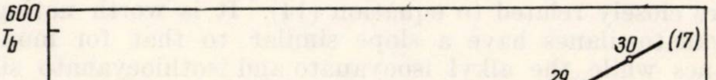

Fig. 7. — Correlation of boiling point and density (number refer to compounds listed in table 6).

From the above correlation it can be inferred that Me^2 values also follow a trend characteristic of molar volumes. The values increase with an increment in the methylene group and in this manner it is possible to deduce the Me^2 value for the Si−R bond. These values are listed in Table 8. There is a rise of 10 units per CH_2 group and by this criterion tetramethyl silane is a rather abnormal compound. The calculations are therefore, based on the values for the ethyl substituted compounds. It is found that the data calculated in this manner agree reasonably with those observed. The branched chain alkyl substituted silanes have a higher density compared with their normal analogues and there is an increment of at least 0.5 unit for branching. The same trend is followed practically in several classes of compounds mentioned herein. Considerable deviation from additivity is noticed in the case of substituents like a phenyl, alkenyl or isocyanate group. The above discussion has classified such compounds as associated. It is therefore suggested that deviation from additivity must be related to association.

Table 8

Me^2 values of Si−X bonds

S. No.	Groups	Me^2 − coefficient
1	$Si-CH_3$	9.19
2	$Si-C_2H_5$	21.15
3	$Si-C_3H_7$	31.08
4	$Si-C_4H_9$	41.06
5	$Si-C_5H_{11}$	51.85
6	$Si-C_6H_5$	86.81
7	$Si-OCH_3$	40.48
8	$Si-OC_2H_5$	49.50
9	$Si-OC_4H_9$	60.73
10	$Si-OC_2H_4OCH_3$	87.96
11	$Si-OCO.CH_3$	78.78
12	$Si-CH=CH_2$	15.68
13	$Si-CH_2=CH-CH_2$	21.11
14	Si−H	3.71
15	Si−OH	35.32
16	Si−Cl	63.28
17	Si−F	32.66
18	Si=O	49.30
19	Si−NH	43.43
20	Si−NCO	100.80 (for electronegative groups). 73.06 (for alkyl groups.)
21	Si−NCs	104.41
22	Si−Si	21.27

The correlation discussed here is thus helpful in accounting for changes in the properties as the substituent groups are varied. These results also indicate a clear dependence of density on the bond character of the silanes, silazanes and siloxanes. It must be mentioned here that the Si—O and Si—N bond energies as observed for the siloxanes and silazanes increase for the straight chain compounds. This has been attributed to electron delocalization involving $(d \rightarrow p)\pi$ bonding. However, small changes or variations in the trend can also be due to small changes in the hybridization of the silicon orbitals and consequently in the geometry of the molecules which might increase or decrease the Si—X bond strength. The halosilanes, the isocyanates and the isothiocyanates, the silazanes and alkoxy and aroxy silanes all have a very small slope for the straight line governing their cohesive energy given by Me^2 and boiling point. The variations noted here can safely be assigned, to changes in their geometry brought about by the introduction of an electronegative group. By virtue of their electron-withdrawing effect such groups induce polarizability in the molecule which would give rise to interpenetration of the molecules. Such compunds would, therefore, be associated while the alkyl silanes having no such groups behave as normal compounds.

Conclusions : The density and boiling point of various groups of organosilicon compounds can be correlated by using their Me^2 values. This parameter is shown to be additive and the departure from additivity is related to association. Thus among the tetraalkyl or trialkyl aryl silanes, the latter are associated. The aryl substituted silanes, in general are different from the alkyls. Among the halides, the monochloro and fluoro silanes are similar but the dichlorides resemble the aryl silanes while the trichlo-silanes are totally different. This behaviour of the chlorides is in contrast with that observed for the alkoxy silanes, where the mono and dialkoxy compounds are different from the trialkoxys. Among the former compounds the predominance of the inductive effect is quite apparent. The same effect is also responsible for separating the halo-isocyanato from the alkyl isocyanato silanes. The last mentioned group has a correlation factor similar to that of the siloxanes which again are grouped according to the number of subunits in the polymeric chain. The similarity of the isocyanates with the siloxanes, then should be related to association.

Revue Roumaine de Chimie, 17, 9, 1599–1609 (1972)

CORRELATION OF THE PHYSICAL PROPERTIES OF ORGANOSILICON COMPOUNDS. II[1]

BOILING POINT, REFRACTIVITY AND DENSITY OF SILANES AND SILOXANES

M. ARSHAD A. BEG

P.C.S.I.R. Laboratories, Karachi—39,
Pakistan

and

IRSHAD A. KHAN

Department of Chemistry, University of Karachi,
Karachi–32

Received June 7, 1971

The boiling point refractivity and density of a series of alkyl silanes, haloalkyl and alkyl halo-silanes, alkoxy, isocyanato and isothiocyanato silanes, silazanes and siloxanes have been correlated by the use of $\sqrt{M/n_D}$. The Mn_D for these molecules have been calculated from those of the various groups and found to agree closely with the observed values. In each group deviations have been noted which are attributed to association.

INTRODUCTION

The previous paper [1] has established certain trends in the properties of the various silanes, silazanes and siloxanes. In general it is found that the replacement of one alkyl group in a tetraalkyl silane by an electronegative group brings in the maximum deviation in the properties. When the second or the third alkyl group is replaced, the properties do not differ in the same manner. The compounds of the type R_3SiX form one class of compounds while R_2SiX_2 and $RSiX_3$ form another. Such a division is particularly noticeable in the alkyl-alkoxy silanes. A similar effect has been noticed in the PMR spectra [2] where it is suggested that this is due to a net decrease in electron density on silicon in the R_3 (alkoxy) Si and an increase otherwise. The inductive effect per alkoxy group has been reported to decrease as the number of these groups increases and the π bonding effect is either unchanged or diminishes with an increasing number of alkoxy groups. In a study of the interaction between the methyl ethoxy silanes and other organic compounds like acetone, amines, alcohols, etc. the deviations from additivity of refractive index are supposed to be due to association. [3] This has also been related to the steric accessibility of the oxygen atom of the alkoxy silanes and to the polarity of the Si-O bond which decreases as the number of alkoxy groups increases.

---

[1] M. A. A. Beg and I. A. Khan *Rev. Roumaine Chim.* (previous paper).
[2] T. Ostdick and P. A. McCusker, *Inorg. Chem.*, **6**, 98 (1967).

A number of workers have studied the bond refractions of the silicon compounds from their molar refractions and the additivity of the atomic refractions has been established. [4,5,6] In a previous paper [7], the refractivity of the phosphines was calculated from the molar refractivity coefficient. Such a coefficient has been found to be very helpful in establishing a pattern for the different series of compounds which have so far included the phosphines, mercaptans and sulphides. [8] Here again a large variety of substituted silanes is available and it will be seen presently that the molar refractivity coefficient is neatly additive.

RESULTS AND DISCUSSION

The refractivity values and related parameters are included in tables 1—7 of the previous paper (Part 1).

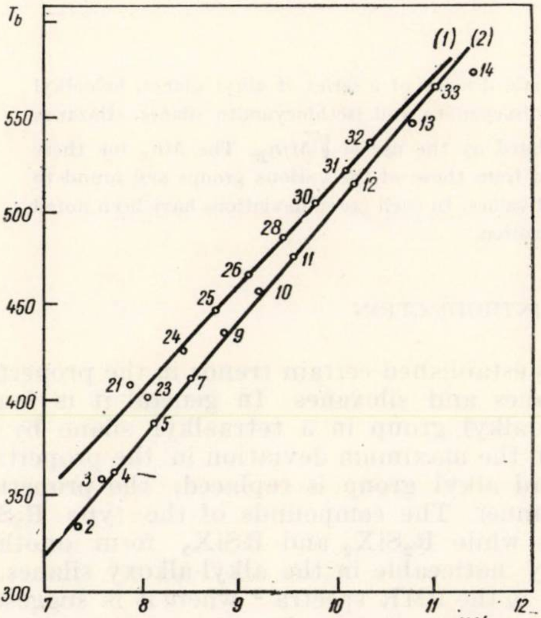

Fig. 1. — Correlation of boiling point and refractivity (numbers refer to compounds listed in table 1).

---

[3] M. G. Voromkov and A. Ya. Deich, *Latvijas PSR Zimeter Akad. Vestes, Kim. Ser.*, **1964**, 145, *Chem. Abstr.*, **61**, 10565 (1964).

[4] P. M. Christopher, *Austral. J. Chem.*, **19**, 2001 (1966).

[5] A. I. Vogel, W. T. Cresswell and J. Leicester, *J. Phys. Chem.*, **58**, 174 (1954).

[6] E. L. Warrick, *J. Amer. Chem. Soc.*, **68**, 2455 (1946).

[7] M. A. A. Beg, *Rev. Roumaine Chim.*, **14**, 503 (1969).

[8] M. A. A Beg and M. A. Hashmi, *Rev. Roumaine Chim.* under publication.

Tetra alkyl and aryl silanes. From Table 2 and figure 1 it might be seen that the correlation of the refractivity and the boiling points classifies these compounds into two groups, governed by the following equations where $\mathrm{Rm} = \frac{\sqrt{M}}{n_D}$

$$T_b = 54.2\ \mathrm{Rm} - 30.5 \quad \ldots\ldots (1)$$

$$T_b = 60.1\ \mathrm{Rm} - 100.2 \quad \ldots\ldots (2)$$

The difference among these classes can be attributed to the number of methylene groups in the chain. Thus the simple compounds with a successive increment of one methylene group form the lower line. With more than one methylene group shielding the silicon atom as in triethyl alkyl silanes the compounds belong to the next higher class. A comparison of 5 with 23, 7 with 24, 9 with 25, 10 with 26, 11 with 28 and 12 with 31 shows that although the compounds have the same molecular weight the difference in refractivity is related to the number of methylene groups directly bonded to the silicon atom. These compounds do not seem to have a significant relation with the odd or even number of carbon atoms as found in the case of hydrocarbons.

It may be noted that for the same molecular weight the refractivity given by $\sqrt{M}/n_D$ is lower for a compact and symmetrical structure compared with an asymmetrical one. Thus trimethyl-pentyl silane (7) has a value of 8.51 but for tetraethyl silane (24) it is 8.41. The molar refractivity given by Mn_D is on the other hand of the reverse order i.e. a symmetrical structure has a lower value than an asymmetrical one. The observed general trend is that the trimethyl alkyl silanes have lower refractivity than triethyl alkyl silanes, which may be attributed to the compactness in the structure of the former class. The abnormal values of Me[2] noted earlier for tetramethyl silanes should in part be due to the packing in this symmetrical molecule.

A further support to this separation due to compactness is provided by the K_n values which are of the order 46 to 50 units while the same for the triethyl series is of the order of 50 to 51 Units. We also note that the Mn_D values rise by a unit of 20.3 per methylene group. If we calculate the molar refractivity coefficient listed in Table 1 by the method of Vogel, the calculated molar refractivity agrees very well with that observed.

Alkyl Halo Silanes. A trend similar to the one for the tetra alkyl silanes is observed for the substituted alkyl silanes e.g. the molar refractivity coefficient listed in table 1 for the chloro alkyl silanes remains constantly at 60.9. This is also substantiated by fig. 2 which gives a straight line for these compounds.

$$T_b = 48.5\ \mathrm{Rm} - 8.4 \quad \ldots\ldots (3)$$

Table 1

Molar refractivity coefficients of various Si − X bonds

S. No.	GROUPS	Molar Refractivity Coefficient
1	Si − CH_3	29.89
2	Si − C_2H_5	51.39
3	Si − C_3H_7	72.01
4	Si − C_4H_9	92.61
5	Si − C_5H_{11}	113.21
6	Si − C_6H_{13}	133.74
7	Si − C_6H_5	137.92
8	Si − OCH_3	52.69
9	Si − OC_2H_5	72.58
10	Si − OC_3H_7	92.24
11	Si − OC_4H_9	113.74
12	Si $O.CO.CH_3$	92.96
13	Si − $OC_2H_4OCH_3$	116.92
14	Si $CH_2 = CH - CH_2$	67.02
15	Si − H	9.56
16	Si − OH	32.30
17	Si − Cl	60.94
18	Si − F	32.19
19	Si = O	43.69
20	Si − NH	46.04
21	Si − NH_2	32.73
22	Si − CH_2Cl	84.07
23	Si − NCO	71.62
24	Si − NCS	105.73
25	Si − Si	28.9

Table 2

Values of s and C in the equation $Me^2 = sRm + C$

Class of Compounds	s	C
Trimethyl alkyl silanes	27.6	−147.4
Triethyl alkyl silanes	27.5	−156.9
Haloalkyl silanes	30.7	−145.2
Alkyl fluoro silanes	29.2	−149.4
Mono and dialkoxy silanes	37.3	−210.8
Trialkoxy silanes	45.5	−306.5
Isothiocyanato silanes	70.0	−586.4
Alkyl isocyanato silanes	174.6	−1255.6
Halo-isocyanato silanes	171.1	−1355.2
Siloxanes with lower chain lengths,	52.8	−353.9
with medium chain lengths,	52.9	−380.1
with higher chain lengths	52.2	−389.5

The slope for this line is slightly lower than that for the tetralkyl silanes which does not indicate any remarkable deviation from the normal. The second group in this class consists of compounds having a polymeric chain with two to three silicon atoms and have a polarizable group

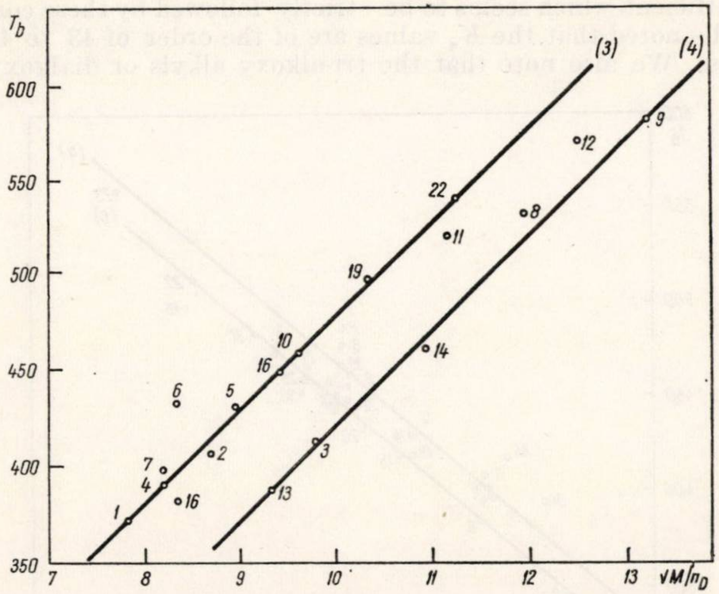

Fig. 2. — Correlation of boiling point and refractivity (numbers refer to compounds listed in table 2).

attached to it. These compounds fall on the straight line given by equation (4).

$$T_b = 53.8 \text{ Rm} - 114.6 \text{ . . . . . } (4)$$

It will be noticed that the slope of this line is similar to methyl alkyl silanes and table 3 does show that the compounds in question are methyl substituted polysilanes. The *Kn* value of these silanes which have been listed in Table 4.

Alkoxy Silanes. The *Kn* values of these silanes have been listed in Table 4 and depicted by fig. 3. A separation is obtained here into two different classes governed by equations (5) and (6)

$$T_b = 42.4 \text{ Rm} + 31.3 \text{ . . . . } (5)$$

$$T_b = 40.7 \text{ Rm} + 26.3 \text{ . . . . } (6)$$

As seen in the earlier correlation of boiling points with Me^2 values, these compounds can again be divided into two groups one with silanes having one or two alkoxy groups and the other with three alkoxy groups. There is a continuous rise in the refractivity with an increase in the chain length of the alkoxy groups. The replacement of an alkyl group by an alkoxy does not give rise to a high increase in refractivity, nevertheless it is in accord with the principle of additivity of the molar refractivity coefficient which seems to be strictly followed by these compounds. It would be noted that the K_n values are of the order of 43 to 46 for the entire class. We also note that the tri-alkoxy alkyls or dialkoxy dialkys have lower boiling points and higher Rm values compared with the trialkyl alkoxy compounds which have the two properties in the reverse order.

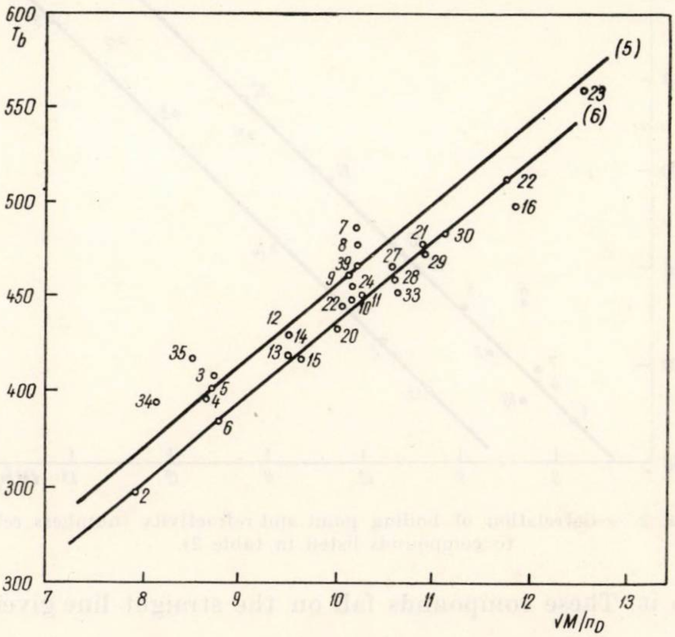

Fig. 3. — Correlation of boiling point and refractivity (numbers refer to compounds listed in table 4).

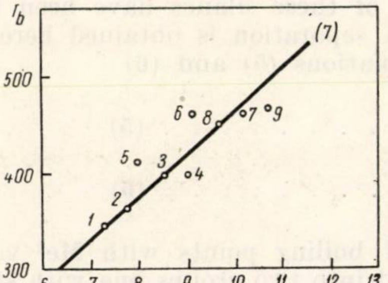

Fig. 4. — Correlation of boiling point and refractivity (numbers refer to compounds listed in table 5).

Silazanes. The refractivity values of the silazanes listed in table 6 and shown in Fig. 4. are $T_b = 44.8\ \mathrm{Rm} + 16.7\ .\ .\ .\ (7)$ and it is seen that for this class K_n has a value of 45—47 but the trialkyl silazanes seem to have higher values of 50—51. However, the additivity of the molar refractivity coefficient is strictly followed here also.

Isocyanate and Isothiocyanate Silanes. Among the isocyanates and isothiocyanates listed in Table 6 and depicted by fig. 5, have the isothiocyanato silanes governed by the equation :

$$T_b = 66.1 \text{ Rm} - 94.35 \tag{8}$$

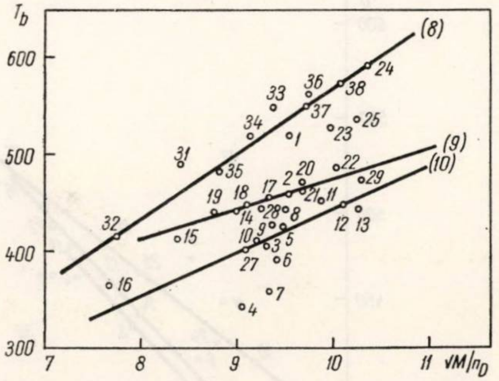

Fig. 5. — Correlation of boiling point and refractivity (numbers refer to compounds listed in table 6).

while the isocyanates which form two groups are governed by equations (9) and (10)

$$T_b = 39.5 \text{ Rm} + 81.3 \tag{9}$$

$$T_b = 49.5 \text{ Rm} - 52.6 \tag{10}$$

It will be noticed here that the slope for the iso-thiocyanates is higher than the classes so far discussed. The straight line given by equation (9) comprises such compounds which have an alkyl group bonded to silicon while that given by equation (10) consists of those which have an electronegative group like fluorine, chlorine or oxygen bonded to it. It will also be seen that the aryl isocyanates do not fall on any of these lines. The principle of additivity of molar refractivity coefficient is followed in all the cases.

Siloxanes. A better correlation is found with the K_n values than with the Me^2 of the siloxanes listed in Table 7 and shown in Fig. 6. Here the compounds can be divided into four sub-groups (1) containing $(CH_3NSiO)_n$ polymers with $n = 3-6$, (2) $[(CH_3)_2 \text{ SiO})]_n$ polymers, $n = 4-9$, (3) $C_2H_5O[(CH_3)_2 \text{ SiO}]_n C_2H_5$ polymers, $n = 1-8$, and (4) $[(CH_3)_2 \text{ SiO}]_n$ having $n > 6$. The rule of additivity is closely followed and we find that the calculated values of the molar refractivity of the siloxanes are quite similar to those observed. These values are governed by the following equations :

$$T_b = 20.8 \text{ Rm} + 211.3 \quad . \; . \; . \; . \; . \; . \; . \quad (11)$$

$$T_b = 25.7 \text{ Rm} + 130.5 \quad . \; . \; . \; . \; . \; . \; . \quad (12)$$

$$T_b = 27.6 \text{ Rm} + 97.2 \quad . \; . \; . \; . \; . \; . \; . \quad (13)$$

$$T_b = 16.5 \text{ Rm} + 159.5 \quad . \; . \; . \; . \; . \; . \; . \quad (14)$$

One notable feature about the K_n values is that it has lower values for the higher polymers and is of the order of 25–26 for a chain of units higher than six. For medium chains it is of the order of 34–37 and for simple compounds it is of the order of 40–45. The efficacy of this constant is therefore of value in determining the molecular weight of a polymer if we know the refractive index and the vapour pressure.

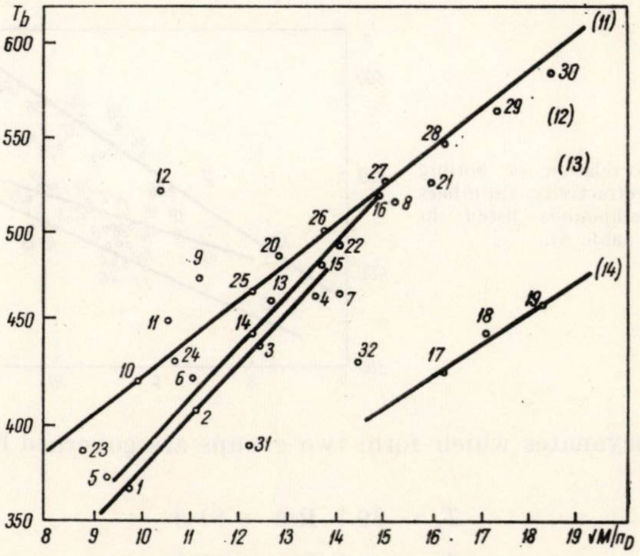

Fig. 6. — Correlation of boiling point and refractivity (numbers refer to compounds listed in table 7).

Correlation of Me² and K_n values

It has been seen above and in the previous paper that the boiling points of the organo-silicon compounds can be correlated with the K_n values and Me [2]. As a natural consequence we have attempted the correlation of the last two properties and we find that the same type of relation exists here as also noted for the sulphides and mercaptans.

It was found in the previous cases that the tetra alkyl and aryl silanes are divided into two classes depending on the substituents i.e. whether it is methyl or a higher alkyl group bonded to silicon. We do find that the silanes having methylene groups intervening the chain are different from those having just the methyl groups. Similarly the organo halo-silanes and the organo-silazanes are divided into groups depending on the interpenetrating effect of the substituent. This is apparent from Figs. 7–12 and from the values of the slopes C and constant s in Table 2 describing the linear relationships depicted in these graphs.

The correlation of these properties gives another constant which has been derived earlier and has been denoted by K_D. It is seen that these values have also the same pattern as those for K_n. For tetralkyl and aryl silanes, these are between 8 and 14 while they are between 12 and

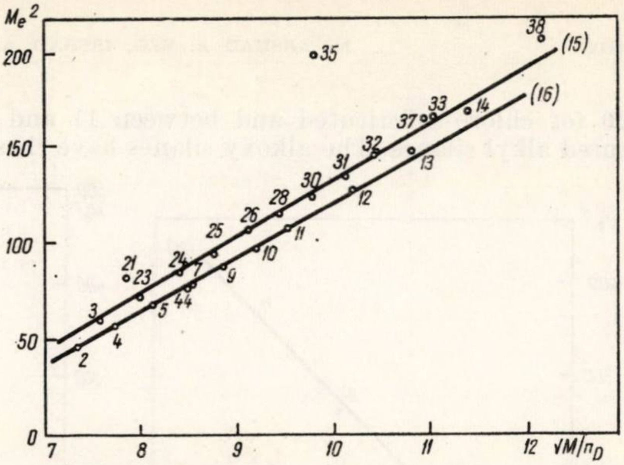

Fig. 7. — Correlation of refractivity and density (numbers refer to compounds listed in table 1).

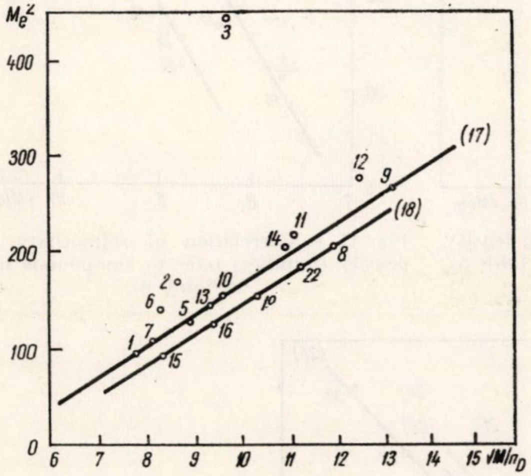

Fig. 8. — Correlation of refractivity and density (numbers refer to compounds listed in table 2).

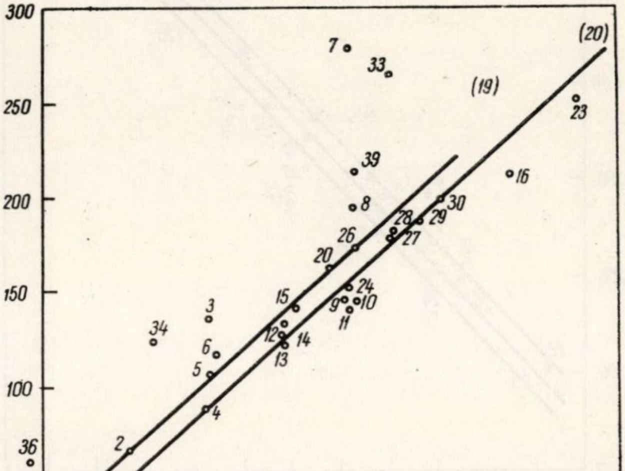

Fig. 9. — Correlation of refractivity and density (numbers refer to compounds listed in table 4).

20 for chloro-substituted and between 11 and 16 for the fluoro substituted alkyl silanes. The alkoxy silanes have these values ranging between 10 and 13 for the methyl compound and 15 to 16 for ethyl compounds. For siloxanes they are between 7 and 12 for the simple compounds and

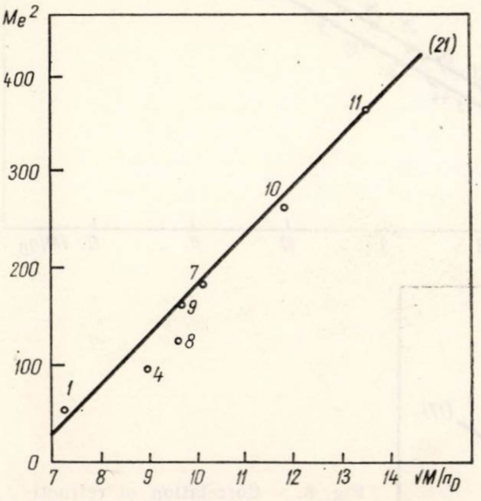

Fig. 10. — Correlation of refractivity and density (numbers refer to compounds listed in table 5).

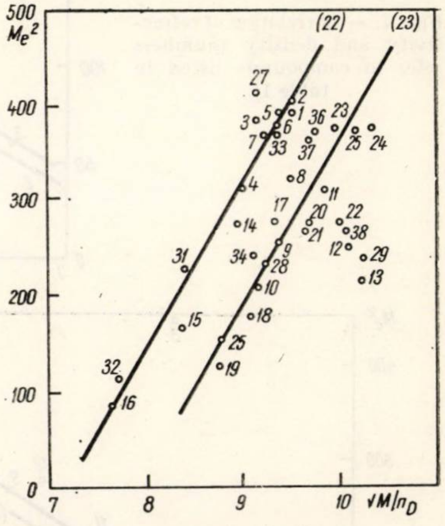

Fig. 11. — Correlation of refractivity and density (numbers refer to compounds listed in table 6).

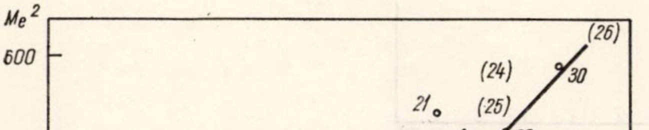

Fig. 12. — Correlation of refractivity and density (numbers refer to compounds listed in table 7).

16 and 32 for polymeric compounds, the value depending on the chain length. The higher polymers have values above 27.

Thus a relation of the density and refractivity also has the same pattern as in the individual cases. The various groups are subdivided in a manner similar to those seen already. A notable feature of these correlations is the observation that the K_n and the K_D values rise with increasing chain length. The increase in the values reminds us of the shift in the UV absorption maxima with increasing chain length of the polysilane. These shifts have been noted to be dependent on the nature of the substituents and a Si—Si bond is essential for an enhanced conjugation with an aromatic or an alkenyl group [9]. Such conjugative interactions have been demonstrated in the case of phenyl and vinyl pentamethylene disilanes. This has been interpreted by us in terms of association in the cases of phosphines, mercaptans, sulphides and during the discussion of the same properties in the present series of compounds.

The agreement of the Me^2 and n_D values calculated from the respective coefficients with those observed is quite close which demonstrates the additivity principle in each case. The exceptions have been attributed to association which have also been indicated by the NMR and UV studies.

[9] H. Sakurai and M. Kumbada, *Bull. Chem. Soc. Japan*, **37**, 1894 (1964).

10 and 32 for polymeric compounds, the value depending on the chain length. The higher polymers have values above 27.

Thus a relation of the density and refractivity also has the same pattern as in the individual cases. The various groups are subdivided in a manner similar to those seen already. A notable feature of these correlations is the observation that the E and the K_p values rise with increasing chain length. The increase in the values reminds us of the shift in the UV absorption maxima with increasing chain length of the polysilane. These shifts have been noted to be dependent on the nature of the substituents and a Si—Si bond is reported for an enhanced conjugation with an aromatic or an alkenyl group.* Such conjugative interactions have been demonstrated in the case of phenyl and vinyl pentamethyldisilanes. This has been interpreted by us in terms of association in the cases of siloxanes, mercaptides, sulphides and through the discussion of the same properties in the present series of compounds.

The agreement of the Mar and n_D values calculated from the respective coefficients with those observed is quite close which demonstrates the additivity principle in each case. The exceptions have been attributed to association which have also been indicated by the NMR and UV studies.

---

* H. Sakurai and M. Kumada, Bull. Chem. Soc. Japan, 37, 1894 (1964).

Revue Roumaine de Chimie, **17**, 9, 1611—1614 (1972)

MORE PROOFS FOR A CHARACTERISTIC BAND IN THE INFRARED SPECTRUM OF SULTAMS

S. H. DOSS*

Received February 10, 1972

Infrared spectra show a band at 1291—1270 cm^{-1} characteristic of the six-membered sultam ring, whether the sultam ring is saturated or unsaturated, substituted or unsubstituted.

It has been suggested that the band in the region 1291—1270 cm^{-1} is connected with the sultam ring since other groups in the various compounds under investigation did not interfere with it. [1] Further supporting proof for this band assignment has also been reported [2] depending on the change of the sultam ring into pyrrol ring, lacking the SO_2 group. It has been observed that the characteristic sultam band (1291—1270 cm^{-1}) and the SO_2 asym. band (1320 cm^{-1}) disappeared. Instead of the SO_2 sym. band at 1130 cm^{-1} another atrophied band shifted to 1118 cm^{-1} was observed (1, 2, 4 aromatic substitution). In this work we would like to add other proofs supporting this observation following the method of elimination. [3] Four model substances containing sultam rings were prepared by published procedures : I : N,N′ — (*p*, *p*′-diphenylene) — bis [2,4-dimethylbutadiene (1,3)] — sultam (1,4), having methyl groups directly attached to the sultam ring; [4] II : N-benzyl—1, 2, 4-trimethylbutadiene (1,3)-sultam (1,4), [5] to give it the aliphatic nature and finally compounds with the benzene ring directly attached to the sultam ring to give it the aromatic nature : III : N, phenyl-2-methyl-4-n-heptylbutadiene (1,3) — sultam (1,4) [5], and IV : N-phenyl-2-methyl-4-n-undecyl-butadiene (1,3)—sultam (1,4) [5].

In all cases, the compounds were of high purity as gauged from the reported physical constants.

On changing compound I to N,N′—(*p*-*p*′-biphenylene-bis-(2,4-dimethyl-pyrrol) (V) [5] the IR-Spectrum showed the complete disappearance of the beak at 1270 cm^{-1} (Fig. 1).

---

* Present address : Organisch-Chemisches Institut der Universität Bonn, Federal Republic of Germany.

[1] S. H. Doss, *Acta Chim. Acad. Sci. Hung.*, in press (1972).

[2] S. H. Doss, *Chem. and Ind.* **1971**, 961.

[3] S. H. Doss and M. W. Müller, *Austral. J. Chem.*, **24**, 2711 (1971).

[4] B. Helferich, R. Dhein ; K. Geist, H. Junger and D. Wiehle ; *Liebigs Ann. Chem.*, **646**, 32 (1961).

[5] B. Helferich and W. Klebert, *Liebigs Ann. Chem.*, **657**, 79 (1962).

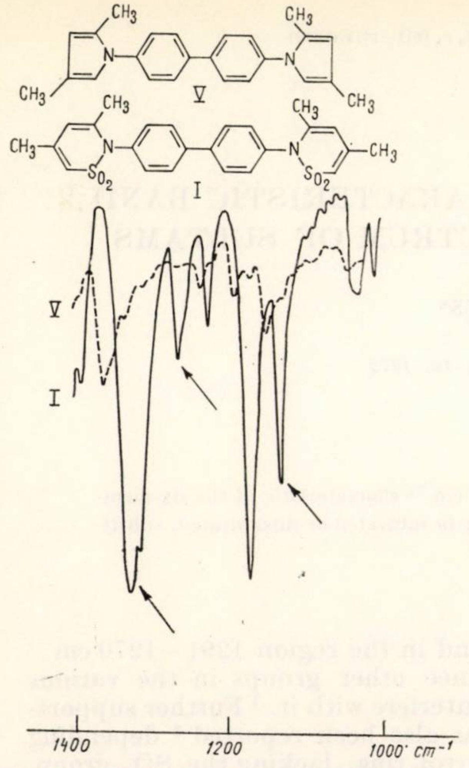

Fig. 1. — IR spectra of compound I containing the sultam ring and compound V containing the pyrrol ring (in KBr).

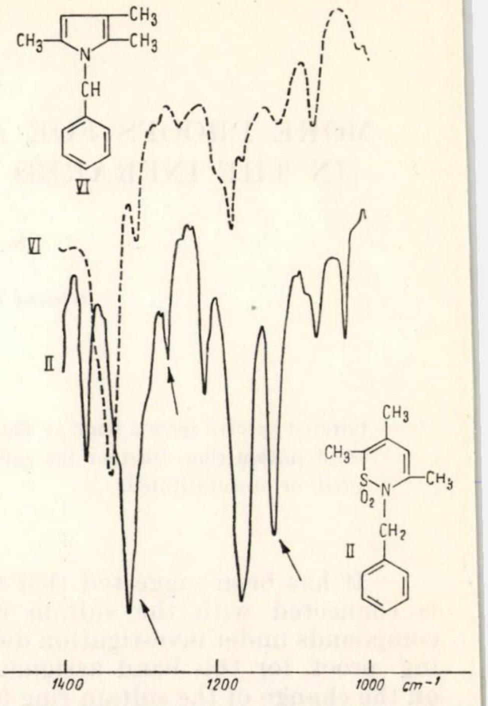

Fig. 2. — IR spectra of compound II containing the sultam ring and compound VI containing the pyrrol ring (in KBr).

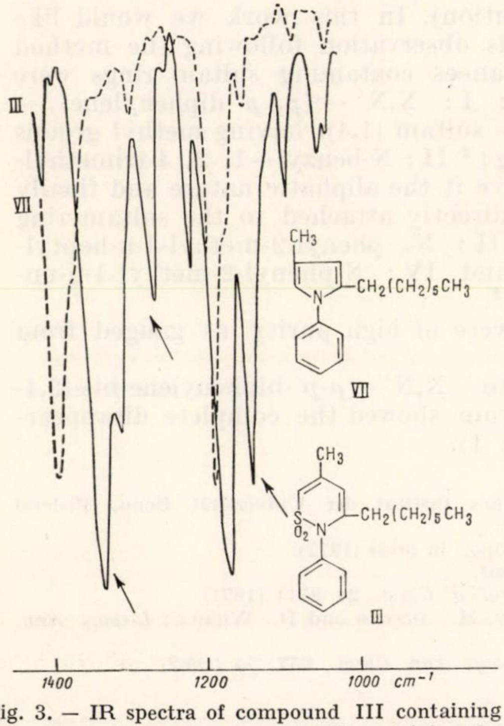

Fig. 3. — IR spectra of compound III containing the sultam ring and compound VII containing the pyrrol ring (in KBr).

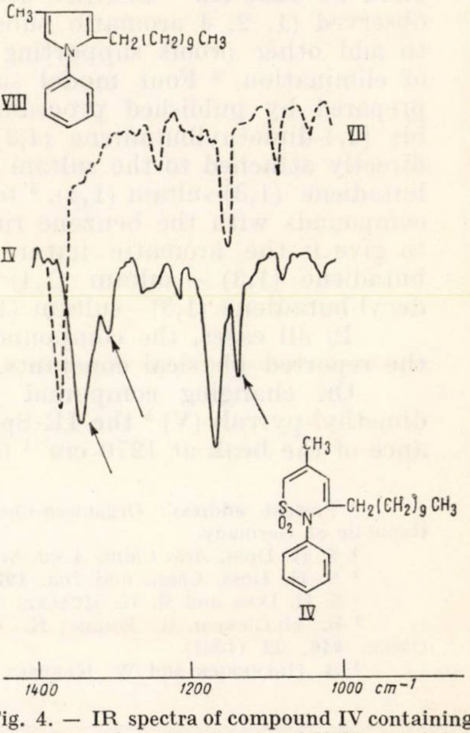

Fig. 4. — IR spectra of compound IV containing the sultam ring and compound VIII containing the pyrrol ring.

By changing compound II to N-benzyl-2, 3, 5-trimethyl-pyrrol (VI)[5] the IR Spectrum showed the complete disappearance of the beak at 1270 cm^{-1} (Fig. 2). The same results were obtained on changing compound III to N-phenyl-2-n-heptyl-4-methyl-pyrrol (VII)[5] (Fig. 3), and compound IV to N-phenyl-2-n-undecyl-4-methyl-pyrrol (VIII)[5] (Fig. 4).

Fig. 5. — IR spectra of compound IX containing the sultam ring, compound XI containing the sultam ring and compound X the sulphonyl amide, intermediate product in the synthesis of XI.

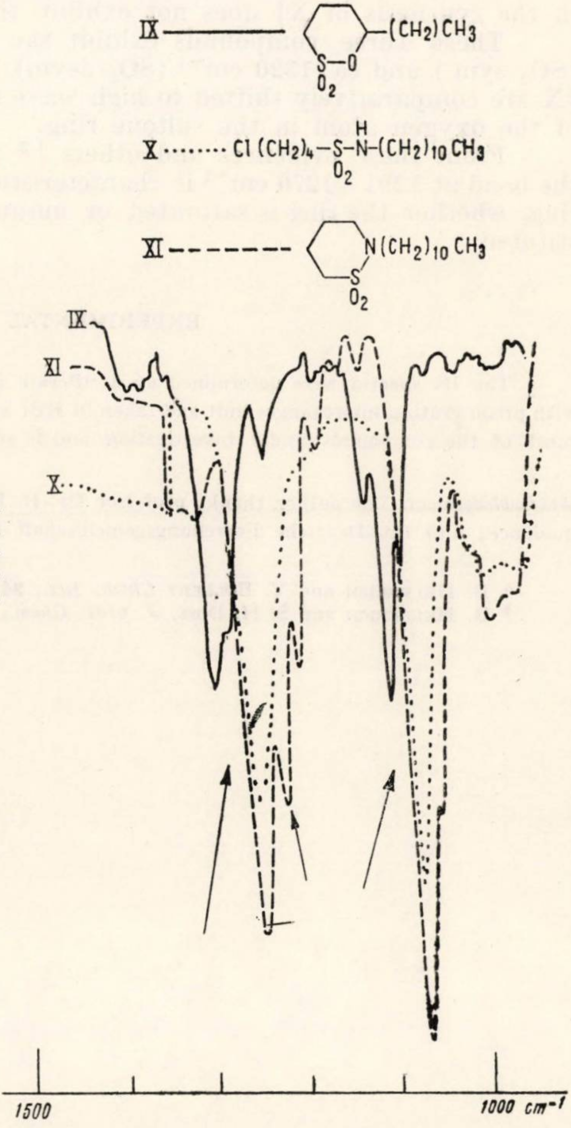

On the other hand, application of the method of elimination of the nitrogen, from the sultam ring, gave analogous results i.e. the disappearance of sultam band. Compound IX, n-hexane-sultone 1,4 [6] and another analogous compound [7] XI containing the sultam ring were prepared by published procedures. Compounds IX and XI possess the same design except the number of (CH_2) groups in the side chain.

Compound XI shows the characteristic sultam band at 1290 cm^{-1} whereas compound IX which has the sultone ring shows no existence of this band (Fig. 5). Compound X which is the intermediate product in the synthesis of XI does not exhibit the band at 1291–1270 cm^{-1}.

These three compounds exhibit the two bands at ca. 1135 cm^{-1} (SO_2 sym.) and ca. 1320 cm^{-1} (SO_2 asym). The two bands of compound IX are comparatively shifted to high wave numbers due to the presence of the oxygen atom in the sultone ring.

From these evidences and others [1,2] we can conclude safely that the band at 1291–1270 cm^{-1} is characteristic of the six-membered sultam ring, whether the ring is saturated or unsaturated, substituted or unsubstituted.

EXPERIMENTAL

The IR spectra were determined on a "Perkin Elmer"-model 221 spectrophotometer with prism grating interchanges unit and taken in KBr and acetonitrile, as the latter dissolved most of the compounds under investigation and is suitable for the region studied.

Acknowledgement. The author thanks professor Dr. B. Helferich for his interest and helpful guidance; also the Deutsche Forschungsgemeinschaft for financial support.

---

[6] B. Helferich and V. Böllert *Chem. Ber.*, **94**, 505 (1961).

[7] B. Helferich and S. H. Doss, *J. prak. Chem.*, in press (1972).

Revue Roumaine de Chimie, 17, 9, 1615–1619 (1972)

ON THE POSSIBILITY OF USING Ag_2S CERAMIC MEMBRANE-ELECTRODE FOR THE DETERMINATION OF THE CONCENTRATION OF SOLUTIONS IN FLOW CONDITIONS. CHROMATOGRAPHIC DETECTOR

C. LITEANU, I. C. POPESCU and H. NAŞCU

DIVISION OF ANALYTICAL CHEMISTRY, BABEŞ-BOLYAI UNIVERSITY,
str. ARANY IANOS 11, CLUJ, ROMANIA

Received December 27, 1971

The paper presents an attempt to use the Ag_2S ceramic membrane-electrode in order to determine the concentration of the flowing electrolyte solutions. This device can also be used as a liquid chromatographic potentiometric detector, as it responds to all the chemical species interacting chemically with Ag^+ or S^{2-}. The electric signal of the detector may be recorded without any previous changes by a high input impedance potentiometric recorder.

An Ag^+ ion selective membrane electrode (ISME) was obtained and studied, [1] based on a procedure for obtaining ion selective membrane electrodes (ISME) from Ag_2S powder. [2]

Its electrochemical properties, and particularly its high response speed has led us to the idea of using it for the analysis of solutions in dynamic conditions. This brings us very near to use it as a chromatographic detector. [3]

The main purpose of the present paper is the study of a device able to record continuously the concentration of species to which ISME is sensitive in a flowing solution of indifferent electrolyte.

EXPERIMENTAL PART AND RESULTS

Detector: The way in which Ag_2S ceramic ISME is adapted for its use in a detector, is described in.[4] Its basic diagram is presented in fig. 1.

---

[1] C. Liteanu, I. C. Popescu and V. Ciovîrnache, *Talanta*, **19**, 985 (1972).

[2] C. Liteanu, I. C. Popescu and S. B. Domşa, Romanian Patent, 67066 (1971).

[3] V. Polesuk, *Amer. Lab.*, **2**, 27 (1970).

[4] C. Liteanu, N. Naşcu and I. C. Popescu, Romanian Patent, **67067** (1971).

The initial volume of the detector (measuring cell) was of 450 μl and was afterwards brought to 25μl, in order to improve the sensitivity. It is worth mentioning that the volume of the detector can be reduced by at least one order of magnitude, without modifying the principle of construction.

Experimental device. The block diagram of the setting up is given in fig. 2.

The constant flow rate through the detector was maintained by using a hydrostatical method.

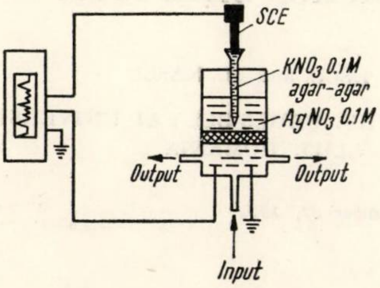

Fig. 1. — Detector.

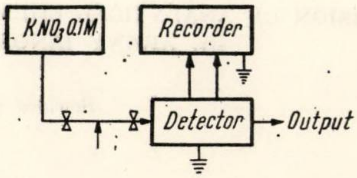

Fig. 2. — Experimental device.

The recording potentiometer Radelkis OH—102 with a high response speed is fitted out with adjustment devices for the rolling speed of the paper, sensitivity, and zero point.

Reagents. Preliminary studies showed the working of the detector as not being adequate if distilled water is used as carrier. An inert electrolyte : 0.1 M KNO_3, was therefore used (fig. 2), as in other studies [5] of the same type.

Solutions (10^{-2} M) for the qualitative and quantitative tests have been prepared from p.a. reagents, at constant ionic strength (J = 0.1 M). To adjust the ionic strength, KNO_3 was used. As a matter of fact, the ionic strength has the same value in the whole experimental device.

Working Method

The flow rate is adjusted to the required value, roughly by means of valve 1 and accurately by means of valve 2 (fig. 2). For both qualitative and quantitative tests, the flow rate has been maintained at the constant value of 5 ml/min since the response speed of the detector is high.[6] 0.2 ml of the 10^{-2} M test solution (fig. 2) were injected rapidly by means of a common syringe of 5 ml. The rolling speed of the paper was of 400 mm/60 min. The working sensitivity may be chosen at will.

RESULTS

Qualitative tests. The types of signals obtained for the detector with a 25 μ 1 volume, are given in fig. 3 (curves a and b).

An estimate of the behaviour of the 25 μl detector for the different tested species, is presented in table 1. In column 2 the type of the

[5] E. Pungor, S. Feher and G. Nagy, *Hung. Sci. Instr.*, **18**, 37 (1970).

[6] T. S. Light and J. L. Swartz, *Analyt. Lett.*, **1**, 825 (1968).

signal obtained is specified, according to the notation used in fig. 3. In column 3 a qualitative measure of the universality of the detector is given, as the ratio of the maximum height of the signal of the tested species, and of the signal for Ag^+ under the same experimental conditions.

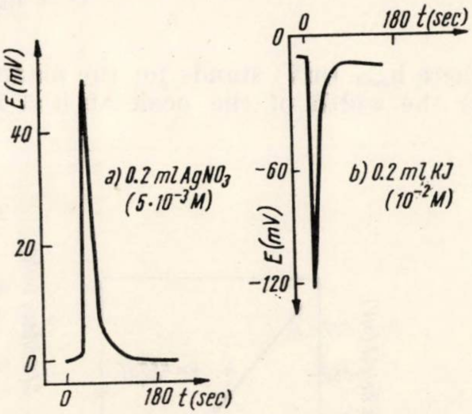

Fig. 3. – Detector responses : a) for Ag^+ ; b) for $X^-(J^-)$.

Table 1

The calitative estimate of the behaviour of the 25μl detector for different species.

Chemical species	Type of signal	The maximum heights ratio of signals (X, 10^{-2} M/Ag^+, 10^{-2}M) (mV)
H^+	a	7/150
NH_4^+	a	—
Cu^{2+}	a	22/150
Hg^{2+}	a	97/150
NH_3	b	2/150
Cl^-	b	6/150
Br^-	b	9/150
J^-	b	30/150
SCN^-	b	11/150
$CH_3CO_2^-$	b	1/150
CO_3^{2-}	b	0.8/150
CrO_4^{2-}	b	6/150
SO_4^{2-}	b	0.7/150
$S_2O_3^{2-}$	b	16/150
$C_2H_4(NH_2)_2$	b	12/150
Phenylalanine	b	—

Quantitative tests. In order to verify the possibility of using this device for the determination of the concentration of solutions in flowing conditions, a calibration curve was plotted for Ag^+, in the case of the 450 μl detector (fig. 4, 5) as well as in the case of the 25 μl detector (figs. 6, 7). The peak area (S) was calculated in both cases (figs. 5, 7) by means of the relation [7]:

$$S = h_{max} \cdot a_{1/2} \qquad (1)$$

where h_{max} (mV) stands for the maximum height of the peak, $a_{1/2}$ (mm) for the width of the peak at $h = 1/2\ h_{max}$.

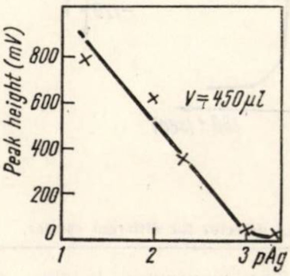

Fig. 4. — Plotting of the peak height *versus* pAg^+ for the 450 µl detector.

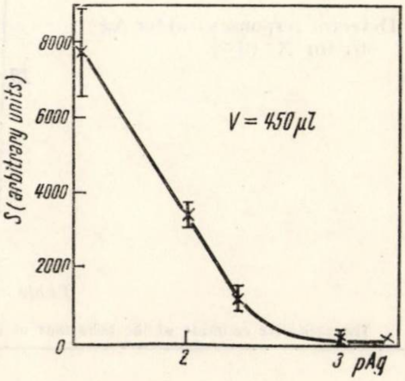

Fig. 5. — Plotting of the peak area (S) *versus* pAg^+ for the 450 µl detector.

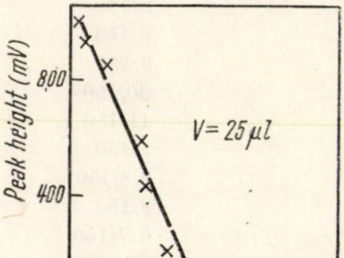

Fig. 6. — Plotting of the peak height *versus* pAg^+ for the 25 µl detector.

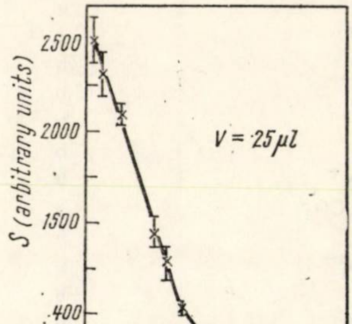

Fig. 7. — Plotting of the peak area (S) *versus* pAg^+ for the 25 µl detector.

---

[7] B. A. RUDENKO, *Zhur. analit. Khim.*, **23**, 341 (1968).

DISCUSSION

The Ag_2S ceramic ISME proved to be Ag^+ selective.[1,2] Therefore it would result that a detector constructed on this basis has a restricted field of application. This would however mean to give an absolute meaning to the concept of ISME selectivity, a mistake pointed out recently by Durst.[8] The data of our qualitative tests point towards the same result, as they show the possibility to detect, to a smaller or greater extent, all the chemical species, which are able to react with Ag^+ and S^{2-} ions.

By comparing figures 5 and 7 it results first that the sensitivity of the detector increases as its volume decreases, which is an easily accountable fact. On the other hand, it seems strange, that the peak area depends on the volume of the detector. Presumably, this is due to the different hydrodynamic conditions in the two measuring cells.

This device can be used either for the determination of the concentration of solutions under flow conditions or in liquid phase chromatography, as a detector. In the first case the ionic strength does not lead to any further complications. In the second case, both the ionic strength and the possibility of irreversibly affecting the active surface of the detector, operate as limiting factors. In both cases, the high electric resistance of the device requires the use of a recording potentiometer with high input impedance.

The remarkable simplicity, the good mechanical resistance, the very low basic noise and the satisfactory reproducibility are all positive characteristics of this device.

In conclusion, based on our experimental data, we may state that the device is suitable for the determination of the concentration of solutions under flow conditions as well as in liquid phase chromatography as a chromatographic detector.

[8] R. A. Durst (ed.), "Ion Selective Electrodes", National Bureau of Standards, Spec. Publ., No. 314, Washington, 1969, p. V.

DISCUSSION

The Ag_2S sensitive ISE proved to be Ag^+ selective.[14] Therefore it would result that a detector constructed on this basis has a restricted field of application. This would however mean to give an absolute meaning to the concept of ISE selectivity, a mistake pointed out recently by [illegible].[5] The [illegible] [illegible] [illegible] [illegible] [illegible] that results, [illegible] the possibilities (however, in particular greater extent) all the chemical species, which are able to react with Ag^+ and S^{2-} ions.

By comparing figures 6 and 7 it results first that the sensitivity of the detector increases as [illegible] decreases, which is an easily accountable fact. On the other hand it seems strange, that the peak area depends on the volume of the detector. Presumably, this is due to the different hydrodynamic conditions in the two measuring cells.

This device can be used either for the determination of the concentration of solutions under flow conditions or in liquid phase chromatography, as a detector. In the first case [illegible] it does not lead to any further complications. In the second case, both the [illegible] and the possibility of irreversibly affecting the active surface of the detector, operate as limiting factors. In both cases, the high electric resistance of the device requires the use of a recording potentiometer with high input impedance.

The remarkable simplicity, the good mechanical resistance, the very low base noise and the satisfactory reproducibility are all positive characteristics of this device.

In conclusion, based on our experimental data, we may state that the device is suitable for the determination of the concentration of solutions under flow conditions as well as in liquid phase chromatography as a chromatographic detector.

[illegible]

Revue Roumaine de Chimie, 17, 9, 1621–1627 (1972)

MÉTHODES DE DÉTERMINATION DE LA VITAMINE B_1 (CHLORHYDRATE DE THIAMINE OU ANEURINE) CARACTÉRISTIQUES SPECTRALES EN VISIBLE ET INFRAROUGE DU PRODUIT OBTENU

GRIGORE TEODORESCU

Institut Polytechnique de Bucarest, Chaire de Chimie inorganique et analytique,
Bucarest, 1, str. Polizu

Reçu le 21 février 1972

On présente des méthodes de détermination de la Vitamine B_1, basées sur sa combinaison avec le reineckate d'ammonium, la dissolution du composé obtenu dans l'acétone, suivie de la précipitation de l'anion reineckate comme reineckate d'argent et titrage de l'excès d'azotate d'argent avec du thiocyanate d'ammonium. Vu que le composé formé est soluble en acétone, résultant une solution colcrée, le composé a été déterminé aussi colorimétriquement. La structure du complexe obtenu a été précisée par détermination de la masse moléculaire, à l'aide des spectres en visible, pour le reineckate d'ammonium et le reineckate de vitamine B_1. La structure du reineckate de VB_1 a été caractérisée aussi par spectre en IR de la vitamine B_1 (VB_1) et de son composé.

La Vitamine B_1 ou le chlorhydrate du chlorure de 3–(4-amino-2-méthylepyrimidyl-5-méthyl)-4-méthyl-5-β-hydroxy-éthyl-thiazole est, comme on sait, la vitamine conditionnant le fonctionnement normal du système nerveux, qui joue un rôle essentiel dans le métabolisme des hydrates de carbone, son absence pouvant déterminer le fonctionnement anormal du système cardio-vasculaire.

La pureté de la vitamine B_1 s'établit usuellement par la détermination de l'acide chlorhydrique existant sous forme de chlorhydrate ou par la détermination du chlore total. Ces méthodes sont indiquées spécialement pour les produits d'une pureté avancée (98%).

PRINCIPE DE LA MÉTHODE

La vitamine B_1 contient deux positions cationisées : une au noyau thiazolique (sel quaternaire de thiazoline) et l'autre au groupement amino de la pyrimidine (comme ion *onium* sous forme de chlorhydrate). Etant donné la structure, nous avons considéré indiquée la méthode de détermination de la pureté de la vitamine par la combinaison des deux positions cationisantes avec le reineckate d'ammonium $NH_4[Cr(NCS)_4(NH_3)_2]$, abrégé $Rc^-NH_4^+$, réactif utilisé par nous à la détermination d'autres produits.[1-14]

Conformément à la structure, la combinaison a lieu avec 2 moles de $Rc^-NH_4^+$, même dans une solution non acidulée, selon le schéma suivant :

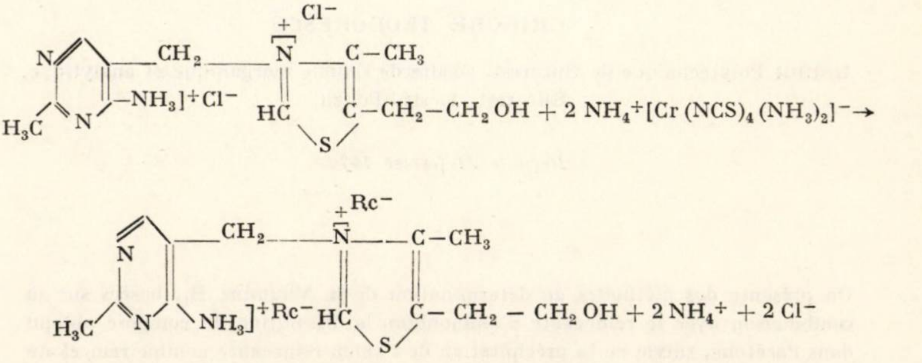
Cl⁻
N
CH₂
C−CH₃
NH₃]⁺Cl⁻
HC
C−CH₂−CH₂OH + 2 NH₄⁺[Cr(NCS)₄(NH₃)₂]⁻→
H₃C
S
Rc⁻
NH₃]⁺Rc⁻
C−CH₂ − CH₂OH + 2 NH₄⁺ + 2 Cl⁻

La réaction de combinaison a été utilisée à la détermination de la VB_1 par les méthodes volumétrique, colorimétrique et spectrale.

1. MÉTHODE VOLUMÉTRIQUE

On précipite la solution aqueuse de vitamine B_1 avec une solution de $Rc^-NH_4^+$ 2% conc., selon l'équation ci-dessus.

Le précipité formé est filtré, lavé et ensuite dissout en acétone.

La solution résultée est traitée par excès de solution d'azotate d'argent 0,1 n. Ainsi le reineckate d'argent précipite conformément à la réaction :

$$[Cr(NCS)_4(NH_3)_2] + Ag^+ \rightarrow Ag[Cr(NCS)_4(NH_3)_2]$$

---

[1] P. Spacu et Gr. Teodorescu, *Rev. Chim. București*, **8** (1), 41 (1957).
[2] Gr. Teodorescu et A. Dinescu, *Bul. Inst. Politeh. Bucureşti*, **26**, (1), 49 (1964).
[3] Gr. Teodorescu et Il. Niculescu, *Bul. Inst. Politeh. Bucureşti*, **29** (1), 43 (1967).
[4] Gr. Teodorescu et Il. Niculescu, *Bul. Inst. Polit. Bucureşti*, **29** (4), 43 (1967).
[5] Gr. Teodorescu, *Bul. Inst. Polit. Bucureşti*, **29** (5), 83 (1967).
[6] Gr. Teodorescu, *Bul. Inst. Polit. Bucureşti*, **29** (6) 55 (1967).
[7] Gr. Teodorescu et Il. Niculescu, *Bul. Inst. Polit. Bucureşti*, **30** (1), 17 (1968).
[8] Gr. Teodorescu, *Bul. Inst. Polit. Bucureşti*, **31** (3), 51 (1969).
[9] Gr. Teodorescu, *Bul. Inst. Polit. Bucureşti*, **31** (4), 45 (1969).
[10] Gr. Teodorescu, *Bul. Inst. Polit. Bucureşti*, **31** (5), 61 (1969).
[11] Gr. Teodorescu et A. Dinescu, *Rev. Chim. (Bucureşti)*, **20**, 727 (1969).
[12] Gr. Teodorescu, *Bul. Inst. Polit. Bucureşti*, **32**, (2), 39 (1970).
[13] Gr. Teodorescu, *Bul. Inst. Polit. Bucureşti*, **32**, (4), 79 (1970).
[14] Gr. Teodorescu, *Bul. Inst. Polit. Bucureşti*, **33**, (1), 67 (1971).

Après filtrage et lavage, l'excès d'azotate d'argent est titré par du thiocyanate d'ammonium en présence de l'alun de fer (II) et d'ammonium.

1.1. *La pratique*

On prend 12 ml de solution de vitamine B_1 avec 0,05 g per 1 ml (totalement 0,6 g de substance) et leur contenu est entraîné quantitativement au balon jaugé à 250 ml avec de l'eau distillée bouillie et refroidie (0,0024 g vitamine B_1 per 1 ml).

A chaque épreuve de 5–16 ml prélevé de la solution obtenue, on ajoute 20 ml d'eau distillée bouillie et refroidie et après, goutte à goutte, sous agitation continuelle, la solution fraîchement préparée de $Rc^- \ NH_4^+$ 2% (25–30 ml). Il précipite le composé cristallin nâcré rose-violet.

Le composé formé est filtré sur un creuset à filtre G_3 entraîné par une solution de $Rc^-NH_4^+$ 0,1% et ensuite lavé 2–3 fois à 4 ml d'eau distillée froide (5°C) et 2 fois à 10 ml d'éther, quand la solution passe incolore.

On dissout directement sur le creuset à filtre le composé avec 20–30 ml d'acétone à 3 reprises, jusqu'à dissolution totale. On lave finalement le creuset à 20–30 ml d'eau distillée et on prend la solution et les eaux de lavage, dans un verre de 250 ml.

On ajoute 100 ml d'eau distillée, 20 ml d'azotate d'argent 0,1 n et 2 gouttes d'acide azotique 2 n.

Le précipité de reineckate d'argent formé est filtré, lavé par décantage à l'eau distillée et le filtrat et les eaux de lavage mis dans un flacon de 750 ml. On ajoute 3–4 ml de solution saturée d'alun de fer (III) et d'ammonium (environ 40 %), 3–4 gouttes d'acide azotique 2 n et on titre l'excès d'azotage d'argent par thiocyanate d'ammonium 0,1 n au facteur connu.

Un ml d'azotate d'argent correspond à 0,01686 g de vitamine B_1 (le chlorhydrate du chlorure sans eau de cristallisation correspondant à une masse moléculaire de $G_m = 337,2$).

Les résultats obtenus sont rapportés au tableau 1.

Tableau 1

Détermination volumétrique de la vitamine B_1 (VB_1)

Solution VB_1 pour analyse	VB_1 épreuve	$AgNO_3$ ajoutée à la précipitation Fo, ln = = 1,0000	NH_4SCN utilisé Fo,ln = = 1,0840	$AgNO_3$ ayant subi la réaction	VB_1 dans l'épreuve déterminée avec du $Rc^- \ NH_4^+$	VB_1 100% dans l'épreuve
ml	g	ml	ml	ml	g	%
5	0,0120	20	19,20	0,71	0,0120	100
6	0,0144	20	19,15	0,85	0,0143	99,58
7	0,0168	20	19,00	1,00	0,0168	100
8	0,0192	20	18,86	1,14	0,0192	100
9	0,0216	20	18,72	1,28	0,0215	99,86
10	0,0240	20	18,58	1,42	0,0239	99,75
11	0,0264	20	18,44	1,56	0,0263	99,62
12	0,0288	20	18,30	1,70	0,0286	99,51
14	0,0336	20	18,02	1,98	0,0333	99,85
16	0,0384	20	17,72	2,28	0,0384	100

2. MÉTHODE COLORIMÉTRIQUE

2.1. *Principe de la méthode colorimétrique*

On précipite la VB_1 avec du $Rc^- NH_4^+$ selon le même procédé dans le rapport molaire 1 :2. Vu que le composé formé est soluble en acétone, résultant une solution colorée en rouge, la VB_1 peut être déterminée aussi colorimétriquement.

2.2. *La pratique*

On applique la méthode des courbes étalon. A cette fin on a employé une solution de $Rc^- NH_4^+$ avec $T = 0{,}0560$ g/ml, dont on a pris des volumes correspondants, dans des ballons jaugés de 100 ml, dilués avec 50 ml d'acétone et complétés avec de l'eau distillée, afin d'obtenir des solutions avec des concentrations $T = 0{,}00028$; 0,000560 ; 0,000840 ; 0,00120. Les déterminations ont été faites à l'aide du photocolorimètre de type B. Lange, en utilisant des filtres verts ($\lambda = 533$ nm) et on a tracé la courbe étalon.

De la solution de VB_1 avec $T = 0{,}00240$ on a prélevé des épreuves entre 0,0144—0,0240 et l'on a précipité avec du $Rc^- NH_4^+$, selon la méthode volumétrique.

Après précipitation, filtrage et lavage, les épreuves ont été quantitativement dissoutes avec de l'acétone, en prenant la solution dans des ballons jaugés à 100 ml. Après l'homogénéisation, les épreuves ont été colorimétrées, les résultats obtenus étant indiqués au tableau 2.

Tableau 2

Résultats du colorimétrage du reineckate de VB_1

VB_1 dans l'épreuve	VB_1 déterminée	Erreur
g	g	%
0,000144	0,000141	−2,07
0,000168	0,000165	−1,81
0,000192	0,000188	−2,12
0,000216	0,000212	−1,89
0,000240	0,000236	−1,69

3. ÉTUDE SPECTRALE

3.1. *Caractérisation du spectre en visible du reineckate de la vitamine B_1*

La structure du composé obtenu est précisée par détermination de sa masse moléculaire, à l'aide de l'absorbance (A) et de l'absorptivité (K).

Une caractéristique commune des spectres en visible du $Rc^- NH_4^+$ et du reineckate de VB_1 réside dans le fait que le maximum d'absorption (λ_{max}) est approximativement le même, $\lambda_{max} = 520-525$ nm (le diagramme au n° 1) pour le $Rc^- NH_4^+$ (dans l'éthanol 95%) et $\lambda_{max} = 530$ nm (le diagramme au n° 2) pour le reineckate de VB_1 (aussi dans l'éthanol 95%).

L'absorptivité (K) a été déterminée conformémement à la relation suivante, sur le $Rc^{-}NH_4^{+}$, dans de l'éthanol 95% à la concentration $c = 0{,}00297$ mole gramme de $Rc^{-}NH_4^{+}$, à une longueur de la courbe $l = 0{,}5$ cm et pour l'absorbance (A) résultée du diagramme (1) et correspondant à la valeur maximale $\lambda_{max} = 520-525$ nm. Etant donné que l'on a travaillé avec $l = 0{,}5$ cm, pour $l = 1$ cm, la valeur (A) devient double

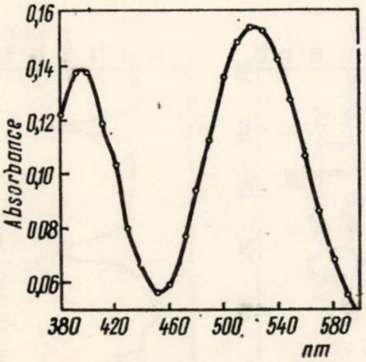

Fig. 1. — Le diagramme d'absorption en visible pour le reineckate d'ammonium.

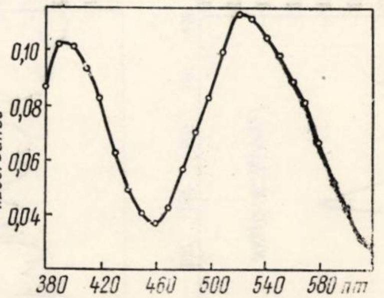

Fig. 2. — Le diagramme d'absorption en visible pour le reineckate de vitamine B_1.

$$K_{\text{éthanol}} = 2 \times 0{,}154/0{,}00297 = 103{,}7$$

La valeur K déterminée pour le $Rc^{-}NH_4^{+}$ peut être considérée, dans les limites des erreurs acceptables, comme étant valable aussi pour le reineckate de VB_1, étant donné que λ_{max} pour le reineckate de VB_1 est égal (ou presque égal) à λ_{max} pour le reineckate (les diagrammes 1 et 2).

La masse moléculaire (M_d) est déterminée selon la relation :

$$M_d = g_1/100 \cdot K/A \cdot l \cdot 1000 \qquad (1)$$

Pour le cas $g_1 = 0{,}1$ g de reineckate de VB_1 per 100 ml solution et $l = 1$ cm, la relation (1) devient :

$$M_d = K/A \qquad (2)$$

Pratiquement, la détermination de l'absorption en visible du reineckate de VB_1 est faite dans de l'éthanol 95%. L'absorbance pour $\lambda_{max} = 530$ nm à la concentration de 0,1% et à une cuve avec $l = 1$ cm (dans les mêmes conditions de travail) est de 0,115. En remplaçant la

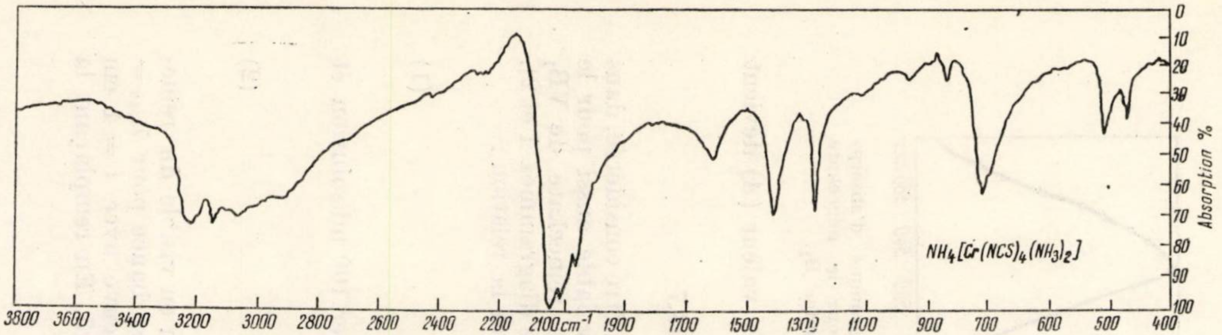

Fig. 3. — Le spectre en IR du reineckate d'ammonium.

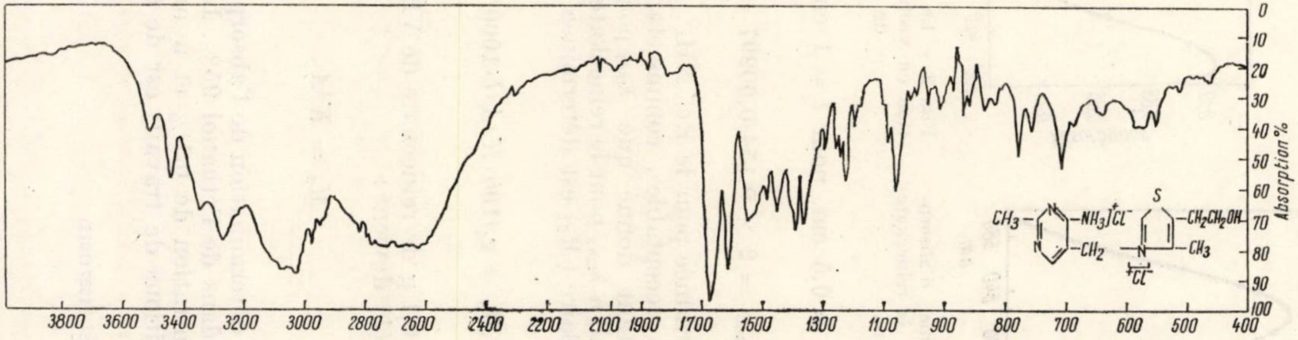

Fig. 4. — Le spectre en IR de la vitamine B_1.

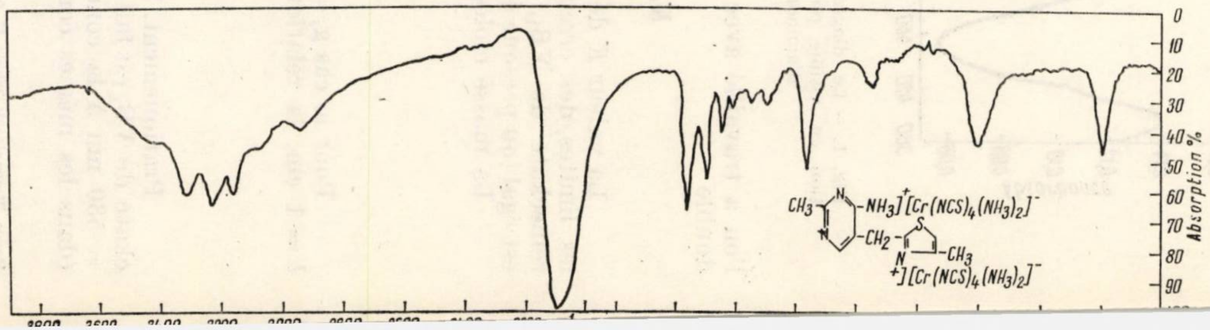

Fig. 5. — Le spectre en IR du

relation (2) on obtient :

$$M_d = K/A = 103,7/0,115 = 901,74$$

La comparaison de cette valeur à celle de la masse moléculaire résultée du calcul $M_c = 902,93$ révèle qu'elles sont assez proches, ce qui démontre l'existence d'un direineckate. Le monoreineckate ayant un $M_c = 584,57$ est nettement différent de la valeur obtenue pour la M_d, ce qui est d'ailleurs normal étant donné que la VB_1 existe sous forme de dichlorhydrate, donc avec deux atomes d'azote cationisés.

3.2. *Caractérisation en infrarouge du reineckate de VB_1*

Le reineckate de VB_1 a été structuralement caractérisé aussi par spectre en infrarouge, que l'on a interprété par comparaison avec le spectre du $Rc^- NH_4^+$ (fig. 3).

Le spectre en IR du composé présente des bandes pouvant être attribuées aux groupements NH_3 et NCS de l'anion reineckate du complexe, retrouvées aussi dans le spectre en IR du reineckate d'ammonium. Elles apparaissent à 497 cm^{-1} $\left(\delta\,NCS\right)$, 1265 cm^{-1} $\left(\delta^{sym}_{\substack{NH_3\\N-H}}\right)$, 2090 cm^{-1} (ν_{C-N}), 3235—3310 cm^{-1} $\left(\nu^{sym}_{\substack{NH_3\\N-H}}\right)$.

Le spectre présente aussi des bandes correspondant à la base organique (fig. 4). Ces bandes, existant à 705 cm^{-1}, 1395 cm^{-1}, 1600 cm^{-1} sont très peu modifiées comme position et intensité dans le spectre en IR du composé étudié (fig. 5).

Revue Roumaine de Chimie, 17, 9, 1629–1633 (1972)

CHARACTERIZATION OF CERAMIC ION-SELECTIVE MEMBRANE ELECTRODES. II. REDOX BEHAVIOUR OF THE Ag_2S MEMBRANE-ELECTRODE

I. C. POPESCU and C. LITEANU
Division of Analytical Chemistry, Babeş-Bolyai University
Str. Arany Janos 11, Cluj, Romania

Received March 3, 1972

New experimental results which prove the existence of a redox behaviour for the Ag_2S ceramic membrane electrode are presented. The working mechanism of the electrode in this case relies on the electronic conductibility of Ag_2S. This electrode can be used with good results in common redox potentiometric titrations but leads to positive errors in automatic redox potentiometric titrations.

The attempts to obtain redox electrodes from more easily available materials than the noble metals (platinum, gold, etc.) and having the same electrochemical qualities, are well known. Among these, studies devoted to redox membrane electrodes occupy a special place. Indeed, by making use of the peculiar techniques for working out membrane electrodes, we can redox test the most different materials, which is by far more difficult in other conditions.

This in principle amounts to the manufacturing of a membrane of the tested substance, separate or in a mixture, a membrane that will be later used to form an electrode. Glass membranes with a variable Fe(II) and Fe(III)[1–9] oxide content, heterogeneous membranes of silicone

---

Part I: C. Liteanu, I. C. Popescu and V. Ciovîrnache, *Talanta*, **19**, 985 (1972)

[1] F. A. Belinskaia and E. A. Materova, *Vestnik Leningrad Univ., ser. Fiz. i Khim.*, **16**, 35 (1957).

[2] O. V. Mazurin, G. A. Pavlova, E. A. Lev and E. K. Leko, *Zhur. tehnk. Fiz.*, **27**, 2704 (1957).

[3] V. V. Barghin and E. A. Antonova, *Tr. Leningr. Tekhnolog. Inst.*, **49**, 55 (1958).

[4] A. A. Beliustin, A. N. Pisarevski, M. M. Mulitz and B. B. Nikolski, *Doklady Akad. Nauk S.S.S.R.*, **154**, 404 (1964).

[5] A. A. Beliustin and A. M. Pisarevski, *Zhur. fiz. Khim.*, **38**, 2913 (1964).

[6] A. A. Beliustin and S. E. Volkov, *Elektrokhimiya*, **3**, 884 (1967).

[7] G. S. Bagdasarova, A. Beliustin, A. M. Pisarevski and M. M. Shultz, *Elektrokhimiya*, **4**, 1239 (1968).

[8] G. S. Bagdasarova, A. A. Beliustin, A. M. Pisarevski, *Elektrokhimiya*, **4**, 1328 (1968).

[9] A. M. Pisarevski, M. M. Schultz, B. P. Nikolski and A. A. Beliustin, *Doklady Akad. Nauk S.S.S.R.*, **187**, 364 (1969).

graphite rubber[10-14] or of epoxidic resins with copper sulphide[15] as well as a membrane of vanadium oxide,[15] were thus examined. All these proved to be able to follow the variations of the redox potential of the adjacent solutions.

For the above materials this feature is the consequence, either of a marked electronic conductivity (graphite, CuS, V_2O_5), or of the presence in the structure of the respective material of a two-valency element (redox glass). It is thus known that Ag_2S presents a noticeable electronic conductivity.[16] This fact enables us to notice that the membrane-electrode of silicone rubber impregnated with Ag_2S could be used for redox measurements.[17]

Certain results proving the existence of a specific redox behaviour of the Ag_2S ceramic membrane-electrode[18] are given below.

EXPERIMENTAL. RESULTS

The Ag_2S membrane-electrode used is shown in figure 1.

A polished platinum electrode (plate : 0.5 cm × 1 cm) was used for comparison.

To estimate the redox electrode function of the Ag_2S membrane-electrode one has measured the e.m.f. (E) of the cells :

(−) | SCE Test solution. | Membrane-electrode (+) (1)

(−) | SCE Test solution, | Pt (+) (2)

by means of a (M.V. 11) electronic potentiometer. The test solution was stirred magnetically. The working temperature was 25° ± 0.1°.

In figure 2 are given the results of the e.m.f. measurements of cells (1) and (2) in $E - \lg \frac{[ox]}{[red]}$ coordinates, for the $Fe(NH_4)_2(SO_4)_2/$ $/Fe_2(SO_4)_3$ redox system, for pH = 0. The total concentration is 0.1 N.

Figures 3—5 give the results of the $E - \log \frac{[ox]}{[red]}$ measurements obtained by measuring the e.m.f. of cells (1) and (2) for the redox system $K_3Fe(CN)_6/K_4Fe(CN)_6$, at pH = 3.30 (fig. 5), pH = 6.20 (fig. 4) and pH = 9.00 (fig. 5). In every case the total concentration was 0.1 N.

---

[10] J. Havas, "The Applications of Ion Selective Membrane Electrodes", Radelkis Electrochemical Laboratory, Budapest, p. VI.

[11] E. Pungor, E. Szepesváry and J. Havas, *Analyt. Lett.*, **1**, 213 (1968).

[12] E. Pungor and E. Szepesváry, *Analyt. Chim. Acta*, **43**, 289 (1968).

[13] F. Farsang, *Hung. Sci. Instr.*, **12**, 22 (1968).

[14] E. Pungor, S. Feher and G. Nagy, *Hung. Sci. Instr.*, **18**, 37 (1970).

[15] I. I. Savin, V. S. Starman, O. A. Zemskaia, A. Ia. Syrchenkov and A. V. Gordievskii, *Zhur. analit. Khim.*, **26**, 1281 (1971).

[16] P. Pascal, "Nouveau Traité de Chimie Minérale", Masson, Paris 1957, vol. VIII, pag. 566.

[17] A. Wesser and E. Pungor, *Acta Chim. Acad. Sci. Hung.*, **64**, 311 (1970).

[18] C. Liteanu, I. C. Popescu and V. Ciovîrnache, *Talanta*, **19**, 985 (1972).

[19] C. Liteanu, ,,Chimie Analitică Cantitativă", Ed. Did. Ped., 5th. ed., Bucharest, 1969, p. 682.

Based on these measurements we have carried out the potentiometric titration of some 0.1 N solutions of Mohr salt with $K_2Cr_2O_7$ 0.1 N, NH_4VO_3 0.1 N, $Ce(SO_4)_2$ 0.1 N and with $KMnO_4$ 0.1 N, at pH = 0, using as indicator electrode the Ag_2S membrane electrode. The results obtained are given in figure 6.

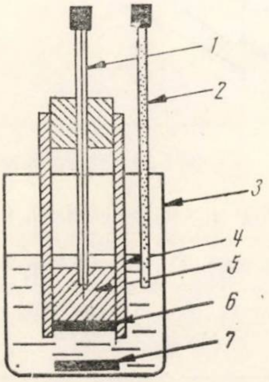

Fig. 1. — Ag_2S membrane electrode; *1*, Pt wire electrode; *2*, SCE; *3*, working cell; *4*, electrode body; *5*, Hg; *6*, Ag_2S membrane.

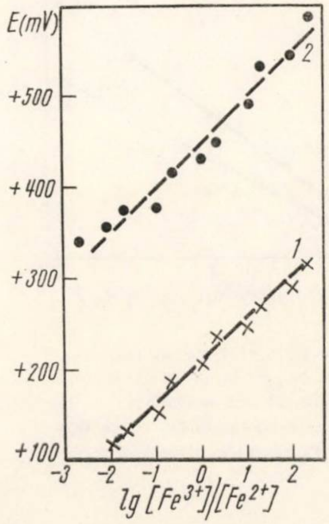

Fig. 2. — Redox electrode function for Fe^{2+}/Fe^{3+} couple, at pH = 0.
1, Ag_2S membrane electrode (slope 47.5 mV); 2, Pt electrode (slope 55.5 mV).

To determine the working readiness of the membrane electrode as redox indicator electrode a series of derivate redox, potentiometric titrations have been carried out with automatic continuous addition of the titrant.

A 5 ml solution of 0.1 N Mohr salt with $K_2Cr_2O_7$ 0.1 N at pH = 0 was titrated. The additional flow capacity of the titrant was of about 6 ml/per minute. The results of the titrations are given on table 1, *versus* those with a bright platinum electrode.

DISCUSSIONS

The measurements carried out actually show that the Ag_2S membrane electrode has noticeable sensitive redox electrode qualities. Thus, on an average, the value of the electrode function slope reaches 65—70% of the theoretical one, for the redox systems used. Moreover, in the equimolecular solutions of $K_3Fe(CN)_6 - K_4Fe(CN)_2$ of different pH, the electrode gives the same potential value (163 ± 15 mV, SCE).

This means that the apparent normal potential of the respective redox system does not depend on the pH, a well-known and ascertained fact for the platinum electrode (210 ± 5 mV, SCE).

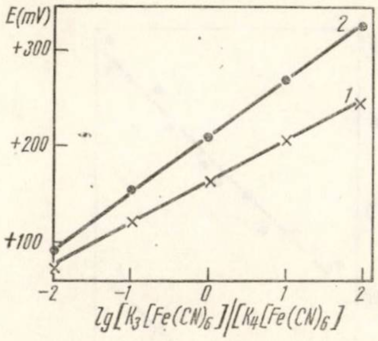

Fig. 3.—Redox electrode function for $[Fe(CN)_6]^{4-}/[Fe(CN)_6]^{3-}$ couple, at pH = 3.30; *1*, Ag_2S membrane-electrode (slope 43.6 mV); *2*, Pt electrode (slope 57.2 mV).

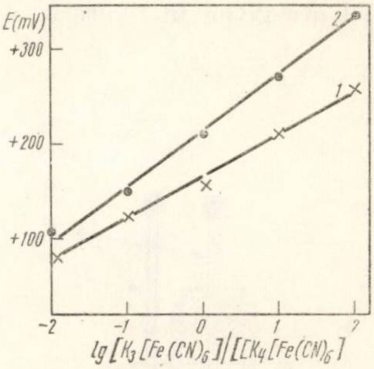

Fig. 4.—Redox electrode function for the $[Fe(CN)_6]^{4-}/[Fe(CN)_6]^{3-}$ couple at pH = 6.20. *1*, Ag_2S membrane-electrode (slope 34.5 mV); *2*, Pt electrode (slope 58.5 mV).

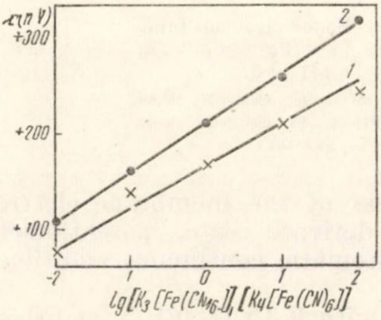

Fig. 5.—Redox electrode function for the $[Fe(CN_6)]^{4-}/[Fe(CN)_6]^{3-}$ couple at pH=9.00; *1*, Ag_2S membrane-electrode (slope 43.6 mV); *2*, Pt electrode (slope 50.0 mV].

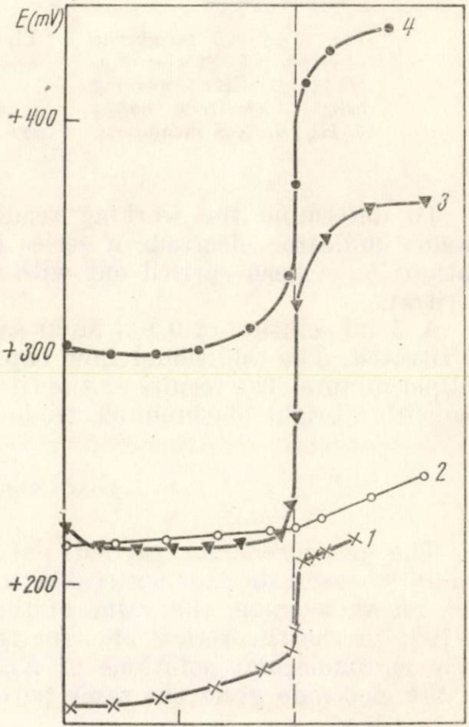

Fig. 6. — Potentiometric titrations of 0.1 N Fe^{2+} with: *1*, 0.1 N $K_2Cr_2O_7$; *2*, 0.1 N NH_4VO_3; *3*, 0.1 N $CeSO_4$; *4*, 0.1 N $KMnO_4$, at pH = 0 using as indicator electrode the Ag_2S membrane electrode.

The fact that the value of the redox electrode function slope of the membrane electrode does not depend significantly on the pH, confirms the hypothesis that, in this case, the functioning of the electrode is based on an electronic mechanism. If the redox sensitivity would be the consequence of a redox reaction to which the sulphide ion participates, one would find a strong dependency of the electrode function on the pH, because this stems from a weak acid.

Table 1

Utilization of the Ag_2S membrane electrode and the bright Pt electrode in the redox automatic titration of Fe^{2+} with $Cr_2O_7^{2-}$

No.	Ag_2S indicator electrode	Pt indicator electrode
	V_e (ml)	V_e (ml)
1	5.30	5.00
2	5.20	4.90
3	5.30	5.00
4	5.10	5.00
5	5.30	5.00
$\overline{V}_e \pm s_{\overline{V}_e} \cdot t_{\alpha,k}$*	$5.24 \pm 3.53 \times 10^{-2}$	$4.98 \pm 5.60 \times 10^{-2}$

$e(\%) = +5.20$

*k = 4
$\alpha = 0.95$

Thus, according to its quality of mixed conductor (ionic and electronic), the silver sulphide offers the possibility of following with satisfactory precision the variations of the redox potential of the adjacent solutions . This is confirmed by the redox potentiometric titrations carried out. The potential leap at equivalence is lesser than the potential leap of a platinum electrode, but it is also reproducible, accurate, and increases as the oxidant used as titrating agent is more energetic (fig. 6). We must point out that this electrode leads to optimum results only when used for the titration of the reductors. This is of course a consequence of the reductor character of silver sulphide.

The response rate of the Ag_2S membrane electrode, tested during the automatic titrations proves to be less than that of the platinum electrode, a fact marked by the positive titration errors in the table.

To conclude, the Ag_2S membrane electrode, presents an incompletely developed redox behaviour, owing to the electronic conductivity of Ag_2S and not to a chemical interference.

NOTE POUR LES AUTEURS

La *Revue Roumaine de Chimie* publie des articles en anglais, français, russe, allemand ou espagnol. Les auteurs sont priés d'envoyer des articles, notes, communications et comptes rendus inédits.

Les manuscrits seront dactylographiés à deux intervalles. Les tableaux seront dactylographiés sur feuilles séparées, de même que la légende des figures. Les diagrammes seront tracés à l'encre de Chine sur papier calque. Les tableaux et les figures seront numérotés par des chiffres arabes, en nombre strictement nécessaire. Prière de ne pas inscrire les mêmes données dans les tableaux et les figures. Les formules chimiques seront incluses dans le texte; en outre, elles seront transcrites sur des feuilles séparées. Les auteurs sont priés d'indiquer les caractères italiques (en soulignant les lettres au crayon), ainsi que tout autre caractère spécial. L'ordre des références bibliographiques sera celui de leur mention dans le texte; le nom de l'auteur sera précédé de l'initiale du prénom; les publications périodiques seront présentées suivant les prescriptions internationales. Les références seront ajoutées à la fin de l'article; elles paraîtront comme des notes, au bas de la page. Le texte sera précédé d'un résumé, comprenant 15 lignes au maximum.

L'entière responsabilité du contenu des articles appartient aux auteurs. On publie des articles dus aux collaborateurs roumains ou étrangers. Les auteurs recevront 50 tirés à part.

PRINTED IN ROMANIA

1972 .DEC 2 9

TRAVAUX PARUS AUX ÉDITIONS DE L'ACADÉMIE DE LA RÉPUBLIQUE SOCIALISTE DE ROUMANIE

P. BALTĂ et E. BALTĂ, **Introducere în chimia fizică a stării vitroase** (Introduction à la chimie physique de l'état vitreux), 1971, 240 p., 15,50 lei.

LYDIA-MARIA VAICUM, **Biodegrabilitatea detergenților** (Biodégrabilité des détergents), 1971, 254 p., 16 lei.

TIBERIU NĂSCUȚIU, **Metode radiometrice de analiză** (Méthodes radiométriques d'analyse), 1971, 346 p., 19,50 lei.

I. ZUGRĂVESCU et L. STOICESCU-CRIVETZ, **Polimeri heterociclici** (Polymères hétérocycliques), 1971, 190 p., 9.50 lei.

CRISTOFOR SIMIONESCU, C. V. UGLEA, **Fracționarea compușilor macromoleculari** (Fractionnement des composés macromoléculaires), 1969, 292 p., 18,50 lei.

I. MAXIM, **Materiale nucleare** (Matériaux nucléaires), 1969, 444 p., 30 lei.

CRISTOFOR SIMIONESCU et CLEOPATRA VASILIU-OPREA, **Mecanochimia compușilor macromoleculari** (La mécanochimie des composés macromoléculaires), 1967, 344 p., 23,50 lei.

CORNEL BODEA et collab., **Tratat de biochimie vegetală**, partea I, **Fitochimie** (Traité de biochimie végétale, Ire partie, Phytochimie), Ier vol., 1964, 747 p. + 4 annexes + 2 pl., 41 lei; IIe vol., 1965, 1262 p., 1 pl., 56 lei; IIIe vol., 1967, 773 p., 35 lei.

V. GHEȚIE et V. MICUȘAN, **Analiza imunochimică. Teorie și practică** (Analyse immunochimique. Théorie et pratique), 1966, 369 p., 28 lei.

R. PORTOCALĂ et L. POPA, **Acizii ribonucleici celulari și virali** (Les acides ribonucléiques cellulaires et viraux), 1966, 375 p., 8 pl., 26 lei.

I.P.I. c. 1619

43 426

Lei 25.—

= 1103

REVUE ROUMAINE DE CHIMIE

TOME 17
N° 10
Octobre 1972

RRCHAX, **17**, *10*, 1635– 1788 (1972)

ÉDITIONS DE L'ACADÉMIE DE LA RÉPUBLIQUE SOCIALISTE DE ROUMANIE

Rev. Roumaine Chim. **17**, *10*, 1635–1788 (1972), Bucarest

COMITÉ DE RÉDACTION

Rédacteur en chef:

I. G. MURGULESCU, membre de l'Académie de la République Socialiste de Roumanie

Rédacteurs en chef adjoints:

A. T. BALABAN et V. EM. SAHINI, membres correspondants de l'Académie de la République Socialiste de Roumanie

Collège de redaction:

C. DRĂGULESCU, RALUCA RIPAN, CR. SIMIONESCU, membres de l'Académie de la République Socialiste de Roumanie; EM. BRATU, ECATERINA CIORĂNESCU-NENITZESCU, P. SPACU, membres correspondants de l'Académie de la République Socialiste de Roumanie; MARGARETA AVRAM, D. I. MARCHIDAN, G. NIAC et D. SĂNDULESCU

La *Revue Roumaine de Chimie* paraît 12 fois par an. Toute commande de l'étranger (fascicules ou abonnements) sera adressée à Întreprinderea de comerţ exterior — Rompresfilatelia B. P. 2001, telex 011631, Bucarest, Roumanie

Les manuscrits, les livres et les revues proposés en échange, ainsi que toute correspondance seront envoyés à la rédaction :

REVUE ROUMAINE DE CHIMIE

23, str. Dumbrava Roşie, Bucarest, Roumanie

ÉDITIONS DE L'ACADÉMIE DE LA RÉPUBLIQUE SOCIALISTE DE ROUMANIE,
3 bis, str. Gutenberg, Bucarest

REVUE ROUMAINE DE CHIMIE

Tome 17, N° 10 Octobre 1972

Page

I. G. MURGULESCU and MELANIA BOZEȘANU, Kinetics of the slow oxidation reaction of methane in dynamic system . . . . 1637–1648 R

D. I. MARCHIDAN and LAURA VASU, The heats of melting in the binary mixtures: $AgCl + AgBr$ and $AgNO_3 + NaNO_3$ 1649–1655

D. I. MARCHIDAN and M. CIOPEC, High temperature enthalpy and related thermodynamic functions of non-stoichiometric uranium oxides 1657–1667

RODICA VÎLCU and NICOLAE GEORGESCU, The oxidation of organic bibasic acids in mixtures of fused salts. I. The decarboxylation of oxalic acid in molten alkali metal nitrates . . . . 1669–1677 R

RODICA VÎLCU and ALIN CIOCHINĂ, Measurement of thermal conductivity by the hot-wire method . . . . 1679–1687 R

S. STERNBERG, VALERIA PETRESCU and I. GALASIU, Chlorine adsorption on active carbon in the molten salts system: $LiCl - KCl$, $PbCl_2 - KCl$, $KCl - NaCl$ 1689–1696

S. STERNBERG et I. GALASIU, L'électrode halogène — charbon dans les électrolytes fondus. VII. L'adsorption du brome sur les électrodes de charbon activé . . . . 1697–1704 Bef

LETIȚIA TOPOR and IVONA MOLDOVEANU, Molecular association of the gaseous magnesium, cadmium and zinc chlorides. 1705–1713

Ș. SOLACOLU and MARIA ZAHARESCU, Phase equilibria of the $CaO - TiO_2 - V_2O_5$ system 1715–1721

P. SPACU and G. D. CISMARU, Electrical conductivity of intermetallic compounds of the praseodymium-thallium system 1723–1728

ILEANA ALBESCU, Contributions to the study of lanthanides with biguanide derivates. III. Europium and gadolinium compounds with paludrine . . 1729–1734

ALICE MARIE GLATZ, A. C. RĂZUȘ, F. BADEA and C. D. NENITZESCU, Aluminiumchloride catalyzed condensation of 1,2-dichloro-cyclohexanes with benzene. Isomerisation of diphenyl-cyclohexanes 1735–1745

EDDA BROSER und CORNEL BODEA, Über Phenothiazone. XIX. 4-Amino- und 4-Amino-Halogen-Phenothiazone . . . . 1747–1753 R

VIOLETA NUȚĂ, D. FELDMAN and CR. I. SIMIONESCU, Photocopolymerization of acrylonitrile with methacrylic esters in the presence of anthraquinone dyes . . . . 1755–1764 R

Page

CAMELIA GEORGETA CĂLIN, ECATERINA DIAMANDESCU and LIVIU MIHAI BĂLOIU, Spectrophotometric determination of the dicyanoaurate(I) ion with paranitral green 1765–176

AGNES BLAZSEK-BODÓ and C. LITEANU, The use of the salt effect in acid-base titration performed in organic medium. III. A study regarding the analytical behaviour of aromatic acids in methyl alcohol in the presence of $Ca(NO_3)_2$ 1771–177

A. DRĂGĂNESCU, I. BICĂ, S. ŞERBAN and ANA MARIA PAVLOVSCHI, Gas chromatographic separation of hydrogen, methane, hydrogen sulphide and carbon disulphide mixtures 1779–1781

I. FLOREA, Spectrophotometrical determination of *ortho*-tolidine with sodium hypochlorite 1783–1787

Rev. Roumaine Chim. **17**, *10*, 1635–1788 (1972), Bucarest

Revue Roumaine de Chimie, **17**, *10*, 1637–1648 (1972)

ORSZÁGOS MŰSZAKI KÖNYVTÁR ÉS DOKUMENTÁCIÓS KÖZPONT

KINETICS OF THE SLOW OXIDATION REACTION OF METHANE IN DYNAMIC SYSTEM

I. G. MURGULESCU and MELANIA BOZEȘANU

Center of Physical Chemistry
Str. Galați 31, Bucharest, Romania

Received May 29, 1972

In the present paper we have studied the kinetics of the slow oxidation reaction of methane in a dynamic system, in the temperature range 583.5–730° and at atmospheric pressure. Two mixtures of methane and oxygen have been studied: $2\ CH_4+O_2$ and CH_4+O_2. It was found that under the experimental conditions, the oxidation reaction of methane is of order 1 with respect to methane and of order 2 with respect to oxygen.

Numerous investigations have dealt with the kinetics of the slow oxidation reaction of methane. Significant contributions in the elucidation of the development and mechanism of this reaction are due to Semenov,[1] Lewis and von Elbe,[2] Axford and Norrish,[3] Norrish and Reagh.[4]

Egret, Sochet and Lucquin,[5] Karmilova, Enicolopian and Nalbandian,[6] Poroikova and Nalbandian[7] have recently brought new contributions to the knowledge of the oxidation kinetics of methane.

To improve the formaldehyde yield, the oxidation has been catalysed in homogeneous system with nitrogen oxides,[8] nitric acid,[9] a.s.o.

In investigating the kinetics of this reaction both statical methods,[3–6] and —more recently — dynamical methods[10,11] have been used.

[1] N. N. Semenov, "Țsepnye Reaktsii", Goskhimtehizdat, Moscow, 1934, p. 102.

[2] B. Lewis and G. von Elbe, "Combustion, Flames and Explosions of Gases", Academic Press Inc, New York and London, 1961, p. 90.

[3] D. W. E. Axford and R. G. Norrish, *Proc. Roy. Soc., A*, **192**, 518 (1948).

[4] R. G. W. Norrish and L. D. Reagh, *Proc. Roy. Soc., A*, **176**, 429 (1940).

[5] J. Egret, L. R. Sochet and M. Lucquin, *Bull. Soc. Chim. France*, **1965**, 2205.

[6] L. V. Karmilova, N. S. Enicolopian and A. B. Nalbandian, *Zhur. fiz. Khim.*, **34**, 550, 990, 1177 (1960).

[7] A. I. Poroikova and A. B. Nalbandian, *Kinetika i Kataliz*, **12**, 849 (1971).

[8] L. V. Karmilova, N. S. Enicolopian and A. B. Nalbandian, *Zhur. fiz. Khim.*, **30**, 798 (1956).

[9] A.B. Nalbandian, I. Iosif and A. I. Schneider, *Rev. Roumaine Chim.*, **13**, 671 (1968).

[10] B. Meriaux and M. Lucquin, *Bull. Soc. chim. France*, **1968**, 3581.

[11] B. Meriaux, M. C. Vandevelde and M. Lucquin, *Bull. Soc. chim. France*, **1970**, 3846.

Although there is a great number of works on the kinetics of the oxidation reaction of methane, the mechanism of this reaction cannot be regarded as wholly elucidated. The present research has aimed at a more complete kinetic characterization of this reaction. Since most of previous studies have been made below 600–650°, in big reactors, in the present paper the experimental temperature has been extended until close to the ignition limit (beyond 700°) in order to set up a continuity between the slow oxidation kinetics and that of living oxidation of methane.

EXPERIMENTAL

The experimental determinations have been made in dynamic regime, at atmospheric pressure, in a cilindrical quartz reactor of 28 cm^3 (∅15 mm.), provided with internal sheath, where the thermocuple (chromel-alumel) is introduced in view of temperature measurement. The reactor was placed in a vertical electrical oven with thermoregulator in order to keep a constant temperature during the determination.

Methane and oxygen of 99.9% purity have been used. From the flasks the gases had been previously passed through the silicagel column to retain water traces. Methane is also passed through a KOH grain column, to hold back CO_2 traces.

The gaseous mixture resulted from the reaction was cooled, on leaving the reactor, to −70° (solid CO_2) in two traps, where the reaction products able to condense were thus kept back (H_2CO, CH_3OH, H_2O). The gaseous reaction products were then analysed with a "Carlo Erba" gas chromatograph, type AtC/t.

Methane, oxygen, carbon oxide and hydrogen have been analysed on silicagel column of 1.5 m in length, while the carbon dioxide on a 25% dimetylsulpholan column impregnated on chromosorb of suitable granulation (30–60 mesh).

Column temperature during the determinations: 36°.

The admixture of products to be condensed was, in its turn, analysed on a 25% polyethyleneglicol column, impregnated on chromosorb of the same granulation.

In all analyses, argon has been used as carrier gas.

RESULTS

The following two mixtures of methane and of oxygen have been studied:

$2\,CH_4 + O_2$ – at 612°, 654°, 702.4° and 730°

$CH_4 + O_2$ – at 583.5°, 612° and 654°

Reaction time: 3–30 sec.

At temperatures higher than the experimental limit temperatures (730° and 654°) the selfignition of the reaction mixture occurs and a living combustion regime sets in. Below minimum experimental temperatures (612° and 583.5°) the reaction proceeds with too small a rate for the experimental technique used.

The development of the reaction is given in Figs 1–6.

In figs. 1, 2 we give the concentration diminutions of methane and oxygen expressed in percents, in terms of time, at experiment temperatures, for the 2 $CH_4 + O_2$ mixture.

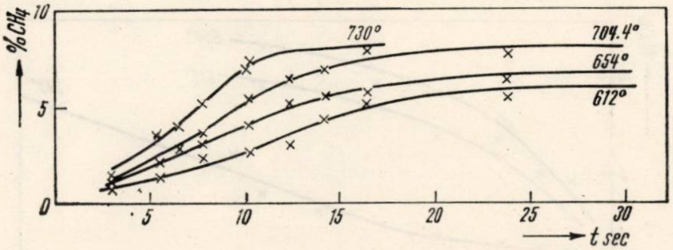

Fig. 1. Concentration diminution of methane for the 2 $CH_4 + O_2$ mixture.

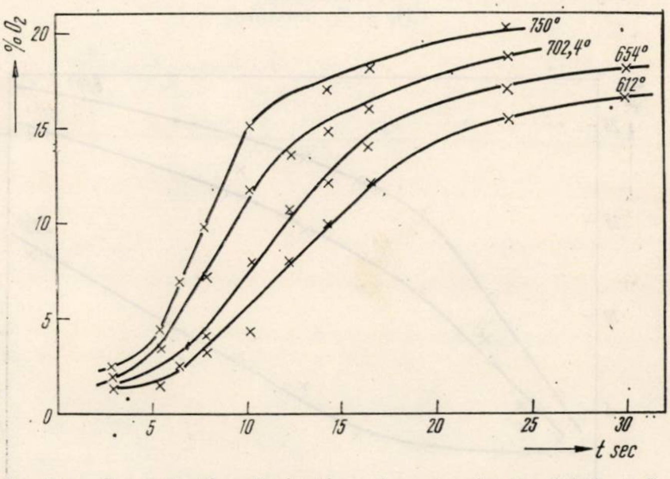

Fig. 2. — Concentration diminution of oxygen for the 2 $CH_4 + O_2$ mixture.

Figures 3, 4 show in the same way the concentration diminutions of the same reactants for the $CH_4 + O_2$ mixture. The shape of the curves of the previous figures (1 and 2) are also roughly found again.

Figures 5 and 6 represent, as a function of time, the cumulation of the gaseous reaction products CO, CO_2, H_2 expressed in percents of the resulting gaseous mixture, for the two CH_4 and O_2 mixtures under investigation.

The last two figures immediately show that the main gaseous reaction product is the carbon oxide. The other two gases CO_2 and H_2, stem from secondary reactions occurring on a small scale.

Figure 7 finally represents the formaldehyde concentration (in moles × 10^{-5}) in the liquid mixture, resulted from an initial mixture made up of 2 $CH_4 + O_2$ for two reaction temperatures (696.5° and 732.2°). The concentration of formaldehyde markedly increases with the reaction temperature.

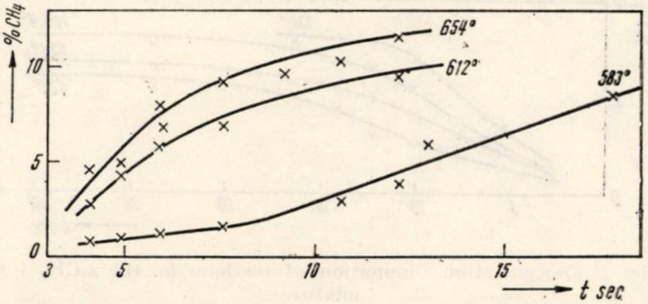

Fig. 3. — Concentration diminution of methane for the $CH_4 + O_2$ mixture.

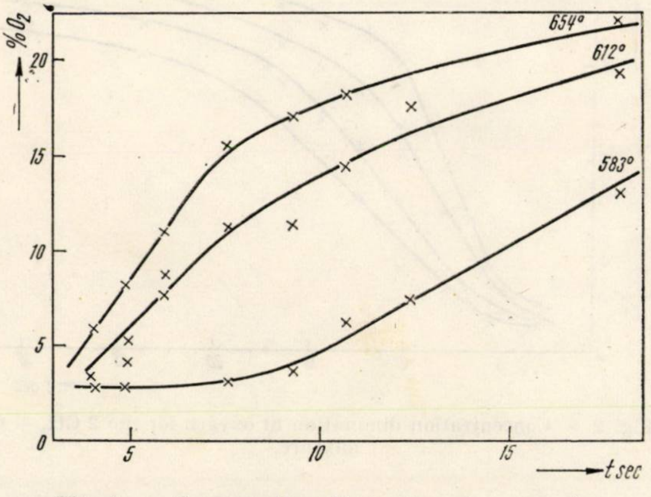

Fig. 4. — Concentration diminution of oxygen for $CH_4 + O_2$ mixture.

DISCUSSION OF RESULTS

The curves in figs. 1—4 have the shape characteristic of chain reactions with degenerated branching. The first portion corresponds to the induction period followed by a portion corresponding to a period of maximum reaction rate and ending by a portion with an almost null rate.

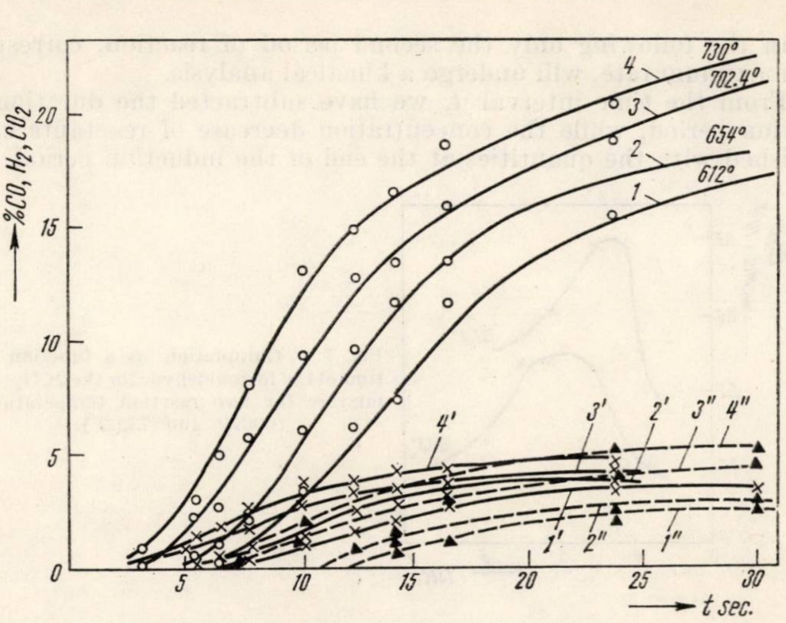

Fig. 5. — Cumulation as a function of time of the gaseous reaction products CO, CO_2, H_2, for the $2CH_4 + O_2$ mixture.
○ —CO(1—4); × —H_2(1′—4′);
▲ —CO_2(1″—4″)

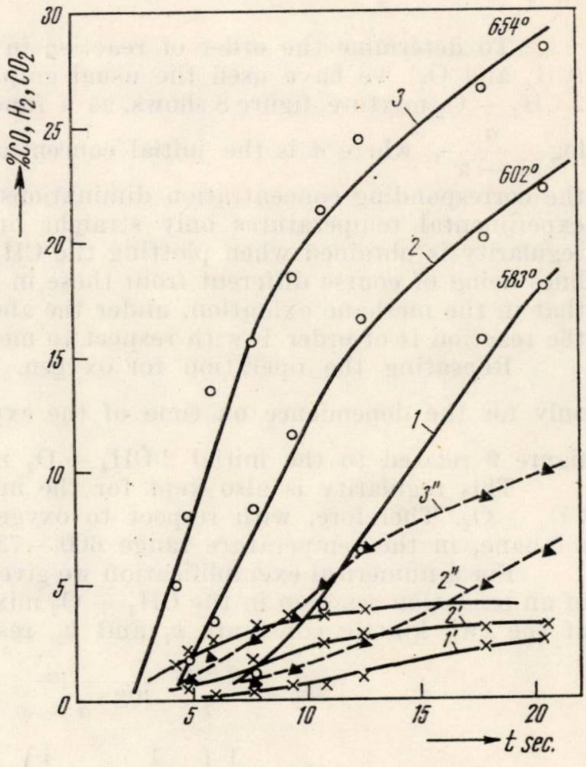

Fig. 6. — Cumulation as a function of time of the gaseous reaction products CO, CO_2, H_2, for the $CH_4 + O_2$ mixture.
○ —CO(1—3); × —H_2(1′—3′);
▲—CO_2(2″—3″)

In the following only the second period of reaction, correspondin to its maximum rate, will undergo a kinetical analysis.

From the time interval t, we have subtracted the duration of th induction period, while the concentration decrease of reactants has bee diminished with the quantities at the end of the induction period.

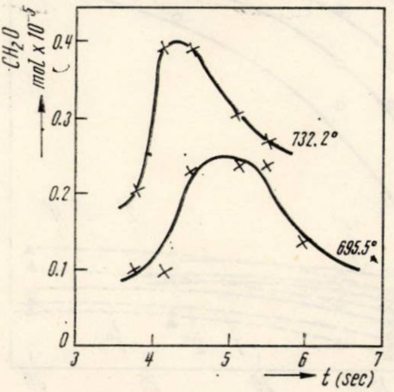

Fig. 7. — Cumulation as a function of time of the formaldehyde for the $2CH_4 + O_2$ mixture for two reaction temperatures (696.5° and 732.2°).

1. KINETICS AND REACTION MECHANISM

To determine the order of reaction in terms of the two reactants (CH_4 and O_2) we have used the usual graphical method. Thus, for the $2\,CH_4 + O_2$ mixture, figure 8 shows, as a function of time t, the expression $\log \frac{a}{a - x}$, where a is the initial concentration of methane, while x — the corresponding concentration diminutions. As seen from fig. 8, for all experimental temperatures only straight lines are obtained. The same regularity is obtained when plotting the $CH_4 + O_2$ mixtures, the straight lines being of course different from those in figure 8. It therefore results that in the methane oxidation, under the above experimental conditions, the reaction is of order 1 with respect to methane.

Repeating the operation for oxygen, straight lines are obtained only for the dependence on time of the expression $\frac{x}{a - x}$, as shown by figure 9 related to the initial $2\,CH_4 + O_2$ mixture.

This regularity is also kept for the initial, equimolecular mixture $CH_4 + O_2$. Therefore, with respect to oxygen, the oxidation reaction of methane, in the temperature range 600°—730° is of order 2.

For a numerical exemplification we give in table 1 the development of an oxidation reaction in the $CH_4 + O_2$ mixture, at 612° and the values of the two kinetic constants k_1 and k_2, resulting from the equations :

$$k_1 = \frac{2.303}{t} \log \frac{a}{a - x}$$

$$k_2 = \frac{1}{t}\left(\frac{1}{a - x} - \frac{1}{a}\right).$$

Both equations are satisfactorily checked up in the period under consideration.

In the experimental conditions of this present work, the methane oxidation with oxygen proceeds according to the overall kinetic equation :

$$-\frac{\mathrm{d}\,(\mathrm{CH_4})}{\mathrm{d}t} = k_3\,(\mathrm{CH_4})\,(\mathrm{O_2})^2 \tag{1}$$

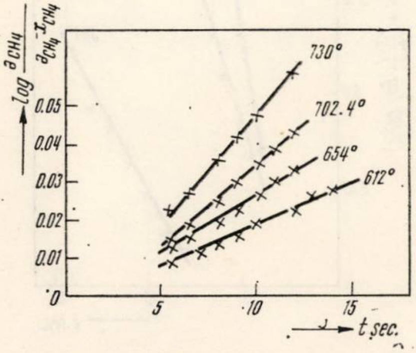

Fig. 8. — Variation of expression log $\frac{a}{a-x}$ as a function of time t, for the $2\,CH_4 + O_2$ mixture.

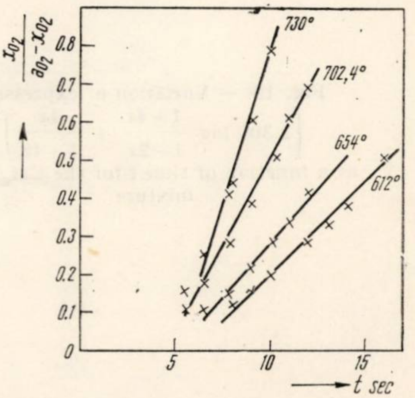

Fig. 9. — Variation of expression $\frac{x}{a-x}$ as a function of time t for the $2\,CH_4+O_2$ mixture.

Table 1

Rate constants for a mixture $CH_4 + O_2$ (ratio 1 : 1) $T = 612°$; $a = 50\%$ (CH_4 and O_2

Time, t (sec.)	$a-x$	k_1, s^{-1}	k_2, $\frac{cm^{-3}}{100}$ percents.s^{-1}
4.5	46.40	0.02620	0.00124
4.9	45.85	0.02788	0.00113
5.5	45.10	0.02763	0.00108
5.9	44.50	0.02841	0.00109
6.0	44.40	0.02878	0.00110
6.5	44.05	0.02620	0.00109
	Average:	0.0275	0.00112

where the magnitudes in brackets represent the usual concentrations. Denoting by a and b the initial concentrations of the reactants, the preceding equation may be written as :

$$\frac{\mathrm{d}x}{\mathrm{d}t} = k_3\,(a - x)\,(b - 2x)^2 \tag{2}$$

x is the diminishing in the methane concentration. Integrating, we get for equimolecular mixtures ($a = b = 1 : 2$) :

$$k_3 = \frac{2}{t}\left(2.303 \log \frac{1-4x}{1-2x} + \frac{4x}{1-4x}\right) \tag{3}$$

In fig. 10 the expression in brackets is plotted with respect to time for the equimolecular mixture $CH_4 + O_2$. At the experimental temperatures, straight lines are obtained according to the requirements of eq. (3).

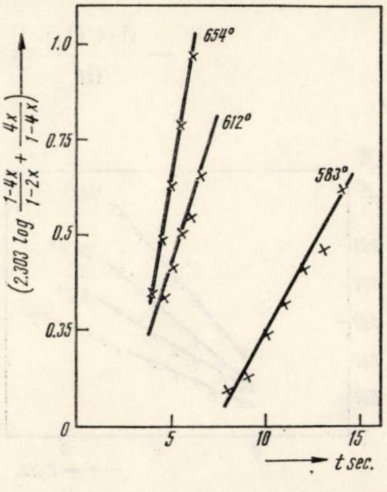

Fig. 10. — Variation of expression $\left(2.303 \log \frac{1-4x}{1-2x} + \frac{4x}{1-4x}\right)$ as a function of time t for the $CH_4 + O_2$ mixture.

The above orders of reaction agree with the data obtained by other researchers [12] and which prove that these values vary with the temperature, beyond 500° the order with respect to methane tending to unity and with respect to oxygen to two.

To account for this behaviour, Enicolopian [13] assumed that the oxidation of hydrocarbons makes up a complex system of chain reactions, developing in several stages, by a great number of simultaneous parallel and consecutive reactions.

Whith the increase in temperature, reactions with great activation energies are becoming prevailing. To explain the variation of the order of reaction with the temperature, Enicolopian has elaborated a comprehensive scheme for the oxidation of hydrocarbons.

By particularizing for the methane oxidation, the consideration of the following main reactions proves sufficient in accounting for the above kinetic data.

$$CH_4 + O_2 \xrightarrow{k_{I}} CH_3 + HO_2 \qquad \text{I}$$

$$CH_3 + O_2 \xrightarrow{k_{II}} H_2CO + OH \qquad \text{II}$$

$$CH_4 + OH \xrightarrow{k_{III}} CH_3 + H_2O \qquad \text{III}$$

$$H_2CO + O_2 \xrightarrow{k_{IV}} HCO + HO_2 \qquad \text{IV}$$

$$HCO + O_2 \xrightarrow{k_{V}} CO + HO_2 \qquad \text{V}$$

$$CH_3 \text{ (wall)} \xrightarrow{k_{VI}} \text{disappearance.} \qquad \text{VI}$$

---

[12] V. Ia. Stern, "Mekhanism okislenie uglevodorodov v gazovoi faze", Izdatelistvo Akademii Nauk S.S.S.R., Moscow, 1960, p. 282.

[13] N. S. Enicolopian, *Zhur. fiz. Khim.*, **33**, 642 (1959).

This reaction system results in :

$$-\frac{d(CH_4)}{dt} = k_{I}(CH_4)(O_2) + k_{III}(CH_4)(OH) \tag{4}$$

By applying to the concentrations of the radicals OH and CH_3 the quasistationarity principle will result,

$$(OH) = \frac{k_{II}(CH_3)(O_2)}{k_{III}(CH_4)}$$

$$(CH_3) = \frac{k_{I}}{k_{VI}}(CH_4)(O_2)$$

while equation (4) becomes :

$$-\frac{d(CH_4)}{dt} = k_{I}(CH_4)(O_2)\left[\frac{k_{II}}{k_{VI}}(O_2) + 1\right]$$

Constant k_{II} is great with respect to k_{VI}, and therefore unity may be neglected as to expression $\frac{k_{II}}{k_{VI}}(O_2)$: thus the preceding equation becomes :

$$-\frac{d(CH_4)}{dt} = \frac{k_{I}\,k_{II}}{k_{VI}}(CH_4)(O_2)^2 \tag{5}$$

where taking $\frac{k_{I}\,k_{II}}{k_{VI}} = k_3$ we find again equation (1) which agrees, as shown above, with the experimental data.

Hoare and Walsh[14] have attempted to explain the same phenomena starting from the hypothesis that at high temperatures also the oxidation of CO to CO_2 starts playing a certain part : this proceeds according to the scheme

$$OH + CO \rightarrow CO_2 + H$$

The hydrogen atoms react with the oxygen according to the scheme

$$H + O_2 \rightarrow OH + O$$

or by a process of triple collision,

$$H + O_2 + M \rightarrow HO_2 + M$$

which is more likely, leading to the growth in the dependence of the total reaction rate on the oxygen concentration, these reactions could also result in the increase of the order of reaction in terms of oxygen and its decrease in terms of methane.

---

[14] D. E. Hoare and A. D. Walsh, Fifth Symposium on Combustion, New York, 1955, p. 474.

Although these considerations have only a qualitative character they may account for the fact that among reaction products we also find CO_2 whose proportion rapidly grows with the prolongation of the contact time accompanied by the almost entire oxygen consumption.

2. INFLUENCE OF TEMPERATURE

The oxidation rate of methane increases with temperature while the industion period decreases. Table 2 gives, for the experimental temperatures, the constants k_1 and k_2, obtained for the two gaseous mixtures under investigation.

Table 2

Kinetic constants k_1 and k_2 at different temperatures

T°K	k_1. s^{-1}	k_2 $\frac{\text{cm}^{-3}}{100}$ percent, s^{-1}
	$2\,CH_4 + O_2$	
885.15	0.00450	0.00145
927.15	0.00690	0.00180
975.55	0.0101	0.00275
1003.15	0.0135	0.00480
	$CH_4 + O_2$	
856.15	0.01467	0.00060
885.15	0.02750	0.00112
927.15	0.04663	0.00160

The values have been used for the graphical determination of the activation energy. Figure 11 where constants k_1 have been used, refers to the $2\,CH_4 + O_2$ mixture. An activation energy of 16,600 cal is deduced. Making use of constants k_2 we find 15,920 cal a value which agrees satisfactorily with the previous one. For the first reactant mixture $2\,CH_4 + O_2$ an average energy of 16,200 cal can be taken.

Reiterating the procedure for the second mixture $CH_4 + O_2$, figure 12 will result; hence, using constants k_1 we deduce an activation energy of 25,500 cal.

Constants k_2 lead to a value somewhat smaller than 22,100 cal. A reasonable value – 25,700 cal – is also obtained by using the values of constants k_3 in figure 10. For the average activation energy of the reaction in the equimolecular mixture $CH_4 + O_2$, the value 24,400 cal. can be taken.

Of course, values in agreement with these data are also obtained from the variation of the reaction rates with the temperature, calculated from the slope of the curves in figures 1–4.

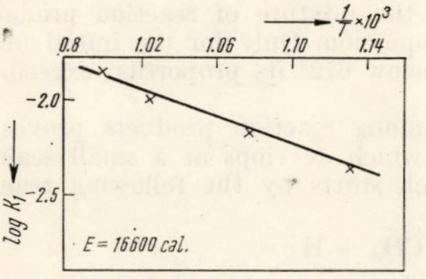

Fig. 11. — Variation of log k_1 as a function of $\frac{1}{T} \times 10^3$ for the $2\,CH_4 + O_2$ mixture.

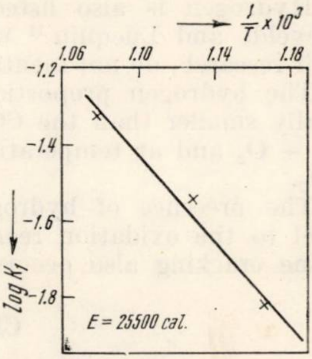

Fig. 12. — Variation of log k_2 as a function of $\frac{1}{T} \times 10^3$ for the $2\,CH_4 + O_2$ mixture.

3. INFLUENCE OF THE $CH_4 : O_2$ RATIO

The ratio between the concentration of the methane and the concentration of the oxygen greatly influences the induction period, the reaction rate and the activation energy.

The induction period of the reaction increases with the oxygen concentration in the initial gaseous mixture. Thus, this is appreciably smaller for the $2\,CH_4 + O_2$ mixture than for the equimolecular mixture $CH_4 + O_2$.

The activation energy increases from 16,600 cal to 24,400 with the passage from the $2\,CH_4 + O_2$ mixture to the equimolecular mixture $CH_4 + O_2$.

4. RELATION BETWEEN THE REACTION TIME AND THE PRODUCTS

The experimental data prove that the duration of reaction and the reaction products are closely linked. Thus, in the induction period, formaldehyde appears, which reaches the maximum amount towards the beginning of this period (fig. 7). In this period the small amounts of methyl alcohol, revealing at a more careful analysis, are most likely developing.

The next period, that of the maximum reaction rate, the main reacting product is represented by the carbon oxide. This forms by the sequence of reactions (II), (IV) and (V). Also in this period the carbon oxide is partially oxidized with CO_2 formation as secondary reaction product (figs. 5 and 6). As expected, the CO_2 concentration in the mixture of reaction products is greater for the equimolecular mixture $CH_4 + O_2$ than for the $2\,CH_4 + O_2$ mixture, poorer in oxygen.

Hydrogen is also listed among the reaction products. Meriaux, Vandevelde and Lucquin[11] who have also used the dynamical method in their research, do not mention hydrogen among the reaction products.

The hydrogen proportion in the mixture of reaction products is generally smaller than the CO_2 proportion. Only for the initial mixture $2\,CH_4 + O_2$ and at temperatures below 612° its proportion exceeds that of CO_2.

The presence of hydrogen among reaction products proves that parallel to the oxidation reaction which develops at a small scale, the methane cracking also occurs which starts by the following reactions.

$$CH_4 \rightarrow CH_3 + H$$

$$CH_4 + H \rightarrow CH_3 + H_2$$

The existence of the cracking process is also confirmed by the presence of some small amounts of ethane and ethylene among the reaction products, revealed on chromatographical analysis. These last hydrocarbon originate, as known,[15,16] due to the reactions:

$$2\,CH_3 \rightarrow C_2H_6$$

$$C_2H_6 \rightarrow C_2H_4 + H_2$$

The presence of the oxygen in the reacting mixture, as shown by Odochian and Schneider,[17] facilitates the initiation of methane cracking.

---

[15] I. G. Murgulescu and I. A. Schneider, *Z. phys. Chem.* (*Leipzig*), **218**, 338 (1961).

[16] R. N. Pease, *J. Amer. Chem. Soc.*, **50**, 1179 (1928), K. I. Leidler and B. W. Wojiechowski, *Proc. Roy. Soc., A*, **260**, 91 (1961).

[17] L. Odochian and I. A. Schneider, *Rev. Roumaine Chim.*, **16**, 1471 (1971).

Revue Roumaine de Chimie, **17**, *10*, 1649 – 1655 (1972)

THE HEATS OF MELTING IN THE BINARY MIXTURES: $AgCl + AgBr$ AND $AgNO_3 + NaNO_3$

D. I. MARCHIDAN and LAURA VASU

Centre of Physical Chemistry
Str. Galaţi 31, Bucharest, Romania

Received April 3, 1972

By means of a differential calorimetric method the heats of melting in the binary mixtures $AgCl + AgBr$ and $AgNO_3 + NaNO_3$ were determined. The results justify the use of a differential calorimetric device for quantitative measurements.

This paper is an extension of the studies [1–3] on heats of melting in binary mixtures and an attempt to establish some regularities.

We have studied two systems. One of them ($AgCl + AgBr$), whose pure components have no transition below melting, forms in the solid state a continuous series of solid solutions. The other ($AgNO_3 + NaNO_3$), has a component with an orientational transition before melting and shows a peritectic point on phase diagram.

We have chosen differential calorimetry owing to its relative suitability for recording data. Differential calorimetry is a method which enables enthalpy changes to be obtained without knowledge of the sample thermal characteristics.

EXPERIMENTAL

The results reported below were obtained with a differential calorimetric assembly similar to that used in a previous work,[2] except the thermocouple beads were located external to the sample container in order to obtain quantitative results. The heating block was in aluminum. Alumina was used as the reference material; the sample and the alumina were both contained in fused silica or Jena cells. The cell holders are in aluminium; between the cell and the cell holder there is a small quantity of alumina and a nickel sheath used as heat distributor. [4] The cell holders rest on the differential thermocouple beads which, in turn, are supported by alumina rods. A third thermocouple records the temperature of the calorimeter block. The whole is enclosed by a cap in order to reduce the heat losses by convection and provide a uniform thermal field.

---

[1] D. I. Marchidan and M. Gambino, *Bull. Soc. chim. France*, **6**, 1954 (1966).
[2] D. I. Marchidan and Cr. Telea, *Rev. Roumaine chim.*, **13**, 1291 (1968).
[3] D. I. Marchidan and Cr. Telea, *Rev. Roumaine chim.*, **14**, 1361 (1969).
[4] M. M. Faktor and R. Hanks, *Trans. Faraday, Soc.*, **63**, 1122 (1967).

Runs were carried out at a heating rate of 2.7°/min. Pure chemicals were used, previously melted in the respective acid atmosphere. To obtain a good mixing the pure substances were melted together before introducing them into the cell.

The enthalpy changes were obtained as the areas under the curve on a differential temperature-time chart, using an X–Y Luxytrace recorder.

RESULTS AND DISCUSSIONS

As Faktor and Hanks [4] showed, in differential calorimetry, the peak area produced by unit enthalpy change in the sample decreases markedly as the temperature increases, the total enthalpy change being :

$$\Delta H = (A + BT^3)\int_0^t \Delta T \, \mathrm{d}t$$

where A and B are the characteristic constants of the calorimeter.

The calorimeter was calibrated using materials of known heats of melting. As the values reported in the literature [2–9] are very different, we chose those calorimetric values that fall on a smooth decreasing curve (Fig. 1) :

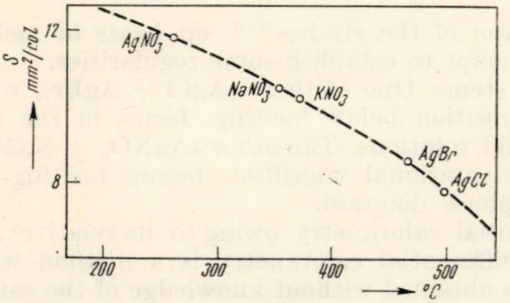

Fig. 1. – Calibration curve, sensitivity (mm²/cal) *vs.* peak temperature.

$$S \text{ (sensitivity, mm}^2\text{/cal)} = 1/(A + BT^3)$$

The sensitivity at the end of the peak is smaller than that at the beginning, so we have used on X-axis the temperature of the top of the peak.

For calibration, we have chosen the following values of the melting heats (in cal/mol) :

$$AgNO_3{}^{5,*} - 2890\,;\ NaNO_3{}^{2,10} - 3600\,;\ KNO_3{}^{*,2} - 2350\,;\ AgCl^{9} - 3100\,;$$
$$AgBr^{\,11,*} - 2200.$$

---

* our results

[5] T. Ozawa, M. Momota and H. Isozaki, *Bull. Chem. Soc. Japan*, **40**, 1583 (1967).

[6] B. R. Curell, *Thermal Analysis*, **2**, 1185 (1969).

[7] K. K. Kelley, *U. S. Bur. Mines Bull.*, **1960**, 584.

[8] J. Janz and F. K. Kelley, *J. Phys. Chem.* **67**, 2848 (1963).

[9] O. Kubachevskii and E. Evans "La thérmochimie en métallurgie", Dunod, Paris, 1964, p. 272.

[10] V. A. Sokolov and N. E. Smidt, *Izvest Sektora Fiz. Khim. Analiza*, **27**, 217 (1956).

[11] U. D. Veriatin, V. P. Mashirev, N. G. Riabtsev, V. I. Tarasov, B. D. Rogoskin, (and I. V. Korobov, "Termodinamicheskie svoistva neorganicheskikh veshestv (spravochinik" Atomizdat, Moscow, 1965, p. 102.

It is worthwhile to notice that most of uncertainty in measuring heats of transition by this method is coming from the calibration. Thus, for the system AgCl + AgBr, if we accept as correct for the pure substance the ΔH_m values which fall on the calibration curve (i.e. 3100 and 2200 cal/mol), the experimental values for mixtures will correspond to the simple additivity (maximum deviation + 2.5% ; Fig. 2). (Every reported value is a result of 4 or 5 runs, mean error 1.5%). But if we choose for AgBr the value $\Delta H_m = 2300$ cal/mol,[9] the maximum deviation will be + 5% (Fig. 3). ΔH_m (calc) were calculated with the relation

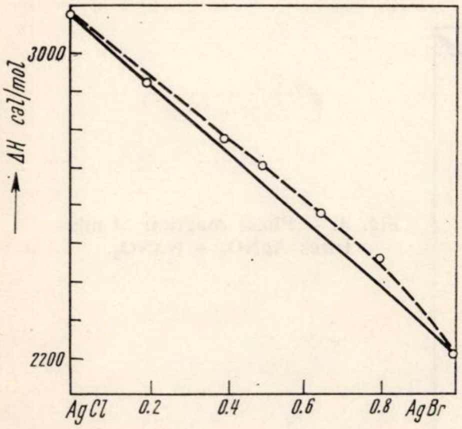

Fg. 2. — Melting heats of mixtures AgCl + AgBr.

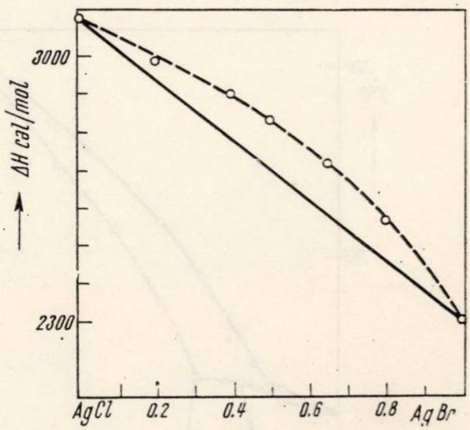

Fig. 3. — Melting heats of mixtures AgCl + AgBr.

$$\Delta H_m(\text{mix}) = x_1 \Delta H_m(\text{AgCl}) + (1 - x_1)\,\Delta H_m(\text{AgBr}).$$

Table 1

Heats of melting of mixtures AgCl + AgBr

System	AgCl + AgBr						
x AgBr	0	0.2	0.4	0.5	0.65	0.8	1.0
ΔH_{m_1} (exp)	3100	2920	2770	2700	2570	2455	$2200^{*,11}$
ΔH_{m_1} (calc)	3100	2920	2740	2650	2510	2380	2200
ΔH_{m_2} (exp)	3100	2985	2900	2830	2710	2560	2300^{9}
ΔH_{m_2} (calc)	3100	2940	2780	2700	2580	2460	2300

*our results

In any case, the deviations seem to be small and positive. This system forms in the solid state a continuous series of solid solutions with a minimum on phase diagram at 65% AgBr (in mols).[12,13]

The other system studied was $AgNO_3 + NaNO_3$. The phase diagram [12] shows a peritectic point at 217°, where the liquid of composition 19.5% mol $NaNO_3$ is in equilibrium with two solid solutions (26% and 38% mol $NaNO_3$).

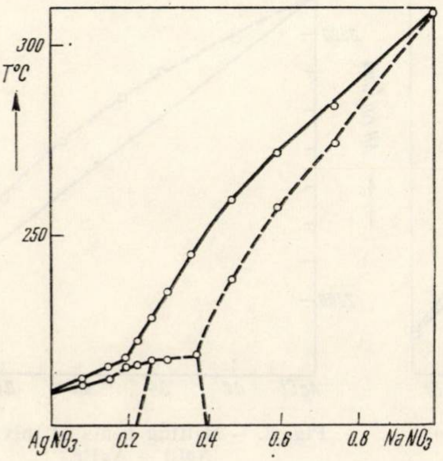

Fig. 4. — Phase diagram of mixtures $AgNO_3 + NaNO_3$.

The results obtained for the second system are very interesting. Both $NaNO_3$ and $AgNO_3$ have phase transitions before melting-at 276° and 159.4° respectively. [14] For $NaNO_3$, crystal form does not change by this transition. [14] From the thermodynamic point of view this is a second order transition. [15] By a phonon description of far infrared spectra of some solid alkali metal nitrates, Wegdam et al. [16] concluded that the anharmonicity in the nitrates is greater than in the alkali halides at comparable temperatures and that it is very important at the second order phase transition. Second order transition of $NaNO_3$ takes place along the rotational coordinate ; the relative positions of the ions do not change.

For $AgNO_3$ the transition at 159.4° is polimorphic. It was described as a "melting of cations lattice". [14] It is a first order transition. [15]

Transitions before melting appear also in mixtures of compositions 80%—40% $NaNO_3$ (in mols). The peak of transition becomes smaller and broader on passing from 80% to 40% $NaNO_3$. Mixtures with high concentration in $AgNO_3$ (0–16% $NaNO_3$) do not present any transition before melting.

---

[12] N. K. Voskresenskaia "Spravochnik po plavkosti sistem iz bezvodnyh neorganicheskikh solei", vol. 1. Izv. Nauk S.S.S.R., Moscow, 1961, p. 56 and 579.

[13] G. M. Lifshitz, *Zhur. obshchei. Khim.*, **26**, 20 (1956).

[14] A. R. Ubbelohde "Melting and Crystal Structure", Oxford Univ. Press., 1965, p. 67 and 73.

[15] P. Cerisier, *Rev. Int. Hautes Tempér. Réfract.*, **8**, 133 (1971).

[16] G. W. Wegdam, J. B. Te Beek, H. Van der Linden and J. Van der Elksen, *J. Chem. Phys.*, **55**, 5207 (1971).

Table 2

Heats of melting of mixtures $AgNO_3$ + $NaNO_3$

System	$AgNO_3 + NaNO_3$					
x $NaNO_3$	0	0.05	0.1	0.15	0.16	0.2
ΔH_m (exp)	2890	3200	3350	3410	2910	2760
ΔH_m (calc)	2890	2925	2960	2990	3000	3030
x $NaNO_3$	0.4	0.5	0.6	0.8	1.0	
ΔH_m (exp)	2580	2520	2560	2950	3600	
ΔH_m (calc)	3170	3245	3310	3460	3600	

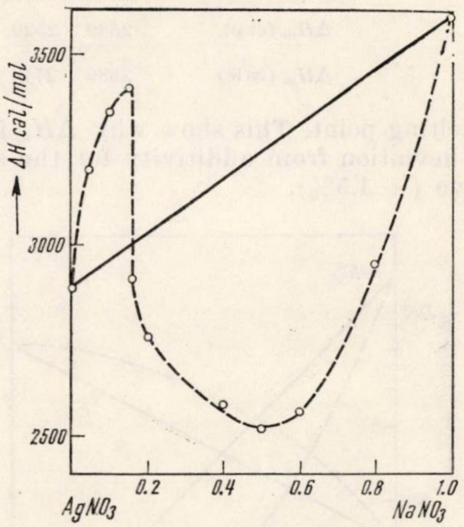

Fig. 5. — Melting heats of mixtures $AgNO_3$ + $NaNO_3$.

The plot of ΔH_m *vs* composition shows at 16% $NaNO_3$ a break of 500 cal/mol. Based on the phase diagram, we divided this plot into three parts :

1. (0–16% $NaNO_3$)—liquid in equilibrium with the solid solution $\alpha = S_1 + AgNO_3$. (S_1 : 16% $NaNO_3$ + 84% $AgNO_3$).

2. (16–38% $NaNO_3$) – liquid in equilibrium with two solid solutions.

3. (38 – 100% $NaNO_3$) – liquid in equilibrium with the solid solution $\beta = S_2 + NaNO_3$. (S_2 : 38% $NaNO_3$ + 62% $AgNO_3$). For mixture with 0–16% $NaNO_3$, with greater ΔH_m, the marked lowering of energy barriers produced by the positional randomization in melting

enables also the orientational randomization to be accomplished. Thus, for these mixtures, the melting transition cumulates the two types of randomization while for other concentrations one of them occurs below the melting point. This show why ΔH_m is greater in this case. The maximum deviation from additivity for the system $AgON_3 + S_1$ is small and positive (+ 4.5%).

Table 3

Heats of melting of mixtures $AgNO_3 + S_1$ and $NaNO_3 + S_2$

System	$AgNO_3 + S_1$				
x $AgNO_3$	1.0	0.67	0.33	0	
ΔH_m (exp)	2890	3200	3350	3410	
ΔH_m (calc)	2890	3060	3240	3410	
System	$NaNO_3 + S_2$				
x $NaNO_3$	0	0.17	0.33	0.67	1.0
ΔH_m (exp)	2580	2520	2580	2950	3600
ΔH_m (calc)	2580	2740	2900	3255	3600

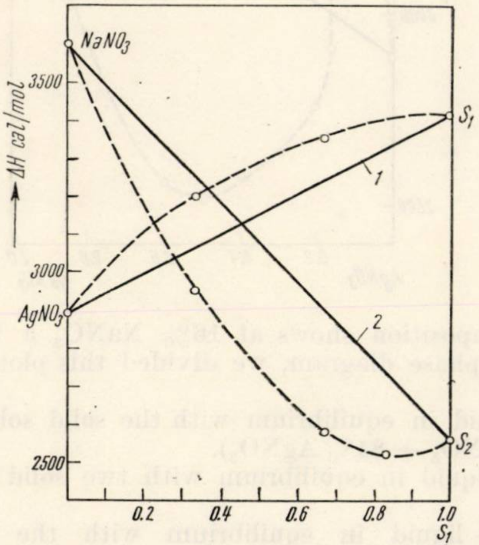

Fig. 6. — Melting beats of mixtures $AgNO_3 + S_1(1)$ and $NaNO_3 + S_2(2)$.

For compositions rich in $NaNO_3$ (system $S_2 + NaNO_3$), where these orientational transitions do take place before melting, the deviation from additivity are negative (maximum deviation − 11%).

CONCLUSIONS

Differential calorimetry is a valuable method to determine enthalpy changes, provided the substances used for calibration have values *a priori* determined by an accurate absolute method. There are few studies in this field, expecially for mixtures. However, there are some thing worthy of remark.

The fact that crystals can exhibit several mechanisms of melting, we suppose, is illustrated by plots of the heat of melting *vs*. composition for binary mixtures.

When positional and orientational disorderings operate simultaneously at the melting point, these diagrams may show slight positive or no deviation from additivity: see AgCl + AgBr or $AgNO_3 + S_1$. When orientational randomization takes place before melting, heat of melting is due only to positional randomization. For these systems the sign of the deviations is negative.

Revue Roumaine de Chimie, 17, *10*, 1657 – 1667 (1972)

HIGH TEMPERATURE ENTHALPY AND RELATED THERMODYNAMIC FUNCTIONS OF NON-STOICHIOMETRIC URANIUM OXIDES

D. I. MARCHIDAN and M. CIOPEC

Centre of Physical Chemistry
P. O. Box 2103, Bucharest, Romania

Received May 6, 1972

High temperature enthalpies of non-stoichiometric uranium oxides $UO_{2.21}$ and $UO_{2,366}$ were measured over a temperature range from 300 K to 1300 K using a drop calorimeter. The sample encapsulated into the platinum container under vacuum, was dropped into a copper block calorimeter with isothermal jacket in order to measure the heat released which was thereafter converted into enthalpies. The least square analysis of the experimental enthalpies data was performed with TERMOX computer program on an IBM System 360/30 computer. With this program four polynomial equations were smoothed from the experimental results. Out of these relations only one was preferred which produces the best fit. Smoothed values of the enthalpies and related thermodynamic functions were calculated and are tabulated at round temperatures.

1. INTRODUCTION

The uranium-oxygen system is one of the most complex metal-oxygen systems that are known. A good knowledge of the uranium-oxygen phase system and of its thermodynamic properties is of paramount importance to the nuclear industry because of the ever-increasing use of uranium oxides as a power reactor fuel.

Although the uranium-oxygen system has been the object of a number of investigations carried out by means of different experimental techniques and methods, many of the thermodynamical data of the stable high temperature oxide phases are not reliable or have not been determined yet.

The enthalpy and heat capacity of non-stoichiometric uranium oxides and their temperature dependence can supply information about thermodynamical aspects of the structural changes. They can specify which transitions take place and at what temperatures and so they allow to characterize the uranium oxides from the thermodynamic point of view.

Previous studies concerning the uranium-oxygen system effected by different experimental techniques (high temperature X-ray techniques, tensimetric, thermogravimetric and effusion methods, calorimetric techniques, EMF measurements) lead to the common conclusion that the following stable phases exist at high temperatures: UO_2 and UO_{2+x} that comes from UO_2 by the inclusion of interstitial oxygen in the fluorite lattice; a cubic or pseudo-cubic phase U_4O_9, coming also from UO_2 by including the interstitial oxygens; an orthorhombic phase, related in structure to U_3O_8.[1–5] Each of these phases exist in a certain range of composition.

Between UO_2 and U_4O_9 there is a series of non-stoichiometric oxides which are single phase at high temperatures, with the fluorite type structure, but disproportionate to UO_{2+x} and U_4O_{9-y} at low temperatures.

A non-stoichiometric oxides comprised between U_4O_9 and U_3O_8 constitute a two-phase region because when x in UO_x exceeds 2.30 the orthorhombic phase is present together with the cubic UO_2 phase.[6] More recently, a number of tetragonal phases have been described in the range $UO_{2.3}$ to $UO_{2.4}$.[7] The α-U_3O_7 phase[8] occurs in the early stages of oxidation of UO_2 at temperatures below 408 K. The O/U ratio of α-U_3O_7 is certainly less than 2.33 and probably less than 2.30. At 453 K, for $O/U > 2.3$, there is a transition to the γ_1 (or β U_3O_7) phase. The conversion is complete for $O/U = 2.33$. The γ_1 phase can be preserved indefinitely below 623 K but above this temperature it transforms to $\gamma_2 + UO_{2.6}$:

$$\gamma_1 \rightarrow \gamma_2 + UO_{2\cdot 6} \qquad (1)$$

The γ_2 phase probably exists over a range of compositions, from 623 K to 983 K. According to eq. (1), γ_1 has a higher oxygen content than γ_2. The probable compositions are:

$UO_{2.33}$ for γ_1
$UO_{2.30}$ for γ_2 at 623 K
$UO_{2.30}$ for γ_2 at 923 K.
Above 873 K reaction (2) occurs:

$$\gamma_2 \rightarrow U_4O_9 + UO_{2.6} \qquad (2)$$

The reversibility of reactions (1) and (2) has not been confirmed, and the thermodynamic stability of the tetragonal phases has not been determined; it is not even known whether these phases are stable or metastable.

Westrum and Grønvold[9] have reported the existence of an oxide $UO_{2.37}$ having a structure of lower than tetragonal symmetry, whereas

---

[1] S. Aronson and J. Belle, *J. Chem. Phys.*, **29**, 151 (1958).

[2] F. Grønvold, *J. Inorg. Nuclear Chem.*, **1**, 357 (1955).

[3] W. Biltz and A. Müller, *Z. anorg. Chem.*, **163**, 257 (1927).

[4] L. E. J. Roberts and A. J. Walter, *J. Inorg. Nuclear Chem.*, **22**, 213 (1961).

[5] P. E. Blackburn, *J. Phys. Chem.*, **62**, 897 (1958).

[6] J. J. Katz and E. Rabinowitch, "The Chemistry of Uranium", Dover Publications, Inc., N. Y., 1951, p. 253.

[7] L. E. J. Roberts, *Quart. Rev.*, **15**, 5 (1961).

[8] "Thermodynamic and Transport Properties of Uranium Dioxide and Related Phases", Technical Reports Series No. 39, IAEA, Vienna, 1965, p. 19.

[9] E. F. Westrum Jr. and F. Grønvold, *Phys. and Chem. Solids*, **23**, 39 (1962).

Belbeoch and co-workers[10] have interpreted the characteristic features of diffraction lines as due to a strained tetragonal structure.

The tetragonal phases are ordered structures based on the fluorite arrangement. Andersen[11] has pointed out the similarity in the neutron diffraction patterns of U_4O_9 and αU_3O_7. The true unit cells of the tetragonal phases are at least as large as that of U_4O_9.

Presently it is difficult to draw a unitary and well founded conclusion on the structure of uranium oxides, as far as there is a great disagreement between the experimental data obtained by different authors. Therefore, it seems of special interest to carry on the study of uranium-oxygen system, regarding especially the non-stoichiometric compounds defined by an O/U ratio varying between 2... 2.25 and 2.25... 2.66 values.

Following our earlier investigations of the thermodynamic properties of non-stoichiometric uranium-oxygen compounds, we have measured the high temperature enthalpies of $UO_{2.21}$ and $UO_{2.366}$.

2. EXPERIMENTAL

Apparatus

The enthalpy measurements in the high temperature range were made by drop calorimetry up to 1300 K with an apparatus described previously.[12,13]

Briefly, the determination procedure and description of the apparatus are the following. The capsule sealed sample is suspended in a furnace until a known temperature is reached. The sample is then dropped into the block type calorimeter with isothermal jacket, which measures the heat evolved by the sample and the container, heat due to the cooling to 298 K. In order to account for the heat content of the capsule and the heat lost while dropping, a similar experiment was carried out with the empty capsule at the same temperature. The difference between the two heat values is a measure of the change in the heat content of the sample from the furnace temperature down to 298 K. The values obtained for a series of temperatures, enable to calculate the enthalpy, whereby the heat capacity, increment in entropy and free energy functions.

The block-type calorimeter with isothermal surrounding jacket consists of a cylindrical block of copper with a central receiving "well", introduced in a brass container. The jacket and calorimeter are immersed into a well-stirred water bath, the temperature of which was controlled within $\pm 0.005°$ by means of a thermo-regulator device.

The change in the block temperature is determined with a thermistor immersed in a calorimeter's hole. The measurement of the temperature increase was made by considering the resistance of a thermistor introduced into a Wheatstone bridge. A 0.001° change brings about a 1.0 Ω change in the thermistor resistance. The thermistor was calibrated in the calorimeter block against a calibrated Beckman thermometer, under similar conditions with those used in the experiments.

---

[10] B. Belbeoch, C. Piekarski and P. Perio, *J. Nuclear Materials*, **3**, 60 (1961).

[11] A. J. Andersen in "Symposium of Reactor Materials", Stockholm, 1959.

[12] D. I. Marchidan and M. Ciopec, *Studii şi Cercetări Chim. Acad. R. S. R.*, **17**, 737 (1969).

[13] D. I. Marchidan and M. Ciopec, *Rev. Roumaine de Chimie*, **16**, 1145 (1971).

The furnace consist of two concentric quartz tubes between which kanthal electric resistance was wound. The furnace core contains a metallic block, the temperature of which was maintained within ±0.5° by a proportional thermo-controller, using a Pt−PtRh control thermocouple. These thermocouples were closed to the sample which is suspended in the central "well" of the metallic block by a 0.1 mm diameter cronix wire, clamped between two solid kanthal electrodes. These electrodes are fixed in a motion-device moving in the X−Y plane that allow adjustment of the positions of the heated sample from outside. In order to accurately release the sample, the current is passed through the suspension wire causing it to vaporize rapidly. Experiments showed that no correction is required for this discharge energy.

The calibration factor of the calorimeter block was determined by supplying a known amount of caloric energy Q and observing the temperature change $\Delta\theta$, of the block which is corrected for heat losses to the isothermal surrounding. The synthetic sapphire, NBS standard reference material 720 was used as a standard substance.[13] A series of 25 runs gave a calibration factor

$$W = 3873.446 \pm 13.016\ (\pm\ 0.3\,\%)\ \text{joules/degree}$$

After one year a series of 11 runs gave a calibration factor

$$W = 3872.666 \pm 3.092\ (\pm 0.1\,\%)\ \text{joules/degree}$$

To prepare uranium oxides $UO_{2.21}$ and $UO_{2.366}$ we started from the uranyl nitrate. A powder which was obtained was pressed and sinterized in nitrogen atmosphere and the O/U ratio was determined by oxydation to U_3O_8 in the air.

A 7.802 g. sample of $UO_{2.21}$ and a 5.8863 g. sample of $UO_{2.366}$ were each introduced in a platinum container of tronconical shape[13] in which the top is connected to a narrow neck welded to a Jena glass ground joint. After filling, the container was attached to a vacuum equipment. After a number of cycles of vacuuming and filling with purified argon (free of oxygen) and after evacuation at 0.3−0.7 Nm^{-2} the glass tube was cut off and closed with gas-oxygen torch close to the body of the container, retaining the vacuum inside. The platinum neck may be pinched shut near the top and sealed by gas-oxygen welding. After each run the capsule was weighed and no weight loss was observed after 39 runs for $UO_{2.21}$ and 45 runs for $UO_{2.366}$.

3. RESULTS OBTAINED. ANALYSIS AND TREATMENT OF DATA

The increase in temperature of the calorimeter block due to the sample was determined for each drop experiment and subsequent correction was made by previously described method.[14]

In order to account for the heat content of the container and the heat lost while dropping, similar experiments were made with the empty container ("black" drop) at the same temperatures. The difference between these two values represents the increase in temperature ΔT of the calorimeter block due to the uranium oxide sample.

The change in the heat content ΔQ of the uranium oxide sample from the furnace temperature down to 298 is

$$\Delta Q = W \,.\, \Delta T \tag{3}$$

---

[14] D. I. Marchidan and M. Ciopec, *Rev. Roumaine de Chimie*, **15**, 1287 (1970).

From the experimental values, enthalpies

$$H_T - H_{298.15} = \Delta Q/n \tag{4}$$

where n is number of moles from uranium oxide sample, were calculated.

The enthalpy values of $UO_{2.21}$ and $UO_{2.366}$ were subject to the least squares analysis in order to obtain a mathematical relationship between enthalpy and temperature, because the variation of this function with temperature above 298.15 K has not been successfully represented by any type of theoretical or empirical equation.

A computer program named TERMOX was written [15] for the least square analysis, which was performed on an IBM computer System 360/30. With this computer program (TERMOX) the empirical equations

$$H_T - H_{298.15} = a + bT + cT^2 \tag{5}$$

$$H_T - H_{298.15} = a + bT + cT^2 + dT^3 \tag{6}$$

$$H_T - H_{298.15} = a + bT + cT^2 + dT^{-1} \tag{7}$$

$$H_T - H_{298.15} = a + bT + cT^2 + dT^{-2} \tag{8}$$

were tested for the best fit of the experimental data. These fitting schemes have been proposed for the enthalpy function of solid substances. [16,17]

From the smoothed equations (Table 1 and Table 2) those for which the standard deviation was minimum and calculated $H_T - H_{298.15}$ for $T = 298.15$ is around zero, were chosen.
For $UO_{2.21}$

$$H_T - H_{298.15} = -21087 + 68.104\ T + 11.037\,(10^{-3})\ T^2 \text{ j/mol} \tag{9}$$

in the temperature range 300—1300 K.

For $UO_{2.366}$

$$H_T - H_{298.15} = -23864 + 79.945\ T + 1.176(10^{-3})\ T^2 \text{ j/mol} \tag{10}$$

in the temperature range 300—775 K, and

$$H_T - H_{298.15} = -10400 + 53.957\ T + 18.629(10^{-3})\ T^2 \text{ j/mol} \tag{11}$$

in the temperature range 775—1300 K.

---

[15] M. Ciopec and D. I. Marchidan, *Rev. Roumaine de Chimie*, **17**, 1139 (1972).

[16] E. H. Buyco and F. F. Davis, *J. Chem. and Eng. Data*, **15**, 518 (1970).

[17] F. Grønvold, N. J. Kveseth, A. Sveen and J. Tichy, *J. Chem. Thermodynamics*, **2**, 665 (1970).

Table 1

Smoothed equations for $UO_{2.21}$ experimental enthalpy data

Smoothed equation	Temperature range (K)	Regression coefficients				Standard deviation	
		a	b	c	d	j/mol	%
$H_T-H_{298.15}=a+bT+cT^2$	300–1300	–21087	68.104	11.037(10⁻³)		±273	±0.84
$H_T-H_{298.15}=a+bT+cT^2 + dT^3$	300–1300	–20156	63.950	16.678(10⁻³)	–2.382(10⁻⁶)	±269	±1.09
$H_T-H_{298.15}=a+bT+cT^2 + dT^{-1}$	300–1300	–23336	71.283	9.649(10⁻³)	4.828(10⁵)	±272	±1.15
$H_T-H_{2^{\circ}8.15}=a+bT+cT^2 + dT^{-2}$	300–1300	–21905	69.624	10.299(10⁻²)	5.290(10⁷)	±272	±1.07

Table 2

Smoothed equations for $UO_{2.386}$ experimental enthalpy data

Smoothed equation	Temperature range (K)	Regression coefficients				Standard deviation	
		a	b	c	d	j/mol	%
$H_T-H_{298.15}= = a + bT+cT^2$	300– 775 775–1300	–23864 –10400	79.945 53.957	1.176(10⁻³) 18.629(10⁻³)		±183 ±568	±0.70 ±0.91
$H_T-H_{298.15}=a + bT + cT^2 + dT^3$	300– 775 775–1300	–37106 172382	155.620 –488.253	––13.794(10⁻²) 54.731(10⁻²)	82.596 (10⁻⁶) –169.553 (10⁻⁶)	±163 ±500	±0.94 ±0.74
$H_T-H_{298.15}= = a+bT+cT^2+ + dT^{-1}$	300– 775 775–1300	–693 –207536	36.782 247.881	27.125(10⁻³) –44.101(10⁻³)	– 40.020 (10) 65.869 (10⁶)	±168 ±492	±0.70 ±0.75
$H_T-H_{298.15}=a+ bT + cT^2 + dT^{-2}$	300– 775 775–1300	–12603 –288113	52.124 417.980	19.904(10⁻³) –113.767(10⁻³)	– 49.182 (10⁷) 45.915 (10⁹)	±170 ±498	±0.69 ±0.75

Table 3

Experimental enthalpy data of $UO_{2.21}$ (mol. wt. = 273.388)

T (K)	$H_T - H_{298.15}$ (j/ mol)		Deviation (calc-obs)	
	observed	calculated qn.(9)	j/mol	%
345.15	3674	3734	60	1.6
347.15	3810	3885	75	1.9
416.15	9253	9166	−87	−1.0
417.15	9390	9243	−147	−1.6
474.65	13880	13725	−155	−1.1
475.15	14016	13764	−252	−1.8
512.65	16738	16727	−11	−0.1
513.65	16874	16806	−68	−0.4
570.15	21229	21330	101	0.5
574.65	21501	21693	192	0.9
654.65	28169	28227	58	0.2
657.15	28441	28434	−7	−0.0
718.15	32932	33415	582	1.7
719.65	33204	33640	436	1.3
785.15	38919	39188	269	0.7
785.95	39191	39257	65	0.2
827.50	42729	42826	97	0.2
827.50	43002	42826	−176	−0.4
866.15	46267	46181	−86	−0.2
918.15	51303	50747	−556	−1.1
918.15	51167	50747	−420	−0.8
971.50	55493	55521	−28	−0.1
977.15	56746	55999	−747	−1.3
1005.65	58787	58564	−223	−0.4
1023.15	60147	59876	271	0.5
1024.15	60556	60238	−318	−0.5
1066.15	63958	64067	109	0.2
1074.15	64639	64801	162	0.3
1077.15	65047	65077	30	0.0
1086.15	65319	65904	585	0.9
1108.65	67905	67982	77	0.1
1117.15	68721	68770	48	0.1
1160.65	72396	72826	430	0.6
1166.15	73348	73342	−6	−0.0
1177.65	74301	74423	121	0.2
1178.15	74573	74470	−103	−0.1
1194.65	75934	76026	92	0.1
1196.15	76342	76167	−175	−0.2
1199.15	76750	76451	−299	−0.4

The fit of the experimental data to the smoothed equations 9—11 is presented in Table 3 and Table 4.

4. DISCUSSION

Experimental enthalpy data, calculated enthalpy and heat capacity data are presented in figures 1 and 2.

The thermodynamic function values derived for each uranium oxide at every 50 K from 300 to 1300 K was calculated with the program TERMOX. The results are listed in tables 5 and 6.

Table 4

Experimental enthalpy data of UO$_{2.366}$ (mol. wt. = 275.884)

T (K)	$H_T - H_{238.15}$ (j/mol)		Deviation (calc-obs)	
	odserved	calculated eqn. (1)	j/mol	%
366.30	5523	5577	54	1.0
367.85	5634	5702	68	1·2
368.15	5716	5727	11	0.2
415.15	9527	9527	0	0.0
415.40	9602	9548	−54	−0.6
472.75	14239	14193	−46	−0.3
474.35	14313	14322	9	0.1
519.80	17969	18009	40	0.2
521.45	18207	18143	−64	−0.4
576.60	22870	22623	−247	−1.1
578.15	22870	22749	−121	−0.5
628.15	26806	26817	11	0.0
632.60	27252	27179	−72	−0.3
671.85	30130	30377	247	0.8
673.45	30312	30508	196	0.6
726.95	34849	34873	24	0.1
727.15	34486	34889	403	1.2
772.15	39024	38566	457	−1.2
		calculated eqn.(11)		
776.26	43380	42709	−671	−1.6
823.65	47192	46679	−513	−1.1
824.95	47010	46789	−221	−0.5
825.25	46829	46814	−14	−0.0
872.45	50096	50854	758	1.5
872.95	50277	50897	620	1.2
928.00	54997	55715	718	1.3
930.00	55541	55892	351	0.6
978.65	60079	60247	168	0.3
980.65	60624	60428	−196	−0.3
1024.15	64617	64400	−217	−0.3
1027.40	64072	64699	627	1.0
1041.25	65887	65980	93	0.1
1071.25	69336	68780	−556	−0.8
1099.90	70970	71484	514	0.7
1107.15	72422	72173	−249	−0.3
1116.60	74963	73075	−1888	−2.6
1152.90	76778	76568	−210	−0.3
1177.90	78955	79002	47	0.1
1216.05	82678	82762	84	0.1
1222.00	83038	83354	316	0.4
1256.15	86942	86773	−169	−0.2
1269.40	87822	88111	289	0.3
1285.90	89468	89787	318	0.4

The curves drawn in Figure 3 do not permit to see any rigorous regularity between heat capacity and stoichiometry. However, a connection between them can be seen by comparing each studied system with literature data.

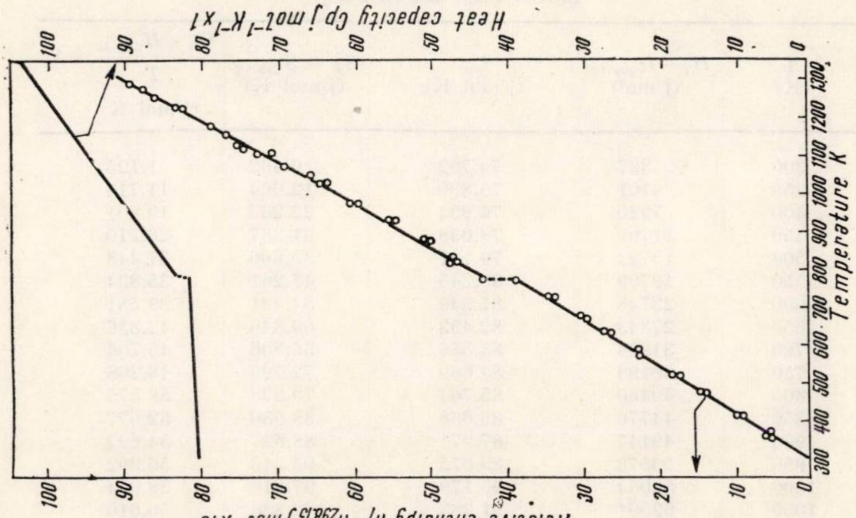

Fig. 2. — Heat capacity and relative enthalpy of $UO_{2.366}$.

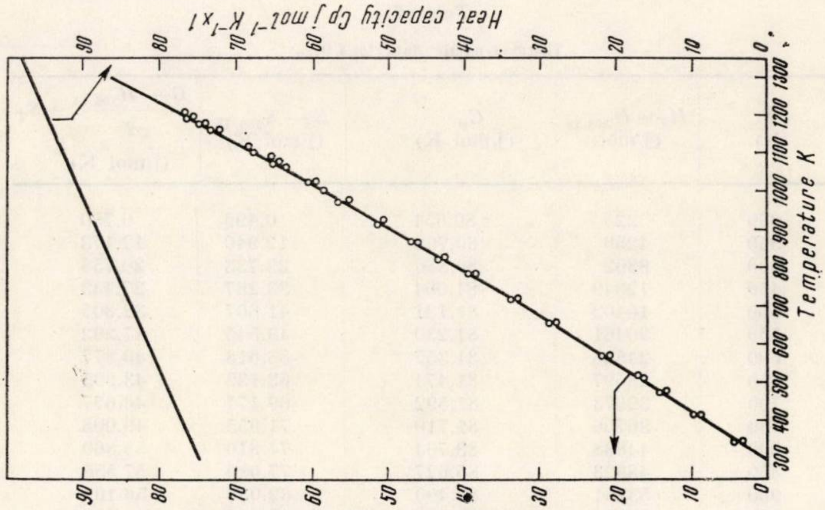

Fig. 1. — Heat capacity and relative enthalpy of $UO_{2.21}$.

Table 5

Thermodynamic data for UO$_{2.21}$

T (K)	$H_T - H_{298.15}$ (j/mol)	C_p (j/mol K)	$S_T - S_{298.15}$ (j/mol K)	$\frac{G_T - H_{298.15}}{T} + S_T$ (j/mol K)
300	337	74.762	0.462	1.125
350	4101	75.830	12.064	11.718
400	7920	76.934	22.262	19.801
450	11795	78.038	31.387	26.210
500	15724	79.141	39.666	31.448
550	19709	80.245	47.261	35.834
600	23748	81.349	54.291	39.581
650	27843	82.453	60.846	42.836
700	31994	83.556	66.996	45.706
750	36199	84.660	72.799	48.266
800	40460	85.764	79.298	50.575
850	44776	86.868	83.530	52.677
900	49147	87.971	88.527	54.607
950	53573	89.075	93.313	56.392
1000	58054	90.179	97.910	58.054
1050	62591	91.283	102.336	56.610
1100	67182	92.386	106.608	61.075
1150	71829	93.490	110.739	62.460
1200	76531	94.594	114.741	63.776
1250	81289	95.698	118.625	65.031
1300	86101	96.801	122.400	66.232

Table 6

Thermodynamic data for UO$_{2.366}$

T (K)	$H_T - H_{298.15}$ (j/mol)	C_p (j/mol K)	$S_T - S_{298.15}$ (j/mol K)	$\frac{G_T - H_{298.15}}{T} + S_T$ (j/mol K)
300	225	80.651	0.499	0.750
350	4260	80.768	12.940	12.173
400	8302	80.886	23.733	20.755
450	12349	81.004	33.267	27.443
500	16402	81.121	41.807	32.805
550	20461	81.239	49.545	37.202
600	24526	81.357	56.618	40.877
650	28597	81.474	63.135	43.995
700	32673	81.592	69.177	46.677
750	36756	81.710	71.955	49.008
800	44688	83.764	74.810	55.860
850	48923	85.627	77.089	57.556
900	53251	87.490	82.036	56.167
950	57672	89.353	86.816	60.707
1000	62185	91.216	91.447	62.186
1050	66793	93.079	95.942	63.613
1100	71494	94.941	100.315	64.994
1150	76287	96.804	104.577	66.337
1200	81174	98.667	108.736	67.645
1250	86154	100.530	112.801	68.923
1300	91227	102.393	116.781	70.175

From figure 3 one can see that the shape of the curve for C_p variation with the temperature for $UO_{2.21}$ places this compound, from the thermodynamic point of view, between $UO_{2.017}$ and $UO_{2.254}$. The behaviour of $UO_{2.21}$ is more similar to that of $UO_{2.254}$ except for the 900–1000 K temperature range in which $UO_{2.21}$ does not undergo any change. Figures 2 and 3 show a discontinuity in the enthalpy and in the heat capacity of $UO_{2.366}$. This discontinuity occurs at 775 K. By increasing the temperature above this value a drastic change in the relative enthalpy and especially, in the heat capacity is brought about.

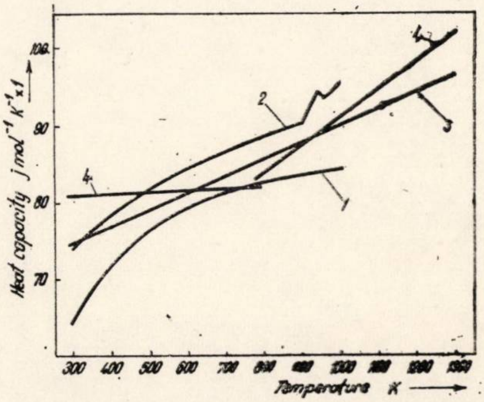

Fig. 3. — Heat capacity of studied uranium oxides and literature data. *1*) C_p for $UO_{2.017}$[17]; *2*) C_p for $UO_{2.254}$[17]; *3*) C_p for $UO_{2.21}$ (present paper); *4*) C_p for $UO_{2.366}$ (present paper).

Lack of structural information did not allow us a rigorous explanation of this phenomenon. Supposedly, a strong structural modification takes place and this generates a new phase. This phenomenon requires a heat contribution of about 4300 j/mol, i.e. 3.7 cal/g.

The thermodynamic behaviour of the studied non-stoichiometric uranium oxides is very different. The heat capacities are influenced by stoichiometry in different ways and proportions. Further investigations are required for the complete thermodynamical characterization of these non-stoichiometric uranium oxides.

Acknowledgments. This work was performed under an International Atomic Energy Agency contract 695/R2/RB. The authors are grateful to the I.A.E.A. for the permission to publish this paper. We wish to express our deep gratitude to Professor I. G. Murgulescu for his interest in our work. Thanks are due to C. Volcovici for his technical assistance.

From figure 3 one can see that the shape of the curve for C_p variation with the temperature for [illegible] places this compound, from the thermodynamic point of view, between [illegible] and [illegible]. The behaviour of [illegible] is more similar to that of [illegible], except for the 900–1000 K temperature range in which [illegible] does not undergo any change. Figures 5 and 6 show a discontinuity in the enthalpy and in the mean capacity of

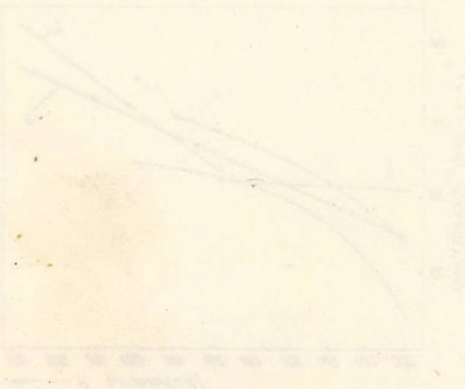

Fig. 6. — Mean heat capacity of uranium oxides [illegible]

[illegible]. This discontinuity occurs at 775 K. By increasing the temperature above this value a drastic change in the relative enthalpy and especially in the heat capacity is brought about.

Lack of structural information did not allow us a rigorous explanation of this phenomenon. Supposedly, a strong structural modification takes place and this generates a new phase. This phenomenon requires a heat contribution of about [illegible] J/mol, i.e. [illegible] cal/g.

The thermodynamic behaviour of the studied non-stoichiometric uranium oxides is very different. The heat capacities are influenced by stoichiometry in different ways and proportions. Further investigations are required for the complete thermodynamical characterization of these non-stoichiometric uranium oxides.

Acknowledgements. This work was performed under an International Atomic Energy Agency contract [illegible]. The authors are grateful to the I.A.E.A. for the permission to publish this paper. We wish to express our deep gratitude to Professor I. G. Murgulescu for his interest in our work. Thanks are due to [illegible] for his technical assistance.

Revue Roumaine de Chimie, **17**, *10*, 1669 – 1677 (1972)

THE OXIDATION OF ORGANIC BIBASIC ACIDS IN MIXTURES OF FUSED SALTS. I

THE DECARBOXYLATION OF OXALIC ACID IN MOLTEN ALKALI METAL NITRATES

RODICA VÎLCU and NICOLAE GEORGESCU

Centre of Physical Chemistry
Str. Galaţi 31, Bucharest, Romania

Received April 22, 1972

The kinetics and the mechanism of oxalate anion decarboxylation in pure nitrate melts, as well as in dichromate solution of molten alkali nitrates is investigated. The dependence of the reaction rate on the flow rate of the purge gas and of the initial CO_3^{2-} concentration is established. The process is studied both by chemical methods and by measuring the evolution in time of the gaseous product CO_2. The decisive step of the decarboxylation is explained in terms of gas — fused salt solution interactions.

INTRODUCTION

Fused electrolytes are generally completely dissociated into ions, and are excellent solvents for salts, metals and gases. [1] They are steadily gaining in technological importance, owing to their high thermal stability, low vapour pressure, good electrical conductivity, low viscosity, extremely wide useful temperature range, and the very high temperatures which can be reached. It is not surprising, therefore, that electrochemical and physico-chemical investigations have recently been intensified with a view of using fused salts in industry and particularly in nuclear technology. [2]

Generally, chemical reactions in fused salts can be divided into three types :

1. Reactions involving participation of the melt and consumption of one or more of its components, with no simple means of regenerating the latter.

2. Reactions in which the melt simply acts as a solvent for the reactants, or in which the components of the melt are formed as by-products, or in which the by-products can be chemically or electrochemically reconverted into the initial compounds. [3]

---

[1] R. Battino and H. L. Clever, *Chem. Rev.*, **66**, 429 (1966).
[2] H. U. Woelk, *Chem. Ing. Tech.*, **32**, 765 (1960).
[3] W. Sundermeyer, *Z. anorg. Chem.*, **314**, 100 (1962).

3. Reactions in which the melt acts as a catalyst.

The study of acid-base as well as of oxidation reactions and their kinetics in fused nitrates is of particular interest. Investigations in this field have been effected by Duke,[4-7] Schlegel[8] as well as by Duke and Lawrence,[9] Duke and Shute[10] and Duke and Iverson.[11] No systematic studies have been accomplished until now on the behaviour of dicarboxylic acids in alkali nitrate melts.

The bibasic acids present a special interest from the point of view of the decarboxylation mechanism as they are directly influenced by the reciprocal positions of the — COOH groups in the molecule.

Considering that oxalic acid is the first term of the aliphatic saturated dicarboxylic acid series where the mutual distance between the —COOH groups is minimum its oxidation in fused alkali nitrate mixtures is investigated in the present work in order to determine the mechanism of the reaction as well as to have a good reference point for further studies of the behaviour of the immediately higher homologs under similar conditions.

EXPERIMENTAL

Chemicals. All substances were Romanian reagent *p. a.* grade "Reactivul". The sodium and potassium nitrates were purified by repeated recrystallizations from water, filtration and further premelting in a dry argon atmosphere. Alkali nitrates as well as potassium oxalate were dried in an oven at 120° for 24 hours before use.

Apparatus. The furnace used for the heating of the reaction cell was similar with that described by Bockris.[12] Constant temperature over a sufficiently long period required by kinetic measurements was ensured by a thermoregulating system consisting of a resistance and an electronic switch actuated by the measuring circuit of the thermocouple mounted between two turns of the heating resistance. The terminals were connected to a variable voltage generator. The thermal inertia of the furnace reduces to a very small value the vertical temperature gradient in the melt.

The temperature both of the melt and of the furnace was measured with chromel-alumel thermocouples.

Procedure. The decarboxylation of oxalate anion in pure fused alkali nitrates has been investigated using both ordinary chemical analysis and a volumetric absorption method. In dichromate solutions of molten nitrates we were limited to the volumetric absorption method, the ordinary chemical analysis being not applicable.

---

[4] F. R. Duke and M. L. Iverson, *J. Amer. Chem. Soc.*, **80**, 5061 (1958).

[5] F. R. Duke and M. Yamamoto, *J. Amer. Chem. Soc.*, **81**, 6378 (1959).

[6] F. R. Duke, "Fused Salts", B. R. Sundheim ed., McGraw-Hill Book Company, New York, 1964, p. 409.

[7] R. N. Kust and F. R. Duke, *J. Amer. Chem. Soc.*, **85**, 3338 (1963).

[8] J. M. Schlegel and F. R. Duke, *J. Phys. Chem.*, **67**, 3487 (1963).

[9] F. R. Duke and W. W. Lawrence, *J. Amer. Chem. Soc.*, **83**, 1271 (1961).

[10] F. R. Duke and E. A. Shute, *J. Phys. Chem.*, **66**, 2114 (1962).

[11] F. R. Duke and M. L. Iverson, *J. Phys. Chem.*, **62**, 417 (1958).

[12] J. O'M. Bockris, T. L. White and T. D. Mackenzie, "Physico-Chemical Measurements at High Temperatures", Butterworths, London, 1959, chap. 13.

Dry purified argon was bubbled through a 40 g $NaNO_3 - KNO_3$ eutectic melt for two hours, to remove any trace of water retained in the molten mixture. The flow rate of the inert gas varied in order to investigate its effect upon the oxidation rate. For each run the flow rate was adjusted to a known constant value and then a weighed sample of potassium oxalate was added to the reaction mixture with the aid of a little spoon laterally attached to the reaction vessel.

In the chemical method, samples were withdrawn at measured time intervals and allowed to solidify on a porcelain plate. Thus, the reaction in the melt was stopped. Then the samples were weighed, dissolved in water and titrated for oxalic anion using a cerimetric analysis method.[13]

Since NO_2^- is a reaction product and its presence interferes with the analysis, a small amount of sulphamic acid was added, so that nitrite was destroyed before the titration of oxalic anion.

The reaction cell built for the volumetric absorption measurements, had dimensions which allowed to follow, under appropiate conditions, the evolution rate of CO_2 from the decarboxylation process. It has been found that, the half-life of the reaction allows the determination of the CO_2 volumes evolved through successive absorptions in KOH solutions. The absorption system represented by a modified Orsat scheme was attached directly to the reaction cell. The reaction rate was followed by adding a weighed amount of potassium oxalate to the alkali nitrate eutectic mixture and measuring successively the volumes of CO_2 produced as a function of time. No nitrogen oxides or carbon monoxide were detected.

RESULTS AND DISCUSSION

The anhydrous potassium salt of oxalic acid reacts with the pure alkali metal nitrate mixture and forms NO_2^-, CO_3^{2-} and CO_2 (gas). When the entire quantity of $K_2C_2O_4$ introduced into the reaction was consumed, the amounts of reaction products were determined and it was established that one mole of each of these substances was produced for every mole of $C_2O_4^{2-}$, which takes part in the oxidation process.

The overall reaction is then :

$$C_2O_4^{2-} + NO_3^- \rightarrow NO_2^- + CO_3^{2-} + CO_2\,(\text{gas}) \qquad (1)$$

During an experiment the reaction melt was purged with argon at a constant flow rate in order to ensure a rapid solvation of potassium oxalate as well as a good mixing. Thus the carbon dioxide was continuously sweept from the reaction mixture and absorbed in the alkali hydroxide solution of the Orsat system.

Preliminary tests were made for the selection of a proper temperature range best suited to a kinetic study.

The process occurs at a slow rate below 315° and at a very fast rate above 370°. Hence, the reaction was studied within this temperature range following the consumption rate of oxalic anion and the volumetric absorption rate of CO_2.

Firstly, it was observed that the reaction rate decreased when the flow rate of the bubbled inert gas increased. For a flow rate of the purging gas of over 0.4 l/min, the course of the decarboxylation is nearly completely quenched.

---

[13] V. R. Wheatley, *Analyst.*, **69**, 207 (1944).

Figures 1 and 2 show the decarboxylation rate as a function of the gas flow rate for two temperatures.

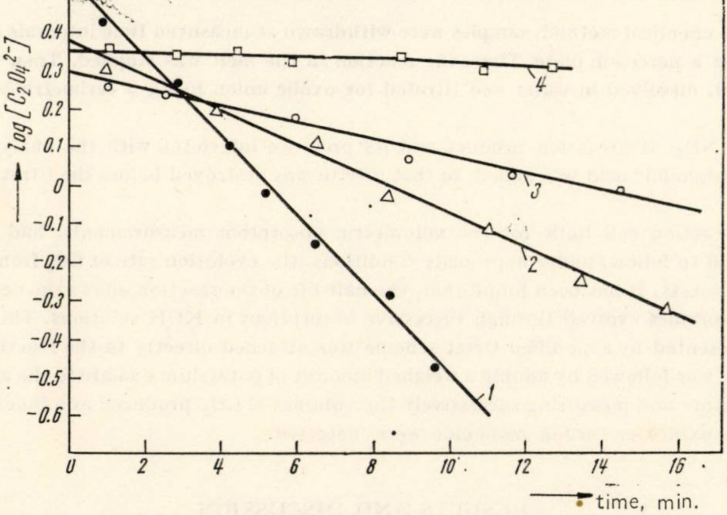

Fig. 1. — Dependence of the decarboxylation rate of oxalate anion in pure alkali nitrate melts on the flow rate of purge argon, at 330°.

1, flow rate : 0.06 l/min ; *2*, flow rate : 0.09. l/min ; *3*, flow rate : 0.15 l/min ; *4*, flow rate : 0.4 l/min.

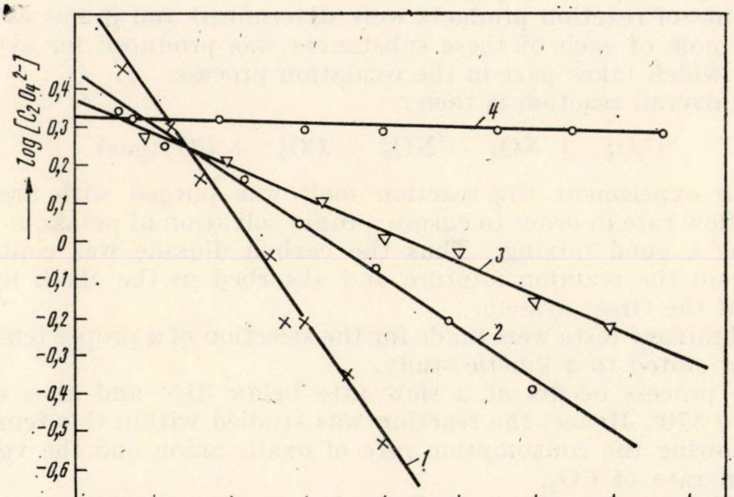

Fig. 2. — Dependence of the decarboxylation rate of oxalate anion in pure alkali nitrate melts on the flow rate of purge argon, at 345°.

1, flow rate : 0.06 l/min ; *2*, flow rate : 0.09 l/min ; *3*, flow rate : 0.15 l/min ; 4, flow rate : 0.4 l/min

A fact worth mentioning is the effect of the initial concentration of CO_3^{2-} ions introduced into the reaction mixture upon the decarboxylation rate of oxalate anion. It was found that by adding, before starting the reaction, K_2CO_3 in different quantities to the pure alkali nitrate melt, the reaction rate decreased, as the concentration of CO_3^{2-} in solution increased. The case is illustrated in Fig. 3.

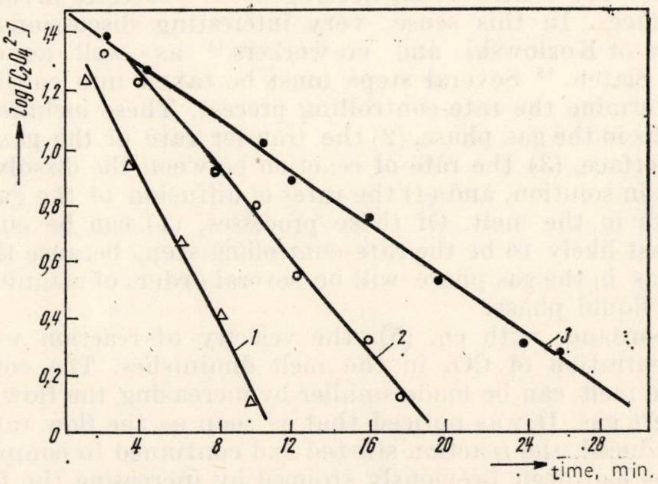

Fig. 3. — Dependence of the decarboxylation rate of oxalate anion in pure alkali nitrate melts on the initial CO_3^{2-} concentration; T: 345°; argon flow rate: 0.09 l/min.
1. CO_3^{2-} : 0 m; 2. CO_3^{2-} : 0.075 m: 3. CO_3^{2-} : 0.1 m.

A reaction mechanism which supports these observations could be:

$$NO_3^- \underset{}{\overset{K_1}{\rightleftharpoons}} NO_2^+ + O^{2-} \quad (2)$$

$$C_2O_4^{2-} + NO_2^+ \xrightarrow{k} NO_2^- + 2CO_2 \quad (3)$$

$$CO_2 + O^{2-} \overset{K_2}{\rightleftharpoons} CO_3^{2-} \quad (4)$$

Considering that it is reaction (3) which governs the decarboxylation rate, the velocity of reaction is:

$$-\frac{d[C_2O_4^{2-}]}{dt} = k\frac{K_i}{K_2}\cdot\frac{[CO_2]}{[CO_3^{2-}]}[C_2O_4^{2-}] \quad (5)$$

where $K_2 = \frac{[CO_2]\cdot[O^{2-}]}{[CO_3^{2-}]}$, $[CO_2]$ representing the concentration of carbon dioxide in the melt.

When the kinetics of the decarboxylation process was studied using the titration of the oxalate ion at measured time intervals, a large percentage of the reaction appeared to obey a first order mechanism.

Thus, a linear relationship was obtained if log $[C_2O_4^{2-}]$ was plotted *vs.* time.

The effect of the carrier gas upon the reaction rate constitutes a part of the very controversial heterogeneous processes involving gas — liquid interfaces. In this sense very interesting discussions are found in the papers of Kozlowski and co-workers [14] as well as of Wiewiorowski and Slaten. [15] Several steps must be taken into consideration in order to determine the rate-controlling process. These include : (1) diffusion of the gas in the gas phase, (2) the transfer rate of the gas across the gas-melt interface, (3) the rate of reaction between the dissolved gas and the reactant in solution, and (4) the rates of diffusion of the gas, reactant, and products in the melt. Of these processes, (1) can be considered as being the least likely to be the rate-controlling step, because the diffusion rate of the gas in the gas phase will be several orders of magnitude greater than in the liquid phase.

In accordance with eq. (5), the velocity of reaction will decrease if the concentration of CO_2 in the melt diminishes. The concentration of CO_2 in the melt can be made smaller by increasing the flow rate of the bubbling inert gas. It was noticed that as soon as the flow rate of argon was again reduced, the reaction started and continued to completion even if the process had been previously stopped by increasing the flow rate of the carrier gas. This shows that in this case, step (4) could be the ratecontrolling process.

It is most likely that the pure fused alkali nitrate mixture contains a certain amount of dissolved CO_2 gas which can remove O^{2-} by forming CO_3^{2-}. The removal of O^{2-} shifts equilibrium (6) to the right thereby maintaining a sufficient concentration of NO_2^+ required for the oxidation reaction.

Therefore, the dependence of the decarboxylation rate on the flow rate of the inert gas seems to indicate the contribution of two factors, between which it is difficult to decide the principal one, namely : (a) the velocity of reaction is determined by the rate of diffusion of CO_2 (g) formed at the surface of the melt, or (b) the velocity of reaction is determined by the solubility of CO_2 (g) in the melt. For step (a), the experimental data now available have ambigous values. The fact that for a limiting value of the flow rate of carrier argon the process is esentially quenched, could be an argument in favour of the existence of an equilibrium between the carbon dioxide in the melt and the reactant, which would indicate step (b) as having the decisive contribution.

Fig. 4 gives the results of volumetric absorption measurements. According to the overall equation of the process (5), we will have a first order kinetics if the plot of log $V_i = f(t)$ is linear.

However a linear relationship was not obtained because the concentration of CO_2 in the melt does not remain constant as the reaction develops.

---

[14] T. R. Kozlowski, R. F. Bartholomew 'and H. M. Garfinkel, *J. Inorg. Nuclear Chem.*, **32**, 401 (1970).

[15] T. K. Wiewiorowski and B. L. Slaten, *J. Phys. Chem.*, **71**, 3014 (1967).

As the decarboxylation proceeds, the partial pressure above the melt increases, thus increasing the concentration of CO_2 in the melt.

The determination of the concentration of CO_2 in the melt under the conditions in which the process was studied, represents a very difficult experimental problem. For this reason only qualitative results could be obtained in melts containing no other Lewis acid.

Although the plots in Fig. 4 are not linear, they do show that the reaction rate of the reaction decreases as the initial concentration of CO_3^{2-} increases.

In order to check that, NO_2^+ is indeed the oxidizing species in the decarboxylation of oxalic anion in fused nitrate melts, experiments were performed at three temperatures : 255°, 275°, and 295° in a dichromate solution of alkali nitrates. The chromate produced was determined in the cooled melt, by dissolving in water and by subsequent precipitation with Ba^{2+} ions. Fig. 5 gives the results.

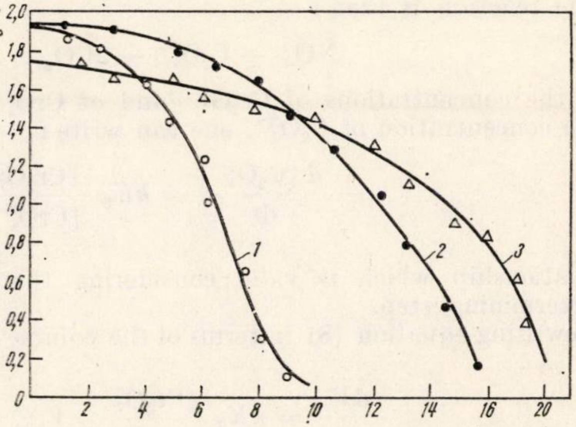

Fig. 4. — Log V_i vs. time for the decarboxylation of $C_2O_4^{2-}$ in a pure alkali nitrate melt.
1, T: 355° 2, T:340°; 3, T: 320°.

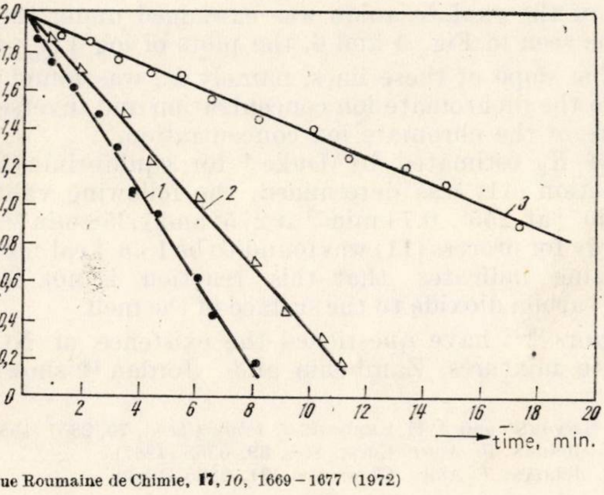

Fig. 5. — Log V_i vs. time for the decarboxylation of $C_2O_4^{2-}$ in alkali nitrate mixture containing $Cr_2O_7^{2-}$ and CrO_4^{2-} ion ; $Cr_2O_7^{2-}$: 0.25 m ; CrO_4^{2-} : 0.15 m
1, T = 295° ; 2, T = 275° ; 3, T = 255°.

Firstly, it should be noted that the working temperature range is considerably lower than in the pure nitrate melts, namely 250–300°, while the reaction rate is much higher. It was also found that two moles of CO_2 were produced for every mole of $C_2O_4^{2-}$ consumed.

Duke and Iverson, [4] report that a rapid equilibrium occurs in fused alkali nitrate mixtures containing $Cr_2O_7^{2-}$ species, namely :

$$Cr_2O_7^{2-} + NO_3^- \overset{K_3}{\rightleftharpoons} NO_2^+ + 2\,CrO_4^{2-} \tag{6}$$

Oxalate anion is oxidized more rapidly in dichromate solutions of molten alkali nitrates, because the concentration of NO_2^+ is much greater than in pure eutectic mixture. Also it is dichromate ion rather than gaseous carbon dioxide which is the oxide ion acceptor.

Therefore, for every mole of $C_2O_4^{2-}$ consumed, two moles of CO_2 are produced.

The reaction is then :

$$NO_2^+ + C_2O_4^{2-} \rightarrow 2CO_2(g) + NO_2 \tag{7}$$

If the concentrations of $Cr_2O_7^{2-}$ and of CrO_4^{2-} are large compared with the concentration of $C_2O_4^{2-}$, one can write :

$$-\frac{d\,[C_2O_4^{2-}]}{dt} = kK_3\,\frac{[Cr_2O_7^{2-}]}{[CrO_4^{2-}]^2}\,[C_2O_4^{2-}], \tag{8}$$

relationship which is valid considering that reaction (11) is the rate determining step.

Rewriting equation (8) in terms of the volume of CO_2 evolved one obtains :

$$\frac{dV_i}{dt} = kK_3\,\frac{[Cr_2O_7^{2-}]}{[CrO_4^{2-}]^2}\,V_{i_{CO_2}} = k'V_{i_{CO_2}} \tag{9}$$

The oxidation rate of the oxalate anion was examined under these conditions and, as can be seen in Fig. 5 and 6, the plots of log V_{iCO_2} *vs.* time are straight lines. The slope of these lines, namely k', was found to be directly proportional to the dichromate ion concentration and inversely proportional to the square of the chromate ion concentration.

Using the values of K_3 estimated by Duke [4] for equilibrium (10) the rate constant for reaction (11) was determined, the following values being obtained : 0.435 min^{-1} at 255°, 0.74 min^{-1} at 275° and 1.258 min^{-1} at 295°. The activation energy for process (11) was found to be 18.8 kcal/mole. This relatively high value indicates that this reaction is not controlled by the diffusion of carbon dioxide to the surface of the melt.

Recently some authors [16,17] have questioned the existence of NO_2^+ ion in fused alkali nitrate mixtures. Zambonin and Jordan [18] showed

---

[16] L. E. Topol, R. A. Osteryoung and J. H. Christie, *J. Phys. Chem.*, **70**, 2857 (1966).

[17] P. G. Zambonin and J. Jordan, *J. Amer. Chem. Soc.*, **89**, 6365 (1967).

[18] P. G. Zambonin and J. Jordan, *J. Amer. Chem. Soc.*, **91**, 2225 (1969).

that at higher concentrations, the O^{2-} ion cannot exist in fused nitrate solution. Their conclusion was established by voltmetric measurements. If we know the equilibrium constants of reactions (6) and (10), we can compute the concentration values of O^{2-} and NO_2^+. Under the working conditions of our experiments these values are about 1×10^{-9} m, and consequently far smaller than the concentrations required for precise voltmetric measurements.

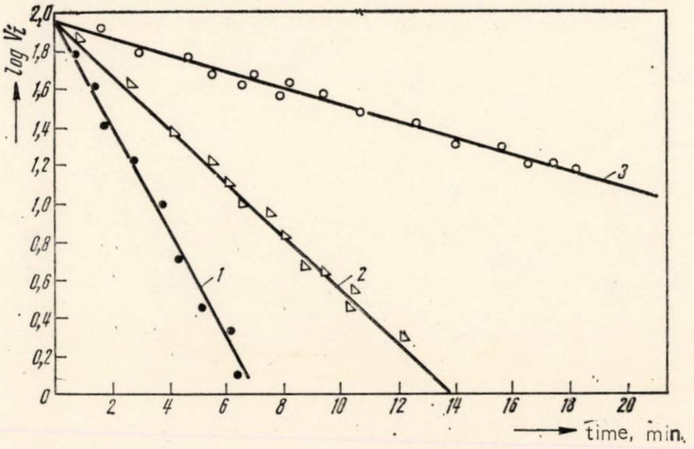

Fig. 6.—Log V_i *vs.* time for the decarboxylation of $C_2O_4^{2-}$ in alkali nitrate melts containing $Cr_2O_7^{2-}$ ions; *T* : 275°.
1. CrO_4^{2-} =0.18 m; *2*. CrO_4^{2-} =0.14 m; *3*. CrO_4^{2-} = 0.09 m.

CONCLUSIONS

1. The decarboxylation of the oxalic anion was examined both in a pure fused alkali nitrate mixture and in a dichromate solution of nitrate melts.

2. In pure nitrate melts, the reaction mechanism is determined by the concentration of the CO_2 produced in the molten phase. The reaction kinetics presents a directly dependence on the flow rate of the carrier inert gas in the reaction mixture.

3. In mixtures containing high concentrations of $Cr_2O_7^{2-}$ and CrO_4^{2-} ions, the reaction follows pseudofirst order kinetics. Under such conditions NO_2^+ species exists at a concentration value corresponding to the equilibrium (10).

4. The oxidizing species of the decarboxylation process is NO_2^+.

and at higher concentrations, the O^{2-} ion cannot exist in fused nitrate solution. This conclusion was established by Kolthoff and [illegible]. If we knew the equilibrium constants of reactions (9) and (10), we could

Fig. 4. Log k vs. time for the decarboxylation of [illegible] in nitrate melts containing Cr_2O_7 [illegible]

[illegible]

compute the concentration values of O^{2-} and NO_2^+. Under the working conditions of our experiments these values are about 1 × 10^{-10}, and consequently far smaller than the concentrations required for precise [illegible] measurements.

CONCLUSIONS

1. The decarboxylation of the oxalic anion was examined both in a pure fused alkali nitrate mixture and in a dichromate solution of nitrate melts.

2. In pure nitrate melts, the reaction mechanism is determined by the concentration of the CO_2 produced in the liquid phase. The reaction kinetics presents a direct dependence on the flow rate of the carrier inert gas in the reaction mixture.

3. In mixtures containing high concentrations of $Cr_2O_7^{2-}$ and CrO_4^{2-} ions, the reaction follows pseudo-first order kinetics. Under such conditions NO_2^+ species exists at a concentration value corresponding to the equilibrium (10).

4. The oxidizing species of the decarboxylation process is NO_2^+

Revue Roumaine de Chimie, **17**, *10*, 1679–1687 (1972)

MEASUREMENT OF THERMAL CONDUCTIVITY BY THE HOT-WIRE METHOD

RODICA VÎLCU and A. CIOCHINĂ

Institute of Physical Chemistry
str. Galaţi 31, Bucharest, Romania

Received May 6, 1972

A hot-wire apparatus of the "potential leads" type has been used to determine the thermal conductivities of some gases and organic vapours. Measurements in the temperature range 30–100° for hydrogen, argon, methane, isopentane methyl and ethyl alcohols, at normal pressure are reported. The experimental data compare favourably with the values resulted from the theoretical evaluation as well as with the literature ones.

1. INTRODUCTION

Thermal conductivity is one of the physical quantities whose measurement is very difficult and requires high precision in the determination of the factors necessary for its calculation. Therefore the data published in the literature show a marked scattering. The reasons for these deviations are various : sometimes they are construction faults of the instruments, and in other cases, particularly with larger temperature drop, heat transfer by natural convection occurs, and so on.

In many engineering calculations involving heat transfer, the knowledge of thermal conductivity appears as an important parameter. The use of thermal conductivity cells is likewise helpful in following the operation of gas generators, and in studying various gaseous reactions such as the combustion of hydrocarbons and the reforming of hydrocarbons with steam.

In this article, we briefly discuss the hot-wire method which has proved sufficiently accurate and adaptable for measurements over a range of experimental conditions.

The experimental setp-up employed for conductivity measurements was tested for hydrogen, argon, methane, isopentane, methyl and ethyl alcohol vapours, at normal pressure between 30–100°.

2. THE HOT-WIRE METHOD

Broadly speaking in this method a metal wire is placed axially in a metal or glass cylinder. The wire acts both as a heater as well as a thermometer. The test gas if filled in the cylinder and the whole assembly is immersed either in a thermostat or a furnace. For the computation of thermal conductivity all one needs to know is the change in the resistance of the axial wire when a certain current heats the wire, in the presence of a gas over its value at zero current. In practically all types of hot-wire cells, the undesirable convection, radiation, end conduction and temperature discontinuity effects are present in varying proportions. The temperature discontinuity and convection effects are brought to minimum by a careful design of the cell, and operating at a proper pressure[1].

The radiation correction is estimated either theoretically on the basis of Stefan-Boltzmann law or by taking differential measurements with and without gas. A small wall efect correction arising because of the finite thickeness of the cell wall is not only small but is also calculable with good accuracy.

The influence of excentricity on the accuracy of the measurements is only a function of the eccentricity itself and not of its direction[2]. In the cylindrical arrangement, we may tolerate some variation in the thickness of the gas layer at the ends when the axial adjustment is correctly made, since the heat transfer areas at the ends are small compared with that of the annulus.

3. APPARATUS

The experimental set-up employed for conductivity measurements containes many independent units. A vacuum pumping installation gas (or vapours) handling unit, a thin-wire variety of the hot-wire cell, electrical circuit for measurement. The conductivity cell was kept in a thermostat bath filled with parafin oil. Efficient stirring, distributed immersion heaters fed by a voltage stabilizer, proper regulation of heaters power, a contact thermometer along with its sensitive relay system made it possible to achieve temperature regulation within ±0.01° in the temperature range 20—100°. A Feussner potentiometer was employed for the electrical measurements. The thermal conductivity cell developed is schematically shown in fig. 1.

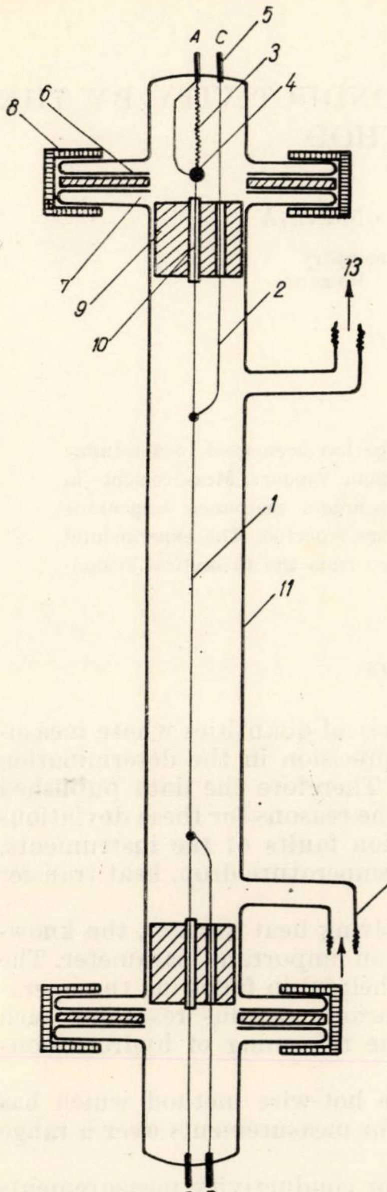

Fig. 1.— The thermal conductivity cell: *1*, hot wire; *2*, potential leads; *3*, tungsten spring; *4*, glass pearl; *4*, tungsten terminals; *6*, rubber gasket; *7*, plane joints; *8*, metal connecting pieces; *9*, teflon stopper; *10*, glass capillary; *11*, calibrated glass tube; *12*, gas inlet; *13*, gas outlet. *A*, *B* current supply terminals; *C*, *D* measuring terminals.

---

[1] G. N. Richter and B. H. Sage, *J. Chem.* and *Eng. Data*, **2**, 61 (1957).

[2] W. Leidenfrost, *Int. J. Heat. Mass. Transfer.*, **7**, 447 (1964).

Fig. 2 reproduces the entire assembly of the set-up employed (except for the electrical circuit).

The boiler and the safety device for water circulation in the cooling system are represented in figs. 3 and 4.

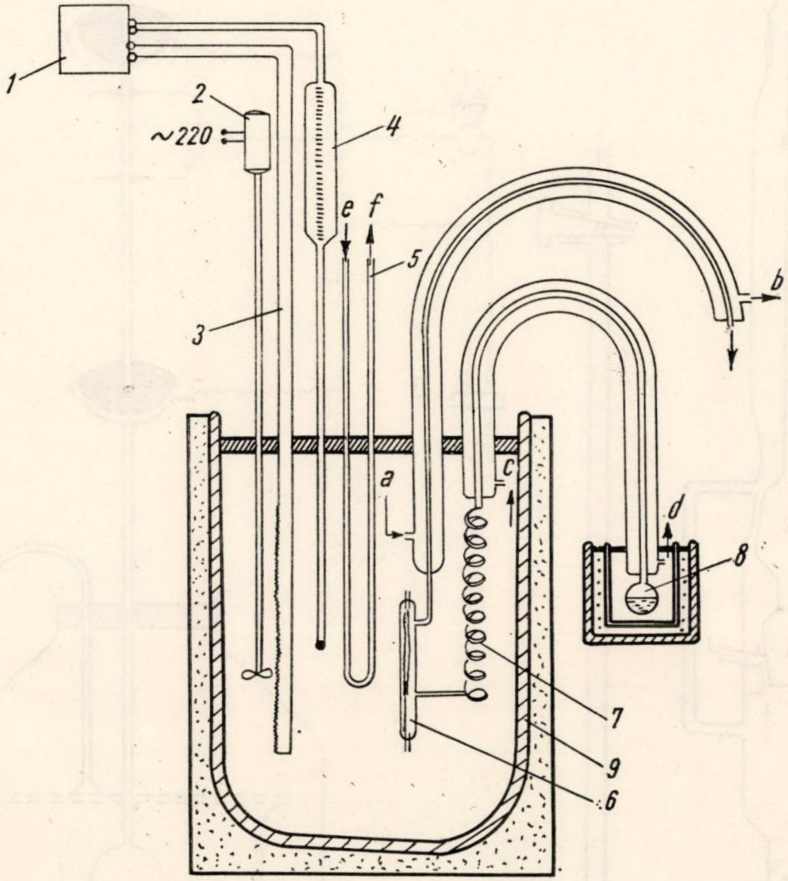

Fig. 2. – Scheme of the experimental set-up

1, thermoregulator; *2*, motor drive with stirrer; *3*, heater; *4*, contact thermometer; *5*, water cooling coil; *6*, measuring cell; *8*, boiler; *9* Dewar vessel: *a*, *b*, *c*, *d*, to the heating., thermostat; *e*, *f*, water cooling.

The "potential leads" thermal conductivity cell used in this work was made of a glass tube of a length of about 16 cm and internal diameter of 6.33 mm. Glass was used to permit a visual check of the position of th axial heating wire, and because it has a relatively small expansion coefficient so that the tube dimensions do not vary significantly over the temperature range used in the present measurements. The wire, of platinum has a diameter of 0.0031 cm.

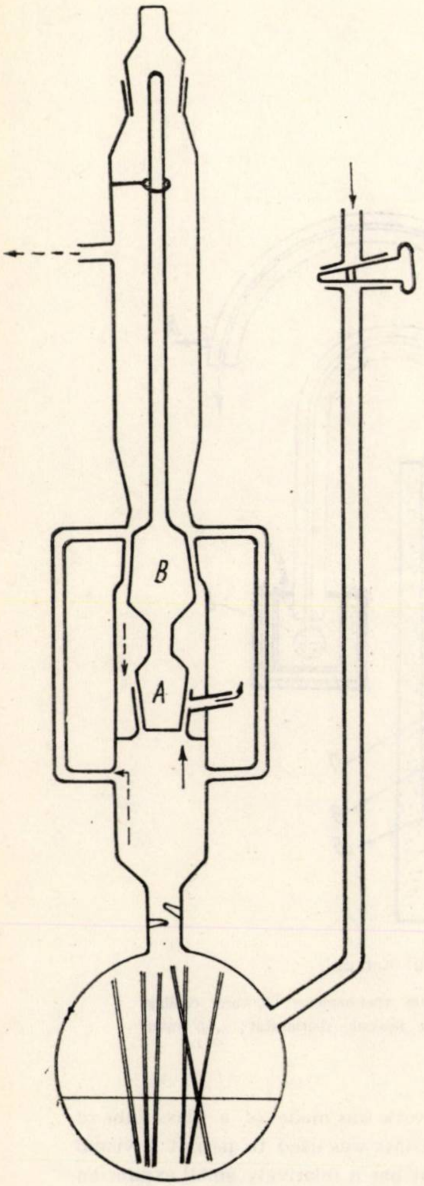

Fig. 3. – Boiler;
A, B, joints

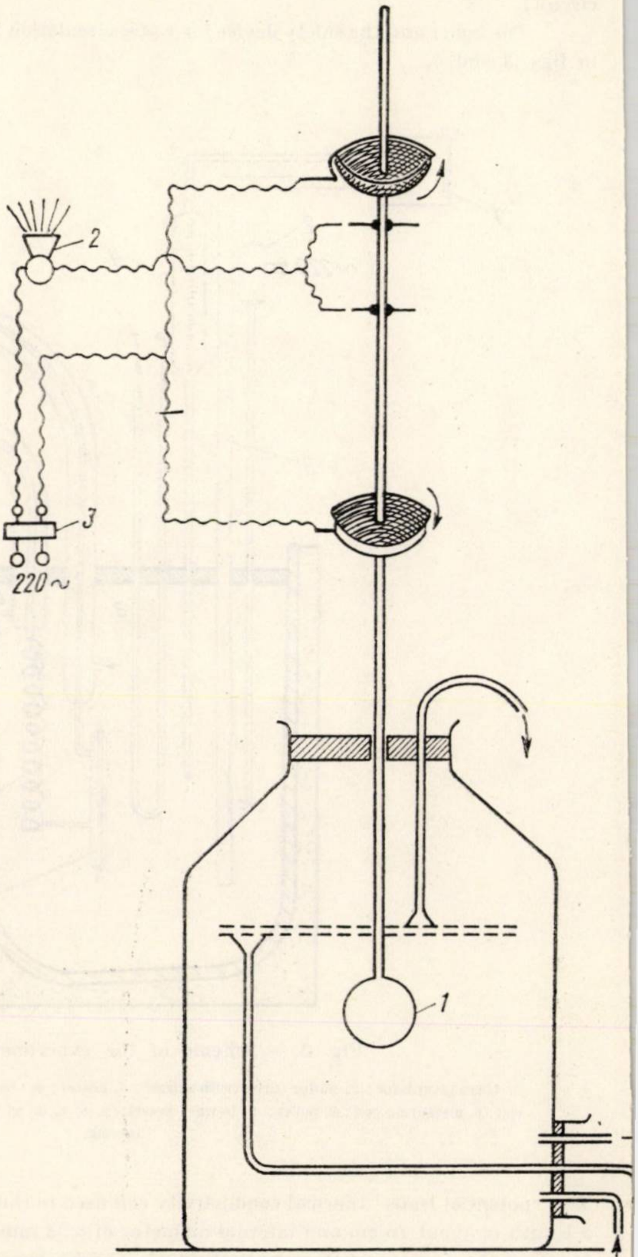

Fig. 4.—Safety device for cooling water circulation·
1, float; *2,* bell; *3,* transformer.

The effective length of the middle portion of the wire was 12.61 cm. at the ends of this portion the potential leads (platinum wire) were soldered.

The axial platinum wire was soldered to a tungsten spring, which accomodates the thermal expansion of the hot wire. The tension of the spring is critical. If this tension is too high, the wire will stretch. A loo low tension will not accomodate the thermal expansion. The ends of the platinum wires were soldered to tungsten leads which pierce both ends of the cell, and are than connected to thick copper leads (outside the cell) to the potentiometer as shown in fig. 5.

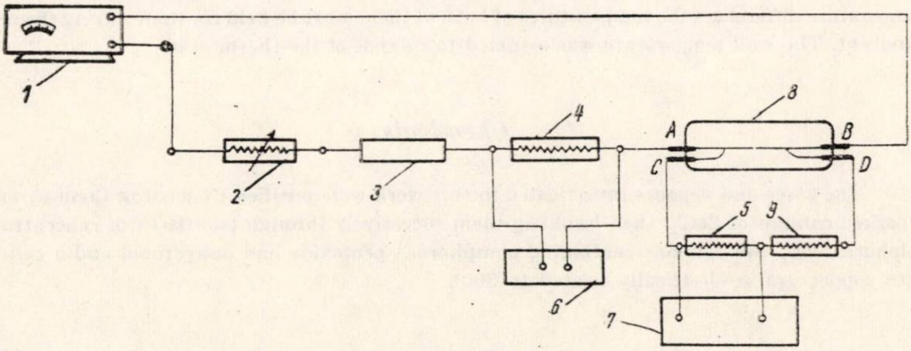

Fig. 5. – Scheme of the electric circuit

1 stabilized voltage supply; *2*, resistance box; *3*, timer; *4*, *5* standard resistances; *6*, *7* potentiometers; *8*, cell; *9*, voltage divider.

Careful investigation of the radiative heat losses *in vacuo* over the temperature range used in these experiments, together with a knowledge of the heat conductivity of glass and the inner and outer radii of the glass wall, enabled an estimate of the inner wall temperature. It has been proved that the inner temperature of the cell wall was equal with the oil thermostat one after the cell had been kept for 30 min in the bath at a constant temperature.

The axial wire was heated by a stabilized voltage source. Suitable resistance boxes in the circuit were used to increase or decrease the heating current as required. The occurate value of the current was obtained by measuring the potential drop across a standard resistance, using a Feussner potentiometer. The temperature of the heating wire was determined by calibration.

The coefficient of thermal conductivity λ was calculated by formula:

$$\lambda = \frac{E \cdot I/J}{2\pi L\ (T_1 - T_2)} \ln \frac{r_2}{r_1} \tag{1}$$

where E is the potential drop across the length L of the heating wire, I is the heating current, J is the mechanical equivalent of heat (to convert energy units in to calories), T_1 and T_2 are the temperatures of the wire and of the wall of the cell, respectively, while r_1 and r_2 are the corresponding radii of the wire and tube.

Convection effects were eliminated by proper design of the cell, and by using appropriately low gas pressures. The radiation and conduction of the potential leads were eliminated simultaneously. For temperatures up to 100°, this was made by extrapolating the plot of λ against $(T_1 - T_2)$ to $(T_1 - T_2) = 0$. This eliminates any errors which may depend on the temperature difference between the wire and the wall. At higher temperatures, the correction was made by measuring the heat loss from te wire *in vacuo*. The „temperature jump" correction was eliminated by working in the pressure range 5 to 6 cm Hg. Careful experiments on the pressure dependence of the thermal conductivity in the range 5 to 15 cm Hg, had shown that this effect was not noticeable, and only becomes important at pressures below 2 cm Hg. The values of I were chosen for each case so that θ, the temperature excess of the wire over that of the bath at a distance z from the centre due to a current I, always remained between 4° and 6°. This precaution is of value in ascribing the average temperature to the gas, and it further eliminates the ïpossible appearance of a pronounced convection effect.

Since the heat transfer from the wire to the wall of the conductivity cell depends on their temperature differences the temperatures of both of them must be held constant during the measurement. The wall temperatute was assumed to be that of the thermostat.

Chemicals

The gases and vapours investigated in this work were purified by passing them through a packed column of $CaCl_2$, then bubbling them succesively through two flasks of concentrated sulphuric acid, two columns containing phosphorous pentoxide and anhydrone, and a column with copper grains electrically heated to 300°.

4. RESULTS

The coefficients of thermal conductivity of gases and vapours are given in tables 1–6 and compared with previous values obtained by other researchers.

Table 1

Thermal conductivity of hydrogen

°t	$\lambda.10^5$ cal/cm.sec. °C	
	our data	literature 3,4
25	—	42,6
25,4	42,1	—
40	—	43,9
50	—	45,5
65	44,8	46.8
74.8	47.8	—
75	—	48.2
95	—	51,0
100	—	51.3

---

[3] P. Gray, *Trans. Faraday, Soc.*, **64**, 1032 (1969).

[4] P. Mukhopadhyay, *Brit. J. Appl. Phys.*, **18**, 1301 (1967).

Table 2

Thermal conductivity of argon

°t	$\lambda.10^5$ cal/cm. sec. °C	
	our data	literature 5, 6
29.3	4.34	—
35	—	4.38
38.4	4.38	—
40	—	4.43
50	4.47	4.55
65	—	4.61
70	—	4.78
78.2	4.85	—
90	—	5.03
100	5.11	5.09

Table 3

Thermal conductivity of methane

°t	$\lambda.10^5$.cal/cm. sec. °C	
	our data	literature 7, 8
30.2	8.28	—
40	—	8.49
45.3	8.78	—
50	—	8.71
60	—	9.20
61.2	9.32	—
75	—	9.76
80	—	9.93
100	—	10.36

---

[5] P. K. Tondon, *Chem. Lett.*, **5**, 619 (1970).

[6] R. S. Gambhir, *Ibdian J. Pure Appl. Phys.*, **5**, 457 (1967).

[7] Ia. M. Naziev, *Zhur. fiz. Khim.*, **6**, 1359 (1965).

[8] W. J. S. Smith, *J. Chem.* and *End. Data*, **5**, 316 (1960).

Table 4

Thermal conductivity of methyl alcohol vaporous

°*t*	$\lambda.10^7$ cal/cm. sec. C°	
	our data	literature 9
30	396.8	397.08
40	—	397.47
40.6	397.21	—
50	—	397.87
60	—	398.16
70	—	398.55
78.1	398.50	—
80	—	398.91
90	—	399.17
100	—	399.53

Table 5

Thermal conductivity of ethyl alcohol vapours

°*t*	$\lambda.10^7$ cal/cm. sec. °C	
	our data	literature 10
30	397.2	397.98
40	—	398.74
50	—	399.5
52.7	399.20	—
60	—	400.07
70	—	400.79
80	—	401.54
86.6	401.50	—
90	—	402.5
100	—	402.77

---

[9] L. A. Bennett and R. G. Vines, *J. Chem. Phys.*, **23**, 1587 (1955).

[10] P. Dumez, *Génie Chimique*, **93**, 143 (1963).

Table 6

Thermal conductivity of isopentane

°t	$\lambda.10^7$ cal/cm. sec. °C	
	our data	literature 11
50	4.10	3.95
68.2	4.62	4.58
75.1	4.81	4.95
84.3	5.03	5.12

Our results are in good agreement with literature data. The investigations will continue on vapours of some more complicated organic compounds as well as on binary mixtures.

Acknowledgements. Thanks are due to Mr. Radu Marin from the Institute of Physical Chemistry for making the thermal conductivity cell and all other glass pieces of the installation.

[11] H. Senftleban, *Z. angew. Phys.*, **17**, 86 (1964).

Revue Roumaine de Chimie, 17, 10, 1689 – 1696 (1972)

CHLORINE ADSORPTION ON ACTIVE CARBON IN THE MOLTEN SALTS SYSTEMS : $LiCl-KCl, PbCl_2-KCl, KCl-NaCl$

S. STERNBERG, VALERIA PETRESCU *, I. GALASIU **

* Polytechnic Institute, str. Polizu 1, Bucharest Romania
** Centre of Physical Chemistry of the Ministry of Education, str. Galaţi 31, Bucharest Romania

Received January 4, 1972

The present paper studies the phenomenon of the electrochemical adsorption of chlorine in the molten salts systems : $LiCl + KCl + 1\% AgCl$, $PbCl_2 + KCl$, $KCl + NaCl$ and $KCl + NaCl + 2\% AgCl$, on an active carbon electrode. The cathodic polarization curves are traced at temperatures between 400—800°. Conclusions are drawn regarding the electrolyte influence on the cathodic polarization curves.

In previous papers[1-3] the electrochemical adsorption of chlorine was studied on active carbone electrodes in the eutectic mixture : AgCl $(x_1 = 0.7)$ + KCl $(x_2 = 0.3)$ – (I). In the present paper this study has been extended to some other systems : $LiCl + KCl + 1\% AgCl$ – (II); $KCl + NaCl$ – (III); $KCl + NaCl + 2\% AgCl$ – (IV); $PbCl_2 + KCl$ – (V) in order to obtain information regarding the electrolyte influence on the process of electrochemical adsorption.

EXPERIMENTAL

The scheme of the experimental outfit used, the working procedure and the obtaining system of the activated carbon have been described in previous papers.[1-3] As in the above mentioned papers, we have used a "semiactivated" carbon.

After a preliminary anodic polarization the active carbon electrode was subjected to a cathodic and galvanostatic polarization, in order to achieve the electrochemical desorption of the adsorbed chlorine. Thus, the potential electrode curves φ *versus* time have been determined at a constant intensity of the current and the halogen quantity was derived from the equations :

$$Q = I \times t \text{ and } a = \frac{Q}{F}$$

---

[1] S. Sternberg and I. Galasiu, *Rev. Roumaine Chim.*, **13**, 991 (1968).
[2] S. Sternberg and I. Galasiu, *Rev. Roumaine Chim.*, **15**, 1169 (1970).
[3] S. Sternberg and I. Galasiu, *Rev. Roumaine Chim.*, in press.

in which Q represents the quantity of the current expressed in coulombs/g, F — Faraday constant, I — the intensity of the cathodic polarization current t — the cathodic polarization time a — gram-atoms of halogen.

The correction for selfdischarge was made as in papers. [1,2]

In the case of the system : LiCl + KCl + 1 %,AgCl, we have used the same electrolyses cell as in the case of the system AgCl + KCl and the electrolyte was an eutectic mixture of LiCl + + KCl having an equimolecular composition to which 1 % AgCl (gravimetric percent) was added. We obtained mixtures having the molar fraction $x_{AgCl} = 0.00388$.

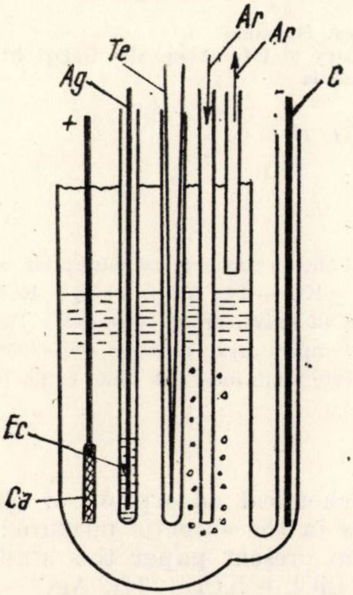

Fig. 1. — Electrolysis cell used for the system KCl + NaCl;

c_a – anode (active carbon); c – cathode (nonactive spectral carbon); E_c – control electrode (Ag rod in the melt NaCl + KCl+ + 2%AgCl); T_e – thermocuple Pt–PtRh; Ar – input and output of the argon.

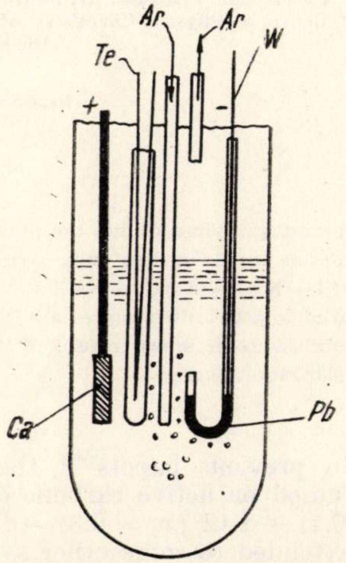

Fig. 2. — Electrolysis cell used for the system $PbCl_2$ + KCl;

c_a – anode (active carbon); w – cathode (wolfram rod in the molten Pb) T_e – termocuple Pt – PtRh; Ar – input and output of the argon.

Some modifications of the electrolysis cells have been made in the case of the systems (III) and (IV). For the system (III) in order to avoid the presence of Ag ions in the anodic space (where the active carbon electrode is) we have used the cell from fig. 1. The other electrode was a spectral (nonactive) carbon placed in the lateral tube of the cell. The electrolyte was an equimolecular mixture of NaCl + KCl. The control electrode was an Ag rod, introduced into an equimolecular mixture of NaCl + KCl, in which 2 % AgCl was added. This electrode is contained in a compact quartz tube (without orifices). The electric current is carried through the quartz membrane practically only by the sodium ions [4].

In the case of the system (IV) we have used a mixture of $PbCl_2$ + KCl with the molar fraction $x_{PbCl_2} = 0.52$. The electrolysis cell used is shown in fig. 2. The cathode is made up of molten Pb, into which a wolfram rod was introduced.

[4] S. Sternberg and C. Herdlicka, *Electrochim. Acta*, **13**, 863 (1968).

RESULTS AND DISCUSSIONS

In fig. 3 the cathodic polarization curves (potential *versus* time) at 700° for the systems (II) and (III) are reproduced. For the sake of comparison, the isotherm obtained for the system (I) was also reproduced. We have considered $\varphi = 0$ — the reversible potential of the carbon-chlorine electrode at a pressure of $p = 1$ atm. In the course of the cathodic polarization the potential becomes negative. In all the cases we have made the correction for the chemical voltage drop IR, that appears at the cathodic polarization. The main process of the cathodic polarization is the ionisation of the adsorbed chlorine at the interface of the activated carbon electrode.

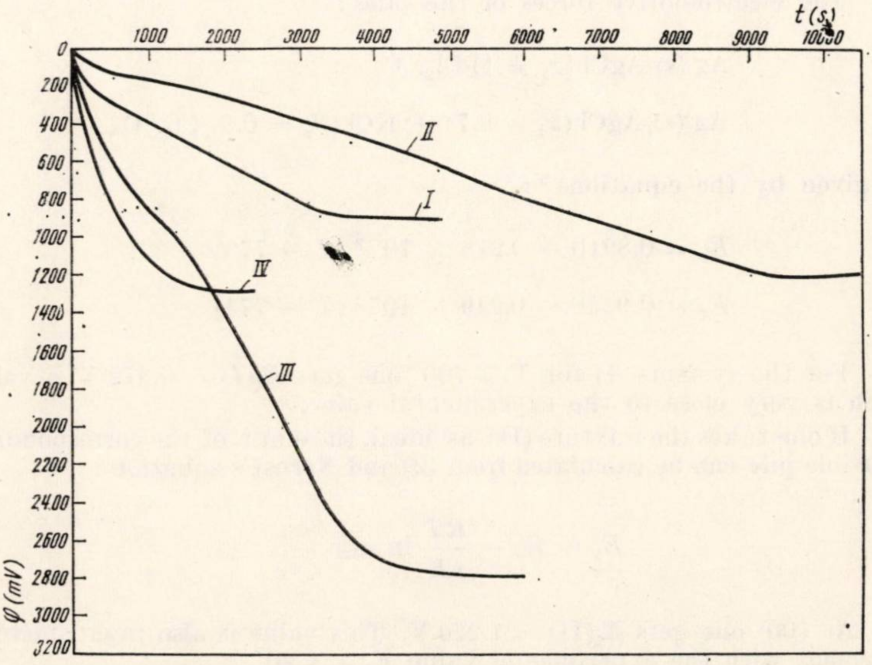

Fig. 3. — Cathodic polarization curves (potential *versus* time) for the systems: (I) — AgCl + KCl (weight of the active carbon $G_C = 2.8$ g); (II) — LiCl+KCl+1%AgCl ($G_C = 3$g); (III) — KCl + NaCl ($G_C = 2.78$g); (IV)—KCl + NaCl + 2%AgCl ($G_C = 2.22$ g); $t = 700°$ C.

$$\mathrm{Cl\,(ads)} + e \rightarrow \mathrm{Cl}^-$$

It should be noticed that all the curves $\varphi - t$ end in a horizontal part at the potentials:

$$\varphi_{(I)} = -\,0{,}88\ \mathrm{V}\,;\ \varphi_{(II)} = -\,1.20\ \mathrm{V}\,;\ \varphi_{(III)} = -\,2.86\ \mathrm{V}.$$

At these potentials the second cathodic process takes place. The approximate values of these potentials can be calculated on the basis of some simple thermo-chemical items.

For the systems (I) and (II) the second cathodic process is the deposition of the Ag ions in accordance with the reaction :

$$Ag^+ + e \rightarrow Ag$$

The electromotive forces of the piles :

$$Ag\,(s)/AgCl\,(x_1 = 1)/Cl_2,\ C \tag{a}$$

$$Ag\,(s)/AgCl\,(x_1 = 0.7) + KCl\,(x_2 = 0.3)/Cl_2,\ C \tag{b}$$

are given by the equations [5] :

$$E_0 = 0.8910 - 0.278 \times 10^{-3}\,(T - 773) \tag{1}$$

$$E_1 = 0.9220 - 0.249 \times 10^{-3}\,(T - 773) \tag{2}$$

For the systems (I) for $T = 700°$ one gets $E_1(I) = 0.872$ V, a value which is very close to the experimental value.

If one takes the mixture (II) as ideal, the e.m.f. of the corresponding reversible pile can be calculated from (2) and Nernst's equation :

$$E_1 = E_0 - \frac{RT}{nF} \ln x_{AgCl} \tag{3}$$

At 700° one gets $E_1(II) = 1.220$ V. This value is also in satisfactory agreement with the experimental value $E_1 \simeq 1.20$.

In the system (III) the second cathodic process is the deposition of the alkaline ions Na^+ or K^+ according to the electrochemical reaction :

$$Na^+ + e \rightarrow Na \text{ or } K^+ + e \rightarrow K$$

The reversible electromotive forces of KCl and NaCl have been calculated by Hamer, Malmberg and Rubin [6] from thermodynamic data and have at 700° the following value : $E_1(III) = 3.550$ V and $E_1(II) = 3.332$ V. The value of $\varphi(III)$ obtained by us experimentally is approximately by 0.450 V more positive than the discharge potential of the Na ion. This behaviour is explainable because the discharge of the alkaline ions from molten salts takes place with an important degree of depolarization. [7]

---

[5] I. Murgulescu and S. Sternberg, *Rev. Chim. Acad. R. P. R.*, **2**, 251 (1957).

[6] W. Hamer, M. Malmberg and B. Rubin, *J. Electrochem. Soc.*, **103**, 8 (1956).

[7] S. Sternberg, C. Herdlicka and M. Terzi, *Rev. Roumaine Chim.*, **11**, 303 (1966).

The apparent capacity of the double layer in zone *ab* of the curve III (see fig. 3) can be calculated from the relation :

$$C = \frac{Q \cdot 10^6}{\Delta\varphi \cdot S}\,\mu F \qquad (4)$$

where S is the surface of the electrode.

It has been shown in a previous paper that the surface of the semi-activated carbon used by us is of about 14 m^2/g. In the present experiment $S = 14 \times 3 = 42\ m^2 = 420\,000\ cm^2$, $Q = 1\,000\ s \times 0.1\ A = 100\ As$ and $\Delta\varphi = 0.83\ V$.

$$C = \frac{100 \times 10^6}{0.83 \times 420\,000} \approx 300\ \mu F/cm^2$$

The capacity of the double layer in the case of the solid electrodes in molten salts is of about 50 $\mu F/cm^2$.[8] Yet, it has been recently shown[9] that the "apparent capacity" of the double layer on platinum electrodes in molten electrolyte of $NaCl + KCl$ is close to the value obtained by us (about 500 $\mu F/cm^2$). Therefore, it is probable that in the zone *ab* of the cathodic polarization curve, the electrode process is controlled by the charging of the double layer.

Curve IV in fig. 3 has been also obtained by using the mixture $KCl + NaCl$, but 2% AgCl was introduced into the cathodic space. On curve IV a horizontal part appears, which corresponds to the discharge of the Ag ion.

The dependence of the desorbed chlorine quantity, function of the temperature, is plotted in fig. 4 for the systems (I) and (II). The quantity Q represents the desorbed chlorine from the surface of the carbon electrode for potentials from $\varphi = 0$ to the discharge potential of the Ag ion, namely $\varphi_{(I)}$ or $\varphi_{(II)}$. In the both systems the adsorbed quantity Q reaches a maximum at 700°. From fig. 4 one can observe that the quantity Q is always greater in system (II) than in system (I).

This behaviour can be explained in the following way : in both systems the chlorine is not completely removed from the carbon electrode at the potentials $\varphi_{(I)}$, $\varphi_{(II)}$ respectively because the Ag ion discharge on the carbon begins at these potentials. As the potential interval is greater in system (II) than in (I) it is to be expected that the quantity of the electrochemically desorbed chlorine should be also greater.

---

[8] E. Ukșe and N. Bukum, *Zhur. fiz. Khim.*, **35**, 2689 (1961).

[9] S. Sternberg and C. Herdlicka, *Rev. Roumaine Chim.*, in press.

The results allow to draw the following conclusions :

The formation of the activated chlorine-carbon electrode is similar to the electrolytes (I), (II) and (III). It is probable that in all the cases the same quantity of chlorine is electrochemically adsorbed on the interface of the carbon electrode, at $\varphi = 0$. The chlorine quantity which is electrochemically desorbed depends on the composition of the electrolyte: the more the second cathodic process develops at a higher electronegative potential, the greater is the electro-chemically desorbed chlorine quantity Q. In order to explore an as large interval of potentials as possible, it is necessary to use such electrolytes in the process of the electrochemical desorption that have no electropositive cations like Ag^+ or Pb^{2+}, which deposit on the cathode before the process of electrochemical desorption is completed.

The experiments made with the system $PbCl_2$ $(x_1 = 0.52) +$ $+ KCl$ $(x_2 = 0.48)$ have led to some results that are different from those previously presented.

Fig. 5 shows some curves potential *versus* time obtained with this system. As a term of comparison, a curve obtained with the system (II) is also presented.

If in the case of the system (II) the curve ends in an horizontal line that marks the discharge of the Ag ions, in the case of the system (V) the potential continues to decrease very slowly so that no stable value is reached, not even after 4—5 hours of cathodic polarization. In this system it was also found that the potential of the chlorine electrode at $p = 1$ at is very close to the reversible one which can be calculated from the e.f.m. $E_1(V)$ of the formation pile :

$$Pb/PbCl_2\,(x_1 = 0.52) + KCl\,(x_2 = 0.48)/Cl_2,\ C$$

$E_1(V)$ can be calculated from the equation [10] :

$$E_1 = 1.210 - 0.60 \times 10^{-3}\,(T - 773)$$

It was also found that in system (V) the charging time and the intensity of the charging current have a strong influence on the chlorine quantity Q obtained in the electrochemical discharging (see fig. 6). In the case of a short charging time the curves Q *versus* temperature are closer to those obtained with the systems (I) and (II). Under these conditions it was found that the curves φ *versus* time are also more similar to those of the systems (I) and (II), the "slow part" of the curves being somewhat, more reduced.

In the case of a long anodic polarization time, "the slow part" of the curves φ *versus* time becomes predominant, the value of Q increases very much, and the maximum points of the curves Q *versus* temperature shift to temperatures smaller than 700°.

---

[10] R. Lorenz and H. Velde, *Z. anorg. Chem.*, **183**, 81 (1929).

Fig. 4. — Dependence of the desorbed chlorine quantity Q function of the temperature t: (I) — system AgCl + KCl; (II) — system LiCl + KCl + 1 %AgCl.

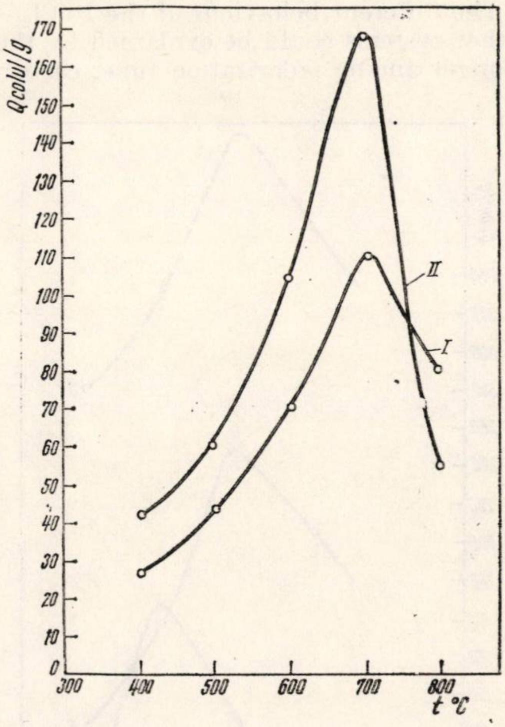

Fig. 5. — Cathodic polarization curves (potential *versus* time) for the systems $PbCl_2$ + KCl (V) and LiCl + KCl + 1 % AgCl (II):

1, System (V), t=500°C, G_C=3 g, long anodic polarization time; *2*, System (V) t = 700°C, G_C = 3 g, long anodic polarization time; *3*, System (V), t=800°C, G_C=3g, long anodic polarization time; *4*, System (V), t = 500°, G_C=3g short anodic polarization; *5*, System (II) t = 500°C, G_C = 3·g.

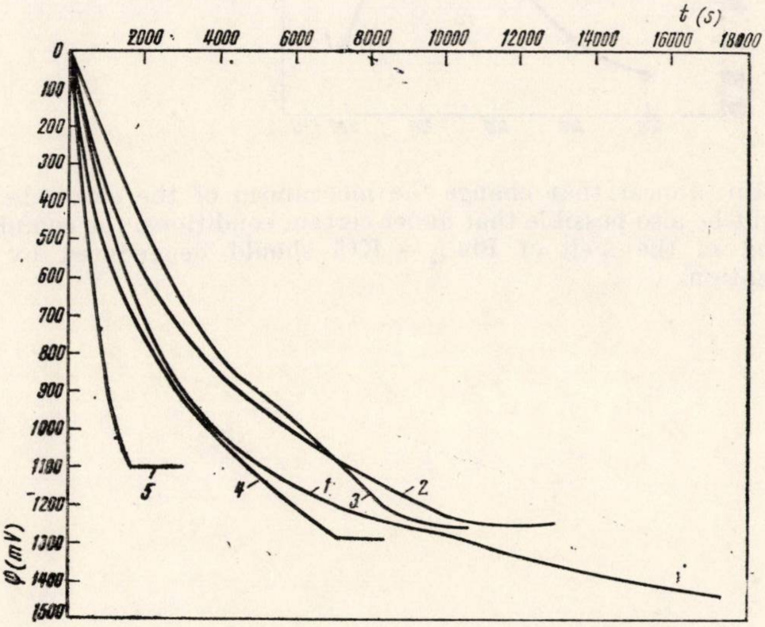

The different behaviour of the $PbCl_2 + KCl$ system as compared to the other systems could be explained by the fact that in this electrolyte, at a longer anodic polarization time, carbon compounds with chlorine or lead (Pb) appear that change the mechanism of the electrode process. It might be also possible that under certain conditions, the complex anions existing in the melt of $PbCl_2 + KCl$ should be reduced by cathodic polarization.

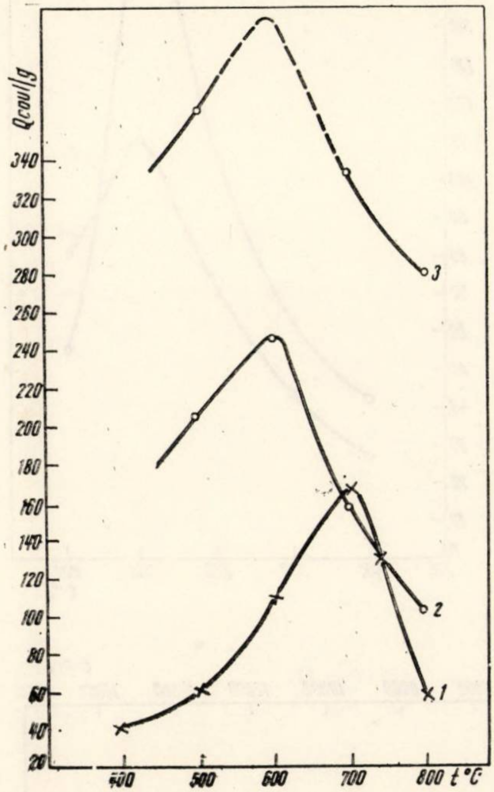

Fig. 6. — Dependence of the desorbed chlorine quantity Q function of the temperature t for the systems : $PbCl_2 + KCl$ (V) and $LiCl+KCl+1\,\%AgCl$ (II) :

1. system (II), time of the anodic polarizatin — 1 hour ; *2*, system (V), time of the anodic polarization — 3 hours ; *3*, system (V), time of the anodic polarization — 1 hour ; the discharge time was measured at the horizontal line.

Revue Roumaine de Chimie, **17**, *10*, 1697 – 1704 (1972)

L'ÉLECTRODE HALOGÈNE—CHARBON DANS LES ÉLECTROLYTES FONDUS. VII[1]

L'ADSORPTION DU BROME SUR LES ÉLECTRODES DE CHARBON ACTIVÉ

S. STERNBERG et I. GALASIU

Centre de Chimie Physique, Bucarest,
31, str. Galaţi

Reçu le 21 mars 1972

On a établi les courbes de polarisation cathodique pour l'électrode brome—charbon actif, pour des températures de 400°—800°. On a trouvé que la quantité de brome adsorbée par le charbon atteint un maximum pour 700°C. On donne aussi un aperçu comparatif des électrodes de chlore, de brome et d'iode sur le charbon actif.

Dans des travaux antérieurs[1,2] on a présenté une méthode électrochimique pour l'étude de l'adsorption du chlore et de l'iode sur les électrodes de charbon actif dans les électrolytes fondus. On a proposé, en outre, un procédé pour la correction de l'auto-désorption thermique de l'halogène sur l'électrode, celle-ci se superposant à la désorption électrochimique, en affectant ainsi l'exactitude des mesures. Maintenant notre étude est étendue au comportement du brome dans ces conditions.

PARTIE EXPÉRIMENTALE

Le schéma de l'installation est présenté dans la figure 1. La cathode c'est une barre en argent de ∅ = 1 mm, l'anode une barre en charbon actif, l'électrolyte fondu un mélange eutectique de AgBr + KBr.

Les charbons actifs ont été préparés à partir d'un mélange homogène de poudre de charbon et goudron de hêtre pressé à environ 700 atmosphères ; puis on calcine à environ 500° dans une atmosphère de gaz inerte pour éliminer les produits volatils.

Ces électrodes que nous considérons comme «semi-activées » ont une surface spécifique d'environ 10—15 m^2/g.

Pour agrandir la surface spécifique on traite les électrodes ainsi obtenues à un mélange de vapeurs d'eau et de bioxyde de charbon à 800°. Il en résulte des charbons actifs d'une surface spécifique de quelques centaines de mètres carrés par gramme, que l'on détermine selon Rubinstein et Afanasyev [3] par adsorption de vapeurs de benzène. Pour immerger complètement le charbon actif dans l'électrolyte on le fixe, à l'aide d'un filet à une barre de charbon spectral. La quantité d'halogène adsorbée sur l'électrode spectrale est négligeable.

---

[1] VIe Partie : S. Sternberg et I. Galasiu, *Rev. Roumaine Chim.*, **15**, 1169 (1970).
[2] S. Sternberg et I. Galasiu, *Rev. Roumaine Chim.*, **13**, 991 (1968).

Pour saturer l'électrode de charbon d'halogène on lui fait subir une électrolyse préliminaire de 20 à 30 minutes à un potentiel correspondant à celui réversible. Pour éliminer de la cellule l'halogène produit pendant l'electrolyse préliminaire, on mène les expériences dans un fort courant d'argon. Après avoir terminé la polarisation anodique, la cellule est connectée à un schéma de polarisation cathodique galvanostatique à l'aide d'un commutateur double qui permet l'inversion de la polarité.

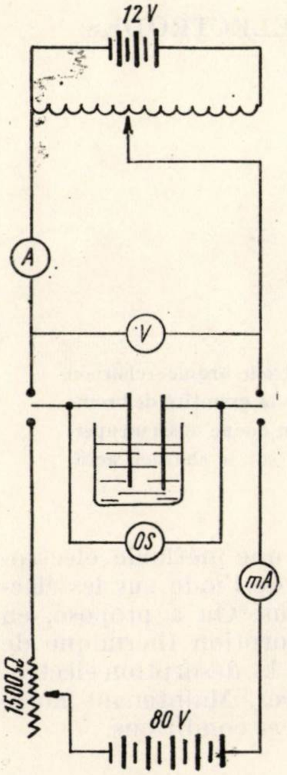

Fig. 1. — Schéma de l'installation.

On a ainsi déterminé les courbes potentiel d'électrode (φ) — temps, à une intensité constante de courant. La quantité d'haolgène a été calculée des relations :

$$Q = I \cdot t \qquad \text{et} \qquad a = \frac{Q}{F}$$

où
Q = quantité de courant exprimée en coulombs ;
F = constante de Faraday ;
I = intensité du courant de polarisation cathodique galvanostatique ;
t = temps de la polarisation cathodique ;
a = atomes-grammes d'halogène.

Le potentiel φ a été mesuré à l'aide d'un oscillographe cathodique à trace rémanente.

Pour l'évaluation de l'autodécharge on a aussi enregistré des courbes potentiel — temps en circuit ouvert.

RÉSULTATS ET DISCUSSIONS

1) L'ÉLECTRODE DE BROME

Dans la figure 2, la courbe *1* représente l'isobare d'adsorption du brome déterminée expérimentalement sur une électrode de charbon semi-activé dans l'eutectique fondu AgBr + KBr. On observe que l'isobare présente un minimum à 500° et un maximum à 700° qui sont dus probablement à la modification de l'énergie de liaison charbon — brome adsorbé.

Ainsi que nous l'avons déjà montré dans les sels fondus, à l'encontre des solutions aqueuses, à cause des hautes températures auxquelles nous travaillions, on enregistre une dépolarisation de l'électrode d'halogène affectant l'exactitude des mesures.

Durant la polarisation cathodique de l'électrode de brome a lieu une réaction de désorption électrochimique

$$\text{Br (ads.)} + e^{-} \rightarrow \text{Br}^{-} \tag{1}$$

---

[3] M. Rubinstein et I. Afanasyev, *Izvest. Akad. Nauk. S. S. S. R., Otdel. khim. Nauk*, **11**, 1294 (1956).

et une dépolarisation de l'électrode due à la désorption thermique

$$2\,\mathrm{Br\,(ads.)} \rightarrow \mathrm{Br}_2 \qquad (2)$$

et à la réaction de recombinaison du brome avec l'argent métallique dissous dans l'électrolyte

$$\mathrm{Ag} + 1/2\,\mathrm{Br}_2 \rightarrow \mathrm{Ag\,Br} \qquad (3)$$

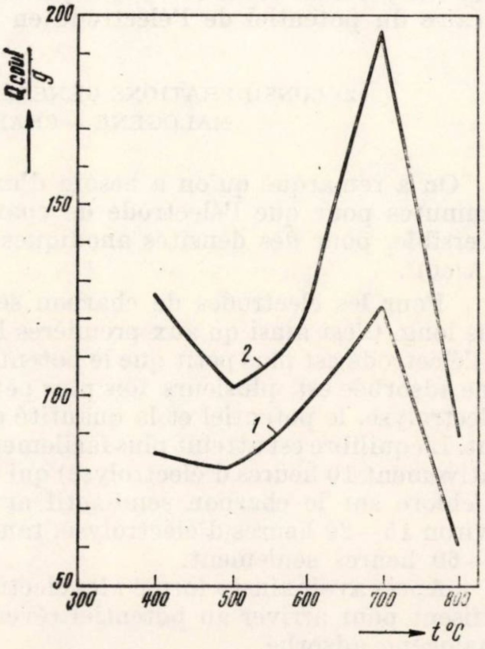

Fig. 2. — Isobare d'adsorption du brome.

1, courbe déterminée expérimentalement ; *2*, courbe corrigée.

Pendant la polarisation cathodique, la réaction (1) prédomine et pour les courbes de décharge en circuit ouvert (les courbes d'autodécharge) agissent les réactions (2) et (3).

Pour obtenir la quantité de brome adsorbée sur l'électrode, il faut ajouter au brome mesuré à l'aide de la polarisation cathodique galvanostatique, le brome perdu entre-temps par l'autodésorption.

A une température donnée, par exemple 600° (figure 3, courbe *1*), la polarisation cathodique dure τ secondes. A ce temps correspond, sur la courbe d'autodécharge (figure 3, courbe *2*), le potentiel $\varphi_{\mathrm{autodécharge}}$. Sur la courbe de polarisation cathodique, à ce potentiel correspond le temps τ' qui doit être ajouté au temps de polarisation cathodique. On procède de la même manière avec tous les points de la courbe 1, obtenant ainsi une nouvelle courbe $\varphi - t$ corrigée, la courbe *1 a*.

La courbe de polarisation cathodique galvanostatique représentant seulement d'une manière approximative le potentiel de l'électrode en fonction de la quantité de brome adsorbée sur l'électrode, la correction obtenue est aussi approximative.

Alors on répète la correction jusqu'à ce que la dernière courbe obtenue se superpose à la précédente (courbe 3). La courbe corrigée *3* représente au fond la variation du potentiel de l'électrode en fonction de la quantité de brome adsorbée sur l'électrode. Dans la figure 2, la courbe *2* représente l'isobare d'adsorption du brome après avoir fait la correction d'autodécharge pour toutes les températures.

La figure 4 représente les isothermes de désorption du brome sur l'électrode de charbon semi-activé à toutes les températures étudiées. Pour des portions étendues de chaque courbe on remarque une dépendance linéaire du potentiel de l'électrode en fonction du temps.

2) CONSIDÉRATIONS GÉNERALES SUR L'ÉLECTRODE HALOGÈNE — CHARBON ACTIVÉ

On a remarqué qu'on a besoin d'un temps de polarisation d'environ 5 minutes pour que l'électrode de charbon spectral touche au potentiel réversible, pour des densités anodiques de courant d'approximativement 1 A/cm^2.

Pour les électrodes de charbon semi-activé ce temps est beaucoup plus long. C'est ainsi qu'aux premières heures de polarisation, le potentiel de l'électrode est plus petit que le potentiel réversible et la quantité d'halogène adsorbée est plusieurs fois plus petite qu'à l'équilibre. En continuant l'électrolyse, le potentiel et la quantité d'halogène sur l'électrode augmentent. L'équilibre est atteint plus facilement pour l'électrode d'iode (approximativement 10 heures d'électrolyse) qui est aussi le plus stable. L'électrode de chlore sur le charbon semi-actif arrive au potentiel réversible après environ 15—20 heures d'électrolyse, tandis que l'électrode de brome après 50—60 heures seulement.

Après avoir ainsi « formé » les électrodes, 20—30 minutes d'électrolyse suffisent pour arriver au potentiel réversible et à une quantité constante d'halogène adsorbé.

On a encore observé qu'après avoir terminé la polarisation cathodique l'électrode « se repose », c'est-à-dire qu'après un certain laps de temps le potentiel de l'électrode augmente jusqu'à une certaine valeur que nous avons nommée « le potentiel rémanent ». Pour l'électrode de chlore, la valeur de ce potentiel est de 400—500 mV, pour l'électrode de brome 60—80 mV, et pour l'électrode d'iode 10—30 mV.

Nous avons montré [1] que l'adsorption des halogènes se fait surtout à la surface de contact entre l'électrolyte et l'électrode et que l'électrolyte ne pénètre pas dans tout le volume des pores du charbon. Bien que, grâce au barbotage de l'argon dans l'électrolyte, la pression partielle de l'halogène dans la cellule d'électrolyse soit quasi nulle, toutefois une certaine quantité d'halogène pénètre à l'intérieur de l'électrode dans la partie des pores non occupée par l'électrolyte. A l'aide de la polarisation cathodique galvanostatique on mesure seulement l'halogène qui se trouve à l'interface électrode — électrolyte, mais après la fin de la polarisation cathodique, l'halogène de l'intérieur des pores diffuse à l'extérieur et confère à l'électrode ce « potentiel rémanent ».

On sait que la tension superficielle des eutectiques AgX + KX diminue dans l'ordre Cl, Br, I ; il résulte alors que l'eutectique AgI + KI qui a la plus petite tension superficielle occupe presque complètement les

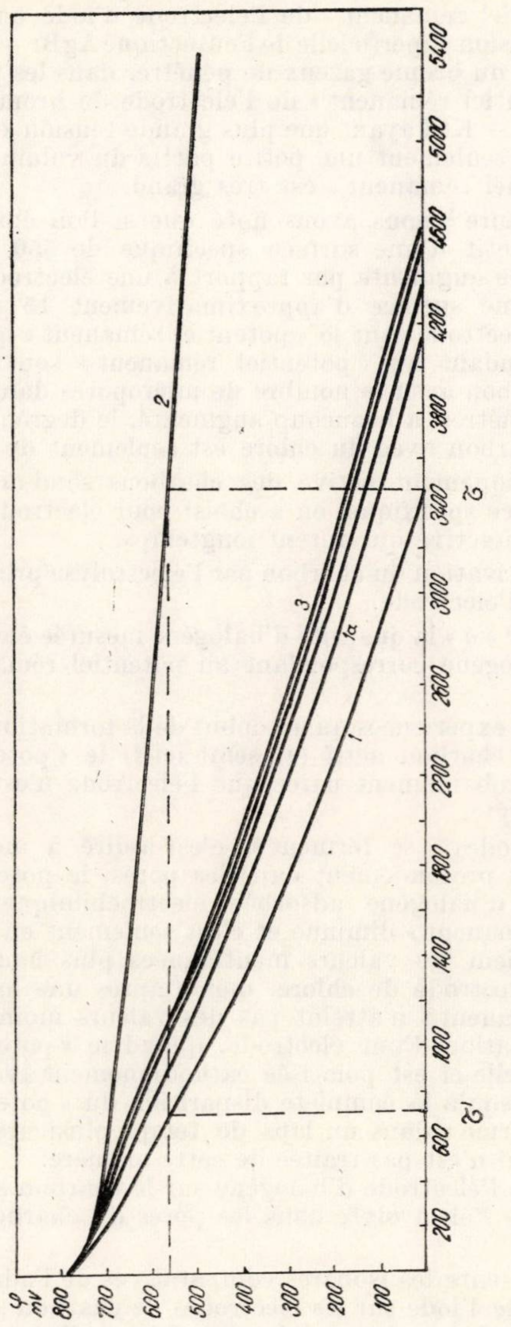

Fig. 3. — Correction pour l'autodécharge à la température de 600°.

1, courbe de polarisation cathodique galvanostatique. Intensité du courant = 0,1 A; *2*, courbe d'autodécharge; *3*, courbe de polarisation cathodique corrigée.

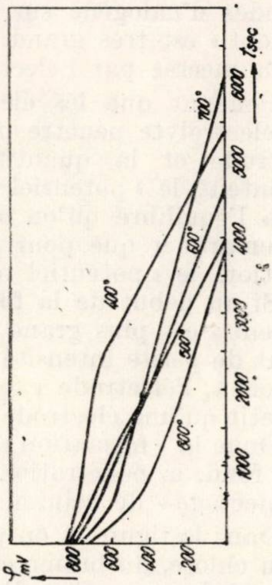

Fig. 4. — Isothermes de désorption du brome à diverses températures.

pores du charbon, ne laissant plus d'espace pour l'iode gazeux, ce qui est démontré par le « potentiel rémanent » de l'électrode d'iode qui est presque nul. Du fait que la tension superficielle de l'eutectique AgBr + KBr est plus grande, la possibilité du brome gazeux de pénétrer dans les pores augmente aussi, et le « potentiel rémanent » de l'électrode de brome est plus élevé ; l'eutectique AgCl + KCl ayant une plus grande tension superficielle occupe probablement seulement une petite partie du volume des pores, tandis que le « potentiel rémanent » est très grand.

Dans une étude antérieure [1] nous avons noté que si l'on emploie une électrode de charbon actif d'une surface spécifique de 550 m^2/g la quantité de chlore adsorbée augmente par rapport à une électrode de charbon semi-actif (ayant une surface d'approximativement 15 m^2/g) seulement de 30%. A cette électrode tant le « potentiel rémanent » que la quantité de chlore correspondant au « potentiel rémanent » sont plus grands. Vu que dans le charbon actif le nombre de micropores dans lesquels l'électrolyte ne peut pénétrer a beaucoup augmenté, le degré apparent de recouvrement du charbon avec du chlore est seulement de 0,03.

La surface électrochimiquement active des charbons semi-activés étant plus proche de la surface spécifique, on a choisi pour électrodes de travail celles de charbon semi-activé qui durent longtemps.

On peut parachever l'activation du charbon par l'électrolyse primaire pendant la « formation » de l'électrode.

On a partout désigné par « *a* » la quantité d'halogène mesurée électrochimiquement sans que l'halogène correspondant au potentiel rémanent y soit compris.

On a observé durant les expériences qu'au début de la formation des électrodes d'halogène sur le charbon actif (et semi-actif) le « potentiel rémanent » est très grand, probablement parce que l'électrode n'est pas assez humectée par l'électrolyte.

Pendant que les électrodes « se forment », c'est-à-dire à mesure que l'électrolyte pénètre plus profondément dans les pores, le potentiel d'électrode et la quantité d'halogène adsorbée électrochimiquement augmentent, le « potentiel rémanent » diminue et c'est seulement en arrivant à l'équilibre qu'on obtient les valeurs mentionnées plus haut. Il faut remarquer que pour l'électrode de chlore, même après une longue utilisation, le « potentiel rémanent » n'atteint pas des valeurs moindres.

Si au début de la formation d'une électrode, quand le « potentiel rémanent » est plus grand, celle-ci est polarisée cathodiquement avec un courant de petite intensité jusqu'à la complète disparition du « potentiel rémanent », l'électrode « se forme » dans un laps de temps plusieurs fois plus petit qu'une électrode qui n'est pas traitée de cette manière.

Donc la « formation » de l'électrode d'halogène sur le charbon signifie, au fond, la pénétration de l'électrolyte dans les pores du charbon et « l'humectage » de celui-ci.

Dans la figure 5 on présente les isobares comparatives de l'adsorption du chlore, du brome et de l'iode sur les électrodes de charbon semi-activé, où la correction d'autodésorption a été faite. Les courbes représentent des valeurs moyennes pour quelques déterminations faites sur des électrodes préparées de la même manière.

Pour tous les charbons actifs que nous avons employés, la forme des isobares est la même et les valeurs absolues varient en fonction de la surface des charbons et du mode de préparation de ceux-ci.

Les maximums et les minimums observés sur les isobares d'adsorption des halogènes sur les électrodes de charbon semi-actif peuvent être expliqués de la manière la plus plausible par le changement de l'énergie d'interaction charbon-halogène adsorbé. Pour cette explication plaide aussi le fait que pour des électrodes encore non formées, les isobares ont la même allure, mais les valeurs du Q sont inférieures à celles de l'équilibre. À mesure que les électrodes se forment, les isobares se déplacent vers les valeurs de l'équilibre.

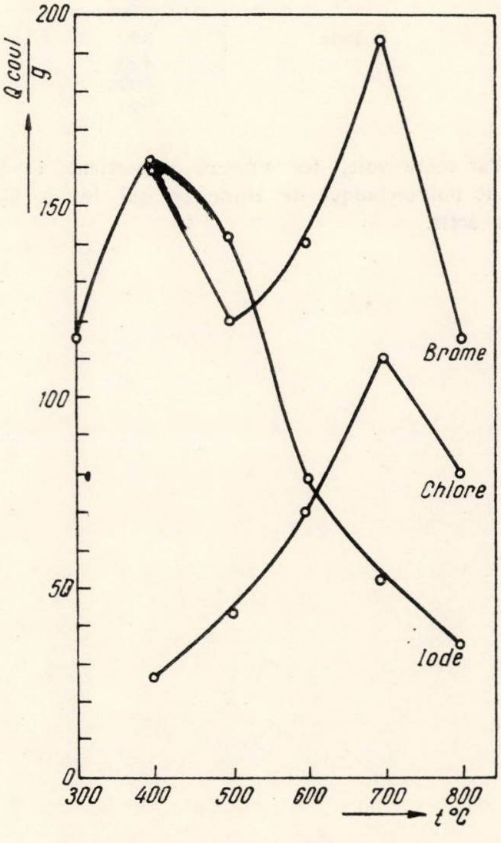

Fig. 5.— Isobares d'adsorption des halogènes sur des électrodes de charbon actif.

On a aussi observé qu'il y a une surtension des halogènes sur des électrodes de charbon actif au-dessous de 600°, surtension qui diminue quand la température augmente et disparaît à 600° ce qui nous montre le tableau 1. On pourrait expliquer cette surtension par le fait que dans les pores du charbon actif l'halogène se trouve à des pressions plus grandes que la pression atmosphérique. La durée de cette surtension après l'interruption du courant d'électrolyse est de 10 à 20 secondes.

Tableau 1

Surtension des halogènes sur des électrodes de charbon actif

Halogène	Température	Surtension mV
Chlore	400	80
	500	40
	600	0
Brome	400	60
	500	30
	600	0
Iode	300	60
	400	30
	500	20
	600	0

Par cette voie, les auteurs remercient le professeur docteur D. Ionescu de l'Institut Polytechnique de Bucarest qui les a aidés à confectionner l'électrode de charbon actif.

Revue Roumaine de Chimie, 17, *10*, 1705 – 1713 (1972)

MOLECULAR ASSOCIATION OF THE GASEOUS MAGNESIUM, CADMIUM AND ZINC CHLORIDES

LETIŢIA TOPOR and IVONA MOLDOVEANU

Center of Physical Chemistry
str. Galaţi 31, Bucharest, Romania

Received May 21, 1972

By using the absolute vapor pressure and the transpiration data, the saturated vapor compositions of the magnesium, cadmium and zinc chlorides were establised. The partial pressures of monomers and dimers as well as their variation with the temperature were deduced. Vaporization enthalpies and entropies of the liquid to monomer and to dimer and the dissociation enthalpies and entropies of the dimers were calculated. From the comparison of these thermodynamic data, the variation of the gaseous phase complexity as a temperature function was deduced.

INTRODUCTION

The association of the alkali halide vapors was thoroughly studied during the last fifteen years, by various methods. For the halides of the 2nd group the studies concerning this problem are less numerous. Provided that the results of an absolute method are combined with those obtained by the transpiration technique, conclusions can be drawn about the vapor composition from vapor pressure measurements. In some cases, the conclusions about the molecular composition of vapors are not in good agreement and depend on the experimental data considered. Such examples are the cadmium [1-3] and zinc [1,2,4] chlorides. The composition of the magnesium chloride vapors in equilibrium with the solid established by mass spectrometry[5] or by torsion effusion[6] studies extrapolated for higher temperatures, does not agree with that obtained by vapor pressure measurements of molten salt [7].

---

[1] H. Bloom and B. Y. Welch, *J. Phys. Chem.*, **62**, 1594 (1958).

[2] H. I. Moss, Thesis Indiana University, 1960, reported by R. L. Seifert in U.S. Atomic Energy Com. Tech. Rept. T I D – 6289 (1960).

[3] F. J. Keneshea and D. D. Cubicciotti, *J. Chem. Phys.*, **40**, 1778 (1964).

[4] F. J. Keneshea and D. D. Cubicciotti, *J. Chem. Phys.*, **40**, 191 (1964).

[5] J. Berkowitz and J. R. Marquart, *J. Chem. Phys.*, **37**, 1853 (1962).

[6] D. L. Hildenbrand, W. E. Hall, F. Ju. and N. D. Potter, *J. Chem. Phys.*, **40**, 2882 (1964).

[7] E. E. Schrier and H. M. Clark, *J. Phys. Chem.*, **67**, 1259 (1963).

A study of the composition of the magnesium, cadmium and zinc chloride vapors was undertaken, using the transpiration method and the previous vapor pressure values obtained by us with the Rodebush-Dixon method.[8]

EXPERIMENTAL

The transpiration apparatus and the required procedure have been described previously [9]. An inert gas is passed over the molten salt held in an isothermal region. The saturated gas-vapor mixture is then passed into a condenser where the vapors are trapped. The amount of the substance condensed and of the carrier gas are determined. The vapor pressure p can be calculated from the following relation :

$$p = \frac{g/\overline{M}}{g/\overline{M} + n_A} P_t \qquad (1)$$

where g is the mg of the salt carried by n_A millimoles of argon in the condenser, $\overline{M}$ is the mean molecular weight of the vapor and P_t is the total pressure in the installation. Using the transpiration data and the vapor pressures p obtained by Redebush-Dixon method, [8] the mean molecular weight has been calculated from relation (1). The amount of the substance carried by the argon and condensed, was determined by potentiometric titration. The total amount of the argon passed during the run was determined with a Mariotte flask. The quartz transpiration cell presented some modifications in regard to the previous one [9] (fig. 1). The wall between the two compartments *a* and *b* of the cell was provided with a much larger opening to avoid the bubbling of the inert gas through the molten salt and hence to carry away into the condenser the liquid drops. In order to avoid the access of the molten salt drops in the condenser, the cell was provided with an aditional tube, *C*, into which the top of the condenser was introduced.

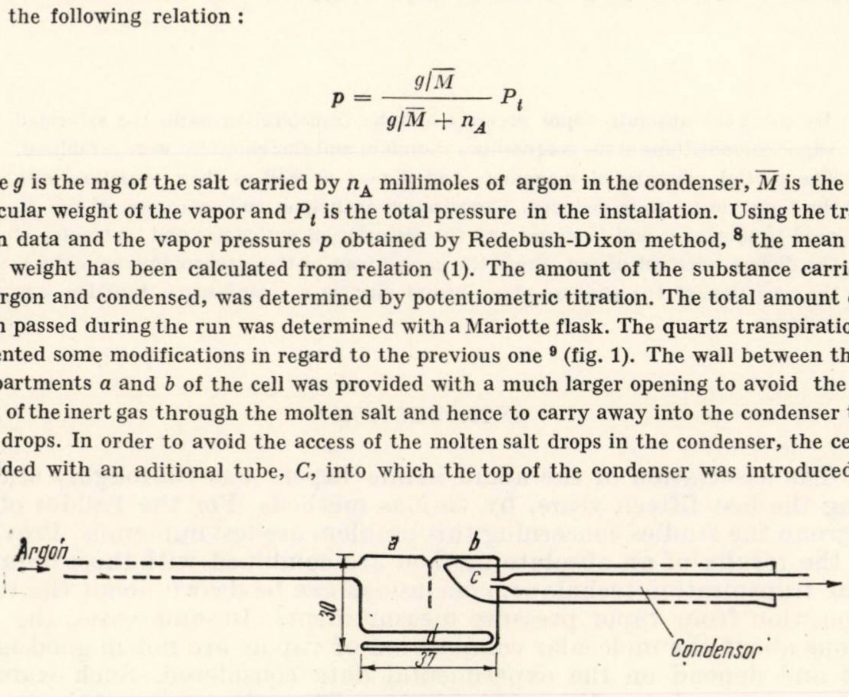

Fig. 1. — Quartz transpiration cell.
a and b – two compartments;
c – an additional tube;
d – tube for the thermocouple.

The temperature was measured by means of a thermocouple Pt—PtRh, introduced into the tube *d*. The highest temperature gradient was 3° and was determined by the thermocouple displacement in tube *d*. During each determination, the temperature was maintained constant within ±1—2° by means of a photo-cell regulator. The method used for purifying the magnesium, cadmium and zinc chlorides was previously described [8].

---

[8] L. Topor, *Rev. Roumaine Chim.*, in the press.

[9] I. G. Murgulescu and L. Topor, *Rev. Roumaine Chim.*, **13**, 1109 (1968).

RESULTS AND DISCUSSIONS

The mean molecular weight $\overline{M}$ of the vapors was determined from relation (1). The mass spectrometric studies have indicated the existence of the monomers and dimers in the $MgCl_2$[5], $CdCl_2$[3] and $ZnCl_2$[4] vapors. Therefore from the mean molecular weight $\overline{M}$ of the vapors, the molar fraction of the monomers x_1 and of the dimers x_2 can be calculated from the relations :

$$\overline{M} = x_1 M + 2\, x_2 M \tag{2}$$

$$1 = x_1 + x_2 \tag{3}$$

M is the molecular weight of the monomer. The partial pressures of the monomers p_1 and of the dimers p_2 was obtained from the expressions :

$$p_1 = x_1 p \tag{4}$$

$$p_2 = x_2 p \tag{5}$$

where p indicates the total vapor pressure determined by the quasi-static method. The variation of the partial vapor pressures with temperature is expressed by the equations of the form :

$$\log p = -\frac{\Delta H_{\text{vap}}}{2.303\, RT} + C \tag{6}$$

obtained by the last squares method using an IBM computer. ΔH_{vap} is the vaporization enthalpy of the liquid to monomers or to dimers at the midtemperature of the experimental interval. From the ratio of the partial pressures, the equilibrium constants K_p for the dissociation reactions :

$$(AX_2)_2 \rightleftarrows 2\, AX_2 \tag{7}$$

were deduced.

From relation :

$$\log\ K_p = -\frac{\Delta H_{\text{dis}}}{2.303\, RT} + \frac{\Delta S_{\text{dis}}}{2.303\, R}$$

where K_p is expressed in atmospheres, the enthalpies ΔH_{dis} and entropies ΔS_{dis} of dissociation were deduced.

Tables 1, 2 and 3 contain the temperatures used, the millimole number of argon carrying g mg of salt into the condenser, the mean molecular weight of the vapor $\overline{M}$ and the average of these molecular weights. After every table, the molecular weight of the salt is indicated.

The mole fraction of dimer in vapor x_2 and the partial pressures of the monomers p_1 and dimers p_2 are calculated by using equations (2), (3), (4), (5) and are summarized in table 4.

Table 1

Trnspiration data and mean molecular weights of the molten $MgCl_2$ vapor *)

T (°C)	n_A (M.M)	g (mg)	$\overline{M}$	Average of mean molecular weights
1017	2.093	7.2	125.99	122.80
1017	2.140	7.2	122.7	
1017	2.846	9.6	123.1	
1015	2.218	5.4	119.93	
1045	2.684	13	125.6	123.52
1045	2.828	13.6	124.7	
1044	4.475	19.5	120.27	
1063.25	2.932	17.4	124.33	123.36
1066	2.081	22.5	122.4	
1081	3.683	27.5	129.79	126.78
1087	3.887	30.6	127.47	
1087	2.539	19.1	123.1	
1094		33.5	126.69	125.98
1096.5	4.072	20.6	128.87	
1094	2.510	10.8	122.43	
1097.5	1.321	20 8	125.28	
1105	2.537	13.6	126.6	124.07
	1.415			
1103	1.293	11.7	121.54	

The $MgCl_2$ molecular weight is 95.2.

A plot of the monomer and dimer pressures as a fonction of 1/T is given in figures 2–4, containing also for comparison, the total vapor pressures obtained by the quasi-static method.[8] The corresponding partial

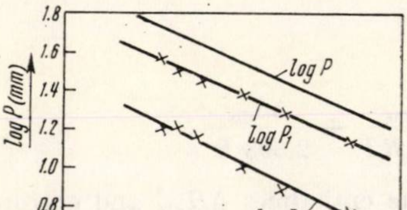

Fig. 2. — Total vapor pressures of $MgCl_2$ and partial vapor pressures of $MgCl_2$ monomer and dimer.

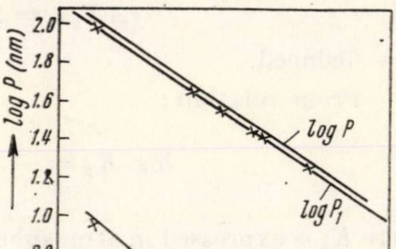

Fig. 3. — Total vapor pressures of $CdCl_2$ and partial vapor pressures of $CdCl_2$ monomer and dimer.

Fig. 4. — Total vapor pressures of $ZnCl_2$ and partial vapor pressures of $ZnCl_2$ monomer and dimer.

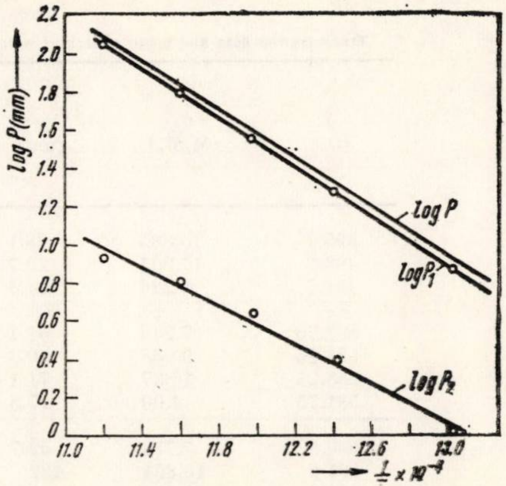

Table 2

Transpiration data and mean molecular weights of the molten $CdCl_2$ vapor*).

T (°C)	n_A (M.M)	g (mg)	$\overline{M}$	Average of the mean molecular weights.
677	2.088	10.9	198.67	
676	2.723	13.0	190.77	193.68
679	2.727	13.8	191.62	
704	3.067	24.2	194.02	
700	3.687	26.9	191.92	
699.5	3.733	27.7	196.75	194.56
699.5	4.141	30.5	195.54	
705	3.567	30.2	202.91	
705	3.693	30.3	196.64	195.5
710	5.628	47.9	187.49	
719.5	4.126	41.8	192.2	
721	7.306	79.3	202.84	196.68
719	4.203	42.5	194.3	
735	2.808	36.6	191.5	
737	2.804	40.4	205.04	
735	2.708	35.5	192.78	197.84
733	3.574	43.7	191.44	
738	3.672	54.1	208.98	
791	4.170	135.1	197.79	
791	4.255	137.0	197.75	198.68
791	2.190	72.0	200.5	

*) The $CdCl_2$ molecular weight is 183.3.

Table 3

Transpiration data and mean molecular weights of the molten $ZnCl_2$ vapor*).

T (°C)	n_A (M.M.)	g (mg)	$\overline{M}$	Average of the mean molecular weights
495.7	15.885	28.1	150.8	152.6
493.2	17.905	29.7	152.8	
494.7	8.226	14.4	154.3	
533.75	9.245	41.1	151.3	152.0
533.25	9.068	40.3	153.2	
533.25	16.37	71.1	149.6	
531.75	4.00	17.3	154	
560.5	7.778	62.7	150.21	151.1
561.5	15.851	132	151.68	
562.5	6.223	51	146.26	
562.5	3.753	32.5	156.34	
588	2.260	32	146.77	148.43
586.2	9.174	126.8	149.35	
588	3.927	57	150.84	
591	4.250	63.7	146.31	
592.3	2.372	37.2	148.88	
619.5	3.379	91.9	146.58	146.00
619.8	2.820	76.6	145.41	
618.8	2.066	90.6	146.03	

*) The $ZnCl_2$ molecular weight is 136.29

Table 4

Molar fractions of the dimers, partial pressures of monomers and dimers in the vapors of the molten Mg, Cd and Zn chlorides.

Substance	T_{mean} (°C)	x_2	p_1 (mmHg)	p_2 (mmHg)
$MgCl_2$	1017	0.290	14.27	5.82
	1045	0.297	19.65	8.31
	1065.5	0.296	24.82	10.43
	1085	0.332	29.14	14.48
	1095.5	0.323	33.04	15.76
	1104	0.303	37.18	16.16
$CdCl_2$	677	0.057	17.76	1.07
	699.5	0.061	25.87	1.68
	705	0.066	28.17	1.99
	720.5	0.073	35.76	2.81
	735.5	0.079	44.83	3.84
	791	0.084	97.83	8.97
$ZnCl_2$	494.7	0.120	7.51	1.02
	533	0.115	18.90	2.46
	561.8	0.109	35.49	4.43
	589.1	0.089	63.64	6.28
	619.5	0.071	112.50	8.60

vapor pressure equations estimated by the least squares method are :

MCl_2

$$\log p_1 = -\frac{8281 \pm 192}{T} + (7.573 \pm 0.143) \tag{8}$$

$$\log p_2 = -\frac{9514 \pm 418}{\mathrm{T}} + (8.137 \pm 0.310) \tag{9}$$

$CdCl_2$

$$\log p_1 = -\frac{6555 \pm 14}{\mathrm{T}} + (8.150 \pm 0.145) \tag{10}$$

$$\log p_2 = -\frac{8260 \pm 283}{\mathrm{T}} + (8.739 \pm 0.285) \tag{11}$$

$ZnCl_2$

$$\log p_1 = -\frac{6451 \pm 7}{\mathrm{T}} + (9.278 \pm 0.008) \tag{12}$$

$$\log p_2 = -\frac{5133 \pm 307}{\mathrm{T}} + (6.734 \pm 0.370) \tag{13}$$

The enthalpies and the entropies of vaporization of the liquid to monomer and dimer (ΔH_1, ΔH_2, ΔS_1, ΔS_2) at the midtemperatures have been obtained from equations 8–13 and are listed in table 5.

Table 5

Vaporization enthalpies and entropies of the liquid magnesium, cadmium and zinc chlorides to monomers and to dimers

Substance	T (°C)	ΔH_1 Kcal/mol	ΔH_2 kcal/mol	ΔS_1 cal/mol. K	ΔS_2 cal/mol. K	References
$MgCl_2$	1017–1104	37.8±0.9	43.5±1.8	21.5±0.6	24.1±1.4	present data
$CdCl_2$	677– 791	29.9±0.1	37.8±1.3	24.1±0.6	26.8±1.3	present data
	558– 767	33.2	26.8	27.2±0.2	16.15±0.9	2
$ZnCl_2$	494.7–619.5	29.5±0.1	23.5± 0.1	29.3±0,03	17.6±1.7	present data
	504	30.8±0.1	21.5± 4	31	14	4
	452.5–625.5	31.6	22.3	31.77±0.1	16.8±0.5	2

From the ratio of the partial pressures, expressed in atmospheres, the equilibrium constants for the dissociation reactions (7) were deduced. By the least square method the following equations were obtained:

$$\mathrm{MgCl_2} \qquad \log K_p = -\frac{7060 \pm 39}{T} + (4.136 \pm 0.029) \tag{14}$$

$$\mathrm{CdCl_2} \qquad \log K_p = -\frac{4846 \pm 0}{T} + (4.677 \pm 1.591) \tag{15}$$

$$\mathrm{ZnCl_2} \qquad \log K_p = -\frac{7781 \pm 4}{T} + (8.954 \pm 0.005) \tag{16}$$

The dissociation enthalpies and entropies have been obtained from equations 14—16 and are presented in table 6 together with other available data.

Table 6

Dissociation enthalpies and entropies of the magnezium, cadmium and zinc chloride dimers

Substance	ΔH_{dis} kcal/mol	ΔS°_D cal/mol. K	References
$MgCl_2$	32.2±0.2	18.8±0.1	Present data
	32.0±4.5	18.8±2	7
$CdCl_2$	22.2±0.0	21.4±7.3	Present data
$ZnCl_2$	35.6±0.0	40.9±0.0	Present data
	40.1±4.0	48.6±5.0	4
	40.9	46.8±0.0	2

The mass-spectrometric studies indicate that magnesium chloride vapors, in equilibrium with the solid, contain about 1 mole % dimer.[5] The extrapolation of these results shows that the vapors contain about 7 mole % dimer at 1400 K.[5,6] These data are in disagreement with the combined boiling-point and transpiration measurements,[7] which point to about 30 mole % dimer for the $MgCl_2$ vapors in equilibrium with the molten salt in the temperature range 1200—1400 K. Our results are in agreement with the last results and show a high dimer concentration of 29—33 mole % (Table 4). The variation of the vapor complexity over the condensed phase as the temperature changes, depends on the values of the enthalpy of dissociation of the dimer and of the enthalpy of vaporization. For the magnesium chloride we have obtained $\Delta H_2 > \Delta H_1 > \Delta H_{\mathrm{dis}}$, therefore the dimer is not very stable. The percentage of the dimer is low at low temperature, but it will increase as the temperature rises, because the partial pressure of dimer will increase more rapidly than that of the monomer as the temperature increases ($\Delta H_2 > \Delta H_1$). There is no good agreement between the entropy values of the gaseous magnesium chloride, calculated by various methods (from molecular constants and from the second-law entropy of vaporization and the entropy of the liquid). This disagreement was attributed by some authors [6] to the presence of a large amount of dimers in the vapors, which were assumed as containing only monomeric species for the calculations of the entropy.

For the $CdCl_2$ saturated vapors, various compositions were obtained by combining the transpiration data of Bloom and Welch [1] and of Moss [2] with those obtained by the boiling point method. [10] For instance, Bloom and Welch have considered that in the $CdCl_2$ vapors no associate species exist, while Moss has admitted the presence of 15% dimers (at temperature about the melting point) this percentage decreasing as the temperature increases. The results of the quasi-static method [3] combined with the transpiration data of Bloom and Welch [1] show an insignifiant percentage of dimers in the vapors. The same quasi-static data combined with the transpiration data of Moss [2] indicate a small amount of dimers at the melting point, which increases up to 10% with rising temperature. The data which we have obtained for the $CdCl_2$ indicated a change of dimer concentration from 5.7% to 8.4% between 677° and 791°. The concentration of gaseous polymers in the $CdCl_2$ saturated vapors is much lower than in the $MgCl_2$ vapors. The comparison of the vaporization and dissociation enthalpy values indicates an increase of the vapor complexity as the temperature rises ($\Delta H_2 > \Delta H_1 > \Delta H_{dis}$) as in the $MgCl_2$ case.

Bloom and Welch [1] have indicated a good agreement between the vapor pressure values of $ZnCl_2$ obtained by the transpiration method assuming only monomers in the gaseous phase and those resulted from the boiling point method. [11] They concluded that the vapors are only made up of monomers. Brewer et al. [12] have suggested the presence of polymers in the zinc chloride vapors and Keneshea, Cubicciotti and Moss, have confirmed Brewer's hypothesis by mass-spectrometric [4] and vapor pressure measurements. [2,4] In the saturated $ZnCl_2$ vapors our results indicate a variation of dimers concentration from 12 moles % to 7.1 moles %, between 494.7° and 611.5°. In opposition to the magnesium and cadmium chlorides, in the saturated $ZnCl_2$ vapors, the dimer percentage decreases as the temperature increases. The same conclusion follows from the comparison of vaporization and dissociation enthalpy values (tables 5 and 6), because $\Delta H_{dis} > \Delta H_1$. The dimer percentage decreases as the temperature increases, because the partial pressure of the monomers increases more rapidly than that of the dimers as the temperature increases ($\Delta H_1 > \Delta H_2$).

---

[10] J. L. Barton and H. Bloom, *J. Phys. Chem.*, **63**, 1785 (1959).

[11] H. Bloom, J. O'M. Bockris, N. E. Richards and R. G. Taylor, J. *Amer. Chem. Soc.*, **80**, 2044 (1958).

[12] L. Brewer, G. R. Somayajulu and E. Brackett, *Chem. Rev.*, **63**, 111 (1963).

temperature increases ($\Delta H_2 > \Delta H_1$). There is no good agreement between the entropy values of the gaseous magnesium chloride, calculated by various methods (from molecular constants and from the second-law entropy of vaporization and the entropy of the liquid). This disagreement was attributed by some authors [5] to the presence of a large amount of dimers in the vapours, which were assumed as containing only monomeric species for the calculations of the entropy.

For the CdCl$_2$ saturated vapours, various compositions were obtained by combining the transpiration data of Bloom and Welch [7] and of Moss [8] with those obtained by the boiling point method. [9] For instance, Bloom and Welch have considered that in the CdCl$_2$ vapours no associate species exist, while Moss has admitted the presence of 15% dimers (at temperatures near the melting point, this percentage decreasing as the temperature increases. The results of the quasi-static method [9] combined with the transpiration data of Bloom and Welch [7] show an insignificant percentage of dimers in the vapours. The same quasi-static data combined with the transpiration data of Moss [8] indicate a small amount of dimers at the melting point, which increases up to 10% with rising temperature. The data which we have obtained for the CdCl$_2$ indicated a change of dimer concentration from 0.7% to 4.4% between 677 and 781°. The concentration of gaseous polymers in the CdCl$_2$ saturated vapours is much lower than in the MgCl$_2$ vapours. The comparison of the vaporization and dissociation enthalpy values indicates an increase of the vapour complexity as the temperature rises ($\Delta H_2 > \Delta H_1$) as in the MgCl$_2$ case.

Bloom and Welch [7] have indicated a good agreement between the vapour pressure values of ZnCl$_2$ obtained by the transpiration method assuming only monomers in the gaseous phase and those resulted from the boiling point method. [9] They concluded that the vapours are only made up of monomers. Brewer et al. [3] have suggested the presence of polymers in the zinc chloride vapour and Keneshea, Cubicciotti and Moss have confirmed Brewer's hypothesis by mass spectrometric [7] and vapour measurements. [8] In the saturated ZnCl$_2$ vapours our results indicate a variation of dimer concentration from 12 moles % to 7.4 moles % between 481° and 631°. In opposition to the magnesium and cadmium chlorides, in the saturated ZnCl$_2$ vapours, the dimer percentage decreases as the temperature increases. The same conclusion follows from the comparison of vaporization and dissociation enthalpy values (tables 5 and 6), because $\Delta H_2 < \Delta H_1$. The dimer percentage decreases as the temperature increases, because the partial pressure of the monomers increases more rapidly than that of the dimers as the temperature increases ($\Delta H_1 > \Delta H_2$).

---

[8] [illegible], J. Phys. Chem., 67, 1383 (1963).

[9] [illegible] Chem., 66, 2040 (1962).

[10] [illegible], Chem. Rev., 48, 11 (1963).

Revue Roumaine de Chimie, 17, 10, 1715–1721 (1972)

PHASE EQUILIBRIA OF THE $CaO-TiO_2-V_2O_5$ SYSTEM

Ş. SOLACOLU and MARIA ZAHARESCU

Centre of Physical Chemistry, str. Dumbrava Roşie 23
Bucharest, Romania

Received March 1, 1972

The phase equilibrium diagram of the system $CaO-TiO_2-V_2O_5$ was established and the limit curves which delimit the areas of primary crystallization of phases and the invariant points were determined. It was established that no ternary compounds are formed in this system. The formation of binary definite compounds which arises in the frame of the ternary system was also studied.

1. INTRODUCTION

The phase equilibria in the ternary system $CaO-TiO_2-V_2O_5$ have not been studied although many data are available on the phase equilibrium diagrams of component binary systems.

The phase equilibria of the system $CaO-V_2O_5$ were established by Morozov[1], who determined the presence in the system of three definite compounds: $CaO.V_2O_5$, $2CaO.V_2O_5$ and $3CaO.V_2O_5$ characterized as a whole by incongruent melting at 778°, 1015° and 1380°.

The system $CaO-TiO_2$ was studied by De Vries, Roy, and Osborn,[2] who report the presence in the system of $3CaO.2TiO_2$, which melts incongruently at the temperature of 1750° and $CaO.TiO_2$ with congruent melting at 1970°. Roth[3] indicates the formation in the system, in addition to $3CaO.2TiO_2$ and $CaO.TiO_2$ of the compound $4CaO.3TiO_2$, characterized by incongruent melting at 1755°. Subsequently, Imlach and Glasser[4] did not succeed in reproducing the synthesis of the compound $4CaO.3TiO_2$. The presence of some narrow fields of solid solutions is also reported in the environment of the definite compounds. The possibility of solid solutions being formed in the system was disputed by Coughanour et al[5] and by Mamykin and Loshkarev.[6] The formation of the definite compounds $CaO.TiO_2$ and $3CaO.TiO_2$ through reactions in solid state was experimentally investigated by Mamykin and Loshkarev[6] and Berezhnoi[7] and was thermodynamically interpreted by Glushkova and Isupova.[8]

---

[1] A. N. Morozov, *Metallurg.*, **13**, 24 (1938).

[2] R. C. DeVries, R. Roy and E. F. Osborn, *J. Phys. Chem.*, **58**, 1069 (1954).

[3] R. S. Roth, *J. Res. Natl. Bur. Stand.*, **61**, 440 (1958).

[4] J. A. Imlach and F. P. Glasser, *Trans. Brit. Ceram. Soc.*, **67**, 581 (1968).

[5] L. W. Coughanour, R. S. Roth and V. A. de Presse, *J. Res. Natl. Bur,. Stand.*, **52,** 37 (1954).

[6] P. S. Mamykin and B. A. Loshkarev, *Ogneupory*, **15**, 215 (1950).

In the system $TiO_2-V_2O_5$ Belyaev and Nestorova[9] notice the small reciprocal isomorphism of compounds which was confirmed by Solacolu *et al.* in subsequent studies.[10,11]

2. EXPERIMENTAL METHODS

The reagents used had a high purity : TiO_2 (anatase) 99.80 %, V_2O_5 – 99.60 % and $CaCO_3$ – 99.10 %. The masses investigated were made up of pulverulent oxides at 60 μ fineness homogenized in aqueous suspension by stirring for one hour in a Fritsch mill.

2.1. DETERMINATION OF FUSION TEMPERATURES

The determination of liquidus temperatures was carried out with a Zeiss high-temperature microscope having a horizontal oven, and the possibility of raising the temperature to 1600°, as described in the experimental technique presented by us in papers.[10,11]

2.2. DETERMINATION OF THE FORMATION OF DEFINITE COMPOUNDS

The thermogravimetric and the thermodifferential analysis were used in order to study the formation of definite oxide compounds. An Erdey-Paulik derivatograph was used with a heating rate of 10°/min, up to the temperature of 1000°.

2.3. PHASE ANALYSIS

The phase analysis was carried out on samples thermally treated by the static method in an oven with kanthal resistance, using the röntgenographic method and the optical microscopy for the identification of phases.

The röntgenographic determinations were carried out by the Debye-Scherrer method on a TUR M–60 apparatus using CuK_α radiation.

Microscopic determinations were carried out with polarized light on powders and thin sections.

---

[7] A. S. Berezhnoi, *Ogneupory*, **15**, 349 (1950).

[8] V. B. Glushkova and E. N. Isupova, *Izv. Akad. Nauk S.S.S.R., Neorg. Mat.*, 9, 1149 (1965).

[9] I. N. Belyaev and A. K. Nestorova, *Zhur. obshohei Khim.*, **22**, 402 (1952).

[10] Ş. Solacolu, R. Dinescu and M. Zaharescu, *Rev. Roumaine Chim.*, **15**, 401 (1970).

[11] Ş. Solacolu, R. Dinescu and M. Zaharescu, *Rev. Roumaine Chim.*, **16**, 351 (1971).

3. EXPERIMENTAL RESULTS

3.1. THE DEFINITE COMPOUNDS IN THE SYSTEM

The phase analysis of binary and ternary masses under investigation led to the identification of the following crystalline phases in the thermal equilibrium : TiO_2 (rutile), V_2O_5, CaO, $CaO.V_2O_5$, $2CaO.V_2O_5$, $3CaO.V_2O_5$, $CaO.TiO_2$ and $3CaO.2TiO_2$. In the system $CaO-TiO_2-V_2O_5$ there has been no evidence of the formation of ternary chemical compounds.

3.1.1. *The system* $CaO-TiO_2$. In the binary system $CaO-TiO_2$ the formation of compounds $CaO.TiO_2$ and $3CaO.2TiO_2$, characterized by röntgen diffraction lines, identical to those reported in the literature,[12] was rendered evident through a reaction in the solid state. It was not possible to obtain the compound $4CaO.3TiO_2$, thereby confirming the results of Imlach and Glasser[4].

3.1.2. *The system* $CaO-V_2O_5$. The existence and the incongruent nature of the following three definite compounds, reported by Morozov[1] was confirmed within the system $CaO-V_2O_5$: $CaO.V_2O_5$, $2CaO.V_2O_5$ and $3CaO.V_2O_5$. The röntgen diffraction lines of the above mentioned compounds, resulting from a reaction in the solid state at 700°, 900° and 1100° respectively, are presented in table 1 and the corresponding microphotographs are represented in figure 1.

$CaO.V_2O_5$ appears as prismatic, elongated pale yellow crystals, presenting an extinction angle of $\sim 43°$.

$2CaO.V_2O_5$ appears as small transparent granulated crystals.

$3CaO.V_2O_5$ presents anisotropic transparent crystals, well developed, in a hexagonal form.

The incongruence of the three mentioned compounds was rendered evident by means of a high temperature microscope. It was noticed that compounds do not melt at a given temperature ; a decomposition is noticed in the liquid phase at the temperature of the corresponding peritectic followed by a gradual melting process which reaches the liquidus temperature.

In this way the incongruent melting temperatures were established at 780, 1015 and 1380°, confirming Morozov's results.[1]

3.1.3. *The system* $TiO_2-V_2O_5$. In the binary system $TiO_2-V_2O_5$, the infinitesimal reciprocal solubility of components as well as the absence of binary compounds was previously identified.[9-10]

3.1.4. *The system* $CaO-TiO_2-V_2O_5$. In the ternary system $CaO-TiO_2-V_2O_5$, the formation of ternary definite compounds was not identified.

Both for binary masses and for ternary masses, the role of V_2O_5 was emphasized as a mineralizer on the polymorphous transformation anatase → rutile, which takes place in the presence of this oxide at a much lower temperature (approx. 600°). The mineralizing effect is due to the isomorphous addition of V_2O_5 in TiO_2 as established in the previous papers, Solacolu et al.[11,10]

---

[12] Inorganic Index to the Powder Diffraction File, ASTM, Philadelphia, 1967, 9–365, 14–151.

Table 1

X-rays diffraction lines of the definite compounds in the CaO – V_2O_5 system

$CaO.V_2O_5$		$2CaO.V_2O_5$		$3CaO.V_2O_5$	
d	I	d	I	d	I
4.8968	s				
4.5025	s				
3.5587	s				
				3.4241	w
				3.2063	s
3.1950	v.s				
		3.0353	s		
2.9760	m.s	2.9377	w		
				2.8642	v.s
		2.7775	s		
				2.6195	v.s
				2.5334	v.w
2.4661	m.s				
2.3421	v.w				
		2.2629	v.w		
		2.1299	v.w		
		1.9876	v.w	1.9632	v.w
				1.9087	v.w
1.8826	w	1.8717	v.w	1.8294	v.w
1.8023	v.w				
		1.7891	w		
1.7262	v.w	1.7384	w	1.7384	s
		1.6793	w		
		1.6515	w	1.6515	w
				1.5837	w

v.s = very strong
s = strong
m.s = middle strong
w = weak
v.w = very weak

Although all initial mixtures of TiO_2 were anatase, when heated in the presence of V_2O_5, its form in reacted masses is found to be rutile. This behaviour was also noticed in the case of related systems $MgO-TiO_2-V_2O_5$,[11] and $BaO-TiO_2-V_2O_5$.[10]

3.2. THE FORMATION OF DEFINITE COMPOUNDS

The formation of definite compounds was analysed starting from initial dry-homogenized mixtures.

By correlating the number and the appearance temperature of thermal effects to the corresponding weight variations and to the röntgenographic analysis, it was possible to deduce the way in which binary compounds were formed from the ternary system.

In the binary system $CaO-V_2O_5$ (figure 2) it is found that regardless of the ratio $CaO : V_2O_5$ in the initial mixture, $CaO . V_2O_5$ is formed in the

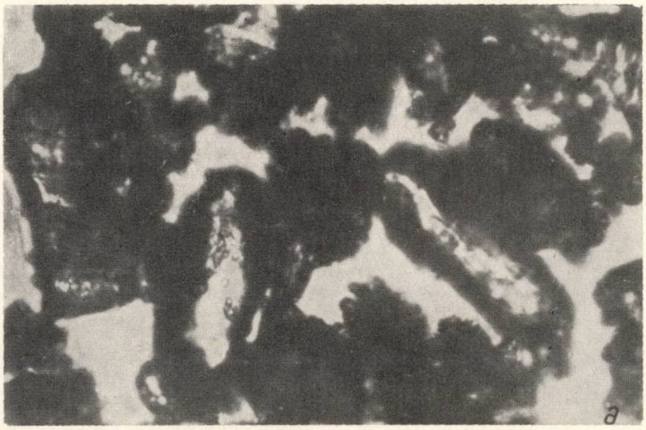

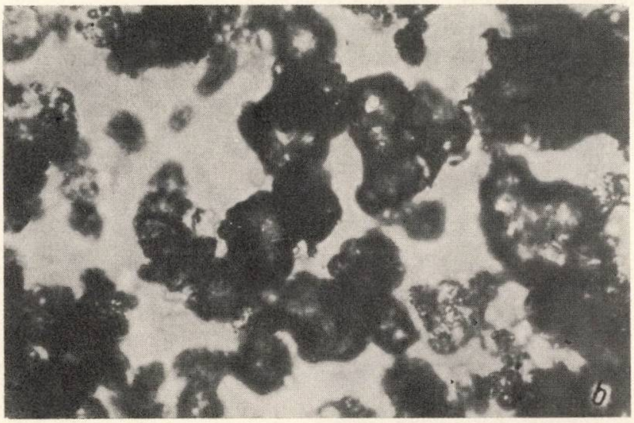

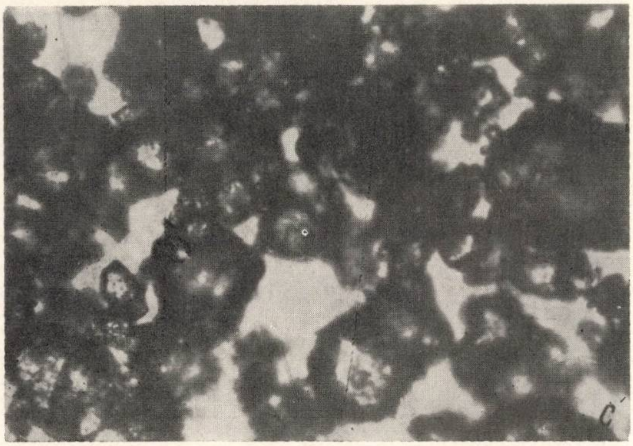

Fig. 1.— Microphotographs of definite compounds in the binary system $CaO - V_2O_5$
1) $CaO.V_2O_5$; *2)* $2CaO.V_2O_5$; *3)* $3\,CaO.V_2O_5$.

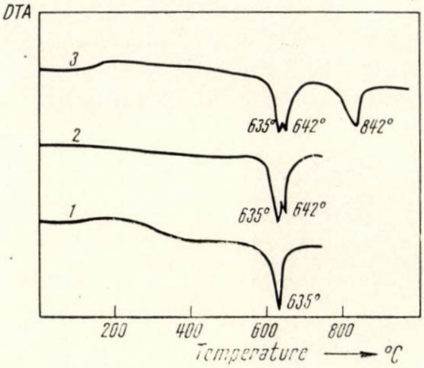

Fig. 2. — Reaction kinetics through the thermodifferential analysis of the definite compounds in the binary system $CaO-V_2O_5$.

1) $CaO.V_2O_5$; *2)* $2CaO.V_2O_5$; *3)* $3CaO.V_2O_5$.

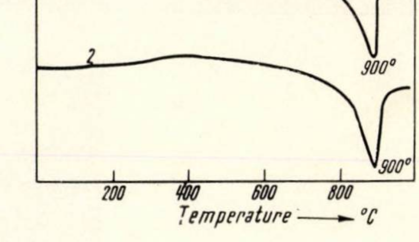

Fig. 3. — Reaction kinetics through the thermodifferential analysis of the definite compounds from the binary system $CaO-TiO_2$.

1) $CaO.TiO_2$; *2)* $3CaO.2TiO_2$.

first phase, at 635° which, in the case of an excess of $CaCO_3$, reacts with this excess, forming $2CaO.V_2O_5$ at 642° and finally the compound $3CaO.V_2O_5$ at 842°.

In the binary system $CaO-TiO_2$ (figure 3) it is found that for all mixtures a single endothermal effect is recorded at the temperature decarbonization of $CaCO_3$; it is accompanied by the formation of the compound corresponding to the stoichiometric proportions of oxides from the masses. For the stoichiometric mixture corresponding to the formation of $3CaO.2TiO_2$ the röntgenographic analysis revealed at the same time the presence of calcium metatitanate. The result obtained indicates that $CaO.TiO_2$ should be considered in this case as an intermediate phase in the formation of $3CaO.2TiO_2$. This is a confirmation of kinetic studies [6,7] which show that the formation rate of $CaO.TiO_2$ is much higher than for $3CaO.2TiO_2$ (at 1400°K, 40 times) and for the latter compound, the initial product of the reaction is $CaO.TiO_2$ subsequently forming $3CaO.TiO_2$, according to the reaction : $2\ (CaO.TiO_2) + CaO \rightarrow \rightarrow 3CaO.2TiO_2$.

3.3. PHASE EQUILIBRIA OF THE SYSTEM $CaO-TiO_2-V_2O_5$

The fusion temperatures determined for ternary mixtures as well as their phase analysis allowed to trace the limit curves which delimit the areas of primary crystallization of phases and the invariant points. The phase equilibrium diagram of the system $CaO-TiO_2-V_2O_3$ is presented in figure 4.

The system is divided into 6 subsystems presented in table 2 namely :

Subsystem I : $TiO_2-V_2O_5-CaO.V_2O_5$ controlled by the eutectic $E_1 = 590°$, with the composition shown in the table.

Subsystem II : $TiO_2-CaO.V_2O_5-2CaO.V_2O_5$ controlled by the eutectic $E_2 = 730°$, having the composition shown in the table.

Subsystem III : $TiO_2-2CaO.V_2O_5-3CaO.V_2O_5$ controlled by the eutectic $E_3 = 940°$ having the indicated composition.

Table 2

Phase equilibria and the invariant points of the $CaO-TiO_2-V_2O_5$ ternary system

Subsystem	Invariant point	Composition %			Melting point (°C)
		CaO	TiO_2	V_2O_5	
I. $TiO_2 - V_2O_5 - CaO \cdot V_2O_5$	E_1	7.5	7.5	85.0	590
II. $TiO_2 - CaO.V_2O_5 - 2CaO.V_2O_5$	E_2	21.0	17.0	62.0	730
III. $TiO_2 - 2CaO.V_2O_5 - 3CaO.V_2O_5$	E_3	29.0	30.0	41.0	940
IV. $TiO_2 - 3CaO.V_2O_5 - CaO.TiO_2$	E_4	32.0	44.0	24.0	1450
V. $3CaO.V_2O_5 - CaO.TiO_2 - 3CaO.2TiO_2$	G_5	52.0	22.0	26.0	1400
VI. $3CaO.V_2O_5 - 3CaO.2TiO_2 - CaO$	E_6	59.0	13.0	28.0	1350

Subsystem IV : TiO_2—$3CaO.V_2O_5$—$CaO.TiO_2$ controlled by the eutectic $E_4 = 1450°$ having the indicated composition.

Subsystem V : $3CaO.V_2O_5$—$CaO.TiO_2$—$2CaO_2.TiO_2$ controlled by peritectic $G_1 = 1400°$ with the composition mentioned in the table.

Subsystem VI : $3CaO.V_2O_5$—$3CaO.2TiO_2$—CaO controlled by the eutectic $E_6 = 1350°$ with the indicated composition.

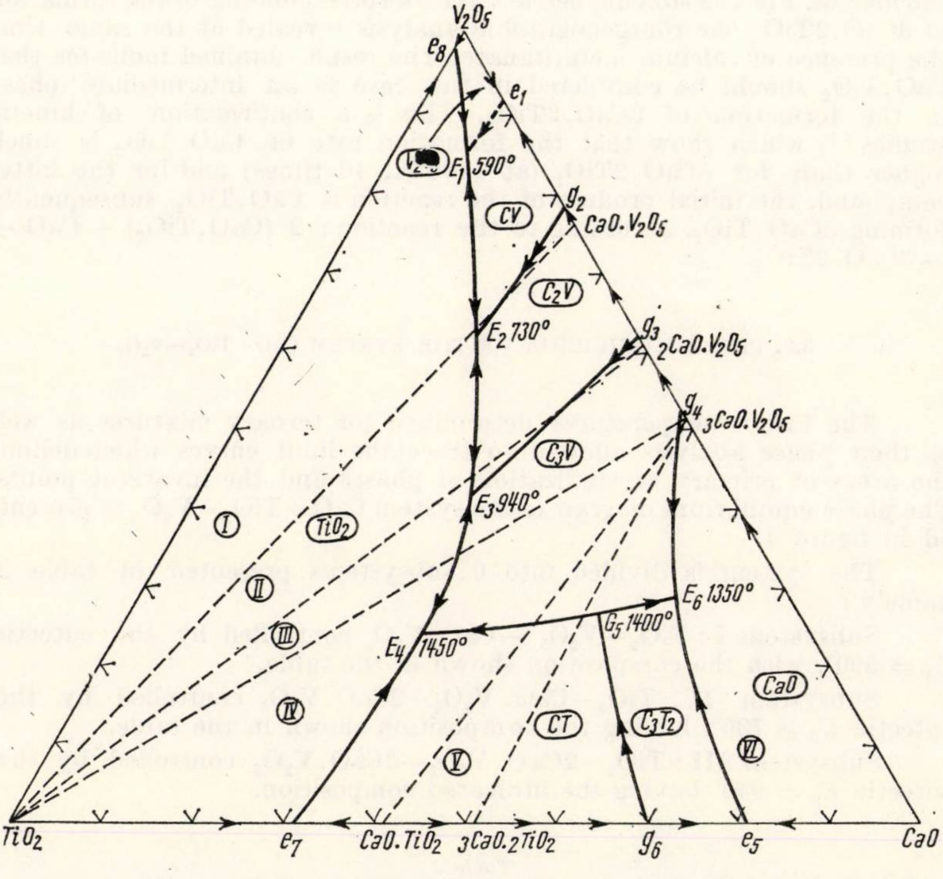
V2O5
e8
e1
V2
E1 590°
g2
CV
CaO.V2O5
C2V
E2 730°
g3
2CaO.V2O5
g4
3CaO.V2O5
C3V
E3 940°
I
TiO2
II
E6 1350°
G5 1400°
III
E4 1450°
CaO
IV
CT
C3T2
V
VI
TiO2
e7
CaO.TiO2
3CaO.2TiO2
g6
e5
CaO

Fig. 4. — Phase equilibrium diagram of the ternary system CaO—TiO_2—V_2O_5. (Ş. Solacolu and M. Zaharescu).

It is found that the areas of primary crystallization of binary compounds as well as ternary eutectics and peritectics are located in the basal area of the ternary system.

The acid area is almost entirely occupied by the primary crystallization field of TiO_2.

Another finding is the strong fusing effect of V_2O_5 on the masses under study, materialized in the low temperatures of the ternary invariant points, compared to those of the invariant points of the system CaO—TiO_2.

4. CONCLUSIONS

1. The phase equilibrium diagram of the system $CaO-TiO_2-V_2O_5$ was established; the fields of primary crystallization of unary and binary compounds V_2O_5, CaO, TiO_2 (rutile), $CaO_2.V_2O_5$, $2CaO.V_2O_5$, $3CaO.V_2O_5$, $CaO.TiO_2$ and $3CaO.2TiO_2$ were established.

2. It was established also that no ternary compounds are formed in this system.

3. Emphasis was laid on the fusing role of V_2O_5 on the masses from the studied system and on the mineralizing role in the transformation anatase → rutile.

4. The formation of binary defined compounds which arise in the frame of the ternary system was established.

Revue Roumaine de Chimie, **17**, *10*, 1715 – 1721 (1972)

Revue Roumaine de Chimie, 17, *10*, 1723 – 1728 (1972)

ELECTRICAL CONDUCTIVITY OF INTERMETALLIC COMPOUNDS OF THE PRASEODYMIUM-THALLIUM SYSTEM

P. SPACU and G. D. CISMARU

Centre of Physical Chemistry
Dumbrava Roşie 23, Bucharest, Romania

Received April 25, 1972

The electrical conductivity of intermetallic compounds of the Pr—Tl system was studied. The conductivity variation within the system confirmed the formation of Pr_5Tl_3, PrTl and $PrTl_3$ compounds and infirmed the existence of the Pr_2Tl compound. An exponential increase of conductivity was observed on increasing the atomic fraction of Tl. Values of $N_{cf}^{2/3}\, l$ product for each compound of Drude's corrected equation were determined.

INTRODUCTION

Among the intermetallic compounds of the Pr—Tl system the first compound studied by Iandelli[1] was PrTl. Vogel and Heumann[2] showed afterwards the formation of Pr_2Tl, PrTl and $PrTl_3$ compounds.

The studies of this system were again devoted to the crystalline structure of intermetallic compounds. Thus, Iandelli [1,3,4] and Palenzona [3,5] show for PrTl the CsCl structure type, and for $PrTl_3$ the $AuCu_3$ structure type. In a study referring to MX_2 compounds these researchers [6] show that the $PrTl_2$ compound does not occur in the Pr—Tl system.

Franceschi and Palenzona[7] studied the crystal structure of a new Pr_5Tl_3 compound and established for this the W_5Si_3 structure type. They showed that it is necessary to revise the possibility of the Pr_2Tl compound existence.

In order to examine the intermetallic compounds that may be formed within the Pr—Tl system and to establish the variation criterion of some properties in the compound series, a study on the conductivity of these compounds was carried out.

---

[1] A. Iandelli, "Atti X Congr. Intern. Chim.", 2, Roma 1938, p. 688—694.
[2] R. Vogel and T. Heumann, *Z. Metallk.*, **35**, 29 (1943).
[3] A. Iandelli and A. Palenzona, *J. Less Common Metals*, **9**, 1 (1965).
[4] A. Iandelli, "Proceedings of the 9th Symposium of the NPL Physical Chemistry of Metals and Alloys", 3F, (1958).
[5] A. Palenzona, *J. Less Common Metals*, **10**, 290 (1966).
[6] A. Iandelli and A. Palenzona, *J. Less Common Metals*, **15**, 273 (1968).
[7] E. Franceschi and A. Palenzona, *J. Less Common Metals*, **18**, 93 (1969).

EXPERIMENTAL

The metals used for preparing the intermetallic compounds were Pr with a purity of 99.9% and Tl with a purity of 99.999%, obtained from Johnson Matthey Ltd. Co., England.

Besides the samples for compounds, where the ratio Pr : Tl was 2 : 1, 5 : 3, 1 : 1 and 1 : 3, other ten samples were prepared where the ratio ranged from 2.3 :1 to 1 : 4; these samples were chosen so that on either side of the supposed compounds two alloys with similar proportions might exist.

Melting of metals introduced into tantalum nacelles was performed in a pure argon atmosphere in a Vacutherm Reichert installation, modified with a tantalum heating element. The installation design was presented in a previous paper [8]. Metal amounts (Pr + Tl) introduced for melting ranged from 1.5 to 2.0 g.

In the beginning, the heating was performed to 400° for 6 hours, then the temperature was increased to 1350° for about 100 minutes. The feeding tension was then suddenly reduced down to 0, bringing about a rapid low temperature down to 200°, followed by a slower cooling down to the room temperature (25°). The slower cooling from 200° to 25° is due to the installation thermal inertia.

Adopting a rapid cooling after melting was necessary since pronounced dendritic formations sometimes 6 mm high occurred with some samples when cooling slowly.

The samples were examined with a metallographic microscope to observe the homogeneity.

In case the compound samples were not homogeneous they were ground and pressed in pellets which were annealed in argon at 300°.

For conductivity determinations parallelepipeds of $10 \times 2 \times 2$ mm were prepared from samples.

The conductivity was determined at 25° by means of Thomson methods and the method of four contacts according to Schnabel [9], using a R–329 double bridge (U.S.S.R.).

Since the samples of intermetallic compounds and alloys presented a pronounced corrosion in air, these were kept in paraffin oil, and conductivity determinations were carried out on samples protected with the same oil or vaseline.

RESULTS AND DISCUSSION

Three singular points, represented by conductivity minima and maxima, resulted from conductivity determinations on samples from the concentration interval studied. Peaks observed on the conductivity — composition curve correspond to Pr_5Tl_3, PrTl and $PrTl_3$ intermetallic compounds. As concerns the Pr_2Tl compound, indicated by Vogel and Heumann,[2] the lack of a minimum conductivity at ratio 2 : 1, compared to alloy conductivity in the interval where the atomic ratio Pr : Tl ranged from 2.3 : 1 to 1.8 : 1, does not confirm the formation of a compound.

The conductivity values show that the criterion of conductivity exponential variation is applied to intermetallic compounds of the Pr—Tl system; the same was also observed with La—Tl [8] and Nd—Tl systems previously studied by the authors.

---

[8] P. Spacu and G. D. Cismaru, *Studii și Cercetări de Chim., Acad. R. P. R.*, **1963**, 399.

[9] P. Schnabel, *Philips Res. Repts.*, **19**, 43 (1964).

Conductivity values in the series of compounds occurring in the Pr—Tl system increase as the atomic fraction of the hyperelectronic element — tallium — increases, according to the following equation:

$$\sigma = A e^{K c_B} \tag{1}$$

where σ is the conductivity; A is a constant for a certain temperature; K is the exponent whose value is given by the line slope and c_B is the concentration of Tl hyperelectronic element expressed by its atomic fraction.

By equation (1) logarithmation and introducing the experimental values the diagrama $\ln \sigma - c_B$ (Fig. 1) is plotted, out of which values of A and K may result, c_B being known:

$$\ln \sigma = \ln A + K c_B \tag{1'}$$

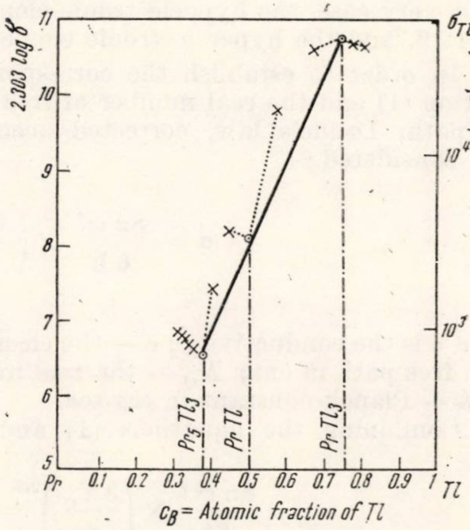

Fig. 1 Exponential variation of conductivity in intermetallic compounds within the Pr—Tl system;

1, ⊙ values corresponding to intermetallic compounds; *2*, values corresponding to alloys in zones between compounds.

The values of conductivity and of A and K for 25° were presented in Table 1.

In the binary intermetallic compounds, formed between a hypoelectronic and a hyperelectronic element according to Pauling's theory [10] on metallic bond, stronger bonds occur than in case of small electronegativity differences, in which some of valence electrons are participating. This leads, on the one side, to the formation of a more compact crystal lattice, and, on the other side, to the reducing in the number of free conduction electrons (N_{ef}) or their mean free path (l) as against pure metals.

---

[10] L. PAULING, "The Nature of the Chemical Bond", 3rd ed., Cornell University Press, New York, 1960, p. 431—432.

Table 1

Values of σ, A and K of equation (1) for intermetallic compounds at 25°

Intermetalic compound	Atomic fraction of Tl c_B	A $[\Omega^{-1} - \mathrm{cm}^{-1}]$	K	σ $[(\Omega^{-1} - \mathrm{cm}^{-1}]$ experimental σ_e	calc. σ_c	$\frac{\sigma_e}{\sigma_c}$
Pr_5Tl_3	0.375	11.20	11.20	7.14×10^2	7.45×10^2	0.958
Pr Tl	0.50			3.29×10^3	3.02×10^3	1.09
Pr Tl_3	0.75			4.76×10^4	5.00×10^4	0,952

It is in that way that the conductivity values of intermetallic compounds may be explained, as they have also been observed experimentally in this very case, the hypoelectronic element being Pr with electronegativity 1.19, and the hyperelectronic element Tl with electronegativity 1.8.

In order to establish the correspondence between the exponential equation (1) and the real number of free electrons, as well as their mean free path, Drude's law, corrected according to quantum theory, has been considered :

$$\sigma = \frac{8\pi\, e^2 l}{6\,\mathrm{h}} \times \left(\frac{3N_{\mathrm{ef}}}{8\pi}\right)^{2/3} \tag{2}$$

where σ is the conductivity ; e — the electron charge in abs. e.s.u. ; l — the mean free path in cm ; N_{ef} — the real number of free electrons in 1 cm³ ; and h — Planck constant in erg/sec.

Combining the equations (1) and (2) :

$$\frac{8\pi\, e^2\, l}{6h} \times \left(\frac{3N_{\mathrm{ef}}}{8\pi}\right)^{2/3} = A e^{Kc_B} \tag{3}$$

where :

$$N_{\mathrm{ef}}^{2/3}\, l = A\left[\left(\frac{3}{\pi}\right)^{1/3} \times \frac{h}{e^2}\right] \times e^{Kc_B} \tag{4}$$

where the paranthesis of the second member is a constant denoted by C.

$$C = \left(\frac{3}{\pi}\right)^{1/3} \times \frac{h}{e^2} = 2.8293 \times 10^{-8}\ \frac{\text{erg-sec}}{(e.s.u)^2} \tag{5}$$

In that case, equation(4) becomes :

$$N_{\mathrm{ef}}^{2/3}\, l = AC\, e^{Kc_B} \tag{6}$$

Therefore the product $N_{ef}^{2/3}\, l$ varies exponentially with the atomic fraction c_B of the hyperelectronic element.

The values of product $N_{ef}^{2/3}\, l$ which characterize the intermetallic compounds, occuring in the Pr — Tl system, were presented in Table 2.

Table 2

Values of product $N_{ef}^{2/3}\, l$ and of constant C of equations (2) and (6) for intermetallic compounds at 25°

Intermetallic compound	Atomic fraction of Tl c_B	C $\frac{\text{erg sec}}{(\text{e.s.u.})^2}$	$A \times C \times 9 \times 10^{11}$ $[\text{cm}^{-1}]$	$N_{ef}^{2/3} l$ $[\text{cm}^{-1}]$	
				of ecuation 2*	of equation 6
Pr_5Tl_3	0.375	$2.8293.10^{-8}$	$2.85.10^5$	1.818×10^7	1.874×10^7
PrTl	0.50			8.375×10^7	7.664×10^7
$PrTl_3$	0.75			1.210×10^9	1.273×10^9

*) Values σ_s from Table 1 were used.

If within the first approximation the mean free path l is considered equal to the distances between the plans of crystal lattice, then the value 3.12 Å (sum of covalent radii of components) may be used for $PrTl_3$, and the lattice constants for the other compounds, that is 3.869 Å for $PrTl^4$, and 4.747 Å for $PrTl_3^4$.

For a clearer illustration the percentage of valence electrons leading the electric current in the intermetallic compounds the value n_{ef} representing the number of free electrons that correspond to 1 atom, was used instead of N_{ef}. The following relation exists between the two values:

$$n_{ef} = \frac{N_{ef}}{N_a} = \frac{N_{ef}\, M}{N.D\, n_a} \tag{7}$$

where N_a is the number of atoms included in 1cm³; M — molecular weight of the compound in grams; N —Avogadro's number 6.0235×10^{23}; D — compound density in gm/cm³; and n_a — number of atoms in the compound formula.

Since in case of values chosen for l, n_{ef} is 4.5×10^{-1} for Pr_5Tl_3, 2.55 for PrTl, and 7.65.10 for PrTl, therefore too low with Pr_5Tl_3 or too high with PrTl, then l has in fact other values.

The limits within which n_{ef} may vary should be considered for determining the possible values of l.

If one admits that at least one part of the valence electrons of each atom participates in the bond of intermetallic compounds, which is similar to the covalent bond with pairs of delocalized electrons according to Pauling's theory [10], then with trivalent elements n_{ef} cannot be but lower or at least equal to $3 (n_{ef} \leqslant 3)$. In order to know the limits within which l might range, its values were calculated for the studied compounds considering some possible values of n_{ef}.

The values obtained for l were mentioned in Table 3.

Table 3

Values of mean free path l with different n_{ef} values for intermetallic compounds at 25°

n_{ef}	0.5	1	1.5	2	2.5	3
Intermetallic compound	$l \times 10^8$ [cm]					
Pr_5Tl_3	2.83	1.78	1.36	1.12	0.97	0.86
PrTl	12.54	7.90	6.03	4.97	4.29	3.80
$PrTl_3$	171.77	102.88	82.57	68.16	58.76	52.02

The cases studied so far show that the mean free path increases from 10^{-8} cm for the compound Pr_5Tl_3 to $10^{-7}-10^{-6}$ cm for the compound $PrTl_3$.

Therefore, the mean free path with the compounds PrTl and $PrTl_3$ is surely higher than the lattice constants. With $PrTl_3$ it reaches values 11–36 times higher, being observed on metallic tallium too, where l is 6.36×10^{-7}, if 3 electrons /atom are participating in the metal conductivity ($\sigma_{Tl} = 5.5 \times 10^4 \ \Omega^{-1} \ cm^{-1}$)[11]. This may be explained, on the one side, by the fact that collectivized electrons are moving according to the laws of wave mechanics, and, on the other side, by deforming the periodicity of crystal potential.

CONCLUSIONS

1. The Pr_5Tl_3, PrTl and $PrTl_3$ intermetallic compounds were identified in the Pr–Tl system by means of conductivity. No conductivity minimum has been noticed for the Pr_2Tl composition, which infirms the occurrence of this compound.

2. The conductivity variation follows an exponential law $\sigma = Ae^{Kc_B}$, where A and K are constants at a constant temperature, and c_B is the atomic fraction of Tl hyperelectronic element.

The increase in conductivity value is observed in the series of intermetallic compounds from Pr_5Tl_3 to $PrTl_3$.

3. The product $N_{ef}^{2/3} \ l$ depends on Kc_B by an exponential equation : $N_{ef}^{2/3} \ l = A \ C \ e^{Kc_B}$. The value of $N_{ef}^{2/3} \ l$ was determined from this equation, as well as the mean free path l of compounds for different n_{ef} values.

---

[11] C. A. HAMPEL, "Rare Metals Handbook", Reinhold Publishing Corporation Chapman& Hall, Ltd., London, 1961.

Revue Roumaine de Chimie, 17, 10, 1729–1734 (1972)

CONTRIBUTIONS TO THE STUDY OF LANTHANIDES WITH BIGUANIDE DERIVATES. III.[1]

EUROPIUM AND GADOLINIUM COMPOUNDS WITH PALUDRINE

ILEANA ALBESCU

Center of Physical Chemistry, str Dumbrava roşie 23
Bucharest, Romania

Received April 24, 1972

The present paper describes new compounds of Eu and Gd with paludrine, N_1-*p*. Cl—phenyl—N_5—iso-propyl-biguanide, of type :

$EuCl_3$.pald $GdCl_3$.2pald $EuCl_3$.3pald $2EuCl_3$.5pald
$GdCl_3$.3pald

The compounds obtained were structurally characterized by means of their electronic and IR spectra.

The present note deals with the preparation of new lanthanide compounds with biguanide derivate, paludrine ($C_{11}N_5H_{16}Cl$), of Eu and Gd, as resulting from the reaction of anhydrous halides of Eu and Gd, or adducts with THF (tetrahydrofuran) of these rare earth ions with paludrine in THF medium. To obtain anhydrous chlorides and THF-adducts, methods reported in literature [2,3] were used.

The following adducts were synthetized :

$$EuCl_3\ 1/2\ \text{THF} \quad \text{and} \quad GdCl_3\ 1^1/_8\ \text{THF},$$

the THF-adduct with Eu being not yet mentioned elsewhere. It should be pointed out that all working operations are to be carried out in the protective medium of inert gas.[4]

---

[1] P. Spacu and I. Albescu, *Rev. Roumaine Chim.*, **16**, 1503 (1971).
[2] J. H. Freeman and M. L. Smith, *J. Inorg. Nuclear Chem.*, **7**, 224 (1958).
[3] K. Rosmanith and C. Auer-Welsbach, *Monatsh*, **96**, 602 (1965).
[4] S. Hertzog and J. Dehnert, *Z. Chem.*, **14**, 1 (1964).

EXPERIMENTAL

1. $EuCl_3.pald$

The adduct or anhydrous chloride is solved by refluxing with THF and the solution obtained is precipitated without heating with the base (paludrine) solution in THF; the molar ratio was 1 : 1 metal salt-ligand. The precipitate becomes crystalline by stirring or if left to stand a period of time. After filtration it is washed with 2–3 ml THF and then dried under vacuum.

2. $GdCl_3.\ 2pald$

A ligand solution in THF is added to a solution of $GdCl_3$–1 1/8 THF, in THF at the molar ratio 1 : 2, the adduct solution being previously prepared by its refluxing with THF till complete dissolution. The precipitate thus obtained as a gel becomes crystalline by stirring. This is filtered and washed with THF to remove basic excess, then dried in vacuum, and since the precipitate still contains THF it is slightly heated in a drying stove at 70°–80° for 30 minutes.

3. $2EuCl_3.\ 5\ pald$

In the same working conditions, using a slight paludrine excess i. e. the molar ratio 1 : 4 adduct-ligand, a well defined crystalline compound is obtained, corresponding to the above chemical formulation.

4. $EuCl_3.\ 3\ pald$ and $GdCl_3.\ 3\ pald$

Compounds of this type are obtained for Eu and Gd, by refluxing their anhydrous salts with paludrine solution in THF at the molar ratio 1 : 3. Filtration, washing and drying are made in the same way as for cases 1 and 2.

Table 1 presents the analytical results and some of the physical properties of these compounds, which are white, stable in air, insoluble in water, alcohol, ether, acetone, THF.

To achieve the best conditions of synthesis, the initial amount of substance used was 0.1–0.5 g $LnCl_3$ (or $LnCl_3.xTHF$), the amount of ligand being then taken according to the corresponding molar ratio.

— It is advisable to work at high concentrations and therefore minimum of solvent (15–20 ml).

— The reaction time and temperature are decisive factors, too high temperature or too long a time being unsuitable because of the secondary products which can occur as impurities.

— The pH was maintained during the reaction at the constant value of 6–6.5.

— The variation of solubility of the anhydrous salts and their adducts explains why some syntheses were carried out using anhydrous lanthanide halide and others using its adduct in THF.

— Owing to the poorer affinity of the lanthanide ion to nitrogen than to oxygen, those syntheses in which rare earth adducts were used, should be carried out in mild conditions, i.e. a slight heating without refluxing of both lanthanide adduct-ligand reagents.

To characterize the new compounds obtained we studied both their electronic spectra in visible and UV range and their IR spectra.

Table 1

Experimental data

Compound	Ln % calc.-found	N % calc.-found	C % calc.-found	H % calc.-found	Crystalline form	Colour	M. P. 0°C
$EuCl_3$.2pald.2T.H.F	23.16 23.14	10.67 10.09	34.77 34.08	4.91 4.08	monoclinic	white	236
2$EuCl_3$.5pald	17.03 16.60	19.62 18.74	37.01 36.24	4.52 5.00	orthorhombic leaflets	white	240
$EuCl_3$.3pald	14.90 14.78	20.60 19.19	38.85 38.53	4.74 4.48	monoclinic	white	240
$GdCl_3$.2pald	20.34 20.00	18.12 18.12	34.17 34.07	4.17 4.37	monoclinic	white	240
$GdCl_3$.3pald	15.30 15.86	20.44 20.01	38.55 37.95	4.75 5.02	orthorhombic	white	240
2$GdCl_3$.5pald	17.51 16.96	19.50 18.91	36.77 35.67	4.49 5.04	monoclinic	white	235

RESULTS AND DISCUSSIONS

The analysis of the electronic spectra leads to the following observations :

— Just as in the case of Nd-compounds, [1] the absorption band at 260 nm of the free ligand due to the phenyl ring occurred in all the compounds, with a slight shift ; the UV bands of the free rare earth ion are masked by the ligand bands up to 360 nm (Figs. 1, 2).

— The changes occurring in the metal bands taking the reference $LnCl_3$[5] and $LnCl_3$.npald, may be briefly summarized as follows :

— In Eu compounds, $EuCl_3$. pald (1), $2EuCl_3$.5pald (2) and $EuCl_3$. 3pald (3), the absorption bands up to 400 nm are the same as those of the free metal ion with only slight shifts.

— The set of bands at 465.1 nm and 465.6 nm of the free ion are shifted to 468 nm in the compound (1) and appear at 464 nm and 470 nm in the compound (2). The bands at 515 nm and 536 nm of Eu^{3+} occur as a single one at 530 nm in the above compounds.

For $EuCl_3$.3pald (3) the band shifts are more evident : the band at 376 nm of $EuCl_3$ is moved to 379 nm and those at 381 nm and 385 nm occur as a single absorption maximum at 386 nm. The bands at 464—465 nm correspond to 465 nm in the above compound, where the absorption maxima at 525 nm and 536 nm cannot be detected.

The ligand influence on the absorption intensity can be followed in all the three compounds 1, 2, 3, the characteristic maximum of central metal ion at 394 nm is lowered, the group of bands at 464—465 nm disappears in (2), and the absorption maxima at 525 nm and 536 nm do not occur in the complex (3).

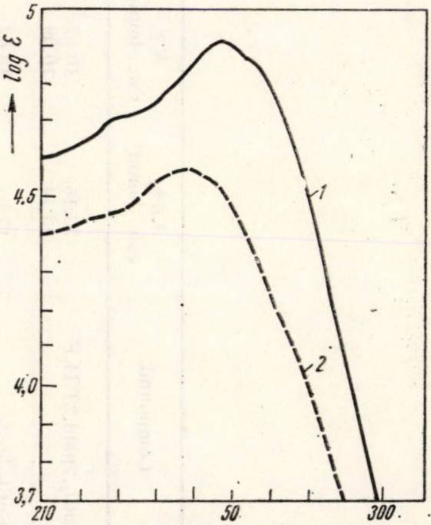

Fig. 1. — UV absorption spectra of : $GdCl_3$.2pald (1) ; $GdCl_3$.3pald (2).

---

[5] C. Stewart and D. Kato, *Analyt. Chem.*, **50**, 164 (1956).

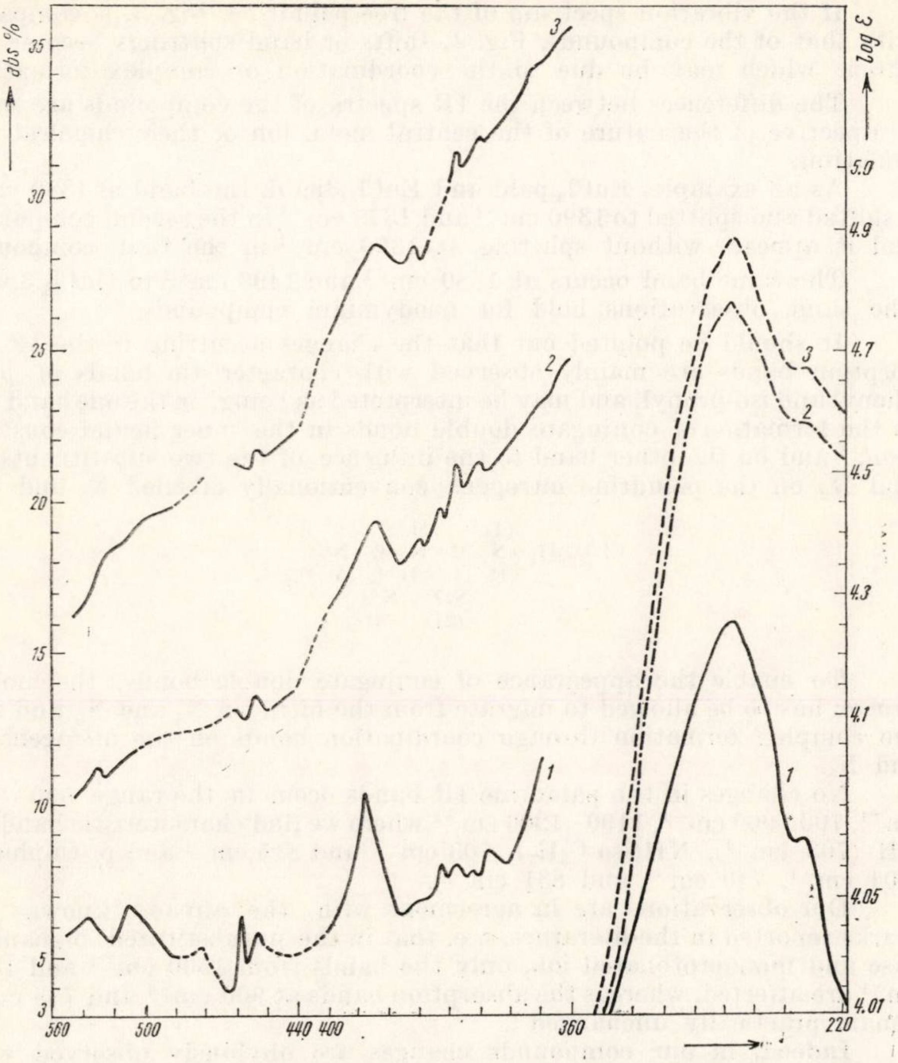

Fig. 2. — UV and visible absorption spectra of : $EuCl_3$.pald (1) ; $2EuCl_3$.5pald (2) ; $EuCl_3$.3pald (3).

The above observations cannot be made on the gadolinium complexes, as the free metal bands occurring in the UV range are overlapped by the absorption maxima of the organic ligand (Fig. 1).

It may be concluded that the small shifts observed with the transitions in the electronic spectra are caused by the coordination and complex formation, $LnCl_3$.npald.

As may be seen below, IR spectra corroborate our last remark.

If the vibration spectrum of the free paludrine, Fig. 3, is compared with that of the compounds, Fig. 4, shifts or band splittings become apparent which may be due to the coordination or complex formation.

The differences between the IR spectra of the compounds are small irrespective of the nature of the central metal ion or their chemical formulation.

As an example, $EuCl_3$.pald and $EuCl_3$.3pald, the band at 1380 cm^{-1} is shifted and splitted to 1390 cm^{-1} and 1375 cm^{-1} in the second compound, and it appears without splitting at 1390 cm^{-1} in the first compound.

The same band occurs at 1380 cm^{-1} and 1400 cm^{-1} in $GdCl_3$.3pald. The same observations hold for neodymium compounds.

It should be pointed out that the changes occurring in the IR absorption bands are mainly observed with characteristic bands of *p*.Cl-phenyl and iso-propyl, and may be interpreted as being, on the one hand due to the formation of conjugate double bonds in the inner ligand constitution, [6] and on the other hand to the influence of the two substituents R_1 and R_2 on the paludrine nitrogens conventionally labelled N_1 and N_5 :

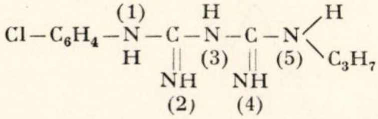

$$\underset{\text{H}}{\overset{}{}}\mathrm{Cl-C_6H_4-}\underset{\text{H}}{\overset{(1)}{\text{N}}}-\underset{\underset{(2)}{\text{NH}}}{\underset{\|}{\text{C}}}-\underset{(3)}{\overset{\text{H}}{\text{N}}}-\underset{\underset{(4)}{\text{NH}}}{\underset{\|}{\text{C}}}-\underset{(5)}{\text{N}}\langle^{\text{H}}_{\mathrm{C_3H_7}}$$

To enable the appearance of conjugate double bonds, the mobile proton has to be allowed to migrate from the nitrogen N_3 and N_5 and also the complex formation through coordination bonds on the nitrogens N_1 and N_5.

No changes in the paludrine IR bands occur in the range 500−600 cm^{-1}, 700−900 cm^{-1}, 1190−1200 cm^{-1} where we find characteristic bands of NH (703 cm^{-1}), NH(iso-C_3H_7), 703 cm^{-1} and 815 cm^{-1} and p. Cl-phenyl (704 cm^{-1}, 740 cm^{-1} and 831 cm^{-1}).

Our observations are in agreement with the already known remarks reported in the literature, i. e. that in the unsubstituted biguanide, base and monoprotonated ion, only the bands from 1500 cm^{-1} and 1460 cm^{-1} are affected, whereas the absorption bands at 900 cm^{-1} and 735 cm^{-1} remain practically unchanged [7].

Indeed, in our compounds changes are obviously observed with those absorption bands in the range 700 cm^{-1} and 900 cm^{-1}, the IR bands lying in the range 1500 cm^{-1} and 1460 cm^{-1} being practically unaffected.

---

[6] C. Stewart, *J. Chem. Phys.*, **30**, 1259 (1959).

[7] M. Takimoto, *J. Chem. Soc. Japan.*, **85**, 168 (1964).

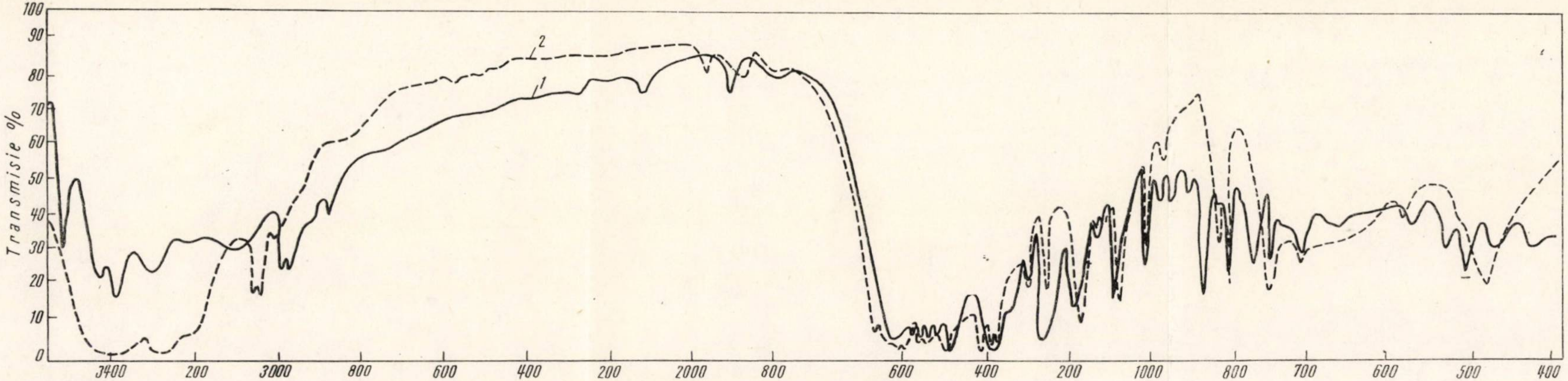

Fig. 3. — IR spectra of : paludrine (1) ; GdCl$_3$.3pald (2).

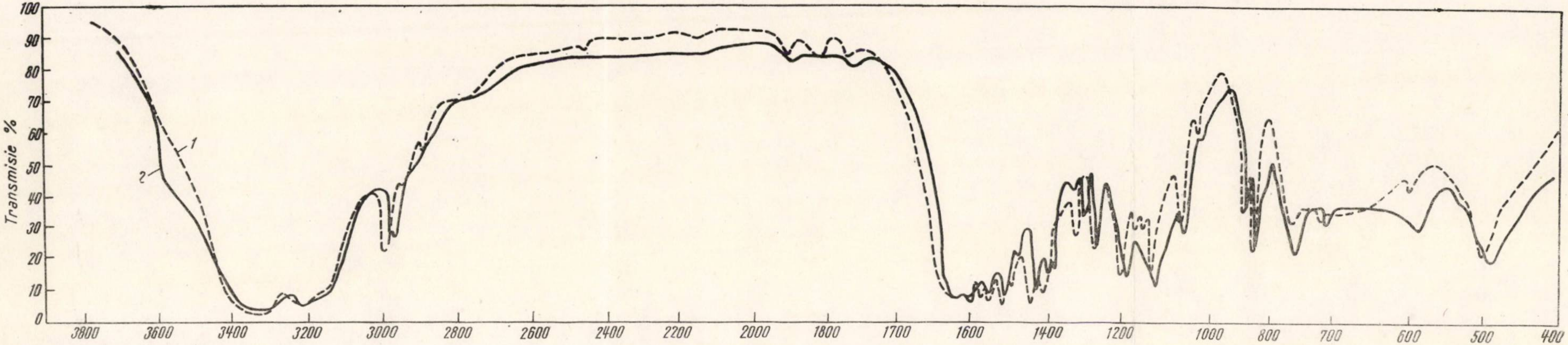

Fig. 4. — IR spectra of : EuCl$_3$.pald (1) ; EuCl$_3$.3pald (2).

Revue Roumaine de Chimie, **17**, *10*, 1735–1745 (1972)

ALUMINIUMCHLORIDE CATALYZED CONDENSATION OF 1,2-DICHLORO-CYCLOHEXANES WITH BENZENE

ISOMERISATION OF DIPHENYL-CYCLOHEXANES

ALICE MARIE GLATZ, A. C. RĂZUŞ, F. BADEA and
C. D. NENITZESCU *
Institute of Organic Chemistry,
Spl. Independenţei 202 B, Bucharest, Romania

Received May 24, 1972

The condensation of *trans*- and *cis*-1,2-dichlorocyclohexanes with benzene and $AlCl_3$ has been studied at 45–50°, the main products being phenylcyclohexane, isomeric diphenylcyclohexanes and small amounts of 1,2-diphenylcyclohexane and diphenyl. The isomerisation of *trans*- and *cis*-1,2- and *trans*-1,4-diphenylcyclohexanes has been also investigated in the same conditions with the arylation reaction. The results are discussed in terms of the reaction mechanism and conformational analysis.

In 1937, Nenitzescu and Curcăneanu[1] have observed that *trans*-1,2-dibromocyclohexane, **1**, on treatment with $AlCl_3$ in benzene at 45–50° gives phenylcyclohexane, **2** (26%), 1,3-diphenylcyclohexane, **3** (43%) and *trans*-1,4-diphenylcyclohexane, **4** (31%):

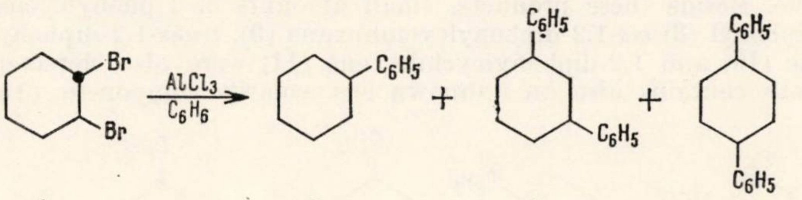

1 **2** **3** **4**

1,2-Diphenylcyclohexanes were not observed.[2] It has been later proved [3] that *trans*-1,2-dibromocyclohexane **1**, with aluminium chloride gives an equilibrium mixture of 1,3- and 1,4-dibromocyclohexanes. The same behaviour has been noted with *trans*-1, 2-dichlorocyclohexane. The isomeric dihalocyclohexanes are possible precursors of the observed isomeric diphenylcyclohexanes.

---

* Deceased 28 Jyly 1970.

[1] C. D. Nenitzescu and D. Curcăneanu, *Ber. dtsch. chem. Ges.* **70**, 346 (1937).

[2] D. N. Kursanov in 1901 (*Liebigs Ann. Chem.*, **318**, 316, 1901) claimed to have obtained only 1,2-diphenycyclohexane in those conditions. It is clear now that he could not have isolated this compound.

[3] C. D. Nenitzescu and I. G. Dinulescu, *Studii şi Cercetări Chim. Acad. R. S. R.*, **7**, 7 (1959).

The development of the physical methods of investigation and especially of the v. p. c.-technique, determined us to reinvestigate these reactions. The purposes of this work were :

a) to determine the exact composition of the reaction mixture in the reaction of *cis*- and *trans*-1,2-dichlorocyclohexanes, with benzene and $AlCl_3$ at 45–50° ;

b) to study the equilibrium between the isomeric diphenylcyclohexanes in the conditions of the arylation reaction.

RESULTS

trans-1,2-Dichlorocyclohexane (**5**), *cis*-1,2-dichlorocyclohexane (**6**), phenylcyclohexane (**2**) and the isomeric diphenylcyclohexane were prepared according to well known procedures described in the literature (s. experimental part). Throught the runs of the phenylation reactions or the isomerisation of the diphenylcyclohexanes, the same ratio cyclohexane-derivatives : $AlCl_3$ (3.2 :1) and the same concentration of the reactantin benzene (0.42 M) were used. The reaction mixture after heating at 45–50° was quenched in ice-aqueous HCl, and worked up in the usual manner. The residue obtained after the evaporation of benzene, was roughly distilled *in vacuo*, the distillate being collected up to 210°/1.5 mm. Both the benzene fraction and the distillate were gas-chromatographically analysed. The benzene is nearly pure and contains only traces of reaction products. No chloroderivatives could be detected ; the disappearence of the reactants is complete within 1 hr.

The formation of phenylcyclohexane (**2**), 1,3-and 1,4-diphenylcyclohexanes, observed by Nenitzescu and Curcăneanu[1], has been confirmed in the condensation of both *cis*- and *trans*-dichlorocyclohexanes with benzene. Beside these products, small amounts of 1-phenylcyclohexene (**7**), diphenyl (**8**) *cis*-1,2-diphenylcyclohexane (**9**), *trans*-1,2-diphenylcyclohexane (**10**) and 1,2-diphenylcyclohexene (**11**) were also detected. The distillate contains also an unhnown less volatile component (Table 1).

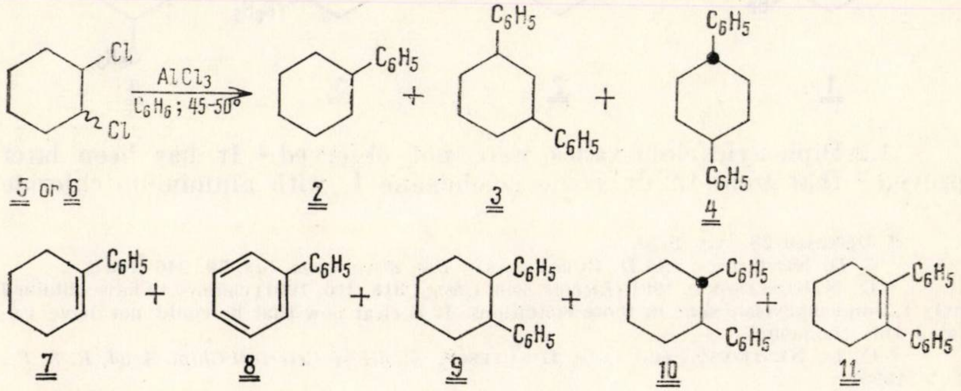

Table 1

Aluminium chloride catalyzed condensation of 1,2-dichlorocyclohexanes with benzene and isomerisation of the diphenylcyclohexanes, at 45–50°[a)]

Run[a)]	Reactant	Time hrs	Products, mole %							
			2	**3**	**4**	**9**	**10**	Minor products[b)]	Unknown	Tar[c]
1	**5**	1	39.6	23.3	11.7	0.6	3.0	2.60	11.4	6
2		6	30.2	24.1	11.6	0.8	3.5	1.63	16.7	27
3		26	24.1	22.4	10.5	1.2	4.0	0.43	16.2	40
4	**6**	1	15.8	36.3	14.6	1.3	4.8	1.63	10.9	12.5
5		6	25.8	28.3	12.0	1.3	4.8	1.78	12.9	40
6		14	27.1	26.4	12.6	1.2	4.3	1.42	10.9	43
7	**9**	1	16.3	12.8	7.9	2.5	5.6	5.55[d)]	36.3	20
8		14	21.7	19.0	9.9	0.7	4.3	3.00	27.2	30.5
9	**10**	1	32.0	15.1	11.9	1.8	18.7	0.80	8.3	20.9
10	**4**	1	24.8	37.2	21.1	0.3	2.7	0.05	10.6	27
11		14	26.5	31.5	15.3	1.5	4.1	0.60	13.4	31.5

Observations : a) In all runs $[\mathrm{Reactant}]_0 = 0.42$ M; Reactant $\mathrm{AlCl_3} = 3.2:1$; except for the last column, the values reported in this table refer to the roughly distilled product of the reaction. The volatile products (mainly solvent) are not recorded.

b) The products recorded in this column are : 1-phyenylcyclohexane (**7**), diphenyl (**8**) and 1,2-diphenylcyclohexene (**11**).

c) Calculated from the resinous material obtained in the distillation and reported to the yield of the residue resulted after the evaporation of the benzene.

d) Consists mainly of 1,2-diphenylcyclohexene, **11**.

The same compounds were formed in the isomerisation of the diphenylated cyclohexanes **4**, **9** and **10** (see Table 1). The proportions between the mentioned reaction products has been determined at different times of reaction. The unknown volatile products are probable a mixture of the isomeric diphenyl-benzenes. Previous works [1] have shown that all phenylcyclohexanes, formed in this reaction, are easily dihydrogenated to the corresponding aromatic compounds. 1,2-Diphenylcyclohexane, **11**, must be regarded as an intermediate in such dehydrogenation reactions.

The tarry unvolatile residue of the distillation represents 6–40% of the overall reaction product obtained after the evaporation of the benzene. The tar increases with the reaction time. After 1 hr it represents only 6% in the phenylation of *trans*-1, 2-dichlorocyclohexane, is larger in the corresponding reaction of the *cis*-derivative (13%) and is more than 20% in the isomerisation of the diphenylcyclohexanes. No attempt has been made to identify the components of the residue. Very probably, the components of the tar are formed through hydride-transfer-reactions which occur in this system (see Discussions).

DISCUSSIONS

1. THE EQUILIBRIUM BETWEEN THE PHENYLATED CYCLOHEXANES

Table 1 shows that regardless on the type of reaction (phenylation of dichlorocyclohexanes or isomerization of the diphenylcyclohexanes) and the initial reactant, a equilibrium between phenylated cyclohexanes is attained at long times of reaction. The equilibrium of the diphenylcyclohexanes is clearly indicated in Table 2 using the data of Table 1.

Table 2

Equilibration of diphenylcyclohexanes in benzene at 45–50° [a]

Reactant	Relative composition of the diphenylcyclohexanes mixture			
	cis-1,2 **9**	*trans*-1,2 **10**	1,3 **3**	1,4 **4**
5 26 hrs	1	3.33	18.7	9.0
6 14 hrs	1	3.60	22.0	10.5
4 14 hrs	1	2.75	21.0	10.2
9 14 hrs	1	6.1	27.0	14.0
Mean b)	1	3.23	20.6	9.9

Obs. a) Data of Table 1 were used
b) The mean values of the first three reactions

As Table 2 shows, equilibrium between the four diphenylcyclohexanes is attained within 14 hrs in the first three reactions. However, starting from *cis*-1,2-diphenylcyclohexane (last reaction, table 2), after 14 hrs, the equilibrium is attained only between 1,3-and 1,4-diphenylcyclohexanes and is not reached between the vicinal diphenylated compounds. Free energy differences between the diphenylcyclohexanes were therefore calculated from the mean values of the first reactions of table 2. The calculated values are compared in table 3 versus free energy differences observed in the corresponding isomerisation of dimethylcyclohexanes.

Table 3

Free energy differences in the isomerisation of diphenyl- and dimethylcyclohexanes

Disubstituted cyclohexane	Number of gauche-interactions	Free energy differences :	
		Diphenycyclohexanes [a]	Dimethycyclohexanes
cis-1,3	0	0	0
trans-1,4	0	0.46	0.45[b]
trans-1,2	1	1.17 (0)	1.11[b] (0)
cis-1,2	3	1.92 (0.75)	– (0.95[c]; 1.46[d])

Observations

a) This work; calculated from the mean values of Table 2.

b) After R. M. Gascogne, *J. Chem. Soc.*, **1958**, 876.

c) After P. Boelhouwer, G. A. M. Diepen, G. van Elk, P.T.H. van Raay and H. I. Waterman, *Brennstoff Chem.*, **39**, 299, (1958); cf. *Chem. Zentr.*, **1959**, 9849.

d) After N. L. Allinger, W. Szkrybalo and F. A. van Catledge, *J. Org. Chem.*, **33**, 784, (1968).

The stability of the diphenyl- and dimethylcyclohexanes decreases in the same order :

cis-1,3 > *trans* 1,4 > *trans*- 1,2 > *cis*-1,2

The differences between the vicinal disubstituted cyclohexanes, on the one hand and the other disubstituted cyclohexanes, on the other hand are easily interpreted considering *gauche*-interactions (Fig. 1).

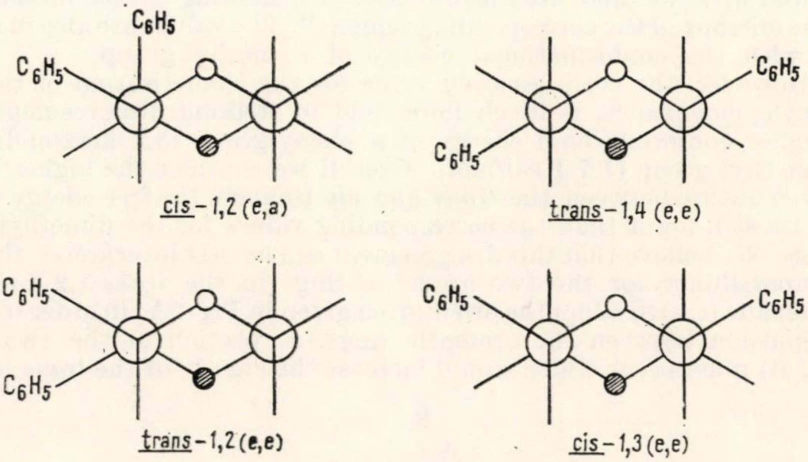

cis-1,2 (e,a) trans-1,4 (e,e)

trans-1,2 (e,e) cis-1,3 (e,e)

Fig. 1. — Stable conformations of the diphenylcyclohexanes.

However, on this basis, the higher stability of *cis*-1,3 is compared to the stability of the 1,4-isomer, cannot be explained. The small free energy differences between the two isomers must be an effect of the entropy of reaction. Indeed, on the isomerization of 1,4-disubstituted cyclohexanes in the corresponding 1,3-isomer two reaction paths are available :

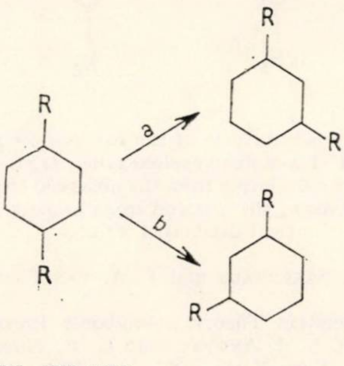

Only one reaction path is possible for the isomerisation of the 1,3-derivative. The entropy difference must be therefore :

$$\Delta S = RT\ln\ 2 \simeq 0.44\ \text{kcal/mol}$$

and must be independent of the nature of the groupR ; this is clearly shown by the figures of Table 3.

The free energy differences between the *trans*-1,2-and *cis*-1,2-disubstituted cyclohexanes need some further comment. In the isomerisation of the dimethylcyclohexanes, the observed experimental values agree quite well with the calculated differences[4a] considering *gauche*-interactions and the entropy of the corresponding isomers[4b]. The values are also in agreement with the conformational energy of a methyl-group.

However, the corresponding value for the isomerisation of the 1,2-diphenylcyclohexanes, is much lower and in striking disagreement with the higher conformational energy of a phenylgroup (3.1 kcal/mol) than for a methyl group (1.7 Kcal/mol). Even if we consider the higher herein observed ratios between the *trans* and *cis* isomers, the free energy differences are still lower than the corresponding values for the dimethylcyclohexanes. We believe that this disagreement can be best interpreted through the impossibility for the two aromatic rings in the *trans*-1,2-diphenylcyclohexane (*e*, *e*) to adopt the orientation given in Fig. 2A ; in order to avoid the repulsion between the aromatic rings, a rotation of the two rings (Fig. 2 B) must occur which would increase the energy of the *trans* isomer.

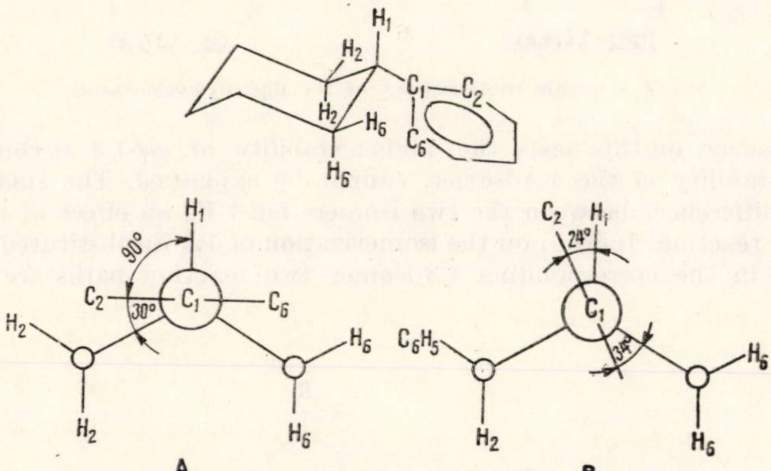

Fig. 2. — Possible orientations of the benzene ring in phenylcyclohexane (*e*) and 1,2-diphenycyclohexane (*e,e*). The angles in orientation B were calculating from the observed free energy differences (Table 3) between the *cis*-and *trans*-isomers and the theoretical calculated value.

[4a] N. L. Allinger, W. Szkrybalo and F. A. van Catledge, *J. Org. Chem.* **33**, 784 (1968).

[4b] M. Hanak, "Conformation Theory", Academic Press, New York, 1965, pp. 109 ; E. L. Eliel, N. L. Allinger, S. J. Angyal and G. A. Morrison, "Conformational Analysis", Interscience Publishers, New York, 1965, pp. 50.

As models show this rotation is not necessary for the *cis* isomer.

2. REACTIVITY OF DIPHENYLCYCLOHEXANES

Phenylcyclohexane equilibrates in its turn with the diphenylcyclohexanes, which is clearly shown in Table 4.

Table 4

Equilibration of diphenylcyclohexanes with phenylcyclohexane in benzene with $AlCl_3$ at 45–50°

Reaction	Relative proportions of :	
	Phenylcyclohexane **2**	Diphenylcyclohexanes (**3**+**4**+**9**+**10**)
5 26 hrs	1	1.58
6 14 hrs	1	1.64
9 14 hrs	1	1.56
4 14 hrs	1	1.60

As a proof for this equilibrium, phenylcyclohexane, in similar conditions, is converted into the diphenylcyclohexanes mixture.

Despite the high excess of the phenylating agent (solvent), phenylcyclohexane is found in the reaction mixture in about the same amount as **3**. That means that **2** is more stable than diphenylcyclohexanes and this must be again related to phenyl-*gauche*-interactions. It can be concluded that the less stable *cis*-1,2-diphenylcyclohexane, **9**, will give the higher proportion of **2**, in the first step of the reaction. However, after 1 hr, the highest proportion of **2** is found in the reaction of *trans*-1,2-diphenylcyclohexanes, **10**, is less for the 1,4-isomer and the lowest for the 1,2-*cis*-diphenylcyclohexane. On the other hand, **9** gives the greatest proportion of dehydrogenated products (alkenes **7**+**11**). These observations need an explanation.

The formation of phenylcyclohexane involves as the first step a dephenylation reaction. The easier this process, the highest the proportion of **2** would be formed. The dephenylation reaction of the isomer **10** might occur faster as only this isomer can form a phenonnium ion, **12**.

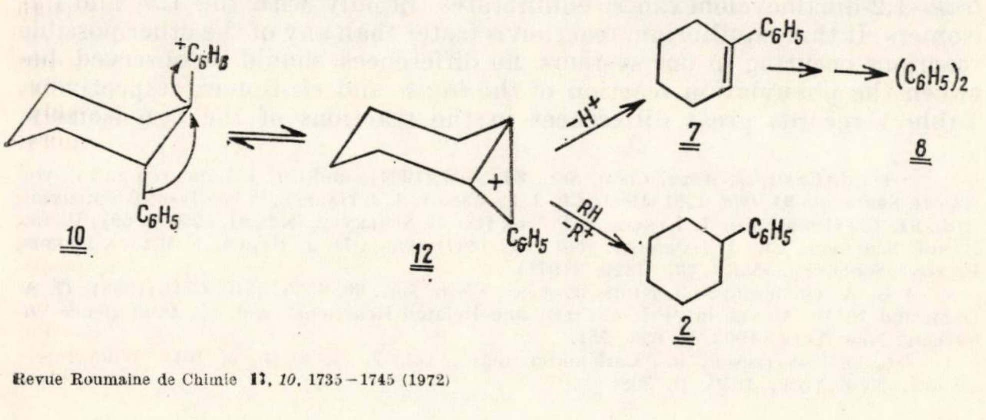

The formation of the phenonium ion **12** is not surprising. Phenonium ions, which may be considered σ-complexes, are commonly encountered in solvolysis reactions.[5] As π-complexes are the most important intermediates in Friedel-Crafts reactions,[6] the occurance of a phenonium ion in such reactions must be at least as probable as in a solvolysis reaction.

Phenonium ion **12** may be transformed in alkene **7** and further in diphenyl, **8**. Another route is its transformation in the reduction product **2**, by intermolecular hydride-shift [7] which seems to be the most important way through which **12** is destroyed (see Table 1). Alkene **7** or anyone of the diphenycyclohexanes is suitable as hydride-ion donor, stable carbonium ions being thus formed :

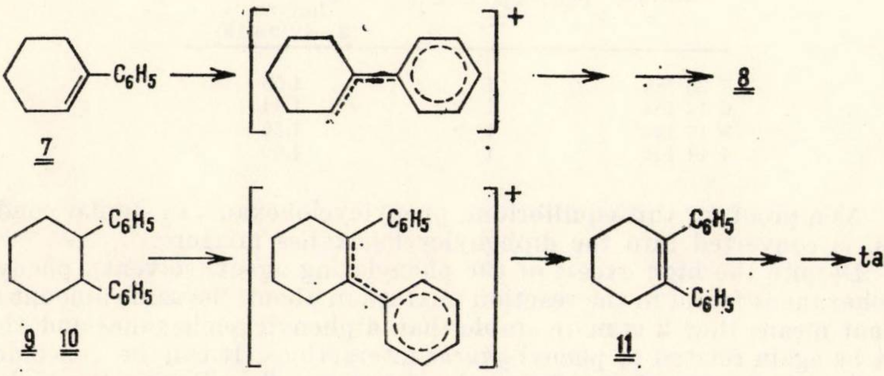

cis-1,2-Diphenylcyclohexane, being dephenylated in a slower reaction, gives probable, in a higher extent this reaction. The formation in a higher yield of tar products and alkene **11** in the isomerisation of **9** is caan indition in this respect.

3. REACTIVITY OF THE DICHLOROCYCLOHEXANES

In presence of $AlCl_3$, Nenitzescu and Dinulescu [2] have observed that *trans*-1,2-dihalocyclohexanes equilibrates rapidly with the 1,3- and 1,4-isomers. If that equilibrium reaction is faster than any of the other possible reactions occuring in our systems, no differences should be observed between the phenylation reaction of the *trans*- and *cis*-isomer, respectively. Table 1 records great differences in the reactions of the two isomers.

---

[5] D. J. Cram, *J. Amer. Chem. Soc.*, **86**, 3767 (1964); and Ch. J. Lancelot and P. von Ragné Schleyer **91**, *ibid.* 4291 (1969). Ch. J. Lancelot, J. J. Harper, P. von Ragné Schleyer; *ibid.*, **91**, 429 (1969); Ch. J. Lancelot, P. von Ragné Schleyer, *ibid.*, **91**, 4296 (1969); P. von Rangé Schleyer, Ch. J. Lancelot, *ibid.*, **91**, 4297 (1969); D. J. Raber, J. Milton Harris, P. von Schleyer, *ibid.*, **93**, 4829 (1971).

[6] G. A. Olah and S. J. Kuhn, *J. Amer. Chem. Soc.*, **80**, 6535, 6540, 6541 (1958); G. A. Olah and M. W. Meyer in "Friedel-Crafts and Related Reactions", vol. 1, Interscience Publishers, New York, 1963, p. 623, 751.

[7] C. D. Nenitzescu, in "Carbonium Ions", vol. 2, G. A. Olah, Ed., Wiley-Interscience, New York, 1970, p. 503.

Thus, after 1 hr, the *trans* isomer **5** gives an essential greater proportion of phenylcyclohexane, **2**, than the *cis*-isomer. Conversely, **6** gives higher yields of the 1,3-diphenylcyclohexane, **3**, and tar products.

It seems therefore that phenylation of the dichlorocyclohexane competes well with their equilibration. The results of this work give no quantitative data regarding the relative reactivity of the two 1,2-dichlorocyclohexanes, their disappearance from the reaction mixture being complete within 1 hr. However, it can be argued that *trans*-1,2-dichlorocyclohexane is faster trapped with benzene than the corresponding *cis* isomer. Indeed, the high amount of phenycyclohexane resulted from **5** is in agreement with the formation in a first step of a halonium ion **13**. Olah et al.[8] have demonstrated that the most stable species from open-chain- and bridged halocarbonium ions is the halonium ion. Such an ion would have a low tendency to pass over in a β- or γ-halocarbonium ion. The chloronium ion **13** cannot be formed directly from the *cis*-isomer. The open ion **14** should instead be formed, and this ion would have a better chance to isomerise in ions **15** and **16** (s. Scheme). The chloronium ion **13** can be transformed in several steps in the phenonium ion **12**, which would account for the similar proportion of **2**, observed after 1 hr in the reactions of **5** and **10**, respectively (Table 1).

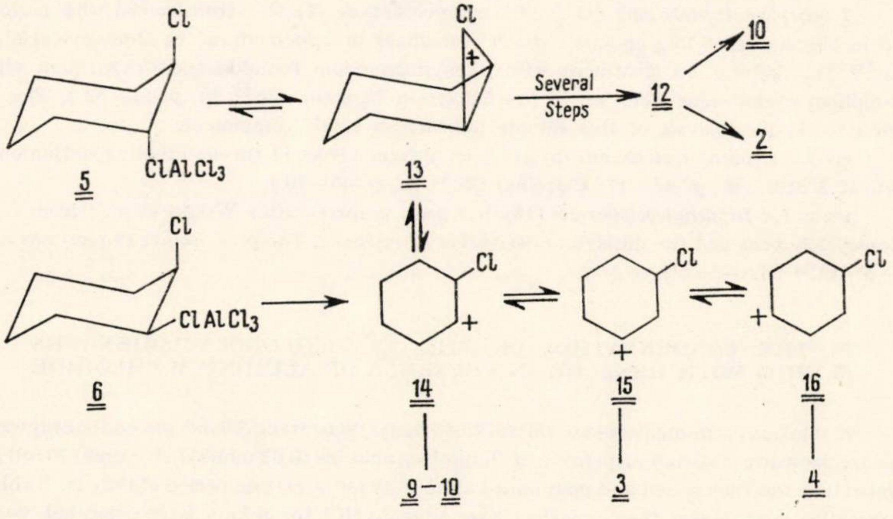

EXPERIMENTAL

All melting points and boiling points are uncorrected. Glpc analyses, performed by Mrs L. Stănescu and Miss D. Georgescu, were carried out on a Carlo Erba instrument (Fractovap Mod.) using a flame ionization detector. For the lower volatile components, a 1.3 m (2 mm diameter) column packed with buthanediol disuccinate on 60–80 mesh Chromosorb W was used ; column temperature 140—190° ; programming speed 3°/min., temperature in vaporisator 320°. Nitrogen as carrier (40 ml/min.). The higher volatile components were analysed on 0.5 m (2 mm diameter) column packed with E 301-silicon grease on 60—80 mesh Chromosorb P ; column temperature 190—225° ; programming speed 3°/min. ; temperature in vaporisator 320° ; nitrogen as carrier (40 ml/min.).

---

[8] H. Böhme and R. Schmitz, *Chem. Ber.*, **88**, 375 (1955).

A. REAGENTS. CHROMATOGRAPHIC STANDARDS

trans-*1,2-Dichlorocyclohexane* (**5**) has been obtained from cyclohexene and chlorine according the method described by Böhme and Schmitz.[8] The purity of the *trans* isomer is about 97% (containing *cis* isomer as single impurity).

cis-*1,2,-Dichlorocyclohexane* (**6**) has been prepared from cyclohexene oxyde and sulfurylchoride in presence of pyridine[9]. The resulted reaction mixture contains (v.p.c.) *cis*-1,2-dichlorocyclohexane, **6** (73.0%), *trans*-1,2-dichlorocyclohexane, **5** (3.6%) and a trichlorocyclohexane (according elementary analysis) in about 23.4% yield. Pure 1,2-dichlorocyclohexane has been isolated from this mixture through preparative gas-chromatography.

Phenylcyclohexane (**2**). Cyclohexanone with phenylmagnesiumbromide afforded 1-phenylcyclohexene[10] **7**. Phenylcyclohexane, **2**, was obtained from **7** through hydrogenation on 5% Pd/C at 3 atm, m. p. 7—7.5° ; b. p. 99°/11 mm (lit.,[11] m. p. 7.5). The v.p.c. analysis of this product reveals a single component.

1,2-Diphenylcyclohexene (**11**). 1-Phenylcyclohexene (**7**) was transformed with performic acid in the corresponding epoxide, which rearranges in acid medium in 2-phenylcyclohexanone.[12] This ketone, on treatment with phenylmagnesium bromide and dehydration affords 1,2-diphenylcyclohexene (**11**) m. p. 51—52° (from ligroine) (lit.[13] m. p. 51—52°). The gas-chromatographic analysis of this sample indicates a single component.

cis-*1,2-Diphenylcyclohexane* (**9**) has been obtained from **11** through hydrogenation on 5% Pd/C at 3 atm., m. p. 46—47° (ligroine) (lit.[13] m. p. 45—46°).

trans-*1,2-Diphenylcyclohexane* (**10**), has been prepared after Wright et al.[14] from 1,4-dichlorocyclohexane and the dinatrium derivative of stylbene. The pure isomer (v.p.c.) has m. p. 54—5° (lit.[14] 54.5—55.5°).

B. THE CONDENSATION OF THE 1,2-DICHLOROCYCLOHEXANES (5 OR 6) WITH BENZENE IN PRESENCE OF ALUMINIUM CHLORIDE

A solution of the dichloro-derivative (0.065 moles) in benzene (70 ml) was added dropwise at room temperature in stirred suspension of aluminium chloride (0.02 moles) in benzene (70 ml) ; the temperature was then raised and maintained at 45—50° for a certain period of time (s. Table 1). The reaction mixture was then quenched in ice-aqueous HCl, the organic layer separated, washed with water, sodium carbonate solution and again with water and afterwards dried over sodium sulfate. Benzene was then removed and the residue distilled *in vacuo* at 210°/1.5 m. A gas-chromatographical analysis of the crude distilate revealed the presence of the components indicated in Table 1. The g.l.p.c. analysis revealed the presence of other few components, present in the distillate in smaller amounts and which could not be identified.

---

[9] J. R. Campbell, J. K. N. Jones and S. Wolfe, *Canad. J. Chem.*, **44**, 2339 (1966).

[10] S. Nametkin, *Ber. dtsch. chem. Ges.*, **56**, 1805 (1923).

[11] F. H. Case, *J. Amer. Chem. Soc.*, **56**, 716 (1934).

[12] S. Goldschmidt and W. L. C. Veer, *Rec. Trav. Chim.*, **67**, 489 (1948).

[13] S. M. Parmerter, *J. Amer. Chem. Soc.*, **71**, 1127 (1949).

[14] J. W. B. Resor, J. G. Smitd and G. F. Wright, *J. Org. Chem.*, **19**, 940 (1954).

From the distillate, *trans*-1,4-diphenylcyclohexane, m.p. 170–171° (lit.[1] 169–170°), could be obtained through crystallization. The ozonolysis of this product gave *trans*-1,4-diphenylcyclohexane dicarboxilic acid (m. p. 309°, sealed tube, lit.[15] 309–310°, *cis*-isomer 168–169°[15]).

The residue of the distillation has no tendency to crystallization. It was not further studied.

C. THE REACTION OF THE DIPHENYLCYCLOHEXANES (**4**, **10** and **11**) IN PRESENCE OF ALUMINIUM CHLORIDE

Diphenylcyclohexane (0.041 moles) and aluminium chloride (0.013 moles) in benzene (100 ml) were treated in a similar way as in experiment B.

The results are reported in Table 1.

[15] W. H. Mills and G. A. Keats, *J. Chem. Soc.*, **1935**, 1373.

Revue Roumaine de Chimie, 17, 10, 1747–1753 (1972)

ÜBER PHENOTHIAZONE. XIX[1]

4-AMINO- UND 4-AMINO-HALOGEN-PHENOTHIAZONE

EDDA BROSER und CORNEL BODEA
Institut für Chemie
Cluj, str. Donath 65–103

Eingegangen am 28. April 1972

Durch Reduktion von 4-Nitro-phenothiazon mit Zink in Eisessig wird das unbeständige, farblose 4-Amino--hydroxy-phenothiazin erhalten, welches an Luft in blaues 4-Amino-phenothiazon übergeht. Die Tieffarbigkeit dieser Substanz wird diskutiert. Werden 7-Halogen-4-nitro-phenothiazone dieser Reduktion unterworfen, entstehen die entsprechenden-Amino-7-halogen-phenothiazone, während bei Reduktion von 2-Halogen-4-nitro-phenothiazonen eine teilweise Enthalogenierung stattfindet.

In einer vorangegangenen Arbeit [2] wurde gezeigt, daß durch Nitrierung von Phenothiazon und Halogenphenothiazonen die Nitrogruppe in Stellung 4 eintritt. Vorliegende Arbeit befaßt sich mit der Reduktion der 4-Nitro- und 4-Nitro-halogen-phenothiazone.

Wird 4-Nitro-phenothiazon (**1**) in heißem Eisessig mit Zinkpulver versetzt, so geht die orangerote Lösung über blau-violett in braun, hellgelb uns schließlich in farblos über. Das farblose Produkt ist unzweifelhaft das durch Reduktion der Nitrogruppe und Aromatisierung des Chinoniminringes gebildete Leukoderivat (**4**). Letzteres (**4**) besitzt eine äußerst große Tendenz zur Oxydation unter Bildung eines blau gefärbten Produktes, so daß das Leukoderivat **4** bei Gegenwart von Luft nicht isoliert werden konnte. Dieser Oxydationsprozeß wird durch Alkalien beschleunigt.

---

[1] XVIII. Mitteilung: T. Panea, C. Bodea und V. Fărcăşan, *Rev. Roumaine Chim.*, **16**, 759 (1971).

[2] C. Bodea, M. Terdic und E. Broser, *Liebigs Ann. Chem.*, **715**, 122 (1968).

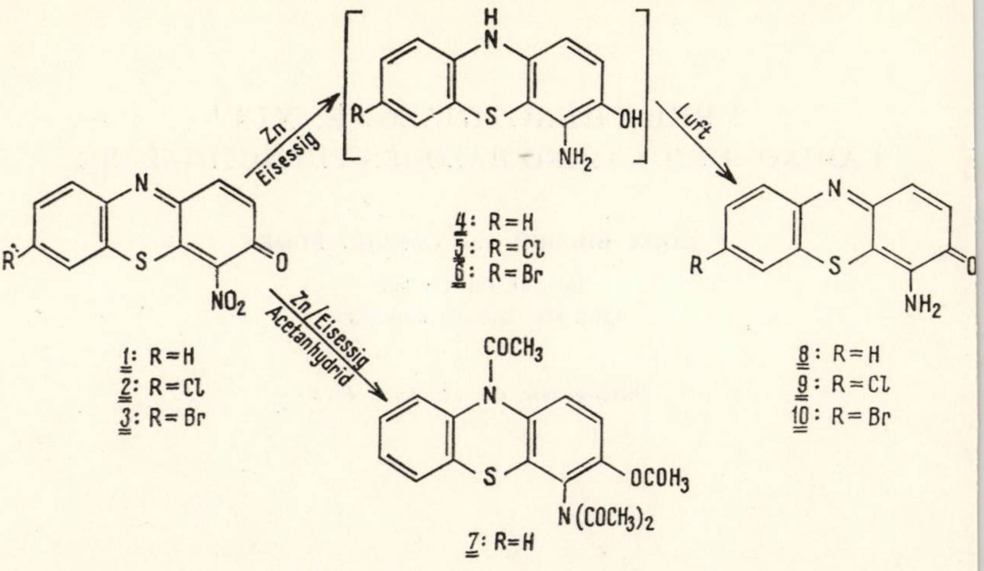

Wird die Reduktion von **1** bei Gegenwart von Essigsäureanhydrid ausgeführt, so kann als Hauptprodukt das farblose Tetraacetylderivat des 4-Amino-3-hydroxy-phenothiazins (**7**) isoliert werden.

Wird das durch Oxydation des Leukoderivates **4** gebildete blaue Produkt aus einer Al_2O_3-Säule mit Toluol eluiert, so erhält man nadelförmige blaue Kristalle mit metallischem Glanz. Es ist bekannt, daß sich 3-Hydroxy-phenothiazin in Gegenwart von Luft zu dem entsprechenden Phenothiazon oxydiert. [3] Im vorliegenden Falle dürfte die Bildung eines Phenothiazons durch das Vorhandensein einer *o*-ständigen elektronenspendenden Aminogruppe begünstigt sein.

Wird die Reduktion von **1** mit $SnCl_2.2H_2O/HCl$ in Eisessig (in Anlehnung an Lit.[4]) durchgeführt, so erhält man unmittelbar eine blaue Verbindung. Diese erwies sich mit der bei der Oxydation des Leukoderivates **4** erhaltenen Verbindung als identisch.

Das IR-Spektrum des blauen Produktes zeigt das Vorhandensein einer Carbonylgruppe bei 1648 cm^{-1} an, in einem für die Phenothiazoncarbonylgruppe charakteristischen Bereich,[5] sowie zwei für die N—H-Valenzschwingung charakteristische Absorptionen bei 3370 bzw. 3475 cm^{-1}.

Die äußerst dunkle Farbe dieses Phenothiazons mit dem langwelligsten Übergang bei 587 nm im Vergleich mit Halogen-,[5] Nitro-,[2] Halogennitro-[2] oder Methyl-phenothiazonen,[6] mit dem langwelligsten Übergang zwischen 480—510 nm, legte das eventuelle Vorhandensein eines Dimeren oder eines Radikals nahe. Doch schlossen genaue Molekularmassenbestimmungen, sowie die Aufnahme der ESR-Spektren, diese Annahme aus. Die Tieffarbigkeit dieser Substanz könnte auch der Bildung einer Imin- d. h. *o*-chinoiden Form **8A** zugeschrieben werden, da bekanntlich *o*-chinoide Derivate tiefer als ihre *p*-Isomere gefärbt sind.

---

[3] C. Craig und M. E. Tate, *Austral. J. Chem.*, **9**, 397 (1957); C. Bodea und M. Răileanu, *Studii și Cercetări Chim. Acad. România Fil. Cluj*, **11**, 325 (1960.)

[4] R. C. Elderfield *et al.*, *J. Amer. Chem. Soc.*, **68**, 1584, 1589 (1946).

[5] M. Terdic, Dissert., Cluj 1968.

[6] M. Terdic, unveröffentlichte Daten.

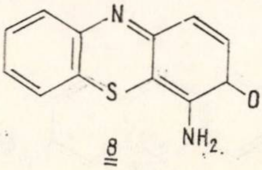

8

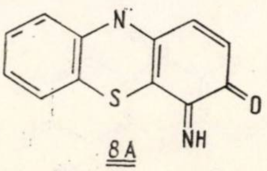

8A

Die beiden N-H-Valenzschwingungen könnten sowohl den beiden sekundären N—H-Gruppen der Imin-Form **8A** als auch der symmetrischen und antisymmetrischen Schwingung der primären NH_2-Gruppe der Amin-Form **8** zugeschrieben werden; die Bandenform spricht für letztere. Monoacetylierung von **8** ergab eine Substanz **11** deren einzige N—H-Valenzschwingung bei 3248 cm^{-1} liegt, demnach stark verschoben in Bezug auf die beiden N—H-Valenzschwingungen der Ausgangssubstanz **8**. Diese Tatsache bekräftigt das Vorhandensein einer primären Aminogruppe. Für Struktur **8** spricht außerdem das durch Kondensation mit Benzaldehyd erhaltene Azomethinderivat **12**, aus dessen IR-Spektrum die N—H-Valenzschwingung fehlt, ein Beweis, daß keine Additionsreaktion des Benzaldehyds an den Chinoniminring [7] stattgefunden hat.

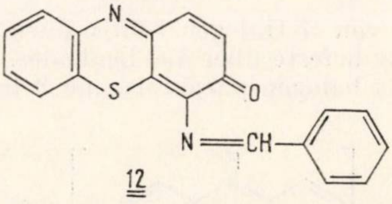

12

Das Vorhandensein einer primären Aminogruppe schließt jedoch die Möglichkeit eines tautomeren Gleichgewichts zwischen **8** und **8A** nicht aus, doch dürfte dieses stark zur Aminform hin verschoben sein.

Die Tieffarbigkeit des 4-Amino-phenothiazons (**8**) kann in Anlehnung an die Arbeiten von Dähne und Leupold [8] über den Zusammenhang zwischen Farbe und Struktur organischer Verbindung, durch das Vorhandensein eines mit einem Polyensystem gekoppelten Polymethinsystems im Molekül erklärt werden, wie dieses aus Mesomeriestruktur **8B** ersichtlich ist. Die Anteiligkeit der für unsubstituiertes Phenothiazon charakteristischen Mesomeriestruktur **13**,[9] wird im Falle des 4-Aminophenothiazons (**8**) zugunsten von **8B** herabgesetzt. Diese Annahme wird durch das Ansteigen der $\nu_{C=O}$ in **8** auf 1648 cm^{-1} im Vergleich zu der des unsubstituierten Phenothiazons von 1638 cm^{-1} bekräftigt. Im 2-Amino[10] und 2-Anilino-phenothiazon[11] liegt die langwelligste Absorption um 480 nm, da in diesem Falle die Elektronenverschiebung der für Phenothiazone charakteristischen Mesomeriestruktur **13** nicht gestört wird; auch ist in diesem Falle mit dem Vorhandensein eines mit einem Polyensystem gekoppelten Polymethinsystems nicht zu rechnen.

---

[7] J. W. Ralls, *Chem. Rev.*, **59**, 331 (1959); J. M. Bruce und E. Cutts, *J. Chem. Soc.*, *C*, **1966**, 449; J. M. Bruce und J. N. Ellis, *ibid.*, **1966**, 1624; J. M. Bruce, D. Creed und J. N. Ellis, *ibid.*, **1967**, 1468.

[8] S. Dähne, D. Leupold, H. E. Nikolajewski, S. Kulpe, H. Paul und R. Radeglia, *Monatsber. deutsch. Akad. Wiss.* Berlin, **9**, 112 (1967).

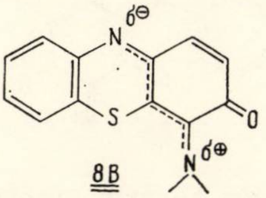

8B

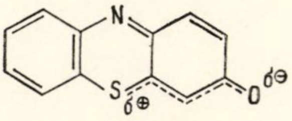

13

Einige Aussagen über den Verlauf der Reduktion des 4-Nitro-phenothiazons (**1**) können aus folgendem Versuch gemacht werden: wird die heiße Eisessiglösung von **1** mit kleineren Mengen Zinkpulver, nur bis zu ihrer Blaufärbung versetzt, und sofort abfiltriert, so kann das blaue Produkt unmittelbar isoliert werden. Diese Tatsache läßt die Annahme zu, daß die Reduktion der Nitrogruppe der der Carbonylgruppe vorausgeht. Weitere diese Reduktionsreaktion betreffenden Untersuchungen sind im Gange.

Die Reduktion von 7-Halogen-4-nitro-phenothiazonen **2** bzw. **3** mittels Zink in Eisessig lieferte über die Leukoderivate **5** bzw. **6** die entsprechenden 4-Amino-7-halogen-phenothiazone **9** bzw. **10**.

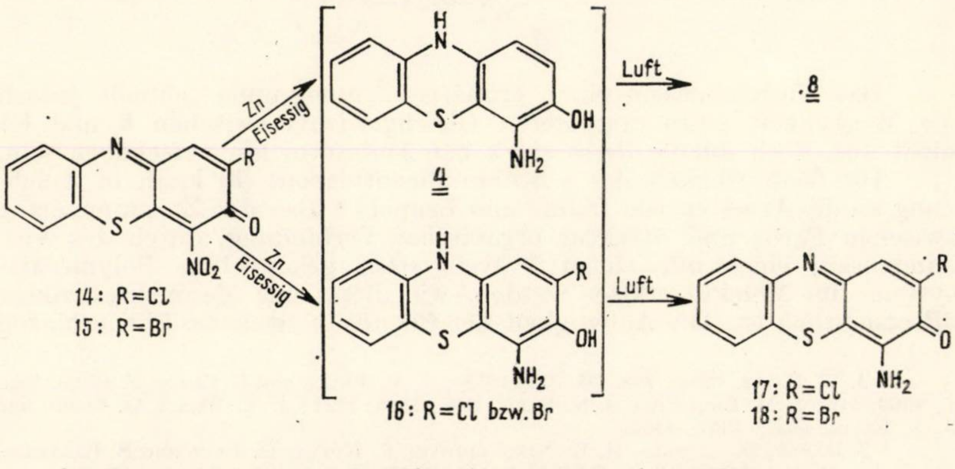

---

[9] C. Bodea und I. Silberg, *Rev. Chim. Acad. România*, **7**, 683 (1962).

[10] D. P. Sevbo und O. F. Ginsburg, *Zhur. org. Khim.*, **4**, 1854 (1968).

[11] C. Bodea und E. Broser, *Rev. Roumaine Chim.*, **14**, 1617 (1969).

Werden hingegen 2-Halogen-4-nitro-phenothiazone **14** bzw. **15** genannter Reduktion unterworfen, erhält man über die entsprechenden Leukoderivate **16** und **4** als Endprodukt ein Gemisch bestehend aus den 4-Amino-2-halogen-phenothiazonen **17** bzw. **18** und 4-Amino-phenothiazon (**8**). Die Reduktion der 2-Halogen-4-nitro-phenothiazone ist demnach von einer teilweisen Enthalogenierungsreaktion begleitet. Es ist anzunehmen, daß die Enthalogenierung an den Leukoderivaten **16** stattfindet, da dasselbe Gemisch von **8** und **17** bzw. **18** erhalten wird, wenn die 4-Amino-2-halogen-phenothiazone **17** bzw. **18** der Reduktion durch Zink in Eisessig und anschließender Oxydation unterworfen werden; auch schreitet die Enthalogenierung mit zunehmender Reduktionszeit fort und ist beim Bromderivat (**18**) weit ausgeprägter als beim Chlorderivat (**17**).

EXPERIMENTELLER TEIL

Die *Schmelzpunkte* sind unkorrigiert. Die IR-*Spektren* wurden als Preßlinge mit einem Spektralphotometer Unicam SP-200-G und in Lösung mit einem Spektralphotometer Carl Zeiss Jena UR-10, die Elektronenspektren mit einem Spektrophotometer Beckman DK 2A aufgenommen. Die *Ausgangsstoffe* **1**, **2** und **3** wurden in einer vorhergehenden Arbeit[2] bereits beschrieben, die Darstellung von 2-Chlor-4-nitro- (**14**) bzw. 2-Brom-4-nitro-phenothiazon (**15**) wird in vorliegender Arbeit angegeben.

4-Amino-phenothiazon (**8**). a) 0,5 g **1** werden in 35 ml siedendem Eisessig gelöst. Der noch heißen orangefarbenen Lösung wird vorsichtig portionsweise Zinkpulver zugegeben, bis diese über blau-violett, gelb schließlich farblos wird. Nach Abfiltrieren der Lösung wird diese mit 5 NaOH-Lsg. alkalisch gemacht, wobei die Lsg. wiederum blau wird. Man schüttelt mehrmals mit Toluol aus, trocknet das mit Wasser gewaschene Extrakt über Na_2SO_4 und reinigt dieses an einer Säule von 400 g Al_2O_3 (Aktiv.-Stufe 3) mit Toluol als Elutionsmittel. Beim Einengen kristallisiert **8** in Form langer dunkelblauer Nadeln vom Schmp. 186–187° aus (nach Waschen mit Äthanol). Ausbeute 44%.

b) 0,5 g **1** werden in 36 ml Eisessig heiß gelöst. Man gibt vorsichtig Zinkpulver bis zur Blaufärbung hinzu, filtriert rasch und macht die Lsg. alkalisch. Aufarbeitung wie a). Ausbeute 13% **8**.

c) Wird eine Lsg. von 0,5 g **1** in 50 ml Eisessig einer eisgekühlten Lsg. von 0,44 g $ZnCl_2H_2O$ in 10 ml konz. HCl zugegeben, alkalisch gemacht und wie bei a) aufgearbeitet, entsteht **8.** Ausbeute 30%.

Die nach a), b) und c) erhaltenen Produkte sind nach Schmp., Mischmp., R_f, IR- und Elektronenspektrum identisch. Anal. $C_{12}H_8N_2OS$ (228,2) *ber.*; C 63,15 H 3,50 N 12,28; *gef.*: C 63,34 H 3,36 N 12,21. IR,Spektrum (in KBr): 1646 (C=0), 3324 bzw. 3406(N–H) cm^{-1}; (in CCl_4): 1648 (C=0), 3370 bzw. 3475 (N–H) cm^{-1}. Elektronenspektrum (in Dioxan): $\lambda(\varepsilon)$: 587 nm (4860), 350,5 nm (12880), 300,5 nm (16310).

4-Acetylamino-phenothiazon (**11**). 0,5 g **8** werden bei Raumtemperatur in 70 ml Essigsäureanhydrid gelöst und 3 Wochen stehengelassen. Die blaue Lsg. wird violett. Man filtriert den gebildeten violetten Niederschlag ab. Ausbeute 93,2%, Schmp. 261–264°. Nach Umkristallisation aus Chloroform wird **11** in Form von violetten Plättchen vom Schmp. 270° erhalten. Anal. $C_{14}H_{10}N_2O_2S$ (270,3) *ber.*: C 62,20 H 3,72 N 10,36; *gef.*; C 62,34 H 3,70 N 10,30. IR-Spektrum (in KBr): 1627 (C=O Chinon), 1700 (C=O Acetyl), 3248 (N–H) cm^{-1}; (in CCl_4):

1630 (C=0 Chinon), 1706 (C=0 Acetyl), 3374 (N—H) cm^{-1}. Elektronenspektrum (in Dioxan) : $\lambda(\varepsilon)$: 515 nm (6960), 360 nm (10990), 284,5 nm (19950), 239 nm (20190).

4-Benzylidenamino-phenothiazon (**12**). Zu 0,1 g **8** in 5 ml Toluol werden 0,05 ml Benzaldehyd zugegeben und 15 Std. unter langsamem Rückfluß gekocht. Nach Zugabe einer kleinen Menge $ZnCl_2$ wird weitere 15 Std. gekocht, abgesaugt, dem Filtrat 15 ml Toluol zugegeben und an einer Säule von 200 g Al_2O_3 (Aktiv.-Stufe 3), mit Toluol als Elutionsmittel, gereinigt. Das violette (an der Al_2O_3-Säule blaue) Hauptprodukt **12**, vom blauen Ausgangsprodukt (**8**) (mit nur wenig niedrigerem R) schwer trennbar, kristallisiert nach Einengen der Toluollsg. in Form dunkler Prismen mit violett-metallischem Glanz vom Schmp. 287° aus. Anal. $C_{19}H_{12}N_2OS$ (316,3) *ber.*; C 72,12 H 3,82 N 8,84; *gef.*; C 72,50 H 3,60 N 8,75 IR-Spektrum (in KBr) : 1624 (C=0) cm^{-1}; (in CCl_4) : 1929 (C=0) cm^{-1}. Elektronenspektrum (in Dioxan) : $\lambda(\varepsilon)$: 557 nm (7130), 331 nm (18150), 293 nm (19750), 252 nm (24840).

3-Acetoxy-4-diacetylamino-10-acetyl-phenothiazin (**7**). 0,5 g **1** werden in einem Gemisch von 20 ml Eisessig und 10 ml Essigsäureanhydrid heiß gelöst. Der heißen Lsg. wird portionsweise Zinkpulver bis zu ihrer Entfärbung zugegeben. Nach 1-stdg.-em Kochen wird filtriert, das Filtrat in Wasser gegossen und der gebildete weiße feine Niederschlag mit Toluol ausgeschüttelt. Der mit Wasser gewaschene und auf Na_2SO_4 getrocknete Toluolextrakt wird eingeengt. Man erhält **7** in Form farbloser Prismen vom Schmp. 167—168° (2maliges Umkristallisieren aus Toluol). Anal. $C_{20}H_{18}N_2O_5S$ (398,4) *ber.* : N 7,04; *gef.*; N 7,07. IR-Spektrum (in KBr) : 1717 (C=0) cm^{-1}; (in CCl_4) : 1729 (C=0) cm^{-1}. Elektronenspektrum (in Dioxan) : $\alpha(\varepsilon)$: 295 nm (2860), 258 nm (10970), 234 nm (25650).

4-Amino-7-chlor-phenothiazon (**9**). Eine Lsg. von 0,1 g **2** in 25 ml heißem Eisessig wird portionsweise mit Zinkpulver versetzt. Anschließend wird 15 Min. unter Rückfluß gekocht, wobei die entstandenen weißen Flocken in Lsg. gehen. Nach Abfiltrieren der gelblichen Lsg. wird mit 5N NaOH-Lsg. alkalisch gemacht und wie **8** aufgearbeitet. Man erhält **9** in Form langer blau-violetter Nadeln vom Schmp. 237,5°. Ausbeute 53%. Anal. $C_{12}H_7ClN_2OS$ (262,7) *ber.* : N 10,62; *gef.* : N 10,52. IR-Spektrum (in KBr) : 1644 (C=0), 3320 bzw. 3410 (N—H) cm^{-1}; (in CCl_4) : 1639 (C=0), 3368 bzw. 3470 (N—H) cm^{-1}. Elektronenspektrum (in Dioxan) : $\lambda(\varepsilon)$: 585 nm (5280), 357 nm (13930), 308 nm (18490).

4-Amino-7-brom-phenothiazon (**10**). 0,1 g **3** wird in 10 ml siedendem Eisessig gelöst und anschließend wie **9** aufgearbeitet und gereinigt. Man erhält 68% **10** in Form blau-violetter Nadeln vom Schmp. über 300°. IR-Spektrum (in KBr) : 1635 (C=0), 3314 bzw. 3411 (N—H) cm^{-1}; (in CCl_4) : 1642 (C=0), 3367 bzw. 3470 (N—H) cm^{-1}. Elektronenspektrum (in Dioxan) : $\lambda(\varepsilon)$: 590 nm (5270), 358,5 nm (14040), 310 nm (17940).

2-Chlor-4-nitro-phenothiazon (**14**). 0,5 g 2-Chlor-phenothiazon werden unter Rühren portionsweise bei Raumtemperatur in 100 ml HNO_3 (d=1,40) eingetragen, wobei die anfangs olivfarbene Lsg. braun wird. Nach 10 Min. weiterem Rühren wird in ca. 800 ml Eis/Wasser gegossen, die gebildete orangefarbene Lsg. mit Toluol extrahiert, der Toluolextrakt gewaschen, über Na_2SO_4 getrocknet und an einer Säule von 300 g Al_2O_3 (Aktiv.-Stuffe 3) gereinigt (Elutionsmittel Toluol). Beim Einengen kristallisiert **14** in Form orangeroter, golden glänzender Prismen vom Schmp. 276—277° aus. Ausbeute 35%. Anal. $C_{12}H_5ClN_2O_3S$ (292,7) *ber.* : N 9,59 Cl 12,12; *gef.* : N 9,33 Cl 11,95. IR-Spektrum (in KBr); 1640 (C=0) cm^{-1}; (in CCl_4) : 1660 (C=0) cm^{-1}. Elektronenspektrum (in Dioxan) : $\lambda(\varepsilon)$: 487 nm (10930), 400 nm (12470), 385 nm (12630), 278, 278,5 nm (19010).

2-Brom-4-nitro-phenothiazon (**15**). Eine Lsg. von 0,5 g 2,Brom-phenothiazon in 100 ml HNO_3 (d=1,40). (s. **13**) wird in Eis/Wasser gegossen wobei ein orangeroter flockiger Niederschlag entsteht, der abgesaugt, mit Wasser gewaschen und getrocknet wird. Ausbeute 62% rohes **14**; braunrote Prismen vom Schmp. 267—268° (2mal aus Eisessig). Nach chromatographischer Reinigung an einer Säule von 400 g Al_2O_3 (Aktiv.-Stufe 3), wobei sich ein Teil der Substanz zersetzt, werden 20,7% reines **15** in Form orangeroter Prismen vom Schmp. 271,5—272° erhalten. Anal., $C_{12}H_5BrN_2O_3S$ (337,0) *ber.* : N 8,31 Br 23,71 ; *gef.* : N 8,12 Br 23,30. IR-Spektrum (in KBr) : 1633 (C=0) cm^{-1}, (in CCl_4) : 1658 (C=0) cm^{-1}. Elektronenspektrum (in Dioxan) : λ(ε) : 488 nm (11070), 402 nm (13520), 390 nm (13580), 281,5 nm (18970).

4-Amino-2-chlor-phenothiazon (**17**). 0,15 g **14** werden in 50 ml heißem Eisessig gelöst, portionsweise Zinkpulver bis zur Entfärbung zugegeben, abfiltriert und das Filtrat mit einer 5N NaOH-Lsg. alkalisch gemacht. Die entstandene blaugrüne Lsg. mit flockigem blauem Niederschlag wird mehrmals mit Toluol ausgeschüttelt un der mit Wasser gewaschene und auf Na_2SO_4 getrocknete Toluolextrakt an einer Säule mit 500 g Al_2O_3 (Aktiv.-Stufe 3) sehr langsam chromatographiert. Als erste wird aus der Säule die grünblaue Hauptverbindung **17** mit Toluol eluiert, welche nach Einengen in Form blaugrüner, rosettenförmig angeordneter Nadeln vom Schmp. 230–231° kristallisiert (Auswaschen mit Äthanol). Ausbeute 60,3. Anal. $C_{12}H_7ClN_2OS$ (262,7) *ber.* : N 10,62 ; *gef.* : N 10,44. IR-Spektrum (in KBr) : 1632 (C=0), 3314 bzw. 3394 (N–H) cm^{-1} ; (in CCl_4) : 1640 (C=0), 3368 bzw. 3470 (N–H) cm^{-1}. Elektronenspektrum (in Dioxan) : λ(ε) : 605 nm (4820), 368 nm (15600), 305 nm (16590).

Als zweite Substanz wird aus der Säule in sehr kleinen Mengen ein blaues Produkt eluiert, das nach Schmp., Mischschmp., R_f, IR- und Elektronenspektrum mit **8** identisch ist.

4-Amino-2-brom-phenothiazon (**18**). 0,2 g **15** werden in 50 ml heißem Eisessig gelöst und wie **17** aufgearbeitet und gereinigt. Als erste wird aus der Säule eine rotviolette, unidentifizierte Substanz eluiert, gefolgt von der grünblauen Hauptverbindung **18**, welche nach Einengen der Toluollsg. in Form rosettenförmig angeordneter blaugrüner Nadeln vom Schmp. über 300°auskristallisiert. Ausbeute 20,2%. IR-Spektrum (in KBr) : 1631 (C=0), 3308 bzw. 3392 (N–H)cm^{-1} ; (in CCl_4) : 1640 (C=0), 3353 bzw. 3448 (N–H)cm^{-1}. Elektronenspektrum (in Dioxan) : λ(ε) : 610 nm (4350), 370 nm (15430), 306,5 nm (15460).

Nach der Hauptverbindung **18** wird aus der Säule eine blaue Substanz eluiert, welche nach Einengen der Toluollsg. in Form langer blauer Nadeln auskristallisiert und nach Schmp., Mischschmp., R_f, IR- und Elektronenspektrum mit **8** identisch ist. Ausbeute 17%.

Für die Aufnahme der IR-Spektren danken wir Frau Erika Hamburg und für die Aufnahme der Elektronenspektren Frl. Magdalena Bossanyi.

Revue Roumaine de Chimie, **17**, *10*, 1747–1753 (1972)

Revue Roumaine de Chimie, **17**, *10*, 1755–1764 (1972)

PHOTOCOPOLYMERIZATION OF ACRYLONITRILE WITH METHACRYLIC ESTERS IN THE PRESENCE OF ANTHRAQUINONE DYES

VIOLETA NUŢĂ, D. FELDMAN and CR. I. SIMIONESCU

Institute of Macromolecular Chemistry "P. Poni",
Aleea Grigore Ghica Vodă 41 A, Jassy, Romania

Received May 3, 1972

Photopolymerization of acrylonitrile (AN) with methacrylic esters such as : methyl methacrylate (MMA), butyl methacrylate (BMA) and lauryl methacrylate (LMA) using as photosensitiser the anthraquinone dye Indanthrene Yellow 3R (IY—3R) was studied. The best conversions depending upon the ratio between monomers and the duration of the process was followed and the reactivities of the comonomers (the reactivity ratios and Q and e parameters) was determined. No reactivity modification was found as the methacrylic ester chain increased.

INTRODUCTION

The coloured polymers directly obtained by synthesis form the object of many papers published in the specialized literature.[1–12]

Simionescu and coworkers [13] have studied the AN photopolymerization in the presence of some anthraquinone dyes and have presented data about the kinetics and the best reaction conditions. The method has the advantage that the photosensitisers used are at the same time dyes of the polymer.

The best synthesis conditions of the AN copolymers yield new data regarding its reactivity with different comonomers.

---

[1] M. Koizumi and A. Watanabe, *Bull. Chem. Soc. Japan*, **28**, 136 (1955).
[2] A. Watanabe and M. Koizumi, *Bull. Chem. Soc. Japan*, **28**, 141 (1955).
[3] G. Oster and Y. Mizutani, *J. Polymer Sci.*, **22**, 173 (1956).
[4] M. Tanyama and G. Oster, *Bull. Chem. Soc. Japan*, **30**, 856 (1957).
[5] A. Watanabe, *Bull. Chem. Soc. Japan*, **32**, 557 (1959).
[6] G. Smets, W. Dewinter and G. Delzenne, *J. Polymer Sci.*, **55**, 767 (1961).
[7] G. Delzenne, S. Toppet and G. Smets, *Bull. Soc. chim. belges*, **71**, 857 (1962).
[8] F. Takemura, *Bull. Chem. Soc. Japan*, **35**, 1073 (1962).
[9] F. Takemura, *Bull. Chem. Soc. Japan*, **35**, 1078 (1962).
[10] Cr. I. Simionescu and C. Ungureanu, *Rev. Roumaine Chim.*, **9**, 10 (1964).
[11] S. Toppet, G. Delzenne and G. Smets, *J. Polymer Sci.*, **A 2**, 1539 (1964).
[12] G. Delzene, W. Dewinter, S. Toppet and G. Smets, *J. Polymer Sci.*, **A 2**, 1069 (1964).
[13] D. Feldman, V. Nuţă and Cr. I. Simionescu, *Rev. Roumaine Chim.*, **14**, 1407 (1969).

In the present paper the AN photochemical copolymerization with methacrylic esters is studied by using as photosensitiser the anthraquinone dye IY-3R, chosen after experiments published in a previous paper.[13]

EXPERIMENTAL

Photochemical copolymerization was experimentally carried out in the mentioned conditions.[13] Monomers and dimethylformamide (DMF) were purified by bidistillation. As reaction medium a mixture of DMF/H_2O 4/11 (v/v) was used. For initiation anthraquinone dye IY-3R of 98% purity, produced by ICECHIM Bucharest, was used.

The experiments were performed at constant temperatures: 40±0.05°.

RESULTS AND DISCUSSIONS

The influence of some factors such as: copolymerization duration, nature and ratio of comonomers was pursued, AN being preserved in all systems as main comonomer.

1. AN-MMA SYSTEM

The variation of the AN/MMA ratio led to the results shown in figure 1.

An increase of the conversion in the copolymer along with the increase of the duration of the process and of the AN/MMA ratio were observed.

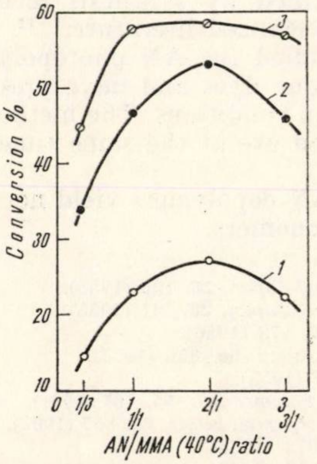

Fig. 1. — Conversion variation depending on AN/MMA ratio

1, duration 1 1/2 hour; *2*, duration 3 hours; *3*, duration 5 hours.

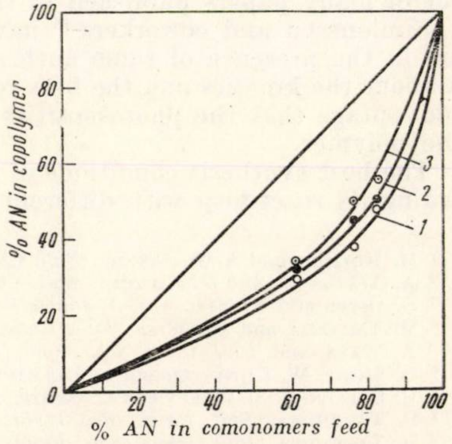

Fig. 2. — Copolymerization diagram AN-MMA

1, duration 15 minutes; *2*, duration 30 minutes; *3*, duration 45 minutes.

At the same time the conversion decreased as a result of the maximum efficiency at the 2/1 ratio and at higher concentrations of AN reached by the monomer. Maximum values are characteristic of all experiments regarding the copolymerization duration. Additional data on the dependence of the copolymerization upon the duration are furnished by the study of the composition of th copolymer obtained (fig. 2).

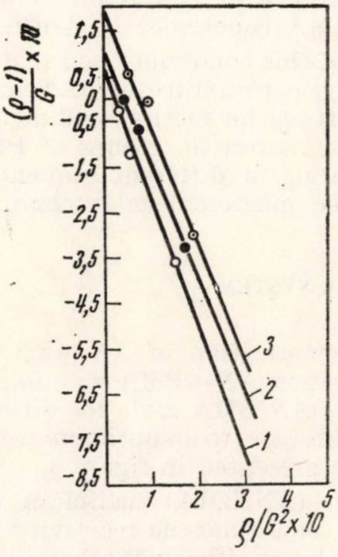

Fig. 3. – Fineman-Ross diagram of AN-MMA system

1, duration 15 minutes; *2*, duration 30 minutes; *3*, duration 45 minutes.

Fig. 4. – IR absorption spectrum of the AN-MMA copolymer.

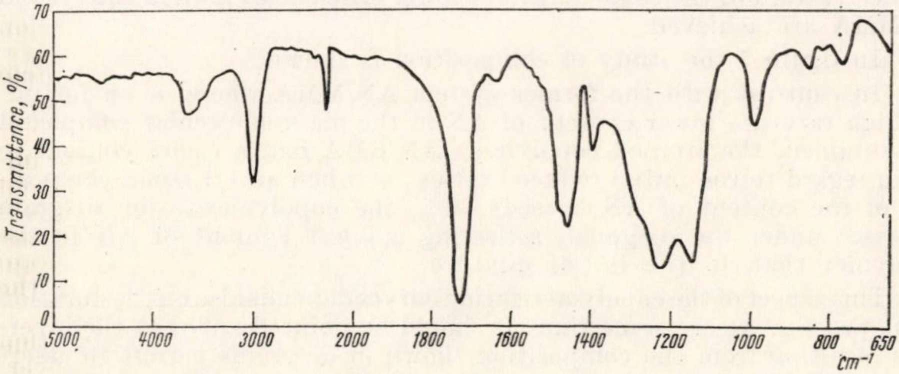

In figure 2 an increase of the AN content in the polymer depending upon the duration of the process was noticed, that is, a lower reactivity of AN in regard to the methacrylic ester. This is very important in the practice in obtaining PAN fibres. It should be pointed out that compositions "rich" in AN (more than 70%), by increasing the duration of copolymerization process are necessary.

The study of the composition for reduced conversions enables the calculation of the reactivity ratios for the given system. In figure 3 a typical example of the diagram Fineman-Ross[14] used to determine the values of r_1 and r_2 is presented.

The synthesis of copolymer AN-MMA is also pointed to by analysis through IR and RMN. As shown in figure 4, the IR spectrum presents the absorption of carbonyl groups at 1724 cm^{-1} and of nitrile groups at 2300 cm^{-1}, characteristic of this type of copolymer.[15]

Similarly, in figure 5 the appearance of characteristic frequencies of the RMN spectrum of the AN-MMA copolymer is shown.[16]

The spectrum is characteristic of this copolymer and it differs as to the aspect of peaks from that of physical mixture of PAN and PMMA. In it we find all the characteristic shiftings for methyn and methyl groups of PAN. The same is true for the characteristic groups of PMMA with slight modifications due to the entering of different sequences of AN, MMA and their derivatives, into the macromolecular chain.

2. AN-BMA SYSTEM

In similar conditions to copolymerization of AN with MMA, the copolymerization of the monomer system AN—BMA was followed. The study of conversion depending on the AN/BMA ratio for different durations of polymerization leads, also in this case, to an optimum ratio between the two comonomers. The results are presented in figure 6.

We notice that for the 2/1 ratio (AN/BMA) maximum conversion in the copolymer is achieved; at the same time the reactivity of the system decreases. For the same durations lower efficiencies than in the system AN-MMA are achieved.

In figure 7 the study of composition is shown.

In contrast with the former system AN/MMA where, even for initial high ratios, a lower content of AN in the macromolecular compound was obtained, the studied copolymers AN/BMA had a richer content in AN in regard to the initial reduced ratios; or when an 1/1 equal composition of the content of AN exceeds 70%, the copolymerization diagram decreases under the diagonal, reflecting a lower content of AN in the copolymer than in the initial mixture.

This aspect of the copolymerization curves depends also on the duration of the process. At the same time, it should be pointed out that the inversions resulting from the composition shown in diagrams permit to assert the possibility of obtaining azeotropic copolymers, products which will contain more and more AN, as the copolymerization duration increases.

For the area in which the initial composition is characterized by a content of more than 70% AN (which presents practical importance) the amount of AN in the copolymer increases along with the reaction duration.

---

[14] M. FINEMAN and S. D. ROSS, *J. Polymer Sci.*, **5**, 259 (1950).

[15] G. GENTILHOMME, A. PIQUET, J. ROSSET and GH. EYROUD, *Bull. Soc. chim. France*, 5, 901 (1960).

[16] J. GUILLOT, A. GUYOT and PHAM QUANG THO, *J. Macromol. Sci. Chem.* **A 2**, 1303 (1968).

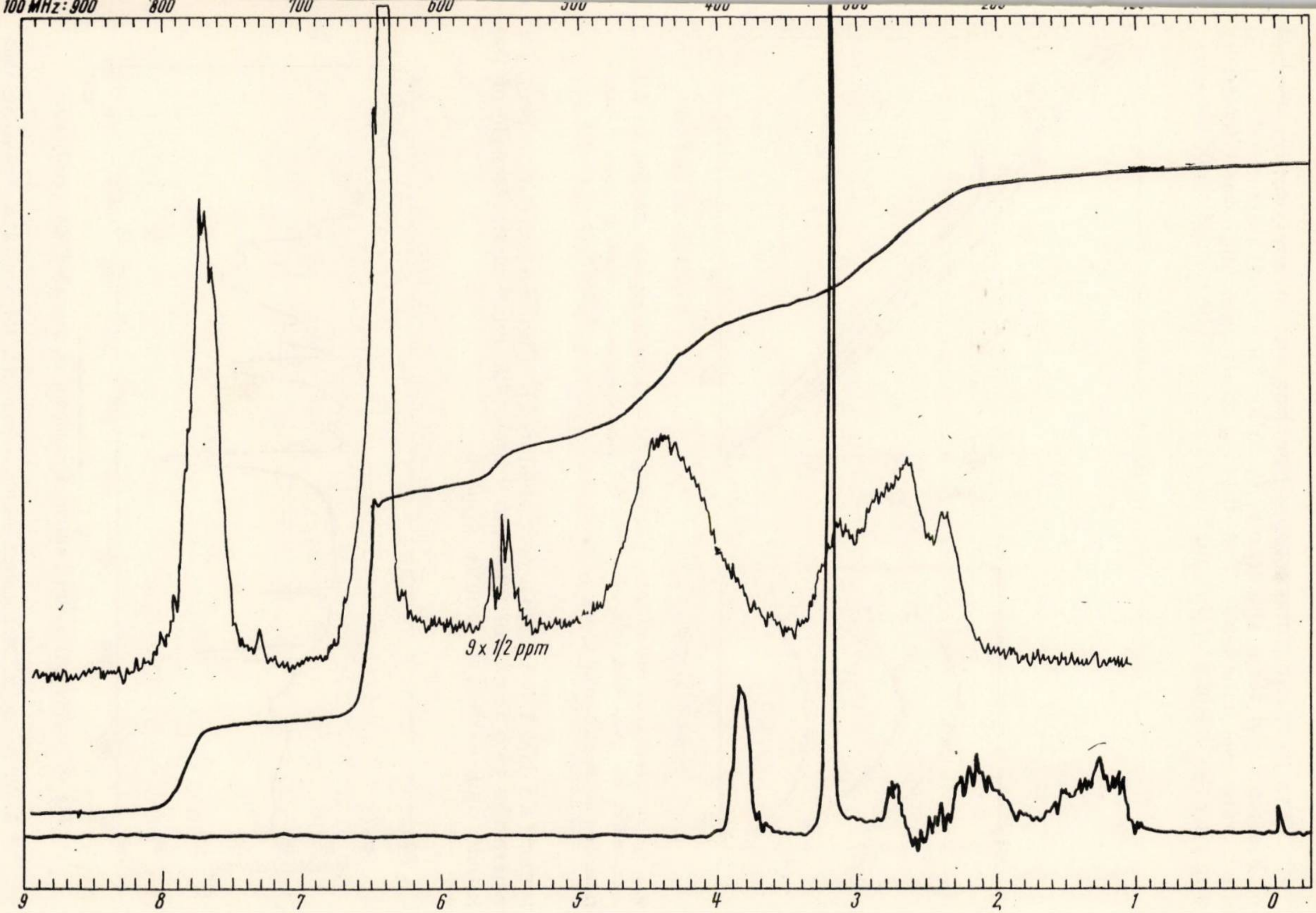

Fig. 5. – RMN spectrum of the AN-MMA copolymer.

With the help of the composition data and by applying the method of Fineman and Ross, the reactivity ratios for the monomer system studied, were also calculated. The drawing of straight lines was effected by applying the method of the smallest squares. [17] The formation of the copolymer (AN-BMA) was also ascertained by IR. Figure 8 presents a spectrum where the two bands of 2300 cm^{-1} and 1725 cm^{-1} characteristic of the nitrile and carbonyl groups appear.

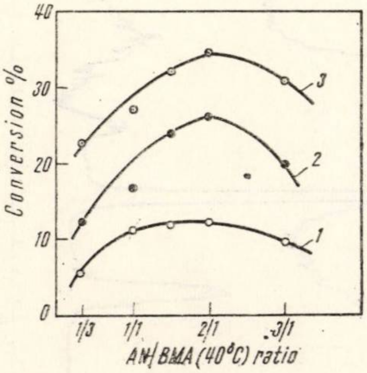

Fig. 6. — Conversion varation depending on AN-BMA ratio

1, duration 1 1/2 hour ; *2*, duration 3 hours ; *3*, duration 5 hours.

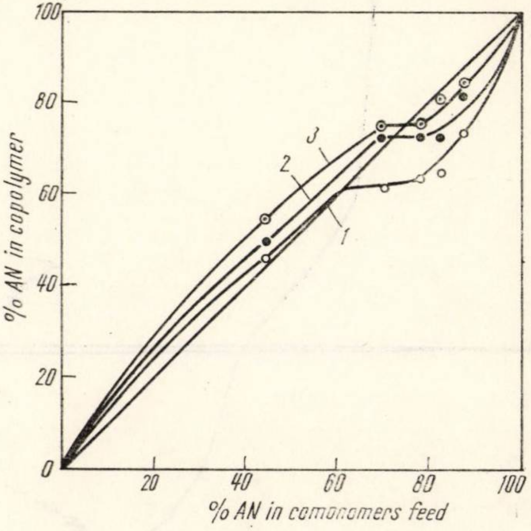

Fig. 7. — Copolymerization diagram AN-BMA

1, duration 30 minutes ; *2*, duration 45 minutes ; *3*, duration 60 minutes.

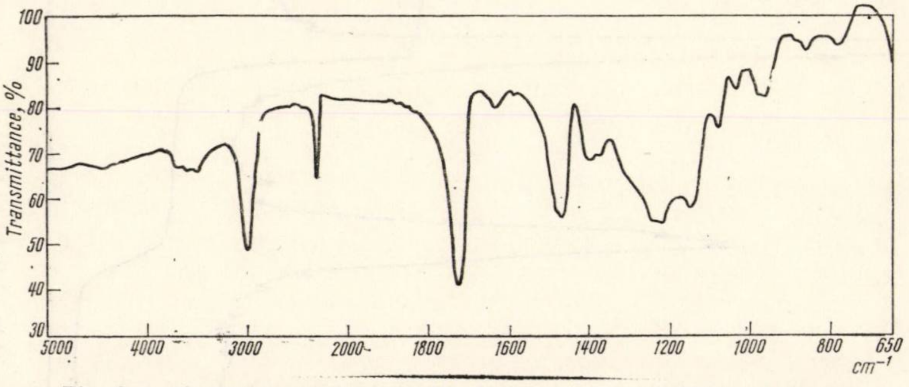

Fig. 8. — Absorption spectrum in IR domain of the AN-BMA copolymer.

---

[17] A. V. Boiarski "Matematică pentru economiști", Ed. Științifică, Bucharest, 1963, p. 291.

3. AN-LMA SYSTEM

In agreement with the former results, in the system AN-LMA an optimum efficiency in the copolymer for the 2/1 ratio AN/LMA (fig. 9) was reached.

As expected, the conversions, even those considered the best ones for this system, implying the copolymerization with a comonomer which has a long lateral chain, are reduced, even at great reaction durations.

The analysis of the composition can produce new data regarding the reactivity of the system (fig. 10).

Similar to AN-BMA and in contrast with AN-MMA, the composition diagrams in figure 10 show the existence of an increased reactivity of AN. Nevertheless, at AN/LMA ratios with more than 80% AN an inflection of the copolymerization curves occurs which shows the formation of products richer in LMA. Even in this case, azeotropic copolymers may be obtained. Evidently, because of the reduced reactivity of the system, the oscillations in the composition will be reduced in accordance with the duration of the process.

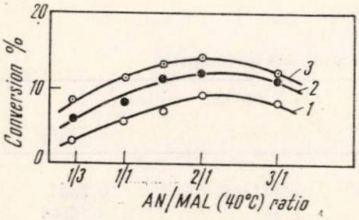

Fig. 9. – Conversion variation depending on AN/IMA ratio

1, duration 1 1/2 hour; *2*, duration 3 hours; *3*, duration 5 hours.

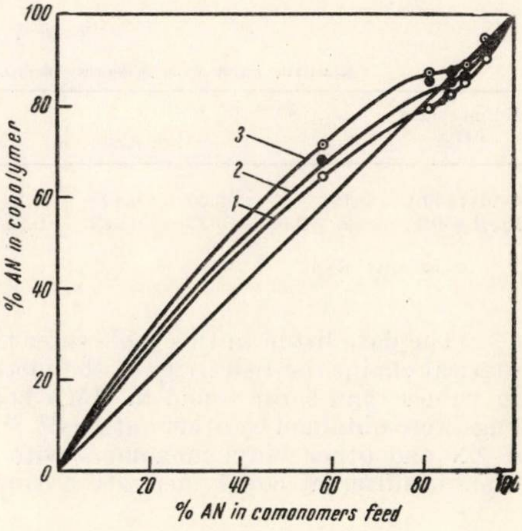

Fig. 10. – Copolymerization diagram AN–IMA

1, duration 1, 1/2 hour; *2*, duration 3 hours; *3*, duration 5 hours.

The IR spectrum shows through the characteristic bands the formation of the copolymer (fig. 11).

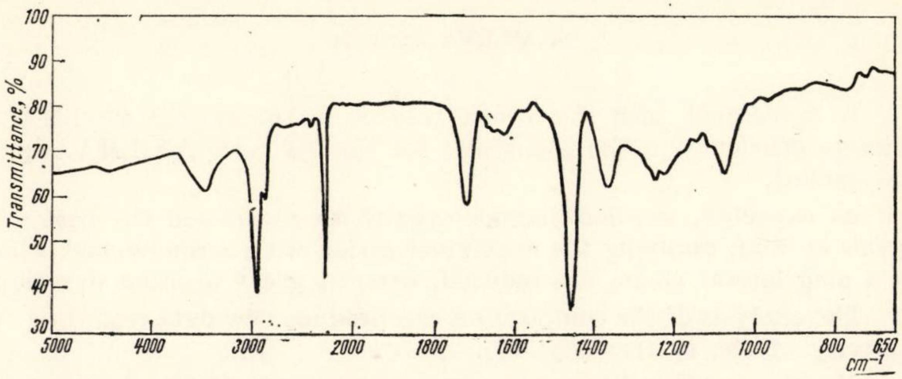

Fig. 11. — IR absorption of the AN-IMA copolymer.

4. REACTIVITY RATIOS

In table 1 the reactivity ratios obtained for the studied systems of comonomers are presented.

Table 1

Reactivity ratios of the monomers. Methacrylate alkyl and acrylonitrile

Methacrylate (M_2)	Present work			Literature values		
	r_1	r_2	r_1r_2	r_1	r_2	r_1r_2
Methyl (40°)	0.19	2.50	0.475	0.1±0.07[a)]	1.351±0.133[a)]	0.1351
Butyl (40°)	0.25±0.09	0.33	0.082	0.31[a]	1.08[a]	0.3348

a) 60° after Ham[18]

The data listed in this table show that along with the increase of the esterical chain, the reactivity of the methacrylic comonomer varies, slighter values than those found in MMA being obtained in BMA. These findings were obtained by other authors[19–24] who studied the copolymerization of AN and other vinyl monomers with different acrylic or methacrylic esters in different copolymerization conditions. For the system AN-MMA the product of the reactivity ratios ($r_1 . r_2$) is much higher than zero ; this fact shows that a regular alternation of the two comonomers does not occur [25].

---

[18] G. Ham, "Copolymerization", Interscience, New York, 1964, p. 703.

[19] C. S. Marvel and R. Schwen, *J. Amer. Chem. Soc.*, **79**, 6003 (1957).

[20] G. G. Cameron, D. H. Grant, N. Grassie and J. E. Lamb, *J. Polymer Sci.*, **36**, 173 (1959).

[21] Takashi Tamikado and Yoshio Iwakura, *J. Polymer Sci.*, **36**, 529 (1959).

[22] E. F. Jordan, Jr., K. M. Doughty and W. S. Port, *J. Appl. Polymer Sci.*, **IV**, 203 (1960).

[23] Tagayuki Otsu, Toshio Ito and Minoru Imoto, *J. Polymer Sci., C 16*, **4**, 2121 (1967).

[24] E. F. Jordan, Jr., R. Bennett, A. C. Shuman and A. N. Wrigley, *J. Polymer Sci., A 1*, **8**, 3113 (1970).

Taking into account the values of these products, the copolymers AN-BMA should present a much more regular alternation.

We remark a difference between the values indicated in literature[18] and those obtained by us. These differences may be accounted for by experimental conditions, such as : synthesis method, medium, reaction temperature, dye purity, a. s. o.

In calculating the reactivity ratios for the system AN-LMA, difficulties were met with, because of the reciprocal insolubility of the two monomers.

Using the equations from [26] and with the help of reactivity data obtained by us, the parameters Q and e values

$$e_2 = e_1 \pm (-\ln r_1 r_2)^{1/2}$$

and

$$Q_2 = Q_1/r_1 \exp \{-e_1(e_1 - e_2)\}$$

were calculated.
The results are presented in table 2.

Table 2

Copolymerization parameters of AN with methacrylate alkyl

Methacrylate (M_2)	Present work		Literature values	
	e_2	Q_2	e_2	Q_2
Methyl	0.353	1.00	0.40[a)]	0.70[a)]
Butyl	−0.380	0.36	−0.23[a)]	0.72[a)]

a) after Younp[26]

For AN we may find in literature [26] the values : $e_1 = 1.20$ and $Q_1 = 0.60$.

CONCLUSIONS

— Photochemical copolymerization of AN with different methacrylic ester monomers, using as photosensitisers anthraquinone dye IY-3R was studied, with a view to obtaining a direct synthesis of some coloured copolymers.

---

[25] G. ODIAN "Principles of Polymerization" McGraw-Hill, New York, 1970, p. 374.

[26] L. J. YOUNG, *J. Polymer Sci.*, **54**, 435 (1961).

— Regardless of the nature of the monomers and the duration of the process, the existence of an optimum comonomer composition at the 2/1 ratio AN/methacrylic ester was found.

— The study of the composition leads to the conclusion that along with the increase of alcoholic rests in the ester compound, the reactivity of the monomers changes. This is in agreement with the data concerning the acrylic esters found by other authors.

— As for the systems with BMA and LMA, in contrast with that of MMA, copolymers richer in AN, even at slight AN/methacrylic ester ratios, were obtained and it is not impossible to obtain azeotropic copolymers.

— The systems of AN-BMA copolymerization yield copolymers which present a more accentuated regularity of sequences.

— The copolymers obtained are coloured in stable shades imparted by the anthraquinone product IY-3R.

Revue Roumaine de Chimie, **17**, *10*, 1765 – 1769 (1972)

SPECTROPHOTOMETRIC DETERMINATION OF THE DICYANOAURATE (I) ION WITH PARANITRAL GREEN

CAMELIA GEORGETA CĂLIN
ECATERINA DIAMANDESCU and LIVIU MIHAI BĂLOIU

Department of Chemistry and Physics
Academy of Economic Studies
Piaţa Romana 6, Bucharest, Romania

Received March 31, 1972

The paper presents the synthesis of a new triphenylmethane basic dyestuff, *p*-dimethylaminobenzene-*p*-nitrobenzene-methane-*p*-quinonedimethylimmonium chloride, called by us "paranitral green". The dyestuff is then used for the spectrophotometric determination of dicyanoaurate(I) ion. The compound dyestuff-$[Au(CN)_2]$ is extracted in benzene and its absorbance is recorded. Lambert-Beer's law is obeyed between 2–50 μg Au/10 cm^3.

I. INTRODUCTION

Gold can be determined from cyanide solutions in three different ways. The first procedure is based on the extraction of gold from the complex ion $[Au(CN)_2]^-$, either by precipitation as Au_2S followed by a gravimetric determination,[1,2] or by cementation with aluminium or tin.[3] This method cannot be used for the analysis of solutions with very small gold amounts.

Another procedure way, more widely used nowaday, is the analysis by atomic absorption spectroscopy, measuring the gold line from 242.8 nm.[4]

The third possibility is based on the determination of the $[Au(CN)_2]^-$ ion, extracting it together with a large basic dyestuff cation into an organic solvent and measuring the absorbance of the organic layer.[5,6] In comparison with the atomic absorption spectroscopy, this method requires a cheaper and more common apparatus.

---

[1] I. I. Kalinichenko and P. A. Sokolova, *Metody Analiza Kern i Tvet. Metallov*, **1953**, 105.

[2] K. A. Karashev, I. A. Kakovski and A. A. Golovin, *Sovremen. Metody Analiza Met. Sbornik*, **1955**, 214.

[3] R. J. Rochat, *Plating*, **36**, 817 (1949).

[4] R. H. Rkewes, *Australian Inst. Mining Met. Proc.*, **221**, 217 (1963).

[5] V. Armeanu, L. M. Băloiu and M. Damian, *Rev. Roumaine Chim.*, **13**, 1617 (1968).

[6] V. Armeanu and L. M. Băloiu, *Analyt. Chim. Acta*, **44**, 230 (1969).

Previous studies show that using triphenyl-methane dyestuffs, no other complex cyanide ion interfers. However on the other hand, the triphenylmethane dyestuffs previously tested [5,7] give with our complex ion highly dissociated compounds ; this means that Lambert-Beer's law is obeyed only over a short concentration range.

The aim of this paper is to describe first the synthesis of a new basic triphenylmethane dyestuff, *p*-dimethylaminobenzene-*p*-nitrobenzene-methane-*p*-quinonedimethylimmonium chloride, called by us "paranitral green", and then to present its use as reagent for the spectrophotometric determination of the $[Au(CN)_2]^-$ ion.

II. EXPERIMENTAL

The dyestuff synthesis is based on an intermolecular condensation between NN-dimethylaniline and p-nitrobenzaldehyde.

A mixture consisting of 11 g *p*-nitrobenzaldehyde, 17.6 g freshly distilled NN-dimethylaniline and 10.2 g anhydrous $ZnCl_2$ is heated in a capsule for six hours on a boiling water bath, stirring continuously. The brown solid mass obtained is treated with 70 cm^3 hot water and passed into a 250 cm^3 long-neck flask. Here, the remained NN-dimethylaniline is stream-distilled for two hours. The leucobase, remained unsolved in the flask, is washed several times with cold water, then recrystallized from ethyl alcohol. Twenty grams yellow crystalline leucobase are obtained.

Five grams leucobase are solved in 35 cm^3 hot 2n hydrochloric acid. The solution, pink-red, is diluted with 350 cm^3 water, then freezed, and a suspension containing 4 g PbO_2 in 15 cm^3 water is added in small portions, followed by a solution of 6 g $ZnCl_2$ in 5 cm^3 water. The dyestuff precipitates almost immediately when a saturated NaCl solution is added ; then it is filtered by sucction, washed with saturated NaCl solution and dried. Four grams dyestuff are obtained as blue-green crystals who are afterwards recrystallized from water.

The dyestuff purity was checked by the $K_2Cr_2O_7$ method.[8] The value we found is 61 %, calculated as dyestuff chloride.

The complex ion $[Au(CN)_2]^-$ was prepared as potassium salt by dissolving the gold(I) cyanide in potassium cyanide solution. [9]

All other reagents were of analytical reagent grade.

The absorption spectra were recorded with a Unicam SP 800 spectrophotometer. All other absorbance measurements were made with a IOR Pulfrich-type colorimeter.

III. PRELIMINARY TESTS

The first problem was to choose the extraction solvent. The polar solvents, as alcohols and ketones, extract the chloride salt of the dyestuff as well as the complex salt. The aliphatic hydrocarbons do not extract the dyestuff in any form. Among the solvents which extract the dyestuff only as dicyanoauric(I) salt, benzene, toluene, ethyl ether, the best results were obtained with benzene, who was then chosen as extraction solvent.

---

[7] V. Armeanu and L. M. Băloiu, Communication at the Scientific Session of the Polytechnic Institute, Bucharest, 1969.

[8] R. P. Lastovski and I. I. Wainstein, "Tehnicheskii analiz v proizvodstve promezhutochinik produktov i krasitelei", Gosudarstvenoe nauchino-tekhnichescoe izdatelstvo khimicheskoi literatury, Moscow, 1958.

[9] H. Bassett and A. S. Corbet, *J. Chem. Soc.*, **125**, 1660 (1924).

The absorbance of the benzene phase is not time-depending, if the aqueous and benzene phases are not together. If the aqueous phase is not removed, a slow decoloration of the benzene layer is observed after a few hours.

The dyestuff is extracted in benzene by the complex ions $[Au(CN)_2]^-$ and $[Au(CN)_4]^-$; the complex cyanide ions containing Ag(I), Cu(II), Zn(II), Cd(II), Hg(II), Pb(II), Fe(III) and Fe(IV) do not interfere.

The dyestuff is extracted also in the presence of tetrahalo-complexes of metals belonging to the third group of the periodical table.

Extracted in benzene as dicyanoauric(I) salt, the dyestuff shows two absorbance maxima corresponding to S−42 and S−66 filters of the IOR Pulfrich-type colorimeter (Table 1). We have chosen the S−66 filter because the absorbance is higher and the measurements with the deep-violet S−42 filter are very tiring.

Table 1

Absorbances of the benzene layer, measured on filters of IOR Pulfrich-type colorimeter (1.05μg Au+0.02 g, dyestuff in 10 cm³ water, 10 cm³ benzene; d=2 cm)

Filter	S−42	S−47	S−61	S−66	S−72
A	0.59	0.21	0.29	0.61	0.30

IV. THE STUDY OF THE COMPOUND FORMED BETWEEN DYESTUFF AND $[Au(CN)_2]$

The compound formed between the dyestuff cation and the complex anion $[Au(CN)_2]^-$ has mainly an ionic character. This can be explained by the fact that both ions are stable systems, electronically satisfied, without any marked donor or acceptor character. None of the two ions has any free bonding orbitals, so that they are not able to establish a covalent bond.

Experimentally, the main ionic character of the compound is proved by the absorption spectra (Fig. 1). The absorption spectra of the aqueous solutions of dyestuff as chloride and dicyanoauric(I) salts (curve 1) are identical; that means that structure, succesion and position of the dyestuff molecular orbitals are not affected on the combination with the complex ion. The shift of the absorption spectrum of the compound extracted in benzene (curve 2), is due to the different polarities of the two solvents.

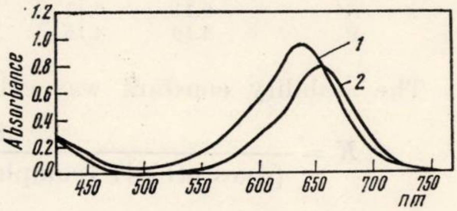

Fig. 1. — Absorbance spectra.

1, absorbance spectra of the compounds dyestuff – halide and dyestuff – dicyanoaurate (I) in water: *2*, spectrum of the compound dyestuff-dicyanoaurate(I) in benzene.

A study of the combination ratio is meaningless ; the single possible ratio is that given by the electric charges of the two ions, i. e. 1 : 1.

The partition constant was determined spectrophotometrically by the double extraction method.[10] The partition constant is :

$$P = \frac{[\text{compound}]_0}{[\text{compound}]_w} = \frac{A/kd}{[\text{compound}]_t - A/kd} \tag{1}$$

because, according to Lambert-Beer's law :

$$[\text{compound}]_0 \cdot k \cdot d = A \tag{2}$$

If the aqueous phase is treated with a new portion of solvent, we obtain for the second extraction :

$$P = \frac{[\text{compound}]'_0}{[\text{compound}]'_w} = \frac{A'/kd}{[\text{compound}]_t - A/kd - A'/kd} \tag{3}$$

where A' is the absorbance of the second benzene portion.

Equations (1) and (3) give :

$$P = \frac{A - A'}{A'} \tag{4}$$

if Lambert-Beer's Law is obeyed in the range $A \div A'$.

The results are given in Table 2.

Table 2

Determination of the partition constant

No.	1	2	3	4	average value
A	0.56	0.88	1.02	1.14	—
A′	0.11	0.17	0.21	0.26	—
P	4.10	4.15	3.85	3.40	3.8

The stability constant was calculated from the equation[11] :

$$K = \frac{A/kd}{[\text{dyestuff}]_t \{P\,[\text{complex ion}]_t - A/kd\,(P+1)\}} \tag{5}$$

where A is the absorbance of a sample containing less dyestuff than required for the total shifting to the right of the compound's formation equilibrium.

---

[10] V. Armeanu, S. Oancea, S. Rusenescu and L. M. Băloiu, *Rev. Roumaine Chim.* **17**, 925 (1972).

[11] L. M. Băloiu, *Rev. Roumaine Chim.*, **17**, 1065 (1972).

Equation (5) was obtained taking into account the two equilibria which appear in the respective system : the combination of the two ions to give the studied compound and the distribution of the compound between aqueous and organic phases.

The reults are given in Table 3.

Table 3

Determination of the stability constant

A (d=2cm)	[Dyestuff]	[Complex ion]$_t$	K
0.22	0.3×10^{-4}	5×10^{-6}	4.3×10^{3}
0.34	0.6×10^{-4}	5×10^{-6}	5.1×10^{3}
0.45	1.2×10^{-4}	5×10^{-6}	4.1×10^{3}
average value			4.5×10^{3}

V. METHOD FOR THE DETERMINATION OF GOLD

Adding different volumes of reagent solution over a constant amount of $[Au(CN)_2]^-$ ions, the absorbance of the benzene layer is brought to a constant level when the ratio dyestuff : gold reaches 1 mg dyestuff for 1 μg Au in 10 cm^3 final aqueous solution, i. e. 0.2 cm^3 0.5% dyestuff solution for 1 μg Au (The method being mainly proposed for the determination of gold, we give concentrations in g Au/cm^3 instead of g $[Au(CN)_2]^-$/cm^3).

The absorbance does not depend on pH, in neutral and acid range. This can be explained by the fact that $[Au(CN)_2]^-$ is the anion of a strong acid,[12] so that the equilibrium between $[Au(CN)_2]^-$ and the dyestuff cation is not affected by a secondary equilibrium between $[Au(CN)_2]^-$ and H^+.

Determination of gold from cyanide solutions is made in the following way. Into a separatory funnel are introduced : the aqueous solution containing gold ; the aqueous solution of the dyestuff, in such an amount as to shift the compound formation equilibrium totally to the right (i.e. 4 cm^3 0.5% dyestuff solution for less than 20 μg Au or 9 cm^3 for 50 μg Au) ; distilled water untill 10 cm^3 ; benzene, 10 cm^3. The separatory funnel is energetically shaken for 1—2 minutes. The aqueous and bezene phases are separated and the absorbance of the benzene solution is measured at 655 nm against a blank consisting of pure benzene.

With 2-cm long cells and an S-66 filter of the IOR colorimeter, gold can be determined in the range 2÷20 μg Au/whole aqueous solution; with 0.5-cm long cells, the range can be extended until 50 μg Au.

The slope of the function absorbance *vs.* gold concentration, for 2-cm long cells and on S-66 filter is 0.058 absorbance unities per 1 μg Au.

---

[12] J. Brigando, *Bull. Soc. chim. France*, **1957**, 503.

Revue Roumaine de Chimie, **17**, *10*, 1771 – 1777 (1972)

THE USE OF THE SALT EFFECT IN ACID-BASE TITRATION PERFORMED IN ORGANIC MEDIUM III *)

A STUDY REGARDING THE ANALYTICAL BEHAVIOUR OF AROMATIC ACIDS IN METHYL ALCOHOL IN THE PRESENCE OF $Ca(NO_3)_2$ **)

AGNES BLAZSEK-BODÓ and C. LITEANU

Medical and Pharmaceutical Institute, Tîrgu-Mureş
str. Gh. Marinescu 38, Tîrgu-Mureş, Romania
and
"Babeş-Bolyai" University, Str. Arany János 11, Cluj, Romania

Received February 29, 1972

The authors studied the effect of the ionic strength in potentiometric titration of certain aromatic acids, performed in methyl alcohol solutions. The ionic strength was assured by adding various amounts of dehydrated $Ca(NO_3)_2$ to the titrated solutions. The increase of the ionic strength was followed in all cases by the rise of the relative acidity of the examined acids, and also by the increase of the potential variation at the equivalence point ($\Delta E_{\pm 1\%}$). The maximal increase of the $\Delta E_{\pm 1\%}$ value was observed by titration of salicylic and mandelic acid (at $I = 4.37$ the value of $\Delta E_{\pm 1\%} = 89$ mV and 97 mV), while with other examined acids at $I = 4.37$, the value of $\Delta E_{\pm 1\%}$ varied between 38–68 mV. It was established that concurrently with the improvement of the circumstances of potentiometric titrations, the relative acidity increased in case of each acid; the maximal values were obtained in case of mandelic acid ($\Delta pK_{a(I_0 - I_{4.37})} = 3.39$).

Apart of the protophylic solvents used for the titration of the aromatic acids slightly soluble in water and slightly dissociating, in most cases differentiating solvents are used, particularly when we are dealing with the differentiated determination of acid mixtures. For this purpose ketones are primarily used,[1-7] the differentiating effect of the alcohols

---

*) Part II, C. Liteanu and Agnes Blazsek-Bodó, *Rev. Roumaine Chim.*, **17**, 1465 (1972).

**) This paper was partly presented at the 2nd Conference of Applied Physical Chemistry, Veszprém (Hungary), 1971.

[1] L. N. Bykova, A. P. Kreshkov, N. A. Kazarian and J. D. Pevzner, *Uspekhi Khim.*, **37**, 676 (1968).

[2] A. P. Kreshkov, L. N. Bykova and N. A. Mhitarian, *Zhur. analit. Khim.*, **14**, 529 (1959).

[3] A. P . Kreshkov, L. N. Bykova and N. A. Kazarian, "Titrarea în mediu neapos", Ed. Tehnică, Bucharest, 1969, p. 36, 52.

[4] A. P. Kreshkov, L. N. Bykova and N. A. Kazarian, *Zhur. priklad. Khim.*, **35**, 1575 (1962).

[5] A. P. Kreshkov, L. N. Bykova, L. N. Kazarian and E. S. Rubtsova, *Zhur. analit. Khim.*, **20**, 492 (1965).

[6] A. P. Kreshkov, L. N. Bykova, N. A. Kazarian and E. S. Rutbsova, *Zhur. prikl. Khim.*, **12**, 1251 (1965).

[7] L. Nyitray, *Gyógyszerészet*, **10**, 215 (1966).

being less expressed. In many instances, however, methyl alcohol or a mixture of methyl alcohol-water – in varying proportions – are suggested for the individual determination of weak acids.[3-6,8,9]

As we know, in any solvent the acidity and basicity scale is determined by its acidity and basicity, as well as by the value of the dielectric constant. The solvents possessing a great dielectric constant are, generally, facilitating the dissociation of HA-type acids, particularly when hydrogen bonds are also formed between the dissolved acid and the solvent.[10]

The standard chemical potential of the acids in mixtures of methyl alcohol and water – of varying proportions – is a function of the concentration of methyl alcohol used. In the case of an increasing methyl alcohol concentration the retrogradation of dissociation of the carboxylic acids may attain values of the order of $\Delta pK = 4.5-5.5$.[11-13] This phenomenon may, first of all, be explained by much smaller dielectric constant of the methyl alcohol ($\varepsilon = 32.6$), as compared with that of the water,[14-16] because the ion product of the methyl alcohol approaches that of the water ($pP_{CH_3OH}) = 16.6$).[17]

The differentiating capacity of a solvent, as well as the acid-base strength of a substance dissolved in a given solvent may be expressed, according to Kreshkov and Bykova[18,19,20] through the relative acidity scale. The relative acidity and basicity scale of the methyl alcohol, thus determined, proved to be 667 mV, a value which also reflects the slight differentiating effect of the methyl alcohol, as well as the considerable decrease noted in the dissociation of the acids which have been dissolved in it.

The correlation equation suggested by Kreshkov and co-workers[19] affords the possibility of determining the pK_a value of the benzoic acid and of its derivatives in different solvents. With its aid and based on the pK_a values determined in water, the dissociation constant of benzoic acid derivatives may be determined in methanol, as follows:

$$pK_{a(CH_3OH)} = 1.31 \times pK_{a(H_2O)} + 4.0$$

The values calculated with the above mentioned equation agree with the values of the dissociation constants determined on the basis of the potentiometric and conductometric measurements.

---

[8] K. E. Burger and E. Schulek, *Talanta*, **4**, 120 (1960).

[9] K. C. Ong, R. A. Robinson and R. G. Bates, *J. Phys. Chem.*, **67**, 1833 (9163).

[10] A. Coulombeau, *Commis. Energ. At.* [*Fr.*] *Serv. Doc., Ser.* "*Bibliogr.*", **1969**, C≡ A–BIB–147; *Chem. Abstr.*, **72**, 6691 (1970).

[11] J. Juillard and N. Simonet, *Bull. Soc. chim. France*, **1968**, 1883.

[12] J. Juillard, *Bull. Soc. chim. France*, **1968**, 1894.

[13] H. Sano, *Bull. Osaka, Ind. Res. Inst.*, **11**, 293 (1960).

[14] G. Charlot and B. Trémillon, "Les réactions chimiques dans les solvants et les sels fondus", Ed. Gauthier-Villars, Paris, 1963, p. 52.

[15] G. Charlot, Les méthodes de la chimie analytique", Ed. Masson, Paris, 1966. p. 489.

[16] L. Meites, "Handbook of analytical chemistry", McGraw-Hill Book, New York, 1963, p. 1–47.

[17] R. Schaal and G. Lambert, *J. Chem. Phys.*, **59**, 1151 (1962).

[18] L. N. Bykova, *Zhur. analit. Khim.*, **24**, 1781 (1969).

[19] A. P. Kreshkov, *Zhur. analit. Khim.*, **23**, 271 (1968).

[20] C. Liteanu and A. Blazsek, *Rev. Roumaine Chim.*, **16**, 835 (1971).

Considering that the methyl alcohol is an adequate solvent of numerous aromatic acids, it seems advisable that in the case of the potentiometric titrations effected in such media, the relative acidic strength of the acid to be determined should be raised through the increase of the ionic strength. Bessière [21] has stated that the completely dissociating salts, present in high concentrations, in solvents with a low dielectric constant, are influencing the acid-base reactions in such a way as if these would take place in solvents with a high dielectric constant. This statement results from our previous observations concerning the realization of optimal conditions for potentiometric titration of aliphatic acids,[20] dicarboxylic and hydroxyacids [22] in methanol; the increase of the ionic strength was assured through addition of anhydrous $Ca(NO_3)_2$.

In order to study the behaviour of aromatic acids in methyl alcohol solutions at high ionic strength, in the present paper we examined the hydroxy-, amino- and nitroderivatives of the benzoic acid. The increase of the relative acidity (pK_a values) of these acids in the given medium, as well as the optimal conditions of the potentiometric titration were determined.

The potentiometric titrations were effected with the aid of a MULTOSKOP V potentiometer, using glass and saturated calomel electrodes.

The method used for calculation of the pK_a values in methanolic solutions with high ionic strength was described in our previous paper. [20] The liquid-junctions potential occurring within the system was established through the application of a benzoic acid standard substance. In our calculations we used the value of acidity constant of benzoic acid in methyl alcohol : $pK_{\text{benzoic ac.}} = 9.4$[3,17,21,23] taking into account the following equation :

$$E_j = E_{1/2(S)} - pK_{a(S)} \times 0.059$$

$E_{1/2(S)}$ being the HNP of the benzoic acid measured in methyl alcohol, $pK_{a(S)}$ being the dissociation constant of the benzoic acid in methyl alcohol:

Our examinations were made with reagents of analytical purity. As standard solutions 0.1 N $NaOCH_3$ in methyl alcohol was used.

The pK_a values of the acids as determined in methanolic solutions with a high ionic strength show a considerable decrease, which indicates the increase of their relative acidity. The modifications of the pK_a values, function of the ionic strength, is illustrated in Figs. 1 and 2. The ΔpK_a values calculated in the cases of $I_0 - I_{0.95}$ and $I_0 - I_{4.37}$ are given in table 1, together with the experimental values of pK_a in methanol compared with the corresponding literature data. [3,17,21,23,24]

As already stated,[21,23] the high ionic strength influences least of all the dissociation of strong acids. Thus in the examined series, in the case

---

[21] J. Bessière, *Bull. Soc. chim. France*, **1968**, 3074.

[22] C. Liteanu and A. Blazse-Bodó, Rev. Roumaine Chim., **17**, 1455 (1972).

[23] A. P. Kreshkov, N. S. Aldarova and N. T. Smolova, *Zhur. obshchei Khim.*, **39**, 1390 (1969).

[24] J. Juillard, *Bull. Soc. chim. France*, **1966**, 1727.

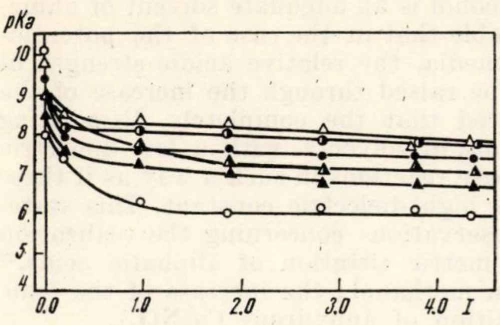

Fig. 1. — Variations of the pK_a values as a function of the ionic strength.

–●– benzoic acid ; –○– salicylic acid ; –▲– acetylsalicylic acid ; – Δ – p-amino-benzoic acid ; –◑– o-amino benzoic acid ; – **Δ** – nicotinic acid

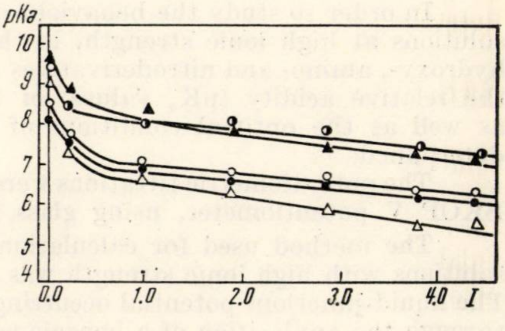

Fig. 2. — Variations of the pK_a values as a function of the ionic strength.

–●– p-nitro benzoic acid ; –○– m-nitro benzoic acid ; –▲– phenylacetic acid ; – Δ – mandelic acid ; –◑– cinnamic acid.

Table 1

Variation of pK_a values function of the ionic strength

Acids	pK_a		$\Delta pK_{a(I_0-I_{0,95})}$	$\Delta pK_{a(I_0-I_{4.37})}$
	Literat.	Determ.		
Benzoic acid	9.40* 10.14** 9.28***	9.40	1.78	2.12
Salicylic acid	8.61**	8.03	1.83	2.27
Acetylsalicylic acid	—	8.52	1.34	2.02
p-Nitrobenzoic acid	8.22**	8.13	1.15	1.86
m-Nitrobenzoic acid	8.22**	8.51	1.41	2.11
p-aminobenzoic acid	9.27**	9.76	1.48	2.22
o-Aminobenzoic acid	—	10.09	2.04	2.48
Phenylacetic acid	—	9.61	1.31	2.33
Mandelic acid	—	9.05	2.31	3.39
Cinnamic acid	—	9.59	1.56	2.34
Nicotinic acid	9.31***	9.03	1.42	2.19

* References [3, 17, 21, 23]
** References [25]
*** References [24]

---

[25] J. D. Tabagua, *Zhur. fiz. Khim.*, **37**, 1545 (1963).

of the *p*-nitrobenzoic acid $\Delta pK_{a(I_0-I_{4.37})} = 1.86$; this value in most acids which have been studied is between $\Delta pK_{a(I_0-I_{4.37})} = 2.0-2.5$, while in the case of the mandelic acid it is $\Delta pK_{a(I_0-I_{4.37})} = 3.39$. Comparing the potentiometric titration curves of the benzoic acid, salicylic acid, mandelic acid and nicotinic acid at different ionic strengths (fig. 3) it may be stated that the high ionic strength influences favourably above all, the titration capacity of the hydroxy groups containing acids.

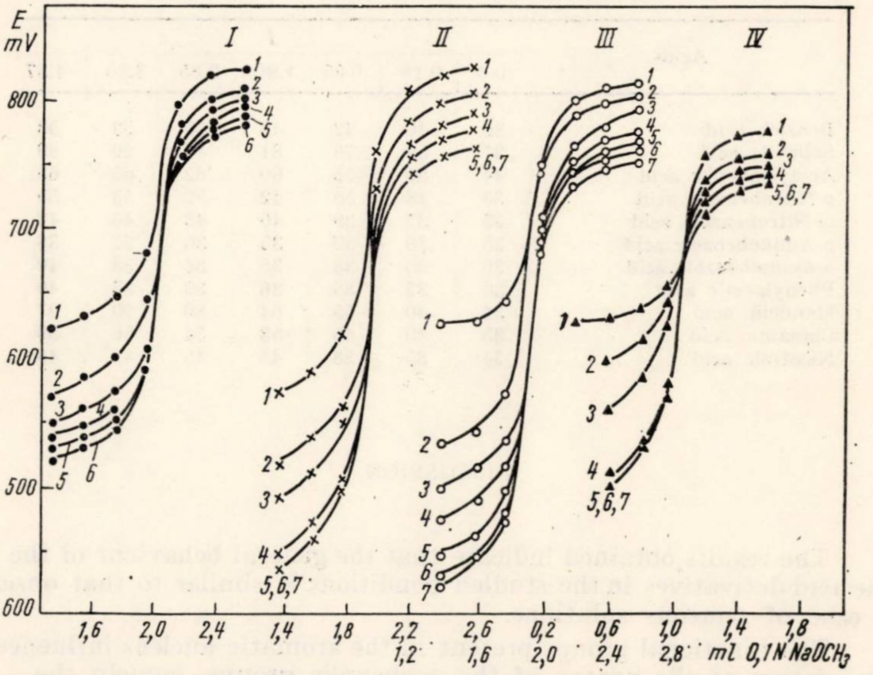

Fig. 3. — Titrations curves of *I*, benzoic acid ; *II* salicylic acid ; *III* mandelic acid and *IV* nicotinic acid at various ionic strengths.
1, $I = 0.0$; *2*, $I = 0.18$; *3*, $I = 0.95$; *4*, $I = 1.90$; *5*, $I = 2.85$; *6*, $I = 3.80$; *7*, $I = 4.37$

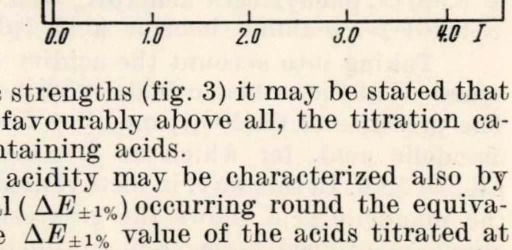

Fig. 4. — Variations of the $\Delta E_{\pm 1\%}$ values as a function of the ionic strength.
—●— benzoic acid ; —×— salicylic acid ; —▲— p-nitro benzoic acid ; —○— p-amino benzoic acid ; —◑— mandelic acid.

The increase of the relative acidity may be characterized also by the value of the jump of potential ($\Delta E_{\pm 1\%}$) occurring round the equivalence point. Table 2 illustrates the $\Delta E_{\pm 1\%}$ value of the acids titrated at various ionic strength, from which the data referring to the benzoic acid, salicylic acid, *p*-nitrobenzoic acid, *p*-aminobenzoic acid, mandelic acid and nicotinic acid are also listed in fig. 4.

Table 2

The potential-modification ($\Delta E_{\pm 1\%}$ mV) occurring round the equivalence point, in the case of aromatic acids titrated at various ionic strengths

Acids	*I*						
	0.0	0.18	0.95	1.90	2.85	3.80	4.37
Benzoic acid	30	40	42	45	55	53	53
Salicylic acid	37	59	73	81	83	90	89
Acetylsalicylic acid	44	50	55	60	62	65	65
p-Nitrobenzoic acid	39	48	50	52	52	53	55
m-Nitrobenzoic acid	25	37	39	40	43	40	42
p-Aminobenzoic acid	25	30	32	35	35	37	38
o-Aminobenzoic acid	30	35	38	38	36	38	40
Phenylacetic acid	30	32	35	36	36	37	40
Mandelic acid	31	40	55	64	80	90	97
Cinnamic acid	35	40	45	53	54	56	59
Nicotinic acid	34	35	38	45	45	43	45

DISCUSSION

The results obtained indicate that the general behaviour of the benzoic acid derivatives in the studied conditions is similar to that observed in case of aqueous solutions.

The functional groups present in the aromatic nucleus influence the dissociation of the proton of the carboxylic groups, namely the $-$ OH and $-NO_2$ groups increase, the $-$ NH_2 groups decrease the relative acidity of the benzoic acid. These statements concerning the aqueous solutions of benzoic acid are valid also in methyl alcohol at various ionic strength. In methyl alcohol, at $I=0$ the following order of decreasing acidity may be established : salicylic acid ($pK_a = 8.03$) >, *p*-nitrobenzoic acid ($pK_a = 8.13$) > *m*-nitrobenzoic acid ($pK_a = 8.51$) >, acetylsalicylic acid ($pK_a = 8.52$) >, nicotinic acid ($pK_a = 9.03$) >, mandelic acid ($pK_a = 9.05$) >, benzoic acid ($pK_a = 9.40$) >, cinnamic acid ($pK_a =$ $= 9.59$) >, phenylacetic acid ($pK_a = 9.61$) >, *p*-aminobenzoic acid ($pK_a =$ $= 9.76$) >, *o*-amino benzoic acid ($pK_a = 10{,}09$).

Taking into account the acidity constant values, it may be established that the aromatic acids examined in methyl alcohol are weak acids. The presence of $Ca(NO_3)_2$ modifies first of all the relative acidity of the mandelic acid, for which at $I = 0.95$ $pK_a = 6.74$, while at $I = 4.37$ $pK_a = 5.66$. In this way, in methyl alcohol solutions, at high ionic strength the mandelic acid shows the greatest acidity, while other acids of the above mentioned series remain unchanged.

The particular behaviour of the mandelic acid in concentrated $Ca(NO_3)_2$ solutions may be explained only through the presence of the hydroxylic group in the lateral chain. We suppose that in these solutions the formation of some complexes with higher dissociation degree occurs :

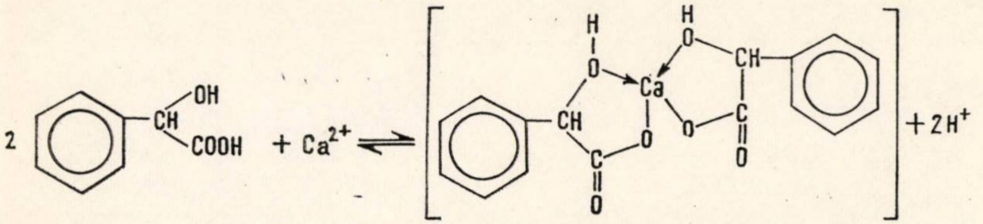

The acidity of the salicylic acid does not show modifications in solutions with high ionic strength, as pronounced as the mandelic acid. The relatively higher acidity of the salicylic acid at $I = 0$ may be explained, as in water, through the formation of intramolecular hydrogen bonds, which exist in the case of the *o*-substituted derivatives ; this enhances the dissociation of the proton belonging to the carboxyl group. However, we consider that the aromatic hydroxy-acids do not form complexes with Ca^{2+} ions, characteristic of the α-hydroxy-derivatives.

The increase in the acidity in the presence of $Ca(NO_3)_2$ may be observed in all acids studied ; substantial variations were established until $I = 0.95$. At higher ionic strength no significant modifications in the dissociation of the acids could be observed. At high ionic strength, the potential jump occurring round the equivalence point similarly rises. This fact facilitates the potentiometric titration of the examined aromatic acids, hardly soluble in water. The difference of $\Delta E_{\pm 1\%(I_0 - I_{4.37})}$ has, generally, fluctuated between 10–25 mV, while more significant changes could be noted in the case of the salicylic acid (52 mV) and that of the mandelic acid (66 mV).

The effect of the neutral salts has been studied above all in the case of aqueous solutions. [26] This effect may be explained through the rise of the proton mobility in these solutions. $Ca(NO_3)_2$ has a powerful methanol binding capacity, its solvatation occurring with four solvent molecules. In concentrated $Ca(NO_3)_2$ solutions the amount of free CH_3OH molecules able to solubilize the acid being small, the relative concentration of the dissolved substance at high ionic strength increases, which besides the increase of the mobility of the protons contributes to the improvement of the titration conditions.

---

[26] E. E. Vinogradov, I. N. Zeicheva, O. N. Samoilov and V. I. Iaskov, *Zhur. fiz. Khim.*, **40**, 2519 (1966).

Revue Roumaine de Chimie, **17**, *10*, 1771–1777 (1972)

the formation of some complexes with higher dissociation degree occurs:

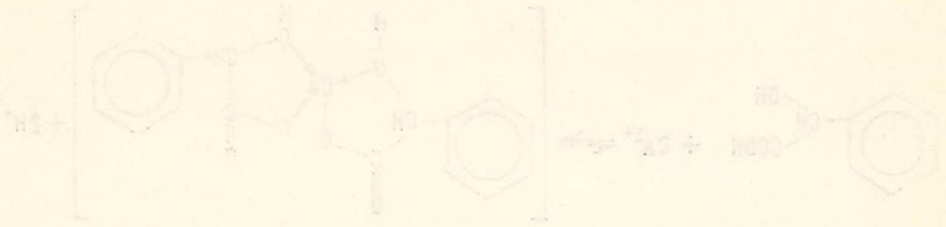

The acidity of the salicylic acid does not show modifications in solutions with high ionic strength, so pronounced as the mandelic acid. The relatively higher acidity of the salicylic acid at $I = 0$ may be explained, as in water, through the formation of intramolecular hydrogen bonds, which exist in the case of the o-substituted derivatives: this enhances the dissociation of the proton belonging to the carboxyl group. However, we consider that the aromatic hydroxy acids do not form complexes with Ca^{2+} ions, characteristic of the α-hydroxy derivatives.

The increase in the acidity in the presence of $Ca(NO_3)_2$ may be observed in all acids studied; substantial variations were established until $I = 0.05$. At higher ionic strength no significant modifications in the dissociation of the acids could be observed. At high ionic strength, the potential jump occurring round the equivalence point similarly rises. This fact facilitates the potentiometric titration of the examined aromatic acids, hardly soluble in water. The difference of ΔE [illegible] has, generally, fluctuated between 10–25 mV, while more significant changes could be noted in the case of the salicylic acid (72 mV) and that of the mandelic acid (60 mV).

The effect of the neutral salts has been studied above all in the case of aqueous solutions.[11] This effect may be explained through the rise of the proton mobility in these solutions. $Ca(NO_3)_2$ has a powerful methanol binding capacity, its solvatation occurring with four solvent molecules. In concentrated $Ca(NO_3)_2$ solution, the amount of free CH_3OH molecules able to solubilize the acid being small, the relative concentration of the dissolved substance at high ionic strength increases, which besides the increase of the mobility of the protons contributes to the improvement of the titration conditions.

---

[10] R. P. [illegible], [illegible], A. N. [illegible] and V. I. [illegible], [illegible] 20, [illegible] (196[illegible]).

[11] [illegible]

Revue Roumaine de Chimie, 17, *10*, 1779–1781 (1972)

GAS CHROMATOGRAPHIC SEPARATION OF HYDROGEN, METHANE, HYDROGEN SULPHIDE AND CARBON DISULPHIDE MIXTURES

A. DRĂGĂNESCU and I. BICĂ

Institute of Physical Chemistry
Str. Galaţi 31, Bucharest, Romania

S. ŞERBAN and ANA MARIA PAVLOVSCHI

"Chimigaz" Institute, Str. Carpaţi 8, Mediaş, Romania

Received April 26, 1972

The H_2, CH_4, H_2S and CS_2 mixture was satisfactorily separated on a 1.5.m column packed with 3% Triton X–305 on silicagel at 140°.

There has been a persistent need for a simple and rapid chromatographic method of analysing H_2, CH_4, H_2S and CS_2 mixtures.

The separation of H_2S from CS_2[1–5] and of H_2 from air and hydrocarbons[6] was performed on different columns.

In this note we are presenting the most satisfactory separation conditions for all the four compounds. This procedure is useful for the analysis of gases resulting during the carbon disulphide synthesis from methane and for other laboratory applications.

EXPERIMENTAL

A Pye model 44, dual-column chromatograph equipped with a thermal conductivity detector and a 1 mV Leeds and Northrup recorder were used. The first two peaks were recorded with a chart speed three times greater than that of the last two. The CS_2 peak is reversed in the experimental conditions chosen.

The carrier gas was argon, at a flow rate of 35 ml/min. The glass columns had a 4 mm internal diameter. All the chromatographic materials were Carlo Erba products, if not otherwise specified.

---

[1] R. Staszewski, J. Janak and T. Pompovski, *Chem. Analit.*, **8**, 897 (1963).
[2] C. T. Hodges and R. F. Matson, *Analyt. Chem.*, **37**, 1065 (1965).
[3] L. G. Berezkina, S. V. Melnicova and N. A. Elefterova, *Khim. Prom.*, **42**, 619 (1966).
[4] E. L. Obermiller and G. O. Charlier, *J. Gas Chromatog.*, **6**, 446 (1968).
[5] E. L. Obermiller and G. O. Charlier, *J. Chromatog. Sci.*, **7**, 580 (1969).
[6] S. A. Greene and H. Pust, *Analyt. Chem.*, **29**, 1055 (1957).

RESULTS AND DISCUSSION

To determine the most satisfactory column and conditions, a number of liquid phases and solid absorbents were examined.

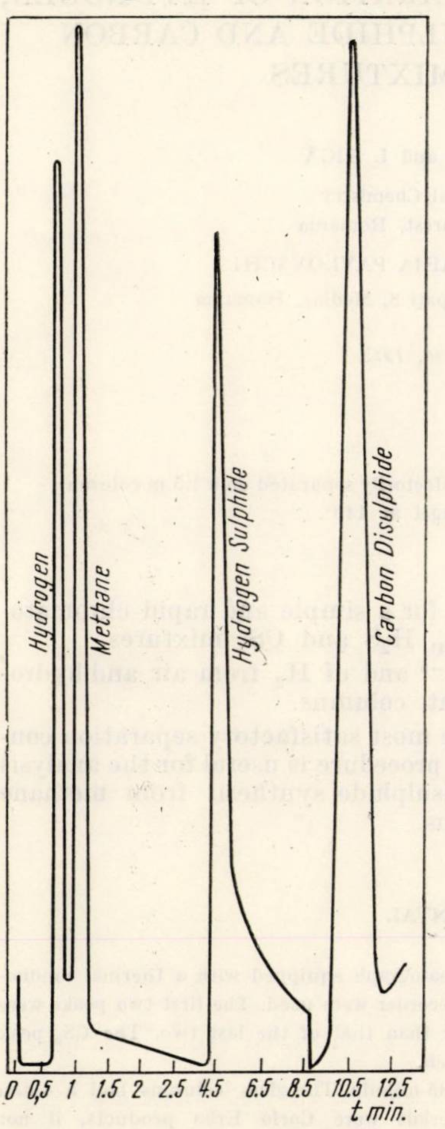

Fig. 1. — Separation of H_2, CH_4, H_2S and CS_2 mixture on a 1.5 m column packed with silica gel.

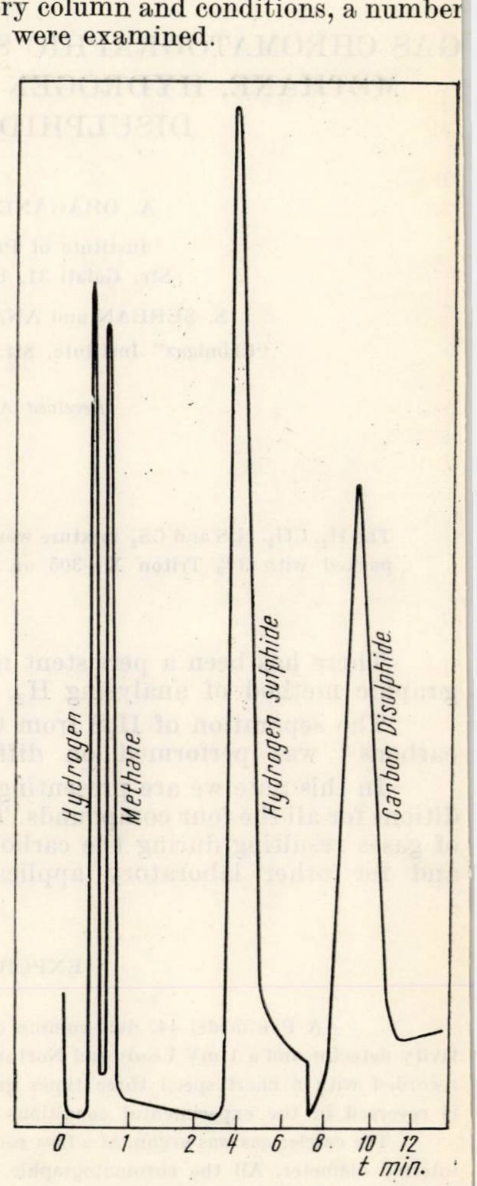

Fig. 2. — Separation of H_2, CH_4, H_2S and CS_2 mixture on a 1.5 m column packed with 3% Triton X−305 coated silica gel.

On a 1.5 m column packed with Molecular Sieve 5Å we obtained a good separation of H_2 and CH_4, but an indeterminate retention of other two compounds.

A 1.5 m column with 15% vaseline oil "low viscosity" on Chromosorb P, 30—60 mesh, at 26° separates only H_2S. It does not separate H_2 from CH_4, while CS_2 is indeterminately retained.

H_2S and CS_2 are separated on a 10% Polyethylene Glycol 1500 on polytrifluorethylene, 30—60 mesh, but CH_4 is not separated from H_2 in the same conditions.

A 5.4 m column packed with 15% Squalan on Chromosorb P, 30—60 mesh, separates H_2, CH_4 and H_2S but CS_2 is retained for more than 20 min at 150°.

All the four compounds are separated on a 1.5 m Porapak Q (Watters Associates Inc.) column, 100—200 mesh. At 125° the analysis is accomplished within 16 min, while at 150° this time is reduced to 9 min, but the separation is not as good as before.

At the same time, we used two silica gel columns of 1 m, respectively 1.5 m length. On the 1 m column at 120—140°, when the analysis time is suitable (less than 10 min) the separation of H_2 from CH_4 is not quite satisfactory. At 140°, the 1.5 m column separates quite well the compounds, but the retention time of CS_2 is beyond 17 min. At 160° this time diminishes to 10.5 min as it can be seen in a typical chromatogram (Fig. 1).

The 3% coated silica gel with various liquid phases leads to the reduction of the analysis time even at lower temperature, the separation performance remaining the same. Octoil S, Silicon Oil DC—702, Didecylphthalate and Triton X—305 have been used as liquid phases at 110°. The analysis time is about 20 min for all the above mentioned liquid phases. At 140° the CS_2 retention time on the Octoil S, Didecylphthalate and Triton X—305 coated silica gel packed column, 1.5 m in length, is about 9 min, but for the DC—702 Silicon Oil the retention time is of about 12 min. The separation of H_2, CH_4, H_2S and CS_2 mixture on the 1.5 m column packed with 3% Triton X—305 on silica gel at 140° is fairly satisfactory as can be seen in Figure 2.

Concluding our experimental results we consider that the last column is the best one for the separation of the mixture under investigation.

Revue Roumaine de Chimie, 17, 10, 1783–1787 (1972)

SPECTROPHOTOMETRICAL DETERMINATION OF *ORTHO*-TOLIDINE WITH SODIUM HYPOCHLORITE

I. FLOREA

Polytechnic Institute "Traian Vuia"
Laboratory of General Chemistry, Str. Remus 14, Timişoara

Received February 19, 1972

A new spectrophotometrical method for *ortho*-tolidine determination with sodium hypochlorite is suggested. The compound is bright-orange and it is extracted with chloroform. Chloroformic solution is yellow and presents two absorption maxima at $\lambda = 428$ nm, and $\lambda = 454$ nm. This method allows the *ortho*-tolidine determination with sodium hypochlorite between 2.12 and 63.6 μg.
Ortho-tolidine determination with sodium hypochlorite can be made in the presence of aniline, *o*-, *m*-, and *p*-toluidine, α-, and β-naphthylamine. The results are good and the sensitivity of the method is appreciable.

In a previous paper [1] we have dealt with the spectrophotometrical determination of benzidine with sodium hypochlorite. In the present paper we use the same reagent for the determination of a benzidine derivative, i. e. *ortho*-tolidine.

In the literature some chromatographical methods for *ortho*-tolidine identification and determination [2–6] are indicated. The iodometrical[7] and volumetrical methods with nitrite [8] are also described.

In this paper we suggest a new spectrophotometrical method for *ortho*-tolidine determination, using as reagent a sodium hypochlorite solution. The method is based on the formation of a bright-yellow quinonediimine [9,10] which is obtained through the oxidazing action of sodium hypochlorite upon an *ortho*-tolidine solution.

[1] I. Florea, *Rev. Roumaine Chim.*, **17**, 915–923 (1972).

[2] I. Gemzova and J. Gasparic, *Coll. Czech. Chem. Comm.*, **31**, 2525 (1966); *Chem. Abstr.*, **65**, 3773 a (1966).

[3] I. Gemzova and J. Gasparic, *Mikrochim. Acta*, **1**, 310 (1966); *Chem. Abstr.*, **65**, 7983 h (1966).

[4] A. Cee and J. Gasparic, *Mikrochim. Acta*, **1**, 295 (1966); *Chem. Abstr.*, **65**, 7983 f (1966).

[5] D. Ader and A. Chrzasczewa, *Med. Pracy*, **8**, 15 (1957); *Chem. Abstr.*, **53**, 19161 d (1959).

[6] G. Ghetti, B. Bartalini, G. Armeli and L. Pozzoli, *Lav. Um.*, **20**, 389 (1968); *Chem. Abstr.*, **71**, 24552 y (1969).

[7] A. Roesler and B. Glasmann, *Chem.-Ztg.*, **27**, 968; *Chem. Zentr.*, **2**, 1147 (1903).

[8] W. Vaubel, *Z. analyt. Chem.*, **35**, 163; *Chem. Zentr.*, **2**, 1147 (1903).

[9] J. D. Johnson and R. Overby, *Analyt. Chem.*, **41**, 1774 (1969).

[10] E. Bishop and G. L. Hartshorn, *Analyst*, **96**, 1 (1971).

The compound extracted with chloroform allows the spectrophotometrical determination of *ortho*-tolidine at λ = 454 nm. The method is suitable for *ortho*-tolidine quantities between 2.12 and 63.63 μg.

The *ortho*-tolidine can be determined with sodium hypochlorite in the same quantities as above in : a) water, b) in the presence of aniline in quantities up to 65 μg, c) in the presence of *o*-, *m*-, and *p*-toluidine in quantities up to 100 μg and d) in the presence of α-, and β-naphthylamine in quantities up to 70 μg.

Benzidine and *o*-dianisidine obstruct the determination.

EXPERIMENTAL

APPARATUS

Spectrophotometrical measurements were made with an UNICAM SP 800 spectrophotometer, at room temperature, using vats of 4, 2 and 1 cm, at λ = 454 nm ; pH of the solution was read at a Multoscop V apparatus Reagents

Ortho-tolidine solution. a) 0.2121 g of *ortho*-tolidine free of impurities obtained after several recrystallizations from water, is dissolved in 1000 ml graduated flask and is completed with alcohol to the mark. *Ortho*-tolidine solution of 1×10^{-3} m is obtained ; 1 ml solution contains 212.1 μg *ortho*-tolidine. b). 20 ml from solution a) is diluted with alcohol to 200 ml ; 1 ml solution contains 21.21 μg *ortho*-tolidine.

Sodium hypochlorite solution was prepared by bubbling chlorine until saturation in a sodium hydroxyde solution ≃ 0.1 m.

Hypochlorous acid solution was prepared by bubbling chlorine until saturation in distilled water.

Solutions of aniline, *o*-, and *m*-toluidine of 1×10^{-3} were prepared from pure and freshly distilled substances. Solutions of *p*-toluidine, α- and β-naphthylamine 1×10^{-3} m were prepared by weighing, from pure substances, recrystallizated from water.

For tests we used amounts between 0.1 and 1 ml in the case of *o*-, *m*-, and *p*-toluidine between 0.1 and 0.7 ml in the case of aniline and between 0.1 and 0.5 ml in the case of α-, and β-naphthylamine.

All solutions mentioned above are preserved in dark bottles.

PROCEDURE

Amounts between 0.1 and 3 ml from solution b) containing *ortho*-tolidine between 2.12 and 63.63 μg are measured with a microbiurette and introduced in a separating funnel ; 25 ml of water, 2 ml of sodium hypochlorite solution, 3 ml of sodium chloride solution 30% are added and stirred for a minute, 6 ml of chloroform is added and stirred strongly for one or two minutes, time in which the chloroformic layer becomes yellow. This layer is then poured into a 25 ml graduated flask. The procedure is repeated twice with the same amount of chloroform and if it is necessary, once or twice again with 3 ml of chloroform as far as the last chloroformic layer remains colourless. The flask is completed with chloroform to 25 ml. If the solution is opalescent, some anhydrous calcium carbonate crystals are added and stirred. The solution becomes clear immediately and the extinction is measured at λ = 454 nm. Chloroform is used as blank test.

RESULTS AND DISCUSSION

ABSORPTION SPECTRUM

Figure 1 presents the absorption curves of the compound formed by mixing of *ortho*-tolidine solution with sodium hypochlorite solution at pH = 8.22 resp. with a hypochlorous acid solution at pH = 3.83. The absorption curves are presenting two absorption maxima at $\lambda = 428$ nm and $\lambda = 454$ nm.

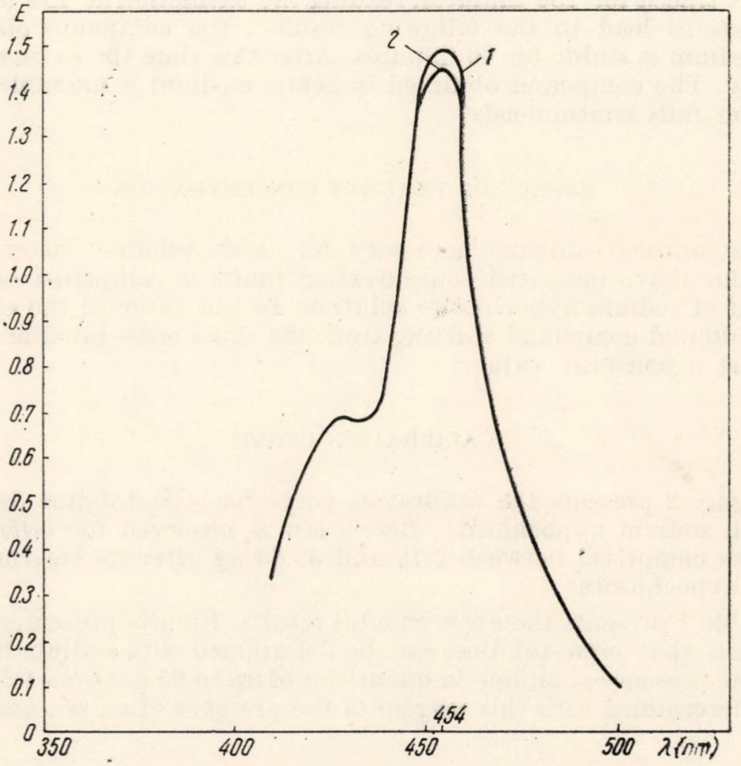

Fig. 1. — Absorption spectrum of the compound extracted with chloroform in vats of 4 cm.

1), 1 ml solution b+25 ml of water + 2 ml of sodium hypochlorite + 3 ml of sodium chloride 30% ; *2*) 1 ml solution b + 25 ml of water + 3 ml of hypochlorous acid.

From the determination performed at different pH values it results that the same chemical compound, both in basic and in acidic medium is formed. The compound in basic medium is useful for the spectrophotometrical determination of *ortho*-tolidine with sodium hypochlorite. The determination is indicated in the case of a mixture of amines. *Ortho*-

tolidine could be determined in the presence of : aniline, *o*-, *m*-, *p*-toluidine, α-, β- naphthylamine in concentrations indicated above. In these cases 4 ml of sodium hypochlorite solution are used for every test.

TIME EFFECT

Colour stability of the compound formed by *ortho*-tolidine oxidation with sodium hypochlorite and hypochlorous acid, extracted with chloroform was traced for 150 minutes, reading the extinction at 454 nm. These investigations lead to the following results : the compound obtained in basic medium is stable for 60 minutes. After this time the extinction falls gradually. The compound obtained in acidic medium is unstable and the extinction falls continuously.

EFFECT OF REAGENT CONCENTRATION

The optimal amount necessary for *ortho*-tolidine determination within the above indicated concentration limits is comprised between 1 and 8 ml of sodium hypochlorite solution. In this interval the extinction of the coloured compound starting from the same *ortho*-tolidine quantity maintains a constant value.

CALIBRATION CURVE

Figure 2 presents the calibration curve for *ortho*-tolidine determination with sodium hypochlorite. Beer's law is observed for *ortho*-tolidine quantities comprised between 2.12 and 63.63 μg after its treatment with sodium hypochlorite.

Table 1 presents the experimental results. Results presented in table 1 establish that *ortho*-tolidine can be determined with sodium hypochlorite in the presence of aniline in quantities of up to 65 g. *Ortho*-tolidine can also be determined with this reagent in the presence of *o*-, *m*-, and *p*-tolui-

Table 1

***Ortho*-tolidine spectrophotometrical determination with sodium hypochlorite**

No.	μg used *ortho*-tolidine	μg used aniline	E $d = 1$ cm	μg found *ortho*-tolidine	E %
1	3.18		0.05	3.12	− 1.88
2	14.85		0.27	14.67	− 1.21
3	55.15		1.05	55.60	+ 0.80
4	25.45		0.46	25.07	− 1.50
5	19.09	9.31	0.34	19.11	+ 1.00
6	12.73	27.92	0.23	12.56	− 1.30
7	38.18	46.53	0.69	38.21	+ 0.98
8	46.66	65.14	0.85	46.75	+21.00

dine in amounts below 100 μg and in the presence of α- and β-naphthylamine in amounts below 70 μg.

The new spectrophotometrical method of *ortho*-tolidine determination with sodium hypochlorite permits the confortable determination of this substance due to the large relative stability of the formed coloured compound extracted with chloroform. *Ortho*-tolidine determination using this method is performed rapidly without any strict pH limits.

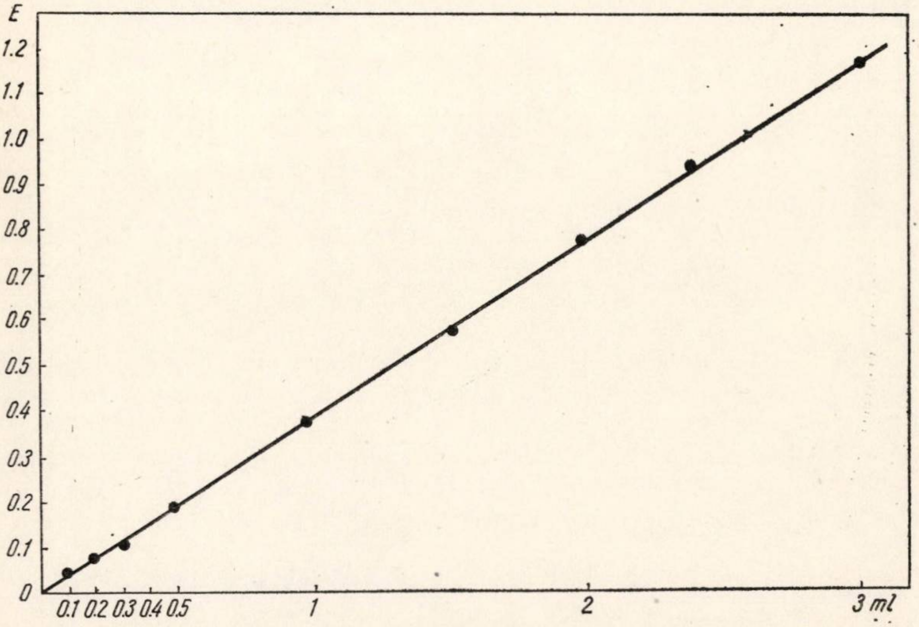

Fig. 2. — Calibration curve.

Ortho-tolidine tests treated with 2 ml of sodium hypochlorite + 3 ml of sodium chloride 30% each.

From the absorption spectrum of the coloured compound formed it results that the ClO^- anion oxidizes *ortho*-tolidine to the same final product both in acidic and basic medium.

Revue Roumaine de Chimie, 17, *10*, 1783–1787 (1972)

MŰSZAKI KÖNYVTÁR ES DOKUMENTÁCIÓS KÖZPONT 1883

NOTE POUR LES AUTEURS

La *Revue Roumaine de Chimie* publie des articles en anglais, français, russe, allemand ou espagnol. Les auteurs sont priés d'envoyer des articles, notes, communications et comptes rendus inédits.

Les manuscrits seront dactylographiés à deux intervalles. Les tableaux seront dactylographiés sur feuilles séparées, de même que la légende des figures. Les diagrammes seront tracés à l'encre de Chine sur papier calque. Les tableaux et les figures seront numérotés par des chiffres arabes, en nombre strictement inécessaire. Prière de ne pas inscrire les mêmes données dans les tableaux et les figures. Les formules chimiques seront incluses dans le texte ; en outre, elles seront transcrites sur des feuilles séparées. Les auteurs sont priés d'indiquer les caractères italiques (en soulignant les lettres au crayon), ainsi que tout autre caractère spécial. L'ordre des références bibliographiques sera celui de leur mention dans le texte ; le nom de l'auteur sera précédé de l'initiale du prénom ; les publications périodiques seront présentées suivant les prescriptions internationales. Les références seront ajoutées à la fin de l'article ; elles paraîtront comme des notes, au bas de la page. Le texte sera précédé d'un résumé comprenant 15 lignes au maximum.

L'entière responsabilité du contenu des articles appartient aux auteurs. On publie des articles dus aux collaborateurs roumains ou étrangers. Les auteurs recevront 50 tirés à part.

PRINTED IN ROMANIA

TRAVAUX PARUS AUX ÉDITIONS DE L'ACADÉMIE DE LA RÉPUBLIQUE SOCIALISTE DE ROUMANIE

P. BALTĂ et E. BALTĂ, **Introducere în chimia fizică a stării vitroase** (Introduction à la chimie physique de l'état vitreux), 1971, 240 p., 15,50 lei.

LYDIA-MARIA VAICUM, **Biodegrabilitatea detergenţilor** (La Biodégrabilité des détergents), 1971, 254 p., 16 lei.

TIBERIU NĂSCUŢIU, **Metode radiometrice de analiză** (Méthodes radiométriques d'analyse), 1971, 346 p., 19,50 lei.

I. ZUVRĂVESCU et L. STOICESCU-CRIVETZ, **Polimeri heterociclici** (Polymères hétérocycliques), 1971, 190 p., 9,50 lei.

I. MAXIM, **Materiale nucleare** (Matériaux nucléaires), 1969, 444 p., 30 lei.

CRISTOFOR SIMIONESCU, C. V. UGLEA, **Fracţionarea compuşilor macromoleculari** (Fractionnement des composés macromoléculaires), 1969, 292 p., p. 18,50 lei.

CRISTOFOR SIMIONESCU et CLEOPATRA VASILIU-OPREA, **Mecanochimia compuşilor macromoleculari** (La mécanochimie des composés macromoléculaires), 1967, 344 p., 23,50 lei.

CORNEL BODEA et collab., **Tratat de biochimie vegetală**, partea I, **Fitochimie** (Traité de biochimie végétale, Ire partie, Phytochimie) Ier vol., 1964, 747 p. + 4 annexes + 2 pl., 41 lei ; IIe vol., 1965, 1262, p., 1 pl., 56 lei, IIIe vol., 1967, 773 p., 35 lei.

V. GHEŢIE et V. MICUŞAN, **Analiza imunochimică. Teorie şi practică** (Analyse immunochimique. Théorie et pratique), 1966, 369 p., 28 lei.

R. PORTOCALĂ et L. POPA, **Acizii ribonucleici celulari şi virali** (Les acides ribonucléiques cellulaires et viraux), 1966, 375 p., 8 pl., 26 lei.

D. PURDELEA et R. VÎLCEANU, **Chimia compuşilor organici ai fosforului şi ai acizilor lui** (La chimie des composés organiques du phosphore et de ses acides), 1965, 540 p., 37 lei.

I.P.I. – c. 1731

43 426

Lei 25

F 1103

06-001

REVUE ROUMAINE DE CHIMIE

Tome 17

N° 11

Novembre 1972

RRCHAX, 17, *11*, 1789—1934 (1972)

ÉDITIONS DE L'ACADÉMIE DE LA RÉPUBLIQUE SOCIALISTE DE ROUMANIE

Rev. Roumaine Chim. 17, *11*, p. 1789—1934 (1972), Bucarest

COMITÉ DE RÉDACTION

Rédacteur en chef:

I. G. MURGULESCU, membre de l'Académie de la République Socialiste de Roumanie

Rédacteurs en chef adjoints:

A. T. BALABAN et V. EM. SAHINI, membres correspondants de l'Académie de la République Socialiste de Roumanie

Collège de rédaction:

C. DRĂGULESCU, RALUCA RIPAN, CR. SIMIONESCU, membres de l'Académie de la République Socialiste de Roumanie ; EM. BRATU, ECATERINA CIORĂNESCU-NENITZESCU, P. SPACU, membres correspondants de l'Académie de la République Socialiste de Roumanie; MARGARETA AVRAM, D. I. MARCHIDAN, G. NIAC et D. SĂNDULESCU

La *Revue Roumaine de Chimie* paraît 12 fois par an. Toute commande de l'étranger (fascicules ou abonnements) sera adressée à Întreprinderea Rompresfilatelia Boîte Postale 2001, telex 011631, Bucarest, Roumanie

Les manuscrits, les livres et les revues proposés en échange, ainsi que toute correspondance seront envoyés à la rédaction :

REVUE ROUMAINE DE CHIMIE
23, str. Dumbrava Roşie, Bucarest, 9, Roumanie

ÉDITIONS DE L'ACADÉMIE DE LA RÉPUBLIQUE SOCIALISTE DE ROUMANIE
3 bis, str. Gutenberg, Bucarest, Roumanie

REVUE ROUMAINE
DE
CHIMIE

Tome 17, N° 11 Novembre 1972

Page

RODICA VÎLCU and NICOLAE GEORGESCU, The decomposition of some transitional metal perchlorates in molten state . . . . 1791—1804 R

G. PANNETIER et D. FĂTU, Contribution à l'étude de la décomposition thermique du coprécipité de carbonate d'argent et de cadmium . . . . 1805—1811

B. J. McALOON and P. G. PERKINS, Semi-empirical LCAOMO theory for infinite systems : tight-binding self-consistent field theory for three-dimensional solids . . . . 1813—1817

ELENA CONSTANTINESCU, Potentiels normaux d'électrode dans des solvants non aqueux . . . . 1819—1827

G. VASU, A double hard core model description of the short-range order in molten alkali halides. I. Viscosity. . . . . 1829—1839

CRISTINA MANDRAVEL und MELANIA GUȚUL, Die Verwendung der Oberflächeneigenschaften für die Charakterisierung der Assoziation des Pyrols in flüssigem Zustand . . . . 1841—1844

ERIKA HAMBURG, RODICA GRECU und M. FERNEA, Kraftkonstantenberechnung an der Aminogruppe des Anilins . . . . 1845—1849

PETRU SPACU and LUCIA ANTONESCU, New molybdenum (V) complexes with biguanide derivatives . . . . 1851—1856 R

MARIA BREZEANU and IOANA JITARU, Coordination compounds with copper-tin bonds. . . . . 1857—1866

ILEANA ALBESCU, Contributions to the study of lanthanides with biguanidine derivatives. IV. Compounds of holmium and ytterbium with paludrine. . 1867—1880

F. KEREK and G. OSTROGOVICH, NMR and UV spectral studies of some 1-aryl-substituted-3-methyl-2-phospholene-oxides . . . . 1881—1887

| J. REICHEL, | B. D. BADER und R. VÎLCEANU, Neue organische Pigmente—Isatinderivate. I. Einführung in die Synthese und Eigenschaften der Verbindungen . . . . 1889—1899

I. OPREAN, V. FĂRCĂȘAN and FLORICA PAIU, Derivatives of furan. XI. Electron impact fragmentation of some 5-substituted 2-(2'-benzothiazolyl)-furans . . . . 1901—1907

MIRCEA E. LUPEȘ, *para*-Intramolecular aromatic rearrangements. II. The mechanism of the N-alkylanilines rearrangement . . . . 1909—1915

A. POP, L. CORMOȘ and LETIȚIA DULĂMIȚĂ, Decomposition of cumene hydroperoxide on silica gel . . . . 1917—1922 R

A. CARPOV, DEMETRA DRĂGAN et I. PETRARIU, Sur l'amination des copolymères macroporeux styrène-divinyl-benzène chlorométhylés avec la diméthyle-2-hydroxyéthyleamine . . . . 1923—1934 R

Rev. Roumaine Chim. **17,** *11,* 1789—1934 (1972), Bucarest

Revue Roumaine de Chimie, 17, *11*, 1791–1804 (1972)

THE DECOMPOSITION OF SOME TRANSITIONAL METAL PERCHLORATES IN MOLTEN STATE

RODICA VÎLCU and NICOLAE GEORGESCU

Centre of Physical Chemistry, Str. Galaţi 31, Bucharest, Romania

Received April 28, 1972

The kinetic parameters and the activation thermodynamic functions of the thermal decomposition reactions of Cu, Mn, Fe, Co and Ni perchlorates have been determined from thermogravimetric analysis (tga) and differential thermal analysis (dta) data. The derivatographic measurements showed that the decomposition mechanism of the perchlorates studied is influenced by the character of the chemical bond between the metallic ion and the complex anion, the process having the possibility to be one-or two-directional, depending on the free energies of formation of the corresponding reaction products.

INTRODUCTION

The development of the explosives, oxidants and solid propellants industry for rockets has incited these last years many research workers, to the study of the thermal decomposition of metallic perchlorates, by different procedures.[1–3]

The thermal decomposition of alkali perchlorates was first studied by Marvin and Woolaver [4]. Similar investigations were performed later by Gordon and Compbell, [5] as well as by Markovitz and Boryta. [6–9] Detailed kinetic measurements were effected mainly on potassium perchlorate, the extremely complex decomposition mechanism of which has been

[1] W. A. Guillory and M. King, *J. Phys. Chem.*, **73**, 4367 (1969).
[2] F. Solymosi and T. Bánságy, *J. Phys. Chem.*, **74**, 15 (1970).
[3] R. J. Acheson and W. M. Iacobs, *Canad. J. Chem.*, **47**, 3031 (1969).
[4] G. G. Marvin and L. B. Woolaver, *Analyt. Chem.*, **17**, 474 (1945).
[5] S. Gordon and C. Campbell, *Analyt. Chem.*, **27**, 1102 (1955).
[6] M. M. Markovitz, *J. Phys. Chem.*, **61**, 505 (1957).
[7] M. M. Markovitz. *J. Phys. Chem.*, **62**, 827 (1958).
[8] M. M. Markovitz and D. A. Boryta, *J. Phys. Chem.*, **64**, 1711 (1960).
[9] M. M. Markovitz and D. A. Boryta, *J. Phys. Chem.*, **69**, 114 (1965).

described by Glasner and Weindenfeld,[10] using a modified Prout-Tompkins [11] rate equation, as well as by other authors. [12-15]

The thermal decomposition of the di- and trivalent metal perchlorates has not yet been studied kinetically and the few experimental data available now concern mainly $Zn(ClO_4)_2$ and $Pb(ClO_4)_2$[16] as well as magnesium and barium perchlorates.

In the present paper we give an account of the results of investigations about the mechanism of the thermal decomposition of Cu, Mn, Fe, Co and Ni perchlorates, as well as the kinetic parameters and the activation thermodynamic functions of the corresponding reactions.

Depending on the cation, Me^{n+}, the residual product of pyrolysis of a hydrated or anhydrous metal perchlorate may be preponderantly a chloride or an oxide in accordance with the general chemical equations :

$$Me^{n+}\,(ClO_4)_n \cdot xH_2O = Me^{n+}\;Cl_n + 2nO_2 + xH_2O \qquad (1)$$

or

$$Me^{n+}\,(ClO_4)_n \cdot xH_2O = \frac{1}{2}\,Me_2^{n+}\,O_n + \frac{n}{2}\,Cl_2 + 1.75\,nO_2 + xH_2O \qquad (2)$$

where $x = 0,1, \ldots$

The pyrolytic behaviour of metal perchlorates is unique when compared with the decompositions of other metal compounds containing decomposable polyatomic anions e. g. metal nitrates [17,18] carbonates [19], sulphates [20,21] and hydroxides.[22]

In contrast with alkali metal perchlorates and barium and silver perchlorates which all decompose in accordance with equation(1), the pyrolysis of the transitional metal perchlorates studied by us, follows, with about the same probability, both general reactions, the residual products of which are the corresponding chlorides and oxides.

In order to compute the kinetic parameters specific of reactions of type (1) and (2), the constants of the different thermal decomposition rates were estimated with the aid of the Prout-Tompkins equation:

---

[10] A. Glasner and L. Weidenfeld, *J. Amer. Chem. Soc.*, **74**, 2467 (1952).

[11] E. G. Prout and F. C. Tompkins, *Trans. Faraday Soc.*, **42**, 468 (1946).

[12] A. E. Harvey, M. T. Edmison, E. O. Jones, R. A. Seybert and K. A. Catto, *J. Amer. Chem. Soc.*, **76**, 3270 (1954).

[13] A. Glasner and A. E. Simchen, *Bull. Soc. chim. France*, **18**, 233 (1951).

[14] T. A. Rodgers and A. Wassink, "Final Summary Report. University of Arkansas", Contract N° DA–23–072–ORD., 1958.

[15] A. E. Simchen, *J. Phys. Chem.*, **65**, 1093 (1961).

[16] A. A. Zinoviev and L. J. Chiudinova, *Zhur. neorg. Khim.*, **1**, 22 (1956). b) F. Solymosi, *Acta Chim. Acad. Sci. Hung.*, **57**, 35 (1968).

[17] P. J. Herley and E. G. Prout, *J. Amer. Chem. Soc.*, **82**, 1540 (1960).

[18] N. V. Sigwick "The Chemical Elements and their Compounds" vol. 1, Oxford, Clarendon Press, 1950, p. 700–701.

[19] A. E. van Arkel, "Molecules and Crystals in Inorganic Chemistry", Butterworths, London, 1949, p. 118–119.

[20] A. G. Ostroff and R. T. Londerson, *J. Inorg. Nuclear Chem.*, **9**, 45 (1959).

[21] R. T. Sanderson, "Chemical Periodicity", Reinhold, New York, 1960, p. 162–165.

[22] H. L. Johnston and T. W. Bauer, *J. Amer. Chem. Soc.*, **73**, 1119 (1951).

$$\log \frac{\alpha}{1-\alpha} = k_{1,2}\, t + C_1 \tag{3}$$

as well as by the equations:

$$\log \frac{1}{1-\alpha} = k_3 t + C_2 \tag{4}$$

and

$$1 - (1-\alpha)^{1/3} = k_4 t \tag{5}$$

In equations (3)—(5), α represents the ratio of the weight, w_t, of the perchlorate sample at the time t, and the initial quantity of perchlorate, W_0.

From the values of the constants of thermal decomposition rates obtained at different temperatures, the activation energies and the activation thermodynamic functions of the decomposition processes were estimated; the last parameters with the aid of the equations supplied by the theory of absolute rates of reaction [23].

The relations used in this case were:

$$\Delta H_0^{\neq} = E - RT \tag{6}$$

for the determination of the activation enthalpy, E being the activation energy of the process experimentally estimated by the Freeman-Carroll method [24], with a precision of ±2 kcal, and:

$$\Delta S_0^{\neq} = R\left[2.303\left(\log A - \log \frac{k}{h} - \log T\right) - 1\right] \tag{7}$$

starting from the equation:

$$A = \varkappa \frac{kT}{h}\, \mathrm{e}^{1 + \frac{\Delta S_0^{\neq}}{R}} \tag{8}$$

In relation (8), $\varkappa$ represents the product of the correction factor of the equilibrium constant and the parameter which describes the reflection of the molecule on the potential barrier.

---

[23] S. Glasstone, K. J. Laidler and H. Eyring, "The Theory of Rate Processes", McGraw-Hill Book Company, New York, 1941, p. 14—28.

[24] E. S. Freeman and B. Carroll, *J. Phys. Chem.*, **62**, 394 (1958).

$\varkappa$ has been considered as equivalent to unity, which is the value normally taken in computations. The other quantities are denoted by the usual symbols A represents the frequency factor in min^{-1}.

Using equation (6) and (7), the free energy of activation, $\Delta G_0^{\neq}$, results immediately :

$$\Delta G_0^{\neq} = \Delta H_0^{\neq} - T\,\Delta S_0^{\neq} \tag{9}$$

EXPERIMENTAL

Materials

Copper, manganese, iron, cobalt, and nickel perchlorates were prepared by the reaction of their carbonates and hydroxides with a 70% solution of perchloric acid. The products were purified by 3–4 recrystallizations from distilled water and dried in vacuum for 3–4 hours at 100–115°, and finally for about 4 hours at 150° (with the exception of $Cu(ClO_4)_2$ which was dried in a single step [25]). The content in perchlorate, ClO_4^-, was estimated by precipitation as nitron perchlorate.[26] Chlorine was determined gravimetrically by precipitation as silver chloride. In order to detect any intermediate product that might have formed during the decomposition, the experiment was interrupted at different times, and an analysis of a sample was effected.

Measuring procedure

The thermal decomposition of perchlorates was investigated thermogravimetrically. As the perchlorates dehydrated in the above way were extremely hygroscopic, they were heated prior to the thermogravimetric experiment, at 110°, in a crucible for 30 minutes in an atmosphere of purified argon.

The TGA and DTA kinetic experiments were perfomed in a DAM – Lyon Ugin-Eyraud thermobalance. The rate of heating was 7–11°/min, and finally maintained at the fixed value of 8°/min. The heating program was achieved with the aid of a RT-64 thermoregulator. The experiments were performed in a controlled argon atmosphere. The final products of the reactions were determined by the usual chemical analysis.

Results

Decomposition of copper perchlorate

The decomposition of copper perchlorate was studied in the temperature range 80°–110°. The pyrolysis can be described by the following two reactions :

$$Cu(ClO_4)_2 \rightarrow CuCl_2 + {}_4O_2$$

---

[25] G. Brauer, "Handbook of Preparative Inorganic Chemistry", vol. 2, Academic Press, New York, 1963, p. 87, 119, 215, 402, 711.

[26] F. P. Treadwell and W. T. Hall, "Analytical Chemistry", vol. 2, John Wiley and Sons, Inc., New York, 1950, p. 181–185.

and

$$Cu(ClO_4)_2 \rightarrow CuO + Cl_2 + 3.5\,O_2$$

The reaction rate constants, k_3, the activation energies, E, calculated from equations (3) and (4), the frequency factor as well as the activation thermodynamic functions which describe the decomposition processes, at different temperatures, are listed in table 1.

The evolution of the thermal decomposition reaction of $Cu(ClO_4)_2$ can be followed in the $\alpha = \alpha(t)$ plot from fig. 1.

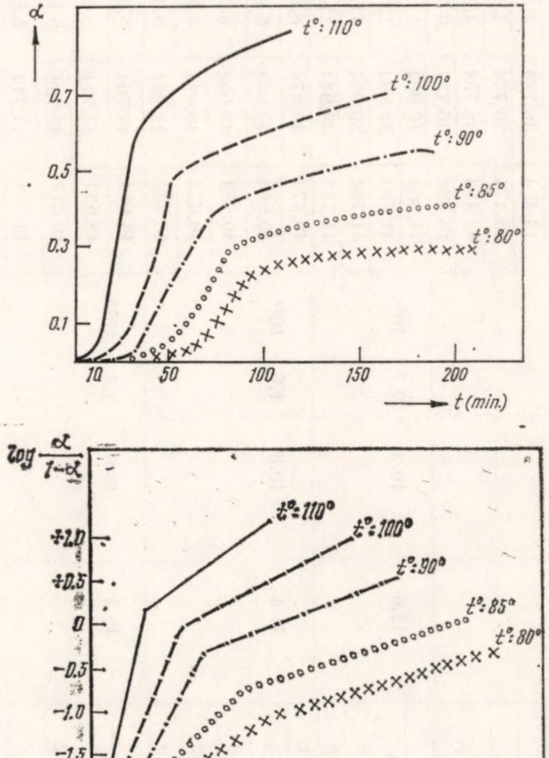

Fig. 1. — Plot of $\alpha = \alpha(t)$ for the thermal decomposition of $Cu(ClO_4)_2$

Unlike the behaviour of alkali metal perchlorates, no formation of the corresponding chlorate, $Cu(ClO_3)_2$, was observed during the reaction.

In the experiments performed with mixtures containing 5–10% of reaction products, it was observed that CuO has no effect on the decomposition rate while in the presence of $CuCl_2$, the process is accelerated as the quantity of copper halide increases.

Revue Roumaine de Chimie, **17**, *11*, 1791–1804 (1972)

Table 1

Kinetic parameters and activation thermodynamic functions of the thermal decompositions of Cu, Mn, Fe, Co and Ni perchlorates

Substance	Temperature °	$k_3 . 10^3$ min^{-1}	Activation energy kcal/mole		Frequency factor min^{-1}	$\Delta H_0^{\neq}$, kcal		$\Delta S_0^{\neq}$ e.u.	$\Delta G_0^{\neq}$, kcal	
			eq. (3)	eq. (4)		eq.(3)	eq.(4)		eq.(3)	eq.(4)
$Cu(ClO_4)_2$	80	8,6	44.2	37.5	1.9×10^{14}	43.494	36.794	4.474	41.914	35.214
	85	13				43.484	36.784	4.446	41.892	35.192
	90	17				43.474	36.774	4.418	41.870	35.170
	100	22				43.454	36.754	4.364	41.826	35.126
	110	25				43.434	36.734	4.312	41.782	35.082
$Mn(ClO_4)_2$	125	4,1	42.6	40.8	9.7×10^{15}	41.804	40.004	12.049	37.008	35.208
	135	5,6				41.784	39.984	12.000	36.888	35.088
	145	7,6				41.764	39.964	11.951	36.768	34.968
	155	11,8				41.744	39.944	11.904	36.648	34.848
$Fe(ClO_4)_3$	90	7,1	41.4	40.8	1.6×10^{15}	40.674	40.074	8.651	37.533	36.933
	95	7,6				40.664	40.064	8.624	37.490	36.890
	100	10,6				40.654	40.054	8.597	37.447	36.847
	115	14,2				40.624	40.024	8.519	37.318	36.718
	135	18,3				40.584	39.984	8.419	37.148	36.548
$Co(ClO_4)_2$	150	6	49.5	48.6	3.3×10^{14}	48.654	47.764	5.212	46.449	45.559
	160	6,8				48.634	47.744	5.165	46.397	45.507
	170	8,2				48.614	47.724	5.120	46.345	45.455
	175	13,3				48.604	47.714	5.098	46.320	45.430
	185	19,2				48.584	47.694	5.054	46.269	45.379
$Ni(ClO_4)_2$	130	4,8	44	42.5	3.7×10^{15}	43.194	42.094	10.109	39.119	38.019
	140	5,17				43.174	41.674	10.061	39.018	37.518
	150	6,8				43.154	41.654	10.013	38.898	37.398
	160	11,5				43.134	41.634	9.967	38.818	37.318
	170	14,2				43,114	41,614	9,921	38,718	37,218

Decomposition of manganese perchlorate

The thermal decomposition of $\mathrm{Mn(ClO_4)_2}$ was investigated in the range between 125 and 155°.

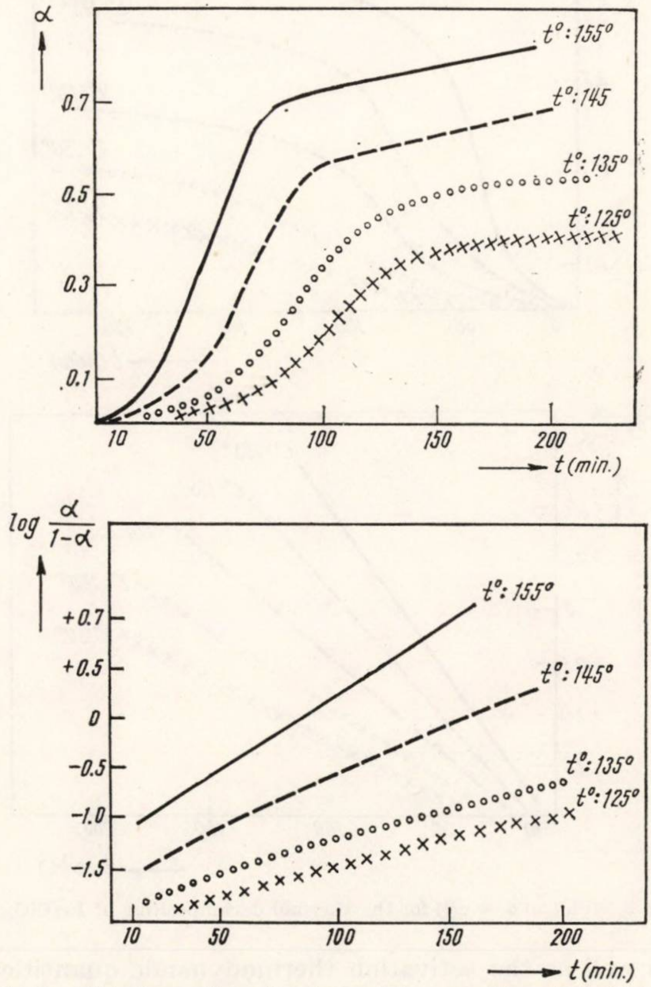

Fig. 2.—Plot of $\alpha = \alpha(t)$ for the thermal decomposition of $\mathrm{Mn(ClO_4)_2}$

The main reaction which takes place is :

$$\mathrm{Mn(ClO_4)_2} \rightarrow \mathrm{MnCl_2} + {}_4\mathrm{O_2}$$

At the same time the following reaction occurred :

$$\mathrm{Mn(ClO_4)_2} \rightarrow \mathrm{MnO} + \mathrm{Cl_2} + 3.5\mathrm{O_2}$$

which played a smaller role.

The kinetic evolution of the process is shown in fig. 2 by the dependence $\alpha = \alpha(t)$, while the kinetic parameters evaluated for the specified

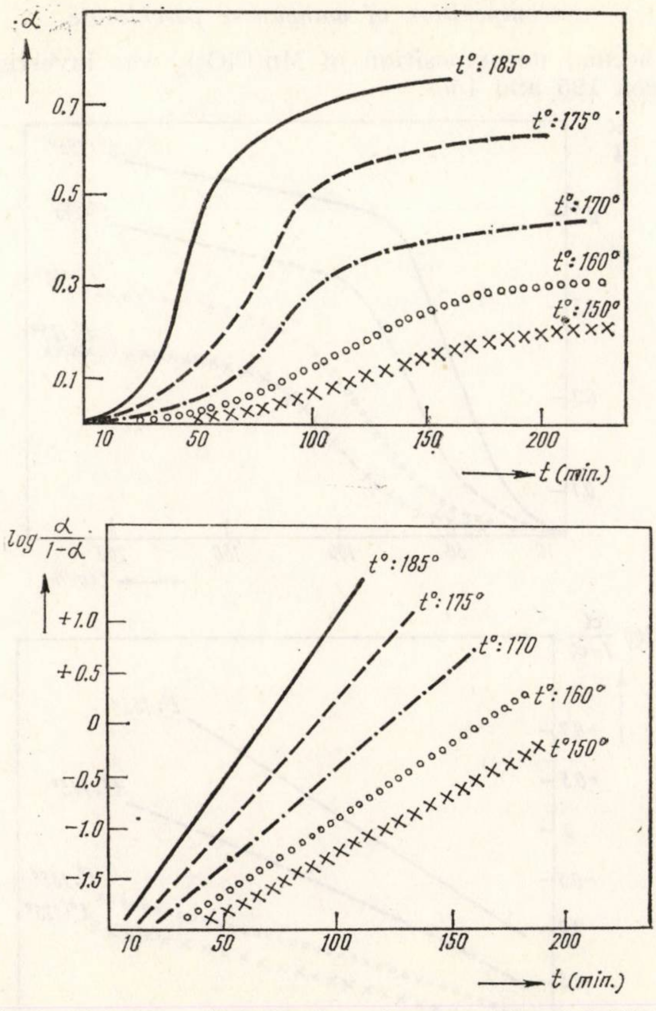

Fig. 3.—Plot of $\alpha = \alpha(t)$ for the thermal decomposition of $Fe(ClO_4)_3$

conditions as well as the activation thermodynamic quantities are listed in table 1.

Decomposition of iron (III) perchlorate

The thermal decomposition of $Fe(ClO_4)_3$ was studied in the range 90°—135°. The pyrolysis can be characterized by the reaction:

$$2Fe(ClO_4)_3 \rightarrow Fe_2O_3 + 3Cl_2 + 10.5\ O_2$$

In this case no $FeCl_3$ formation as reaction product was observed. The parameters which characterize the evolution of the reaction are listed in table 1, while the $\alpha - t$ curves, at different temperatures, are plotted in fig. 3.

Decomposition of cobalt (II) *perchlorate*

The thermal decomposition of $Co(ClO_4)_2$ was studied between 150° and 185°. The pyrolysis process takes place mainly in accordance with the reaction.

$$Co(ClO_4)_2 \rightarrow CoCl_2 + {}_2O_2$$

while the reaction:

$Co(ClO_4)_2 \rightarrow CoO + Cl_2 + 3.5\ O_2$ occurred to a smaller extent.

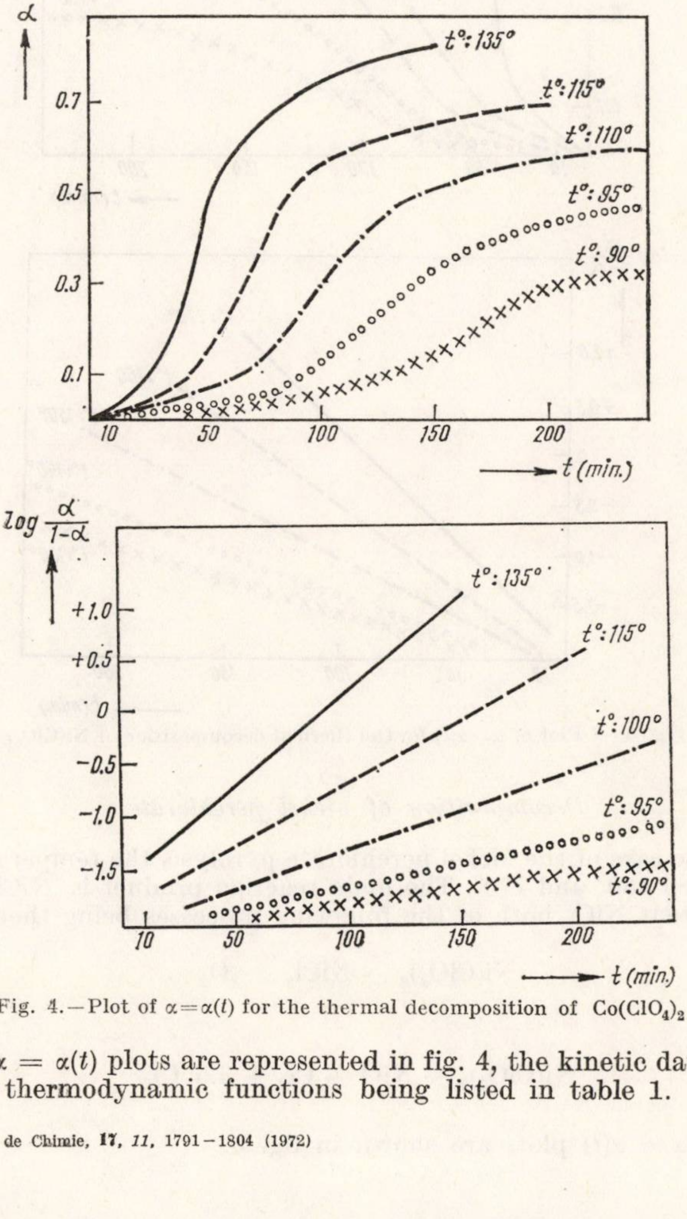

Fig. 4.—Plot of $\alpha=\alpha(t)$ for the thermal decomposition of $Co(ClO_4)_2$

The $\alpha = \alpha(t)$ plots are represented in fig. 4, the kinetic data and the activation thermodynamic functions being listed in table 1.

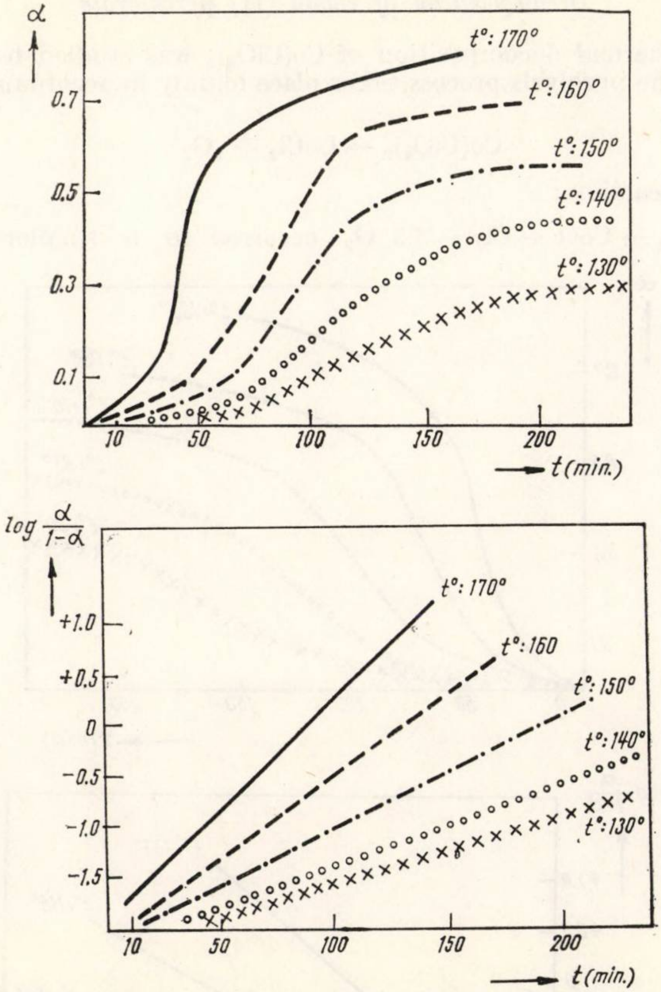

Fig. 5. — Plot of $\alpha = \alpha(t)$ for the thermal decomposition of $Ni(ClO_4)_2$

Decomposition of nickel perchlorate

In the case of the nickel perchlorate pyrolysis the temperature range was between 130° and 170°. The main reaction product is $NiCl_2$ and to a smaller extent NiO, both of the following processes being then possible :

$$Ni(ClO_4)_2 \rightarrow NiCl_2 + {}_2O_2$$

and

$$Ni(ClO_4)_2 \rightarrow NiO + Cl_2 + 3.5\ Cl_2$$

The $\alpha = \alpha(t)$ plots are shown in fig. 5.

The kinetic data as well as the activation thermodynamic functions are listed in table 1. An acceleration of the reaction rate in the presence of 10% $NiCl_2$ in the starting material was observed, while NiO brings no remarkable contribution to the development of the process.

DISCUSSION

Between the ionic radii, electronegativities and polarizing powers of the cations, as well as the crystal structures and phase changes of metal perchlorate salts studied here, there exist great differences. However, according to the results obtained, all these perchlorates show very high decomposition rates at temperatures below 200°, unlike alkali metal perchlorates which decompose at higher temperatures.

It has been found that the single compound which has a different thermal behaviour as regards the reaction product, is $Fe(ClO_4)_3$, which gave by decomposition only Fe_2O_3, without any corresponding chloride.

Indeed, if we consider the general reactions :

$$Me(ClO_4)_2 \rightarrow MeCl_2 + 4O_2 \tag{10}$$

and

$$Me(ClO_4)_2 \rightarrow MeO + Cl_2 + 3.5\ O_2 \tag{11}$$

we have obviously :

$$\Delta G^0_{(10)} = \Delta G^0_{MeCl_2} - \Delta G^0_{Me(ClO_4)_2} \tag{12}$$

and

$$\Delta G^0_{(11)} = \Delta G^0_{MeO} - \Delta G^0_{Me(ClO_4)_2} \tag{13}$$

Since $\Delta H^0_{298(Fe_2O_3)} > \Delta H^0_{298(FeCl_3)}$ [27] (−196.8 kcal and −95.7 kcal respectively), it is clear that reaction (11) is distinctly favoured in comparison with reaction (10).

For the other four perchlorates studied here, the differences between the equivalent heats of formation of the corresponding chlorides and oxides are not considerable, as can be seen from table 2. Therefore, the possible kinetic pathways of the decomposition process are bidirectional, according to the experimental data.

As a general rule it would appear that the nature of the main pyrolysis product of a metal perchlorate depends on the relative ionic characteristics of the corresponding chloride and oxide. Consequently, most polyvalent metal perchlorates, except those of the alkaline earths following magnesium, would be expected to yield through decomposition, oxides rather than chlorides. This is particularly clear in the case of Fe, where

---

[27] C. E. WICKS and F. E. BLOCK, "Thermodynamic Properties of 65 Elements. Their Oxides. Halides, Carbides and Nitrides", Bull. 605 Bureau of Mines, U. S. Dept. of Int., Washington, 1963, p. 58–59.

$FeCl_3$ has chemical bonds which display marked covalent properties. A similar situation was observed on the decomposition of $Al(ClO_4)_3\ 6H_2O$.[4,16]

In the case of Mn^{2+}, Co^{2+} and Ni^{2+} perchlorates the distribution of the reaction products is about the same, the main process being however the one which leads to the formation of the corresponding chloride.

Table 2

Equivalent heats of formation for the Cu, Mn, Fe, Co and Ni oxides and chlorides (after [27])

Oxides	ΔH°_{298} kcal/mole	chlorides	ΔH°_{298} kcal/mole
CuO	−37.5	$CuCl_2$	−53.4
CoO	−57.3	$CoCl_2$	−77.8
Fe_2O_3	−196.8	$FeCl_3$	−95.7
NiO	−57.3	$NiCl_3$	−73.0
MnO	−92.05	$MnCl_2$	−115.19

A somewhat different behaviour, which requires a more detailed discussion, occurred at the decomposition of $Cu(ClO_4)_2$. According to the data found in the literature,[22,27] at the decomposition temperature (90°) – when more than 40% of the initial quantity of $Cu(ClO_4)_2$ is already thermally dissociated, the free energies of formation of $CuCl_2$ and CuO are very close to each other. An early TGA study [20] of copper perchlorate hexahydrate led to the conclusion that copper oxide was formed in accordance with the following sequence of reactions:

$$Cu(ClO_4)_2 . 6H_2O \rightarrow Cu(OH)_2 + {}_2HClO_4 + {}_4H_2O \qquad (14)$$

$$Cu(OH)_2 \rightarrow CuO + H_2O \qquad (15)$$

However, this reaction course does not appear to be likely in view of the fact that pure anhydrous copper perchlorate is actually prepared by dehydration of the hydrate between 60–90° and, on the other hand, it has been shown that there exists a notable temperature difference between complete dehydration(95°) and rapid decomposition(115–120°).

At the same time the decomposition products, either in the case of anhydrous salt or of the hexahydrate perchlorate, are practically the same, and $Cu(OH)_2$ would not be expected to decompose at moderate temperatures, the dissociation pressure of water shown by copper hydroxide being rather low at 90–100° ($\sim$18 mm)[21].

Since the free energies of formation of copper chloride and oxide are comparable, a reversible interconversion of these two compounds is possible through the equilibrium process:

$$CuO_{(solid)} + Cl_{2(gas)} \rightleftharpoons CuCl_{2(solid)} + {}_{1/2}O_{2(gas)} \qquad (16)$$

$$\Delta G^0_{(16)} = \Delta G^0_{CuCl_2} - \Delta G^0_{CuO} = \Delta G^0_{(10)} - \Delta G^0_{(11)} = - RT \ln (P^{1/2}_{O_2}/P_{Cl_2}) \qquad (17)$$

Experimental studies accomplished as far back as in 1906 by Haber and Fleischman,[28] as well as by Hirschkind,[29] have shown that equilibrium (16) is achievable in practice. A somewhat similar situation occurs in the case of magnesium perchlorate [30].

Thus, it follows that the composition of the vapour phase in contact with the decomposing copper perchlorate is the main factor determining the nature and the distribution of the reaction products.

Under the essentially ireversible conditions of the usual DTA or TGA experiments, it seems reasonable that the important factor should be the composition of the vapour phase in immediate contact with the pyrolysing substance, i. e. the ratio of the pressures of the instantaneously evolved gaseous decomposition products.

Below 110°, the breakdown of Cu $(ClO_4)_2$ by a reaction of type (10) will yield an exceedingly oxygen-rich atmosphere which would then tend to convert the chloride into oxide in accordance with the reverse of reaction(16). The extent of conversion of the chloride into oxide is dependent on the rate of oxygen-chlorine exchange, as well as on the time period of the oxygen gas evolution.

Thus, below 110°, the distribution of the reaction products is governed by the following reactions:

$$Cu(ClO_4)_{2(liq)} \rightarrow CuCl_{2(solid)} + {}_4O_{2(gas)} \qquad (18)$$

and

$$CuCl_{2(solid)} + {}_{1/2}O_{2(gas)} \rightarrow CuO_{(solid)} + Cl_{2(gas)} \qquad (19)$$

Above 110°, the decomposition resulting in the formation of copper oxide, seems to be the most probable:

$$Cu(ClO_4)_2 \rightarrow CuO + Cl_2 + {}_{7/2}O_2 \qquad (20)$$

In the case of $Cu(ClO_4)_2$, the decomposition mechanism differs from that of other perchlorates by the fact that the reaction becomes extremely rapid, after a short induction period. During the rapid period about 50% of the initial material is consumed. It may be supposed that the acceleration of the reaction was due to the melting of the material.

---

[28] F. Haber and F. Fleischmann, *Z. anorg. Chem.*, **51**, 336 (1906).

[29] W. Hirschkind, *Z. anorg. Chem.*, **67**, 113 (1909).

[30] K. K. Kelley, "Energy Requirements and Equilibria in the Dehydration, Hydrolysis and Decomposition of Magnesium Chloride", Bureau of Mines Technical Paper 676, U.S. Government Printing Office, Washington, D.C., 1945, p. 18–20.

The melting point of the pure $Cu(ClO_4)_2$ is 82.5°. According to our observations, the melting process begins at about 75°, during the initial part of the reaction.

This could be explained by the formation of an eutectic in the binary system $Cu(ClO_4)_2 - CuCl_2$.

From the mechanistic point of view the decompositions of manganese, cobalt and nickel perchlorates are similar.

All the reactions are mildly self-catalytic. All three substances melted during the reaction.

Unlike alkali perchlorates, there are marked differences between the activation energies of the decomposition processes.

In the case of decomposition reactions of (10) type, the activation energies are higher ($Co(ClO_4)_2$, $Ni(ClO_4)_2$). For clear bidirectional processes ($Cu(ClO_4)_2$), the activation energy is lower.

No chlorate or chloride was found in the decomposition reactions studied.

Correlations between the effective electric field strength of the cations, crystal structure and thermal stabilities of the Cu, Co, Ni, Mn and Fe perchlorates will form the object of a future paper.

Revue Roumaine de Chimie, 17, *11* 1805–1811 (1972)

CONTRIBUTION À L'ÉTUDE DE LA DÉCOMPOSITION THERMIQUE DU COPRÉCIPITÉ DE CARBONATE D'ARGENT ET DE CADMIUM

G. PANNETIER et D. FĂTU *

Laboratoire de Cinétique Chimique de l'Université de Paris VI, 1, rue Guy de la Brosse,
75-Paris 5°, France

Reçu le 1er avril 1972

Les analyses thermogravimétrique et thermique différentielle montrent que la décomposition thermique du coprécipité $Ag_2CO_3-CdCO_3$ commence et se déroule dans un domaine de température moins élevé que celui correspondant à la pyrolyse du carbonate d'argent pur. La présence de carbonate de cadmium, dans une proportion de 0,1 %, dans le coprécipité $Ag_2CO_3-CdCO_3$ suffit à modifier considérablement la cinétique de décomposition. Le processus de vieillissement et la présence de vapeur d'eau modifient les décompositions du carbonate d'argent et du coprécipité.

INTRODUCTION

Dans une étude antérieure,[1] nous avons montré que la morphologie des produits de la décomposition thermique du coprécipité $Ag_2CO_3-CdCO_3$ est influencée par les conditions de préparation et de pyrolyse des carbonates.

Etant donné que les courbes de thermogravimétrie et d'analyse thermique différentielle du coprécipité $Ag_2CO_3-CdCO_3$ se trouvaient déplacées vers des températures inférieures à celles du carbonate d'argent pur, il nous a paru intéressant de chercher à mettre en évidence la modification des paramètres cinétiques du processus de décomposition du système $Ag_2CO_3-CdCO_3$ en fonction de la proportion en carbonate de cadmium.

Nous ne reviendrons pas sur les techniques expérimentales et l'appareillage utilisés, décrits dans une note antérieure.[1]

Les paramètres cinétiques, à savoir : l'énergie apparente d'activation « E », l'ordre de réaction « *n* » et le coefficient préexponentiel « *Z* », ont été calculés à l'aide des données fournies par le dépouillement des courbes d'analyse thermogravimétrique (A.T.G.) et d'analyse thermique différentielle (A.T.D.) tracées dans des conditions non isothermes.

---

* Adresse habituelle : Chaire de Cinétique Chimique, Université de Bucarest, 13, Bd. Republicii, Roumanie.

[1] G. Pannetier et D. Fătu, *Rev. Roumaine. Chim.*, **17**, 225 (1972).

MÉTHODES DE CALCUL UTILISÉES

Dans le cas d'un processus simple, de type :

$$A(s) \rightarrow B(s) + C(g) \uparrow$$

la vitesse de décomposition exprimée par la dérivée du degré de transformation « α » par rapport au temps « t » est souvent formulée :

$$\frac{\mathrm{d}\alpha}{\mathrm{d}t} = Z\,\mathrm{e}^{-E/RT}\,(1-\alpha)^n \tag{1}$$

où R— constante des gaz ; T — température absolue.

Le degré de transformation représente par définition la fonction du réactif solide décomposé, ou bien la fraction de composante volatile éliminée par pyrolyse.

Dans les techniques d'A.T.G. et d'A.T.D. l'échantillon est chauffé selon une loi linéaire, de sorte que la vitesse de chauffage est maintenue constante

$$\frac{\mathrm{d}T}{\mathrm{d}t} = \beta \tag{2}$$

En combinant les relations (1) et (2) il en résulte :

$$\frac{\mathrm{d}\alpha}{\mathrm{d}T} = \frac{Z}{\beta}\,\mathrm{e}^{-E/RT}\,(1-\alpha)^n \tag{3}$$

ou encore :

$$\log\frac{\mathrm{d}\alpha/\mathrm{d}T}{(1-\alpha)^n} = \log(Z/\beta) - \frac{E}{2{,}303R}\cdot\frac{1}{T} \tag{4}$$

Si l'on dispose d'une thermobalance équipée d'un dérivateur, on peut enregistrer directement la vitesse de décomposition $\mathrm{d}\alpha/\mathrm{d}T$, ce qui permet de calculer les paramètres cinétiques à l'aide de l'équation(4).

Dans le cas contraire, il est préférable d'utiliser une méthode d'intégration. Plusieurs auteurs [2-5] ont élaboré des méthodes qui consistent à intégrer l'équation (3) par des procédés approchés.

---

[2] D. W. van Krevelen, C. van Heerden et F. J. Huntjes, *Fuel*, **30**, 253 (1951).

[3] A. W. Coats et P. J. Redfern, *Analyst*, **88**, 906 (1963).

[4] A. W. Coats et P. J. Redfern, *Nature*, **21**, 68 (1964).

[5] H. Horowitz et G. Metzger, *Analyt. Chem.*, **35**, 1464 (1963).

Ces inconvénients peuvent être évités si l'on utilise un programme[6] de chauffage qui obéit à une loi hyperbolique du type :

$$T = \frac{1}{a - bt} \tag{5}$$

avec «a» et «b» -constantes.

Dans ces conditions, on peut intégrer exactement l'équation (3) et l'on obtient finalement :

$$\left\{ \begin{array}{l} -\log \left[\dfrac{1 - (1 - \alpha)^{1-n}}{1 - n} \right]_{n \neq 1} \\ -\log \left[- \ln (1 - \alpha) \right]_{n = 1} \end{array} \right\} = \frac{E}{2{,}303R} \, \frac{1}{T} - \log \frac{ZR}{\beta E} \tag{6}$$

Cette relation nous a permis de calculer les paramètres cinétiques à partir des données thermogravimétriques.

Les renseignements fournis par l'analyse thermique différentielle peuvent également servir pour des études cinétiques. Dans ce but, il est utile d'exprimer la vitesse de réaction et le degré de décomposition dans l'équation (4) en fonction de grandeurs accessibles sur la courbe d'A.T.D. Les calculs[7] conduisent à l'expression :

$$\frac{\Delta \log \Delta T}{\Delta \log (A/a_r)} = \frac{E}{2{,}303R} - \left[\frac{\Delta (1/T)}{\Delta \log (A/a_r)} \right] - n \tag{7}$$

où

Δ = le symbole des différences finies.

ΔT = la différence de température entre l'échantillon et la substance de référence.

A = l'aire totale du pic A.T.D.

a_r = l'aire du pic d'A.T.D. comptée à partir d'un instant « t » jusqu'à la fin de la réaction.

Les résultats obtenus par ce procédé ont été comparés à ceux obtenus par la méthode de Kissinger.[8]

Afin de tester la validité de l'équation(3) pour le processus étudié, nous avons appliqué une méthode plus générale, élaborée indépendamment par Ozawa[9] et Flynn et Wall.[10] Ce procédé exige l'enregistrement de plusieurs courbes d'A.T.G., en utilisant des vitesses de chauffage différentes. Si les données expérimentales obéissent à l'équation :

$$\left[\frac{\mathrm{d} \log \beta}{\mathrm{d}\,(1/T)} \right]_{\alpha = \mathrm{ct}} = 0{,}457 \frac{E}{R} = \text{constante} \tag{8}$$

---

[6] D. Fătu et E. Segal, *Rev. Roumaine Chim.*, **16**, 343 (1971).

[7] D. Fătu, *J. Thermal. Anal.*, **1**, 285 (1969).

[8] H. Kissinger, *Analyt. Chem.*, **29**, 1702 (1957).

[9] T. Ozawa, *Bull. Chem. Soc. Japan*, **38**, 1881 (1965).

[10] J. H. Flynn et L. A. Wall, *Polymer Letters*, **4**, 323 (1966).

on peut conclure que la décomposition thermique envisagée représente un processus unique, caractérisé par une seule valeur de l'énergie d'activation.

RÉSULTATS ET DISCUSSION

Nous avons rassemblé (fig. 1) les courbes thermogravimétriques de la décomposition des carbonates d'argent et de cadmium.

La courbe théorique a été calculée dans l'hypothèse où la décomposition des carbonates d'argent et de cadmium, contenus dans le coprécipité, se déroulerait indépendamment l'une de l'autre. En d'autres termes, la courbe théorique 4 représente une combinaison linéaire pondérée des courbes *1* et *3* en tenant compte des pourcentages de Ag_2CO_3 et $CdCO_3$, contenus dans le coprécipité. La courbe théorique est très proche de celle correspondant à la décomposition de l'Ag_2CO_3. Pourtant, l'expérience montre que la courbe expérimentale (1) ne coïncide guère avec la courbe théorique (4), ce qui montre que la présence du carbonate de cadmium modifie d'une façon évidente le processus de pyrolyse du carbonate d'argent.

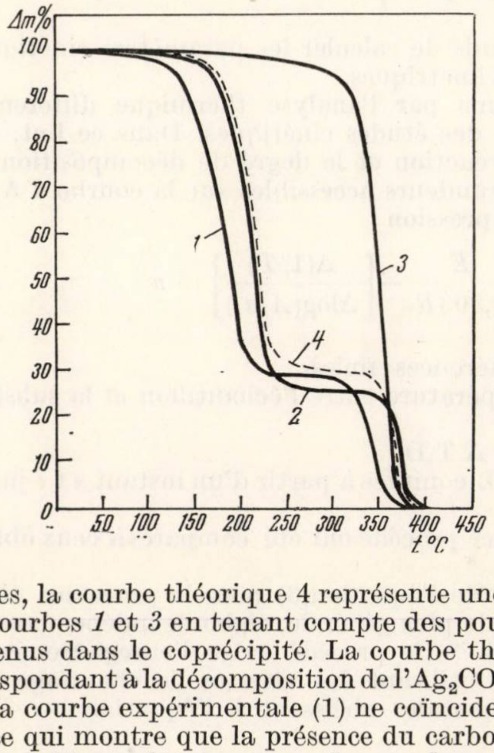

Fig. 1. — Courbes thermogravimétriques :
1, du coprécipité $Ag_2CO_3-CdCO_3$ contenant 7,1% de $CdCO_3$; $m_1 = 0,12759$g. 2, d'Ag_2CO_3 pur ; $m_2 = 0,12826$ g .3, de $CdCO_3$ pur ; $m_3 = 0,12863$ g. 4, la courbe d'A.T.G. théorique pour le coprécipité $Ag_2CO_3-CdCO_3$ (7,1%). B = 5°C/mn, atmosphère — N_2.

Il est bien établi que la pyrolyse de l'Ag_2CO_3 comporte deux étapes conduisant à la formation de Ag_2O et Ag avec élimination de CO_2 et de O_2 respectivement.

On peut, d'ailleurs, vérifier aisément sur la courbe *2*, que le rapport des pertes de masse pour les deux étapes satisfait la relation :

$$\frac{\Delta m_{\mathrm{II}}}{\Delta m_{\mathrm{I}}} = \frac{\frac{1}{2} M_{O_2}}{M_{CO_2}} = 0,36 \tag{9}$$

où M_{O_2} et M_{CO_2} sont respectivement les poids moléculaires de l'oxygène et du dioxyde de carbone ce qui est conforme au schéma :

$$Ag_2CO_3 \rightarrow Ag_2O + CO_2$$

$$Ag_2O \rightarrow 2Ag + \frac{1}{2} O_2$$

Au premier abord, en examinant la courbe *1* de la pyrolyse du coprécipité $Ag_2CO_3-CdCO_3$ on pourrait conclure que ce processus comporte également deux étapes.

Toutefois, l'analyse thermique différentielle permet d'établir que dans ce cas la décomposition thermique est plus complexe. Le premier pic situé à 175° (fig. 2, courbe *1*) correspond à la décomposition de l'Ag_2CO_3 contenu dans le coprécipité et semble être un processus unique. On retrouve ce processus sur la courbe de décomposition de l'Ag_2CO_3 pur (fig. 2, courbe *2*) à une température plus élevée (187°).

Vers 288° commence la décomposition d'une faible quantité d'oxyde d'argent formée par pyrolyse d'Ag_2CO_3.

L'argent métallique final forme avec l'oxyde d'argent non décomposé une solution solide, qui est plus stable que l'oxyde d'argent pur, de sorte que le processus de décomposition cesse pratiquement.

La solution solide Ag_2O-Ag a été mise en évidence par Faivre[11] à l'aide des données radiocristallographiques. Quant aux processus situés à 324° et 352°, ceux-ci correspondent aux décompositions du carbonate de cadmium et de la solution solide Ag_2O-Ag, respectivement. Les trois derniers processus sont partiellement superposés.

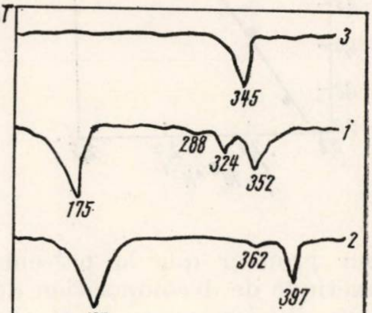

Fig. 2. — Courbes A. T. D. pour les décompositions :
1, du mélange $Ag_2CO_3-CdCO_3$ 7,1% ; $m_1=0{,}01477$ g. 2, d'Ag_2CO_3 ; $m_3=0{,}01591$g. 3, du $CdCO_3$; $m_3=0{,}01076$ g. $\beta=2{,}5$°C/mn ; atmosphère — N_2.

La formation de la solution solide Ag_2O-Ag et la pyrolyse du $CdCO_3$ contenu dans le coprécipité, bien que caractérisées par des effets thermiques aisément décélables sur la courbe d'A.T.D. sont accompagnées d'une faible perte de masse. C'est la raison pour laquelle ces processus ne sont pas résolus sur la courbe d'A.T.D.

---

[11] R. Faivre, *Comptes Rend.*, **210**, 398 (1940).

On peut observer que sur la courbe d'A.T.D. correspondant à la pyrolyse du coprécipité $Ag_2CO_3-CdCO_3$ on retrouve, déplacés vers des températures inférieures, tous les processus enregistrés pendant la décomposition des carbonates d'argent et de cadmium non mélangés.

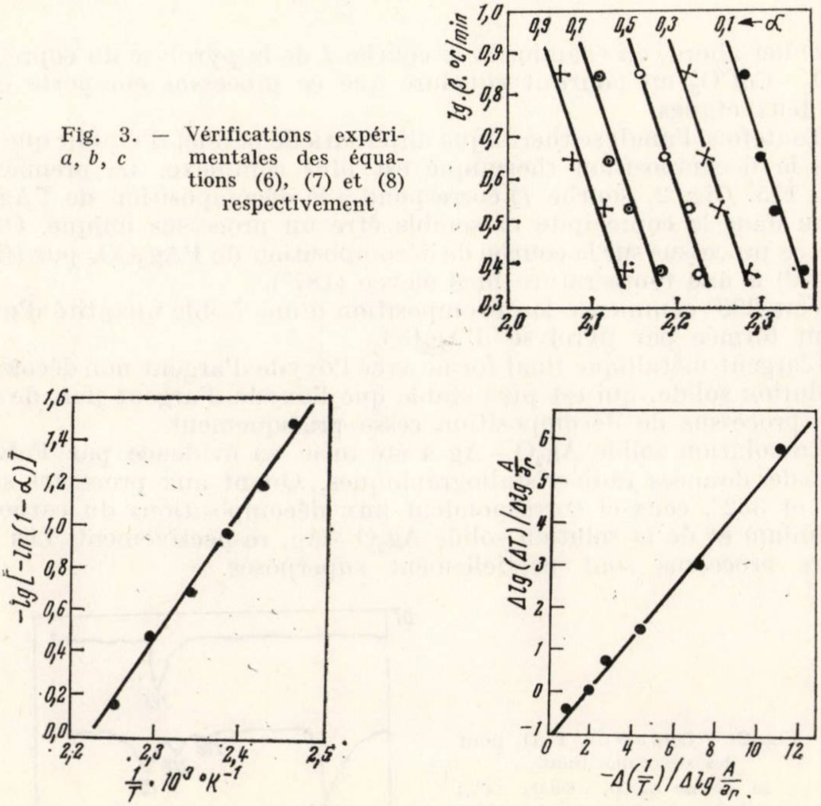

Fig. 3. — Vérifications expérimentales des équations (6), (7) et (8) respectivement

a, *b*, *c*

Pour prouver que la présence du carbonate de cadmium influe sur la cinétique de décomposition du carbonate d'argent, on a calculé les paramètres cinétiques pour la décomposition de l'Ag_2CO_3 pur et contenant divers pourcentages de $CdCO_3$.

Les figures 3 *a*, *b*, *c*, établissent la vérification expérimentale des équations (6), (7), (8), pour la décomposition de l'Ag_2CO_3 (schéma réactionnel I).

Les valeurs moyennes des paramètres cinétiques lors de l'addition de $CdCO_3$ sont rassemblées dans le tableau 1.

On peut remarquer l'influence des faibles pourcentages de carbonate de cadmium sur la cinétique de déconposition du carbonate d'argent.

La présence de l'ion Cd^{2+} dans la maille du carbonate d'argent, même dans de faibles proportions, a comme conséquence un accroissement de la concentration des défauts ponctuels, ce qui favorise la décomposition thermique et la réactivité en général.

Le processus de vieillissement est important dans le cas de carbonate d'argent et se traduit par l'augmentation des valeurs des paramètres cinétiques : $n = 1, 3$, $E = 39,2$ *k*cal/mole, $Z = 1,6 . 10^{17}$ s^{-1}.

Tableau 1

Paramètres cinétiques pour le processus :
$Ag_2CO_3 - Ag_2O + CO_2$

Pourcentage de $CdCO_3$ contenu dans l'Ag_2CO_3	n	E(*k*cal/mole)	$Z(s^{-1})$
0,0	1,1	28,6	$1,2.10^{13}$
0,1	0,87	26,7	$9,2.10^{11}$
0,5	0,76	23,0	$2,6.10^{10}$
1,0	0,68	22,4	$5,4.10^{9}$
7,1	0,66	21,4	$4,3.10^{9}$

Dans le cas du carbonate de cadmium, Pavlyutchenko et Prodan [12] ont observé une augmentation de l'énergie d'activation due au processus de vieillissement.

D'autre part, si le coprécipité $Ag_2CO_3-CdCO_3$ (7,1%) n'est pas séché en présence d'anhydride phosphorique on ne peut observer des valeurs de l'énergie apparente d'activation que de l'ordre de 16,4 *k*cal/mole,ce qui prouve que non seulement la présence du carbonate de cadmium, mais aussi l'humidité diminue l'énergie d'activation, en agissant sur le processus de nucléation.[1]

Les paramètres cinétiques des processus de formation de la solution solide Ag_2O-Ag, des décompositions de Ag_2O et de $CdCO_3$ n'ont pas été évaluées, à cause du chevauchement de ces étapes.

CONCLUSIONS

La cinétique de la décomposition du carbonate d'argent est modifiée d'une façon évidente par les impuretés (traces de $CdCO_3$), l'humidité et le processus de vieillissement des réactifs.

Les résultats contradictoires rencontrés parfois dans la littérature sont dus au fait que les divers auteurs ont utilisé des réactifs de pureté et de degré de vieillissement différents.

---

[12] M. M. PAVLYUCHENKO et E. A. PRODAN, « Gheteroghenye khimiceskie reactii », Izd. Nauka i tekhnika, Minsk, 1965, p. 79.

Revue Roumaine de Chimie, 17, 11, 1805–1811 (1972)

Revue Roumaine de Chimie, **17**, *11*, 1813 – 1817 (1972)

SEMI-EMPIRICAL LCAOMO THEORY FOR INFINITE SYSTEMS: TIGHT-BINDING SELF-CONSISTENT FIELD THEORY FOR THREE-DIMENSIONAL SOLIDS

B. J. McALOON and P. G. PERKINS

Department of Pure and Applied Chemistry
University of Strathclyde
Glasgow, C. 1, Scotland

Received June 7, 1972

Equations are derived which enable the Fock matrices to be constructed for any three-dimensional polymer. Under the tight-binding approximation, the evaluation of the matrices leads to a self-consistent field solution of the band-structure problem for the system.

Calculations by the LCAO MO SCF *ab initio* methods have now been well established on a molecular level.[1] By contrast, however, virtually no *ab initio* three-dimensional solid-state calculations have yet been performed. This is due to the fact that solid-state calculations are much more computationally demanding than their molecular counterparts and indeed, at present, three-dimensional *ab initio* solid-state calculations, even with a relatively small unit cell basis set, are outwith the capabilities of the largest computers. Clearly, therefore, a different method of approach must be made to three-dimensional SCF solid-state calculations and in considering these, such methods should possess the quality that, while being less computationally demanding than the *ab initio* approach, they preserve essentially the latter's important feature of self-consistency. It is well known that the time-consuming problem of three- and four- centre integral evaluation is circumvented by the zero differential overlap approximation inherent in CNDO theory.[2] Since in the CNDO approach the starting wave function is a correctly antisymmetrised product of one-electron LCAO molecular orbitals, the technique also involves the self-consistent iteration of the calculated wave function to a prespecified limit. Hence, because of its ready application to tight-binding calculations, which has previously been shown,[3,4] we feel that the CNDO method will assume increasing value. Accordingly, we present herein a generalization of the tight-binding theory, based on the LCAO MO SCF CNDO approximations, for three-dimensional solid-state problems.

---

[1] Richards, Walker and Hinckley, " A Bibliography of *ab initio* Calculations for Molecules", Oxford University Press, 1971.

[2] J. A. Pople, D. P. Santry and G. A. Segal, *J. Chem. Phys.*, **43**, 5129, (1965).

[3] B. J. McAloon and P. G. Perkins, *J. Chem. Soc.*, (*Faraday*), in press.

[4] B. J. McAloon and P. G. Perkins, *J. Chem. Soc.*, (*Faraday*), submitted for publication

THEORY

The translational symmetry of a three-dimensional lattice of $N_1 \times N_2 \times N_3$ identical unit cells, each contained in the volume spanned by the three lattice vectors $\boldsymbol{t}_1$, $\boldsymbol{t}_2$ and $\boldsymbol{t}_3$ and each containing n orbitals, can be expressed group theoretically by defining the $N_1 \times N_2 \times N_3$ translational operators $\mathbf{R}_{i+j+k}(i = 1, -N_1, j = 1, -N_2, k = 1, -N_3)$ which interchange equivalent points in the lattice. We further suppose the lattice to be subject to the Born-Von Kármánn periodic boundary conditions. The operators R can be used in conjunction with the projection operator technique to construct symmetry orbitals, $b_r(p)$, which transform under one of the irreducible representations of the translational group,

$$b_r(p) = \sum_{i=1}^{N_1} \sum_{j=1}^{N_2} \sum_{k=1}^{N_3} \Gamma(\mathbf{R}_{i+j+k})^{p*}_{l_q} \mathbf{R}_{i+j+k} \varkappa_r(\mathbf{R}_{i\boldsymbol{t}_1+j\boldsymbol{t}_2+k\;{}_3}) \tag{1}$$

where $\Gamma(\mathbf{R}_{i+j+k})^{p*}_{l_q}$ represents the complex conjugate of the lth matrix element of the q-dimensional irreducible representation p between two arbitrary orthonormal functions in the set $f(p)$. The operators $\mathbf{R}_{i+j+k}$ appearing in these matrix elements operate on the function $\chi_r(\mathbf{R}_0)$ at the chosen centre of the coordinate system and displace it to an equivalent point at the vector distance $i\boldsymbol{t}_1 + j\boldsymbol{t}_2 + k\boldsymbol{t}_3$ in real space. Since these translational operators commute with each other, the translational group is abelian and all irreducible representations p are one-dimensional. This means that $l = q = 1$ and $p = 1, \ldots N_1\, N_2\, N_3\;\; N_1 N_2 N_3$. Each matrix $\Gamma(\mathbf{R}_{i+j+k})$ is therefore diagonalised for each $\mathbf{R}_{i+j+k}$ and so facilitates the construction of the Bloch sums defined by equation(1). The above set of functions $f(p)$ can in fact be chosen arbitrarily because matrix elements $\Gamma(\mathbf{R}_{i+j+k})^p_{lq}$ arising from different sets of functions, $f(p)$ and $g(p)$, say, are related by a similarity transformation.

The choice of matrix element $\Gamma(\mathbf{R}_{i+j+k})^p_{lq}$ is here of the form

$$\exp\left(2\pi i \left(\underset{N_1}{m_1 i} + \underset{N_2}{m_2 j} + \underset{N_3}{m_3 k}\right)\right.$$

where, for $i = 1,\ 2,\ 3$,

$$(-N_i + 1)/2 \leqslant m_i \leqslant (N_i - 1)/2 \quad \text{if } N_i \text{ odd}$$

$$(-N_i + 1)/2 \leqslant m_i \leqslant N_i/2 \quad \text{if } N_i \text{ even}$$

Thus the matrix element is

$$\begin{aligned} &\exp\ (2\pi i(h_1 i + h_2 j + h_3 k) \\ &= \exp\ i(\boldsymbol{k}_{h_1} + \boldsymbol{k}_{h_2} + \boldsymbol{k}_{h_3})\ .\ (\mathbf{R}_i + \mathbf{R}_j + \mathbf{R}_k) \\ &= \exp\ i\boldsymbol{k}.\mathbf{R}_n\ \ldots \end{aligned} \tag{2}$$

where $\boldsymbol{k}$ and $\mathbf{R}_n$ are defined as

$$\boldsymbol{k} = \boldsymbol{k}_{h_1} + \boldsymbol{k}_{h_2} + \boldsymbol{k}_{h_3} = 2\pi(h_1\boldsymbol{b}_1 + h_2\boldsymbol{b}_2 + h_3\boldsymbol{b}_3) \tag{3}$$

$$\mathbf{R}_n = \mathbf{R}_i + \mathbf{R}_j + \mathbf{R}_k = i\boldsymbol{t}_1 \pm j\boldsymbol{t}_2 + k\boldsymbol{t}_3 \tag{4}$$

and where, to satisfy equations (2)

$$\boldsymbol{b}_i \cdot \boldsymbol{t}_j = \delta_{ij} \qquad i,\ j = 1,\ 2,\ 3 \tag{5}$$

Using equations (3), (4) and (5) it can easily be shown that,

$$\boldsymbol{b}_1 = \frac{\boldsymbol{t}_2 \times \boldsymbol{t}_3}{\boldsymbol{t}_1 \cdot (\boldsymbol{t}_2 \times \boldsymbol{t}_3)},\ \ \boldsymbol{b}_2 = \frac{\boldsymbol{t}_3 \times \boldsymbol{t}_1}{\boldsymbol{t}_1 \cdot (\boldsymbol{t}_2 \times \boldsymbol{t}_3)},\ \boldsymbol{b}_3 = \frac{\boldsymbol{t}_1 \times \boldsymbol{t}_2}{\boldsymbol{t}_1 \cdot (\boldsymbol{t}_2 \times \boldsymbol{t}_3)}$$

The vectors $\boldsymbol{b}_1$, $\boldsymbol{b}_2$, and $\boldsymbol{b}_3$ are the vectors of the reciprocal space and are identical to the vectors used in the classical method for construction of the Brillouin zones in the $\boldsymbol{k}$-space.

From equations (1), (2), (3) and (4) the (normalised) Bloch functions are now of the form

$$\begin{aligned} \boldsymbol{b}_r(\boldsymbol{k}_{h_1},\ \boldsymbol{k}_{h_2},\ \boldsymbol{k}_{h_3}) = \frac{1}{N_1 N_2 N_3} \sum_i \sum_j \sum_k \exp\ i(\boldsymbol{k}_{h_1} + \boldsymbol{k}_{h_2} + \\ + \boldsymbol{k}_{h_3}) \cdot (\mathbf{R}_i + \mathbf{R}_j + \mathbf{R}_k)\ a_r(\mathbf{R}_{it_1 + jt_2 + kt_3}). \\ r = 1 \ldots n \end{aligned} \tag{6}$$

If these Bloch functions are now permitted to interact *via* a Hartree-Fock Hamiltonian, and using the notation of our previous work, it can be shown that the $\boldsymbol{k}$-dependent diagonal and off-diagonal elements of the interaction matrix derived from the associated LCAO MO SCF CNDO secular equations are given by

$$\begin{aligned} F_{pp}(\boldsymbol{k}_{h_1},\ \boldsymbol{k}_{h_2},\ \boldsymbol{k}_{h_3}) = -\, I_p - \sum_{\substack{\mathrm{B} \\ \text{all atoms}}} z_B \gamma_{sp} + \gamma_{pp} + \\ + \sum_i \sum_j \sum_k \exp -\, i(\boldsymbol{k}_{h_1} + \boldsymbol{k}_{h_2} + \boldsymbol{k}_{h_3}) \cdot (\mathbf{R}_i + \mathbf{R}_j + \mathbf{R}_k) \times \end{aligned}$$

$$\times A \times S_{pq}(\mathbf{R}_{i+j+k}) \times I_p +$$

$$+ \frac{1}{N_1 N_2 N_3} \sum_{\boldsymbol{k}'_{h_1}} \sum_{\boldsymbol{k}'_{h_2}} \sum_{\boldsymbol{k}'_{h_3}} \sum_{i} \sum_{j} \sum_{k} \sum_{l} P_{ll}(\boldsymbol{k}'_{h_1}, \boldsymbol{k}'_{h_2}, \boldsymbol{k}'_{h_3}) < pp \mid ll, (\mathbf{R}_{i+j+k}) >$$

$$- \frac{1}{2N_1 N_2 N_3} \sum_{\boldsymbol{k}'_{h_1}} \sum_{\boldsymbol{k}'_{h_2}} \sum_{\boldsymbol{k}'_{h_3}} \sum_{i} \sum_{j} \sum_{k} P_{pp}(\boldsymbol{k}'_{h_1}, \boldsymbol{k}'_{h_2}, \boldsymbol{k}'_{h_3})$$

$$\times \cos \{[(\boldsymbol{k}_{h_1} - \boldsymbol{k}'_{h_1}) + (\boldsymbol{k}_{h_2} - \boldsymbol{k}'_{h_2}) + (\boldsymbol{k}_{h_3} - \boldsymbol{k}'_{h_3})] \cdot$$

$$\cdot [\mathbf{R}_i + \mathbf{R}_j + \mathbf{R}_k]\} < pp \mid pp (\mathbf{R}_{i+j+k}) > \tag{7}$$

$$F_{pq}(\boldsymbol{k}_{h_1}, \boldsymbol{k}_{h_2}, \boldsymbol{k}_{h_3}) = \sum_{i} \sum_{j} \sum_{k} \exp - i (\boldsymbol{k}_{h_1} + \boldsymbol{k}_{h_2} + \boldsymbol{k}_{h_3}) \cdot$$

$$\cdot (\mathbf{R}_i + \mathbf{R}_j + \mathbf{R}_k) \times A \times S_{pq}(\mathbf{R}_{i+j+k}) \sqrt{I_p I_q} -$$

$$- \frac{1}{2N_1 N_2 N_3} \sum_{\boldsymbol{k}'_{h_1}} \sum_{\boldsymbol{k}'_{h_2}} \sum_{\boldsymbol{k}'_{h_3}} \sum_{i} \sum_{j} \sum_{k} P_{qp}(\boldsymbol{k}'_{h_1}, \boldsymbol{k}'_{h_2}, \boldsymbol{k}'_{h_3}) \times$$

$$\times \exp i [(\boldsymbol{k}_{h_1} - \boldsymbol{k}'_{h_1}) + (\boldsymbol{k}_{h_2} - \boldsymbol{k}'_{h_2}) + (\boldsymbol{k}_{h_3} - \boldsymbol{k}'_{h_3})] \cdot$$

$$\cdot [\mathbf{R}_i + \mathbf{R}_j + \mathbf{R}_k] < pp \mid qq (\mathbf{R}_{i+j+k}) > \tag{8}$$

while the total electronic energy per unit cell of lattice is given as

$$E = \frac{1}{N_1 N_2 N_3} \sum_{\boldsymbol{k}'_{h_1}} \sum_{\boldsymbol{k}'_{h_2}} \sum_{\boldsymbol{k}'_{h_3}} < \Psi_l^{*} (\boldsymbol{k}'_{h_1}, \boldsymbol{k}'_{h_2}, \boldsymbol{k}'_{h_3}) \mid H_N (1)$$

$$+ \sum_{m}^{\mathrm{occ}} \sum_{\boldsymbol{k}_{h_1}} \sum_{\boldsymbol{k}_{h_2}} \sum_{\boldsymbol{k}_{h_3}} (2) J_{m,\, \boldsymbol{k}_{h_1}, \boldsymbol{k}_{h_2}, \boldsymbol{k}_{h_3}} - K_{m,\, \boldsymbol{k}_{h_1} \boldsymbol{k}_{h_2}, \boldsymbol{k}_{h_3}} \mid \Psi_l (\boldsymbol{k}'_{h_1}, \boldsymbol{k}'_{h_2}, \boldsymbol{k}'_{h_3}) > \tag{9}$$

Here, $H_N(1)$, $J_{m\, \boldsymbol{k}_{h_1} \boldsymbol{k}_{h_2} \boldsymbol{k}_{h_3}}$ and $K_{m\, \boldsymbol{k}_{h_1}, \boldsymbol{k}_{h_2}, \boldsymbol{k}_{h_3}}$ represent the one-electron operators and the coulomb and exchange operators respectively and $\Psi_l(\boldsymbol{k}'_{h_1} \boldsymbol{k}'_{h_2} \boldsymbol{k}'_{h_3})$ represents the LCAO Bloch function,

$$\Psi_l(\boldsymbol{k}_{h_1}, \boldsymbol{k}_{h_2}, \boldsymbol{k}_{h_3}) = \sum_{r=1}^{n} C_{lr}(\boldsymbol{k}_{h_1} \boldsymbol{k}_{h_2} \boldsymbol{k}_{h_3})\, b_r(\boldsymbol{k}_{h_1}, \boldsymbol{k}_{h_2}, \boldsymbol{k}_{h_3}) \tag{10}$$

Calculations of the total nuclear energy per unit cell of lattice cannot be effected by the usual point nuclear charge repulsion summation, *i.e.*,

$$V(r) = \sum_{A \neq B} \sum \frac{Z_A Z_B}{r_{AB}} \tag{11}$$

because by imposing the periodic boundary conditions the lattice has been transposed into a set of infinitesimally intertwining loops. We therefore suggest that the required nuclear energy $V(r)$ is obtained from a Madelung series

$$V(r) = A + \frac{B}{r} + \frac{C}{r^2} + \text{higher terms} \tag{12}$$

We note from equations (7) and (8) that the $N_1 \times N_2 \times N_3$ labelled wave functions initially interact through the two electron coulomb and exchange operators. This requires that the wave function be calculated at each point in the Brillouin zone, which in turn leads, therefore, to the problem of diagonalising $N_1 \times N_2 \times N_3$ determinants in order to achieve the required solution.

This problem is much simplified, however, firstly by noting the Hermitian property of the Hamiltonian, and secondly, by using the fact that Ψ is wave-vector-dependent, *i. e.*,

$$\Psi = \Psi(\boldsymbol{k}_{h_1}, \boldsymbol{k}_{h_2}, \boldsymbol{k}_{h_3}) \tag{13}$$

Therefore, the allowed permutations of these reciprocal vectors yield the same value of E in equation (8). By combining the two features above, the minimum number of diagonalisations of the matrices which must be effected is reduced from $N_1 \times N_2 \times N_3$ to N'. Typical reductions are shown in the Table 1.

Table 1

Symmetry reduction effect

N_1	N_2	N_3	$N_1\ N_2\ N_3$	N'
3	3	3	27	6
5	5	5	125	19
7	7	7	343	44

We thank Albright and Wilson Ltd. for a Maintenance Grant (to B. McA).

Revue Roumaine de Chimie, **17**, *11*, 1819 – 1827 (1972)

POTENTIELS NORMAUX D'ÉLECTRODE DANS DES SOLVANTS NON AQUEUX*

ELENA CONSTANTINESCU

Chaire de Thermodynamique et d'Électrochimie, Université de Bucarest, 13, Bd. Republicii

Reçu le 30 mai 1972

On déduit une équation pour le calcul des potentiels normaux d'électrode dans des solvants non aqueux à partir des données spectroscopiques et thermochimiques. Les résultats obtenus sont comparés avec les données expérimentales.

Ce travail s'inscrit sur la ligne des recherches que nous avons effectuées antérieurement en vue d'établir des équations pour le calcul des potentiels normaux d'électrode[1,2] pour des systèmes Me, $Me^{(+)n}$ et X, $X^{(-)n}$ à partir des données spectroscopiques et thermochimiques.**

Compte tenu de l'intérêt toujours croissant pour les études électrochimiques des solvants non aqueux nous avons considéré utile d'étendre ces équations aux solvants non aqueux également.

Ainsi nous avons calculé les potentiels standard des différentes électrodes dans une série de neuf solvants, par rapport au potentiel de l'électrode standard d'hydrogène dans le solvant considéré, potentiel pris comme zéro conventionnel.

Les valeurs ainsi calculées sont comparées à celles correspondant aux mêmes systèmes en milieu aqueux.

Le potentiel normal d'électrode représente, comme on le sait, la tension électrique réversible d'une cellule galvanique, réalisée à l'aide d'une électrode donnée et d'une électrode standard d'hydrogène :

$$\mathrm{Me}/\mathrm{Me}^{(+)n}\,(a_{\mathrm{Me}^{(+)n}} = 1)\,||H^+\,(a_{\mathrm{H}^+} = 1)/H_2\,(\mathrm{g},\ 1\ \mathrm{atm}).$$

---

[1] I. G. Murgulescu et E. Constantinescu, *Rev. Roumaine Chim.*, **12**, 199 (1967).

[2] I. G. Murgulescu et E. Constantinescu, *Rev. Roumaine Chim.*, **12**, 223 (1967).

* Ouvrage communiqué à la deuxième Conférence républicaine de chimie-physique générale et appliquée – septembre 1970.

** Dans ce travail on a noté par Me, le métal.

Il paraît, à première vue, que la réaction électrochimique :

$$\mathrm{Me}\,(s) + n\mathrm{H}^+\,(a_{\mathrm{H}^+} = 1) = \mathrm{Me}^{(+)n}\,(a_{\mathrm{Me}^{(+)n}} = 1) + \frac{n}{2} H_2\,(\mathrm{g},\ 1\ \mathrm{atm}) \quad (1)$$

qui se produit dans la cellule est la même pour n'importe quel solvant. Mais il faut rappeler que tant les ions de métaux que ceux d'hydrogène sont solvatés et que par conséquent l'énergie libre de réaction dépend de la nature du solvant.

Malgré l'évidence de cette situation, on a été longtemps persuadé que les potentiels normaux étaient indépendants du solvant, ou que, si cette dépendance existait, elle serait sans importance. Cela s'explique par le fait que la plupart des travaux plus anciens dans ce domaine comme par exemple ceux de Sackur [3] Neustadt, Abegg [4] et d'autres ont été particulièrement consacrés aux alcools, surtout aux alcools méthylique et éthylique en tant que solvants très proches de l'eau.

Il est évident qu'il est pour nous d'un plus grand intérêt d'effectuer les mesures ou les calculs des potentiels d'électrode dans des solvants qui diffèrent par leurs propriétés chimiques et physiques. C'est pourquoi nous avons choisi, à côté des solvants qui contiennent l'oxhydryl-méthanol éthanol, le butanol, l'alcool isoamylique, des solvants basiques-ammoniac et hydrazine, des solvants acides—acide formique et aussi l'acétone et l'acétonitrile.

La méthode de calcul des potentiels normaux d'électrode, établie au début pour les milieux aqueux [1] a été transposée aux solvants non aqueux. On a eu recours aux cycles conjugués des transformations suivants :

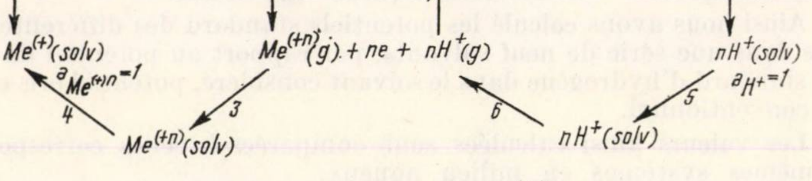

Fig. 1. — Systèmes Me, $\mathrm{Me}^{(+)n}$.

Les modifications n'interviennent que là où il s'agit des ions en phase liquide, c'est-à-dire là où les ions hydratés sont remplacés par les ions solvatés.

L'absence des valeurs des énergies libres de dilution des ions solvatés, dans les différents solvants, de même que la contribution peu importante du terme qui contient les énergies de dilution dans l'équation finale de calcul — ainsi qu'il a résulté pour l'eau — conduit finalement à la fusion dans une seule étape des processus partiels 3 et 4 dans le cas du métal et

[3] O. Sackur, *Z. Elektrochem*, **11**, 387 (1905).

[4] S. Neustadt et R. Abegg, *Z. phys. Chem.*, **69**, 486 (1909).

5 et 6 dans le cas de l'hydrogène, de sorte que les cycles deviennent rectangulaires :

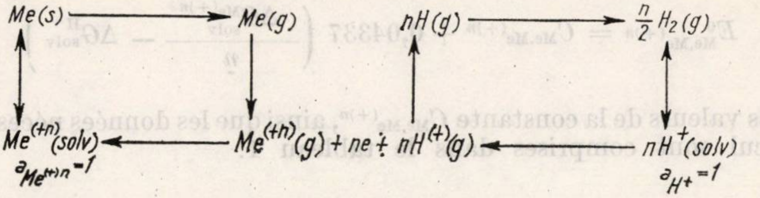

Fig. 2. – Systèmes Me, $\mathrm{Me}^{(+)n}$.

Compte tenu de toutes ces modifications, – l'équation antérieurement établie[1] aura la forme :

$$E^0_{\mathrm{Me,\,Me}^{(+)n}} = \frac{\lambda^0 - \frac{n}{2} D^0_{\mathrm{H}_2}}{nF} + \frac{\frac{5}{2}(n-1)\,RT\ln T}{nF} + \frac{RT}{nF}\left[\int_0^T \frac{\mathrm{d}T}{RT^2}\int_0^T\left(Cp_{\mathrm{Me}(s)} - \frac{n}{2}C_{p_{\mathrm{H}_2(g)}}\right)\mathrm{d}T\right] + \tag{2}$$

$$+ \frac{RT}{nF}\left[-\,i_{\mathrm{Me}(g)} + n\left(i_{\mathrm{H}} - \frac{i_{\mathrm{H}_2}}{2}\right)\right] + \frac{\sum\limits_1^n I_i - nI_{\mathrm{H}}}{n} + \frac{\Delta G^{\mathrm{Me}^{(+)n}}_{\mathrm{solv}} - n\Delta G^{\mathrm{H}^+}_{\mathrm{solv}}}{nF}$$

En introduisant les valeurs numériques de R et F et celles caractéristiques de l'hydrogène, de sorte que E^0 résulte en volts, on obtient, à 25° (298,16°K) :

$$(E^0_{\mathrm{Me,Me}^{(+)n}})^{\mathrm{volts}} = \left(\frac{\sum\limits_1^n I_i}{n} - 13{,}59\right)^{\mathrm{volts}} + 0{,}04337\left(\frac{\lambda_0}{n} - 51{,}62\right)^{k\mathrm{cal}}$$

$$+ \, 0{,}02567\left[\frac{5}{2}\left(1 - \frac{1}{n}\right)\ln T - \frac{i}{n}\mathrm{Me}(g) + 10{,}87 - \frac{5{,}26}{2} - 9{,}915 + \right. \tag{3}$$

$$\left. + \frac{1}{n}\int_0^T \frac{\mathrm{d}T}{RT^2}\int_0^T C_{p_{\mathrm{Me}(s)}}\mathrm{d}T\right] + 0{,}04337\left(\frac{\Delta G^{\mathrm{Me}^{(+)n}}_{\mathrm{solv}}}{n} - \Delta G^{\mathrm{H}^+}_{\mathrm{solv}}\right)^{k\mathrm{cal}}$$

Tous les termes de l'équation (3) à l'exception du dernier, sont indépendants de la nature du solvant et par conséquent, pour le même système d'électrode, ils peuvent être inclus dans une constante $C_{\mathrm{Me,Me}^{(+)n}}$ l'équation (3) prenant une forme simple :

$$E^0_{\mathrm{Me,Me}^{(+)n}} = C_{\mathrm{Me,Me}^{(+)n}} + 0{,}04337 \left(\frac{\Delta G^{\mathrm{Me}^{(+)n}}_{\mathrm{solv}}}{n} - \Delta G^{\mathrm{H}^+}_{\mathrm{solv}} \right), \tag{4}$$

Les valeurs de la constante $C_{\mathrm{Me,Me}^{(+)n}}$, ainsi que les données nécessaires à son calcul sont comprises dans le tableau 1.

Tableau 1

Paramètres de calcul de l'équation (3)

Electrode	$\sum_1^n I_i$ volts	λ° kcal/mole	$\int_0^T \frac{\mathrm{d}T}{RT^2} \int_0^T C_{p_{\mathrm{Me}(s)}} \mathrm{d}T$	$i_{\mathrm{Me}(g)}$	$C_{\mathrm{Me,Me}^{(+)n}}$
Li, Li+	5,40	38,05	1,01	13,77	– 9,149
Na, Na+	5,14	25,97	3,28	15,56	– 9,921
K, K+	4,34	21,59	4,69	16,36	–10,894
Rb, Rb+	4,17	19,91	5,04	17,53	–11,159
Cs, Cs+	3,89	19,05	7,26	18,20	–11,436
Ag, Ag+	7,54	67	2,82	17,88	– 5,813
Ca, Ca++	18,01	47,4	2,65	15,70	– 5,823
Zn, Zn++	27,24	31,4	2,56	16,44	– 1,566
Cd, Cd++	25,89	27,03	3,35	17,25	– 2,336
Electrode	I_{H} volts	$D^0_{\mathrm{H}_2}$ kcal/mole	$\frac{1}{2} \int_0^T \frac{\mathrm{d}T}{RT^2} \int_0^T C_{p_{\mathrm{H}_2}} \mathrm{d}T$	i_{H}	i_{H_2}
H, H+	13,59	103,24	9,915	10,87	5,26

Pour évaluer les potentiels normaux d'électrode nous avons utilisé les énergies libres de solvatation des ions individuels d'après Izmailov, [5] compris dans le tableau 2.

Les résultats sont présentés dans le tableau 3.

Avant de discuter les résultats il faut montrer brièvement comment nous avons évalué les potentiels normaux des halogènes X, $X^{(-)n}$.

Nous admettons que la réaction électrochimique :

$$X^- \ (a_{X^-} = 1) + \mathrm{H}^+ \ (a_{\mathrm{H}^+} = 1) = \frac{1}{2} X_2 \ (\mathrm{g,\ 1\ atm}) + \frac{1}{2} \mathrm{H}_2 \ (\mathrm{g,\ 1\ atm}) \tag{5}$$

qui a lieu dans une cellule galvanique du type général :

$$(\mathrm{g,\ 1\ atm}) \ X_2/X^- \ (a_{X^-} = 1) \parallel \mathrm{H}^+ \ (a_{\mathrm{H}^+} = 1) \ / \ \mathrm{H}_2 \ (\mathrm{g,\ 1\ atm}).$$

---

[5] N. A. Izmailov, *Doklady Akad. Nauk SSSR*, **149**, 1364 (1963).

Tableau 2

Énergies libres de solvatation $\Delta G^{Me^{(+)n}}_{solv}$ (kcal/ion.g)

Ion	CH_3OH	C_2H_5OH	C_4H_9OH	$C_5H_{11}OH$	CH_3COCH_3	CH_3CN	HCOOH	NH_3	N_2H_4
H^+	252,5	251,5	251,5	252,0	252,0	249,0	243,0	278,0	274,5
Li^+	115,0	113,0	114,5	115,5	115,0	114,5	113,5	121,0	113,5
Na^+	92,0	89,0	88,5	85,0	80,0	90,5	91,5	96,5	92,0
K^+	75,0	72,5	69,0	69,5	68,0	75,0	73,0	77,0	75,0
Rb^+	69,0	66,5	60,0	65,0	62,0	70,5	70,0	71,0	70,0
Cs^+	59,5	58,5	57,0	57,0	57,0	61,5	61,0	63,0	61,5
Ag^+	106,0	106,0	106*	106*	108*	115,0	111,00	131,5	128,5
Ca^{++}	366*	360*	362*	360*	362*	350,0	358,0	355,5	363,0
Zn^{++}	479,0	472,0	472*	470*	468*	472,0	471,0	530,0	508,5
Cd^{++}	415,0	413,5	416*	412*	414*	412,0	413,0	457,0	446,5

* Valeurs d'après Khomutov.[6]

---

[6] N. E. Khomutov, *Zhur. fiz. Khim.*, **9**, 2223 (1968).

Tableau 3

Potentiels normaux d'électrode (volts)

Electrode	H_2O	CH_3OH	C_2H_5OH	C_4H_9OH	$C_5H_{11}OH$	CH_3COCH_3	CH_3CN	$HCOOH$	NH_3	N_2H_4
Li, Li^+	−3,001 −3,01	−3,186 −3,095	−3,143 −3,042	−3,207 —	−3,229 —	−3,207 —	−3,316 −3,23	−3,533 −3,48	−2,253 −2,24	−2,167 −2,20
Na, Na^+	−2,694 −2,713	−2,960 −2,728	−2,873 −2,657	−2,851 —	−2,678 —	−2,461 —	−3,047 −2,87	−3,350 −3,42	−2,059 −1,85	−2,006 −1,83
K, K^+	−2,950 −2,925	−3,196 −2,921	−3,131 —	−2,979 —	−2,979 —	−2,914 —	−3,347 −2,16	−3,521 −3,36	−2,176 −1,98	−2,241 −2,02
Rb, Rb^+	−2,923 −2,925	−3,200 −2,912	−3,135 —	−2,853 —	−3,049 —	−2,918 —	−3,417 −3,17	−3,656 −3,45	−2,181 −1,93	−2,290 −2,01
Cs, Cs^+	−2,919 −2,923	−3,066 —	−3,066 —	−3,001 —	−2,979 —	−2,979 —	−3,304 −3,16	−3,543 −3,44	−2,112 −1,95	−2,199 —
Ag, Ag^+	+0,793 +0,799	+0,541 +0,764	+0,498 —	+0,498 —	+0,519 —	+0,433 —	−0,001 +0,23	−0,088 +0,17	+0,541 +0,83	+0,519 —
Ca, Ca^{++}	−2,863 −2,87	−2,809 —	−2,722 —	−2,765 —	−2,700 —	−2,744 —	−2,614 −2,75	−3,047 −3,20	−1,475 −1,74	−1,790 −1,91
Zn, Zn^{++}	−0,729 −0,763	−1,002 −0,74	−0,894 —	−0,894 —	−0,829 —	−0,785 —	−1,002 0,74	−1,241 −1,05	−1,002 −0,53	−0,688 −0,41
Cd, Cd^{++}	−0,371 −0,402	−0,385 −0,43	−0,395 —	−0,449 —	−0,331 —	−0,375 —	−0,471 −0,47	−0,753 −0,75	−0,189 −0,20	−0,113 −0,10
Cl, Cl^-	+1,314 +1,339	+1,436 +1,116	+1,371 +1,048	+1,327 —	+1,306 —	+1,284 —	+0,893 —	+1,284 —	+2,325 —	+2,411 —
Br, Br^-	+1,078 +1,066	+1,171 +0,887	+1,106 +0,777	+1,171 —	+1,033 —	+1,171 —	+0,803 —	+0,911 —	+2,190 —	+2,277 —
I, I^-	+0,534 +0,536	+0,714 +0,357	+0,584 +0,305	+0,562 —	+0,627 —	+0,541 —	+0,432 —	+0,345 —	+1,777 —	+1,625 —

peut être représentée à l'aide de deux groupes conjugués de transformations :

$$\begin{tikzcd}
X^{-}(solv) \arrow[r] \arrow[d, leftrightarrow, "a_{X^{-}}=1"] & X^{-}(g) \arrow[d] & H^{+}(solv) \arrow[rr, leftrightarrow] \arrow[d, "a_{H^{+}}=1"] & & \frac{1}{2}H_2(g) \\
\frac{1}{2}X_2(g) & X(g)+e \arrow[l] & +\,H^{+}(g) \arrow[rr] & & H(g) \arrow[u]
\end{tikzcd}$$

Fig. 3. — Systèmes X, $X^{(-)n}$.

Les processus sont analogues à ceux imaginés dans le cas des systèmes Me, $\mathrm{Me}^{(+)n}$, le métal étant remplacé par l'halogène. Il s'ensuit que :

$$E^0_{X,X^-} = (A_{\mathrm{e}}^{X^-} - I_{\mathrm{H}}) - \frac{1}{F}\left(\frac{1}{2}D^0_{\mathrm{H}_2} + \frac{1}{2}D^0_{X_2}\right) + \frac{5RT}{F}\ln T$$

$$-\frac{RT}{F}\left[\frac{1}{2}\int_0^T \frac{\mathrm{d}T}{RT^2}\int_0^T (C_{p_{\mathrm{H}_2(g)}} + C_{p_{X_2(g)}})\,\mathrm{d}T\right] + \frac{RT}{F}(i_X + i_{\mathrm{H}}) \qquad (6)$$

$$-\frac{RT}{F}\left(\frac{i_{\mathrm{H}_2}}{2} + \frac{i_{X_2}}{2}\right) - \frac{1}{F}\,(\Delta G^{X^-}_{\mathrm{solv}} + \Delta G^{\mathrm{H}^+}_{\mathrm{solv}})$$

De même que pour les métaux, tous les termes de l'équation (6), qui ne dépendent pas des propriétés du solvant, sont compris dans une constante notée cette fois-ci par C_{X,X^-}, de sorte que, finalement, on obtient :

$$E^0_{X,X^-} = C_{X,X^-} - 0{,}04337\,(\Delta G^{X^-}_{\mathrm{solv.}} + \Delta G^{\mathrm{H}^+}_{\mathrm{solv.}}) \qquad (7)$$

Les valeurs de la constante C_{X,X^-} ainsi que les données nécessaires à son calcul sont inscrites dans le tableau 4.

Tableau 4

Paramètres de calcul de l'équation (6)

Electrode	A_{e}^{X-} volts	$D^0_{X_2}$ $k$cal/mole	$\frac{1}{2}\int_0^T \frac{\mathrm{d}T}{RT^2}\int_0^T C_{p_{X_2}}\,\mathrm{d}T$	i_X	i_{X_2}	$C_{X,X-}$
Cl, Cl⁻	3,78	57,08	11,669	16,91	16,93	−12,681
Br, Br⁻	3,52	45,44	12,375	18,13	19,47	−12,707
I, I⁻	3,16	35,55	12,677	18,82	20,83	−12,861

On a utilisé les énergies libres de solvatation des ions individuels d'halogènes toujours d'après Izmailov, [5] tableau 5.

Tableau 5

Énergies libres de solvatation $\Delta G^{X(-)n}_{\text{solv.}}$ (kcal/ion.g)

Ion	CH_3OH	C_2H_5OH	C_4H_9OH	$C_5H_{11}OH$	CH_3COCH_3	CH_3CN	$HCOOH$	NH_3	N_2H_4
Cl^-	73,0	72,5	71,5	70,5	70,0	64,0	79,0	68,0	73,5
Br^-	67,5	67,0	68,5	64,8	68,0	62,5	71,0	65,5	71,0
I^-	60,5	58,5	58,0	59,0	57,0	57,5	61,5	59,5	59,5

Les résultats obtenus sont insérés dans le tableau général 3.

Pour chaque élément, les valeurs calculées dans cette étude sont inscrites sur la première ligne horizontale, suivies immédiatement, en dessous, pour la comparaison, des données de la littérature, extraites du tableau général présenté par Strehlow. [7]

Si les potentiels standard sont classés dans le même ordre pour tous les solvants, on obtient un parallélisme de leurs valeurs.

Pour le même système d'électrode, quand on passe de l'eau aux alcools les variations des valeurs des potentiels standard ne sont pas trop grandes.

On obtient une toute autre image [8] en passant des alcools à des solvants d'une nature tout à fait différente, comme par exemple à l'ammoniac liquide ou à l'hydrazine, solvants aux propriétés basiques fortement prononcées et possédant, en conséquence, une puissante affinité pour le proton, affinité qui trouve son expression dans la formation des ions stables du type NH_4^+ et $N_2H_5^+$, ainsi que dans une série de particularités de comportement des solutions en NH_3 (1) et N_2H_4 qui prouvent un accroissement appréciable de l'énergie de solvatation du proton dans ces solvants.

On connaît d'autre part la capacité de l'ammoniac et de l'hydrazine de former de nombreux complexes et cristaux solvatés. La variation du potentiel atteint pour certains cas 1 volt, ce qui prouve l'augmentation brusque de l'énergie de solvatation des ions correspondants.

L'acide formique est, au contraire, un solvant « typiquement acide » ayant une capacité de former des complexes très petite. C'est pourquoi la série des tensions standard dans ce solvant est plus proche de celle dans l'eau.

L'acétonitrile possède une certaine acidité, pas trop prononcée. En effet, quoique l'acétonitrile forme avec les HBr, et $HClO_4$ et avec d'autres acides différentes combinaisons, la stabilité de celles-ci est très petite et l'affinité protonique de l'acétonitrile est probablement plus petite que celle de l'eau.

D'autre part, CH_3-CN étant le dérivé organique de l'HCN le plus simple, les deux possèdent une capacité nettement prononcée de former des complexes avec les ions des métaux lourds.

---

[7] J. J. Lagowski, « The Chemistry of Non-Aqueous Solvents », vol. I, Academic Press, Inc. New York-Londres, 1966, p. 131, 134.

[8] V. A. Pleskov, *Uspekhi Khim.*, **16**, 254 (1947).

Ainsi s'explique le déplacement du potentiel de l'argent en direction négative.

La littérature offre un nombre trop restreint de données expérimentales à l'aide desquelles on puisse comparer les valeurs calculées, à cause des difficultés qu'on a à effectuer des mesures dans les solvants non aqueux. [7]

Tandis que dans les cellules galvaniques en milieux-aqueux — les erreurs systématiques de mesure des tensions électriques sont beaucoup inférieures à 1 mV, cette situation est presque exceptionnelle en milieux non aqueux.

En beaucoup de cas les potentiels d'électrode dans des solvants non aqueux ne sont pas aussi stables que dans l'eau. Les fluctuations peuvent être attribuées parfois à l'empoisonnement de l'électrode par le solvant ou par les impuretés contenues dans le solvant.

Certains solvants tel que l'acétonitrile peuvent être réduits sur une électrode de platine-hydrogène, surtout si l'électrode est fortement platinée. Le produit de réduction éthylamine diminue sérieusement la concentration de l'ion d'hydrogène à l'électrode.

La dissociation incomplète peut sérieusement limiter la précision de l'extrapolation à la dilution infinie des données de tension électrique (surtout dans les milieux à constante diélectrique faible).

Il faut également effectuer les mesures dans les cellules galvaniques contenant les solutions dans le même solvant, afin d'éviter les incertitudes liées à l'existence des potentiels de diffusion, incertitudes beaucoup plus grandes quand les solvants sont différents.

L'absence des données certaines concernant les valeurs de l'énergie libre de solvatation des ions individuels, expliquée en grande mesure par l'insuffisance de nos connaissances sur la structure des liquides et par l'imperfection de nos représentations sur le mécanisme de solvatation, rend a priori impossible le calcul précis des potentiels normaux d'électrode.

L'accumulation ultérieure d'un matériel expérimental correct concernant les potentiels d'électrode dans des solutions non aqueuses d'une part, ainsi que l'obtention de valeurs certaines pour les énergies libres de solvatation des ions individuels d'autre part permettront à l'avenir une comparaison rigoureuse des potentiels dans différents solvants. Les calculs pourraient aussi être étendus, dans les mêmes conditions, à des mélanges de solvants.

Revue Roumaine de Chimie, 17, *11*, 1829 – 1839 (1972)

A DOUBLE HARD CORE MODEL DESCRIPTION OF THE SHORT-RANGE ORDER IN MOLTEN ALKALI HALIDES I VISCOSITY

G. VASU

Centre of Physical Chemistry
Str. Galaţi no. 31, Bucharest, Romania

Received June 20, 1972

A simple geometrical model for molten alkali halides is given, in order to account for the local short range order due to the coulombian forces in the melt. The model consists in assuming that all the ions in the melt are interacting with each other as hard core particles, but in such a way that the shortest distance between two like ions exceeds by a $\sqrt{2}$ factor the shortest distance between two unlike ions; by this prescription, the model leads to a NaCl crystalline structure in the solid state. On this basis it is assumed that the model will reproduce fairly well the liquid state structure in the neighbourhood of the melting point. By using the scaled particle theory of fluids, the contact correlation functions are obtained. These functions are then used in a Chapmann-Enskog formalism for viscosity computations. Results are fairly well for the molten alkali halides where the volume increase on melting is close to 15%.

1. INTRODUCTION

In the last decade, a great variety of researches have been devoted to the study of molten salts, resulting in a detailed information on both equilibrium and nonequilibrium properties of these systems, as well as in some valuable structural information obtained mainly from X-ray and neutron diffraction techniques. Some theoretical results have also been obtained, but there seems to be an important hiatus between the two trends followed by the theory. Thus, there is a class of works [1-4] which make use of the scaled particle theory of hard sphere fluids developed by Reiss, Frish, Helfand and Lebowitz.[5,6] All these works are based in some

---

[1] H. Reiss and S. W. Mayer, *J. Chem. Phys.*, **34**, 2001 (1961).

[2] F. H. Stillinger, *J. Chem. Phys.*, **35**, 1581 (1961).

[3] S. W. Mayer, *J. Chem. Phys.*, **40**, 2429 (1964).

[4] S. Y. Yoshim and B. B. Owens, *J. Chem. Phys.*, **41**, 2032 (1964).

[5] H. Reiss, H. L. Frisch and J. L. Lebowitz, *J. Chem. Phys.*, **31**, 369 (1959).

[6] E. Helfand, H. Reiss, H. L. Frisch and J. L. Lebowitz, *J. Chem. Phys.*, **32**, 119 (1960).

way on Stillinger's approximation [2] that some properties of monoatomic molten salts are nearly equal to the corresponding properties of a hypothetical fluid of uncharged ion cores at the same overall particle density, and also that the mean correlation function $g_m(r)$ for all particles in the melt (i. e. irrespective of their type) is well approximated by the pair correlation function of the hypothetical fluid.

On the opposite side, other authors have claimed that Coulomb forces in the melt must determine a solid-like structure where some kind of defects are included.[7] A refinement has been made by Murgulescu and Vasu,[8] by accounting for the relaxation of the lattice and polarization of the ions around vacancies in conjunction with McLellan's free volume theory.[9] They have obtained a good agreement for the equilibrium properties of molten alkali halides within a formalism which is exempt from adjustable parameters; similar results were obtained later by Eyring *et al.* [10] in an improved significant structure theory. Recently, a very simple and effective formula for the compressibility and expansion coefficients of molten salts has been established by Murgulescu, who has also given a very thorough analysis for the viscosity of these systems in therms of structure.[11,12]

It should be observed that not only standpoints are different among these works; the difference is a more fundamental one. For example, in the case of molten alkali halides, the coordination number, solid-like theories are consistent with, is nearly six, likely five of less, which is in agreement with experimental data.[13] On the other hand, the coordination number in a fluid of uncharged cores is nearly twelve, likely ten or less, but it is not five ! Doubtless, one cannot expect to have a faultless equivalence between ionic dense fluids and fluids of uncharged cores, though this is efficient in explaining equilibrium properties. Particularly, it seems that this approximation cannot account for the viscosity of molten alkali halides. For instance, let us take the molten CsCl (ionic radii are nearly equal in this case); it has been found [14] that a simple hard core model would account for its viscosity, only that the common diameter which was assigned to all the ions turned out to be greater than the real diameters of both Cs^+ and Cl^-. This is tantamount to saying that movements in the melt are considerably hindered than in ordinary fluids, so that the specific structure of the melt must be considered.

In view of these facts, a simple geometrical model is proposed here, which hopefully gives a better structural description for these melts. An extension of the scaled particle theory in the form given for mixtures of simple fluids by Lebowitz, Helfand and Praestgaard[15] is then made, and the correlation functions obtained are used for viscosity computations.

---

[7] H. Bloom and J. O' M Bockris, "Structural Aspects of Ionic Liquids", in "Fused Salts" edited by B. R. Sundheim, McGraw-Hill Book Company, New York and London, 1964, p. 1–62.

[8] I. G. Murgulescu and G. Vasu, *Rev. Roumaine Chim.*, **11**, 681 (1966).

[9] A. G. McLellan, *J. Chem. Phys.*, **40**, 567 (1964).

[10] Wei-Chea Lu, T. Ree, G. V. Gerrard and H. Eyring, *J. Chem. Phys.*, **49**, 797 (1968).

[11] I. G. Murgulescu, *Rev. Roumaine Chim.*, **14**, 965(1969); *ibid.* **15**, 1463 (1970); **17**, 603 (1972).

[12] I. G. Murgulescu, *J. Chim. phys.*, October 1969, special number, p. 43.

[13] G. J. Janz, "Molten Salts Handbook", Academic Press, New York, and London, 1967, p. 376–377.

[14] G. Vasu, *Rev. Roumaine Chim.*, **14**, 167 (1969).

Before further going, we shall mention the very interesting theory of transport phenomena in ionic melts given by Rice[16] and Berne & Rice[17]. We shall make use here of the structural description of molten salts given by them, which for our purposes will be formulated in a more quantitative way.

2. THE DOUBLE HARD CORE MODEL

The model to be given here is intended to replace the coulombian forces in the melt by some fictitious hard core interactions in a way leading to nearly the same structure. It is assumed that the structure of the melt will be accurately enough predicted, once the hard core interactions are determined by requiring them to lead to the real crystalline structure of the alkali halides. This requirement will be fulfiled by supposing that ions of opposite charges interact with each other as hard spheres of radius r, while identical ions (e. g. a pair of cations, or a pair of anions) are interacting as hard spheres of a radius R, say R equal to γr. Indeed, if one takes γ equal to $\sqrt{2}$, the compact structure of such a system of particles will surely be a NaCl type one.

Thus, the model consists in the statement that identical neighbouring ions — which are imagined as second order neighbours — cannot approach closer than a minimum distance. But it must be observed that the minimum distance between the second order neighbours is, in fact, a consequence of the thermodynamical equilibrium and not a parameter straightforwardly related to the potential energy. Consequently, by predetermining its value a structural statement is made. It is certain that second order neighbours in crystals of alkali halides are prevented to approach one another at shorter distances than $2r\sqrt{2}$ (where $2r$ is the anion-cation contact separation), but in melts they can come closer. Hence, for melts the γ factor must be somewhat less than $\sqrt{2}$, and so much the less as the density decreases and the structural order is lost. But having no other criterion, the value $\sqrt{2}$ for γ will be used throughout this work.

Before further going, a closer examination of the model may be useful. As it is shown in Fig. 1, all the ions are pictured as consisting of two concentric hard cores, so that the inner (or outer) hard cores are relevant to interactions between the pairs of unlike (or like) ions. Now, we can assume that the fundamental event in the dynamics of a pair of unlike ions is the collision of the inner hard cores. As to the outer hard cores, they are only a way to account for the structure of the melt in statistical computations, and their collisions are not to be considered as real dynamical events. Of course, all these approximations are drastically enough and the model may be expected to fail at lower densities. On the contrary, at high densities the structure seems to be fairly well described and good values for the contact correlation function of the inner hard cores — i.e. for the contact correlation function of unlike ions — are expected to result. Moreover, in this limit collissions of unlike ions are the only relevant dynamical events, collisions of like ions being prevented as a result of the solid-like short-range order. Consequently, the model seems to be suited for computations of transport phenomena in molten alkali halides at higher densities.

---

[15] J. L. Lebowitz, E. Helfand and E. Praestgaard, *J. Chem. Phys.*, **43**, 774 (1965).

[16] S. A. Rice, *Trans. Faraday Soc.*, **58**, 499 (1962).

[17] B. Berne and S. A. Rice, *J. Chem. Phys.*, **40**, 1347 (1964).

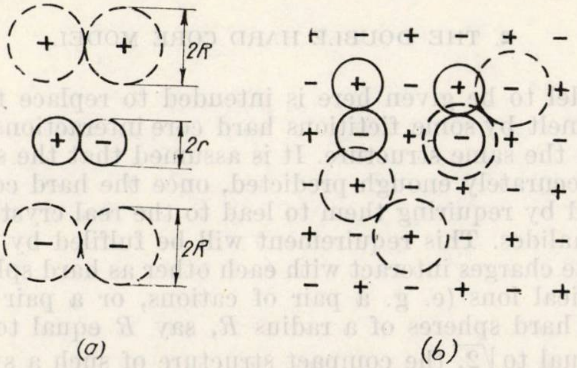

Fig. 1. — Double hard core model.
(a) Model of hard core interactions replacing the coulombian forces in the melt; (b) compact crystalline structure of the model particles.

Now, an extension of the scaled particle theory[15] can be readily given for the present double hard core model. The melt of alkali halides consists of two types of particles at equal concentrations, so that the coupling of a pair of scaled particles — a scaled cation and a scaled anion — must be investigated. A double hard core structure composed of an inner hard core of radius r_s and an outer hard core of radius R_s will be associated with any ion. In this way, there are two scaling parameters r_s and R_s, but one of them will be excluded by relating R_s to r_s as follows :

$$R_s = r_s \sqrt{2} \tag{1}$$

Let us consider a scaled cation. Because of the rigid core repulsion, the centres of all the cations of the melt are excluded from a spherical volume of a radius $R + R_s$ centered on the scaled cation. Similarly, the centres of all the anions are excluded from a similar spherical volume of a radius $r + r_s$. Therefore, a scaled cation can be treated as a cationic cavity of radius $R + R_s$ centered on an anionic cavity of radius $r + r_s$. Of course, for a scaled anion things are symmetrically reversed.

Now, we shall follow closely the usual procedure.[15] It consists in scaling r_s from $- r$ up to $+ r$. In the present case, especially interesting are the negative values of r_s for which

$$-r < r_s < -r(\sqrt{2}-1)/(\sqrt{2}+1), \tag{2}$$

because solute ions which have r_s in this range can run throughout the entire volume of the melt, and they will never collide two host ions simultaneously. But then, the reversible work $W(r_s)$ for coupling such an ion in a fixed point of the melt can be obtained exactly in the same manner as in [15]. Taking into account that $R_s + R = (r_s + r)\sqrt{2}$, in the present case one obtains

$$W(r_s) = -kT \ln \{1 - (4\pi/3)\, n\, (2\sqrt{2}+1)\, (r_s + r)^3\} \tag{3}$$

for all r_s satisfying (2). In the above equation $n = N/V$ is the particle density, which in alkali halides is the same for cations as for anions, i. e.

$$n_1 = n_2 = n. \tag{4}$$

Now, we look for a continuation of $W(r_s)$ in the physical domain $r_s > 0$. It will be assumed here that (3) remains a good approximation in the narrow domain $-r(\sqrt{2}-1)/(\sqrt{2}+1) < r_s < 0$, while for $r_s > 0$ the usual form [15] of $W(r_s)$ will be assumed:

$$W(r_s) = A + Br_s + Cr_s^2 + D\, r_s^3, \qquad r_s > 0. \tag{5}$$

The A, B and C are coefficients to be determined by matching the equations (5) and (3) at r_s equal to zero, so as to ensure the continuity of $W(r_s)$ and its first and second derivatives, while D will be obtained by requiring $W(r_s)$ to approach asymptotically the pressure work for creating a cavity at $r_s \gg r$. It results

$$W(r_s) = kT \left\{ -\ln(1-\xi_3) + \frac{6\xi_2}{1-\xi_3}\, r_s + \left[\frac{12\xi_1}{1-\xi_3} + \frac{18\xi_2^2}{(1-\xi_3)^2} \right] r_s^2 \right\} + \frac{p}{2}\, \frac{4\pi}{3}\, (2\sqrt{2}+1)\, r_s^3, \quad r_s > 0 \tag{6}$$

where

$$\xi_l = (\pi n/6)\, (2\sqrt{2}+1)\, (2r)^l, \qquad l = 1,\ 2,\ 3. \tag{7}$$

There is a strong resemblance between (7) and Eq. (2.7) of. [15] In the pressure work term of the above equation, $p/2$ stands for the partial pressure which anions or cations exert on the inner or outer spherical shell of the solute particle.

The chemical potential of the melt, defined for a pair of oppositely charged ions, may now be easily obtained ; taking into account (4) we have :

$$\mu = 2kT \ln \, [nh^3 (2\pi kT)^{-3/2} (m_1 m_2)^{-3/4}] + 2\, W(r), \tag{8}$$

where h is Planck's constant. The first term in (8) is the translational free energy for two ions of masses m_1 and m_2, and the second is the reversible work needed for coupling them completely in the melt.

From (6), (7), and (8) it results :

$$\begin{aligned} \mu = 2k\,T \ln[nh^3 (2\pi kT)^{-3/2} (m_1 m_2)^{-3/4}] + 2k\,T\,\{- \ln(1 - \xi_3) + \\ + (12\,\xi_3 - 3\xi_3^2) / [2\,(1 - \xi_3^2)]\} + p\,\xi_3/n. \end{aligned} \tag{9}$$

By substituting (9) in the thermodynamical equation

$$(\partial p \,/\, \partial n)_T = n\,(\partial \mu \,/\, \partial n)_T \tag{10}$$

the following equation of state is obtained :

$$p = 2nkT\,(1 + \xi_3 + \xi_3^2)\,(1 - \xi_3)^{-3}. \tag{11}$$

This result is very similar to those obtained for a liquid of hard spheres by the scaled particle theory[5,6,15] ; the difference comes only from the equation (7) defining ξ_3.

The contact correlation functions can also be obtained by the scaled particle theory. Let $g(2r)$ be the contact correlation function of unlike ion pairs, and $G(2R)$ that of like ion pairs (the last one has the same value for pairs of cations or anions, because in the present model the geometry of these particles is perfectly symmetrical). Let us assume that a scaled cation of a radius r_s in the range (2) has been coupled in the melt ; this cation is equivalent to a cavity of radius $R_s + R$ equal to $(r_s + r)\sqrt{2}$ wherefrom all the cations are excluded, and a concentric cavity of radius $r_s + r$ wherefrom all the anions are excluded. Let $C(r_s + r,\ R_s + R)$ denote such a complex cationic cavity, and let $p_0(r_s + r,\ R_s + R)$ be the probability of his occurrence in the melt. If r_s is in the range (1) and R_s equals r_s 2, the cavity $C(r_s + r\ ,\ R_s + R)$ cannot be occupied simmultaneously by two particles, so that :

$$p_0\,(r_s + r,\ R_s + R) = 1 - (4\pi/3)\, n\, [(r_s + r)^3 + (R_s + R)^3]. \tag{12}$$

As usual[18] the negative rate of p_0, i. e. $-\,(\partial p_0/\partial r_s)\,\mathrm{d}r_s$, is the probability of finding a cavity $C(r_s + r,\ R_s + R)$ and the centre of an anion in the spherical shell between $r_s + r$ and $r_s + r + \mathrm{d}r_s$; by dividing it to p_0 we obtain the conditional probability for having an anion in the shell of internal radius $r_s + r$ and external radius $r_s + r + \mathrm{d}r_s$ in the presence of a cationic cavity. But this conditional probability is also related to $g(r_s + r)$ and it results :

---

[18] H. L. FRISCH, "Advances in Chemical Physics", vol. 6, ed. by I. PRIGOGINE, Interscience Publishers, New York, 1964, p. 229.

$$4\pi (r_s + r)^2 \, n g (r_s + r) \, \mathrm{d}r_s = -[\partial \ln p_0 (r_s + r,\ R_s + R)/\partial r_s] \, \mathrm{d}r_s.$$

Using (12) we obtain :

$$g (r_s + r) = \{1 - (4\pi/3) \, n \, [(r_s + r)^3 + (R_s + R)^3]\}^{-1},$$

$$-r < r_s < r(\sqrt{2} - 1)/(\sqrt{2} + 1) \tag{13}$$

Equation (13) gives the contact correlation function of the scaled ion and the opposite charged ions, and it is a rigorous result. In the same way, by varying the radius R_s we obtain the contact correlation function of the scaled ion and the ions of the same charge in the melt, i. e. $G(R_s + R)$. If r_s is in the range (2), we obtain :

$$G (R_s + R) = g (r_s + r), \tag{14}$$

where $R_s = r_s \sqrt{2}$.

We shall assume now that (13) and (14), which are rigorous for $r_s < -r(\sqrt{2}-1)/(\sqrt{2}+1)$, remain also good approximations up to $r_s = 0$, while for $r_s > 0$ we write as usual[15] :

$$g (r_s + r) = \frac{p/2}{nkT} + \frac{b}{r_s + r} + \frac{c}{(r_s + r)^2}, \quad r_s > 0. \tag{15}$$

By matching (15) and (13) at $r_s = 0$ so as to ensure the continuity of $g(r_s + r)$ and its first derivative, we obtain :

$$g (r_s + r) = \frac{p}{2nkT} \frac{r_s^2}{(r_s + r)^2} + \frac{2 + \xi_3}{(1 - \xi_3)^2} \frac{r}{r_s + r} - \frac{1 + 2\xi_3}{(1 - \xi_3)^2} \frac{r^2}{(r_s + r)^2}, \quad r_s > 0. \tag{16}$$

Similarly, by writing :

$$G(R_s + R) = \frac{p/2}{nkT} + \frac{B}{R_s + R} + \frac{C}{(R_s + R)^2}, \quad R_s > 0$$

and requiring the continuity of G and $\mathrm{d}G/\mathrm{d}R_s$ at $R_s = 0$, it results :

$$G (R_s + R) = g(r_s + r), \text{ where } R_s = r_s \sqrt{2} > 0. \tag{17}$$

As usual, there is an exact equation connecting the contact correlation functions and the derivative of the reversible work W[15]; for our model we have:

$$\mathrm{d}W/\mathrm{d}r_s = 4\pi n^0 kT[(r_s + r)^2 g(r_s + r) + (R_s + R)^2 G(R_s + R)(\mathrm{d}R_s/\mathrm{d}r_s)], \quad (18)$$

where the factor $\mathrm{d}R_s/\mathrm{d}r_s$ accounts for the fact that a variation $\mathrm{d}r_s$ of the inner hard core entails a variation $\mathrm{d}R_s$ of the outer hard core, according to (1). By using (1), (6), (16), and (17), it can be verified at once that (18) is satisfied identically by our results. Therefore, the approximation (6) is consistent with (16) and (18).

Substituting r_s equal to r into (16) and using (7) and (11) we obtain the contact correlation function at complete coupling:

$$g(2r) \equiv g_{12}(2r) = [1 - (\xi_3/2) + (\xi_3/2)^2](1 - \xi_3)^{-3}. \quad (19)$$

This is the main result of this work. According to the present model, we think the value $g(2r)$ given by (19) to be a good approximation for the contact correlation function of oppositely charged ion pairs in the melt, denoted as usual by $g_{12}(2r)$. Of course, from (17) we may write down immediately the contact correlation function of the outer hard cores, $G(2R)$. But, as mentioned, the outer hard cores are only fictitious; they are only a means to account for the local short-range order in the ionic melt. The outer hard cores collision is not a real dynamic event and consequently $G(2R)$ has no significance in connection with the transport phenomena.

Thus, the double hard core model presented here leads to Eq. (19) for the anion-cation contact correlation function. As to the real anion-anion and cation-cation contact correlation functions g_{11} and g_{22}: they are not to be confounded with $G(2R)$ and it is consistent with our model to consider them zero. Indeed, let R_+ and R_- be the ionic radii so that the shortest anion-cation separation $2r$ will be approximately R_+ plus R_-. Then, according to our model, two like ions cannot approach each other closer than $2(R_+ + R_-)$; but this exceeds both $2R_+$ and $2R_-$. This means that the present model will be valid only if one can assume that the real hard cores of two like ions are never in contact with one another, i.e. the contact correlation functions for two like ions are zero:

$$g_{11}(2R_+) = g_{22}(2R_-) = 0; \quad (20)$$

The assumption leading to (20) has been first put forward by Rice.[16]

3. VISCOSITY

In a previous paper,[14] the viscosity of molten alkali halides has been discussed in terms of the Dymond & Alder formalism,[19] and it has been pointed out the need for a better calculation of the contact correlation

[19] J. H. Dymond and B. J. Alder, *J. Chem. Phys.*, **45**, 2061 (1966).

functions. The same formalism will be applied here, and we shall use the contact correlation functions given by (19) and (20). We shall calculate the viscosity of molten alkali halides starting from Thorne's formula [20] for the viscosity of rigid sphere mixtures:

$$\eta = \frac{5}{2} kT \Biggl[b_{-1-1} \frac{n_1}{n_2} \Bigl(1 + \frac{4\pi}{15} n_1 g_{11} \sigma_{11}{}^3 + \frac{8\pi}{15} \frac{m_2}{m_1+m_2} n_2 g_{12} \sigma_{12}{}^3)^2 -$$

$$- 2b_{1-1} \Bigl(1 + \frac{4\pi}{15} n_1 g_{11} \sigma_{11}{}^3 + \frac{8\pi}{15} \frac{m_2}{m_1+m_2} n_2 g_{12} \sigma_{12}{}^3 \Bigr) \Bigl(1 + \frac{4\pi}{15} n_2 \sigma_{22}{}^3 g_{22} +$$

$$+ \frac{8\pi}{15} \frac{m_1}{m_1+m_2} n_1 g_{12} \sigma_{12}{}^3 \Bigr) + b_{11} \frac{n_2}{n_1} \Bigl(1 + \frac{4\pi}{15} n_2 g_{22} \sigma_{22}{}^3 +$$

$$+ \frac{8\pi}{15} \frac{m_1}{m_1+m_2} n_1 g_{12} \sigma_{12}{}^3 \Bigr)^2 \Biggr] \Bigl[g_{12} (b_{11} b_{-1-1} - b^2{}_{1-1}) \Bigr]^{-1} +$$

$$+ \frac{4}{15} (\pi kT)^{1/2} \left[m_1{}^{1/2} n\,{}_1^2 g_{11} \sigma_{11}^4 + 2 \left(\frac{2m_1 m_2}{m_1+m_2} \right)^{1/2} n_1 n_2 g_{12} \sigma_{12}^4 + m_2^{1/2}\, n_2^2\, g_{22}\, \sigma_{22}^4 \right], \quad (21)$$

where

$$b_{11} = b'_{11} + \frac{n_1 g_{11}}{n_2 g_{12}} b''_{11},\ b_{-1-1} = b'_{-1-1} + \frac{n_2 g_{22}}{n_1 g_{12}}\ b''_{-1-1},$$

$$b_{1-1} = -\frac{32}{3} \left[\frac{\pi m_1 m_2 kT}{2(m_1+m_2)^3} \right]^{1/2} \sigma_{12}^2,$$

$$b'_{11} = \frac{16}{3}\ (5m_1 + 3m_2) \left[\frac{\pi m_2 kT}{2m_1(m_1+m_2)^3} \right]^{1/2} \sigma_{12}^2,\ b''_{11} = 8 \left(\frac{\pi kT}{m_1} \right)^{1/2} \sigma_{11}^2,$$

$$b'_{-1-1} = \frac{16}{3}\ (5m_2 + 3m_1) \left[\frac{\pi m_1 kT}{2m_2(m_1+m_2)^3} \right]^{1/2} \sigma_{12}^2,\ b''_{-1-1} = 8 \left(\frac{\pi kT}{m_2} \right)^{1/2} \sigma_{22}^2. \quad (22)$$

In the above equations m_1 and m_2 are the masses of the particles, and σ_{ij} are the distances between the centers of two particles i and j at contact with each other. Of course, σ_{ij} are to be thought of as some effective temperature dependent hard core diameters. In conformity with our model, σ_{12} must be taken as $2r$, and it is useful to point out the equation connecting $n\sigma_{12}{}^3$ and the parameter ξ_3 defined by (7):

$$\xi_3 = (\pi/6)\,(2\sqrt{2} + 1) n\, \sigma_{12}^3. \quad (23)$$

---

[20] S. Chapman and D. J. Cowling, "The Mathematical Theory of Non-Uniform Gases", University Press, Cambridge 1960, p. 231.

Now, in the case of molten alkali halides near the melting point, a great simplification results owing to the approximation $g_{11}=g_{22}=0$. Combining (20), (21), (22), and (23), the following equation for the molten alkali halides viscosity is obtained:

$$\eta = \frac{0.419\,\xi_3^2\, g_{12}(\sigma_{12})}{\sigma_{12}^2}\left(\frac{m_1 m_2 kT}{m_1+m_2}\right)^{1/2}\left\{1+\frac{0.993}{\xi_3 g_{12}(\sigma_{12})}+\right. \tag{24}$$
$$\left.+\left[1+0.375\frac{m_1 m_2}{(m_1+m_2)^2}\right]\frac{0.475}{[\xi_3 g_{12}(\sigma_{12})]^2}\right\}.$$

The only problem to be elucidated is the value of the effective hard core diameter σ_{12}. We are constrained here to calculate it by starting from the potential of ionic interaction. The method has been given in a previous paper,[21] and considerations developed there can be resumed in the following equation:

$$\varphi(\sigma_{12}) = \varphi(a) + kT \tag{25}$$

where $\varphi(r)$ is the potential of interaction, and a is the mean distance between two neighbouring particles. The kT term arises by projecting the relative movement of two colliding particles on the symmetry axes and taking the respective component of the mean kinetic energy. It is this kinetic energy which is converted into the potential one during the collision and therefore it is determining for the mean distance of the shortest approach (we have in mind an approximate solution of the collision problem). For our purpose, we shall identify $\varphi(r)$ with the potential energy of the repulsive forces between anions and cations, which can be written in the form[22]:

$$\varphi(r) = \frac{\alpha e^2}{6\,\varkappa\sigma_0}\left(\frac{\sigma_0}{r}\right)^{\varkappa} \tag{26}$$

where σ_0 is the nearest neighbours distance in the crystal and α is the Madelung constant. To simplify, I shall take the repulsion exponent $\varkappa$ equal to ten. Now, let us assume that the nearest neighbours distance does not vary sensibly by melting, i. e. that a equals σ_0. Then we obtain from (25) and (26)

$$\sigma_{12} = \sigma_0\,[1 + 60kT\sigma_0/\alpha e^2]^{-10}. \tag{27}$$

Now, the viscosity of molten alkali halides can be immediately computed from (19), (24), and (27). The values of the liquid volume, temperature and nearest neighbours distance used in computations, and the results obtained are given in table 1. In the last column it is also given the ratio $\Delta V_f/V_s$ of the volume increase by melting ΔV_f to the solid volume at the melting point V_s. This ratio can give a measure of the loss of short-range order by melting. It can be seen that the smaller $\Delta V_f/V_s$ is, i. e. the smaller the structural change by melting is, the better the computed viscosities are. This trend can be easily understood in connection with the structural assumptions made in our model (see discussion below Fig. 1)

---

[21] G. Vasu, *Rev. Roumaine Chim.*, **15**, 1011 (1970).

[22] C. Kittel, "Introduction to Solid State Physics" Wiley, New York, 1956, p. 72.

Table 1

Molten alkali halides viscosity at the melting point

	V (cm^3)	T (K)	σ_0 (Å)	η (cP)		$\frac{\Delta V_f}{V_s}$, %
				calculated	experimental [23]	
NaCl	37.74	1.073	2.78	0.37	1.44	25.8
NaBr	43.94	1.020	2.93	0.43	1.38	25.5
KCl	48.80	1.043	3.14	0.80	1.20	16.3
KBr	56.03	1.007	3.29	0.92	1.19	16.8
RbCl	53.93	995	3.28	1.16	1.31	15.0
RbBr	61.16	965	3.43	1.59	1.48	14.9

Acknowledgements. The author wishes to express his gratitude to Professor I. G. Murgulescu for his interest and the very illuminating discussions he had with him during the preparation of this work.

---

[23] Ref. 13, pp. 39, 54 and 55.

Revue Roumaine de Chimie, **17**, *11*, 1841 – 1844 (1972)

DIE VERWENDUNG DER OBERFLÄCHENEIGENSCHAFTEN FÜR DIE CHARAKTERISIERUNG DER ASSOZIATION DES PYROLS IN FLÜSSIGEM ZUSTAND

CRISTINA MANDRAVEL und MELANIA GUŢUL

von der Fakultät für Physik und Chemie der Universität Bukarest

Eingegangen am 12. Juli 1971

In dieser Arbeit werden die Ergebnisse der Bestimmungen über die Veränderungen der Oberflächeneigenschaften von reinem Pyrol mit der Temperatur mitgeteilt. Man erhält die Werte der verbundenen Oberflächenenergien und des Assoziationsfaktors, man korreliert die Angaben der Fachliteratur mit den gemessenen Werten der verschiedenen spezifischen Eigenschaften der Pyrol-Luft-Oberfläche.

Die Arbeiten, welche in den letzten Jahren über die Chemie des Pyrols erschienen sind, beweisen ein wachsendes Interesse entweder für das Studium seiner Eigenschaften in Wechselbeziehung mit seinem aromatischen Charakter,[1–6] oder für die Bestimmung seiner kennzeichnenden Eigenschaften, was die komplexe Charakterisierung des flüssigen Zustandes [7–13] betrifft.

In dieser letzten Richtung haben wir ein Studium über die Veränderungen der Oberflächeneigenschaften des Pyrols mit der Temperatur und die Korrelation dieser Oberflächeneigenschaften mit der Assoziation des Pyrols in flüssigem Zustand vorgenommen.

---

[1] A. Treibs und H. G. Koln, *Liebigs Ann. Chem.*, **606**, 166 (1957).

[2] A. Treibs, *Rev. Chim. Acad.* **6**, 1345 (1962).

[3] R. K. Kind, E. M. Lauglin und A. R. Ubbelode, *Trans. Faraday Soc.*, **56**, 331 (1960).

[4] H. Lumbroso und G. Pappalardo *Bull. Soc. chim. France*, **1961**, 131.

[5] L. B. Kier, *Tetrahedron Letters*, **37**, 3273 (1965).

[6] G. G. Le Fèvre, R. Y. W. Le Fèvre, B. P. Rao, und M. R. Smith, *J. Chem. Soc.*, 1959, 1188.

[7] S. Hirano, M. Suzuki und T. Nogucki, *J. Chem. Soc. Japan.*, **55**, 514 (1952).

[8] J. P. Mc Cullough und D. R. Dauslin, *J. Amer. Chem. Soc.*, **81**, 5884 (1959).

[9] R. Fauquenbergue, L. Raczy und E. Constant, *Compt. rend.*, **264**, 1213 (1967).

[10] D. W. Scott, W. T. Berg, D. R. Douslin und Y. P. Mc Cullough, *J. Phys.* Chem., **71**, 2263 (1967).

[11] M. Gomel und H. Lumbroso, *Bull. Soc. chim. France*, **1962**, 2200.

[12] N. E. Hill, *Proc. Roy Soc.* (A), **240**, 101 (1957).

[13] N. Gagnoli, *Ann. Chim.* (*Ital.*), **48**, 839 (1958).

EXPERIMENTELLES

Das verwendete Pyrol (Riedel von Haën AG – Hannover, p.a.) wurde vor jeder Bestimmung destilliert, die Reinheit des Pyrols durch Dichte- und Brechungsindex-Bestimmungen charakterisiert ($\rho_4^{20} = 0,969$, $n^{20} = 1,5085$).

Die Dichtebestimmungen wurden durch die pyknometrische Methode in Thermostatierungsbedingungen mit einer Genauigkeit von ± 0,01° ausgeführt. Die Oberflächenspannug wurde stalagmometrisch bestimmt, in denselben Thermostatierungsbedingungen, u.zw. unter Bedingungen, bei welchen die erhaltenen Werte die statische Oberflächenspannung darstellen (entsprechend der Einstellung des Adsorptionsgleichgewichts). Die Meßergebnisse sind in Tabelle 1 angegeben.

Tabelle 1

Die Werte der Oberflächenspannung und das spezifische Volumen abhängig von der Temperatur im Falle des reinen Pyrols

Nr.	σ (dyn.cm^{-1})	$V_{s\,(\mathrm{cm^3 g^{-1}})}$	TK
1	33,25	1,035	293,16
2	32,52	1,036	298,16
3	32,22	1,039	303,16
4	31,97	1,041	308,16
5	31,36	1,043	313,16
6	31,02	1,045	318,16
7	30,64	1,048	323,16

DISKUSSIONEN

Reines Pyrol hat bei 20° eine Oberflächenspannung von 33,25 dyn cm^{-1}, welche dem Wert einer wenig assozierten Flüssigkeit entspricht und ist in guter Übereinstimmung mit dem in der Arbeit [13] für reines Pyrol angegebenen Wert von 33,24 dyn cm^{-1}.

Anhand der Abhängigkeit zwischen Oberflächenspannung und Temperatur haben wir den Wert der Größe $\left(\frac{d\sigma}{dT}\right)_p = -0,07$ dyn/cm. Grad berechnet, welche die Größe der verbundenen Oberflächenenergie darstellt. Aufgrund der Werte der Oberflächenspannung (bzw. der freien Oberflächenenergie) laut einer Gleichung vom Typ Gibbs-Helmholtz kann man den Wert ΔU_s erhalten, der für Pyrol bei 20°, 53,72 dyn cm^{-1}, oder $12,89.10^{-7}$ cal. cm^{-2} darstellt.

Vergleicht man diesen Wert mit ΔU_s des Wassers bei derselben Temperatur ($3,5.10^{-6}$ cal. cm^{-2}), so bemerkt man, daß der Wert der gesamten Oberflächenenergie entsprechend größer ist im Falle des Wassers, wo der Beitrag der intermolekularen van der Waalsschen Kräfte und die Verbindungen durch Wasserstoffbrücken bedeutsamer ist.

Berücksichtigt man den Wert der Verdampfungs-Standardenthalpie des Pyrols aus Arbeit[10] so ergibt sich der Wert des Innendrucks und der Stärke der Oberflächenschicht Gibbs an der Pyrol-Wasser-Trennfläche berechnet, sowie auch eine Reihe von anderen thermodynamischen Eigenschaften, welche in Tabelle 2 dargestellt sind.

Tabelle 2

Die berechneten Werte der verschiedenen thermodynamischen Eigenschaften welche für die Trennschicht Pyrol-Luft spezifisch sind

$\Delta S_s = -\left(\frac{d\sigma}{dT}\right)_p$ (dyn.cm^{-1}.grd.$^{-1}$)	0,07				
ΔU_s (dyn.cm^{-1})	53,72	53,43	53,38	53,27	43,25
$T_{(K)}$	293,16	298,16	303,16	313,16	323, 16
π (Innendruck) (dyn.cm^{-2})	6.15.10^9				
δ (Oberflächenschicht) (Å)	0,705				
P_e (Parackor) (cm (dyn.cm^{-1})$^{1/4}$	165,7				
$\varkappa$ (Assoziationsfaktor)	1,49				
k^* (dyn.cm^{-1}.grd^{-1})	−0,1				
σ_s^* (dyn.cm^{-1})	37,10				

* – Die Werte von k und σ_s stellen die Konstanten aus der Gleichung $\sigma = \sigma_S - k\,(T - T_S)$ dar (wo T_S der Wert der Erstarrungstemperatur des Pyrols ist[8]), die für wenig assozierte Flüssigkeiten anwendbar ist. Die Konstanten sind graphisch bestimmt.

Für die Flüssigkeiten, die durch die Substraktion von zwei aus der Gleichung Eötwos abgeleiteten Gleichungen assoziert sind und für zwei nicht zu weit entfernte Temperaturen konkretisiert, kann man folgende Beziehung ableiten :

$$\sigma_1\,(\varkappa M V_{sp1})^{2/3} - \sigma_2\,(\varkappa M V_{sp2})^{2/3} = k_E\,(T_2 - T_1)$$

wobei :

σ_1, σ_2 — die Oberflächenspannungen bei den Temperaturen T_1, T_2‘
V_{sp1}, V_{sp2} — die spezifischen Volumina unter denselben Bedingungen,
M — die Molekularmasse,
k_E — die Eötwos Konstante,
$\varkappa$ — den Wert des Assoziationsfaktors darstellen.

Diese Beziehung wurde für die Berechnung des Assoziationsfaktors des Pyrols verwendet, für welchen man den Wert 1,46 im Intervall 20–45° erhält.

Wenn man die Ergebnisse der Forschung der Pyrollösungen in CCl_4 und des reinen Pyrols durch Hertz-Spektroskopie [9] in demselben Temperaturgebiet ausgeführt vergleicht, woraus man ableiten kann, daß die Statistik der Kettenverbindung der Pyrolmoleküle nicht wahrscheinlich ist und daß die Dimerenverbindungen vorherrschen, und wenn man auch die Arbeiten über den scheinbaren Moment im flüssigen Pyrol,[11,12] welcher die große Wahrscheinlichkeit des Vorhandenseins der orthogonalen cyklischen Dimere des Pyrols zuläßt (im Tmperaturgebiet 16–83°) berücksichtigt, dann erscheint der von uns ermittelte Wert als vollständig begründet.

Revue Roumaine de Chimie, **17**, *11*, 1845–1849 (1972)

KRAFTKONSTANTENBERECHNUNG AN DER AMINOGRUPPE DES ANILINS

ERIKA HAMBURG, RODICA GRECU und M. FERNEA

aus dem Chemischen Forschungsinstitut, Cluj, str. Donath 65–103 und dem
Recheninstitut der Akademie, Cluj, str. Republicii 37

Eingegangen am 7. Juni 1971

Mit Hilfe der *G*- und *F*-Matrix Methode von Wilson u. Mitarb. wurden die Kraftkonstanten der NH_2-Gruppe des Anilins berechnet. Die Berechnung der Normalschwingungen wurde aufgrund folgender Voraussetzungen gemacht : a) Anilin hat annähernd eine Symmetrie C_s ; b) Winkel τ zwischen der Fläche des Benzolrings und der Aminogruppe hat den Wert von 38°22′.

EINLEITUNG

Mit dem Infrarotspektrum des Anilins haben sich viele Autoren befaßt doch die Zuordnung der Schwingungsfrequenzen der Aminogruppe von Anilin wurde nur von einigen Autoren besprochen.$^{1-5}$ Wir nahmen uns vor, in dieser Arbeit die Kraftkonstanten der Aminogruppe des Anilins zu berechnen und die berechneten Schwingungsfrequenzen so wie deren frühere Zuordnungen zu kommentieren.

Da für Anilin bisher keine Diffraktionsstudien gemacht wurden, und deshalb die Frage, ob Anilin planar oder nicht planar sei nicht endgültig gelöst wurde, setzen wir unserer Arbeit die zur Zeit wahrscheinlichste Annahme voraus, daß die Struktur des Anilins in der Form $R-NH_2$ (R=Phenyl) einen Übergang zwischen der planaren (Symmetrie C_{2v}) und der pyramidalen (Symmetrie C_{3v}) Konfiguration bildet,$^{6-8}$ und so gehört Anilin zu der Symmetriegruppe C_s.

In diesem Falle ist theoretisch die Zahl der infrarotaktiven Normalschwingungen für das System $R-NH_2$, in Klasse A' vier, und in Klasse A''

---

[1] S. Califano und R. Moccia, *Gazz. chim. Ital.*, **87**, 805 (1957).
[2] J. C. Evans, *Spectrochim. Acta*, **16**, 428 (1960).
[3] M. Tsuboi, *Spectrochim. Acta*, **16**, 505 (1960).
[4] J. M. Lebas, *J. Chim. phys.*, **59**, 1072 (1962).
[5] C. Belorgeot, P. Quintard und J. Gerbier, *Compt. rend.*, **B 269**, 1105 (1969).
[6] A. Julg und P. Carles, *J. Chim. phys*, **62**, 1134 (1965).
[7] D. G. Lister, und J. K. Tyler, *Chem. Commun.*, **6**, 152 (1966).
[8] J. C. Brand, D. R. Williams und T. J. Cook, *J. Mol. Spectroscopy*, **20**, 193, 359 (1966).

zwei. Tabelle 1 enthält alle Normalschwingungen und die ihnen zugeordneten Frequenzen für Anilin und deuteriertes Anilin.

Tabelle 1

Berechnete und gefundene Schwingungfrequenzen der NH_2-Gruppe von Anilin und deuteriertem Anilin in Tetrachlorkohlenstofflösung

Species		Schwingungsart		Frequenzwerte in cm^{-1}				
				Literatur	Literatur	Literatur	Diese Arbeit	Berechnet
Anilin	A′	NH_2	sym. Valenzschw.	3395	3401	3395	3400	3405
		CN	Valenzschw.	1247	1278	1276	1280	1237
		NH_2	Deformationsschw.	1619	1618	1619	1620	1622
		NH_2	Schaukelschw.	—	570	~700	605	585
	A″	NH_2	asym. Valenzschw.	3478	3485	3481	3485	3487
		NH_2	Torsionsschw.	1055	1054	1114	1116 oder 1050	1006
Deuteriertes Anilin	A′	ND_2	sym. Valenzschw.	2430	2485 2466 2440		2480 2462 2428	2469
		CN	Valenzschw.	1300	1303	1301	1305	1314
		ND_2	Deformationsschw.	1079	1152	1150	1078	1068
		ND_2	Schaukelschw.	—	420	—	—	445
	A″	ND_2	asym. Valenzschw.	2600	2592		2595	2583
		ND_2	Torsionsschw.	797	750	797	750 oder 800	728

Es geht aus dieser Tabelle hervor, daß die von verschiedenen Autoren angegebenen Zuordnungen sehr unterschiedlich sind. Im Gegensatz zu Evans,[2] welcher der NH_2 Schaukelschwingung die Absorptionsbande bei 570 cm^{-1} zuordnet, beobachten Belorgeot und Mitarb.[5] im fernen Infrarotspektrum des Anilins diese Schwingung bei 130 cm^{-1}. Die von Evans[2] angegebene Zuordnung scheint im Vergleich mit den Zuordnungen der Schwingungen von der Aminogruppe[9-13] aus anderen Verbindungen korrekt zu sein. Paillous[14] hat die Normalschwingungen des Benzolkerns einer Serie von monosubstituierten Benzolderivaten inklusiv des Anilins mit der Annahme berechnet, daß diese Moleküle planar seien, wobei die Substituenten für einen Massenpunkt genommen wurden. Als Ergebnis der Rechnungen wurde hier bewiesen, daß sich die charakteristischen Schwingungen desBenzolkerns leicht von den Normalschwingungen

---

[9] A. P. Gray und R. C. Lord, *J. Chem. Phys.*, **26**, 690 (1957).

[10] E. L. Wu, G. Zerbi, S. Califano und B. Crawford, Jr., *J. Chem. Phys.*, **35**, 2060 (1961).

[11] J. C. Evans, *J. Chem. Phys.*, **22**, 1228 (1954).

[12] Yu. I. Mushkin und A. I. Finkelstein, *Optika i Spektroskopia*, **13**, 289 (1962).

[13] K. Nakamoto, J. Fujita, R. A. Condrate und Y. Morimoto, *J. Chem. Phys.*, **39**, 423 (1963).

[14] J. K. Paillous, *J. Chim. Phys.*, **57**, 1048 (1960).

der Substituentengruppen separieren lassen. Aufgrund dieser Ergebnisse nehmen wir bei unseren Rechnungen den Teil $>C-NH_2$ des Anilinmoleküls in Betracht.

RECHENMETHODE, ERGEBNISSE UND DISKUSSION

Das von uns erwählte Vierpunktproblem (System $R-NH_2$) mit einer Symmetrie C_s, hat notwendigerweise eine Zahl von 6 Innerkoordinaten: Δr_1, Δr_2, ΔR, $\Delta\alpha$, $\Delta\beta_1$ und $\Delta\beta_2$. Abbildung 1 zeigt die Struktur und die Bezeichnung der inneren Koordinaten des Anilins.

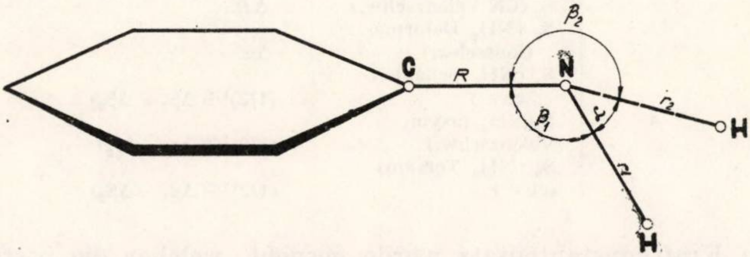

Abb. 1. – Innerkoordinaten für die NH_2-Gruppe des Anilins.

Eine Transformation der inneren Valenzkoordinaten in Symmetriekoordinaten ist vorteilhaft, da durch diese der physikalische Sinn der Schwingungsfrequenzen besser vertreten ist und andererseits bieten die Symmetriekoordinaten wie bekannt auch den mathematischen Vorteil, das Wilsonsche [15] Säkulargleichungssystem

$$\det (GF - E\lambda) = 0 \qquad (1)$$

entsprechend den Symmetrieklassen in Determinanten niedrigeren Grades aufzuspalten. Die Symmetriekoordinaten sind in Tabelle 2 angegeben.

Die Elemente der Matrix G wurden nach der Methode von Decius [16] berechnet. Als Masse von R wurde die reduzierte Masse des Phenyls genommen. Für Kernabstände und Winkel wurden folgende Werte eingesetzt: $r = 1{,}05$ Å, $R = 1{,}43$ Å; $\alpha = 112°$ (dieser Wert wurde mit der Annahme berechnet,[12] daß die symmetrische und antisymmetrische Valenzschwingung der Aminogruppe von den anderen Schwingungen unabhängig ist); $\beta = 112°{,}51'$ (entsprechend der Größe $\tau = 46°$ welche mit Hilfe der elektronischen Spektren gefunden wurde [8]) und $\beta = 116°$ (der von Evans [2] angegebene Winkelwert).

---

[15] E. B. Wilson, Jr., J. C. Decius und P. C. Cross, ,,Molecular Vibrations. The Theory of Infrared and Raman Vibrational Spectra'', Mac Graw-Hill Book Co. Inc., New York, Toronto, London, 1955.

[16] J. C. Decius, *J. Chem. Phys.*, **16**, 1025 (1948).

Es wurde die im gewöhnlichen Urey-Bradley-Kraftfeld[17] beschriebene Potentialfunktion mit den bekannten Symbolen K, H und F bzw. F' für Valenz-, Winkeldeformations-, bzw. Interaktionskraftkonstanten, angewandt.

Tabelle 2

Symmetriekoordinaten der Atomgruppe $>C-NH_2$ (Symmetrie C_s)

Species	Schwingungsart	Symmetriekoordinaten
A'	S_1 (NH_2 sym. Valenzschw.)	$(1/2)^{1/2}(\Delta r_1 + \Delta r_2)$
	S_2 (CN Valenzschw.)	ΔR
	S_3 (NH_2 Deformationsschw.)	$\Delta\alpha$
	S_4 (NH_2 Schaukelschw.)	$(1/2)^{1/2}(\Delta\beta_1 + \Delta\beta_2)$
A''	S_5(NH_2 (asym. Valenzschw.)	$(1/2)^{1/2}(\Delta r_1 - \Delta r_2)$
	S_6 (NH_2 Torsionsschw.)	$(1/2)^{1/2}(\Delta\beta_1 - \Delta\beta_2)$

Ein Kraftkonstantensatz wurde gesucht, welcher die beste Übereinstimmung zwischen gefundenen und berechneten Frequenzwerten für Anilin und ebenso auch für deuteriertes Anilin gibt. Eindeutige Kraftkonstanten können im Prinzip nur dann ausgerechnet werden, wenn isotope Moleküle herangezogen werden, da die Zahl der Frequenzen sich hierbei verdoppelt, während angenommen werden kann, daß die Potentialfunktion die gleiche bleibt.

Die Übertragbarkeit der Urey-Bradley Kraftkonstanten in Betracht nehmend, haben wir für die erste Näherung der Matrix F Kraftkonstantenwerte angewandt, welche für die Aminogruppe anderer Moleküle in der Literatur angegeben wurden.[10,12–14,18,19] Die Rechnungen wurden in mehreren Etappen durchgeführt, wobei die Elemente der Matrix F so lange verändert wurden, bis die erhaltenen Eigenwerte λ befriedigend waren. Die Eigenwerte der Säkulargleichung (1) wurden mit Hilfe der Rechenanlage DACCICC I des Recheninstituts aus Cluj berechnet. Da das Produkt GF im allgemeinen eine unsymmetrische Matrix ist, haben wir diese Produkt-Matrix jedesmal mit Anwendung der Methode von Wilson und Mitarb.[15] (Kapitel 9) bei der Hand symmetrisiert.

Die Kraftkonstanten sind in Tabelle 3, die berechneten Schwingungsfrequenzen in Tabelle 1, angegeben. Die besten Ergebnisse erhielten wir mit dem Winkelwert $\beta = 116°$.

Aufgrund dieser Ergebnisse ordnen wir der ND_2 Winkeldeformationsschwingung die Absorptionsbande bei 1078 cm^{-1} aus dem Infrarotspektrum des deuterierten Anilins zu. Der große Unterschied zwischen gefundenen und berechneten Frequenzwerten für die Nickschwingung

---

[17] T. Shimanouchi, *J. Chem. Phys.*, **17**, 245, 848 (1949).

[18] M. S. Barvinok und Yu. S. Barsahavsky, *Zhur. neorg. Khim.*, **6**, 851 (1961).

[19] J. E. Stewart, *J. Chem. Phys.*, **30**, 1259 (1959).

(A'') von NH_2 bzw. ND_2 kann seinen Grund in einer schlechten Zuordnung der Schaukelschwingung NH_2 haben, oder auch darin, daß eine zweite Torsionsschwingung nicht in Betracht genommen wurde. Evans[2] hat dieser Schwingung eine Bande bei 220 cm^{-1} im Anilinspektrum zugeordnet, Belorgeot und Mitarb.[5] fanden diese Schwingung bei 59 cm^{-1} und ordneten die Bande von 220 cm^{-1} einer Kernschwingung des Benzols zu.

Tabelle 3

UBFF Kraftkonstanten in mdyn/Å

$K(N-H) = 6{,}44$
$K(C-N) = 6{,}03$
$H(H-N-H) = 0{,}58$
$H(C-N-H) = 0{,}23$
$F(H\ldots H) = 0{,}05$
$F(C\ldots H) = 0{,}11$
$F'(H\ldots H) = -0{,}005$
$F'(C\ldots H) = -0{,}011$

EXPERIMENTELLES

Für die Aufnahme des Infrarotspektrums wurde Anilin *p.a.* (Merck) benutzt, das deuterierte Anilin wurde mit Hilfe eines Isotopenaustausches mit D_2O erhalten. Die Infrarotspektren des Anilins, deuterierten Anilins und deren Tetrachlorkohlenstofflösungen wurden im Bereich von 4000—400 cm^{-1}, mit Hilfe eines Infrarotspektrofotometers UR 10, der Firma Carl Zeiss-Jena, mit LiF-, NaCl- und KBr-Prismen aufgenommen.

Revue Roumaine de Chimie, **17**, *11*, 1851–1856 (1972)

NEW MOLYBDENUM (V) COMPLEXES WITH BIGNUAIDE DERIVATIVES

PETRU SPACU and LUCIA ANTONESCU

Faculty of Chemistry, Laboratories of Inorganic Chemistry, University of Bucharest, Spl. Independenţei 89, Bucharest, Romania

Received May 5, 1972

Biguanidonium salts of molybdenum (V) of the type $(\mathrm{R\ Big\ H})_2\ [\mathrm{Mo_2O_4Cl_4(H_2O)_2}]$, have been prepared (where R Big = N^1– phenyl-biguanide, N^1– *p*-chloro-phenyl-biguanide and N^1-*p*-chloro-phenyl-N^5-isopropyl-biguanide). All compounds are light brown, hardly soluble in common organic solvents and greatly stable in air. The oxidation state +5 of molybdenum has been ceriometrically determined. Some chemical, magnetic and spectral properties are also described. A dimer structure with oxygen bridges is evidenced in agreement with the low magnetic moments.

In recent years, many papers have been published concerning the coordination chemistry of some metals in a high oxidation state such as Fe (III), V (IV) and Mo (V). The interest for such compounds has been undoubtedly stimulated by the development of the theory of the chemical bond in complex combinations and as a tool used for the interpretation of their magnetic and spectral properties.

In order to enlarge the range of molybdenum (V) compounds under investigation, some research workers have been concerned with the synthesis and characterization of some complex combinations where the central molybdenum atom is bound to one or several chloride ions.[1–12]

---

[1] P. Spacu, M. Brezeanu, O. Constantinescu and I. Pascaru. *J. Less-Common Metals*, **19**, 1 (1969).

[2] P. C. H. Mitchell and R. J. P. Williams, *J. Chem. Soc.*, **1962**, 4570.

[3] P. C. H. Mitchell, *J. Inorg. Nuclear Chem.*, **25**, 963 (1963).

[4] P. Marzilii and D. Buckingham, *Austral. J. Chem.*, **19**, 2259 (1966).

[5] R. L. Dutta and B. Chatterjee, *J. Indian Chem. Soc.*, **44**, 685 (1967).

[6] R. L. Dutta and B. Chatterjee, *J. Indian Chem. Soc.*, **46**, 228 (1969).

[7] R. L. Dutta and B. Chatterjee, *J. Indian Chem. Soc.*, **44**, 759 (1967).

[8] R. L. Dutta and B. Chatterjee, *J. Indian Chem. Soc.*, **47**, 673 (1970).

[9] G. Spengler and J. Gäusheimer, *Angew. Chem.*, **69**, 523 (1957).

[10] D. A. Edwards, *J. Inorg. Nuclear Chem.*, **27**, 303 (1965).

[11] W. M. Carmichael and D. A. Edwards, *J. Inorg. Nuclear Chem.*, **32**, 1199 (1970).

[12] L. Larson and F. W. Moore, *Inorg. Chem.*, **5**, 801 (1966).

These last years, some quaternary ammonium salts of the following form were prepared :

$R_2[Mo_2O_4Cl_2(OH)_2(H_2O)_2]$ [13] where $R = NH_4^+$

$R_4[Mo_2O_4Cl_2(OH)_4]$ [13,14] $R = PyH^+$

$R_2[Mo_2O_4Cl_4(H_2O)_2]$ [13,14,15] $R = NH_4^+$, PyH^+ and Me_4N^+

The present paper carries on the study on some complexes of Mo (V) as oxy—chloro— compounds with certain substituted biguanide derivatives.

The formation of biguanidonium salts of the type $(R\ Big\ H)_2[Mo_2O_4Cl_4(H_2O)_2]$ is ascertained.

EXPERIMENTAL

Solutions of Mo (V) have been obtained by $Na_2MoO_4.2H_2O$ reduction with $N_2H_4.HCl$.

Substituted biguanide derivatives, as chlorhydrates R Big .HCl, were prepared according to literature.[16] (R Big = N^1-phenyl-biguanide $C_8H_{11}N_5$ — denoted PhBig, N^1-*p*-chloro-phenyl-biguanide $C_8H_{10}N_5Cl$ denoted Cl—PhBig and N^1-*p*-chloro-phenyl-N^5-isopropyl-biguanide or paludrine $C_{11}H_{16}N_5Cl$ denoted Pald).

Molybdenum has been gravimetrically determined with 8-hydroxyquinoline, subsequent to the decomposition of compounds with hydrogen peroxide in ammonia medium. Nitrogen has been determined by microcombustion using Pregl's method, while chlorine by precipitation with 5% $AgNO_3$ in the presence of HNO_3.

The oxidation state of molybdenum has been determined by titration in acid medium with cerium sulphate (IV) in the presence of ferroin as indicator.

Visible and UV electronic spectra have been recorded in DMF for solutions with concentrations of 10^{-2} M and 10^{-4} M, respectively, using a UNICAM SP 800 D spectrophotometer, and in solid state a VSU_1 spectrophotometer, to which a device for reflectance has been adapted.

IR spectra have been recorded with a UR_{10} Zeiss — Jena spectrophotometer using the technique of KBr pelletted powders.

The magnetic susceptibilities have been measured on solids samples using the Gouy method.

Thermodifferential and thermogravimetric analyses have been carried out for temperatures ranging from 0 to 600°.

PREPARATION

The biguanidonium salts of the ion μ-dioxo-bis [oxo-dichloro-aquomolybdate (V)] have been obtained starting from 1g $Na_2MoO_4.2H_2O$, to which 15 ml of conc. HCl and 1.5 g of $N_2H_4.HCl$ have been added. Heating was needed until obtaining a clear green solution, due to the formation of the $[MoOCl_5]^{2-}$ ion. The solution was evaporated until it reached half of its volume and the colour passed from green to red-brown.

---

[13] B. Jezowska-Trzebiatowska and M. Rudolf, *Roczniki Chem.*, **44**, 745 (1970).

[14] B. Jezowska-Trzebiatowska and M. Rudolf, *Bull. Acad. Polon. Sci. Ser. Sci. Chim.*, **17**, 419 (1969).

[15] R. M. Wing and K. P. Callahan, *Inorg. Chem.*, **8**, 871 (1969).

[16] H. King and J. M. Tonkin, *J. Chem. Soc.*, **1964**, 1063.

To the brown solution, the aqueous concentrated solution of biguanide chlorhydrate in a molar ratio 1 : 1 of molybdenum: ligand (1 g Pald. HCl, 0.9 g Cl–Ph Big.HCl and 0.8 g Ph Big. HCl, respectively) was added. The solution is kept cool for 2–3hrs and then hydrazine hydrate is added dropwise under stirring. At pH = 3–4 the bulk precipitation of the brown compounds (1–3) takes place. These compounds had been filtered off, washed with a very small amount of water and air dried. Analytical results are listed in table 1 and correspond to the general formula : (R BigH)$_2$ [$Mo_2O_4Cl_4(H_2O)_2$]. The same compounds have been obtained even if the ratio Mo : RBig was 1 : 2. The compounds are hardly soluble in alcohol, acetone, ether, etc. and dissolve easily enough in DMF and DMSO.

Attempts to obtain oxi-chloro-molybdates (V) by using substituted biguanide derivatives with alkyl radicals did not lead to positive results.

Table 1

Elemental analysis data

Compounds	Mo %		N %		Cl %	
	calcd.	found	calcd.	found	calcd.	found
PhBigH)$_2$[$Mo_2O_4Cl_4(H_2O)_2$]	24.33	24.12	17.73	17.93	17.98	18.02
(Cl–PhBigH)$_2$[$Mo_2O_4Cl_4$ ($H_2O)_2$]	22.33	22.46	16.28	16.42	16.52	16.45
(Pald H)$_2$[$Mo_2O_4Cl_4(H_2O)_2$]	20.36	20.47	14.84	14.96	15.05	15.26

IR spectra

The wave numbers of the main bands and the most probable assignment for the 400–4000 cm^{-1} range are given in table 2.

Table 2

Main bands and probable assignments in IR spectra (cm^{-1})

(Ph Big H)$_2$ [$Mo_2O_4Cl_4(H_2O)_2$]

3320	3170	1650	1535	1500	1100	955	730	635	550
(water, ligand)	water	NH_2	CN	NCN	NH_2	Mo=0	MoO_2Mo (ligand)	MoO_2Mo	

(Cl–Ph Big H)$_2$ [$Mo_2O_4Cl_4(H_2O)_2$]

3320	3160	1650	1535	1495	1100	955	730	620
(water, ligand)		NH_2	CN	NCN	NH_2	Mo = 0	MoO_2 Mo (ligand)	MoO_2Mo

(Pald H)$_2$ [$Mo_2O_4Cl_4(H_2O)_2$]

3320	3200	1645	1535	1500	1100	965	730	620
(water, ligand)		NH_2	CN	NCN	NH_2	Mo=0	MoO_2Mo (ligand)	MoO_2Mo

The strong absorption bands at 955–965 cm^{-1}, appearing in all synthetized compounds, are assigned to the molybdenum – terminal oxygen stretching vibration.[17,18]

The strong band at 730 cm^{-1} appears with an intensity greater than in biguanidonium chloride used as ligand and it is assigned to the vibration of the di-oxo-bridge 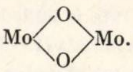 $\mathrm{Mo}\langle^{\mathrm{O}}_{\mathrm{O}}\rangle\mathrm{Mo}$.[15,19]

The bands at 620–630 cm^{-1} in compounds (1–3) and the band at 550 cm^{-1} in compound (1) are also characteristic of the stretching vibration modes associated to the di-oxo-bridge.[15,20]

The main vibrations characteristic of the IR spectra of biguanide derivatives, respectively vibrations of the CN, NCN and NH_2 groups,[21] are found again in biguanidonium oxi-chloromolybdates (V) which have been prepared.

However, the IR spectra of these compounds are very much like those of the complex biguanidonium oxalates previously prepared[22] (R Big H)$_2$ $[Mo_2O_4(C_2O_4)_2(H_2O)_2]$ excepting, of course, the bands characteristic of the vibrations of the oxalate ion. This is still another confirmation of the fact that we have here dimers compounds, too, whereas the bond between the two adjacent Mo (V) ions also occurs by two oxygen bridges.

The broad bands at frequencies greater than 3000 cm^{-1} are due to 0–H stretching vibrations, but these overlap the bands given by biguanides in this range, so that the assignment is not sure enough.

IR spectra below 400 cm^{-1} have not been given, although the Mo–N and Mo–Cl stretching modes generate bands in the 220–270 cm^{-1} range, since no assignment can be performed to biguanide derivatives also presenting bands around 250 cm^{-1}.

Visible and UV electronic spectra

Since spectra recorded on solutions (DMF and DMSO) for the 260–1000 nm range, are quite similar to those on the solid state (reflexion) we give in table 3, the absorption maxima for the electronic spectra in DMF.

Table 3

Electronic spectra of the compounds (in DMF)

	λ_{max} (nm)	Wave number (10^{-3} cm^{-1})
(Ph Big H)$_2$ $[Mo_2O_4Cl_4(H_2O)_2]$	680	14.7
	445	22.4
	402	24.8
	268	37.3
(Cl–Ph Big H)$_2$ $[Mo_2O_4Cl_4(H_2O)_2]$	675	14.8
	450	22.2
	400	25.0
	268	37.3
(Pald H)$_2$$[Mo_2O_4Cl_4(H_2O)_2]$	680	14.7
	454	22.0
	404	24.7
	270	37.0

Probable transitions will be later discussed.

---

[17] C. G. Barraclough, J. Lewis and R. S. Nyholm, *J. Chem. Soc.*, **1959**, 3552.
[18] F. A. Cotton and R. M. Wing, *Inorg. Chem.*, **4**, 867 (1965).
[19] P. C. H. Mitchell, *Quart. Rev.*, **20**, 103 (1966).
[20] W. P. Griffith, *J. Chem. Soc. (A).*, **1969**, 211.
[21] M. Tahimotto, *Nipon Kagaku Zasshi*, **85**, 168 (1964).
[22] L. Antonescu, *Analele Univ. București*, in press.

DISCUSSION

In a previous note,[22] we have established that starting from $Na_2MoO_4 \cdot 2H_2O$ in aqueous solution, reduced with $N_2H_4 \cdot HCl$ to Mo (V), in the presence of oxalate ions, the complex anion $[Mo_2O_4(C_2O_4)_2(H_2O)_2]^{2-}$, well known in literature, is forming, from which, by adding biguanide derivatives, biguanidonium salts of the following form are obtained : $(RBig\,H)_2[Mo_2O_4(C_2O_4)_2(H_2O)_2]$.

If the reduction reaction of sodium molybdate was carried out in strong hydrochloric solutions (> 8 M HCl), we should initially obtain an intense green solution with $[MoOCl_5]^{2-}$ and $[MoOCl_4(H_2O)]^-$ ions. Subsequent to HCl evolving on heating and due to hydrolysis, the composition of the ions in solution is changing with the conversion from green to red — brown.

According to literature data, [23-27] it should be assumed that in our reaction conditions, hydrolysis occurs as follows :

$$[MoOCl_5]^{2-} + H_2O \rightleftharpoons [MoOCl_4(H_2O)]^- + Cl^-$$

$$2[MoOCl_4(H_2O)]^- \rightleftharpoons [Mo_2O_3Cl_8]^{4-} + 2H^+ + H_2O$$

$$[Mo_2O_3Cl_8]^{4-} + H_2O \rightleftharpoons [Mo_2O_2(OH)_2Cl_6]^{2-} + 2Cl^-$$

$$[Mo_2O_2(OH)_2Cl_6]^{2-} + 2H_2O \rightleftharpoons [Mo_2O_2(OH)_4Cl_4]^{2-} + 2H^+ + 2Cl^-$$

$$[Mo_2O_2(OH)_4Cl_4]^{2-} \rightleftharpoons [Mo_2O_4Cl_4(H_2O)_2]^{2-}$$

To the red-brown solution, biguanide derivatives R Big. HCl have been added in concentrated aqueous solutions and after a few hours the pH was brought to 3—4. At this pH the equilibrium of the last above reaction is most likely shifted to the right, since the brown compounds (Table 1) show some characteristics which make us consider them as biguanidonium salts with the general formula $(R\ Big\ H)_2\ [Mo_2O_4Cl_4(H_2O)_2]$.

Thus, IR spectra have clearly stressed the existence of di-oxo-bridges, whereas the thermodifferential and thermogravimetric analyses point quantitatively to the water molecules in the coordination sphere, the thermograms being, for the first stage, quite similar to those of biguanidonium oxalates $(R\ Big\ H)_2\ [Mo_2O_4(C_2O_4)_2(H_2O)_2]$.

Also, IR spectra and thermodifferential and thermogravimetric analyses have removed the formulation as compounds of the form $Mo_2O_3Cl_4L_2$,[3,6], analogous to those with 2,2′-dipyridyl and 1,10—phenanthroline, the biguanide derivatives being able to act also as nitrogen—donor ligands.[28]

In all synthetized compounds, the oxidation state + 5 of molybdenum has been ceriometrically checked up. Evidence of the existence of pentavalent molybdenum and of the already mentioned hydrolysis me-

---

[23] B. Jezowska-Trzebiatowska and M. Rudolf, *Roczniki Chem*, **41**, 453 (1967).

[24] A. B. Blake, F. A. Cotton and J. S. Wood, *J. Amer. Chem. Soc.*, **86**, 3024 (1964).

[25] J. P. Simon and P. Souchay, *Bull. Soc. chim. France*, **1956**, 1402.

[26] G. P. Haight, *J. Inorg. Nuclear Chem.*, **24**, 663 (1962).

[27] R. Colton and G. G. Rose, *Austral. J. Chem.*, **21**, 883 (1968).

[28] C. Gheorghiu and L. Antonescu, *Analele Univ. București*, in press.

chanism has been brought by the obtainment, on treating with conc. HCl, of green solutions, from which green compounds containing the ions $[MoOCl_5]^{2-}$ or $[MoOCl_4(H_2O)]^-$ crystallized.

Magnetic moments at 290°K take values from 0.5 to 0.7 B.M. anomalously low for Mo (V) and which are explained by the coupling of electron spins of the two adjacent Mo (V) ions bound by oxygen bridges and due to direct metal – metal interactions.

If we dwell upon electronic spectra (Table 3) it becomes apparent that the absorption maxima can be well related to the formulation given to the synthetized compounds.

Thus, as shown by Haight[26] in a spectrophotometric study of $[MoOCl_5]^{2-}$ ion dimerization on hydrolysis, the shape of the curves is to a great extent maintained, as the absorption spectrum of Mo (V) occurs in HCl solution of concentrations form 12 M to 1 M. Subsequent to hydrolysis, with the appearance of new dimer species, a decrease in the intensity of the bands under study also takes place, the electronic transitions remaining, probably, the same. The standpoint adopted by us also for the interpretation of electronic absorption spectra of other Mo (V) complexes with biguanide derivatives [22,28] induces us, as in the case of oxi-chloro compounds, to proceed to the assignment of bands with respect to those given for the $[MoOCl_5]^{2-}$ and for its ammonium salt respectively.[29]

As in the case of the complex oxalates of Mo (V) the changes occurring on the hydrolysis of the $[MoOCl_5]^{2-}$ ion, are accompanied by the lowering of absorption in the visible range and the shift to somewhat higher frequencies, due to the higher splitting of t_{2g} orbitals. The splitting could be caused to the interaction of (dxz, dyz) orbitals of the metal with the π orbitals of the terminal oxygen, bridge – oxygen and chlorine. Hence, the broad band of low intensity at 14,700–14,800 cm^{-1} in the compounds $(R\ Big\ H)_2\ [Mo_2O_4Cl_4(H_2O)_2]$ is considered as corresponding to the maximum at about 14,000 cm^{-1} in $(NH_4)_2\ [MoOCl_5]$ and, like this, it is assigned to a $(dxy)^1 \rightarrow (dxz, dyz)^1$ transition. The band at 23,000 cm^{-1} in $(NH_4)_2$ $[MoOCl_5]$ corresponding to a $(dxy)^1 \rightarrow (dx^2-y^2)^1$ transition is found again at 22,000–22,400 cm^{-1} in the biguanidonium salts obtained by us.

All three compounds still present at 25,000 cm^{-1} a band of high intensity which, according to the values of the calculated extinction coefficients, is looked upon as a charge transfer transition similar to the band at 26,700 cm^{-1} in $(NH_4)_2[MoOCl_5]$.

At about 37,000 cm^{-1} another intense broad band appears, that could originate in the overlapping of charge transfer bands at 32,100 cm^{-1} and 35,700 cm^{-1} in $(NH_4)_2[MoOCl_5]$ with the internal transitions of R Big. HCl at about 39,000 cm^{-1}.

In conclusion, based on observations made in accordance with the synthesis method, on the properties of the compounds, on TG and DTA results, on magnetic and spectral measurements, the synthetized compounds have been formulated as biguanidonium salts $(R\ Big\ H)_2\ [Mo_2O_4Cl_4(H_2O)_2]$, where the two molybdenum (V) atoms are hexacoordinated and bound by a di-oxo-bridge.

---

[29] H. B. Gray and C. R. Hare, *Inorg. Chem.*, **1**, 363 (1962).

Revue Roumaine de Chimie, **17**, *11*, 1857 – 1866 (1972)

COORDINATION COMPOUNDS WITH COPPER-TIN BONDS

MARIA BREZEANU and IOANA JITARU

University of Bucharest, Laboratory of Inorganic Chemistry, Splaiul Independenţei 87,
Bucharest, Romania

Received June 7, 1972

In the system $CuCl_2-SnCl_2$-choline chloride, two series of compounds of the Cu (I) and Cu (II) as well as a series of oxygen adducts of Cu (I) compounds, corresponding to the general formulas : $(choline)_3\ [Cu(SnCl_3)_nCl_{4-n}](n = 1,\ 2,\ 3,\ 4)$; $(choline)_2[Cu(SnCl_3)_nCl_{4-n}]\ (n=1,\ 2)$ and $(eholine)_3\ [Cu(SnCl_3)\ _nCl_{4-n}(O_2)](n=1,\ 2,\ 3,\ 4)$ have been synthesized. The compounds have been characterized by elementary chemical analysis, IR, electronic and EPR spectra, magnetical measurements as well as determinations of molecular electrical conductivity and thermodifferential analysis. The data have been interpreted in terms of the assignment of the nature, stereochemistry and stability of the compounds under investigation.

The present paper is part of a more comprehensive study on the capacity of quaternary ammonium ions, derived from aminoalcohols, to stabilize a series of complex anions and on the other hand, to function as cationic ligands with respect to the ions of transitional metals.

By using some choline salts we succeeded in characterizing a series of cobalt and copper halogen and pseudohalogen complexes.[1,2]

In order to stabilize as choline salts a series of complex anions which should contain $SnCl_3^-$ as ligand, we attempted to study the system $CuCl_2-SnCl_2$-choline chloride.

The literature points to a relative small number of coordination compounds, especially of platinum metals, containing this ligand.[3]

In previous studies we succeeded in characterizing a series of Co(II) complex compounds containing the ligand $SnCl_3^-$, of the general formula $[Co(SnCl_3)_nCl_{4-n}]^{2-}$ $(n = 1,\ 2,\ 3,\ 4)$.[4,5]

---

[1] M. Brezeanu and I. Ailincăi, *Anal. Univ. Bucureşti*, **10**, 35 (1969).

[2] M. Brezeanu and I. Ailincăi, *Anal. Univ. Bucureşti*, in press.

[3] R. D. Cramer, R. V. Lindsey, C. T. Prewitt and U. G. Stolberg, *J. Amer. Chem. Soc.*, **87**, 658 (1965).

[4] M. Brezeanu and L. Patron, *Anal. Univ. Bucureşti*, in press.

[5] M. Brezeanu and L. Patron, *Anal. Univ. Bucureşti*, in press.

From copper, the literature points only to $Cu(SnCl_3)(PPh_3)_3$[6] isolated in solid state, as well as to a kinetic study of the system $CuCl_2-SnCl_2-HCl$, in view of elucidating the reduction mechanism of copper by $SnCl_2$[7,8].

In the system $CuCl_2-SnCl_2$ — choline chloride we succeeded in characterizing three series of complex compounds corresponding to the Cu(I), Cu(II), as well as series of oxygen adducts of the first compounds, with the general formulas:

$(choline)_3\ [Cu(SnCl_3)_n\,Cl_{4-n}]$ (n = 1, 2, 3, 4)

$(choline)_3\ [Cu(SnCl_3)_n\,Cl_{4-n}\,(O_2)]$ (n = 1, 2, 3, 4) and

$(choline)_2\ [Cu(SnCl_3)_n\,Cl_{4-n}]$ (n = 1, 2).

These compounds have been characterized by elementary chemical analysis, IR, electronic and EPR spectra, magnetical determinations, measurements of molecular electrical conductivity and thermodifferential analysis.

RESULTS AND DISCUSSIONS

Carrying out the synthesis in ~3 M HCl alcoholic solution, at $CuCl_2 : SnCl_2$ ratios, ranging from 1 :1 to 1 :10, we have succeeded in isolating four white Cu(I) compounds of the general formula $(choline)_3[Cu(SnCl_3)_nCl_{4-n}]$ (n = 1, 2, 3, 4). All these compounds hate the property to turn yellow on air exposure.

For each of the four complexes the change in colour is accompanied by an increase in weight. On heating to over 100° the reverse phenomenon occurs, i. e. the initial colour and weight restoring (the loss in weight corresponds to the recorded growth). The cycle white $\rightleftarrows$ yellow may be repeated several times.

On the basis of this reversibility, as well as of the fact that the increase or decrease in weight corresponds to one O_2 molecule per Cu atom we have formulated these compounds as oxygen adducts of the Cu(I) complexes. Additional evidences, supporting this formulation, will be brought in the following.

It has been also noticed that the easiness of the colour conversion depends on the composition of the complex, i. e. it decreases with the growth in the number of $SnCl_3^-$ groupings.

This could be explained, on the one hand, by the electronic and steric peculiarities of the $SnCl_3^-$ ligand and, on the other hand, by the nature of the $M-O_2$ interaction. Thus, the $SnCl_3^-$ ligand is a good π acceptor and in the $M-O_2$ bond, the π interaction has the predominant contribution. In this way, the behaviour of these compounds may be correlated to a modification in the charge density on the central metallic ion.

It could be thus predicted a decrease in the charge density on the Cu(I) ion with the increase in the number of $SnCl_3^-$ ligands. This might explain the lowering in the same direction of the tendency of these complexes to oxygenation and of the stability of the adducts (as shown by the thermal derivatograms).

---

[6] J. A. Dilts and M. P. Johnson, *Inorg. Chem.*, **5**, 2079 (1966).

[7] T. L. Nunes, *Inorg. Chem.*, **9**, 1325 (1970).

[8] T. L. Nunes and R. E. Powell, *Inorg. Chem.*, **9**, 1912 (1970).

If the white Cu(I) complex compounds are not separated at once, but only after a few days, some yellow compounds will be obtained. The nature of these compounds is different in terms of the $CuCl_2 : SnCl_2$ ratio. Thus, for 1 : 1 and 1 : 2 ratios the obtained complexes correspond to the general formula : $(choline)_2\ [Cu(SnCl_3)_nCl_{4-n}]$ (n=1, 2) i. e. are Cu (II) complexes.

For 1 : 3 and 1: 4, $CuCl_2 : SnCl_2$ ratio, oxygen adducts of some Cu(I) complexes are obtained, whose composition has not been defined so far.

This behaviour allows to conclude that for complexes with one or two $SnCl_3^-$ ligands, respectively, the Cu(I) to Cu(II) oxidation in solution is possible, while, in the given experimental conditions, oxidation is no longer possible for the complexes with three or four $SnCl_3^-$ ligands, respectively.

To get some information on the nature of these complexes, we have followed the behaviour of some of them in DMF, a solvent with relatively high coordination ability. Under these conditions, the $(choline)_2[Cu(SnCl_3)Cl_3]$ fixes two solvent molecules leading to $(choline)_2\ Cu(SnCl_3)Cl_3(DMF)_2$, while the oxygen adduct, $(choline)_3[Cu(SnCl_3)Cl_3(O_2)]$ remains unchanged and it is found as such, after the evaporation of the solvent excess. This behaviour could be interpreted as pointing to a coordinative unsaturation of the first complex (the presence of some vacant positions in the coordination sphere). The fact that the oxygen adduct does not bind DMF, points to the existence of a relatively stable configuration, that does not allow the penetration of other molecules.

The formulation of some of these compounds as oxygen adducts is supported by a preparative evidence.

With that end in view, two syntheses of the compound $(choline)_3\ [Cu(SnCl_3)_2Cl_2]$ have been simultaneously carried out, the former, in normal conditions, the latter, in CO_2 atmosphere.

Left in the air, the former compound rapidly changes in colour (about one hour) while the compound kept in CO_2 atmosphere remains unchanged for about twenty four hours.

The literature points to some Cu(I) complex compounds [9] with the property of binding reversibly the oxygen. To this, an important contribution reverts to the ligands field.

The specified behaviour of $(choline)_3\ [Cu(SnCl_3)_nCl_{4-n}]$ leads to the conclusion that the $SnCl_3^-$ ion belongs to the ligands which seem to be highly efficient in achieving the conditions of a reversible oxygen binding.

To obtain additional data on the nature, stereochemistry and stability of the compounds under study, the IR, electronic and EPR spectra, magnetical determinations, measurements of molecular electrical conductivity and thermal derivatograms have been carried out.

---

[9] E. Bayer and P. Schretzmann, *Structure and Bonding*, **2**, 181 (1967).

Electronic spectra. Based on the diagram of the energy levels of an ion with d^9 configuration, such as Cu(II), a relatively simple spectrum is to be expected. Nonetheless, most Cu(II) complex compounds show intricate and generally difficult assigning spectra. This could be assigned, on the one hand, to a Jahn-Teller distorsion and, on the other hand, to a spin-orbit coupling (the Cu(II) spin-orbit coupling constant is great enough (-830 cm^{-1}) not to be neglected).

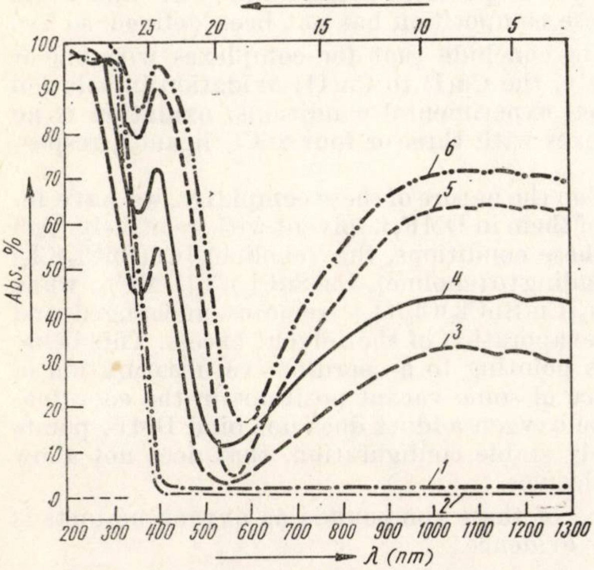

Fig. 1. — Electronic spectra of the compounds: *1*, $(choline)_3$ $[Cu(SnCl_3)_4]$, white; *2*, $(choline)_3[Cu(SnCl_3)_3Cl]$, white; *3*, $(choline)_3$ $[Cu(SnCl_3)_4(O_2)]$, yellow; *4*, $(choline)_3[Cu(SnCl_3)_3Cl(O_2)]$, yellow; *5*, $(choline)_3[Cu(SnCl_3)_2Cl_2(O_2)]$, yellow; *6*, $(choline)_3$ $[Cu(SnCl_3)Cl_3(O_2)]$, yellow.

The electronic spectra of the compounds $(choline)_3$ $[Cu(SnCl_3)_nCl_{4-n}]$ (Fig. 1) reveal that these do not absorb in the visible range, as expected for a d^{10} system. In the near UV range, a relatively intense band appears which may be assigned to a M→L charge transfer.

Fig. 2 represents the electronic visible and UV spectra of the two Cu(II) compounds and for comparison the $(enH)_2$ $[CuCl_4]$ spectrum. As noticed, the spectra of these complexes are very similar (both as to the position of the band and its shape) and may be fairly well interpreted in terms of a strongly distorted tetrahedral configuration. In the 800—1100 nm range, a broad band appears which is sufficiently structured as to distinguish the maxima corresponding to the three transitions theoretically provided for a D_{4h} pattern.

In the near UV range ($\lambda = 410$ nm) both complexes show a relatively intense band assigned to a L → M charge transfer.

The spectra of the four oxygen adducts are different from those of the analogous Cu(II) tetracoordinated complexes, both by the position and by the shape of the band. (Fig. 1).

---

[10] I. F. JONUG, R. D. GILLORD and G. WILLKINSON, *J. Chem., Soc. (A)*, **1964**, 5176.

These spectra can be fairly well interpreted based on a trigonal bipyramidal pentacoordinated structure, with two theoretically provided transitions.

However, for a complex compound with unequivalent ligands, as the studied compounds, a distorsion is predicted leading to an additional splitting.

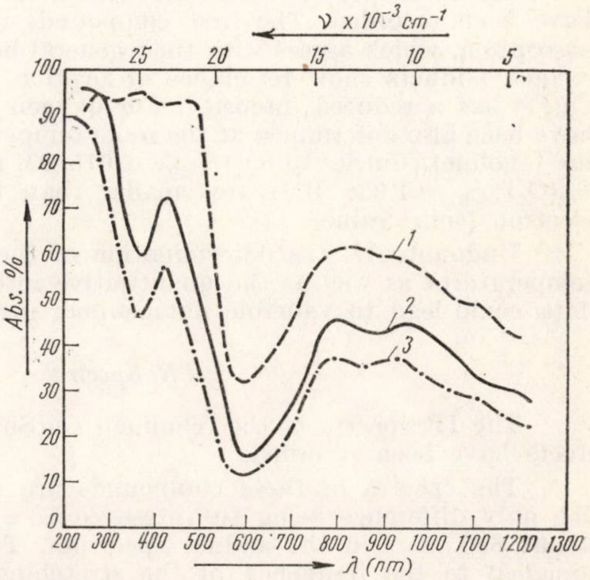

Fig. 2. — Electronic spectra of the compounds: *1*, $(enH)_2[CuCl_4]$; *2*, $(choline)_2[Cu(SnCl_3)Cl_3]$; *3*, $(choline)_2[Cu(SnCl_3)_2Cl_2]$.

Since the various possible transitions are very close, the result will be a broad absorption band, which may be also experimentally established ($\lambda = 1000-1300$ nm).

A band in the near UV range ($\lambda = 302$ nm) also appears in the spectra of these compounds. It is characteristic that this band appears at the same frequency as in the Cu(II) complex compounds. Generally, the position of the charge transfer band is first determined by the oxidation state of the central metallic ion and, to a small extent, by the configuration of the complexes. This allows to assume that in the oxygen absorption, the charge transfer from copper to oxygen, $Cu \rightarrow O_2$, is equivalent to one electron:

$$[Cu(d^{10})(SnCl_3)_nCl_{4-n}]^{3-} + O_2 \rightleftarrows [Cu(d^{10})(SnCl_3)_nCl_{4-n}(O_2)]^{3-} \rightleftarrows$$
$$\rightleftarrows [Cu(d^9)(SnCl_3)_n Cl_{4-n}(O_2^-)]^{3-}$$

In other words, in oxygen adducts, copper is likely to be found as bivalent ion. This assumption has to be undoubtedly checked also, by other determinations.

The natural compounds of oxyhemocyanine type [9] show a pentacoordinated structure. This is an additional evidence for the assigned structure on the basis of electronic spectra of the oxygen adducts under study.

EPR Spectra and Magnetical Measurements

The EPR spectra of the Cu(I) complexes and of their oxygen adducts have been recorded. The first compounds do not show any resonance absorption, which agrees with their general behaviour. The corresponding oxygen adducts show resonance absorption, but the signal assigned to Cu(II) has a reduced intensity. For oxygen adducts magnetic moments have been also determined at the room temperature. The obtained values for $(\text{choline})_3[\text{Cu}(\text{SnCl}_3)_4(\text{O}_2)]$ $\mu_{\text{eff}}=1.075$ BM and for $(\text{choline})_3\text{Cu}(\text{SnCl}_3)_2\text{Cl}_2(\text{O}_2)]$$\mu_{\text{eff}} = 1.058$ BM) are smaller than those provided for an odd electron (spin value).

Undoubtedly, the determination of the magnetic moments at low temperatures as well as the quantitative interpretation of EPR spectral data could lead to valuable data supporting this assumption.

IR Spectra

The IR spectra of the $(\text{choline})_3[\text{Cu}(\text{SnCl}_3)_4]$ and of its oxygen adducts have been recorded.

The spectra of these compounds are comparatively very similar, the only difference being the presence of a somewhat intense band at about 850 cm^{-1} in the adduct spectrum. This band could be possibly assigned to the frequency of the stretching mode, $\nu_{\text{Cu-O}_2}$.

We have also attempted to use these data in view of establishing the presence of the σ-bonded SnCl_3 ligand.

In the studied compounds, the absorption assigned to the two σ-bonded SnCl_3^- vibrations appear at frequencies comparable to those noticed for the compound $\text{Cu}(\text{SnCl}_3)(\text{PPh}_3)^6$ ($\nu_{\text{sym}}=310$ cm^{-1}, $\nu_{\text{asym}} = 285$ cm^{-1}).

Thermal Derivatograms

To obtain more precise data regarding the thermal stability of oxygen adducts, their thermal derivatograms have been recorded.

The comparative examination of thermal derivatograms of oxygen adducts and of Cu(I) and Cu(II) complexes allows to establish the presence of an additional endoeffect for the first compounds.

Figs 3 a and b represent the thermal derivatograms of the compound $(\text{choline})_3[\text{Cu}(\text{SnCl}_3)_4]$ and of its oxygen adduct. The additional endoeffect noticed on the DTA curve of the adduct occurs prior to the decomposition of the complex. It corresponds to the temperature of 120° and it is accompanied by a weight loss of $\sim 2.90\%$ noticed both on the TG and on the DTG curve.

In the derivatograms of the adducts $(\text{choline})_3[\text{Cu}(\text{SnCl}_3)\text{Cl}_3(\text{O}_2)]$ and $(\text{choline})_3[\text{Cu}(\text{SnCl}_3)_2\text{Cl}_2(\text{O}_2)]$ no distinct endoeffect appears. Most likely in this case the exoeffect corresponding to the decomposition of the complexes starting around 180° covers the endoeffect of oxygen removal. This behaviour confirms the statement that the stability of oxygen adducts increases from $(choline)_3[Cu(SnCl_3)_4(O_2)]$ to $(choline)_3[Cu(SnCl_3)Cl_3(O_2)]$.

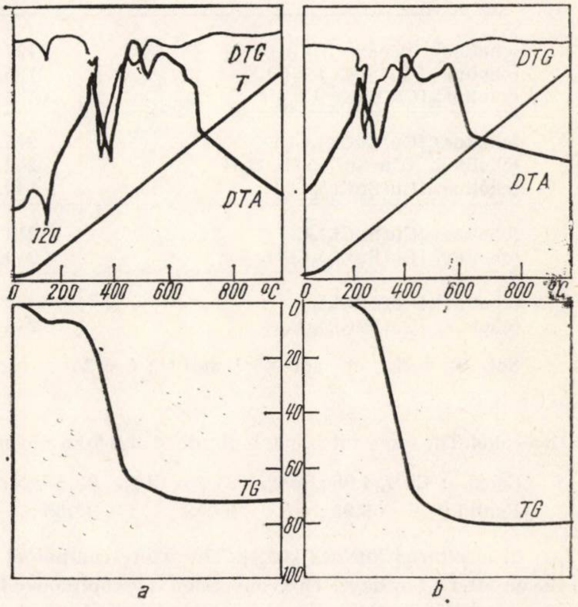

Fig. 3. – Derivatograms of the compounds:
(*a*) $(choline)_3[Cu(SnCl_3)_4(O_2)]$;
(*b*) $(choline)_3[Cu(SnCl_3)_4]$.

Molecular Conductivities

The formulation of the studied compounds has been confirmed by the determination of their molecular electrical conductivities.

Table 1 shows that the Cu(I) compounds and their oxygen adducts are 1 : 3 electrolytes, while the Cu(II) compounds, 1 : 2 electrolytes. The assignment of the electrolyte type occurred according to data for the complexes with $SnCl_3$ as ligand.[10-12]

EXPERIMENTAL

I. Synthesis of Compounds

1. $(choline)_3[Cu(SnCl_3)_4]$. To a solution obtained by solving 0.25 g $CuCl_2.2H_2O$ in 5 ml. alcohol, 0.7 ml ~ 3M HCl, 2.66 g solid $SnCl_2.2H_2O$ and 0.96 g solid choline chloride is added (molar ratio $Cu^{2+} : Sn^{2+}$: choline = 1 :8 :4). The formed white substance is filtered off and washed

---

[11] D. J. PHILLIPS and S. Y. ZYREE, *J. Amer. Chem. Soc.*, **83**, 1806 (1961).

[12] J. V. QUAGLIANO, J. FUJITA, G. FRANZ, D. J. PHILLIPS, J. A. WALMSLE and S. Y. TYREE, *J. Amer. Chem. Soc.*, **83**, 3370 (1961).

Table 1

Molecular conductivities of studied compounds

Compound	Solvent DMF	Nature of the electrolyte
$(\text{choline})_3\,[Cu(SnCl_3)Cl_3]$	197.2	1 :3
$(\text{choline})_3[Cu(SnCl_3)Cl_3(O_2)]$	195.8	1 :3
$(\text{choline})_2[Cu(SnCl_3)Cl_3]$	135.2	1 :2
$(\text{choline})_3[Cu(SnCl_3)_2Cl_2]$	215.3	1 :3
$(\text{choline})_3\,[Cu(SnCl_3)_2Cl_2(O_2)]$	202.8	1 :3
$(\text{choline})_2[Cu(SnCl_3)_2Cl_2]$	142.8	1 :2
$(\text{choline})_3[Cu(SnCl_3)_3Cl]$	213.6	1 :3
$(\text{choline})_3[Cu(SnCl_3)_3Cl(O_2)]$	210.2	1 :3
$(\text{choline})_3[Cu(SnCl_3)_4]$	222.6	1 :3
$(\text{choline})_3[Cu(SnCl_3)_4(O_2)]$	218.7	1 :3

Sol. 10^{-3} M, in $cm^2\ \Omega^{-1}\ mol^{-1}$; $t = 25°$

with alcohol. The same substance is obtained also for a molar ratio Cu^{2+} : Sn^{2+} : choline = 1 :10 :4.

Calcd. : Cu %, 4.98 ; Sn %, 37.20 ; Cl %, 33.33 ; N %, 3.29 ;
Found : 3.95 ; 37.13 ; 32.85 ; 3.58.

2. *$(choline)_3[Cu(SnCl_3)_4(O_2)]$*. The white compound $(\text{choline})_3\ [Cu(SnCl_3)_4]$ turns yellow in the air after a few days. This conversion is accompanied by a weight increase of 2.83 %. Heated to about 120° the yellow compound returns the initial white one, the whole change being accompanied by a weight loss of 2.54 %. The white compound turns again yellow in the air, with a weight increase of 2.75 %.

Calcd. : Cu %, 4.85 ; Sn %, 36.29 ; Cl %, 32.51 ; N %, 3.21 ; O_2 %, 2.56 ;
Found : 4.10 ; 36.80 ; 32.40 ; 3.30 ; 2.83.

3. *$(choline)_3[Cu(SnCl_3)_3Cl]$*. To a solution obtained by solving 0.25 g $CuCl_2 . 2\ H_2O$ in 5 ml alcohol, 0.7 ml ~ 3M HCl, 1,33 g solid $SnCl_2 . 2H_2O$ and 0.96 g solid choline chloride is added (molar ratio Cu^{2+} : Sn^{2+} : choline = 1 : 4 : 4). The formed white substance is filtered off and washed with alcohol.

Calcd. : Cu %, 5.84 ; Sn %, 32.76 ; Cl %, 32.62 ; N %, 3.86 ;
Found : 5.15 ; 32.43 ; 32.54 ; 4.10.

4. *$(choline)_3[Cu(SnCl_3)_3Cl(O_2)]$*. The white compound $(\text{choline})_3[Cu(SnCl_3)_3Cl]$ turns yellow by air exposure and gains about 3.15 % in weight.

Calcd. : Cu %, 5.68 ; Sn %, 31.83 ; Cl %, 31.69 ; N %, 3.75 ; O_2 %, 2.93 % ;
Found : 4.89 ; 31.94 ; 31.93 ; 4.05 ; 3.15.

5. *$(choline)_3[Cu(SnCl_3)_2Cl_2]$*. To a solution obtained by solving 0.25 g $CuCl_2 . 2H_2O$ in 5 ml alcohol, 0.7 ml ~ 3 M HCl 0. 99 g solid $SnCl_2 . 2H_2O$ and 0.96 g solid choline chloride is added (molar ratio Cu^{2+} : Sn^{2+} : choline = 1 : 3 : 4). The obtained white substance is filtered off and washed with alcohol.

Calcd. : Cu %, 7.09 ; Sn %, 26.46 ; Cl %, 31.61 ; N %, 4.67 ;
Found : 6.30 ; 26.05 ; 31.75 ; 4.90.

6. $(choline)_3[Cu(SnCl_3)_2Cl_2(O_2)]$. The white compound $(\mathrm{choline})_3$ $[\mathrm{Cu(SnCl_3)_2Cl_2}]$ turns yellow in the air, after a few hours. The conversion is accompanied by weight increase of 3.20 %.

Calcd. : Cu %, 6.83 ; Sn %, 25.55 ; Cl %, 30.52 ; N %, 4.52 ; O_2 %, 3.56 ;
Found : 6.00 ; 25.70 ; 30.75 ; 4.70 ; 3.20 ;

7. $(choline)_3[Cu(SnCl_3)Cl_3]$. To a solution obtained by solving 0.25 g $\mathrm{CuCl_2.2H_2O}$ in alcohol, 0.7 ml ~ 3 M HCl, 0.33 g solid $\mathrm{SnCl_2.2H_2O}$ and 0.96 choline chloride solved in a minimum amount of alcohol is added (molar ratio $\mathrm{Cu^{2+}}$: $\mathrm{Sn^{2+}}$: choline 1 : 1 : 4). The formed white compound is filtered off and washed with alcohol.

Calcd. : Cu %, 8.98 ; Sn %, 16.77 ; Cl %, 30.06 ; N %, 5.93 ;
Found : 8.00 ; 17.15 ; 30.25 ; 6.10.

8. $(choline)_3[Cu(SnCl_3)Cl_3(O_2)]$. By air exposure, the white compound $(\mathrm{choline})_3$ $[\mathrm{Cu(SnCl_3)Cl_3}]$ rapidly turns yellow ; conversion is accompanied by an increase in weight of 4.10 %.

Calcd. : Cu %, 8.59 ; Sn % , 16.03 ; Cl %, 28.76 ; N %, 5.68 ; O_2 %, 4.52 ;
Found : 7.65 ; 16.55 ; 29.10 ; 5.80 ; 4.10.

9. $(choline)_2[Cu(SnCl_3)Cl_3]$. To a solution obtained by solving 0.25 g $\mathrm{CuCl_2.2H_2O}$ in 5 ml alcohol, 1 ml ~ 5 M HCl, 0.33 g solid $\mathrm{SnCl_2.2H_2O}$ and 0.96 g solid choline chloride is added. The obtained white compound is kept in solution for a few days. The primarily colourless solution turns yellow-green in time, while the white substance turns yellow ; it is then filtered off and washed with alcohol.

Calcd. : Cu %, 10.53 ; Sn %, 19.67 ; Cl %, 35.25 ; N %, 4.64 ;
Found : 9.70 ; 19.85 ; 35.20 ; 4.80.

10. $(choline)_2[Cu(SnCl_3)_2Cl_2]$. Dissolve in 5 ml alcohol 0.25 g $\mathrm{CuCl_2.2H_2O}$, add 1.5 ml ~ 5M HCl, 0.66 g solid $\mathrm{SnCl_2 . 2H_2O}$ and 0.96 g solid choline chloride. The obtained white compound is kept in solution for a few days. The primarily colourless solution turns yellow – green in time, while the white substance turns yellow ; it is then filtered off and washed with alcohol.

Calcd. : Cu %, 8.01 ; Sn %, 29.94 ; Cl %, 35.77 ; N %, 3.53 ;
Found : 7.20 ; 30.35 ; 35.65 ; 3.73.

11. $(choline)_2Cu(SnCl_3)Cl_3(DMF)_2$. Dissolve some portion of $(\mathrm{choline})_2$ $[\mathrm{Cu(SnCl_3)Cl_3}]$ compound in a minimum amount of DMF. After evaporation of solution the obtained yellow-orange compound is washed with ether several times.

Calcd. : Cu %, 8.47 ; Sn %, 15.82 ; Cl %, 28.38 ; N %, 7.47 ;
Found : 7.40 ; 15.20 ; 28.50 ; 7.75.

II. *Electronic Spectra*

The electronic spectra were recorded at room temperature using a spectrophotometer $\mathrm{VSU_1}$, and as reference the magnesium oxide.

III. *Infrared Spectra*

The ir spectra were measured with a Perkin Elmer spectrophotometer using both Nujol mulls and potassium bromide technique.

IV. *Magnetical Measurements*

Magnetic susceptibility measurements were made by the Gouy method on finely powdered samples, at room temperature.

V. *Molecular Conductivities*

Conductivity measurements were made at 25°, in 10^{-3} M, N, N,dimethylformamide solutions, using a Conductometer II (Czechoslovakia) with a unit cell with $K = 0.52$.

VI. *Thermal Derivatograms*

Derivatograms were recorded in 20–1000° range, using a Paulik-Paulik-Erdey derivatograph (Hungary) with concomitant registering of T, TG, DTG, DTA curves. The curves recorded in air, heating velocity was 5°/min., sensibility of the heating system was 100 mg. and the standard was calcined Al_2O_3.

Revue Roumaine de Chimie, 17, *11*, 1867–1880 (1972)

CONTRIBUTIONS TO THE STUDY OF LANTHANIDES WITH BIGUANIDINE DERIVATIVES. IV[1]

COMPOUNDS OF HOLMIUM AND YTTERBIUM WITH PALUDRINE

ILEANA ALBESCU

Center of Physical Chemistry, str. Dumbrava Roşie 23, Bucharest, Romania

Received June 10, 1972

The present paper points to the synthesis and the physico-chemical study of some new Ho and Yb compounds with paludrine. In order to establish the constitution of the new compounds with this ligand in the series Nd-Yb, the results of these studies are discussed in the light of experimental data from previous works.

As a sequel of the study dealing with the obtainment of new lanthanides compounds with biguanidine derivatives, i.e. paludrine, the Ho and Yb syntheses, the electronic and the vibration spectra are briefly described; the study is supplemented with the thermal analysis and the differential thermal analysis of a representative compound from the series of the newly obtained combinations i. e. $HoCl_3.3$pald.

For the above elements, the same synthesis method as for elements of the previous notes [1-3] has been applied.

The following types of compounds have been obtained:

$HoCl_3$. 2pald	$2HoX_3$.5pald	HoX_3.3pald
	$2YbX_3$.5pald	X=Cl,Br
	X=Cl,Br	

Anhydrous halides as well as their adducts with THF, prepared according to literature [4-6] have been used for the syntheses.

The following adducts have been synthetized:

$HoCl_3$ 1.3/4 THF $YbCl_3$ 1.1/2 THF $YbBr_3$ 3 THF

---

[1] Part I: I. Albescu, *Rev. Roumaine Chim.*, in press.
[2] P. Spacu and I. Albescu, *Rev. Roumaine Chim.*, **16**, 1503 (1971).
[3] P. Spacu and I. Albescu, *Z. Chem.*, **10**, 470 (1970).
[4] J. H. Freeman and M. L. Smith, *J. Inorg. Nuclear Chem.*, **7**, 224 (1958).
[5] R. Schuster, *Dissertation*, Greifswald, 1965.
[6] R. Schuster, *Z. Chem.*, **1**, 1 (1967).

EXPERIMENTAL

1. $HoCl_3 . 2\,pald$

The synthesis method used for the similar compound with Nd and Gd [1,3] has been applied.

2. $2LnX_3 . 5\,pald$ Ln = Ho, Yb X = Cl, Br

A paludrine solution in THF is precipitated with an adduct (or anhydrous halide) solution, in an excess of ligand, the molar ratio being 1 : 4 adduct (salt) — ligand. Synthesis occurs without heating i. e. in conditions similar to those at 1.

3. $LnX_3 . 3\,pald$ Ln = Ho, Yb X = Cl, Br

The anhydrous halide or the adduct are solved by THF refluxing and with this solution we precipitate a ligand solution in THF discontinuing the refluxing. The ratio of reactants is 1 : 3 for chlorides and 1 : 6 for bromides.

The reaction between $LnX_3.nTHF$ (X = Cl, Br) and the ligand enables the formation of compounds by replacing the THF molecules by paludrine only in the case of chlorides and not for bromides; in the same types of compounds from the bromides of lanthanides these are obtained only from the anhydrous halide, $LnBr_3$, but not from the respective adducts. This bears wittness as to a more pronounced possible labilization of the M—O bond in the series of adducts chlorides and hence the possibility to replace THF molecules by paludrine more easily than in the series of bromide adducts where the M—O bond is stronger.

The new combinations are stable in air and show as crystalline powder, insoluble in water, alcohol, ether, acetone, THF.

Analytical results are listed in table 1.

Table 1

Experimental data

Compound	Ln % calc. found.	N % calc. found.	C % calc. found.	H % calc. found.	Crystal shape	Colour	Melt. p. 0°C
$HoCl_3 . 2pald$	21.18 22.01	17.99 18.15	33.92 34.19	4.14 5.01	orthorhombic acicular cryst.	white	238
$2HoCl_3 . 5pald$	18.22 17.94	19.33 19.02	36.47 36.62	4.45 4.01	orthorhombic cryst.	,,	238
$2YbCl_3 . 5pald$	18.93 17.93	19.20 18.28	36.14 34.24	4.41 4.69	,, ,,	,,	238
$HoCl_3 . 3pald$	15.85 15.58	20.57 20.33	38.85 37.94	4.69 4.85	orthorhombic cryst.	cream-coloured	240
$YbCl_3 . 3pald$	16.64 15.73	20.20 19.45	38.11 37.78	4.65 4.05	,,	white	240
$YbBr_3 . 3pald$	14.74 14.55	17.90 17.80	33.76 33.38	4.12 4.58	rectangular plates	,,	231
$2YbBr_3 . 5pald$	16.53 17.02	16.72 16.70	31.54 32.00	3.85 4.05	,,	,,	238

The electronic spectra, Figs. 1, 2 and the IR spectra, Table 2, as well as the thermal behaviour, Figs. 3, 4, have been studied in order to establish the structure of the new compounds.

GENERAL DISCUSSION

As for combinations of the same type presented in previous studies, the same remarks regarding the electronic spectra are valid also for the UV range; the band of the free ligand at 260 nm will appear while the

Table 2

IR spectra of chlorocomplexes of Ho with paludrine (cm^{-1})

$HoCl_3$ 1.3/4 THF	Paludrine	$HoCl_3 . 2pald$	$HoCl_3 . 3pald$
	3472		
	3390		
3333		3333	3333
	3279		
		3208.1	3249.7
		3141.5	
	3077		3041.5
	2959		
	2857		
2300	2326	2350	
		2125	
	2085		
	1887		
1643		1643	1647
			1629
	1613		
			1619
		1596	1596
1550–15	1550–15		1560
		1536	1536
		1500	1500
	1481		1464
		1420	1420
			1387
	1370	1377.1	1377.1
	1299		1294.7
		1268	
	1250		1250
	1183		1180.5
	1170	1173	
	1130–11		1131.9
		1094.4	1118
	1087		1094.4
			1078
	1011	1011	1011
	970.9	971	971
	941		
	900		
	865.8	844	844.4
	800	825	826.6
	744	722.3	722
	704–10		
	670–80		672

Table 3

Transition energies of the Nd^{3+} ion in its complexes with paludrine, compared

Ground state $Nd^{3+} = {}^4I_{9/2}$

Excited levels	$[Nd(H_2O)_6](NO_3)_3$		$NdCl_3$. 2 pald		δ	$2NdCl_3$. 5 pald		δ
	$\tilde{\nu}_{max}$ cm^{-1}	λ_{max} nm	$\tilde{\nu}_{max}$ cm^{-1}	λ_{max} nm		$\tilde{\nu}_{max}$ cm^{-1}	λ_{max} nm	
$^4F_{3/2}$	11695	855	11627	860	0.5	11627	860	0.5
$^2H_{9/2}$	12739	785	12658	790	0.64	12658	790	0.64
$^4F_{7/2}$	13699	730	13513	740	1.37	13550	738	1.1
$^4F_{9/2}$	14925	670	14705	680	1.49	14925	670	0
$^2H_{11/2}$	16129	620	16129	620	0	—	—	—
$^4G_{5/2}$	17391	575	17241	580	0.87	17391	575	0
$^4G_{7/2}$	19231	520	19231	520	0	19231	520	0
$^2G_{9/2}$	19802	505	—	—	—	—	—	—
$^4G_{9/2}$	21277	470	—	—	—	—	—	—
$^4G_{11/2}$	21882	457	—	—	—	—	—	—
$P_{1/2}$	23365	428						
	24038	416			$\delta_m = 0.97$			$\delta_m = 0.74$

bands characteristic of the free metallic ion will be covered in this region by the ligand band.

We shall remark the appearance of an inflexion at about 230 nm also noticed for all compounds studied in the series Nd—Yb, sometimes rather shifted to higher frequencies close to the sensitivity limit of the apparatus.

To establish the covalence degree in the new paludrine compounds, we have compared the electronic spectra according to the type of compound, to those of the respective aquaions determined in similar experimental conditions.

Since the character of the discussions is similar for all compounds, we present the results only for Nd, Dy and Ho, Tables 3, 4, 5.

The UV and visible spectra may be assigned both to the electronic transitions in the system of π electrons of the ligand and to the electronic transitions of the own f^n configuration of the central metallic ion.

The assignment of transitions occurred by comparing the spectrum of every compound to the spectra of the ligand and of the free metallic ion. The above tables show the most likely assignment of absorption bands; the

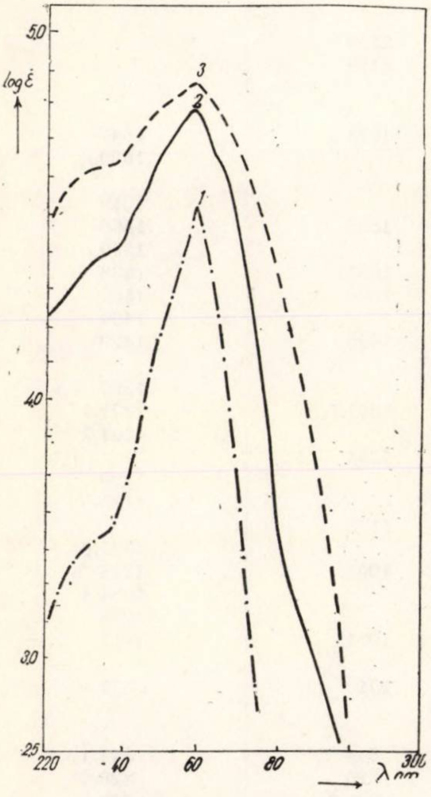

Fig. 1. — Absorption spectra in the UV range of the Ho compounds:
HoCl$_3$.2pald; 2, 2HoCl$_3$. 5pald; 3, HoCl$_3$. 3pald

with those occurring in the aquocomplex, $[Nd(H_2O)_6]^{3+}$, taken as standard

δ=covalence degree

NdCl$_3$.3 pald		δ	2 NdBr$_3$.5 pald		δ	Nd Br$_3$.3 pald		δ
$\tilde{\nu}_{max}$ cm^{-1}	λ_{max} nm		$\tilde{\nu}_{max}$ cm^{-1}	λ_{max} nm		$\tilde{\nu}_{max}$ cm^{-1}	λ_{max} nm	
11627	860	0.5	11627	860	0.5	11627	860	0.5
12658	790	0.64	12658	790	0.64	12658	790	0.64
13513	740	1.37	13513	740	1.37	13550	738	1.1
14925	670	0	14705	680	1.49	14925	670	0
—	—	—	16129	620	0	—	—	—
17241	580	0.87	17391	575	0	17241	580	0.87
19231	520	0	19231	520	0	19231	520	0
—	—	—	—	—	—	—	—	—
—	—	—	—	—	—	—	—	—
21505		1.75	21739	460	0.65	—	—	—
		δ_m=1.02			δ_m =0.85			δ=0.78

assignment of transitions for the metallic ion occurring according to literature data.[7-9]

As shown by the tables the frequencies of spin forbidden transitions for the f^n configuration of the central ion are shifted subsequent to coordination.

Table 4

Transition energies of the Dy^{3+} ion in its complexes with paludrine, compared with those occurring in the aquocomplex $[Dy_6 (H_2O)]^{3+}$, taken as standard

Ground state $Dy^{3+} = {}^6H_{15/2}$ δ=covalence degree

Excited levels	$[Dy(H_2O)_6]$ $(NO_3)_3$		DyCl$_3$.pald		δ	DyCl$_3$.3pald		δ
	$\tilde{\nu}_{max}$ cm^{-1}	λ max nm	$\tilde{\nu}$ max cm^{-1}	λ_{max} nm		$\tilde{\nu}_{max}$ cm^{-1}	λ_{max} nm	
${}^6F_{9/2}$	9090.9	1100	9259.2	1050	2.86	9259.2	1050	2.86
?	9523.8	1050						
${}^6H_{5/2}$	10309	970	—	—	—	—	—	—
${}^6F_{7/2}$	11173	895	11111	900	0.56	11111	900	0.56
${}^6F_{5/2}$	12539	797.5	12500	800	0.31	12500	800	0.31
${}^6F_{3/2}$	13333	750	13330	750	0	13513	740	(—)
	21097	474	21551	464	(—)	21551	464	(—)
	22222	450	22123	452	0.44	21978	455	1.11
${}^4G_9$	23474	426	23696	422	(—)	masked	—	—
	25125	398	25316	395		24937	401	0.75
			25641	390	(—)			
J=11/2	25839	387	25906	386	(—)	25445	393	1.55
	27472	364	27100	369	1.37	27322	366	0.55
			27472	364	0			
					δ_m = 1.10			δ_m = 1.07

---

[7] M. A. Eliashevitchi, *J. Chem. Phys.*, **39**, 2134 (1963).

[8] C. K. Jørgensen, *Acta Chem. Scand.*, **11**, 981 (1957).

[9] G. Gramberg, *Z. Phys.*, **159**, 125 (1960).

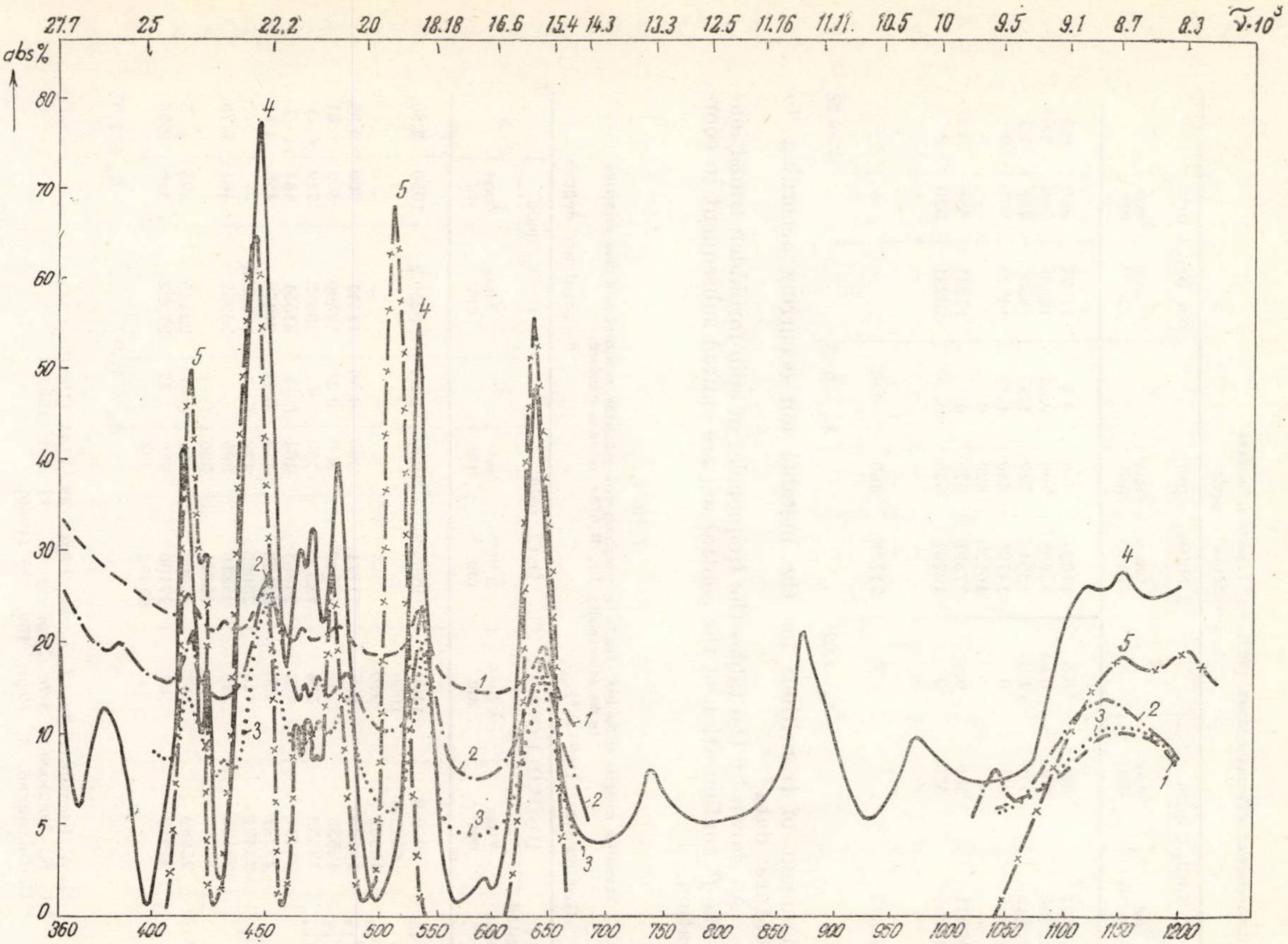

Fig. 2. — Absorption spectra in the visible range of the Ho compounds:
1, $HoCl_3$. 2pald; *2*, $2HoCl_3$. 5pald; *3*, $HoCl_3$. 3pald; *4*, $[Ho(H_2O)_8](NO_3)_3$; *5*, $HoCl_3$

Table 5

Transition energies of the Ho^{3+} ion in its complexes with paludrine. compared with those occurring in the aquocomplex, $[Ho(H_2O)_6]^{3+}$, taken as standard

Ground state $Ho = {}^5I_8$ δ = covalence degree

Excited levels	$[Ho(H_2O)_6](NO_3)_3$		$HoCl_3 . 2pald$		δ	$2HoCl_3 . 5pald$		δ	$HoCl_3 . 3pald$		δ
	$\tilde{\nu}_{max}$ cm^{-1}	λ_{max} nm	$\tilde{\nu}_{max}$ cm^{-1}	λ_{max} nm		$\tilde{\nu}_{max}$ cm^{-1}	λ_{max} nm		$\tilde{\nu}_{max}$ cm^{-1}	λ_{max} nm	
$^5I_6$	8695.6	1150	8658	1155	0.43	8771.9	1140	1.79	8620.6	1160	0.87
	8928.5	1120									
?	10309	970	masked inflexion								
$^5I_5$	11494	870	,,			masked inflexion					
$^5I_4$	13513	740	,,								
$^5F_5$	15686	637	15673	638	0.08	15625	640	0.39	15625	640	0.39
$^5F_4$	18691	535	18691	535	0	18690	535	0	18691	535	0
$^5F_3$	20790	481	20746	482	0.21	20661	484	0.62	20661	484	0
$^5F_2$	21231	471	—	—	—	21186	472	0.21	21186	472	0.21
$^3K_8$	21459	466	21459	466	0	21459	466	0	21367	468	0.43
F_1	22271	449	22222	450	0.22	22222	450	0.22	22222	450	1.41
?	23584	424	23255	430	1.41	—	—	—	23255	430	1.41
$^5G_5$	24096	415	24038	416	0.24	23923	418	0.72	24038	416	0.24
$^3K_7$	26315	380	—	—	—	25906	386	1.58	—	—	—
					$\delta_m = 0.43$			$\delta_m = 0.79$			$\delta_m = 0.55$

This phenomenon can hardly be interpreted in the case of lanthanides complexes; appreciations in this sense are but for a few cases and only for electronic configurations with few electrons (f^2, f^3).[10]

It is therefore preferred the appreciation as a whole of the nefelauxetic effect from the shift of absorption bands with respect to a reference complex $[Ln(H_2O)_6]^{3+}$.

The covalence degree δ has been calculated according to the relation :

$$\delta = \frac{\tilde{\nu}_{\mathrm{aquo}} - \tilde{\nu}_{\mathrm{complex}}}{\tilde{\nu}_{\mathrm{complex}}} \cdot 100$$

where $\tilde{\nu}_{\mathrm{aquo}}$ and $\tilde{\nu}_{\mathrm{complex}}$ are the frequencies of the same transition in the complex i. e. of the reference aquaion.

It should be noted that δ defines the covalence degree in relative value and as percent it can assume negative values if the chemical bonds of the complex have a smaller covalence degree than those in the aquaion and positive if it is greater than these.

It is obvious that not every transition will be affected in the chemical bond, but only those where the *f* orbitals, which might eventually enter chemical bonds with the ligands, are implied.

The shifts for the present complexes are small and therefore we have considered only those exceeding the recording errors of the apparatus.

Since the discussions bear a general character, we have calculated an δ_m (average) of these shifts for the same bands appearing in the complexes under investigation. The positive values of δ show that the chemical bonds in the complexes under study have a higher covalence degree than those of the chemical bonds in the respective aquaion.

For the IR spectra, Table 2, the discussions have a character similar to those in the case of previously studied elements (Sm, Nd, Eu, Dy, Gd).

In the whole series of compounds of the general form, $LnX_3 \cdot$ npald, there is a clear distinction between the spectrum of the free ligand and that of the compounds as regards some shifts, splittings or merging of bands, phenomena which might occur subsequent to the formation of the complex.

The literature[11] identifies in general the following characteristic frequencies : 740, 703, 831 cm^{-1} (p.Cl-phenyl), 704,815 cm^{-1} ($=N-N=$ in secondary amines, (iso-C_3H_7)NH), 1220, 1020 cm^{-1} ($=C=N-$), 1191, 1171, 1190 cm^{-1} (secondary C (iso-$C_3H_7)_2$NH).

The following can be noticed in the compounds under study, irrespective of the number of ligand molecules :

— The low frequencies at 941,900,800 cm^{-1} in the ligand (paludrine) disappear in the compounds [2], the band at 3390 cm^{-1}, pronounced in the ligand, disappears in all compounds.

— The frequencies at 744 and 704 cm^{-1} in the paludrine are converted into a single peak which appears at 720 cm^{-1} strongly marked in all compounds.[3]

---

[10] C. K. Jørgensen, R. Pappalardo and E. Rittershaus, *Z. Naturforsch*, **19a**, 424 (1964).

[11] C. Stewart, *J. Chem. Phys.*, **30**, 1259 (1959).

— An apparent conversion appears between 400—600 cm^{-1} namely the frequencies at 460,505 and 530 cm^{-1} in the ligand are converted into a single more pronounced band at 490 cm^{-1} in the compounds.[1]

Shifts, splittings and mergings of bands accompanied by intensity changes may be also noticed; thus, the band at 570 cm^{-1} shifts to 580 cm^{-1}, that at 970 to 980 cm^{-1}, 2990 to 2980 cm^{-1} and 3000, while 2970 to 2980 cm^{-1}.

The band at 870 cm^{-1} strong in the basis splits in the compounds and passes to 835 cm^{-1} (strong) and 850 cm^{-1} (weak). Similarly the band at 1380 cm^{-1} in the paludrine splits into two bands in the compounds, appearing at 1380 cm^{-1} and 1420 cm^{-1} as strong bands [1-3].

Another shift accompanied by splitting occurs at 1130 cm^{-1} (paludrine) passing into 1140 and 1120 cm^{-1}.[1]

No important distinction, except for the magnitude of shifts are remarked in the spectrum of the same type of compounds on passing from one element to the other in the series of lanthanides under study and no specific regularity has been therefore outlined.

In the series of compounds of the same element there are insignificant distinctions; the discussions regarding Eu and Dy compounds are valid also for Ho and Yb.

As regards the 600—220 cm^{-1} domain, because both the ligand and the halides of lanthanides (chloride or bromide) show characteristic bands in this spectral range (248—250 cm^{-1}) it is hardly appreciable whether we have to do with the M—X or the M—N bond.

The influence of the halogen for similar compounds points to a slight shift of the band at 490 cm^{-1} to higher frequencies in the case of Br-compounds.

Taking account of the foregoing, of the analysis of UV, IR and visible absorption spectra, we shall attempt to hypothetically appreciate the constitution of the new lanthanides combinations with paludrine.

Generally viewed, the spectral changes occur in 4 regions i.e. 500—600 cm^{-1}, 700—900 cm^{-1}, 1000—1400 cm^{-1} and 1900—2300 cm^{-1}.

In a work published in 1958,[12] where the structure of biguanidine is also discussed, the authors state that the conjugated system C=N—C=N present in pald HCl (b) and which may also appear in the basic paludrine due to possible limit forms(d) (see the scheme) absorbs at 230—233 nm.

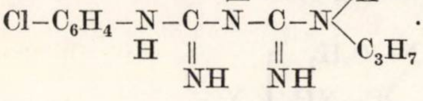

$Cl-C_6H_4-\underset{H}{N}-\underset{\underset{NH}{\|}}{C}-\overset{H}{N}-\underset{\underset{NH}{\|}}{C}-N\langle^{H}_{C_3H_7} \cdot HCl$;

(a)

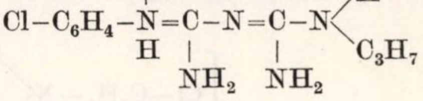

$Cl-C_6H_4-\underset{H}{\overset{+}{N}}=\underset{\underset{NH_2}{|}}{C}-N=\underset{\underset{NH_2}{|}}{C}-N\langle^{H}_{C_3H_7}$

(b)

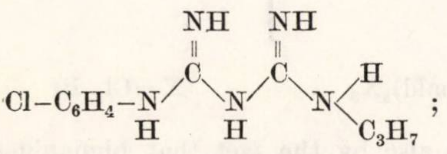

;

(c)

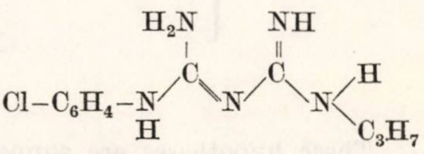

(d)

---

[12] R. C. Hirt and R. G. Schmidt, *Spectrochim. Acta*, **12**, 127 (1958).

This band is found again in the new compounds under study, sometimes as a slight inflexion, or strongly shifted to higher frequencies,close to the sensitivity limit of the apparatus.

Due to the passage from paludrine to LnX_3.pald compounds, in the IR spectrum the change appears in the same region $700-800$ cm^{-1}as for the passage from paludrine to paludrine HCl; whence the similitude in the spectra of these compounds and that of paldHCl but differing from that of paludrine.

This allows us to assume that the system of conjugated double bonds is the same in the compounds, too. To regard as possible the appearance of the system of conjugated double bonds, we assume mobility of the H atoms from the N_3 and N_5 nitrogen atoms, as well as the formation of the complex by the lanthanide bonding to N_1 and N_5.

Actually, the changes in the spectrum, subsequent to the formation of paludrine compounds, occur around 700, $700-900$, $500-600$ cm^{-1}. However, the affecting of the band at 700 $cm^{-1}$is characteristic of the NH grouping. On the other hand, the frequencies at $820-750$ cm^{-1}, assigned to propylamine, and 710 and 750 cm^{-1} assigned at p. Cl-phenyl, are also affected, i. e. the radicals neighbouring the nitrogen atoms to which the bonding of lanthanide is assumed on complex formation. This also implies a perturbation in the system of π electrons, neighbouring the N_1 nitrogen atom.

In conclusion, the changes appearing in the spectrum on the formation of paludrine complexes, occur at frequencies characteristic of p.Cl-phenyl and iso-propyl and could be interpreted in terms of the formation of a system of conjugated double bonds. This could be also due to the influence of the two substituents from the N_1 and N_5 nitrogen atoms.

Our remarks also agree with some literature data[13] which conclude that in the nonsubstituted biguanide base and monoprotonated ion, merely the bands at 1500 and 1460 cm^{-1} are affected, while those at 900 and 735 cm^{-1} keep unchanged; nonetheless, in the compounds obtained by us perturbations occur even at the 700 cm^{-1} band and not at that at 1500cm^{-1}.

For the close visible and IR domain, as regards the absorption spectrum of the compounds, there are obvious differences in the spectrum of the free ion and that in the compound.

We are therefore justified in assuming the lanthanides compounds with paludrine as complexes of the following form:

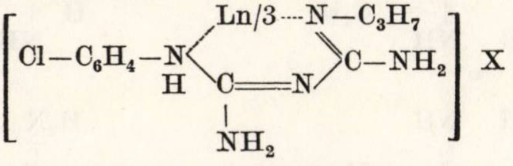

$Ln(pald)_3X_3$ $X=Cl, Br$

These hypotheses are supported also by the fact that biguanides substituted at the nitrogen N_3 atom cannot form any complexes; this proves the necessity of the mobility of the H atom from this nitrogen for the formation of the system of conjugated double bond.

---

[13] M. Takimoto, *J. Chem. Soc. Japan*, **85**, 168 (1964).

The above formulation also agrees with the data referring to paludrine structure by the X—ray method.[14] The spatial form would allow the participation in the chemical bond with the metal only of the N_1 and N_5 atoms and to a smaller extent of N_2 and N_4 atoms for which the frequencies would not be perturbed.

The newly obtained compounds have been also studied by thermal and the differential thermal analysis. Since the results can be generalized, a single representative compound $[Ho(pald)_3]Cl_3$ will be discussed. Figs. 3 and 4 represent the curves of thermal decomposition of paludrine and of the respective compound.

The comparison of thermograms, ligand-compound, shows differences which confirm the formation of the compound. Thus the phase transformation which corresponds to 115° on the DTA curve of the ligand is no longer found in the compound.

To the endothermal decomposition process of the ligand that starts at 190° corresponds a maximum decomposition rate at 250°. A second endothermal decomposition process follows with a maximum rate at 360° which does not exist in the free ligand.

Unlike paludrine, two exothermal processes appear with maximum at 460° and 540°, the former corresponding, most likely, to the loss of the last part of the ligand.

The organic base is weakly enough bound to the metal; the decomposition of the compound starts at about 190° and after the TG curve the loss of the ligand may be calculated, which corresponds to a decrease in weight of 74% as against 73.83% theoretically calculated; at 510°, $HoCl_3$ appears corresponding to a 25.8% amount, while between 500° and 600° the formation process of HoOCl takes place, as compared to 620°, the formation temperature of HoOCl indicated by literature,[15] which corresponds to an amount of 20.3%; Ho_2O_3 finally forms, which appears at 710° and which corresponds to 18% as against 18,6% theoretically calculated.

By comparing the DTA curve of the compound to that of pald. HCl we find also by this method a similarity as regards both the appearance of the two endothermal processes, in the compound and in paldHCl, and the location of the two maxima (250° and 360° for the compound, 240°, 340° for pald HCl).

The thermal study stresses the same aspects which may give some clues as to the structure of the new compounds.

Therefore, by this physico-chemical method, too, the assumptions on the structure of the new compounds are in the same sense as those resulting from spectral studies.

---

[14] C. J. Brown, *J. Chem. Soc.*, **1967**, 60.

[15] R. Mobeus and F. Matthess, *J. Less. Common. Metals*, **10**, 254 (1966).

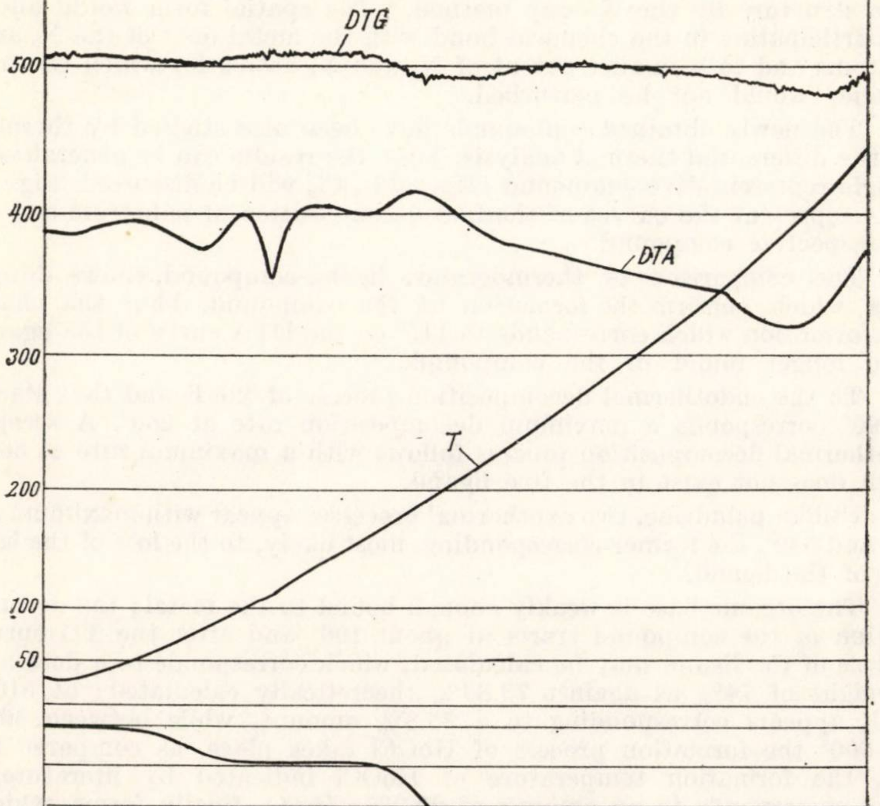

Fig. 3. — Thermal decomposition curves of the paludrine.

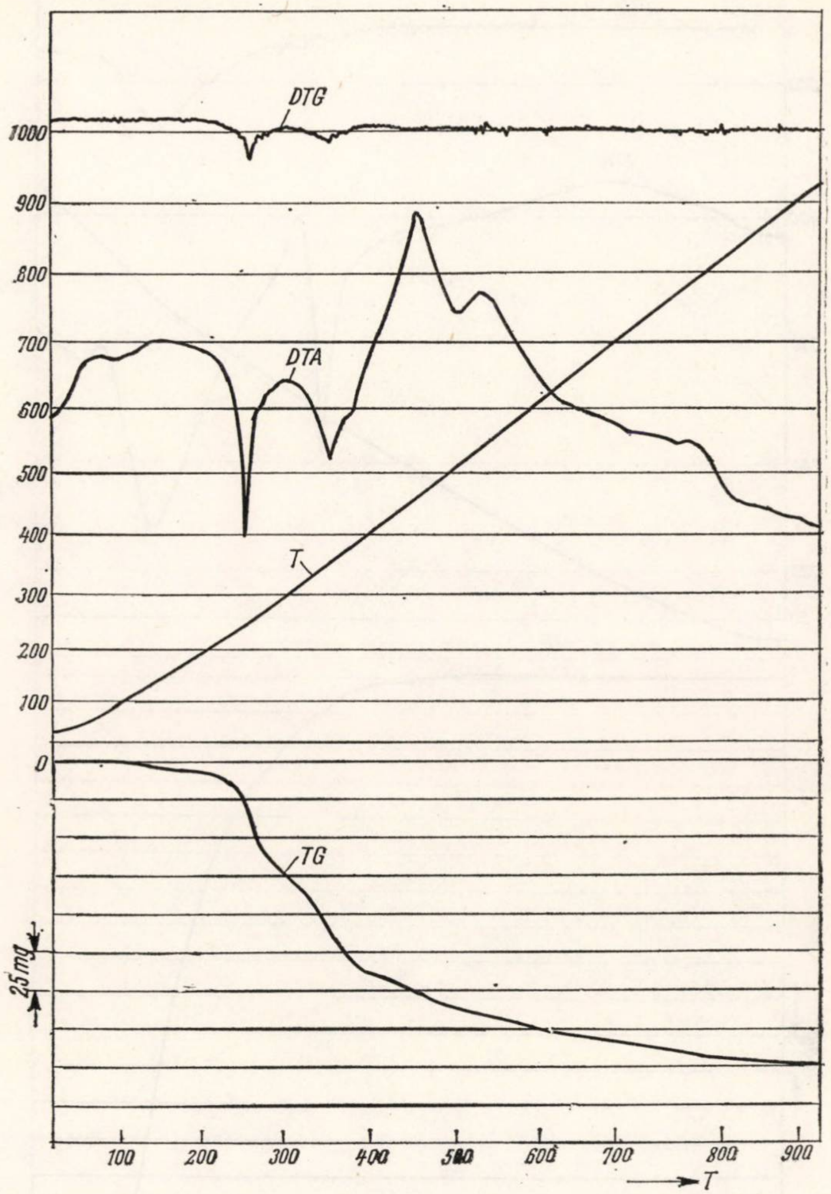

Fig. 4. – Thermal decomposition curves of $HoCl_3$.3pald.

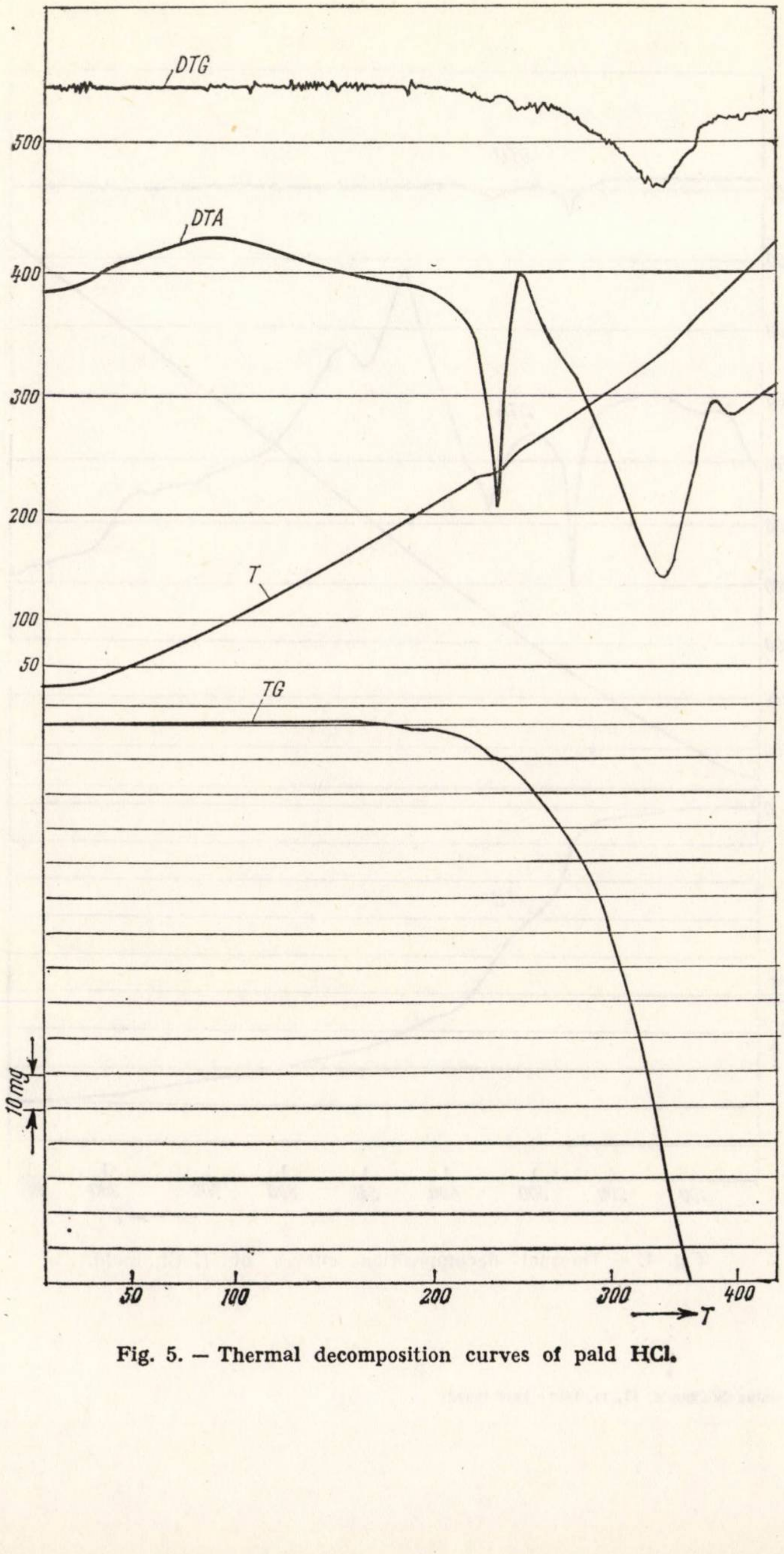

Fig. 5. – Thermal decomposition curves of pald HCl.

Revue Roumaine de Chimie, **17**, *11*, 1881 – 1887(1972)

NMR AND UV SPECTRAL STUDIES OF SOME 1-ARYL-SUBSTITUTED-3-METHYL-2-PHOSPHOLENE-OXIDES

F. KEREK and G. OSTROGOVICH

Laboratory of Organic Chemistry, The "Traian Vuia" Polytechnic Institute,
Timişoara, Romania

Received December 27, 1971

The NMR and UV spectra of seven various 1-aryl-3-methyl-2-phospholene-oxides have been recorded and are discussed. The value of about 25 cps of the coupling constants of the phosphorus atom with vinylic protons points to the $\Delta^{2,3}$ position of the phospholene ring double bond. The linear correlation of the bathochromic shift values ($\delta\lambda_{max}$) with "normal" substituent constants (σ°) showed a low conjugative interaction between the benzene ring and the phosphoryl group.

★

1. INTRODUCTION

In our previous paper,[1] the syntheses and catalytic activity (in converting isocyanates into carbodiimides and CO_2) of some 1-aryl-3-methyl-phospholene-oxides ($I_a \ldots I_g$)*) were reported. Recently we succeeded in splitting the racemic I_g by means of camphor-π-sulphonic acid.[2]

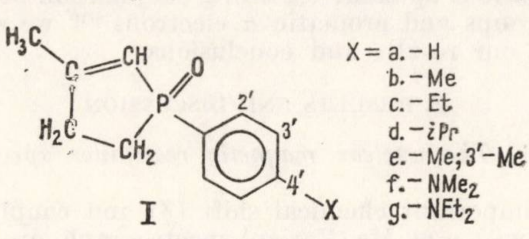

I

For compounds I_{b-g} two questions needed further investigations:
— the position $\Delta^{2,3}$ or $\Delta^{3,4}$ of the phospholene ring double bond;
— the conjugation between the benzene ring and the phosphoryl group.

*) Except I_f whose synthesis and catalytic study were performed latter.

[1] G. Ostrogovich, F. Kerek, A. Buzas and N. Doca, *Tetrahedron*, **25**, 1875 (1969).

[2] G. Ostrogovich and F. Kerek, *Angew. Chem.*, **83**, 496 (1971).

[3] W. B. McCormack, U. S. Pat., 2.663.737 (1953); *Chem. Abstr.*, **49**, 7601 (1953); Org. Syntheses (Edited by B. B. McCusick) Vol. 43., J. Wiley, New York, 1963.

[4] a. T. W. Campbell, J. J. Monagle and V. Foldi, *J. Amer. Chem. Soc.*, **84**, 3573 (1962); b. J. J. Monagle, T. W. Campbell and H. F. McShane, *ibid.*, **84**, 4288 (1962).

In the first item it was accepted [1,3-6] for many years (making a formal analogy with common Diels Alder reactions) that in phospholene rings resulted from phosphorus dihalides and a diene (eq. 1), the double bond must have the $\Delta^{3,4}$ position (II).

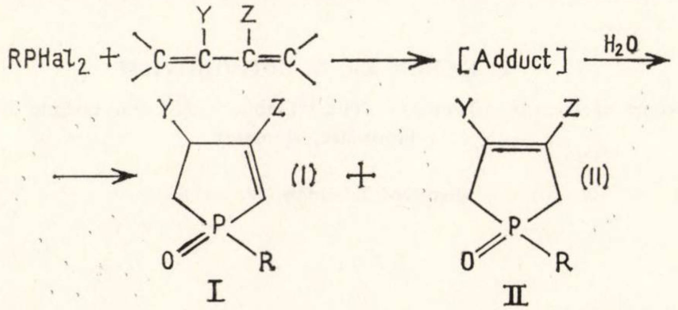

Later on NMR measurements [7,8] showed that both isomers may result. Moreover, Quin *et al.*[8] had demonstrated that reaction (1) has frequently a good stereospecifity. Thus, for example, by $R = -C_6H_5$; $Hal = -Cl$; $Y = H$; $Z = CH_3$ (eq. 1) it resulted only isomer *I*. The use of phosphorous dibromides ($Hal = Br$) with the same R = phenyl and $Z = CH_3$; $Y = H_1$ caused the formation of 3-phospholene derivatives (II). The same isomer resulted in $R = C_6H_5$; $Hal = Cl$ and $Y = Z = CH_3$, due perhaps to double bonds localization by methyl groups.

Thus, it has been conclusively shown that the position of the double bond in diene-phosphorus dihalide adducts is controlled by structural features of both participants in the reaction.[8d] Most probably in every case it results primarily the normal 3-phospholene adduct, which may suffer (or not) a rearrangement of the double bond.

From the various opinions regarding conjugation between a P atom, or phosphoryl groups and aromatic π electrons [9,10] we shall quote only those related to our results and conclusions.

2. RESULTS AND DISCUSSION

2.1. *The nuclear magnetic resonance spectra*

The most important chemical shift (δ) and coupling constant (J) values, obtained with a 60 Mc (Varian) spectrograph, are given in table 1.

---

[5] W. Ballon, U. S. Pat., 2.853.518; *Chem. Abstr.*, **53**, 5202 (1959).

[6] B. A. Arbuzov, A. O. Vizel, *Doklady Akad. Nauk. SSSR. Himia*, **158**, 1105 (1964).

[7] *a.* U. Hasserodt, K. Hunger and F. Korte, *Tetrahedron*, **19**, 1563 (1963); *b.* H. Weitkamp and F. Korte, *Z. analyt. Chem.*, **204**, 245 (1964).

[8] *a.* L. D. Quin, J. A. Peters, C. E. Griffin and M. Gordon, *Tetrahedron Letters*, **1964**, 3689; *b.* L. D. Quin, J. P. Gratz and R. Montgomery, *ibid.*, **1965**, 2187; *c.* L. D. Quin and T. Barket, *Chem. Comm.*, **1967**, 914; *d.* L. D. Quin, J. P. Gratz and T. P. Barket, *J. Org. Chem.*, **33**, 1034 (1968).

[9] R. F. Hudson, "Structure and Mechanism in Organo-Phosphorus Chemistry", Acad. Press, New York, 1965, p. 58–70.

[10] P. Mauret, J. P. Fayet, M. C. Labarre, *Compt. rend.*, **265**, 65 (1967).

Table 1

Chemical shift (δ) and coupling constant (J) values of some 1-aryl-substituted-2-phospholene oxides (I)

I	Phospholene ring					Benzene ring				Substituent X				
	H (2)		CH_3 (3)	CH_2 (4)	CH_2 (5)	H^A 2′; 6′ H^B 3′; 5′	AB	PA	PB	$-CH_3$		$-CH_2$		CH
X	$\delta^{i)}$	J_{P-H}	δ	$\delta^{ii)}$	$\delta^{ii)}$	$\delta^{ii)}$	J	J	J	δ	J	δ	J	δ/J
a	5.89	25.0	2.08	2.1–2.4	2.4–3.1	7.3–7.9	–	–	–	–	–	–	–	–
b	5.88	25.0	2.06	2.1–2.4	2.4–2.9	7.0–7.7	–	–	–	2.38	–	–	–	–
c	5.94	25.0	2.10	2.1–2.5	2.4–3.0	7.2–7.8	–	–	–	1.27	7.75	2.72	7.75	–
d	5.92	24.9	2.08	2.1–2.4	2.4–2.8	7.1–7.8	–	–	–	1.26	7.0	–	–	2.85 / 7.0
e	5.92	24.9	2.08	2.1–2.4	2.5–3.0	7.1–7.8	–	–	–	2.30 2.35	–	–	–	–
f	5.90	24.7	2.06	2.0–2.4	2.4–2.9	7.57 ; 6.77	9.0	12.0	2.6	3.00	–	–	–	–
g	5.88	24.8	2.03	2.0–2.40	2.4–2.9	7.48 ; 6.70	9.0	11.5	2.4	1.16	7.0	3.37	7.0	–

i) all δ values given in ppm ($\delta_{TMS}=0$) and J values in cps.

ii) complex multiplet in the given ppm range, except benzene ring protons by I_f and I_g

The δ and J values of the phospholene ring protons show their general constancy, which means a small electronic influence of the R-group on the phospholene ring. The most important coupling constant values are those between the vinyl proton and the phosphorus atom : J_{P-H}. According to [7,8], the values around 25 cps which have been obtained denoted undoubtedly a $\Delta^{2,3}$ position of the double bonds which means that our compounds have a 2-phospholenic structure. The coupling constant value of a P atom and a vinyl proton in β position is greater : $30 \div 33$ cps.[11] It must be noted that for compounds I_a and I_f a small 3-phospholene isomer content was detected through a vinyl H peak by 5.62 resp.5.56 ppm, splitted with $J = 31.5$ resp. 30.9 cps.

The methylene protons of the phospholene ring gave in every case a complex multiplet due to their supplementary splitting with phosphorus atom ($J = 1.5 \div 1.7$ cps). The same observation is true for the aromatic protons. However for compounds I_f and I_g it is easy to recognize the ABX feature of these protons, with $J_{AB} = 9.0$ cps as well as $J_{PA} = 12.0$ and 11.5 respectively $J_{PB} = 2.6$ and 2.4 cps with phosphorus atom (where A are the protons in 2′, 6′ position and B those in 3′, 5′). These data are in agreement with similar ones measured by aromatic phosphine oxides.[12,13]

2.2. *UV spectra*

Compounds $I_a - I_e$ have the characteristic benzene like UV spectra with a strong primary band below 200 mμ and the characteristic secondary band ^1L_b in the 254–281 mμ range.

Similar observations were reported for I_a[7] and some aromatic phosphine oxides.[14]

The spectra of I_f and I_g differed considerably from these, having a stronger secondary band at 274, respectively 277 mμ. The exact wavelength and extinction values measured in cyclohexane solution are given in table 2.

It is most probable that in compounds I_f and I_g the +M acting dialkylamino groups determined mainly the observed bathochromic shifts. However the (−) mesomeric action of the phosphorus "d" orbitals on the aromatic π electrons (in their excited state) may contribute to this shift, and determine especially the increase of the absorption. Thus the unsubstituted N,N-dimethylaniline absorbed at 251 mμ with $\varepsilon = 15{,}5000$,[15] while I_f has a stronger maximum with $\varepsilon = 23{,}380$ at 273.8 mμ. In order to estimate quantitatively this interaction similarly to Monagle *et al.*[16] the observed bathochromic shift values $\delta\lambda_{\max} = (\lambda^{x}_{\max} - \lambda^{a}_{\max})$

---

[11] H. Fingold, *Ann. New York Acad. Sci.*, **70**, 875 (1958).

[12] J. B. Hendrickson, M. L. Maddox, J. J. Sims and H. D. Kaesz, *Tetrahedron*, **20**, 449 (1964).

[13] C. E. Griffin, *Tetrahedron*, **20**, 2399 (1964).

[14] H. H. Jaffe, *J. Chem. Phys.*, **22**, 1430 (1954).

[15] J. Burgers, M. A. Hoefnagel, P. E. Verkade, H. Visser and B. M. Wepster, *Rec. Trav. chim.*, **77**, 491 (1958).

[16] J. J. Monagle, J. V. Mengenhauser and David Jones Jr., *J. Org. Chem.*, **32**, 2477 (1967).

Table 2

Absorption maxima and extinction values of some 1-aryl-3-methyl-phospholene oxides

I	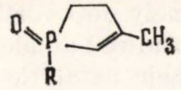	λ_{max} mμ	ε 1000 cm²/mol	log ε
a	H_5C_6-	254.0 259.2 265.0 271.6	333 473 650 562	2.52 2.67 2.81 2.75
b	$4'-Me-H_4C_6-$	(258) 263.5 270.0 777.2	310 440 512 377	2.49 2.64 2.71 2.58
c	$4'-Et-H_4C_6-$	(257.0) 263.5 269.7 276.8	300 410 480 383	2.48 2.61 2.68 2.58
d	$4'-iPrH_4C_6-$	(257.0) 263.5 269.0 275.5	315 458 490 352	2.50 2.66 2.69 2.55
e	$3',4'-Me_2H_3C_6-$	— 266.0 272.3 281.4	— 490 550 480	— 2.70 2.74 2.68
f	$4'-Me_2N-H_4C_6-$	273.8	23380	4.37
g	$4'Et_2N-H_4C_6-$	277.5	28900	4.45

were related, to some Hammett-like substituent constants. In our case it resulted a linearity only with "normal substituent constants" (σ°) given by Taft,[17] as it is shown in Fig. 1.

(Observation : Lacking a given σ° constant for $-NEt_2$ we used the value $\sigma^\circ = -0.44$ recommended for $-NMe_2$ by,[17] and for $-CHMe_2$ the corresponding Hammett standard σ value[18] which may differ insignificantly from the real σ° constants). It is known that these σ° values are designated for substituted aryl systems with broken conjugation between benzene ring and the reaction center Z ($R-C_6H_4-CH_2-Z$).[17] In the field of phosphor-organic compounds, these σ° values gave also good linear correlation for dissociation constants of substituted arylphosphonic acids.[19]

---

[17] R. W. Taft, *J. Phys. Chem.*, **64**, 1805 (1960).

[18] J. E. Leffler and E. Grunwald, "Rates and Equilibria of Organic Reactions", J. Wiley, New York, 1963, chap. 7.

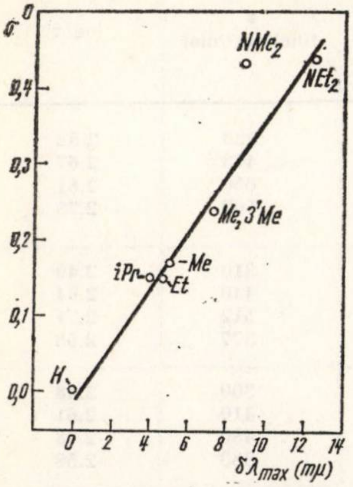

Fig. 1. — Correlation diagram of the normal substituent constants (σ°) with bathochromic shift($\delta\lambda_{max}$) values.

It is extremely noteworthy that our compounds I_{a-g} showed an identical linear correlation of their catalytic activity (in converting phenyl isocyanate into diphenyl carbodiimide) with these "normal" substituent constants.[1]

The same result of two completely different methods proved the validity of these σ° values in characterizing the electronic influences in the aryl-substituted phospholene rings.

By organophosphorous derivatives due to the various constitutional and steric factors the linear free energy relationships are more complicated than for the common, first-row element contained organic compounds.[20] In such circumstances it is more suitable to establish for each compound, classes and reaction types corresponding to the σ value set.

2.3. *Conclusion*

The 25 cps value of the coupling constant of the vinyl proton and the P atom demonstrated a 2-phospholene structure of compounds $I_a—I_g$. From the analysis of their UV spectra it results that no conjugation, in its classical sense, exists between the benzene ring and the phosphoryl group, but only a d-π^* interaction.

3. EXPERIMENTAL

Compounds $I_a - I_g$ (except I_f) were prepared according to eq. 1, as described in paper.[1] The *p*-dimethylaminophenyl-dichloro-phosphine was obtained by heating alone equimolar amounts of dimethylaniline and PCl_3 in a steam bath for 9 hours (yield 58 %).[21] The mixture of the purified dichloro-phosphine and the freshly distilled isoprene was allowed to stay 10 days in dried N_2 atmosphere in the presence of small amounts of Cu — stearate (as polymerization inhibitor).

---

[19] M. I. Kabachnik, T. A. Mastriakova and T. A. Melenteva, *Zhur. obsch. Khim.*, **32**, 267 (1962).

[20] M. I. Kabachnik, "Khimiya i prymenenie fosfororganicheskikh soedineni", Izd. Akad. Nauk S.S.S.R., Moscow, 1962, p. 24.

[21] M. P. Viont, *J. Rech. Centr. natl. recherche sci.*, No. 28, p. 15 (1954); *Chem. Abstr.*, 7077c (1956).

After the hydrolysis and drying (as described in[1] for I_g) it was distilled *in vacuo*, having b.p.$_{4-5\ \mathrm{mm}}$ = 230–235°. By combustion analysis it was found: C – 66.2%; H – 7.3%; P – 13.3%; N – 12.9% compared to those required: C – 66.38%; H – 7.65%; P – 13.18%; N – 5.97%.

UV spectra were recorded in dried and freshly distilled cyclohexane *p.a.* (Reanal) in 0.1–0.5 cm length cells with a UNICAM SP–800 spectrograph. For all spectra Holmium-glass etalons were used (with 279.4 and 287.5 mμ standard peaks).

The NMR spectra were recorded in deuterochloroform solutions with a Varian A 60 MC spectrograph using TMS as internal standard.

★

Acknowledgement. We are grateful to Mr. Filip Chiraleu from the Institute of Organic Chemistry, Bucharest, for his invaluable help in recording the NMR spectra.

Revue Roumaine de Chimie, 17, 11, 1889–1899 (1972)

NEUE ORGANISCHE PIGMENTE–ISATINDERIVATE. I EINFÜHRUNG IN DIE SYNTHESE UND EIGENSCHAFTEN DER VERBINDUNGEN

|J. REICHEL,| B. D. BADER* und R. VÎLCEANU

Aus dem Zentrum für chemische Forschungen, Timişoara, Bd. Mihai Viteazul, 24;
*Forschungslaboratorium der Industriellen Gruppe für Petrochemie Piteşti, Şos.
Giurgiului, 127

Eingegangen am 26. Januar 1972

Es wird eine Reihe von neuen Verbindungen des Isatins, ihre Herstellung sowie ihre Eigenschaften beschrieben. Die Verbindungen können als hochwertige organische Pigmente für Kunststoffe eingesetzt werden, wie es Färbeversuche auf Polyäthylen bewiesen.

EINLEITUNG

Die hervorragende Entwicklung der organischen Pigmente in den letzten Jahren wird von einer Reihe von zusammenfassenden Arbeiten[1–5] unterstrichen, welche den heutigen Stand der Forschung, so wie die Entwicklungsrichtlinien dieser Pigmente wiedergeben.

Die wichtigsten Anwendungsgebiete – Kunststoffe, Lacke und Druckfarben – fordern organische Pigmente von höchster Qualität und besonderen Echtheiten an. Die ersten organischen Pigmente mit hohen Echtheiten und universeller Anwendungsmöglichkeit stellten die Phthalocyanine dar, deren Nuancen aber auf blau und grün begrenzt blieben. Alle darauffolgenden Versuche verliefen mit dem Ziel, gleichwertige Pigmente mit den aus der Phthalocyaninepalette fehlenden Farben aufzufinden. Die in letzter Zeit aus der Dioxazin-, Quinacridon-, Perylene-Reihe erschienenen Pigmente sind eben das Ergebnis der Versuche, den hervorragenden Eigenschaften der Phthalocyanine gleichzukommen und um andere Farbtöne darzustellen.Einer der letzten Erfolge in diesem Gebiet ist die von Pugin und van der Crone [6,7] entwickelte

---

[1] H. Gärtner, *J. Oil Colour Chemists Assoc.*, **46**, 13 (1963).

[2] J. Lenoir, *Peintures, Pigments, Vernis*, **35**, 303 (1959); **38**, 384 (1962); **39**, 536, 615 (1963).

[3] G. M. Reiner, *Pitture e Vernici*, **42**, 51 (1966).

[4] N. V. Shah, *J. Soc. Dyers and Colourists*, **83**, 220 (1967).

[5] Z. B. Stefanska, *Chemik (Gliwice)*, **21**, 45 (1968).

[6] A. Pugin und J. van der Crone, *Official Dig. Federation Soc. Paint Technol.*, **37**, 1071 (1965); *Farbe Lack*, **72**, 206 (1966).

[7] Geigy A. G., Brit. Pat. 833548, 1960; Ger. Pat. 1113276, 1961. A. Pugin, U. S. Pat. 2973358, 1961; U. S. Pat. 3076815, 1963.

Synthese der Pigmente der Tetrachlorisoindolinon-Reihe, welche heute einen wichtigen Platz im Rahmen der hochwertigen Pigmente einnehmen.

In der vorliegenden Arbeit wird eine neue Reihe von Pigmenten beschrieben, deren sehr gute Eigenschaften sie für das Färben von Kunststoffen empfehlen. Den Ausgangspunkt zur Synthese dieser Pigmente stellte die Idee dar, strukturell ähnliche Verbindungen mit denen der Tetrachlorisoindolinon-Reihe herzustellen.

ALLGEMEINES

Die vom Isatin(I) abgeleiteten Pigmente gehören einer Reihe aus der Literatur bekannten Verbindungen an, und zwar die α- und β-Anile sowie Dianile des Isatins, mit aromatischen oder aliphatischen primären Monoaminen gebildet. [8,9] Anile des Isatins aus Diaminen, in welchen beide Aminogruppen durch je einen Isatinrest substituiert werden und eine Azomethin-Typ Bindung bilden, sind aus der Literatur nicht bekannt. Die einzige beschriebene Reaktion dieser Art ist die Kondensation des Isatins mit aromatischen *ortho*-Diaminen, welche zur Bildung eines Phenazin-Ringes führt. [9,10]

Zur Verwirklichung der Kondensation des Isatins mit Diaminen gingen wir von einem ähnlichen Prozeß in der Phthalimid-Reihe aus, in welchem die Kondensation von bei einer der Ketongruppen chloriertem Phthalimid mit Diaminen in einem chlorierten Lösungsmittel verläuft.[7]

Derivate des am Heterozyklus chlorierten Isatins sind aus der Literatur bekannt. So wird die Möglichkeit das Isatin entweder bei der Ketongruppe in Stellung 2, oder bei der in Stellung 3 zu chlorieren, wie folgend beschrieben:

— in Stellung 2 — wobei man 2-Chlorindolenin-3-on (Isatin-2-chlorid) (II) erhält, durch Chlorierung mit PCl_5 in Chlorbenzol bei 100—105° und Vervollständigung der Reaktion mit SO_2Cl_2 bei 60°.[9,11,12]

— in Stellung 3 — wobei man 3,3-Dichlorindolin-2-on oder 3,3-Dichloroxindol (3,3-Dichlorisatin) (III) erhält, durch Chlorierung mit PCl_5 in Benzol bei Zimmertemperatur.[13,14]

KONSTITUTION UND SYNTHESE DER VERBINDUNGEN

Die von den Autoren synthetisierten und als Pigmente vermuteten, vom Isatin abgeleiteten Verbindungen sind Kondensationsprodukte der primären Diamine, vor allem aromatische, mit zwei chlorierten Isatinmolekülen. Daraus ergeben sich zwei isomere Reihen von Verbindungen: eine von dem in Stellung 3 chlorierten Isatin wobei man Verbindun-

---

[8] R. Stolle, R. Bergdoll, M. Luther, A. Auerhahn, und W. Waker, *J. prakt. Chem.*, **128**, 1, (1930).

[9] W. C. Sumpter, *Chem. Rev.*, **34**, 393 (1944).

[10] N. P. Buu-Hoi und G. Saint-Ruf, *Bull. Soc. chim. France*, **1960**, 1920.

[11] E. Kambli, *Helv. Chim. Acta*, **24**, 93 (1941).

[12] A. von Bayer, *Ber. dtsch. chem. Ges.*, **12**, 456 (1879).

[13] A. Hantzsch, *Ber. dtsch. chem. Ges.*, **54B**, 1221, 1257 (1921).

[14] B. H. Nicolet und J. J. Pelc, *Ber. dtsch. chem. Ges.*, **51**, 2336 (1918).

gen der allgemeinen Formel (IV) erhält, die andere von dem in Stellung 2 chlorierten Isatin wobei Verbindungen der Formel (V) entstehen. Im Falle der vom Isatin-2-chlorid abgeleiteten Kombinationen (V) besteht die Möglichkeit einer Tautomerie (Va, Vb), auf welche wir in einer folgenden Arbeit zurückkommen werden.

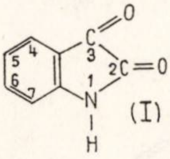

(I)

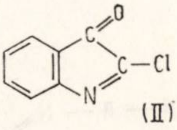

(II)

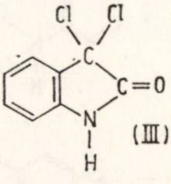

(III)

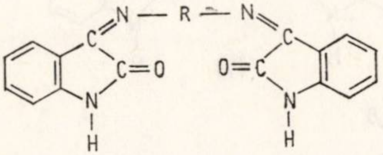

(IV)

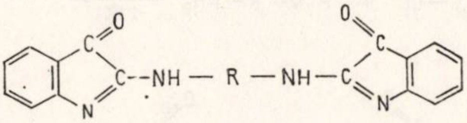

(Va)

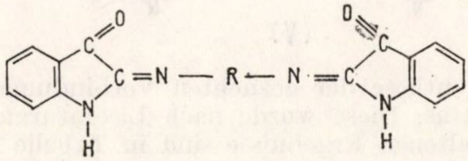

(Vb)

Die Pigmente besitzen die allgemeine Strukturformel (IV) und (V).

Wenn man R als einen in Stellung 1 und 4 substituierten Benzolring ansieht, so wird die Nomenklatur der Kondensationsprodukte wie folgend lauten:

Bis-(Indolin-2-on-3-yliden)-phenylendiamin-1,4 (IV),

Bis-(Indolenin-3-on-2-yl)-phenylendiamin-1,4 (Va).

Vom chemischen Standpunkt aus können die durch Kondensation des Isatins in Stellung 2 erhaltenen Derivate als substituierte Amidine angesehen werden, wo einer der Substituenten aus einer Acyl-Gruppe besteht, während die durch Kondensation in Stellung 3 erhaltenen Derivate als substituierte Azomethine bezeichnet werden können, in denen einer der Substituenten eine Acylamino-Gruppe darstellt.

Die Synthese der Pigmente aus der Isatin-Reihe geht von chlorierten Derivaten des Isatins aus, welche mit einem Diamin nach Schema 1 oder

2 kondensieren. Chlorierte Derivate des Isatins werden ihrer höheren Reaktionsfähigkeit wegen in Kondensationsreaktionen mit primären Aminen verwendet.

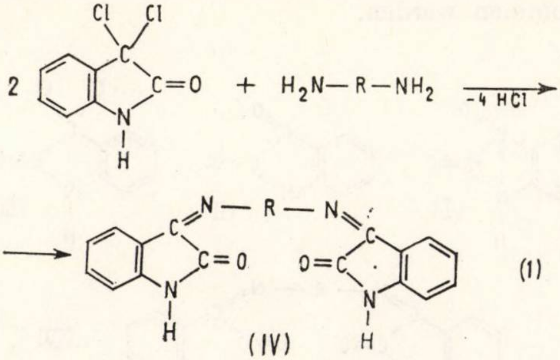

(IV) (1)

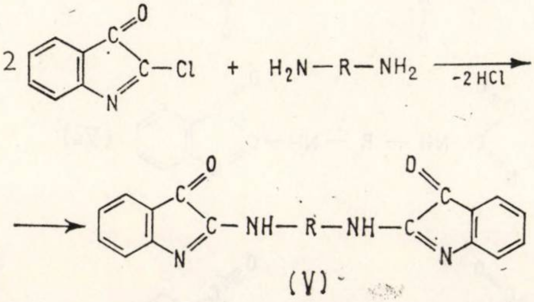

(V) (2)

Der erste Schritt der Synthese der gesuchten Verbindungen besteht in der Chlorierung des Isatins. Diese wurde nach Literaturangaben vorgenommen, einige der erhaltenen Ergebnisse sind in Tabelle 1 zusammengefaßt.

Tabelle 1

Reaktionsbedingungen und Ergebnisse der Isatinchlorierung

Molarverhältnis PCl_5/Isatin	Lösungsmittel	Temperatur °C	Zeit h	Reinigung mit	Ausbeute		Chlor-Analyse	
					Literatur	Experiment	% Berechnet	% Erhalten-
Isatin-2-chlorid								
1,41 :1	Chlorbenzol	124	3,0	Chlorbenzol+ Äthyläther	73	88	21,4	21,15
1,23 :1	,,	124	3,5	,,	73	91	21,4	21,12
1,17 :1	,,	124	3,0	,,	73	84,5	21,4	20,84
3,3-Dichlorisatin 1,41:1	Benzol	20–25	3,0	$C_2H_5OH+H_2O$ Rekrist. aus Äthyläther	80	85,5	35,05	34,84
1,23 :1	,,	20–25	5,0	,,	80	87,5	35,05	34,75

Den nächsten Schritt stellt die Kondensation der erhaltenen chlorierten Derivate des Isatins mit aromatischen Diaminen dar, welche in einem organischen Lösungsmittel wie 1,2-Dichlorbenzol oder 1,2,4-Trichlorbenzol, bei einer Temperatur von 160—180°, während 2—4 Stunden stattfindet. Die in der Kondensation verwendeten Diamine, sowie die erhaltenen Farbtöne sind in Tabelle 2 zusammengefaßt.

In Tabelle 3 werden die Reaktionsbedingungen, die in der Kondensation erzielten Ausbeuten, sowie die Elementaranalyse der Produkte gezeigt.

Tabelle 2

Die Abhängigkeit der Farbtöne der Kondensationsprodukte von der Natur de Diamine

Verwendete Diamine	Durch Kondensation erhaltene Farbtöne mit Chlorisatin des Typs :	
	II	III
1,4-Phenylendiamin	braun	gelb-braun
1,3-Phenylendiamin	braun-schwarz	kaffeebraun
2,4-Toluilendiamin	dunkelbraun	braun
Benzidin	rotbraun	hell rotbraun
o-Tolidin	dunkel rotbraun	kaffeebraun
o-Dianisidin	braun	braun
1,4-Diaminoanthrachinon	schwarzbraun	schwarzbraun
1,5-Diaminoanthrachinon	schwarzbraun	rotbraun

Nach Beendigung der Kondensation wird das Reaktionsgemisch warm filtriert und nachher mit heißem Lösungsmittel und Azeton auf dem Filter gewaschen. Man erhält ein fein verteiltes Produkt von brauner Farbe, dessen Farbton sich je nach der Art des verwendeten Diamins und des chlorierten Isatins ändert, so wie es aus Tabelle 2 ersichtlich ist.

Bemerkenswert ist die Tatsache, daß alle vom Isatin-2-chlorid abgeleiteten Verbindungen einen dünkleren Farbton, als diejenigen die vom 3,3-Dichlorisatin abstammen, aufweisen.

Wenn man die Ergebnisse aus Tabelle 1 und 3 verfolgt, wird ersichtlich, daß die Totalausbeute der beiden Synthesephasen 70—80% darstellt, wobei kleinere Werte nur in der Phenylendiamin-Reihe erzielt werden. Gleichzeitig kann man folgende optimale Reaktionszeiten festsetzen :

3,5 Stunden für Chlorierung in Stellung 2 des Isatins;
5,0 Stunden für Chlorierung in Stellung 3 des Isatins;
2,5 Stunden für die Kondensation der Chlorisatine mit Diaminen.

ANALYSE DER SYNTHESEPRODUKTE UND BESTIMMUNG EINIGER IHRER EIGENSCHAFTEN

Die Syntheseprodukte wurden neben der Elementaranalyse, deren Ergebnisse in Tabelle 3 wiedergegeben sind, einem Studium durch IR-Spektroskopie, Spektralanalyse im UV- und sichtbaren Bereich, sowie durch Differential-Thermoanalyse unterworfen.

Tabelle 3

Ergebnisse der durchgeführten Syntheseversuche

Symbol	Ausgangssubstanzen		Lösungsmittel	Kondensationszeit, *h*	Ausbeute %	Bruttoformel	Elementaranalyse					
	Chlorisatin	Diamin					% berechnet			% gefunden		
							C	H	N	C	H	N
Struktur nach Formel Va												
VI	Isatin-2-chlorid	1-4-Phenylendiamin	*o*–DCB	3,0	83	$C_{22}H_{14}N_4O_2$	72,1	3,82	15,3	71,8	3,84	14.9
VII	,,	1,3-Phenylendiamin	*o*–DCB	2,75	54	,,	72,1	3,82	15,3	71,6	3,80	15,0
VIII	,,	2,4-Toluilendiamin	*o*–DCB	2,5	82	$C_{23}H_{16}N_4O_2$	72,6	4,21	14,7	72,1	4,30	14,4
IX	,,	Benzidin	*o*–DCB	2,5	94	$C_{28}H_{18}N_4O_2$	75,9	4,07	12,6	75,5	4,10	12,4
X	,,	*o*-Tolidin	TCB	2,5	87	$C_{30}H_{22}N_4O_2$	76,6	4,68	11,9	76,1	4,59	12,0
X	,,	*o*-Tolidin	*o*–DCB	3,0	93	,,	76,6	4,68	11,9	76,4	4,60	11,8
XI	,,	*o*-Dianisidin	*o*–DCB	2,0	90	$C_{30}H_{22}N_4O_4$	71,7	4,38	11,1	71,5	4,42	11,0
XII	,,	1,4-Diaminoanthrachinon	*o*- DCB	3,0	63	$C_{30}H_{16}N_4O_4$	72,5	3,23	11,3	72,4	3,20	11,0
XIII	,,	1,5-Diaminoanthrachinon	*o*- DCB	2,0	86	,,	72,5	3,23	11,3	72,2	3,15	11,1
Struktur nach Formel IV												
XIV	3,3-Dichlorisatin	1,4-Phenylendiamin	TCB	3,0	90	$C_{22}H_{14}N_4O_2$	72,1	3,82	15,3	71,8	3,86	15,1
XV	,,	Benzidin	TCB	3,0	92	$C_{28}H_{18}H_4O_2$	75,9	4,07	12,6	75,7	4,00	12,6
XVI	,,	*o*-Tolidin	*o*–DCB	3,0	95	$C_{30}H_{22}N_4O_2$	76,6	4,68	11,9	76,5	4,67	11,4
XVI	,,	*o*-Tolidin	TCB	3,0	97	,,	76,6	4,68	11,9	76,3	4,66	11,6
XVII	,,	1,5-Diaminoanthrachinon	TCB	2,5	86	$C_{30}H_{16}N_4O_4$	72,5	3,23	11,3	72,3	3,20	11,2

Bemerkung: *o*–DBC = 1,2–Dichlorbenzol
TCB = 1,2,4–Trichlorbenzol

Durch IR-Spektroskopie wurden die wichtigsten charakteristischen Absorptionsbänder, und zwar ν_{NH}, $\nu_{C=N}$, $\nu_{C=O}$, der hergestellten Verbindungen verfolgt. In Tabelle 4 werden einige erhaltene Werte zusammengefaßt.

Die für die charakteristischen Absorptionsbänder bestimmten Werte bestätigen die vermutete Struktur der Verbindungen. Eine Diskussion der Absorptionsbänder in bezug auf die Struktur der Verbindungen wird in einer der folgenden Arbeit geführt werden.

Tabelle 4

Die wichtigsten Absorptionsbänder des IR-Spektrums

Untersuchte Verbindungen	Absorptionsmaxima, cm^{-1}		
	ν_{NH}	$\nu_{C=O}$	$\nu_{C=N}$
VI	3400 2850	1715	1610
IX	3400 2850	1710	1605
XIII	3400 sehr breit	1720	1600
XIV	3400 3200	1730	1710
XV	3400 3200	1710	1710

Da bei dem Studium der Verbindungen durch Spektralanalyse im UV- sichtbaren Bereich auf einige Schwierigkeiten gestoßen wurde, die hauptsächlich auf die unzulängliche Löslichkeit in Dimethylformamid in welchem die Spektren ausgeführt wurden, zurückzuführen sind, haben wir unsere Bestimmungen auf die Diphenyl- und Anthrachinon-Reihe beschränkt. In Tabelle 5 werden die Absorptionsmaxima für die untersuchten Verbindungen wiedergegeben.

Alle Verbindungen aus Tabelle 5 zeigen im UV-Bereich Absorptionsbänder zwischen 282—306 mμ auf, welche dem Band bei 295 mμ des Absorptionsspektrums des Isatins sehr nahe liegen.[9,15]

Was die Lichtabsorption bei größeren Wellenlängen anbelangt, kann man bemerken, daß nur die Verbindungen X und XI aus Tabelle 5 ein dem Isatin bei 416 mμ nahestehendes Absorptionsband aufweisen. Gleichzeitig ist ersichtlich, daß die Verbindungen IX—XIII ein Absorptionsmaximum zwischen 440 und 520 mμ besitzen. Es muß ebenfalls unterstrichen werden, daß durch Einführung eines Auxochroms in den Diphenylrest, eine Verschiebung nach höheren Wellenlängen des langwelligsten Absorptionsmaximums zu verzeichnen ist. Diese Verschiebung scheint kaum von der Natur des Auxochroms beeinflußt zu werden.

---

[15] A. MANGANI und R. PASSERINI, *Gazz. chim. Ital.*, **85**, 840 (1955).

Bei den Verbindungen XV und XVI aus Tabelle 5 ist neben einer Absorption bei 300 mμ, eine intensive Lichtabsorption bei 346 mμ und eine weniger intensive zwischen 446 und 460 mμ zu verzeichnen. Auch in diesem Falle ist eine leichte Verschiebung des langwelligsten Maximums nach höheren Wellenlängen bei Verbindung XVI bemerkbar, welche höchstwahrscheinlich auch durch die Einführung eines Auxochroms in den Diphenylrest zu erklären ist.

Tabelle 5

Lichtabsorptionsmaxima im UV- und sichtbaren Bereich

Untersuchte Verbindungen	λ_{max}, μ	log ε_{max}
IX	297	4,483
	440	3,880
X	295	4,289
	400	3,508
	490	3,271
XI	282	4,452
	393	4,036
	490	3,742
XII	300	4,396
	470	3,861
	550	3,816
XIII	320	4,235
	482	3,850
XV	306	3,809
	345	3,588
	446	2,951
XVI	300	4,062
	346	3,774
	460	3,235

In Abb. 1 werden die Spektren der Verbindungen IX und X aus Tabelle 5 aufgeführt und zum Vergleich wird das Spektrum des Isatins danebengestellt.

Zur Bestimmung der Anwendungsmöglichkeit der Syntheseprodukte als Pigmente für Kunststoffe, wurden diese zwecks Ermittlung ihrer Thermostabilität, Löslichkeit in organischen Lösungsmitteln und Beständigkeit gegen Chemikalien, geprüft.

Das Verhalten bei hohen Temperaturen wurde auf einer thermogravimetrischen Waage untersucht. Die Ergebnisse der Thermoanalyse im Hinblick auf die Thermostabilität werden durch die in Tabelle 6 zusammengefaßten Werte veranschaulicht.

Aus den in Tabelle 6 enthaltenen Werten wird ersichtlich, daß alle untersuchten Verbindungen bis zu Temperaturen von 280—300° thermisch stabil sind. Bei höheren Temperaturen beginnt eine leichte Zersetzung, die bei 440—470° ein Maximum erreicht, wobei aber die Verbindungen nicht schmelzen. Das Ausbleiben eines Schmelzpunktes so wie die hohe Zersetzungstemperatur weisen auf wahrscheinlich durch intermolekulare Wasserstoffbindungen stark assoziierte Verbindungen hin. Dieses Thema wird in einer künftigen Arbeit behandelt werden.

Tabelle 6

Ergebnisse der Thermoanalyse

Untersuchte Verbindungen	TG-Kurve % Verlust bei		DTG Maximum °C	exotherme DTA-Spitze °C
	30–X°C	X–750°C		
IX	X=300°C			
	3,0	90,0	482	470
X	X=318°C			
	2,5	85,0	442	440
XI	X=281°C			
	2,0	88,0	482	465
XIV	X=286°C			
	4,0	85,0	470	450
XVI	X=282°C			
	2.5	90,0	470	445

Zwecks Bestimmung der Löslichkeit der Syntheseprodukte wurden Versuche in einer Reihe von organischen Lösungsmitteln unternommen, wobei eine vollkommene Unlöslichkeit der Verbindungen in folgenden Lösungsmitteln beobachtet wurde: Azeton, Äthyläther, Petroläther, Methanol, Äthanol, Isopropanol, n-Butylazetat, Azetessigsäureäthylester, Hexan, Heptan, Benzol, Toluol, Xylol, Methylenchlorid, Chloroform, Chlorbenzol, *o*-Dichlorbenzol, Trichlorbenzol, Nitrobenzol, Azetonitril, Dibutylphthalat, Dioxan und 1-Chlornaphthalin. Eine geringe Löslichkeit von ungefähr 1% besitzen die Verbindungen in Anilin, Pyridin und Dimethylformamid. Bessere Löslichkeit zwischen 2–5% wurde nur in Dimethylsulfoxyd verzeichnet.

Die Löslichkeitsuntersuchungen führen zur gleichen Schlußfolgerung wie die Ergebnisse der Thermoanalyse, und zwar das Vorhandensein von kräftigen intermolekularen Assoziationen.

Weiterhin wurde das Verhalten der Verbindungen gegen Säuren und Basen getestet, indem sie bei Zimmertemperatur mit HCl 1,2n, NaOH 2,5n, $NaHCO_3$ 1,5n und konzentrierter H_2SO_4 behandelt wurden. Die chemische Stabilität war in den ersten drei Fällen ausgezeichnet, während mit konzentrierter Schwefelsäure eine vollkommene Löslichkeit bemerkt wurde. Durch Einführen dieser konzentrier-

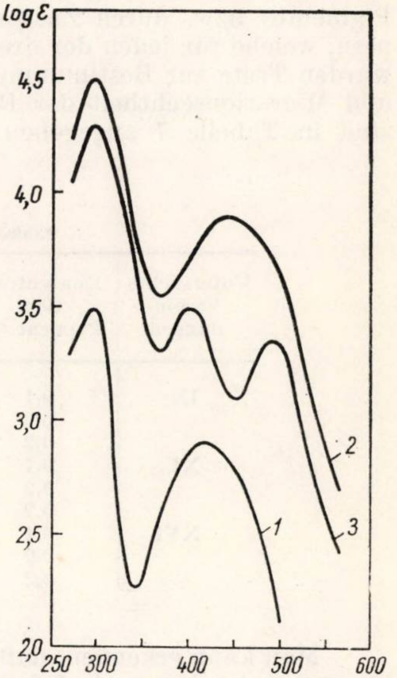

Abb. 1. — Lichtabsorptionsspektren.

1, Isatin; *2* und *3*, Kondensationsprodukte zwischen Isatin-2-chlorid und Benzidin beziehungsweise *o*-Tolidin.

ten H_2SO_4-Lösungen in Wasser, wurden sehr feine stabile Suspensionen erhalten, welche auf ausgezeichnete Dispergierung hinweisen. Diese Bemerkung ist ein Hinweis, daß die untersuchten Verbindungen mit ähnlichen Ergebnissen wie Phthalocyanine und Dioxazine einer sauren Pastifikation unterworfen werden können. Dieses Verfahren ist von höchster Wichtigkeit für die Herstellung von für Färbungen verwendbare pigmentäre Formen.

Zur Ermittlung der Anwendungsmöglichkeit der Syntheseprodukte für Pigmentierung von Kunststoffen wurden Färbeversuche auf Hochdruck-Polyäthylen unternommen. Nach einer trockenen Vormischung des Polyäthylengranulates mit dem Pigment, wurde die eigentliche Einfärbung auf einem Zweischneckenextruder Werner-Pfleiderer vorgenommen. Zwecks Einfärbung wurden drei Verbindungen aus der Diphenyl-Reihe ausgesucht. Die Konzentration des Pigmentes bei allen diesen Einfärbungen war 0,2%, wobei eine transparente Färbung erzielt wurde.

Das eingefärbte Polyäthylengranulat wurde anschließend zum Spritzgießen von Probekörpern verwendet.

Bei allen untersuchten Verbindungen wurden außer der Konzentration von 0,2%, eine verminderte Konzentration von 0,1% Pigment zur Färbung verwendet. Gleichzeitig wurde durch Zugabe von Titandioxyd auch eine Deckfärbung erprobt. Auf den drei, durch Konzentration des Pigmentes bzw. durch Zusatz von Titandioxyd verschiedenen Probekörpern, welche für jeden der drei ausgesuchten Pigmente vorhanden waren, wurden Teste zur Bestimmung der Lichtechteit auf einem Xenotest-Gerät und Migrationsechtheit der Pigmente ausgeführt. Die erhaltenen Werte sind in Tabelle 7 angegeben.

Tabelle 7

Echtheitsuntersuchungen der Pigmente

Untersuchte Verbindungen	Konzentration Pigment, %	Konzentration TiO_2, %	Lichtechtheit	Migrationsechtheit
IX	0,1	—	7	sehr gut
	0,2	—	6–7	sehr gut
	0,2	0,8	6	sehr gut
XI	0,1	—	6–7	sehr gut
	0,2	—	6	gut
	0,2	0,8	5	gut
XVI	0,1	—	7–8	sehr gut
	0,2	—	7	sehr gut
	0,2	0,8	6–7	sehr gut

Man kann erkennen, daß sowohl die Lichtechteit als auch die Migrationsechtheit der vom 3,3-Dichlorisatin abstammenden Verbindungen höher als die der vom Isatin-2-chlorid erhaltenen Verbindungen liegen und daß durch Substitution im Diamin der vom Isatin-2-chlorid abgeleiteten Reihe ein leichtes Absinken der obengenannten Echtheiten bemerkbar wird.

Allgemein genommen kann man die Licht- und Migrationsechtheiten als gut bezeichnen und wenn man noch die sehr gute Thermostabilität hinzuzählt, wird die Anwendungsmöglichkeit der untersuchten Verbindungen als Pigmente für Kunststoffe offensichtlich.

EXPERIMENTELLER TEIL

Die untersuchten Verbindungen VI—XIII wurden nach folgendem Verfahren synthetisiert:

In einem mit Rührwerk und Rückflußkühler versehenen Dreihalskolben wurden 1 Teil Isatin mit 1, 5—2 Teilen PCl_5 und 2 Teilen Chlorbenzol 2,5—3,5 Stunden bei Rückfluß erhitzt. Nach raschem und energischem Abkühlen (bis —10°) wurde das Gemisch abfiltriert und der Rückstand mit kaltem Äthyläther gewaschen und gut abgesaugt. Das erhaltene Isatin-2-chlorid, welches noch Äther enthält, wird sofort weiterverarbeitet, indem es mit ungefähr der fünffachen Menge von *o*-Dichlorbenzol in einem mit Rührwerk und Rückflußkühler versehenen Dreihalskolben aufgerührt, wird. Dazu wird ca. 80% der stöchiometrisch berechneten Menge des Diamins hinzugefügt und bei Rückfluß des Dichlorbenzols 2—4 Stunden lang erhitzt. Das Gemisch wird heiß abfiltriert und der Rückstand mit heißem Lösungsmittel und Azeton gewaschen.

Die Verbindungen XIV—XVII wurden folgendermaßen hergestellt:

In einem mit Rührwerk und absteigendem Kühler versehenen Dreihalskolben werden 1 Teil Isatin mit 1,8—2 Teilen PCl_5 und 2 Teilen Benzol 5—10 Stunden bei Zimmertemperatur gerührt. Der erhaltene braune Brei wird abgesaugt und der Rückstand mit Äthanol und Wasser gewaschen. Das erhaltene 3,3-Dichlorisatin kann aus Benzol oder Äthyläther umkristallisiert werden. Die Kondensation des Chlorisatins mit dem Diamin erfolgt wie im oben beschriebenen Beispiel.

Die IR-Spektren der untersuchten Verbindungen wurden wegen Unlöslichkeit in den üblichen IR-Lösungsmitteln, an Kaliumbromid-Preßlingen ausgeführt und auf einem Perkin-Elmer 621-Spektrophotometer aufgenommen.

Die Untersuchung der Verbindungen durch Spektralanalyse im UV- und sichtbaren Bereich erfolgte auf einem Pye-Unicam SP 800 Spektrophotometer in Dimethylformamidlösung, welche eine Konzentration an der zu untersuchenden Substanz von 9.10^{-3} bis 3.10^{-5} Mol/l besaß.

Die Thermoanalyse der Verbindungen wurde auf einer thermogravimetrischen Waage Typ Mettler in statischer Luft bei einer Aufwärmungsgeschwindigkeit von 4°/ Minute ausgeführt.

Revue Roumaine de Chimie, 17, *11*, 1901 – 1907 (1972)

DERIVATIVES OF FURAN. XI[1]. ELECTRON IMPACT FRAGMENTATION OF SOME 5-SUBSTITUTED 2-(2′-BENZOTHIAZOLYL)-FURANS

I. OPREAN, V. FĂRCĂŞAN and FLORICA PAIU

Department of Chemistry, "Babeş-Bolyai" University
str. Arany Janos 11, Cluj, Romania

Received February 8, 1972

The mass spectra of some 2-(2′-benzothiazolyl)-furans (I, III, IV, V and VI) and of 2-phenylbenzothiazole (II) have been recorded. The behaviour of the 2-(2′-benzothiazolyl)-furans towards electron impact is characterized by a dominant process of fragmentation, which involves the furan ring, producing a characteristic ion of m/e 172.

As a part of our researches in the furan series, we have prepared derivatives of 2-(2′-benzothiazolyl)-furan (I), in order to obtain, by investigating their physical and chemical behaviour, more information about the interaction of the furan and the benzothiazole rings in 2-(2′-benzothiazolyl)-furan (I).

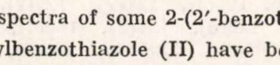

I : R = H; III : R = CHO
IV : R = NO_2 ; V : R = COOH
VI : R = Br.

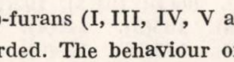

II

This paper deals with the mass spectra of some of these compounds. We considered it of interest to find out to what extent the characteristic fragmentation modes of furans,[2-6] thiazoles,[7-9] or benzothiazoles [10,11] are also present in the case of 2-(2′-benzothiazolyl)-furan (I), and what is

---

[1] Part X : V. Fărcăşan and F. Paiu, *Stud. Univ. Babeş-Bolyai, Chim.*, **16**, 111 (1971).

Table 1

Mass spectral data m/e (I%) of 2-(2′-benzothiazolyl) furans*)

I	44(5), 51(2), 58(3), 63(4), 69(12), 77(3), 82(5), 92(2), 105(3), 105,5(5) 108(21), 109(2), 139(2), 167(2), 184(4), 209(2), 210(18), 211(100,M), 212(16), 213(6).
II	44(2), 45(3), 51(2), 58(2), 63(4), 69(11), 70(2), 71(3), 82(4), 100,5(7), 102(2), 108(5), 128(3), 129(2), 140(2), 145(4), 146(4), 147(2), 172(15), 173(22), 174(3), 200(7), 201(100,M), 202(13), 203(5).
III	41(6), 43(6), 44(6), 45(2), 51(2), 55(4), 56(2), 57(4), 60(4), 63(2). 67(2), 68(2), 69(7), 70(2), 71(3), 73(4), 81(3), 82(3), 83(2), 85(2), 91(3), 95(2), 100,5(3), 101(2), 108(3), 128(3), 129(2), 137(2), 140(2), 145(5), 146(3), 172(24), 173(9), 174(2), 200(6), 201(8), 228(19), 229(100,M), 230(16), 231(6).
IV	43(2), 44(9), 45(7), 50(2), 51(3), 52(2), 55(2), 57(3), 58(2), 63(6), 64(3), 65(2), 69(12), 70(4), 73(2), 75(2), 76(4), 77(2), 80(5), 82(5), 83(2), 90(2), 96(4), 101(3), 102(2), 107(2), 108(4), 121(2), 127(2), 128(8), 133(2), 134(8), 135(3), 140(4), 145(11), 146(6), 159(3), 160(4), 162(12), 163(2), 170(2), 172(55), 173(9), 174(3), 186(2), 188(11), 189(2), 200(2), 214(3), 216(14), 217(3), 229(5), 230(2), 246(100,M), 247(14), 248(6).
V	41(3), 43(2), 44(4), 45(4), 50(2), 51(2), 55(2), 63(3), 69(5), 75(2), 77(2), 82(3) 83(2), 85(2), 108(5), 127(3), 128(4), 134(2), 135(10), 136(2), 140(2), 145(8) 146(6), 160(8), 161(16), 162(3), 171(2), 172(34), 173(10), 174(2), 189(3) 200(12), 201(3), 216(2), 228(3), 245(100,M), 246(19), 247(8).
VI	41(2), 44(7), 45(19), 50(13), 51(6), 52(2), 55(3), 57(2), 58(5), 62(4), 63(17), 64(12), 69(50), 70(10), 71(2), 72,5(2), 73(2), 74(4), 75(8), 76(6), 77(6), 78(2), 80(2), 81(5), 82(13), 85,5(5), 86(19), 86,5(2), 87(2), 88(2), 90(6), 93(3), 94(2), 95(2), 96(4), 101(7), 102(7), 107(4), 108(14), 117(4), 118(2), 119(5), 120(2), 121(2), 122(3), 125,5(4), 126(2), 126,5(5), 127(7), 128(21), 129(2), 133(2), 134(3), 139,5(9), 140(10), 140,5(13), 141(2), 144(2), 145(25), 146(12), 147(3), 159(3), 170(4), 171(3), 172(100), 173(16), 174(6), 200(17), 201(4), 251(40), 252(6), 253(43), 254(6), 255(2), 279(94,M), 280(11), 281(92,M), 282(13), 283(5).

*) The peaks corresponding to 1% relative intensities were not tabulated.

---

[2] R. I. Reed and W. K. Reid, *J. Chem. Soc.*, **1963**, 5933.

[3] H. Budzikiewicz, C. Djerassi, and D.H. Williams, ''Mass Spectrometry of Organic Compounds'', Holden-Day Inc., 1968, p. 615.

[4] R. Grigg, M. W. Sargent, D. H. Williams and J. A. Knight, *Tetrahedron*, **21**, 3441 (1965).

[5] K. Heyns, R. Stute and H. Scharmann, *Tetrahedron*, **22**, 2223 (1966).

[6] C. Mercier, *Bull. Soc. chim. France*, **1969**, 145.

[7] *Idem*, 2, p. 634.

[8] G. M. Clarke, R. Grigg and D. H. Williams, *J. Chem. Soc.* (*B*), **1966**, 339.

[9] M. J. Rix and B. R. Webster, *Org. Mass. Spectrom.*, **5**, 311 (1971).

[10] B. J. Millard and A. F. Temple, *Org. Mass. Spectrom.*, **1**, 285 (1968).

[11] H. Ogura, S. Sugimoto and T. Itoh, *Org. Mass. Spectrom.*, **3**, 1341, (1970).

the influence of a substituent in position 5 of I upon the fragmentation process.

In order to simplify the interpretation of the mass spectra of our compounds, we recorded also the spectrum of a model compound, namely 2-phenylbenzothiazole (II).

Details of the spectra are summarized in Table 1.

Compound II — a typical aromatic one — exhibits a very simple spectrum, dominated by a peak at m/e 211 (the molecular ion). By loss of a neutral molecule of benzonitrile, the parent ion afforded the most abundant fragment of the spectrum m/e 108 (*a*), which further fragmented in a manner similar to that observed in the case of thiophenol,[12] by deletion of C_2H_2 or C_3H_3 producing the ions of m/e 82 (*b*) and m/e 69 (*c*), respectively (see Scheme 1).

A less important fragmentation mode involves the elimination of a molecule of hydrogen cyanide from the parent ion to form the ion of m/e 184 (4%) (*d*). This process can be rationalized by postulating a cleavage of the S—C bond followed by the transfer of a hydrogen atom and finally elimination of hydrogen cyanide (see Scheme 1). Both the expulsion of a neutral molecule and the stability of the ion *d* may account for the fulfilment of the energetical requirements of such a reaction.

In the spectrum of II, interesting features are the very low abundance (1%) of ions originating from the molecular ion by elimination of S or C=S fragments, characteristic of benzothiazole derivatives,[11,12] and the relatively prominent peak (18%) corresponding to the M⊕ -1 ion (m/e 210).

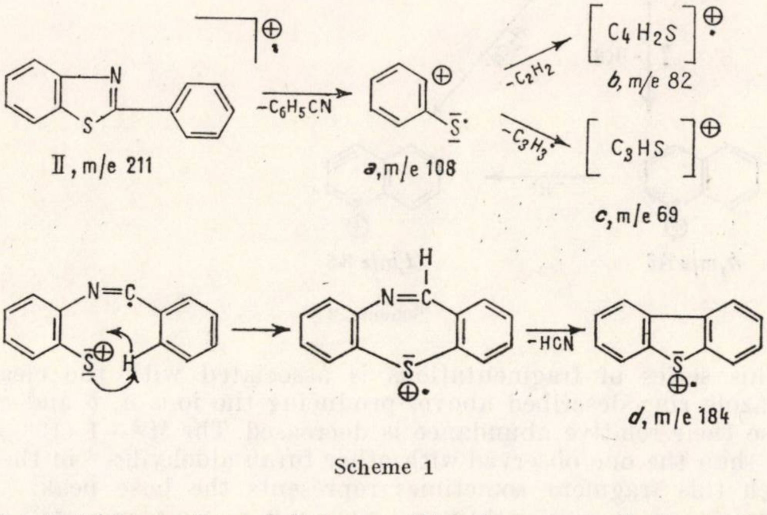

Scheme 1

The 2-(2′-benzothiazolyl)-furan (I) behaves similarly to 2-phenylbenzothiazole (II) in that the ions of m/e 108, 82 and 69 (*a*, *b*, *c*) are present in the mass spectrum, and to furan [2-6] by the cleavage of CO or

---

[12] D. G. Earnshaw, G. L. Cook and G. U. Dinneen, *J. Phys. Chem.*, **68**, 296 (1964).

$H\dot{C}O$ fragments producing the most abundant ions m/e 173 (*e*) and m/e 172 (*f*), respectively (see Scheme 2).

Most probably a subsequent fragmentation of *e* and *f* gives rise to the ions m/e 146 (formulated by us as *g* or *h*) and m/e 145 (*i*).

As expected, in the case of 2-(2′-benzothiazolyl)-5-formyl-furan (III), the molecular ion, the base peak in the spectrum, cleaves similarly to aromatic aldehydes,[13] producing the ions m/e 228 (*j*), 201 (*k*) and 200 (*l*), which undergo a further fragmentation, observed also in the case of I, to afford the ions m/e 173 (*e*) and m/e 172 (*f*) (see Scheme 3).

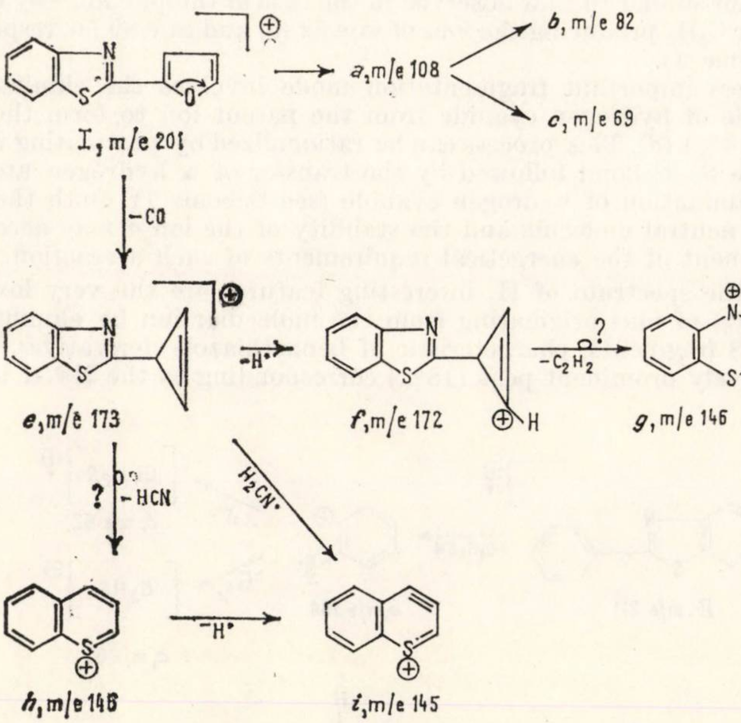

Scheme 2

This series of fragmentations is associated with the cleavage of the thiazole ring described above, producing the ions *a*, *b* and *c*, but in this case their relative abundance is decreased. The $M^{\oplus}-1$ (19%) peak is smaller than the one observed with other furan aldehydes [4] in the spectra of which this fragment sometimes represents the base peak.

The spectrum of 2-(2′-benzothiazolyl)-5-nitrofuran (IV) exhibits the distinctive features of an aromatic nitro derivative [14] – namely the presence of the $M^{\oplus}-O$ (*m*), $M^{\oplus}-NO$ (*n*), $M^{\oplus}-NO_2$ (*l*) and $M^{\oplus}-NO-CO$ (*o*) ions – and those of the 2-(2′-benzothiazolyl)-furans described above.

---

[13] *Idem*, 3, p. 162.
[14] *Idem*, 3, p. 515.

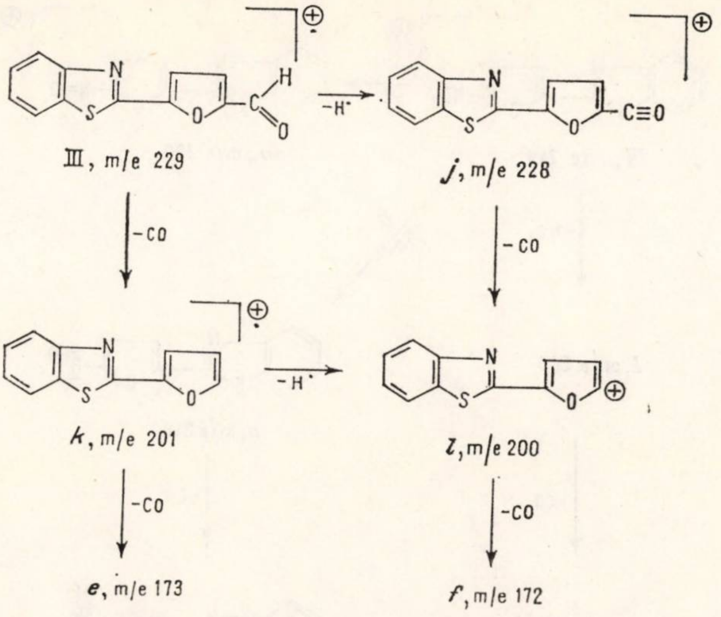

Scheme 3

The dominant fragment of the spectrum is the ion of m/e 172 (55%) (see Scheme 4).

The 2-(2′-benzothiazolyl)-5-carboxifuran (V) shows the expected mass spectrometric behaviour for an aromatic carboxylic acid.

In the spectrum of 2-(2′-benzothiazolyl)-5-bromofuran (VI), the relative abundance of the ionic fragments is higher as compared to that of the compounds I, III, IV and V (see Table 2), so that the base peak corresponds to the ion of m/e 172 (*f*) (see Scheme 5). The molecular ion ejects the CO molecule with retention of the bromine atom, to give rise to an ion of m/e 251/253 (*p*). This is the most intense $M^{\oplus}-CO$ peak of the whole series investigated here.

From the above data, some general conclusions can be drawn.

— The 2-(2′-benzothiazolyl)-furan system is very stable; the molec-

Table 2

Relative intensities of the main fragments in the mass spectra of the 2-(2′-benzothiazolyl) furans

Compound	Molecular weight	$M^{\oplus}$	$M^{\oplus}-1$	$M^{\oplus}-CO$	$M^{\oplus}-HCO$	$M^{\oplus}-R$	172	146	145	134	108
I	201	100	7	22	15	7	15	4	4	1	5
III	229	100	19	8	6	6	24	3	5	—	3
IV	246	100	—	1	—	2	55	6	11	8	4
V	245	100	1	1	2	12	34	6	8	2	5
VI	279/281	94/92	—	41/43	—	17	100	13	25	3	14

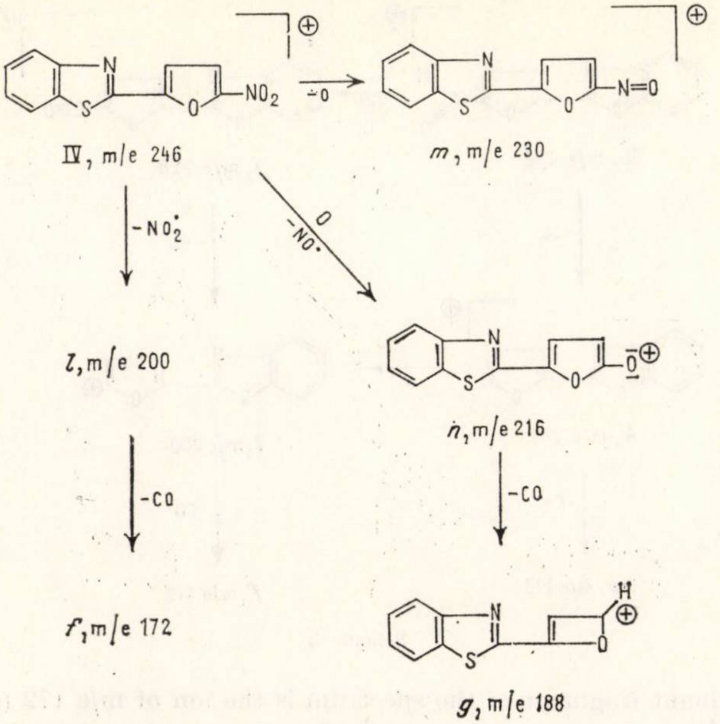
IV, m/e 246
-O
m, m/e 230
-NO$_2$
-NO
l, m/e 200
n, m/e 216
-CO
-CO
f, m/e 172
g, m/e 188

Scheme 4

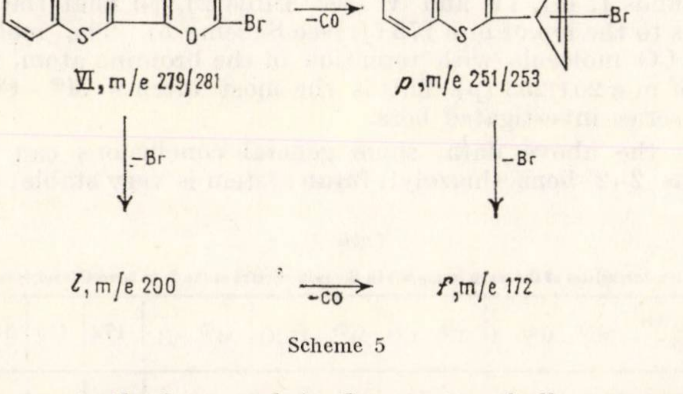
VI, m/e 279/281
-CO
p, m/e 251/253
-Br
-Br
l, m/e 200
-CO
f, m/e 172

Scheme 5

ular ion represents the base peak in the spectra of all compounds except VI.

— Of the two heterocycles the electron impact fragmentation involves preferentially the furan ring and, as a result, the most abundant fragment in all cases except I is that of m/e 172. The corresponding peak may be used for the identification of the 2-(2′-benzothiazolyl)-furans.

— The peaks at m/e 145 and 146 are also distinctive, but less intense than the peak at m/e 172.

— Some fragments which are characteristic of benzothiazole (m/e 134, 108) are of little importance in the case of our compounds.

— The fragmentation of the substituted derivatives is that expected for the corresponding aromatic analogoues.

EXPERIMENTAL

The substances I,[15], II,[16] III,[1] IV,[17] V,[18] and VI,[19] were prepared by literature methods.

The purity of the substances was checked by TLC on silica gel.

The mass spectra were recorded using a Varian SM—1 with direct inlet system mass spectrometer. The source temperature, was 180—200°. The ionizing energy was 70 eV.

Acknowledgements. The authors are grateful to Dr. W. Schäfer ("Max Planck Institut für Biochemie", Munich) for providing the facilities for the recording of mass spectra ; one of us (I.O.) thanks the "Alexander von Humboldt" foundation for financial support.

---

[15] V. Fărcăşan and C. Makkay, *Studii şi Cercetări Chim. Fil. Cluj*, **10**, 145 (1959).

[16] P. Jacobsen, *Ber. dtsch. chem. Ges.*, **19**, 1068 (1886).

[17] V. Fărcăşan and F. Paiu, *Stud. Univ. Babeş-Bolyai, Chim.*, **11**, 107 (1966).

[18] V. Fărcăşan, F. Paiu and I. Balász, *Stud. Univ. Babeş-Bolyai, Chim.* **15**, 97 (1970).

[19] V. Fărcăşan, *Studii şi Cercetări Chim. Fil. Cluj*, **13**, 103 (1962).

Revue Roumaine de Chimie, **17**, *11*, 1901—1907 (1972)

Revue Roumaine de Chimie, **17**, *11*, 1909–1915 (1972)

PARA-INTRAMOLECULAR AROMATIC REARRANGESMENTS. II.[1]
THE MECHANISM OF THE N-ALKYLANILINES REARRANGEMENT

MIRCEA E. LUPEȘ

Aleea Stanila 4, Bucharest 57, Romania

Received April 4, 1972

This paper represents an extension of the "adjacent electron localization" theory on the mechanism of the other reaction in the class of *para*-intramolecular aromatic rearrangements : the rearrangement of the N-alkylanilines. According to this theory the key-intermediate of the reaction is the compound formed by a metal halide addition to that carbon atom of the benzene ring adjacent to the amino group (the carbon atom thus becoming sp^3 hybridized). This intermediate rearranges to *p*-alkylanilines by a cyclic transition state in which the benzene ring adopts a boat shape (whose geometry is discussed too). The whole hypothesis is consistent with experimental data described in literature.

1. INTRODUCTION

By "*para*-intramolecular aromatic rearrangements" we understand those migrations from the side chain to the nucleus which brought about intramolecularly, *directly* to the *para* position (being different in this way from other intramolecular aromatic rearrangements — as the 0-allylphenols rearrangement leading to *p*-allylphenols is — where the *para* isomer does not form directly but through the *ortho* one).

The explanation of such a reaction type implies getting over special stereochemical difficulties, which only now are to be solved satisfactorily. The mechanism of these rearrangements seems to consist of a new type of intermediate formation by "adjacent electron localization" of a π-electron pair to that carbon atom of the aromatic nucleus adjacent to the substituted amino group (the other two π-electron pairs remaining in a pentadienyl cation form). The so-formed intermediate, analogous to that formed in the electrophilic aromatic substitution, rearranges by a cyclic transition state in which the aromatic nucleus adopts a boat shape (bringing the reactionable positions in a favourable stereochemical situation which permits a direct reaction).

---

[1] Part I of this series will be considered : M. E. Lupeș, *Rev. Roumaine Chim.*, **17**, 1253 (1972).

Until now, this mechanism has already been used in the explanation of the N-anilinesulfonic acid rearrangement leading to *p*-anilinesulfonic acid [2] and in the benzidine rearrangement leading to *p*-semidine. [1] It is thus extremely likely that other *para*-intramolecular aromatic rearrangements, such as N-alkylanilines, N-haloacylanilides, N-nitroanilines and N-nitrosoanilines ones, should follow the same mechanism (which thus seems to have a more general application). The object of this series of papers is to prove such a possibility.

2. THE REARRANGEMENT OF THE N-ALKYLANILINES

Just a century ago, Hofmann and Martius [3] have discovered that N-alkylaniline hydrohalides, warmed in a sealed tube at high temperatures (200—300°), give rearranged products with the alkyl group to the nucleus. In 1919, Reilly and Hickinbottom [4a,4b] discovered that N-alkylaniline (free base) complexes with metal halides rearranges similarly. Nevertheless, it was soon seen that the two rearrangements are not at all identical, they being basically different.

Thus, by warming of the N-alkylaniline hydrohalides the migrating alkyl group isomerizes, the primary and secondary groups turning into tertiary ones. That is why N-isobutylaniline hydrobromide gives *p*-*tert*-butylaniline hydrobromide,[4e] and N-isoamylaniline hydrobromide gives *p*-*tert*-amylaniline hydrobromide.[4g] On the other hand, N-alkylaniline hydrohalides with an optically active alkyl group racemize. Thus, the optically active N-(α-phenethyl)-aniline hydrochloride gives optically inactive *o*- and *p*-(α-phenethyl)-aniline hydrochlorides.[5] Afterwards, N-alkylaniline hydrohalides give — besides the normal products of rearrangement — alkenes, alkyl halides and aniline. Thus, N-isobutylaniline hydrobromide (in the presence of dry $CoBr_2$ or $ZnBr_2$) gives aniline as the main product and a neutral oil composed of polymerized alkenes[4e]; N-ethyl-, N-propyl-, N-butyl-, N-isobutyl-, and N-isoamylanilines hydrobromides give alkenes and alkyl bromides (whose relative ratio depends on the kind of the alkyl group and temperature)[4f]; N-isoamylaniline hydrobromide gives great amounts of trimethylethylene and, as the main product, aniline [4g]; N-methylaniline hydrobromide gives a great deal of methyl bromide[4h]; N-*tert*-butyl- and *N*-*tert*-hexylaniline hydrohalides give besides aniline, isobutylene and 3-methyl-2-pentene, respectively.[4i] Finally, certain N-alkylaniline hydrohalides give "cross-products". Thus, N, N-dibenzyl-

[2] Z. Vrba and Z. J. Allan, *Tetrahedron Letters*, **1968**, 4507.

[3] *(a)* A. W. Hofmann and C. A. Martius, *Ber. dtsch. chem. Ges.*, **4**, 742 (1871); *(b)* A.W. Hofmann, *ibid.*, **5**, 704 (1872); (*c*) A. W. Hofmann, *ibid.*, **7**, 526 (1874).

[4] (*a*) J. Reilly and W. J. Hickinbottom, *Chem. News*, **119**, 161 (1919); (*b*) J. Reilly and W. J. Hickinbottom, *J. Chem. Soc.*, **117**, 103 (1920); (*c*) W. J. Hickinbottom, *ibid.*, **1927**, 64; (*d*) W. J. Hickinbottom and A. C. Waine, *ibid.*, **1930**, 1558; (*e*) W. J. Hickinbottom and G. H. Preston, *ibid.*, **1930**, 1566; (*f*) W. J. Hickinbottom and S. E. A. Ryder, *ibid.*, **1931**, 1281; (*g*) W. J. Hickinbottom, *ibid.*, **1932**, 2396; (*h*) W. J. Hickinbottom, *ibid.*, **1934**, 1700; (*i*) W. J. Hickinbottom, *ibid.*, **1937**, 404; (*j*) W. J. Hickinbottom, *ibid.*, **1937**, 1119.

[5] H. Hart and J. R. Kosak, *J. Org. Chem.*, **27**, 116 (1962).

aniline hydrochloride give a mixture of *p*-benzyl-, 2,4-dibenzyl- and 2,4,6-tribenzylaniline hydrochlorides.[6]

The rearrangement of the N-alkylaniline (free base) — metal halides complexes takes place in two different ways, depending on the kind of alkyl group. When this group is a tertiary one (and sometimes secondary and even primary one) the rearrangement is the same as in the case of hydrohalides. Thus, N-*tert*-butyl- and N-*tert*-hexylaniline complexes with $CoCl_2$ or $CoBr_2$ give by warming rapid evolution of isobutylene and 3-methyl-2-pentene, respectively[4i]; N-cyclohexyl- and N-*sec*-octylaniline complexes with $CoCl_2$ and $CoBr_2$ give by warming great amounts of alkenes too.[4j] Then, N-benzylaniline complex with $CoCl_2$ gives "cross-products" as 2, 4-dibenzylaniline.[4j] Finally, optically active N-(α-phenethyl)-aniline complex with $ZnCl_2$ gives by warming optically inactive products.[5] On the contrary, when the alkyl group is a primary one (and sometimes secondary) the rearrangement takes place without formation of alkenes or alkyl halides and without alkyl group isomerization. Thus, N-isobutylaniline (free base) complexes with $CoBr_2$ or $ZnBr_2$ give high yields of *p*-isobutylaniline [4e]; N-isoamylaniline (free base) complexes with $CdCl_2$, $CoCl_2$ or $CoBr_2$ give *p*-isoamylaniline[4g]; N-(*n*-amyl)-, N-(*n*-hexyl)-, N-(*n*-heptyl)-, N-(*n*-octyl)-, N-(*n*-dodecyl)-, and N-cetylaniline (free bases) complexes with $CoCl_2$ or $CoBr_2$ give *p*-rearranged products too, without alkene elimination or alkyl group isomerization.[4j] A modern proof that alkyl group does not isomerize has been brought by the rearrangement of N-(ethyl-1-C^{14})-aniline complexes with $CoCl_2$, $ZnCl_2$, $NiCl_2$, $AlCl_3$ and $CdCl_2$.[7a] However this process could take place, partially at least, the rearrangement with and without the alkyl group isomerization being perhaps competitive, Molera and his co-workers [7b] finding that the rearrangement of the N-(*n*-propyl-1-c^{14})- aniline with $CoCl_2$ and $ZnCl_2$ gives both *p*-propyl- and *p*-sopropylaniline.

3. THE MECHANISM OF THE N-ALKYLANILINE INTRAMOLECULAR REARRANGEMENT

As a result of the above mentioned short review of the experimental data known in literature, one can see that the N-alkylanilines rearrange in two different ways:

A. The hydrohalide catalysed rearrangements of all the N-alkylanilines and the metal halides catalysed rearrangements of the N-alkylanilines with tertiary alkyl groups (and sometimes secondary or even primary ones) are going with alkyl group isomerization or racemization, alkenes and alkyl halides evolution and "cross-products" formation. For that reason the mechanism is very likely an *intermolecular* one.[4h,5,8]

---

[6] P. J. Drumm, W. F. O'Connor and J. Reilly, *J. Amer. Chem. Soc.*, **62**, 1241 (1940).

[7] (*a*) M. J. Molera, J. M. Gamboa and M. del Val Cob, *Anales real soc. españ. fís. y quím.* (*Madrid*), **55 B**, 493 (1959); *Chem. Abstr.*, **54**, 2221 (1960); (*b*) M. J. Molera, J. M. Gamboa, M. del Val Cob and N. Ortin *ibid.*, **59 B**, 379 (1963); *Chem. Abstr.*, **60**, 4033 (1964).

[8] Y. Ogata, H. Tabuchi and K. Yoshida, *Tetrahedron*, **20**, 2717 (1964).

B. The metal halides catalyzed rearrangements of the N-alkylanilines with primary alkyl groups (and sometimes secondary ones) going — partially at least [7b] — without alkyl group isomerization or alkene and alkyl halide formation. That is why the mechanism is assumed to be *intramolecular* and its elucidation represents the main object of this paper.

As one can see the nature of the substrate decides the inter-or intramolecular path for the rearrangement of the N-alkylaniline complexes. Those that have alkyl groups which can form stable carbocations react intermolecularly. This is the case with tertiary groups, with some secondary groups and even with primary ones (when these form carbocations stabilized by conjugation such as benzyl and α-phenylethyl). On the contrary, those that have alkyl groups which cannot form stable carbocations react — partly at least — intramolecularly.

3.1. Theories of the Mechanism

A first attempt to account for the mechanism of the metal halides catalyzed rearrangement of the N-alkylanilines is due to Bennett and Chapman [9] who came to the conclusion that the intermediate of this reaction is the alkyl halide (which would be the intermediate of the intermolecular rearrangement of the hydrohalides too). Later on, Hickinbottom [4h] has assumed that the two types of rearrangement have also a common intermediate : the alkyl carbocation. In the case of the intramolecular rearrangement the apparence of such a intermediate is very unlikely (Hickinbottom's opinion was that the intermediary formed carbocation does not suffer internal changes due either to the stabilizing effect of the metal halide or to the fact that this cation reaction with the nucleus would have been catalysed by the metal halide).[4h]

As to the proper going of the reaction Hickinbottom considers corectly the fact that the reaction is produced *directly* into the *para*- position (and not first into the *ortho* one) as otherwise the ratio of *ortho* isomer should be greater than the *para* one and small alkyl group migration (methyl and even ethyl) would not be possible but through a considerable distorsion of the molecule. It was also proved in other similar rearrangements (the intramolecular rearrangements of N-anilinesulfonic acid [2] and N-nitroaniline[10]) that the migration takes place *directly* in the *para* position and not through intermedium of the *ortho* position (the so-called "cartwheel" mechanism).

According to all the above mentioned facts we do think that the intramolecular rearrangement of the N-alkylanilines are proceeding quite differently.

3.2. The "Adjacent Electron Localization" Theory

In the previous work [1] we have applied this theory to the explanation of the benzidine rearrangement mechanism, but the same theory fits very well to the here discussed mechanism too. It has thus for a long time been known[11] that the N-alkylanilines (I) give — with certain metal halides — complexes (II) in which the metal atom is bound to the nitrogen atom by a coordinative bond. These complexes are less stable than that obtained, for example, from primary arylamines. That is why, in the first step of the rearrangement these complexes (II) can give — due to the high temperature demanded by the reaction — "active" complexes (III) in which the metal halide has migrated (either inter- or intramolecularly) to that carbon atom of the benzene nucleus adjacent to the amino group. This is possible by a π-electron pair localization in the adjacent position (the other two π-electron pairs remaining in a pentadienyl cation form), that brings about a change in the adjacent carbon atom hybridization from sp^2 to sp^3, thus giving a first approach of the alkyl group to the *para* position of the nucleus (see Fig. 2). The "active" complex (III) is the key-intermediate of the intramolecular rearrangement of N-alkylanilines. The necessary activation energy for its formation cannot be too great (Fig. 1) as the benzene conjugation does not disappear completely but it is replaced by a pentadienylic one (similar to the electrophilic aromatic substitution).

---

[9] G. M. Bennett and A. W. Chapman, *Ann. Reports*, **1930**, 124.

[10] W. N. White and J. R. Klink, *J. Org. Chem.*, **35**, 965 (1970).

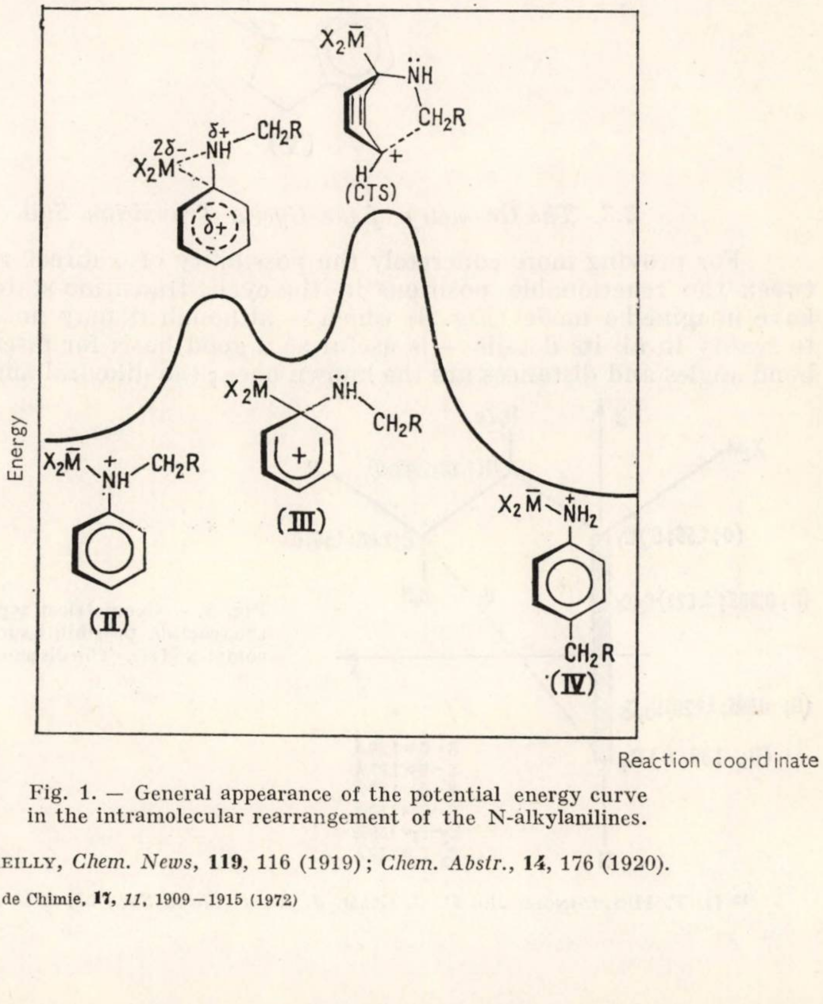

Fig. 1. — General appearance of the potential energy curve in the intramolecular rearrangement of the N-alkylanilines.

---

[11] J. Reilly, *Chem. News*, **119**, 116 (1919); *Chem. Abstr.*, **14**, 176 (1920).

In the second step of the rearrangement the alkyl group migrates into the *para* position of the nucleus by a cyclic transition state (CTS) in which the benzene ring adopts a boat shape. In this transition state the reactionable positions are brought to such a distance that permits a direct reaction (see Fig. 3). Thus, the complicated stereochemical problem of this reaction is easily got over without implying a special chemical bond.

The energetical motivation for the formation of such a cyclic transition state (CTS), in which is destroyed even the cyclopentadienyl conjugation and the aromatic nucleus adopts the boat form, is not known yet. However, Hefelfinger and Cram [12] have recently discovered an extremely important fact : /2.2/-metaparacyclophane treated with acetyl chloride and $AlCl_3$ gave the stable compound (V), through a (III)-like intermediate. This exceptional discovering seems to confirm decisively our theory of he mechanism.

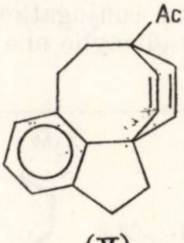

(V)

3.3. *The Geometry of the Cyclic Transition State*

For proving more concretely the possibility of a direct reaction between the reactionable positions in the cyclic transition state (CTS) we have imagined a model (Fig. 3) which – although it may not correspond to reality in all its details – is useful as a good basis for discussion. The bond angles and distances are the known ones ; the dihedral angle between

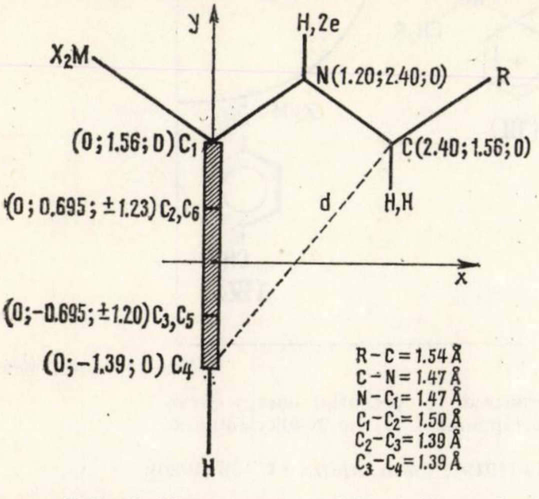

Fig. 2. – Geometrical representation of the reaction possibilities in the "active" complex (III). The distance $d = 3.73$ Å.

---

[12] D. T. HEFELFINGER and D. J. CRAM, *J. Amer. Chem. Soc.*, **93**, 4754 (1971).

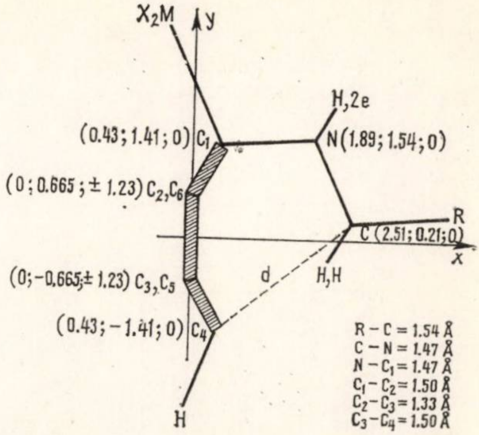
X₂M
y
H,2e
(0.43; 1.41; 0) C₁
N(1.89; 1.54; 0)
(0; 0.665; ± 1.23) C₂,C₆
R
C (2.51; 0.21; 0)
x
(0; −0.665; ± 1.23) C₃,C₅
d
H,H
(0.43; −1.41; 0) C₄
H
R − C = 1.54 Å
C − N = 1.47 Å
N − C₁ = 1.47 Å
C₁ − C₂ = 1.50 Å
C₂ − C₃ = 1.33 Å
C₃ − C₄ = 1.50 Å

Fig. 3. — Geometrical representation of the reaction possibilities in the cyclic transition state (CTS). The distance $d = 2.64$ Å.

the boat shape planes is about 150°, an extension for which there is practical no tension in the cycle.

The calculation shows that the p-C_4 distance in the cyclic transition state is maximum 2.64 Å (given the same distance in the N-alkyl aniline complex (II) and in the "active" complex (III) is 4.95 Å and 3.73 Å, respectively), this distance being able to become much shorter by possible deformation of bond angles.

4. CONCLUSIONS

The analysis of both the experimental data and the theories of the mechanism in the literature has confirmed our initial assumption that the mechanism under study can be well explained by the "adjacent electron localization" theory. As far as we know, such a theory of the mechanism for the N-alkylaniline intramolecular rearrangement has not yet been proposed anywhere, although recently Allan[13] has suggested the application of this theory in the explanation of other *para*- intramolecular aromatic rearrangements.

---

[13] Z. J. ALLAN, *Tetrahedron Letters*, **1971**, 4225.

Revue Roumaine de Chimie, 17, *11*, 1917–1922 (1972)

DECOMPOSITION OF CUMENE HYDROPEROXIDE ON SILICA GEL

A. POP, L. CORMOŞ and LETIŢIA DULĂMIŢĂ

General Chemical Technology Department, Faculty of Chemistry
str. Arany János 11, Cluj, Romania

Received October 23, 1971

In order to improve the yield of phenol, the decomposition of cumene hydroperoxide has been tested on different solid catalysts. In the present paper this reaction was followed on indigenous silica gel. A thermogravimetric investigation is made on microporous and macroporous silica gel. The kinetics of the cumene hydroperoxide decomposition reaction is investigated on silica gel submitted to thermal treatment at different temperatures. The kinetic data are correlated with the catalytic activity.

Looking for new, more advantageous and more economical ways to obtain phenol is justified by the fact that increasingly large quantities of phenol are required as raw material by various branches of the chemical industry.

The modern method of manufacturing phenol, the "cumene" procedure uses the hydroperoxide of cumene as intermediate, which is then decomposed by 10% sulphuric acid. In the industry practice this procedure presents certain disadvantages such as : a partial acidic resination of phenol and acetone, an alkalic resination during the neutralization, formation of rather large quantities of by-products, corrosion of the equipment due to the presence of sulphuric acid, the necessity to concentrate the cumene hydroperoxide and others.

In order to avoid at least part of these difficulties of the "cumene" procedure, new possibilities of the cumene hydroperoxide decomposition have been tested lately, especially in heterogeneous catalysis.

Ion exchange resins [1-10], natural silicates [11-14] and a few synthetic alumino-silica gel systems [14-16] were tested.

Kucher and Soroka [17] made a preliminary study of the cumene hydroperoxide decomposition on bentonitic clays and various sorts of silica gel. In the case of silica gel, they observed with a single exception, only adsorption phenomena while the cumene hydroperoxide decomposition did not take place.

In the present paper the authors investigated the properties of indigenous microporous and macroporous silica gel in the following model reaction :

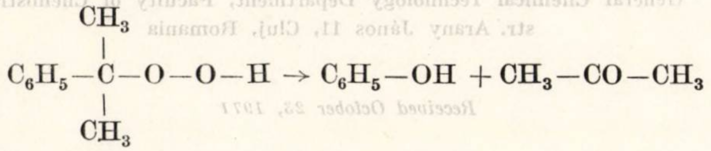

$$C_6H_5-\overset{\displaystyle CH_3}{\underset{\displaystyle CH_3}{\overset{|}{\underset{|}{C}}}}-O-O-H \rightarrow C_6H_5-OH + CH_3-CO-CH_3$$

EXPERIMENTAL

The catalyst used for the cumene hydroperoxide decomposition reaction was silica gel "Ionosil" type I, manufactured by "Uzinele Ocna-Mureş".

Before utilization, the silica gel was granulated and categorized. In all our experiments we used the category between 0.1—0.2 mm to make sure that the decomposition process is not influenced by the size of the catalyst granules. Then, the silica gel was purified by repeated wash-

---

[1] O. A. Kolmakov, I. A. Miasnikova, M. A. Barembaum, N. A. Golitina, and I.S. Izmailova, *Trudy po Khim. i Khim. Tehnol.*, **1**, 701 (1958).

[2] O. A. Kolmakov, I. A. Miasnikova, M. A. Barembaum, N. A. Golitina and I. S. Izmailova, *Trudy po Khim. i Khim., Tehnol.*, **1**, 43 (1958).

[3] V. Ia. Jablokov, V. A. Susunov and O. A. Kolmakov, *Trudy po Khim. i Khim. Tehnol. Gorki*, **1959**, 24.

[4] G. A. Razuvaev, V. A. Susunov and V. A. Sokolov, *Doklady Akad. Nauk. S.S.S.R.* **139**, 1128 (1961).

[5] V. A. Susunov, V. A. Jablokov and N. A. Jablokova, *Trudy po Khim. i Khim. Tehnol.*, **4**, 441 (1961).

[6] I. Vodnar, *Rev. Chem.* (*Bucureşti*), **21**, 549 (1970).

[7] A. Teichert, Z. Leszczynski and H. Radoniewicz, *Przemysl. Chem.*, **36**, 664 (1957).

[8] A. Teichert, Z. Leszczynski and H. R. Radoniewicz, Pat. Pol., 42. 393, 30 Sept. 1959, *Chem. Abstr.*, **55**, 7357 f (1961).

[9] I. Vodnar, G. I. Kulcsar, E. Toth and C. Pleşa, *Rev. Chim.* (*Bucureşti*), **19**, 120 (1968).

[10] I. Vodnar, *Rev. Chim.* (*Bucureşti*), **19**, 533 (1968).

[11] Société des usines chimiques Rhone-Poulenc. Pat. Brit., 724.009, 16 Febr. 1955, *Chem. Abstr.*, **50**, 4214 b (1956).

[12] H. Sodoman, B. Hauschutz and M. Hanke, Pat. Ger., 1.136.713, 20 Sept. 1962, *Chem. Abstr.*, **58**, 4471 c (1963).

[13] S. Carra, *Chimica e Industria*, **45**, 1087 (1963).

[14] Z. Leszczynski, *Przemysl. Chem.*, **44**, 488 (1965).

[15] A. Pop, P. Kröbl, L. Cormoş and Gh. Lengyel, *Stud. Univ. Babeş-Bolyai*, *Chem.*, **1967**, 89.

[16] E. I. Pollitzer, J. I. Lower and G. J. Illingwath, Pat. U. S., 3.305.590. *Chem. Abstr.*, **67**, 2881 v (1967).

[17] P. V. Kucher and V. A. Soroka, *Zhur. priklad. Khim.*, **34**, 1753 (1961).

ings[18] with aqueous 1 : 1 solution of HCl, in order to remove the cations K, Na, Ca and especially Fe. These acidic washings are advantageous because they maintain the small pores in the gel, i. e. a large specific area. By such washings the iron content of silica gel can be reduced up to 5 p.p.m. Afterwards, the samples were washed with distilled water until they became acid free, dried in an oven at 105° and subjected to thermal treatment at different temperatures.

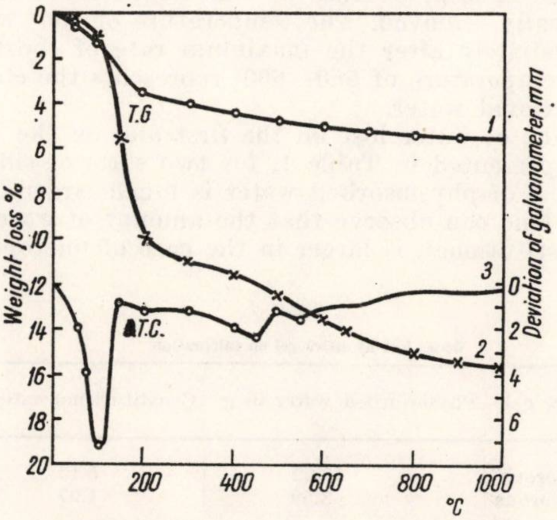

Fig. 1. — T. G. and D. T. G. curves.
1, T.G. curve for macroporous silica gel ; *2*, T.G. curve for microporous silica gel ; *3*. D.T.G. curve for microporous silica gel.

In order to establish the temperatures at which the activation of the samples is made, we performed thermogravimetric and differential thermogravimetric analyses. These diagrams are presented in Fig. 1.

The dehydration process of microporous and macroporous silica gel was followed by a thermobalance[19] while the temperature increase of the system was of 10 degrees per minute, using samples of 0.7–1.2 g.

RESULTS AND DISCUSSIONS

We found that the water which is physiosorbed on the active centres of the silica gel is lost in the interval 50–220° with a maximum dehydration rate at 100–110° for microporous silica gel and at 150° for macroporous silica gel. Beyond 220–230° the loss of the constitutional water begins. This results from two surface or internal hydroxyl groups and is lost gradually up to 950°. The rate of water loss increases gradually up to 600°, the greatest part of the constitutional water being lost in the temperature range 220–600°. The rate reaches a maximum at 440°. Between 600 and 700° the rate of water loss remains constant and begins to decrease gradually beyond this temperature.

---

[18] J. Fraissard, "Contribution à l'étude de la structure et des propriétés des gels de silice". Doctoral thesis, Paris, 1961.

[19] W. B. Innes, *Analyt. Chem.*, **28**, 332 (1956).

Depending on these data, we chose the temperatures for the thermal treatment, to which the silica gel samples were subjected. The temperature of 220° was chosen, because at this temperature the physiosorbed water is practically removed. The temperature of 450° was chosen since it follows immediately after the maximum rate of constitutional water loss while the temperature of 580–600° represents the end of the largest loss of constitutional water.

The amount of water lost on the first and on the second stage of dehydration is presented in Table 1, for two sorts of silica gel. In both cases the amount of physiosorbed water is much larger than the constitutional water. One can observe that the amount of water, both physiosorbed and constitutional, is larger in the case of microporous silica gel.

Table 1

Water lost by silica gel on calcination

Silica gel	Physiosorbed water in g	Constitutional water in g
Microporous	10.22	5.13
Macroporous	3.59	1.97

The catalytic activity of silica gel in the above mentioned model reaction was determined by the cumene hydroperoxide decomposition reaction, according to a statical method described earlier.[15] The conversions obtained at 30 and 40°, after 100 minutes are given in Table 2, for the solid systems submitted to thermal treatment at different temperatures. The same Table contains also the corresponding specific areas determined by the BET method.

Table 2

Conversion as a function of the thermal treatment

No. exp.	Calcination temperature	Conversion %		Specific area m^2/g	Conv. at $40°C/m^2.10^2$
		30°	40°		
1	220	16.08	23.91	485.3	4.92
2	350	16.43	25.11	468.8	5.35
3	450	15.38	22.81	434.7	5.24
4	580	15.92	23.42	430.1	5.44
5	700	10.98	16.22	314.2	5.13
6	800	4.02	6.29	129.8	4.83
7	950	1.82	2.48	63.4	3.91
8	1050	—	—	11.3	—

From the data presented in Table 2 we can establish that by applying an increasing calcination temperature, the content of constitutional water varies with the specific area. The decrease of the specific area due to the action of high temperature, is accompanied by the loss of an equivalent amount of water. Consequently, the degree to which the surface is covered by hydroxyl groups remains constant. Thus, we can explain the fact that the specific catalytic activity of silica gel, referred to a unit surface, practically does not vary with the calcination temperatures up to 600–650°.

A gradual decrease of the catalyst activity is observed beyond 600°, along with a considerable decrease of the specific area. Beyond this temperature a destruction of the pore walls occurs leading to gradually larger pores and beyond 950° even a process of pore-closing takes place. This is consistent with the decrease of the conversion rate beyond 600°.

It is well known that the highest activity of silica gel is observed with microporous silica gel [20–22] which has a large specific area. This is confirmed also by the model reaction investigated by us since the decomposition takes place on microporous silica gel, but not on macroporous silica gel with a specific area of 129.8 m^2/g.

Tests which were made on silica gel submitted to thermal treatment at 200–220° give results which cannot be taken into account, although the surface of the silica gel is large, since in our opinion most active centres are occupied by physiosorbed water.

In order to investigate the kinetics of hydroperoxide decomposition on microporous silica gel, experiments were performed on systems submitted to thermal treatment at 420 and 580°, and working at temperatures of 20, 30 and 40°. These data are presented in Fig. 2. The kinetics is of first order

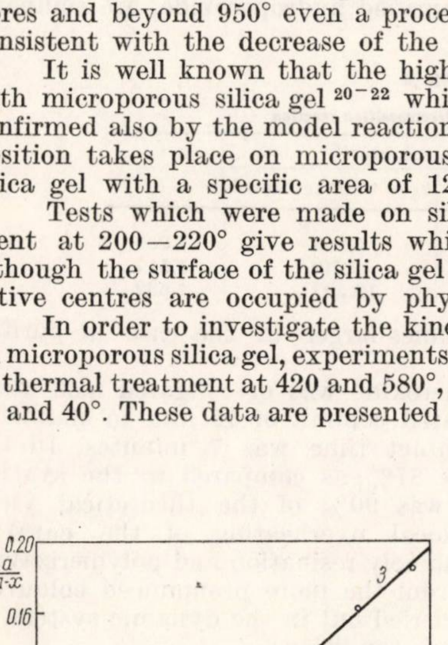

Fig. 2. — Linearization of first order kinetic curves.

1 – For the temperature of 20° 2 – For the temperature of 30°; 3 – For the temperature of 40°.

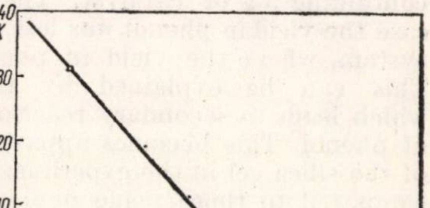

Fig. 3. — Graphical determination of the activation energy, based on Arrhenius equation.

[20] V. Aristov, B. G. Dzhavodov and I. Kiselev, *Koll. Zhur.*, **30**, 183 (1968).

[21] A. V. Kiselev, *Doklady Akad. Nauk S. S. S. R.*, **52**, 64 (1948).

[22] A. V. Kiselev, *Zhur. fiz. Khim.*, **5**, 595 (1949).

Revue Roumaine de Chimie, **17**, *11*, 1917–1922 (1972)

with regard to hydroperoxide and the activation energy calculated from Fig. 3 is of 10.41 kcal/mole. The amount of hydroperoxide in the system was determined iodometrically.[23] Experiments were carried out with 1 g catalyst and 25 ml cumene hydroperoxide solution, corresponding to a concentration of 0.723 mole/l.

The technical hydroperoxide, purified by a method given in the literature [24] was dissolved in cumene which was purified by distillation. In the case of the system subject to thermal treatment at 580°, experiments were carried out also with technical cumene hydroperoxide. The rate constants obtained with technical and purified hydroperoxide, are compared în Table 3.

Table 3

Kinetics of the decomposition reaction

Working temperature °	$k \times 10^{-4}$. minute^{-1}		$\frac{k_1}{k_2}$
	k_1 – CHP pure	k_2 – CHP technical	
20	5.368	3.353	1.601
30	11.683	7.701	1.517
40	20.420	12.507	1.632

The reaction rate about 1.6 times larger in the case of purified cumene hydroperoxide.

The decomposition of hydroperoxide was investigated also under dynamic conditions, on a thermostated column of 12 mm in diameter, containing 5 g of catalyst. The contact time was 7 minutes. In this case the yield in phenol was less, only 87%, as compared to the statical system, where the yield in phenol was 90% of the theoretical yield. This can be explained by the local overheating of the catalyst which leads to secondary reactions namely resination and polymerization of phenol. This becomes apparent from the more pronounced colouring of the silica gel in the experiments carried out in the dynamic system, as compared to those made under static conditions.

However, we found that the silica gel can be regenerated on heating with methyl alcohol, or by treating it with overheated water vapours, which leads to a desorption of phenol from the silica gel surface.

CONCLUSIONS

The decomposition of cumene hydroperoxide on microporous silica gel occurs according to a first order kinetics.

On macroporous silica gel only adsorption phenomena occur and the decomposition reaction does not take place.

The decomposition rate of purified cumene hydroperoxide is larger than that of technical grade.

The yield in phenol is larger under a statical regime, as compared to a dynamic regime.

---

[23] H. Hook and H. Kropf, *Angew. Chem.*, **69**, 313 (1957).

[24] B. D. Krujalov and B. I. Golovanenko, "Obţinerea simultană a fenolului şi acetonei", Ed. de Stat Tehnico-Ştiinţifică de Literatură Chimică, Moscova 1963, p. 116.

Revue Roumaine de Chimie, 17, *11*, 1923–1934 (1972)

SUR L'AMINATION DES COPOLYMÈRES MACROPOREUX STYRÈNE-DIVINYL-BENZÈNE CHLOROMÉTHYLÉS AVEC LA DIMÉTHYL-2-HYDROXYÉTHYLAMINE

A. CARPOV, DEMETRA DRĂGAN et I. PETRARIU

Institut de chimie macromoléculaire « Petru Poni », Jassy

Reçu le 4 septembre 1971

On a étudié les conditions optimales de la synthèse d'un échangeur d'anions fortement basique de type II adsorbant. On a effectué la réaction d'amination à l'aide de la diméthyl-2-hydroxyéthylamine en milieu aqueux et dans des solvants organiques et on a étudié aussi l'influence des différents paramètres de la réaction sur le degré de transformation de l'échangeur d'anions. Les caractéristiques physico-chimiques de l'échangeur d'anions synthétisé conformément aux conditions optimales ont été estimées par analyse élémentaire, titrage pH-métrique, spectres IR, analyse thermogravimétrique et thermodifférentielle, détermination de la capacité d'adsorption des ions organiques.

Par l'introduction des groupements d'ammonium dans les copolymères gel styrène-divinylbenzène, à l'aide de la triméthylamine (TMA) et de la diméthyl-2-hydroxyéthylamine (DHEA),[1-4] on a obtenu des échangeurs d'anions fortement basiques. Par convention, on a dénommé l'échangeur obtenu par amination avec la TMA, échangeur d'anions fortement basiques de type I, et celui obtenu avec la DHEA, échangeur d'anions fortement basiques de type II.

La différence de basicité des amines qui ont participé à l'amination (TMA – pKa = 9,907 et DHEA – pKa = 9,31) [5] se maintient dans une certaine mesure aussi dans le cas des échangeurs d'anions fortement basiques obtenus à l'aide de celles-ci. Par conséquent, les échangeurs d'ani-

---

[1] Wm. C. Bauman et R. Mc Kellar (Dow Chemical Co). U. S. Pat. 2614099 (1952) ; *Chem. Abstr.*, **47**, 2401 c (1953).

[2] J. Gh. Hwa (Rohm and Haas Co), Pat. Fr. 1 140 490, 1957.

[3] A. G. Greer et M. E. Gilwood (Permutit Co), U. S. 2 788 331 (1957) ; *Chem. Abstr.*, **51**, 17025 b, 1957.

[4] E. F. Riener (Rohm and Haas Co) Pat. Fr. 1 193 700, 1959.

[5] D. D. Perrin « Dissociation Constants of Organic Bases in Aqueons Solution », Londres, Butterworths, 1965, p. 15, 19.

ons de type II, à cause de leur basicité un peu plus basse, ont une moindre affinité vis-à-vis des anions inorganiques et organiques ; mais ils présentent une tendance de rétention des ions OH^- et se régénèrent plus rapidement, et dans une mesure accrue, avec une quantité plus petite de NaOH que celle utilisée pour les échangeurs d'anions de type I.

Dans un ouvrage antérieur [6], on a donné certaines précisions sur la synthèse des échangeurs d'anions gel de type II ; dans le présent travail, nous nous proposons d'étudier la synthèse des échangeurs d'anions macroporeux de type II adsorbants, utilisant des copolymères ternaires macroporeux styrène-acrylonitrile (AN)-divinylbenzène (DVB) obtenus en présence du toluène, de poursuivre l'influence des facteurs conditionnant la réaction d'amination avec la DHEA et d'insister sur le rôle joué par le diméthylformamide (DMF) dans cette réaction. Noda et Kagawa ont étudié l'influence du DMF seulement sur la réaction d'amination à l'aide des trialkylamines.[7]

MATÉRIAUX ET MÉTHODES

– Copolymères macroporeux styrène-1,25 % AN-27 % DVB, obtenu en présence de toluène comme partenaire inerte.[8]

Après la copolymérisation les perles obtenues ont été lavées à l'eau, tamisées par voie humide entre 0,31 – 0,65 mm et le toluène extrait à l'acétone dans un appareil Soxhlet. Les caractéristiques du copolymère étaient les suivantes :

Coefficient de toluène	Coefficient de méthanol	Densité apparente	Densité spécifique
1,7619	0,4449	1,0182	1,1283

– Monochlorodiméthyléther (MCDE) redistillé avant l'utilisation (*p. e.* = 56 – 60°, n_D^{25} = = 1,3949 et ρ_{25} = 1,062).

– Chlorure de zinc pur, déshydraté par fusion, avant l'utilisation.

– Diméthyl-2-hydroxyéthylamine (N,N-diméthyléthanolamine) (DHEA) pure Fluka, avec ρ_{25} = 0,89, fraîchement distillée.

– Benzène, N-N-diméthylformamide (DMF) *p. a.*

– Acilan Naphtolrot 6 B 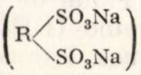

$\left(R\begin{matrix}\diagup SO_3Na\\ \diagdown SO_3Na\end{matrix}\right)$

La chlorométhylation du copolymère macroporeux a été effectuée à l'aide de MCDE en présence du chlorure de zinc dans le rapport molaire copolymère /MCDE/ $ZnCl_2$ = 1/10/0,7, pendant 5h, à 40°. On a lavé au méthanol et ensuite à l'eau le copolymère chlorométhylé (Co – CM) jusqu'à l'élimination totale du chlore ionique.

Le copolymère chlorométhylé (Co – CM) avait un contenu de 13,30 % Cl, correspondant à un degré de transformation molaire de 66,47 %.

La réaction d'amination à la DHEA a été effectuée en milieu de DMF, benzénique ou aqueux, ou en solutions aqueuses de différentes concentrations volumétriques de DMF, en ajoutant l'amine sous l'agitation continue dans le ballon de réaction où se trouvait le copolymère chlorométhylé dans un bain thermostaté à la température choisie.

---

[6] I. Petrariu, C. Luca et M. Dima, *Rev. Chim.* (*București*), **19**, 576 (1968).

[7] I. Noda şi I. Kagawa, *Kogyo Kagaku Zasshi*, **66**, 857 (1963) ; *Chem. Abstr.*, **60**, 6947 a (1964).

[8] J. R. Millar, D. G. Smith, W. E. Marr et T. R. E. Kressman, *J. Chem. Soc.* **1968**, 218.

Après la réaction, les perles d'échangeurs d'anions obtenues ont été lavées avec une solution de HCl 4 % et ensuite à l'eau, jusqu'à la disparition du chlore ionique des eaux de rinçage.

Le copolymère aminé, selon les conditions optimales décrites dans la partie « Résultats et discussions », contenait 3,10 %N (capacité d'échange = 2,20 méq/g) qui correspond à un degré de transformation molaire de 70,67 %. On a exprimé dans tous les cas le degré de transformation (DT) du Co—CM dans la réaction avec la DHEA, par la capacité d'échange (CE) calculée à partir du contenu en azote des échangeurs d'anions obtenus.

— La stabilité chimique de l'échangeur d'anions vis-à-vis des oxydants et des hydroxydes alcalins a été évaluée par détermination de la capacité d'échange, avant et après le traitement d'un échantillon avec l'H_2O_2 30 %, pendant 10h, à 80°, ou avec une solution 10 N de NaOH (dans un rapport échangeur d'anions/solution = 1/20 g/g).

La capacité d'échange des échantillons a été déterminée par titrage pH-métrique, effectué à l'aide d'une solution de HCl 1 M, sur un échantillon d'échangeur d'anions sous forme hydroxyle, qui se trouvait dans une solution de NaCl 1 M. On a travaillé en atmosphère d'azote, à 20° et avec un rapport échangeur d'anions/solution NaCl 1 M = 1/100 g/g.

Les valeurs du pH ont été mesurées à l'aide d'un pH-mètre type 22-Radiometer-Copenhague et d'une électrode combinée verre-calomel.

La valeur de la stabilité chimique de l'échantillon en solution a été calculée par la formule :

$$X = \frac{CE_{apD} \cdot 100}{CE_{avD}}$$

où

CE_{apD} = capacité d'échange après dégradation ;
CE_{avD} = capacité d'échange avant dégradation.

Les analyses d'azote ont été effectuées d'après Kjeldahl (méthode semi-microanalytique).

— Les spectres IR des échangeurs d'anions ont été enregistrés avec un spectrophotomètre Unicam SP—200, les échantillons étant préparés par pastillage avec du KBr.

On a estimé la stabilité thermique par analyse thermogravimétrique et thermodifférentielle à l'aide d'un dérivatographe F. Paulik, J. Paulik et L. Erdey, en présence de l'air, avec une vitesse de chauffage de 9,8°/mn.

— Pour apprécier les propriétés adsorbantes des échangeurs d'anions synthétisés on a étudié la dynamique d'adsorption du colorant Acilan Naphtolrot 6B sur l'échangeur d'anions sous forme de Cl.[9] A cette fin on a utilisé un photocolorimètre Spekol Carl Zeiss Jena.

RÉSULTATS ET DISCUSSIONS

Dans une série d'essais préliminaires on a établi que le rapport molaire Co—CM/DHEA=1/2 représente la valeur maximale pour laquelle, dans les conditions données de réaction, on ne constate plus une croissance significative du degré de transformation. C'est pourquoi, dans toutes les expérimentations effectuées pour établir l'influence des autres facteurs sur le degré d'amination, on a utilisé cette valeur du rapport molaire Co—CM/DHEA.

Pour trouver les conditions optimales d'amination, on a effectué une série d'essais sur l'influence de la nature du solvant sur le degré de transformation, c'est-à-dire sur la capacité d'échange de l'échangeur d'anions obtenu (calculé d'après le contenu en azote). Parmi les solvants organiques qui influencent favorablement la réaction de quaternisation du copolymère styrène—DVB chlorométhylé avec les amines tertiaires, on a choisi le DMF et le benzène.

---

[9] F. Martinola et G. Naumann, *Angew. Makromol. Chemie*, 4/5, 185 (1968).

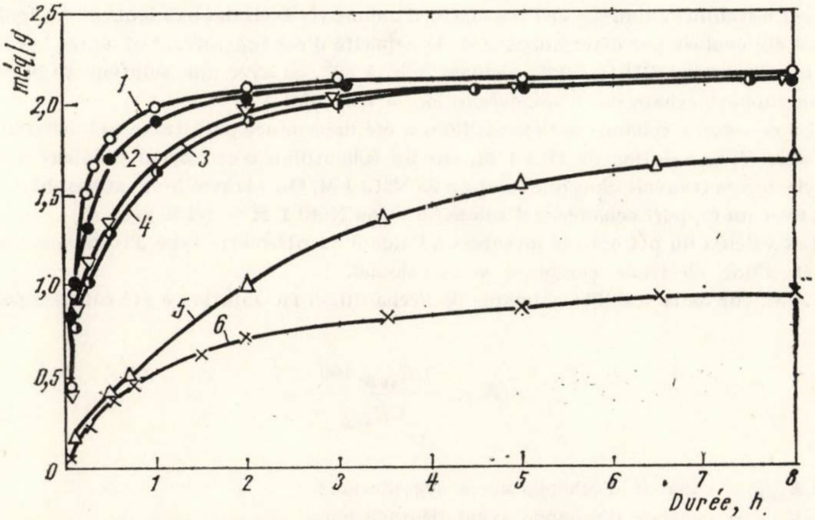

Fig. 1. — Influence de la nature du solvant sur la valeur du degré de transformation (exprimé comme capacité d'échange calculée d'après le contenu en azote).

Conditions de réaction : rapport molaire CoCM/DHEA = 1/2 ; concentration de l'amine dans la solution 9,1% ; rapport gravimétrique CoCM/solvant = 1/15 ; 1, DMF, 50° ; 2, benzène, 50° ; 3, DMF, 40° ; 4, benzène, 40° ; 5, solution aqueuse 5% de DMF, 40° ; 6, eau 50°.

Dans la figure 1 on observe qu'à une température modérée de réaction (40—50°), l'amination avec la DHEA se déroule en DMF et benzène presque identiquement courbes (*1—4*) et on obtient en 2—3 heures la valeur maximale de degré de transformation (CE = 2,20 méq/g).

Des différences peu significatives apparaissent seulement aux premiers stades de la réaction. On peut comparer la courbe *6* qui indique la variation du degré de transformation, exprimé comme CE, quand la réaction d'amination s'effectue dans l'eau et la courbe *5* qui montre l'influence positive de l'addition d'une petite quantité de DMF dans l'eau sur l'accroissement de la vitesse de réaction.

Ainsi, au cas de l'amination dans une solution de 5% DMF dans l'eau (courbe *5*), pour les conditions mentionnées dans la figure 1, on réalise la valeur maximale de la capacité d'échange après 12—14 h, tandis qu'au cas de la réaction effectuées dans l'eau (courbe *6*) sont nécessaires 48 h.

Dans une autre série d'expériences, on a suivi l'influence de la température du milieu réactionnel sur la valeur du degré de transformation exprimé comme CE.

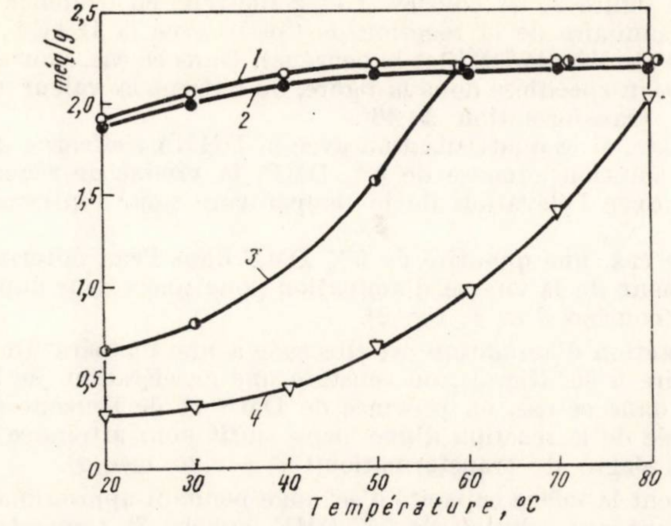

Fig. 2. – Variation du degré de transformation en fonction de la température.

Conditions de réaction : rapport molaire CoCM/DHEA = 1/2 ; concentration de l'amine en solution = 9,1% ; durée de la réaction 5 h ; 1, DMF ; 2, benzène ; 3, solution aqueuse de DMF ; 4, eau.

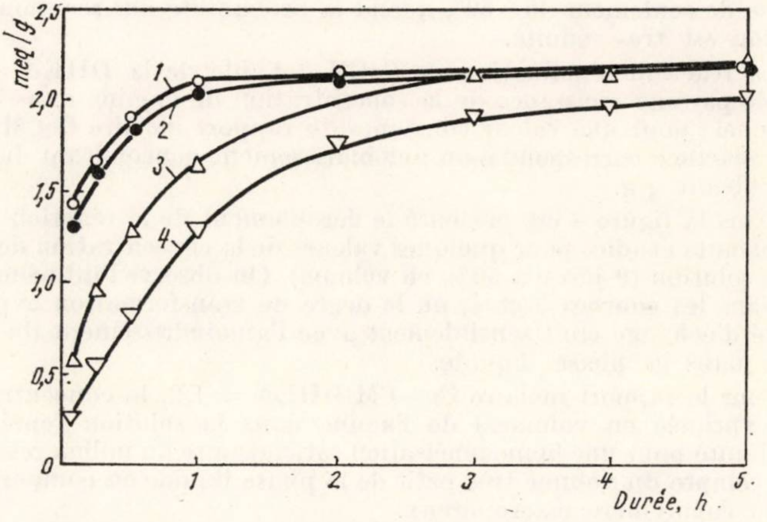

Fig. 3. – Variation du degré de transformation en fonction de la durée de la réaction à 80°.

Conditions de réaction : rapport molaire CoCM/DHEA = 1/2 ; Concentration de l'amine en solution = 9,1%. 1, DMF ; 2, benzène ; 3, solution aqueuse 5% de DMF ; 4, eau.

Dans la figure 2, les courbes *1* et *2* mettent en évidence aussi un déroulement similaire de la réaction de CoCM avec la DHEA, dans les deux solvants étudiés (le DMF et le benzène). Dans ce cas, pour les conditions de réaction spécifiées dans la figure, on obtient la valeur maximale du degré de transformation à 40°.

Par contre, si la quaternisation avec la DHEA s'effectue dans l'eau ou dans une solution aqueuse de 5% DMF, la vitesse de réaction croît sensiblement avec l'élévation de la température pour l'intervalle de 20 à 60°.

Dans ce cas, une quantité de 5% DMF dans l'eau détermine aussi un accroissement de la vitesse d'amination pour une valeur donnée de la température (courbes *3* et *4*, fig. 2).

Si la réaction d'amination est effectuée à une température plus élevée, c'est-à-dire à 80° (fig. 3), on constate une accélération de la vitesse de réaction; dans ce cas, en présence de DMF et de benzène (courbe *1* et *2*) une durée de la réaction d'une heure suffit pour atteindre la valeur maximale du degré de transformation(CE = 2,20 méq/g).

On obtient la même capacité d'échange pendant approximativement 3 h, en utilisant une solution de 5% DMF (courbe *3*). Cependant, à 80°, la réaction d'amination peut s'effectuer aussi dans l'eau avec un degré de transformation élevé (capacité d'échange 2,00 méq/g, courbe *4*).

Pourtant, dans ces conditions sont possibles des réactions de dégradation chimique des groupements ammonium avec formation de groupements aminiques d'une moindre basicité et l'échangeur d'anions n'est plus monofonctionnel. Par conséquent, on préfère utiliser une température de synthèse de seulement 40—50°, quand la probabilité des réactions de dégradation est très réduite.

La réaction d'amination de CoCM à l'aide de la DHEA est aussi favorisée par une croissance de la concentration de l'amine dans le milieu réactionnel; pour une valeur constante du rapport molaire CoCM/DHEA, cette croissance correspond à un amoindrissement concomitant du rapport CoCM/solvant g/g.

Dans la figure 4 est présenté le déroulement de la réaction dans les trois solvants étudiés pour quelques valeurs de la concentration de l'amine dans la solution (9 jusqu'à 50% en volume). On observe l'influence la plus nette dans les courbes *3* et *4*, où le degré de transformation exprimé en capacité d'échange croît sensiblement avec l'amoindrissement du contenu en eau dans la phase liquide.

Pour le rapport molaire Co—CM/DHEA = 1/2, la concentration de 50% (exprimée en volumes) de l'amine dans la solution représente la valeur limite pour une homogénéisation satisfaisante du milieu réactionnel, tenant compte du volume très petit de la phase liquide en comparaison de celui du copolymère macroporeux.

D'après la figure 5 on peut conclure que dans le cas de l'utilisation du DMF et du benzène comme solvants pour un rapport CoCM/solvant = 1/2 g/g et une concentration de l'amine en solution de 37,5%, la réaction avec la DHEA est bien accélérée et on peut obtenir la valeur maximale du degré de transformation (CE = 2,20 méq/g) dans 5 h à 22° (courbes *3* et *4*) et dans une heure à 40° (courbes *1* et *2*).

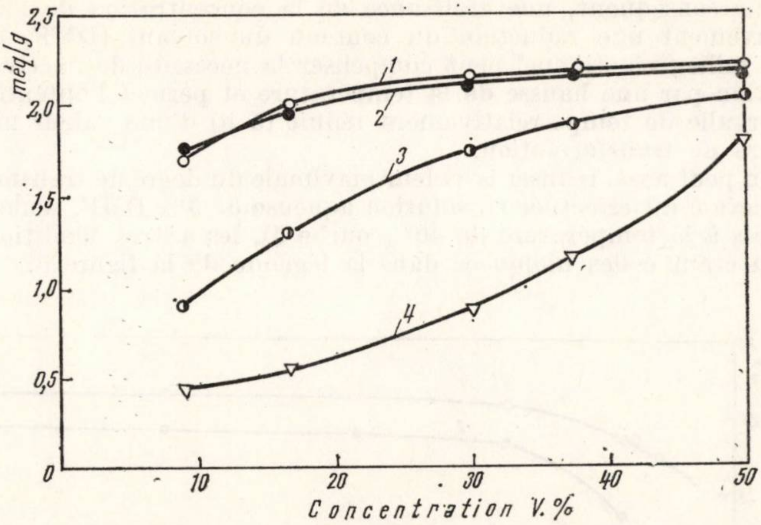

Fig. 4. — Variation du degré de transformation en fonction de la concentration de l'amine en solution.

Conditions de réaction : rapport molaire CoCM/DHEA = 1/2 ; température = 40°. 1, DMF, 2h ; 2, benzène, 2 h ; 3, solution aqueuse 5% de DMF, 2 h ; 4, eau, 5 h.

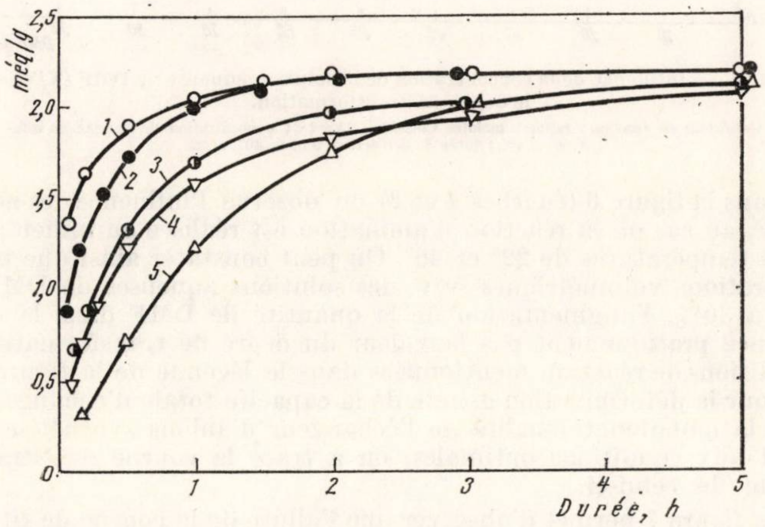

Fig. 5. — Variation du degré de transformation en fonction de la durée de la réaction, pour une concentration de l'amine en solution de 37,5 %, à 22° et à 40°.

Conditions de réaction : rapport molaire CoCM/DHEA = 1/2 ; rapport gravimétrique CoCM/solvant = 1/2 ; 1, DMF, 40° ; 2, benzène, 40° ; 3, DMF, 22° ; 4, benzène, 22° ; 5, solution aqueuse en DMF, 40°.

Par conséquent, une croissance de la concentration de l'amine et respectivement une réduction du contenu du solvant (DMF, benzène) dans le milieu réactionnel peut compenser la nécessité de l'activation de la réaction par une hausse de la température et permet l'obtention dans un intervalle de temps relativement réduit (5 h) d'une valeur maximale du degré de transformation.

On peut aussi réaliser la valeur maximale du degré de transformation si la réaction est effectuée en solution aqueuse de 5% DMF, seulement en 5 h, mais à la température de 40° (courbe 5), les autres conditions de la réaction étant celles indiquées dans la légende de la figure 5.

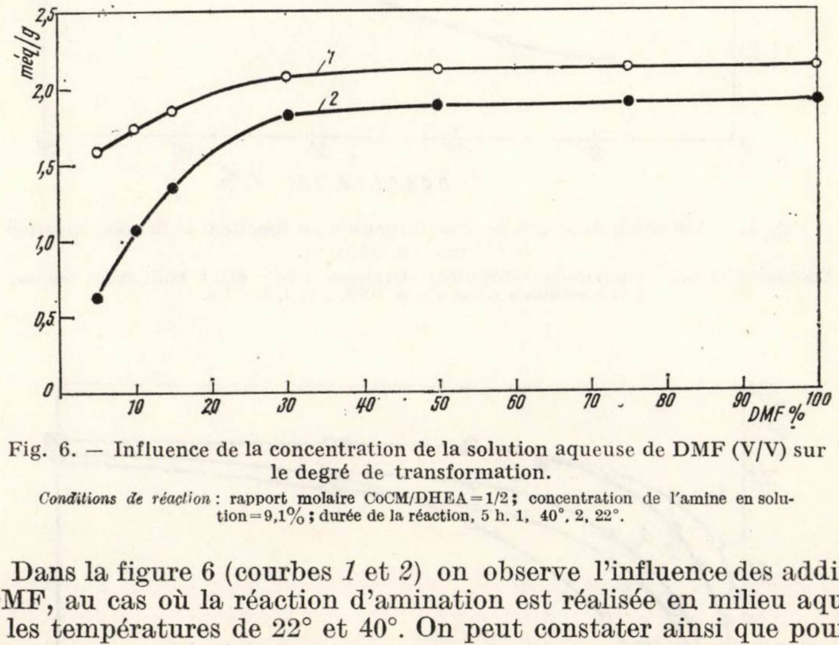

Fig. 6. — Influence de la concentration de la solution aqueuse de DMF (V/V) sur le degré de transformation.

Conditions de réaction : rapport molaire CoCM/DHEA = 1/2 ; concentration de l'amine en solution = 9,1% ; durée de la réaction, 5 h. 1, 40°, 2, 22°.

Dans la figure 6 (courbes *1* et *2*) on observe l'influence des additions de DMF, au cas où la réaction d'amination est réalisée en milieu aqueux, pour les températures de 22° et 40°. On peut constater ainsi que pour des concentrations volumétriques v/v des solutions aqueuses de DMF supérieures à 30%, l'augmentation de la quantité de DMF dans la solution n'influence pratiquement pas la valeur du degré de transformation dans les conditions de réaction mentionnées dans la légende de la figure 6.

Pour la détermination exacte de la capacité totale d'échange et pour évaluer la monofonctionnalité de l'échangeur d'anions synthétisé conformément aux conditions optimales, on a tracé la courbe de titrage pH-métrique de celui-ci.

La figure 7 permet d'observer que l'allure de la courbe de titrage est spécifique des échangeurs d'anions fortement basiques de type II.

Pour comparaison, on a titré aussi d'Amberlite IRA-910 (échangeurs d'anions fortement basiques macroporeux de type II). La détermination des groupements faiblement basiques, par voie pH-métrique pour les deux échangeurs d'anions présentés dans la figure 7, a donné des valeurs inférieures à 5% de la capacité d'échange totale. Il s'ensuit que les deux échangeurs d'anions sont pratiquement monofonctionnels.

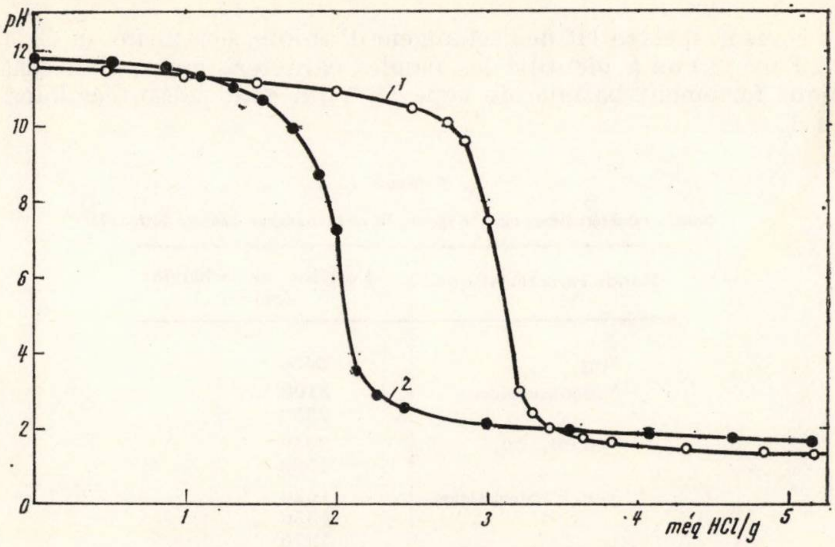

Fig. 7. — Courbes de titrage pH-métrique.

1. —○— Amberlite IRA-910. 2. —●— l'échangeur d'anions de type II synthétisé.

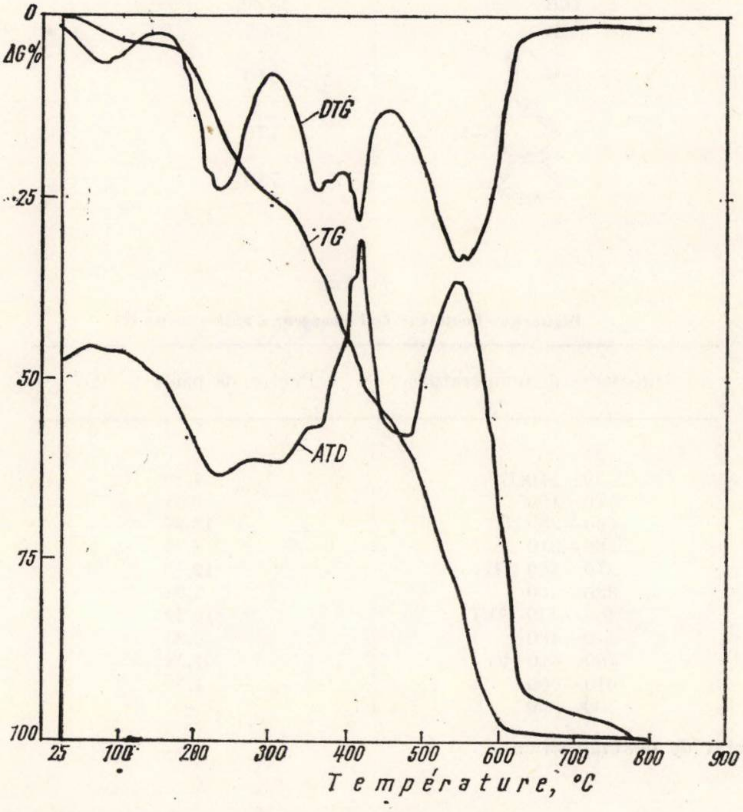

Fig. 8. — Décomposition thermique de l'échangeur d'anions synthétisé.

Dans le spectre IR de l'échangeur d'anions sous forme de Cl^- (CE = = 2,20 méq/g) on a identifié les bandes caractéristiques d'un échangeur d'anions fortement basique de type II [10] qui sont présentées dans le tableau 1.

Tableau 1

Bandes caractéristiques dans le spectre IR de l'échangeur d'anions (forme Cl)

Bande caractéristique	Position de la bande (cm^{-1})
ν_{OH}	3450
$\nu_{CH(aromatique)}$	3100 2850
$\nu_{CH(CH_2,\ CH_3)}$	2950 1585
$\nu_{-C=C-(aromatique)}$	1620 1350 1370
$\delta_{CH(CH_2,\ CH_3)}$	1385 1460
γ_{CH}	1220
δ_{OH}	1095
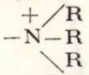	910
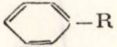	770
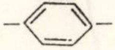	710

Tableau 2

Destruction thermique de l'échangeur d'anions (forme Cl)

Intervalle de température	Pertes de poids % ΔG
25–50	–
50–110(I)	1,58
110–190*	2,11
190–280 (II)	15,87
280–310	4,23
310–380 (III)	12,70
380–400	4,24
400–440 (IV)	10,52
440–480	6,34
480–610 (V)	41,27
610–700	1,5
700–900	–

*) Point de décomposition.

---

[10] D. Whittington et J. R. Millar, *J. Appl. Chem.*, **18**, 122 (1968).

Les données de l'analyse thermogravimétrique et thermodifférentielle pour le même échangeur d'anions sont indiquées dans la figure 8 et le tableau 2.

On constate que l'échangeur d'anions sous forme de Cl est stable pendant le chauffage dans l'air jusqu'à 50° ; en continuant le chauffage jusqu'à 900°, on peut distinguer cinq processus de décomposition exothermique indiqués dans le tableau 2 par chiffres romains. Entre 200°–600° se produit la décomposition massive de l'échangeur d'anions qui perd dans cet intervalle de température plus de 96% de son poids initial.

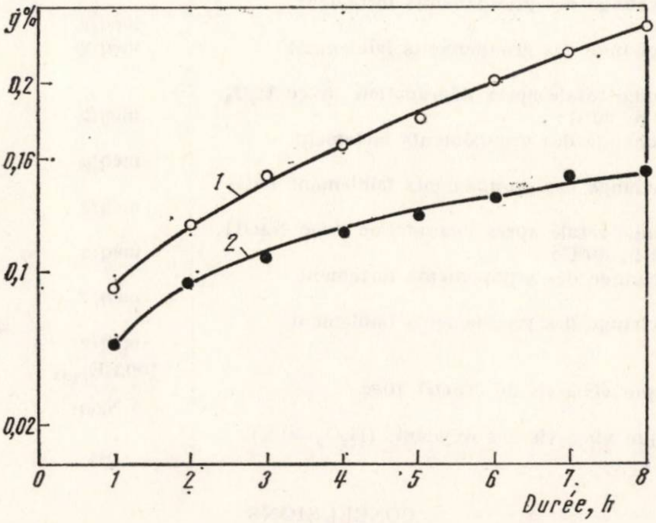

Fig. 9. — Dynamique de l'adsorption du colorant Acilan Naphtolrot 6 B ; g% grammes colorant sur 100 g échangeur d'anions.
1, –○– Amberlite IRA-910 ; 2, –●– échangeur d'anions de type II.

La figure 9 présente la dynamique de l'adsorption du colorant Acilan Naphtolrot 6 B sur l'échangeur d'anions synthétisé, en comparaison de l'Amberlite IRA-910.

La figure 9 révèle que l'allure des courbes est semblable et que la valeur de l'adsorption du colorant, pour une durée de contact de 8 h, représente pour l'échangeur d'anions synthétisé 67% de l'adsorption déterminée dans les mêmes conditions pour l'Amberlite IRA-910. La quantité de colorant retenue et la vitesse d'adsorption plus grande de l'Amberlite IRA-910 sont déterminées probablement par la valeur plus grande de la CE de celui-ci (3,30 méq/g).

Les caractéristiques physico-chimiques de l'échangeur d'anions fortement basique obtenu par amination avec de la DHEA sont présentées dans le tableau 3.

Tableau 3

Caractéristiques physico-chimiques de l'échangeur d'anions de type II (forme Cl)

Dénomination de la caractéristique	Unité de mesure	Valeur
Granulosité	mm	0,31–0,65
Poids volumétrique (humidité 19,98%)	kg/l	0,708
Contenu total d'azote déterminé par analyse élémentaire	%N	3,10
Capacité d'échange totale (calculée d'après le contenu d'azote)	méq/g	2,20
Capacité d'échange déterminée par titrage pH-métrique :	méq/g	2,20
a. Capacité d'échange des groupements fortement basiques	méq/g	2,10
b. Capacité d'échange des groupements faiblement basiques	méq/g	0,10
Capacité d'échange totale après dégradation avec H_2O_2 30%, 10 h, 80°C :	méq/g	1,78
a. Capacité d'échange des groupements fortement basiques	méq/g	1,40
b. Capacité d'échange des groupements faiblement basiques	méq/g	0,38
Capacité d'échange totale après dégradation avec NaOH, 10 N, 10 h, 80°C :	méq/g	1,99
a. Capacité d'échange des groupements fortement basiques	méq/g	1,11
b. Capacité d'échange des groupements faiblement basiques	méq/g	0,88
Stabilité chimique vis-à-vis du NaOH 10%	$\frac{100.CE_{apD}}{CN_{avD}}$	90,5
Stabilité chimique vis-à-vis des oxydants (H_2O_2 30%)	,,	81,8
Domaine du pH	pH	0–12

CONCLUSIONS

— On a étudié les conditions optimales d'obtention d'un échangeur d'anions macroporeux adsorbant par amination avec de la DHEA (échangeur d'anions de type II).

— On a trouvé que les solvants organiques (DMF, benzène) sont des milieux d'amination meilleurs que l'eau et que l'addition de DMF dans la solution aqueuse d'amines accélère sensiblement la vitesse de réaction.

— Dans le cas d'un rapport molaire CoCM/DHEA constant, l'élévation de la concentration de l'amine dans la phase liquide, respectivement un amoindrissement du rapport gravimétrique CoCM/solvant, a un effet favorable sur la vitesse de réaction.

— L'échangeur d'anions, synthétisé conformément aux conditions optimales établies, a été caractérisé par détermination de la nature et du nombre des groupements fonctionnels par titrage pH-métrique, spectrophotométrie IR et analyse thermogravimétrique et thermodifférentielle. Ces déterminations indiquent que l'échangeur d'anions obtenu est pratiquement monofonctionnel.

— On a établi aussi que l'échangeur d'anions macroporeux adsorbant présente une bonne résistance chimique vis-à-vis de l'H_2O_2 et du NaOH 10 N et des propriétés adsorbantes comparables à l'Amberlite IRA–910.

CORRIGENDA

The following corrections are to be made in the paper "The proton magnetic resonance spectrum of thioacridone", published in N⁰ 8, 1972, of this journal:

1) On page 1426, in the last column of Table 1, the words: "saturated solution" and "DMS—d_6 solution" will be lowered by one line, respectively.

2) On page 1427, the formulas IV and VI should read:

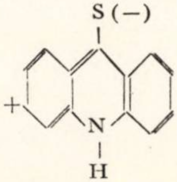

IV

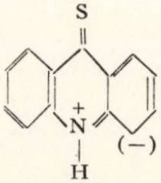

VI

3) On page 1429, line 4 from the top should read: is connected to the above mentioned desactivating process.

4) On page 1429, formula XI should read:

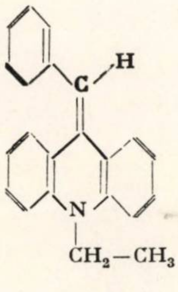

XI

5) On page 1430, line 3 from the botom should read: $\rangle C{=}S$ group a character of a simple bond, in the case of thioacridone.

6) On page 1432, line 6 from the botom should read:

. . . protons of 10-ethyl-9 (o-methyl-benzal) 9,10-dihydroacridine (XI,

7) On page 1433, the heading of Table 3 should read:

Deshielding effect of cyclic groups $\rangle C{=}X$ on the protons in *ortho* position ($H_{1,8}$)

8) On page 1434, line 9 from the top should read:

. . . . . . degree of the double bond: $\rangle C{=}X \leftrightarrow \underset{(+)\,|\,(-)}{\overset{|}{-C-}}X$, respectively to

NOTE POUR LES AUTEURS

La *Revue Roumaine de Chimie* publie des articles en anglais, français, russe, allemand ou espagnol. Les auteurs sont priés d'envoyer des articles, notes, communications et comptes rendus inédits.

Les manuscrits seront dactylographiés à deux intervalles. Les tableaux seront dactylographiés sur feuilles séparées, de même que la légende des figures. Les diagrammes seront tracés à l'encre de Chine sur papier calque. Les tableaux et les figures seront numérotés par des chiffres arabes, en nombre strictement nécessaire. Prière de ne pas inscrire les mêmes données dans les tableaux et les figures. Les formules chimiques seront incluses dans le texte ; en outre, elles seront transcrites sur des feuilles séparées. Les auteurs sont priés d'indiquer les caractères italiques (en soulignant les lettres au crayon), ainsi que tout autre caractère spécial. L'ordre des références bibliographiques sera celui de leur mention dans le texte ; le nom de l'auteur sera précédé de l'initiale du prénom ; les publications périodiques seront présentées suivant les prescriptions internationales. Les références seront ajoutées à la fin de l'article ; elles paraîtront comme des notes, au bas de la page. Le texte sera précédé d'un résumé, comprenant 15 lignes au maximum.

L'entière responsabilité du contenu des articles appartient aux auteurs.On publie des articles dus aux collaborateurs roumains ou étrangers. Les auteurs recevront 50 tirés à part.

PRINTED IN ROMANIA

TRAVAUX PARUS AUX ÉDITIONS DE L'ACADÉMIE DE LA RÉPUBLIQUE SOCIALISTE DE ROUMANIE

I. ZUGRĂVESCU et L. STOICESCU-CRIVETZ, **Polimerii hetero-ciclici** (Polymères hétérocycliques), 1971, 190 p., 9,50 lei.

CRISTOFOR SIMIONESCU et CLEOPATRA VASILIU-OPREA, **Mecanochimia compușilor macromoleculari** (La mécanochimie des composés macromoléculaires), 1967, 344 p., 23,50 lei.

I. V. MAXIM, **Materiale nucleare** (Matériaux nucléaires), 1969, 444 p., 30 lei.

CORNEL BODEA et collab., **Tratat de biochimie vegetală**, partea I, **Fitochimie** (Traité de biochimie végétale, Ier partie, Phytochimie), Ier vol., 1964, 747 p. + 4 annexes + 2 pl., 41 lei, IIe vol., 1265, 1962 p., 1 pl., 56 lei, IIIe vol., 1967, 773 p., 35 lei.

V. GHEȚIE et V. MICUȘAN, **Analiza imunochimică. Teorie și practică** (Analyse immunochimique. Théorie et pratique), 1966, 369 p., 28 lei.

R. PORTOCALĂ et L. POPA, **Acizii ribonucleici celulari și virali** (Les acides ribonucléiques cellulaires et viraux), 1966, 375 p., 8 pl., 26 lei.

D. PURDELA et R. VÎLCEANU, **Chimia compușilor organici ai fosforului şi ai acizilor lui** (La chimie des composés organiques du phosphore et de ses acides), 1965, 540 p., 37 lei.

SILVIA IONESCU, **Reacții chimice induse de radiațiile ionizante** (Réactions chimiques produites par les radiations ionisantes), 1963, 271 p., 15 lei.

MARIETA NICOLAE, **Fizico-chimia proceselor fotografice** (Physico-chimie des processus photographiques), 1964, 426 p. + 4 pl., 35 lei.

CRISTOFOR SIMIONESCU, MARGARETA GRIGORAŞ et AGATA CERNĂTESCU-ASANDEI, **Chimia lemnului din R. P. R.** (La chimie du bois en Roumanie), 1964, 239 p. + 6 pl., 27 lei.

I.P.I. — c. 1860

43 426

Lei 25.—

F1103

REVUE ROUMAINE DE CHIMIE

TOME 17
N° 12
Décembre 1972

RRCHAX, 17, *12*, 1935–2088 (1972)

ÉDITIONS DE L'ACADÉMIE DE LA RÉPUBLIQUE SOCIALISTE DE ROUMANIE

Rev. Roumaine Chim. 17, *12*, p. 1935–2088 (1972), Bucarest

COMITÉ DE RÉDACTION

Rédacteur en chef:

I. G. MURGULESCU, membre de l'Académie de la République Socialiste de Roumanie

Rédacteurs en chef adjoints:

A. T. BALABAN et V. E. SAHINI, membres correspondants de l'Académie de la République Socialiste de Roumanie

Collège de rédaction:

C. DRĂGULESCU, RALUCA RIPAN, CR. SIMIONESCU, membres de l'Académie de la République Socialiste de Roumanie; EM. BRATU, ECATERINA CIORĂNESCU-NENITZESCU, P. SPACU, membres correspondants de l'Académie de la République Socialiste de Roumanie; MARGARETA AVRAM, D. I. MARCHIDAN, G. NIAC et D. SĂNDULESCU

La *Revue Roumaine de Chimie* paraît 12 fois par an. Toute commande de l'étranger (fascicules ou abonnements) sera adressée à Întreprinderea de comerț exterior — Rompresfilatelia B. P. 2001, telex 011631, Bucarest, Roumanie

Les manuscrits, les livres et les revues proposés en échange, ainsi que toute correspondance seront envoyés à la rédaction :

REVUE ROUMAINE DE CHIMIE

23, str. Dumbrava Roşie, Bucarest, Roumanie

ÉDITIONS DE L'ACADÉMIE DE LA RÉPUBLIQUE SOCIALISTE DE ROUMANIE

3 bis, str. Gutenberg, Bucarest, Roumanie

REVUE ROUMAINE DE CHIMIE

Tome 17, N° 12 Décembre 1972

Page

D. OANCEA and C. PODINĂ, The kinetics of the isotopic exchange reactions between sodium iodide and benzyl iodide in hydroxylic solvents 1937–1949

C. I. GHIRVU, On the electronic structure of *o*-, *m*-, and *p*-chloronitrobenzene 1951–1961

MIGUEL MARTÍN y RAMÓN CARBÓ, Derivados del Miracil-D: relación actividad carcinoestatica-estructura electrónica localizada 1963–1967

H. L. JINDAL, N. P. BANSAL and KRISHNA BANSAL, A. C. Chronopotentiometry: a theoretical study of an irreversible electrode process preceded by a chemical reaction 1969–1975

J. ZSAKÓ, V. VOICULESCU, I. GĂNESCU and A. POPESCU, Kinetics and mechanism of substitution reactions of complexes. XLV. Solvation of the $[Cr(NCS)_4(m\text{-xylidine})_2]^{\ominus}$ ion in ethanol-water mixtures 1977–1984

C. LITEANU and T. HODIȘAN, Thin layer thermochromatography. V. Influence of the temperature gradient on the resolution of some amino-acids in thin layer chromatography 1985–1989 84

B. D. BADER und R. VÎLCEANU, Neue organische Pigmente — Isatinderivate. II. Synthese durch direkte Kondensierung 1991–1996

A. BARABÁS, Bis-(thenoyl-trifluoroacetonato)-beryllium 1997–2002

CR. I. SIMIONESCU, SILVIA IOAN, I. BENEDEK et N. ASANDEI, Réactions de copolymérisation à l'aide des dérivés organiques du titane-alcoyle-aluminium. VI. Étude par la diffusion de la lumière des copolymères acrylonitrile-styrolène obtenus à l'aide des catalyseurs homogènes Ziegler-Natta 2003–2011

NATALIA SIMIONESCU, ELENA MARIA CĂLUGĂRU and D. FELDMAN, Vinyl acetate — acrylic acid copolymers . . . . 2013–2020 R

C. V. UGLEA et PROFIRA ANDREESCU, Étude comparative des méthodes de calibrage de la chromatographie sur gel perméable. 2021–2032

I. NANU und I. GROS, Untersuchungen von Styrol–α-Methylstyrol–Divinylbenzol-Copolymeren und Kationenaustauschern durch Thermoanalyse . 2033–2041 R

Rev. Roumaine Chim. 17, *12*, 1935–2088 (1972) Bucarest

G. OSTROGOVICH and M. SAFTA, Studies in the s-triazine field (new series). V. Phenyl substituted 1,3-dimethyl-6-(β-styryl)-formoguanamide (-1*H*, 3*H*-s-triazin-2,4-dione) and the corresponding *p*-dimethylamino-β-styryl hemicyanine: 1,3,5-trimethyl-6-(*p*-dimethylamino-β-styryl)-formoguanamidium iodide 2043–2054

M. SAFTA, F. CHIRALEU, A. T. BALABAN and G. OSTROGOVICH, Quantitative study of active methyl groups in C-methyl-s-triazines. I. Hydrogen exchange kinetics of 6-methyl-s-triazine-2,4 (1*H*, 3*H*)-dione and its N-methyl derivatives (Studies in the s-triazine field. New series, VI) . . 2055–2065

INDEX DES AUTEURS 2067–2078

INDEX DES SUJETS 2078–2087

Revue Roumaine de Chimie, **17**, *12*, 1937 – 1949 (1972)

THE KINETICS OF THE ISOTOPIC EXCHANGE REACTIONS BETWEEN SODIUM IODIDE AND BENZYL IODIDE IN HYDROXYLIC SOLVENTS

D. OANCEA and C. PODINĂ

Faculty of Chemistry of the Bucharest University, Physical Chemistry Department,
Bd. Republicii 13, Bucharest, Romania

Received May 10, 1972

The kinetics of the isotopic exchange reactions between sodium iodide and benzyl iodide in *n*-propyl and *n*-butyl alcohols was studied. The results, together with the similar data reported in literature for the same reaction occurring in methyl and ethyl alcohols, are discussed on the basis of both the collision and transition state theories in solution. The rate constant of the isotopic exchange exhibits a maximum in *n*-propyl alcohol. This result could be explained in view of the compensatory behaviour of the enthalpy and entropy of activation. By using different concentrations of sodium iodide, it was found that ionic pairing occurred in these solvents at higher concentrations of ionofore.

The solvent effect on the ion-dipole reactions is a basic feature of the kinetics and mechanisms of these reactions and extensive work has consequently been carried out in this field. In the first quantitative correlations, the solvent has been looked as a continuous isotropic dielectric which alters the interactions between the reacting species, according to the electrostatic laws. [1] Often, the theories resulted from this simple reasoning could not explain satisfactorily the solvent effect.[2]

The accumulation of the new experimental data led, in the course of time, to the new points of view regarding this matter.

The study of the ion-molecule reactions in the gas phase,[3,4] as well as the calculation of the complete potential energy surfaces for an ion-dipole reaction in the gas phase [5] have shown that the activation energy of these reactions approach zero. However, the activation energy of the ion-dipole reactions in solution lays between[6] 10 and 30 kcal. mol^{-1}, and, in the light of these data, it seems that it is mainly due to the solvent effects.[5] The way in which the solvent acts is not yet entirely cleared up, but there are arguments that besides the changes of the electrostatic interactions, the solvent presence manifests itself by a reorganization occurring along the reaction coordinate.[7,8] It is apparent that the classical electrostatic theories of the solvent effects on the ion-molecule reactions in solution must be carefully used. Thus, when the reactions occur in structurally unlike solvents, as for instance protic and dipolar aprotic solvents, the electrostatic model, in which the main feature of the solvent is its dielectric constant, cannot be used. It has been pointed out that protic — dipolar aprotic solvent effects on the rates of the ion-dipole reactions can be reasonably explained on the basis of the specific solvation of the reactants and transition state.[2]

---

[1] E. S. Amis, "Solvent Effects on Reaction Rates and Mechanisms", Academic Press, New York, 1966, chap. 2.

[2] A. J. Parker, *Chem. Revs.*, **69**, 1 (1969).

[3] F. W. Lampe, J. L. Franklin and F. H. Field, *Progr. React. Kinetics*, **1**, 67 (1961).

[4] P. F. Knewstubb, "Mass Spectrometry and Ion-Molecule Reactions", Cambridge Univ. Press, Cambridge, 1969, chap. 1.

[5] E. A. Moelwyn-Hughes, "Physical Chemistry", 2^{-nd} ed., Pergamon Press, 1961, chap. 24.

However, in the similar solvents, a satisfactory accord between theory and experiment has been found, though the microscopic dielectric constant around the reactant particles differs from the macroscopic value because of the dielectric saturation effects.[9]

It must be emphasized that, in this case, only the changes brought about by the solvent on the electrostatic interactions between the reactant species are taken into account, while the solvation phenomena occurring during the formation of the transition state are disregarded. From this point of view, the satisfactory agreement between the theory and experiment would be somewhat fortuitous, particularly since the experiments have been carried out mainly in the solvent mixtures, where, it is well known, selective solvation occurs.[10,11] As a result of the selective solvation of the ionic species in the solvent mixtures, the solvent composition near the ions is changed and, consequently, the local dielectric constant differs from its macroscopic value.

The selective solvation can be avoided by using pure solvents instead of their mixtures. On the other hand, these pure solvents must have similar structures in order to keep the specific solvation as constant as possible. Primary saturated alcohols fulfil these requirements and, at the same time, their dielectric constants change appreciably on going from an alcohol to another, mainly for the first members of the class.

The kinetic study of the reaction between alcoxide ions and benzyl halides in these solvents[12-14]

$$RO^- + PhCH_2X \rightarrow PhCH_2OR + X^- \tag{1}$$

---

[6] E. A. Moelwyn-Hughes, "The Kinetics of Reactions in Solution", 2nd ed., Oxford Univ. Press, Oxford, 1947, chap. 3.

[7] E. F. Caldin, *J. Chem. Soc.*, **1959**, 3345.

[8] C. D. Ritchie, G. A. Skinner and V. G. Badding, *J. Amer. Chem. Soc.*, **89**, 2063 (1967).

[9] R. M. Noyes, *J. Amer. Chem. Soc.*, **84**, 513 (1962).

[10] J. Padova, *J. Phys. Chem.*, **72**, 796 (1968).

[11] J. B. Hyne, *J. Amer. Chem. Soc.*, **82**, 5129 (1960).

[12] I. G. Murgulescu, D. Oancea and G. Mincu, *Rev. Roumaine Chim.*, **14**, 3 (1969).

[13] I. G. Murgulescu and D. Oancea, *ibid.*, **15**, 299 (1970).

[14] I. G. Murgulescu and D. Oancea, *ibid.*, **15**, 1635 (1970).

has shown that good linear correlations of the rate constants towards the reciprocal of the dielectric constant could be obtained. However, in this case, the change of the rate constant on going from an alcohol to another might be due to both the structural changes of the alcoxide ion and solvent effects. Although the charge of the alcoxide ion is strongly localized on the oxygen atom, the alcoxide ions have different structures because of the different sizes of the hydrocarbonate chains.

On the other hand, the kinetic study of the isotopic exchange reaction between iodide ion and benzyl iodide

$$\overset{*}{I}^- + PhCH_2I \rightleftharpoons PhCH_2\overset{*}{I} + I^- \qquad (2)$$

carried out by Stillson and Kahn[15] in methyl and ethyl alcohols, has indicated a similar behaviour as compared to the reactions between methoxide or ethoxide ions and benzyl iodide in the respective alcohols.[14] This similitude consists in an increase of the rate constant on going from methyl to ethyl alcohol. At the same time, the rate constant of the reaction between benzyl iodide and alcoxides originating in higher alcohols decreases when the hydrocarbonate chain of the alcohol increases. So, the rate constant of the reaction (1) exhibits a maximum value in ethyl alcohol. Since this behaviour can be attributed to the combined contributions of the solvent and structural changes, a study of a similar ion-dipole reaction occurring in the same solvents, but keeping the same ion throughout the solvents, would indicate the preponderant factor associated with the appearance of this maximum.

With that end in view, we have studied the kinetics of the isotopic exchange between iodide ion and benzyl iodide in *n*-propyl and *n*-butyl alcohols. In the longer chain alcohols, ionic pairing can easily occur, causing a decrease in the rate constant since an ion pair is generally less reactive than a free ion. The decrease in the rate constant as a result of the ionic pairing was not observed in the systems involving alcoxide ions. Such a behaviour is somewhat to be expected since the alcoxide ions are good hydrogen bond acceptors and hence strongly solvated in hydroxylic solvents. As the iodide ion is comparatively a weaker hydrogen-bond acceptor it is less solvated and leads easier to the formation of the ion pairs. This is why our study was carried out only in *n*-propyl and *n*-butyl alcohols, the easiness of the ion pair formation increasing in the higher alcohols.

EXPERIMENTAL

Benzyl iodide was prepared by the reaction of benzyl chloride with sodium iodide in acetone solution.[16] The crude product was recrystallized three times from ethyl alcohol, obtaining a crystalline and colourless product (m.p. = 27°). All the other substances used in this study were of analitical reagent grade. The maximum water content in alcohols was determined by Karl-Fischer method and was found to be less than 0.02 %. I^{131} with a half-life period of 8 days was used as tracer. The active sodium iodide aqueous solution obtained from Institute of Atomic Physics in Bucharest, was evaporated to dryness and the residue dissolved either in *n*-propyl or *n*-butyl alcohol. The activities of the solutions were adjusted in the linear range of the counter. The isotopic exchange reactions were followed in a reaction vessel which was previously described.[13] In order to obtain the rate data, aliquots of 1 cm^3 were withdrawn at different time intervals and were thoroughly shaken with 2 cm^3 water and 7 cm^3 carbon tetrachloride. By centrifugation two phases were separated and their activities were then measured.

---

[15] P. Stillson and M. Kahn, *J. Amer. Chem. Soc.*, **75**, 3579 (1953).

[16] G. H. Coleman and C. R. Hauser, *J. Amer. Chem. Soc.*, **50**, 1196 (1928).

RESULTS AND DISCUSSIONS

The isotopic exchange law in its logarithmic form is given by [17]

$$-\ln(1-F) = R\cdot([\mathrm{PhCH_2I}]+[\mathrm{NaI}])\cdot t/[\mathrm{PhCH_2I}]\cdot[\mathrm{NaI}] \qquad (3)$$

where $[\mathrm{PhCH_2I}]$ and $[\mathrm{NaI}]$ are the total (active and inactive) concentrations of benzyl iodide and sodium iodide, respectively, in $\mathrm{mol.l^{-1}}$, F is the exchange fraction at the time t given by

$$F = A^t_{\mathrm{PhCH_2I}}/A^{\infty}_{\mathrm{PhCH_2I}} \qquad (4)$$

where $A^t_{\mathrm{PhCH_2I}}$ and $A^{\infty}_{\mathrm{Ph\,CH_2I}}$ are the activities of the organic phase at the time t and at the equilibrium ($t=\infty$), respectively, and R is the exchange rate between sodium iodide and benzyl iodide.

The plot $\log(1-F)$ against t must be a straight line with a negative slope, passing through the origin.

The rate constants of the substitution reactions were calculated by using the equation

$$R = k_2\,[\mathrm{PhCH_2I}]\cdot[\mathrm{NaI}] \qquad (5)$$

The exchange rate R can be calculated either from eq. (3) if the exchange half time $t_{1/2}$ is determined experimentally,[15] or from the slope ($\mathrm{tg}\alpha$) of the plot $\log(1-F)$ against t. This slope is given by

$$\mathrm{tg}\alpha = R\,([\mathrm{PhCH_2I}]+[\mathrm{NaI}])/2.303\,[\mathrm{NaI}]\cdot[\mathrm{PhCH_2I}] \qquad (6)$$

Combining (5) and (6), it is seen that

$$k_2 = 2.303.\mathrm{tg}\alpha/([\mathrm{NaI}]+[\mathrm{PhCH_2I}]). \qquad (7)$$

---

[17] G. FRIEDLANDER and J. W. KENNEDY, "Introduction to Radiochemistry", John Wiley and Sons. Inc., New York, 1949, p. 285.

The rate constants were calculated from eq. (7) and the exchange rates from eq. (6) by using the slopes — $\mathrm{tg}\alpha$ — obtained from experimental data by the least squares method.

The isotopic exchange given by eq. (2) can occur following three possible routes : a simple SN_2 or SN_1, or a mixed mechanism.[15] The plot $R/[PhCH_2I]$ against [NaI] might give a straight line passing through the origin and with the slope equal to k_2 (the rate constant of the bimolecular SN_2 exchange) in the first case, a straight line parallel to abscissa and with the intercept equal to k_1 (the rate constant of the unimolecular SN_1 exchange) in the second case, and a straight line with the slope k_2 and intercept k_1 in the last case. It was experimentally found that the reaction occurred through a SN_2 mechanism.

At the same time, since ionic pairing can occur in these solvents, the experimental rate constant will be given by [18,19]

$$k_2 = k_f \cdot \alpha + k_p \cdot (1 - \alpha) \tag{8}$$

where α is the dissociation degree of the ion pair, k_f and k_p are rate constants for the exchange occurring through the free ions or ion pairs, respectively. If the dissociation degree of the ion pair is known either from the experimental determinations or by making use of the existing theories of electrolyte solutions, a straight line with $(k_f - k_p)$ slope and k_p intercept must be obtained when k_2 is plotted against α.

Since the experimental determinations of α meet with difficulties in the range of the small concentrations and, on the other hand, the computed values are somewhat doubtful, we prefered to work at successive dilutions of sodium iodide. At higher dilutions, sodium iodide is entirely dissociated and k_f can be obtained by extrapolation at infinite dilution.

In the present study iodide ion was present as sodium iodide, while in the methyl and ethyl alcohols as potassium iodide.[15] For this reason we followed at first the influence of the cation on the isotopic exchange between iodide ion and benzyl iodide in ethanol. When sodium iodide was used, the mean value of the rate constant at 27.3° was 1.73 $\mathrm{l.mol^{-1}.min^{-1}}$, as compared to 1.72 $\mathrm{l.mol^{-1}.min^{-1}}$ found at the same temperature when potassium iodide was used.[15] It can be seen that no cation influence was observed and, therefore, our rate data can be undoubtly compared with the similar data obtained in methyl and ethyl alcohols.

The results of the kinetic measurements at different temperatures in *n*-propyl and *n*-butyl alcohols are given in tables 1 and 2, respectively. A kinetic run in *n*-propyl alcohol at 27° is also given in table 3.

The plots log $(1-F)$ against t are illustrated in fig. 1 for the same system.

The rate constants of the isotopic exchange decreases when concentration of sodium iodide increases. In the range of small concentrations

---

[18] N. N. Lichtin and K. N. Rao, *J. Amer. Chem. Soc.*, **83**, 2417 (1961).

[19] P. Beronius, U. Isacsson and Ann-Margret Nilson, *Acta Chem. Scand.*, **24**, 189 (1970).

Table 1

The rate constants of the isotopic exchange in *n*-propyl alcohol

$t°$	[NaI] (mol.l^{-1})	[$PhCH_2I$] (mol.l^{-1})	$10^3 \times$ tgα (min^{-1})	k_2 (l. mol^{-1} min^{-1})
17.0	0.0040	0.0213	8.57	0.780
17.0	0.0040	0.0158	7.00	0.814
17.0	0.0040	0.0124	5.70	0.798
27.0	0.0096	0.0152	21.2	1.98
27.0	0.0060	0.0265	29.5	2.09
27.0	0.0040	0.0097	13.5	2.28
27.0	0.0033	0.0249	28.6	2.33
27.0	0.0020	0.0232	25.2	2.30
27.0	0.0010	0.0149	17.1	2.47
37.0	0.0060	0.0111	42.8	5.81
37.0	0.0040	0.0113	37.1	5.58
37.0	0.0020	0.0120	36.0	5.90
37.0	0.0010	0.0046	14.7	6.02

Table 2

The rate constants of the isotopic exchange in *n*-butyl alcohol

$t°$	[NaI] (mol. l^{-1})	[$PhCH_2I$] (mol. l^{-1})	$10^3 \times$ tg α (min^{-1})	k_2 (l. mol^{-1}. min^{-1})
24.0	0.0010	0.0058	4.58	1.55
24.0	0.0025	0.0107	9.00	1.57
24.0	0.0049	0.0134	12.0	1.54
34.0	0.0010	0.0101	19.4	4.03
34.0	0.0025	0.0073	16.6	3.90
34.0	0.0035	0.0110	24.8	3.94
34.0	0.0049	0.0097	23.7	3.78
44.0	0.0010	0.0091	45.5	10.5
44.0	0.0010	0.0069	37.8	11.0

Table 3

A kinetic run for the isotopic exchange reaction in *n*-propyl alcohol at 27°; [NaI] = 0.0040 M; [$PhCH_2I$] = 0.0097 M; tgα = = 13.5×10^{-3} min^{-1}; k_2 = 2.28 l.mol^{-1}.min^{-1}

t (min.)	$A^{t}_{PhCH_2I}$	F	log $(1 - F)$
5	472	0.1841	−0.088
15	1008	0.3932	−0.217
26	1470	0.5733	−0.370
50	2008	0.7831	−0.664
75	2301	0.8974	−0.989
300	2564	1.0000	—

the rate constant keeps a constant value. This behaviour was attributed to ion pairs formation. At small concentrations, the plot R/[$PhCH_2I$] against [NaI] gives a straight line passing through the origin, which falls off at higher concentrations, as can be seen from fig. 2. From these plots, the concentration ranges where ion pairing was avoided could be established. The mean values of the rate constants were calculated disregarding those values determined at higher concentration at which ion pairing could occur.

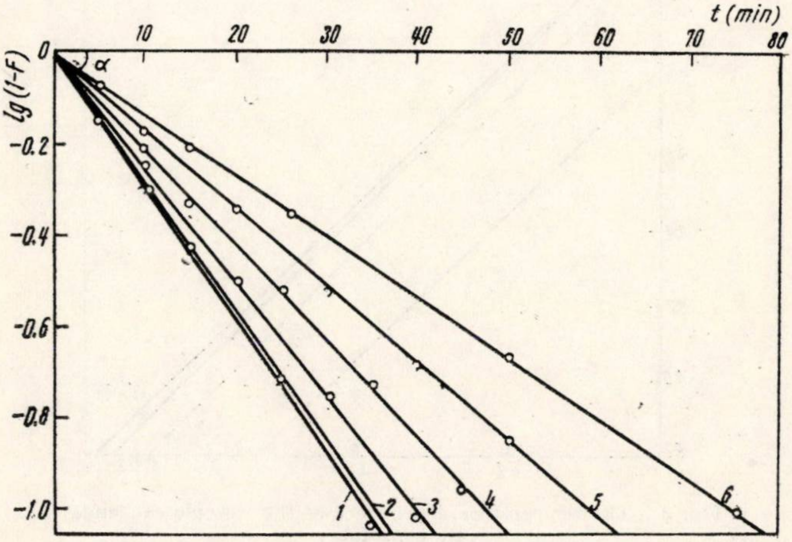

Fig. 1. — The isotopic exchange law for the system NaI* + $PhCH_2I$ in *n*-propyl alcohol at 17°. The lines have the following slopes ($10^2 \times tg\alpha$) :
1) 2.95; 2) 2.86; 3) 2.52; 4) 2.12; 5) 1.71; 6) 1.35.

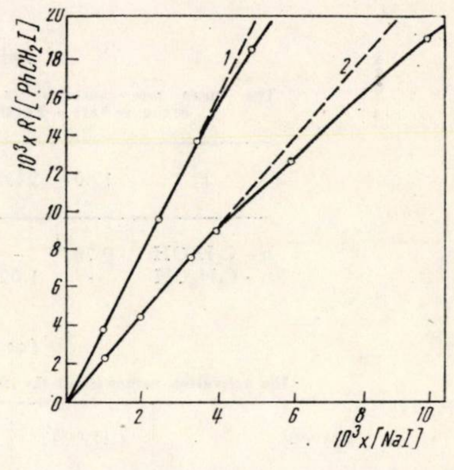

Fig. 2. — Deviations from the isotopic exchange law because of the ion pairs formation :
1) in n-C_4H_9OH at 34°; 2) in n-C_3H_7OH at 27°.

The mean rate constants at the different working temperatures are listed in table 4. The plots log k_2 against the reciprocal of absolute temperature are given in fig. 3. In table 5 there are recorded the activation parameters obtained from Arrhenius equation. In the same table there are also recorded the corresponding activation parameters reported for the same reaction in methanol and ethanol.[15] In order to compare the rate constants at the same temperature, they were calculated by interpolation at 30°, and were also listed in table 5. It can be seen from this

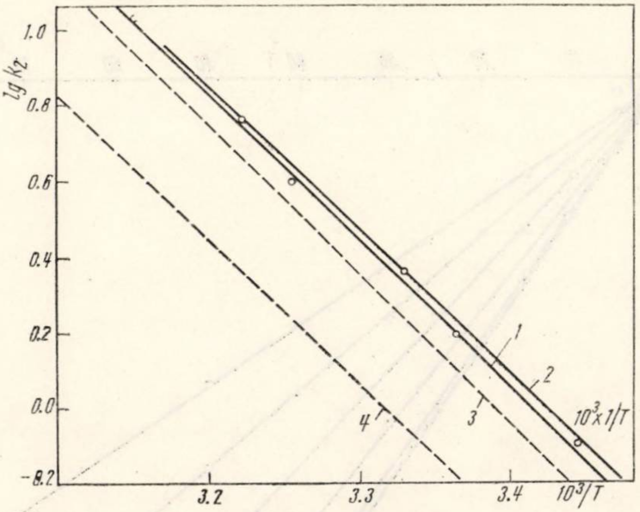

Fig. 3.—The temperature dependence of the isotopic exchange rate constants:
1) n-C_4H_9OH; 2) n-C_3H_7OH; 3) C_2H_5OH; 4) CH_3OH.

Table 4

The mean rate constants (in $l.mol^{-1}.min^{-1}$) of the isotopic exchange $NaI^* + PhCH_2I \rightleftarrows NaI + PhCH_2I^*$

$t°$	17.0	24.0	27.0	34.0	37.0	44.0
$n-C_3H_7OH$	0.797	—	2.28	—	5.74	—
$n-C_4H_9OH$	—	1.55	—	3.96	—	10.8

Table 5

The activation parameter of the isotopic exchange in different alcohols

Solvent	CH_3OH^a	$C_2H_5OH^a$	$n-C_3H_7OH$	$n-C_4H_9OH$
E_a ($kcal.mol^{-1}$)	16.200	17.300	17.550	18.100
$10^{-13} \times A$ ($l.mol^{-1}.min^{-1}$)	0.0630	0.769	1.35	3.22
$k_2^{30°}$ ($l.mol^{-1}.min^{-1}$)	1.15	2.32	2.97	2.78
$\Delta F^{\ddagger}$ ($kcal.mol^{-1}$)	15.940	15.500	15.420	15.450
$\Delta H^{\ddagger}$ ($kcal.mol^{-1}$)	15.600	16.700	16.950	17.500
$\Delta S^{\ddagger}$ (E.U.)	−1.12	3.96	5.07	6.84

a) ref. 15.

table that the rate constant of the isotopic exchange reaches a maximum in *n*-propyl alcohol. The presence of this maximum is due to the simultaneous increase of both the activation energy and preexponential factor. The increase of the activation energy when the hydrocarbonate chain of the alcohol increases is beyond the experimental error which is smaller than 500 cal.mol^{-1}. The preexponential factor increases more sharply for the lower alcohols, but its increase for the higher alcohols, although visible, is within the experimental errors. So, the presence of the maximum results from the exponential dependence of the rate constant upon the activation energy. As a matter of fact, the compensatory behaviour of the activation parameters has been long ago recognized.[20]

The changes of the activation parameters which occur when the solvent is changed can be explained from the point of view of the collision theory in solution. The collision theory of the chemical reactions in solution [21a,b,c] has proved that, as a result of the cage effect, the overall collision frequency, Z_{ov}, between the reactant particles A and B in a solvent S is given by the product of the encounter frequency, Z_{en}, by the collission frequency per encounter, Z_c

$$Z_{ov} = Z_{en} \cdot Z_c \tag{9}$$

Both Z_{en} and Z_c are dependent on the solvent viscosity, but while Z_{en} decreases, Z_c increases when the solvent viscosity increases. The reactions whose rates are dependent on the total number of collisions would be independent on the viscosity changes.[21,b] At the same time, an increase in the solvent viscosity must decrease the rates of the diffusion controlled reactions and increase the rates of the kinetically controlled reactions.[21,c] Since the viscosity of the alcohols increases when the hydrocarbonate chain increases, the frequency factor must increase in the same way. It can be seen from table 5 that the experimental data confirm these expectations.

On the other hand, the increase of the activation energy with the increase in the hydrocarbonate chain of the alcohol can be explained assuming that the hydrocarbonate chains of the alcohol molecules, which solvate iodide ion, point outwards giving rise to an external cage made up from hydrocarbonate chains. When the reacting molecules approach the ions, repulsive forces take place because of this cage, which cause an increase in the activation energy. When the hydrocarbonate chain increases in length, this external sheath becomes a better screen which prevents the approach of the solvated reacting species.

---

[20] S. Winstein and A. H. Fainberg, *J. Amer. Chem. Soc.*, **79**, 5937 (1957).

[21a] A. M. North, "The Collision Theory of Chemical Reactions in Liquids", Methuen, London, 1964.

[21b] J. E. Leffler and E. Grunwald, "Rates and Equilibria of Organic Reactions", John Wiley and Sons. Inc., New York and London, 1964, chap. 4.

[21c] I. D. Clark and R. P. Wayne, in "Comprehensive Chemical Kinetics", edited by C. H. Bamford and C. F. H. Tipper, Elsevier Publ. Comp., Amsterdam, 1969, vol. 2, chap 4.

At the same time, although the electrostatic theories of the solvent effects on the chemical reactions in solution are often in disagreement with the experiment, we tried to discuss the obtained results in terms of these theories relying on the chemical similitude of the alcoholic solvents which minimizes the specific effects. It is preferably, in this case, to use the transition state theory. The rate constant is then given by

$$k_2 = (kT/h)\cdot \exp(-\Delta F^{\ddagger}/RT) \tag{10}$$

where

$$\Delta F^{\ddagger} = \Delta H^{\ddagger} - T\Delta S^{\ddagger}. \tag{11}$$

The activation parameters at 30° were calculated as follows

$$\Delta F^{\ddagger} = 2.303\, RT\,[\log (kT/h) - \log k_2^{30}] \tag{12}$$

$$\Delta H^{\ddagger} = E_a - RT \tag{13}$$

$$\Delta S^{\ddagger} = 2.303\, R[\log A - \log (kT/h) - \log e] \tag{14}$$

The activation free energy and the activation entropy were calculated taking 1 mol/cm^3 as the standard state. The results are listed in table 5 (the rate constants used in these calculations were expressed in cm^3 mol^{-1} sec^{-1}).

The free energy of activation as well as the entropy and enthalpy of activation can be split up into an electrostatic $\Delta F^{\ddagger}_{el}$ and a nonelectrostatic $\Delta F^{\ddagger}_0$ contribution

$$\Delta F^{\ddagger} = \Delta F^{\ddagger}_0 + \Delta F^{\ddagger}_{el} \tag{15}$$

From eqs. (11) and (15) the activation entropy and enthalpy can be calculated as follows

$$\Delta S^{\ddagger} = \Delta S^{\ddagger}_0 - \mathrm{d}\,(\Delta F^{\ddagger}_{el})/\mathrm{d}T \tag{16}$$

$$\Delta H^{\ddagger} = \Delta H^{\ddagger}_0 + \Delta F^{\ddagger}_{el} - T\cdot \mathrm{d}(\Delta F^{\ddagger}_{el})/\mathrm{d}T \tag{17}$$

The electrostatic contribution of the activation free energy for an ion — dipole reaction has been calculated starting from different points of view.[22] The most frequently utilized results are given by eqs. (18 a, b and c)

$$\Delta F^{\ddagger}_{el} = N_0 Z \varepsilon \mu \cdot \cos\theta / D r_0^2 \tag{18a}$$

$$\Delta F^{\ddagger}_{el} = (N_0 Z \varepsilon \mu_x \cdot \cos\theta / D r_x^2)\cdot(1 - \mu_s \cdot r_x^2/\mu_x \cdot r_s^2) \tag{18b}$$

$$\Delta F^{\ddagger}_{el} = [N_0 (Z\varepsilon)^2/2]\cdot[(1/D) - 1]\cdot[(1/r_i) - (1/r_{\ddagger})] \tag{18c}$$

---

[22] S. W. BENSON, "The Foundations of Chemical Kinetics", McGraw-Hill Comp., New York, 1960, chap. 15.

In eq. (18a) the electrostatic contribution of the activation free energy is given by the electrostatic energy required to bring an ion of charge $Z\varepsilon$ from infinite to the reaction distance r_0 near the reacting dipole of dipole moment μ_x, under the angle θ, in the medium of dielectric constant D. In this case the reference state is a hypothetic medium with $D = \infty$.

In eq. (18b) it has been considered that $\Delta F^{\ddagger}_{el}$ arises from the displacement in the solvent sheath of the ion of a solvent molecule of dipole moment μ_s and radius r_s by a reactant solute molecule of dipole moment μ_x and radius r_x, in the medium of dielectric constant D.

In eq. (18c) it has been considered that the whole change in $\Delta F^{\ddagger}_{el}$ is due to the dielectric solvation of both reactant ion of radius r_i and transition state of radius $r_{\ddagger}$, neglecting the change brought about by the solvation of the reactant dipole which is comparatively smaller. In this case the reference state is the gas phase with $D = 1$.

It must be specified that for the considered reaction, the substitution occurs by nucleophilic attack of the iodide ion on the opposite sign end of benzyl iodide dipole, so that $Z\varepsilon \cos \theta < 0$, the electrostatic contribution being attractive.

Eqs. (18a) and (18c) indicate that the plot log k_2 versus $1/D$ must be a straight line with a positive slope in disagreement to the experimental findings. Although in the eq. (18b) certain structural effects which occur during the formation of the transition state are considered in addition, the plot log k_2 versus $(1/D)(1 - \mu_s r_x^2/\mu_x r_s^2)$ exhibits also a maximum, as can be seen from fig. 4.

If the same correlation is tested for higher temperatures, although at 60° the plot is not yet a straight line, the maximum disappears (the rate constants were calculated in this case by extrapolation). This behaviour originates in the compensatory action of the enthalpy and entropy of activation which can be illustrated following their changes against dielectric properties of the alcohols.

According to eqs. (16), (17) and (18b) it is evident that

$$\Delta S^{\ddagger} = \Delta S^{\ddagger}_0 - (N_0 Z \varepsilon \cos\theta\, \mu_x/r_x^2)\,(1 - \mu_s r_x^2/\mu_x r_s^2)\,(L/D) \tag{19}$$

$$\Delta H^{\ddagger} = \Delta H^{\ddagger}_0 - (N_0 Z\varepsilon \cos\theta\, \mu_x/r_x^2)(1 - \mu_s r_x^2/\mu_x r_s^2)\,(LT - 1)/D \tag{20}$$

where L results from the temperature dependence of dielectric constant :

$$D = C \cdot \exp(-LT) \tag{21}$$

The plots $\Delta S^{\ddagger}$ versus $f(L/D)$ and $\Delta H^{\ddagger}$ versus $f(LT - 1)/D$ are given in figs. 5 and 6, respectively, where f stands for the expression $(1 - \mu_s r_x^2/ /\mu_x r_s^2)$.

Taking into account that $Z\varepsilon\cos\theta < 0$, eqs. (19) and (20) indicate that from the above plots, straight lines with positive slopes must be obtained, in agreement with the experiment. When eqs. (18a) and (18c) are used, the same behaviour is obtained. From the slopes of the resulted lines, calculated by the least squares method, the corresponding parameters r_0 and $r_{\ddagger}$ were calculated obtaining the following results:

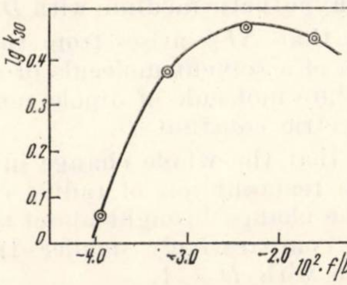

Fig. 4. — The change of the isotopic exchange rate constant brought about by the solvent effects (f stands for $1 - \mu_s\ r_x^2/\mu_x\ r_s^2$).

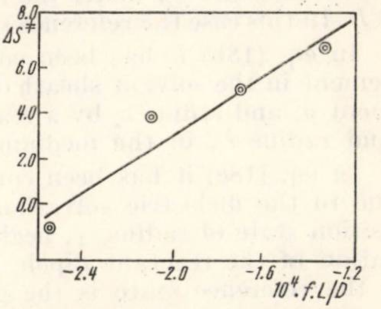

Fig. 5. — Activation entropy dependence on the structural and dielectric properties of the solvents.

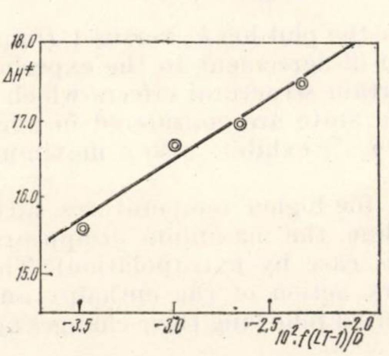

Fig. 6. — Activation enthalpy dependence on the structural and dielectric properties of the solvents.

$r_0 = 2.0$ Å (when $\cos\theta = 1$) and $r_{\ddagger} = 3.5$ Å. The data needed in these calculations are given in table 6.

Table 6

Physical properties needed in solvent effect correlation

	D_{30^0} ref. 12	$10^3.L$ (grd^{-1}) ref.[23]	r (Å) ref. 12	(D) ref.[24]
CH_3OH	31.53	6.08	2.03	1.69
C_2H_5OH	23.72	6.23	2.29	1.69
n-C_3H_7OH	18.96	6.75	2.50	1.66
n-C_4H_9OH	16.17	7.72	2.67	1.63
$PhCH_2I$	—	—	2.98 [14]	1.59 [14]
I^-	—	—	2.16 [25]	—

---

[23] „Handbook of Chemistry and Physics'', 41^{-st} ed., Chemical Rubber Publ., 1959–1960.

[24] C. P. Smyth, "Dielectric Behaviour and Structure", McGraw-Hill Book Comp., New York, 1955, p. 301.

[25] L. Pauling, "The Nature of the Chemical Bond", Cornell Univ. Press, New York, 1948, p. 346.

Having in view the simplifying assumptions, it can be concluded that there is a good agreement between theory and experiment. Because of the chemical similitude of the alcoholic solvents, the electrostatic theories of the solvent effect on the ion — dipole reactions are able to explain reasonably the trend of the change in the activation parameters. Comparatively, none of the semi-empirical parameters which describe the solvent polarity [26,27] could be used to give a reasonable explanation to the experimental data. The presence of a maximum, which is more pronounced at lower temperatures and disappears at higher temperatures can be explained on the basis of the specific solvation occurring in the alcoholic solvents. The alcohol molecules are made up from a polar hydroxyl group of small size and a nonpolar hydrocarbonate chain. The solvation of the ionic species is ensured mainly by the polar group of the solvent molecule because of both ion — dipole interaction and hydrogen bond formation. The solvation is more pronounced at lower temperatures and decreases gradually when temperature increases. So, at higher temperatures, by diminution of the specific solvent effects, the continuous dielectric model of the solvent becomes closer to reality and the theories resulted from this model lead to a better accord with experimental data.

[26] C. Reichardt, *Angew Chem. Intern. Edn.*, 4, 29 (1965).

[27] F. Fowler, A. Katritzky and R. J. Rutherford, *J. Chem. Soc.*, **B**, **1971**, 460.

Revue Roumaine de Chimie, 17, *12*, 1951–1961 (1972)

ON THE ELECTRONIC STRUCTURE OF *o*-, *m*-, AND *p*-CHLORONITROBENZENE

C. I. GHIRVU
The "Al. I. Cuza" University, Physical Chemistry Laboratory, Calea 23 August 11, Jassy, Romania

Received April 26, 1972

The charge densities and the bond orders, calculated by the CNDO method were compared with those obtained by the ASMO–CI–LCAO method in the Pariser-Parr-Pople's (PPP) approximation. The CNDO type calculations have been performed for *o*-, *m*-, and *p*- chloronitrobenzene by using the standard approximations of the method. The two sets of data are slightly different due perhaps to the contribution given by other valence electrons, in addition to those having π-character.

INTRODUCTION

During the past twenty years the PPP type method was shown to have a great power in explaining many characteristic features of π-electron chemistry. [1,2] As is well known, the basis of this method is the model of σ – π separability, the π-electron orbitals having a different symmetry with respect to the molecular plane than do σ-electron orbitals. The σ – π separability, however, is physically consistent only in the case of planar aromatic hydrocarbons. The failure of this method increases when the quantum-mechanical treatment of both nonplanar and polar molecular systems is requested. Therefore, a model of such kind cannot be ever accurate.

On the other side the "*ab initio*" methods [3] have limited practical applications due to the computation difficulties.

During the last years an increasing practical importance was given to the calculation methods taking account of all valence electrons.[4] Such a method, which we are referring to, is the CNDO method elaborated by Pople and his co-workers. [5–8]

---

[1] R. Pariser and R. G. Parr, *J. Chem. Phys.*, **21**, 466, 767 (1953).
[2] J. A. Pople, *Trans. Faraday Soc.*, **49**, 1735 (1953).
[3] L. C. Allen, *Rev. Mod. Phys.*, **32**, 275 (1960).
[4] C. I. Ghirvu, *Studii și cercetări chim.*, Acad. R.S.R., **19**, 461 (1971).
[5] J. A. Pople, D. P. Santry and G. A. Segal., *J. Chem. Phys.*, **43**, S129 (1965).
[6] J. A. Pople and G. A. Segal, *J. Chem. Phys.*, **43**, S136 (1965).
[7] J. A. Pople and G. A. Segal, *J. Chem. Phys.*, **44**, 3389 (1966).
[8] D. P. Santry and G. A. Segal, *J. Chem. Phys.*, **47**, 158 (1967).

In the present paper this method was used to calculate the charge densities and the bond orders for *o*-, *m*-, and *p*-chloronitrobenzene. The calculated results were compared with those previously obtained by using the PPP type method.

CALCULATION METHOD

The CNDO method is an approximate SCF–LCAO–MO theory taking account of all valence electrons, but the calculations are considerable reduced compared with those of a full SCF-LCAO-MO type treatment.[9] The approximations introduced in the CNDO method are similar with those of the PPP type, but the former divides the total number of electrons into the valence and the core electrons.

In this paper the CNDO/2 variant,[7] which is a slight modification of the former, CNDO/1, has been used. For brevity we shall give only a very short presentation of the CNDO method. For details we are referring to the original papers or to a recent review of them.[4]

Let ψ_i be a molecular orbital and φ_ν an atomic one. In the CNDO method φ_ν are valence orbitals. The LCAO-MO approximation starts with

$$\psi_i = \sum_\nu c_{\nu i}\varphi_\nu \tag{1}$$

Roothaan[9] used this approximation in the Hartree-Fock equations[10,11] and obtained the well-known relations

$$\sum_k F_{\mu k} c_{ki} = \sum_k S_{\mu k} c_{ki}\varepsilon_i \tag{2}$$

where (in atomic units),

$$F_{\mu k} = H_{\mu k} + G_{\mu k} \tag{3}$$

$$H_{\mu k} = <\varphi_\mu \,|\, -\frac{\Delta^2}{2} - \sum_A V_A(r) \,|\, \varphi_k> \tag{4}$$

$$G_{\mu k} = \sum_{\lambda,\,\sigma} P_{\lambda\sigma}\left[<\mu\lambda|\hat{g}|\nu\sigma> - \frac{1}{2}<\mu\sigma|\hat{g}|\nu\lambda>\right] \tag{5}$$

$$<\mu\lambda|\hat{g}|\nu\sigma> = \iint \varphi_\mu^*(1)\varphi_\lambda^*(2)\,\frac{1}{r_{12}}\,\varphi_\nu(1)\,\varphi_\sigma(2)\,d\tau_1\,d\tau_2 \tag{6}$$

$$S_{\mu\nu} = <\varphi_\mu \,|\, \varphi_\nu> \tag{7}$$

$$P_{\lambda\sigma} = 2\sum_i^{\text{occ}} c_{i\lambda}^* c_{i\sigma} \tag{8}$$

---

[9] C. C. J. Roothaan, *Rev. Mod. Phys.*, **23**, 69 (1951).
[10] D. R. Hartree, *Proc. Cambridge Phil. Soc.*, **24**, 89, 111, 426 (1928).
[11] V. Fock, *Z. Physik*, **61**, 126 (1930).

In Eq. (2) ε_i represents the orbital energy corresponding to the molecular orbital ψ_i, being a theoretical estimation of the corresponding ionization potential. $H_{\mu\nu}$ is the matrix element of the one-electron Hamiltonian including the kinetic energy and the potential energy, $V_A(r)$, in the field of the core, $G_{\mu\nu}$ is the matrix element of the potential due to other valence electrons and, as it is seen from Eq. (5), it depends on molecular orbitals via $P_{\lambda\sigma}$.

The approximations of the CNDO/1 method are

1. $$S_{\mu\nu} = \delta_{\mu\nu} \Rightarrow \sum_{\mu} c_{\mu i} c_{\mu j} = \delta_{ij} \tag{9}$$

2. $$<\mu\lambda|\hat{g}|\nu\sigma> = <\mu\lambda|\hat{g}|\nu\sigma> \delta_{\mu\lambda}\delta_{\lambda\sigma} = \gamma_{\lambda\mu} \tag{10}$$

3. The integrals $\gamma_{\mu\nu}$ are not depending on the actual form of the atomic orbitals φ_μ and φ_ν but only on the atoms which they belong to. So, if φ_μ belongs to atom A and φ_ν to atom B, then

$$\gamma_{\mu\nu} = \gamma_{AB} \tag{11}$$

4. If φ_μ and φ_ν belong to the same atom A, then

$$<\mu/V_B|\nu> = <\mu|V_B|\nu> \delta_{\mu\nu} = V_{AB} \tag{12}$$

and V_{AB} has the same value for all valence electrons of the atom A.

5. $$H_{\mu\nu} = \beta_{\mu\nu} = \beta^0_{AB} S_{\mu\nu} \tag{13}$$

where φ_μ and φ_ν are centered on different atoms, $S_{\mu\nu}$ is the overlap integral given by Eq. (7), and β^0_{AB} is a parameter depending only upon the nature of the atoms A and B.

Within these approximations the matrix elements $F_{\mu\gamma}$ become

$$F_{\mu\mu} = U_{\mu\mu} + \left(P_{AA} - \frac{1}{2} P_{\mu\mu}\right)\gamma_{AA} + \sum_{B \neq A} (P_{BB}\gamma_{AB} - V_{AB}) \tag{14}$$

$$F_{\mu\nu} = \beta^0_{AB} S_{\mu\nu} - \frac{1}{2} P_{\mu\nu}\gamma_{AB} \tag{15}$$

($\mu \neq \nu$, centered on different atoms),

where $U_{\mu\mu}$ is the diagonal matrix element of φ_μ with the one-electron Hamiltonian containing only the core of its own atom, and

$$P_{AA} = \sum_{\mu}^{A} P_{\mu\mu}, \sum_{\mu} P_{\mu\mu} = 2N \tag{16}$$

$2N$ being the number of valence electrons.

The matrix elements of the CNDO/2 method, which have been used in the present paper, are slightly different compared with those given by Eqs. (14) and (15), being

$$F_{\mu\mu} = -\frac{1}{2}(I_\mu + A_\mu) + \left[(P_{AA} - Z_A) - \frac{1}{2}(P_{\mu\mu} - 1)\right]\gamma_{AA} + \qquad (17)$$

$$+ \sum_{B \neq A} (P_{BB} - Z_B)\,\gamma_{AB},$$

$F_{\mu\nu}$ being given by Eq. (15).

In these relations I_μ and A_μ are the ionization potential and the electron affinity, respectively, both averaged over the corresponding valence states.

The physical significance of the CNDO approximations is the invariance of the results to transformations among atomic orbitals on a given atom.

RESULTS AND DISCUSSIONS

As it was stated above, the charge densities and the bond orders of the *o*-, *m*-, and *p*-chloronitrobenzene were calculated by using the CNDO/2 variant of the CNDO method. All the necessary parameters were chosen as indicated by the authors of the method.[5-8] The CNDO results were compared with those previously obtained [12] by using a modified PPP method due to Roos and Skancke.[13]

In the Roos and Skancke's modification of the PPP type method the one-electron parameter is made dependent on the surroundings to the atom which is referred to. At the same time, the core resonance integrals and the two-electron two-center Coulomb repulsion integrals between neighbours are expressed by linear distance dependent relations

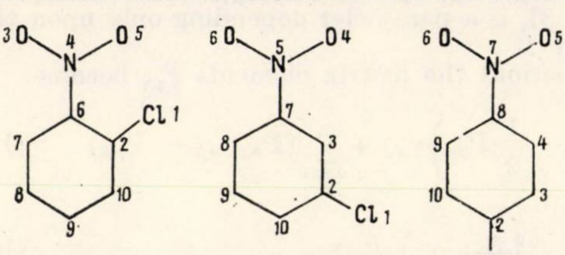

Fig. 1. — Numbering of atoms for chloronitrobenzenes.

$$\beta_{\mu\nu} = \beta^0_{\mu\nu} + \delta^\beta_{\mu\nu}(R_{\mu\nu} - R^0_{\mu\nu}) \qquad (18$$

$$\gamma_{\mu\nu} = \gamma^0_{\mu\nu} + \delta^\gamma_{\mu\nu}(R_{\mu\nu} - R^0_{\mu\nu}) \qquad (19$$

where $\delta^\beta_{\mu\nu}$ and $\delta^\gamma_{\mu\nu}$ are semi-empirical parameters. The numbering of th atoms which we are concerned with in the present paper is given in Figure 1

---

[12] C. I. Ghirvu and O. Gropen, *Acta Chem. Scand.*, **25**, 1011 (1971).

[13] B. Roos an P. N. Skancke, *Acta Chem. Scand.*, **21**, 233 (1967).

The CNDO π-electron charges and their comparison with those previously obtained by the PPP type method are given in Table 1. From Table 1 it can be observed that the two sets of values are slightly different. However, a careful analysis of these data shows that the CNDO results are more realistic. We can see, for instance, that the CNDO charge density in the *meta* position of the nitro group is greater than that corresponding to the *ortho* position, which is the reverse case in the Roos-Skancke's modification of the PPP method. It should be, however, emphasized, that the Roos-Skancke's parametrisation of the PPP method gave a very good agreement between calculated and experimental transition energies.[12] This observation for the nitro group is also valid for the corresponding positions of the chlorine atom.

Table 1

Calculated π-electron charges

Atom	Molecule					
	o-chloronitrobenzene		*m*-chloronitrobenzene		*p*-chloronitrobenzene	
	PPP[a)]	CNDO	PPP[a)]	CNDO	PPP[a)]	CNDO
1	1.9745	1.9668	1.9724	1.9735	1.9812	1.9748
2	1.1708	0.9810	1.0189	1.0004	1.2108	0.9781
3	1.6704	1.5275	1.0627	0.9743	0.8477	0.9893
4	0.7117	0.9603	1.6683	1.5272	1.2389	0.9821
5	1.6686	1.5293	0.7183	0.9608	1.6817	1.5278
6	0.8059	1.0499	1.6684	1.5288	1.6817	1.5278
7	1.0960	0.9814	0.8339	1.0518	0.6885	0.9610
8	0.9277	0.9883	1.0836	0.9698	0.5828	1.0426
9	1.0600	0.9748	0.9384	0.9977	1.2398	0.9821
10	0.9143	0.9912	1.0349	0.9670	0.8477	0.9893

[a)] ref [12]

The theoretical bond orders and the calculated and observed bond lengths are given in Tables 2, 3, 4.

Table 2

Calculated Bond Orders and Bond Lengths in *o*-chloronitrobenzene

Bond	Bond Order		Calculated Bond Length (Å)		$\Delta R' = \lvert R_{PPP} - R_{CNDO} \rvert$
	PPP	CNDO	PPP	CNDO	
1–2	0.1431	0.1742			
2–6	0.6330	0.6321	1.403	1.403	0.000
2–10	0.6405	0.6317	1.402	1.403	0.001
3–4	0.6466	0.6907	1.209	1.201	0.008
4–5	0.6482	0.6877	1.208	1.201	0.007
4–6	0.2241	0.2117	1.418	1.420	0.002
6–7	0.6450	0.6617	1.401	1.398	0.003
7–8	0.6546	0.6531	1.399	1.399	0.000
8–9	0.6683	0.6682	1.397	1.397	0.000
9–10	0.6733	0.6756	1.396	1.395	0.001

Table 3

Bond Orders and the calculated and observed Bond Lengths in *m*-chloronitrobenzene

Bond	Bond Order		Bond Length (Å)			$\Delta R = \vert R_{\text{obs}} - R_{\text{calc}} \vert$		$\Delta R' = \vert R_{\text{PPP}} - R_{\text{CNDO}} \vert$
	PPP	CNDO	Calculated		Observed	PPP	CNDO	
			PPP	CNDO				
1−2	0.1634	0.1599			1.790			
2−3	0.6484	0.6329	1.400	1.403	1.390	0.010	0.013	0.003
2−10	0.6696	0.6492	1.398	1.400	1.380	0.018	0.020	0.002
3−7	0.6454	0.6609	1.401	1.398	1.410	0.009	0.012	0.003
4−5	0.6469	0.6909	1.208	1.201	1.250	0.042	0.049	0.007
5−6	0.6469	0.6898	1.209	1.201	1.220	0.011	0.019	0.008
5−7	0.2329	0.2071	1.416	1.421	1.480	0.064	0.059	0.005
7−8	0.6421	0.6548	1.401	1.399	1.430	0.029	0.031	0.002
8−9	0.6570	0.6523	1.399	1.399	1.380	0.019	0.019	0.000
9−10	0.6623	0.6756	1.396	1.395	1.400	0.004	0.005	0.001

Table 4

Calculated Bond Orders and Bond Lengths for p-chloronitrobenzene

Bond	Bond Order		Calculated Bond Length (Å)		$\Delta R' = \lvert R_{PPP} - R_{CNDO} \rvert$
	PPP	CNDO	PPP	CNDO	
1–2	0.1210	0.1574			
2–3	0.6487	0.6485	1.400	1.400	0.000
2–10	0.6487	0.6485	1.400	1.400	0.000
3–4	0.6639	0.6603	1.397	1.398	0.001
4–8	0.5947	0.6550	1.410	1.399	0.011
5–7	0.6412	0.6902	1.210	1.201	0.009
6–7	0.6412	0.6902	1.210	1.201	0.009
7–8	0.2037	0.2080	1.421	1.421	0.000
8–9	0.5947	0.6550	1.410	1.399	0.011
9–10	0.6639	0.6603	1.397	1.398	0.001

The obtained bond orders have been used to estimate the corresponding bond distances. For this purpose the following semi-empirical relations have been applied [13,14,15]

$$R_{\mu\nu}(\mathrm{C,\ C}) = 1.517 - 0.18\, p_{\mu\nu} \tag{20}$$

$$R_{\mu\nu}(\mathrm{C,\ N}) = 1.458 - 0.18\, p_{\mu\nu} \tag{21}$$

$$R_{\mu\nu}(\mathrm{C,\ O}) = 1.325 - 0.18\, p_{\mu\nu} \tag{22}$$

In these equations, $p_{\mu\nu}$ is the mobile bond order between atoms μ and ν, and the constants are dependent upon the nature of the corresponding bonds. Unfortunately, the only available experimental data are those for *m*-chloronitrobenzene.[16]

In order to get a good comparison between the two sets of calculated bond distances and between the former and those experimentally observed we introduced the quantity

$$\Delta R = \lvert R_{\mathrm{exp}} - R_{\mathrm{calc}} \rvert \tag{23}$$

In the cases where the experimental results were not available the only quantity

$$\Delta R' = \lvert R_{\mathrm{PPP}} - R_{\mathrm{CNDO}} \rvert \tag{24}$$

was given in the corresponding tables.

From Tables 2, 3, 4 a good agreement between the two sets of calculated data can be observed. In the case of *m*-chloronitrobenzene we

---

[14] I. Fischer-Hjalmars and M. Sundbom, *Acta Chem. Scand.*, **22**, 607 (1968).

[15] O. Gropen and P. N. Skancke, *Acta Chem. Scand.*, **23**, 2685 (1969).

[16] E. M. Gopalakrishna, *Z. Krist.*, **121**, 378 (1965).

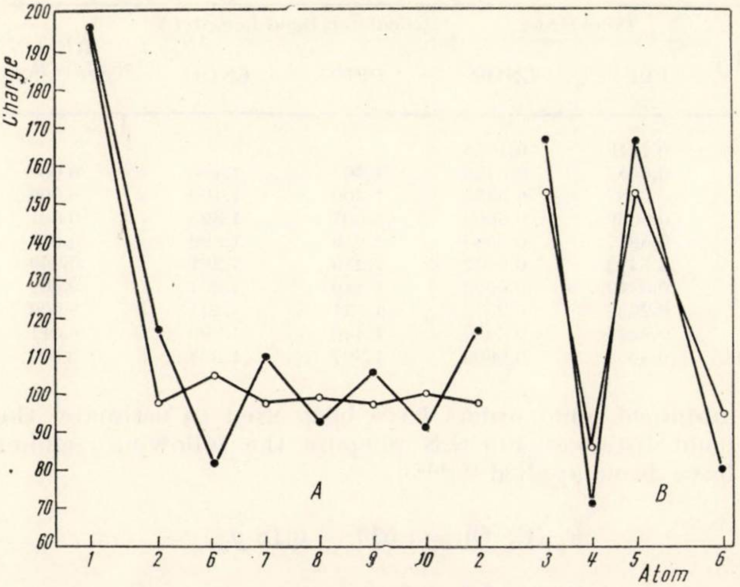

Fig. 2. — Diagram of charge distribution in *o*-chloronitrobenzene :

○ CNDO; ● PPP

A. In the ring, B. In the substituent.

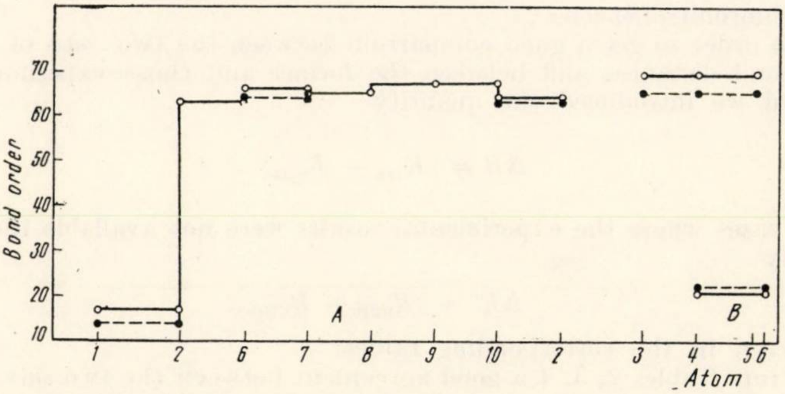

Fig. 3. — Diagram of bond order distribution in *o*-chloronitrobenzene :

○ CNDO; ● PPP

A. In the ring, B. In the substituent.

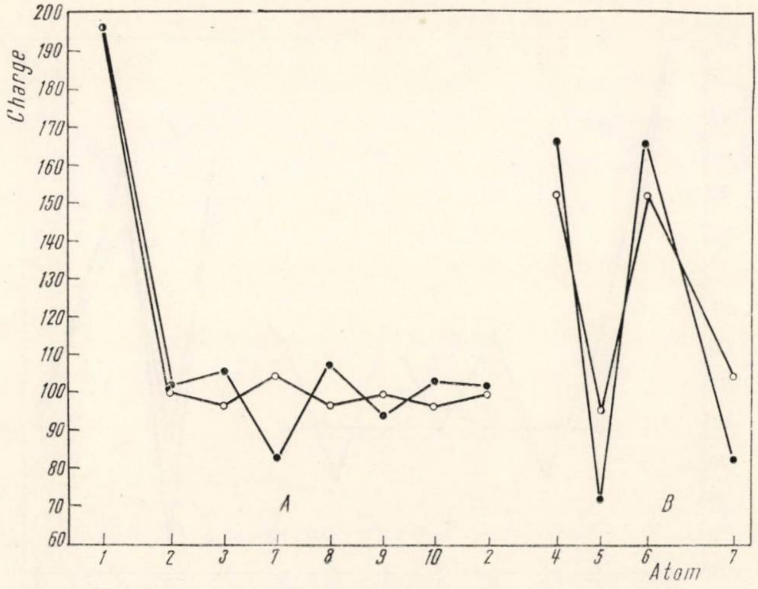

Fig. 4. — Diagram of charge distribution in *m*-chloronitrobenzene:

○ CNDO; ● PPP
A. In the ring, B. In the substituent.

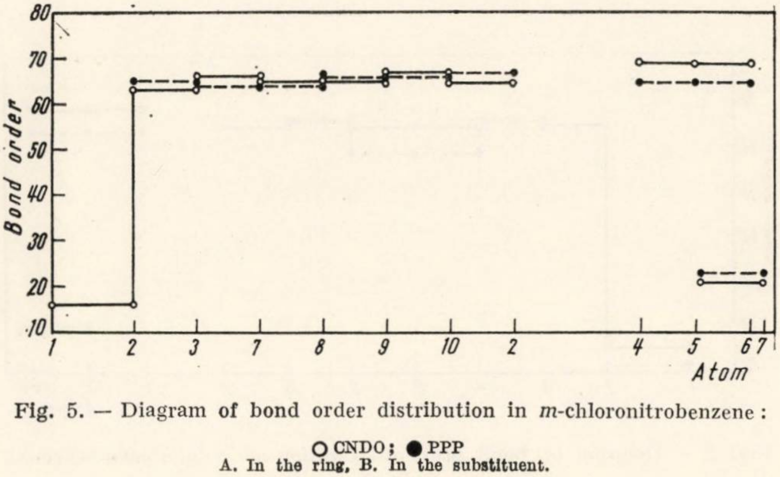

Fig. 5. — Diagram of bond order distribution in *m*-chloronitrobenzene:

○ CNDO; ● PPP
A. In the ring, B. In the substituent.

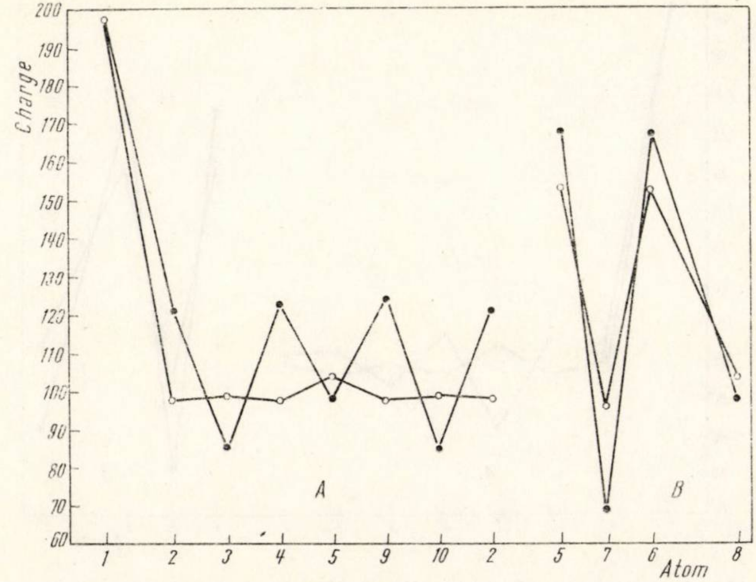

Fig. 6. — Diagram of charge distribution in *p*-chloronitrobenzene:

○ CNDO; ● PPP
A. In the ring, B. In the substituent.

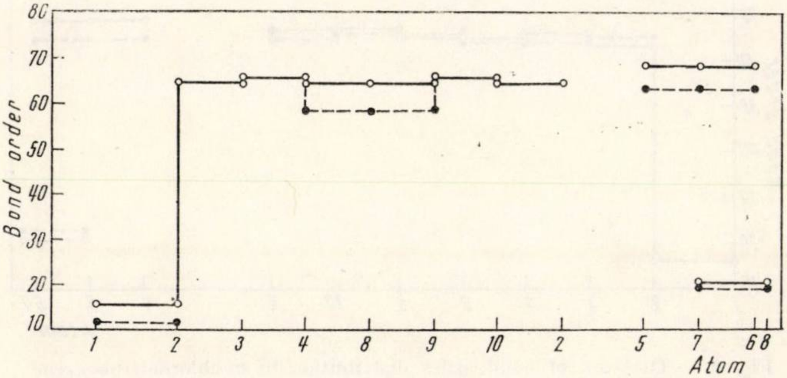

Fig. 7. — Diagram of bond order distribution in *p*-chloronitrobenzene:

○ CNDO; ● PPP
A. In the ring, B. In the substituent.

got also a satisfactory agreement between the calculated and experimental results.

In order to get further comparison between the results obtained by the CNDO and PPP methods we draw diagrams of the charges and bond order distributions over the molecular frame. The explanation of these diagrams is given in the Figures 2—7, where a distance between atoms proportional to that calculated by the CNDO method was considered.

From these diagrams one can observe that both in the ring and in the substituent, and in all cases, the CNDO charges are more uniformly distributed among atoms compared with those of the PPP method. In the case of the bond orders we observe that the two distributions are very close each other.

We can conclude that the CNDO method gave significantly better results for charge distributions than the PPP method did, but both methods gave similar results for bond distances.

[illegible] calculated and experimental results.

In order to get further insight between the results obtained by the CNDO and PPP methods, we drew diagrams of the charge and bond order [illegible] form. The explanation of these diagrams is given in the Figures 2–3, where correlations between [illegible] by the CNDO method were considered.

From these diagrams we can observe that both [illegible] the CNDO [illegible] results compare with those of the PPP method [illegible].

We can [illegible] that the CNDO [illegible] the PPP method [illegible] methods give similar results [illegible].

Revue Roumaine de Chimie, 17, 12, 1963 – 1967 (1972)

DERIVADOS DEL MIRACIL-D : RELACIÓN ACTIVIDAD CARCINOESTÁTICA-ESTRUCTURA ELECTRÓNICA LOCALIZADA

MIGUEL MARTÍN y RAMÓN CARBÓ

Sección de Química Cuántica
Departamento de Química Orgánica
Instituto Químico de Sarriá
Barcelona —17—
Instituto de Biología Fundamental
Universidad Autónoma de Barcelona

En trabajos anteriores, se ha puesto a punto una metodología para el estudio de las relaciones actividad biológica-estructura electrónica, mediante un método MO-LCAO. En este trabajo se aplica dicha técnica a una familia de derivados del Miracil-D.

INTRODUCCIÓN

El Miracil-D (1-dietil-amino-4-metil-10-tioxantenona) y sus derivados han sido repetidamente ensayados en ciertos tipos de neoplasmas, presentando actividad carcinoestática.

Se supone que el mecanismo de acción transcurre a través de un complejo formado entre el DNA y el derivado del Miracil-D, interrumpiéndose de esta manera la síntesis del mismo.

Experimentalmente se comprueba inhibiendo la formación de RNA en el Bacillus subtilis, o del DNA en el Escherichia coli[1].

En este trabajo se lleva a cabo un estudio del primer caso, mediante un método MO-LCAO empírico, intentando con ello encontrar una relación entre la estructura electrónica localizada de los derivados del Miracil-D y su ponder de inhibición.

MÉTODO

Los datos experimentales de la actividad se han obtenido del trabajo realizado por Hirschberg et al.[1]

---

[1] E. Hirschberg, I. B. Weinstein, N. Gersten, E. Marner, T. Finkelstein, y R. Carchman, *Cancer Research*, **28**, 606 (1968).

La inhibición ha sido calculada por este autor mediante la fórmula:

$$R = 25\ 10^{-5}/x$$

x es la concentración molar de compuesto necesaria para inhibir en un 50 %, o en un orden superior, el desarrollo del Bacillus subtilis, pasados 20 minutos después de la adición de los productos.

La estructura electrónica localizada se estudia mediante el método de Del Re,[2,3] ampliamente utilizado en problemas de este tipo, como puede apreciarse en las referencias que se citan.[4,6] Dicho método calcula la distribución de carga sigma (Q_i), así como un parámetro relacionado con la energía del sistema electrónico localizado.

En el método de Del Re, se estudia cada enlace aisladamente de los demás. De esta manera el cálculo se reduce a la resolución de determinantes 2×2.

Para cada átomo I, la integral de Coulomb se expresa como

$$\alpha_I = \alpha_0 + \delta_I \beta_0$$

en donde α_0 y β_0 son valores de referencia y δ_I es un parámetro que depende de los átomos con los que se encuentra enlazado el centro I. La integral de resonancia, β_{IJ} para cada enlace I – J se evalúa mediante

$$\beta_{IJ} = \varepsilon_{IJ} \beta_0$$

ε_{IJ} depende del carácter de los átomos enlazados. El problema se reduce, pues, al cálculo de dichos parámetros. Para ello se emplea el sistema de ecuaciones

$$\delta_I = \delta_{O.I} + \sum_J \gamma_{IJ} \delta_J \qquad (I = 1, N)$$

siendo $\delta_{O.I}$ y γ_{IJ} parámetros empéricos.

Las cargas netas sobre cada átomo, Q_I, se obtienen a partir de las ecuaciones

$$Q_{IJ} = (\delta_J - \delta_I)/2\varepsilon_{IJ}$$

$$Q_I = \sum_J Q_{IJ}$$

La aportación a la energía total de cada enlace se calcula mediante

$$E_{IJ} = \alpha_0 + [\delta_I + \varepsilon_{IJ}(Q_{IJ} + \sqrt{1 + Q_{IJ}^2})]\beta_0$$

La energía que aporta cada átomo se calcula mediante

$$E_I = 2 \sum_J E_{IJ}$$

y la energía total

$$E = \sum_{I=1}^{N} E_I$$

---

[2] G. Del Re, *J. Chem. Soc.*, **1958**, 4031.

[3] R. Carbó, *Theoret. Chim. Acta*, **18**, 170 (1970).

[4] R. Carbó y M. Pardillos, *Afinidad*, **27**, 513 (1970).

[5] R. Carbó, *Anales real Soc. españ Fis. Quim.* **12**, 945 (1970).

[6] G. Del Re y B. Pullman, *J. Chim. phys.*, **62**, 943 (1965).

En las expresiones anteriores el símbolo $\sum_J$ se refiere únicamente a los átomos enlazados al I. Los parámetros empleados se encuentran en la tabla 1.

Tabla 1

Parámetros para el método de Del Re

ATOMO	δ_{OI}	*ENLACE*	ε_{IJ}
H	0.0	H–C	1.0
C	0.07	H–N	0.45
N	0.24	C–C	1.0
O	0.40	C–N	1.0
S	0.07	C–S	0.75
Cl	0.35	C–O	0.95
		C–C1	0.60

$\gamma_{HX} = 0.4$
$\gamma_{XH} = 0.3$
$\gamma_{IJ} = \gamma_{JI} = 0.2$ (I,J = C, N, O)
$\gamma_{CS} = 0.2$; $\gamma_{SC} = 0.4$

De esta manera, al introducir las cargas de los átomos que sufren sustitución, así como E en la correlación, se tienen en cuenta dos factores que pueden determinar la actividad: La variación de la distribución electrónica debida a la sustitución y el efecto estérico producido por los distintos R_1, R_2, R_3, R_4, (véase la figura 1), simulado por la variación de E.

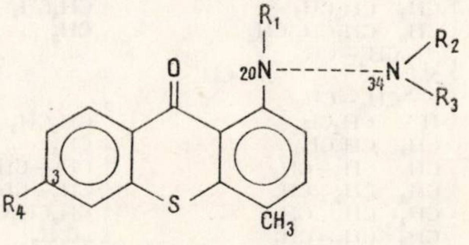

Fig. 1.— Derivados del Miracil-D.

Con los valores de estas variables y los datos de actividad, se realiza un estudio de correlación multilineal, según las técnicas empleadas normalmente.

La ecuación obtenida se somete a los controles estadísticos habituales, es decir, coeficiente de regresión multilineal, significación estadística, cálculo de errores, etc.

RESULTADOS Y CONCLUSIONES

En la ecuación (1) se encuentra la relación hallada según el método apuntado anteriormente. De los resultados del análisis estadístico, se deduce que dicha ecuación se ajusta al objetivo de encontrar una expresión matemática, que una la inhibición del desarrollo-bacteriano con la estructura electrónica localizada de los diversos derivados del Miracil-D.

$$\log R = 3.350\, Q_3 - 5.659\, Q_{20} - 0.888\, Q_{34} + 0.0143\, E - 2.839 \qquad (1)$$

r	n° derivados	$\bar{e}_r$	$F_{4,15}$	Nivel de significación
0.920	20	16.6%	20.7	99.9%

Para más detalles véanse las Tablas 2 y 3.

a) En el trabajo experimental del cual se han extraído los datos numéricos [1] se concluían, de una manera intuitiva, las siguientes relaciones actividad-estructura.

Tabla 2

Estructuras estudiadas

Compuesto N°	R_1	N . . . N	R_2	R_3	R_4	Actividad (Ref [1])
1	H	CH_2-CH_2	$CH-CH_3$	CH_2-CH_3	H	6
2	H	CH_2-CH_3	H	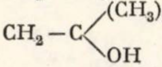 $CH_2-C{<}^{(CH_3)_2}_{OH}$	H	12
3	H	CH_2-CH_2	CH_2-CH_3	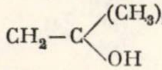 $CH_2-C{<}^{(CH_3)_2}_{OH}$	H	12
4	H	$CH_2-CH_2-CH_2$	CH_3	CH_3	H	9
5	H	$CH_2-CH_2-CH_2$	CH_2-CH_3	CH_2-CH_3	H	16
6	H	$CH_2-CH_2-CH_2$	CH_2CH_2OH	CH_2CH_2OH	H	6
7	H	$CH_2-CHOH-CH_2$	CH_2CH_3	CH_2-CH_3	H	5
8	H	$CH_2CH_2CH_2CH_2$	CH_2CH_3	CH_2-CH_3	H	18
9	H	$CH(CH_3)CH_2CH_2CH_2$	CH_2CH_3	CH_2CH_3	H	25
10	CH_3	CH_2CH_2	CH_2CH_3	CH_2CH_3	H	1
11	CH_3	$CH(CH_3)CH_2$	CH_3	CH_3	H	1
12	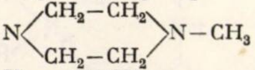 $N{<}\begin{matrix}CH_2-CH_2\\CH_2-CH_2\end{matrix}{>}N-CH_3$				H	1
13	H	CH_2CH_2	CH_2CH_3	$CH_2CHOHCH_3$	Cl	21
14	CH_3	CH_2CH_2	CH_3	CH_3	Cl	3
15	CH_3	CH_2-CH_2	CH_2-CH_2	CH_2CH_3	Cl	4
16	CH_3	CH_2-CH_2	CH_2-CH_3	CH_2CH_2OH	Cl	3
17	CH_2	CH_2-CH_2	CH_2CH_2OH	CH_2CH_2OH	Cl	6
18	CH_2	CH_2-CH_2	nC_4H_9	nC_4H_9	Cl	18
19	CH_3	CH_2-CH_2	CH_2CH_3	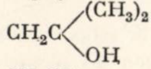 $CH_2C{<}^{(CH_3)_2}_{OH}$	Cl	8
20	CH_3	$CH_2CH_3CH_2$	CH_2CH_3	CH_2CH_3	Cl	6

* Ver la figura 1.

b) La sustitución en el nitrógeno 20, (ver figura 1), disminuye la actividad, excepto si está sustituído por un cloro en la posición 3.

La prolongación de la cadena lateral, entre los dos nitrógenos induce un aumento en el poder inhibidor.

Estas mismas conclusiones se ven corroboradas por este trabajo, a través de la ecuación (1):

a) Al ser sustituído el H del N_{20} por un resto alquilo, aumenta la carga de Del Re, haciéndose menos negativa, por lo que, bajo el punto de vista de dicha ecuación, se traducirá en una menor actividad, ya que su coeficiente es negativo.

Sin embargo, al sustituir la posición 3 por un cloro, aumenta la aportación de Q_3 al logaritmo de la variable que mide la inhibición,

Tabla 3

Valores utilizados y resultados de la correlación

Compuesto Nº	Valores de las variables				Log. actividad	
	Q3	Q34	Q20	E	Calculada	Experimental
1	−0.0310	−0.3650	−0.2043	109.6679	0.877	0.778
2	−0.0310	−0.3649	−0.3548	110.7798	1.027	1.079
3	−0.0310	−0.3650	−0.2030	125.0403	1.096	1.079
4	−0.0310	−0.3658	−0.2003	103.0880	0.784	0.954
5	−0.0310	−0.3658	−0.2053	116.2727	0.978	1.204
6	−0.0310	−0.3642	−0.2013	120.6456	1.036	0.778
7	−0.0310	−0.3659	−0.2035	118.4399	0.998	0.699
8	−0.0310	−0.3676	−0.2054	122.8758	1.073	1.255
9	−0.0310	−0.2119	−0.2054	129.4737	1.177	1.398
10	−0.0310	−0.2138	−0.2044	117.3442	0.121	0.
11	−0.0310	−0.2135	−0.1997	118.7577	0.148	0.
12	−0.0310	−0.3650	−0.2012	101.9825	−0.093	0.
13	0.1194	−0.2119	−0.2027	118.4228	1.506	1.322
14	0.1194	−0.2119	−0.1194	104.1478	0.360	0.477
15	0.1194	−0.2119	−0.2044	117.3325	0.625	0.602
16	0.1194	−0.2119	−0.2024	119.5189	0.654	0.477
17	0.1194	−0.2119	−0.2004	121.7053	0.684	0.778
18	0.1194	−0.2119	−0.2049	143.7403	1.004	1.255
19	0.1194	−0.2119	−0.2034	145.0987	1.034	0.903
20	0.1194	−0.2127	−0.2053	123.9372	0.725	0.778

contrarrestando, por lo tanto, la disminución de actividad debida a la sustitución en el nitrógeno.

b) También se ve reflejada en esta ecuación el aumento de actividad por prolongación de la cadena lateral, va que al aumentar su numero de carbones, aumenta el parámetro *E*, el cual al ir afectado por un coeficiente positivo, aumenta la actividad.

Revue Roumaine de Chimie, 17, *12*, 1969–1975 (1972)

A.C. CHRONOPOTENTIOMETRY: A THEORETICAL STUDY OF AN IRREVERSIBLE ELECTRODE PROCESS PRECEDED BY A CHEMICAL REACTION

H. L. JINDAL*, N. P. BANSAL* and KRISHNA BANSAL**

* Ramjas College, University Enclave, Delhi-7 (INDIA)

** Department of Mathematics, Janki Devi Mahavidyalaya, Poorvi Marg, New Delhi

Received June 10, 1972

Theoretical relationships for a.c. chronopotentiometry for a case where the irreversible electrode process is preceded by chemical reaction are derived. It is also shown that for a limiting case where the rate of chemical reaction is very fast, the relationship is reduced to that where no chemical reaction occurs prior to the electrode reaction.

INTRODUCTION

In chronopotentiometry, electrolysis of a solution containing a depolarizer and an excess of an indifferent electrolyte is carried out at constant current and variations of the potential of a polarizable (micro) electrode *versus* a depolarized reference are recorded as a function of time. The diffusion equations representing different electrode processes have been solved [1] under appropriate boundary and initial conditions and mathematical relationships worked out. Although the applications of chronopotentiometry have been known since the early work of Weber [2], Sand [3], Cottrell [4], Karaoglanoff [5] and Butler and Armstrong [6], active interest in application of this technique to analytical problems was taken only after the comprehensive work of Gierst and Julliard [7], who also devised an ingenious experimental arrangement for oscillographic recording of potential-time curves. Potentialities of this technique as an important analytical tool in aqueous and non-aqueous media have been recently reviewed[8-10].

---

[1] P. Delahay "New Instrumental Methods in Electrochemistry", Interscience Publishers, Inc., New York, 1954, Chap. 8.

[2] H. F. Weber, *Wied. Ann. Physik.*, **7**, 536 (1879).

[3] H. J. S. Sand, *Phil. Mag.*, **1**, 45 (1901).

[4] F. G. Cottrell, *Z. phys. Chem.*, **42**, 385 (1902).

[5] Z. Karaoglanoff, *Z. Electrochem.*, **12**, 5 (1906).

[6] J. A. V. Butler and G. Armstrong, *Proc. Roy. Soc.* **A139**, 406 (1933); *Trans. Faraday Soc.*, **30**, 1173 (1934).

[7] L. Gierst and A. Juliard, *J. Phys. Chem.*, **57**, 701 (1953).

In determining the transition-time (τ) from d.c. chronopotentiograms arbitrary methods are employed which introduce some uncertainty in τ measurement. It has been shown[11] that superimposition of alternating current of constant amplitude on the constant direct electrolysis current (a.c. chronopotentiometry) greatly improved the precision in τ measurement. Theoretical principles for reversible[11,12] and irreversible[13] electrode processes for a.c. chronopotentiometry have been reported.

In the present communication, the diffusion equations representing an irreversible electrode process preceded by a chemical reaction have been solved under appropriate conditions for a.c. chronopotentiometry.

THEORETICAL ANALYSIS

Consider the electrode process

$$X \underset{k_b}{\overset{k_f}{\rightleftharpoons}} \mathrm{Ox} \xrightarrow{\mathrm{ne}} \mathrm{R}$$

where a substance Ox, in equilibrium with another substance X, is being reduced at markedly less cathodic potentials than X. The rate of reduction of Ox to R depends upon the rate of the chemical transformation X $\rightleftharpoons$ Ox and also on the rate of mass transfer of the involved species.

The differential equations representing the above electrode process are

$$\frac{\partial C_{\mathrm{O}x}(x,\ t)}{\partial t} = D_{\mathrm{Ox}} \frac{\partial^2 C_{\mathrm{Ox}}(x,\ t)}{\partial x^2} + k_f\, C_x(x,\ t) - k_b\, C_{\mathrm{Ox}}(x,\ t) \qquad (1)$$

$$\frac{\partial C_x(x,\ t)}{\partial t} = D_x \frac{\partial^2 C_x(x,\ t)}{\partial x^2} - k_f\, C_x(x,\ t) + k_b\, C_{\mathrm{Ox}}(x,\ t) \qquad (2)$$

where C's are the concentrations, D's are the diffusion coefficients of the species, x is the distance from the electrode surface and k's are the formal rate constants (conventional rate constants in sec^{-1}) for the transformation X $\rightleftharpoons$ Ox for the forward and backward steps, respectively.

---

[8] D. G. Davis, "Electroanalytical Chemistry", Vol. I, A. J. Bard, Ed., Marcel Dekker, Inc., New York, 1966.

[9] N. P. Bansal, Ph. D. Thesis, University of Delhi (1972).

[10] J. J. Lingane, *Analyst*, **91**, 1 (1966).

[11] Y. Takemori, T. Kambara, M. Senda and I. Tachi, *J. Phys. Chem.*, **61**, 968 (1957).

[12] N. P. Bansal and H. L. Jindal, Paper presented at the Convention of Chemists (1971), held at Institute of Science, Bombay.

[13] H. C. Gaur and H. L. Jindal, *J. Electroanalyt. Chem.*, **14**, 297 (1967).

To obtain the boundary conditions the flux to the reducible species (Ox) in a.c. chronopotentiometry is expressed as the sum of direct current and alternating current components

$$\left[\frac{\partial C_{\mathrm{Ox}}(x, t)}{\partial x}\right]_{x=0} = \frac{i}{nFq\,D_{\mathrm{Ox}}} + \frac{A\sin\omega t}{nFq\,D_{\mathrm{Ox}}} \tag{3}$$

and also because the substance X is not reduced at the electrode ; flux of X is equal to zero at the electrode surface

$$\left[\frac{\partial C_{\mathrm{X}}(x, t)}{\partial x}\right]_{x=0} = 0 \tag{4}$$

where i is the constant d.c., A the amplitude of a.c. of frequency ω, q the area of the electrode and nF the charge involved in the reduction of the one mole of Ox.

The initial conditions are

$$\frac{C_{\mathrm{Ox}}(x, 0)}{C_{\mathrm{X}}(x, 0)} = K \tag{5}$$

$$C_{\mathrm{Ox}}(x, 0) + C_{\mathrm{X}}(x, 0) = C^{\circ} \tag{6}$$

where K is the equilibrium constant for the chemical reaction $\mathrm{X} \rightleftarrows \mathrm{Ox}$ and C° is the initial bulk concentration of X.

To solve the differential equations (1) and (2) under the boundary and initial conditions (3)–(6), several substitutions are to be made and also for the sake of simplicity it is assumed that the diffusoin coefficients of Ox and X are equal i.e. $D_{\mathrm{Ox}} = D_{\mathrm{X}} = D$.

The following functions are to be introduced

$$\Psi(x, t) = C_{\mathrm{Ox}}(x, t) + C_{\mathrm{X}}(x, t) \tag{7}$$

$$\Phi(x, t) = C_{\mathrm{X}}(x, t) - \frac{k_b}{k_f} C_{\mathrm{Ox}}(x, t) \tag{8}$$

Using the Laplace transformation, it can be shown (see appendix) that the transforms corresponding to the equations (1) and (2) are

$$\overline{\Psi}(x, S) = \frac{C^{0}}{S} + M\exp\left[-x\frac{S^{1/2}}{D^{1/2}}\right] \tag{9}$$

$$\overline{\Phi}(x, S) = N\exp\left[-x\frac{(S + k_b + k_f)^{1/2}}{D^{1/2}}\right] \tag{10}$$

The integration constants M and N are determined from the transforms of the boundary conditions (see appendix) giving

$$\overline{\Psi}(x,\ S) = \frac{C^0}{S} - \frac{i}{n\,F\,q\,D^{1/2}\,S^{3/2}} \exp\left[-x\frac{S^{1/2}}{D^{1/2}}\right]$$

$$-\frac{A}{n\,F\,q\,S^{1/2}\ D^{1/2}} L[\sin\ \omega t]\ \exp\left[-x\ \frac{S^{1/2}}{D^{1/2}}\right] \tag{11}$$

$$\overline{\Phi}\,(x,\ S) = \frac{i^{k_b/k_f}}{n\,F\,q\,D^{1/2}\ S\,(S+k_b+k_f)^{1/2}} \exp\left[-x\ \frac{(S+k_f+k_b)^{1/2}}{D^{1/2}}\right]$$

$$+\frac{A^{k_b/k_f}\,L[\sin\ \omega t]}{n\,F\,q\,D^{1/2}\,(S+k_b+k_f)^{1/2}} \exp\left[-\ x\frac{(S+k_b+k_f)^{1/2}}{D^{1/2}}\right] \tag{12}$$

where $L\ (\sin\omega\ t)$ denotes the Laplace transform of sin ωt. For the sake of simplicity we calculate here the interfacial concentrations only; putting $x = 0$ in (11) and (12) one obtains

$$\overline{\Phi}(0,\ S) = \frac{C^0}{S} - \frac{i}{n\,F\,q\,D^{1/2}\ S^{3/2}} - \frac{A}{n\,F\,q\,D^{1/2}\ S^{1/2}}\,L\,[\sin\ \omega t] \tag{13}$$

$$\overline{\Phi}\ (0,\ S) = \frac{i^{k_b/k_f}}{n\,F\,q\,D^{1/2}\ S\,(s+k_b+k_f)^{1/2}} +$$

$$+\ \frac{A^{k_b/k_f}}{n\,F\,q\ D^{1/2}\,(S+k_b+k_f)^{1/2}}\,L\,[\sin\ \omega t) \tag{14}$$

By inverse transformation and by applying the method of convolution one obtains the functions $\Psi(0,\ t)$ and $\Phi(0,\ t)$. Thus (see appendix)

$$\Psi(0,\ t) = C^0 - \frac{2\,i\,t^{1/2}}{n\,F\,q\ D^{1/2}\ \pi^{1/2}} - \frac{A\sin\,(\omega t - \pi/4)}{n\,F\,q\ D^{1/2}\ \ \omega^{1/2}} \tag{15}$$

and

$$\Phi\,(0,\ t) = \frac{i^{k_b/k_f}}{n\,F\,q\ D^{1/2}\,(k_b+k_f)^{1/2}}\ \mathrm{erf}\ \{t^{1/2}\,(k_b+k_f)^{1/2}\}$$

$$+\ \frac{A^{k_b/k_f}}{n\,F\,q\ D^{1/2}\ \{(k_b+k_f)^2+\omega^2\}^{1/2}}\left[\frac{\pm\ \omega\ \sin\ \omega t \mp [\{(k_b+k_f)^2+\omega^2\}^{1/2}-(k_b+k_f)]\cos\ \omega t}{[2\,\{(k_b+k_f)^2+\ \omega^2\}^{1/2} - 2\,(k_b+k_f)]^{1/2}}\right] \tag{16}$$

where the notation "erf" in (17) represent the error function having the quantity within brackets as argument. In view of the definition of the functions $\Psi(x, t)$ and $\Phi(x, t)$, the concentration $C_{\mathrm{Ox}}(0, t)$ and $C_{\mathbf{X}}(0, t)$ can be calculated from equations resulting from putting $x = 0$ in (7) and (8) and from the relations (15) and (16) as

$$C_{\mathrm{Ox}}(0, t) = \frac{k_f}{k_f + k_b}\left\{C^0 - \frac{2\,i\,t^{1/2}}{n F q D^{1/2}\pi^{1/2}} - \frac{A \sin(\omega t - \pi/4)}{n F q D^{1/2}\omega^{1/2}}\right\} -$$

$$- \frac{i k_b \operatorname{erf}\{t(k_b + k_f)\}^{1/2}}{n F q D^{1/2}(k_b + k_f)^{3/2}} - \frac{A k_b}{n F q D^{1/2}(k_b + k_f)\{(k_b + k_f)^2 + \omega^2\}^{1/2}} \times$$

$$\times \left[\frac{\pm\,\omega \sin \omega t \mp [\{(k_b + k_f)^2 + \omega^2\}^{1/2} - (k_b + k_f)] \cos \omega t}{[2\{(k_b + k_f)^2 + \omega^2\}^{1/2} - 2(k_b + k_f)]^{1/2}}\right] \tag{17}$$

$$C_{\mathbf{X}}(0, t) = \frac{k_b}{2k_f}\left\{C^0 - \frac{2\,i\,t^{1/2}}{n F q D^{1/2}\pi^{1/2}} - \frac{A \sin(\omega t - \pi/4)}{n F q D^{1/2}\omega^{1/2}}\right\} +$$

$$+ \frac{i^{k_b/k_f} \operatorname{erf}\{t(k_b + k_f)\}^{1/2}}{2n F q D^{1/2}(k_b + k_f)^{1/2}} + \frac{A^{k_b/k_f}}{2n F q D^{1/2}\{(k_b + k_f)^2 + \omega^2\}^{1/2}} \times$$

$$\times \left[\frac{\pm\,\omega \sin \omega t \mp [\{(k_b + k_f)^2 + \omega^2\}^{1/2} - (k_b + k_f)] \cos \omega t}{[2\{(k_b + k_f)^2 + \omega^2\}^{1/2} - 2(k_b + k_f)]^{1/2}}\right] \tag{18}$$

Equations (17) and (18) represent the concentrations of the species Ox and X at the electrode surface at any time 't'. Since the reduction Ox to R is irreversible, the variation of electrode potential with time during the course of electrolysis can be calculated by the method adopted by Gaur and Jindal.[13]

By putting $K = \dfrac{k_f}{k_b} = \propto$ in (17) and (18) one has

$$C_{\mathrm{Ox}}(0, t) = C^0 - \frac{2i\,t^{1/2}}{n F q D^{1/2}\pi^{1/2}} - \frac{A \sin(\omega t - \pi/4)}{n F q D^{1/2}\omega^{1/2}}$$

and

$$C_{\mathbf{X}}(0, t) = 0$$

showing that, as expected, this equation representing $C_{\mathrm{Ox}}(0, \mathrm{t})$ for $K = \propto$ is the same as derived earlier [13], for a case of an irreversible electrode process where no chemical reaction precedes the electrode process. This also gives a check for the above derivation for $C_{\mathrm{Ox}}(0, t)$.

APPENDIX

From the functions $\Psi(x, t)$ and $\Phi(x, t)$ defined by equations (7) and (8) one easily gets the following values of $C_{\mathrm{Ox}}(x, t)$ and $C_{\mathrm{X}}(x, t)$

$$C_{\mathrm{Ox}}(x, t) = \frac{\Psi(x, t) - \Phi(x, t)}{1 + k_b/k_f} \tag{i}$$

$$C_{\mathrm{X}}(x, t) = \frac{\Phi(x, t) + k_b/k_f\, \Psi(x, t)}{1 + k_b/k_f} \tag{ii}$$

Recalling the assumption $D_{\mathrm{Ox}} = D_{\mathrm{X}} = D$, made earlier, and using the newly defined functions $\Psi(x, t)$ and $\Phi(x, t)$, the differential equations represented by (1) and (2) are transformed into

$$\frac{\partial \Psi(x, t)}{\partial t} = D \frac{\partial^2 \Psi(x, t)}{\partial x^2} \tag{iii}$$

$$\frac{\partial \Phi(x, t)}{\partial t} = D \frac{\partial^2 \Phi(x, t)}{\partial x^2} - (k_f + k_b)\, \Phi(x, t) \tag{iv}$$

With the initial and boundary conditions as

$$\Psi(x,\ 0) = C^0 \tag{v}$$

$$\Phi(x,\ 0) = 0 \tag{vi}$$

$$\frac{\partial \Psi(0,\ t)}{\partial x} - \frac{\partial \Phi(0,\ t)}{\partial x} = \frac{i}{n\,F\,q\,D}\left(1 + \frac{k_b}{k_f}\right) + \frac{A \sin \omega t}{n\,F\,q\,D}(1 + k_b/k_f) \tag{vii}$$

$$\frac{\partial \Phi(0,\ t)}{\partial x} = -\frac{k_b}{k_f}\frac{\partial \Psi(0,\ t)}{\partial x} \tag{viii}$$

Taking the Laplace transform with respect to the variable t, equations (i) and (ii) are converted into the following ordinary differential equations

$$D \frac{\partial^2 \overline{\Psi}(x, S)}{\partial x^2} - S\, \overline{\Psi}(x,\ S) + C^0 = 0 \tag{ix}$$

$$D \frac{\partial^2 \Phi(x,\ S)}{\partial x^2} - (S + k_b + k_f)\, \overline{\Phi}(x,\ S) = 0 \tag{x}$$

The solutions of equations (ix) and (x) $[\overline{\Psi}(x,\ S)$ and $\overline{\Phi}(x,\ S)$ are bound for $x \rightarrow \infty]$ have been given above in equations (9) and (10).

The integration constants M and N are evaluated by satisfying the Laplace transforms of the boundary conditions (vii) and (viii) which are given by

$$\frac{\partial\overline{\Psi}(0,\ S)}{\partial x} - \frac{\partial\overline{\Phi}(0,\ S)}{\partial x} = \frac{i}{n F q D S}\left(1 + \frac{k_b}{k_f}\right) + \\ + \frac{A}{n F q D}\left(1 + \frac{k_b}{k_f}\right) L\,[\sin\ \omega t] \qquad \text{(xi)}$$

$$\frac{\partial\overline{\Phi}(0,\ S)}{\partial x} = -\frac{k_b}{k_f}\,\frac{\partial\overline{\Psi}(0,S)}{\partial x} \qquad \text{(xii)}$$

where $L\ [\sin\ \omega t]$ represents the Laplace transform of $\sin\ \omega t$. Thus from equations (9), (10), (xi) and (xii) one gets

$$M = -\frac{i}{n F q D^{1/2} S^{3/2}} - \frac{A}{n F q D^{1/2} S^{1/2}} L[\sin\omega t) \qquad \text{(xiii)}$$

$$N = \frac{i^{k_b/k_f}}{n F q D^{1/2} S (S + k_b + k_f)^{1/2}} + \frac{A\, k_b/k_f}{n F q D^{1/2} (S + k_b + k_f)^{1/2}}\, L\,[\sin\ \omega t] \qquad \text{(xiv)}$$

Putting these values of M and N into (9) and (10), we get equations (11) and (12). By inverse transformation of (13) and (14) one finally obtains the functions $\Psi(0,\,t)$ and $\Phi(0,\,t)$ represented by (15) and (16). The inverse transform of all the terms except the last in equation (13) can be found from standard tables while that of the last term is obtained by applying the method of convolution, from which

$$L^{-1}\left[\frac{1}{S^{1/2}} L\{\sin\ \omega t\}\right] = \frac{1}{\omega^{1/2}} \sin\,(\omega t - \pi/4) \qquad \text{(xv)}$$

The inverse transform of the first term of the right hand side in equation (14) is available in mathematical tables while that of the second term is again obtained by convolution.

$$L^{-1}\left[\frac{L\{\sin\ \omega t\}}{(S + k_b + k_f)^{1/2}}\right] = \\ = \frac{\pm\,\omega \sin\ \omega t \mp [\{(k_b + k_f)^2 + \omega^2\}^{1/2} - (k_b + k_f)] \cos\ \omega t}{\{(k_b + k_f)^2 + \omega^2\}^{1/2}\, [2\{(k_b + k_f)^2 + \omega^2\}^{1/2} - 2\,(k_b + k_f)]^{1/2}} \qquad \text{(xvi)}$$

Acknowledgements : The authors are thankful to Prof. I. G. Murgulescu for going through the manuscript and to him and Dr. H. C. Gaur for helpful suggestions.

Revue Roumaine de Chimie, **17**, *12*, 1969 – 1975 (1972)

Revue Roumaine de Chimie, 17, 12, 1977–1984 (1972)

KINETICS AND MECHANISM OF SUBSTITUTION REACTIONS OF COMPLEXES. XLV

SOLVATION OF THE $[Cr(NCS)_4\,(m\text{-xylidine})_2]^{\ominus}$ ION IN ETHANOL-WATER MIXTURES

J. ZSAKÓ*, V. VOICULESCU**, I. GĂNESCU**, and A. POPESCU**

* Faculty of Chemistry, Babeş-Bolyai University, str. Arany János 11, Cluj
** Faculty of Chemistry of the Craiova University, Calea Bucureşti 165, Craiova

Received February 19, 1972

Solvation kinetics of $[Cr(NCS)_4\,(m\text{-xylidine})_2]^{\ominus}$ has been studied in ethanol-water mixtures at different temperatures. The first stage of the solvation consists of two competitive reactions : two $NCS^{\ominus}$ ions are exchanged, presumably, for water molecules and in paralel an *m*-xylidine molecule for ethanol, the latter in a second-order reaction, accelerated by hydrogen ions. The exchange of the amine is followed by the substitution of the first two $NCS^{\ominus}$ ions. The third and fourth $NCS^{\ominus}$ ions are substituted only in neutral and not very acid solutions. Kinetic parameters have been derived for reactions (1), (2) and (4). The influence of solvent composition and of acidity is discussed.

INTRODUCTION

In our previous papers [1–6] the solvation kinetics of some $[Cr(NCS)_4\,(\text{amine})_2]^{\ominus}$ type complexes has been studied in ethanol-water mixtures, with the following amines : aniline, *p*-toluidine, *p*-ethylaniline, *p*-anisidine and *p*-phenetidine.

The first stage of the solvation consists of two competitive reactions, viz. of the exchange of the first $NCS^{\ominus}$ ion or of an amine molecule A for solvent molecules ROH, i.e.

$$[Cr(NCS)_4A_2]^{\ominus} + ROH = [Cr(NCS)_3A_2ROH] + NCS^{\ominus} \tag{1}$$

$$[Cr(NCS)_4A_2]^{\ominus} + ROH = [Cr(NCS)_4A\ ROH]^{-} + A \tag{2}$$

---

[1] J. Zsakó, Cs. Várhelyi and I. Gănescu, *Rev. Roumaine Chim.*, **13**, 577 (1968).

[2] J. Zsakó, Cs. Várhelyi, I. Gănescu and J. Turós, *Acta Chim. Acad. Sci. Hung.*, **61**, 167 (1969).

[3] J. Zsakó, Cs. Várhelyi, I. Gănescu and L. Zöldi, *Monatsch. Chem.*, **99**, 2235 (1968).

[4] J. Zsakó, *Stud. Univ. Babeş Bolyai Chem.*, **15**, 93 (1970).

[5] J. Zsakó, I. Gănescu, Cs. Várhelyi and Al. Popescu, *Rev. Chim. Min.*, **7**, 927 (1970).

[6] J. Zsakó, I. Gănescu, Cs. Várhelyi and Al. Popescu, *Z. anorg. Chem.* **380**, 2,16 (1971).

Reaction (1) seems to be of mechanism S_N1, and is followed presumably by the practically instantaneous reaction

$$[Cr(NCS)_3A_2ROH] + ROH = [Cr(NCS)_2A_2(ROH]_2]^{\oplus} + NCS^{\ominus} \quad (3)$$

Reaction (2) seems to be of mechanism S_N2. It is accelerated by the presence of mineral acids and is followed by the reactions

$$[Cr(NCS)_4A\ ROH)^{\ominus} + ROH = [Cr(NCS)_3A(ROH)_2] + NCS^{\ominus} \quad (4)$$

$$[Cr(NCS)_3A(ROH)_2] + ROH = [Cr(NCS)_2A(ROH)_3]^{\oplus} + NCS^{\ominus} \quad (5)$$

Reaction (4) is perfectly analogous with reaction (1), its kinetic parameters are very close to those characteristic of reaction (1) and reaction (5) is presumably also instantaneous.

In neutral solutions the third and the fourth NCS^- ions are substituted too, according to the equations

$$[Cr(NCS)_2A_2(ROH)_2]^{\oplus} + ROH = [Cr(NCS)A_2(ROH)_3]^{\textcircled{2+}} + NCS^{\ominus} \quad (6)$$

$$[Cr(NCS)_2A(ROH)_3]^{\oplus} + ROH = [Cr(NCS)A(ROH)_4]^{\textcircled{2+}} + NCS^{\ominus} \quad (7)$$

$$[Cr(NCS)A_2(ROH)_3]^{\textcircled{2+}} + ROH = [CrA_2(ROH)_4]^{\textcircled{3+}} + NCS^{\ominus} \quad (8)$$

$$[Cr\ NCS\ A(ROH)_4]^{\textcircled{2+}} + ROH = [CrA(ROH)_5]^{\textcircled{3+}} + NCS^{\ominus} \quad (9)$$

One cannot exclude even the possibility that the second amine molecule may be exchanged. Thus, other reactions may be involved, too.

Kinetic parameters of reactions (1) and (4) are not influenced sensibly by the nature of the amine molecule, but the rate of reaction (2) depends on the nucleophilic character of the amine, viz. it has lower values if A is *p*-anisidine or *p*-phenetidine, than in the case of the other amines studied.

RESULTS AND DISCUSSIONS

In the present paper the solvation of the complex ion with A = = *m*-xylidine has been studied at different temperatures and in ethanol-water mixtures containing 37,7, 48.5, 72.7 and 97.0 p.c. in volume ethanol. The concentration of the non-transformed complex ion and of the $NCS^{\ominus}$ ions liberated have been followed in time. The concentration of the non-transformed complex ion bas been determined colorimetrically and since the validity of Beer's law has been observed, the graphical plot of log E has been performed (E stands for the extinction of the sample) in order to derive rate constants. This graphical plot gives very good straight lines, which shows the overall reaction to be of first order. Some examples are given in Fig. 1. Rate constants derived from the slope of these straight lines are presented in Table 1. The graphical plot of log k/T values versus $1/T$ enabled us to derive the apparent activation energy and entropy values. Both systematically decrease with increasing ethanol content of the solvent, as is seen from Table 1.

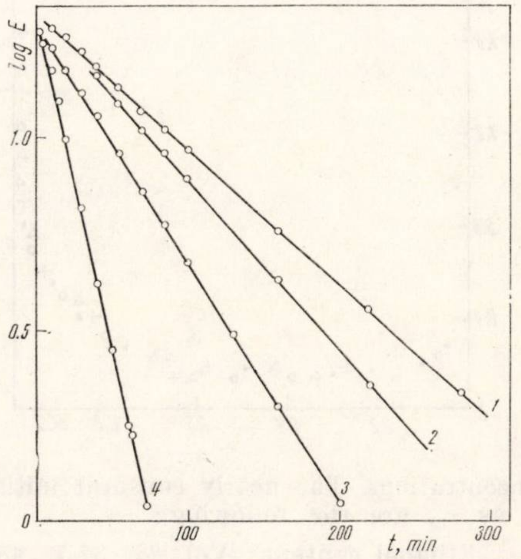

Fig. 1. – Determination of overall rate constants k.

1, 48.5% EtOH, 40°C; 2, 72.7% EtOH, 40°C; 3, 97.0% EtOH, 40°C; 4, 48.5% EtOH, 50°C.

In order to find the share of reactions (1) and (2) in the overall reaction, the ratio between the concentration C_1 of NCS^- ions liberated and the complex transformed, $r = C_1/(c_0 - c)$, has been determined (c_0 and c stand for the initial and actual concentration of the complex ion studied). As in the case of the earlier investigated complexes, a finite zero-time $NCS^{\ominus}$-ion concentration has been found and in order to estimate the concentration of NCS^- liberated, C_1-values have been corrected with the zero-time values, obtained by means of extrapolation of experimental data.

Table 1

Kinetic parameters of the overall process

EtOH content %Vol.	$k \times 10^3$, sec^{-1}				$\Delta H^{\neq}$ kcal/mole	$\Delta S^{\neq}$ e.u.
	40°C	45°C	50°C	55°C		
37.7	0.099	0.238	0.542	1.19	33.2	29.1
48.5	0.138	0.307	0.696	1.45	31.5	24.3
72.7	0.176	0.380	0.800	1.74	30.4	21.4
97.0	0.240	0.515	1.08	2.21	29.6	19.3

Similarly to the analogous complexes, the ratio has a practically constant value at the beginning of the solvation process and it depends only on the ethanol content of the solvent and not on the temperature. The plot of r versus transformation degree α of the complex is visualized by Fig. 2. The shape of the $r-\alpha$ curves is also similar for other ethanol concentrations. The nearly constant initial r values, which are referred to as r_0, are the following:

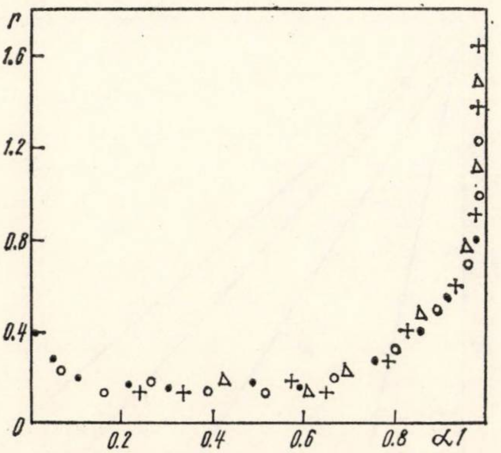

Fig. 2. – Ratio $r = C_1/(c_0 - c)$ as function of transformation degree α. 48.5 % EtOH: 40°C; ○45°C; + 50°C; △65°C

Ethanol content /Vol. %/	37.7	48.5	72.7	97.0
r_0	0.27	0.16	0.090	0.050

The small r_0 values show that reaction (2) plays an important part in the overall process. By using the above given r_0 values, the rate constants k_1 and k_2 of reactions (1) and (2) can be derived from the overall first-order rate constant k. In order to diminish the influence of experimental errors, calculations have been carried out by using corrected k values, derived from $\Delta H^{\neq}$ and $\Delta S^{\neq}$ values given in Table 1, instead of the experimentally determined ones. In these calculations reaction (3) has been presumed to be instantaneous. This presumption seems to be sound, since in the case of the Reinecke salt, with $A = NH_3$ [7] and also in the case of the analogous benzylamine derivative, [8] where the amine molecules are not substituted, $r_0 \approx 2$ has been observed, which means the practically simultaneous exchange of the first two NCS^- ligands. By adopting this reaction scheme, the individual first-order rate constants k_1 and k_2 can be calculated according to the following formulae

$$k_1 = k\frac{r_0}{2} \quad \text{and} \quad k_2 = k\left(1 - \frac{r_0}{2}\right) \tag{10}$$

---

[7] A. W. Adamson, *J. Amer. Chem. Soc.*, **80**, 3183 (1958).

[8] J. Zsakó, Cs. Várhelyi, I. Gănescu and D. Oprescu, "Proceedings of the Thirteenth International Conference on Coordination Chemistry" Cracow-Zakopane, Poland, 1970, Vol. **I**, p. 25.

Results are given in Table 2. Rate constants k_1 are a little larger than for the analogous complexes studied earlier and show a systematic decrease with increasing ethanol content. This variation is much larger than previously observed. First-order rate constants k_2 increase in parallel with the ethanol content and the ratio of k_2 to molar concentration of ethanol is practically constant for a given temperature. One may presume the amine molecules to be substituted only by ethanol on an S_N2 pathway. The corresponding second-order rate constants k_2' are given in the same Table 2. These values are close to k_2' obtained for the analogous complexes with $A = p$-toluidine and p-ethylaniline,[4,5] even a little higher.

Table 2

Rate constants of reactions (1) and (2)

EtOH content % Vol.	Rate const.	Temperature			
		40°C	45°C	50°C	55°C
37.7		1.35	3.17	7.26	16.2
48.5	$k_1 \times 10^5$	1.10	2.48	5.46	11.7
72.7	sec^{-1}	0.783	1.72	3.68	7.74
97.0		0.600	1.29	2.69	5.52
37.7		0.865	2.03	4.65	10.4
48.5	$k_2 \times 10^4$	1.27	2.85	6.27	13.5
72.7	sec^{-1}	1.66	3.65	7.81	16.4
97.0		2.34	5.02	10.5	21.5
37.7		1.135	0.318	0.727	1.63
48.5	$k_2 \times 10^4$	0.154	0.346	0.762	1.64
72.7	$\text{sec}^{-1}\text{mol}^{-11}$	0.135	0.296	0.633	1.33
97.0		0.142	0.305	0.637	1.31

The influence of acidity upon the solvation kinetics has been studied in solutions with 37.7 p.c. ethanol, by adding various amounts of perchloric acid. Results obtained are given in Table 3. The general picture is the same as observed in our previous papers: k_1, r_0, $\Delta H^{\neq}$ and $\Delta S^{\neq}$ decrease with the increasing in perchloric acid concentration, i.e. reaction (1) is hindered and reaction (2) is, on the contrary, promoted. At concentration higher than 10^{-2} M, the rate constant k_1 is practically not influenced by the acidity. Generally, increasing acidity and increasing ethanol content make k_1 and k_2 vary in the same direction, but a partial reaction order can be found only in the case of k_2 and only for ethanol. The order effects involve presumably different pre-equilibria.

The kinetic parameters $\Delta H^{\neq}$ and $\Delta S^{\neq}$ of the overall reaction decrease when the part played by reaction (2) increases. This suggests the idea, that both $\Delta H^{\neq}$ and $\Delta S^{\neq}$ of reaction (1) are higher than the same parameters for reaction (2). We could not derive their individual values, since our experimental data were too scattered to evidence the influence of temperature upon the initial ratio r_0.

In order to obtain pieces of information concerning the second stage of the solvation process, i.e. reactions (4)—(9), the excess concentration c_{ex} of NCS$^{\ominus}$ ions has been calculated by subtracting from the experimental free NCS$^{\ominus}$ concentrations the theoretical C_1, calculated from k_1 values, taking into account the instantaneous reaction (3) too. Results expressing the influence of temperature, ethanol content and of the acidity on this excess concentration, are given in Figs. 3—5. From these figures it is

Table 3

Influence of perchloric acid upon the kinetic parameters. 37.7% EtOH

[HClO$_4$] mole/l	Rate const.	Temperature 40°C	45°C	50°C	55°C	$\Delta H^{\neq}$ kcal/mol	$\Delta S^{\neq}$ e.u.	r_0
10^{-4}	$k \times 10^3$ sec^{-1}	0.111	0.246	0.536	1.39	31.0	22.5	0.140
10^{-3}		0.132	0.300	0.645	1.31	30.6	21.3	0.090
10^{-2}		0.165	0.341	0.766	1.57	30.5	21.4	0.035
10^{-1}		0.195	0.423	0.873	1.80	29.5	18.8	0.025
10^{-4}	$k_1 \times 10^5$ sec^{-1}	0.784	1.75	3.81	8.08			
10^{-3}		0.603	1.33	2.85	5.98			
10^{-2}		0.280	0.614	1.31	2.75			
10^{-1}		0.245	0.523	1.10	2.25			
10^{-4}	$k_2 \times 10^3$ sec^{-1}	0.104	0.232	0.506	1.07			
10^{-3}		0.128	0.282	0.605	1.27			
10^{-2}		0.157	0.345	0.738	1.55			
10^{-1}		0.194	0.414	0.867	1.77			

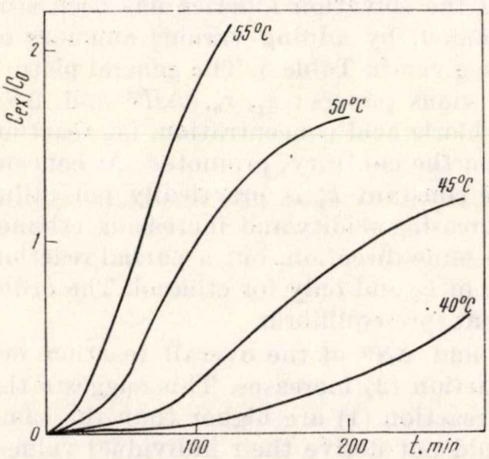

Fig. 3. — Influence of temperature on the excess NCS⁻ concentration. 37.7% EtOH.

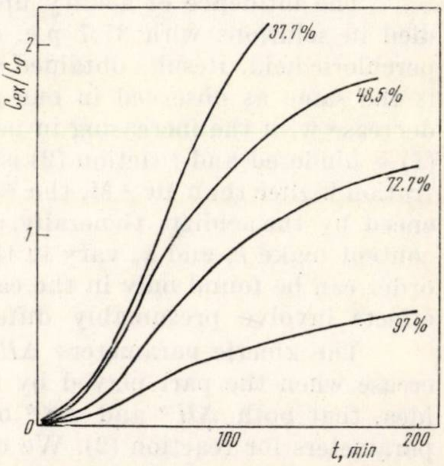

Fig. 4. — Influence of the ethanol content on the excess NCS⁻ concentration. 55°C.

apparent, that the third and fourth NCS⊖ ions are also substituted in neutral and in not very acid solutions.

But the rate of this reaction decreases considerably with increasing ethanol content. NCS⊖ ions are exchanged presumably for water molecules, which may be involved in the reaction mechanism too.

Table 4

Rate constants of reaction (4) in acid solutions $k_4 \times 10^5$, sec^{-1}. 37.7% EtOH

t°C	[HClO$_4$], mole/l	
	10^{-1}	10^{-2}
40	0.29	0.30
45	0.59	0.60
50	1.18	1.15
55	2.30	2.35

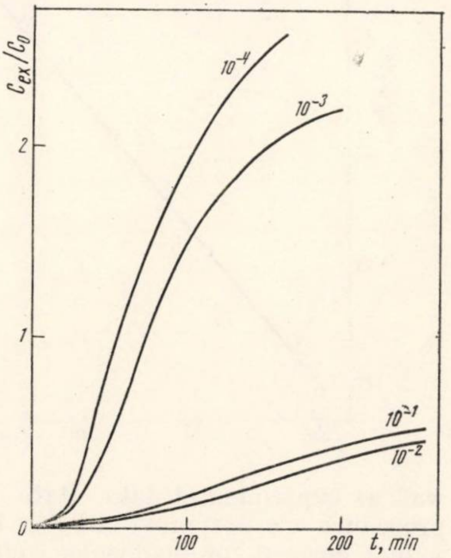

Fig. 5. — Influence of the perchloric acid concentration (in mole/l) on the excess NCS⊖ concentration. 37.7% EtOH, 55°C.

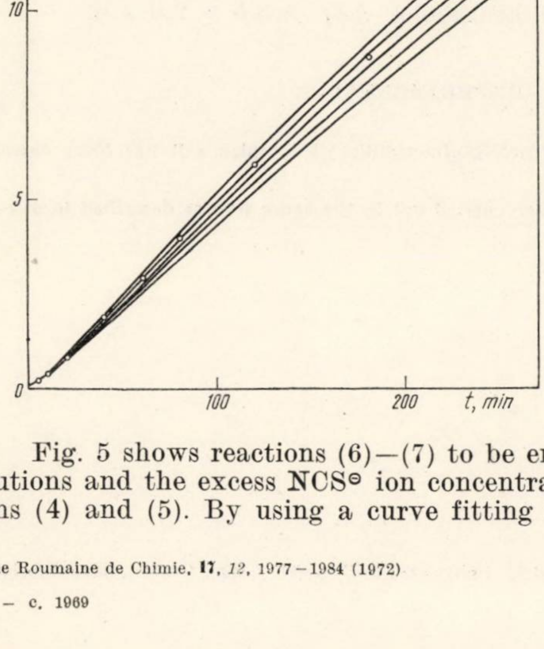

Fig. 6. — Deriving of k_4 by means of the curve fitting method. 37.7% EtOH. 55°C conc. of HClO$_4$ = 10^{-1} M.
Presumed $k_4.10^5$ values:
1, 2.0; 2, 2.1; 3, 2.2; 4, 2.3; 5, 2.4.

Fig. 5 shows reactions (6)—(7) to be entirely hindered in very acid solutions and the excess NCS⊖ ion concentration to be due only to reactions (4) and (5). By using a curve fitting method, described earlier,[4-6] rate constants k_4 of reaction (4) can be derived from the c_{ex}-time curves for concentration of $HClO_4 = 10^{-2}$ and 10^{-1} M, on the presumption that reaction (5) was instantaneous. The procedure is illustrated by Fig. 6, showing several theoretical curves calculated for different k_4 values, as well as experimental data. Rate constants k_4 derived by means of this procedure are presented in Table 4. Values obtained are very close to k_4 values derived for analogous complexes studied earlier.[4-6]

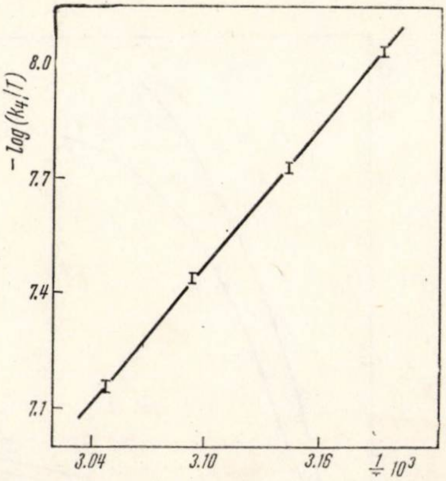

Fig. 7. — Determination of $\Delta H_4^{\neq}$ and $\Delta S_4^{\neq}$ in acid solutions. 37.7% EtOH.

The plot of $\log k_4/T$ versus $1/T$, given in Fig. 7, shows a good linearity and enabled us to derive, by means of the least square method, the following kinetic parameters of reaction (4)

$$\Delta H_4^{\neq} = 27.4 \pm 0.6 \text{ kcal/mole}, \quad \Delta S_4^{\neq} = 3.5 \pm 2.0 \text{ e.u.}$$

EXPERIMENTAL

The synthesis of the *m*-xylidine $H[Cr(NCS)_4(m\text{-xylidine})_2]$ complex salt has been described in our previous paper.[9]

Kinetic measurements have been carried out in the same way as described in our previous paper.[5]

---

[9] I. Gănescu, Al. Popescu and M. Proteasa, *Coll. Czech. Chem. Comm.*, **36**, 3088 (1971).

Revue Roumaine de Chimie, **17**, *12*, 1985 – 1989 (1972)

THIN LAYER THERMOCHROMATOGRAPHY. V*

INFLUENCE OF THE TEMPERATURE GRADIENT ON THE RESOLUTION OF SOME AMINO-ACIDS IN THIN LAYER CHROMATOGRAPHY

C. LITEANU and T. HODIŞAN

"Babeş-Bolyai" University, Department of Chemistry
Analytical Chemistry Department – Cluj, Str. Arany Janos, 11

Received May 12, 1972

The paper deals with the influence of the temperature gradient on the resolution of the following amino-acid mixtures : leucine + phenyl-alanine, alanine + glutamic acid, and arginine + cystine. The resolution of the components taken into consideration increases with the growth of the temperature gradient a fact in good agreement with the theoretical views. An empirical relation between resolution and temperature gradient was found, allowing us to determine the very weak resolutions, and the values of the temperature gradient for which, from a theoretical point of view, the resolution of the components considered should be "infinite" $\left(\frac{1}{R_s} = 0\right)$.

It is known that, the dimension rendering the efficiency of a closed or open chromatographic column (paper or thin layer) is the resolution [1,2] or the separation function. [3,4] In literature we often find that the degree of separation capacity of two or more substances depends on the number of theoretical plates realized in the column. In fact Martin and Synge [5] have already demonstrated in 1941 that the chromatographic separation of two components is not exclusively determined by the number of theoretical plates of the column.

De Ligny [6–9] and co-workers have dealt, in a series of papers, with the problem of efficiency in chromatographic separation of two components

---

[*] Part I, T. Hodişan and C. Liteanu, *Stud. Univ. Babeş-Bolyai, Chem.*, **17**, 73 (1972).

[1] T. Ellerington, "Gas Chromatography", D. H. Desty(ed), Butterworths, London 1958.

[2] W. J. Jones and R. Kieselbach, *Analyt. Chem.*, **30**, 1590 (1958).

[3] J. C. Giddings, *Analyt. Chem.*, **32**, 1707 (1960).

[4] H. Sevensson, *J. Chromatog.*, **25**, 266 (1966).

[5] A. J. P. Martin and R. L. M. Synge, *Biochem. J.*, **35**, 1358 (1941).

[6] C. L. De Ligny and A. G. Remijnse, *Rec. Trav. chim.*, **86**, 421 (1967).

[7] C. L. De Ligny, H. M. Schmidt and W. De Vries, *Rec. Trav. chim.*, **82**, 1061 (1963).

[8] C. L. De Ligny H. M. Schmidt and W. De Vries, *Rec. Trav. chim.*, **82**, 1071 (1963).

[9] C. L. De Ligny, H. M. Schmidt and W. De Vries, *Rec. Trav. chim.*, **82**, 1076 (1963).

in paper and thin layer chromatography. The authors define[8] the efficiency E by the following relation

$$E = \frac{R_s^2}{\sqrt{l_1 l_2}} \tag{1}$$

where : R_s is the resolution of the two components considered, and l_1 and l_2 are the distances measured on the densitogram from the starting point to the point of maximum concentration. But we know that the following relation exists between the resolution and the separation function F : $F = R_s^2$, thus $E = R_s^2/\sqrt{l_1 l_2} \simeq F/l$. Otherwise said, the separation efficiency E is nothing else than the separation function referred to the length unit of the column.

From a theoretical point of view, the problem of resolution in thin layer and paper chromatography with a temperature gradient was dealt with in a previous paper.[10]

EXPERIMENTAL

To study the influence of the temperature gradient on the resolution in thin layer chromatography, several pairs of amino-acids were chosen, which, in isothermic conditions, present separate difficulties.[11] One has therefore chosen the following couples : a) leucine + phenylalanine b) alanine + glutamic acid and c) arginine + cystine.

Microcrystalline cellulose (Merck) was used as support, and the highest phase of the n-butanol-acetic acid — water (4 : 1 : 5 v/v) mixture as eluent. The developments were carried out at different gradients and the value of each one is included in the figure. In each case the temperature of the eluent in the room was 20°.

After development, for the visualizing of the zones, the chromatograms were sprayed with a 0.2% alcoholic solution of ninhydrine. All the chromatograms were photographed on the same film and in the same conditions. The readings of the film were made by transmission, for each 0.1 mm with a G II Schnellphotometer type microphotometer and then the respective densitograms were plotted. The obtained results are given in figures 1 to 3, in which the transmittance (T) is represented in divisions read by a microphotometer, versus the distance in mm on which the zone extends itself.

The resolution was calculated from the plotted curves by means of the following relation : $R_s = \Delta z/2(\sigma_1 + \sigma_2)$, where Δz is the distance between maximum concentrations, measured on the densitogram, and σ is the standard deviation of the peak on the densitogram.

As is known, according to the normal distribution law, the standard deviation, σ, represents half of the curve breadth between the inflexion points, or a quarter of the curve breadth at the base, limited by the tangents drawn through the inflexion points. These reasons were also transposed in the case of chromatographic peaks which have a similar form to the normal distribution curve.

---

[10] S. Gocan and C. Liteanu, *Rev. Roumaine Chim.*, **17**, 661 (1972).

[11] T. Hodişan and C. Liteanu, *Stud. Univ. Babeş-Bolyai, Chem.*, **17**, 73 1972).

Dybczynski[12] suggests that the breadth of the chromatographic peak should be measured at the 0.368 value of the maximum height. In fact, this value better reflects the size of the resolution for the symmetrical curves as well as for the asymmetrical ones.

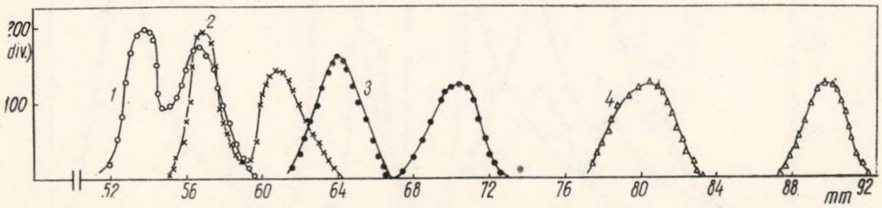

Fig. 1. — Shape of the densitograms of the leucine-phenylalanine mixture at different temperature gradients :

1, t.grad. = 0(t = 20°); R_s = 0.79;
2, t.grad. = 0.55(t_i = 20°); R_s = 0.95;
3, t.grad. = 1.11(t_i = 20°); R_s = 1.44;
4, t.grad. = 1.66(t_i = 20°); R_s = 2.17.

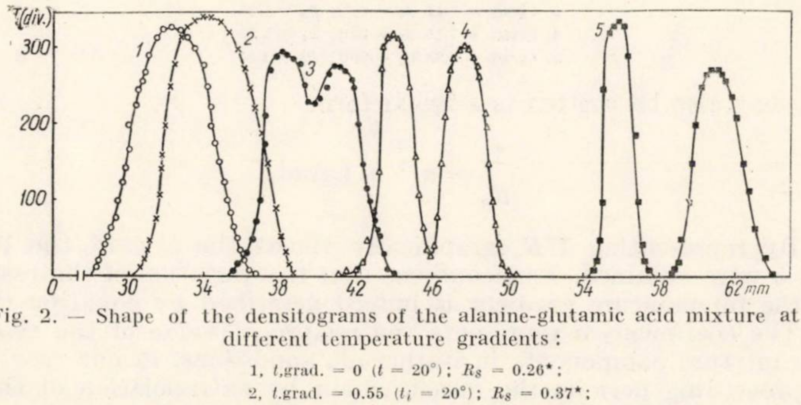

Fig. 2. — Shape of the densitograms of the alanine-glutamic acid mixture at different temperature gradients :

1, t.grad. = 0 (t = 20°); R_s = 0.26*;
2, t.grad. = 0.55 (t_i = 20°); R_s = 0.37*;
3, t.grad. = 1.11 (t_i = 20°); R_s = 0.53;
4, t.grad. = 1.66 (t_i = 20°); R_s = 1.02;
5, t.grad. = 1.94 (t_i = 20°); R_s = 1.58.

---

* The respective values were determined by extrapolation the line giving the $1/R_s$ variation with the temperature gradient (fig. 5).

The results obtained are given in figure 4.

This figure shows that the resolution grows with the temperature gradient, a fact actually confirming the thoeretical considerations about the acting mechanism of the temperature gradient.[10]

The shape of the curves in figure 4 suggests the idea that between the resolution and the temperature gradient there might exists an empirical relation of the following form

$$R_s = \frac{1}{a + b\ t.\mathrm{grad.}} \tag{2}$$

---

[12] R. Dybczynski, *J. Chromatog.*, **14**, 79 (1964).

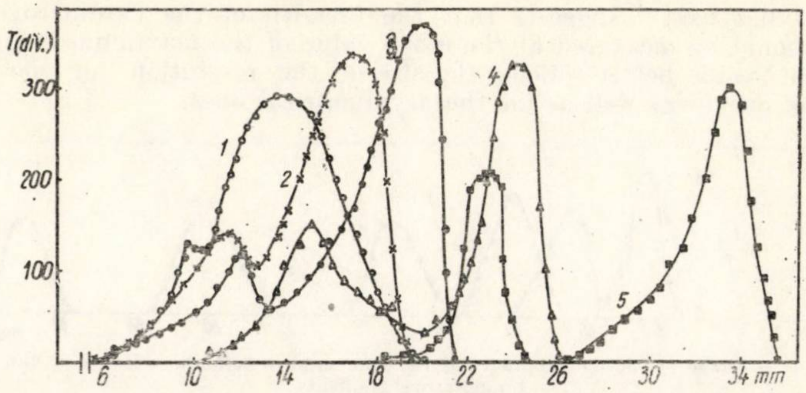

Fig. 3. — Shape of the densitograms of the arginine-cystine mixture at different temperature gradients :

1, t.grad. = $0 (t = 20°)$; $R_S = 0.52$;
2, t.grad. = 0.55 ($t_i = 20°$); $R_S = 0.70$;
3, t.grad. = 1.11 ($t_i = 20°$); $R_S = 1.02$;
4, t.grad. = 1.66 ($t_i = 20°$); $R_S = 1.26$;
5, t.grad. = 1.94 ($t_i = 20°$); $R_S = 1.96$;

which may also be written in a linear form

$$\frac{1}{R_S} = a + b \ \ t.\mathrm{grad}. \tag{3}$$

By representing $1/R_S$ graphically versus the t. grad. the lines in figure 5 were obtained. This confirms that the variation of the resolution with the temperature gradient is indeed described by equation (2).

The coefficient a represents the reciprocal value of the resolution of the mixture components in isothermic conditions, in our case at 20°. This proceeding permits the measurement by extrapolation of the very low resolutions, which cannot be determined by the shape of the elution curve. As for two components $\alpha_1 \neq \alpha_2$, there results theoretically, from the analysis of the terms of the resolution equation [10]

$$R_S = \frac{\Delta R_f \cdot \sqrt{L}}{2(\sqrt{R_{f_1} \cdot H_1} + \sqrt{R_{f_2} \cdot H_2})} \tag{4}$$

that the resolution always differs from zero, even if on the densitogram two peaks are not evident.

By analysing the form of the chromatographic peak obtained at 20° for the temperature gradient 0.55°/cm, one notices a broadening of the latter, confirming the fact that the resolution has increased. The values of the resolution obtained by extrapolation are 0.26 for a temperature gradient of 0 and respectively 0.37 for a temperature gradient of 0.55°/cm.

Meanwhile equation (3) permits, on the one hand, the measurement of the temperature gradient corresponding to an optimum separation resolution ($R_S = 1.0$ corresponds to a 98% separation of the com-

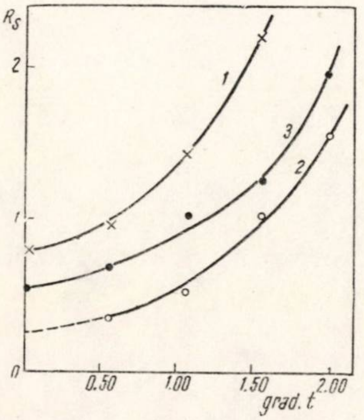

Fig. 4. — Variation of the resolution of:

1, leucine-phenylalanine;
2, alanine-glutamic acid;
3, arginine-cystine, with the temperature gradient.

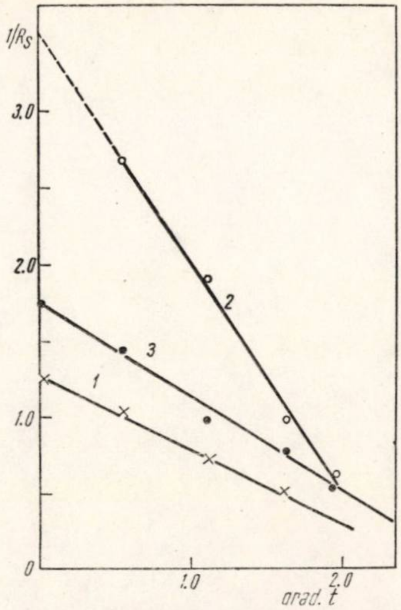

Fig. 5. — Variation of the reciprocal value of the resolution with the temperature gradient, for the same mixtures:

1, leucine-phenylalanine;
2, alanine-glutamic acid;
3, arginine-cystine.

ponents), and on the other hand, the determination of the gradient value for which, from a theoretical point of view, the resolution of the considered components should be "infinite" ($1/R_S = 0$).

In isothermic working conditions, there is no sense to associate the "infinite" value to the resolution, as it would thus correspond to a chromatographic column of infinite length, but in the conditions of the temperature gradient, it was shown [13] that the supplementary eluent volume. ΔV, passing through the column and participating to the repartition processes, may be infinite, for a well-determined value of the temperature gradient. This does not signify anything else but that the length of such a column is practically infinite. On a column of infinite length one can achieve an "infinite" resolution. Hence, in the conditions of the temperature gradient one could speak about an "infinite" resolution i.e. $1/R_S = 0$, ($R_S = \infty$).

This is practically achieved when the average evaporation rate of the eluent found in the column above the zone (participating to the repartition) [14] is equal to the speed with which it goes through the zone,

---

[13] C. Liteanu and S. Gocan, *Bull. Soc. chim. France*, **1970**, 4527.

[14] S. Gocan, C. Ciupală-Costea, T. Hodişan and C. Liteanu, *Rev. Roumaine Chim.* **16**, 1069 (1971).

Revue Roumaine de Chimie, 17, 12, 1991–1996 (1972)

NEUE ORGANISCHE PIGMENTE–ISATINDERIVATE. II[1]

SYNTHESE DURCH DIREKTE KONDENSIERUNG

B. D. BADER und R. VÎLCEANU

aus dem Forschungslaboratorium der industriellen Gruppe für Petrochemie, Piteşti, Şos. Giurgiului, 127; und von der chemischen Forschungsstelle Timişoara, Bdul Mihai Viteazul, 24

Eingegangen am 14. März 1972

Es wird eine neue Synthesemethode der Isatinderivate durch direkte Kondensierung des Isatins mit Diaminen in Polyphosphorsäure beschrieben.

In einer vorhergehenden Arbeit [1] wurde eine neue Reihe von organischen Pigmenten mit guten Echtheiten beschrieben, welche vom Isatin abgeleitet wurden und den allgemeinen Formeln (I) und (II) entsprechen :

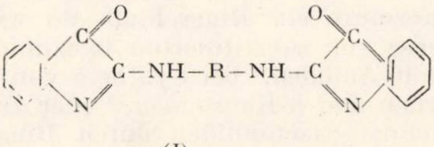

(I)

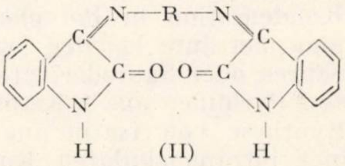

(II)

Die Synthese dieser Verbindungen ist im allgemeinen aber umständlich, vor allem wegen der Chlorierungsphase im Heterozyklus des Isatins. Da aber schon die Synthese des Isatins als Verfahren eine Reihe von schwierigen Prozessen erfordert, haben sich unsere Bemühungen auf das Auffinden einer neuen und direkten Kondensierungsmöglichkeit des Isatins mit Diaminen konzentriert.

ALLGEMEINES

Die bestehenden Literaturangaben bringen keine Hinweise betreffend Derivate die durch Kondensierung des Isatins mit Diaminen dargestellt werden können, Hinweise welche auch in bezug auf andere ähnliche Heterozyklen wie Benzimidazol, Benzothiazol und Benzoxazol fehlen.

---

[1] I. Mitt., J. Reichel, B. D. Bader und R. Vîlceanu, *Rev. Roumaine Chim.*, **17**, 1889 (1972).

Anderseits wurden eine Reihe von Syntheseversuchen von Schiffbasen aus aromatischen Ketonen und aromatischen Aminen beschrieben, welche in Gegenwart von Zinkchlorid,[2,3] Phosphoroxychlorid oder Phosphortrichlorid[4] vollzogen wurden. Gleichzeitig gibt es Angaben, die über die Herstellung von Isatin-3-anilen[5,6] berichten, Verbindungen welche folgender Formel (III) entsprechen:

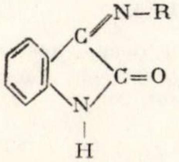

(III) wo R = aromatischer Rest

Da uns der besondere Erfolg, mit welchem die Polyphosphorsäure als Kondensationsmittel in einer Vielfalt von Reaktionen der organischen Chemie angewandt wird,[7] ins Auge fiel, haben wir den Versuch unternommen, die direkte Kondensation des Isatins mit aromatischen primären Diaminen mit Hilfe der Polyphosphorsäure durchzuführen. Die gefundene Synthesemöglichkeit und ihre Verfahren stellen das Thema einer Patentanmeldung[8] dar.

Die Anwendung der Polyphosphorsäure als Kondensationsmittel in mit Wasserabspaltung verlaufenden Reaktionen, bei der Herstellung von Kondensationsprodukten mit Bildung von C=N-Bindungen, wird ziemlich häufig in der Literatur beschrieben. In den meisten Fällen folgt der Kondensation in Polyphosphorsäure ein Ringschluß. So wird die Polyphosphorsäure bei der Synthese von substituierten Benzimidazolen aus Säuren oder Säurederivaten mit Aniliden,[9] bei Synthese von substituierten Pyridinen aus β-Ketonitrilen und β-Ketamiden,[10] oder auch bei der Synthese von Isatin aus Isonitrosoazetaniliden durch Ringschluß in einer intramolekularen Kondensation[11] verwendet.

Bei Reaktionen die in Polyphosphorsäure verlaufen, werden hauptsächlich Polyphosphorsäuren mit einem Gehalt von 82–85% Phosphorpentoxyd verwendet. Diese stellen eigentlich Gemische von verschiedener Zusammensetzung dar, welche vom Gehalt an Phosphorsäureanhydrid abhängig ist. So zum Beispiel, besitzt die Polyphosphorsäure mit 84% P_2O_5, welche wir in unserer Synthese verwendet haben, nach

---

[2] W. M. Foley, *J. Amer. Chem. Soc.*, **74**, 5489 (1952).

[3] G. Reddelien, *Ber. dtsch. chem. Ges.*, **42**, 4759 (1909), **43**, 2476 (1910).

[4] A. W. Weston und R. L. Michels, *J. Amer. Chem. Soc.*, **73**, 1381 (1951).

[5] G. B. Crippe und S. Pietra, *Gazz. chim. Ital.*, **81**, 195 (1951).

[6] W. C. Sumpter, *Chem. Rev*, **34**, 393 (1944).

[7] F. Uhlig und H. R. Synder, „The Polyphosphoric Acid as Reactant in Organic Chemistry", in: „Advances in Organic Chemistry", Bd. I, Interscience Publ., New York – London, 1960.

[8] Patentanmeldung R. S. România (B. D. Bader), Nr. 67849, 1971.

[9] D. W. Hein, R. J. Alheim und J. J. Leavitt, *J. Amer. Chem. Soc.*, **79**, 427 (1957).

[10] C. R. Hauser und C. J. Eby, *J. Amer. Chem. Soc.*, **79**, 725, 728 (1957).

[11] F. Piozzi und G. Favini, *Atti Accad. naz. Lincei, Rend. Classe Sci. fis. mat. nat.*, **18**, 647 (1955).

Angaben von Huhti und Gartaganis[12] folgende Zusammensetzung: Orthophosphorsäure und Pyrophosphorsäure 15%, Polyphosphorsäuren mit n = 1 bis 7 um 65% und höhere Polyphosphorsäuren 20%. In der nachstehenden Formel wird die Bedeutung des obengebrauchten Faktors n (ein sogenannter Polymerisationsfaktor) angezeigt:

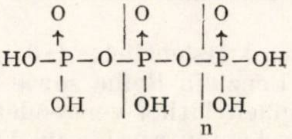

$$HO-\underset{OH}{\overset{\overset{O}{\uparrow}}{P}}-O\left[-\underset{OH}{\overset{\overset{O}{\uparrow}}{P}}-O-\right]_n\underset{OH}{\overset{\overset{O}{\uparrow}}{P}}-OH$$

VERSUCHE UND ERGEBNISSE

Von der Idee ausgehend, die direkte Kondensation des Isatins mit Diaminen durchzuführen um Verbindungen der allgemeinen Formel (II) zu erhalten, haben wir verschiedene, in der Literatur angegebene Kondensationsmittel versucht. Der Versuch, Phosphortrichlorid als Kondensationsmittel[4] in der Reaktion des Isatins mit *o*-Tolidin anzuwenden, führte zum respektiven 3-Anil von orangegelber Farbe, dessen Struktur sich mit der, des durch Erwärmen in Alkohol von Isatin mit *o*-Tolidin erhaltenen 3-Anils als identisch bewies, was auch durch die Identität der IR-Spektren erwiesen wurde.

Die Anwendung der Polyphosphorsäure als Kondensationsmittel und Reaktionsmedium führte zu den erwünschten Reaktionsprodukten. Die Kondensation wurde bei Temperaturen von 100 bis 150° mit Überschuß von Isatin durchgeführt.

Die Reaktion verläuft nach folgendem Schema:

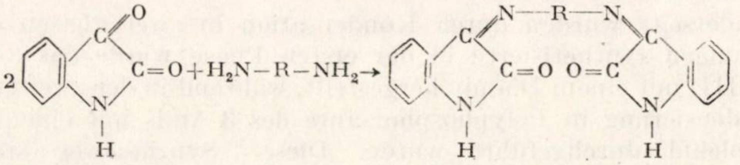

In einem mit Rührwerk und Heizhaube versehenen Kolben wurde die berechnete Menge Polyphosphorsäure auf 60° erwärmt. Unter ständigem Rühren und weiterem Erwärmen wird die nötige Menge Isatin eingeführt, wobei sich ein dunkelweichselrotes Gemisch bildet. Bei 100—110° wird das Diamin eingerührt, wobei man eine Verdunkelung der Farbe des Gemisches sowie einen Temperaturanstieg von 10—15°, welcher auf einen exothermen Effekt schließen läßt, bemerken kann. Es wird nun bis auf 140—150° aufgewärmt und bei dieser Temperatur 2—3 Std. lang gerührt. Nach Beendigung der Reaktion wird das Gemisch auf 60—70° abgekühlt und mit Eiswasser verdünnt bis die Konzentration an Orthophosphorsäure annähernd auf 75% absinkt. Das erhaltene Gemisch wird nun auf einem Nutschefilter abgesaugt, der Rückstand wird mit Wasser aufgerührt, aufgekocht und heiß filtriert. Der Niederschlag wird am Filter mit heißem Wasser bis zur neutralen Reaktion gewaschen.

---

[12] A. L. Huhti und P. A. Gartaganis, *Canad. J. Chem.*, **34**, 785 (1956).

Die in der Kondensation verwendeten Diamine, das molare Verhältnis der Ausgangsverbindungen, die Reaktionsdauer, die Ausbeuten sowie die Elementaranalysen der Reaktionsprodukte werden in Tabelle 1 wiedergegeben.

Desgleichen werden in Tabelle 2 die Farbtöne angezeigt, welche durch Gebrauch von verschiedenen Diaminen in der Kondensation erhalten werden.

Aus den Tabellen wird ersichtlich, daß in jenen Kondensationen, in welchen Diamine der Benzidin-Reihe sowie Diamino-Diphenylmetan, Diphenylsulfon oder -Diphenyläther verwendet werden, die Ausbeuten sehr gut sind. Kleinere Ausbeuten werden im Falle der Verwendung von Anthrachinondiaminen (wahrscheinlich wegen der Unlöslichkeit in Polyphosphorsäure der Diamine) und zum Teil von Phenylendiaminen (wahrscheinlich wegen der teilweisen Löslichkeit der Reaktionsprodukte in der bei der Verdünnung der Polyphosphorsäure erhaltenen konzentrierten Phosphorsäure) erhalten. Gleichzeitig kann man bemerken, daß durch Substitution im Diamin mit verschiedenen Substituienten (Cl, CH_3, CH_3O) eine Verschiebung der Farbtöne zu dünkleren Tönen eintritt, Effekt welcher insbesondere in der Benzidin-Reihe ersichtlich ist.

Da die Literaturangaben [6] vor allem die Beteiligung der Ketongruppe aus Stellung 3 des Isatins in direkten Kondensationen anzeigen, haben wir vermutet, daß die synthetisierten Kondensationsprodukte die in Formel II angezeigte Struktur besitzen. Diese Vermutung wurde durch ihr IR-Spektrum bestätigt, welches sich mit dem IR-Spektrum der durch Kondensation des 3,3-Dichlorisatins mit denselben Diaminen hergestellten Verbindungen deckt, was auf die Identität der untersuchten Produkte schließen läßt.

Anderseits wurden durch Kondensation in zwei Phasen dieselben Verbindungen synthetisiert : in der ersten Phase wurde das 3-Anil des Isatins (III) mit einem Diamin hergestellt, während in der zweiten Etappe die Kondensierung in Polyphosphorsäure des 3-Anils mit einem zweiten Isatinmolekül durchgeführt wurde. Dieser Syntheseweg stellt desgleichen einen Beweis für die vermutete Struktur der Kondensationsprodukte dar.

Da die synthetisierten Verbindungen sich mit einer der beiden von uns früher beschriebenen Reihen von Produkten [1] als identisch erwiesen, hatten wir nochmals die Möglichkeit ihre ausgezeichnete Thermostabilität, Unlöslichkeit in fast allen organischen Lösungsmitteln, sowie ihr Färbevermögen an Kunststoffen zu beobachten.

Das Trennungsverfahren der Produkte aus dem Reaktionsgemisch durch Verdünnung ihrer Lösung in einer konzentrierten Säure stellt gleichzeitig einen sauren Pastifikationsprozeß dar und lieferte dadurch äußerst fein dispergierte Produkte.

Diese fein disperse Form der Produkte eignete sich besser zum Pigmentieren von Kunststoffen als diejenige der Verbindungen, welche bei der Kondensation des 3,3-Dichlorisatins mit Diaminen erhalten wurde.

Tabelle 1

Reaktionsbedingungen und Ergebnisse betreffend Sybthese der Verbindungen

In der Kondensation verwendete Diamine	Verhältnis Ausgangsprodukte/Polyphosphorsäure	Molarverhältnis Diamin/Isatin	Kondensationszeit, h	Ausbeute gegenüber Diamin %	Bruttoformel	Elementaranalyse							
						% berechnet				% gefunden			
						C	H	N	S/Cl	C	H	N	S/Cl
1,4-Phenylendiamin	1 : 10	1 : 4	2,5	90,0	$C_{22}H_{14}N_4O_2$	72,1	3,82	15,3	—	71,9	3,71	14,9	—
1,3-Phenylendiamin	1 : 10	1 : 4	2,5	82,0	idem	72,1	3,82	15,3	—	71,8	3,75	14,9	—
2,4-Toluylendiamin	1 : 10	1 : 3	2,0	75,0	$C_{23}H_{17}N_4O_2$	72,6	4,21	14,7	—	72,1	4,11	14,6	—
Benzidin	1 : 10	1 : 4	3,0	95,7	$C_{28}H_{18}N_4O_2$	75,9	4,07	12,6	—	75,4	4,00	12,3	—
Benzidin	1 : 10	1 : 4	2,0	91,2	idem	75,9	4,07	12,6	—	75,7	3,95	12,4	—
o-Tolidin	1 : 9	1 : 4	3,0	94,5	$C_{30}H_{22}N_4O_2$	76,6	4,68	11,9	—	76,2	4,55	11,3	—
o-Tolidin	1 : 10	1 ; 3	2,0	84,5	idem	76,6	4,68	11,9	—	76,1	4,58	11,6	—
o-Dianisidin	1 : 8	1 : 3	2,0	83,0	$C_{30}H_{22}N_4O_4$	71,7	4,38	11,1	—	71,6	4,15	11,0	—
o-Dianisidin	1 : 10	1 : 4	3,0	90,3	idem	71,7	4,38	11,1	—	71,4	4,23	10,8	—
3,3-Dichlorbenzidin	1 : 10	1 : 4	2,0	76,1	$C_{28}H_{16}N_4O_2Cl_2$	65,3	3,13	10,9	Cl = 13,9	65,0	3,10	10,8	13,85
2,6-Diaminopyridin	1 : 10	1 : 4	2,0	90,1	$C_{21}H_{13}N_5O_2$	68,8	3,54	19,1	—	67,1	3,41	19,0	
4,4′-Diaminodiphenylsulfon	1 : 8	1 : 3	2,0	81,8	$C_{28}H_{18}N_4O_4S$	66,5	3,56	11,1	S = 6,33	66,3	3,42	10,8	6,28
4,4′-Diaminodiphenyläther	1 : 8	1 : 3	2,0	77,9	$C_{28}H_{18}N_4O_3$	72,9	3,93	12,2	—	72,8	3,80	12,1	—
4,4′-Diaminodiphenylmethan	1 : 8	1 : 3	2,0	80,6	$C_{29}H_{20}N_4O_2$	76,3	4,39	12,3	—	75,9	4,21	12,0	—
1,4-Diaminoanthrachinon	1 : 10	1 : 4	2,0	60,6	$C_{30}H_{16}N_4O_4$	72,5	3,23	11,3	—	72,2	3,05	11,0	—
1,5-Diaminoanthrachinon	1 : 10	1 : 2,8	2,0	55,0	idem	72,5	3,23	11,3	—	71,2	3,13	10,9	—
3,6-Diaminodiphenylenoxyd	1 : 11	1 : 4	2,0	64,8	$C_{28}H_{16}N_4O_3$	73,2	3,51	12,3	—	73,0	3,38	12,1	—

Tabelle 2

Abhängigkeit der erhaltenen Farbtöne von der Natur des verwendeten Diamins

In der Kondensation verwendetes Diamin	Erhaltener Farbton
1,4-Phenylendiamin	gelbbraun
1,3-Phenylendiamin	kaffeebraun
2,4-Toluylendiamin	braun
Benzidin	helles rotbraun
o-Tolidin	kaffeebraun
o-Dianisidin	braun
3,3-Dichlorbenzidin	helles rotbraun
4,4'-Diaminodiphenylsulfon	kaffeebraun
4,4'-Diaminodiphenylähter	gelbbraun
4,4'-Diaminodiphenylmethan	braun (graustichig)
2,6-Diaminopyridin	braunstichig schwarz
3,6-Diaminodiphenylenoxyd	rotbraun
1,4-Diaminoanthrachinon	schwarzbraun
1,5-Diaminoanthrachinon	rotbraun

Revue Roumaine de Chimie, 17, 12, 1997–2002 (1972)

BIS-(THENOYL-TRIFLUOROACETONATO)-BERYLLIUM

A. BARABÁS

Institute of Atomic Physics, P.O. Box 35, Bucharest

Received June 22, 1972

Bis-[3-(2′-thenoyl)-1,1,1-trifluoroacetonato]-beryllium was synthetized and characterized by m.p., IR, UV and ^{1}H-NMR spectra. Complexation simplifies the spin pattern of the thienyl protons (*ABX* in the free ligand) to a first-order *AMX* multiplet.

INTRODUCTION

The beryllium complex of 3-(2′-thenoyl)-1,1,1-trifluoroacetone (ttaH, I) was first prepared by Berg and Truemper.[1] The complexation equilibrium between ttaH and Be^{2+} was studied by solvent extraction.[2] It seems however that no detailed report on the properties of the bis-[3-(2′-thenoyl)-1,1,1-trifluoroacetonato]-beryllium (tta_2Be, II) was published. In our laboratory this compound was investigated as part of a more extended research on 1,3-diketonates of beryllium and boron.[3-5]

EXPERIMENTAL PART

Commercial ttaH was used. It was not further purified when used for synthesis of tta_2Be, but samples for spectroscopic measurements were recrystallized from carbon tetrachloride.

The synthesis of tta_2Be was effected as follows: 3 g of sodium acetate were added to a solution of 0.4 g (5 mmoles) of $BeCl_2$ in 20 ml of water. Into this solution 2.2 g (10 mmoles) of ttaH in 5 ml of methanol were introduced, which resulted in the formation of an oily layer. The mixture was shaken till all oil was converted into a white precipitate. This precipitate was filtered off, washed with water, dried in air and recrystallized from benzene-ligroin, giving pure tta_2Be, m.p. 164° (corr.), lit[1]. m.p. 169°.

Electronic spectra were recorded in 1,2-dichloroethane solution with an Optica-Milano CF 4 spectrophotometer. Infrared spectra were recorded in nujol mulls with a Perkin-Elmer 457 instrument.

---

[1] E. W. Berg and I. T. Truemper, *J. Phys. Chem.*, **64**, 487 (1960).

[2] H. J. de Bruin and R. B. Temple, *Austral. J. Chem.*, **15**, 153 (1962).

[3] A. Barabás, E. Işfan, M. Roman, M. Paraschiv, E. Romaş and A. T. Balaban, *Tetrahedron*, **24**, 1133 (1968), and earlier work cited therein.

[4] A. Barabás, E. Işfan, E. Romaş and A. Trestianu, *Rev. Roumaine Chim.*, **14**, 253 (1969).

[5] A. Trestianu, H. Niculescu-Majewska, I. Bally, A. Barabás and A. T. Balaban, *Tetrahedron*, **24**, 2499 (1968).

Proton magnetic resonance spectra were recorded in $CDCl_3$ solution with internal TMS standard. Two basic frequencies were used : spectra at 60 MHz were recorded with a Perkin Elmer R 12 instrument ; spectra at 80 MHz, including double resonance experiments, were recorded with a TESLA BS-487-B spectrometer.

RESULTS AND DISCUSSION

Strong IR-absorption bands assigned to individual vibrations in the free ligand and in the complex molecule are shown in Table 1. Assignments were done empirically by comparison with similar compounds.[3,4,6–9]

Table 1

Assigned major IR-absorption bands in thenoyl-trifluoroacetone (ttaH, I) and bis-(thenoyl-trifluoroacetonato)-beryllium (tta_2Be, II). Wave numbers (cm^{-1}) are given

ttaH	tta_2Be	Assignments
	Chelate ring frequencies	
3100 mw	3100 mw	$\nu C-H$
1650–	1578 vs	$\nu C.....O....M$ ($M = H, Be$)
–1560 vs	1550 vs	ν_{as}, C....C.....C
1460 vs	1455 vs	ω O.....C.....C......C......O
1310 s	1305 s	ν_s, C.....C.....C
—	950 s	ν_{as}, BeO_4, normal to symmetry axis
—	810 s	ν_{as}, BeO_4, axial
—	509 m	δ, BeO_4
	Thiophene ring frequencies	
1650–	1620 vs	skeletal modes
–1560 vs		
1520 shs	1510 s	
1410 vs	1410vs	
1355 s	1355 s	
1250 vs	1255 s	
860 s	860 m	
718 vs	720 s	$\delta C-H$, out-of-plane
678 m	681 m	
	CF_3 frequencies	
1230 s	1232 s	$\nu C-F$
1190 vs	1190 vs	
585 m	590 m	$\delta C-F$
552 w	525 w	
460 mw	460 mw	C–F, rocking

[6] E. Funck, *Ber. Bunsenges. Physik. Chem.*, **68**, 617 (1964) ; **71**, 170 (1967).

[7] H. Musso and H. Junge, *Tetrahedron Letters*, **1966**, 4003, 4009.

[8] A. R. Katritzky, *Quart. Rev.*, **13**, 353 (1959).

[9] I. H. Rosatzin, *Spectrochim. Acta*, **19**, 1107 (1963).

Electronic absorption bands of ttaH and tta$_2$Be are shown below (λ_{max}, nm):

ttaH, (I)	280,	*325,*	*352*
tta$_2$Be, (II)	281,	*350,*	*360*

Most intense are the italicized double bands at longer wavelength. These were attributed [3,4,10,11] to the $\pi \rightarrow \pi^*$ transition in the delocalized system including the chelate ring and the thienyl group, see formulae (I) and (II).

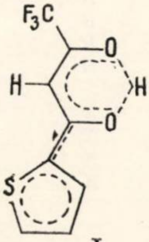

I

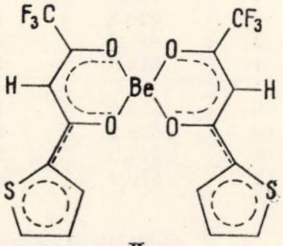

II

The bathochromic shift of this absorption band due to complexation is a standard feature with metallic 1,3-diketonates. [3,4]

Proton magnetic resonance spectra of ttaH and tta$_2$Be will be discussed in more detail. The free ligand, ttaH, appears fully enolized, the chelated proton giving a somewhat broadened signal at $\delta = 14.35$ ppm. Evidently, no signal appears in this region of the spectrum of tta$_2$Be. The methinic proton of the chelate ring resonates at $\delta = 6.44$ ppm in ttaH and at $\delta = 6.56$ ppm in tta$_2$Be. This slight deshielding of ligand protons due to complexation occurs invariably for a large number of metallic 1,3-diketonates of various structures. It was attributed to long-range anisotropic effects due to intramolecular electric fields.[5,12,13]

Complexation changes the spectrum of the thienyl protons in an interesting way. This three-spin system appears as an ABX multiplet in the free ligand, ttaH, see Table 2. The chemical shifts and coupling constants could be calculated in the usual way,[14] giving a calculated spectrum in fair agreement with the experimental one both for line positions and intensities. In the complex II, tta$_2$Be, the thienyl protons afford a simpler spectrum, a first-order multiplet of the AMX type, see Table 3. Chemical shifts and coupling constants could be measured directly. This interpretation was verified experimentally, using double resonance techniques, see Fig. 1.

[10] J. P. Collman, *Angew. Chem.*, **77**, 155 (1965).

[11] G. N. LaMar, *Acta Chem. Scand.*, **20**, 1359 (1966).

[12] J. A. S. Smith and E. J. Wilkins, *J. Chem. Soc. A*, **1966**, 1749.

[13] J. C. Hammel, J. A. S. Smith and E. J. Wilkins, *ibid.*, **1969**, 1461.

[14] E. D. Becker, "High-Resolution NMR, Theory and Chemical Applications", Academic Press, New York, 1969.

Table 2

NMR-signals of the thienyl protons in thenoyl-trifluoroacetone (ttaH, I) in $CDCl_3$ solution at 80 MHz

Line no.	Frequency (Hz)	Relative intensity	Attribution
8	628.0	1.21	*A*
6	626.7	1.30	*A*
7	624.0	1.45	*A*
5	623.0	1.97	*A*
4	622.0	1.87	*B*
2	620.8	1.24	*B*
3	617.3	1.58	*B*
1	616.0	1.19	*B*
9	579.2	1.90	*X*
10	575.2	1.49	*X*
11	574.2	1.34	*X*
12	570.2	1.00	*X*

Calculated parameters

	δ_A	δ_B	δ_X	J_{AB}	J_{AX}	J_{BX}
(Hz)	625.5	619.0	574.7	1.2	3.9	4.9
(ppm)	7.83	7.74	7.18			

$$\frac{\delta_A - \delta_B}{J_{AB}} = 5.5$$

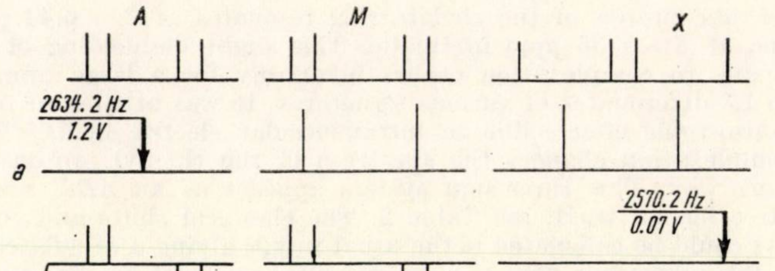
A
M
X
2634.2 Hz
1.2 V
a
2570.2 Hz
0.07 V
2574.2 Hz
0.07 V
b
2575.2 Hz
0.07 V
2579.2 Hz
0.07 V

Fig. 1. — Double resonance experiments on the thienyl multiplet in tta_2 Be, (II). Irradiation frequencies and energies are given.
a, decoupling; b, INDOR.

Table 3

NMR-signals of the thienyl protons in bis-(thenoyl-trifluoroacetonato)-beryllium (tta_2Be, II) in $CDCl_3$ at 80 MHz

Line no.	Frequency (Hz)	Relative intensity	Attribution
8	636.6	1.13	*A*
6	635.6	1.20	*A*
7	632.7	1.37	*A*
5	631.6	1.36	*A*
4	624.0	1.31	*M*
2	623.0	1.16	*M*
3	619.0	1.43	*M*
1	618.0	1.18	*M*
9	579.1	1.35	*X*
10	575.2	1.40	*X*
11	574.2	1.40	*X*
12	570.2	1.00	*X*

Measured parameters

	δ_A	δ_M	δ_X	J_{AM}	J_{AX}	J_{MX}
(Hz)	634.1	621.0	574.7	1.0	4.0	5.0
(ppm)	7.92	7.76	7.18			

$$\frac{\delta_A - \delta_M}{J_{AM}} = 13.0$$

An examination of the chemical shifts in Tables 2 and 3 reveals that complexation simplifies the thienyl resonance pattern by deshielding preferentially the proton *A* (with about 0.1 ppm), whereas the chemical shifts of *B* (*M*) and *X* remain practically unchanged. Leaving coupling constants unaltered (within an experimental error of ± 0.2 Hz), complexation will increase the $\delta_A - \delta_B/J_{AB}$ ratio (see Tables 2 and 3), thus transforming the *ABX* spin pattern into a first-order one, *AMX*.

An assignment of the thienyl spectrum in ttaH and tta_2Be can be attempted now. The magnitude of the coupling constants suggests that both J_{AX} and J_{BX} are due to vicinal coupling; consequently *X* must be the proton from position 4 of the thiophene ring (see formula III). This is in agreement with the low value of J_{AB} (J_{AM}), suggesting that protons *A* and *B* (*M*) are more distant within the ring, thus corresponding to positions 3 and 5. Finally, as complexation alters specifically the chemical shift of *A*, leaving *B* (*M*) and *X* mostly unchanged, it seems logical to assign proton *A* to position 3, *ortho*- towards the chelate ring. As shown in Table 4, this above assignment agrees with literature data[15,16] for a series of related 2-thenoyl compounds.

---

[15] R. A. Hoffman and S. Gronowitz, *Arkiv. Kemi*, **16**, 501, 515, 539 (1961).

[16] A. D. Cohen and K. A. McLauchlan, *Discuss. Faraday Soc.*, **34**, 132 (1962).

Table 4

Chemical shifts and coupling constants of the thienyl ring protons in some 2-thenoyl compounds[15,16]

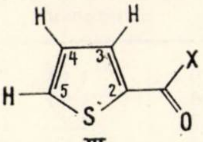

III

X	δ (ppm)			J (Hz)		
	H3	H4	H5	3–4	3–5	4–5
CH_3	7.54	6.97	7.44	3.6	1.1	5.0
C_2H_5	7.53	6.96	7.44	3.6	1.2	5.0
OCH_3	7.67	6.92	7.36	3.6	1.3	5.0
OH	7.76	7.04	7.60	3.5	1.2	4.9
Cl	7.85	7.03	7.60	3.4	1.4	5.0

The additional deshielding of proton 3 (*A*), due to complexation may be ascribed to the long-range anisotropic effect of intramolecular electric fields, discussed above.

Acknowledgements. Part of this work was done during a visit of the author at the laboratory of Prof. J.A.S. Smith, University of Warwick, Coventry, England. Further, gratitude is expressed to Prof. A. T. Balaban and Alice Vasilescu from the Institute of Atomic Physics and to M. Elian from the Institute of Organic Chemistry, Bucharest, for their valuable help.

Revue Roumaine de Chimie, 17, 12, 2003–2011 (1972)

RÉACTIONS DE COPOLYMÉRISATION À L'AIDE DES DÉRIVÉS ORGANIQUES DU TITANE-ALCOYLE-ALUMINIUM. VI*

ÉTUDE PAR LA DIFFUSION DE LA LUMIÈRE DES COPOLYMÈRES ACRYLONITRILE-STYROLÈNE OBTENUS À L'AIDE DES CATALYSEURS HOMOGÈNES ZIEGLER-NATTA

CR. I. SIMIONESCU, SILVIA IOAN, I. BENEDEK et N. ASANDEI

Institut de Chimie macromoléculaire «P. Poni», Aleea Gr. Ghica Vodă, 41/A,
Jassy, Roumanie

Reçu le 12 mai 1972

Le travail expose les résultats de la recherche par la diffusion de la lumière des copolymères acrylonitrile-styrolène, préparés à l'aide du système catalytique soluble, de type Ziegler-Natta : dichlorure du bis (cyclopentadiényle)-titane-triéthylaluminium ($Cp_2TiCl_2-AlEt_3$).

L'étude des copolymères par la diffusion de la lumière permet d'obtenir des données structurelles caractéristiques des macromolécules en solution.

On a démontré que pour les copolymères ayant une distribution compositionnelle, la masse moléculaire moyenne en poids M_w, déterminée par la diffusion de la lumière, dépend de la nature du solvant utilisé. [1]

Selon la théorie de Benoit, l'étude d'un copolymère binaire (sans connaître ses caractéristiques structurelles, telles que hétérogénéité en masse et en composition) requiert l'utilisation, au moins, de trois solvants différents. Pour chaque solvant, on obtient la masse moléculaire apparente, la masse moléculaire en poids réelle étant reliée à cette masse apparente par une dépendance complexe, contenant les incréments de l'indice de réfraction des homopolymères et du copolymère.

En général, on considère qu'un copolymère azéotrope est homogène en composition. Similairement on suppose l'existence d'une composition homogène au cas des copolymères obtenus à des conversions réduites.

---

* Ce travail représente une partie de la thèse soutenue par I. Benedek.

Le travail V a été publié dans l'*European Polymer J.*, **7**, 1561 (1971), signé par Cr. I. Simionescu, N. Asandei et I. Benedek.

[1] H. Benoit, *Ber. Bunsengesellschaft Phys. Chem.*, **70**, 286 (1966).

Ces hypothèses permettent l'application d'un traitement simplifié à l'étude des copolymères acrylonitrile-styrolène[2] et acrylonitrile méthylméthacrylate,[3] selon la méthode appliquée aux homopolymères, c'est-à-dire par l'emploi d'un seul solvant.

Les avantages de ces recherches à un seul solvant sont très importants notamment au cas des copolymères de l'acrylonitrile, pour lesquels le nombre de solvants est très réduit.

Les résultats de l'étude des copolymères d'acrylonitrile par diffusion de la lumière diffèrent selon la nature du copolymère.

Shimura et ses collaborateurs [4] démontrent par l'étude d'un copolymère azéotrope, acrylonitrile-styrolène, que la composition de ce copolymère est homogène par rapport aux copolymères industriels. D'autres chercheurs [5,6] constatent une composition hétérogène aux copolymères azéotropes styrolène-méthylmétacrylate.

Ce travail comprend les résultats de l'investigation, par la diffusion de la lumière, des copolymères acrylonitrile-styrolène préparés à l'aide des catalyseurs sur la base de dichlorure de bis (cyclopentadiényle)-titane-triéthylaluminium.

PARTIE EXPÉRIMENTALE

Matériaux

Le copolymère acrylonitrile-styrolène a été préparé selon les méthodes indiquées par la littérature.[7]

Solvants utilisés : diméthylformamide (DMF), diméthylacétamide (DMA), diméthylsulfoxyde (DMSO), tétrahydrofuranne (THF), benzène (Bz), dioxanne (Dx), ester (acétylacétique (EST), chloroforme (Cl), bromobenzène (BB), mélange benzène-diméthylsulfoxyde 1 : 1 vol. (Am), méthyl-éthyl-cétone (EMC) purifiés par séchage et distillation.

Incréments de l'indice de réfraction

Pour les homopolymères on a utilisé les valeurs de l'incrément de l'indice de réfraction données par la littérature. Pour les copolymères les valeurs correspondantes ont été calculées par additivité, et vérifiées à l'aide d'un interféromètre Zeiss.

Les solvants habituels du polyacrylonitrile (PAN) sont : DMF, DMSO et carbonate d'éthylèneglycole. Ces solvants dissolvent également les copolymères à teneur élevée en acrylonitrile. Au cas des copolymères acrylonitrile-styrolène se pose le problème de l'insolubilité du polystyrolène (PS) dans le DMSO. Ainsi la détermination de l'incrément de l'indice de réfraction par voie expérimentale n'est plus possible.

Pour écarter cette difficulté, on a préparé des oligomères du styrolène qui, solubles dans le DMSO, permettent la mesure directe de ν, par extrapolation des valeurs obtenues.

---

[2] Y. Shimura, *J. Polymer Sci.*, **A2 4**, 423 (1966).

[3] Y. Shimura, *Bull. Chem. Soc. Japan*, **40**, 273 (1967).

[4] Y. Shimura, *J. Polymer Sci.*, **B2**, 403 (1964).

[5] M. Leng et H. Benoit, *J. Chim. phys.*, **58**, 480 (1961).

[6] D. Froelich, *Thèse*, Univ. Strasbourg, 1966.

[7] Cr. I. Simionescu, N. Asandei, I. Benedek et C. Ungurenaşu, *European Polymer J.*, **6**, 925 (1970).

Le tableau 1 indique la variation de l'incrément de l'indice de réfraction du polystyrolène dans le DMSO, en fonction de la masse moléculaire des oligomères.

Comme l'on peut voir sur le tableau 1, les valeurs de l'incrément de l'indice de réfraction diminuent au fur et à mesure que la masse moléculaire augmente, se rapprochant de la valeur calculée par additivité pour le polystyrolène à masse moléculaire élevée. Ainsi la dernière valeur $\nu = 0{,}0579$ ml/g (pour un oligomère de $M = 1500$) se confond avec la valeur théorique $\nu = 0{,}0574$ ml/g donnée par la littérature.[8]

Tableau 1

Variation de l'incrément de l'indice de réfraction du polystyrolène en DMSO, en fonction de la masse moléculaire

N°	M	ν ml/g
1	210	0,0714
2	321	0,0600
3	1500	0,0579
4	500000	0,0574

Sur la figure 1 est illustrée la variation de l'incrément de l'indice de réfraction du PAN, PS et P(AN–S), en fonction de l'indice de réfraction des solvants utilisés.

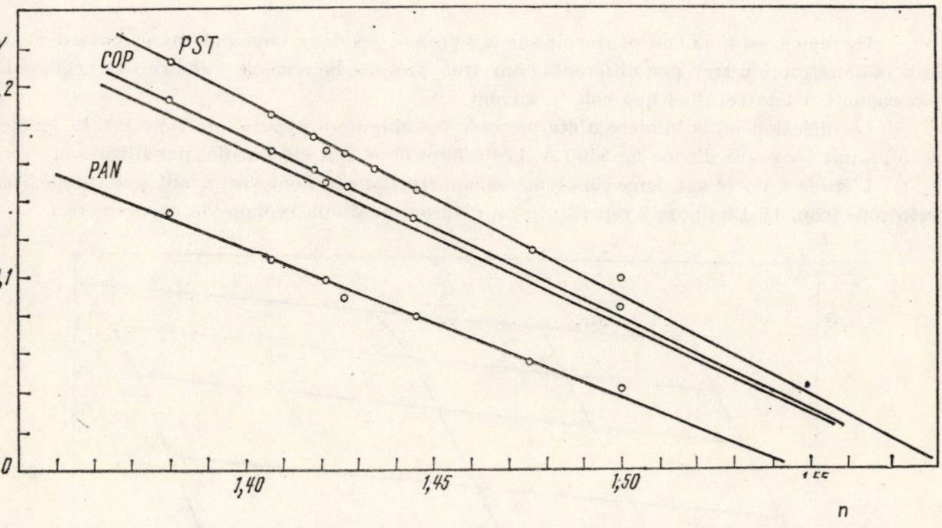

Fig. 1. — Variation de l'incrément d'indice de refraction des homopolymères et des copolymères sur la base de S et AN, en fonction de l'indice de réfraction des solvants utilisés.

Il ressort de l'analyse de la figure 1 que les solvants du copolymère, notamment les solvants communs aux deux homopolymères (*p.e.* DMF, DMA), sont trop peu nombreux et possèdent des indices trop voisins pour que l'on puisse construire avec une précision satisfaisante l'équation de la parabole :

---

[8] J. C. Galin, *Thèse*, Univ. Strasbourg, 1967.

$$M_{\text{app}} = M_w + 2P\,\frac{\nu_A - \nu_B}{\nu} + Q\left(\frac{\nu_A - \nu_B}{\nu}\right)^2 \tag{1}$$

Dans l'expression ci-dessus M_{app} est la masse moléculaire apparente du copolymère dans les solvants différents ; ν_A, ν_B et ν sont les incréments de l'indice de réfraction des homopolymères, respectivement du copolymère ; P et Q sont des paramètres caractérisant l'hétérogénéité en masse et l'hétérogénéité compositionnelle :

$$P = \frac{\Sigma c_i M_i\,\delta x_i}{\Sigma c_i} \quad (2) \qquad\qquad Q = \frac{\Sigma c_i M_i\,\delta x_i^2}{\Sigma c_i} \quad (3)$$

Dans les relations (*2*) et (*3*), c_i désigne la concentration d'un polymère ayant la masse moléculaire M_i, $\delta x_i = x_i$ définissant l'écart en composition de la molécule « *i* », par rapport à la composition moyenne.

Par une raison similaire, les équations ne peuvent pas être rigoureusement résolues ainsi que les valeurs obtenues pour M_w, P et Q puissent satisfaire les conditions de la théorie :

$$-\,xM_w \leqslant P \leqslant (1 - x)M_w \tag{4}$$

$$0 \leqslant Q \leqslant (1 - x(1 - x))M_w \tag{5}$$

De même, comme l'on peut voir sur la figure 1, les deux homopolymères possèdent des indices de réfraction trop peu différents pour que l'un des incréments d'indice soit négligeable par rapport à l'autre, quel que soit le solvant.

La diffusion de la lumière a été mesurée à l'aide d'un appareil de type P.C.L. Peaker, à 25°, à une longueur d'onde de 5460 Å. Les échantillons ont été purifiés par filtration.

L'étude a porté sur deux copolymères non fractionnés dont l'un ayant une composition azéotrope (cop. 1). La figure 2 représente un diagramme Zimm typique du copolymère 1.

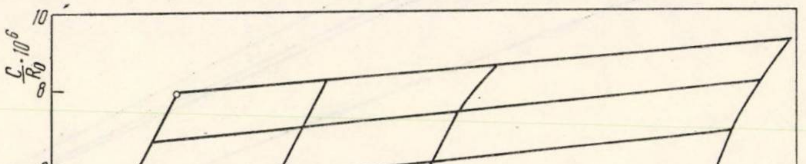

Fig. 2. – Diagramme Zimm du cop. 2 en DMA.

RÉSULTATS ET DISCUSSIONS

Les données expérimentales obtenues par la diffusion de la lumière, pour les copolymères acrylonitrile-styrolène, sont réportées dans le tableau 2.

Tableau 2

Caractéristiques structurelles des copolymères poly(acrylonitrile-styrolène) obtenus par la diffusion de la lumière

Cop.	S % g	Solvant	$M_{app} \cdot 10^{-5}$	$(R_0^{-2})^{1/2}$ Å	Q/Q_{max}	$A_2 \cdot 10_3$
Cop. 1	76,2	DMF	4,500	1240		0,325
		MEC	6,240	710		0,240
		THF	4,980			
		Bz	3,080			
		Dx	9,463		0,335	
		EST	5,624			
		Cl	7,790			
		BB	4,650			
Cop. 2	71,8	DMF	6,563	1360	0,265	0,308
		Cl		810		0,139
		DMA	5,830	800		0,343
		DMSO	6,640	590		0,056
		Am	7,997	580		0,019

$(R_0^2)^{1/2}$ désigne le rayon de giration, et A_2 le second coefficient viriel. M_w Q et P ont les valeurs $1{,}1614 \cdot 10^6$, $0{,}704 \cdot 10^6$ et $-0{,}855 \cdot 10^6$ pour le Cop. 1, respectivement $1{,}36 \cdot 10^6$, $0{,}705 \cdot 10^6$ et $-0{,}877 \cdot 10^6$ pour le Cop. 2.

La représentation des masses moléculaires apparentes figurant dans le tableau 1, en fonction de $(\nu_A - \nu_B)/\nu$ (selon l'équation 1) permet d'obtenir deux paraboles, correspondant aux deux copolymères (fig. 3).

La masse moléculaire moyenne en poids et les coefficients de la polydispersité P et Q sont déterminés à l'aide des paramètres de la parabole.

Les valeurs de P, Q et θ/θ_{max} (voir tableau 2), démontrent l'hétérogénéité de la composition de nos copolymères, même au cas du copolymère azéotrope.

Selon la théorie de la polymérisation, les copolymères obtenus aux conversions réduites, ou ayant une composition azéotrope, se caractérisent par une polydispersité négligeable. Par conséquent pour ces polymères la masse moléculaire déterminée par la diffusion de la lumière ne devrait dépendre que dans une mesure réduite de la nature du solvant. En réalité, les produits obtenus par catalyse Ziegler-Natta possèdent une polydispersité illustrée par les valeurs θ/θ_{max} situées entre 0,2 et 0,4.

Une telle hétérogénéité structurelle (en masse et en composition) peut être expliquée en supposant dans le processus de la préparation de ces polymères la concurrence d'espèces catalytiques différentes.

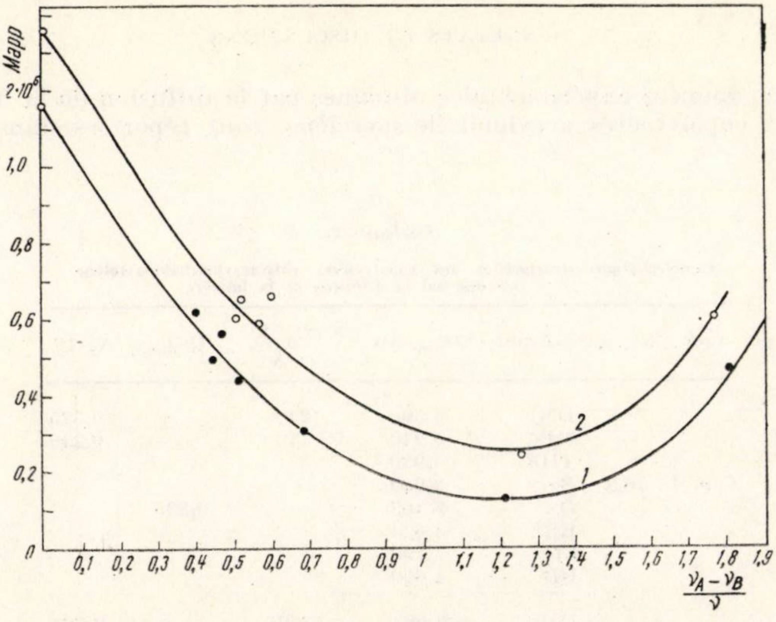

Fig. 3. — Distribution des masses moléculaires apparentes en fonction de $(\nu_A - \nu_B)/\nu$.
1, cop. 1; 2, cop. 2.

Les homopolymères (PAN et PS) sont caractérisés par une hétérogénéité similaire. Le tableau 3 donne les résultats d'un fractionnement brut pour le PS préparé par catalyse Ziegler-Natta.

Tableau 3

Résultats du fractionnement brut d'un PS préparé par catalyse Ziegler-Natta homogène

Nº	Fraction % g	M_n
1	57	14200
2	22	27100
3	18	1530
4	Polymère non fractionné	19800

Les données du tableau 3 illustrent que le PS que nous avons obtenu présente une forte distribution de la masse moléculaire. À l'aide des données de la diffusion de la lumière et des mesures viscosimétriques, nous avons calculé les paramètres de polydispersité pour les PS et PAN (voir tableau 4).

Les valeurs rassemblées sur le tableau 4 démontrent une hétérogénéité accentuée de la masse moléculaire. Les données de la littérature, concernant les polymères obtenus par catalyse homogène Ziegler-Natta,

Tableau 4

Données structurelles obtenues par la diffusion de la lumière et par viscosimétrie pour les homopolymères et copolymères sur la base de l'AN et du S

Polymère	Solvant	$M_w \cdot 10^{-5}$	$M_w \cdot 10^{-5}$ visc.	$M_n \cdot 10^{-5}$	$[\eta]$	M_w/M_n	Relation viscosimétrique	K'	Réf.
PS	MEC	2,000	—	0,533	0,209	3,77	$[\eta] = 3{,}05.10^{-4}M_n^{0,60}$	—	9
,,	MEC	—	0,602	—	—	1,13	$[\eta] = 3{,}90.10^{-4}M_w^{0,58}$	—	10
PAN	DMF	4,559	—	2,140	3,900	2,13	$[\eta] = 3{,}92.10^{-4}M_n^{0,75}$	0,50	11
,,	DMF	—	2,834	—	—	—	$[\eta] = 2{,}09.10^{-4}M_n^{0,76}$	—	12
Cop. 2	DMF	6.563	3,080	—	2,120	—	$[\partial] = 1{,}20.10^{-4}M_w^{0,77}$	0,44	2
,,	DMSO	6,540	—	—	0,540	—	—	0,35	
,,	Am	7,997	—	—	1,898	—	—	0,25	
,,	Cl	6,105	—	—	0,920	—	—	0,20	

M_w visc désigne la masse moléculaire en poids déterminée par viscosimétrie, $[\eta]$ la viscosité intrinsèque, K la constante de Huggins déterminée par viscosimétrie.

respectivement par celle hétérogène, sont les suivantes[13,14] : $Q = 2-6$; $8-40$; $35-290$. Selon Billmeyer,[15] pour les polymères de coordination $Q = 8-30$. Par conséquent, les valeurs expérimentales que nous avons obtenues sont en bon accord avec les données de la littérature.

A partir des résultats de la diffusion de la lumière, on peut calculer également le facteur stérique σ (facteur caractérisent l'empêchement stérique de la rotation libre autour de la liaison simple C—C, d'une chaîne flexible dans l'état non perturbé). On utilise la relation suivante[16] :

$$\sigma = (L_0^2)/(L_{0f}^2) \tag{6}$$

où (L_0^2) est la distance quadratique moyenne non perturbée entre les extrémités de la chaîne, et (L_{0f}^2) est la même distance, si l'on admet la rotation complètement libre.

A l'aide de nos données, on obtient le facteur stérique égal à 2,06. Cette valeur de σ est en bon accord avec les valeurs indiquées par la littérature pour le PS ($\sigma = 2{,}27$)[17] et pour le P (AN—S) radicalaire ayant une composition voisine ($\sigma = 2{,}22 \pm 0{,}05$)[2].

---

[9] C. E. H. Bawn, R. F. J. Freeman et A. K. Kamaliddin, *Trans. Faraday Soc.*, **46**, 1107 (1950).

[10] P. Outer, C. I. Caer et B. H. Zimm, *J. Chim. phys.*, **18**, 830 (1950).

[11] H. Leighton et H. Peebles, *J. Amer. Chem. Soc.*, **80**, 5603 (1958).

[12] H. Inagaki, K. Hayashi et T. Matsuo, *Makromol. Chem.*, **84**, 80 (1965).

[13] J. Boor Jr., ,,Macromolecular Reviews », vol. 2, Interscience Publishers, New York, 1967, p. 121.

[14] E. A. Fushman, V. I. Tzvetkova et N. M. Chirkov, *Doklady Akad. Nauk. S.S.S.R.*, **164**, 1085 (1965).

[15] F. W. Billmeyer Jr., *J. Polymer Sci.*, **C8**, 162 (1965).

[16] M. Kurata et W. H. Stockmayer, *Fortschr. Hochpolym.-Forsch.*, **3**, 196, (1963).

[17] W. R. Krigbaum, *J. Polymer Sci.*, **28**, 213 (1958).

Des données structurelles supplémentaires sont fournies par l'étude viscosimétrique de nos polymères. L'analyse du tableau 4 montre qu'en bon accord avec la littérature,[18] la constante de Huggins, obtenue par nous, est plus petite que celle obtenue aux homopolymères. A ce propos il faut mentionner que la valeur réduite de ces constantes dénote l'existence des chaînes macromoléculaires non ramifiées.

CONCLUSIONS

Nos recherches démontrent que l'étude des copolymères binaires sur la base de l'AN se heurte à la difficulté de trouver des solvants adéquats. Dans le cas idéal, quand on trouve trois bons solvants (solvants pour les deux homopolymères et également pour le copolymère), l'incrément de l'indice de réfraction peut être déterminé directement ou par additivité. Comme l'on peut voir sur les courbes *1* et *2* dans la figure 3, les points correspondant aux bons solvants sont rassemblés dans un intervalle étroit, à cause de la différence plus petite entre les indices de ces solvants. Ainsi la parabole ayant l'expression :

$$M_{\text{app}} = f\left(\frac{\nu_A - \nu_B}{\nu}\right)$$

ne peut être tracée rigoureusement.

Pour d'écarter ces difficultés, une bonne partie de chercheurs se limitent à l'étude de certains copolymères homogènes de l'AN, auxquels on puisse appliquer le traitement à un seul solvant.

L'étude de nos résultats montre que, malgré l'utilisation des copolymères obtenus à des conversions réduites, respectivement à composition azéotrope, un tel calcul simplifié pourrait conduire à des résultats erronés.

C'est pourquoi, on a utilisé un grand nombre de solvants (même si quelques-uns ne sont pas des solvants pour le PAN), ce qui a permis la détermination de la masse moléculaire moyenne en poids M_w, et des paramètres d'hétérogénéité.

L'étude des copolymères AN-S préparés par catalyse homogène Ziegler-Natta illustre le fait que ces copolymères présentent, similairement aux homopolymères, une hétérogénéité structurelle prononcée. Les données montrent une hétérogénéité tant en ce qui concerne la masse que la composition, indifféremment si l'on obtient des copolymères azéotropes ou habituels obtenus même à des conversions réduites.

Ainsi on conclut que nos copolymères diffèrent des copolymères AN-S radicalaires (étudiés par Shimura [4]).

---

[18] W. H. Stockmayer L. D. Moore Jr. M. Fixman et B. M. Epstein, *J. Polymer Sci.*, **16**, 517 (1955).

L'hétérogénéité des copolymères a été caractérisée par les valeurs P, Q et $Q/Q_{\max}$. Cette hétérogénéité peut être expliquée en admettant la concurrence de différents mécanismes dans la synthèse de ces copolymères.[7]

On a également déterminé par la diffusion de la lumière les caractéristiques structurelles : $(\bar{R}_0^2)^{1/2}$, A_2, σ. Nos valeurs sont en bon accord avec celles de la littérature concernant les copolymères statistiques AN-S.

En conclusion, on constate que la catalyse homogène Ziegler-Natta conduit à des copolymères statistique AN-S, possédant des chaînes linéaires et une hétérogénéité accentuée en ce qui concerne la masse et la composition.

Revue Roumaine de Chimie, **17**, *12*, 2013–2020 (1972)

VINYL ACETATE – ACRYLIC ACID COPOLYMERS

NATALIA SIMIONESCU, ELENA MARIA CĂLUGĂRU and D. FELDMAN

"Petru Poni" Institute of Macromolecular Chemistry
Yassy, Aleea Gr. Ghica Vodă 41 A

Received April 24, 1972

In aqueous medium, using potassium peroxydisulphate as initiator, the reactivity ratios for the pair of monomers vinyl acetate (VAc)-acrylic acid (AA) were determined at the following temperatures: 65, 70, 75 and 80°. The influence of the content of AA in the starting mixture of monomers in the range of concentrations from 1 to 10% on the conversion, on the copolymers composition and on their viscosity in dimethyl formamide (DMF) was studied. For 4% AA in the copolymerization process was studied dependent upon the duration of the reaction. The composition and the specific viscosity of the copolymers were followed. The copolymer homogeneity rises with the increasing reaction temperature and with the duration of the process.

Polyvinyl acetate finds a large technical use owing to its precious properties (transparency, photostability, good solubility in the majority of organic solvents, adhesiveness to glass, porcelain, ceramics, wood, leather, metals and plastics). At the same time it has some shortcomings, like a low glass transition temperature ($T_g = 27°$), a low thermostability, a low resistance, a low stability to chemicals and water.

It is known that to increase the adhesiveness of some polymers and copolymers, one proceeds to the introduction of the carboxyl group into the macromolecular chain. The copolymerization of vinyl acetate with unsaturated acids is mentioned in the literature. In this way, Ushakov and co-workers,[1] to rise the glass transition temperature of polyvinyl acetate, synthesized vinyl acetate – crotonic acid copolymers, by radical copolymerization with benzoyl peroxide.

Other research workers studied the copolymerization of the same vinylic monomer with the acrylic, methacrylic and itaconic acids. Thus, Johanson [2] obtained and described five copolymers of vinyl acetate with crotonic acid. Other authors [3] determined the reactivity ratios for this system.

---

[1] S. N. Ushakov and E. M. Lawrentiewa, *Zhur. prikled. Khim.*, **31**, 1686 (1958).
[2] S. Johanson, *Svensk Kemisk Tidskrift*, **60**, 122 (1948).
[3] E. Chapin, G. Ham and C. Mills, *J. Polymer Sci.*, **4**, 597 (1949).

The patents literature also points to the obtaining of adhesives from vinyl acetate copolymers. Some patents [4,5] describe the synthesis of some vinyl acetate copolymers with crotonic acid andrespectively with itaconic acid, acrylic acid or maleic acid.

The emulsion copolymerization of vinyl acetate with the crotonic, acrylic, methacrylic acids, maleic anhydride [6,7] has been used to obtain some latexes for the protection of classic materials.

The literature mentions the following values for the pair of monomers : acrylic acid (M_1) and vinyl acetate (M_2), at 70° temperature $r_1 = 2.0$ and $r_2 = 0.1$ [8]; by the successive approximation method one found for the reactivity ratios, $r_1 = 10 \pm 1$ and $r_2 = 0.01 \pm 0.003$. [9]

One knows that the temperature and the reaction medium have a significant effect on the kinetics of the polymerization process, as they affect the rate of reaction, the molecular weight as well as the properties of the obtained product. As the reactivity ratios r_1 and r_2 represent the main parameters of this process, it was interesting to study the influence of the temperature and the reaction medium on these ratios. The r_1 and r_2 being known for a certain domain of the temperature, one can determine the value of the ratio for other temperatures. Moreover, the determination of the reactivity ratios at different temperatures allows to compute the difference between the activation energies of the radical reactions with its own monomer and with the strange one.

This work was undertaken in order to determine reactivity ratios for the vinyl acetate—acrylic acid pair in aqueous medium, in the presence of potassium peroxydisulphate like initiator, at the following temperatures : 65, 70, 75 and 80°. It was also studied the influence of the content of acid comonomer in the starting monomers mixture on the copolymerization process, as well as the variation of the conversion of the monomers and of the composition of the copolymers depending on the reaction time.

EXPERIMENTAL

Monomers. VAc was purified by repeated distillation ; one used the fraction which distills between 71 and 72°. AA was twice distilled in vacuum ; the fraction boiling at 44—45° and 12 mm Hg was collected.

The copolymerization. In all experiments the copolymerization of VAc with AA was performed in aqueous medium at a constant stirring, using the components in the following ratios :

— monomers : water (by weight) . . . . 1 : 3
— initiator (% against to monomers mixture) 0.2

All components have been introduced at the beginning in the reaction vessel.

---

[4] N. Şakato and J. Koizumi, Japan Pat. 6827, 426 (1968) ; *Chem. Abstr.*, **70**, 58403v (1969).

[5] Soc. Rhodiatoce S. p. A., Ital. Pat. 794, 464 (1967) ; *Chem. Abstr.*, **70**, 58651z (1969).

[6] R. Ozawa, T. Yamashita and S. Hayashi, Jap. Pat. 1474, May 8, 1962 ; *Chem. Abstr.*, **60**, 10927D (1964).

[7] A. E. Corey and F. H. Norris, Brit. Pat. 923, 850, Apr. 18, 1963 ; *Chem. Abstr.*, **59**, 822H (1963).

[8] T. Alfrey, Jr., J. J. Bohrer and H. Mark, "Copolymerization", Interscience Publishers, New York, 1952, p. 35.

[9] J. Bourdais, *Bull. Soc. chim. France*, **1955**, 485.

The separation and the analysis of the copolymers. The obtained products have been separated by decantation and filtering and, then, washed with bidistilled water and dried at 40—45° in vacuum. After bringing at a constant weight, the water-soluble part has been extracted for 24 hours in Soxhlet. From the water-insoluble parts, after drying, have been prepared solutions in dimethyl formamide (DMF); their viscosity has been determined at 20° with an Ubbelohde viscometer (capillary I). The AA content of the dissolved in DMF copolymer was proved by a direct titration of carboxyl groups with a 0.1 n KOH alcoholic solution in the presence of phenolphthalein.

RESULTS AND DISCUSSIONS

The influence of the reactivity ratios. With the object of determining the reactivity ratios for VAc (M_2) and AA (M_1), one made copolymerizations at different $M_2 : M_1$ molar ratios in the starting mixture. In table 1 there are presented the necessary data of VAc with AA copolymerization for computing the reactivity ratios at different temperatures. To establish the conversion, the water-insoluble fraction was used. When the reaction time was 30 minutes, the value of the conversion was less than 4%.

It was remarked a slight conversion decrease with the increase of the AA content in the starting mixture of comonomers from 0 to 5%.

In table 2 there are given the values of r_1 and r_2 computed by the Fineman and Ross method.[10] These values confirm that AA is the more active monomer because it is bounding to its own radical and to VAc radical faster than VAc. The examination of the values of the $r_1 r_2$ products shows an increase of the homogeneity tendency of the copolymer chain at the same time with the increase of the copolymerization temperature.

Admitting, that VAc has $Q_2 = 0.026$ and $e_2 = -0.22$,[11] there were computed by Alfrey and Price method,[12] the AA specific activity and polarity. These values continuously decrease with the increase of the copolymerization temperature. By means of Arrhenius' relation $K = \mathrm{A}e^{-E/RT}$ one gets for r_1 the equation

$$r_1 = \text{const. exp.}\left(-\frac{E_{11} - E_{12}}{RT}\right),$$

$$\lg\, r_1 = \lg\, \text{const} + \frac{E_{12} - E_{11}}{2.303R}\, \frac{1}{T}$$

In figure 1 there is plotted the relation $\lg r_1 = f(1/T)$. From the slope of the straight line one obtains the difference between the activation ener-

---

[10] M. Fineman and S. D. Ross, *J. Polymer Sci.*, **5**, 259 (1950).

[11] L. J. Young, *J. Polymer. Sci.*, **54**, 446 (1961).

[12] T. Alfrey, Jr. and C. C. Price, *J. Polymer Sci.*, **2**, 101 (1947).

Table 1

Kinetic data of Vinyl Acetate (M_2) with Acrylic Acid (M_1) copolymerization at different temperatures. (initiator potassium peroxydisulphate 9.2% ; duration of the reaction 30 minutes)

$M_2 : M_1$ moles %	65°			70°			75°			80°		
	Ψ g%	−COOH g%	$m_2 : m_1$ moles%	Ψ g%	−COOH g %	$m_2 : m_1$ moles%	Ψ g%	−COOH g %	$m_2 : m_1$ moles%	Ψ g%	−COOH g %	$m_2 : m_1$ moles %
98.81 : 1.19	1.49	16.62	70.71 : 29.29	1.58	14.86	72.85 : 27.15	3.73	12.12	77.67 : 22.33	3.86	15.06	72.51 : 27.49
97.63 : 2.37	1.93	21.30	61.81 : 38.19	1.67	21.17	62.03 : 37.97	3.35	18.07	67.46 : 32.54	2.12	19.53	64.97 : 35.03
96.44 : 3.56	1.11	27.59	51.43 : 48.57	1.36	24.34	56.76 : 43.24	2.46	23.82	57.61 : 42.39	2.34	22.32	59.34 : 40.66
95.27 : 4.73	0.92	—	—	1.22	29.37	48.57 : 51.43	0.93	26.78	52.75 : 47.25	1.36	26.48	51.64 : 48.36
94.17 : 5.83	0.41	28.87	49.37 : 50.63	—	—	—	1.20	29.26	48.75 : 51.25	1.44	28.56	49.86 : 50.14
92.92 : 7.08	1.36	32.69	43.26 : 56.74	—	—	—	—	—	—	1.64	29.91	47.69 : 52.31
91.75 : 8.25	1.42	34.10	40.54 : 59.46	0.78	32.94	42.89 : 57.11	—	—	—	—	—	—

Obs. Ψ = copolymer yield (the water-insoluble part).
−COOH = the COOH contentin copolymer.

Table 2

Reactivity ratios of AA (r_1) and VAc (r_2) and the activity factors Q_1 and e_1 at different temperatures

Temp. °C	r_1	r_2	$r_1 \cdot r_2$	Q_1	e_1
65	10.0	0.020	0.20	0.96	1.048
70	9.5	0.025	0.23	0.78	0.979
75	9.0	0.030	0.27	0.67	0.924
80	8.5	0.035	0.29	0.60	0.900

gies of M_1 radical reaction with the strange monomer and with its own one, as follows

$$E_{12} - E_{11} = 10\,927 \ \text{J/grad mol.}$$

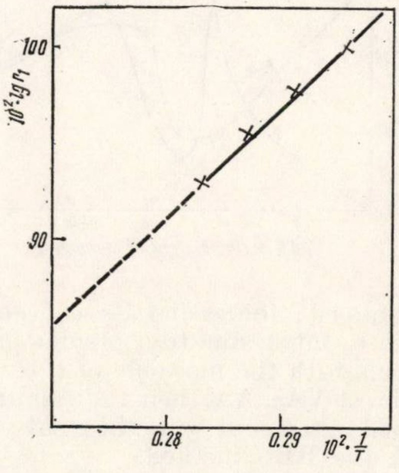

Fig. 1. — The relation between the ratio of copolymerization and the temperature.

The influence of AA content in the starting mixture on VAc polymerization. These two comonomers, in different gravimetric ratios, were copolymerized in aqueous medium (monomer-water ratio 1 : 3) at 65° temperature, using as initiator 0.2 % potassium peroxydisulphate ; the reaction time was 5 hours. The polymerization and the separation of the obtained copolymers were carried out as mentioned above. Experimental data show that in the same reaction conditions the polymerization rate of VAc decreases after the introduction of the more active monomer in the starting mixture.

Starting from 5 % AA content the rate of copolymerization increases again. The negative influence of AA when it is in small amounts on the rate of VAc polymerization can be explained by the fact that AA monomer is more active than VAc due to its greater double bond polarization produced by the carboxyl group. But, at the same time, the radicals of these two comonomers manifest an inverse activity. Because of a great rate of addition of AA molecules to VAc radicals at small concentrations of AA are formed less active macroradicals of AA; the decrease of the rate of addition of VAc molecules to AA macroradicals in comparison with that of VAc molecules to the own radicals determines the decrease of the total rate of copolymerization.

As it results from figure 2, a minimum of the conversion (curve 1) corresponding to 5% AA content in the starting mixture of monomers is obtained; increasing its concentration, the rate of copolymerization increases much due to a greater probability of interaction of AA macroradicals with the molecule of this monomer. Our conclusions on the reactivities of VAc, AA, their radicals and of the copolymers macroradicals are in good agreement with the results obtained by B. Rånby and co-worker,[13] using the RES method.

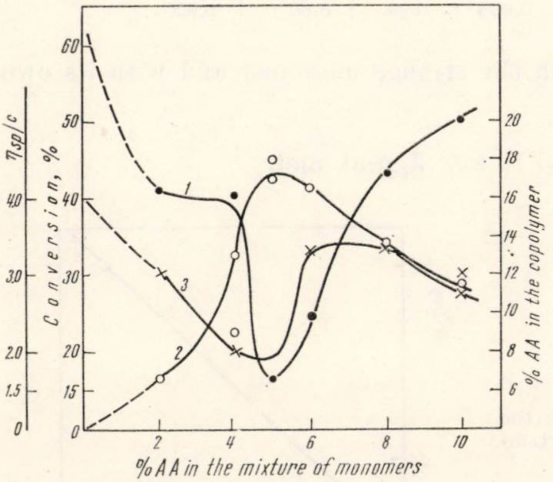

Fig. 2. — The influence of the acrylic acid content in the mixture of monomers on the : conversion (curve 1), composition (curve 2) and viscosity of copolymers (curve 3); time of copolymerization 5 hours; temperature 65°.

In our synthesis conditions, the amount of AA in copolymer is for all ratios superior to that from the starting mixture; as is seen from curve 2 (Fig. 2), at 5% AA in the starting mixture of monomers, after 5 hours (time of reaction) a copolymer with 18% medium content of the acid comonomer is obtained. For 5—10% AA added initially, the copolymer composition changes again in the sense of the decreasing of this amount. The η_{sp}/c values mark a minimum for 5% AA amount in the starting mixture of monomers.

The variation of the conversion and composition. With the object of following the conversion in time, one effectuated a series of copolymerizations at 65° temperature, with an amount of 4% AA in the starting mixture of monomers, respectively, a molar AA/VAc ratio equal to 0.0496.

---

[13] K. Takakura and B. Rånby, *J. Polymer Sci.*, Part C, **1969**, 939.

From the examination of the experimental data presented in table 3, it results that in the obtained product of copolymerization, the amount of the water-soluble fraction decreases with the duration of the reaction. We have not determined the composition of this fraction, but the literature indicates, for a similar range of concentrations, the absence of AA macroradicals.[13]

Table 3

The variation of the yield depending on the duration of the process. (VAc : AA : water = 96 : 4 : 300 p. weight; 0.2% potassium peroxydisulphate; temperature 65°)

Duration min.	Raw product yield %	From 100g raw product, the fraction	
		soluble in water %	insoluble in water %
30	3.20	73.92	26.08
60	4.91	48.88	51.12
90	6.47	36.78	63.22
150	9.48	30.71	69.29
180	16.40	32.62	67.58
240	35.00	7.80	92.20
300	43.25	10.15	89.85
420	75.00	7.27	92.73

The composition of the water-insoluble fraction has been established, after dissolving in DMF, by determining the carboxyl-group content. The specific viscosities of the copolymers were also determined in DMF solutions. The obtained results are represented in figure 3. Curve 1 shows the variation of the monomers conversion in the water-insoluble copolymer. Thus, as it results from curve 1, in the starting stages, the copolymerization takes place with the preponderant participation of the more active comonomer (AA). The content of acid comonomer in the copolymer, decreases gradually, in time, and at high conversion it gets near to the value from the starting mixture. At the obtained copolymers, the decrease of the specific viscosity with the extension of the reaction duration is noticed, especially at the beginning of copolymerization; this is explained

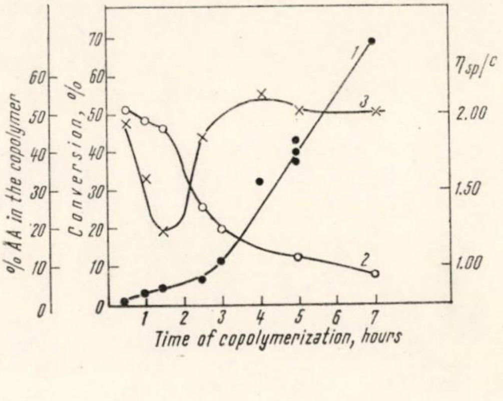

Fig. 3. — The variation of the conversion (curve 1), of the acrylic acid content (curve 2) and of the viscosity (curve 3) depending on the time of copolymerization (0.2 % $K_2S_2O_8$; the ratio monomer : water = 1 : 3; 4% acrylic acid in the mixture of monomers ; temperature 65°).

by the inhomogeneity of the copolymers composition (in the indicated conditions). At longer durations of reaction (3 hours), the variation of the viscosity becomes less pronounced. This observation has also been made by other researchers [14] for the copolymerization of some pairs of monomers with more different activities.

CONCLUSIONS

1. With the increase of the reaction temperature from 65 to 80°, the product of the reactivity ratios of AA and VAc increases and accordingly some copolymers with a more homogeneous distribution of the comonomers in the macromolecular chain are obtained.

2. For the range comprised between 2 and 10% AA in the starting mixture of monomers, at 65° and at a duration of 5 hours, a 5% content of AA determines the smallest copolymerization rate, the maximum percent (18%) of acid monomer in the copolymer, and the η_{sp}/c ratio registers a minimum value.

3. By the copolymerization of a monomers mixture with 4% AA the conversion after 7 hours reaches a 70% value; the obtained copolymer has a content of 7% AA and η_{sp}/c is about 2.

---

[14] A. JA. DRINBERG, B. M. FUNDILER and E. A. WOLYNSKAJA, *Zhur. priklad. Khim.*, **32**, 2075 (1959).

Revue Roumaine de Chimie, **17**, *12*, 2021–2032 (1972)

ÉTUDE COMPARATIVE DES MÉTHODES DE CALIBRAGE DE LA CHROMATOGRAPHIE SUR GEL PERMÉABLE

C. V. UGLEA et PROFIRA ANDREESCU

Institut de Chimie Macromoléculaire « Petru Poni », 41 A, Aleea Grigore Ghica Vodă, Jassy, Roumanie

Reçu le 3 février 1972

On présente des données obtenues par analyses effectuées sur de nombreux polymères (polyacrylonitrile, polyacétate de vinyle, poly-α-méthylestyrène, polystyrène, polyéthylèneglycol et copolymère ternaire d'acrylonitrile, acétate de vinyle et α-méthylestyrène à l'aide de la chromatographie sur gel perméable. La détermination des courbes de calibrage pour tous ces produits permet de conclure que par l'utilisation des méthodes universelles de calibrage on obtient des données approximatives. On aboutit à des conclusions permettant une bonne interprétation des gel-chromatogrammes, de même que la sélection du paramètre général de calibrage.

INTRODUCTION

La chromatographie sur gel perméable (CGP), nouvelle méthode d'analyse rapide et efficiente, utilisée dans de nombreux domaines de la chimie et de la biologie, est considérée aujourd'hui dans la chimie macromoléculaire la meilleure méthode pour la détermination et la répartition du poids moléculaire en divers polymères. Bien que convenable par la rapidité, l'application de la CGP est pourtant partiellement limitée, faute d'une solution optimale pour l'interprétation des données expérimentales. L'étape la plus importante c'est le « calibrage », qui est la détermination d'une relation entre le volume d'élution V_{EL} et le poids moléculaire. La variation du logarithme du poids moléculaire en fonction de V_{EL} conduit à un diagramme linéaire qui, pour un système polymère-solvant-température, pourrait être exprimé par la relation

$$\log M = A - BV_{EL} \tag{1}$$

Les constantes A et B sont spécifiques de chaque système. Habituellement, pour le calibrage sont utilisés les étalons avec la distribution du poids moléculaire très étroite ($M_w/M_n \simeq 1,1$). En ce qui concerne les composés macromoléculaires synthétiques, il est très difficile d'obtenir de telles épreuves à l'exception du polystyrène et du polyéthylèneglycol pour lesquels la firme Waters Assoc., USA s'est chargée de fournir des étalons à poids moléculaire connu et distribution restreinte ($M_w/M_n = 1{,}1$). La réalisation de tels étalons pour d'autres polymères n'est possible que par fractionnement préparatif (précipitation ou dissolution successive). Outre le fait que la séparation par telles méthodes exige un long intervalle de temps, les fractions ainsi obtenues présentent des caractéristiques qui peuvent imprimer au calibrage des inexactitutes inhérentes aux méthodes classiques de fractionnement. C'est pourquoi, l'un des buts principaux des recherches en ce domaine c'est de calibrer un système chromatographique des colonnes pour toutes les combinaisons polymère-solvant-température avec les étalons de polystyrène ou de polyéthylèneglycol.

L'application de ce « calibrage primaire » (relation 1) effectuée avec les étalons du polystyrène sur d'autres polymères qui diffèrent par la structure chimique pour obtenir une interprétation quantitative des données expérimentales exige un « paramètre général de calibrage ». Moore et Hendrickson [1] ont proposé comme paramètre général de calibrage « le facteur Q », obtenu par la division du poids moléculaire par la longueur de la chaîne calculée à l'aide des angles de valence et de la distance entre les atomes formant la chaîne principale du polymère. L'application de ce procédé a démontré que les erreurs possibles peuvent revêtir des valeurs importantes, ce qui nous conduit à la conclusion que le facteur Q n'est pas une constante et, comme suite, il ne peut pas être pris pour paramètre général de calibrage.

L'analyse du principe sur lequel repose la séparation par CGP montre que la forme et les dimensions de la particule du soluté déterminent la sélection des espèces moléculaires et leur apparition dans l'effluent à des volumes d'élution différents. Il est évident que le paramètre général de calibrage doit refléter le volume de la particule du soluté ; de plus, il doit être sensible aux variations des dimensions de la particule, variations imposées par les transformations du système gel-solvant-température où se produit la séparation.

Conformément à l'équation d'Einstein pour la viscosité intrinsèque, c'est le produit $[\eta]\ M$ qui détermine le volume hydrodynamique effectif de la macromolécule. En partant de cette idée, par la représentation du $\log\ [\eta]\ M$ par rapport à V_{EL} Grubisic et coll.[2] ont obtenu, pour les composés macromoléculaires linéaires ou ramifiés, chimiquement différents, des courbes de calibrage communes.

Coll et Gilding [3] ont proposé, comme paramètre général de calibrage la grandeur $M\ [\eta]/f_{(\varepsilon)}$, dont le facteur $f_{(\varepsilon)}$ résulte de la relation :

$$f_{(\varepsilon)} = 1 - 2{,}63\varepsilon + 2{,}86\varepsilon^2 \tag{2}$$

$$\varepsilon = (2a - 1)/3 \tag{3}$$

a étant l'exposant de l'équation de Mark-Houwink.

---

[1] J. C. Moore et J. G. Hendrickson, *J. Polymer Sci.*, *C*, **8**, 233 (1965).
[2] Z. Grubisic, P. Remp et H. Benoit, *J. Polymer Sci.*, *B*, **5**, 753 (1967).
[3] H. Coll et D. K. Gilding, *J. Polymer Sci.*, *A—2*, **8**, 89 (1970).

Le facteur $f_{(\varepsilon)}$ a l'origine dans la relation proposée par Ptitsyn et Eizner[4] :

$$[\eta] = \Phi_0 f_{(\varepsilon)} 6^{3/2} \, (\bar{R}^2) \, 3^{3/2}/M, \tag{4}$$

où $\bar{R}^2$ représente la moyenne des carrés du rayon de giration et $\Phi_0 = 2{,}86 \cdot 10^{23}$.

La méthode de Grubisic présente pourtant un inconvénient assez important ; dans un bon solvant le volume proposé s'avère moins grand, tandis que dans les conditions thêta ce volume est plus grand que les dimensions réelles de la pelote macromoléculaire.

Compte tenu de l'influence du solvant, le facteur $f_{(\varepsilon)}$ donne des corrections au calibrage et le rapport $[\eta]M/f_{\varepsilon}$, constitue, jusqu'à présent, la grandeur dont le spectre de sensibilité renferme, dans la plus grande mesure, les phénomènes qui se déroulent pendant la séparation par CGP.

Notre but c'est de présenter les résultats obtenus pour une série de polymères, résultats donnés par l'application comparative des méthodes de calibrage indiquée par la relation (1), par Grubisic, par Coll et Gilding et par une méthode empirique appliquée dans notre laboratoire.

PARTIE EXPÉRIMENTALE

Les polymères analysés représentent cinq homopolymères et un copolymère ternaire. Les homopolymères polystyrène et polyéthylèneglycol constituent les étalons fabriqués par Waters Assoc., USA. Les trois autres homopolymères formés par les mêmes monomères qui entrent dans la composition du copolymère ternaire ont été obtenus dans notre laboratoire.

Le but suivi par la sélection de ces polymères est la réalisation d'un test sur les méthodes universelles de calibrage dans l'analyse des composés macromoléculaires avec une structure chimique différente et la connaissance du comportement du copolymère ternaire et l'influence de la non-homogénéité chimique sur les résultats obtenus par CGP.

A. Polymères analysés

1. Polyacrylonitrile (PAN), obtenu dans notre laboratoire par la polymérisation en milieu aqueux. L'initiation a été réalisée avec du persulfate d'ammonium (0,65 % envers le monomère) et avec du métabisulfite de sodium (1,7 fois la quantité de persulfate). La proportion en monomère est de 11 % envers le milieu. Le processus de polymérisation a été effectué sous agitation, à 60°, pendant 90 minutes. La moyenne numérique du poids moléculaire, déterminée par osmométrie, $\overline{M}_n = 90\,000$.
2. Polyacétate de vinyle (PAV), produit BDL (Angleterre), $\overline{M}_n = 29\,000$.
3. Poly-α-méthylestyrène (PMS), produit obtenu par la polymérisation de l'α-méthylestyrène dans une solution de dichloréthane, comme initiateur étant utilisé le $SnCl_4$, $\overline{M}_n = 98\,000$.
4. Copolymère ternaire (CT) d'acrylonitrile-acétate de vinyle-α-méthylestyrène, produit industriel, $\overline{M}_n = 58\,000$ et composition chimique 92,4 moles % acrylonitrile, 6,1 moles % acétate de vinyle et 1,5 % moles d'α-méthylestyrène.
5. Polystyrène, (PS), étalon, standard, produit par Waters Assoc., USA.
6. Polyéthylèneglycol (PEG), étalon standard, produit par Waters Assoc., USA.

---

[4] O. B. Ptitsyn et Yu. E. Eizner, *Soviet. J. Tech. Phys* (*Engl. Transl.*,), **4**, 1020 (1960).

B. *Fractionnement*

Les polymères (excepté le PS et le PEG) ont été fractionnés par précipitation successive pour obtenir les fractions les plus homogènes possibles qui puissent être utilisées comme étalons dans le calibrage. Nous allons présenter brièvement les conditions dans lesquelles s'est déroulée la séparation. Tous les polymères (PAN, PAV, PMS et CT) ont été fractionnés dans le système solvant/non-solvant (S/NS) diméthyleformamide (DMF)/*n*-heptane (H) à T°C = = 75. L'addition du NS a lieu sous agitation avec un biuret thermostaté à la même température. La décantation une fois achevée, le précipité obtenu a été de nouveau dissous et ensuite totalement reprécipité. La quantité prélevée de chaque produit a été de 4–5 g, chaque épreuve étant divisée en 7–8 fractions, excepté le CT dont on a obtenu 12 fractions.

C. *Caractérisation des fractions*

Pour chaque fraction nous avons déterminé le poids moléculaire moyen en nombre $\overline{M}_n$ et la viscosité intrinsèque $[\eta]$. De plus, pour les fractions séparées du CT nous avons déterminé la composition chimique.

a) La viscosité intrinsèque des fractions et des étalons à été déterminée en DMF, à 25°, à l'aide d'un viscosimètre à niveau suspendu, pourvu d'une boule de dilution. L'extrapolation à concentration nulle a été réalisée graphiquement par quatre points.

b) *Osmométrie*. La moyenne numérique du poids moléculaire des fractions (excepté le PS et le PEG) à été déterminée en DMF, réactif *p.a.* fraîchement bidistillé, à 25°, avec un osmomètre Pinner-Stabin pourvu d'une membrane Pecel 600. Dans le cas du PAN, avant d'être bidistillé, le solvant à été déionisé par passage à travers une colonne à échangeurs d'ions, et les données obtenues ont été vérifiées à l'osmomètre Melabs, les résultats étant entièrement reproductibles.

D. *Chromatographie sur gel perméable*

Les gel-chromatogrammes des épreuves non fractionnées, des fractions et des étalons ont été réalisés à l'aide du gel-chromatographe Waters Model 200, avec une série de quatre colonnes ayant une perméabilité de 10^6 Å, 10^3 Å, 500 Å et 250 Å. Comme solvant a été utilisé le DMF bidistillé, la température de travail étant 50°, la vitesse d'élution 1 ml/mn et le temps d'injection 2 minutes.

Les caractéristiques des fractions séparées et des étalons sont présentées dans les tableaux 1–6. Les constantes K et a de la relation Mark-Houwink sont obtenues par la représentation de log M_n, par rapport à log $[\eta]$. Les données obtenues sont présentées dans le tableau 7.

Tableau 1

Caractéristiques des fractions séparées du polyacrylonitrile

N° de la fraction	V_{EL}/5 ml	M_n	$[\eta]_{dl/g}$
1	26,20	9 000	0,30
2	24,80	22 000	0,30
3	23,20	52 000	1,35
4	22,90	65 000	1,60
5	22,80	82 000	1,90
6	22,50	106 000	2,30
7	22,40	115 000	2,45

Tableau 2

Caractéristiques des fractions séparées du polyacétate de vinyle

N° de la fraction	V_{EL}/5 ml	M_n	$[\eta]_{dl/g}$
1	25,70	24 000	0,248
2	25,40	25 000	0,365
3	25,30	29 000	0,372
4	25,15	34 000	0,410
5	25,05	34 500	0,421
6	24,90	35 000	0,453
7	24,70	39 300	0,465
8	24,45	51 000	0,572

Tableau 3

Caractéristiques des fractions séparées du poly-α-méthylestyrène

N° de la fraction	V_{EL}/5 ml	M_n	$[\eta]_{dl/g}$
1	26,40	62 000	0,052
2	25,95	81 000	0,068
3	25,75	85 000	0,074
4	25,60	89 000	0,087
5	25,35	125 000	0,100
6	25,00	156 000	0,120
7	24,55	186 000	0,160
8	23,73	364 000	0,215

Tableau 4

Caractéristiques des fractions séparées du copolymère ternaire

N° de la fraction	V_{EL}/5 ml	M_n	$[\eta]_{dl/g}$	Composition chimique		
				AN*	AV**	MS***
1	25,70	14 000	0,52	91,00	5,90	3,10
2	23,25	66 000	1,30	90,00	6,00	4,00
3	23,20	70 000	1,34	91,00	6,00	3,00
4	22,90	106 000	1,72	91,00	6,00	2,80
5	22,60	148 000	2,11	91,10	6,10	2,80
6	22,30	173 000	2,32	91,10	6,20	2,70
7	22,20	176 000	2,48	91,50	6,10	2,40
8	21,95	204 000	2,56	91,50	5,90	2,60
9	21,85	209 000	2,60	91,90	5,90	2,20
10	21,65	226 000	2,72	92,00	6,10	1,90
11	21,40	244 000	2,85	93,40	6,00	0,60
12	21,20	262 000	2,98	93,60	6,00	0,40

* Déterminé par une méthode chimique.
** Déterminé par spectroscopie en IR.
*** Déterminé par différence.

Tableau 5

Caractéristiques des étalons du polystyrène

N° de la fraction	V_{EL}/5 ml	M_n	$[\eta]_{dl/g}$
1	28,75	4 600	0,026
2	27,20	9 700	0,073
3	26,75	19 100	0,110
4	25,50	49 000	0,190
5	24,50	96 200	0,285
6	23,80	164 000	0,370
7	22,50	392 000	0,770
8	20,40	773 000	1,240
9	19,80	1 780 000	1,890

Tableau 6

Caractéristiques des étalons du polyéthylèneglycol

N° de la fraction	V_{EL}/5 ml	M_n	$[\eta]_{dl/g}$
1	30,00	790	0,0335
2	29,00	1 220	0,0415
3	27,80	2 020	0,0548
4	26,60	3 900	0,0595

Tableau 7

Valeurs des constantes K et a de la relation Mark–Houwink pour les polymères analysés

Polymère	a	K
PAN	0,756	$3{,}65.10^{-4}$
PAV	0,618	$6{,}71.10^{-4}$
PMS	0,535	$1{,}84.10^{-4}$
CT	0,602	$16{,}20.10^{-4}$
PS	0,644	$1{,}92.10^{-4}$
PEG	0,551	$0{,}08.10^{-4}$

RÉSULTATS ET DISCUSSIONS

La représentation des données conformément à la relation (1) (fig. 1), selon la méthode de Grubisic (fig. 2) et celle de Colle et Gilding (fig. 3) permet la caractérisation du comportement des polymères analysés durant la séparation par CGP. On remarque (fig. 1) que les points caractérisant chacun des polymères s'ordonnent sur des droites tout à fait différentes, la courbe de calibrage de chaque produit constitue un paramètre spécifique de la nature chimique du composé macromoléculaire investigué. C'est toujours ici (fig. 1) que l'on constate que la courbe de calibrage garde sa valeur pour un certain polymère à travers l'entier domaine du poids moléculaire, excepté le CT qui présente une « rupture » due, probablement, à la variation de la composition chimique des fractions séparées par précipitation successive (tableau 4).

La représentation des données selon la méthode proposée par Grubisic (fig. 2) conduit à un diagramme qui diffère du premier par le fait

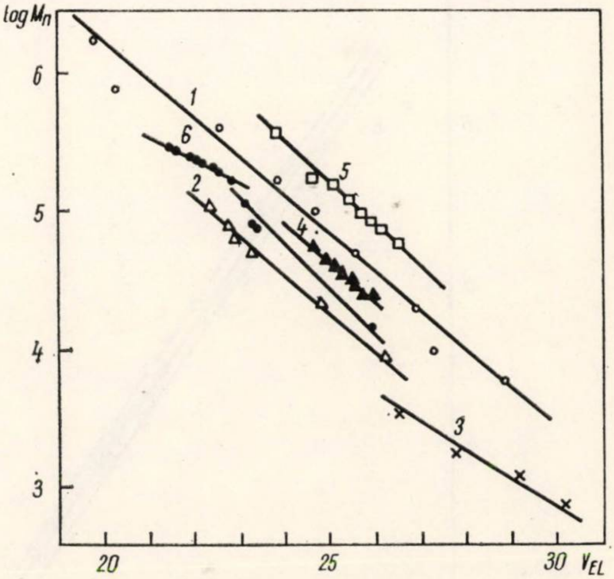

Fig. 1.— Calibrage conformément à la relation (1); 1, PS; 2, PAN; 3, PEG; 4, PAV: 5, PMS; 6, CT.

que, indépendamment de la structure chimique du polymère, les points obtenus présentent tous la tendance de s'accumuler sur une même droite. L'analyse de la distribution des points sur le diagramme réalisé en appliquant cette méthode relève quelques aspects particulièrement intéressants. L'ensemble (excepté les points obtenus pour PEG) des données expérimentales se situent entre les limites définies par PMS (côté droit du diagramme, noté par des carreaux blancs) et PAN (côté gauche du diagramme, indiqué par des triangles blancs). Ce comportement pourrait être justifié par l'analyse du principe sur lequel s'appuye la méthode proposée par Grubisic. L'évaluation du volume hydrodynamique de la particule du soluté à l'aide du produit $[\eta]\ M$ peut être approximative à cause de la dépendance de la viscosité intrinsèque de la nature du système polymère—solvant. C'est un fait connu que, en partant de l'état thêta jusqu'à la configuration élargie, la viscosité intrinsèque passe à travers un domaine de valeurs qui reflètent la variation du volume de soluté en solution. Autrement dit pour certaines valeurs de produit [5] $[\eta]\ M$ le volume macromoléculaire sera plus grand dans un bon solvant que dans les conditions thêta. Comme suite V_{EL} sera, dans ces deux cas extrêmes, plus grand ou plus petit que le volume prévu par le calibrage qui repose sur le produit

---

[5] E. F. Casassa et Y. Tagami, *Macromolecules*, **2**, 14 (1969).

$[\eta]$ M. Nous remarquons dans le tableau 7 que la valeur de l'exposant a pour PAN est 0,756 et pour PMS est 0,532. De ces données il résulte que le système PMS–DMF est très rapproché de l'état thêta, tandis que dans le système PAN–DMF la chaîne macromoléculaire a une configuration élargie, similaire à celle du système polymère–bon solvant. Par conséquent pour certaines valeurs de poids moléculaire le volume de la pelote macromoléculaire reste toujours plus grand dans le cas de PAN et plus petit dans le cas de PMS.

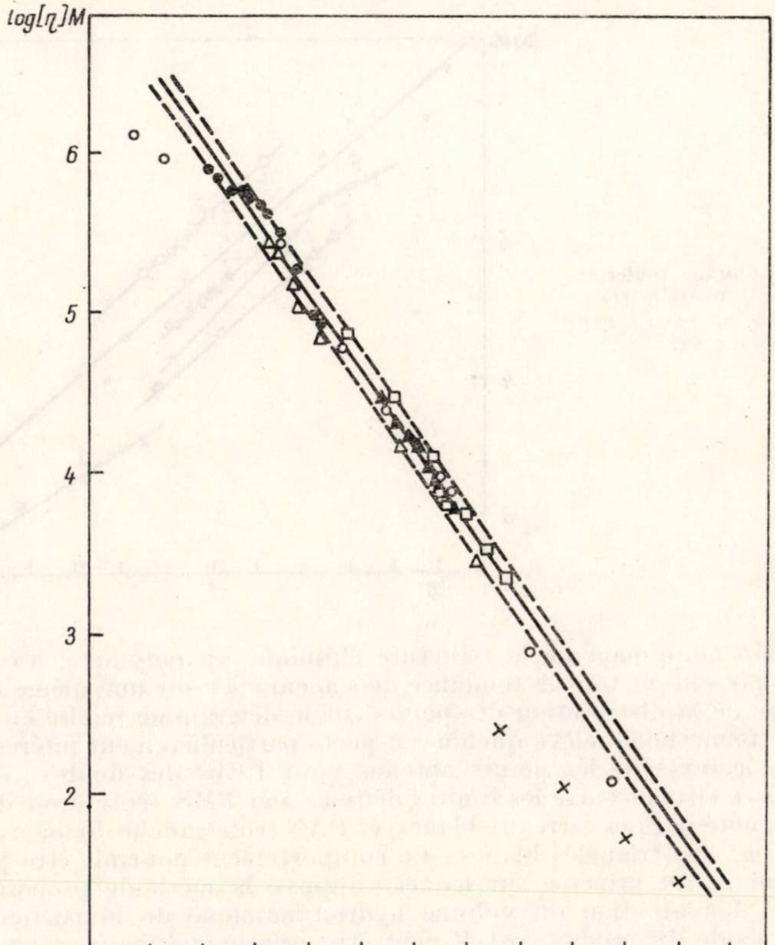

Fig. 2. – Calibrage conformément à la méthode proposée par Grubisic; les symboles gardent la signification indiquée dans la figure 1.

Des résultats obtenus par la caractérisation du CT[6] il ressort que la solubilité en DMF des copolymères ternaires d'AN avec AV et MS dans lesquels AN est majoritaire dépend de la composition chimique. Le tableau 4 montre que les fractions séparées par précipitation successive sont différentes tant selon le poids moléculaire que selon la composition chimique. Etant donné que la composition chimique influence directement le comportement dans la solution des polymères et donc le volume de la pelote macromoléculaire, nous considérons que la distribution plus élargie des points correspondant au CT est déterminée par la dépendance de la configuration des espèces par rapport au contenu d'AN.

---

[6] C.V. Uglea, V. Lupu et F. Săndescu, *Rev. Roumaine Chim.*, **16**, 1399 (1971).

Dans le cas des poids moléculaires petits (<5000) cette méthode ne garde pas ses qualités ce qui nous suggère que, dans ce domaine, la valeur de V_{EL} est déterminée par d'autres facteurs et non pas par le volume hydrodynamique du soluté macromoléculaire.

Le diagramme de la fig. 3 contient les données obtenues par l'application de la méthode proposée par Coll et Gilding [3]; dans ce cas les points se rangent sur une seule droite aussi mais dans le domaine des poids moléculaires plus grand ou très petit la distribution des points est plus considérable. L'introduction de l'exposant *a* de la relation de Mark-Houwink dans le paramètre général de calibrage mène, selon notre opinion, à une grandeur plus sensible envers des transformations qui ont lieu pendant le passage des polymères par les colonnes CGP, à condition que la valeur des poids moléculaires contenus dans l'épreuve analysée soit plus grande que 10 000.

Si on reprend la relation $[\eta]\ M = KV$ en y faisant intervenir la valeur de la viscosité intrinsèque de l'équation $[\eta] = KM^a$, on obtient :

$$K'M^{(a+1)} = KV \qquad (5)$$

où pour éliminer toute confusion on a noté la constante K de la relation Mark-Houwink par K'.

La représentation de la valeur du membre gauche de cette relation par rapport à V_{EL} conduit au diagramme réproduit dans la figure 4. L'emploi de ce calibrage mène à des résultats similaires aux données obtenues par l'application de la méthode proposée par Grubisic; y font l'exception les points du PEG et deux points correspondant au PAN

Au cas où les étalons font défaut, il faut que le calibrage soit effectué à l'aide des fractions obtenues par les méthodes classiques de fractionnement. Il faut aussi remarquer que, le plus souvent, ces fractions présentent une courbe spécifique de polydispersité dont la largeur est semblable à celle de l'épreuve non fractionnée (fig. 5). Dans le cas des polymères chimiquement non homogènes les méthodes de fractionnement classiques séparent les espèces moléculaires tant selon la poids moléculaire que selon leur composition chimique (tableau 4). Il est très probable que l'inexactitude du processus du fractionnement et la distribution large des fractions soient la cause des défauts pour les courbes de calibrage établies avec les étalons obtenus par fractionnement selon les méthodes classiques. Dans le cas des polymères chimiquement non homogènes la

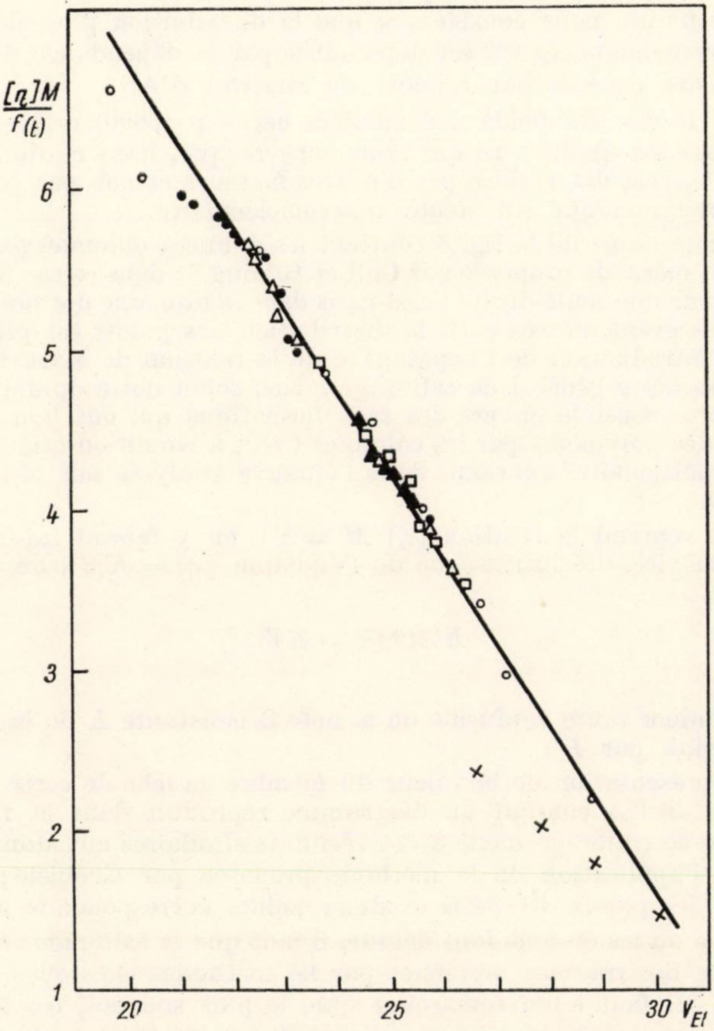

Fig. 3. — Calibrage conformément à la méthode de Coll et Gilding ; les symboles gardent la signification indiquée dans la figure 1.

sélection d'un système S/NS moins sensible envers la composition chimique et la caractérisation rigoureuse des fractions représentent, pour le moment, une manière de travail obligatoire pour obtenir des étalons standards satisfaisants pour le CGP.

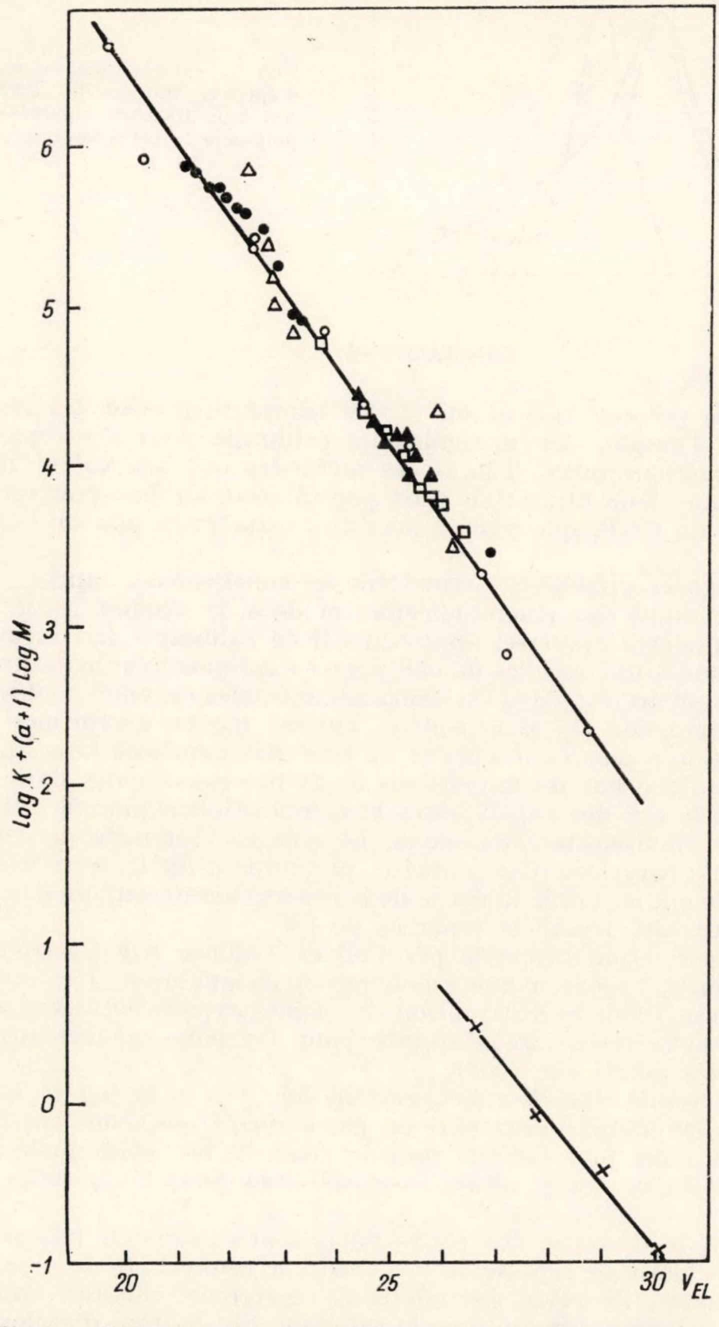

Fig. 4. — Calibrage conformément à la méthode empirique appliquée dans notre laboratoire ; les symboles gardent la signification indiquée dans la figure 1.

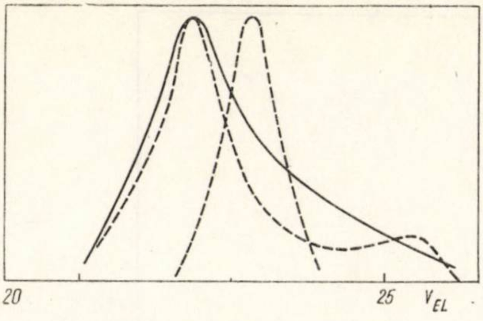

Fig. 5. — Gel-chromatogrammes d'épreuve initiale du PAN et des deux fractions séparées de ce polymère (courbes interrompues).

CONCLUSIONS

Dans le présent travail on étudie comparativement les résultats obtenus par l'emploi des méthodes de calibrage pour l'interprétation des gel-chromatogrammes. Toutes ces méthodes ont une valeur limitée, qui conditionne leur utilisation tant par rapport au but poursuivi par l'application du CGP, que par rapport aux caractéristiques de l'épreuve analysée.

Les données présentées permettent les conclusions ci-après.

— Le volume des macromolécules et donc le produit $/\eta/M$ représente un paramètre universel approximatif de calibrage. Les inexactitudes des méthodes universelles de calibrage s'expliquent par la nature compliquée de la séparation dans les domaines extrêmes du poids moléculaire.

— L'expression $/\eta/\,M$ considérée comme moyen d'exprimer le volume de la pelote macromoléculaire ne peut pas exprimer tous les paramètres qui influencent les dimensions de la macromolécules dans la solution. Dans le cas des copolymères la composition chimique influe sur la valeur de la viscosité intrinsèque. Le sens et l'intensité de cette influence ont un caractère occasionnel et proprement dit ils sont inconnus. Il est possible que se soit là la cause de la répartition irrégulière des points correspondant aux fractions séparées de CT.

— La correction proposée par Coll et Gilding par l'introduction de la fonction $f_{(\varepsilon)}$ mène à une amélioration insignifiante. Par l'application de cette méthode la distribution des points expérimentaux se réduit, mais la méthode reste insatisfaisante pour les poids moléculaires très grands ou plus petits que 10 000.

— Nos essais d'utiliser l'expression log $K(a + 1)$ log M donnent des résultats similaires à ceux obtenus par d'autres méthodes universelles Ce procédé s'avère plus indiqué pour le domaine des poids moléculaires grands mais donne des résultats insatisfaisants pour les valeurs petits de M.

— Dans le domaine des petits poids moléculaires ou très petits le volume moléculaire ne représente pas encore le seul critère de séparation.

Selon nous, l'analyse des composés macromoléculaires chimiquement non homogènes impose pour le calibrage l'utilisation d'étalons dont la structure soit la même que l'épreuve analysée et l'application de la méthode d'obtenir la courbe de calibrage par la représentation de log M par rapport à V_{EL}.

Revue Roumaine de Chimie, 17, 12, 2033–2041 (1972)

UNTERSUCHUNGEN VON STYROL–α-METHYLSTYROL–DIVINYLBENZOL–COPOLYMEREN UND KATIONENAUSTAUSCHERN DURCH THERMOANALYSE

ION NANU und IOSIF GROS

von der Technischen Hochschule, Timişoara
und vom Chemischen Kombinat, Oraşul Victoria

Eingegangen am 10. April 1972

Die am Netzwerk festgelegten Vinylgruppen in Copolymeren des Divinylbenzols mit Styrol und α-Methylstyrol sind dank eines exothermen Effektes, dessen Maximum bei 140–160° liegt, thermoanalytisch bestimmbar. Wie die Versuchsergebnisse zeigen, kann die Anzahl der nicht umgesetzten Doppelbindungen des Divinylbenzols verringert und praktisch zum Verschwinden gebracht werden, wenn das Ausgangsmonomerengemisch eine entsprechende Menge α-Methylstyrol enthält. Thermoanalytische Untersuchungen stark saurer, aus Styrol-Divinylbenzol-Copolymeren mit und ohne Zusatz von α-Methylstyrol hergestellten Kationenaustauscher ergaben, daß die Methylgruppe der α-Methylstyrolbausteine die thermische Stabilität der Kationenaustauscher beeinflußt.

Im Rahmen von Arbeiten, die die Herstellung von Copolymeren des α-Methylstyrols und deren Verwendung bei der Synthese von neuen Ionenaustauschertypen zum Ziele hatten, wurde das Verhalten von α-Methylstyrol bei der radikalischen Copolymerisation mit Styrol und Divinylbenzol untersucht. Es ist bekannt,[1–4] daß α-Methylstyrol in Systemen mit radikalischem Polymerisationsmechanismus durch eine gewisse Reaktionsträgheit gekennzeichnet ist und es ist auch zu erwarten, daß diese nicht nur die Reaktionskinetik, sondern auch die Struktur der Copolymeren beeinflußt.

Bei der radikalischen Polymerisation und Copolymerisation des Divinylbenzols reagiert ein Teil des Monomeren nur mit einer der beiden Vinylgruppen, so daß die vernetzten Polymeren noch eine gewisse Menge

[1] G. E. Lowry, *J. Polymer Sci.*, **31**, 187 (1958).
[2] P. Wittmer, *Makromol. Chem.*, **103**, 188 (1967).
[3] G. Smets, *Bull. Soc. chim. belges*, **59**, 13 (1950).
[4] I. Nanu, I. Gros und H. Kolck, *Bul. şt. şi tehnic IPT, seria chimie*, **16** (1971) (in Druck).

ungesättigter Gruppen enthalten. Die Bestimmung dieser Gruppen gestaltet sich deshalb als schwierig, weil vernetzte Copolymere unlöslich sind und dadurch die Diffusion von Reagenzien zu den Vinylgruppen erheblich behindert wird. Versuche zur qualitativen und auch quantitativen Erfassung dieser Doppelbindungen wurden von Breitenbach und Fucik [5] mittels IR-Spektroskopie, sowie von Kühnle und Funke [6] titrimetrisch, mit Quecksilberacetat unternommen. In letzterem Fall wurden sowohl poröse als auch nicht poröse Copolymere verwendet, die zwecks Verbesserung der Diffusion der Reagenzien zu den Vinylgruppen durch Emulsionspolymerisation hergestellt wurden.

Ziel der vorliegenden Arbeit ist es, durch Thermoanalyse die nicht umgesetzten Doppelbindungen in Suspensionscopolymerisaten qualitativ zu bestimmen und gleichzeitig festzustellen, welche Veränderungen die Styrol—Divinylbenzol-Copolymeren und die daraus hergestellten stark sauren Kationenaustauscher durch Zusatz von α-Methylstyrol zum Monomerengemisch erfahren.

EXPERIMENTELLER TEIL

Die differentialthermoanalytischen (DTA) und die thermogravimetrischen (TG) Untersuchungen wurden mit einem Gerät der Firma Setaram, des Typs GD-10, im Bereich 20—500°, bei einer Aufheizgeschwindigkeit von 5°/min, in inerter Atmosphäre (Helium) durchgeführt. Es wurde deshalb bei geringer Aufheizgeschwindigkeit gearbeitet, da sich die zu untersuchenden Polymeren wegen ihrer rigiden Netzwerkstrukturen nur langsam abbauen lassen und gleichzeitig die Diffusion der Abbauprodukte erschwert ist. Die gewählte Aufheizgeschwindigkeit befindet sich innerhalb der Grenzen, die im allgemeinen für die Analyse von Polymeren empfohlen werden.[7,8]

Die Monomeren Styrol und α-Methylstyrol waren von analytischer Reinheit, Divinylbenzol (technisch) bestand etwa zu 55 % aus *p*-und *m*-Divinylbenzol und zu 45 % aus *p*- und *m*-Aethylvinylbenzol. Die Monomeren wurden vor Gebrauch durch Waschen mit 10 %iger NaOH-Lösung entstabilisiert, mit kalziniertem Na_2SO_4 getrocknet und unter Vakuum destilliert. Die Reinheit der Monomeren wurde gaschromatographisch geprüft.

Die untersuchten Copolymeren waren perlförmig und wurden durch Copolymerisation in wäßriger Suspension hergestellt.[9] Durch Sulfonierung dieser Copolymeren mit Schwefelsäure [10] wurden dann die stark sauren Kationenaustauscher erhalten.

Für die IR-spektroskopische Untersuchung wurden KBr-Perßlinge (1 Gew.-% Untersuchungsmaterial) verwendet. Die Spektren wurden auf einem Perkin-Elmer-Spektrographen mit NaCl-Prisma (INFRACORD 137) aufgenommen.

---

[5] J. W. Breitenbach und J. Fucik, *Monatsh.*, **99**, 2436 (1968).
[6] D. Kühnle und W. Funke, *Makromol. Chem.*, **139**, 255 (1970).
[7] J. S. Double, *Plast. Inst. Trans. and J.*, **34**, 73 (1966).
[8] I. A. Schneider, *Makromol. Chem.*, **117**, 41 (1968) und **125**, 201 (1969).
[9] H. Knall und I. Gros, *Materiale Plastice*, **5**, 182 (1968).
[10] O. Popa, I. Gros und H. Knall, *Materiale Plastice*, **2**, 269 (1965).

VERSUCHSERGEBNISSE UND DISKUSSION

A. STYROL – α-METHYLSTYROL – DIVINYLBENZOL – COPOLYMERE

Zur Bestimmung des Divinylbenzolgehaltes und somit des Vernetzungsgrades von Copolymeren wird vielfach das Quellvermögen des Copolymeren in Toluol [11–14] herangezogen. Mit steigender Vernetzung nimmt das Quellvermögen ab.

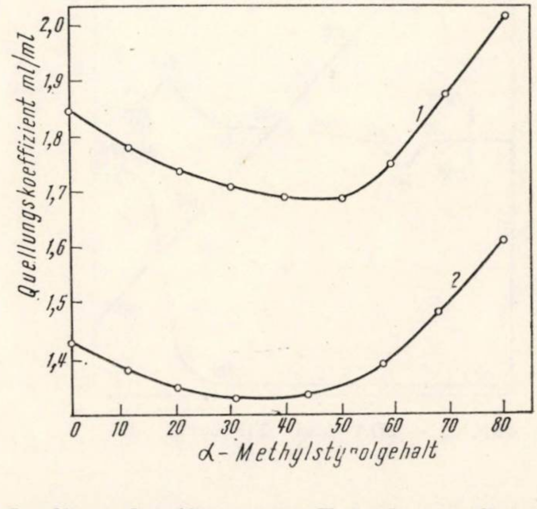

Abb. 1. – Abhängigkeit des Quellungskoeffizienten von α-Methylstyrol-Styrol-Divinylbenzol-Copolymeren vom α-Methylstyrolgehalt des Anfangsmonomerengemisches. Kurve *1* – für Monomerengemische mit 10 % Divinylbenzol; Kurve *2* – für Monomerengemische mit 20 % Divinylbenzol.

Aus Abb. 1, in der der Quellungskoeffizient in Toluol von Copolymeren mit einem Divinylbenzolgehalt von 10 und 20% in Abhängigkeit des α-Methylstyrolgehaltes des Anfangsmonomerengemisches dargestellt wurde, ist ersichtlich, daß mit steigendem α-Methylstyrolgehalt das Quellvermögen anfangs abnimmt, dann aber bei Gehalten von über 40% steil ansteigt. In diesem Zusammenhang sei erwähnt, daß bei großen α-Methylstyrolgehalten (über 40%) die Kettenübertragungsreaktionen überhand nehmen,[3] somit mit kürzeren Ketten und folglich auch mit einem Ansteigen des Quellvermögens zu rechnen ist.

Der erste Teil dieser Kurven, mit dem wir uns in vorliegender Arbeit näher beschäftigen, läßt auf eine zusätzliche Vernetzung der α-Methylstyrol enthaltenden Copolymeren schließen. Es muß also entgegen aller Erwartungen angenommen werden, daß mit dem Ansteigen des α-Methylstyrolgehaltes in den Copolymeren die Anzahl der nicht umgesetzten Vinylgruppen abnimmt. Dieses Verhalten kann dadurch erklärt werden, daß

---

[11] G. Naumann, *Plaste u. Kautschuk*, **2**, 74 (1955).

[12] K. Dusek, *Chem. prûmysl.*, **13**, 436 und 662 (1963).

[13] E. F. Gurm, *J. Polymer Sci., Part A–2*, **5**, 799 (1967).

[14] O. Popa, I. Gros und H. Knall, *Rev. Chim.* (*București*), **17**, 78 (1966).

mit dem Zusatz von α-Methylstyrol zum Styrol—Divinylbenzol-Monomerengemisch die Copolymerisationsgeschwindigkeit gedrosselt wird, bei gleichbleibendem Divinylbenzolgehalt also ein größerer Anteil dieses Monomeren mit beiden Doppelbindungen reagieren kann und somit ein höherer Vernetzungsgrad erreicht wird. Diese Annahme konnte mit Hilfe der Thermoanalyse bestätigt werden.

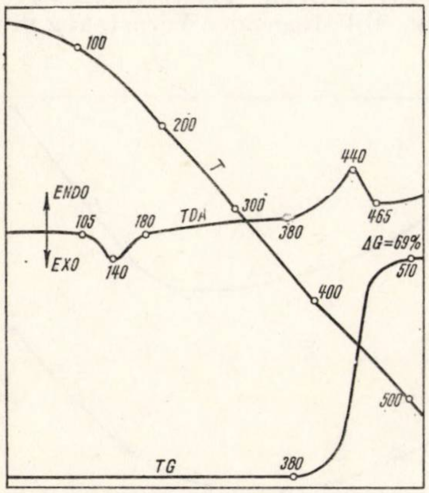

Abb. 2. — TDA- und TG-Kurve des Polydivinylbenzols.

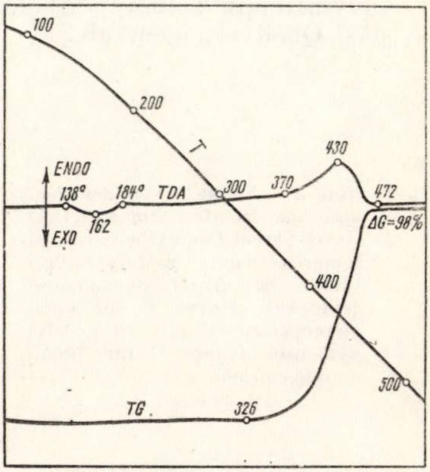

Abb. 3. — TDA- und TG-Kurve eines aus Styrol (83 %) und Divinylbenzol (17 %) hergestellten Copolymeren.

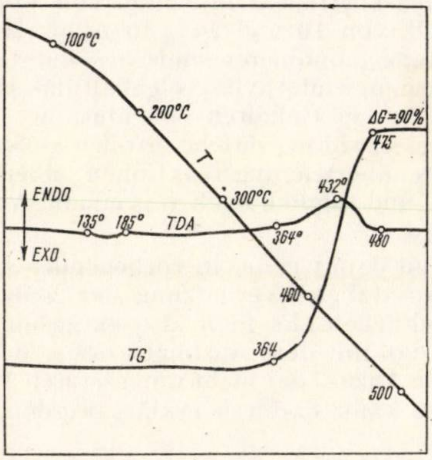

Abb. 4. — TDA- und TG-Kurve eines aus Styrol (73,5 %), α-Methylstyrol (9,5 %) und Divinylbenzol (17 %) hergestellten Copolymeren.

In den Abbildungen 2—4 sind die Thermogramme dreier charakteristischer Copolymeren wiedergegeben, bei deren Herstellung folgende Monomerengemische verwendet wurden:

— 100 % Divinylbenzol (Abb. 2)

— 17% Divinylbenzol und 83% Styrol (Abb. 3)

— 17% Divinylbenzol, 9,5% α-Methylstyrol und 73,5% Styrol (Abb. 4)

In allen drei Fällen tritt außer einem endothermen Effekt im Temperaturbereich 360—480° der auf den thermischen Abbau der Copolymeren zu etwa 70—95% zurückzuführen ist, im Bereich von 100—180° ohne Gewichtsverlust ein exothermer Effekt auf. Dieser ist beim Polydivinylbenzol (Abb. 2) am stärksten ausgeprägt und nimmt mit der Verringerung des Divinylbenzolgehaltes im Copolymeren ab (Abb. 3). Enthält das Copolymere bei gleichbleibendem Divinylbenzolgehalt neben Styrol auch α-Methylstyrol (Abb. 4), ist der exotherme Effekt sehr diskret und kann bei größeren α-Methylstyrolgehalten (15% und darüber) nicht mehr wahrgenommen werden. Ähnliches Verhalten konnte auch bei Copolymeren des Divinylbenzols mit α-Methylstyrol, die kein Styrol enthalten, festgestellt werden.

Es ist naheliegend, den exothermen Effekt als Begleiterscheinung von Umwandlungsreaktionen der noch vorhandenen Doppelbindungen anzusehen. Als weiteres Beweismaterial können die Ergebnisse folgender Versuche gewertet werden:

a) Erwärmen der Probe in inerter Atmosphäre.

Proben von α-Methylstyrol—Divinylbenzol-Copolymeren wurden in Glasampullen unter Stickstoffatmosphäre eingeschlossen und etwa 30 Minuten lang bei 180° erwärmt. Vor und nach der thermischen Behandlung der Proben wurden die Quellungskoeffizienten bestimmt (Tabelle 1) und die IR-Spektren aufgenommen (Abb. 5).

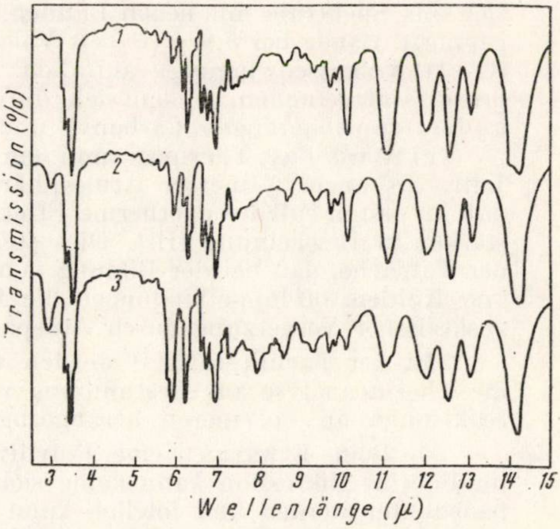

Abb. 5. — IR-Spektren eines α-Methylstyrol- Divinylbenzol-Copolymeren. Spektrum *1* — vor thermischer Behandlung; Spektrum *2* — nach Erwärmung bei 180° in Stickstoffatmosphäre; Spektrum *3* — nach Erwärmung bei 180° in Luft.

Der etwa um 12—15% geringere Quellungskoeffizient der thermisch behandelten Proben läßt auf eine zusätzliche Vernetzung schließen, die zweifellos durch das Abreagieren der anfangs nicht umgesetzten Doppelbindungen des Divinylbenzols zustande gekommen ist.

Tabelle 1

Abnahme des Quellungskoeffizienten in Toluol nach thermischer Behandlung der Copolymeren in inerter Atmosphäre

Copolymeres Nr.	Zusammensetzung der Copolymeren (Mol– %)		Quellungskoeffizient (ml/ml)	
	α-Methylstyrol	Divinylbenzol	vor Erwärmung	nach Erwärmung
1	62,1	37,9	1,39	1,18
2	40,9	59,1	1,22	1,07

Beim Vergleich der IR-Spektren eines Copolymeren (Copolymere Nr. 2/Tabelle 1) vor (Abb. 5, Spektrum 1) und nach der thermische Behandlung (Abb. 5, Spektrum 2) ist bei der erwärmten Probe eine deut liche Abnahme der für die Vinylgruppe charakteristischen Absorption banden zu erkennen. Es handelt sich hauptsächlich um die Banden b 6,1 μ (C = C Valenzschwingung) und 10,1 μ (= *C* – *H* Deformation schwingung).

b) Erwärmen der Proben in Luft.

Das IR-Spektrum eines in Luft bei 180° erwärmten Copolymere (Abb. 5, Spektrum 3) weist gegenüber dem Spektrum der nicht erwärm ten Probe bedeutende Unterschiede auf. Einerseits nehmen, wie bei de thermischen Behandlung in inerter Atmosphäre, die für die Vinylgrupp charakteristischen Absorptionsbanden ab, andererseits wieder bereicher sich das Spektrum mit neuen Banden, von denen besonders die gut au geprägte Bande bei 5,8 μ (C = 0 Valenzschwingung) und eine bei 2,9 (O—H Valenzschwingung) auffallen. Es hat somit ein Oxydation prozeß stattgefunden, bei dem sich durch Anlagerung von Luftsauersto an die Doppelbindungen, Carbonyl- und Carboxylgruppen gebildet habe

c) Wird das Thermogramm ein und derselben Probe sowohl i Luft, als auch in inerter Atmosphäre (He) aufgenommen, zeigt sic daß im ersten Fall der exotherme Effekt im Temperaturbereich 100—18 stärker in Erscheinung tritt. Dies steht in guter Übereinstimmung m der Tatsache, daß bei der Bildung von C=O Bindungen durch Reaktio von Kohlenstoffdoppelbindungen die Reaktionswärme größer ist als b zusätzlicher Vernetzung durch Aufspalten derselben.

In der Fachliteratur [15] werden weitere Fälle angeführt, in dene die Thermoanalyse zur Bestimmung von Vernetzungs- und Oxydation reaktionen an Polymeren herangezogen wird.

d) Beim Erwärmen einer Polydivinylbenzol-Probe von 20 bis 20 im Boëtius-Mikroskop kann keine sichtbare Veränderung des Polymere beobachtet werden und folglich kann der exotherme Effekt auch nic einem physikalischen Prozeß zugeschrieben werden.

Die Versuchsergebnisse (a—d) haben somit eindeutig bewiese daß der exotherme Effekt im Temperaturbereich 100—180° auf das Vo handensein von Doppelbindungen im Netzwerk des Copolymeren zurückzuführen ist. Seine bis zum Verschwinden reichende Abnahme beim Zusatz von α-Methylstyrol zum Styrol-Divinylbenzol-Monomerengemisch zeigt somit, daß dadurch Bedingungen geschaffen werden, unter denen der Vernetzer mit beiden Vinylgruppen reagieren kann und als Folge Copolymere entstehen, die eine viel geringere Menge nicht umgesetzter Doppelbindungen enthalten als diejenigen, bei deren Herstellung nur Styrol-Divinylbenzol-Monomerengemische verwendet wurden.

---

[15] B. Ke, „Newer Methods of Polymer Characterization", Intersc. Publ. New Yor 1964, S. 404—412.

Zur Zeit wird die Einsatzmöglichkeit der Thermoanalyse bei der quantitativen Bestimmung von Vinylgruppen in vernetzten Copolymeren geprüft.

B. STARK SAURE KATIONENAUSTAUSCHER

Bei der Herstellung der stark sauren Kationenaustauscher wurden sowohl Styrol — Divinylbenzol — α-Methylstyrol-Copolymere, als auch solche ohne α-Methylstyrol-Zusatz verwendet.

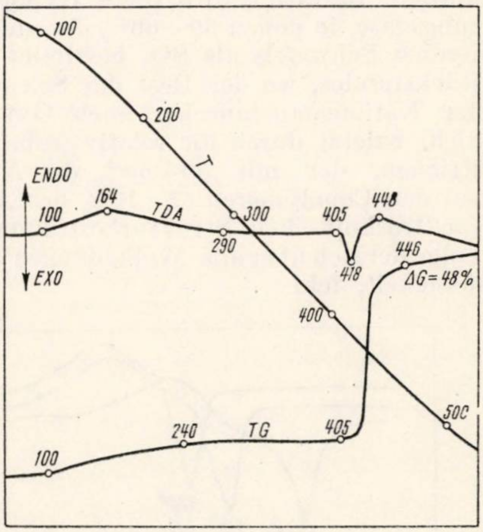

Abb. 6. — TDA- und TG-Kurve eines stark sauren Kationenaustauschers, für dessen Herstellung ein Monomerengemisch bestehend aus α-Methylstyrol (19%), Styrol (64%) und Divinylbenzol (17%) copolymerisiert wurde.

Für die Thermoanalyse wurden die Kationenaustauscher entsprechend vorbereitet, indem sie zuerst in die Na-Form überführt und nachher 16 Stunden lang bei 105° getrocknet wurden.

Die TDA- und TG-Kurven von Kationenaustauschern verschiedener Zusammensetzung sind einander sehr ähnlich. Ein typisches Thermogramm ist in Abb. 6 wiedergegeben; es stammt von einem Kationenaustauscher, für dessen Herstellung folgendes Monomerengemisch copolymerisiert wurde : 17% Divinylbenzol, 64% Styrol und 19% α-Methylstyrol.

Der durch die TG-Kurve im Temperaturbereich 100—240° angedeutete und durch Wärmeaufnahme (Maximum der TDA-Kurve bei

155—165) gekennzeichnete Gewichtsverlust von 4—8% ist auf die Hydratwasserabgabe der $NaSO_3$-Gruppen zurückzuführen. Durch Bestimmung der Austauschkapazität einer bei 200° erhitzten Probe konnte der Beweis erbracht werden, daß in diesem Temperaturbereich noch keine Zersetzung des Kationenaustauschers eintritt. Das dem Maximum der TDA-Kurve entsprechende Temperaturinterval (155—165°) stimmt mit den von anderen Autoren für verschiedene Kationenaustauschertypen gefundenen Werten gut überein.[16-20].

Änderungen in der Struktur des Kationenaustauschers und Zersetzungsreaktionen treten erst im Temperaturbereich 400—450° auf. Der aus der TG-Kurve resultierende Gewichtsverlust beträgt hierbei 35—45%. Die sich anfangs abspielenden Reaktionen finden unter Wärmeabgabe statt, wie aus dem Verlauf der TDA-Kurve mit dem scharf abgezeichneten Maximum bei 410—420° ersichtlich ist; sie werden jedoch bei höheren Temperaturen von endothermen Reaktionen abgelöst.

Durch Sulfongruppen ausgelöste Oxydationsreaktionen am Skelett des Kationenaustauschers und Vernetzungsreaktionen unter Bildung von Sulfonen könnten für den exothermen Effekt verantwortlich gemacht werden. Bestätigt wird diese Hypothese durch die Analyse der Zersetzungsgase, in denen 30—60% des anfangs im Kationenaustauscher vorliegenden Schwefels als SO_2 bestimmt werden konnte, und des verkokten Rückstandes, wo der Rest des Schwefels gefunden wurde. Daß im Falle der Kationenaustauscher auch Oxydationsreaktionen stattfinden, wird nicht zuletzt durch die relativ große Menge verkokten Rückstandes unterstrichen, der mit 50—60% des Anfangsgewichtes viel höher liegt als bei den Copolymeren (2—10% des Anfangsgewichtes). Versuche zur IR-spektroskopischen Strukturbestimmung dieser Rückstände schlugen, in Folge der sich über alle Wellenlängen erstreckenden, fast totalen Undurchlässigkeit, fehl.

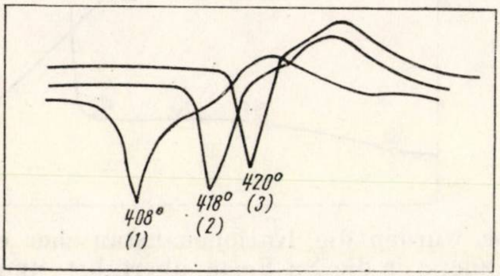

Abb. 7. — Verschiebung der exothermen Maxima stark saurer Kationenaustauscher mit dem α-Methylstyrolgehalt des Ausgangsmonomerengemisches. Kurve *1*, 39% α-Methylstyrol; Kurve *2*, 19% α-Methylstyrol; Kurve *3*, 0% α-Methylstyrol.

Position und Größe des exothermen Maximums sind von der Zusammensetzung des Ausgangscopolymeren abhängig. In Abb. 7 sind die exothermen Maxima dreier Kationenaustauscher wiedergegeben, bei deren

---

[16] Ju. A. Leikin, A. V. Smirnov, A. B. Davankov und V. V. Korschak, *Vysokomol. Soedineniya*, **10**, 157 (1968).

[17] J. M. Marchevskaja, *Zhur. fiz. Khim.*, **39**, 2489 (1965).

[18] W. Tischer, *Z. phys. Chem. (Leipzig)*. **246**, 42 (1971).

[19] N. G. Perashkina, V. S. Soldatov und N. I. Sudarikova, *Plast. massy*, **1966/4**, 60.

[20] J. Inczédy, ,,Analytische Anwendungen von Ionenaustauschern'', Akadémiai Kiadó, Budapest, 1964, S. 36.

Herstellung Monomerengemische mit dem selben Divinylbenzolgehalt (17%), aber verschiedenen α-Methylstyrol- und Styrolgehalten als Ausgangspunkt dienten. Je nach dem α-Methylstyrolgehalt befinden sich die Maxima bei 420° (Abwesenheit von α-Methylstyrol, Peak 3), 418° (19% α-Methylstyrol, Peak 2) und 408° (39% α-Methylstyrol, Peak 1). Diese Verschiebung des Maximums gegen niederere Temperaturwerte, bei steigendem α-Methylstyrolgehalt, steht in Übereinstimmung mit der geringeren Stabilität des Poly-α-Methylstyrols im Vergleich zum Polystyrol,[21] sowie mit dem Vorhandensein von leicht oxydierbaren CH_3-Gruppen im Poly-α-Methylstyrol. Bei der Thermoanalyse von Copolymeren des 2-Methyl-5-Vinylpyridins mit Styrol konnten Leikin und Mitarbeiter [16] ebenfalls ein besonderes Verhalten durch die anwesenden CH_3-Gruppen feststellen.

Herrn Ing. S. Şerban, Direktor des Forschungsinstitutes „Chimigaz" Mediaş, danken wir für die nützlichen Aussprachen und für die Erlaubnis, die Thermoanalysen in diesem Institut durchführen zu können.

---

[21] D. W. Brown und L. A. Wall, *J. Phys. Chem.*, **62**, 848 (1958).

Revue Roumaine de Chimie, 17, 12, 2043–2054 (1972)

STUDIES IN THE s-TRIAZINE FIELD (NEW SERIES).V[1]

PHENYL SUBSTITUTED 1,3-DIMETHYL-6-(β-STYRYL)-FORMOGUANAMIDE (-1*H*, 3*H*-s-TRIAZIN-2,4-DIONE) AND THE CORRESPONDING *p*-DIMETHYLAMINO-β-STYRYL HEMICYANINE : 1,3,5-TRIMETHYL-6-(*p*-DIMETHYLAMINO-β-STYRYL)-FORMOGUANAMIDIUM IODIDE

G. OSTROGOVICH, M. SAFTA

Organic Chemistry Laboratory, Polytechnic Institute, Timişoara, str. Bocşa 6

Received July 7, 1972

Preparation of 1,3,6-trimethyl-1*H*,3*H*-s-triazin-2,4-dione (**2**) by alkylation of 6-methyl-1*H*, 3*H*-s-triazin-2,4-dione (**1**) with dimethylsulphate in alkaline aqueous solution as well as preparation of 1,3,5,6-tetramethyl-1*H*,3*H*,5*H*-s-triazinium-2,4-dione iodide (**3**) (by quaternarization of compound **2** with ICH_3), was described. From the condensation reaction of the active methyl base (**2**), performed in acid (H_2SO_4) or base (piperidine) catalysis with 11 aromatic aldehydes, a series of 1,3-dimethyl-6-(β-styryl)-formoguanamides, variously substituted at the phenyl nucleus, was obtained. By condensation of p-dimethylaminobenzaldehyde with **3** in weak acid (acetic acid) or base (piperidine) catalysis, the hemicyanine 15 was obtained.

In a previous study concerning the preparation and electronic spectra of some 6-(*p*-X-β-styryl)-1*H*,3*H*-s-triazin-2,4-dione and of the conjugated acids resulting from their protonation with sulphuric acid, we noticed that the respective bases are sparingly soluble in most solvents and insoluble in water. The spectrophotometric study was therefore performed in a vol. 50% aqueous-alcoholic solvent in which however concentrations greater than 4.10^{-4} Mol/l could not be obtained and for which an acidity function H_0, was not established.

In order to obtain similar, more soluble compounds, we synthetised the corresponding 1,3-dimethylated compounds (with an aprotic s-triazinic part of the molecule). With this in mind we first accomplished the methylation of NH groups of methyl-formo-(so called aceto-) "guanamide" = 6-methyl-1*H*,3*H*-s-triazin-2,4-dione (**1**). We thus prepared the N^1, N^3-dimethyl derivative (**2**) and on the other hand we carried out also the complete methylation of base **2**, synthetizing the N^1,N^3,N^5-trimethylic quaternary compound **3** (1, 3, 5, 6-tetramethyl-1*H*, 3*H*, s-triazinium-2,4-dione iodide) from which we obtained further the p-dimethylamino-β-styryl-s-triazine hemicyanine **15**.

---

[1] G. Ostrogovich and M. Safta, *Rev. Roumaine Chim.*, **15**, 799 (1970).

The N^1, N^3-dimethylated triazine **2** was prepared in our laboratory starting from acetoguanamide **1**, with Me_2SO_4

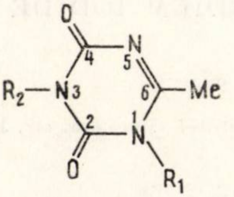

1 $R_1 = R_2 = H$

2 $R_1 = R_2 = Mt$

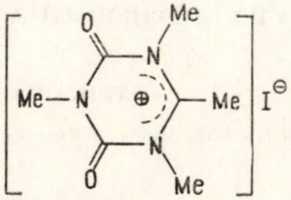

3

This compound was first obtained by Piskala starting also from acetoguanamide but with diazomethane [2]. We noticed some disadvantages of the method described by Piskala — inherent for alkylation with diazomethane — which make difficult the preparation of greater amounts of the product as well as the fact that on the methylation of **1** with this agent, besides product **2**, 1-methyl-2,4-dimethoxy-s-triazine and 1,6-dimethyl-4-methoxy-1*H*-s-triazin-2-dione also result as secondary products.

We therefore used dimethylsulphate in alkaline medium, a procedure successfully applied to hydroxi-purine and pyrimidine[3-4] N-methylation and which allowed us to obtain product **2** in a 87% yield (brutto). The pure product has m.p. = 99—100° (Piskala: 98—99°).

On the other hand, subjecting this compound to methylation with JCH_3 in sealed tube, on a steam bath for several hours, we were also able to synthetize, with very good yield the new quaternary compound **3**, very soluble in water and with m.p. = 185—187°. This is the next higher homologue (in position 6) of 1,3,5-trimethyl-formoguanamidium (-1*H*, 3*H*-s-triazinium-2,4-dione) iodide obtained for the first time by Gut and Piskala, [5] also with ICH_3.

Compound **2** was further condensed with a series of benzoic mono- and di-substituted aldehydes, obtaining the 6-(β-styrylic) compounds, corresponding to formulae **4**—**14**

---

[2] A. Piskala, *Coll. Czech. Chem. Comm.*, **28**, 2365 (1963).

[3] a. E. Fischer, *Chem. Abstr.*, II, 157 (1897); *Ber dtsch. chem. Ges.*, **30**, 3009 (1897).
b. H. Biltz, *Liebigs, Ann. chem.*, **70**, 431 (1923); *J. prakt. Chem.*, **118**, 206 (1928).
c. K. Bredereck, *Chem. Ber.*, **83**, 201 (1950).

[4] E. Wittenburg, *Chem. Ber.*, **99**, 2380 (1966).

[5] A. Piskala and J. Gut, *Coll. Czech. Chem. Comm.*, **29**, 2794 (1964).

(4.–11.)

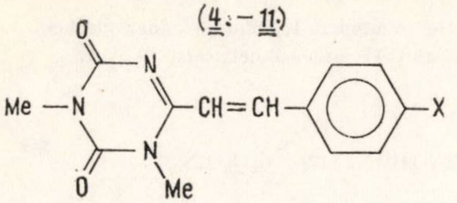

(12.–14.)

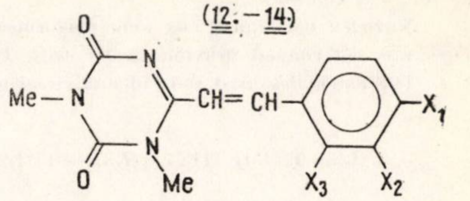

	X		X
4	NMe_2	8	Cl
5	NH_2	9	Ip
6	OMe	10	H
7	OH	11	NO_2

	X_1	X_2	X_3
12.	OH	OMe	H
13	O — CH_2 — O		H
14	Cl	H	Cl

In all cases the condensation follows with good yields both in acid catalysis (H_2SO_4), by refluxing on boiling steam bath with 96% ethanol as solvent, and in base catalysis (piperidine), maintaining the equimolar mixture of the two reagents in melt at 150°, on a calcium chloride saturated solution bath.

Bases were obtained in acid catalysis either by isolation of salts, dissolution in aqueous sulphuric acid and neutralization with ammonia to pH 2—4, or by direct neutralization of the reaction mixture without previous isolation of the salts.

In order to obtain the hemicyanine **15**, the quaternary salt 1,3,5-trimethyl-6-(*p*-dimethylamino-β-styryl)-1*H*,3*H*-s-triazinium-2,4-dione iodide, **3**, was condensed with *p*-dimethyl-aminobenzaldehyde by heating in glacial acetic acid or in methanol in the presence of piperidine.

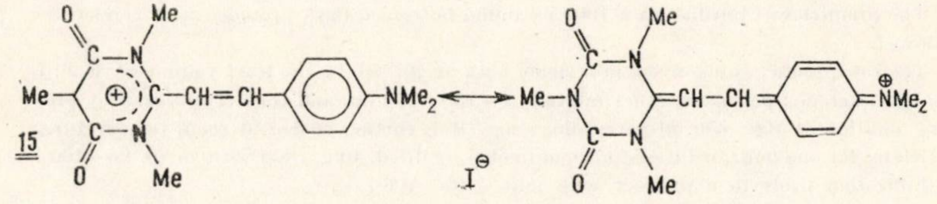

15

Hemicyanine **15** appears as needle-shaped crystals with m.p. 142—143°C (decomp.) and is very soluble in polar solvents.

EXPERIMENTAL

We present preparative and analytical data concerning the above mentioned compounds, which are all new, except **1** and **2**.

Prior to analysis, products were maintained at least 48 hours in a vacuum desiccator (20 mm Hg column).

Nitrogen determinations were performed by the semimicro-Kjeldahl-Wagner method, $SO_4^{2\ominus}$ was determined gravimetrically with $BaSO_4$, and $I^{\ominus}$ argentometrically as AgI.

The aldehydes used were of analytical purity.

1,3,6-TRIMETHYL-1*H*,3*H*-s-TRIAZIN-2,4-DIONE (2) : $C_6H_9O_2N_3$

0.1 Moles (12.7 g) of **1** are added to 100 ml aqueous solution of potassium hydroxide containing 0.2 moles (12 g) KOH. This procedure is performed in a three-necked flask, on a cooling waterbath, and provided with stirring, dropping funnel and thermometer.

After complete dissolution of **1**, 0.30 moles (30 ml) dimethylsulphate are added, high speed stirring is started and the pH is checked and maintained within the range 8—8.5 by adding a solution containing 0.30 moles (18 g) KOH dissolved in 150 ml water. Optimum reaction temperature is between 40—45°. The pH value is checked with special indicator paper (pH = 7.2—9.7).

After 30—45 minutes the pH remains practically constant without any KOH addition. For completion of the methylation another 0.15 moles (15 ml) of dimethylsulphate are added, continuing the processes as described, for about 1 hour, the optimum temperature being maintained without external cooling.

The system was allowed to reach the ambient temperature, was finally acidified with diluted sulphuric acid up to pH 5—6 and was then concentrated in vacuum to 100—120 ml (up to the appearance of turbidity). If necessary, the potassium sulphate crystals formed are redissolved by adding a minimum amount of water and are then extracted 7—8 times with 80 ml chloroform. The extracts are dried over calcium chloride, then filtered and the chloroform distilled. The chloroform concentrate is passed to a 100 ml round-bottomed flask and is then distilled in vacuum for an advanced elimination of the solvent taking care of the final product temperature not to exceed 60—70°. On cooling the product solidifies : it is then ground and maintained for a while in a 20 mm Hg vacuum over paraffin for the elimination of the last chloroform traces. Yield 13.5 g (87%).

The product was purified in a 1000 ml round-bottomed flask provided with condenser, as follows :

The raw product is dissolved on a steam bath at 40—50° in the least volume of a 2 : 1 metyhl-ethyl-ketone : petroleum ether mixture (~ 150—250 ml) and then crystallized by progressive addition of 400—600 ml petroleum ether. It is further cooled at room temperature, then with ice for one hour, is filtered off and finally air dried. 10 g yield with m. p. 96—100°. Recrystallization leads to a product with m.p. = 99—100°.

Compound **2** is a colourless, very thin flake shaped product, readily soluble in any solvent (especially polar) except petroleum ether.

Found : N, 27.0.

Calculated for $C_6H_9N_3O_2$, N, 27.08%.

Purity control as well as the alkylation reaction control was pursued by paper cromatography using n-butanol : acetic acid : water = 4 : 1 : 1 as solvent (R_f value of **2** = 0.65)[2], and as reagent for identification of **2** an alcoholic solution, 3% in p-dimethylaminobenzaldehyde and 1 N in H_2SO_4[6]. We thus ascertained that work under the above described conditions (pH = 8 — 8.5) is leading exclusively to **2** (free of any of the corresponding 0-methylated tautomers).

---

[6] M. Safta and G. Ostrogovich, *J. Chromatog*, **69** (**1**), 219 (1972).

1,3,5,6-TETRAMETHYL-1*H*,3*H*-*s*-TRIAZINIUM-2,4-DION IODIDE (3) : $C_7H_{12}O_3N_3I$

5.10^{-3}moles (= 0.775 g) of **2** are dissolved in $2,4.10^{-1}$ moles (= 15 ml) methyl iodide with one drop of mercury added, in a thick walled sealed tube (~ 2.5 × 35 cm) . It is heated for 6 hours on steam bath then allowed to stand overnight at room temperature. It is cooled with ice, filtered on a G_3 sintered glass crucible, and air dried. Yield = 2.7 g (91 %).

Purification was performed by recrystallization as follows :

The product is crystallized from a concentrated ethanolic solution prepared at room temperature (2.7 g/100 ml), as colourless, very thin needles by ethyl ether addition (250 ml). Kept cool overnight it yields 2.2 g product of with m.p. : 185–187°C.

The compound is soluble in water, sparingly soluble in ethanol, insoluble in acetone, ether and hydrocarbons.

Calculated : M = 297.15	N : 14.14 ;	I : 42.71 %
Found :	N : 14.2 ;	I : 42.6 %
	N : 14.4 ;	I : 42.7 %

1,3-DIMETHYL-6 (*p*-DIMETHYLAMINO-β-STYRYL) 1*H*,3*H*-s-TRIAZINIUM-2,4-DION BISULPHATE (4*A*) : $C_{15}H_{10}O_2N_4.H^{\oplus}HSO_4^{\ominus}$

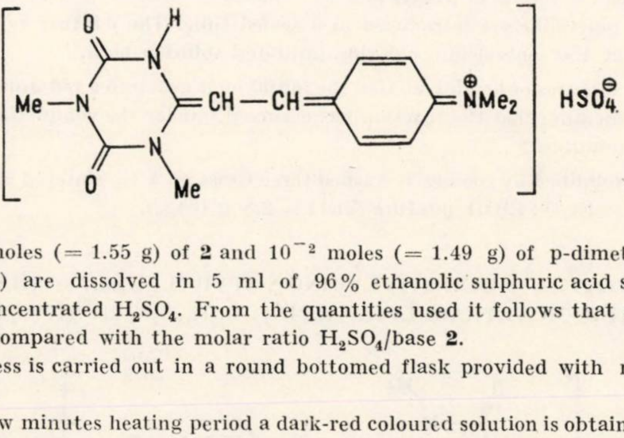

a. 10^{-2} moles (= 1.55 g) of **2** and 10^{-2} moles (= 1.49 g) of p-dimethylaminobenzaldehyde (p-DAB) are dissolved in 5 ml of 96 % ethanolic sulphuric acid solution, containing 0.75 ml concentrated H_2SO_4. From the quantities used it follows that a 35 % excess of H_2SO_4 is used compared with the molar ratio H_2SO_4/base **2**.

The process is carried out in a round bottomed flask provided with reflux condenser on steam bath.

After a few minutes heating period a dark-red coloured solution is obtained. After 3 hours the reaction is practically completed. It is allowed to stand overnight, cooled with ice filtered and washed twice with 1–2 ml of 2 : 1 ethyl ether (Et_2O) : ethanol (EtOH) mixture. Yield = = 2.7 g (70) % : dark red coloured needles with bright metallic shining.

b. In very high purity the bisulphate was obtained as follows : 1 g of recrystallized base **4** (see bellow) is dissolved by heating (reflux) in 2.5 ml H_2SO_4 2M in water: ethanol (1 : 1 vol) and allowed to cool at room temperature. Filtered next day it yields 0.7 g **4** *A* with m.p. = 244– –245°

Calculated : M = 384.41	N : 14.58 ;	$SO_4^{2\ominus}$: 24.98 %
Found :	N : 14.6 ;	$SO_4^{2\ominus}$: 24.6 %
	N : 14.7 ;	$SO_4^{2\ominus}$: 24.7 %

1,3-DIMETHYL-6-(*p*-DIMETHYLAMINO-β-STYRYL)-1*H*,3*H*-s-TRIAZIN-2,4-DIONE (*4*) : $C_{15}H_{18}O_2N_4$

a. *From bisulphate 4A*

4A bisulphate obtained as described above, is dissolved in 5 ml of 1M H_2SO_4. The solution is diluted with 10 ml of water, then neutralized with concentrated ammonia and further with diluted ammonia up to pH ≃ 4, thus leading to complete precipitation of the orange coloured base. It is cooled with ice and filtered. Yield = 2 g, i.e. practically 100 %.

For a more advanced purification it might be recrystallized from n-butanol : formamide = 1 : 1 (1g from 18 ml) or from n-butanol : dimethylsulfoxide = 1 : 1. Cooled slowly it is allowed to stand overnight, at room temperature. It is filtered on a G_2 sintered glass crucible and washed with a 2 : 1 = Et_2O : EtOH mixture (three times with 1 ml). 0.8 g of orange coloured needles are yielded with m.p. = 271 – 272°, insoluble in water, sparingly soluble in alcohols and acetone, very soluble in dimethylsulfoxide (DMSO) and formamide.

Calculated :	M = 286.33	N : 19.57 %
Found :		N : 19.5 %
		N : 19.4 %

b. *Base (piperidine) catalysed synthesis*

10^{-2} moles (= 1.49 g) of pDAB and 10^{-2} moles (= 1.55 g) of **3** as well as 3 drops of freshly distilled piperidine are introduced in a sealed tube. The mixture is melted and kept for 30 minutes at 150° on calcium chloride saturated solution bath.

After few minutes of heating at 150° the initial melt gets into a red-orange coloured crystalline mass, indicating that the reaction has occurred but for the completion heating is prolonged for 30 minutes.

The melt solidified by cooling is washed three times on a G_2 sintered glass crucible with 2 ml of a 2 : 1 = Et_2O : EtOH mixture Yield = 2.8 g (84 %).

1,3-DIMETHYL-6-(*p*-DIMETHYLAMINO-β-STYRYL)-1*H*,3*H*-s-TRIAZINIUM-2,4-DION TETRASULPHATE (*4B*) : $C_{15}H_{18}O_2N_4.2H^{\oplus}(HSO_4)_2^{2\ominus}$

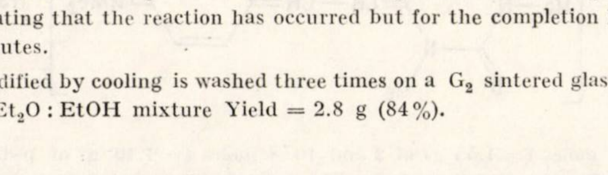

1.5 g of base **4** are dissolved, under heating, in 3.5 ml of 5M ethanolic H_2SO_4. By slow cooling, overnight standing, further ice cooling and filtering, colourless, highly hygroscopic needles are obtained (∼ 0.5 g).

Calculated :	M = 482.48	N : 11.61 ;	$SO_4^{2\ominus}$ 39.82 %
Found :		N : 11.5 ;	$SO_4^{2\ominus}$ 39.6 %
		N : 11.6 ;	$SO_4^{2\ominus}$ 39.5 %

1,3-DIMETHYL-6-(*p*-AMINO-β-STYRYL)-1*H*,3*H*-s-TRIAZIN-2,4-DIONE (5): $C_{13}H_{15}O_2N_5$

a. *Acid catalysed* (H_2SO_4) *synthesis*

10^{-2} moles (1.55 g) of base **2** and 10^{-2} moles (1.21 g) of p-aminobenzaldehyde (Fluka) are dissolved under heating in 4 ml of sulphuric acid solution in 96% ethanol, containing $1.5.10^{-2}$ moles H_2SO_4 (0.83 ml conc. H_2SO_4). It is refluxed for 3 hours. The base is isolated from the red-brown solution containing the corresponding bisulphate by dilution with 20 ml 1M H_2SO_4 and careful neutralization with ammonia up to pH = 3. It is cooled filtered and dried; yield = 2.1 g (∼ 82%)

Recrystallization from a 1 : 1 = dimethylsulfoxide : n-butanol mixture leads to 0.5 g brown prisms with m.p. = 267–269°, very soluble in polar organic solvents alcohols, acetone, DMSO), sparingly soluble in water.

The solutions are more or less fluorescent.

Calculated:	M = 258.27	N: 27.12%
Found:		N: 27.0%
		N: 26.9%

b. *Base* (*piperidine*) *catalysed synthesis*

Same proportions of reagents **2** and p-amino-benzaldehyde, and same procedure described above for base **4** are used.

Yield (brutto) = 2.4 g (93%).

1,3-DIMETHYL-6-(*p*-METHOXY-β-STYRYL)-1*H*,3*H*,-s-TRIAZINIUM-2,4-DION BISULPHATE (6A): $C_{14}H_{15}O_3N_3.H^{\oplus}HSO_4^{\ominus}$

10^{-2} moles of **2** and 10^{-2} moles (= 1.2 ml) of p-methoxybenz-aldehyde are dissolved by heating in 4 ml H_2SO_4 solution in 96% ethanol containing $1.5.10^{-2}$ moles H_2SO_4 and refluxed for 3 hours. A yellow coloured precipitate is obtained after a few minutes. The reaction mass is cooled and filtered through a G_2 sintered glass crucible. The precipitate is washed twice with 0.5 ml of a 2 : 1 = Et_2O : EtOH mixture. Yield = 2.2 g (∼ 59%); orange prisms with m.p. = = 261–263°.

Calculated:	M = 371.36	N: 11.32;	$SO_4^{2\ominus}$ 25.87%
Found:		N: 11.2;	$SO_4^{2\ominus}$ 26.0%
		N: 11.3;	$SO_4^{2\ominus}$ 24.0%

1,3-DIMETHYL-6-(*p*-METHOXY-β-STYRYL)-1*H*,3*H*-s-TRIAZIN-2,4-DIONE (6): $C_{14}H_{15}O_3N_3$

a. *From bisulphate* **6** *A*:

2 g of **6***A* are suspended in 5 ml water and neutralized with ammonia. It is cooled and filtered. After drying, 1.4 g of product are obtained (∼ 96%).

Recrytallization is carried out from 15 ml of a 2 : 1 = n-butanol : formamide mixture, the solution is cooled slowly and is then standing overnight. The yellow crystals are washed twice with 2 ml of Et_2O : EtOH = 2 : 1. Yield 1.2 g (44 %) with m.p. = 247—248°. The product is very soluble in aprotic polar organic solvents (DMSO, DMF, F) and sparingly soluble in water and ethanol.

Calculated :	M = 273.28	N : 15.36 %
Found :		N : 15.4 %
		N : 15.3 %

b. *Base (piperidine) catalysed synthesis*

5.10^{-3} moles (= 0.78 g) of **2** and 5.10^{-3} moles (0.6ml) of p-methoxybenzaldehyde are taken and the procedure is performed as described for **4**. After dissolution in 2—3 ml of 2 : 1 Et_2O : EtOH and filtration, 0.9 g (yield = 6.6 %) are resulting.

1,3-DIMETHYL-2,4-DIOXO-6-(*p*-HYDROXY-β-STYRYL)-1*H*,3*H*-s-TRIAZIN-2,4-DION BISULPHATE (7*A*) : $C_{13}H_{13}O_3N_3.H^{\oplus}SO_4^{\ominus}$

Proceeding as described for **6***A* and taking 10^{-2} moles of the two reactants (1.22 g p-hydroxybenzaldehyde), 2.5 g of salt **7***A* are obtained (yield = 70 %) as yellow coloured prismatic crystals. They melt with decomposition at 310°.

Calculated :	M = 357.34	N : 11.76 ;	$SO_4^{2\ominus}$ 26.88 %
Found :		N : 11.5 ;	$SO_4^{2\ominus}$ 27.0 %
		N : —	$SO_4^{2\ominus}$ 26.8 %

1,3-DIMETHYL-6-(*p*-HYDROXY-β-STYRYL)-1*H*,3*H*-2-TRIAZIN-2,4-DIONE (7) : $C_{13}H_{13}O_3N_3$

a. *From bisulphate* 7 *A*

2.5 g of salt **7***A* are suspended in 20 ml of 1 : 9 ethanol water mixture and neutralized with ammonia to pH ≃ 4.

Yield = 1.8 g (100 %)

It is recrystallized by slow cooling from 160 ml of 2 : 1 = ethylcelosolve : water mixture. It is allowed to stand overnight filtered and washed with 3—4 ml of 2 : 1 = Et_2O : EtOH. 0.9 g of small, needleshaped, yellow crystals with m.p. = 284—286°, very soluble in ethanol, acetone, insoluble in water and ethylic ether, are obtained.

Calculated :	M = 259.26	N : 16.21 %
Found :		N : 16.1 %
		N : 16.2 %

b. *Base (piperidine) catalysed synthesis*

The procedure is similar to that described for compound **4**, starting with 10^{-2} moles. Dissolution of the reaction mass is performed with 1 ml of 2 : 1 = Et_2O : EtOH, three times. It is isolated from the brown-viscous liquid by filtration through a G_3 sintered glass crucible and one washing with 1 ml of 2 : 1 = Et_2O : EtOH. Yield = 1.1 g (42 %).

1,3-DIMETHYL-6-(*p*-CHLORO-β-STYRYL)-1*H*,3*H*-s-TRIAZIN-2,4-DIONE (**8**) : $C_{13}H_{12}O_2N_3Cl$

a. *Acid catalysed synthesis*

By direct neutralization of the reaction mass obtained by the procedure described for the preparation of base **5**, without a previous dilution with 1M H_2SO_4, filtration on G_2 sintered glass crucible and washing twice with 1–2 ml of a 1 : 2 = EtOH : Et_2 O mixture, 2 g of base **8** (yield 72%) have resulted.

Recrystallization from n-propanol (~ 150 ml) yields 1.25 g of light yellow coloured needles with m.p. = 249–250°, soluble in ethanol, insoluble in ether and water.

Calculated :	M = 277.71	N : 15.13%
Found :		N : 14.9%
		N : 14.8%

b. *Base* (*piperidine*) *catalysed synthesis*

The procedure was identical to that for base **4**, starting with 5.10^{-3} moles of the two reactants, **2** and p-chlorobenzaldehyde (0.705 g). The resulting melt was extracted twice, as being warm, with 1 ml acetone. Yield = 0.8 g (~ 57%).

1,3-DIMETHYL-6-(*p*-ISOPROPYL-β-STYRYL)-1*H*,3*H*-s-TRIAZIN-2,4-DIONE (**9**) : $C_{16}H_{19}O_2N_3$

a. *Acid catalysed synthesis*

The reaction solution obtained as that for synthesis of compound **5** (10^{-2} moles cuminaldehyde ~ 1.5 ml) is diluted with 10–15 ml water and neutralized with NH_3 up to pH = 2, when base **9** precipitates. It is cooled, filtered and washed two-three times with 4–5 ml. Et_2O : EtOH = 2 : 1. Yield = 1.6 (56%)

Recrystallization of the raw product from ethanol (20 ml) gives 0.6 g colourless needles, insoluble in water, soluble in ethanol.

Calculated :	M = 285.34	N : 14.73%
Found :		N : 14.8%
		N : 14.8%

b. *Base* (*piperidine*) *catalysed synthesis*

The procedure was identical to that described for compound **4** but carrying the reaction for two hours.

The viscous mass resulting after cooling was taken with a small amount (~ 5 ml) of ethanol and then dissolved in 15 ml ethanol, in a flask provided with reflux condenser, on steam bath. The reaction product was crystallizing from the cooling solution, as colourless needles. After cool overnight standing the product was filtered on a G_2 sintered glass crucible and washed with 1–2 ml of a 2 : 1 = ether : ethanol mixture, yielding 0.8 g (27%).

1,3-DIMETHYL-6-(β-STYRYL)-1*H*,3*H*-s-TRIAZIN-2,4-DIONE (**10**) : $C_{13}H_{13}O_2N_3$

a. *Acid catalysed synthesis*

The synthesis was performed as for compound **5** (10^{-2} moles of benzaldehyde = 1 ml). The reaction solution is neutralized with HN_3 up to pH = 2.5, the sticky mass filtered off and washed with 1 ml acetone. Yield 1.1 g (45%).

By recrystallization from ethanol (14 ml) and cooling with ice, 0.4g are obtained. A second recrystallization leads to a product with m.p. =202–203° as colourless prismatic crystals, very soluble in polar organic solvents (ethanol, acetone, etc.) and insoluble in water.

Calculated : M = 242.25 N : 17.35%
Found : N : 17.2%
N : 17.1%

b. *Base (piperidine) catalysed synthesis*

It is performed as for the synthesis of **9**. The reaction liquid is mixed, three times, on hot water-bath, with 2 ml of 96% ethanol. The clear solution thus obtained is allowed to stand overnight, then cooled with ice. A twice washing of the crystals obtained by filtration, with 0.5 ml of acetone leads to 0.8 g (yield 33%) of product with m.p. = 201–203°.

1,3-DIMETHYL-6-(*p*-NITRO-β-STYRYL)-1*H*,3*H*-s-TRIAZIN-2,4-DIONE (**11**) : $C_{13}H_{12}O_4N_4$

b. *Base catalysed synthesis*

The preparation is carried out after the procedure described for **5** using 10^{-2}moles of the two reaction partners (=1.51 g p-nitrobenzaldehyde). The reaction proceeds quickly, namely in 5 minutes. After other 10 minutes of heating, it is cooled, and the brown coloured product obtained is twice taken with 2 ml acetone, filtered and washed with 2 ml of acetone. Yield = 2.3 g (80%).

A higher purification is performed by a dispersion of the raw, fine-grinded product, in 5–7 ml acetone, followed by filtration.

Crystallization is ready from nitromethane (~ 50 ml). A second recrystallization gives 0.5 g of product with m.p. = 294–296°C as yellow-brown rhombic crystals, sparingly soluble in acetone and ethanol.

Calculated : M = 228.26 N : 19.09%
Found : N : 19.1%
N : 19.0%

1,3-DIMETHYL-6-(3′-METHOXY-4′-HYDROXY-β-STYRYL)-1*H*,3*H*-s-TRIAZIN-2,4-DIONE (**12**) : $C_{14}H_{15}O_4N_3$

a. *Acid catalysed synthesis*

10^{-2} moles of reactants (1.52 g vanilline) are taken and handled as for preparation of **6***A*. After washing of salt **12***A* thus obtained on a G_2 sintered glass crucible, with 2–3 ml of 2 : 1 = Et_2O : EtOH, 3g (77%) of product are yielded.

The finelly grinded product is suspended in 20 ml water and neutralized up to pH = 4 It is further cooled with ice, filtered and dried. Yield = 2.2 g (98 %)

Base **12** may be recrystallized from nitromethane (2.2 g/150 ml). Crystals isolated by filtration on G_2 are washed with 2–3 ml of a 1 : 2 = EtOH : Et_2O mixture. 1.5 g of dark-yellow flakes are yielded, insoluble in water and ether, soluble in EtOH.

Calculated : M = 290.29 N : 14.48 %
Found : N : 14.5 %
N : 14.4 %

b. *Base (piperidine) catalysed synthesis*

Performing with 5.10^{-3} moles of both reaction partners (0.76 g vanilline and 0.78 g of **2**) in the same conditions as described for preparation of **4**, then washing the reaction mass on a G_2 sintered glass crucible with 1–2 ml of a 2 : 1 = Et_2O : EtOH mixture 1.1 g (~76 %) of product are obtained.

1,3-DIMETHYL-6-(3′,4′-DIOXI-METHYLENE-β-STYRYL)-1*H*,3*H*-s-TRIAZIN-2,4-DIONE (13) : $C_{14}H_{14}O_4N_3$

a. *Base (piperidine) catalysed synthesis*

Following the procedure described for preparation of **4** a mixture of 10^{-2} moles (1.1g) of piperonal and 10^{-2} moles of **2** are maintained at 150° for 20 minutes. A longer heating time causes a marked browning of the melt and a lowering of the yield.

The resulting brown melt is taken twice with 3 ml of acetone, filtered on a G_3 filtering crucible, where it is washed with another 2–3 ml acetone for complete removing of the brown coloured impurities. Yield = 1.9 g (66 %).

Recrystallization is ready from a 1 : 2 = DMSO : n-butanol mixture by slow cooling. A second recrystallization yields 1.4 g of yellow flakes with m.p. = 289–290°, insoluble in water, sparingly soluble in ethanol and acetone, very soluble in DMSO.

Calculated : M = 288.87 N : 14.58 %
Found : N : 14.8 %
N : 14.6 %

1,3-DIMETHYL-6-(2′,4′-DICHLORO-β-STYRYL)-1*H*, 3*H*-s-TRIAZIN-2,4-DIONE (14) $C_{13}H_{11}O_2N_3Cl_2$

2.4 g of **14**A bisulphate, obtained with a 58 % yield from the reaction of 10^{-2} moles of **2** and 10^{-2} moles of 2,4-dichlorobenzaldehyde (= 1.75 g), following the procedure described for preparation of salt **6**A and performing with 3 ml ethanolic solution of H_2SO_4, are finely grinded and suspended in 10 ml water. The pH of the solution is brought to 3, then filtration is followed by drying. Yield = 18 g (100 %).

Crystallization is performed from a 1 : 1 = DMSO : n-butanol mixture (150 ml). By slow overnight cooling, 1.7 g of colourless parallelipipedic crystals with m.p. = 291–292.5°. are yielded.

Calculated : M = 313.16 N : 13.42 %
Found : N : 13.4 %
N : 13.6 %

1,3,5-TRIMETHYL-6-(*p*-DIMETHYLAMINO-β-STYRYL)-1*H*,3*H*,-s-TRIAZINIUM-2,4-DION IODIDE (15) : $C_{16}H_{21}O_2N_4I$

a. *Acid catalysed synthesis*

10^{-3} moles (= 0.297 g) of 3 and 10^{-3} moles (= 0.147 g) of pDAB are dissolved, on steam bath with stirring, in 0.5 ml of glacial acetic acid. The red solution thus obtained is heated for 30 minutes on steam bath, at 90°. After cooling, 2 ml of aquo-methanolic solution, containing 25% vol. methanol and 0.2 g KI are added. It is allowed to stand cool for 48 hours and the dark red-green shining, needle shaped crystals settled are then filtered and dried. Yield = = 0.2 g (47%).

The product is readily soluble on chloroform, acetone, ethanol and acetic acid, and sparingly soluble in water. It melts with decomposition at 142—143°.

Calculated :	M = 428.28	N : 13.09 :	I : 29.63 %
Found :		N : 12.9 ;	I : 29.5 %
		N : 12.8 ;	I : 29.6 %

b. *Base (piperidine) catalysed synthesis*

10^{-3} moles (= 0.297 g) of 3 and 10^{-3} moles (= 0.147 g) of pDAB are dissolved on heating in 0.5 ml ethanol containing a drop of piperidine. The reaction is performed in a 5 ml flask provided with condenser. It is further refluxed on steam bath, at 75° for 30 minutes. It is cooled and 2 ml aqueous acetic acid solution (25% volume acetic acid) containing 0.2 g KI are added to the reaction solution thus obtained. It is allowed to stand cool for 48 hours, then filtered and dried. Yield = 0.2 g (47%).

Revue Roumaine de Chimie, 17, 12, 2055 – 2065 (1972)

QUANTITATIVE STUDY OF ACTIVE METHYL GROUPS IN C-METHYL-s-TRIAZINES. I.

HYDROGEN EXCHANGE KINETICS OF 6-METHYL-s-TRIAZINE-2,4(1*H*,3*H*)-DIONE AND ITS N-METHYL DERIVATIVES (STUDIES IN THE s-TRIAZINE FIELD. NEW SERIES, VI*)

M. SAFTA*, F. CHIRALEU**, A. T. BALABAN*** and G. OSTROGOVICH*

* Department of Organic Chemistry, Polytechnic Institute, Timişoara, str. Bocşa, 6
** Institute of Organic Chemistry, Bucharest, Spl. Independenţei 202 B
*** Institute of Atomic Physics, P.O. Box 35, Bucharest

Received July 7, 1972

The $C_{(6)}$-methyl group of 6-methyl-s-triazine-2,4(1*H*, 3*H*)-dione (**1**) and of its 1,6-dimethyl- (**2**) and 1,3,6-trimethyl-derivative (**3**) undergoes ready deuterium exchange in buffered D_2O solutions. The kinetic parameters were determined by NMR both for the acid-catalyzed (for **1**, **2** and **3**) and the base-catalyzed reactions (for **3**), evidencing the pH dependence of the rate constants. Compounds **1** and **2** are not methyl-deuterated in basic catalysis. 1,3,5,6-Tetramethyl-2,4-(1*H*, 3*H*)-dione-s-triazinium iodide (**4**) exchanges the hydrogens too fast to follow kinetically. The pK values of **1**–**3** were determined, and a modified procedure for preparing **2** was described.

Previous studies [1,2,3] revealed that the C-methyl-group of 6-methyl-s-triazine-2,4 (1*H*, 3*H*)-dione (2,4-dioxo-6-methyl-tetrahydro-s-triazine) and its 1,3-dimethylderivative [4] readily enter condensation reactions with aromatic aldehydes. Acid catalysts are as effective as basic catalysts (piperidine).[3,4]

The purpose of the present paper is to find a quantitative determination of the activity of $C_{(6)}$-methyl groups in 6-methyl- (**1**), 1,6-dimethyl- (**2**), and 1,3,6-trimethyl-s-triazine-2,4(1*H*,3*H*)-dione (**3**).

---

* Previous part in the series, preceding paper.

[1] N. V. Khromov-Borisov and E. V. Kisareva, *Zhur. obshchei Khim.*, **29**, 3010 (1959).

[2] P. W. Hickmott, *J. Appl. Chem.*, **16**, 227 (1966).

[3] G. Ostrogovich and M. Safta, *Rev. Roumaine Chim.*, **15**, 799 (1970).

[4] G. Ostrogovich and M. Safta, *Rev. Roumaine Chim.*, **17**, 2043 (1972).

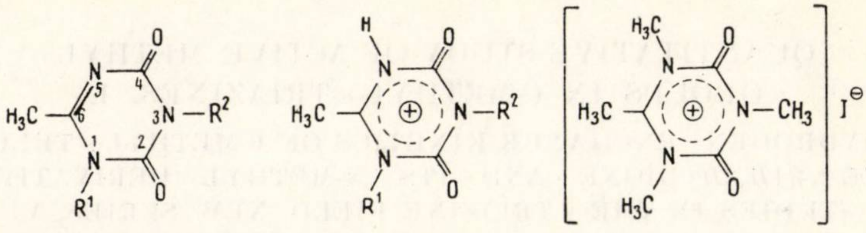

1 $R^1=R^2=H$ **1A**
2 $R^1=CH_3$, $R^2=H$ **2A**
3 $R^1=CH_3$; $R^2=CH_3$ **3A**

This purpose was achieved by investigating their hydrogen exchange in deuterium oxide. The exchange was followed by PMR at various pH values and temperatures. Literature surveys [5] indicate few similar studies of aromatic N-heterocycles with active methyl groups, where the H—D exchange was correlated with the pH.[6,7] In the present case, however, a wide range of pH values had to be investigated because compounds **1** and **2** are amphoteric : A. Ostrogovich had shown that **1** may be titrated sharply with alkali in the presence of phenolphthalein.[8]

PROTONATION EQUILIBRIA OF COMPOUNDS 1, 2, AND 3

The UV spectrum of **1** is presented in fig. 1 at various acidities in the range from pH = 4.5 to $H_0 = -0.56$. On protonation a hypochromic and hipsochromic effect on the absorption maximum of **1** is apparent : the conjugate acid (**1A**) has $\lambda_{max} = 225$ nm.

An isobestic point at 222 nm can be noticed. At pH > 3 no **1A** can be detected spectroscopically ; on decreasing the pH at 1.30, appreciable concentrations of **1A** appear, and at acidities higher than 2N H_2SO_4 ($H_0 = -0.26$) compound **1** is practically completely protonated. For the other compounds (**2** and **3**) similar λ_{max} values are formed in the order **2** > **3** > **1** (table 1).

For the determination of *pK* values (expressed as pK_a of the conjugate acids of **1**—**3**) the pH-metric method described by Albert and Serjeant [9] was employed, with an average error of ± 0.03 pH units. As is seen from table 1, all three compounds have similar pK_a values. The basicity decreases in the same order **2** > **3** > **1**. This order results from a combination of steric and inductive effects of methyl groups and of the symmetry of the molecule. The difference between the basicity of **1** and

[5] M. Bologa and E. Gârd, *Studii şi Cercetări chim. Acad. R.S. România*, **19**, 1329 (1971).

[6] T. J. Batterham, D. J. Brown and N. M. Paddon-Row, *J. Chem. Soc.* B, **1967**, 171.

[7] J. Mc. Andless and R. Stewart, *Canad. J. Chem.*, **48**, 263 (1970).

[8] A. Ostrogovich, *Gazz. chim. Ital.*, **44**, II, 572 (1914).

[9] A. Albert and P. T. Serjeant "Ionization Constants of Acids and Bases. A Laboratory Manual", Methuen and Co. London, Wiley, New York, 1962.

the other compounds, smaller than for other nitrogen heterocycles,[10] is probably due to the symmetry of **1A**, similarly to the situation in N-methyl derivatives of guanidine.[11]

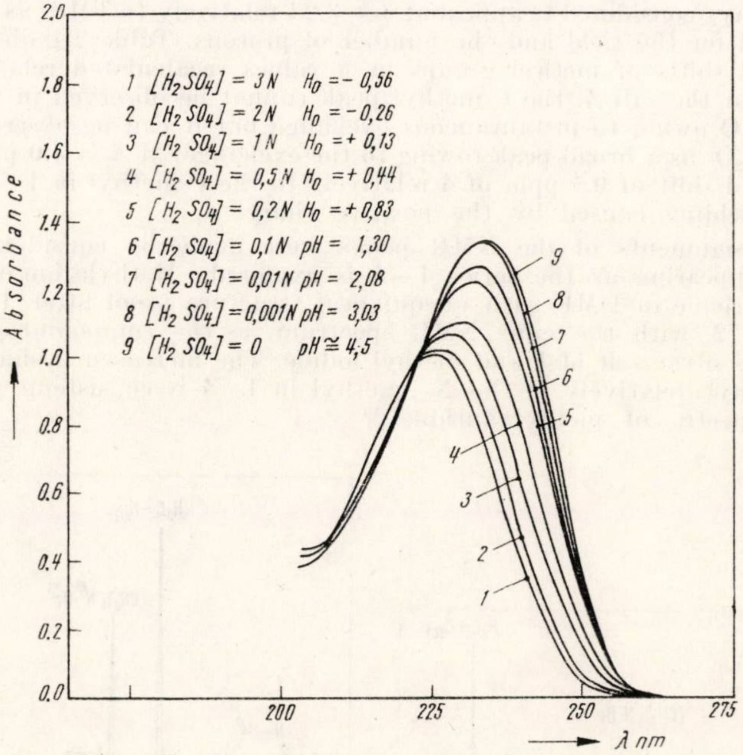

Fig. 1. — UV Absorption spectra of **1** ($2 \cdot 10^{-5}$ molar) in sulphuric acid of various concentrations (cell width 0.5 cm).

Table 1

Values of pK_a and absorption maxima of 1, 2 and 3 in water at room temperature

Compound	pK_a	λ_{max} nm
1	1.13	238
2	1.21	243
3	1.18	241

---

[0] D. D. Perrin "Dissociation Constants of Organic Bases in Aqueous Solution", Butterworths, London, 1965.

[11] S. J. Angyal and W. K. Warburton, *J. Chem. Soc.*, **1951**, 2492.

PMR SPECTRA

Figures 2a–d present proton magnetic resonance spectra of **1**, **2**, **3** and **4** in D_2O, with tetramethylammonium bromide (whose peak was always considered to appear at $\delta = 3.24$ relatively to TMS) as internal standard for the field and the number of protons. Table 2 indicates the chemical shifts of methyl groups in δ values recalculated relatively to TMS. For the salt **4**, the C-methyl peak cannot be observed in non-buffered D_2O owing to instantaneous exchange but it can be observed (fig. 2e) in H_2O as a broad peak (owing to the exchange) at $\delta = 3.0$ ppm. The downfield shift of 0.5 ppm of **4** relatively to the C-methyl in **1**–**3** is due to deshielding caused by the positive charge.

Assignments of the NMR peaks were made by considering new peaks appearing as the series **1**–**4** is explored. Methylation of **1** with diazomethane in DMF with unequivocal structure proof after Piskala[12] afforded **2**, with the same NMR spectrum as the compound prepared from the silver salt of **1** and methyl iodide. The increased deshielding of $N_{(1)}$-methyl relatively to the $N_{(2)}$-methyl in **1**–**4** is consistent with the NMR spectra of methylxanthines.[13]

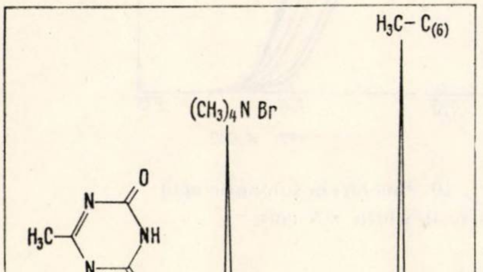

Fig. 2a – Proton magnetic resonance spectrum of **1** in D_2O.

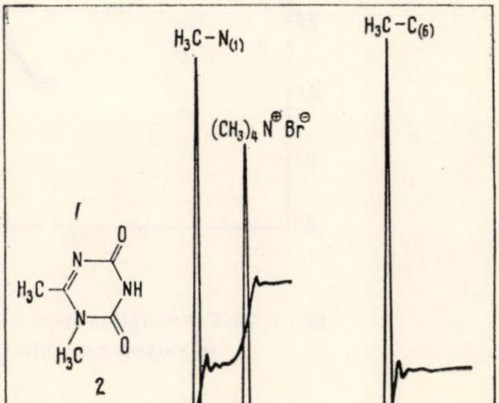

Fig. 2b – Proton magnetic resonance spectrum of **2** in D_2O.

---

[12] A. Piskala, *Coll. Czech. Chem. Comm.*, **28**, 2365 (1963).

[13] J. C. N. Ma and E. W. Warnhoff, *Canad. J. Chem.*, **43**, 1849 (1965).

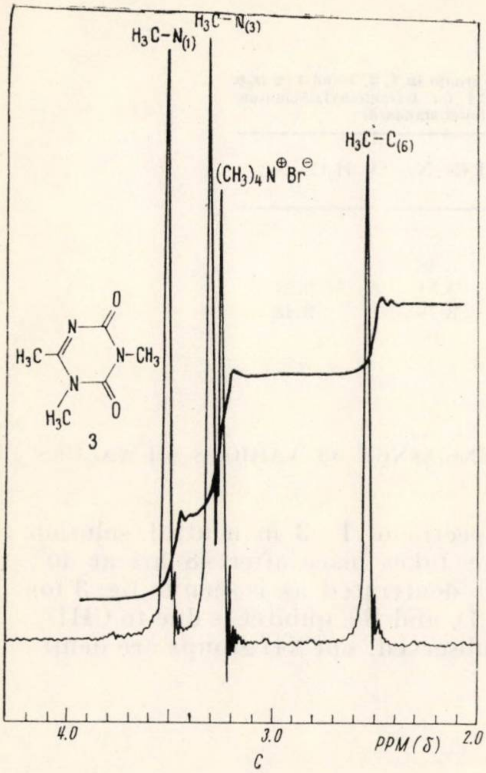

Fig. 2c – Proton magnetic resonance spectrum of **3** in D_2O.

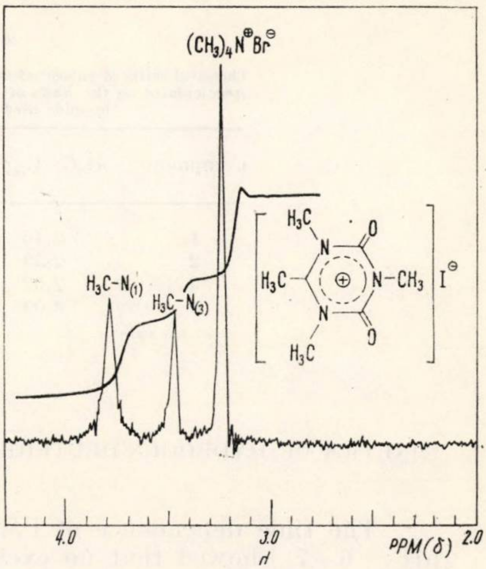

Fig. 2d – Proton magnetic resonance spectrum of **4** in D_2O.

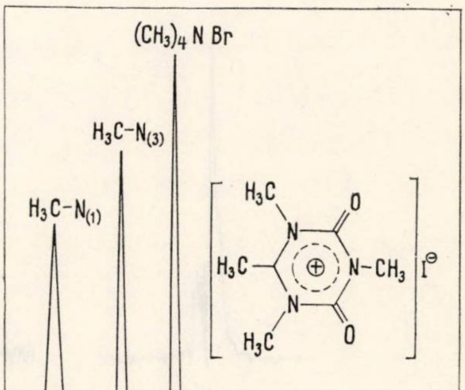

Fig. 2e – Proton magnetic resonance spectrum of **4** in H_2O.

Table 2

Chemical shifts (δ values) of methyl groups in 1, 2, 3 and 4 in D_2O (recalculated on the basis of δ = 3.24 for tetramethylammonium bromide used as internal standard)

Compound	$H_3C-C_{(6)}$	$H_3C-N_{(1)}$	$H_3C-N_{(3)}$
1	2.40	—	—
2	2.53	3.48	—
3	2.52	3.51	3.31
4	3.02[a]	3.79	3.48

a. In water.

KINETICS OF HYDROGEN-DEUTERIUM EXCHANGE AT VARIOUS pH VALUES

The time dependence of PMR spectra of **1**—**3** in neutral solution (pH = 6—7) showed that no exchange takes place after 48 hrs at 40°. However at pH$\leqslant$4, the $C_{(6)}$-methyl is deuterated as is seen in fig. 3 for **1** (pH = 3.3) : the triplet is due to CH_2D, and the quintet is due to CHD_2. No exchange of N-methyl groups was observed, but NH groups are deuterated instantaneously.[14]

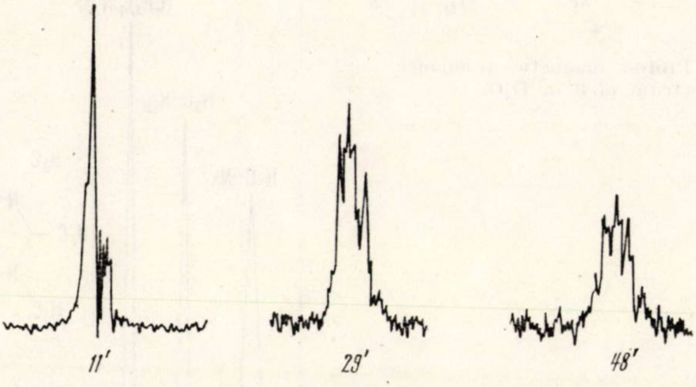

Fig. 3. — $C_{(6)}$-methyl peak of compound **1** in D_2O at pH 3.3 and 38° after various deuteration times : 11,29 and 48 minutes.

Table 3 presents the kinetic parameters for the exchange of $C_{(6)}$-methyl groups in **1**—**3**. These parameters were determined using buffered D_2O media at various temperatures. As an example, figure 4 represents the time dependence of the logarithm of the integrated intensity of the PMR C-methyl peak of **3**. A linear dependence holds.

---

[14] V. K. Pogorelyi and I. P. Gragerov, *Uspekhi Khim.*, **39**, 1856 (1970).

Thus the reaction is a first order one in **3**, during the whole process, therefore table 3 also gives the half-life $T_{1/2}$.

Table 3

Kinetic data for the hydrogen exchange of 1, 2 and 3 in D_2O

Compound	t °C	pH	k.10^5 sec^{-1}	$T_{1/2}$ sec	ΔE kcal/mol	$H^{\ddagger 298}$ kcal/mol	$\Delta S^{\ddagger 298}$ e.u.
1	87.5	3.95	161	430	16.1	15.6	−14.8
	59	3.95	23	3040			
	38	3.95	4.5	15400			
	38	3.5	9,8	7960			
	38	3.3	23	3020			
	38	2.07	147	471			
	38	1.4	400	173			
	38	1.07	1160	60			
2	87.5	3.95	394	176	13.7	13.1	−19.5
	72	3.95	189	366			
	59	3.95	62	1115			
	38	3.95	18	3770			
	38	3.3	114	608			
	38	2.07	597	116			
3	87.5	3.95	247	280	15.00	14.5	−16.8
	72	3.95	105	660			
	59	3.95	45	1600			
	38	3.95	9	7520			
	38	2.07	341	203			
	38	3.3	45	1540			
	38	4.5	6	11770			
	38	8.3	4.6	15000			
	38	9.5	52	1320			
	38	10.3	22	314			
	38	10.6	400	171			

Figure 5 illustrates the influence of the acidity by plotting log k at 38° *versus* pH. An approximately linear plot is observed in the pH range from 1 to 5 for all three methyl-triazinediones **1**—**3**.

Table 3 indicates that at the same acidity the rate of exchange decreases in the same order as the basicity **2** > **3** > **1** (as shown by $T_{1/2}$ at pH = 3.95 and the same temperature). This is due to the fact that the exchange proceeds *via* protonated forms, whose concentration depends on the basicity.

The acid-catalyzed exchange involves protonation of the free base **5**(**1**—**3**) to afford the conjugate acid **5A.** Proton loss from the methyl group of the latter results in the methylene base **6**, a tautomer of the initial base **5**, which is the active intermediate in the deuteration. Owing to the close values of pK of **1**–**3**, the Brönsted relationship[15] could not be used to investigate whether the reaction is a specific or a general acid catalysis.

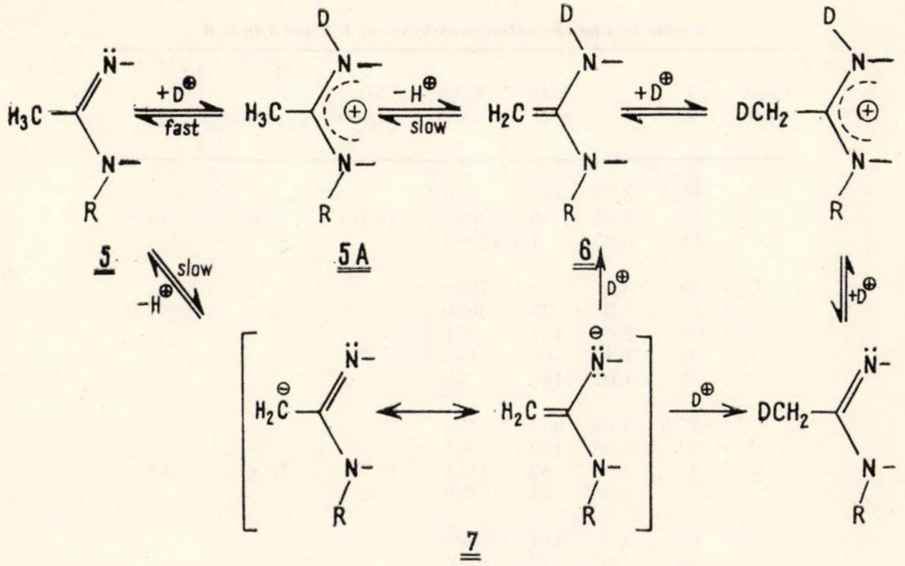

H_3C
N
N
R
$+D^{\oplus}$
fast
H_3C
D
N
N
R
$-H^{\oplus}$
slow
H_2C
D
N
N
R
$+D^{\oplus}$
DCH_2
D
N
N
R
5
5A
6
slow
$-H^{\oplus}$
$D^{\oplus}$
$+D^{\oplus}$
$H_2C^{\ominus}$
N
N
R
H_2C
N
N
R
$D^{\oplus}$
DCH_2
N
N
R
7

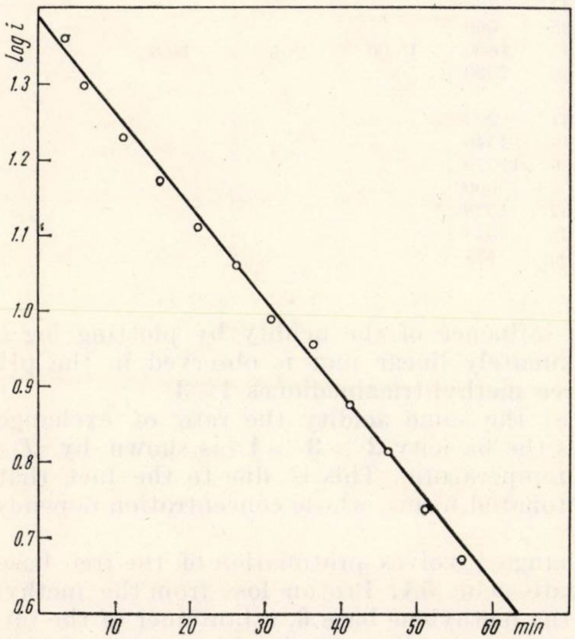

Fig. 4. — Time dependence of the logarithm of integrated NMR peak intensities for the $C_{(6)}$-methyl group of 3 in D_2O at 38° and pH 3.3

---

[15] R. P. Bell "The Proton in Chemistry", Cornell Univ. Press, New York, 1959; "Acid-Bases Catalysis", Oxford Univ. Press, 1941.

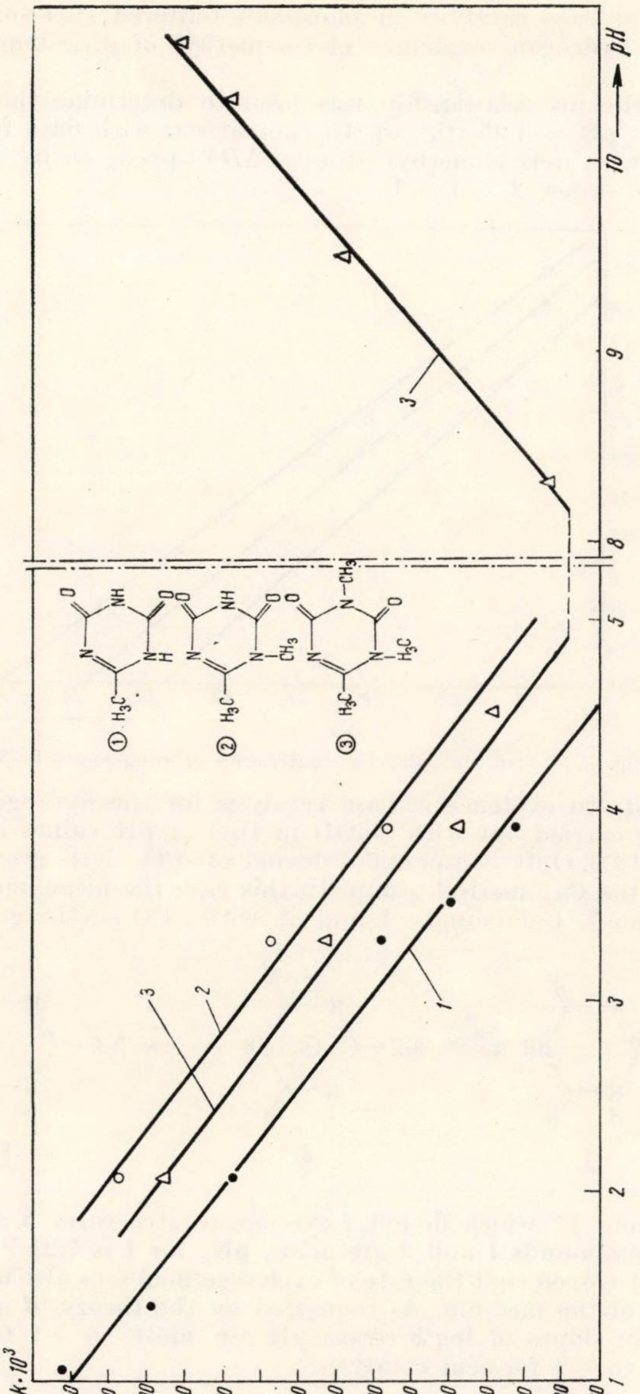

Fig. 5. — Plot of logarithm of rate constants at 38° *versus* pH for compounds **1**, **2** and **3**.

A general base catalysis in phosphate-buffered D_2O solutions was found in the hydrogen exchange of $C_{(7)}$-methyl of 6,7,8-trimethyllumazine.[7]

The Arrhenius relationship was used to determine the activation parameters at pH = 3.95 (fig. 6). In comparison with data for other N-heterocycles with active methyl groups, $\Delta H^{\ddagger}$ appear to be smaller and maintain the order **2** < **3** < **1**.

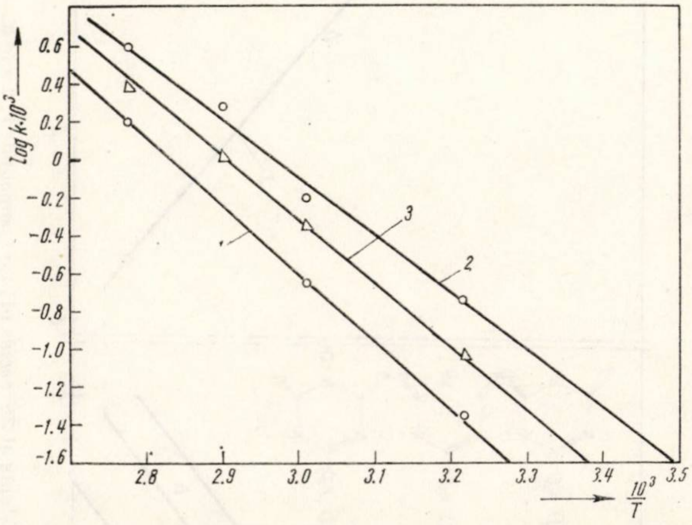

Fig. 6. — Arrhenius plot for deuteration of compounds **1**—**3**.

Attempts to evidence a base catalysis for the hydrogen exchange of **1**—**3** were carried out with NaOD in D_2O at pH values in the range from 8.3 to 10.6. Only compound **3** devoid of -CO—NH- groups presents exchange of the $C_{(6)}$ -methyl group. In this case the mechanism probably involves anion **7**. Compounds **1** and **2** with -CO—NH- groups afford different anions **8***) which do not rearrange to structures **9** analogous to **7**. Indeed, compounds **1** and **2** are acids, pK_a for **1** is 7.21.[16] From table 3 and fig. 5 it is seen that the rate of exchange increases also on increasing the basicity of the medium. As requested by the theory of acid-base catalysis,[15] the slopes of log *k versus* pH are close to —1 for base catalysis, and to +1 for acid catalysis.

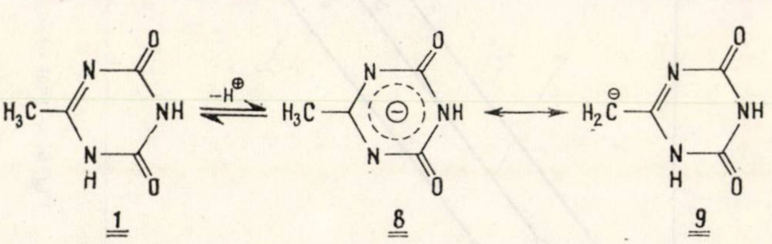

---

[16] J. Jonas and J. Gut, *Coll. Czech. Chem. Comm.*, **27**, 716 (1962).

* In the scheme the anion of **1** was formulated.

Compound **4** is deuterated instantaneously even at +2° : no trace of the $C_{(6)}-CH_3$ group was seen in a few seconds after dissolution in cold D_2O. The pH of the solution (without added buffer) is ca. 1 owing to the acidity of **4**. In **4**, in addition to the positive charge, the strong —E effect of carbonyl groups makes this C-methyl the fastest exchangeable group in heterocyclics.[5] Also compounds **1**—**3** undergo faster exchange than most other heterocycles with active methyl groups.

For obtaining a quantitative measure of the enormous increase in the rate of deuteration brought about by quaternization, the NMR spectra of **4** in very strongly acid solution and at low temperature were recorded. The following half-lives were indeed obtained at −10° in $D_2O + P_2O_5$: 2 minutes for 2.5 M D_3PO_4, 3 minutes for 5M D_3PO_4.

EXPERIMENTAL PART

Compound **1** was prepared by cyclization of 1,5-diacetylbiuret in concentrated aqueous alkali.[17] Compounds **3** and **4** were prepared as described previously.[4]

1,6-*Dimethyl-s-triazine*-2,4(1*H*, 3*H*)-*dione*

(**2**) was prepared from the silver salt of **1** and methyl iodide, modifying the procedure of A. Ostrogovich [18] (who had employed sealed tubes and methanol solutions) and obtaining better yields and a purer product.

In a flask with stirrer, efficient reflux condenser and dropping funnel, a mixture of 200 ml toluene and 100 ml dioxan is introduced and heated to reflux temperature. Finely powdered and dry silver salt of **1** (11.7 g, 50 mmoles) is introduced. Methyl iodide (0.4 moles, 57 g, 25 ml) is added dropwise with good stirring for 30 min. After 2 hrs' refluxing under stirring the hot solution is filtered with suction.

The filtrate is kept overnight in the refrigerator affording 2.5 g crystalline **2**. If the residue on the filter is again suspended and methylated, another 1.0 g of **2** can be obtained. Total yield 3.5 g, 50%. The product **2** crystallizes in colourless prisms which are insoluble in toluene, ether or acetone, sparingly soluble in ethanol, soluble in water. It may be recrystallized from 60 ml 96% ethanol, m.p. 223—224°. Found N, 29,6%. Calc. for $C_4H_5N_3O_2$, N,29.7%.

1,3-*Dideutero*-6-d_3-*methyl-s-triazine*-2,4(1*H*, 3*H*)-*dione*

Compound **1** (5 mmole, 0.635 g) is heated at 100° on the water bath for 6 hrs in a test tube with 4 ml D_2O acidified with 2—3 drops of acetic acid. After cooling the deuterated product is filtered off and dried in vacuum over KOH, yield 0.4 g, 62%, m.p. 296°.

Nuclear magnetic resonance spectra were recorded with a Varian A 60A with 5% solutions in D_2O (molar ratio substrate : solvent 1 : 50) with weighed amounts of tetramethylammonium bromide as internal standard. (N-methyl groups were also found to be reliable standards for the number of protons).

Ultraviolet absorption spectra were recorded with a Unicam SP 800 spectrophotometer.

The determination of pK_a values was effected with a Radelkis OP—205 pH-meter using a glass electrode ; the pH values were not converted into pD values. Buffers were prepared from 1N D_3PO_4 obtained from P_2O_5 and D_2O, and from 1N NaOD prepared from Na and D_2O.

Nitrogen analyses were semimicro Kjeldahl-Parnas-Wagner analyses. Melting points were determined on a Boetius hot stage.

---

[17] G. Ostrogovich, *Bul. St. şi Techn. Inst. Polit. Timişoara* (in press).

[18] A. Ostrogovich, *Gazz. chim. Ital.*, **2**, 27, 416 (1897).

1883

F 1103

Revue Roumaine de Chimie, 17, 12, 2067–2087 (1972)

MŰSZAKI KÖNYVTÁR ÉS DOKUMENTÁCIÓS KÖZPONT 1883

INDEX DU TOME 17, 1972

INDEX DES AUTEURS

Page

A

Aamland E., voir Bratland D. . . . 41
Adorian I. and S. Sternberg, Thermodynamic excess functions in molten mixtures of potassium chloride with alkaline-earth chloride 1361
Agherghinei I., voir Crusos A. . . . 565
Albescu I., Contributions to the study of lanthanides with biguanide derivates. III. Europium and gadolinium compounds with paludrine . 1729
— , Contributions to the study of lanthanides with biguanidine derivates. IV. Compounds of holmium and ytterbium with paludrine . . 1867
Alevra V. and D. Ciomârtan, M. Ionescu, Influence of the preparation method on the structure and physical properties of alumina. I. Aluminium hydroxides 1163
— and D. Ciomârtan, M. Ionescu, Influence of the preparation method on the structure and physical properties of alumina. II. Aluminium oxides 1379
Andreescu P., voir Uglea C.V. . . . 2021
Andrei C., voir Nanu I. 741
— , voir Nanu I. 1043
Angelis G. de, voir Campanella L.. . 1087
Antonescu L., voir Spacu P.. 1851
Armeanu V. and S. Oancea, S. Rusenescu, L. M. Băloiu, Determination of the partition constant of compounds used in spectrophotometric analysis 925
Arsenie I., voir Popa L. I. 937
Arshad A., Beg M. and I. A. Khan, Correlation of the physical properties of organosilicon compounds. I. Boiling point and density of substituted silanes and siloxanes and the additivity of density. 1579
— and I. A. Khan, Correlation of the physical properties of organosilicon compounds. II. Boiling point, refractivity and density of silanes and siloxanes 1599

Page
Asandei N., voir Simionescu Cr. . . 2003

B

Bacaloglu I., voir Bacaloglu R.. . . 747
Bacaloglu R. and Fl. Neamţiu, I. Bacaloglu, G. Ostrogovich, Infrared spectra of amidic derivatives of carbonic acid. VI. Substituted 1,5-benzylidine guanylureas (free bases and sulphates) 747
Badea F., voir Glatz A. M. 1735
— , voir Voicu M. 1551
— , voir Voicu M. 1563
Bader B. D., voir Reichel J.. . . . 1889
— und R. Vilceanu, Neue organische Pigmente-Isatinderivate. II. Synthese durch direkte Kondensierung.. 1991
Bagrii V. A., voir Delimarskii Yu. K. 111
Balaban A. T., Chemical graphs. XIV. Valence isomers of [12] annulene. 865
— , Chemical graphs. XV. Degenerate Cope rearrangements of valence isomers of annulenes 883
— , Chemical graphs. XVII. (Aromaticity. X) *cata*-condensed polycyclic hydrocarbons which fulfill the Hückel rule but lack closed electronic shells 1531
— , Determination of hyperfine coupling constants from ESR spectra of organic free radicals. . . . 9
— and N. Negoiţă, Factors affecting stability and equilibria of free radicals. VII. Arenesulphonyl-phenyl-nitroxides and 1-arenesulphonyl-2,2-diphenylhydrazyls 1227
— , voir Safta M. 2055
Balasubrahmanyam K., voir Janz G. J. 187
Bălăceanu G., voir Oncescu T.. . . 213
Băloiu L. M., Determination of the stability constant of compounds used in spectrophotometric analysis 1065
— , voir Armeanu V. 925
— , voir Călin C. G. 1765

Baltă E., Etude de la réaction d'alkylation du colorant azoïque benzothiazolique à l'aide de l'analyse thermique différentielle 1241

Baltă P., New theoretical data on the structural chemical equilibrium in molten glass 969

— and L. Dollingher, M. Cîrstea, Phototropic glasses on B_2O_3 basis 25

Balthazár-Vass K., voir Erdey-Grúz T. 137

Banciu M. and P. Buck, E. Ciorănescu, C. D. Nenitzescu, Solvolysis of Δ^2-cyclobutenylethyl-β-tosylate and Δ^2-cyclobutenylpropyl-γ-tosylate . 1393

Bansal K., voir Jindal H. L.. 1969

Bansal N. B., voir Jindal H. L.. . . . 1969

Barabás A., Bis-(thenoyl-trifluoroacetonato)-beryllium 1997

Bâtcă-Cerbu A., Study on the behaviour of the NaA type zeolite in the presence of nitrates of some bivalent cations dissolved in molten sodium nitrate 855

Benedek I., voir Simionescu Cr. I.. . 2003

Beyer H. und D. Kalló, G. Schay, Zur kinetischen Untersuchung der katalytischen Krackung von Propan. . 29

Bhatnagar V. M., Spectroscopic observations on nickel (II) perchlorate complexes 477

Bică I., voir Drăgănescu A.,. 1779

Bîndeanu St., voir Gocan S.. . . . 669

Biradar N. S. and V. H. Kulkarni, A spectroscopic study of oxovanadium (V) complexes with multidentate Schiff bases. II. 481

Bîrhală Al., voir Topor D.. 961

Blazsek-Bodó A., voir Liteanu C. 1465

— and C. Liteanu, The use of the salt effect in acid-base titration performed in organic medium. III. A study regarding the analytical behaviour of aromatic acids in methyl alcohol in presence of $Ca(NO_3)_2$ 1771

Bliznakov G. and S. Delineshev, On the binding energy of small clusters of atoms 35

Bockris J. O'M, voir Woon kie Paik 405

Bodea C., voir Broser E.. 1747

Boe G. H., voir Bratland D.. 41

Bojan N., voir Pascu N. 505

Bonciocat N., voir Radovici O. . . 253

Bozeşanu M., voir Murgulescu I. G. 1637

Bratland D. and G. H. Bøe, K. Grjotheim, H. Revnsvik, E. Aamland, Some introductory investigations on electrolytic deposition of Y-Al and Y-Mg alloys 41

Bratu Em. A. and G. Jinescu, Heat transfer in vibrated fluidized layers 49

Brenet J. et P. Dantzer, P. Mirabel, J. Guion, Evaluation de la nature des interactions ioniques dans les mélanges binaires de sels fondus à anion commun et comportant des cations polarisables 57

Brezeanu M. and I. Jitaru, Coordination compounds with copper-tin bonds 1857

— , voir Teodorescu M. 1191

Březina M., voir Koryta J. 171

Broser E. und C. Bodea, Über Phenothiazone. XIX. 4-Amino-und 4-Amino-Halogen-Phenothiazone . . 1747

Buck P., voir Banciu M. 1393

Bucur A., voir Voicu M. 1563

C

Călin C. G. and E. Diamandescu, L. M. Băloiu, Spectrophotometric determination of dicyanoaurate (I) ion with paranitral green. 1765

Calu C., voir Duca Al.. 125

Călugăru E. M., voir Simionescu N. . 2013

Campanella L. and G. de Angelis, Electrochemical behaviour of isonicotinic acid in aqueous solution. . 1087

— and E. Chiacchierini, M. Palchetti, Polarographic and oscillopolarographic behaviour of dipicolinic acid 647

Caproşu M., voir Zugrăvescu I. . . 397

Carbó R., voir Martín M.. 1963

Carpov A. et D. Drăgan, I. Petrariu, Sur l'amination des copolymères macroporeux styrène-divinyl-benzène chlorométhylés avec la diméthyle-2-hydroxy-éthyle amine . . 1923

Caşcaval C. N. et I. A. Schneider, Étude par chromatographie pyrolytique de quelques polymères vinyliques 835

Cenuşe Z, voir Vîlcu R. 367

Cerchez M., voir Dinescu R.. 643

Chemla M., Relation diffusion-conductivité dans les solutions d'électrolytes et applications structurales . 63

Chiacchierini E., voir Campanella L. 647

Chiraleu F., voir Moraru M. . . . 1235

— , voir Safta M. 2055

Chirulescu T. and C. Ciobanu, Gh. Şerban, Reduction studies on nickel oxide catalysts 1509

Ciobanu C., voir Chirulescu T. . . . 1509

Ciochină A., voir Vîlcu R. 1679

Ciomârtan D., voir Alevra V. . . . 1163

— , voir Alevra V. 1379

— , voir Spacu P. 977

Ciopec M., voir Marchidan D. I. . . 1657

— and D. I. Marchidan, The use of the digital computer in the pheno-

menological thermodynamics. I. Termox — program for processing experimental data from the thermodynamical measurements of oxides 1139
— and D. I. Marchidan, The use of the digital computer in phenomenological thermodynamics. II.. . 1313
Ciorănescu E., voir Banciu M. . . . 1393
Cîrstea M., voir Baltă P. 25
Cismaru D. and C. Radovici, Kinetic equations for reactions taking place in powders. I. Complete form of the equation for spheric particles. . . 69
Cismaru G. D., voir Spacu P. . . . 947, 1723
Ciurea L., voir Sahini V. Em. . . . 273
Comptes Rendus, 589, 590, 765, 1281, 1283, 1483
Constantinescu E., Potentiels normaux d'électrode dans des solvants non aqueux 1819
Constantinescu M. and E. Segal, Memory effects in oxygen and hydrogen photosorption on thin zinc oxide films 83
Constantinescu M., voir Zuca Șt. . 385
Contineanu M., voir Oncescu T. . . 213
Comșa G. and W. Groth, The influence of gas adsorption on the surface recombination of nitrogen atoms on stainless steel 77
Coriciuc C. i G. Csomontanyi, S. Popa, Issledovanie zauglerojivania nekotorykh katalizatorov degidrirovaniya alkilaromaticheskikh uglevorodov 533
Cormoș L., voir Pop A. 1917
Costeanu G. et O. Landauer, L'influence du solvant sur la vitesse de réaction. L'hydrolyse acide du formiate, de l'acétate et du propionate de n-butyle dans le solvant mixte eau-alcool éthylique 1331
— et O. Landauer, L'influence du solvant sur la vitesse de réaction. L'hydrolyse acide du formiate, de l'acétate et du propionate de n-butyle dans le solvant mixte eau-acétone 1339
— et O. Landauer, L'influence du solvant sur la vitesse de réaction. L'hydrolyse acide du formiate, de l'acétate, et du propionate de n-butyle dans le solvant mixte eau-dimétylsulfoxyde 1347
— et C. Mateescu, L'influence du solvant sur la vitesse de réaction. L'hydrolyse alcaline de l'acétate, du propionate et du butyrate de n-butyle dans le solvant mixte eau-acétone 95
— et C. Mateescu, L'influence du solvant sur la vitesse de réaction. L'hydrolyse alcaline de l'acétate du propionate et du butyrate de n-butyle dans le solvant mixte eau-tétrahydrofuranne 1353
Crețu Șt. , voir Iovu M.. 1417
Crivei L., voir Pascu N.. 505
Crusos A. et C. Uglea, I. Agherghinei, Étude de la polydispersité du polychlorure de vinyle par chromatographie sur gel perméable pendant la destruction mécano-chimique . . 565
Csomontanyi G., voir Coriciuc C.. . 533
— et A. Panovici, Étude de la déshydratation du méthylphénylcarbinol sur diverses masses de contact. 525
Cuiban Fl., Reductive cyclization of α-and β-(o-nitrophenyl)-substituted amides 897

D

Dantzer P., voir Brenet J. 57
Dărîngă M., voir Simionescu Cr. . 303
Deleanu Th. et I. V. Ionescu, V. Nahorniak, D. A. Isăcescu, Déduction d'une classification des transitions de phase 103
Delimarskii Yu. K. i A. V. Gorodskii, V. A. Bagrii, Issledovanie differentsialnogo soprotivlenia electroda pri bolshikh poliarizatsiyakh 111
Delineshev S., voir Bliznakov G.. . 35
Demetrescu C., Recherches sur la cyclisation des N_1-acyl-N_4-aryl-thiosemicarbazides. II. Nouveaux p-fluorodiphénylsulfonyl-5-aryl-amino- 1, 3, 4-thiadiazoles et 1, 2, 4, -mercaptotriazoles à intérêt thérapeutique. . 1013
— et I. Șaramet, Recherches sur la cyclisation des acyl-aryl-thiosemicarbazides 1, 4-disubstituées. V. Nouveaux N_1-diphénylsulfonyl-N_4-aryl-thiosemicarbazides et 1, 2, 4-mercapto-triazoles à action antivirale 115
Demetrescu I., voir Murgulescu I. G. 595
Diamandescu E., voir Călin C. G. . 1765
Dima M., voir Maxim S. 1437, 1447
Dimonie V., voir Gavăt I. 559
Dinescu R. et M. Cerchez, Formules de calcul du nombre des sous-systèmes contenus dans les systèmes chimiques binaires, ternaires et quaternaires 643
— , voir Solacolu Ș. 311
Dollingher L., voir Baltă P. . . . 25
Donescu D., voir Gavăt I. 559

Doss S. H., More proofs for a characteristic band in the infrared spectrum of sultams 1611
— , The proton magnetic resonance spectra of sultams 905
Drăgan D., voir Carpov A. 1923
Drăgan S., voir Maxim S. 1437, 1447

Drăgănescu A. and I. Bică, S. Şerban, A. M. Pavlovschi, Gas chromatographic separation of hydrogen, methane, hydrogen sulphide and carbon disulphide mixtures . . . 1779
Drăgulescu C. and A. Nimară, I. Julean, Contributions to the bismuth hydrolysis study. II. Spectrophotometric and polarographic investigations on bismuthyl perchlorate hydrolysis. 1181
— , voir Policec S. 231
— und P. Tribunescu, O. Grecu, Lösungsgleichgewicht von MgO aus Serpentinen durch Einwirkung von CO_2 und Wasser 1517
Drimuş I. et A. Lupu, Oxydation du *n*-dodécane en phase liquide par l'oxygène moléculaire en présence des catalyseurs métalliques pseudo-homogènes. I. L'effet des naphténates des métaux alcalins et alcalino-terreux 1409
Druţă I., voir Zugrăvescu I.. 397
Duca Al. et C. Calu, Méthodes de détermination du rhénium dans les molybdénites. La détermination polarographique du rhénium à côté des traces de molybdène 131
Dulămiţă L., voir Pop A. 1917
Dumitrescu S., voir Simionescu Cr. 303, 547

E

Emschwiller G., Sur la production de tétracyanoferrates 131
Erdey-Grúz T. und E. Kugler, I. Nagy-Czakó, K. Balthazár-Vass, Überführungszahlen und Temperaturkoeffizienten der Leitfähigkeit einiger Elektrolyte in Gemischen von Dioxan mit Wasser 137

F

Fărcăşan V., voir Oprean I.. 1901
Fătu D., voir Pannetier G. 225, 1805

Feldman D., voir Nuţă V. 1755
— , voir Simionescu N. 2013
— et C. V. Uglea, V. Nuţă, M. Popa, Caractérisation du polychlorure de vinyle. Relation viscosité intrinsèque — poids moléculaire . . 1033
Fellner P., voir Grĭotheĭm K. . . . 819
Ferando M., voir Ionescu M.. . . . 179
Ferloni P. and C. Telea, P. Franzosini, M. Rolla, Demixing phenomena in methyl formate + paraffinic or olefinic hydrocarbon binary mixtures 145
Fernea M., voir Hamburg E. 1845
Fink P., voir Popescu A. 511
Florea I., Spectrophotometrical determination of *ortho*-tolidine with sodium hypochlorite 1783
— , Spektrophotometrische Dosierung des Benzidins mit Natriumhypochlorit und mit Unterchloriger Säure 915
—, Über das 2-Äthoxy-6,9-Diaminoakridin-Molybdatophosphat . . 1457
Florianovici G. M., voir Kolotyrkin Ya. M. 161
Franzosini P., voir Ferloni P. . . . 145
Frumkin A. N. i E. V. Stenina, N. V. Nikolaeva-Fedorovich, G. N. Petukhova, V. A. Yusupova, Polarographic maxima of the third kind. II. Borneol 155

G

Găgescu D., voir Zuca Şt. 1497
Galasiu I., voir Sternberg S. . . . 1689, 1697

Gălăţeanu-Titieni M., voir Mánok F. 675
Gănescu I., voir Zsakó J. 1977
Gavăt I. et V. Dimonie, D. Donescu, M. Munteanu, I. Isăcescu, Polymérisation rapide de l'ε-caprolactame en présence de composés organo-métalliques 559
Georgescu N., voir Vîlcu R. . . . 1669, 1791

Ghirvu C. I., On the electronic structure of *o*-, *m*-, and *p*-chloronitrobenzene 1951
Glatz A. M. and A. C. Răzuş, F. Badea, C. D. Nenitzescu, Aluminiumchloride catalyzed condensation of 1,2-dichloro-cyclohexanes with benzene. Isomerisation of diphenyl-cyclohexanes 1735
Gocan S., voir Liteanu C. 497
— and C. Liteanu, Some considerations about the resolution by paper and thin layer chromatography with temperature gradient 661
— , and C. Liteanu, T. Hodişan, H. Naşcu, Şt. Bîndeanu, Temperature gradient chromatography as compared to unidimensional multiple chromatography 669

Goia I., voir Panea I. 1423
Görbe I., voir Nagy P.. 1115
Gorodskii A. V., voir Delimarskii Yu. K. 111
Grecu O., voir Drăgulescu C. . . . 1523
Grecu R., voir Hamburg R. 1845
Grjotheim K., voir Bratland D. . . 41
— , I. K. Matiasovskii, P. Fellner, Poluchenie splavov cremniya posredstovom elektroliza krilolito-kremtsezemtsogo rasplava 819
Gros I., voir Nanu I. 2033
Groth W., voir Comșa G.. 77
Grovu M., voir Simionescu Cr. . . 303, 547
Guion J., voir Brenet J.. 57
Guțul M., voir Mandravel C. . . . 1841

H

Hamburg E. und R. Grecu, M. Fernea, Kraftkonstantenberechnung an der Aminogruppe des Anilins. 1845
Herdlicka C., voir Sternberg S. . . 343
Herția D. I. and Ivanov Al., About the exact development of atomic and molecular wave functions . . 621
Hessett B. and P. G. Perkins, The reorganisation energy of $TiCl_4$. . . 611
Hibaum G., voir Krugliak Yu. A. . 781
Hodișan T., voir Gocan S. 669
— , voir Liteanu C.. . . 497, 1985

I

Ioan S., voir Simionescu Cr. 2003
Ionescu I. V., voir Deleanu Th.. . . 103
Ionescu M., voir Alevra V. . . . 1163, 1379
Ionescu M. and M. Ivănescu, M. Ferando, Chemical changes in cereals by shrivelling 179
Ionescu M., voir Makkay C. 1005
— , voir Panea I.. 1423
Ionescu S. G., voir Murgulescu I. G. 423
Iovu M., Aromatic bis-ethers. III. Condensation of sodium dimethylphenoxides with dichloromethylated derivatives 1261
—and N. Miclovici, Șt. Crețu, Aromatic bis-ethers. IV. Condensation of sodium cyclohexylphenoxides with dichloromethylated derivatives 1417
Isăcescu D. A., voir Deleanu Th.. . 103
Isăcescu I., voir Gavăt I. 559
Ivănescu M., voir Ionescu M. . . . 179
Ivanov Al., voir Herția D. I. . . . 621
— , voir Sahini V. Em. 617

J

Janachkova I. und M. Staewski, Derivatographische untersuchung eines Dreikomponenten-Oxydsystems $MnO_2-CO_2O_3-Ni_2O_3$ 1375
Jantz G. J. and K. Balasubrahmanyam, Some applications of laser Raman spectroscopy in fused salt studies 187
Jindal H. L. and N. P. Bansal, K. Bansal, A. C. Chronopotentiometry : a theoretical study of an irreversible electrode process preceded by a chemical reaction. . . 1969
Jinescu G., voir Bratu Em. 49
Jitaru I., voir Brezeanu M. 1857
Julean I., voir Drăgulescu C. . . . 1181

K

Kalló D., voir Beyer H.. 29
Kerek F. and G. Ostrogovich, NMR and UV spectral studies of some 1-aryl - substituted - 3 - methyl - 2 - phospholene-oxides 1381
Khan I. A., voir Arshad A. Beg M. 1579, 1599
Kiss E., voir Pascu N., ... 505
Kolotîrkin, Ya. M. i G. M. Florianovici, G. S. Raskin, Vliyanie sostąva rastovara na kinetiku rastvoreniya khroma v kislykh sredakh pri katodnoi poliyarizatsii 161
Kondratiev V. N., On the mechanism of the nitrogen atom reaction with ethylene 167
Koryta J. and M. Březina, N. Kříž, Electrode processes of hydrogen peroxide on platinum electrode in alkaline and acid medium 171
Krause A., Über zwei verschiedene katalytische Hydrierungs-reaktionen des Naphthols und deren Mechanismen 539
— , Mechanismus der katalytischen Bildung von langkettigen Kohlenwasserstoffen und oxidischen organischen Nebenprodukten aus CO und H_2. 543
Kříž N., voir Koryta J. 171
Krugliak Yu. A. i G. Hibaum, N. E. Radomyselskaia, Elektronnaia struktura osnovnogo sostoiania benzilnogo radikala v ravnoveskoi konfiguratsii 781

Kudesia V. P., Kinetics and mechanism of bromination of crotonic acid by aqueous bromine 841

Kugler E., voir Erdey-Grúz T., . . 137

Kulkarni V. H., voir Biradar N. S. 481

L

Landauer O., voir Costeanu G.. . . 1331, 1339, 1347

Leancă M., voir Simionescu Cr.. . . 303

Lepădatu G. I., An MO approach to the stabilization problem of the coordination clusters 863

— , voir Spacu P. 335

Leroy J. M. et G. Tridot, Applications de la microanalyse par sonde électronique à la catalyse hétérogène . . 519

Liteanu C. und A. Blasek-Bodó, Die Verwendung des Salz-effektes in nicht wäßrigen Lösungen bei acidobasischen Titrationen. II. Studium über das analytische Verhalten einiger Dicarbonsäuren und Hydroxysäuren in methanolischen Lösungen in Gegenwart von $Ca(NO_3)_2$ . . . 1465

— , voir Blazsek-Bodó A. . . . 1771

— , voir Gocan. S. 661, 669

— and S. Gocan, T. Hodişan, H. Naşcu, C. Măruţoiu, The influence of the temperature gradient on the form of the elution curves and of the height of the theoretical plate in column chromatography with ion exchangers 497

— and T. Hodişan, Thin layer thermochromatography. V. Influence of the temperature gradient on the resolution of some amino-acids in thin layer chromatography. . . . 1985

— , voir Popescu I. C. 1629

— and I. C. Popescu, H. Naşcu, On the possibility of using Ag_2S ceramic-membrane electrode for the determination of the concentration of solutions in flow conditions. Chromatographic detector 1615

Lupeş M. E., *para*-Intramolecular aromatic rearrangements. II. The mechanism of the N-alkylanilines rearrangement 1909

— , The mechanism of the benzidine rearrangement. 1253

Lupu A., voir Drimuş I. 1409

Lupu D., voir Micu-Semeniuc R. . . 993

M

Macarovici Const. Gh., voir Micu-Semeniuc R. 981, 993

— , voir Morar Gh. 1061

— et Gh. Morar, Étude de la cinétique de la réaction $Bi_2O_3 + TiO_2$ avec formation de $Bi_4Ti_3O_{12}$ . . . 1051

— et Gh. Morar, L'obtention de combinaisons complexes mixtes de Ti(IV) et Bi(III) avec les acides oxalique et tartrique pour leur conversion aux oxydes mixtes correspondants 847

Makkay C. and F. Makkay, M. Ionescu, Polarographic behaviour of some cyclohexanone derivatives. . 1005

Makkay F., voir Makkay C. 1005

— , voir Zsakó J.. 1071

Malinovský M., voir Matiašovský K. 801

— , voir Paučirová M. 809

Mandravel C. und M. Guţul, Die Verwendung der Oberflächeneigenschaften für die Charakterisierung der Assoziation des Pyrols in flussigem Zustand 1811

Mandric Gh. and V. Ţăranu, Synthesis of polyurethane elastomers, starting materials and intermediates. XI. Synthesis of nitrodiisocyanates . . . 571

Mánok F. und CS. Várhelyi, M. Gălăţeanu-Tiţieni, Polarographische Untersuchung des UO_2^{2+}-Oxalsüre-Systems 675

Marchidan D. I., voir Ciopec M. 1139, 1313

— and M. Ciopec, High temperature enthalpy and related thermodynamic functions of non-stoichiometric uranium oxides 1657

— and S. Matei, Thermodynamic data for some non-stoichiometric uranium oxides by solid-state EMF technique 195

— and S. Matei, Thermodynamic data for some uranium oxides with nonstoichiometric compositions . . . 1187

— and L. Pandele, Thermal properties of Alurom aluminium heat content at high temperatures . . 1327

— and L. Pandele, A. Nicolescu, Thermal properties of alumina TA 600. Heat content at high temperature 1493

— and L. Vassu, The heats of melting in the binary mixtures : $AgCl + AgBr$ and $AgNO_3 + NaNO_3$. . 1649

Marcu Gh. und V. Săcelean, Indirekte Bestimmungen mit Hilfe der β^--Rückstrahlung. IV. Die Bestimmung von K^+ und NH_4^+ mit $Na_2Pb[Me^{II}(NO_2)_6]$ 489

— und V. Săcelean, Indirekte Bestimmung von K^+ und NH_4^+ durch die β^--Strahlen Absorption . 705

— und CS. Várhelyi, I. Müller, Neue Kobalt (III)-Chelate mit einem vierzähnigen Komplexbildner . . . 711

Markov B. F., Calcul des énergies d'excès intégrales libres des systèmes ternaires de sels fondus sur la base des systèmes binaires. . . . 203
Martin M. y R. Carbó, Derivados del miracil-D ; Relacion actividad carcinoestatica-estructura electronica localizada 1963
Măruţoiu C., voir Liteanu C. 497
Marx Fr., voir Nuţiu M.. 1551
Mateescu C., voir Costeanu G. . 95, 1353
Matei S., voir Marchidan D. I . 195, 1487
Matiašovský K., voir Grĭotheĭm K. 819
— , voir Paučĭrová M. 809
— and M. Paučírová , M. Malinovský, Contribution to the study of the structure and the thermodynamic properties of molten compounds of the type M_3AlF_6. I. Structure 801
Mavrodin M., Nouveaux réactifs pour le dosage spectrophotométrique de l'uranium 1199
Mavrodin-Tărăbîc M., voir Radovici O. 1153
Maxim S. and Ig. Poinescu, S. Drăgan, M. Dima, Chloromethylation of ternary macroporous copolymers . . 1437
— and Ig. Poinescu, S. Drăgan, M. Dima, Synthesis of anion exchangers based on macroporous ternary copolymers. 1447
McAloon B. J. and P. G. Perkins, Semi-empirical LCAOMO theory for infinite systems : tight-binding selfconsistent field theory for three-dimensional solids 1813
Miclovici N., voir Iovu M.. 1417
Micu-Semeniuc R. et Const. Gh. Macarovici, Combinaisons complexes avec dérivés biphényliques. XXVI. Cyanates métalliques simples et complexes avec dérivés diaminobiphényliques 981
— et Const. Gh. Macarovici, D. Lupu, Combinaisons complexes avec dérivés diaminobiphényliques. XXVII. Cyanates complexes du Cu(II) 993
Mihail R., External catalytic reactions on bluff surfaces 683
Mirabel P., voir Brenet J.. 57
Moldoveanu I., voir Topor L. . . . 1705
Morar Gh., voir Macarovici Const. Gh. 847
— , voir Macarovici Const. Gh. . 1051
— et Const. Gh. Macarovici, Le dosage complexométrique du mélange bismuth-titane 1061
Moraru M. and F. Chiraleu, Spectra-stereochemistry correlations for bicyclic rigid arylidenecyclohexanones 1235
Müller I., voir Marcu Gh. 711
Munteanu M., voir Gavăt I. 559
Murgulescu I. G. and M. Bozeşanu, Kinetics of the slow oxidation reaction of methane in dynamic system 1637
— and I. Demetrescu, Kinetics of reactions of benzhydryl chloride and benzyl bromide with secondary alcohols 595
— and T. Oncescu, S. G. Ionescu, On the photolysis of $[Mn(C_2O_4)_2(H_2O)_2]K$ in dimethylformamide. I. 423
— and L. Popescu, Thermodynamic properties from electromotive force measurements with formation cells in molten salts. AgBr+CsBr mixture 1287
— and E. Sălăgeanu, Some physico-chemical properties of simple molten salts. III. 603
— and M. Şerban, On the viscosity of molten metals 431

N

Nagy P. and I. Görbe, A. Szurkos, The polarographic reduction of methyl-substituted N-ethyl pyridinium ions. A HMO treatment . . 1115
Nagy-Czakó I., voir Erdey-Grúz T. 137
Nahorniak V., voir Deleanu Th.. . . 103
Nalbandian A. B., O nekotorykh rezultatakh issledovaniya reactsii okisleniya metana, initsiirovanogo azotnoi kislotoi 209
Nanu I. and C. Andrei, Copolymers of conjugated dienes with maleic acid monoesters. V. Copolymerization of isoprene with monocyclohexylmaleate and monobenzylmaleate 741
— and C. Andrei, Copolymers of conjugated dienes with maleic acid monoesters. VI. Constants Q and e in the copolymerization of isoprene with maleic acid monoesters . . . 1013
— und I. Gros, Untersuchungen von Styrol-*o*-Methylstyrol-Divinylbenzol-Copolymeren und Kationenaustauschern durch Thermoanalyse 2033
Naşcu H., voir Gocan S. 669
— , voir Liteanu C.. . . . . . . 497, 1621
Neamţiu Fl., voir Bacaloglu R. . . 747
Negoiţă N., voir Balaban A. T. . . 1227
Negoiu D. and Z. Toma, The determination of osmium as $[Os(thio)_6][Cr(NH_3)_2(NCS)_4]_3$ 1083

Nenitzescu C. D., voir Banciu M.. . . 1393

— , voir Glatz A.-M. 1735

Nicolau C., Méthode microbiologique de détermination quantitative de l'acide *para*-aminobenzoïque, vitamine H_1 755

Nicolau C, Short-lived free radicals in aqueous solutions of purines . . . 411

Nicolescu A., voir Marchidan D. I. 1493

Nicolaeva-Fedorovich N. V., voir Frumkin A. N. 155

Nimară A., voir Drăgulescu C. . . . 1181

Nuţă V., voir Feldman D. 1033

— and D. Feldman, Cr. I. Simionescu, Photocopolymerization of acrylonitrile with methacrylic esters in the presence of anthraquinone dyes 1755

Nuţiu M. and Fr. Marx, G. Ostrogovich, Studies of the biuret reaction. VII. Crystalline structure of the natrium-copper(II)-tetracyanurate hexahydrate and of its two anhydrous states 1545

— , voir Simon Z.. 573

Oancea D. and C. Podină, The kinetics of the isotopic exchange reactions between sodium iodide and benzyl iodide in hydroxylic solvents . . . 1937

Oancea S., voir Armeanu V. 925

Odochian L. and I. A. Schneider, Some aspects of methane cracking kinetics in static conditions. III. The influence of the coal deposit . . . 441

Olteanu M. and M. Stan, Conductometric study of some mercuric complexes 1525

Olteanu M., voir Zuca Şt. 1497

Onaca I., voir Radovici O. 1153

Oncescu T., and M. Contineanu, G. Bălăceanu, Kinetics and mechanisms of the thermal decomposition of diphenyldiazomethane in the absence of solvent. I. 213

— , voir Murgulescu I. G. . . . 423

Oprean I. and V. Fărcăşan, F. Paiu, Derivatives of furan. XI. Electron impact fragmentation of some 5-substituted 2-(2'-benzothiazolyl)-furans 1901

Ostrogovich G., voir Bacaloglu R. . 747

— , voir Kerek F. 1881

— , voir Nuţiu M. 1551

— , voir Safta M. 2055

— and M. Safta, Studies in the s-triazine field (new series). V. Phenyl substituted 1,3-dimethyl-6-(β-styryl)-formoguanamide (-1H 3H-s-triazin-2,4-dione) and the corresponing *p*-dimethylamino-β-styryl hemicyanine : 1, 3, 5-trimethyl-6- (*p*-dimethylamino-β-styryl)-formoguanamidium iodide 2013

— , voir Simon Z.. 573

P

Paiu F., voir Oprean I. 1901

Palchetti M., voir Campanella L. . 647

Pandele L., voir Marchidan D. I. 1327, 1493

Panea I. and I. Goia, M. Ionescu, Acridone. XLI. The proton magnetic resonance spectrum of thioacridone 1423

Pannetier G. et D. Fătu, Contribution à l'étude de la décomposition thermique du coprécipité de carbonate d'argent et de cadmium. . . 1805

— et D. Fătu, Étude de la morphologie des produits de la décomposition thermique du coprécipité : $Ag_2CO_3-CdCO_3$ 225

Panovici A., voir Csomontanyi G. . 525

Pascu N. und V. Săcelean, L. Crivei, E. Kiss, N. Bojan, Studium des Verhaltens von Fe^{3+}, Co^{2+} und Ni^{2+} auf dem Kationenaustauscher Vionit CS—3 im Medium von organischem Lösungsmittel—HCl—H_2O 505

Paučírová M. and M. Malinovský, K. Matiašovský, Contribution to the study of the structure and the thermodynamic properties of molten compounds of the type M_3AlF_6. II. Thermodynamic properties . . 809

— , voir Matiašovský K. 801

Pavlovschi A. M., voir Drăgănescu A. 1779

Pelloni-Tamaş V. and N. Rădulescu, R. Simionovici, The solvent effect on UV spectra of some aminopyridine derivatives 931

Perişanu St., voir Vîlcu R. 447

Perkins P. G., The electronic structure of some molecules and ions containing carbon, silicon, oxygen and sulphur. I. 773

— , voir Hessett B. 611

— , voir McAloon B. J. 1813

Petrariu I., voir Carpov A. 1923

Petrescu V., voir Sternberg S. . . 1689

Petrovanu M., voir Zugrăvescu I. . . 397

Petukhova G. N., voir Frumkin A. N. 155

Piontelli R., On some definitions and conventions in electrochemistry . 461

Ploştinaru S., voir Spacu P. . . . 697

Podină C., voir Oancea D. 1937

Poinescu Ig., Transformations chimiques du polychlorure de vinyle. II. Synthèses de polyélectrolytes réticulés avec des groupes sulfoniques à base de polychlorure de vinyle arylé avec des polyalkalylbenzènes 727

— , Transformations chimiques du polychlorure de vinyle. III. Synthèses de polyélectrolytes réticulés avec groupes sulfoniques sur la base du polychlorure de vinyle arylé avec des hydrocarbures aromatiques polynucléaires 1125

— , voir Maxim S. 1437, 1447

Policec S. and T. Simonescu, C. Drăgulescu, Simultaneous spectrophotometric determination of gallium and indium 231

Pop A. and L. Cörmoş, L. Dulămiţă, Decomposition of cumene hydroperoxide on silica gel 1917

Popa L. I. et I. Arsenie, Recherches sur l'obtention du hafnium de pureté nucléaire. I. 937

Popa M., voir Feldman D. 1033

Popa S., voir Coriciuc C. 533

Popescu A. und A. Szabo, P. Fink, IR-Untersuchungen der Adsorption an Mischoxid-Katalysatoren . . . 511

Popescu A., voir Zsakó J., ... 1977

Popescu I., voir Voiculescu N. . . 719

Popescu I. C., voir Liteanu C. . . . 1621

— and C. Liteanu, Characterization of ceramic ion-selective membrane electrodes. II. Redox behaviour of the Ag_2S membrane electrode 1629

Popescu L., voir Murgulescu I. G. . 1287

Popescu-Haş D., voir Solacolu Ş. . . 319

Popescu-Tucsek V., voir Radovici O. 253

Pourbaix M., Signification du potentiel de protection lors de la corrosion par piqures, de la corrosion intergranulaire et de la corrosion fissurante sous tension 239

Prissiajnyi V. and V. Vasilescu, Ultrasonic velocity and reciprocal fused salts systems : Cd, Pb, Cl, Br . . 455

Puri A., voir Teoreanu I. 471

R

Rădoi I., Die Anordnung der Grenzschicht an zylindrischen Elektroden bei erzwungener Konvektion . . 1367

Radomyselskaia I. E., voir Krugliak Yu. A. 781

Radovici C., voir Cismaru D. . . . 69

Radovici O. and N. Bonciocat, V. Popescu-Tucsek, Some kinetic aspects of the anodic oxidation of silicon in ethylene glycol 253

— et M. Mavrodin - Tărăbîc, I. Onaca, I. Solacolu, L'étude de la réduction de l'oxygène sur les électrodes poreuses en argent 1153

Rădulescu N., voir Pelloni-Tamaş V. 931

Raskin G. S., voir Kolotyrkin Ya. M. 161

Răzuş A. C., voir Glatz A.-M. . . 1735

Reichel J. und B. D. Bader, R. Vîlceanu, Neue organische Pigmente-Isatinderivate. I. Einfürhung in die Synthese und Eigenschaften der Verbindungen 1889

Rensvik H., voir Bratland D. . . . 41

Ripan R. und CS. Várhelyi, Über α-Dioximinkomplexe der Übergangsmetalle. XXXV. Kobalt (III)-bis-dimethyl-glyoximin-Chelate mit *cis*-geometrischer Konfiguration . 259

Rolla M., voir Ferloni P. 145

Rossini F. D., Compilations of data for chemical thermodynamics 267

Rusenescu St., voir Armeanu V. . . 925

S

Săcelean V., voir Marcu Gh. . . . 489, 705

— , voir Pascu N. 505

Safta M. and F. Chiraleu, A. T. Balaban, G. Ostrogovich, Quantitative study of active methyl groups in C-methyl s-triazines, I. : Hydrogen exchange kinetics of 6-methyl-s-triazine-2,4 (1H, 3H)-dione and its N-methyl derivatives (Studies in the s-triazine field, New series. VI) 2055

— , voir Ostrogovich G. 2043

Sahini V. Em. and L. Ciurea, Infrared spectra of carbonyl aromatic ion radicals. I. Carbonyl stretching frequency and force constant changes due to the formation of anion radicals from benzophenone, fluorenone, phenanthrenequinone and anthraquinone 273

— and V. Tufoi, Al. Ivanov, Some considerations about the stability of complex combinations of cobalt 617

Sălăgeanu E., voir Murgulescu I. G. 603

Sanesi M., The heats of adsorption of some hydrocarbons on zirconia 285

Şaramet I., voir Demetrescu C. . . 115

Schay G., voir Beyer H. 29

Schneider I. A., Über die dynamische Thermogravimetric bei komplexen Abbauprozessen 291
— , voir Caşcaval C. N. 835
— , voir Odochian L. 441
Schultz P., voir Vîlceanu R. . . . 361
Segal E., Cinétique des réactions superficielles en courant, accompagnées d'une augmentation du nombre des molécules. IV. 633
— , voir Constantinescu M. . . . 83
Şerban Gh., voir Chirulescu T. . . . 1509
Şerban M., voir Murgulescu I. G. . 431
Şerban S., voir Drăgănescu A. . . 1779
Simionescu Cr. et S. Dumitrescu, M. Grovu, Étude sur la polymérisation des dérivés acétyléniques. XII. Cinétique de la photopolymérisation du phénylacétylène . . . 547
— und S. Dumitrescu, M. Leancă, M. Dărîngă, M. Grovu, Studium der Polymerisation von Acetylenderivaten. XV. Die übermolekulare Struktur der Polymere 303
— et S. Ioan, I. Benedek, N. Asandei, Réactions de copolymerisation à l'aide des dérivés organiques du titane-alcolye aluminium. VI. Étude par la diffusion de la lumière des copolymères acrylonitrile-styrolène obtenus à l'aide des catalyseurs homogènes Ziegler-Natta 2003
— , voir Nuţă V. 1755
Simionescu N. and E. M. Călugăru, D. Feldman, Vinyl acetate — acrylic acid copolymers 2013
Simionovici R., voir Pelloni-Tamaş V. 931
Simion Z. and M. Nuţiu, G. Ostrogovich, The study of the biuret reaction. VI. Electronic spin resonance of some copper (II)-complexes with cyanuric acid and succinimide 573
Simionescu T., voir Policec S. . . . 231
Skinner H. A. and Y. Virmani, High-temperature microcalorimetry : the thermal decomposition of $Cr(CO)_6$ and of $Mo(CO)_6$ 467
Sokolova I. D., voir Zuca Şt. . . 1497
Solacolu I., voir Radovici O. . . . 1153
Solacolu Ş. und R. Dinescu, M. Zaharescu, Die thermischen Phasengleichgewichte des Systems $SrO-V_2O_5$ 311
— et D. Popescu-Haş, Coordination de l'ion Al^{3+} dans les structures vitrocéramiques du système $Na_2O-MgO-Al_2O_3-SiO_2$ ayant le fluor comme agent de nucléation . . . 319
— und D. Ţenţulescu, Struktur der gezogenen Glasfasern aus dem System $Na_2O-ZnO-SiO_2$ . . . 1219
— and M. Zaharescu, Phase equilibria of the $CaO-TiO_2-V_2O_3$system 1715
Soria J. and J. Turkevich, Electron paramagnetic resonance study of nitroxides in dioxane water system 329
Spacu P. and L. Antonescu, New molybdenum (V) complexes with biguanide derivatives 1851
— and D. Ciomârtan, M. Teodorescu, Roentgenographic studies of $Fe(II)phen_2\,(NCS)_2$ 977
— and G. D. Cismaru, Behaviour of uranium compounds on heating. Thermal decomposition of ammonium uranates 947
— and G. D. Cismaru, Electrical conductivity of intermetallic compounds of praseodynium-thallium system 1723
— and C. I. Lepădatu, Molecular orbital patterns for *f*-clusters 335
— and S. Ploştinaru, Mixed ligand lanthanide chloromandelates containing *o*-phenanthroline and 5,6-dimethylphenanthroline 697
— , voir Teodorescu M. 1191
Staewski M., voir Janachkova Y. . 1375
Stan M., voir Olteanu M. 1531
Stannett V., voir Vlagiu I. 379
Stenina E. V., voir Frumkin A. N. . 155
Sternberg S., voir Adorian I. . . . 1361
— et I. Galasiu, L'électrode halogène-charbon dans les électrolytes fondus. VII. L'adsorption du brome sur les électrodes de charbon activé 1697
— and C. Herdlicka, Interdiffusion coefficient of the silver ion in molten alkali chlorides by the chronopotentiometric method 343
— and V. Petrescu, I. Galasiu, Chlorine adsorption on active carbon in the molten salts systems : $LiCl-KCl$, $PbCl_2-KCl$, $KCl-NaCl$ 1689
— and M. Terzi, Surface tension of the reciprocal molten salt pairs (Na, Ag, Cl, Br) 1147
Suciu G. C., Notes on pyrolysis . . 353
Szabo A., voir Popescu A. 511
Szurkos A., voir Nagy P. 1115

T

Ţăranu V., voir Mandric Gh.. . . . 571
Telea C., voir Ferlloni P. 145
Ţenţulescu D., voir Solacolu Ş. . . 1219
Teodorescu Gr., Determination of codeine phosphate. Visible and IR spectra of the compound obtained by the combination with ammonium reineckate 1475
— , Méthodes de détermination de la vitamine B_1 (chlorhydrate de

thiamine ou aneurine). Caractéristiques spectrales en visible et infrarouge du produit obtenu 1621

Teodorescu M. and M. Brezeanu, P. Spacu, Cobalt complexes with 2,9-dimethyl-1,10-phenanthroline . 1191

— , voir Spacu P. 977

Teoreanu I, Considérations générales sur l'apparition des propriétés liantes 1211

— und A. Puri, Studium der Anregung der Hochofenschlacke mit Natronsilikat und Natronfluosilikat 471

Terzi M., voir Sternberg S. 1147

Toma Z., voir Negoiu D. 1083

Topor D. and Al. Bîrhală, Cryolite bath ratio by X-ray diffraction . 961

Topor L., Vapour pressures of molten magnesium, cadmium and zinc chlorides 1503

— and I. Moldoveanu, Molecular association of the gaseous magnesium, cadmium and zinc chlorides 1705

and J. Wypartowicz, Vapour pressures of molten cadmium bromide and cadmium iodide 831

Tribunescu P., voir Drăgulescu C. . 1517

Tridot G., voir Leroy J. M. 519

Tufoi V., voir Sahini V. Em. 617

Turkevich J., voir Soria J. 329

U

Ubbelohde A. R., Ionic melts as model liquids 357

Uglea C. V. et P. Andreescu, Étude comparative des méthodes de calibrage de la chromatographie sur gel perméable 2021

— , voir Crusos A. 565

— , voir Feldman D. 1033

V

Várhelyi Cs., voir Mánok F. . . . 675

— , voir Marcu Gh. 711

— , voir Ripan R. 259

Vasilescu V., voir Prissiajnyi V. . . 455

Vasu G., A double hard core model description of the short-range-order in molten alkali halides. I. Viscosity 1829

Vasu L., voir Marchidan D. I. . . 1649

Vîlcu R. and Z. Cenuşe, Thermodynamic excess functions in liquid-vapour equilibria in the *n*-heptane-toluene system 367

— and A. Ciochină, Measurement of thermal conductivity by the hot-wire method 1679

— and N. Georgescu, The oxidation of organic bibasic acids in mixtures of fused salts. I. The decarboxylation of oxalic acid in molten alkali metal nitrates . . . 1669

— and N. Georgescu, The decomposition of some transitional metal perchlorates in molten state . . 1791

— and Şt. Perişanu, Application of the Allen-Skinner bond energy scheme to aromatic hydrocarbons and to amines 447

Vîlceanu R., voir Bader B. D. . . 1991

— , voir Reichel J. 1889

— und P. Schultz, Kinetische Untersuchung basischer Esterverseifungen in wäßriger Lösung mit einem pH-metrischen Titrationsverfahren. Basische Hydrolyse der Dialkylphosphite in wäßriger Lösung 361

Virmani Y., voir Skinner H. A. . . 467

Vlagiu I. and V. Stannett, Initial studies on the radiation induced grafting of styrene to polyethylene terephthalate fibers 379

Vodnár J., Hydroperoxidation of organic compounds at the liquid/gas interface. III. Hydroperoxidation of phenylcyclohexane with oxygen 581

Voicu M. and F. Badea, Kinetics of solvolytic reactions. II. Acetolysis of 5H-dibenzo [a, d] cycloheptene-5-yl-methyl tosylate under thermodynamic control 1551

— and F. Badea, A. Bucur, Kinetics of solvolytic reactions. III. Intermediates involved in the acetolysis of 5H-dibenzo [a, d] cycloheptene-5-yl-methyl tosylate and 9,10-bis(hydroxymethyl)-9,10-dihydroanthracene ditosylate 1563

Voiculescu N. et I. Popescu, Réactions des ligands coordinés. I. L'action des composés organoaluminiques sur les bisdiméthylglyoximates de nickel, palladium et cuivre et sur la diméthylglyoxime non coordinée 719

Voiculescu V., voir Zsakó J. . . . 1977

W

Warren K. D., Strong field spin-orbit matrices for d^3 configurations in tetragonal symmetry 1293

Wohl A., Prinzipielle Betrachtungen über die Wirksamkeit einiger Reinigungsmethoden durch Adsorption. II. Mathematische Modelle 1267

Woon kie Paik and J. O'M. Bockris, Ellipsometric and reflectance measurements for the determination of optical properties and thickness of a light-absorbing thin film . . . 405

Wypartowicz J., voir Topor L. . . . 831

Yusupova V. A., voir Frumkin A. N. 155

Z

Zaharescu M., voir Solacolu Ș. . . 311

— , voir Solacolu Ș. 1715

Zsakó J. und F. Makkay, Linearisation der potentiometrischen Titrationskurven. I. Fällungstitrationen . . 1071

— and V. Voiculescu, I. Gănescu, A. Popescu, Kinetics and mechanism of substitutions reactions of complexes. XLV. Solvation of the $[Cr(NCS)_4\ (m\text{-xylidine})_2]^-$ ion in ethanol-water mixtures. 1977

Zuca Șt. and M. Constantinescu, The self-diffusion coefficients in some molten nitrates 385

— and I. D. Sokolova, D. Găgescu, M. Olteanu, Density and electrical conductivity of melted metaphosphates 1497

Zugrăvescu I. et M. Petrovanu, M. Caproșu, I. Druță, Sur le méthyl-1-phtalazinium-carbéthoxyméthylure. III. 397

INDEX DES SUJETS

A

A. C. Chronopotentiometry : a theoretical study of an irreversible electrode process preceded by a chemical reaction, H. L. Jindal, N. P. Bansal and K. Bansal 1969

Acridone. XLI. The proton magnetic resonance spectrum of thioacridone, I. Panea, I. Goia and M. Ionescu 1423

Alumina. I. Aluminium hydroxides, Influence of the preparation method on the structure and physical properties of —, V. Alevra, D. Ciomârtan and M. Ionescu. 1163

Alumina. II. Aluminium oxides, Influence of the preparation method on the structure and physical properties of —, V. Alevra, D. Ciomârtan and M. Ionescu. 1379

Aluminiumchloride catalyzed condensation of 1,2-dichlorocyclohexanes with benzene. Isomerisation of diphenyl-cyclohexanes, A. M. Glatz, A. C. Răzuș, F. Badea and C. D. Nenitzescu 1835

Aminopyridine derivatives, The solvent effect on UV spectra of some -, V. Pelloni-Tamaș, N. Rădulescu and R. Simionovici 931

Anodic oxidation of silicon in ethylene glycol, Some kinetic aspects of the-, O. Radovici, N. Bonciocat and V. Popescu-Tucsek 253

Anregung der Hochofenschlake mit Natronsilikat und Natronfluosilikat, Studium der —, I. Teoreanu und A. Puri 471

Aromatic bis-ethers. III. Condensation of sodium dimethylphenoxides with dichloromethylated derivatives, M. Iovu 1261

Aromatic bis-ethers. IV. Condensation of sodium cyclohexylphenoxides with dichloromethylated derivatives, M. Iovu, N. Miclovici and S. Crețu 1417

Aromatic rearrangements. II. The mechanism of the N-alkylanilines rearrangement, *para*-Intramolecular —, M. E. Lupeș 1909

1-Aryl-substituted-3-methyl-2-phospholene-oxides, NMR and UV spectral studies of some —, F. Kerek and G. Ostrogovich 1881

Assoziation des Pyrols in flüssigem Zustand, Die Verwendung der Oberflächeneigenschaften für die Charakterisierung der —, C. Mandravel und M. Guțul 1841

2-Äthoxy-6,9-Diaminoakridin-Molybdatophosphat, Über das —, I. Florea 1457

Atomic and molecular wave functions, About the exact development of —, D. I. Herția and Al. Ivanov. . . 621

B

Benzhydryl chloride and benzyl bromide with secondary alcohols, I. G. Murgulescu and I. Demetrescu . 595

Benzidine rearrangement, The mechanism of the —, M. E. Lupeş. . . 1253

Binary mixtures : AgCl + AgBr and $AgNO_3$ + $NaNO_3$, The heats of melting in the —, D. I. Marchidan and L. Vasu 1649

Binding energy of small clusters of atoms, On the —, G. Bliznakov and S. Delineshev 35

Bis-(theonyl-trifluoroacetonato)-beryllium, A. Barabás 1997

Bismuth hydrolysis study. II. Spectrophotometric and polarographic investigations on bismuthyl perchlorate hydrolysis, Contributions to the —, C. Drăgulescu, A. Nimară and I. Julean 1181

Bismuth-titane, Le dosage complexométrique du mélange —, Gh. Morar et Const. Gh. Macarovici 1061

Biuret reaction. VI. Electronic spin resonance of some copper (II) — complexes with cyanuric acid and succinimide, The study of the —, Z. Simon, M. Nuţiu and G. Ostrogovici 573

Biuret reaction. VII. Crystalline structure of the natrium-copper (II)-tetracyanurate hexahydrate and of its two anhydrous states, M. Nuţiu, Fr. Marx and G. Ostrogovich. . 1545

Bond energy scheme to aromatic hydrocarbons and to amines, Application of the Allen-Skinner —, R. Vîlcu and Şt. Perişanu . . . 447

Bromination of crotonic acid by aqueous bromine, Kinetics and mechanism of —, V. P. Kudesia 841

C

C-methyl s-triazines. I : Hydrogen exchange kinetics of 6-methyl-s-triazine-2,4 (1H, 3H)-dione and its N-methyl derivatives (Studies in the s-triazine field, New series. VI), Quantitative study of active methyl groups in —, M. Safta, F. Chiraleu, A. T. Balaban and G. Ostrogovich 2055

Chemical changes in cereals by shrivelling, M. Ionescu, M. Ivănescu and M. Ferando 179

Chemical graphs. XIV. Valence isomers of [12] annulene, A. T. Balaban 865

Chemical graphs. XV. Degenerate Cope rearrangements of valence isomers of annulenes, A. T. Balaban . . 883

Chemical graphs. XVII. (Aromaticity. X) *cata*-condensed polycyclic hydrocarbons which fulfill the Hückel rule but lack closed electronic shells, A. T. Balaban 1531

Chromatographic detector, On the possibility of using Ag_2S ceramic-membrane electrode for the determination of the concentration of solutions in flow conditions, C. Liteanu, I. C. Popescu and H. Naşcu. . . 1615

Chromatographie sur gel perméable, Étude comparative des méthodes de calibrage de la —, C. V. Uglea et P. Andreescu 2021

Cinétique de la réaction $Bi_2O_3 + TiO_2$ avec formation de $Bi_4Ti_3O_{12}$, Étude de la—, Const. Gh. Macarovici et Gh. Morar 1051

Cinétique des réactions superficielles en courant, accompagnées d'une augmentation du nombre des molécules. IV., E. Segal 633

Cobalt complexes with 2,9-dimethyl-1,10-phenanthroline, M. Teodorescu, M. Brezeanu and P. Spacu 1191

Codeine phosphate. Visible and IR spectra of the compound obtained by the combination with ammonium reineckate, Determination of —, Gr. Teodorescu 1475

Colorant azoïque benzothiazolique à l'aide de l'analyse thermique différentielle. Etude de la réaction d'alkylation du —, E. Baltă. 1241

Column chromatography with ion exchanger, The influence of the temperature gradient on the form of the elution curves and of the height of the theoretical plate in —, C. Liteanu, S. Gocan, T. Hodişan, H. Naşcu and C. Măruţoiu. 497

Combinaisons complexes avec dérivés biphényliques. XXVI. Cyanates métalliques simples et complexes avec dérivés diaminobiphényliques, R. Micu-Semeniuc et Const. Gh. Macarovici 981

Combinaisons complexes avec dérivés diaminobiphényliques. XXVII. Cyanates complexes du Cu(II), R. Micu-Semeniuc, Const. Gh. Macarovici et D. Lupu 993

Combinaisons complexes mixtes des Ti(IV) et 2i(III) avec les acides oxalique et tartrique pour leur conversion aux oxydes mixtes corres-

pondants, L'obtention de —, Const. Gh. Macarovici et Gh. Morar 847

Complex combinations of cobalt, Some considerations about the stability of —, V. Em. Sahini, V. Tufoi and Al. Ivanov 617

COMPTES RENDUS, 589, 590, 765, 1281, 1283, 1483

Coordination clusters, An MO approach to the stabilization problem of the —, C. I. Lepădatu 863

Coordination compounds with copper-tin bonds, M. Brezeanu and I. Jitaru 1857

Copolymères macroporeux styrène-divinyl-benzène chlorométhylés avec la diméthyle-2-hydroxy-éthyle amine, Sur l'amination des —, A. Carpov, D. Drăgan et I. Petrariu 1923

Copolymérisation à l'aide des dérivés organiques du titane-alcoyle aluminium. VI. Étude par la diffusion de la lumière de copolymères acrylonitrile-styrolène obtenus à l'aide des catalyseurs homogènes Ziegler-Natta, Reactions de —, Cr. I. Simionescu, S. Ioan, I. Bendek et N. Asandei 2003

Copolymers, Chloromethylation of ternary macroporous —, S. Maxim, Ig. Poinescu, S. Drăgan and — M. Dima 1437

Copolymers of conjugated dienes with maleic acid monoesters. V. Copolymerization of isoprene with monocyclohexylmaleate and monobenzylmaleate, I. Nanu and C. Andrei 741

Copolymers of conjugated dienes with maleic acid monoesters. VI. Constants Q and e in the copolymerization of isoprene with maleic acid monoesters, I. Nanu and C. Andrei 1043

Copolymers, Syntheses of anion exchangers based on macroporous ternary —, S. Maxim, Ig. Poinescu, S. Drăgan and M. Dima 1447

Cryolite bath ratio by X-ray diffraction, D. Topor and A. Bîrhală 961

Cumene hydroperoxide on silica gel, Decomposition of —, A. Pop, L. Cormoş and L. Dulămiţă 1917

Cyclisation des acyl-aryl-thiosemicarbazides 1,4-disubstituées. V. Nouveaux N_1-diphénylsulfonyl-N_4-arylthiosemicarbazides et 1, 2, 4-mercapto-triazoles à action antivirale, Recherches sur la —, C. Demetrescu et I. Şarameţ 115

Cyclisation des N_1-acyl-N_4-aryl-thiosemicarbazides. II. Nouveaux *p*-fluorodiphényl-sulfonyl-5-arylamino-1, 3, 4-thiadiazoles et 1, 2, 4-mercaptotriazoles à intérêt thérapeutique, Recherches sur la —, C. Demetrescu 1013

Cyclohexanone derivatives, Polarographic behaviour of some —, C. Makkay, F. Makkay and M. Ionescu 1005

Décomposition thermique du coprécipité : $Ag_2CO_3-CdCO_3$, Étude de la morphologie des produits de la —, G. Pannetier et D. Fătu 225

Décomposition thermique du coprécipité de carbonate d'argent et de cadmium, Contribution à l'étude de la —, G. Pannetier et D. Fătu 1805

Demixing phenomena in methyl formate + paraffinic or olefinic hydrocarbon binary mixtures. P. Ferloni, C. Telea, P. Franzosini and M. Rolla 145

Déshydratation du méthylphénylcarbinol sur diverses masses de contact, Étude de la —, G. Csomontanyi et A. Panovici 525

Dicyanoaurate (I) ion with paranitral green, Spectrophotometric determination of —, C. G. Călin, E. Diamandescu and L. M. Băloiu 1765

Diffusion-conductivité dans les solutions d'électrolytes et applications structurales, Relation —, M. Chemla 63

α-Dioximinkomplexe der Übergangsmetalle. XXXV. Kobalt (III)-bis-dimethylglyoximin-Chelate mit *cis*-geometrischen Konfiguration, Über —, R. Ripan und Cs. Várhelyi 259

Dreikomponenten-Oxydstems MnO_2-CO_2O_3-Ni_2O_3, Derivatographische Untersuchung eines — I. Janachkova und M. Staevski 1375

E

Electrochemical behaviour of isonicotinic acid in aqueous solution, L. Campanella and D. De Angelis 1087

Electrochemistry, On some definitions and convections in —, R. Piontelli 461

Électrode halogène-charbone dans les électrolytes fondus. VII. L'adsorption du brome sur les électrodes de charbon activé, L'—, S. Sternberg et I. Galasiu 1697

Electrolytic deposition of Y-Al and Y-Mg alloys, Some introductory investigations on —, D. Bratland, G. H. Bøe, K. Grjotheim, H. Rensvik and E. Aamland 41

Electron paramagnetic resonance study of nitroxides in dioxane water system, J. Soria and J. Turkevich 329

Electronic structure of *o*-, *m*-, and *p*-chloronitrobenzene, C. I. Ghirvu 1951
Electronic structure of some molecules and ions containing carbon, silicon, oxygen and sulphur. I., P. G. Perkins 773
Elektroden bei erzwungener Konvektion, Die Anordnung der Grenzschicht an zylindrischen —, I. Rădoi 1367
Elektronaia struktura osnovnogo sostoiania benzilnogo radikala v ravnovesnoi konfigurasii, Yu. A. Krugliak, G. Hibaum i N. E. Radomyselskaia 781
Énergies d'excès intégrales libres des systèmes ternaires de sels fondus sur la base des systèmes binaires, Calcul des —, B. F. Markov. . . 203
Esterverseifungen in wässriger Lösung mit einem pH-metrischen Titrationoverfahren. Basische Hydrolyse der Dialkylposphite in wässriger Lösung, Kinetische Untersuchung basicher —, R. Vîlceanu und P. Schulz 361
External catalytic reactions on bluff surfaces, R. Mihail. 683

F

Free radicals. VII. Arenesulphonyl-phenyl-nitroxides and 1-arenesulphonyl-2,2-diphenyl-hydrazyls, Factor affecting stability and equilibria of —, A. T- Balaban and N. Negoiţă 1227
Furan. XI. Electron impact fragmentation of some 5-substituted 2-(2'-benzothiazolyl)-furans, Derivatives of —, I. Oprean, V. Fărcăşan and F. Paiu 1901

G

Gallium and indium, Simultaneous spectrophotometric determination of —, S. Policec, T. Simionescu and C. Drăgulescu 231
Gas adsorption on the surface recombination of nitrogen atoms on stainless steel, G. Comşa and W. Groth 77
Gas chromatographic separation of hydrogen methane, hydrogen sulphide and carbon disulphide mixtures, A. Drăgănescu, I. Bică, S. Şerban and A. M. Pavlovschi 1779
Glasfasern aus dem System $Na_2O-ZnO-SiO_2$, Struktur der gezogenen —, Ş. Solacolu und D. Ţenţulescu 1219

H

Hafnium de pureté nucléaire. I., Recherches sur l'obtention du —, L. I. Popa et I. Arsenie 937
Heat transfer in vibrated fluidized layers, Em. A. Bratu and G. I. Jinescu 49
Heats of adsorption of some hydrocarbons on zirconia, The —, M. Sanesi 285
Hydrierungsreaktionen des Naphthols und deren Mechanismen, Über zwei verschiedene katalytische —, A. Krause. 539
Hydrolyse acide du formiate, de l'acétate et du propionate de *n*-butyle dans le solvant mixte eau-acétone, L'influence du solvant sur la vitesse de réaction. L' —, G. Costeanu et O. Landauer 1339
Hydrolyse acide du formiate, de l'acétate et du propionate de *n*-butyle dans le solvant mixte eau-alcool éthylique, l'influence du solvant sur la vitesse de réaction. L' —, G. Costeanu et O. Landauer 1331
Hydrolyse acide du formiate, de l'acétate et du propionate de *n*-butyle dans le solvant mixte eau-diméthylsulfoxyde, L'influence du solvant sur la vitesse de réaction. L' —, G. Costeanu et O. Landauer. . 1347
Hydrolyse alcaline de l'acétate, du propionate et du butyrate de *n*-butyle dans le solvant mixte eau-tétrahydrofuranne, L'influence du solvant sur la vitesse de réaction. L' —, G. Costeanu et C. Mateescu 1353
Hydroperoxidation of organic compounds at the liquid /gas interface/. III. Hydroperoxidation of phenylcyclohexane, with oxygen, I. Vodnár 581
Hyperfine coupling constants from ESR spectra of organic free radicals, Determination of —, A. T. Balaban 9

I

Indirekte Bestimmung von K^+ und NH_4^+ durch die β^--Strahlen Absorption, Gh. Marcu und V. Săcelean 705
Indirekte Bestimmungen mit Hilfe der β^--Rückstrahlung. IV. Die Bestimmung von K^+ und NH_4^+ mit $Na_2Pb[Me^{11}(NO_2)_6]$, Gh. Marcu und V. Săcelean 489
Infrared spectra of amidic derivatives of carbonic acid. VI. Substituted 1,5-benzylidine guanylureas (free

bases and sulphates), R. Bacaloglu, Fl. Neamţiu, I. Bacaloglu and G. Ostrogovich 747

Infrared spectra of carbonyl aromatic ion radicals. I. Carbonyl stretching frequency and force constant changes due to the formation of anion radicals from benzophenone, fluorenone, phenanthrenequinone and anthraquinone, V. Em. Sahini and L. Ciurea 273

Interdiffusion coefficient of the silver ion in molten alkali chlorides by the chronopotentiometric method, S. Sternberg and C. Herdlicka . . 343

Intermetallic compounds of praseodymium-thallium system, Electrical conductivity of —, P. Spacu and G. D. Cismaru 1723

Ion-selective membrane electrodes. II. Redox behaviour of the Ag_2S membrane electrode, I. C. Popescu and C. Liteanu 1629

Ionic melts as model liquids, A. R. Ubbelohde 357

Isotopic exchange reactions between sodium iodide and benzyl iodide in hydroxylic solvents, The kinetics of the —, D. Oancea and C. Podină . . 1937

Issledovanie differentsialnogo soprotivlenia elektroda pri bolshikh polarizatsial, Yu. K. Delimarsckii, A. V. Gorodisckii i V. A. Bagrii . . . 111

K

Katalytischen Krackung von Propan, Zur kinetischen Untersuchung der —, H. Beyer, D. Kalló und G. Schay 29

Katodnoi poliarizatsii, Vlianie sostava rastvora na kinetiky rastvorenia broma v kislikh sredakh pri katodnoi poliarizatsii, Ya. M. Kolotyrkin, G. M. Florianovichi i. G. S. Raskin 161

Kinetic equations for reactions taking place in powders. I. Complete form of the equations for spheric particles, D. Cismaru and C. Radovici. . . 69

Kobalt (III)—Chelate mit einem vierzähnigen Komplexbildner, Neue —, Gh. Marcu, Cs. Várhelyi und I. Müller 711

Kohlenwasserstoffen und oxidischen organischen Nebenprodukten aus CO und H_2, Mechanismus der katalytischen Bildung von langkettigen —, A. Krause 543

Kraftskonstantenberechnung an der Aminogruppe des Anilins, E. Hamburg, R. Grecu und M. Fernea. . 1845

Lanthanides with biguanide derivatives. III. Europium and godolinium compounds with paludrine, Contributions to the study of —, I. Albescu 1729

Lanthanides with biguanidine derivatives. IV. Compounds of holmium and ytterbium with paludrine, Contributions to the study of —, I. Albescu 1867

Ligands coordinés. I. L'action des composés organoaluminiques sur les bisdiméthylglyoximates de nickel, palladium et cuivre et sur la diméthylglyoxime non coordinée, Réactions des —, N. Voiculescu et I. Popescu 719

Light-absorbing thin film, Ellipsometric and reflectance measurements for the determination of optical properties and thickness of a —, Woon kie Paik and J. O'M. Bockris. . . 405

Linearisation des potentiometrischen Titrationskurven. I. Fällungstitrationen, J. Zsakó und F. Makkay . 1071

Lösungsgleichgewicht von MgO aus Serpentinen durch Einwirkung von CO_2 und Wasser, C. Drăgulescu, P. Tribunescu und O. Gogu . . 1517

M

Mélanges binaires de sels fondus à anion commun et comportant des cations polarisables. Évaluations de la nature des interactions ioniques dans les —, J. Brenet, P. Dantzer, P. Mirabel et J. Guion 57

Mercuric complexes, Conductometric study of some —, M. Olteanu and M. Stan 1525

Metaphosphates, Density and electrical conductivity of melted —, Şt. Zuca, I. D. Sokolova, D. Găgescu and M. Olteanu 1497

Methane cracking kinetics in static conditions. III. The influence of the cool deposit, Some aspects of —, L. Odochian and I. A. Schneider 441

Methane in dynamic system, Kinetics of the slow oxidation of —, I. G. Murgulescu and M. Bozeşanu. . 1637

Méthode microbiologique de détermination quantitative de l'acide *para*-aminobenzoïque, vitamine H_1, C. Nicolau 755

Méthyl-1-phtalazinium-carbéthoxyméthylure. III., Sur le —, I. Zugrăvescu, M. Petrovanu, M. Caproşu et I. Druţă 397

Microanalyse par sonde électronique à la catalyse hétérogène, Applications de la —, J.—M. Leroy et G. Tridot 519

Microcalorimetry; the thermal decomposition of $Cr(CO)_6$ and of $Mo(CO)_6$, High temperature —, H. A. Skinner and Y. Virmani 467

Miracil—D; Relacion actividad carcinoestatica-estructura electronica localizada, Derivados del —, M. Martin y R. Carbó 1963

Mischoxid-Katalysatoren, IR-Untersuchungen der Adsorption an —, A. Popescu, A. Szabo und P. Fink 511

Mixed ligand lanthanide chloromandelates containing *o*-phenanthroline and 5,6-dimethylphenanthroline, P. Spacu and S. Ploştinaru . . 697

Molecular association of the gaseous magnesium, cadmium and zinc chlorides, L. Topor and I. Moldoveanu 1705

Molecular orbital patterns for f-clusters, P. Spacu and C. I. Lepădatu 335

Molten alkali halides. I. Viscosity, A double hard core model description of the short-range order in —, G. Vasu 1829

Molten alkali metalnitrates. The oxidation of organic bibasic acids in mixtures of fused salts. I. The decarboxylation of oxalic acid in —, R. Vîlcu and N. Georgescu 1669

Molten cadmium bromide and cadmium iodide, Vapor pressures of —, L. Topor and J. Wypartowicz . . . 831

Molten compounds of the type M_3AlF_6. I. Structure, Contribution of the study of the structure and the thermodynamic properties of —, K. Matiašovský, M. Paučirová and M. Malinovský 801

Molten compounds of the type M_3AlF_6. II. Thermodynamic properties, Contribution to the study of the structure and the thermodynamic properties of —, M. Paučírová, M. Malinovský and K. Matiašovský. . 809

Molten glass, New theoretical data on the structural chemical equilibrium in —, P. Baltă. 969

Molten metals, On the viscosity of —, I. G. Murgulescu and M. Şerban 431

Molten mixtures of potassium chloride with alkaline-earth chloride, Thermodynamic excess functions in —, I. Adorian and S. Sternberg . . 1361

Molten nitrates, The self-diffusion coefficients in some —, Şt. Zuca and M. Constantinescu 385

Molten salt pairs (Na, Ag, Cl, Br), Surface tension of the reciprocal —, S. Sternberg and M. Terzi . . . 1147

Molten salts. III, Some physico-chemical properties of simple —, I. G. Murgulescu and E. Sălăgeanu . 603

Molten salts systems: LiCl—KCl, $PbCl_2$—KCl, KCl—NaCl, Chlorine adsorbtion on active carbon in the —, S. Sternberg, V. Petrescu and I. Galasiu 1689

Molybdenum (V) complexes with biguanide derivatives, New —, P. Spacu and L. Antonescu. . . 1851

N

Nickel oxide catalysts, Reduction studies on —, T. Chirulescu, C. Ciobanu and Gh. Şerban. 1509

Nickel (II) perchlorate complexes, Spectroscopic observations on —, V. M. Bhatnagar 477

Nitrogen atom reaction with ethylene, On the mechanism of the —, V. N. Kondratiev 167

Nitrogen atom reaction with ethylene, On the mechanism of the —, J. Koryta, M. Březina and N. Kříž 171

O

Okisleniya metana, initsiirovannogo azotnoi kislotoi, O nekotorykh rezultatakh issledovaniya reaktsii —, A. B. Nalbandian 209

Organosilicon compounds. I. Boiling point and density of substituted silanes and siloxanes and the additivity of density, Correlation of the physical properties of —, M. Arshad A. Beg and I. A. Khan 1579

Organosilicon compounds. II. Boiling point, refractivity and density of silanes and siloxanes, M. Arshad A. Beg and I. A. Khan. 1599

Osmium as $[Os(thio)_6][Cr(NH_3)_2(NCS)_4]_3$ The determination of —, D. Negoiu and Z. Toma 1083

Oxavanadium (V) complexes with multidentate Schiff bases. II., A spectroscopic study of —, N. S. Biradar and V. H. Kulkarni. 481

Oxydation du n-dodécane en phase liquide par l'oxygène moléculaire en présence des catalyseurs métalliques pseudo-homogènes. I. L'effet des naphténates des métaux alcalins et alcalino-terreux, I. Drimuş et A. Lupu. 1409

P

Phase equilibria of the $CaO-TiO_2-V_2O_5$ system, Ş. Solacolu and M. Zaharescu 1715
Phasengleichgewichte des Systems $SrO-V_2O_5$, Die thermischen —, S. Solacolu, R. Dinescu und M. Zaharescu 311
Phenomenological thermodynamics. I. Termox-program for processing experimental data from the thermodynamical measurements of oxides, The use of the digital computer in the —, M. Ciopec and D. I. Marchidan 1139
Phenomenological thermodynamics. II., The use of the digital computer in —, M. Ciopec and D. I. Marchidan . 1313
Phenothiazone. XIX. 4-Amino- und 4-Amino-Halogen-Phenothiazone, E. Broser und C. Bodea 1747
Photocopolymerization of acrylonitrile with methacrylic esters in the presence of anthraquinone dyes, V. Nuţă, D. Feldman and Cr. I. Simionescu 1755
Photolysis of $[Mn(C_2O_4)_4(H_2O)_2]K$ in dimethylformamide. I., On the —, I. G. Murgulescu, T. Oncescu and S. G. Ionescu 423
Photosorption on thin zinc oxide films, Memory effects in oxygen and hydrogen —, M. Constantinescu and E. Segal 83
Phototropic glasses on B_2O_3 basis, P. Baltă, L. Dollingher and M. Cîrstea 25
Pigmente-Isatinderivate. I. Einführung in die Synthese und Eigenschaften der Verbindungen, Neue organische —, I. Reichel, B. D. Bader und R. Vîlceanu 1889
Pigmente-Isatinderivate. II. Synthese durch direkte Kondensierung, Neue organische —, B. D. Bader und R. Vîlceanu 1991
Polarographic maxima of the third kind. II. Borneol, A. N. Frumkin, E. V. Stenina, N. V. Nikolaeva-Feodorovici, G. N. Petukhova and V. A. Yusupova 155
Polarographic and oscillopolarographic behaviour of dipicolinic acid, L. Campanella, E. Chiacchierini and M. Palchetti 647
Polarographic reduction of methylsubstituted N-ethyl pyridinium ions. A HMO treatment, P. Nagy, I. Görbe and A. Szurkos 1115
Polarographische Untersuchung des UO_2^{2+}-Oxalsäure-Systems, F. Mánok, Cs. Várhelyi und M. Gălăţeanu-Titieni 675
Poluchenie splavov kremnia posredstvom elektroliza kriolitokremnezemnogo rasplava, K. Griotheim, K. Matiasovski i P. Fellner. . . . 819
Polychlorure de vinyle. Relation viscosité intrinsèque-poids moléculaire, Caractérisation du —, D. Feldman, C. V. Uglea, V. Nuţă et M. Popa 1033
Polychlorure de vinyle. II. Synthèses de polyélectrolytes réticulés avec des groupes sulfoniques à base de polychlorure de vinyle arylé avec des polyalkylbenzènes, Transformations chimiques du—, Ig. Poinescu 727
Polychlorure de vinyle. III. Synthèses de polyélectrolytes réticulés avec groupes sulfoniques sur la base du polychlorure de vinyle arylé avec des hydrocarbures aromatiques polynucléaires, Ig. Poinescu 1125
Polydispersité du polychlorure de vinyle par chromatographie sur gel perméable pendant la destruction mécano-chimique, Étude de la —, A. Crusos, C. V. Uglea et I. Agherghinei 565
Polymères vinyliques, Étude par chromatographie pyrolytique de quelques, — C. N. Caşcaval et I. A. Schneider 835
Polymerisation von Acetylenderivaten. XV. Die übermolekulare Struktur der Polymere, Studium der —, Cr. Simionescu, S. Dumitrescu, M. Leancă, M. Dărîngă und M. Grovu 303
Polymérisation des dérivés acétyléniques. XII. Cinétique de la photopolymérisation du phénylacétylène, Étude sur la —, Cr. Simionescu, S. Dumitrescu et M. Grovu 547
Polymérisation rapide de l'ε-caprolactame en présence de composés organo-métalliques, I. Gavăt, V. Dimonie, D. Donescu, M. Munteanu et I. Isăcescu. 559
Polyurethane elastomers, starting materials and intermediates. XI. Synthesis of nitrodiisocyanates, Synthesis of —, Gh. Mandric and V. Ţăranu 571
Potentiel de protection lors de la corrosion par piqûres, de la corrosion intergranulaire et de la corrosion fissurante sous tension, Signification du —, M. Pourbaix. 239
Potentiels normaux d'électrode dans des solvants non aqueux, E. Constantinescu. 1819

Propriétés liantes, Considérations générales sur l'apparition des —, I. Teoreanu 1211

Purines, Short-lined free radicals in aqueous solutions of —, C. Nicolau 411

Pyrolysis, Notes on —, G. C. Suciu 353

R

Radiation induced grafting of styrene to polyethylene terephthalate fibers, Initial studies on the —, I. Vlagiu and V. Stannett 379

Raman spectroscopy in fused salt studies, Some application of laser —, G. J. Janz and K. Balasubrahmanyam 187

Réduction de l'oxygène sur les électrodes poreuses en argent, L'étude de la —, O. Radovici, M. Mavrodin-Tărăbîc, I. Onaca et I. Solacolu 1153

Reductive cyclization of α-and β-(o-nitrophenyl)-substituted amides, Fl. Cuiban 897

Reinigungsmethoden durch Adsorption. II. Mathematische Modelle, Prinzipielle Betrachtungen über die Wirksamkeit einiger —, A. Wohl 1267

Reorganization energy of TiCl$_4$, The —, B. Hessett and P. G. Perkins. . . 611

Resolution by paper and thin layer chromatography with temperature gradient, Some considerations about the —, S. Gocan and C. Liteanu 661

Rhénium dans les molybdénites. La détermination polarographique du rhénium à côté des traces de molybdène, Méthodes de détermination du — , A. Duca et C. Calu. 125

Roentgenographic studies of [Fe(II) phen$_2$(NCS)$_2$], P. Spacu, D. Ciomârtan and M. Teodorescu . . . 977

S

Salt effect in acid-base titration performed in organic medium. III. A study regarding the analytical behaviour of aromatic acids in methyl alcohol in the presence of Ca(NO$_3$)$_2$, The use of the —, A. Blazsek-Bodó and C. Liteanu 1771

Salzeffektes in nichtwässrigen Lösungen bei acido-basischen Titrationen. II. Studium über das analytische Verhalten einiger Dicarbonsäuren und Hydroxysäuren in methanolischen Lösungen in Gegenwart von Ca(NO$_3$)$_2$, Die Verwendung des —, C. Liteanu und A. Blazsek-Bodó 1465

Semi-empirical LCAOMO theory for infinite systems: tightbinding self-consistent field theory for three-dimensional solids, B. J. McAloon and P. G. Perkins 1813

Solvolysis of Δ^2-cyclobutenyl-ethyl-β-tosylate and Δ^2-cyclobutenylpropyl-γ-tosylate, M. Banciu, P. Buck, E. Ciorănescu and C. D. Nenitzescu 1393

Solvolytic reactions. II. Acetolysis of 5H-dibenzo [a, d] cycloheptene-5-yl-methyl tosylate under thermodynamic control, Kinetics of —, M. Voicu and F. Badea 1551

Solvolytic reactions. III. Intermediates involved in the acetolysis of 5H-dibenzo [a, d] cycloheptene-5-yl-methyl tosylate and 9,10-bis (hydroxymethyl)-9, 10-dihydroanthracene ditosylate, Kinetics of —, M. Voicu, F. Badea and A. Bucur 1563

Spectra-stereochemistry correlations for bicyclic rigid arylidenecyclohexanones, M. Moraru and F. Chiraleu 1235

Spectrophotometric analysis, Determination of the stability constant of compounds used in —, L. M. Băloiu 1065

Spectrophotometric analysis, Determination of the partition constant of compounds used in —, V. Armeanu, S. Oancea, S. Rusenescu and L. M. Băloiu 925

Spectrophotometrical determination of *ortho*-tolidine with sodium hypochlorite, I. Florea 1783

Spektrophotometrische Dosierung des Benzidins mit Natriumhypochlorit und mit Unterchloriger Säure, I. Florea 915

Structures vitrocéramiques du système $Na\ O-MgO-Al_2O_3-SiO_2$ ayant le fluor comme agent de nucléation. Coordination de l'ion Al^{3+} dans les —, Ş. Solacolu et D. Popescu-Haş 319

Styrol-α-Methylstyrol-Divinylbenzol-Copolymeren und Kationenaustauschern durch Thermoanalyse, Untersuchungen von —, I. Nanu und I. Gros 2033

Substitution reactions of complexes. XLV. Solvation of the $[Cr(NCS)_4(m\text{-xylidine})_2]^-$ ion in ethanol-water mixtures, J. Zsakó, V. Voiculescu, I. Gănescu and A. Popescu 1977

Sultams, More proofs for a characteristic band in the infrared spectrum of—, S. H. Doss 1611

Sultams, The proton magnetic resonance spectra of—, S. H. Doss . . 905

Systèmes chimiques binaires, ternaires et quaternaires, Formules de calcul du nombre de sous-systèmes contenus dans les —, R. Dinescu et M. Cerchez 643

T

Temperature gradient chromatography as compared to unidimensional multiple chromatography, S. Gocan, C. Liteanu, T. Hodişan, H. Naşcu and St. Bîndeanu 669

Tétracyanoferrates, Sur la production de —, G. Emschwiller 131

Tetragonal symmetry, Strong field spin-orbit matrices for d^3 configurations in —, K. D. Warren . . 1293

Thermal conductivity by the hot-wire method, Measurement of —, R. Vîlcu and A. Ciochină 1679

Thermal decomposition of diphenyldiazomethane in the absence of solvent. I. Kinetics and mechanisms of the—, T. Oncescu, M. Contineanu and G. Bălăceanu 213

Thermal properties of alumina TA 600. Heat content at high temperature, D. I. Marchidan, L. Pandele and A. Nicolescu 1493

Thermal properties of Alurom aluminium heat content at high temperatures, D. I. Marchidan and L. Pandele 1327

Thermodynamic data for some nonstoichiometric uranium oxides by solid-state EMF technique, D. I. Marchidan and S. Matei 195

Thermodynamic data for some uranium oxides with nonstoichiometric compositions, D. I. Marchidan and S. Matei 1487

Thermodynamic excess functions in liquid-vapour equilibria in the *n*-heptane-toluene system, R. Vîlcu and Z. Cenuşe 367

Thermodynamic properties from electromotive force measurements with formation cells in molten salts. AgBr + CsBr mixture, I. G. Murgulescu and L. Popescu 1287

Thermodynamics, Compilations of data for chemical —, F. D. Rossini 267

Thermogravimetrie bei komplexen Abbauprozessen, Über die dynamische —, I. A. Schneider . . . 291

Thin layer thermochromatography. V. Influence of the temperature gradient on the resolution of some amino-acids in thin layer chromatography, C. Liteanu and T. Hodişan 1985

Transitional metal perchlorates in molten state, The decomposition of some—, R. Vîlcu and N. Georgescu 1791

Transitions de phase, Déduction d'une classification des —, Th. Deleanu, I. V. Ionescu, V. Nahorniak et D. A. Isăcescu 103

s-Triazine field (new series). V. Phenyl substituted 1,3-dimethyl-6-(β-styryl)-formoguanamide (-1H 3H-*s*-triazine-2,4-dione) and the corresponding *p*-dimethylamino-β-styryl hemicyanine : 1,3,5-trimethyl-6-(*p*-dimethylamino-β-styryl)-formoguanamidium iodide, Studies in the —, G. Ostrogovich and M. Safta 2043

U

Überführungszahlen und Temperaturkoeffizienten der Leitfähigkeit einiger Elektrolyte in Gemischen von Dioxan mit Wasser, T. Erdey-Grúz, E. Kugler, I. Nagy-Czakó und K. Balthazár-Vass 137

Ultrasonic velocity and compressibility in reciprocal fused salts systems : Cd, Pb//Cl, Br, V. Prissiajnyi and V. Vasilescu 455

Uranium compounds on heating. Thermal decomposition of ammonium uranates, Behaviour of —, P. Spacu and G. D. Cismaru 947

Uranium, Nouveaux réactifs pour le dosage spectrophotométrique de l' —, M. Mavrodin 1199

Uranium oxides, High temperature enthalpy and related thermodynamic functions of nonstoichiometric —, D. I. Marchidan and M. Ciopec 1657

V

Vapour pressures of molten magnesium, cadmium and zinc chlorides, L. Topor 1503

Verhaltens von Fe^{3+}, Co^{2+} und Ni^{2+} auf dem Kationenaustauscher Vionit CS—3 im Medium von organischem Lösungmittel—HCl—H_2O, N. Pascu, V. Săcelean, L. Crivei, E. Kiss und N. Bojan 505

Vinyl acetate-acrylic acid copolymers, N. Simionescu, E. M. Călugăru and D. Feldman 2013
Vitamine B_1 (chlorhydrate de thiamine ou aneurine). Caractéristiques spectrales en visible et infrarouge du produit obtenu, Gr. Teodorescu 1621
Vitesse de réaction. L'hydrolyse alcaline de l'acétate, du propionate et du butyrate de *n*-butyle dans le solvant mixte eau-acétone, L'influence du solvant sur la —, G. Costeanu et C. Mateescu 95

Z

Zauglerojivaniya nekotorykh katalizatorov deghidrirovaniya alkilaromaticheskikh uglerodov, Issledovanie—, C. Coriciuc, G. Csomontanyi i S. Popa 533
Zeolite in the presence of nitrates of some bivalent cations dissolved in molten sodium nitrate, Study on the behaviour of the NaA type—, A. Bâtcă-Cerbu. 855

Revue Roumaine de Chimie, 17, *12*, 2067–2087 (1972)

CORRIGENDUM

In Rev. Roumaine Chim., **17**, *1*, *2* (1972), on page 19, read lower instead of lover in the caption of fig. 4.

NOTE POUR LES AUTEURS

La *Revue Roumaine de Chimie* publie des articles en anglais, français, russe, allemand ou espagnol. Les auteurs sont priés d'envoyer des articles, notes, communications et comptes rendus inédits.

Les manuscrits seront dactylographiés à deux intervalles. Les tableaux seront dactylographiés sur feuilles séparées, de même que la légende des figures. Les diagrammes seront tracés à l'encre de Chine sur papier calque. Les tableaux et les figures seront numérotés par des chiffres arabes, en nombre strictement nécessaire. Prière de ne pas inscrire les mêmes données dans les tableaux et les figures. Les formules chimiques seront incluses dans le texte; en outre, elles seront transcrites sur des feuilles séparées. Les auteurs sont priés d'indiquer les caractères italiques (en soulignant les lettres au crayon), ainsi que tout autre caractère spécial. L'ordre des références bibliographiques sera celui de leur mention dans le texte; le nom de l'auteur sera précédé de l'initiale du prénom; les publications périodiques seront présentées suivant les prescriptions internationales. Les références seront ajoutées à la fin de l'article; elles paraîtront comme des notes, au bas de la page. Le texte sera précédé d'un résumé comprenant 15 lignes au maximum.

L'entière responsabilité du contenu des articles appartient aux auteurs. On publie des articles dus aux collaborateurs roumains ou étrangers. Les auteurs recevront 50 tirés à part.

PRINTED IN ROMANIA

1973 MAR 14

TRAVAUX PARUS AUX ÉDITIONS DE L'ACADÉMIE DE LA RÉPUBLIQUE SOCIALISTE DE ROUMANIE

P. BALTĂ et E. BALTĂ, **Introducere în chimia fizică a stării vitroase**, (Introduction à la chimie physique de l'état vitreux), 1971, 240 p., 15,50 lei.

LYDIA-MARIA VAICUM, **Biodegrabilitatea detergenților** (La Biodégrabilité des détergents), 1971, 254 p., 16 lei.

TIBERIU NĂSCUȚIU, **Metode radiometrice de analiză** (Méthodes radiométriques d'analyse), 1971, 346 p., 19,50 lei.

I. ZUGRĂVESCU et L. STOICESCU-CRIVETZ, **Polimeri heterociclici** (Polymères hétérocycliques), 1971, 190 p., 9,50 lei.

CRISTOFOR SIMIONESCU, C. V. UGLEA, **Fracționarea compușilor macromoleculari** (Fractionnement des composés macromoléculaires), 1969, 292 p., p. 18,50 lei.

I. MAXIM, **Materiale nucleare** (Matériaux nucléaires), 1969, 444 p., 30 lei.

CRISTOFOR SIMIONESCU et CLEOPATRA VASILIU-OPREA, **Mecanochimia compușilor macromoleculari** (La mécanochimie des composés macromoléculaires), 1967, 344 p., 23,50 lei.

CORNEL BODEA et collab., **Tratat de biochimie vegetală, partea I, Fitochimie** (Traité de biochimie végétale, Ire partie, Phytochimie), Ier vol., 1964, 747 p. + 4 annexes + 2 pl., 41 lei ; IIe vol., 1965, 1262, p., 1 pl., 56 lei ; IIIe vol., 1967, 773 p., 35 lei.

V. GHEȚIE et V. MICUȘAN, **Analiza imunochimică. Teorie și practică** (Analyse immunochimique. Théorie et pratique), 1966, 369 p., 28 lei.

R. PORTOCALĂ et L. POPA, **Acizii ribonucleici celulari și virali** (Les acides ribonucléiques cellulaires et viraux), 1966, 375 p., 8 pl., 26 lei.

I.P.I. – c. 1969

43 426

Lei 25.—